UEMK 2019

4th INTERNATIONAL ENERGY & ENGINEERING CONGRESS

24-25 OCTOBER 2019

MAVERA CONGRESS & ART CENTER
GAZIANTEP UNIVERSITY, TURKEY

http://uemk.gantep.edu.tr

UEMK 2019

PROCEEDINGS BOOK

24-25 October 2019

Mavera Kongre ve Kültür Merkezi

GAZIANTEP UNIVERSITY

DEPARTMENT OF ENERGY SYSTEMS ENGINEERING

TURKEY

UEMK 2019

BİLDİRİLER KİTABI

24-25 Ekim 2019

Mavera Kongre ve Kültür Merkezi

GAZİANTEP ÜNİVERSİTESİ

ENERJİ SİSTEMLERİ MÜHENDİSLİĞİ BÖLÜMÜ

TÜRKİYE

4th INTERNATIONAL ENERGY & ENGINEERING CONGRESS 2019

PROCEEDINGS BOOK

4. ULUSLARARASI ENERJİ & MÜHENDİSLİK KONGRESİ 2019

BİLDİRİLER KİTABI

ISBN

978-975-7375-47-0

Onaylanma Tarihi

28/10/2019

Editör

Doç. Dr. Adem ATMACA

Gaziantep Üniversitesi

Mühendislik Fakültesi

Enerji Sistemleri Mühendisliği Yayınları

Gaziantep/ TÜRKİYE

Tel: +90 342 360 1200-3999

Fax: +90 342 360 1013

e-posta: gaun.uemk@gmail.com

web-site: http://uemk.gantep.edu.tr/

TABLE OF CONTENTS

SPONSORS


GAZİANTEP UNIVERSITY
1973


REPUBLIC OF TURKEY MINISTRY OF ENERGY AND NATURAL RESOURCES


EPDK
ENERJİ PİYASASI
DÜZENLEME KURUMU


BÜYÜKŞEHİR
GAZİANTEP


SANKO ENERJİ


Springer


LİMİTSİZ ENERJİ
"Doğandan Gelen Enerji"


DOW

CHAIRS

HONORORIAL CHAIR of UEMK 2019

Prof. Dr. Ali GÜR

Rector of Gaziantep University

TURKEY

CHAIR of UEMK 2019

Assoc. Prof. Dr. Adem ATMACA

Energy Systems Engineering

Gaziantep University

TURKEY

ORGANIZING COMMITTEE

Assoc. Prof. Dr. Adem Atmaca

Prof. Dr. Bin Chen

Dr. Fatih Balcı

Dr. Martin Brabant

Assoc. Prof. Dr. Nihat Atmaca

Dr. Serap Sur Çelik

Ahmet Kılıç

Ali Erdem Rende

Furkan Kuzudişli

Gökçe Yürekli

Hande Topalbekiroğlu

Hanse Özel

Harun Taştan

Kübra İbolar

Merve Çamcı

Miraç Anıl Tunç

Nihal Turgut

Nisan Şafak Güler

Okan Dengiz

Zehra Kardaş

Rıdvan Candemir

Yusuf Yapıcı

Yunus Emre Kandemir

Ahmed Talha Hız

Suat Köksüz

Ebru Gedik

CONGRESS TOPICS

Energy

Modeling of Energy and Systems

Energy Transport, Power & Fuels

Energy Systems

Energy Supply and Demand

Renewable Energy Resources and Technologies

Energy Audit and Rational Use of Energy

Advanced Energy Technologies

Energy-Saving Technologies

Electrical and Electronics Engineering

Civil Engineering and green buildings

Climate Change and Global Warming

Environmental engineering, Environmental Systems and Telecommunications

Environmental Safety and Health

Water Resources and Future Conflicts

Solid Waste, Waste Treatment and Management

Soil pollution

Air Pollution Control

Noise and Vibration Control

Planning & Sustainable Development Policy

Environmental Policy, Planning and Economy

Energy Policy, Planning and Economics.

Computer engineering

Global Climate Change

International cooperation to reduce carbon emissions

Industrial Engineering, Sustainable Materials

More Sustainable Product Design

Science for Sustainable Development

Social Security, Process Safety and Hazard Management

Waste Assessment and Treatment

Sustainable Urban Development

Mechanical Engineering

Mechanical and Structural Sustainability

Sustainable Chemical ProcessesTools to plan, design and operate integrated green technology

Adsorption and Gas Storage Materials

Sustainable Agriculture and Organic Farming; Green Agriculture Technology

Food engineering, Food Safety and Organic Food

Nanotechnology for Sustainability

Life Cycle Assessment

Computation, Modeling and Simulation, Ecological Sustainability

Management, Green Economy and Sustainable Economic Development

Natural Sciences

PREFACE

ÖNSÖZ

Dünya, ekonomide ve enerji sektöründe dengelerin değiştiği ve son derece dinamik olduğu bir dönemden geçmektedir. Düşük maliyetli ve büyük petrol kaynaklarının bulunduğu Orta Doğu'da yaşanan gelişmeler, küresel enerji güvenliğini uluslararası gündemin üst sırasına taşımaktadır. Diğer yandan enerji talebi ve çevre ilişkisi önemini korumakta, en zengin kaynaklara sahip ülkeler için bile enerji verimliliği ve çevresel etki ana gündemi oluşturmaktadır.

Ülkelerin kalkınma, refah ve gelişmelerini sağlamada birincil derecede önemli olan enerji, uluslararası sistemde en stratejik araçlardan biri haline gelmiştir. Enerji politikaları kısa vadede enerji kaynaklarının uluslararası pazarlara güvenli biçimde ulaşmasını, arz ve fiyatlama gibi konuları ele alırken, uzun vadede ise kalkınma planlamalarını ve politikalarını içermektedir. Enerji kaynaklarına sahip olmak, enerji üretebilmek ve elde edilen enerjiyi pazara ulaştıracak taşıma yollarını kontrol altında tutmak, günümüzde devletlerin dış politika yapımında ağırlık verdikleri konular arasındandır. Enerji güvenliği, ulusal ve küresel boyutta, devletlerin önümüzdeki dönemlerde de dış politikalarına yön veren temel konulardan biri olmayı sürdürecektir.

Küresel mali kriz nedeniyle birçok ülke ekonomisinin daralma gösterdiği bir dönemde Türkiye ekonomisi, 2008 yılındaki yavaşlamanın ve 2009 yılındaki küçülmenin ardından toparlanarak önemli oranda büyüme sağlamıştır. Bu ekonomik büyümenin sağlanmasında enerji sektörü hayati bir rol oynamaktadır. 2003-2016 arasında birincil enerji arzımızın yılda ortalama %4,2 büyümüş olması ekonominin enerji tüketimiyle beraber büyüdüğünü göstermektedir.

Türkiye, gelişmekte olan ülkeler içerisinde geçtiğimiz 15 yıllık dönemde enerji talep artışının en hızlı gerçekleştiği ülkelerden biri olmuştur. Bu durumda Ülkemizin belirlediği enerji stratejisi, çok kritik ve uzun dönemli etkileri olacak bir konudur. Aynı zamanda ekonomik gelişme ile paralel olarak enerji ile birlikte doğal kaynakların yönetimi de stratejik önemini korumaktadır.

2015-2019 Milli Enerji ve Maden Politikası Stratejimiz doğrultusunda başta yerli kömür olmak üzere rüzgâr, güneş, hidrolik, jeotermal gibi yerli ve yenilenebilir enerji

kaynaklarımızın enerji portföyündeki payının artırılmasına yönelik çabalarımız çevreci bir anlayış ve sürdürülebilirlik ilkesi doğrultusunda yoğunlaştırılmıştır.

Bölgelerarası petrol ve doğal gaz ticaretinin rotalarına göre 2030 Yılına kadar petrol ticaretinin iki kat artması beklenirken bölgeler arası gaz ticaretinin üç kat artacağı tahmin edilmektedir.

Türkiye, mevcut uluslararası boru hatları ile hem ihtiyaçlarını karşılayıp gelir sağlıyor hem de enerji kaynaklarının transferine aracılık ederek stratejik önemini artırıyor. Türkiye, hayata geçirilecek uluslararası boru hattı projeleriyle de Orta Asya, Hazar ve Orta Doğu bölgelerindeki zengin doğal gaz ve petrol rezervlerini Avrupa'nın ana tüketim merkezlerine ulaştıran en önemli enerji köprülerinden biri olacak.

Küresel iklim değişiyor ve ekosistem, insan sağlığı ve ekonomiye yönelik giderek artan kritik riskler getiriyor. Bu değişimler, dünya çapındaki insan faaliyetlerinin bir sonucu olarak atmosfere yüksek miktarlarda sera gazı salındığından dolayı gerçekleşiyor. Bu faaliyetler arasında hepsinden önemlisi elektrik üretimi, ısınma ve taşımacılık için fosil yakıtların yakılması var. Fosil yakıtların yanması da çevreye ve insan sağlığına zararlı hava kirleticilerin salınmasına neden oluyor.

Küresel olarak enerji kullanımı, insan faaliyetlerinden açığa çıkan sera gazı emisyonları arasında açık ara en büyük kaynağı temsil ediyor. Küresel sera gazı emisyonlarının neredeyse üçte ikisi, ısınma, elektrik, taşımacılık ve sanayide kullanılacak enerji için fosil yakıtların yanmasıyla ilişkilendiriliyor.

Enerji krizi ve enerji savaşları 20.yy'dan beri üzerine çokça çizilip konuşulan iki kavram. Artan nüfus oranı ve daha konforlu bir yaşam isteği enerji krizlerine yol açarken, enerji savaşları daha siyasi bir konu olarak karşımıza çıkıyor. Sömürgeciliğin doğuşundan bu yana süregelen zamanda, zengin enerji kaynaklarına sahip toprakların paylaşımı konuşunda bir güç savaşı yaşanmıştır.

Süper güç diye tabir edilen devletler ve terör grupları enerji odaklı bir strateji izlemektedir. Bundan dolayı yaşanan uluslararası siyasi krizlerin ve çatışmaların temel sebeplerine baktığımızda enerji faktörünün olduğu görülür. Türkiye'nin artan elektrik ihtiyacının karşılanması amacı doğrultusunda önemli yatırımlar gerçekleştirilirken, ülkenin toplam kurulu gücünde ve dolayısıyla elektrik üretiminde son 30 yılda kayda değer bir artış yaşandı. 1980'li yılların ortasında 10.000 MW'ın altında olan kurulu güç, 2018 sonu itibariyle 88.550 MW seviyesine çıktı.

Önümüzdeki yirmi-otuz yıl için petrol ve doğalgaz arzında rezervler açısından bir sorun olmasa da yeni rezervlerin aranması, üretilmesi, tüketiciye ulaştırılması gibi konular, uluslararası ilişkileri etkileyen temel problem alanları olmaya devam edecek görünmektedir.

Bu sene dördüncüsü düzenlenen konferansımız kamu, özel sektör ve akademik kurumları biraraya getirerek karşılıklı görüş alış verişinde bulunma fırsatı vermiştir. Enerji sektörü ve çevre başta olmak üzere mühendislik teknolojileri konularında yapılan güncel akademik çalışmalar, yaklaşık 50'si yurt dışından olmak üzere 300'e yakın katılımcı tarafından sunulmuştur. Gerçekleştirilen olan oturumlarda, enerji piyasaları, sanayide enerji verimliliği, yenilenebilir enerji teknolojileri ile makine, inşaat, gida ve elektrik elektronik mühendisliklerinin kapsamına giren birçok farklı alanda sorunlar tartışılacak ve akademik çözüm önerileri ortaya konulmuştur. Kongremiz Mavera Kongre ve Sanat Merkezi'nde bulunan 5 farklı salonda, toplam 18 oturumda yapılmış olup, 300'e yakın katılımcı hocamız 167 akademik bildiri sunmuştur.

Organizasyon Komitesi Başkanı

Doç.Dr. Adem ATMACA

Enerji Sistemleri Mühendisliği Bölüm Başkanı

Gaziantep Universitesi

Ekim 2019

FULL PAPERS, ABSTRACTS and POSTERS

EFFECT OF TEMPERATURE ON ANAEROBIC DIGESTION OF SEWAGE SLUDGE

Soukaina Aitlahyane*, Zehor Aityacine
Laboratoire génie de l'Environnement Ressources Faculté des sciences et techniques, Université Sultan Moulay Slimane, Béni Mellal, aitlahyanesoukaina@gmail.com

Hafida Hanine
Laboratoire de biointerface et biofilm Faculté des sciences et techniques, Université Sultan Moulay Slimane, Béni Mellal.

Brahim Lekhlif
Hydrologie traitement et épuration des eaux et changement climatiques Ecole Hassania des ingénieurs.

ABSTRACT: In Morocco, the volumes of wastewater discharged were estimated at 470 Mm^3 per year in 1994 and would reach 900 Mm^3 per year by 2020 (Ministry of Agriculture and Agricultural Development, Morocco 2008). Like developing countries, most wastewater is discharged into the natural environment without treatment. Nevertheless, in recent years, the increase in demand for water for human, industrial and agricultural consumption and the repeated droughts in Morocco have raised awareness among decision-makers to consider wastewater as a significant water resource, hence the need to consider a national wastewater treatment programme. As part of this policy, ONEE has set up several wastewater treatment plants at various sites. Many water treatment plants have been built and the State plans to increase the number of WWTPs nationwide to 280 water treatment plants by 2020. Wastewater treatment generates, on the one hand, clean, sanitized water discharged into the receiving environment or ready for reuse by various processes (bacterial beds, activated sludge, infiltration-percolation), and on the other hand, huge quantities of wastewater sludge that constitute an economic and environmental problem on a national scale. As a result, sludge management systems were sought. Among these sectors, we find anaerobic digestion, which seems an attractive option for the degradation of fermentable waste into useful products such as biogas and high quality compost. In this context, we carried out an experimental study on the anaerobic digestion of fermentable sludge. Two tests were installed, one with heating and the other without heating. The results of the physico-chemical analyses showed that anaerobic digestion with heating gave the best results in terms of:
- Production of biogas.
- A pH value of 7.8 shows that we have a favorable environment for anaerobic digestion and that the methanogen process has been successfully completed.
- A reduction in COD and Organic Matter of 80% and 81% respectively, which clearly shows the reduction in organic load.

Keywords: Wastewater treatment sludge, bio-methanization, physico-chemical characterization, anaerobic digestion.

THE DISINFECTION BY-PRODUCTS (THMS) LEVELS IN DRINKING TAP WATER AT MOSTAGANEM REGION (NORTHERN WEST ALGERIA)-ALGERIA

BENHAMIMED EL-Attafia

Department of Biology, Faculty of Natural and Life Sciences, Abdelhamid Ibn Badis University of Mostaganem, Algeria, elattafia.benhamimed@univ-mosta.dz

ABSTRACT: Chlorine is commonly used for the disinfection of drinking water in Algeria. During chlorination, chlorine reacts with organics matter in water to form the chlorination by-products including trihalomethanes. The high concentration autorised in drinking water is 100µg/l. These are carcinogenic compounds for humans. This problem leads us to undertake a study about hyperchloration and trihalomethanes analysis in drinking water, especially in Mostaganem region. For this, 18 samples of tap water are collected and analyzed using headspace solid-phase microextraction during the year 2017. The results obtained have shown that the maximal concentration is 172.61µg/l was in Achaacha region and 17.54µg/l in Salamandre area. It was concluded that the drinking tap water distributed in Mostaganem region, contains a considerable amount of Trihalomethanes, chlorodibromomethane and bromoform are in majority, this could impact directly on consumer's health during a long period of time.

Key words: Analyse, tap water, Trihalomethanes, Mostaganem.

SYNTHESIS AND CHARACTERIZATION OF ACTIVATED CARBON PRODUCED FROM WASTE HUMAN HAIR MASS USING CHEMICAL ACTIVATION

Meryem Dokumacı
Recep Tayyip Erdogan University
Engineering Faculty
Department of Energy Systems Engineering Rize, Turkey
meryemdokumacii@gmail.com

Safak Cam
Recep Tayyip Erdogan University
Faculty of Arts and Sciences,
Department of Chemistry
Rize, Turkey
safak.cam.36@gmail.com

Vagif Nevruzoğlu
Recep Tayyip Erdogan University
Engineering Faculty
Department of Energy Systems Engineering, Rize, Turkey
vagif.nevruzoglu@erdogan.edu.tr

Derya Bal Altuntaş
Recep Tayyip Erdogan University
Engineering Faculty
Department of Bioengineering, Rize, Turkey
derya.balaltuntas@erdogan.edu.tr

ABSTRACT: In this study, hair waste was converted into active carbon for the first time and its characteristics were analyzed. As chemical activation tool, zinc chloride ($ZnCl_2$) was impregnated and then carbonized under different temperatures (250-300°C). Scanning Electron Microscope (SEM) images showed increase in the pores density, radius and volume of pores. X-ray diffraction analysis (XRD) showed that the samples had an amorphous structure. In Fourier transform infrared (FT-IR) spectroscope analysis, C=C and N-H vibrations observed in 1515-1520 cm^{-1} wave number of protein molecules were found to disappear with the increase in temperature. With Raman spectroscopy, the behaviours of D peak at 1344 cm^{-1} wave number and G peak at 1566 cm^{-1} wave number expressing structure layout in carbonized structures were analyzed depending on the temperatures. Between these intensities, (ID/IG) rate was found to differ in direct proportion to temperature. XRD spectrums showed that the samples are converted into a more irregular crystal structure. All these results implied that the waste hair mass could be used as an adsorbant material.

Key words: Human hair, chemical activation, carbonization, active carbon.

***Corresponding author:** derya.balaltuntas@erdogan.edu.tr

REFERENCES

Berndt, T. J. (2002). Friendship quality and social development. Current Directions in Psychological Science, 11, 7-10.

Banat FA. Al-Asheh S. (2001). The use of human hair waste as a phenol biosorbent. Adsorpt. Sci. Technol, 19, 599–608

Gupta A. (2014). Human Hair "Waste" and Its Utilization: Gaps and Possibilities. J. Waste Manag., 1–17

THE EFFECTS OF ALCOHOL ADDITION TO FUEL ON PISTON WEAR IN A TWO-STROKE ENGINE

Salih özer
Muş Alparslan University, Faculty of Engineering and Architecture, Mechanical Engineering s.ozer@alparslan.edu.tr

ABSTRACT: In this study, the effects of adding 20% by volume of methanol and ethanol into the fuel of a motorized scythe with a two-stroke gasoline engine, which is also used as a hand tool, were investigated. The effects of the added fuels obtained on this purpose on the fuel consumption value on the engine, the amount of drowsiness, piston and piston wear are investigated. For this reason, the effects of the motor scythe have been investigated for 50 hours and 100 hours. With the addition of methanol and ethanol, it was determined that the fuel consumption value compared to gasoline and the amount of wear increased when the wear increased.

Key words: Two-stroke engine, Alcohol, Abrasion.

İKİ ZAMANLI BİR MOTORDA YAKITINA ALKOL İLAVESİNİN PİSTON AŞINMASINA ETKİLERİ

ÖZET: Bu çalışmada el aleti olarak da geçen iki zamanlı benzinli bir motora sahip motorlu tırpananın yakıtının içerisine hacimce %20 oranında metanol ve etanol ilavesinin etkileri incelenmiştir. Bu amaçla elde edilen ilave edilen yakıtların motor üzerindeki yakıt tüketim değerine, kuruntu bırakma miktarına, piston ve segman aşıntılarına etkileri incelenmiştir. Bu nedenle motorlu tırpan normal çalışma sürelerinde 50 saat ve 100 saatlik sürelerde çalıştırılarak etkileri incelenmiştir. Metanol ve etanol ilavesi ile benzine göre yakıt tüketim değerinin ve aşınmanın arttığı kuruntu miktarının ise azaldığı tespit edilmiştir.

Anahtar sözcükler: İki zamanlı motor, Alkol, Aşınma

GİRİŞ

Enerji makinelerin iş yapabilme kabiliyeti olarak tanımlanmaktadır. Makineler iş yaparken enerji kaynağı olarak katı, sıvı ve gaz yakıtlarını kullanmaktadır. Dünyada bu tür yakıtlar petrol kökenlidir. Bu nedenle petrole alternatif olabilecek yakıtlar üzerinde arayışlar artmaktadır. Bu alanın başında da içten yanmalı motorlarda kullanılan yâda kullanılabilecek potansiyele sahip çok çeşitli biyolojik kökenli yakıtlarla ilgili yayınlar

artmaktadır. Bunun yanında kendisi petrol üretemeyip dışarıdan petrol alan ülkelerde de kendi kaynakları ile üretilebilecek yakıt arayışları devam etmektedir. Bu aşamada çalışmalar hem yerli kaynaklarla üretilebilen hem de çevreci yakıtlar üzerinde durmaktadır (Bayraç ve ark. 20018).

Fakat yapılan çalışmalar kullanım alanlarının büyüklüğü göz önünde bulundurularak genelde büyük silindir hacmine sahip dört zamanlı motorlarda denenmektedir. Fakat günlük hayatta kullandığımız birçok el aletinde (jeneratör, çapalama makinesi, sulama makinesi, çim makinesi, ilaçlama makinesi vb.) de içten yanmalı motorlar kullanılmaktadır (MAPAS 2019). Bu tür el aletleri birçok iş yeri ve fabrikada sıklıkla kullanılmaktadır. Bu tip el aletleri sürekli taşınması gerektiği için küçük motor hacimlerine sahip motorlar kullanılmaktadır. Benzinli yâda dizel seçenekleri ile satışa sunulan bu ev tipi araçlarda taşıtlarda kullanılan yakıtlar kullanılmaktadır. Bir içten yanmalı motor yakıtın yakıldığı alan altındaki pistonu ile itme gücü sağlanarak çalışmaktadır. Silindir içerisinde yakılan yakıtın yanma sonrası oluşturduğu itme gücü ile el aletine hareket enerji aktarılmaktadır. İçten yanmalı motorlar çalışma koşullarına göre iki yada dört zamanlı olarak adlandırılmaktadır. El tipi aletler sürekli taşınması gerektiği için genellikle kompakt ve hafif motorlar olan iki zamanlı motorlar tercih edilmektedir. El tipi aletlerde kullanılan iki zamanlı motorlarda ekstra bir yağlama sistemi olmayıp yakıt içerisine katılan yağlama yağı ile segmanların yağlama işlemi gerçekleştirilmektedir (Mengi 2004). Yağlama işleminde de genel olarak yakıt içerisine 1:50 oranında katılan 2T diye tabir edilen yağlar karıştırılmaktadır. Bu yağlar motorun uzun süren çalışması esnasında bazen görevini yerine getiremeyip adhezyon oluşmasına neden olabilmektedir. Aşınma tipinin en basiti olan adhezyon demirin demir ile sürtünmesi ile oluşup sürtündüğü parçalara zarar vermektedir. İçten yanmalı motorlarda segmanın gömlek ile sürtünmesi yada pistonun silindir gömleği ile sürtünmesi piston ve segmanlara zarar verebilmektedir. Bu durumda çalışan motorlar zamanla güçten düşerek çalışamaz duruma gelebilmektedir (Kaleli 2019). Alkoller bitkisel kaynaklardan üretilebilmektedir. Genel olarak taşıtlarda en çok kullanılan alternatif yakıt olarak ön plana çıkmaktadırlar. Günümüzde birçok ülkede %15'lere kadar benzin içerisine katılarak kullanılan örnekleri mevcuttur (Onurbaşavcıoğlu 2013).

Daha önce yapılan çalışmalar incelendiğinde alkollerin yüksek oktan sayısının motorun çalışmasında iyileşmelere neden olduğu, hatta sıkıştırma oranının artırılması ile motor gücünde artışların görülebileceği bildirilmiştir (Balki ve ark.2012; Thahur et al. 2017). Benzin içerisine alkol ilavesi ile yapılan birçok çalışma ise belirli bir oranda kullanıma kadar motor performansı açısından olumsuzlukların oluşmadığını belirtmektedir (Wua et al., 2011). Yapılan çalışmalar emisyonlar açısından benzine alkol ilavesinde bazı iyileştirmelerin oluştuğunu da göstermektedir (Yüksek ve ark. 2019).

Zulfattah et al. (2019), iki zamanlı tek silindirli bir motorda buji tırnak sayısının ve yakıt içerisine kattıkları ilave biyolojik yağların emisyonlara etkilerini incelemişlerdir.

Etkilerini görebilmek için deney motorunu rölanti, orta gaz kolu konumu ve tam gaz kolu konumunda çalıştırarak emisyon parametrelerini incelemişlerdir. Tırnak sayısının artması ile emisyonların değiştiğini bildirmişlerdir.

Raviteja, et al. (2019), iki zamanlı motora sahip insansız hava aracında yakıt katkısı olarak alkol türü olan nitrometanın itme, devir, tork, güç, frene özgü yakıt tüketimi ve fren ısıl verimi gibi motor etkilerini incelemişler ve metanol ilavesinin sonuçları ile kıyaslamışlardır. Elde ettikleri veriler göstermiştir ki kütlece %40 karışım oranlarında metanol yakıtana göre nitrometan ilavesiyle motor itişinde yaklaşık% 24 artış görülmüştür.

Bu çalışmada iki zamanlı tek silindirli 3 hp'lik benzinli bir motora sahip çim biçme makinesinde gerçekleştirilmiştir. Bu motorların bir yağlama sistemi olmayıp yağ benzin yada dizel yakıtının içerisine doğrudan karıştırılarak segmanların yağlama işlemi gerçekleştirilmektedir. Bu çalışmada da benzin içerisine hacimsel olarak %20 oranında etanol ve metanol ilave edilmesinin piston ve segman aşıntısına ile yakıt tüketim değerine etkisi incelenmiştir. Her bir yakıt karışımı ile motorun 50 ve 100 saat doğal çalıştırılma koşullarında çalışması sağlanmıştır.

YÖNTEM

Bu çalışmada tek silindirli, iki zamanlı benzinli bir motorlu çim tırpanı kullanılmıştır. Makinenin bazı teknik özellikleri Tablo 1'de verilmektedir. Kullanılan motorlu tırpan makinesi şekil 1'de gösterilmektedir. Deneylerde kullanılan metanol ve etanol %99,6 saflık oranındadır. Deney yakıtlarının özellikleri Tablo 2 ve 3'de verilmektedir.

Tablo 1. Motorlu Tırpanın Teknik Özellikleri (STHİL 2019).

STHIL FS460	
Silindir Hacmi	45,60 cm^3
Motor Gücü	3 HP
Toplam Ağırlık	8,5 kg
Benzin Deposu	0,75 lt

Tablo 2. Motor yağının özellikleri (OPET 2019a).

FULLTRAC 2T	
Viskozite (mm^2/s)	42,3
Yoğunluk (g/m3)	0,873
Parlama noktası (^oC)	180
Akma Noktası (^oC)	-12

Tablo 3. Kullanılan yakıtların özellikleri (Özer, 2014; OPET2019b; Onurbaşavcıoğlu ve ark.2013) .

	Benzin	Metanol	Etanol
Kimyasal Formülü	C_5H_{10}-$C_{12}H_{26}$	CH_3OH	C_2H_5OH
Yoğunluk (g/m^3)	0,732-0,755	0,796	0,788
Parlama Noktası (^{o}C)	-45 - -13	-40 - -21	12 - 20
Isıl Değer (Mj/kg)	44,3	20,11	26,9
Oktan Sayısı	95	108,7	108,6
Viskozite (mm2/s)	0,37-0,44	0,59	1,19

Üretici firma bu ürünü için benzin içerisine 1:50 oranında yağlama yağı ilave edilmesini önermektedir (STHİL 2019b). Yakıt karışımları için öncelikle benzin ve alkol karışımları oluşturulmuştur. Benzin içerisine hacimce %20 oranında etanol ve metanol ilave edilmiştir. Hazırlanan bu karışıma 1:50 oranında yağ ilave ederek deneylerde kullanılacak yakıtlar hazırlanmıştır. Yakıtlar günlük olarak hazırlanmış ve çalışma boyunca süreler bir kronometre ile kayıt altına alınarak toplam çalışma süresi tespit edilmiştir. Yakıt tüketim değerinin ölçülmesi için bir depo yakıtın tükenme süresi kronometre yardımı ile ölçülmüştür.

Şekil 1. Motorlu tırpanın görünüşü.

Her bir yakıt karışımının kullanımından önce motorun piston ve segman seti yenilenmiştir. Tüm pistonlar ve segman setlerinde yerli üretim olan Episan markalı ürünler kullanılmıştır. Takılan ve sökülen motor piston ve segman setleri şekil 2'de gösterilmektedir. Belirlenen kullanım sürelerinden sonra motor piston ve segman seti sökülerek tortulu ve tortulardan temizlenmiş şekilde 0,0000 hassasiyetindeki bir terazide tartılmıştır. Deneyler tüm yakıt karışımları için tekrarlanmıştır. Oluşturulan karışımlar grafiklerde B100 (%100 benzin) BE20 (%80 benzin+%20 Etanol) ve BM20 (%80 benzin+%20 Metanol) olarak ifade edilmektedir.

(a) (b)

Şekil 2. Sökülen (a) ve Takılan (b) piston ve segmanlar.

Şekil 3. Adhezyona maruz kalmış piston.

BULGULAR

Şekil 4'de alkol ilavesinin yakıt tüketimine etkisi verilmektedir. Yakıt tüketim değeri motorun rölanti durumu yada tam gaz durumuna göre değişiklik gösterebilmektedir. Bu nedenle yakıt tüketim değeri motorun tam gaz kolu konumunda çalıştırılması ile ölçülmüştür. Gaz kolu düğmesi tam gaza getirilerek 0,75 litrelik deponun bitmesi sağlanmış ve bu sürede kronometre ile ölçüm yapılmıştır. Yakıt tüketim değeri yakıtların ısıl değeri ile doğru orantılıdır. Yapılan çalışmalar ısıl değeri düşük yakıtlardan daha fazla tüketilmesi gerektiğini bildirmektedir. Deney sonuçları literatürde daha önce yapılmış birçok çalışma ile benzerlik göstermiştir.

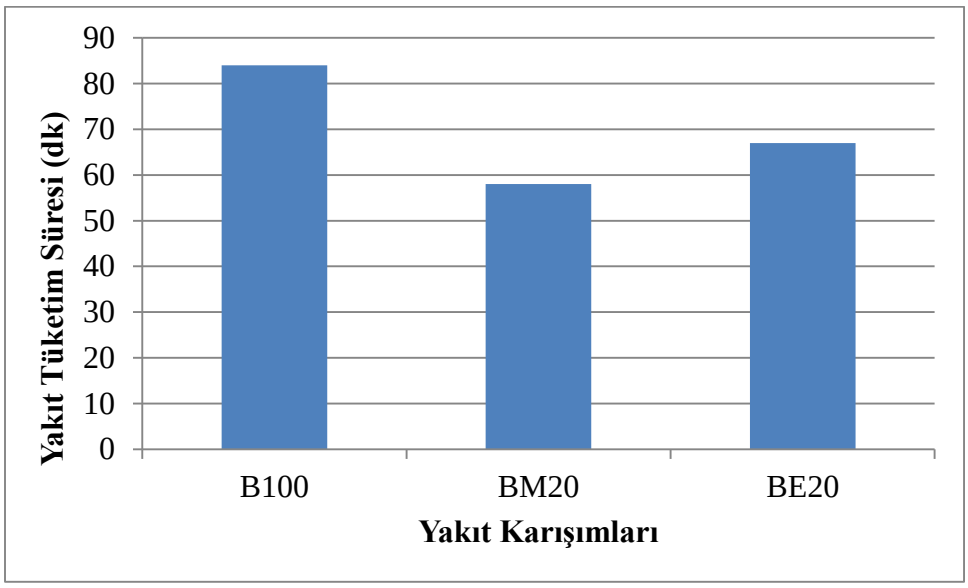

Şekil 4. Bir depo (0,75 lt) yakıt karışımının tüketim süresi.

Şekil 5'de 50 ve 100 saatlik kullanım sonrasında piston ve segmanlardaki toplam kuruntu miktarı gösterilmektedir. Motorun çalışma süresi uzadıkça piston ve segmanlardaki kuruntu miktarında artış görülmüştür. Benzin içerisine alkol ilavesi ile birlikte kuruntu miktarında azalma görülmüştür. Bu durumu benzin içerisine ilave edilen alkoller ile yakıt karışımındaki toplam karbon (C) miktarındaki azalmanın neden olduğu düşünülmektedir. Ayrıca alkoller yakıtların viskozitesini düşürmekte ve benzin içerisindeki yağın çözülmesine de neden olmaktadır. Bu durumda kuruntu miktarını azaltmış olabilir.

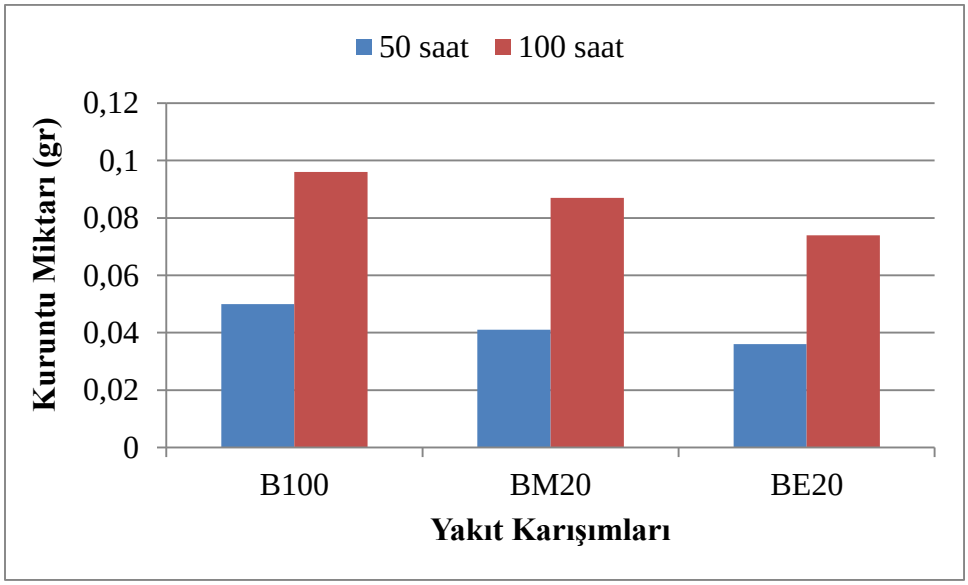

Şekil 5. Toplam kurunu miktarı değişimi.

Motorun 50 saatlik ve 100 saatlik kullanımı sonrasında kuruntulardan temizlenerek tartılan piston ve segmanlardaki ilk duruma göre değişimi Şekil 6'da verilmiştir. Kullanım süresinin artması ile aşıntı miktarının arttığı görülmektedir. Bilindiği gibi pistonlar çalışma esnasında silindir gömleğine dayanarak çalışmaktadır. Bu nedenle yağlamanın zayıfladığı noktalarda aşınmanın olması beklenilen bir durumdur. Alkol ilavesi ile birlikte aşıntı miktarında artış olmuştur. Bu durum yakıtların viskozitesindeki azalma ile açıklamak mümkündür. Azalan viskozite değeri yağlamanın tam manasıyla gerçekleşmesine engel olmaktadır. Bu nedenle alkol kullanımı benzine göre sürtünmeyi arttırmaktadır.

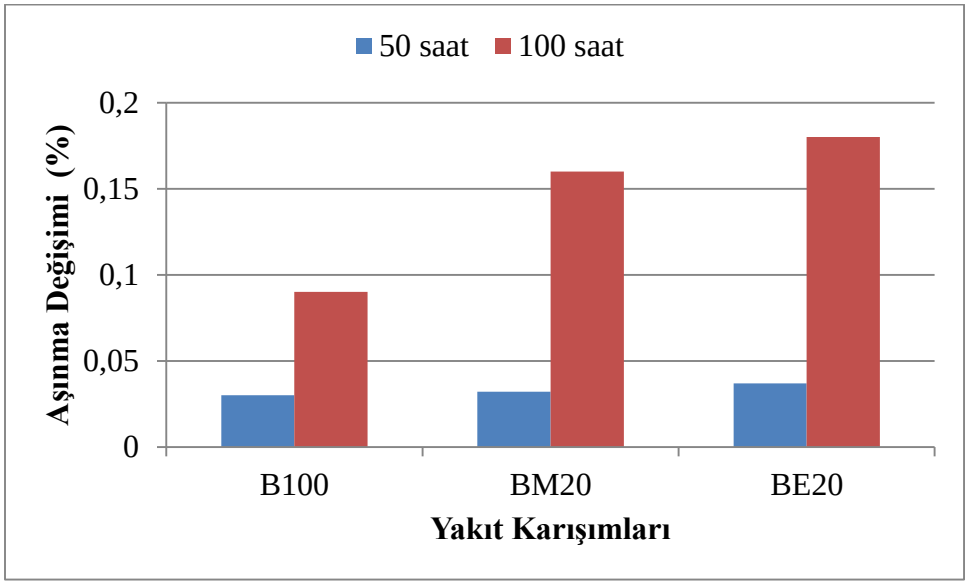

Şekil 6. Toplam aşıntı miktarı değişimi.

Yapılan çalışmada ayrıca ilk çalıştırma durumunda benzine göre daha iyi bir performans elde edildiği görülmektedir. Bu durum alkollerin buharlaşma sıcaklıklarının benzine göre daha düşük olmasından kaynaklanmaktadır. Elle çekilerek ilk ateşlemenin sağlandığı bu araçlarda yakıtların bu özelliği önemli bir avantaj getirmektedir.

SONUÇLAR VE ÖNERİLER

Bu çalışmada el aletlerinde kullanılan iki zamanlı bir motorda alkol ilave edilmesinin etkileri incelenmiştir. Elde edilen sonuçlar göstermektedir ki;

- İki zamanlı motora sahip bir el aletinde hacimce %20 oranında alkol ilave edilerek çalıştırılabilir.
- Alkol ilavesi ile birlikte yağlamada aksilikler olmakta ve aşınma miktarı artmaktadır.
- Motorun ürettiği kuruntu miktarında azalma görülmektedir.

Bu çalışmanın devamı niteliğinde emisyonlar ile ilgili çalışmalar da yapılmalıdır. Bu nedenle emisyonlar açısından da incelenerek deneyler tekrarlanmalıdır.

KAYNAKLAR

Kaynaklar

Balki, M. K., Sayın, C., Çanakcı, M., (2012). Farklı Alkol Yakıtların Buji Ateşlemeli Bir Motorun Performans, Emisyon ve Yanma Karakteristiklerine Etkisinin Deneysel İncelenmesi, 12. Uluslararası Yanma Sempozyumu, (ICS 2012), Mayıs 228-234.

Bayraç, N.H., Çelikay, F., Çildir, M. (2018). Küreselleşme Sürecinde Sürdürülebilir Enerji Politikaları. Ekin Basım Yayın Dağıtım, Bursa.

Kaleli, H. (2019). İçten yanmalı motorlarda aşınma, yağlama ve soğutma. https://www.yeniatmaca.com/blogs/icten-yanmali-motorlarda-asinma-yaglama-ve-sogutma.pdf, (Erişim: 26.06. 2019).

MAPAS (2019), İki zamanlı motorların çalışması ve bakım koşulları, http://mapas.com.tr/blog/2-zamanli-benzinli-motor-calistirma-ve-bakimi/304, (Erişim: 26.06. 2019).

Mengi, M., (2004). Modern İki zamanlı motorlarda verimi artırma yöntemlerinin incelenmesi, Yüksek Lisans Tezi, İstanbul Teknik Üniversitesi.

Onurbaşavcıoğlu, A., Atasoy, Z. D., Türker, U., Koçtürk, D., (2013). Tarımsal Kökenli Yenilebilir Enerjiler: Biyoyakıtlar, Nobel Yayınevi, Ankara.

OPET (2019a). Yağlama Yağının Teknik Özellikleri, http://www.opetfuchs.com.tr/urun/fulltrac-2t, (Erişim Tarihi: 26.06.2019).

OPET (2019b). https://www.opet.com.tr/files/PDF/Urun/Ultra-Force-95-Oktan-urun-teknik-ozellikleri.pdf, (Erişim Tarihi: 26.06.2019).

Özer, S., (2014). Alkollerin içten yanmalı motorlarda alternatif yakıt olarak kullanılması. Uludağ Üniversitesi Mühendislik-Mimarlık Fakültesi Dergisi, 19 (1): 97-114.

Raviteja, S., Ramakrishna, P.A., Ramesh, A., (2019). Performance Enhancement of a Small Two-Stroke Engine Using Nitromethane Blends", Journal of Propulsion and Power 35(3):1-10.

STHİL (2019a). Motorlu Tırpanın Özellikleri. https://www.sadal.com.tr/Product?productId=211, (Erişim Tarihi: 26.06.2019).

STHİL (2019b). Motorlu tırpan kullanım kılavuzu. http://admin2.sadal.com.tr/Upload/Image/STIHL%20FS%20%20460%20C-M-49f19e52492a4d7d890d56e7fd02b04e.pdf, (Erişim Tarihi: 26.06.2019).

Thakur, A. K., Kaviti, A. K., Mehra, R., Mer, K.K.S. (2017). Progress in performance analysis of ethanol-gasoline blend on SI engine, Renewable and Sustainable Energy Reviews, 69, 324-340.

Yüksel, T., Temizer, İ., Can, İ., Koca, F., (2019). Benzinli bir motorda ısıtılmış biyoetanolün ikincil yakıt olarak kullanılmasının etkileri", Fırat Üniversitesi Mühendislik Bilimleri Dergisi, 31 (1): 67-77,

Zulfattah Z.M., Zulkifli, N.W.M., Masjuki, H.H., Harith, M.H. Syahir, A.Z. Norain, I., Jumaidin, R., Yusoff M.N.A.M, Azham A., Jamshaid, M., Arslan, A. (2019). Effect of bio-

based lubricant towards emissions and engine breakdown due to spark plug fouling in a two-stroke engine, Journal Of Cleaner Production, 221 (1): 215-223.
Wua, X., Daniel, R., Tianb, G., Xub, H., Huanga, Z., Richardson, D., (2011). Dual-injection: The Flexible, Bi-Fuel Concept for Spark-Ignition Engines Fuelled with Various Gasoline and Biofuel Blends, Applied Energy, 88, 2305-2314.

NUMERICAL STUDY OF EFFECT OF SERPENTINE FLOW FIELD ON PEM FUEL CELL STACK

Elif EKER KAHVECİ
Engineering Faculty, Mechanical Engineering Department
Sakarya University
Sakarya, TURKEY
eeker@sakarya.edu.tr

Imdat TAYMAZ
Engineering Faculty, Mechanical Engineering Department
Sakarya University
Sakarya, TURKEY
taymaz@sakarya.edu.tr

ABSTRACT: In this study, a 3-cell PEM fuel cell stack model that has serpentine flow channels with 150 cm^2 active layer has been developed to show contour plots of molar concentrations of reactant gases, temperature and protonic potential. The model equations were solved using the commercial CFD software ANSYS Fluent® 16.2 and Gambit® 2.4.6 as a pre-processor. It was found from simulations that H_2 concentration on the anode side in did not cause a visible decrease from the inlet to the outlet because of excessive flow rate required for chemical reactions. Also as shown in the figures clearly, the oxygen decreased and water concentration increased from the inlet of the channels to the outlet of the channels due to the reactions on the cathode side.

Key words: CFD, PEM fuel cell stack, Molar concentration distribution

INTRODUCTION

Fuel cell that is expected to provide clean and efficient form of power generation by definition is an electrochemical device which changes chemical energy into electrical energy. Additionally PEM fuel cell are the most promising clean energy technologies in many applications like portable, automotive and stationary due to their high power density at low operating temperatures among the fuel cells.

Modelling plays a very significant role in determining the best configuration for the reactant transport and the optimum operating conditions of PEM fuel cell in order to improve the performance. In literature, several modelling work has been investigated in order to understand the effect of operating and design parameters to the PEM fuel cell performance.

Kahveci and Taymaz (2018) established a 3-D single PEM fuel cell model that was operated in 333–353K, the pressure range of 1–3atm, gas diffusion layer (GDL) porosity range of 0.3–0.6, both anode and cathode relative humidity range (RH) of 10–100% to investigate the performance. The current density and power density was measured according to these varying operation parameters. Also they compared simulation results with the experimental data reported in literature. It showed good agreement between the model and experimental results.

Sezgin et al. (2016) observed a 3-D model of High Temperature PEM fuel cell by using COMSOL Multiphysics. Also they compared their results with experimental results 0.133 m/s H_2 velocity, 1.3 m/s air velocity for 10 S/m proton conductivity at 160°C cell temperature.

Shao et al. (2019) built a 2-D PEMFC model described by the Butler-Volmer equation, Darcy's law and Maxwell-Stefan equations, to simulate the current density distribution and liquid water distribution in cathode by using COMSOL Multiphysics. Their results are that to achieve a more efficient water management to pretend the flooding in the cathode in the PEMFC, the material with appropriate smaller porosity should be used or a higher air mass flow rate should be applied in cathode to remove the produced liquid water in time.

Carcadea et al. (2019) investigated numerically the effect of the catalyst microstructure on a 5 cm^2 PEM fuel cell performance. They found that a higher platinum loading and a lower particle radius were recommended to achieve better performance.

Wilberforce et al. (2019) studied a 3-D single serpentine model of PEM fuel cell in order to obtain the effect of humidification of reactive gases comparing with experimental results. They found that simulation with 100% relative humidity of oxygen and air showed a better results than the use of pure oxygen. Also flow rate of gases and their flow patterns played an important role in the improvement of water management and fuel cell performance.

Park and Li (2007) performed a 3-D numerical simulation covering the entire flow channel and GDL in a serpentine PEM fuel cell to understand the effect of cross leakage flow on pressure distribution. The simulation indicated that permeability and thickness of GDL were the two most important parameters influencing the cross flow and the resultant pressure drops.

Solati et al. (2019) investigated the influence of different configurations of catalyst, gas diffusion and membrane on the performance of the radial fuel cell. The maximum net power of the cell at the voltage of 0.5 V was found to be 1.594 W and 1.037 W for the R4C

and R2CV models, respectively, and showed that it is possible to increase the cell power through modifying the configuration of the layers without any additional cost.

Wei et al. (2019) developed a 3-D PEMFC having 25 cm^2 active layer to investigate the effects of flow mode and relative humidity on cell performance. They found that membrane conductivity was improved from 10.35 to 11.11 S/m by using counter flow mode instead of co-flow mode. Also with high RH (%100) the membrane would contain more water and have a high conductivity.

Dawes et al. (2009) developed a 3-D PEM fuel cell model to investigate the effects of water flooding on cell performance parameters. It was determined that the GDL permeability had little or no effect on the current densities due to the diffusion dominated nature of the gas flow. Although the diffusivity model improved the power of model, a multiphase model would represent a significant improvement.

Qin et al. (2018) established a fuel cell stack model based on the flow network method to determine the pressure and mass distributions of the reactant gas and coolant streams by the flow network method incorporating the cross flow effect. The optimal designs for the fuel cell stack obtained as the cathode flow channel with a cross section of 0.25×0.25mm2 ,the cooling channel with a width of 2.16 mm, a depth of 0.6 mm ,a the mass flow rate of 1.992x10-2 kg/s.

In this study a structured grid scheme was employed which was built with a pre-processing software, GAMBIT 2.4.6. Then, the grid was imported into finite volume based commercial software, ANSYS-FLUENT 16.2. The PEMFC Module is an add-on module based on FLUENT CFD package for computations. This 3-D PEM fuel cell stack model with 3x70x70 mm^2 active layer has been investigated by determining the current density, oxygen ,hydrogen and water molar concentration distributions took into account the mass, momentum, energy, species, charge conservation equation as well as combines electrochemistry reaction inside the fuel cell.

METHODS

In paper, the model presented is a 3-D, isothermal, single-phase, steady-state model that resolves coupled transport processes in membrane, catalyst layers, gas diffusion layers and reactant flow channels of a PEM fuel cell (Fig.1). Dimensions of PEM fuel cell model components are given at Table 1.

Table 1 Dimensions of PEM Fuel Cell Model

Parameter	Value (mm)
Gas channel depth	1

Gas channel width	1
Rib width	1
GDL thickness	0.2232
Catalyst layer thickness	0.0287
Membrane thickness	0.23

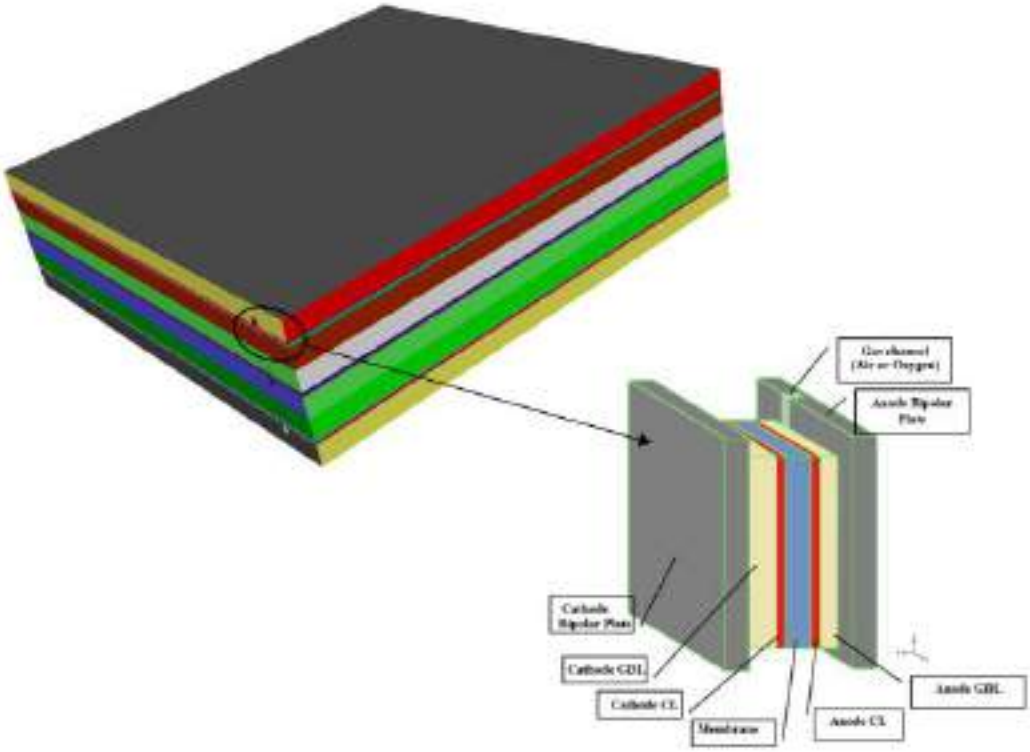

Figure 1. PEM Fuel Cell Stack and Its Components

Modeling Approach

Basic equations used during fuel cell operation are as follows:

Conservation of mass equation:

$$\nabla.(\rho\vec{u}) = S_m \quad (1)$$

The source terms are;

$$S_m = S_{H_2} + S_{wv_p} + S_{wl_p} + S_{awv_e} \quad (2)$$

$$S_m = S_{O_2} + S_{wv_p} + S_{wl_p} + S_{cwv_e} \quad (3)$$

$$S_{H_2} = -\frac{M_{H_2} A_{cv} I}{2F} \quad (4)$$

$$S_{O_2} = -\frac{M_{O_2} A_{cv} I}{4F} \quad (5)$$

Momentum transport equation:

$$\nabla.(\rho\vec{u}\vec{u}) = -\nabla P + \nabla.(\mu\nabla\vec{u}) + S_{p,i} \quad (6)$$

Here β is the permeability. $S_{p,i}$ is the sink source term for porous media in x, y and z-directions;

$$S_{p,i} = -\left(\sum_{j=1}^{3} \frac{1}{\beta_j}\mu u_j\right) \quad (7)$$

Species transport equation:

$$\nabla.(\rho m_n\vec{u}) = \nabla.(J_n) + S_s \quad (8)$$

Here n denotes for H_2, O_2 water vapor and liquid water. The source terms are the same as those of the conservation of mass equation. The diffusion mass flux (J) of species n in n-direction is:

$$J_{\xi,n} = -\rho D_{\varepsilon,n}\frac{\partial m_{K,n}}{\partial \xi} \quad (9)$$

Energy equation:

$$\nabla.(\rho\vec{u}h) = \nabla.(k\nabla T) + S_h \quad (10)$$

The source term S_h can be obtained by energy losses and heat source by phase change. The heat source from the electrochemical reaction:

$$S_{he} = h_{rxn}\left[\frac{IA_{cv}}{2F}\right] - IV_{cell}A_{cv} \quad (11)$$

The local current density of the cell is calculated from the open circuit voltage (V_{oc}) and the losses;

$$I = \frac{\sigma_m}{t}\{V_{oc} - V_{cell} - \eta\} \quad (12)$$

Where t is the membrane thickness and σ_m is the membrane conductivity and defined as;

$$\sigma_m = \left(0.514\frac{M_{m,dry}}{\rho_{m,dry}}C_{wa} - 0.326\right).exp\left(1268\left(\frac{1}{T_0} - \frac{1}{T}\right)\right) \quad (13)$$

The procedure to model PEM fuel cell is (Fig.2);

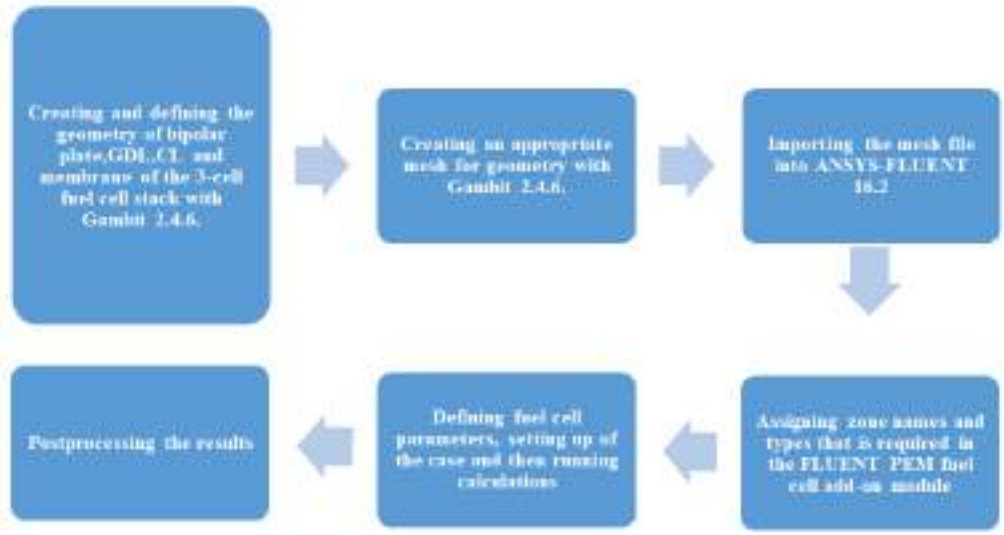

Figure 2. Modeling Procedure of PEM Fuel Cell

Solution Algorithm

The solution strategy was based on the SIMPLE algorithm. Momentum equations were solved for the velocity followed by solving the equation of continuity, which updates the pressure and the flow rate. A HP-PC-Intel®Xeon® CPU E5-2650v2@2.6 GHz, 2.6 GHz, 64 GB was used to solve the set of equations. The computational time for solving the set of equations was about 476 min. Physical and electrochemical parameters are shown in Table 2, operating and boundary conditions of PEMFC model are given in Table 3.

Table 2 Physical and Electrochemical Parameters of PEM Fuel Cell Model

Anode			**Cathode**		
Parameter	**Value**	**Unit**	**Parameter**	**Value**	**Unit**
Reference current density	10000	A/ m^2	Reference current density	20	A/ m^2
Reference concentration	1	$kmol/m^3$	Reference concentration	1	$kmol/m^3$
Reference diffusivity	3e-05	m^2/s	Reference diffusivity	3e-05	m^2/s
GDL viscose resistance	1e+12	1/ m^2	GDL viscose resistance	1e+12	1/ m^2
GDL porosity	0.5	-	GDL porosity	0.5	-
Catalyst porosity	0.5	-	Catalyst porosity	0.5	-
Catalyst surface/volume	200000	1/m	Catalyst surface/volume	200000	1/m
Concentration exponent	0.5	-	Concentration exponent	1	-

Exchange coefficient	2		Exchange coefficient	2	-
Open circuit voltage	2.85	V			
Active layer	0.015	m^2			
Membrane equivalent weight	1100	kg/kmol			

Boundary Conditions

Boundary conditions are set as follows: constant mass flow rate at the channel inlet (mass flow inlet type) and constant pressure condition at the channel outlet (pressure outlet type). The membrane-GDL interface was defined as a wall. The anode voltage was grounded (V = 0) and the cathode voltage was adjusted 2.7 V, 2.4 V, 2.1 V, 1.8 V, 1.5 V, 1.2 V respectively less than the open-circuit potential (2.85 V). Boundary of PEM fuel cell stack model is given at Fig. 3. The current density values which correspond to each voltage value in the simulation results were noted. Both anode and cathode terminals were assigned wall boundaries. Hydrogen and oxygen velocities are evaluated from the chemical stoichiometric ratio, operational pressure and temperature by the following equations:

$$u_{a,in} = \zeta_a \frac{I_{ref}}{n_e . F} . A_{MEA} . \frac{1}{X_{H_2,in}} . \frac{R . T_{in,cell}}{P_{a,in}} . \frac{1}{A_{ch}} \quad (14)$$

$$u_{c,in} = \zeta_c \frac{I_{ref}}{n_e . F} . A_{MEA} . \frac{1}{X_{O_2,in}} . \frac{R . T_{in,cell}}{P_{c,in}} . \frac{1}{A_{ch}} \quad (15)$$

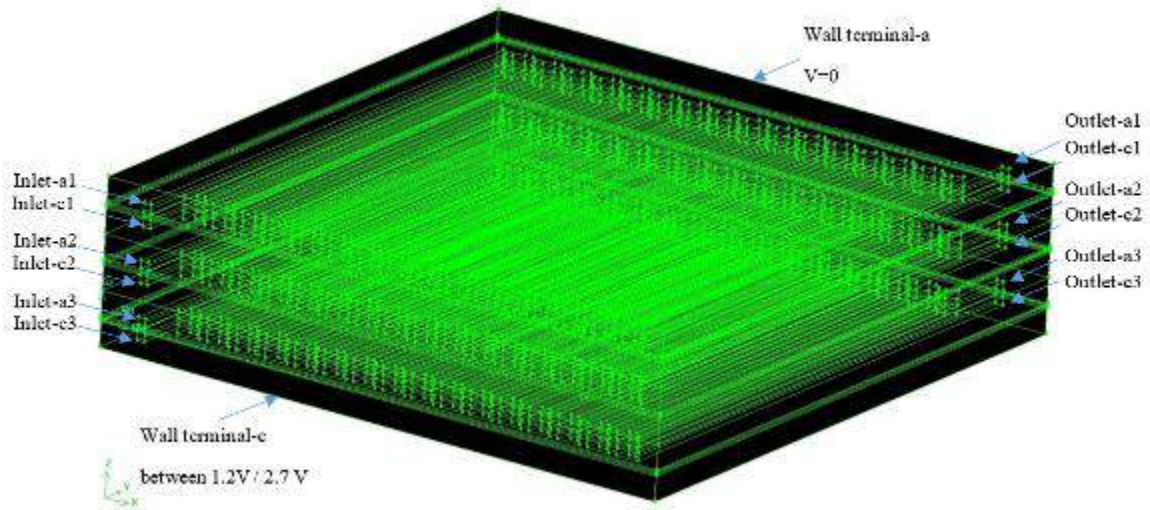

Figure 3. Boundary of PEM Fuel Cell Stack Model

Table 3. Operating and Boundary Conditions of PEM Fuel Cell Model

Zone	Parameter	Unit	Value
Anode	Operation pressure	kPa	200
	Operation temperature	K	333
	RH_a	%	100
	Mass flow rate	kg/s	1.659×10^{-3}
	Mass fraction of H_2	-	0.378
	Mass fraction of H_2O	-	0.622
Cathode	Operation pressure	atm	200
	Operation temperature	K	333
	RH_c	%	100
	Mass flow rate	kg/s	2.910×10^{-2}
	Mass fraction of O_2	-	0.247
	Mass fraction of H_2O	-	0.0097

Mesh Independence Study

A grid independence test was carried out to determine the number of optimum meshes and to check that the results are independent of the grid. The number of cells for tests, the grids were 45150, 697200 and 5107200 respectively. As shown in the Fig. 4, no considerable difference in the results for the number 2 and number 3 grids and thus the results of the number 2 grid are used for the simulations. The computational time for solving the set of equations was about 476 min for number 2 grid model.

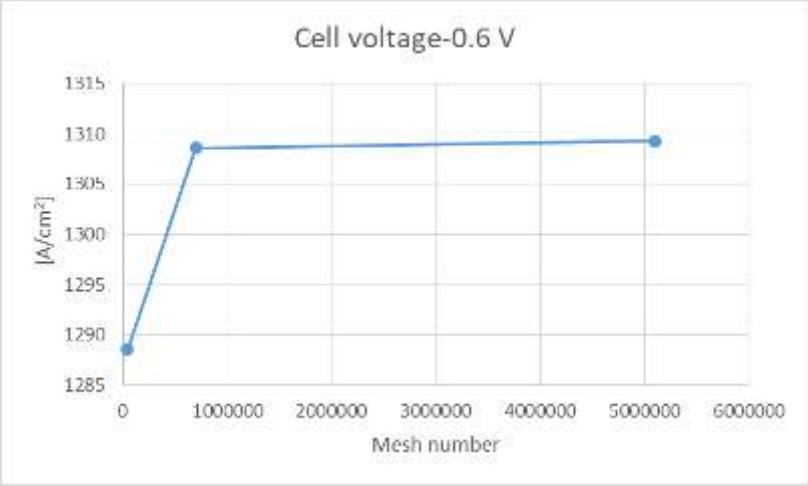

Figure 4. Mesh Independence Study for Three Different Grid

RESULTS AND FINDINGS

The fact that the H_2 concentration on the anode side in the Fig. 5 does not cause a visible decrease from the inlet to the outlet is due to the fact that the flow rate is higher than the required for chemical reactions. Similar results were obtained in single-cell analysis at previous studies. As shown in Fig. 6, due to the reactions on the cathode side, the oxygen concentration decreases from the inlet of the channels to the outlet of the channels.

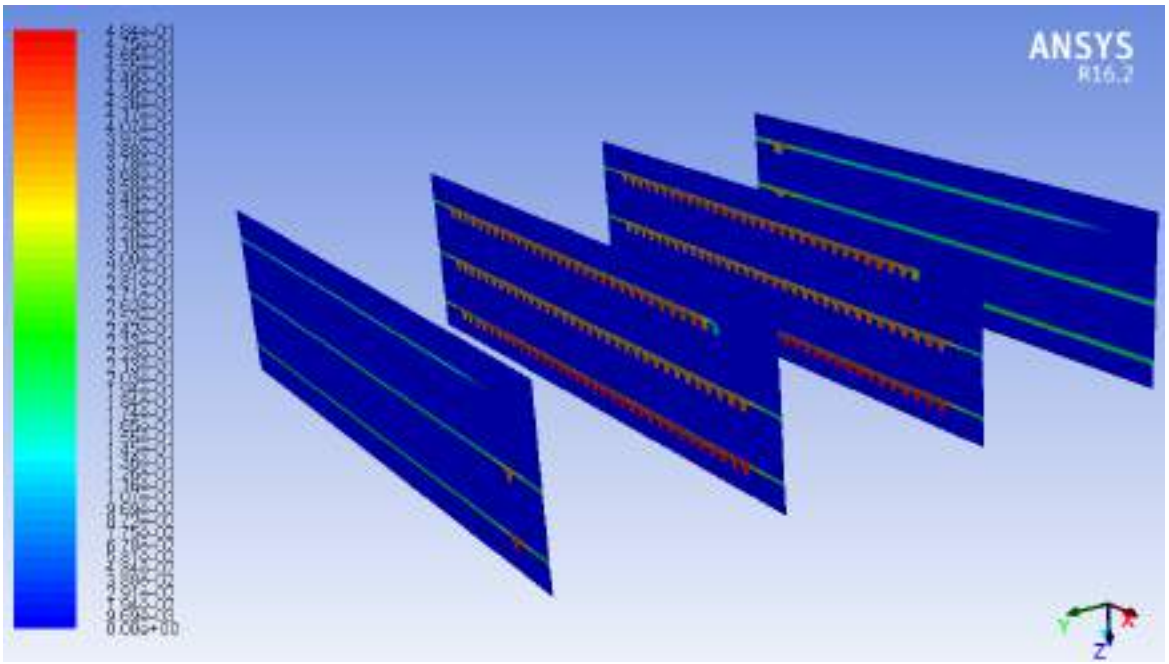

Figure 5. Molar Concentration Distributions of H_2 for Given Operating Conditions at 0.6 V in 3-Cell Fuel Cell Stack.

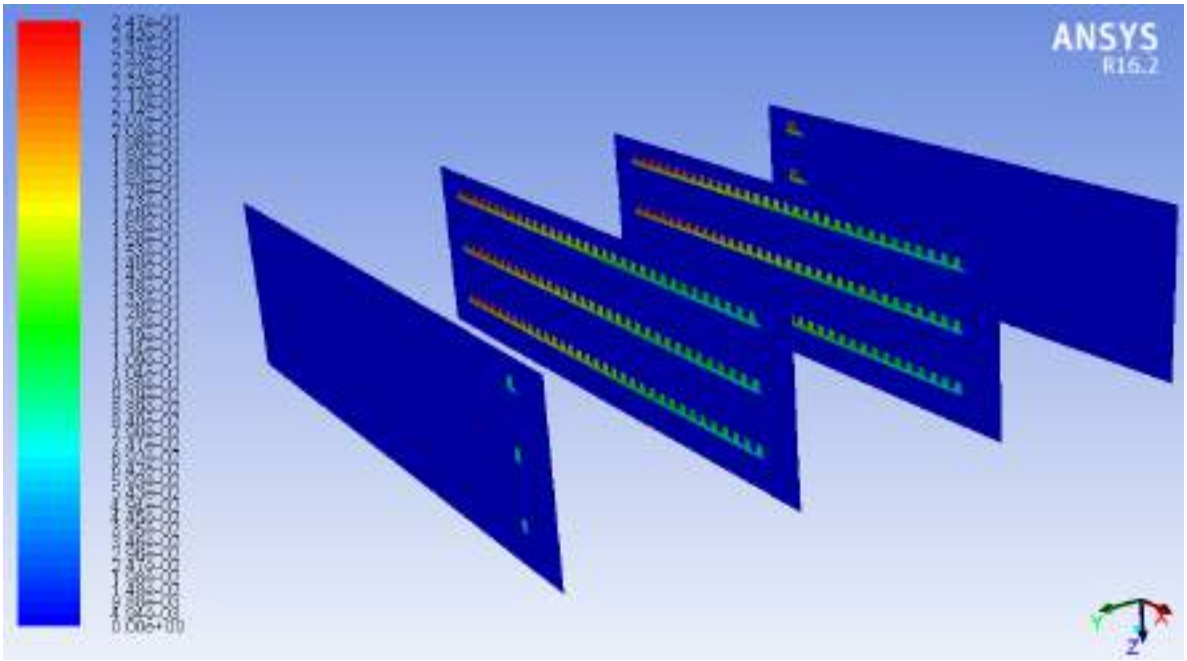

Figure 6. Molar Concentration Distributions of O_2 for Given Operating Conditions at 0.6 V in 3-Cell Fuel Cell Stack.

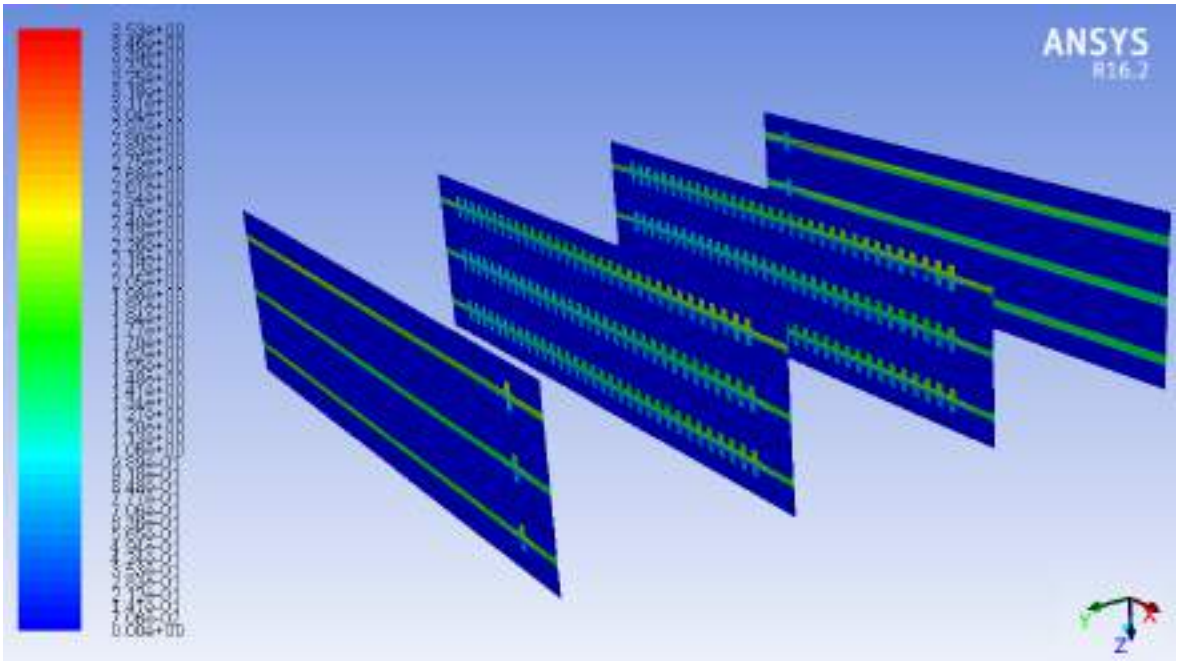

Figure 7. Molar Concentration Distributions of H_2O for Given Operating Conditions at 0.6 V in 3-Cell Fuel Cell Stack.

It is observed as shown in Fig. 7 that the largest amount of water molar concentration was obtained in the mid region of anode side and the water observed at the anode region is due to the fact that the hydrogen gas is fully humidified. Also in Fig. 7, it is seen that the water formed as a result of the reactions on the cathode side creates an increase from the inlet to the outlet and does not create an excessive change on the anode side and provides the desired humidity in the membrane layers.

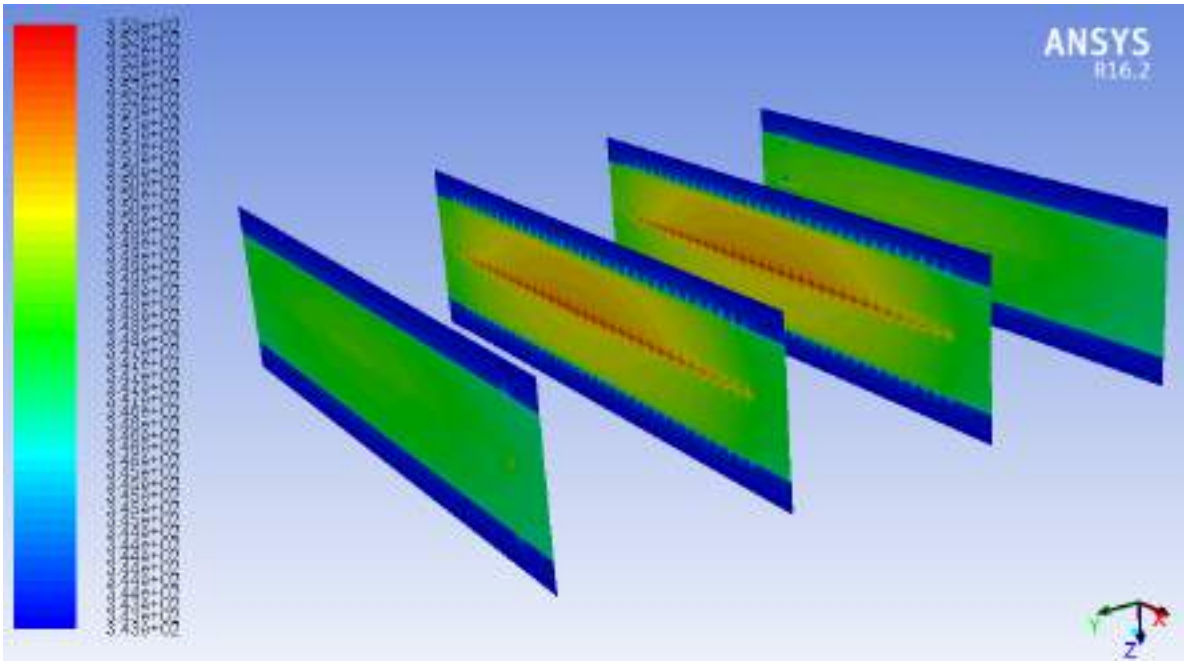

Figure 8. Temperature Distributions for Given Operating Conditions at 0.6 V in 3-Cell Fuel Cell Stack.

The temperatures in the middle layers are higher than the temperature of the components of the edge cells, because the temperature cannot be removed as a result of the reactions. (Fig.8)

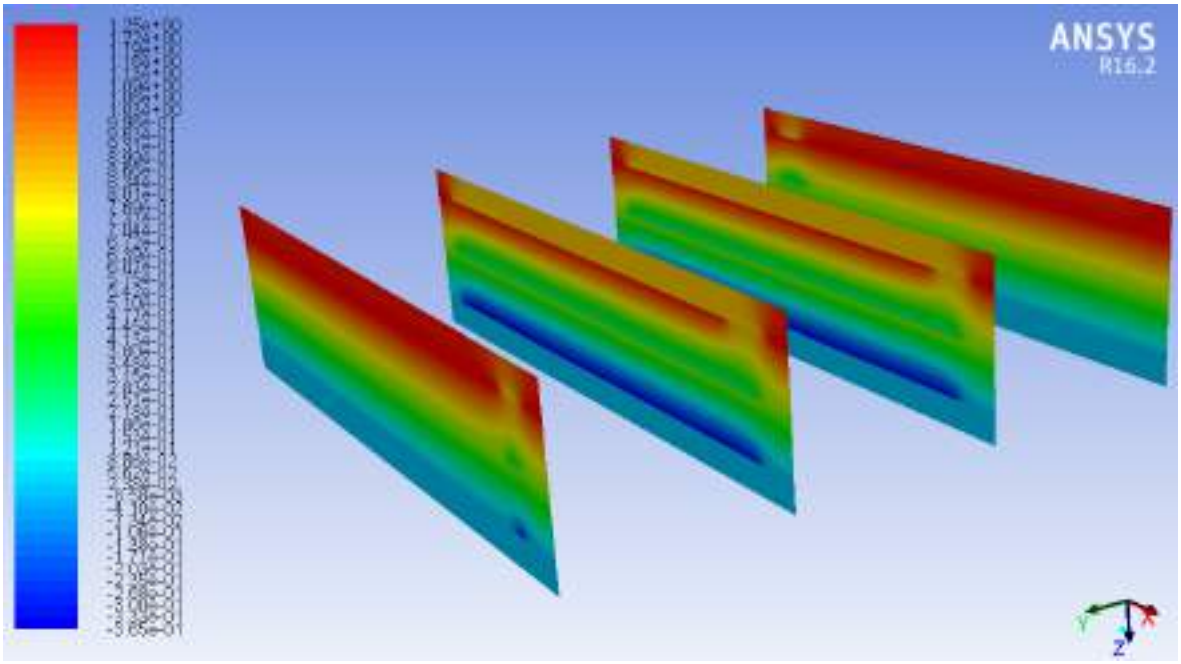

Figure 9. Contours of Protonic Potential for Given Operating Conditions at 0.6 V in 3-Cell Fuel Cell Stack.

It is shown that the protonic potential for given operating conditions at 0.6 V in 3-cell Fuel cell stack from anot side to cathode side in Fig.9. It is expected that the protonic potential shows an increasing properties from the anode to the cathode, since the reactions take place on the cathode side.

CONCLUSIONS

In this study a 3-D CFD model of PEM fuel cell stack with serpentine flow channels was developed to investigate stack temperature, molar concentration of reactant gases at each cell. The temperature and mass flow distributions in the fuel cell stack have been obtained from the modeling. The structured grid scheme was employed which was built with a pre-processing software, GAMBIT 2.4.6. Then, the grid was imported into finite volume based commercial software, ANSYS-FLUENT 16.2. The PEMFC Module is an add-on module based on FLUENT CFD package for computations. The distributions of oxygen, hydrogen and water molar concentration were taken into account the mass, momentum, energy, species, charge conservation equation as well as combines electrochemistry reaction inside the fuel cell. In the numerical study, verification was performed under the highest operating conditions obtained from the experiments in previous studies.

ACKNOWLEDGEMENTS

This study was supported by project number of 216M045 from Scientific and Technological Research Council of Turkey (TUBITAK).

REFERENCES

Carcadea, E., Varlam, M., Marinoiu, A., Raceanu, M., Ismail, M.S., Ingham, D.B. (2019).Influence of catalyst structure on PEM fuel cell performance–A numerical investigation. International Journal of Hydrogen Energy, 44(25)12829-12841. doi.org/10.1016/j.ijhydene.2018.12.155.

Dawes, J.E., Hanspal, N.S., Family, O.A., Turan, A. (2009). Three-dimensional CFD modelling of PEM fuel cells: An investigation into the effects of water flooding. Chemical Engineering Science, 64, 2781-2794. doi:10.1016/j.ces.2009.01.060

Kahveci, E.E., Taymaz, I. (2018). Assessment of single-serpentine PEM fuel cell model developed by computational fluid dynamics. Fuel, 217, 51-58.doi.org/10.1016/j.fuel.2017.12.073.

Qin,Y., Liu,G., Chang,Y., Du,Q. (2018).Modeling and design of PEM fuel cell stack based on a flow network method. Applied Thermal Engineering, 144,411-442.doi.org/10.1016/j.applthermaleng.2018.08.050.

Park, J., Li, X. (2007). An experimental and numerical investigation on the cross flow through gas diffusion layer in a PEM fuel cell with a serpentine flow channel. Journal of Power Sources, 163(2), 853-863. doi.org/10.1016/j.jpowsour.2006.09.083.

Sezgin,B.,Caglayan,D.G.,Devrim,Y.,Steenberg,T.,Eroglu,I. (2016). Modeling and sensitivity analysis of high temperature PEM fuel cells by using Comsol Multiphysics. International Journal of Hydrogen Energy, 41(23), 10001-10009. doi.org/10.1016/j.ijhydene.2016.03.142.

Shao, Y., Xu, L., Liu, J., Ouyang, M. (2019).Numerical modeling and performance prediction of water transport for PEM fuel cell. Energy Procedia, 158, 2256-2265. 10.1016/j.egypro.2019.01.186.

Solati, A., Nasiri, B., Mohammadi-Ahmar, A., Mohammedi, K., Safari, A.H. (2019). Numerical investigation of the effect of different layers configurations on the performance of radial PEM fuel cells. Renewable Energy, 143, 1877-1889. 10.1016/j.renene.2019.06.003.

Wilberforce, T.,Ijaodola, O., Khatib, F.N., Ogungbemi, E.O., Hassan,Z.E.,Thompson, J.,Olabi,A.G. (2019).Effect of humidification of reactive gases on the performance of a proton exchange membrane fuel cell. Science of the Total Environment, 688,1016-1035.doi.org/10.1016/j.scitotenv.2019.06.397.

Wei, G., Lu, J., Zhang, F., Yan, X., Zhang, J. (2019).Analyze the effect of flow mode and humidity on PEMFC performance by equivalent membrane conductivity. International Journal of Energy Research,43,1-14.doi.org/10.1002/er.4592.

INVESTIGATION OF SUITABILITY OF HIGH PERFORMANCE CARBON DERIVED FROM TEA WASTE BIOMASS TO TRANSISTOR APPLICATIONS

Saliha Nur BIÇAKÇI
Department of Energy Systems Engineering, Recep Tayyip Erdogan University, Fener-Rize, 53100, Turkey
salihanur.bicakci@gmail.com

Asst. Prof. Dr. Gökçen AKGÜL
Department of Energy Systems Engineering, Recep Tayyip Erdogan University, Fener-Rize, 53100, Turkey
gokcen.akgul@erdogan.edu.tr

ABSTRACT: Carbon materials are studied in high-tech electronics such as diodes, transistors similar devices (Feng et al., 2018). The use of porous carbon materials in electronic devices and their application in energy storage areas are important in terms of developing more economical methods and reducing the dimensions. Although a large number of carbon channel transistors have been reported in the literature in recent years, transistor applications of carbon from biomass as porous carbon are limited. Most of the carbon materials are originated from fossil sources that are diminishing. So, renewable carbon resources are gaining importance. Biomass is the only renewable carbon resource. It can be converted to carbonized material called biochar by pyrolysis. However, in order to apply the biochar to carbon-based electrical devices, its structure needs to be improved. In this study, biochar obtained from industrial tea wastes was converted to high performance and n-dopped carbon material (graphene-like) by chemical and physical methods (Roy, 2017; Smith et al., 2019). The upper contact / upper door structured field effect transistors (FETs) were made by using these carbon materials that silver paint was used as contact point paste (Koç et al., 2019;). The newly derived carbon materials were characterized by SEM, XRD, Raman Spectroscopy, FT-IR, TGA methods. The current – voltage (I-V) characteristics of the developed FETs were determined.

Key words: industrial tea waste, carbon, field effect transistor

Acknowledgement: We gratefully acknowledge the financial support provided by Recep Tayyip Erdoğan University, Scientific Research Projects Coordinator Unit (BAP) (Project No: FYL-2018-970).

ÇAY ATIĞI BİYOKÜTLESİNDEN TÜRETİLEN YÜKSEK PERFORMANS KARBONUN TRANSİSTÖR UYGULAMALARINA UYGUNLUĞUNUN ARAŞTIRILIMASI

ÖZET: Diyotlar, transistörler ve benzeri aygıtlar gibi ileri teknoloji alanlarında karbon malzemeler çalışılmaktadır (Feng vd., 2018). Gözenekli karbon materyallerin elektronik aygıtlarda kullanımı ve enerji depolama alanlarında uygulamaları da daha ekonomik yöntemler geliştirilmesi ve boyutların küçültülmesi bakımından önemlidir. Son yıllarda literatürde çok sayıda karbon kanallı transistör rapor edilmiş olsa da, gözenekli karbon olarak biyokütleden elde edilen karbonun transistör uygulamaları sınırlı sayıdadır. Karbon malzemelerin çoğu, giderek tükenmekte olan fosil kaynaklardır. Bu sebeple yenilenebilir karbon kaynakları önem kazanmaya başlamaktadır. Biyokütle tek yenilenebilir karbon kaynağıdır. Piroliz yöntemi ile biyokömür olarak adlandırılan karbonize materyale dönüştürülebilir. Ancak biyokömürün karbon tabanlı elektriksel aygıtlara uygulanabilmesi için yapısının geliştirilmesi gerekmektedir. Bu çalışmada, endüstriyel çay atıklarından elde edilen biyokömür, kimyasal ve fiziksel yöntemlerle yüksek performans ve n-katkılı karbon materyale (grafen benzeri) dönüştürülmüştür (Roy, 2017; Smith vd., 2019;). Oluşturulan bu karbon ile üst kontak / üst kapı yapılı alan etkili transistörler gümüş boya kullanılarak kontakları gerçekleştirilmiş ve karakterizasyonları yapılmıştır (Koç vd., 2019). Yeni türetilen karbon materyal SEM, XRD, Raman Spektroskopisi, FT-IR, TGA yöntemleriyle karakterize edilmiştir. Geliştirilen alan etkili karbon transistörün akım-gerilim (I-V) karakteristikleri belirlenmiştir.

Anahtar sözcükler: endüstriyel çay atığı, karbon, alan etkili transistör

Teşekkür: Bu proje Recep Tayyip Erdoğan Üniversitesi, Bilimsel Araştırma Projeleri Koordinatör Birimi (BAP) (Proje No: FYL-2018-970) tarafından desteklenmiştir.

KAYNAKLAR

Feng, X. et al., 2018. All carbon materials pn diode. Nature Communications, 9, 3750, 1-7.
Koç, M.M. et al., 2019, Electrical characterization of solar sensitive zinc oxide doped amorphous carbon photodiode. Optik - International Journal for Light and Electron Optics 178, 316-326.
Roy, S., 2017. Synthesis of graphene oxide using tea-waste biochar as green substitute of graphite and its application in de-fluoridation of contaminated water. AJCR, 1, 1, 1-19.
Smith, A.T., La Chance, A.M. Zeng, S., Liu, B. and Sun, L., 2019. Synthesis, properties, and applications of graphene oxide/reduced graphene oxide and their nanocomposites. Nano Materials Science, 1(1), 31-47.

DEVELOPMENT SEMICONDUCTIVE CARBON MATERIAL from BIOMASS and ITS DIODE APPLICATIONS

Sözer SÖZER
Department of Energy Systems Engineering, Recep Tayyip Erdogan University, Fener-Rize, 53100, Turkey
sozerszer@gmail.com

Asst. Prof. Dr. Gökçen AKGÜL
Department of Energy Systems Engineering, Recep Tayyip Erdogan University, Fener-Rize, 53100, Turkey
gokcen.akgul@erdogan.edu.tr

ABSTRACT: Electronic devices generally consist of circuits containing semiconductor materials. Semiconductor materials can be organic and/or inorganic, such as polymers and metal oxides [1]. Current studies are being conducted on the use and development of carbon in semiconductor technology [2]. Recently, unlike nano-carbon or graphene materials, the use of porous carbon materials in electronic devices and their applications in energy storage areas have been among the research subjects in terms of developing more economical and greener methods [3]. Porous carbon, also called as biochar, can be obtained by pyrolysis of biomass, a renewable energy source. Biochar is generally amorphous, rich in surface functional groups, and its electrical conductivity is negligible [4]. However, the carbon structure can be developed into graphite / graphene-like structures by thermal and / or chemical methods. The presence of surface functional groups also facilitates N and / or P type doping onto the structure. In addition, the mineral elements existing in the biomass also enhance the semiconductivity properties.
Diodes are the simplest and most basic semiconductor devices with one P type and one N type sides. Applying porous and doped carbon to diodes can produce electronic devices with advantages such as directing signals, providing flexibility, low power consumption, high switching speed, diminishing dimensions and lower cost [5].

Key words: yarı iletken karbon, biyokütle, diyot

YARI İLETKEN KARBON MATERYALİN BİYOKÜTLEDEN GELİŞTİRİLMESİ ve DİYOT UYGULAMALARI

ÖZET: Elektronik aygıtlar genellikle yarı iletken malzemeler içeren devrelerden oluşmaktadır. Yarı iletken malzemeler polimerler ve metal oksitler gibi organik ve inorganik temelli olabilmektedir [1]. Karbonun yarı iletken teknolojisinde kullanımı ve geliştirilmesi yönünde güncel çalışmalar yapılmaktadır [2]. Son zamanlarda, nano-karbon veya grafen materyallerinden farklı olarak, gözenekli karbon materyallerin

elektronik aygıtlarda kullanımı ve enerji depolama alanlarında uygulamaları da daha ekonomik ve çevreci yöntemler geliştirilmesi bakımından araştırma konuları arasında yer almıştır [3]. Gözenekli karbon, biyokömür olarak da adlandırılır, yenilenebilir enerji kaynağı olan biyokütlenin pirolizi ile elde edilebilir. Biyokömür genellikle amorf yapıdadır, yüzey fonksiyonel gruplarınca zengindir ve elektriksel iletkenliği ihmal edilecek düzeyde düşüktür [4]. Ancak karbon yapısı grafit/grafen benzeri yapılara termal ve/veya kimyasal yöntemlerle geliştirilebilir. Yüzey fonksiyonel grupların varlığı, yapıya N ve/veya P tipi katkılmayı da kolaylaştırır. Ayrıca biyokütlenin içerdiği mineral elementler de yarı iletkenlik özelliğini geliştirici yönde etki eder.
Diyotlar, yapısında bir adet P tipi ve bir adet N tipi yarı iletken bulunan en basit ve temel yarı iletken aygıtlardır. Gözenekli ve katkılanmış karbonun diyotlarda uygulanması ile sinyallerin doğrultulması, esneklik sağlanması, düşük güç tüketimi, yüksek anahtarlama hızı, boyutların küçültülmesi ve düşük maliyet gibi avantajlara sahip elektronik aygıtlar üretilebilir [5].

Anahtar sözcükler: yarı iletken karbon, biyokütle, diyot

KAYNAKLAR

[1] Ahmad, S. (2014). Organic semiconductors for device applications: Current trends and future prospects. Journal of Polymer Engineering, 34(4), 279–338. doi:10.1515/polyeng-2013-0267
[2] Kreupl, F. (2015). Advancing CMOS with carbon electronics, 1–6. doi:10.7873/date2014.250
[3] Rahimi, R., Ochoa, M. ve Ziaie, B. (2016). Direct Laser Writing of Porous-Carbon/Silver Nanocomposite for Flexible Electronics. ACS Applied Materials and Interfaces, 8(26), 16907–16913. doi:10.1021/acsami.6b02952
[4] Gabhi, R. S., Kirk, D. W. ve Jia, C. Q. (2017). Preliminary investigation of electrical conductivity of monolithic biochar. Carbon, 116, 435–442. doi:10.1016/j.carbon.2017.01.069
[5] Semple, J., Georgiadou, D. G., Wyatt-Moon, G., Gelinck, G. ve Anthopoulos, T. D. (2017). Flexible diodes for radio frequency (RF) electronics: A materials perspective. Semiconductor Science and Technology, 32(12). doi:10.1088/1361-6641/aa89ce.

DEVELOPMENT OF BORON DOPED SUPERCAPACITOR ENERGY STORAGE MATERIALS from BIOMASS

Ayşenur GÜNDOĞDU
Department of Energy Systems Engineering, Recep Tayyip Erdogan University, Fener-Rize, 53100, Turkey
gundogdu.aysenur@hotmail.com

Asst. Prof. Dr. Gökçen AKGÜL
Department of Energy Systems Engineering, Recep Tayyip Erdogan University, Fener-Rize, 53100, Turkey
gokcen.akgul@erdogan.edu.tr

ABSTRACT: Energy is a key part of modern economies. Possession of energy is necessary for rising living standards, having larger economies, social and economic development. Increasing the use of renewable and sustainable energy sources and developing energy storage technologies are very important for meeting the increasing energy demand of human beings as well as reducing the negative factors of climate change and environmental pollution.
Supercapacitors are energy storage devices with high power density, fast charging and discharging properties, also known as ultracapacitors or electrochemical double layer capacitors [1]. Electrodes are the most important components that affect the performance of supercapacitors. Metal oxides, polymers and carbon-based materials are used as electrode materials [2]. It is aimed to develop carbon energy storage material that uses biomass as an alternative, renewable, sustainable, domestic and clean carbon source. It is proposed to produce supercapacitor material with high energy storage capacity, high galvanostatic charge-discharge cycle and low impedance properties by boron doping of biochar which is obtained by pyrolysis of biomass. Developing energy storage systems by using entirely domestic resources are targeted.

Key words: supercapacitor, biomass, boron

Acknowledgement: We gratefully acknowledge the Boron Institute for the bursary support program (2019).

BİYOKÜTLEDEN BOR KATKILI SÜPERKAPASİTÖR ENERJİ DEPOLAMA MALZEMELERİNİN GELİŞTİRİLMESİ

ÖZET: Enerji, modern ekonomilerin anahtar parçalarından bir tanesidir. Yaşam standartlarının artması, daha büyük ekonomilere sahip olma, sosyal ve ekonomik kalkınma gibi nedenlerle enerjiye sahip olmak gereklidir. Fosil kaynakların giderek

tükendiği ve sebep olduğu iklim değişikliğinin etkilerinin iyice hissedildiği günümüzde yenilenebilir ve sürdürülebilir enerji kaynaklarının kullanımının artması ve enerji depolama teknolojilerinin geliştirilmesi, hem insanoğlunun artan enerji ihtiyacının karşılanması hem de iklim değişikliği ve çevre kirliliğine neden olan negatif faktörlerin azaltılması için çok önemlidir.
Süperkapasitörler; ultrakapasitörler veya elektrokimyasal çift tabakalı kapasitörler olarak da bilinen, yüksek güç yoğunluğu, hızlı şarj ve deşarj özellikleri olan enerji depolama araçlarıdır [1]. Süperkapasitörlerdeki performansı etkileyen en önemli parça elektrotlardır. Elektrot materyali olarak metal oksitler, polimerler ve karbon esaslı malzemeler kullanılır [2]. Alternatif, yenilenebilir, sürdürülebilir, yerli ve temiz karbon kaynağı olarak biyokütlenin kullanıldığı enerji depolama materyali geliştirilmesi hedeflenmektedir. Biyokütlenin pirolizi ile elde edilen ve yüzey fonksiyonel gruplarınca zengin olan "biyokömürün" bor katkılanması ile enerji depolama kapasitesi yüksek, galvanostatik şarj-deşaj döngüsü çok ve impedansı düşük süperkapasitör materyali üretilmesi amaçlanmıştır. Böylece tamamen yerli kaynaklar kullanılarak enerji depolama sistemlerinin geliştirilmesi hedeflenmektedir.

Anahtar sözcükler: superkapasitör, biyokütle, bor

Teşekkür: Bu çalışma BOREN burs programı tarafından desteklenmektdir.

KAYNAKLAR

[1] Kalyani, P., Anitha, A., 2013. Biomass carbon & its prospects in electrochemical energy systems. Int. J. of Hydrogen Energy, 38, 4034-4045.

[2] Guerrero, M.A. et al., 2009. Supercapacitors: Alternative Energy Storage Systems. Przeglad Elektrotechnıczny, 85(10), 188-195.

MODELLING of DIRECT CARBON FUEL CELL USING BIOCHAR as FUEL

Fatma Gül NİŞANCI
Department of Energy Systems Engineering, Recep Tayyip Erdogan University, Fener-Rize, 53100, Turkey
f.g.nisanci@gmail.com

Asst. Prof. Dr. Gökçen AKGÜL
Department of Energy Systems Engineering, Recep Tayyip Erdogan University, Fener-Rize, 53100, Turkey
gokcen.akgul@erdogan.edu.tr

Asst. Prof. Dr. Rasim Volga OVALI
Department of Material Science and Nanotechnology Engineering, Recep Tayyip Erdogan University, Fener-Rize, 53100, Turkey

ABSTRACT: Due to the diminishing fossil fuel reserves of the world and the increasing need for energy, there has been a growing interest in technologies that use energy efficiently. Fuel cells are one of them. Direct carbon fuel cells (DCFC) are systems operating at high temperatures, using solid carbon as fuel, and converting chemical energy in carbon by electrochemical reactions into electricity. The fuel cell performance using biochar derived from biomass as renewable, clean and alternative carbon fuel was determined by modeling with Matlab program. In this study, the direct carbon fuel cell-solid model of Liu et al. [1] was referenced and biochar was accepted as fuel [2, 3]. The effects of cell temperature, electrical conductivity, density and particle size of carbon on fuel cell voltage were determined by Matlab modeling. During modeling, 3 main losses affecting fuel cell performance were evaluated; activation losses due to electrochemical reaction, ohmic losses due to ionic and electronic conductivity and concentration losses due to mass transfer. The high performance values for DCFC were found to be close to the graphite fuel used systems when having high electrical conductivity biochar has been used. It can be concluded that the use of biochar with high electrical conductivity as a fuel in DCFCs increases the fuel cell performance.

Key words: Direct Carbon Fuel Cell (DCFC), Matlab, Modeling, Biochar

BİYOKÖMÜR YAKITI KULLANILAN DOĞRUDAN KARBON YAKIT PİLİNİN MODELLENMESİ

ÖZET: Dünyanın azalan fosil yakıt rezervleri ve enerjiye olan ihtiyacın artması nedeniyle enerjinin verimli kullanıldığı teknolojilere ilgi artmıştır. Yakıt pilleri bunlardan bir tanesidir. Doğrudan karbon yakıt pilleri (DCFC) yüksek sıcaklıkta çalışan, yakıt olarak

katı karbonu kullanan ve karbondaki kimyasal enerjiyi elektrokimyasal reaksiyonlarla elektriğe dönüştüren sistemlerdir. Yenilenebilir, temiz ve alternatif karbon yakıt olarak biyokütleden türetilen biyokömürün kullanıldığı yakıt pili performansı, Matlab programı ile modellenerek belirlenmiştir. Bu çalışmada Liu vd. [1]'nin doğrudan karbon yakıt pili katı modeli referans olarak alınmıştır. Biyokömün DCFC'lerde yakıt olarak kullanılmasının uygun olduğu bulunmuştur [2, 3]. Hücre sıcaklığının, karbonun elektriksel iletkenliğinin, yoğunluğunun ve parçacık büyüklüğünün yakıt pili gerilimi üzerindeki etkileri bu çalışmada Matlab modelleme ile belirlenmiştir. Modelleme yapılırken yakıt pili performansını etkileyen 3 ana kayıp değerlendirilmiştir; elektrokimyasal reaksiyondan kaynaklanan aktivasyon kayıpları, iyonik ve elektronik iletime bağlı omik kayıplar ve kütle transferi nedeniyle oluşan konsantrasyon kayıplarıdır. Biyokütlenin elektriksel iletkenliğinin yüksek olduğu değerlerde grafit kullanılan sistemlere yakın performans değerleri bulunmuştur. Elektriksel iletkenliği yüksek olan biyokömürün DCFC'ler de yakıt olarak kullanılmasının yakıt pili performansını arttırdığı söylenebilir.

Anahtar sözcükler: Doğrudan Karbon Yakıt Pilleri (DCFC), Matlab, Modelleme, Biyokömür

KAYNAKLAR

[1] Liu, Q., Tian, Y., Xia, C., Thompson L.T., Liang, B. and Li, Y., 2008. Modeling and simulation of a single direct carbon fuel cell. Journal of Power Sources, 185, 1022–1029. DOI:10.1016/j.jpowsour.2008.08.100

[2] Yu, J., Zhao, Y. and Li, Yongdan., 2014. Utilization of corn cob biochar in a direct carbon fuel cell. Journal of Power Sources, 270, 312-317.

[3] Gabhi, R.S., Kirk, D.W. and Jia, C.Q., 2017. Preliminary investigation of electrical conductivity of monolithic biochar. Carbon, 116, 435-442.

INVESTIGATION OF APPLICABILITY OF RENEWABLE CARBON IN ELECTRICAL CIRCUIT

İpek Nur AYDİN
Department of Energy Systems Engineering, Recep Tayyip Erdogan University, Fener-Rize, 53100, Turkey
aydinipeknur@gmail.com

Asst. Prof. Dr. Gökçen AKGÜL
Department of Energy Systems Engineering, Recep Tayyip Erdogan University, Fener-Rize, 53100, Turkey
gokcen.akgul@erdogan.edu.tr

ABSTRACT: Electric circuits are the electrical systems that are needed at every level of our daily life. It is used in many fields such as cooling, heating, lighting, sound production, motion and communication. Transmission of electrons through conductive channels is provided in electrical circuits. Conductive metals are generally used in conductive channels such as gold, silver and copper. The use of conductive carbon materials in electrical circuits for more environmentally friendly, economic, domestic and renewable circuits is being investigated [1-3]. In this study, carbon material (biochar) was derived from industrial tea waste biomass - a renewable biomass energy source - by pyrolysis. Carbon composites were prepared impregnation of conductive metals. Biochar, rich in surface functional groups, is very advantageous in the production of carbon composite materials. As next step, an ink of carbon composite was prepared with ethyl cellulose / terpinol then applied as an electrical circuit through a circuit pattern. Detailed characterization of the derived material was performed, such as SEM, XRD, FTIR and the conductivity of the electrical circuit was determined. Thus, renewable, sustainable, alternative organic electricity circuit has been developed by using local and domestic biomass energy source.

Key words: electrical circuit, renewable carbon, tea waste

Acknowledgement: We gratefully acknowledge the financial support provided by TUBITAK 2209A (project no: 1919B011803642)

YENİLENEBİLİR KARBONUN ELEKTRİK DEVRESİNDE UYGULANABİLİRLİĞİNİN ARAŞTIRILMASI

ÖZET: Elektrik devreleri, günlük yaşantımızın her alanında ihtiyaç duyulan ve kullanımı en üst düzeyde olan elektriksel sistemlerdir. Soğutma, ısıtma, aydınlatma, ses üretimi, hareket, haberleşme gibi birçok alanda kullanılmaktadır. Elektirk devrelerinde elektronların iletken kanallardan geçerek iletimi sağlanır. İletken kanallarda genellikle

altın, gümüş, bakır gibi iletken metaller kullanılır. Daha çevreci, ekonomik, yerli ve yenilenebilir devreler için iletken karbon materyallerin elektrik devrelerinde kullanımı araştırılmaktadır [1-3]. Bu çalışmada yenilenebilir biyokütle enerji kaynağı olan çay fabrika atığı biyokütlesinden piroliz ile biyokömür karbon materyali türetilmiştir. İletken metallerle katkılanarak elektriksel iletkenliği geliştirilmiş karbon kompozitleri geliştirilmiştir. Yüzey fonksiyonel gruplarınca zengin olan biyokömür, kompozit materyallerin türetilmesi açısından oldukça avantajlıdır. Daha sonra etil selüloz/terpinol ile mürekkebi hazırlanan karbon materyal, çıkarılan kalıp üzerinden elektrik devresi olarak uygulanmıştır. Türetilen materyalin SEM, XRD, FTIR gibi detaylı karekterizasyonları yapılmış, elektrik devresinin iletkenliği belirlenmiştir. Böylece yenilenebilir, sürdürülebilir, altenatif organik elektrik devresinin yerel ve yerli biyokütle enerji kaynağı kullanılarak geliştirilebileceği gösterilmiştir.

Anahtar sözcükler: elektrik devresi, yenilenebilir karbon, çay atığı

Teşekkür: Bu proje Tübitak 2209-A (proje no: 1919B011803642) Üniversite Öğrencileri Araştırma Projeleri Destekleme Programı kapsamında desteklenmiştir.

KAYNAKLAR

[1] Massey, M.K., Kotsialos, A., Volpati, D., Vissol-Gaudin, E., Pearson, C., Bowen, L.,Petty, M. C. (2016). evolution of electronic circuits using carbon nanotube composites. Scientific Reports, 6, 1–7. doi:10.1038/srep32197

[2] Lawes, S., Riese, A., Sun, Q., Cheng, N. ve Sun, X. (2015). Printing nanostructured carbon for energy storage and conversion applications. Carbon, 92, 150–176. doi:10.1016/j.carbon.2015.04.008

[3] Zhong,X., Hu, H., and Fu, H. (2018). Self-cleaning, chemically stable, reshapeable, highly conductive nanocomposites for electrical circuits and flexible electronic devices. ACS Appl. Mater. Interfaces, 10, 25697−25705.

THICKNESS EFFECT OF MEMBRANE AND CATALYST LAYER ON THE PEM FUEL CELL PERFORMANCE

Safiye Nur ÖZDEMİR
Department of Mechanical Engineering, Sakarya University, Sakarya-Turkey
safiyeozdemir@sakarya.edu.tr

İmdat TAYMAZ
Department of Mechanical Engineering, Sakarya University, Sakarya-Turkey
taymaz@sakarya.edu.tr

ABSTRACT: Proton exchange membrane fuel cells (PEMFCs) are considered as promising alternative energy sources when the optimal performance criteria is supplied. Membrane or catalyst layer's thickness is one of the design parameters affecting system performance in PEM fuel cells using pure hydrogen on the anode side and air on the cathode side. In this study, a three dimensional, steady-state and single-phase numerical model was developed by using ANSYS FLUENT 18.1, a CFD software with a Fuel Cell and Electrolysis Module based on finite volume method in order to investigate the thickness effect of membrane and catalyst layer on the performance of the PEM fuel cell. Modeling findings are presented in the form of polarization curves, which show the effects of the different design parameters on the performance of the PEMFC. As a result of this study, it is observed that the cell performance is improved as the membrane or catalyst layer's thickness decreases.

Key words: Computational Fluid Dynamics, Membrane Thickness, Catalyst Layer's Thickness, Cell Performance

INTRODUCTION

A fuel cell is an electrochemical energy converter that converts the chemical energy of the fuel directly into electricity without combustion process. Fuel cells operate quietly compared to internal combustion engines, cleaner, more efficient, simple structured modern energy carriers. They can be classified by electrolyte type and can be listed as follows: proton exchange membrane fuel cell (PEMFC), solid oxide fuel cell (SOFC), molten carbonate fuel cell (MCFC), phosphoric acid fuel cell (PAFC) and alkaline fuel cells (AFC) (Sharaf and Orhan 2014; Ding et al. 2013). Among several types of fuel cells, the proton exchange membrane fuel cells (PEMFCs) are the most promising and attractive energy technologies for stationary and portable transportation applications based on its high power density, low noise, harmless and long-lasting.

Most of the studies related to the operating parameters affecting the cell performance have been conducted in the literature (Freire et al. 2014; Khazaee et al. 2012; Ahmadi et al. 2016; Caglayan et al. 2016). Optimum design of the flow channels within the bipolar plates is a key parameter affecting the overall performance of the fuel cell. During the last twenty years, lots of studies have been performed in order to enhance the cell performance by designing a novel flow field (Bilgili et al. 2015; Shen et al. 2018; Kuo et al. 2008; Afshari et al. 2017; Soong et al. 2005).

Jourdani et al. (2017) developed a three-dimensional PEMFC model to analyze the membrane thickness effect on the single PEMFC performance. Four different membrane thicknesses (125e-6 m, 100e-6 m, 75e-6 m, 50e-6 m) have been studied in order to get the best cell performance after the model validation. It is recorded that, the performance of PEMFC depends strongly on the characteristics of the membrane. Numerical results indicated that higher current densities are obtained using a thinner membrane.

Xia et al. (2018) carried out numerical simulations by using a three-dimensional model of high-temperature PEMFC in COMSOL to investigate the effects of the physical parameters (operating temperature, membrane's thickness and catalyst layer's thickness) on the cell performance. Cell performance is enhanced as the operating temperature increases. It could be drawn from this study, better cell performance has been obtained with a thinner membrane and catalyst layer.

Fadzillah et al. (2015) developed a two-dimensional simulation model by using MATLAB to determine the effects of the gas diffusion layer's thickness and porosity on the cell performance. Simulation results indicated that thinner GDL produced a higher-performance cell. Higher porosity GDL corresponds to better cell performance.
Lee et al. (2004) investigated the effects of the gas diffusion layer's thickness and fabrication method on cell performance. The main goal of this study is to find the optimum gas diffusion layer's thickness and to analyze the characteristics of the electrodes fabricated by several methods.

Ferng et al. (2014) investigated the effects of the different parameters which are PBI loading, operating temperature, gas flow rate, electrode thickness and porosity, and acid doping level to improve the performance of a PBI-based PEMFC. It could be drawn from this study, thinner electrode thickness, higher acid doping level and smaller porosity positively affect the performance of the PBI-based PEMFC.

METHODS

Numerical Model

In this study, numerical simulations are performed based on a single-phase, single-channel proton exchange membrane PEM fuel cell with a conventional flow field by using a commercial flow solver ANSYS FLUENT 18.1 PEM fuel cell add-on module. The PEM fuel cell model consists of major components that are porous membrane, two straight gas flow channels, two catalyst layers (CLs), two gas diffusion layers (GDLs). The geometry of the single-channel PEM fuel cell is generated by using ANSYS Design-Modeler. Parameters of the PEM fuel cell used in the numerical model are shown in Table 1. The mesh structure is created by using ANSYS Meshing for generated geometry. Zone names and types are specified because it is required in the ANSYS FLUENT PEM fuel cell add-on module. Mesh file is uploaded on ANSYS FLUENT, set up the case, set the operating and boundary conditions and run the calculations. Postprocess the results. The model is validated compared to an experimental data is provided in this paper. The model is constructed to replicate the cell employed by Wang et al. (2003). The numerical model has been analyzed by changing one parameter. Three different membrane thicknesses have been selected to see the effects of the membrane thickness on the cell performance. In this same way, the numerical model is analyzed under the three different catalyst layer's thicknesses to see the effect of the catalyst layer's thickness. F-Cycle of Multigrid cycle setting and BCGSTAB (Bi-Conjugate Gradient Stabilization Method) are used to converge the solution for species, potential and saturation equations. The current density values are recorded by taking individual solution for the cell potential values that are 0,45V, 0,50V, 0,55V, 0,60V, 0,65V, 0,70V, 0,75V, 0,80V, 0,85V and 0,90V. Figure 1 shows a good agreement between the simulation and experimental data.

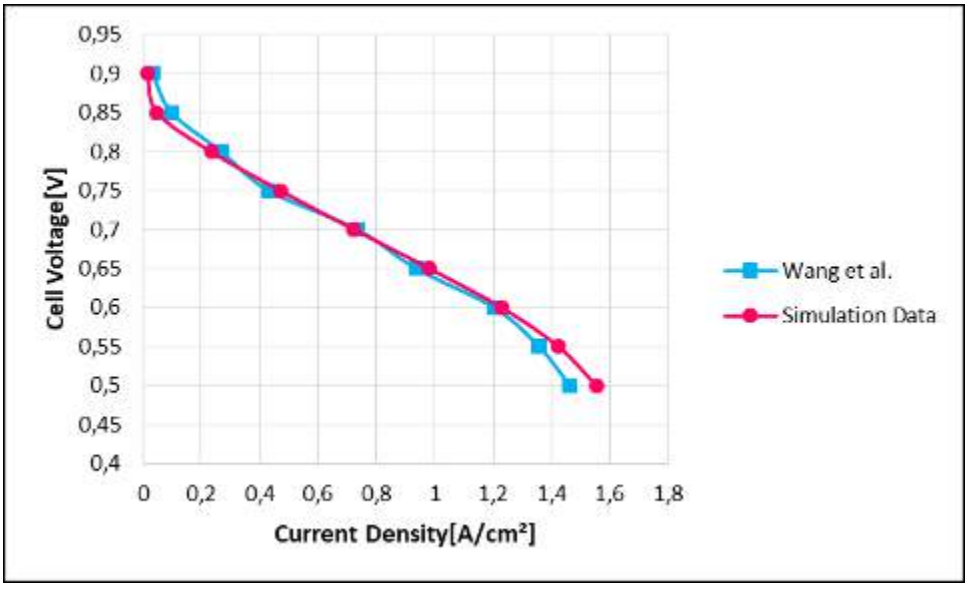

Figure 1. Validation of Simulation Data with Experimental Data

Table 1. Geometric and Electrochemical Parameters

Parameters	Value	Unit
Channel width	1	mm

Channel depth	1	mm
Channel length	70	mm
Active area(XxZ)	0,00021	m^2
Catalyst layer thickness	0,01, 0,02, 0,03	mm
GDL thickness	0,3	mm
Membrane thickness	0,075, 0,1, 0,125	mm
Operating temperature	343	K
Operation pressure	300	kPa
Mass flow rate on the anode side	6e-07	kg/s
Mass flow rate on the cathode side	5e-06	kg/s
Gas diffusion layer porosity	0,5	-
Anodic exchange coefficient at the	1/2	-
Cathodic exchange coefficient at	1/2	-
Anodic exchange coefficient at the	2	-
Cathodic exchange coefficient at	2	-
Reference diffusivity of H_2	3e-05	m^2/s
Reference diffusivity of O_2	3e-05	m^2/s
Viscous resistance of GDL	1e+12	$1/m^2$
Surface/Volume ratio of CL	200000	1/m

Governing Equations

In the CFD model development, the following assumptions are used;
1. The PEM fuel cell operates at steady-state conditions.
2. 3D domain, the single-phase model is presumed.
3. The gas flow regime is laminar and incompressible due to the low velocities.
4. Reactants and products are considered to be ideal gases.
5. The gas diffusion layers, catalyst layers, and membrane are assumed as isotropic and homogeneous.
6. Viscous dissipation and buoyancy effects are negligible.
7. The membrane is impermeable to the water and reactant gases.
8. There is no contact resistance at the interfaces between the different layers.
9. The electrochemical reaction is governed by the Butler-Volmer equation in PEMFC modeling.
10. The membrane is completely moistened and its proton concentration is constant. partial differential equations used for the numerical analysis as follows: mass, momentum, energy, species and charge conservation equations. The gas transport equations for three-dimensional PEMFC can be expressed as follows:

Conservation of mass:

The general conservation of mass is expressed for all processes which are fluid flow, phase change, electrochemical reactions, etc. in fuel cells as follows:

$$\nabla \cdot (\varepsilon \rho v) = 0 \tag{1}$$

Where v, ε, ρ, ∇ are the velocity vector, porosity, density and del operator, respectively.

Conservation of momentum:

$$\nabla \cdot (\varepsilon \rho v v) = -\varepsilon \nabla p + \nabla \cdot (\varepsilon \mu^{eff} \nabla v) + S_m \tag{2}$$

Where p is the fluid pressure, μ^{eff} is dynamic viscosity and S_m is the source term that varies in each region of the fuel cell. In gas channels, the source term of the momentum equation is expressed as $S_m = 0$. In the porous regions, the source term is represented as follows:

$$S_m = -\frac{\mu}{k}\varepsilon^2 v \tag{3}$$

Where k is the permeability of the gas diffusion layers or catalyst layers, ε is the porosity coefficient respectively.

Conservation of energy:

$$(\rho c_p)_{eff} (v \cdot \nabla T) = \nabla \cdot (k_{eff} \nabla T) + S_e \tag{4}$$

Where c_p, T, k and S_e are the specific heat capacity, temperature, thermal conductivity and source term of the energy equation, respectively.

Conservation of species:

$$\nabla \cdot (\varepsilon v C_k) = \nabla \cdot (D_k^{eff} \nabla C_k) + S_k \tag{5}$$

In the porous medium, D_k^{eff} is a function of porosity which is described as a common relationship is given by the Bruggeman model,

$$D_{k,eff} = D_k \varepsilon^{1,5} \tag{6}$$

Where D_k is the species diffusion coefficient. Species volumetric source terms for the PEMFC are expressed as follow:

Source term for hydrogen:

$$S_k = -\frac{M_{w,H_2}}{2F} R_{an} \quad (7)$$

Source term for oxygen:

$$S_k = -\frac{M_{w,O_2}}{4F} R_{cat} \quad (8)$$

Source term for water:

$$S_k = \frac{M_{w,H_2O}}{2F} R_{cat} \quad (9)$$

Conservation of charge:

$$\nabla \cdot (\varepsilon v \phi_e) = -S_\phi \quad (10)$$

RESULTS AND FINDINGS

Thickness Effect of Membrane

The membrane thickness is a key parameter affecting cell performance. In this paper, numerical analyses are carried out to investigate the effect of membrane thickness on the cell performance in three different values which are taken as 0,075 mm, 0,1 mm and 0,125 mm. All other parameters are kept constant. To see the effect of membrane thickness on polarization curve, a total of 30 different boundary conditions are defined in FLUENT. Figure 2 shows the change of current density compared to the cell potential. Power density based on a cell potential is represented as Figure 3. The results indicated that better cell performance can be obtained by using a thinner membrane. Figure 4 shows the largest molar water concentration in the PEMFC at 0,075 mm for the same voltage level. The electrochemical reaction has been accelerated as the membrane thickness decreased. Water formation is increased, and thus ionic resistance is reduced.

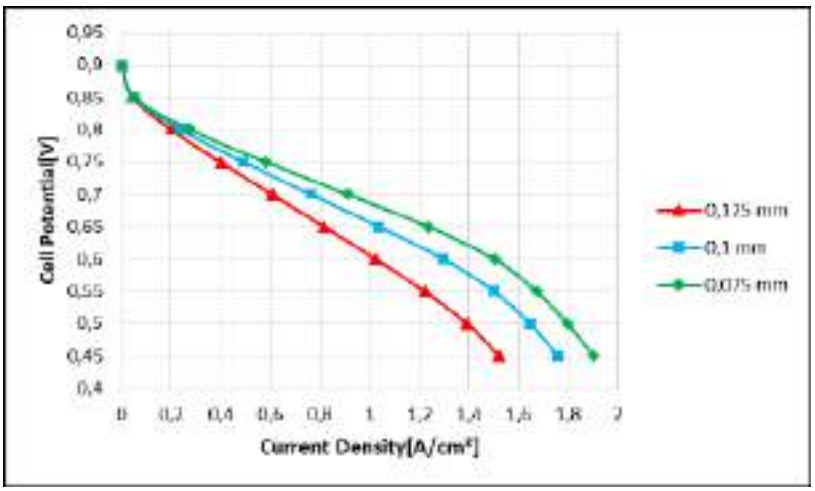

Figure 2. Cell Performance at Different Membrane Thicknesses with I-V Graph

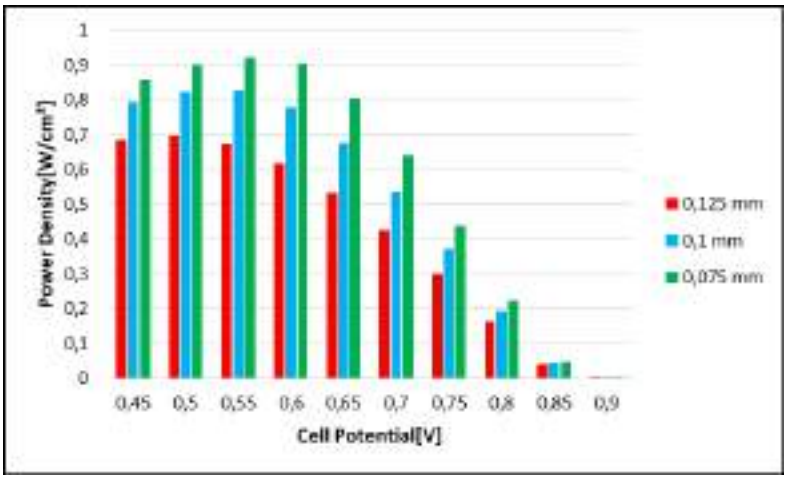

Figure 3. Cell Performance at Different Membrane Thicknesses with V-P Graph

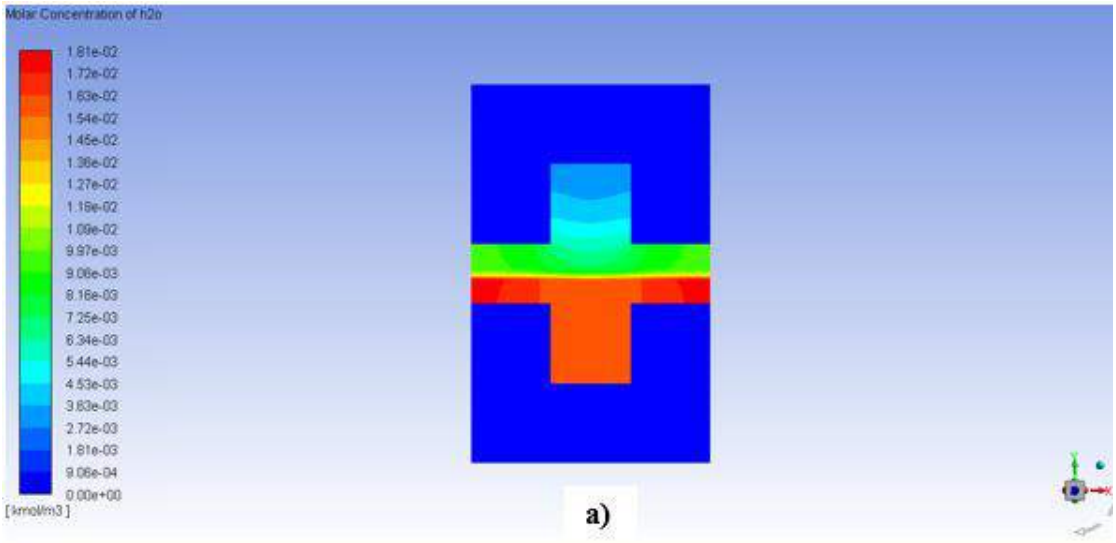
Molar Concentration of h2o
1.81e-02
1.72e-02
1.63e-02
1.54e-02
1.45e-02
1.36e-02
1.27e-02
1.18e-02
1.09e-02
9.97e-03
9.06e-03
8.16e-03
7.25e-03
6.34e-03
5.44e-03
4.53e-03
3.63e-03
2.72e-03
1.81e-03
9.06e-04
0.00e+00
[kmol/m3]

a)

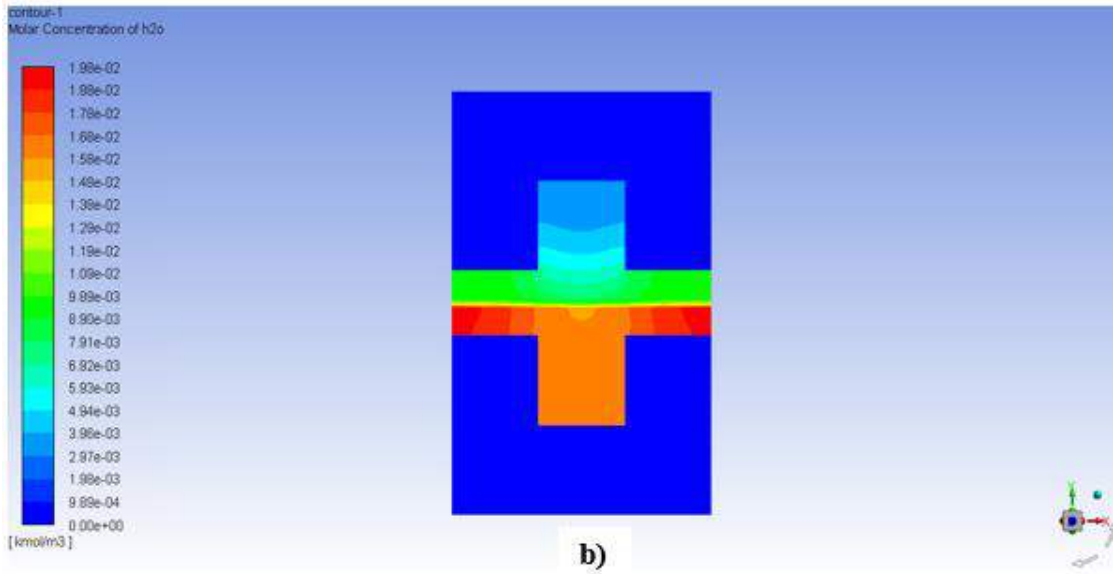
contour-1
Molar Concentration of h2o
1.98e-02
1.88e-02
1.78e-02
1.68e-02
1.58e-02
1.48e-02
1.38e-02
1.29e-02
1.19e-02
1.09e-02
9.89e-03
8.90e-03
7.91e-03
6.92e-03
5.93e-03
4.94e-03
3.96e-03
2.97e-03
1.98e-03
9.89e-04
0.00e+00
[kmol/m3]

b)

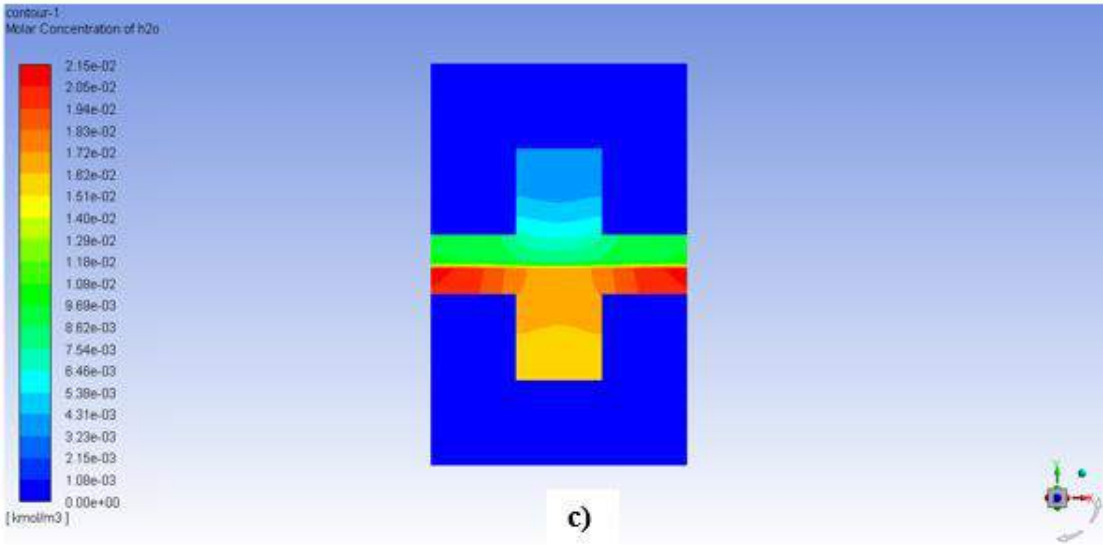
contour-1
Molar Concentration of h2o
2.15e-02
2.05e-02
1.94e-02
1.83e-02
1.72e-02
1.62e-02
1.51e-02
1.40e-02
1.29e-02
1.18e-02
1.08e-02
9.69e-03
8.62e-03
7.54e-03
6.46e-03
5.38e-03
4.31e-03
3.23e-03
2.15e-03
1.08e-03
0.00e+00
[kmol/m3]

c)

Figure 4. Contours of Molar Concentration of H_2O : a) 0,125 mm, b) 0,1 mm, c) 0,075 mm

Thickness Effect of Catalyst Layer

The operating temperature and operating pressure are set as 343 K, 300 kPa respectively, and the proton exchange membrane has a thickness of 0,1 mm. Numerical analyses are performed to investigate the effects of the three different values (0,01 mm, 0,02 mm and 0,03 mm) on cell performance. Figure 5 shows the change of current density compared to the cell potential. Power density based on a cell potential is represented in Figure 6. For the effect of catalyst layer's thickness, the thinner catalyst layer results in best performance of PEMFC.

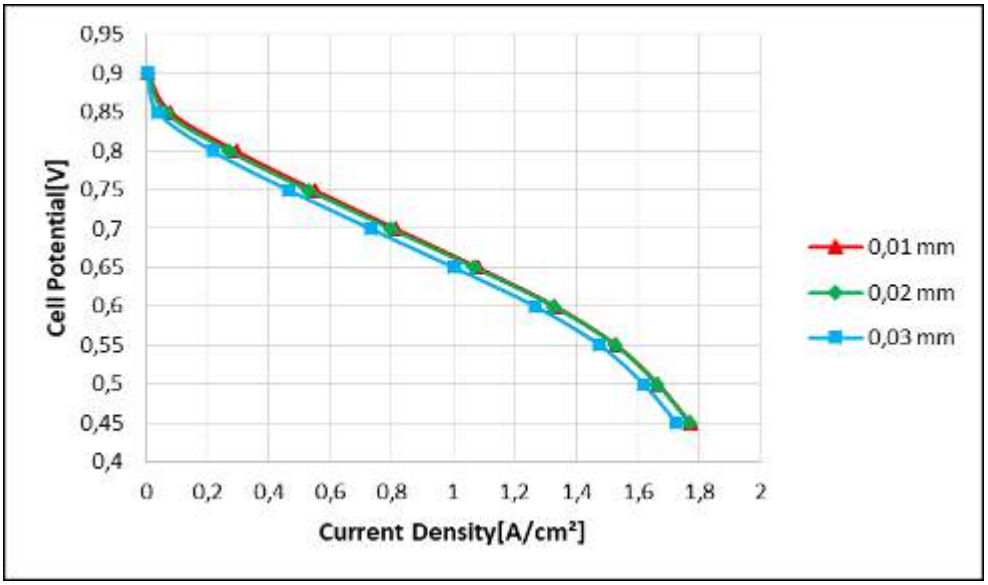

Figure 5. Cell Performance at Different Catalyst Layer's Thicknesses with I-V Graph

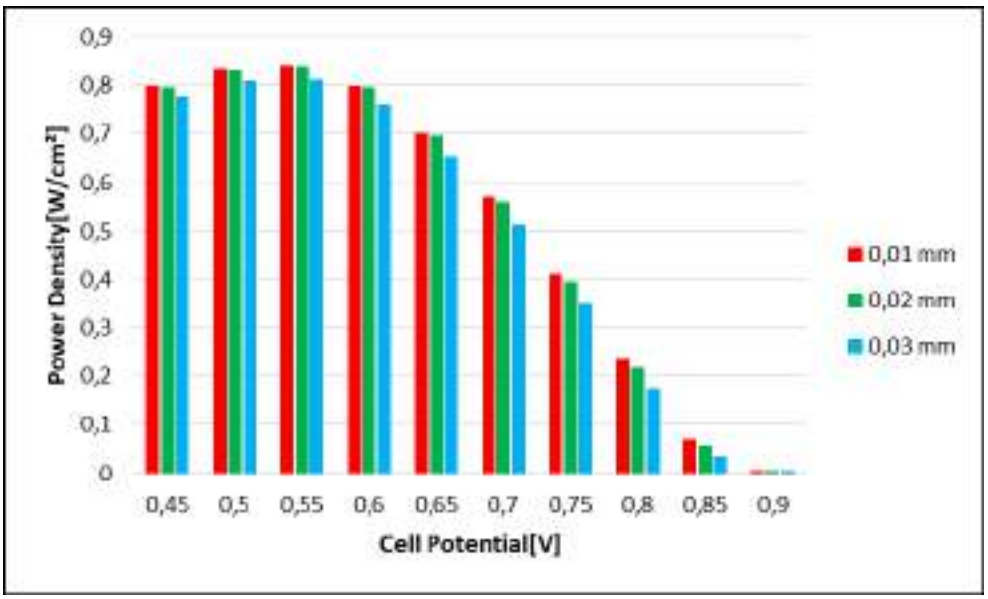

Figure 6. Cell Performance at Different Catalyst Layer's Thicknesses with V-P Graph

CONCLUSION

In this present paper, a 3-D computational model containing a conventional straight flow field is developed to investigate the thickness effects of membrane and catalyst layer on the performance of PEMFC. The numerical model is developed by using ANSYS FLUENT 18.1, a CFD software. The simulation model is validated with experimental data. The governing equations were solved by the finite volume method. Effective cell performance is achieved with decrease of membrane thickness provided that enough humidification. Membrane thicknesses are selected as 0,075 mm, 0,1 mm and 0,125 mm, respectively. The temperature is taken as 343 K. The operating temperature should not be too high because of overheating of membrane. The maximum current density is obtained as 1,90354 A/cm² when the cell potential is 0,45 V and the value of membrane thickness is 0,075 mm. The maximum power density is obtained as 0,91947 W/cm² when the cell potential is 0,55 V and the value of membrane thickness is 0,075 mm. When the catalyst layer's thickness decreases from 0,03 mm to 0,01 mm, improved cell performance has been obtained according to the numerical results. The maximum current density has been obtained as 1,77042 A/cm², when the cell potential is 0,45 V and the values of the catalyst layer and membrane thicknesses are 0,01 mm and 0,1 mm, respectively.

REFERENCES

Sharaf, O. Z. and Orhan, M. F. (2014) 'An overview of fuel cell technology: Fundamentals and applications', Renewable and Sustainable Energy Reviews. Elsevier, 32, pp. 810–853.

Ding, Y., Bi, X., Wilkinson, D.P., 2013. Numerical Analysis on Performance of Polymer Electrolyte Membrane Fuel Cells. Chemical Engineering Science, V.100, p.445-455
Freire, L. S. et al. (2014) 'Influence of operational parameters on the performance of PEMFCs with serpentine flow field channels having different (rectangular and trapezoidal) cross-section shape', International Journal of Hydrogen Energy. Elsevier Ltd, 39(23), pp. 12052–12060.
Khazaee, I., Ghazikhani, M., and Mohammadiun, M. (2012) 'Sharif University of Technology Experimental and thermodynamic investigation of a triangular channel geometry PEM fuel cell at different operating conditions', Scientia Iranica. Elsevier B.V., 19(3), pp. 585–593.
Ahmadi, N. et al. (2016) 'Analysis of the operating pressure and GDL geometrical configuration effect on PEM fuel cell performance', Journal of the Brazilian Society of Mechanical Sciences and Engineering. Springer Berlin Heidelberg, 38(8), pp. 2311–2325.
Caglayan, D. G. et al. (2016) 'Three-dimensional modeling of a high temperature polymer electrolyte membrane fuel cell at different operation temperatures', International Journal of Hydrogen Energy. Elsevier Ltd, 41(23), pp. 10060–10070.
Bilgili, M., Bosomoiu, M. and Tsotridis, G. (2015) 'Gas flow field with obstacles for PEM fuel cells at different operating conditions', International Journal of Hydrogen Energy. Elsevier Ltd, 40(5), pp. 2303–2311.
Shen, J. et al. (2018) 'Performance investigation of PEMFC with rectangle blockages in Gas Channel based on field synergy principle', Heat and Mass Transfer/Waerme- und Stoffuebertragung. Heat and Mass Transfer.
Kuo, J. K., Yen, T. S. and Chen, C. K. (2008) 'Improvement of performance of gas flow channel in PEM fuel cells', Energy Conversion and Management, 49(10), pp. 2776–2787.
Afshari, E., Mosharaf-Dehkordi, M., and Rajabian, H. (2017) 'An investigation of the PEM fuel cells performance with partially restricted cathode flow channels and metal foam as a flow distributor', Energy. Elsevier Ltd, 118, pp. 705–715.
Soong, C. Y. et al. (2005) 'Analysis of reactant gas transport in a PEM fuel cell with partially blocked fuel flow channels', Journal of Power Sources, 143(1–2), pp. 36–47.
Jourdani, M., Mounir, H. and Marjani, A. (2017) 'Three-Dimensional PEM Fuel Cells Modeling using COMSOL Multiphysics', 11(4), pp. 427–442.
Soong, C. Y. et al. (2005) 'Analysis of reactant gas transport in a PEM fuel cell with partially blocked fuel flow channels', Journal of Power Sources, 143(1–2), pp. 36–47.
Xia, L. et al. (2018) 'Investigation of parameter effects on the performance of high-temperature PEM fuel cell', International Journal of Hydrogen Energy. Elsevier Ltd, 43(52), pp. 23441–23449.
Fadzillah, D. M., Nee, C. L. and Rosli, M. I. (2015) 'The model development of gas diffusion layer for PEM fuel cell', International Journal of Mechanical and Mechatronics Engineering, 15(5), pp. 83–89.
Lee, H. K. et al. (2004) 'A study on the characteristics of the diffusion layer thickness and porosity of the PEMFC', Journal of Power Sources, 131(1–2), pp. 200–206.

Ferng, Y. M., Su, A. and Hou, J. (2014) 'Parametric investigation to enhance the performance of a PBI-based high-temperature PEMFC', Energy Conversion and Management, 78, pp. 431–437.
Wang, L. et al. (2003) 'A parametric study of PEM fuel cell performances', International Journal of Hydrogen Energy, 28(11), pp. 1263–1272.

THE INVESTIGATION OF FRESHWATER AND SEAWATER IN KAMIL ABDUS LAGOON AS PART OF WATER POLLUTION CONTROL

Burak YANIK
Marmara University
burakdincer9@hotmail.com

Esin BOZKURT KOPUZ*
Marmara University
esin.bozkurt@marmara.edu.tr

Yeşim GÜRTUĞ
Marmara University
yesim.gurtug@marmara.edu.tr

ABSTRACT: Lagoons should be protected against potential pollutants and hazards as they are used extensively for recreational purposes such as fishing and swimming. In this study, temperature, pH and salinity were measured onsite weekly at three stations in the south of the Kamil Abduş Lagoon (Station 1), north (Station 2) and in the Marmara Sea (Station 3) between 7 November 2018 and 16 April 2019. Water samples were also collected and prepared in the laboratory and heavy metal concentrations (Cu, Cd, Cr, Pb, Ni, Zn, As, Co, Fe, Mn, Se, Ba, Al) were determined by ICP-OES. The temperature varies between 4 and 16.9 °C at stations 1 and 2, while it is between 8.6 and 17.4°C at Station 3. The salinity values at Station 3 where sea water is measured are generally higher than lake salinity values at Station 1 and 2. According to the Water Pollution Regulation, both the pH values of seawater at the station no. 3 and of fresh water at stations 1 and 2 are suitable. The pH ranges at station 1 and 2 indicate the Class I water quality of the lagoon. Stations 1 and 2 were suitable for the fresh water limit of the pH in the EPA Aquatic Life Criteria table, while station 3 exceeded slightly the salt water limit by 8.62 on 20 March 2019. Within the scope of the General Quality Criteria of Sea Water Regulation, at station 3, copper, cadmium, chromium, lead, nickel and arsenic concentrations are below the limit value, but zinc concentration has exceeded the limit value. According to the Quality Criteria of Inland Water Resources, copper, cadmium, chromium, iron, manganese, barium, aluminum I., arsenic, cobalt II, lead, nickel, zinc III., Selenium IV. water quality class.

Key words: sea water, freshwater, lagoon, heavy metal, water quality.

Acknowledgement: This work was supported by Research Fund of the Marmara University. Project Number: FEN-C-YLP-110718-0405

KAMİL ABDUŞ LAGÜNÜ'NDE TATLI VE TUZLU SUYUN SU KİRLİLİĞİNİN KONTROLÜ YÖNETMELİĞİ KAPSAMINDA İNCELENMESİ

ÖZET: Lagünler balıkçılık, plaj gibi rekreasyon amacıyla yoğun bir şekilde kullanıldıklarından dolayı potansiyel kirletici ve tehlikeli kaynaklarına karşı korunmalıdır. Bu çalışmada haftalık olarak 7 Kasım 2018 ve 16 Nisan 2019 tarihleri arasında Kamil Abduş Lagünü'nün güneyinde (İstasyon 1), kuzeyinde (İstasyon 2) ve Marmara Denizi'nde (İstasyon 3) üç istasyonda sıcaklık, pH ve tuzluluk yerinde ölçüldü. Ayrıca su örnekleri toplanarak laboratuvarda hazırlanıp ağır metal konsantrasyonları (Cu, Cd, Cr, Pb, Ni, Zn, As, Co, Fe, Mn, Se, Ba, Al) ICP-OES cihazıyla belirlendi. İstasyon 1 ve 2'de sıcaklık 4 ile 16,9 °C arasında, İstasyon 3'te 8,6 ile 17,4 °C arasında değişmektedir. Deniz suyunun ölçüldüğü İstasyon 3'teki tuzluluk değerleri İstasyon 1 ve 2'deki göl tuzluluk değerlerinden genellikle daha yüksektir. Su Kirliliği Yönetmeliği'ne hem 3 nolu istasyondaki deniz suyunun hem de 1 ile 2 nolu istasyonlardaki tatlı suyun pH değerleri uygundur. 1 ve 2 nolu istasyonlardaki pH aralıkları lagünün I. Sınıf su kalitesini göstermektedir. EPA Akuatik yaşam kriter tablosundaki pH'ın tatlı su sınırına 1 ve 2 nolu istasyonlar uygunken tuzlu su sınırını 3 nolu istasyon sadece 20 Mart 2019'da 8,62 değeri ile çok az aşmıştır. Su Kirliliği Yönetmeliği deniz suyunun genel kalite kriterleri kapsamında 3 nolu istasyonda bakır, kadmiyum, krom, kurşun, nikel ve arsenik konsantrasyonları limit değerin altındadır fakat çinko konsantrasyonu limit değeri aşmıştır. Kıta İçi Su Kaynaklarının Kalite Kriterlerine göre bakır, kadmiyum, krom, demir, mangan, baryum, alüminyum I., arsenik, kobalt II., kurşun, nikel, çinko III., selenyum IV. su kalite sınıfına girmektedir.

Anahtar sözcükler: deniz suyu, tatlı su, lagün, ağır metal, su kalitesi.

Teşekkür: Bu çalışma Marmara Üniversitesi Bilimsel Araştırma Projeleri Koordinasyon Birimince Desteklenmiştir. Proje Numarası: FEN-C-YLP-110718-0405

GİRİŞ

Kamil Abduş Lagünü (Tuzla Balık Gölü), Kocaeli Yarımadası'nın güneybatısıyla Tuzla Yarımadası'nın kuzeyinde konumlanmaktadır. Lagün alanı kıyı bölgesi olduğundan dalga ve akıntıların etkisindedir. Denizden bir kıyı kordonu ile ayrılır. Lagün bir dereyle beslenmekle birlikte özellikle lodoslu havalarda deniz sularının istilası sonucu suları yükselmektedir (Atalay, Ekinci& Bayrak, 2015).

Marmara denizinde 1970 ile 2018 yılları arasında aylık ortalama deniz suyu sıcaklığı 8 ve 24,1°C aralığında değişmektedir (Tarım ve Orman Bakanlığı Meteoroloji Genel Müdürlüğü, 2019). Tuzluluk Karadeniz'de ‰18, Marmara denizinde ‰22 civarındadır.

Kamil Abduş Lagünü denizle bağlantısı olan bir göl olduğundan kendine has ekolojiye sahiptir (Acar, 2003). Kamil Abduş Lagünü coğrafi konumu bakımından mineral su kaynaklarından etkilenmektedir (Ateş Can, 2014 ve Şenol, 2012). Ayrıca Marmara denizinin kıyı morfolojisi sebebiyle Kamil Abduş Lagünü su seviyesi değişimlerinden de etkilenmektedir (Ertek, 2016, Alpar, 2016, Ceylan ve Ceylan, 2010).
Lagün alanındaki doğal ormanlar tahribat sonucu ortadan kalkmıştır. Değişik kuş türleri de tehlike altındadır. Kamil Abduş Lagünü, son yıllarda yapılaşmanın artması ve atık girdisinin kontrol altına alınamaması sonucu bataklık olma tehlikesiyle karşı karşıya gelmiştir. Tuzla tersanelerinin lagüne yakınlığından dolayı tersaneden çıkan atıklar ve Umur Deresi'nin aktığı dönemlerde taşıdığı endüstriyel atıklar lagüne karışmıştır. Lagünün hidrografik yapısında ortaya çıkan ani değişimler biyolojik yapıyı da etkilemiş, ani ölümlere sebep olmuştur. Kıyıda yapılan dolgu alanları, tersane ve limanlar dalgaların aşındırma ve biriktirme faaliyetlerinde kesintilere sebep olmuştur. Bunun sonucunda yapay alanın arkasındaki doğal kıyının gelişimi durmuştur.

Kamil Abduş Lagünü'ndeki tüm bu olumsuz koşullar lagünü kurtarmaya yönelik çalışmaların yapılmasını zorunlu hale getirmiştir. Lagün alanı çevresel ve doğal kültürel özelliklerinden dolayı Kültür ve Tabiat Varlıklarını Koruma Kurulu'nca doğal parka dönüştürülmüş ve 1. Derece sit alanı ilan edilmiştir. Bu nedenle lagünde ve lagünün Marmara Denizi ile bağlantısındaki plajda su kalitesi oldukça önemlidir. DSİ, İBB, Tuzla Belediyesi ve İstanbul Çevre Vakfı'nca sürdürülen Tuzla Ekolojik Diriliş Projesi dâhilinde lagüne doğal su sirkülasyonunun tekrar kazandırılması amaçlanmış, bu proje vasıtasıyla lagünün birçok canlı türüne tekrar yaşam alanı olması bir nebze de olsa sağlanmıştır (Atalay vd., 2015).

Su Kirliliği Kontrolü Yönetmeliği pH limitleri (Tablo 1), deniz suyundaki element konsantrasyonları limitleri (Tablo 2) ve kıta içi su kaynaklarının kalite kriterleri (Tablo 3) bu çalışmada Kamil Abduş Lagününün değerlendirilmesinde kullanılmıştır (EPA Quality Criteria for Water, 1986 ve Gazete, 2004 a,b,c).

Tablo 1. pH Limit Değerleri (EPA Quality Criteria for Water, 1986 ve Gazete, 2004a, b, c)

EPA		SKKY kontrolü göllerin		SKKY	SKKY kıta içi su kaynakları			
Tatlı su	Tuzlu su	Rekreasyon	Çeşitli kullanımlar	Deniz suyu	I. Sınıf	II. Sınıf	III. Sınıf	IV. Sınıf

6,5-9	6,5-8,5	6,5-8,5	6-10,5	6,0-9,0	6,5-8,5	6,5-8,5	6,0-9,0	6,0-9,0 dışında

Tablo 2. SKKY Deniz Suyunun Genel Kalite Kriterleri (Gazete, 2004b)

Element	Limit (µg/L)
Bakır	10
Kadmiyum	10
Krom	100
Kurşun	100
Nikel	100
Çinko	100
Arsenik	100

Tablo 3. SKKY Kıta İçi Su Kaynaklarının Sınıflarına Göre Kalite Kriterleri (Gazete, 2004c)

Element	I. Sınıf	II. Sınıf	III. Sınıf	IV. Sınıf
Bakır (µg Cu/L)	20	50	200	> 200
Kadmiyum (µg Cd/L)	3	5	10	> 10
Krom (toplam) (µg Cr/L)	20	50	200	> 200
Kurşun (µg Pb/L)	10	20	50	> 50
Nikel (µg Ni/L)	20	50	200	> 200
Çinko (µg Zn/L)	200	500	2000	> 2000
Arsenik (µg As/L)	20	50	100	> 100
Kobalt (µg Co/L)	10	20	200	> 200
Demir (µg Fe/L)	300	1000	5000	> 5000
Mangan (µg Mn/L)	100	500	3000	> 3000
Baryum (µg Ba/L)	1000	2000	2000	> 2000
Alüminyum (µg Al/L)	300	300	1000	> 1000
Sıcaklık (°C)	25	25	30	> 30

Kamil Abduş Lagünü'nde 1990 yılında Orhon ve Kıratlı tarafından yapılan çalışmada lagündeki çözünmüş oksijenin düşük, Ni ve Fe haricindeki ağır metallerin uygun değerlerde olduğu tespit edilmiştir (Acar, 2003). Kayhan ve Özhatay'ın çalışmasında ise Kamil Abduş Lagünü'nde kadmiyum (Cd), alüminyum (Al) ve demir (Fe) birikimi insan, balık, kuş ve diğer canlılar açısından incelenmiştir. Dünya Sağlık Örgütü (WHO), Avrupa Komisyonu (CEU) ve T.C. Çevre ve Şehircilik Bakanlığı standartlarıyla karşılaştırılmıştır.

Cd değerlerinin yüksek, Al ve Fe değerlerinin ise normal düzeylerde olduğu belirtilmiştir (Kayhan ve Özhatay, 2004).

İstanbul'daki göller; Terkos, Ömerli, Elmalı, Alibey, Darlık, Samandıra (Aydos), Sazlıdere, Çatalca Büyükkokmuşgöl ve Küçükkokmuşgöl iken lagünler Büyükçekmece, Küçükçekmece ve Kamil Abduş Lagünü'dür. Bu göllerin arasında Kamil Abduş Lagünü flora ve fauna açısından 1. Derece Doğal Sit olarak tescil edildiğinden (T.Ü.İ.K., 2014) ve lagünün Marmara denizi ile bağlantısında plaj bulunduğundan su kalitesi oldukça önemlidir.

İstanbul'da Marmara denizinde rekreasyon amacıyla kullanılan 3 plajdaki su kalitesi parametrelerinden nikel ve kurşun ağır metalleri 2009 yılında Su Kalitesi Yönetmeliğindeki limit değerlerin altında gözlenmiştir (Bozkurt vd., 2014).

Meksika'nın Pasifik kıyılarında 2013-2014 yıllarında pH, iletkenlik, tuzluluk, ağır metal konsantrasyonları (arsenik, bakır, kadmiyum, krom, civa, nikel, kurşun ve çinko) limit değerlerin altında (Pérez-Moreno vd., 2016) iken Endonezya'nın Palu kıyılarında ağır metal konsantrasyonları (çinko ve kurşun) limit değerlerin üzerindedir (Rahmadani vd., 2015).

Güllük Lagünü'nde Haziran 2011 ve Mayıs 2012 tarihleri arasında yapılan çalışmada sıcaklık, pH, iletkenlik ve tuzluluk değerleri normal seviyelerde tespit edilmiş olup, çözünmüş oksijen değerlerinin lagünün kimi bölgelerinde yaşamı güçleştirecek kadar düşük olduğu belirlenmiştir (Özdemir ve Alparslan, 2013).

Balık Gölü'nde (Samsun) 2010 yılında ilkbahar (Nisan/Mayıs) ve sonbahar (Ekim/Kasım) karışım dönemlerinde yapılan çalışmada; sonbahar döneminde tuzluluğun artması sonucu iletkenliğin de arttığı, tuzluluktaki artışın sebebinin sonbahar döneminde denizle bağlantıyı sağlayan boğazdan gölün iç kesimlerine giren tuzlu su olduğu, pH ve çözünmüş oksijen değerlerinin doğal koruma alanları bazında kritik düzeylerde olduğu ve gölün III.sınıf su kalitesine sahip olduğu tespit edilmiştir (Cüce vd., 2011).

Romanya'daki Razim-Sinoie Lagün Sistemi'nde 2016 yılında Mayıs ve Ağustos olmak üzere iki dönemde yapılan çalışmada; pH değerleri bazik sulara yakın olarak ölçülmüş, Golovita, Zmeica ve Sinoie göllerinde krom değerlerinin araştırılan diğer metallere (Cu, Zn, Fe, Mn, Ni) nazaran yüksek olduğu tespit edilmiştir. Çalışmada sistemdeki çevresel koşulların iyi olduğu ve su örneklerinin de bunu yansıttığı belirtilmiştir (Catianis vd., 2018).

Akyatan Lagünü'nde Aralık 2007 ve Kasım 2008 tarihleri arasında yapılan çalışmada; lagün boyunca alkali bir ortam (pH dolayısıyla) tespit edilmiştir (Demir vd., 2014).

Arnavutluk'taki Karavasta Lagünü'nde 2013 yılında yapılan çalışmada; pH, 3. ve 4. İstasyonlarda yüksek bulunmuştur. Buna sebep olarak fitoplankton yoğunluğundan kaynaklanan yüksek fotosentez oranı gösterilmiştir. Çözünmüş oksijen değerlerinin iyi bir biyolojik verimliliği işaret ettiği belirtilmiştir. Sudaki bakır ve krom konsantrasyonları yüksek, kadmiyum ve çinko konsantrasyonları düşük bulunmuştur. Bakır konsantrasyonunun yüksek olmasına sebep olarak lagün çevresinde yapılan tarımsal faaliyetler gösterilmiştir (Koto vd., 2014).

Meksika'nın Karayip kıyılarında (Akumal kasabası) Eylül 2007 ve Eylül 2008 tarihleri arasında yapılan çalışmada; en yüksek sıcaklık deniz suyunda, en düşük sıcaklıklar kaynaklarda ve Lagartos Lagünü'nde ölçülmüştür. En yüksek pH deniz suyunda, en düşük pH ise Akumal Körfezi'nin güneyindeki bir kaynakta tespit edilmiştir. Akumal Körfezi'ndeki sualtı kaynağı en düşük tuzluluğa sahip olup, en yüksek değerler deniz suyunda elde edilmiştir (Hernández-Terrones vd., 2015).

Karagöl'de (Sivas) Kasım 2011 ve Kasım 2012 tarihleri arasında yapılan çalışmada; göl sıcaklık ve iletkenlik bakımından iyi durumda (SKKY göre I.sınıf) bulunmakla birlikte pH değerleri suyun bazik karakterde olduğunu (SKKY göre I – III. Sınıf) göstermektedir. Göl suyu Cd ve Pb elementleri bakımından I. Sınıftır. Cu elementi kışın tespit edilmezken ilkbaharda birden artış gösterdiği görülmüştür. Buna sebep olarak göl çevresindeki meyve bahçelerinde bakım ve budama işlemlerinde kullanılan bordo bulamacı (göztaşı) gösterilmiştir. Dolayısıyla Cu elementi açısından gölün su kalitesi SKKY göre II. Sınıftır. Fe elementi kış aylarında düşük seviyelerdeyken ilkbaharda en yüksek değerine ulaşmıştır. Bu bakımdan gölün su kalitesi SKKY göre I. Sınıftır (Mutlu vd., 2013).

Uluabat Gölü'nde Haziran 2008 ve Mayıs 2009 tarihleri arasında yapılan çalışmada sıcaklık ve iletkenliğin yazın maksimum, kışın minimum değerlerde olduğu gözlenmiştir. pH değerleri göl sularının bazik karakterde olduğunu göstermektedir. Çözünmüş oksijen değerleri kış mevsiminde yüksek, yaz mevsiminde düşük seviyelerde gözlenmiştir (İleri vd., 2014).

Tecer Gölü'nde (Sivas) Mart 2011 ve Şubat 2012 tarihleri arasında yapılan çalışmada; sıcaklık uygun değerlerde bulunmuş olup (SKKY göre I.Sınıf), pH değerlerine göl suyu biraz bazik olarak (SKKY göre I – II.Sınıf) nitelendirilmiştir. Çözünmüş oksijen uygun seviyelerde olup (SKKY göre I.Sınıf), iletkenlik değerlerine göre de su kalitesi SKKY göre I.Sınıftır. Göl suları Pb değerleri açısından SKKY göre II.Sınıf, Cd değerleri açısından ise III.Sınıf olarak nitelendirilmiştir. Cu değerleri kışın iz seviyelerdeyken ilkbaharda birden artış göstermiştir. Buna sebep olarak (yine Sivas'ta bulunan Karagöl'de olduğu gibi) göl çevresindeki meyve bahçelerinde bakım ve budama işlemlerinde kullanılan bordo bulamacı (göztaşı) gösterilmiştir. Bundan dolayı su kalitesi Cu değerleri açısından SKKY göre II.Sınıf özelliği göstermektedir (Mutlu vd., 2018).

Arnavutluk'ta Butrinti Lagünü'nde 2011 yılı Ağustos ayı boyunca yapılan çalışmada pH değerleri lagün suyunun bazik karakterde olduğunu göstermekte olup, çözünmüş oksijen değerlerinin lagünün biyolojik verimliliğini olumlu etkilediği belirtilmiştir. Pb değerlerinin bir istasyon hariç AB standartlarının (7,2 µg/L) altında olduğu, yine Cd değerlerinin de standart değerin (1 µg/L) altında ölçüldüğü belirtilmiştir. Cr değerleri yüzeyde WHO limit değerinin (50 µg/L) altında iken dipte sadece iki istasyonda bu değerin üzerindedir. Cu değerlerinin de aynı şekilde limit değerlerin altında olduğu tespit edilmiştir (Topi vd., 2012).

Kolombiya, Cartagena Körfezi'nde Eylül 2014 ve Ağustos 2015 tarihleri arasında Tosic ve diğ. tarafından yapılan çalışmada tuzluluğun yağmur mevsiminde azaldığı tespit edilmiştir. Buna sebep olarak da aynı dönemde kanaldan körfeze yapılan tatlı su deşarjı gösterilmiştir. Sıcaklığın hem yüzey sularında hem de dip sularında kuru/rüzgârlı mevsim boyunca düşük olduğu belirlenmiştir. Yağmur mevsimi boyunca derinlerde çözünmüş oksijen değeri 4 mg/L'nin altına düşerken, mevsim geçişlerinde yüzeye yakın sularda da benzer durum görülmüştür (Tosic vd, 2017).

Tunus Lagünü'nün güney kısmında Abidi ve diğ. tarafından Temmuz 2013 ve Şubat 2014 olmak üzere iki farklı dönemde gerçekleştirilen çalışmada, sıcaklık ve tuzluluk değerlerinin mevsimsel olarak değişkenlik gösterdiği görülmüştür. pH değerleri lagün sularının bazik karakterde olduğunu göstermektedir (Abidi vd., 2018).

Meksika'nın Karayip kıyılarındaki Bacalar Lagünü'nde Tobón Velázquez ve diğ. tarafından Kasım 2016 ve Haziran 2017 olmak üzere iki farklı dönemde gerçekleştirilen çalışmada, düşük iletkenlik değerlerinin bir tatlı su sistemini işaret ettiği belirtilmiş olup, sıcaklık değerlerinin iki dönemde de stabil olduğu gözlenmiştir. pH değerleri göl sularının yer yer asidik karakterde olduğunu göstermektedir (Tobón Velázquez vd., 2019).

Fransa'da Bages-Sigean ve Canet-St.Nazaire lagünlerinde Vouvé ve diğ. tarafından Mart 2009, Haziran-Temmuz 2009 ve Ekim 2009 olmak üzere üç farklı dönemde gerçekleştirilen çalışmada, tuzluluk değerlerinin Bages-Sigean Lagünü'nün kuzey kısmının tatlı su etkisi altında, güney kısmının ise deniz etkisi altında olduğunu gösterdiği belirtilmiş olup; en yüksek tuzluluk değerinin Canet-St.Nazaire Lagünü'nde elde edildiği görülmüştür. pH değerleri lagünlerdeki suyun çoğunlukla bazik karakterde olduğunu göstermektedir. Cu değerleri Bages-Sigean Lagünü'nün güney kısmında yüksekken lagünün kuzey kısmında Cd değerleri yüksektir. Canet-St.Nazaire Lagünü'nde Cu değerleri Bages-Sigean Lagünü'nden daha yüksek olup, Cd değerleri hemen hemen aynı seviyededir (Vouvé vd., 2014).

Arnavutluk'ta Narta Lagünü'nde Kotori ve diğ. tarafından Eylül 2013 tarihinde yapılan çalışmada; pH değerleri normal seviyelerde tespit edilmiştir (Kotori vd., 2015).

Adıyaman'da Gölbaşı Gölü'nde Uçkun tarafından Ağustos 2017 ve Kasım 2017 olmak üzere iki farklı dönemde gerçekleştirilen çalışmada; gölün su kalitesi fizikokimyasal parametreler açısından I.sınıf olarak belirlenmiştir. Hem Ağustos hem de Kasım dönemlerinde en yüksek konsantrasyona sahip olan metalin krom olduğu tespit edilmiştir. Sudaki toplam metal konsantrasyonunun Ağustos döneminde Kasım dönemine göre genelde daha yüksek olduğu belirtilmiştir. Ağustos ve Kasım dönemleri arasında krom ve çinko konsantrasyonlarında belirgin farklılıklar tespit edilmiştir. Ancak, sudaki metal konsantrasyonlarının EPA'ya ait içme sularında izin verilen maksimum ağır metal konsantrasyonları limit değerlerinin altında olduğu ilave edilmiştir (Alkan, 2019).

İskenderun Körfezi'nde Göycıncık ve diğ. tarafından Kasım 2014 ve Mart 2015 tarihleri arasında yapılan çalışmada; Al, Cr, Fe, Cu, Se konsantrasyonlarının yüksek, Ni ve As konsantrasyonlarının düşük olduğu tespit edilmiştir (Tarım ve Köy İşleri Bakanlığı'nın "Su Ürünleri Yönetmeliği"nde belirtilen limit değerlere göre). Elde edilen sonuçlara göre İskenderun Körfezi'nin Al, Cr, Fe, Cu, Se yönünden kirlenmeyle karşı karşıya kaldığı belirtilmiştir. Ancak Ni ve As konsantrasyonlarının kimi aylarda farklılıklar gösterdiği tespit edilmiş olup; bunun sebebinin arıtılmış ve arıtılmamış suların bölgeye deşarjı ve liman ve insan kaynaklı faaliyetlerin oluşturduğu mevsimsel farklılıklar olduğu ifade edilmiştir. Özellikle K istasyonundan alınan örneklerde Ni, Fe, Cr ve Al konsantrasyonlarının diğer istasyonlara göre oldukça yüksek olduğu gözlenmiştir. Buna sebep olarak bölgeye yapılan evsel atık kaynaklı deşarjlar gösterilmiştir (Göycıncık vd., 2018).

Bafa Gölü'nde Kara tarafından 2018 yılı Nisan ayında yapılan çalışmada; göldeki ağır metal konsantrasyonları ölçülmüş, göl suları S.K.K.Y'ye göre 1.sınıf olarak tespit edilmiştir. Ayrıca toksik ve antropojenik olabilen As, Cd, Cr, Pb, Co ve Ni elementlerine ait konsantrasyon değerlerinin Yerüstü Su Kalitesi Yönetmeliği'ndeki yıllık ortalama ve maksimum çevresel kalite standartlarına uygun olduğu belirtilmiştir. Al, Cu ve Zn konsantrasyonları bazı ölçüm noktalarında standartların biraz üzerinde ölçülmüştür. Ayrıca gölde ölçülen element konsantrasyonlarının sulama ve hayvansal içme suyu kullanım amaçları için uygun değerlerde olduğu tespit edilmiştir (Kara, 2019).

Eğirdir Gölü'nde Bulut ve Kubilay tarafından Nisan 2013 ve Ocak 2014 tarihleri arasında yapılan çalışmada; sıcaklık değerlerinin standartlara uygun olduğu, pH değerlerinin biraz yüksek olmasına karşın (göl çevresindeki kireç taşlarından dolayı) standartları aşmadığı tespit edilmiştir (Bulut ve Kubilay, 2019).

Tunus'da Gabes Körfezi'nde El Zrelli ve diğ. tarafından 2013 yılı Eylül ayında yapılan çalışmada; pH değerleri 3 istasyonda (CE, LG ve GH1) standartların altında tespit edilmiş; bunun sebebi olarak endüstri kaynaklı deşarjlar gösterilmiştir. Yine aynı istasyonlarda su sıcaklığının standartları aştığı, Cd, Zn ve Cr konsantrasyonlarının da yüksek değerlerde olduğu belirtilmiştir (El Zrelli vd., 2018).

İspanya'da Mar Menor Lagünü'nde Pérez-Ruzafa ve diğ. tarafından Ocak 2010 – Haziran 2012, Şubat 2016 - Aralık 2017 ve Ocak 2018 - Kasım 2018 olmak üzere üç farklı dönemde gerçekleştirilen çalışmada, sıcaklık ve tuzluluk değerlerinin ötrofikasyon aşamaları boyunca uygun değerlerde olduğu belirtilmiştir (Pérez-Ruzafa vd., 2019).

İran'da Gomishan Lagünü'nde Basatnia ve diğ. tarafından Temmuz 2010 ve Aralık 2010 tarihleri arasında yapılan çalışmada; su sıcaklığının Temmuz ayı hariç uygun değerlerde olduğu, pH değerlerinin de standartlara uygun olduğu tespit edilmiştir. Tuzluluk değerlerinin ölçüm periyodu boyunca artış gösterdiği, ancak Hazar Denizi'nden büyük miktarlarda su girişi olduğu zamanlarda gölün orta kısımlarında düşüş gösterdiği belirtilmiştir. Çözünmüş oksijen özellikle gölün kuzey kesimlerindeki iyi havalanmadan dolayı yüksek değerlerde ölçülmüştür (Basatnia vd., 2018).

Kolombiya'da Juan Polo Lagünü'nde Baldiris-Navarro ve diğ. tarafından 2001 ve 2015 yılları arasında yürütülen çalışmada; pH değerlerinin standartlara uygun olduğu belirtilmiş; tuzluluk değerlerinin geniş bir aralıkta (%2 – 53,2) değişim gösterdiği, bunun lagünün çoğunlukla yağmurlu mevsimde gerçekleşen tuzlanmasının bir işareti olduğu ve sebep olarak da lagün ile deniz arasında devamlı bir etkileşimin olmayışı gösterilmiştir (Baldiris-Navarro vd., 2018).

Küba'da El Cobre Blue Lagünü'nde Rodríguez Gámez ve diğ. tarafından Şubat 2017 ve Nisan 2017 tarihleri arasında yapılan çalışmada; su sıcaklığı değerlerinin standartlara uygun olduğu, pH değerlerinin ise standartların altında olduğu tespit edilmiştir. Özellikle pH değerlerinden dolayı göl suları ortalama düzeyde asidik ve fazlasıyla oligohalin olarak nitelendirilmiştir. Çözünmüş oksijen değerleri ise standartların üzerinde tespit edilmiştir (Gámez vd., 2019).

YÖNTEM

Kamil Abduş Lagünü'nde, çevresel kirliliğin araştırılması amacıyla sahada belirlenen 3 istasyonda (Şekil 1a) 6 ay boyunca her hafta sıcaklık, pH ve tuzluluk ölçülerek su numunesi toplanmıştır ve laboratuvarda hazırlanan numunelerde ağır metal konsantrasyonları İndüktif Eşleşmiş Plazma Optik Emisyon Spektrometresi (ICP-OES) cihazıyla (Şekil 1b) belirlenmiştir. Birinci istasyon tersane yakınındaki lagünün kuzeyi, ikinci istasyon lagünün güneyi ve üçüncüsü Marmara Denizi'ne girilen Tuzla Halk Plajı'dır.

Polietilen şişeler %40 nitrik asit içeren deiyonize su içinde 24 saat bekletildikten sonra deiyonize su cihazından (ELGA purelab) su ile 3 kez çalkalanmış (Şekil 2a) ve etüvde (Binder) kurutulmuştur. Numuneler, 3-4 m uzunluğundaki teleskopik çubuğun tepesine tutturulmuş olan beher kullanılarak (Şekil 2b), yüzeyin 50 cm altında bir derinlikten alınmıştır. Numune şişeleri, deniz suyu ile üç kez çalkalandıktan sonra, şişeler tamamen doldurulmuştur. Deniz suyunun sıcaklık, pH ve tuzluluk değerleri denizin altına batırılmış ölçüm cihazının (WTW) probları ile belirlenmiştir (Şekil 2c). Daha sonra, Strickland & Parsons, 1968'deki yöntemlere göre analiz için Marmara Üniversitesi laboratuvarına transfer edilmek üzere örnekler buz üzerinde saklanmıştır. Laboratuvarda, örnekler 0,45 µm PTFE filtreden (Sartorius) steril şırınga ile süzülmüştür (Şekil 2d). Mikropipet (Brand) kullanılarak (Şekil 2e) %2 nitrik asit (Merck) ilave edilmiş ve cihazda analiz başlayana kadar buzdolabında saklanmıştır. Tüm numunelerde (Şekil 2f) ICP-OES (Spectro Blue marka) cihazı ile metal konsantrasyonları belirlenmiştir.

İndüktif Eşleşmiş Plazma Optik Emisyon Spektrometresi (ICP-OES) tekniği ile plazma içerisinden geçirilen numunelerin ışığının optik özelliklerine bağlı olarak dalga boylarına göre elementlerin kalitatif ve kantitatif analizi yapılır. Katı numuneler ekstraksiyon ya da parçalama sonrası cihaza verilirken sıvı ve gazlar doğrudan verilir. Bu teknik numunenin plazmanın yaklaşık 6000-10000 °C sıcaklığına maruz kalarak gaz fazına geçtiğinde atomların emisyon ölçümüne dayanır. Numune çözeltisinin plazma yüksek ısısı ile iyonlaşarak kütle ağırlıklarına göre elementlerin tayinini yapan İndüktif eşleşmiş plazma-kütle spektrometresi (ICP-MS) tekniğinde ppt dedeksiyon limitinde ölçüm yapılabilirken ICP-OES'te ppb seviyesinde ölçüm yapılabilir. Gaz faz atomlarının konsantrasyonunu ölçmek için ışığın absorpsiyonunun kullanıldığı Atomik Absorpsiyon Spektrometresinde katot ve anot arasında yüksek bir voltaj geçirilir ve metal atomları belli bir emisyon spektrumuyla ışık üretir. ICP; Atomik Absorpsiyon Spektrometresinden daha hızlıdır ve aynı anda 69 elementi analiz edebilir.

Şekil 1. (a) Araştırma Alanı: 1. İstasyon Kamil Abduş Lagününün Tersane Yakınındaki Kuzeyi, 2. İstasyon: Lagünün Güneyi Ve 3. İstasyon: Tuzla Halk Plajı (b) ICP-OES cihazı

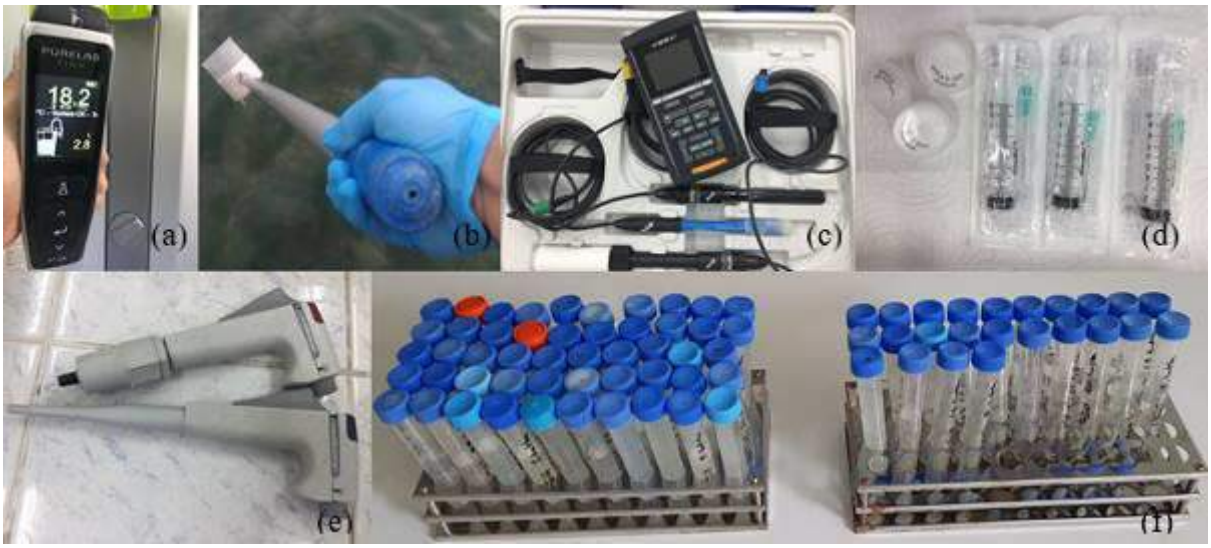

Şekil 2. (a) Deiyonize Su Cihazı, (b) Numune Toplama Aparatı, (c) Sıcaklık, pH Ve Tuzluluk Ölçüm Cihazı, (d) Filtre Ve Şırıngalar, (e) Mikropipetler (f) Laboratuvarda Hazırlanan Numuneler

BULGULAR

Lagünde sıcaklık değerleri Kasım ayında 13,3 ve 16,9°C arasında, Aralık ayında 6,2 ve 10,2°C arasında, Ocak ayında 4,0 ve 9,7°C arasında, Şubat ayında 6,5 ve 11,2°C arasında, Mart ayında 9,7 ve 15,9°C arasında ve Nisan ayında 14,5 ve 19,1°C arasında ölçülmüştür (Şekil 3a). pH değerleri Kasım ayında 7,40 – 8,28 arasında, Aralık ayında 8,02 – 8,16 arasında, Ocak ayında 8,10 – 8,22 arasında, Şubat ayında 8,16 – 8,29 arasında, Mart ayında 8,22 – 8,36 arasında ve Nisan ayında 8,11 – 8,19 arasında ölçülmüştür (Şekil 3b). Tuzluluk değerleri ölçüm süresi boyunca 19,68 – 23,24 değerleri arasında değişiklik göstermiştir (Şekil 3c).

Denizde ise sıcaklık değerleri Kasım ayında 14,7 ve 17,4°C arasında, Aralık ayında 8,9 ve 12,8°C arasında, Ocak ayında 9,1 ve 10,8°C arasında, Şubat ayında 9,1 ve 9,7°C arasında, Mart ayında 8,6 ve 12,7°C arasında ve Nisan ayında 15,4 ve 16,3°C arasında ölçülmüştür. pH değerleri Kasım ayında 8,36 – 8,40 arasında, Aralık ayında 8,06 – 8,29 arasında, Ocak ayında 6,75 – 8,24 arasında, Şubat ayında 8,25 – 8,51 arasında, Mart ayında 8,35 – 8,62 arasında ve Nisan ayında 8,34 civarında ölçülmüştür. Tuzluluk değerleri ölçüm süresi boyunca 19,68 – 23,24 değerleri arasında değişiklik göstermiştir.

Alüminyum, arsenik, baryum, krom, mangan, demir, kobalt, nikel, bakır, çinko, kurşun, kadmiyum, selenyum konsantrasyonları sırasıyla 0,574-266,102, 2,765-25,808, 0,474-55,185, 0,638-9,732, 0,413-97,097, 1,191-187,333, 0,479-13,271, 1,017-127,92, <0,1818, 1,725-942,685, 4,706-30,75, 0,098-2,132, 0,937-28,411 aralığındadır (Şekil 4).

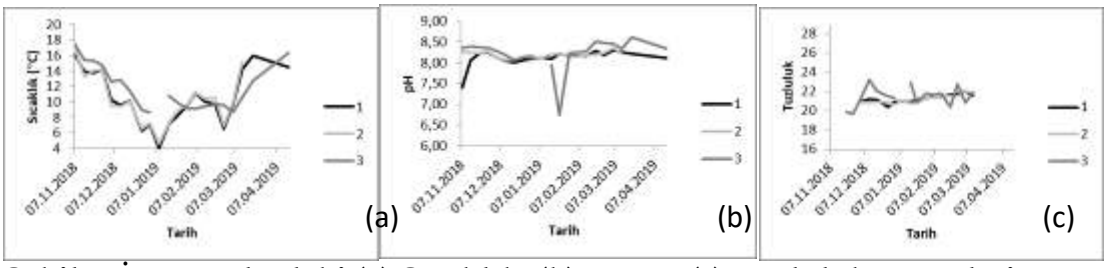

Şekil 3. İstasyonlardaki (a) Sıcaklık, (b) pH Ve (c) Tuzluluk Değerleri

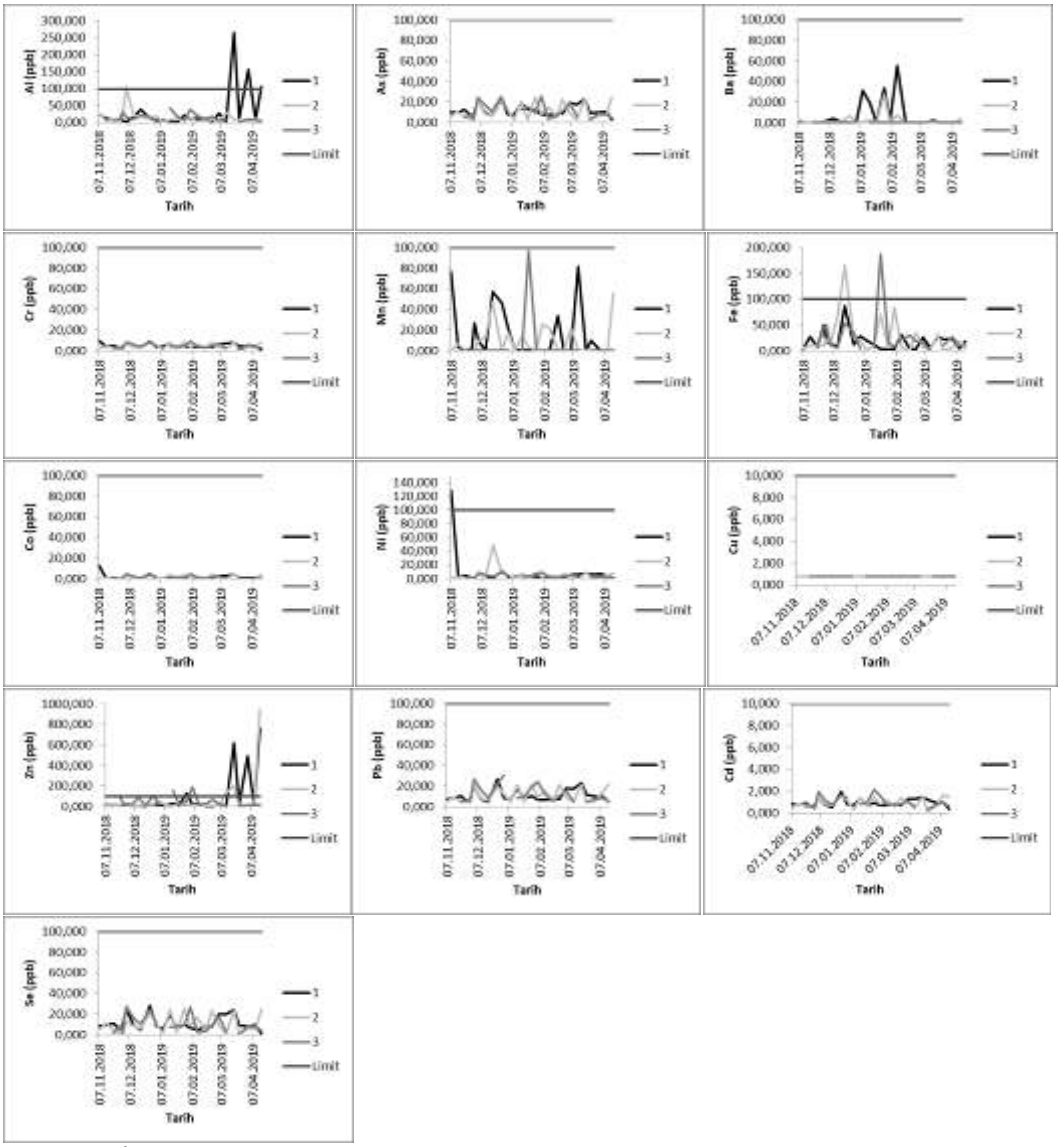

Şekil 4. İstasyonlardaki Ağır Metal Konsantrasyonları

2009 yılında Küçüksu, Fenerbahçe ve Suadiye sahillerinde Bozkurt ve diğ. yapılan çalışma ile kıyaslandığında; sıcaklık değerleri Şubat ayında Küçüksu ve Fenerbahçe sahillerine göre yüksek, Suadiye sahili ile uyumludur. Mart ayında Küçüksu sahiline göre yüksek, Fenerbahçe ve Suadiye sahilleri ile uyumludur. Nisan ayında üç sahile göre de düşüktür. pH değerleri Şubat ve Mart aylarında üç sahile göre de yüksektir. Nisan ayında üç sahille de uyumludur. Ni ve Pb değerleri üç sahile göre de düşüktür.

2013 yılında Meksika'da Playa Blanca, El Calvario ve Troncones kıyılarında Pérez-Moreno ve diğ. tarafından yapılan çalışma ile kıyaslandığında; sıcaklık ve iletkenlik değerleri üç kıyıya göre de düşüktür. pH değerleri sonbaharda Playa Blanca ve El Calvario kıyılarına göre yüksek, Troncones kıyısına göre düşüktür. Kışta Playa Blanca

kıyısına göre düşük, El Calvario ve Troncones kıyılarına göre yüksektir. İlkbaharda üç kıyıya göre de yüksektir. As değerleri üç kıyıya göre de yüksek olup Cd, Cu, Cr, Ni, Pb ve Zn değerleri üç kıyıya göre de düşüktür.

2013 yılında Karavasta Lagünü'nde Topi ve diğ. tarafından yapılan çalışma ile kıyaslandığında; sıcaklık ve pH değerleri tüm istasyonlara göre düşüktür. İletkenlik değerleri 1 ve 2. İstasyonlarla uyumlu, diğer istasyonlara göre yüksektir. Cu ve Cr değerleri tüm istasyonlara düşük olup Cd ve Pb değerleri tüm istasyonlara göre yüksektir.

2010 yılında Gomishan Lagünü'nde Basatnia ve diğ. tarafından yapılan çalışma ile kıyaslandığında; sıcaklık değerleri Kasım ve Aralık aylarında lagünle uyumludur. pH ve iletkenlik değerleri her iki ayda da lagüne göre yüksektir.

2014 yılında İskenderun Körfezi'nde Göycıncık ve diğ. tarafından yapılan çalışma ile kıyaslandığında pH değerleri Kasım, Aralık, Şubat ve Mart aylarında tüm istasyonlarda körfeze göre yüksek olup Ocak ayında düşüktür. Cr, Fe, Ni, Cu ve As değerleri tüm istasyonlara göre düşüktür.

2011 yılında Tecer Gölü'nde Mutlu ve diğ. tarafından yapılan çalışma ile kıyaslandığında; pH, tuzluluk ve iletkenlik değerleri ilkbahar, sonbahar ve kış mevsimlerinde göle göre yüksektir. Pb değerleri ilkbahar ve kış mevsimlerinde göle göre yüksek olup sonbahar mevsiminde göle göre düşüktür. Cd değerleri ilkbahar ve sonbahar mevsimlerinde göle göre düşük olup kış mevsiminde göle göre yüksektir. Cu değerleri üç mevsimde de göle göre düşüktür. Fe değerleri ilkbahar mevsiminde göle göre düşük olup sonbahar ve kış mevsimlerinde göle göre yüksektir.

SONUÇ

Su Kirliliği Yönetmeliği'ndeki deniz suyunun genel kalite kriterlerine göre 3 nolu istasyondaki deniz suyunun 6,75 ve 8,62 aralığı içindeki pH değerleri uygundur. Su Kirliliği Yönetmeliği'ndeki göller, göletler, bataklıklar ve baraj haznelerinin doğal koruma alanı ve rekreasyon kullanımında ötrofikasyon kontrolü sınır değerlerine göre 1 ve 2 nolu istasyonlardaki tatlı suyun 7,4 ve 8,36 aralığı içindeki pH değerleri de uygundur.
Su Kirliliği Kontrolü Yönetmeliği kıta içi su kaynaklarının sınıflarına göre kalite kriterlerine göre pH lagünün I. sınıf su kalitesini göstermektedir.
EPA Akuatik yaşam kriter tablosundaki pH'ın tatlı su sınırına 1 ve 2 nolu istasyonlar uygunken tuzlu su sınırını 3 nolu istasyon sadece 20 Mart 2019'da 8,62 değeri ile aşmıştır.
Su Kirliliği Yönetmeliği deniz suyunun genel kalite kriterleri kapsamında 3 nolu istasyonda bakır, kadmiyum, krom, kurşun, nikel ve arsenik konsantrasyonları limit

değerin altındadır fakat çinko konsantrasyonu 27.12.2018, 16.01.2019, 5.2.2019 tarihlerinde limit değeri aşmıştır.
Kıta İçi Su Kaynaklarının Kalite Kriterlerine göre bakır, kadmiyum, demir, mangan, baryum, alüminyum I., arsenik, kobalt II., kurşun, nikel, çinko III., selenyum IV. su kalite sınıfına girmektedir.
İnsanların balıkçılık vb. rekreasyon amacıyla kullanımı ve su canlılarının yaşamı açısından önemli olan Kamil Abduş Lagünü'nün korunması gerekmektedir.

KAYNAKLAR

Acar, H. (2003). Göllerin ekolojisini etkileyen faktörlerin araştırılması ve Tuzla (Kamil Abduş) Gölü örneği.
Alkan Uçkun, A. (2019) Investigation of Toxic Metal Contamination in Water and Sediments of Gölbaşı Lake (Adıyaman). Adıyaman University Journal of Science 8(2).
Alpar, B. (2016). Sea level changes along the turkish straits system and climate change. The Sea of Marmara: Marine Biodiversity, Fisheries, Conservation and Governance, 831.
Atalay, İ., Ekinci, D., Bayrak, M. (2015). Türkiye Kıyılarındaki Bazı Sulak Alanların Antropojenik Süreçlere Bağlı Ekolojik Sorunları. IV. Ulusal Jeomorfoloji Sempozyumu. Bildiriler Kitabi, Samsun.
Ateş Can, S. (2014). Robert oerley and Tuzla mineral springs. METU Journal of the Faculty of Architecture, 31(1).
Baldiris-Navarro, I., Sanchez-Aponte, J., Gonzalez-Delgado, A., Acosta-Jimenez, J.C. ve Jimenez, A.R. (2018) Multivariable statistical evaluation of water quality in Juan polo coastal lagoon (Colombian Caribbean). Contemporary Engineering Sciences 11(27), 1339-1348.
Basatnia, N., Hossein, S.A., Rodrigo-Comino, J., Khaledian, Y., Brevik, E.C., Aitkenhead-Peterson, J. ve Natesan, U. (2018) Assessment of temporal and spatial water quality in international Gomishan Lagoon, Iran, using multivariate analysis. Environmental Monitoring and Assessment 190(5), 314.
Bozkurt, E., Eliri, Ö., Kesiktaş, M. (2014) Analysis of Heavy Metals in Seawater Samples Collected From Beaches of Asian Side of Istanbul. Journal of Recreation and Tourism Research (JRTR) 1(1), 39-47.
Bulut, C. ve Kubilay, A. (2019) Seasonal change of water quality in Egirdir Lake (Isparta/Turkey). Ege Journal of Fisheries and Aquatic Sciences 36(1), 13-23.
Catianis, I., Secrieru, D., Pojar, I., Grosu, D., Scrieciu, A., Pavel, A.B. ve Vasiliu, D. (2018) Water Quality, Sediment Characteristics and Benthic Status of the Razim-Sinoie Lagoon System, Romania. Open Geosciences 10(1), 12-33.
Ceylan, M., & Ceylan, M. A. (2010). Türkiye kıyılarında tombololaların oluşumu dağılışı ve fonksiyonel özellikleri konusunda bir araştırma. Marmara Coğrafya Dergisi, (22), 205-232.

Cüce, H., Bakan,G., Akıncı, H. (2011) Balık Gölü (Kızılırmak Deltası, Samsun) Su Kalitesinin Konumsal Analizi, 3.
Demir Yetis, A., Selek, Z., Seckin, G. ve Davutluoglu, O.I. (2014) Water quality of Mediterranean coastal plains: conservation implications from the Akyatan Lagoon, Turkey. Environmental Monitoring and Assessment 186(11), 7631-7642.
El Zrelli, R., Rabaoui, L., Ben Alaya, M., Daghbouj, N., Castet, S., Besson, P., Michel, S., Bejaoui, N. ve Courjault-Rade, P. (2018) Seawater quality assessment and identification of pollution sources along the central coastal area of Gabes Gulf (SE Tunisia): Evidence of industrial impact and implications for marine environment protection. Marine Pollution Bulletin 127, 445-452.
EPA Quality Criteria for Water (1986). Gold Book National Recommended Water Quality Criteria - Aquatic Life Criteria Table. https://www.epa.gov/wqc/national-recommended-water-quality-criteria-aquatic-life-criteria-table
Ertek, T. A. (2016). Coastal geomorphology of Sea of Marmara and its islands. The Sea of Marmara: Marine Biodiversity, Fisheries, Conservation and Governance, 290.
Gámez, O.R., Laffont-Schwob, I., Prudent, P., Vassalo, L., Rodriguez, I.A., Macias, R.P., Petit, M.E., Ibarra, A.T.A., Masotti, V., Perraud-Gaime, I. ve Rodriguez, A.A. (2019) Assessment of water quality from the Blue Lagoon of El Cobre mine in Santiago de Cuba: a preliminary study for water reuse. Environmental Science and Pollution Research, 26(16), 16366-16377.
Gazete, R. (2004a). Su Kirliliği Kontrolü Yönetmeliği. TC Çevre ve Şehircilik Bakanlığı, Karar, 8289, Tablo 2: göller, göletler, bataklıklar ve baraj haznelerinin ötrofikasyon kontrolü sınır değerleri, http://www.mevzuat.gov.tr/Metin.Aspx?MevzuatKod=7.5.7221&sourceXmlSearch=&MevzuatIliski=0
Gazete, R. (2004b). Su Kirliliği Kontrolü Yönetmeliği. TC Çevre ve Şehircilik Bakanlığı, Karar, 8289, Tablo 4: Deniz suyunun genel kalite kriterleri http://www.mevzuat.gov.tr/Metin.Aspx?MevzuatKod=7.5.7221&sourceXmlSearch=&MevzuatIliski=0
Gazete, R. (2004c). Su Kirliliği Kontrolü Yönetmeliği. TC Çevre ve Şehircilik Bakanlığı, Karar, 8289, Tablo1: Kıtaiçi su kaynaklarının sınıflarına göre kalite kriterleri, http://www.mevzuat.gov.tr/Metin.Aspx?MevzuatKod=7.5.7221&sourceXmlSearch=&MevzuatIliski=0
Göycıncık, S., Danahaliloğlu, H. ve Karayiğit, H.B. (2018) İskenderun Körfezi Deniz Suyunun Eser Element Düzeylerinin Araştırılması. Karadeniz Fen Bilimleri Dergisi 8(2), 39-48.
Hernández-Terrones, L.M., Null, K.A., Ortega-Camacho, D. ve Paytan, A. (2015) Water quality assessment in the Mexican Caribbean: Impacts on the coastal ecosystem. Continental Shelf Research 102, 62-72.
İleri, S., Karaer, F., Kâtip, A., Onur, S. (2014) Sığ Göllerde Su Kalitesi Değerlendirmesi, Uluabat Gölü Örneği. Uludağ Üniversitesi Mühendislik-Mimarlık Fakültesi Dergisi 19(1).

Kara, M. (2019) Bafa Gölü Sularında Element Konsantrasyonlarının Belirlenmesi ve Su Kalitesi Açısından Değerlendirilmesi. BEÜ Fen Bilimleri Dergisi 8(1).
Kayhan, F.E., Özhatay, E. (2004) The Determination of Some Chemical Pollution Parameters (Cd, Al, Fe) in Tuzla Balık Lake, DPÜ Fen Bilimleri Enstitüsü Dergisi, (7).
Kayhan, F.E., Özhatay, E. (2004) The Determination of Some Chemical Pollution Parameters (Cd, Al, Fe) in Tuzla Balık Lake, DPÜ Fen Bilimleri Enstitüsü Dergisi, (7).
Koto, R., Bani, A., Topi, T., Topi, M. (2014) Water Quality and Heavy Metal Content of Karavasta Lagoon in Albania. Fresenius Environmental Bulletin 23(12).
Kotori, P., Hasanaj, L. ve Kane, S. (2015) Physical-Chemical Parameters and Assessment of Pollution Through Bioindicators of Narta Lagoon, Sustainable Development of Sea-Corridors and Coastal Waters, Bölüm 5, 47-55.
Mutlu, E., Kutlu, B., Demir, T., Yanık, T. (2018) Assessment of metal concentrations and physicochemical parameters in the waters of Lake Tecer, Kastamonu Universitesi Orman Fakültesi Dergisi 18(1).
Mutlu, E., Yanık, T., Demir, T. (2013) Karagöl (Hafik-Sivas) 'ün Su Kalitesinin İncelenmesi, Alınteri Zirai Bilimler Dergisi 24(1), 35-45.
Özdemir, N., Engin, A. (2013) Güllük Lagünü'nün Su Kalitesi Yönünden İncelenmesi, Güllük Körfezi Bakteriyolojisi TÜBİTAK Proje Çalıştayı, 10 Mayıs 2013, Güllük, Muğla, 53.
Pérez-Ruzafa, A., Campillo, S., Fernández-Palacios, J.M., García-Lacunza, A., García-Oliva, M., Ibañez, H., Navarro-Martínez, P.C., Pérez-Marcos, M., Pérez-Ruzafa, I.M., Quispe-Becerra, J.I., Sala-Mirete, A., Sánchez, O. ve Marcos, C. (2019) Long-Term Dynamic in Nutrients, Chlorophyll a, and Water Quality Parameters in a Coastal Lagoon During a Process of Eutrophication for Decades, a Sudden Break and a Relatively Rapid Recovery, Frontiers in Marine Science, (6).
Rahmadani, T., Sabang, S. M., Said, I. (2015) Analisis Kandungan Logam Zink (Zn) Dan Timbal (Pb) Dalam Air Laut Pesisir Pantai Mamboro Kecamatan Palu Utara, Jurnal Akademika Kimia, 4(4), 197-203.
Şenol, C. (2012). İstanbul'un içme suyu havzalarının ekolojik sorunları. III. Ulusal Jeomorfoloji Sempozyumu. Bildiriler Kitabi, Hatay.
T.Ü.İ.K. (2014) Seçilmiş Göstergelerle İstanbul (2013), Türkiye İstatistik Kurumu Matbaası, Eylül 2014, Ankara, Türkiye.
Tarım ve Orman Bakanlığı Meteoroloji Genel Müdürlüğü, 2019, https://www.mgm.gov.tr/FILES/resmi-istatistikler/denizSuyu/Marmara-DenizSuyu-Sicakligi-Analizi.pdf
Tobón Velázquez, N.I., Rebolledo Vieyra, M., Paytan, A., Broach, K.H. ve Hernández Terrones, L.M. (2019) Hydrochemistry and carbonate sediment characterisation of Bacalar Lagoon, Mexican Caribbean. Marine and Freshwater Research 70(3), 382.
Topi, T., Bani, A., Malltezi, J., Sulce, S. (2012) Heavy Metals in Soil, Sediments, Mussels and Water From Butrinti Lagoon (Albania). Fresenius Environmental Bulletin 21(10).

Tosic, M., Restrepo, J.D., Lonin, S., Izquierdo, A. ve Martins, F. (2019) Water and sediment quality in Cartagena Bay, Colombia: Seasonal variability and potential impacts of pollution, Estuarine, Coastal and Shelf Science, (216), 187-203.
Vouvé, F., Buscail, R., Aubert, D., Labadie, P., Chevreuil, M., Canal, C., Desmousseaux, M., Alliot, F., Amilhat, E., Faliex, E., Paris-Palacios, S. ve Biagianti-Risbourg, S. (2014) Bages-Sigean and Canet-St Nazaire lagoons (France): physico-chemical characteristics and contaminant concentrations (Cu, Cd, PCBs and PBDEs) as environmental quality of water and sediment, Environmental Science and Pollution Research, 21(4), 3005-3020.

MICRON-SIZED COAL PARTICLES AS A NOVEL FUEL ADDITIVE FOR DIESEL ENGINE APPLICATION

Abdülvahap ÇAKMAK
Department of Motor Vehicles and Transportation Technologies, Kavak Vocational School, Samsun University
abdulvahap.cakmak@samsun.edu.tr

Hakan Özcan
Department of Mechanical Engineering, Ondokuz Mayıs University
ozcanh@omu.edu.tr

ABSTRACT: This research investigates the effect of addition micron-sized coal particles to diesel fuel on engine performance and emissions. Micron-sized coal particles used in this study was prepared by the mechanical ball milling process. The obtained coal particles were characterized by Scanning Electron Microscopy (SEM) and energy dispersive X-rays (EDX) analysis. The micron-sized coal particles were dispersed in a mass fraction of 300 ppm with diesel fuel and B20 by ultrasonication and the resulted fuels were labeled as D+C and B20+C, respectively. Pure diesel (D) and B20 without coal particles were used to set baseline data for comparison. Engine performance and emission tests were performed at a constant engine speed of 1500 rpm and full engine load. Addition of micron-sized coal particles to diesel fuel improved the brake thermal efficiency by 6.3% and reduced the NOx emissions by 11.8%. Improvement in engine performance and exhaust emissions were also observed for B20+C fuel.

Keywords: Micron-sized coal particles, Nano-additives, Diesel engine, Biodiesel, Performance and emissions

INTRODUCTION

The diesel engine is the most efficient internal combustion engine widely used in car, bus, truck, railroad, marine, industrial and agricultural applications (Pulkrabek, 1997). However, diesel-powered vehicles and equipment emit a big amount of pollutants such as NOx and PM which cause serious health and environmental hazards (Bhandarkar, 2013; Heywood, 1988). Therefore, a major concern has been raised for scientists to find an effective way of reducing pollutant emissions. There are some methods of reducing pollutant exhaust emissions: exhaust gas recirculation (EGR), after-treatment methods, fuel injection/combustion system design and fuel modification. Nevertheless, among these methods fuel modification is the more effective and cheaper countermeasure to high emissions, agreed by many researchers (Chen et al., 2018).

With the advancement in nanotechnology in recent years enabled production different of type and size particles that considered one of the best fuel additive to improve fuel properties, combustion and exhaust emissions (Mehregan & Moghiman, 2018; Saxena et al., 2017). That is why many studies have been conducted on nanoparticle additives. Chen et al. (2018) investigate the effects of aluminum oxide, carbon nanotube (CNT), and silicon oxide nanoparticles on combustion characteristics, engine performance and emissions of a diesel engine. The results indicated that brake specific fuel consumption for CNT blends decreased up to 19.8% and thermal efficiency for aluminum oxide blends enhanced by 18.8%. CNT resulted in a significant improvement in NOx emissions while CNT blends were the least stable fuel. According to Mehregan and Moghiman (2018), manganese oxide and cobalt oxide addition to B20 fuel resulted in a reduction in brake specific fuel consumption, NOx and CO emissions while thermal efficiency considerably increased compared to those of base fuel. An experimental study on zinc oxide (ZnO) and ethanox as additives with biodiesel in CI conducted by Ashok et al. (2017). The study revealed that due to the catalytic effect of nanoparticles ZnO improved the engine efficiency by 4.7% and reduced NOx emissions by 12.6% at full load. In addition, ethanox resulted in a maximum decrease in NOx emissions of 17.8% by inhibiting the formation of free radicals. Annamalai et al. (2016) investigated the effects of using cerium oxide (CeO_2) nanoparticles as an additive in biodiesel-water emulsion fuel on engine combustion, performance, and exhaust emissions. The findings indicated that the addition of cerium oxide nanoparticles to emulsion ensured a drastic reduction in CO, HC and NOx emissions and smoke opacity. Moreover, owing to the large surface area to volume ratio of nanoparticles, the evaporation, and atomization rate of the fuel enhanced which eventually led to an improvement in brake thermal efficiency. Devarajan et al. (2019) analyzed the engine performance and emissions biodiesel-fueled engine with the addition of copper oxide (CuO) nanoparticles. Copper oxide nanoparticles were blended with mahua oil biodiesel at a mass fraction of 100 ppm. It was observed that the inclusion of copper oxide nanoparticles to biodiesel reduced the NOx, CO, HC, and smoke emissions. Besides, CuO nanoparticles improved engine performance parameters. Sivakumar at al. (2018) studied the effects of aluminum oxide (Al_2O_3) nanoparticles as an additive to biodiesel fuel on a diesel engine parameters, and showed that the addition of 100 ppm aluminum oxide to biodiesel fuel resulted in reduced CO, HC, and smoke emissions while an increase was observed in NOx emissions. The blending aluminum oxide particles to biodiesel produced better engine performance than that of the base fuel. Wu et al. (2018) investigated the effect of carbon coated aluminum (Al@C) nanoparticles as a fuel additive to biodiesel-diesel blends on diesel engine performance and exhaust emissions. It was determined that adding of carbon coated aluminum nanoparticles reduced brake specific fuel consumption, NOx and CO emissions. However, with the addition of carbon coated aluminum nanoparticles, the emissions of particulate number increased. By further analyzing exhaust gas it was noticed that after combustion the carbon coated aluminum nanoparticles transformed into alumina particles.

The overall results concluded from the previous studies indicated that the addition of nanoparticles to diesel/biodiesel fuel results in the more homogeneous fuel-air mixture, more complete combustion, which ultimately leads to better thermal efficiency and fewer exhaust emissions. However, the matter of concern with the addition of nanoparticles as a fuel additive is that extra metal oxide emissions emitted from the burning of metallic nanoparticles (Soudagar et al., 2018). This results in a possible risk related to human health and environment because of exposure of metal oxide particles as an additional pollutant released into the atmosphere (Saxena et al., 2017). In addition, the inclusion of nanoparticles to fuel could result in an increase in fuel cost (Gumus et al., 2016). Therefore, it is necessary to find new organic particles that do not lead to extra harmful emissions and also to make economic fuel additives for commercial applications. Within this context, this present study which is presented for the first time, according to the best of the author's knowledge, focused on the investigation of micron-sized coal particles as a fuel additive that could overcome the drawbacks of the addition of nano-sized metallic particles.

METHODS

The easily and economically available coal supplied from a mining company in Çorum, Turkey is chosen for micron-sized coal particles preparation. Firstly, coal pieces without any pre-treatment were ground into about a size of 5 mm and then filled into the stainless steel mill jar of the ball milling machine. In the next step, coal pieces were milled for a one-half hour with a rotating speed of 1200 rpm. The grounded micron-sized coal particles are used as a fuel additive. A photographic view of coal particles before and after the milling process is shown in Figure 1.

Figure 1. A Photographic View of Coal Particles Before (a) and After (b) Milling Process

The characterization of coal particles was done by combined techniques of Scanning Electron Microscope (SEM) and energy dispersive X-ray (EDX) analysis. The SEM image and the spectrum of EDX analysis of the coal particles are presented in Figure 2 and

Figure 3, respectively. As seen in Figure 2, coal particles have a different diameter and almost spherical shape. The diameter of randomly selected three coal particles was measured as 240 nm, 530 nm, and 570 nm. Due to less milling time, the diameter of coal particles has not been obtained in nano-scale (<100 nm). EDX results in Figure 3, indicates that more than one peaks appear in the spectrum due to many chemical substances inside the coal particles. One can see that the highest three peaks belong to carbon, oxygen, and iron, respectively. Also, it can be concluded that silicon, sulfur, aluminum, calcium and magnesium and potassium present in the coal particles. But the mass ratios presented in the spectrum may not indicate the exact mass ratios of substances since EDX analysis is not a sensitive method to determine the elemental composition of a matter.

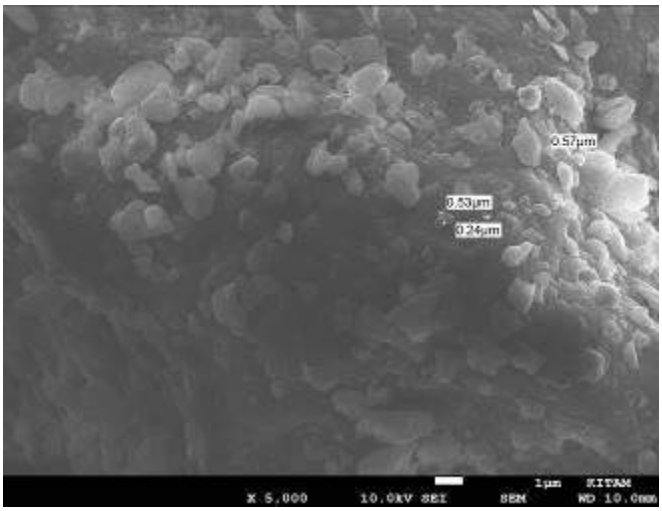

Figure 2. The SEM Image and of Coal Particles

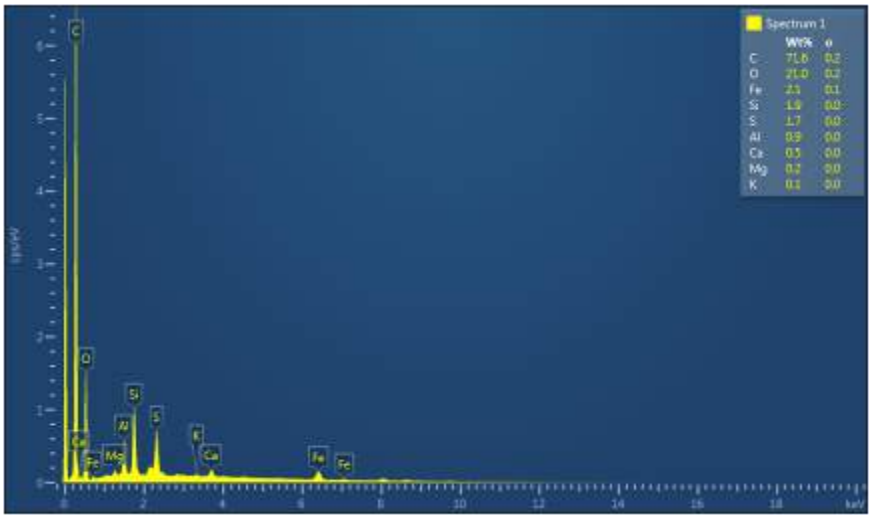

Figure 3. EDX spectrum of Coal Particles

Produced micron-sized coal particles dispersed in diesel (D) and a diesel-biodiesel blend (B20) fuel at a mass concentration of 300 ppm by ultrasonication process at 40 kHz for the time duration of 30 min. At the end of the ultrasonication process, as seen in Figure 4, a darker liquid fuel formed due to the physical color of coal particles. Micron-sized coal particles dispersed fuels were labeled as D+C and B20+C and pure diesel fuel and B20 (20% corn oil biodiesel +80% diesel fuel by volume) was selected as base fuel.

The engine performance and emissions test were conducted on a test setup consisting of a 4-stroke diesel engine, Eddy current dynamometer, exhaust gas analyzer, and related measurement instruments. The engine used in this study was a single-cylinder, natural aspirated, water-cooled, direct injection diesel engine with a cylinder bore of 87.5 mm, a stroke of 110 mm and a compression ratio of 17.5:1. Rated engine power is 3.5 kW at full engine load and 1500 rpm. A schematic sketch of the experimental setup is shown in Figure 5. Engine performance and emissions test were performed at full engine load and 1500 rpm engine speed. The selected engine operating parameters yielded the same amount of brake power output for each fuel to make a comparison. Exhaust gas analyzer was used to measure the volumetric concentrations of CO and NOx emissions. Before measurements, the engine was allowed to run for 30 minutes until the engine cooling water temperature and exhaust gas temperature has reached steady-state values and all data were measured subsequently at least three times. The average values were taken into consideration to reduce the experimental uncertainties. Measurements were first done for base fuels namely D and B20. After collection the base data, the engine was run with D+C and B20+C fuel. The uncertainties of the measured and calculated quantities are presented in Table 1.

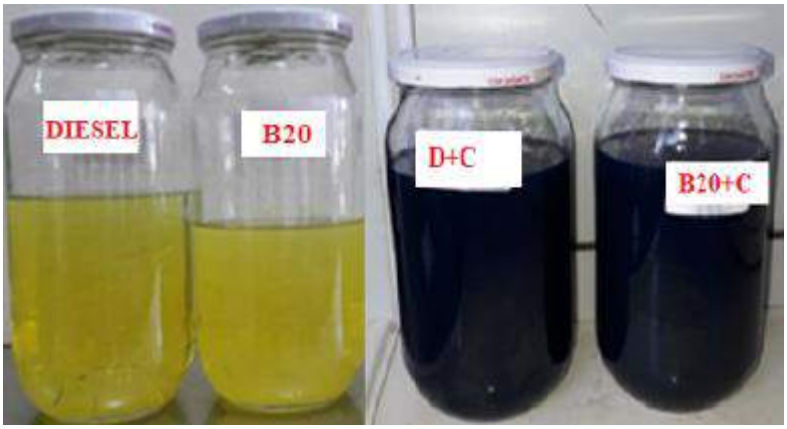

Figure 4. The Images of Prepared Test Fuels

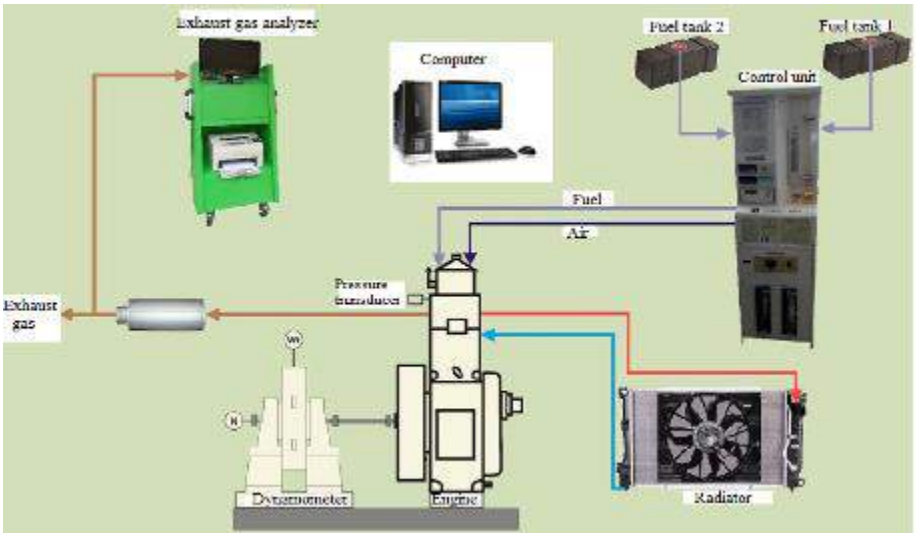

Figure 5. Experimental Setup

Table 1. The Uncertainties of the Measured and Calculated Quantities

Parameter	Measurement Range	Resolution	Uncertainty
Brake torque	0-90 Nm	0.1 Nm	±1.5 %
Engine speed	0-9999 rpm	1 rpm	±0.06 %
Air flow rate	-	-	<±0.8 %
Fuel flow rate	-	-	<±0.7 %
Temperature	-	0.1 °C	1 °C
Brake thermal efficiency	-	-	<±0.9 %
CO	0-10 % vol.	0.001 %	±3%
NOx	0-4000 ppm	1 ppm	± 25 ppm

RESULTS AND FINDINGS

Brake thermal efficiency (BTE) of the test fuels presented in Figure 6. Brake thermal efficiency is a significant performance parameter used to identify the engine's capability to convert fuel chemical energy into useful work. It can be clearly seen in this figure that B20 base fuel presented higher BTE than that of base diesel fuel. In spite of the low heating value of B20 fuel, the oxygen in the chemical structure of the biodiesel could improve the combustion quality, and thus enhance the BTE. The BTE results revealed that the inclusion of micron-sized coal particles in both D and B20 presented an improvement in BTE compared to base fuels. Addition of 300 ppm coal particles to D and B20 resulted in an increase in BTE by 6.32% and 3.34%, respectively. This increase in BTE could be due to the catalytic effect of coal particles. In addition, adding micron-sized coal particles could improve the fuel properties such as thermal conductivity, evaporation rate and

thus it provides short ignition delay and more complete combustion. Similar increases in BTE by adding nanoparticles to fuel were observed by many researchers (Chen et al., 2018; Gumus et al., 2016; Mehregan & Moghiman, 2018).

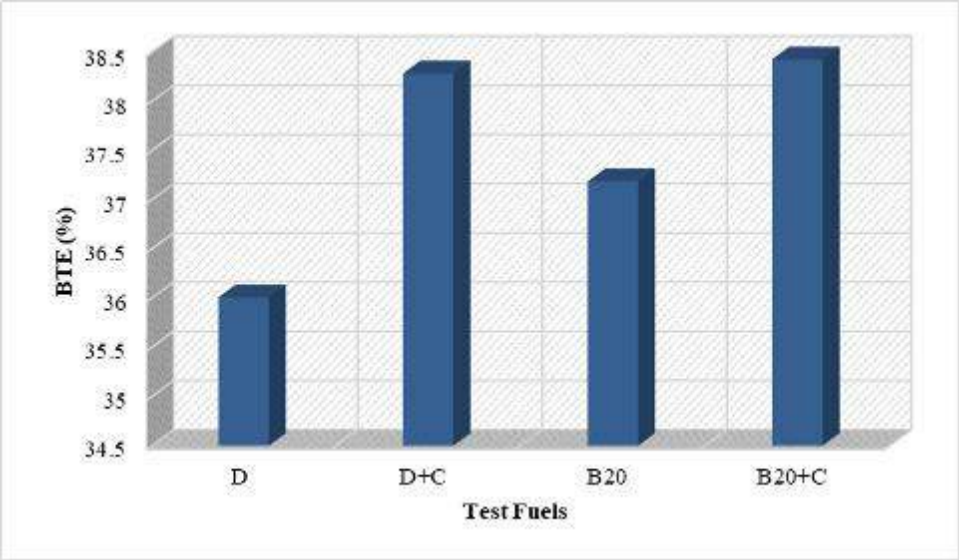

Figure 6. Brake Thermal Efficiency

The measured exhaust temperature (EGT) of test fuels is shown in Figure 7. The highest exhaust temperature was measured for diesel fuel owing to its high heating value. But this is not the only reason for high exhaust temperature. The presence of oxygen in the fuel could increase the fuel oxidation rate and decrease ignition delay, which contributes more effective power production. In addition, low exhaust gas temperature could be considered as the indication of the more efficient conversion of the heat energy into effective power. This finding could be confirmed by BTE results, in other words, the fuel that gives low exhaust temperature leads to an increment in BTE. Inclusion of micron-sized coal particles in base fuels led to a decrease in exhaust gas temperature because of its catalytic effect. Addition of 300 ppm coal particles to D and B20 resulted in a decrease in EGT by 2.84% and 1.80%, respectively.

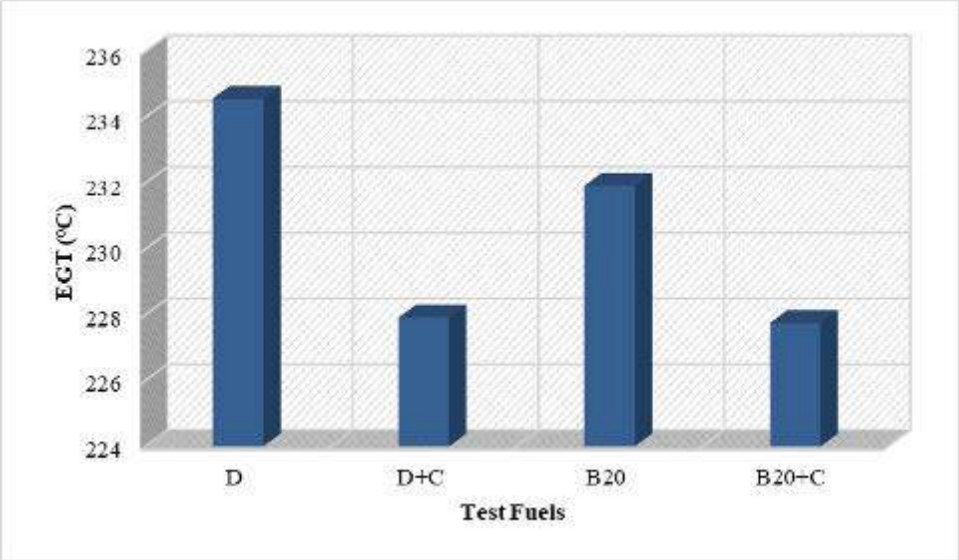

Figure 7. Exhaust Gas Temperature

Figure 8 shows the CO emissions for test fuels. CO emission value for D and B20 was measured as 0.14% and 0.16%, respectively. The potential reasons for high CO emission for B20 could be its high fuel consumption, high viscosity, high density, and lower volatility of biodiesel. At full engine load, due to low energy content more B20 fuel must be injected in the cylinder in order to produce the equal brake power when compared to diesel fuel, so there would not be enough time to completely burn of all injected fuel. High viscosity and low volatility of the biodiesel could worsen the fuel-air mixing process. As a result, CO emission increased. It is noticed also in Figure 8 that adding of micron-sized coal particles to base fuels led to different behavior in CO emissions. It was determined that the inclusion of 300 ppm coal particles in diesel fuel led to an increase in CO emissions by 12.85%. This was due to the increase in the carbon content of the base fuel (Chen et al., 2018). However, the addition of coal particles to B20 fuel presented lower CO emission by 15.63% compared to base B20 fuel. In spite of an increase in the carbon content of B20 fuel owing to coal particle adding, the influence of oxygen in the biodiesel and catalytic effect of coal particles resulted in a decrease in CO emissions.

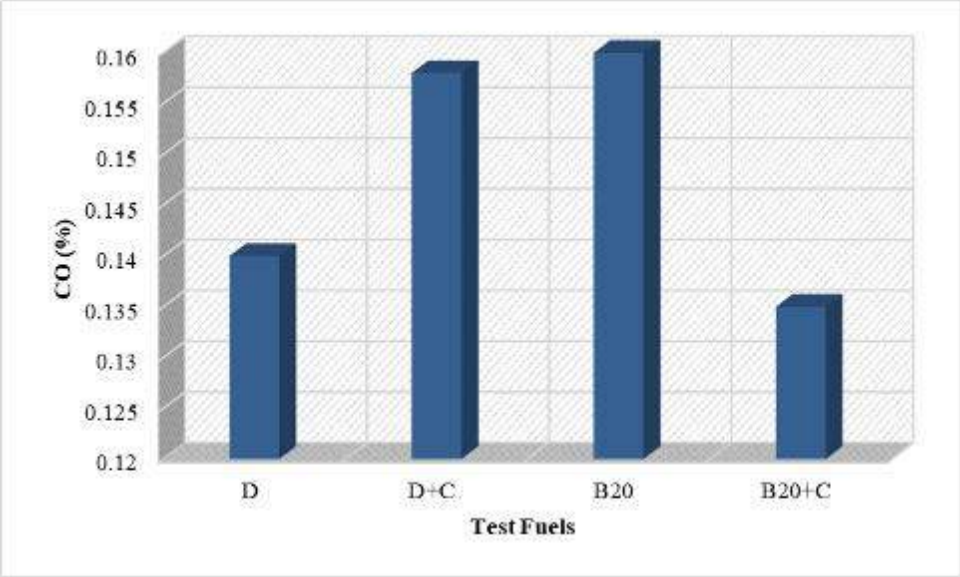

Figure 8. CO emissions

All fuels that include micron-sized coal particles presented a decrease of NOx emissions as shown in Figure 9. This was caused by the catalytic effect of coal particles that accelerate the combustion rate. Micron-sized coal particles could reduce the ignition delay thus less fuel being burned in the premixed combustion phase, resulting in low NOx emissions (Heywood, 1988). Addition of 300 ppm micron-sized coal particles to D and B20 resulted in a decrease in NOx emissions by 11.79% and 3.37%, respectively. The trend observed in NOx emissions is in agreement with the results concluded from research using nanoparticles (Debbarma & Misra, 2018; Pandian et al., 2017; Paramashivaiah et al., 2018).

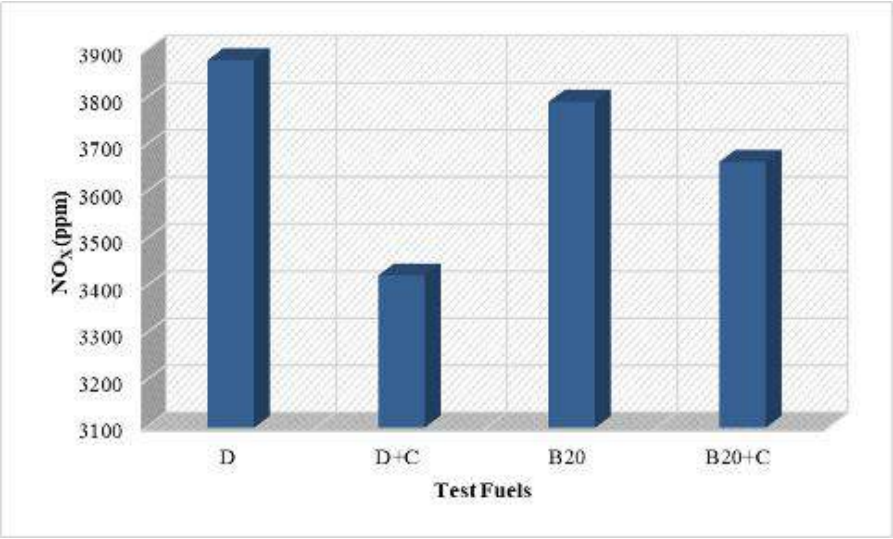

Figure 9. NO_X emissions

CONCLUSIONS

This study revealed that micron-sized coal particles could have the potential to replace metal-based nanoparticles. Along with this, the coal particle could overcome the side effects of metal nanoparticles. The obtained results from this study showed that the addition of coal particles to diesel and B20 fuel resulted in an improvement in brake thermal efficiency and NO_X emissions. In the frame of engine experiments, no issues related to the engine functionality were observed. This observation indicates that micron-sized coal particles can be used in a CI without any modification.

RECOMMENDATIONS

Since this study is the first research on using micron-sized coal particles as a fuel additive, could not be done a comprehensive experimental study, however, Authors are planning to make further research on this subject. Further studies are required to determine coal particle size and its dosage value, which will provide the optimum engine performance and exhaust emissions. Another aspect should be investigated is the stability of coal particles added fuels. In addition, an economic analysis of coal particle use should be done.

ACKNOWLEDGMENTS

This study was supported by the Project Management Office of Ondokuz Mayis University (Project number: PYO.MUH.1904.19.016). Abdülvahap ÇAKMAK thanks TUBİTAK for his doctoral scholarship (TUBİTAK-BİDEB: 2211-C).

REFERENCES

Annamalai, M., Dhinesh, B., Nanthagopal, K., SivaramaKrishnan, P., Isaac JoshuaRamesh Lalvani, J., Parthasarathy, M., & Annamalai, K. (2016). An assessment on performance, combustion and emission behavior of a diesel engine powered by ceria nanoparticle blended emulsified biofuel. Energy Conversion and Management, 123, 372–380. https://doi.org/10.1016/J.ENCONMAN.2016.06.062

Ashok, B., Nanthagopal, K., Mohan, A., Johny, A., & Tamilarasu, A. (2017). Comparative analysis on the effect of zinc oxide and ethanox as additives with biodiesel in CI engine. Energy, 140, 352–364. https://doi.org/10.1016/J.ENERGY.2017.09.021

Bhandarkar, S. (2013). Vehicular Pollution, Their Effect on Human Heatlh and Mitigation Measures. Vehicle Engineering(VE), 1(2).

Chen, A. F., Akmal Adzmi, M., Adam, A., Othman, M. F., Kamaruzzaman, M. K., &

Mrwan, A. G. (2018). Combustion characteristics, engine performances and emissions of a diesel engine using nanoparticle-diesel fuel blends with aluminium oxide, carbon nanotubes and silicon oxide. Energy Conversion and Management, 171, 461–477. https://doi.org/10.1016/J.ENCONMAN.2018.06.004

Debbarma, S., & Misra, R. D. (2018). Effects of Iron Nanoparticle Fuel Additive on the Performance and Exhaust Emissions of a Compression Ignition Engine Fueled With Diesel and Biodiesel. Journal of Thermal Science and Engineering Applications, 10(4), 041002. https://doi.org/10.1115/1.4038708

Devarajan, Y., Nagappan, B., & Subbiah, G. (2019). A comprehensive study on emission and performance characteristics of a diesel engine fueled with nanoparticle-blended biodiesel. Environmental Science and Pollution Research, 26(11), 10662–10672. https://doi.org/10.1007/s11356-019-04446-1

Gumus, S., Ozcan, H., Ozbey, M., & Topaloglu, B. (2016). Aluminum oxide and copper oxide nanodiesel fuel properties and usage in a compression ignition engine. Fuel, 163, 80–87. https://doi.org/10.1016/J.FUEL.2015.09.048

Heywood, J. B. (1988). Internal combustion engine fundamentals.

Mehregan, M., & Moghiman, M. (2018). Effects of nano-additives on pollutants emission and engine performance in a urea-SCR equipped diesel engine fueled with blended-biodiesel. Fuel, 222, 402–406. https://doi.org/10.1016/J.FUEL.2018.02.172

Pandian, A. K., Ramakrishnan, R. B. B., & Devarajan, Y. (2017). Emission analysis on the effect of nanoparticles on neat biodiesel in unmodified diesel engine. Environmental Science and Pollution Research, 24(29), 23273–23278. https://doi.org/10.1007/s11356-017-9973-6

Paramashivaiah, B. M., Banapurmath, N. R., Rajashekhar, C. R., & Khandal, S. V. (2018). Studies on Effect of Graphene Nanoparticles Addition in Different Levels with Simarouba Biodiesel and Diesel Blends on Performance, Combustion and Emission Characteristics of CI Engine. Arabian Journal for Science and Engineering, 43(9), 4793–4801. https://doi.org/10.1007/s13369-018-3121-6

Pulkrabek, W. W. (1997). Engineering Fundamentals of the Internal Combustion Engine (No. 621.43). Pearson New International Edition. Pearson Higher Ed.

Saxena, V., Kumar, N., Saxena, V. K. (2017). A comprehensive review on combustion and stability aspects of metal nanoparticles and its additive effect on diesel and biodiesel fuelled CI engine. Renewable and Sustainable Energy Reviews, 70, 563–588.

Sivakumar, M., Shanmuga Sundaram, N., Ramesh kumar, R., & Syed Thasthagir, M. H. (2018). Effect of aluminium oxide nanoparticles blended pongamia methyl ester on performance, combustion and emission characteristics of diesel engine. Renewable Energy, 116, 518–526. https://doi.org/10.1016/J.RENENE.2017.10.002

Soudagar, M. E. M., Nik-Ghazali, N.-N., Abul Kalam, M., Badruddin, I. A., Banapurmath, N. R., & Akram, N. (2018). The effect of nano-additives in diesel-biodiesel fuel blends: A comprehensive review on stability, engine performance and emission characteristics. Energy Conversion and Management, 178, 146–177. https://doi.org/10.1016/J.ENCONMAN.2018.10.019

Wu, Q., Xie, X., Wang, Y., & Roskilly, T. (2018). Effect of carbon coated aluminum nanoparticles as additive to biodiesel-diesel blends on performance and emission characteristics of diesel engine. Applied Energy, 221, 597–604. https://doi.org/10.1016/J.APENERGY.2018.03.157.

A SURROGATE MODEL FOR AN OLD PROBLEM: LARGE DEFLECTIONS OF CANTILEVERS

Hakan ÖZBAŞARAN
Eskişehir Osmangazi University, Department of Civil Engineering, Eskişehir/TURKEY
ozbasaran@ogu.edu.tr

ABSTRACT: Exceeding of the allowable stress, loss of stability and large deflections are the leading problems in design of beams. In most cases, beams fail due to excessive stress under increasing loads. However, depending on the mechanical properties of the structural material and the cross-section geometry, some beams can make undesired large deflections without exceeding allowable stress limits. The Euler-Bernoulli beam theory, which is a useful simplification to calculate the deflection curves of laterally loaded beams, leads to acceptable results for small deflections. Unfortunately, this theory fails in large deflection analysis due to invalid assumptions. Solution of the large deflection problems mostly involves calculation of integrals and/or dealing with long equations. This paper revisits the large deflection analysis of highly flexible beams and presents a surrogate model to reduce the computational cost of the exhaustive procedures involving large deflection analysis such as optimization with metaheuristics.

Key words: beam; cantilever; large deflection; deflection curve; surrogate model

INTRODUCTION

Since Bernoulli presented the first precise formulation of elastica in 1691 (Levien, 2008), many studies are conducted on the deflection of highly flexible beams. However, it would be appropriate to mention some of the latest studies. Barten (1945) presented the solution for large deflection of the cantilever beam subjected to a concentrated load at its free end. Bisshopp and Drucker (1945) introduced the solution of large deflection problem for a cantilever beam which is subjected to a concentrated load acting at its free end in terms of elliptic integrals. Mattiasson (1980) provided the numerical solutions of large deflection problems for various systems including a cantilever beam subjected to a concentrated load acting at its free end. De Bona and Zelenika (1997) presented an analytical solution for the large deflections of slightly curved cantilever strips. Lee (2002) studied the large deflection of cantilever beams that include material and geometrical non-linearities; a numerical solution is presented by using a fifth order Runge-Kutta method. Belendéz et al. (2002, 2003) conducted numerical and experimental studies on large deflections of cantilevers. Kumar et al. (2004) presented genetic algorithms for large deflection analysis of simply supported and cantilever beams; validating the accuracy of

presented method by numerical solutions. Caire and Vaz (2007) investigated the large deflection of a cantilever beam made of linear viscoelastic material that is subjected to a concentrated load at its free end; the numerical solutions are obtained by shooting method and a fourth order Runge-Kutta algorithm. Chen (2010) proposed an integral approach for bending of cantilever beams which can be used to calculate large deflections of even non-uniform beams under arbitrarily distributed loads. Scarpello and Ritelli (2011) provided analytical solutions for large deflections of highly-flexible beams under various loading cases concerning Lauricella hypergeometric functions and validated the analytical results. Tari (2013) presented an approximate analytical solution for the large deflections of cantilever beams under combined tip point loading. This paper presents a surrogate model to calculate (approximately) the deflection curves of highly-flexible beams with less computational effort. Consider the beam given in Figure 1.

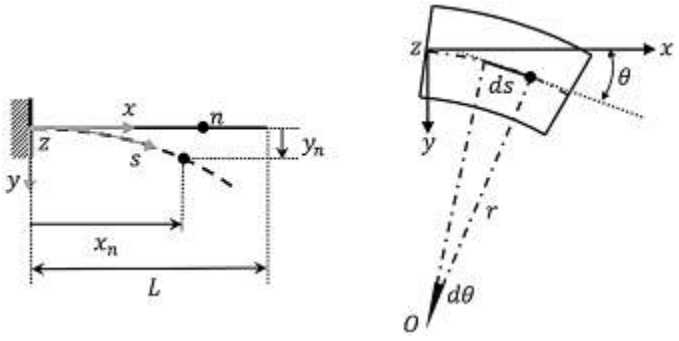

(a) (b)

Figure 1. a) Deflected Cantilever Beam, b) Detailed View of the Deflection Curve Near Point "n"

In Figure 1, n is an arbitrary point on the beam. x_n and y_n indicate the x and y coordinates of the point n on the deflected beam, respectively. z is the axis of bending, L is the cantilever length, s is the longitudinal axis of the deflected cantilever, θ is the angle between the x axis and the tangent of the curvature, dθ is the angle between the normals of the infinitesimal part (ds) of the deflection curve. Finally, r is the radius of the curvature. The infinitesimal length of the deflected beam can be calculated as $ds = rd\theta$. Thus, with the assumption of "beam length remains the same" (which means that the s coordinate of a random point on the beam is same for both unloaded and loaded configurations) and "shear forces have no effect on deflection", following equation can be written by using the well-known relation between curvature and bending moment (Timoshenko, 1940).

$$\left|\frac{d\theta}{ds}\right| = \frac{M_z}{EI_z} \tag{1}$$

where E is the Young's modulus, I_z is the moment of inertia, and M_z is the bending moment about z axis. It can be seen from Equation 1 that the rotation function varies with respect to the form of the bending moment gradient. Four common loading cases are considered in this study (Figure 2), which produce moment gradients of various orders.

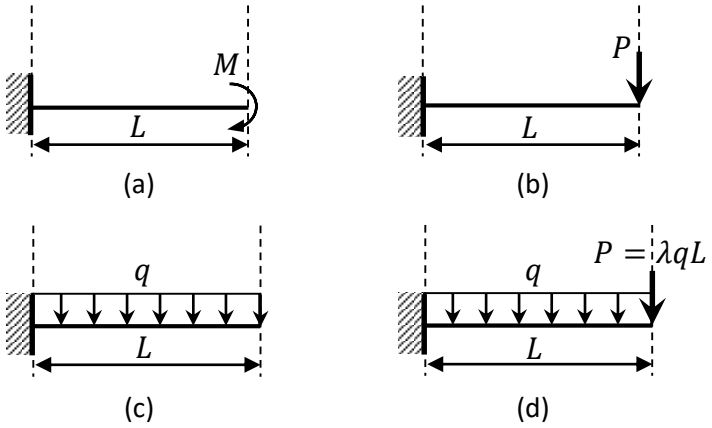

Figure 2. Considered Loading Cases a) Constant Moment (Case I), b) Concentrated Load at Free End (Case II), c) Uniformly Distributed Load (Case III), d) Combined Loading of Concentrated Load at Free End and Uniformly Distributed Load (Case IV)

In Figure 2a, M is the magnitude of the bending moment. Similarly, P is the magnitude of the concentrated load in Figure 2b, and q is the magnitude of uniformly distributed load in Figures 2c and 2d. Finally, λ is the concentrated load multiplier in Figure 2d. Following equilibrium equations that relate the deformation to the load magnitude can be written for Case I (Equation 2), Case II (Equation 3), Case III (Equation 4), and Case IV (Equation 5).

$$EI\frac{d\theta}{ds} - M = 0 \tag{2}$$

$$EI\frac{d^2\theta}{ds^2} - P\cos\theta = 0 \tag{3}$$

$$EI\frac{d^2\theta}{ds^2} - q(L-s)\cos\theta = 0 \tag{4}$$

$$EI\frac{d^2\theta}{ds^2} - [q(L-s) + \lambda qL]\cos\theta = 0 \tag{5}$$

Equation 2 can be solved for θ by implementing the boundary condition that the rotation is zero at fixed end ($\theta = 0$ at $s = 0$). Boundary conditions for Equations 3, 4, and 5 are "rotation is 0 at fixed end ($\theta = 0$ at $s = 0$) and bending moment is 0 at free end ($d\theta/ds = 0$ at $s = L$)"; these equations (Equations 3, 4, and 5) can be solved numerically by shooting method (Stoer and Bulirsch, 1992). Then, x and y coordinates of any point on the deflected

beam can be calculated by Equations 6 and 7, respectively with a numerical integration method such as Simpsons' rule (Adams, 1999).

$$x(s) = \int_0^s cos\,\theta\, ds \tag{6}$$

$$y(s) = \int_0^s sin\,\theta\, ds \tag{7}$$

THE SURROGATE MODEL

The form of the deflection curve depends on the load magnitude, cantilever length, Young's modulus, and the moment of inertia. The dimensionless coefficients for each considered loading case are developed to be used in the surrogate model (see Table 1). It can be said that the deflection curves of two beams having the same c values under the same loading case is identical.

Table 1. Dimensionless c Coefficients

Loading Case	c
Case I	$\frac{2ML}{EI_z}$
Case II	$\frac{PL^2}{2EI_z}$
Case III	$\frac{2qL^3}{3EI_z}$
Case IV	$\frac{2qL^3(1+2\lambda)}{3EI_z}$

First, the equilibrium equations for considered loading cases (Equations 2, 3, 4, and 5) are solved numerically for various c values and interpolating rotation functions are constructed. Then, $s/L - x/L$ and $s/L - y/L$ curves for each loading case are obtained with respect to c by substituting corresponding functions into Equations 6 and 7, respectively. It is found that for any value of c, position of a point on the deflection curve of a cantilever beam can be approximated by the bivariate polynomials given in Equations 8 and 9.

$$x(c,s) = L\sum_{i=1}^{n}\sum_{j=1}^{n} K_{ij}^{x} c^{i-1}\left(\frac{s}{L}\right)^{j-1} \tag{8}$$

$$y(c,s) = L\sum_{i=1}^{n}\sum_{j=1}^{n} K_{ij}^{y} c^{i-1}\left(\frac{s}{L}\right)^{j-1} \tag{9}$$

In Equations 8 and 9, K_{ij}^{x} and K_{ij}^{y} are the elements of the coefficient matrices K^{x} and K^{y}. Note that taking $n = 5$ is adequate to obtain satisfactory approximations.

TUNING

The K_{ij}^{x} and K_{ij}^{y} matrices are calculated for the values of c between 0.5 and 5.0; the smallest considered c value is determined by comparing the difference of the obtained deflection curves with the presented study and the Euler-Bernoulli beam theory. The deflection curve of the cantilever beams are obtained with respect to c with 0.05 intervals by the numerical procedure explained in the introduction part. Each deflection curve is obtained precisely by calculating x and y coordinates of 100 nodes. Then, Equations 8 and 9 are fitted to three-dimensional $c - s/L - x/L$ and $c - s/L - y/L$ data with the Jaya Algorithm (Venkata Rao, 2016). The relation between c and the deflection curve for Case I is given in Figure 3.

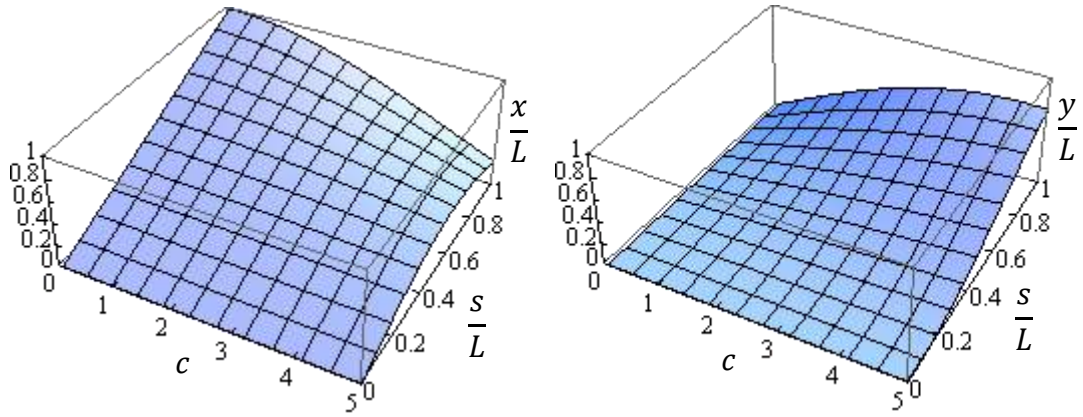

Figure 3. The "c – Deflection Curve" Relation for Case I
a) $c - s/L - x/L$, b) $c - s/L - y/L$

In Figure 3a, the relative x coordinates (x/L) are nearly equal to the relative s coordinates (s/L) for small smaller values of c. The x/L ratio significantly decreases by increasing c (as expected). The K^{x} and K^{y} matrices to determine the surfaces presented in Figures 3a and 3b are given in Equations 10 and 11, respectively.

$$K^{x} = \begin{bmatrix} -0.04415 & 10001 & -13.123 & 31.066 & -24.581 \\ 0.24174 & -10.166 & 71.629 & -169.23 & 133.56 \\ -0.31872 & 13.375 & -94.038 & -195.06 & -174.29 \\ 0.15561 & -6.5113 & 45.651 & -107.20 & 83.924 \\ -0.01574 & 0.61534 & -3.9213 & 7.4232 & -1.6580 \end{bmatrix} 10^{-5} \qquad (10)$$

$$K^y = \begin{bmatrix} -0.00575 & 0.13550 & -0.14717 & -2.4476 & 5.7702 \\ 0.01750 & -0.16928 & 2496.8 & 22.413 & -38.439 \\ 0.00560 & -0.95731 & 12.275 & -48.359 & 65.183 \\ -0.02710 & 1.4765 & -13.011 & 39.995 & -96.820 \\ 0.01541 & -0.70629 & 5.4384 & -14.547 & 14.014 \end{bmatrix} 10^{-5} \quad (11)$$

Figure 4 presents the relation between the presented dimensionless coefficient (c) and deflection curve components (x/L and y/L) for Case II.

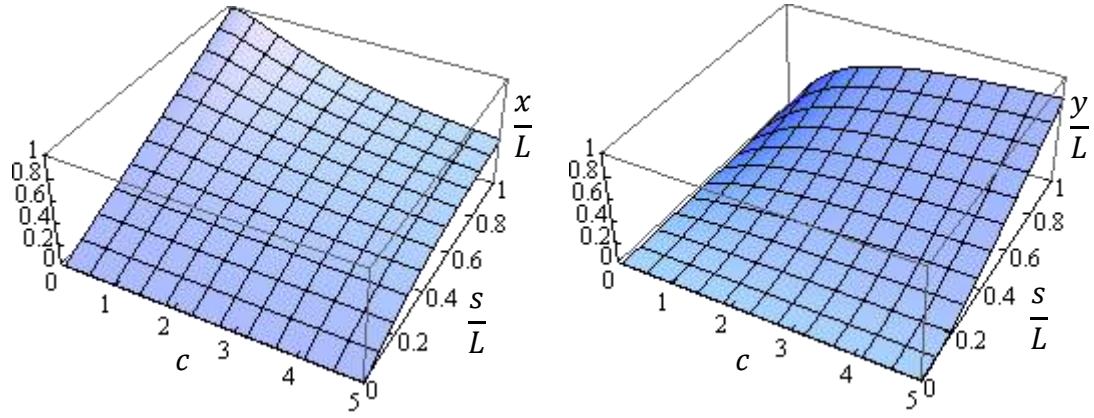

Figure 4. The "c – Deflection Curve" Relation for Case II
a) $c - s/L - x/L$, b) $c - s/L - y/L$

The K^x and K^y matrices are given in Equations 12 and 13, respectively for the plots given in Figures 4a and 4b.

$$K^x = \begin{bmatrix} 0.11104 & 9997.1 & 4.5063 & 591.37 & -311.43 \\ -0.22374 & -2.9105 & 123.80 & -3967.7 & 2042.0 \\ -2.9918 & 151.68 & -1284.6 & 1309.8 & -381.43 \\ 0.78495 & -36.520 & 279.44 & -61.016 & -39.487 \\ -0.06242 & 2.7950 & -20.470 & -6.3897 & 8.8000 \end{bmatrix} 10^{-5} \quad (12)$$

$$K^y = \begin{bmatrix} -0.28538 & 12.833 & -151.74 & 202.33 & -68.265 \\ 1.4621 & -60.897 & 11286 & -3917.2 & 23.091 \\ -0.96090 & 22.455 & -2880.8 & -1322.3 & 1231.1 \\ -0.02927 & 7.0351 & 392.55 & 499.63 & -331.75 \\ 0.01344 & -1.0492 & -22.147 & -45.567 & 27.497 \end{bmatrix} 10^{-5} \quad (13)$$

Similarly, the "c – deflection curve" relation for uniformly distributed load along the beam (Case III) is presented in Figure 5.

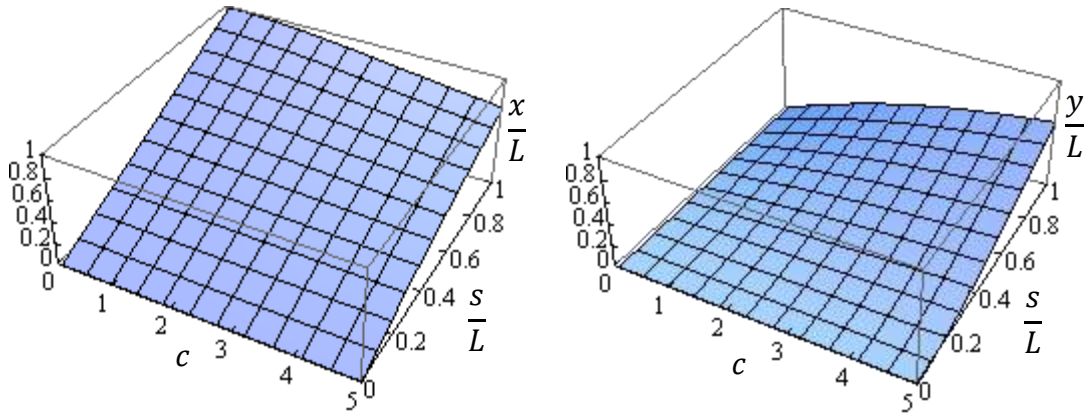

Figure 5. The "c – Deflection Curve" Relation for Case III
a) $c - s/L - x/L$, b) $c - s/L - y/L$

The K^x and K^y matrices given in Equations 14 and 15 are for the surface plots presented in Figures 5a and 5b, respectively.

$$K^x = \begin{bmatrix} -0.01965 & 10000 & -6.3753 & -3.5438 & 3.6387 \\ 0.12426 & -5.4326 & 38.879 & 29.007 & -26.490 \\ -0.86194 & 41.170 & -336.19 & -111.48 & 145.67 \\ 0.12610 & -5.2592 & 35.667 & 47.139 & -36.229 \\ -0.00574 & 0.21145 & -1.1818 & -3.6368 & 2.4140 \end{bmatrix} 10^{-5} \quad (14)$$

$$K^y = \begin{bmatrix} -0.01444 & 0.42982 & -9.6231 & -7.8642 & 6.7851 \\ 0.07472 & -2.1664 & 3799.4 & -2455.7 & 587.92 \\ -0.08538 & 2.3471 & -55.397 & -58.508 & 46.695 \\ -0.05947 & 2.6528 & -54.706 & 20.043 & 0.99480 \\ 0.00628 & -0.25375 & 5.0238 & -0.58629 & -0.82585 \end{bmatrix} 10^{-5} \quad (15)$$

The form of the deflection curve varies due to the value of the concentrated load multiplier (λ) for Case IV. Therefore, different K^x and K^y matrices will be obtained for each λ value to build an accurate surrogate model. In this study, the results are presented for $\lambda = 0.5$ (Figure 6).

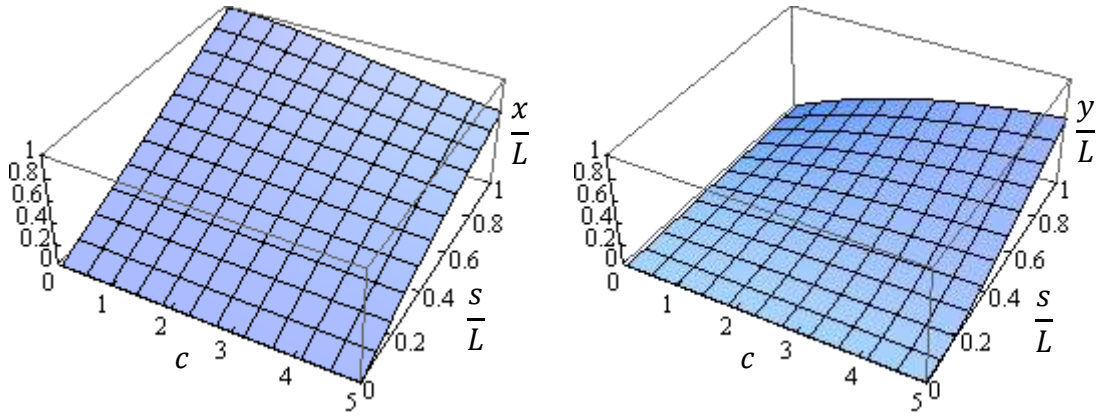

Figure 6. The "c – Deflection Curve" Relation for Case IV
a) $c - s/L - x/L$, b) $c - s/L - y/L$

Finally, the K^x and K^y matrices are given in Equations 16 and 17 to obtain the surfaces given in Figures 6a and 6b, respectively.

$$\mathrm{K}^x = \begin{bmatrix} -0.01594 & 10000 & -5.3594 & -0.39736 & 1.6016 \\ 0.09815 & -4.3068 & 30.941 & 31.576 & -24.937 \\ -0.68692 & 31.774 & -250.45 & -424.74 & 285.71 \\ 0.09057 & -3.5500 & 22.293 & 122.53 & -71.364 \\ -0.00370 & 0.11617 & -0.47215 & -9.3590 & 5.1576 \end{bmatrix} 10^{-5} \quad (16)$$

$$K^y = \begin{bmatrix} -0.00091 & -0.24091 & -14.882 & -24.174 & 15.674 \\ -0.00214 & 1.6845 & 3829.8 & -1734.0 & 222.61 \\ 0.01707 & -2.8634 & -97.048 & -195.01 & 121.45 \\ -0.05280 & 2.3946 & -49.975 & 26.717 & -3.7837 \\ 0.00461 & -0.18193 & 5.0204 & -0.20548 & -0.93486 \end{bmatrix} 10^{-5} \quad (17)$$

VALIDATION

In this part, the results obtained by the presented model and a finite element analysis (FEA) software are compared. The ABAQUS software is utilized for finite element analysis; one dimensional cantilever beam models are generated and loads are applied to the beams that satisfy certain c values. The x and y coordinates of the deflection curve of each numerical example are noted. The results are presented in the plot given in Figure 7 for $c = 1.0$.

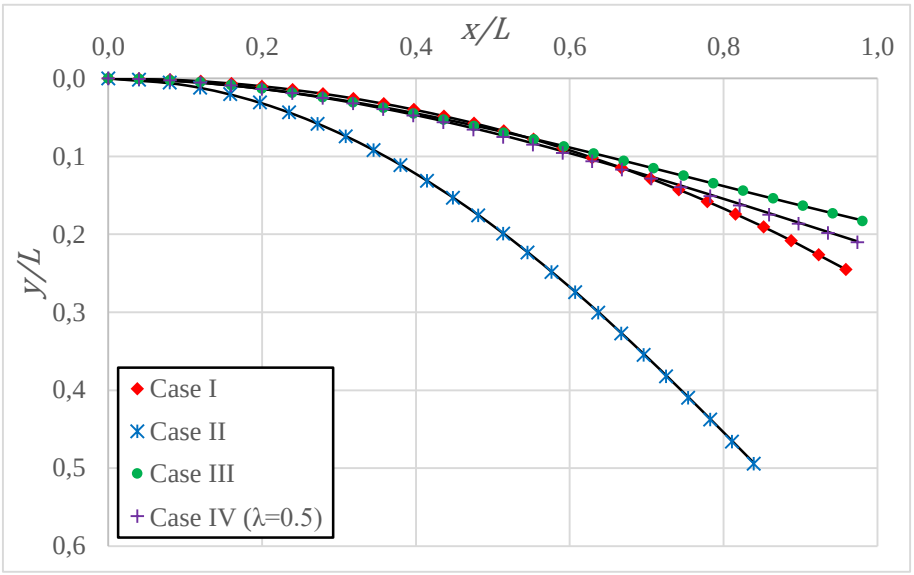

Figure 7. The deflection curves for $c = 1.0$

In Figure 7, the ticks indicate the values obtained by ABAQUS software. The continuous lines show the deflection curves obtained by the surrogate model presented in this study. The deflection curves for $c = 2.0$ is given in Figure 8.

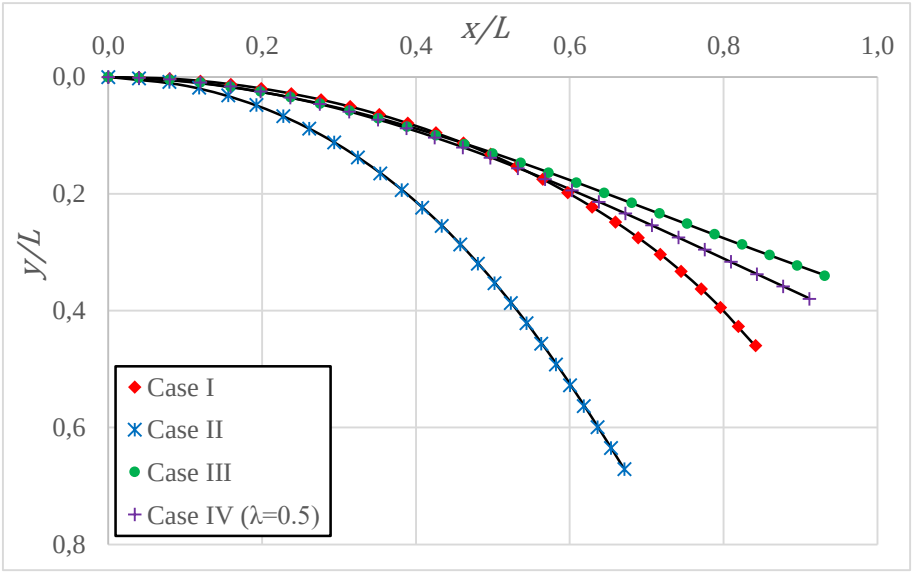

Figure 8. The deflection curves for $c = 2.0$

Finally, the deflection curves for $c = 4.0$ are as presented in Figure 9.

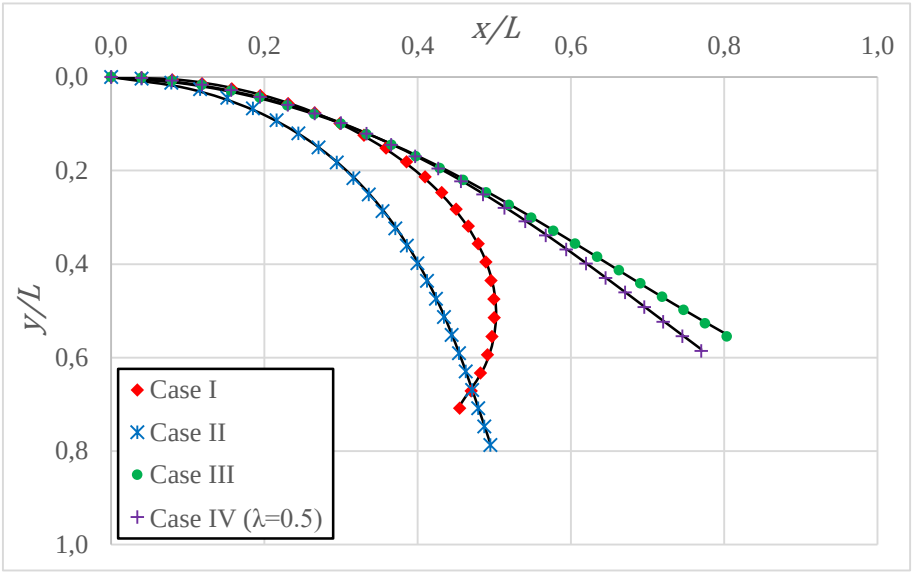

Figure 9. The deflection curves for $c = 4.0$

It can be seen from Figures 7, 8, and 9 that the results obtained by the surrogate model perfectly coincide with the finite element solutions.

CONCLUSION

A surrogate model to calculate the deflection curves of highly flexible cantilever beams is presented. The relation between the deflection curve shape and the loading case is modeled by bivariate polynomials introducing dimensionless coefficients that involve the load magnitude, cantilever length, Young's modulus of the material, and the moment of inertia of the beam section with respect to the bending axis. The values for parameters of the surrogate model are provided for constant moment, concentrated load at free end, uniformly distributed load, and combined loading of concentrated load at free end and uniformly distributed load cases with respect to the introduced dimensionless coefficients. Finally, the results obtained by the presented model are validated through finite element analysis. It is shown that the presented model provide nearly identical solutions to those obtained with the ABAQUS software. The presented surrogate model can be used to reduce the computational cost in applications such as structural optimization.

REFERENCES

Adams, R.A. (1999). Calculus "A Complete Course" Fourth Edition. Addison-Wesley.
Barten, H.J. (1945). On the deflection of a cantilever beam. Quarterly of Applied Mathematics, 2, 168-171; 3, 275-276.

Belendéz, T., Neipp, C., Belendéz, A. (2002). Large and small deflections of a cantilever beam. European Journal of Physics, 23(3), 371-379.
Belendéz, T., Neipp, C., Belendéz, A. (2003). Numerical and experimental analysis of a cantilever beam: a laboratory project to introduce geometric nonlinearity in mechanics of materials. International Journal of Engineering Education, 19(6), 885-892.
Bisshopp, K.E., & Drucker, D.C. (1945). Large deflections of cantilever beams. Quarterly of Applied Mathematics, 3, 272-275.
Caire, M., & Vaz, M.A. (2007). Large deflections of a linear viscoelastic cantilever beam subjected to a concentrated end load. Proceedings of the 19th International Congress of Mechanical Engineering, Brazil.
Chen, L. (2010). An integral approach for large deflection cantilever beams. International Journal of Non-Linear Mechanics, 45, 301-305.
De Bona, F., & Zelenika, S. (1997). A generalized elastica-type approach to the analysis of large displacements of spring strips. Proceedings of the Institution of Mechanical Engineers (Part C), 211, 509-517.
Kumar, R., Ramachandra, L.S., Roy, D. (2004). Techniques based on genetic algorithms for large deflection analysis of beams. Sadhana, 29(6), 589-604.
Lee, K. (2002). Large deflections of cantilever beams of non-linear elastic material under a combined loading. International Journal of Non-Linear Mechanics, 37, 439-443.
Levien, R. (2008). The elastica: a mathematical history. Technical Report No. UCB/EECS 2008-103, EECS Department, University of California, Berkeley.
Mattiasson, K. (1980). Numerical results from large deflection beam and frame problems analysed by means of elliptic integrals. International Journal for Numerical Methods in Engineering, 17(1), 145-153.
Scarpello, G.M., & Ritelli, D. (2011). Exact solutions of nonlinear equation of rod deflections involving the Lauricella hypergeometric functions. International Journal of Mathematics and Mathematical Sciences, Article ID: 838924.
Stoer, J. & Bulirsch, R. (1992). Introduction to Numerical Analysis. Second ed., New York: Springer-Verlag.
Tari, H. (2013). On the parametric large deflection study of Euler–Bernoulli cantilever beams subjected to combined tip point loading. International Journal of Non-Linear Mechanics, 49, 90-99.
Timoshenko, S. (1940). Strength of Materials: Part I. Second ed., D. Van Nostrand Company Inc.
Venkata Rao, R. (2016). Jaya: A simple and new optimization algorithm for solving constrained and unconstrained optimization problems. International Journal of Industrial Engineering Computations, 7, 19-34.

TRIANGULAR LAYOUT DETECTION IN 2D TRUSS OPTIMIZATION

Hakan ÖZBAŞARAN
Eskişehir Osmangazi University, Department of Civil Engineering, Eskişehir/TURKEY
ozbasaran@ogu.edu.tr

Batuhan ŞANLI
Eskişehir Osmangazi University, Department of Civil Engineering, Eskişehir/TURKEY
batuhansanli@gmail.com

ABSTRACT: Due to limited resources and growing demand, more researchers have been interested in studying optimal design of structures including trusses in the last decade. The trusses are structural systems formed by connecting bars with hinged ends. These lightweight systems are useful to provide efficient solutions for large-span structures. Depending on the design variables, efficient designs for truss systems can be obtained by using size, shape, and topology optimization procedures. Contrary to size and shape optimization, topology optimization of trusses involves adding and removing of the members to obtain an optimum design, which may lead to unfavorable topological configurations that have structural defects such as kinematic instability and overlapping members. Accepting these unfavorable forms as proper design candidates and submitting them to the finite element analysis software may dramatically increase the optimization time and/or lead to infeasible final designs. This preliminary study is the very first part of a project on identifying and repairing the unfavorable truss design candidates before the structural analysis step. In this paper, an algorithm to detect 2D trusses that are formed by triangular cells, which is the fundamental form for many popular truss topology configurations, is presented. The performance of the presented algorithm is evaluated through computer-generated candidates.

Key words: truss, design, triangular layout, kinematic stability

INTRODUCTION

Truss systems have been commonly used especially in large-span structures. In these structural systems, the loads are applied directly to the nodes where at least two members are connected. Therefore, the shear force and bending moment on the members are almost zero; only axial forces (tensile and compression only) apply. Since the load carrying capacity is much more than that of solid systems considering the structural weight, the truss systems are more advantageous in terms of both strength and economy. Examples of these efficient systems include bridges, large industrial buildings, factories, stadiums, and sports halls. Truss systems can be classified into two as planar and spatial

trusses. The planar truss systems, which is the main concern of the study, is a two-dimensional lattice system with co-planar members. The simplest internally stable planar truss is a triangular cell, which can be constructed by connecting three straight members to each other from their ends to form a triangle.

The optimal design of trusses can be carried out through three different procedures as size, shape, and topology optimization. The size optimization process searches for the minimum weight design by altering the sections of the members. The most favorable node positions are investigated in the shape optimization process. Finally, the truss topology optimization is to explore the design space for the best member count and connectivity configuration for the given loads and constraints. The constraints may be stress, deflection, stability, etc. depending on the application.

A considerable number of studies have been conducted on topology optimization of trusses and detection of unfavorable topological forms. Cazacu and Grama (2014) have proposed an algorithm for topology optimization that works together with the Finite Element Method. In their tests using MATLAB, they mentioned the importance of the penalty function to be used in the genetic algorithm to solve the problem. Cui et al. (2018) proposed an approach to determine the intersecting and overlapping bars; they have also provided the mathematical definition of intersections and overlaps. Recently, Shakya et al. (2018) developed an algorithm that removes kinematically unstable and useless zero-stress bars from the system. Bekdaş et al. (2015) formulated a structural optimization approach based on the Flower Pollination Algorithm. Assimi et al. (2017) presented a genetic algorithm approach to the simultaneous size and topology optimization of trusses. They aimed to achieve minimum weight by adhering to the maximum permissible stress and deflections. In earlier period, Zhou (1996) wrote an article on stress and local buckling constraints and optimization of truss system topology. However, he pointed out that the solution made in this way may behave unstable and that the solution may be different from the real optimal solution. In addition to Zhou's study, Rozvany (1996) added system stability constraints to the formulation to prevent the seemingly optimal but unstable solutions. However, it is shown in his examples that even these modified formulations can lead to a non-optimal solution. Recently, Larsen et al. (2018) proposed a method for obtaining a near-optimal frame structure based on the solution of a topology optimization model based on homogenization. The Michell (1904) method, which was developed by considering the least weight truss problem, leaded to the solutions close to the optimal solution with a relatively low operational cost.

There are popular predefined topological configurations for planar trusses (see Figure 1) that are commonly used to build structural systems for roofs and bridges; most of these topological forms can be formed by joining triangular cells. In this study, the planar trusses that can be formed by connecting triangular cells are called as “trusses that have triangular layout”. All trusses given in Figure 1 except the “Fink” have triangular layout

(assuming that the top cord of the "Bowstring" is constructed by straight bars). Note that the "Fink" is constructed by connecting two triangular layout trusses sharing a node with a bar.

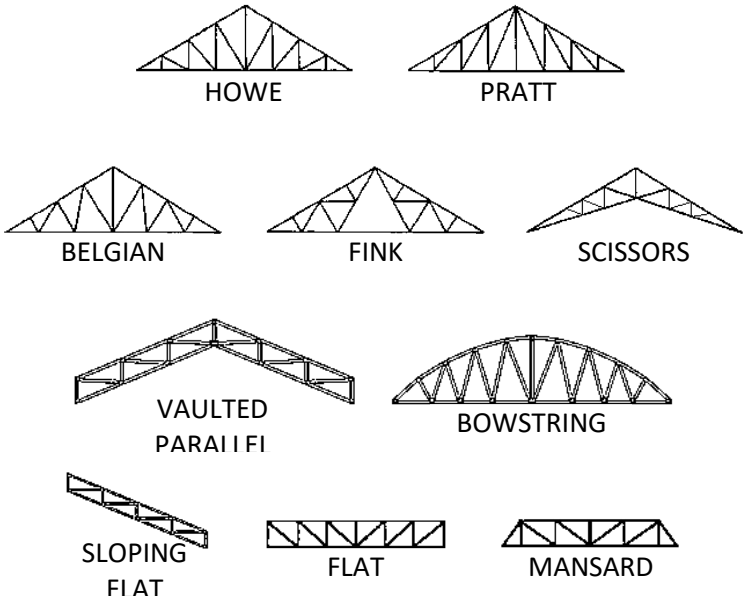

Figure 1. Common Planar Trusses (Karagöz et al., 2015)

This study presents an algorithm to detect truss systems with triangular layout. The presented algorithm may be used in topology optimization applications to force the final design to have a triangular layout, which is mostly preferred in engineering practice for the construction ease. In addition, this algorithm naturally checks the kinematic stability of the candidates before submitting it to the structural analysis (saving a significant amount of computational effort) since the trusses with triangular layout are internally stable. The following part summarizes the kinematic stability of planar trusses.

KINEMATIC STABILITY OF PLANAR TRUSSES

Kinematics is the branch of physics that examines the movement of bodies, regardless of the forces that cause or result from these movements. The members of a structural system should be assembled to construct a kinematically stable structure. The first condition is that the system meets the stiffness condition. The number of the unknowns in a truss system is the sum of the number of the bars (c) and the number of the support reactions (r). Since all of the members of the two-dimensional trusses are straight bars on the same plane, the forces acting on each joint is in the same plane and intersect with each other. For this reason, the rotation and the torque balance at the joints is provided. Only the equilibrium equations $\sum Fx = 0$ and $\sum Fy = 0$ are required to be satisfied. On the other hand, the total number of the equations is 2d, where d is the number of the nodes in the truss system. Thus, by comparing the number of unknowns (c + r) with the total number of

equations, it can be found whether the system has enough bars and support reactions to build a stable form as a preliminary test as follows:

$$c + r \geq 2d \qquad (1)$$

If Equation 1 is not satisfied, it can be said that the system is certainly unstable (the system does not have enough bars to construct a load bearing structure). However, a truss system may be unstable even though it passes the above mentioned test (Figure 2); Therefore, Equation 1 is a necessary but not sufficient condition for kinematic stability of planar trusses. In such cases, it is possible to decide whether the system is stable by observation or force analysis.

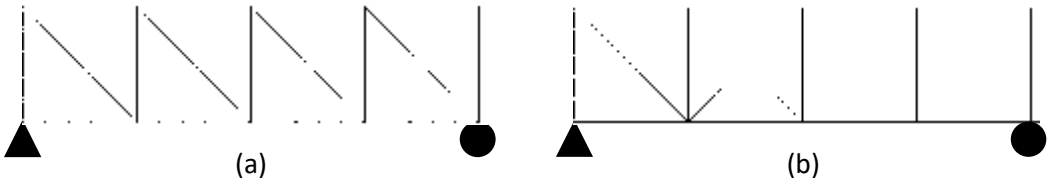

Figure 2. Two Planar Trusses Having Same Number of Nodes, Bars, and Support Reactions
a) Stable, b) Unstable

It should be reminded that constructing the global elastic stiffness matrix of a truss and conducting a positive definiteness test is an exact but computationally expensive method to determine if the system is kinematically stable or not. As told above, it can be said that a truss system is internally stable if it can be formed by joining triangular cells; however, this does not mean that a truss system candidate is certainly unstable if it has a non-triangular layout. Note that the bars 1-2 and 1-4 are not members of a triangular cell in the simple truss given in Figure 3.

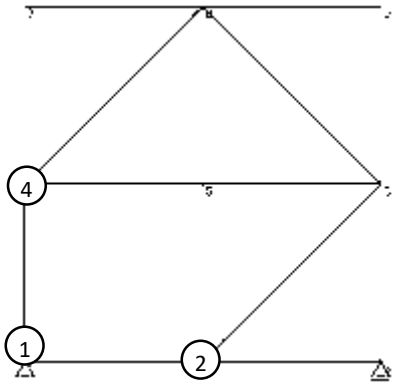

Figure 3. A Kinematically Stable Planar Truss with a Non-Triangular Layout

THE ALGORITHM

An efficient algorithm should be robust and computationally inexpensive. As the number of operations increases the required processing power and time increase as well. The authors do not claim that a more efficient algorithm than the presented one in this study cannot be found to accomplish the mentioned task. However, it can be said that it does its job by using an acceptable amount of computational power considering the applications in the field. The steps of the presented algorithm is as follows:

1. Node and bar lists are generated.
The algorithm does not use the coordinates of the nodes. This sometimes cause detection of a triangular cell of which nodes lie on the same line. It is well-known that this condition is unfavorable since constructing trusses with overlapping bars is not possible in real-world. However, theoretically, this unfavorable form is internally stable. The nodes list consist of node numbers as n = (1, 2, …) and the bars list stores the start and the end nodes of the bars as b = ((1,2), (1,4), (2,3), (2,4), …). An additional empty list is generated for the bars that are components of the triangular cells as b_t = ().
2. The first element of the nodes list is selected.
In fact, it is not necessary to start from the first element of the nodes list; a random node can be selected.
3. The bars in the b and b_t lists connected to the selected node are determined.
Consider that the node "1" is selected. The bars in the "b" list that are connected to node 1 are determined and added to another list called "b_n" as b_n = ((1,2), (1,4), …).
4. The other node (other than the selected one) of the bars are extracted and listed.
This list would be in the form o_n = (2, 4, …) for selected node 1.
5. The bars in the lists b and b_t that connect the nodes in the o_n list are checked.
The bar (2,4) in the b list connects the nodes 2 and 4 of the o_n list.
6. The bars detected in the 5th step and the relevant bars are appended to the b_t list (by avoiding duplication) and removed from b list (if it is there).
For example, consider that the bar (2,4) is detected in the 5th step. The bars (1,2), (1,4), and (2,4) should be added to the b_t list and removed from the b list. This means that the mentioned bars are the components of at least one triangular cell.
7. The algorithm proceeds by selecting the next node in the nodes list (n) and returning to step 3.
If no nodes are left. Then proceed to the next step.
8. The design candidate is categorized.
If no bars are left in the b list (all of the bars are moved to the b_t list) this means that all bars in the system are the components of at least one triangular cell. Therefore, it can be said that the considered system has a triangular layout. If there are bars left in the b list, the considered system has a non-triangular layout. The bars left in the b list may be removed (if possible) or connected to a random triangular cell as a fast repairing procedure.

Since the presented algorithm does not benefit from the coordinates of the nodes, the collinear nodes cannot be detected. This may lead to undesired results in some conditions. Consider the "Fink" truss given in Figure 4.

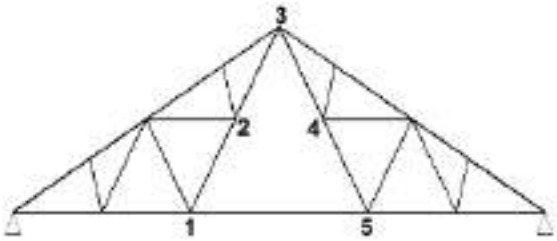

Figure 4. A Stable Planar Truss with a Non-Triangular Layout

The vertices (1,3), (1,5), and (3,5) in Figure 4 form a triangle for sure. However, the bars (1,3), (1,5), and (3,5) do not exist. The (1,3) vertex is formed by the collinear (1,2) and (2,3) bars. Similarly, the vertex (3,5) is formed by the bars (3,4) and (4,5). Since the proposed algorithm detects the triangular cells formed by three bars, the 1-3-5 cell cannot be detected.

The performance of the algorithm is tested through 10000 randomly generated planar truss candidates. Figure 5 presents the ratio of unstable designs to the total number of generated candidates.

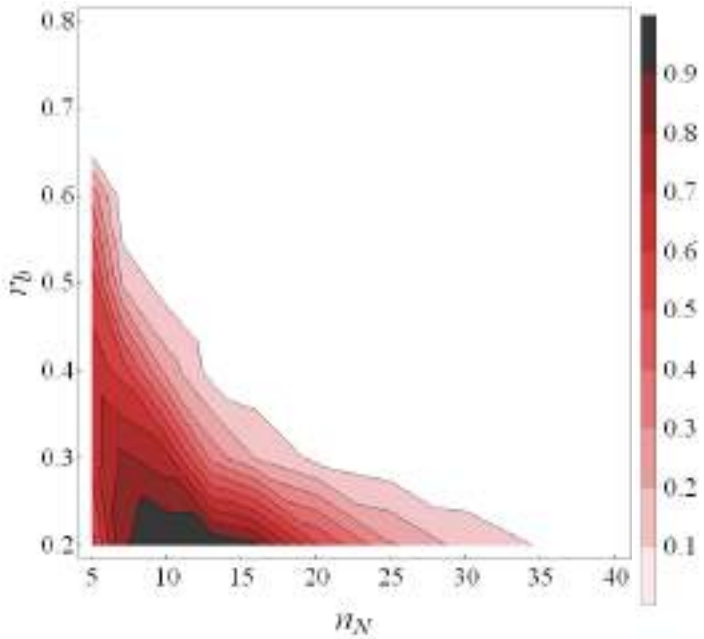

Figure 5. The Ratio of the Unstable Forms

In Figure 5, the n_N is the available number of the nodes, and the symbol r_b is for the ratio of the number of bars in the generated candidate to the maximum number of the available

bars (considering the number of the available node number n_N). For example if the number of available nodes is 10, the ground structure of this node configuration has (10×9)/2=45 bars. If the r_b is 0.4, it means that the candidate is generated by using 0.4×45=18 of the 45 available bars. The plot in Figure 5 shows that if the r_b is over 0.65 or the number of available nodes (n_N) is over 35, (surprisingly) no unstable candidates are generated. The criterion given in Equation 1, which is a necessary but not sufficient condition for kinematic stability, is usually used as a rapid evaluation method to eliminate unstable forms before sending them to structural analysis module. However, as mentioned before in the manuscript (see Figure 2), there may be unstable design candidates that satisfy the criterion in Equation 1 (Figure 6).

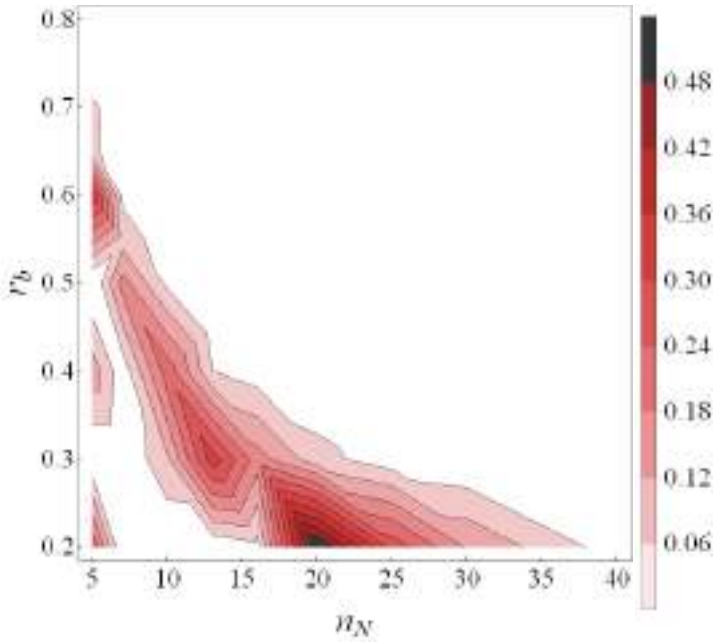

Figure 6. The Ratio of the Unstable Candidates That Satisfy the Criterion in Equation 1

It is seen from Figure 6 that a considerable percent of the unstable candidates in the generated set satisfy Equation 1. The ratio of unstable candidates satisfying the Equation 1 reaches up to 48% for certain r_b – n_N configurations. As the final plot, Figure 7 presents the ratio of unstable forms that have triangular layout.

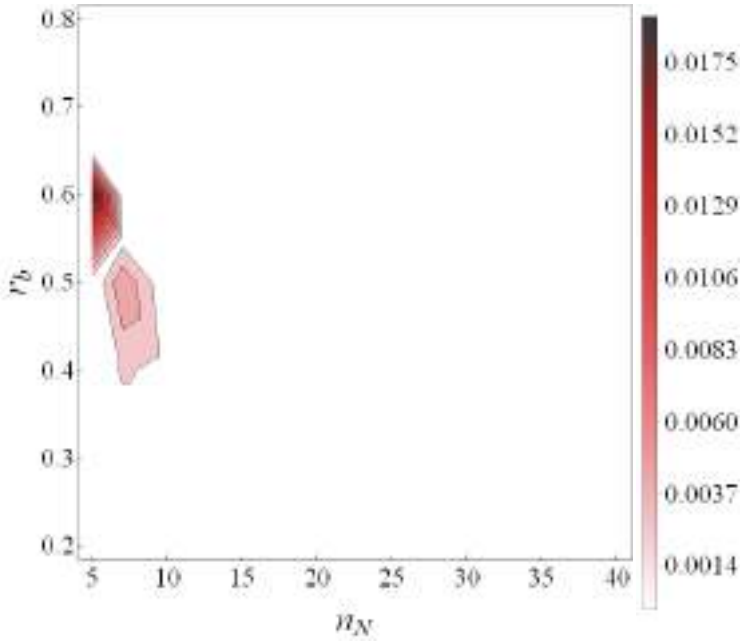

Figure 7. The Ratio of the Unstable Forms having Triangular Layout

The plot given in Figure 7 summarizes the performance of the presented algorithm in detecting kinematically unstable candidates. It is crucial to write here that the main objective of the proposed algorithm is not about identifying kinematic instability; however, it mostly comes with the triangular layout as a gift. It is seen from Figure 7 that a small ratio of candidates that have triangular layout are unstable (below 2% percent at most). These topological configurations may be formed by unconnected triangular cells, or triangular cells that share one node in some cases.

CONCLUSION

This paper is the preliminary study of a geometrical inspection method to eliminate unfavorable shapes in truss topology and shape optimization problems. An algorithm to detect truss design candidates that have triangular layout is proposed. The presented triangular layout detection method does not require the coordinates of the nodes; the node-bar connectivity information is sufficient. However, it should be stated that there are cases in which the proposed algorithm identifies the unfavorable forms as triangular layouts. As a bonus feature of trusses formed by triangular cells, the kinematic stability constraints are naturally satisfied (mostly). It is shown through numerical experiments conducted on 10000 randomly generated planar truss topologies that the proposed algorithm successfully categorizes the design candidates.

ACKNOWLEDGEMENTS

The second author (Batuhan ŞANLI) is an undergraduate student in Eskişehir Osmangazi University, Department of Civil Engineering. The first author congratulates his effort to prepare this paper.

REFERENCES

Assimi, H., Jamali, A., Nariman-zadeh, N. (2017). Sizing and topology optimization of truss structures using genetic programming. Swarm and Evolutionary Computation, 37, 90-103. doi:10.1016/j.swevo.2017.05.009

Bekdaş, G.¸ Nigdeli, S.M., Yang X.S. (2015). Sizing optimization of truss structures using flower pollination algorithm. Applied Soft Computing, 37, 322-331. doi:10.1016/j.asoc.2015.08.037

Cazacu, R., & Grama, L. (2014). Steel truss optimization using genetic algorithms and FEA. Procedia Technology, 12, 339-346. doi:10.1016/j.protcy.2013.12.496

Cui, H., An, H., Huang, H. (2018). Truss topology optimization considering local buckling constraints and restrictions on intersection and overlap of bar members, Structural and Multidisciplinary Optimization, 58(2), 575-594. doi:10.1007/s00158-018-1910-x

Karagöz, Ö., Özbaşaran, H., Doğan, M., Gönen, H., Ünlüoğlu E. (2015). Betonarme taşıyıcı sistem – çelik kafes çatı etkileşimi: Deprem davranışı. 6. Çelik Yapılar Sempozyumu. Eskişehir, Turkey.

Larsen, S.D., Sigmund, O., Groen, J.P. (2018). Optimal truss and frame design from projected homogenization-based topology optimization. Structural and Multidisciplinary Optimization, 57(4) 1461-1474. doi:10.1007/s00158-018-1948-9

Michell, A.G.M. (1904). The limits of economy of material in frame-structure. The Philosophical Magazine: Structure and Properties of Condensed Matter, 8(47), 589-597. doi:10.1080/14786440409463229

Rozvany, G.I.N. (1996). Difficulties in truss topology optimization with stress, local buckling and system stability constraints. Structural Optimization, 11(3-4), 213-217. doi:10.1007/BF01197036

Shakya, A., Nanakorn, P., Petprakob, W. (2018). A ground-structure-based representation with an element-removal algorithm for truss topology optimization. Structural and Multidisciplinary Optimization, 58(2), 657-675. doi:10.1007/s00158-018-1917-3

Zhou, M. (1996). Difficulties in truss topology optimization with stress and local buckling constraints. Structural Optimization, 11(2), 134-136. doi:10.1007/BF01376857.

CONCEPTUAL DESIGN METHODOLOGY FOR FOLDABLE MOBILE SHELTERS

Jumana ALRAHAL*, Mustafa ÖZAKÇA

Department of Civil Engineering, Faculty of Engineering, University of Gaziantep, Gaziantep, Turkey.

*Corresponding author: jumanarahal2016@gmail.com

ABSTRACT: Prefabricated and quick-to-install shelters can provide victims of harsh natural and man-made disasters with the opportunity to survive. Seeking to cater for this need and to reflect the topic of the mobile sheltering system, this paper focuses on the case study development of a foldable, modular mobile shelter, from emergency scenarios to the permanent phase. The purpose of this paper is to propose a lightweight foldable and modular shelter that can be considered for the post-disaster shelter response and can be replaced, upgraded in size and geometrical configuration, and stored in a very short period of time. Using the folding technique, the specific mobile shelter structure investigated in this study has the ability to transform from a compact closed form to a large living space open form. The suggested structure of these shelters are incrementally expandable through adding more modular units to its ends and sides. Furthermore, this paper examines the feasibility of the proposed concept and structure systems through a literature review, design-based research and digital model development.

Keywords: Incremental architecture, foldable structure, shelter design.

Introduction

Natural and manmade disasters have caused considerable damage to buildings. Many homes have been damaged and rendered unusable, causing a high number of displaced people. Thus, housing reconstruction programs take a significant role in disaster recovery and temporary shelters are essential suppliers and a critical part of disaster recovery. In this sense, shelters should provide homeless victims with privacy, safety and comfort to restart their daily activities and return to normal life as soon as possible after a disaster [1].

After the Second World War, governments were trying to develop urgent solutions to the drastic housing problem. With the support of the industries, architects and engineers, alternative solutions such as prefabricated buildings, mobile architecture and modular, transformable structures were developed. These alternative solutions expanded with the need for affordable, rapidly-constructed housing [2]. The need for shelter and housing reconstruction program was not limited to the post-war period; however, it became the main issue after every disaster. To coordinate activities associated with the right to have a proper shelter, Global Shelter Cluster (GSC) was established in 2005 by the Inter-

Agency Standing Committee (IASC) of United Nations and is co-instructed worldwide by United Nations High Commissioner for Refugees (UNHCR) and International Federation of the Red Cross and Red Crescent Societies (IFRC/RCS) in natural disaster situations. GSC is responsible for emergency urgent requirements (such as plastic, sheeting, tents, cash, etc.) and long-term requirements (such as mobile shelters, building or reconstruction of houses and related matters). Moreover, a shelter cluster is responsible for site planning and settlement design working in close cooperation with other clusters [3]. Given that the reconstruction, or resettlement, generally takes between 2 to 15 years [4].

Bashawri et.al [5] reviews the categories of sheltering/housing which are divided into emergency shelter, temporary shelter, temporary housing, transitional/progressive shelter, and permanent housing (see Figure 1).

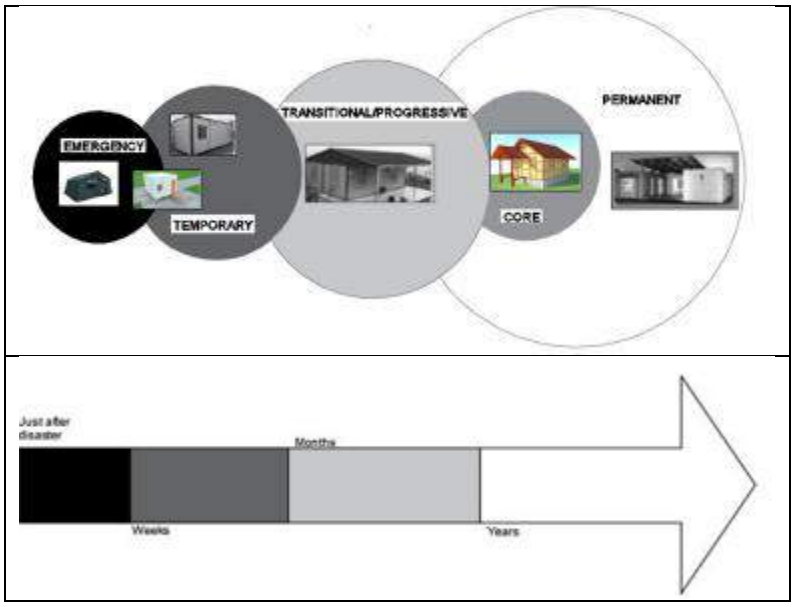

Figure 1 Categories of sheltering/housing systems

The existing evacuation shelters are usually complicated, take too much time to be constructed and are usually made of heavy materials. Many of them cannot be deployed or folded in a configurable geometric order, transportation becomes more difficult and storage for future use is particularly problematic. Asefi and Sirus [6] review the shelter both with and without transformable elements. Examples for shelters with transformable elements are folding bamboo house, recover accordion shelter and portable, retractable tent. Many researchers and engineers keep searching for a better alternative design for emergency shelter. During the design of a better shelter, they take the local culture and traditions into account and use materials available near to affected site.
As a result, researchers started to investigate sustainable solutions. One possible shelter solution is supplying affected families with the means to start reconstruction directly

after the disaster through the foldable transitional shelter approach as shown in Figure 2. In fact, the foldable transitional shelter can be considered as incremental process, not a final product, but an ongoing process. It supports the post-disaster affected families as they seek to sustain alternative options for recovering the damage, starting just after the disaster, and achieve a durable permanent house in a progressive manner within a limited period of time [7].

Figure 2 An incremental foldable transitional shelter and construction process

The transitional shelter can begin just after the disaster by distributing a foldable shelter package. Further support, such as cash or further material distribution, enables incremental building and upgrading of shelter towards the permanent house as presented in Figure 2. However, the period this process can take depends mainly on the economic situation and size of the family.

Additionally, the transitional shelter is grounded on five characteristics which are defined by IOM [7]. These shelters are upgradable, reusable, relocatable, resalable and recyclable. Consequently, the mobile transitional shelter is expected to be a continuous process for months and even years. The mobile transitional shelter offers the opportunity to link relief and future development perspectives towards a sustainable solution [7].

As a response for the increasing need for decent, more sustainable sheltering system, this research aims to suggest a design of a mobile shelter following a modular methodology and innovate an easy foldable unit that can fold in a short time. The suggested shelter will be well equipped for quick deployment immediately after the disaster. The suggested design is controlled to be light, so that it can be compactly folded in a package to make transportation easier. Moreover, it has the capability to be expanded as needed. The suggested mobile shelter design has objectives (such as security, size, lifespan, relief, and privacy) and limitations (such as cost, quantity, timeliness, materials availability, cultural appropriateness, and construction skills).

Foldable Mobile Structure Design Methodology

The term 'foldable structure' can be used to describe a structure that can be transformed from a compressed 'folded' form to a larger 'expanded' form [8]. Since folding is a relatively simple and rapid process to acquire three-dimensional shape, it has attracted

many architects to implement this technology in designing a wide range of structures, from extended roofs to exceptional building structures. In addition, with the possibility of combining it with parametric graphic tools, folding technology significantly accelerates the design cycle. More specifically, the existing application of folding technology in architectural design is basically focused on structural design and surface design [9].

The folding technique is generally used in the pre-hinged structure system. In foldable structures, in order to facilitate the folding process, static elements (plates) are connected by movable joints, which converts them into kinetic components. Taking this into consideration, it is understood that movable joints not only are a connection between two plates but also must transfer loads permitting relative motion in some directions while constraining motion in others [2]. A review of current challenges regarding foldable structures is presented and different mechanical modelling of foldable structures is investigated by Lebée [10]. Rigid folding, in which all the deformation is concentrated in the hinges while the faces between the folds remain flat, is adopted in this study.

Modular design (construction) can be defined as: A module is a unit whose structural elements are powerfully connected among themselves and relatively weakly connected to elements in other units. Obviously there are degrees of connection, so there are gradations of modularity [11].

The modular design grid described by Smith [12] and adopted in this current study is a geometric configuration system that enables building components and module elements to have standard dimensions. These configuration systems are generally based on square and rectangular structure, thus creating linear, component-like, flat-panel and box-like modules, though not necessarily. Structural systems are often placed on an axial grid, and panels and modules are deployed on a modular grid. Although this is effective from a design standpoint, there are problems in adjusting how other materials and elements are connected to the main module. If each column, beam, or structural element is in a different dimension, the 2D and 3D grid loses the ability to have a standardized panel or filling element associated with the frame with a standardized connection. When a major structural system is connected to another enclosure or interior system on the axis grid, special connections are necessary to be made.

Every building is designed in accordance with specific parameter sets such as use, size, material etc. Traditionally, this set of parameters is fixed earlier at the design process. However, the modular design features changeability of parameters into the current design process. Use of folding and interlocking techniques will improve the system flexibility for easy assembling, transportation, restoration and expansion. This leads to a more dynamic and flexible design where "late change", such as adding a kitchen unit to a base mobile shelter, does not result in the difficult laborious manual integration of a new element into an existing design [13].

The incremental housing is a step-by-step process and is designed to be one part of the sustainable response. It starts with a primary core shelter which can be a bedroom unit or a bare lot with the possibility of connecting more units. It is not quick, immediate or

complete but the owner manages housing expansion based on his needs and resources. The implementation of the incremental strategy is not as simple as ready-set-go. However, one of the most important issues that must be tackled by possible policies is to provide a starter house core to provide families with shelter and offer flexibility [14].

Design Example: Winged Shelter

Module description

The Winged shelter is a foldable housing unit which consists of an expandable parallelogram. The four symmetrical folded plates are the wings which are connected to long sides of the parallelogram by hinge joint system. Each wing is joined by two foldable plates. One of these two foldable plates is folded to the long edge of the wing, and the other is folded into the short edge of the wing using a hinge system so that it can freely rotate at a 90 degree angle. Figure 3 shows folded and unfolded Winged shelter unit.

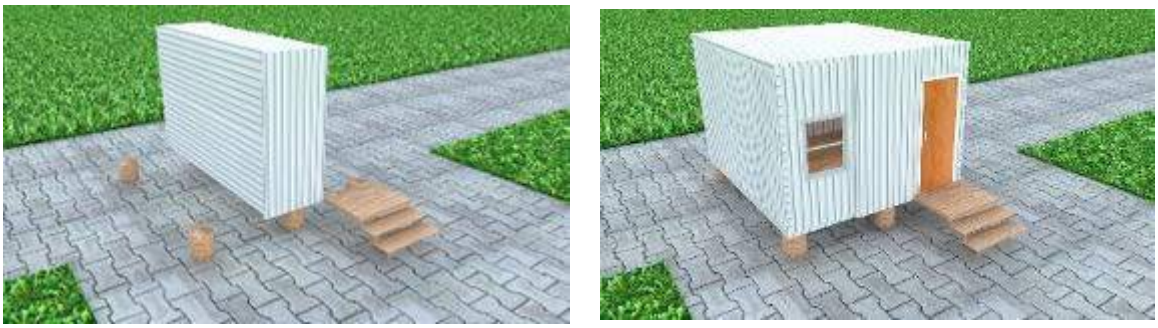

(a) (b)

Figure 3 Winged shelter design (a) folded unit, (b) unfolded (after erected) unit

Geometry and dimension

The suggested shelter structure is derived from a simple technique of folding. When Winged shelter design is erected (opened), the base unit will be 400 cm long, 358 cm wide, 269 cm high. The unit supports 14.32 m^2 living floor area. The plane and sections views of the Winged shelter design is shown in Figure 4. The shape of this design is a parallelogram. It is a purely geometric shape which consists of flat sides. Flat surfaces give the ability to use standard prefabricated panels. In addition, they have flexibility to create openings like doors and windows to provide good lighting conditions to the unit.

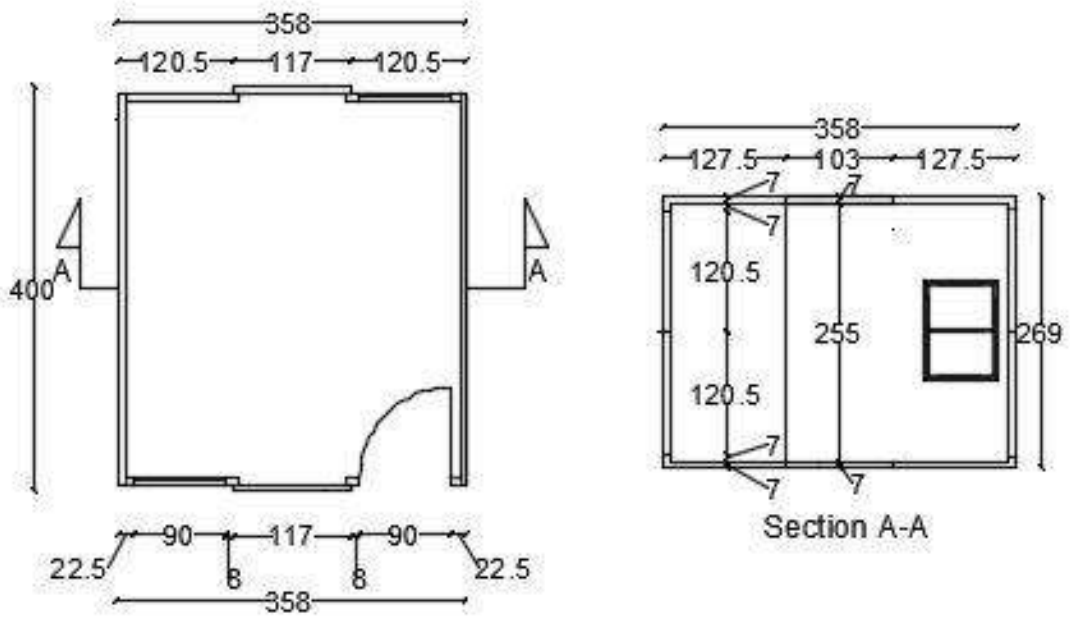

Figure 4 The plane and section view of Winged design (All dimensions are in cm)

Conceptual design

The basic idea of the concept is using folding and interlocking technology with the same modular composition system unit. The use of folding techniques makes the system more flexible, easily transportable, restorable and expandable.

As shown step by step in Figure 5, the installation procedure begins with the preparation of the foundation and ground where the unit will be placed as shown in image1. Next, the wings are unfolded at a 90 degree angle to form the roof and floor as shown in image 2 and 3. After that, each wing is unfolded from the long edge at a 90 degree angle to form side walls (see image 4 and 5). It is noted that two plates from two different wings meet to form a side wall. The result of this step is two opposite walls of the unit. Then, the second plates of two of the wings are unfolded to the short edge at a 90 degree angle to make two vertical plates forming the backside walls as shown in image 6 and 7. Finally, the second plates of the other two wings are unfolded at a 90 degree angle to form front window and door panels as shown in image 8 and 9. In this case, the desired erected (unfolded) unit is ready to shelter people. The unit can be unfolded to make it available within an hour by only three persons.

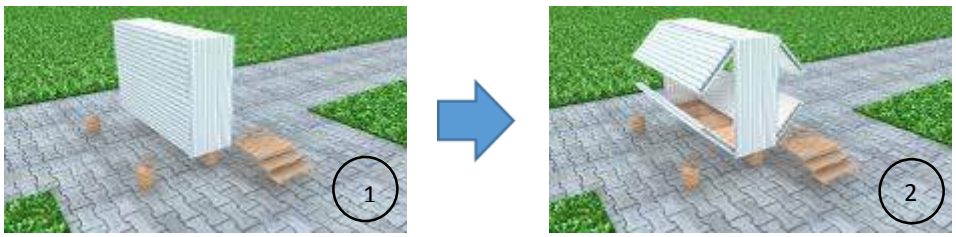

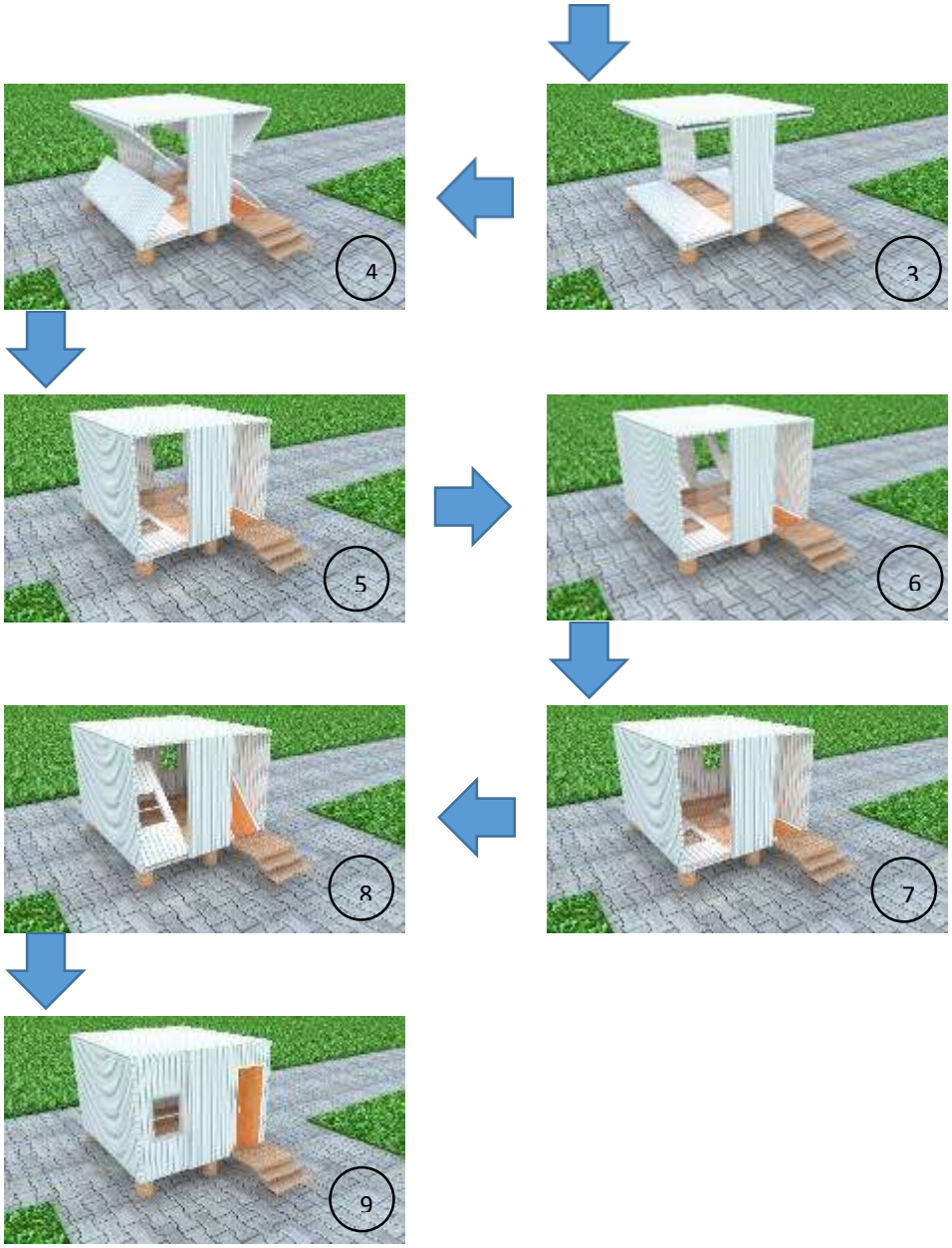

Figure 5 Unfolding process of Winged shelter unit

Transportation

In order to minimize the transportation cost and fast delivery of the unit and to maximize the number of units carried in one transportation container to a remote campsite, the folded unit dimension must fit the transportation container (the maximum height of the package should be less than 2.69 m), depending on the internal standard container dimensions (12.03 length, 2.35m width, 2.69m height).

The suggested shelter structure can be folded into a small package to facilitate transportation. The package dimension of the basic unit is 400cm long, 117cm wide, and

269 cm high. Six basic unit packages can fit in a standard transportation container and be delivered up at a time as shown in Figure 6.

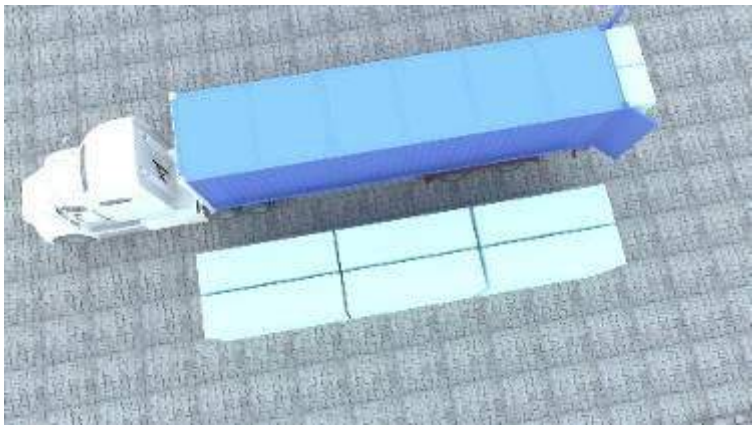

Figure 6 Transportation of Winged shelter units

Incremental housing process

After receiving relief, affected families usually begin looking for more space to be used for daily activities. In incremental housing concept, the base unit is considered as the first step to be used in emergencies. Families can expand their shelter according to their needs, such as adding a bathroom or a kitchen unit or both.

The expansion will occur according to incremental architecture, which is a step-by-step process using addition, subtraction and substitution to obtain the required configuration. The core structure which is a bedroom with a baby-room space unit; this phase is called emergency phase (is a place for people to live temporarily when they cannot live in their previous residence, similar to homeless shelters) see Figure 7. The unit in the emergency phase (single unit) has the following features:

- Easily and quickly transported
- Easy to set up and quick to construct
- The unit can fit for 3 to 4 people
- Relocatable as necessary
- Upgradable size

(a) (b)

Figure 7 The first level of **e**xpansion of Winged shelter design, (a) main module (emergency phase), (b) Plan of the main module

When it is required, it is possible to connect additional modules (including bathroom, kitchen or another bedroom) to the core structure. This phase represents the temporary phase (double unit) and is illustrated in Figure 8
In this phase, one of the modules contains a kitchen and a bathroom, separate from each other. The unit in this temporary phase has the following features:

- People at this stage will begin searching for a larger area to cover more purposes such as a kitchen, a bathroom and a living room etc.
- The added unit can easily function as a kitchen or a bathroom by connecting it to the water supply system in the site or providing a water tank for each shelter.
-

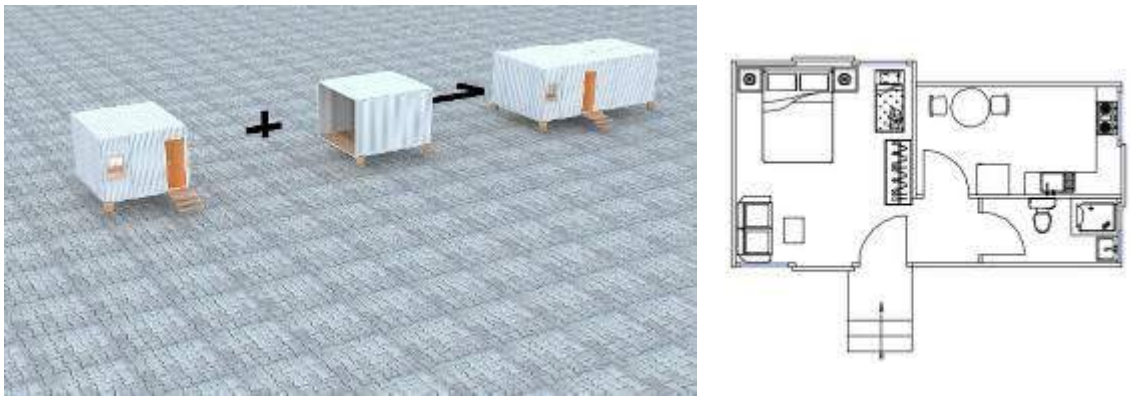

(a) (b)

Figure 8 The second level of expansion of Winged shelter design, (a) Two module (temporary phase), (b) Plan view of two modules.

The third level of expansion program is called the transitional or semi-permanent phase (triple unit) in which we add another module to the unit in the previous phase (temporary phase). In this phase one of the modules represents the entrance - a living room with a

dining room space unit as shown in Figure 9. The system in the transitional or semi-permanent phase has the following features:

- After a long recovery from the disaster, the transitional stage will require more space for different purposes. 2-3 years later, users of this shelter will need more area to improve their living conditions. Systems designed to provide better living conditions can be upgraded not only horizontally but also vertically.
- Needs for more area increase by time. At this stage, the family can upgrade their unit size in order to have more space for living and dining area. However, adding more units will depend on the size and economic situation of each family.
- Adding an entrance to enhance privacy and protection.
-

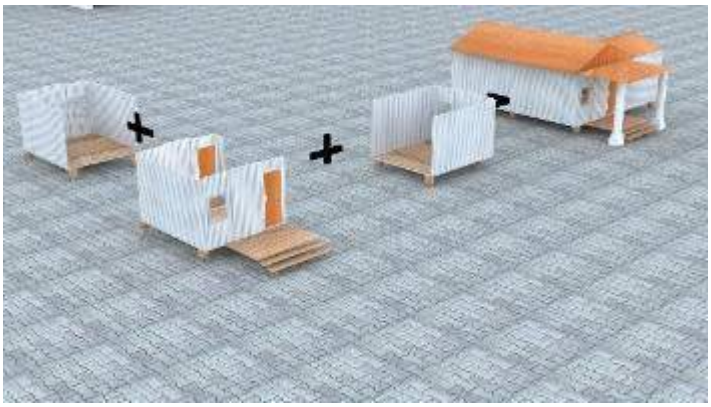

(a)

(b)

Figure 9 The third level of **e**xpansion of Winged shelter design, (a) Three modules (transitional phase), (b) Plane of three modules

In the fourth level of expansion program, the permanent housing phase happen by adding another module to the transitional phase. In this phase, one of the modules contains a baby room and a bathroom using a separator between them as shown in Figure 10. The system in the permanent or final phase (quadruple unit) has the following features:

- This stage may come after years of use. The system should be more durable to work permanently and provide better life conditions.
- Adding more space is possible in this stage, and the unit is upgradable to ensure the space necessary for standard living conditions. Still, adding more units depends on the number of family members and their economic condition.
- In this stage the unit could be connected to the electric power system in the site or provided with solar panels system to each unit as a solution for a more sustainable house. Moreover, each unit is designed to be easily connected to the water distribution system.

(a) (b)

Figure 10 The fourth level of **e**xpansion of Winged shelter design, (a) Four modules (permanent phase), (b) Plan view of four modules

Conclusion

A creative idea for foldable mobile shelter is proposed for various purposes, especially as temporary residences. The main advantage of this design, which is different from the existing temporary shelter systems, is that they can be folded in a very compact form with an opening and closing mechanism. These modular design can also be repaired and maintained making them more effective and efficient compared to regular temporary shelters. It is also possible to expand the structure as necessary by connecting additional units.

One of the main features of the proposed structure is that it is designed to cover all of the disaster recovery phases, so mobile shelter units can be utilized from the emergency phase up to the last phase, the permanent housing phase. To serve both short-term and long-term sheltering plans, these structures were designed to include the following features: ıt is easy to transport and set up, the area is adequate to accommodate 3 to 4 people during emergencies, and it can be relocated as necessary and upgradable in size and living conditions. To add more, structure storage is very simple since the structure is foldable to reach a much smaller size than the original size, which makes it easy to transport.

This paper also shows that it is possible to optimize the architectural functionality of the sheltering system while, at the same time, maintain its structural stability through the utilization of folding techniques in the design and implementation of the proposed sheltering systems.

Finally, shelter solutions should provide the opportunity for affected families to gradually move from emergency, temporary solutions to durable, permanent ones within the shortest possible time, taking into consideration the accessibility to the extra resources necessary.

References

[1] Félix D, Branco JM, Feio A. Temporary housing after disasters: A state of the art survey. Habitat International 2013; 40: 136-141.

[2] Werner C.D.M. Transformable and transportable architecture: analysis of buildings components and strategies for project design. MSc, Escuela Técnica Superior de Arquitectura de Barcelona, Universitat Politècnica de Catalunya, Spain, 2013.

[3] UNHCR, United Nations High Commissioner for Refugees. Handbook for emergencies. 4nd ed. Genova, Switzerland: 2015.

[4] do Nascimento JIG. Transitional Architecture in Emergency Scenarios: Click house case study: modular shelter made of advanced composite materials. MSc, Instituto Superior Técnico of the University of Lisbon, Lisboa, Portugal, 2015.

[5] Bashawri A, Garrity S, Moodley K. An overview of the design of disaster relief shelters. Procedia Economics and Finance 2014; 18: 924-931.

[6] Asefi M, Sirus FA. Transformable shelter: Evaluation and new architectural design proposals. Procedia-Social and Behavioral Sciences 2012; 51: 961-966.

[7] International Organization for Migration (IOM). Transitional Shelter Guidelines. Shelter Centre. Geneva Switzerland, 2012.

[8] Farrugia P. Kinematic analysis of foldable structures. PhD diss., University of Surrey, England, United Kingdom, 2008.

[9] Shen T, Nagai Y. An Overview of Folding Techniques in Architecture Design. World Journal of Engineering and Technology 2017; 5: 12-19.

[10] Lebée A. From folds to structures, a review. International journal of space structures. 2015 Jun; 30(2):55-74.

[11] Baldwin YC, Clark BK. Design Rules, The Powerity of Modularity. The MIT Press Cambridge, Massachusetts, London, England: 2000.

[12] Smith RE. Prefab Architecture: A Guide to Modular Design and Construction. New Jersey, USA: John Wiley and Sons, Inc., Hoboken, 2010.

[13] Bakbak D, Özakça M, Göğüş MT. Design of Transitional Shelter Using Foldable Panels. Architecture in Emergency: Rethinking the refugee crisis conference; 17–19

November 2016; , İstanbul Kultur University, Turkey.

[14] Goethert, R. Incremental housing. Monday Developments, **9**, 23–25. Retrieved from http://web.mit.edu, 2010.

UTILISATION OF GLYCEROL ETHERS IN A DIESEL ENGINE

Abdülvahap ÇAKMAK
Department of Motor Vehicles and Transportation Technologies, Kavak Vocational School, Samsun University
abdulvahap.cakmak@samsun.edu.tr

Murat KAPUSUZ
Department of Mechanical Engineering, Ondokuz Mayıs University
muratkapusuz@hotmail.com.tr

Hakan ÖZCAN
Department of Mechanical Engineering, Ondokuz Mayıs University
ozcanh@omu.edu.tr

ABSTRACT: The aim of this study is to explore the usability of glycerol ethers as a future bio-renewable fuel in a diesel engine. In this context, an experimental study was carried out to synthesize glycerol ethers and investigate the effect of glycerol ethers on diesel engine performance and emissions. Glycerol ethers were synthesized by etherification reaction of glycerol with tert-butyl alcohol (TBA) in a stainless steel batch reactor. Produced glycerol ethers were mixed by 2 vol. % with a biodiesel-diesel blend to research glycerol ethers usage as fuel in a diesel engine. Engine performance and emissions tests were performed on a single-cylinder research diesel engine and the results revealed that the addition of glycerol ethers in the fuel caused an average increase in brake specific fuel consumption by 2.17 % and NOx emissions by 1.79 %. However, a reduction was observed in CO emissions by 2.71 % and HC emissions by 48.99 %, due to the addition of glycerol ethers in the diesel-biodiesel blend.

Keywords: Glycerol ethers, Oxygenated fuel, Biodiesel, Diesel engine, Performance, Emissions

INTRODUCTION

Today, the world energy supply is heavily depending on petroleum products and fossil fuels. But the limited reserves of fossil resources, increasing petroleum products cost and environmental issues resulted in the need to find alternative fuels that will be renewable and environment-friendly fuel. Biodiesel is one of the best alternative fuel for diesel engine application since it has many advantages over petroleum-based diesel fuel. Biodiesel is a renewable fuel produced from vegetable oils, animal fats or waste oils by the transesterification reaction. It is a biodegradable, non-toxic fuel and it contains no

sulfur and aromatic compounds in its composition (Singh & Singh, 2010). Without any fuel system and engine modification in a diesel engine, biodiesel can be used in 100% concentration or it can be blended in any ratio with diesel fuel. Biodiesel has a higher flash point than that of diesel fuel, which makes it safer for handle and transportation (Al-Zuhair, 2007). Due to oxygen in molecular structure, it improves the fuel oxidation rate and thus lowers exhaust emissions and increase engine efficiency. In addition, it has a high cetane number and good lubricity property (Singh & Singh, 2010). Thanks to the above-mentioned advantages of biodiesel, it has been an alternative for petroleum-based diesel fuel. Therefore, countries around the world are using biodiesel produced different sources. Moreover, in order to reduce dependence on limited petroleum reserves the blending ratio of biodiesel is being progressively increased. For example, the Europe Union has set a target to increase biofuels use up to 10% for transportation in 2020 (Phillips et al., 2018). In Turkey, biodiesel produced from local sources could be mixed up to 7 vol.% with diesel fuel. Because biodiesel is a leading solution for diesel engine application, its production experienced sustainable growth over two decades. Since 2000-2017 global biodiesel production has increased from 0.78 billion liters to 32.6 billion liters (IEA, 2018). Additionally, it is estimated that biodiesel production can reach up to 39 billion liters in 2027 (OECD/FAO, 2018).

In the biodiesel production process, glycerol occurs as a by-product approximately 10 wt. % of produced biodiesel. (Rahmat et al.2010; Spooner-Wyman et al., 2010). As a result of the increasing of biodiesel production, also the production of glycerol will grow proportionally (Beatrice et al., 2014). The main problem associated with increasing biodiesel production is the surplus glycerol which could not be completely used in glycerol related industries, which could lead to improper disposal of glycerol into the environment. (Rahmat et al., 2010). So, the key challenge emerged is the evaluation of excess glycerol. However, it is demonstrated that excess glycerol can be transformed into oxygenated fuels could be used in conventional internal combustion engines (Karinen & Krause, 2006; Klepáþová et al., 2003).

Etherification of glycerol with tert-butyl alcohol (TBA) or isobutene has emerged the most effective route to convert excess glycerol into oxygenated fuel additives. The etherification of glycerol yields mono-ethers, di-ethers, and tri- ether of glycerol which considered as potential oxygenated fuel (Klepáčová et al., 2005; Klepáþová et al., 2003). Although there are many studies deal with etherification of glycerol (Chang & Chen, 2011; Frusteri et al., 2009; Kiatkittipong et al., 2011; Klepáčová et al., 2006; Ozbay et al., 2010; Ozbay et al., 2013), only a few studies related to the effect of glycerol ethers on engine performance and emissions are found in the existing literature (Beatrice et al., 2014; Beatrice et al., 2015; Frusteri et al., 2013). The aim of this research study is to investigate the effects of glycerol ethers on performance and emissions of a diesel engine fueled with a diesel-biodiesel blend. Unlike previous studies, in this work produced glycerol ethers were mixed with biodiesel since glycerol ethers can improve the cold fuel

properties of biodiesel (Klepáþová et al., 2003; Noureddini et al., 1998), this can be the novelty of this presented study.

METHODS

In this research, glycerol ethers were synthesized by etherification reaction of glycerol with TBA at a presence of Amberlyst-15 catalyst since the glycerol ethers are not commercially available. For this purpose, a 0.5 L stainless steel batch reactor was designed and manufactured. A photograph of the batch reactor was given in Figure 1. Glycerol (purity ≥ 99%, TEKKİM), TBA (purity ≥ 99.5%, Merck) and Amberlyst-15 (dry form, Dow Chemical Company) were the chemicals for synthesis glycerol ethers. The esterification reaction conditions such as alcohol/glycerol molar ratio, amount of catalyst, reaction time, reaction temperature and stirring speed, which gives high glycerol conversion and high ether selectivity were determined from the previously published studies (Frusteri et al., 2009b; Klepáčová et al., 2006; Nagabhatla Viswanadham & Saxena, 2013). The etherification reaction conditions selected for this study were below:

- TBA/Glycerol molar ratio: 4:1
- Amount of Amberlyst-15: 7.5 wt. % / glycerol
- Reaction temperature: 90 ℃
- Reaction time: 3 h
- Stirring speed: 1200 rpm

The reaction procedure was the following: a defined amount of glycerol, TBA and Amberlyst-15 were loaded into the reactor and the reactor was flushed with nitrogen gas to obtain an inert environment. Then, the reactor was heated up to reaction temperature and the reaction started immediately by running the magnetic stirring. At the end of the reaction, the reactor was cooled down to the room temperature to obtain all compounds in the liquid phase. The Amberlyst-15 catalyst was removed from the product by the vacuum filtration method. In order to purify the products, a distillation process was done. Sufficient amounts of glycerol ethers were produced with the same method by repeating experiments.

Figure 1. The Batch Reactor Used for Glycerol Ether Synthesis

Since glycerol is produced about 10 wt. % of total biodiesel production, a blending ratio of 10 vol. % was chosen in this study. This blending ratio does not alter fuel characteristics greatly and it contributes to sustainable biodiesel production. Produced glycerol ethers were blended with biodiesel in 10 vol. % and this resulted in a biodiesel-glycerol ether mixture (10 vol. % glycerol ethers + 90 vol. %biodiesel). This blend was mixed with firstly a magnetic stirrer and then by ultrasonication process at 40 kHz for the time duration of 30 min. Then, the glycerol ethers-biodiesel blend was mixed with diesel fuel in the concentration of 20 vol. % and this blended fuel designated as B20_GTBE. At the final stage, B20_GTBE fuel consists of 80 vol. % diesel fuel, 18 vol. % biodiesel and 2 vol. % glycerol ethers. B20 selected as a reference fuel and it was formed by adding of biodiesel into diesel fuel (20 vol. % biodiesel + 80 vol.% diesel). Some important fuel properties of B20_GTBE and B20 fuel were measured and presented in Table 1.

Table 1. The Properties of B20_GTBE and B20 Fuel

Property	Test method	Unit	B20_GTBE	B20
Density@15 °C	TS EN ISO 12185	kg/m^3	846.0	847.9
Cloud point	TS 2834 EN 23015	°C	-4	-4
Cold filter plugging point (CFPP)	TS EN ISO 116	°C	-14	-14
Cetane index	TS EN ISO 4264	-	52.5	52
Distillation Temperature	TS EN ISO 3405	T10 (°C)	204	217
		T50 (°C)	302	294
		T90 (°C)	344	343

As seen in Table 1, using glycerol ethers by 2 vol. % rate resulted in no significant changes in determined fuel properties. A slight decrease in fuel density and no changes in cold flow properties of test fuels were observed. Due to the low boiling temperature of glycerol ethers the distillation temperature (T10) of the B20_GTBE decreased.

Engine performance and emission tests were performed on a single-cylinder four-stroke diesel engine. The test engine has a stroke volume of 661.5 cm^3 and a compression ratio of 17.5:1. Test engine fitted with the mechanical fuel injection system with an injection pressure of 200 bar. At full engine load and a speed of 1500 rpm, the maximum brake power output of the engine is 3.5 kW. The engine was connected to an Eddy current dynamometer to load engine. External engine cooling system was used to decrease parasitic loads without influencing the engine load conditions. Each test fuels were supplied to the engine by separate fuel tanks. The engine was operated at a constant speed of 1500 rpm and at 25%, 50%, 75%, and 100% engine load. An exhaust gas analyzer was used to measure the emissions of CO, HC, CO_2, and NOx. In figure 2, the experimental layout was illustrated and in Table 2 experimental uncertainties were presented.

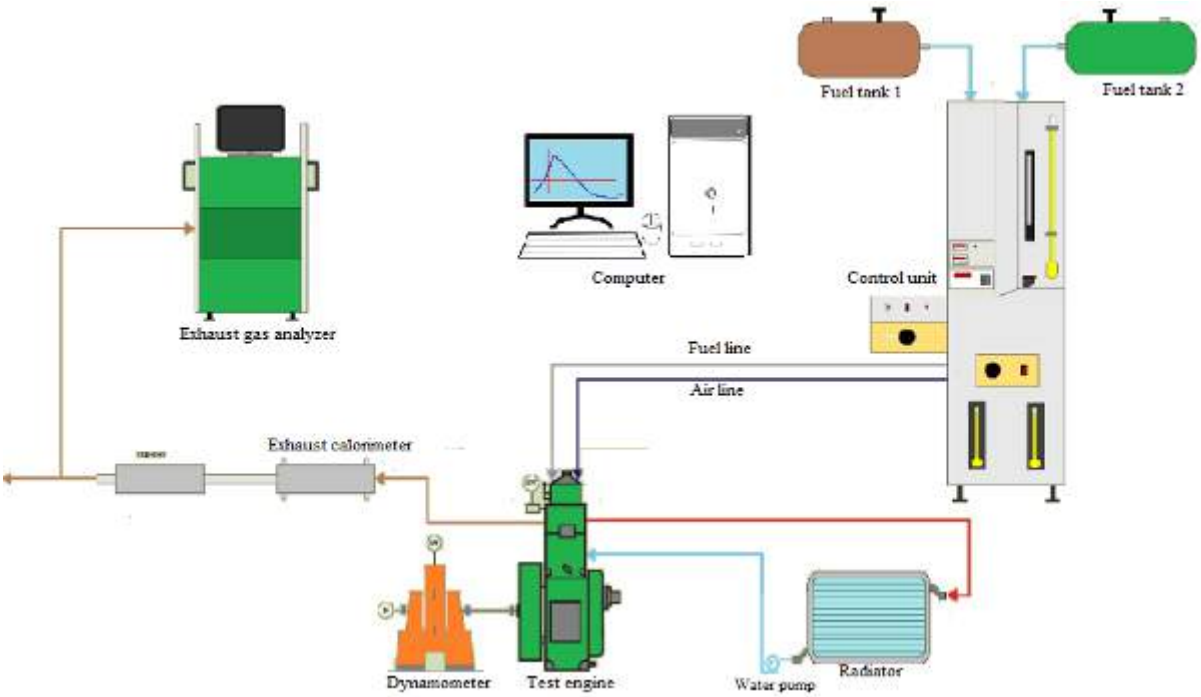

Figure 2. Test Setup Layout

Table 2. The Uncertainties of the Measured and Calculated Parameters

Parameter	Measurement Range	Resolution	Uncertainty
Brake torque	0-90 Nm	0.1 Nm	±1.5 %
Engine speed	0-9999 rpm	1 rpm	±0.06 %

Air flow rate	-	-	<±0.8 %
Fuel flow rate	-	-	<±0.7 %
Temperature	-	0.1 ℃	1 ℃
Brake thermal efficiency	-	-	<±0.9 %
CO	0-10 % vol.	0.001 %	±3%
HC	0-4000	1 ppm	± 8 ppm
CO_2	0-20 % vol.	0.01%	±3%
NOx	0-4000 ppm	1 ppm	± 25 ppm

RESULTS AND FINDINGS

Since each fuel was tested at the same engine speed and loads, test fuels produced the same brake power at the same test condition. Hence, the comparison of the engine performance was made based on brake specific fuel consumption (BSFC) and brake thermal efficiency (BTE). The variation of brake specific fuel consumption and brake thermal efficiency for test fuels were presented in Figure 3. It was noticed that BSFC decreased while BTE increased with increasing the engine load for both fuels, as expected. This was due to an increase in the amount of injected fuel in the cylinder that enhances engine power. In addition, as increase engine load, the heat loss per cycle through the cylinder wall decreased and this consequently reduced the BSFC and increased BTE. It can be seen in this figure that B20_GTBE presented slightly higher brake specific fuel consumption than that of B20. It was determined that the addition of 2 vol. % glycerol ethers in fuel caused an average increase in BSFC by 2.14% because of the lower heating value of glycerol ethers. Glycerol ethers did not show a significant effect on brake thermal efficiency in spite of the lower heating value of glycerol ethers. The reasons for this may be extra oxygen content of the fuel due to the addition of glycerol ethers in the biodiesel. Moreover, the low distillation temperature of the glycerol ether could reduce the ignition delay, which led to an improvement in fuel combustion. Thus, B20_GTBE presented nearly the same thermal efficiency with B20 and differences in brake thermal efficiency were less than the calculated uncertainties of BTE.

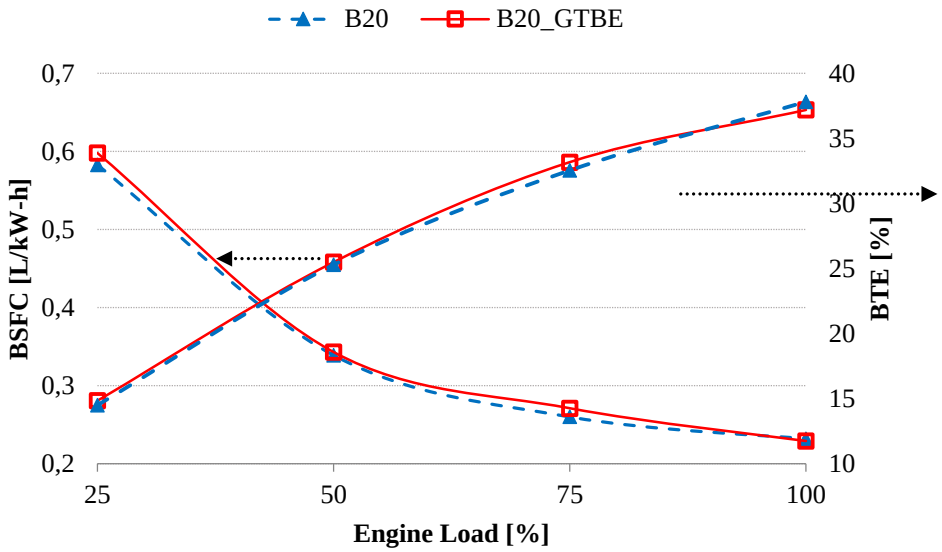

Figure 3. Comparison of Engine Performance for Test Fuels

Figure 4. shows the variation of exhaust gas temperature of test fuels. The exhaust temperature with B20_GTBE was lower than that of B20 at all engine loads. Besides, an average decrease of 1.36% in exhaust temperature was determined with the use of glycerol ethers. The decrease in exhaust temperature can be attributed to lower energy content and shorter ignition delay for B20_GTBE compared to B20. Therefore, B20_GTBE caused a lower combustion temperature, resulting in a lower exhaust temperature compared with B20.

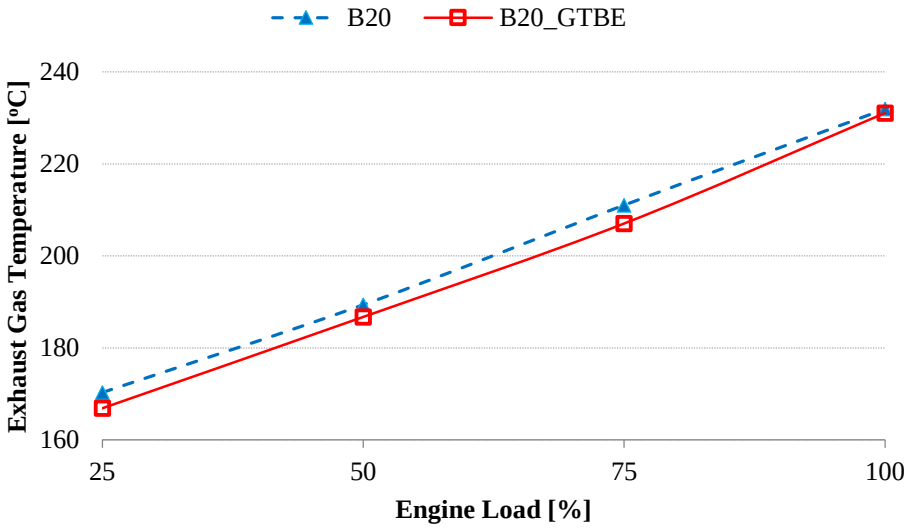

Figure 4. Comparison of Exhaust Temperature for Test Fuels

The variation of CO and HC emissions of test fuels was illustrated in Figure 5 and Figure 6, respectively. Both CO and HC emissions decreased with the use of glycerol ethers. It

was determined that B20_GTBE fuel resulted in an average reduction in CO and HC emissions by 2.71% and 48.99%, respectively, compared to B20. These findings are a typical result of oxygenated fuel since this may be due to better combustion in case of oxygen contained fuels (Beatrice et al., 2015; Behçet et al., 2015; Cakmak et al., 2018). Glycerol ethers contain about 39 mol. % oxygen in chemical structure (Beatrice et al., 2014) and the oxygen atoms weakly bonded two carbon atoms (Kaul et al., 2015). The weakly bonded oxygen atoms in glycerol ethers further aid the fuel oxidation process by it reduces the local fuel-rich zone. This resulted in less HC and CO emissions for B20_GTBE fuel. Additionally, the lower distillation temperature of glycerol ethers might facilitate the breakdown of the fuel molecule, which enhances the combustion efficiency.

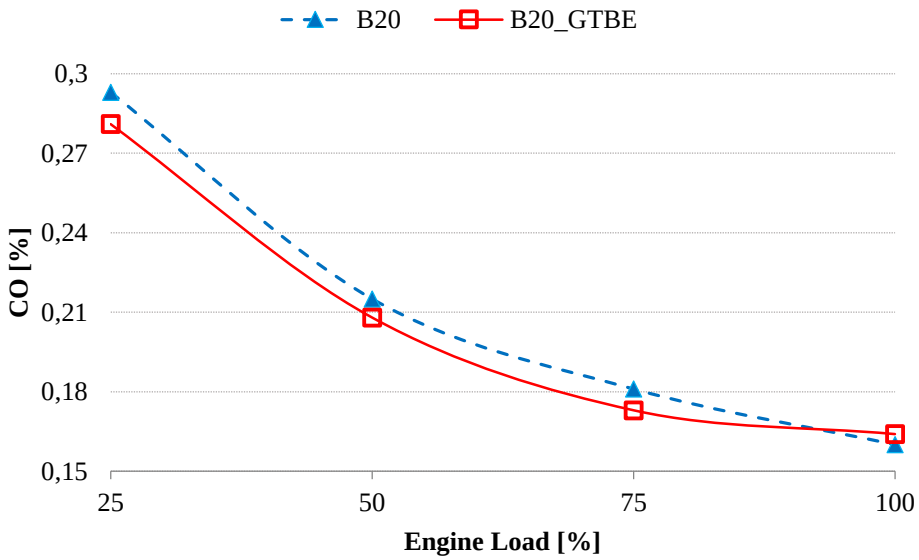

Figure 5. Comparison of CO Emissions for Test Fuels

CO_2 emissions of test fuel presented in Figure 7. As seen in this figure both fuels resulted in nearly the same level of CO_2 emissions. The fuel impact on CO_2 emissions was not significant and the differences between CO_2 emissions value were in the range of measurement uncertainties for CO_2.

The effect of test fuels on NO_X emissions was presented in Figure 8. An average increase of 1.79 % in NO_X emissions was found when the engine fuelled with B20_GTBE as compared to B20. The NO_X values of test fuels were close to each other up to 75% engine load however, beyond this load B20_GTBE led to an increase in NO_X emission level. Because of the lower heating value of glycerol ethers, more fuel must be injected at full engine load to run the engine at the same test condition compared to that of B20 operation. This led to a further increase in cylinder temperature and oxygen concentration in the cylinder and thus high NO_X emissions. Moreover, due to the improved combustion quality as a result of fuel borne-oxygen, more NO_X emissions were formed in the case of glycerol ethers use.

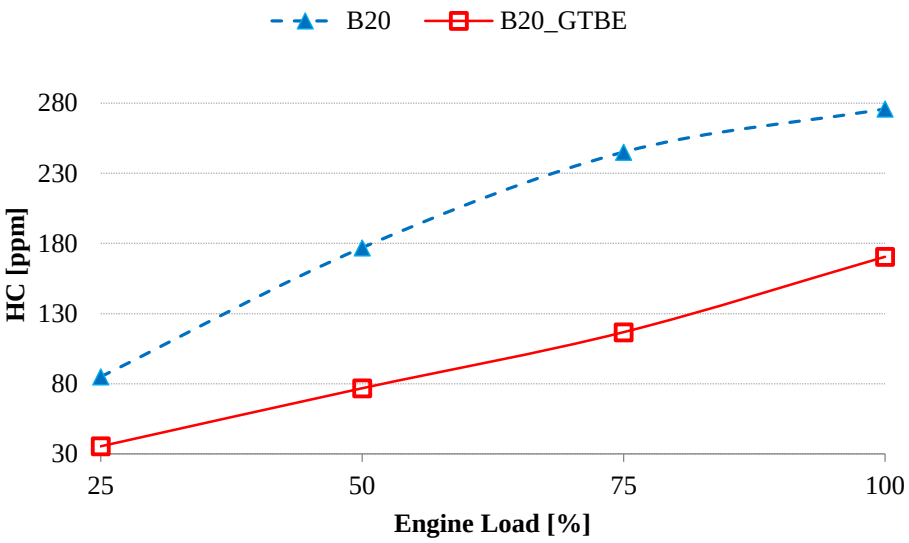

Figure 6. Comparison of HC Emissions for Test Fuels

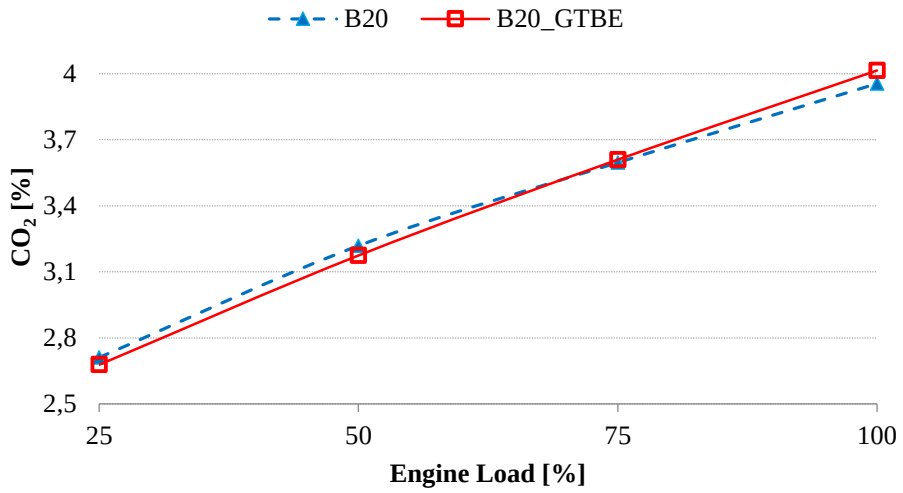

Figure 7. Comparison of CO_2 Emissions for Test Fuels

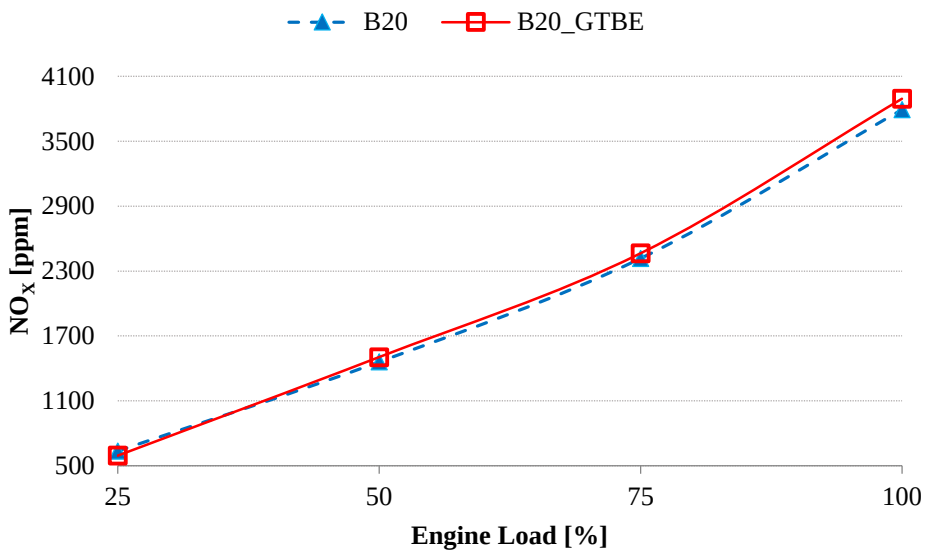

Figure 8. Comparison of NO_X Emissions for Test Fuels

CONCLUSION

In this research study, glycerol ethers were synthesized and added to a diesel-biodiesel blended fuel to investigate the usability of glycerol ethers in a diesel engine. The results of this study revealed the possibility to use glycerol ethers at a concentration of 2 vol. % in a diesel-biodiesel blend without any significant influence- on fuel properties, engine performance, and exhaust emissions. In addition, this study indicated that excess glycerol originated from biodiesel production could be turned into oxygenated fuel and could be used as a fuel additive in diesel engines. It is evident that by evaluating excess glycerol in fuel production in this way, environmental pollution caused by excess glycerol will be prevented.

RECOMMENDATIONS

It is recommended to investigate the economic analysis of production and use of glycerol ethers. Because of appropriate fuel properties, glycerol ethers could also be used as a fuel additive to gasoline and thus studies in this field should be conducted.

ACKNOWLEDGMENTS

This study was supported by the Project Management Office of Ondokuz Mayis University (Project number: PYO.MUH.1904.19.016). Abdülvahap ÇAKMAK has been awarded a doctoral scholarship by the Scientific and Technical Research Council of Turkey (TUBİTAK-BİDEB: 2211-C).

REFERENCES

Al-Zuhair, S. (2007). Production of biodiesel: possibilities and challenges. Biofuels, Bioproducts and Biorefining, 1(1), 57–66. https://doi.org/10.1002/bbb.2

Beatrice, C., Di Blasio, G., Guido, C., Cannilla, C., Bonura, G., & Frusteri, F. (2014). Mixture of glycerol ethers as diesel bio-derivable oxy-fuel: Impact on combustion and emissions of an automotive engine combustion system. Applied Energy, 132, 236–247. https://doi.org/10.1016/J.APENERGY.2014.07.006

Beatrice, C., Di Blasio, G., Lazzaro, M., Mancaruso, E., Marialto, R., Sequino, L., & Vaglieco, B. M. (2015). Investigation of the combustion in both metal and optical diesel engines using high-glycerol ethers/diesel blends. International Journal of Engine Research, 16(1), 38–51. https://doi.org/10.1177/1468087414561482

Behçet, R., Oktay, H., Çakmak, A., & Aydin, H. (2015). Comparison of exhaust emissions of biodiesel-diesel fuel blends produced from animal fats. Renewable and Sustainable Energy Reviews, Vol. 46, pp. 157–165. Elsevier Ltd.

Cakmak, A., Kapusuz, M., Ganiyev, O., & Ozcan, H. (2018). Effects of Methyl Acetate as Oxygenated Fuel Blending on Performance and Emissions of SI Engine. Environmental and Climate Technologies, 22(1), 55–68. https://doi.org/10.2478/rtuect-2018-0004

Chang, J.-S., & Chen, D.-H. (2011). Optimization on the etherification of glycerol with tert-butyl alcohol. Journal of the Taiwan Institute of Chemical Engineers, 42(5), 760–767. https://doi.org/10.1016/J.JTICE.2011.02.011

Frusteri, F., Arena, F., Bonura, G., Cannilla, C., Spadaro, L., & Di Blasi, O. (2009a). Catalytic etherification of glycerol by tert-butyl alcohol to produce oxygenated additives for diesel fuel. Applied Catalysis A: General, 367(1–2), 77–83. https://doi.org/10.1016/J.APCATA.2009.07.037

Frusteri, F., Arena, F., Bonura, G., Cannilla, C., Spadaro, L., & Di Blasi, O. (2009b). Catalytic etherification of glycerol by tert-butyl alcohol to produce oxygenated additives for diesel fuel. Applied Catalysis A: General, 367(1–2), 77–83. https://doi.org/10.1016/J.APCATA.2009.07.037

Frusteri, F., Cannilla, C., Bonura, G., Spadaro, L., Mezzapica, A., Beatrice, C., … Guido, C. (2013). Glycerol Ethers Production and Engine Performance with Diesel/Ethers Blend. Topics in Catalysis, 56(1–8), 378–383. https://doi.org/10.1007/s11244-013-9983-7

IEA. (2018). Key World Energy Statistics 2018. Retrieved from https://webstore.iea.org/key-world-energy-statistics-2018

Karinen, R. S., & Krause, A. O. I. (2006). New biocomponents from glycerol. Applied Catalysis A: General, 306, 128–133. https://doi.org/10.1016/j.apcata.2006.03.047

Kaul, S., Behera, B., Negi, M. S., Porwal, J., Kanojia, P., Tripathi, D., … Bangwal, D. (2015). Efficacy of a bio-additive on the exhaust emissions of petrodiesel. Biomass Conversion and Biorefinery, 5(4), 387–395. https://doi.org/10.1007/s13399-014-0155-1

Kiatkittipong, W., Intaracharoen, P., Laosiripojana, N., Chaisuk, C., Praserthdam, P., & Assabumrungrat, S. (2011). Glycerol ethers synthesis from glycerol etherification with tert-butyl alcohol in reactive distillation. Computers & Chemical Engineering, 35(10), 2034–2043. https://doi.org/10.1016/J.COMPCHEMENG.2011.01.016

Klepáčová, K., Mravec, D., & Bajus, M. (2006). Etherification of glycerol with tert-butyl

alcohol catalysed by ion-exchange resins. Chemical Papers, 60(3), 224–230. https://doi.org/10.2478/s11696-006-0040-x

Klepáčová, Katarína, Mravec, D., Bajus, M., & Klepáčová, K., Mravec, D., & Bajus, M. (2005). tert-Butylation of glycerol catalysed by ion-exchange resins. Applied Catalysis A: General, 294(2), 141-147. https://doi.org/10.1016/J.APCATA.2005.06.027

Klepáþová, K., Mravec, D., Hajekova, E., & Bajus, M. (2003). Etherification of glycerol. Petroleum and Coal, 45, 1-2.

Noureddini, Hossein; Dailey, W R.; and Hunt, B. A. (1998). Production of ethers of glycerol from crude glycerol - The by-product of biodiesel production. Papers in Biomaterials., 18, 1–14. Retrieved from https://digitalcommons.unl.edu/cgi/viewcontent.cgi?article=1019&context=chemeng_biomaterials

OECD/FAO. (2018). OECD Agriculture statistics (database). Retrieved from http://dx.doi.org/10.1787/agr-outl-data-en.

Ozbay, N., Oktar, N., Dogu, G., & Dogu, T. (2010). Conversion of Biodiesel By-Product Glycerol to Fuel Ethers over Different Solid Acid Catalysts. International Journal of Chemical Reactor Engineering, 8(1). https://doi.org/10.2202/1542-6580.2149

Ozbay, N., Oktar, N., Dogu, G., & Dogu, T. (2013). Activity Comparison of Different Solid Acid Catalysts in Etherification of Glycerol with tert-Butyl Alcohol in Flow and Batch Reactors. Topics in Catalysis, 56(18–20), 1790–1803. https://doi.org/10.1007/s11244-013-0116-0

Phillips, S., Flach, B., Lieberz, S., Lappin, J., & Bolla, S. (2018). EU Biofuels Annual 2018. Retrieved from https://gain.fas.usda.gov/Recent GAIN Publications/Biofuels Annual_The Hague_EU-28_7-3-2018.pdf

Rahmat, N., Abdullah, A. Z., & Mohamed, A. R. (2010). Recent progress on innovative and potential technologies for glycerol transformation into fuel additives: A critical review. Renewable and Sustainable Energy Reviews, 14(3), 987–1000. https://doi.org/10.1016/J.RSER.2009.11.010

Singh, S. P., & Singh, D. (2010). Biodiesel production through the use of different sources and characterization of oils and their esters as the substitute of diesel: A review. Renewable and Sustainable Energy Reviews, 14(1), 200–216. https://doi.org/10.1016/j.rser.2009.07.017

Spooner-Wyman, J. K., Appleby, D. B., Yost, D. M., Rahmat, N., Abdullah, A. Z., & Mohamed, A. R. (2010). Recent progress on innovative and potential technologies for glycerol transformation into fuel additives: A critical review. Renewable and Sustainable Energy Reviews, 14(3), 987–1000. https://doi.org/10.1016/J.RSER.2009.11.010

Viswanadham, N. and Saxena, S. K. (2013). Etherification of glycerol for improved production of oxygenates. Elsevier. Retrieved from https://www.sciencedirect.com/science/article/pii/S0016236112004772

Viswanadham, Nagabhatla, & Saxena, S. K. (2013). Etherification of glycerol for improved production of oxygenates. Fuel, 103, 980–986. https://doi.org/10.1016/J.FUEL.2012.06.057.

TEMPERATURE DEPENDENT DYNAMIC VISCOSITY OF VEGETABLE OIL-BIODIESEL BLENDS

Mert Gülüm
Department of Mechanical Engineering, Karadeniz Technical University
gulum@ktu.edu.tr

Abdülvahap ÇAKMAK
Department of Motor Vehicles and Transportation Technologies, Kavak Vocational School, Samsun University
abdulvahap.cakmak@samsun.edu.tr

Atilla BİLGİN
Department of Mechanical Engineering, Karadeniz Technical University
bilgin@ktu.edu.tr

ABSTRACT: Vegetable oils can be considered as an alternative or emergency fuel for diesel engine due to the oxygen content in the molecular structure and biodegradability, renewability and superior lubrication properties. However, vegetable oils result in operational and durability problems for the long-term operation because of being much more viscous than diesel fuel. To overcome this drawback, the blending of vegetable oils with diesel fuel or alcohol is one of the most widely used techniques. Therefore, in this study, (1) corn oil biodiesel (COB) was produced by the transesterification reaction, (2) corn oil (CO) was mixed with corn oil biodiesel on the volume basis of 10%, 15%, 20%, 30% and 40%, (3) dynamic viscosities the binary blends were measured at different temperatures (10°C-70°C) according to DIN 53015, (4) the variations in viscosity of binary blends vs. temperature were evaluated, and (5) the rational model as a function of temperature were fitted to the experimental data measured by the authors. According to results, the best correlation was obtained by the rational model with the low error of 1.2115% and the high minimum R^2 value of 0.9993.

Keywords: Corn oil, Biodiesel, Viscosity, Binary blends, Rational model

INTRODUCTION

Increase in demand for energy to satisfy the need for modernization of the world has resulted in the depletion of fossil fuel reserve along with increased global temperature and anthropogenic climate change (Owusu & Asumadu-Sarkodie, 2016). This present global scenario has risked the inventory of fossil fuel resources and has pushed the planet to rely on renewable energy sources (Höök & Tang, 2013). Biodiesel is one such promising

renewable biofuel which is known for its environmental friendliness, non-toxicity, non-aromatic, high biodegradability and improved combustibility along with reduced emissions of HC, CO, and PM (Srinivasan, Shankar, & Jambulingam, 2019). Moreover, the continuous use of petroleum increases the amount of carbon dioxide released into the atmosphere. However, if pure or blend biodiesel is used as fuel, the amount of released carbon dioxide can be reduced (Çakmak & Bilgin, 2017; Srinivasan et al., 2019). Generally, the transesterification process is used for the production of biodiesel. In this process, vegetable oil or animal fat is treated with alcohol in the presence of a catalyst at a particular reaction time and temperature (Srinivasan et al., 2019).

Viscosity is one of the most significant fuel properties because it affects atomization quality, the size of fuel droplets and jet penetration, all of which affect the quality of combustion. High viscosity causes poor fuel atomization and incomplete combustion increases engine deposits, requires more power to pump the fuel, and causes more problems in cold weather, as viscosity increases with decreasing temperature. Viscosity also affects injectors and fuel pump lubrications (Mert Gülüm & Bilgin, 2017).

For the correct development of the models which can be used the engine combustion, it is required the knowledge of the thermophysical properties (such as viscosity) of biodiesel blends (Ramírez-Verduzco, 2011). In addition, given the difficulty of obtaining the basic properties of the blends by measurement, the ability to calculate these properties using regression models is very useful (Candeia et al., 2009). Although the measurements or predictions of the viscosity of pure biodiesel or blends are not new, we have focused either on a specific type of biodiesel fuel or on vegetable oil-biodiesel blends. At present, no report is available on deriving regression equations for the viscosities of the corn oil-corn oil biodiesel. The objectives of this study were to address these issues.

MATERIALS and METHODS

The transesterification reaction for producing biodiesel was performed with the molar ratio of methanol to the oil of 9:1 and catalyst (NaOH) concentration of 0.90% for 60 minutes at 50°C and atmospheric pressure with a continuous stirring speed of 500 rpm. It shall be noted here that the optimum reaction parameters were previously determined by the author (Gülüm, 2014; Gülüm, Bilgin, & Çakmak, 2015) to produce COB having the lowest viscosity.

Dynamic viscosities of corn oil-corn oil biodiesel (CO-COB) (CO10COB-CO40COB) were measured at several temperatures (10°C-70°C) using Haake Falling Ball Viscometer, Haake Water Bath and stopwatch in accordance with DIN 53015 standard. The viscosity measurements were performed three times for each sample, and the results were averaged. More details on dynamic viscosity can be also found in the author's previous study (Mert Gülüm & Bilgin, 2016).

RESULTS AND FINDINGS

Figure 1 illustrates the comparisons between the experimental data and calculated values of dynamic viscosities of corn oil-corn oil biodiesel binary blends according to temperature. The calculated results show similar patterns with the experimental data for all blends measured by the authors: the binary blends demonstrate nonlinearity temperature dependence behavior, and at a fixed temperature increase of oil fraction in blend increases viscosity since the viscosity of the oil is greater than that of biodiesel. As the temperature increases, the average intermolecular forces decrease which in turn reduce the resistance to follows and result in lower viscosity. In these figures, the symbols show viscosity data measured by the authors at the corresponding temperature and oil fraction while the lines correspond calculated values from the regression model. The rational model (Eq. 1) was suggested to predict the viscosity variation with temperature for different corn oil-corn oil biodiesel binary blends. The mathematical form of the rational model was given as respectively:

$$\mu(T) = (a + T)/(b + c \cdot T) \qquad (1)$$

where T is blend temperature (K), and a, b and c are regression constants. It can be seen that the rational model successfully represents the viscosity variation vs. temperature throughout all studied temperature in terms of qualitative behavior. In other words, the calculated values from the rational model are close to the measurements. Table 1 lists dynamic viscosity data of the binary blends measured by the authors, percent relative errors between measured data and calculated values from Eq. (1), and regression constants and correlation coefficients (R^2). The maximum errors coming from Eq. (1) were computed as 1.2115% and 0.9469 with the minimum R^2 value of 0.9993, respectively. These results show that the rational model (Eq. 1) developed to describe the variation in viscosity as a function of temperature shows an excellent agreement with the experimental dynamic viscosity data in terms of quantitative behavior.

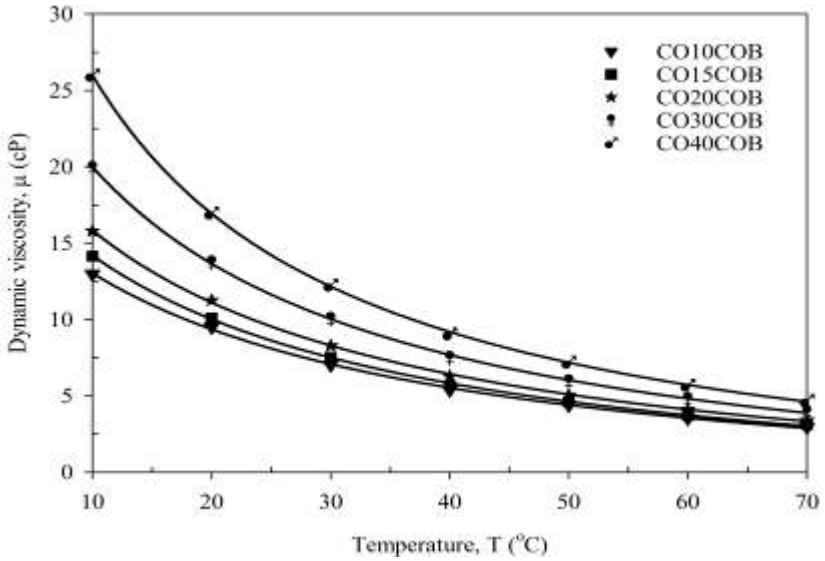

Figure 1. Viscosities of Corn Oil (CO)-Corn Oil Biodiesel (COB) Binary Blends as a Function of Temperature for the Author's Measurements

Table 1. Dynamic Viscosity Data of Corn Oil-Corn Oil Biodiesel Blends at Different Temperatures Measured by the Author, Regression Constants, R^2 and Statistical Parameters.

CO fraction	Measured viscosity, μ (cP)						
	Temperature, T (°C)						
X (%)	10	20	30	40	50	60	70
10	12.978	9.516	7.022	5.390	4.398	3.539	2.955
15	14.155	10.113	7.534	5.683	4.603	3.694	3.120
20	15.796	11.251	8.279	6.278	5.052	4.107	3.411
30	19.952	13.776	10.061	7.507	5.975	4.820	3.978
40	25.979	16.955	12.234	9.042	7.188	5.685	4.678

Table 1. (Continued)

CO fraction	Eq.	Regression constants			R^2	AARD (%)	OARD (%)
X (%)		a	b	c			
10	Eq. (1)	-1.713e2	-8.582	-3.8e-1	**0.9993**	1.1482	0.9469
15		-1.750e2	-7.780	-3.852e-1	0.9995	**1.2115**	
20		-1.759e2	-6.911	-3.564e-1	0.9996	1.0752	
30		-1.712e2	-5.055	-3.008e-1	0.9997	1.0454	
40		-1.823e2	-3.677	-2.954e-1	0.9999	0.6611	

$AARD(\%) = \sum_{i=1}^{n} \frac{ARD_i(\%)}{n}$, $OARD(\%) = \frac{1}{N_s}\sum_n AARD(\%)$ where n is the number of experimental data points of a given blend at various temperature and N_s is the number of systems being investigated.

CONCLUSION

In this study, the variation in viscosity corn oil-corn oil biodiesel binary blends with respect to temperature was determined. Viscosity measurements were performed according to DIN 53015 standards. The rational model, previously suggested by the authors, was fitted to the viscosity data of corn oil-corn oil biodiesel binary blends measured by the authors. According to results, the rational model is determined to be the better predictor since the low error values arising from the rational model were determined as 1.2115% and 0.9469%.

REFERENCES

Çakmak, A., & Bilgin, A. (2017). Performance and Emissions of a Single Cylinder CI Engine Running on Corn Oil Methyl Ester-Diesel Blends. Journal of Clean Energy Technologies, 5(4), 280–284. https://doi.org/10.18178/JOCET.2017.5.4.383

Candeia, R. A., Silva, M. C. D., Carvalho Filho, J. R., Brasilino, M. G. A., Bicudo, T. C., Santos, I. M. G., & Souza, A. G. (2009). Influence of soybean biodiesel content on basic properties of biodiesel–diesel blends. Fuel, 88(4), 738–743. https://doi.org/10.1016/J.FUEL.2008.10.015

Gülüm, M. (2014). Experimental investigation of the effect of various production parameters on the some fuel properties of produced biodiesels from corn and hazelnut oils. Karadeniz Technical University.

Gülüm, Mert, & Bilgin, A. (2016). Two-term power models for estimating kinematic viscosities of different biodiesel-diesel fuel blends. Fuel Processing Technology, 149, 121–130. https://doi.org/10.1016/J.FUPROC.2016.04.013

Gülüm, Mert, & Bilgin, A. (2017). Measurements and empirical correlations in predicting biodiesel-diesel blends' viscosity and density. Fuel, 199, 567–577. https://doi.org/10.1016/J.FUEL.2017.03.001

Gülüm, Mert, Bilgin, A., & Çakmak, A. (2015). Comparıson of optımum reactıon parameters of corn oıl bıodıesels produced by usıng sodıum hydroxıde (NAOH) and potassıum hydroxıde (KOH). Journal of the Faculty of Engineering and Architecture of Gazi University., 30(3), 503–511.

Höök, M., & Tang, X. (2013). Depletion of fossil fuels and anthropogenic climate change—A review. Energy Policy, 52, 797–809. https://doi.org/10.1016/J.ENPOL.2012.10.046

Owusu, P. A., & Asumadu-Sarkodie, S. (2016). A review of renewable energy sources, sustainability issues and climate change mitigation. Cogent Engineering, 3(1). https://doi.org/10.1080/23311916.2016.1167990

Ramírez-Verduzco, L. F., García-Flores, B. E., Rodríguez-Rodríguez, J. E., & del Rayo

Jaramillo-Jacob, A. (2011). Prediction of the density and viscosity in biodiesel blends at various temperatures. Fuel, 90(5), 1751–1761. https://doi.org/10.1016/J.FUEL.2010.12.032

Srinivasan, G. R., Shankar, V., & Jambulingam, R. (2019). Experimental study on influence of dominant fatty acid esters in engine characteristics of waste beef tallow biodiesel. Energy Exploration & Exploitation, 37(3), 1098–1124. https://doi.org/10.1177/0144598718821791.

INVESTIGATION THE EFFECT OF TEMPERATURE ON DENSITIES OF CORN OIL (CO)-DIESEL FUEL (DF) BLENDS

Mert Gülüm
Department of Mechanical Engineering, Karadeniz Technical University
gulum@ktu.edu.tr

Abdülvahap ÇAKMAK
Department of Motor Vehicles and Transportation Technologies, Kavak Vocational School, Samsun University
abdulvahap.cakmak@samsun.edu.tr

Atilla BİLGİN
Department of Mechanical Engineering, Karadeniz Technical University
bilgin@ktu.edu.tr

ABSTRACT: Fuel crisis because of a dramatic increase in vehicular population and environmental concerns have renewed interest in the scientific community to look for alternative fuels of bio-origin such as vegetable oils. Vegetable oils have become more attractive recently because of its environmental benefits and the fact that it is made from renewable resources. In this study, densities of corn oil-commercially available petrodiesel fuel blends have been investigated. The effect of temperature on the densities of blends was examined. The blends (CO10DF, CO15DF, CO30DF, and CO40DF) were prepared on a volume basis and their densities were measured by following ISO test method between 278.15 K-368.15 K. Regression equations were fitted to the measurements for identifying of variations of densities with respect to temperature

Keywords: Corn oil, Density, Diesel, Regression equations

INTRODUCTION

The scarcity of conventional fossil fuels and the concern of environmental protection, the utilization of biofuel from bio-renewable resources have attracted increasing worldwide interest. With recent increases in petroleum prices, there is renewed interest in vegetable oil and their derivatives as alternative fuels for diesel engines. As an alternative fuel vegetable oil is one of the renewable fuels. Vegetable oils have become more attractive recently because of its environmental benefits and the fact that it is made from renewable resources (Behçet, Oktay, Çakmak, & Aydin, 2015; Demirbas, 2008). When Rudolf Diesel invented the diesel engine more than a century ago, he demonstrated the principle of compression ignition engine by employing peanut oil as fuel and suggested that

vegetable oils would be the future fuel for diesel engines. However, petroleum was discovered later, which replaced vegetable oils as engine fuel due to its abundant supply and low price (Agarwal, Kumar, & Agarwal, 2008). The major problem associated with the use of pure vegetable oils as fuels, for Diesel engines is caused by high fuel viscosity and density in compression ignition and resulting injector fouling and other engine problems. The disadvantages of vegetable oils as diesel fuel are: (a) higher density, (b) higher viscosity, (c) higher pour point, (d) higher flash point, (e) higher cloud point, (f) higher density, and (g) the reactivity of unsaturated hydrocarbon chains (Demirbas, 2008).

As the use of vegetable oil becomes more widespread, researchers have shown a strong interest in modeling the combustion process in the engine in order to understand the fundamental characteristics of vegetable oil combustion. They often use physical properties (such as density) of vegetable oil as input data in their combustion models. Regression equations as a function of temperature, percentage of blend and the chemical structure have been generally used to calculate these properties without measurements (Gülüm & Bilgin, 2016; Ramírez-Verduzco, 2011).

The main objective of the present study is to investigate the effect of temperature (T) on the densities of corn oil (CO)-diesel fuel (DF) blends. Therefore five corn oil-diesel fuel samples were prepared by mixing the corn oil with commercially available Ultra Force Euro Diesel fuel on a volume base of %10, %15, %30 and %40 and the resulted fuel samples were labeled as CO10DF, CO15DF, CO30DF, and CO40DF, respectively. In addition, a regression equation was fitted to the measurements to estimate their densities

METHODS

Density measurement

The densities of CO10DF, CO15DF, CO30DF, and CO40DF were determined at different temperatures (278.15 K-368.15 K) by means of Eq. (1) and measurements in accordance with ISO 4787 standard:

$$\rho_{blends} = \frac{m_{total} - m_{pycnometer}}{m_{water}} \rho_{water} \quad (1)$$

where ρ and m represent density and mass, respectively. In order to minimize measurement errors, all the measurements were conducted three times for each sample and the results were averaged. Also, an uncertainty analysis was carried out depending on the sensitivities of measurement devices.

Uncertainty analysis

The results obtained from experimental studies are generally calculated from measured physical quantities. These quantities have some uncertainties due to uncertainties of measuring tools and measurement systems. Therefore, uncertainty analysis should be

applied to proving the reliability of the calculated results. In this study, uncertainties of the measured density values were determined by the method proposed by Kline and McClintock given in According to this method (Holman, 2001), if the result R is a given function of the independent variables x_2, x_2, x_3, .., x_n and w_1, w_2, w_3, …, w_n are the uncertainties of each independent variables, then the uncertainty of the result w_R is calculated by using the equation:

$$w_R = \left[\left(\frac{\partial R}{\partial x_1}\cdot w_1\right)^2 + \left(\frac{\partial R}{\partial x_2}\cdot w_2\right)^2 + \left(\frac{\partial R}{\partial x_3}\cdot w_3\right)^2 + \cdots + \left(\frac{\partial R}{\partial x_n}\cdot w_n\right)^2\right]^{1/2} \quad (2)$$

According to Eq. (2), the highest uncertainty for measured densities was determined as 0.0417%, which means that the results are highly reliable.

RESULTS AND FINDINGS

Figure 1 shows the effects of temperature on densities of corn oil-diesel fuel blends. As shown in the figure, the densities, as expected, decrease with increasing temperature and there are similar trends for all fuels and the blends in the studied temperature range. According to the distributions of measured data, the following exponential model was tried to represent the variations of densities with temperature.
The exponential model:

$$\rho = \rho(T) = ae^{bT} + ce^{dT} \quad (3)$$

where T is the temperature in K and a, b, c, and d are regression constants.
Table 1 lists the measured and calculated (from Eq. (3)) densities of the blends, % errors between them, regression constants and correlation coefficients. For the exponential model, the maximum error was computed as 0.0875%. The minimum R value is 0.9998 for the exponential model. According to these results, the qualitatively and quantitatively the best agreement of the calculated and measured density values is captured by the exponential model for the investigated temperature ranges.

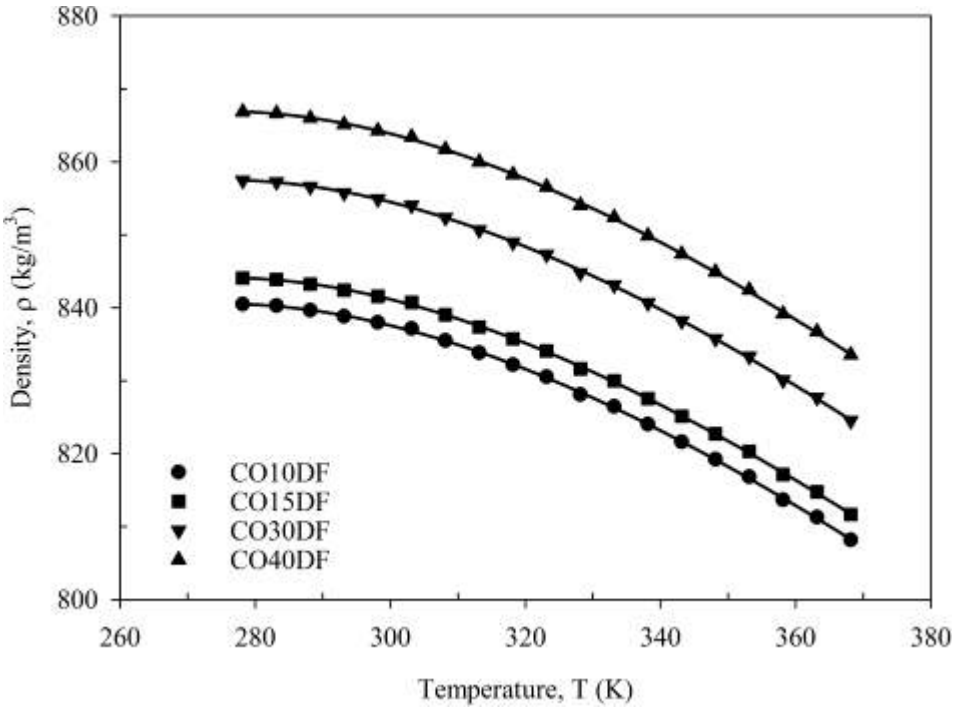

Figure 1. Variation of the Density of Corn Oil-Diesel Fuel Blends with Respect to Temperature

Table 1. The measured density data, relative errors, and regression constants and correlation coefficients of the exponential model

Oil fraction X (%)	**Measured,** $\rho\ (kg/m^3)$								
	Temp., $T\ (K)$								
	278.15	283.15	288.15	293.15	298.15	303.15	308.15	313.15	318.15
10	840.50	840.29	839.66	838.81	837.98	837.15	835.49	833.82	832.17
15	844.09	843.88	843.25	842.41	841.57	840.73	839.06	837.39	835.74
30	857.49	857.27	856.63	855.77	854.92	854.07	852.37	850.68	849.00
40	866.88	866.66	866.01	865.15	864.29	863.43	861.71	860.00	858.30

Table 1. (Continued)

Oil fraction X (%)	**Measured, ρ (kg/m³)**									
	Temperature, T (K)									
	323.15	328.15	333.15	338.15	343.15	348.15	353.15	358.15	363.15	368.15
10	830.53	828.07	826.44	824.01	821.60	819.20	816.81	813.64	811.29	808.17
15	834.08	831.62	829.98	827.54	825.15	822.70	820.31	817.12	814.76	811.63
30	847.32	844.81	843.15	840.67	838.21	835.76	833.32	830.09	827.69	824.51
40	856.60	854.07	852.39	849.88	847.39	844.91	842.45	839.18	836.76	833.54

Table 1. (Continued)

Oil fraction X (%)	Eq.	Regression constants				R
		a	**b**	**c**	**d**	
10	Eq. (3)	1.271e3	1.123e-3	-2.1e3	1.136e-2	0.9999
15		1.276e3	1.123e-3	-2.109e3	1.136e-2	0.9999
30		1.296e3	1.123e-3	-2.143e3	1.136e-2	**0.9998**
40		1.311e3	1.123e-3	-2.166e3	1.136e-2	0.9999

Table 1. (Continued)

Eq.	Relative errors (%)			
	Oil fraction, X (%)			
	10	15	30	40
Eq. (3)	0.0474	0.0100	0.0144	0.0561
	0.0382	0.0010	0.0224	0.0473
	0.0502	0.0129	0.0103	0.0593
	0.0614	0.0226	0.0004	0.0685
	0.0446	0.0068	0.0156	0.0522
	0.0039	0.0330	0.0555	0.0119
	0.0399	0.0035	0.0184	0.0488
	0.0562	0.0190	0.0035	0.0636
	0.0502	0.0124	0.0095	0.0574
	0.0244	0.0117	0.0342	0.0326
	0.0801	0.0428	0.0217	**0.0875**
	0.0192	0.0176	0.0392	0.0264
	0.0398	0.0030	0.0184	0.0474
	0.0436	0.0069	0.0141	0.0517
	0.0328	0.0026	0.0245	0.0415
	0.0082	0.0284	0.0487	0.0162
	0.0675	0.0317	0.0102	0.0756
	0.0151	0.0206	0.0417	0.0227
	0.0473	0.0113	0.0097	0.0552

CONCLUSION

In this study, the effect temperature on the densities of blends of corn oil with commercially available Ultra Force Euro Diesel fuel was experimentally investigated. The exponential model has been developed for estimating densities at various temperatures and biodiesel percentages. According to results, the exponential model well represents the density-temperature relationship. The minimum correlation coefficient (R) and the maximum relative errors are 0.9998 and 0.0875% for the exponential model.

REFERENCES

Agarwal, D., Kumar, L., & Agarwal, A. K. (2008). Performance evaluation of a vegetable oil fuelled compression ignition engine. Renewable Energy, 33(6), 1147–1156.

Behçet, R., Oktay, H., Çakmak, A., & Aydin, H. (2015). Comparison of exhaust emissions of biodiesel-diesel fuel blends produced from animal fats. Renewable and Sustainable

Energy Reviews, Vol. 46, pp. 157–165.
Demirbas, A. (2008). Relationships derived from physical properties of vegetable oil and biodiesel fuels. Fuel, 87(8–9), 1743–1748. https://doi.org/10.1016/J.FUEL.2007.08.007
Gülüm, M., & Bilgin, A. (2016). Two-term power models for estimating kinematic viscosities of different biodiesel-diesel fuel blends. Fuel Processing Technology, 149, 121–130.
Holman, J. P. (2001). Experimental methods for engineers. In McGraw-Hill series in mechanical engineering (7th ed.). Boston.
Ramírez-Verduzco, L. F., García-Flores, B. E., Rodríguez-Rodríguez, J. E., & del Rayo Jaramillo-Jacob, A. (2011). Prediction of the density and viscosity in biodiesel blends at various temperatures. Fuel, 90(5), 1751–1761. https://doi.org/10.1016/J.FUEL.2010.12.032.

UNDERGRADUATE INDUSTRIAL CONTROL LABORATORY EXPERIMENTAL SETUP: PART 2 TEMPERATURE CONTROL WITH PLC

Cengiz TEPE
Electronic and Electrical Engineering
Ondokuz Mayıs University
ctepe@omu.edu.tr

Ertuğrul Furkan SAVAŞTAER
Electronic and Electrical Engineering
Ondokuz Mayıs University
savastaer.furkan@gmail.com

İlyas EMİNOĞLU
Electronic and Electrical Engineering
Ondokuz Mayıs University
ilyase@omu.edu.tr

ABSTRACT: In this study, industrial temperature control experiment setup that teaches the use of PLC is introduced for the students who take industrial automation course and their contributions are explained to the students. Temperature control with PLC is one of the widely used applications in the industry. Therefore, in this study, it is aimed to teach students how to control temperature with PLC.
The temperature of the resistance in the water tank is controlled by s7 1200 PLC. The control and monitoring of the reference and output temperature of the system is carried out via the human-machine interface. The temperature of the water is continuously measured by the PT100 temperature sensor and transferred to the PLC. Thanks to PID algorithm in PLC, water temperature is kept at reference value. The human-machine interface can also be used to observe the arrival of the water temperature to the reference value. All of the devices used in this study are widely used in industrial automation systems today. With this experiment, electrical-electronic, control, mechatronics and mechanical engineering students gain professional experience and knowledge before starting their business life.

Key words: PLC, temperature control, industrial automation, PID, control engineering.

LİSANS ENDÜSTRİYEL KONTROL LABORATUVARI DENEY DÜZENEĞİ: BÖLÜM 2 PLC İLE SICAKLIK DENETİMİ

ÖZET: Bu çalışmada endüstriyel otomasyon dersini alan öğrenciler için PLC kullanımını öğreten endüstriyel sıcaklık denetimi deney düzeneği tanıtılmakta ve öğrencilere katkıları açıklanmaktadır. PLC ile sıcaklık kontrolü endüstride yaygın olarak kullanılan uygulamalardan bir tanesidir. Bu sebepten dolayı bu çalışmada öğrencilere PLC ile sıcaklık kontrolünün nasıl yapıldığının öğretilmesi amaçlanmaktadır.
Gerçeklenen bu deney düzeneğinde su tankındaki rezistansın sıcaklığı s7 1200 PLC ile kontrol edilmektedir. Referans ve sistemin çıkış sıcaklığının kontrolü ve gözlemlenmesi insan-makine arayüzü üzerinden yapılmaktadır. Suyun sıcaklığı PT100 sıcaklık sensörü ile sürekli ölçülüp PLC ye aktarılır. PLC deki PID algoritması sayesinde su sıcaklığı referans değerinde tutulmaya çalışılır. İnsan-makine arayüzü ile suyun sıcaklığının referans değerine gelişi de gözlemlenebilmektedir. Bu çalışmada kullanılan cihazların tümü günümüzde endüstriyel otomasyon sistemlerinde yaygın olarak kullanılmaktadır. Yapılan bu deney düzeneği ile elektrik-elektronik, kontrol, mekatronik ve makine mühendisliği bölümü öğrencileri iş hayatlarına başlamadan önce mesleki tecrübe ve bilgi birikimi kazanmaktadırlar.

Anahtar sözcükler: PLC, sıcaklık kontrolü, endüstriyel otomasyon, PID, kontrol mühendisliği

GİRİŞ

Günümüzde PLC ile sıcaklık kontrolü birçok endüstride yaygın olarak kullanılmaktadır. Demir-çelik gibi metallerin eritilip şekillendirilmesinde, gıda sektöründe besinlerin pişirilip dondurulmasında, tavuk çiftliklerindeki kuluçka makinalarında (Velagic, Osmic, Lutvica, & Kadic, 2010) yerlerini örnek olarak gösterebiliriz.
Günümüzde sıcaklık kontrol sistemlerini tasarlamaya ve geliştirmeye yönelik birçok çalışma bulunmaktadır. Yusuf çalışmasında sıcaklık kontrolü gerekebilecek tüm sistemlerde uygulanabilecek bir otomatik kontrol sistemi tasarlamış ve simüle etmiştir. Method olarak Ziegler and Nichols PID (Proportional Integral Derivative) ayarlama metodu (Shahrokhi & Zomorrodi, 2013), PLC olarak OMRON CJIM-CPU22 ve Citect SCADA' nın Schneider Electric v 7.3 adlı yazılımını kullanmıştır (Al Yusuf, 2018). Rata çalışmasında belli miktardaki bir sıvıyı ısıtmak için kullanılacak olan rezistansı kontrol etmek için çözümler sunmuş ve bu çözümlerin avantaj ve dezavantajlarını belirlemiştir. PLC olarak XC-CPU101 PLC, HMI olarak EATON'dan XV102 HMI ve sıcaklık sensörü olarak ta LM35 kullanmıştır (Rata & Rata, 2016). Weibin ve Qingjian çalışmalarında sıvı sıcaklığını kontrol etmek için PID kontrolü ile Bulanık kontrolü beraber kullanmışlardır. Kontrol sürecinin belli bir adımına kadar bulanık kontrol kullanılmış, sonrasında sıcaklık değeri istenen değere yaklaştığında PID kontrole geçilmiştir. Çalışmalarını MATLAB üzerinden simüle etmişlerdir (Weibin & Qingjian, 2010). Gulpanich ve arkadaşların çalışmalarında bir büyük bir de küçük endüstriyel fırının sıcaklık kontrolü deneysel olarak sağlamışlardır. İlk önce iki fırında aynı ayarlama metoduyla kontrol edilmiş (The

Cohen-Coon PID ayarlama metodu) (Shahrokhi & Zomorrodi, 2013). Sonrasında her iki fırın içinde özelleştirilmiş kontrol yaklaşımları geliştirerek fırınların istenilen sıcaklıklara daha kısa sürede ulaşmalarını sağlamışlardır. Çalışmalarında PLC olarak Siemens S7-300'den FB58 "TCONT_CP" adlı bloğu ve sıcaklık sensörü olarak PT100 kullanmışlardır (Gulpanich, Krongratana, Srimuang, Tipsuwanporn, & Wongvanich, 2017). Velagic ve arkadaşları çalışmalarında bir kuluçka makinesi sisteminin hem simülasyonu hem de deneysel düzeneğini kurup alınan sonuçları karşılaştırmışlardır. Çalışmalarında Schneider'in Modicon M340 adlı modüler PLC'sini, NTC sıcaklık sensörünü ve Magelis XBT GT4330 adlı HMI'yı kullanmışlardır (Velagic et al., 2010). Yang ve Bian çalışmalarında bulanık kontrol ile PID kontrolünün beraber kullanılmasının sadece PID kontrolünün kullanılmasından daha verimli olduğunu deneysel olarak kanıtlanmaya çalışılmışlardır. Çalışmalarında PLC olarak Delta PLC (DVP-28SV) sıcaklık kontrolörü olarak DTC1000 kullanmışlardır (Yang & Bian, 2012). Bunların dışında bizim çalışmamızdaki gibi PLC eğitimi ihtiyacını karşılamaya yönelik çalışmalarda bulunmaktadır. Alves ve arkadaşları kurdukları PLC deney düzeneği sayesinde sıvı sıcaklığını kontrol edebilmektedirler (Alves, Brandão, & Oliveira, 2019).
Bu araştırma kapsamında ise, lisans ve yüksek lisans endüstriyel kontrol laboratuvarında kullanılmak üzere PLC ile sıcaklık denetimi deney düzeneği tasarımı ve gerçeklemesi yapılmıştır. PLC ve sıcaklık denetiminin endüstri sektöründeki yaygın kullanımı ve bu bağlamda PLC kullanımını iyi bilen donanımlı mühendis ihtiyacı, öğrencilerin mezun olduktan sonra daha rahat iş bulabilmesi için bu deney düzeneğine duyulan ihtiyacın önemini ortaya koymuştur.
Bu çalışmada, Siemens S7-1200 PLC, 30cm x 30cm x 50cm boyutlarında su tankı, 200 W'lık ısıtıcı, endüstriyel PT100 sıcaklık sensörü, ktp700 insan-makine arayüzü ve PID algoritması kullanılmıştır.

YÖNTEM

Bu çalışmada tasarlanan ve gerçeklenen deney düzeneğinin öbek çizgesi Şekil 1'de ve deney düzeneği Şekil 2'de verilmiştir. Deney düzeneğinde kullanılan devre elamanları: a) Siemens s7 1200 PLC ve Tia portal v15, b) KTP 700 HMI arayüzü, c) Su tankı ve rezistans, d) Katı hal rölesi, e) PT100 sıcaklık sensörü, f) PT100 dönüştürücüdür.

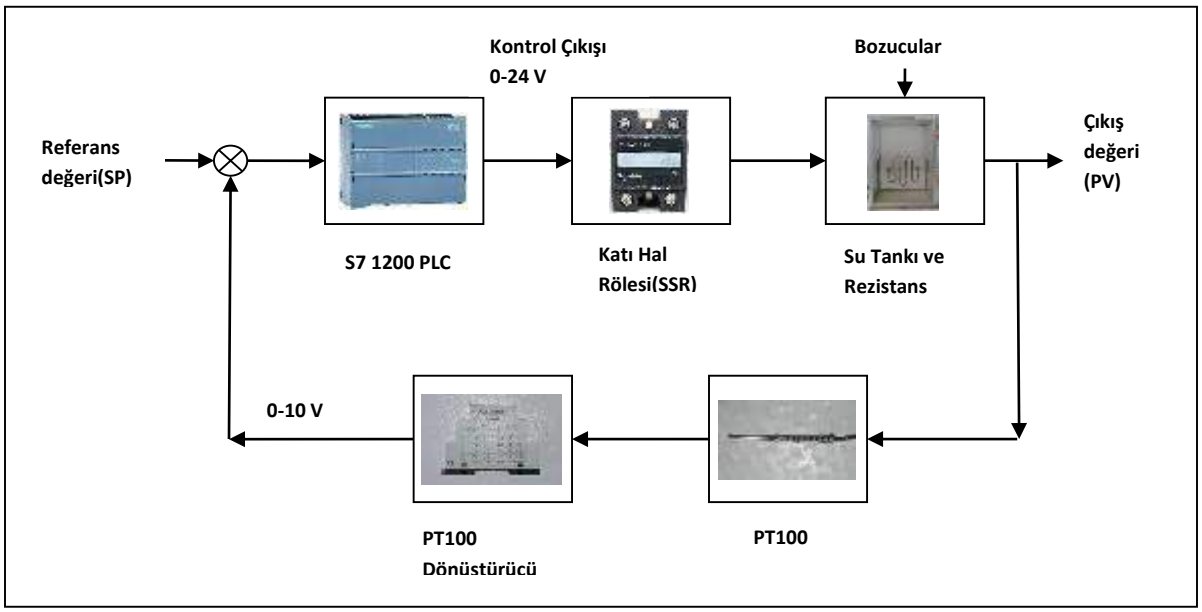

Şekil 1. PLC Sıcaklık Kontrolü Blok Şeması

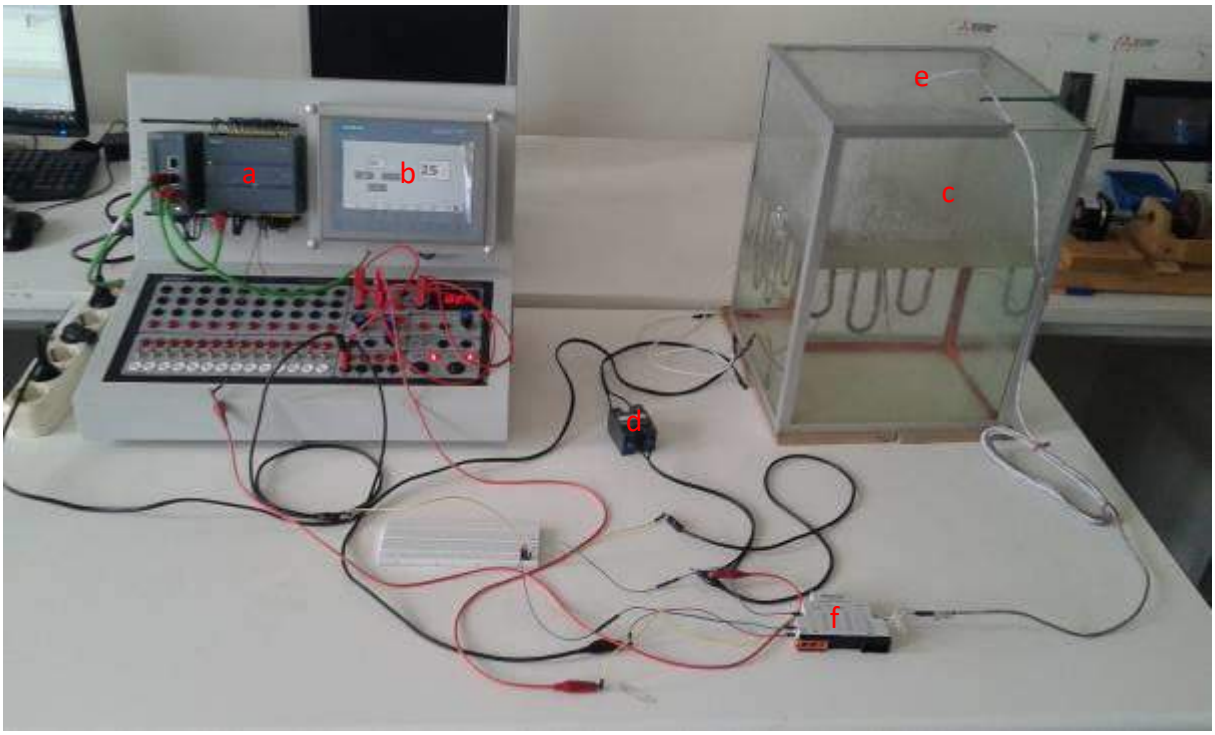

Şekil 2. Deney Düzeneğini Oluşturan Cihazlar

S7 1200 PLC ve TIA Portal v15

Bu çalışmada S7-1200 CPU 1214C DC/DC/DC PLC kullanılmıştır. 120/230V AC **voltaj** ile çalışır. Bu modelden 24 V besleme alınabilir. Ancak besleme akımı 1.5 A ile sınırlıdır. Analog giriş sayısı 2'dir. Analog çıkışı bir tanedir. Dijital giriş sayısı 14'tür.

Bunlardan 6'sı yüksek hızlı sayıcıdır. Dijital çıkış sayısı 10'dur. Bunlardan 4'ü yüksek hızlı sayıcıdır. Ethernet haberleşme protokolünü kullanılmaktadır. Bu çalışmada bir adet analog giriş, bir adet hızlı sayıcı çıkışı ve PLC yazılım programı olarak TIA Portal V15 kullanılmıştır.

KTP 700 HMI

Dokunmatik panel veya operatör paneli gibi adlandırmalar ile kullanılan i**nsan-makine arayüzleri** Endüstriyel Otomasyon sektöründe yaygın bir şekilde kullanılmaktadır.
Bu çalışmada KTP 700 insan-makine arayüzü kullanılmıştır. Besleme gerilimi 24 V DC'dir.
İnsan-makine arayüzü üzerinde referans sıcaklık değerini girmek için butonlar ve çıkış sıcaklık değerlerini okumak için metin editörü kullanılmıştır(Şekil 3).

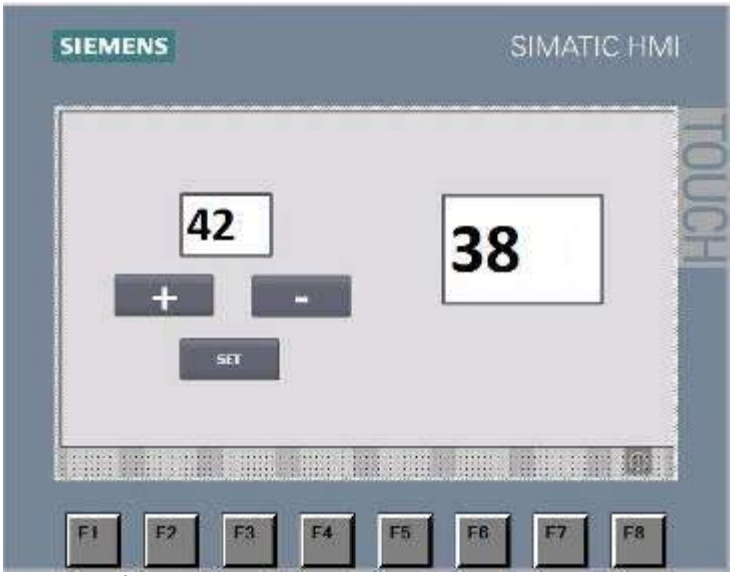

Şekil 3. İnsan-Makine Arayüzü

Su Tankı Ve Rezistans

Bu çalışmada 30cm x 30cm x 50cm ölçülerinde su tankı, 200 W gücünde rezistans kullanılmıştır(Şekil 4). Su tankının üzerindeki açıklıktan su eklenerek dış bozucu verilmektedir. Suyun sıcaklığı 0-100 ^{o} C arasında ısıtılabilmektedir.

Şekil 4. Su Tankı Ve Rezistans

Katı Hal Rölesi (SSR)

Katı hal rölesi mikro elektronik ve güç elektroniği devre elemanlarından oluşan mekanik olarak temassız bir elektronik anahtardır. Katı hal rölesinin girişi, büyük bir akım yükünü sürmek için küçük bir kontrol sinyali kullanır. Deney düzeneğinde kullanılan katı hal rölesinin akımı 50 A'dir. Katı hal rölesinin bağlantı şeması Şekil 5'de gösterilmiştir.

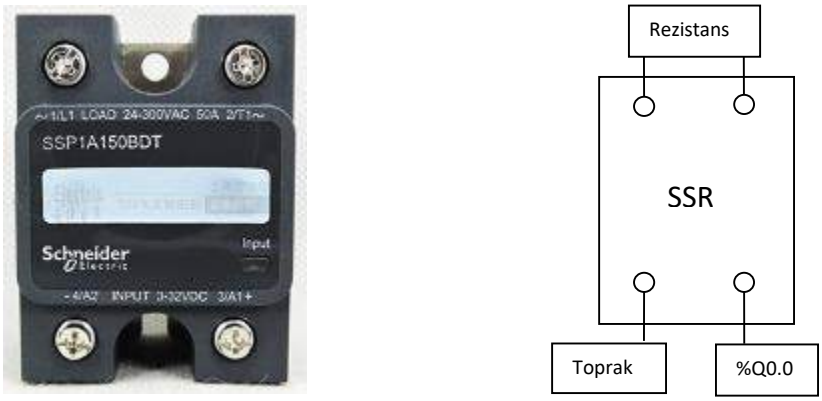

Şekil 5. SSP1A150BDT Katı Hal Rolesi-SSR(Solid State Relay)

PT100

PT100'lere Rezistans termometre adı da verilir(Şekil 6). Endüstride ve laboratuvarlarda yaygın olarak kullanılmaktadır. Özellikle hassas değer alınmak istenilen yüksek sıcaklıklarda, PT100 tercih edilirler. PT100 iletken bir telin direnç değerinin sıcaklıkla değişmesinden istifade edilerek oluşturulan bir sıcaklık algılayıcısıdır. 0 ^{o}C devreye

100ohm'luk direnç uygular. Sıcaklık artışına göre değişen direnç değeriyle bulunduğu ortamdaki sıcaklık ölçülür("<pt100_datasheet.pdf>,").

Şekil 6. PT100 Sıcaklık Sensörü

PT100 Dönüştürücü

Kullanılan PLC de RTD modülü olmadığı için Klemsan Ascon 321 adlı PT100 dönüştürücü kullanılmıştır. Bu dönüştürücünün bağlantı şeması Şekil 7'de verilmiştir. Bu dönüştürücü ile PT100'ün sıcaklıkla değişen direnç değeri 0-10 V arası değere dönüştürülmüştür. Bu gerilim değeri giriş olarak PLC'ye verilmiştir.

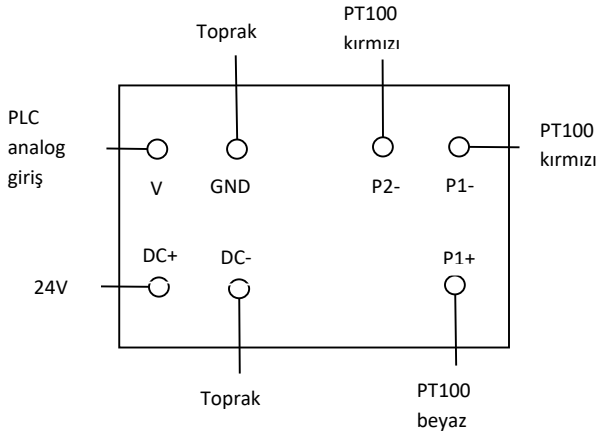

Şekil 7. Klemsan ASCON 321 PT100 Dönüştürücü

PLC Programı

Ana Blok Programı

Şekil 8'deki network 1 de PT100 dönüştürücüsünden gelen 0-10 V arası gerilim 0-27648 arasında karşılık gelen değere dönüştürülür. Sonrasında bu değer 0-100 ^{o}C aralığındaki tamsayı değerine çevrilir.

Şekil 8. Ana Blok Network 1

Şekil 9'da network 2 ile HMI ara yüzündeki referans sıcaklık değeri değiştirilir.

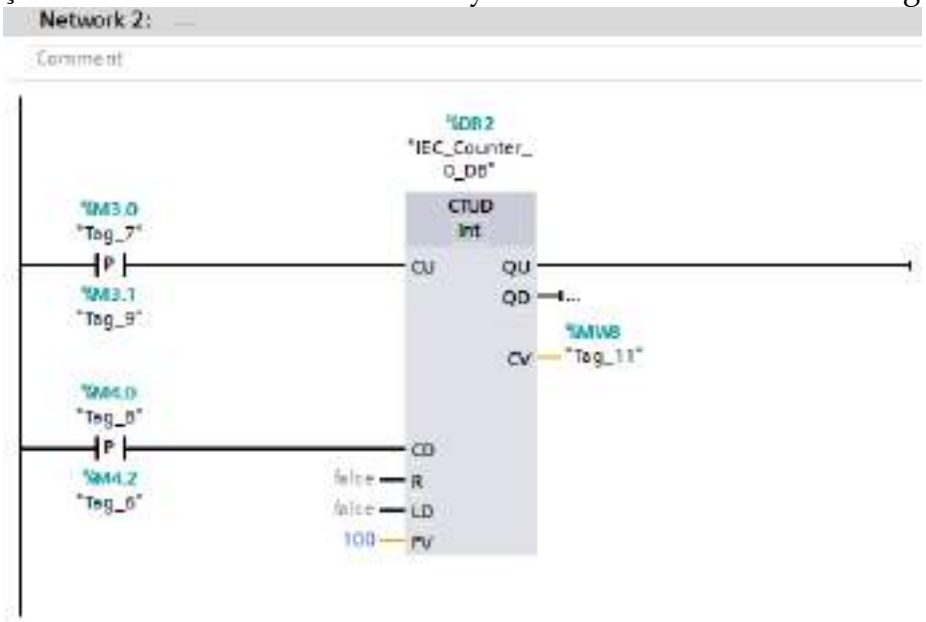

Şekil 9. Ana Blok Network 2

Şekil 10 daki network 3'te ise referans tamsayı değeri gerçel sayı değerine dönüştürülür.

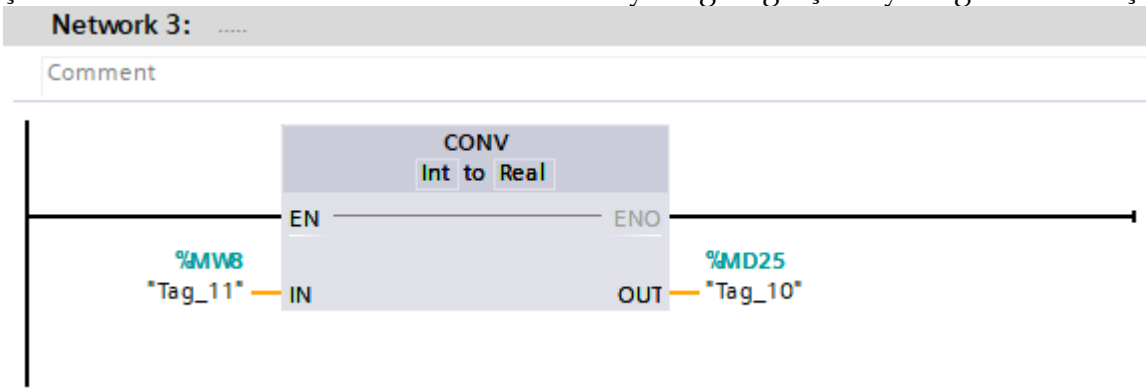

Şekil 10. Ana Blok Network 3

PID Blok Programı

Şekil 11'deki network 1'de referans değerinin reel değeri ile PT100'den gelen 0-100 arası reel değer PID bloğundan geçerek SSR'a gidecek çıkışa dönüşür.

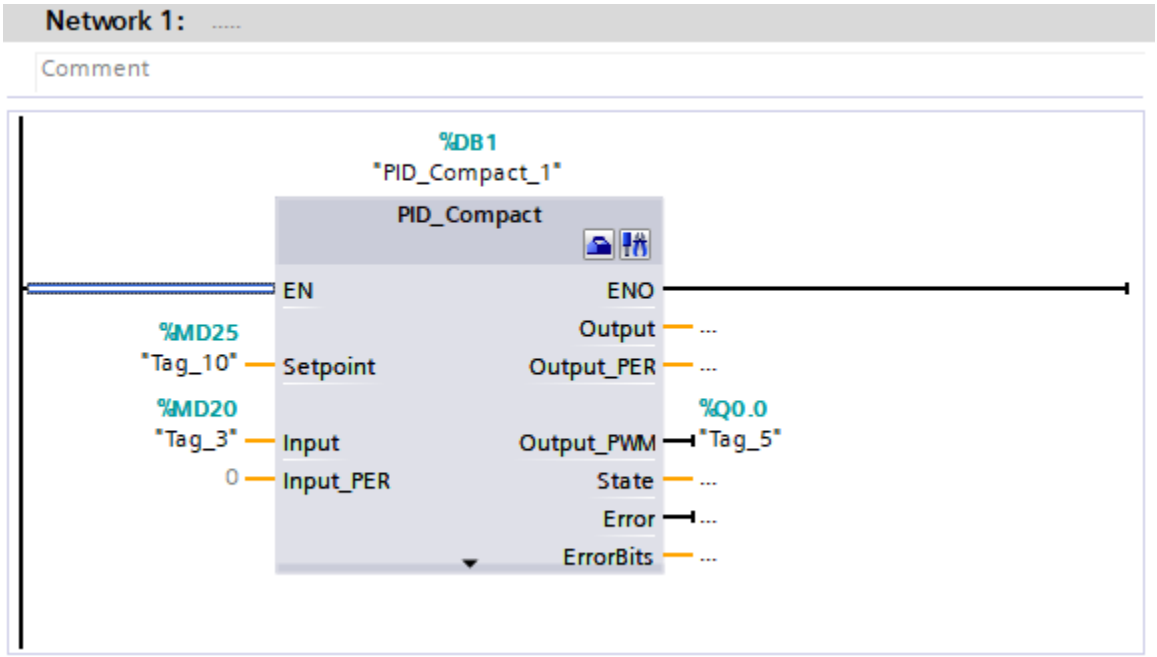

Şekil 11. PID Blok Network 1

PLC programında kullanılan etiket ve adresler Tablo 1'de verilmiştir.

Tablo 1. Blok Diyagramı Etiket Ve Adresleri

Etiketler	PLC Adres	Açıklamaları
Tag_1	%IW64	PT100'den çıkan 0-10 V arası değerin 0-27648 arasında karşılık gelen değeri
Tag_2	%MD10	0-27648 arasındaki değerin %'lik karşılığı
Tag_3	%MD20	% değerinin reel karşılığı
Tag_4	%MW10	Reel değerin integer karşılığı
Tag_5	%Q0.0	SSR'ye giden PLC çıkışı
Tag_6	%M4.2	Referans değeri azaltma butonu bırakma
Tag_7	%M3.0	Referans değeri arttırma butonu basma
Tag_8	%M4.0	Referans değeri azaltma butonu basma
Tag_9	%M3.1	Referans değeri arttırma butonu bırakma
Tag_10	%MD25	Referans değerinin reel hali
Tag_11	%MW8	Referans değerinin integer hali

BULGULAR

Sıvı sıcaklık kontrolü deneyinde referans değeri 42 ºC ayarlanmıştır. Şekil 12'de görüldüğü üzere su tankının içindeki suyun sıcaklığı 38 ºC'ken referans değerinin 42 ºC ayarlanmasıyla yaklaşık 130 saniyede 42 ºC ulaşmıştır. 280. saniyede su tankına bozucu olarak soğuk su ilave edilmiş ve suyun sıcaklığı tekrar 33 ºC'ye düşürülmüştür. Sonrasın 325. Saniyede su sıcaklığı tekrar 42 ºC'ye ulaşmıştır.
Deney düzeneğinde PID kodunda kullanılan katsayılar deneme yanılma Kp: 0.05, Ki: 0.06, Kd: 0.0 şeklinde bulunarak ayarlanmıştır.

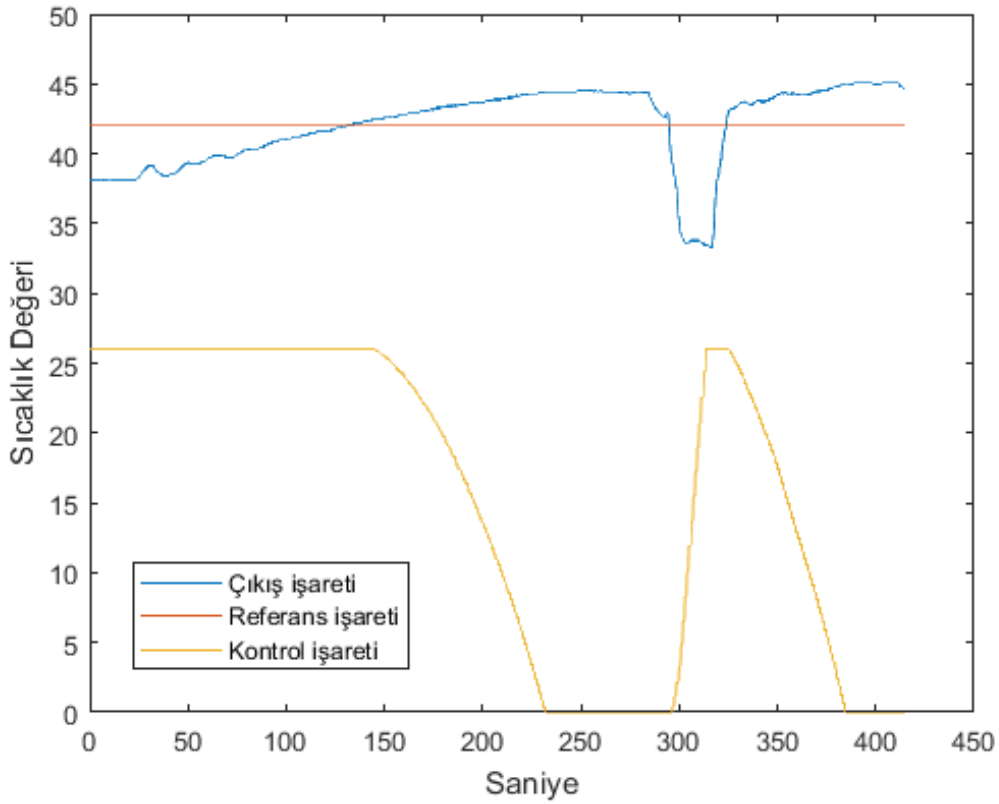

Şekil 12. Çıkış-Referans Ve Kontrol İşareti Tablosu

SONUÇ

Bu çalışma, öğrencilere PLC kullanma ve program tasarlama becerilerini kazandırmayı amaçlamaktadır. Deney düzeneğindeki cihazların endüstri sektöründe yaygın olarak kullanılması öğrencilere eğitim ortamlarında öğrendiklerini iş hayatlarında uygulamalarına olanak sağlayacaktır.

Kaynaklardaki çalışmaların bazılarında sıcaklık sensörü olarak lm35 ("<lm35_datasheet.pdf>,") kullanmıştır. Kontrol algoritması olarak PID kontrolü ile birlikte bulanık mantık (Weibin & Qingjian, 2010), (Yang & Bian, 2012) kullanılmıştır.
Bu çalışmada ise endüstri sektöründe en çok tercih edilen sıcaklık sensörlerinden biri olduğu için PT100 sıcaklık sensörü kullanılmıştır. Kontrol algoritması olarak kullanımının kolay olması, iyi sonuçlar vermesi ve sanayide hala tercih edilmesi nedenlerinden dolayı PID algoritması kullanılmıştır.

Bu çalışma sonucunda elektrik-elektronik, kontrol, mekatronik ve makine mühendisliği bölümü öğrencileri suyun sıcaklık denetimini, PT100 kullanımını, katı hal röle kullanımı, rezistans sürmeyi, PLC programlamayı, PLC ile analog veri girişi, PLC ile birlikte transmitter kullanmayı, PLC ile PID modülü kullanmayı kendileri uygulayarak öğrenmişlerdir.

ÖNERİLER

PT100 yerine başka sıcaklık sensörleri ve PID yerine farklı kontrol algoritmaları kullanılarak tekrarlanabilir. Ayrıca PLC programlamada merdiven diyagramı yerine fonksiyon blok diyagramı, komut listesi gibi programlama biçimleri kullanılarak programlanabilir.

TEŞEKKÜR

Bu çalışma Ondokuz Mayıs Üniversitesi tarafından Bilimsel Araştırma Projesi kapsamında desteklenmektedir (PYO.MUH.1906.17.002). Çalışmalarda destek olan lisans öğrencisi Mustafa Özçelik'e teşekkür ederiz.

KAYNAKLAR

Al Yusuf, S. (2018). Development of PLC and SCADA based Integrated Thermal Control System with Self/Auto-tuning Feature. Paper presented at the 2018 Condition Monitoring and Diagnosis (CMD).
Alves, L. F., Brandão, D., & Oliveira, M. A. (2019). A multi-process pilot plant as a didactical tool for the teaching of industrial processes control in electrical engineering course. The International Journal of Electrical Engineering & Education, 56(1), 62-91.
Gulpanich, S., Krongratana, V., Srimuang, A., Tipsuwanporn, V., & Wongvanich, N. (2017). PLC-based industrial temperature controller with different response times. Paper presented at the 2017 17th International Conference on Control, Automation and Systems (ICCAS).
<lm35_datasheet.pdf>.

<pt100_datasheet.pdf>.
Rata, G., & Rata, M. (2016). Temperature control solution with PLC. Paper presented at the 2016 International Conference and Exposition on Electrical and Power Engineering (EPE).
Shahrokhi, M., & Zomorrodi, A. (2013). Comparison of PID controller tuning methods. Department of Chemical & Petroleum Engineering Sharif University of Technology, 1-2.
Velagic, J., Osmic, N., Lutvica, K., & Kadic, N. (2010). Incubator system identification and temperature control with PLC & HMI. Paper presented at the Proceedings ELMAR-2010.
Weibin, C., & Qingjian, M. (2010). Based on PLC temperature PID-Fuzzy control system design and simulation. Paper presented at the 2010 International Conference on Information, Networking and Automation (ICINA).
Yang, Y., & Bian, H. (2012). Design and Realization of Fuzzy Self-tuning PID Water Temperature Controller Based on PLC. Paper presented at the 2012 4th International Conference on Intelligent Human-Machine Systems and Cybernetics.

UNDERGRADUATE INDUSTRIAL CONTROL LABORATORY EXPERIMENTAL SETUP: PART 1 FLOW RATE CONTROL WITH PLC

Cengiz TEPE
Electronic and Electrical Engineering
Ondokuz Mayıs University
ctepe@omu.edu.tr

Osman Can ÇALIŞKAN
Electronic and Electrical Engineering
Ondokuz Mayıs University
osmancaneem@gmail.com

İlyas EMİNOĞLU
Electronic and Electrical Engineering
Ondokuz Mayıs University
ilyase@omu.edu.tr

ABSTRACT: The aim of this study is to enable the personnel who are knowledgeable about industrial automation systems in electrical-electronics, control, mechatronics and mechanical engineering department design and can use them. For this purpose, Flow Control Experience System was prepared and realized for PLC Industrial Control Laboratories. The clearness of other important points in PLC applications is the most accurate analysis and the fastest way to reach. The work plan on this page describes how to achieve a more stable and faster PID address than an ordinary system on a computer with a PLC-enabled operation.
This system is S7-1200 PLC as control unit, flow meter giving panel adjustment in single room system, inverter for driveable motor at variable speeds, asynchronous motor and pump for flooding system, valve ventilation as disruptor. Production history in an industry where experience is used. Recognize and work with devices that are used in the industry before starting a career.

Key words: Flow control, PLC, PID, Induction Motor, Flow

LİSANS ENDÜSTRİYEL KONTROL LABORATUVARI için DENEY DÜZENEĞİ TASARIMI: BÖLÜM 1 PLC ile AKIŞ DENETİMİ

ÖZET: Bu çalışma elektrik-elektronik, kontrol, mekatronik ve makine mühendisliği bölümü öğrencilerinin endüstriyel otomasyon sistemleri hakkında bilgi sahibi olmasını

ve sistemde yer alan araçları istenilen düzeyde kullanabilmelerini amaçlamaktadır. Bu amaç doğrultusunda Lisans Endüstriyel Kontrol Laboratuvarları için PLC ile Akış Denetim Deney Düzeneği tasarlanmış ve gerçeklenmiştir. PLC uygulamalarında diğer önemli nokta sistemin en doğru kararlılığa en hızlı şekilde ulaşabilmesidir. Bu bağlamda çalışma kapsamında PLC ile akış kontrolü gerçekleştirilecek olan bir sistemin PID kullanılarak sıradan bir sistemden daha hızlı ve doğru bir karalılığa ulaşması anlatılmaktadır.
Bu çalışmada kontrol ünitesi olarak S7-1200 PLC, tek hall sensör çıkışı veren debi ölçer, motorun değişken devirlerde sürülmesi için invertör, sisteme su basmak için asenkron motor ve pompa, bozucu olarak ise vana kullanılmıştır. Deney düzeneğinde kullanılan ürünlerin tamamı endüstride kullanılan ürünlerden oluşmaktadır. Böylece öğrencilere, meslek hayatına başlamadan önce endüstride kullanılan cihazları tanıma ve bu cihazlarla çalışma imkanı sunulmuştur.

Anahtar sözcükler: Akış kontrolü, PLC, PID, Asenkron motor, Debi

GİRİŞ

Son yıllarda Türkiye'de ve dünyada PLC uygulamalarının giderek yaygınlaştığı görülmektedir. PLC tabanlı sistemlerin endüstride başarılı sonuçlar elde etmesi bu durumun oluşmasında önemli bir faktördür. Endüstriyel alanda çeşitli uygulamalarda PLC kullanılarak akış kontrolü sağlanmaktadır. Kompleks veya basit olarak tasarlanmış sistemlerde yer alan akış kontrolü, inovasyona açık bir şekilde endüstriyel uygulamaların geniş bir alanında mevcuttur. Akış kontrolü su tedarik ağları, kanalizasyon sistemleri, kimya sanayi, petrol aktarım tesisleri gibi birçok alanda önemli bir rol oynamaktadır. Endüstriyel uygulamaların kullanım amaçlarının anlaşılabilmesi için mühendislik bilgilerinin edinildiği ilk yer olan üniversitelerde verilen eğitimin nitelikli olması gerekmektedir. Nitelikli eğitim ise teorik bilgilerin yanında uygulamalı faaliyetlerin gerçekleşmesi ile mümkündür. Bu bağlamda teorik olarak PLC eğitiminin yanında uygulamalı eğitim de önemli bir unsur haline gelmiştir (Geaney & O'Mahony, 2015; Gevorkov, Vodovozov, Lehtla, & Bakman, 2015; Q. X. Liu, 2016; Y. Liu & He, 2011; Özerdem, 2016; E. Priyanka, Maheswari, & Thangavel, 2018; Rajeswari, Suresh, & Rajeshwari, 2013; Shankar, 2008). Geverkov ve Bakman çalışmalarında PLC tabanlı bir sistem için akış kontrol uygulaması gerçekleştirmişlerdir. Çalışmalarında ABB AC500 PLC kullanmış olup, değişken frekanslı santrifüj pompa motorunun devrini kontrol etmek için invertörü, sistemin kararlılığını ölçmek için ise PID yi kullanmışlardır (Gevorkov et al., 2015). Liu ise çalışmasında uzman PID sistemine dayalı bir akış kontrol işlemi gerçekleştirmiştir. Bu sistemde S7-1500 PLC ana kontrolör olarak görev yapmaktadır (Q. X. Liu, 2016). Liu ve He çalışmalarında S7-200 PLC kullanarak su şebekesi için otomatik kontrol sistemi tasarlamışlardır. Tasarlanan sistem sıcaklık, basınç ve akış hızını kontrol etmiştir (Y. Liu & He, 2011). Priyanka ve arkadaşları çalışmalarında

bulanık mantık PID kullanarak PLC tabanlı bir petrol boru hattı sisteminin çevrimiçi akış kontrolünü sağlamışlardır. Sistem kaskat PID ile bulanık mantık PID için gerçeklenmiş olup, uygulanan PID türüne göre çıkış cevabının dengeye ulaşma süresi gözlemlenmiştir (E. Priyanka et al., 2018). Rajeswari çalışmasında PLC ve SCADA kullanarak ilaçlarda su depolama ve dağıtım sistemi gerçekleştirmiştir. Allen Bradley Micrologix 1200 PLC kullanmıştır. Sistem ilaç sanayi için kaliteli su teminatını gerçekleştirmektedir. Sistem tarafından pH, sıcaklık, basınç, iletkenlik ve akış hızı kontrolü sağlanmıştır (Rajeswari et al., 2013). Shankar çalışmasında PLC ve SCADA kullanarak kompleks bir kazan kontrol sistemi tasarlamıştır. Tasarladığı sistem için Allen Bradley 1000 PLC kullanmış ve sistemde yer alan SCADA ekranının PLC ile bağlantısını yaparak kazan için belirlenen parametrelerin sürekli olarak takibini gerçekleştirmiştir. Yapılması gereken işlemleri devreye sokmak için kazan AC motor ile kontrol edilmiştir. Sistemin karalılığı PID kontrol ile sağlanmaktadır (Shankar, 2008). Cai ve arkadaşları yüksek sıcaklıkta ve yüksek hızda bir rüzgar tüneli için iki üniteli bir yakıt deposunun koordineli besleme işleminin akış kontrolünü gerçekleştirmişlerdir. Uygulamanın kontrolü PLC tabanlıdır. Sisteme bulanık PI adaptif çapraz bağlanma ve PI çapraz bağlanma algoritması uygulamışlardır (Cai, Yang, & Liu, 2016). Priyanka ve arkadaşları PLC tabanlı PID denetleyicisi kullanarak benzin nakil hatlarının izlenmesi üzerine bir çalışma gerçekleştirmişlerdir. Çalışmalarında kararlılık metotları olan Ziegler Nichols PID, Simple IMC-PID ve Shams IMC-PID algoritmalarını kıyaslamışlardır (E. B. Priyanka, Maheswari, & Meenakshipriya, 2016).

Bu çalışmada, gerçeklenen deney düzeneğinde S7-1200 PLC üzerinden sürülen invertör aracılığıyla üç fazlı asenkron motorun devri kontrol edilerek motora bağlı olan su pompası ile sisteme su basılmıştır. Bu sistemde suyun debisi PID algoritması kullanılarak kontrol edilmiştir. Uygulanan bu yöntem ile sistemin hızlı ve doğru çıkış tepkesi oluşturması sağlanmıştır. Deney düzeneğine harici olarak eklenen valf ile bozucu etki oluşturulmuştur.

Laboratuvar ortamında fiziksel bir gerçeklikle ele alınan bu çalışma teorik bilgilerin pratiğe dökülmesi adına uygun bir ortam oluşturacaktır. Yalnızca teorik olarak verilen derslerin kaliteli mühendis grupları oluşturabilmesi için güncel dünya koşullarında yeterli olmayacağı bilinmektedir. PLC ile ilgili deney setlerinin uygulama alanlarının arttırılması öğrencilerin mühendislik alanında derinlemesine bilgi edinip öğrendiklerini meslek hayatlarında uygulayabilmelerini sağlayacaktır. Bu amaç doğrultusunda çalışma kapsamında tasarlanan akış deney düzeneği, endüstriyel bir PLC uygulamasının anlaşılabilir ve gerçek hayata uygulanabilir olmasında öğrenciler için bir basamak oluşturması açısından önem taşımaktadır.

YÖNTEM

Deney Düzeneği Tasarımı

Deney Seti Araçları

Şekil 1'de deney düzeneğinin blok diyagramı yer almaktadır. Şekil 2'de gösterilen deney düzeneği içeriğinde kullanılan devre elemanları; a) S-7 1200 PLC, b) KTP 700 HMI arayüz, c) asenkron motor, d) invertör, e) akış ölçer sensör, f) tampon devresi, g) bozucu vana ve h) akış hattıdır.

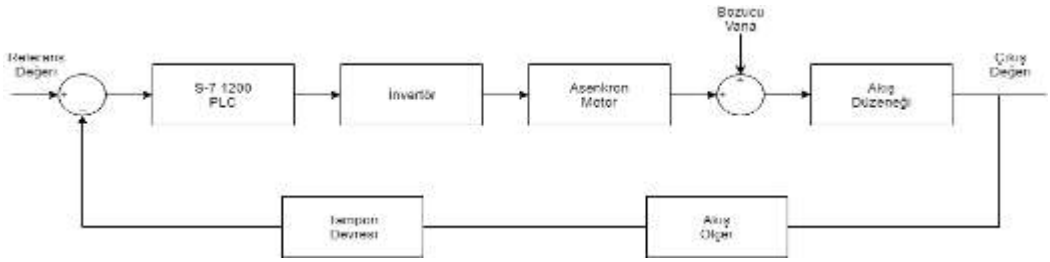

Şekil 1. Deney Düzeneği Blok Diyagramı

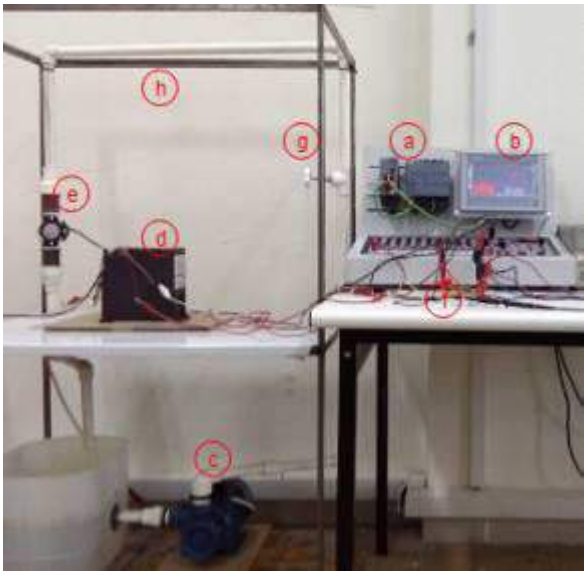

Şekil 2. Deney Düzeneği

S-7 1200 PLC ve TIA Portal

Siemen PLC'lerin S7-200-300-400-1200-1500 olmak üzere farklı modelleri bulunmaktadır. Bu çalışmada S7-1200 CPU 1214C DC/DC/DC PLC kullanılmıştır. S7-1200'ün En belirgin özelliklerden biri de PPI haberleşme portu yerine Profinet yani Ethernet haberleşme protokolünü kullanmaktadır. Standart olarak her S7 1200 PLC üzerinde 14 sayısal giriş ve 10 sayısal çıkış bulunmaktadır. Ayrıca 2 adet 0-10 V analog giriş ve 4 adet PWM çıkışı vardır. S-7 1200 PLC'lerin yan modülleri de bulunmaktadır. Bunlar standart giriş/çıkış modülleri ve haberleşme modülleridir. PLC yazılım programı olarak TIA Portal V15 kullanılmıştır. TIA Portal giriş/çıkış, insan-makine arayüzü, sürücüler, hareket kontrolü ve motor yönetimi sistemlerini bir bütün halinde sunar. Ortak veri yönetimi ve akıllı

kütüphane sistemi sayesinde kapsamlı yazılım ve donanım fonksiyonları verimli bir şekilde tüm otomasyon görevlerini yerine getirebilir.

KTP-700 HMI Arayüz

İnsanların makineler ile iletişim kurabilmesi günümüzde önemli bir unsur haline gelmiştir. Bunun sonucu olarak insan-makine arayüzü kavramı ortaya çıkmıştır. Bir HMI, diğer adı ile insan-makine arayüzü, kullanıcıların, makine ve üretim tesisleri ile iletişim kurmasına olanak sağlayan bir aygıt ya da yazılımdır. Bu şekilde, operatör üretim sürecini kontrol etmek için gerekli tüm araçlara sahip olmaktadır. Bu çalışmada insan-makine arayüzü olarak KTP-700 yer almaktadır. KTP-700'ün ekran boyutları 214x158x39mm'dir. Dokunmatik ekran olarak TFT ekran yer almaktadır. Etnernet haberleşme protokolünü kullanmaktadır. TIA Portal V15 ile programlanabilmektedir. Besleme gerilimi 24V DC'dir. Bu çalışmada akış hızını gösterebilmek için bar grafiği ve metin editörü kullanılmıştır. Bar grafiği 0-50Lt/dk arasında ölçeklendirilmiştir. Referans değer Şekil 3'te yer alan 'Set Akis Hizi' metin editörü ile sisteme girilmektedir.

Şekil 3. KTP 700 HMI Arayüz

İnvertör

Elektriksel gücü dönüştürme elemanı olarak tanımlanabilen invertör, güç dönüştürücü ya da evirici olarak da adlandırılmaktadır. AC frekans invertörü, motor sürücü veya motor kontrol ünitesi olarak adlandırılır. AC elektrik motorlarının hız, akım ve rotor pozisyonu gibi parametrelerini kontrol etmek için kullanılan devre elemanıdır. Bir invertör, değişken hız kontrolünü sağlamak için motor sargılarına uygulanan gerilimin frekansını değiştirir ve buna bağlı olarak gerilimin genliğini değişir. Bu değişime bağlı olarak motorun devri değişir. Şekil 4'te invertörün bağlantıları yer almaktadır. Deney setinde kullanılan sürücü 1.5kW gücündedir. Sürücü besleme gerilimi 200-240 volt arasındadır. PLC'den gelen 0-10V değişken işaret değerine göre asenkron motora aktarılan gerilim 0-50Hz aralığında değişmektedir. Frekans değişimi ile asenkron motorun devri kontrol edilmektedir. Şekil 5'te yer alan invertörün ön panel görünümündeki girişler; a) 12 numaralı pin 24V girişi, b) 18 numaralı pin motor başlatma anahtarı, c) 53 numaralı pin 0-10V gerilim girişi, d) 55 numaralı pin invertör toprağıdır.

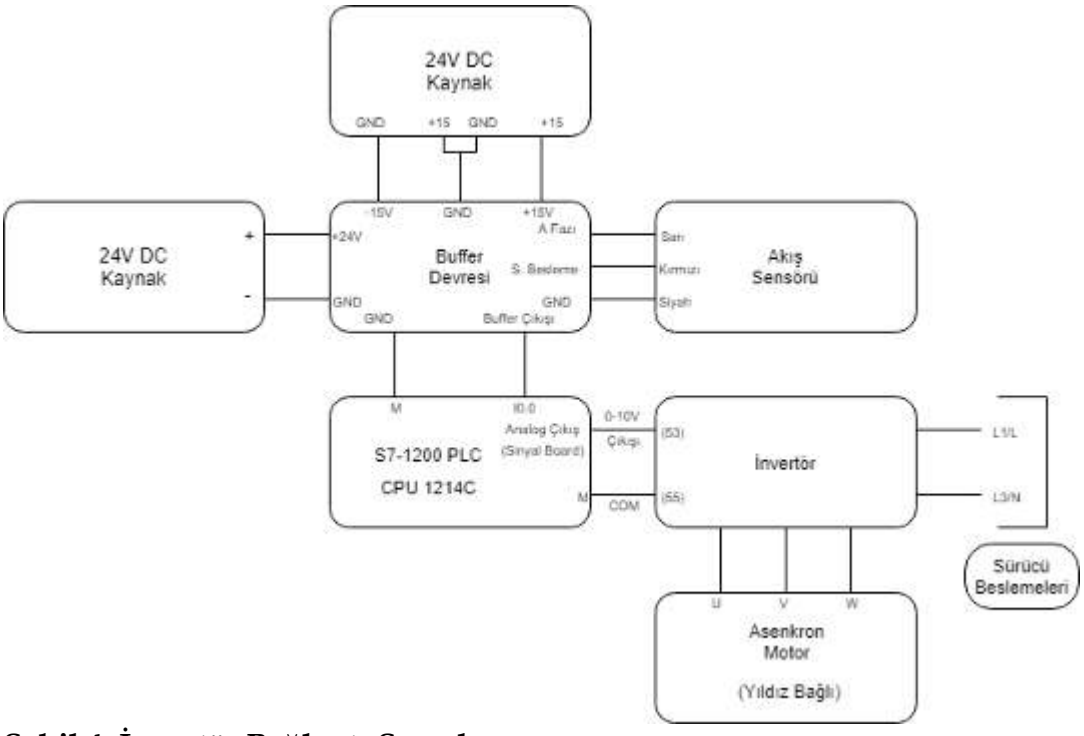

Şekil 4. İnvertör Bağlantı Şemaları

Şekil 5. İnvertör Ön Panel Görünümü

Asenkron Motor

Genel olarak AC motorlar; kaldırma, kaydırma, pompa, sürme ve delme işlemleri için gerekli olan itici gücü sağlar, endüstriyel ve ticari uygulamalardaki diğer işlemleri yerine getirir. Deney düzeneğinde yer alan asenkron pompa motoru sıvının sürekli olarak akışını gerçekleştirmektedir. Bu işlemi yerine getirirken sürücüden aldığı frekans değerine göre artan, azalan veya sabit bir devirde dönmektedir. Deney düzeneğinde yer alan asenkron motor yıldız bağlı, 50Hz, 3 fazlı, 2850 d/dk nominal hızlı ve 800W gücündedir.

Şekil 6. Asenkron Motor

Akış Ölçer Sensör

Deney düzeneğinde dakikada 2-100Lt/dk ölçüm yapabilen bir akış ölçer kullanılmıştır. Sensörün çıkışı şekil 9'da görüleceği üzere 5-24 V arası kare dalga şeklindedir. Bu çalışmada sensör 24V ile beslenmiştir. Akış sensörü için debi değeri denklem 1'deki formül ile hesaplanır.

$$Q=F \times 60 / 4{,}8 \qquad (1)$$

Burada F : 1 saniyedeki kare dalga sayısı, Q : debi

Sensör PLC'ye bağlandığında çıkış gerilimi 24V'tan 6V değerine düşmektedir. Bu sebepten dolayı akış ölçer çıkışında Şekil 8'de gösterilen tampon devresi kullanılarak gerilim düşümü engellenmiştir. Tampon devresi giriş gerilimini koruyarak çıkışa aktaran devrelerdir. Bu devrelerin en önemli özelliği giriş empedansının çok yüksek, çıkış empedansının düşük olmasıdır.

Şekil 7. Akış Ölçer Sensör

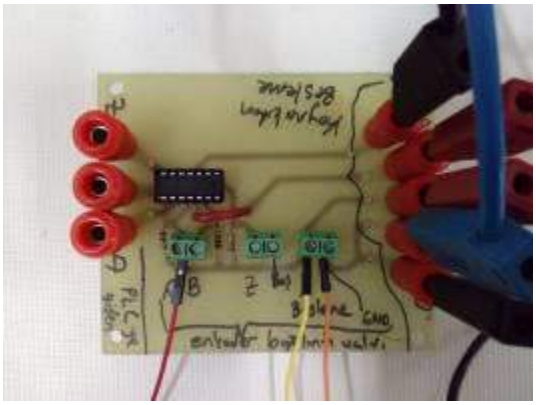

Şekil 8. Tampon Devresi

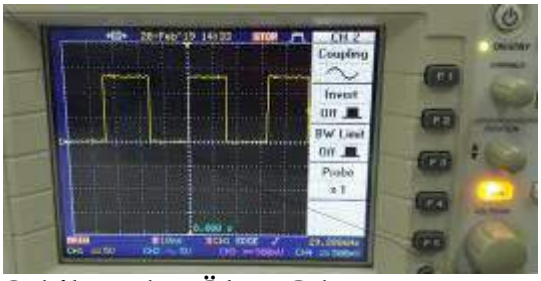

Şekil 9. Akış Ölçer Çıkışı

PLC Program

Ana Blok Program

TIA Portal V15 yazılımı ile programlama yapılırken fonksiyon blok yöntemi kullanılmıştır. Şekil 10'da yer alan network 1'de gösterilen bir hızlı sayıcı bloğudur. Akış ölçerden gelen kare dalga sinyallerini saymak için kullanılır. I0.0 girişi kullanılmıştır.

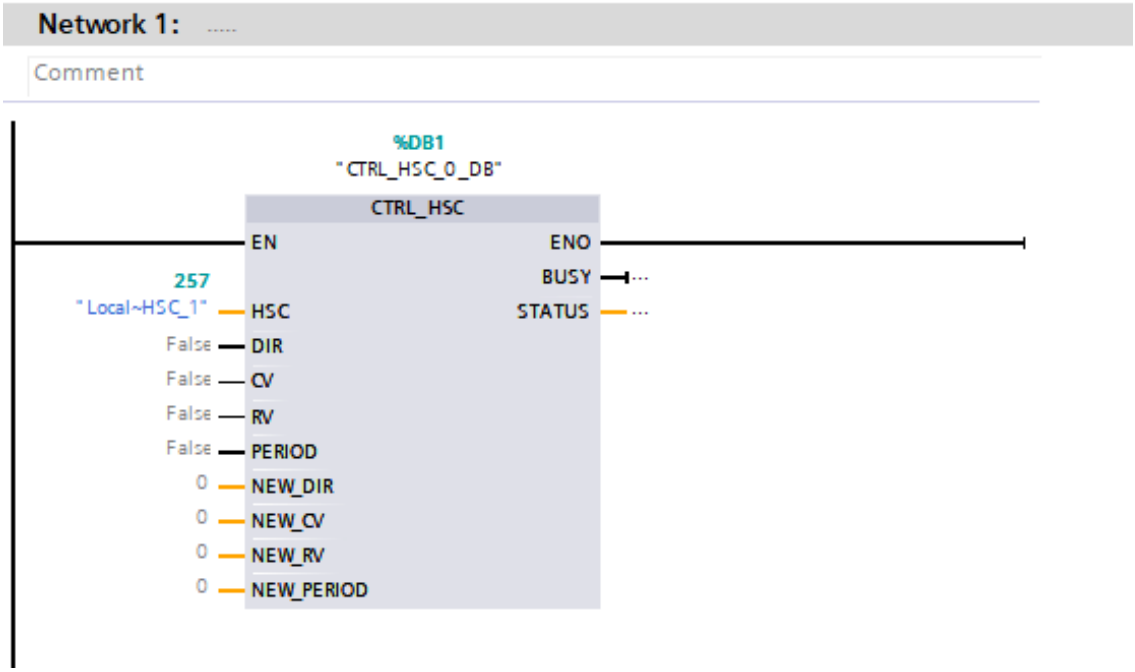

Şekil 10. Ana Blok Diyagramı Network 1

Şekil 11'de yer alan network 2'de gösterilen CONV bloğu ID1000 adresindeki tam sayıyı gerçel sayıya dönüştürmek için kullanılmıştır. Elde edilen sayı MUL bloğunda 10 ile çarpılmış ve DIV bloğunda 4.8'e bölünmüştür. Böylelikle akış ölçerin çıkışındaki kare dalgalar PLC içerisindeki hesaplamalar sonucu çıkışta 0-10V aralığında değer alır.

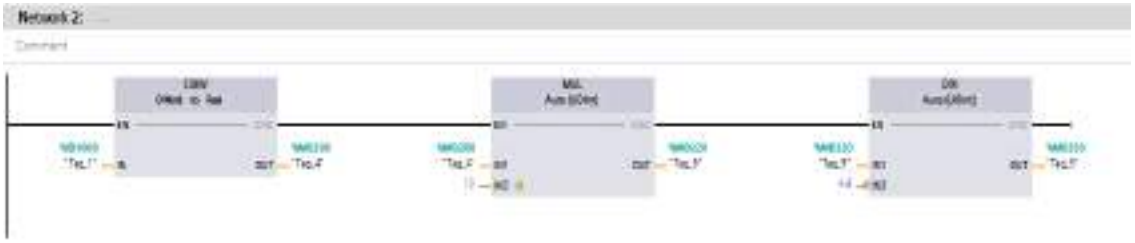

Şekil 11. Ana Blok Diyagramı Network 2

PID Bloğu

Şekil 12'de gösterilen PID bloğunda Tag_6 sistemin ulaşmasını istediğimiz referans değerini temsil etmektedir. Bu değer HMI arayüz ile sisteme girdiğimiz 'Set Akis Hizi' değeridir. Sistemden gelen veriler neticesinde anlık olarak hesaplanan akış hızı değeri Tag_5 kısmında bulunmaktadır. Giriş ve referans karşılaştırılması sonucunda çıkış cevabı olan Tag_8 üretilmektedir. Tag_8 0-10V arasına değişken bir gerilimdir. Bu değer sürücüye gönderilir. Sistemin hangi akış değerinde seyrettiğini ise yine HMI arayüzde yer alan 'Akis Hizi' bölümü ile takip edilmektedir.

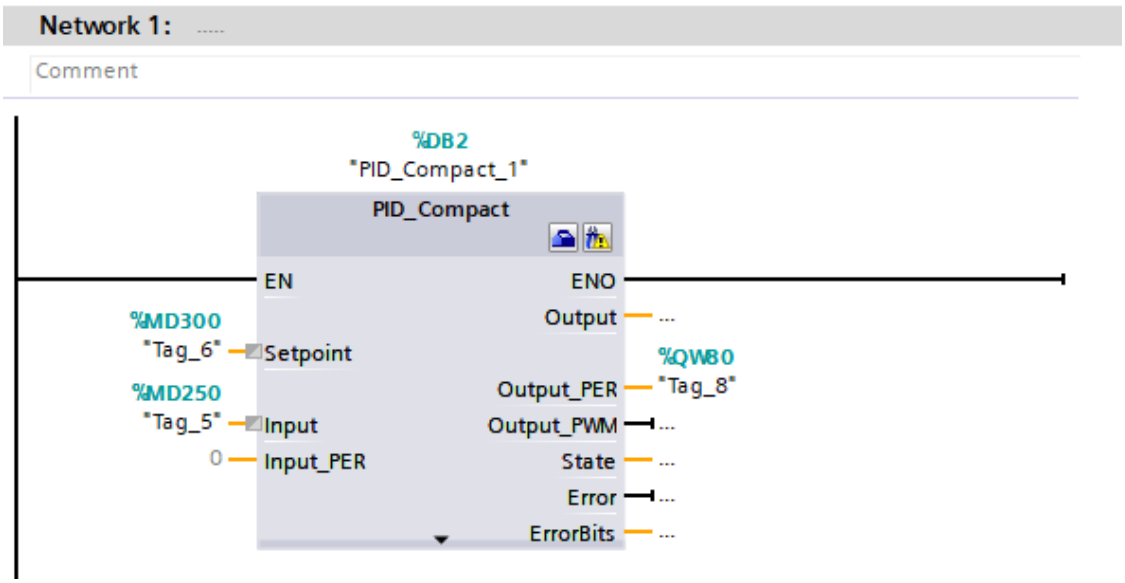

Şekil 12. PID Bloğu Network 1

Blok Diyagramı Etiket ve Adresleri

Aşağıdaki tabloda TIA PORTAL V15 yazılımında kullanılan etiketler, adresler ve adreslerin görevleri hakkında bilgi verilmiştir.

Tablo 1. PLC Etiketleri ve Adresleri

Etiketler	PLC Adresi	Açıklamaları
Local ~HSC_1	%I0.0	Akış ölçerden gelen kare dalgaların sayıldığı adres.
Tag_1	%ID1000	Kare dalgaların atandığı adres.
Tag_4	%MD200	Reel verilerin 10 ile çarpıldığı adres.
Tag_5	%MD250	Akış ölçerin kare dalgalarının 0-10V arası tanımlanması.
Tag_6	%MD300	Referans olarak girilen değer.
Tag_8	%QW80	Çıkış işaretinin adresi.
Tag_9	%MD220	Reel verilerin 4.8 ile bölündüğü adres.

BULGULAR

Akış hızı kontrol deneyinde referans değer olarak 20Lt/dk değeri ayarlanmıştır. Akış kontrol ünitesi çalıştırıldıktan yaklaşık 120 saniye sonra ulaşması beklenen referans değeri elde edilmiştir. 300.sn'de bozucu valf açılarak suyun debisi 15Lt/dk değerine

kadar indirilmiştir. Bu işlem uygulandıktan sonra bozulan işaretin 30sn içinde tekrar eski konumu olan 20Lt/dk değerine ulaştığı gözlemlenmiştir. 360. sn'den sonra bozucu valf kapatılarak suyun debisinin referans değerin üzerine çıkması sağlanmıştır. Bu işlemin ardından debi değeri 30sn kadar sonra tekrar eski referans değerine ulaşmıştır. PID algoritması ile sistem bozucu etkilere karşı ayarlanan referans değerine doğru bir şekilde oturmuştur. PID bloğunda yer alan katsayı değerleri deneme yanılma ile Kp: 1, Ki: 20, Kd: 0 şeklinde bulunarak ayarlanmıştır. Bu çalışmada endüstriyel ortamda geçerliliği halen devam eden, iyi sonuçlar veren ve kullanımının basit olmasından dolayı en sık tercih edilen denetim olan PID algoritması kullanılmıştır.

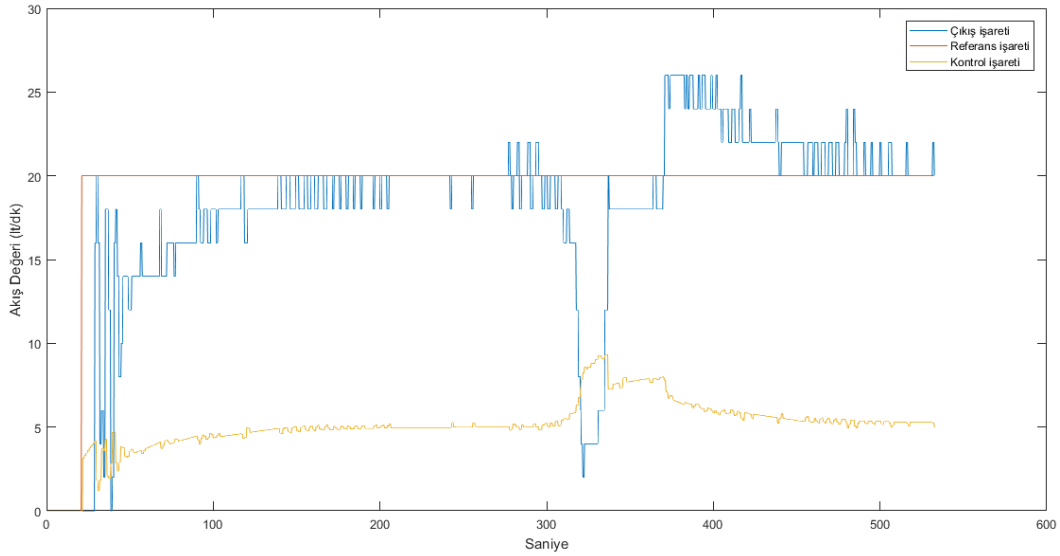

Şekil 13. Çıkış-referans İşaretinin Kontrol İşaretine Göre Değişimi

SONUÇ

Bu çalışma sonucunda elektrik-elektronik, kontrol, mekatronik ve makine mühendisliği bölümü öğrencileri suyun debi (Lt/dk) ölçümünü, akış sensörü kullanımını, asenkron motorun (devir/dakika) kontrolünü, PLC programlamayı, PLC çıkışından analog veri gönderimini, PLC hızlı sayıcı ile kare dalga okumayı, PLC ile PID modülü kullanmayı, PLC ile invertör kullanımını, invertör ile asenkron motor hız denetimini, sensör çıkışlarında tampon devre elamanı kullanımını kendileri uygulayarak öğrenmişlerdir.

ÖNERİLER

Bu çalışma farklı akış sensörleri ve PLC'ler kullanılarak tekrarlanabilir. Kontrol algoritması PID yerine bulanık mantık PID, kaskat PID ve uzman PID gibi yöntemler kullanılabilir.

TEŞEKKÜR

Bu çalışma Ondokuz Mayıs Üniversitesi tarafından Bilimsel Araştırma Projesi kapsamında desteklenmektedir (PYO.MUH.1906.17.002). Çalışmalarda destek olan lisans öğrencisi Mustafa ÖZÇELİK'e teşekkür ederiz.

KAYNAKLAR

Cai, C., Yang, Y., & Liu, T. (2016). Coordinated control of fuel flow-rate for a high-temperature high-speed wind tunnel. Proceedings of the Institution of Mechanical Engineers, Part G: Journal of Aerospace Engineering, 230(13), 2504-2514. doi: 10.1177/0954410015626737

Geaney, G., & O'Mahony, T. (2015). Design and evaluation of a remote PLC laboratory. International Journal of Electrical Engineering & Education, 53(3), 212-223. doi: 10.1177/0020720915622468

Gevorkov, L., Vodovozov, V., Lehtla, T., & Bakman, I. (2015). PLC-based flow rate control system for centrifugal pumps. Paper presented at the 2015 56th International Scientific Conference on Power and Electrical Engineering of Riga Technical University (RTUCON).

Liu, Q. X. (2016). Design of flow control system based on expert pid. Paper presented at the 2016 International Symposium on Computer, Consumer and Control (IS3C).

Liu, Y., & He, X. (2011). Design of automatic control system for waterworks based on PLC. Paper presented at the 2011 2nd International Conference on Artificial Intelligence, Management Science and Electronic Commerce (AIMSEC).

Özerdem, Ö. C. (2016). Design of two experimental setups for programmable logic controller (PLC) laboratory. International Journal of Electrical Engineering & Education, 53(4), 331-340. doi: 10.1177/0020720916630325

Priyanka, E., Maheswari, C., & Thangavel, S. (2018). Online monitoring and control of flow rate in oil pipelines transportation system by using PLC based Fuzzy-PID Controller. Flow Measurement and Instrumentation, 62, 144-151.

Priyanka, E. B., Maheswari, C., & Meenakshipriya, B. (2016). Parameter monitoring and control during petrol transportation using PLC based PID controller. Journal of Applied Research and Technology, 14(2), 125-131. doi: 10.1016/j.jart.2016.03.004

Rajeswari, V., Suresh, L. P., & Rajeshwari, Y. (2013). Water storage and distribution system for pharmaceuticals using PLC and SCADA. Paper presented at the 2013 International Conference on Circuits, Power and Computing Technologies (ICCPCT).

Shankar, K. G. (2008). Control of boiler operation using PLC–SCADA. Paper presented at the Proceedings of the International MultiConference of Engineers and Computer Scientists.

THE PERFORMANCE AND EMISSION ANALYSIS OF BIODIESEL PRODUCED FROM SAFFLOWER SEED OIL IN A SINGLE CYLINDER DI DIESEL ENGINE

İlker ÖRS
Cihanbeyli Vocational School, Selcuk University, Konya, Turkey
Automotive Application and Research Center, Selcuk University, Konya, Turkey
ilker.ors@selcuk.edu.tr

Murat CİNİVİZ
Technology Faculty, Selcuk University, Konya, Turkey
Automotive Application and Research Center, Selcuk University, Konya, Turkey
mciniviz@selcuk.edu.tr

Bahar SAYIN KUL
Technology Faculty, Selcuk University, Konya, Turkey
bsayin@selcuk.edu.tr

ABSTRACT: In this study, biodiesel fuel produced from safflower oil was blended in 20% and 50% with diesel fuel. The diesel fuel, biodiesel and blend fuels were tested in a single-cylinder, direct injection, four-stroke, natural aspirated diesel engine under four different engine loads and 1400 rpm engine speed. Besides, important fuel analyses of test fuels have been performed. It was found that biodiesel use resulted in slightly increment on break specific fuel consumption (up to 25.1%). However, 20% biodiesel fuel addition resulted in slightly increment on break thermal efficiency (up to 2.31%). The biodiesel also increased NOx emissions and decreased carbon monoxide, smoke and hydrocarbon emissions for the all engine loads.

Key words: biodiesel, engine performance, exhaust emissions, diesel engine

INTRODUCTION

Diesel engines are preferred nowadays in so many sectors owing to the fact that it has better fuel economy, higher efficiency, more reliability, lower fuel cost, and longlasting capacity. Exhaust emissions from these engines are very badly affecting the human health and habitat from so many times. Moreover, due to the rise in automobile numbers on roads the fossil fuels are depleting at an alarming rate which may result in its permanent deterioration in the near future. To overcome this, researchers, and analysts are trying to find an alternative fuel which can increase the performance characteristics of the engine and decrease exhaust emissions (Goga, Chauhan, Mahla, & Cho, 2019). Vegetable oils

have been observed to be main alternative fuels for diesel engines. But, when vegetable oils use direct, they lead to some problems in engines. These problems are arised to high density, viscosity, and poor volatility of vegetable oils. According to previous researches, biodiesel production with transesterification is the best way to use vegetable oil as a fuel in existing diesel engines. Thus, an alternative diesel fuel having lower density and viscosity can obtain. But, nevertheless it has still higher viscosity and density that exceed the standard values for conventional diesel fuel (Aydın, 2016; Chang et al., 1996; Puhan, Vedaraman, Ram, Sankarnarayanan, & Jeychandran, 2005; Szybist, Song, Alam, & Boehman, 2007; Tat et al., 2000).

Many studies in literature presented that engine performance parameters of B20 and B50 fuels are lower than that diesel fuel due to biodiesel's lower calorific values compare to diesel fuel (Çelebi & Aydın, 2018; Ilkılıç, Aydın, Behcet, & Aydin, 2011; Shrivastava, Verma, & Pugazhendhi, 2019). However, there are also studies showing that thermal efficiency values of these fuels are higher than diesel fuel owing to their oxygen content provides the proper burning of the fuel (Abed, El Morsi, Sayed, El Shaib, & Gad, 2018; Sharma & Murugan, 2015; Sidhu, Roy, & Wang, 2018). There are also studies using pure biodiesel as fuel. As performance results of these studies, higher viscosity and lower calorific value caused a drop in engine performance values (Alagu et al., 2019; Asokan, Prabu, Bade, Nekkanti, & Gutta, 2019; Channapattana, Kantharaj, Shinde, Pawar, & Kamble, 2015). On the other hand, some researchers have suggested that B100 fuel improved engine performance (Jindal, Nandwana, Rathore, & Vashistha, 2010; Muralidharan, Vasudevan, & Sheeba, 2011). Many researchers have shown that CO, HC and smoke opacity emissions were decreased, and NOx emissions was increased by use of biodiesel due its oxygen content (Abed et al., 2018; EL_Kassaby & Nemit_allah, 2013; Mohanraj & Mohan Kumar, 2013; Pali, Kumar, & Alhassan, 2015)

The production of biodiesel from vegetable oils is made from species such as: castor bean, soybean, cotton, sunflower, safflower, moringa, among others that have properties and energy efficiency like the mineral diesel (de Oliveira et al., 2018). Biodiesel has some negative properties such as high density and viscosity, bad cold flow properties etc. Especially, high viscosity limit the use of biodiesel as pure fuel. Previous studies have shown that some modifications such as injection pressure and time must make on engine after 20% biodiesel content.

In this study, safflower oil which can be produced with lower cost than other oil plants has been used for production of biodiesel. The obtained biodiesel has been blended different ratio with diesel fuel, and besides, it used in diesel engine as pure fuel. The results of engine performance and exhaust emission parameters obtained with use of these fuels presented.

MATERIALS AND METHODS

In the tests, a direct injection diesel engine, whose technical characteristics are given in Table 1, was used. The engine's injection pressure, injection advance, valve times were set according to values obtained from manufacturer.

Table 1. The technical properties of test engine

Test Engine	
Engine type	4-stroke, direct injection
Cylinder number	Single
Cylinder volume (cm^3)	510
Diameter × stroke (mm)	85x90
Compression rate	17.5 / 1
Maximum engine torque (Nm)	36@1400 rpm
Injector pressure (bar)	190

Biodiesel used in tests was produced from safflower seed oil with conventional transesterification method. It was blended %20 and 50% with diesel fuel as volumetric. Thus, four test fuels were occurred as D100, B20, B50 and B100. Table 2 shown some important fuel properties of test fuels.

Table 2. Important fuel properties of test fuels

Fuels / Properties	**Diesel fuel**	**B20**	**B50**	**B100**
Density (kg/m^3, at 15°C)	831.96	842.33	859.74	885.6
Viscosity (mm^2/s, at 40 °C)	2.767	3.015	3.763	4.353
LHV (MJ/kg)	45.609	42.234	41.364	38.258
Cetane index	47.89	49.14	49.88	51.17
CFPP (°C)	-18	-16.5	-15	-12

LHV: Lower Heating Value
CFPP: Cold Filter Plugging Point

Tests were conducted under four different engine load values as 25%, 50%, 75% and 100% (full load) at constant 1400 rpm engine speed which obtained of maximum engine torque value.

RESULTS AND FINDINGS

Specific fuel consumption is the amount of fuel consumed at a given time to achieve a certain power. Thermal efficiency indicates the transformation ratio of the chemical energy of the fuel burned in the combustion chamber to the mechanical energy. Therefore, both terms are very important for interpretation of performance parameters.

In Figure 1, the changes in brake specific fuel consumptions (BSFC) and thermal efficiency are shown. The main reason for the reduction up to 25.1% in BSFC values as a result of using biodiesel can be explained by the fact that biodiesel has a low calorific value than diesel fuel, which gives rise to the requirement that more fuel be consume in order to obtained the same engine power.

The content of oxygen in biodiesel has been caused an increase by 2.31% on thermal efficiency for B20 fuel compare to diesel fuel. But, brake thermal efficiency values for other test fuels used of biodiesel have been decreased by 1.28% and 3.9% respectively for B50 and B100 fuels due to rise of drop in their calorific values.

The major reason for the formation of CO emissions in internal combustion engines is the deficiency of the amount of oxygen in combustion chamber. Therefore, CO emissions for all test fuels decreased up to 32.1% with increase of biodiesel ratio in test fuels owing to approximately 10% oxygen in biodiesel. CO emission values increased depending on increase of engine load as shown in Figure 2 due to decrease of air amount entered in cylinder.

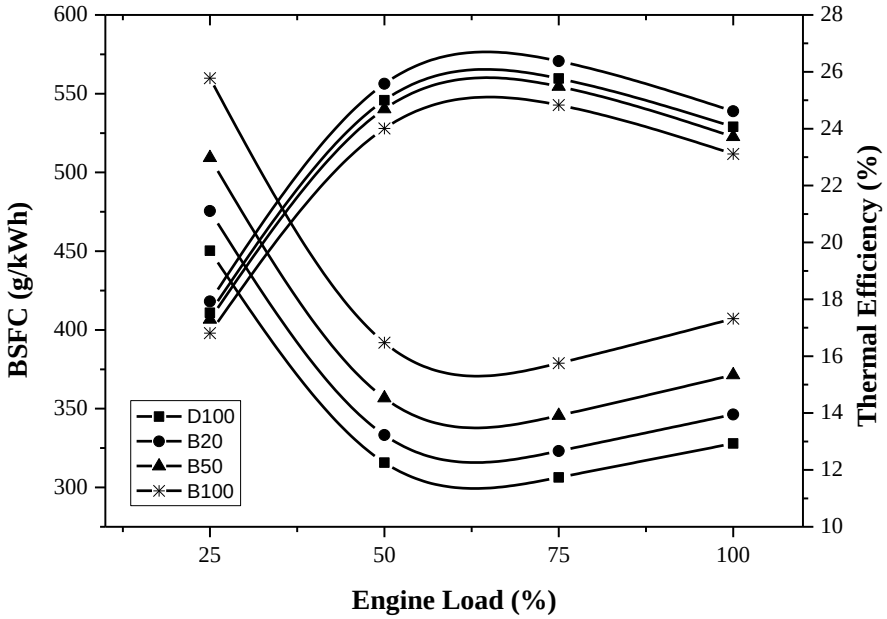

Figure 1. BSFC and thermal efficiency values of test fuels

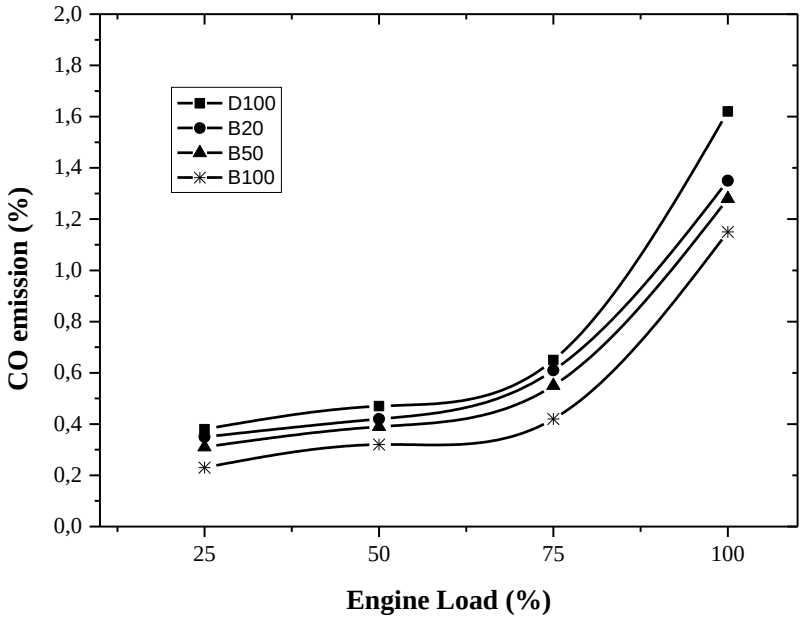

Figure 2. CO emission values of test fuels

Changes of HC and NOx emission have been shown in Figure 3. Both emission parameters are depending on temperature of end of combustion in cylinder as basic. When biodiesel decreased HC emissions up to 30.62% owing to combustion efficiency improved thanks to its oxygen content, NOx emission was increased up to 18.67% with use of biodiesel due to same reason. Because, excess oxygen caused to reaction with O atoms of more N atoms at high temperature.

Smoke opacity values with use of biodiesel fuel decreased up to 23.55% as seen in Figure 4. Because, smoke opacity is happened by rich mix. So, solid carbon particles are occurred at the zone of intensive HC fuel during combustion due to deficient oxygen. But, oxygen content of biodiesel is prevented occur of these particles owing to better combustion efficiency.

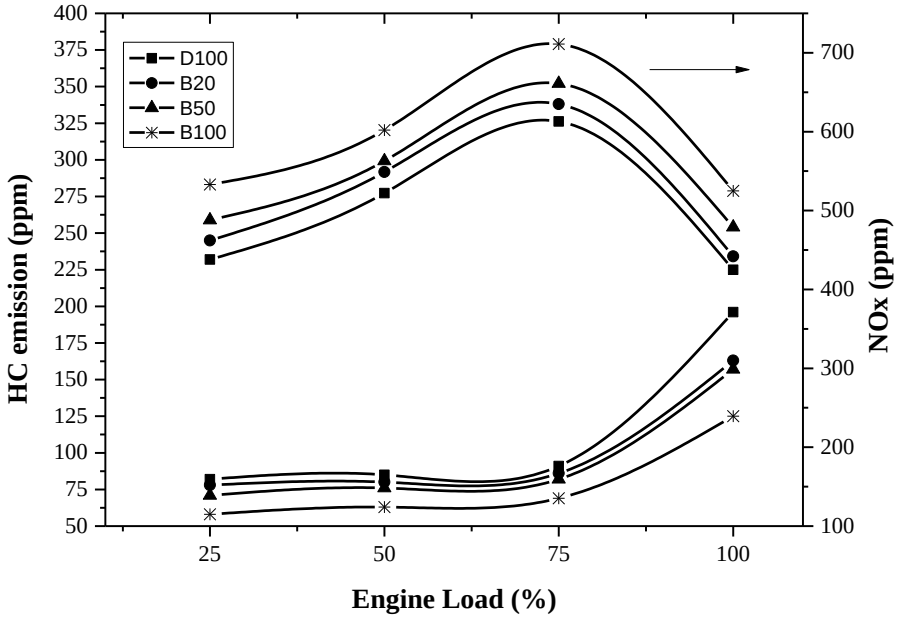

Figure 3. HC and NOx emission values of test fuels

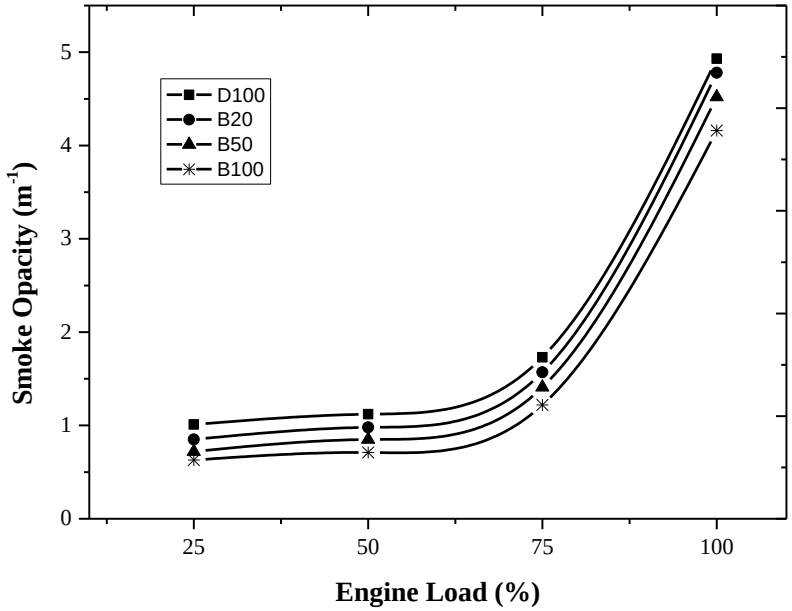

Figure 4. Smoke opacity values of test fuels

CONCLUSION

The results obtained using diesel fuel, biodiesel and their blends are as follows.

- Biodiesel decreased BSFC values due to its low calorific value.

- Although thermal efficiency of B50 and B100 fuels are lower according to diesel fuel due to their low calorific values, B20 fuel increased thermal efficiency owing to combustion improved by oxygen in fuel.
- The oxygen content of biodiesel has been caused a decrease in all exhaust emission parameters except NOx.
- Especially, B20 fuel could be used easily without any modification in diesel engines in order to it improved both exhaust emissions and thermal efficiency. But, some engine parameters such as injection pressure, injection time, injectors of different form and other changes on fuel system need to change for use of high ratio biodiesel.

REFERENCES

Abed, K., El Morsi, A., Sayed, M., El Shaib, A., & Gad, M. (2018). Effect of waste cooking-oil biodiesel on performance and exhaust emissions of a diesel engine. Egyptian Journal of Petroleum, 27, 985-989.

Alagu, K., Venu, H., Jayaraman, J., Raju, V. D., Subramani, L., Appavu, P., & Dhanasekar, S. (2019). Novel Water Hyacinth biodiesel as a potential alternative fuel for existing unmodified diesel engine: Performance, Combustion and Emission characteristics. Energy, 179, 295-305.

Asokan, M., Prabu, S. S., Bade, P. K. K., Nekkanti, V. M., & Gutta, S. S. G. (2019). Performance, combustion and emission characteristics of juliflora biodiesel fuelled DI diesel engine. Energy, 173, 883-892.

Aydın, H. (2016). Scrutinizing the combustion, performance and emissions of safflower biodiesel–kerosene fueled diesel engine used as power source for a generator. Energy Conversion and Management, 117, 400-409.

Chang, D. Y., Van Gerpen, J. H., Lee, I., Johnson, L. A., Hammond, E. G., & Marley, S. J. (1996). Fuel properties and emissions of soybean oil esters as diesel fuel. Journal of the American Oil Chemists' Society, 73(11), 1549-1555.

Channapattana, S., Kantharaj, C., Shinde, V., Pawar, A. A., & Kamble, P. G. (2015). Emissions and performance evaluation of DI CI-VCR engine fuelled with honne oil methyl ester/diesel blends. Energy Procedia, 74, 281-288.

Çelebi, Y., & Aydın, H. (2018). Investigation of the effects of butanol addition on safflower biodiesel usage as fuel in a generator diesel engine. Fuel, 222, 385-393.

de Oliveira, C. V. K., Santos, R. F., Siqueira, J. A. C., Baricatti, R. A., Lenz, N. B. G., Cruz, G. S., . . . Klajn, F. F. (2018). Chemical characterization of oil and biodiesel from four safflower genotypes. Industrial crops and products, 123, 192-196.

EL_Kassaby, M., & Nemit_allah, M. A. (2013). Studying the effect of compression ratio on an engine fueled with waste oil produced biodiesel/diesel fuel. Alexandria engineering journal, 52(1), 1-11.

Goga, G., Chauhan, B. S., Mahla, S. K., & Cho, H. M. (2019). Performance and emission characteristics of diesel engine fueled with rice bran biodiesel and n-butanol. Energy Reports, 5, 78-83.

Ilkılıç, C., Aydın, S., Behcet, R., & Aydin, H. (2011). Biodiesel from safflower oil and its application in a diesel engine. Fuel processing technology, 92(3), 356-362.
Jindal, S., Nandwana, B., Rathore, N., & Vashistha, V. (2010). Experimental investigation of the effect of compression ratio and injection pressure in a direct injection diesel engine running on Jatropha methyl ester. Applied Thermal Engineering, 30(5), 442-448.
Mohanraj, T., & Mohan Kumar, K. M. (2013). Operating characteristics of a variable compression ratio engine using esterified tamanu oil. International Journal of Green Energy, 10(3), 285-301.
Muralidharan, K., Vasudevan, D., & Sheeba, K. (2011). Performance, emission and combustion characteristics of biodiesel fuelled variable compression ratio engine. Energy, 36(8), 5385-5393.
Pali, H. S., Kumar, N., & Alhassan, Y. (2015). Performance and emission characteristics of an agricultural diesel engine fueled with blends of Sal methyl esters and diesel. Energy Conversion and Management, 90, 146-153.
Puhan, S., Vedaraman, N., Ram, B. V., Sankarnarayanan, G., & Jeychandran, K. (2005). Mahua oil (Madhuca Indica seed oil) methyl ester as biodiesel-preparation and emission characterstics. Biomass and Bioenergy, 28(1), 87-93.
Sharma, A., & Murugan, S. (2015). Potential for using a tyre pyrolysis oil-biodiesel blend in a diesel engine at different compression ratios. Energy Conversion and Management, 93, 289-297.
Shrivastava, P., Verma, T. N., & Pugazhendhi, A. (2019). An experimental evaluation of engine performance and emisssion characteristics of CI engine operated with Roselle and Karanja biodiesel. Fuel, 254, 115652.
Sidhu, M. S., Roy, M. M., & Wang, W. (2018). Glycerine emulsions of diesel-biodiesel blends and their performance and emissions in a diesel engine. Applied Energy, 230, 148-159.
Szybist, J. P., Song, J., Alam, M., & Boehman, A. L. (2007). Biodiesel combustion, emissions and emission control. Fuel processing technology, 88(7), 679-691.
Tat, M. E., Van Gerpen, J. H., Soylu, S., Canakci, M., Monyem, A., & Wormley, S. (2000). The speed of sound and isentropic bulk modulus of biodiesel at 21 C from atmospheric pressure to 35 MPa. Journal of the American Oil Chemists' Society, 77(3), 285-289.

INVESTIGATION OF ENERGY QUALITY IN FABRIC DYING FACILITIES

Ahmed KADİFECİ
University of Kahramanmaraş Sütçü İmam Granduate School of Natural and Applied Sciences Department of Electric-Electronic Engineering
akadifeci@gmail.com

ABSTRACT: The most common type of energy found in many forms on earth is electrical energy. Countries' energy consumption per capita is taken as the reference for development. The quality standards of such an important consumption item are determined by a number of internationally accepted guidelines. As a result of the advancement of technology, non-linear loads, which increase the density of use, adversely affect the quality of energy due to the semiconductor components they contain. In the textile dyeing sector, which is one of the most important parts of the textile industry, non-linear loads are used in almost every step from the beginning of the manufacturing process to the end. In this thesis, energy quality measurement of low voltage side of 4 different transformers of a fabric dyeing factory in Kahramanmaraş province is aimed to investigate the effect of the machines used on energy quality.

Key words: energy quality, harmonics, flicker, ts en 50160

KUMAŞ BOYA TESİSLERİNDE ENERJİ KALİTESİNİN İNCELENMESİ

ÖZET: Yeryüzünde birçok formda bulunan enerji türlerinden en sık kullanılanı elektrik enerjisidir. Ülkelerin gelişmişlik belirtisi olarak kişi başına düşen enerji tüketimi referans alınmaktadır. Bu kadar önemli bir tüketim kaleminin kalite standartları uluslararası arenada kabul görmüş bir takım yönergelerle belirlenmiştir. Teknolojinin ilerlemesi sonucu kullanım yoğunluğu artan lineer olmayan yükler, içerdikleri yarı iletken bileşenlerden dolayı enerji kalitesine olumsuz etki etmektedir. Tekstil endüstrisinin en önemli parçalarından biri olan kumaş boyama sektöründe ise imalat sürecinin başından sonuna kadar neredeyse her adımda lineer olmayan yükler kullanılmaktadır. Bu tezde, Kahramanmaraş ilinde faaliyet gösteren bir kumaş boya fabrikasının 4 ayrı trafosunun alçak gerilim tarafında enerji kalitesi ölçümü yapılarak kullanılan makinelerin enerji kalitesine etkisinin incelenmesi hedeflenmiştir.

Anahtar sözcükler: enerji kalitesi, harmonikler, fliker, ts en 50160.

EFFICIENCY ESTIMATION OF ENERGY GENERATING COUNTRIES WITH SOLAR POWER PLANTS BY DATA ENVELOPMENT ANALYSIS

Ufuk ALTINSOY
Department of Industrial Engineering, Engineering Faculty,
Kırıkkale University,Yahsihan, Kırıkkale,Turkey
altinsoyufuk@gmail.com

Erdem AKSAKAL
Department of Industrial Engineering, Engineering Faculty,
Atatürk University, Yakutiye Erzurum,Turkey
erdem.aksakal@atauni.edu.tr

ABSTRACT: Increasing population in the world, constantly developing technology, concerns about economic development and the reduction of fossil resources together with the increase in prices, and the damage caused to the ecological environment cause the countries to search for energy sources which may be an alternative to their primary energy resources. In this sense, solar energy, which is an unlimited source and has no harm to the ecological environment, is a strong alternative to classical energy sources. Countries that are dependent on non-renewable energy resources in energy production strengthen their investments in solar power generation. In this study, the efficiency status of the 9 countries that are considered as samples were evaluated with Data Envelopment Analysis (DEA) and the potential improvement targets were determined in order to enable ineffective countries to reach the effective level.

Keywords: Data Envelopment Analysis, Solar Energy System, Energy Efficiency, Photovoltaic Energy

GÜNEŞ ENERJİSİ SANTRALLERİ İLE ENERJİ ÜRETEN ÜLKELERİN ETKİNLİKLERİNİN VERİ ZARFLAMA ANALİZİ İLE BELİRLENMESİ

ÖZET: Dünya üzerindeki nüfusun artması, sürekli gelişen teknoloji, ekonomik kalkınma kaygıları ve bunlarla beraber fosil kaynakların azalması, fiyatlarındaki artışlar ve ekolojik çevreye verdiği zararlar ülkelerin birincil enerji kaynaklarına alternatif olabilecek enerji kaynakları aramasına neden olmaktadır. Bu anlamda sınırsız bir kaynak olan ve ekolojik çevre düzenine hiçbir zararı olmayan güneş enerjisi, klasik enerji kaynakları karşısında güçlü bir alternatif olarak karşımıza çıkmaktadır. Enerji üretiminde yenilenemeyen enerji kaynaklarına bağımlı olan ülkeler, güneş enerjisinden elektrik üretimine yönelik yatırımlarını güçlendirmektedir. Bu çalışmada, örneklem olarak ele alınan 9 ülkenin Güneş Enerji Santrallerinden (GES) enerji üretimindeki etkinlik durumları Veri Zarflama Analizi (VZA) ile değerlendirilmiş, etkin olmayan ülkelerin etkin seviyeye gelebilmeleri için potansiyel iyileştirme hedefleri belirlenmiştir.

Anahtar Kelimeler: Veri Zarflama Analizi, Güneş Enerji Sistemi, Enerji Verimliliği, Fotovoltaik Enerji

GİRİŞ

Dünya genelinde ülkelerin enerji ihtiyacının karşılanmasında yakın zamana kadar sıklıkla fosil yakıtlar ve nükleer santraller yardımıyla elde edilen enerji kullanılmaktaydı. Özellikle nükleer enerjinin ortaya çıkardığı problemler ve gelişen teknoloji ile beraber insana ve doğaya saygılı olacak yeni kaynak arayışları da ortaya çıkmıştır. Bu bağlamda ekonomik olduğu kadar kesintisiz ve temiz bir kaynak olan güneş, enerji üretiminde kullanılmaya başlamıştır. (Koç ve ark. 2018) Güneş enerjisi, kurulum ve kullanım kolaylığı olmasının yanı sıra çevreyi kirletmemesi ve zararlı atık oluşturmaması gibi özelliklere sahip bir yenilenebilir enerji kaynağıdır (T.C. Enerji ve Tabii Kaynaklar Bakanlığı). Güneş enerjisinin yenilenebilir enerji kaynaklarından biri olarak da ifade edilmesi sürekli bir kaynak olmasından ileri gelmektedir.

Gelişmiş ülkeler kadar gelişmekte olan ülkeler de güneş enerjisinden faydalanmakta ve bu fayda oranını her geçen gün daha ileriye taşıyacak şekilde çalışmalar ortaya koymaktadırlar. (Taktak ve Mehmet, 2018). Bu bağlamda evrensel olarak ele alınmaya başlanan bu enerji türü, ülkelerin ekonomik ve politik olarak dikkate alacağı bir araç halini de almıştır. Özellikle artan dünya nüfusu ile ortaya çıkan elektrik ihtiyacı güneş enerjisinin öneminin giderek artmasına sebep olmuştur. Çevremize, geleceğimize ve insanlığa zararı olmayacak şekilde enerji ihtiyacının karşılanması, yenilenebilir enerji kaynaklarından birinin kullanılması sayesinde mümkün olabilmektedir. Yenilenebilir enerji kaynaklarının kullanımı ile çevreye daha az zarar veren sonuçların elde edilmesiyle günümüz dünyasının büyük problemlerinden biri olan iklim değişikliğinin önlenmesi hususunda da önemli mesafeler kaydetmek mümkün olabilecektir.

Ülkemiz bulunduğu konum itibariyle, güneş enerjisi bakımından yüksek bir potansiyele sahiptir. Türkiye'nin güneş alma süresi sene içerisinde değişiklik gösterse de yıllık olarak yaklaşık 2 bin 741 saat (günlük ortalama 7,5 saat),olarak belirlenmiştir. Yıllık toplam gelen güneş enerjisi 1.527 kWh/m².yıl (günlük ortalama 4,18 kWh/m².gün) olduğu tespit edilmiştir. Günümüzde güneş enerjisinden çok farklı biçimlerde ve alanlarda yararlanılmaktadır. Bunlar arasında elektrik üretmek üzere güneş ışığını doğrudan elektrik enerjisine çeviren Fotovoltaik (PV) enerji sistemleri kullanılmaktadır (T.C. Enerji ve Tabii Kaynaklar Bakanlığı).

Çalışmamızda kullanacağımız yöntem olan Veri Zarflama Analizi (VZA) üretim, hizmet ve finans sektörleri gibi dinamik olan uygulama alanlarına sahiptir. Enerji konusunda literatürde VZA ile ilgili çeşitli çalışmalar bulunmaktadır. Çalışmamızın özünü oluşturan Fotovoltaik enerji sistemlerinin VZA ile beraber kullanıldığı makaleleri incelediğimizde;

Cucchiella ve Gastaldi (2014) VZA ile İtalya'daki fotovoltaik teknolojinin etkinliği, kurulu güç kapasitesi, güneş ışınımı, işletme ve yatırım yoğunluğunu girdi; enerji şiddeti ve kaçınılan CO2 miktarını çıktı olarak ele alarak değerlendirmişlerdir. Sueyoshi ve Goto (2014) Almanya ile ABD arasında hangi ülkenin daha verimli bir şekilde yenilenebilir enerji sağladığını fotovoltaik elektrik santrallerini karşılaştırarak incelemişlerdir. Mostafaeipour ve ark. (2016) Khuzestan vilayetindeki seçili 14 alanı fotovoltaik güç santrallerinin yapımı üzerine teknik-ekonomik bir fizibilite çalışmasında sıralamak için VZA, Kurumsal Karne ve Oyun Teorisi'nden oluşan bir bütünleşik yaklaşımı kullanmışlardır. Sueyoshi ve Goto (2017) çalışmalarında projeksiyon ve referans setinde benzersiz bir optimal çözüm varsayımı altında ölçeğe getiri tipinin nasıl sınıflandırılacağını VZA çerçevesinde incelemiştir. Uygulama olarak ise Amerika Birleşik Devletleri (ABD) ve Almanya'da sıklıkla "mega güneş parkları" olarak adlandırılan büyük fotovoltaik enerji santrallerindeki ölçeğe getiri tiplerinin sınıflandırmasında önerilen yaklaşımı kullanmışlardır. Villiers ve Vermeulen (2017) çalışmalarında bir fotovoltaik tesisin enerji dönüşüm performansını değerlendirmek için VZA çalışmasının sonuçlarını geleneksel yöntemlerle elde edilen sonuçlar ve yerel hava koşullarının tesis performansı üzerindeki etkilerini referans alarak incelemişlerdir. Khanjarpanah ve ark. (2018) bütünleşik bir enerji santralinin kurulması için uygun yerleşimin belirlenmesinde çift sınır ağ temelli VZA kullanan hem tek dönemli hem de çok dönemli programlamanın yapıldığı yeni bir algoritma önermişlerdir.

Bu çalışmanın amacı Güneş Enerji Santralleri (GES) ile enerji üreten ülkelerin faaliyetlerinde etkin olup olmadıklarının VZA yöntemi ile değerlendirilmesidir. Çalışmanın çıktısında etkin olmayan ülkelerin, etkin olmak için ulaşmaları gereken sınıra dair gereken iyileştirme hedefleri de belirlenmeye çalışılmıştır.

MATERYAL VE YÖNTEM

VZA, benzer girdi değişkenleri kullanarak benzer çıktı değişkenleri elde eden, birimler arasında etkinlik analizi yapan non-parametrik bir yöntemdir. VZA ile yapılan analizde karar verme birimleri, verimliliği en iyi olan etkin karar verme birimine göre kıyaslama yapılır. Fakat VZA; Farrell (1957)' in ağırlıklandırılmış çıktı değişkenlerinin ağırlıklandırılmış girdi değişkenleri ile oranlanması sonucunda yapılan performans ve etkinlik ölçümü ile ortaya çıkmıştır.
VZA yöntemiyle aynı girdi ve çıktı değişkenleri benzer olan karar verme birimlerinin etkinlik ölçümü yapılabilir. Model çözüldükten sonra KVB'den etkinlik değeri 1 olanlar etkin KVB olarak kabul edilir. Etkinlik değeri 1'in altında ise etkin olmayan KVB olarak kabul edilir. Bu aşamadan sonra etkinlik skoru 1'in altında olan KVB etkinlik değeri 1 olan KVB' ne benzetilmeye çalışılır (Banker ve Thrall, 1992). Diğer bir ifadeyle etkin olmayan KVB etkin olan KVB (referans küme) gibi etkin olabilmek için referans olarak belirlenen KVB' nin girdi ve çıktı değişkenlerinin değerlerini hedeflemesi gerekmektedir.

Bu sayede etkin olmayan KVB için potansiyel iyileştirmeler hesaplanır ve bu hesaplamalar aşağıdaki formülle yüzde olarak hesaplanabilir.
PI (%) =((Hedef Değer-Gerçekleşen Değer) / (Gerçekleşen Değer)) x 100
VZA, "girdiye yönelimli" ve "çıktı yönelimli" olmak üzere ikiye ayrılır. Bu iki model temel olarak birbirine benzer ancak girdi yönelimli VZA modelleri mevcut çıktının elde edilebilmesi için en az girdi değişkenin kullanılması gerektiğini, çıktıya yönelimli VZA modelleri ise mevcut girdi değişkeni ile maksimum ne kadar çıktı değişkeni üretilmesi gerektiğini hesaplar (Banker ve Thrall, 1992).
VZA ilk defa Charnes-Cooper-Rhodes (1978) tarafından ortaya koyulmuştur. Charnes-Cooper-Rhodes'un adlarının baş harflerinden oluşan CCR modeli ölçeğe göre sabit getiri altında KVB'lerinin etkinlik durumunu ölçmeyi hedeflemektedir. CCR modeli aşağıdaki gibi gösterilmektedir (Banker ve Thrall, 1992).

UYGULAMA

Çalışmanın amacı Güneş Enerji Santralleri(GES)'den enerji üreten ülkelerin bu kapsamda yaptıkları faaliyetleri etkin olarak yapıp yapmadıklarını ortaya koyabilmektir. Ayrıca etkin olmayan ülkelerin etkin olmayışlarının sebeplerini bularak etkin sınıra ulaşabilmeleri için iyileştirme hedefleri belirleyebilmektir.

Çalışmada Fotovoltaik enerji sistemleri ile enerji üreten 9 Avrupa ülkesi (Avusturya, Belçika, Danimarka, Finlandiya, Norveç, Portekiz, İspanya, İsveç, Türkiye) ele alınmış ve Veri Zarflama Analizi ile etkinlik analizi yapılmıştır.

Çalışmada kullanılan verilere ''Uluslararası Enerji Şirketi'' resmi internet sitesinde yayınlanmış 2018 yılı Fotovoltaik Güç Sistemleri Programı yayınından ulaşılmıştır.

Kullanılan girdi ve çıktı değişkenleri elde edilebilen, güvenilir ve doğruluk ihtimali yüksek veriler doğrultusunda, daha önceki çalışmalarda kullanım şekilleri dikkate alınarak belirlenmiştir. Kullanılan girdiler, Toplam Kurulu Güç (MW), Nüfus (Milyon), Enerji Tüketimi (TWH)'dir. Kullanılan çıktılar ise Enerji üretimi (TWH), Kişi Başına Düşen Enerji Miktarı (%), Gayri Safi Milli Hâsıla (Milyar $)'dır.

Etkinlik analizine başlamadan önce çalışma açısından önemli olabilecek değişkenin göz ardı edilmemesine ve verimlilik açısından ilişkisiz olan değişkenin çalışmaya dâhil edilmemesine dikkat edilmeye çalışılmıştır. Tablo 2'de çalışmada kullanılacak girdi ve çıktı değişkenleri gösterilmektedir.

Tablo 2: Analizde kullanılan girdi ve çıktı kümesi

Girdi Değişkenleri	**Çıktı Değişkenleri**
Toplam Kurulu Güç **(X_1)**	Enerji Üretimi **(Y_1)**

Nüfus **(X_2)**	Kişi Başına Düşen Enerji Miktarı **(Y_2)**
Enerji Tüketimi**(X_3)**	Gayri Safi Milli Hasıla **(Y_3)**

Yapılan çalışmada etkinlik ve verimlilik analizinde son dönemlerde çok sık uygulama alanı bulunan VZA yöntemi kullanılmıştır.
Model, yazılımı Huberts Virtos tarafından geliştirilmiş olan Şekil 1'de gösterilen OSDEA-GUI programı kullanılarak çözülmüştür. Kullanılan programın anlaşılması kolay bir ara yüze sahip olması, yapılan analizi daha önceki yapılanlar ile karşılaştırma imkânı sağlaması, kontrol edilemeyen belirsiz değişkenler kullanarak analiz yapabilmesi imkânın olması, sınırsız değişken ve sınırsız KVB kullanabilmesi öne çıkan özelliklerindendir.

Şekil 1: OSDEA-GUI Programı

Yapılan etkinlik analizi bazı girdi değişkenleri (güneşlenme süresi, nüfus) üzerinde kontrolün az olduğunun değerlendirilmesi ve mevcut çıktının iyileştirilmesi için en az girdinin kullanılmasını hedeflemesi sebebiyle "Çıktı Yönelimli CCR Modeli" ile gerçekleştirilmiştir.
Girdi Yönelimli CCR Sabit Getirili Modeli ile yapılan hesaplamalar neticesinde Güneş Enerjisi Santrallerinden elektrik üreten 9 Avrupa ülkesinden Avusturya, Belçika, Danimarka, Norveç, İsveç'in etkin, Finlandiya, Portekiz, İspanya, Türkiye'nin etkin olmadığı görülmüştür. Analize ait etkinlik skorları Tablo 3' te görüldüğü gibidir.

Tablo 3: Girdiye yönelimli CCR modeline göre etkinlik skorları

Karar Verme Birimi (KVB)		Etkinlik Skoru	Etkinlik Durumu
Avusturya	**(KVB_1)**	**1**	**Etkin**

Belçika	**(KVB2)1**	**Etkin**
Danimarka	**(KVB3)1**	**Etkin**
Finlandiya	**(KVB4)0.924195802**	**Etkin değil**
Norveç	**(KVB5)1**	**Etkin**
Portekiz	**(KVB6)0,741201476**	**Etkin Değil**
İspanya	**(KVB7)0,607226019**	**Etkin Değil**
İsveç	**(KVB8)1**	**Etkin**
Türkiye	**(KVB_9)0,541496966**	**Etkin Değil**

VZA'da etkin sınıra ulaşamayan KVB için etkin sınıra ulaşabilmeleri için referans kümeleri oluşturmaktadır. Referans kümelerinde bulunan etkin KVB etkin olmayan KVB için ne gibi tedbirler alınması gerektiği konusunda karar vericilere yol göstermektedir. Tablo 4'te etkinlik değeri 1'in altında olan etkin olmayan KVB için referans olabilecek etkin KVB' leri gösterilmektedir.

Tablo 4: Etkin olmayan karar verme birimleri için referans kümeleri

KVB	Refarans KVB
KVB_1	**KVB_1**
KVB_2	**KVB_2**
KVB_3	**KVB_3**
KVB_4	**KVB_3, KVB_5, KVB_8**
KVB_5	**KVB_5,**
KVB_6	**KVB_1, KVB_3, KVB_8**
KVB_7	**KVB_1, KVB_3, KVB_8**
KVB_8	**KVB_8**
KVB_9	**KVB_1, KVB_3, KVB_8**

Etkin olmayan KVB için gösterilen referans KVB'nin lambda değerleri Tablo-5'te gösterilmiştir. Lambda değerleri birden fazla referans birimine sahip etkin olmayan KVB'nin hangi referans biriminin girdi ve çıktı değerlerini hedef alarak etkin sınıra ulaşmaya çalışacağını belirtir.

Tablo 5: Etkin olmayan karar verme birimleri Lambda değerleri

KVB	KVB_1	KVB_2	KVB_3	KVB_5	KVB_8
KVB_1	1	0	0	0	0
KVB_2	0	1	0	0	0
KVB_3	0	0	1	0	0
KVB_4	0	0	0,053155332	0,614491232	0,01425787
KVB_5	0	0	0	1	0
KVB_6	0,000608698	0	0,560897089	0	0,216801225
KVB_7	0,007110234	0	5,613745876	0	0,662901072
KVB_8	0	0	0	0	1
KVB_9	0,004460523	0	3,45728485	0	0,854662926

KVB'nin referans kümesini oluşturan etkin KVB'lerine ait lambda değerleri etkin girdi ve çıktı değerlerine ulaşmak için katkı oranını ifade etmektedir. İspanya'nın referans kümesini oluşturan ülkelere ait lambda değerleri toplamı için toplam lambda değeri 6,283757182 (0,007110234+5,613745876+0,662901072) yani %63' lük etki oranına sahiptir. İspanya'nın etkin sınıra ulaşması için 3 referans kümesi vardır. Fakat Danimarka'nın etki değeri Avusturya ve İsveç'e kıyasla daha fazla olduğu görülmektedir. Bu sebeple İspanya etkin sınıra ulaşabilmek için Danimarka'yı referans alacaktır.

Etkinlik değerleri 1'in altında olan KVB'leri için yapılacak iyileştirmeler ile etkin sınıra ulaşılabilir. Bu durum VZA'nın sağladığı en önemli faydadır. Etkinlik değeri altında kalan KVB'lerinin etkin olan KVB'lerine benzemek için ulaşmaya çalıştığı hedefe potansiyel iyileştirme hedefi denir. Potansiyel iyileştirme hedef değerleri Tablo 6'da verilmiştir.

Tablo 6: Girdi ve çıktı değişkenlerine ait hedef değerler

KVB	X_1	X_2	X_3	Y_1	Y_2	Y_3
KVB_4	80	3,533966846	86	0,053155332	27,050544 8	14,06628332
KVB_6	581	5,538873061	48	1,349160831	29,681538 2	92,28164915
KVB_7	5331	40,37547809	268	14,821499255	215,735155	875,5260812
KVB_9	3427	29,33048306	228	9,233662067	156,972255	553,4988261

Finlandiya, Portekiz, İspanya, Türkiye; girdi ve çıktı değişkenlerinde Tablo 6'da gösterilen değerlere göre değişiklik yapılması halinde etkin sınıra ulaşacaktır. Örneğin

Finlandiya enerji üretimini 1,349 TWh'e yükseltirse, GSMH 29,6 Milyar $ olursa ve kişi başına düşen enerji miktarı 92,281 W/Kişi seviyesine ulaştırırsa etkin seviyeye ulaşabilir. Finlandiya'da olduğu gibi diğer etkin olmayan ülkeler de yapılacak iyileştirmelerle etkin seviyeye ulaşabilir.

SONUÇ

Çalışmada örneklem olarak ele alınan 9 ülkede (KVB) Güneş Enerjisinden PV yöntemi ile enerji elde etmeye yönelik etkinlik analizi yapılmıştır. Yapılan değerlendirme neticesinde 5 ülkenin 'ETKİN' olduğu 4 ülkenin 'etkin olmadığı' sonucuna ulaşılmıştır. Analiz neticesinde etkin olmayan ülkelerin etkin olabilmesi için gerekli olan potansiyel iyileştirme hedefleri tespit edilmiştir. Standart VZA yaklaşımında etkin sınırda yer almayan bir karar birimi ancak bütün girdiler hedef değerlere getirildiğinde etkin sınıra gelebilmektedir. Oysa bu durum gerçekte mümkün olmayabilir. Örneğin GSMH'yi arttırmak hemen yapılabilecek bir durum değildir. Buna müdahale etme olasılığı vardır ama kısa vadede elde edilebilecek bir sonuç değildir. Bu noktada VZA'nin her bir girdi ve çıktıyı odak noktası alarak gerçekleştirilen bir türü olan Ölçüt Odaklı VZA'nin gerçekleştirilmesi hedeflerin sadece bir girdiye veya çıktıya yönelik olarak belirlenmesi daha ulaşılabilir bir bakış açısı sunmaktadır.

KAYNAKLAR

Banker, R. D. ve Thrall, R. M., (1992). Estimation of returns to scale using data envelopment analysis. European Journal of Operational Research, **62**, 1, 74-84.
Charnes, A., Cooper, W. W. ve Rhodes, E., (1978). Measuring the efficiency of decision making units, European journal of operational research, **2**, 6, 429-444.
Charnes, A., Cooper, W. W. ve Rhodes, E., (1981). Evaluating program and managerial efficiency: an application of data envelopment analysis to program follow through. Management science, **27**, 6, 668-697.
Cingi, S. ve Tarım, A. (2000). Türk banka sisteminde performans ölçümü Dea-Malmquist Tfp endeksi uygulaması. Türkiye Bankalar Birliği Araştırma Tebliğleri Serisi, 1, 1-34.
Cucchiella, F., & Gastaldi, M. (2014). Data envelopment analysis to evaluate photovoltaic plants in Italy. In Advanced
Materials Research (Vol. 827, pp. 435-440). Trans Tech Publications.
De Villiers, A., & Vermeulen, H. J. (2017, June). Sector performance monitoring in utility-scale solar farms using data
envelopment analysis. In 2017 IEEE PES PowerAfrica (pp. 192-197). IEEE.
Farrell, M.J. (1957). The Measurement of Productive Efficiency. Journal of the Royal Statistical Society, **120**, 253-290.
Khanjarpanah, H., Jabbarzadeh, A., & Seyedhosseini, S. M. (2018). A novel multi-period double frontier network DEA

to sustainable location optimization of hybrid wind-photovoltaic power plant with real application. Energy
Conversion and Management, 159, 175-188.
Koç, A., Yağlı, H., Koç, Y., & Uğurlu, İ. (2018). Dünyada ve Türkiye'de Enerji Görünümünün Genel Değerlendirilmesi.
Mostafaeipour, A., Qolipour, M., & Mohammadi, K. (2016). Evaluation of installing photovoltaic plants using a hybrid
approach for Khuzestan province, Iran. Renewable and Sustainable Energy Reviews, 60, 60-74.
Sueyoshi, T., & Goto, M. (2014). Photovoltaic power stations in Germany and the United States: A comparative study by
data envelopment analysis. Energy Economics, 42, 271-288.
Sueyoshi, T., & Goto, M. (2017). Measurement of returns to scale on large photovoltaic power stations in the United
States and Germany. Energy Economics, 64, 306-320.
Taktak, F., & Mehmet, I. L. I. (2018). Güneş Enerji Santrali (GES) Geliştirme: Uşak Örneği. Geomatik, 3(1), 1-21.
T.C. Enerji ve Tabii Kaynaklar Bakanlığı - Güneş. (n.d.). Retrieved from https://www.enerji.gov.tr/tr-TR/Sayfalar/Gunes.

EXPERIMENTAL INVESTIGATION OF EFFECTS ON ENGINE PERFORMANCE AND EXHAUST EMISSION PARAMETERS OF TERNARY FUEL BLEND AS DIESEL-BIODIESEL-BUTANOL

Murat CİNİVİZ
Technology Faculty, Selcuk University, Konya, Turkey
Automotive Application and Research Center, Selcuk University, Konya, Turkey
mciniviz@selcuk.edu.tr

İlker ÖRS
Cihanbeyli Vocational School, Selcuk University, Konya, Turkey
Automotive Application and Research Center, Selcuk University, Konya, Turkey
ilker.ors@selcuk.edu.tr

Bahar SAYIN KUL
Technology Faculty, Selcuk University, Konya, Turkey
bsayin@selcuk.edu.tr

ABSTRACT: In this study, 5% isobutanol were added in 20% safflower biodiesel and 80% diesel fuel blend, and performance (brake specific fuel consumption and thermal efficiency) and exhaust emission parameters (CO, HC, NOx and smoke opacity) have been investigated in a single cylinder diesel engine. As results, isobutanol addition improved cold flow properties, effected negatively engine performance, CO and HC emissions, and it decreased NOx and smoke opacity values.

Key words: biodiesel, isobutanol, engine performance, exhaust emissions, diesel engine

INTRODUCTION

The renewables energy sector is seeing increased growth especially because of the changing governmental legislations aimed at improving energy security and curbing greenhouse gas emissions (Abbas & Ansumali, 2010). Biodiesel is a viable alternative fuel for diesel engines because it is widely available, non-toxic and renewable (Wei, Cheung, & Ning, 2018). Previous studies have demonstrated that the addition of biodiesel to diesel leads to higher fuel consumption and higher nitrogen oxides (NOx) emission, lower carbon monoxide (CO), unburnt hydrocarbon (HC) and particulate matter (PM) emissions, while there is little change in the brake thermal efficiency (BTE) (Agarwal, Gupta, & Dhar, 2017; Shahir, Jawahar, & Suresh, 2015). Biodiesel can be produced from vegetable oil (or) animal fat primarily by micro emulsions with alcohols, thermal cracking

and Transesterification with short chain alcohols in the presence of a catalyst (Prabu, Asokan, Roy, Francis, & Sreelekh, 2017). Although, nowadays, biodiesel can blend at every ratio with diesel fuel, it was presented that especially blended 20% biodiesel content can use without any modification in diesel engines (Aktaş & Şahin, 2009; Van Gerpen, Peterson, & Goering, 2007).

The alcohols are used for decrease of higher NOx emission of biodiesel and improve of its cold flow properties. Methanol (Yilmaz & Sanchez, 2012), ethanol (Krishna, Salam, Tongroon, & Chollacoop, 2019), isopropyl (Tsai et al., 2014), butanol (Hosseinzadeh-Bandbafha, Tabatabaei, Aghbashlo, Khanali, & Demirbas, 2018) and pentanol (Chen, Su, He, & Xie, 2019) are alcohols use of the most commonly. These alcohols contents C atoms respectively between 1-5 number (methanol CH_4, ethanol C_2H_6, isopropyl C_3H_8, butanol C_4H_{10} and pentanol C_5H_{12}). In general, high carbon alcohols are chooses due to better mixes with diesel engine fuels.

Goga et al. added 10 and 20% butanol in blend containing 20% rice bran biodiesel by volume at their study. As results, they presented that biodiesel increased brake specific fuel consumption (bsfc), besides, it increased further with butanol addition. Although, both biodiesel and butanol decreased CO and smoke emissions, biodiesel increased NOx emission, and butanol increased HC emission (Goga, Chauhan, Mahla, & Cho, 2019). According to Wei et al., butanol decreased NOx and smoke emissions, although it increased CO emission due to effected negatively combustion. Besides, low butanol addition was decreased HC emission but it increased with rise of butanol in blend (Wei et al., 2018). Karabektas et al. presented the effects of 5 – 20% butanol addition to the diesel fuel on the performance and emissions. They reported that the HC, CO and NOx emissions decreased by rise of the amount of butanol in blend (Karabektas & Hosoz, 2009). Kumar and Pali , butanol at 5 – 20% mixed with biodiesel produced from Jatropha by volumetric, and were tested in a DI diesel engine. The improve for engine performance and the significantly reduce for exhaust emissions due to reduced viscosity and more oxygen content in the fuels with addition of butanol (Kumar & Pali, 2016). Siwale et al. reported the effect of butanol-diesel blends on exhaust emissions in a diesel engine. As a result of their study, an important reduction in soot was observed as the ratio of butanol in the blend (Siwale et al., 2013).

In this study, %20 biodiesel from safflower oil as volumetric blended with diesel fuel. Then, 5% butanol added in this blend fuel for lower NOx emissions and kinematic viscosity. The effects on engine performance and exhaust emissions of both biodiesel and butanol investigated.

MATERIALS AND METHODS

Biodiesel was produced with conventional transesterification method from safflower seed oil. B20 test fuel was occurred with blend of 80% diesel fuel plus 20%biodiesel. The B20Bu5 ternary blend fuel was obtained with 5% isobutanol addition in this blend. Some properties of the all test fuels given in Table 1.

Table 1. Some fuel properties of test fuels

Fuels / Properties	Diesel fuel	B20	B20Bu5
Density (kg/m³, at 15°C)	831.96	842.33	839.76
Viscosity (mm²/s, at 40 °C)	2.767	3.015	3.634
LHV (MJ/kg)	45.609	42.234	41.122
Cetane index	47.89	49.14	48.55
CFPP (°C)	-18	-16.5	-17.5

LHV: Lower Heating Value
CFPP: Cold Filter Plugging Point

Tests were conducted in a single cylinder and direct injection diesel engine at four engine load (25-50-75-100%). The features of gas analyzer used during tests presented Table 2.

Table 2. The features of gas analyzer

Gases / Features	Measuring range	Precision
CO (%)	0-15	± 0.02 ppm
HC (ppm)	0-2000	± 4 ppm
NOx (ppm)	0-5000	± 25 ppm
Smoke opacity (m^{-1})	0-10	± 2% absolute

RESULTS AND FINDINGS

Figure 1 has been shown bsfc and thermal efficiency values of test fuels as engine performance parameters. B20 fuel's bsfc values is higher average 5.56% than diesel fuel due to lower LHV of biodiesel compare to diesel fuel. The bsfc values obtained with isobutanol addition increased according to B20 fuel by average 3%. However, biodiesel caused an increase of average 2.31% for thermal efficiency owing to decreased of pomp leaks due to its high density. But, isobutanol addition decreased thermal efficiency values

by average 2.9% due to its lower LHV value. Besides, its latent evaporation heat is higher than diesel fuel and biodiesel. Therefore, homogeny of fuel blend injected in combustion chamber is worse. This case caused to a decrease in combustion efficiency.

The variation of CO emission values of test fuels according to engine load has been shown in Figure 2. Biodiesel decreased CO emission by 12.5% owing to oxygen in its content. However, isobutanol increased CO emission values by 6.6% compare to B20 fuel due to its lower cetane number and higher evaporation heat.

Figure 3 has been shown NOx and HC emissions of test fuels. Biodiesel increased NOx values by 4.5% according to diesel fuel due to its oxygen content and higher exhaust gas temperature value. However, NOx emission was decreased by 2.8% with isobutanol addition owing to its lower exhaust gas temperature. The oxygen in biodiesel's content caused a decrease by 10.35% in HC emission according to diesel fuel. But, worsening combustion with isobutanol addition was increased HC emission by 2.7% compare to diesel fuel.

The oxygen content of both biodiesel and isobutanol caused a cleaner combustion. Therefore, smoke opacity values obtained with biodiesel and isobutanol addition were decreased 6.94% and 16.38% respectively according to diesel fuel as shown in Figure 4.

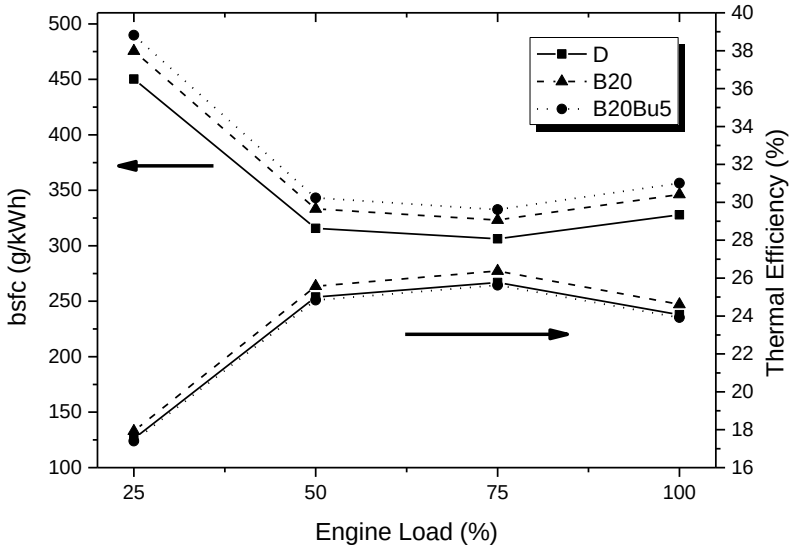

Figure 1. bsfc and thermal efficiency values of test fuels

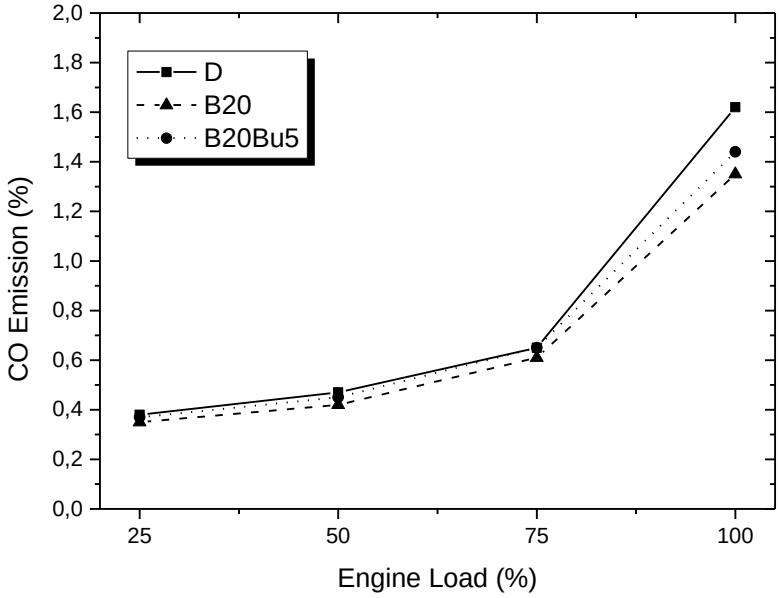

Figure 2. The variation of CO emission values of test fuels

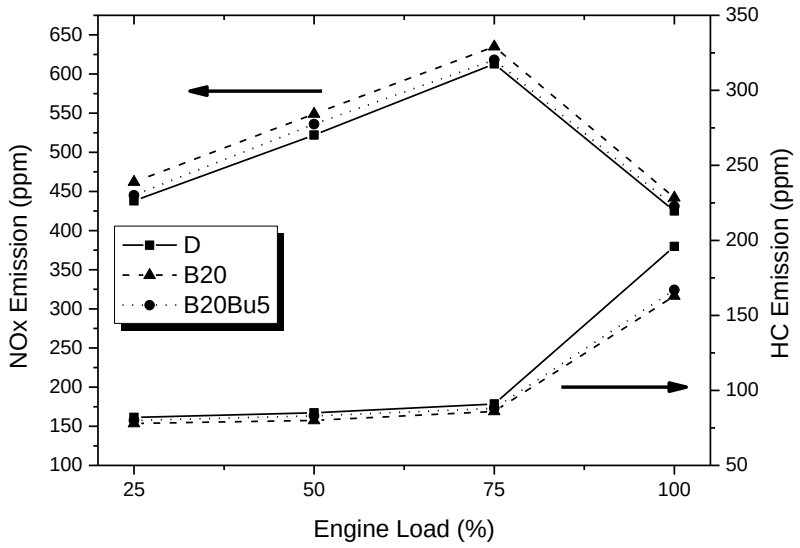

Figure 3. NOx and HC emissions values of test fuels

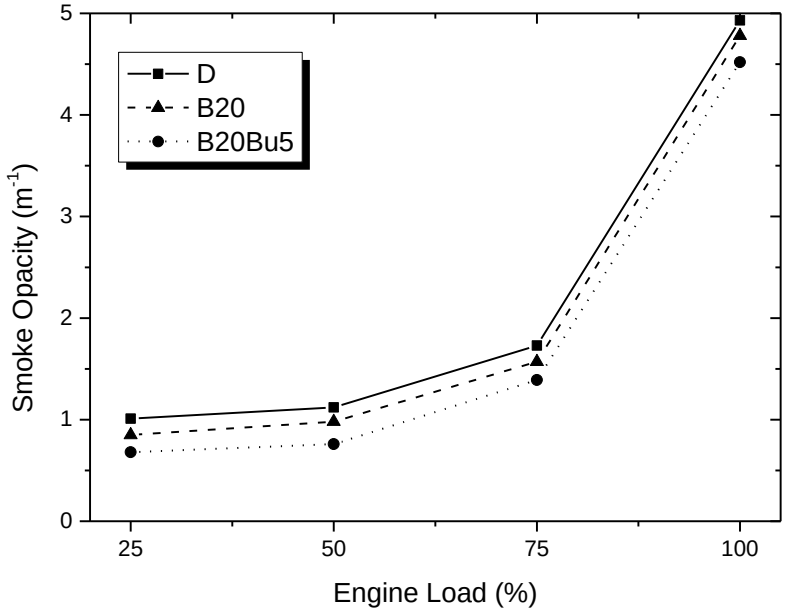

Figure 4. Smoke opacity values of test fuels

CONCLUSION

Biodiesel is an optimal alternative fuel for diesel engines. But, although biodiesel's better emission parameters according to diesel fuel, its bad cold flow properties make it difficult to use. Therefore, the addition of isobutanol as an alcohol having a high carbon atom helped to solve these problems. Although isobutanol effected performance and some emission parameters as negatively, it has been caused lower NOx and smoke opacity values. Besides, homogeny of fuel blend was provided a long time due to isobutanol has high C atom numbers.

REFERENCES

Abbas, A., & Ansumali, S. (2010). Global potential of rice husk as a renewable feedstock for ethanol biofuel production. BioEnergy Research, 3(4), 328-334.

Agarwal, A. K., Gupta, J. G., & Dhar, A. (2017). Potential and challenges for large-scale application of biodiesel in automotive sector. Progress in Energy and Combustion Science, 61, 113-149.

Aktaş, A., & Şahin, Ö. (2009). Dizel/biyodizel karışımı ile çalışan bir motorun performans ve emisyonlarını iyileştirmek için hidrojen kullanılması. Uludağ University Journal of The Faculty of Engineering, 14(1), 87-97.

Chen, H., Su, X., He, J., & Xie, B. (2019). Investigation on combustion and emission characteristics of a common rail diesel engine fueled with diesel/n-pentanol/methanol blends. Energy, 167, 297-311.

Goga, G., Chauhan, B. S., Mahla, S. K., & Cho, H. M. (2019). Performance and emission characteristics of diesel engine fueled with rice bran biodiesel and n-butanol. Energy Reports, 5, 78-83.
Hosseinzadeh-Bandbafha, H., Tabatabaei, M., Aghbashlo, M., Khanali, M., & Demirbas, A. (2018). A comprehensive review on the environmental impacts of diesel/biodiesel additives. Energy Conversion and Management, 174, 579-614.
Karabektas, M., & Hosoz, M. (2009). Performance and emission characteristics of a diesel engine using isobutanol–diesel fuel blends. Renewable energy, 34(6), 1554-1559.
Krishna, S. M., Salam, P. A., Tongroon, M., & Chollacoop, N. (2019). Performance and emission assessment of optimally blended biodiesel-diesel-ethanol in diesel engine generator. Applied Thermal Engineering, 155, 525-533.
Kumar, N., & Pali, H. S. (2016). Effects of n-Butanol Blending with Jatropha Methyl Esters on Compression Ignition Engine. Arabian Journal for Science and Engineering, 41(11), 4327-4336.
Prabu, S. S., Asokan, M., Roy, R., Francis, S., & Sreelekh, M. (2017). Performance, combustion and emission characteristics of diesel engine fuelled with waste cooking oil bio-diesel/diesel blends with additives. Energy, 122, 638-648.
Shahir, V., Jawahar, C., & Suresh, P. (2015). Comparative study of diesel and biodiesel on CI engine with emphasis to emissions—a review. Renewable and Sustainable Energy Reviews, 45, 686-697.
Siwale, L., Kristóf, L., Adam, T., Bereczky, A., Mbarawa, M., Penninger, A., & Kolesnikov, A. (2013). Combustion and emission characteristics of n-butanol/diesel fuel blend in a turbo-charged compression ignition engine. Fuel, 107, 409-418.
Tsai, J.-H., Chen, S.-J., Huang, K.-L., Lin, W.-Y., Lee, W.-J., Lin, C.-C., . . . Kuo, W.-C. (2014). Emissions from a generator fueled by blends of diesel, biodiesel, acetone, and isopropyl alcohol: Analyses of emitted PM, particulate carbon, and PAHs. Science of the total environment, 466, 195-202.
Van Gerpen, J. H., Peterson, C. L., & Goering, C. E. (2007). Biodiesel: An alternative fuel for compression ignition engines: American Society of Agricultural and Biological Engineers.
Wei, L., Cheung, C., & Ning, Z. (2018). Effects of biodiesel-ethanol and biodiesel-butanol blends on the combustion, performance and emissions of a diesel engine. Energy, 155, 957-970.
Yilmaz, N., & Sanchez, T. M. (2012). Analysis of operating a diesel engine on biodiesel-ethanol and biodiesel-methanol blends. Energy, 46(1), 126-129.

SUSTAINABLE GREEN BUILDING ASSESSMENT FOR SHOPPING MALLS

Emine Elif NEBATİ
İstanbul sabahattin zaim üniversitesi
elif.nebati@gmail.com

İsmail EKMEKÇİ
İstanbul ticaret üniversiesi
iekmekci@ticaret.edu.tr

ABSTRACT: Competition in shopping malls, which have an important place in our social life, is increasing day by day. Therefore, management must be vital and sustainable in order to achieve success in shopping malls. In particular, it is necessary to create a safe, comfortable and clean environment for visitors and tenants, monitoring of technical services, water efficiency and energy optimization should be prioritized. In the long term, sustainability has been observed to have positive effects on both investment and the environment. Green building certificates are one of the innovative and sustainable practices that have recently become widespread. It can be said that the concept of green building is emphasized especially with the definitions of sustainable and ecological buildings. It is of great importance for both today and the future that many different units, from ventilation to lighting, heating and cooling, to building automation, create sustainable and green investments in line with a common principle. It can be said that especially in recent years, green building certification systems, which are rapidly becoming widespread in the World and Turkey, it contribute positively to the environmental performance of buildings. LEED and Breeam certificates are also some of these systems. In this study, based on all these developments, the criteria for measuring the building performance of shopping centers under the name of green building are discussed. A model was proposed based on expert opinions and literature studies. The selected criteria have been taken into consideration in many national and international green building certification systems such as ÇEDBİK, LEED, BREEAM and have been developed with some changes. With the correct structuring in shopping malls, a significant contribution can be made to the sustainable success of the shopping malls, to the profitability of both tenants and investors, and to a more effective assessment of their performance.

Key words: Green buildings, Shopping malls, Performance measurement.

PID CONTROL DESIGN FOR A COOLING SYSTEM

Baris SANDAL
Istanbul University-Cerrahpasa
bsandal@istanbul.edu.tr

Yuksel HACIOGLU
Istanbul University-Cerrahpasa
yukselh@istanbul.edu.tr

Nurkan YAGIZ
Istanbul University-Cerrahpasa
nurkany@istanbul.edu.tr

ABSTRACT: The aim of this study is to introduce a PID controlled system model for heating, ventilation and air conditioning (HVAC) that works under the disruptive effect for summer cooling operations. While HVAC system models generally include several parts of the HVAC system and/or zone model, this study deals with a zone and full model of HVAC system. The indoor air temperature and relative humidity values in the zone were acquired from two calculation loops linked to each other. Mathematical models of the air handling unit (AHU) elements from mixing box to air duct, the single zone, the disturbance effect and the proportional–integral–derivative (PID) control approach, forming our HVAC system are presented. The indoor air temperature was held within acceptable limits by a PID controller via controlling the flow of cold water passing through the cooling coil. It was observed that there is no need for humidification due to high humidity in summer weather conditions. The overall system was simulated under the summer conditions of Istanbul, Turkey and the results demonstrated that the system is successful in regulating the zone temperature at the desired level.

Key words: Cooling, Dynamic Model, Disturbance, PID Controller

INTRODUCTION

While developing HVAC technologies, attention is given to many features such as being eco-friendly, reducing energy costs, delivering high efficiency and enabling comfort conditions. It is aimed at obtaining the most suitable design by making simulations in the design stage in order to reach the determined goals. The most realistic model of the identified system should be used for reliable simulation results.

Any model proposed for an element of the HVAC system is expected to give accurate results when simulated within the operating range of the entire system. Due to the nonlinear behavior of cooling coils, they are more difficult to model than other

components and are complicated enough to be used only in numerical simulations. Jin, Cai, Wang and Yao (2006) developed the model presented by Wang, Shi and Cai (2004) and proposed a simpler, dynamic cooling coil unit (CCU) model with six parameters and a broad variety of operation range. Wemhoff (2012) proposed a calibration methodology to optimize the PID coefficients to reduce the energy consumption of the system. It is observed that calibrated integral and proportional coefficients increase energy saving and derivative coefficient has negligible effect. Geng (1993) examined the performance of the tuning rules based on open-loop parameters and based on ultimate parameters in the HVAC control system with disturbances and processing time delays. Wang, Shi and Cai (2001) developed a simple and effective PID autotuner that can be applied to HVAC systems. The PID controller is designed based on gain- and phase-margin specifications, the autotuner identifies a second order plus dead time model based on two continuous relay feedback experiments. Koçal and Muğan (2017) designed a simulation in MATLAB Simulink environment for the HVAC system of the whole ship they dealt with and obtained the desired temperature and humidity conditions for the spaces by adding PID controller to the model.

In order to develop dynamic models based on mass and energy transfer of HVAC system components, it is necessary to understand in detail the physics and operating principles of the entire system. Each element that forms the HVAC system (AHU elements, zone and outdoor weather conditions) has distinct features and is usually non-linear. The operating mode and parameters (e.g. thermal, flow, structural) of each also differ. In this study, natural ventilation was added to the HVAC system model as time-varying disturbance and PID controller attempted to maintain indoor air conditions at requested intervals. This article is organized as follows: Mathematical models of HVAC system, relative humidity, disturbance effect and PID control approach are introduced, then numerical results are discussed and the concluding remarks are presented.

METHODS

The detailed dynamic mathematical model of the single zone HVAC system is given in detail, the system is exposed to disturbing effect and the temperature and relative humidity values are regulated with the PID controller. Components of the HVAC system such as PID controller, disturbing effect, zone, mixing box, circulation air fan, cooling coil, humidifier, air duct are modeled. The disturbing effect is caused by natural ventilation, opening the window at a certain time and remaining open for a certain time to the variable wind speed outdoor air. Outdoor air is very hot and humid in summer conditions, so the cooling coil is the most important component of AHU in summer operating mode, as it reduces both temperature and humidity to ensure comfort conditions. The humidifier will not activate because the humidity is high in summer operating conditions. The study contains some acceptances; it is assumed that there is no friction in the air flow, it is assumed that the air mixes completely in the zone, the outdoor conditions do not change over time, the properties of components of the HVAC system

and fluids used do not change with the temperature. The overall HVAC system used in this study is shown in Figure 1.

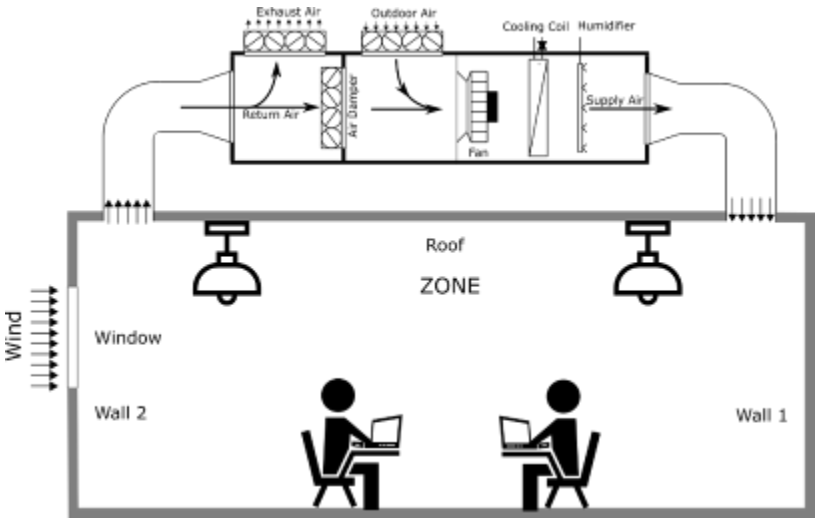

Figure 1. The Overall HVAC System

The zone model is a very significant component of the HVAC system, where this causes most of the heat and humidity loads to be encountered, and this area's comfort requirement must be encountered. Thermal loads are heat gains that transfer from boundaries (walls and roof), heat generated within the zone (individuals and equipment) and heat caused by disturbing impact. The load of humidity is created by the individuals in the area and the disturbing effect. Face-to-face walls have same thermal effects at the zone. As shown in Figure 1, East-West walls were referred as Wall 1 and North-South walls were referred as Wall 2. Energy and mass balance equations of the zone are given below (Tashtoush, Molhim and Al-Rousan, 2005).

$$C_z \frac{dT_z}{dt} = \dot{V}_a \, \rho_a \, c_{p,a} \left(T_{d,o} - T_Z\right) + 2U_{w1} \, A_{w1} \, (T_{w1} - T_z) + U_R \, A_R \, (T_R - T_z) + 2 \, U_{w2} \, A_{w2} \, (T_{w2} - T_z) + q + q_{nv} \quad (1)$$

$$C_{w1} \frac{dT_{w1}}{dt} = U_{w1} \, A_{w1} \, (T_z - T_{w1}) + U_{w1} \, A_{w1} \, (T_{out} - T_{w1}) \quad (2)$$

$$C_{w2} \frac{dT_{w2}}{dt} = U_{w2} \, A_{w2} \, (T_z - T_{w2}) + U_{w2} \, A_{w2} \, (T_{out} - T_{w2}) \quad (3)$$

$$C_R \frac{dT_R}{dt} = U_R \, A_R \, (T_z - T_R) + U_R \, A_R \, (T_{out} - T_R) \quad (4)$$

$$V_z \frac{dW_z}{dt} = \dot{V}_a \left(W_{h,o} - W_z\right) + \frac{P}{\rho_a} + d_{nv} \quad (5)$$

The zone model has been defined by three variables: T_z , $T_{w1,2}$, W_z. Equation 1. states that the rate of change of energy in the zone, Equations 2., 3. and 4. states the rate of change of energy through walls, and Equation 5. states the rate of change of humidity content in the zone.

In the mixing box, dampers adjust the mixture of outdoor air and return air, energy consumption and fresh air requirement are the fundamental criteria for determining the mixing ratio. The mixing ratio is constant in this study and the mixture occurs under adiabatic circumstances.

$$\dot{m}_{ret}\, c_{p,a}\, T_{ret} + \dot{m}_{out}\, c_{p,a}\, T_{out} = \dot{m}_{mix}\, c_{p,a}\, T_{mix,o} \quad (6)$$

$$\dot{m}_{ret} + \dot{m}_{out} = \dot{m}_{\mathrm{mix}} \quad (7)$$

$$T_{mix,o} = \frac{\dot{m}_{ret}\, T_{ret} + \dot{m}_{out}\, T_{out}}{\dot{m}_{ret} + \dot{m}_{out}} \quad (8)$$

$$W_{mix,o} = \frac{\dot{m}_{ret}\, W_{ret} + \dot{m}_{out}\, W_{out}}{\dot{m}_{ret} + \dot{m}_{out}} \quad (9)$$

Air motion throughout the system is provided by the fan. The fans are usually driven by AC electric motors and are placed together with the fan in the air stream to improve effectiveness. The heat generated on the motor side passes into the air, which was assumed that the air temperature increases by approximately 1 °C during the fan inlet and outlet.

$$T_{fan,o} = T_{mix,o} + 1 \quad (10)$$

The cooling coil is a water-to-air heat exchanger used to decrease air temperature and humidity. The cold water provided to the cooling coil is supplied at a continuous temperature by the chiller. On the air side of the cooling coil, air temperature drops below the saturation temperature and condensation occurs after this point. After this point, the air temperature is further decreases and separates as saturated air from the cooling coil. Because of this change in phase, thermal calculations are complex, and different approaches will need to be used to calculate the amount of humidity remaining in the air and condensed water. This two-phase process makes the cooling coil the most difficult component to model within the HVAC system (Jin, Cai, Wang & Yao, 2006).

$$\frac{dT_{cw,o}}{dt} + c_1 \dot{m}_{cw}\left(T_{cw,o} - T_{cw,i}\right) = \frac{c_2\, \dot{m}_a^{\ell}}{1 + c_3\left(\frac{\dot{m}_a}{\dot{m}_{cw}}\right)^{\ell}}\left(T_{cc,o} - T_{cw,o}\right) \quad (11)$$

$$\frac{dT_{cc,o}}{dt} + c_4 \dot{m}_a\left(T_{cc,o} - T_{cc,i}\right) = -\frac{c_5\, \dot{m}_a^{\ell}}{1 + c_3\left(\frac{\dot{m}_a}{\dot{m}_{cw}}\right)^{\ell}}\left(T_{cc,o} - T_{cw,o}\right) \quad (12)$$

A transient thermal model developed by Clark, Hurley and Hill (1985) for the duct unit is used.

$$\frac{dT_{d,o}}{dt} = \frac{\left(h_{d,i} + h_{d,o}\right)\dot{m}_a\, c_{p,a}}{h_{d,i}\, m_d\, c_d}\left(T_{d,i} - T_{d,o}\right) \quad (13)$$

In the summer season, it is essential to maintain humidity at certain interval in locations where the outdoor climate is humid because the relative humidity value has a major impact on the thermal comfort conditions. During the cooling operation, relative humidity is expected to be about 25%-60% to ensure comfort conditions, you need to use more power to maintain this value low. The following formulas can be used to calculate

the relationship between humidity and relative humidity in partial pressures. (Baird, 2001)

$$\varphi = \frac{p_w}{p_{ws}} \quad (14)$$

$$W = \frac{M_w}{M_{da}} = 0.62198 \frac{p_w}{p - p_w} \quad (15)$$

$$p_w = \frac{W\,p}{0.62198 + W} \quad (16)$$

$$ln\, p_{ws} = \frac{C_8}{T} + C_9 + C_{10}T + C_{11}\mathrm{T}^2 + C_{12}T^3 + C_{13}\, ln\, T \quad (17)$$

$$W_s = 0.62198 \frac{p_{ws}}{p - p_{ws}} \quad (18)$$

Although new buildings are designed windowless and glass exterior, most of the current structures have windows that open to the outdoor. Natural ventilation caused by opening the window while the zone air condition is in balance will cause the HVAC system to alter its working behavior to handle this disturbing effect. The volumetric flow rate, the heat and humidity load created by the air entering the zone can be calculated by the following relations. In the study, wind speed varies with a certain frequency. (Edwards, 2005)

$$\dot{V}_{nv} = 0.025\, A_{wdo}\, V_{wind}\, f_{wind} \quad (19)$$

$$q_{nv} = \dot{V}_{nv}\, \rho_a\, c_{p,a}(T_{out} - T_z) \quad (20)$$

$$d_{nv} = \dot{V}_{nv}\, (W_{out} - W_z) \quad (21)$$

With the development of control systems, the PID control approach has become commonly used in industrial applications. The difference between the value of the control variable and the set value, which is the required value to be realized, is taken as the error term in the closed loop control. The response of the PID control approach consists of proportion, integration and derivation components and their coefficients. The coefficients are tuned system-specific ones, and the control signal can be given as below. (Arslan, Hacioglu, Taskin & Yagiz, 2015)

$$u(t) = K_p \left(e(t) + \frac{1}{T_i} \int e(\tau) d\tau + T_d \frac{de(t)}{dt} \right) \quad (22)$$

Here the control signal is equal to the mass flow rate of cold water.

RESULTS AND FINDINGS

The values of some of the desired, initial and systemic properties used in the analyzes are given below:

- Desired indoor conditions: T_z=24 °C, ϕ=60 %
- Outdoor conditions: T_{out}=33 °C, W_{out}=0.02744 kg/kg (dry air)
- Wind conditions: V_{wind}=5 km/h, f_{wind}= 0,1 Hz

- The disturbance effect (opening of window) starts at 100th minute and lasts 2 minute.
- Volume flow rate of the supply air: $\dot{V}_a$ =0.0634 m^3/s
- The heat gains in the zone: 2 people each 0.15 kW, 2 lamps and 2 laptops total 1 kW
- The initial conditions of zone at t=0 are set to T_z (0)=T_{out} and W_z (0)=W_{out}

Figure 2 illustrates the volumetric flow rate of air entering the zone due to natural ventilation caused by opening the window at 100th minute and keeping it open for 2 minutes. This flow acts as a disturbance to the system.
The temperature of the cold water supplied to the cooling coil is constant in both controlled and uncontrolled system analysis. In the uncontrolled model, the cold water flow rate was determined using the trial and error method to bring the zone temperature to the desired level. When designing the PID controller, PID coefficients were identified in multiple trials based on the designer's expertise. In the first moments of the cooling process, it is seen that the temperature of the zone reaches the desired temperature without a controller later than the system with PID controller (Figure 3). Shortly after reaching a steady state, the system is subjected to a disturbing effect. In these moments, it was later that the uncontrolled system delivered the zone temperature to the desired level compared to the system with the PID controller. The system with the controller acted in a short time by increasing the cold water flow rate. The mass flow rate of cold water passing through the cooling coil in the systems with and without controller is shown in Figure 4.
Figure 5 shows the relative humidity of the zone for controlled and uncontrolled systems. Relative humidity is the proportion of humidity in the air to the highest amount of humidity available at that temperature. Therefore, its value is based on temperature and humidity. In summer operating conditions, humidification is not necessary as the humidity of outdoor air is usually high. When the humidity is high, it already condenses as it passes through the cooling coil, thereby reducing relative humidity and providing thermal comfort conditions. Initially, the humidity value in all points of the system is equal to the humidity of the outdoor air. No control algorithm is designed to adjust relative humidity in this study. Relative humidity values are calculated from the zone's humidity content and temperature. Relative humidity calculation begins with the start of the cooling process. The relative humidity is high owing to the high humidity at the beginning, the cooling coil condenses in a short time and approaches its normal values.

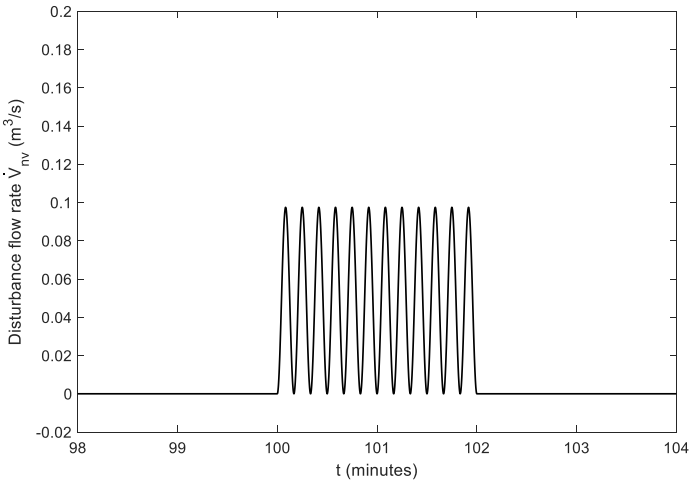

Figure 2. Volumetric Flow Rate of Naturel Ventilation to the Zone

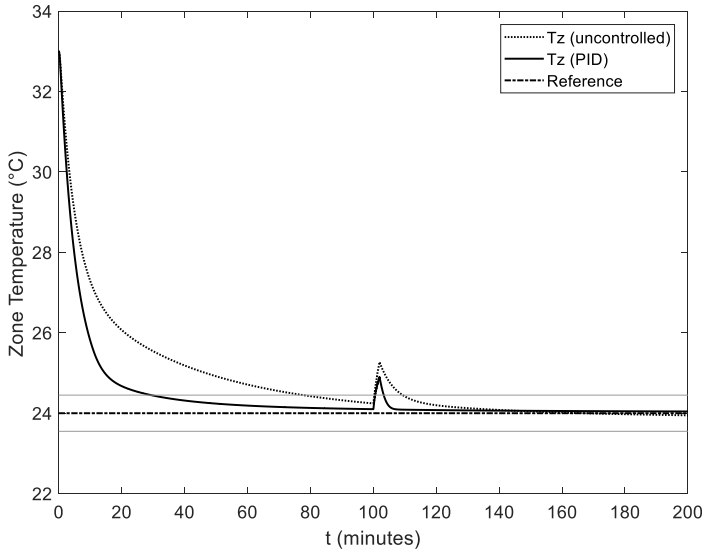

Figure 3. Zone Temperature for PID Controlled and Uncontrolled Systems

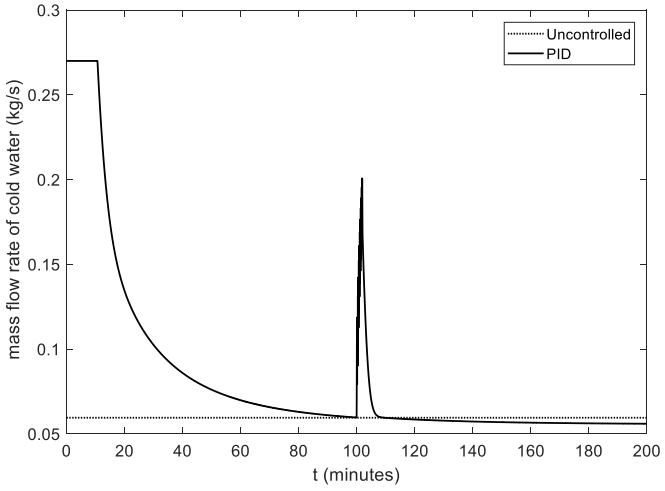

Figure 4. Mass Flow Rate of Cold Water Used by PID Controlled and Uncontrolled Systems

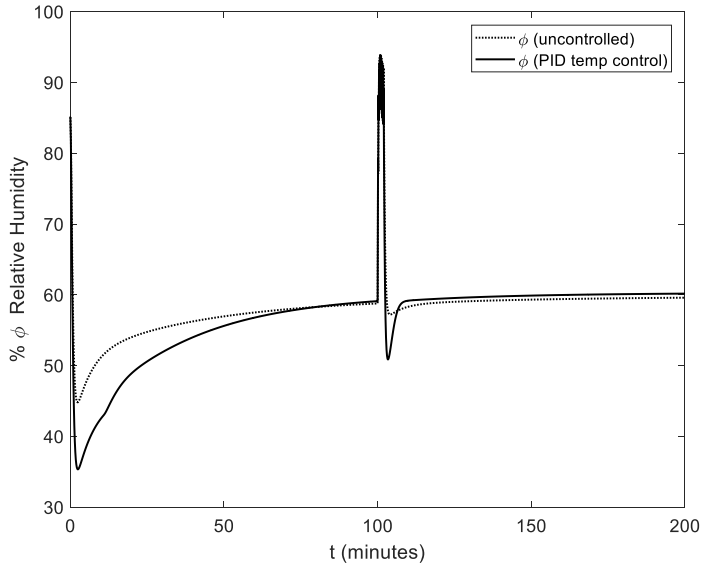

Figure 5. Relative Humidity of Zone for PID Controlled and Uncontrolled Systems

CONCLUSION

In this study, the proposed HVAC model has been subjected to disturbing effects in two systems as uncontrolled and PID controlled and various calculations have been made in summer conditions of Istanbul. The results have confirmed that the proposed HVAC model can provide a suitable platform for determining and analyzing the performance of the controllers to be used in the cooling process. When the calculation results were examined; it was observed that the disturbing effects significantly changed the temperature and relative humidity, that the system must have a controller to deal with this situation and there was no need to operate the humidifier in moist outdoor locations. Finally, it was seen that PID controller performed well in the presence of disturbance.

RECOMMENDATIONS

Due to climate change induced by global warming, the need for cooling has increased in the hotter summer months. With improvements in computer technology, we can now more easily evaluate complicated procedures such as air conditioning. In this way, efforts can be made to increase energy efficiency and thermal comfort.

REFERENCES

Arslan, Y. Z., Hacioglu, Y., Taskin, Y., & Yagiz, N. (2015). Control of a Biomimetic Robot Hand Finger: Classical, Robust, and Intelligent Approaches. In M. Habib (Ed.), Handbook of Research on Advancements in Robotics and Mechatronics (pp. 475-499). Hershey, PA: IGI Global.

Baird, J. (Ed.). (2001). ASHRAE 2001 HVAC Fundamentals Handbook. Atlanta, GA: American Society of Heating, Refrigerating, and Air-Conditioning Engineers.

Clark, D. R., Hurley, C. W., & Hill, C. R. (1985). Dynamic models for HVAC system components. ASHRAE Trans, 91(1), 737-751.

Edwards, R., (2005). Handbook of Domestic Ventilation, Elsevier Butterworth Heinemann.

Geng, G., & Geary, G. M. (1993). On performance and tuning of PID controllers in HVAC systems. Proceedings of IEEE International Conference on Control and Applications, 2, 819-824.

Jin, G., Cai, W., Wang, Y., & Yao, Y. (2006). A simple dynamic model of cooling coil unit. Energy Conversion and Management, 47(15-16), 2659-2672.

Koçal, T., & Muğan, A. (2017). PID Control of Humidity and Temperature Exchange in a Ship. Gemi Ve Deniz Teknolojisi, 22(209), 44-54. Retrieved from http://dergipark.org.tr/gdt/issue/34371/379733

Tashtoush, B., Molhim, M., & Al-Rousan, M. (2005). Dynamic model of an HVAC system for control analysis. Energy, 30(10), 1729-1745.

Wang, Y., Cai, W., Soh, Y., Li, S., Lu, L., & Xie, L. (2004). A simplified modeling of cooling coils for control and optimization of HVAC systems. Energy Conversion and Management, 45(18-19), 2915-2930.

Wang, Y., Shi, Z., & Cai, W. (2001). PID autotuner and its application in HVAC systems. Proceedings of the 2001 American Control Conference., 3, 2192-2196. Arlington, VA, USA

Wemhoff, A. (2012). Calibration of HVAC equipment PID coefficients for energy conservation. Energy and Buildings, 45, 60-66.

SUPPRESSION OF BONY STRUCTURES FROM CHEST ROENTGENS USING INDEPENDENT COMPONENT ANALYSIS

Emre ÖZER
Eskisehir Osmangazi University/Eskisehir Vocational School/Department of Motor Vehicles and Transportation Technologies
eozer@ogu.edu.tr

Semih ERGİN
Eskisehir Osmangazi University/Faculty of Engineering and Architecture/Department of Electrical and Electronics Engineering
sergin@ogu.edu.tr

ABSTRACT: Among cancer types, lung cancer is the most common type of cancer. Chest X-ray images are commonly used to detect the disease. Early detection of lung nodules increases the success of treatment. On chest X-ray images, ribs surrounding the lungs make it difficult to identify nodules. Therefore, the ribs must be suppressed. In this study, we present a technique based on Independent Component Analysis (ICA) for the suppression of ribs. Images used in the study Japanese Society of Radiological Technology (JSRT) database.

Key words: rib suppression, chest x-ray, independent component analysis, JSRT dataset

INTRODUCTION

Among cancer types, lung cancer is the most common cancer in the world and in our country and has the highest mortality rate (Arınç et al., 2005; Stewart & Wild, 2014). Nodules are small tissue masses in the lung that are seen as round, bright spots. Although not all of these masses cause cancer, they are found in cancer patients and are called malignant. Identification of nodules is important for cancer risk. Computed tomography (CT), Magnetic Resonance Imaging (MRI) or X-ray imaging can also be used in lung imaging. X-ray imaging is widely used to be economical.

Chest X-ray images include both the lungs and ribs surrounding it. Since we are interested in the lung, it is important to detect and suppress ribs in the image. Difficulties encountered in this process; the nodules are white in color similar to the bones and the parts behind the bones are difficult to detect. There are many rib suppression studies in the literature (Ahmed et al., 2007; Nguyen & Dang, 2015; Suzuki, Abe, MacMahon, & Doi, 2006). Independent component analysis method is applied to various biomedical applications such as EEG and MEG (Hyvärinen & Oja, 2000). A chest X-ray image can be

considered as a linear combination of soft tissue and bones. Starting from this point, we applied independent component analysis method to the images we preprocessed in our study and suppressed the bones. There are different types of ICA algorithm (Hyvarinen, 1999). In this study, we used fast fixed point algorithm (Fast ICA).

In this research, we apply the method (Nguyen & Dang, 2015) that presents the usage of ICA in ribs suppression. When the ribs are suppress in the image, the soft tissue remains. In this case, it saves time for radiologists and doctors and also simplifies their work.

Independent Component Analysis

This technique was presented by Aapo Hyvärinen and several different implementations of ICA can be found in the literature (Hyvärinen & Oja, 2000). Independent component analysis attempts to decompose a multivariate signal into independent signals. ICA is sometimes known as blind signal separation. It is not known both the source signals and which way they are mixed. It is an effective method for finding independent and non-Gaussian components. The basic linear mixing model can be expressed mathematically as follows;

$$\mathbf{x}=A\mathbf{s} \quad (1)$$

Where **x** is the observation vector, **s** is the source vector; A is the mixing matrix. The goal is to estimate unknown A and **s** values using the observation vector **x**. The source and the number of independent components are considered equal, so that the matrix A is found as a square matrix. After estimating the matrix A, computing its inverse, W, and obtaining the independent component by:

$$s = W x \quad (2)$$

METHODS

ICA requires multiple observation vectors as input. In our case we have only one original image. So we need to create the second image artificially. One of the images is taken from the database and the normalization process is applied and the second image is the histogram equalization image. The method used can be summarized as in Figure 1. All operations and codes are implemented in the MATLAB environment.

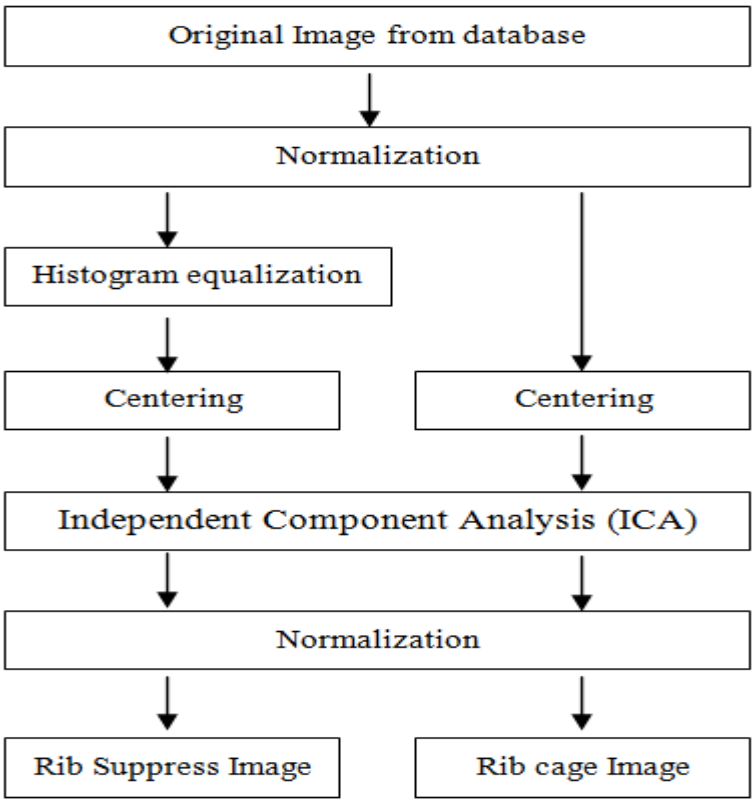

Figure 1. Method

The image used in the study was randomly selected from the JSRT database. The normalization process is a pre-processing step so the overall image was first enhanced. Histogram equalization method increases the contrast of image.

RESULTS AND FINDINGS

JSRT Database

JSRT database, 154 abnormal and 93 normal standard digital image databases with a total of 247 chest X-rays. The size of all X-ray images is 2048 x 2048 matrix size and 0.175mm pixels. The density range is 12 bits, 4096 grayscale. The database also contains information on nodule size (mm), age, sex, definitive diagnosis, degree of fineness, anatomical position of the nodule, x and y coordinates of the nodule center in the digital image, benign or malignant.

A random image is selected from the database is named as the original image. Original image is shown in Figure 2.

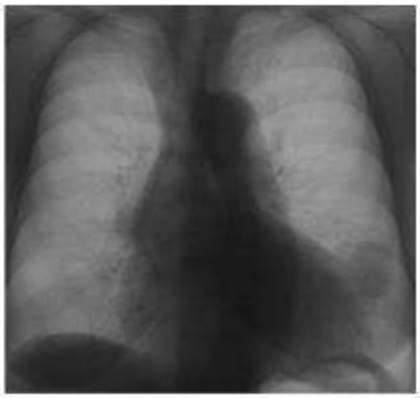

Figure 2. Original Image

Normalization method was applied to improve overall image contrast and to strengthen the edges. This is local normalization, which makes the image a zero average and a unit variable. Figure 3. shows the image after normalization.

Figure 3. Normalization Applied Image

Histogram equalization was used to obtain at least one non-Gaussian signal and to increase the image construction. Figure 4. shows the histogram equalization image.

Figure 4. Histogram Equalization Applied Image

Images from two channels were one by one centralized. The next step is independent component analysis. Each image was transformed into a vector when applying ICA.

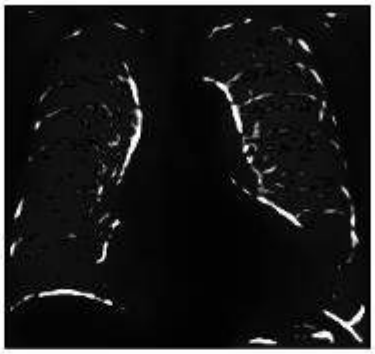

Figure 5. Rib cage Image After Rib Suppression Process

Figure 6. The Lung Roentgen Image After Rib Suppression Process

After ICA, normalization was performed to the images. The image of the ribs is shown in Figure 5. and the image of rib suppress is shown in Figure 6.As shown in Figure 6. the ribs are successfully suppressed.

CONCLUSION

ICA is the available method for rib suppression. In the method we used, there was no reduction in the image size, so there was no loss of information in the image. We can apply Fast ICA so that the data was initially made zero mean and whitened. Histogram equalization ensures at least one non-gauss source, one of the main ideas of the ICA method, and also convergence of ICA. Normalization applied after Independent Component Analysis makes the suppression more clear. In the future, it is aimed to detect the disease due to nodule detection using suppressed images of the bones.

REFERENCES

Ahmed, B., Rasheed, T., Khan, M. A., Cho, S. J., Lee, S., & Kim, T.-S. (2007). Rib suppression for enhancing frontal chest radiographs using independent component analysis. Paper presented at the International Conference on Adaptive and Natural Computing Algorithms.
Arınç, S., Özvaran, M. K., Güngör, N., Çelik, O., Soğukpınar, Ö., Çolak, F., & Baran, R. (2005). Hastanemizde tanı alan akciğer kanserli olguların epidemiyolojik ve histolojik özellikleri. Turkiye Klinikleri Archives of Lung, 6(4), 149-152.
Hyvarinen, A. (1999). Survey on independent component analysis. Neural computing surveys, 2(4), 94-128.
Hyvärinen, A., & Oja, E. (2000). Independent component analysis: algorithms and applications. Neural networks, 13(4-5), 411-430.
Nguyen, H. X., & Dang, T. T. (2015). Ribs suppression in chest x-ray images by using ICA method. Paper presented at the 5th International Conference on Biomedical Engineering in Vietnam.
Stewart, B., & Wild, C. P. (2014). World cancer report 2014.
Suzuki, K., Abe, H., MacMahon, H., & Doi, K. (2006). Image-processing technique for suppressing ribs in chest radiographs by means of massive training artificial neural network (MTANN). IEEE Transactions on medical imaging, 25(4), 406-416.

DIELECTRIC CHARACTERIZATION OF ORGANIC LIQUIDS UNDER CONFINEMENT: A STUDY OF ACETONITRILE

Adil Nadir KAPLANSEREN
Pamukkale University
akaplanseren09@posta.pau.edu.tr

Can TUNCER
Pamukkale University
ctuncer11@posta.pau.edu.tr

Mehmet ORHAN
Pamukkale University
morhan@pau.edu.tr

Tahir CAGIN
Texas A&M University
tcagin@tamu.edu

ABSTRACT: Use of organic liquids, such as Acetonitrile, in electrolyte solutions of supercapacitors are common due to low viscosities. In such applications, nanostructured surfaces enable high surface area to volume ratio in favor of capacitance as well. Therefore, effect of confinement on dielectric properties of acetonitrile is investigated numerically. For this purpose, Single Walled Carbon Nanotubes (SWCNTs) were filled with the acetonitrile by employing the isothermal-isobaric ensemble followed by canonical ensemble molecular dynamics simulations for investigating interactions between the acetonitrile and SWCNTs. Several interesting features of the acetonitrile were identified as the diameter of CNTs becomes smaller. First of all, two distinct regions were identified i.e., a core region along the longitudinal direction dominated by rarefaction effects and an interface region with relatively high density of fluid. Secondly, a preferred coordination between each pair of the C (methyl group carbon), C (nitrile group carbon) and N atoms and an ordering in the vicinity of wall are observed contrary to those of larger tubes. Last but not least, enhancement in the volume of the rarefied core in cooperation with anti-parallel dipole alignment encouraged by interface effects leads to decrease in dielectric constant considerably.

Key words: Acetonitrile, SWCNT, Molecular Dynamics, Dielectric relaxation

INTRODUCTION

Despite both theoretical and experimental studies about dielectric phenomenon of neat Acetonitrile and its mixtures are available for a long time, the microscopic point of view about its behavior under confinement is not well understood if one considers its usage in electrolyte solutions in favor of lower viscosity. Uniform translational diffusion, relatively high dielectric permittivity and conductivity of the acetonitrile are other advantages for capacitors applications [1, 2, 3]. The use of less viscous organic solvents with ionic liquids promotes penetration in nano pores, which greatly enhances the operating voltage, the energy density and higher rate scalability of the capacitor [4, 5, 6, 7, 8]. Lithium perchlorate in acetonitrile enabling obstruction free nano pores [9], hybrid capacitors operating high temperatures with high cycle performance [10, 11] and nano porous carbons in an electrolyte containing acetonitrile showing good performance under extreme conditions [12] are some applications pointing out importance of acetonitrile in such a fast developing technology of supercapacitors.

Although there are wide range of interests for Acetonitrile, studies investigating its dielectric behavior in molecular scale is rather limited. Recently, in reference [13], short time behavior of Acetonitrile is determined by libration of molecules and, with a larger time, the molecular motion is influenced by rotational diffusion. Investigating the capability and accuracy of some proposed models compared with the experiments [14, 15, 16, 17], structure organization of ACN and ionic liquid mixtures in nanoscale [18], dielectric relaxation of mixtures including ACN [19, 20, 21] are some studies appeared in last two decades.

Although we could not address all studies concerning with the role of ACN in electrolyte mixtures and its interaction with nano-structured electrodes, use ACN in reducing the viscosity of electrolytes seems to be significant. To the author's knowledge, there is no study addressing dielectric relaxation phenomena in confinement. These are the reasons why this study aims to investigate dielectric properties and structural organization ACN in SWCNTs. The second part of our study is organized as follows. After briefly mentioning computational methodology in the next section, dielectric properties are given each separate section followed by a conclusion.

MODELING AND COMPUTATIONAL METHODOLOGY

Acetonitrile was represented by a six-site model which is composed of three methyl hydrogen atoms (H), a methyl carbon atom (C1), a nitrile carbon atom (C2), and a nitrogen atom (N). Forces acting on each atom were determined by considering intra and intermolecular potentials. Intramolecular force constants and geometry parameters of the ACN were adopted from DREIDING/A force field with some revisions [22]. Pairwise interaction was taken account for the computation of intermolecular potentials. Both intra and intermolecular force field parameters are given in Table 1.

Intramolecular forces acting each atom of carbon nanotube was calculated using the many-body Tersoff Potential [23]. All simulations were carried on the large scale atomic/molecular massively parallel simulator LAMMPS [24]. Simulations were

performed in two stages. In the first stage of the simulations, armchair Single-Walled Carbon NanoTubes (SWCNTs) with five different diameters were filled with ACN. In the second stage, systems of ACN filled SWCNTs were simulated. According to type of mentioned stages the following computational strategies were employed. Details of resulting ACN-CNT systems and densities were tabulated in Table 2.

Table 1. Force Field Parameters For Acetonitrile

Harmonic Bond Stretch Parameters	**r_{eq} (Å)**	**k_{ij} ((kcal/mol)/Å²)**
H-C1	1.090	665.0
C1-C2	1.450	700.0
C2-N	1.192	2500.0
Harmonic angle bend parameters	**θ_{eq} (deg)**	**k_{ij} ((kcal/mol)/rad²)**
H-C1-H	109.471	100.0
H-C1-C2	109.471	100.0
C1-C2-N	180.000	55.0
Lennard-Jones parameters	**ϵ (kcal/mol)**	**σ (Å)**
C1	0.0950	3.457
C2	0.0950	3.457
H	0.0152	2.2147
N	0.1490	3.292

Table 2: Geometries Of Systems And Densities Of Confined ACN

System	**System Dimensions (Å)**	**Number of ACN Molecules**	**Density of ACN (kg/m3)**
Bulk ACN	50.88 x 50.88 x 50.88	1500	777.0
ACN + CNT (10,10)	d = 13.55, l = 98,38	576	460.61
ACN + CNT (15,15)	d = 20.33, l = 98,38	1620	575.77
ACN + CNT (20,20)	d = 27.11, l = 98,38	3204	640.54
ACN + CNT (25,25)	d = 33.89, l = 98,38	5088	650.98
ACN + CNT (30,30)	d = 40.67, l = 98,38	7644	679.18

Simulations of ACN Inside CNT

CNTs were located on a rectangular parallelepiped box where periodic boundary conditions were imposed in each direction. The longitudinal length of the box was set to 98.38 Å so that interactions of ACN molecules with surround are taken place just on each open ends of CNTs. Simulation procedure for ACNCNT couple is the same as that of filling process with some exceptions. Systems were well equilibrated over 300 ps after the temperature was set to 298 K within 60 ps, and then data were collected in every 5 fs and over 110 ps and 300 ps velocities and positions of ACN molecules respectively. Molecular strain rate 100 tensors were recorded in every 0.5 fs over 1.5 ns while center of mass velocity of CNT was removed in every 150 fs. In the proceeding sections, structure, dynamic and transport properties of ACN will be exhibited systematically.

RESULTS AND FINDINGS

Dielectric Relaxation

In this section, the authors will discuss dielectric phenomenon of the ACN under confinement. For this purpose, the system is assumed to be an isotropic, polarizable, homogeneous and continuous media. Furthermore, an external and frequency dependent electric field, **E** (ω), is acting on it. Now, electric displacement vector can be written as the sum of externally acting electric field and polarization field - i.e.

$$\mathbf{D}(\omega) = \epsilon_0 \mathbf{E}(\omega) + \mathbf{P}(\omega) \quad (1)$$

where ϵ_0 stands for dielectric constant of vacuum. If the dielectric properties of the system are assumed to be linear and isotropic, the polarization, **P**, is proportional to the electric field, **E**, and given by

$$\mathbf{P}(\omega) = \epsilon_0 \chi(\omega) \mathbf{E}(\omega) \quad (2)$$

where $\chi(\omega)$ denotes the frequency dependent dielectric susceptibility. Substituting Eqn 2 into Eqn 1 leads to

$$\mathbf{D}(\omega) = \epsilon_0 (1+ \chi(\omega)) \mathbf{E}(\omega) = \epsilon_0 \epsilon \mathbf{E}(\omega) = \epsilon_\alpha(\omega) \mathbf{E}(\omega) \quad (3)$$

$$\epsilon(\omega) = \frac{\epsilon_\alpha(\omega)}{\epsilon_0} \quad (4)$$

where $\epsilon_\alpha(\omega)$ and $\epsilon(\omega)$ are called complex absolute permittivity and complex relative permittivity of the system respectively. The complex relative permittivity is written simply

$$\epsilon(\omega) = 1 + \chi(\omega) \quad (5)$$

whose real and imaginary parts, $\epsilon(\omega) = \epsilon'(\omega) - i\,\epsilon''(\omega)$, correspond to the relative permittivity and the dielectric loss of the system respectively.

Dense system approach

In the first case, when one considers the system as a general case that a system is dense and each dipole moment is correlated with each other, then the system is assumed to exhibit a collective dynamics in which there is a dipole-dipole interaction among the molecules. With application of linear response theory for equilibrium, the electric susceptibility in 3D is given by

$$\chi(\omega) = \frac{1}{3k_BT}\frac{\langle \boldsymbol{M}(0)\cdot\boldsymbol{M}(0)\rangle}{V\epsilon_0}\mathcal{L}_{i\omega}\{-\dot{\Phi}\} \quad (6)$$

where the operator $\mathcal{L}_{i\omega}$ stands for Fourier-Laplace transform, i.e.

$$\mathcal{L}_{i\omega}\{-\dot{\Phi}\} = \int_0^\infty e^{-i\omega t}\left(\frac{-d\Phi(t)}{dt}\right)dt \quad (7)$$

and **M**(t) is vectorial sum of dipole moments of constituent molecules at time t. k_B and T stand for Boltzmann constant and thermodynamic temperature respectively. V is the volume enclosed by CNTs. In this case, the correlation function is treated as

$$\Phi(t) = \frac{\langle \boldsymbol{M}(0)\cdot\boldsymbol{M}(t)\rangle}{\langle \boldsymbol{M}(0)\cdot\boldsymbol{M}(0)\rangle} \quad (8)$$

In Eq. 8, the system is assumed to be a dense system where all interactions among the molecules have been taken account. Thus, Eq. 6 leads to a solution, complex permittivity, that interaction of the dipole moment of each molecule is correlated with other molecules.

Dilute system approach

In the second case, cross terms between the dipole moments on different molecules are vanished and the system is assumed to be a dilute system in which the dynamics of each dipole moment is independent from the others. In such case, the correlation function is expressed in terms of orientation of the dipole moment of each molecule
such that

$$\Phi(t) = \frac{\langle \sum_{i=1}^{Nm}\boldsymbol{u}_i(0)\cdot\boldsymbol{u}_i(t)\rangle}{\langle \sum_{i=1}^{Nm}\boldsymbol{u}_i(0)\cdot\boldsymbol{u}_i(0)\rangle} \quad (9)$$

followed by the electric susceptibility

$$\chi(\omega) = \frac{1}{3k_BT}\frac{\langle \sum_{i=1}^{Nm}\boldsymbol{u}_i(0)\cdot\boldsymbol{u}_i(0)\rangle}{V\epsilon_0}\mathcal{L}_{i\omega}\{-\dot{\Phi}\} \quad (10)$$

Where N_m and **u** are the number of the molecules in the system and the dipole moment of each molecule respectively.

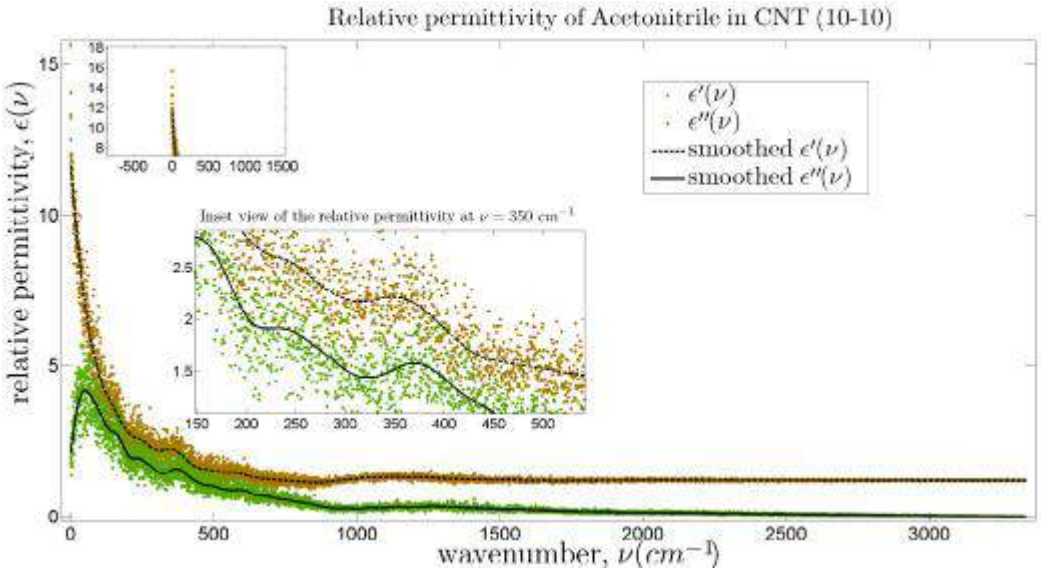

Figure 1: Dielectric Constant As A Function Of Correlation Time. The Line Shape Is A Smoothed Curve Of Its Relatively Noisy Counterpart. There Are Some Local Maxima Affected by Mode Frequencies of The ACN.

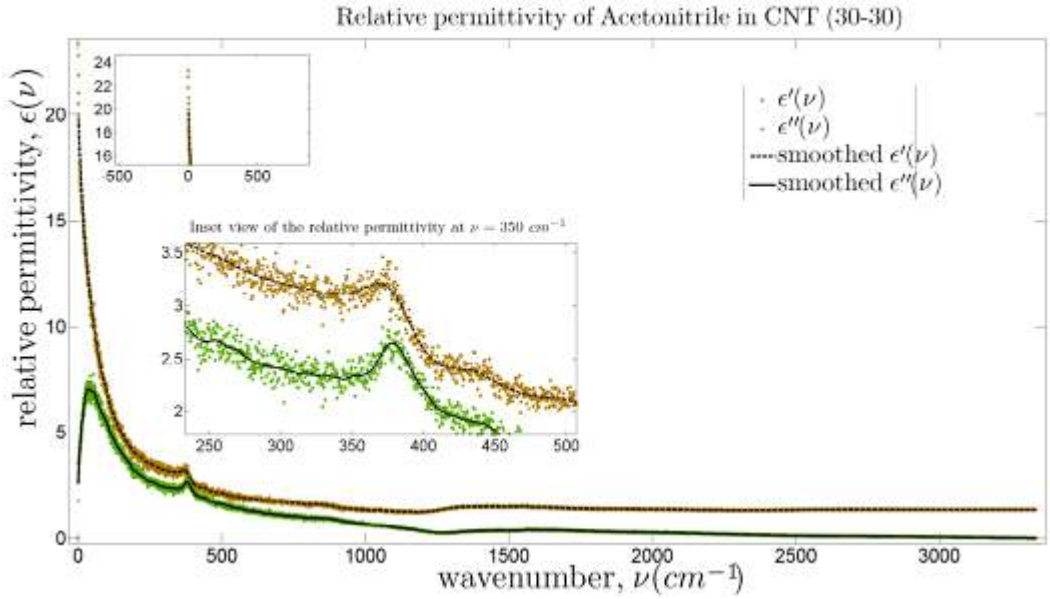

Figure 2: Dielectric Constant As A Function Of Correlation Time.

Table 3: Dielectric Constants Obtained From Fourier-Laplace Analyses

	(10-10)	**(15-15)**	**(20-20)**	**(25-25)**	**(30-30)**	**Bulk(Calculated)**
Interacting Molecules	13.49	16.01	16.70	17.62	17.67	30.30

Non-interacting Molecules	16.23	19.81	21.79	22.01	22.92	38.00

The dielectric permeability and loss for the non-interacting approximation of the ACN molecules inside the smallest and largest tubes are shown in Fig. 1 and 2 respectively. In both cases, the permeability diminishes monotonically while the dielectric loss of each case becomes maximum in a certain frequency. The permeability decreases sharply in a fairly small frequency increment where the maximum loss occurs. A strong sensitivity of the dielectric constant on the C1-C2-N bending (e-symmetry) was observed in both tubes. Other modes that affect the relaxation phenomenon were C1-H bending (e-symmetry) and C1-C2 stretching (a_1-symmetry) modes. Our results show that, a remarkable decrease in static dielectric constant of ACN, $\epsilon(0)$, is observed as compared with the bulk state. The dielectric constant computed for the CNT (10-10) is 29.18 % smaller than that of the largest tube. Size dependent variation of dielectric constant under the assumptions of interacting and non-interacting molecules is summarized in Table 3.

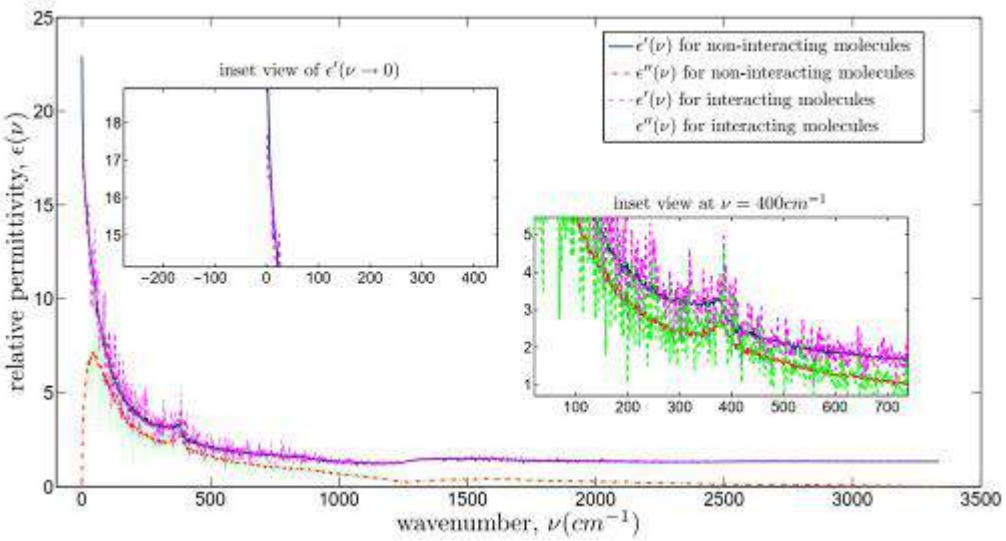

Figure 3: A Comparison Of The Dielectric Relaxations Resulting From Approximations Of Interacting And Non-interacting Molecules Inside CNT (30-30).

In order to make clear why such increase in dielectric constant was observed with increasing diameters of tubes, Kirkwood correlation factor, g factor, was introduced;

$$g = \sum_{i=1}^{N_m} \langle cos\ \theta ij \rangle \quad (8)$$

Where θ_{ij} denotes the angle between the orientations of the i^{th} and the j^{th} dipole. The calculated correlation factor for increasing radii in each CNT is shown in Fig. 4. At first glance, it can be observed that there is no correlation between the i^{th} molecule and the others within the first half of the radius of the CNT (10-10). This is due to strong rarefaction effects observed in the core of this CNT.

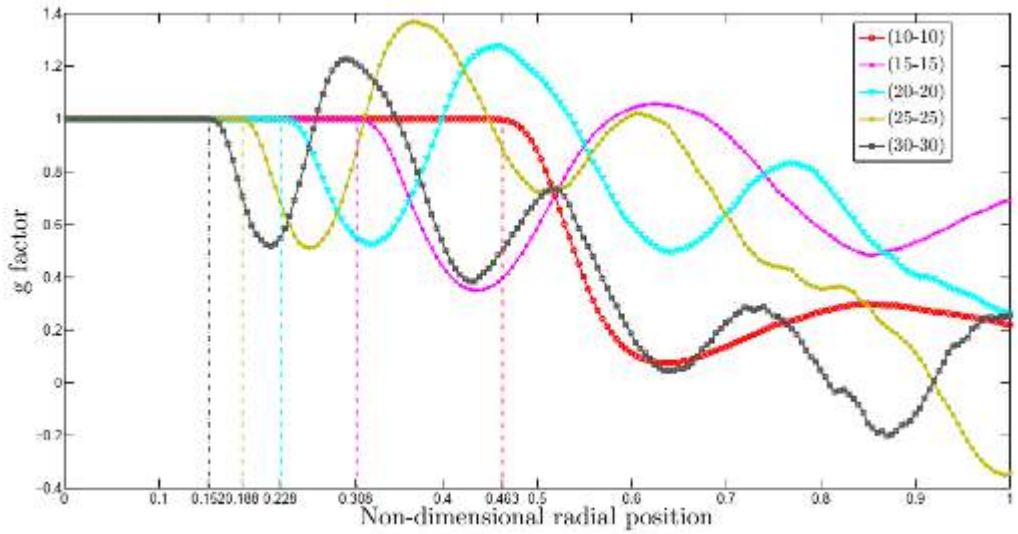

Figure 4: Radial Variation Of Kirkwood Correlation Factor Calculated From The Eq. 5. Note That The Radius Of Each CNT Is Set To Unity. Coloured Lines Denote The Radius Of Rarefaction That Observed In The Core Region Of The Tubes.

This region wherein rarefaction effects are observed becomes smaller with increasing sizes of CNTs. Beyond this critical radius, correlations starts to develop and can be represented as continuous functions. The molecules tend to direct themselves in opposite direction in the vicinity of the wall. In other words, there is an antiparallel orientation just on the region of fluid-wall interface of each CNT, which is rather limited for the CNT (15-15). It is very clear that the coupled dynamics of both rarefaction and the confinement effect decreases the dielectric constant enormously. Although the confinement in a smaller CNT encourages self-organized and directed dipoles in the direction free to move, in the axial direction for cylindrical structures, a dominant rarefaction effect tries to align rather limited number of molecules opposite to those of surface region. We believe that the main reason for sharp drops in dielectric constant is increasing fractional volume of rarefaction with smaller sizes of the CNTs.

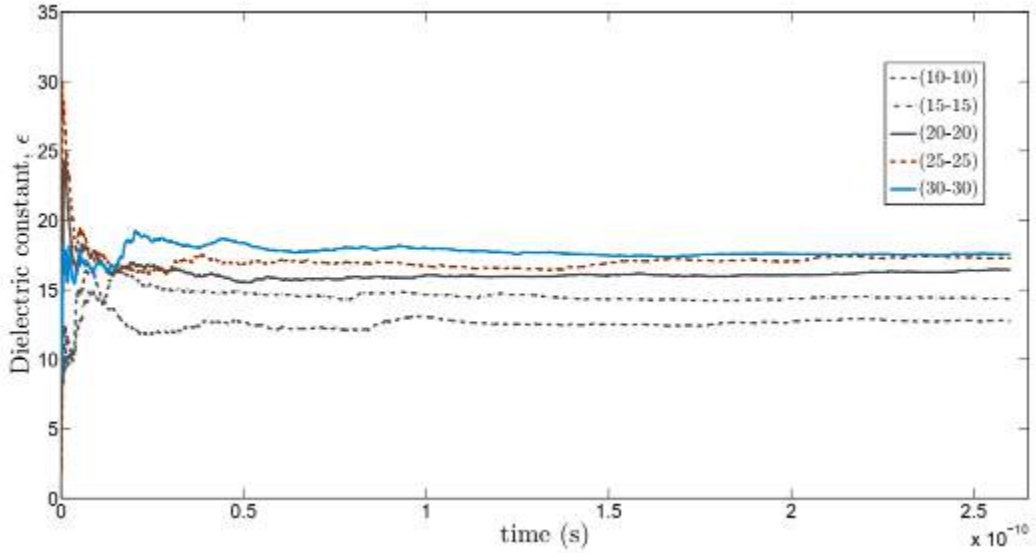

Figure 5: Dielectric Constant Obtained From The Fluctuation Formula.

Table 4: Inertial and Relaxation Times For The Liquid Acetonitrile. Biexponential Function Was Utilized For The Fitting The Correlation Functions.

	A	τ_m (s)		B	τ_n (s)		Debye relaxation time (s) $\langle\tau\rangle = \frac{A\tau_m^2+B\tau_n^2}{A\tau_m+B\tau_n}$
CNT(10-10),(R^2 = 0.9698)	0.8750	$5.078\ 10^{-13}$	x	0.1250	$2.030\ 10^{-11}$	x	1.735×10^{-11}
CNT(15-15),(R^2 = 0.9597)	0.9577	$3.181\ 10^{-13}$	x	0.0423	$2.072\ 10^{-11}$	x	1.545×10^{-11}
CNT(20-20),(R^2 = 0.9893)	0.9603	$3.481\ 10^{-13}$	x	0.0397	$2.589\ 10^{-11}$	x	1.962×10^{-11}
CNT(25-25),(R^2 = 0.9937)	0.9790	$3.829\ 10^{-13}$	x	0.0210	$3.463\ 10^{-11}$	x	2.298×10^{-11}
CNT(30-30),(R^2 = 0.9924)	0.9775	$3.283\ 10^{-13}$	x	0.0225	$2.480\ 10^{-11}$	x	1.586×10^{-11}
Bulk (calculated)	0.7100	$1.077\ 10^{-13}$	x	0.2900	$2.110\ 10^{-12}$	x	1.900×10^{-12}

Furthermore, calculated Debye relaxation times for each system are approximately an order of magnitude greater than the bulk value (see Table 4 for calculated results). From Table 4, it can be realized that the computed dipole time correlation function data noticeably deviate from the bulk Debye relaxation behavior. Although the faster component of dielectric relaxation τ_m is smaller than τ_n, the coefficient of the faster component, the coefficient a, seems to manage relaxation phenomena. The calculated time evolution of the dipole correlation function showed that the diffusive and slower response is missed in the initial phase of the time evolution. Although the mean

relaxation time is two order of magnitude more than the inertial component, τ_m, the dynamics of the system is dominated by the rotational diffusion of molecules and inertial effects which are taken place in a short time. In addition to the relaxation time, molecular reorientation dynamics in acetonitrile was analyzed through the time correlation function

$$C_l(t) = \langle P_l\,(\bar{u}(0)\cdot\,\bar{u}(t))\,\rangle \qquad (6)$$

where P_l represents l_{th} Legendre polynomial and $\bar{u}(t) = u(t) / u(t)$ is the unit vector of the dipole moment. The correlation functions associated with the Legendre polynomials are

$$C_1\,(t) = \langle \cos\theta\,(t)\rangle \qquad (7)$$

$$C_2 = \frac{1}{2}\cdot\langle 3\cdot cos^2\,\theta(t) - 1\rangle \qquad (8)$$

where $\cos\theta(t) = \bar{u}(t)\cdot\bar{u}(0)$. The fitting coefficients and corresponding times were tabulated in Table 5 and 6.

Table 5: l=1.

	A	**τ_m (s)**	**B**	**τ_n (s)**	**Debye relaxation time (s) $\langle\tau\rangle = \frac{A\tau_m^2+B\tau_n^2}{A\tau_m+B\tau_n}$**
CNT (10-10) (R^2 =0.9821)	0.6608	8.216×10^{-12}	0.3392	4.220×10^{-11}	3.285×10^{-11}
CNT (15-15) (R^2 =0.9940)	0.7316	7.490×10^{-12}	0.2684	2.910×10^{-11}	2.019×10^{-11}
CNT (20-20) (R^2 =0.9858)	0.8604	6.675×10^{-12}	0.1396	4.093×10^{-11}	2.375×10^{-11}
CNT (25-25) (R^2 =0.9994)	0.8922	4.701×10^{-12}	0.1078	2.080×10^{-11}	1.030×10^{-11}
CNT (30-30) (R^2 =0.9819)	0.9062	3.642×10^{-12}	0.0938	3.337×10^{-11}	1.811×10^{-11}
Bulk (experimental)	-	-	-	-	-

Table 6: l=2

	A	**τ_m (s)**	**B**	**τ_n (s)**	**Debye relaxation time (s) $\langle\tau\rangle = \frac{A\tau_m^2+B\tau_n^2}{A\tau_m+B\tau_n}$**

CNT (10-10) (R^2 =0.9992)	0.804	3.662×10^{-12}	0.196	3.906×10^{-11}	2.922×10^{-11}
CNT (15-15) (R^2 =0.9960)	0.887	4.072×10^{-12}	0.113	3.441×10^{-11}	1.980×10^{-11}
CNT (20-20) (R^2 =0.9525)	0.853	1.614×10^{-12}	0.147	3.348×10^{-11}	2.651×10^{-11}
CNT (25-25) (R^2 =0.9954)	0.947	1.337×10^{-12}	0.053	6.274×10^{-11}	4.580×10^{-11}
CNT (30-30) (R^2 =0.9979)	0.956	1.212×10^{-12}	0.044	6.492×10^{-11}	4.653×10^{-11}
Bulk (experimental)	-	-	-	-	1.020×10^{-12}

Coating carbon nanotubes to the electrode materials is trending technique to increase specific surface area of the electrode accessible to electrolyte ions to increase capacitance. Use of porous nano-structures is becoming a conventional technique. Nevertheless, there is no consensus about the optimal value of the pore size. If we remember the radius of rarefied region whose value approximately an half of the radius of the CNT(10-10) (see Figure 4 for detailed view), we can eventually realize that the distance between the atom whose potential well is the maximum among the others and C atoms of the cnt will be simply :

$\delta_r = r_{pore} - \sqrt{\sigma_{atom\ having\ the\ maximum\ potential\ well} \cdot \sigma_{atoms\ of\ CNT}}$. In our calculations δ_r is equal to 3.373 Å which is almost equal to an half of the radius of pore (in our case 0.50 $r_{CNT(10-10)}$ = 3.387Å) Therefore, we propose a relation, such that

$$r_{min\ of\ pore} > 2\sqrt{\sigma\sigma_C} \quad (9)$$

in order to eliminate increase in viscosity, the volume of rarefied region within the pore and to ensure occupancy of solvent molecules and ions in the pore. In Eqn.9, $r_{min.\ of\ pore}$, σ and σ_C refer the minimum radius of the pore on the electrode surface, the Lennard-Jones equilibrium distance of the atom whose potential well is the maximum of the atoms of constituent molecules/ions and Lennard-Jones equilibrium distance of the C atom of the CNT respectively. Investigation of the pore size may be beneficial for the industry and is left to another study for more details.

CONCLUSION

The authors have presented the results of molecular dynamics simulations of acetonitrile in SWCNTs with diameters spanning from 13.55 to 40.67Å. The temperature is set to 298 K in all cases. We have discussed how the confinement effect changes the structure, dynamic and transport properties of the acetonitrile. Our observations are summarized as follows. With respect to the bulk state, a rarefied region with increasing volume and an interface region are identified in smaller nanotubes. The confinement forms an interfacial layer of pairwise interaction in smaller tubes too. The volume of influence of

these two distinctive regions according to density of the fluid plays a vital role in the structure, transport and electrical properties of the acetonitrile. The last but the not least, dielectric properties of the ACN seems to be very sensitive both rarefaction and confinement effects. The magnitude of the dielectric constant is a function of the size of the dilute volume; i.e., increasing size which drops down the dielectric constant cooperating with the confinement effect. An antiparallel arrangement of dipoles seems to be the other reason for lower values of dielectric constant. We have used two different methods in the simulation of dielectric relaxation. In the first one, the system is treated as a system composed of interacting molecules. In the other, the system is treated as individual molecules which do not affect each other. The results of both approximations are totally different. Our simulations for the bulk state show that the assumption of non-interacting particles gives better result which constitutes well with the experimental data. Moreover, we observed that the relaxation time of the acetonitrile increases considerably compared with experiments. The relaxation process is mainly based on rotational diffusion.

REFERENCES

[1] Abdallah, T., Lemordant, D., & Claude-Montigny, B. (2012). Are room temperature ionic liquids able to improve the safety of supercapacitors organic electrolytes without degrading the performances? Journal of Power Sources,201, 353-359. doi:10.1016/j.jpowsour.2011.10.115

[2] Kalugin, O. N., Chaban, V. V., Loskutov, V. V., & Prezhdo, O. V. (2008). Uniform Diffusion of Acetonitrile inside Carbon Nanotubes Favors Supercapacitor Performance. Nano Letters,8(8), 2126-2130. doi:10.1021/nl072976g

[3] Palm, R., Kurig, H., Tõnurist, K., Jänes, A., & Lust, E. (2013). Influence of Different Organic Solvent Additives on 1-ethyl-3-methylimidazolium Tetrafluoroborate Electrolyte Based Electrical Double Layer Capacitors. Journal of The Electrochemical Society,160(10). doi:10.1149/2.046310jes

[4] Frackowiak, E. (2006). Supercapacitors based on carbon materials and ionic liquids. Journal of the Brazilian Chemical Society,17(6), 1074-1082. doi:10.1590/s0103-50532006000600003

[5] Frackowiak, E., Lota, G., & Pernak, J. (2005). Room-temperature phosphonium ionic liquids for supercapacitor application. Applied Physics Letters,86(16), 164104. doi:10.1063/1.1906320

[6] Pilathottathil, S., Thasneema, K. K., Thayyil, M. S., Pillai, M. P., & Niveditha, C. V. (2017). A high voltage supercapacitor based on ionic liquid with an activated carbon electrode. Materials Research Express,4(7), 075503. doi:10.1088/2053-1591/aa7116

[7] Tsai, W., Taberna, P., & Simon, P. (2014). Electrochemical Quartz Crystal Microbalance (EQCM) Study of Ion Dynamics in Nanoporous Carbons. Journal of the American Chemical Society,136(24), 8722-8728. doi:10.1021/ja503449w

[8] Kötz, R., Hahn, M., Ruch, P., & Gallay, R. (2008). Comparison of pressure evolution in supercapacitor devices using different aprotic solvents. Electrochemistry Communications, 10(3), 359-362. doi:10.1016/j.elecom.2007.12.016
[9] Fleischmann, S., Jäckel, N., Zeiger, M., Krüner, B., Grobelsek, I., Formanek, P., Presser, V. (2016). Enhanced Electrochemical Energy Storage by Nanoscopic Decoration of Endohedral and Exohedral Carbon with Vanadium Oxide via Atomic Layer Deposition. Chemistry of Materials,28(8), 2802-2813. doi:10.1021/acs.chemmater.6b00738
[10] Lee, B., & Yoon, J. R. (2015). Influence of Mixed Solvent on the Electrochemical Property of Hybrid Capacitor. Journal of Nanoscience and Nanotechnology,15(11), 8849-8853. doi:10.1166/jnn.2015.11542
[11] Mo, D., Zhou, W., Ma, X., & Xu, J. (2015). Facile electrochemical polymerization of 2-(thiophen-2-yl)furan and the enhanced capacitance properties of its polymer in acetonitrile electrolyte containing boron trifluoride diethyl etherate. Electrochimica Acta,155, 29-37. doi:10.1016/j.electacta.2014.12.110
[12] Chen, X. Y., He, Y. Y., Song, H., & Zhang, Z. J. (2014). A multi-template carbonization approach to hierarchically nanoporous carbon for high-performance supercapacitors. Journal of Solid State Electrochemistry,19(1), 179-186. doi:10.1007/s10008-014-2593-x
[13] Stoppa, A., Nazet, A., Buchner, R., Thoman, A., & Walther, M. (2015). Dielectric response and collective dynamics of acetonitrile. Journal of Molecular Liquids,212, 963-968. doi:10.1016/j.molliq.2015.03.045
[14] Mountain, R. D. (1997). Shear viscosity and dielectric constant of liquid acetonitrile. The Journal of Chemical Physics,107(10), 3921-3923. doi:10.1063/1.474767
[15] Guàrdia, E., Pinzón, R., Casulleras, J., Orozco, M., & Luque, F. J. (2001). Comparison of Different Three-site Interaction Potentials for Liquid Acetonitrile. Molecular Simulation,26(4), 287-306. doi:10.1080/08927020108024509
[16] Orhan, M. (2014). Dielectric and Transport Properties of Acetonitrile at Varying Temperatures: A Molecular Dynamics Study. Bulletin of the Korean Chemical Society,35(5), 1469-1478. doi:10.5012/bkcs.2014.35.5.1469
[17] Nikitin, A. M., & Lyubartsev, A. P. (2007). New six-site acetonitrile model for simulations of liquid acetonitrile and its aqueous mixtures. Journal of Computational Chemistry, 28(12), 2020-2026. doi:10.1002/jcc.20721
[18] Bardak, F., Xiao, D., Hines, L. G., Son, P., Bartsch, R. A., Quitevis, E. L., Voth, G. A. (2012). Cover Picture: Nanostructural Organization in Acetonitrile/Ionic Liquid Mixtures: Molecular Dynamics Simulations and Optical Kerr Effect Spectroscopy (ChemPhysChem 7/2012). ChemPhysChem,13(7), 1601-1601. doi:10.1002/cphc.201290029
[19] Shere, I., Pawar, V., & Mehrotra, S. (2007). Temperature dependent dielectric relaxation study of acetonitrile with chlorobenzene at microwave frequency using time domain reflectometry. Journal of Molecular Liquids,133(1-3), 116-119. doi:10.1016/j.molliq.2006.07.002

[20] Bernardi, E., & Stassen, H. (2004). Molecular dynamics simulations of acetonitrile/dimethyl sulfoxide liquid mixtures. The Journal of Chemical Physics,120(10), 4860-4867. doi:10.1063/1.1644540
[21] Jellema, R., Bulthuis, J., & Zwan, G. V. (1997). Dielectric relaxation of acetonitrile-water mixtures. Journal of Molecular Liquids,73-74, 179-193. doi:10.1016/s0167-7322(97)00066-4
[22] Mayo, S. L., Olafson, B. D., & Goddard, W. A. (1990). DREIDING: A generic force field for molecular simulations. The Journal of Physical Chemistry,94(26), 8897-8909. doi:10.1021/j100389a010
[23]-Tersoff, J. (1990). Erratum: Modeling solid-state chemistry: Interatomic potentials for multicomponent systems. Physical Review B,41(5), 3248-3248. doi:10.1103/physrevb.41.3248.2
[24] Plimpton, S. (1995). Fast Parallel Algorithms for Short-Range Molecular Dynamics. Journal of Computational Physics,117(1), 1-19. doi:10.1006/jcph.1995.1039

EFFECT OF CURING CONDITIONS ON THE MECHANICAL PROPERTIES OF CONVENTIONAL CONCRETE WITH HYBRID FIBER

Kazim TURK
Department of Civil Engineering, Inonu University
kazim.turk@inonu.edu.tr

Mahmut BASSURUCU
Department of Construction Technology, Darende Vocational High School, Malatya Turgut Ozal University
mahmut.bassurucu@ozal.edu.tr

ABSTRACT: In this study, the effects of curing conditions on the mechanical properties of hybrid fiber reinforced concrete were investigated experimentally. Three type conventional concrete mixtures with no fiber, fiber and hybrid fiber having approximately same slump value were designed. Later, specimens produced from these concrete mixtures were exposed to different curing regimes namely standard 23±2 °C, sealed and air curing conditions. After 7 and 28 curing days, the mechanical tests were performed to determine compressive, splitting tensile, flexural strength and ultrasonic pulse velocity. Finally, the specimens cured in water had the best mechanical properties and energy absorption capacity while those of specimens cured in air were the worst. Moreover, the specimens cured in sealed condition had similar mechanical properties compared to the specimens cured in water.

Key words: Macro Steel Fiber, Micro Steel Fiber, Curing Conditions, Compressive Strength, Flexure Strength

INTRODUCTION

Concrete is the most widely used as building material today due to its desired shape, economical and easy to find. Conventional concrete is produced by mixing aggregate, cement and water. The compressive strength of the concrete was increased considerably as results of many studies carried out by researchers and it became a material that benefited from this feature. As concrete strength increases, axial deformation capacities increase. After the peak, the stress drop is sudden and a brittle fracture is observed because of its high compressive strength. For this purpose, fiber reinforcement is used in concrete to eliminate these problems that occur in concrete, and thus, increase in the tensile strength and ductility of the concrete is provided.

The first studies on fiber reinforced concrete were carried out in 1950 to understand the mechanical properties of fiber reinforced concrete (Hannant, 1987). Fiber reinforced concrete is defined as concrete containing randomly directed fibers (Bentur, 1989). In today's construction industry, fiber-reinforced concrete is used in many applications such as industrial slabs, bridges, aircraft runways and precast elements. Fiber-reinforced concrete, which consists of a mixture of multiple discontinuous fiber types and conventional concrete matrix, is defined hybrid fiber-reinforced concrete (Ding et al. 2010). The view of hybrid fiber in concrete mixture was first proposed by Rossi et al. (1987). The combination of micro fibers that controls the initiation and spread of micro-cracks and macro fibers that control macro-cracks in hybrid fiber-reinforced concrete provide important advantages in terms of mechanical properties [Mobasher and Cheng, 1996].

Appropriate curing plays an important role in success optimum performance/full potential from a given concrete mixture (BCA, 1993). The study carried out by Bentz et al. shows that curing conditions have important effect on the rate of hydration of cement. In the study conducted by Yazicioglu et al., the engineering properties of self-compacting concrete (SCC) under different curing conditions were investigated experimentally. Portland cement concrete and two types of SCC i.e., SCC with fly ash and SCC with silica fume, concrete specimens are prepared and cured in three different curing conditions, namely water, sealed and air cured for the different periods of 3, 7, 14 and 28 days. The conclusions indicated that water cured specimens always give the highest values followed by those cured as sealed and in air irrespective of type and age of concrete.

The essential aim of this study is to search the influence of different curing conditions on the engineering properties of hybrid and single containing fiber concrete in comparison with normal concrete by using determined test methods.

MATERIALS AND METHODS

Materials and mixture proportions

For this study, CEM I 42.5 Type I Portland cement was used for all mixtures and the chemical composition and physical properties of Portland cement was showed in Table 1. Two different groups of aggregates were used. In the first one, the aggregate sizes were in the range of 0-5 mm and its specific gravity and water absorption values were 2.53 and 1.90%, respectively. The aggregate sizes of the second were 5 to 15 mm. The specific gravity of that group was 2.62 and water absorption was 0.50%. The grading of the total aggregate was showed in Table 2 and as can be seen the maximum aggregate size was 16 mm. The specific gravity of plasticizer based polymer used in all concrete mixtures was 1.09. Moreover, to improve the tensile strength of mixtures, macro and micro steel fibers were added to concrete mixtures as single and hybrid. The geometry of macro (Dramix 65/60) and micro (OL 13/.16) steel fibers showed in Figure 1. The properties of their geometry and mechanical were shown in Table 3. Three concrete types were selected,

namely control concrete without fiber, concrete containing only macro fiber of 1% (MAC1.00) and the concrete containing 0.80% macro and 0.20% micro fiber named hybrid fiber (MAC0.80). Details of the concrete mix compositions and properties of fresh concretes were showed in Table 4.

Table 1. Chemical composition of portland cement used in concretes (%)

Composition	SiO_2	Al_2O_3	Fe_2O_3	CaO	MgO	SO_3	K_2O	Na_2O	Specific gravity (g/cm^3)
PC	19.41	5.58	3.67	58.85	2.12	3.16	0.69	0.61	3.15

Table 2. The grading of the total aggregate

Sieve size (mm)	16	8	4	2	1	0.5	0.25	0.125
Aggregate (% passing)	100.00	59.80	39.19	23.74	13.34	9.40	6.11	3.80

(a) (b)

Figure 1. Shape of macro and micro fibers used in the mixtures

Table 3. Properties of the macro and micro fibers

Fiber	**Diameter (mm)**	**Length (mm)**	**Aspect Ratio**	**Tensile Strength (MPa)**	**Elastic Modulus (GPa)**	**Density (kg/m^3)**
Macro (Dramix 65/60)	0.92	60	65	2300	210	7850
Micro (OL 13/.16)	0.15	13	87	3000	200	7200

Table 4. Concrete Mixes (kg/m^3)

Mixture Name	Cement	Water	Steel Fiber		Aggregate Normal		Plasticizer	Slump (mm)
			Macro	Micro	0-5 mm	5-15 mm		
CONTROL	350	200	0	0	1025	684	8	12
MAC1.00	350	200	78.5	0	1004	670	12	12
MAC0.80	350	200	62.8	14.4	1001	668	12	9

Specimen preparation and curing of specimens

All concrete specimens were cast on a vibrating table to ensure optimum compaction. The compressive strength and ultrasonic pulse velocity of the concrete mixtures were evaluated by using three cube specimens with the dimensions of 100x100x100 mm according to ASTM C39 and ASTM C597-16, respectively. To specify splitting tensile strength as per ASTM C496, cylinder specimens with the dimensions of Ø100x200 mm were used. The flexural tensile strength of the concrete mixtures were evaluated by applying four point bending test by using 80x100x300 mm prismatic specimens according to ASTM C1609. In the following day of casting, the concrete specimens were de-moulded and located in three different curing conditions, namely standard 23±2 °C water, sealed and air cured for the periods of 7 and 28 days. At the end of each curing period, a total of three specimens from all concrete mixture were tested for each mechanical property. All tests during this study were performed at 7 and 28 days for all curing conditions. The performance of MAC1.00 and MAC0.80, have been examined with respect to relevant properties of control concrete.

RESULTS AND DISCUSSIONS

Compressive Strength

The results obtained from compressive strength tests for control concrete, MAC1.00 and MAC0.80 for all concrete ages and curing conditions were showed in Figure 2-4, respectively. It can be seen from these figures that at 7 and 28 curing days, the compressive strength of the MAC1.00 mixture containing macro steel fiber showed little reduction for all curing regimes compared to the control concrete specimens. Moreover, in the mixture of, the inclusion of micro steel fibers to MAC0.80 mixture had a positive effect on compressive strength. It was also displayed that the highest compressive strength values were derived from standard water curing followed by the sealed and air

curing regimes irrespective of the concrete types. But the compressive strength values of mixtures exposed to sealed curing conditions were close to that of the mixtures exposed to standard curing. Moreover, the effect of curing regimes on the compressive strength of the mixtures was seen in general at 28 days while the compressive strength values of the mixtures at 7 days were close to other. Based on the results of the 28-days the control mixture compressive strength for water curing, the compressive strength of the mixture with single fiber decreased with 6.7% and that of the hybrid fiber reinforced mixture increased with 6% for water curing condition. Similar results were found by Pierre (2000) that the compressive strength of the concrete of the steel fibre-reinforced was studies on changes approximate by ±25%. In the literature, it was observed in the studies on the hybrid fiber reinforced concretes that the micro fibers were more effective in preventing the formation and spreading of micro cracks in the concrete specimens exposed to the load, thus, improving the compressive strength of the concrete (Sahmaran et al., 2005).

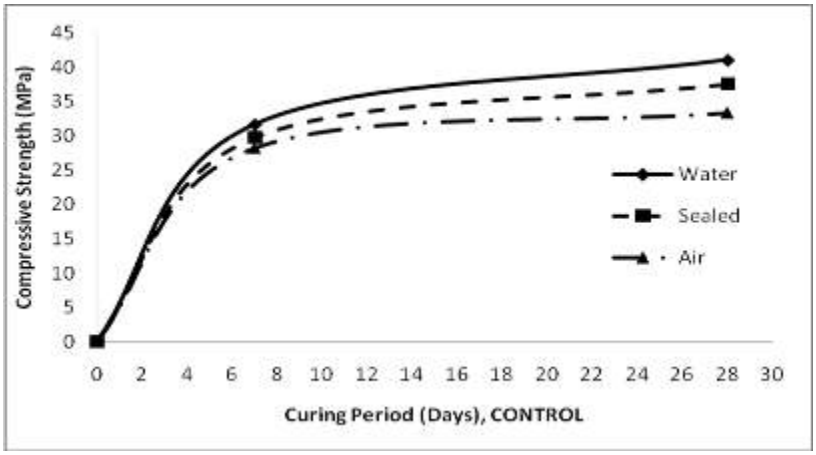

Figure 2. Compressive strength results for control concrete

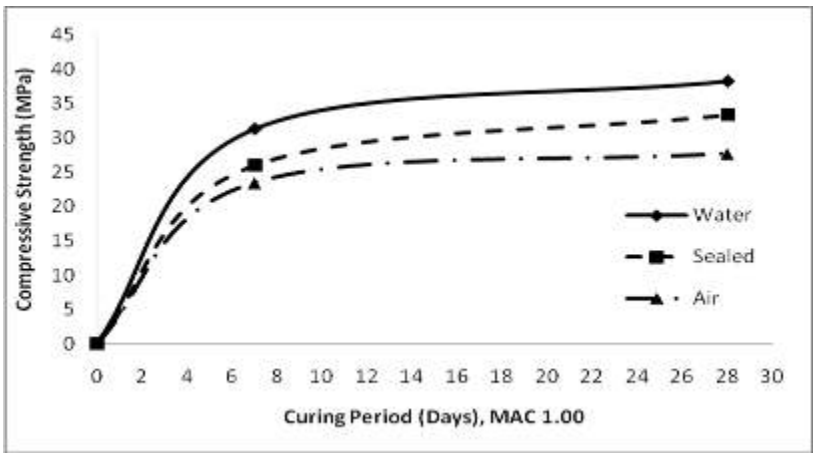

Figure 3. Compressive strength results for MAC 1.00

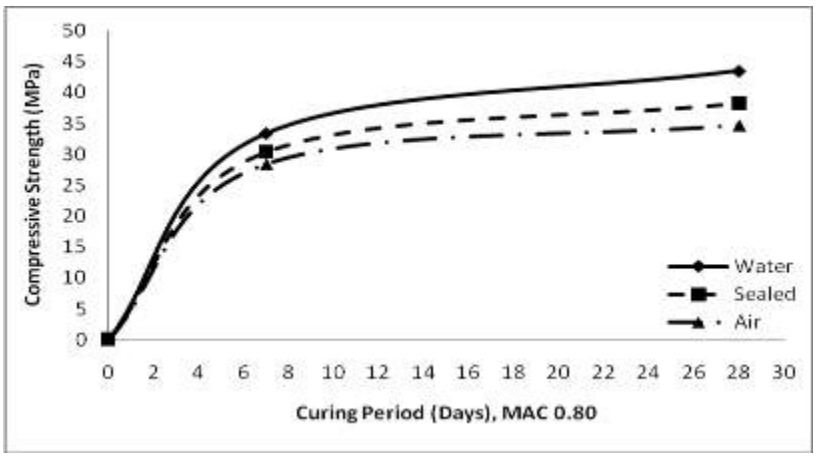

Figure 4. Compressive strength results for MAC 0.80

Splitting tensile strength

The splitting tensile strength results for the three types of concrete, control concrete, MAC1.00 and MAC0.80, for three different curing methods at the 7 and 28 days curing periods were given in Figure 5-7, respectively. It was showed in these figures that the improvement of splitting tensile strengths of MAC1.00 was the highest followed MAC0.80 and control concrete. Based on the results of the 28-days the control mixture splitting tensile strength for water curing, the splitting tensile strength of the mixture with single fiber increased with 64% and that of the hybrid fiber reinforced mixture increased with 28% for water curing condition. Similar results were found by Mazaheripour et al. (2011) that fiber reinforcement to concrete increased the splitting tensile strength of concrete. When the effect of curing methods on the splitting tensile strength of concretes were investigated, it was seen that the highest values were obtained from water cured specimens followed by sealed and air cured specimens, regardless of concrete type.

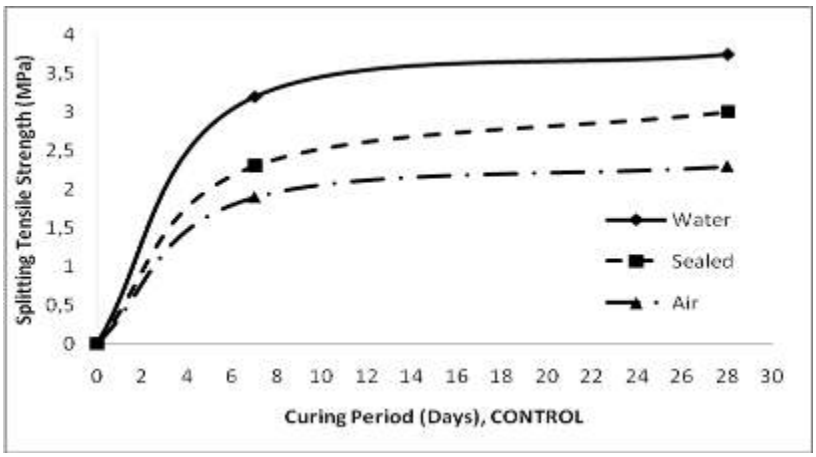

Figure 5. Splitting tensile strength results for control concrete

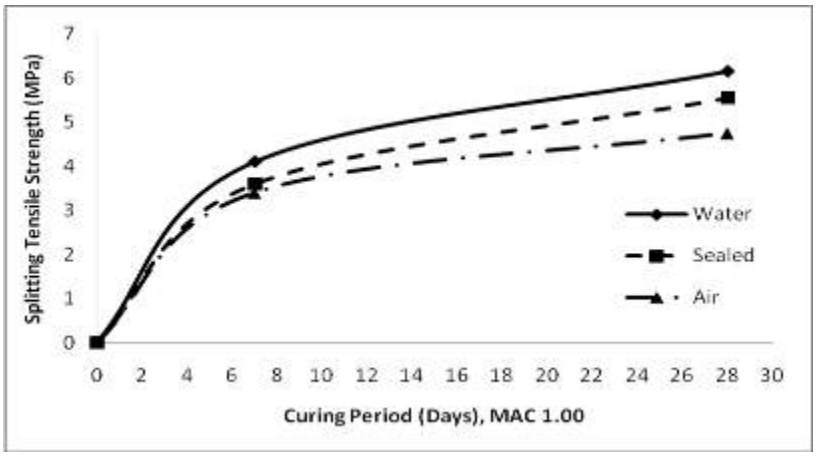

Figure 6. Splitting tensile strength results for MAC 1.00

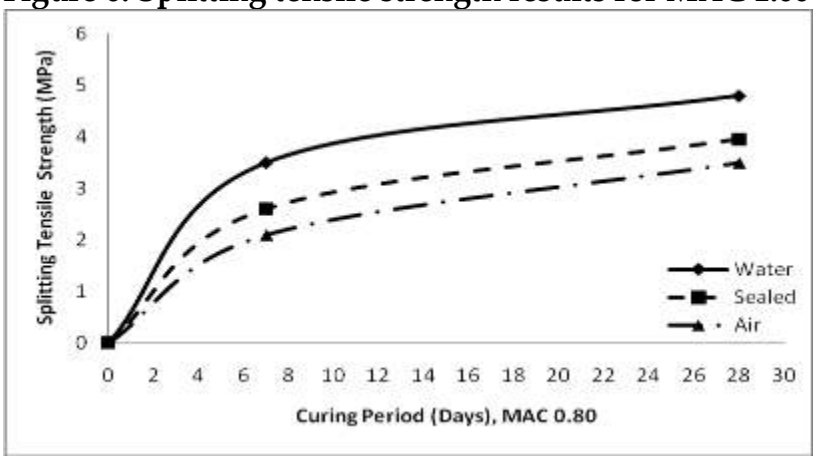

Figure 7. Splitting tensile strength results for MAC 0.80

Flexural tensile strength and Energy Absorption Capacity

The flexural tensile strength results for the three types of concrete, control concrete, MAC1.00 and MAC0.80, in three different curing methods for the 7 and 28 days curing periods were given in Figure 8-10, respectively. It was showed in these figures that the improvement of flexural tensile strengths of MAC1.00 was the highest followed MAC0.80 and control concrete. It was also displayed that the highest flexural tensile strength values were derived from water cured specimens followed by the sealed and air cured specimens irrespective of the concrete types. Based on the results of the 28-days the control mixture flexural tensile strength for water curing, the flexural tensile strength of the mixture with single fiber increased with 59% and that of the hybrid fiber reinforced mixture increased with 26% for water curing condition.

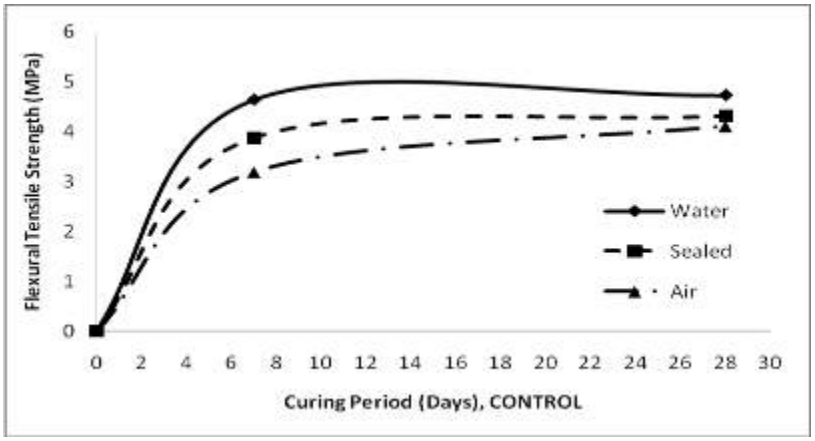

Figure 8. Flexural tensile strength results for control concrete

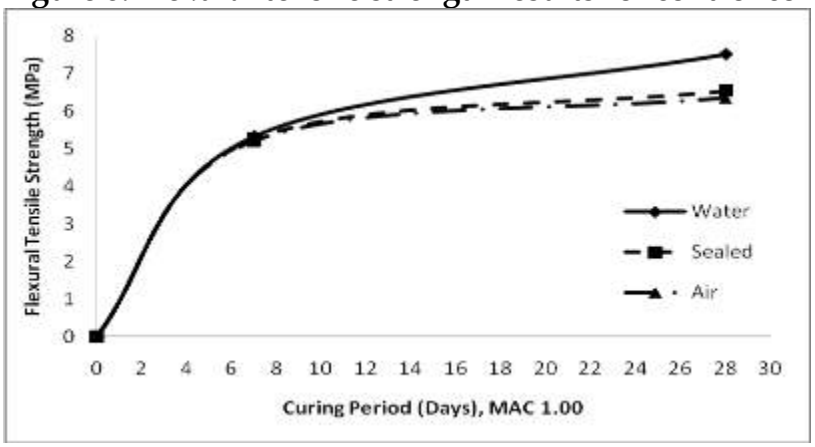

Figure 9. Flexural tensile strength results for MAC 1.00

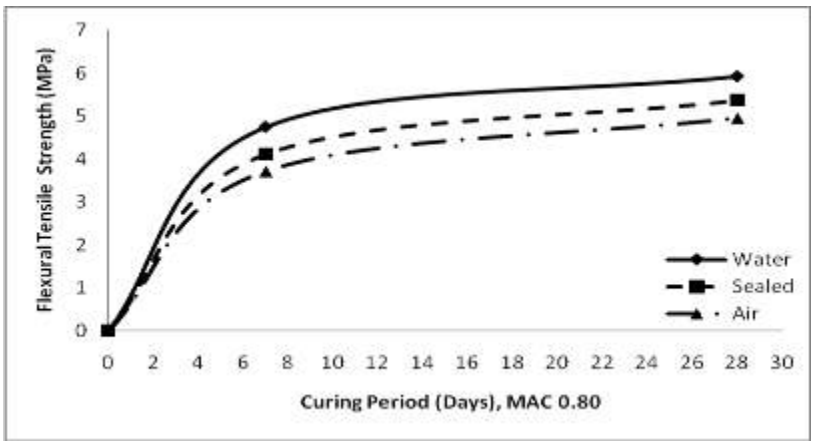

Figure 10. Flexural tensile strength results for MAC 0.80

The energy absorption capacity results for three types of control concrete, MAC1.00 and MAC0.80, for three different curing methods at the 7 and 28 days curing periods were showed in Figure 11-13, respectively. It was seen in these figures that the values of energy absorption capacity of MAC1.00 were the highest followed MAC0.80 and control concrete. For water curing, compared to the results of the 28-days the control mixture energy absorption capacity with 1163 N.mm, the concrete with the single fiber extremely increased with 20238 N.mm and that of the energy absorption capacity with the hybrid fiber increased with 16066 N.mm. The reason for this was that the fibers generate a mechanism with higher energy absorption capacity by preventing crack initiation and growth with effective bridging (Bentur and mindess, 1990).

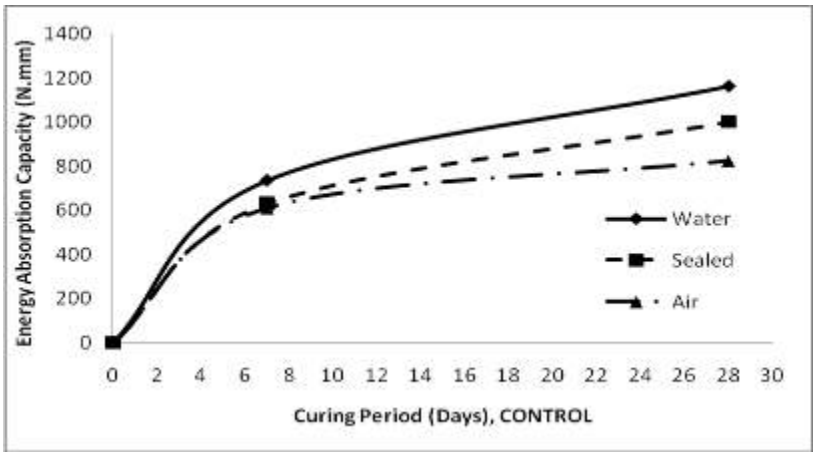

Figure 11. Energy absorption capacity results for control concrete

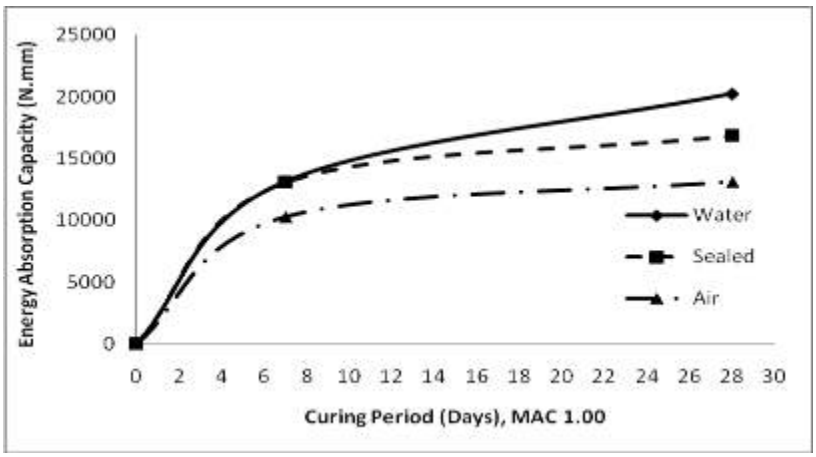

Figure 12. Energy absorption capacity results for MAC 1.00

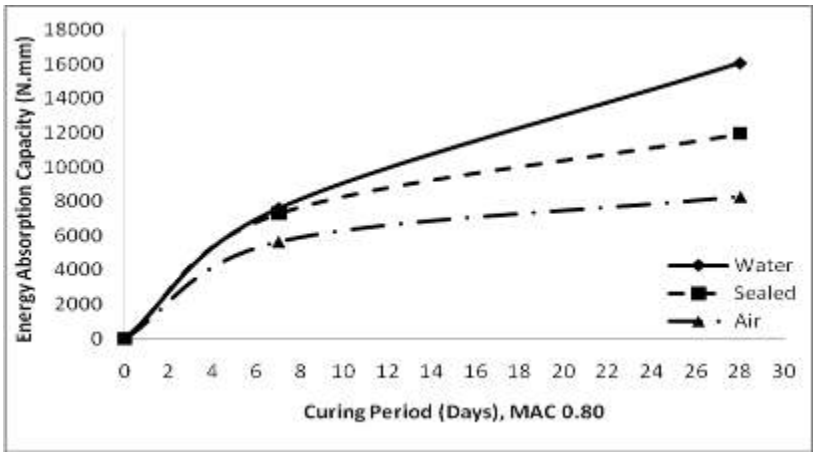

Figure 13. Energy absorption capacity results for MAC 0.80

Ultrasonic pulse velocity (UPV)

Figure 14-16 show the UPV test results for control concrete, MAC1.00 and MAC0.80 concretes, respectively, at 7 and 28 days for all curing conditions. The highest UPV values were attained from the MAC1.00 followed by control concrete and MAC 0.80 concretes. Water cured concrete specimens for all concrete types gave the highest values then followed by sealed and air cured concrete specimens also indicated the role of moisture degree on the hydration development (Yazicioglu, 2006).

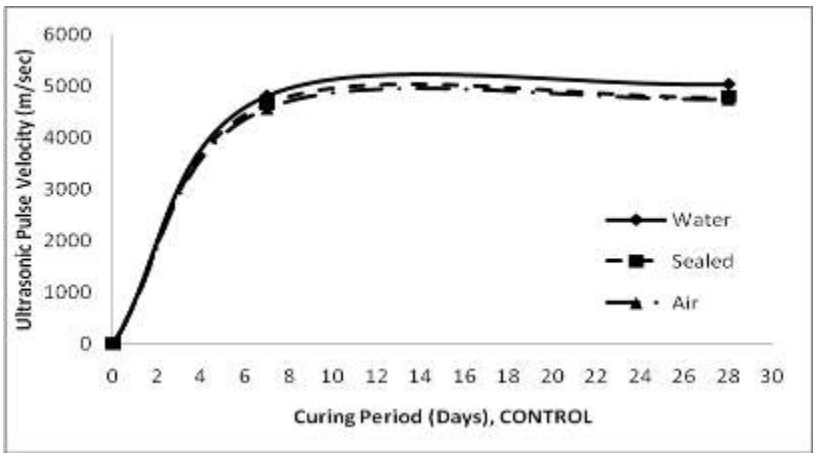

Figure 14. Ultrasonic pulse velocity results for control concrete

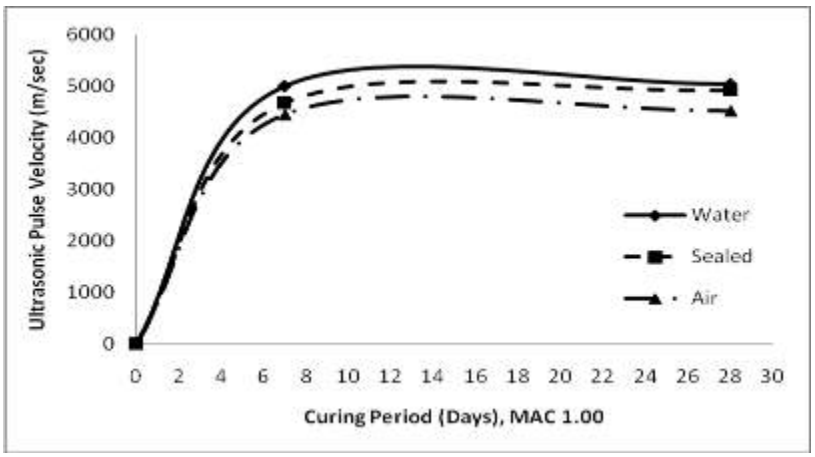

Figure 15. Ultrasonic pulse velocity results for MAC 1.00

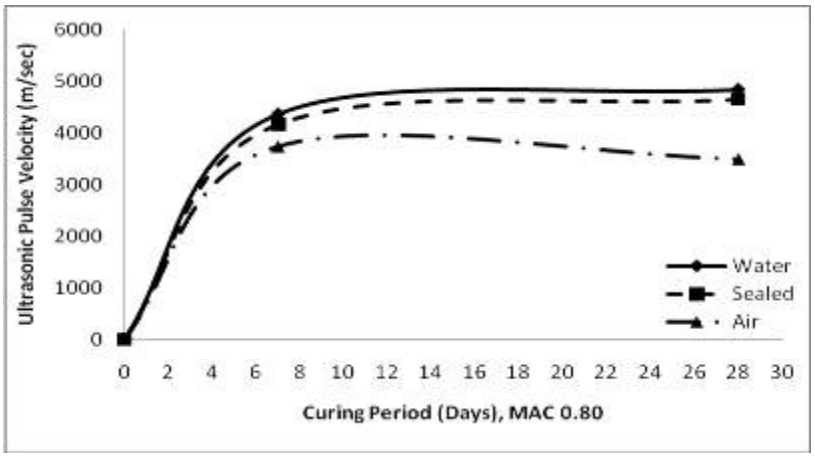

Figure 16. Ultrasonic pulse velocity results for MAC 0.80

Comparison of tensile and compressive strength

The flexural tensile and compressive strength results of control, MAC1.00 and MAC0.80 concretes were showed in Figure 17, on the basic of the curing method applied. It is showed in this figure that as the concrete compressive strength increased, the flexural tensile strength also increased. In general, the correlation between the values of compressive strength and flexural tensile strength were well with R^2 values of over 0.90. The MAC1.00 obtained the highest values while the control concrete and MAC0.80 concretes were near.

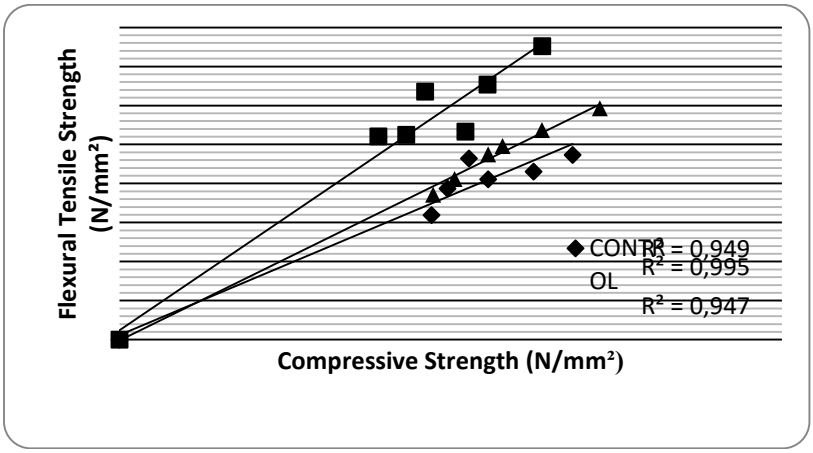

Figure 17. Comparison of compressive and flexural strength of concrete

CONCLUSIONS

Based on the experimental study carried out, the following conclusions can be drawn: It was also displayed that the highest values of mechanical properties for all curing ages were obtained from standard water curing followed by the sealed and air curing regimes irrespective of the concrete types. Also, the mechanical properties values of mixtures exposed to sealed curing conditions were close to that of the mixtures exposed to standard curing. Hybrid fiber reinforced concrete mixtures had higher the compressive strength, splitting tensile strength, flexural tensile strength and energy absorption capacity for all curing conditions at 7 and 28-day compared to control concrete. Concrete mixtures with only macro reinforced fiber had highest the values of splitting tensile strength, flexural tensile strength, energy absorption capacity and ultrasonic pulse velocity while the compressive strength of the mixtures with hybrid fiber was highest in all concrete mixtures.

RECOMMENDATIONS

In hybrid fiber reinforced conventional concretes, the dosage of the plasticizer can be reduced by using super plasticizer instead of the normal plasticizer. In this case, it is be thought that the setting retardant effect resulting from the excessive dosage of the normal plasticizer in the concrete will be eliminated.

ACKNOWLEDGEMENT

In this study, the financial support was provided by Scientific Research Projects Committee of Inonu University, Turkey (Project No: FBA-2017-776). Their support was gratefully acknowledged.

REFERENCES

ASTM C39 (2018). . Standard Test Method for Compressive Strength of Cylindrical Concrete Specimens, ASTM International, West Conshohocken, PA.

ASTM C496 (2016). . Standard Test Method for Splitting Tensile Strength of Cylindrical Concrete Specimens, ASTM International, West Conshohocken, PA.

ASTM C597-16 (2016). . Standard Test Method for Pulse Velocity Through Concrete, ASTM International, West Conshohocken, PA.

ASTM C1609 (2019). . Standard Test Method for Flexural Performance of Fiber-Reinforced Concrete, ASTM International, West Conshohocken, PA.

Bentur, A., Mindess, S., (1990). Fiber – reinforced cementitious composites. 1st ed. Elsevier Applied Science, London and New York.

Bentur, A. (1989). Fiber – reinforced cementitious materials. Material Science of Concrete,Westerville, Ohio, The American Ceramic Society, 223-285.

Bentz, D. P., Synder, K. A., Stutzman, P. E., (1997). Hydration of Portland cement: The effect of curing conditions, presented at the 10th Int. Congr. Chemistry of Cement, Sweden.

British Cement Association (BCA) (1993). Curing, Concrete Series, Crowthorne, UK, 9.

Ding, Y. N., You, Z., Jalali, S., (2010). Hybrid fiber influence on strength and toughness of RC beams. Composite Structures, 92(9), 2083-2089.

Hannant, D. J. (1987). Fiber cements and fiber concrete. Chichester, UK:Wiley.

Mazaheripour, H., Ghanbarpour, S., Mirmoradi, S. H., Hosseinpour, I., (2011). The effect of polypropylene fibres on the properties of fresh and hardened lightweight self-compacting concrete. Construction and Building Materials, 25(1), 351-358.

Mobasher, B., Li Cheng, Y., (1996). Mechanical properties of hybrid cement based composites. American Concrete Institute Materials Journal , 93(3), 284-292.

Pierre, R., (2000). Ultra High Performance Fibre Reinforced Concretes: An overview, Fifth RILEM Symposium on Fibre-Reinforced Concretes, Lyon, France.

Rossi, P., Acker, P., Malier, Y., (1987). Effect of steel fibres at two different stages: the material and the structure. Material and Structures, 20(6), 436-439.

Sahmaran, M., Yurtseven, A., Yaman, I., (2005). Workability of hybrid fiber reinforced self-compacting concrete. Building and Environment , 40, 1672-1677.

Yazicioglu, S., Caliskan, S., Turk, K., (2006). Effect of curing conditions on the engineering properties of self-compacting concrete. Indian Journal of Engineering & Materials Sciences, 13, 25-29.

Turk, K., Caliskan, S., Yazicioglu, S., (2007). Capillary water absorption of self-compacting concrete under different curing conditions. Indian Journal of Engineering & Materials Sciences, 14, 365-372.

NUMERICAL INVESTICATION OF STRUCTURAL BEHAVIOR OF STEEL FRAMES UNDER FIRE LOAD

Aslıhan ALGÜL Mustafa ÖZAKÇA
University of Gaziantep, Gaziantep, TURKEY
aslihanalgl@gmail.com, ozakca@gantep.edu.tr

ABSTRACT: The fire event in steel structures is a critical point to be focused on. For that reason, steel structures are of particular importance in terms of fire. In these structures, the shape changes occurring during the fire are in the foreground. Steel structures have taken place in many standards on the world. Structures that can withstand up to 540°C in regulations related to fire, are characterized as durable. However, steel which has mentioned has resistance to a certain limit should not be ignored. This steel reaches half of the yield stress at room temperature at 550°C and is observed in a laboratory environment where it resist to various fire conditions. The resistance to fire time is the interval at which a structure continues to fulfill what is expected of a particular fire load. Steel structures are used especially in industrial structures. This is because the structures must have a wide span and a long height. Industrial building systems have a serious loss of life and property when the fire occurs. In order to avoid this event, design should be done based on fire and ıt should be aimed to delay the collapse period. It has been observed that these measures have greatly reduced the hazards of fire that may arise.

Keywords: Steel Structures, Fire design, Industrial Building Systems

INTRODUCTION

Fire makes a constant danger to humans. During history, it has caused to change the historical textures, so it has lead the substances to receive new forms. The fire is in all forms of housing, office, school, factory, etc. Therefore, it can occur in anywhere at any moment. Since the possibility of a fire is always in question, the important thing is to find the elements which can cause to have a fire and take prevention in order to interfere with the fire. One of the weakest features of the steel is very sensitive to heat. Steel is not flammable as being material. When the heat goes up, rapid decreases occur of its strength and elasticity modulus. Especially, the decrease in strength values of the steel becomes obvious when the heat is above 200 °C [1]. Among the most important uses of steel structures are industrial structures. Among the reasons why industrial structure are made up of steel construction is that it is possible to cross wide openings without columns and easy to assemble conveyor and monorail lines in industrial structures.
The biggest disadvantage of steel structures in this regard is fire. The resistance of steel at high temperature decreases very quickly. In industrial structures, thinner, fibre-style materials cause the temperatures in the fire to rise suddenly and the strength of steel structures to drop very quickly. This period up to the collapse of the structure is very

important in terms of avoiding the loss of both human and property with minimal damage. I did this study to measure the effect of the scissors system in the industrial structure on this time.

THE RELATION OF STEEL STRUCTURE AND FIRE

The high temperatures encountered in fires lead to significant changes in mechanical properties of steel building materials and significant expansion in these materials. Experiments have shown that when the temperature increases, the flow limit in carbon steel is decreased and no residual flow limit is formed after a certain temperature. This means that when compared to normal temperatures, plastic shape changes begin to take place under lower stresses and the total shape change is greater under the same strain. After the tensile strength of steel increases slightly at 150 ~ 300 °C, it decreases rapidly at higher temperatures and falls below the safety strain at 550 °C, which is easily accessed in fires.

Steel is very sensitive to heat, although it is not flammable as material, and rapid decreases can be observed in strength and elasticity modulus as heat rises. When the steel is unprotected, there can be seen some losses in its own strength and changes in own shape, while it is starting to soften at high temperatures. Therefore, it is mandatory to protect steel structural elements against fire. The resistance of unprotected steel to the fire is limited to 60 minutes. This time is the highest value, and normally this limit is even lower. The required fire resistance in steel structures is expressed in the form of fire-resistant classes which are F30 (30-59 min.), F60 (60-89 min.), F90 (90-119 min.), F120 (120-179 min.) and F180 (180 min.). This fire- resistance varies depending on the number of floors of the building, its intended use, type, fire load, and the positive effect of sprinkler systems. These deadline periods represent neither the actual fire wait times nor the time required for the escape of residents of the building. Time parameters are basically made to compare buildings for fire safety and demonstrate the durability of structural steel elements in laboratory conditions.

THE STUDIES OF FIRE ON THE STEEL

There has been a lot of work done in the world about fires in buildings. The main reason why these studies are widespread on steel is that steel structures lose their strength very quickly under high temperatures. In general, studies have shown that this temperature value has completely lost its strength of steel material after reaching 1000 degrees. We can examine the studies on this subject in two groups

Experimental Studies: In our country, experimental studies related to fire are limited. This requires a lot of budget .This is not available in our country at the moment.

Theoretical Studies: Many different programs can be used when working on fire. In the study below, a theoretical study was conducted using the SAFIR program.

Built in Geneva, Switzerland, the Hans-Wilsdorf is a unique steel bridge. This structure is vital in terms of its resistance to fire load. Therefore an analysis was conducted through the SAFIR program to measure the sensitivity of the structure to fire. This analysis made the event more descriptive by FDS simulation of a truck burning on the bridge, resulting in significant results.

As a result of the analysis, we have come to the conclusion that Hans-Wilsdorf bridge is safe in fire situations and that the structure has a really satisfactory attitude towards fire with many simulations being studied.

- This result is obtained partly because the different scenarios develop in open air.
- The CFD analysis was very helpful and confirmed the assumed maximal temperature expected using simplified analytcal models
- The possibility to get adrabratic temperature values from the FDS model to be introduced in to the SAFIR model was very helpful [6].

Welded steel frame is one of the most suitable traditional engineering structures used today. However, the economic fire designs of these buildings are important issue. The aim of the current research is to examine the complex structural behavior of a single layer of an industrial structure during fire. This analysis focuses on advanced numerical techniques that make the system's fire resistance more economical using the SAFIR program. This analysis outlines a complex research program to improve the FEM based design method of steel frames installed by fire action.

This possibilities and advantages of combined analysis methods are presented and discussed on paper that can make the design of steel frames easier and faster for static loads and fire action. The paper presents two modelling levels to analyse steel frames under fire action and to consider the time depend joint characteristics, which can lead to a more accurate approximation of the real structural behaviour.

ANALYSED STRUCTURES

The most widely used types of frames in industrial structures are portal frame and truss frame. Both types of frames provide sufficient stability and adequate continuity by regulations. When determining which one will by used during the design process, the material supply time, affordability, manufactoring time, labor cost, location of cranes, monarays and conveyorlines within the structure determine the type of frames.

Portal frame is short manufactoring time and low cost of workmanship are the most important reason why the portal frames are preferred. IPE and INP profiles are often used when choosing frames in portal frames due to the fact that IPE and INP profiles are more economical (the ratio of kg/m is lower than other) than HEA and HEB profiles.

Truss frame is one of the most important reason for choosing truss frame is that it is much more economical than Rolling trusses in wide opening. When making this comparison, the cost of labor should be checked. Because of manufacturing time is long and workmanship is hard. In general, pipe and box profiles are preferred when selecting

corner benches in the upper and lower headers and connectors. The material supply time is not long (since most of materials produced in Turkey are corner pipe nd box profiles). It is also suitable for welded and bolted connections.

When examining the effect of frame differences in industrial structures under the fire load, first we need to design the industrial structure. For this purpose, the regulations in SAP2000 defines the clearance and axle dimensions of the structure, earthquake, snow and wind loads and determines sections of the industrial structure.

The structure consisting of 6 axles with a gap of 15m in the industrial structure subject to this thesis is designed as if it will be built on the site of Civil Engineering Department of Gaziantep University and the required ground by the regulations, seismicity wind and snow load coefficients are selected accordingly.

These sections are created in the WIZARD (It is the program which is used to create TEM files for the SAFIR program) after the sections are determined in the same aperture and axle ranges in the types of truss and portal frames. To create TEM files, TEM files are formed by sizing and analyzing them with using SAFIR.

A sequential analysis is used to properly analyze a structure under fire. Figure 4.1 schematically shows the steps of nonlinear sequential analysis. The first stage of loading is the application of gravitational loads that are assumed to be static, smooth and constant throughout the analysis. A fake earthquake load then follows in the form of a pushover that reaches its maximum value and returns to zero in a short time

Before fire loading, the properties of the structures are set to the reference temperature, but during the fire the mechanical properties change with the temperature. In this study, sequential seismic and fire analyzes were carried out using SAP2000 for thrust analysis and SAFIR for sequential analysis, including the model shown in.

Turkey's earthquake regulations and American regulations are exactly the same except for very small differences. Since Turkey does not have a design code in SAP2000 program, we choose the AISC 360-10 design code from the American regulation.

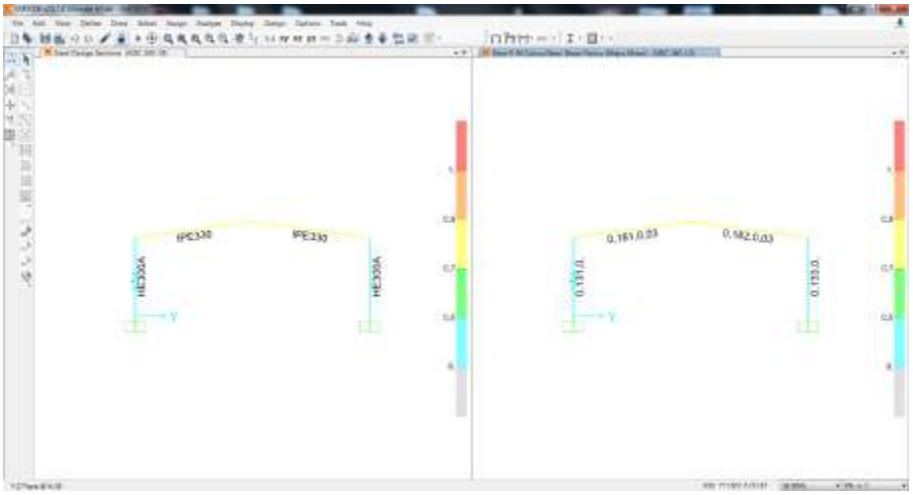

Figure 1.Portal Frame Analysis Result in SAP2000 (Determination of cross section)

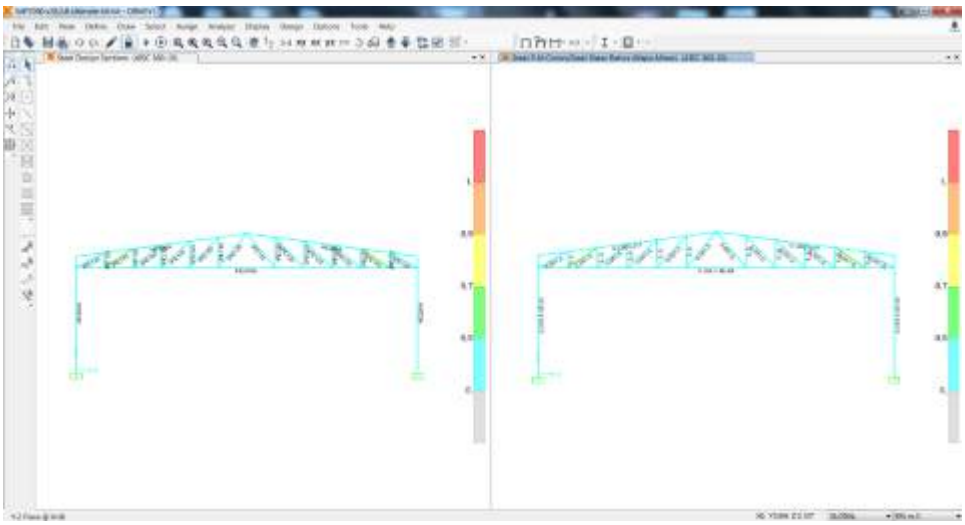

Figure 2.Truss Frame Analysis Result in SAP2000 (Determination of cross section)

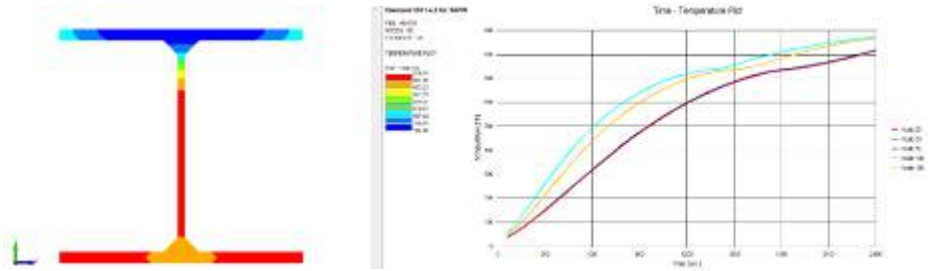

Figure 3. Analysis Result in SAFIR for HEA300

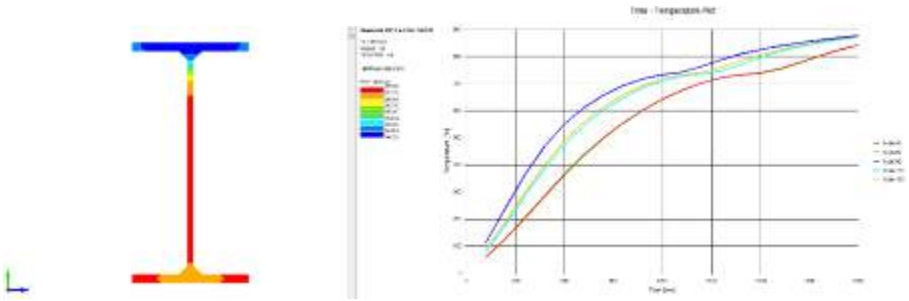

Figure 4. Analysis Result in SAFIR for IPE330

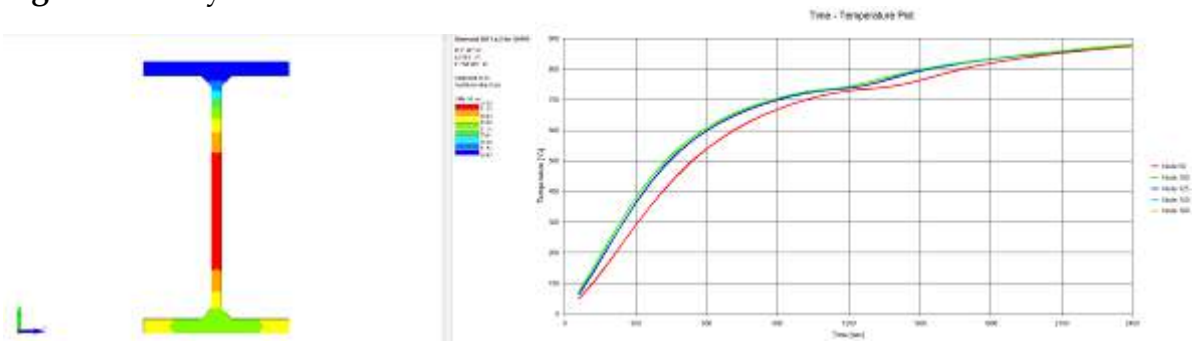

Figure 5. Analysis Result in SAFIR for IPE120

CONCLUSION

Steel structures are used in industrial structures because of their desired opening and usage areas (monorail, conveyor lines, etc.) The disadvantage of steel structures is that they do not have resistance to heat. This study was carried out to measure fire resistance times of two different truss systems with the same opening, height and axle ranges. For this purpose, in the static analysis program, sections of the industrial structure that should be used under seismicity, wind and snow loads were determined. Then, TEM files of the column and truss system were created and the system was analyzed in thermal analysis program. The program provides convenience to the design engineer in terms of cross sectional effects, design criteria and account summary tables of the elements. The designer is able to analyze the results of the data efficiently. In addition, the program clearly states the formulations used in analysis with manual.

REFERENCES

[1] Arda, T.S. ve Yardımcı, N. (1995), Çelik Yapı Elemanlarının Yangın Mukavemeti, İstanbul, 50s

[2] TS7486 Yangından Korunma-Terimler(1989), Türk Standartları Enstitüsü, Ankara.

[3] Özcan O., Sağman N. ve İnce, A. (2000), Yangınla Mücadele Eğitimi Ders Kitabı, İtfaiye Eğitim Merkezi Yayınları, İstanbul.

[4] Eric Tonicello, Sylvain Desanghere, Olivier Vassart,Jean Marc Franssen (2012) Fire Analysis Of A New Steel Bridge, Conference: 7 th International Conference on Structures at Zürich

[5] Fire Behaviour of Steel Industrial Hall, Laszlo Horvath,Balazs Kövesdi,Laszlo Dunai, Budapest University of Technology and Economics,Department of Structural Engineering 1111 Budapest. http://www3.hamk.fi/metnet/Budapest%202015/P04Paper_Horvath_Kovesdi_Dunai.pdf

[6] J.M. Franssen.(2012) User's Manuel for SAFIR 2011 A Computer, Program for Analysis of Structures Subjected to Fire.

CHALLENGES ON SMART THERMOSTAT SYSTEMS IN INTELLIGENT BUILDINGS

Ataberk KEŞKİŞOĞLU
Atılım University, Department of Mechanical Engineering, Ankara, Turkey
ataberk.keskisoglu@gmail.com

Cihan TURHAN
Atılım University, Department of Energy Systems Engineering, Ankara, Turkey
cihan.turhan@atilim.edu.tr

ABSTRACT: The main purpose of Heating, Ventilating and Air-Conditioning (HVAC) systems is to increase thermal comfort for occupants. Alongside developing technology in intelligent building sector, HVAC systems still consume 30-50% of total energy consumption of the buildings. For this reason, smart thermostats become popular in order to decrease energy consumption while building a personalized network between the occupants and HVAC systems. On the other hand, smart thermostats bring large security and efficiency concerns for the occupants. A smart thermostat generally includes temperature sensor, a user interface for displaying and receiving information to and from an occupant, a communication port with HVAC system, a processor, and a transceiver. Large numbers of expensive sensors are used to gather personalized data and communication between the occupant and HVAC system is satisfied via wireless technologies. The privacy and security of these systems are always question marks. To this aim, this paper addresses some significant challenges on using smart thermostat systems and potential threats for the occupants. The main challenges on smart thermostats can be counted as privacy, security and complexity of devices for the occupants.

Key words: smart thermostats, intelligent systems, security, advanced HVAC systems

INTRODUCTION

Heating, Ventilating and Air-Conditioning (HVAC) systems provide thermal comfort and air-conditioning for occupants and buildings, respectively (Ashrae, 2017). Buildings are responsible for 40% of total energy consumption share in Europe while HVAC systems consume approximately 30-50% of total energy in buildings (EU, 2018). Occupant activity and behavior play vital role on energy consumption of HVAC systems. For this reason, smart thermostats received an increasing attention with the development of intelligent building concept in the last decade. Siroky et al. (Široký, Oldewurtel, Cigler,

& Prívara, 2011) indicated that improving control algorithms of HVAC systems is more cost-effective than changing HVAC equipment with efficient ones. Smart thermostats are control systems for intelligent buildings in order to satisfy better thermal environment to the occupants (Nguyen & Aiello, 2013). The control parameters are generally indoor air temperature and flow rate. In spite of occupants use these devices to save money, smart thermostats learn occupant behaviors by proper Artificial Intelligent (AI) methods and allow occupant to control parameters remotely, in conclusion save energy (Fig.1).

Figure 1. Overview of working principle of smart thermostats

A smart thermostat generally includes temperature sensor, a user interface for displaying and receiving information to and from an occupant, a communication port with HVAC system, a processor, and a transceiver. Furthermore, smart thermostats use communication procedures such as Wi-Fi, Radio-Frequency (RF) and Bluetooth which allow occupant wireless control over HVAC system. In addition, the occupant follows and controls thermal comfort parameters even on smart phones and personal computers. In conclusion, the data is stored in a web-server. Thus, thermostat learns occupant behaviors by using existing data in server. Moreover, smart thermostats understand the absence/presence of occupants with the help of Passive Infrared (PIR) sensors to decrease energy consumption when the occupant is outside of building. Gruber et al. (2015) showed that 20% of energy usage can be decreased in buildings by using PIR sensors. However, the ability to reliably detect occupancy states is limited by the lack of sensing technologies (Pisello & Asdrubali, 2014). Additionally, intense caution is requested to develop control algorithm which lays on presence of occupants since more energy can be required to satisfy fully thermal comfortable environment again when occupant come back.

With the development of smart thermostats, energy engineers and architects find an opportunity to monitor energy consumption of building; on the other hand, occupants are able to interact with intelligent building. Although there are some studies on developing smart systems for intelligent buildings in literature (Feldmeir, 2009; (Ranjan

& Scott, 2016), (Turhan, 2018)), smart thermostats are also highly used in industrial applications (Google Nest, 2018; Ecobee, 2019; Honeywell, 2019) (Fig.2).

Figure 2. Examples of commercially available smart thermostats

Smart thermostat producers offer different options to the occupants not only energy control of HVAC system but also water and gas leakage controls in building. However, smart thermostats require expert users due to their complex control mechanisms. Many occupants are aware of advantageous and features of these intelligent systems ((Danassis, Siozios, Korkas, Soudris, & Kosmatopoulos, 2017)). Moreover, according to Peffer et al. (Peffer, Perry, Pritoni, Aragon, & Meier, 2013), occupants find interfaces of smart thermostats quite confusing. Smart thermostats use wireless communication technologies which can be easily intercepted by unauthorized users. Security is a serious problem on vulnerable and unreliable device such as smart thermostats. Moreover, occupants have privacy concern since the system stores there is no occupant in the building. A potential attacker could reach this information by using the wireless network. (Worthy, Matthews, & Viller, 2016) stated that trust on smart thermostats is the biggest limitation on intelligent buildings.

(Awojobi & Chang, 2017) indicated that the need of smart thermostats will be increased by 30% in 2020 compared to 2015. However, smart thermostats are still expensive since they include large number of sensors. The costs of smart thermostats vary between 249$ and 469$ (Burrough & Gill, 2015). The high price is an obstacle on growing demand. Considering the increase on elderly population in Europe, adaptation of smart thermostats is a vital challenge to create intelligent buildings.

This paper proposes to address some significant challenges on using smart thermostats in intelligent buildings. The focus is on not only privacy and security concerns but also social and economic aspects. The knowledge of these challenges would help occupants and smart thermostat producers to make better and more secure environments in intelligent buildings.

CHALLENGES ON SMART THERMOSTATS

Smart thermostats become popular in the early of 21th century. After development of technology in building sector, these systems are seen as the best commercial energy saving system for buildings. The advantages of smart thermostats are being an occupant centric HVAC control system and continuous communication between occupants and electronic devices in intelligent building. These devices decrease energy consumption of buildings by learning occupant behaviors and schedules. On the other hand, smart thermostats have some serious security gaps and these gaps could be potential threats for the occupants. Challenges on smart thermostats can be stated as privacy, security and other challenges such as operational and occupant centric errors and some threats are discussed in detail on this section.

Privacy

Smart thermostats learn behavioral patterns of occupants who live their routine life in their home. These patterns play a significant role for energy savings. Smart thermostat systems are collecting occupants both daily behavioral and environmental data ((Hernandez, Arias, Buentello, & Jin, 2014). The collected data are then converted into zeros and ones (0s and 1s) and are sent to microcontrollers to generate meaningful outputs. Smart thermostats are integrated with HVAC systems of intelligent buildings, thus, they increase energy efficiency of the building with corresponding outputs. However, collected data or/and internet servers (Malar & Prabhu, 2019). Previous works (Hou et al., 2016) showed that these collected data were also sent to 3rd parties which create privacy concerns for occupants. Moreover, privacy concerns include privacy risks due to pairing and discovery protocols that leak information about devices in the home (Demeure, Caffiau, Elias, & Roux, 2015)These systems can allow an attacker to remotely track occupant's life. Another problem is in shared intelligent homes. The occupants can track their home-friend's daily routine life via internet services. For instance, a baby monitor in an intelligent building was hacked by an attacker in 2013 and baby was tracked by a spy for two months (Hill, 2013). Similar attacks can be seen for smart thermostats.

Security

Smart thermostats communicate between occupants and HVAC systems by using RF, Bluetooth and Wi-Fi communication procedures(Davidson, Rezwana, & Hoque, 2019). Each communication procedures have their own advantages and disadvantages in terms of security. RF is beneficial when a Wi-Fi network is not available or reachable. Wi-Fi technology is significant when a machine to machine (M2M) communication is needed with remote control. RF procedure is more secure than Wi-Fi technology; however, the

procedure can be easily interrupted with external sources and might cause some energy consumption problems (Decoutere, Carchon, Dehan, & Mercha, 2005). Smart thermostats generally use Wi-Fi network which allows many electronic devices to connect same link (Zeng, Mare, Roesner, & Allen, 2017). The occupant uses a password to access Wi-Fi connected electronic devices. However, many authors indicated that occupants have security concerns with their internet connected smart thermostats(Manic, Amarasinghe, Rodriguez-Andina, & Rieger, 2016). For example, smart thermostats uses eco-mode (sleeping mode) when the occupant leaves the building and thus decrease energy consumption. However, GPS technique or PIR sensors are used to understand absence/presence of occupants and these data are stored in web-servers. Some attackers can reach this information and understand if the home is unoccupied or occupied and even understand that how many occupants live in that intelligent building. These systems have security gaps that can be hacked to remotely accessible (Lee, Lin, & Owe, 2019). Once it is hacked it gives continuous information about occupants' location, motion activity within the home or sleeping condition.

Other challenges

1. Smart thermostats have structural errors which lead energy consumption increase and thermal discomfort (Nägele, Kasper, & Girod, 2017). Big limitations of smart thermostats are their sleeping or eco-modes. These modes are activated with the occupant absence and/or sensing no motion in the building. Smart thermostat would be useless when occupant who has an amnesia or a baby that requires intense care during whole night. Smart thermostat cannot learn extreme behaviors which creates thermal discomfort and more energy consumption.

2. Some smart thermostats track location of occupants via GPS technologies in order to adjust set-temperature of HVAC system. However, a guest in intelligent building can ruin training period of smart thermostat. For instance, if the occupant deactivates the system, it will lead more energy consumption. If the occupant uses smart thermostat, the behavioral pattern will be guest's pattern. This training error will affect testing period and lead wrong decisions for HVAC system.

3. All smart thermostat systems use operation networks. The main module of these devices acts like the brain of the network and unfortunately can only deal with limited tasks. Considering the aim of smart thermostat is to decrease energy consumption and increase thermal comfort, the main module must be connected in the main room for energy efficiency. The challenge is if an occupant lives in a residence which has more than one room, the set-temperature of HVAC system will only be adjusted for the main room. Producers still sell extra parts apart from the main system just for plugging the other

rooms. Therefore, it will not only increase energy consumption but also the canalize occupants to buy extra sensors.

4. Behavioral patterns update itself once a week(Moustaka, Theodosiou, Vakali, Kounoudes, & Anthopoulos, 2019). Extreme or intense conditions are always ignored in smart thermostats. For example, an occupant could be sick and could need extra care for heating/cooling condition. In current systems, these possibilities are ignored and it will be annoying for the occupants to set temperature manually.

5. Smart thermostats use memory cards in their systems. Memory card contains all the collected data for intelligent building. Then, they provide communication between the occupants and HVAC system. However, memory cards are a big threat for these systems. Firstly, all smart thermostats require power for proper operation. Most of the cases, the power is supplied from batteries or directly from the city grid. Batteries could be a problem for the zones that cannot be changed easily. Secondly, if the thermostat is connected to city grid and the electricity goes off, smart thermostats reboot themselves. The challenge is losing behavioral patterns of occupants and the system needs to train itself again. This period is very time-consuming and requires more energy. Another issue is the internet crashes. Continuous data transfer is obtained from the occupants such as their location and clock information etc. Case of connection lost, smart thermostat systems will not operate accurately and cause thermal discomfort or energy loss.

6. Smart thermostats use occupancy detectors. Occupancy detectors are often falsely triggered by pets. Especially cats are curious animals, they will try to attack or play with smart thermostat systems. Also, some of the smart thermostat systems are integrated with security systems which have PIR sensors. False movement detection may not only trigger smart thermostat systems but also security system of building. Since smart thermostat systems are beneficial because of their energy-saving potential, a false trigger may cause a serious decrease in energy saving potential.

7. Smart thermostats learn occupant behaviors. These behaviors are updated once a week when smart thermostats sense a difference in the occupant's behavior. If the occupant has not any daily routine, these systems become unreliable. If smart thermostat system cannot develop meaningful data, HVAC system will use more energy.

8. One of the main challenges of smart thermostat is initial cost. Main thermostat system is around $250 but it is not 100% effective when occupants only have this system alone. For higher effectiveness companies are selling additional sensors for each room. Each sensor is around $80. Higher energy efficiency requires large number of sensors, therefore, investment costs are high and the pay-back periods are long.

9. For highest efficiency, smart thermostat systems are continuously communicating with occupants via Mobil applications installed into smart phones. This communication requirement causes some problems where the elder population is higher such as European countries (Europe Populatin, 2019).Elder occupants use less technology compared with younger populations. Separate from this situation, most of the old people do not have smart phones, which are required for efficiency gain in smart thermostat systems. The setup process of smart thermostat systems is also complicated for elders. It requires several cable connection, Wi-Fi or radiofrequency settings, etc. Therefore, these systems are not easily integrated with elders and would not be beneficial for them.

10. Thermal comfort is necessary for humans, animals, and plants. Almost all systems are designed for thermal comfort of occupants, however, thermal comfort of pets and plants are also significant. Smart thermostat systems go sleeping or eco-modes when occupants are not present in the building. Animals and plants do not have any chance to change their location. Eco-mode settings would be harmful for them. Humidity would change fast or temperature would be unbearable.

RECOMMANDATIONS

In this section, some recommendations are indicated about the challenges of smart thermostats. Some minor changes on the system can be effective to overcome problems mentioned above.

Privacy

Occupant behavioral data is stored both in the cloud network and memory card of smart thermostat systems. Some attackers can easily hack internet-connected systems. Cloud transmission is obtained by a Wi-Fi network and has security vulnerability by an external interruption. Ethernet cables are not easy to interrupt and may be used for the internet connection of smart thermostats. Smart thermostat system uses mobile applications to communicate with occupants. Smart phones became mainstream and reached out to almost everybody in the 21st century. Malwares are getting developed for smart phones too. Since smart thermostat systems got all your behavioral data it is highly risky for occupants to carry these pieces of information with them. We recommend companies to encrypt their data and develop an encrypted mobile application for the occupant. Companies should also create a secure network for domestic communication between smart systems.

Security

RF communication is more secure than Wi-Fi communication. On the other hand, RF can be interrupted with other electronic devices in intelligent building. For instance, all microwaves outflow radiation which interferes with the RF. Similarly, television receivers use RF and transmitters also interfere with the RF. The recommendations are a careful installation of these electronic devices and get regular maintenance. This solution will decrease interruptions and develop a smooth communication path. Creating a secure internet network is vital if smart thermostat uses Wi-Fi communication between occupants and HVAC systems. To shatter security concerns of occupant, producers should generate a secure internet and Wi-Fi networks for just smart thermostat systems.

Another security issue is GPS module of smart thermostat systems. GPS is required for pre-heating of residences or post-deactivate of HVAC systems. Any external interfere will provide occupants current position information to 3rd parties. Occupants can de-activate this module and create a message-based communication. Occupants should be able to communicate with the system via short message services (SMS). After leaving/arriving the building, occupants could send SMS to smart thermostat systems and adjust the set-temperature. A simple notification will be sent to occupants for reminding to use this service.

Other challenges

Behavioral pattern is focused on occupants in intelligent building but the system often fails when a guest exists. The training period of smart thermostat becomes longer and time-consuming. Producers can add extra devices which are operated according to guest's schedule. It is worth to note that smart thermostat should take into multi-user interactions consideration.

Most of the smart thermostats update themselves once a week when smart thermostats sense a difference in the occupant's behavior. Update periods can be shortened by the producers in order to decrease energy consumption since daily routines of occupant can change time to time.

Occupancy detection is satisfied with the help of PIR sensors in smart thermostat systems. PIR sensors can be falsely triggered by pets. Producers should include more sensitive sensors that discriminate occupants from pets.

Pets and babies are often curious which often try to reach smart thermostat systems. For security, producers should install the smart thermostat systems higher. Thus, pets and babies could not reach the smart thermostat easily.

Smart thermostats are operated from main module in main room. The main module is sold around $250 and each separate sensor is sold about $80 for other rooms. Producers should decrease the cost of sensors.

Producers should take elderly population into account for smart thermostat systems. The interfaces can be more user-friendly for elders. External guidance can be required.

CONCLUSIONS

Smart thermostats are highly becoming popular in intelligent building sector. Alongside the convenience of these systems, smart thermostats bring occupants privacy, security and other concerns. The aim of this paper is to highlight challenges on smart thermostats in intelligent buildings. The research shows that Wi-Fi communication procedure exemplifies a big challenge for smart thermostats. Occupants carry security and privacy concerns while using these systems. Another big challenge is growing elderly population in Europe. Old population requires external guidance to use and understand interfaces of smart thermostats. Although there are some publications that investigate the challenges on smart systems in intelligent buildings, more researches are needed to understand challenges. The knowledge of these challenges would help occupants and smart thermostat producers to make better and more secure environments in intelligent buildings.

REFERENCES

Europe Population. Retrieved from https://www.worldometers.info/world-population/europe-population/ (Date accessed 21.08.2019)
Google Nest Smart-Thermostat. Retrieved from https://nest.com/ (Date accessed 21.08.2019)
Ecobee Smart-Thermostat. Retrieved from https://www.ecobee.com/ (Date accessed 21.08.2019)
Honeywell Smart-Thermostat. Retrieved from https://www.honeywellhome.com/en/products/wi-fi-thermostats (Date accessed 21.08.2019)
Hill, K. (2013, August 27). 'Baby Monitor Hack' Could Happen To 40,000 Other Foscam Users. Retrieved from https://www.forbes.com/sites/kashmirhill/2013/08/27/baby-monitor-hack-could-happen-to-40000-other-foscam-users/#3e11d7158b5a
Ashrae. (2017). ASHRAE Handbook Series. Retrieved from https://www.ashrae.org/technical-resources/ashrae-handbook/description-2017-

ashrae-handbook-fundamentals
Awojobi, A., & Chang, H. (2017). Security and Privacy Issues with Smart Thermostats – A First Look.
Burrough, M., & Gill, J. (2015). Smart thermostat security: turning up the heat. Retrieved from https://burrough.org/papers/523-Final-Paper.pdf
Danassis, P., Siozios, K., Korkas, C., Soudris, D., & Kosmatopoulos, E. (2017). A low-complexity control mechanism targeting smart thermostats. Energy and Buildings, 139, 340–350. https://doi.org/10.1016/J.ENBUILD.2017.01.013
Davidson, C., Rezwana, T., & Hoque, M. A. (2019). Smart Home Security Application Enabled by IoT: BT - Smart Grid and Internet of Things (A.-S. K. Pathan, Z. M. Fadlullah, & M. Guerroumi, eds.). Cham: Springer International Publishing.
Decoutere, S., Carchon, G., Dehan, M., & Mercha, A. (2005). Passive on-chip components: Trends and challenges for RF applications. Microelectronic Engineering, 82(3–4), 503–513. https://doi.org/10.1016/J.MEE.2005.07.050
Demeure, A., Caffiau, S., Elias, E., & Roux, C. (2015). Building and Using Home Automation Systems: A Field Study. https://doi.org/10.1007/978-3-319-18425-8_9
EU. (2018). Energy performance of buildings and Directive 2012/27/EU on energy efficiency (Text with EEA relevance). Official Journal of the European Union, 156(75), 1–17. Retrieved from https://eur-lex.europa.eu/legal-content/EN/TXT/PDF/?uri=CELEX:32018L0844&from=EN
Hernandez, G., Arias, O., Buentello, D., & Jin, Y. (2014). Smart Nest Thermostat : A Smart Spy in Your Home. Black Hat USA, 1–8.
Hou, L., Zhao, S., Xiong, X., Zheng, K., Chatzimisios, P., Hossain, M. S., & Chen, W. (2016). Internet of Things Cloud: Architecture and Implementation. IEEE Communications Magazine, 54(11), 32–39. https://doi.org/10.1109/MCOM.2016.1600398CM
Lee, M.-C., Lin, J.-C., & Owe, O. (2019). PDS: Deduce elder privacy from smart homes. Internet of Things, 7, 100072. https://doi.org/10.1016/J.IOT.2019.100072
Malar, M. B. B. A., & Prabhu, J. (2019). An analysis of security issues in cloud computing. International Journal of Civil Engineering and Technology, 10(2), 2138–2153.
Manic, M., Amarasinghe, K., Rodriguez-Andina, J. J., & Rieger, C. (2016). Intelligent Buildings of the Future: Cyberaware, Deep Learning Powered, and Human Interacting. IEEE Industrial Electronics Magazine, 10(4), 32–49. https://doi.org/10.1109/MIE.2016.2615575
Moustaka, V., Theodosiou, Z., Vakali, A., Kounoudes, A., & Anthopoulos, L. G. (2019). Enhancing social networking in smart cities: Privacy and security borderlines. Technological Forecasting and Social Change, 142, 285–300. https://doi.org/10.1016/J.TECHFORE.2018.10.026
Nägele, F., Kasper, T., & Girod, B. (2017). Turning up the heat on obsolete thermostats: A simulation-based comparison of intelligent control approaches for residential heating systems. Renewable and Sustainable Energy Reviews, 75, 1254–1268. https://doi.org/https://doi.org/10.1016/j.rser.2016.11.112

Nguyen, T. A., & Aiello, M. (2013). Energy intelligent buildings based on user activity: A survey. Energy and Buildings, 56, 244–257. https://doi.org/10.1016/J.ENBUILD.2012.09.005

Peffer, T., Perry, D., Pritoni, M., Aragon, C., & Meier, A. (2013). Facilitating energy savings with programmable thermostats: evaluation and guidelines for the thermostat user interface. Ergonomics, 56(3), 463–479. https://doi.org/10.1080/00140139.2012.718370

Pisello, A. L., & Asdrubali, F. (2014). Human-based energy retrofits in residential buildings: A cost-effective alternative to traditional physical strategies. Applied Energy, 133, 224–235. https://doi.org/10.1016/J.APENERGY.2014.07.049

Ranjan, J., & Scott, J. (2016). ThermalSense: determining dynamic thermal comfort preferences using thermographic imaging. https://doi.org/10.1145/2971648.2971659

Široký, J., Oldewurtel, F., Cigler, J., & Prívara, S. (2011). Experimental analysis of model predictive control for an energy efficient building heating system. Applied Energy, 88(9), 3079–3087. https://doi.org/10.1016/J.APENERGY.2011.03.009

Turhan, C. (2018). Development of energy-efficient personalized thermal comfort driven control in HVAC systems. Retrieved from http://openaccess.iyte.edu.tr/handle/11147/7166

Worthy, P., Matthews, B., & Viller, S. (2016). Trust me: Doubts and concerns living with the internet of things. DIS 2016 - Proceedings of the 2016 ACM Conference on Designing Interactive Systems: Fuse, 427–434. https://doi.org/10.1145/2901790.2901890

Zeng, E., Mare, S., Roesner, F., & Allen, P. G. (2017). End User Security and Privacy Concerns with Smart Homes End User Security & Privacy Concerns with Smart Homes. (Soups). Retrieved from https://www.usenix.org/conference/soups2017/technical-sessions/presentation/zeng.

EFFECT OF SHEAR SPAN AND REINFORCEMENT RATIO ON NORMAL AND HIGH STRENGTH REINFORCED CONCRETE ONE WAY SLAB

Sara Sh. Alhilali
Department of Civil Engineering, University of Gaziantep, Turkey
sara.alhilali@mail2.gantep.edu.tr

Bahaa H. Al-Abbas
Department of Civil Engineering, University of Kerbala, Iraq
bahaa.hussain@uokerbala.edu.iq

Mustafa ÖZAKÇA
Department of Civil Engineering, University of Gaziantep, Turkey
ozakca@gantep.edu.tr

ABSTRACT: This paper investigates the flexural behavior, ultimate load carrying capacity, deflection, and cracking for High-Strength Concrete (HSC) and Normal-Strength Concrete (NSC) one way solid slab. For this, reinforced concrete slabs with rectangular in cross-section and nominally 3500 mm long, 600 mm width, and 150 mm thickness with a clear span (distance between supports) of 3300 mm are analyzed. Nonlinear finite element analysis (FEA) under four points loading are carried out. These types of slabs could be analyzed numerically by using software program ANSYS19.1. The parameters studied in this research are the concrete strength (NSC with f_c'=34 MPa and HSC with f_c' =52 and f_c' =70 MPa), different shear span to effective depth ratios (a/d), and effective of tensile longitudinal reinforcement ratio. The results indicated that increasing the amount of reinforcement ratio for HSC improved the peak load carrying capacity and reducing the mid-span deflection ductility as compared to NSC with the same reinforcement configuration. The numerical findings also point out that the ultimate capacity of these slabs reduces with increasing the ratio (a/d) for (6, 8, and 10) respectively. Peak load obtained from FEA were verified by comparison with previous experimental research and had good correlation with the experimental result.

Keywords: reinforced concrete slab, ANSYS, flexural behavior, nonlinear finite element.

INTRODUCTION

The one way solid slab is a unique efficient structural system. The possibility of producing one-way simply supported slab with NSC and HSC has opened now opportunities for structural designers. It is economically important and widely used in structural applications such as roofs, floors, and walls. A significant amount of research

has previously focused on behavior of reinforced concrete members built with HSC (Li & Aoude 2019, Mohebi et al 2019, Al-Shamiri et al 2019).

In the past many of researchers studies on the structural behavior of HSC and NSC simply supported slab. Al-Azzawi, & Abed (2017) tested one way solid slab for different shear span to depth ratios (a/d) (2, 2.5, and 3) and the results showed that the ultimate load carrying capacity of the slab reduces with increasing the ratio (a/d) under flexural failure. Mahmoud (2015) have carried out the nonlinear FEA of 16 flat-slab models using ANSYS10 software for studying the shear reinforcement behavior on flat slab. In this research parameters studied are slab thickness and punching shear reinforcement. Shehab et al (2017) carried out experimental work and nonlinear FEA by using ANSYS program for studying the opening ratio effect on solid one way slab. They showed that the FEA results had a good agreement with the experimental results. Al-Azzawi & Abed (2006) reported a series of modeling by software ANSYS for simply supported solid NSC (concrete strength as 25, 38, and 45 MPa) slab. They reported that, the compressive strength increases caused increase in cracking and peak load. Qin et al (2017) studied on effect of different reinforcement ratio on the flexural performance. They noted that ductility of reinforced concrete beam specimens are reduced by decreasing the hybrid reinforcement ratio.

The objective of paper is to investigate the flexural behavior, ultimate load carrying capacity, deflection, and cracking for HSC and NSC one way solid slab using nonlinear FEA.

ANALYTICAL PROGRAM

The analytical program consisted of analyses of 27 full-scale one-way spanning slab. All slabs were rectangular in cross-section and nominally 3500 × 600 × 150 mm with a clear span of 3300 mm as shown in Figure 1. These slabs specimens were separated to three sets according to concrete strength in which f_c' =34 MPa for NSC , f'_c= 52 MPa and f'_c= 70 MPa for HSC and each of them included three types of shear span to effective depth ratio (a/d) (6, 8, and 10) and different steel reinforcement ratio (0.22, 0.34 and 0.5). Details and description of analyzed specimens are shown in Table 1.

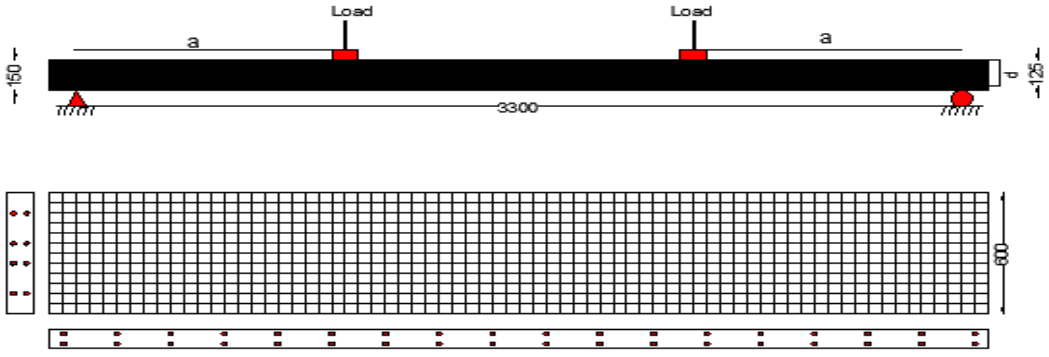

Fig.1 Details of specimens

Table 1 Description of specimen

Group	NSC	HSC		Top steel reinforcement		Bottom steel reinforcement		$\frac{As}{Ac}$%
1	S34-6-1	S52-6-1	S70-6-1	4ø8@150	18ø8@200	18ø8@200	4ø8@150	0.22
	S34-6-2	S52-6-2	S70-6-2	4ø8@150	18ø8@200	18ø8@200	4ø10@150	0.34
	S34-6-3	S52-6-3	S70-6-3	4ø8@150	18ø8@200	18ø8@200	4ø12@150	0.50
2	S34-8-1	S52-8-1	S70-8-1	4ø8@150	18ø8@200	18ø8@200	4ø8@150	0.22
	S34-8-2	S52-8-2	S70-8-2	4ø8@150	18ø8@200	18ø8@200	4ø10@150	0.34
	S34-8-3	S52-8-3	S70-8-3	4ø8@150	18ø8@200	18ø8@200	4ø12@150	0.50
3	S34-10-1	S52-10-1	S70-10-1	4ø8@150	18ø8@200	18ø8@200	4ø8@150	0.22
	S34-10-2	S52-10-2	S70-10-2	4ø8@150	18ø8@200	18ø8@200	4ø10@150	0.34
	S34-10-3	S52-10-3	S70-10-3	4ø8@150	18ø8@200	18ø8@200	4ø12@150	0.50

ELEMENT TYPE AND MESHING

The 3D finite element program, ANSYS R 19.1, was used in this study to simulate the flexural behavior of twenty seven reinforced concrete one-way slabs. A nonlinear FEA modeling has been carried out by using ANSYS parametric design language (APDL), which generally based on mesh of a continuous domain into a set of discrete subdomains, called element representing the steel reinforcement and concrete. In this study, the discrete element was used to simulate reinforcement, where the reinforcement is modelled using link element connected to the mesh of concrete nodes as shown in Figure 2. Also, the concrete exists in the same regions occupied by the reinforcement, generally full bond is assumed between the concrete and steel bar reinforcement.

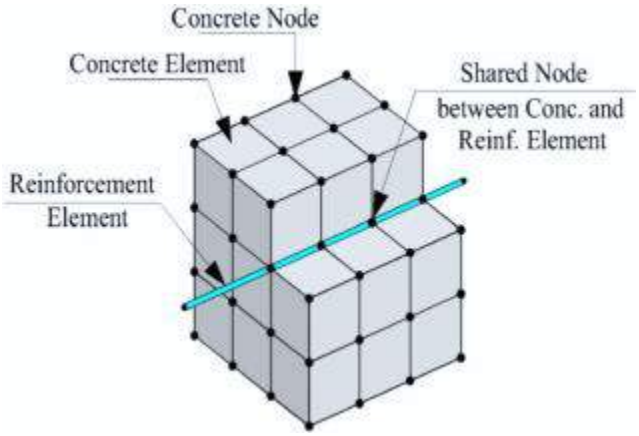

Fig.2 Discrete model for reinforced concrete

Concrete was modeled using (SOLID65) 3D 8-node solid elements. The feature of this element is the ability to account the behavior of nonlinear material, and also capable of prevent the perpendicular cracking in three directions creep, plastic deformation and crushing. The element having three degrees of freedom at each node in the x, y & z directions is defined by eight nodes as shown in Figure 3(a). The steel reinforcement are represented by (LINK180), this element is a uniaxial tension–compression have three degrees of freedom at each node, and also capable of plastic deformation. Figure 3(b) explain the geometry of LINK180. The element (SOLID185) as shown in Figure 3(c) is used for modeling the steel plates with three degrees of freedom at each node in the x, y & z directions. The element is capable of hyper elasticity, plasticity, stress stiffening, large deflection, creep, and large strain capabilities.

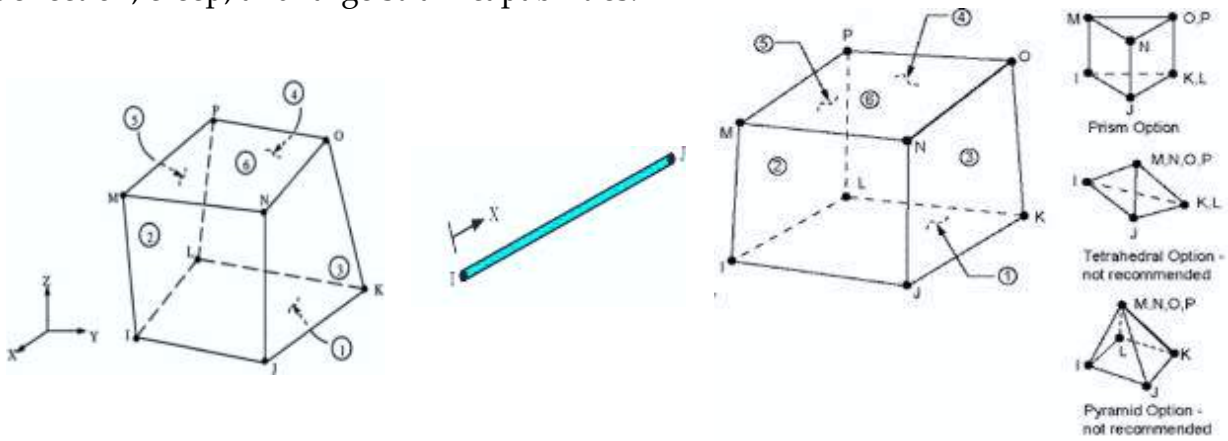

(a) SOLID65 (b) LINK180 (c) SOLID185

Fig.3 The type of element used for FEA modelling

Four types of concrete mesh solid slab are used to find the best mesh density (1260, 2400, 5040, & 9000 element) as shown in Figure 4.

MATERIAL MODELS

Multi-linear isotropic properties are required for solid65 element to model the behavior of concrete. The failure of concrete define by multi-linear material uses von Mises criterion along with the (Warnk & Willam 1974). Modulus of elasticity of concrete (E_c) based on Eq (1) for NSC & HSC.

$Ec = 4700\sqrt{fc'}$ for NSC and $Ec = 5700\sqrt{fc'}$ for HSC (1)

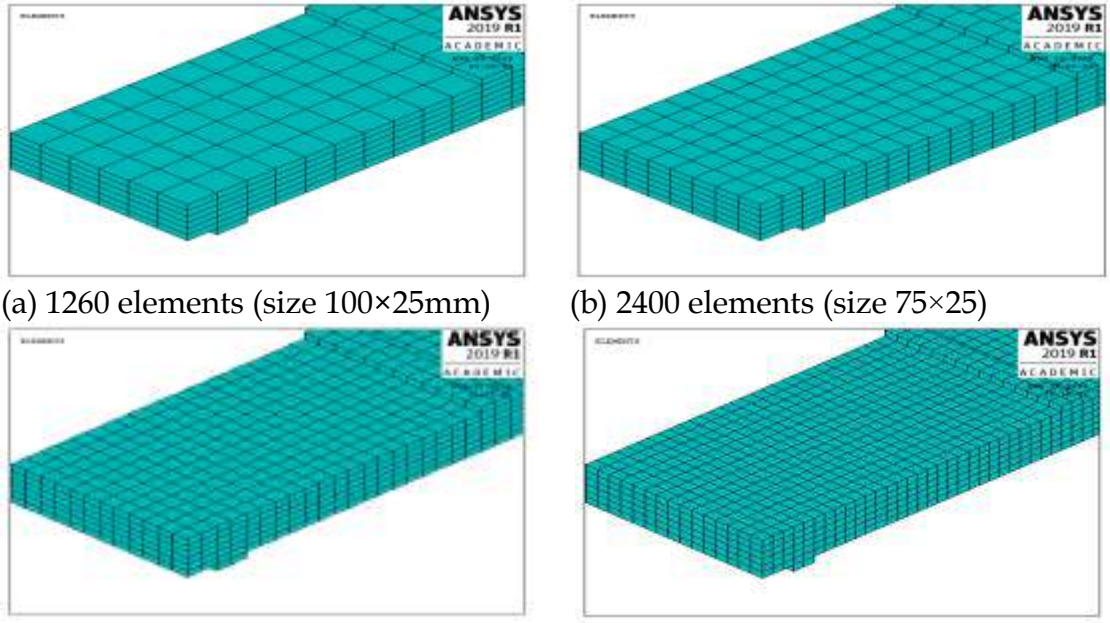

(a) 1260 elements (size 100×25mm) (b) 2400 elements (size 75×25)

(c) 5040 element (size 50×25) (d) 9000 element (size 35×25)

Fig.4 Finite element meshing

The compressive strength of concrete considered in present study was 34, 52 & 70 MPa with 0.2 Poisson's ratio. The uniaxial stress-strain relationship for NSC in compression as shown in Figure 5(a) are required for software and construct in Eq (2) (Gere and Timoshenko, 1997)

$$f = \frac{Ec*\varepsilon}{1+(\frac{\varepsilon}{\varepsilon_o})^2} \qquad \varepsilon_0 = \frac{2fc'}{Ec} \qquad E_c = \frac{f}{\varepsilon_0} \qquad (2)$$

While the stress-strain curve for HSC shown in Figure 5(b) using Eq 3 (Sargin 1971).

$$f_c = \frac{f'_c A\left(\frac{\varepsilon}{\varepsilon_{co}}\right)+(D-1)(\frac{\varepsilon}{\varepsilon_{co}})^2}{1+(A-2)\left(\frac{\varepsilon}{\varepsilon_{co}}\right)+D(\frac{\varepsilon}{\varepsilon_{co}})^2} \qquad E_{it} = 5975\sqrt{fc'} \quad D = 0.65 - 7.25f_c^{`}10^{-3} \quad A = \frac{E_{it}*\varepsilon_{co}}{f_c^{`}} \qquad \varepsilon_{co} = 0.0024 \qquad (3)$$

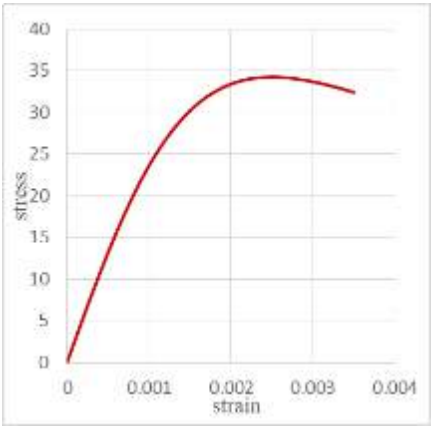

(a) Stress-strain curve for NSC, (Gere and Timoshenko1997)

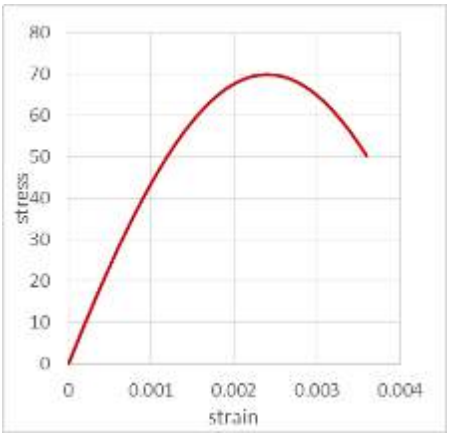

(b) Stress-strain curve for HSC, (Sargin 1971)

Fig.5 Stress strain curve for NSC and HSC

The shear transfer coefficients are ranged from (0.0 to 1.0), with 0.0 for smooth crack and 1.0 for rough crack. The various values attempted for shear transfer coefficients open crack Bt and closed crack Bc within a range between (0.15 to 0.9) for Bt and (0.5 to 0.9) for Bc. In this study, Bt and Bc were set to 0.2 and 0.8 respectively (Shehab & El-Awady, 2017). These values were achieving a good converging results. The uniaxial cracking strength is calculated using (Al-Azzawi & Abed, 2017):

$$f'ct = o.5\sqrt{fc'} \qquad (3)$$

The steel reinforcement element was assumed to be bilinear isotropic inelastic material and agreeing in tension and compression as shown in Figure 6. Poisson's ratio of 0.3 was used for all reinforcement types, LINK180 and SOLID185 in linear isotropic material, while the young modulus was 200 GPa for desecrate steel bar and 2000 GPa for support plate.

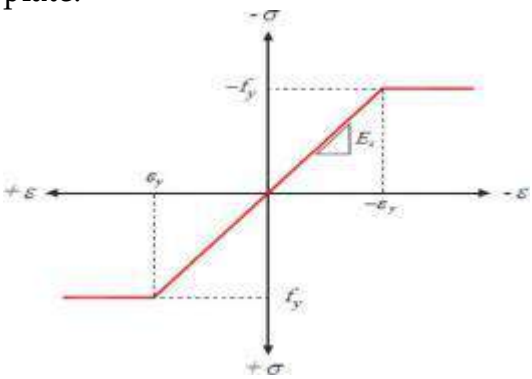

Fig.6 Stress-strain curve for steel

LOADS AND BOUNDARY CONDITIONS

The model acts the same way as the experimental slabs, boundary conditions were applied at four steel plates have 25 mm thickness, 100 mm width and 600 mm long. These modeled by SOLID185 element which located under the slabs to prevent local cracking in concrete, and over the surface of slabs with the required locations for applied loading as shown in Figure 7(a). The external loads were applied as concentrated load on mid top nodes of plate as a $(\frac{p/2}{13})$ for each node as shown in Figure 7(b). The model of steel plate at support have three degrees of freedom ux, uy, and uz. These are restrained with a centerline of the steel plate as a simply supported slab. Displacement is used to model the boundary condition in this ANSYS models, the left end were pinned by putting the value of the displacement degrees of freedoms for y and z directions to be equal zero and the roller support was created by putting the value of the displacement degrees of freedoms for y directions to be equal zero.

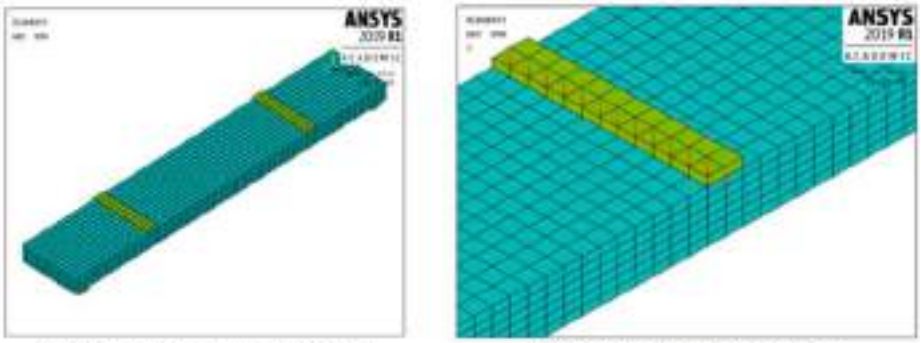

(a) Location of supports and loading (b) Distribution of loads on nodes

Fig. 7 Applied loads

ANALYSIS AND DISCUSSION OF RESULTS

Initially, a comparison has been achieved to proof the accuracy of present FEA model. These is done by modeling the same specimen and boundary condition for one way solid slab in a previous experiment research (Shehab & El-Awady 2017) as shown in Figure 8. The nonlinear FEA are carried out. The loads up to failure was done incrementally by the Modified Newton-Raphson method. Therefore the load step size is done by divided the applied load in to a series of load increments. The results were indicated that the FEA in this study have a good agreement with the previous experimental work as shown in Figure 9.

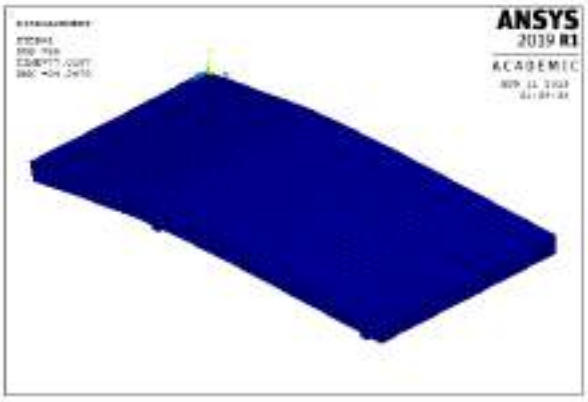

Fig. 8 The cantilever end one way solid reinforced concrete slab (Shehab & El-Awady 2017)

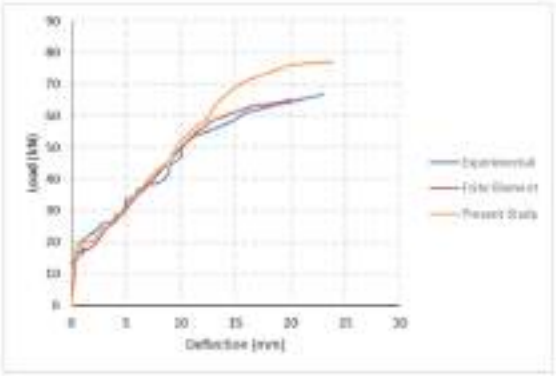

Fig. 9 Verification of Results with (Shehab & El-Awady 2017)

After verifying present FEA model, the flexural behavior, ultimate load carrying capacity, deflection, and cracking for HSC and NSC simple supported one way solid slab investigated in detail. First of all convergence analyses are carried out. The optimum results are obtained when the model have adequate number of elements. This is achieved when an increase in the mesh density cannot cause significant effect on the results as shown in Figure 10. Therefore, in this study can be concluded that the different elements number can be neglected when the number increase from (5040) to (9000), since (50mm) was selected in the modelling of all slabs.

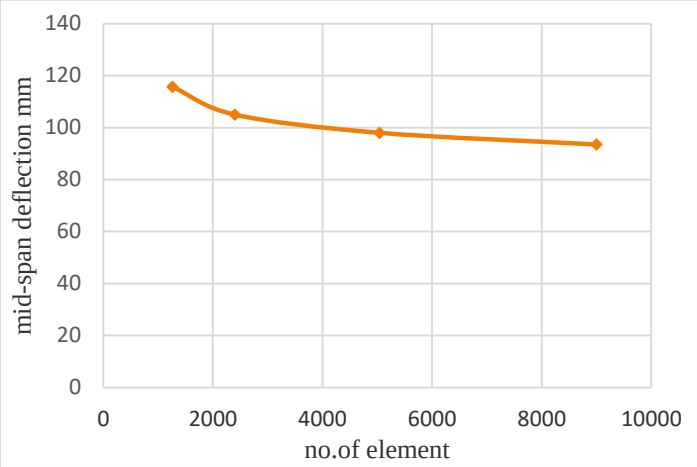

Fig. 10 Convergence of results

The FEA are repeated for three type of concrete ($f_c' = 34$, $f_c' = 52$, and $f_c' = 70$ MPa). The vertical deflection in y direction corresponding to ultimate slab strength is obtained at the center of the mid-span. The main cracks for modeling slabs specimens obvious at middle third as line with width of the slab from bottom face, all slabs exhibited flexural failure as shown in Figure 11. The equivalent normal stresses in longitudinal steel reinforcement was exceed the yielding of 420 N/mm² in all slabs sections as shown in Figure 12. Results are presented in Table 2. The minimum 11.61 kN and maximum 28.37 kN crack loads occurred at the specimens S34-10-1 and S70-6-3 respectively. The cracking load increases when the strength of concrete and reinforcement ratio increase and (a/d) ratio decreases. The similar behavior is observed for peak load. The minimum 5.55 mm and maximum 20.30 mm cracking deflections found at the specimen S52-10-3 and S70-6-1 respectively. It is noted that cracking deflection and peak load deflection decreases when the reinforcement ratio and (a/d) ratio increase.

The load of (19.477, 23.85, and 27.6425) kN are caused the first crack in the mid-span location with deflection of (16.3721, 18.4165, 20.306) mm slabs (S34-6-1, S52-6-1, and S70-6-1) respectively. The increasing in applied load resulted in more distributed crack in constant zone of moment. A peak load of (36.95, 38.45, and 41.463) were reached after considerable yielding of stress with deflection of (119.116, 194.687, and 221.895) respectively. The cracking loads, deflection at first crack, ultimate loads and ultimate deflections for slabs in (a/d) ratio equal to 8 and 10 are decreasing in compare with (a/d) ratio equal to 6, with notes that whenever the load increasing the deflection increased also for the same (a/d) ratio and different in concrete strength as shown in Table 2. The failure mode behavior for crack patterns are similar for all groups and shown in specimens up to compression.

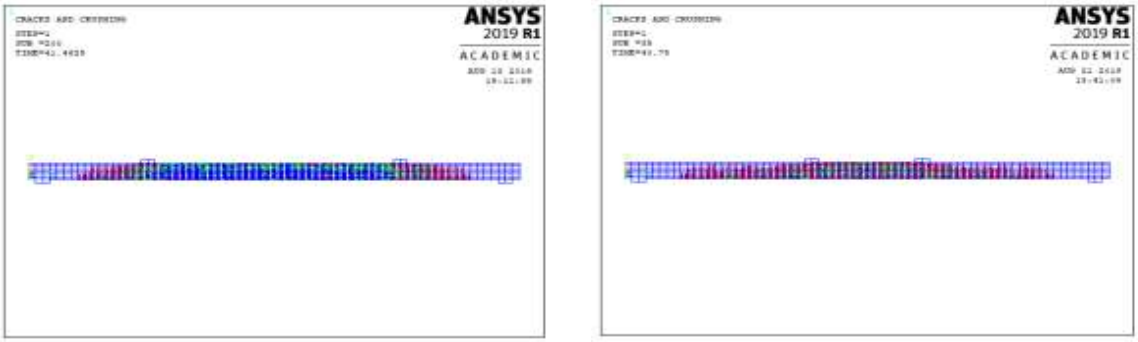

(a) S70-6-1 (b) S52-10-3

Fig. 11 Crack pattern

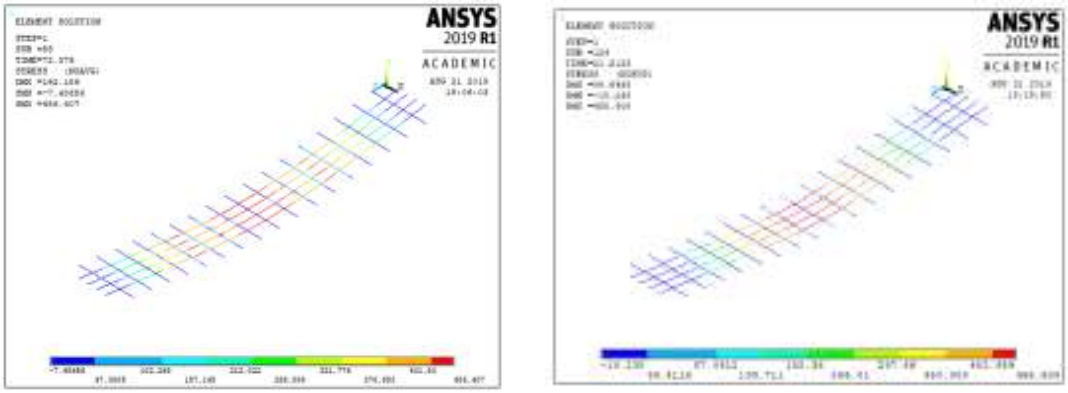

(a) S70-6-3 (b) S34-10-1

Fig.12 Equivalent normal stresses in longitudinal steel reinforcement

Table 2 Results of FEA

Specimen	Cracking load (kN)	Cracking deflection (mm)	ultimate load (kN)	ultimate deflection (mm)
S34-6-1	19.47	16.37	34.48	129.96
S34-6-2	19.78	11.10	47.98	98.65
S34-6-3	20.10	8.13	64.91	89.65
S52-6-1	23.85	18.41	38.45	194.68
S52-6-2	24.04	12.55	52.84	139.58
S52-6-3	24.35	9.42	68.35	95.42
S70-6-1	27.64	20.30	41.46	221.89
S70-6-2	27.76	13.78	56.06	183.26
S70-6-3	28.37	10.94	71.37	163.60
S34-8-1	14.53	12.01	26.16	106.98
S34-8-2	14.76	8.97	36.36	88.72
S34-8-3	15.26	7.08	47.96	67.42

S52-8-1	17.79	14.16	30.99	161.59
S52-8-2	17.99	9.78	41.99	139.39
S52-8-3	18.19	7.35	51.99	82.50
S70-8-1	20.60	16.19	33.40	211.73
S70-8-2	20.76	12.84	45.09	172.74
S70-8-3	21.01	8.52	59.36	154.01
S34-10-1	11.61	9.25	21.21	88.68
S34-10-2	11.85	6.66	28.95	67.91
S34-10-3	12.01	5.53	39.23	56.47
S52-10-1	14.17	11.58	26.42	152.22
S52-10-2	14.37	6.62	31.57	81.37
S52-10-3	14.75	**5.55**	40.75	73.37
S70-10-1	16.46	11.18	27.96	206.57
S70-10-2	16.78	8.19	36.36	150.68
S70-10-3	16.80	6.58	43.00	68.74

PARAMETRIC STUDY

A) **Effect of** (a/d): The analyzing of reinforced concrete solid slab is carried with different values of shear span to effective depth ratio. Three values of a/d are used as (6, 8, & 10) for normal and high strength concrete and these results are shown in Figure 13 which indicated that the increasing of (a/d) ratio the ultimate load decrease with decrease the deflection for the same reinforcement ratio and concrete strength solid slab.

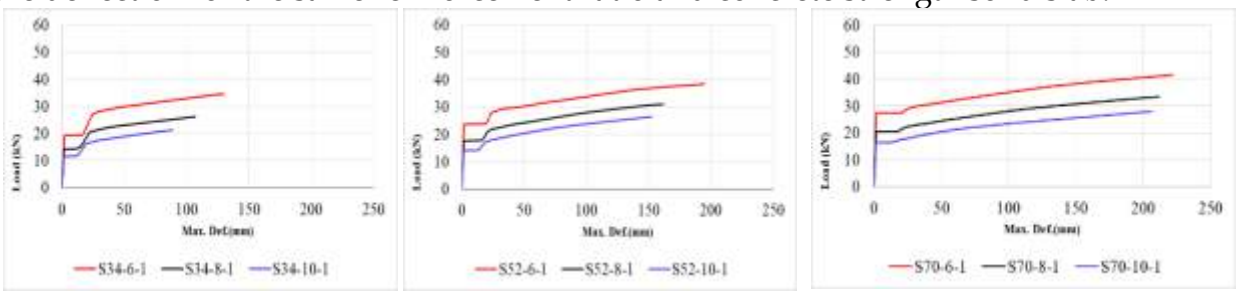

(a) f'_c=34MPa and reinforcement ratio 0.22 (b) f'_c=52MPa and reinforcement ratio 0.22 (c) f'_c=70MPa and reinforcement ratio 0.22

Fig.13 Effect of (a/d) ratio

B) **Effect of compressive strength**: The concrete slab under (a/d) equal (6, 8, and 10) was selected to investigate the influence of concrete grade on load-deflection behavior curve for the slab. It has been done by using different value of compressive strength as (f'_c =34, f'_c =52, and f'_c =70) MPa. The results shown in Figure 14 obtain from these study explained that the increases of concrete stiffness caused increasing in cracking and ultimate loads with increasing the mid-span deflection.

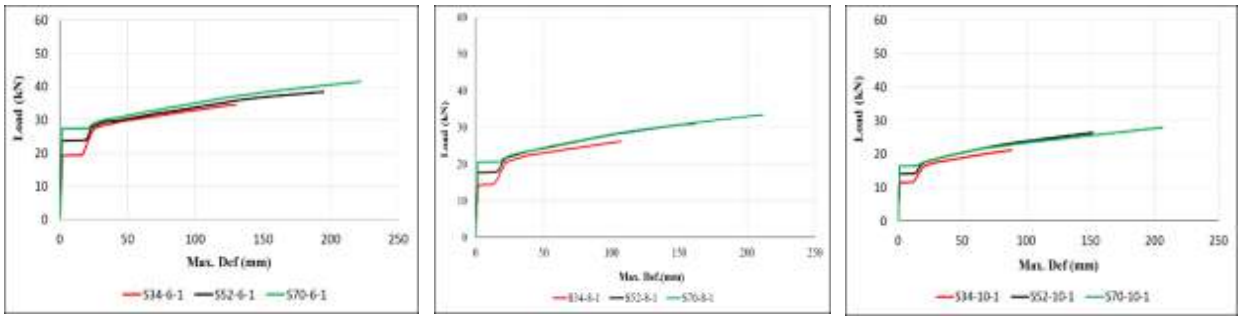

(a) (a/d) ratio = 6 and reinforcement ratio 0.22 (b) (a/d) ratio = 8 and reinforcement ratio 0.22 (c) (a/d) ratio =10 and reinforcement ratio 0.22

Fig.14 Effect of f_c'

C) **Effect of steel reinforcement ratio**: Three types of steel bar size ø8, ø10, and ø12 are corresponding to reinforcement ratios 0.22, 0.34, and 0.5 respectively. The results shown in Figure 15 explained for the NSC & HSC the ultimate load for slab section was improved against less of deflection in the same (a/d) ratio with the increased of steel reinforcement, while these increasing for different (a/d) ratio are decreased the peak load and deflection.

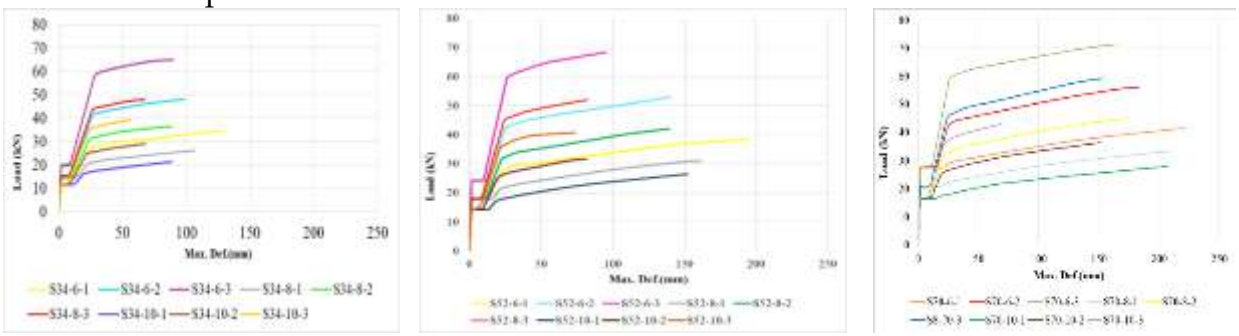

(a) f_c' =34MPa (b) f_c' =52MPa (c) f_c' = 70MPa

Fig. 15 Effect of reinforcement ratio

CONCLUSIONS

- The increasing of (a/d) ratio from 6 to 8 and 10 for the same concrete strength and reinforcement ratio lead to decreasing the ultimate load and mid-span deflection.

- The longitudinal steel bars at tension zone caused increasing in the peak load and reduction in deflection if the bar size are increasing from ø8 to ø10 and ø12 respectively.

- The concrete grade have an influence on cracking, ultimate strength, and deformed shape. The change of concrete properties from normal to high strength results

in increase the concrete strength and deflection, while the (a/d) and reinforcement ratio are remain constant.

- In high strength concrete solid slab the f_c' equal to 70 MPa have more stiff results if we compared with f_c' equal to 52 MPa.

- The FEA with increasing reinforcement ratio (As/Ac) from 0.22 to 0.34 and 0.5 respectively lead to decreasing in ultimate load and deflection for the different (a/d) ratio in RC slab

- The cracks for one way solid RC slab commenced at middle third with flexural failure mode.

- Maximum ultimate deflection equal 221.89 mm in specimen of (S70-6-1) due to the increase in compressive strength beside minimum steel reinforcement this allow specimen to more deform with ductility more than others. The vice versa with respect to the specimen (S34-10-3) which have the minimum ultimate deflection (56.47mm)

REFERENCES

ACI318-14 (2014). Building Code Requirements for Structural Concrete (ACI 318-14) and Commentary, Detroit, U.S.A.
Al-Azzawi, A. A. & Abed, S. A. (2006). Numerical analysis of reinforced concrete hollow-core slabs. ARPN Journal of Engineering and Applied Sciences, **11**(5), 9284=9296.
Al-Azzawi, A. A. & Abed, S. A. (2017). Investigation of the behavior of reinforced concrete hollow-core thick slabs. Comput. Concrete, **19**(5), 567-577.
Al-Shamiri, A. K., Kim, J. H., Yuan, T. F., & Yoon, Y. S. (2019). Modeling the compressive strength of high-strength concrete: An extreme learning approach. Construction and Building Materials, **208**, 204-219.
Li, Y., & Aoude, H. (2019). Blast response of beams built with high-strength concrete and high-strength ASTM A1035 bars. International Journal of Impact Engineering, **130**, 41-67.
Mohebi, Z. H., Bahnamiri, A. B., & Dehestani, M. (2019). Effect of polypropylene fibers on bond performance of reinforcing bars in high strength concrete. Construction and Building Materials, **215**, 401-409.
Mahmoud, A. M. (2015). Finite element implementation of punching shear behaviors in shear-reinforced flat slabs. Ain Shams Engineering Journal, **6**(3), 735-754.
Qin, R., Zhou, A., & Lau, D. (2017). Effect of reinforcement ratio on the flexural performance of hybrid FRP reinforced concrete beams. Composites Part B: Engineering, **108**, 200-209.
Sargin, M., Ghosh, S. K., & Handa, V. K. (1971). Effects of lateral reinforcement upon the strength and deformation properties of concrete. Magazine of Concrete Research, **23**(75-76), 99-110.

Shehab, H. K., Eisa, A. S., & El-Awady, K. A. (2017). Strengthening of cutouts in existing one-way Spanning RC Flat slabs using CFRP sheets. International Journal of Concrete Structures and Materials, **11**(2), 327-341.

INNOVATIVE AND ENVIRONMENTALLY FRIENDLY TWO DIMENSIONAL MATERIAL: BOROPHENE

Hakan ÇELEBİ
Aksaray University
hakanaz.celebi@gmail.com

İsmail ŞİMŞEK
Aksaray University

Tolga BAHADIR
Aksaray University

Şevket TULUN
Aksaray University
stulun@aksaray.edu.tr

Melayib BİLGİN
Aksaray University

ABSTRACT: After the discovery of graphene, numerous theoretical and experimental studies have been conducted to explore alternative two-dimensional (2D) materials in both energy and the environment. In these examinations, more efficient than graphene, mechanical, electronic and optical properties are tried to synthesize a variety of two-dimensional materials (silicene, almanen, stanen, phosphorene, arsenene, antimonene and borophen etc.). The main focus of these synthesis studies is not only to discover new materials, but also to integrate these materials into nano-scale applications in different fields and to improve their performance. In addition to developments in the production of new two-dimensional materials recently, there have been exciting developments in borofen synthesis. borofen has various potential applications due to its unique physical and chemical properties. In this review, physicochemical structure of boron, similarity with carbon, synthesis methods are examined with emphasis on the literature. In addition, other materials used, the development process and application areas of borofen (energy and environmental sectors) were evaluated.

Keywords: boron; borofen; energy applications; two-dimensional materials

YENİLİKÇİ VE ÇEVRE DOSTU İKİ BOYUTLU MALZEME: BOROFEN

ÖZET: Grafenin keşfinden sonra, hem enerji hem de çevre alanında alternatif iki boyutlu (2B) materyalleri araştırmaya yönelik çok sayıda teorik ve deneysel çalışma yapılmıştır. Bu incelemelerde, grafenden daha verimli, mekanik, elektronik ve optik özelliklerinin üst seviyede olduğu çeşitli iki boyutlu malzemeler (silisen, almanen, stanen, fosforen, arsenen, antimonen ve borofen gibi) sentezlenmeye çalışılmıştır. Bu sentezleme çalışmalarının ana odağı sadece yeni malzemeleri keşfetmek değil aynı zamanda, bu malzemeleri farklı alanlarda nano ölçekli uygulamalara entegre etmek ve performanslarını artırmakta büyük önem taşımaktadır. Yeni iki boyutlu malzemelerin üretimindeki gelişmelere ek olarak, son zamanlarda borofen sentezi ile ilgili heyecan verici gelişmeler de yaşanmıştır. Borofen eşsiz fiziksel ve kimyasal özellikleri nedeniyle çeşitli potansiyel uygulamalara sahiptir. Bu derlemede, literatürde yapılan çalışmalara vurgu yaparak borun fizikokimyasal yapısı, karbon ile olan benzerliği, sentezleme yöntemleri incelenmiş ayrıca kullanılan diğer materyaller, borofenin gelişim süreci ve uygulama alanları (enerji ve çevre sektörleri) değerlendirilmiştir.

Anahtar sözcükler: bor; borofen; enerji uygulamaları; iki boyutlu malzemeler

GİRİŞ

Grafenin mekanik ve ısı iletimi özelliklerinden dolayı silisen, almanen, fosforen, geçiş metali diklorojenitler, arsenen ve antimonen gibi iki boyutlu malzemeler, son on yılda büyük ölçüde ilgi çekmeye başlamıştır. İki boyutlu (2B) materyaller, dikkate değer ve geniş potansiyel uygulamaları nedeniyle şu anda en ilginç araştırma konuları arasında sayılmaktadır (Ma vd., 2016; Elia vd., 2016; Mortazavi vd., 2016; Ji vd., 2016; Bhimanapati vd., 2015; Zhu vd., 2015). Bu yeni malzeme sınıfına ilgi, başarılı grafen üretiminden ve düzlem biçimindeki karbon atomlarının petek kafesinden kaynaklanmaktadır. Eşsiz fiziksel ve kimyasal özellikleri nedeniyle, 2B malzemeler, elektronik cihazlarda, enerji ve çevre alanında geniş uygulama potansiyeli göstermektedir (Osumi vd., 2016; Larcher & Tarascon, 2015; Raccichini vd., 2015). Bu iki boyutlu (2B) malzemeler, elektronik, fotonik, enerji dönüşümü ve depolama ve biyomedikal teknolojilerde geniş bir uygulama yelpazesinde kullanılan istisnai fiziksel özelliklere sahiptirler. Borofen, grafenin bor atomu analoğudur (Feng vd., 2016; Mannix vd., 2015; Ogitsu vd., 2013). Borun, malzemelerin özelliklerini ayarlamak için yaygın olarak bir katkı maddesi olarak kullanıldığı bilinmektedir. Saf bor, basit düzlemsel moleküller ve kafes benzeri fullerenler oluşturan, karbona belirgin şekilde benzer yapısından dolayı nanomalzeme alanında büyük önem arz etmektedir (Şekil 1). Daha önce yapılan deneysel ve teorik çalışmalar, iki boyutlu (2D) bor tabakalarının, bor atomuna benzer bir atomik yapı ortaya koyduğunu göstermektedir. Bugüne kadar, nano-yapılı bor allotroplarının deneysel araştırmaları, oldukça seyrektir. Bununla birlikte, sayısız teorik çalışma borofeni incelemiştir (Li vd., 2015; Le & Nguyen, 2015; Zhang vd., 2015; Peng vd., 2015; Shirodkar

vd., 2015). Periyodik tablodaki beşinci element olarak, bor $2s^22p^1$'in zemin durum yapılandırmasına sahip üç değerlik elektronuna sahiptir. Bu form borun karmaşık polimorfik yığın yapılar ve nanoskopik kümeler ve ayrıca farklı elementlere sahip çok sayıda bileşik oluşturmasını sağlar (Mortazavi vd., 2016; Peng vd., 2016).

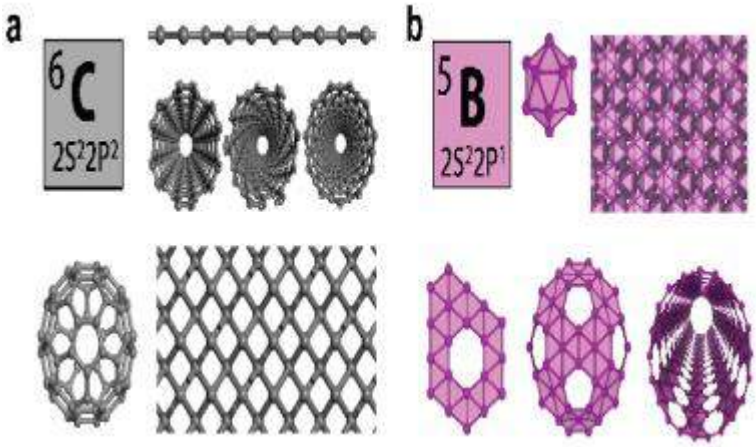

Şekil 1. Karbon ve bor arasındaki kimyanın paralelliği (Wang vd., 2019).

Elementel Bor ve Borofen Sentezi

Metaloid grup içerisinde yer alan bor (Şekil 2) genişletilmiş kovalent ağlar oluşturmak için en düşük Z elementi olarak karşımıza çıkmaktadır. Periyodik tabloda grup III'te tek metal element olma özelliğinin yanında düşük yoğunluklu (2.34-2.52 g/cm^3), yüksek erime noktası (>2000 ^0C), büyük kütle modülü (185-227 GPa), yüksek sertlik gibi özellikleri ile bilim adamlarının dikkatini çekmektedir (Ranjan vd., 2019; Campell vd., 2018; Weng vd., 2018; Sun vd., 2017; Wang, 2016). Düzlemsel bor molekülleri ve kafes benzeri bor kümelerinin varlığı borun karbonun özelliklerinin çoğunu sergilediğini göstermektedir. Bununla birlikte, yalnızca karbona benzerlikten dolayı, borun tek başına grafen benzeri bir iki boyutlu yapı oluşturabileceği kesin değildir. Bor karbon ile karşılaştırıldığında bir elektrondan yoksun olduğundan, bir bal peteği borlu tabaka kararsızdır ve sadece bazı metal diboridlerin yüzeyinde var olabilir. Periyodik tablodaki berilyum ve karbon arasında konumlandırılmış olan bor, hem metal hem de metal olmayan kimyasal özelliklere sahip anahtar bir elementtir. Bu eşsiz doğası nedeniyle, normal iki-orta-iki elektronlu bağlardan çok merkezli iki elektronlu bağlara kadar değişen çok sayıda bağlanma düzenine sahip olan bor atomları arasında zengin bir çeşitlilikte bağlanma konfigürasyonları oluşabilir (Liu vd., 2018; Karmodak & Jemmis, 2018; Penev vd., 2016; Mannix vd., 2015; Feng vd., 2016). İlk olarak 2015 yılında özel bir yöntemle sentezlenen borofende bor atomları 4'lü veya 5'li olarak bağlanmakta ve özel desen oluşturmaktadır. Sentezlemenin gerçekleşmesi ve iki boyutlu malzemenin elde edilmesi için gümüş, altın ve bakır gibi destek materyallerine ihtiyaç vardır. Literatürde yapılan birçok çalışmada bu maddeler test edilmiş olup özellikle gümüşün (Ag-111)

yüksek sıcaklık (450-700 ^{0}C) ve vakum altında en iyi borofen sentezini oluşturduğu gözlenmiştir (Kiraly vd., 2019; Peköz vd., 2018; Yi vd., 2017; Piazza vd., 2014; Zhai vd., 2014). Borofen ve bor arasındaki büyük enerji farkı nedeniyle, borofen sentezlenmesi zor olduğundan yüksek sıcaklık, basınç ve vakum kesinlikle kullanılmak zorundadır. Ayrıca, bor, doğada sadece üç boyutlu formlarda bulunur ve borofenin bu durumda üretimi araştırmacılar açısından büyük önem taşımaktadır.

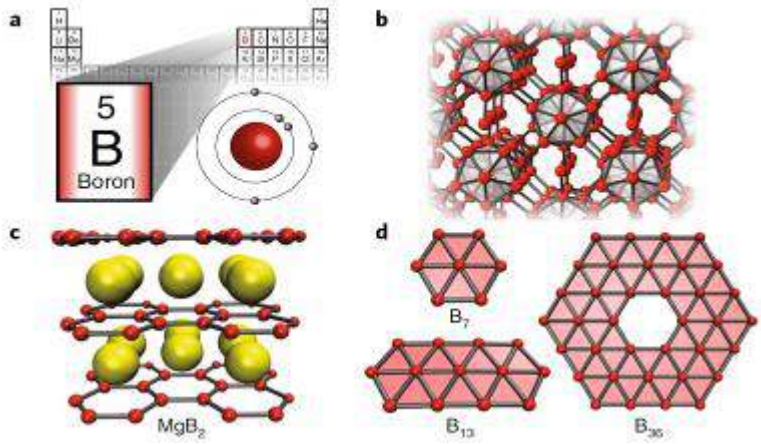

Şekil 2. Bor yapısı ve kimyasının temelleri. a, konumu periyodik cetvel tablosundaki boronun ve yörünge diyagramının üç değerlikli dış kabuk. b-d, Atomik yapı modelleri (Mannix vd., 2018).

Borofenin Fiziksel ve Kimyasal Özellikleri

Borofen, Şekil 3'te vurgulanan bir dizi benzersiz özelliğe sahiptir. Bir Ag (111) yüzeyinde buharlaşma yoluyla sentezlenen borofen, yapısal anizotropi ve polimorfizm sergiler, bu da metaliklik, mekanik esneklik, şeffaflık ve süper iletkenlik kombinasyonu içeren 2B malzemelere özgü bir dizi özellik ile sonuçlanmaktadır (Peköz vd., 2018; Mannix vd., 2018; Ranjan vd., 2018; Feng vd., 2017; Mannix vd., 2015). Özellikle enerji sektörü açısından enerjinin depolanması için belirli özelliklerin üst seviyede olması gerekmektedir.

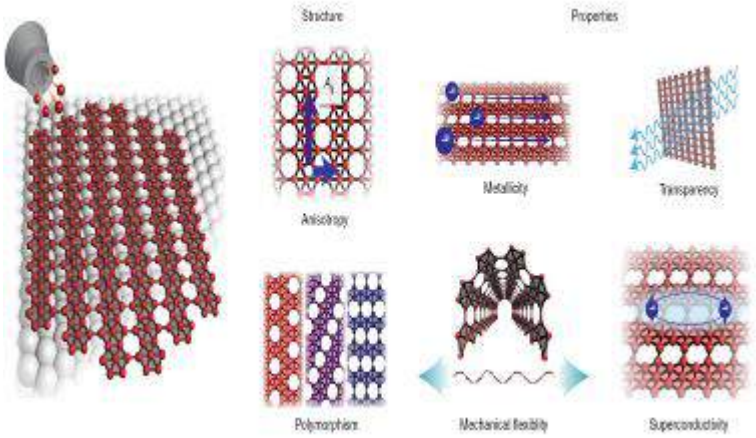

Şekil 3. Borofen yapısının özeti ve özellikleri (Mannix vd., 2018).

Borofenlerin mekanik özellikleri güçlü B-B bağları ve benzersiz atom yapısı nedeniyle, yüksek nitelikli olarak bildirilmiştir. Elastik sabitler (c_{11}, c_{22}, c_{12}), katman modülü, kayma modülü (Ɣ), Young modülü ve Poisson oranı (ƴ) gibi mekanik parametreler, borofen ve yaygın 2D malzemeler için Tablo 1'de listelenmiştir (Peköz vd., 2018; Wang vd., 2016; Feng vd., 2016; Gao vd., 2016). Borofen'in mekanik özellikleri, kimyasal modifikasyon, katman sayısı ve sıcaklıktan olumlu ya da olumsuz olarak etkilenmektedir. Bu nedenle Tablo 1 'de belirtilen parametreler kontrollü bir şekilde incelenmelidir. Özellikle, kimyasal modifikasyon, borofen'in mekanik özellikleri üzerinde güçlü bir etkiye sahiptir (Feng vd., 2017; Gao vd., 2017; Khanifaev vd., 2017). Sentezlemede kullanılan gümüş vb. malzemelerin etkisi dikkatlice değerlendirilmelidir. Isı iletkenliği, nano cihazların performansı ve uzun ömürlülüğü için önemli bir fiziksel parametredir (Mir vd., 2016; Jiang vd., 2016; Kou vd., 2016). Borofen'in termal iletkenliği incelenmiş olup anizotropik karakterdedir. Çeşitli çalışmalarda borofenin süper iletkenlik özellikleri bildirilmiştir (Peköz vd., 2018; Padilha vd., 2016). Bu özelliği sayesinde enerji alanında (pil üretimi) diğer iki boyutlu malzemelere göre avantaj elde etmektedir. Ayrıca bu özelliklerinin yanında günümüzde araştırmacılar borofenin elektronik ve optik özelliklerini de derinlemesine incelemektedirler (Zhong vd., 2019; Kumar vd., 2018; Higuchi vd., 2017; Shukla vd., 2017).

Tablo 1. Borofen ve yaygın iki boyutlu malzemelerin bazı stratejik fiziksel ve kimyasal parametre değerleri (Peköz vd., 2018).

2D Malzemeler	c_{11}	c_{22}	c_{12}	G	Ɣ	ƴ
Borofen	333.50	576.00	21.50	157.00	453.66	0.051
Grafen	348.75	348.75	61.00	143.88	338.08	0.175

Fosforen	186.80	44.61	31.23	41.82	103.64	0.434
Silisen	68.30	68.30	23.30	22.50	60.60	0.341
Germanen	46.40	46.10	13.10	16.70	42.70	0.282

Borofenin Uygulama Alanları

Borofenin enerji ve arıtma malzemesi olarak uygulanması son yıllarda büyük önem kazanmış olup özellikle yenilenebilir enerji alanında aktif olarak değerlendirilmektedir. Borofen grafenden daha esnek daha güçlü olmasıyla öne çıkmaktadır. Oldukça hafif ve reaktif niteliktedir. Böylece elektron depolamak gibi işlemlerde kullanıma elverişlidir. Bu durum ise borofeni lityum, sodyum, potasyum, aliminyum ve magnezyum iyon bataryaları için oldukça işlevli bir anot haline getirmektedir (Chen vd., 2018; Jiang vd., 2018; Zhao vd., 2016). Ayrıca yüksek yüzey aktivitesi ve diğer malzemelerden daha hafif olmasından dolayı umut verici bir elektrot kaynağı ve süper bir kapasitör olmaktadır (Kumar vd., 2018; Mannix vd., 2018; Kondo, 2017). En hafif 2D malzeme olan borofen aynı zamanda hidrojen yakalama ve tutma açısından en iyi materyal olarak dikkat çekmektedir. Ağırlığının %15'ine kadar hidrojen tutabilen nitelikte olup katalizör olarak da kullanılmakta ve bu sayede hidrojen atomlarının hidrojen iyonlarına dönüşmesini sağlamaktadır (Wang vd., 2019). Bu durum ise su tabanlı enerji sistemleri için yeni bir uygulama teknolojisidir. Hidrojen depolama ile ilgili birçok çalışmada borofen incelenmiştir. Borofen, sensör sektöründe de geniş bir uygulama potansiyeli göstermektedir (Mannix vd., 2018; Shukla vd., 2017; Peng vd., 2017). Borofen'in etanol, formaldehit ve hidrojen siyanür tespiti için bir sensör olarak kullanılabileceği çeşitli çalışmalarda bildirilmiştir. Bazı metallerin (Li, Na, K, Ca, Mg, Al) borofen üzerindeki adsorpsiyon yetenekleri ile ilgili yapılan çalışmalarda başarılı sonuçlar elde edilmiştir (Şekil 4) (Zhang & Cheng, 2019; Rao vd., 2017). Bu sonuçlar ışığında çevre kirliliğinde büyük yer tutan su ortamlarındaki ağır metallerin ve diğer kirletici gruplarının adsorpsiyon yöntemi ile arıtımında borofen yeni bir adsorbent malzeme olarak karşımıza çıkmaktadır. Su sektöründe hem arıtım hem de içme suyu kalitesi açısından günümüzde kullanılan klasik membran reaktörlerin dizaynında da grafen, borofen gibi iki boyutlu malzemeler kullanılarak daha fazla verim ve kaliteli su elde edilebilir.

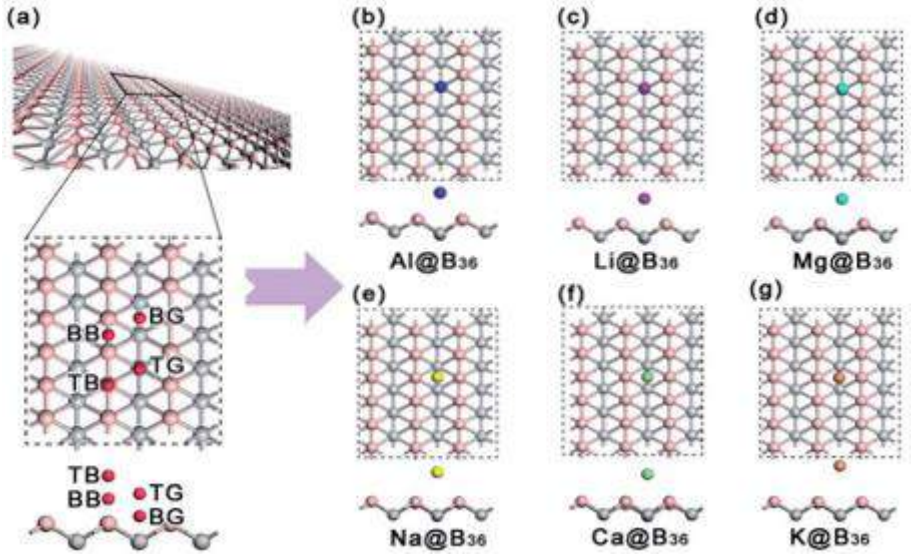

Şekil 4. Borofen ve metal adsorpsiyonu. (a) Borofen (pembe ve gri toplar) modeli ve adsorpsiyon bölgeleri (kırmızı toplar). (b) Al, (c) Li, (d) Mg, (e) Na, (f) Ca, (g) bir süper hücrede 36 bor atomundan (B36) oluşan bir borofen yüzeyindeki K (Rao vd., 2017).

SONUÇ

Borofen yeni gelişmekte olan iki boyutlu bir malzemedir ancak bazı güçlü özelliklerinden (mekanik, elastik, hafiflik, yüzey alanı, termal iletkenlik, anizotropik vb.) dolayı enerji alanında ve su arıtımında uygulanabilirliği söz konusudur. Bu avantajlı yapısının yanında özellikle reaktif olması demek ayrıca paslanmaya da açık olması demektir. Bu sebeple borofenin iyi korunması gerekmektedir. Bir diğer dezavantaj da bu materyalin sadece küçük boyutlarda üretilmesi ve büyük boyutlarda üretiminin pahalı olmasıdır. Sürekli artan küresel nüfus ve kademeli olarak fosil enerjinin tükenmesiyle birlikte, çevre kirliliğini artışı yeni enerji depolama sistemlerinin ve arıtma teknolojilerinin gelişmesine yol açmaktadır. Bu noktada ise mevcut malzemeler yerine nano ölçekte iki boyutlu malzemeler ön plana çıkmaktadır. İki boyutlu borofen gibi malzemelerle yeni tip enerji depolama sistemleri (şarj edilebilir piller, hidrojen ve doğal gaz depolama ortamları ve süper kapasitörler vb.) geliştirilmeye çalışılmaktadır. Aynı zamanda modern toplumlarda ve tüm dünyada, yüksek performanslı ve düşük maliyetli enerji ve arıtım uygulamaları önem arz etmektedir. Enerji sektörünün yanında su arıtımı ile ilgili olarak ta borofen kirliliklerin verimli gideriminde umut veren literatür çalışmaları ortaya koymaktadır.

KAYNAKLAR

Bhimanapati, G. R., Lin, Z., Meunier, V., Jung, Y., Cha, J., Das, S., Xiao, D., Son, Y., Strano, M. S., Cooper, V. R., Liang, L., Louie, S. G., Ringe, E., Zhou, W., Kim, S. S., Naik, R. R., Sumpter, B. G., Terrones, H., Xia, F., Wang, Y., Zhu, J., Akinwande, D., Alem, N., Schuller,

J. A., Schaak, R. E., Terrones, M., Robinson, J. A. (2015). Recent advances in two-dimensional materials beyond graphene. ACS Nano, 9, 11509-11539.
Campbell, G. P., Mannix, A. J., Emery, J. D., Lee, T. L., Guisinger, N. P., Hersam, M. C., Bedzyk, M. J. (2018). Resolving the chemically discrete structure of synthetic borophene polymorphs. Nano Letters, 18, 2816-2821.
Chen, X., Shen, X., Li, B., Peng, H. J., Cheng, X. B., Li, B. Q., Zhang, X. Q., Huang, J. Q., Zhang, Q. (2018). Ion-solvent complexes promote gas evolution from electrolytes on a sodium metal anode. Angewandte Chemie International Edition, 57, 734-737.
Elia, G. A., Marquardt, K., Hoeppner, K., Fantini, S., Lin, R., Knipping, E., Peters, W., Drillet, J. F., Passerini, S., Hahn, R. (2016). An overview and future perspectives of aluminum batteries. Advanced Materials, 28, 7564-7579.
Feng, B., Sugino, O., Liu, R. Y., Zhang, J., Yukawa, R., Kawamura, M., Limori, T., Kim, H., Hasegawa, Y., Li, H., Chen, L., Wu, K., Kumigashira, H., Komori, F., Chiang, T. C., Meng, S., Matsuda, I. (2017). Dirac fermions in borophene. Physical Review Letters, 118, 096401.
Feng, B., Zhang, J., Zhong, Q., Li, W., Li, S., Li, H., Cheng, P., Meng, S., Chen, L., Wu, K. (2016). Experimental realization of two-dimensional boron sheets. Nature Chemistry, 8, 563-568.
Gao, M., Li, Q. Z., Yan, X. W., Wang, J. (2017). Prediction of phononmediated superconductivity in borophene. Physical Review B, 95, 024505.
Higuchi, T., Heide, C., Ullmann, K., Weber, H. B., Hommelhoff, P. (2017). Light-field-driven currents in graphene. Nature, 550, 224-228.
Ji, J., Song, X., Liu, J., Yan, Z., Huo, C., Zhang, S., Su, M., Liao, L., Wang, W., Ni, Z., Hao, Y., Zeng, H. (2016). Two-dimensional antimonene single crystals grown by van der waals epitaxy. Nature Communications, 7, 13352.
Jiang, H. R., Lu, Z., Wu, M. C., Ciucci, F., Zhao, T. S. (2016). Borophene: a promising anode material offering high specific capacity and high rate capability for lithium-ion batteries. Nano Energy, 23, 97-104.
Jiang, N., Li, B., Ning, F., Xia, D. (2018). All boron-based 2D material as anode material in Li-ion batteries. Journal of Energy Chemistry, 27, 1651-1654.
Karmodak, N., & Jemmis, E. D. (2018). Metal templates and boron sources controlling borophene structures: An Ab initio study. Journal of Physical Chemistry,122, 2268-2274.
Khanifaev, J., Pekö̈z, R., Konuk, M., Durgun, E. (2017). The interaction of halogen atoms and molecules with borophene. Physical Chemistry Chemical Physics, 19, 28963-28969.
Kiraly, B., Liu, X., Wang, L., Zhang, Z., Mannix, A. J., Fisher, B. L., Yakobson, B. I., Hersam, M. C., Guisinger, N. P. (2019). Borophene synthesis on Au(111). ACS Nano, 13, 3816-3822.
Kondo, T. (2017). Recent progress in boron nanomaterials. Science and Technology of Advanced Materials, 18, 780-804.
Kou, L., Ma, Y., Tang, C., Sun, Z., Du, A., Chen, C. (2016). Auxetic and ferroelastic borophane: a novel 2D material with negative possion's ratio and switchable dirac transport channels. Nano Letters, 16, 7910-7914.

Kumar, K. S., Choudhary, N., Jung, Y., Thomas, J. (2018). Recent advances in two-dimensional nanomaterials for supercapacitor electrode applications. ACS Energy Letters, 3, 482-495.
Larcher, D., & Tarascon, J. M. (2015). Towards greener and more sustainable batteries for electrical energy storage. Nature Chemistry, 7, 19-29.
Le, M. Q., & Nguyen, D. T. (2015). The role of defects in the tensile properties of silicene. Applied Physics A, 118, 1437-1445.
Li, X. B., Xie, S. Y., Zheng, H., Tian, W. Q., Sun, H. B. (2015). Boron based two-dimensional crystals: theoretical design, realization proposal and applications. Nanoscale, 7, 18863-18871.
Liu, X., Zhang, Z., Wang, L., Yakobson, B. I., Hersam, M. C. (2018). Intermixing and periodic self-assembly of borophene line defects. Nature Materials, 17, 783-788.
Ma, F., Jiao, Y., Gao, G., Gu, Y., Bilic, A., Chen, Z., Du, A. (2016). Graphene-like two-dimensional ionic boron with double dirac cones at ambient condition. Nano Letters, 16, 3022-3028.
Mannix, A. J., Zhang, Z., Guisinger, N. P., Yakobson, B. I., Hersam, M. C. (2018). Borophene as a prototype for synthetic 2D materials development. Nature Nanotechnology, 13, 444-450.
Mannix, A. J., Zhou, X. F., Kraly, B., Wood, J. D., Alducin, D., Myers, B. D., Liu, X., Fisher, B. L., Santiago, U., Guest, J. R., Yacaman, M. J., Ponce, A., Oganov, A. R., Hersam, M. C., Guisinger, N. P. (2015). Synthesis of borophenes: anisotropic, two-dimensional boron polymorphs. Science, 350, 1513-1516.
Mir, S. H., Chakraborty, S., Jha, P. C., Warna, J., Soni, H., Jha, P. K., Ahuja, R. (2016). Two-dimensional boron: lightest catalyst for hydrogen and oxygen evolution reaction. Applied Physics Letters, 109, 053903.
Mortazavi, B., Fan, Z., Pereira, L. F. C., Harju, A., Rabczuk, T. (2016). Amorphized graphene: A stiff material with low thermal conductivity. Carbon, 103, 318-326.
Mortazavi, B., Rahaman, O., Dianat, A., Rabzcuk, T. (2016). Mechanical responses of borophene sheets: a first-principles study. Physical Chemistry Chemical Physics, 18, 27405-27413.
Ogitsu, T., Schwegler, E., Galli, G. (2013). Bernstein, M. (2002). At the crossroads of the chemistry of boron and the physics of frustration. Chemical Reviews, 113, 3425-3449.
Osumi, S., Saito, S., Dou, C., Matsuo, K., Kume, K., Yoshikawa, H., Awaga, K., Yamaguchi, S. (2016). Boron-doped nanographene: Lewis acidity, redox properties, and battery electrode performance. Chemical Scinece, 7, 219-227.
Padilha, J. E.; Miwa, R. H.; Fazzio, A. (2016). Directional Dependence of the Electronic and Transport Properties of 2D Borophene and Borophane. Physical Chemistry Chemical Physics, 18, 25491-25496.
Peköz, R., Konuk, M., Kilic, M. E., Durgun, E. (2018). Two-dimensional fluorinated boron sheets: mechanical, electronic, and thermal properties. ACS Omega, 3, 1815-1822.
Penev, E. S., Kutana, A., Yakobson, B. I. (2016). Can two-dimensional boron superconduct. Nano Letters, 16, 2522-2526.

Peng, B., Zhang, H., Shao, H., Ning, Z., Xu, Y., Ni, G., Lu, H., Zhang, D. W., Zhu, H. (2017). Stability and strength of atomically thin borophene from first principles calculations. Materials Research Letters, 5, 399-407.
Peng, B., Zhang, H., Shao, H., Xu, Y., Zhang, R., Zhu, H. (2016). The electronic, optical, and thermodynamic properties of borophene from first-principles calculations. Journal of Materials Chemistry C, 4, 3592-3598.
Peng, Q., Han, L., Wen, X., Liu, S., Chen, Z., Lian, J., De, S. (2015). Mechanical properties and stabilities of a-boron monolayers. Physical Chemistry Chemical Physics, 17, 2160-2168.
Piazza, Z. A., Hu, H. S., Li, W. L., Zhao, Y. F., Li, J. (2014). Planar hexagonal B36 as a potential basis for extended single-atom layer boron sheets. Nature Communications, 5, 3113.
Raccichini, R., Varzi, A., Passerini, S., Scrosati, B. (2015). The role of graphene for electrochemical energy storage. Nature Materials, 14, 271-279.
Ranjan, P., Agrawal, S., Sinha, A., Rao, T. R., Balakrishnan, J., Thakur, A. D. (2018). A low-cost non-explosive synthesis of graphene oxide for scalable applications. Scientific Reports, 8, 12007.
Ranjan, P., Sahu, T. K., Bhushan, R., Yamijala, S. SRKC., Late, D. J., Kumar, P., Vinu, A. (2019). Freestanding borophene and its hybrids. Advanced Materials, 31, 1900353.
Rao, D., Zhang, L., Meng, Z., Zhang, X., Wang, Y., Qiao, G., Shen, X., Xia, H., Liu, J., Lu, R. (2017). Ultrahigh energy storage and ultrafast ion diffusion in borophene-based anodes for rechargeable metal ion batteries. Journal of Materials Chemistry A, 5, 2328-2338.
Shirodkar, S. N., Waghmare, U. V., Fisher, T. S., Grao-Crespo, R. (2015). Engineering the electronic bandgaps and band edge positions in carbon-substituted 2D boron nitride: a first-principles investigation. Physical Chemistry Chemical Physics, 17, 13547-13552.
Shukla, V., Warna, J., Jena, N. K., Grigoriev, A., Ahuja, R. (2017). Toward the realization of 2D borophene based gas sensor. The Journal of Physical Chemistry, 121, 26869-26876.
Sun, X., Liu, X., Yin, J., Yu, J., Li, Y., Hang, Y., Zhou, X., Yu, M., Li, J., Tai, G., Guo, W. (2017). Two-dimensional boron crystals: structural stability, tunable properties, fabrications and applications. Advanced Functional Materials, 27, 1-22.
Wang, H., Li, Q., Gao, Y., Miao, F., Zhou, X. F., Wan, G. (2016). Strain effects on borophene: ideal strength, negative Possion's ratio and phonon instability. New Journal of Physics, 18, 73016.
Wang, L.S. (2016). Photoelectron spectroscopy of size-selected boron clusters: from planar structures to borophenes and borospherenes. International Reviews Physical Chemistry, 35, 69-142.
Wang, Z. Q., Lü, T. Y., Wang, H. Q., Feng, Y. P., Zheng, J. C. (2019). Review of borophene and its potential applications. Frontiers Physics, 14, 33403.
Weng, Q., Li, G., Feng, X., Nielsch, K., Golberg, D., Schmidt, O. G. (2018). Electronic and optical properties of 2D materials constructed from light atoms. Advanced Materials, 30, 1801600.

Yi, W. C., Liu, W., Botana, J., Zhao, L., Liu, Z., Liu, J. Y., Miao, M. S. (2017). Honeycomb boron allotropes with dirac cones: a true analogue to graphene. Journal of Physical Chemistry Letters, 8, 2647.

Zhai, H. J., Zhao, Y. F., Li, W. L., Chen, Q., Bai, H., Hu, H. S., Piazza, Z. A., Tian, W. J., Lu, H. G., Wu, Y. B., Mu, Y. W., Wei, G. F., Liu, Z. P., Li, J., Li, S. D. (2014). Observation of an all-boron fullerene. Nature Chemistry, 6, 727-731.

Zhang, Y., & Cheng, X. (2019). Hydrogen adsorption property of Na-decorated boron monolayer: a first principles investigation. Physica E: Low-dimensional Systems and Nanostructures, 107, 170-176.

Zhang, Z., Yang, Y., Gao, G., Yakobson, B. I. (2015). Two-dimensional boron monolayers mediated by metal substrates. Angewandte Chemie International Edition, 54, 13022-13026.

Zhao, T., Wang, Q., Jena, P. (2016). Cluster-inspired design of high-capacity anode for Li-ion batteries. ACS Energy Letters, 1, 202-208.

Zhong, C., Wu, W., He, J., Ding, G., Liu, Y., Li, D., Yang, S. A., Zhang, G. (2019). Two-dimensional honeycomb borophene oxide: strong anisotropy and nodal loop transformation. Nanoscale, 11, 2468.

Zhu, F. f., Chen, W. j., Xu, Y., Gao, C. l., Guan, D. d., Liu, C. h., Qian, D., Zhang, S. C., Jia, J. f. (2015). Epitaxial growth of two-dimensional stanene. Nature Materials, 10, 1020-1025.

THE ROLE OF SAFETY CONCERN AND NUTRITIONAL QUALITY IN ORGANIC FOOD

Chi-Ching LEE

İstanbul Sabahattin Zaim University,The Faculty of Engineering and Natural Sciences, The Department of Food Engineering, Halkalı Cad. No: 2 Halkalı, Küçükçekmece, İstanbul 34303, Turkey

chi.lee@izu.edu.tr

ABSTRACT: Global consumption and market of organic food products are boosting significantly over the past several decades. According to previous studies, the reasons include of the concern of the quality and safety in conventional food products, the development of health consciousness, the awareness of contamination in the food chain and environment, animal welfare and ethical motives, and personal life values. Organic agriculture is well-defined in the regulation of the European Union, the United States, Australia, Japan, and other many countries. Based on the definition of UN Food and Agriculture Organization (FAO), the main characteristics of organic agriculture are production of high nutritional quality foodstuffs in sufficient quantity, promotion of animal respect and natural cyclic systems, no use of chemical fertilizers/ pesticide/ herbicide, maintenance of environmental sustainability, and avoidance of genetically modified (GM) crops. The aim of this study is to evaluate and compare the nutritional value of organic and conventional food. Moreover, the toxicological and microbiological data will be reviewed including contamination of pathogenic microorganisms, phytochemicals, and mycotoxins. For the nutritional quality of organic food, they contain more polyunsaturated acid, more minerals like iron magnesium, and more antioxidants such as phenolic compounds and salicylic acid than the conventional produce. For animal products, organic beef contains more lean meat than conventional counterparts. For food safety concern, the contamination of pathogenic microorganisms and mycotoxins is no significant difference between organic and conventional foodstuffs. The phytochemical residue was not detected among more than 94% of organic food. However, 41% of usual food products were examined to have chemical contaminants. In summary, organic farming systems showed the capacity to provide foods with high quality standards. I recommend that the global organic agriculture should be developed and improved continuously to accomplish sustainable food production for the benefit of all mankind.

Keywords: organic food, nutritional quality, food safety, contaminants.

DETECTION OF SCHIZOPHRENIA ON EEG SIGNALS BY USING RELATIVE WAVELET ENERGY AS A FEATURE EXTRACTOR

Zülfikar ASLAN
Fen Bilimleri Enstitüsü, Dicle Üniversitesi, Diyarbakır, Türkiye
zulfikaraslan27@gmail.com

Mehmet AKIN
Elektrik-Elektronik Mühendisliği, Mühendislik Fakültesi, Dicle Üniversitesi, Diyarbakır
makin@dicle.edu.tr

ABSTRACT: Detecting diseases by use of EEG signals has been a widely used technique in the literature and still one of the most prominent research topics. In this study, feature extraction is done by using Relative Wavelet Energy method on EEG recordings of healthy samples and schizophrenia patients in order to investigate performance of the method on detecting the schizophrenia disease. In the first step, low band components of the signal are obtained by using wavelet transformation. Then, Relative Wavelet Energy method is applied to each of these bands in order to extract features. These features are fed to the K-Nearest Neighbors (KNN) algorithm to evaluate the classification performance. As a result, extracted features helped the classifier to classify with a performance of nearly 90% accuracy.

Key words: Wavelet, Relative Wavelet Energy, Schizophrenia, Knn

EEG SİNYALLERİNDE GÖRECELİ DALGACIK ENERJİSİ YÖNTEMİYLE ÖZELLİK ÇIKARIMI YAPILARAK ŞİZOFRENİ TESPİTİ

ÖZET: EEG sinyalleri üzerinden hastalık tespiti literatürde pek çok uygulama alanı bulmuş ve halen önemini koruyan konulardan birisidir. Bu çalışmada, şizofreni hastası ve sağlıklı bireylere ait EEG sinyalleri üzerinde göreceli dalgacık enerjisi yöntemiyle özellik çıkarımı yapılarak şizofreni tespitindeki başarımı gözlemlenmiştir. İlk olarak sinyal öncelikle dalgacık dönüşümü uygulanarak sinyalin alt bant bileşenleri elde edilmiştir. Sonrasında elde edilen bu alt bant bileşenlerine göreceli dalgacık dönüşümü enerjisi yöntemi uygulanarak özellik çıkarımları yapılmıştır. Elde edilen özellik değerleri knn (en yakın k komşu) sınıflandırma algoritması kullanılarak başarımları

değerlendirilmiştir. Sonuç olarak elde edilen özellik çıkarımları ile 90% civarında başarı elde edildiği gözlemlenmiştir.

Anahtar sözcükler: Dalgacık Dönüşümü, Göreceli Dalgacık Dönüşümü Enerjisi, Şizofreni, En yakın k komşu

GİRİŞ

Şizofreni, belirli beyin sistemleri ve fonksiyonlarından ziyade, beyindeki psişik aktiviteyi bozan bir hastalıktır. Araştırmacılar uzun zamandır şizofreninin insan beyni üzerindeki değişimleri ile ilgilenmektedir. İnsan beynindeki histolojik ve fizyolojik değişiklikler hakkında önemli veriler bilgiler elde etmişlerdir. Şizofreninin farklı evrelerinde beynin farklı kısımları arasındaki ilişkilerin olduğunu tespit etmişlerdir(Lewis and Gonzalez-Burgos 2000; Selemon and Goldman-Rakic 1999). Şizofreni, nüfusun % 1'inin yaşadığı zihinsel bir hastalıktır. Amerikan Psikiyatri Birliği'nin (American Psychiatric Association 1994; WHO 2011) tanı kriterlerine göre, hastalar yanılgı, halüsinasyonlar veya düzensiz konuşma gibi bazı karakteristik semptomlar göstermektedir.

Şizofrenik hastaların EEG sinyallerinin analizi literatürde de önemli bir yer bulmuştur. Bazı araştırmalarda (Jeong et al. 1998; Shao, Fan, and Li 2007), iki şizofrenik hasta grubunun ve kontrol katılımcılarının EEG sinyallerine doğrusal olmayan yöntemler uygulanmıştır. İki grup arasındaki sonuçlar, dinamik süreçte farklılıklar göstermiştir. Hornero ve diğ. (Hornero et al. 2006) katılımcılardan zaman serileri oluşturmak için rastgele boşluk tuşuna basmalarını istemişlerdir. Elde edilen sonuçlar şizofrenik hastalar tarafından oluşturulan zaman serilerinin kontrol grubuna göre daha düşük bir karmaşıklığa sahip olduğunu göstermiştir.

İlginç bir testte, rasgele sayı üretimi için (Rosenberg et al. 1990), katılımcılardan birkaç kez 1'den 10'a kadar bir sayı seçmeleri istenmiştir. Sayıların üretiminin bir kuraldan yoksun olması, yani mümkün olduğunca rastgele olması gerekiyordu. Bu yapılan çalışmada şizofreni hastalarının tekrarlı olmaya meyilli olduklarını buldular. Pressman ve diğ. (Pressman, A., Peled, A., & Geva 2000) şizofreni hastalarında çalışma belleği görevi sırasında senkronizasyon değişim yeteneği olmadığını gösterdiler. Böylece beyin aktivitesinde, özellikle frontal ve temporal kanallarda bir fark olduğunu belirtmişlerdir. Cherif ve diğ. (Cherif et al. 2004) şizofreni hastalarının sağlıklı katılımcılarla karşılaştırıldığında gözünü tek bir yerde tutma görevlerinde anormallik gösterdiklerini belirtmişlerdir. Gaser ve diğ. (Gaser et al. 1999) şizofrenik hastalarda yapısal beyin değişikliklerini tasvir etmişlerdir. Ayrıca, Keil ve ark. (Keil et al. 1998) şizofrenik hastalarda ritmik parmak salınımları göstermişlerdir. Paulus ve diğ. (Paulus, Geyer, and Braff 1999) , şizofreni ve kontrol grubu olan hastalarda ikili yanıt elde etmek için bir uyaranın 500 rasgele sağ veya sol görünüşünü öngörmekten oluşan basit bir seçim görevi

gerçekleştirmiştir. Karşılıklı ve çaprak karşılıklı olarak bilgi uyguladıktan sonra, hastalar tarafından oluşturulan yanıt dizilerinin kontrol grubundakilerden daha yüksek derecede bir bağımlılık gösterdiğini göstermişlerdir. Sabeti ve diğ. (Sabeti et al. 2007) şizofrenik ve sağlıklı kişilerden elde edilen EEG sinyallerine PCA tabanlı özellik çıkarım yaptıktan sonra, elde edilen özellik değerlerini sınıflandırmışlardır. Borisov ve diğ. (Borisov et al. 2005) 39 sağlıklı ve 45 şizofreni hastası olmak üzere 84 genç bireyden alınan EEG sinyallerini, kafa derisindeki yerleşim yerlerine göre kategorize etmiş ve ilgili kanallardan alınan sinyallerden özellik çıkarım yaparak sınıflandırma işlemi uygulamıştır. Kategorize edilmiş kanalların sınıflandırma başarımları karşılaştırılmıştır.

Bu çalışmada öncelikle elimizde bulunan sağlıklı ve şizofreni hastası bireylere ait EEG kayıtları öncelikle dalgacık dönüşü ile alt bant kanallarına ayrılmış sonrasında ise bu alt bant kanallarına göreceli dalgacık dönüşümü enerjisi yöntemi uygulanarak özellik çıkarımları yapılmıştır. Farklı Daubechies türünde (dB2, dB6 gibi) dalgacık dönüşümü yapılarak en iyi başarım sonucunu veren özellikler elde edilmiştir. Elde edilen bu alt bant kanallarına göreceli dalgacık dönüşüm enerjisi yöntemi uygulanarak özellik çıkarımları yapılmıştır. Elde edilen özellik değerleri en yakın k komşu sınıflandırma algoritması ile sınıflandırılmıştır. Farklı n değerleri için sonuçlar değerlendirilmiş ve en iyi başarım olarak 90% civarında başarım elde edilmiştir.

Veri Seti

Bu çalışmada kullanılan şizofreni hastalığını içeren EEG kayıtları, benzer şizofrenik bozukluğa sahip 45 çocuğa aittir. Tüm hastaların tanıları Ruh Sağlığı Araştırma Merkezi (MHRC) uzmanları tarafından doğrulanmıştır. MHRC muayenesi yapılan hastaların hiçbirisi kemoterapi görmemiştir. Hastaların en küçüğü 10 yıl 8 aylık ve en büyüğü de 14 yaşındadır. Kontrol grubu (sağlıklı örnekler) ise en küçüğü 11 yaş ve en büyüğü 13 yaş 9 aylık olan 39 sağlıklı öğrenciyi içermektedir. Her iki gruptaki çocukların ortalama yaşı 12 yıl 3 aydır (Borisov et al. 2005).
EEG kayıtları, denekler uyanık, rahat ve gözleri kapalı iken kafalarına bağlı 16 elektrot ile alınmıştır. Her kanaldan alınan veri 7680 uzunluğunda tek boyutlu bir dizi yapısındadır.

YÖNTEM

39 sağlıklı ve 45 şizofreni hastası bireylerden alınan 16 kanallı EEG verisi üzerinde öncelikle Dalgacık dönüşümü uygulanarak alt bant kanalları elde edilmiştir. Sonrasında elde edilen bu alt bant kanalları üzerinde göreceli dalgacık dönüşümü enerjisi yöntemi kullanılarak özellik çıkarımları yapılmıştır. Elde edilen özellik vektörleri en yakın k komşu sınıflandırma algoritmasıyla sınıflandırılmıştır. Bu çalışmada uygulanan yöntem Şekil1' de gösterilmektedir.

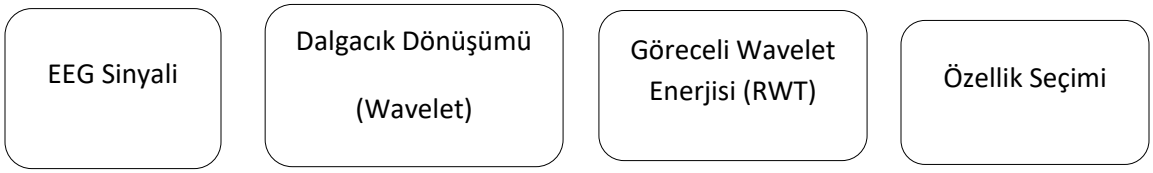

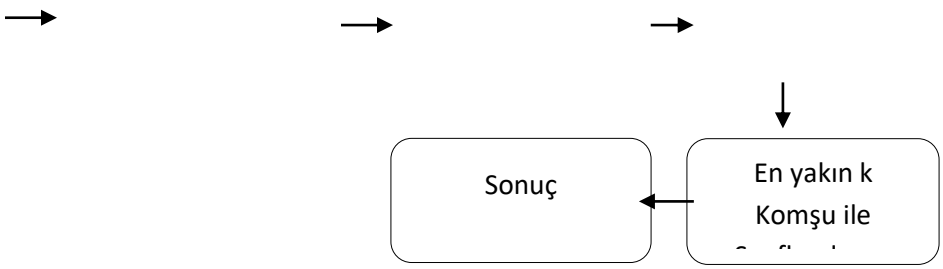

Şekil 1. Bu çalışmada kullanılan metot ve yöntemlere ait işlem süreçleri.

Dalgacık Dönüşümü (Wavelet)

Wavelet serisi veya dönüşümü, verilen bir fonksiyonun ortonormal (birbirine dik birim uzunluklu) terimlerin toplamı olarak ifade edilmesidir. Elde edilen bu seri, en popüler zaman-frekans dönüşümlerinden biridir (Graps 1995). Daha biçimsel olarak ifade edilirse, Φ(x) wavelet için bir çevrim fonksiyonu gibi düşünüldüğünde,

$$\Phi_{(s,l)}(x) = 2^{\frac{-s}{2}}\Phi(2^{-s}x - 1) \quad (1)$$

Φ(x), s ve l tam sayı değişkenleri yardımıyla dönüşümün ölçeğini ve yayılmasını kontrol edeceğimiz bir fonksiyon olarak tanımlanır. Örneğin bu çalışmada kullanılan Daubechies wavelet kategorisindeki dönüşümler bu şekilde çalışmaktadır. s değişkeni genişliği, l değişkeni ise konum indeksini vermektedir. Böylece, farklı terimler ile dönüştürülecek uzayın baz vektörlerini elde etmiş oluruz. Dönüştüreceğimiz uzayın tamamını kaplamak için bu terimlerin bir toplamı kullanılmaktadır.

$$W(x) = \sum_{k=-1}^{N-2}(-1)^k c_{k+1}\Phi(2x + k) \quad (2)$$

W(x) ölçekleme fonksiyonu, ck ise wavelet katsayılarıdır. Bu katsayılar, aşağıdaki kısıtları sağlamaktadır:

$$\sum_{k=0}^{N-1} c_k = 2\ , \sum_{k=0}^{N-1} c_k c_{k+2l} = 2\delta_{l,0} \quad (3)$$

δ, delta fonksiyonunu, l ise konum indeksini göstermektedir. Bahsedilen kısıtları sağlayan katsayılar belirlenerek, wavelet istenen probleme adapte olabilmektedir. Böylece bir f(x) fonksiyonu, istenen derecede ve sayıda terimin toplamı olarak wavelet dönüşümü şeklinde elde edilebilmektedir. Elde edilen bu terimler, verilen sinyalin farklı

bileşenlerini temsil etmektedir ve bu bileşenler ayrı ayrı analiz edilerek, orijinal sinyalde görünür olmayan pek çok özellik ortaya çıkarılabilmektedir. Şekil 2'de bir sinyalin dalgacık dönüşümü sonrasında detaylı ve yaklaşım bileşenlerine ayrılması gösterilmektedir.

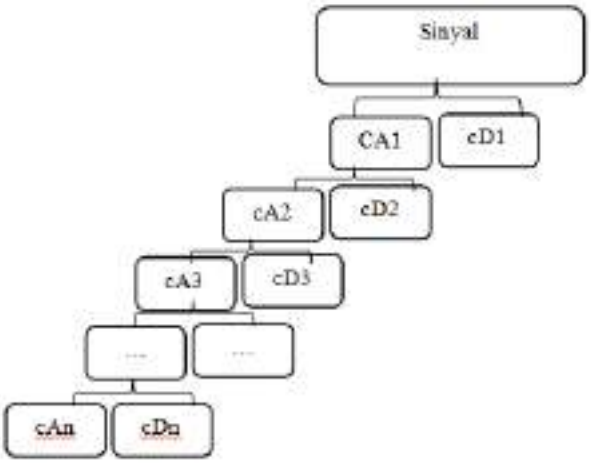

Şekil 2. Bir Sinyalin Dalgacık Dönüşümü İle Detaylı Ve Yaklaşımlı Alt Bant Kanallarına Ayrılması (Garg et al. 2011).

Bu çalışmada sağlıklı ve şizofreni bireylere ait EEG sinyallerine Daubechies türünde wavelet dönüşümü yapılmış ve bu dönüşüm sonrası elde edilen farklı bileşenler (örneğin db2 veya db6) analiz edilerek, bu bileşenler üzerinde göreceli dalgacık dönüşümü enerjisi yöntemi uygulanarak en iyi başarım sonucunu veren özellikler çıkarılmıştır.

Göreceli Dalgacık Dönüşümü Enerjisi (Relative Wavelet Energy)

Dalgacık katsayılarının farklı ölçeklerdeki entropileri, katsayıların taşıdığı bilgi içeriğini ortaya çıkarmak için ölçülür. Dalgacık entropisi, sinyalin düzen / düzensizlik derecesinin bir ölçüsüdür ve doğrusal olmayan sinyallerin gizli dinamik özelliklerini gösterir (Rosso et al. 2006; Rosso, Martin, and Plastino 2002). Verilen ayrık sinyal x (n) anında k ve j ölçeğinde dönüştürülür. Yüksek frekans bileşenli dalgacık katsayısı Dj (k) 'ye ve düşük frekanslı bir bileşen dalgacık katsayısı Aj (k) sahiptir. Dj (k) ve Aj (k) sinyal bileşeninde bulunan bilgilerin frekans bantları aşağıdaki şekilde elde edilir.

$$\left.\begin{array}{l} D_j(k): [2^{-(j+1)} f_s \, , 2^{-j} f_s] \\ A_j(k): [0, 2^{-(j+1)} f_s] \end{array}\right\} \quad \text{Where } j=1,2,3,\ldots\ldots,J \tag{4}$$

fs örnekleme frekansıdır. (1,…, N) 'den farklı ayrışma seviyesindeki enerji, dalgacık ayrıntı katsayıları Dj (k) ve dalgacık yaklaşık katsayısı Aj (k)' nin enerjisidir.

Her ayrışma seviyesindeki enerji,

$$E_j = \sum_k |D_j(k)|^2 \quad (5)$$

$$E_{N+1} = \sum_k |A_j(k)|^2 \quad (6)$$

Ortalama dalgacık Enerjisi detay katsayıları

$$\bar{E}_j = \frac{1}{N_j} \sum_j |D_j(k)|^2 \quad (7)$$

Nj, j seviyesindeki dalgacık ayrıntı katsayılarının sayısıdır.

$$\bar{E}_{N+1} = \frac{1}{N_j} \sum_j |A_j(k)|^2 \quad (8)$$

Ortalama dalgacık Enerjisi yaklaşık katsayıları,

Daha sonra, dalgacık ayrışmasından sonra sinyalin toplam enerjisi,

$$E_{total} = \sum_{j=1}^{N+1} \bar{E}_j \quad j = 1,2,\ldots,N+1 \quad (9)$$

Böylece göreceli dalgacık enerjisi (RWE),

$$\rho_j = \frac{\bar{E}_j}{E_{total}} \quad (10)$$

$\sum_j \rho_j = 1$ ve dağılım ρ_j zaman ölçeği yoğunluğu olarak düşünülebilir. Bu, farklı frekans bantlarındaki sinyal enerjisi dağılımını karakterize etmek için bilgi sağlar (Kumar, Dewal, and Anand 2012).

En Yakın k Komşu Sınıflandırma Algoritması (kNN)

En basit sınıflandırma tekniklerinden biri, en yakın k komşu sınıflandırıcısıdır. Bir girdi özellik vektörü X'in sınıflandırılması, en yakın k eğitim vektörlerini uygun bir mesafe metrik değerine göre belirleyerek yapılır. Vektör X daha sonra, bu en yakın komşuların çoğunluğunun ait olduğu sınıfa atanır (Latifoğlu et al. 2008; Sengur 2008). kNN algoritması, en yakın komşuluklarda bir mesafe fonksiyonu ve bir oylama fonksiyonuna

dayanmaktadır, kullanılan metrik Öklid uzaklığıdır. En yakın k komşu sınıflandırıcısı, optimum değerler k (Duda, Hart, and Stork 1998) için iyi bir performans sergilediği söylenen klasik parametrik olmayan denetimli sınıflandırmacıdır.
Çoğu öğreticili öğrenme algoritması gibi, kNN algoritması bir eğitim aşamasından ve bir test aşamasından oluşur. Eğitim aşamasında, veri noktaları n-boyutlu bir alanda verilir. Bu eğitim veri noktalarında, sınıflarını belirten onlarla ilişkili etiketler bulunur. Test aşamasında, etiketlenmemiş veriler verilir ve algoritma etiketlenmemiş noktaya en yakın k (en önceden sınıflandırılmış) veri noktalarının listesini oluşturur. Algoritma daha sonra o listenin çoğunluğunun sınıfını döndürür (Hall 1998; Morgan, D. P., & Scofield 1991) .
En yakın k komşu algoritması aşağıdaki adımlardan oluşmaktadır (El-Dahshan, Hosny, and Salem 2010) :
1.Uygun bir mesafe metriğini belirleyin.
2.Eğitim aşamasında: P tüm eğitim verilerini P çiftlerine (seçilen özelliklere göre) depolayın, burada P = {(y_i, c_i), i = 1, ..., n}, y_i bir eğitim modeli Eğitim verileri seti, c_i karşılık gelen sınıf ve n, eğitim kalıpları miktarıdır.
3.Test aşamasında: Yeni özellik vektörü ile depolanan tüm özellikler (eğitim verileri) arasındaki mesafeleri hesaplayın.
4. En yakın komşular seçilir ve yeni örneği sınıf için oy kullanmaları istenir. Test aşamasında verilen doğru sınıflandırma algoritmanın doğruluğunu değerlendirmek için kullanılır. Eğer bu tatmin edici değilse, makul bir doğruluk düzeyi elde edilinceye kadar k değeri ayarlanabilir.

BULGULAR

Sağlıklı ve hasta bireylerden alınan 16 kanallı EEG kayıtlarından her birine öncelikle Daubechies türünde dalgacık dönüşümü uygulanmaktadır. Dalgacık dönüşümü sonucunda elde edilen alt bant kanallarından en iyi performansı veren Daubechies türünü belirlemek için farklı Daubechies (db2, dB6 gibi) türleri denenmiştir. En iyi başarım sonucu verecek olan dalgacık dönüşümü ile elde edilen değerler üzerinde, sonrasında göreceli dalgacık dönüşüm enerjisi yöntemi kullanılarak özellik çıkarımı yapılmıştır.

Her bireye ait 16 kanallı EEG verisinde her kanaldan alınan veri 4780 uzunluğu tek boyutlu bir dizidir. Özellik çıkarımı sonucunda her kanaldan 218 uzunluğunda özellik vektörleri elde edilmiş. Elde edilen özellik vektörleri en yakın k komşu sınıflandırma algoritması kullanılarak sınıflandırılmıştır. Farklı k değerleri için farklı başarım sonuçları elde edilmiştir ve sonuçlar Şekil 3'de gösterilmektedir. Şekilde de görüldüğü üzere en yüksek başarım k=1 değeri için 94,1% olarak elde edilmiştir. Ancak sınıflandırma işleminde çapraz doğrulama (Cross Validation=10 değeri için) yapıldığında başarım oranı 95,2% olarak elde edilmiştir.

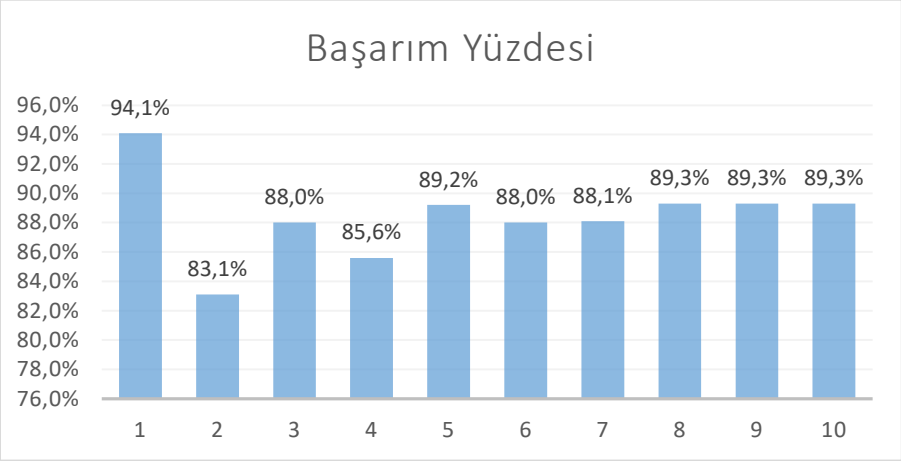

Şekil 3. Farklı n Değerleri İçin En Yakın k Komşu Sınıflandırma Algoritmasının Başarım Sonuçları.

SONUÇ

Bu çalışmada şizofreni hastalığına sahip hastaların EEG kayıtları Dalgacık dönüşümü ve göreceli dalgacık enerjisi metotlarıyla analiz edilmiştir. Bu analiz sonucu elde edilen özellikler, bir sınıflandırıcıya verilerek, ilgili özelliklerin hastalığı ayırt edici özelliğe sahip olup olmadıkları incelenmiştir. Sonuç olarak, kullanılan en yakın k komşu sınıflandırıcısında başarım 90% civarında elde edilmektedir. Bu da bize ilgili analiz yönteminin EEG sinyalindeki tanı amaçlı önemli özellikleri koruyabildiğini göstermektedir. Çalışmada kullanılan metot bize şizofreni hastalarının normal bireylerden ayırt edilebilmesini sağlayacak bir uzman sistem tasarlanabileceğini göstermekte ve bu yöndeki çalışmaları teşvik edici olarak öne çıkmaktadır. Sonraki çalışmalarda, bu çalışmadaki metodoloji baz alınarak, şizofreni hastalığının teşhisi, tespiti veya buna benzer alanlarda klinik çalışanlara yardımcı olabilecek karar destek sistemlerinin geliştirilmesi oldukça olası görünmektedir.

KAYNAKLAR

American Psychiatric Association. 1994. "Diagnostic and Statistical Manual of Mental Disorders American Psychiatric Association." *Washington, DC*.

Borisov, S. V., A. Ya Kaplan, N. L. Gorbachevskaya, and I. A. Kozlova. 2005. "Analysis of EEG Structural Synchrony in Adolescents with Schizophrenic Disorders." *Human Physiology*.

Cherif, R., A. Nait-Ali, J.F. Motsch, and M.O. Krebs. 2004. "A Parametric Analysis of Eye Tremor Movement during Ocular Fixation, Applied to Schizophrenia."

Duda, Richard O, Peter E Hart, and David G Stork. 1998. "Pattern Classification (2nd Ed .)." *Computational Complexity*.

El-Dahshan, El Sayed Ahmed, Tamer Hosny, and Abdel Badeeh M. Salem. 2010. "Hybrid Intelligent Techniques for MRI Brain Images Classification." *Digital Signal Processing: A Review Journal*.

Garg, Girisha, Vijander Singh, J R P Gupta, and A P Mittal. 2011. International Journal of Biomedical Signal Processing *RELATIVE WAVELET ENERGY AS A NEW FEATURE EXTRACTOR FOR SLEEP CLASSIFICATION USING EEG SIGNALS*.

Gaser, Christian et al. 1999. "Detecting Structural Changes in Whole Brain Based on Nonlinear Deformations Application to Schizophrenia Research." *NeuroImage*.

Graps, Amara. 1995. "An Introduction to Wavelets." *IEEE Computational Science and Engineering*.

Hall, M. 1998. "Correlation-Based Feature Selection for Machine Learning." Waikato Uni.

Hornero, Roberto et al. 2006. "Variability, Regularity, and Complexity of Time Series Generated by Schizophrenic Patients and Control Subjects." *IEEE Transactions on Biomedical Engineering*.

Jeong, Jaeseung et al. 1998. "Nonlinear Analysis of the EEG of Schizophrenics with Optimal Embedding Dimension." *Medical Engineering and Physics*.

Keil, Andreas, Thomas Elbert, Brigitte Rockstroh, and William J. Ray. 1998. "Dynamical Aspects of Motor and Perceptual Processes in Schizophrenic Patients and Healthy Controls." *Schizophrenia Research*.

Kumar, Yatindra, Mohan Lal Dewal, and Radhey Shyam Anand. 2012. "Relative Wavelet Energy and Wavelet Entropy Based Epileptic Brain Signals Classification." *Biomedical Engineering Letters*.

Latifoğlu, Fatma, Kemal Polat, Sadik Kara, and Salih Güneş. 2008. "Medical Diagnosis of Atherosclerosis from Carotid Artery Doppler Signals Using Principal Component Analysis (PCA), k-NN Based Weighting Pre-Processing and Artificial Immune Recognition System (AIRS)." *Journal of Biomedical Informatics*.

Lewis, David A., and Guillermo Gonzalez-Burgos. 2000. "Intrinsic Excitatory Connections in the Prefrontal Cortex and the Pathophysiology of Schizophrenia." *Brain Research Bulletin*.

Morgan, D. P., & Scofield, C. L. 1991. "Neural Networks and Speech Processing." *In Neural Networks and Speech Processing* Springer(Boston, MA.): (pp. 329-348).

Paulus, Martin P., Mark A. Geyer, and David L. Braff. 1999. "Long-Range Correlations in Choice Sequences of Schizophrenic Patients." *Schizophrenia Research*.

Pressman, A., Peled, A., & Geva, A. B. 2000. "SYNCHRONIZATION ANALYSIS OF MULTI-CHANNEL EEG OF SCHIZOPHRENIC DURING WORKING-MEMORY TASKS." *In 21st IEEE Convention of the Electrical and Electronic Engineers in Israel. Proceedings (Cat. No. 00EX377)* April: 337–41.

Rosenberg, Stewart et al. 1990. "Random Number Generation by Normal, Alcoholic and Schizophrenic Subjects." *Psychological Medicine*.

Rosso, O. A. et al. 2006. "EEG Analysis Using Wavelet-Based Information Tools." *Journal of Neuroscience Methods*.

Rosso, O. A., M. T. Martin, and A. Plastino. 2002. "Brain Electrical Activity Analysis Using Wavelet-Based Informational Tools." *Physica A: Statistical Mechanics and its Applications*.
Sabeti, M., R. Boostani, S. D. Katebi, and G. W. Price. 2007. "Selection of Relevant Features for EEG Signal Classification of Schizophrenic Patients." *Biomedical Signal Processing and Control*.
Selemon, Lynn D., and Patricia S. Goldman-Rakic. 1999. "The Reduced Neuropil Hypothesis: A Circuit Based Model of Schizophrenia." *Biological Psychiatry*.
Sengur, Abdulkadir. 2008. "An Expert System Based on Principal Component Analysis, Artificial Immune System and Fuzzy k-NN for Diagnosis of Valvular Heart Diseases." *Computers in Biology and Medicine*.
Shao, Chenxi, Jinfeng Fan, and Shaobin Li. 2007. "Nonlinear Characteristics and Qualitative Analysis of Sleep EEG." In *2007 1st International Conference on Bioinformatics and Biomedical Engineering, ICBBE*,.
WHO. 2011. "International Statistical Classification of Diseases and Related Health Problems - 10th Revision." *World Health Organisation*.

URBAN TRANSFORMATION PROJECT USING ANALYTICAL HIERARCHY PROCESS (AHP): CASE OF SANLIURFA

Mehmet TOPDAĞ
Şanlıurfa Büyükşehir Belediyesi İmar ve Şehircilik Dai. Bşk.
mehmet.topdag@sanliurfa.bel.tr

Hüseyin Zahit SELVİ, İlkay BUĞDAYCI
Necmettin Erbakan Üniversitesi Mühendislik Mimarlık Fakültesi Harita Mühendisliği Bölümü, hzselvi@erbakan.edu.tr , ibugdayci@erbakan.edu.tr

ABSTRACT: As a natural result of developing science and technology, it can be said that it is very easy to access data today. However, it is very important to reach the most accurate data in the shortest time. Particularly in the decisions such as urban transformation and disaster management where decisions are very important, it is necessary to make the right decision by considering all the necessary criteria. It is known that analyzing spatial data with the support of GIS (Geographical Information System) makes a significant contribution to decision-makers. Multi-criteria decision-making methods can provide significant contributions, especially when multiple criteria affect the decision. Urban transformation projects are located the complex problems in which more than one spatial criteria affect the decision-making process. In this study, it is aimed to determine the areas where priority urban transformation is needed from Yesildirek, Sehitlik, Hizmali, Karakoyun neighborhoods in Haliliye District of Sanliurfa Province by Analytical Hierarchy (AHP), which is a multi-criteria decision making method. Thus, the importance of using GIS and multi-criteria decision making methods will be introduced in order to make an accurate urban transformation decision according to objective criteria.

Key Words: Geographical Information Systems, Urban Transformation, multi criteria data analysis

ANALİTİK HİYERARŞİ YÖNTEMİYLE (AHP) KENTSEL DÖNÜŞÜM UYGULAMASI: ŞANLIURFA ÖRNEĞİ

ÖZET: Gelişen bilim ve teknolojinin doğal sonucu olarak, günümüzde veriye ulaşmanın oldukça kolay olduğu söylenebilir. Ancak bu verilerden en doğrusuna en kısa sürede ulaşmak oldukça önem taşımaktadır. Özellikle belirlenen kararların çok önemli olduğu kentsel dönüşüm, afet yönetimi gibi kararlarda gerekli tüm kriterlerin dikkate alınarak

doğru karar verilmesi gerekmektedir. Mekânsal verilerin CBS (Coğrafi Bilgi Sistemi) desteğiyle analiz edilmesinin, karar vericilere önemli katkı sağladığı bilinmektedir. Özellikle birden fazla kriterin, kararı etkilediği durumlarda, çok kriterli karar verme yöntemleri önemli katkılar sunabilmektedir. Kentsel dönüşüm projeleri de birden fazla mekânsal kriterin karar verme sürecini etkilediği karmaşık problemler arasında yer almaktadır. Bu çalışmada çok kriterli karar verme yöntemlerinden Analitik Hiyerarşi (AHP) yöntemiyle, Şanlıurfa İli Haliliye İlçesinde bulunan Yeşildirek, Şehitlik, Hızmalı, Karakoyun mahallelerinden, öncelikli Kentsel Dönüşüme ihtiyaç duyulan alanların belirlenmesi amaçlanmaktadır. Böylece objektif kriterlere göre doğru bir kentsel dönüşüm yapılabilmesi için CBS ve çok kriterli karar verme yöntemlerinin kullanılmasının önemi ortaya konulacaktır.

Anahtar kelimeler: Coğrafi Bilgi Sistemi, Kentsel Dönüşüm, Çok Kriterli Veri Analizleri.

GİRİŞ

Kentler, toplumsal olarak sürekli bir gelişmeyi içerisinde barındıran ve toplumda yer alan bireylerin, yerleşme, barınma, eğlenme gibi temel yaşamsal ihtiyaçlarının karşılandığı; pek az sayıda bireyin tarımsal faaliyetlerde bulunduğu; nüfus önünden kırsaldan daha yoğun olan ve insanların sosyalleşebildiği yerleşme birimidir (Keleş, 1987;70). Kentler, toplumsal yaşama biçim verirler.

Kentlerde tıpkı diğer varlıklar gibi, doğan, büyüyen, gelişen ve eskiyen toplumsal birimlerdir. Kentsel dönüşüm, birçok etmene bağlı olarak, sosyal yaşamın her anında ve alanında sürekli bir değişim özelliğini barındıran süreç olarak tanımlanmakta olup; makro ölçekten, mikro ölçeğe uzanan ve bir bütünlük arz eden kavram olan dönüşüm olgusunun birçok faktörünü (sosyal, psikolojik, kültürel, politik, ekonomik, felsefi vb.) bir arada barındırmaktadır (Arabulan, 2015: 8).

Kentsel dönüşüm ifadesi ilk olarak, 18. yüzyıldan itibaren ortaya çıkan ve endüstri devriminin sonucunda oluşan, sosyal ve ekonomik çöküntü bölgelerinin rehabilite edilmesi ve yenileştirmesi amacıyla gerçekleştirilen çalışmaların genel bir ifadesi olarak tanımlanabilmektedir. Kentsel dönüşüm çalışmaları, kentin nüfus yoğunluğunda artma olduğu ya da dar gelir gruplarının iyi olmayan şartlarda yaşam sürdürdüğü konut ve endüstri alanlarında, şehre ekonomik yönde olumlu biçimde katkı sağlayacak projelerin geliştirilmesi biçiminde uygulanabildiği görülebilmektedir (Özkul, 2017: 5).
Daha açık bir ifadeyle kentsel dönüşüm ve gelişim uygulamaları, kentlerin eskiyen, yıpranmış ve sefalet yuvası haline gelmiş bölgelerinin daha sağlıklı, modern, yaşanabilir alanlar haline getirilmesi; kentin büyümesi ile kent içinde kalan sanayi alanlarının kentin dışına çıkarılması sonucu boşalan yerlerin halkın yararına düzenlenmesi, yıpranmış kent alanlarının restorasyonu yapılarak, toplumun hizmetine kazandırılması ve olası bir doğal

afet sonrasında zarar görme riski olan alanların iyileştirilmesi gibi nedenlerle gerçekleştirilmektedir.

Örneğin deprem, Türkiye`nin önemli bir gerçeği konumundadır ve kimi dönemlerde maalesef mal ve can ayıplarına neden olmaktadır. Depremlerin bir doğa olayı olarak ciddi afetlere dönüşmesi kentsel dönüşüm süreçlerinde depreme dayanıklı, güvenli konutların yapılmasını önemli bir amaç haline getirmektedir. (TMMOB, 2012).

Karar verme pozisyonundaki idarecilerin, yeni yaşam alanlarını oluşturma ve kaçak yapılaşma ile mücadele noktasındaki gecikmeleri, gecekondu yerleşkelerinin oluşmasının temel sebeplerindendir.

Gecekondu yaşam alanı, plansız, fen ve bilim normlarına uymayan düzensiz bir yaşam alanı oluşturmaktadır. Diğer yandan bölgenin alt yapısının yetersiz oluşu, çevresel etmenlere bağlı olarak sağlık sorunlarına neden olabilmektedir. Günümüzde bilhassa gecekondu alanları için, görmek istediğimiz modern kent görüntüsünü, kentsel dönüşüm projeleri ile kazanabildiği, yukarıdaki tanımlamalardan anlaşılabilmektedir. Ancak kentsel dönüşüm projeleri için, gerek projelendirme noktasında, gerek inşaat maliyeti göz önünde bulundurulduğunda; yüksek bir bütçenin ayrılması gerektiği aşikârdır.

Kentte yer alan bütün bir gecekondu alanının dönüşümü mümkün olamıyor ise, idare tarafından öncelikli kriterler belirlenerek bu doğrultuda Çok Kriterli Veri Analizleri Yönetimleriyle, var olan gecekondu alanlarından öncelikli dönüşüme ihtiyaç duyulan alanların belirlenmesi gerekmektedir.

Şanlıurfa İli 1980'li yıllar ile birlikte, özellikle GAP çalışmalarının doğal sonucu olarak sulu tarıma geçilmesiyle, tarımsal anlamda cazibeli bir konuma gelmiştir. Ancak geçen zamanın etkisiyle nüfus ve sanayideki gelişime paralel olarak kentleşme oranı % 50 lerden, % 92 oranlarına yükselmiştir. Bu süre zarfındaki kentleşme oranında anormal artış, kentleşmeyle beraber, çevre sorunları ve sosyolojik sorunların önünü açmıştır (URL 1).

Bu çalışma ile, Şanlıurfa Büyükşehir Belediye Başkanlığı tarafından 5393 sayılı Belediye kanunun 73. maddesi gereği, kentin çöküntü, eskimiş bölgelerinden kentsel dönüşüm ihtiyaç duyulan öncelikli olarak dönüşümün yapılması gereken alanların tespiti amaçlanmaktadır.

Kentsel dönüşüme ihtiyacı bulunan alanlar;

Plansız ve ruhsatsız alanlar, diğer bir ifadeyle gecekondu alanları,

Planlı alanlarda yer alan ruhsatsız yapılar olarak belirlenmiştir.

Kentsel dönüşümün genel amaçları aşağıdaki şekilde sıralanabilir;

Kentin geçmişten bu yana sahip olduğu kimlik ile fiziki şartlar arasında bir bağın oluşturulması gerekmektedir. Kentlerin birtakım sorunları yaşamalarının ve kötü koşulları altında yaşama durumunun ortaya çıkmasının en önemli nedenlerinden biri, toplumsal alanda görülen sorunlardır. Bu nedenle kentsel dönüşüm projelerinin oluşturulmasında toplumsal (sosyal ve ekonomik) sorunların incelenmesi, çözüm önerilerinin geliştirilmesi ve elde edilen sonuçlar dikkate alınarak düzenlenmesi gerekir.

Kentler doğası gereği, birçok fiziksel özellikle birlikte sürekli bir değişim süreci içerisindedir. Bu nedenle, kentsel dönüşüm projeleri, fiziksel unsurlarda meydana gelen değişimlere cevap vermeyi hedefler. Daha açık olmak gerekirse, kentsel dönüşüm değişen koşullara bağlı olarak, kentin alt yapı ve üst yapı gibi, değişen fiziki ihtiyaç ve özelliklerine cevap vermeyi amaçlar.
Kentsel dönüşüm, kentte yaşayan insanların yaşam standartlarını yükseltmeyi, daha sağlıklı yaşam çevreleri oluşturmayı ve refah bir yaşam sağlamayı amaçlar.
Kentlerde meydana gelen sorunlar, sadece fiziksel ve sosyal alanlarda görülmemektedir. Bunlara benzer bir şekilde ekonomik alanda görülen bir takım sorunlar, kentlerin ya da kent içerisindeki bazı bölgelerin çöküntü haline gelmesi ile sonuçlanmaktadır. Kentsel dönüşüm projeleri yolu ile kentin ya da kentin bazı bölgelerinde görülen ekonomik sorunların çözülmesi ve bu sayede kent içerisinde yaşayan bireylerin yaşam standartlarının geliştirilmesi amaçlanmaktadır.
Kentsel dönüşüm ve gelişim projelerinin bir diğer önemli hedefi, şehirdeki plansızlaşmanın ve düzensizliğin ortadan kaldırılmasıdır. Kentsel dönüşüm projeleri ile kentsel yaşam alanların daha etkin ve verimli bir biçimde kullanılması, yaşam alanlarındaki gereksiz yayılmaların önüne geçilmesi amaçlanır (Şişman ve Kibaroğlu, 2009: 2).

Kentsel dönüşüm çalışmaları, başından sonuna dek uzun bir süreç içerisinde gerçekleşir. Bu süre zarfında birçok noktada kararsız kalınabilecek durumlar oluşabilmektedir. Bu sorunlar çok kriterli karar verme teknikleri yardımıyla, objektif ve doğru karar verme imkanı veren mekânsal analizlerle çözülebilmektedir. Bu çalışmada çok kriterli karar verme yöntemlerinden Analitik Hiyerarşi (AHP) yöntemiyle seçenekler arasından öncelikli dönüşüm alanının belirlenmesi sağlanacaktır.

Bütün bu amaçlara ulaşacak doğru bir kentsel dönüşüm uygulaması ise sübjektiflikten uzak objektif kriterlerle uygulama yapılarak mümkün olabilir. Bu kapsamda gelişen teknoloji ve imkânlar daha sağlıklı ve doğruluğu yüksek analizler yapmaya imkan tanımaktadır. Bu noktada coğrafi bilgi sistemlerinin dönüşüm süreçlerinde kullanılması önemli avantajlar sağlamaktadır.

1.Yöntem

1.1 Analitik Hiyerarşi Yöntemi (AHP):

Çok kriterli karar verme teknikleri, karar verme pozisyonunda yer alan idarecilerin birbirinden bağımsız çok sayıda seçenekler arasında, en uygun seçeneği seçebileceği yöntemleri barındırır. Seçenekler arasında karar verme durumuyla karşılaşıldığında, bu seçeneklerden en olası olanın seçilmesi gerekir. Lineer cebir programlama, dinamik programlama ve döküm kontrolü gibi gelişim gösteren yeni sayılabilecek pek çok yöntem, en nihai çözüme/karara ulaşmak amacına hizmet etmektedir. Bu yöntemler ilerleyen zamanlarda, çok kriterli karar verme adı altında toplanmıştır (Çetinsaya, 2004).

Yalnızca 1 adet kriter ölçü alınarak alternatifler değerlendirilebilirken, karar verme işi göreceli olarak daha kolay yapılabilmektedir. Fakat kriter sayısının artması ile birlikte, karar verme işlemi çok daha zor boyutlara ulaşabilmektedir. AHP kullanımı, seçenekler ile alt seçenekler arasında ikili mukayeseye dayanarak, birbirilerine olan üstünlüklerin belirlenmesi ile sonuca ulaştırır. Bu bilgiler ışığında, belirlenen kriterlere bağlı olarak en etkin seçimin alternatifler arasında yapılabilmesini sağlar. AHP de, hiyerarşik yapının (Şekil 1) oluşturulması ilk adımdır. Belirlenen amaç doğrultusunda kriterler ve ona ait olan alt bilgileri içeren hiyerarşik yapı oluşturulur. Hiyerarşiye bakıldığında en tepede nihai amacın, ortada ele alınacak kriterlerin ve en altta ise değerlendirilecek alternatiflerin olduğu görülmektedir.

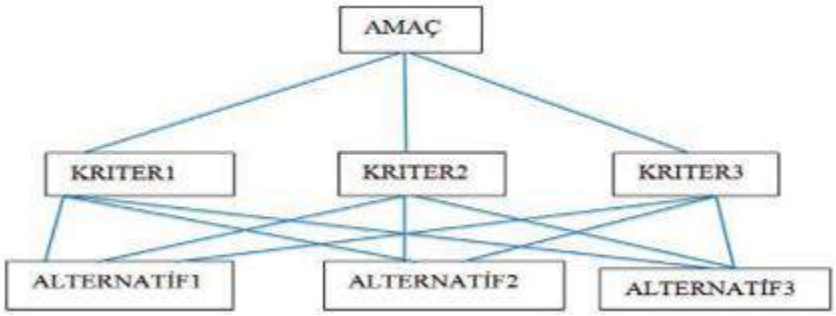

Şekil 1: Hiyerarşik Yapı

1.2. Seçenekler

Ülkemizde kentsel dönüşüme yönelik yerel yönetimler tarafından benimsenen tanım ve amaç; sağlıksız ve eskimiş konutlar ile birlikte, plansız olarak gelişmiş yerleşimlerin, kent merkezlerinde kalan sanayi alanlarının kaldırılması sonucu tamamen atıl vaziyette kalan ya da iyileştirilmesi ve yeni ihtiyaçlar doğrultusunda tekrardan halka kazandırılması gereken kentsel fonksiyonların, yeni ihtiyaçlar doğrultusunda geliştirilmesi ve yenilenmesi yoluyla yerleşim yerlerinin günümüz koşullarına uygun biçimde daha yaşanabilir, sürdürülebilir ve modern kent merkezleri halini almasıdır (Demirkıran 2008,8s.).
Yukarıdaki tanıma göre Şanlıurfa Büyükşehir Belediyesi sınırları içerinde kalan Şehitlik, Hızmalı, Karakoyun ve Yeşildirek mahallelerinin kentsel dönüşüme ihtiyaç duyacağı gözlemlenebilmektedir. Bu çalışmada Şanlıurfa ili Haliliye İlçesi sınırlarında kalan, Şekil 2 de belirtilen bu mahallelerde, belirlenen kriterlere göre en uygun çalışma alanın belirlenmesi hedeflenmektedir.

Şekil 2: Kentsel Dönüşüm Alanlarının Kent İçindeki Konumları

2.1. Kriterlerin Belirlenmesi ve Uygunluk Haritalarının Oluşturulması

En uygun dönüşüm alanının belirlenmesi sürecinde, dikkat edilmesi gereken hususların belirlenmesi ve irdelenmesi ile ikili mukayeseler büyük önem arz etmektedir. Bu kapsamda çalışma alanı seçilirken deprem, sıcaklık, nemlilik, hakim rüzgar yönü unsuru, yağış miktarı gibi beklenmedik olası durumlarda dikkate alınmış ve incelenmiştir. Bütün bu çalışmalar ışığında veri karmaşasını önlemek ve çalışmanın işlevselliği ve anlaşılırlığını sağlamak amacıyla farklı alanlarda farklı özellik gösteren kriterler hesaplamaya katılmıştır.

Bu noktada öncelikli dönüşüm alanının belirlenmesi sürecinde;
1-Mülkiyet bilgisi (Özel, kamu)
2-Parsel bilgileri
3-Yapı miktarı (kat adetleri)
4-Yapının yıpranma oranları

5-Kent merkezindeki konumları
6- Maliyet
7-Jeolojik
8-Eğim
9-Sıcaklık kriterleri üzerinde durulacaktır.
AHP Hiyerarşik yapısı oluşturulduktan sonra kriterlerin kendi aralarında ikili mukayesesi ile karşılaştırma karar matrisleri oluşturulur. Bu matrislerin oluşturulmasında (Saaty, 1980) tarafından önerilen 1-9 önem skalası kullanılmaktadır.

Tablo 1: Önem Skalası

Önem Derecesi	**Tanım**	**Açıklama**
1	Eşit derecede önemli	İki seçenek eşit derecede öneme sahiptir.
3	Orta derecede önemli	Tecrübe ve yargı, bir kriteri diğerinden önemli saymaktadır.
5	Kuvvetli derecede önemli	Tecrübe ve yargı, bir kriteri diğerine karşı oldukça üstün saymaktadır.
7	Çok kuvvetli derecede önemli	Bir kriter, diğer bir kriterden üstün sayılmaktadır.
9	Kesin önemli	Bir kriteri diğer bir kriterden üstün olduğunu ortaya koyan çok sayıda kanıt bulunmaktadır.
2-4-6-8	Ara değerler	Anlaşma gerektiğinde kullanılabilecek iki ardışık yargı arasındaki değerleri ifade etmektedir.

Şekil 3: Yeşildirek Mülkiyet Haritası

Şekil 4:Şehitlik Hızmalı Karakoyun (ŞHK) Bölgesi Mülkiyet Haritası

Şekil 3 ve Şekil 4 te Kentsel dönüşüm alanlarının mülkiyet dokusu ortaya çıkarılmış olup, mülkiyet dağılımı incelenebilmektedir.

Bu işlem sırasında Kadastro müdürlüğünden alınan mülkiyet sınırları ile tapu kayıt bilgileri birbirine entegre edilmiştir.

Yapılan incelemede, söz konusu alanın büyük çoğunluğunu özel mülkiyet oluştururken, kalan kısımlar sırasıyla Şanlıurfa Büyükşehir Belediyesi ile Toplu Konut İdaresi Başkanlığı adına kayıtlıdır. Mülkiyet dokusu bilhassa kamulaştırma noktasında önem arz ederken, diğer yandan imar planı yapım aşamasında da dikkate alınması gereken önemli bir husustur. Kamulaştırma işlemi yapılırken yapılan tespitlere göre; Şehitlik-Hızmalı-Karakoyun bölgesi ortalama arsa m² rayiç bedeli 40-50 TL iken, Yeşildirekte ise 120-150 TL dolaylarındadır (URL2). Şekil 4 te verilen alana dair belirlenen diğer kriterlerin dağılımı ArcGIS yazılımı marifetiyle hazırlanarak ortaya çıkarılmıştır.
Diğer analizler ise bölgenin halihazır haritası çıkartılarak; yapı kat sayısı, yapı niteliği (nitelikli yapı-niteliksiz yapı), yapı kullanım haritaları (Ticaret-konut-depo vs), yapı kat sayısı analizleri yine ArcGIS yazılımı marifetiyle çıkartılmıştır (Şekil 5).

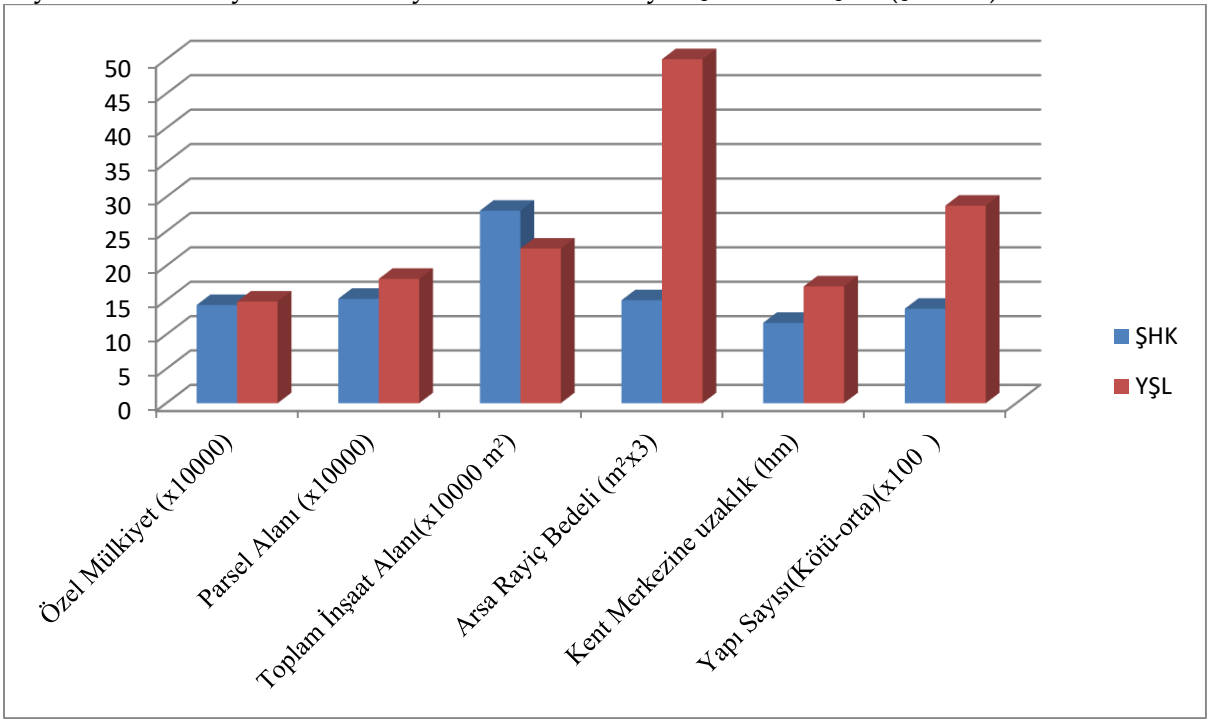

Şekil 5:Yeşildirek (YŞD) ve Şehitlik-Hızmalı-Karakoyun (ŞHK) Bölgesi Karşılaştırılmalı Analizleri

Elde edilen bulguları kullanarak önem skalası ile matrisler oluşturulmuştur. Bu noktada önem arz eden kriterler ile daha az önem arz eden kriterler 1-9 rakamları arasında puanlanmış olup; sonuç olarak kriter ağırları oluşturulmuştur (Tablo 2).

Tablo 2: Önem Skalası Matrisi

	K1	K2	K3	K4	K5	K6	K7	K8	K9
Mülkiyet (K1)	5	5/3	5/4	5/4	5/2	5/9	5	5	5
Parsel Sayısı (K2)	3/5	3	3/4	3/4	3/2	3/9	3	3	3
Yapı Adedi (K3)	4/5	4/3	4	4/4	4/2	2/9	2	2	2
Yapı Durumu (K4)	4/5	4/3	4/4	4	4/2	4/9	4	4	4

Kent Merkezine Göre Konumları (K5)	2/5	2/3	2/4	2/4	2	4/9	2	2	2
Maliyet (K6)	9/5	9/2	9/4	9/4	9/2	9	9	9	9
Jeolojik(K7)	1/5	1/3	1/4	1/4	1/2	1/9	1	1	1
Eğim (K8)	1/5	1/3	1/4	1/4	1/2	1/9	1	1	1
Sıcaklık (K9)	1/5	1/3	1/4	1/4	1/2	1/9	1	1	1

Yukarıdaki matris önem skalası marifetiyle 1 ila 9 rakamları arasında puanlanarak oluşturulmuştur. Puan sistemine göre 9 puanı, kriterler içerisinde en önemli olanı simgelemektedir.

Puanlamada uzman görüşleri de dikkate alınarak; mülkiyet kriteri 5, parsel sayısı 3, yapı kat adedi 4, yapı durumu kriteri 4, kent merkezine göre konumları 2, maliyet ise 9 rakamı ile puanlanmıştır. Jeolojik durum, eğim ve sıcaklık değerleri ise bölgesel anlamda standart olarak kabul edilmektedir ve 1 rakamı ile puanlanmıştır.

Jeolojik durum; MTA verilerine göre araştırma sahası barınak yapımı için uygun özelliklere sahip olan kalker ve bazalt kayaçlar yönünden zengindir. temeli oluşturan Bazalt ve Alüvyonal zemin jeolojik ve jeoteknik özellikleri, literatür bilgileri ve arazi gözlemleri birlikte değerlendirildiğinde, bu malzemenin temel oluşturmada herhangi bir sorun yaratmayacağı anlaşılmış ve uygun yerleşim alanlarındandır (URL 4).

Eğim analizi; Çalışma alanı ve yakın çevresinin eğimi %13 yani yaklaşık yatay durumdadır. Çalışma alanındaki jeolojik birimlerin tekdüze bir özellik gösterdiği belirlenmiştir (URL3).

Sıcaklık analizi; İklim bölgeye has karasal iklimdir. Bölgede kışlar soğuk ve yağışlı, yazlar sıcak ve kurak geçmektedir. Kontinental (kara) iklim özelliğinden ötürü sıcaklık farklılıkları görülmektedir. Bölgede en soğuk aylar Ocak-Şubat ayları olup, ortalama sıcaklık derecesi 11.5 °C; en sıcak aylar ise Temmuz-Ağustos olup ortalama sıcaklık derecesi 46.3 °C ve yıllık ortalama sıcaklık derecesi 18.2 °C dir (URL 5).

Maliyet kriterinin projenin yürütülmesi noktasında, en önemli kriter olduğu açık biçimde görülmektedir (Şekil 6).

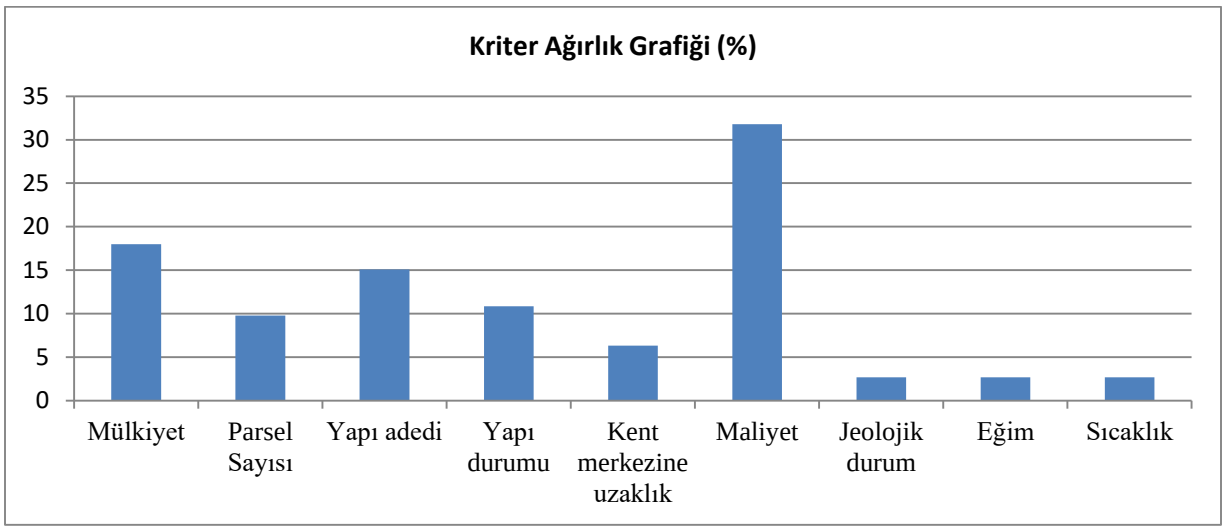

Şekil 6: Kriter Ağırlıkları

SONUÇ

Kentsel dönüşüm ve gelişim projelerinin öncelikli olarak, bütüncül bir dönüşüm ile birlikte bölgeye yeni bir çehre kazandırdığı aşikârdır. Özellikle şehrin merkezinde kalarak prestij kazanan; fakat kentin eskimiş, düzensiz, estetik bir görüntüye sahip olmayan; daha genel bir ifadeyle sorun teşkil eden bölgelerin yenilenmesine imkan sağlamaktadır.

Kent merkezinde bulunan gecekondu alanları, kent merkezinin dışında kalan ya da kırsalda yer alan gecekondu bölgelerine yönelik getirilebilecek çözümlerle çözülemez. Bu nedenle kentsel dönüşüm uygulanabilecek bölgelerde, uyumlu ve modern bir kent imajı ile bütünleşebilecek, bulunduğu kente prestij kazandırabilecek tasarımlarla şekillenen dönüşüm işlemi tasarlanmalıdır. Diğer yandan barındırdıkları gecekondulu nüfusun sosyal, yaşamsal, ekonomi ve diğer problemlerini çözüme kavuşturmalıdır. Dönüşüm ancak sağlıklı veri envanteri, akılcı çözüm ve sağlam bir irade ile sağlanabilmektedir. Dönüşüm uygulamalarında coğrafi bilgi sistemlerinin kullanımı, sağlıklı projelerin tasarımı noktasında önem arz etmektedir. Bu noktadan yola çıkılarak bölgelerin, kadastral durumları, halihazır durumları vs. kriterleri tek tek ele alınmıştır. Kriterlerden maliyet kısmı üzerinde yapılan araştırmada; Şehitlik-Hızmalı-Karakoyun (ŞHK) bölgesinin ortalama arsa rayiç bedeli (m^2) 40-50 TL, Yeşildirek (YŞD) bölgesi ise ağırlıklı olarak (m^2) 120-150 TL olduğu Haliliye İlçe Belediye Başkanlığından öğrenilmiştir (URL2).

Bu çalışmada yapılan bütün mekânsal analizlere altlık teşkil etmesi bakımından, CBS ye atfedilen önem bir kez daha gözler önüne serilmiştir. Çalışma alanında AHP yöntemiyle yapılan mekânsal analizler sonucunda Şehitlik-Hızmalı-Karakoyun bölgesinin % 59, Yeşildirek bölgesinin % 41 oranında öncelikli dönüşüme ihtiyaç duyduğu sonucuna varılmıştır (Şekil 7).

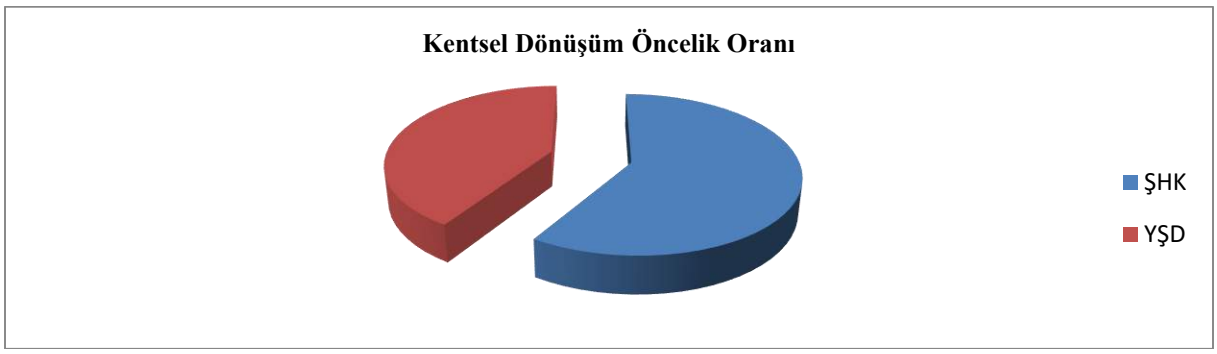

Şekil 7:Sonuç Grafiği

Ayıca karar verme pozisyonundaki idarecilerin, herhangi bir kararsızlık anında problemlere karşı çözüm için ihtiyaç duyulan ve bu ihtiyaçları bilimsel ve matematiksel temele dayanan ikili mukayeseler ile AHP yönteminin ne denli işlevli bir yöntem olduğu görülmektedir.

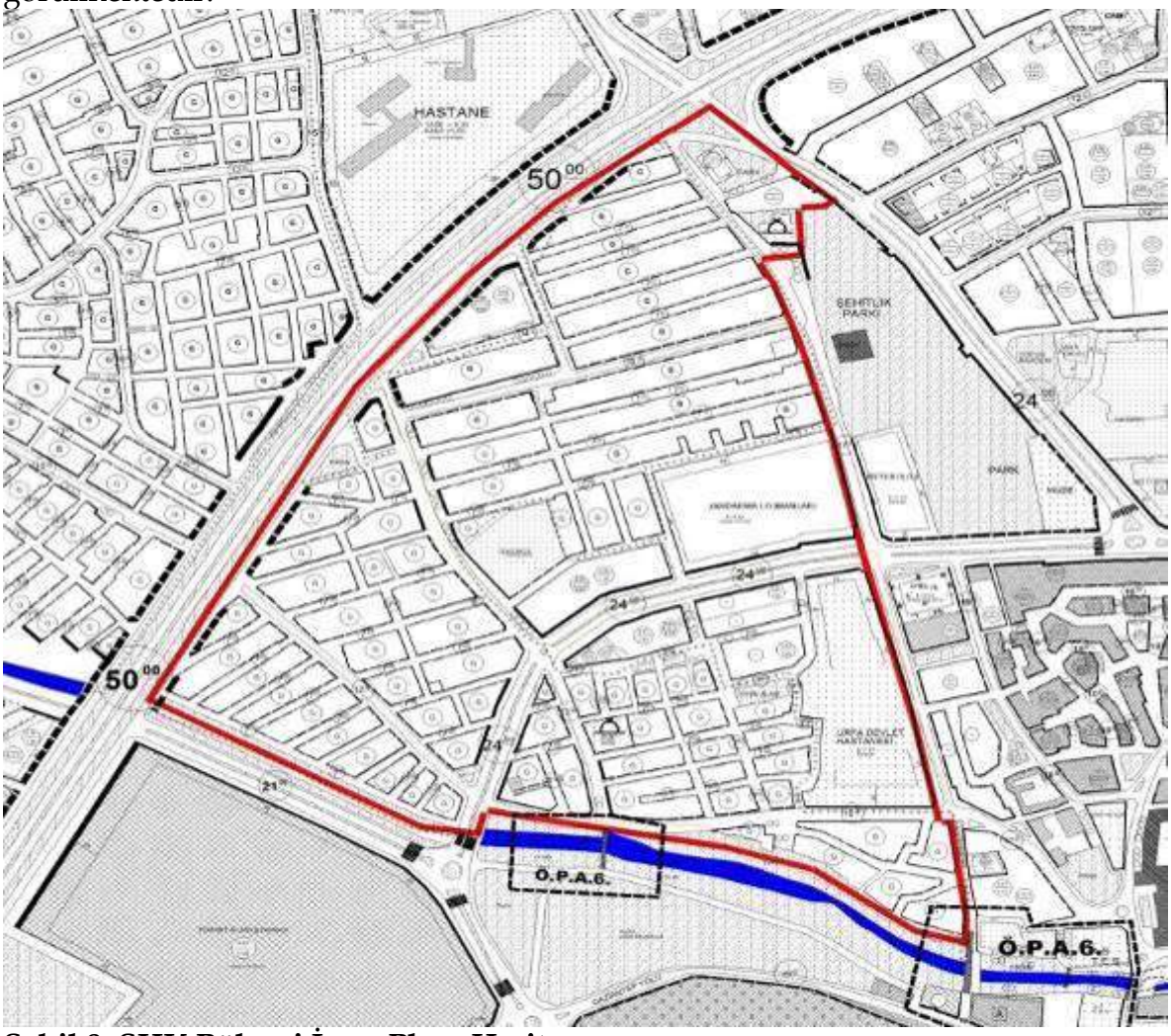

Şekil 8: ŞHK Bölgesi İmar Planı Haritası

KAYNAKLAR

Arabulan, S. (2015). Kentsel Dönüşüm Kapsamında Kimliğin Yeniden Kazanımı: Edirne - Karaağaç Örneği, Basılmamış Doktora Tezi, Trakya Üniversitesi Fen Bilimleri Enstitüsü, Edirne.

Çetinsaya, V., 2004. "Çok Kriterli Kaynak Tahsisi Problemlerinin Optimizasyonunda Bulanık Karar Verme Yöntemlerinin Uygulanması", Yıldız teknik Üniversitesi, Fen Bilimleri Enstitüsü Yüksek Lisans Tezi.

Daşkıran, F., Ak, S. (2015). 6306 Sayılı Kanun Kapsamında Kentsel Dönüşüm, Yönetim ve Ekonomi Araştırmaları Dergisi, Cilt: 13, Sayı: 3.

Demirkıran S. (2008). Türkiye'de Kentsel Dönüşüm Uygulamalarında Yerel Yönetimin rolü konulu Yüksek Lisans Tezi.

Keleş R. (1984) "Kentlesme Ve Konut Politikası", Ankara, Ankara Üniversitesi Siyasal Bilgiler Fakültesi Yayınları.

Saaty T.L.,1980. "The Analytic Hierarcy Process" New York, McGraw-Hill.

Şişman, A., Kibaroğlu, D. (2009). Dünyada Ve Türkiye'de Kentsel Dönüşüm Uygulamaları, TMMOB Harita ve Kadastro Mühendisleri Odası 12. Türkiye Harita Bilimsel ve Teknik Kurultayı, Ankara.

TMMOB, (2012). Kentsel Dönüşüm Nedir?, TMMOB İnşaat Mühendisleri Odası, Ankara.

Özkul, M. (2017). Dünyada Ve Türkiye'de Kentsel Dönüşüm Projelerinin Finansman Yöntemleri, Uzmanlık Tezi, İller Bankası Anonim Şirketi, Ankara

URL1: https://www.karacadag.gov.tr/Planlama/Dosya/www.karacadag.gov.tr_31_BX0B70CW_sanliurfa_kentlesme_yasam_kalitesi_ve_kentsel_donusum_danisma_toplantisi_2014__2018.pdf

URL 2: https://www.turkiye.gov.tr/haliliye-belediyesi-arsa-rayic

URL 3: https://www.sanliurfa.bel.tr/birim/8/142/imar-ve-sehircilik-dairesi-baskanligi

URL 4: http://www.mta.gov.tr/v3.0/

URL 5: https://www.mgm.gov.tr/veridegerlendirme/il-ve-ilceler-istatistik.aspx?m=SANLIURFA.

APPLICATION OF ENERGY AND EXERGY ANALYSES TO AN SI ENGINE OPERATED AT DIFFERENT ENGINE LOADS WITH BIOFUEL-GASOLINE BLENDS

Bahar SAYIN KUL
Selcuk University, Mechanical Engineering Department, Konya, Turkey
bsayin@selcuk.edu.tr

İlker ÖRS
Selcuk University, Department of Motor Vehicles and Transportation Technologies, Konya, Turkey
ilker.ors@selcuk.edu.tr

Murat CİNİVİZ
Selcuk University, Mechanical Engineering Department, Konya, Turkey
mciniviz@selcuk.edu.tr

ABSTRACT: In this study, energy and exergy analyzes were applied to a single cylinder four stroke SI engine operated with base gasoline, biofuel-gasoline blends under different test conditions. The blends abbreviated as E10 and M10 prepared to contain 90% gasoline-10% ethanol, 90% gasoline-10% methanol. The engine test carried out under different engine loads varied from 2 Nm to 4 Nm for 2500 constant engine speed. It is found that maximum energy and exergy efficiencies are obtained as by 0.161, 0.201, 0.148% and 0.148, 0.186, 0.137% at 2.5 Nm for gasoline, E10, M10 respectively. Exergy destruction rate increases with increase in engine load and load-averaged values of gasoline, E10, M10 are found as 3.23, 2.91, 3.28 kW.

Key words: Ethanol, Methanol, Gasoline, Energy Analysis, Exergy Analysis

INTRODUCTION

Alcohols such as ethanol and methanol are two interesting liquid biofuels with widespread usage for spark ignition (SI) engine powered vehicles (El-Emam & Desoky, 1985; Kowalewicz, 1993; Yüksel & Yüksel, 2004).One of the most important common characteristics of these fuels is that they can be used directly without requiring any major changes in the construction of the engine. But it seems that the operation of the engine at different test conditions with these alcohols is limited only by energy analysis. Energy

analysis has narrow ability to take into account irreversibility effects such as mixing of the different reactants during the chemical reactions, heat transfer between molecules at different temperatures, friction and combustion processes, expansion of gases, turbulent flow inside the cylinder (Moran, Shapiro, Boettner, & Bailey, 2010; Zheng & Caton, 2012). Exergy analysis is essential for more accurate assessment of the amount of losses from the engine. Some exergy-based studies based on SI engine operation with these alcohols are presented below. Sayin, Hosoz, Canakci, and Kilicaslan (2007) carried out engine tests for gasoline fuels with different research octane numbers at different engine speeds in a four-cylinder, four-stroke SI engine. According to the results of energy and exergy analysis applied to the engine using engine test data, gasoline of 91-RON has been found to provide better energetic and exergetic performance. It has been stated that exergy rates were slightly lower than the related energy rates and the main contribution to inefficiencies in the system is combustion. Doğan, Erol, Yaman, and Kodanli (2017) studies the fuels prepared by blending ethanol with gasoline in various ratios in a SI engine operated at in various engine speeds in terms of the first and second laws of thermodynamics. According to the results, the highest exergy and energy efficiencies were observed in 3000 rpm on average. It is stated that combustion is a more effective parameter on the irreversibility of the test engine, while less effective parameters are heat transfer, friction and mixtures. Sezer, Altin, and Bilgin (2008) studied on the usage of the oxygenated fuels, which are isooctane, methanol and ethanol, in a SI engine by means of exergy analysis. It is one of the results of the study that oxygenated fuels are more appropriate from an exergy point of view due to being caused less entropy production and less heat loss. Exergy destruction by using methanol and ethanol was found to be lower than isooctane. Caton (2012) provides an overview of exergy destruction depending on engine operating parameters and various fuels, two of which are ethanol and methanol. It has been determined that of the parameters that have the greatest effect on exergy destruction are the equivalence ratio, EGR and inlet oxygen concentration. Differences between fuels in terms of exergy destruction have been associated with the complexity of the fuel molecule and the presence of an oxygen atom.
This study is based on investigating the terms of energy and exergy are affected presents how the terms of energy and exergy are affected by single cylinder four stroke air cooled SI engine operation under various engine loads with different test fuels for constant engine speed of 2500 rpm. The engine was fueled with gasoline as reference, E10 and M10 formed by blending 10% ethanol-90% gasoline and 10% methanol-90% gasoline.

MATERIAL AND METHOD

Experimental setup consists of test engine, test unit compatible with test engine, dynamometer, exhaust gas analyser and thermocouples. Test engine is single cylinder, four stroke, air-cooled SI engine with external carburation and swept volume of 0.148 L. Its maximum brake torque and brake power 4.5 Nm and 1.2 kW respectively. During the tests carried out by varying engine load and test fuels, the data of fuel flow rate, air flow

rate, exhaust emissions, ambient temperature, surface temperature, exhaust temperature were noted on test unit. Temperatures were read with the help of K type thermocouples. The carbon monoxide (CO) and carbon dioxide (CO_2), hydrocarbon (HC), nitrogen oxide (NO_x) emissions was measured by Mobydic 5000 exhaust gas analyzer. When gasoline, one of the test fuels, is supplied from an oil station and others were formed by blending ethanol and methanol with gasoline in the specified proportions. During the application of the mass, energy and exergy balances, formulated as in Eq. (1-3), SI engine is thought to be as an open thermodynamic system with continuous flow.

$$\dot{m}_f + \dot{m}_a = \dot{m}_{exh} \quad (1)$$

$$\dot{E}_f = W + \dot{E}_{exh} + \dot{E}_{lost} \quad (2)$$

$$\dot{A}_f = \dot{A}_W + \dot{A}_{exh.} + \dot{A}_{ht} + \dot{A}_{dest.} \quad (3)$$

The parameters needed for exergy balance are calculated by the following related equations.

$$\dot{A}_f = \dot{m}_f H_u (1.0401 + 0.1728\frac{h}{c} + 0.0432\frac{o}{c} + 0.2169\frac{\alpha}{c}(1 - 2.0628\frac{h}{c})) \quad (4)$$

$$A_W = \dot{W} \quad (5)$$

$$\dot{A}_{exh} = \dot{m}_{i,exh}[(\sum_{i=1}^{n} a_i \left\{(\overline{h_i} - \overline{h_{0i}}) - T_a(\overline{s_i} - \overline{s_{0i}})\right\}) + (\overline{R}T_a \sum_{i=1}^{n} a_i \ln\frac{y_i}{y_i^e})] \quad (6)$$

$$\dot{A}_{ht} = \sum (1 - \frac{T_a}{T_{es}})\dot{E}_{lost} \quad (7)$$

By replacing an exergy term in the exergy balance, the exergy destruction rate attributed to irreversibilities, is calculated.

RESULTS AND FINDINGS

Energy exergy distributions for gasoline, E10 and M10 fuels are presented in the following figures. When both the energy and exergy distributions of all test fuels were examined, a gradual increase was observed with the increase of the load for both distributions. The meaning of increased fuel energy and exergy rate with the addition of ethanol and methanol when the lower heating values decreases is: the flow rate of fuel entering the engine to obtain the same power has increased. It has been found that the lost energy rate has the largest share among the energy distributions. In terms of exergy distributions, the term with the highest rate is exergy destruction. Exergy rate through heat transfer is the term following exergy destruction as second one. Exhaust exergy was the next term in the ranking.

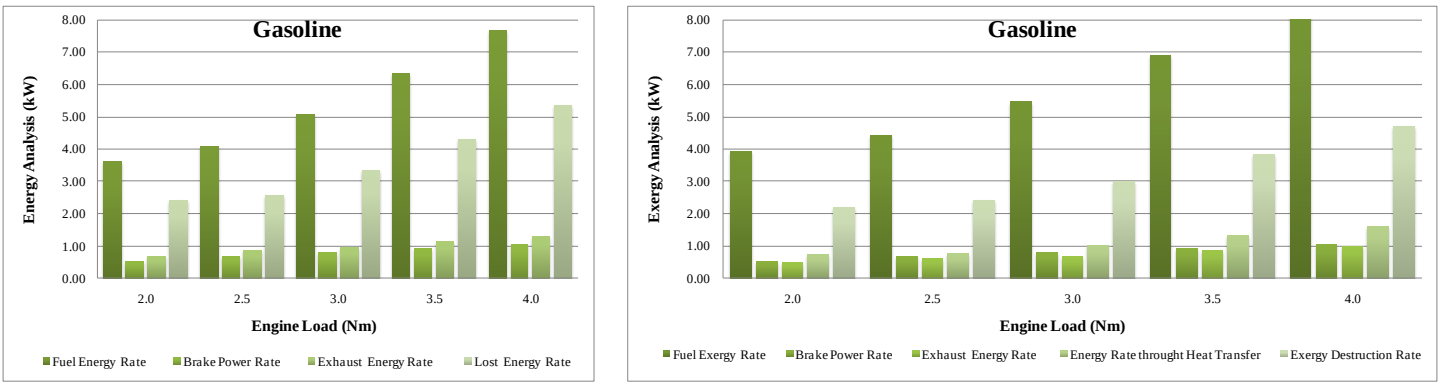

Figure 1. Energy and exergy distribution with engine load for gasoline

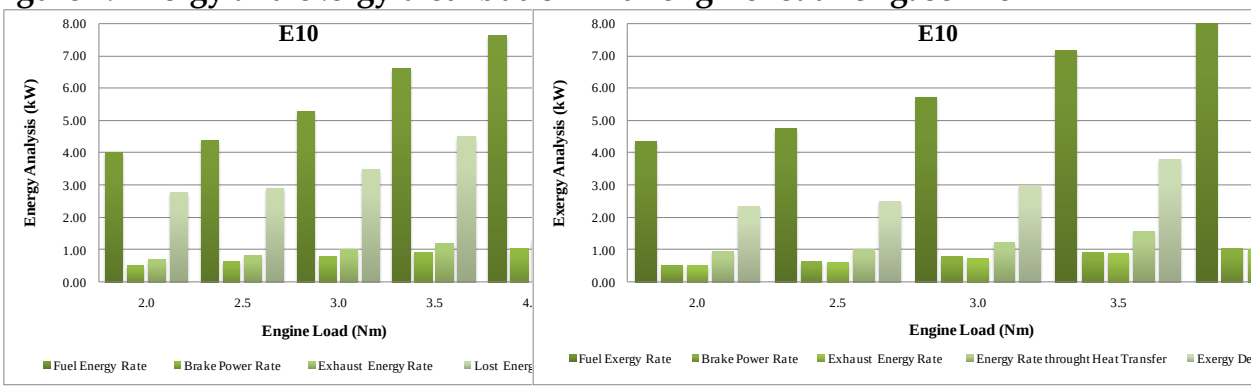

Figure 2. Energy and exergy distribution with engine load for E10

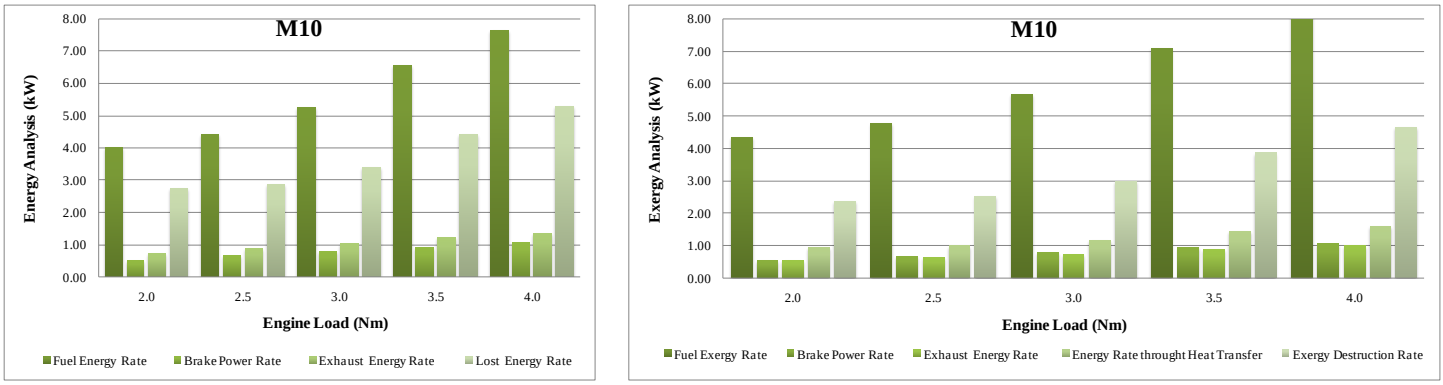

Figure 3. Energy and exergy distribution with engine load for M10

Energetic efficiency is determined as the ratio of brake power to the fuel energy rate of engine while the exergetic efficiency is an expression of how much of the exergy rate of the fuel entering the engine is converted into effective power exergy rate. As can be seen in Figure 4, which includes a comparison of energetic and exergetic efficiencies, firstly the increase and then the decreases occurred due to the increase in engine load. Both efficiencies reached the highest values for almost all test fuels around the load of 2.5 Nm. It is observed that the exergy yields are lower in energy yields in any case. Averages of energy efficiencies are 14.84, 14.08, 14.12% and averages of exergetic efficiencies are 13.69,

12.98, 13.00 % by load for gasoline, E10 and M10 respectively. That is, both ethanol addition and metanol addition reduce energetic and exergetic efficiencies, but further reduction occurs in the case of the usage of methanol in fuel.

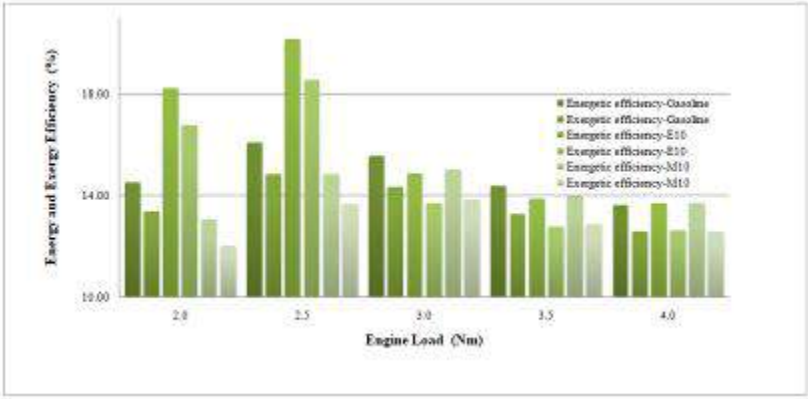

Figure 4. Energetic and exergetic efficiencies with engine load

CONCLUSION

The results of this study investigating the energetic and exergetic performance of a single cylinder four stroke SI engine fueled with gasoline, E10 (10% ethanol and 90% gasoline) and M10 (10% methanol and 90% gasoline) . Engine was operated with these at various engine loads of 2, 2.5, 3, 3.5,4 Nm and constant engine speed of 2500 rpm are as follows.
It was observed that all energy and energy parameters were affected in ascending direction by increasing engine load.
Although fuel energy and exergy rate increases with ethanol or methanol addition, losses also increases while engine brake power remains constant (for engine operation with different fuels under the same load).
Exergy rates have been found to have a similar tendency with the related energy rates.
Among exergy terms, the order from highest to low is as follows: exergy destruction rate, exergy rate through heat transfer and exhaust exergy rate while the lost energy rate is remarkable for energy analysis.
The addition of alcohol reduced both energy and exergy yields. Ethanol may be preferred instead of metanol as alcohol since energetic and exergetic efficiencies are slightly higher.

REFERENCES

Caton, J. A. (2012). Exergy destruction during the combustion process as functions of operating and design parameters for a spark-ignition engine. *International Journal of Energy Research, 36*(3), 368-384.
Doğan, B., Erol, D., Yaman, H., & Kodanli, E. (2017). The effect of ethanol-gasoline blends on performance and exhaust emissions of a spark ignition engine through exergy analysis. *Applied Thermal Engineering, 120*, 433-443. doi:https://doi.org/10.1016/j.applthermaleng.2017.04.012

El-Emam, S. H., & Desoky, A. A. (1985). A study on the combustion of alternative fuels in spark-ignition engines. *International Journal of Hydrogen Energy, 10*(7), 497-504. doi:https://doi.org/10.1016/0360-3199(85)90079-5

Kowalewicz, A. (1993). Methanol as a fuel for spark ignition engines: a review and analysis. *Proceedings of the Institution of Mechanical Engineers, Part D: Journal of Automobile Engineering, 207*(1), 43-52.

Moran, M. J., Shapiro, H. N., Boettner, D. D., & Bailey, M. B. (2010). *Fundamentals of engineering thermodynamics*: John Wiley & Sons.

Sayin, C., Hosoz, M., Canakci, M., & Kilicaslan, I. (2007). Energy and exergy analyses of a gasoline engine. *International Journal of Energy Research, 31*(3), 259-273.

Sezer, I., Altin, I., & Bilgin, A. (2008). Exergetic analysis of using oxygenated fuels in spark-ignition (SI) engines. *Energy & Fuels, 23*(4), 1801-1807.

Yüksel, F., & Yüksel, B. (2004). The use of ethanol–gasoline blend as a fuel in an SI engine. *Renewable Energy, 29*(7), 1181-1191.

Zheng, J., & Caton, J. A. (2012). Second law analysis of a low temperature combustion diesel engine: Effect of injection timing and exhaust gas recirculation. *Energy, 38*(1), 78-84. doi:https://doi.org/10.1016/j.energy.2011.12.034.

FLEXURAL STRENGTH OF AUTOCLAVED AERATED CONCRETE PANELS REINFORCED WITH STEEL REBARS

Derya BAKBAK
The Grand National Assembly of Turkey (TBMM)
derya.bakbak@tbmm.gov.tr

Ahmet Emin KURTOGLU
Istanbul Rumeli University
aemin.kurtoglu@rumeli.edu.tr

ABSTRACT: Autoclaved aerated concrete (AAC) provides superior material characteristics such as high thermal insulation and low density. Also, AAC is considered to be environment friendly and it reduces the design and transportation costs thanks to lightweight nature. In this study, reinforced aerated concrete panels (RAACPs) were tested by cyclic and monotonic loading procedures. Two point bending test is applied using universal testing machine with a maximum capacity of 500 kN. Displacement controlled testing procedure is conducted both for monotonic and cyclic loading. Load and mid-span deflection are measured. The results show that ultimate load is higher for monotonic loading case and is achieved slightly faster as compared to cyclic loading. The performance of RAACPs under seismic loading is expected to be superior since the performance under cyclic loading is close to that of monotonic loading. This superior performance is attributed to the low density and homogenous nature of AAC. Thus, this provides a significant advantage in the areas where earthquake risk exist.

Key words: lightweight concrete, autoclaved aerated concrete, reinforced concrete panel, cyclic loading

INTRODUCTION

Autoclaved aerated concrete (AAC) is a type of lightweight concrete made of cement or lime mortar containing air voids entrapped in the matrix by means of an expansion agent. It has been used in the construction industry for non-structural and structural applications since mid-1920s. By volume, 70-80% of AAC consists of air voids, resulting in lower density which minimizes the design cost and labor (Thongtha, 2014). The materials generally used in the production of AAC are (i) siliceous material (silica flour or finely ground siliceous sand), (ii) binding material (Portland cement with quick lime),

(iii) aluminum powder and (iv) entrapping agent (Desai, 2002). AAC is considered to be environmentally friendly material as it reduces 70% and 40% energy per material volume as compared to normal concrete and bricks, respectively. It also provides high thermal insulation and eliminate the requirement of using extra insulation material (Qu and Zao 2017, Bonakdar 2013).

Production of AAC panel elements with reinforcement can offer an alternative for low-rise precast construction. 60% of new building constructions in Europe are built with different types of AAC elements (Taghipour et al., 2018). In the housing industry in China, reinforced AAC materials for exterior walls are preferred to other materials (Taghipour et al., 2018).

For reinforced AAC (RAAC) elements, steel bar cages are manufactured by spot-welding of steel bars to the U-shaped links. The cages are treated with protective coating against corrosion. Earlier studies on the mechanical properties of RAAC members are very limited. Matsumura (1984) investigated the Shear behavior of reinforced autoclaved lightweight cellular concrete members. Aroni and Cividini (1989) studied the shear strength of reinforced slabs made of autoclaved aerated concrete without shear reinforcement. Alengaram et al. (2010) studied on foamed aerated concrete reinforced beams with palm kernel shell as aggregate. Taghipour et al. (2018) studied the seismic behavior of reinforced AAC vertical load-bearing wall panels under constant axial load and two-way cyclic lateral displacement excursions. Kurtoglu and Bakbak (2019) proposed models to predict the shear strength of reinforced aerated concrete slabs via support vector machines and artificial neural networks.

EXPERIMENTAL WORK

Reinforced AAC panels (RAACPs) were produced by YTONG Gaziantep firm, Gaziantep, Turkey. All production processes are made in accordance with TS EN 12602 standard. Two panel specimens were prepared. (Fig. 1) Both specimens had identical properties such as mechanical performance, reinforcement geometry and placement. Each RAACP specimen has a dimension of 1000 mm length, 600 mm width and 200 mm depth. Top and bottom reinforcement details are shown in Fig. 1.

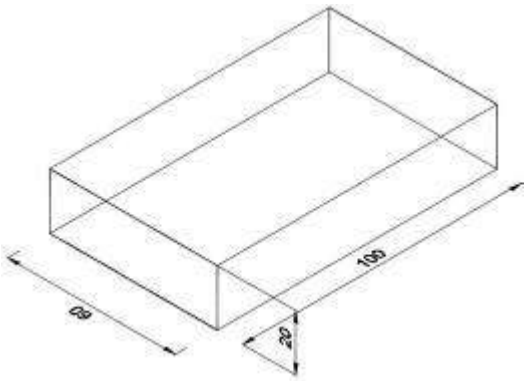

Slab Dimensions

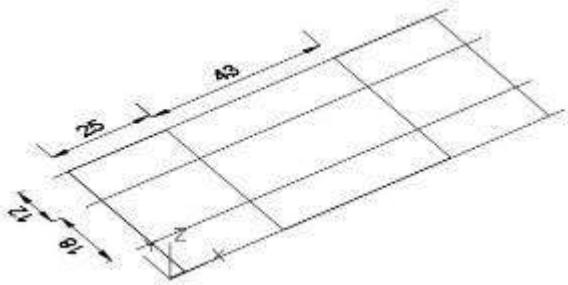

Top Reinforcement

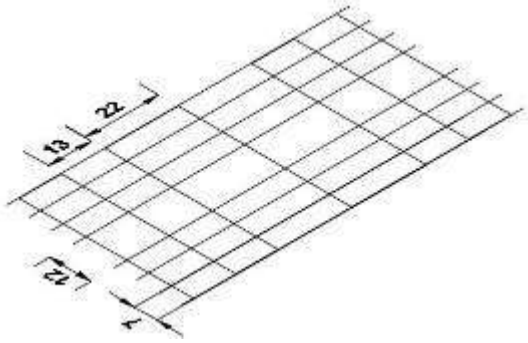

Bottom Reinforcement

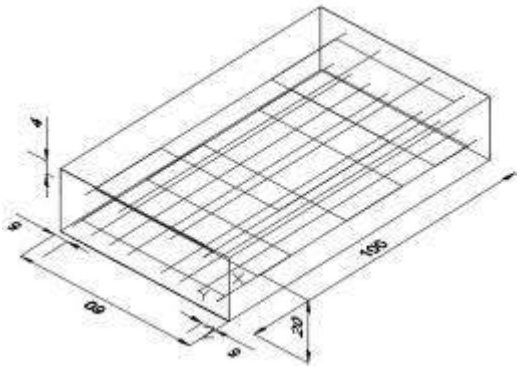

Reinforcement Configuration

Figure 1 Schematic Design and Reinforcement Configuration (Dimensions in cm)

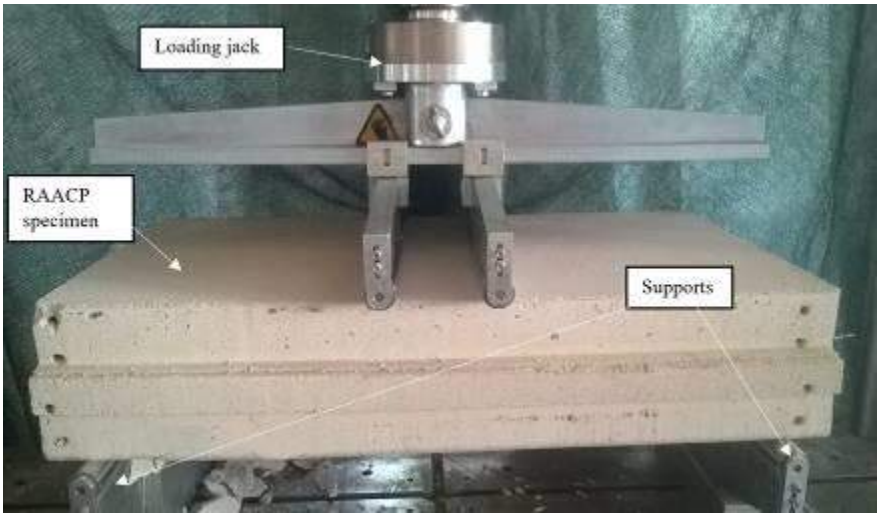

Figure 2 Test Setup

Fig. 2 shows the test setup for two point bending tests of RAACP specimens. A universal testing machine with a capacity of 500 kN was used. One specimen was subjected to monotonic loading with a rate of 5 mm/min while the other specimen was subjected to

cyclic loading based on displacement controlled manner with 5 mm increments. Thus, for the first cycle, the specimen was loaded until 5 mm deflection is reached and then unloaded. For the next cycle, specimen was loaded until 10 mm deflection and unloaded. This incremental loading was continued until failure.

RESULTS AND DISCUSSION

Maximum load capacities of RAACPs are measured as 44.93 kN for monotonic loading case, and 43.41 kN for cyclic loading case. The specimen reached the maximum mid-span deflections of 3.72 mm and 4.14 mm, for monotonic and cyclic loading cases, respectively. Fig. 3 shows that loading cases yield similar load-displacement response except for small differences. The ultimate load is higher for monotonic loading case and is achieved slightly faster as compared to cyclic loading case.

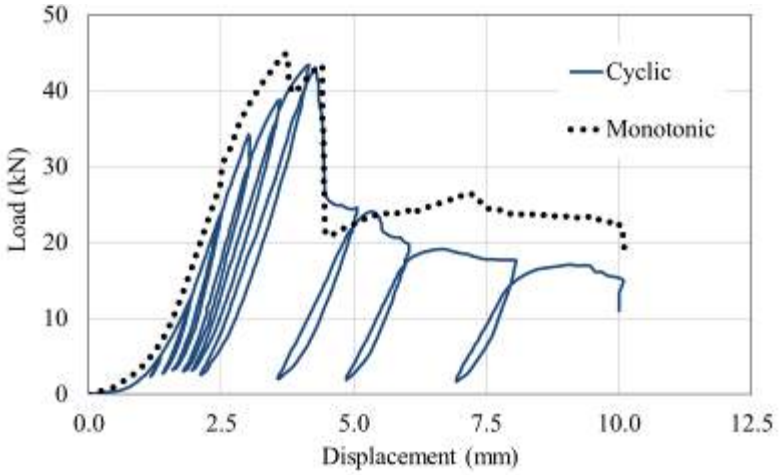

Figure 3 Load-Displacement Curves

Figures 4 and 5 show that similar failure types are observed for both loading conditions. Since the performance under cyclic loading is close to that of monotonic loading, the performance of RAAC panels under seismic loading is expected to be superior. This superior performance can be attributed to the low density and homogenous nature of autoclaved aerated concrete. Thus, this provides a significant advantage in the areas where earthquake risk exist.

Figure 4 Failed RAACP (cyclic loading)

Figure 5 Failed RAACP (monotonic loading)

ACKNOWLEDGMENTS

Authors would like to thank YTONG Gaziantep firm and Dr. Ali Khaled HUSSEIN for their support and sponsorship of the tests.

REFERENCES

Alengaram, U. J., Mahmud, H., Jumaat, M. Z., & Shirazi, S. M. (2010). Effect of aggregate size and proportion on strength properties of palm kernel shell concrete. *International Journal of the Physical Sciences*, *5*(12), 1848-1856.

Aroni, S., & Cividini, B. (1989). Shear strength of reinforced aerated concrete slabs. *Materials and Structures*, *22*(6), 443-449.

Bonakdar, A., Babbitt, F., & Mobasher, B. (2013). Physical and mechanical characterization of fiber-reinforced aerated concrete (FRAC). *Cement and Concrete Composites*, *38*, 82-91.

Desai, S. (2002). Reinforced autoclaved aerated concrete roof slabs. In *Innovations and Developments In Concrete Materials And Construction: Proceedings of the International Conference held at the University of Dundee, Scotland, UK on 9–11 September 2002* (pp. 523-532). Thomas Telford Publishing.

Kurtoğlu, A. E., & Bakbak, D. (2019). Modeling the Shear Strength of Reinforced Aerated Concrete Slabs via Support Vector Regression. *International Journal of Engineering Technologies*, *5*(1), 6-14.

Kurtoğlu, A. E., & Bakbak, D. (2019). Shear Resistance of Reinforced Aerated Concrete Slabs: Prediction via Artificial Neural Networks, *Journal of Sustainable Construction Materials and Technologies*, In press.

Matsumura, A. (1984). Shear strength and behavior of reinforced autoclaved lightweight cellular concrete members. *Trans. Architect. Inst. Jpn*, *343*, 13-23.

Taghipour, A., Canbay, E., Binici, B., Aldemir, A., Uzgan, U., & Eryurtlu, Z. (2018). Seismic behavior of reinforced autoclaved aerated concrete wall panels. *ce/papers*, *2*(4), 259-265.

Thongtha, A., Maneewan, S., Punlek, C., & Ungkoon, Y. (2014). Investigation of the compressive strength, time lags and decrement factors of AAC-lightweight concrete containing sugar sediment waste. *Energy and Buildings*, *84*, 516-525.
TS EN 12602, (2011). Önyapımlı donatılı gazbeton yapı elemanları, *Türk Standartları Enstitüsü*, (in Turkish).

Qu, X., & Zhao, X. (2017). Previous and present investigations on the components, microstructure and main properties of autoclaved aerated concrete–A review. *Construction and Building Materials*, *135*, 505-516.

DECENTRALIZED CONTROL STRATEGY FOR FUEL CELL INVERTERS WITH GRID INTEGRATION

Mustafa İNCİ
İskenderun Technical University, Department of Mechatronics Engineering, 31200, İskenderun, Hatay
mustafa.inci@iste.edu.tr

ABSTRACT: In order to simplify the grid connection of fuel cells and obtain high performance, this study presents a single-stage cascaded fuel cell inverter system with grid interconnection. For this, a decentralized power flow control strategy is performed in a single stage cascaded fuel cell inverter system. In the system structure, inputs of cascaded inverters are directly connected to each fuel cell stack, and inverters are series-connected at the output-side. This output is integrated with an electrical grid. With this topology, additional dc-dc converter is eliminated from the system, and presented a low-cost solution with a reliable structure is presented. For this, a module control strategy based on current control is implemented in each inverter structure. The performance results of the system are obtained by using Simulink program. In the designed system, it is connected to local resistive loads, which become active at different durations. In this way, the system is tested for different load conditions. Simulation results show the applicability of the designed system under changeable load conditions. Also, harmonic analysis of supplied current is performed up to 25^{th} component.

Key words: Decentralized control, fuel cells, single-stage system, grid integration.

INTRODUCTION

With the changes in the energy industry, interest in the renewable energy field is increasing day by day. Renewable energy supported by photovoltaic systems, wind turbines and fuel cells, has become more important over the years (Dhakouani, Znouda, & Bouden, 2019; Samy, Barakat, & Ramadan, 2019). Among these, the obvious advantages of fuel cells make them applicable in a variety of applications. Fuel cells are devices with superior features such as high efficiency and low emissions (İnci & Türksoy, 2019). In recent years, fuel cells with increasing power ratings have been applied for the integration of electrical grids with single or photovoltaic/wind energy units (Sun, Jin, Pan, Shen, & Lee, 2019). The integration of electrical grids with fuel cells and/or photovoltaic/wind units are known as grid-connected renewable systems.

In conventional grid-connected systems, fuel cells are connected to utility-grids through dc-dc converter, inverter, filter and transformer (optional) (Hatziadoniu, Lobo, Pourboghrat, & Daneshdoost, 2002; Kyoungsoo & Rahman, 1998; Mazumder, Burra, Huang, Tahir, & Acharya, 2010), as shown in Figure 1. For conventional PV systems, dc voltages at fuel cells' outputs are generally stepped up to higher voltage levels, and centralized inverter is used to convert dc voltage into ac voltage for the grid integration (Chandrasekaran & Gokdere, 2004; Nymand & Andersen, 2010). However, the system reliability is fairly low and a central inverter is required for this structure type (Luo et al., 2018).

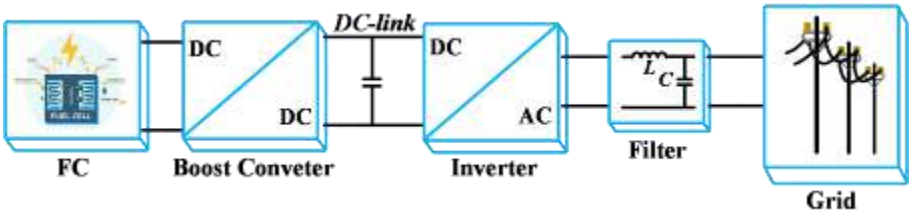

Figure 1. Conventional grid-connected fuel cell system

In order to improve the system stability and reduce the system cost, a grid-connected single-stage fuel cell inverter system is proposed in this paper. In this study, a high step-up dc-dc conversion is eliminated and additional dc-dc converter is removed in the system structure, which increases system reliability with a low-cost solution (Jafarian, Kim, & Parkhideh, 2018). In the presented system, the output voltage of each module is controlled independently and each inverter is connected to separate output filter (Al-Shetwi, Sujod, & Blaabjerg, 2018). The key properties of the grid-connected single-stage PV inverter system in this study are described as follows:

Total output voltage of fuel cell inverters at the point of common coupling (PCC) is equal to the summation of produced ac voltages of each fuel cell inverter. The complete number of fuel cell inverter is specified by the operating voltage of local fuel cell stacks.

Single-stage grid-connected fuel cell system reduces dc / dc power conversion connection (Luo et al., 2018). Also, it has a high conversion efficiency, low-cost advantages and suitable for medium power applications.

Compared with a conventional system, the system reliability is increased. Also, the presented system can generate output voltage/current with low distortion through multi-inverter control.

The paper structure is organized as follows: The system configuration and system elements are given in "System structure". The control strategy is presented in "Module Control Method". The performance and case studies are given in "Simulation results". A short brief is given in "Conclusion".

SYSTEM STRUCTURE

In this section, the system configuration and components of single-stage grid-connected fuel cell system are presented in detail.

System Configuration

The structure of single-stage grid-connected fuel cell inverter system is presented in Figure 2. As shown in the circuit scheme, the complete system consists of *n* single-stage fuel cell with inverter units, which are series tied to electrical grid (Jafarian et al., 2018; Luo et al., 2018). In fuel cell inverters, each fuel cell stacks are directly connected to the inputs of H-bridge inverters (Wang et al., 2019).

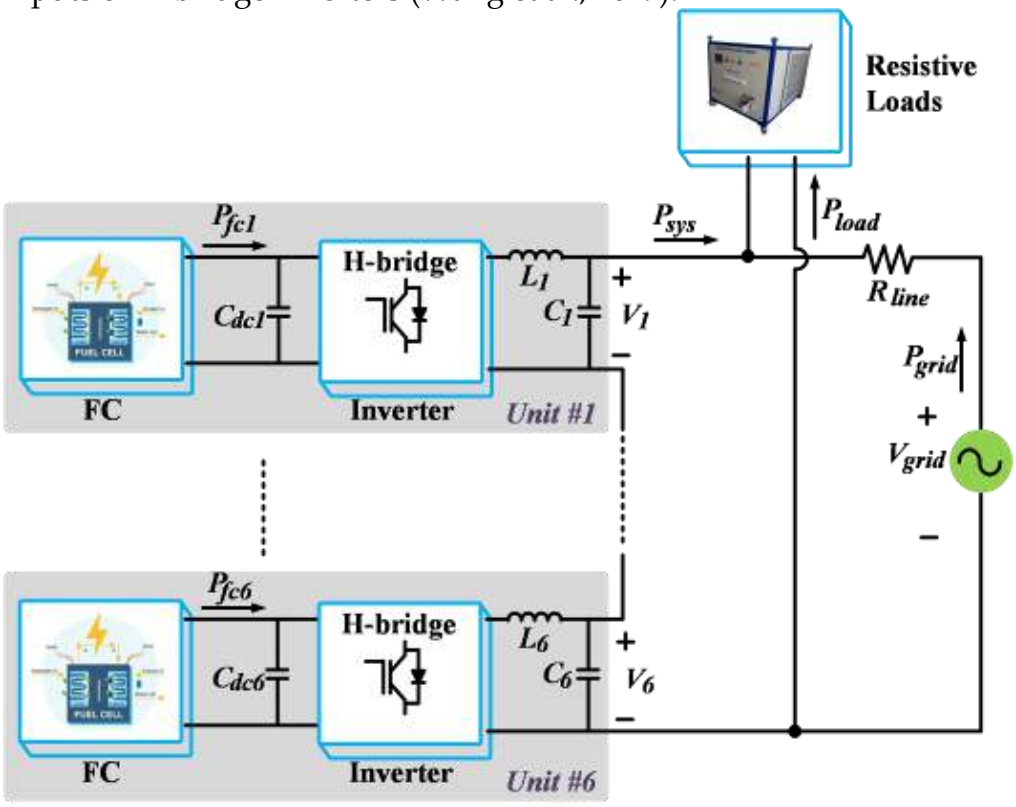

Figure 2. Single-stage fuel cell system consisting of six modules

The obtained power value is equal to the sum of each sub-module. Ignoring the power losses in single-stage cascaded fuel cell system, the obtained system power (P_{sys}) is expressed as:

$$P_{sys} = \sum_{n=1}^{6} P_{fcn} = P_{fc1} + P_{fc2} + P_{fc3} + P_{fc4} + P_{fc5} + P_{fc6} \quad (1)$$

The power exchange at the point of common coupling is also defined in Eq. (2). If system power (P_{sys}) is higher than load power (P_{load}), the excess power is supplied to grid-side. In contrary, the required power is absorbed from grid in order to provide sufficient power for connected loads.

$$\Sigma P = P_{sys} + P_{load} + P_{grid} = 0 \quad (2)$$

System Components

In the designed system, proton exchange membrane fuel cell (PEMFC) is used in the energy generation unit, which is high efficient (İnci & Türksoy, 2019). The dynamic operation of PEMFC is expressed according to open-circuit voltage (V_{oc}), internal resistive voltage (V_{ohmic}) and polarization voltage (V_d) (Chen, Han, Li, Liu, & Peng, 2014; Li, Chen, Liu, Zhou, & Ma, 2015).

$$V_{fc} = V_{oc} - V_{\Omega} - V_d \quad (3)$$

The extended-expression of V_{oc} is given as (Li et al., 2015):

$$V_{oc} = K_c \left[V_o + (T - 298)\frac{-44{,}43}{zF} + \frac{RT}{zF} \ln\left(\frac{P_{H_2} P_{O_2}^{1/2}}{P_{H_2O}} \right) \right] \quad (4)$$

K_c is a fixed numeric quantity in $(kmol/(sA)^{-1})$.

T is the temperature in Kelvin.

F is faraday.

V_o is an electromotive force for a pressure value.

The ohmic overvoltage is given below:

$$V_{ohmic} = i_{fc} R_{ohmic} \quad (5)$$

V_d is the absolute polarization overvoltage and expressed below(Li et al., 2015):

$$V_d = N \times A \times \ln(i_{fc} / i_o) \quad (6)$$

N is the quantity of cells.

A is Tafel slope

i_o is exchange current.

The nominal power rating of PEMFC is 3.12 kW which its operating point is defined as 60 A, 52 V. The electrical characteristics of used PEMFC is introduced in Figure 3.

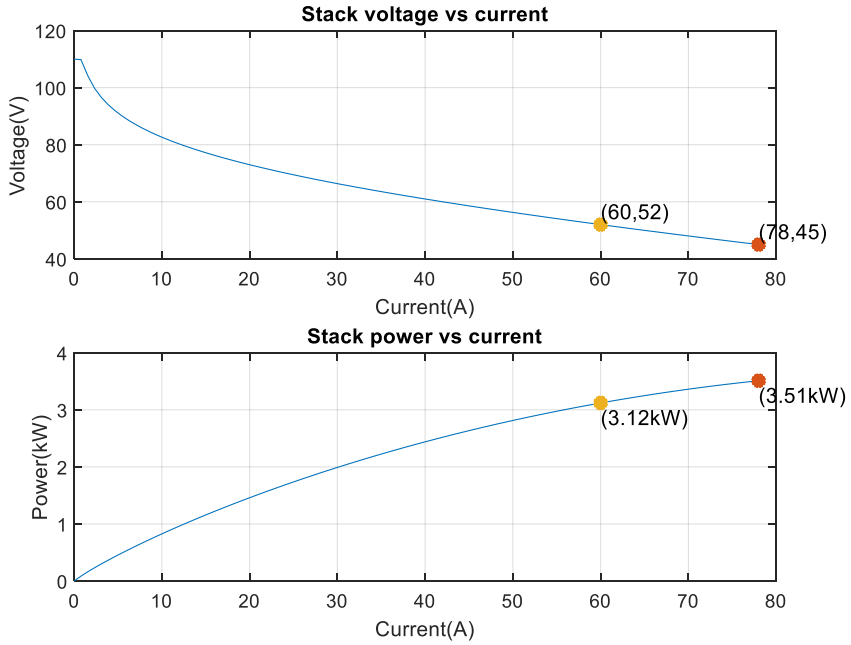

Figure 3. Electrical characteristics of PEMFC in the designed system

The most well-known inverter structure to generate a single-phase ac voltage is H-bridge inverter, also called as a full-bridge inverter. The equivalent scheme of an H-bridge inverter is shown in Figure 4. As shown in the scheme, it includes four switching elements in order to convert dc voltage into ac voltage.

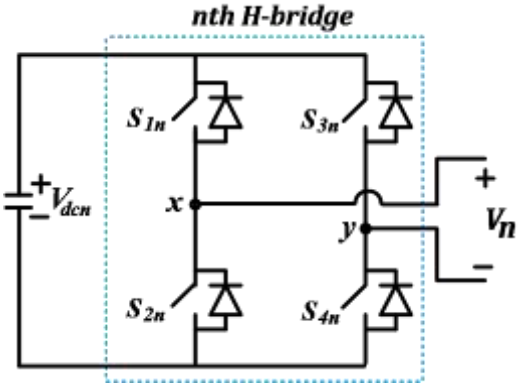

Figure 4. H-bridge inverter connected to the single-stage cascaded fuel cell system

In an H-bridge inverter topology, the output ac voltage (V_n) is the difference between two points. It is expressed as (Kang, Park, Cho, & Kim, 2005):

$$V_n = V_x - V_y \quad (7)$$

Dc energy generated by the fuel cell is converted into ac form by using inverter units. In the system, full (H) bridge inverter is used as dc-ac converter. The output voltage of an H-bridge inverter is defined as (Kim, 2017):

$$V_n(t) = \sum_{n=1}^{\infty} V_n \sin(n\omega_o t + \theta_n) \quad (8)$$

An H-bridge inverter provides ac load voltage with rms value corresponding to ninety percent of input dc voltage (Kim, 2017).

$$V_{n1\_rms} = \frac{1}{\sqrt{2}} \frac{4V_{dc}}{\pi} = 0.9V_{dc} \quad (9)$$

The single-stage fuel cell inverters are series-connected, the voltage at point of common coupling is the summation of output voltages. It is calculated as:

$$V_{sys} = \sum_{n=1}^{6} V_n \quad (10)$$

For the designed system, n is 6. Therefore, output voltage is:

$$V_{sys} = \sum_{n=1}^{6} V_n = V_1 + V_2 + V_3 + V_4 + V_5 + V_6 \quad (11)$$

MODULE CONTROL METHOD

This section presents the decentralized power flow control method used in the single-stage fuel cell system. In cascaded system structure, it includes six series inverter modules, and it is aimed to control each inverter module smoothly by keeping dc-link voltage constant at 52 V. In the designed system, total power supplied to load/grid is the sum of power values of each module. For this, all modules are designed and controlled symmetrically. Figure 5 introduces the detailed control block of the decentralized control method for each module (Jafarian et al., 2018; Luo et al., 2018).

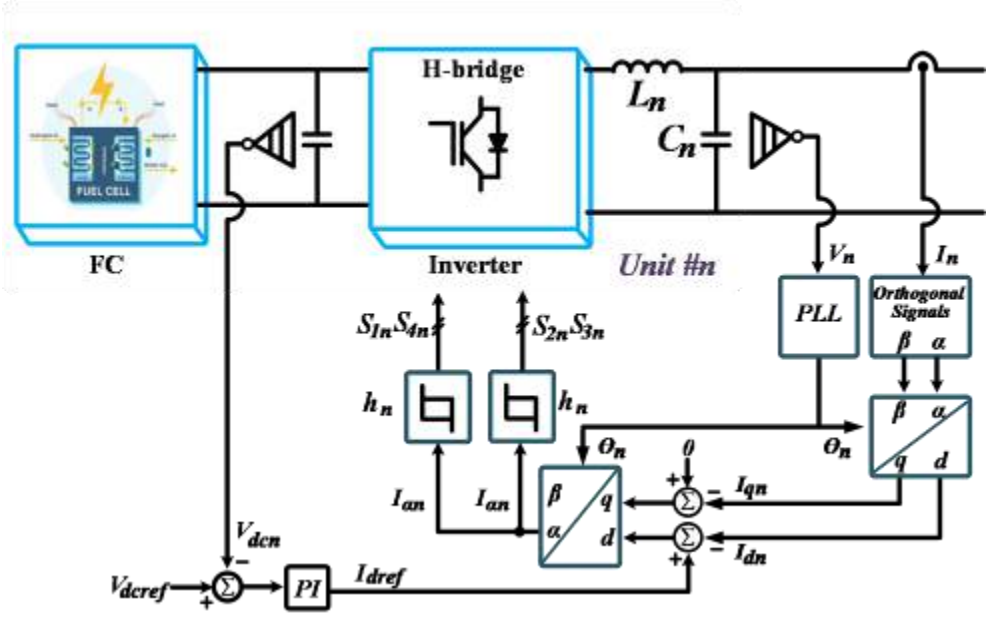

Figure 5. The scheme of the decentralized control method for the designed system

According to the scheme of decentralized control, power flow is controlled by using dc-link voltage, module inverter voltage, and system current. The system current is directly used to control power flow exchange from fuel cell units to grid/load. In order to integrate with grid, inverter output voltage is used to generate phase angle information and to track grid voltage. Also, dc-link voltage is used to keep dc-link voltage at a defined voltage and to generate the reference value of d-component of system current through a proportional-integral control (Malakondareddy, Senthil Kumar, Ammasai Gounden, & Anand, 2019; Turksoy, Hames, Teke, & Latran, 2018). First of all, α/β components of the inverter current (I_n) are converted to d and q components in two-frame transformation (Ahmad & Singh, 2018; Yao & Xiao, 2013).

$$\begin{bmatrix} I_{dn} \\ I_{qn} \end{bmatrix} = \begin{bmatrix} \cos(\omega t) & \sin(\omega t) \\ -\sin(\omega t) & \cos(\omega t) \end{bmatrix} \begin{bmatrix} I_{n\alpha} \\ I_{n\beta} \end{bmatrix} \quad (12)$$

I_{dn} and I_{qn} are rearranged in Eqs. (13-14).

$$I_{dn} = I_{n\alpha}\cos(\omega t) + I_{n\beta}\sin(\omega t) \quad (13)$$

$$I_{nq} = -I_{n\alpha}\sin(\omega t) + I_{n\beta}\cos(\omega t) \quad (14)$$

The error currents between reference and actual currents are calculated in dq frame(Gayathri Devi & Keshavan, 2019).

$$I_{derrorn} = I_{dref} - I_{dn} \quad (15)$$

$$I_{qerrorn} = I_{qref} - I_{qn} \quad (16)$$

The reference current value is calculated by using dq to αβ conversion.

$$\begin{bmatrix} I_{\alpha n} \\ I_{\beta n} \end{bmatrix} = \begin{bmatrix} \cos(\omega t) & -\sin(\omega t) \\ \sin(\omega t) & \cos(\omega t) \end{bmatrix} \begin{bmatrix} I_{derror,n} \\ I_{qerror,n} \end{bmatrix} \quad (17)$$

According to the dq to αβ conversion, α-output defined the error signal $(I_{error} = I_{\alpha})$ due to single-phase system.

$$I_{\alpha n} = I_{derrorn}\cos(\omega t) - I_{qerrorn}\sin(\omega t) \quad (18)$$

And finally, the generated reference error is implemented in a hysteresis modulation technique to generate triggering signals of H-bridge module (Chatterjee & Mohanty, 2018). The switching is performed according to the hysteresis rule below:

$$Switching = \begin{cases} I_{\alpha n} > h & S_{1n}, S_{4n} \\ I_{\alpha n} < h & S_{2n}, S_{3n} \end{cases} \quad (19)$$

where h_n indicates the hysteresis bands implemented in each module. Each hysteresis band in modules have different values.

SIMULATION RESULTS

This part presents the simulation results of the designed system. The energy generation units include six PEMFCs in the ratings of 3.12 kW. It means that the total power value is

equal to 18.72 kW for nominal condition. Fuel cells are connected to single-phase 220 Vrms/50 Hz electrical grid, which its peak value is 311 V. Also three loads (load 1=4 Ω, load 2=5 Ω, load 3= 3 Ω) are connected to the point of common coupling. For this, the system is modeled by using Simulink environment program.

The designed system is tested for different load situations. The situations are given as follows:
State 1: no-load condition between 0.0 s and 0.5 s
State 2: load 1 is active between t=0.5 s and 1.0 s
State 3: load 1 and load 2 are active between t=1.0 s and 1.7 s
State 4: load 2 is active between t=1.7 s and 2.1 s
State 5: load 2 and load 3 are active between t=2.1 s and 2.5 s

Figure 6 presents the fuel cell voltage and inverter voltage for each module. Fuel cell voltage is equal to 52 V at output. Inverter converts fuel cell voltage in dc form into ac form. Figure 7 shows system currents, load currents and grid currents for five states.

It is clear that loads don't draw currents from the system/grid for first state. All of system currents flow into the grid-side. When load 1 becomes active at t=0.5 s, the current value increases at load-side. The excess power is supplied to grid for state 2. In state 3, Load 2 turns on at t=1.0 s, and the loads consume more power compared to previous states.

Thus, the grid current reduces to lower values in comparison with state 2. In state 4, load 1 is turned off while load 2 is active. Therefore, the excess power supplied to grid increases. In state 5, load 2 and load 3 become active. This state cause more power consumed by loads.

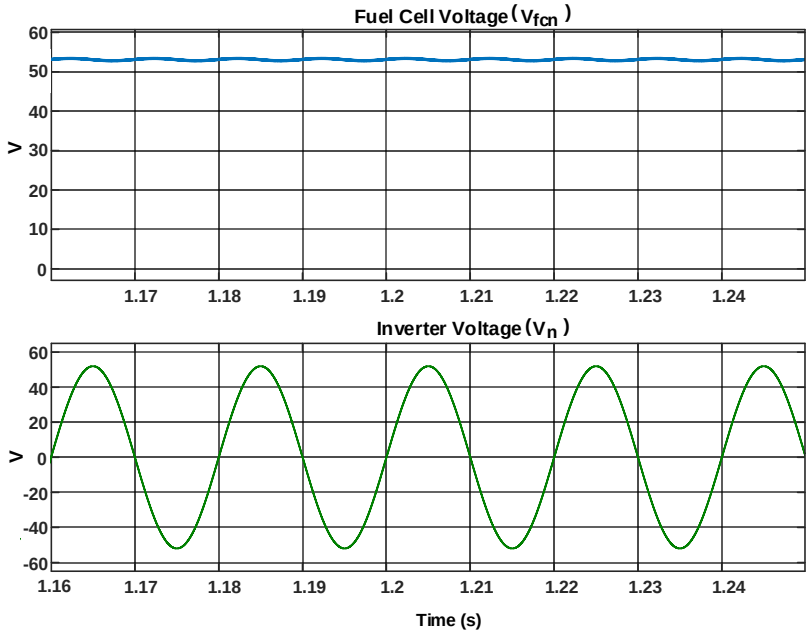

Figure 6. Fuel cell and inverter voltages for each module

Figure 8 shows the curve of load currents versus grid currents for different states. For state 1, grid current is 118.2 A while load current is zero. In state 2, load current increases to 78.1 A and grid current decreases to 39.3 A. The current values of load and grid are 140.5 A and 24.1 A for state 3, respectively. In state 4, 117.4 A and 54.7 A are values of load and grid currents. In state 5, the values of load/grid currents are 166.3 and 47.9 A.

The power values of system, load and grid are presented in Figure 9. As shown in the results, it is performed at no-load condition for first state. The system power is constant and it is equal to 18.1 kW for all states. The supplied power to grid is 18.4 kW. Then, load 1 is active and consumed load power increases. Load power is equal to 12.1 kW for state 1. When load 2 is turned on, the consumed load power increases to 21.9 kW. Also, the extra power is consumed from grid and its value 3.45 kW. In state 4, load 2 is active and excess power is supplied to grid. In state 5, load 2 and load 3 are in on-state. In this state, a power in the rating of 7.5 kW is consumed from the grid.

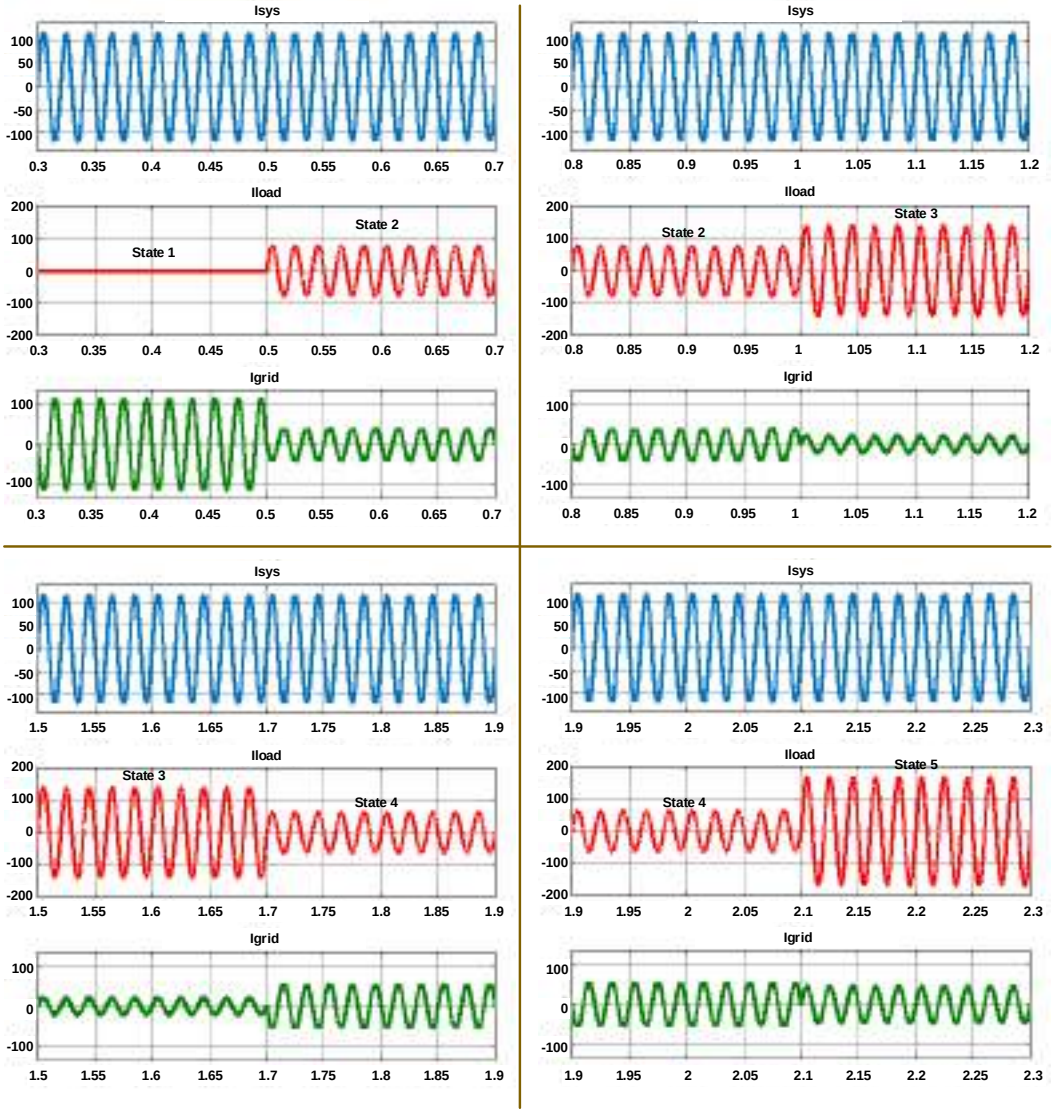

Figure 7. System currents, load currents and grid currents for five states

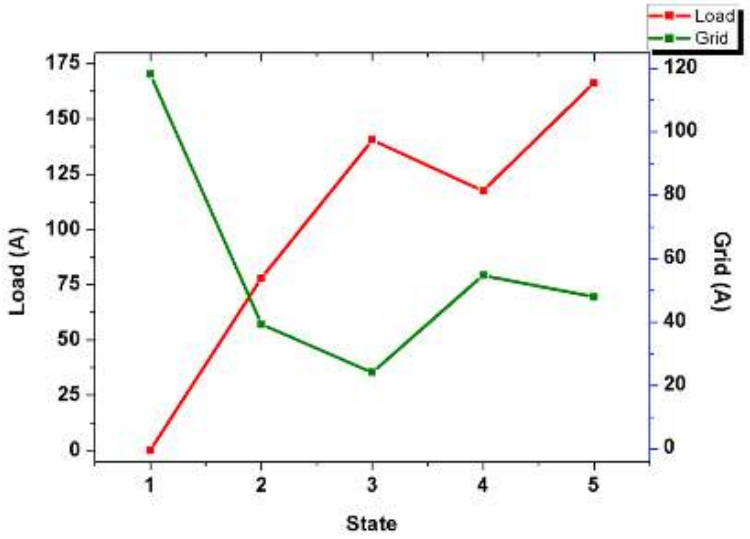

Figure 8. Load current versus grid current

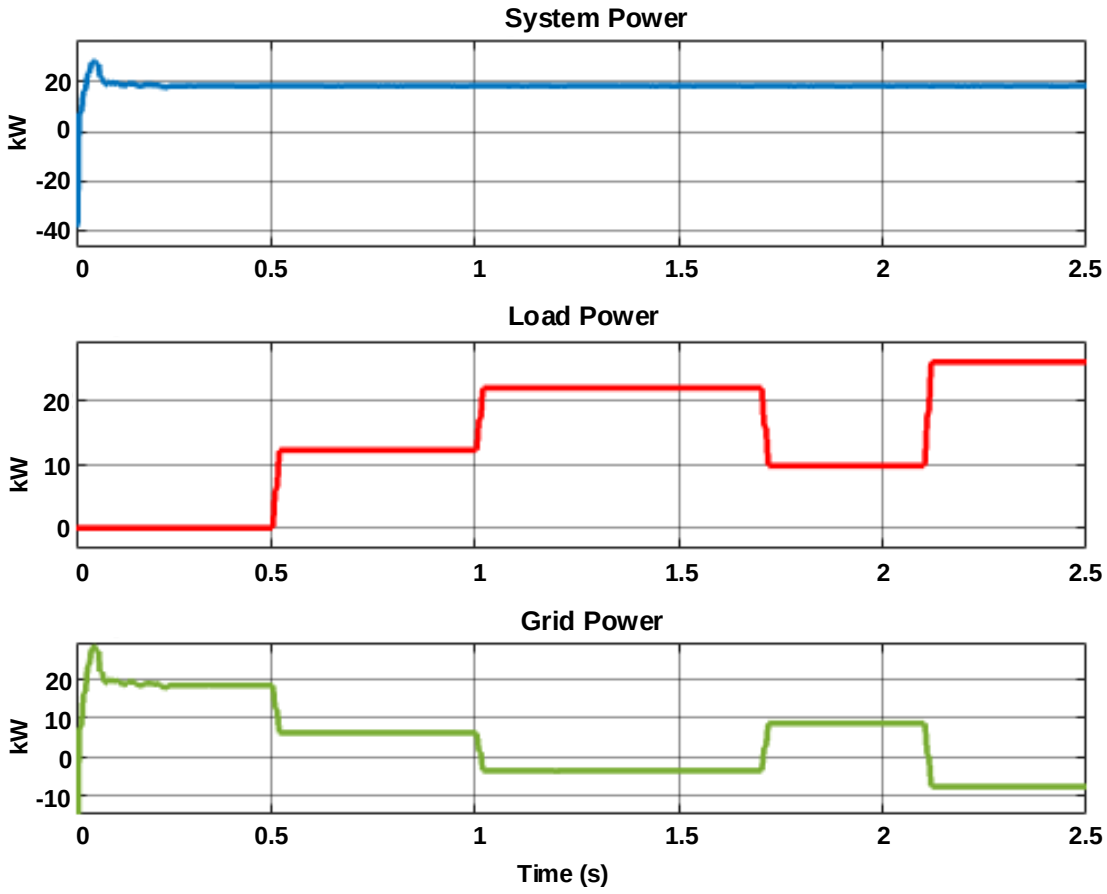

Figure 9. Power values for system, load and grid

The harmonic spectrum of grid current is also presented in Figure 10. It shows that total harmonic distortion value of grid current is 1.43%, which is less than the limits defined in IEEE 519 Standards. Also, it is calculated up to 25th harmonics. THD analysis of current has been performed for two periods between t=2.0 s and t=2.04 s.

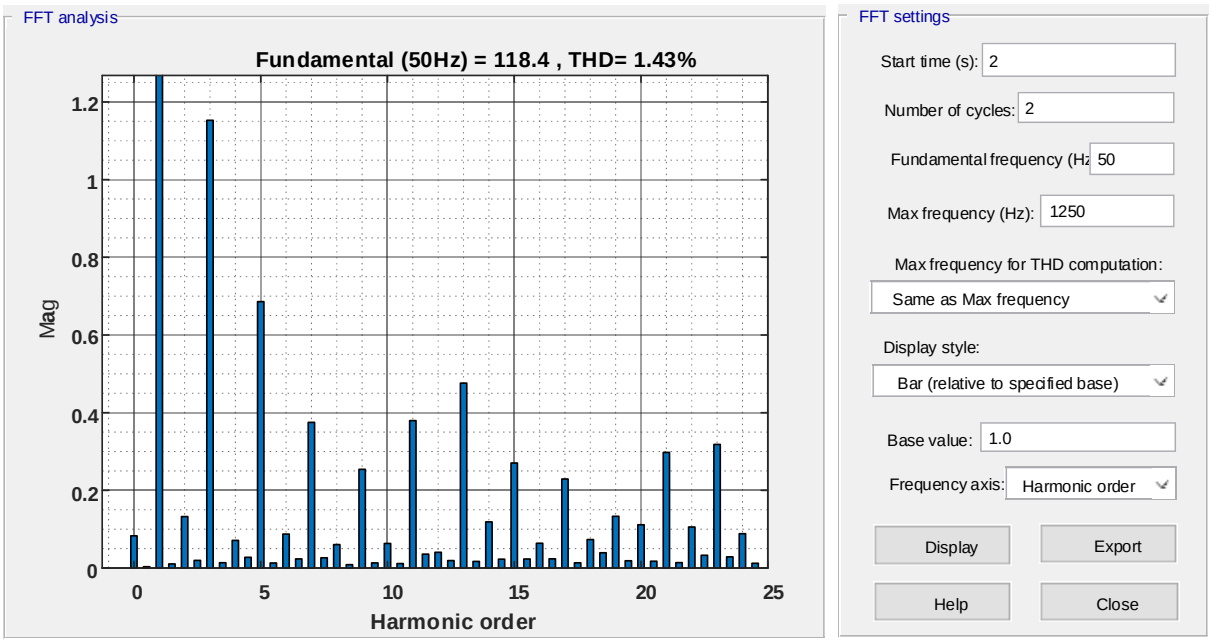

Figure 10. THD analysis of system current for two periods between 2.0 s and 2.04 s

CONCLUSION

In this study, a single-stage cascaded fuel cell inverter system with a module control strategy is presented for the grid integration. In the system, six fuel cells in the rating of 3.12 kW are used as energy generation units. Total output power is obtained as approximately 18.72 kW. For the grid integration, fuel cells are integrated into utility-grid through H-bridge inverters with the elimination of dc-dc boost converters. Therefore, it presents a low-cost and reliable structure in comparison with conventional systems. For the operation of system, a current control based scheme is used to control the active/reactive power and dc-link voltage at each output. The system is performed under different load conditions through Simulink program. The case studies show good results for system operation. The power flows have been tested for different conditions. At no-load condition, all power is supplied to grid-side. When a low power is consumed by loads, the excess power is supplied to utility-grid. In contrast, the required power is provided from the grid-side. In addition to power results, the waveforms of system current, load current and grid current are presented in detail. And finally, THD analysis of system current is performed up to 25th harmonics. THD value at system current is observed as 1.43%.

REFERENCES

Ahmad, Z., & Singh, S. N. (2018). Improved modulation strategy for single phase grid connected transformerless PV inverter topologies with reactive power generation capability. *Solar Energy, 163*, 356-375. doi:https://doi.org/10.1016/j.solener.2018.01.039

Al-Shetwi, A. Q., Sujod, M. Z., & Blaabjerg, F. (2018). Low voltage ride-through capability control for single-stage inverter-based grid-connected photovoltaic power plant. *Solar Energy, 159*, 665-681. doi:https://doi.org/10.1016/j.solener.2017.11.027

Chandrasekaran, S., & Gokdere, L. U. (2004, 20-25 June 2004). *Integrated magnetics for interleaved DC-DC boost converter for fuel cell powered vehicles.* Paper presented at the 2004 IEEE 35th Annual Power Electronics Specialists Conference (IEEE Cat. No.04CH37551).

Chatterjee, A., & Mohanty, K. B. (2018). Current control strategies for single phase grid integrated inverters for photovoltaic applications-a review. *Renewable and Sustainable Energy Reviews, 92*, 554-569. doi:https://doi.org/10.1016/j.rser.2018.04.115

Chen, W., Han, Y., Li, Q., Liu, Z., & Peng, F. (2014). Design of proton exchange membrane fuel cell grid-connected system based on resonant current controller. *International Journal of Hydrogen Energy, 39*(26), 14402-14410. doi:https://doi.org/10.1016/j.ijhydene.2014.02.103

Dhakouani, A., Znouda, E., & Bouden, C. (2019). Impacts of energy efficiency policies on the integration of renewable energy. *Energy Policy, 133*, 110922. doi:https://doi.org/10.1016/j.enpol.2019.110922

Gayathri Devi, B., & Keshavan, B. K. (2019). A novel hybrid Phase Shifted-Modified Synchronous Optimal Pulse Width Modulation based 27-level inverter for grid-connected PV system. *Energy, 178*, 309-317. doi:https://doi.org/10.1016/j.energy.2019.03.173

Hatziadoniu, C. J., Lobo, A. A., Pourboghrat, F., & Daneshdoost, M. (2002). A simplified dynamic model of grid-connected fuel-cell generators. *IEEE Transactions on Power Delivery, 17*(2), 467-473. doi:10.1109/61.997919

İnci, M., & Türksoy, Ö. (2019). Review of fuel cells to grid interface: Configurations, technical challenges and trends. *Journal of Cleaner Production, 213*, 1353-1370. doi:https://doi.org/10.1016/j.jclepro.2018.12.281

Jafarian, H., Kim, N., & Parkhideh, B. (2018). Decentralized Control Strategy for AC-Stacked PV Inverter Architecture Under Grid Background Harmonics. *IEEE Journal of Emerging and Selected Topics in Power Electronics, 6*(1), 84-93. doi:10.1109/JESTPE.2017.2773079

Kang, F.-s., Park, S.-J., Cho, S. E., & Kim, J.-M. (2005). Photovoltaic power interface circuit incorporated with a buck-boost converter and a full-bridge inverter. *Applied Energy, 82*(3), 266-283. doi:https://doi.org/10.1016/j.apenergy.2004.10.009

Kim, S.-H. (2017). Chapter 7 - Pulse width modulation inverters. In S.-H. Kim (Ed.), *Electric Motor Control* (pp. 265-340): Elsevier.

Kyoungsoo, R., & Rahman, S. (1998). Two-loop controller for maximizing performance of a grid-connected photovoltaic-fuel cell hybrid power plant. *IEEE Transactions on Energy Conversion, 13*(3), 276-281. doi:10.1109/60.707608

Li, Q., Chen, W. R., Liu, Z. X., Zhou, G. H., & Ma, L. (2015). Active control strategy based on vector-proportion integration controller for proton exchange membrane fuel cell grid-connected system. *IET Renewable Power Generation, 9*(8), 991-999. doi:10.1049/iet-rpg.2014.0245

Luo, C., Su, M., Hou, X., Han, H., Sun, Y., & Yang, Y. (2018, 22-25 May 2018). *A Decentralized Power Control of Cascaded Single-Stage PV Inverters for Grid-connected Applications.* Paper presented at the 2018 IEEE Innovative Smart Grid Technologies - Asia (ISGT Asia).

Malakondareddy, B., Senthil Kumar, S., Ammasai Gounden, N., & Anand, I. (2019). An adaptive PI control scheme to balance the neutral-point voltage in a solar PV fed grid connected neutral point clamped inverter. *International Journal of Electrical Power & Energy Systems, 110*, 318-331. doi:https://doi.org/10.1016/j.ijepes.2019.03.012

Mazumder, S. K., Burra, R. K., Huang, R., Tahir, M., & Acharya, K. (2010). A Universal Grid-Connected Fuel-Cell Inverter for Residential Application. *IEEE Transactions on Industrial Electronics, 57*(10), 3431-3447. doi:10.1109/TIE.2009.2038943

Nymand, M., & Andersen, M. A. E. (2010). High-Efficiency Isolated Boost DC–DC Converter for High-Power Low-Voltage Fuel-Cell Applications. *IEEE Transactions on Industrial Electronics, 57*(2), 505-514. doi:10.1109/TIE.2009.2036024

Samy, M. M., Barakat, S., & Ramadan, H. S. (2019). Techno-economic analysis for rustic electrification in Egypt using multi-source renewable energy based on PV/ wind/ FC. *International Journal of Hydrogen Energy*. doi:https://doi.org/10.1016/j.ijhydene.2019.04.038

Sun, L., Jin, Y., Pan, L., Shen, J., & Lee, K. Y. (2019). Efficiency analysis and control of a grid-connected PEM fuel cell in distributed generation. *Energy Conversion and Management, 195*, 587-596. doi:https://doi.org/10.1016/j.enconman.2019.04.041

Turksoy, A., Hames, Y., Teke, A., & Latran, M. B. (2018). A novel adaptive switching method to reduce DC-Link capacitor ripple in PV based grid-connected inverter. *Solar Energy, 173*, 702-714. doi:https://doi.org/10.1016/j.solener.2018.08.002

Wang, X., Li, Q., Chen, W., Wang, W., Pu, Y., & Yu, J. (2019). Parallel interaction influence of single-stage photovoltaic grid-connected/hydrogen production multi-inverter system based on modal analysis. *International Journal of Hydrogen Energy, 44*(11), 5143-5152. doi:https://doi.org/10.1016/j.ijhydene.2018.10.046

Yao, Z., & Xiao, L. (2013). Control of Single-Phase Grid-Connected Inverters With Nonlinear Loads. *IEEE Transactions on Industrial Electronics, 60*(4), 1384-1389. doi:10.1109/TIE.2011.2174535.

INVESTIGATION OF WOB AND RPM FOR DIFFERENT BIT TYPES USED IN WESTERN RAMAN DRILLINGS

Ömer İMİR
Institute of Science
omer.imir@batman.edu.tr

ABSTRACT: In this study, weight on bit that are used with the different types of bits were examined in Western Raman oil field which is the Turkey's largest oil production fields. With the purpose of this (with the scope of this), weight on bit (WOB), revolutions per minute (RPM) and ROP (rate of penetration) values () given to insert, standard, and PDC bit that are used in similar wells were analyzed. For this purpose, in the second stage of the drillings carried out in the Western Raman field, the data of fourteen wells including five wells drilled with PDC drill bit 8 ½'' in diameter, five wells drilled with standard bit and four wells drilled with insert bit were utilized, and the performance of these bits were evaluated in terms of quality. Upon comparing and analyzing the graphs created based on these data, the PDC (Poly-Crystalline Diamond Compact) drill bit was found to be much more efficient than insert and standard drill bits in terms of time and correspondingly cost.

Key words: WOB, RPM, West Raman, ROP, bit, drilling

BATI RAMAN SONDAJLARINDA KULLANILAN FARKLI MATKAP TİPLERİ İÇİN WOB VE RPM DEĞERLERİNİN İNCELENMESİ

ÖZET: Bu çalışmada, Türkiye'nin en büyük petrol üretim sahası olan Batı Raman'da farklı tip matkaplar ile yapılan sondajlarda matkaba verilen ağırlık değerleri incelendi. Bu kapsamda aynı sahada benzer kuyularda kullanılan insert, standart ve PDC (Çok Kristalli Elmas Kompakti) matkaplara verilen ağırlık (WOB), dönme hızı (RPM) ve sondaj ilerleme hızı (ROP) değerleri analiz edilmiştir. Bu amaçla Batı Raman sahasında yapılan sondajların ikinci aşamasında 8 ½'' çapında PDC matkap ile kazılan beş kuyu, standart matkap ile kazılan beş kuyu ve insert matkap ile kazılan dört kuyu olmak üzere toplam on dört kuyunun verileri kullanılmıştır ve bu matkapların WOB açısından performansları niteliksel olarak değerlendirilmiştir. Kullanılan bu veriler ile oluşturulan grafikler karşılaştırılıp analiz edilerek, PDC matkabın zaman ve buna bağlı olarak

maliyet açısından insert ve standart matkaba göre çok daha avantajlı olduğu tespit edilmiştir.

Anahtar sözcükler: WOB, RPM, Batı Raman, ROP, matkap, sondaj

GİRİŞ

Petrol, doğalgaz ve jeotermal sektöründe en önemli faktörlerden biri kuyu sondajındaki zaman ve buna bağlı olarak maliyettir. Sondaj endüstrisinin hedefi, güvenlik ve çevre standartlarından ödün vermeden (Sivagnanam, 2014) çok masraflı bir faaliyet olan sondajın maliyetini minimize etmektir.

Matkap, sondaj dizisi sonunda bulunan, kayaçları ezme ve kesme işlemini yapan önemli bir alettir (Özbayoğlu, 2011). Sondaj mühendisliğinde en önemli konulardan biri optimum matkap seçimidir. Ayrıca optimum matkabın iyi bir performans göstermesi için de optimum çalışma parametreleri ile kullanılması lazım. Belirli bir sondaj için matkabın seçimi, sondaj işlemi sırasında beklenen çalışma koşullarının yanı sıra kazılacak formasyonun yapısına göre değişmektedir. Bir matkabın performansı; WOB, RPM, çamur özellikleri ve hidrolik verimliliği de dahil olmak üzere çeşitli çalışma parametrelerinin bir fonksiyonudur (Özbayoğlu, 2011).

Bu çalışmada döner konlu (insert, standart) ve sabit başlı (PDC) matkap tiplerinin WOB-sondaj ilerleme hızı ilişkisi incelenecektir. Uygun matkap seçimi, WOB ve RPM değerleri için referans kuyu verileri ve formasyon özellikleri kullanılmalıdır. Referans kuyu verileri; kullanılan matkabın özellikleri, kazılan formasyon özellikleri (sertlik, aşındırma, baskı mukavemeti, litoloji), ROP (ilerleme hızları), WOB, RPM, debi ve kullanılan matkapların metre maliyetlerinden oluşur. Matkap seçimi, WOB ve RPM değerleri belirlenirken bahsedilen bütün bu parametreler gözden geçirilerek değerlendirilmektedir. Bu çalışmada Türkiye'nin en büyük petrol üretim sahası olan Batı Raman'da yapılan sondajlarda kullanılan insert, standart ve PDC matkap tipleri WOB-sondaj ilerleme hızı açısından tartışılmıştır. Bu çalışma kapsamında; WOB, RPM(dönme hızı), ROP (sondaj ilerleme hızı) parametreleri dikkate alınarak, bu sahada kullanılan PDC, insert ve standart matkapların performansları, kullanılan parametrelerin etkileri açısından değerlendirilmiştir. Bu tez çalışmasının amacı, bu değerlendirmelerin sonucunda düşük WOB yüksek ilerleme hızına sahip matkap tipini tespit etmektir.

Bu amaçla sondajın ikinci aşamasında 8 ½ " 'lik insert matkapla kazılan dört kuyu, standart matkapla kazılan beş kuyu ve PDC matkapla kazılan beş kuyunun gerçek WOB, RPM ve ROP verileri kullanılarak analizler yapılmış ve değerlendirilerek yorumlanmıştır. İnceleme alanında ki kuyularda kullanılan matkapların performansları,

karşılaşılan sorunlar ve çözümüne yönelik önlemlerinin alınması ile ilgili öneriler tartışılmıştır.

Batı Raman Sahası

1961 yılında keşfedilen Batı Raman sahası, Türkiye'nin Güneydoğu Bölgesinde yer almaktadır. Petrol, kretase çağından heterojen bir karbonat formasyonundan üretilmektedir ve Garzan Formasyonu olarak tanımlanmaktadır. Garzan formasyonunun brüt kalınlığı 64 m'dir (Babadağlı ve ark., 2009). Şekil 1'deki yer buldurunda görüldüğü gibi Batı Raman petrol sahası yaklaşık 18 km uzunluk ve 2 ila 4 km genişliğinde bir alana sahiptir. Sahanın ortalama gözenekliliği % 18 civarındadır ve esas olarak matriks, vug ve çatlaklardan oluşmaktadır (Babadağlı ve ark., 2009). Matriks, 10 md ila 100 md arasında değişen geçirgenliğe sahiptir. Rezervuardan üretilen petrol 9,7 ile 15,1 arasında değişen bir API gravitesi ile çok ağır bir ham petroldür. Petrolün viskozitesi rezervuar koşullarında 450 ila 1000 cp arasında değişmektedir ve bu durum petrolün gözeneklerde ilerlemesini zorlaştırmaktadır (Babadağlı ve ark., 2009).

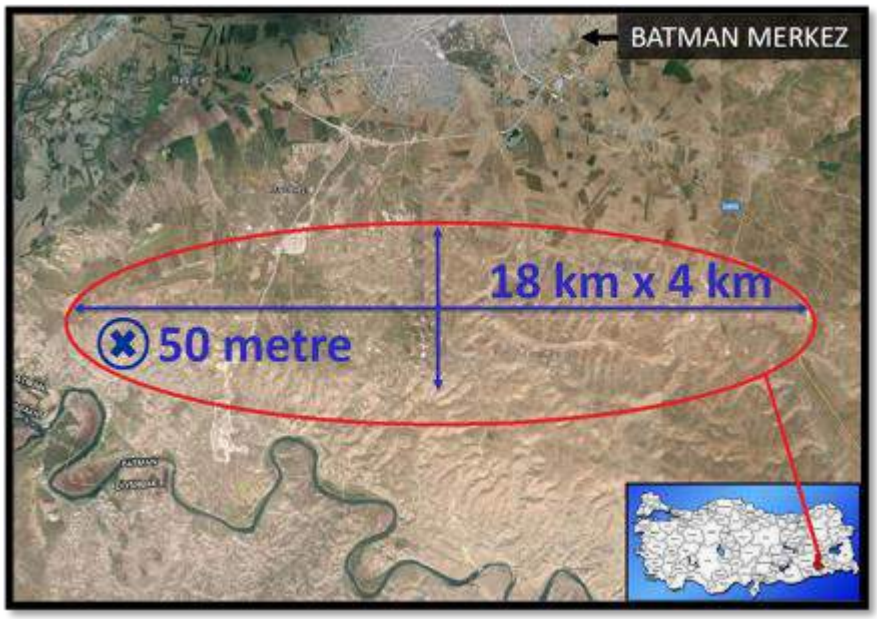

Şekil 1. İnceleme Alanı Yer Bulduru (TPAO, 2018)

Matkap Parametreleri

Sondaj ilerleme hızını etkileyen en önemli araçlardan biri matkap tipidir. Matkaplar: kendi ekseni etrafında dönerken, sondaj dizisi ile üzerinde döndüğü formasyonu kırıp öğüten gereçlerdir. Bir başka değişle matkap; dizinin en alt ucuna takılan ve üstüne ağırlık ve dönme hareketi verilmek suretiyle delme işlemini gerçekleştiren elaman olarak tanımlanır. Kuyu sondajlarının sağlıklı ve hızlı yapılabilmesi için ideal matkap

seçilmelidir. Matkabın da en iyi performansı gösterebilmesi için en iyi çalışma parametrelerinde kullanılmalıdır. Matkap çalışma parametreleri olan WOB (matkaba verilen ağırlık), RPM (dönme hızı) ve jet hızı sondaj mühendisi tarafından değiştirilebilir parametrelerdir. Bu yüzden mühendisin sahip olduğu bilgi birikimi ve tecrübesi önem kazanmaktadır. Bu çalışmada WOB ve RPM değerleri incelenecektir.

Matkaba Verilen Ağırlık (WOB)

Sondaj dizisinin ağırlığının bir kısmı matkaba verilir. Bu ağırlığa WOB (matkaba verilen ağırlık) denir. Genel olarak matkaba DC'lerin (drill collar) çamur içindeki ağırlığının % 75'i verilir. WOB (matkaba verilen ağırlık) kayacın basınç mukavemetine, formasyon sertliğine ve matkap tipine bağlıdır. WOB kayacın basınç mukavemetinden fazla olmamalıdır. Yoksa döner konlu matkabın dişleri kayaç üzerinde sürtünerek yüzeysel bir aşınmaya neden olur. Bu da matkap dişlerinin kırılmasına veya sondaj dizisinde bükülmeler sonucu sapmalara ve sıkışmalara neden olur. WOB'un düşük olması da kayaca yeterince batmayarak üzerinde kaymasına sebep olacak ve sondaj ilerleme hızını düşürecektir (Yünsel, 2001).

WOB sondaj sırasında ROP'yi (ilerleme hızını) kontrol etmede önemli bir parametre olarak kabul edilir. Düzgün olarak kontrol edilen WOB, sadece sondaj süresini azaltmakla kalmaz, aynı zamanda matkap ömrünü de uzatmada önemli bir faktördür (Wang ve ark., 2018). Döner konlu matkaplar yumuşak formasyonlarda az, sert formasyonlarda yüksek WOB ile çalışırlar (Özkara ve Derman, 2013).

Genellikle ilerleme hızı aşağıdaki bağıntıya yakın bir bağıntıyla bulunur (Göktekin, 1983);

$$v = K\frac{R^{0.5}*W}{d} \qquad (1)$$

Formül (1)'de; v, ilerleme hızını (m/saat); K, kayacın delinebilirliğini gösteren bir katsayı; R, matkabın dönme hızını (devir/dakika); w, matkaba verilen ağırlığı (ton); d, ise kuyu çapını (inç) ifade etmektedir.

WOB ve RPM'in ROP üzerindeki etkisi hem laboratuvarda hem de sahada çok sayıda araştırmacı tarafından incelenmiştir. Sabit tutulan diğer tüm sondaj değişkenleri ile deneysel olarak elde edilen WOB'a karşı ROP'nin değişimi grafiği, Şekil 1.'de gösterilmiştir.
Şekil 2.'de WOB eşik noktasına (b noktası) gelmeyene kadar belirgin bir şekilde ROP artışı gözlenmemiştir.
b-c noktaları arasında daha hızlı bir ROP artışı vardır. Çünkü b noktası kazmaktan öğütme ve kesme işlemine geçiş noktasıdır (Özbayoğlu, 2011). d noktasında optimum WOB seviyesine gelmiştir.

d noktasından sonra WOB arttırıldığı halde (d-e arası) ROP düşmeye başlamıştır. Bunun sebebi olarak yüksek WOB'te matkap saplanması olarak tanımlanır Özbayoğlu, 2011).

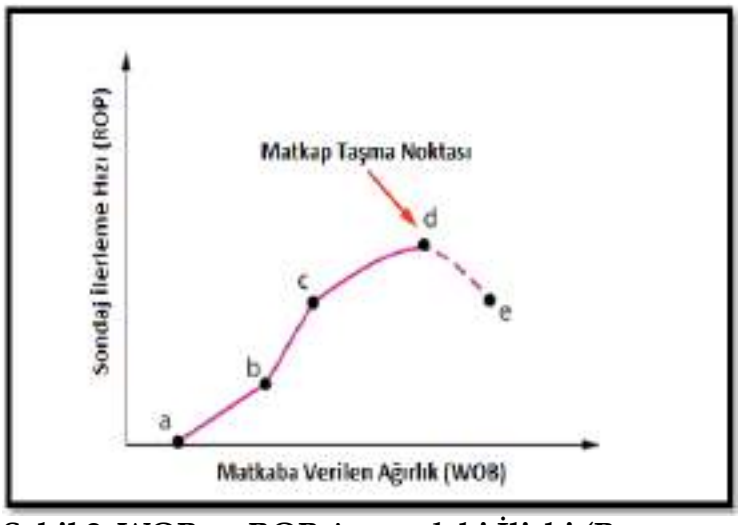

Şekil 2. WOB ve ROP Arasındaki İlişki (Bourgoyne ve ark., 1991)

Dönme Hızı (RPM)

Matkaba dönme hareketi döner masa (rotary table) veya top drive aracılığıyla sondaj dizisinin döndürülmesiyle aktarılır. Bu yöntemler dik kuyular için kullanılmaktadır. Yönlü kuyularda ise dönme hareketi dizinin tümünün döndürülmesi yerine, direk olarak çamur motoru matkaba dönme hareketini aktararak sadece matkabın dönmesini sağlar.

Dönme hızı (RPM) dakikada matkabın dönme sayısıdır. Birimi 1/dakika'dır. Dönme hızı sondaj ilerleme hızını etkileyen önemli matkap çalışma parametrelerindendir. Özellikle yumuşak formasyonlarda, bu iki kavram arasında doğrusal bir ilişki vardır. Sondaj sırasında yumuşak formasyonlar için yüksek dönme hızı, orta ve sert formasyonlar için ise düşük dönme hızı daha verimli olmaktadır (Şekil 3.). Bu yüzden dönme hızı formasyon tipine göre belirlenmelidir (Ergin ve ark., 2016). Aşırı dönme hızı matkabın aşınmasına, dişlerinin çatlamasına ve kırılmasına sebep olabilir (Yibudongha ve Izuwa, 2017).
İyi bir ilerleme hızı için RPM ve matkaba verilen ağırlık (WOB) sürekli olarak takip edilmelidir. Genellikle matkaplar sert ve aşındırıcı formasyonlarda yüksek WOB ve düşük RPM'de, yumuşak formasyonlarda ise, düşük WOB ve yüksek RPM'de daha iyi performans gösterirler (Moore, 1986).

Şekil 4.'te RPM (dönme hızı) ve ROP (sondaj ilerleme hızı) arasındaki ilişki görülmektedir. Genellikle düşük RPM lerde, ROP lineer (doğrusal) olarak artmaktadır. RPM yükseldikçe (b noktasından sonra) ROP'nin artışına etkisi azalır ve c noktasında optimum seviyeye ulaşır (Özbayoğlu, 2011).

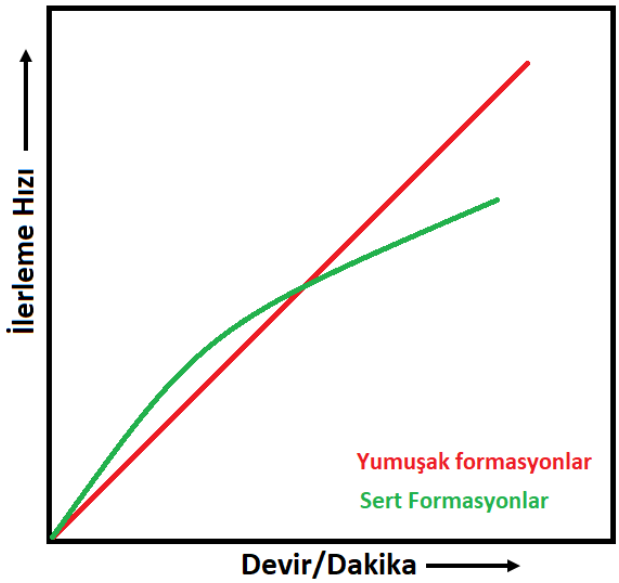

Şekil 3. Dönme Hızı İle İlerlemenin Formasyon Sertliğine Göre Değişimi (Moore, 1986)

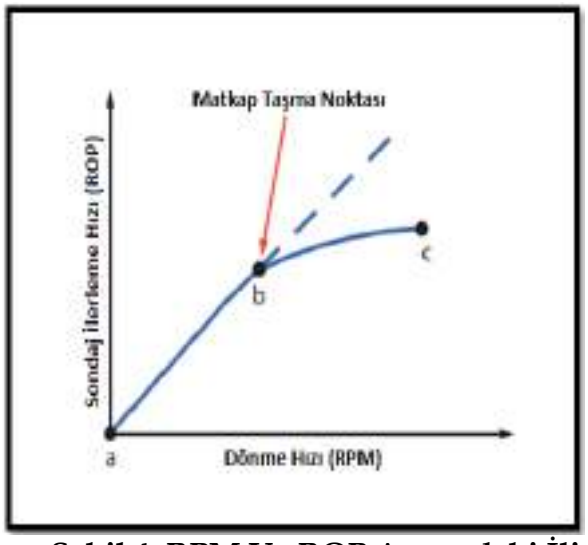

Şekil 4. RPM Ve ROP Arasındaki İlişki (Bourgoyne Ve Ark., 1991)

YÖNTEM

Bu çalışmada Türkiye'nin en büyük petrol üretim sahası olan Batı Raman'da döner konlu (insert, standart) ve sabit başlı (PDC) matkap ile yapılan sondajların performansları WOB ve ROP açısından tartışılmıştır. Bu kapsamda sondajın ikinci aşaması PDC, döner konlu insert ve standart matkapla sondajı yapılan kuyuların WOB ve ROP verileri kullanılmıştır. Bu amaçla sondajın ikinci aşaması 8 ½" 'lik insert matkapla kazılan dört

kuyu, standart matkapla kazılan beş kuyu ve PDC matkapla kazılan beş kuyunun gerçek sondaj verileri kullanılarak analizler yapılmış ve değerlendirilerek yorumlanmıştır.

İnceleme alanında ki kuyularda kullanılan matkapların performansları, karşılaşılan sorunlar ve çözümüne yönelik önlemlerinin alınması ile ilgili öneriler tartışılmıştır.

BULGULAR

Tablo 1.'de görüldüğü gibi WOB matkap tipine bağlı olarak değişmiştir. Çünkü matkabın çalışma performanslarından ve yapısından dolayı WOB matkap tipine göre değişebilmektedir. Çizelge 5.5'te görüldüğü üzere, PDC matkapla yapılan sondajlarda ortalama 4,5 ton ağırlık ile en düşük WOB'un uygulandığı görülmektedir. Sonrasında ortalama 9,8 ton ağırlıkla standart matkap gelmektedir.

En yüksek WOB'a sahip insert matkap ise ortalama 10,9 ton ağırlık ile sondaj yapabilmiştir. Bu durumda inceleme alanında WOB açısından en iyi performansı gösteren matkap tipi en düşük WOB ile PDC daha sonra standart en sonda insert matkap olarak belirlenmiştir.

Tablo 1. İncelenen tüm kuyuların sondaj ilerleme hızı ve WOB ortalamaları (TPAO, 2018)

MATKAP TİPİ: PDC		
KUYU ADI	**Sondaj Hızı (ort), m/s**	**WOB (ort), ton**
P-1	8,7	5,1
P-2	9,0	3,8
P-3	8,2	4,6
P-4	9,4	3,8
P-5	10,7	5,1
ORTALAMA	**9,2**	**4,5**
MATKAP TİPİ: STANDART		
KUYU ADI	**Sondaj Hızı (ort), m/s**	**WOB (ort), ton**
S-1	8,7	10,3
S-2	6,9	10,9
S-3	6,2	8,4
S-4	5,3	9
S-5	7,3	10,5

ORTALAMA	**6,9**	**9,8**
MATKAP TİPİ: INSERT		
KUYU ADI	**Sondaj Hızı (ort), m/s**	**WOB (ort), ton**
İ-1	4,9	9,3
İ-2	5,5	12
İ-3	5,6	11,4
İ-4	5,4	10,8
ORTALAMA	**5,4**	**10,9**

SONUÇ

1. Bu çalışmada Batman ili Batı Raman Petrol sahasında yapılan sondaj çalışmalarında kullanılan standart, insert ve PDC matkapların sondaj performasnları değerlendirilmiştir. Çalışmada ulaşılan sonuçlar aşağıdaki gibi özetlenebilir.

2. Bu çalışma kapsamında Batı Raman Petrol sahasında sondajı yapılan 14 kuyunun 8 ½" çapında matkap ile yapılan sondajın ikinci aşaması, performans ve WOB ve ROP parametreleri açısından değerlendirilmiştir.

3. Sahada kullanılması planlanan matkapların seçiminde daha önceden kazılmış referans kuyulardan alınan veriler ve formasyon tipi değerlendirilerek uygun matkap seçimi gerçekleştirilmiştir. Daha önceleri bu sahada standart ve insert matkap ile sondaj yapılırken PDC matkapların sektöre girmesiyle birlikte PDC matkaplar Batı Raman petrol sahasında kullanılmaya başlanmış ve yüksek performans alınmıştır. Bunun neticesinde Batı Raman kuyularının sondaj süresi kısalmış ve maliyetlerde azalma görülmüştür.

4. Batı Raman Petrol sahasında kazılan kuyuların WOB ve ROP verileri her üç matkap tipi için değerlendirilmiş ve sonuç olarak PDC matkap kullanımı her anlamda daha verimli olduğu ve düşük maliyetli kuyular kazılmasına sebep olmuştur.

5. Genellikle PDC matkaplar insert ve standart matkaba göre düşük WOB'te daha iyi performans gösterdiği bilinmektedir. Batı Raman petrol sahasında da bu durum görülmüştür. İncelediğimiz on dört kuyuda sondajın ikinci aşamasında her üç tip matkabın WOB ortalaması hesaplanmış ve insert matkapla yapılan sondajın WOB ortalaması 10,85 ton, standart matkapla yapılan sondajın WOB ortalaması 9,80 ton ve PDC matkapla yapılan sondajın WOB ortalaması 4,47 ton olduğu görülmüştür.

KAYNAKLAR

Yünsel, T.Y. (2001). Rotary (Döner) Sondajlarda Matkap Çalışma ve Kaya Parametrelerinin İlerleme Hızı Üzerine Etkileri. *Yüksek Lisans Tezi, Çukurova Üniversitesi, Maden Mühendisliği Ana Bilim Dalı,* Adana.

Wang, C., Liu, G., Li, J., Zhang, T., Jiang, H., Ling, X., & Ren, K. (2018). New methods of eliminating downhole WOB measurement error owing to temperature variation and well pressure differential. Journal of Petroleum Science and Engineering, 171, 1420-1432.

Özkara, H., Derman, Ş.O., (2013). Sondaj Matkapları. TPAO Sondaj Daire Başkanlığı, Sondaj Uygulamaları Eğitimi, Belek, Antalya

Göktekin, A., (1983). Sondaj tekniği. *TC İTÜ Kütüphanesi*.

Ozbayoglu, E. (2011). Rotary Drilling Bits. In: Fundamentals of Drilling Engineering, Ed.: Mitchell, R.F., Miska, S.Z., 1. *Edition, Society of Petroleum Engineers, USA, p.: 311*

Bourgoyne, A.T. Chenevert, M.E., Millheim, K.K., and Young, F.S. Jr. (1991). Applied Drilling Engineering. *Textbook Series, SPE, Richardson, Texas 2: 113–189*.

Sivagnanam, M., (2014), PDC Drill Bit Redesign and Simulation for Optimized Performance. M.Sc., Unıversıty Of Calgary, İnstitute Of Science, 163, Alberta.

Babadagli, T., Sahin, S., Kalfa, U., Celebioglu, D., Karabakal, U., & Topguder, N. N. (2009). Evaluation of steam injection potential and improving ongoing CO2 injection of the Bati Raman field, Turkey. Journal of Petroleum Science and Engineering, 68(1-2), 107-117.

Wang, C., Liu, G., Li, J., Zhang, T., Jiang, H., Ling, X., & Ren, K. (2018). New methods of eliminating downhole WOB measurement error owing to temperature variation and well pressure differential. Journal of Petroleum Science and Engineering, 171, 1420-1432.

TPAO, (2018), TP Batman Sondaj Müdürlüğü, 11554511-622.03-E.64438 sayı 25.09.2017 tarihli Bilgi ve Belge Talepleri konulu resmi yazı ile alınan veriler, Batman

Yibudongha Y., and Izuwa N., C., 2017, Bıt Performance Evaluatıon: A Case Study Of Fıeld A, Nıger Delta, Nıgerıa, 1,2 Department of Petroleum Engineering, Federal University of Technology, Owerri, Nigeria 1 Drilling Engineer, NPDC, Benin, Nigeria

Moore, P.L. 1986, Drilling Practices Manuel, Second Edition, Oklahama.

UTILIZATION OF *MALUS FLORIBUNDA* JUICE AS A POTENTIAL FOOD INGREDIENT: FOAM STABILITY, DRYING KINETICS AND POWDER PROPERTIES

Hulya CAKMAK
Hitit University, Department of Food Engineering
hulyacakmak@hitit.edu.tr

ABSTRACT: The aim of this study was to determine the optimum foam formulation for producing *Malus floribunda* fruit juice foams by employing faba bean protein concentrate (FB) and maltodextrin (MD) as potential foaming agent and wall material. Also the juice with optimum foam formulation was dried with foam-mat drying method in microwave oven in order to decrease the drying time thus energy efficiency, besides the quality of foam powders was evaluated.
FB had a positive surface charge (>25.5 mV) at the natural pH (2.91±0.02) of *Malus floribunda* juice, therefore the juice was directly used in foam production. Depending on the experimental design, the FB level was significantly improved the foam stability with respect to density response ($p<0.05$), however MD level had no effect on both density and foaming capacity ($p>0.05$). The optimum amount of FB (10% w/w) was further used in foam-mat drying, and the drying period was shortened nearly 31% compared to the control sample. Among the tested thin layer models, Midilli et al. model had the best fit (Adj-R^2> 0.99) to the experimental drying data of *Malus floribunda* juice and foams.
The redness (18.85±0.16) and brightness (62.93±0.27) of *Malus floribunda* foam powders with FB was significantly higher than the control and MD added sample ($p<0.05$). Moreover, the *Malus floribunda* fruit juice powders produced with foam mat drying had higher color intensity with good flowability which had the potential to use as coloring agent or functional ingredient in different food matrices.

Key words: Malus floribunda, foam stability, drying, powder.

EFFECT OF HYDROGEN ON IMPACT RESPONSE OF DUCTILE CAST IRON

Hina NAJAM
Abdullah Gul University, 38080 Kayseri, Turkey
hina.najam@agu.edu.tr

Burak BAL
Abdullah Gul University, 38080 Kayseri, Turkey
burak.bal@agu.edu.tr

Baris Cetin
FNSS Defense Systems Co, 06830 Ankara, Turkey
cetin.baris@fnss.com.tr

ABSTRACT: The effect of hydrogen on the impact response of EN-GJS-600-3 ductile cast iron was investigated by conducting charpy V-notch impact tests on uncharged and hydrogen pre-charged samples. Before the impact tests, micro vickers hardness tests were carried out on uncharged and hydrogen charged samples for determining the correlation between material hardness and impact toughness. Results indicated an increase in the hardness value by the hydrogen uptake which resulted from solution hardening caused by hydrogen. However, only a slight difference was observed in the material impact toughness with the impact toughness of hydrogen charged specimen being slightly greater than the uncharged one.

Key words: Hydrogen, impact test, micro hardness, impact toughness, solution hardening

INTRODUCTION

Ductile cast iron is widely used as a material for pipes in the city gas pipelines and is also a prospective material for hydrogen gas pipes (Matsunaga, Usuda, Yanase, & Endo, 2013). There are many studies that focus on the properties of cast iron under uniaxial tensile loading (Matsunaga, Matsuno, & Hayashida, 2011; Matsunaga, Usuda, Yanase, & Endo, 2014; Usuda, Matsuno, Matsunaga, Yanase, & Endo, 2013). However, uptil now very few studies focus on the effect of hydrogen on the toughness of these steels under impact loading.
In many materials especially high strength steels, hydrogen has known to cause embrittlement of the steels. Hydrogen embrittlement (HE) is characterized as a severe

material degradation process which results in ductility loss of the specimen and may cause sudden catastrophic material failure (Cialone & Asaro, 1979; Koyama, Akiyama, Lee, Raabe, & Tsuzaki, 2017; Symons, 1994).
To understand the effect of hydrogen on the impact response of EN-GJS-600-3 is of vital importance as to design hydrogen gas pipelines, the materials ability to distort under impact in the presence of hydrogen must be carefully examined. That way, suitable materials can be designed that have the ability to survive under those conditions.
In the present study, the effect of hydrogen on the impact toughness of EN-GJS-600-3 ductile cast iron is determined. For this purpose, impact tests have been conducted on notched specimens at room temperature with and without hydrogen to elucidate the effect of hydrogen on the material toughness under impact loading.

METHODS

EN-GJS-600-3 specimens were firstly machined to the charpy impact test specifications. The dimensions of the machined specimens were measured to be 55mm long with a square cross section of 10mm. A 2mm deep notch was produced on one surface of the specimen. The notch was produced exactly in the center of the specimen with an angle of 45 degrees. The technical drawing of the specimen is shown in Figure 1.

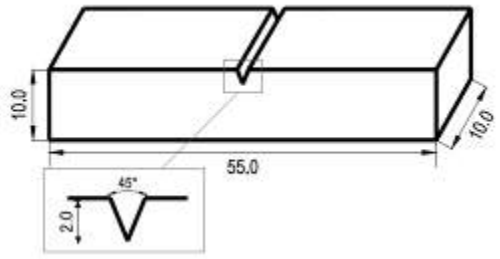

Figure 1. Specimen geometry used for the present study

Before carrying out hydrogen pre-charging process, all sides of the specimen were firstly mechanically grinded using sandpapers with particle size of P400 to P2500 in order to remove the residual stresses produced by the machining process and have even distribution of the scratch lines. Then mechanical polishing was carried out on the specimens surface using monocrystalline diamond suspension powder of 6um and then 1um for removing the surface scratches. After mechanical polishing, 3 notched specimens were put for hydrogen pre-charging in electrochemical solution consisting of 3%NaCl + 3g/L NH_4SCN. The current density for the pre-charging process was taken as 60A/m^2. One end of the DC power supply was connected to a conductive metal piece while other end was connected to the Pt electrode. The hydrogen pre-charging process was carried

out for 5 hours and 40 mins at room temperature. The schematic outline of the equipment used for hydrogen pre-charging is shown in Figure 2.

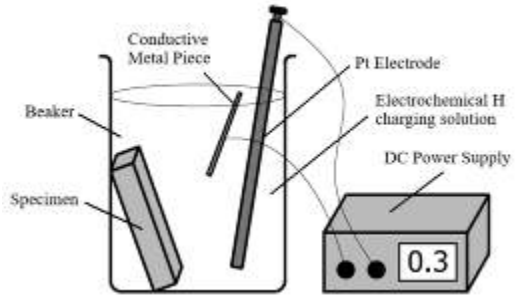

Figure 2. Schematic outline of the equipment used for hydrogen pre-charging

Vickers Hardness tests were performed on uncharged and hydrogen charged samples at a distance of 3mm from the notch. For the hardness tests, 6 points were taken around the notch and average taken for determining the material hardness. For the vickers hardness tests, 1 kgf was applied on the material by the indentor for 10s. After the hardness tests, impact tests were carried out on 3 uncharged and 3 hydrogen pre charged samples for repeatability of the data. Average was taken for the 3 obtained values in order to determine the impact energy. The impact tests were carried out at room temperature using AIT-300-EN impact testing machine.

RESULTS AND FINDINGS

The hardness test results for the uncharged and hydrogen charged samples are shown in Table 1.

Table 1. Hardness test results for uncharged and hydrogen charged sample

	Point 1	Point 2	Point 3	Point 4	Point 5	Point 6	Average	Standard Deviation (%)
HV (Uncharged)	227.4	224.4	246.1	192.3	256.1	255.5	233.6	10.4
HV (H+ Charged)	250.7	189.6	246.1	277.8	236.8	271.2	245.4	12.8

From Table 1, it can be seen that the hardness of hydrogen charged sample is greater than uncharged one. The difference in the hardness values for the 6 points accross the notch for the uncharged and hydrogen charged case as seen from the percentage standard deviation values can be due to surface inhomogenities as well as the presence of inculsions in the material.
The increase in the hardness of the specimen by hydrogen charging has been reported in many studies before (El-Amoush, 2008; Murakami, Kanezaki, & Mine, 2010; Stępień & Kupka, 2008). The increase is probably due to solution hardening caused by the presence

of hydrogen atoms occupying the interstitial sites in the lattice (Stępień & Kupka, 2008). The presence of interstitial hydrogen in the material induces lattice strains in it due to lattice distortion caused by the intersitial hydrogen atoms. The lattice strains creates a barrier to dislocation motion which in turn, increases the material yield strength and hence results in material hardening.
The impact test results for uncharged and hydrogen charged EN-GJS-600-3 samples are shown in Table 2.
Table 2. Impact test results for uncharged and hydrogen charged samples

	Test 1	Test 2	Test 3	Average	Standard Deviation (%)
Energy absorbed (J) (Uncharged)	3.8	3.8	4.0	3.87	3.10
Energy absorbed (J) (H+ Charged)	3.9	4.9	3.9	4.23	13.71

From Table 2, a difference of 0.36J can be seen in the energy absorbed by the specimen before fracture for the uncharged and hydrogen charged case. Moreover, in both the cases, very poor impact toughness values are observed due to high strength but insignificant ductility of EN-GJS-600-3. It is interesting to note that hydrogen uptake increased the microhardness values whereas, a negligible difference was observed in the material impact toughness as indicated by Table 2. The only possible reason behind it can be attributed to high deformation rate associated with the impact testing. As the specimen fractured within milliseconds, hydrogen didn't get enough time to diffuse to the crack tip from the graphite/ matrix interface and deterioate the specimen ductility during the deformation process. The slight increase in the material impact toughness results from the increased yield strength of the hydrogen charged specimen due to solution hardening as discussed previously. However, high deformation rate as well as the solution hardening alone cannot explain the increase in impact toughness of the material by hydrogen uptake since detailed microstructural analysis needs to be done to support the theory. Moreover, the fracture surface of the specimen must be carefully examined by using high magnification microscope such as scanning electron microscope (SEM) to confirm that hydrogen uptake didn't result in the specimen ductility loss during the fracture process.

CONCLUSIONS

The effect of hydrogen on the impact response of EN-GJS-600-3 ductile cast iron was investigated by conducting impact tests with and without hydrogen pre-charging. Microhardness tests were performed on the uncharged and hydrogen charged sample prior to impact testing for determining correlation between material hardness and impact toughness. According to the present study, the following conclusions were obtained:

Hydrogen charging led to a marked increase in the material hardness while negligible difference was observed in the material impact toughness with the impact toughness of hydrogen charged specimen being slightly greater than the uncharged one. The increase in hardness can be attributed to solid solution hardening casued by interstitial hydrogen present in the material. Slight increase in the material impact toughess by the hydrogen uptake can be attributed to high deformation rate and solid solution hardening. However, this alone cannot explain the difference as detailed microstructural analysis needs to be done to confirm the theory.

REFERENCES

Cialone, H., & Asaro, R. J. (1979). The role of hydrogen in the ductile fracture of plain carbon steels. *Metallurgical Transactions A*, *10*(3), 367–375. https://doi.org/10.1007/BF02658347

El-Amoush, A. S. (2008). An investigation of hydrogen-induced hardening in 7075-T6 aluminum alloy. *Journal of Alloys and Compounds*, *465*(1–2), 497–501. https://doi.org/10.1016/J.JALLCOM.2007.10.126

Koyama, M., Akiyama, E., Lee, Y.-K., Raabe, D., & Tsuzaki, K. (2017). Overview of hydrogen embrittlement in high-Mn steels. *International Journal of Hydrogen Energy*, *42*(17), 12706–12723. https://doi.org/10.1016/J.IJHYDENE.2017.02.214

Matsunaga, H., Matsuno, K., & Hayashida, K. (2011). Effect of Hydrogen on Tensile Properties of a Ductile Cast Iron. In *Supplemental Proceedings* (pp. 447–454). Hoboken, NJ, USA: John Wiley & Sons, Inc. https://doi.org/10.1002/9781118062173.ch56

Matsunaga, H., Usuda, T., Yanase, K., & Endo, M. (2013). Ductility loss in Hydrogen-charged Ductile Cast Iron. Chinese Society of Theoretical and Applied Mechanics. Retrieved from https://kyushu-u.pure.elsevier.com/en/publications/ductility-loss-in-hydrogen-charged-ductile-cast-iron

Matsunaga, H., Usuda, T., Yanase, K., & Endo, M. (2014). Ductility Loss in Ductile Cast Iron with Internal Hydrogen. *Metallurgical and Materials Transactions A*, *45*(3), 1315–1326. https://doi.org/10.1007/s11661-013-2109-9

Murakami, Y., Kanezaki, T., & Mine, Y. (2010). Hydrogen Effect against Hydrogen Embrittlement. *Metallurgical and Materials Transactions A*, *41*(10), 2548–2562. https://doi.org/10.1007/s11661-010-0275-6

Stępień, K., & Kupka, M. (2008). Effect of hydrogen on room-temperature hardness of B2 FeAl alloys. *Scripta Materialia*, *59*(9), 999–1001. https://doi.org/10.1016/J.SCRIPTAMAT.2008.07.002

Symons, D. M. (1994). *An investigation into the effects of hydrogen on the fracture and deformation of Alloy X-750*. West Mifflin, PA (United States). https://doi.org/10.2172/10195743

Usuda, T., Matsuno, K., Matsunaga, H., Yanase, K., & Endo, M. (2013). Hydrogen-Induced Ductility Loss in Cast Irons. *Materials Science Forum*, *750*, 260–263. https://doi.org/10.4028/www.scientific.net/MSF.750.260.

THE EFFECTS OF METHYLPARABEN AND PROPYLPARABEN ON EARLY DEVELOPMENTAL STAGES AND TRANSCRIPTIONAL PROFILES OF ZEBRAFISH

Ceyhun Bereketoglu
Biology, The Life Science Center, School of Science and Technology, Örebro University, SE-701 82 Örebro, Sweden.
Iskenderun Technical University, Faculty of Engineering and Natural Sciences, Department of Biomedical Engineering, Hatay, Turkey
ceyhunbereketoglu@gmail.com,

Ajay Pradhan
Biology, The Life Science Center, School of Science and Technology, Örebro University, SE-701 82 Örebro, Sweden.
ajay.pradhan@oru.se

ABSTRACT: Parabens are preservatives used in various commercial products such as food, cosmetics and pharmaceuticals. Parabens have been shown to accumulate in the environment and have negative impacts on animals as well as human health. In this study, we performed a comprehensive research to determine the effects associated with propylparaben (PP) and methylparaben (MP) on early developmental stages of zebrafish. We analyzed developmental abnormalities, hatching, and mortality as well as gene expression profiles in the embryos exposed to both compounds. We showed that both MP (≥ 100 μM) and PP (≥10 μM) are toxic to the embryos in a dose-dependent manner and resulted in developmental abnormality. We observed several malformations including spinal defects, pericardial edema, and pigmentation defects in response to both MP and PP treatments. These data indicate that PP is more toxic than MP. We used 1 and 10 μM doses of MP and PP to determine gene expression profiles. We showed that several genes involved in different physiological pathways such as stress response, cell cycle and DNA damage, inflammation, fatty acid metabolism and endocrine functions were affected by MP and PP. The gene expression analysis demonstrate that parabens may cause toxicity by inducing oxidative stress, DNA double-strand breaks, apoptosis as well as by altering fatty acid metabolism. Altogether, this study provides considerable information on the adverse effects of MP and PP using different physiological endpoints.

Keywords: toxicity, gene expression, stress response, development abnormality.

Acknowledgements: This study was supported by Knowledge Foundation, Sweden and Örebro University.

TURKEY'S ELECTRICITY CONSUMPTION FORECASTING with ARTIFICIAL NEURAL NETWORKS

Şeyma EMEÇ
Ataturk University
seyma.yayla@atauni.edu.tr

Gökay AKKAYA
Ataturk University
gakkaya@atauni.edu.tr

ABSTRACT: Sensitive information on future demand for electrical energy helps countries and companies greatly. In this way, planning of development works is made easier and wrong planning and misuse of resources can be prevented. Artificial neural networks (ANN) model was developed by using MATLAB software to forecast Turkey's future electrical energy in this study. In the forecasting of electrical energy, the values of independent variables such as gross domestic product (GDP), population, export, import and installed capacity between 1990 and 2016 were used in the model. Then, model 3000 was run for iteration. The results showed that the developed ANN model made demand forecast with high accuracy and the R value expressing the forecast performance was 99,259%.

Key words: Artificial Neural Networks, Demand forecasting, Electrical Energy

INTRODUCTION

Energy sources become more important due to the increase in population and industrialization in the world. Therefore, energy is seen as one of the basic building blocks of economic development. Electrical energy has the most flexible structure among energy items due to its advantages such as ease of use, being able to convert to other energy types at any time and its prevalence in daily life.

Plans on demand, supply, transmission, distribution and pricing are of great importance for the healthy development of the electricity sector. One of the most important problems of planning to be made is future demand information. Failure to store electrical energy increases the importance of accuracy level in demand forecasting. It is clear that the more accurate the estimations to be made are, the more valid the planning studies will be.

There is a large increase in energy and particularly electricity use in parallel with Turkey's rapid population growth and economic growth. Accurate and reliable forecasting of electricity demand will play an important role in determining the energy strategy of our country. (Turker and Koksal, 2008). In this context, Turkey's net electrical power demand forecasting has been made using the method of ANN in this study.

LITERATURE REVIEW

Many methods such as time series (Amarawickrama and Hunt, 2008), regression model (Bessec and Fouquau, 2008), genetic algorithm (Lee and Tong, 2011), fuzzy logic (Kucukali and Baris, 2010), artificial neural networks (Hamzaçebi *et al.,* 2017) are used in literature for energy demand forecasting. Many studies have shown that artificial neural networks (ANNs) give as much or even better results as traditional methods (Hill et al., 1996; Sharda and Patil, 1992; Tang et al., 1991) in future forecasting.

There are many studies forecasting Turkey's electrical energy demand using artificial neural. In the study of Hamzaçebi and Kutay (2004), they forecasted electrical energy for 2003-2010, Hamzaçebi (2007) forecasted electrical energy on a sectoral basis for 2005-2020, Kavaklıoğlu (2011) calculated electrical energy forecasting for 2007-2026 using 4 input variables (population, imports, exports and gross national product) in his study, Kavaklıoğlu *et al*. (2009) used GSHM, population, exports, imports for 2007-2027 electrical energy forecasting. Bilgili *et al.* (2012) forecasted electrical energy in residential and industrial sector in 2008-2015 and took into account input variables, installed capacity, gross electricity generation and population. Özden and Öztürk (2018) forecasted seasonal electrical energy for 2014-2016 and Hamzaçebi *et al.* (2017) forecasted seasonal electrical energy for 2015-2018, Başoğlu and Bulut (2017) seasonal electrical energy short-term electricity demand in their studies.

METHODS

Artificial Neural Networks

ANN is a generalization of the mathematical model of human perception and biological nerves. ANN is a combination of artificial nerve cells that are developed by inspiration from biological nerve cells. The most important features of ANN are modeling of nonlinear structures, parallel distributed structure, learning and generalization ability, applicability for different problems and having fault tolerance.

ANN does not require any prior knowledge between input and output variables. The input information and the output information corresponding to the information are provided to the network and the network is allowed to learn the relationship between

the input-output variable. This learning process is called consultative learning. In the solution of the present problem, back propagation algorithm from the consultative learning method was used. Learning of an artificial neural network by back propagation algorithm consists of two stages including forward and backward calculation. In the forward calculation, the input variables that come to the network are processed by weight matrices and the output values are calculated. Then, backward propagation of the network and the network weights are rearranged based on minimizing the error value between the output value produced by the network and the actual value. This process continues until the network produces the desired output.

ANN can be used for both cause and effect forecasting and time series forecasting methods. For a forecasting problem based on the cause-effect relationship, the inputs of ANN express the independent variable. The output is dependent variable. The nonlinear functional relationship determined by ANN can be written as in Equation 1.

$$Y = f(x_1, x_2, ..., x_n)$$

In the above equation, $x_1, x_2, ..., x_n$ is 'n unit' independent variable and Y is the dependent variable. For a time series-based forecasting problem, ANN's inputs consist of historical observation values of the data series, while the output represents the future forecasting value. The nonlinear relationship determined by ANN can be written as in Equation 2.

$$Y_{t+1} = f(Y_t, Y_{t-1}, ..., Y_{t-n})$$

Application

In the literature, it is seen that the independent variables used in the studies conducted with forecasting methods based on cause-effect relationship differ. In this study, independent variables that can be added to the model in order to forecast the model to be established with ANN and the net energy demand reliably and steadily, and independent variables such as "gross domestic product (GDP), population, export, import and installed power capacity" that reached to enough historical observation values were added to the model.

After data were used for independent variables (GDP: WorldBankData, 2019; Population: Turkey Population, 2019; Installed power, TEIASa, 2019; Exports and Imports, TEIASb, 2019) obtained from official sources from 1990 to 2016 and the model was established by Matlab Neural Network Toolbox software. 70% of the available data were used for training, 15% for verification and 15% for test set. Both input and output data were converted to the range of [0,1] by simple normalization process.

Since the number of single hidden layers in the literature is sufficient for achieving successful results, the single hidden layer was preferred (Zhang *et al.*, 1998). The number

of neurons in the hidden layer was determined by trial and error method to give the best results for training and verification sets.

The following is the structure of the ANN developed within the scope of the study (Figure 1):

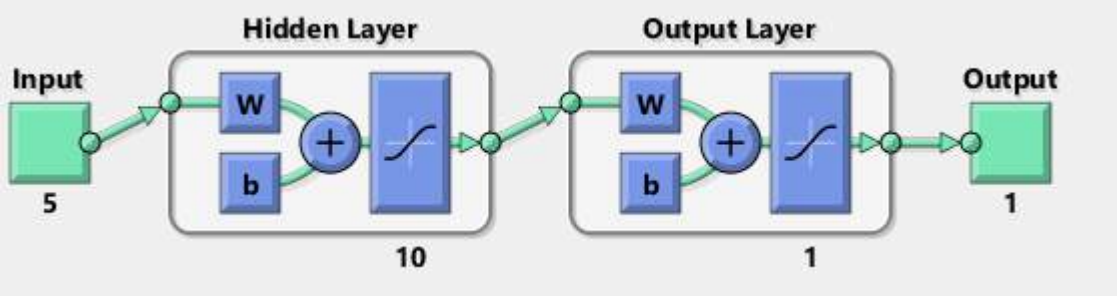

Figure 1. The structure of the ANN developed within the scope of the study

RESULTS AND FINDINGS

In this study, GDP, population, exports, imports and the installed capacity of the input variables are used to forecast the future electricity demand of Turkey. Feed forward backpropagation method was used in the model and the model 3000 was run for iterations. The prediction performance of the developed ANN model has showed in Figure 2. The R value represents the correlation coefficient. The correlation coefficient is used to express the relationship between the variables. The R value is between +1 and -1. When R is equal to +1, there is a positive strong linear relationship. When R is equal to -1, there is a negative, weak linear relationship. Where R is equal to 0, there is no relationship between variables. As a result, it is reflected in the graphs that learning and testing process in the network is successful, so R value was found to be 99,259% and the error was found 0.0016.

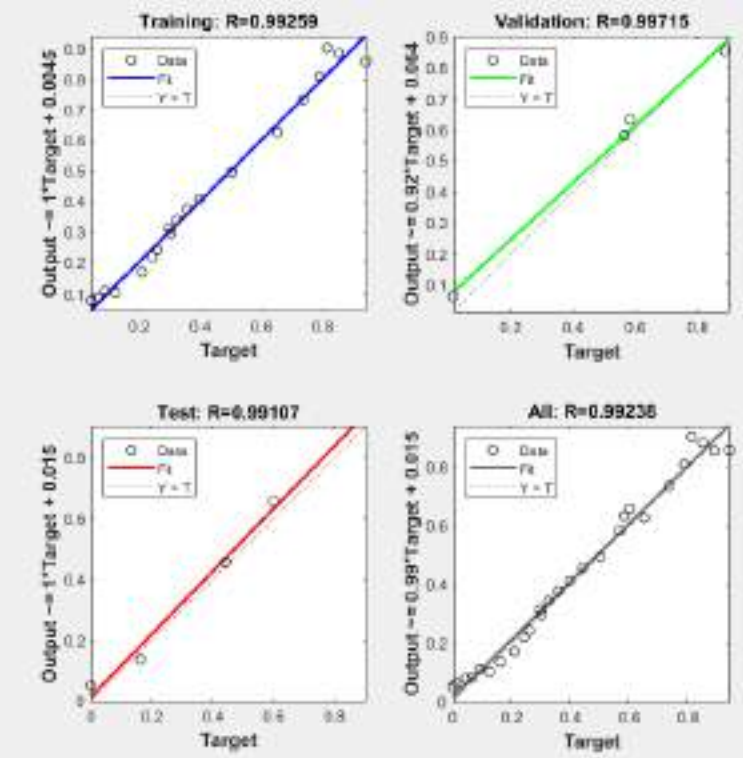

Figure 2. The prediction performance of the developed ANN model

After the network was trained with historical data and achieved successful results, electricity demand forecast for 2020 was made. Turkey's electricity demand for 2020 forecasted as 277.595 (*10^9) kWh.

CONCLUSIONS

In the electricity sector, it is important to make accurate forecasts of demand, to provide supply of electricity without any problem and to use the resources correctly. Accurate forecasting of values requires forecasts based on expert systems for such random elements. In this study, electricity demand forecasting was made with the help of artificial neural networks method which is widely used in literature. The obtained results showed that ANN technique can be used as a forecasting tool and it gives very good results.

ANN techniques allow working with less data. However, they can sometimes produce negative results as they have a black box feature. Therefore, when they are used as a forecasting tool, attention should be paid to the suitability of the established network model to the nature of the problem.

RECOMMENDATIONS

Future studies can develop and forecast a new model using different independent variables. The results obtained can be compared with other forecasting methods and the results can be discussed. The distribution of the electrical energy forecasting according to the sectors can be forecasted.

REFERENCES

Amarawickrama, H. A., & Hunt, L. C. (2008). Electricity demand for Sri Lanka: a time series analysis. *Energy*, *33*(5), 724-739.

Başoğlu, B., & Bulut, M. (2017). Kısa dönem elektrik talep tahminleri için yapay sinir ağları ve uzman sistemler tabanlı hibrit sistem geliştirilmesi. *Journal of the Faculty of Engineering and Architecture of Gazi University*, *32*(2), 575-583.

Bilgili, M., Sahin, B., Yasar, A., & Simsek, E. (2012). Electric energy demands of Turkey in residential and industrial sectors. *Renewable and Sustainable Energy Reviews*, *16*(1), 404-414.

Bessec, M., & Fouquau, J. (2008). The non-linear link between electricity consumption and temperature in Europe: a threshold panel approach. *Energy Economics*, *30*(5), 2705-2721.

Hamzaçebi, C., Es, H. A., & Çakmak, R. (2017). Forecasting of Turkey's monthly electricity demand by seasonal artificial neural network. *Neural Computing and Applications*, 1-15.

Hamzaçebi, C., & Kutay, F. (2004). Yapay sinir ağlari ile türkiye elektrik enerjisi tüketiminin 2010 yilina kadar Tahmini. *Gazi Üniversitesi Mühendislik-Mimarlık Fakültesi Dergisi*, *19*(3).

Hamzaçebi, C. (2007). Forecasting of Turkey's net electricity energy consumption on sectoral bases. *Energy policy*, *35*(3), 2009-2016.

Hill, T., O'Connor, M., & Remus, W. (1996). Neural network models for time series forecasts. *Management science*, *42*(7), 1082-1092.

Kavaklioglu, K., Ceylan, H., Ozturk, H. K., & Canyurt, O. E. (2009). Modeling and prediction of Turkey's electricity consumption using artificial neural networks. *Energy Conversion and Management*, *50*(11), 2719-2727.

Kavaklioglu, K. (2011). Modeling and prediction of Turkey's electricity consumption using Support Vector Regression. *Applied Energy*, *88*(1), 368-375.

Kucukali, S., & Baris, K. (2010). Turkey's short-term gross annual electricity demand forecast by fuzzy logic approach. *Energy policy*, *38*(5), 2438-2445.

Lee, Y. S., & Tong, L. I. (2011). Forecasting energy consumption using a grey model improved by incorporating genetic programming. *Energy conversion and Management*, *52*(1), 147-152.

ÖZDEN, S., & ÖZTÜRK, A. (2018). Yapay sinir ağları ve zaman serileri yöntemi ile bir endüstri alanının (ivedik OSB) elektrik enerjisi ihtiyaç tahmini. *Bilişim Teknolojileri Dergisi*, *11*(3), 255-261.

Sharda, R., & Patil, R. B. (1992). Connectionist approach to time series prediction: an empirical test. *Journal of Intelligent Manufacturing*, *3*(5), 317-323.
Tang, Z., De Almeida, C., & Fishwick, P. A. (1991). Time series forecasting using neural networks vs. Box-Jenkins methodology. *Simulation*, *57*(5), 303-310.
WorldBankData (2019). World Development Indicators. Retrieved September 10, 2019 from https://databank.worldbank.org/source/world-development-indicators/Type/TABLE/preview/on#.
Türker, L., Köksal, M.A.(2008). TÜRKİYE'NİN UZUN DÖNEM ELEKTRİK TALEBİ VE BUNA BAĞLI CO2 EMİSYONUNUN TAHMİNİ. *Hava Kirliliği ve Kontrolü Ulusal Sempozyumu*, 22-25 Ekim 2008, HATAY.
Turkey Population (2019). Population Information Turkey by Provinces and Districts. Retrieved September 05, 2019 from. https://www.nufusu.com/ulke/turkiye-nufusu.
Turkish Electricity Transmission (TEIAS)a. Turkey installed power for 1990-2016. Retrieved September 03, 2019 from. https://www.teias.gov.tr/tr/i-kurulu-guc-0 .
Turkish Electricity Transmission(TEIAS)b. Turkey exports and imports for 1990-2016. Retrieved September 03, 2019 from. https://www.teias.gov.tr/tr/v-ithalat-ihracat-0.
Zhang, G., Patuwo, B. E., & Hu, M. Y. (1998). Forecasting with artificial neural networks: The state of the art. *International journal of forecasting*, *14*(1), 35-62.

FUZZY CHINESE POSTMAN PROBLEM AND AN APPLICATION

Özlem ÇOMAKLI SÖKMEN
Erzurum Technical University
ozlem.sokmen@erzurum.edu.tr

Mustafa YILMAZ
Ataturk University
mustafay@atauni.edu.tr

ABSTRACT: Arc routing problems are the problems used to determine the shortest path or paths that returns to the starting vertex by traversing all arcs or edges on a graph at least once. Chinese Postman Problem (CPP), one of the arc routing problems; can be defined as the problem of returning to the starting point after a postman traverses all connections on the defined network. In this study, Fuzzy CPP (FCPP) was applied on an example problem since factors such as traffic density and weather conditions changed the arrival time between two vertices. In the problem, the objective function coefficients are considered as fuzzy and triangular fuzzy numbers were used. The mathematical model established in the study; was solved using GAMS, a high-level programming language used for the solution of modeling and optimization problems.

Key words: fuzzy chinese postman problem, triangular fuzzy number, arc routing problem

INTRODUCTION

Chinese Postman Problem (CPP) first studied in 1962 by a Chinese mathematician called Mei-Ko Kwan, may be defined as the delivery of mails that a postman receives from the post office in the shortest possible path by traversing all streets/roads in the city and returning to the post office which is the starting vertex after the delivery is completed (Ahujava *et al.* 1993, Eiselt *et al.* 1995). CPP may be used in several areas such as mail delivery, garbage collection, snow and ice controls on streets and highways, road gritting, snow removal and street cleaning operations, school bus and police patrol vehicles routing, water and newspaper distribution, effective web site determination (Thimbleby 2003). Expenditures of public and private enterprises in these areas are increasing day by day and reach to high amounts. Due to insufficient planning and faulty investments, a significant amount of resources is extravagantly spent in these areas. Therefore, the importance of such problems is increasing and is being the subject of many researches.

Studies of researchers in these areas help to increase the possibility of implementation by finding more effective solutions and thus to provide significant savings (Emel *et al.* 2003).

A feature of today's problems is time constraint. When defining and solving problems, the optimum solution and the most accurate definition may not be necessary considering the time spent. In this context, defining problems with net values is no longer an obligation. the method that eliminates this requirement is Fuzzy Logic. In fuzzy logic, there are membership functions that show the amount of membership to these definitions instead of definitions such as 1-0 as in classical logic. The main difference between fuzzy logic and classical logic is that mathematics in the known sense allows only extreme values. This is why it is difficult to model and control complex systems with classical mathematical methods, because the data should be complete. Fuzzy logic saves one from this necessity (Memmedova and Keskin 2009). Some of the studies on Fuzzy routing problems are given in Table 1.

Table 1. Literature Research

Author(s) and Publishes Year	Type of Problem	Fuzzy Number	Method of Defuzzification
Botzheim (2009) *et al.*	Fuzzy Traveling Salesman Problem (FTSP)	Triangular	Center of Gravity
Kumar and Gupta (2012)	Fuzzy Assignment Problem And FTSP	Trapezoidal	Yager's Ranking Index
Dhanasekar *et al*. (2013)	FTSP	Triangular and Trapezoidal	Fuzzy Hungarian Method
Dingar and Sundari (2014)	FTSP	Trapezoidal	Linear Ranking Fonction
Srinivasan and Geetharamani (2014)	FTSP	Triangular and Trapezoidal	Yager's Ranking Technique

Crisan and Nechita (2008)	FTSP	Triangular	Center of Mass Method
Yahya Mohamed and Divya (2016)	FTSP	Octagonal	Robust Ranking Technique

When the related literature is examined, it is seen that there has not been a study conducted on Fuzzy Chinese Postman Problem (FCPP) before. In real life problems, transportation time between the two centers varies greatly due to various reasons such as weather conditions, traffic density and traffic accidents. Therefore, the objective function coefficients representing the arrival time between two vertices are considered as triangular fuzzy numbers (TFNs) in this study. Robust's Ranking Method frequently used in the literature in order to defuzzificate (Defuzzification) the used triangular fuzzy numbers was used. The proposed model was applied on a small size sample problem. It is aimed to make the new problem type developed to be the first study in the literature and to increase its applicability.

METHODS

Fuzzy Chinese Postman Problem

CPP may be defined as the problem of returning to the starting point after a postman traverses all connections on the defined network for the distribution and collection of letters. In this type of problem, the problem turns into FCPP when the objective function coefficient values showing the arrival time between two vertices are considered as fuzzy.

On a graph G = (V, E); where edge (i, j) establishes a connection between vertices i and j. Mathematical model, parameters and variables for CPP are given in following (Yılmaz *et al.* 2017). In this model, the model is valid for FCPP when the objective function coefficients are considered as fuzzy.
Variables;
x_{ij} : The main decision variable which represents the number of times arc (i,j) is traversed in each cycle using vehicle starting from node i ending at node j. The variable is integer.
x_{ji} : Decision variable which represents the number of times arc (j,i) is traversed in each cycle using vehicle starting from node j ending at node i. The variable is integer.

Parameters;
$\tilde{C}_{ij}$: The length for traversing arc (i,j). (Fuzzy times are used instead of distance.)
V: Set including all nodes in the network,

E: Set including all edges in the network,
n: Total number of nodes in network.
The entire formulation can be seen in the following,

$$\text{Min:} \sum_{i=1}^{n}\sum_{j=1}^{n} \tilde{C}_{ij}\, x_{ij} \qquad (1)$$

Subject to

$$\sum_{j=1}^{n} x_{ij} - \sum_{j=1}^{n} x_{ji} = 0 \quad ; i = 1,2,\dots,n \quad \forall_i \in V \qquad (2)$$

$$x_{ij} + x_{ji} \geq 1 \quad \forall (i,j) \in E \qquad (3)$$

$$x_{ij}, x_{ji} \geq 0 \text{ and integer} \qquad (4)$$

The fuzzy objective function (1) minimizes the total length of route R that is covered by track inspection vehicle. Eq. (2) is flow conservation at each node constraint which guarantees the creation of a tour of the network for the vehicle. Eq. (3) ensures that each arc that exists is covered at least once during each cycle regardless of its direction using the vehicle. Eq. (4) is restriction on the variables.

Fuzzy Set

The characteristic function μ_A of a crisp set $A \subseteq X$ assigns a value either 0 or 1 to each member in X . A function $\mu\tilde{a}$ such that the value assigned to the element of the universal set X fall within a specified range i.e $\mu\tilde{a} : X \rightarrow [0,1]$. The assigned value indicates the membership grade of the element in the set A . The function $\mu\tilde{a}_{(x)}$ is called the membership function and the set $\tilde{A} = \{(x, \mu\tilde{a}_{(x)}; x \in X)\}$ defined by $\mu\tilde{a}_{(x)}$ for each $x \in X$ is called a fuzzy set (Prabha and Shanmugavel 2016).

Linguistic Variables

Linguistic variables are variables that can take words in a language as a variable value. For example, it is expressed in words such as "hot" or "cold". The most important feature that distinguishes fuzzy logic from other systems is that it allows the use of linguistic variables (Özkan 2003). Linguistic variables are used to express very complex or poorly defined situations quantitively (Chen *et al*. 2005).

Triangular fuzzy number (TFNs)

A TFN $\tilde{A}$ is specified by three parameters (a_1, a_2, a_3) and is defined by its continuous membership function $\mu_{\tilde{A}(x)} : X \rightarrow [0, 1]$ as follows (Giri *et al.* 2015):

$$\mu_{\tilde{A}}(x) = \begin{cases} \frac{x-a_1}{a_2-a_1} & \text{for } a_1 \leq x \leq a_2 \\ \frac{x-a_1}{a_2-a_1} & \text{for } a_2 \leq x \leq a_3 \\ 0 & \text{otherwise} \end{cases}$$

Robust's Ranking Method

Yager's ranking technique which satisfies compensation, linearity, additivity properties and provides results which consists of human intuition. For a convex fuzzy number ã, the Robust's Ranking Index is defined by (Yager 1978, Nagarajan and Solairaju 2010, Prabha and Vimala 2016);

$R(\tilde{a}) = \int_0^1 (0.5)\,(a_\alpha^L, a_\alpha^U) d\,\alpha$
Where (a_α^L, a_α^U) = {(b-a) α + a, c – (c-b) α} which is the α – level cut of the fuzzy number ã.

Application

In this study, a 5-vertices FCPP is discussed. The objective function coefficients are considered as fuzzy and triangular fuzzy numbers are used since the factors such as weather conditions, traffic density, traffic accidents, construction and repair works change the arrival time between two vertices. In this problem, it is aimed to create the shortest path by traversing every edge at least once. Membership functions for traffic density, which is a fuzzy verbal variable, are formed as less dense, normal and very dense. The fuzzy cost matrix and mathematical model of the sample problem is given below.

$$[\tilde{C}_{ij}]_{5x5} = \begin{pmatrix} - & (16,25,64) & (16,36,49) & (4,9,16) & (4,49,64) \\ (16,25,64) & - & (4,49,81) & (1,4,9) & (9,36,49) \\ (16,36,49) & (4,49,81) & - & - & (4,25,81) \\ (4,9,16) & (1,4,9) & - & - & - \\ (4,49,64) & (9,36,49) & (4,25,81) & - & - \end{pmatrix}$$

$Min\ \check{z} =$ R(16, 25, 64)x_{12} + R(16, 36, 49) x_{13}+ R(4, 9, 16) x_{14}+ R(4, 49, 64) x_{15}+ R(16, 25, 64) x_{21}+ R(4, 49,81) x_{23} + R(1, 4, 9) x_{24}+ R(9, 36, 49) x_{25} + R(16, 36, 49) x_{31} + R(4, 49, 81) x_{32} + R(4, 25, 81) x_{35}+ R(4, 9, 16) x_{41} + R(1,4,9) x_{42} + R(4, 49, 64) x_{51} + R(9, 36, 49) x_{52} + R(4, 25, 81) x_{53}

Subject to

$\sum_{j=1}^{n} x_{ij} - \sum_{j=1}^{n} x_{ji} = 0 \quad ; \ i = 1,2, \ldots, n \quad \forall_i \in V$

$x_{ij} + x_{ji} \geq 1 \quad \forall (i,j) \in E$

$x_{ij}, x_{ji} \geq 0$ and integer

RESULTS AND FINDINGS

In this study; Robust's Ranking Method is used to convert the triangular fuzzy numbers in the cost matrix into crisp values and the results are given.

$R(\tilde{a}) = \int_0^1 (0.5)\,(a_\alpha^L, a_\alpha^U) d\,\alpha$
Where (a_α^L, a_α^U) = {(b-a) α + a, c – (c-b) α};

Therefore, R(16, 25, 64) = $R(\tilde{C}_{12}) = \int_0^1 (0.5)\,\{(25-16)\alpha + 16,\ 64 - (64-25)\alpha\} d\alpha$

$R(\tilde{C}_{12}) = \int_0^1 (0.5)\,\{(9\alpha + 16), 64 - 39\alpha) d\alpha = \int_0^1 (0.5)\,(80 - 30\alpha)\, d\alpha = 32.5$

Similarly, R(16, 36, 49) = $R(\tilde{C}_{13})$ = 34.25, R(4, 9, 16) = $R(\tilde{C}_{14})$ = 9.5, R(4, 49, 64) = $R(\tilde{C}_{15})$ = 41.5,

R(16, 25, 64) = $R(\tilde{C}_{21})$ = 32.5, R(4, 49, 81) = $R(\tilde{C}_{23})$ = 45.75, R(1, 4, 9)) = $R(\tilde{C}_{24})$ = 4.5,

R(9, 36, 49) = $R(\tilde{C}_{25})$ = 32.5, R(16, 36, 49) = $R(\tilde{C}_{31})$ = 34.25, R(4, 49, 81) = $R(\tilde{C}_{32})$ = 45.75,
R(4, 25, 81) = $R(\tilde{C}_{35})$ = 33.75, R(4, 9, 16) = $R(\tilde{C}_{41})$ = 9.5, R(1, 4, 9) = $R(\tilde{C}_{42})$ = 4.5,
R((4, 49, 64) = $R(\tilde{C}_{51})$ = 41.5, R(9, 36, 49) = $R(\tilde{C}_{52})$ = 32.5, R(4, 25, 81) = $R(\tilde{C}_{53})$ = 33.75.

Defuzzifying the triangular fuzzy numbers by using Yager's ranking technique, we have;

Table 2. Defuzzifying by Yager's ranking technique

Nodes	1	2	3	4	5
1	-	32.5	34.25	9.5	41.5
2	32.5	-	45.75	4.5	32.5
3	34.25	45.75	-	-	33.75
4	9.5	4.5	-	-	-
5	41.5	32.5	33.75	-	-

According to the crisp values obtained using the Robust's Ranking Method, the problem was solved and the optimal route and duration were found in GAMS Program. The fuzzy optimum route obtained is R = 1–4–2–5–3–2–1–3–5–1 and the value of fuzzy objective function Min $\tilde{z}$ =268.

CONCLUSION

In this study, an FCPP whose objective function coefficients are triangular fuzzy numbers is discussed. Since the arrival time between the two vertices is not constant in real life problems due to various reasons (such as weather conditions, traffic density, traffic accidents, construction and repair works), fuzzy times are used instead of distance in the objective function. The triangular fuzzy numbers were clarified by Robust's Ranking Method to obtain crisp values. According to the obtained values, CPP was solved in GAMS Program and optimum route and time were found. When the related literature is examined, it is seen that no study has been conducted on FCPP before. Considering the large amounts of money spent annually for routing problems and wastes due to wrong planning, the importance of studies in this field is seen.

RECOMMENDATIONS

In future studies, triangular fuzzy numbers can be defuzzificated with different defuzzification methods and the results obtained can be compared. Moreover, the problem may be solved using trapezoidal fuzzy numbers in objective function coefficients and different techniques to defuzzificate them. Moreover, different types of CPP may be fuzzificated and applied to real-life problems.

REFERENCES

Ahuja, R. K., Magnanti, T. L., & Flows, J. O. N. (1993). Theory, algorithms, and applications. In *Network flows*.

Botzheim, J., Földesi, P., & Kóczy, L. T. (2009, July). Solution for Fuzzy Road Transport Traveling Salesman Problem Using Eugenic Bacterial Memetic Algorithm. In *IFSA/EUSFLAT Conf.* (pp. 1667-1672).

Chen, C. T., Lin, C. T., & Huang, S. F. (2006). A fuzzy approach for supplier evaluation and selection in supply chain management. *International journal of production economics*, *102*(2), 289-301.

Crisan, G. C., & Nechita, E. (2008). Solving fuzzy TSP with ant algorithms. *International Journal of Computers, Communications and Control*, *3*, 228-231.

Dhanasekar, S., Hariharan, S., & Sekar, P. (2013). Classical Travelling Salesman Problem (TSP) based Approach to Solve Fuzzy TSP using Yager's Ranking. *International Journal of Computer Applications*, *975*, 8887.

Dingar, D. S., & Sundari, K. T. (2014). Neighboring Optimal Solution for Fuzzy Travelling Salesman Problem. *International Journal of Engineering Research and General Science*, *2*(4).

Eiselt, H. A., Gendreau, M., & Laporte, G. (1995). Arc routing problems, part I: The Chinese postman problem. *Operations Research*, *43*(2), 231-242.

Emel, G. G., Taşkın, Ç., & Dinç, E. (2003). Yönsüz Çinli Postacı Problemi: Polis Devriye Araçları İçin Bir Uygulama.

Giri, P. K., Maiti, M. K., & Maiti, M. (2015). Fully fuzzy fixed charge multi-item solid transportation problem. *Applied Soft Computing*, *27*, 77-91.

Kumar, A., & Gupta, A. (2012). Assignment and travelling salesman problems with coefficients as LR fuzzy parameters. *International Journal of applied science and engineering*, *10*(3), 155-170.

Memmedova, N., & Keskin, İ. (2009). Hayvancılıkta Bulanık Mantık Uygulamaları (Derleme). *Selcuk Journal of Agriculture and Food Sciences*, *23*(47), 89-95.

Nagarajan, R., & Solairaju, A. (2010). Computing improved fuzzy optimal Hungarian assignment problems with fuzzy costs under robust ranking techniques. *International Journal of Computer Applications*, *6*(4), 6-13.

Özkan, M. M. (2003). *Bulanık hedef programlama*. Ekin Kitabevi.

Prabha, S. K., & Vimala, S. (2016). Implementation of BCM for Solving the Fuzzy Assignment Problem with Various Ranking Techniques. *Asian Research Journal of Mathematics*, *1*(2), 1-11.

Srinivasan, A., & Geetharamani, G. (2013). Method for solving fuzzy assignment problem. *Applied Mathematical Sciences*, *7*(113), 5607-5619.

Thimbleby, H. (2003). Explaining code for publication. *Software: Practice and Experience*, *33*(10), 975-1001.

Yager, R. R. (1979, January). Ranking fuzzy subsets over the unit interval. In *1978 IEEE conference on decision and control including the 17th symposium on adaptive processes* (pp. 1435-1437). IEEE.

Yahya Mohammed, S., & Divya, M. (2016). Solving fuzzy travelling salesman problem using octagon fuzzy numbers with α-cut and ranking technique. *IOSR journal of mahthematics*, 12(6), 52-56.

Yılmaz, M., Çodur, M. K., & Yılmaz, H. (2017). Chinese postman problem approach for a large-scale conventional rail network in Turkey. *Tehnički vjesnik*, *24*(5), 1471-1477.

DEVELOPMENT OF SCADA SYSTEM FOR AN INDUSTRIAL NATURAL GAS COMPRESSOR STATION

Orhan OKAY
Kahramanmaraş Sütçü İmam Üniversitesi Elektrik-Elektronik Mühendisliği Bölümü
okayorhan02@gmail.com

Ö.Fatih KEÇECİOĞLU
Kahramanmaraş Sütçü İmam Üniversitesi Elektrik-Elektronik Mühendisliği Bölümü
fkececioglu@ksu.edu.tr

Ahmet GANİ
Kahramanmaraş Sütçü İmam Üniversitesi Elektrik-Elektronik Mühendisliği Bölümü
agani@ksu.edu.tr

ABSTRACT: In this study, an industrial natural gas compressor station was connected to SCADA (Supervisory Control and Data Acquisition) system and its automation was realized. With the SCADA system, the parameters of an industrial natural gas compressor station can be remotely controlled to prevent possible failures. In the event of a malfunction in the system, the system automatically stops or warns the operator with warning lamps. In this study, critical parameters for an industrial natural gas compressor station can be monitored continuously and interventions can be intervened remotely. With the SCADA system developed for an industrial natural gas compressor station, the facility was controlled and managed with a small number of technical personnel by intervening the failures in the facility without wasting time. With the developed SCADA system, human errors are minimized so that possible work accidents are minimized and the facility is operated safely.

Keywords: Industrial Natural Gas Compressor, SCADA

ENDÜSTRİYEL BİR DOĞAL GAZ KOMPRESÖR İSTASYONU İÇİN SCADA SİSTEMİNİN GELİŞTİRİLMESİ

ÖZET: Bu çalışmada, endüstriyel bir doğal gaz kompresör istasyonu SCADA (Supervisory Control and Data Acquisition: Denetleme Kontrol ve Veri Toplama) sistemi ile irtibanlandırılarak otomasyonu gerçekleştirilmiştir. SCADA sistemi ile endüstriyel bir

doğal gaz kompresör istasyonu'nun parametrelerinin, uzaktan kumanda edilmesi sağlanarak olası arızalar gerçekleşmeden önlenebilmektedir. Sistemde arıza oluşması durumunda ise sistem ya otomatik olarak duruşa geçmekte ya da operatörü ikaz lambaları ile uyarmaktadır. Bu çalışmada endüstriyel bir doğal gaz kompresör istasyonu için kritik öneme sahip parametreler sürekli izlenerek, meydana gelebilecek arızalara uzaktan müdahale edilebilmektedir. Endüstriyel bir doğal gaz kompresör istasyonu için geliştirilen SCADA sistemi ile birlikte, tesiste oluşabilecek arızalara zaman kaybedilmeden müdahale edilerek, az sayıda teknik personel ile işletme kontrol edilmiş ve yönetilmiştir. Geliştirilen SCADA sistemi ile insan hataları en aza indirgenmekte böylelikle oluşabilecek iş kazaları da minimuma indirilerek, tesisin güvenli işletilmesi sağlanmaktadır.

Anahtar sözcükler: Endüstriyel Doğal Gaz Kompresörü, SCADA

1. GİRİŞ

Günümüzde hızla gelişen teknolojinin ilerlemesi, fiziksel iş gücünün küçülmesi yeni yöntem ve modellerini ortaya çıkarmaktadır. Bu yöntem ve modeller bilginin öne çıktığı iletişim çağı 21. yüzyılın ürünü olan ve artık birçok sektörün vazgeçemediği SCADA (Supervisory Control and Data Acquisition) sistemleri, işlevselliğini kanıtlamış, güven duyulan ve bu sebeple günümüzde oldukça yaygın hale gelmiş ve teknolojik açıdan büyük mesafeler kat etmiştir (Kul,2009 ; Özkara,2009). SCADA yazılım ürünleri endüstriyel işletmelerde sistemsel bir alt yapı görevini üstlenerek, işletme içerisi ile dışarısına ait ağlara bağlanarak işletmenin tüm segmentlerinde uyum içerisinde çalışmasına olanak sağlamaktadır. Endüstriyel otomasyon sistemleri tasarım açısından üç bölüm altında incelenebilir. Endüstriyel kumanda sistemleri, geribeslemeli kontrol sistemleri ve veri iletişim sistemleri. Endüstriyel kumanda sistemleri, en küçük üretim birimlerinin çalışma koşullarını (devreye girme ve devreden çıkma) düzenleyen lojik temelli sistemlerdir. Geribeslemeli kontrol sistemleri, çeşitli üretim süreçlerinin her türlü bozucu etkiye karşı, sürecin istenen değerlerde çalışmasını sağlayan sistemlerdir. Veri iletişim sistemleri ise birimler arasında bilginin güvenilir ve hızlı akışını sağlayan donanım ve yazılım sistemleri olup bu amaçla günümüzde yaygın olarak SCADA yazılımları kullanılır (Kurtulan,1999). SCADA, işletme içerisindeki bütün personele reel zamanlı ve ayrıntılı bilgiye diledikleri zaman erişebilme imkânı sağlamaktadır. Bu çalışmada, SCADA sistemi geliştirilerek endüstriyel bir doğal gaz kompresör istasyonu'ndan en verimli şekilde yararlanılması hedeflenmektedir.

2. ENDÜSTRİYEL BİR DOĞAL GAZ KOMPRESÖR İSTASYONU

Endüstriyel bir doğal gaz kompresör istasyonu, boru hattı içinde taşınan doğal gazın taşınması sırasında uzak mesafeler sebebiyle ve özellikle kış aylarında doğal gaza artan

talebe göre düşen boru hattı basıncını tekrar belirli bir basınç değerine çıkararak, boru hattının doğal gaz taşıma kapasitesini artırmak dolayısıyla doğal gaz arzını karşılamak amacıyla kurulan endüstriyel tesislerdir. Endüstriyel bir doğal gaz kompresör istasyonu 7 ana bölümden oluşmaktadır.

Endüstriyel bir doğal gaz kompresör istasyonu bölümleri;

İstasyon Giriş ve Çıkış, Pig Alma ve Atma İstasyonu, Bypass Sistemi

Filtreleme Sistemi

Gaz Sıkıştırma (Türbin ve Kompresör Grubu) Sistemi

Gaz Soğutma Sistemi

Tahliye (Relief, Blowdown) ve Recycle (Geri Çevrim) Sistemi

Ölçüm Sistemi

Yardımcı Tesisler (Yakıt gazı ve Yardımcı ekipmanlar Gaz Skidleri, Hava Kompresörleri, Isı Merkezi ve Jeneratörler) Sistemi

Endüstriyel bir doğal gaz kompresör istasyonu'nun daha iyi anlaşılabilmesi için 7 ana bölümü detaylı olarak incelenecektir.

Şekil 1. Endüstriyel Bir Doğal Gaz Kompresör İstasyonu'nu Genel Görünümü

2.1.İstasyon Giriş ve Çıkış, Pig Alma ve Atma Istasyonu, Bypass Sistemi

Şekil 2. İstasyon Giriş ve Çıkış, Pig Alma ve Atma İstasyonu, Bypass Sistemi

Ana iletim boru hattı içinden gelen doğal gaz, istasyon giriş vanasından geçerek istasyona giriş yapar. İstasyona giriş yaptıktan sonra filtrelerde (siklon ve separatör) temizliği yapılan, türbin ve kompresör grubunda sıkıştırılan, gaz soğutma sisteminde soğutuculardaki soğutulan ve son olarak ölçümü yapılan doğal gaz, istasyon çıkış vanasından geçerek ana iletim boru hattına verilir. Pig alma /atma istasyonları boru hattı temizliği ve boru hattında hasar tespiti için kurulan istasyonlardır. Pig alma/atma istasyonları içerisinde ana iletim boru hattından gelen veya ana iletim boru hattına verilecek olan piglerin yerleştirilmesi için pig kovanları bulunmakta ve normal şartlarda gaz basıncı olmaması gerekmektedir. Her bir pig kovanı üzerinde ayrıca gaz basıncını okumak için mekanik manometre, pig atıldığında gelen pigi haber veren pig alındı sinyal anahtarı, pig kovanı içerisindeki fazla basıncın otomatik olarak tahliyesi için PSV (Pressure Safety Valve;Basınç Emniyet Vanası) ve pig kovanı içerisindeki gazın tahliyesi için drain (boşaltım) ve vent (tahliye) vanaları bulunmaktadır. İstasyon bypass sistemi, istasyon bypass vanasından, bu vananın bypass hattı üzerindeki iki adet kontrol vanasından, iki adet basınç transmitterinden, aynı vana üzerindeki fark basınç anahtarından ve mekanik manometrelerinden oluşur. İstasyon çalışırken bypass vanası kapalı durumdadır. Ancak istasyonda kritik arıza durumlarında veya istasyonun çalışmasına ihtiyaç duyulmadığı dönemlerde, istasyon giriş ve çıkış vanaları otomatik/manuel kapatılarak, bypass vanası otomatik/manuel açılarak,ana iletim boru hattı içerisindeki doğal gaz sevkiyatı bypass sistemi üzerinden devam eder. İstasyon doğal gazdan izole edilmiş olur.

2.2. Filtreleme Sistemi

Şekil 3. Filtreleme Sistemi (Siklon ve Ayırıcı-Separatör Filtreleri)

İstasyona, ana iletim boru hattı içerinden gelen doğal gazda bulunabilecek katı ve sıvı partikülleri temizlemek amacıyla genellikle siklon ve seperator (ayırıcı) olmak üzere istasyonda iki kademe filtreleme sistemi bulunmaktadır. İlk kademe siklon filtrelerdir. Bu kademe yerçekimi prensibine göre çalışan dikey siklon tipi filtrelerdir. Bu filtreler yoğunluk farkına göre gazın içindeki pislikleri ayırır ve doğal gaz buradan ikinci kademe filtresi olan ayırıcı kısmına gönderilir. Ayırıcı kısmında ise kovan içinde dizayn değerlerine göre belirli miktarda kartuş vardır. Doğal gaz bu kartuşların içerisinden geçerek filtrelenmiş olur ve basınçlandırılmak üzere türbin/kompresör grubuna gönderilir. Bu kartuşlar genel olarak 3 μm'den büyük partükülleri % 99,8 oranında temizleme kabiliyetine sahiptir.

2.3. Gaz Sıkıştırma (Türbin ve Kompresör Grubu) Sistemi

Şekil 4. Gaz Türbini /Gaz Kompresörü

Türbin ve kompresör grubu istasyonun ana ekipmanıdır. Doğal gazın sıkıştırılarak transfer edildiği gaz kompresörü ve gaz kompresörünün tahrik elemanı olarak kullanılan gaz türbinleri ve bunların yardımcı donanımlarından oluşur.

2.3.1 Gaz Kompresörü

İstasyonda bulunan gaz kompresörlerinin görevi; gazın hacminin indirgenmesi yolu ile gazın basıncını yükseltmektir. Kompresörde gazın hacminin düşürülmesi yani sıkıştırılmasının sonucu olarak gazın basıncı yükselir ve bu basınç artışı gazın başka bir yere aktarılmasını mümkün kılar. Gaz kompresöründeki gazın sıkıştırılması termodinamik bir olaydır. Gazın sıkıştırılması sonucu basınç ve hacimdeki değişim ile gaz enerjilendirilmiş olur. Tipik olarak kompresör istasyonlarında kullanılan kompresörler santrifüj tip olmakla birlikte uygulama alanlarına göre farklı tipte kompresörler bulunmaktadır.

2.3.2 Gaz Türbini

Gaz türbini; yanma ile açığa çıkan ısı enerjisini mekanik enerjiye çevirmeye yarayan bir makinedir. Gaz türbini temelde ısı enerjisinin termodinamik çevrimlerle mekanik enerjiye dönüştürüldüğü bir motordur. Isı enerjisinin mekanik enerjiye dönüştürülmesi Brayton çevrimi olarak bilinen, termodinamik süreçten oluşan çevrim yolu ile olur. Bunlar;

- Sıkıştırma: Atmosferik hava burada sıkıştırılır. Sıkıştırılan hava yakıtla karıştırıldığı yanma odasına akar.

- Yanma: Sıkıştırılan havaya yakıt (doğal gaz) püskürtülerek ateşlenir ve yanma gerçekleşir. Türbin çalıştığı süre boyunca yanma sürekli devam eder.
- Genişleme: Yanma odasında üretilen sıcak gaz hızla genleşir ve gazın basıncı sabit kalırken, gaz hacmi ve akış hızı büyük ölçüde artar. İçinde gazın genleştiği, ısısının, hızının ve basınç enerjisinin büyük kısmını gaz jeneratörü ve güç türbini rotorlarını döndürmek için kullanır. Böylece, genişleyen gaz türbin rotor kanatlarının içinden geçerken mekanik enerji üretilir.
- Egzoz: Genişleyen yanma gazı (hava ve yanan gazlar) atmosfere verilir.

Bu çalışmada endüstriyel bir doğal gaz kompresör istasyonu için çift şaftlı endüstriyel tip gaz türbini anlatılmaktadır. İstasyonda gaz türbini gazın sıkıştırıldığı gaz kompresörü için sürücü olarak kullanılır. Gaz türbinine start, gaz basıncıyla çalışan motor veya elektrikli motor ile verilir. Atmosferden filtrelenerek temin edilen hava, belirli kademeli aksiyel akışlı türbin kompresöründen geçerek sıkışır ve hava türbin grubu üzerinde dairesel olarak bulunan dizayna göre belirli adette yanma odasına püskürtülür. Yakıt gazı istasyon ana iletim hattından temin edilen türbin dizayn değerlerine ayarlanan belirli bir basınçtaki doğal gaz ile atmosferik hava, yanma odasında dizayna göre belirli adette elektrikli manyeto ile yakılarak ısı enejisi elde edilir. Yanma ile ortaya çıkan enerji yine sıkıştırılarak gaz türbininin sabit kanatçıklarından püskürtülerek hareketli kanatçığı çevirir. Böylece yanma ile ortaya çıkan enerji, kanatçıkların döndürülmesiyle mekanik enerjiye dönüşmüş olur. Bu enerji, starter motoru ile dönen şafta hareket verir. Sıcak gaz, önce dizayna ve kullanılan marka-model türbine göre değişkenlik gösteren (devir/dakika) hızla dönen gaz jeneratörünü, daha sonra arada bir bağlantı olmaksızın iki kademeli, güç türbinini çevirir. Güç türbini, bir şaftla, gaz kompresör kısmına bağlıdır. Kompresöre iletilen güç, ana hattan gelen gazı sıkıştırmada kullanılır. Böylelikle ana hattan alınan gaz talep edilen basınca ve akışa göre ayarlanarak gaz iletimi sağlanmış olur.

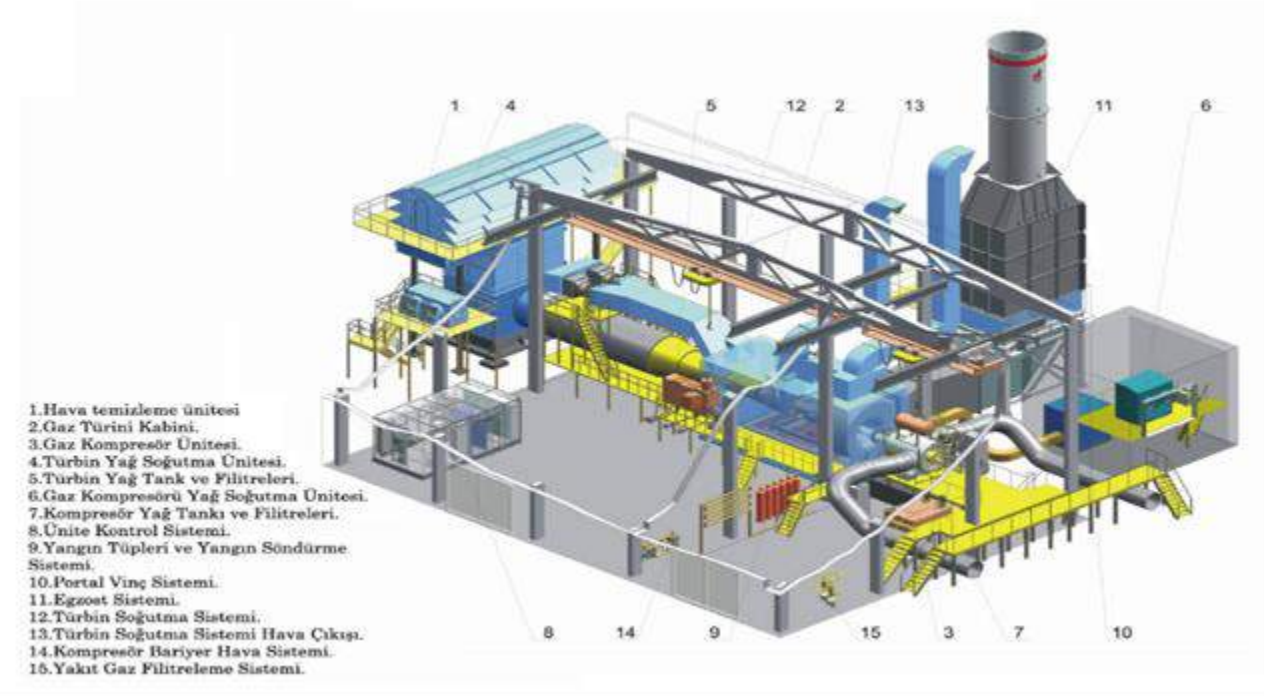

Şekil 5. Türbin-Kompresör Paketi

2.4. Gaz Soğutma Sistemi

Şekil 6. Gaz Soğutma Sistemi

Bilindiği üzere sıkışan gazlar ısınır, gaz kompresöründen sıkışmış olarak çıkan gazın sıcaklığı, giriş gazı sıcaklığına göre oldukça yüksektir. Sıcak gazın ana hatta verilmesi durumunda, sıcak gazın soğuk gaza göre fazla yer kaplamasından dolayı boru hattı taşıma performansı düşecektir. Bu sebeple, boru hattındaki gazın sıcaklığının yüksek

olması talep edilmez. Bunun için istasyonda, kompresör üniteleri çıkışında gaz soğutma sistemi mevcuttur.

2.5. Tahliye ve Geri Çevrim Sistemi

Tahliye ve geri çevrim sistemleri tamamıyla istasyon güvenliği için kurulmuş ekipmanlardır. İstasyonda,bulunan tahliye vanaları, altlarındaki manuel izolasyon vanalarından ve ana tahliye vanalarından oluşur. Tamamıyla mekanik şekilde çalışan tahliye vanaları, gaz soğutucu sonrasında sıkıştırılmış olan doğal gaz basıncı, tahliye vanalarda ayarlanan basınç (bar) değerini aştığı durumlarda tahliye vanaları otomatik olarak açar ve istasyonun mekanik güvenliği açısından yüksek basınçlı doğal gazı atmosfere vererek istasyonu boşaltır. Normal durumlarda tahliye vanası altındaki manuel vanalar açık tutulur. İstasyonda bulunan tahliye vanaları da yine istasyon güvenliği açısından, istasyon içini boşaltmak amacıyla, istasyon kontrol sistemi tarafından otomatik olarak açılan vanalardır. Bu vana sistemleri de aynı şekilde altta manuel izolasyon vanaları ve üstte tahliye vanasından ve aktüatör grubundan oluşmaktadır. İstasyondaki geri çevrim vanası, özellikle kompresör üniteleri devreye alma-çıkarma ve kararsızlık durumlarında, türbin ve kompresör grubunu korumak amacıyla çıkış tarafındaki bir miktar gazın dolayısıyla basıncın istasyon giriş kısmına aktarılması maksadıyla kurulmuştur. Bu şekilde türbin ve kompresör grubu girişlerine yeteri kadar gaz temini sağlanarak büyük hasarlar verebilecek istenilmeyen durumlardan korunulmuş olunur. İstasyon geriçevrim vanası, istasyon kontrol sistemi tarafından otomatik kontrol edilebildiği gibi manuel olarak da kullanılabilir.

Şekil 7. Tahliye (Relief, Blowdown) Vanaları

Şekil 8. Geri Çevrim Vanası

2.6. Ölçüm Sistemi

İstasyonda, istasyon çıkış vanasından önce sevk edilen gazı ve türbin/kompresör grubununda yakılan gazı ölçmek için kurulan sistemlerdir. Ölçümde kullanılan ekipmanlar primer ekipmanlar ve sekonder ekipmanlar olarak 2'ye ayrılmaktadır. Primer ekipmanlar gazın geçiş hızı veya kütlesine göre temel şartlardaki hacmini

hesaplarken, sekonder ekipmanlar ise hesaplanan bu hacmin akışkan gazın basınç, sıcaklık ve gaz bileşen değerlerinin kullanılarak bilinen bir standarda dönüştürülmesini sağlamaktadır. Primer ve sekonder ekipmanlardan aldığı veriye göre, gazın anlık, saatlik ve günlük periyotlarda hacim, kütle, enerji vb. toplam miktar geçişini hesaplayan hacim dönüştürücü ekipman olan akış bilgisayarları(flow computer) sistemde önemli bir yer tutmaktadır.

Doğal Gaz Ölçüm Ekipmanları

Primer Ölçüm Ekipmanları ;
-Orifis Plakaları(orifice plates),
-Akış Nozulları (Flow Nozzles),
-Pilot Tüpleri (Pilot Tubes),
-Rotarimetreler ,
-Türbinmetreler (Turbine Meters),
-Ultrasonikmetreler (Ultrasonic Meters) vs.

Sekonder Ölçüm Ekipmanları ;
-Basınç Transmitteri ,
-Sıcaklık Transmitteri ,
-Gaz Kromatografı vb.

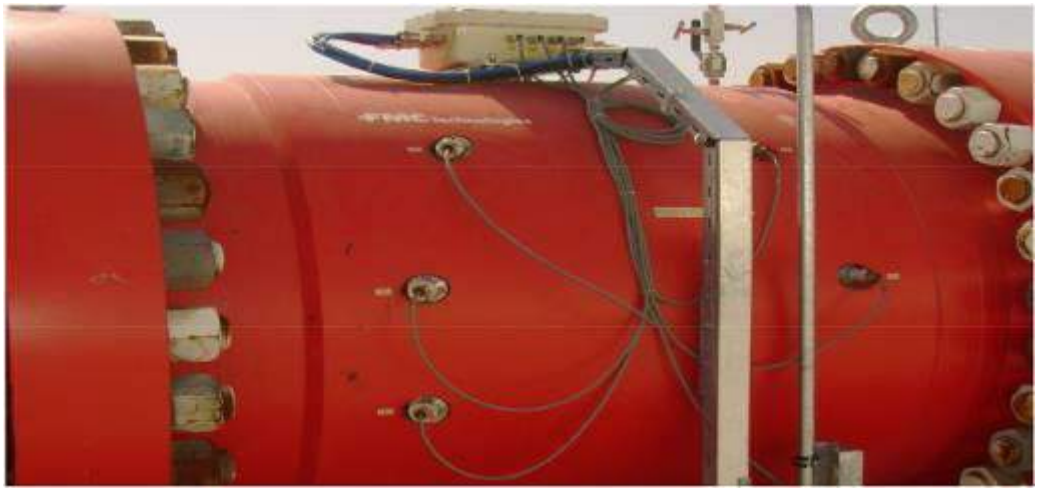

Şekil 9. Ultrasonikmetre

2.7. Yardımcı Tesisler (Yakıt Gazı ve Yardımcı Ekipmanlar Gaz Skidleri, Hava Kompresörleri, Isı Merkezi ve Jeneratörler) Sistemi

Endüstriyel doğal gaz kompresör istasyonlarında, türbin/kompresör grubuna yakıt gazı temin etmek amacıyla genellikle basınç düşürme istasyonu bulunmaktadır. Bu istasyon filtreleme sisteminden sonra aldığı gazı tekrar filtreler, ısıtır ve ayarlanan basınç değerine düşürür. Türbin/kompresör grubu yakıt gazı hattına ait ölçüm sisteminde ölçümü yapılan gaz türbin/kompresör grubuna gönderilir. İstasyonda, jeneratöre, kazan dairesine ve diğer binalara (kontrol binası, idari bina vb. gibi) yakıt gazı temin etmek maksadıyla genellikle bir basınç düşürme istasyonu daha bulunmaktadır. İstasyondaki bazı vanalar (Geriçevrim, Tahrik, Yakıt gazı vanaları vb.) hava aktüvatörlü olarak kullanılabilir. Bunlara hava temin etmek, türbin/kompresör grubu start ve duruşlarında yağlama yağı ile sızdırmazlık gazını ayırmak için tampon vazifesi gören havayı temin etmek, istasyonun çeşitli yerlerinde ekipman temizliğinde kullanılacak havayı temin etmek amacıyla hava kompresörleri bulunur. Üretilen havanın içindeki yağ, su vb. havalı sistemlere zarar verecek maddelerden ayırmak için hava kurutucu kullanılır. Genellikle hava kompresörlerden üretilen hava önce içindeki sıvılardan yoğunluk farkından dolayı ayrılmak üzere hava tankına, sonra da hava kurutucularından geçerek sisteme gönderilir. Bu tür istasyonların genellikle sürekli olarak çalışması veya çalışmaya hazır olması istendiğinden sisteme kesintisiz elektrik temin etmek amacıyla jeneratör kullanılır. Elektrik kesintilerinde ve dalgalanmalarında jenaratör istasyonu beslemektedir. Enerji kesilmelerinde jeneratörün devreye girip yükü üstlenmesine kadar geçen sürede sistemin enerjisiz kalmaması için sistemi belirli bir süre besleyebilecek kesintisiz güç kaynağı bulunmaktadır. İstasyonda genellikle, basınç düşürme sisteminde gazı ısıtmak, binalara ısınma amaçlı sıcak su temin etmek amacıyla kazan, pompa grupları ve ilgili diğer müştemilat kullanılır.

Şekil 10. Türbin Fuel Gaz Skidi

Şekil 11. Yardımcı Binalar Gaz Skid

Şekil 12.Hava Kompresörleri ve Hava Kurutucuları

3. SCADA

3.1. SCADA Tanımı ve Uygulama Alanları

SCADA ingilizceden dilimize katılan teknik bir terim olup açıklaması "Supervisory Control And Data Acquisition" kelimelerinin baş harflerinin birleşmesi ile oluşan bir kısaltmadır, Türkçe anlamı "Denetleme Kontrol ve Veri Toplama" anlamına gelmektedir. Bileşen sayısı çok fazla olan bir sistemin takibi, çalışmasının denetlenmesi, uzaktan veya manuel kontrol edilebilmesi ve sistemin optimizasyonu için gerekli verilerin toplanması için kurulan basit ve kolay sistemlerden karmaşık sistemlere kadar bu işi yapan sistemlere verilen ortak addır (Gaushell ve Darlington 1987). SCADA sistemi çok geniş bir kullanım alanına sahip olmasının yanı sıra artık gündelik hayatımızda çoğu yerde biz görmesek de karşımıza çıkmaktadır. Başlıca kullanım alanları arasında tehlikesi yüksek

iş sektörlerinden olan kimya endüstrisi, petrokimya endüstrisi, doğalgaz ve petrol boru hatlarında kullanılmakta, diğer yandan elektrik, su dağıtım sistemleri ve hatlarında da izleme ve takip yapılmaktadır.

3.2. SCADA Yapısı

SCADA sisteminin ana yapısını üç başlıkta toplayabiliriz. İlki uzaktan kontrol birimi dediğimiz veri toplama ve uç kontrol birimleridir. İkincisi bölgelerin birbiri ile etkileşim ve haberleşme yapabilmesi için bir iletişim sistemi olmalıdır. Üçüncüsü ise tüm uç noktaların toplandığı bir bilgisayar ile kontrolün sağlandığı, izlendiği ve yönetildiği kontrol merkez sistemidir(MTU). SCADA sistemini tasarlarken kurulacak yapıyı istediğiniz gibi hayal edebilirsiniz (Strauss,2003).

3.3. SCADA İşlevleri

SCADA sistemleri izleme, kontrol, veri analizi ile beraber raporlama ve kayıt yapabilmektedir. Bunun için sistemin bir veri tabanına bağlı olması gerekmektedir. Bu işlevlerin gerçekleşebilmesi için sistemdeki girdi ve çıktı bilgilerinin bir veri tabanında tanımlanması gerekir. Bu bilgiler sistemde bulunan yazılım sayesinde bir takım alarm ve sınırlamalar ile değişkenlerin kontrolünü ve izlenmesini sağlamaktadır. Bu kontrol sayesinde örneğin bir proseste katkı madde miktarını görülmesi ile prosesteki ürünün kalitesi hakkında bilgi alabilir veya üretilen malzeme miktarı ile üretim verimliliği hakkında da bilgi sahibi olunabilmektedir. Bütün bunlarla beraber olarak üretim hattındaki bir makine veya motor durumu hakkında bilgide sağlanarak bakım-onarım amaçlı bilgilerde edinilebilmektedir. SCADA sisteminin kuruluşu amacı ile sistemde nelerin takibi ve kontrolü sağlanmak istenmişse an ve an istenilen talebin kontrolü durumu izlenebilmektedir. Tüm prosese ait bütün istatistikleri görülebilmesi ile mevcut sistemde iyileştirme yapmaya da olanak sağlamaktadır (Karataş,2018).

Şekil 13. SCADA Organizasyon Şeması

3.4. SCADA Yapısı ve Temel Elemanları

3.4.1. Ana Terminal Birimi (MTU)

Ana Terminal Üniteleri SCADA sisteminde geniş bir alana yayılmış Uzak Terminal Birimlerinin koordineli çalışması, Uzak Terminal Birimlerinden gelen bilgilerin yorumlanması, kullanıcılara sunulması, ayrıca kullanıcıların isteklerini Uzak Terminal Birimlerine ileterek merkezi kumandanın sağlanması işlevlerine SCADA sisteminde merkezi sistem birimi yerine getirir. (Megep,2007).

Ana terminal ünitelerinin görevleri:

-Uzak terminal ünitelerinden gelen verilerin toplanması
-Toplanmış verilerin yazılım programları ile işlenerek ekrana veya yazıcıya gönderilmesi
-Sistemde kontrol edilecek cihazlara kontrol komutu gönderilmesi
-Belli olaylar karşısında alarm üretme ve gelen alarmları operatöre en hızlı şekilde iletme
-Meydana gelen olayları ve verileri zaman sırasına göre kaydetme
-Başka bilgisayar sistemleri ile iletişimde olma
-Dağıtım yönetim sistemi ve enerji yönetim sistemi gibi üst seviye uygulama programlarını çalıştırma
-Yazıcı, çizici, haberleşme birimleri gibi ek birimlerin kontrolü.

3.4.2. Uzak Terminal Birimi (RTU)

RTU (bazen uzak telemetri ünitesi olarak adlandırılır) başlıktan da anlaşıldığı gibi; monitör ve kontrol aletleri merkez istasyondan uzakta bulunan, genellikle, mikroişlemci

bazlı, kendi başına veri kazanımı ve kontrol ünitesidir. En önemli görevi; uzak noktalardaki işlem aletleriyle veri kazanımı ve kontrol sağlamak ve de bu verileri merkez istasyonuna transfer etmektir. Konfigurasyonunu ve kontrol programlarını, bazı merkez istasyonlardan etkin bir figürde yükleyebilme özelliğine sahiptir. Bunun dışında bazı RTU programlama ünitelerini, yerinde düzenleyebilme imkanı mümkündür. Genel olarak RTU bazı merkez istasyonlarla, geri iletişim kurmasına rağmen, diğer RTU'larla karşılıklı iletişim kurması da mümkündür. RTU, merkez istasyonlardan ulaşılamayan diğer RTU'lara, röle istasyon (bazen depolayıcı ve ileri istasyon olarak belirtilir) olarak da görev yapabilmektedir. (EMO,2012)

Uzak terminal biriminin görevleri;

-Bilgi toplama ve depolama
-Kontrol ve kumanda
-İzleme (monitoring)
-Arıza yeri tespiti ve izolasyonudur.

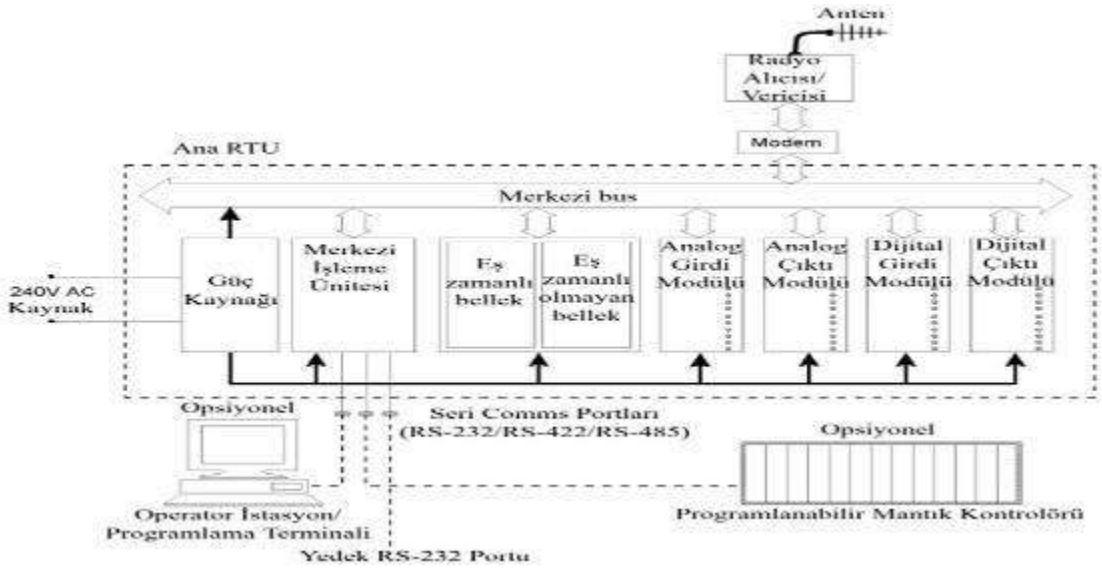

Şekil 14. RTU donanım yapısı

3.4.3. İletişim Ağlari ve Protokolleri

İletişim, bir noktadan başka bir noktaya, karşılıklı olarak, veri veya haberin gönderilmesi işlemidir. SCADA sisteminde sistemin işlemesi için iletişim hayati öneme sahiptir. SCADA sisteminde hız performansı tamamen iletişim ağı ile ilintilidir. SCADA sisteminde araçlar ve cihazların birbiri ile haberleşmesi kablolar vasıtası ile gerçekleşmektedir. Veri yolu bu kablolar üzerindeki iletken ile veya toprak dönüş hattı üzerinden gerçekleşmektedir. Dünya üzerinde çoğu sistem ve projede artık bir standart olan bir arabirim vardır. İletişimde kullanılan bu ara birimler RS-232 ve RS-485'tir.

3.4.4. Veri Toplama Üniteleri

Kontrol üniteleri SCADA sistemlerinin diğer önemli birimidir. Kontrol üniteleri kontrol odası seviyesinden çeşitli yardımcı işletmelerin kontrol ünitelerinden işletme ve yönetim seviyesine kadar tüm veri ve bilgileri yüksek hızlarda işleyecek bir yapıya sahiptir. Kontrol alt birimlerine, işletme ünitelerine, çalışma sahasına ait enstrumantasyon ve dedektörlere bağlanarak gerekli bilgi ve veri alış verişini sağlamaktadır.

3.4.5. Yazılım

Elektronik cihazlarda tanımlanmış bir işi veya değişik ve çeşitli görevler yapma amaçlı tasarlanmış elektronik aygıtların birbirleriyle haberleşebilmesini ve uyumunu sağlayarak görevlerini ya da kullanılabilirliklerini geliştirmeye yarayan makine komutlarıdır. Yazılım, elektronik aygıtların belirli bir işi yapmasını sağlayan programların tümüne verilen isimdir.

3.4.5. Merkez Kontrol Odası

SCADA sisteminin kurulu olduğu ve izleme yapıldığı alandır.Tesiste oluşabilecek arızaları veya tesisin kararlı olup olmadığı hakkında tüm bilgilerin görülebileceği ve aynı zamanda zaman kaybedilmeden müdahale edildiği yerdir.Bu oda genelde bilgisayarlar ve monitörlerden oluşmakta olup gerekmesi halinde terminaller, yazıcılar ve alarmlar ile desteklenebilirler.

4. ENDÜSTRİYEL BİR DOĞAL KOMPRESÖR İSTASYONU İÇİN SCADA GELİŞTİRİLMESİ

Bu çalışmada endüstriyel bir doğal gaz kompresör istasyonunun sistem otomasyonu için kullanılan SCADA yazılımı Emerson firmasına ait DeltaV yazılımıdır. DeltaV yazılım uygulamaları DeltaV Explorer ve Kontrol Studiodur. Exploring DeltaV sistem yapılanmasını görmek ve düzenlemek için kullanılır. Control Studio'da ise kontrol algoritmaları ve blokları yer almaktadır. SCADA donanımı olarakta Delta V MD(RTU) serisi kontrolür kullanılmaktadır.

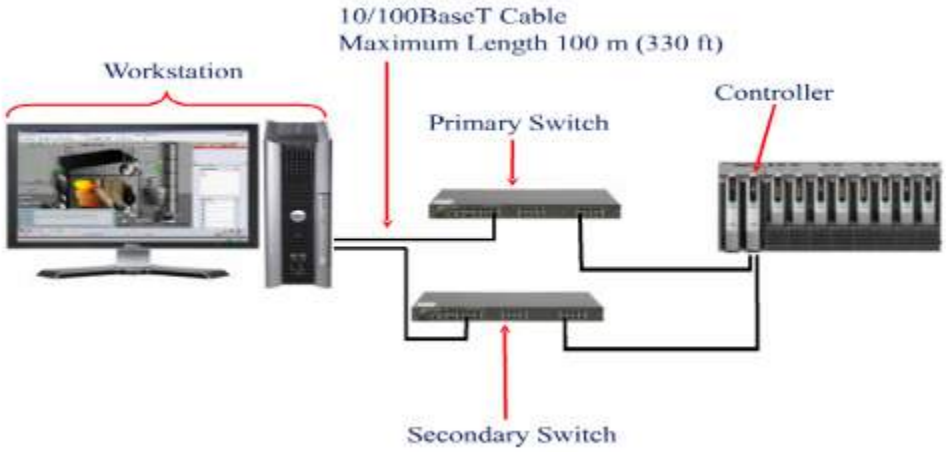

Şekil 15 . Delta V Sistem yapısı

Şekil 16 . Delta V M serisi kontrolör

Şekil 17 . RTU paneli I/O kartlar (Delta V M serisi kontrolör)

Endüstriyel Bir Doğal Gaz Kompresör İstasyonu'da SCADA Sistemi ile haberleşen 3.Parti Ekipmanlar ;

Ünite Kontrol Panelleri: Sadece Türbin/Kompresör sistemini kontrol eden panellerdir. İçerisinde SIEMENS marka S-7 400 PLC'ler kullanılmaktadır.Ünite Kontrol Panelleri Türbin/Kompresör sistem sahasından gelen verileri MODBUS RS-485 haberleşme ile SCADA'ya aktarmaktadırlar.

Flow computer (Akış Bilgisayarı): Akış Bilgisayarı, gaz ölçümünde kullanılacak cihazlar olup, gaz hatlarına bağlı sayaç, transmitter ve gaz kromatograf gibi ekipmanlardan alınan verilerin işlenmesi ve gazın enerji değerlerine çevrilmesinde ve bu değerlerin saklanmasında kullanılır. SCADA sistemi ile Modbus RS-485 ile haberleşmektedir.

Gaz kromatografı: Gaz kromatograf cihazı doğal gaz içindeki bileşenleri ayırarak analiz etmek üzere konfigüre edilmiş cihazdır. Gaz analizi C_1' den C_6+' ya kadar karbon bileşenleri ile N_2 ve CO_2' yi kapsar. SCADA sistemi ile Modbus RS-485 ile haberleşmektedir.

Gaz Algılama Paneli: Endüstriyel bir doğal gaz kompresör istasyonu'nda kapalı alanlarda doğal gaz boru hattında gaz kaçağı kontrolü gaz dedektörleri ile yapılmaktadır.Gaz dedektörleri tipik olarak besleme voltajı 24 V_{DC} olup çıkış akımı 4-20 mA'dir.Gaz algılama paneli gaz dedektörlerinden (sahadan) almış olduğu bilgiyi MODBUS RS-485 ile SCADA'ya aktarmaktadır.

Endüstriyel Bir Doğal Gaz Kompresör İstasyonun'da Tipik olarak bulunan Enstrümanlar;

-Basınç, Sıcaklık, Seviye, Fark basınç vb. Transmitterları (Analog girişler) tipik olarak 24 V_{DC} besleme voltajı ile çalışmakta olup çıkış olarak 4-20 mA üretmektedirler.

-Seviye, Basınç, Sıcaklık, Pozisyon vb. Anahtarlar (Dijital girişler) tipik olarak kuru kontak veya 24 V_{DC} enerjili kontak olarak çalışmaktadırlar.

-Vanalar ;Küresel ,Plug ,Akış oransal vb. vanalar.

- Hız problar , vibrasyon probları da kompresör istasyonunda kullanılan enstrumanlar arasında yer almaktadır.

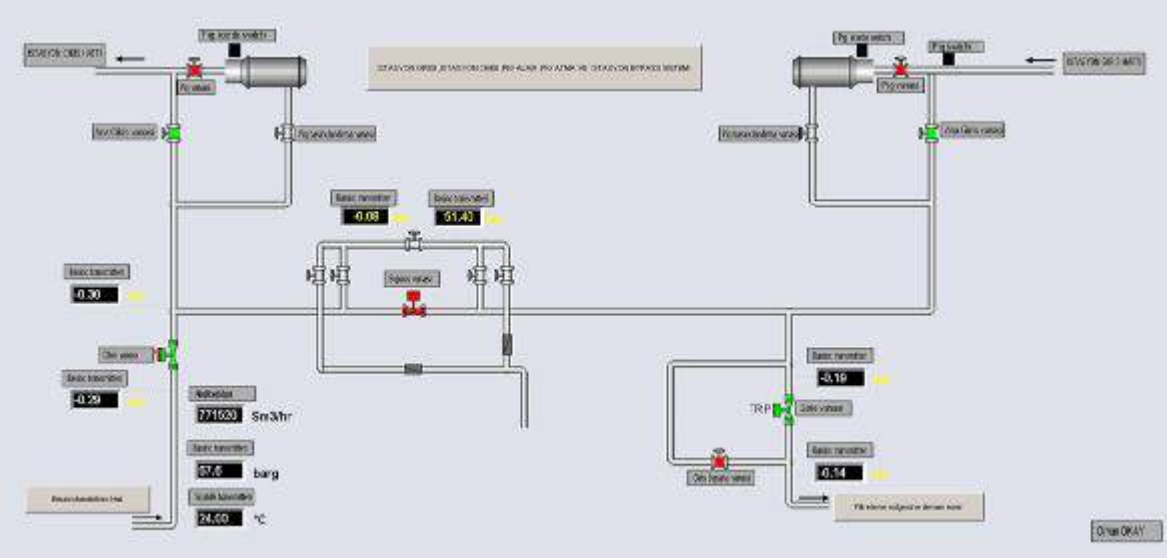

Şekil 18 . SCADA İstasyon Giriş ve Çıkış, Pig Alma ve Atma İstasyonu, Bypass Sistemi Görünümü

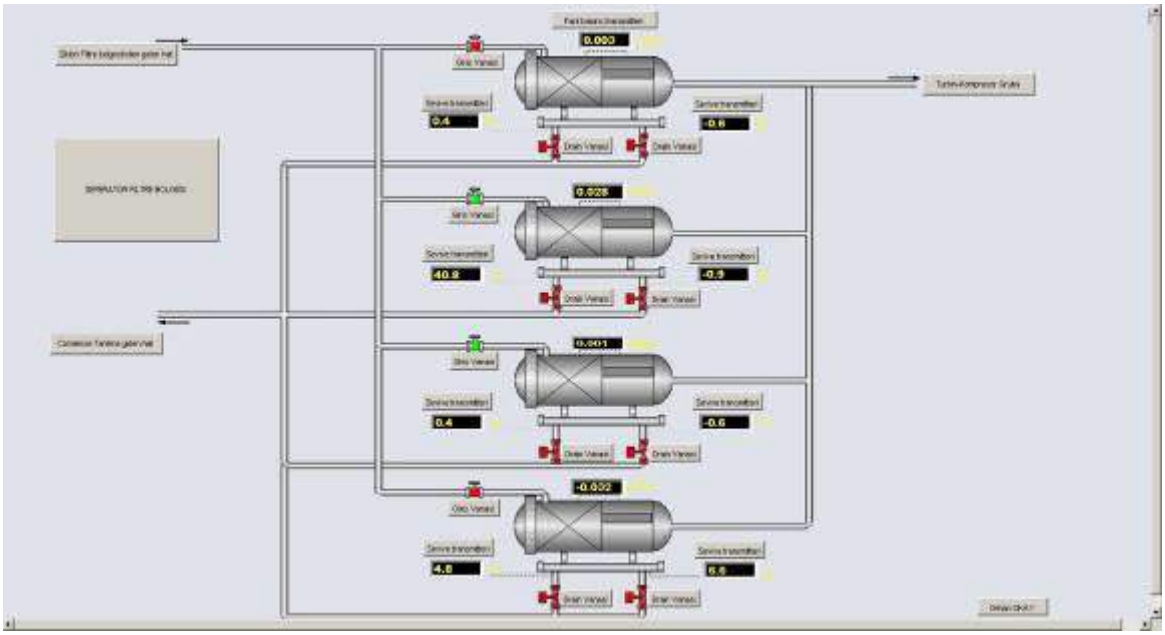

Şekil 19. SCADA İstasyon Filtreleme Sistemi Görünümü

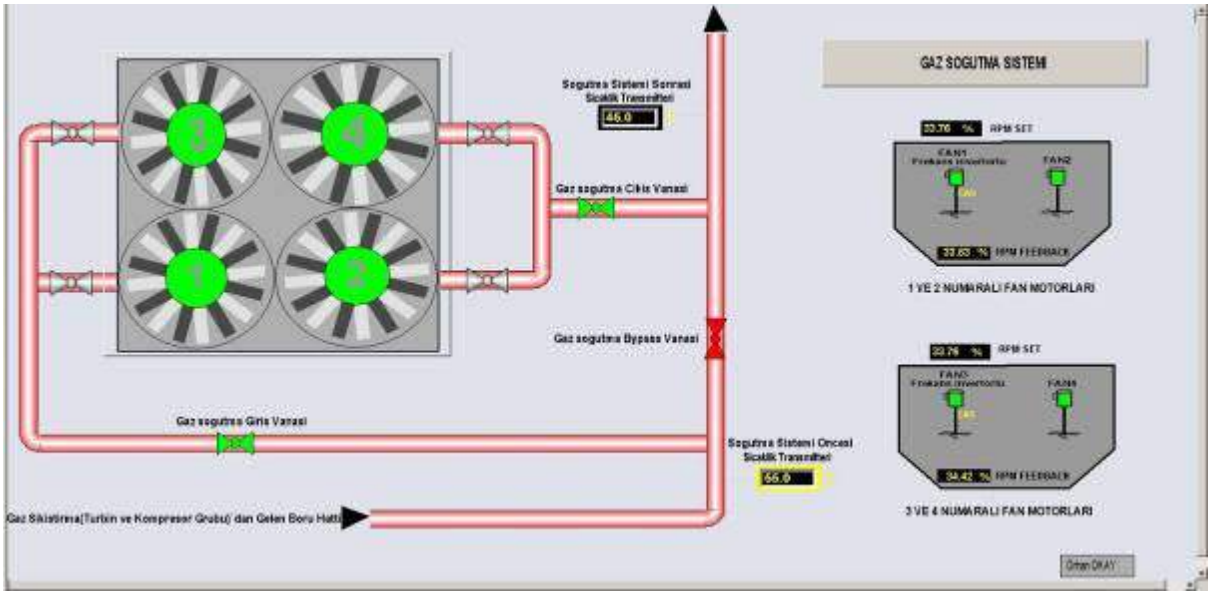

Şekil 20. SCADA Gaz Soğutma Sistemi Görünümü

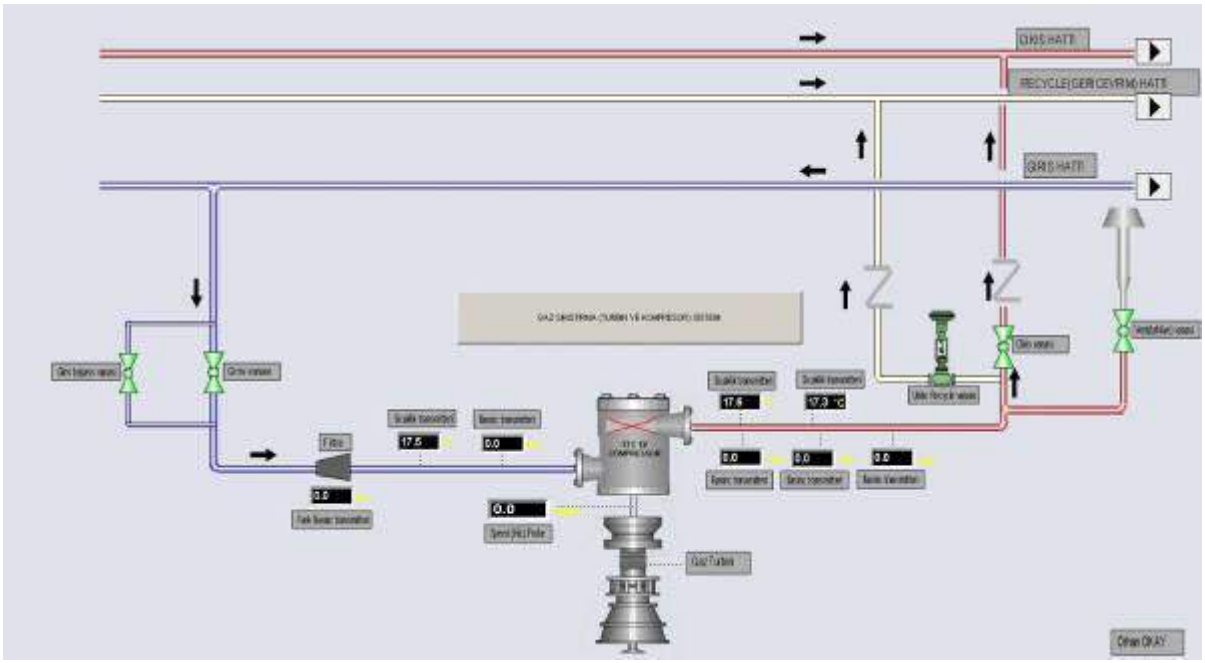

Şekil 21. SCADA Türbin Kompresör Grubu Görünümü

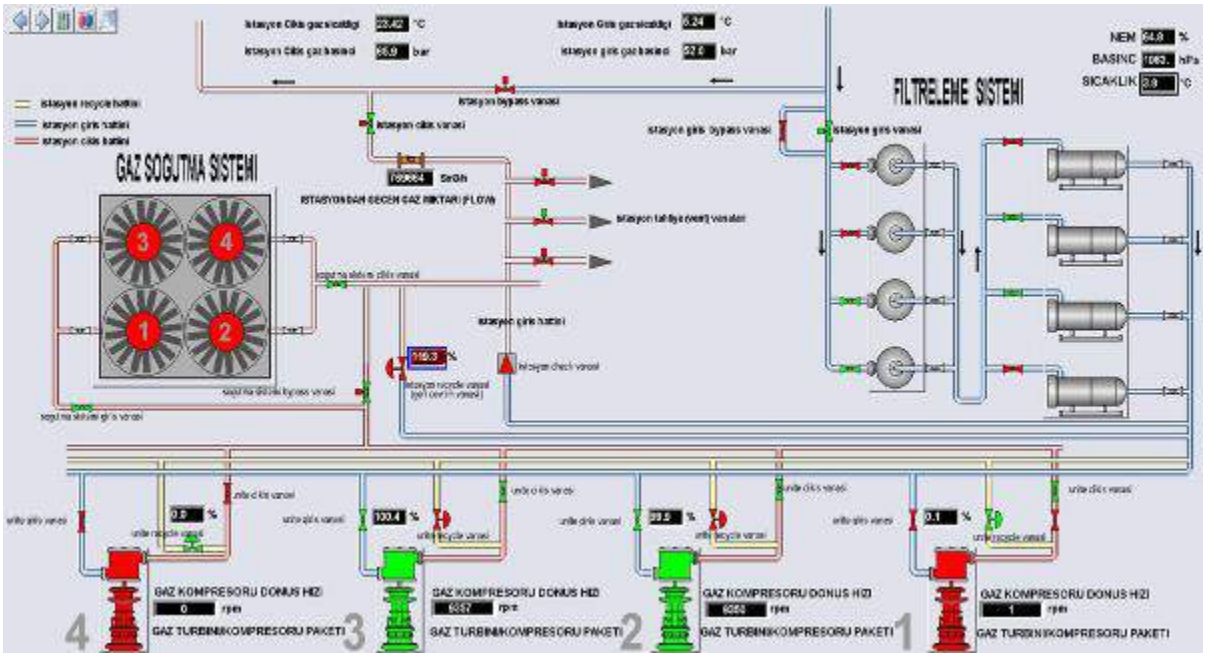

Şekil 22 . SCADA Ana Ekran Görünümü

5. SONUÇLAR

Bu çalışmada endüstriyel bir doğal gaz kompresör istasyonu için kritik öneme sahip parametreler (basınç, sıcaklık, seviye, hız ,vibrasyon vs. değerleri) sürekli izlenebildiğinden kontrol altında tutularak , meydana gelebilecek olası arızalara zaman kaybetmeden müdahale edilmeye imkan sağlanmıştır. Böylelikle tehlikesi yüksek tesis sınıfında yer alan endüstriyel bir doğal kompresör istasyonu için geliştirilen SCADA sistemi ile insan hataları en aza indirgenmekte ve oluşabilecek iş kazaları da minumuma indirilerek az sayıda teknik personel ile kontrol edilip yönetilmiştir. Geliştirilen SCADA sistemi tesisin verimli ve güvenli işletilmesine olanak sağlamıştır.

6. KAYNAKLAR

Gaushell, D.J. Darlington, H.T. (1987) "Supervisory Control and Data Acquisition", Proceeding of IEEE

Elektrik Mühendisleri Odası, (2012) Kontrol Sistemleri-SCADA.

Karataş, M,Y.,(2018) "388 Adet 110 KVA Dizel Jeneratör Grubunda SCADA Uygulamaları ve Analizi", Yüksek Lisans Tezi, İstanbul Aydın Üniversitesi Fen Bilimleri Enstitüsü, İstanbul.

Kul, N., **(**2009**)** "1500 KVA Gücünde 6.3 KV Çıkış Gerilimli Jeneratör Grubu ve Yüksek Gerilim Kesicilerinin PLC-SCADA ile Uzaktan İzlenmesi", Yüksek Lisans Tezi, Karadeniz Teknik Üniversitesi, Fen Bilimleri Enstitüsü, Trabzon.

Kurtulan, S. (1999). PLC ile Endüstriyel Otomasyon (Birinci Baskı)." Türkiye: Birsen Yayınevi, 1-2.

MEGEP (2007). Elektrik-Elektronik Teknolojisi SCADA Sistemleri.

Özkara, A**., (**2009). " Bir Orta Gerilim Dağıtım Sisteminin SCADA ile İzlenmesi ", Yüksek Lisans Tezi, İstanbul Teknik Üniversitesi, Fen Bilimleri Enstitüsü, İstanbul

Strauss, C., (2003). "Practica Electrical Network Automation and Communication Systems ", Elsevier, İngiltere, 108-118.

OVERVIEW OF AKSARAY'S SOLAR ENERGY STATUS

Hakan ÇELEBİ
Aksaray University, Faculty of Engineering, Department of Environmental Engineering
hakanaz.celebi@gmail.com

Şevket TULUN
Aksaray University, Faculty of Engineering, Department of Environmental Engineering
sevkettulun@gmail.com

İsmail ŞİMŞEK
Aksaray University, Faculty of Engineering, Department of Environmental Engineering
ismailsimsek83@hotmail.com

Tolga BAHADIR
Aksaray University, Faculty of Engineering, Department of Environmental Engineering
tolgabahadir61@gmail.com

Melayib BİLGİN
Aksaray University, Faculty of Engineering, Department of Environmental Engineering
melayib@gmail.com

ABSTRACT: Energy is both a source of life for living things and an essential production input for the economic and social development of countries. It is important for our country to reduce its dependence on non-renewable energy sources by using renewable and inexhaustible energy sources such as solar, wind, geothermal, wave and tidal energy as in the world. Since solar energy is not dependent on foreign sources in terms of raw materials, it is not affected by the economic problems that may arise. Solar energy is the sun's radiation reaching the world and is the most easily available energy source. Aksaray is a very rich city in terms of the diversity and potential of renewable energy sources. Aksaray has high sunbathing potential due to its geographical location. As in the whole world, the use of solar energy is increasing day by day in Aksaray. In this study, the current state of Aksaray solar energy has been evaluated by evaluating from different statistical data sources.

Key words: Aksaray, Renewable Energy, Solar Energy, Energy Distribution.

AKSARAY'IN GÜNEŞ ENERJİSİ DURUMUNA GENEL BAKIŞ

ÖZET: Enerji hem canlıların yaşam kaynağı hem de ülkelerin ekonomik ve sosyal alanda gelişimi için temel bir üretim girdisidir. Ülkemizin dünya genelinde olduğu gibi, güneş, rüzgâr, jeotermal, dalga ve gelgit enerjisi gibi yenilenebilir ve tükenmez enerji kaynakları kullanarak, yenilenemeyen enerji kaynaklarına bağımlılığını azaltması önemlidir. Güneş enerjisi hammadde açısından dışa bağımlı olmadığından ortaya çıkabilecek ekonomik olumsuzluklardan etkilenmemektedir. Güneş enerjisi, güneşin dünyaya ulaşan radyasyonu olup en kolay temin edilebilen enerji kaynağıdır. Aksaray, yenilenebilir enerji kaynaklarının çeşitliliği ve potansiyeli açısından oldukça zengin bir şehirdir. Aksaray coğrafi konumundan dolayı yüksek oranda güneşlenme potansiyeline sahiptir. Tüm dünyada olduğu gibi Aksaray'da da güneş enerjisinin kullanımı her geçen gün artmaktadır. Bu çalışmada Aksaray'ın güneş enerjisinin mevcut durumu farklı istatistik veri kaynaklarından incelenerek değerlendirilmiştir.

Anahtar sözcükler: Aksaray, Yenilenebilir Enerji, Güneş Enerjisi, Enerji Dağılımı.

GİRİŞ

Küreselleşme, ülkelerin ekonomik olarak ilerlemesi ve insan nüfusunun hızla artış göstermesi gibi nedenlerle enerjiye olan talep her geçen gün artış göstermektedir. Ortaya çıkan bu enerji talebinin karşılanmasında kullanılan petrol, gaz ve kömür gibi fosil kökenli yakıtlar ise küresel ısınma, asit yağmurları ve ozon tabakasının incelmesi gibi çevresel problemlere neden olmaktadır. (Yılmaz, 2018; Yılmaz, 2019; Lee vd., 2017; Wang ve Jiang 2017). Fosil yakıtların kullanımı ile elde edilen enerji miktarı dünya enerji arzının yaklaşık olarak ¾'ünü karşılamaktadır (Abdul-Wahab ve ark., 2019). Fosil yakıt kullanımına bağlı olarak ortaya çıkan çevresel problemlerin önlenebilmesi amacıyla güneş, rüzgar, jeotermal, biyokütle, dalga, vb. gibi yenilenebilir enerji kaynaklarının kullanımının arttırılması gerekmektedir (Wahab vd., 2019).

Güneş enerjisi en önemli yenilenebilir enerji kaynaklarından biri olarak kabul edilmektedir. (Abdul-Wahab ve ark., 2019). Güneş enerjisini, güneşin çekirdeğinde meydana gelen bazı gaz reaksiyonlarının sonucu olarak ortaya çıkan enerji olarak tanımlayabiliriz. Uzay alanında oluşan bu enerjinin derecesi, ortalama 1370 W/m²'dir. Bunu başka bir şekilde ifade edecek olursak Dünyamız 120 petawat hızında güneş enerjisi alıyor, bu da bir gün içinde güneşten elde edilebilecek tüm enerjinin yirmi yıl boyunca dünyanın enerji ihtiyacını karşılayabileceği anlamına gelmektedir (Abdul-Wahab ve ark., 2019; URL-1,2019). Ancak yeryüzüne ulaşan bu enerjinin miktarı atmosferik kayıplardan ötürü 0 ile 1100 W/m² aralığında farklılık göstermektedir. Güneş ışımasının minimum miktarı bile sektörün ihtiyacından çok yüksek seviyeler de olup, bu

enerjiden faydalanma ile ilgili araştırmalar 1970 yıllarından sonra artış göstermiştir. Bu enerji tüm dünyada çevre açısından pozitif bir görüş kazanmıştır (URL-1, 2019). Güneş enerjisi sürekli mevcut olan ve sonu olmayan bir enerji kaynağıdır ve bu enerjinin kullanımı sonucunda herhangi bir emisyon oluşumu söz konusu değildir. Yeryüzü şekilleri nedeniyle verim farklılığı olabilmekle birlikte her bölgede bu enerji kaynağından yararlanmak mümkündür.

Türkiye'de Kullanılan Enerji Kaynakları

TEİAŞ (Türkiye Elektrik İletim A.Ş.)'ın 2017 yılı verilerine göre ülkemizde elektrik üretiminde kullanılan kaynaklarını incelediğimizde toplamda %70.37'lik bir oranda fosil kökenli kaynaklardan elektrik enerji üretildiğini görmekteyiz (Şekil 1). 2000-2017 yılları arasında üretilen enerji, kaynak bazında değerlendirildiğinde ürettiğimiz enerjinin ortalama olarak %54.8'ini ithal etmekteyiz ve bu ithalat ettiğimiz kaynak tamamen fosil kökenli kaynak durumundadır. Bu verileri değerlendirdiğimizde elektrik enerjisi üretiminde maalesef dışa bağımlı durumda olduğumuz sonucuna ulaşılmaktadır (URL-2, 2019; Kaplan ve Aladağ, 2016; Kaya ve Kılıç, 2015; Erdil ve Erbıyık, 2015).

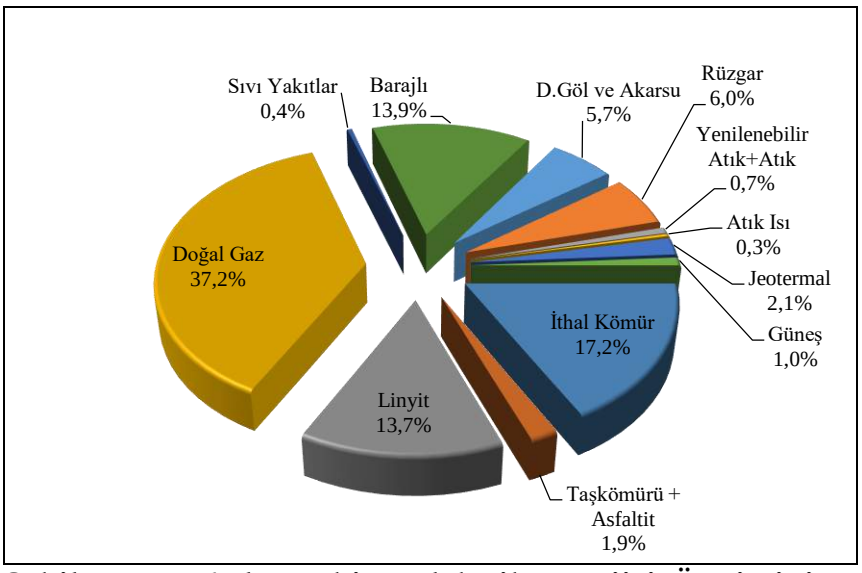

Şekil 1. 2017 Yılı Türkiye Elektrik Enerjisi Üretiminin Kaynaklara Göre Dağılımı (URL-2, 2019)

Yenilenebilir enerji kaynakları arasında güneş enerjisi ile üretilen elektriğin toplamdaki payı % 0.97'dir. Yenilenebilir enerji kaynaklarını kendi içerisinde değerlendirdiğimizde ise güneş enerjisi kaynaklı olarak 2017 yılında 2889.3 GWh'lik bir elektrik enerjisi üretimi gerçekleştirilmiştir. Bu üretim gücüyle 5. sırada bulunan güneş ülke ekonomisinin dışa bağımlılığından uzaklaşmasında % 3.31'lik bir oranda katkı sağlamıştır (Şekil 2) (URL-2, 2019).

TEİAŞ'ın 2000-2017 yılları arası derlemiş olduğu verilerine göre ülkemizde güneşten elektrik üretilmesine 2014 yılında başlanmış ve bu dönemde güneşin toplam enerji üretimine olan katkısı % 0.007 oranında olmuştur. 2017 yılında bu oran % 0.97'ye çıkmış ve diğer kaynaklarla karşılaştırıldığında oldukça fazla miktarda bir artış meydana gelmiştir (URL-2, 2019). Ayrıca diğer yenilenebilir enerji kaynakları ile karşılaştırma yapıldığında güneş, Türkiye'de en fazla kullanım potansiyeline sahip olan enerji kaynağı olarak karşımıza çıkmaktadır (Taktak ve Ilı, 2018).

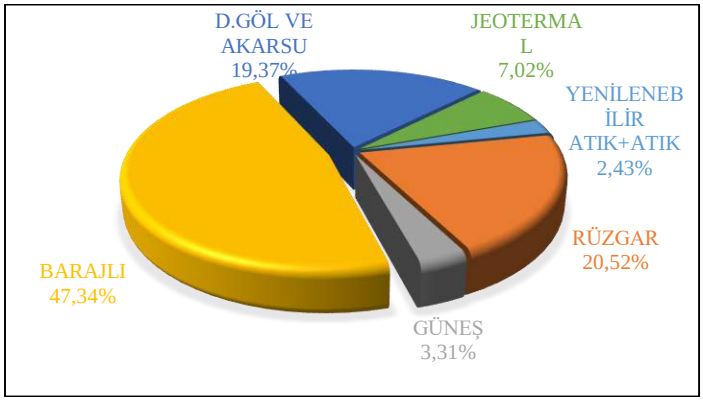

Şekil 2. 2017 Yılı Türkiye Yenilenebilir Enerji Kaynakları Dağılımı (URL-2, 2019)

Türkiye'deki Güneş Enerjisi Potansiyeli

Güneş enerjisini, dünya ve ülkemiz için değerlendirdiğimizde sınırsız bir enerji kaynağı olarak karşımıza çıkmaktadır. Ülkemizde güneşten ısı ve elektrik enerjisinin elde edilmesi, giderek artan bir konudur. Türkiye, güneş enerjisini kullanma açısından küresel arenada önemli bir konumdadır. Şekil 3'te, Türkiye'nin güneşten ısı enerjisi olarak yararlanma konusunda dünyada 4. olduğu ifade edilmektedir. Ülkemizin topografik, jeolojik, meteorolojik vd. konumlarının uygunluğu, sosyo-ekonomik yaklaşımlar, bölgesel uygulamalar ve ülkenin enerji politikalarından ötürü bu enerjinin kullanımı açısından önemli bir yere sahip durumdayız (Erdin ve Özkaya, 2019; Uğurlu ve Gökçöl, 2017; URL-3, 2016; Şimşek ve Şimşek, 2013). Ülke olarak güneşten termal enerji kaynağı olarak faydalanmakta dünya dördüncüsü olmamıza rağmen, güneşten elektrik enerjisi üretmek konusunda aynı başarıyı gösterebilmiş değiliz.

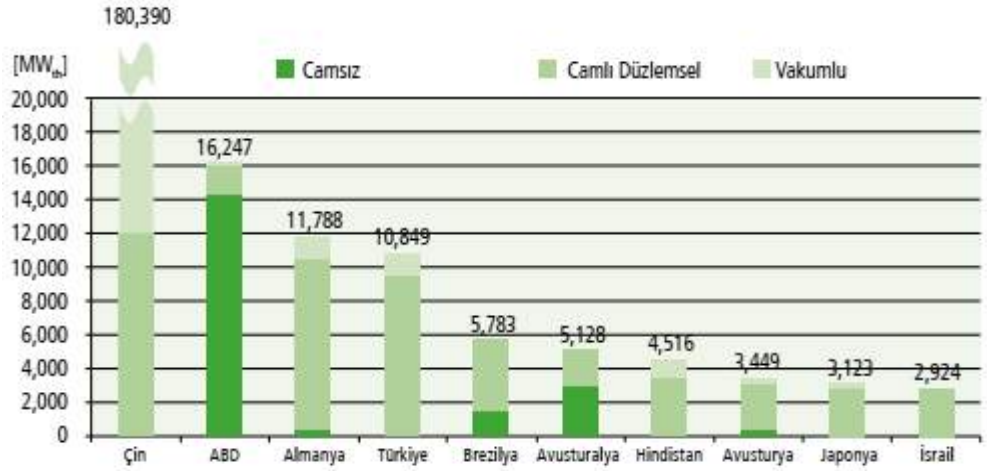

Şekil 3. Global Platformda Aktif Isıl Enerji Dağılımı (URL-3, 2016)

Ülkemizin, sıcak su gücü bakımından dünyada 4. sırada bulunmasına rağmen, güneşten elektrik enerjisinin üretilmesi yönündeki çalışmalar yeterli seviyeye ulaşamamıştır. Bu durum ise ülkelerin maksimum seviyede ekonomik ve uygulanabilir çalışmalarına göre şekil alabilmektedir. Türkiye'de yapılan yatırım teşvikleri ile güneşten elektrik enerjisi üretimiyle ilgili olan çalışmalar pozitif yönde gelişme göstermiştir. Ayrıca, bu konu hakkında hem yatırımcıların bilinçlendirilmesi hem de yasal kuralların güncellenmesi ve ekonomik destekler sayesinde ulusal ve uluslararası ölçekte bu enerji için santrallerin hızla kurulmasının önü açılmıştır (URL-3, 2016).

Türkiye'nin güneş kuşağında yer alması sebebiyle sahip olduğu güneş enerjisi potansiyeli oldukça fazladır. Yetkili kurum ölçümlerine göre yaklaşık güneşlenme süresi 7.50 saat/gün, ortalama toplam ışınım şiddeti ise 4.18 kWh/m^2/gün olduğu belirlenmiştir (URL-4, 2019). Ülkemizde en fazla güneşlenme süresi yaz mevsiminde Temmuz ayında, en az güneşlenme süresi ise kış mevsiminde Aralık aylarında gerçekleşmektedir (Şekil 4). Avrupa ülkeleri ile karşılaştırıldığında Türkiye'de güneşlenme süresi birçok Avrupa ülkesinden fazladır. Buna rağmen Avrupa ülkeleri Türkiye'ye oranla güneş enerjisinden daha fazla faydalanmaktadır. Ülkemiz yenilenebilir enerji kaynakları açısından dünyanın en zengin ülkelerinden birisidir. Güneşten yılda 380 milyar kWh/yıl elektrik enerjisi elde edebilme potansiyelimiz bulunmaktadır. (Bektaş ve Yılmaz, 2014).

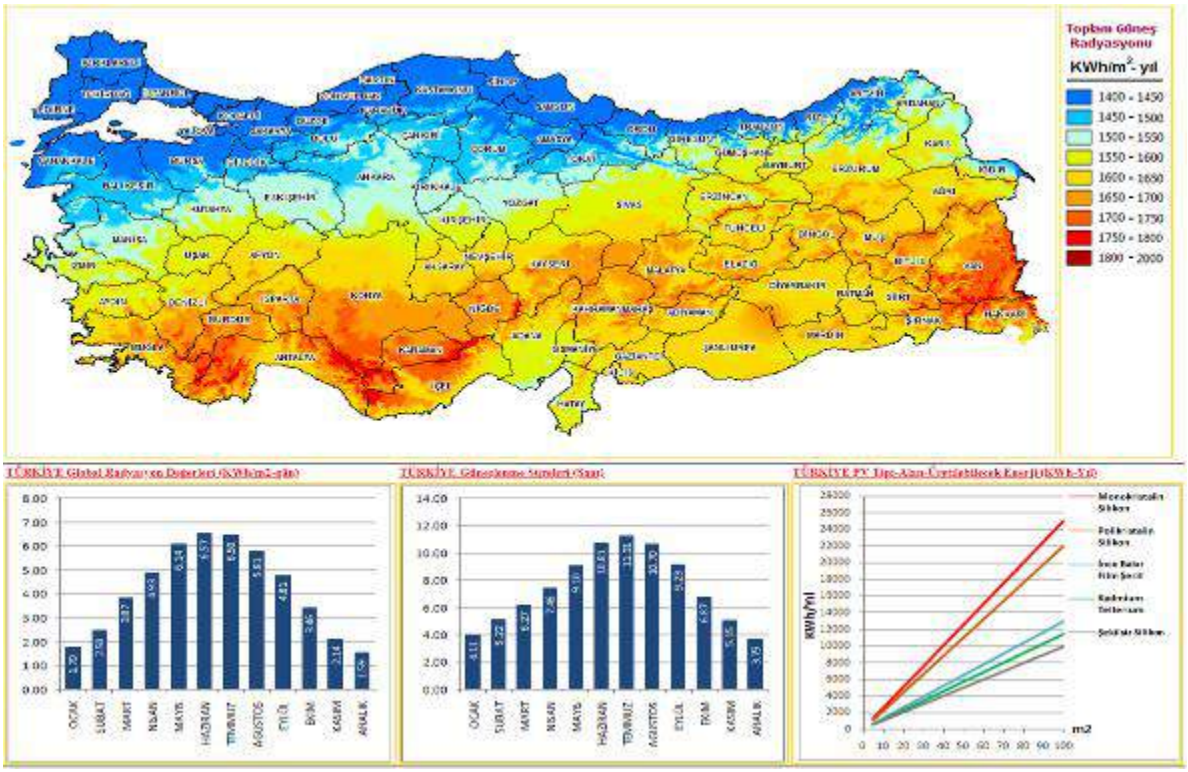

Şekil 4. Türkiye Güneş Enerjisi Durumu (URL-4, 2019)

Aksaray'ın Güneş Enerjisi Potansiyeli

Aksaray ili 7.626 km² yüz ölçümüne sahip İç Anadolu bölgesinde yer almaktadır. Aksaray ilinin güneş enerjisi potansiyeli yıllık olarak ortalama 1600-1700 kWh/m²/yıl aralığındadır. Bu değere bakıldığında güneş enerjisi potansiyelinin oldukça iyi olduğu anlaşılmaktadır. Şekil 5'de Aksaray ili güneş enerjisi potansiyel atlası verilmiştir (URL-4, 2019). Şekil 4'deki verilere göre Aksaray ilinin ortalama güneşlenme süresi 7.91 saat/gün, ortalama toplam ışınım şiddeti ise 4.32 kWh/m²/gün olduğu belirlenmiştir. Her iki değer Türkiye geneli ile karşılaştırıldığında Türkiye ortalamasından yüksek olduğu sonucuna varılmaktadır.

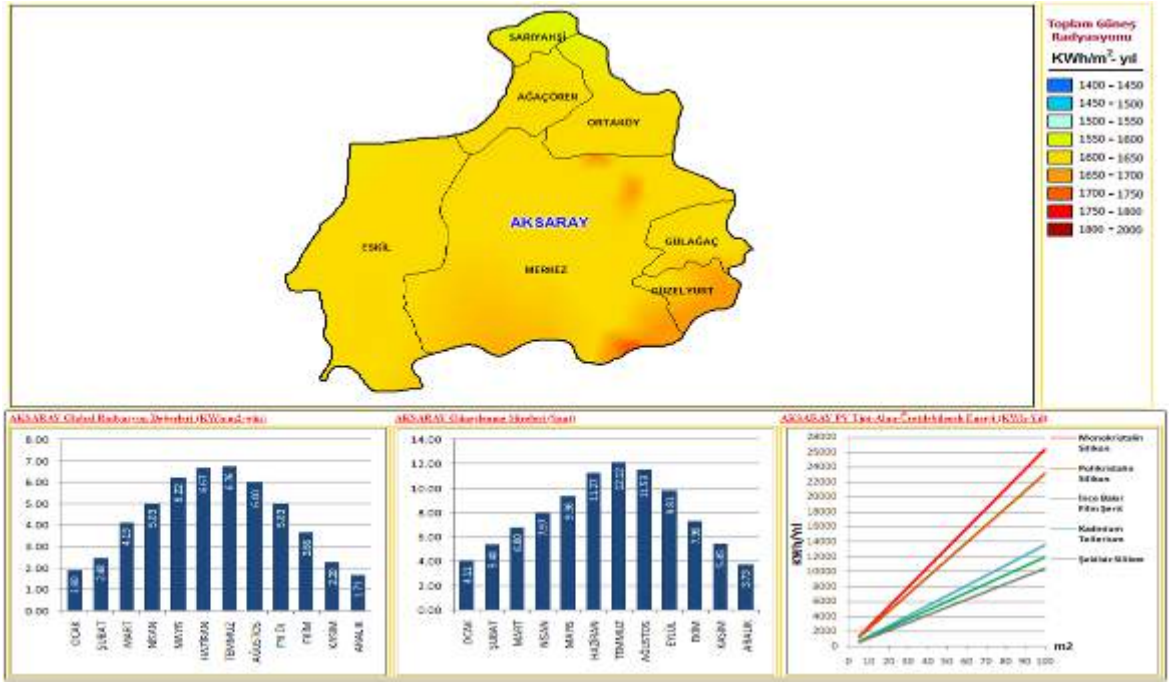

Şekil 5. Aksaray Güneş Enerjisi Durumu (URL-4, 2019)

Aksaray'da Bulunan Güneş Enerjisi Santralleri

TEİAŞ'ın Temmuz-2019 verilerine göre Türkiye'de toplam 6410 adet güneş enerjisi santrali bulunmaktadır. Aksaray ili sınırları içerisinde aktif halde ve yapım aşamasında bulunan güneş enerjisi santrallerinin listesi Tablo 1'de verilmiştir. Aksaray ili sınırları içerisinde 5 adet toplamda 13.2 MW kurulu güce sahip ve bir adet de 10 MW kurulu güce sahip olacak yapım aşamasında olan güneş üretim santrali bulunmaktadır. Türkiye'deki toplam güneş enerjisi santrali kurulu gücünün 5095 MW olduğu düşünülürse Aksaray ilinin güneşten enerji üretimine olan payı % 0.46 oranında olmaktadır

Tablo 1. Çalışma Alanı Kurulu Güç Dağılım (URL-5, 2019)

Faaliyetteki Enerji Sistemleri	
Aksaray İncesu Köyü Güneş Enerji Santrali	7.00 MW
Yapılcanlar Tarım Aksaray GES	3.00 MW
Sancak Enerji Aksaray İncesu GES	2.00 MW
Taşlıgöl Elektrik Güneş Enerji Santrali	1.00 MW
Aksaray Belediyesi Güneş Enerji Santrali	0.20 MW
Kurulu Olmayan Enerji Sistemleri	

Seg Elektrik Enerji		Aksaray Santrali	Eskil	Güneş	10.00 MW

SONUÇ VE DEĞERLENDİRME

Artan nüfusla birlikte büyüyen ekonomi, artan endüstrileşme ve gelişen teknoloji ülkelerin ihtiyaç duyduğu enerji miktarı da artmaktadır. Ülkemizin yeterli oranda enerji kaynağına sahip olamaması nedeniyle, enerjiyi ithal etmek zorunda kalmakta ve ithal ettiği kaynağa ödemiş olduğu bedel yaklaşık olarak toplam ülke ithalatımızın 1/5'ini oluşturmaktadır. Bu nedenle başta güneş olmak üzere, yenilenebilir enerji kaynakları bakımından zengin olan ülkemizde bu kaynakların aktif olarak kullanılması önem arz etmektedir. Aksaray İli, güneş enerjisi açısından mevcut konumu ve sahip olduğu güneş enerjisi potansiyeli açısından Türkiye'nin önde gelen illerinden birisidir. Aksaray İli'nin güneşlenme süresi (7.91 saat/gün) ve güneş radyasyonu (4.32 kWh/m^2/gün) değerlerine göre ülkemiz ortalamasının üzerinde bir güneş enerjisi elde etme değerine sahip olup, gelecek dönemlerde güneş tarlası yatırımlarının yapılabileceği bir konumda bulunmaktadır. Gelecek yıllarda fosil kökenli kaynakların rezervlerinin azalmaya başlayacak olması nedeniyle yenilenebilir enerji kaynaklarına verilecek önem artacaktır. Günümüzde güneş enerjisi santrallerinin ilk yatırım maliyetlerinin yüksek olduğu bilinmektedir. Teknolojik gelişmelerle birlikte bu maliyetlerin zamanla azalacağı düşünülmektedir.

KAYNAKLAR

Abdul-Wahab, S., Charabi, Y., Al-Mahruqi, A. M., Osman, I., Osman, S. (2019). Selection of the best solar photovoltaic (PV) for Oman. *Solar Energy, 188,* 1156-1168.

Bektaş, Y., Yılmaz, F. (2014). Aksaray ilinin güneş enerjisi potansiyelinin incelenmesi. XI. International HVAC+R Technology Symposıum. 8-10 May 2014, İstanbul, TÜRKİYE.

Erdil, A., Erbıyık, H. (2015). Renewable energy sources of Turkey and assessment of sustainability. *Procedia-Social and Behavioral Sciences, 207,* 669-679.

Erdin, C., Özkaya, G. (2019). Turkey's 2023 Energy strategies and investment opportunities for renewable energy sources: Site selection based on ELECTRE. *Sustainability, 11,* 2136.

Journal of Cleaner Production, 143, 452-461.

Kaplan, Y. A., Aladağ, C. (2016). The importance of the different kinds of energy sources for energy future of Turkey. *EPJ Web of Conferences 128,* 05002.

Kaya, D., Kılıç, F. C. (2015). New markets for renewable industries: Developing countries – Turkey, its potential and policies. *Journal of Energy in Southern Africa, 6,* 25-35.

Lee, C.Y., Lee, M.K., Yoo, S.H. (2017). Willingness to pay for replacing traditional energies with renewable energy in South Korea. *Energy, 128*, 284-290.

Özdemir, R. (2019). Güneş enerjisi sektörü. Ahiler Kalkınma Ajansı Aksaray Yatırım Destek Ofisi, Erişim tarihi: 04.09.2019. http://investinaksaray.com/assets/ilgilidosyalar/Gunes-Enerjisi-Sektor-Raporu_1.pdf
Şimşek, H A., Şimşek, N. (2013). Recent incentives for renewable energy in Turkey. *Energy Policy, 63*, 521-530.
Taktak, F., Ilı, M. (2018). Güneş enerji santrali (GES) geliştirme: Uşak örneği. *Geomatik Dergisi, 3 (1)*, 1-21.
Uğurlu, A., Gökçöl, C. (2017). An overview of Turkey's renewable energy trend. *Journal of Energy Systems, 1,* 148-158.
URL-1, (2019). Güneş enerjisi ve teknolojileri. Erişim tarihi: 20.08.2019. http://www.yegm.gov.tr/yenilenebilir/g_enj_tekno.aspx
URL-2, (2019). 2017 yılı Türkiye elektrik enerjisi üretiminin kaynaklara göre dağılımı. Erişim tarihi: 04.09.2019. https://www.teias.gov.tr/tr/iii-elektrik-enerjisi-uretimi-tuketimi-kayiplar-0
URL-3, (2016). Aksaray yenilenebilir enerji (Güneş Enerjisi) ihtisas endüstri bölgesi ilanına yönelik fizibilite raporu. Erişim tarihi: 05.09.2019 https://www.ahika.gov.tr/assets/upload/dosyalar/ahika_2016_aksaray-yenilenebilir-enerji-ihtisas-endustri-bolgesi-fizibilite-raporu.pdf
URL-4, (2019). Yenilenebilir Enerji Genel Müdürlüğü, Güneş Enerjisi Potansiyeli. Erişim tarihi: 04.09.2019. http://www.yegm.gov.tr/MyCalculator/Default.aspx
URL-5, (2019). Erişim tarihi: 04.09.2019. https://www.enerjiatlasi.com/gunes-enerjisi-haritasi/aksaray
Wahab, A., Hassan, A., Qasim, M. A., Ali, H. M., Babar, H., Sajid, M. U. (2019). Solar energy systems-potential of nanofluids. *Journal of Molecular Liquids, 289,* 111049.
Wang, R., Jiang, Z. (2017). Energy consumption in China's rural areas: a study based on the village energy survey.
Yılmaz, F. (2018). Thermodynamic performance evaluation of a novel solar energy basedmultigeneration system. *Applied Thermal Engineering, 143,* 429-437.
Yılmaz, F. (2019). Energy, exergy and economic analyses of a novel hybrid ocean thermal energy conversion system for clean power production. *Energy Conversion and Management, 196,* 557-566.

THE EFFECT OF THRUST BEARING FAILURES ON HYDROELECTRIC POWER PLANTS AND INVESTIGATION OF SOLUTION METHODS

Gökhan KAHRAMAN
Munzur Üniversitesi Mühendislik Fakültesi Makine Mühendisliği Bölümü
gokhankahraman@munzur.edu.tr

ABSTRACT: Renewable energy has a very important place in the economy of countries. Because renewable energy sources meet the energy needs of countries, they do not need fossil fuels. Thus, they reduce the dependence of the economy on foreign sources. In addition, renewable energy sources do not emit carbon to nature and thus contribute positively to the environment. Renewable energy is derived from water, wind, solar, thermal and biogas. Although the generation of electricity from wind and solar energy among these types of energy has increased considerably in our country lately, no renewable energy is as common as electricity production from water power. The production of electricity using the potential power of water is called hydraulic energy. Hydraulic energy can be obtained in dams with or without dams. Hydroelectric power plants consist of forced pipes, turbines and generators that transmit pressurized water to the turbine wheel. Between the turbine and generator parts there is a shaft that transmits the movement. The shaft is supported by axial and radial bearings. The radial bearings limit the movement of the shaft in the horizontal direction, while the axial bearings carry the entire load on the shaft, thereby rotating the shaft. The bearings in hydroelectric power plants operate according to the hydrodynamic or hydrostatic lubrication principle. Cooling and maintenance of such deposits are of great importance for the healthy operation of hydroelectric power plants. This is because any failure of such bearings can cause hydraulic turbines to fail to produce energy for a long time. Being unable to generate energy for long periods in hydroelectric power plants, which is a renewable energy source, causes great damage to the national economy. In this study, the maintenance and maintenance of the bearing bearings in the vertical turbines used in hydroelectric power plants are investigated. In addition, the bearing bed failures occurring in such plants are examined and solution methods are presented to eliminate these failures. This study will be useful for the operation of all hydroelectric power plants.

Keywords; Renewable energy, Hydroelectric power plant, Thrust bearing

HİDROELEKTRİK SANTRALLERDE TAŞIYICI YATAK ARIZALARININ ENERJİ ÜRETİMİNE ETKİSİ VE ÇÖZÜM YÖNTEMLERİNİN ARAŞTIRILMASI

ÖZET: Yenilenebilir enerji ülkelerin ekonomisinde çok önemli bir yere sahiptir. Çünkü yenilenebilir enerji kaynakları ülkelerin enerji ihtiyaçlarını karşılarken fosil yakıtlara ihtiyaç duymazlar. Böylece ekonominin dışa bağımlılığını azaltmış olurlar. Ayrıca yenilenebilir enerji kaynakları doğaya karbon salınımında bulunmadıkları için çevreye pozitif katkı sağlarlar. Yenilenebilir enerji su, rüzgâr, güneş, termal ve biyogaz gibi enerjilerden elde edilir. Bu enerji türlerinden rüzgâr ve güneş enerjisinden elektrik üretimi ülkemizde son zamanlarda kayda değer bir şekilde artmasına rağmen henüz hiçbir yenilenebilir enerji su gücünden elektrik üretimi kadar yaygın değildir. Suyun potansiyel gücünden faydalanılarak elektrik üretimine hidrolik enerji denilmektedir. Hidrolik enerji barajlı veya barajsız HES'lerde elde edilebilmektedir. Hidroelektrik santraller basınçlı suyu türbin çarkına ileten cebri boru, türbin ve generatör kısmından oluşmaktadır. Türbin ve generatör kısımları arasında haraketi ileten bir şaft bulunmaktadır. Şaft eksenel ve radyal yataklarla yataklanmıştır. Radyal yataklar şaftın yatay yöndeki haraketini sınırlamakta, eksenel yataklar ise şaft üzerindeki bütün yükü taşıyarak şaftın dönmesini sağlamaktadır. Hidroelektrik santrallerindeki yataklar hidrodinamik veya hidrostatik yağlama prensibine göre çalışmaktadır. Bu tür yatakların soğutulması ve bakımı hidroelektrik santrallerin sağlıklı işletilmesi için büyük önem arz etmektedir. Çünkü bu tür yataklarda oluşacak herhangi bir arıza hidrolik türbinlerin uzun süre enerji üretememesine neden olabilir. Yenilenebilir bir enerji kaynağı olan hidroelektrik santrallerinde uzun süreler enerji üretememek ülke ekonomisine büyük zararlar verir. Bu çalışmada, hidroelektrik santrallerde kullanılan dikey türbinlerde bulunan taşıyıcı yatakların teknik açıdan sağlıklı işletilebilmesi için dikkat edilmesi gerekenler ve yapılması gereken bakımlar araştırılmıştır. Ayrıca bu tür santrallerde oluşan taşıyıcı yatak arızaları incelenerek oluşan bu arızaları gidermek için çözüm yöntemleri sunulmuştur. Bu çalışma tüm hidroelektrik santrallerin işletilmesinde faydalı olacaktır.

Anahtar kelimeler; Yenilenebilir enerji, Hidroelektrik santral, Taşıyıcı yatak.

GİRİŞ

Enerji, sosyo-ekonomik gelişme ve yaşam standardını yükseltmede hayati bir rol oynamaktadır[1]. Enerji üretimini artırırken yenilenebilir enerji kaynaklarını kullanmak ülkelerin dışa bağımlılığını azaltır ve yenilenebilir enerji kaynakları sayesinde enerji üretirken çevreyi kirletmeyiz[2]. Yenilenebilir enerjinin dünyada en yaygın kullanılanı hidrolik enerjidir. Hidroelektrik santrallerin ekonomik ve çevresel faydaları ve aynı zamanda dünya çapındaki potansiyelleri, dünyanın enerji ihtiyacına önemli bir katkı sağlar[3]. Bu sebeplerden dolayı hidroelektrik enerji üretimini artırmak ayrıca mevcut hidroelektrik santrallerin verim ve kapasitelerini yükseltmek büyük öneme sahiptir. Bilim adamları hidroelktrik santrallerin verim ve üretim miktarlarını artırmak için

çalışmaktadır[4, 6]. Hidroelektrik santraller belirli bölümlerden oluşurlar[7]. Bu bölümlerin en önemlilerden bir tanesi taşıyıcı yataklardır[8, 10].

MATERYAL VE YÖNTEM

Hidroelektrik santrallerde kullanılan taşıyıcı yataklar lokmalı tip taşıyıcı yataklardır. Bu tip taşıyıcı yataklar taşıyıcı yatak çemberi üzerinde lokmaların dizilişleriyle imal edilirler. Hidrodinamik yağlamalı lokmalı taşıyıcı yataklar daha iyi yağlandıkları ve daha iyi soğuyabildikleri için çok büyük yüklerde kullanılabilirler. Şekil 1'de dikey şaftlı hidro türbinlerde hidrodinamik yağlamalı yatakların konumu şematik olarak gösterilmektedir.

Şekil 1. Dikey şaftlı hidro türbinlerde hidrodinamik yağlamalı yatakların şematik gösterimi

Şekil 1'de görüldüğü gibi hidroelektrik santrallerde dikey bir şaft 3 adet hidrodinamik yağlamalı yatakla desteklenmektedir. Bunlardan generatör ve türbin kılavuz yataklar şafta gelen radyal yükleri yataklamaktadır. Taşıyıcı yatak ise şaft üzerindeki eksenel yükleri yataklamaktadır. Şaft üzerine gelen eksenel yükler generatör ve türbin çarkının oluşturduğu yükler olup radyal yüklerden çok daha fazladır. Türbin-generatör ünitesinin ürettiği enerji ne kadar fazla ise eksenel yükler o kadar fazla olur. Bu durum taşıyıcı yatakların önemini artırmaktadır. Şekil 2'de 150 MW gücünde dikey Francis türbinine ait taşıyıcı yatak ve taşıyıcı yatak ringi görülmektedir.

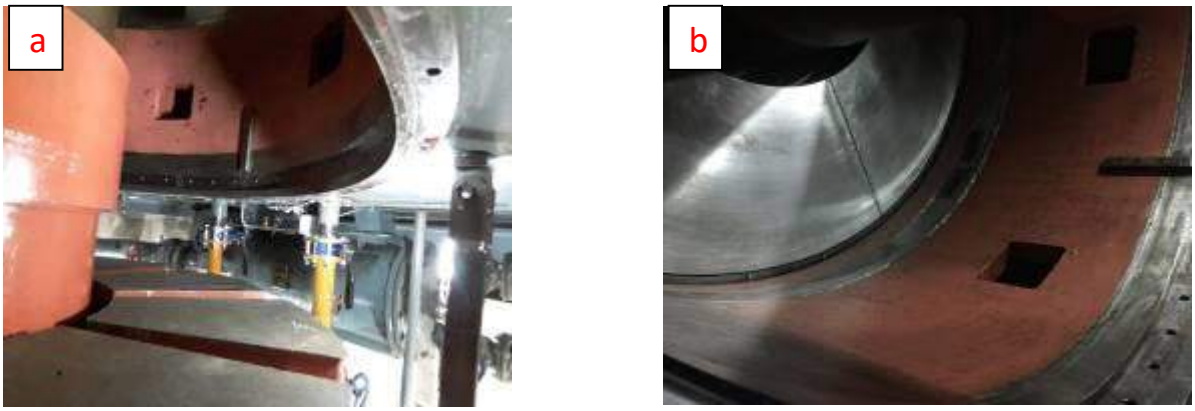

Şekil 2. a)Taşıyıcı yatak lokması, b)Taşıyıcı yatak ringi

Şekil 2'de hidroelektrik santrallere ait taşıyıcı yatak lokması ve ringi görülmektedir. Hidrolik santrallerde bulunan taşıyıcı yataklar hidrostatik ve hidrodinamik yağlama prensibine göre çalışırlar. Türbin-generatör ünitesi enerji üretimi için devreye alınırken taşıyıcı yatak yağ pompası lokma ile ring arasına lokmaların içerisine açılan kanallar vasıtası ile basınçlı yağ gönderir.

Basınçlı yağ lokma ile ring arasında belli bir mesafe oluşturarak şaftın ilk hareketinde kuru sürtünmeyi engeller. Şaft nominal devrinin %30'una ulaştığında taşıyıcı yatak yağ pompası devreden çıkar ve bu devirden sonra hidrodinamik yağlama başlar.

Türbin-generatör ünitesi tam üretim kapasitesine ulaştığında taşıyıcı yatak yağ filmi üzerinde oluşan yük maksimum seviyeye ulaşır. Bu durum lokmaların ve yağ filminin sıcaklığının artmasına neden olur. Eğer yeterli kapasitede soğutma gerçekleşmezse yağ filminde delinmeler ve taşıyıcı yatak lokmaları üzerindeki beyaz metalde deformasyonlar oluşur. Bu deformasyonlar hidroelektrik santralin uzun süreler enerji üretememesine neden olarak ülke ekonomilerine büyük zararlar verir. Deformasyona uğramış taşıyıcı yatak lokması şekil 3'te görülmektedir.

Şekil 3. Taşıyıcı yatak lokması beyaz metal deformasyon başlangıcı

Çok büyük miktarlarda deformasyona uğrayan taşıyıcı yatak lokmaları değiştirilmelidir veya beyaz metali yeniden dökülerek kullanılmalıdır. Çünkü özellikle beyaz metal ortalarındaki üzerindeki derin çizikler yağ filmini bozarak yatağın sağlıklı çalışmasını engelleyecektir. Taşıyıcı yatak lokmalarının darbeleri absorbe edebilmeleri için her lokmanın altında şekil 4'te gösterilen yaylar bulunmaktadır.

Şekil 4.Taşıyıcı yatak lokmalarında darbe emici yaylar

Şekil 4'te gösterilen yaylar türbin generatör ünitesine gelebilecek herhangi bir mekaniksel veya elektriksel darbeyi absorbe ederek taşıyıcı yatak lokmalarına gelebilecek zararı engellemektedir.

SONUÇLAR

Hidroelektrik santrallerde taşıyıcı yatağın kontrollü bir şekilde çalıştırılması ünitelerin verimli ve arızalanmadan çalışabilmesi açısından büyük önem teşkil etmektedir. Bir

hidroelektrik santralinde taşıyıcı yatak arızalarından kaçınma çareleri aşağıda maddeler halinde verilmektedir.
İlk çalışma esnasında taşıyıcı yatak yağ filmi basıncı yeterli seviyede olmalıdır. Bu basıncı taşıyıcı yatak yağ pompası oluşturduğu için pompanın bakımı periyodik şekilde yapılmalıdır.
Türbin-generatör ünitesinin elektrik üretimi esnasında yatak sıcaklıkları periyodik olarak kontrol edilmeli sıcaklık göstergesinin üzerindeki sinyal ve trip fonksiyonları doğru sıcaklık değerlerine ayarlanmalıdır.
Taşıyıcı yataklar belli periyotlarda indirilerek lokma yüzeyleri kontrol edilmeli ve yükseklik ayarları ölçülmelidir.
Zarar gören yatak lokmaları yenisi ile değiştirilmeli veya beyaz metali yeniden dökülmelidir.

KAYNAKLAR

Gökçöl C, Dursun B, Alboyacı B, Sunan E.(2009). Importance of biomass energy as alternative to other sources in Turkey. Energy Policy 424-431.
Lejeune A, Hui SL. (2012). Hydropower: a multi benefit solution for renewable energy. Comprehensive Renewable Energy, 6 15–47.

Yuksek O.,Komurcu M.I., Yuksel I., Kaygusuz K. (2006). The role of hydropower in meeting Turkey's electric energy demand, Energy Policy, Volume 34, Issue 17 3093-3103.

J.C.Galvis, J.M. Yusta Loyo, (2011). Cost assessment of efficiency losses in hydroelectric plants, Electric Power Systems Research, 81 1866-1873.

Barros C.P., Peypoch N., (2007). The determinants of cost efficiency of hydroelectric generating plants: A random frontier approach, Energy Policy, 35 4463-4470.

Barros C.P., (2008). Efficiency analysis of hydroelectric generating plants: A case study for Portugal, Energy Economics, 30 59-75.

Momcilvic D, Odanovic Z, Mitrovic R, Atanasovska I, Vuherer T.(2012). Failure analysis of hydraulic turbine shaft. Engineering Failure Analysis 20:54–66.

Peixoto T.F., Cavalca K.L., (2019). Investigation on the angular displacements influence and nonlinear effects on thrust bearing dynamics, Tribology International, 131 554-566.

Wang W., Allaire P.E., (2018). Theoretical and experimental study on the static and dynamic characteristics of tilting-pad thrust bearing, Tribology International, 123 26-36.

Gropper D., Wang L., (2018). Numerical analysis and optimization of surface textures for a tilting pad thrust bearing, Tribology International, 124 134-144.

ANALYSIS OF RESEARCHES DEALING WITH ANAEROBIC DIGESTION ON THE WORLD AND TURKEY

Elanur ADAR
Artvin Coruh University
aelanur@artvin.edu.tr

ABSTRACT: Anaerobic digestion is a technology that provides both stabilization of wastes/wastewater and allows the production of energy. Like every treatment/disposal method, the anaerobic digestion method has some disadvantages as well as its advantages. Some of these disadvantages include low treatment efficiency, long reaction time, and the need for treatment of the resulting liquid products, sensitivity to environmental conditions and so on. Despite these disadvantages, it is a widely used method.
The aim of this study is to analyze realized how much of the studies on anaerobic digestion, which is widely used as full-scale, in the world and in Turkey. Web of Science and Scopus sites were used for this purpose. Different titles (anaerobic digestion, mesophilic, thermophilic, manure, sewage sludge, etc.) were taken into consideration and analyzed for the last 5 years. It has determined which countries do most of the researches and how much study carries out in Turkey. In addition, the data between 1975-2019 were taken into consideration. As a result of the research, it was observed from Scopus that the first study was conducted in 1928. The first study deals with distillery slop wastewater treatment in the USA. Commonly treated sludge and animal manure (poultry) studies were carried out in the USA in 1947 and 1963, respectively. Considering the researches in the last 5 years, China is the country in the first place in all work areas; Turkey has carried out studies on the most manure treatment. The majority of these studies conducted in Turkey are conducted in the ITU, Bosphorus and Adıyaman University. As a result, more studies on different wastes should be realized in Turkey.

Key words: anaerobic digestion, analysis, research, world, Turkey

DÜNYADA VE TÜRKİYE'DE ANAEROBİK ÇÜRÜTME İLE İLGİLİ ARAŞTIRMALARIN ANALİZİ

ÖZET: Anaerobik çürütme, hem atıkların/atıksuların stabilizasyonunu sağlayan hem de enerji eldesine imkan sağlayan bir teknolojidir. Her arıtım/bertaraf metodu gibi anaerobik çürütme metodu da avantajlarının yanısıra bazı dezavantajlara sahiptir. Bu dezavantajlarının bazıları düşük arıtım verimi, uzun reaksiyon süresi, oluşan sıvı

ürünlerin arıtım gereksinimi, çevresel şartlara karşı duyarlı olması vb. dir. Bu dezavantajlarına rağmen yaygın şekilde de kullanılan bir yöntemdir.
Bu çalışmanın amacı yaygın şekilde tam ölçekli olarak kullanılan anaerobik çürütme ile ilgili dünya'da ve Türkiye'de ne kadar çalışmaların gerçekleştiğini analiz etmektir. Bu amaç içinde Web of Science ve Scopus sitelerinden faydalanılmıştır. Farklı başlıklar (anaerobik çürütme, mezofilik, termofilik, gübre, arıtma çamuru vb.) dikkate alınmıştır ve son 5 yıl için analiz edilmiştir. Hangi ülkelerin en çok araştırma yaptığı ve Türkiye'de ne kadar çalışma yürütüldüğü belirlenmiştir. Ayrıca 1975-2019 arası veriler de dikkate alınmıştır.
Araştırma sonucunda da ilk çalışmanın 1928 yılında yapıldığı Scopus'tan belirlenmiştir. İlk çalışma ABD'de içki fabrikası atık suyu arıtımı ile ilgilidir. Yaygın şekilde arıtılan çamur ve hayvan gübresi (kümes) ile ilgili çalışmalar ise sırasıyla 1947'de ve 1963'de ABD'de gerçekleştirilmiştir. Son 5 yıldaki araştırmalar ele alındığında, Çin tüm çalışmalarda ilk sırada yer alan ülkedir; Türkiye ise en çok gübre arıtımı ile ilgili çalışmalar gerçekleştirmiştir. Türkiye'de gerçekleştirilen bu çalışmaların çoğunluğu ise İTÜ, Boğaziçi ve Adıyaman üniversitelerinde yürütülmüştür. Sonuç olarak, Türkiye'de farklı atıklar ile daha fazla çalışmalar gerçekleştirilmelidir.

Anahtar sözcükler: anaerobik çürütme, analiz, araştırma, dünya, Türkiye

GİRİŞ

Anaerobik çürütme, atık/atıksuların arıtımı için yaygın şekilde kullanılan bir yöntemdir. Bu yöntem arıtımın yanısıra bertaraf edilmesi gereken atığın hacmini/kütlesini azaltmakta (%30-50) (Nges & Liu, 2010), atığın stabilizasyonu sağlanmakta ve yenilebilir enerji elde edilmektedir. Bu açıdan da anaerobik çürütme sürdürülebilir arıtım metodu olduğu söylenebilir. Ayrıca düzenli depolama yükünü de azaltmaktadır (Vindis, Mursec, Janzekovic & Cus, 2009)(Aich & Ghosh, 2016). Anaerobik çürütme, oksijenin olmadığı uygun şartlar altında (optimum pH, sıcaklık, mikroorganizma sayısı-türü, alkalinite, nütrient içeriği, vb.) organik içerikli atıkların/atıksuların ayrıştırılması işlemidir. Bu yöntem biyokütle enerjisi eldesi sağlamaktadır. Organik içeriğin mikroorganizmalar aracılığı ile ayrıştırılması ile biyogaza dönüştürülmekte ve %40-70 metan, %30-60 karbondioksit, %0-3 hidrojen sülfür ile çok az miktarda azot ve hidrojen içerir (Çetinkaya, 2018). Biyogazın içeriği substratın özelliği ve işletme şartları gibi birçok parametreye bağlıdır. Oluşan biyogaz enerjiye çevrilerek sistem içi veya dışı kullanılabilmektedir. Çakir & Stenstrom, (2005) uygun şartlar sağlandığı taktirde oluşan gazın metan içeriğinin enerjiye çevrilmesi ile önemli ekonomik kazanç sağlanabildiği ve elde edilen enerjinin tesisin enerji tüketiminin %28 oranını karşıladığını ifade etmektedir. Oluşan sıvı ve katı ürün toksik bileşenler içeriğine göre (patojen mikroorganizma, ağır metaller vb.) gübre olarak değerlendirilmektedir.

Anaerobik çürütme sistemi mezofilik (35-37 °C) ve termofilik (55-60 °C) sıcaklıklarda çalıştırılabilmektedir (Vindis, Mursec, Janzekovic & Cus, 2009). Avrupa'daki beraber çürütme tesislerinde indirgenmiş termofilik sıcaklık (47°C) yaygın şekilde kullanılmaktadır. Beraber çürütme farklı atıkların uygun oranlarda karıştırılması ile ayrıştırılmasıdır. Farklı atık/atıksuların beraber çürütülmesi daha fazla mikroorganizma türü ve sayısı, artan stabilizasyon ve böylece de artan metan oluşumu demektir (Vindis, Mursec, Janzekovic & Cus, 2009).
Bu çalışmanın amacı yaygın şekilde tam ölçekli olarak kullanılan anaerobik çürütme ile ilgili dünya'da ve Türkiye'de ne kadar çalışmaların gerçekleştiğini analiz etmektir. Bu amaç içinde başlıca Web of Science ve Scopus sitelerinden faydalanılmıştır. Farklı başlıklar (anaerobik çürütme, beraber çürütme, mezofilik, termofilik, gübre, arıtma çamuru vb.) dikkate alınmıştır ve son 5 yıl için analiz edilmiştir. Hangi ülkelerin en çok araştırma yaptığı ve Türkiye'de ne kadar çalışma yürütüldüğü belirlenmiştir. Ayrıca 1975-2019 arası veriler de dikkate alınmıştır.

YÖNTEM

Anaerobik çürütme ile ilgili Dünya'da ve Türkiye'de ne kadar çalışmaların gerçekleştiğini belirlemek için Web of Science, Scopus ve YÖK tez merkezi sitelerinden faydalanılmıştır. YÖK tez merkezinden ilk gerçekleştirilen tez çalışması hakkında bilgi edinmek için faydalanılmıştır. Son 5 yıllık veriler Web of Science sitesinden temin edilmiştir; ve bu verilerde SCI, ESCI ve Book Citation Index çalışmaları dikkate alınmıştır. Web of Science sitesinde 1975'den beri gerçekleştirilen çalışmalar yer aldığı ve Scopus sitesinde ise 1928 yılından itibaren verilerin olduğu gözlenmiştir. Bu sebeple de Scopus sitesinden de faydalanılmıştır. 1975-2019 arası toplamda ne kadar çalışma gerçekleştirildiği de yine Web of Science sitesinden alınmıştır.
Bu veriler, sunulurken de en çok çalışma yapan 5 ülke ele alınmıştır. Türkiye'de ise hangi üniversitelerde çalışmaların gerçekleştiği ele alınmıştır.
Bu sitelerden araştırma yapılırken de konu+başlık ve başlık+başlık olarak bazı anahtar kelimeler yazılmıştır. Anahtar kelime olarak anaerobik çürütme (AÇ), beraber çürütme (BÇ), mezofilik (M), termofilik (T), nanopartikül (NP), nano atık (NA), gübre (G), sığır gübresi (SG), tavuk gübresi (TG), arıtma çamuru (Aça), katı atık (KA), gıda atığı (GA), enerji (E), biyogaz (B), metan (Me), atık (A) ve atık su (AS) seçilmiştir. Atık türlerinden bunların seçilmesinin sebebi ise nanopartikül ve nano atık hariç diğerlerinin en yaygın çürütülen atıkların olmasıdır.

BULGULAR

İlk Çalışmalar

Araştırma sonucunda da anaerobik çürütme ile ilgili ilk çalışmanın 1928 yılında yapıldığı Scopus'tan belirlenmiştir. İlk çalışma ABD'de içki fabrikası atık suyu arıtımı ile ilgilidir. Bu çalışma sonrası 1941 yılında Japonya'da endüstriyel atıklar ile ilgili bir çalışma

gerçekleştirilmiştir. Yaygın şekilde arıtılan çamur ve hayvan gübresi (kümes) ile ilgili çalışmalar ise sırasıyla 1947'de ve 1963'de ABD'de gerçekleştirilmiştir.
YÖK Tez Merkezi'nde ise 1994 yılına ait ilk tez çalışması mevcuttur. Bu tez yüksek lisans tezi olup anaerobik çürütmeye metallerin etkisi çalışılmıştır.

Dünya Genelindeki 1975-2019 Yılları Arası ve Son 5 Yılda Yapılmış Çalışmalar

Şekil 1'de dünya genelindeki 1975-2019 yılları arasında ve son 5 yılda yapılmış çalışmaların sayısı verilmiştir. Bu veriler verilirken de konu+başlık ve başlık+başlık anahtar kelimeler kullanılmıştır. 1975-2019 yılları arası anaerobik çürütme ile ilgili çalışmaların toplam sayısı 6147, son 5 yılda 2908 çalışma yapılmıştır. Yaklaşık %47'si son 5 yılda gerçekleştirilmiştir. Enerji, metan ve biyogaz kelimeleri taratıldığında ise en çok biyogaz ifadesi tercih edilmiştir. İşletme sıcaklık şartlarından mezofilik ve termofilikte ise termofilik daha fazla kullanılmıştır. Bunun sebebi mezofilik şartlar yaygın şekilde kullanıldığı için özellikle belirtilmemesi olabilir. Ele alınan atık türlerinden ise çoktan aza sırasıyla atık, çamur, atık su, gübre ve nanopartikül/atık ile ilgili çalışmalar gerçekleştirilmiştir. Atık türlerinden katı atıktan çok gıda atığı ile çalışmalar gerçekleştirilmişken gübre başlığı altında ise sığır gübresi ile ilgili çalışmalar daha çok gerçekleştirilmiştir. En az çalışma ise nano-partikül/atık ile gerçekleştirilmiştir.

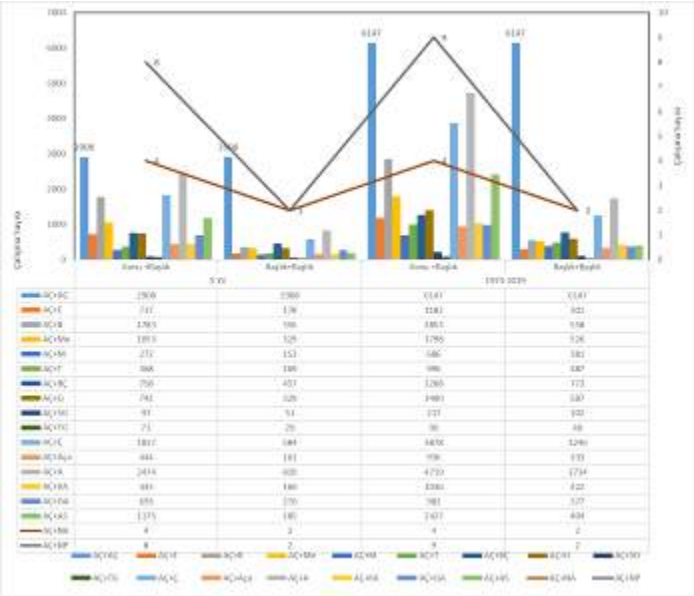

Şekil 1. Dünya Genelindeki 1975-2019 Yılları Arası ve Son 5 Yılda Yapılmış Çalışma Sayısı

Dünya ve Türkiye Genelindeki Son 5 Yılda Yapılmış Çalışmalar
Dünya ve Türkiye genelindeki son 5 yıldaki yapılmış çalışma sayıları tespit edilirken konu+başlık olarak anahtar kelimeler Web of Science sitesinden taratılmıştır. AÇ terimi konu olarak taratıldığında 10423 çalışma olduğu gözlenmiştir. Termofilik çalışmaların

daha çok yapıldığı; nanopartikül ve nano atık ile ilgili ise sırasıyla 8 ve 4 tane çalışmanın olduğu görülmüştür. Bu çalışmaların hepsi ise yurtdışında gerçekleştirilmiştir. Türkiye'de gübre ile çalışmaların fazla olduğu özellikle de tavuk gübresi ile çalışmaların gerçekleştirildiği tespit edilmiştir.

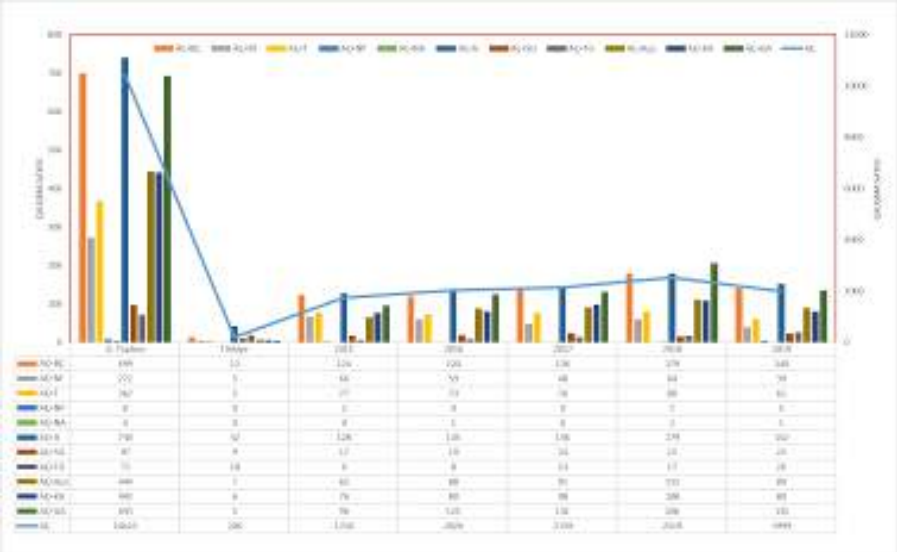

Şekil 2. Dünya ve Türkiye Genelindeki Son 5 Yılda Yapılmış Çalışma Sayısı

Şekil 3'te ise son 5 yılda anaerobik çürütme ile ilgili gerçekleştirilmiş çalışmaların ülkelere göre dağılımı ele alınmıştır. En çok çalışma yapan 5 ülkenin toplam % ne kadar çalışma yaptığı hakkında fikir vermektedir. Konu+başlık olarak ifadelerin taratılması sonucunda tüm aramalarda en çok çalışma yapan ülke Çin; Türkiye gübre, sığır gübresi ve tavuk gübresi ile ilgili çalışmalarda ilk 5'te yer alan ülke olduğu sonucuna ulaşılmıştır. Nanopartikül ile ilgili çalışmalar Çin, ABD, Avustrulya ve Hindistan'da gerçekleştirilmişken nano atık ile ilgili çalışmalar Çin ve Danimarka'da gerçekleştirilmiştir. Genellikle de çalışmaların çoğu Çin, ABD, İtalya, İspanya, Almanya ve Japonya'da gerçekleştirilmiştir.

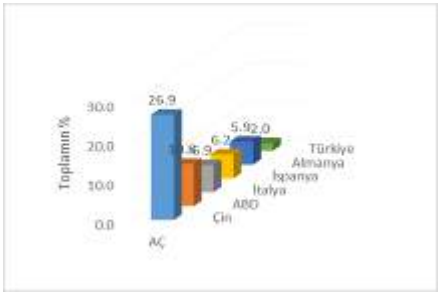

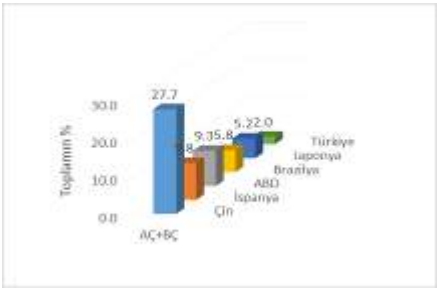

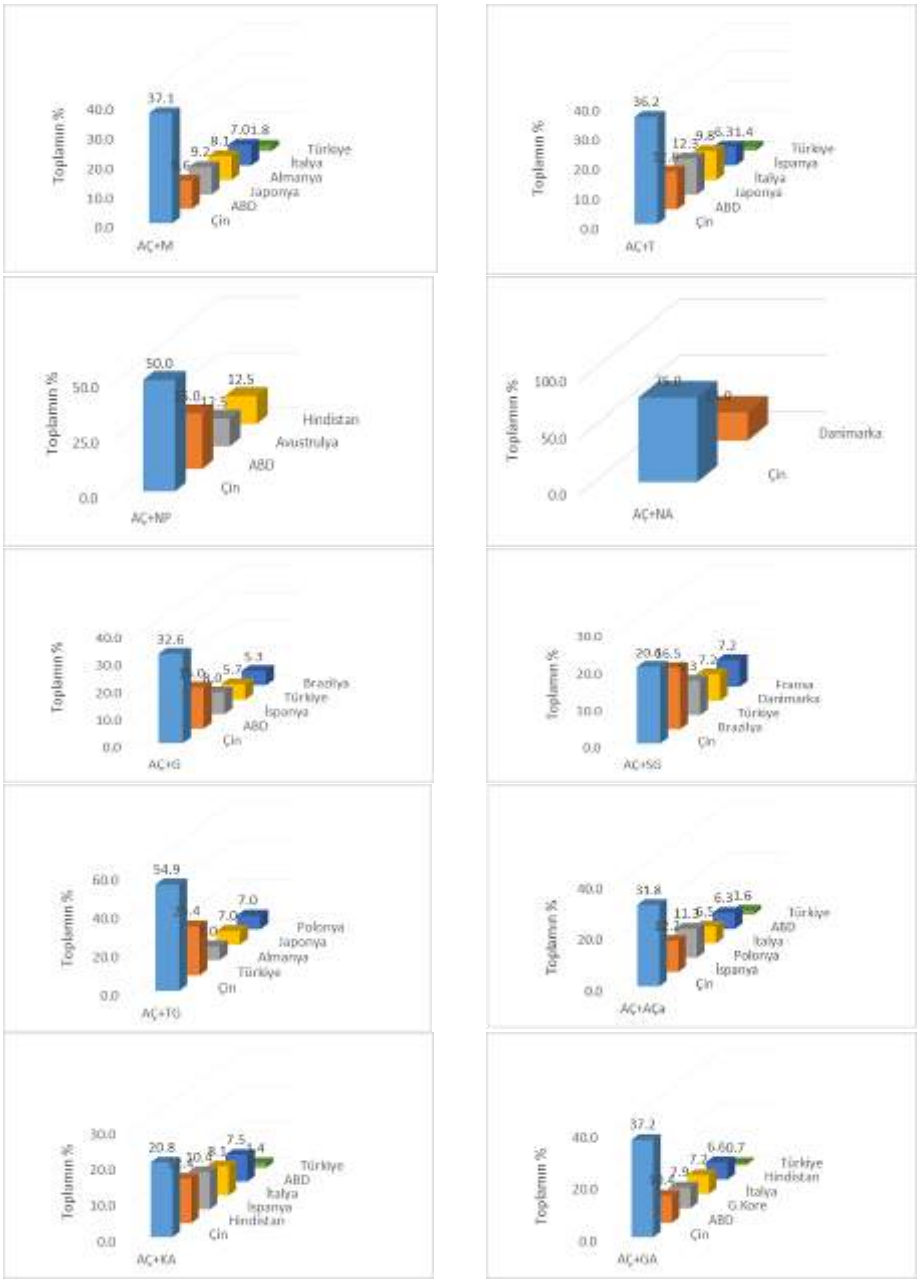

Şekil 3. Dünya Genelinde Son 5 Yılda Yapılmış Çalışma Sayısının Ülkelere Göre Dağılımı

Şekil 4'teki veriler ise Türkiye'de son 5 yılda yapılmış çalışma sayısının yıllara göre dağılımını göstermektedir. Anaerobik çürütme ile ilgili çalışmalar en çok 2018 yılında gerçekleştirildiği, en çok çalışmaların gübre özellikle de tavuk gübresi ile çalışıldığı ve nanopartikül/atık ile ilgili hiç çalışmanın yapılmadığı gözlenmiştir. Türkiye'de gerçekleştirilen bu çalışmaların çoğunluğu ise İTÜ, Boğaziçi ve Adıyaman üniversitelerinde yürütülmüştür.

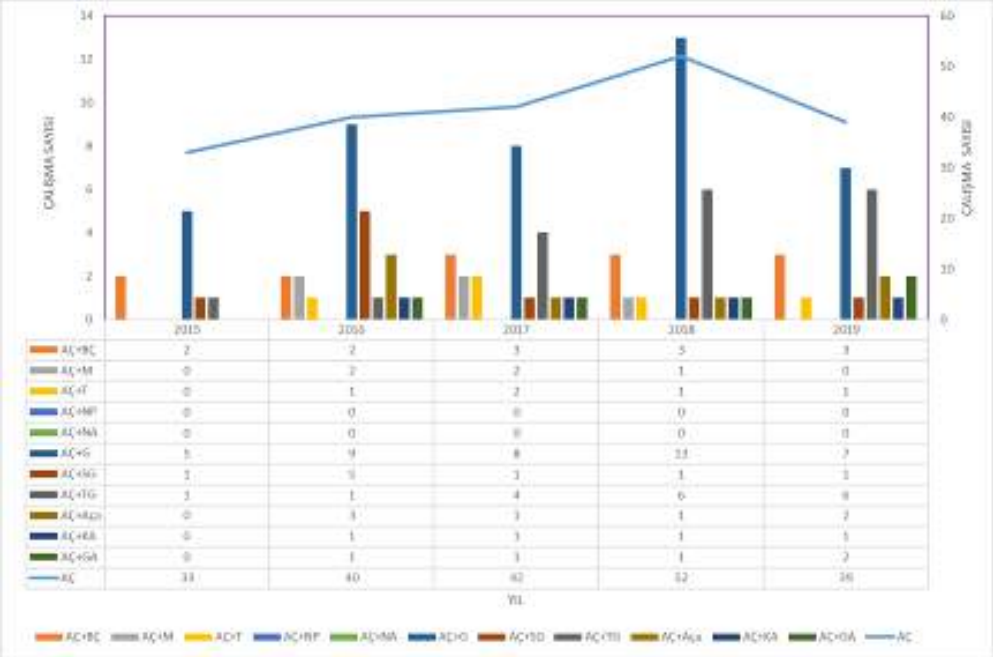

Şekil 4. Türkiye'de Son 5 Yılda Yapılmış Çalışma Sayısı

SONUÇ

Her arıtım/bertaraf metodu gibi anaerobik çürütme metodu da avantajlarının yanısıra bazı dezavantajlara sahiptir. Bu dezavantajlarının bazıları düşük arıtım verimi, uzun reaksiyon süresi, oluşan sıvı ürünlerin arıtım gereksinimi, çevresel şartlara karşı duyarlı olması vb. dir. Bu dezavantajlarına rağmen yaygın şekilde de kullanılan bir sürdürülebilir arıtım yöntemidir. Tam ölçekli kullanılan gelişmiş bir teknolojidir. Farklı anahtar kelimeler dikkate alınarak gerçekleştirilen bibliyometrik analiz sonucunda çalışmaların çoğusu Çin'de gerçekleştirildiği, nanopartikül/nano atık ile ilgili çalışmaların toplamda 12 civarında olduğu ve bu çalışmaların da başlıca Çin olmak üzere ABD, Avustrulya, Danimarka ve Hindistan'da gerçekleştirildiği tespit edilmiştir. Mezofilik sıcaklıklarda anaerobik çürütme daha az işletme maliyeti ve yüksek stabilite avantajları sağlamasından dolayı yaygın şekilde kullanılmasına rağmen çalışmaların çoğu termofilik ile yapıldığı tespit edilmiştir. Bunun sebebi mezofilik sıcaklıklar yaygın şekilde kullanıldığı için özellikle başlıkta ifade edilmediğinden dolayı olduğu düşünülmektedir.

Türkiye'de anaerobik çürütme ile ilgili çalışmaların az olduğu, gübre ile ilgili çalışmalar (özellikle de tavuk gübresi) hariç ilk 5 ülke içerisinde yer almamaktadır. Günümüzün de güncel konularından olan nanopartikül veya nanoatıkların etkisi ile ilgili çalışmaların olmadığı görülmüştür. Bu sebeple de Türkiye'de özellikle de farklı atıkların beraber çürütülmesi ve nanopartikül/nano atıkların anaerobik çürütülmesi ile çalışmalara yoğunluk verilmesi gerektiği söylenebilir.

KAYNAKLAR

Aich, A., & Ghosh, S. K. (2016). Application of SWOT Analysis for the Selection of Technology for Processing and Disposal of MSW. *Procedia Environmental Sciences*, *35*, 209–228. https://doi.org/10.1016/j.proenv.2016.07.083

Çakir, F. Y., & Stenstrom, M. K. (2005). Greenhouse gas production: A comparison between aerobic and anaerobic wastewater treatment technology. *Water Research*, *39*(17), 4197–4203. https://doi.org/10.1016/j.watres.2005.07.042

Çetinkaya, A. Y. (2018). Süt Endüstrisi Atıksuyunun Biyometanizayon Potansiyelinin İncelenmesi. *Journal of Polytechnic*, *0900*(2), 457–460. https://doi.org/10.2339/politeknik.403974

Nges, I. A., & Liu, J. (2010). Effects of solid retention time on anaerobic digestion of dewatered-sewage sludge in mesophilic and thermophilic conditions. *Renewable Energy*, *35*(10), 2200–2206. https://doi.org/10.1016/j.renene.2010.02.022

Vindis, P; Mursec, B, Janzekovic M, Cus, F. (2009). The impact of mesophilic and thermophilic anaerobic digestion on biogas production. *Journal of Achievements in Materials and Manufacturing Engineering*, *36*(2).

THE EFFECT OF LOW IRRADIANCE ON THE HARMONICS IN STAND-ALONE PHOTOVOLTAIC SYSTEM

Hasan CANGİ
HasCan Engineering Company
hasancangi@yahoo.com

Süleyman ADAK
Mardin Artuklu University
suleymanadak@yahoo.com

ABSTRACT: Photovoltaic (PV) systems have been increasingly used in the generation of electrical energy, either as a means of providing electricity in areas where there is stand-alone systems, or by providing electricity to the grid connected systems. In this study the effect of low irradiance has been investigated on the harmonic components for stand-alone PV systems. Pyranometer was installed for controlled data acquisition system and used to collect the spectral irradiance data. It is clear that total harmonics distortion (THD) is very sensitive to be changed in solar irradiance condition. The THD values are high up to 130 % in the morning and evening hours when the solar irradiance is low and also when the solar irradiance is affected by sudden changes like passing clouds. But when the solar irradiance is high during the day, the current THD value gets reduced below the value of 10%. Also, fluctuating solar irradiance resulted in reduction of active power generated by off-grid PV system reducing the overall efficiency of the solar system.

Key words: Off-grid system, power quality, solar irradiance, harmonics, renewable energy sources

INTRODUCTION

Due to the increasing fuel prices and related environmental concerns, renewable energies become an important source to supply electricity to buildings and industrial sectors. The energy demand in the world is consistently increasing, and new types of energy sources must be found in order to supply the future energy demands. Renewable sources of energy such as solar, wind, geothermal have gained popularity owing to consuming of conventional energy sources such as coal, gas and oil. Solar energy is one of the cleanest

forms of energy sources and the main energy resource for all of the life processes, and the basic condition causing varied physical phenomenon and processes in the atmosphere. Photovoltaic (PV) array, which converts sunlight to electrical power [1-3]. The use of photovoltaic systems as clean source of energy from the sun has been quicly increasing. Solar PV is most popular owing to its significant advantages, such as no fuel costs, no pollution, no noise, and little maintenance. The principle of off-grid solar system is as given in figure 1.

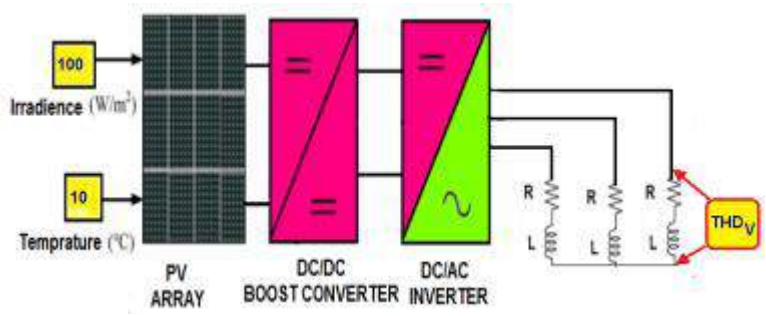

Figure 1. Off-Grid Solar System Principle Scheme

HARMONICS IN SOLAR SYSTEM

Harmonic currents are being generated by nonlinear electronic loads, or non-sinusoidal sources. Harmonic currents flowing through power system impedances generate voltage harmonics and distort the supply voltage. The nth harmonic is equal to n times the fundamental frequency, namely n*f, where n is a positive integer. When n is a positive fractional number, an inter-harmonic (n*f) is generated. Inverters produce aforementioned harmonics that affects Total Harmonic Distortion (THD), Distortion Factor (DF) and Power Factor (PF). Harmonics increase heat losses, power bills, and reduce system efficiency in power system. Inverters, DC/DC boost converter, and battery chargers are the most significant harmonic sources in PV power systems [2-4]. Non-linear waveform of inverter output voltage is given as an example in equation (1).

$$\begin{aligned} v(\omega t) = {} & 12.77\sin(\omega t - 1.1) + 1.527\sin(2\omega t + 4.576) + 0.1905\sin(3\omega t + 84.34) \\ & + 0.6921\sin(4\omega t - 58.38) + 1.049\sin(5\omega t + 144.1) \\ & + 0.8947\sin(6\omega t - 43.75) + 0.4659\sin(7\omega t + 95.75) \\ & + 0.4967\sin(8\omega t - 30.89) + 0.8114\sin(9\omega t - 73.87) \\ & + 0.8356\sin(10\omega t + 142.1) + 0.5985\sin(11\omega t - 43.58) \\ & + 0.49.24\sin(12\omega t128.4) + 0.7028\sin(13\omega t - 43.36) \end{aligned} \quad (1)$$

Graphics of equation (1) is as given in fig. 2.

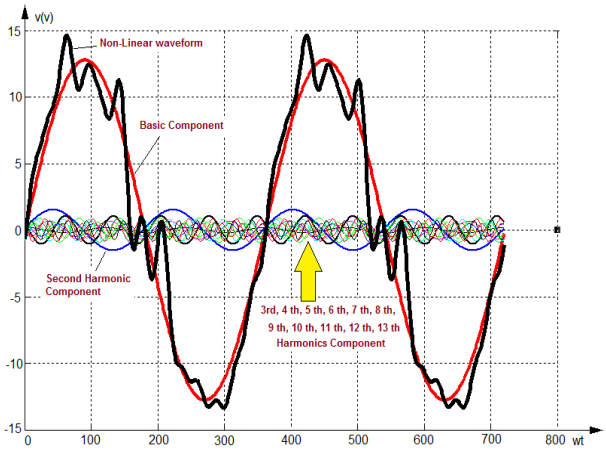

Figure 2. Nonlinear Waveform and Their Harmonic Components

The decrease in harmonics is also proportional to an increase in solar irradiation levels. Harmonics have become increasingly necessary to calculate their influence when making any additions or changes to an power systems. As these higher frequency harmonic currents flow through the power system, they can cause, overheating and system hardware damage, such as:

Overheating of electrical distribution equipment such as cables, transformers, battery PV panels.
High voltages and circulating currents is caused by as a result ofharmonic resonance,
Increased internal energy losses in connected such as, PV array, DC/DC convereter and solarinverter.
Causing elements failure owing to hingh total harmonic distortion.
Shortened life span of solar device,
False triggers at power electronics device,
Errors measurements in the measuring,
Fires in wiring and distribution systems,
Crest factors and related to problems,
Lower solar system power factor.

PV systems incorporate power electronic interfaces, which generate a level of harmonics potentially leading to current and voltage distortion. High frequency harmonics that appear due to power semi-conductors switching are reduced by selecte the optimal carrier frequency. Total harmonic distortion for voltage is the summation of all harmonic components of the current waveform compared against the fundamental component of the voltage wave,

$$THD_v = \frac{\sqrt{V_2^2+V_3^2+V_4^2+\cdots+V_n^2}}{V_1} \quad (2)$$

In the off-grid mode, the voltage and current harmonics are the biggest power quality issues in off-grid PV system. THDv was used to characterize the power quality of solar power systems. In power systems, lower THDv means reduction in peak currents, heating, emissions, and core loss in motors. Harmonic distortion can have detrimental effects on electrical equipment. Unwanted distortion can increase the current in power systems which results in higher temperatures in neutral conductors and distribution transformers. These higher order harmonics can also interfere with communication transmission lines since they oscillate at the same frequencies as the transmit frequency. Due to the fast growth of photovoltaic installations, concerns are rising about the harmonic distortion generated from PV inverters. Solar photovoltaic generation depends extensively on power converters to produce alternating current output for interconnection purposes [5, 6]. Thus, the harmonic issue is an important aspect affecting the integration of PV generation. It is not necessary to reach power quality levels defined by several international standards in off-grid power systems, but only good power quality allows electrical devices to function in their given manner without loss of performance or possible damage [7-9].

APPLICATION OF MATLAB/SIMULINK IN SOLAR SYSTEM

The photovoltaic array converts the sunlight into electricity. The photovoltaic array consists of parallel and series of photovoltaic modules. The cell is grouped together to form the panels or modules. The model of photovoltaic array is obtained from the photovoltaic cells and depends on how the cells are connected [8-10]. Because no power is provided during the hours of darkness, the stand alone systems must generate and store sufficient energy during the day to satisfy the peak daily load. The storage should also be sufficient to cover several days when no sunlight is available. Batteries are normally used as a buffer to provide the necessary storage to guarantee short term continuity of supply by storing surplus energy during the day for use during the night and during periods of overcast skies [11-12]. Unfortunately it is not practical to store the summer's surplus energy for use during the winter. Fig. 3 shows the change of solar irradians throughout the day.

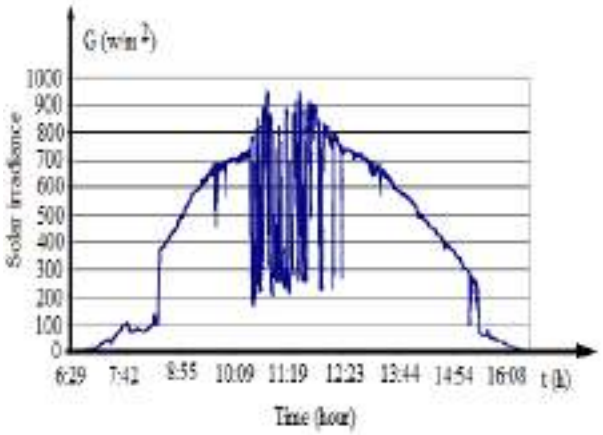

Figure 3. Changing of Solar Irradiance in Long the Day

It has been shown that current THD increases with a decrease in solar irradiation (W/m^2) levels and that current THD decreases with an increase in inverter output current or power. The topologic structure of the management PV system is shown in Fig.4, which consists of PV array, DC/DC converter and inverter, which connects at inductive R-L load.An ideal switch is used in DC/DC bosst converter so as to observe the output without any kind of loss across the switch. The voltage and current produced at the terminals of a PVcan feed a DC/DC converter, and connect to an inverter to produce AC current. Stand alone solar system which consists of PV Array, battery bank, DC/DC boost converter, charge controller, solar inverter, and inductive R-L load. Then main emphasis is to be placed on the photovoltaic system, the modeling and simulation photovoltaic array, the MPPT control and the DC/DC converter, total harmonic distortion values depend on PWM's carrier frequency will be analyzed and evaluated. The step of modeling with Matlab/Simulink of the photovoltaic system is shown respectively and simulation results are provided.The Simulink model of the PV could be used in the future for extended study with different DC/DC converter topology and solar inverter. In the following we will examine a system implementation with two microcontrollers. One will be responsible for the battery charge controller with MPPT and the other one with the DC/DC boost converter, DC/AC power inverter and R-L load. The proposed system is modeled and simulated under Matlab/Simulink under low irradiance. Stand alone solar PV system schematic diagram of this system is given in Fig.4.

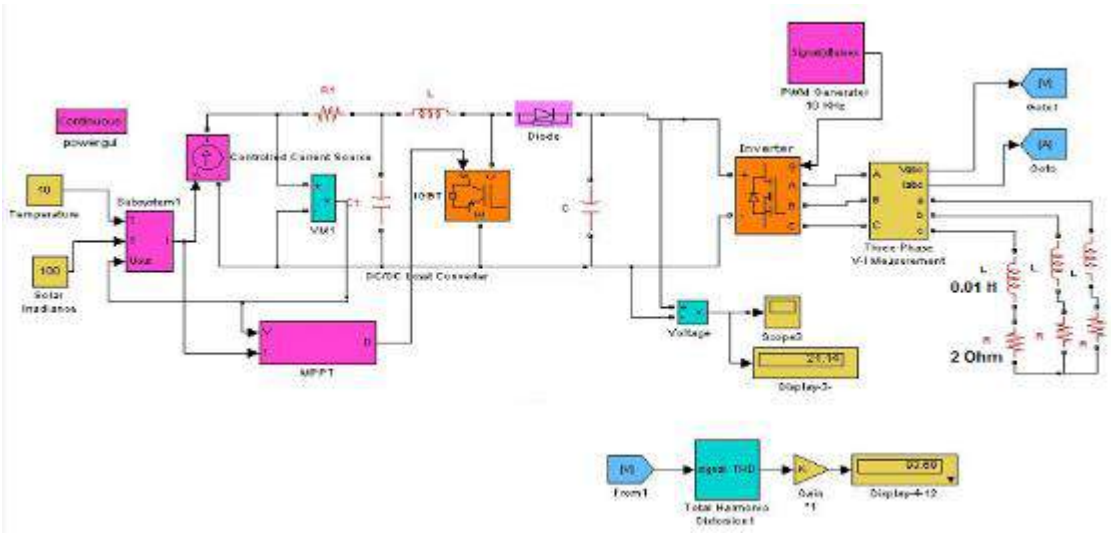

Figure 4. Principle Scheme of Stand Alone Solar System (for 100 (w/m², 10 ⁰C)

Power quality is considered to be one of the important criteria for the design of any electric power generation system. Hence it is necessary to identify and analyse the factors that are responsible for the deterioration of power quality. In this regard, it was found that fluctuating solar irradiance has strong inter-relation with power quality index. The solar irradiance dependent level of harmonic distortion due to off- grid PV system was investigated. One inherent problem with PV systems, however, is the necessity to convert the PV array's direct current to the electrical grid's alternating current, which is implemented by means of pulse-width modulation (PWM). Such electronic switching introduces more distortion into the grid which already contains some harmonics that are caused by nonlinear loads. DC link in solar system contains pulsation. Large electrolytic capacitors are connected to the DC link so as to absorb this pulsation so that the DC link voltage ripple can be kept small. Fig.4. shows a Matlab/Simulink diagram of typical solar PV renewables sources of energy. The integrated system has PV array as sources of energy. Therefore, the characteristic of energy storage for a PV system will be explained as well as some specification and standards for a off- grid connected PV system. The effect of fluctuating solar irradiance on the harmonics component of solar photovoltaic system was examined. It was clear that current THD is very sensitive to changes in solar irradiance condition. Table 1 shows the value of the harmonic components in the photovoltaic system.

Table 1. Harmonic Components Of Output Solar Inverter

Off- Grid Solar System Harmonics Component at Low Solar Irradiance		
Harmonics Component	Amplitude (V)	phase angle (Degree)

1	12.77	-1.1
2	1.527	4.567
3	0.1905	84.34
4	0.6921	-58.38
5	1.049	144.1
6	0.8947	-43.75
7	0.4659	95.75
8	0.4967	-30.89
9	0.8114	-73.87
10	0.8356	142.1
11	0.5985	-43.58
12	0.4924	128.4
13	0.7028	-43.36
14	0.7979	139
15	0.6662	-53.17
16	0.5246	125.3
17	0.6373	92.18
18	0.761	-43.83
19	0.7037	139.4
20	0.5661	-47.44
21	0.5987	133.2
22	0.7272	-42.03
23	0.7217	135
24	0.646	-57.51
25	0.5813	-70.54
26	0.6866	130.9
27	0.7254	-42.36
28	0.6428	135.3
29	0.5812	-47.44
30	0.6536	135.8
31	0.718	-40.12
32	0.6703	121.9
33	0.5935	167.4
34	0.6278	-51.09
35	0.7022	135.5
36	0.689	120.78
37	0.613	131.3
38	0.6819	137
39	0.6012	-45.89
40	0.6986	-44.95

Presence of harmonics leads to overloading of consumers electrical installation, terminal voltage rise and flicker, increased heating of neutral conductors, increased induction motor and transformer heating as well as saturation effects in the core, interferences on telecommunication lines, protective relays malfunction and failure of power factor correction capacitors. Hence it is important to identify the causes for harmonic generation along with its nature of influence in the off-grid PV systems performance to ensure the satisfactory operation, design of component ratings, protection settings and optimization of controller present in off-grid PV system . Normally harmonics is created due to any non linear nature of characteristics. The level of harmonic distortion in currents and voltages caused by off-grid PV systems is the subject of several international standards. When the PV inverters operate under low solar insolation and low power levels, more unwanted harmonics are generated. This has a huge impact on the power quality of the grid as well as capital and maintenance costs. The main aim of this work is to analyze the harmonic components at low radiation. The amplitudes of output inverter harmonic components are given in Fig 5.

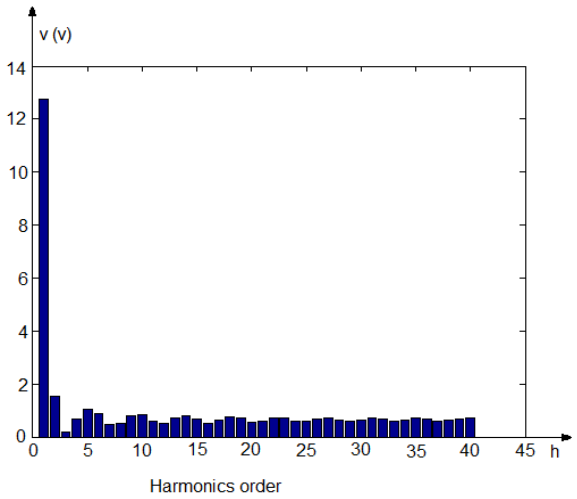

Figure 5. Spectrum of Voltage Harmonic Inverter

The problems caused by the harmonics are well defined; we cannot justify an incident on the installation due to their presence. The effects can be shown instantly switch failure, incorrect operations in static equipment, etc. and in the long term capacitor battery resonance, transformer overheating, conductors and motors, measurement errors from measurement instruments, thermal losses, etc. By exceeding the maximum conductor isolation temperature by only 10^{o}C motors and transformers reduce their working life practically by half. There are two operational modes in the system according to the different working statuses of PV panels, battery and mains supply.Solar electric or photovoltaic technology is one of the biggest renewable energy resources to generate electrical power and the fastest growing power generation in the world. Matlab / Simulation has been done to examine the harmonic components at low irradiance.

CONCLUSION

At low solar irradiance condition, the current THD increases significantly high from 10% to 130% which is above the recommended standard. By comparing the results of voltage THD, it can be reduced that fluctuating solar irradiance plays some role in the distortion of the voltage waveform and hence the power quality. Also, fluctuating solar irradiance resulted in reduction of active power generated by off-grid PV system reducing the overall efficiency of the solar system. It has been investigated that the low solar irradiance has a significant impact on the harmonic components of the output of stand-alone PV system. The total harmonic distortion value is increased at low irradiance.

REFERENCES

Parthasarathy, S., & Anandkumar, N. V. (2017). Effect of Fluctuating Solar Irradiance on the Quality of Power Generated by Solar Photovoltaic System. *International Journal of Advanced Engineering Research and Technology (IJAERT) Volume 5 Issue 9, ISSN No.:* 2348 – 8190.

Rustemli, S., & Cengiz, M. S. (2015). Active filter solutions in energy systems. *Turk J Elec Eng & Comp Sci, 23*: 1587 – 1607 doi:10.3906/elk-1402-212.

Wang, F., Duarte, J. L., Hendrix, M. A. M., & Ribeiro, P. F. (2011). Modeling and analysis of grid harmonic distortion impact of aggregated DG inverters. *IEEE Trans. Power Electron., vol. 26, no. 3*, (pp. 786–797)

Kececioglu, O. F., Acikgoz, H., Yildiz, C., Gani, A., & Sekkeli, M. (2017). Power Quality Improvement Using Hybrid Passive Filter Configuration for Wind Energy Systems. *Journal of Electrical Engineering Technology, 12,* 2370-2375. DOI: 10.1016/j.sbspro.2015.06.211.

Kaushika, N. D., Nalin, K., Gautam., & Kshitiz, K. (2005). Simulation model for sizing of stand-alone solar PV system with interconnected array. *Solar Energy Materials & Solar Cells. 85,* pp. 499–519.

Watson, N. R., & Arrillaga, J. (2003). Harmonics in large systems. *Electric Power Systems Research, 66 (1),* pp. 15-29.

Ozdemir, A., & Ferikoglu, A. (2004). Low cost mixed-signal microcontroller based power measurement technique. *IEE Proceedings-Science Measurement and Technology,151,* 253-258. Doi: 10.1049/ip-smt:20040242 –JUL.

İzgi, E., Oztopal, A., Durna, B., Kaymak, M. K., & Şahin, A. D. (2012). Short–mid-term solar power prediction by using artificial. *Solar Energy, vol.86,* pp.725-733.

Dugan, R. C., McGranaghan, M. F., Santoso, S., & Beaty, H. W. (2004). Electrical Power Systems Quality, Second Edition. *McGraw-Hill*.

Nema, S., Nema, R. K., & Agnihotri, G. (2010). Matlab/Simulink based study of photovoltaic cells/modules/array and their experimental verification. *International journal of Energy and Environment, vol.1, No.3,* pp.487-500.

Cangi, H., & Adak, S. (2015). Analysis of solar inverter THD according to PWM's carrier frequency. *International Conference on Renewable Energy Research and Applications (ICRERA);* DOI: 10.1109/ICRERA.2015, 7418694.

Oliva A. R., & Balda, J. C. (2003). A PV dispersed generator: a power quality analysis within the IEEE 519. *IEEE Trans. on Power Delivery , 18, 2* 525-530.

CHARPY IMPACT BEHAVIOR OF GLASS FIBER REINFORCED COMPOSITE PIPES FABRICATED BY CONTINUOUS FILAMENT WINDING TECHNIQUE

Özkan ÖZBEK
Gaziantep University, Mechanical Engineering Department, 27310, Gaziantep, Turkey, ozkanozbek@gantep.edu.tr

Ömer Yavuz BOZKURT
Gaziantep University, Mechanical Engineering Department, 27310, Gaziantep, Turkey, oybozkurt@gantep.edu.tr

Mehmet Sami KANAT
Akbor Boru Sanayi ve Ticaret Limited Şirketi, Aksaray, Turkey, msamikanat68@gmail.com

ABSTRACT: In the current work, damage resistance of filament wound glass fiber/epoxy resin reinforced composite pipes is studied. Composite pipes with different diameters 600, 700, 800, 900 and 1000 mm were manufactured using continuous filament winding technique. Damage resistance was evaluated by subjecting samples to low velocity impact loading at an energy level of 15 J using Kögel 3/70 Charpy impact test system. Five specimens were tested for each diameter of composite pipes. The damage analysis, using optical inspection, was conducted to understand the cause, extent and type of damage. Results of the tests are reported in terms of absorbed energy and impact toughness. The comparison of absorbed energy and impact toughness show that damage resistance of the samples are increased with an increase in diameter.

Key words: charpy, continuous filament winding, glass fiber

INTRODUCTION

In the last few decades, polymer-based composite materials, which have emerged as a result of the search for new material development, have started to be widely used in applications due to their superior properties such as high specific strength and stiffness compared to classical metallic-based engineering materials. Today, they have been used in a variety of engineering field ranging from daily life tools to space industry. Depending on the area of application, they can be subjected to low velocity impact loading in cases

of many unpredictable event such as work accident, natural disaster etc. Therefore, the determination of energy absorption capabilities of composite materials in an impact event has a crucial importance before the usage in applications.

A considerable amount of studies devoted to low impact behaviors of composite materials are present in the literature [1-3]. Caminero et al. [4] studied the effects of stacking sequences on the Charpy impact and flexural responses of carbon fiber reinforced composite laminates. Two main lay-up as cross ply and angle-ply were analyzed. The samples having $[\pm 45]_{3s}$ sequences showed the best energy absorption capability due to its pseudo-ductile behavior. Splitting, matrix cracking and delamination were observed as failure modes. Bulut [5] investigated the influence of graphene nanopellets inclusion on the Charpy impact characteristics of basalt fiber reinforced composite laminates. He stated that the 0.1 wt % nanoparticle addition were improved the material response because of high bonding strength at the interphase between nanoparticle-epoxy-fiber interactions. Demirci et al. [6] investigated the Charpy impact behaviors of arc shaped samples. The samples produced by filament winding method had the six layer with ± (55°) winding angles. Basalt and glass fibers were used as reinforcement. They conducted the experiments at different notch-depth ratios. The delamination damage in glass reinforced composites was observed to be more dominant than basalt reinforced samples. Reis et al. [7] explored the influence of nanoclay content on impact response of Kevlar fiber reinforced epoxy composites to determine the ideal amount (wt.%) of nanoclay for the best impact response.

In the current work, damage resistance of filament wound glass fiber/epoxy resin reinforced composite pipes is studied. To this aim, the pipes with different diameters 600, 700, 800, 900 and 1000 mm were manufactured using continuous filament winding technique and exposed to impact loading on Charpy test machine.

MATERIALS AND METHODS

Sample Preparation

The glass roving fiber with 2400 tex and 17 µm monofilament diameter, provided from Cam Elyaf A. Ş., Turkey, was used as reinforcement material. For matrix component of composite pipes, the polyester resin (BOYTEK PW05) and its hardener were mixed with the stoichiometric weight ratio of 98:2, respectively. Composite pipes were manufactured by a continuous filament winding machine shown in Figure 1. The machine has 2 motion capability as mandrel translation and mandrel rotational movements. All production stages were performed on the winding machine in Akbor San. ve Tic. Ltd. Şti., Aksaray, Turkey. Firstly, release wax application was performed to mandrel and glass wool was wrapped to obtain smooth surface inside of the sample. Then prepared resin mixture was deposited and the wrapping process of the reinforcements with 100 number of glass fibers together was conducted. The silica sand was used for strengthening in the middle

part of the pipe. Finally, glass fibers was again wrapped and finally glass wool was applied on the outer surface as seen in Figure 1.

Figure 1. Continuous filament winding technique

The all samples were cut on the longitudinal axis of the pipe as shown in Figure 2. The thickness and naming information of the glass fiber reinforced composite pipes were given in Table 1.

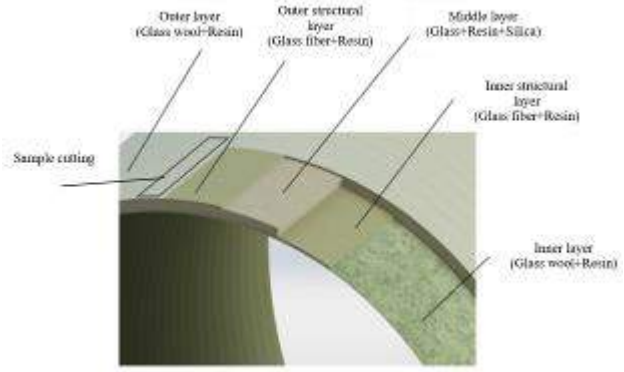

Figure 2. The pipe structure

Table 1. The naming and thickness information of glass fiber reinforced composite pipes

Diameter, mm	Naming	Thickness, mm
600	G06	9.43 ± 0.05
700	G07	11.66 ± 0.08
800	G08	13.46 ± 0.08
900	G09	13.43 ± 0.06
1000	G10	17.68 ± 0.05

Charpy Impact Test

Charpy impact experiments were conducted to determine low velocity impact characteristics of glass fiber reinforced pipes. All experiments were performed in accordance with ISO 179/92 standard [8]. A Köger 3/70 Charpy test machine having 15.0 J capacity, shown in Fig. 3, were employed to measure impact energy of each sample. Also, schematic illustration of Charpy impact experiment was given in Fig.4.

Figure 3. Kögel 3/70 Charpy impact tester

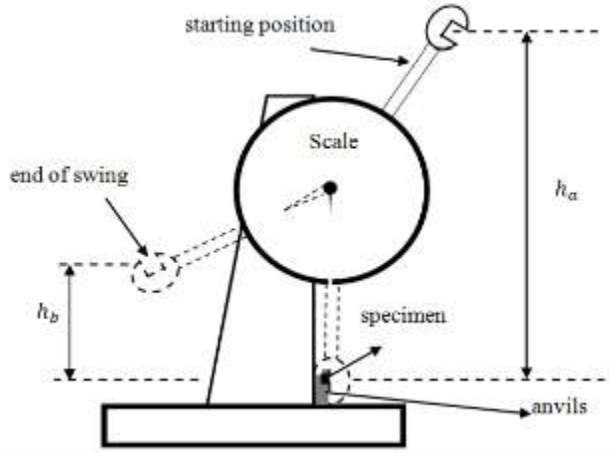

Figure 4. Schematic illustration of Charpy impact test

The samples having 55 mm x 10 mm dimensions in length and width, shown in Fig. 5, were prepared as unnotched and subjected to flatwise impact loading. For each pipe diameter, five number of samples were tested to ensure experimental reliability. All tests were performed at standard weather conditions. The absorbed impact energy and impact toughness of samples were determined according to following equations:

$E = E_a - E_b$ (1)

$a_{cu}=E/(bh)$ (2)

where, E, E_a, E_b, a_{cu}, h and b represent the absorbed impact energy, potential energy of the weighted pendulum before and after impact (shown in Fig. 3), impact toughness, thickness and width of the test sample, respectively. Average values and standard deviations for the absorbed impact energy and impact toughness were used to assess the effect of pipe diameter.

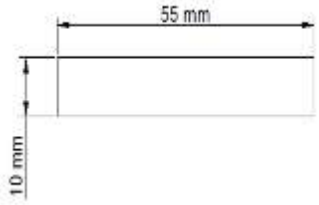

Figure 5. The dimensions of Charpy samples

RESULTS AND DISCUSSIONS

Charpy impact test was performed to determine the low velocity impact behaviors of glass fiber reinforced composite pipes. Energy absorption and impact toughness of the samples obtained from the longitudinal axis of the pipe with different diameters were given in Figure 6 and Figure 7, respectively. The increase in diameter value improved the absorption energy and impact toughness of the samples. Maximum impact energy and impact toughness values were obtained from G10 samples as 14.35 J and 25.28 kJ/m^2, respectively. The improvements in percentage at G10 in terms of energy and toughness were achieved as 65% and 77.4% compared to G06 samples. The diameter increase of the pipe is thought to be due to the fact that the sample is slightly flatter within the required dimensions. Thickness values also played an important role on the impact responses.

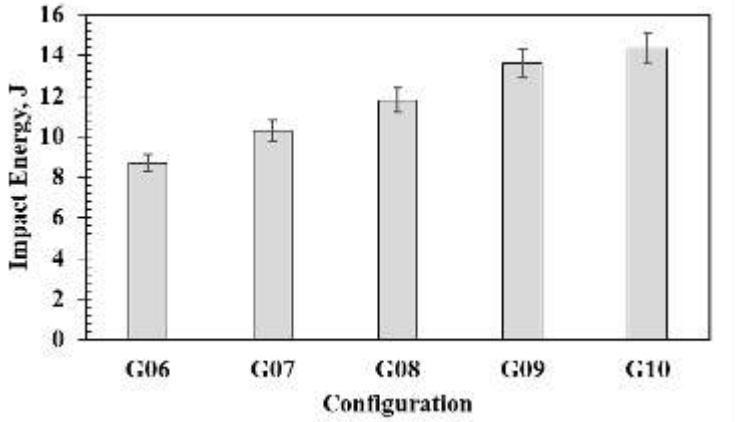

Figure 6. Absorbed energy

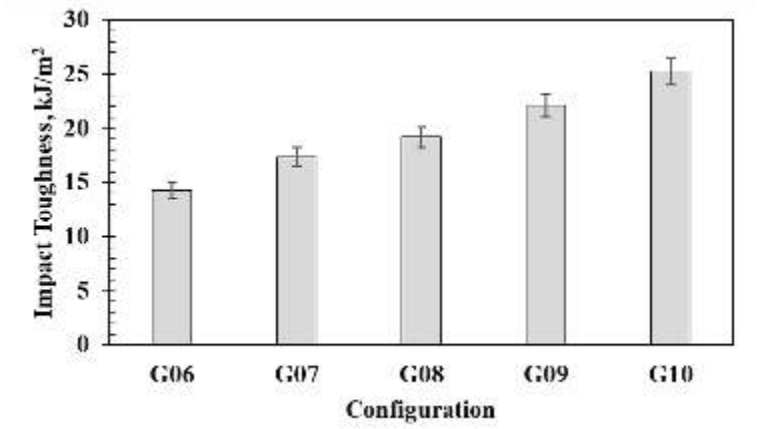

Figure 7. Impact toughness

Figure 8 shows the fracture shapes and failure modes of the samples after the Charpy impact experiments. Increase in impact strength and energy as the diameter increases lead to more destructive fractures. In addition, silica sand in mid region was directly separated after fiber breakage in outer side of sample resulted with the crack propagated to inner side. The most destructive fractures were generally observed in G10 samples with a diameter of 1000 mm. The combination of matrix fragmentation, layer delamination and fiber breakage were seen as failure modes of the samples.

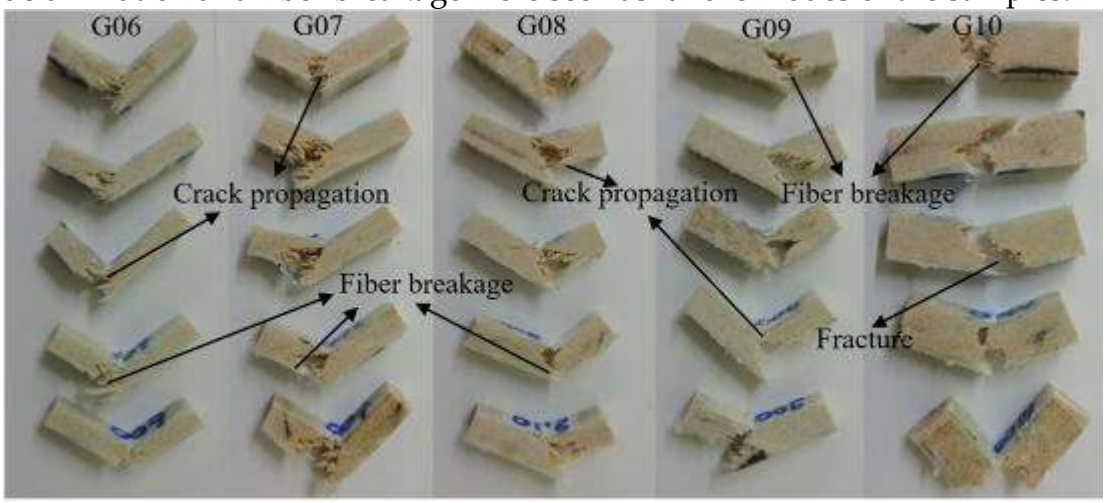

Figure 8. Fracture shapes and failure modes

CONCLUSION

In this study, the effect of pipe diameter on the low velocity characteristics of glass fiber composite pipes fabricated by continuous filament winding technique samples were investigated. Charpy impact experiments were evaluated to obtain impact behaviors in terms of absorbed energy and impact toughness. The results showed that the pipe diameter had very significant influences on examined parameters. Higher pipe diameter

with thicker material resulted with the higher energy absorption and impact toughness. Maximum impact energy and impact toughness values were obtained from G10 samples as 14.35 J and 25.28 kJ/m^2, respectively. The improvements in percentage at G10 in terms of energy and toughness were achieved as 65% and 77.4% compared to G06 samples. Matrix fragmentation, delamination of layers and fiber breakage were observed as failure modes. With higher load carrying capacity led to more catastrophic failures especially in samples with 1000 mm diameter. In conclusion, pipe diameter proved the magnificent effect on low velocity behaviors of the filament wound composite pipes.

REFERENCES

[1] Zhong, Y., & Joshi, S. C. (2015). Impact behavior and damage characteristics of hygrothermally conditioned carbon epoxy composite laminates. *Materials & Design* (1980-2015), 65, 254-264.

[2] Farsani, R. E., Khalili, S. M. R., & Daghigh, V. (2014). Charpy impact response of basalt fiber reinforced epoxy and basalt fiber metal laminate composites: Experimental study. *International Journal of Damage Mechanics*, 23(6), 729-744.

[3] Hufenbach, W., Ibraim, F. M., Langkamp, A., Böhm, R., & Hornig, A. (2008). Charpy impact tests on composite structures–an experimental and numerical investigation. *Composites Science and Technology*, 68(12), 2391-2400.

[4] Caminero, M. A., Rodríguez, G. P., & Muñoz, V. (2016). Effect of stacking sequence on Charpy impact and flexural damage behavior of composite laminates. *Composite Structures*, 136, 345-357.

[5] Bulut, M. (2017). Mechanical characterization of Basalt/epoxy composite laminates containing graphene nanopellets. *Composites Part B: Engineering*, 122, 71-78.

[6] Demirci, M. T., Tarakçıoğlu, N., Avcı, A., & Erkendirci, Ö. F. (2014). Fracture toughness of filament wound BFR and GFR arc shaped specimens with Charpy impact test method. *Composites Part B: Engineering*, 66, 7-14.

[7] Reis, P. N. B., Ferreira, J. A. M., Zhang, Z. Y., Benameur, T., & Richardson, M. O. W. (2013). Impact response of Kevlar composites with nanoclay enhanced epoxy matrix. *Composites Part B: Engineering*, 46, 7-14.

[8] ISO, I, 179–1, Plastics—Determination of Charpy Impact Properties, Part 1: Non-Instrumented Impact Test, *International Organization for Standardization: Geneva*, Switzerland, 2010.

NOMENCLATURE

D thermal duct diameter (m)
L thermal duct lenght (m)
$\dot{m}$ mass flow rate (kg s^{-1})
p perimeter (m)
Pr Prandtl number

q heat flux (W m^{-2})
q' heat transfer per unit of length (W m^{-1})
Q heat transfer rate
Re Reynolds number
S entropy generation rate per unit length (W m^{-1} K^{-1})
T temperature (K)
W water
x axial coordinate (m)

Greek symbols

ϕ nanoparticles volume concentration (%)
ν kinematic viscosity (m^2s^{-1})
ΔT temperature difference (K)

Subscripts

bf base fluid
gen generation
nf nanofluids
p particles
t thermal
T total

SECOND LAW OPTIMIZATION OF WATER-PROPYLENE GLYCOL/ Al_2O_3 NANOFLUID FLOW IN VARIOUS SHAPES AND AREAS OF THERMAL DUCTS

Nurullah Arslanoglu
Bursa Uludag University, Faculty of Engineering, Dept. of Mechanical Eng., Bursa, Turkey
narslanoglu@uludag.edu.tr

Abdulvahap Yigit
Bursa Uludag University, Faculty of Engineering, Dept. of Mechanical Eng., Bursa, Turkey
avahap@uludag.edu.tr

ABSTRACT: Water/propylene glycol (W/PG)-based Al_2O_3 nanofluids flow entropy generation in a circular cross-section thermal duct and under constant uniform heat flux thermal boundary condition was analytically investigated for turbulent regime. In addition, this study investigated the entropy generation characteristics of various particle volume fraction, and cross section shape and area of thermal ducts for W/PG (60:40)-Al_2O_3 nanofluid flow. Furthermore, thermodynamic performance of Water/propylene glycol and Water/ ethylene glycol fluid flow was compared. Consequently, $N_{s,a}$ values of W/PG- Al_2O_3 nanofluids are smaller than 1 from Re=3000 to Re=10392(ϕ=1%), 9007(ϕ=3%), 8241(ϕ=5%). The optimum Re numbers, where the entropy generation is minimum, are 7217(ϕ=0), 7162(ϕ=1%), 6998(3%), 6838 (5%). The thermal ducts are ranked in order from lowest to highest entropy generation: circular, square, triangle. It is found that total entropy generation increases with the increasing cross-sectional area and the entropy generation of water/propylene glycol fluid flow is higher than water/ethylene glycol fluid flow.
Key words: Entropy generation, water-propylene glycol/Al_2O_3, nanofluids

INTRODUCTION

Nanofluids are obtained by suspending nanoparticles (less than 100 nm) in the basic fluid. The scope is to improve the heat transfer properties of the base fluid. Especially, nanofluids will be used thermal systems in the future. But, nanoparticles increase the viscosity of the base fluid. This causes increasing friction factor. The studies related to heat transfer, friction characteristics, and entropy generation analysis of nanofluids in literature are summarized below.

Heat transfer and friction factor characteristics of water/propylene glycol-based CuO nanofluids were investigated in a circular tube fitted with and without helical inserts. Experiments were carried out different Re numbers and volume concentrations. Correlations were developed for predicting Nu number and friction factor [Naik and Sundar, 2014]. The effect of nanoparticle concentration (0–1%) and temperature on thermal conductivity and viscosity of ceria–propylene glycol nanofluids was investigated. The ceria–propylene glycol nanofluids are suitable for cooling applications [Prabhakaran et al. 2016]. 20% PG (propylene glycol)-water was used as the working fluid. As a result, the thermal conductivity increased with increasing volumetric concentration of nanofluid. The increasing of the solar collectors efficiency is from the greatest to the least: MWCNT, CuO, Al_2O_3, TiO_2 and SiO_2 nanofluids [Kim et al., 2016]. In the case of 2% nanoparticle addition, the thermal conductivity increased by 16% and the viscosity decreased by 47%. The sand-propylene glycol-water nanofluid could be used as a heat transfer fluid in solar collectors [Manikandan and Rajan, 2016].

Studies investigating the effect of different cross-sectional types of channels on entropy generation are available in the literature. Optimum duct geometry was determined by using second-law analysis. Circular duct exhibits lowest total entropy generation compared to triangular and rectangular duct geometries [Sahin, 1998].

Entropy generation was obtained for semi-cylindrical ducts for laminar flow and subjected to constant wall heat flux. The effect of heat flux rate, Reynolds number and cross sectional area on entropy generation was investigated. The cross-sectional area and the wall heat flux were found to have a significant effect on entropy generation [Oztop, 2005]. The effect of cross section shape on entropy generation minimization was studied for fully developed laminar and turbulent flow [Jankowski, 2009]. The entropy generation was investigated in the hexagonal channel for fully developed laminar convection. Water and engine oil were used as the working fluid [Jarungthammachote, 2010]. The effect of cross section shape on entropy generation minimization was examined. Circular, square and triangle cross section shapes were considered. The Al_2O_3-water and MWCNT-water nanofluids were used as the working fluid. Circular duct produces lowest total entropy generation compared to other considered shapes [Leong ve Ong, 2014] .

According to minimal entropy generation principle, the optimum design conditions of thermal systems are obtained when entropy generation is minimized. Because entropy generation indicates the irreversibility of thermal system, minimizing entropy generation makes the thermal systems more efficient [Bejan, 1996].

Numerous studies are available in the literature about entropy generation minimization of thermal systems to find their optimum design conditions. Entropy generation of the Al_2O_3-water and ethylene glycol- Al_2O_3 nanofluids was investigated in a circular pipe subjected constant wall heat flux boundary conditions. It is found that increase the thermal performance of the Al_2O_3-water nanofluids with Re numbers less than 40000 and ethylene glycol- Al_2O_3 nanofluids flow with $Re<11$. Optimum conditions were represented for both laminar and turbulent regimes [Moghaddami et al., 2011].

Three different diameters (0.1 mm, 1mm, and 10 mm) were studied. It is found that fluid flow irreversibility is dominant at lower tube diameter, heat transfer irreversibility is dominant at higher tube diameter [Singh et al., 2010]. Entropy generation of Al_2O_3-water nanofluid was obtained in circular tube under constant wall heat flux boundary condition for turbulent flow. The study was carried out under different parameters (i.e. constant Re, fixed mass flow rate and constant velocity). Low nanoparticle concentration is required to decrease the total entropy generation when the velocity is kept constant [Bianco et al., 2014]. Entropy generation analysis of Al_2O_3-water nanofluids was found in square section tubes for turbulent flow. The optimum Re numbers were obtained for Al_2O_3-water nanofluids flow [Bianco et al., 2011]. Entropy generation analysis of nanofluid flow was carried out in a circular tube for laminar regime. Tube was immersed in an isothermal external fluid. Water-Al_2O_3 and ethylene glycol- Al_2O_3 were selected as working nanofluids. The effect of the non-dimensional temperature differences, external Biot number, and volume fraction on the entropy generation was investigated. The addition of nanoparticles is only useful for small Reynolds numbers and for less viscous fluids [Anand, 2015].

The water has a higher freezing point and lower boiling point a compared to ethylene glycol-water mixture. In addition, the viscosity of the ethylene glycol is higher than the viscosity of the ethylene glycol-water mixture, thus reducing the required pumping power. Thus, ethylene glycol is preferred as antifreeze in automobile radiators and solar energy systems. But, the use of propylene glycol is recommended to avoid adverse effects caused by ethylene glycol. Because, propylene glycol, which is much less toxic than ethylene glycol [Ethylene Glycol and Propylene Glycol Toxicity, 2017]. However, there are no studies comparing the performance of thermal systems using ethylene glycol and propylene glycol as antifreeze in the literature.

In present study, entropy generation minimization of a mixture of ethylene glycol-water and propylene glycol-water fluid flow was carried out. Thermodynamic performance of two different fluids was compared. In addition, a variety of cross section shape is important in thermal system design and can be used to enhance the thermal performance. Also, this study investigated the entropy generation characteristics of various particle volume fraction, and cross section shape of thermal ducts for W/PG (60:40)-Al_2O_3 nanofluid flow. Furthermore, effect of cross sectional-area of ducts on entropy generation was investigated. There are no studies investigating the entropy generation characteristics of various particle volume fraction, cross section shape and area for turbulent flow in literature.

In present study, W/PG (60:40)-Al_2O_3 nanofluid flow entropy generation in a circular cross-section thermal duct under turbulent regime and constant uniform heat flux was analytically investigated. As a result, the Re numbers ranges in which the addition of nanoparticles to W/PG is advantageous in terms of thermodynamics were obtained under turbulent regimes. In addition, the optimum Re numbers, where the entropy generation is minimum, were obtained.

METHODOLOGY

Description of problem

In present study, W/PG (60:40)-Al_2O_3 nanofluid flow entropy generation through a circular thermal duct was investigated. The circular pipe is shown in Fig. 1, subjected to a constant heat flux of q= 9450 W/m^2 has a diameter of 16 mm and a length of 1 m. W/PG -Al_2O_3 flow is investigated for turbulent flow conditions. Nanoparticles concentration ranged from 0% up to 5%.

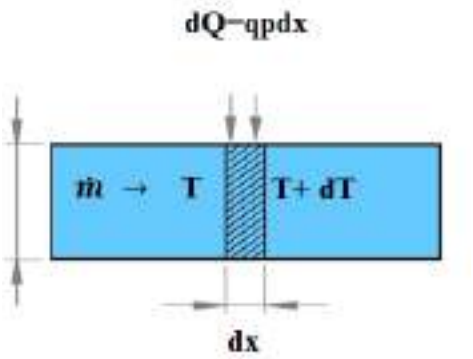

Fig.1. The Schematic Of The Physical System Under Investigation

The temperature rise along the pipe is small and the thermal properties of the base fluid and nanoparticles are obtained at the mean temperature (303 K). Since the variation of thermal conductivity and viscosity is less than 2.5% with 5 ^oC temperature change, temperature-dependent changes of the nanofluid properties are neglected [Das et al., 2003]. Thermal properties of base fluid and Al_2O_3 nanoparticles are found Table 1 [ASHRAE, 2009; Pak and Cho, 1998].

Table 1. Properties Of Base Fluid And Al_2O_3 Nanoparticles [ASHRAE, 2009; Pak and Cho, 1998]

Material	Density kg/m^3	Viscosity kg/m. s	Thermal conductivity W/mK	Specific heat J/kgK
(W/PG) (60:40)	1031.03	0.00312	0.392	3735
Al_2O_3	3880	-	36	773

Thermophysical properties of nanofluids

The thermophysical properties of the W/PG (60:40)-Al_2O_3 nanofluid may be calculated as depend on nanoparticle volume concentration, base fluid and nanoparticles properties. The nanofluid density is obtained following equation:

$$\rho_{nf} = (1-\phi)\rho_{bf} + \phi\rho_p \quad (1)$$

Specific heat is calculated by following equation by assuming the thermal equilibrium between the nanoparticles and the base fluid [Buongiorno, 2006]:

$$Cp_{nf} = \frac{(1-\phi)\rho_{bf}Cp_{bf}+\phi\rho_p Cp_p}{\rho_{nf}} \quad (2)$$

These equations were validated (1-2) by experimentally [Pak and Cho, 1998; Xuan and Roetzel, 2000]. And for the W/PG (60:40)-Al_2O_3 nanofluid, thermal conductivity and viscosity can be obtained by [Maxwell, 1891; Brinkman, 1952]:

$$k_{nf} = k_f\left[\frac{k_p+2k_{bf}+2\phi(k_p-k_{bf})}{k_p+2k_{bf}-\phi(k_p-k_{bf})}\right] \quad (3)$$

$$\mu_{nf} = \frac{\mu_{bf}}{(1-\phi)^{2.5}} \quad (4)$$

GOVERNING EQUATIONS

The entropy generation of the W/PG (60:40)-Al_2O_3 nanofluid flow in a circular duct is investigated analytically in present study. The principle of Bejan [Bejan, 1996] was used for entropy generation analysis.

There are two entropy source for W/PG (60:40)-Al_2O_3 nanofluid flow through the duct. These sources are heat transfer and fluid friction and are defined as follows:

$$S_{gen,T} = S_{gen,t} + S_{gen,f} \quad (5)$$

To determine the effect of the two entropy sources on the total entropy generation, the Bejan number (Be), a dimensionless parameter, is considered.

$$Be = \frac{S_{gen,t}}{S_{gen,T}} \quad (6)$$

The Be number changes from 0 to 1. The high values of Be number indicate that the thermal entropy is dominant.

The two irreversibility sources given in Eq. 5 are calculated as follows:

$$S_{gen,T} = \frac{q'\Delta T}{T^2} + \frac{\dot{m}}{\rho T}\left(-\frac{dP}{dx}\right) \quad (7)$$

Eq. (7) gives the local total entropy generation for per unit length. In Eq. (7), the first term indicates the thermal entropy generation, and the second term represents the frictional entropy generation.

When Eq. (7) is integrated, it is obtained as follows [Bejan, 1996]:

$$S_{gen,T} = \frac{q'^2}{4T^2\,\dot{m}c_p}\frac{D}{St} + \frac{2\dot{m}^3 f}{\rho^2 TDA^2} \quad (8)$$

Eq. (8) can be defined for circular-cross section duct, as follows:

$$S_{gen,T} = \frac{q'^2}{\pi k T^2 Nu} + \frac{32\dot{m}^3 f}{\pi^2\rho^2 TD^5} \quad (9)$$

Thus, thermal and frictional entropy generation are expressed as :

$$S_{gen,t} = \frac{q'^2}{\pi k T^2 Nu} \quad (10)$$

$$S_{gen,f} = \frac{32\dot{m}^3 f}{\pi^2 \rho^2 T D^5} \quad (11)$$

In Eq. (9), the mean temperature which is the average of the inlet and outlet temperatures is calculated [Moghaddami et al., 2011]. Nu number and friction factor are calculated for turbulent flow conditions. Governing equations for turbulent flow are given below.

Nusselt number can be determined as follows [Gnielinski, 1976]:

$$Nu = \frac{\left(\frac{f}{8}\right)(Re - 1000)Pr}{1 + 12.7\left(\frac{f}{8}\right)^{0.5}\left(Pr^{\frac{2}{3}} - 1\right)} \quad (12)$$

Where

$$Re = \frac{uD}{\nu} \quad (13)$$

$$Pr = \frac{\mu C_p}{k} \quad (14)$$

$$St = \frac{Nu}{RePr} \quad (15)$$

The friction factor (f) of the fluid flow can be obtained as follows [Petukhov, 1970]:

$f = (0.79lnRe - 1.64)^{-2}$ (16)

To measure the efficiency of the heat transfer augmentation technique, its performance should be compared to the original thermal system. Since present study is related to the entropy generation, the corresponding augmentation number is augmentation entropy generation number, defined as [Bejan, 1996]:

$$N_{s,a} = \frac{S_{gen,a}}{S_{gen,o}} = \frac{Entropy\ generated\ in\ system\ with\ nanofluids}{Entropy\ generated\ in\ system\ with\ basefluids\ only} \quad (17)$$

The $N_{s,a}$ value lower than 1 is desirable in view of thermodynamics [Bejan, 1996]. As mentioned before, present study investigates the entropy generation characteristics of various shapes of cross section ducts and effect of cross sectional-area on entropy generation was investigated for W/PG (60:40)-Al_2O_3 nanofluid flow. For this, the hydraulic diameters of different geometries are determined by using Table 2 [Cengel, 2003].

Table 2. Different cross-section shapes [Cengel, 2003]

Cross section	Diagram	Perimeter	Area	Hydraulic Diameter
Circular	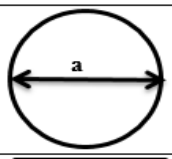	πa	$\frac{\pi a^2}{4}$	a
Square	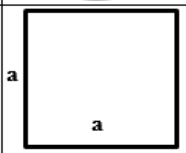	$4a$	a^2	a
Equilateral Triangle	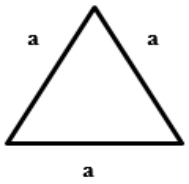	$3a$	$\frac{\sqrt{3}}{4}a^2$	$\frac{\sqrt{3}}{3}a$

RESULTS and DISCUSSIONS

Entropy generation of W/PG (60:40)-Al_2O_3 nanofluid

Fig. 2 shows that the thermal, frictional, and total entropy generation versus Re number for turbulent regimes, respectively. Fig. 2a shows that thermal entropy decreases with increasing Re number. As the Re number increases, the thermal entropy decreases because of the improvement of the heat transfer properties of pure W/PG and W/PG - Al_2O_3 nanofluid.

Furthermore, adding Al_2O_3 nanoparticles to the W/PG increases the thermal conductivity, so the thermal entropy decreases. W/PG-Al_2O_3 nanofluid (ϕ=5%) has the lowest thermal entropy while pure W/PG has the highest thermal entropy.

Fig. 2b illustrates that frictional entropy increases with increasing Re number. Because, the mass flow rate increases with increasing Re number. This causes an increase in frictional entropy. In addition, adding Al_2O_3 nanoparticles to the pure W/PG increases the viscosity, thus frictional entropy increases. W/PG - Al_2O_3 nanofluid (ϕ=5%) has the highest frictional entropy while W/PG (ϕ=0) has the lowest frictional entropy.

Fig. 2c demonstrates that total entropy generation for W/PG - Al_2O_3 nanofluid flow for turbulent conditions. At the beginning, the total entropy decreases with the addition of Al_2O_3 nanoparticles, since thermal entropy is dominant.

As the Re number increases, the addition of Al_2O_3 nanoparticles increases total entropy in order to frictional entropy is dominant. For the same reason, the total entropy decreases with the increase of the Re number at the beginning, then the total entropy increases at the higher Re numbers. The optimum Re numbers, where the entropy

generation is minimum, are 7217(ϕ=0), 7162(ϕ=1%), 6998(3%), 6838 (5%) under turbulent regime. It is found that adding Al_2O_3 nanoparticles to propylene glycol -water decreases the optimum Reynolds numbers. Similar results were found by Moghaddami et al. [Moghaddami et al., 2012]. They found that adding Al_2O_3 nanoparticles to pure water decreases the optimum Reynolds numbers.

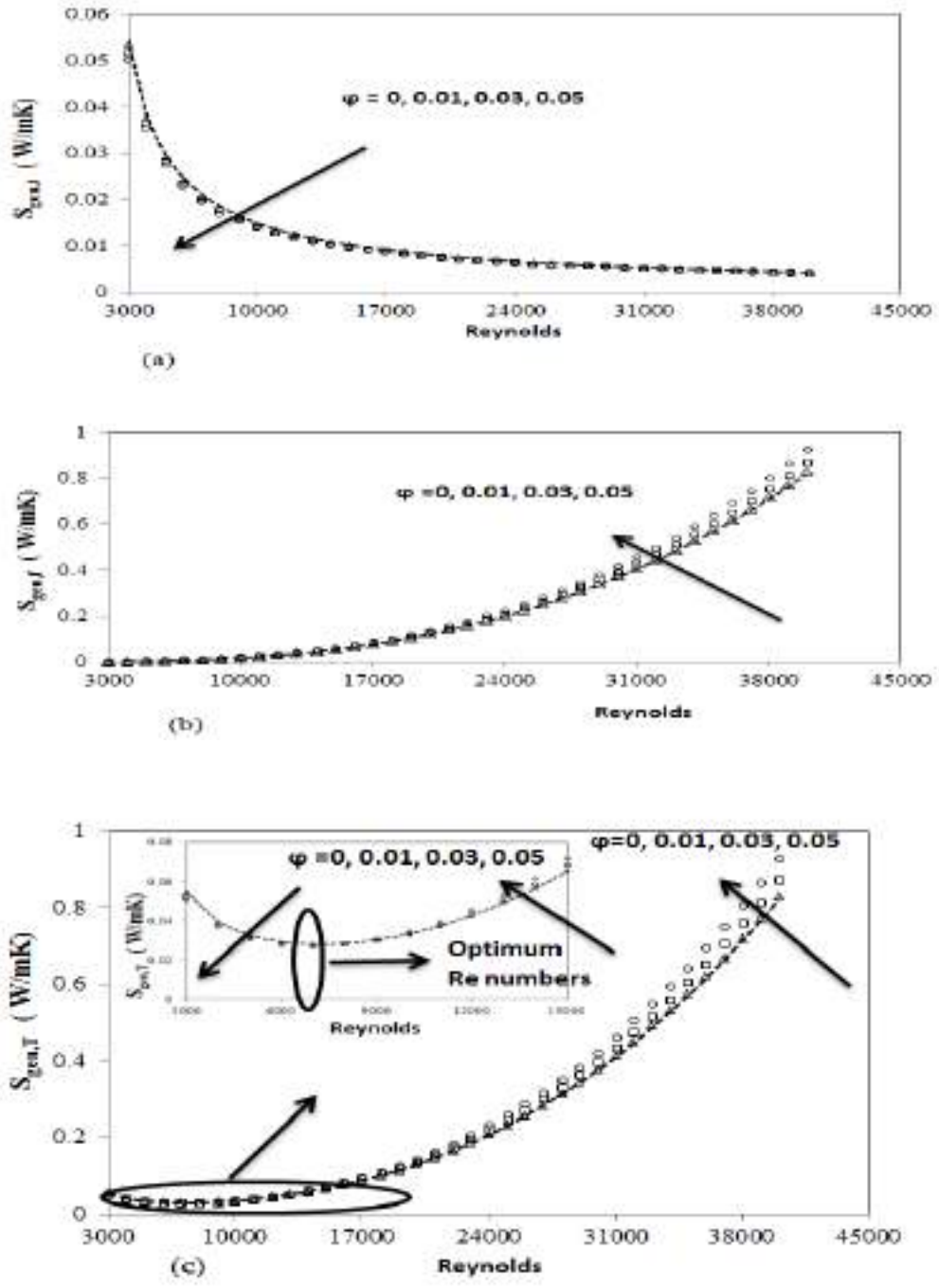

Fig. 2. Entropy Generation Versus Re Number (a) Thermal Entropy Generation, (b) Frictional Entropy Generation, (c) Total Entropy Generation

Figure 3 shows that the variation of the Be number versus Re number. The Be number decreases with increasing Re number. The heat transfer irreversibility decreases with the addition of Al_2O_3 nanoparticles, and the Be number decreases.

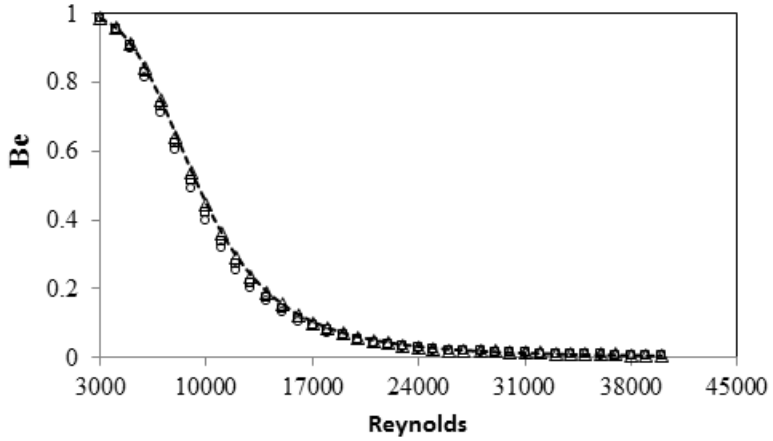

Fig.3. Variation of Bejan Number Versus Re Number.

Fig. 4 demonstrates that the augmentation entropy generation number versus Re number. $N_{s,a}$ values of W/PG- Al_2O_3 nanofluids are smaller than 1 from Re=3000 to Re=10392(ϕ=1%), 9007(ϕ=3%), 8241(ϕ=5%). This means, it is thermodynamically advantageous, adding Al_2O_3 nanoparticles to the pure W/PG from Re=3000 to Re=10392(ϕ=1%), 9007(ϕ=3%), 8241(ϕ=5%) in turbulent regime. Because, thermal entropy is dominant at these reynolds number ranges. In the turbulent flow, frictional entropy is dominant beyond the considered Re number for each concentrations and increases with increasing Re number. It is not thermodynamically advantageous, adding Al_2O_3 nanoparticles to pure W/PG beyond the considered Re number for each concentrations in the turbulent flow conditions.

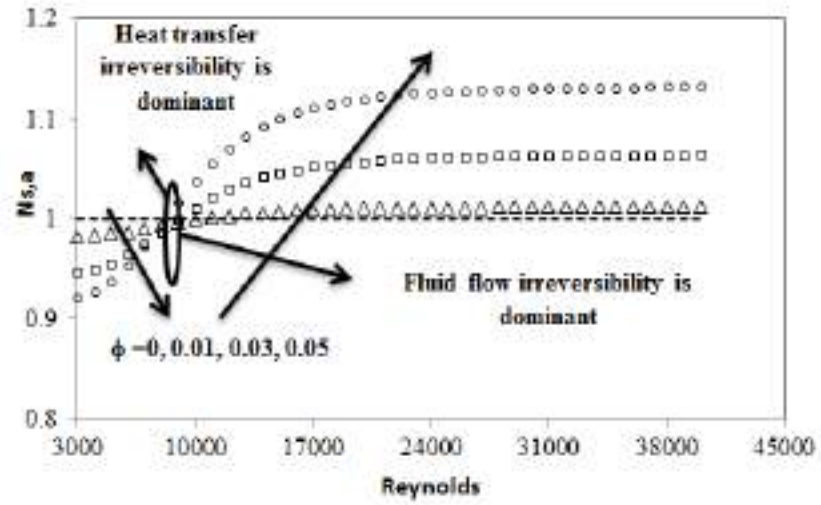

Fig.4. Augmentation Entropy Generation Number Of W/PG-Al_2O_3 Nanofluid Versus Re Number

Effect of particle volume fraction, and cross section shape, area of thermal ducts

Fig. 5 represents that total entropy generation of W/PG (60:40)-Al_2O_3 nanofluid with respect to particle volume fraction. It is found that total entropy generation increases with the increase of particle volume fraction for all cross section shapes. Because, when the volume fraction increases in turbulent regime, viscosity increases.

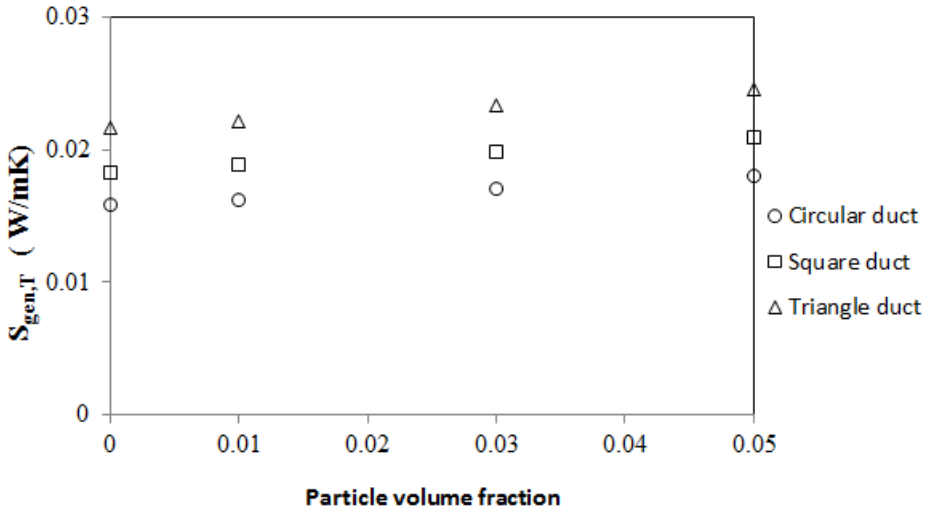

Fig.5. Effect Of Particle Volume Fraction On Entropy Generation For Various Cross-Section Shapes (A= 0.015 m^2)

Fig. 6 shows that cross section shape and area effect on total entropy generation. In this study, the hydraulic diameters were calculated for same cross-section area. Fig. 6 shows that the thermal duct with the lowest entropy generation is the circular channel. This is followed by square and triangular ducts, respectively. The reason of this, the highest hydraulic diameter belongs to the circular channel for same cross-section area. As the hydraulic diameter increases, the Re number increases. As the Re number increases, the friction factor reduces, so the total entropy reduces. The same result is seen for the same volumetric concentration in Fig. 5. Similar results were found [Leong ve Ong, 2014]. They found that thermal duct with the lowest entropy generation is the circular channel for laminar flow conditions. Figure 6 shows that total entropy generation increases with increasing cross-sectional area. Because, as the cross-sectional area increases, the mass flow rate increases. As a result, the total entropy increases.

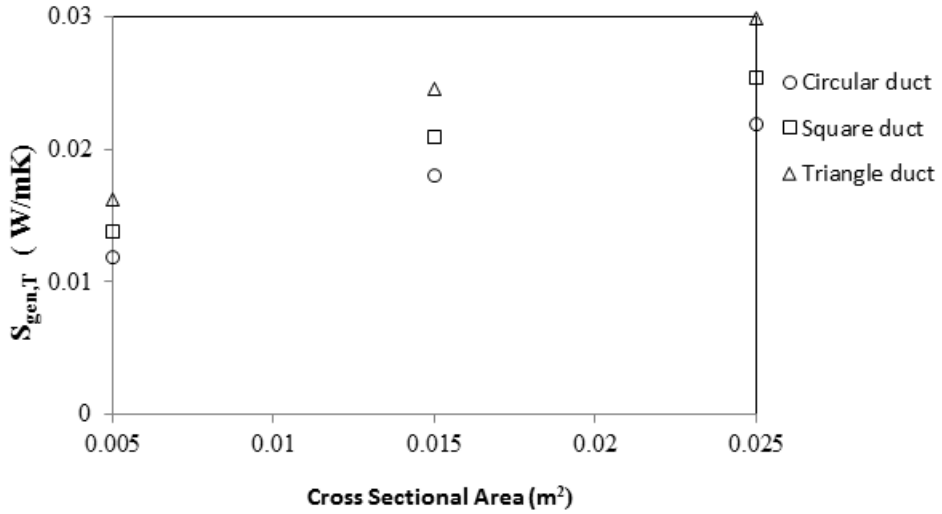

Fig.6. Effect Of Cross Sectional Area On Entropy Generation For Various Cross Sectional Shapes (ϕ=5%)

Comparison of entropy generation for W/EG and W/PG fluid flow

Fig.7. shows that total entropy generation of W/EG and W/PG fluid flow for turbulent flow. In both fluid flow, initially the total entropy decreases and then increases. The entropy generation of W/PG fluid flow is higher than W/EG fluid flow. Because, thermal conductivity of PG is lower than EG, and viscosity of PG is higher than EG, thermal properties of PG are worse than EG. The frictional entropy is dominant for high Re numbers. In order to W / PG' s higher viscosity, the entropy generation of W / PG flow more increases. If it is desired to use PG as antifreeze, the thermal properties of the W / PG mixture can be improved by reducing the volumetric concentration of PG. Fig. 7 shows that in the case of using 30% PG or 40% EG is used as antifreeze, the entropy generation are almost the same for water mixture.

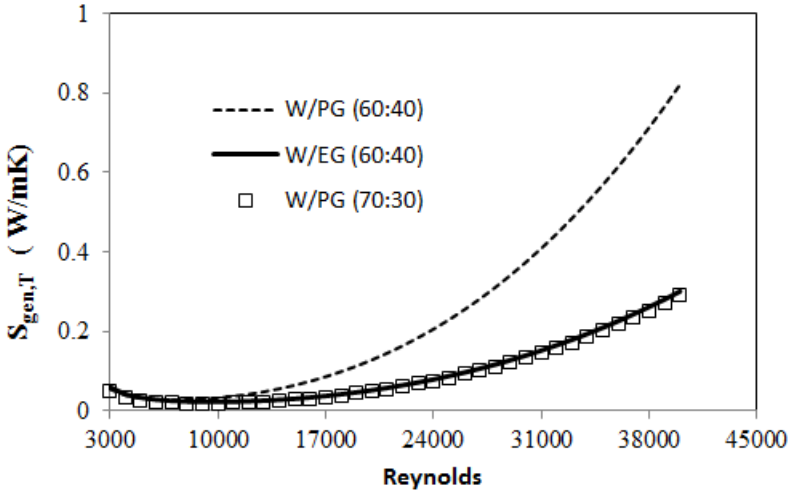

Fig. 7. Comparison Of Entropy Generation For W/PG And W/EG Fluid Flow

CONCLUSION

In present study, W/PG (60:40)-Al_2O_3 nanofluid flow entropy generation in a circular cross-section thermal duct under turbulent regime and constant uniform heat flux was analytically investigated. In addition, this study investigates the entropy generation characteristics of various particle volume fraction and cross section shape and area for W/PG (60:40)-Al_2O_3 nanofluid flow. Furthermore, thermodynamic performance of W/PG and W/EG fluid flow was compared.

Whether the addition of Al_2O_3nanoparticles in turbulent flow is thermodynamically advantageous depends on the Re number and the volumetric concentration of Al_2O_3 nanoparticles.

$N_{s,a}$ values of W/PG- Al_2O_3 nanofluids are smaller than 1 from Re=3000 to Re=10392(ϕ=1%), 9007(ϕ=3%), 8241(ϕ=5%). It is not thermodynamically advantageous to add Al_2O_3 nanoparticles to pure W/PG beyond the considered Re number for each concentrations in the turbulent regime.

The optimum Re numbers, where the entropy generation is minimum, are 7217(ϕ=0), 7162(ϕ=1%), 6998(3%), 6838 (5%) for turbulent flow regime. It is shown that adding Al_2O nanoparticles to propylene glycol-water mixture decreases the optimum Reynolds numbers.

The thermal ducts are ranked in order from lowest to highest entropy generation: circular, square, triangle.

Total entropy generation increases with the increasing cross-sectional area.

The entropy generation of W/PG fluid flow is higher than W/EG fluid flow.

In the case of using 30% PG or 40% EG as antifreeze, the entropy generation are almost the same for water-glycol mixture.

REFERENCES

Anand, V. (2015). Entropy generation analysis of laminar flow of a nanofluid in a circular tube immersed in an isothermal external fluid. *Energy 93, 154-164.*

ASHRAE Handbook – Fundamentals (SI edition), (2009). Atlanta: American Society of Heating, Refrigerating and Air-Conditioning Engineers Inc.

Bejan, A. (1996). *Entropy Generation Minimization*. Boca Taron: CRC Press.

Bianco, V., Manca, O., Nardini, S. (2014). Entropy generation analysis of turbulent convection flow of Al_2O_3–water nanofluid in a circular tube subjected to constant wall heat flux. *Energy Convers. Manage. 77, 306–314.*

Bianco, V., Nardini, S., Manca, O. (2011). Enhancement of heat transfer and entropy generation analysis of nanofluids turbulent convection flow in square section tubes. *Nanoscale Res. Lett. 6, 252.*

Brinkman, H.C. (1952). The viscosity of concentrated suspensions and solutions. *The Journal of Chemical Physics, 20, 571–581.*
Buongiorno, J. (2006). Convective transport in nanofluids. *ASME J. Heat Transfer 128, 240–250.*
Cengel, Y.A. (2003). *Heat Transfer: A Practical Approach*. New York: McGraw- Hill.
Das, S.K., Putra, N., Thiesen, P., Roetzel, W. (2003). Temperature dependence of thermal conductivity enhancement of nanofluids. *Trans. ASME, J. Heat Transfer 125, 567–574.*
Ethylene Glycol and Propylene Glycol Toxicity, Public Health Service, U.S. Department of Health and Human Services, Public Health Service in Atlanta, GA. Retrieved from https://www.atsdr.cdc.gov/csem/csem.asp?csem=12&po=2.
Gnielinski, V. (1976). New equations for heat and mass transfer in turbulent pipe flow and channel flow. *Int. Chem. Eng. 16, 359–368.*
Jankowski, T.A. (2009). Minimizing entropy generation in internal flows by adjusting the shape of the cross-section. *International Journal of Heat and Mass Transfer 52, 3439–3445.*
Jarungthammachote, S. (2010). Entropy generation analysis for fully developed laminar convection in hexagonal duct subjected to constant heat flux. *Energy 35, 5374–5379.*
Kim, H., Ham, J., Park, C. Cho, H. (2016). Theoretical investigation of the efficiency of a U-tube solar collector using various nanofluids. *Energy 94, 497–507.*
Leong, K.Y., Ong, H.C. (2014). Entropy generation analysis of nanofluids flow in various shapes of cross section ducts. *Int. Commun. Heat Mass 57, 72–78.*
Manikandan, S., Rajan, K.S. (2016). Sand-propylene glycol-water nanofluids for improved solar energy collection. *Energy 113, 917-929.*
Maxwell, J.C. (1891). *A Treatise on Electricity and Magnetism*. UK: Clarendon Press.
Moghaddami, M., Shahidi, S.E., Siavashi, M. (2012). Entropy generation analysis of nanofluid flow in turbulent and laminar regimes. *J. Comput. Theor. Nanosci. 9, 1–10.*
Moghaddami, M., Mohammadzade, A., Varzane Esfehani, S.A. (2011). Second law analysis of nanofluid flow. *Energy Convers. Manage. 52, 1397–1405.*
Naik, M.T., Sundar, L.S. (2014). Heat transfer and friction factor with water/propylene glycol-based CuO nanofluid in circular tube with helical inserts under transition flow regime. *Heat Transfer Eng. 35,53–62.*
Oztop, H.F. (2005). Effective parameters on second law analysis for semicircular ducts in laminar flow and constant wall heat flux. *Int. Comm. Heat Mass Transfer 32, 266–274.*
Pak, B.C., Cho, Y.I. (1998). Hydrodynamic and heat transfer study of dispersed fluids with submicron metallic oxide particles. *Exp. Heat Transfer 11,151– 170.*
Petukhov, B.S. (1970). Heat transfer in turbulent pipe flow with variable physical properties. in: J.P. Harnett (Ed.), *Advances in Heat Transfer, vol. 6, Academic Press, New York, 504–564.*
Prabhakaran, M., Manikandan, S., Suganthi, K.S., Vinodhan, V.L., Rajan, K.S. (2016). Development and assessment of ceria–propylene glycol nanofluid as an alternative to propylene glycol for cooling applications. *Applied Thermal Engineering 102, 329-335.*
Sahin, A.Z. (1998). Irreversibilities in various duct geometries with constant wall heat flux and laminar flow. *Energy 23, 465-473.*

Singh, P.K., Anoop, K.B., Sundararajan, T., Das, S.K. (2010). Entropy generation due to flow and heat transfer in nanofluids. *Int. J. Heat Mass Transfer, 53, 4757– 4767.*
Xuan, Y., Roetzel, W. (2000). Conceptions for heat transfer correlation of nanofluids. *International Journal of Heat and Mass Transfer 43, 3701–3708.*

COMPARISON OF CAPITAL COST FLOWS OF 1 MW SOLAR POWER PLANT WITH AND WITHOUT SOLAR TRACKING SYSTEM

Mert Gürtürk
Department of Energy Systems Engineering, Technology Faculty, Fırat University, 23119 Elazig, Turkey, m.gurturk@gmail.com

ABSTRACT: In this study, the cost analysis is used to determine the capital cost flow of two different solar power plants. PV panels at one of these solar power plants are located at fixed collector angle, whereas the other one with the same operating conditions has a solar tracking system. Although both PV solar power plants operate under similar conditions, there are many differences in terms of economic parameters. These parameters can be used for the economic feasibility of solar power plant for investors. Some of these parameters are capital cost flow, operation and maintenance cost, total capital investment, present value factor, annual capital cost, salvage value. The results obtained from both economic analyzes were compared according to the parameters considered.

Keywords: Economic analysis; solar power plant; renewable energy; solar energy

INTRODUCTION

The investment costs of the solar power plant are very important for investors. However, studies about economic analysis of solar power plants are very rare and investments in solar power plants are increasing in many parts of the world. Generally, economic analysis about solar power plant based on the PV module is carried out by big organizations, councils and intuitions. One of those reports about economic analysis worldwide is published by The World Energy Council. That organization publishes very detail report on solar energy in every year. In that report, many parameters are considered such as solar energy, information about the sector, the latest economic data and so on (Khetarpal, 2016). In the same perspective, The European Union is also publishing a similar report. In that report, up-to-date information on the solar energy sector in the European Union member countries is shared. Also, evaluation of policies of the other countries on solar energy can be found in that report (Jäger-waldau, 2016). Reports of national institutes on the solar energy sector can be found in the literature. Those reports are handled mainly economic data and policies of investors, governments and producers. One of those national institutes is the National Renewable Energy

Laboratory. That institute has shared the latest technological developments, studies about the solar cell, economic data and recent investments on a national basis (National Renewable Energy Laboratory, 2018). However, those institutions and councils are not considering specific economic data. For example, levelized cost analysis is used for determining capital cost flows of two different solar power plants. In the previous study, one of these solar power plants was designed as PV panels placed at fixed collector angle (Gürtürk, 2019). The other solar energy plant considered in this study is designed with a solar tracking system. In the literature, many studies about the solar tracking system can be found (Mousazadeh et al., 2009). Those studies are about novel solar tracking system design, tracking the sun at low error rates, advantages and disadvantages of solar tracking systems and so on. For example, researchers have studied on passive solar tracking (Clifford & Eastwood, 2004) and they said that azimuth-elevation and tilt-roll tracking mechanism method have been most used (Chong & Wong, 2009). As can be seen, any study about economic advantages and disadvantages of solar tracking systems cannot be found in the literature. However, very limited analysis which was about the economic benefits of solar tracking system has been carried out in the literature (Bhagat, 2016).

MATERIAL AND METHODS

The levelized cost analysis considers many economic parameters. These parameters show capital cost flow, cost of operating and maintenance, total capital investment, present value factor, annual capital cost, salvage value. These parameters are calculated as follows,

$\dot{Z}$ is the capital cost flow (Bejan, Tsatsaronis, & Moran, 1996; Gürtürk, 2019; Gürtürk, Oztop, & Hepbasli, 2015).

$$\dot{Z} = \dot{Z}^{CI} + \dot{Z}^{OM} \quad (1)$$

where $\dot{Z}^{CI}$ is the hourly levelized cost of capital investment. $\dot{Z}^{OM}$ is the hourly levelized cost of operating and maintenance of the solar power plant.

$$\dot{Z}^{CI} = \frac{AC}{\tau} \quad (2)$$

Hourly levelized operating and maintenance cost ($\dot{Z}^{OM}$) is calculated by using Eq. (3) (Bejan et al., 1996; Gürtürk, 2019; Gürtürk & Oztop, 2016; Gürtürk et al., 2015).

$$\dot{Z}^{OM} = \frac{OM}{\tau} \quad (3)$$

Many parameters are considered for the levelized cost analysis and these parameters are shown in Table 1 (Gürtürk, 2019).

Table 1. Economical parameters of solar power plants with and without a solar tracking system for 1 MW power (US$) (Gürtürk, 2019)

	Without a solar tracking system	With a solar tracking system

Parameters		
PV modules (270 W)	594,000.00	594,000.00
Inverter	98,600.00	98,600.00
Other system components	237,726.00	237,726.00
Other costs	226,437.00	226,437.00
Solar tracking system	-	115,676.33
TOTAL COST	***1,156,763.34***	***1,272,439.67***

These costs parameters considered in the study may vary. For example, land structure, panel type used and transportation costs may affect initial investment costs. At the same time, the variability of global economic parameters should be considered. Especially when macroeconomic parameters are considered, their effects on costs may vary. In summary, it should be noted that the values in table 1 are not constant and depend on the reasons explained above.

RESULTS AND DİSCUSSİON

In this study, a levelized cost analysis was carried out for determining capital cost flows of two different solar power plants which are designed as PV panels placed at fixed collector angle and with solar tracking system. Considering the data in Turkey, foreign currency loan interest rates for both system are taken into consideration as 6%. Results obtained from the economic analysis shows in Table 2.

Table 2. Results obtained from the economic analysis (US$)

Parameters	Without a solar tracking system	With a solar tracking system
Present worth	1,130,855.909	1,272,439.67
Salvage value	115,676.344	127,243.96
Present value factor	2.28E-08	2.28E-08
Effective discount rate	6%	6%
Annual capital cost	89,878.39	98,866.22
Capital recovery factor	0.079	0.079
Hourly levelized cost of capital investment	10.26 (US$/h)	11.28 (US$/h)
Hourly levelized cost of operating and maintenance	5.79 (US$/h)	7.84 (US$/h)
Capital cost flow	16.05 (US$/h)	19.13 (US$/h)

It can be said that the initial investment cost is high for both systems. However, it is seen that the initial investment cost of a solar energy plant which has a solar tracking system, is higher. Many published reports indicate that prices are still high due to the need for raw materials in the production of photovoltaic panels. Although the initial investment cost of solar power plants is high, the cost of a power plant with a solar tracking system seems to be the most important barrier. Also, the costs of operating and maintenance of the solar tracking systems are high too. It is observed that the solar tracking systems increase the total power output at a rate between 20 - 40% (Samsamoddin Naghavi Chalehtori & M. Funde, 2015). When solar power plants are considered according to economic values, the most important parameter is the first investment cost. The investors want to decrease this parameter, and they chose solar power plants which are designed as PV panels placed at fixed collector angle. Results obtained from the analysis show that capital cost flow of the solar power plant which is designed as PV collectors placed at fixed collector angle is 16.05 (US$/h). The capital cost flow of the other system which is designed solar tracking system is 19.13 (US$/h). When costs of operating and maintenance of both systems are compared, cost of operating and maintenance of the solar power plant which is designed solar tracking system is higher. Costs of operating and maintenance of both systems were calculated as 5.79 (US$/h) for the fixed system (Gürtürk, 2019) and 7.84 (US$/h) with a solar tracking system. When present worthies of both systems are compared, it was calculated as 1,130,855.909 (US$) for the fixed system and 1,272,439.67 (US$) with the solar tracking system. Actually, there is no significant difference between the two values. If a solar tracking system is used in the solar power plant, increasing 19% at capital cost flow of the system and increasing 35.4% at an hourly levelized cost of operating and maintenance occurs.

More detailed analysis can be found in the literature. According to the cost situation, the level of investment feasibility was determined by using different methods. There is no significant difference between the systems where PV panels are fixed and combined with a single axis solar tracking system. However, dual-axis solar tracking systems cause significant differences (Honrubia-Escribano et al., 2018). The effect of these differences on initial investment cost and maintenance operating costs was clearly seen in this study. However, the investability of PV power plants integrated with fixed and dual-axis solar tracking systems varies depending on the capacity. The location where the power plant will be installed has a great impact on these parameters. When the installed capacity of the solar power plant increases, the investment viability of the solar tracking system increases. S If this factor is taken into consideration, preferring solar tracking system in solar power plants with an installed capacity of 1 MW will provide significant advantages. However, in developing countries, solar tracking systems are generally not preferred due to efforts to reduce initial investment costs and lack of incentives for solar tracking systems.

CONCLUSIONS

In this study, levelized cost analysis is used for determining capital cost flows of two different solar power plants and conclusion obtained from this study are illustrated following,

• Solar tracking system causes a significant increase at an hourly levelized cost of operating and maintenance. This increasing is 35.4%.
• The capital cost flow of the solar power plant which is designed solar tracking system is calculated as 19.13 (US$/h).
• The annual capital cost of the solar power plant which is designed solar tracking system is 98,866.22 (US$).
• When present worthies of both systems are compared, there is no significant difference between the values. The solar power plant which is designed solar tracking system is 1,272,439.67 (US$). This study can be combined with any solar radiation forecasting methods for determining net profit and costs of both systems.

REFERENCES

Bejan, A., Tsatsaronis, G., & Moran, M. (1996). *Thermal Desgn and Optimization*. New York: John Wiley & Sons.

Bhagat, A. K. (2016). An Analysis of Economic Benefits of Solar Tracking Systems, *3*(07), 48–51.

Chong, K. K., & Wong, C. W. (2009). General formula for on-axis sun-tracking system and its application in improving tracking accuracy of solar collector. *Solar Energy*, *83*(3), 298–305. https://doi.org/10.1016/j.solener.2008.08.003

Clifford, M. J., & Eastwood, D. (2004). Design of a novel passive solar tracker, *77*, 269–280. https://doi.org/10.1016/j.solener.2004.06.009

Gürtürk, M. (2019). Economic feasibility of solar power plants based on PV module with levelized cost analysis. *Energy*, *171*, 866–878. https://doi.org/10.1016/j.energy.2019.01.090

Gürtürk, M., & Oztop, H. F. (2016). Exergoeconomic analysis of a rotary kiln used for plaster production as building materials. *Applied Thermal Engineering*, *104*, 486–496. https://doi.org/10.1016/j.applthermaleng.2016.05.106

Gürtürk, M., Oztop, H. F., & Hepbasli, A. (2015). Comparison of exergoeconomic analysis of two different perlite expansion furnaces. *Energy*, *80*, 589–598. https://doi.org/10.1016/j.energy.2014.12.015

Honrubia-Escribano, A., Ramirez, F. J., Gómez-Lázaro, E., Garcia-Villaverde, P. M., Ruiz-Ortega, M. J., & Parra-Requena, G. (2018). Influence of solar technology in the economic performance of PV power plants in Europe. A comprehensive analysis. *Renewable and*

Sustainable Energy Reviews, *82*(July 2017), 488–501. https://doi.org/10.1016/j.rser.2017.09.061

Jäger-waldau, A. (2016). *PV Status Report 2016*. https://doi.org/10.2790/749737

Khetarpal, D. (2016). World Energy Resources: Solar 2016. *World Energy Council*, 78. Retrieved from https://www.worldenergy.org/wp-content/uploads/2017/03/WEResources_Solar_2016.pdf

Mousazadeh, H., Keyhani, A., Javadi, A., Mobli, H., Abrinia, K., & Sharifi, A. (2009). A review of principle and sun-tracking methods for maximizing solar systems output, *13*, 1800–1818. https://doi.org/10.1016/j.rser.2009.01.022

National Renewable Energy Laboratory. (2018). efficiency-chart @ www.nrel.gov. Retrieved February 16, 2018, from https://www.nrel.gov/pv/assets/images/efficiency-chart.png

Samsamoddin Naghavi Chalehtori, S., & M. Funde, A. (2015). Econometric analysis of solar tracker systems in India , a case study. *International Jounrnal of Applied Engineering Research*, *10*(April), 31590–31593.

ESTIMATION OF GREENHOUSE GAS EMISSION FROM A DISSOLVED AIR FLOTATION TANK

Pelin YAPICIOĞLU
Harran University
pyapicioglu@harran.edu.tr

ABSTRACT: Greenhouse gases emissions have been increased, in recent years. One of the greenhouse gases emission resources is the industrial wastewater treatment plants. Dissolved air flotation process is implemented for fats, oil and grease and organic material removal from industrial wastewater. Dissolved air flotation tank is one of the main greenhouse gas emitter units in a dairy industry wastewater treatment plant. In this study, the off-site greenhouse gas emissions of a DAF tank located in a dairy wastewater treatment plant were estimated. The off-site emission was estimated from chemical consumption and electricity consumption. This paper aims to determine the off-site emissions for dissolved air flotation process in a dairy wastewater treatment plant. The results revealed that electricity consumption was the major source of the off-site greenhouse gas emission in the tank with the value of 3752.35 kg CO_2e/d. The off-site emission due to the chemical use was 119.51 kg CO_2e/d. Total off-site emission was 3871.86 kg CO_2e/d.

Key words: greenhouse gas, wastewater treatment plant, DAF, off-site emission.

INTRODUCTION

Greenhouse gases emissions have been increasing in the atmosphere because of the industrial, domestic and anthropogenic activities in last decades (Kyung et al., 2015). Wastewater treatment plants have been regarded as one of the greenhouse gases emissions resources in recent year (Kyung et al., 2015; Corominas et al., 2012; Yerushalmi et al., 2013; Yapıcıoğlu, 2018). Carbon dioxide (CO_2) and methane (CH_4) and nitrous oxide (N_2O) are the main greenhouse gases emitting from wastewater treatment plants due to the applying treatment process (biological, chemical or biochemical processes etc), sludge dewatering and stabilization process (incineration, anaerobic digestion, composting etc.), chemical use (added chemical materials for wastewater and sludge treatment process (coagulants, flocculants), for nitrification and denitrification (methanol, etc.), for alkalinity and pH adjustment), energy consumption (electricity consumption, air

consumption, etc.), and maintenance and transport activities (Kyung et al., 2015; Metcalf and Eddy, 2014; Yapıcoğlu, 2018).

Greenhouse gases emissions can be categorized as the on-site emissions and the off-site emissions (Parravicini et al., 2016; Yapıcıoğlu, 2018). The on-site emissions in the plants are the emitting emissions in the sewage collection system, the emissions in the result of the existing treatment processes and the emissions in the discharge point of the treated water. The off-site GHGs emissions are formed by the electricity consumption, air consumption, transportation, chemical use and sludge stabilization and disposal process (Parravicini et al., 2016; Yapıcıoğlu, 2018). In particular, the industrial wastewater plants emit the large amounts of greenhouse gas emissions because of highly organic wastewater content and applying treatment processes. The dairy industry is one of them.

The dairy industry is one of the most pollutant plants due to the wastewater generated and discharging highly organic wastewaters (Ozturk et al., 2003; Demirel et al., 2005). Chemical oxygen demand (COD), fats, oil and grease (FOG) and total suspended solids (TSS) are the major pollution indicators of the dairy wastewaters. (Speece, 1996; Yapıcıoğlu &Filibeli, 2017). The dairy wastewater has a highly organic content and fats oil and grease concentration. Dissolved Air flotation (DAF) is widely used for FOG removal from dairy wastewater. Falletti et al., 2014; Pereira et al., 2018). DAF process is applied before the secondary treatment which generally tends to be anaerobic treatment configurations (Castillo et al., 2017). Dissolved air flotation process is a type of flotation process that separates fats, oils and grease and other organic substances from wastewater (Behin & Bahrami, 2012; Chung et al., 2000). The most significant parameters in order to obtain high treatment efficiencies in DAF involve determining the volume of microbubbles occurring in the DAF tank and the coagulation and flocculation processes that depend on the pH of the media, the doses and the types of coagulants and flocculants (alum, ferric chloride etc.) used (Pereira et al., 2018; Edzwald, 2010).

In this study, the off-site greenhouse gas emissions of a DAF tank located in a dairy wastewater treatment plant were estimated. The off-site emission was estimated from chemical consumption and electricity consumption. The main aim of this study is to estimate the off-site emissions for dissolved air flotation process in a dairy wastewater treatment plant.

METHODS

Description of the Dairy Industry

The dairy industry is located in an organized industrial zone in Turkey. The main products are drinking milk, fruit juice, cream, milk powder, yoghurt and butter. The wastewater characterization of the dairy industry is given in Table 1. The wastewater analysis results were obtained using Standard Methods (APHA 1999). The wastewater treatment plant is a full-scale plant.

Figure 1 demonstrates the wastewater treatment process flow scheme in the plant. In DAF process, fats, oil, grease and suspended organic materials removal have been obtained. After wastewater is treated, then the effluent is discharged to the Organized Industrial Zone Central Sewage System.

Table 1. Influent Dairy Wastewater Characterization

Parameter	Value
COD (mg/L)	12000
FOG (mg/L)	350
TSS (mg/L)	350
pH	6
Flow Rate (Q) (m^3/d)	2100

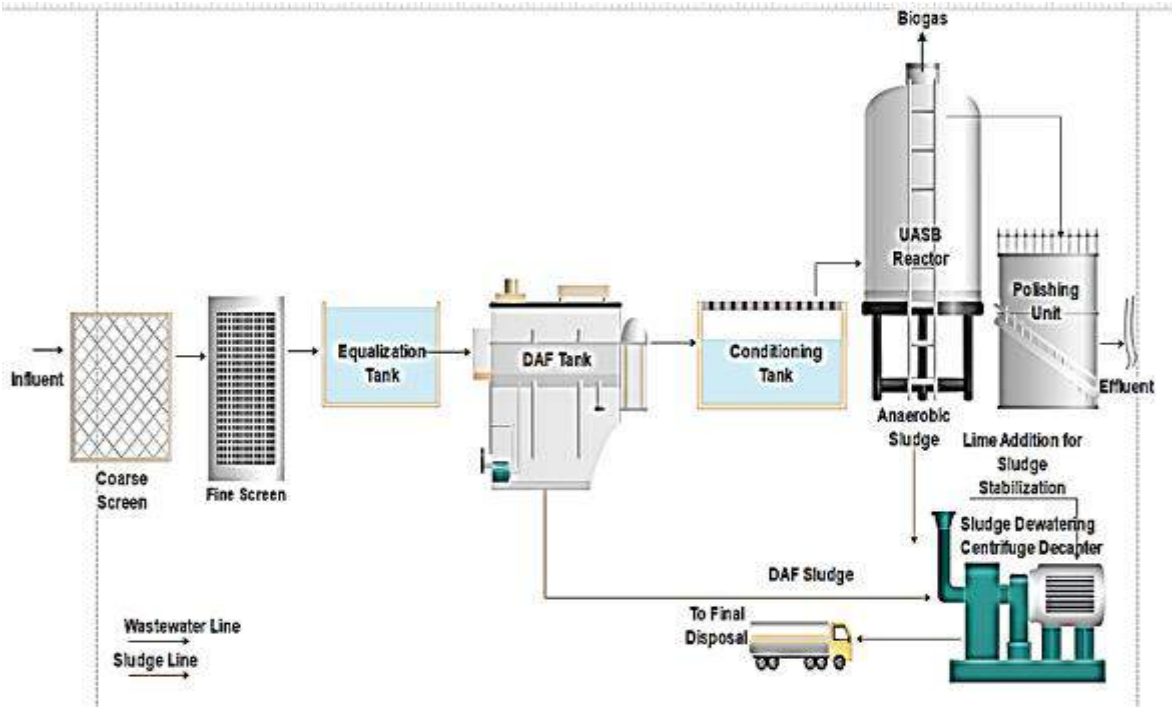

Figure 1. Wastewater Flow Scheme of the Dairy Industry WWT

Dissolved Air Flotation Process

DAF systems are designed and planned to remove suspended solids, carbonaceous materials, and fats, oil and grease from a wastewater mass. Pollutant substances are treated with the use of dissolved air in a wastewater system generated by injecting air under high pressure into a recycle stream of clarified DAF effluent by a blower. This recycle stream is then mixed with the inlet in an internal contact tank where the dissolved air comes out in the form of the bubbles that attach to the pollutants (Metcalf & Eddy, 1991). The bubbles and organic materials rise to the tank surface and form a floating bed of material that is removed by a surface skimmer. The principles of dissolved air flotation (DAF) are bubble formation and size, bubble-particle interactions, measures of supplied air, and modeling of the reaction and clarification zones of the flotation tank (Edzwald, 2010). The feed wastewater of the DAF tank is often supported with a coagulant such as ferric chloride or aluminum sulfate, polyaluminum chloride (PAC) etc. to agglomerate the colloidal particles, and a flocculant (polyelectrolyte etc.) to conglomerate the particles into heavier flocks.

In this study, a DAF tank was continually operated in a full-scale wastewater treatment plant under specific varying conditions to achieve the highest treatment efficiency. DAF unit is a type of cross-flow plate pack tank. In the DAF system, the ferric chloride was used as the coagulant. Table 2 shows the data used to estimate greenhouse gas emissions corresponded to the DAF tank.

Table 2. Data Set of DAF Tank

Parameter	Value
Ferric chloride dose (D, mg/L)	21
Electricity consumption (CE, kWh)	7550

Estimation of Off-site Greenhouse Gas Emissions

In this study, there are two components of off-site greenhouse gas emissions were considered. Electricity consumption for the operation of DAF tank in the WWTP was used to estimate the off-site GHG emissions. The other component is the emission from chemical use.

The off-site emission corresponded to the electricity consumption was figured out by multiplying electricity consumption (CE) (kWh) of the DAF tank and the emission factor ($EF_{electricity}$) of the electricity consumption related to Turkey (kg CO2e/kWh). Electricity demand of the DAF tank was ensured from the electricity bills and the electricity meter

in the plant. $EF_{electricity}$ is 0.497 kg CO_2e/kWh (IEA, 2016). The calculation model is given in Eq.1.

$P_{off\text{-}site\ ,electricity} = CE \times EF_{electricity}$ (Eq. 1) (Kyung et al., 2015)

The other off-site emission was resulted from chemical use in DAF tank. It can be estimated by means of daily chemical consumption ($M_{chemical}$) (kg/d) and the emission factor of chemical substance ($EF_{chemical}$) (Kyung et al., 2015). The off-site emission can be ensured by multiplying chemical consumption and the emission factor. The emission factor of ferric chloride is 2.71 kgCO2e/kg ferric chloride (Ashrafi et al., 2013, Kyung et al., 2015, Yerushalmi et al., 2013). The off-site emission of the chemical use can be calculated via Eq.2 and Eq.3.

$P_{off\text{-}site\ ,chemical} = M_{chemical} \times EFc_{hemical}$ (Eq. 2) (Kyung et al., 2015)

$M_{chemical} = Q \times D$ (Eq.3)

Total off-site emission is the sum of off-site emissions from electricity and chemical consumption. Eq.4 shows the calculation tool.

$P_{off\text{-}site} = P_{off\text{-}site\ ,electricity} + P_{off\text{-}site\ ,chemical}$

RESULTS AND FINDINGS

The results reveled that off-site emission due to electricity consumption was higher than chemical use. It can be originated from using the blower to obtain air to operate the DAF tank. This process consumes huge amounts of electricity. The off-site emission corresponds to the electricity consumption is 96.9% of the total off-site emission.

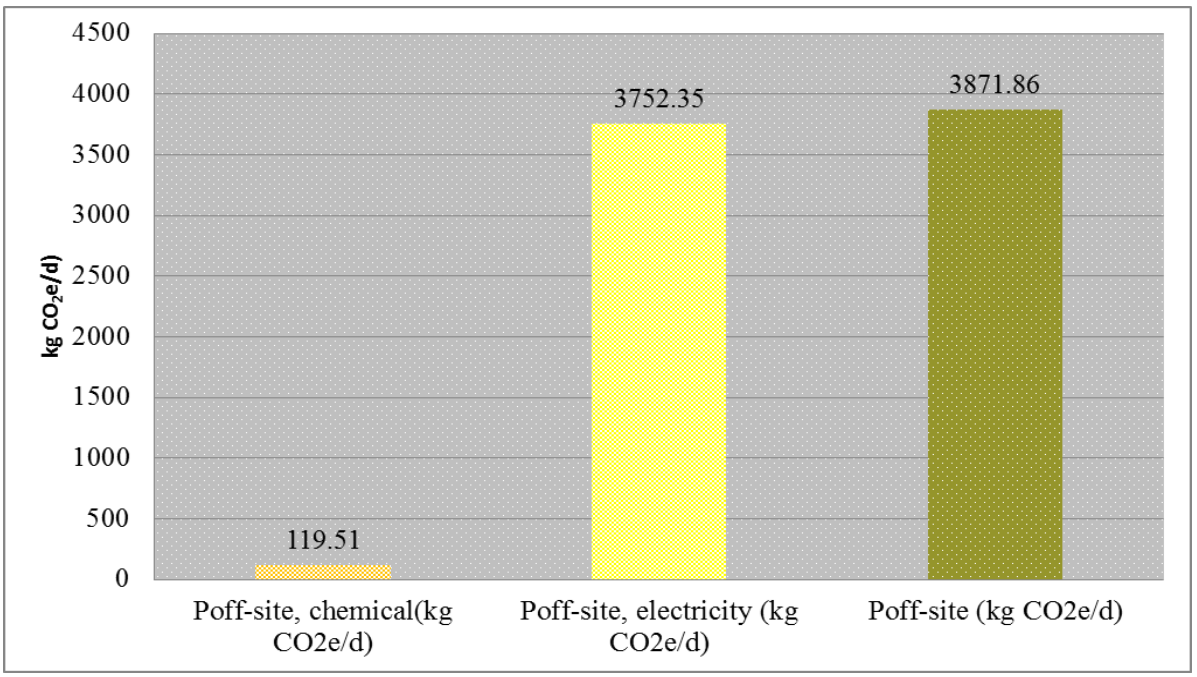

Figure 2. Off-site Emissions from DAF tank

The electricity consumption was the major source of the off-site emissions in DAF tank with the value of 3752.35 kg CO_2e/d. The off-site emission due to the chemical use was 119.51 kg CO_2e/d. Total off-site emission was 3871.86 kg CO_2e/d from DAF tank. Figure 2 shows the comparison of the emissions.

Kyung et al. (2015) performed a similar study for a municipal plant. They oppositely reported that chemical use is the major source of off-site emissions in the hybrid plant (2.698 ± 336 kg CO2e/d), and that this amounts to 58.8% of total off-site emissions (4,591 ± 576 kg CO_2e/d). It can be said that dissolved air process can have lower off-site emissions than a municipal wastewater treatment plant.

CONCLUSION

Dissolved air flotation tank is a unit that emits greenhouse gas emissions in a dairy industry wastewater treatment plant. Electricity consumption and chemical use cause the

off-site emissions in a DAF tank. Electricity consumption leads to the maximum off-site emissions with the value of 3752.35 kg CO_2e/d .The off-site emission due to the chemical use was 119.51 kg CO_2e/d. Total off-site emission was 3871.86 kg CO_2e/d from DAF tank. Electricity consumption is the major resource of off-site emissions from DAF tank. It can be originated from using air blower in DAF tank. Electricity consumption should take under control to decrease the emissions from DAF tank.

RECOMMENDATIONS

In the literature, the researches related to greenhouse gas emissions from dissolved air flotation process are limited. These researches on this topic should be increased.

REFERENCES

American Public Health Association, American Water Works Association, (1999). *Standard Methods for the Examination of Water and Wastewater,* USA.

Ashrafi, O., Yerushalmi, L. & Haghighat, F. (2013). Application of dynamic models to estimate greenhouse gas emission by wastewater treatment plants of the pulp and paper industry. *Environmental Science and Pollution Research, 20(3),* 1858–1869.

Behin, J. & Bahrami, S. (2012). Modeling an industrial dissolved air flotation tank used for separating oil from wastewater. *Chemical Engineering and Processing, 59*, 1– 8.

Castillo, A., Vall, P., Garrido-Baserba, M., Comas, J. & Poch, M. (2017). Selection of industrial (food, drink and milk sector) wastewater treatment technologies: a multi-criteria assessment. *Journal of Cleaner Production, 143,* 180-190.

Chung, Y., Choi, Y.C., Choi, Y.H. & Kang, H.S. (2000). A demonstration scaling-up of the dissolved air flotation. *Water Research*, *34,* 817–824.

Corominas, L., Flores-Alsına, X., Snip, L. & Vanrolleghem, P.A. (2012). Comparison of different modeling approaches to better evaluate greenhouse gas emissions from whole wastewater treatment plants. *Biotechnology and Bioengineering, 109*(11), 2854–2863.

Demirel, B., Yenigun, O., & Onay, T.T. (2005). Anaerobic treatment of dairy wastewaters: a review. *Process Biochemistry, 40 (8)*, 2583–2595.

Edzwald, J.K. (2010). Dissolved air flotation and me. *Water Research*, *44,* 2077-2106.

Falletti, L., Conte, L., Zaggia, A., Battistini, T. & Garosi, D. (2014). Food industry wastewater treatment plant based on flotation and MBBR. *Modern Environment Science and Engineering, 1,* 562-566.

Kyung, D., Kim, M., Chang, J. & Lee, W. (2015). Estimation of greenhouse gas emissions from a hybrid wastewater treatment plant. *Journal of Cleaner Production*, *95*,117–123.

Metcalf & Eddy, Inc. (1991) *Wastewater Engineering: Treatment, Disposal, and Reuse*. 3rd Ed., McGraw-Hill, New York.

Metcalf & Eddy, (2014). *Wastewater Engineering: Treatment and Resource Recovery* 5th ed, Boston, USA, McGraw-Hill.

Ozturk, I., Eroglu, V., Ubay, G. & Demir, I. (2003). Hybrid upflow anaerobic sludge blanket reactor (HUASBR) treatment of dairy effluents. *Water Science and Technology*, *28*, 77–85.

Parravicini, V., Svardal, K. and Krampe, J. (2016). Greenhouse gas emissions from wastewater treatment plants. *Energy Procedia*, *97*, 246–253.

Pereira, M.S., Borges, A.C., Heleno, F.F., Squillace, L.F.A. & Faroni, L.R.D. (2018). Treatment of synthetic milk industry wastewater using batch dissolved air flotation. *Journal of Cleaner Production, 189,* 729-737.

Speece, R.E. (1996). Anaerobic biotechnology for industrial wastewaters, USA, Archae Press.

Yapıcıoğlu, P., & Filibeli, A. (2017). Proceedings from IATS '17: The 8th International Advanced Technologies Symposiu. Elazığ, Turkey.

Yapıcıoğlu, P. (2018). Greenhouse Gases Emissions Minimization of Wastewater Treatment, MSc thesis, Harran University Graduate School of Natural and Applied Sciences Department of Environmental Engineering, 96pp.

Yerushalmi, L., Ashrafi, O. & Haghighat, F. (2013). Reductions in greenhouse gas (GHG) generation and energy consumption in wastewater treatment plants. *Water Science and Technology*, *67(5),* 1159–1164.

ENERGY COST ESTIMATION IN TERMS OF ORGANIC LOADING FOR A MEAT PROCESSING INDUSTRY WASTEWATER TREATMENT PLANT

Pelin YAPICIOĞLU
Harran University
pyapicioglu@harran.edu.tr

ABSTRACT: Wastewater treatment plants are operated in order to minimize hazardous organic materials discharges to the receiving bodies. These plants can be considered as one of the major energy consumers by municipalities and authorities. Energy demand of a plant is based mainly on the treated wastewater volume and organic loading. In this study, the effects of organic loading on energy cost for a meat processing wastewater treatment plant were investigated. The aim of the study is to reveal the role of design parameters in terms of organic loading on energy management. Energy cost indicator has been calculated for the assessment. This indicator was figured out for both design organic loading and operational organic loading. The results revealed that energy cost indicator of operational organic loading was higher than the design one. Their values were 6.88 x 10^{-3} and 8.06x 10^{-6}, respectively. If plants are operated in design parameters, energy cost of the plant can be minimized.

Key words: energy cost, meat processing wastewater, BOD, organic loading.

INTRODUCTION

Wastewater treatment plants are operated in order to protect the water bodies from harmful wastewater discharges (Metcalf &Eddy, 1991; Metcalf & eddy, 2014). These facilities are regarded as one of the major energy consumers by the municipalities and authorities (Castellet-Viciano et al., 2018). Electricity consumption causes to the greenhouse gases emissions in the wastewater treatment plants (Kyung et al., 2015, Yapıcıoğlu, 2018a, Parravicini et al., 2016). Electricity and air consumption in a plant leads to the off-site greenhouse gases emissions therefor electricity consumption should take under control for the minimization of greenhouse gas emissions to the atmosphere (Kyung et al., 2015, Yapıcıoğlu, 2018a). Also, energy cost locates in the top of the wastewater treatment plant's operations costs list.

Energy demand mainly depends on the wastewater volume and organic loading in a wastewater treatment plant (Metcalf & Eddy, 1991). These two operational parameters detect the energy requirement and energy costs of a plant. Operational parameters of the wastewater treatment plants do not match with the design parameters for many times. It can be originated from production capacity variations for the industrial wastewater treatment plants. This mismatch has a negative effect on the performance of the plants and their energy costs. Organic loading varies due to the production capacity and amount and the variation of products types. Meat processing industry is the facilities that have high organic wastewater loadings (Yapıcıoğlu, 2018b).

This paper aims to reveal the role of design parameters in terms of organic loading on energy management. The impact of design organic loading for a meat processing wastewater treatment plant on energy cost were researched and benchmarked with the operational organic loading.

METHODS

Description of the Meat Processing Industry

The meat industry is located in an organized industrial zone in Turkey. The main products being processed are sujuk, sausage, meatball, raw meat, döner and jambon. The main wastewater generating points of the industry are the slaughterhouse, rendering unit, and intestinal washing process. The data set of this industry is given in Table 1. The wastewater analysis results were performed using Standard Methods (APHA 1998).

Figure 1 shows the existing wastewater treatment process in the plant. Biological treatment method is used as extended aeration activated sludge system to remove organic and suspended materials from the wastewater.

Table 1. Data Set of Meat Processing Industry

Parameter	Value
BOD, $_{operational}$ (g/m^3)	2.554
BOD, $_{design}$ (g/m^3)	3.025
Operational Flow Rate (Q) (m^3/d)	2800
Design Flow Rate (q) (m^3/d)	4000

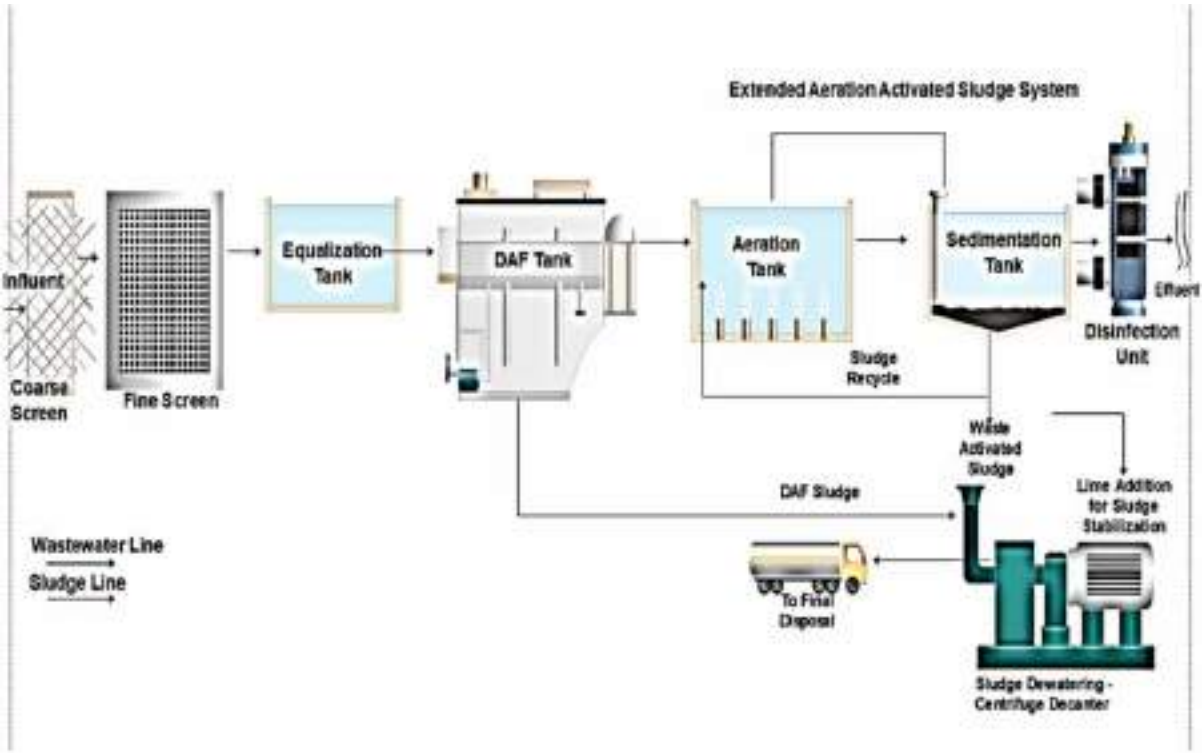

Figure 1. Wastewater Flow Diagram of the Meat Processing Industry Wastewater Treatment Plant

Energy Cost Indicator (ECI) Term

Energy cost assessment depends on the model developed by Hernandez-Sancho et al. (2011a). In this methodology, the performance index (Z) and energy cost indicator (ECI) which is derived from "Z" have been figured out.

The performance index (Z) comprises operational flow rate (Q) (m^3/d) and the design flow of the plant (q) (m^3/d). Eq. 1 indicates the calculation of the performance index (Castellet-Viciano et al., 2018).

$$Z = [(q-Q) / Q] \times 100 \quad \text{(Eq.1)} \quad (1)$$

Energy cost indicator (ECI) has been derived from the performance index, the tool contains the volume of wastewater treated per year (V) (m^3/year) and biological oxygen demand (BOD) (g/m^3). In this study, ECI values related to design organic loading ($ECI_{\text{organic loading, design}}$) and operational organic loading ($ECI_{\text{organic loading, operational}}$) were

calculated and benchmarked. In this term, variable parameter is BOD that means to the required oxygen amount for the stabilization of organic materials in the wastewater. It also corresponds to the organic loading. In Eq. 2, the calculation model of ECI for small scale WWTPs was given (Castellet-Viciano et al., 2018; Hernandez-Sancho et al. , 2011a).

$$ECI=1983.10^{6}\ V^{0.717}\ e^{(-14.327\ BOD+0.660Z)} \quad \text{(Eq.2)} \quad (2)$$

RESULTS AND FINDINGS

The results showed that energy cost indicator of operational organic loading was higher than the design one whose values were 6.88×10^{-3} and 8.06×10^{-6}, respectively. Figure 2 demonstrates the comparison of the indicators.

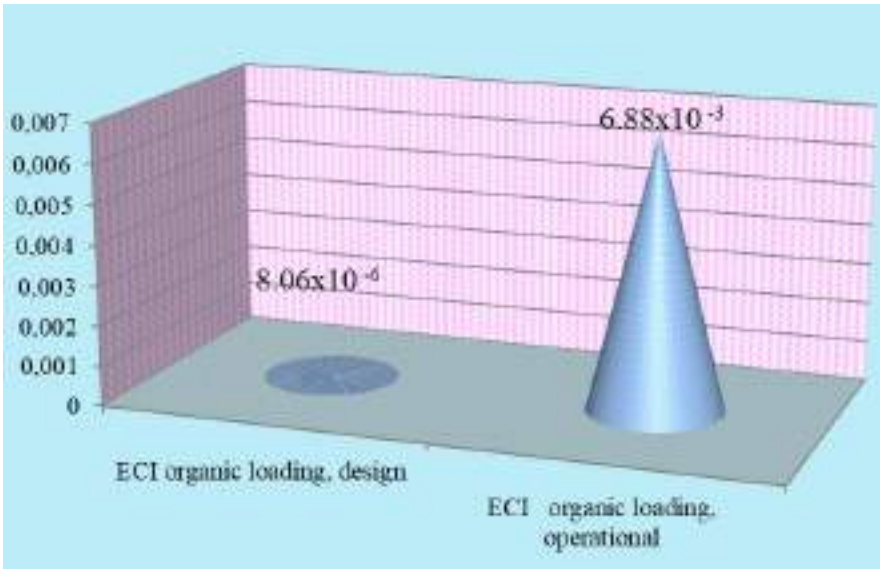

Figure 2. Energy Cost Indicators of Meat Processing Industry

BOD is the meaning of biological oxygen demand for the stabilization of the organic materials. It is an indicator parameter of organic loading in a wastewater sample. According to the model, if organic loading is lower, the cost indicator is higher, oppositely. So if the plants are operated under the design parameters, energy cost indicator would be lower.

There are many study corresponds to this topic. The use of cost functions has been applied in general in the literature. Most of developed models for the wastewater treatment process have been applied to estimate the operational and maintenance cost of the process. Hernandez-Sancho et al. (2011b) studied a cost modelling methodology using statistical information from a sample of 341 wastewater treatment plants in Spain. Castellet-Viciano et al. (2018) researched the effect of design flow as the design parameters on energy costs for small, middle and large scale of WWTPs. They reported

that Z was 0.20, 0.40, 0.60 and 0.80 for small-scale plants. Similarly, Z value was 0.428 for a small scale wastewater treatment plant, in this study. Molinos-Senante et al. (2013) applied a cost function model to estimate the cost of the sludge and waste management. Similarly, cost functions for extended aeration and activated sludge also contain the volume of wastewater treated and the biological oxygen demand removal efficiency in %. Plumlee et al. (2014) estimated the cost of the advanced treatment, and in near future Yumin et al. (2016) estimated the operational cost of WWTPs in rural areas.

CONCLUSION

This study shows that energy cost indicator and the performance index can be used as an approach tool to evaluate the energy costs of a wastewater treatment plant.

The results demonstrate that energy cost indicator of operational organic loading was higher than the design one. Their values were 6.88×10^{-3} and 8.06×10^{-6}, respectively.

If organic loading that is closed with BOD parameter is lower, the energy cost indicator is higher, oppositely. So if the plants are operated under the design parameters, energy cost indicator would be lower.

RECOMMENDATIONS

There are limited studies to this topic in the literature. The energy cost assessments of the meat processing industry wastewater treatment plants should be increased.

REFERENCES

American Public Health Association, American Water Works Association, (1999). *Standard Methods for the Examination of Water and Wastewater,* USA.

Castellet-Viciano, L., Torregrossa, D. & Hernández-Sancho, F. (2018). The relevance of the design characteristics to the optimal operation of wastewater treatment plants: Energy cost assessment. *Journal of Environmental Management, 222*,275–283.

Hernandez-Sancho, F., Molinos-Senante, M. & Sala-Garrido, R. (2011a). Cost modelling for wastewater treatment processes. *Desalination*, *268*, 1–5.

Hernández-Sancho, F., Molinos-Senante, M. & Sala-Garrido R. (2001b). Energy efficiency in Spanish wastewater treatment plants: a non-radial DEA approach. *Science of Total Environment, 409*,2693–2699.

Kyung, D., Kim, M., Chang, J. & Lee, W. (2015). Estimation of greenhouse gas emissions from a hybrid wastewater treatment plant. *Journal of Cleaner Production*, *95*,117–123.

Metcalf & Eddy, Inc. (1991) *Wastewater Engineering: Treatment, Disposal, and Reuse*. 3rd Ed., McGraw-Hill, New York.

Metcalf & Eddy, (2014). *Wastewater Engineering: Treatment and Resource Recovery* 5th ed, Boston, USA, McGraw-Hill.

Molinos-Senante, M., Hernandez-Sancho, F. & Sala-Garrido, R. (2013). Cost modeling for sludge and waste management from wastewater treatment plants: an empirical approach for Spain. *Desalination and Water Treatment*, 51, 5414–5420.

Parravicini, V., Svardal, K. and Krampe, J. (2016). Greenhouse gas emissions from wastewater treatment plants. *Energy Procedia*, *97*, 246–253.

Plumlee, M.H., Stanford, B.D., Debroux, J., Hopkins, D.C. & Snyder, S.A. (2014). Costs of advanced treatment in water reclamation. *Ozone Sci. Eng.*, *36*, 485–495.

Yapıcıoğlu, P. (2018a). Greenhouse Gases Emissions Minimization of Wastewater Treatment, MSc thesis, Harran University Graduate School of Natural and Applied Sciences Department of Environmental Engineering, 96pp.

Yapıcıoğlu, P. (2018b). Environmental impact assessment for a meat processing industry in Turkey: wastewater treatment plant. *Water Practice & Technology*, *13(3),* 692-704.

Yumin,W., Lei, W. & Yanhong, F. (2016). Cost function for treating wastewater in rural regions. *Desalination and Water Treatment, 57*, 17241–17246.

ESTIMATION OF GREENHOUSE GAS EMISSION FROM EXTENDED AERATION ACTIVATED SLUDGE PROCESS

Pelin YAPICIOĞLU
Harran University
pyapicioglu@harran.edu.tr

ABSTRACT: Greenhouse gases emissions have been increasing, in the recent times. One of the greenhouse gases emission resources is the meat processing industrial wastewater treatment plants. Extended aeration activated sludge process is applied for organic materials removal from industrial wastewater. Extended aeration activated sludge system consists of an aeration tank and a sedimentation tank. Aeration tank is the main greenhouse gas emitter units in a meat processing industry wastewater treatment plant. In this study, the off-site greenhouse gas emissions of extended aeration activated sludge process in a meat processing wastewater treatment plant were estimated. The off-site emission was estimated from electricity consumption and chemical use. This paper aims to determine the off-site emissions for extended aeration process in a meat processing wastewater treatment plant. The results revealed that electricity consumption was the major source of the off-site greenhouse gas emission for this process with the value of 4014.77 kg CO_2e/d. The off-site emission due to the chemical use was 100.87 kg CO_2e/d. Total off-site emission was 4115.64 kg CO_2e/d.

Key words: greenhouse gas, meat processing industry, wastewater treatment plant, extended aeration process, off-site emission.

INTRODUCTION

Greenhouse gas emissions have increased in the atmosphere due to the industrial, domestic and anthropogenic activities in last decades (Kyung et al., 2015). Wastewater treatment plants have been considered as one of the greenhouse gases emissions resources recently (Kyung et al., 2015; Corominas et al., 2012; Yerushalmi et al., 2013; Yapıcıoğlu, 2018). Carbon dioxide (CO_2), methane (CH_4) and nitrous oxide (N_2O) are the main greenhouse gases which emits from wastewater treatment plants to the atmosphere due to applying treatment process (biological, chemical or biochemical processes etc), sludge dewatering and disposal process (anaerobic digestion, incineration etc.), chemical use (added chemical materials for wastewater and sludge treatment process (coagulants, flocculants), for nitrification and denitrification (methanol, etc.), for alkalinity and pH

adjustment), energy consumption (electricity consumption, air consumption, etc.), and maintenance and transport (Kyung et al., 2015; Metcalf and Eddy, 2014; Yapıcoğlu, 2018).

Greenhouse gases emissions can be classified as the on-site emissions and the off-site emissions (Parravicini et al., 2016; Yapıcıoğlu, 2018a). The on-site emissions in the plants are the emitting emissions in the wastewater collection system, the emissions originated from the existing treatment processes and the emissions in the discharge point of the treated water. The off-site GHGs emissions comprise from the electricity consumption, air consumption, transportation, chemical use and sludge stabilization and disposal process (Parravicini et al., 2016; Yapıcıoğlu, 2018a). Especially, the industrial wastewater plants emit the huge amounts of greenhouse gas emissions due to highly organic wastewater content and existing treatment processes. The meat processing industry is one of them.

The meat processing industry discharges large volumes of wastewater in many countries that is in need of considerable treatment if its release to the environment is to be sustainable (Johns 1995, Yapıcıoğlu 2018b). The organic materials and total suspended solids concentration is very high and has a highly contaminating effect in the meat processing wastewater (Ruiz et al. 1997; Yapıcıoğlu 2018b). The wastewater majorly includes organics, pathogenic and non-pathogenic viruses and bacteria, and detergents and disinfectants (Debik & Coskun 2009; Lecompte & Mehrvar 2014). There are several methods for the treatment of meat processing wastewater, with most focusing on biological processes such as activated sludge, stabilization ponds and aerobic reactors (Davarnejad & Nasiri 2017). The common treatment method is extended aeration activated sludge process for meat processing wastewater. In this process carbon and nitrogen removal can be ensured (Metcalf & Eddy, 2014).

In this study, the off-site greenhouse gas emissions of aeration tank in extended aeration activated sludge process applied in meat processing wastewater treatment plant were estimated. The off-site emission was estimated from chemical consumption (added methanol for denitrification) and electricity consumption in the aeration tank. The main aim of this study is to estimate the off-site emissions for extended aeration tank in a meat processing industry wastewater treatment plant.

METHODS

Description of the Meat Processing Industry

The meat industry is located in an organized industrial zone in Turkey. The main products being processed are sujuk, sausage, meatball, raw meat, döner and jambon. The main wastewater generating points of the industry are the slaughterhouse, rendering unit, and intestinal washing process. The wastewater characterization of this plant is given in Table 1. The wastewater analysis results were performed using Standard Methods (APHA 1998).

Figure 1 demonstrates the existing wastewater treatment process in the plant. Biological treatment method is applied as extended aeration activated sludge system to remove organic and suspended materials from the wastewater.

Table 1. Influent Wastewater Characteristics of the Meat Industry

Parameter	Value
COD (mg/L)	5293
BOD (mg/L)	2554
TSS (mg/L)	2122
FOG (mg/L)	329
pH	7.29

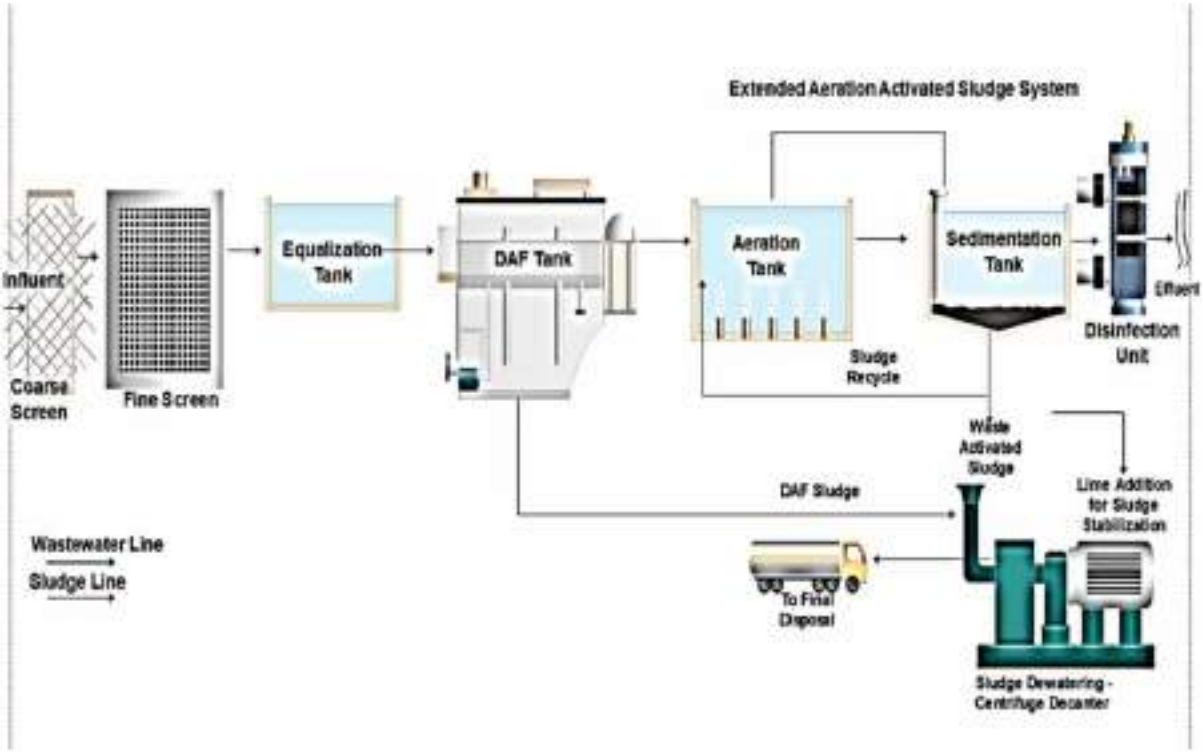

Figure 1. Wastewater Flow Diagram of the Meat Processing Industry Wastewater Treatment Plant

Extended Aeration Activated Sludge Process

Extended aeration activated sludge process is a type of biological treatment. It consists of an aeration tank and sedimentation tank. The wastewater hydraulic retention time is in the range of 18-24 hours. Organic materials are removed with the help of microorganisms in the aeration tank. Air is pumped in to the aeration tank for the respiration of the microbial mass (Metcalf &Eddy, 1991).

In this study, the hydraulic retention time in the aeration tank is 24 hours. Carbon and nitrogen (nutrient) removal can be ensured with this process. For denitrification, methanol is added to the aeration tank. Table 2 shows the data used to estimate greenhouse gas emissions corresponded to the aeration tank.

Table 2. Data Set of Aeration Tank

Parameter	Value
Methanol dose (kg/d)	65.5
Electricity consumption (CE, kWh)	8078

Estimation of Off-site Greenhouse Gas Emissions

In this study, there are two components of off-site greenhouse gas emissions were considered. Electricity consumption for the operation of aeration tank in the plant was used to estimate the off-site emissions. The other component is the emission from methanol (chemical) use for denitrification.

The off-site emission corresponded to the electricity consumption was figured out by multiplying electricity consumption (CE) (kWh) of the aeration tank and the emission factor ($EF_{electricity}$) of the electricity consumption related to Turkey (kg CO_2e/kWh). Electricity demand of the aeration tank was ensured from the electricity bills and the electricity meter in the plant. $EF_{electricity}$ is 0.497 kg CO_2e/kWh (IEA, 2016). The calculation model is given in Eq.1 (Kyung et al., 2015)

$$P_{off\text{-}site\ ,electricity} = CE \times EF_{electricity} \quad \text{(Eq. 1)}$$

The other off-site emission was resulted from methanol use for denitrification to ensure nitrogen removal in aeration tank. It can be estimated by means of daily chemical consumption ($M_{chemical}$) (kg/d) and the emission factor of chemical substance ($EF_{chemical}$) (Kyung et al., 2015). The off-site emission can be ensured by multiplying chemical consumption and the emission factor. The emission factor of methanol is 1,54 kgCO_2e/kg methanol (Ashrafi et al., 2013, Kyung et al., 2015, Yerushalmi et al., 2013). The off-site emission of the chemical use can be calculated with the help of Eq.2 (Kyung et al., 2015).

$$P_{off\text{-}site\ ,chemical} = M_{chemical} \times EFc_{Chemical} \quad \text{(Eq. 2)}$$

Total off-site emission is the sum of off-site emissions from electricity and chemical consumption. Eq.3 shows the calculation tool.

$$P_{off\text{-}site} = P_{off\text{-}site\ ,electricity} + P_{off\text{-}site\ ,chemical} \quad \text{(Eq.3)}$$

RESULTS AND FINDINGS

The results show that the off-site emission due to electricity consumption was higher than chemical use. It can be originated from using blower to obtain air to operate the aeration tank. This process consumes huge amounts of electricity to ensure air for the respiration of microorganisms. The off-site emission corresponds to the electricity consumption is 97.5% of the total off-site emission.

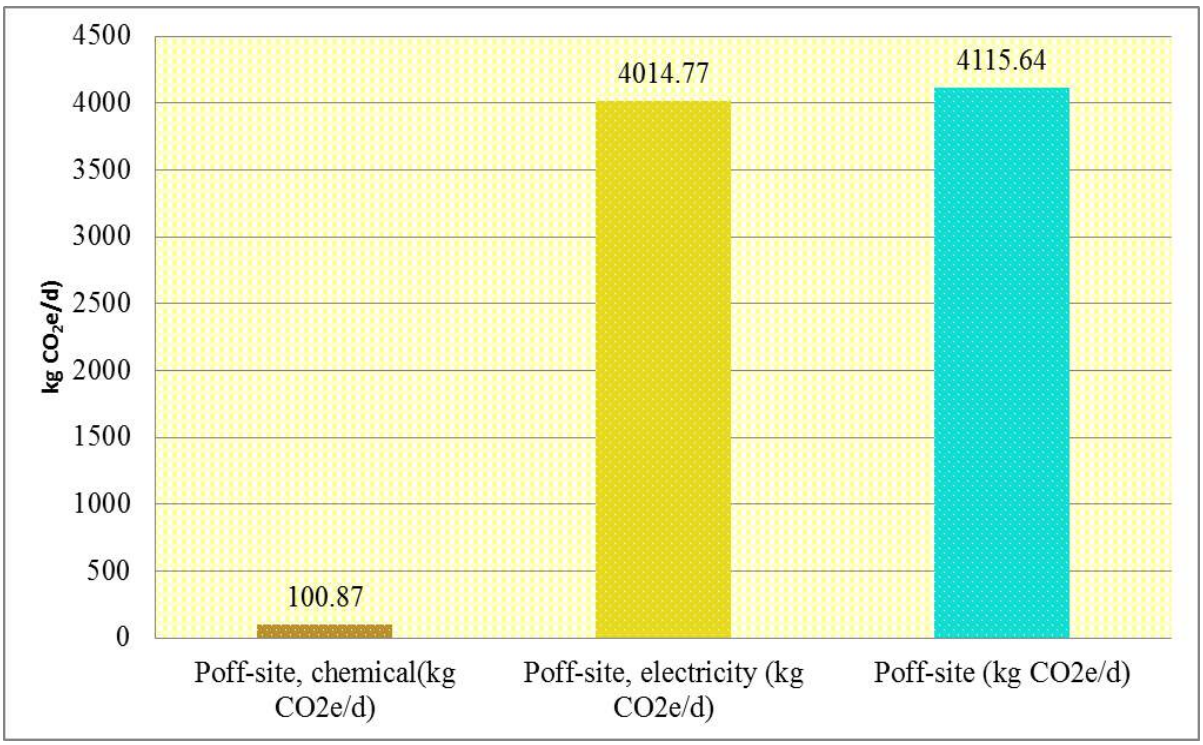

Figure 2. Off-site Emissions from aeration tank

The electricity consumption was the major source of the off-site emissions in the aeration tank with the value of 4014.77 kg CO_2e/d. The off-site emission due to the chemical use was 100.87 kg CO_2e/d. Total off-site emission was 4115.64 kg CO_2e/d from the aeration tank. Figure 2 indicates the comparison of the emissions.

Kyung et al. (2015) performed a similar study for a municipal plant. They oppositely reported that chemical use is the major source of off-site emissions in the hybrid plant (2.698 ± 336 kg CO2e/d), and that this amounts to 58.8% of total off-site emissions (4,591 ± 576 kg CO_2e/d). It can be said that extended aeration process can have similar off-site emissions with a hybrid municipal wastewater treatment plant. It is originated from nutrient removal for both processes.

CONCLUSION

Extended aeration activated sludge process is the biological treatment method that releases greenhouse gases to the atmosphere in a meat processing industry wastewater treatment plant. Aeration tank is a unit that emits greenhouse gas emissions in a meat

processing industry wastewater treatment plant. Electricity consumption and chemical use cause the off-site emissions in the aeration tank.

Electricity consumption causes to the highest off-site emissions with the value of 4014.77 kg CO_2e/d .The off-site emission due to the chemical use was 100.87 kg CO_2e/d. Total off-site emission was 4115.64 kg CO_2e/d from the aeration tank.

Electricity consumption is the major source of the off-site emissions from the aeration tank. It can be originated from using air blower for the respiration of the microbial committee that is responsible for the stabilization of the organic materials. Electricity consumption should take under control to decrease the emissions from the aeration tank.

RECOMMENDATIONS

In the literature, the studies related to greenhouse gases emissions from meat processing industry are limited. These researches on this topic should be increased.

REFERENCES

American Public Health Association, American Water Works Association, (1999). *Standard Methods for the Examination of Water and Wastewater,* USA.
Ashrafi, O., Yerushalmi, L. & Haghighat, F. (2013). Application of dynamic models to estimate greenhouse gas emission by wastewater treatment plants of the pulp and paper industry. *Environmental Science and Pollution Research, 20(3),* 1858–1869.
Corominas, L., Flores-Alsına, X., Snip, L. & Vanrolleghem, P.A. (2012). Comparison of different modeling approaches to better evaluate greenhouse gas emissions from whole wastewater treatment plants. *Biotechnology and Bioengineering, 109(11),* 2854–2863.
Davarnejad, R. & Nasiri, S. (2017). Slaughterhouse wastewater treatment using an advanced oxidation process: optimization study. *Environmental Pollution, 223*, 1–10.
Debik, E. & Coskun, T. (2009). Use of the Static Granular Bed Reactor (SGBR) with anaerobic sludge to treat poultry slaughterhouse wastewater and kinetic modeling. *Bioresource Technology, 100(11),* 2777–2782.
IEA, 2016. World Energy Statistics 2016. Key world energy statistics http://www.iea.org/statistics/topics/energybalances/.
Johns, M. R. (1995). Developments in wastewater treatment in the meat processing industry: a review. *Bioresource Technology*, *54(3)*, 203–216.
Kyung, D., Kim, M., Chang, J. & Lee, W. (2015). Estimation of greenhouse gas emissions from a hybrid wastewater treatment plant. *Journal of Cleaner Production*, *95*,117–123.

Lecompte, B. C. F. & Mehrvar, M., (2014). Cost-effectiveness analysis of TOC removal from slaughterhouse wastewater using combined anaerobiceaerobic and UV/H_2O_2 processes. *Journal of Environmental Management,134,* 145–152.

Metcalf & Eddy, Inc. (1991) *Wastewater Engineering: Treatment, Disposal, and Reuse*. 3rd Ed., McGraw-Hill, New York.

Metcalf & Eddy, (2014). *Wastewater Engineering: Treatment and Resource Recovery* 5th ed, Boston, USA, McGraw-Hill.

Parravicini, V., Svardal, K. and Krampe, J. (2016). Greenhouse gas emissions from wastewater treatment plants. *Energy Procedia*, *97*, 246–253.

Ruiz, I., Veiga, M. C., Santiago, P. & Blazquez, R. (1997). Treatment of slaughterhouse wastewater in a UASB reactor and ananaerobic filter. *Bioresource Technology, 60(3)*, 251–258.

Yapıcıoğlu, P. (2018a). Greenhouse Gases Emissions Minimization of Wastewater Treatment, MSc thesis, Harran University Graduate School of Natural and Applied Sciences Department of Environmental Engineering, 96pp.

Yapıcıoğlu, P. (2018b). Environmental impact assessment for a meat processing industry in Turkey: wastewater treatment plant. *Water Practice & Technology*, *13(3),* 692-704.

Yerushalmi, L., Ashrafi, O. & Haghighat, F. (2013). Reductions in greenhouse gas (GHG) generation and energy consumption in wastewater treatment plants. *Water Science and Technology*, *67(5),* 1159–1164.

UNMANNED AERIAL VEHICLES IN THE CONSTRUCTION INDUSTRY: APPLICATIONS AND IMPLICATIONS

Volkan ARSLAN
Zonguldak Bulent Ecevit University, Department of Civil Engineering, Zonguldak, Turkey
volkanarslan@beun.edu.tr

Serdar ULUBEYLI
Zonguldak Bulent Ecevit University, Department of Civil Engineering, Zonguldak, Turkey
ulubeyli@beun.edu.tr

Aynur KAZAZ
Akdeniz University, Department of Civil Engineering, Antalya, Turkey
akazaz@akdeniz.edu.tr

ABSTRACT: An unmanned aerial vehicle (UAV) is an aircraft system that is controlled autonomously or by a pilot on the ground. The use of UAVs has started in military operations and transferred to the commercial use in numerous industries. In these industries, UAVs were usually utilized in mapping applications, environmental change monitoring, disaster prevention response, resource exploration, etc. Despite their many advantages, the construction industry incorporates with this technology slowly. However, the technological development of UAVs leads the construction industry to adapt these devices in order to provide time and cost savings during the execution process of construction activities. It was known that some civil engineering works, such as management of river facilities, monitoring for bridge degradation, and quality inspections, were conducted using UAVs. This is because UAVs simplify and improve the execution process in construction. Moreover, efficient monitoring and reviewing activities in construction projects may be beneficial to save time and money for contractors. Therefore, the aim of this study was to investigate UAVs and their related usage areas in the construction industry. For this purpose, a detailed literature review was presented and the existing UAV practices in the construction industry were examined. The obtained results may help both researchers and practitioners be aware of the current situation of UAVs and determine future expectations from UAVs in the construction industry.

Key words: construction industry, unmanned aerial vehicle

INTRODUCTION

An unmanned aerial vehicle (UAV) is an aircraft system that is controlled autonomously or by a pilot on the ground (Liu et al., 2014). This vehicle is also known as an unmanned aerial system, a remotely piloted vehicle, or a drone in the literature (Siebert & Teizer, 2014). The use of UAVs has started in military operations and transferred to the commercial use in numerous industries (Dupont, Chua, Tashrif, & Abbott, 2017). In these industries, UAVs were usually utilized in mapping applications, environmental change monitoring, disaster prevention response, resource exploration, etc. (Liu et al., 2014). The technological development of UAVs leads the construction industry to adapt these devices in order to provide time and cost savings during the execution process of construction activities (Herrmann, 2018). Despite their many advantages, the construction industry incorporates with this technology slowly (Holt, Benham, & Bigelow, 2015). It was known that some civil engineering works, such as management of river facilities, monitoring for bridge degradation, and quality inspections, were conducted using UAVs. This is because UAVs simplify and improve the execution process in construction. Moreover, efficient monitoring and reviewing activities in construction projects may be beneficial to save time and money for contractors. Therefore, the aim of this study was to investigate UAVs and their related usage areas in the construction industry. For this purpose, a detailed literature review was presented and the existing UAV practices in the construction industry were examined.

UAV SYSTEM AND DESIGN

There are four different types of UAVs, namely, multirotor, fixed-wing, single-rotor, and fixed-wing hybrid (Figure 1). The application area of multirotor UAVs which have more than two rotors is larger than any other kinds. Especially quadcopters (Figure 2) have advantageous features such as robustness, high maneuverability, and low purchase and maintenance costs (Li & Liu, 2019). In addition, UAVs' hardware and software components can be designed in accordance with their purpose of usage. In this context, their system design, system implementation, control mechanism, and software properties become crucial (Liu et al., 2014). However, the most significant disadvantages of UAVs are insufficient battery life and low wind resistance (Cajzek & Klanšek, 2016). Considering advantages, disadvantages, design condition, terms of use, and capabilities of UAVs, this technology may provide new opportunities for the construction industry.

Figure 1. Type of UAVs

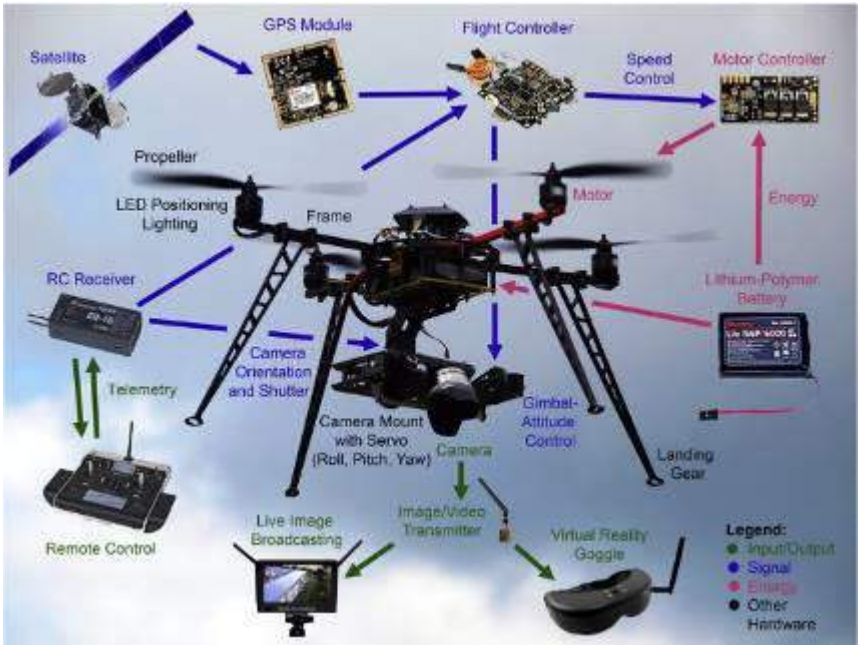

Figure 2. A Sample of Quadcopter

RESEARCH METHOD

In this study, the investigation and examination process of current practices of UAVs in the construction industry was carried out by utilizing past studies. During the process of evaluation of past studies, a systematic review of construction-related UAV studies was conducted. The UAV technology is regarded as a new concept in the construction industry. Therefore, the number of studies considering UAV in the construction industry is relatively low, indeed. Consequently, all of the gathered research papers were analyzed, categorized, and explained in the next section.

LITERATURE REVIEW

The construction industry is known with its slower adaptation of the emerging technologies (Holt et al., 2015). From this perspective, research efforts on the UAV technology can be described as new. Table 1 presents past studies considering UAV applications in the construction industry. In Table 1, studies were categorized and listed in accordance with their authors, publication dates, and areas of usage of UAVs.

Table 1. Past Studies on UAVs in the Construction Industry

Author and Date	Area of Usage
Siebert & Teizer (2014)	Earth-moving Operations
Gheisari, Irizzarry, & Walker (2014)	Health and Safety
Wen & Kang (2014)	Quality Control
Morgenthal & Hallermann (2014)	Quality Control
Hubbard et al. (2015)	Material Tracking
Lin, Han, & Golparvar-Fard (2015)	Quality Control
Tuttas, Braun, Borrmann, & Stilla (2015)	Quality Control
Fernandez Galarreta, Kerle, & Gerke (2015)	Structural Damage Assessment
Vacanas et al. (2016)	On-site Data Collection
Wang, Chen, & Yin (2016)	Vehicle Detecting and Tracking
Meouche et al. (2016)	Land Surveying
Fang, Chen, Cho, & Zhang (2016)	Material Tracking
Fleming et al. (2016)	Earth-moving Operations
Yasin, Zaidi, & Nawi (2016)	Quality Control
Liu, Jennesse, & Holley, (2016)	Quality Control
Dupont et al. (2017)	Productivity
Bang, Kim, & Kim (2017)	On-site Data Collection
Hamledari, McCabe, & Davari (2017)	Quality Control
McCabe et al. (2017)	Quality Control
Moeini et al. (2017)	Quality Control
Howard, Murashov, & Branche (2018)	Health and Safety
Kim & Irizarry (2019)	Human Performance
Gheisari & Esmaeili (2019)	Health and Safety
Kim, Park, Cho, & Kang (2019)	On-site Data Collection
Ham & Kamari (2019)	On-site Data Collection
Ficapal & Mutis (2019)	Quality Control

Mahami (2019)	Quality Control
Liu, Chen, Hu, & Zhang (2019)	Health and Safety
Kim, Liu, Lee, & Kamat (2019)	Health and Safety
Moon, Chung, Kwon, Seo, & Shin (2019)	Equipment Planning
Kang, Park, & Suh (2019)	Material Tracking
Julge, Ellmann, & Köök (2019)	Earth-moving Operations

The number of UAV studies in the construction industry tends to increase in recent years. Especially in 2019, a significant effort was shown in order to determine or evaluate the performance of UAVs in construction practices. Past studies can be categorized considering the area of usage of UAVs, such as (i) earth-moving operations, (ii) health and safety, (iii) quality control, (iv) material tracking, (v) structural damage assessment, (vi) on-site data collection, (vii) vehicle detecting and tracking, (viii) land surveying, (ix) productivity, (x) human performance, and lastly, (xi) equipment planning. Among these publications, three (i.e., quality control, health and safety issues, and on-site data collection) are the most common topics that researchers have had concerned.

Several authors in the literature discussed the usage of UAVs in quality control works in the construction industry. Wen & Kang (2014) presented an ongoing study that aims to increase the possibility of discovering the unfound problem on construction projects by the help of UAVs. Morgenthal & Hallermann (2014) investigated the application of UAVs for the visual inspection and damage detection on civil structures. Lin, Han, & Golparvar-Fard (2015) suggested a framework for the automated monitoring process that utilizes UAVs in construction projects. Tuttas, Braun, Borrmann, & Stilla (2015) introduced an approach that uses UAVs and BIM to compare as-planned and as-built situation of buildings. Liu, Jennesse, & Holley, (2016) proposed to use UAVs to reduce the total cost, minimize the planned time, and mitigate the risk of adverse safety conditions in order to inspect a portion of curtain walls to validate the efficacy of a building. Yasin, Zaidi, & Nawi (2016) intended to explore the viability of the UAV application for the building inspection with the advantage it has especially in inspecting and collecting the data at difficult to reach some areas such as roof, ceiling, gutter, and in recording the data for large building projects. McCabe et al. (2017) examined the potential of using UAVs to monitor indoor construction sites. Hamledari, McCabe, & Davari (2017) tried to automatically detect components of an interior partition using three image databases including an UAV, a smartphone, and publically available sources on the internet. Moeini et al. (2017) examined the application and integration of BIM and UAV throughout the monitoring process of construction projects. Mahami (2019) targeted to develop an automatic imaging network design which uses UAVs to improve the efficiency and accuracy of the automated construction progress monitoring.

From the perspective of health and safety issues, UAVs can reveal a solution for construction projects. Gheisari, Irizzarry, & Walker (2014) conducted a research to

determine (1) the effectiveness and frequency of using UAVs in improving safety operations or hazardous situations, (2) ideal UAV technical features, and (3) enablers and barriers for using UAVs to monitor and control on-site construction activities. Howard, Murashov, & Branche (2018) described UAVs according to their use in construction, potential risks for workers, the effect for the risk mitigation, and the impact on health and safety professionals. Liu, Chen, Hu, & Zhang (2019) introduced a safety inspection method that integrates UAV and BIM. Kim, Liu, Lee, & Kamat (2019) presented an UAV-assisted visual monitoring method to prevent struck-by accidents in construction projects.

In order to have a good construction management performance, collecting data from a construction site may be considered as a vital aspect. Vacanas et al. (2016) explored the combined use of BIM and UAV technologies in order to achieve efficient and accurate as-built data from a construction site. Bang, Kim, & Kim (2017) proposed a method to generate a panorama of a construction site by using UAVs. Kim, Park, Cho, & Kang (2019) discussed enabling UAVs to gather data in a time-efficient manner in construction activities. Ham & Kamari (2019) aimed to use UAVs to create a new method which automatically retrieves photo-worthy frames containing construction-related contents in order to have the data from construction sites.

The earth-moving operations topic is a major issue in the construction industry. Siebert & Teizer (2014) evaluated the performance of UAV systems in large excavation and earth moving construction sites. Fleming et al. (2016) presented a novel imaging and software application that utilizes UAVs, and used this application in an excavation project in downtown San Francisco. Julge, Ellmann, & Köök (2019) carried out a study to develop a method to monitor road construction earthworks. In their work, UAVs were utilized as a surveying technique that enables generating point clouds, 3D surface models, and orthophoto mosaics. Land surveying is also a critical issue for construction excavation works. Meouche et al. (2016) aimed to extract a vectorized plan utilizing an UAV for a small site and to investigate the possibility of an official land surveyor exploiting and certificating it. Moreover, Moon, Chung, Kwon, Seo, & Shin (2019) indicate that inaccurate information regarding the terrain in construction projects represents a major challenge to the earthwork process. In this regard, they proposed a method for generating and merging hybrid point cloud data acquired from laser scanning and UAV-based image processing to conduct a better equipment management process in construction works.

In terms of supply chain and total quality management in construction, material tracking emerges as a successful technology to provide the identification of materials. Hubbard et al. (2015) revealed findings of an initial feasibility study on combining RFID technologies with UAV technologies to improve supply chain management in construction. Fang, Chen, Cho, & Zhang (2016) introduced a point cloud-vision hybrid approach to track mobile assets on construction sites. Kang, Park, & Suh (2019) proposed an UAV-based

system that carries an RFID reader in the air for locating RFID tags attached to materials on the ground. Similarly, Wang, Chen, & Yin (2016) states that using UAVs as devices for the traffic data collection exhibits many advantages in collecting traffic information. From this point of view, they proposed a new vehicle detecting and tracking system based on image data collected by an UAV.

A natural disaster can have a great impact on buildings. Therefore, a structural damage assessment is a critical process and should be handled carefully. Fernandez Galarreta, Kerle, & Gerke (2015) benefitted from UAVs to conduct a damage assessment based on multi-perspective, overlapping, and very high-resolution oblique images.

Dupont et al. (2017) approached UAVs from a different perspective. In their study, the potential of UAVs in linking BIM to the real world to improve the productivity was explored. In addition, they presented a technical review of main challenges of using UAVs in the construction sector. Moreover, Kim & Irizarry (2019) evaluated UAV operators' performance and identified the relationship between their performance and experience in the construction industry.

DISCUSSION AND CONCLUSION

UAV technologies have undergone an exponential growth and have become much more affordable (Goessens, Mueller, & Latteur, 2018). With the increasing availability of camera-equipped devices of UAVs, large numbers of high-quality images or video footages are constantly collected to document as-is status of construction job sites (Ham & Kamari, 2019). Thus, the application of the UAV technology in the construction industry tends to increase in recent years. However, there is still much to do to investigate, examine, and evaluate advantages and disadvantages of the application of UAVs in the construction industry. From this perspective, past studies concerning the UAV application in the construction industry were reviewed in this study through a detailed classification.

According to aforementioned studies, researchers have tried to utilize UAVs in quality control works particularly. In addition, health and safety and on-site data collection are the other major issues for researchers. However, all of these research efforts have potential to be investigated in a detailed manner. This is because new technology concepts have always potential to improve the performance of construction firms. Consequently, the UAV technology has been found to be beneficial and useful in the construction industry. Therefore, it can easily be asserted that the number of construction-related UAV studies has a serious potential to increase in the near future.

REFERENCES

Bang, S., Kim, H., & Kim, H. (2017). UAV-based automatic generation of high-resolution panorama at a construction site with a focus on preprocessing for image stitching. *Automation in Construction*, *84*(August), 70–80. https://doi.org/10.1016/j.autcon.2017.08.031

Cajzek, R., & Klanšek, U. (2016). An unmanned aerial vehicle for multi-purpose tasks in construction industry. *Journal of Applied Engineering Science*, *14*(2), 314–327. https://doi.org/10.5937/jaes14-10918

Dupont, Q. F. M., Chua, D. K. H., Tashrif, A., & Abbott, E. L. S. (2017). Potential Applications of UAV along the Construction's Value Chain. *Procedia Engineering*, *182*(3), 165–173. https://doi.org/10.1016/j.proeng.2017.03.155

Fang, Y., Chen, J., Cho, Y. K., & Zhang, P. (2016). A point cloud-vision hybrid approach for 3D location tracking of mobile construction assets. *ISARC 2016 - 33rd International Symposium on Automation and Robotics in Construction*, (ISARC), 613–620. https://doi.org/10.22260/isarc2016/0074

Fernandez Galarreta, J., Kerle, N., & Gerke, M. (2015). UAV-based urban structural damage assessment using object-based image analysis and semantic reasoning. *Natural Hazards and Earth System Sciences*, *15*(6), 1087–1101. https://doi.org/10.5194/nhess-15-1087-2015

Ficapal, A., & Mutis, I. (2019). Framework for the Detection, Diagnosis, and Evaluation of Thermal Bridges Using Infrared Thermography and Unmanned Aerial Vehicles. *Buildings*, *9*(8), 179. https://doi.org/10.3390/buildings9080179

Fleming, K. L., Hashash, Y. M. A., McLandrich, S., O'Riordan, N., & Riemer, M. (2016). Novel Technologies for Deep-Excavation Digital Construction Records. *Practice Periodical on Structural Design and Construction*, *21*(4), 1–10. https://doi.org/10.1061/(ASCE)SC.1943-5576.0000295

Gheisari, M., & Esmaeili, B. (2019). Applications and requirements of unmanned aerial systems (UASs) for construction safety. *Safety Science*, *118*(May), 230–240. https://doi.org/10.1016/j.ssci.2019.05.015

Gheisari, M., Irizzarry, J., & Walker, B. (2014). UAS4SAFETY: The Potential of Unmanned Aerial Systems for Construction Safety Applications. *Construction Research Congress 2014*, 1801–1810. https://doi.org/10.1061/9780784413517.176

Goessens, S., Mueller, C., & Latteur, P. (2018). Feasibility study for drone-based masonry construction of real-scale structures. *Automation in Construction*, *94*(August), 458–480. https://doi.org/10.1016/j.autcon.2018.06.015

Ham, Y., & Kamari, M. (2019). Automated content-based filtering for enhanced vision-based documentation in construction toward exploiting big visual data from drones. *Automation in Construction*, *105*(May), 102831. https://doi.org/10.1016/j.autcon.2019.102831

Hamledari, H., McCabe, B., & Davari, S. (2017). Automated computer vision-based detection of components of under-construction indoor partitions. *Automation in Construction*, *74*, 78–94. https://doi.org/10.1016/j.autcon.2016.11.009

Holt, E. A., Benham, J. M., & Bigelow, B. F. (2015). Emerging technology in the construction industry: Perceptions from construction industry professionals. *ASEE Annual Conference and Exposition, Conference Proceedings*, *122nd ASEE* (122nd ASEE Annual Conference and Exposition: Making Value for Society). https://doi.org/10.18260/p.23933

Howard, J., Murashov, V., & Branche, C. M. (2018). Unmanned aerial vehicles in construction and worker safety. *American Journal of Industrial Medicine*, *61*(1), 3–10. https://doi.org/10.1002/ajim.22782

Hubbard, B., Wand, H., Leasure, M., Ropp, T., Lofton, T., & Hubbard, S. (2015). Feasibility Study of UAV use for RFID Material Tracking on Construction Sites. *51st ASC Annual International Conference Proceedings*, (1995), 669–676.

Julge, K., Ellmann, A., & Köök, R. (2019). Unmanned aerial vehicle surveying for monitoring road construction earthworks. *Baltic Journal of Road and Bridge Engineering*, *14*(1), 1–17. https://doi.org/10.7250/bjrbe.2019-14.430

Kang, S., Park, M. W., & Suh, W. (2019). Feasibility study of the unmanned-aerial-vehicle radio-frequency identification system for localizing construction materials on large-scale open sites. *Sensors and Materials*, *31*(5), 1449–1465. https://doi.org/10.18494/SAM.2019.2266

Kim, D., Liu, M., Lee, S. H., & Kamat, V. R. (2019). Remote proximity monitoring between mobile construction resources using camera-mounted UAVs. *Automation in Construction*, *99*(December 2018), 168–182. https://doi.org/10.1016/j.autcon.2018.12.014

Kim, P., Park, J., Cho, Y. K., & Kang, J. (2019). UAV-assisted autonomous mobile robot navigation for as-is 3D data collection and registration in cluttered environments. *Automation in Construction*, *106*(July), 102918. https://doi.org/10.1016/j.autcon.2019.102918

Kim, S., & Irizarry, J. (2019). Human Performance in UAS Operations in Construction and Infrastructure Environments. *Journal of Management in Engineering*, *35*(6), 04019026. https://doi.org/10.1061/(asce)me.1943-5479.0000715

Li, Y., & Liu, C. (2019). Applications of multirotor drone technologies in construction management. *International Journal of Construction Management*, *19*(5), 401–412. https://doi.org/10.1080/15623599.2018.1452101

Lin, J. J., Han, K. H., & Golparvar-Fard, M. (2015). A Framework for Model-Driven Acquisition and Analytics of Visual Data Using UAVs for Automated Construction Progress Monitoring. *Computing in Civil Engineering 2015*, 156–164. https://doi.org/10.1061/9780784479247.083

Liu, D., Chen, J., Hu, D., & Zhang, Z. (2019). Dynamic BIM-augmented UAV safety inspection for water diversion project. *Computers in Industry*, *108*, 163–177. https://doi.org/10.1016/j.compind.2019.03.004

Liu, J., Jennesse, M., & Holley, P. (2016). Utilizing Light Unmanned Aerial Vehicles for the Inspection of Curtain Walls: A Case Study. *Construction Research Congress 2016: Old and New Construction Technologies Converge in Historic San Juan - Proceedings of the 2016*

Construction Research Congress, CRC 2016, 2651–2659. https://doi.org/10.1061/9780784479827.264

Liu, P., Chen, A. Y., Huang, Y. N., Han, J. Y., Lai, J. S., Kang, S. C., … Tsai, M. H. (2014). A review of rotorcraft unmanned aerial vehicle (UAV) developments and applications in civil engineering. *Smart Structures and Systems*, *13*(6), 1065–1094. https://doi.org/10.12989/sss.2014.13.6.1065

Mahami, H., Nasirzadeh, F., Hosseininaveh Ahmadabadian, A., Esmaeili, F., & Nahavandi, S. (2019). Imaging network design to improve the automated construction progress monitoring process. *Construction Innovation*, *19*(3), 386–404. https://doi.org/10.1108/CI-07-2018-0059

McCabe, B. Y., Hamledari, H., Shahi, A., Zangeneh, P., & Azar, E. R. (2017). Roles, Benefits, and Challenges of Using UAVs for Indoor Smart Construction Applications. *Congress on Computing in Civil Engineering, Proceedings*, *2017-June*, 349–357. https://doi.org/10.1061/9780784480830.043

Meouche, R., Hijazi, I., Poncet, P. A., Abunemeh, M., & Rezoug, M. (2016). UAV photogrammetry implementation to enhance land surveying, comparisons and possibilities. *International Archives of the Photogrammetry, Remote Sensing and Spatial Information Sciences - ISPRS Archives*, *42*(2W2), 107–114. https://doi.org/10.5194/isprs-archives-XLII-2-W2-107-2016

Michele Herrmann, J. D. (2018). Regulation of unmanned aerial vehicles and a survey on their use in the construction industry. *Construction Research Congress 2018: Construction Information Technology - Selected Papers from the Construction Research Congress 2018*, *2018-April* (Herrmann 2016), 758–764. https://doi.org/10.1061/9780784481264.074

Moeini, S., Oudjehane, A., Edition, S., Baker, T., & Hawkins, W. (2017). Application of an interrelated UAS -BIM system for construction progress monitoring, inspection and project management 1. *PM World Journal*, *VI*(VIII), 1–13. Retrieved from www.pmworldjournal.net

Moon, D., Chung, S., Kwon, S., Seo, J., & Shin, J. (2019). Comparison and utilization of point cloud generated from photogrammetry and laser scanning: 3D world model for smart heavy equipment planning. *Automation in Construction*, *98*(June 2017), 322–331. https://doi.org/10.1016/j.autcon.2018.07.020

Morgenthal, G., & Hallermann, N. (2014). Quality assessment of Unmanned Aerial Vehicle (UAV) based visual inspection of structures. *Advances in Structural Engineering*, *17*(3), 289–302. https://doi.org/10.1260/1369-4332.17.3.289

Siebert, S., & Teizer, J. (2014). Mobile 3D mapping for surveying earthwork projects using an Unmanned Aerial Vehicle (UAV) system. *Automation in Construction*, *41*, 1–14. https://doi.org/10.1016/j.autcon.2014.01.004

Tuttas, S., Braun, A., Borrmann, A., & Stilla, U. (2015). Validation of BIM components by photogrammetric point clouds for construction site monitoring. *ISPRS Annals of the Photogrammetry, Remote Sensing and Spatial Information Sciences*, *2*(3W4), 231–237. https://doi.org/10.5194/isprsannals-II-3-W4-231-2015

Vacanas, Y., Themistocleous, K., Agapiou, A., & Hadjimitsis, D. (2016). The combined use of Building Information Modelling (BIM) and Unmanned Aerial Vehicle (UAV) technologies for the 3D illustration of the progress of works in infrastructure construction projects. *Fourth International Conference on Remote Sensing and Geoinformation of the Environment (RSCy2016)*, *9688*(August 2016), 96881Z. https://doi.org/10.1117/12.2252605

Wang, L., Chen, F., & Yin, H. (2016). Detecting and tracking vehicles in traffic by unmanned aerial vehicles. *Automation in Construction*, *72*, 294–308. https://doi.org/10.1016/j.autcon.2016.05.008

Wen, M. C., & Kang, S. C. (2014). Augmented reality and unmanned aerial vehicle assist in construction management. *Computing in Civil and Building Engineering - Proceedings of the 2014 International Conference on Computing in Civil and Building Engineering*, 1570–1577. https://doi.org/10.1061/9780784413616.195

Yasin, M. F. M., Zaidi, M. A., & Nawi, M. N. M. (2016). A review of Small Unmanned Aircraft System (UAS) advantages as a tool in condition survey works. *MATEC Web of Conferences*, *66*. https://doi.org/10.1051/matecconf/20166600038.

THE USE OF INTERNET OF THINGS IN THE CONSTRUCTION INDUSTRY

Volkan ARSLAN
Zonguldak Bulent Ecevit University, Department of Civil Engineering, Zonguldak, Turkey, volkanarslan@beun.edu.tr

Serdar ULUBEYLI
Zonguldak Bulent Ecevit University, Department of Civil Engineering, Zonguldak, Turkey, ulubeyli@beun.edu.tr

Aynur KAZAZ
Akdeniz University, Department of Civil Engineering, Antalya, Turkey, akazaz@akdeniz.edu.tr

ABSTRACT: In recent years, a new technology concept, Internet of Things (IoT), has drawn a great interest. This technology aims to share information across platforms enabling innovative applications. Moreover, it can be considered as a network of sensors, actuators, or machines to facilitate real-time communications between these items in the environment of computer applications. Several industries, such as telecommunication, automotive, healthcare, and logistics, have experienced its advantages and IoT is nowadays beginning to attract attention of the construction industry. Studies on IoT in the construction industry are relatively new. However, there are a few examples of the IoT usage in the construction industry, such as the communication of machines for the optimization of construction works, the coordination of project partners to share information, risk management applications, smart cities, and so on. Therefore, the purpose of this research is to analyze the IoT technology and its practical implications in the construction industry. To this aim, a detailed literature review was conducted and current IoT applications were investigated in detail.

Key words: construction industry, internet of things

INTRODUCTION

The construction industry is known as one of the largest industries in the world. However, it can also be considered as one of the most conservative industry in terms of the adaptation of new methods or technologies. The developing technologies force the

construction industry to utilize novel approaches to overcome cost and time overruns of construction projects (Louis & Dunston, 2018). Internet of Things (IoT), an example of these approaches, is one of the most recent technologies that has drawn a great interest in several industries, such as telecommunication, automotive, healthcare, and logistics, and is nowadays beginning to attract attention of the construction industry (Niu, Anumba, & Lu, 2019). IoT can be described as the interconnection of sensing and actuating devices providing the ability to share information across platforms through a unified framework, developing a common operating picture for enabling innovative applications (Gubbi, Buyya, Marusic, & Palaniswami, 2013). Moreover, it can be considered as a network of sensors, actuators, or machines to facilitate real-time communications between these items in the environment of computer applications (Shahinmoghadam & Motamedi, 2019). Scientific studies on IoT in the construction industry are relatively new. However, there are a few examples of the IoT usage in the construction industry, such as the communication of machines for the optimization of construction works, the coordination of project partners to share information, risk management applications, smart cities, and so on. Therefore, the purpose of this research is to analyze the IoT technology and its practical implications in the construction industry. To this aim, a detailed literature review was conducted and current IoT applications were investigated in detail.

IoT CONCEPT AND DEFINITION

IoT was first introduced by Kevin Ashton in 1998 and has gained increasingly more attention in the academia and industry (Santucci, 2009). The concept of IoT is the environment of things or objects which can interact with each other and corporate with their neighbors via radio-frequency identification (RFID) tags, sensors, actuators, mobile phones, etc., for pre-determined objectives (Giusto, Iera, Morabito, & Atzori, 2010). There are numerous definitions for IoT in the literature, but from a broader perspective, it is a "world-wide network of interconnected objects uniquely addressable, based on standard communication protocols" (Bandyopadhyay & Sen, 2011). The IoT concept is the convergence of three different visions such as (i) things oriented vision, (ii) internet oriented vision, and (iii) semantic oriented vision (Atzori, Iera, & Morabito, 2010). The things oriented vision represents how to integrate generic objects into a common framework. From this perspective, IoT can be evaluated as a tool for autonomous data capture, event transfer, network connectivity and interoperability. The perspective of internet oriented vision directs a network-oriented definition, which enables to connect a large number of communicating devices. Lastly, the semantic oriented vision has a key role to overcome the problem of dealing with the huge information generated by IoT due to the extremely high number of items involved in the future internet (Bandyopadhyay & Sen, 2011). The general concept of the IoT technology that includes main concepts, technologies, and standards was presented in Figure 1, and more detailed information can be found in the study of Atzori et al. (2010).

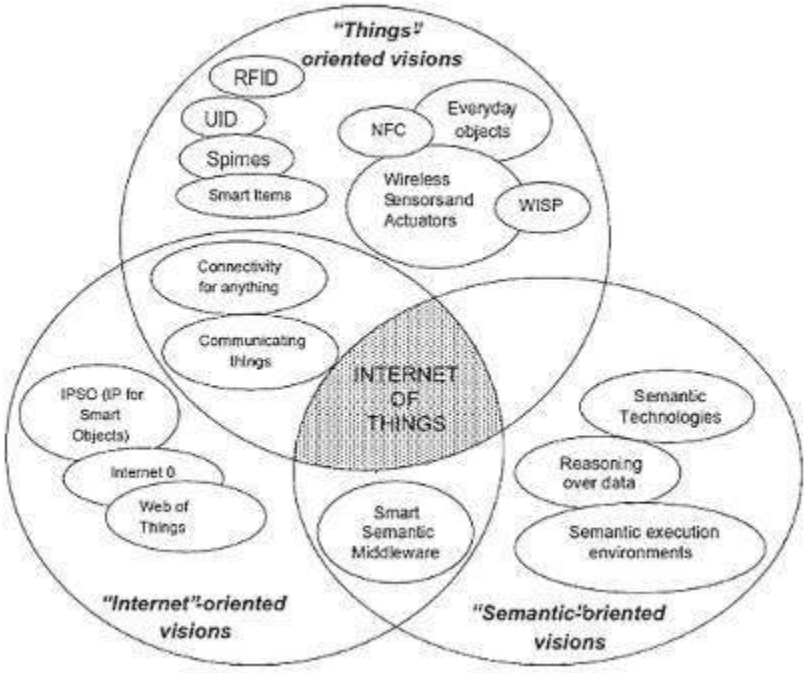

Figure 3. General Concept of IoT (Atzori et al., 2010)

Application of IoT

The IoT technology has a great potential to affect and direct future perspectives of numerous industries. Up to date, some industries (i.e., aerospace and aviation, automotive, telecommunications, medical and healthcare, independent living, pharmaceutical, retail, logistics and supply chain management, manufacturing, environment monitoring, transportation, agriculture and breeding, media, entertainment, insurance, and recycling) have benefitted from IoT (Atzori et al., 2010, Bandyopadhyay & Sen, 2011). From the perspective of the construction industry, IoT is a relatively new and unknown concept. However, in the past decade, some research efforts were shown in terms of smart buildings, communities, cities, and infrastructures. Several researchers have also tried to utilize IoT to overcome health and safety problems in the construction industry. Moreover, many other researchers have paid significant attention on the IoT technology for a better project or construction management performance. In this respect, practical applications of IoT in the construction industry was investigated through a literature review in the following section.

LITERATURE REVIEW

In this section, past studies regarding applications of IoT in the construction industry were reviewed and explained to reveal the current situation of IoT researches in the construction industry. For this purpose, academic databases were utilized to search

relevant studies. After that, these researches were analyzed and then sorted chronologically.

Kortuem et al. (2010) worked on an alternative architectural model for IoT as a system of smart objects or autonomous physical/digital objects augmented with sensing, processing, and network capabilities. From their point of views, there are three smart object types such as (i) activity-aware objects, (ii) policy-aware objects, and lastly, (iii) process-aware objects. They believe that these types represent fundamental design and architectural principles of smart objects and can be integrated into the IoT technology. As a result, they claimed that smart objects that were made into building blocks could cooperate with and form IoT.

Ghimire et al. (2017) state that the interaction between internet and real world objects have a significant potential to become an issue of major importance in business. In this regard, they claim that the IoT technology can be utilized in order to optimize the systematic process of business. Therefore, a framework was provided to decrease the time for decision-making and thus to have a better project management performance in construction industry. In conclusion, the new generation of IoT-based situational-aware computing applications were found to be beneficial to solve communication problems in dynamic site conditions.

Park et al. (2017) studied to clarify the user experience and motivations of IoT technologies, considering a smart home environment. In this context, they proposed a research model in which there are five potential user factors and a technology acceptance model. For this purpose, a questionnaire survey was conducted with 40 smart home users. The findings reveal that users' attitude toward IoT technologies is the greatest predictor of their intention to use. In addition, the perceived compatibility and cost showed notable impacts on the use intention.

Teizer et al. (2017) presented the concept of the integration of IoT and environmental and localization data in a cloud-based BIM platform. They exhibited the usage of the IoT technology and a lean and injury-free construction management approach. In this task, it was aimed to facilitate higher quality, on-time project delivery, and safe value creation processes. Toward this aim, they conducted two case studies. In the first case study, a test of the developed IoT concept focused on tracking several trades in a building construction project was run. In the second one, the developed IoT concept focused on measuring the brightness level at work stations was tested. Finally, the possibility to collect and visualize actual project data in real-time and the potential for the implementation of connected, digital, and smart technologies in construction management were revealed.

Zhou and Ding (2017) aimed to present an IoT-based safety barrier warning system for a better health and safety performance in underground construction projects. To this aim, they investigated hazard energies and their coupling mechanisms and analyzed scenarios for avoiding unsafe behaviors and unsafe status of construction equipment and workers' environment. The proposed system was implemented in a metro tunnel construction in China and the obtained results showed that the safety performance was improved and that the occurrence of accidents caused by the hazard energy on site could be prevented.

Zhong et al. (2017) introduced a multi-dimensional IoT-enabled Building Information Modelling (BIM) platform (MITBIMP) to achieve real-time visibility and traceability in the prefabricated construction. BIM is a powerful tool for the digital presentation and currently supports the planning, design, construction, operation, and maintenance of most physical infrastructures. Therefore it is very useful in the prefabrication-based construction (Azhar, 2011). However, they identified several challenges (i.e., incomplete, inaccurate, and inadequate data, confined data sharing, poor visibility and traceability of the construction process) when using BIM in Hong Kong. To overcome these challenges, they implemented the IoT technology to BIM applications and presented MITBMIP. The results have some significant contributions. First of all, smart construction objects which can collaborate with IoT to ease operations were presented. Second, a multi-dimensional BIM platform was created in order to provide opportunities to stakeholders to share information. Third, through the proposed platform, a better monitoring process was provided for end users. Lastly, traditional 3D BIM applications were extended by utilizing IoT in the process of prefabrication.

Ding et al. (2018) discussed to use BIM and IoT together in order to deal with the uncontrollability and inefficiency problem of the construction progress, quality, and cost in traditional steel bridge construction projects. They state that the collaboration and information sharing among designer, fabricator, constructor, and maintainer is in a dynamic manner during the lifecycle of steel bridges. Therefore, better information and communication technologies should be implemented to overcome the existing problems. To do so, they decided to utilize BIM and IoT together during steel bridge lifecycle activities. A steel construction in which IoT and BIM technology was utilized together is called as the smart steel bridge construction. The smart steel bridge construction was considered in three smart components, namely, smart steel bridge, smart construction site, and smart construction process. These components and participating parties of the smart steel bridge construction conduct a comprehensive process in order to build a smart environment using several instruments. Thus, an opportunity for an efficient digital collaboration throughout the construction lifecycle of a steel bridge was provided.

Kanan et al. (2018) aimed to design an autonomous system based on IoT that monitors, localizes, and warns site laborers who avail within danger zones. For a better health and safety performance, the proposed design considers (i) the real-time alerting of potential

hazards, (ii) indexing of potential hazards for analysis and for the overall improvement of site safety, (iii) the seamless integration of heterogeneous sensors in a middleware IoT platform, and (iv) the introduction of a reliable low-cost and low-power energy harvesting scheme. Then, two IoT-based autonomous, power saving, and real-time sensing systems were determined. These were (i) the back over accidents prevention system (ii) the smart alerting system for potential hazard avoidance. Consequently, it was revealed that the proposed design has a potential to reduce the risk of construction site accidents with low capital and operational costs.

Louis and Dunston (2018) intended to build a framework using the IoT technology to assist the real-time decision-making on the construction site. A practical and sensor-agnostic implementation of operation-level decision-making by utilizing IoT networks was then introduced. From their perspective, the developed framework has potential to improve the operation performance for earthmoving operations in construction. This is because the framework utilizes the IoT infrastructure to first determine equipment state of entities that perform the construction process and to communicate with the same to a discrete-event model of the operation. Consequently, it was stated that the provided framework may help decision makers in the process of decision-making and can increase scientific planning and control methods in the domain of construction project management.

Xu et al. (2018) proposed an integrated cloud-based IoT platform for prefabricated construction works through exploiting the concept of cloud asset. This platform was designed to operate to enable small and medium enterprises to adopt IoT technologies economically and flexibly. For this purpose, they explained the working principle of the cloud-based IoT system firstly. They then adopted the model in a real time prefabricated construction project in Hong Kong. In conclusion, it is believed that the proposed compatible and scalable cloud-based IoT platform may improve the current information and automation level in the construction industry.

Reja and Varghese (2019) targeted to identify the potential usage of the IoT technology for various construction projects and to discuss the potential of 5G technology in order to improve the performance of the IoT technology in terms of construction management issues. In accordance with this target, they carried out a comparative study of current IoT applications in the construction industry and analyzed advantages and shortcoming of IoT in construction. They concluded that the effective use of IoT in the construction environment is not an easy task and that the continuous improvement of IoT is needed in the near future for better applications.

Park et al. (2019) implemented an IoT-based system to prevent the dangerous situation of construction works on job sites. This system works in accordance with sensors and a deep learning system in order to solve the falling problems of construction workers. From

their point of views, this system is suitable for construction sites with various radio interference factors. Based on the findings, they believe that an objective safety guideline could be established for workers at the construction site using the IoT technology.

Table 1. Past Studies on IoT in the Construction Industry

Author and Date	Approach
Kortuem et al. (2010)	Smart Objects
Ghimire et al. (2017)	Decision-making
Park et al. (2017)	Smart Home
Teizer et al. (2017)	BIM Integration
Zhou and Ding (2017)	Health and Safety
Zhong et al. (2017)	BIM Integration
Ding et al. (2018)	BIM Integration
Kanan et al. (2018)	Health and Safety
Louis and Dunston (2018)	Decision-making
Xu et al. (2018)	Prefabricated Construction
Reja and Varghese (2019)	5G Integration
Park et al. (2019)	Health and Safety
Mehata et al. (2019)	Health and Safety

Mehata et al. (2019) utilized smart wearable devices using the IoT technology in detecting the fall of workers and in sending the notification in case of a need for an immediate aid. To do so, they developed a system which monitors the hearth rate and temperatures of workers and thereby warns regarding abnormal health conditions. They tested their system in two different cases, namely, (i) heart beat and temperature sensor and (ii) fall detection. As a result, the proposed system ensures the good health monitoring and fall detection for construction workers.

According to these thirteen past studies concerning the use of IoT in the construction industry, the number and extent of studies seem to be scarce. In Table 1, these studies were categorized in accordance with their approaches of the IoT technology chronologically.

DISCUSSION AND CONCLUSION

The IoT technology has a huge application area when it is used in other technologies such as sensing, identification and recognition, hardware, software and cloud platforms, communication and networks, software and algorithms, positioning, data processing solutions, power and energy storage, security mechanisms, etc. (Čolaković & Hadžialić,

2018). This technology utilizes advantages of intelligent devices, smart mobile devices, single board computers, and different types of sensors and actuators (Dehury & Sahoo, 2016). From this perspective, the awareness about benefits of IoT is rapidly increasing due to the current technology trend in the construction industry (Kanan et al., 2018). Therefore, the IoT technology has a great potential to become more popular in the future.

Aforementioned past studies reveal that IoT has a potential to be utilized in order to solve decision-making and health and safety problems in the construction industry. For this purpose, especially sensors and monitoring systems can be used or developed by construction companies. Considering the poor health and safety performance of construction firms, minimizing or eliminating construction incidents may be possible by using such a new technology in construction sites. In this respect, the help of IoT applications may decrease the number of occupational accidents caused by construction machines. Similarly, using IoT-based technologies may improve the monitoring activities for construction workers in construction sites.

In addition to decision-making and health and safety problems, the IoT technology can also be used to improve the construction management performance. In this context, it was shown that IoT has a potential to provide time and money savings and better quality in construction works. The application of BIM in construction projects has had a great impact on construction management practices. Furthermore, the integration of IoT and BIM may increase the positive effect of technologic developments in the construction industry. Similarly, the IoT technology enabled the emergence of smart objects and smart homes. Thus, construction firms have a chance to enhance their performance in terms of economic, sustainable, and environmentally-friendly practices. Lastly, the 5G technology, which is expected to arise in the near future, may be integrated with the IoT technology in order to expand application opportunities of this technology.

Consequently, IoT is a novel technology and has a potential to be used in the construction industry to improve several issues under the construction management topic. By applying the IoT technology, the construction industry may benefit from its application practices in a positive manner. The system of IoT can be integrated with different applications which are already in use in construction. For future studies, additional research efforts can be carried out in order to improve the performance of smart or intelligent building, smart objects, health and safety precautions, monitoring systems, quality control, etc.

REFERENCES

Atzori, L., Iera, A., & Morabito, G. (2010). The Internet of Things: A survey. *Computer Networks*, *54*(15), 2787–2805. https://doi.org/10.1016/j.comnet.2010.05.010

Azhar, S. (2011). Building information modeling (BIM): Trends, benefits, risks, and challenges for the AEC industry. *Leadership and Management in Engineering*, *11*(3), 241–252. https://doi.org/10.1061/(ASCE)LM.1943-5630.0000127

Bandyopadhyay, D., & Sen, J. (2011). Internet of things: Applications and challenges in technology and standardization. *Wireless Personal Communications*, *58*(1), 49–69. https://doi.org/10.1007/s11277-011-0288-5

Čolaković, A., & Hadžialić, M. (2018). Internet of Things (IoT): A review of enabling technologies, challenges, and open research issues. *Computer Networks*, *144*, 17–39. https://doi.org/10.1016/j.comnet.2018.07.017

Dehury, C. K., & Sahoo, P. K. (2016). Design and implementation of a novel service management framework for IoT devices in cloud. *Journal of Systems and Software*, *119*, 149–161. https://doi.org/10.1016/j.jss.2016.06.059

Ding, K., Shi, H., Hui, J., Liu, Y., Zhu, B., Zhang, F., & Cao, W. (2018). Smart steel bridge construction enabled by BIM and Internet of Things in industry 4.0: A framework. *ICNSC 2018 - 15th IEEE International Conference on Networking, Sensing and Control*, 1–5. https://doi.org/10.1109/ICNSC.2018.8361339

Ghimire, S., Luis-Ferreira, F., Nodehi, T., & Jardim-Goncalves, R. (2017). IoT based situational awareness framework for real-time project management. *International Journal of Computer Integrated Manufacturing*, *30*(1), 74–83. https://doi.org/10.1080/0951192X.2015.1130242

Giusto, D., Iera, A., Morabito, G., & Atzori, L. (2010). *The Internet of Things*. Springer.

Gubbi, J., Buyya, R., Marusic, S., & Palaniswami, M. (2013). Internet of Things (IoT): A vision, architectural elements, and future directions. *Future Generation Computer Systems*, *29*(7), 1645–1660. https://doi.org/10.1016/j.future.2013.01.010

Kanan, R., Elhassan, O., & Bensalem, R. (2018). An IoT-based autonomous system for workers' safety in construction sites with real-time alarming, monitoring, and positioning strategies. *Automation in Construction*, *88*(December 2017), 73–86. https://doi.org/10.1016/j.autcon.2017.12.033

Kortuem, G., Kawasar, F., Fitton, D., & Sundramoorthy, V. (2010). Smart Objects as Building Blocks for the Internet of Things. *Internet Computing*, *14*(1), 44–51.

Louis, J., & Dunston, P. S. (2018). Integrating IoT into operational workflows for real-time and automated decision-making in repetitive construction operations. *Automation in Construction*, *94*(August 2017), 317–327. https://doi.org/10.1016/j.autcon.2018.07.005

Mehata, K. M., Shankar, S. K., Karthikeyan, N., Nandhinee, K., & Robin, H. P. (2019). IoT Based Safety and Health Monitoring for Construction Workers. In *1st International Conference on Innovations in Information and Communication Technology (ICIICT)*. IEEE. https://doi.org/10.1007/bf00677603

Niu, Y., Anumba, C., & Lu, W. (2019). Taxonomy and Deployment Framework for Emerging Pervasive Technologies in Construction Projects. *Journal of Construction Engineering and Management*, *145*(5), 1–13. https://doi.org/10.1061/(ASCE)CO.1943-7862.0001653

Park, E., Cho, Y., Han, J., & Kwon, S. J. (2017). Comprehensive Approaches to User Acceptance of Internet of Things in a Smart Home Environment. *IEEE Internet of Things Journal*, *4*(6), 2342–2350. https://doi.org/10.1109/JIOT.2017.2750765

Park, M., Park, S., Song, M., & Park, S. (2019). IoT-based Safety Recognition Service for Construction Site. *2019 Eleventh International Conference on Ubiquitous and Future Networks (ICUFN)*, 738–741. https://doi.org/10.1109/icufn.2019.8806080

Reja, V. K., & Varghese, K. (2019). Impact of 5G Technology on IoT Applications in Construction Project Management? *Proceedings of the 36th International Symposium on Automation and Robotics in Construction (ISARC)*, (ISARC). https://doi.org/10.22260/isarc2019/0029

Santucci, G. (2009). From internet to data to internet of things. *In Proceedings of the International Conference on Future Trends of the Internet.* Luxembourg.

Shahinmoghadam, M., & Motamedi, A. (2019). Review of BIM-centered IoT deployment: State of the Art, Opportunities, and Challenges. *Proceedings of the 36th International Symposium on Automation and Robotics in Construction (ISARC)*, (ISARC), 1268–1275. https://doi.org/10.22260/isarc2019/0170

Teizer, J., Wolf, M., Golovina, O., Perschewski, M., Propach, M., Neges, M., & König, M. (2017). Internet of Things (IoT) for integrating environmental and localization data in Building Information Modeling (BIM). *ISARC 2017 - Proceedings of the 34th International Symposium on Automation and Robotics in Construction*, (ISARC), 603–609.

Xu, G., Li, M., Chen, C. H., & Wei, Y. (2018). Cloud asset-enabled integrated IoT platform for lean prefabricated construction. *Automation in Construction*, *93*(September 2017), 123–134. https://doi.org/10.1016/j.autcon.2018.05.012

Zhong, R. Y., Peng, Y., Xue, F., Fang, J., Zou, W., Luo, H., … Huang, G. Q. (2017). Prefabricated construction enabled by the Internet-of-Things. *Automation in Construction*, *76*, 59–70. https://doi.org/10.1016/j.autcon.2017.01.006

Zhou, C., & Ding, L. Y. (2017). Safety barrier warning system for underground construction sites using Internet-of-Things technologies. *Automation in Construction*, *83*(May), 372–389. https://doi.org/10.1016/j.autcon.2017.07.005.

CO-HYDROTHERMAL TREATMENT OF LIGNITE AND WOOD SAWDUST

Sibel BAŞAKÇILARDAN KABAKCI
Yalova University, Energy Systems Engineering Department, Engineering Faculty
sibel.kabakci@yalova.edu.tr

Medya Hatun TANIŞ
Yalova University, Department of Energy Systems Engineering, Institute of Science
tansmedyahatun@gmail.com

ABSTRACT: While energy directly affects the growth of a country's economy, it also contributes to the social and cultural development of societies. In order to revive and grow the economy, local resources should be included in energy production and cleaner energy production methods should be preferred. In this way, it is possible to produce energy by using processes that have less impact on the environment by using local resources. High humidity, high ash content and low calorific value are the major disadvantages of using the low-grade coal without any pre-treatment. Particularly, high moisture and high volatile content make it disadvantageous to use the biomass resources. Hydrothermal treatment which is an effective thermochemical pre-treatment method, which can be applied to fuels to enhance their fuel properties. This study mainly investigates the production of coal-biomass hydrochars and discusses the benefits of applying hydrothermal treatment to lignite, biomass and their blend. In the experimental study Soma lignite, wood sawdust (obtained from poplar tree) and their blend (50%, wt.%) were hydrothermally treated at 230 °C for 90 min. Fuel properties of Soma lignite, poplar sawdust and their blend and their corresponding hydrochars were evaluated in terms of heating value, ultimate analysis, proximate analysis and combustion properties. It was observed that hydrothermal process caused changes in moisture, fixed carbon and ash contents of both the blend. As fuels, all hydrochars had higher fixed carbon content and higher heating values compared to their original samples. When coal-biomass blend was compared with its hydrochar, it was observed that fixed carbon content increased by 85% and heating value increased by 12%. Ignition temperatures and burnout temperatures of all hydrochars showed higher values when compared their raw samples, except the coal-biomass blend. The hydrochar of the blend showed lower ignition temperature (293.6 °C) and lower burnout temperature (707.7 °C) when compared to raw blend (315.4 °C and 715.4 °C respectively).

Key words: hydrothermal treatment, coal-biomass blends, hydrochar, fuel properties.

DETERMINATION OF EPILEPTIC EEG SİGNALS USING MULTIWAVELET TRANSFORM AND RECURRENCE QUANTIFICATION ANALYSIS METHODS

Andaç İMAK
Elektrik-Elektronik Mühendisliği
Munzur Üniversitesi
Tunceli, Türkiye
andacimak@munzur.edu.tr

Ömer Faruk ALÇİN
Elektrik-Elektronik Mühendisliği
Bingöl Üniversitesi
Bingöl, Türkiye
ofalcin@bingol.edu.tr

Melih Cevdet İNCE
Elektrik-Elektronik Mühendisliği
Fırat Üniversitesi
Elazığ, Türkiye
mcince@firat.edu.tr

ABSTRACT: Epilepsy is a neurological disease characterized by recurrent seizures. Electroencephalogram (EEG) is an indispensable tool in the diagnosis of epilepsy because it contains valuable information about different physiological conditions of the brain. The resulting detect these signals are integrated with epilepsy models are made to the local health system aims to develop a lot of work. Proposed in this study, the effects of the features obtained by using Multisignal Wavelet Packet and Recurrence Quantification Analysis methods in the differentiation of epileptic EEG signals were observed. Attributes obtained from the methods were classified with Extreme Learning Machine, Support Vector Machines, K-Nearest Neighbors algorithm and Decision Trees. In addition, for the system with the best performance results, the Receiver Operating Characteristic curve which is commonly used in the classification assessment in medical diagnostic tests was analysed and the performance of the classifier was made. Finally, it was compared with the studies using the same data set in the literature.

Key words: Multisignal Wavelet Packet, Recurrence Quantification Analysis, Electroencephalogram (EEG) signals, Epilepsy

ÇOKLU DALGACIK DÖNÜŞÜMÜ VE TEKRARLILIK ÖLÇÜM ANALİZİ YÖNTEMLERİ KULLANILARAK EPİLEPTİK EEG SİNYALLERİNİN SAPTANMASI

ÖZET: Epilepsi tekrarlayan nöbetlerle karakterize edilen bir nörolojik hastalıktır. Elektroensefalogram (EEG) beynin farklı fizyolojik durumlar ile ilgili değerli bilgiler içermesinden dolayı epilepsi tanısında vazgeçilmez bir araçtır. Bundan dolayı epilepsi tespitinde yerel sağlık sistemlerine entegre modeller geliştirmeyi amaçlayan çalışmalar yapılmaktadır. Önerilen bu çalışmada Çoklu Dalgacık Dönüşümü (CDD) ve Tekrarlılık Ölçüm Analizi (TÖA) yöntemleri kullanılarak elde edilen özniteliklerin epileptik EEG sinyallerinin ayırt edilmesindeki etkileri, performansları gözlemlenmiştir. Yöntemlerden elde edilen öznitelikler Aşırı Öğrenme Makinesi (AÖM), Destek Vektör Makinesi (DVM), En Yakın K-Komşu Algoritması (KNN) ve Karar Ağaçları (KA) ile sınıflandırılmıştır. Ayrıca en iyi başarım sonuçları elde edilen sistem için tıpta tanı testlerinde sınıflandırma değerlendirmesinde yaygın olarak kullanılan Alıcı İşlem Karakteristikleri (ROC) eğrisi ile analizleri yapılarak sınıflandırıcının performans değerlendirmesi yapılmıştır. Son olarak da literatürdeki aynı veri seti kullanılarak yapılan çalışmalar ile karşılaştırılmıştır.

Anahtar sözcükler: Çoklu Dalgacık Dönüşümü (CDD), Tekrarlılık Ölçüm Analizi (TÖA), Elektroensefalogram (EEG) sinyali, Epilepsi

GİRİŞ

Küresel hastalık yükünün %0.6'sını oluşturan epilepsi, beyindeki binlerce veya milyonlarca nöronun ani elektrik boşalması sonucu oluşan nörolojik bir bozukluktur. Bu rahatsızlık kısa süreli istemsiz hareketlerin oluşturduğu tekrarlayan nöbetlerle karakterize edilmektedir. Dünya Sağlık Örgütünün (WHO) yaptığı analizlere göre düşük ve orta gelirli ülkelerde her 1000 kişide 7 ile 14 arasında epilepsi hastası olduğu tespit edilmiştir [1].

Elektroensefalogram (EEG), klinik ortamda beyin hastalıklarını teşhis etmek ve elektriksel aktivitesini incelemek için non-invaziv, düşük maliyetli ve etkili bir tekniktir [2]. Uzmanlar tarafından EEG cihazı yardımıyla beyindeki elektriksel faaliyetlerin izlenmesi genellikle 24 saat gibi uzun süreli bir zamana ihtiyaç duyulmaktadır. Ancak sinyallerin içerisinde bulunan gözlem noktalarının tümü karar verme konusunda katkı sağlamamaktadır [3]. Özellikle çok sayıda hasta göz önünde bulundurularak uzmanlar için epilepsi tespiti hem zaman alıcı hem de yanıltıcı bir süreç oluşturabilmektedir [4]. Aynı zamanda EEG sinyallerinin görsel analizi çok objektif bir işlem değildir. Aynı EEG sinyalleri için farklı uzmanlar çelişkili teşhisler verebilmektedir. Yapılan son bir araştırmada dört eğitimli uzmanlar arası duyarlılığın yalnızca % 92'sinin elde edildiğini göstermiştir [5]. Bu nedenle, epilepsinin otomatik tespiti için büyük bir talep vardır ve bu durum teşhis için gereken zamanı büyük ölçüde azaltabilir.

Otomatik tanı tespit sistemlerine ihtiyaç doğrultusunda bilimsel araştırmalar 1970 yılının başlarında EEG ve Beyin Bilgisayar Arayüz (BBA) sistemleri ile insanın yaşam kalitesini etkileyen epilepsi hastalığının tespiti üzerine de çalışmalar başlamıştır. Epileptik nöbetleri saptamak amacıyla birçok EEG sinyal analizi ve işleme tekniği ortaya çıkmıştır. Genel olarak bu yöntemler temelde sınıflandırılma aşaması için öznitelik çıkarma yöntemleri ile sinyalin çeşitli özelliklerine odaklanılır. Literatürde bu sorunu ele alan çeşitli yöntemler sunulmuştur. Yapılan çalışmaların büyük bir çoğunluğunda Kaliforniya Bonn Üniversitesi Epileptoloji Bölümünde erişime açık EEG epileptik veri seti kullanılmıştır. Andrzejak ve ark. deterministik kaos teorisi ile lineer olmayanlığın, karmaşık zamansal davranışa yol açtığı basit deterministik dinamikleri ele almaktadır. Epileptojenik bölgelerden gelen EEG sinyallerinin diğer bölgelerdeki EEG sinyallere oranla lineer olmayan analizlerin faydalı nöbet tespit bilgisini sağlayabileceğini gösteren lineer stokastik dinamiklere dikkat çekmiştir [6]. Acharya ve ark. normal, iktal ve preiktal EEG sinyallerini sınıflandırmak için Hurst üssü, en büyük Lyapunov üssü, fraktal boyut ve yaklaşık entropi gibi kaotik özellikleri kullanmışlardır. Sınıflandırma algoritması olarak DVM ve Gaussian Karma Modeli (GKM) algoritmalarının kullanıldığı bu çalışmada GKM ile daha iyi sonuçlar elde edildiği tespit edilmiştir [7]. Srinivasan ve ark. EEG sinyallerinden özelliklerin çıkarılmasında, zaman ve frekansa dayalı beş öznitelik kullanmışlardır. Elman tekrarlayan sinir ağlarının sınıflayıcı olarak kullanıldığı sistemde yüksek doğruluk oranları elde edilmiştir [8]. Kannathal ve ark. farklı entropi değerleri ve uyarlanabilir bir nöro-bulanık çıkarım algoritması tabanlı bir çalışma gerçekleştirmiştir [9]. Polat ve Güneş KA algoritmaları ve hızlı bir Fourier dönüşüm tabanı içeren bir hibrit model önerdiler [10]. Chua ve ark. normal, iktal ve preiktal EEG sinyallerini ayırt etmek için çeşitli daha yüksek dereceli spektral özellikler kullandılar ve ayrıca yüksek konsantrasyon seviyesine sahip çeşitli sınıflar için çıkarılan özniteliklerin ayırt edici aralıklar olduğunu gösterdiler [11]. Tzallas ve ark. epilepsi tanısı için yapay sinir ağları ile birlikte zaman-frekans dönüşüm özelliklerine sahip Wigner-Ville dönüşümünü önermişlerdir [12]. Acharya ve arkadaşları TÖA yönteminin sinyal hakkında doğru bilgi edinileceği üzerine dikkat çekmiştir. TÖA ile elde edilen öznitelikler normal ve iktal EEG sinyallerinin ayırt edilmesi üzerine DVM tabanlı bir sistem önermişlerdir [13]. Onay ve arkadaşı epileptik EEG sinyallerinin tespitinde Hilbert-Huang dönüşümü ile elde edilen fonksiyonlarının tekrarlılık grafiğinden faydalanmıştır. Elde edilen özniteliklerin DVM ile sınıflandırılması üzerine bir çalışma gerçekleştirmişlerdir [14]. Orhan ve arkadaşları Ayrık Dalgacık Dönüşümü (ADD) ile elde ettikleri öznitelikleri KNN algoritması ile kümeleyerek çok katmanlı sinir ağı giriş olarak kullanıp daha iyi sonuçlar elde etmeye çalışmışlardır [15]. Liang ve arkadaşları epileptik EEG sinyallerinin sınıflandırılması için yaklaşık entropi özniteliklerini kullanmışlardır. Ayrıca hızlı bir Fourier Dönüşümü kullanılarak hesaplanan EEG güç spektrumları eklenerek performansın arttırılması amaçlanmıştır. Elde edilen bu öznitelikler Temel Bileşen Analizi ile en iyi özellikler seçilerek çeşitli doğrusal ve doğrusal olmayan yöntemler tarafından sınıflandırılmıştır [16].

Literatürdeki çalışmalarda öznitelik çıkarımı aşamasında ayarlanabilir pencere yapısından dolayı düşük ve yüksek frekanslı bileşenler açısından iyi bir frekans çözünürlük sağlandığı için dalgacık dönüşümü temelli birçok çalışmada mevcuttur. Subaşı normal ve epileptik EEG sinyallerini tespit etmek amacıyla ADD kullanılarak frekans alt bantlarına ayrıştırıldı. Daha sonra bu alt-bant frekanslarının mutlak değerlerinin ortalaması, ortalama gücü, standart sapma ve bitişik alt bandın mutlak değer otalamalarından oluşan 4 adet öznitelik elde edilmiş olup hibrit bir sistem ile sınıflandırılmıştır [17]. Swami ve ark. ADD kullanarak shanon entropy ve standart sapmalarının hesaplanması ile elde edilen öznitelikler DVM ile sınıflandırılması üzerine bir çalışma gerçekleştirmişlerdir [18]. Wang ve ark. epileptik nöbet tespiti için üç aşamalı hiyerarşik bir elektroensefalogram (EEG) sınıflandırma sistemi önerilmiştir. En iyi bazlı dalgacık paket entropisi yöntemini kullanarak elde edilen öznitelikler ikinci aşamada KNN sınıflandırıcı ile hiyerarşik bilgi tabanına yönelik eğitim aşaması gerçekleştirmişlerdir. Son olarak sınıflandırıcının en üst düzey ayrımcı kuralları kullanarak sınıflandırma aşaması test edilmiştir [19]. Guo ve ark. EEG sinyallerinden ADD ile düşük ve orta frekans göreceli bir dalgacık enerjisi algoritması ile iki adet öznitelik elde etmişlerdir. Daha sonrasında elde edilen bu özniteliklerin üç katmanlı ileri beslemeli bir sinir ağı mimarisi ile sınıflandırılması üzerine bir sistem önerdiler [20]. Bir başka çalışmada ise Guo ve ark. CDD yöntemine dikkat çekmiştir. CDD kullanarak elde edilen frekans alt bantlarının yaklaşık entropi özniteliklerini kullanarak yapay sinir ağları ile sınıflandırmışlardır [21]. Peker ve arkadaşları çalışmalarında karmaşık sınıflandırıcılara dayanan EEG sinyallerinden epilepsi tanısı için yeni bir yöntem önermektedir. Çift ağaçlı karmaşık dalgacık dönüşümü kullanılarak elde edilen EEG frekans alt bantlarından istatistiksel ölçümlere dayanarak maksimum, minimum, aritmetik ortalama, standart sapma, ortanca değer olmak üzere beş öznitelik elde etmişlerdir. Son olarak bu öznitelikler karmaşık değerli sinir ağlarına girdi boyutu olarak sunulmuştur [24].

Bu çalışmada, literatürde bahsedilen çalışmalarla benzer olarak Kaliforniya Bonn Üniversitesi Epileptoloji Bölümünde erişime açık EEG epileptik veri seti kullanılmıştır. CDD ve TÖA temelli bir yaklaşım önerilmiştir. CDD kullanılarak EEG sinyallerinin sadece yakınsama katsayılarını değil, aynı zamanda detay katsayılarını da ayrıştırmak amaçlanmıştır. Önerilen yönteme ek olarak daha yüksek bir performans sağlaması için kısa ve durağan olmayan verileri analiz etmek için uygun TÖA yöntemi kullanılmıştır. Önerilen iki yaklaşımdan elde edilen öznitelikler ayrı ayrı ve birlikte AÖM, DVM, KNN, KA ile sınıflandırılmıştır. En iyi başarım elde edilen sistemin literatürdeki çalışmalar ile karşılaştırılması yapılmıştır. Ayrıca tıpta tanı testlerinde sınıflandırma değerlendirmesinde yaygın olarak kullanılan ROC eğrisi ile yapılan çalışmalarda en iyi başarım sonuçları elde edilen sistemin sınıflandırma performansı gösterilmiştir.

Çalışmanın ikinci bölümünde uygulama adımları, veri seti ve teorik bilgiler anlatılmıştır. Üçüncü bölümde deneysel sonuçlar analiz edilerek literatürdeki çalışmalar ile karşılaştırılması sunulmuştur. Son bölümde ise çalışmanın sonuç kısmına yer verilmiştir.

YÖNTEM

Önerilen çalışma öznitelik çıkarma ve sınıflandırma olmak üzere iki ana aşamadan oluşmaktadır. İlk aşamada TÖA ve CDD metotları kullanılarak EEG sinyallerini temsil eden öznitelikler elde edilmiştir. Öznitelik çıkarma aşaması bir sinyalin karakteristik özelliklerini ortaya çıkarma açısından en önemli adımlardan bir tanesidir. İkinci aşamada ise sinyallerden oluşturulan ikili gruplarda özniteliklerin makine öğrenmesi yöntemleri üzerindeki başarımları irdelenmiştir. Sonuç olarak en iyi başarım sonucu elde edilen sınıflandırıcının ayrıca ROC analizi ile performansı gözlemlenmiştir. Şekil 1'de önerilen metodun kısa bir diyagramı gösterilmiştir.

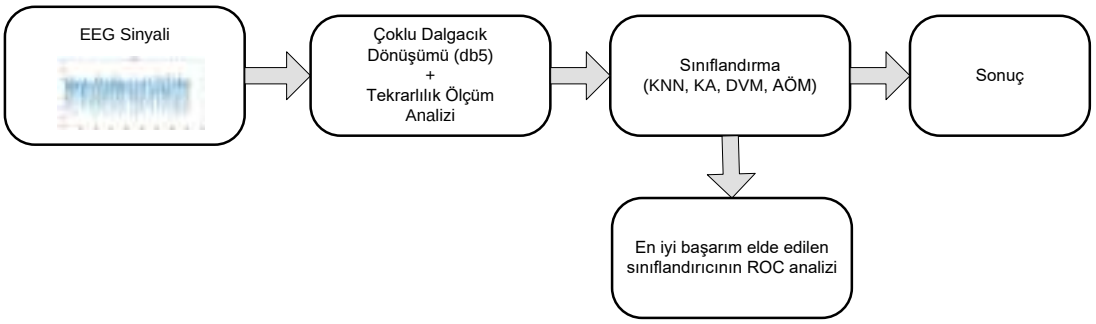

Şekil 1. Önerilen Metot Diyagramı

Veri Seti

Bu çalışmada veri kümesi olarak kullanılan EEG sinyalleri, Bonn Üniversitesi Epileptoloji Bölümü veritabanından elde edilmiştir. Tüm veriler A, B, C, D ve E olarak adlandırılan 23.6 sn tek kanallı beş kümeden oluşmakla birlikte her bir küme 100 adet sinyal içermektedir. Tasarımlar, 12 bitlik bir analog dijital dönüştürücü ile dönüştürüldükten sonra 173.61-Hz örnekleme frekansıyla (toplam 4097 örnek) bir dijital ortama aktarılmıştır. A ve B kümeleri, sırasıyla sağlıklı gönüllülerden alınan ve sırasıyla gözler açık ve kapalı olan EEG kayıtlarından oluşmaktadır. C kümesi nöbetten önce beynin hipokampal karşıt hemisferinden elde edilen EEG kayıtlarından oluşur. D kümesi nöbet öncesi epileptojenik bölgeden elde edilen ve E kümesi ise hasta nöbet anındayken elde edilen EEG kayıtlarından oluşmaktadır [25].

Çoklu Dalgacık Dönüşümü

A Coifman ve arkadaşları çoğullaştırma yaklaşımları ve dalgacık arasındaki bağlantıyı genelleştirerek Çok Boyutlu Dalgacık Dönüşümü (CDD) olarak adlandırılan bir yöntem önermişlerdir [26]. CDD, 1-D dalgacık ayrışmasının genelleştirilmesini temsil etmektedir.

Orijinal sinyal uzayı $\Omega_{0,0}$ yani ağacın kökünü temsil ettiğini varsayarsak, CDD bir alt uzay dal olarak düşünülebilir. Genel bir gösterimde düğüm $\Omega_{j,k}$ olarak ifade edildiğinde buradaki j ölçeği ve k ölçek içindeki alt bant endeksini ifade etmektedir. Dalgacık dönüşümü ile yaklaşım uzayı $\Omega_{j,k} \rightarrow \Omega_{j+1,2k}$, $\{\Phi_{j+1}(t\text{-}2^{j+1}k\}_{k\epsilon Z}$ ve ayrıntı uzayı $\Omega_{j,k} \rightarrow \Omega_{j+1,2k+1}$, $\{\psi_{j+1}(t\text{-}2^{j+1}k\}_{k\epsilon Z}$ olmak üzere iki ortogonal alt uzayı olarak ayrıştırılır. Denklem (1)'de yaklaşım uzayı, Denklem (2)'de de ayrıntı uzayı matematiksel olarak şu şekilde ifade edilmektedir:

$$\Phi_{j,k}(t) = \frac{1}{\sqrt{|2^j|}} \Phi\left(\frac{t-2^j k}{2^j}\right) \quad (1)$$

$$\psi_{j,k}(t) = \frac{1}{\sqrt{|2^j|}} \psi\left(\frac{t-2^j k}{2^j}\right) \quad (2)$$

Burada $\Phi_{j,k}(t)$, $\psi_{j,k}(t)$ dalgacık ve ölçeklendirme fonksiyonları, j ölçeği, k alt bant endeksini ve 2^j ise ölçekleme parametresi olarak bilinmektedir [27].

A CDD'nün, dalgacık dönüşümü arasındaki fark sonraki ayrıklaştırma seviyeleri için CDD sadece yakınsama katsayılarını değil, aynı zamanda detay katsayılarını da ayrıştırmaktadır. Bu işlem J kere tekrarlamaktadır. Bu tekrarlanma N adet orijinal sinyaldeki örnek sayısında $J \leq log_2 N$ olacak şekilde şartı sağlaması gerekmektedir. Tekrarlama işleminin sonucunda JxN boyutunda bir katsayı matrisi elde edilir. Böylece $j = 1, 2, \ldots, J$ çözünürlük seviyesinde N adet örnek sayısına sahip bir sinyalden katsayılar 2^j'lik bir ölçeklendirme ile bloklara bölünmüştür. Bu tekrarlamalı süreç, bir ikili dalgacık paket dönüşümü benzeri bir yapı oluşturmaktadır. Ağacın düğümleri farklı frekans özelliklerine sahip alt uzayları temsil etmektedir [27]. CDD'ne örnek Şekil 2'de üç ayrışma seviyesi ile şematik olarak gösterilmiştir.

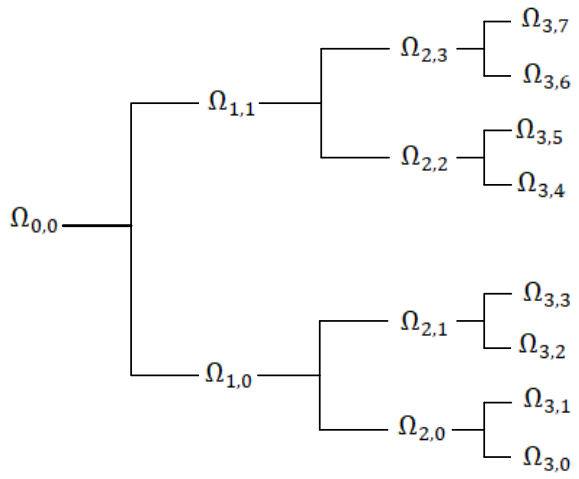

Şekil 2. j=3 İçin Alt Uzaylara Ayrışma Şeması

Tekrarlılık Ölçüm Analizi

Zaman serisi dinamiğinin temsili faz uzayının yeniden oluşturulmasını sağlar. Tekrarlılık durumlarının zamana bağlı davranışını göstermek için Tekrarlılık Noktalarının (TN) oluşturduğu NxN'lik grafiğin temel adımları şu şekildedir;

$R_{i,j} = \theta(\varepsilon - (||X_i - X_j||)$ i,j=1,…,N
(3)
Burada; ε: Önceden tanımlanmış bir kesme mesafesi,
$||\cdot||$: Öklid formu,
N: Toplamda bulunan nokta sayısı,
θ: Bir yoğunluk fonksiyonudur.
X_i'ninci nokta X_j'ninci nokta arasındaki uzaklık bir ε eşik değerinin altına ise $R_{i,j}$=1 yani nokta olan X_i merkezli bir küre tanımlanır. Aksi takdirde $R_{i,j}$=0 olur.
Tekrarlılık Ölçüm Analizi (TÖA) tekniği, tekrarlılık grafiğinin karakteristik yapılarının niceliksel analizine izin veren yöntemdir. Elde edilen tekrarlılık grafiklerinden aşağıdaki karakteristik parametreleri dikkate alınmıştır [28]:

Tekrarlılık Noktoları (RR)

Tekrarlılık grafiğinde tekrarlama noktalarını karakterize eden genel göstergedir. Tekrarlama noktalarının yoğunluğunu gösterir [29].

Belirlilik (DET)

Köşegen çizgiler üzerinde konumlanmış tekrar noktalarının yüzdesidir. Bu çizgiler, sistemin durumlarının benzer evrim zamanlarını temsil etmektedir [30].

Ortalama köşegen çizgi uzunluğu (L)

Bu parametre, sistemin farklılaşmasının ortalama öngörme süresini veya tersini belirtir [30].

Entropi (ENTR)

Çapraz hatların uzaklıklarının olasılıksal dağılım değerleridir [30]. Kullanılan niceliksel parametrelerin denklemleri Tablo 1'de gösterilmiştir.

Tablo 1. TÖA Parametreleri

Parametre	Denklemi
RR	$\frac{1}{N^2}\sum_{i,j=0}^{N} R_{i,j}$ (4)
DET	$\frac{\sum_{i=l_{min}}^{N} lP(l)}{\sum_{i,j}^{N} R_{i,j}}$ (5)
L	$\frac{\sum_{i=l_{min}}^{N} lP(l)}{\sum_{i,j}^{N} Pl}$ (6)
ENTR	$-\sum_{l=l_{min}}^{N} P(l)lnP(l)$ (7)

Tablodaki denklemlerde bulunan l_{min} minimum köşegen çizgi uzunluğu, P(l) l uzunluklu köşegen çizgilerin histogramını temsil etmektedir.

Aşırı Öğrenme Makinesi

Aşırı Öğrenme Makinesi (AÖM), sinir ağı yapıları arasında basit bir mimariye sahip model olan Tek Gizli Katmanlı İleri Beslemeli TGKİB ağ yapısı için basit bir öğrenme yöntemidir [31]. Gradyan temelli geri yayılımlı algoritmalarda öğrenme sürecinde iteratif işlemler ile ağırlıklar ve eşik değerlerinin en uygun değerini buluncaya kadar değişmektedir [32]. AÖM ise uygulama sürecinde rastgele oluşturulmuş girdi ağırlıklarını ve eşik değerlerini kullanarak çıktı ağırlıklarını en küçük kareler yöntemi ile hesaplayarak eğitimini tamamlamış olur. Bu sayede AÖM hızlı bir öğrenme ve genelleme performansı avantajlarıyla benzersiz bir optimal çözüm üretir [33].

Girişler $X_i = [X_1, X_2, \dots X_N]^T \in R^N$ vektörü ve karşılık gelen istenen çıkışlar ise $Y_i = [Y_1, Y_2, \dots Y_N]^T \in R^N$ vektörü ile gösterilmiştir. Gizli katmanda M adet nörona ve $g_{(x)}$ aktivasyon fonksiyonuna sahip TGKİB ağ için matematiksel gösterim aşağıdaki gibi ifade edilmektedir.

$\sum_{i=1}^{M} \beta_i g(W_i X_j + b_i) = Q_j$, j=1,2,…,N (8)

N adet nöron sayısına sahip TGKİB ağ yapısında $w_i = [w_{i1}, w_{i2}, \dots, w_{im}]^T$ gizli nöron ile giriş nöronları birbirine bağlayan giriş ağırlık vektörü, $\beta_i = [\beta_{i1}, \beta_{i2}, \dots, \beta_{im}]^T$ gizli nöron ile çıkış nöronlarını birbirine bağlayan çıkış ağırlık vektörü, b_i eklenen eşik değerini ve $Q_j = [Q_1, Q_2, \dots, Q_j]^T$ ise beklenen çıkışı ifade etmektedir. TGKİB ağ yapısında Q_j ve Y_j arasındaki hatayı en aza indirmeyi hedeflemektedir. Beklenen çıkış ile olması istenilen çıkış ilişkisi arasında;

$\sum_{j=1}^{N} ||Q_j - Y_j|| = 0$ (9)

Şeklinde matematiksel olarak ifade edilmektedir. Hatanın sıfıra yaklaştığı varsayılırsa TGKİB ağ yapısı için matematiksel gösterim de olması istenilen çıkış eşitliği ile mevcut β_i, w_i ve b_i için (8) eşitliği;

$\sum_{i=1}^{M} \beta_i g(W_i X_j + b_i) = Y_j$, j=1,2,…,N (10)

Şeklinde tanımlanabilir. Burada tüm parametrelerinin ayarlanması gerektiğine dair geleneksel sinir ağı yapılarından farklı olarak öğrenme aşamasında giriş ağırlıkları ve gizli katman eşik değeri rastgele seçilerek H gizli katman çıkış matrisi elde edilmektedir.

$$H=\begin{bmatrix} g(W_1 X_1 + b_1) & \cdots & g(W_M X_1 + b_M) \\ \vdots & \ddots & \vdots \\ g(W_1 X_N + b_1) & \cdots & g(W_M X_N + b_M) \end{bmatrix}_{NxM} \quad (11)$$

Şeklinde yazılabilir [34, 35]. Eşitlik (10)'daki matematiksel ifadeden yola çıkılarak *N* adet denklemin daha sade bir halde gösterimi;

$H\beta = Y$ (12)

Eşitlik (12)'deki doğrusal bir denklemi tek seferde çözümleyip β çıkış ağırlıklarının elde edilerek eğitimini tamamlaması için;

$\beta = H^{\dagger} Y$ (13)

H NxN'lik bir kare matris ise tersi alınabilir ve $H^{\dagger} = H^{-1}$ eşitliği yazılabilmektedir. Fakat genellikle gizli nöron sayısı M, farklı eğitim örnek sayısı N'den (M<<N) çok daha azdır. Bu yüzden H matrisi kare matris olmayabilir. β değerini elde etmek için H matrisinin Moore-Penrose Genelleştirilmiş Tersi yöntemi kullanılmaktadır. En küçük kareler yöntemlerinden biri kullanılarak önerilen öğrenme algoritması sadece en küçük eğitim hatasını değil, aynı zamanda en küçük ağırlık seviyesine ulaşma eğilimindedir. Çünkü ağırlıklar ne kadar küçük olursa ağın genel performansı da doğru orantılı olarak iyi olmaktadır [36].

Destek Vektör Makineleri

Destek vektör makineleri (DVM) ilk olarak 1995'te Cortes ve Vapnik tarafından sınıflandırma ve regresyon için kullanılan, danışmanlı öğrenme yaklaşımıyla çalışan bir öğrenme algoritması olarak önerilmiştir. Genel olarak DVM'nin çalışma prensibi sınıf etiketleri bilinen iki sınıfa ait örneklerin, eğitim ve test verileri olmak üzere iki gruba ayrılıp; eğitim verisi sonucu elde edilen bir karar fonksiyonu sayesinde test verilerinin sınıflandırılması işlemidir [37].

Karar Ağaçları

Bir şartın kendisinden başka bir şarta bağlı olduğu sezgisel bir yöntem olarak önerilmiştir. Tümevarım yöntemi ile benzer örüntüleri bulmak için kullanılabilecek bir denetimli öğrenme algoritmasıdır. Doğru tahmin elde etmek için pek çok if-then yapısına tabi tutarak en iyi sırayı bulmaya çalışır [38].

En Yakın K-Komşu Algoritması

Sınıf etiketleri belirli olan bir eğitim örneği kümesine dahil edilecek yeni bir örneğin hangi sınıfa ait olacağını mesafeye dayalı olarak sınıflandırma yapan denetimli bir

öğrenme algoritmasıdır. Söz konusu bu yöntemin çalışma prensibi dahil edilecek örneğin, belirlenen bir k değerinde eğitim örnekleri arasındaki uzaklıkları hesaplanmaktadır. Genel olarak baskın sınıfa dahil olmaktadır. Denetimli bir öğrenme olduğundan dolayı gürültü parametrelerin varlığında sorun yaratabilmektedir [39].

Alıcı İşlem Karakteristikleri (ROC) Eğrisi

Tespit sistemlerinin bilimsel araştırma alanında önemli bir hale gelmesinden dolayı performans değerlendirmesinde ROC analizinin kullanımı giderek yaygınlaşmaktadır. Doğru pozitiflerin yanlış pozitiflere olan kesri olarak ifade edilebilir. Bir ROC eğrisi, farklı eşik değerleri için dikey eksen üzerinde doğru pozitifler (duyarlılık) ve yatay eksen üzerinde yanlış pozitiflerin (1-özgüllük) oranlarının yer aldığı bir eğridir [40]. ROC uzayı grafiği Şekil 3'te gösterilmiştir.

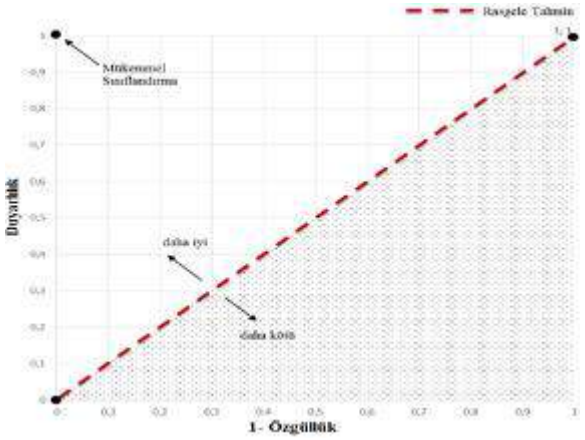

Şekil 3. ROC Uzay Grafiği

ROC eğrisi altında kalan alan ise sistemin doğruluğunu belirtmektedir. ROC uzayı grafiğinde iyi bir performansta sırasıyla (0.0), (0.1) ve (1.1) noktalarından geçen bir eğri oluşturmaktadır.

BULGULAR

Deneysel çalışma EEG veri seti epilepsi krizi var veya yok olacak şekilde 7 farklı durumun sınıflandırma problemine yönelik yapılmıştır. Önerilen yöntemde, çoklu dalgacık dönüşümü ve tekrarlılık ölçüm analizi yöntemi kullanılarak öznitelikler çıkarılmıştır. Elde edilen bu öznitelik çıkarma yöntemlerinin etkisi ayrı ayrı ve birlikte 7 farklı durumda test edilmesi için AÖM, KA, DVM ve KNN makine öğrenmesi yöntemleri kullanılmıştır.

Çalışmada ilk olarak CDD'nde j=5 alınarak her bir sinyale ait 5x63 lük bir öznitelik matrisi elde edildi. Her bir özelliğe ait 5 adet parametrenin ortalaması alınarak bir sinyale ait 1x63 adet öznitelik çıkarılmıştır. Elde edilen öznitelikler KA, DVM, KNN ve AÖM

(gizli katman nöron sayısı 2000 ve aktivasyon fonksiyonu sigmoid) ile sınıflandırılmıştır. Önerilen özniteliklerinin sınıflandırıcılar üzerindeki başarım sonuçları Tablo 2'de verilmiştir.

Tablo 2. CDD Özniteliklerinin Başarım Sonuçları

Sınıflandırıcı	Doğruluk (%)						
	A-E	AB-E	CD-E	A-CDE	ACD-E	AB-CDE	ABCD-E
KA	99.50	99.30	96	98	97.30	97	98
DVM	99.50	100	98	99.30	99	99.20	98.60
KNN	99.50	99.70	98	99.30	98.80	98.80	99
AÖM	100	99.67	99	99.75	99.25	99.80	99.40

Çalışmada ikinci olarak TÖA ile elde edilen özniteliklerden RR, DET, L ve ENTR'den oluşan 4 adet öznitelik kullanılmıştır. Her bir sinyale ait elde edilen bu 4 adet öznitelik KA, DVM, KNN ve AÖM (gizli katman nöron sayısı 1000 ve aktivasyon fonksiyonu tribas) ile sınıflandırılmıştır. Önerilen özniteliklerinin sınıflandırıcılar üzerindeki başarım sonuçları Tablo 3'te verilmiştir.

Tablo 3. TÖA Özniteliklerinin Başarım Sonuçları

Sınıflandırıcı	Doğruluk (%)						
	A-E	AB-E	CD-E	A-CDE	ACD-E	AB-CDE	ABCD-E
KA	95	96.30	81	95.30	86.80	93.80	87.80
DVM	97.50	96.70	87	95.80	91	96.20	89.40
KNN	98	96.70	85.30	95.30	89	94.40	99
AÖM	99	98.33	87	97.25	89.25	97.40	90.20

Deneysel çalışmada son olarak da önerilen yöntem, CDD ve TÖA ile elde edilen öznitelikler birleştirilerek 67 adet öznitelik elde edilmiştir. Bu öznitelikler KA, DVM, KNN ve AÖM ile sınıflandırılmıştır. Önerilen yaklaşım başarım sonuçları Tablo 4'te verilmiştir.

Tablo 4. CDD + TÖA Özniteliklerinin Başarım Sonuçları

Sınıflandırıcı	Doğruluk (%)						
	A-E	AB-E	CD-E	A-CDE	ACD-E	AB-CDE	ABCD-E
KA	100	99.30	95	97.80	97	98	97.80
DVM	100	99.70	98	99.30	98.80	99.60	98.40
KNN	100	99.70	98	100	98.50	99.60	98.40
AÖM	**100**	**100**	**99.33**	**100**	**99.50**	**99.80**	**99.40**

Öznitelik çıkarma yöntemlerinin ayrı ayrı ve birlikte kullanılarak elde edilen başarım oranları karşılaştırma yapıldığında, CDD ve TÖA birlikte kullanılması ile daha iyi sonuçlar elde edilmiştir. Ayrıca CDD ve TÖA yöntemleri birlikte kullanılarak elde edilen özniteliklerin Tablo 4'e bakıldığında AÖM diğer sınıflandırıcılara kıyasla daha iyi bir performans yakaladığı kaydedilen başarım sonuçlarından gözlemlenmektedir.
Önerilen yaklaşımda CDD ve TÖA tabanlı EEG sinyallerinin AÖM ile sınıflandırılmasında, sınıflandırıcının gizli katman nöron sayısı 2000 ve gizli katmanda sigmoid aktivasyon fonksiyonu ampirik yöntemlerle seçilmiştir. Oluşturulan 7 durumda da yapılan testin hatasını daha iyi tahmin edebilmek için 10 kat çaprazlama kullanılarak doğruluk, duyarlılık ve özgüllük oranı Tablo 5'te gösterilmiştir.

Tablo 5. Önerilen (CDD+TÖA) Özniteliklerin AÖM Üzerindeki Başarım Sonuçları

Durum	Doğruluk (%)	Duyarlılık (%)	Özgüllük (%)
A-E	100	100	100
AB-E	100	100	100
CD-E	99.33	99.05	100
A-CDE	100	100	100
ACD-E	99.50	99.34	100
AB-CDE	99.80	99.51	100
ABCD-E	99.40	99.26	100

Tablo 5'e bakıldığında en yüksek başarım oranı A-E, AB-E, A-CDE durumları için %100 ve en düşük başarım oranı ise %99.33 olarak CD-E durumunda elde edilmiştir. AÖM'nin tüm durumlar için ROC eğrileri sırasıyla Tablo 6'da verilmiştir.

Tablo 6. Önerilen Yöntemin 7 Durum İçin ROC Eğrisi

|A|-|E|	|AB|-|E|
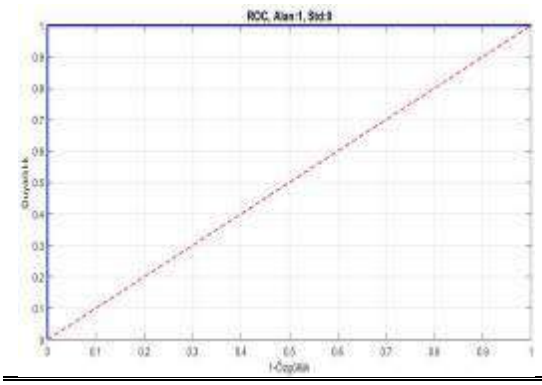	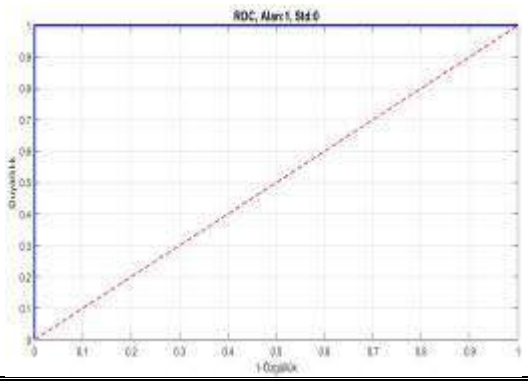

|CD|-|E|

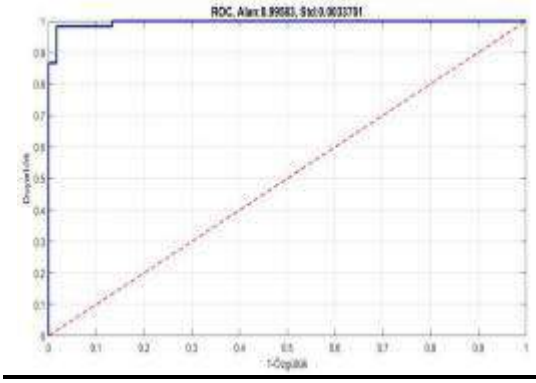

|A|-|CDE|

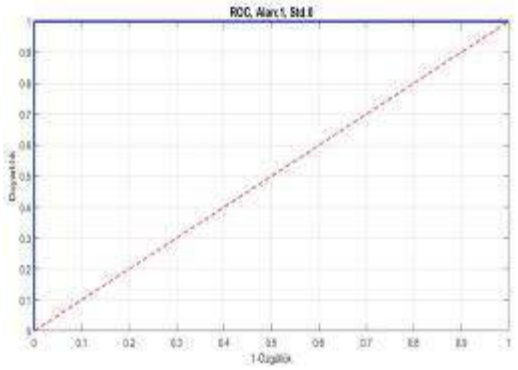

|ACD|-|E|

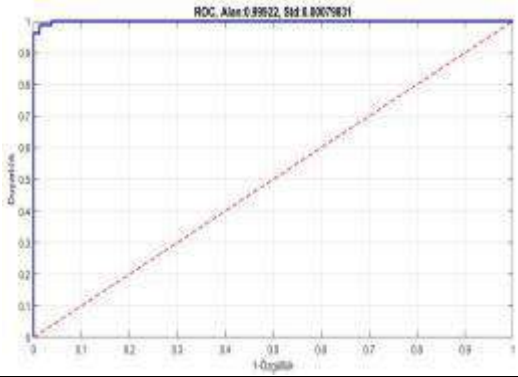

|AB|-|CDE|

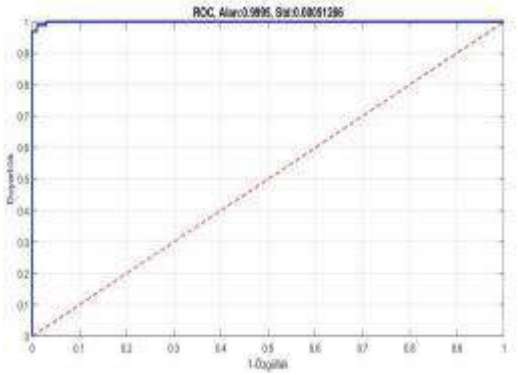

|ABCD|-|E|

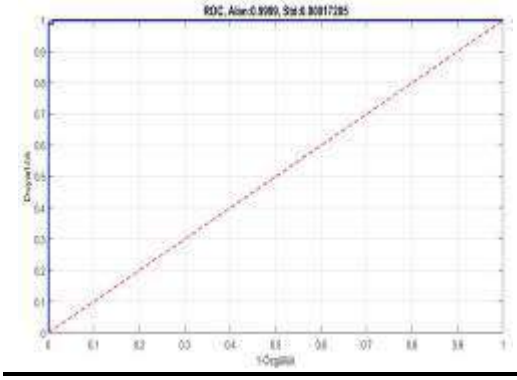

ROC eğrilerinde sınıflandırıcının iyi bir performans göstermesi için koordinat olarak sırasıyla (0.0), (0.1) ve (1,1) noktasına yakın geçmesi istenmektedir. Tablo 6'da analiz sonuçları incelendiğinde sınıflandırıcının önerilen öznitelik çıkarma yöntemleri ile ikili grupları iyi bir şekilde ayır ettiği gözlemlenmektedir. Ayrıca deneysel çalışmadan elde edilen sonuçlar literatürde aynı veri setini ve aynı durumları dikkate alan çalışmalarla da karşılaştırılmıştır. Karşılaştırmalı sonuçlar ABCD-E ve A-E durumları için sırasıyla Tablo 7'de verilmiştir.

Tablo 7. ABCD-E ve A-E Durumları İçin Karşılaştırma Tablosu

Yazar	Yöntem	Durum	Veri Seçimi	Doğruluk
Tzallas ve ark. [12]	Wigner-Ville Dönüşümü+ Yapay Sinir Ağı	ABCD-E	%50 eğitim, %50 test	%97.73
Orhan ve ark. [15]	ADD+ Çok Katmanlı Sinir Ağı	ABCD-E	%50 eğitim, %50 test	%99.60
Liang ve ark. [16]	ADD-Yaklaşık Entropi+ Doğrusal veya Doğrusal Olmayan Sınıflandırıcı	ABCD-E	%60 eğitim, %40 test	%98.51
Guo ve ark. [21]	CDD–Yaklaşık Entropi+ Çok katmanlı Sinir Ağı	ABCD-E	%50 eğitim, %50 test	%98.27
Peker ve ark. [24]	Çift Ağaçlı Karmaşık Dalgacık Dönüşümü +Karmaşık Değerli Sinir Ağı	ABCD-E	10 kat çaprazlama	%99.15
Önerilen Sistem	***TÖA- CDD+ AÖM***	***ABCD-E***	***10 kat çaprazlama***	***%99.40***
Srinivasan ve ark. [8]	Zaman-Frekans Domeni Özellikleri+ Tekrarlayan Sinir Ağı	A-E	%60 eğitim, %40 test	%99.60
Kannathal ve ark. [9]	Entropi+ Uyarlamalı Sinirsel Bulanık Çıkarım Sistemi	A-E	%60 eğitim, %40 test	%92.22
Polat ve Güneş [10]	Hızlı Fourier Dönüşümü+ KA	A-E	10 kat çaprazlama	%98.72
Tzallas ve ark. [12]	Wigner-Ville Dönüşümü+ Yapay Sinir Ağı	A-E	%50 eğitim, %50 test	%100
Subaşı [17]	ADD+ Hibrit Sistem	A-E	%60 eğitim, %40 test	%94.50
Swami ve ark. [18]	ADD+ DVM	A-E	10 kat çaprazlama	%99.53

Wang ve ark. [19]	ADD+ Hiyerarşik Sınıflandırma Sistemi	A-E	10 kat çaprazlama	%99.44
Guo ve ark. [20]	ADD+ Çok Katmanlı Sinir Ağı	A-E	10 kat çaprazlama	%95.20
Guo ve ark. [21]	CDD–Yaklaşık Entropi+ Çok katmanlı Sinir Ağı	A-E	%50 eğitim, %50 test	%99.85
Önerilen Sistem	***TÖA- CDD+ AÖM***	***A-E***	***10 kat çaprazlama***	***%100***

Literatürde aynı veri seti, farklı sinyal işleme ve makine öğrenmesi yöntemi kullanılarak önerilen çalışmalarla birlikte Guo ve ark. [21] önerdiği CDD ve yaklaşık entropi özniteliklerinin çok katmanlı bir sinir ağı yapısı kullanılarak yapılan sınıflandırma çalışması ile karşılaştırma yapılmıştır. Önerilen sistemde 10 kat çaprazlama yapılarak rastgele ayırma yaklaşımının farklı sonuçlar üretme ihtimalini ortadan kaldırarak sistemin güvenilirliğinin arttırılması hedeflenmiştir. Yapılan bu karşılaştırma sonucunda genel olarak hem veri seçimi hem de başarım sonucu olarak önerilen yöntemin epilepsi ve normal EEG sinyallerinin sınıflandırılmasında yararlı bir parametre olarak sunulabileceği geçerliliğini göstermektedir.

SONUÇ

Gelişen teknolojiyle birlikte her alanda olduğu gibi biyomedikal alanda da önemli gelişmeler gerçekleştirilmektedir. Dünyadaki en yaygın nörolojik hastalıklarından biri olarak görülen epilepsi hastalığının tespitindeki zorluklardan dolayı bu alandaki bilimsel araştırmalar nöbetlerin saptanması üzerine yoğunlaşmıştır. Böylece nöbet tespitinde nörofizyologlara yardımcı olmakla birlikte hastanın nöbet başlangıcında süreci uyarılarak ciddi yaralanmaların önlenebilmesi ile yaşam kalitesini yükseltmeyi hedefleyen bir tanı aracı amaçlanmıştır.

Önerilen öznitelik çıkarma yöntemleri ve ikinci aşamasında KA, DVM, KNN ve AÖM ile sınıflandırılarak iyi bir başarım ve kısa sürede sonuçlanması hedeflenmiştir. Genel olarak en yüksek %100 (A-E, AB-E, A-CDE) ve en düşük %99.33 (CD-E) ile iyi sonuçlar AÖM ile kaydedilmiştir. Kullanılan öznitelik çıkarma yöntemleri ve AÖM ile tanı kararının çok kısa sürede, iyi başarım oranı vermesi sağlanmıştır. Yöntemin literatürde aynı veri seti kullanılarak yapılan çalışmalarla kıyasla iyi bir başarım göstermesi ile birlikte tek gizli katmanlı ileri beslemeli ağ mimarisine sahip AÖM' nin medikal tanı sistemlerinde iyi bir

genelleme performansı elde etmek için öğrenme algoritması olarak kullanılabileceğini göstermiştir.

KAYNAKLAR

[1] World Health Organization (2019). Retrieved September 22, 2019 from https://www.who.int/en/news-room/fact-sheets/detail/epilepsy
[2] Stam, C. J., Pijn, J. P. M., Suffczynski, P., & Da Silva, F. L. (1999). Dynamics of the human alpha rhythm: evidence for non-linearity?. *Clinical Neurophysiology*, 110, 1801-1813.
[3] Gotman, J. (1999). Automatic detection of seizures and spikes. *Journal of Clinical Neurophysiology,* 16, 130-140.
[4] Tzimourta, K. D., Astrakas, L. G., Tsipouras, M. G., Giannakeas, N., Tzallas, A. T., & Konitsiotis, S. (2017, June). Wavelet based classification of epileptic seizures in EEG signals. In *2017 IEEE 30th International Symposium on Computer-Based Medical Systems (CBMS)* (pp. 35-39). IEEE.
[5] Wilson, S. B., Scheuer, M. L., Plummer, C., Young, B., & Pacia, S. (2003). Seizure detection: correlation of human experts. *Clinical Neurophysiology,* 114, 2156-2164.
[6] Andrzejak, R. G., Widman, G., Lehnertz, K., Rieke, C., David, P., & Elger, C. E. (2001). The epileptic process as nonlinear deterministic dynamics in a stochastic environment: an evaluation on mesial temporal lobe epilepsy. *Epilepsy research*, *44*, 129-140.
[7] Acharya, U. R., Chua, C. K., Lim, T. C., Dorithy, & Suri, J. S. (2009). Automatic identification of epileptic EEG signals using nonlinear parameters. *Journal of Mechanics in Medicine and Biology*, *9*, 539-553.
[8] Srinivasan, V., Eswaran, C., & Sriraam, A. N. (2005). Artificial neural network based epileptic detection using time-domain and frequency-domain features. *Journal of Medical Systems*, *29*, 647-660.
[9] Kannathal, N., Choo, M. L., Acharya, U. R., & Sadasivan, P. K. (2005). Entropies for detection of epilepsy in EEG. *Computer Methods and Programs in Biomedicine,* 80, 187-194.
[10] Polat, K., & Güneş, S. (2007). Classification of epileptiform EEG using a hybrid system based on decision tree classifier and fast Fourier transform. *Applied Mathematics and Computation,* 187, 1017-1026.
[11] Chandran, V., Acharya, R., & Lim, C. M. (2007, August). Higher order spectral (HOS) analysis of epileptic EEG signals. In *2007 29th Annual International Conference of the IEEE Engineering in Medicine and Biology Society* (pp. 6495-6498). IEEE.
[12] Tzallas, A. T., Tsipouras, M. G., & Fotiadis, D. I. (2007). Automatic seizure detection based on time-frequency analysis and artificial neural networks. *Computational Intelligence and Neuroscience,* 2007.

[13] Acharya, U. R., Sree, S. V., Chattopadhyay, S., Yu, W., & Ang, P. C. A. (2011). Application of recurrence quantification analysis for the automated identification of epileptic EEG signals. *International journal of neural systems*, *21*, 199-211.
[14] Onay, F. K. & Cemal, K. (2014, November). İçsel Mod Fonksiyonlarının Tekrarlılık Grafiği Kullanılarak EEG Sinyallerinde Epileptik Nöbetin Algılanması. *In 2014 27th Bilgisayar ve Biyomedikal Mühendisliği Sempozyumu* (pp. 613-617).
[15] Orhan, U., Hekim, M., & Ozer, M. (2011). EEG signals classification using the K-means clustering and a multilayer perceptron neural network model. *Expert Systems with Applications,* 38, 13475-13481.
[16] Liang, S. F., Wang, H. C., & Chang, W. L. (2010). Combination of EEG complexity and spectral analysis for epilepsy diagnosis and seizure detection. *EURASIP journal on advances in signal processing,* 2010, 853434.
[17] Subasi, A. (2007). EEG signal classification using wavelet feature extraction and a mixture of expert model. *Expert Systems with Applications*, *32*, 1084-1093.
[18] Swami, P., Godiyal, A. K., Santhosh, J., Panigrahi, B. K., Bhatia, M., & Anand, S. (2014, December). Robust expert system design for automated detection of epileptic seizures using SVM classifier. In *2014 International Conference on Parallel, Distributed and Grid Computing* (pp. 219-222). IEEE.
[19] Wang, D., Miao, D., & Xie, C. (2011). Best basis-based wavelet packet entropy feature extraction and hierarchical EEG classification for epileptic detection. *Expert Systems with Applications*, *38*, 14314-14320.
[20] Guo, L., Rivero, D., Seoane, J. A., & Pazos, A. (2009, June). Classification of EEG signals using relative wavelet energy and artificial neural networks. In *Proceedings of the first ACM/SIGEVO Summit on Genetic and Evolutionary Computation* (pp. 177-184). ACM.
[21] Guo, L., Rivero, D., & Pazos, A. (2010). Epileptic seizure detection using multiwavelet transform based approximate entropy and artificial neural networks. *Journal of neuroscience methods*, *193*, 156-163.
[24] Peker, M., Sen, B., & Delen, D. (2015). A novel method for automated diagnosis of epilepsy using complex-valued classifiers. *IEEE journal of biomedical and health informatics,* 20, 108-118.
[25] Andrzejak, R. G., Widman, G., Lehnertz, K., Rieke, C., David, P., & Elger, C. E. (2001). The epileptic process as nonlinear deterministic dynamics in a stochastic environment: an evaluation on mesial temporal lobe epilepsy. *Epilepsy research,* 44, 129-140.
[26]Coifman, R. R., Meyer, Y., & Wickerhauser, V. (1992). Wavelet analysis and signal processing. In *In Wavelets and Their Applications*, Jones and Barlett, pp. 153-178.
[27] Mallat, S. (2008). A wavelet tour of signal processing: The sparse way, third edition. *Academic Press,* pp. 386-387.
[28] Stangalini, M., Ermolli, I., Consolini, G., & Giorgi, F. (2017). Recurrence quantification analysis of two solar cycle indices. *Journal of Space Weather and Space Climate*, 7 (A5), 1-13.
[29] Eckmann, J. P., Kamphorst, S.O. & Ruelle, D. (1987). Recurrence plots of dynamical systems. *EPL (Europhysics Letters),* 4, 973-977.

[31] Huang, G. B., Zhu, Q. Y. & Siew, C. K. (2006). Extreme learning machine: theory and applications. *Neurocomputing,* 70, 489-501
[32] Ertuğrul, Ö. F., & Kaya, Y. (2014). A detailed analysis on extreme learning machine and novel approaches based on ELM. *American Journal of computer science and engineering,* 1, 43-50.
[33] Alcin, O. F., Sengur, A., Ghofrani, S. & Ince, M.C. (2014). GA-SELM: Greedy algorithms for sparse extreme learning machine. *Measurement,* 55, 126-132.
[34] Huang, G. B., Zhu, Q. Y. & Siew, C. K. (2004). Extreme learning machine: a new learning scheme of feedforward neural networks. *IEEE International Joint Conference on Neural Networks, Budapest, 25-29 July*, 2, 985-990.
[35] Alçin, Ö.F., Şengür, A., & İnce, M.C. (2015). İleri-geri takip algoritmasi tabanli seyrek aşiri öğrenme makinesi. *Gazi Üniversitesi Mühendislik-Mimarlık Fakültesi Dergisi,* 30, 111-117.
[36] Huang, G. B., Zhu, Q. Y. & Siew, C. K. (2006). Extreme learning machine: theory and applications. *Neurocomputing,* 70, 489-501.
[37] Varady, P., Micsik, T., Benedek, S. & Benyo, Z. (2002). A novel method for the detection of apnea and hypopnea events in respiration signals. *IEEE Trans. Biomed. Eng.,* 49, 936–942.
[38] Emel, G.G. & Taşkın, Ç. (2005). Veri madenciliğinde karar ağaçları ve bir satış analizi uygulaması. *Eskişehir Osmangazi Üniversitesi Sosyal Bilimler Dergisi,* 6, 221-239.
[39] Desai, U. (2017, May). Automated detection of cardiac health condition using linear techniques. In *2017 2nd IEEE International Conference on Recent Trends in Electronics, Information & Communication Technology (RTEICT)* (pp. 890-894). IEEE.
[40] Spackman, K.A. (1989). Signal detection theory: Valuable tools for evaluating inductive learning. *In Proceedings of the sixth international workshop on Machine learning,* pp. 160-163.

CRASHWORTHINESS OF BASALT FIBER REINFORCED COMPOSITE PIPES SUBJECTED TO QUASI-STATIC LATERAL COMPRESSION

Özkan ÖZBEK
Gaziantep University, Mechanical Engineering Department, 27310, Gaziantep, Turkey
ozkanozbek@gantep.edu.tr

Ömer Yavuz BOZKURT
Gaziantep University, Mechanical Engineering Department, 27310, Gaziantep, Turkey
oybozkurt@gantep.edu.tr

Ahmet ERKLİĞ
Gaziantep University, Mechanical Engineering Department, 27310, Gaziantep, Turkey
erklig@gantep.edu.tr

ABSTRACT: This paper aimed to explore the failure modes and crashworthiness characteristics of basalt fiber reinforced pipes (BFRP) subjected to quasi-static lateral compression. Experimental investigations were performed on various fiber orientation angles (±40°, ±55°, and ±70°) of the basalt FRP fabricated by filament winding technique. Fracture mechanisms of pipe samples were discussed to understand failure modes. The increase in fiber orientation resulted with increase in energy absorption capability and load carrying capacity. The pipe sample with ±70° fiber orientation angle showed the maximum specific energy absorption of 3.07 J/g. Maximum values of initial peak load and mean crushing loads were also obtained from the sample with ±70° fiber orientation angle. This is attributed to fiber closer position against to direction of application loading. In addition, failure modes and crack propagation were investigated on crushing history at different stroke values of load-displacement curves. For all samples, mid-surface of samples were observed as damage region beginning with a buckling behavior of the vertical walls. In conclusion, fiber orientation angle had a significant influences on the crashworthiness characteristics of filament wound BFRP.

Key words: crashworthiness, basal fiber, fiber orientation angle, filament winding

INTRODUCTION

In recent years, polymer based composites have been an interesting class of materials used in applications due to their excellent mechanical characteristics such as higher specific strength and stiffness, better damping, longer service life which are the limitations of classical engineering materials. Furthermore, they may offer the higher specific energy absorption with lightweight structures in a crash event. While metallic crash absorber materials show the phenomenon of plastic deformation, progressive collapse in a brittle manner [1] is forming for composite materials. The use of thin-walled tubular composites decreasing the size and mass of the material or reducing negative inertial effects have been a creative way to achieve higher ability to absorb energy in crushing applications.

At present, a considerable amount of scientific papers devoted to energy absorption capabilities of thin walled composites are seen in the literature [2-4]. Mahdi et al. [5] investigated the effects of fiber orientation angle on the crashworthiness characteristics of E-glass/epoxy reinforced composite pipes. The six different fiber orientation angles were considered as 0°, 15°, 30°, 45°, 60° and 75°. 15°/-75° and 75°/-15° were being recommended for better load carrying and energy absorption capability. Sebaey and Mahdi [6] examined the crashworthiness behaviors of glass/epoxy composite tubes fabricated by filament winding. The samples were compressed after impacted by Charpy impact tester. Various places such as side, top, down were exposed to impact energy with more than one time. They explained that top impacted samples had less sensitivity to impact damage compared to side impacted ones. Kim et al. [7] researched the crushing behaviors of composite tubes. Carbon/epoxy, kevlar/epoxy and interply carbon-kevlar/epoxy composite tubes were utilized to obtain specific energy absorption, maximum peak load, mean crushing load. According to results, carbon/epoxy provided to the best energy absorption capability with the value of 81.7%. Also, kevlar /epoxy gave the worst specific absorption in their studies.

The main emphasis of this paper is the effects of the fiber orientation angle on the crashworthiness characteristics of basalt fiber reinforced composite pipes fabricated by filament winding technique. The samples having different fiber orientation angles (±(40°), ±(55°), ±(70°)) has been subjected to quasi-static lateral compression loadings and compared with each configurations based on the load carrying capacity, energy absorption capability.

MATERIALS AND METHODS

Sample Preparation

The basalt roving fiber with 2.4K linear density (tex), shown in Figure 1, are used as reinforcement and are procured from Tila Kompozit company, Turkey. The mechanical properties of the basalt fiber reinforcement are given in Table 1.

Figure 1. Basalt roving fiber

Table 1. Mechanical properties of basalt fiber reinforcement

Tensile strength (MPa)	Tensile modulus (GPa)	Elongation at break (%)	Filament diameter (μm)	Specific density (g/cm^3)
3200	90	3.1	13	2.78

For the matrix component of pipes, the epoxy (EPIKOTE MGS LR160 resin) and hardener (EPIKURE Curing Agent MGS LH260S), which are supplied from Dost Kimya A.Ş., Turkey, are mixed with a stoichiometric weight ratio of 100:35, respectively.

The filament winding technique, shown in Figure 2, is used to produce all considered pipe samples. The fabrication process of fiber reinforced composite pipes can be categorized into three distinct steps as preliminary preparations, process conducting and post processing. As preliminary preparations, release wax is applied on the mandrel and release agent film is wrapped at first. Afterwards, release wax is again implemented to pull out the mandrel from the pipe at the end of the winding process. The glass wool is exerted to obtain smooth surface inside the samples. Fiber reinforcement is placed with helping of resin bath and rollers. By using epoxy and hardener, resin mixture is prepared and deposited into the resin bath tank. Then the process at desired parameters is begun by loading the motion codes to machine, as seen in Figure 3.

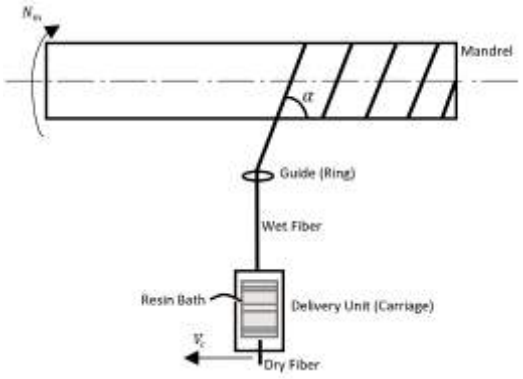

Figure 2. Filament winding technique

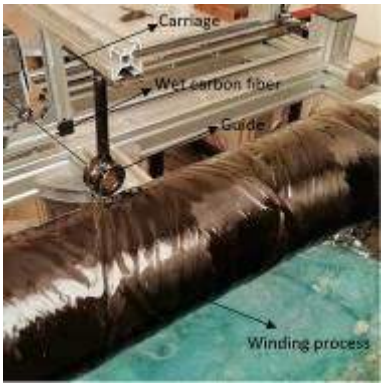

Figure 3. Fabrication of composite pipes

After process is completed, a heat shrinkage tape is wrapped on the mandrel and curing procedure is performed by heating the samples when it is rotating. Sanding and polishing as post processing can be conducted to obtain aesthetic appearance on the sample. The thickness and length values of the samples were measured as 4.00 ± 0.20 mm and 170 ± 0.5 mm for all fiber orientations. Also, fiber mass fractions were determined as 59.95%, 63.40% and 66.01% for ±(40°), ±(55°) and ±(70°) fiber orientation angles, respectively.

Quasi-static Lateral Compression

The lateral crushing experiments on Shimadzu AG-X Series universal testing machine with 30 tones capacity, as shown in Fig. 4, were performed between two flat steel plates as quasi-static lateral compression tests, which to obtain crashworthiness parameters of basalt fiber reinforced composite pipes. All samples exposed to 12.5 mm/min loading rate were compressed into 35 mm. At least five number of experiments for each fiber orientation angle are evaluated to ensure experimental reliability.

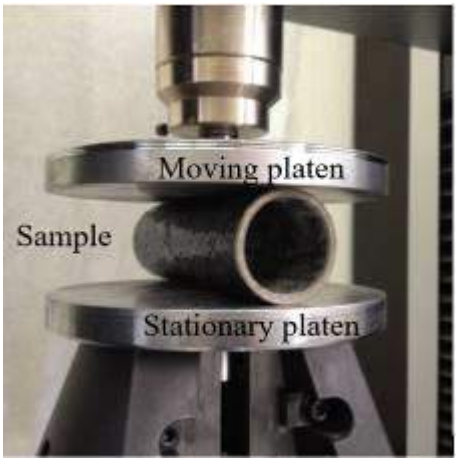

Figure 4. Quasi-static lateral compression

Three distinctive stages, shown in Figure 5, are considered in crushing process [8]. The material behaves elastically in pre-crushing stage and initial peak load is noted. After that, post-crushing presents the propagation of crushing in progressive or catastrophic manner. This stage is the crucial to measure crashworthiness parameters except initial peak load and to understand failure mechanisms. Lastly, when load increases suddenly which means densification phase, crushing process is finished.

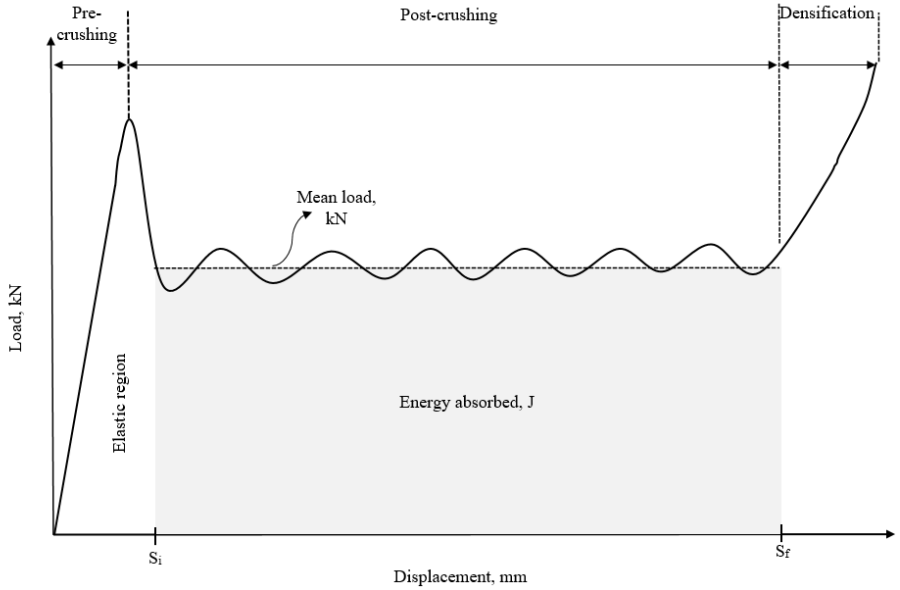

Figure 5. Typical load-displacement curve of crushing process

The crashworthiness parameters of the samples are calculated by considering load-displacement curves obtained from experiments. Total energy absorption, E is the area under load-displacement curve between crush distances, which is shown in Figure 5, and calculated by integration of load, P as seen Eqn. (1);

$$E = \int_{S_i}^{S_f} P(s)\, ds \tag{1}$$

where Si and Sf represents the initial and final stroke values in compression after the first initial peak load. Also, mean load is found from the integration of each load value depending on stroke, P(s) in crushing propagation stage as in Eqn. (2);

$$P_m = \frac{\int_{S_i}^{S_f} P(s)\, ds}{S_f} \tag{2}$$

Crushing load efficiency, ηf, which is the percentage ratio of mean load and initial peak load. It is obtained from Eqn. (3);

$$\eta_f = 100(P_m/P_i) \tag{3}$$

where the peak load (P_i), is the initial peak load in the load-displacement curve. Specific energy absorption, E_s is the absorbed energy per unit mass of crushing sample and calculated with Eq. (4);

$$E_s = \frac{E}{m_{crush}} = \frac{\int_{S_i}^{S_f} P(s)\, ds}{m_{crush}} \quad (4)$$

RESULTS AND DISCUSSIONS

Load-displacement Response and Failure Modes

The load-displacement curves and the crushing history of the lateral loading application at different fiber orientations of the considered pipes were given in Figure 6 and Figure 7, respectively. For all examined samples, mid-surface of samples were observed as damage region beginning with a buckling behavior of the vertical walls. This buckling allowed and encouraged the cells to readjust its position which causes a vertical crack at the samples mid plane [9]. Furthermore, first failure mode can be given as matrix cracking that triggers delamination of the layers. Most of the samples showed the fiber debonding failure mode as lateral loading continued.

There were irregular ups and downs in the graphs, caused from individual breaks in each layer. As the surface contact with the load was worse than the cross-sectional flatness, cyclic load-displacement graphs could not be obtained. Higher fiber orientation angle resulted with the increase in load carrying capacity as reported in İsmail's study [10].

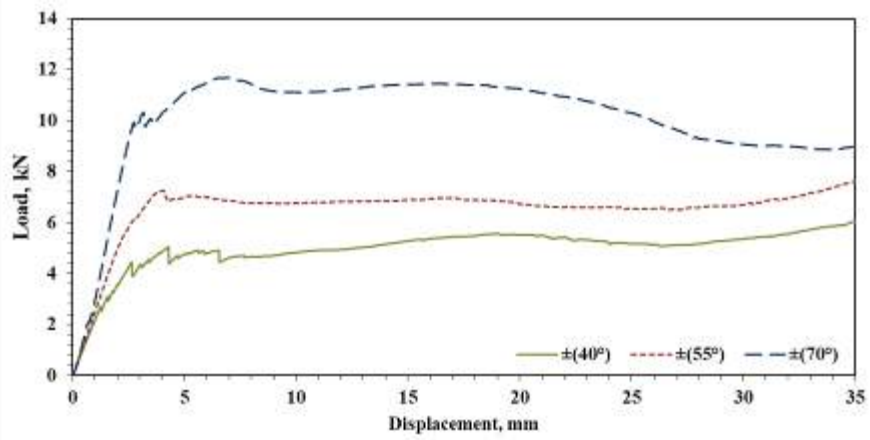

Figure 6. Load-displacement curves

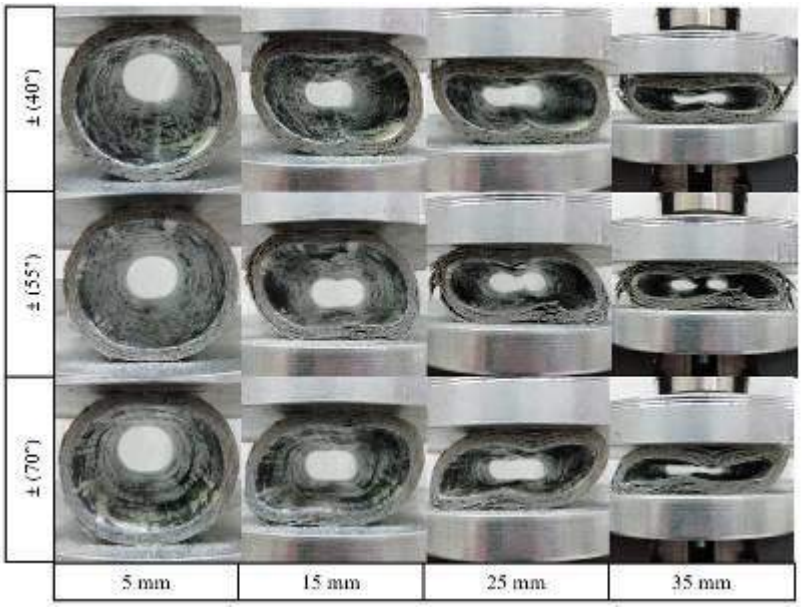

Figure 7. Crushing history

After crushing application, the samples returned back an amount because of spring back effect. But, they did not take the original circular characteristics shapes due to plastic deformation and failure inside the samples. The last appearances of the samples with respect to fiber orientation angle were given in Figure 8 as top and side view. The failure process was initiated with the matrix cracking and proceeding of delamination. Buckling of the samples, which caused the vertical cracks in mid plane, had the crucial role for fiber breakage. Fiber breakage failures, especially for ±(55°) and ±(70°) were achieved as longitudinal cracks that happened a left and right sides of the samples. Lastly, the combination of fiber debonding, matrix cracking, delamination and fiber breakage of failures were observed in all samples as seen on crushed samples.

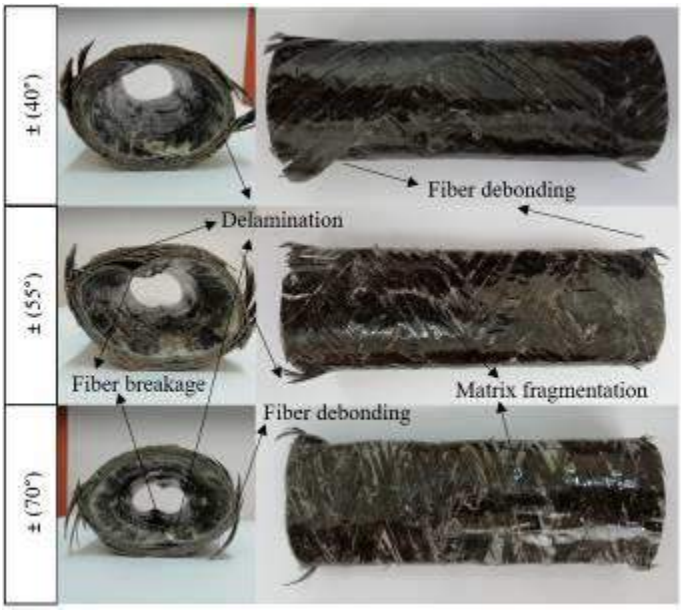

Figure 8. Fracture shapes and failure modes of crushed samples

Crushing Load Efficiency

The initial peak load and the mean crushing load, which are references for the spring back values and the crush load stability, were shown in Figure 9. BFRP at ±(70°) fiber orientation exhibited the maximum initial peak and mean crushing load values as 10.33 kN and 10.55 kN due to fiber approaching to loading direction. The lateral crushing load efficiency values for samples of ±(40°), ±(55°) and ±(70°) fiber orientations were presented in Figure 10. In general cases of the lateral crushing application, mean load was greater than the initial peak load values. Consequently, more than 100% load efficiency, especially in ±(40°) and ±(70°) samples, took place on the results. It can be said that higher fiber orientation angle resulted in decrease for crushing load efficiency.

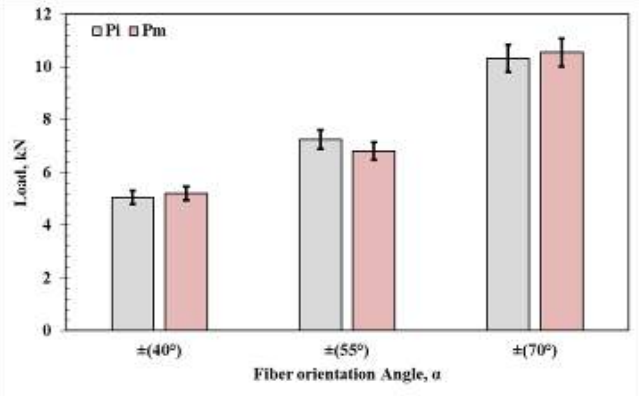

Figure 9. Initial peak and mean crushing loads

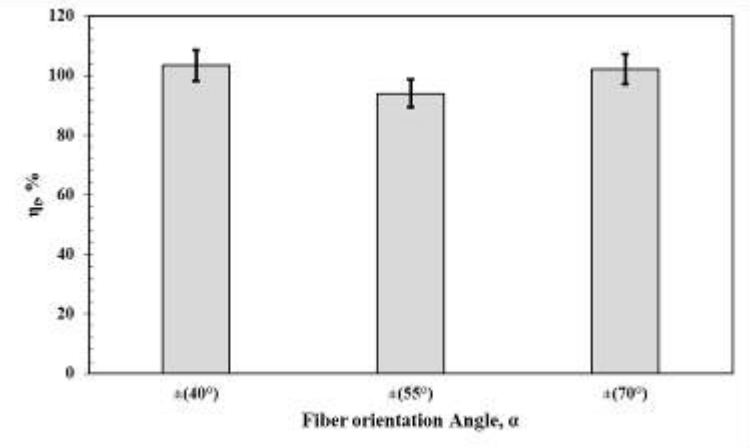

Figure 10. Crushing load efficiency

Energy Absorption

Total absorption energy and specific absorbed energy of the samples with different fiber orientation angles were presented in Figure 11 and Figure 12, respectively. Maximum values of total energy absorption and specific absorbed energy as 335.91 J and 3.07 J/g was obtained from the sample having ±(70°) fiber orientation. This is attributed to fiber dominant effects on loading when direction of fiber is closer. The improvements in percentage at ±(70°) angle in terms of total energy absorption and specific absorbed energy were achieved as 110% and 106% compared to sample having ±(40°) fiber orientation.

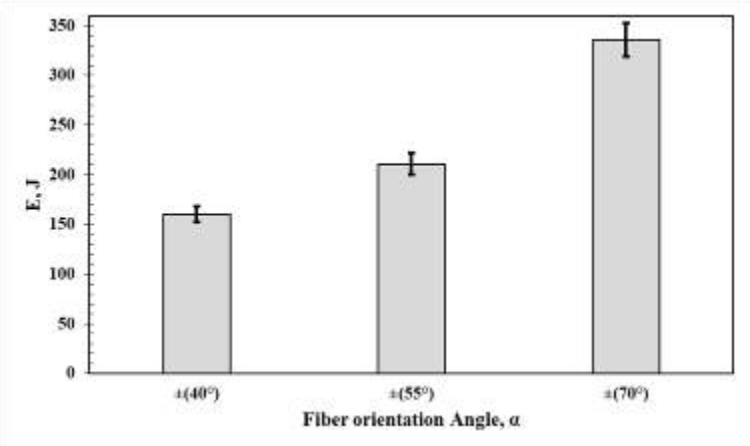

Figure 11. Total energy absorption

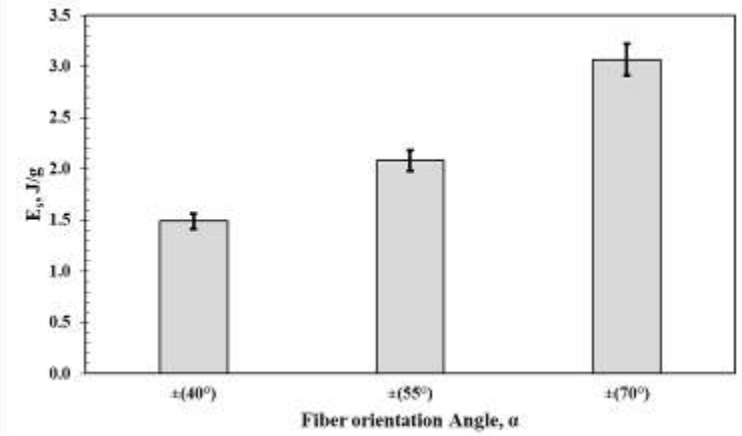

Figure 12. Specific absorbed energy

CONCLUSION

In this study, the effect of fiber orientation angle on the crashworthiness characteristics of basalt fiber composite pipes fabricated by filament winding technique were investigated. Quasi-static lateral compression tests were evaluated to obtain crushing parameters in terms of load carrying capacity, energy absorption capability, failure modes. The results showed that the fiber orientation angle had very significant influences on examined parameters. Higher fiber orientation angle resulted with the higher load carrying capacity and energy absorption capability. Maximum specific absorbed energy was achieved from ±(70°) fiber orientation angle as 3.07 J/g. The improvements in percentage at ±(70°) angle in terms of total energy absorption and specific absorbed energy were achieved as 110% and 106% compared to sample having ±(40°) fiber orientation. Lastly, the combination of fiber debonding, matrix cracking, delamination and fiber breakage of failures were observed in all samples as seen on crushed samples. In conclusion, fiber orientation angle proved the magnificent effect on crashworthiness behaviors of the basalt fiber reinforced filament wound composite pipes.

REFERENCES

Hou, T., Pearce, G. M. K., Prusty, B. G., Kelly, D. W., & Thomson, R. S. (2015). Pressurised composite tubes as variable load energy absorbers. *Composite structures*, 120, 346-357.
Pickett, L., & Dayal, V. (2012). Effect of tube geometry and ply-angle on energy absorption of a circular glass/epoxy crush tube–A numerical study. *Composites Part B: Engineering*, 43(8), 2960-2967.
Hu, D., Zhang, C., Ma, X., & Song, B. (2016). Effect of fiber orientation on energy absorption characteristics of glass cloth/epoxy composite tubes under axial quasi-static and impact crushing condition. *Composites Part A: Applied Science and Manufacturing*, 90, 489-501.

Alkbir, M. F. M., Sapuan, S. M., Nuraini, A. A., & Ishak, M. R. (2014). Effect of geometry on crashworthiness parameters of natural kenaf fibre reinforced composite hexagonal tubes. *Materials & Design*, 60, 85-93.

Mahdi, E., Hamouda, A. A., & Sebaey, T. A. (2014). The effect of fiber orientation on the energy absorption capability of axially crushed composite tubes. *Materials & Design* (1980-2015), 56, 923-928.

Sebaey, T. A., & Mahdi, E. (2016). Crashworthiness of pre-impacted glass/epoxy composite tubes. *International Journal of Impact Engineering*, 92, 18-25.

Kim, J. S., Yoon, H. J., & Shin, K. B. (2011). A study on crushing behaviors of composite circular tubes with different reinforcing fibers. *International Journal of Impact Engineering*, 38(4), 198-207.

Roslan, M. N., Yahya, M. Y., Ahmad, Z., Rashid, A., Hani, A., & Wang, W. X. (2018). Energy Absorption Capacity of Basalt Sandwich Composite Cylinder Subjected to Axial Compression Loadings. *In Materials Science Forum* (Vol. 917, pp. 7-11). Trans Tech Publications.

Mahdi, E., & Sebaey, T. A. (2014). Crushing behavior of hybrid hexagonal/octagonal cellular composite system: Aramid/carbon hybrid composite. Materials & Design, 63, 6-13.

Ismail, A. E., & Sahrom, M. F. (2015). Lateral crushing energy absorption of cylindrical kenaf fiber reinforced composites. International Journal of Applied Engineering Research, 10(8), 19277-19288.

DEVELOPMENT OF MULTIFERROIC MATERIALS FOR SPINTRONICS APPLICATIONS

Ramazan TOPKAYA
Department of Electrical Electronics Engineering,
Iğdır University, Iğdır, Turkey
ramazan.topkaya@igdir.edu.tr

Adem KOÇYİĞİT
Department of Electrical Electronics Engineering,
Iğdır University, Iğdır, Turkey
adem.kocyigit@igdir.edu.tr

ABSTRACT: The multiferroic materials having both ferromagnetic and ferroelectric properties have drawn a great interest because of the potential device applications in magnetoelectronics, optoelectronics and spintronics (Baek, 2017; Basu, 2008). Some of the applications: non-volatile memory elements, sensors, spin wave generators, spintronic devices whose spins are controlled with electric field, solar cells (Wang, 2004; Wolf, 2001). It should be developed the perfect multiferroic materials and structures for these applications. Due to the fact that these materials can be controlled both electric and magnetic fields, a lot of nanoscale devices can be easily fabricated. In this study, the multiferroic $BiFeO_3$ powders were synthesized by using sol-gel method. Structural, morphological and magnetic properties of these materials were characterized. Magnetization measurements revealed that undoped and Ni doped $BiFeO_3$ powders have ferromagnetic behaviour. It has been realized that $BiFeO_3$ powders annealed in air atmosphere can be useful for spintronic applications.

Key words: Multiferroic, Ferromagnetic, Ferroelectric, Spintronics

REFERENCES

Baek, S. H., Choi, S., Kim, T. L., & Jang, H. W. (2017). Domain engineering in $BiFeO_3$ thin films. *Current Applied Physics, 17*(5), 688-703.
Basu, S. R., Martin, L. W., Chu, Y. H., Gajek, M., Ramesh, R., Rai, R. C., Musfeldt, J. L. (2008). Photoconductivity in $BiFeO_3$ thin films. *Applied Physics Letters, 92*(9), 091905.
Wang, J., Zheng, H., Ma, Z., Prasertchoung, S., Wuttig, M., Droopad, R., Ramesh, R. (2004). Epitaxial $BiFeO_3$ thin films on Si. *Applied Physics Letters, 85*(13), 2574-2576.

Wolf, S. A., Awschalom, D. D., Buhrman, R. A., Daughton, J. M., von Molnár, S., Roukes, M. L., Treger, D. M. (2001). Spintronics: A Spin-Based Electronics Vision for the Future. *Science, 294*(5546), 1488-1495.

OPTICAL TWEEZING POTENTIAL OF INTEGRATED VORTEX BEAM EMITTER

Kenan ÇİÇEK
Iğdır Üniversitesi
Kenan.cicek@igdir.edu.tr

Adem KOÇYİĞİT
Iğdır Üniversitesi

ABSTRACT: The angular momentum of light consists of two distinct components, namely orbital angular momentum (OAM) and spin angular momentum (SAM). SAM is related to the polarization of light and OAM, however, depends on the field spatial distribution and can be associated with a light beam that has helical wavefront. OAM is another degree of freedom of light that can be utilized in so many applications ranging from communication to biomedical. However, for the last decade optical tweezers employing OAM beams become more and more relevant in research. Many techniques have been used to generate OAM beams in laboratory since 1992 in which its existence was confirmed. Most of these techniques are large, bulky and laboratory base that are unpractical for optical manipulation applications. However, with the features of compactness and the combability of current CMOS technology, integrated vortex beam emitter seems more suitable for daily life optical tweezers. Thus, in this study, we address the possibility of using integrated vortex beam emitter as the source of an optical tweezer. We perform a set of simulation via Lumerical-FDTD tools and analyzed the output force related to the emitted power. As the result of the study, we realize that, the integrated vortex beam emitter needs improvement in terms of power output to perform a proper optical manipulation.

Key words: Orbital angular momentum of light, vortex beam emitter, optical tweezers.

TEMPERATURE STABILITY OF PVA-Borax GEL ELECTROLYTE FOR SUPERCAPACITORS

Serkan DEMİREL
Igdir University, Electric and Energy Department, 76002 Igdir, Turkey
serkan.demirel@igdir.edu.tr

ABSTRACT: In this study, the capacitive performance and temperature stability properties have been investigated of PVA-Borax gel as electrolyte for supercapacitors. In the experimental studies, identical graphite rods were used as electrodes to create a capacitor. The cyclic-voltammetry (cv) measurements have been showed that permanent current plateaus and rectangular shapes at different scanning speeds. That plateaus and rectangular shapes are show the production of supercapacitor via PVA-Borax electrolyte. The capacitance has been calculated as 0.23 F/g at room temperature. Temperature stability measurements have been made between 20-80 ^{o}C and it was observed that the capacity value decreased to about 0,15 F/g at 80 ^{o}C. According to charge-discharge cycles measurements, the PVA-Borax electrolyte also showed rechargeable electrolyte property.

Key words: PVA-Borax, Electrolyte, Supercapacitor.

BEHAVIOR OF SULFATE-REDUCING BACTERIA IN SINGLE-STAGE ANAEROBIC DIGESTERS PRETREATED WITH OZONE

Sera TUNCAY, Environmental Engineering Department, Middle East Technical University, sera.tuncay@metu.edu.tr

Merve AKCAKAYA, Environmental Engineering Department, Middle East Technical University, merve.akcakaya@metu.edu.tr

Bulent ICGEN, Environmental Engineering Department, Middle East Technical University, bicgen@metu.edu.tr

ABSTRACT: Anaerobic digestion is a solid stabilization process commonly used at both municipal and industrial wastewater and sludge treatment. Anaerobic digesters convert the microbiological cells and other solids generated during the treatment process to a stable end product and also produce methane-rich biogas as an energy source through the degradation of organic matter. Microbial population dynamics involved in anaerobic digestion are not well-studied yet due to the requirement of an extensive investigation of microorganisms, their mechanisms and their relations to each other. There are four successive stages of anaerobic digestion as hydrolysis, acidogenesis, acetogenesis and methanogenesis which are governed by hydrolytic microorganisms, acidogens, acetogens and methanogens. Ozone pretreatment to anaerobic digestion promotes the hydrolysis stage by enhancing methane production ability of methanogens. In anaerobic digestion, sulfates and other sulfur oxides are easily reduced to sulfides especially to hydrogen sulfide (H_2S) by sulfate-reducing bacteria (SRB). In the presence of sulfate at considerable levels, this sulfate reduction process dominates over methanogenesis since sulfate reducers and methanogens compete for the similar substrates. Besides, H_2S as the end-product of the process, has an inhibitory effect to methanogens and other microbial communities because of its toxicity. In this study, 0.03, 0.06 and 0.09 g O_3/g TSS ozone doses were applied to single-stage mesophilic anaerobic digesters in order to observe the improvement in methane production. The effects of these ozone doses on SRB and their role in methane production were examined. Community analysis for the sulfate reducers were performed with Fluorescence *in situ* Hybridization (FISH) method. As a result of the study, sulfate reducers dominated for the digester pretreated with 0.03 g O_3/g TSS ozone dose day by day, while sulfate reducers in the other digesters remained same and did not show a significant change during the operation.

Keywords: Ozone pretreatment, single-stage mesophilic anaerobic digester, sulfate-reducing bacteria, FISH

Acknowledgement: This work was supported by The Scientific and Technological Research Council of Turkey (TUBITAK) through the project number 116Y181.

COMPOSITES USED AS DENTAL BIOMATERIALS IN HUMAN BODY; A REVIEW

Efe Çetin YILMAZ
Kilis 7 Aralık University, Engineering Faculty, Department of Mechanical Engineering, Kilis, TURKEY, efecetinyilmaz@msn.com

ABSTRACT: In recent years, composite materials have become an increasingly popular type of material in many fields such as aerospace, healthcare, defense industry. Thanks to the improvements in the matrix structure of the composite materials, it has been provided to have superior biocompatibility, mechanical and aesthetic properties. It has become a highly preferred material group in the field of dentistry, especially in the treatment of restoration. The bio-composite materials used in the human body exhibit different mechanical and aesthetic behaviors on the living tissue depending on the chemical composition and filler structure they contain. However, because the experiments on living tissue were too long, costly and ethical problems arose, they directed the researchers to in vitro test methods to determine the mechanical and aesthetic behavior of these materials. The human body has a complex and continuous structure. Therefore, it has been quite difficult to simulate a material placed in the human mouth in the oral environment. In this area, various chewing test test methods have been developed which can model human oral environment. The aim of this study is to evaluate the development of composite materials used in the mouth and the effects of the filling material on the mechanical and aesthetic behaviors of the composite material.

Key words: bio-composite, restorative material, in vitro, simulation

İNSAN VÜCUDUNDA DİŞ BİYOMALZEMESİ OLARAK KULLANILAN KOMPOZİTLER; BİR İNCELEME

ÖZET: Son yıllarda kompozit malzemeler havacılık, sağlık, savunma sanayi gibi birçok alanda giderek kullanımı artan bir malzeme türü olmuştur. Kompozit malzemelerin matris yapısındaki gelişmeler ile üstün biyo-uyumluluk, mekanik ve estetik özelliklere sahip olması sağlanmıştır. Diş hekimliği alanında da özellikle restorasyon tedavisinde çokça tercih edilen bir malzeme grubu olmuştur. İnsan vücudunda kullanılan biyo-kompozit malzemeler içerdikleri kimyasal birleşimi ve doldurucu yapısına bağlı olarak canlı doku üzerinde farklı mekanik ve estetik davranışlar sergilemektedir. Ancak, canlı doku üzerindeki deneylerin çok uzun zaman alması, maliyetli olması ve etik sorunların ortaya çıkması nedeniyle araştırmacıları bu malzemelerin mekanik ve estetik davranışlarını belirlemede laboratuvar ortamı (in vitro) test yöntemlerine yöneltmiştir.

İnsan vücudu karmaşık ve sürekli bir yapıya sahiptir. Bu nedenle insan ağız içerisine yerleştirilen bir malzemenin ağız ortamında simüle edilmesi oldukça zor bir durum olmuştur. Bu alanda, insan ağız ortamını modelleyebilen çeşitli çiğneme test deney yöntemleri geliştirilmiştir. Bu çalışmanın amacı, ağız içerisinde kullanılan kompozit malzemelerin gelişimi ve kompozit malzemenin doldurucu yapısının mekanik ve estetik davranışları üzerindeki etkilerinin değerlendirilmesidir.

Anahtar sözcükler: biyo-kompozit, restoratif malzeme, in vitro, simülasyon

GİRİŞ

Işıkla sertleşen diş kompozit malzemelerinin, doğal diş yapısına benzemesi, kolay işlenebilir olması ve gelişmiş mekanik kabiliyetlerinden dolayı kesici ve öğütücü dişlerin eski haline getirilmesinde yaygın olarak kullanılmaktadır (Alsharif, Akil, Abd El-Aziz, & Bin Ahmad, 2014; Angeletaki, Gkogkos, Papazoglou, & Kloukos, 2016; Rodriguez, Kriven, & Casanova, 2019). Kompozit malzemeler diş hekimliği alanında 1960 yılından bu yana sürekli bir gelişim göstererek giderek kullanımı artmıştır (Fugolin & Pfeifer, 2017). Doğrudan diş restorasyonları (direct tooth restorations) için kompozitlerin piyasaya sürülmesinden bu yana önemli evrimi, endikasyonlarının klasik olarak yalnızca amalgamlarla restore edilmiş daha büyük posterior restorasyonlara genişlemesini sağlamıştır (Fugolin & Pfeifer, 2017). Bu alanda gelişimlerin büyük bir kısmı kompozitlerin mekanik özelliklerinin (özellikler aşınma dirençleri) iyileşmesiyle daha geniş alanda dolgu sistemlerinin elde edilmesiyle gerçekleşmiştir (Ferracane, 2011). Kompozit malzemelerin aşınma davranışının belirlenmesi amacıyla literatürde birçok in vitro (labaratuvar) ortam deneyleri geliştirilmiştir (Injeti et al., 2019; E. Yilmaz & R. Sadeler, 2018; E. C. Yilmaz, 2019; E. C. Yilmaz & R. Sadeler, 2018a; E. Ç. Yilmaz, 2019). Kompozit malzemelerin mekanik ve kimyasal özellikleri sürekli bir gelişim gösterse de canlı doku üzerinde yeterli oranda 10 yıl kullanım ömrü olduğu rapor edilmiştir (Demarco, Correa, Cenci, Moraes, & Opdam, 2012).

Kompozit malzemelerin gelişim periyoduna bakıldığında; 2000'li yılların başında, bugüne kadar sadece metakrilat kimyasına, daha özel olarak BisGMA (bisfenol A glisidil dimetakrilat), TEGDMA (trietilen glikol dimetakrilat), BisEMA (etoksile bisfenol) esaslı olan organik matrisin daha da geliştirilmesi üzerinde duruldu (Fugolin & Pfeifer, 2017). Bununla birlikte kompozit malzemelerde polimerizasyon büzülmesinin ve gerilmenin azaltılması ortak amacı ile alternatif monomerler geliştirilmeye başlanmıştır (Fugolin & Pfeifer, 2017). Bu alandaki gelişimlerin temel amacı kompozit malzemelerin matris yapısındaki gerilmeleri en aza indirgemek olmuştur. Ağız içerisine yerleştirilen bir kompozit malzemenin çiğneme hareketi sırasında karmaşık ve sürekli olarak mekanik yüklemelere maruz kaldığı görülecektir. Bu mekanik yüklemelerin kompozit malzemenin matris yapısındaki istenmeyen gerilmelerin azaltılması ve karşı malzeme

(insan dişi) benzer elastik davranış göstermesi üzerine odaklanmıştır. Kompozit malzemenin matris yapısında bu gelişimler ile elde edilen yeni monomerler ya halka açıcı polimerleştirilebilir kısımlara (siloran kimyasına dayanan yalnızca ticari örnek olan Filtek LS'dir) ya da molar büzülme katsayısını azaltmada başarılı olduklarını kanıtlayan daha yüksek moleküler ağırlıklı moleküller elde edilebiliyordu (Fugolin & Pfeifer, 2017). Şekil 1 bu monomer yapılarının örnek kimyasal yapılarını göstermektedir.

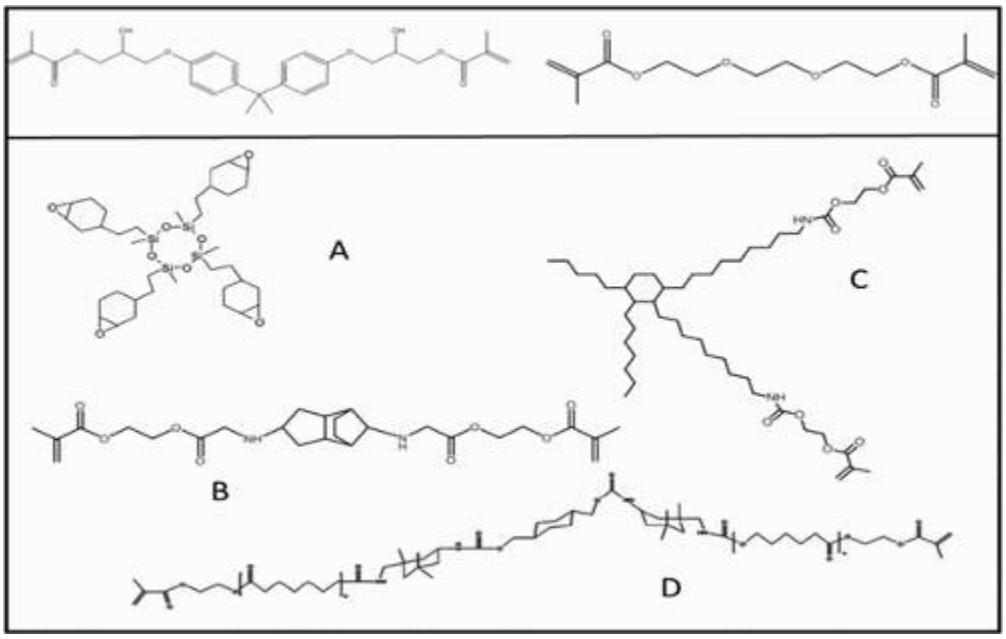

Şekil 1. Üst Kutucuk : Bisgma (Bisfenol A Glisidil Dimetakrilat) (Solda) Ve TEGDMA (Trietilen Glikol Dimetakrilat) (Sağda) Moleküler Yapıları. Alt: Halen Ticari Ürünlerde Kullanılan Alternatif Monomerlerin Moleküler Yapısı. (A) Oxirane (Filtek LS; 3M-ESPE), (B) TCD-Üretan (Venus Diamond; Heraeus Kulzer), (C) Dimerasit Dimetakrilat (N'Durance; Confidental-Septodont) Ve (D) Dupont DX-511 (Kalore; GC America (Fugolin & Pfeifer, 2017)

Son zamanlarda, kompozit malzemelerin matris ve arayüz yapılarında, reçine geliştirmedeki odak, metakrilatlarda bulunan ester bağlarının tükürük ve bakteri enzimleri tarafından mevcut hidrolizinin yanı sıra, tükürük ve bakteri enzimleriyle metakrilatlarda mevcut olan hidroliz de dahil olmak üzere, oral ortamdaki restorasyonun genel direncini arttırmaya yönelmiştir (Wu, Weir, Melo, & Xu, 2015). Ayrıca, bulk-fill dolgu ve kendinden yapışkanlı kompozitler gibi daha az uygulama basamağı gerektirmesi nedeniyle kullanımı daha kolay materyaller geliştirmek için çok çaba sarf edilmiştir (Fugolin & Pfeifer, 2017).

Bulk-fill reçine kompozitleri piyasaya, hem akıcı hem de konvansiyonel / şekillendirilebilir viskozitelerde şeklinde sürülmüştür (Fugolin & Pfeifer, 2017). Bu kompozit malzemeler daha büyük ve derin restorasyonlarda tercih edilmiştir (E. C. Yilmaz & R. Sadeler, 2018b). Bu yapılarda elde edilen klinik başarılar, sistemin optimizasyonunu (yeni foto başlatıcılar veya daha fazla geleneksel foto başlatıcı konsantrasyonu), doldurma sisteminin modifikasyonlarını (daha büyük doldurucular veya daha fazla saydam doldurucular) veya farklı kimyasalların dahil edilmesini içeren farklı yollarla elde edilmiştir (Miletic, Pongprueksa, De Munck, Brooks, & Meerbeek, 2017). Akışkan bulk-fill kompozit dolgu malzemeleri genellikle, şekillendirilebilir malzemelerden daha düşük dolgu yüküne sahiptir ve okluzal katmanın oklüzal yükleme altında daha güçlü ve aşınmaya karşı daha dayanıklı olması beklenen daha yüksek oranda doldurulmuş bir kompozitin bir "kapağı" (cap) ile doldurulmasını gerektirir (Fugolin & Pfeifer, 2017). Literatürden bir örnek vermek gerekirse, SureFil (Dentsply) kompozit malzemesi üreticiye göre, bu ürün, daha düşük dolgu maddesi içeriğine ek olarak, büzülmeyi azaltmaya yardımcı olan yüksek molekül ağırlıklı (849 g / mol) yeni bir UDMA bazlı monomer içerir (Fugolin & Pfeifer, 2017). Üreticinin "polimerizasyon modülatörü" olarak adlandırdığı monomerin yeni kısmı, bir oligomerik türün omurgasına gömülü fotoaktif gruplardan oluşur (Fugolin & Pfeifer, 2017).

Kompozit malzemelerde gerilmeyi azaltan dolgu maddeleri, diş restoratif malzeme arayüzünde boşluk oluşumunu önlemedeki faydalarından dolayı araştırmaların odağı olmaya devam etmektedir. Bununla birlikte, büzülme azaltma üzerine yoğunlaşmak yerine, mevcut stratejilerin çoğu, polimer ağında gerilmeyi aynı anda azaltabilen ve mekanik özellikleri ve monomer dönüşümünü koruyan ya da arttıran bir tür modifikasyon önerir (Bacchi & Pfeifer, 2016). Bu moleküller, hafif koşullar altında bir tıklama reaksiyonu ile sentezlenir ve sekonder vinil monomer matrisi ile zincir transfer reaksiyonlarına katılmak için mevcut olan kolye tiyol fonksiyonelliklerine sahiptir (Fugolin & Pfeifer, 2017). Bu anlamda, tiyoüretanlar, klasik thiol-ene reaksiyonlarında görüldüğü gibi gecikmiş jelasyon / vitrifikasyona yol açan stres azaltma mekanizmasına dayanır (Boulden et al., 2011). Aynı zamanda, sert thio-carbamate bağlarının ağa dahil edilmesinden kaynaklanan ağ takviyesi sağlarlar (Lowe, Hoyle, & Bowman, 2010). Yüksek oranda doldurulmuş kompozitlerde kullanıldığında, tiyoüretanların polimerizasyon stresini% 50'ye kadar düşürdüğü ve kırılma tokluğunun 2 kat arttığı gösterilmiştir (Bacchi, Nelson, & Pfeifer, 2016) . Diğer nano-boyutlu ön-polimerleştirilmiş parçacıklar da önemli bir büzülme / gerilme azaltma göstermiştir ve malzeme modifikasyonu için oldukça kuyruklu bir platform temsil etmektedir (Moraes et al., 2011) Kompozit malzemenin içerdiği çok işlevli monomerler, daha sonra ağa bir çapraz bağ olarak dahil edilen bir "allyl disulfide moiety" (diğer olası örnekler arasında) içerir. Şekil 2 bu açıklamayı özetlemiştir. Sonuç olarak, Net çapraz bağlanma yoğunluğu esasen değişmeden kalırken, bu alil bağı, gerilmenin yayılmasıyla kırılabilir ve yeniden düzenlenebilir (Fugolin & Pfeifer, 2017). Nihayetinde, polimerizasyon gerilimi,

geleneksel camsı ağlarla karşılaştırılabilir mekanik özellikler korunarak yerleştirilebilir ve sonuçta azaltılabilir (Park, Kloxin, Abuelyaman, Oxman, & Bowman, 2012).

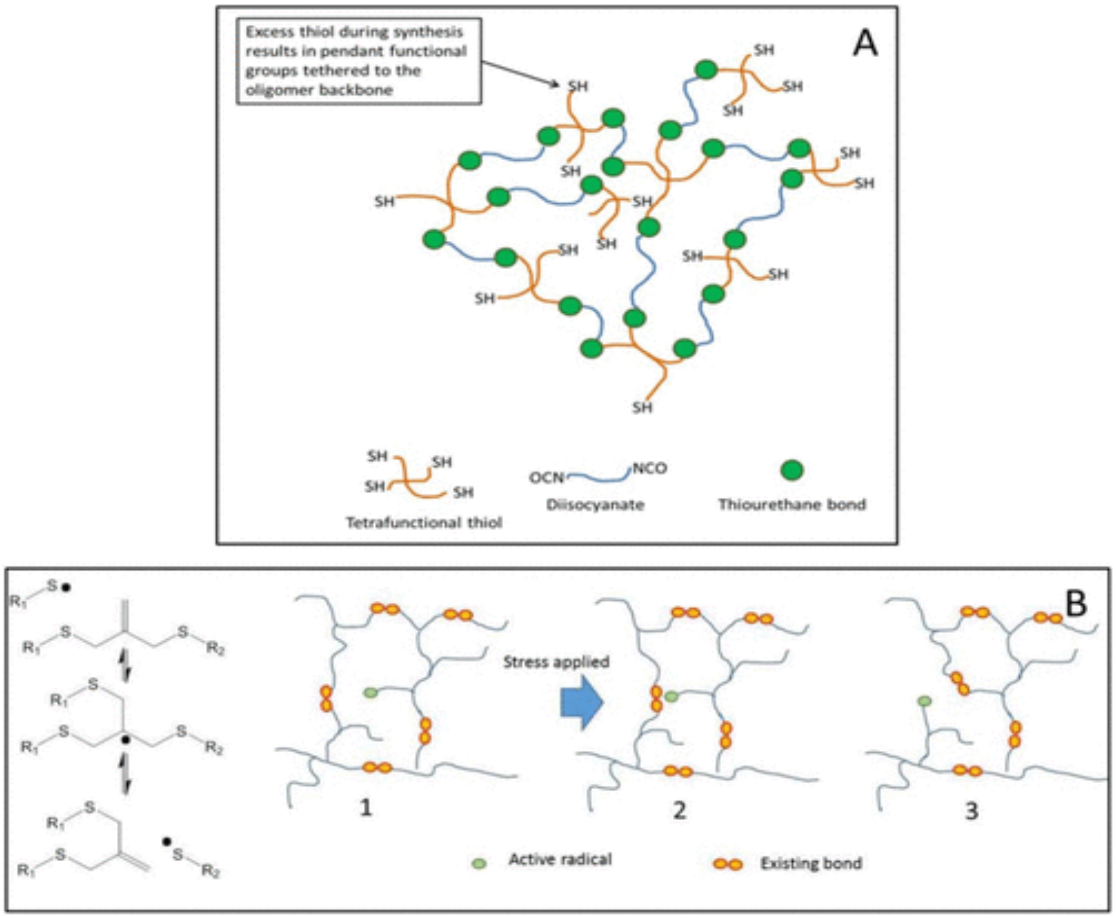

Şekil 2. Tiyoüretan oligomerleri (thiourethane oligomers) (A) ilave parçalanma zinciri transferi (B) oluşturulan kovalent adapte edilebilir ağların kullanımıyla stresin azalmasına yol açan ağ modifikasyonları için diyagramın gösterimi (Fugolin & Pfeifer, 2017)

SONUÇ

Literatürde yapılana araştırmalara göre kompozit malzemelerin üstün mekanik ve kimyasal davranışları nedeniyle biyo-malzeme olarak canlı vücudunda kullanımı önümüzdeki yıllarda giderek artacaktır. Ancak geliştirilen yeni kompozit malzemelerin canlı doku testleri öncesinde laboratuvar testlerinin yapılması büyük önem arz etmektedir. Bu nedenle, araştırmacıların insan vücudunu modelleyebilen yeni test mekanizmaları geliştirmeleri önemli olacaktır.

KAYNAKLAR

Alsharif, S. O., Akil, H. B., Abd El-Aziz, N. A., & Bin Ahmad, Z. A. (2014). Effect of alumina particles loading on the mechanical properties of light-cured dental resin composites. *Materials & Design, 54*, 430-435. doi:10.1016/j.matdes.2013.07.069

Angeletaki, F., Gkogkos, A., Papazoglou, E., & Kloukos, D. (2016). Direct versus indirect inlay/onlay composite restorations in posterior teeth. A systematic review and meta-analysis. *Journal of Dentistry, 53*, 12-21. doi:10.1016/j.jdent.2016.07.011

Bacchi, A., Nelson, M., & Pfeifer, C. S. (2016). Characterization of methacrylate-based composites containing thio-urethane oligomers. *Dental Materials, 32*(2), 233-239. doi:10.1016/j.dental.2015.11.022

Bacchi, A., & Pfeifer, C. S. (2016). Rheological and mechanical properties and interfacial stress development of composite cements modified with thio-urethane oligomers. *Dental Materials, 32*(8), 978-986. doi:10.1016/j.dental.2016.05.003

Boulden, J. E., Cramer, N. B., Schreck, K. M., Couch, C. L., Bracho-Troconis, C., Stansbury, J. W., & Bowman, C. N. (2011). Thiol-ene-methacrylate composites as dental restorative materials. *Dental Materials, 27*(3), 267-272. doi:10.1016/j.dental.2010.11.001

Demarco, F. F., Correa, M. B., Cenci, M. S., Moraes, R. R., & Opdam, N. J. M. (2012). Longevity of posterior composite restorations: Not only a matter of materials. *Dental Materials, 28*(1), 87-101. doi:10.1016/j.dental.2011.09.003

Ferracane, J. L. (2011). Resin composite-State of the art. *Dental Materials, 27*(1), 29-38. doi:10.1016/j.dental.2010.10.020

Fugolin, A. P. P., & Pfeifer, C. S. (2017). New Resins for Dental Composites. *Journal of Dental Research, 96*(10), 1085-1091. doi:10.1177/0022034517720658

Injeti, V. S. Y., Nune, K. C., Reyes, E., Yue, G., Li, S. J., & Misra, R. D. K. (2019). A comparative study on the tribological behavior of Ti-6Al-4V and Ti-24Nb-4Zr-8Sn alloys in simulated body fluid. *Materials Technology, 34*(5), 270-284. doi:10.1080/10667857.2018.1550138

Lowe, A. B., Hoyle, C. E., & Bowman, C. N. (2010). Thiol-yne click chemistry: A powerful and versatile methodology for materials synthesis. *Journal of Materials Chemistry, 20*(23), 4745-4750. doi:10.1039/b917102a

Miletic, V., Pongprueksa, P., De Munck, J., Brooks, N. R., & Meerbeek, B. (2017). Curing characteristics of flowable and sculptable bulk-fill composites. *Clinical Oral Investigations, 21*(4), 1201-1212. doi:10.1007/s00784-016-1894-0

Moraes, R. R., Garcia, J. W., Barros, M. D., Lewis, S. H., Pfeifer, C. S., Liu, J. C., & Stansbury, J. W. (2011). Control of polymerization shrinkage and stress in nanogel-modified monomer and composite materials. *Dental Materials, 27*(6), 509-519. doi:10.1016/j.dental.2011.01.006

Park, H. Y., Kloxin, C. J., Abuelyaman, A. S., Oxman, J. D., & Bowman, C. N. (2012). Novel dental restorative materials having low polymerization shrinkage stress via stress relaxation by addition-fragmentation chain transfer. *Dental Materials, 28*(11), 3-9. doi:10.1016/j.dental.2012.06.012

Rodriguez, H. A., Kriven, W. M., & Casanova, H. (2019). Development of mechanical properties in dental resin composite: Effect of filler size and filler aggregation state. *Materials Science & Engineering C-Materials for Biological Applications, 101*, 274-282. doi:10.1016/j.msec.2019.03.090

Wu, J. L., Weir, M. D., Melo, M. A. S., & Xu, H. H. K. (2015). Development of novel self-healing and antibacterial dental composite containing calcium phosphate nanoparticles. *Journal of Dentistry, 43*(3), 317-326. doi:10.1016/j.jdent.2015.01.009

Yilmaz, E., & Sadeler, R. (2018). Effect of artificial aging environment and time on mechanical properties of composite materials. *Journal of Dental Research and Review, 5*(4), 111-115. doi:10.4103/jdrr.jdrr_50_18

Yilmaz, E. C. (2019). Effects of thermal change and third-body media particle on wear behaviour of dental restorative composite materials. *Materials Technology*. doi:10.1080/10667857.2019.1611201

Yilmaz, E. C., & Sadeler, R. (2018a). Investigation of three-body wear of dental materials under different chewing cycles. *Science and Engineering of Composite Materials, 25*(4), 781-787. doi:10.1515/secm-2016-0385

Yilmaz, E. C., & Sadeler, R. (2018b). Investigation of Two- and Three-Body Wear Resistance on Flowable Bulk-Fill and Resin-Based Composites. *Mechanics of Composite Materials, 54*(3), 395-402. doi:10.1007/s11029-018-9750-8

Yilmaz, E. Ç. (2019). Effect of Sliding Movement Mechanism on Contact Wear Behavior of Composite Materials in Simulation of Oral Environment. *Journal of Bio- and Tribo-Corrosion, 5*(3), 63. doi:10.1007/s40735-019-0258-0.

EFFECT OF TEMPERATURE CHANGE AND DWELL TIME ON SURFACE ROUGHNESS OF COMPOSITE MATERIAL IN ARTIFICIAL SALIVA MEDIUM

Efe Çetin YILMAZ
Kilis 7 Aralık University, Engineering Faculty, Department of Mechanical Engineering, Kilis, TURKEY, efecetinyilmaz@msn.com

ABSTRACT: The aim of this study was to investigate the effect of different thermal cycle and dwell time tests on the surface roughness of two different composite materials in artificial saliva medium. Estelite Flow Quick and Charisma Opal composite materials were produced under the conditions recommended by the manufacturer. Composite test samples were divided into 3 groups as control, 1200 thermal and 3000 thermal cycle test procedures for 10 seconds and 30 seconds dwell time respectively. The surface roughness values of the composite materials were measured after each test procedure with using non-contact profilometer. In addition, surface roughness behavior of composite materials was analyzed at the micro and macro level. As a result of this study, with the increase in the number of thermal cycles and dwell time, an increase in surface roughness was observed in both materials. However, there was no linear relationship between the number of thermal cycles and surface roughness values. In this study scope, it is possible to say that the organic matrix structure of the composite material affects the surface roughness behavior.

Keywords: composite biomaterial, surface roughness, thermal cycle, dwell time

INTRODUCTION

Composite materials have been used as dental biomaterials since the mid-1960s (Cao, Zhao, Gong, & Zhao, 2013). There are many different composite materials for direct dental restorations, including classic hybrid and nano-filled composite materials, silicones and compomers. However, differences in the monomer system, filler composition and matrix filler chemistry between these materials can lead to different mechanical performances and may also take into account the differences in the resistance of the materials to chemical and mechanical degradation (Hahnel, Henrich, Burgers, Handel, & Rosentritt, 2010; Manhart, Kunzelmann, Chen, & Hickel, 2000). It has been reported that the damage to the composite materials may be caused by the deterioration of the matrix and fillers, or by mechanical and environmental loads, interfacial bones dissolution, micro-cracking or filling material. particle fracture which can reduce the possibility of in vivo survival of composite restorations (Drummond, 2008).

The superior mechanical and aesthetic properties of the composite materials increase the use of biomaterials. However, it has been reported that composite materials still have insufficient wear resistance in clinical studies (Hickel & Manhart, 2001). The term wear can generally be defined as loss of volume of a material. The wear mechanism in the intra-tribological process may be due to many factors such as composite material mechanic behavior, antagonist material, lubrication medium, chewing parameter. As long as the composite materials used as biomaterials remain within the body, changes in their mechanical properties are inevitable. Because the body contains a complex and continuous structure. This structure can affect the hardness and surface roughness behavior of the composite material. The change of the surface roughness behavior of the composite material will affect the wear mechanism. Surface roughness in restorative materials is an important parameter affecting wear. If the surface roughness of the composite material has a value of 0.2erem and above, it is clinically a risk (Bollen, Lambrechts, & Quirynen, 1997; Marghalani, 2010; Yilmaz & Sadeler, 2017). Finishing and polishing are carried out after filling into these materials in order to minimize surface roughness. In this way, the sensitivity of the composite restorative material to the wear mechanism will be reduced. Another parameter affecting the mechanical properties of composite resins has been found to be caused by hydrolytic disturbances. In this process, the durability of the composite material is evaluated by exposing the composite material to thermal cycles and artificial oral fluid for a long time in vivo treatment process (Cho, Yi, & Heo, 2002; Yilmaz & Sadeler, 2017) The aim of this study was to investigate the effect of different thermal cycle and dwell time tests on the surface roughness of two different composite materials in artificial saliva medium.

MATERIAL AND METHOD

In this study, detailed information about the tested composite materials is summarized in Table 1. Three groups (control, 12000 thermal cycles and 3000 thermal cycles) of specimens of 2 mm X 6 mm (height X diameter) were produced from each composite material. Composite samples were hardened in laboratory conditions with the blue light polarization technique and under the conditions recommended by the manufacturer. After this process, the surface roughness of all samples was minimized by finishing and polishing technique.

The chemical components of artificial saliva used in thermal cycling and dwell time tests are shown in Table 2 (Sutiman, Mareci, Nechita, Iordache, & Rosca, 2007). The pH of this solution was measured to be about 5.7 (Yilmaz & Sadeler, 2017). This ratio is within the range of artificial oral conditions (in vitro).

The surface roughness of the tested samples was determined using a three-dimensional non- contact profilometer (Bruker-Contour GT 3D). The wear area of the composite samples was scanned with dimensions of 4 mm x 4 mm, with a step of 12 µm along the x-axis, 12 µm along with the y-axis and measurement speed of 1000 µm / s. The

average measurement time was approximately 25 minutes. The average roughness value obtained over the area of wear was recorded as the surface roughness of the sample.

Table 1. The chemical properties composite materials

Composite Material	Manufacturer	Monomer	Filler Structure	Filler Loading
Estelite Flow Quick	Tokuyama Dental Corp., Tokyo, Japan. /Nanofill	Bis-MPEPP, TEGDMA, UDMA	Silica-zirconia filler and silica-titania filler (0.04-0.06 µm).	71/53
Charisma Opal	Heraeus Kulzer GmbH, Hanau, Germany. / Nanohybrid	Bis-GMA , EBADMA	Barium aluminium glass (0.02-2 microns), highly dispersive silica (0.02-0.07 microns)	58 / 64

Table 2 The chemical components of artificial saliva used in thermal cycling and dwell time tests

Component	NaCI	KCI	$CaCl_2.2H_2O$	$Na_2S.9H_2O$	$NaH_2PO_4.2H_2O$	Urea
Qantity g/L	0,4	0,4	0,795	0,005	0,69	1

RESULTS AND FINDINGS

The surface roughness value of the composite materials after thermal test and dwell time procedures (control, 1200 thermal and 3000 thermal cycles for 10 and 30 sn dwell time) is shown in Table 3. The increase in surface roughness values was observed with the increasing number of thermal cycles in both composite materials. Figure 1 shows an example of surface roughness determination with using scanned with dimensions of 4 mm x 4 mm, with a step of 12 µm along the x-axis, 12 µm along with the y-axis and measurement speed of 1000 µm / s. method.

Table 3 The surface roughness value of the composite materials after thermal test and dwell time procedures (µm)

Composite Material / Test Procedure	Estelite Flow	Charisma Opal	
Control Group	0.11	0.09	**Dwell time procedure**
1200 thermal cycles	0.15	0.12	10 seconds
	0.17	0.13	30 seconds
3000 thermal cycles	0.21	0.17	10 seconds
	0.26	0.18	30 seconds

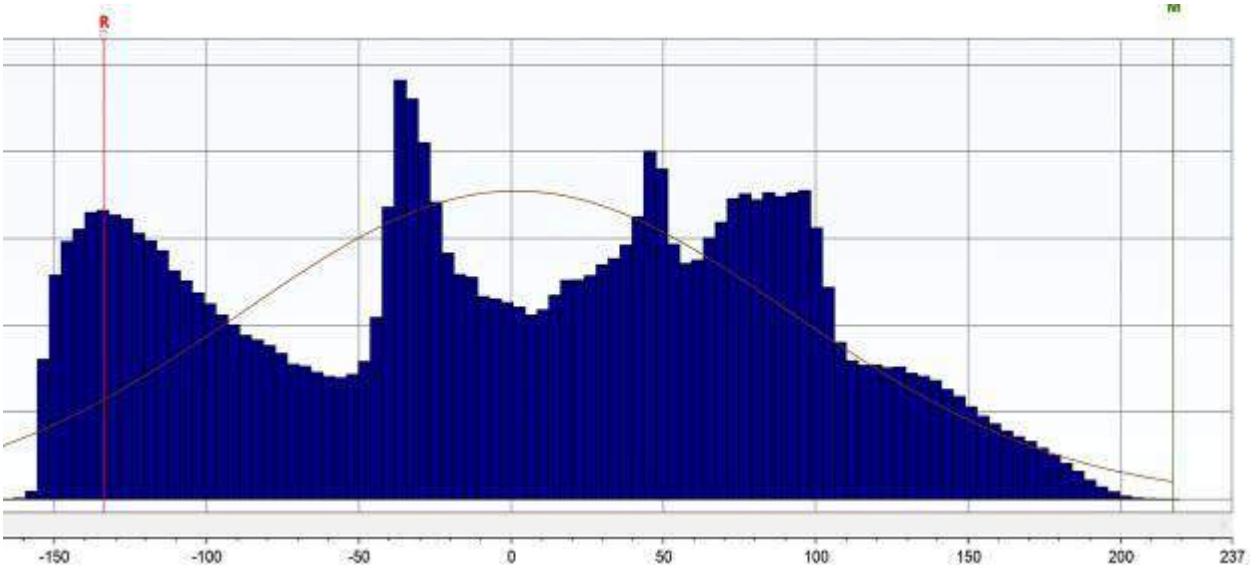

Figure 1. Example of surface roughness determination of composite material

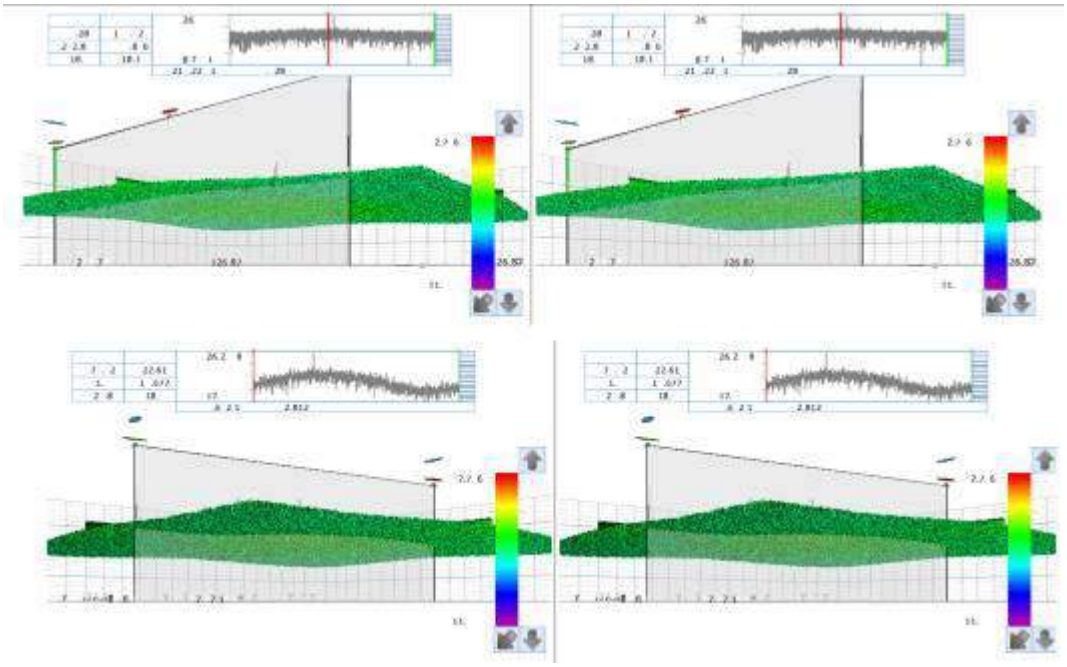

Figure 2 Example of microstructure analysis of composite material

Figure 3 and figure 4 shows the microstructure of the Estelite Flow and Charisma Opal composite material after 3000 thermal cycles and 30 seconds dwell time test procedure. In previous studies, it has been seen that thermal cycling experiments have significantly affected the surface roughness and chemical internal structure of composite resin materials (Dos Santos et al., 2015) It has been observed that the thermal structure of the composite materials subjected to thermal cycling experiments caused microcracks in the matrix structure due to thermal expansion and these cracks caused damage to the filling matrix interface (Ozcan et al., 2013)

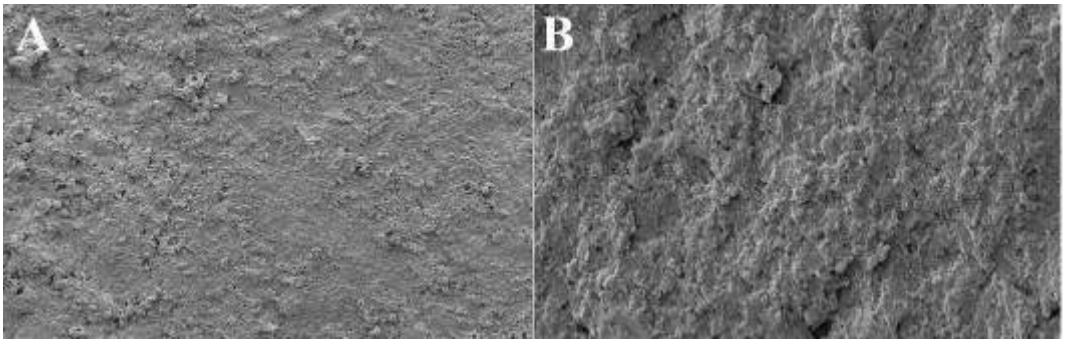

Figure 3. The microstructure of the Estelite Flow composite material after 3000 thermal cycles and 30 seconds dwell time test procedure. (left figure 5kV, 1600x mag. 50µm, right figure: 5kV, 6000x mag. 10 µm reference line)

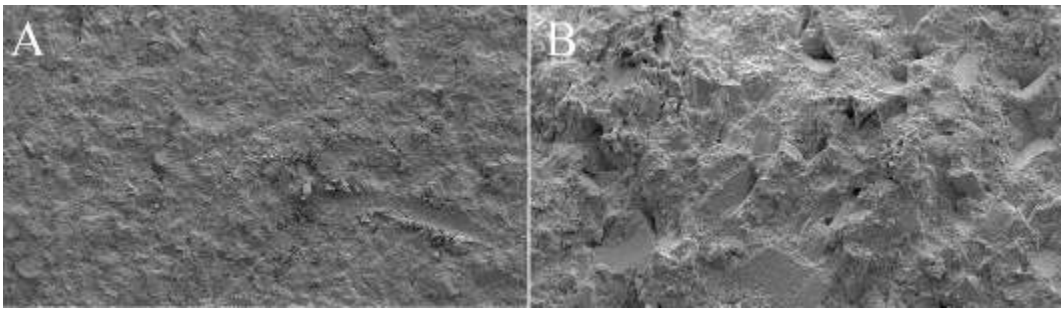

Figure 4. The microstructure of the Charisma Opal composite material after 3000 thermal cycles and 30 seconds dwell time test procedure (left figure 5kV, 6000x mag. 50 µm, right figure: 5kV, 12000x mag. 4 µm reference line).

CONCLUSION

The following evaluations were made with the findings obtained in this study.

The increase in the number of thermal cycles and dwell time resulted in an increase in surface roughness in both composite materials. However, the Estelite Flow composite material showed better surface roughness resistance when comparing the two composite materials after thermal and dwell time test procedures.

It has been observed that the composite material containing TEGDMA or TEGMA component is more sensitive to thermal cycling and dwell time test procedures. Therefore, it can be concluded that the wear properties of composite materials having this structure are affected when it is considered as a mechanism to increase wear in the intra-oral tribology.

REFERENCES

Bollen, C. M. L., Lambrechts, P., & Quirynen, M. (1997). Comparison of surface roughness of oral hard materials to the threshold surface roughness for bacterial plaque retention: A review of the literature. *Dental Materials, 13*(4), 258-269. doi:Doi 10.1016/S0109-5641(97)80038-3

Cao, L. Q., Zhao, X. Y., Gong, X., & Zhao, S. L. (2013). An in vitro investigation of wear resistance and hardness of composite resins. *International Journal of Clinical and Experimental Medicine, 6*(6), 423-430.

Cho, L. R., Yi, Y. J., & Heo, S. J. (2002). Effect of tooth brushing and thermal cycling on a surface change of ceromers finished with different methods. *Journal of Oral Rehabilitation, 29*(9), 816-822. doi:DOI 10.1046/j.1365-2842.2002.00877.x

Dos Santos, P. H., Catelan, A., Guedes, A. P. A., Suzuki, T. Y. U., Godas, A. G. D., Briso, A. L. F., & Bedran-Russo, A. K. (2015). Effect of thermocycling on roughness of nanofill, microfill and microhybrid composites. *Acta Odontologica Scandinavica, 73*(3), 176-181. doi:10.3109/00016357.2014.971868

Drummond, J. L. (2008). Degradation, fatigue, and failure of resin dental composite materials. *Journal of Dental Research, 87*(8), 710-719. doi:Doi 10.1177/154405910808700802

Hahnel, S., Henrich, A., Burgers, R., Handel, G., & Rosentritt, M. (2010). Investigation of Mechanical Properties of Modern Dental Composites After Artificial Aging for One Year. *Operative Dentistry, 35*(4), 412-419. doi:10.2341/09-337-L

Hickel, R., & Manhart, J. (2001). Longevity of restorations in posterior teeth and reasons for failure. *J Adhes Dent, 3*(1), 45-64.

Manhart, J., Kunzelmann, K. H., Chen, H. Y., & Hickel, R. (2000). Mechanical properties of new composite restorative materials. *Journal of Biomedical Materials Research, 53*(4), 353-361. doi:Doi 10.1002/1097-4636(2000)53:4<353::Aid-Jbm9>3.0.Co;2-B

Marghalani, H. Y. (2010). Effect of Finishing/Polishing Systems on the Surface Roughness of Novel Posterior Composites. *Journal of Esthetic and Restorative Dentistry, 22*(2), 127-138. doi:10.1111/j.1708-8240.2010.00324.x

Ozcan, M., Valandro, L. F., Pereira, S. M. B., Amaral, R., Bottino, M. A., & Pekkan, G. (2013). Effect of Surface Conditioning Modalities on the Repair Bond Strength of Resin Composite to the Zirconia Core / Veneering Ceramic Complex. *Journal of Adhesive Dentistry, 15*(3), 207-210. doi:10.3290/j.jad.a29717

Sutiman, D. M., Mareci, D., Nechita, T. M., Iordache, I., & Rosca, J. C. M. (2007). The electrochemical behaviour of some unnoble alloys in fusayama artificial saliva. *Macedonian Journal of Chemistry and Chemical Engineering, 26*(1), 57-63.

Yilmaz, E., & Sadeler, R. (2017). Yapay Ağız Sıvısında Termal Çevrimin Kompozit Restoratif Malzemelerinin Yüzey Pürüzlülüğü Üzerindeki Etkisi. *Technological Applied Sciences, 12*(2), 38-42.

WEAR MECHANISMS OF INTRA-ORAL TRIBOLOGY; REVIEW

Efe Çetin YILMAZ
Kilis 7 Aralık University, Engineering Faculty, Department of Mechanical Engineering, Kilis, TURKEY, efecetinyilmaz@msn.com

ABSTRACT: The term wear can generally be defined as the loss of material that occurs after the interaction of at least two materials. Tooth wear is a complex and continuous physiological process that results from various tribological interactions within the oral cavity. In this process, biomaterials placed in the mouth can be exposed to several wear mechanisms simultaneously. These wear mechanisms significantly affect the mechanical, aesthetic and biological behavior of biomaterials. Predicting the mechanical and biological behavior of biomaterials in the oral tribological process before the treatment process will contribute to the formation of a more satisfactory treatment process. For this reason, in vitro test mechanisms have been developed in order to simulate the oral tribological process. The aim of this study was to investigate and evaluate the wear mechanisms in the oral tribological process during chewing cycle motion.

Key words: wear, biomaterial, chewing simulation

AĞIZ-İÇİ TRİBOLOJİDE AŞINMA MEKANİZMALARI; BİR İNCELEME

ÖZET: Aşınma terimi genel olarak en az iki malzemenin etkileşimi sonrasında meydana gelen malzeme kaybı olarak tanımlanabilir. Diş aşınması, ağız boşluğu içindeki çeşitli tribolojik etkileşimler sonucu oluşan karmaşık ve sürekli bir fizyolojik süreçtir. Bu süreçte ağız içerisine yerleştirilen biyomalzemeler eş zamanlı olarak birçok aşınma mekanizmasına maruz kalabilirler. Bu aşınma mekanizmaları biyomalzemelerin mekanik, estetik ve biyolojik davranışlarını önemli derecede etkilemektedir. Tedavi sürecinden önce biyomalzemelerin ağız içi tribolojik süreçte mekanik ve biyolojik davranışlarını tahmin edebilmek daha tatminkâr tedavi sürecinin oluşmasına katkı sağlayacaktır. Bu sebeple ağız içi tribolojik süreci simüle edebilmek amacıyla birçok laboratuvar ortam (in vitro) test mekanizmaları geliştirilmiştir. Bu çalışmanın amacı çiğneme hareketi sırasında ağız içi tribolojik süreçte meydana gelen aşınma mekanizmalarını araştırmak ve değerlendirmektir.

Anahtar sözcükler: aşınma, biyomalzeme, çiğneme test simülasyonu

GİRİŞ

Vücut içerisine yerleştirilen biyomalzemeler karmaşık ve sürekli bir yapı içerisinde çeşitli aşınma ve yorulma mekanizmalarına maruz kalırlar. Bu yorulma ve aşınma mekanizmaları biyomalzemelerin vücut içerisindeki fonksiyonlarını önemli derecede etkileyebilmektedir. Biyomalzemelerin aşınması karmaşık ve tahmin edilemeyen bir süreçtir. Ağız içi tribolojide genel anlamda dört temel aşınma mekanizmasının meydana geldiğinin söylemek mümkündür (Heintze, 2006; E. C. Yilmaz & Sadeler, 2018a, 2018b). Bu aşınma mekanizmaları diş ve biyomalzemenin direkt teması ile gerçekleşen two-body aşınma mekanizması, arada yemek parçacıklarının varlığı ile three-body aşınma mekanizması, korozif etki nedeniyle korozyonlu aşınma ve tekrarlı yüklemelerin neden olduğu yorulmalı aşınma mekanizması olarak adlandırılabilir. Bu aşınma mekanizmaları çiğneme hareketi boyunca sürekli ve karmaşık bir yapıda bulunabilir (E. Yilmaz et al., 2018; E. Ç. Yilmaz, 2019).

Çiğneme hareketi aşınmayı belirleyen temel iki aşınma sürecini içerir. Bu aşınma süreçleri biyomalzeme ve karşı malzemenin (genellikle diş malzemesi) direkt teması ile gerçekleşir ve bu süreçte malzemeler arası geçiş olabilir veya yüzey aşınmaları meydana gelebilir. Diğer süreçte ise çiğneme hareketi işlemi sırasına biyomalzeme ve karşı (antagonist) olarak adlandırılan malzeme arasına üçüncü aşındırıcı parçacıklar (genellikle yemek parçacıkları) dahil olur. Bu işlem sürecinde bu parçacıklardan ortaya çıkan asidik etki ve aşındırıcı özellikler nedeniyle korozif etki ve aşınma bölgeleri oluşmaya başlar. Bu süreç çiğneme hareketi sürecinde sürekli yeninden tek başına veya bir arada tekrar edebilir. Dolayısıyla ağız içerisine yerleştirilmiş bir biyomalzeme karmaşık ve sürekli bir yapı içerisinde yorulma ve aşınma mekanizmalarına maruz kalabilmektedir.

Çiğneme hareketi sırasında karşı malzeme ağız içeresindeki yiyecek tabakasını hapseder ve dişler birbirinden geçerken öğütme işlemi başlar. Bu öğütme işlemi sırasında karşılıklı iki malzeme arasında aşınma ve yorulma mekanizmaları meydana gelmeye başlar. Şekil 1 de bu işlem süreci özetlenmiştir. Çiğneme döngüsü hazırlık, ezme ve kayma hareketi olarak üç bölüme ayrılabilir (DeLong, 2006). Hazırlık aşamasında, çene yemek parçacıkları ile temas edecek şekilde konumlandırılmıştır. Çene açma hareketi ile başlar ve dişler gıda parçacıkları ile temas edene kadar kapanma hareketi boyunca devam eder. Normalde, bu aşamada hiçbir oklüzal kuvvet dahil değildir (yapışkan yiyecekler bir istisnadır) (DeLong, 2006). Ezme aşaması hazırlık aşamasını takip eder ve dişlerin gıda parçacıkları ile üç gövdeli bir etkileşimini temsil eder. Bu aşamada gıda parçacıklarından ortaya çıkan korozif etki malzemelerin aşınma yüzeyini etkiler. Dişler ilk önce gıda

parçacıkları temas ettiğinde başlar ve diş-diş teması olana kadar veya çene açılmaya başlayana kadar (hazırlık aşamasının başlangıcı) devam eder. İlk temasta, kuvvet gıda parçacıkları boyunca dağıtılır. Dişlerin yaşadığı kuvvetin büyüklüğü, yiyecek parçacıklarının sertliğine bağlıdır. Yiyecek parçacıkları sıkıştırıldıkça, çiğneme kuvveti, gıda parçacıkları yüzeyinden kesici dişler ve öğütücü dişler üzerinde dağıtılmaya başlanır (DeLong, 2006). Mühendislik açısından temas yüzeyi arttıkça, birim alandaki kuvvet azalacağı bir gerçektir. Her zaman çiğneme sırasında meydana gelmeyen kayma aşaması dişe dişle temasla başlar (eğer varsa yiyecek parçacıklarının tam penetrasyonu) ve çene açılmaya başlayana kadar (hazırlık aşamasının başlangıcı) devam eder (DeLong, 2006). Temas halinde, çiğneme kuvveti okluzal temas bölgesinde yoğunlaşmaktadır. Diş-diş teması ve besin parçacıklarının varlığı nedeniyle, hem iki hem de üç vücut aşınma mekanizması meydana gelmektedir.

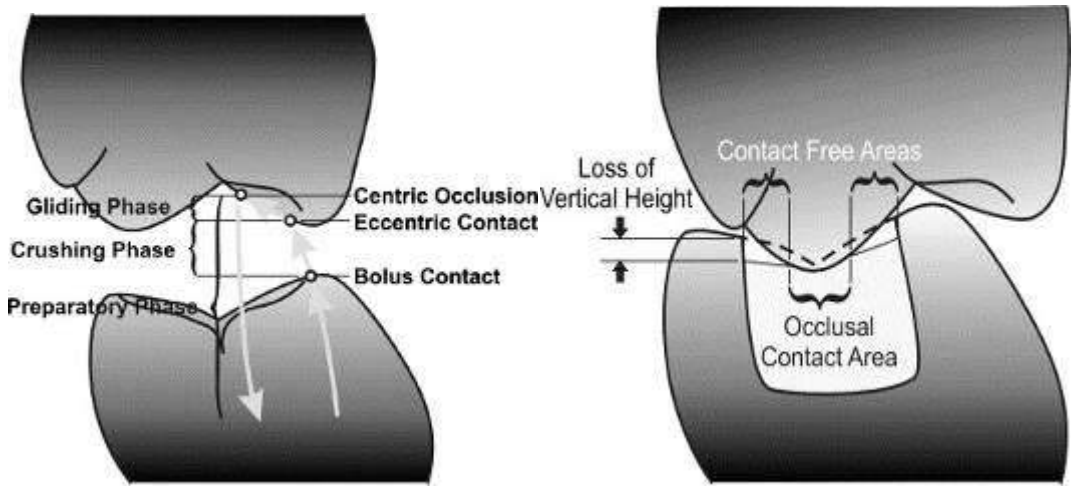

Şekil 1. Çiğneme hareketi sırasında meydana gelen aşınma mekanizmalarının gösterimi (DeLong, 2006)

2. Direkt-Temas Aşınma Mekanizması (Two-Body Wear Mechanism)

Bu aşınma mekanizmasının in vitro test düzeneği genel olarak canlı doku / yapay tükürük veya su gibi sıvı kayganlaştırıcılar olmadan yapılır. Birleşme yüzeyleri temas yükü madde kaybı altında kaydığından reçine matrisinin zıt yüzeyinin sert özellikleri ve yorulma aşınması nedeniyle aşınması nedeniyle oluşabilir (Iwasaki et al., 2014; Kruzic, Arsecularatne, Tanaka, Hoffman, & Cesar, 2018) Farklı doldurucu tipine sahip kompozit malzemelerin mikro yapıları şekil 2 de gösterilmiştir (Koottathape, Takahashi, Iwasaki, Kanehira, & Finger, 2012). Bir kompozit içine daha yüksek bir dolgu maddesi doldurulması, reçine matrisinin aşınmasını azaltabilir (Heintze, 2007). Bu süreçte daha yüksek bir kırılma tokluğu, yorulmayı azaltabilen mikroyapıda çatlak ilerlemesini

geciktirebilir (Kruzic et al., 2018). Genel olarak, bir diş kompozitinin iki gövdeli aşınması, dolgu maddesi oranı ve kırılma tokluğu ile doğrudan ilişkilidir (Heintze, 2007). İki cisim aşınmasına ilişkin önemli eğilimler aşağıdaki gibi özetlenmiştir.

Matrise yeterli dolgu maddesi yapışması aşınma direnci için esastır; aslında, arayüz bağlanma destekli çatlak başlatma / çoğaltma işleminin yol açtığı yorulma aşınması mekanizması nedeniyle zayıf ara yüz bağlaması olan kompozitler daha yüksek oranda aşınmaktadır (Kruzic et al., 2018; Shinkai, Taira, Suzuki, & Suzuki, 2016). Buna karşılık, yeterli arayüz bağ kuvveti ile, yeraltı çatlak ilerlemesi yavaştır ve sığ ve yorulma aşınma mekanizmaları yüksek aşınma kaybına neden olmaz (Kruzic et al., 2018).

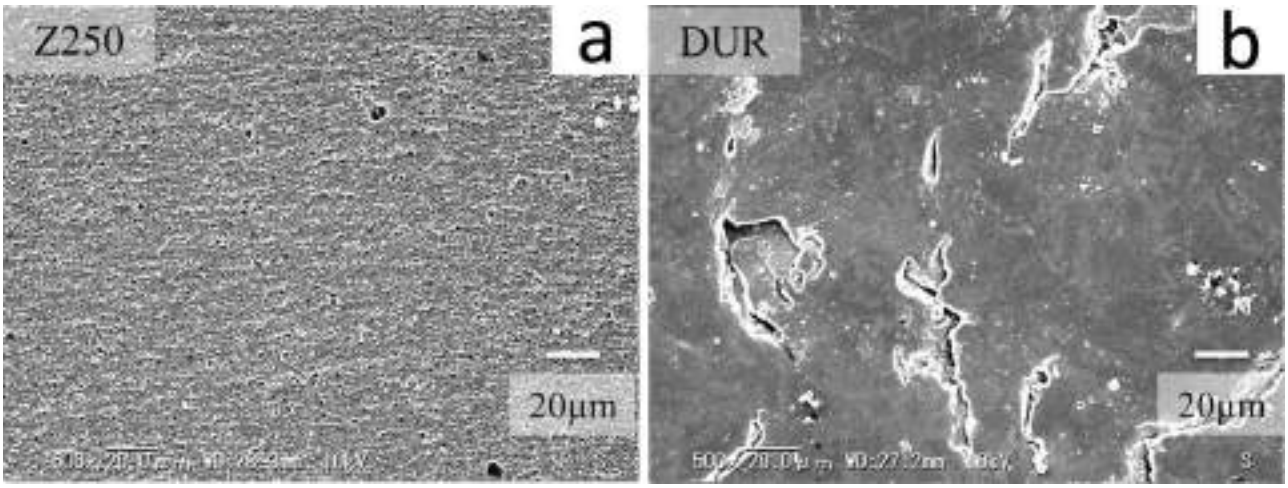

Şekil 2. Farklı tip kompozit malzemelerin 10.000 direkt-temas (two-body) çiğneme testi sonrasındaki mikro yapılarının gösterimi (Koottathape et al., 2012)

3. Aşındırıcı Ortam Mekanizması (Three-Body Wear Mechanism)

Laboratuvar ortamında three-body aşınma mekanizmasını simüle etmek amacıyla kompozit numune ve karşı malzeme arasında gıda parçacıklarını simüle eden üçüncü bir vücut ortamı ile yük altında kayan temas halindedir (Lambrechts, Debels, Van Landuyt, Peumans, & Van Meerbeek, 2006).
Genel olarak üçüncü vücut ortamı olarak aşağıda belirtilen sulu süspansiyonlar kullanılmaktadır.
*öğütülmüş pirinç / darı / haşhaş tohumu;
*polimetil metakrilat (PMMA) veya cam boncuklar;
*alümina parçacıkları (Benetti, Larsen, Dowling, & Fleming, 2016)

Literatürdeki çalışmalardan elde edilen sonuçlar kapsamında aşağıdaki değerlendirmeler yapılmıştır.

Daha büyük dolgu maddesi yüklü kompozitler, daha yumuşak matrisin aşınması nedeniyle daha az üç gövde aşınması gösterir (Kruzic et al., 2018; Lambrechts et al., 2006). Bunun nedeni dolgu maddesi partikülleri arasındaki büyük boşlukların matrisi aşınmaya (dolgu maddesinin dökülmesine ve dolayısıyla daha fazla aşınmaya maruz bırakmasıdır (Shinkai et al., 2016).

Nispeten daha büyük dolgu maddelerine sahip (örneğin, mikro dolgu veya hibrit malzemeler) olan kompozelerle karşılaştırıldığında, nano dolgu maddelerine sahip olanlar (örneğin, nano dolgu maddesi) üstün üç-gövde aşınma direnci gösterir (Kruzic et al., 2018)

Yukarıdaki eğilimler, iki vücut aşınmasına göre üç vücut aşınmasını anlamak için biraz daha basit bir resim çiziyor gibi gözükse de, yine de belirli mekanizmalar ve test koşullarıyla ilgili komplikasyonlar vardır. Örneğin, aşınma hızları mutlaka sabit değildir ve aşınma döngüleri ile artabilir veya bunun tersine ilk aşamada daha büyük aşınma olabilir ve bunu takiben sabit aşınma oranına sahip bir faz (De Souza, Goutianos, Skovgaard, & Sorensen, 2011; Kruzic et al., 2018). İkinci durumda, ilk aşamadaki yüksek aşınma (~ 100.000 devire kadar) mekanik olarak, daha sonra sabit bir durum durumuna ulaşan numune hazırlama sırasında kullanılan taşlama / cilalama işlemleri nedeniyle başlangıçtaki yüzey hasarına bağlanır.

KAYNAKÇA

Benetti, A. R., Larsen, L., Dowling, A. H., & Fleming, G. J. P. (2016). Assessment of wear facets produced by the ACTA wear machine. *Journal of Dentistry, 45*, 19-25. doi:10.1016/j.jdent.2015.12.003

De Souza, J. A., Goutianos, S., Skovgaard, M., & Sorensen, B. F. (2011). Fracture resistance curves and toughening mechanisms in polymer based dental composites. *Journal of the Mechanical Behavior of Biomedical Materials, 4*(4), 558-571. doi:10.1016/j.jmbbm.2011.01.003

DeLong, R. (2006). Intra-oral restorative materials wear: Rethinking the current approaches: How to measure wear. *Dental Materials, 22*(8), 702-711. doi:10.1016/j.dental.2006.02.003

Heintze, S. D. (2006). How to qualify and validate wear simulation devices and methods. *Dental Materials, 22*(8), 712-734. doi:10.1016/j.dental.2006.02.002

Heintze, S. D. (2007). Systematic reviews: I. The correlation between laboratory tests on marginal quality and bond strength. II. The correlation between marginal quality and clinical outcome. *Journal of Adhesive Dentistry, 9*, 77-106.

Iwasaki, N., Takahashi, H., Koottathape, N., Kanehira, M., Finger, W. J., & Sasaki, K. (2014). Texture of composite resins exposed to two- and three-body wear in vitro. *J Contemp Dent Pract, 15*(2), 232-241.

Koottathape, N., Takahashi, H., Iwasaki, N., Kanehira, M., & Finger, W. J. (2012). Two- and three-body wear of composite resins. *Dental Materials, 28*(12), 1261-1270. doi:10.1016/j.dental.2012.09.008

Kruzic, J. J., Arsecularatne, J. A., Tanaka, C. B., Hoffman, M. J., & Cesar, P. F. (2018). Recent advances in understanding the fatigue and wear behavior of dental composites and ceramics. *Journal of the Mechanical Behavior of Biomedical Materials, 88*, 504-533. doi:10.1016/j.jmbbm.2018.08.008

Lambrechts, P., Debels, E., Van Landuyt, K., Peumans, M., & Van Meerbeek, B. (2006). How to simulate wear? Overview of existing methods. *Dental Materials, 22*(8), 693-701. doi:10.1016/j.dental.2006.02.004

Shinkai, K., Taira, Y., Suzuki, S., & Suzuki, M. (2016). In vitro wear of flowable resin composite for posterior restorations. *Dental Materials Journal, 35*(1), 37-44. doi:10.4012/dmj.2015-080

Yilmaz, E., Sadeler, R., Duymu, #351, , Z., #214, . . . an, A. (2018). Effect of ambient pH and different chewing cycle of contact wear on dental composite material. *Dentistry and Medical Research, 6*(2), 46-50. doi:10.4103/dmr.dmr_26_18

Yilmaz, E. C., & Sadeler, R. (2018a). Investigation of three-body wear of dental materials under different chewing cycles. *Science and Engineering of Composite Materials, 25*(4), 781-787. doi:10.1515/secm-2016-0385

Yilmaz, E. C., & Sadeler, R. (2018b). Investigation of Two- and Three-Body Wear Resistance on Flowable Bulk-Fill and Resin-Based Composites. *Mechanics of Composite Materials, 54*(3), 395-402. doi:10.1007/s11029-018-9750-8

Yilmaz, E. Ç. (2019). Effect of Sliding Movement Mechanism on Contact Wear Behavior of Composite Materials in Simulation of Oral Environment. *Journal of Bio- and Tribo-Corrosion, 5*(3), 63. doi:10.1007/s40735-019-0258-0.

INVESTIGATION OF THE EFFECT OF ARTIFICIAL AGING ENVIRONMENT TEMPERATURE ON MECHANICAL BEHAVIOR OF BIO-COMPOSITE MATERIAL WITH NANO FILLER

Efe Çetin YILMAZ
Kilis 7 Aralık University, Engineering Faculty, Department of Mechanical Engineering, Kilis, TURKEY, efecetinyilmaz@msn.com

Recep SADELER
Atatürk University, Engineering Faculty, Department of Mechanical Engineering, Erzurum, TURKEY, receps@atauni.edu.tr

ABSTRACT: The aim of this study was to investigate the effect of artificial aging ambient temperature on the mechanical behavior of nano filler Supreme bio composite material used as restoration material in oral tribological environment as biomaterial. In this study, 2 mm wide X 13 mm diameter cylindrical test specimens were prepared in nano-filled Supreme composite material. Test specimens are artificial saliva (0.4 NaCl + 0.4 KCl + 0.795 CaCl2.2H2O + 0.005 Na2S.9H2O + 0.69 NaH2PO4.2H2O + 1 Urea (grams / liter) at 5 °C, 37 °C and 55 °C ambient temperatures After the artificial aging test procedure, surface roughness values of the test specimens were determined by 2D profilometer After the test procedures, it was obtained that the Supreme bio-composite material with nano filler showed higher surface roughness behavior with increasing temperature. It was concluded that temperature increase has an effect on increasing the hydraulic degradation mechanism of bio-composite material in artificial aging environment.

Key words: Bio-composite, Artificial aging, Surface roughness

YAPAY YAŞLANDIRMA ORTAM SICAKLIĞININ NANO DOLDURUCULU BIO-KOMPOZİT MALZEMESİNİN MEKANİK DAVRANIŞI ÜZERİNDEKİ ETKİSİNİN İNCELENMESİ

ÖZET: Bu çalışmanın amacı, yapay yaşlandırma ortam sıcaklığının biyomalzeme olarak ağız içi tribolojik ortamda restorasyon malzemesi olarak kullanılan nano dolduruculu Supreme biyo-kompozit malzemesinin mekanik davranışı üzerindeki etkisinin incelenmesidir. Bu çalışma kapsamında nano-dolduruculu Supreme kompozit malzemesinde 2 mm genişliğinde X 13 mm çapında silindirik biçimde test numuneleri hazırlanmıştır. Test numuneleri yapay tükürük (0,4 NaCI + 0,4 KCI + 0,795 $CaCl_2.2H_2O$

+ 0,005 $Na_2S.9H_2O$ + 0,69 $NaH_2PO_4.2H_2O$ + 1 Urea (gram/litre) ortamında 5 °C, 37 °C ve 55 °C ortam sıcaklıklarında 7 gün süresince yapay yaşlandırma işlemine maruz bırakılmıştır. Yapay yaşlandırma test prosedürü sonrasında test numunelerini yüzey pürüzlülük değerleri 2D profilometre ile belirlenmiştir. Test prosedürleri sonrasında nano dolduruculu Supreme bio-kompozit malzemesinin sıcaklık artışı ile daha yüksek yüzey pürüzlülüğü davranışı gösterdiği elde edilmiştir. Bu çalışma sonrasında elde edilen veriler ile sıcaklık artışının yapay yaşlandırma ortamında biyo-kompozit malzemesinin hidrolik bozunma mekanizmasını artırıcı bir etki oluşturduğu sonucuna varılmıştır.

Anahtar sözcükler: Bio-kompozit, Yapay yaşlandırma, Yüzey pürüzlülüğü

GİRİŞ

Son yıllarda mavi ışık teknolojisi ile polorisazyon olabilme kabiliyetine sahip farklı doldurucu yapılarında kompozit malzemelerin kullanımı giderek artmaktadır (Kurachi, Tuboy, Magalhaes, & Bagnato, 2001). Diş kompozit malzemeleri, genellikle reçine matrisi, inorganik dolgu maddeleri ve bir silan birleştirme maddesi olan heterojen malzemelerdir (Yilmaz et al., 2018). Kompozit malzeme reçine matrisine dahil edilen dolgu maddesi parçacıklarının miktarı ve büyüklüğü, her bir kompozit tipini ve sonuçta en avantajlı klinik uygulamasını belirleyebilir. Canlı doku üzerinde kompozit malzemelerde meydana gelene hasarın, matris ve dolgu maddelerinin bozulmasından kaynaklanabileceği veya kompozit restorasyonların in vivo hayatta kalma olasılığını azaltabilecek mekanik ve çevresel yükler, ara yüzey bağlanma, mikro çatlama veya dolgu partikülü kırılmasından kaynaklanabileceği bildirilmiştir (Hahnel, Henrich, Burgers, Handel, & Rosentritt, 2010a).

Literatürde bazı kaynaklarda kompozit sınıflandırmaları, kompozit malzemenin viskozitesini ve kararlılığını tanımlayan özelliklere odaklanırken (örneğin, flowable or packable), diğer kaynaklarda diş kompozitlerinin mekanik özelliklerini göz önünde bulundurarak, mikro yapı sınıflandırmalarını dikkate alınmaktadır (Kruzic, Arsecularatne, Tanaka, Hoffman, & Cesar, 2018)

Mikro doldurulmuş kompozitler. Silika parçacıkları içerir (0.01 ila 0.04 μm) ve küçük parçacık büyüklüğü nedeniyle yüksek derecede cilalanabilir. Düşük mukavemetlerinden dolayı ön veya servikal restorasyonlarda kullanılırlar (Kruzic et al., 2018).

Hibrit kompozitler. Bu kompozitlere dolgu maddesi yüklemesi ağırlıkça% 75'tir ve iki tür parçacık içerir: buzlu cam (1.0 ila 10 um) ve kolloidal silika. Kolloidal silika, toplam

dolgu yükünün% 20'si kadardır. Bu kompozitler, piyasada daha yeni mikro- / nano-hibrit ve nano-doldurulmuş kompozitler ile değiştirilmektedir(Kruzic et al., 2018).

Mikro / nano hibrit kompozitler. Bunlar evrensel (ön ve arka) malzemelerdir. Posterior restorasyonlar için gerekli güç ve aşınma direncine ve ayrıca anterior restorasyonlar için gerekli cilalanabilirlik ve estetiğe sahiptirler. Bu malzemeler, mikro ölçekli ve nano ölçekli (~ 20 nm) parçacıkların bir kombinasyonudur. Tipik bir dolgu maddesi doldurma yüklemesi, ağırlıkça% 78, mikro-hibrit dolgu için 1 ila 3.5 um ve nano hibrid için 0.4 ila 1 um aralığındadır(Kruzic et al., 2018).

Nano doldurulmuş kompozitler. Bunlar ayrıca, tek tek ya da reçine matrisinde topak halinde dağılmış nano dolgulu üniversal restoratörlerdir. Nano doldurucular, 5 ila 20 nm arasındadır ve kümeler, 0.6 ila 1.4 um arasında değişmektedir. Son kompozitlerin bazıları,% 92'ye kadar çok yüksek dolgu yüküne sahiptir(Kruzic et al., 2018).

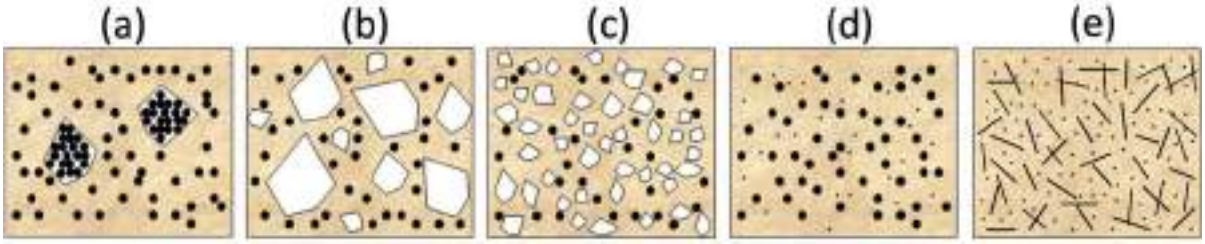

Şekil 1. Çeşitli reçine bazlı dental kompozitler sınıfları arasındaki mikroyapısal farklılıkları gösteren şematik yapı (a) Mikro doldurma; (b) Hibrit; (c) Mikro / nano hibrid; (d) Nano doldurulmuş; (e) Kısa elyaf takviyeli (Kruzic et al., 2018).

MATERYAL VE YÖNTEM

Supreme biyo-kompozit malzemesinin mekanik davranışı üzerindeki etkisinin incelenmesidir. Bu çalışma kapsamında nano-dolduruculu Supreme kompozit malzemesinde 2 mm genişliğinde X 13 mm çapında silindirik biçimde test numuneleri hazırlanmıştır. Yapay yaşlandırma testleri için tablo 2 de belirtilen yapay tükürük kimyasal bileşenleri kullanılmıştır. (Sutiman, Mareci, Nechita, Iordache, & Rosca, 2007). Bu çözeltinin pH oranı yaklaşık 5,7 olarak ölçülmüştür. Bu oran yapay ağız ortam (in vitro) çalışma şartları aralığındadır. Bu çalışmada test edilen nano dolduruculu Supreme kompozit malzemesinin mekanik ve kimyasal özellikleri Tablo 2 de gösterilmiştir.

Tablo 1. Yapay yaşlandırma ortamının kimyasal bileşenlerinin gösterimi

Bileşen	NaCI	KCI	$CaCl_2.2H_2O$	$Na_2S.9H_2O$	$NaH_2PO_4.2H_2O$	Urea

Miktar g/L	0,4	0,4	0,795	0,005	0,69	1

Tablo 2. Nano dolduruculu Supreme kompozit malzemesinin mekanik ve kimyasal özelliklerinin gösterimi

Materials	**Manufacturer**	**Composition**		
		Monomer	**Filler /Filler average size**	**Filler Weight %/Vol%**
Filtek Supreme XT/ FIL	3M ESPE,St. Paul, MN,USA Nanofilled	Bis-GMA, UDMA, BisEMA, TEGDMA	Nanosilica Zirconia/silica Nanoclusters (nanoparticle size) (5-20nm)	78 / 60

SONUÇ VE TARTIŞMA

Bu çalışmada test edilen nano dolduruculu Supreme kompozit malzemesinin yapay yaşlandırma testlerinden sonra yüzey pürüzlülük değerleri 5 °C de 0.11(0.03) µm, 37 °C için 0.13 (0.02) µm ve 55 °C de 0.16 (0.05) µm olarak elde edilmiştir. Şekil 2 nano dolduruculu Supreme kompozit malzemesinin yapay yaşlandırma testlerinden sonra yüzey pürüzlülük değerinin 2D profilometre örneğini göstermektedir. Şekil 3 yapay yaşlandırma ortam sıcaklığının 55 °C olduğu testlerden sonra nano dolduruculu Supreme kompozit malzemesinin yüzeyinden alınan mikro yapı analizini göstermektedir.

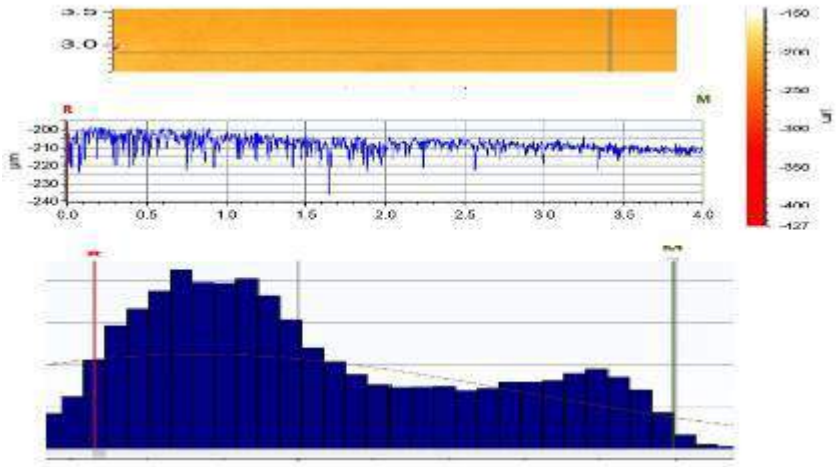

Şekil 2. Nano dolduruculu Supreme kompozit malzemesinin yapay yaşlandırma testlerinden sonra yüzey pürüzlülük değerinin 2D profilometre örneğini gösterimi

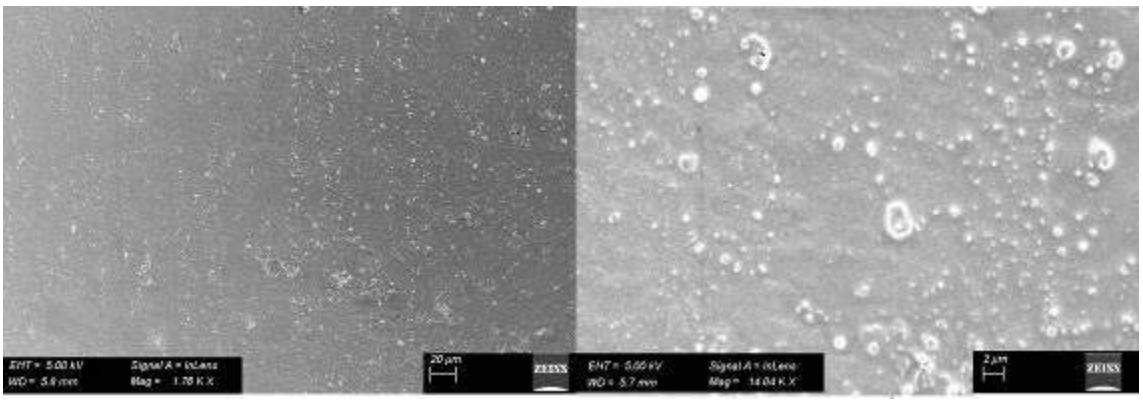

Şekil 3. 3 yapay yaşlandırma ortam sıcaklığının 55 °C olduğu testlerden sonra nano doldurucu lu Supreme kompozit malzemesinin yüzeyinden alınan mikro yapı analizinin gösterimi

Kompozit malzemelerin farklı monomer yapısına, farklı doldurucu oranlarına ve iç yapıdaki farklı kimyasal bağlara sahip olmaları bu malzemelerin birbirinden farklı mekanik özelliklere sahip olmalarını sağlamıştır. Ayrıca bu yapılardaki farklılıklar bu malzemelerin farklı mekanik bozunma mekanizmalarına duyarlılık gösterdiği gözlemlenmiştir. Daha önceki çalışmalarda kompozit malzemenin matriks yapında meydana gelen bozulmalardan dolayı in vivo tedavi sürecinde kompozit malzemenin yapı bütünlüğünde önemli derecede hasar aldığı rapor edilmiştir.(Hahnel, Henrich, Burgers, Handel, & Rosentritt, 2010b) Kompozit malzemenin rezin matriks yapısının kimyasal bağ çiftlerinde ve doldurucu parçacıkların karakteristikleri rezin kompozitin yüzey pürüzlüğünü doğrudan etkileyen parametrelerdir.(Marghalani, 2010a)
Restoratif malzemelerde yüzey pürüzlüğü aşınmayı etkileyen önemli bir parametredir. Eğer kompozit malzemenin yüzey pürüzlülüğü 0,2µm ve üzerinde bir değere sahipse klinik olarak bir risk oluşturmaktadır.(Bollen, Lambrechts, & Quirynen, 1997) Yüzey pürüzlülüğünün en aza indirgemek için bu malzemelere doldurma işlemi sonrasında bitirme ve cilalama işlemi uygulanmaktadır.(Marghalani, 2010b) Böylelikle bu işlem ile kompozit restoratif mazlemenin aşınma mekanizmasına karşı duyarlılığı azaltılmış olacaktır. Kompozit rezinlerin mekanik özelliklerini etkileyen bir diğer parameter hidrolitik bozulmalardan kaynaklı olduğu görülmüştür. Bu durumun in vivo tedavi sürecinde kompozit malzemenin uzun sürelerde termal çevrimlere ve ortamdaki yapay ağız sıvısına maruz bırakılarak kompozit malzemenin dayanıklılığı test edilerek yorumlanmaktadır.(Dos Santos et al., 2015)Bu durumlara ek olarak termal çevrim ortamında diş fırça mekanizmaları da kullanılarak kompozit rezinlerin dayanıklıları test edilerek yorumlanamaya çalışılmıştır (Cho, Yi, & Heo, 2002).

DEĞERLENDİRME

Bu çalışma sonucunda elde edilen in vitro deney verileri kapsamında, Supreme bio-kompozit malzemesinin sıcaklık artışı ile daha yüksek yüzey pürüzlülüğü davranışı gösterdiği elde edilmiştir. Ayrıca, sıcaklık artışının yapay yaşlandırma ortamında biyo-kompozit malzemesinin hidrolik bozunma mekanizmasını artırıcı bir etki oluşturduğu sonucuna varılmıştır.

KAYNAKÇA

Bollen, C. M. L., Lambrechts, P., & Quirynen, M. (1997). Comparison of surface roughness of oral hard materials to the threshold surface roughness for bacterial plaque retention: A review of the literature. *Dental Materials, 13*(4), 258-269. doi:Doi 10.1016/S0109-5641(97)80038-3

Cho, L. R., Yi, Y. J., & Heo, S. J. (2002). Effect of tooth brushing and thermal cycling on a surface change of ceromers finished with different methods. *Journal of Oral Rehabilitation, 29*(9), 816-822. doi:DOI 10.1046/j.1365-2842.2002.00877.x

Dos Santos, P. H., Catelan, A., Guedes, A. P. A., Suzuki, T. Y. U., Godas, A. G. D., Briso, A. L. F., & Bedran-Russo, A. K. (2015). Effect of thermocycling on roughness of nanofill, microfill and microhybrid composites. *Acta Odontologica Scandinavica, 73*(3), 176-181. doi:10.3109/00016357.2014.971868

Hahnel, S., Henrich, A., Burgers, R., Handel, G., & Rosentritt, M. (2010a). Investigation of mechanical properties of modern dental composites after artificial aging for one year. *Oper Dent, 35*(4), 412-419. doi:10.2341/09-337-L

Hahnel, S., Henrich, A., Burgers, R., Handel, G., & Rosentritt, M. (2010b). Investigation of Mechanical Properties of Modern Dental Composites After Artificial Aging for One Year. *Operative Dentistry, 35*(4), 412-419. doi:10.2341/09-337-L

Kruzic, J. J., Arsecularatne, J. A., Tanaka, C. B., Hoffman, M. J., & Cesar, P. F. (2018). Recent advances in understanding the fatigue and wear behavior of dental composites and ceramics. *J Mech Behav Biomed Mater, 88*, 504-533. doi:10.1016/j.jmbbm.2018.08.008

Kurachi, C., Tuboy, A. M., Magalhaes, D. V., & Bagnato, V. S. (2001). Hardness evaluation of a dental composite polymerized with experimental LED-based devices. *Dental Materials, 17*(4), 309-315. doi:Doi 10.1016/S0109-5641(00)00088-9

Marghalani, H. Y. (2010a). Effect of filler particles on surface roughness of experimental composite series. *Journal of Applied Oral Science, 18*(1), 59-67. doi:Doi 10.1590/S1678-77572010000100011

Marghalani, H. Y. (2010b). Effect of Finishing/Polishing Systems on the Surface Roughness of Novel Posterior Composites. *Journal of Esthetic and Restorative Dentistry, 22*(2), 127-138. doi:10.1111/j.1708-8240.2010.00324.x

Sutiman, D. M., Mareci, D., Nechita, T. M., Iordache, I., & Rosca, J. C. M. (2007). The electrochemical behaviour of some unnoble alloys in fusayama artificial saliva. *Macedonian Journal of Chemistry and Chemical Engineering, 26*(1), 57-63.

Yilmaz, E., Sadeler, R., Duymu, #351, , Z., #214, . . . an, A. (2018). Effect of ambient pH and different chewing cycle of contact wear on dental composite material. *Dentistry and Medical Research, 6*(2), 46-50. doi:10.4103/dmr.dmr_26_18.

SOLAR ENERGY TECHNOLOGY IN RENEWABLE ENERGY

Fatma AVLİ FIRIŞ
AKEDAŞ Elektrik Dağıtım A.Ş.
fatma.avlifiris@akedasdagitim.com.tr

Sabri Murat KISAKÜREK
AKEDAŞ Elektrik Dağıtım A.Ş.
murat.kisakurek@ akedasdagitim.com.tr

ABSTRACT: The concept of energy and the supply, security, accessibility and sustainability of energy resources have been one of the most important issues in the world. Due to traditional fossil fuels used to meet the increasing energy demand by gaining momentum all over the world and the economic and political problems associated with being dependent on the source countries constitute the perception that the existing energy resources should be changed. Energy sources developed as an alternative to these traditional fuels are called renewable energy sources; hydraulic, wind, solar, geothermal, biomass-waste and wave. Also, the studies related to the use of renewable energy sources are accelerating in our country and important developments are experienced in this field. Our country has a very high potential in terms of solar energy which is among the renewable energy sources. In this study, the current potential of solar energy in our country and photovoltaic solar energy technologies that convert solar energy into electrical energy are discussed. One of the results obtained in the study; In order to evaluate the solar energy potential of our country, investments in this area should be accelerated and another result is the increase in the installed power in the field of photovoltaic solar energy, the generation of electricity and the capture of grid parity of the photovoltaic electricity, and the formation of the market in the domestic photovoltaic module. In addition, it is predicted that photovoltaic module costs will be decreased and their efficiency will be increased in the light of R & D studies and technological developments.

Key words: Renewable energy, solar energy, photovoltaic technology.

YENİLENEBİLİR ENERJİDE GÜNEŞ ENERJİSİ TEKNOLOJİSİ

ÖZET: Enerji kavramı ve enerji kaynaklarının temini, güvenliği, erişilebilirliği ve sürdürülebilirliği konuları, geçmişten günümüze kadar dünyada en önemli meselelerden

biri olmuştur. Dünya üzerinde ivme kazanarak artan enerji ihtiyacının karşılanmasında kullanılan geleneksel fosil kökenli yakıtların sınırlı oluşları ve kaynak ülkelere bağımlı olmanın beraberinde getirdiği ekonomik ve siyasi sorunlar, mevcuttaki enerji kaynaklarında değişiklik yoluna gidilmesi gerektiği algısını oluşturmaktadır. Bu geleneksel yakıtlara alternatif olarak geliştirilen enerji kaynakları, yenilenebilir enerji kaynakları olarak isimlendirilen; hidrolik, rüzgâr, güneş, jeotermal, biokütle-atık ve dalga olarak sıralanabilen kaynaklardır. Bunlara paralel olarak ülkemizde de yenilenebilir enerji kaynaklarının kullanımı ile ilgili çalışmalar hızlanarak devam etmekte ve bu alanda önemli gelişmeler yaşanmaktadır. Ülkemiz, yenilenebilir enerji kaynakları içerisinde yer alan güneş enerjisi açısından oldukça yüksek bir potansiyele sahiptir. Bu çalışmada güneş enerjisinin ülkemizdeki mevcut potansiyeli ve güneş enerjisini elektrik enerjisine dönüştüren fotovoltaik güneş enerjisi teknolojileri ele alınmıştır. Çalışmada elde edilen sonuçlardan biri; ülkemizin güneş enerjisi potansiyelinin değerlendirilmesi adına bu alandaki yatırımların hızlandırılması gerektiği olup bir diğer sonuç ise fotovoltaik güneş enerjisi alanında kurulu güç artışı, elektrik üretimi ve fotovoltaik elektriğinin şebeke paritesini yakalamasıyla bu alanda pazar oluşacağı, pazar oluşumunun yerli fotovoltaik modül üretiminin başlamasını sağlayacağıdır. Ayrıca Ar-Ge çalışmalarının ve teknolojik gelişmelerin ışığında fotovoltaik modül maliyetlerinin azalıp verimliliklerinde artış sağlanacağı öngörülmüştür.

Anahtar sözcükler: Yenilenebilir enerji, güneş enerjisi, fotovoltaik teknolojisi.

FREQUENCY DEPENDENT CHARACTERIZATION OF THE AL/CRN/N-SI DEVICE

Murat YILDIRM
Selcuk University, Faculty of Science, Department of Biotechnology, 42130 Konya, Turkey, muratyildirim@selcuk.edu.tr

Adem KOCYIGIT
Igdir University, Engineering Faculty, Department of Electrical Electronic Engineering, 76000 Igdir, Turkey, adem.kocyigt@igdir.edu.tr

ABSTRACT: The Al/*n*-Si metal semiconductor heterojunction with coronene (CRN) interfacial layer was fabricated by physical vapor deposition (PVD) technique and characterized by *C-V* measurements depending on various frequency measurements from 10 kHz to 1 MHz at room temperature. Furthermore, the photocapacitance measurements were performed on the device under various illumination intensities from 20 mW to 100 mW by 20 mW steps. While the capacitance values decreased with increasing frequency, the conductance values increased. Thus, the *C-V* and *G-V* characteristics of the Al/CRN/*n*-Si device showed that the capacitance and conductance values are strong function of the frequency and voltage. In addition, various electrical parameters of the Al/CRN/*n*-Si device were extracted from C^{-2}–*V* plots and discussed in the details. The device exhibited excellent photocapacitance behavior under light illumination. The Al/CRN/*n*-Si device can be employed photocapacitance applications.

Keywords: Coronene film, Al/CRN/*n*-Si device, *C-V* characteristics, photocapacitance

INTRODUCTION

Coronene is an organic semiconductor material with six benzene rings (Barış, Karadeniz, & Erdal, 2017). It has light emitting capabilities and suitable transport mechanism for organic electronics applications (Petrushenko & Petrushenko, 2019; Zhang, Zheng, & Shen, 1999). Therefore, the coronene can be used as interfacial interlayer between the metal and semiconductor to obtain optoelectronic devices such as photodiodes and light emitting diodes.

Metal semiconductor contacts have been investigated due to their importance in the semiconductor technology (Bilgili, Güzel, & Özer, 2019; A. Kocyigit, Orak, Çaldıran, & Turut, 2017; Adem Kocyigit, Yılmaz, Aydoğan, & İncekara, 2019). Sometimes interfacial

layers such as insulator, semiconductor polymer or metal oxide are inserted between the metal and semiconductor to the electrical properties of the contacts (Gökçen, Altuntaş, Altındal, & Özçelik, 2012; Yildiz, Altindal, & Kanbur, 2008). Among this interfacial layers, organic semiconductors are very popular depending on their adjustable conductivity and environmentally friendly structure (Chandrakala, Ramaraj, Shivakumaraiah, Madhu, & Siddaramaiah, 2012; Jiang et al., 2017). The coronene also can be used as interfacial control layer between the metal and semiconductor. Pakma *et al*. (Pakma, Çavdar, Koralay, Tuğluoğlu, & Faruk Yüksel, 2017) used coronene as interfacial layer for Al metal and *n*-Si semiconductor device. The coronene layer was obtained by spin coating technique. The device was characterized by *I-V* measurements under dark and various illumination conditions at room temperature and *C-V* measurements for 1 MHz frequency. They concluded that the coronene can used for optoelectronic and solar cell applications. Xiao *et al*. (Xiao et al., 2011) were fabricated coronene nanowires by reprecipitation method and characterized them by various instruments. They prepared thin film of the coronene nanowires on rGO/SiO2/Si electrode and obtained a strong photoresponse. Furthermore, the quartz/ITO/p-coronene/n-SiC/Ti (10 nm)/Au device was obtained, and it exhibited strong electroluminescence emission better than inorganic layers through of the coronene nanowires.

In this study, coronene interfacial organic layer were deposited by physical vapor deposition on the *n*-Si substrate to obtain metal semiconductor Al/CRN/*n*-Si device. The Al/CRN/*n*-Si device was characterized by *C-V* measurements for various frequencies from the 10 kHz to 1 MHz at room temperature. Furthermore, photocapacitance behavior of the Al/CRN/*n*-Si device was investigated under various illumination intensities.

METHODS

To fabrication of the Al/CRN/*n*-Si device was firstly started with cutting and cleaning of the Si wafer (*n*-type) semiconductor and substrate. The wafer has (100) direction and 7.3 x 10^{15} cm^{-3} carrier concentration according to producer. The wafer obtained as 1.5 cm x 1.0 cm piece and then cleaned with acetone, water and propanol according to RCA cleaning procedures. For removing native oxide layer and impurities on the surface of the Si wafer, the pieces were submerged into HF:H_2O (1:1) solution for just 30 seconds. Aluminum was sputtered back surface of the piece as ohmic contact, and they were annealed in N_2 atmosphere for 5 minutes at 500 °C. For preparing coronene layer on Si substrate the PVD technique were employed. Then another Al layer was sputtered on the coronene layer and, the Al/CRN/*n*-Si device was obtained. The schematic illustration of the fabricated device has been given in Fig. 1.

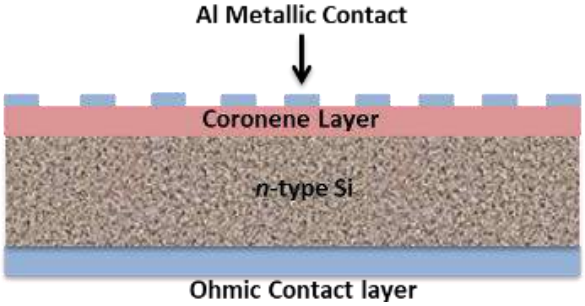

Figure 1. The Al/CRN/*n*-Si device as a schematic illustration

While the Keithley 4200 SCS was employed for *C-V* and *G-V* measurements, the FYtronix FY-5000 Photovoltaic Characterization System was used to light exposure to the devices for photocapacitance measurements.

RESULTS AND DISCUSSION

Fig. 2 presents frequency dependent *C-V* graphs of the Al/CRN/*n*-Si for the -5 V and +5 V voltage range. The device exhibited peaks at inversion region and their position shifted towards to depletion region via increasing frequency. While the peak behavior of the Al/CRN/*n*-Si device can be attributed to series resistance or interface states, decreasing at the peak intensities can be depended on the interface states not able to following ac signal for higher frequencies (Doğan, Yildirim, Orak, Elagöz, & Turut, 2015; Korucu, Turut, Turan, & Altindal, 2013; Şafak-Asar, Asar, Altındal, & Özçelik, 2015). The negative capacitance of the Al/CRN/*n*-Si device at the 10 kHz frequency can be ascribed to the injection of the minority carriers to the polarization or measurement errors (Gökçen et al., 2012). Furthermore, the capacitance values did not change at the accumulation region with changing frequency and voltage.

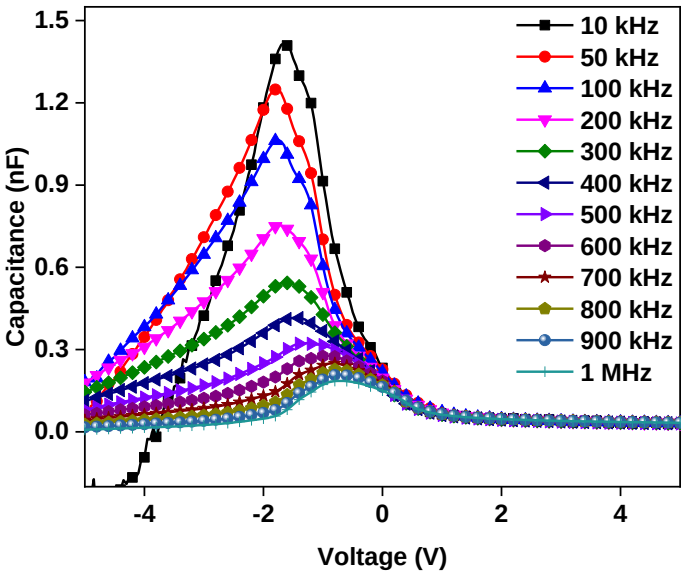

Figure 2. The *C*–*V* plots of the Al/CRN/*n*-Si device as a function of frequency

The *G*-*V* graphs of Al/CRN/*n*-Si device have been displayed in Fig. 3 for changing frequency in the range of 10 kHz and 1 MHz. The conductance values increased with increasing frequency at inversion region and suddenly decreased at depletion region. There is no change at accumulation region for the Al/CRN/*n*-Si device with changing frequency and voltage. The increase at the conductance values via increasing frequency at the same voltage values can be attributed to existence interface states (Al Orainy & Hendi, 2014). On the other hand, the device exhibited linearly decreasing profile for the 10 kHz, 50 kHz and 100 kHz frequencies from -5 V to -1 V or from inversion to depletion region. However, the conductance values of the device stayed constant and decreased suddenly towards to depletion region for higher frequencies than 100 kHz.

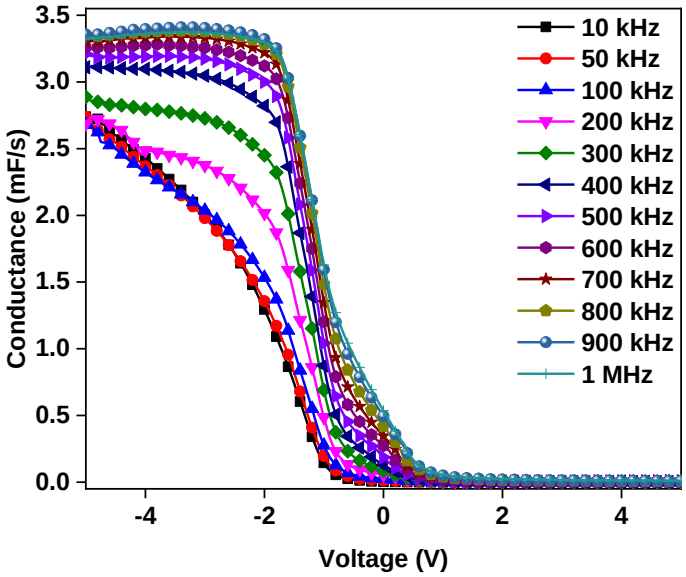

Figure 3. The G–V plots of the Al/CRN/n-Si device as a function of frequency

R_i–V graphs of the Al/CRN/n-Si device have been indicated in Fig. 4 for various frequencies from 10 kHz to 1 MHz. The R_i values are higher for 10 kHz and effective at inversion, depletion and accumulation regions, but they decreased with increasing frequency. Furthermore, R_i values showed peaks (inset of Fig. 4) at around depletion regions due to interface states effects (Baraz, Yücedağ, Azizian-Kalandaragh, & Altındal, n.d.). The resistances values decreased with increasing frequency because charges cannot follow ac signal towards to high frequencies (Orak, Kocyigit, & Alindal, 2017).

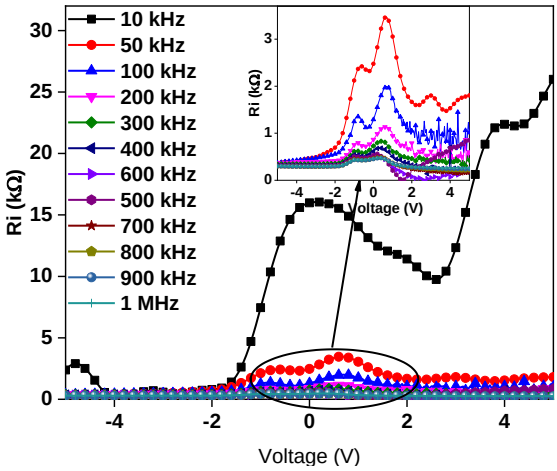

Figure 4. The Ri–V plots of the Al/CRN/n-Si device as a function of frequency

Fig. 5 indicates the C^{-2}-V graphs of the Al/CRN/n-Si device for various frequencies. The C^{-2}-V plots illustrated almost straight lines for wide range voltages from 5 V to 1 V. The deviations from the linearity can be attributed to interfacial layer effect (R. H., 2014). The x- intercept and slope of the C^{-2}-V plots are used to calculate doping concentration of the donor atoms (N_d), Fermi energy level (E_F), width of the depletion region (W_d), maximum electric field (E_m) and barrier heights (Φ_b). (Sze, 1981). These parameters provide to understand the Al/CRN/n-Si device properties and listed in Table 1 for various frequencies.

The barrier heights are calculated by the next equation from the C^{-2}–V plots:

$$\Phi_b(C-V) = (V_d + E_F) - \Delta\Phi \qquad (1)$$

where V_d and $\Delta\Phi$ show diffusion potential ($V_d = V_i + kT/q$) which is determined by the sum of the x-intercept of the C^{-2}–V plot and kT/q, and image force barrier lowering, respectively. The $\Delta\Phi$ values are neglected for intermediated interfacial layers.

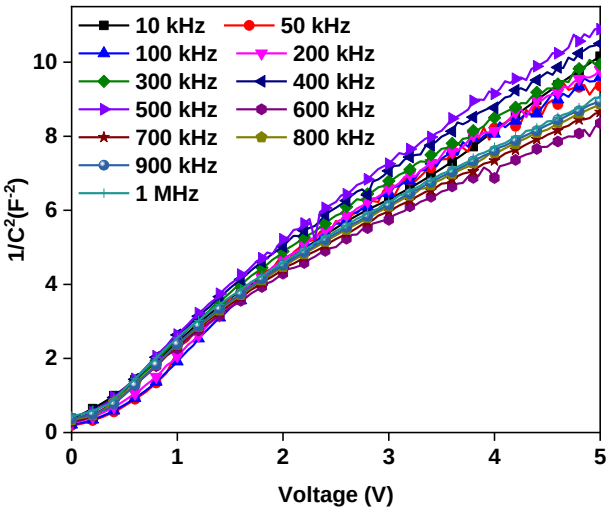

Figure 5. The C^{-2}–V plots of the Al/CRN/n-Si device as a function of frequency

The E_F is calculated by the following equation:

$$E_F = \frac{KT}{q} Ln\left(\frac{N_v}{N_d}\right) \quad (2)$$

where N_v is given by:

$$N_v = 4.82 \text{ x } 10^{15} T^{3/2} \left(\frac{m_e^*}{m_0}\right)^{3/2} \quad (3)$$

where m_0 and m_e are mass and efficient mass of the electron, respectively.

The Φ_b and N_d values were discussed in below for changing frequency via Figs. The E_F values stayed almost same and increased up to 500 kHz frequency and then decreased with increasing frequency. The E_m and W_d values generally increased by increasing frequency according to Table 1.

Table 1. Some electrical parameters of the Al/CRN/n-Si device for various frequencies

f (kHz)	N_d (10^{15} cm^{-3})	R_s (Ω)	Φ_b (eV)	E_F (eV)	E_m (×10^4 V/cm)	W_d (×10^{-4} cm)	N_{ss} (10^{10} eV^{-1} cm^{-2})
10	1.051	364.58	0.684	0.196	1.23	0.79	7.61
50	1.088	357.63	0.812	0.195	1.41	0.87	6.01
100	1.108	348.92	0.884	0.195	1.51	0.91	6.34
200	1.111	326.03	0.959	0.195	1.59	0.96	7.02
300	1.112	307.33	1.087	0.195	1.73	1.04	7.19
400	1.045	288.13	1.000	0.196	1.58	1.01	8.23
500	9.893	283.12	0.918	0.198	1.46	0.99	9.44
600	1.420	276.77	1.442	0.189	2.32	1.09	11.58
700	1.349	270.16	1.358	0.190	2.18	1.07	12.60

800	1.313	265.39	1.332	0.191	2.13	1.08	13.32
900	1.297	262.12	1.319	0.191	2.10	1.08	14.04
1000	1.296	264.89	1.363	0.191	2.14	1.10	13.67

Series resistance (R_s) and interface states (N_{ss}) are other important parameters to understand the electrical properties of the metal semiconductor devices. Series resistance (R_s) is obtained by Nicollian and Brews method and given via below formula at strong accumulation region (Nicollian & Brews, 2003):

$$R_s = \frac{G_{ma}}{G_{ma}^2 + (\omega C_{ma})^2} \qquad (4)$$

To explain the interaction between the frequency and N_{ss}, Hill-Coleman method is used. The N_{ss} is addressed by below equation depending on measured capacitance (C_m) and conductance (G_m) (Hill & Coleman, 1980):

$$N_{ss} = \frac{2}{qA} \frac{(G_m/\omega)_{max}}{((G_m/\omega)_{\max}/C_{0x})^2 + (1 - C_m/C_{0x})^2} \qquad (5)$$

where □ and A□ are angular frequency and contact area, respectively. The C_{0x} represent the interface capacitance and given for strong accumulation region by below equation:

$$C_{0x} = C_{ma}\left[1 + \frac{G_{ma}^2}{(\omega C_{ma})^2}\right] \qquad (6)$$

The N_{ss} and R_s values were calculated and tabulated at Table 1 for various frequencies. While the Fig. 6a shows frequency dependent profile of the Φ_b and N_d values, Fig. 6b exhibits changing of the N_{ss} and R_s values with changing frequency. The Φ_b and N_d values have almost same profile for changing frequency, but the N_{ss} and R_s values have almost reverse profile. While the effect of N_{ss} is more important at lower frequencies, R_s values are more effective at higher frequencies (Bilkan, Altındal, & Azizian-Kalandaragh, 2017). The R_s values also decreased with increasing frequency due to reordering of the interface states under applied bias voltages (Zeyrek, Acaroğlu, Altındal, Birdoğan, & Bülbül, 2013).

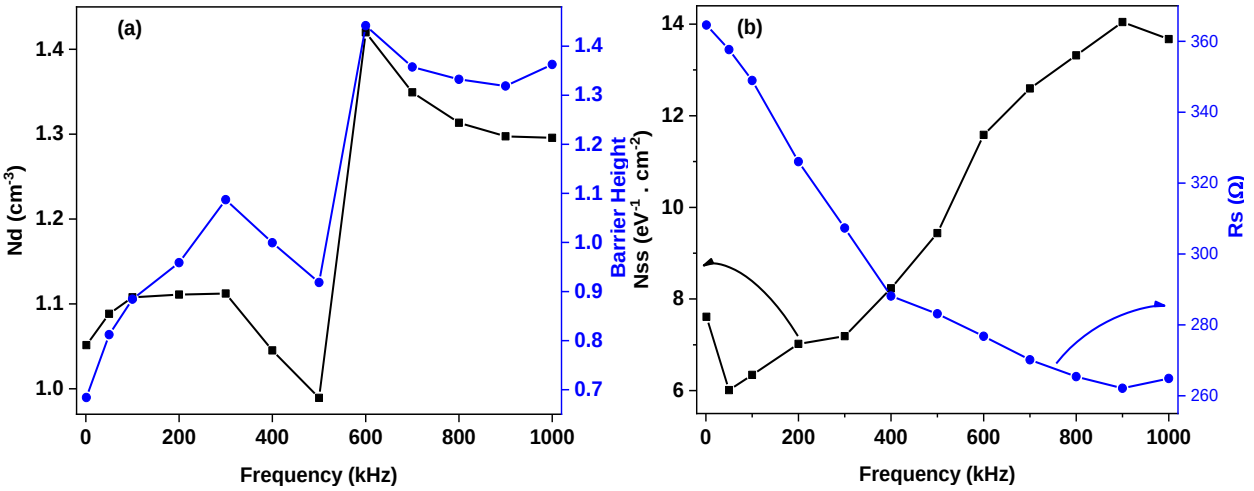

Figure 6. a) The N_d and Φ_b b) N_{ss} and R_s versus frequency plots of the Al/CRN/n-Si device

Capacitance and conductance transient measurements of the Al/CRN/n-Si device for various frequencies have been indicated in Fig. 7a and 7b, respectively to understand the photocapacitance behavior of the device. The device has photocapacitance property with increasing linearly by illumination intensities. However, the conductance behavior of the device is not linearly changed by increasing illuminations.

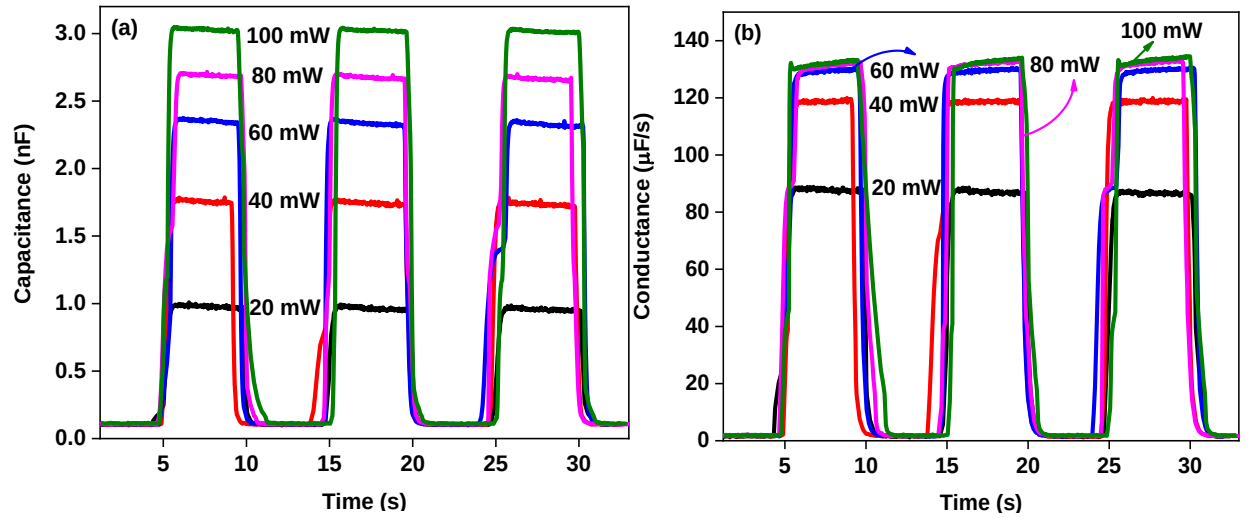

Figure 7. a) Capacitance and b) conductance transient profile of the Al/CRN/n-Si device for various illumination intensities

CONCLUSION

We fabricated the Al/CRN/n-Si device by PVD technique and characterized its electrical properties by the C-V measurements for various frequencies at room temperature. In

addition, we studied photocapacitance behaviors of the Al/CRN/*n*-Si device by capacitance transient measurements for various illumination intensities. The device exhibit capacitance and conductance properties at inversion region depending on the series resistance and interface states. While the capacitance values decreased with increasing frequency, the conductance values increased. The resistance values of the device are effective at lower frequency. The C^{-2}-V plots provide to calculate various electrical parameters such as doping concentration of the donor atoms (N_d), Fermi energy level (E_F), width of the depletion region (W_d), maximum electric field (E_m) and barrier heights (Φ_b) and discussed in details depending on the frequency changes. The electrical parameters as well as capacitance, conductance and resistance values affected from the frequency changes. Furthermore, the device has linearly photocapacitance behavior and can be employed for capacitor and optoelectronic applications.

REFERENCES

Al Orainy, R. H., & Hendi, A. A. (2014). Fabrication and electrical characterization of CdO/p-Si photosensors. *Microelectronic Engineering*, *127*, 14–20. https://doi.org/10.1016/j.mee.2014.02.014

Baraz, N., Yücedağ, İ., Azizian-Kalandaragh, Y., & Altındal, Ş. (n.d.). Determining electrical and dielectric parameters of dependence as function of frequencies in Al/ZnS-PVA/p-Si (MPS) structures. *Journal of Materials Science: Materials in Electronics*, *28*(2). https://doi.org/10.1007/s10854-016-5662-3

Barış, B., Karadeniz, S., & Erdal, M. O. (2017). Preparation of coronene nanowires and its properties. *Materials Letters*, *205*, 70–74. https://doi.org/10.1016/j.matlet.2017.05.137

Bilgili, A. K., Güzel, T., & Özer, M. (2019). Current-voltage characteristics of Ag/TiO2/n-InP/Au Schottky barrier diodes. *Journal of Applied Physics*, *125*(3), 035704. https://doi.org/10.1063/1.5064637

Bilkan, Ç., Altındal, Ş., & Azizian-Kalandaragh, Y. (2017). Investigation of frequency and voltage dependence surface states and series resistance profiles using admittance measurements in Al/p-Si with Co3O4-PVA interlayer structures. *Physica B: Condensed Matter*, *515*, 28–33. https://doi.org/10.1016/J.PHYSB.2017.04.002

Chandrakala, H. N., Ramaraj, B., Shivakumaraiah, Madhu, G. M., & Siddaramaiah. (2012). The influence of zinc oxide-cerium oxide nanoparticles on the structural characteristics and electrical properties of polyvinyl alcohol films. *Journal of Materials Science*, *47*(23), 8076–8084. https://doi.org/10.1007/s10853-012-6701-y

Doğan, H., Yildirim, N., Orak, I., Elagöz, S., & Turut, A. (2015). Capacitance-conductance-frequency characteristics of Au/Ni/n-GaN/undoped GaN Structures. *Physica B: Condensed Matter*, *457*, 48–53. https://doi.org/10.1016/j.physb.2014.09.033

Gökçen, M., Altuntaş, H., Altındal, Ş., & Özçelik, S. (2012). Frequency and voltage dependence of negative capacitance in Au/SiO2/n-GaAs structures. *Materials Science in Semiconductor Processing*, *15*(1), 41–46. https://doi.org/10.1016/j.mssp.2011.08.001

Hill, W. A., & Coleman, C. C. (1980). A single-frequency approximation for interface-state density determination. *Solid-State Electronics*, *23*(9), 987–993. https://doi.org/10.1016/0038-1101(80)90064-7

Jiang, X., Wang, Z., Han, W., Liu, Q., Lu, S., Wen, Y., … Cao, G. (2017). High performance silicon–organic hybrid solar cells via improving conductivity of PEDOT:PSS with reduced graphene oxide. *Applied Surface Science*, *407*, 398–404. https://doi.org/10.1016/j.apsusc.2017.02.193

Kocyigit, A., Orak, I., Çaldıran, Z., & Turut, A. (2017). Current–voltage characteristics of Au/ZnO/n-Si device in a wide range temperature. *Journal of Materials Science: Materials in Electronics*. https://doi.org/10.1007/s10854-017-7646-3

Kocyigit, Adem, Yılmaz, M., Aydoğan, Ş., & İncekara, Ü. (2019). The effect of measurements and layer coating homogeneity of AB on the Al/AB/p-Si devices. *Journal of Alloys and Compounds*, *790*, 388–396. https://doi.org/10.1016/J.JALLCOM.2019.03.179

Korucu, D., Turut, A., Turan, R., & Altindal, Ş. (2013). Origin of forward bias capacitance peak and intersection behavior of C and G/w of Ag/p-InP Schottky barrier diodes. *Materials Science in Semiconductor Processing*, *16*(2), 344–351. https://doi.org/10.1016/j.mssp.2012.09.015

Nicollian, E. H., & Brews, J. R. (2003). *MOS (metal oxide semiconductor) physics and technology*. Wiley-Interscience.

Orak, I., Kocyigit, A., & Alindal, S. (2017). Electrical and dielectric characterization of Au/ZnO/n-Si device depending frequency and voltage. *Chinese Physics B*, *26*(2), 028102-028102–028107. https://doi.org/10.1088/1674-1056/26/2/028102

Pakma, O., Çavdar, Ş., Koralay, H., Tuğluoğlu, N., & Faruk Yüksel, Ö. (2017). Improvement of diode parameters in Al/n-Si Schottky diodes with Coronene interlayer using variation of the illumination intensity. *Physica B: Condensed Matter*, *527*, 1–6. https://doi.org/10.1016/J.PHYSB.2017.09.101

Petrushenko, I. K., & Petrushenko, K. B. (2019). Optical properties of bilayer quantum dot models based on coronene and its BN analogues with a BODIPY dye: Theoretical TD-CAM-B3LYP-D3 investigation. *Spectrochimica Acta - Part A: Molecular and Biomolecular Spectroscopy*, *206*, 498–505. https://doi.org/10.1016/j.saa.2018.08.033

R. H., A. O. (2014). Electrical characterization of a Schottky diode based on organic semiconductor film. *Journal of Optoelectronics and Advanced Materials*, *16*(7–8), 793–797. Retrieved from http://apps.webofknowledge.com/full_record.do?product=WOS&search_mode=GeneralSearch&qid=1&SID=E5YCEgA2NPDBaCXk2pV&page=1&doc=2

Şafak-Asar, Y., Asar, T., Altındal, Ş., & Özçelik, S. (2015). Investigation of dielectric relaxation and ac electrical conductivity using impedance spectroscopy method in (AuZn)/TiO2/p-GaAs(110) schottky barrier diodes. *Journal of Alloys and Compounds*, *628*, 442–449. https://doi.org/10.1016/j.jallcom.2014.12.170

Sze, S. M. (1981). *Physics of Semiconductor Devices* (2. edition). Newyork: Wiley.

Xiao, J., Yang, H., Yin, Z., Guo, J., Boey, F., Zhang, H., & Zhang, Q. (2011). Preparation, characterization, and photoswitching/light-emitting behaviors of coronene nanowires. *J.*

Mater. Chem., *21*(5), 1423–1427. https://doi.org/10.1039/C0JM02350G
Yildiz, D. E., Altindal, Ş., & Kanbur, H. (2008). Gaussian distribution of inhomogeneous barrier height in Al/ SiO2/p-Si Schottky diodes. *Journal of Applied Physics*, *103*(12), 124502. https://doi.org/10.1063/1.2936963
Zeyrek, S., Acaroğlu, E., Altındal, Ş., Birdoğan, S., & Bülbül, M. M. (2013). The effect of series resistance and interface states on the frequency dependent C–V and G/w–V characteristics of Al/perylene/p-Si MPS type Schottky barrier diodes. *Current Applied Physics*, *13*(7), 1225–1230. https://doi.org/10.1016/j.cap.2013.03.014
Zhang, R., Zheng, H., & Shen, J. (1999). Blue light-emitting diodes based on coronene-doped polymers. *Synthetic Metals*, *105*(1), 49–53. https://doi.org/10.1016/S0379-6779(99)00056-9.

TEMPERATURE DEPENDENT DIELECTRIC CHARACTERISTICS OF THE AL/CU:TIO_2/*N*-SI DEVICE

Adem KOCYIGIT
Igdir University, Engineering Faculty, Department of Electrical Electronic Engineering, 76000 Igdir, Turkey
adem.kocyigt@igdir.edu.tr

Murat YILDIRM
Selcuk University, Faculty of Science, Department of Biotechnology, 42130 Konya, Turkey
muratyildirim@selcuk.edu.tr

ABSTRACT: In this study, Cu doped (10%) TiO_2 thin film was deposited on the *n*-Si by spin coating technique to use the film as interfacial layer for metal semiconductor heterojunction. Thus, Al/Cu:TiO_2/*n*-Si device was fabricated and its dielectric properties was investigated by impedance spectroscopy technique for wide range temperature from 80 K to 400 K by 40 K intervals and ±5 voltages. Temperature dependent dielectric constant (ε'), dielectric loss (ε''), loss tangent (tan δ), the real and imaginary parts of electric modulus ($M'$and M'') and ac electrical conductivity (σ) were extracted from the *C-V* measurements and discussed in the details for a wide range temperatures. The results highlighted that all dielectric parameters was not so changed from the measurement temperatures, and the device can be employed for a wide range temperatures.

Keywords: Dielectric properties, Al/Cu:TiO_2/*n*-Si heterojunction, Cu doped TiO_2 thin film

INTRODUCTION

Schottky devices or heterojunctions are obtained with contacting of the metal and semiconductor (Bilgili, Güzel, & Özer, 2019; Dahlan et al., 2015; Zeyrek, Acaroğlu, Altındal, Birdoğan, & Bülbül, 2013). The rectifiers, diodes and inverters are some of the technological applications of the Schottky devices (Cifci, Bakir, Meyer, & Kocyigit, 2018; Koo et al., 2017). To control the electrical properties or current transport mechanism of these devices an oxide or insulator layers are deposited between the semiconductor and metal (Kumar, Mondal, Kumar, & Koteswara Rao, 2015; Tataroğlu, Yücedağ, & Altindal, 2008). This insulator or oxide interfacial layer provide to increase of the dielectric

properties of these devices (Ahmet Kaya, Altındal, Asar, & Sönmez, 2013). For that reason, the Schottky devices can be investigated by the dielectric characterization to understand the polarization and conduction mechanism of the Schottky devices according to ionic, electronic, surface and dipolar polarization (Orak, Kocyigit, & Alindal, 2017). The surface and dipolar polarization are shown up lower frequencies below 1 MHz (Ahmet Kaya et al., 2013). As an oxide layer, TiO_2 has high electrochemical activity, wide band gap and low cost can used as interfacial layer Schottky devices due to its good properties (Rawat et al., 2016). The temperature dependent electrical characterization of the Schottky devices is really important to determine the device stability for various temperatures (Kocyigit, Orak, & Turut, 2018). The device properties should be investigated depending on temperature for that reason.

We deposited Cu doped TiO_2 thin film as interfacial layer for Schottky device and fabricated Al/Cu:TiO_2/*n*-Si device. The impedance spectroscopy was operated to obtain dielectric properties of the Al/Cu:TiO_2/*n*-Si device for wide range temperature and voltages. The dielectric constant, dielectric loss, loss tangent, real and imaginary parts of the electric modulus and ac electric conductivity was determined and discussed in the details as a function of the temperature and voltage.

METHODS

Titanium (IV) isopropoxide was used as host material for Cu doped TiO_2 thin film. It was solved in mixed of 1 mL acetylacetone and 35 mL alcohol solvents as precursor solution. The copper (II) nitrate was employed as Cu source and dissolved in 10 mL alcohol in a different vessel to achieve 10% Cu doping. The solutions were stirred 30 minutes and mixed in a vessel and stirred again 30 minutes. For stabilization, 2 mL glacial acetic acid (CH_3CO_2H, Sigma-Aldrich), 2 mL deionized water and 20 mL alcohol was dropped in the mixed solution and stirred 5 hours. Meanwhile, the *n*-type Si wafer was cut and cleaned in acetone and propanol by ultrasonic cleaner and immersed in HF:H_2O (1:1) solution to remove oxide layer and impurities for 30 seconds. Al layer was vaporized the back surface of the wafer pieces and annealed in N_2 atmosphere for 5 minutes at 450 °C. The obtained solution was deposited on front surface of the Si wafer pieces by spin coater at 3000 rpm as three layers. An Al layer were evaporated on Cu doped TiO_2 thin film surface as 100 nm thicknesses by thermal evaporator as rectifying contact via hole array mask. The impedance spectroscopy technique was employed by a computer Keithley 4200 SCS instrument in a temperature controlled cryostat from 80 K to 400 K by 40 K intervals at 500 kHz frequency.

RESULTS AND DISCUSSION

To understand the polarization and conduction mechanism of the Al/Cu:TiO_2/*n*-Si device, we extracted the real dielectric constant (ε'), imaginary dielectric constant (ε'')

and ac electric conductivity (σ) from the *C-V* measurements for wide range temperature from 80 K to 400 K and voltage range of ±5 voltages. While the imaginary dielectric constant reveals absorbed energy because of the frictional dampening, the real dielectric constant exhibits strength of the dipole against to applied electric field and stored energy (Karataş, 2008). The real and imaginary dielectric constants are obtained as parts of complex dielectric constant or complex permittivity.

The Equation (1) shows complex permittivity formula depending on the real and imaginary dielectric constants (Shiwakoti, Bobby, Antony, & Asokan, 2016):

$$\varepsilon *= \varepsilon' - j\varepsilon'' = \frac{C}{C_0} - j\frac{G}{\omega C_0} \quad \textbf{(1)}$$

where the C_0 and j are capacitance of free capacitor and imaginary root, respectively. The C and G represent the measured capacitance and conductance. We can type the formula of the ε' and ε'' by the following equations (Demirezen, 2013):

$$\varepsilon' = \frac{C}{C_0} = \frac{Cd_i}{\varepsilon_0 A} \quad \textbf{(2)}$$

$$\varepsilon'' = \frac{G}{\omega C_0} = \frac{Gd_i}{\varepsilon_0 \omega A} \quad \textbf{(3)}$$

where ε_0 is permittivity of the vacuum, the d_i is thickness of the interfacial layer, and A shows contact area At enough high forward biases for the maximum capacitance value is called to interlayer capacitance and given by $C_{ac} = C_i = \varepsilon'\varepsilon_0 A/d_i$ formula. The ratio of the real and imaginary dielectric constant is named as loss tangent (tan δ) and addressed by next equations:

$$\tan\delta = \frac{\varepsilon'}{\varepsilon''} = \frac{G}{\omega C} \quad \textbf{(4)}$$

The temperature dependent dielectric constant profile of the Al/Cu:TiO_2/n-Si device has been shown in Fig. 1 for the voltage range of the -5 V and +5 V. The ε' values increased up to around 1.7 and exhibited peaks at inversion region. The peak intensities at the ε' values decreased towards to inversion region with increasing temperature depending on the interface states (Yahia, Fadel, Sakr, Shenouda, & Yakuphanoglu, 2012). The presence of the peaks can be attributed to surface polarization and particular density distribution of N_{ss} or series resistance effect (R_s) (Kocyigit et al., 2018). Furthermore, the ε' values stayed almost 0.9 – 1.1 at depletion and accumulation regions for various temperatures. The dispersion of the ε' values with changing temperature can be attributed to that Maxwell–Wagner type interfacial polarization (Yang, Chao, Liang, Wei, & Yang, 2015). In fact, the charge carriers accumulated at boundaries and caused to increase interfacial and surface charge polarization (Kyritsis, Pissis, & Grammatikakis, 1995).

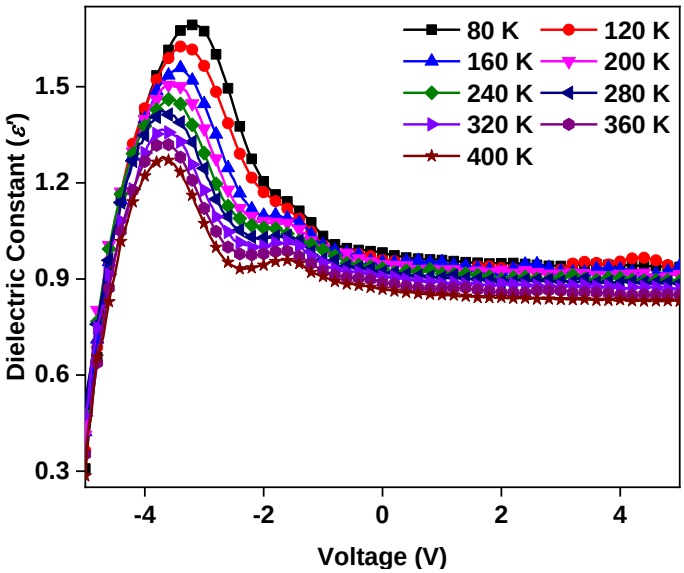

Figure 1. The dielectric constant versus voltage plot of the Al/Cu:TiO_2/*n*-Si device for various temperature

Fig. 2 displays temperature dependent ε'' profile of the Al/Cu:TiO_2/*n*-Si device for inversion, depletion and accumulation regions or -5 and +5 voltage ranges. The ε'' values decreased linearly from 22.0 to 0 in the inversion regions and then stayed constant at depletion and accumulation regions. The temperature changes almost did not affect the ε'' values for the given temperature range. This results confirmed that the Al/Cu:TiO_2/*n*-Si device is stable for temperature changes and can be used for a wide range temperature without losing energy (Karataş & Kara, 2011).

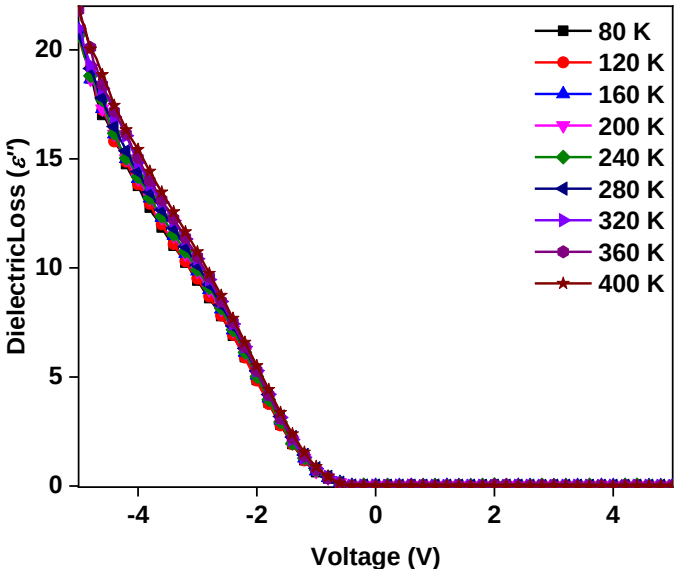

Figure 2. The dielectric loss versus voltage plot of the Al/Cu:TiO_2/*n*-Si device for various temperature

The tan δ versus voltage plots of the Al/Cu:TiO_2/n-Si device have been shown in Fig. 3 for various temperature. The tan δ values decreased exponentially from 87.0 to 0 by the changing biases from inversion to depletion regions. The temperature changes slightly affected the tan δ values at inversion region, and the tan δ values exhibited peaks at with increasing temperature (inset of Fig. 3). The changes at the tan δ values can be attributed to decreasing series resistance and polarizations (Demirezen, 2013; Ahmet Kaya et al., 2013).

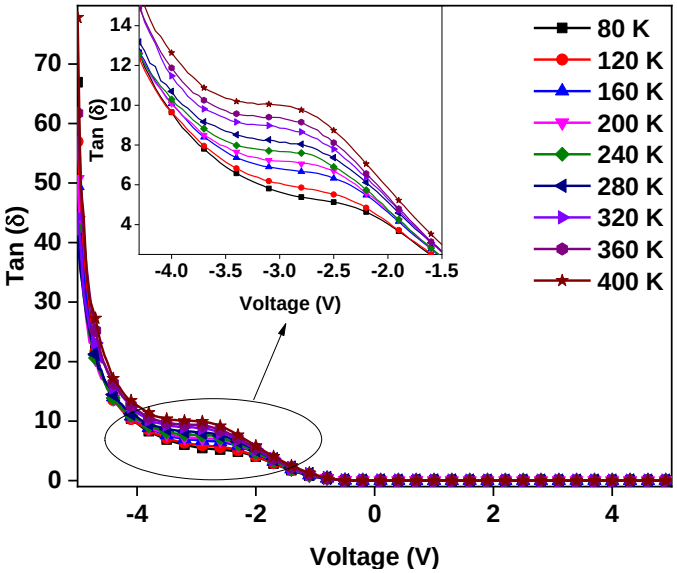

Figure 3. The tangent loss versus voltage plot of the Al/Cu:TiO_2/n-Si device for various temperature

The inverse of the complex permittivity gives the complex electric modulus depending on the relation of the $\varepsilon^*=1/M^*$. The Complex electric modulus is addressed by the following equation depending on the $\varepsilon'$and ε'' values as below (Demirezen, 2013):

$$M^* = \frac{1}{\varepsilon^*} = \frac{\varepsilon'}{\varepsilon'^2 + \varepsilon''^2} + j\frac{\varepsilon''}{\varepsilon'^2 + \varepsilon''^2} = M' + jM'' \quad \textbf{(5)}$$

The temperature dependent real electric modulus (M') profile of the Al/Cu:TiO_2/n-Si device has been given in Fig. 4 for the wide range voltages from -5 V to +5 V. The M' values remained almost 0 up to -2 V voltages or strong inversion region and then suddenly increased to around 1.0 value and then stayed constant towards to accumulation region. When the M' values did not change at the inversion with changing temperature, they slightly increased at the depletion and accumulation regions for various temperatures.

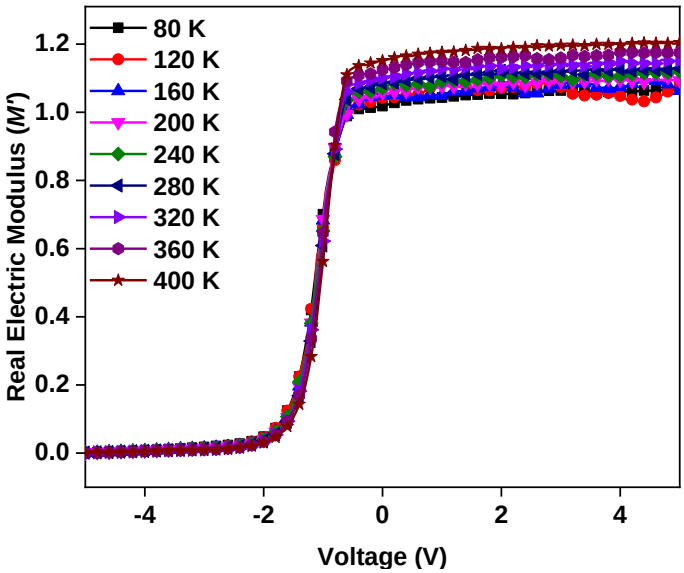

Figure 4. The real electric modulus versus voltage plot of Al/Cu:TiO_2/*n*-Si device for various temperature

Fig. 5 displays M''-V plots of the Al/Cu:TiO_2/*n*-Si device for various temperature. The M'' values increased exponentially from -5 V to -1.7 V and showed peaks at low inversion region. The The M'' values stayed constant at depletion and accumulation regions at zero. The exhibiting peaks at the M'' values can be attributed to that particular distribution of the charges at surface states or relaxation time (A. Kaya et al., 2016).

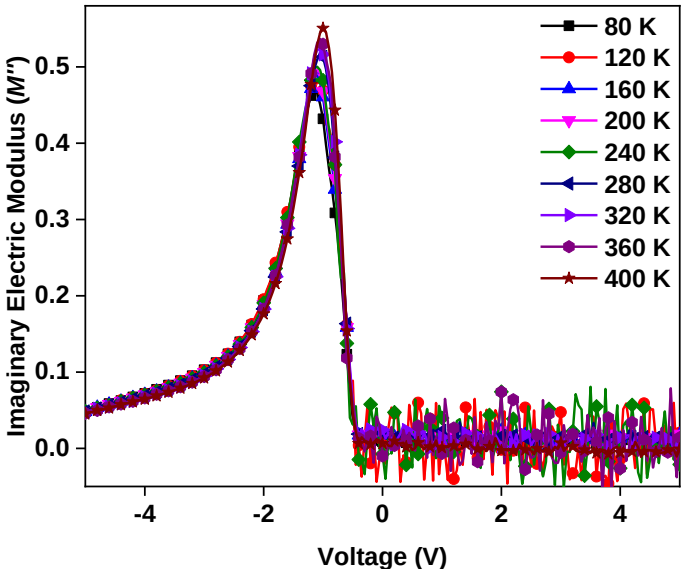

Figure 5. The imaginary part of electric modulus versus voltage plot of the Al/Cu:TiO_2/*n*-Si device for various temperature

The σ is given by next equation depending on the imaginary parts of the dielectric constant, ε_0 and ω:

$$\sigma = \left(\frac{d}{A}\right)\omega C \tan\delta = \varepsilon''\omega\varepsilon_0 \quad (6)$$

Fig. 6 indicates the σ-V graph of the Al/Cu:TiO_2/n-Si device for various temperatures. The σ values decreased almost linearly from inversion to depletion region and stayed at zero at depletion and accumulation regions. They slightly increased with increasing temperature at the inversion region (inset of the Fig. 6). The slightly increase at σ values by the increasing temperature in depletion region can be depended on the increasing eddy current (Nezhadesm-Kohardafchahi et al., 2018).

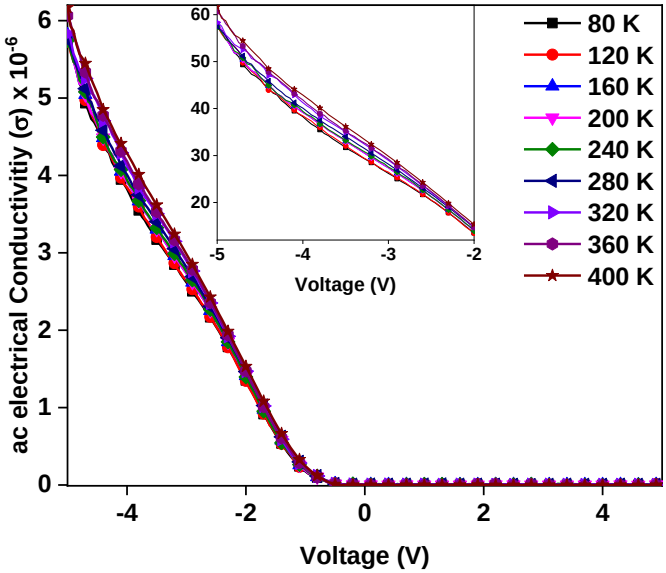

Figure 6. The ac electric conductivity versus voltage plot of the Al/Cu:TiO_2/n-Si device for various temperature

CONCLUSION

The TiO_2 thin film with the Cu dopant were deposited on the Si wafer to fabricate Al/Cu:TiO_2/n-Si device by spin coating technique. The dielectric properties of the Al/Cu:TiO_2/n-Si device was studied by impedance spectroscopy technique in the temperature range of 80 K and 400 K by 40 K steps at 500 kHz frequency. The C-V and G-V data were employed to extract the dielectric parameters of the Al/Cu:TiO_2/n-Si device. The ε'' values did not affect from the temperature changes, but the ε' and tan δ values increased at inversion region by changing temperature. However, the voltage changes at the depletion and accumulation regions did not change the ε', ε'' and tan δ values. The M'' values exhibited peaks at inversion region and the peaks intensities slightly increased by the increasing temperature and shifted towards to depletion region. The σ values decreased from inversion to depletion region down to zero and stayed constant at the depletion and accumulation regions. The results revealed that the Al/Cu:TiO_2/n-Si device can be employed in the wide range temperatures for switching applications.

REFERENCES

Bilgili, A. K., Güzel, T., & Özer, M. (2019). Current-voltage characteristics of Ag/TiO2/n-InP/Au Schottky barrier diodes. *Journal of Applied Physics*, *125*(3), 035704. https://doi.org/10.1063/1.5064637

Cifci, O. S., Bakir, M., Meyer, J. L., & Kocyigit, A. (2018). Morphological and electrical properties of ATSP/p-Si photodiode. *Materials Science in Semiconductor Processing*, *74*, 175–182. https://doi.org/10.1016/J.MSSP.2017.10.039

Dahlan, A. S., Tataroğlu, A., Al-Ghamdi, A. A., Al-Ghamdi, A. A., Bin-Omran, S., Al-Turki, Y., … Yakuphanoglu, F. (2015). Photodiode and photocapacitor properties of Au/CdTe/p-Si/Al device. *Journal of Alloys and Compounds*, *646*, 1151–1156. https://doi.org/10.1016/j.jallcom.2015.06.068

Demirezen, S. (2013). Frequency- and voltage-dependent dielectric properties and electrical conductivity of Au/PVA (Bi-doped)/n-Si Schottky barrier diodes at room temperature. *Applied Physics A*, *112*(4), 827–833. https://doi.org/10.1007/s00339-013-7605-7

Karataş, Ş. (2008). Studies on electrical and the dielectric properties in MS structures. *Journal of Non-Crystalline Solids*, *354*(30), 3606–3611. https://doi.org/10.1016/J.JNONCRYSOL.2008.03.028

Karataş, Ş., & Kara, Z. (2011). Temperature dependent electrical and dielectric properties of Sn/p-Si metal–semiconductor (MS) structures. *Microelectronics Reliability*, *51*(12), 2205–2209. https://doi.org/10.1016/J.MICROREL.2011.03.041

Kaya, A., Alialy, S., Demirezen, S., Balbaşı, M., Yerişkin, S. A., & Aytimur, A. (2016). The investigation of dielectric properties and ac conductivity of Au/GO-doped PrBaCoO nanoceramic/n-Si capacitors using impedance spectroscopy method. *Ceramics International*, *42*(2), 3322–3329. https://doi.org/10.1016/j.ceramint.2015.10.126

Kaya, Ahmet, Altındal, Ş., Asar, Y. Ş., & Sönmez, Z. (2013). On the Voltage and Frequency Distribution of Dielectric Properties and ac Electrical Conductivity in Al/SiO 2 /p-Si (MOS) Capacitors. *Chinese Physics Letters*, *30*(1), 017301. https://doi.org/10.1088/0256-307X/30/1/017301

Kocyigit, A., Orak, İ., & Turut, A. (2018). Temperature dependent dielectric properties of Au/ZnO/ *n* -Si heterojuntion. *Materials Research Express*. https://doi.org/10.1088/2053-1591/aab2e3

Koo, J. H., Jeong, S., Shim, H. J., Son, D., Kim, J., Kim, D. C., … Kim, D.-H. (2017). Wearable Electrocardiogram Monitor Using Carbon Nanotube Electronics and Color-Tunable Organic Light-Emitting Diodes. *ACS Nano*, *11*(10), 10032–10041. https://doi.org/10.1021/acsnano.7b04292

Kumar, A., Mondal, S., Kumar, S. G., & Koteswara Rao, K. S. R. (2015). High performance sol–gel spin-coated titanium dioxide dielectric based MOS structures. *Materials Science in Semiconductor Processing*, *40*, 77–83. https://doi.org/10.1016/j.mssp.2015.06.073

Kyritsis, A., Pissis, P., & Grammatikakis, J. (1995). Dielectric relaxation spectroscopy in poly(hydroxyethyl acrylates)/water hydrogels. *Journal of Polymer Science Part B: Polymer*

Physics, *33*(12), 1737–1750. https://doi.org/10.1002/polb.1995.090331205
Nezhadesm-Kohardafchahi, S., Farjami-Shayesteh, S., Badali, Y., Altındal, Jamshidi-Ghozlu, M. A., & Azizian-Kalandaragh, Y. (2018). Formation of ZnO nanopowders by the simple ultrasound-assisted method: Exploring the dielectric and electric properties of the Au/(ZnO-PVA)/n-Si structure. *Materials Science in Semiconductor Processing*, *86*, 173–180. https://doi.org/10.1016/j.mssp.2018.06.030
Orak, I., Kocyigit, A., & Alindal, S. (2017). Electrical and dielectric characterization of Au/ZnO/n-Si device depending frequency and voltage. *Chinese Physics B*, *26*(2), 028102-028102–028107. https://doi.org/10.1088/1674-1056/26/2/028102
Rawat, G., Somvanshi, D., Kumar, H., Kumar, Y., Kumar, C., & Jit, S. (2016). Ultraviolet Detection Properties of p-Si/n-TiO2 Heterojunction Photodiodes Grown by Electron-Beam Evaporation and Sol–Gel Methods: A Comparative Study. *IEEE Transactions on Nanotechnology*, *15*(2), 193–200. https://doi.org/10.1109/TNANO.2015.2512565
Shiwakoti, N., Bobby, A., Antony, B., & Asokan, K. (2016). Interface state density and dielectric properties of Au/n-GaP Schottky diode. *Journal of Vacuum Science & Technology B, Nanotechnology and Microelectronics: Materials, Processing, Measurement, and Phenomena*, *34*(5), 051206. https://doi.org/10.1116/1.4961907
Tataroğlu, A., Yücedağ, İ., & Altindal, Ş. (2008). Dielectric properties and ac electrical conductivity studies of MIS type Schottky diodes at high temperatures. *Microelectronic Engineering*, *85*(7), 1518–1523. https://doi.org/10.1016/j.mee.2008.02.005
Yahia, I. S., Fadel, M., Sakr, G. B., Shenouda, S. S., & Yakuphanoglu, F. (2012). Effect of the frequency and temperature on the complex impedance spectroscopy (C–V and G–V) of p-ZnGa2Se4/n-Si nanostructure heterojunction diode. *Journal of Materials Science*, *47*(4), 1719–1728. https://doi.org/10.1007/s10853-011-5951-4
Yang, L., Chao, X., Liang, P., Wei, L., & Yang, Z. (2015). Electrical properties and high-temperature dielectric relaxation behaviors of NaxBi(2−x)/3Cu3Ti4O12 ceramics. *Materials Research Bulletin*, *64*, 216–222. https://doi.org/10.1016/j.materresbull.2014.12.060
Zeyrek, S., Acaroğlu, E., Altındal, Ş., Birdoğan, S., & Bülbül, M. M. (2013). The effect of series resistance and interface states on the frequency dependent C–V and G/w–V characteristics of Al/perylene/p-Si MPS type Schottky barrier diodes. *Current Applied Physics*, *13*(7), 1225–1230. https://doi.org/10.1016/j.cap.2013.03.014.

PRODUCTION OF COBALT-NICKEL ALLOY THIN FILMS BY ORGANIC COUMARIN INVESTIGATION OF THE STRUCTURAL AND THE MAGNETIC PROPERTIES

Rasim ÖZDEMİR
Kilis 7 Aralık University, Department of Electricity and Energy
rsmozdemir@gmail.com

ABSTRACT: Cobalt-nickel (CoNi) alloy thin films were successfully produced by the electrodeposition method, using organic coumarin ($C_9H_6O_2$) additive. Cobalt sulphate, nickel sulphate, nickel chloride, boric acid contents in bath composition were taken constant. The parameters affecting the production such as current, voltage, ambient temperature, pH, were kept constant. The organic coumarin was varied from 0.07 Mol.Lt^{-1} to 0.022 Mol.Lt^{-1}. The structural and magnetic properties of the produced thin films were examined. For this purpose; The chemical properties (Cyclic Voltammetry, CV), morphological properties (Scanning Electron Microscope, SEM), crystal structures (X-Ray Diffractometer, XRD), the amount of substance content (Inductive Coupled Plasma, ICP) and magnetic properties (Vibrating Sample Magnetometer, VSM) of the film were investigated. It was seen that, in the production of the CoNi alloy, the coumarin has a significant effect on the amount of substance deposited in the film and on the crystal structure properties. As the amount of coumarin was increased, the cobalt content in the thin film decreased and the nickel content increased. When the amount of coumarin in the bath composition was increased, it was seen that the crystalline structure (Face Centered Cubic, FCC) formed in thin films convert to amorphous structure. Magnetization measurements were performed in the range of +75000 Oe and -75000 Oe and hysteresis loops were obtained. Coercivity, saturation magnetization and permanent magnetism values were found from the hysteresis loops. When the amount of coumarin in the bath composition increased, the coercivity value (147-228 Oe) increased but the saturation magnetization (79-15 emu/g) and permanent magnetization (31-1.4 emu/g) value decreased. It was seen that coumarin exchange had a great effect on the magnetic properties and crystal structure of the CoNi thin film.

Key words: electrodeposition, coumarin, additive, cobalt-nickel, magnetization.

KOBALT-NİKEL ALAŞIM İNCE FİLMLERİN ORGANİK KUMARİNLE ÜRETİMİ YAPISAL VE MANYETİK ÖZELLİKLERİNİN İNCELENMESİ

ÖZET: Kobalt-nikel (CoNi) alaşım ince filmler elektrodepolama yöntemiyle organik kumarin ($C_9H_6O_2$) ek katkı maddesi kullanılarak başarıyla üretildi. Banyo kompozisyonu içerisindeki kobalt sülfat, nikel sülfat, nikel klorür, borik asit miktarı sabit alındı. Üretime etki eden akım, gerilim, ortam sıcaklığı, pH, gibi parametreler sabit tutuldu. Organik kumarin 0.07 $Mol.Lt^{-1}$ ile 0.022 $Mol.Lt^{-1}$ aralığında değiştirildi. Üretilen ince filmlerin yapısal ve manyetik özellikleri incelendi. Bu amaçla; kaplama banyosu kimyasal özellikleri (Dönüşümlü Voltametri, CV), morfolojik özellikleri (Taramalı Elektron Mikroskopu, SEM), kristal yapıları (X ışını difraktometresi, XRD), filmin içeriğindeki madde miktarı oranı (İndüktif Eşleşmiş Plazma, ICP) ve manyetik özellikleri (Titreşimli Örnek Manyetometre, VSM) araştırıldı. Kumarin maddesinin, CoNi alaşımın üretiminde, filmde depolanan madde miktarı ve kristal yapı özellikleri üzerine büyük etki ettiği görüldü. Kumarin miktarı arttıkça ince film içerisindeki kobalt madde miktarı azaldı nikel madde miktarı ise arttı. Banyo kompozisyonu içerisindeki kumarin madde miktarı arttırıldığında, ince filmlerde oluşan kristal yapının (Yüzey Merkezli Kübik, FCC) amorf yapıya dönüşmesine neden olduğu görüldü. Manyetizasyon ölçümleri, +75000 Oe ve -75000 Oe aralığında gerçekleştirildi ve histerezis eğrileri elde edildi. Histerezis eğrilerinden koersivite, doyum manyetizasyonu ve kalıcı mıknatıslık değerleri bulundu. Banyo kompozisyonu içerisindeki kumarin miktarı arttığında koersivite değeri (147-228 Oe) arttı, ancak doyum manyetizasyonu (79-15 emu/g) ve kalıcı mıknatıslık değeri (31-1.4 emu/g) azaldı. Kumarin değişiminin CoNi ince filmin manyetik özellikleri ve kristal yapısı üzerinde büyük etkiye sahip olduğu görüldü.

Anahtar sözcükler: elektrodepolama, kumarin, ek katkı, kobalt-nikel, manyetizasyon.

CONTRIBUTION OF THE INVESTIGATION OF SMALL WIND AND SOLAR ENERGY SYSTEMS TO TURKEYS ENERGY PRODUCTION

Hüseyin ÖZDEN
Ege University
Huseyin.ozden@ege.edu.tr

ABSTRACT: Almost all of the fossil-based energy source is imported and used in electrical power generation in Turkey. Increases in expected energy consumption in the near future, environmental pollution and a decrease in fossil energy reserves are increasing the importance of wind and solar energy. Today, Mega and Giga Watt wind power machines, power plants technology, its installation and maintenance is imported and costs are very high. In order to contribute to the search for alternative solutions to such problems, low power wind and solar power generation systems that are simple and economical to construct and install were investigated. In the project study, residential, farm type low energy wind turbines were designed. The expected contribution of low energy generation systems to the country's total electricity generation system is presented for discussion. In our country where the production is simple and economical, the installation of low-energy wind turbines and photovoltaic panels that can be produced easily even in a workshop will meet most of the electrical energy needs of the houses. The contribution of low-energy wind and solar generation systems to the country's total energy production should not be underestimated. It is proposed to encourage the construction of domestic energy production systems in our country. Project work; The aim of the study is to contribute to scientific studies on energy production and energy supplementation of residential and farm type low energy wind turbines and photovoltaic panels.

KEYWORDS: Energy, Renewable Energy, Wind Turbine Design, Low Power, Research

DÜŞÜK GÜÇLÜ RÜZGÂR VE GÜNEŞ ENERJİSİ SİSTEMLERİNİN TÜRKİYENİN ENERJİ ÜRETİMİNE KATKISININ ARAŞTIRILMASI

ÖZET: Fosil bazlı enerji kaynaklarının tamamına yakını Türkiyede ithal edilmektedir ve elektrik enerji üretim santrallerinde kullanılmaktadır. Yakın gelecekte beklenen enerji tüketiminde artışlar, çevre kirliliği ve fosil enerji rezervlerindeki azalma, rüzgâr ve güneş enerjilerin önemi artırıyor. Günümüzde Mega ve Giga Watt gücündeki rüzgâr enerji makinaların, santrallerin teknolojisi kurulumu ve bakımları ithal olup maliyetleri çok

yüksektir. Bu gibi sorunlara alternatif çözüm arayışlarına katkı sağlamak amacıyla, yapımı ve kurulumu basit ve ekonomik olan düşük güçlü rüzgâr ve güneş enerji üretim sistemleri araştırılmıştır. Proje çalışmasında konut, çiftlik tipi düşük enerjili rüzgâr türbinleri tasarlanmıştır. Ülkenin toplam elektrik enerji üretim sisteminde düşük enerji üretim sistemlerin beklenen katkıları tartışmağa sunulmaktadır. Yapımların basit ve ekonomik olan ülkemizde bir atölyede dahi rahatlıkla üretilebilecek düşük enerjili rüzgâr türbinlerin ve fotovoltaik panellerin konutlarda monte edilmesi ile konutların elektrik enerji ihtiyacının büyük kısmını karşılayacaktır. Düşük enerjili rüzgâr ve güneş üretim sistemlerinin ülkenin toplam enerji üretimine olan katkısı küçümsenmemelidir. Ülkemizde yerli enerji üretim sistemlerin yapımları teşvik edilmesi önerilmiştir. Proje çalışması; konut ve çiftlik tipi düşük enerjili rüzgâr türbinlerin ve fotovoltaik panellerin enerji üretimi ile enerji takviyesi konulu bilimsel çalışmalara katkı sağlaması amaçlıdır.

Anahtar Sözcükler: Enerji, Yenilenebilir Enerji, Rüzgâr Türbin Tasarımı, Düşük Güçlü, Araştırma

BUCKLING OF NANOBEAMS USING ADOMIAN DECOMPOSITION METHOD

Safa Bozkurt COŞKUN
Kocaeli University
sb.coskun@kocaeli.edu.tr

Servet MERT KUTSAL
Kocaeli University
servet.mert@ kocaeli.edu.tr

ABSTRACT: In this study, Adomian Decomposition Method (ADM) is applied to investigate the stability of nanobeams based on non-local Euler-Bernoulli beam theory. ADM is an analytical approximation technique that has been successfully applied in recent years to important problems of mathematics, physics and engineering. The method is very straightforward and the results by using ADM in the studies available in the literature has shown its efficiency. ADM solutions in this study are compared with other available results in the literature and a very good agreement is observed. Presented technique is very effective in the stability analysis of nanobeams.

Key words: nonlocal Euler-Bernoulli beam theory, Adomian decomposition method, buckling; nano beam

INTRODUCTION

The nano-sized structures such as nano-beams, nanoplates and nano-shells are commonly used as components in NEMS (nanoelectromechanical systems) devices that play a significant role in nanotechnology. These structures have thus received great attention in scientific community and the interest to the field has been accelerating due to outstanding physical and mechanical properties of nanomaterials. Both experimental and theoretical simulation studies have shown that the size effect has a major role on mechanical properties when the dimensions of structural elements become very small. Hence, nonlocal elasticity concept (Eringen, 1972) has been widely applied to take small length scale effect into account.

Peddieson *et al*. (2003) performed a pioneering work on the application of non-local elasticity theory to investigate bending, buckling and vibration of nano sized beams. Wang *et al*. (2006) considered elastic buckling analysis of micro- and nano-rods/tubes based on Eringen's nonlocal elasticity theory and the Timoshenko beam theory. Reddy (2007) reformulated various beam theories using the nonlocal differential constitutive relations of Eringen. Pradhan and Phadikar (2009) conducted structural analysis of nonhomogeneous nanotubes has been carried out using nonlocal elasticity theory. Akgöz and Civalek (2011) proposed higher-order continuum theories for the buckling analysis of single walled carbon nanotubes. Ghannadpour *et al*. (2013) studied the bending, buckling and vibration analyzes of nonlocal Euler beams. Tuna and Kırca (2016) examined the buckling and vibration characteristics of nonlocal Euler–Bernoulli beams analytically. Tuna and Kırca (2017) developed finite element formulations for static bending, linear buckling and free vibration analysis of nanobeam structures by utilizing the integral form of Eringen nonlocal model. Zhu et al. (2017) adopted Eringen's two-phase nonlocal integral model to obtain analytical solutions for the buckling problem of Euler-Bernoulli beams. Chakraverty and Behera (2017) provided theoretical information on bending, buckling and vibration of nanobeams and nanoplates. Ghannadpour (2018) investigated bending, buckling and vibration behaviors of nonlocal Timoshenko beams using a variational approach.

In this study elastic stability of nanobeams is investigated using nonlocal Euler-Bernoulli beam theory via ADM (Adomian, 1994). Nondimensional buckling load parameters are computed for the beams with various boundary conditions and the influence of scaling effect parameter is discussed.

NONLOCAL EULER BEAM THEORY FOR STABILITY

Euler-Bernoulli beam theory (EBT) is based on following displacement field Reddy (2007), Chakraverty and Behera (2017).

$$u_1 = -z\frac{\partial w}{\partial x} \qquad u_2 = 0 \qquad u_3 = w(x,t) \tag{1}$$

where (u_1, u_2, u_3) are the displacements along x-, y-, and z-coordinates, respectively, and w is the transverse displacement of the point (x, 0) on the mid-plane (z = 0) of the beam. The only non-zero strain of EBT is

$$\varepsilon_{xx} = -z\frac{\partial^2 w}{\partial x^2} \tag{2}$$

Governing equation of Euler-Bernoulli nanobeam may be written neglecting transverse force as

$$\frac{\partial^2 M}{\partial x^2} - N\frac{\partial^2 w}{\partial x^2} = m_0\frac{\partial^2 w}{\partial t^2} \tag{3}$$

where N is axial compressive force, $M = \int_A z\sigma_{xx}dA$ and $m_0 = \int_A \rho dA = \rho A$. According to Eringen's nonlocal theory (Eringen 1987), the constitutive relation for Euler–Bernoulli nanobeam is given by (Reddy 2007)

$$M - \mu\frac{\partial^2 M}{\partial x^2} = -EI\frac{\partial^2 w}{\partial x^2} \tag{4}$$

where E is Young's modulus and I is the second moment of area about y-axis. It may be noted here that $\mu = (e_0 a)^2$ is the nonlocal parameter, where e_0 and a denote material constant and internal characteristic length, respectively. Using Eqs. (3) and (4), the nonlocal form of M may be written as

$$M = -EI\frac{\partial^2 w}{\partial x^2} + \mu\left(N\frac{\partial^2 w}{\partial x^2} + m_0\frac{\partial^2 w}{\partial t^2}\right) \tag{5}$$

Governing equation in terms of displacement is rewritten as

$$-EI\frac{\partial^4 w}{\partial x^4} + \mu\frac{\partial^2}{\partial x^2}\left(N\frac{\partial^2 w}{\partial x^2} + m_0\frac{\partial^2 w}{\partial t^2}\right) - N\frac{\partial^2 w}{\partial x^2} = m_0\frac{\partial^2 w}{\partial t^2} \tag{6}$$

If we ignore the dynamic effects, Eq.(6) becomes

$$EI\frac{\partial^4 w}{\partial x^4} = \mu\frac{\partial^2}{\partial x^2}\left(N\frac{\partial^2 w}{\partial x^2}\right) - N\frac{\partial^2 w}{\partial x^2} \tag{7}$$

Constant axial compressive force lead to the following form for governing equation.

$$EI\frac{\partial^4 w}{\partial x^4} = N\frac{\partial^2}{\partial x^2}\left(\mu\frac{\partial^2 w}{\partial x^2} - w\right) \tag{8}$$

Introducing the nondimensional terms $X = x/L$, $\bar{W} = W/L$, $\bar{N} = NL^2/EI$ and $\alpha = e_0 A/L$ dimensionless governing equation is obtained as follows:

$$\frac{d^4\bar{W}}{dX^4} = \bar{N}\frac{d^2}{dX^2}\left(\alpha^2\frac{d^2\bar{W}}{dX^2} - \bar{W}\right) \tag{9}$$

where $\bar{N}$ is nondimensional buckling load parameter and α is scaling effect parameter.

ADOMIAN DECOMPOSITION METHOD (ADM)

ADM calculates an analytical approximate solution as a series summation with a rapid convergence. We consider the following differential equation for the application of the method.

$$Lu + Ru + Nu = g(x) \tag{10}$$

where *L* is the linear operator which is highest order derivative, *N* is the nonlinear operator, *R* is remainder of linear operator including derivatives of less order than *L*, *u* represents the unknown variable and *g(x)* is the source function. The solution for Eq.(10) is

$$u = f(x) - L^{-1}(Ru) - L^{-1}(Nu) \quad (11)$$

where L^{-1} is the inverse operator for the linear operator *L*. *f(x)* is the summation of integral of the source term and the terms arising from given conditions of the problem. ADM approximates the solution as the summation of an infinite series as

$$u(x) = \sum_{n=0}^{\infty} u_n(x) \quad (12)$$

The nonlinear operation *Nu* is represented by Adomian polynomials, A_i, for the specific nonlinearity.

$$Nu = \sum_{n=0}^{\infty} A_n(u_0, u_1, \ldots, u_n) \quad (13)$$

The relation for the calculation of Adomian polynomials is given as follows.

$$A_n = \frac{1}{n!}\frac{d^n}{d\lambda^n} N\left(\sum_{n=0}^{\infty} \lambda^k u_k\right),\ n > 0 \quad (14)$$

Application of the method lead to following recursive algorithm for the components of solution. $u_0(x) = f(x)$ (15)

$$u_{n+1}(x) = -L^{-1}\left[Ru_n - A_n\right],\ n \geq 0 \quad (16)$$

SOLUTION PROCEDURE

After the application of ADM to Eq.(9), following successive approximations are obtained

$$\bar{W}_0 = \bar{W}(0) + \bar{W}'(0)X + \bar{W}''(0)\frac{X^2}{2} + \bar{W}'''(0)\frac{X^3}{6} \quad (17)$$

$$\bar{W}_n = L^{-1}\left\{N\frac{d^2}{dX^2}\left(\alpha^2\frac{d^2\bar{W}_{n-1}}{dX^2} - \bar{W}_{n-1}\right)\right\},\qquad n \geq 1 \quad (18)$$

N^{th} order ADM solution to the problem is

$$\bar{W}(X) = \sum_{n=0}^{N} \bar{W}_n(X) \quad (19)$$

For the stability problems, three different beams are considered. The beam with both ends pinned (PP), the beam with both ends clamped (CC) and the beam with one end pinned and other end clamped (CP). According to type of the support at the beam's end we use the displacement function and apply it to the specific boundary conditions at both ends of the beam, hence, four equations in four unknowns are obtained. These equations can be represented in matrix form as

$$\left[M\left(\bar{N}\right)\right]\{\psi\} = \{0\} \quad (20)$$

where $\{\psi\} = \left\langle \bar{W}(0) \quad \bar{W}'(0) \quad \bar{W}''(0) \quad \bar{W}'''(0) \right\rangle^T$. For a nontrivial solution, determinant of coefficient matrix must be zero. Determinant of coefficient matrix yields a characteristic equation in terms of nondimensional buckling load parameter $\bar{N}$. Positive real roots of this equation are the nondimensional buckling loads for the case considered.

NUMERICAL RESULTS

Below nondimesional buckling loads for PP, CP and CC nanobeams are compared with the available results in literature (Wang *et al*., 2006; Pradhan and Padikar, 2009; Ghannadpour *et al*., 2013; Tuna and Kırca, 2016; Tuna and

Kırca, 2017; Zhu *et al*., 2017) for $\alpha = 0.05$ and $\alpha = 0.2$. Numerical work revealed that tenth order solution is adequate for computing the critical buckling load for PP beam when $\alpha = 0.05$, while the required number of terms are doubled for the same beam when $\alpha = 1$. For CC and CP beams required order of solutions is triple the order of solution for PP beam. Buckling load parameters decreases with the increasing scale parameter. Table 1, Table 2 and Table 3 summarize the comparisons for PP, CP and CC nanobeams respectively. For all the cases $L/d = 10$ is assumed.

Table 1. Nondimensional buckling load parameter $\bar{N}$ for PP beam with various scaling effects α

α	ADM	Wang *et al*. (2006)	Pradhan and Padikar (2009)	Ghannadpour *et al*. (2013)	Tuna and Kırca (2016)	Tuna and Kırca (2017)	Zhu *et al*. (2017)
0.05	9.63195	9.6319	-	-	9.6319	9.6319	9.6261
0.2	7.07608	7.0760	-	7.0760	7.0761	7.0776	-
1	0.90780	-	0.9080	0.9080	-	-	-

Table 2. Nondimensional buckling load parameter $\bar{N}$ for CC beam with various scaling effects α

α	ADM	Wang *et al*. (2006)	Pradhan and Padikar (2009)	Ghannadpour *et al*. (2013)	Zhu *et al*. (2017)
0.05	35.93206	35.9321	-	-	30.5311
0.2	15.30679	15.3068	-	15.3068	-
1	0.97310	-	0.9753	0.9753	-

Table 3. Nondimensional buckling load parameter $\bar{N}$ for CP beam with various scaling effects α

α	ADM	Wang *et al*. (2006)	Pradhan and Padikar (2009)	Ghannadpour *et al*. (2013)	Tuna and Kırca (2016)	Tuna and Kırca (2017)	Zhu *et al*. (2017)
0.05	19.22054	19.2205	-	-	17.537	17.547	17.5333
0.2	11.16973	11.1699	-	11.1697	9.2784	9.2899	-
1	0.95262	-	0.9528	0.9528	-	-	-

CONCLUSION

In this study elastic stability of nanobeams is studied using nonlocal Euler-Bernoulli beam theory. ADM is employed in the analysis and solutions are computed for the nondimensional buckling load parameters. The results obtained using ADM is in very good agreement with the various solutions available in the literature. It is demonstrated that ADM is an effective technique to apply on elastic stability problems of nano beams.

REFERENCES

Adomian, G. (1994). *Solving Frontier Problems of Physics: The Decomposition Method*. Springer Netherlands.

Akgöz, B. & Civalek, Ö. (2011). Buckling Analysis Of Cantilever Carbon Nanotubes Using The Strain Gradient Elasticity And Modified Couple Stress Theories. *Journal of Computational and Theoretical Nanoscience, 8*(9), 1821-1827.

Chakraverty, S. & Behera, L. (2017). *Static and Dynamic problems of nanobeams and nanoplates*. World Scientific Publishing Co., Singapore.

Eringen, A. C. (1972). Nonlocal polar elastic continua. *International Journal of Engineering Science, 10*, 1-16.

Eringen, A. C. (1987). Theory of nonlocal elasticity and some applications. *Res. Mech., 21*, 313-342.

Ghannadpour, S. A. M., Mohammadi, B. & Fazilati, J. (2013). Bending, buckling and vibration problems of nonlocal Euler beams using Ritz method. *Composite Structures, 96*, 584-589.

Ghannadpour, S. A. M. (2018). Ritz Method Application to Bending, Buckling and Vibration Analyses of Timoshenko Beams via Nonlocal Elasticity. *Journal of Applied and Computational Mechanics, 4*(1), 16-26.

Peddieson, J., Buchanan, G. R. & McNitt, R. P. (2003). Application of nonlocal continuum models to nanotechnology. *International Journal of Engineering Science, 41*, 305-312.

Pradhan, S. C. & Phadikar, J. K. (2009). Bending, buckling and vibration analyses of nonhomogenous nanotubes using GDQ and nonlocal elasticity theory. *Structural Engineering and Mechanics, 33* , 193–213.

Reddy, J. N. (2007). Nonlocal theories for bending, buckling and vibration of beams. *International Journal of Engineering Science, 45*, 288-307.

Tuna, M. & Kırca, M. (2016). Exact solution of Eringen's nonlocal integral model for vibration and buckling of Euler–Bernoulli beam. *International Journal of Engineering Science, 107*, 54-67.

Tuna, M. & Kırca, M. (2017). Bending, buckling and free vibration analysis of Euler-Bernoulli nanobeams using Eringen's nonlocal integral model via finite element method. *Composite Structures, 179*(1), 269-284.

Wang, C. M., Zhang, Y. Y., Ramesh, S. S. & Kitipornchai, S. (2006). Buckling analysis of micro- and nano-rods/tubes based on nonlocal Timoshenko beam theory. *Journal of Physics D: Applied Physics, 39*(17), 3904-3909.

Zhu, X., Wang, Y. & Dai, H. H. (2017). Buckling analysis of Euler–Bernoulli beams using Eringen's two-phase nonlocal model. *International Journal of Engineering Science, 116*, 130-140.

VIBRATION OF NANOBEAMS USING ADOMIAN DECOMPOSITION METHOD

Safa Bozkurt COŞKUN
Kocaeli University
sb.coskun@kocaeli.edu.tr

Servet MERT KUTSAL
Kocaeli University
servet.mert@ kocaeli.edu.tr

ABSTRACT: In this study, a semi analytical technique called Adomian Decomposition Method (ADM) is applied to investigate free vibration of nanobeams based on non-local Euler-Bernoulli beam theory. ADM has been successfully used in linear/nonlinear variable coefficient solutions of ordinary/partial differential equations. All the steps of the ADM are very straightforward and the boundary conditions can be implemented in the computed analytical solution easily. ADM solutions are compared with other available results and perfect agreement is observed. Presented technique is very effective in the vibration analysis of nanobeams.

Key words: nonlocal Euler-Bernoulli beam theory, Adomian decomposition method, vibration; nano beam

INTRODUCTION

In recent years, nanomaterials has been widely used in engineering and nanotechnology. Among these materials beam type structures play a significant role in nanotechnology. Beam type structural elements are broadly utilized in civil, mechanical and aerospace engineering and recently beams have also been used in nanoelectromechanical systems. Since vibration is an important issue, dynamic analysis of beam structures has been carried out by numerous researchers. Hence, mechanical behavior of nanobeams for accurate investigation of vibration characteristics has drawn great attention to researchers worldwide. In the study of mechanical behavior atomistic, semi-continuum and continuum models are used. Experimental and atomistic simulation works revealed that at nanoscale, the small length scale effect may be considered. Hence, nonlocal elasticity theory by Eringen (1972) has been widely applied to take small length scale effect into account.

A pioneering work conducted by Peddieson *et al*. (2003) on the application of non-local elasticity theory to analyze bending, buckling and vibration of nanobeams. Xu (2006) used the integral equation approach and the non-local elasticity theory to investigate the

free transverse vibrations of nano-to-micron scale beams. Reddy (2007) reformulated various beam theories using the nonlocal differential constitutive relations of Eringen. Wang *et al*. (2007) considered the free vibration problem for micro/nano beams using Eringen's nonlocal elasticity theory. Murmu and Pradhan (2009) vibration response of nanocantilever is investigated using differential quadrature method. Murmu and Adhikari (2010) considered vibration analysis of double-nanobeam-systems. Roque *et al*. (2011) employed meshless methods to study bending, buckling and free vibration of Timoshenko nanobeams. Behera and Chakraverty (2015) applied differential quadrature method to investigate free vibration of nanobeams based on different beam theories. Chakraverty and Behera (2017) provided theoretical information on bending, buckling and vibration of nanobeams and nanoplates. Jena and Chakreverty (2018) studied free vibration of nanobeams based on non-local Euler–Bernoulli beam theory via differential transformation method. Akgöz and Civalek (2018) considered thermo-elastic vibrational behavior of thick microbeams embedded in a two-parameter elastic foundation.

In this study free vibration of nanobeams is investigated using nonlocal Euler-Bernoulli beam theory. ADM (Adomian, 1994) is used in the solution process of governing equation. First five free vibration frequencies are computed and the influence of scaling effect parameter is discussed.

NONLOCAL EULER-BERNOULLI BEAM THEORY FOR FREE VIBRATION

Euler-Bernoulli beam theory (EBT) is based on following displacement field Reddy (2007), Chakraverty and Behera (2017).

$$u_1 = -z\frac{\partial w}{\partial x} \qquad u_2 = 0 \qquad u_3 = w(x,t) \tag{1}$$

where (u_1, u_2, u_3) are the displacements along x-, y-, and z-coordinates, respectively, and w is the transverse displacement of the point (x, 0) on the mid-plane (z = 0) of the beam. The only non-zero strain of EBT is

$$\varepsilon_{xx} = -z\frac{\partial^2 w}{\partial x^2} \tag{2}$$

In the absence of transverse force and axial compressive force, governing equation of Euler-Bernoulli nanobeam may be written as

$$\frac{\partial^2 M}{\partial x^2} = m_0\frac{\partial^2 w}{\partial t^2} \tag{3}$$

where $M = \int_A z\sigma_{xx}dA$ and $m_0 = \int_A \rho dA = \rho A$. According to Eringen's nonlocal theory (Eringen 1987), the constitutive relation for Euler–Bernoulli nanobeam is given by (Reddy 2007)

$$M - \mu\frac{\partial^2 M}{\partial x^2} = -EI\frac{\partial^2 w}{\partial x^2} \tag{4}$$

where E is Young's modulus and I is the second moment of area about y-axis. It may be noted here that $\mu = (e_0 a)^2$ is the nonlocal parameter, where e_0 and a denote material constant and internal characteristic length, respectively. Using Eqs. (3) and (4), the nonlocal form of M may be written as

$$M = -EI\frac{\partial^2 w}{\partial x^2} + \mu m_0 \frac{\partial^2 w}{\partial t^2} \quad (5)$$

Governing equation in terms of displacement is rewritten as

$$-EI\frac{\partial^4 w}{\partial x^4} + \mu m_0 \frac{\partial^4 w}{\partial x^2 \partial t^2} = m_0 \frac{\partial^2 w}{\partial t^2} \quad (6)$$

If we assume the generalized displacements as

$$w(x,t) = W(x)e^{i\omega t} \quad (7)$$

Eq.(6) becomes

$$-EI\frac{\partial^4 W}{\partial x^4} - \omega^2 \mu m_0 \frac{\partial^2 W}{\partial x^2} = -\omega^2 m_0 W \quad (8)$$

Introducing the nondimensional terms $X = x/L$, $\bar{W} = W/L$, $\lambda^2 = \rho A \omega^2 L^4 / EI$ and $\alpha = e_0 A/L$ dimensionless governing equation is obtained as follows:

$$\frac{\partial^4 \bar{W}}{\partial X^4} + \alpha^2 \lambda^2 \frac{\partial^2 \bar{W}}{\partial X^2} = \lambda^2 \bar{W} \quad (9)$$

where □² is frequency parameter and □ is scaling effect parameter.

ADOMIAN DECOMPOSITION METHOD (ADM)

ADM applied successfully to a number of problem in physics (Adomian, 1994). The method provides an analytical approximate solution as a series summation approaching the exact solution rapidly. Consider a differential equation of the following form.

$$Lu + Ru + Nu = g(x) \quad (10)$$

where L is the linear operator which is highest order derivative, N is the nonlinear operator, R is remainder of linear operator including derivatives of less order than L, u represents the unknown variable and $g(x)$ is the source function. The solution for Eq.(10) is

$$u = f(x) - L^{-1}(Ru) - L^{-1}(Nu) \quad (11)$$

where L^{-1} is the inverse operator for the linear operator L. $f(x)$ is the summation of integral of the source term and the terms arising from given conditions of the problem. The solution is produced as an infinite series as

$$u(x) = \sum_{n=0}^{\infty} u_n(x) \quad (12)$$

The nonlinear Nu is represented by an infinite series of specially generated Adomian polynomials, A_i, for the specific nonlinearity.

$$Nu = \sum_{n=0}^{\infty} A_n \left(u_0, u_1, \ldots, u_n\right) (13)$$

Adomian polynomials can be calculated by means of following expression.

$$A_n = \frac{1}{n!}\frac{d^n}{d\lambda^n} N\left(\sum_{n=0}^{\infty} \lambda^k u_k\right),\ n > 0 (14)$$

The components of solution can be generated with the following algorithm recursively.

$$u_0(x) = f(x) (15)$$

$$u_{n+1}(x) = -L^{-1}\left[Ru_n - A_n\right],\ n \geq 0 (16)$$

SOLUTION PROCEDURE

After the application of ADM to Eq.(9), following successive approximations are obtained

$$\bar{W}_0 = \bar{W}(0) + \bar{W}'(0)X + \bar{W}''(0)\frac{X^2}{2} + \bar{W}'''(0)\frac{X^3}{6} (17)$$

$$\bar{W}_n = L^{-1}\left\{-\lambda^2\alpha^2 \frac{d^2\bar{W}_{n-1}}{dX^2} + \lambda^2\bar{W}_{n-1}\right\},\qquad n \geq 1 (18)$$

N^{th} order ADM solution to the problem is

$$\bar{W}(X) = \sum_{n=0}^{N} \bar{W}_n(X) (19)$$

Three different beams are considered in this study. The beam with both ends pinned (PP), the beam with both ends clamped (CC) and the beam with one end pinned and other end clamped (CP). After the application of boundary conditions, four equations in four unknowns may be written with respect to the boundary conditions of the problem. These equations can be represented in matrix form as

$$\left[M(\lambda)\right]\{\psi\} = \{0\} (20)$$

where $\{\psi\} = \left\langle \bar{W}(0) \quad \bar{W}'(0) \quad \bar{W}''(0) \quad \bar{W}'''(0) \right\rangle^T$. For a nontrivial solution, determinant of coefficient matrix must be zero. Determinant of coefficient matrix yields a characteristic equation in terms of □. Positive real roots of this equation are the frequency parameters of free vibration for the case considered.

NUMERICAL RESULTS

Below first five frequency parameters of PP, CP and CC nanobeams are compared with the analytical solutions available in literature (Wang *et al*., 2007). Although, a third order solution is enough for first and twentieth order solution is required for fifth frequency parameters for □ = 0.1, by the choose of □ = 0.7 the convergence for the first frequency parameter is satisfied with the fifth order solution while the twenty-fifth order solution is required for the convergence for fifth mode of vibration. Frequency parameters decreases with the increasing scale parameter. Table 1, Table 2 and Table 3 summarize

the comparisons for PP, CP and CC nanobeams respectively. For all the cases $L/d=10$ is assumed as given in Wang *et al*. (2007).

Table 1. First five frequency parameters $\sqrt{\lambda}$ for PP beam with various scaling effects α

	$\alpha=0.1$		$\alpha=0.3$		$\alpha=0.5$		$\alpha=0.7$	
Mode	ADM	Wang *et al.* (2007)	ADM	Wang *et al.* (2007)	ADM	Wang *et al.* (2007)	ADM	Wang *et al.* (2007)
1	3.06853	3.0685	2.68000	2.6800	2.30223	2.3022	2.02125	2.0212
2	5.78167	5.7817	4.30134	4.3013	3.46040	3.4604	2.95848	2.9585
3	8.03999	8.0400	5.44225	5.4422	4.29406	4.2941	3.64855	3.6485
4	9.91611	9.9161	6.36300	6.3630	4.98200	4.9820	4.22340	4.2234
5	11.51115	11.5111	7.15677	7.1568	5.58250	5.5825	4.72734	4.7273

Table 2. First five frequency parameters $\sqrt{\lambda}$ for CC beam with various scaling effects α

	$\alpha=0.1$		$\alpha=0.3$		$\alpha=0.5$		$\alpha=0.7$	
Mode	ADM	Wang *et al.* (2007)	ADM	Wang *et al.* (2007)	ADM	Wang *et al.* (2007)	ADM	Wang *et al.* (2007)
1	4.59446	4.5945	3.91837	3.9184	3.31532	3.3153	2.88934	2.8893
2	7.14025	7.1402	5.19631	5.1963	4.15608	4.1561	3.54624	3.5462
3	9.25832	9.2583	6.23169	6.2317	4.93279	4.9328	4.19964	4.1996
4	11.01580	11.0160	7.04819	7.0482	5.52129	5.5213	4.68165	4.6816
5	12.51960	12.5200	7.79551	7.7955	6.09667	6.0963	5.16861	5.1689

Table 3. First five frequency parameters $\sqrt{\lambda}$ for CP beam with various scaling effects α

	$\alpha=0.1$		$\alpha=0.3$		$\alpha=0.5$		$\alpha=0.7$	
Mode	ADM	Wang *et al.* (2007)	ADM	Wang *et al.* (2007)	ADM	Wang *et al.* (2007)	ADM	Wang *et al.* (2007)
1	3.82089	3.8209	3.28284	3.2828	2.78993	2.7899	2.43644	2.4364
2	6.46488	6.4649	4.76676	4.7668	3.83250	3.8325	3.27757	3.2776
3	8.65169	8.6517	5.83714	5.8371	4.61046	4.6105	3.92008	3.9201
4	10.46875	10.4690	6.71428	6.7143	5.26316	5.2632	4.46439	4.4644
5	12.01778	12.0180	7.47730	7.4773	5.83850	5.8384	4.94642	4.9464

CONCLUSION

In this study free vibration of nanobeams is investigated using nonlocal Euler-Bernoulli beam theory. To this aim ADM is employed and twenty-fifth order solutions computed for the first five vibration frequency parameters of free vibration. The results obtained using ADM is excellent agreement with the analytical solutions available in the literature. It is shown that ADM is an effective technique to apply on vibration problems of nano beams. Another great advantage of the technique is that it provides the frequencies in successive orders. It is not that easy in analytical solutions even for constant coefficient governing differential equations.

REFERENCES

Adomian, G. (1994). *Solving Frontier Problems of Physics: The Decomposition Method*. Springer Netherlands.
Akgöz, B. & Civalek, Ö. (2018). Vibrational characteristics of embedded microbeams lying on a two-parameter elastic foundation in thermal environment. *Composites Part B: Engineering, 150*, 38-77.
Behera, L. & Chakraverty, S. (2015). Application of Differential Quadrature method in free vibration analysis of nanobeams based on various nonlocal theories. *Computers and Mathematics with Applications, 69*(12), 1444-1462.
Chakraverty, S. & Behera, L. (2017). *Static and Dynamic problems of nanobeams and nanoplates*. World Scientific Publishing Co., Singapore.
Eringen, A. C. (1972). Nonlocal polar elastic continua. *International Journal of Engineering Science, 10*, 1-16.
Eringen, A. C. (1987). Theory of nonlocal elasticity and some applications. *Res. Mech., 21*, 313-342.
Jena, S. K. & Chakraverty, S. (2018). Free vibration analysis of Euler–Bernoulli nanobeam using differential transform method. *International Journal of Computational Materials Science and Engineering, 07*(03), 1850020.
Murmu, T. & Adhikari, S. (2010). Nonlocal transverse vibration of double-nanobeam-systems. *Journal of Applied Physics, 108*, 083514.
Murmu, T. & Pradhan, S. (2009). Small-scale effect on the vibration of nonuniform nanocantilever based on nonlocal elasticity theory. *Physica E, 41(8)*, 1451-1456.
Peddieson, J., Buchanan, G. R. & McNitt, R. P. (2003). Application of nonlocal continuum models to nanotechnology. *International Journal of Engineering Science, 41*, 305-312.
Reddy, J. N. (2007). Nonlocal theories for bending, buckling and vibration of beams. *International Journal of Engineering Science, 45*, 288-307.
Roque, C. M. C., Ferreira A. J. M. & Reddy, J. N. (2011). Analysis of Timoshenko nanobeams with a nonlocal formulation and meshless method. *International Journal of Engineering Science, 49(9)*, 976-984.
Wang, C. M., Zhang, Y. Y. & He, X. Q. (2007). Vibration of nonlocal Timoshenko beams. *Nanotechnology, 18*, 105401.
Xu, M. (2006). Free transverse vibrations of nano-to-micron scale beams. *Proceedings of the Royal Society A:Mathematical, Physical and Engineering Sciences, 462(2074)*, 2977-2995.

A CONCEPTUAL DECISION MAKING MODEL PROPOSAL FOR R&D PROJECT SELECTION

Zeynep Didem UNUTMAZ DURMUŞOĞLU
Gaziantep University
unutmaz@gantep.edu.tr

Alptekin DURMUŞOĞLU
Gaziantep University
durmusoglu@gantep.edu.tr

ABSTRACT: One of important functions of technology management (TM) research area is to present the required tools and techniques for "the correct selection of new R&D projects among the alternatives". Many new technology project proposal prepared by R&D unit of companies located in our country and USA are evaluated by the executives and the projects that are thought to be promising are selected and implemented. This selection decision is usually executed by the heuristic approaches in the light of the experiences of executives. At the end, many projects that are predicted to be successful end with failure while the projects that may be probably successful are disclaimed. In this study, an analytical model frame is formed to be used in the evaluation of R&D projects among the alternatives. In the proposed model, fuzzy DEMATEL method will be used to determine interrelations among selection criteria whereas TOPSİS will be implemented to find out the hierarchy of criteria.

Key words: R&D project selection, DEMATEL, TOPSİS

AR&GE PROJESİ SEÇİMİ İÇİN KAVRAMSAL BİR KARAR VERME MODELİ ÖNERİSİ

ÖZET: Teknoloji yönetimi (TY) çalışma alanının önemli fonksiyonlarından biri de "yeni AR&GE projelerinin, alternatifler arasından doğru seçilmesi için" gerekli araçların ve tekniklerin uygulayıcılara sunulmasıdır. Ülkemizde ve ABD'de firmaların AR&GE birimleri tarafından hazırlanan birçok yeni teknoloji proje önerisi, firma üst yöneticileri tarafından değerlendirilmekte ve en çok başarı vaat ettiği düşünülen projeler seçilerek uygulama aşamasına geçilmektedir. Bu seçim kararı genellikle yöneticilerin tecrübeleri ışığında sezgisel yöntemler ile yürütülmektedir. Nihayetinde, başarılı olacağı öngörülen birçok proje, başarısızlıkla sonuçlanmakta, başarılı olması muhtemel bazı projelerden ise vazgeçilmektedir. Bu çalışmada, yeni AR&GE projesi alternatiflerinin

değerlendirilmesinde kullanılmak amacıyla analitik bir modelin çerçevesi çizilmektedir. Önerilen modelde, seçim kriterleri arasındaki etkileşimi belirlemek için bulanık DEMATEL yöntemi, önerilen modeldeki kriter hiyerarşilerini incelemek için ise bulanık hiyerarşik TOPSİS yöntemi kullanılacaktır.

Anahtar sözcükler: AR&GE proje seçimi, DEMATEL, TOPSİS

GİRİŞ

"Varlığını sürdürebilmenin" yenilikçiliğe bağlı olduğu birçok işletmede, "yeni ürünler ve süreçler geliştirmek" rekabetçi kalabilmenin tek yolu olmuştur. Bu tip işletmeler için AR&GE, stratejik yönetim çerçevesinde içselleştirilmiş bir fonksiyona sahip olmalıdır. Ancak bir işletme için teknik anlamda mükemmel yeterliliklere sahip olunsa bile göz ardı edilmemesi gereken kısıtlı kaynaklar söz konusudur. AR&GE projesi seçim kararı kısıtlı organizasyonel kaynakların (para, insan, enerji vb.) doğru dağıtılmasını esas alır. Bu nedenle AR&GE projelerinin doğru seçimi ve fonlanması, firmaların hayatta kalabilmesi için kritik öneme sahiptir. Bu kritik önem ulusal düzeyde ülkelerin refahı açısından da oldukça önemlidir. Hızlı değişimin çevrelediği günümüz dünyasında, AR&GE, ulusların geleceklerine yaptıkları bir yatırımdır. Bu çerçevede ülkeler öz kaynaklarının optimum dağılımını belirlemek için gerçekçi ve analitik bir yaklaşıma ihtiyaç duymaktadır. Optimum kaynak dağılımının yanı sıra dikkate alınması gereken diğer önemli faktörler seçilen projenin başarıyla sonuçlanmasına ve kazanç oluşturacağına yönelik öngörülerin isabetli olmasıdır.

Bilimsel yazın, AR&GE seçim kararına yönelik oldukça çok sayıda yöntem geliştirilmesine karşın bunların ancak bazılarının gerçekten kullanıldığını işaret etmektedir. Bu yöntemlerle ilgili temel eleştiri, yöntemlerin stratejik unsurları dikkate almadığı ve matematiksel olarak oldukça karmaşık oldukları yönündedir. Bu çalışma ile hedeflenen, bahsedilen eleştirileri dikkate alan, kısıtları yok saymayan analitik, çok kriterli bir karar verme yönteminin kavramsal olarak sunulmasıdır.

BİLİMSEL YAZIN TARAMASI

Bu bölüm, bilimsel yazında yer alan AR&GE projesi değerlendirme yöntemlerinin gelişimini genel başlıklar halinde sunmak üzere hazırlanmıştır. Bilimsel yazına 40 yılı aşkın süredir konu olan AR&GE projesi seçimi konusunun bu denli ilgi çekmiş olması açıklanmaya muhtaçtır. Konunun bu denli ilgi çekmesinde ilk akla gelen sebepler şunlardır:

- AR&GE projesi seçimi problemi ürün geliştirme departmanlarının sıklıkla karşılaştığı zorlu bir problemdir. Her ne kadar birçok araştırma yapılmış olsa da, konu gelecek için önemli fırsatların olduğu geniş bir çalışma konusudur.

- AR&GE projesi seçimi için önerilen çözümler diğer bazı alanlar için de çözüm değeri taşıyabilir. Örneğin; bulunacak bir çözüm, firmaların sıklıkla karşılaştığı "teknoloji seçimi" problemi için de tatmin edici bir düzeyde olabilir. Çünkü AR&GE projesi ve teknoloji seçimi ortak özelliklere sahip süreçlerdir.
- Kamu kurumları aracılığıyla fonlanan AR&GE çalışmalarının değerlendirilmesinde, kamuoyunu ikna edebilecek nesnellikte adil bir değerlendirme sistemi arayışı söz konusudur. Bu nedenle teknik unsurları dikkate alan ve popülizmi dışlayan şeffaf yöntemler üzerinde çalışmalar sürdürülmektedir.

AR&GE projesi seçimi için uygulanan yöntemlerin sınıflandırılmasında genel olarak iki ana görüşün etkisinde kalınmıştır. Bunlardan ilki Baker, Freeland, ve Pound (Baker & Freeland, 1975; Pound, 1964) tarafından ortaya atılan sağlanacak faydanın öngörülmesi üzerine kurulu yaklaşımdır. İkincisi ise Baker, Freeland, ve Pound tarafından ortaya atılan opsiyonların teknik analizine dayalı yöntemlerin sınıflandırılmasıdır (Kocaoglu, 1992; Souder & Mandakovic, 1986). Her iki görüşün de ortaya koyduğu sınıflandırmalar dikkate alındığında AR&GE projesi seçimi için bilimsel yazında sunulan yöntemleri altı değişik kategori de toplamak mümkündür. Şekil 1 de görüldüğü üzere; bu yöntemler, fayda ölçüm metotları, matematiksel modeller, benzetim ve sezgisel modeller, bilişsel yaklaşımlar, gerçek alternatifler ve amaca mahsus tasarlanmış modellerdir. Burada ismi anılan her yaklaşım problemi kendine özgü bir şekilde ele aldığından, yöntemlerin yine kendilerine özgü farklı avantajları ve dezavantajları söz konusudur. Problemi bir karar problemi olarak ele alan yaklaşımlar birbirinden farklı alternatiflerden birinin en iyi kararı almak üzere seçilmesine odaklanırken, maliyetler çoğu zaman göreceli bir değerlendirme ile (hâlbuki öngörülen maliyetler sayısal olarak ifade edilebilmektedir) sadece ağırlıklandırılmış bir faktör olarak ele alınmaktadır. Bir diğer yandan problemi bir optimizasyon problemi gibi ele alan yaklaşımlar ise projenin başarısına yönelik uzman öngörülerini dışlayan ve salt nesnel verileri dikkate alan teknik çözümler üretebilmektedir. Bu nedenle farklı yaklaşımların görece dezavantajlı yönlerini dengeleyecek melez yaklaşımlar önerilmesinin problemin daha sağlıklı ele alınmasını sağlayacağı ifade edilebilir.

Fayda Ölçümü Amaçlı Modeller

Karşılaştırmalı Modeller: Karşılaştırmalı modeller bir grup proje önerisinin önceden belirlenmiş kriterler eşliğinde birbirleriyle kıyaslanarak değerlendirilmesi üzerine kuruludur (Milosevic, 2003). Bu modeller bir grup uzmanın proje önerilerini kıyaslaması üzerine kurulur. Bu nedenle değerlendirmeler yüksek derecede öznellik içerir. Karşılaştırmalı modellerin de kendi içinde değişik biçimlerde sınıflandırılması mümkündür. Bu çalışmada ele alınan alt sınıflar şu şekildedir:

Skorlama Yaklaşımları: Skorlama yöntemleri aday projelerin sıralanması için geliştirilmiş metotlardır. Her aday proje sırasıyla bir kritere göre puanlanır ve tüm puanlar toplanarak

proje skoru hesaplanır. Çok kriterli karar verme yöntemlerinin önemli bir kısmı da bu kategoride sınıflandırılabilir. Analitik hiyerarşi prosesi (AHP) bu yaklaşımlardan biridir. AHP'nin AR&GE projesi seçimi kullanımına çeşitli çalışmalarda rastlamak mümkündür (Amer & Daim, 2011; Khorramshahgol, Azani, & Gousty, 1988; M. J. Liberatore, 1987; Lockett, Hetherington, Yallup, Stratford, & Cox, 1986; Suh, Suh, & Baek, 1994; Unutmaz Durmuşoğlu, 2018; Wang, Kocaoglu, Daim, & Yang, 2010). Hiyerarşik yapıdaki faktörlerin birbirleriyle etkileşimlerini dikkate alan analitik ağ süreci (ANP) yaklaşımı da proje seçiminde kullanılmakta olan bir yöntemdir (Iskin, Daim, Kayakutlu, & Altuntas, 2012). Veri zarflama analizinin çok kriterli bir değerlendirmenin ardından proje skorlama ve sıralamada kullanıldığı özgün çalışmalar da mevcuttur (Karasakal & Aker, 2017).

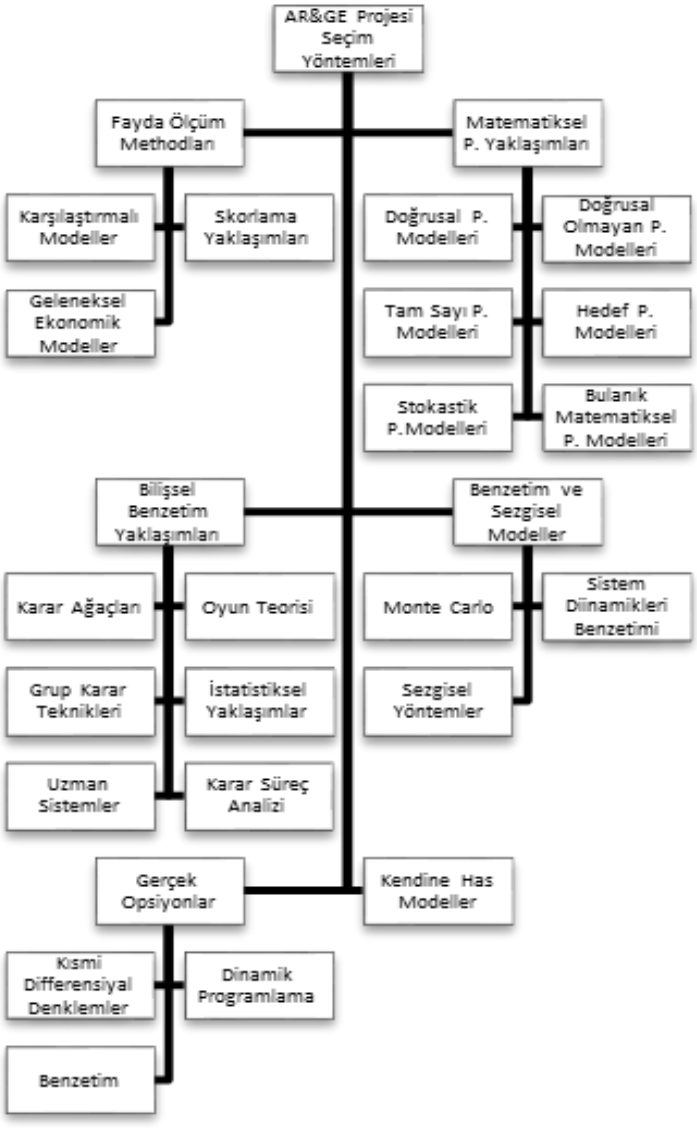

Şekil 1. AR&GE Projesi Seçiminde Kullanılan Yöntemler

Matematiksel Programlama Yaklaşımları

Doğrusal Programlama Modelleri: Doğrusal programlama modelleri doğrusal programlamayı proje seçiminde kullanan sayısal modellerdir. Bu konuda ilk geliştirilen model Asher'in geliştirdiği modeldir (Asher, 1962). Bu modelde profesyonel çalışan gücü düşünülerek (çalışanların oluşturacağı maliyet kısıtları tanımlanmıştır) AR&GE projesinden sağlanacak ekonomik fayda optimize edilmeye çalışılmıştır.

Doğrusal Olmayan Programlama Modelleri: Aslında uygulamada Blanning'in risk getiri modelinde (Blanning, 1981) olduğu gibi birçok karar modeli doğası gereği doğrusal değildir. Blanning'in modelinde toplam beklenen getirinin, toplam getiri ile toplam riskin çarpımından farkı (kayıtsızlık eğrisinin doğrusal eğimi çarpan katsayı olarak kullanılır) en çoklanmaya çalışılır.

Tam Sayı Programlama Modelleri: En klasik örneklerinden biri Paolini ve Glaser (Paolini & Glaser, 1977) tarafından gerçekleştirilmiştir. Model seçilecek projeden elde edilecek faydanın en çoklanması için kurulmuştur. Model kısıtları müsait araştırmacı sayısı, teknisyen sayısı ve sermaye harcamasıdır. Projenin gerçekleştirilip gerçekleştirilmeyeceği değişkeni 0 ve 1 gibi tam sayı değerleri alabilmektedir.

Hedef Programlama Modelleri: Hedef programlama ile proje seçiminde, karar vericinin, hedeflerini durumsal gerçeklerle karşılaşınca koyduğu varsayılır. Bu varsayım hedef programlama yaklaşımını birçok yaklaşımına göre daha gerçekçi kılar. Winkofsky ve arkadaşlarının (Winkofsky, Baker, & Sweeney, 1981) modeli bu yaklaşımın en iyi örneklerindendir. Bu modelde AR&GE kaynaklarının dağıtımıyla ilgili bireysel karar noktaları belirlenir ve proje için önemli faktörler önceliklendirilir. Daha öncelikli faktörlerde elde edilen tatmin düzeyi daha az öncelikli faktörlerin tatminin düzeyinden önemlidir. Bu nedenle model sıralı basamakların çözümüyle sağlanır.

Stokastik Programlama Modelleri: Şans kısıtlı programlamanın kullanıldığı modellerdir. Charnes ve Stedry (Charnes & Stedry, 1966), bu yaklaşımı AR&GE projesi seçiminde ilk kez kullananlardır. Gerekli AR&GE seviyesi ile gerçekleştirilebilecek AR&GE seviyesi modelde dikkate alınmaktadır. Gerçekleştirilebilecek AR&GE seviyesi tesadüflerden etkilenmektedir. Her AR&GE aktivitesinin tamamlanması için gerekli minimum seviyeyi yakalanmalı ve yakalanan seviye gerçekleştirilebilecek AR&GE seviyesinden fazla olmamalıdır.

Bulanık Matematiksel Programlama Modelleri: AR&GE projesi seçim problemlerinin girdileri "yüksek" "düşük" "orta" gibi bulanık olabilir. Bu girdiler uygun bir şekilde matematiksel modelde yer alabilirler. Weber ve arkadaşları (Weber, Werners, &

Zimmermann, 1990) geliştirdikleri modelde hedef fonksiyonun maksimizasyonu yerine belirli bir istenilen seviyeyi aşmasını hedeflemişlerdir. Bu modelde kısıtlar da bulanık olup doğrusal modelleme ile çözülmüştür.

Bilişsel Benzetim Yaklaşımları

Karar Ağaçları: Karar ağacı analizleri zaman içinde gerçekleşecek, çoğunlukla belirsizlik içeren AR&GE projesi yatırım kararlarının gösteriminde kullanılır. Genellikle bir karar ağacında karar vericinin karşılaşabileceği durumlar ve alternatifler ile bu durumların gerçekleşebilme olasılıkları yer alır (Martino, 1995). Alternatiflerin dizilimi ve bu dizilimlere karşıt gelen olasılıklara göre çözümler oluşturulur.

Oyun Teorisi Temelli Yaklaşımlar: Oyun teorisi temelli modeller, rakiplerin nasıl davranacağını da dikkate alarak (rasyonel davranış sergileyecekleri varsayımı ile) AR&GE kaynakları dağıtımı stratejilerinin değerlendirilmesini sağlarlar. Örneğin, patentlerde rekabet edilen bir firmanın AR&GE harcaması kalıpları incelenebilir (Grossman & Shapiro, 1985).

Grup Karar Verme Teknikleri: Grup karar verme teknikleri, sistematik olarak alanında uzman olan kişilerden bilgi toplanması ve birleştirilmesine dayanır. Bu nedenle, bu teknikler, (en azından daha karmaşık modeller için uzman bilgisinin derlenmesinde) pratikte AR&GE projesi seçimi için uygun ve gerçekçi çözümler sağlarlar (Khorramshahgol vd., 1988). Delfi yöntemi, bu yöntemlerden en yaygın kullanıma sahip olanlardandır.

İstatistiksel Yaklaşımlar: AR&GE proje performansını etkileyen faktörlerin belirlenmesinde istatistiksel yöntemlerin uygulandığı yaklaşımlardır. Kümeleme analizleri, regresyon ve diskriminant analizi proje seçiminde yaygın olarak kullanılan yöntemlerdir. Diskriminant analizi, belirli proje özellikleri için kestirim değerleri sunarak, projelerin sınıflandırılmasını sağlar. Regresyon analizinde ise AR&GE performansıyla girdi değişkenler arasında ilişkiler kurulmaya çalışılır. AR&GE projesi seçiminde regresyon kullanan çalışmalara rastlamak mümkündür (Cooper, 1981; Schwartz & Vertinsky, 1977; Stahl & Harrell, 1983). Benzer özelliklere sahip AR&GE projelerinin aynı kümelerde toplanmaya çalışıldığı kümeleme yaklaşımında, kümeler için skorlama yapılarak proje seçimi yapılır (Mathieu & Gibson, 1993).

Uzman Sistemler: Uzman sistemler, AR&GE müdürünün karar süreçlerinin kısmen taklit edilerek projenin değerlendirildiği sistemlerdir (Hall & Nauda, 1990). Bir uzman sistem, bahsedilen taklit işlemini, bir bilgisayar yazılımı ara yüzü ile sağlar. Liberatore ve Stylianou (Matthew J. Liberatore & Stylianou, 1993) çalışmalarında bilgi tabanlı karar destek sistemlerinin AR&GE projelerinde yeterli karar desteği verebilecek bir yapıya sahip olup/olamayacağını araştırmak amaçlı bir uzman sistem oluşturmuştur. Uygulama deneyimi, sistemin karar desteği sağlamakta faydalı olduğunu göstermiş

ancak ilerde daha gelişmiş çoklu uzman sistemlere ihtiyaç olduğunu işaret etmiştir (Matthew J. Liberatore & Stylianou, 1993).

Karar Süreç Analizi: Karar süreç analizinin amacı genel yönetsel politikalar hakkında bilgi edinimi ve AR&GE sürecine dâhil olan grupların hiyerarşik organizasyon yapısını yansıtmaktır. Schmidt ve Freeland (Schmidt & Freeland, 1992) çalışmalarında, AR&GE projesi seçiminde optimizasyon yaklaşımlarının organizasyonel bağlamı dikkate almadığını bu nedenle karar noktalarından karar süreçlerine doğru gerçekleşen bir yön arayışını ifade etmişlerdir. Yazarlar (Schmidt & Freeland, 1992) ayrıca, karar süreç analizlerinin bu anlamda sonuçlardan ziyade sürecin içeriğine dönük bir kavrama geliştirmeye çalıştırdığına dikkati çekmişlerdir.

Benzetim ve Sezgisel Modeller

Monte Carlo benzetim çalışmaları AR&GE projelerindeki tüm rassal unsurların olasılıklarını kullanarak, hedef değerlere ve kullanılacak kaynaklara ait genel olasılığı ortaya koyarlar (Martino, 1995; Souder & Mandakovic, 1986). Versapalainen ve Lauro (Vepsalainen & Lauro, 1988) çalışmalarında, Monte Carlo benzetimini kullanarak rasyonel rakip firma stratejilerinin projeyi seçen firma üzerindeki etkilerini olasılıksal olarak incelemiştir.

Sistem dinamikleri benzetimin de ise, geri besleme döngüleriyle belirli bir AR&GE sonucu ortaya çıkacak ürünle pazarda yaşanacak değişiklikler senaryo bazlı olarak incelenebilmektedir (Milling, 1996). Fox ve Baker'ın gerçekleştirdiği çalışmada (Fox & Baker, 1985) ise hipotetik bir firmanın, hipotetik bir pazardaki AR&GE süreci, sistem dinamikleri ile modellenerek politika değişiklerinin etkisi test edilmiştir.
Matematiksel modellerle kıyaslandığında, sezgisel modeller genellikle en iyi olması gerekmeyen kabul edilebilir çözümleri de kabul ederler. Matematiksel modelin çok fazla değişkeni içermesi veya zorlayıcı kısıtlara sahip olması, çözüm için oldukça uzun zaman beklemeyi gerektirebilmektedir. Mandakovic ve Souder çalışmalarında, 1000 değişkenli, 400 bütçe kısıtına sahip bir AR&GE projesi seçimi problemini, Toyoda sezgiselini kullanılarak makul bir sürede çözmüş ve elde edilen çözümün de bilinen optimuma çok da uzak olmadığını göstermişlerdir (Mandakovic & Souder, 1985).

Gerçek Opsiyonlar Analizleri

Gerçek (reel) opsiyonlar yaklaşımında, finansal opsiyonlar yerine, AR&GE projelerine ve daha geniş anlamda AR&GE stratejilerine uygun opsiyonlar değerlendirilir. Projenin başka bir tarihe ertelenmesi, projenin beklenenden erken ya da geç bitmesi gibi opsiyonlarda değerlendirilmeye dâhil edilir. Bu nedenle gerçek opsiyonlar yaklaşımı, işin doğasında olan belirsizlikleri ve aktif karar gerektiren stratejileri dikkate alan dinamik bir proje değerlendirme aracıdır (Luehrman, 1998).

Kendine Has Modeller

Özel amaçlarla geliştirilmiş, yapısal olmayan modellerdir. İlgili yaklaşımlar AR&GE projesinin türüne, uygulama alanına ve sektöre uygun olarak kendine özgü bir şekilde oluşturulur.

MEVCUT YAKLAŞIMLARIN DEĞERLENDİRİLMESİ

Bilimsel yazın bölümünde açıklandığı üzere AR&GE projesi değerlendirilmesinde kullanılmak üzere birçok model ve metot ortaya konulmuştur. Bu kadar çok önerilmiş model olmasına karşın AR&GE projesi seçimi problematik olarak kalmış sadece birkaç model yaygın kabul görmüştür (Meade & Presley, 2002). Liberatore ve Titus, AR&GE projelerinin seçiminde kullanılan yöntemlerle ilgili gerçekleştirdikleri ampirik çalışmada, şirketlerin geleneksel finansal yöntemlerle diğer bazı metotları birleştirerek kullandıklarını tespit etmişlerdir (Matthew J. Liberatore & Titus, 1983). Ayrıca, proje, kaynak ve kriter çeşitliliği nedeniyle doğrusal ve tam sayılı programlamanın yaygın olarak kullanılmadığını belirtmiştirler. Bir diğer önemli tespitleri ise birçok yöneticinin, mevcut yöntemlerin karar kalitesini artırmadığına inandığı olmuştur. Benzer tespitler başkaca çalışmalarda (Bordley, 1999; Fahrni & Spätig, 1990; Lockett, Stratford, Cox, Hetherington, & Yallup, 1987) da belirtilmiştir. Baker ve Freeland (Baker & Freeland, 1975) mevcut yöntemlerdeki zayıflıkları şöyle sıralamıştır:

1) Çoklu ve birbirine bağımlı kriterlerin yetersiz değerlendirilmesi
2) Projeler arası iç ilişkilerin değer katkısı ve kaynak kullanımına göre yetersiz değerlendirilmesi
3) Risk ve belirsizliklerin yeterli olmayan bir şekilde değerlendirilmesi
4) Para dışı boyutların tanımlanması ve değerlendirilmesindeki yetersizlikler
5)AR&GE yöneticilerinin modelleri anlaşılmasını ve uygulanılmasını zor bulması yönündeki algıları

Bu ve benzeri zayıflıkların önemli bir çoğunluğu yeni çalışmalarda da tam anlamıyla çözümlenememiş ve alternatif yöntemlerin geliştirilmesi için araştırmalar yapılması gereğini doğurmuştur. Bir sonraki bölümde, önerilen kavramsal model ile ortaya konulmaya çalışılan yaklaşım bu problemleri çözmede nasıl katkılar sağlayabileceği tartışılmıştır.

KAVRAMSAL MODEL

AR&GE projesi ve buna benzer daha birçok proje seçimi uygulamalarında seçim problemlerinin çözümü için çok kriterli karar verme (ÇKKV) yöntemlerini kullanmak mümkündür. Kriterlerin neler olduğu ve ne tip bir hiyerarşik bir yapıya sahip olduğunun belirlenmesi için deneyimli ve birikimli uzmanlar grubuyla çalışılması önemlidir. Bir diğer zorluk da bu kriterlere uygun ağırlıkların verilmesidir. Kriterler ve ağırlıkların belirlenmesi problem çözmek için gerekli olan ana çerçevenin oluşturulmasını sağlayacaktır. Mevcut AR&GE projesi seçeneklerini kurulan ana çerçeve vasıtasıyla değerlendirerek bir sıralama elde etmek mümkündür. Bu çalışma kapsamında sunulan kavramsal model, klasik ÇKVV yaklaşımlarında sıklıkla karşılaşıldığı bilinen zorlukları gidermek için birden fazla yöntemi ve teoriyi bütünleştiren melez/entegre bir modeldir.

Şekil 2. Önerilen Kavramsal Modelin Uygulama Adımları

Önerilen modelin uygulanmasında izlenecek adımlar Şekil 2'de sunulmaktadır. Önerilen karar verme modeli alternatif projelerin listelenmesiyle başlamaktadır. Alternatif projelerin değerlendirilmesine başlamadan önce ilk basamak değerlendirme kriterlerinin belirlenmesidir. Bu çalışmanın ana konusu olan AR&GE projesi seçimi problemi için kriterlerin belirlenmesinde ilgili uzmanlardan Delfi tekniği ile veri toplanılması önerilmektedir. Delfi tekniğinin esası, dikkatlice seçilmiş uzmanların, birbirlerinden habersiz şekilde etkileşimini sağlamaktır. Bu kapsamda hazırlanan anket soruları

uzmanlara iletilerek ortak görüşler derlenmeye çalışılmalı ve izleyen turlarda ise tartışmalı hususlarda netliğin sağlanması amaçlı toplantılar düzenlenmelidir. Bu modelde ayrıca hiçbir öznel değerlendirmeye tabii tutulması ihtiyacı duyulmayan maliyet, kapasite vb kriterler daha sonra kullanılmak üzere bir kenarda tutulmaktadır. Burada amaçlanan maliyet gibi parasal bir unsurun, AR&GE konusunun "yenilik içermesi kriteri" gibi öznel bir ölçeklendirmeyle birlikte ele alınmasını önlemektir. Ayrıca, maliyetin doğrudan kriter olarak değerlendirildiği ÇKKV modellerinde, maliyet genelde karardaki en büyük kriter ağırlığına sahip olmakta ve maliyet üzerine bir karar inşa edilmektedir. Oysaki AR&GE projelerinde kesinlik kazanmamış ve tam olarak öngörülemeyen bir kazanç söz konusudur. Bu kazancın büyüklüğü maliyetten çok daha büyük olabilir. Modeli iki ayrı aşamada ele alarak projelerin oluşturacakları muhtemel faydaları maliyete ezdirmemektir.

Bu kavramsal modelde, ilk olarak kriterlerin ağırlıklarının belirlenmesinde bulanık DEMATEL yöntemi, daha sonra ise alternatiflerin sıralanması için bulanık TOPSİS yöntemi kullanılacaktır. ÇKKV problemlerinde, bulanık kavramların/sözel ölçütlerin sıklıkla veri olarak yer alması, reel değerlerle analiz yapılmasını ve gerçeğin olduğu gibi modellenmesini zorlaştırdığından (Chen, 2000), analizlerde bulanık yöntemler kullanılacaktır. Kriterlerin birbiriyle etkileşimi ve hiyerarşik yapısının tespitinde kullanılacak olan DEMATEL yöntemi karmaşık ilişkilerin yapısının görselleştirilmesi amacıyla geliştirilmiş bir yöntemdir (Büyüközkan & Çifçi, 2012). DEMATEL yönteminde kriterler "sebep" ve "etki" kriterleri olarak iki gruba ayrılırlar. Sebep kriterlerinin etki grubu üzerindeki gücü kriter ağırlıklarının belirlenmesinde kullanılmaktadır (Baykasoğlu, Kaplanoğlu, Durmuşoğlu, & Şahin, 2013). Hwang and Yoon (1981) tarafından geliştirilen TOPSİS yöntemi ise bu kavramsal model kapsamında, seçeneklerin ideal pozitif ve ideal negatif çözüme olan mesafelerine göre sıralanmasında kullanılacaktır. TOPSİS yönteminin en önemli avantajı, kriter ağırlıklarının belirlenmesi gibi önemli hususta daha az uzman görüşüne ihtiyaç kalmasını sağlamasıdır (Gupta & Barua, 2018).

Öznel değerlendirmeler gerektiren tüm değerlendirmeler DEMATEL modelinde hesaplanarak alternatifler için toplam fayda skoru belirlenmektedir. Elde edilen toplam fayda skoru ile toplam maliyet ve diğer teknik özellikler gibi nesnel veriler ise daha sonra normalize edilerek TOPSİS yöntemine dâhil edilmekte ve alternatifler öznel ve nesnel veriler ışığında sıralanmaktadır.

SONUÇ

AR&GE projesi seçim problemi, özellikle gelişmekte olan ülkeler için kritik öneme sahip bir problemdir. Kısıtlı kaynakların ülkelerin refahını artıracak şekilde doğru projelere tahsisi elzem niteliktedir. Özellikle kamu destekli projelerde seçimin hangi analitik

yöntemlerle yapıldığı, kriterlerin ve ağırlıklarının neler olduğu kamu şeffaflığının ve kaynakların doğru kullanıldığının ispatı olarak toplumla paylaşılmalıdır. Bu kapsamda doğru kararın verilmesi için kullanılacak olan yöntem analitik temelleri olan ancak oldukça fazla sayıda öngörüyü de kapsayacak (başarı/başarısızlık; kazanç beklentisi vb) bir model olmak durumundadır. Bu çalışmada öznel ve nesnel değerlendirmeleri öncelikle ayrı değerlendiren daha sonra ise birlikte ele alınmasını sağlayan analitik melez bir yöntem önerilmiştir. DEMATEL metodu ile öznel değerlendirme gerektiren kriterlerin ağırlıkları belirlenmekte ve kriterlerin önem dereceleri sıralanmaktadır. Nesnel veriler analizin ilk kısmında dikkate alınmamakta, pozitif ideal çözüm ve negatif ideal çözümlerin TOPSİS yöntemiyle hesaplanması sırasında devreye sokulmaktadır. Nesnel ile öznel kriterlerin ilk aşamada birbiriyle kıyaslanmasının farklı ölçeklere sahip olmaları sebebiyle adaletsiz olacağı düşünülmektedir. Bu çalışmada kavramsal olarak sunulan modelin başarımı hiç şüphesiz çalışmada yer verilecek uzmanların tecrübeleri ve bilgi birikimiyle yakından ilintilidir. Bu nedenle "doğru uzmanları" bulma hususunda özenle durulmalıdır. Gelecek çalışmalarda, burada sunulan kavramsal modelin somut ve gerçek bir modele çevrilmesi ve test edilmesi mümkündür.

KAYNAKLAR

Amer, M., & Daim, T. U. (2011). Selection of renewable energy technologies for a developing county: A case of Pakistan. *Energy for Sustainable Development*, *15*(4), 420-435. https://doi.org/10.1016/j.esd.2011.09.001

Asher, D. T. (1962). A Linear Programming Model for the Allocation of R and D Efforts. *IRE Transactions on Engineering Management*, *EM-9*(4), 154-157. https://doi.org/10.1109/IRET-EM.1962.5007697

Baker, N., & Freeland, J. (1975). Recent Advances in R&D Benefit Measurement and Project Selection Methods. *Management Science*, *21*(10), 1164-1175. https://doi.org/10.1287/mnsc.21.10.1164

Baykasoğlu, A., Kaplanoğlu, V., Durmuşoğlu, Z. D. U., & Şahin, C. (2013). Integrating fuzzy DEMATEL and fuzzy hierarchical TOPSIS methods for truck selection. *Expert Systems with Applications*, *40*(3), 899-907. https://doi.org/10.1016/j.eswa.2012.05.046

Blanning, R. W. (1981). Variable-Base Budgeting for R&D. *Management Science*, *27*(5), 547-558. https://doi.org/10.1287/mnsc.27.5.547

Bordley, R. F. (1999). Keeping It Sophisticatedly Simple in R&d Project Management. *The Engineering Economist*, *44*(2), 168-183. https://doi.org/10.1080/00137919908967515

Büyüközkan, G., & Çifçi, G. (2012). A novel hybrid MCDM approach based on fuzzy DEMATEL, fuzzy ANP and fuzzy TOPSIS to evaluate green suppliers. *Expert Systems with Applications*, *39*(3), 3000-3011. https://doi.org/10.1016/j.eswa.2011.08.162

Charnes, A., & Stedry, A. C. (1966). A Chance-Constrained Model for Real-Time Control in Research and Development Management. *Management Science*, *12*(8), B-353. https://doi.org/10.1287/mnsc.12.8.B353

Chen, C.-T. (2000). Extensions of the TOPSIS for group decision-making under fuzzy environment. *Fuzzy Sets and Systems*, *114*(1), 1-9. https://doi.org/10.1016/S0165-0114(97)00377-1

Cooper, R. G. (1981). An empirically derived new product project selection model. *IEEE Transactions on Engineering Management*, *EM-28*(3), 54-61. https://doi.org/10.1109/TEM.1981.6448587

Fahrni, P., & Spätig, M. (1990). An application-oriented guide to R&D project selection and evaluation methods. *R&D Management*, *20*(2), 155-171. https://doi.org/10.1111/j.1467-9310.1990.tb00693.x

Fox, G. E., & Baker, N. R. (1985). Project Selection Decision Making Linked to a Dynamic Environment. *Management Science*, *31*(10), 1272-1285. https://doi.org/10.1287/mnsc.31.10.1272

Grossman, G. M., & Shapiro, C. (1985). *Dynamic R&D Competition* (Working Paper Sy 1674). https://doi.org/10.3386/w1674

Gupta, H., & Barua, M. K. (2018). A framework to overcome barriers to green innovation in SMEs using BWM and Fuzzy TOPSIS. *Science of The Total Environment*, *633*, 122-139. https://doi.org/10.1016/j.scitotenv.2018.03.173

Hall, D. L., & Nauda, A. (1990). An interactive approach for selecting IR&D projects. *IEEE Transactions on Engineering Management*, *37*(2), 126-133. https://doi.org/10.1109/17.53715

Hwang, C. L., & Yoon, K. (1981). *Multiple attributes decision making methods and applications*. Springer Berlin.

Iskin, I., Daim, T., Kayakutlu, G., & Altuntas, M. (2012). Exploring renewable energy pricing with analytic network process—Comparing a developed and a developing economy. *Energy Economics*, *34*(4), 882-891. https://doi.org/10.1016/j.eneco.2012.04.005

Karasakal, E., & Aker, P. (2017). A multicriteria sorting approach based on data envelopment analysis for R&D project selection problem. *Omega*, *73*, 79-92. https://doi.org/10.1016/j.omega.2016.12.006

Khorramshahgol, R., Azani, H., & Gousty, Y. (1988). An integrated approach to project evaluation and selection. *IEEE Transactions on Engineering Management*, *35*(4), 265-270. https://doi.org/10.1109/17.7449

Kocaoglu, D. F. (Ed.). (1992). *Management of R&D and engineering*. Amsterdam ; New York: North-Holland.

Liberatore, M. J. (1987). An extension of the analytic hierarchy process for industrial R amp;D project selection and resource allocation. *IEEE Transactions on Engineering Management*, *EM-34*(1), 12-18. https://doi.org/10.1109/TEM.1987.6498854

Liberatore, Matthew J., & Stylianou, A. C. (1993). The Development Manager's Advisory System: A Knowledge-Based DSS Tool for Project Assessment*. *Decision Sciences*, *24*(5), 953-976. https://doi.org/10.1111/j.1540-5915.1993.tb00498.x

Liberatore, Matthew J., & Titus, G. J. (1983). The Practice of Management Science in R&D Project Management. *Management Science*, *29*(8), 962-974. https://doi.org/10.1287/mnsc.29.8.962

Lockett, G., Hetherington, B., Yallup, P., Stratford, M., & Cox, B. (1986). Modelling a Research Portfolio Using AHP: A Group Decision Process. *R&D Management*, *16*(2), 151-160. https://doi.org/10.1111/j.1467-9310.1986.tb01168.x

Lockett, G., Stratford, M., Cox, B., Hetherington, B., & Yallup, P. (1987). Modelling a research portfolio using AHP — a group decision process. *Mathematical Modelling*, *8*, 142-148. https://doi.org/10.1016/0270-0255(87)90558-6

Luehrman, T. A. (1998). Investment Opportunities as Real Options: Getting Started on the Numbers. *Harvard Business Review*, *76*. Geliş tarihi gönderen https://hbr.org/1998/07/investment-opportunities-as-real-options-getting-started-on-the-numbers

Mandakovic, T., & Souder, W. E. (1985). An Interactive Decomposable Heuristic for Project Selection. *Management Science*, *31*(10), 1257-1271. https://doi.org/10.1287/mnsc.31.10.1257

Martino, J. P. (1995). *Research and Development Project Selection*. Wiley.

Mathieu, R. G., & Gibson, J. E. (1993). A methodology for large-scale R&D planning based on cluster analysis. *IEEE Transactions on Engineering Management*, *40*(3), 283-292. https://doi.org/10.1109/17.233190

Meade, L. M., & Presley, A. (2002). R&D project selection using the analytic network process. *IEEE Transactions on Engineering Management*, *49*(1), 59-66. https://doi.org/10.1109/17.985748

Milling, P. M. (1996). Modeling innovation processes for decision support and management simulation. *System Dynamics Review*, *12*(3), 211-234. https://doi.org/10.1002/(SICI)1099-1727(199623)12:3<211::AID-SDR105>3.0.CO;2-8

Milosevic, D. Z. (2003). *Project Management ToolBox: Tools and Techniques for the Practicing Project Manager* (1 edition). Hoboken, N.J: Wiley.

Paolini, A., & Glaser, M. A. (1977). Project Selection Methods that Pick Winners. *Research Management*, *20*(3), 26-29.

Pound, W. H. (1964). Research project selection: Testing a model in the field. *IEEE Transactions on Engineering Management*, *EM-11*(1), 16-22. https://doi.org/10.1109/TEM.1964.6446389

Schmidt, R. L., & Freeland, J. R. (1992). Recent progress in modeling R&D project-selection processes. *IEEE Transactions on Engineering Management*, *39*(2), 189-201. https://doi.org/10.1109/17.141276

Schwartz, S. L., & Vertinsky, I. (1977). Multi-Attribute Investment Decisions: A Study of R&D Project Selection. *Management Science*, *24*(3), 285-301. https://doi.org/10.1287/mnsc.24.3.285

Souder, W. E., & Mandakovic, T. (1986). R&D Project Selection Models. *Research Management*, *29*(4), 36-42. https://doi.org/10.1080/00345334.1986.11756981

Stahl, M. J., & Harrell, A. M. (1983). Identifying operative goals by modeling project selection decisions in research and development. *IEEE Transactions on Engineering Management*, *EM-30*(4), 223-228. https://doi.org/10.1109/TEM.1983.6448624

Suh, C.-K., Suh, E.-H., & Baek, K.-C. (1994). Prioritizing telecommunications technologies for long-range R&D planning to the year 2006. *IEEE Transactions on Engineering Management*, *41*(3), 264-275. https://doi.org/10.1109/17.310141

Unutmaz Durmuşoğlu, Z. D. (2018). Assessment of techno-entrepreneurship projects by using Analytical Hierarchy Process (AHP). *Technology in Society*, *54*, 41-46. https://doi.org/10.1016/j.techsoc.2018.02.001

Vepsalainen, A. P. J., & Lauro, G. L. (1988). Analysis of R&D portfolio strategies for contract competition. *IEEE Transactions on Engineering Management*, *35*(3), 181-186. https://doi.org/10.1109/17.7438

Wang, B., Kocaoglu, D. F., Daim, T. U., & Yang, J. (2010). A decision model for energy resource selection in China. *Energy Policy*, *38*(11), 7130-7141. https://doi.org/10.1016/j.enpol.2010.07.031

Weber, R., Werners, B., & Zimmermann, H.-J. (1990). Planning models for research and development. *European Journal of Operational Research*, *48*(2), 175-188. https://doi.org/10.1016/0377-2217(90)90372-I

Winkofsky, E. P., Baker, N. R., & Sweeney, D. J. (1981). A Decision Process Model of R&D Resource Allocation in Hierarchical Organizations. *Management Science*, *27*(3), 268-283.

HYBRID MULTI-LEVEL INVERTER BASED PHOTOVOLTAIC APPLICATION.

Omar AL-BASRI
Department of Electric and Electronic Engineering, Gaziantep University, Gaziantep 27310, Turkey, Omarsat84@yahoo.com

Ergun ERÇELEBİ
Department of Electric and Electronic Engineering, Gaziantep University, Gaziantep 27310, Turkey, ercelebi@gantep.edu.tr

ABSTRACT: Multi-level inverter performance is high when compared to conventional two-level inverter. This due to their reduced harmonics distortion , less electromagnetic interference ,reduced common mode voltage and higher dc link voltages .yet the main drawbacks of multi-level inverter are complex pulses with modulations control , balancing of capacitor voltages and increased number of switches .The study and simulation of three phase nine level inverter using only twelve switches and feed by photovoltaic panels is focused here in this paper . This paper also present control technique for nine level inverter topology.

Key words: Cascade multilevel inverter, Photovoltaic, Buck – boost dc to dc converter, Perturb and observe maximum power point method.

INTRODUCTION

Resent research studues have witnessed a huge increasing interest to multi-level power conversion.These researchers involve the introduction of new inverter topologies and unique modulation teqniques .But the most widly used of multi level inverter topologies are multi-cell inverter [1],diode clamped inverter[8]-[5] and flying capacitor inverter [6].Some of the applications included for these inverters are industrial drives flexable ac transmission system[7],traction applications in the transport industrry and grid integration of non-conventional energy sources.
Becouse of the values of all voltage sources are the same ,the nine level twelive switches topology is a symetrical topology however there are several asymetrical topologies that need voltage sources of different values.The results of this asymmetry have aspicific relations between them concerning the need of dc voltages and also the difference in the rating of the semiconductor switches .
This paper presents study and simulation of nine level new multi level inverter topology named by the reversing voltage (RV) .
This topology differs from conventional topologies becouse it requre less number of component ,not only this it is more efficient since the inverter operate at line frequency

.As result there is no need for all frequency to work in high frequency. This leads to simpler and reliable control of the inverter .In this paper the dc source will represented by solar panals
instead of conventional sourses so this paper will handeled also Interview of photovoltaic system and their maximum power point Algorithm and components.
In section I, introduction to multi-level inverter is discussed. In section II, we discussed the nine level multilevel inverter. In section III, Interview of photovoltaic system. Our proposed inverter results is discussed in section IV whereas conclusions are drawn in section VI.

INTERVIEW OF NINE LEVEL-TWELVE SWITCH INVERTER

There are two seperated parts as an output voltage in this hybirid multi-level inverter .The first part is named "level generator "whitch is responsible for level generation in positive polarity .To produce required levels , high-frequency switches are required in this part .
The other part is named "polarity generation" whitch is responsible for generating the polarity of the output voltage .polarity generator operates at line frequency . In order to produce the multi-level voltage output ,this topology mergs the two parts (low frequency and high frequency) .
The positive levels are generated by the level generator (high frequency part)to generate a complete multilevel output . this part is then feed to apolaity genrator (full bridge inverter)and this will generate the required polarity for the output.
Accordingly, this process will reduce the number of the semiconductor switches whitch responsible to generate the output voltage levels in negative and positive polarities .
In figure one shown below the proposed nine level twilve switches is shown at the left of this figure the level generator is lockated whitch consists of eight switches and four dc sources that we will repalce them with solar panal sources while in the right side of the figure the polarity generator occupied its place whitch consists of conventioal h bidge unit the out put of level generator will be the input to polarity generator ,more over there is no need of using isolation component between the polarity and level part .

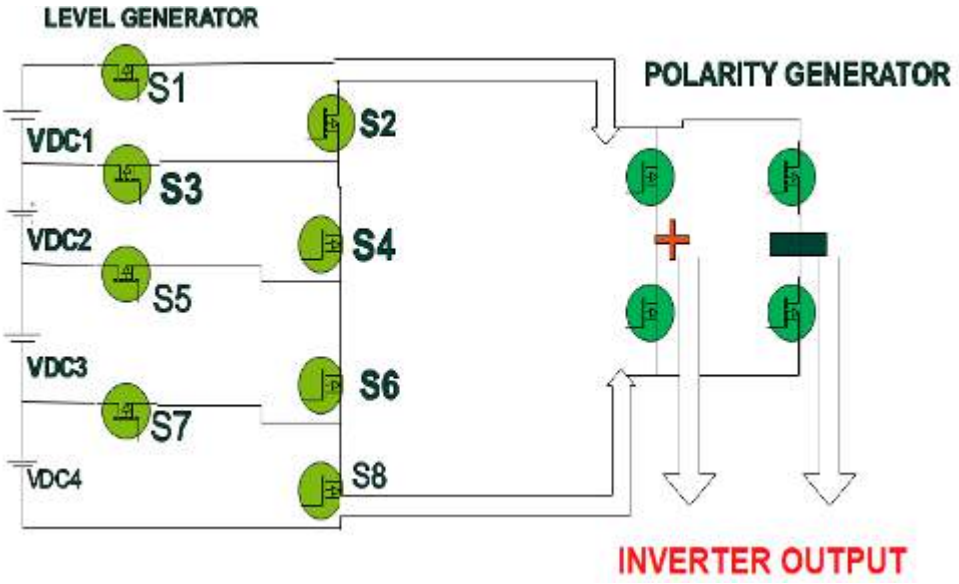

Figure 1. Nine Level Twelve Switch Inverter

Five possible switching states to control the inverter . The level generator produces the required output possitive voltage levels as follows :

1- Zero output level :Switches S2,S4,S6,S8 are ON with short circuit the input of the polarity generator .Results in the generation of zero voltage.

2- Vdc output level: Switches S2,S4,S6,S7 are ON with all other high frequency swithches are off results in generation of Vdc voltage level.

3- Two Vdc output level: Switches S2,S4,S5 are ON with all other high frequency swithches are off results in generation of two Vdc voltage level.

4- Three Vdc output level: Switches S2,S3 are ON with all other high frequency swithches are off results in generation of three Vdc voltage level.

5- Four Vdc output level: Switches S1 are ON with all other high frequency swithches are off results in generation of fourVdc voltage level.

The modulation teqnique whitch is used to generate nine level output is based on sinisodal pulse with modulation method(spwm) .

In this teqnique the reference signals have the same amplitude and the same frequency to line frequency .

They are in phase with each other with an offset equal to the value of the magnitude of the carrier signal.

These references signals will be compared with the carrier signal to produce pulses required for the switches of the inverter circuit figure 2 shows the refereces signal with the carrier signal .

The ratio of the amplitude of the reference signal to the amplitude of carrier signal defined as the modulation index for inverter .

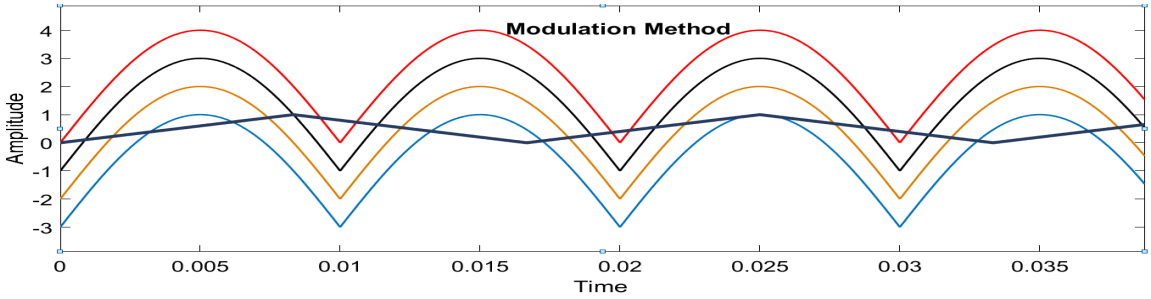

Figure 2. Modulation Method

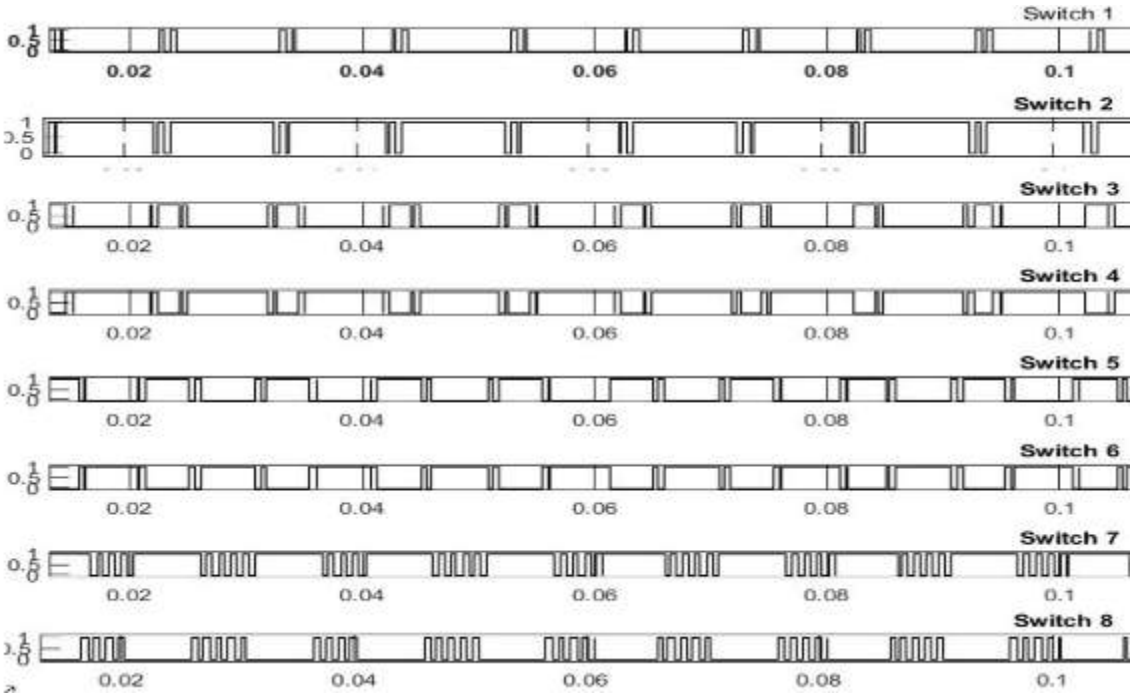

Figure 3. Gate Pulses for Level Genration Switches

INTERVIEW OF PHOTOVOLTAIC SYSTEM

In general, solar cells generate potential from solar energy through photovoltaic modules made up of silicon cells. And since the output of these cells is always very low, a photovoltaic array is formed to increase the potential total output. An array can consist of solar cells connected in series or in parallel to increase the voltage or current generated by the module. The array is positioned to provide maximum output power at a specific point. This is called the maximum power point depending on the load, temperature and illumination. According to this characteristic, the photovoltaic module cannot operate at the maximum power point due to external effects, so one of the maximum power point tracking algorithms is used. The operating point should be close to the maximum power point area that should be used with the DC-DC converter to maintain the panel [4]. These

techniques include the constant voltage MPPT algorithm, the perturbation and observation (P & O) MPPT algorithm, and the incremental conductance (INC) MPPT algorithm [8]. The cuk converter combined with buck-boost, mppt algorithm is the construction of the maximum power point tracking and solar charge controller [7] to ensure that the module runs in it. This article uses the following components:

1-buck-boost dc-dc converter
2-perturb and observe algorithm

Buck –Boost Dc-Dc Converter

Typically, a DC-DC converter is an electronic circuit that can generate various levels of DC voltage and uses many conversion processes such as mode, linearity, and magnetism [7].
Some of the most well-known topologies are step-down, step-up, and buck-boost converters for buck converters whose output voltage is lower than the input voltage. On the other hand, in the boost converter, the output voltage is used larger than the input voltage. As is clear from the title of this converter, the buck-boost type can operate in the buck mode and boost mode.
As mentioned earlier, this type of converter and (mppt) algorithm will be used to implement the If the current in the converter does not go to zero, this converter can be put into a continuous conduction mode (ccm) of two operating modes, and once the converter current reaches the zero region of the converter current, the other operating modes are , Called discontinuous operation mode (dcm) during the period, different from all formula models
In this article, using continuous conduction mode (ccm), the output voltage is calculated as:

$vo = vi * D/(1-D)$ (1)

While in discontinuous conduction mode (dcm)the output vol
tage is calculated as:

$vo = vi\ D^2/2Io$ (2)

Where D is the duty ratio which will fed to the controlling switch and vo in both modes n average values is the current through the load. In continuous conduction mode (ccm) when D > 0.5 it will operate in buck mode while when D< 0.5 it will be in boost mode. In fig. it shows the diagram of the buck boost converter

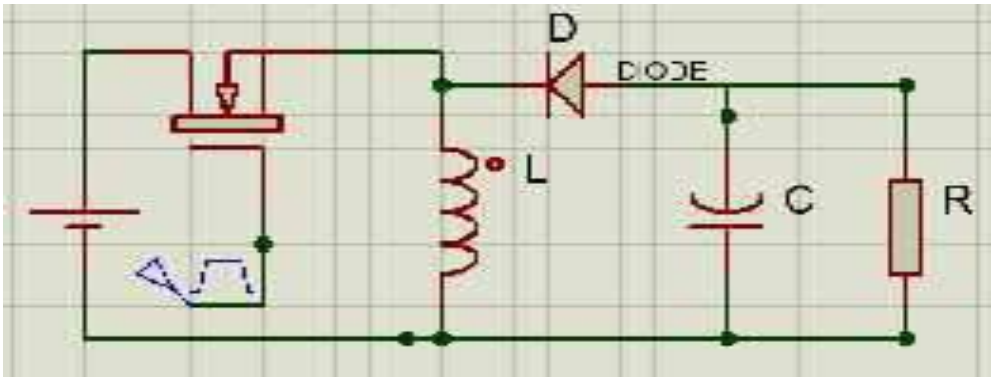

Figure 4. Buck Boost DC-DC Converter

inductor, and the current path passes through the diode (D) and capacitor (C).
Because this article uses a buck-boost DC-DC converter, there are several reasons for choosing a buck-boost converter model for this task.

- Ability to run buck mode and boost mode
- Easy design
- Reduce costs
- Reduce power loss
- Fewer components required

One feature of this type of converters is the output of this converter has the opposite polarity with respect to it is input.

Perturb And Observe Maximum Power Point Tracking Algorithm (P&O Mppt)

Solar cells are considered the most advertised source of renewable energy because of their availability and the positive impact of this energy on the environment.
This solar energy affected by weather conditions, such as temperature, irradiance, shading etc.
Many techniques, such as Constant Voltage MPPT, perturbation and observation Algorithm and Incremental conductance (INC) MPPT algorithm, etc are used to solve this problem and ensure that the PV module operates at or near its maximum point figure 5 show the (iv) characteristic of pv cell and its maximum power point (mpp) location.
This work will be simple and fair based on the use of perturbation and observation methods. Figure 6 shows the flowchart for this technique. The symbol of the last increment and the power of one step are used to determine the next decision. Increasing the voltage on the left side of the MPP increases power, and decreasing the voltage on the right-side increases power.

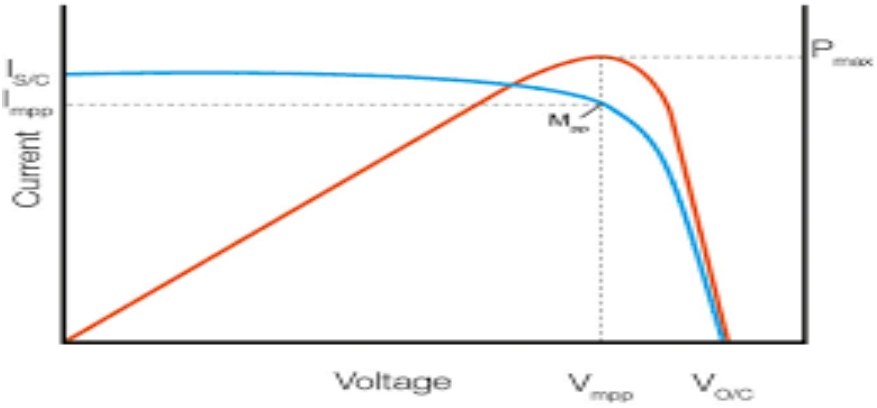

Figure 5. Current And Voltage Characteristic Of Solar

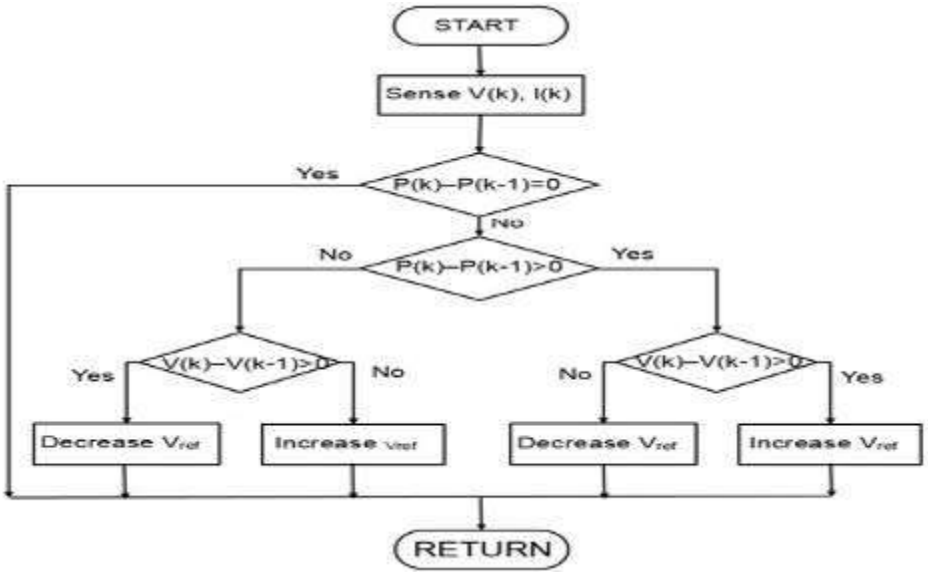

Figure 6. Chart Flow Of Perturb And Observe Method

One of the disadvantages of this approach is that the operating point does not reach this point close to the maximum point exactly, and one of the processes that improves the accuracy of the method is to reduce the step time (dt), The module takes time to work in it.

SIMULATION RESULTS

Simulation results in MATLAB 2016A are used to prove the operation of the proposed inverter with the pv module which is used to charge the batteries continuously and it is type is bpsx150 , the pv panel generate it is maximum power at vmpp = 34.5v and Imax

= 4.35 A .so due to the symmetric the all pv panels should give the same voltages,e.g 54 volt will be the voltage of of each pv module in results the dc to dc converter will operate in boost d >0.5 in figure it shows the duty cycle of the pv module.

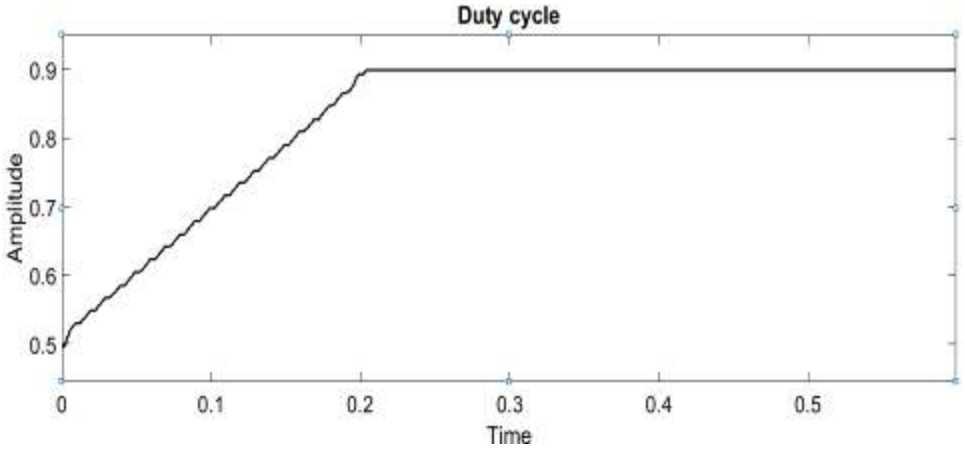

Figure 7. Duty Cycle of Buck Boost Converter

The voltage of the batteries is shown in figure (8) shown below:

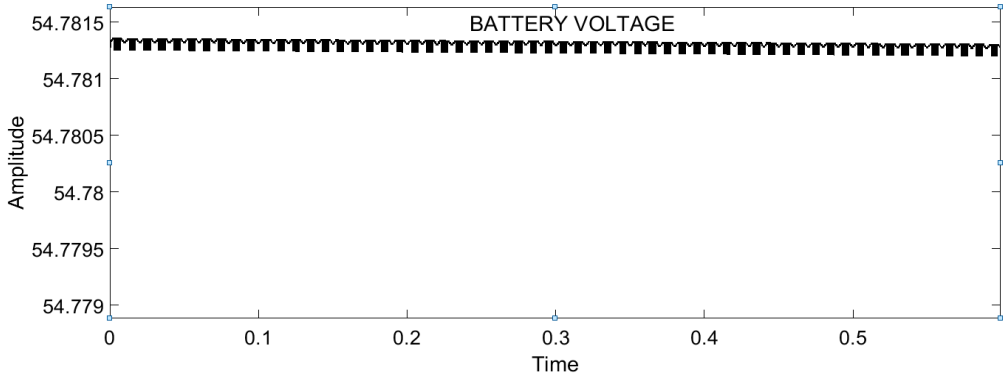

Figure 8. Battery Output Voltage

Figures (9) show the final output waveform (nine levels)

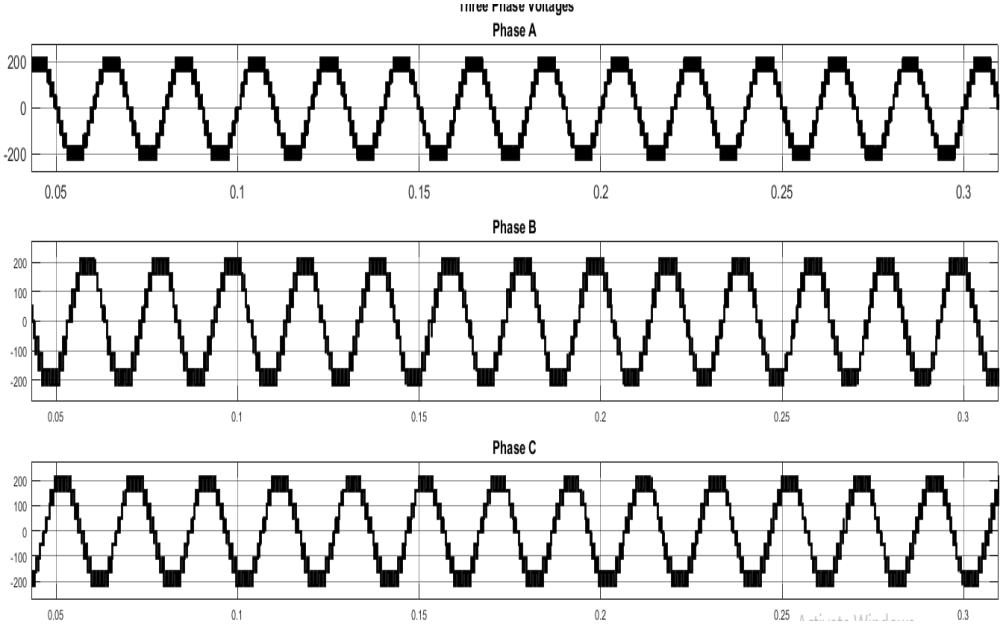

Figure 9. Three Phase Output Of Nine Level Output Voltage

CONCLUSION

In this work an improvement in the cascade inverter is done this improvement includes two points: the first is related to the number of the output levels witch increased by using minimum number of dc sources and semiconductor switches and the second concern with the amount of power which drawn from each DC source is equalized .this inverter is working perfectly with direct connect batteries and pave panels as shown in the simulation result shows the performance of the proposed inverter.

REFERENCES

[1] Adam, G. P., & Williams, B. W. (2014). New emerging voltage source converter for high-voltage application: hybrid multilevel converter with dc side H-bridge chain links. *IET Generation, Transmission & Distribution*, *8*(4), 765-773. doi:10.1049/iet-gtd.2013.0076

[2] Agelidis, V., Baker, D., Lawrance, W., & Nayar, C. (n.d.). A multilevel PWM inverter topology for photovoltaic applications. *ISIE '97 Proceeding of the IEEE International Symposium on Industrial Electronics*. doi:10.1109/isie.1997.649027

[3] Babaei, E. (2011). Charge Balance Control Methods for a Class of Fundamental Frequency Modulated Asymmetric Cascaded Multilevel Inverters. *Journal of Power Electronics*, *11*(6), 811-818. doi:10.6113/jpe.2011.11.6.811

[4] Bahravar, S., Babaei, E., & Hosseini, S. H. (2012). New cascaded multilevel inverter topology with reduced variety of magnitudes of dc voltage sources. *2012 IEEE 5th India International Conference on Power Electronics (IICPE)*. doi:10.1109/iicpe.2012.6450408
[5] Calais, M., Borle, L., & Agelidis, V. (n.d.). Analysis of multicarrier PWM methods for a single-phase five level inverter. *2001 IEEE 32nd Annual Power Electronics Specialists Conference (IEEE Cat. No..01CH37230)*. doi:10.1109/pesc.2001.954308
[6] Cintron-Rivera, J. G., Li, Y., Jiang, S., & Peng, F. Z. (2011). Quasi-Z-Source inverter with energy storage for Photovoltaic power generation systems. *2011 Twenty-Sixth Annual IEEE Applied Power Electronics Conference and Exposition (APEC)*. doi:10.1109/apec.2011.5744628
[7] Ding, K., Cheng, K., & Zou, Y. (2012). Analysis of an asymmetric modulation method for cascaded multilevel inverters. *IET Power Electronics*, *5*(1), 74. doi:10.1049/iet-pel.2010.0370
[8] Farokhnia, N., Fathi, S., Yousefpoor, N., & Bakhshizadeh, M. (2012). Minimisation of total harmonic distortion in a cascaded multilevel inverter by regulating voltages of DC sources. *IET Power Electronics*, *5*(1), 106. doi:10.1049/iet-pel.2011.0092
[9] Hossain, M. K., & Ali, M. H. (2014). Low voltage ride through capability enhancement of grid connected PV system by SDBR. *2014 IEEE PES T&D Conference and Exposition*. doi:10.1109/tdc.2014.6863248
[10] Kouro, S., Leon, J. I., Vinnikov, D., & Franquelo, L. G. (2015). Grid-Connected Photovoltaic Systems: An Overview of Recent Research and Emerging PV Converter TechNo.logy. *IEEE Industrial Electronics Magazine*, *9*(1), 47-61. doi:10.1109/mie.2014.2376976
[11] Linus, R. M., & Damodharan, P. (2015). Maximum power point tracking method using a modified perturb and observe algorithm for grid connected wind energy conversion systems. *IET Renewable Power Generation*, *9*(6), 682-689. doi:10.1049/iet-rpg.2014.0070
[12] Manjrekar, M., & Lipo, T. (n.d.). A hybrid multilevel inverter topology for drive applications. *APEC '98 Thirteenth Annual Applied Power Electronics Conference and Exposition*. doi:10.1109/apec.1998.653825
[13] Osborn, D. (2013). Wind Power Grid Integration wind power grid integration : Transmission Planning wind power grid integration transmission planning. *Renewable Energy Systems*, 1740-1768. doi:10.1007/978-1-4614-5820-3_90
[14] Sung-Jun Park, Feel-Soon Kang, Man Hyung Lee, & Kim, C. (2003). A new single-phase five-level PWM inverter employing a deadbeat control scheme. *IEEE Transactions on Power Electronics*, *18*(3), 831-843. doi:10.1109/tpel.2003.810837
[15] Rao, S. N., Kumar, D. V., & Babu, C. S. (2013). New multilevel inverter topology with reduced number of switches using advanced modulation strategies. 2013 International Conference on Power, Energy and Control (ICPEC). doi:10.1109/icpec.2013.6527745
[16] Syed Abdul Moiz, M. (2019). *Study and Simulation of Seven Level - Ten Switch Inverter Topology*. International Journal Of Research, VIII(2236-6124), 778-803.

[17] Thilaga, S., & Kumar, S. (2013). Simulation and Analysis of Seven Switch Nine-Level Hybrid Cascaded Inverter for Fuel Cell Applications. Applied Mechanics And Materials, 367, 199-203. doi: 10.4028/www.scientific.net/amm.367.199.

DESIGN OF AN EXPERIMENTAL SETUP FOR DETERMINING FRICTION PARAMETERS OF LINEAR PNEUMATIC CYLINDERS

Mustafa DAĞDELEN
Çukurova University, Mechanical Engineering Department
mdagdelen@cu.edu.tr

Mehmet İlteriş SARIGEÇİLİ
Çukurova University, Mechanical Engineering Department
msarigecili@cu.edu.tr

ABSTRACT: The friction resistance characteristics should be identified clearly to ensure precise control of linear pneumatic cylinders. There are many friction models [Tran et al. (2015); Schroeder and Singh (1993); Liu et al. (2011); Kosari and Moosavian (2015); Belforte et al. (2003)] developed for pneumatic cylinders available in the literature. In this study, an experimental setup designed to determine the parameters of the Static-Coulomb-Stribeck-Viscous friction model [Kosari and Moosavian (2015)] for a given pneumatic cylinder will be presented. In the experimental setup, there is a compressor for driving piston rod, a pressure regulating valve for adjusting the pressure and two speed control valves for controlling the speed of piston rod. For controlling the direction of motion of piston rod, a control card is utilized where a solenoid valve, two-way relay card as well as control buttons are connected to this card. While the net force acting on the piston rod can be calculated with the pressure sensors connected to the inlet and outlet ports, the linear potentiometer connected to the piston rod can provide instant position information of the piston rod and thus speed and acceleration information. The desired friction parameters can easily be found from the experiments by transferring the data to the computer via the control card.

Key words: Pneumatic cylinder, friction model, parameter estimation, experimental setup

Acknowledgement: This project is funded by "ÖYP Coordination" in Çukurova University.

REFERENCES

Tran, X., Dao, H., & Tran, K. (2015). A new mathematical model of friction for pneumatic cylinders. *Proceedings of the Institution of Mechanical Engineers, Part C: Journal of Mechanical Engineering Science, 230*(14), 2399-2412. doi:10.1177/0954406215594828.

Schroeder, L. E., & Singh, R. (1993). Experimental Study of Friction in a Pneumatic Actuator at Constant Velocity. *Journal of Dynamic Systems, Measurement, and Control*, 115(3), 575. doi:10.1115/1.2899143.

Liu, H., Chen, J., Tao,G. (2011).Parameter identification and analysis of pneumatic cylinders friction model based on experiments. *Proceedings of the 8th JFPS International Symposium on Fluid Power*,pp.276-284, 25-28 Oct., OKINAWA.

Kosari, H., Moosavian, S.A.A., 2015. Friction Compensation in a Pneumatic Actuator Using Recursive Least Square Algorithm. *5th Australian Control Conference (AUCC)*, 5th-6th Nov., Gold Coast, Australia, pp. 81-86.

Belforte, G., Mattiazzo, G., Mauro, S., & Tokashiki, L. R. (2003). Measurement of friction force in pneumatic cylinders. *Tribotest*, 10(1), 33-48. doi:10.1002/tt.3020100104.

EFFECT OF HEAT TREATMENT PROCESS ON PHASE TRANSFORMATION OF NEW TYPE ZIRCONIA BASED SOLID ELECTROLYTE SYSTEM

Aynur GÜRBÜZ
Mersin University, Advanced Technology Education Research and Application Center, Ciftlikkoy Campus, 33343, Yenisehir/Mersin/Turkey
aynurgurbuz@mersin.edu.tr

Serdar YILMAZ
Mersin University, Department of Physics, Ciftlikköy Campus, 33343, Yenisehir/Mersin/Turkey
Mersin University, Department of Nanotechnology and Advanced Materials, Ciftlikköy Campus, 33343, Yenisehir/Mersin/Turkey
syilmaz@mersin.edu.tr

ABSTRACT: In this study, heat treatment procedure was investigated of $(Yb_2O_3)_x(Y_2O_3)_y(ZrO_2)_{1-x-y}$ solid electrolyte ternary system for x=0.2,0.4,0.8 and y=0.2,0.4,0.8. The heat treatment steps for stabilizing of high temperature doped Zirconia Oxide based systems is an important parameter. Also the cubic phase of these electroceramic systems uses in many application such as SOFCs, oxygen sensors and thermal barrier materials as a solid state electrolyte. In the sintering procedure not only the gradual heat treatment but also only one step heating is open to research. For this reason in this study we compared the gradual heat treatment and one-step heating effect on microstructure and crystal formation of the samples calcined at 750 °C for 2 hours. In the first group of materials, the gradual heat treatment was applied consecutively at 900, 1000 and 1100 °C for 24 h and in the second group only one-step heating applied at 1000 and 1100 °C for 24 h. The grain structures of the samples sintered at different temperatures and times were examined by FE-SEM. There was no difference in grain structure and size between the two groups. The crystal structures of the samples were examined by XRD. When XRD data were analyzed, cubic structure formation was observed at all of synthesized powders. Because there is no difference between two group materials, it is proposed that the one-step sintering is efficient and the optimum synthesis temperature for the synthesis of $(Yb_2O_3)_x(Y_2O_3)_y(ZrO_2)_{1-x-y}$ solid electrolyte was proposed as 900 °C for 24 h which is lowest sintering temperature.

Key Words: Electroceramic, Solid Electrolyte, Sintering, ZrO_2
Acknowledgement: This study is supported by the Mersin University (project no: 2018-1-TP3-2795).

AUTOMATIC RECOGNITION OF VINE LEAF DISEASES USING DEEP LEARNING AND CONVOLUTIONAL NEURAL NETWORKS

Ahmet Alkan, KSÜ, Department of Electrical &Electronics Engineering, Kahramanmaraş, aalkan@ksu.edu.tr

Muhammed Üsame Abdullah, KSÜ, Department of Electrical &Electronics Engineering, Kahramanmaraş, ousalab@gmail.com

Hanadi Omaish Abdullah, GAÜN, Department of Civil Engineering,Gaziantep, hanadi@gantep.edu.tr

Muhammed Assaf, KSÜ, Department of Agriculture Engineering, Kahramanmaraş, agro.assaf81@gmail.com

ABSTRACT: Grape production for grape juice and grape are a very important economic issue in and around Syria. There are vast vineyards in this area. Quality is also very important in grape production as it is in most areas today. The aim of this research is to improve the accuracy of detection of diseases in vine leaves and to develop a system to help Syrian and Turkish farmers, Agricultural Engineers. The proposed system will be useful for the early identification of diseases to be processed later and thus contribute to raising the efficiency and quality of crops of this type of fruit. In this study, images (600 pictures) of vine leaves were collected from farmers and the internet. These images were processed using MATLAB 2018B. The proposed methodology will be able to increase the effective and healthy grape leaves and grape growth in Syria and nearby areas. Also, this new technique will provide researchers and international farmers with disease diagnosis which can be used in the production of high-quality grapes. Deep learning and Convolutional Neural Network (CNN) technologies and transfer learning algorithm were used to increase the accuracy of disease detection in grape leaves to produce high-quality grapes. In this research CUDA code and GPU processing were used for Accelerate processing. After this step, we became able to build a system capable of detecting five types of diseases and natural/healthy condition automatically and rapidly. The experimental studies showed that the total recognition of the accuracy of the proposed system reached to 91.1%.

Key words: Convolutional Neural Network(CNN), CUDA code, Deep learning, transfer learning, GPU processing.

INTRODUCTION

The plant diseases recognition with deep learning is considered one of the most advanced and modern techniques. Here is a summary of research into these techniques:

Reis et al, presented a simple system for the detection, which works in the natural environment, for vine, in color images range, they used of one a simple technique which based on image processing, this technique is work on recognizing between white and red grapes, this system which based on this technique is also to work at night, which can be using in help the working of harvesting robot. The system presented here represents part of an effort that is being made by their team to help introducing PA (Precision Agriculture) and PV (Precision Viticulture) in the farmers' every day (Reis *et al*, 2012).

Mohanty et al ,used deep learning for classification of 14 crop species with 26 diseases (or healthy) they used dataset consist of 54.000 images from PlantVillage which it is open access. They reported the obtained results will help in the diagnosis of cases and the identification of diseases automatically *(Mohanty et al , 2016).*

K. Muthukannan et al, used feed forward neural network (FFNN) which is one kind of the artificial neural network algorithm (ANN) to solve complex problems by modelling complex input-output relationships. They used Learning Vector Quantization (LVQ) is a supervised version of vector quantization that can be used for labeled input data. The inputs were 118 images, this leads to the classification stage in output, in addition to this ,they used radial basis function network (RBF) were tested for two different diseased leaf image classifications such as bean and bitter gourd leaves *(K. Muthukannan et al,2015).*

Thanki et al , used machine learning, for example on machine learning approaches which they used, the support vector machine (SVM) *(Ahmet, A. (2011))*, neural network models and clustering models. To predict specific diseases and classify various diseases from the input plant leaf images of different plants, and for the quantification of disease severity in plants, they used images from potato and tomato leaves, and they can classification for leaf identification and disease detection, this leads to meet the new challenges in the field of agriculture *(Thanki et al ,2018) .*

S. E. A. Raza and et al, used thermal imaging by thermal camera, which provides a fast and non-destructive way of scanning plants, for diseased regions, Thermal imaging used to study the effect of disease, on the thermal profile of a plant, and they developed a machine learning system, to remotely detect plants infected, they used support vector machine (SVM), which it is one of kind machine learning, where it used to classification between diseases leaves and healthy leaf *(Raza and et al,2015).*

As can be seen from the studies above, transfer learning based deep learning and in particular the use of digital image processing has made the detection of leaf diseases possible. This study contributes to the developments in this field by presenting a new technique based on deep learning to increase the accuracy of disease detection in vine

leaves for greater efficiency of high-quality grape production. To the best of our knowledge, there have been no studies of this kind in the literature on image processing research.

For this, in our research, we will try to present a new technique, to increase accuracy for detection of diseases in vine leaves for contributing in obtaining high-quality grape production, this new technique is based on deep learning.

MATERIALS

We have used 600 images of vine leaves that were collected from farmers and internet. A sample of dataset is shown Figure 2. We have employed Matlab2018A, Neural Network Toolbox . As an CNN network we have used Alexnet which is a pre-trained network and contain 25 layers. The first five layers are convolutional layers and the final three layers are fully connected layer as can be seen in the Figure 1.
The first layer, the image input layer, requires input images for size 227-by-227-by-3, where 3 is the number of color channels
net = alexnet;
net.Layers

```
ans =
  25x1 Layer array with layers:

     1   'data'     Image Input                 227x227x3 images with 'zerocenter' normalization
     2   'conv1'    Convolution                 96 11x11x3 convolutions with stride [4  4] and padding [0  0  0  0]
     3   'relu1'    ReLU                        ReLU
     4   'norm1'    Cross Channel Normalization  cross channel normalization with 5 channels per element
     5   'pool1'    Max Pooling                 3x3 max pooling with stride [2  2] and padding [0  0  0  0]
     6   'conv2'    Convolution                 256 5x5x48 convolutions with stride [1  1] and padding [2  2  2  2]
     7   'relu2'    ReLU                        ReLU
     8   'norm2'    Cross Channel Normalization  cross channel normalization with 5 channels per element
     9   'pool2'    Max Pooling                 3x3 max pooling with stride [2  2] and padding [0  0  0  0]
    10   'conv3'    Convolution                 384 3x3x256 convolutions with stride [1  1] and padding [1  1  1  1]
    11   'relu3'    ReLU                        ReLU
    12   'conv4'    Convolution                 384 3x3x192 convolutions with stride [1  1] and padding [1  1  1  1]
    13   'relu4'    ReLU                        ReLU
    14   'conv5'    Convolution                 256 3x3x192 convolutions with stride [1  1] and padding [1  1  1  1]
    15   'relu5'    ReLU                        ReLU
    16   'pool5'    Max Pooling                 3x3 max pooling with stride [2  2] and padding [0  0  0  0]
    17   'fc6'      Fully Connected             4096 fully connected layer
    18   'relu6'    ReLU                        ReLU
    19   'drop6'    Dropout                     50% dropout
    20   'fc7'      Fully Connected             4096 fully connected layer
    21   'relu7'    ReLU                        ReLU
    22   'drop7'    Dropout                     50% dropout
    23   'fc8'      Fully Connected             1000 fully connected layer
    24   'prob'     Softmax                     softmax
    25   'output'   Classification Output       crossentropyex with 'tench' and 999 other classes
```

Figure1. Layers in the Alexnet

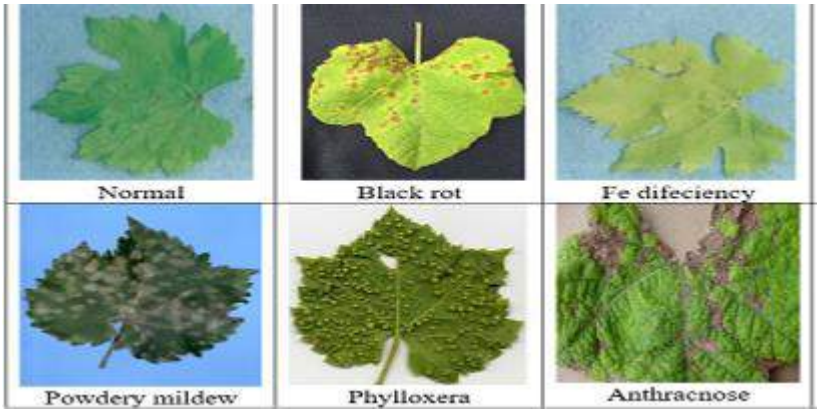

Figure 2. A sample of dataset

In this study was used transfer learning that based on deep learning, but what is transfer learning and why we used it ?
Transfer learning is an efficient solution for many problems. Training requires some data and computer time, but much less than training from scratch, and the result is a network suited to our specific problem , we benefited from pretrained network (Alexnet as example) in new building for our network , Figures 3,4 *(www.mathwork.com, n.d,2017)*.

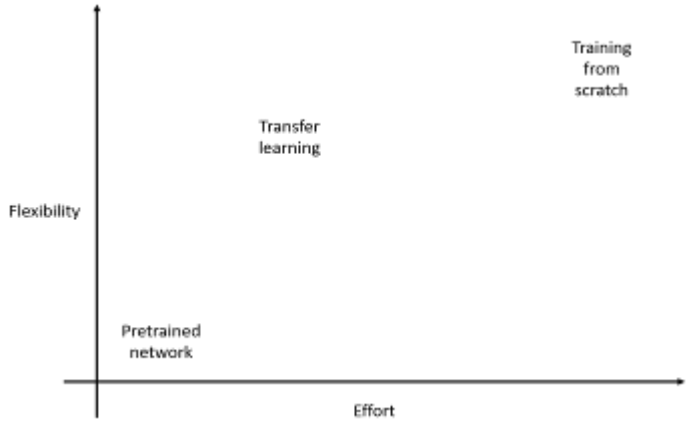

Figure 3. Transfer learning between pretrained network and training from scratch

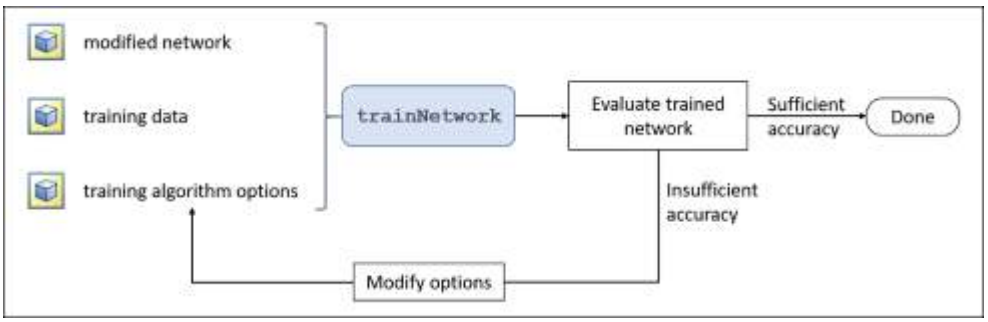

Figure 4. Typical workflow for transfer learning

METHODS

Pre-Processing of the Images :

We have resized the images to 227*227*3 where 3 is the number of color channels, This process is done by Matlab2018B and manually, We can do this through Paint program or another photo editing program Figure.5 .

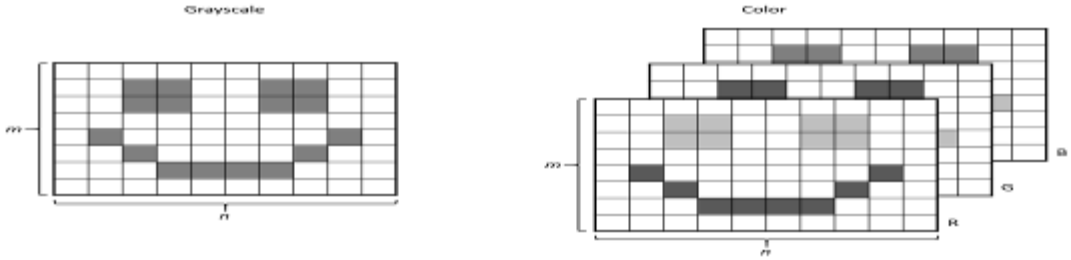

Figure 5. The deference between grayscale and color images

Training and Testing Stages:

After above step and by Alexnet network and transfer learning code, where we can run the new code with new data and new inputs. At this stage, all legacy network data will be erased and replaced with new our data, where our data are 600 images with 6 categories (There are five kinds of diseases and a normal condition, each category contain 100 images).

The new code will run automatically in training network stage and testing stage. We used Alexnet based on CUDA code which work with Nvidia productions, and all processing operations can be done with GPU, that helps to accelerate the processing and achieve a high accuracy. Figure.6 is shown stages of processing of diseases in vine leaves by Deep learning.

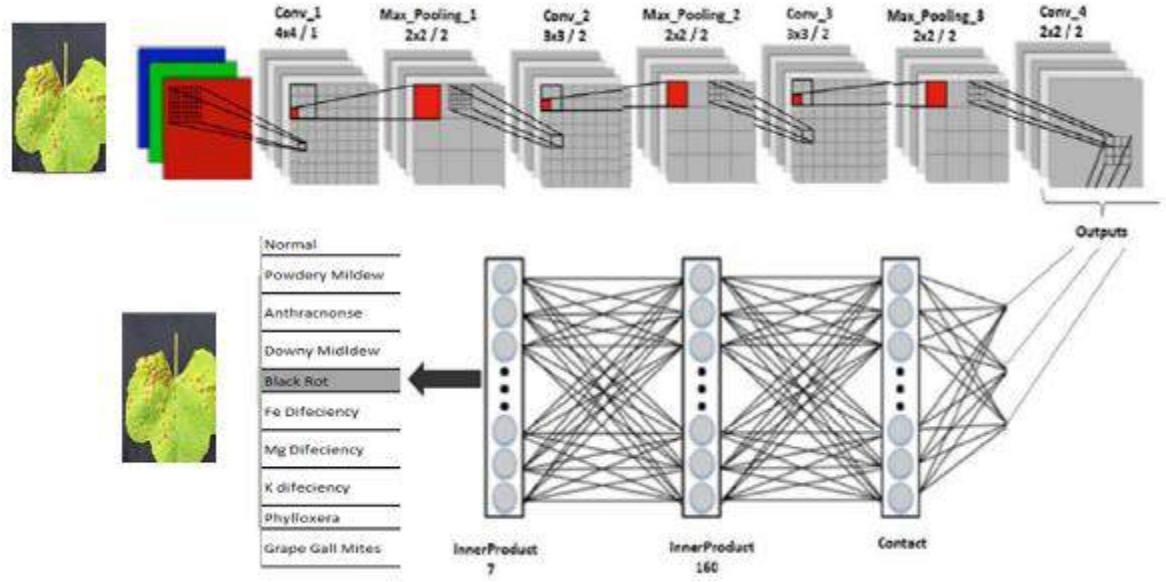

Figure 6. stages of processing of diseases in vine leaves by Deep learning

RESULTS AND FINDINGS

In the system, which we have proposed, we can confirm the results by some commands in Matlab 2018B We knew the number of randomly selected images for the testing phase by the following command in Matlab 2018B:

Vine Actual = testImages.Labels ;
>> vinePreds = classify(myNet,testImages)
vinePreds =
180×1 categorical array

Now for knowing how many images is correct and identical to the category to which it belongs by next command we knew this :

>> numCorrect = nnz(vinePreds == vineActual)
numCorrect = 164
>> fracCorrect = numCorrect/numel(vinePreds)
fracCorrect =
accuracy = 0.9111

Where: Accuracy =Total number of vine images correctly /Total number of vine images used for testing
According to this : 164/180=0.91111
For a confusion matrix Figure7.This figure shows the number of correct and incorrect images when testing stage

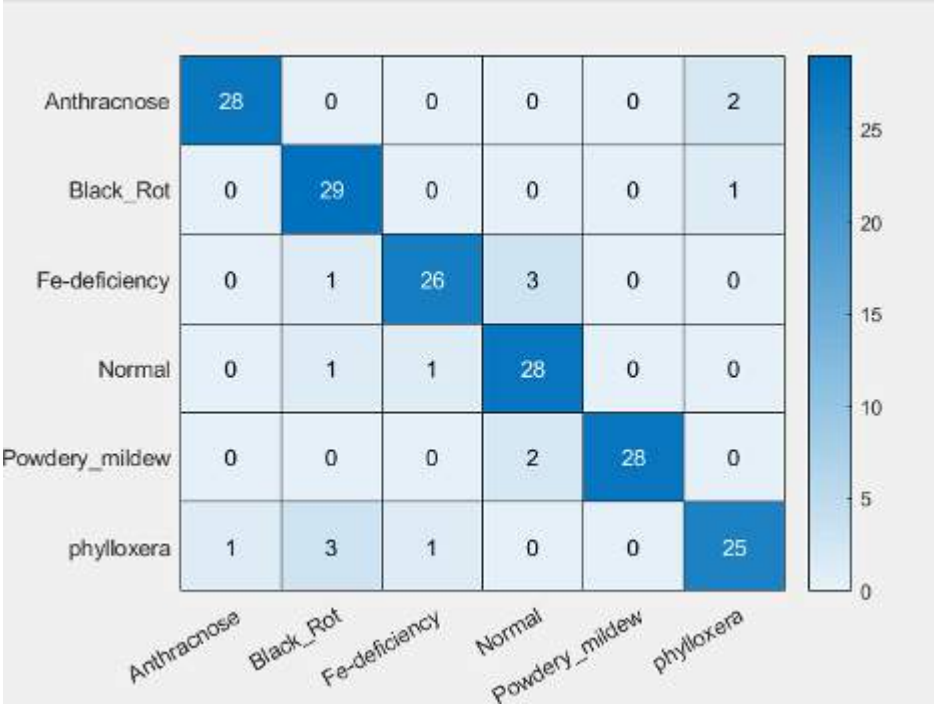

Figure7. Confusion matrix

CONCLUSION

In this project we have used deep learning and transfer learning for detection the diseases of vine leaves automatically , these diseases are defined by five types of diseases(Anthracnose, Black Rot, Fe-deficiency, Phylloxera, Powdery mildew) and Normal type .Finally, the proposed system obtained the accuracy of 91.1%. So that this system can detect/recognize diseases automatically and rapidly, therefore our proposed system will be helpful for the farmers and scientists that study in related areas.

RECOMMENDATIONS

For future projects, we aspire to expand with the other diseases for vine leaves also, we aspire to transform this system to work on mobile devices in order to be of greater benefit to farmers and agricultural engineers. Also , Also the used methodology may be used/ applied to the different images for the different analyses for the different plants.

ACKNOWLEDGMENT

This research is sponsored by CARA organization (from Uk for Academics). This research has won a small grant from Cara, so the authors of this research thank Cara for sponsoring this research.

REFERENCES

Reis, M.J.C.S., Morais, R., Peres, E., Pereira, C., Contente, O., Soares, S., Valente, A., Baptista, J., Ferreira, P.J.S.G., Bulas Cruz, J., (2012). Automatic detection of bunches of grapes in natural environment from color images. J. Appl. Log. 10, 285–290. https://doi.org/10.1016/j.jal.2012.07.004

Mohanty, S. P., Hughes, D. P., & Salathé, M. (2016). Using Deep Learning for Image-Based Plant Disease Detection. Frontiers in Plant Science, 7. https://doi:10.3389/fpls.2016.01419

Muthukannan, K., Latha, P., Pon Selvi, R., Nisha, P., (2015). Classification of diseased plant leaves using neural network algorithms. ARPN J. Eng. Appl. Sci. 10, 1913–1919.

Thanki, R., Borra, S., Dey, N., Ashour, A.S., (2018). Machine Learning Based Plant Leaf Disease Detection and Severity Assessment Techniques: State-of-the-Art, Lecture Notes in Computational Vision and Biomechanics. https://doi.org/10.1007/978-3-319-65981-7_1.

Raza, S.E.A., Prince, G., Clarkson, J.P., Rajpoot, N.M.,(2015). Automatic detection of diseased tomato plants using thermal and stereo visible light images. PLoS One 10, 1–20. https://doi.org/10.1371/journal.pone.0123262.

www.mathwork.com,n.d. https://matlabacademy.mathworks.com/R2017b/portal.html?course=deeplearning&s_tid=course_dlor_start.

Ahmet, A. (2011). Analysis of knee osteoarthritis by using fuzzy c-means clustering and SVM classification. Scientific Research and Essays, 6(20), 4213–4219. doi:10.5897/sre11.068.

FACIAL EXPRESSION RECOGNITION USING CONVOLUTIONAL NEURAL NETWORKS

Ahmet Alkan, KSÜ, Department of Electrical &Electronics Engineering, Kahramanmaraş, aalkan@ksu.edu.tr

Muhammed Üsame Abdullah, KSÜ, Department of Electrical &Electronics Engineering, Kahramanmaraş, ousalab@gmail.com

Hanadi Omaish Abdullah, GAÜN, Department of Civil Engineering,Gaziantep hanadi@gantep.edu.tr

ABSTRACT: The face recognition technique using deep learning is one of the most advanced and modern techniques. Face recognition have been used for security purposes such as sensitive security centers, airports, metro stations, tramway stations, and any other crowded places. Identification of the facial expressions using convolutional neural networks is a novel technology, and it was intended to be used to recognize facial expressions on social media sites. However, as far as we know, facial recognition has not been studied together with facial expression in previous research. So, this research introduces a convolutional neural network based deep learning technique to recognize faces and facial expressions together.
The aim of this research is to introduce new technology to use in companies, institutions and schools, in order to aid psychiatrists when there are large numbers of staff, employees or students, need to follow their psychological situations. In this research, images of five people (four males and one female) with eight emotional state expressions (anger, happiness, surprise, disgust, concentration, sadness, and fear) were used. These images were taken from publicly available MMI dataset which is available to those working in higher education institutions and is provided on the condition that it is being used only for educational and research purposes. 1200 images were processed using convolutional neural networks (CNNs) developed on MATLAB2018-a environment. Obtained results on the used database showed that the proposed system capable of recognizing facial expressions related to the emotional states and faces (the names of people for the five people mentioned above), with the excellent accuracy.

Keywords: Deep learning ,CNN, Facial Expression .

INTRODUCTION

Face recognition technology and recognizing facial expressions with deep learning is considered one of the most advanced and modern techniques. Here is a brief summary of research related to these techniques:

Veena Mayya and et al., proposed a method to automatically recognize facial expressions. Their method was based on Deep Convolutional Neural Network (DCNN) that focuses on recognizing the facial expressions of an individual from a single image. The feature extraction time is significantly reduced by using general purpose graphic processing unit (GPGPU). They used images from CK+ Dataset (Japanese Female Facial Expression) and JAFFE Dataset for many facial expressions such as, anger, disgust, fear, happiness, neutral, sadness and surprise expressions *(Veena Mayya and et al,2016)*.

Abir Fathallah and et al., have used Deep Neural Networks (DNN) based on Convolutional neural networks (CNN) for Automated Facial Expression Recognition. They fine-tuned their architecture with the Visual Geometry Group model (VGG) to improve results. To evaluate their architecture, they tested it with many large public databases (CK+, MUG, and RAFD).

The results obtained showed that the CNN approach is very effective in image expression recognition on many public databases which represented an improvement in facial expression analysis *(Abir Fathallah and et al,2017)*.

Dinh Viet Sang and et al., have applied recent advances in deep learning to propose effective deep Convolutional Neural Networks (CNNs) that can accurately interpret semantic information available in faces in an automated manner without hand-designing of features descriptors. They used the FERC-2013 dataset provided on the Kaggle facial expression recognition competition. The dataset consists of 35,887 gray images of 48x48 resolution. Kaggle has divided these images into 28,709 training images, 3589 public test images and 3589 private test images *(Dinh Viet Sang and et al,2017)*.

Shraddha Arya and et al., proposed a method for face recognition based on Deep learning and Linear Discriminant Analysis (LDA), where typical structures of face recognition system consist of three major steps, obtaining face data, extracting facial features and recognition of faces. In the first phase, the face images are partitioned into multiple face parts. This step is termed as the pre-processing of images. Secondly, the images are processed for feature extraction to apply the LDA algorithm. Finally, the neural network is proposed to perform training on extracted face features and classes and the trained model is used for recognizing the faces *(Shraddha Arya and et al,2018)*.

Hayfaa Hussein and et al., in their research, they relied on the geometric features of facial expressions with relatively low complexity. They used three databases of different faces images, namely VDMFP, BINED, and MMI. These databases contain images of different facial expressions in different imaging conditions. These images were rotated around a central point. then these images were processed and features were extracted using deep learning *(Hayfaa Hussein and et al,2018)*.

Examining the summarized previous studies, we can reach the conclusion that most of the research focused on face recognition without focusing on facial expression

recognition, or have been focused on facial expression without focusing on face recognition , therefore in the current study we presented new technique for recognize the facial expression and faces for the five people mentioned above .

MATERIALS

In this research we have used 1200 images belonging to five people these pictures are distributed over eight psychological/emotional expressions so that each person has eight facial expressions (anger, happiness, surprise, disgust, concentration, sadness, and fear) and therefore we have 40 categories in each category 30 pictures, It should be noted that the images were obtained from a base and after we pledged to use them only for scientific and research purposes, we then classified facial expressions and we put fake names of the five people (Mary, Mechil , Mario, Jon, Frank)

A sample of dataset is shown Figure 1. We have employed Matlab2018A, Neural Network Toolbox. As an CNN network we have used Alexnet which is a pre-trained network and contain 25 layers. The first five layers are convolutional layers and the final three layers are fully connected layer as can be seen in the Figure 1.

The first layer, the image input layer, requires input images for size 227-by-227-by-3, where 3 is the number of color channels.

Figure 1. A sample of dataset

Convolutional Neural Networks (CNNs) are one of the most popular and novel neural network architectures. They are extremely successful at image processing, but also for many other tasks (such as speech recognition, natural language processing, and more). The state of the art CNNs are pretty deep (dozens of layers at least), so they are part of Deep Learning.

In this study transfer learning that is based on deep learning has been employed for the analysis. Transfer learning is an efficient solution for many problems. Training requires some data and computer time, but much less than training from scratch, and the result is a network suited to our specific problem we benefited from pretrained network (Alexnet as example) in new building for our network , Figures 2,3 *(www.mathwork.com, n.d,2017)*.

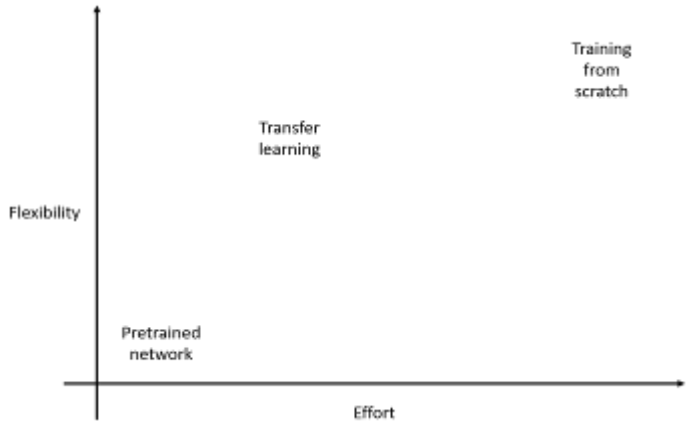

Figure 2. Transfer learning between pretrained network and training from scratch

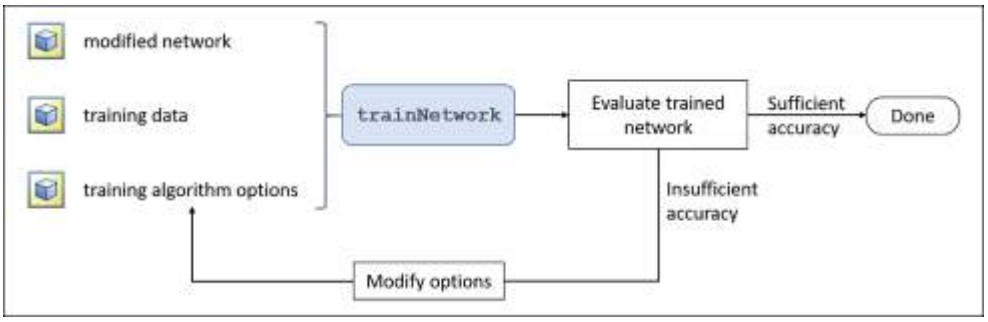

Figure 3. Typical workflow for transfer learning

METHODS

Pre-Processing of the Images:

Image database have been used by resizing/reducing the dimension of them to 227*227*3 where 3 is the number of color channels. This dimension reduction is needed for the proposed deep learning based CNNs.[1]

Training and Testing Stages:

After above preprocessing step, we have applied the data into Alexnet network and transfer learning code, where we can run the new code with new data and new inputs. At this stage, all legacy network data will be erased and replaced with new our data,

where our data are 1200 images with 40 categories (for five people with eight facial expressions, each category contain 30 images). we selected 70% from images (840 images) for training stage and 30% from images (360 images) for testing stage.
The developed code will run automatically in training network stage and testing stage. We have used Alexnet based on CUDA code which work with Nvidia productions, and all processing operations can be done with GPU, that helps to accelerate the processing and achieve a high accuracy. Stages of the developed facial expressions and face recognition system is shown in figure 4.

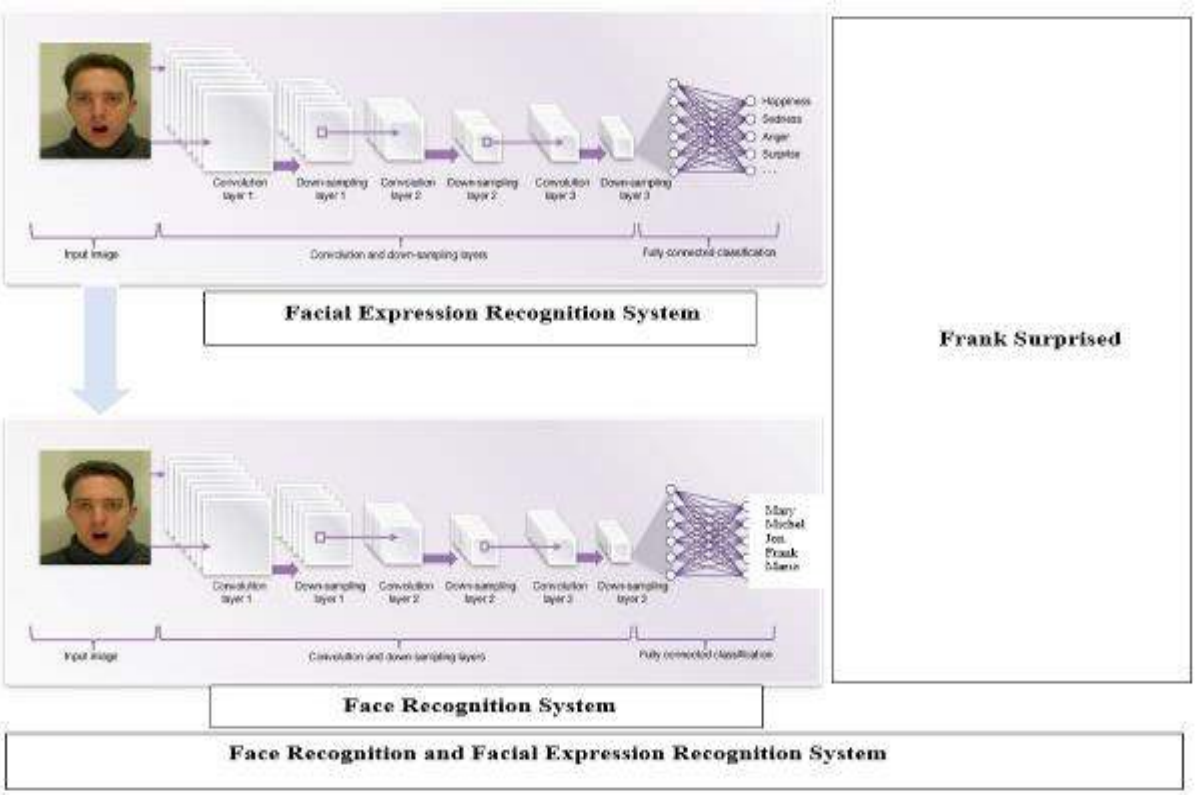

Figure 4. Processing stages of the proposed system by using CNN based Deep learning

RESULTS AND FINDINGS

In the proposed system, the system was reduced to 227*227*3 by reducing its dimensions (Ahmet, A. (2011)) and classified with CCN based deep learning. 70% of the dataset was used for the training of the system. After the training process was completed, the test process was completed using the remaining 30% dataset.

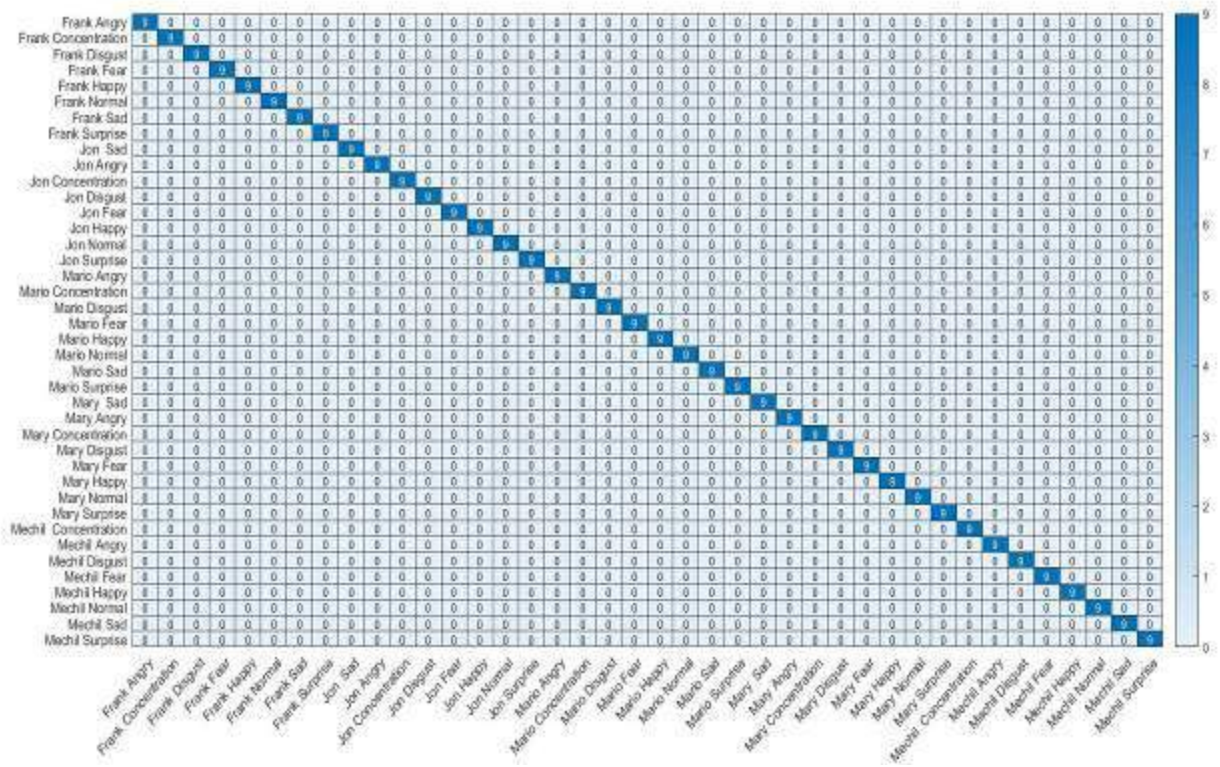

Figure 5. confusion matrix

When the accuracy of the test process was calculated, an excellent classification performance (100% classification accuracy) was obtained. With the proposed system, both the face of the person and the emotional state of the person whose face is recognized have been classified very successfully. Figure 5. shows the confusion matrix that includes the number of correct and incorrect images on testing stage, where the X-axis represents the predicted situations and the Y-axis represents the actual situations.

CONCLUSIONS

In this study to recognize the facial expressions and faces automatically, we have proposed a system employed used convolutional neural networks and transfer learning, these faces with fake names are five people (Mary-Mechil -Mario -Frank -Jon) and eight facial expressions are anger, happiness, surprise, disgust, concentration, sadness, and fear. Finally, the proposed system obtained the accuracy of 100%. So that this system can detect/recognize facial expressions and faces automatically and rapidly, therefore our proposed system will be helpful for the psychiatrists and scientists that study in related areas.

RECOMMENDATIONS

For future projects, we plan to expand this research to include recognizing a much larger number of people, based on our own database, in order to provide more help for psychiatrists and contribute to accelerating the solution of psychological problems for students, workers, and employees or the target groups in this research.

REFERENCES

V. Mayya, R. M. Pai, and M. M. Manohara Pai.(2016). "Automatic Facial Expression Recognition Using DCNN," Procedia Comput. Sci., vol. 93, no. September, pp. 453–461.

A. Fathallah, L. Abdi, and A. Douik.(2017). "Facial Expression Recognition via Deep Learning," 2017 IEEE/ACS 14th Int. Conf. Comput. Syst. Appl., pp. 745–750.

Sang, D. V., Van Dat, N., & Thuan, D. P. (2017). Facial expression recognition using deep convolutional neural networks. 2017 9th International Conference on Knowledge and Systems Engineering (IEEE /KSE). doi:10.1109/kse.2017.8119447.

A. A. M.E, Shraddha Arya.(2018)."Face Recognition with Partial Face Recognition and Convolutional Neural Network," vol. 7, no. January, pp. 91–94.

Hussein, H., Angelini, F., Naqvi, M., & Chambers, J. A. (2018). Deep-Learning Based Facial Expression Recognition System Evaluated on Three Spontaneous Databases. 9th International Symposium on Signal, Image, Video and Communications (ISIVC). doi:10.1109/isivc.2018.8709224 .

www.mathwork.com,n.d.
https://matlabacademy.mathworks.com/R2017b/portal.html?course=deeplearning&s_tid=course_dlor_start.

Ahmet, A. (2011). Analysis of knee osteoarthritis by using fuzzy c-means clustering and SVM classification. Scientific Research and Essays, 6(20), 4213–4219. doi:10.5897/sre11.068.

THERMODYNAMIC ANALYSIS OF HYBRID GEOTHERMAL POWER PLANT SUPPORTED WITH BIOMASS USING DIFFERENT BIOMASSES

Mustafa Alper YERLİKAYA
Erzincan Binali Yıldırım Üniversitesi
Alperyk24@hotmail.com

Prof Dr. Ahmet TANDIROĞLU
Erzincan Binali Yıldırım Üniversitesi
atandıroglu@erzincan.edu.tr

ABSTRACT: The concept of energy and the sustainability of energy resources have been one of the most important issues and problems on a global scale from the past to the present. With all the technological developments, different fossil energy sources have been used over time (coal, oil, natural gas, etc.). Furthermore, considering the damages it causes to the environment and humanity, the demand for renewable energy sources, which are environmentally friendly, increased. One of these renewable energy sources is biomass. Biomass energy has started to gain importance as it has an impact on the solution of the global environmental and air pollution problems. In developing and energy-needly countries, especially Turkey which has high potential of waste and animal, the value given to biomass should increase in order to decrease dependence on importing energy since herbal animal and other waste are in biomass class too.
After an overview of the kinds of biomass energy in Turkey in this study the most efficient and economic was chosen by comparison. Then a model of biomass supported hybrid geothermal power plant was examined and calculations were made using certain data and assumptions. It is aimed to generate electrical energy from geothermal energy known as alternative energy source by increasing energy efficiency by using more efficient and economical biomass.

Key words: Thermodynamic Analysis, Geothermal Energy, Hybrid Geothermal Power Plant, BioMass.

FARKLI BİOKÜTLELER KULLANAN BİOKÜTLE DESTEKLİ JEOTERMAL ENERJİ SANTRALİNİN TERMODİNAMİK ANALİZİ

ÖZET: Enerji kavramı ve enerji kaynaklarının sürdürülebilir olması geçmişten günümüze kadar evrensel boyutta en önemli konulardan ve sorunlardan biri olmuştur. Teknolojik gelişmelerle birlikte zaman içerisinde çok farklı fosil enerji (kömür, petrol, doğalgaz vb.) kaynakları kullanılmıştır. Fosil enerji kaynaklarının çevreye ve insanlığa

vermiş olduğu zararları da göz önüne alınınca, çevre dostu olan yenilenebilir enerji kaynaklarına talep artmıştır. Bu yenilenebilir enerji kaynaklarından biri de biokütledir. Küresel bir sorun olan çevre ve hava kirliliği sorunlarının çözümünde de etkisi olduğundan biokütle enerjisi önem kazanmaya başlamıştır. Bitkisel, hayvansal ve diğer atıklarda biokütle sınıfında olduğundan gelişmekte ve enerji ihtiyacı çok olan ülkelerde ve özellikle hayvansal ve atık olarak önemli bir biokütle potansiyeline sahip olan Türkiye'de de enerjide dışa bağımlılığın azaltılması için biokütleye verilen değerin artması gerekmektedir.

Bu çalışmada Türkiye'deki biokütle enerji çeşitlerine genel bir bakış yapıldıktan sonra aralarında bir kıyaslama yapılarak en verimli ve ekonomik olanı seçilmiştir. Çalışmada, biokütle destekli hibrit jeotermal enerji santralinin bir modeli incelenmiş ve belli veriler ve kabuller kullanılarak hesaplamalar yapılmıştır. Alternatif enerji kaynağı olarak bilinen jeotermal enerjiden, daha verimli ve ekonomik biokütleler kullanılarak enerji verimi arttırılarak elektrik enerjisi üretmek amaçlanmıştır.

Anahtar sözcükler: Termodinamik Analiz, Jeotermal Enerji, Hibrit Jeotermal Enerji Santrali, Biokütle.

HYDROCHEMICAL INVESTIGATION OF HOT AND MİNERAL WATERS IN EMİR GEOTHERMAL FIELD (KULA, MANİSA)

Özgün DEMİREL
Pamukkale University
ozgun_demirel@hotmail.com

Ali GÖKGÖZ
Pamukkale University
agokgoz@pau.edu.tr

ABSTRACT: Emir geothermal field is located 13 km northeast of Kula district of Manisa province. The aim of this study is to determine the chemical composition of thermal waters in the Emir geothermal field and to provide an approach to reservoir temperature. The basement rock of the study area is the Upper Cretaceous Vezirler melange composed of serpentinite, chert, mudstones and limestone blocks. Melange is unconformably overlain by the conglomerates and sandstones of Kurtköyü formation and by the Yeniköy formation composed of conglomerates-sandstone-siltstone-claystone-clayey and sandy limestone-marl-tuffite alternations. Both formations are Miocene in age. These formations are overlain by the Lower Pliocene Ahmetler formation (Balçıkdere member), which consists of conglomerate-sandstone-claystone-marl and limestone intercalations. Qaternary is represented by the Asartepe formation, which consists of Quaternary conglomerate-sandstone intercalations and the Kula volcanics made up basalt, slag and tuffs, travertine and alluvium. There are three geothermal drillings in the Emir geothermal field, eight thermal springs and one mineral water resource. Temperatures of the thermal waters vary between 21.1 and 63.3°C, electrical conductivities 3840 to 5210 µS/cm and pH values varybetween 6.56 and 7.69. The cation arrangement is Na> Mg> Ca> K and the anion arrangement is HCO_3>Cl>SO_4. Na concentration of the thermal waters is 720-1025 mg/l, HCO_3 concentration is between 2500-3480 mg/l and they are generally are of the Na-HCO_3 type. Chalcedony and quartz geothermometers applied to approach the reservoir temperature of the thermal waters of the study area. Chalcedony geothermometers yielded reservoir temperatures ranging from 80 to 125°C and quartz geothermometers ranging from 102-150°C.

This work was supported by PAU BAP Coordinator (Project No: 2018FEBE049).

Key words: Emir, Kula, geothermal, hydrochemistry, geothermometer

EMİR JEOTERMAL SAHASI (KULA, MANİSA) SICAK VE MİNERALLİ SULARININ HİDROKİMYASAL İNCELEMESİ

ÖZET: Emir jeotermal sahası Manisa ilinin Kula ilçesinin 13 km kuzeydoğusunda yer alır. Bu çalışmanın amacı Emir jeotermal sahasındaki sıcak suların kimyasal kompozisyonlarını belirlemek ve rezervuar sıcaklığına yaklaşım sağlamaktır. İnceleme alanının temelini serpantinit, çört ve çamurtaşlarıyla kireçtaşı bloklarından meydana gelen Üst Kretase yaşlı Vezirler melanjı oluşturur. Melanj üzerine uyumsuz olarak çakıltaşı ve kumtaşından oluşan Kurtköyü formasyonu ile çakıltaşı-kumtaşı-silttaşı-kiltaşı-killi ve kumlu kireçtaşı-marn-tüfit ardalanmasından oluşan Yeniköy formasyonu gelir. Her iki formasyon da Miyosen yaşlıdır. Bu formasyonlar üzerinde çakıltaşı-kumtaşı-kiltaşı-marn ve kireçtaşı ardalanmasından oluşan Alt Pliyosen yaşlı Ahmetler formasyonu (Balçıkdere üyesi) bulunur. Kuvaterner çakıltaşı-kumtaşı ardalanmasından oluşan Asartepe formasyonu, bazalt, cüruf ve tüflerden oluşan Kula volkanitleri, traverten ve alüvyonla temsil edilir. Emir jeotermal sahasında üç jeotermal sondaj, sekiz termal kaynak ve bir maden suyu kaynağı bulunur. Termal suların sıcaklıkları 21,1 ile 63,3°C, elektriksel iletkenlikleri 3840 ile 5210 µS/cm ve pH değerleri 6,56 ile 7,69 arasında değişir. Katyon dizilimi Na>Mg>Ca>K, anyon dizilimi ise HCO_3>Cl>SO_4 şeklindedir. Sıcak suların Na derişimi 720-1025 mg/l, HCO_3 derişimi de 2500-3480 mg/l arasında olup hidrokimyasal olarak genellikle Na-HCO_3 tipindedirler. İnceleme alanı termal sularının rezervuar sıcaklığına yaklaşımda bulunmak için kalsedon ve kuvars jeotermometreleri uygulanmıştır. Kalsedon jeotermometreleri 80-125°C, kuvars jeotermometreleri ise 102-150°C arasında değişen rezervuar sıcaklıkları vermiştir.

Bu çalışma PAÜ BAP Koordinatörlüğü tarafından desteklenmiştir (Proje No: 2018FEBE049).

Anahtar sözcükler: Emir, Kula, jeotermal, hidrokimya, jeotermometre.

EXPERIMENTAL INVESTIGATION OF A SOLAR DISH COLLECTOR WITH SPIRAL COIL TUBE HEAT EXCHANGER FOR HOT WATER PRODUCTION

Devrim AYDIN
Eastern Mediterranean University
devrim.aydin@emu.edu.tr

ABSTRACT: In the last decade, solar energy technologies are gaining attention due to their potential for reducing environmental emissions and enhancing sustainability in residential and industrial applications. In this regard, solar collector systems are widely used for hot water production in buildings. Currently, flat plate collectors are mostly used collector type; however their efficiency dramatically drops in winter period when the hot water demand is at its peak. Consequently, present study is concerned with the design and development of a parabolic dish collector as an alternative to flat plate collectors. The proposed collector consists of a parabolic dish, a receiver made up of a black painted spiral coil tube heat exchanger and a glass glazing. In the system, a 50 L water tank is also used and the water is circulated between the collector and the water tank by employing a water pump.
System is tested on the coldest days of the year (10-13 December 2018) and highest water temperature of 42 °C is achieved. The average and maximum instantaneous thermal efficiencies of collector were obtained as 48% and 76% respectively.

Key words: solar energy, parabolic dish, water heating, thermal energy analysis, efficiency

INTRODUCTION

With the growing emphasis on energy conservation, renewable energy sources have received increasing attention (Tian and Zhao, 2013). The term "renewable energy" is not a new concept to the environment, but rapidly it continues to emerge as an alternative to fossil fuels and all other deleterious energy resources. Solar energy, which is one of the most abundant renewable source have the potential to meet the total global energy demand. However, only 0.02% of that energy is utilized in the present day (Devabhaktuni et al., 2013). Nevertheless, since the initial implementation of solar systems, numerous projects have been completed and the developments in the field of solar energy are ongoing. Among all renewable sources, solar energy is considered as one of the most economic and efficient alternative.

Solar systems are basically converts solar irradiation into useful form of energy such as heat or electricity. In solar thermal applications, solar collectors or concentrators are used to gather the solar radiation. The radiation energy can then be used for space/water

heating and for producing process heat in residential and industrial applications (Mekhilef et al., 2011). In the literature, several studies investigating different type of solar collector performances have been completed previously. Bellos & Tzivanidis (2018) studied flat plate collector performance experimentally and numerically under Athens conditions. Average efficiency of the investigated system was found 54.2%. Zhang et al. (2016) investigated a multi-purpose flat place solar collector for air and water heating. The overall efficiency of the collector in combined air-water heating mode reached to 73.4%.

Nikolić and Lukić (2015) studied a double exposure flate plate collector for water heating. Results showed that double exposure collector provides an efficiency enhancement of 18.4% when compared to conventional flat plate collector. Fan et al. (2019) investigated a novel solar collector with V-corrugated multi-channel absorber. Thermal efficiency of the new collector was found in the range of 69-74%, while the efficiency of conventional solar collectors is determined as 58-69% for the same operating conditions.

Jowzi et al. (2018) investigated evacuated tube collector performance with cylindrical absorbers in Greece. It is obtained that; four evacuated tube collectors connected in series can produce a maximum of 5.6 kW thermal energy. Xu et al. (2019) carried out experimental studies on evacuated tube collector performance under China climate conditions. Thermal efficiency of the developed collector was found between 43-55%.

Teles et al. (2019) numerically investigated the performance enhancement with the use of sun-tracking in evacuated tube solar collector applications in Brazil climate. The efficiencies of tracking and non-tracking evacuated tube collector were found 73% and 42% respectively. In another study, Budihardjo and Morrison (2009) performed comparative investigations between vacuum tube and flat plate collector in Sydney. The thermal performance of the vacuum tube collector was found higher while its sensitivity to the size of the storage tank was found lower compared to the flat plate collector.

Despite several studies have been performed on flat plate and vacuum tube collectors, research on dish type concentrating solar water heaters is very limited in the literature. Such type of solar systems is mostly investigated for high temperature applications such as in solar thermal power plants. Different than the previous research, in present study, a dish type concentrating solar water heater using spiral coil tube heat exchanger is investigated for residential applications under North Cyprus climate conditions.

METHODS

System Design and Operation

The proposed parabolic dish solar water heating unit consists of four main components namely; solar dish, copper coil receiver, support frame and water tank, as illustrated in Figure 1. In the system, receiver is made up of a horizontally aligned copper coil which is fitted inside a cylindrical glass glazing. With such design, it is targeted to enhance the

receiver area to eliminate the tracking requirement and to enhance the heat transfer rate to the water across the copper coil heat exchanger. During the system operation water is circulated between the water tank and receiver by using a water pump. Mass flow rate of water across the system is also controlled by using a water valve as illustrated in Figure 1.

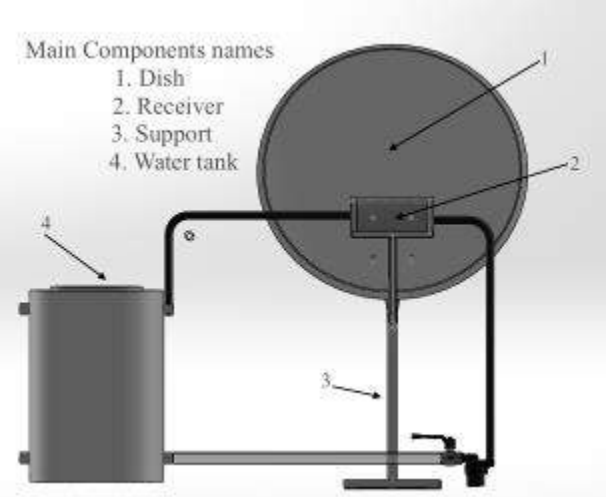

Figure 1. CAD Design of Solar Dish Water Heating System

Parabolic dish is the main component of the design that is made up of aluminum sheet metal. It is covered with reflective aluminum tape for enhancing the reflected radiation on to the receiver. The parabolic dish is of 800 mm diameter (*Dc*) with a depth (*h*) of 80 mm and a focal length (*F*) of about 500 mm as shown in Figure 1.

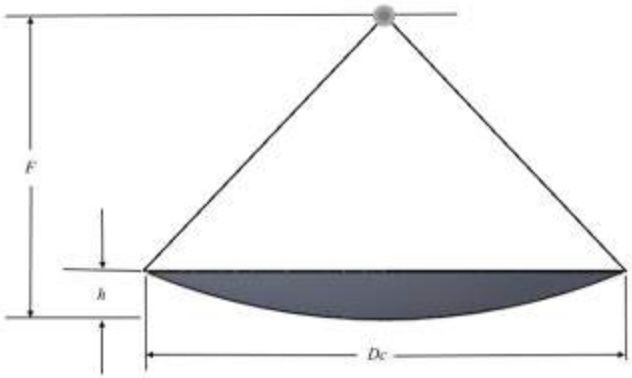

Figure 2. Design of Parabolic Dish Unit

The manufactured and assembled solar dish water heating system is illustrated in Fig. 3-a. During the experimental testing, dish is faced to south and system is operated between 10:00-14:30 hours. The detailed view of the copper coil heat exchanger (receiver) is presented in Fig. 3-b. The copper pipe is processed in turning machine to obtain the coil type configuration and the final product is painted to black for enhancing the absorptivity

of the coil. The coil is placed inside a transparent cylindrical glass glazing and placed horizontally at the focal point of receiver. As the receiver is aligned in horizontal direction, the change of the focal point of dish in horizontal direction, due to the movement of sun, is tolerated and the focal point remained on the coil heat exchanger during the testing.

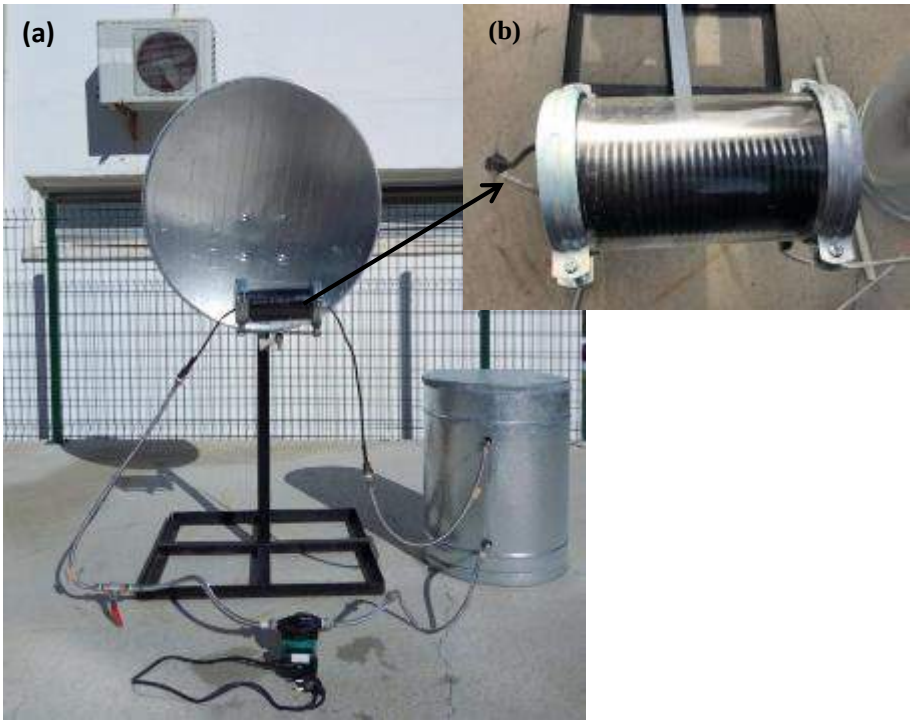

Figure 3. (a) Assembled Solar Dish Water Heating System (b) Detailed View of Copper Coil Receiver

Experimental Measurement and Data Logging

Temperature readings at the inlet and the exit of the collector, ambient temperature and tank temperature changes with time were closely monitored during the study. PCE-T 390 digital thermometer (Figure 4-a) is used for this purpose. This data logger has four channels and can be connected to different type of thermocouples (K/J/T//E/R/S). The instrument is powered by UM3/AA (1.5V) x 6 batteries or DC 9V adapter or it can be easily connected the PC computer interface. The temperature sensors are able to measure temperatures in the range of -50°C to approximately 1000 °C with an accuracy of ±0.4% + 1 °C. During the experiments solar radiation was also measured by using a pyranometer (Figure 4-b). It can measure the total radiation with a scope of 180 degree. The data is recorded in voltage and later converted into energy per unit area.

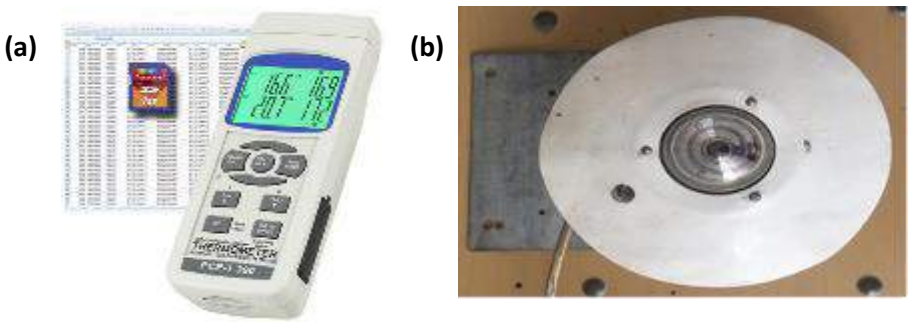

Figure 4. (a) Image of PCE-T390 Digital Thermometer, (b) Pyranometer

Three different experiments were performed and temperatures were recorded during the tests. The tank is filled with water and outlet water temperature form the tank (at the bottom) is assumed to be equal to the inlet temperature to the collector (T1). T2 is the water temperature in the tank, T4 is the water outlet temperature from the collector receiver and T3 is the ambient temperature. Figure 5 shows the schematic of the sensor positions in the system. The mass flow rate of water during the first two experiments is set to 0.00525 kg/s and in the last experiment it is set to 0.00277 to investigate the impact of water mass flow rate on system efficiency.

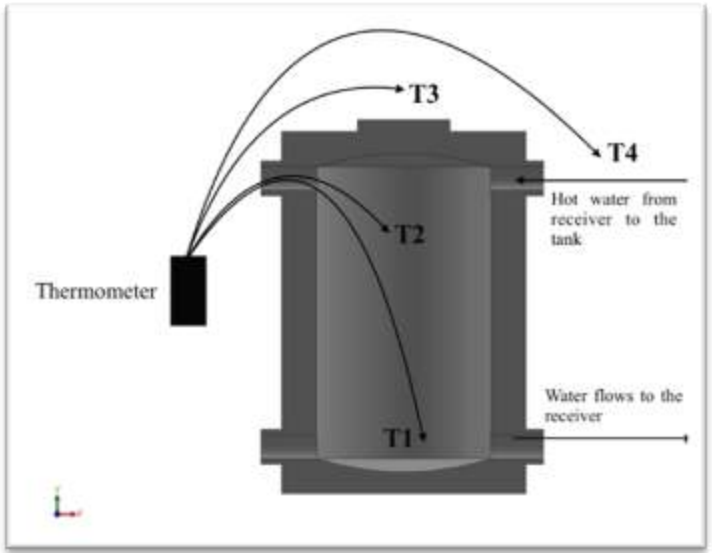

Figure 5. Schematic view of the water tank and illustration of sensor positions

Design Parameters of the Solar Dish Collector

A mathematical analysis was performed based on the dish dimensions to calculate the values that satisfy the need for the design criteria.

The concentration ratio index (C) is defined as the ratio of aperture area (A_c) to the area of the receiver (A_r). This concentration index indicates that the higher the ratio, the higher the temperature to be reached with the concentrator. Among the rest of the collectors

parabolic dish is known or characterized as the best collectors with higher concentration ratio. C is defined in Equation (1).

$$C = \frac{Ac}{Ar} \quad (1)$$

The collector area A_c can be calculated by the following equation:

$$A_c = \frac{\pi Dc\hat{}2}{4} \quad (2)$$

While the receiver area is the surface area of the cylindrical receiver and is given by:

$$A_r = \pi Dl \quad (3)$$

Where D is the diameter of the cylinder with a value of 0.12m, and it has a length l of 0.21m.
Therefore A_c = 0.503 m^2 and A_r = 0.0792 m^2, then;

$$C = \frac{0.503}{0.0792} = 6.34$$

The half acceptance angle (John and Nidhi, 2015, Alarcón et al. 2013) is given by:

$$\emptyset = \sin^{-1}\sqrt{\frac{1}{C}} = 23.40° \quad (4)$$

The optimum rim angle (John and Nidhi, 2015, Alarcón et al. 2013) is given by:

$$\psi = 90 - \emptyset = 66.6° \quad (5)$$

Thermodynamic Analysis of the Solar Dish Collector

The available solar energy that can be obtained from the reflection can be calculated by:

$$Q_s = I_g \,.A_c \quad (6)$$

While the total amount of heat from the parabolic dish reflected to the receiver aperture area can be defined as the optical efficiency by the available solar energy is defined by Equation (7) below:

$$Q_{abs} = \eta_{opt} \,.I_g \,.A_c \quad (7)$$

Where, η_{opt} is the optical efficiency of the dish collector, A_c is the dish collector aperture area and I_g is the solar irradiation intensity. The optical efficiency for most solar collectors is 60 - 70 % (Alarcón et al. 2013)
The estimated useful energy is calculated by:

$$Q = \dot{m}_w.C_p.\Delta T \quad (8)$$

Where, $\dot{m}_w$ mass flow rate of water, C_p is the specific heat capacity of water and ΔT is change in the final and initial temperature. While the thermal efficiency of the collector can be calculated by Equation (9) and is defined as the ratio of the useful delivered energy to the incident energy falling to the concentrator surface (John and Nidhi, 2015);

$$\eta_{c,therm} = \frac{Q}{Qabs} \quad (9)$$

The energy balance over the absorber leads to Eq. (10). According to the equation, absorbed heat by the receiver is equal to the total of heat gain by water and the heat losses.

$$Q_{abs} = Q + Q_{losses} \quad (10)$$

The efficiency (η) of most solar collectors' is between 40-60% (Alarcón et al. 2013). Gained useful energy can be calculated by:

$$Q = \eta .I_g .A_c \quad (11)$$

This shows that Equations (8) and (11) are equal and yield:

$$Q = \eta .I_g .A_c = \dot{m}_w.C_p.\Delta T \quad (12)$$

The instantaneous thermal efficiency is given by;

$$\eta = \frac{Q}{Ig .Ac} \quad (13)$$

RESULTS AND FINDINGS

This section presents the results obtained from the performed experiments. The testing was conducted in three different days; Dec 10, Dec 11 and Dec 13. On the first two days, mass flow rate of water is set to 0.00525 kg/s and in the final day of testing it is set to 0.00277 kg/s. By applying high and low water flow rates, it was aimed to analyze the impact of flow rate on the solar dish efficiency.

Results for 10th December 2018

The system was tested for almost 4.5 hours of that day, which is from 10:00 to 14:30. During the experiments four different sensor locations were used. T1 (collector inlet temp) is the temp of the water inlet to the heat exchanger and it is also assumed equal to the bottom temperature in the tank, while T4 (collector outlet temp) represents the hot water temperature at the exit of the dish receiver. T2 (water tank temp) is the surface water temperature inside the tank, and T3 is the ambient temperature.

Figure 6 a-d represents the temperature, solar radiation, energy and efficiency variations obtained during the experiment. The average temperature increase of water across the dish was determined as 6.3 °C whereas maximum water temperature inside the tank was reached to 37.7 °C from the initial temperature of 17.7 °C (See: Figure 6-a). As shown in Figure 6-b, solar radiation varied between 764 and 887 W/m² while average heat transfer rate to the water was calculated as 139.1 W (Figure 6-c). Accordingly, based on the data presented in Fig 6-d, average efficiency of the dish was found 32.7% during the operation.

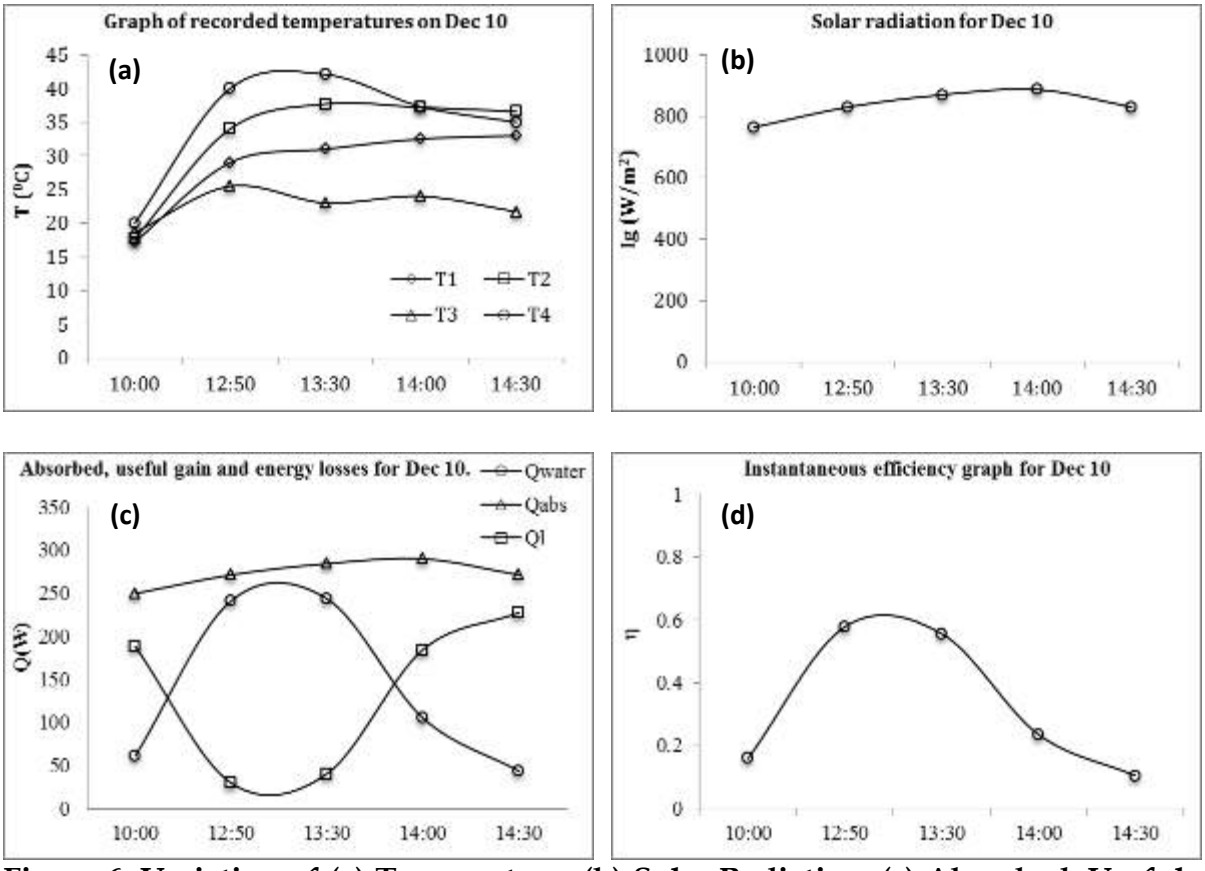

Figure 6. Variation of (a) Temperature, (b) Solar Radiation, (c) Absorbed, Useful and Lost Energy, and (d) Efficiency During the Experiment On 10th December

Results for 11th December 2018

On 11th December, system is tested under similar operating conditions to validate the results obtained in initial testing. Temperature, solar radiation, energy and efficiency variations of the second day testing were illustrated in Fig. 7. The average temperature increase and rate of heat gain across the dish were found 9.1°C (See: Figure 7-a) and 199.7 W (See: Figure 7-c), which were higher than the values obtained in the first day of testing. On the other hand average solar radiation is measured as 811 W/m2 (See: Figure 7-b) on the second they which was slightly less than the average solar radiation in first day. As a result, as presented in Figure 7-d, efficiency of the dish varied in the range of 24.5%→58.3% and the average efficiency is obtained as 48.3% on that day.

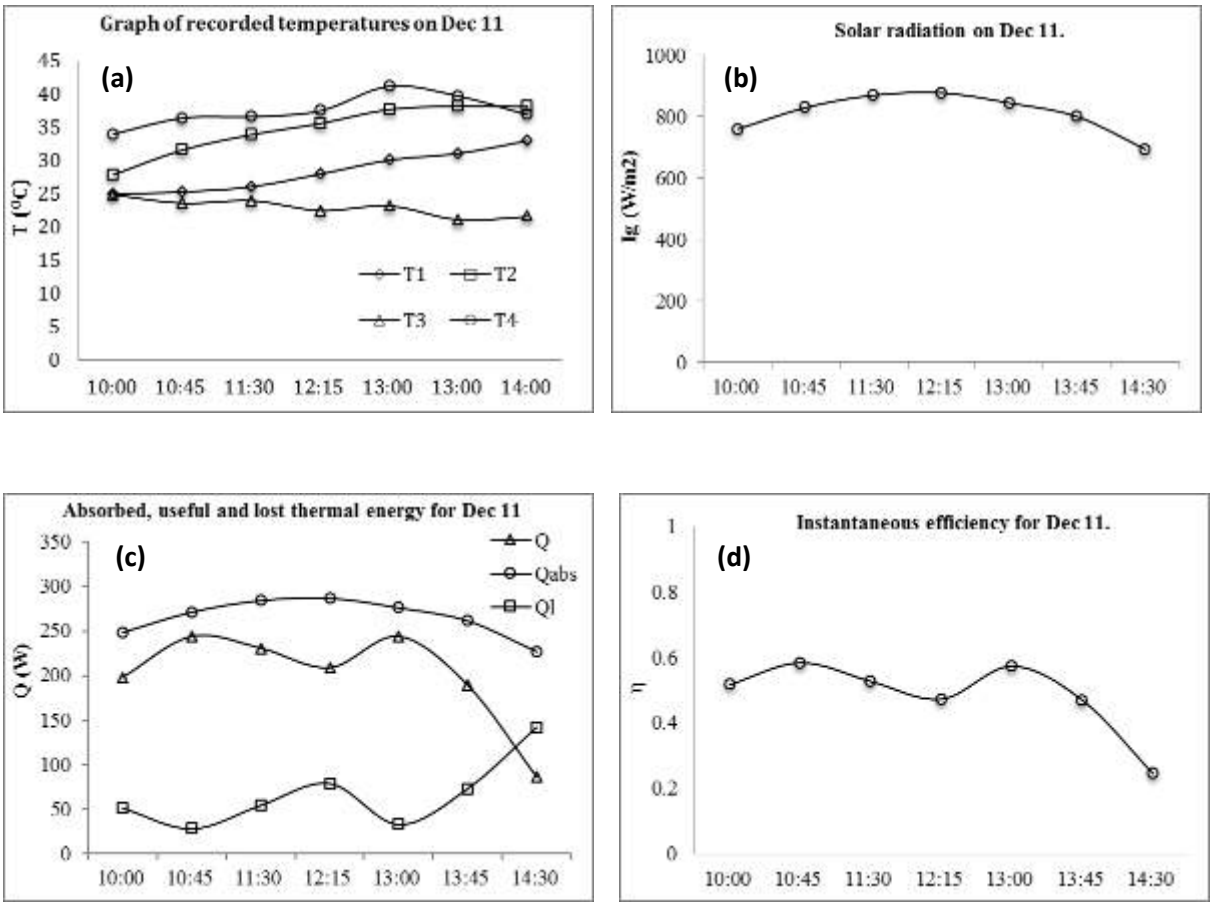

Figure 7. Variation of (a) Temperature, (b) Solar Radiation, (c) Absorbed, Useful and Lost Energy, and (d) Efficiency During the Experiment On 11th December

Results for 13th December 2018

In the last day of testing, mass flow rate of water is reduced to 0.00277 kg/s to see the impact of flow rate on solar dish water heater performance (See: Figure 8). Besides, in this testing, receiver temperature was also measured to demonstrate the highest temperature

obtained with spiral coil heat exchanger. According to the testing results average temperature lift and rate of heat gain of water across the dish were achieved as 7.1 °C (Figure 8-a) and 153.9 W (Figure 8-b) respectively, while the maximum receiver temperature reached to 116 °C at around 11:45 am (Figure 8-e). During the experiments average solar intensity is measured as 810.1 W/m² (Figure 8-b), and it was in close approximation with the intensity on the second day of testing. Accordingly efficiency of the dish water heater is obtained as 37.3% (Figure 8-d), which was higher than the first day but lower than the second day of testing.

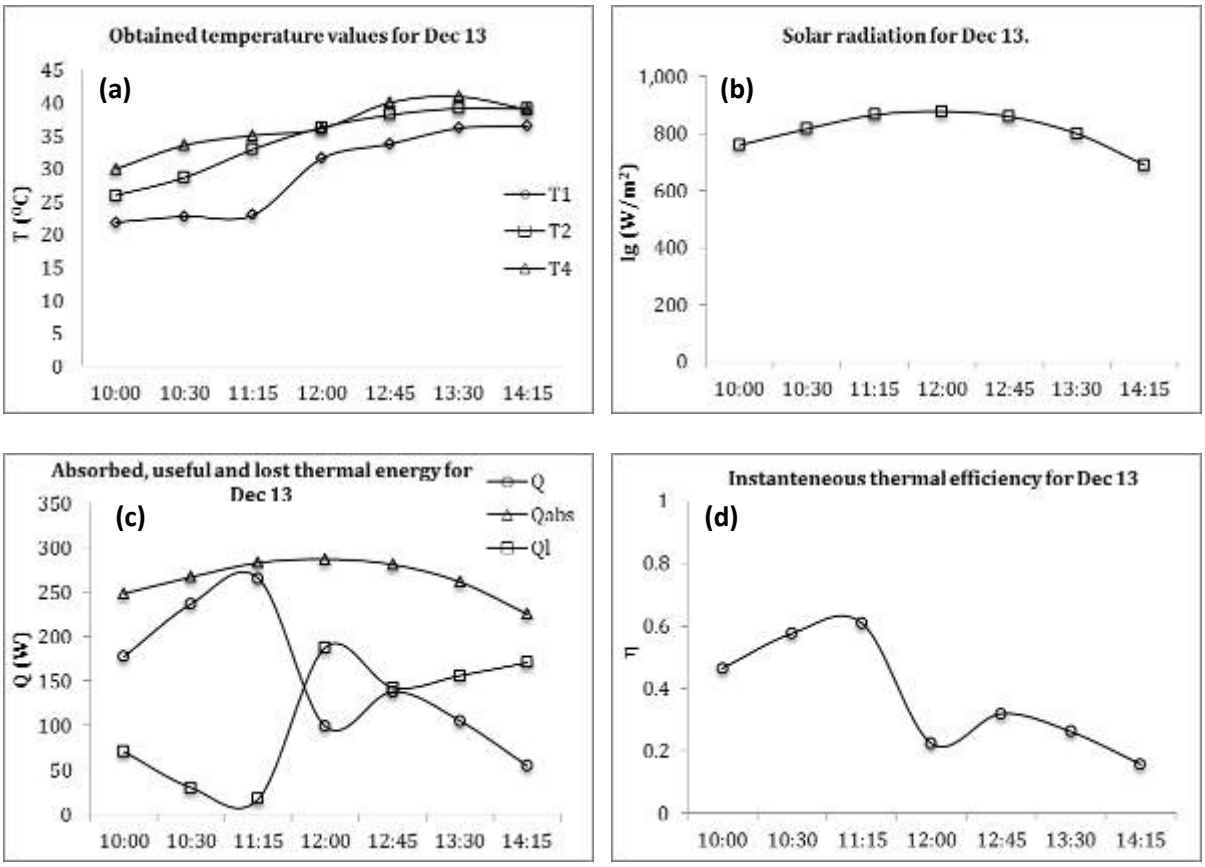

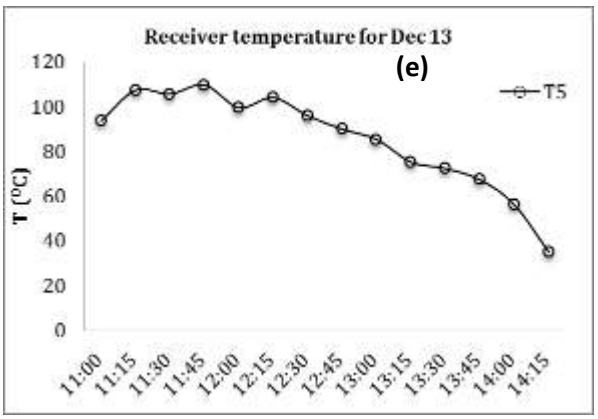

Figure 8: Variation of (a) Temperature, (b) Solar Radiation, (c) Absorbed, Useful and Lost Energy, (d) Efficiency, and (e) Receiver Temperature during the Experiment On 13th December

CONCLUSION

In this study, a solar dish unit with copper coil receiver is designed and experimentally investigated for residential water heating applications. System is tested under different solar radiation and water mass flow rate conditions. The summary of the testing results are presented in Table 1. According to the study results, maximum hot water temperature inside the tank is achieved in the first day of testing, while maximum rate of heat gain is obtained in the last day. However the highest average of heat gain across the dish is achieved in Day 2. Results showed that both solar radiation and mass flow rate of water significantly effects the system performance. More specifically, it could be stated that; dish system provides higher efficiency at lower solar radiation conditions ($\eta_{day3} > \eta_{day1}$) and higher mass flow rates ($\eta_{day2} > \eta_{day3}$). However further studies are required for optimizing the operating parameters (mass flow rate, dish size, receiver configuration, water tank volume etc.) of the investigated solar dish system.

Table 1. Summary of the Testing Results

	Dec 10	Dec 11	Dec 13
m_w (kg/s)	0.00525	0.00525	0.00277
I_g (W/m^2)	836.2	811.4	809.1
$T1_{average}$ (^{O}C)	28.5	33	29.4
$T2_{average}$ (^{O}C)	32.6	34.7	34.3
$T4_{max}$ (^{O}C)	42.1	41.2	40.1
$T4_{average}$ (^{O}C)	34.8	37.3	36.4
Q_{max} (W)	243.5	243.5	265.5
$Q_{average}$ (W)	139.1	200	153.9
η	0.33	0.48	0.37

RECOMMENDATIONS

This study presents a water heating system using solar dish unit for building application. As such systems are low cost, efficient and require less space compared to flat plate collectors, they demonstrate a potential to be employed in building water heating applications in the future. However deep research on numerical modelling, experimental validation through pilot applications and economic feasibility analysis of such systems is required to bring them to the market level.

REFERENCES

Tian, Y., & Zhao, C. Y. (2013). A review of solar collectors and thermal energy storage in solar thermal applications. *Applied Energy*, *104*, 538-553.

Devabhaktuni, V., Alam, M., Depuru, S. S. S. R., Green II, R. C., Nims, D., & Near, C. (2013). Solar energy: Trends and enabling technologies. *Renewable and Sustainable Energy Reviews*, *19*, 555-564.

Mekhilef, S., Saidur, R., & Safari, A. (2011). A review on solar energy use in industries. *Renewable and Sustainable Energy Reviews*, *15(4)*, 1777-1790.

Bellos, E., & Tzivanidis, C. (2018). Development of an analytical model for the daily performance of solar thermal systems with experimental validation. *Sustain. Energy Technol. Assessments*, *28*, 22–29.

Zhang, D., Li, J., Gao, Z., Wang, L., & Nan, J. (2016). Thermal performance investigation of modified flat plate solar collector with dual-function. *Applied Thermal Engineering*, *108*, 1126–1135.

Nikolić, N., & Lukić, N. (2015). Theoretical and experimental investigation of the thermal performance of a double exposure flat-plate solar collector. *Solar Energy*, *119*, 100–113.

Fan M., et al. (2019). A comparative study on the performance of liquid flat-plate solar collector with a new V-corrugated absorber. *Energy Conversion and Management*, *184*, 235–248.

Jowzi, M., Veysi, F., & Sadeghi, G. (2018). Novel experimental approaches to investigate distribution of solar insolation around the tubes in evacuated tube solar collectors. *Renewable Energy*, *127*, 724–732.

Xu, L.-C., Liu, Z.-H., Li, S.-F., Shao, Z.-X., & Xia, N. (2019). Performance of solar mid-temperature evacuated tube collector for steam generation. *Solar Energy*, *183*, 162–172.

Teles, M. de P. R., Ismail, K. A. R., & Arabkoohsar, A. (2019). A new version of a low concentration evacuated tube solar collector: Optical and thermal investigation. *Solar Energy*, *180*, 324–339.

Budihardjo, I., & Morrison, G. L. (2009). Performance of water-in-glass evacuated tube solar water heaters. *Solar Energy*, *83*, 49–56.

John, G. A., & Nidhi, M. J. (2015). *Design and simulation of parabolic dish collector for hot water generation.* Retrieved December 13, 2018 from http://troindia.in/journal/ijcesr/vol2iss9/20-24.pdf

Alarcón, J. A., Hortúa, J. E., & Lopez, A. (2013). Design and construction of a solar collector parabolic dish for rural zones in Colombia. *Tecciencia, 7(14)*, 14-22.

INVESTIGATION OF CRYSTAL STRUCTURE OF $BaCeO_3$ BASED NEW TYPE ELECTROCERAMICS DEPENDING ON TEMPERATURE AND Gd ADDITIVE AMOUNT

Çiğdem ÇELEN
Institute of Natural and Applied Sciences, Department of Nanotechnology and Advanced Materials, Mersin University, Mersin, Turkey
cigdemcelen@gmail.com

Serdar YILMAZ
Faculty of Arts and Sciences, Department of Physics, Mersin University, Mersin, Turkey
Institute of Natural and Applied Sciences, Department of Nanotechnology and Advanced Materials, Mersin University, Mersin, Turkey
syilmaz@mersin.edu.tr

ABSTRACT: The rapid development in urbanization and industrialization as a result of the increase of the world population increases energy consumption. Consequently, the need for energy increases day by day. The use of fossil fuels to meet the energy needs also damages the ecological balance and thus reduces the quality of human life. Because of these negative effects, new, sustainable, safe and non-polluting alternative energy sources are extremely important to search. The most remarkable renewable energy source is hydrogen energy among the alternative energy sources to fossil fuels. The fuel cells are clean and efficient electricity generating systems therefore they have been working hard in recent years. A fuel cell has three important components: anode, electrolyte and cathode. The most important (main) part of these components is the electrolyte of the ceramic fuel cell. The materials used for electrolyte in the proton conductive solid oxide fuel cell (PC-SOFC) are called proton conductive solid/ceramic oxide. Perovskite compounds (ABO_3) have structure flexibility that can contain both large(A position) and small(B position) cations. They are also suitable to form void and other crystal motifs in atomic size. Because of these properties, it can be used as a solid electrolyte in PSYH as used in many fields. In this study, electroseramics which can be used as solid electrolyte with the general formula of $BaCe_{(1-x)}M_xO_3$ have Perovskite ($ABMO_3$) structure which are doped in different stoichiometric ratios were synthesized by using sol-gel(Pechini) method. Where A; Barium(Ba), B; Cerium(Ce), while M is the Zirconium(Zr), Yttrium(Y) and Gadolinium(Gd) cations which settle into the lattice by doping. These synthesized materials were heat treated at three different temperatures, 900^{o}C, 1100^{o}C and 1300^{o}C. Crystal structures were determined by XRD analysis on the synthesized powder materials. As a result of XRD analysis, the solid electrolytes synthesized were found to have perovskite structure.

Keywords: Protonic Ceramic Fuel Cells, Solid Electroseramics, Perovskite, Barium Cerate.

Acknowledgement:
This study is supported by the Department of Scientific Research Project of Mersin University "2019-1-TP3-3424" (Mersin, Turkey).

$BaCeO_3$ TABANLI YENİ TİP ELEKTROSERAMİKLERİN SICAKLIK VE Gd KATKI MİKTARINA BAĞLI OLARAK KRİSTAL YAPILARININ İNCELENMESİ

Çiğdem ÇELEN
Fen Bilimleri Enstitüsü, Nanoteknoloji ve İleri Malzemeler Bölümü, Mersin Üniversitesi, Mersin, Türkiye
cigdemcelen@gmail.com

Serdar YILMAZ
Fen Edebiyat Fakültesi, Fizik Bölümü, Mersin Üniversitesi, Mersin, Türkiye
Fen Bilimleri Enstitüsü, Nanoteknoloji ve İleri Malzemeler Bölümü, Mersin Üniversitesi, Mersin, Türkiye
syilmaz@mersin.edu.tr

ÖZET: Dünya nüfusunun artmasının sonucu olan kentleşme ve sanayileşmedeki hızlı gelişim, enerji tüketimini arttırmaktadır. Buna bağlı olarak her geçen gün enerji ihtiyacı artmaktadır. Enerji ihtiyacını karşılamak için fosil yakıtların kullanılması ekolojik dengeye de zarar vermekte ve dolayısıyla insanın yaşam kalitesini düşürmektedir. Bu olumsuz etkilerden dolayı, yeni, sürdürülebilir, güvenli ve çevreyi kirletmeyen alternatif enerji kaynaklarının araştırılması son derece önemlidir. Fosil yakıtlara alternatif olan yenilenebilir enerji kaynakları arasında en dikkat çekici olanı Hidrojen enerjisidir. Yakıt Hücrelerinin temiz ve etkili elektrik üreten sistemler olmalarından dolayı son yıllarda oldukça fazla çalışılmaktadır. Bir yakıt hücresinde anot, elektrolit ve katot olmak üzere üç önemli bileşen vardır. Bu bileşenler içinde en önemli (ana) kısım seramik yakıt hücresinin elektrolitidir Proton iletken katı oksit yakıt hücresinde (PC-SOFC) elektrolit için kullanılan materyallere proton iletken katı / seramik oksit denir. Perovskit bileşikler (ABO_3) hem büyük (A konumu) hem de küçük (B konumu) katyonları yapısında bulundurabilecek yapı esnekliğine sahiptirler. Ayrıca boşluk oluşumuna ve atomik boyutta diğer kristal motiflerin oluşmasına elverişlidirler. Bu özelliklerden dolayı birçok alanda kullanıldığı gibi PSYH'lerde de katı elektrolit olarak kullanılabilmektedir. Bu çalışmada sol-jel (Pechini) yöntemi kullanılarak farklı stokiyometrik oranlarda katkılanmış Perovskit ($ABMO_3$) yapılı $BaCe_{(1-x)}M_xO_3$ genel formülüne sahip katı elektrolit olarak kullanılabilecek elektroseramikler sentezlenmiştir. Burada A; Baryum (Ba), B; Seryum iken M ise katkılama ile örgüye yerleşen Zirkonyum (Zr), Yitriyum (Y) ve

Gadolinyum (Gd) katyonlarıdır. Sentezlenen malzemelere 900^{o}C, 1100^{o}C ve 1300^{o}C olmak üzere üç farklı sıcaklıklarda ısıl işlem uygulanmıştır. Sentezlenen toz malzemelere XRD analizi yapılarak kristal yapıları tespit edilmiştir. XRD analizi sonucunda sentezlenen katı elektrolitlerin perovskit yapıda olduğu tespit edilmiştir.

Anahtar kelimeler: Protonik Seramik Yakıt Hücreleri, Katı Elektroseramikler, Perovskit, Baryum Serat.

TEŞEKKÜR
Bu çalışma; Mersin Üniversitesi Bilimsel Araştırma Proje Birimi tarafından (2019-1-TP3-3424) desteklenmiştir (Mersin, Türkiye).

MINICHANNEL EVAPORATOR DESIGN FOR ELECTRONIC COMPONENTS IN COMPUTER COOLING APPLICATIONS

Mehmet Harun SÖKÜCÜ*
Gebze Technical University
Friterm Termik Cihazlar Inc.
mehmetharun@gtu.edu.tr, mehmetharun@friterm.com

Mustafa Fazıl SERİNCAN
Gebze Technical University
mfserincan@gtu.edu.tr

Hüseyin ONBAŞIOĞLU
Friterm Termik Cihazlar Inc.
huseyinonbasioglu@friterm.com

ABSTRACT: In parallel with the developments in electronic component production the heat dissipation amount of the chips has increased considerably. Electronics cooling is one of the most critical concerns in reliable operation of computers. Conventionally, some applications available for electronics cooling such as radiation, free convection, force air - liquid cooling and evaporation. Especially the cooling methods used for military applications and supercomputers need to be designed specially in order to obtain reliable operating temperatures for electronic components. Conventional cooling methods for electronic components may be inadequate in harsh operating environments. At this point, active cooling techniques may be considered such as vapor compression refrigeration (VCR) system. In this study, a vapor compression refrigeration system for computers which need powerful cooling applications have been studied for maintaining the chip surface temperature below the critical value of 85 ^{o}C. At the same time a calculation module, for evaporator optimization and design, has been developed. The minichannel evaporator design calculations were done by selecting from heat transfer and pressure drop equations from the literature. Then, the chips which generates 100 - 500 W heat power will be modeled experimentally in the test apparatus which will be formed by producing the designed evaporators. Chip surface temperatures will be measured according to constant evaporation temperature and variable condensation capacity and the results will be compared with the generated calculation module.

Key words: Computer cooling, Minichannel evaporator, Calculation module, VCR

EFFECTS OF AIR POLLUTION ON HUMAN HEALTH AND AIR POLLUTION PROBLEM IN GAZIANTEP

Rukiye DOĞANYİĞİT
Vocational School of Health Services, Gaziantep University,
Gaziantep, Turkey
rdoganyigit@gantep.edu.tr

ABSTRACT: Air pollution refers to a phenomenon in which pollutants that are present in various forms in the atmosphere have reached a level that harms humans and other living beings. Human beings are the main reason for this pollution. Human activities form the main source of pollutants (e.g. traffic, industry, heating systems). Natural environment factors also have an influence on pollution, either positively or negatively. Air pollution is one of the top ten risk factors against health throughout the world, which makes it an important problem. Air pollution still exceeds safe limits worldwide, particularly in big metropolitans, despite regular monitoring facilities and measures taken. It is usually originated from industrial activities, fossil fuel use in domestic settings and vehicle exhaust emission. Although there is a decrease in air pollution in big cities of Turkey due to use of natural gas, it is still a serious health concern. In Gaziantep, because of a rapid increase in its population recently, wrong urbanization and a relative increase in industrialization, air pollution leads to dangerous levels, particularly in the winter.
In the study, first of all, literature studies were conducted and the causes of air pollution and the problems caused by increasing air pollution for human and environmental health were tried to be concretized. In the study; The annual air pollution monitoring data of Gaziantep province in the recent years were examined and the level of air pollution in the province and the studies on the reduction of air pollution in the province were examined

Key words: Gaziantep city, air pollutants, air pollution sources, lung health.

HAVA KİRLİLİĞİNİN İNSAN SAĞLIĞI ÜZERİNE ETKİLERİ VE GAZİANTEP İLİNDE HAVA KİRLİLİĞİ SORUNU

ÖZET: Atmosferde çeşitli şekillerde bulunan kirleticilerin, insan ve diğer canlılara zarar verecek düzeye erişmesi biçiminde tanımlanan hava kirliliğinin temel sorumlusu insandır. İnsanın yaptığı beşeri faaliyetler kirleticilerin temel kaynağını (trafik, sanayi ve ısınma sistemleri vs.) oluştururken, doğal çevre faktörleri de kirliliğin etkisini olumlu

veya olumsuz biçimde etkilemektedirler. Hava kirliliği, dünya genelinde sağlığa yönelik ilk on risk faktörlerinden olup, önemli bir sorun teşkil etmektedir. Türkiye'deki hava kalitesi de endişe verici boyutlara ulaşmıştır. Hava kirliliği düzeyleri düzenli olarak izlenmesine ve mücadele edilmesine rağmen, bütün dünyada, başta büyük metropoller olmak üzere halen kabul edilen sınırların üzerinde seyretmektedir. Kirlilik özellikle endüstriyel tesislerden, konutlarda ısınma amaçlı yakıt tüketiminden ve motorlu taşıt egzozlarından kaynaklanmaktadır. Ülkemizde doğal gaz kullanımıyla büyük kentlerde hava kirliliğinde nispeten bir gerileme olmasına rağmen, halen ciddi bir sorun olarak varlığını sürdürmektedir. Gaziantep'te son yıllarda hızlı nüfus artışı, yanlış kentleşme ve nispeten artan sanayileşme nedeniyle özellikle kış aylarında hava kirliliği ciddi boyutlara ulaşmaktadır.
Çalışmada öncelikle literatür çalışması yapılarak hava kirliliğinin nedenleri, artan hava kirliliğinin insan ve çevre sağlığı için oluşturduğu sorunlar somutlaştırılmaya çalışılmıştır. Çalışmada ayrıca; Gaziantep ilinin son yıllardaki yıllık hava kirliliği izleme verileri incelenerek ilin hava kirliliği bakımından hangi düzeyde olduğu ve ilde hava kirliliğinin azaltılması konusunda yapılan çalımalar incelenmiştir.

Anahtar sözcükler: Gaziantep şehri, hava kirleticileri, hava kirliliği kaynakları, akciğer sağlığı,

GİRİŞ

Çevre; insanların ve diğer canlıların yaşamları boyunca karşılıklı olarak etkileşim içinde bulunduğu, biyolojik, kimyasal, sosyal, ekonomik ve kültürel bütün faaliyetlerini devam ettirdiği bir ortamdır.

Ne yazık ki bütün canlılar için önemli olan çevre, sanayinin dünyada hızla gelişmesine paralel olarak, ham madde ihtiyacının karşılanması için doğal kaynakların tüketilmeye başlanması, üretim atıklarının hızla artması ve insanların bilinçsizce doğaya zarar vermesi sonucunda hızla kirletilmeye, tahrip edilmeye kısacası yok edilmeye başlanmıştır. Günümüze gelindiğinde ise çevre sorunları ciddi problemler doğurmaya başlamış ve tüm canlı yaşamı için tehlikeli bir hal almıştır (Çay ve Çelik 2015).

Çevre sorunlarının başında bütün canlıları tehdit eden hava kirliliği problemi gelmektedir. Atmosfer çok hızlı hareket eden ve akışkan dinamik bir yapı gösterdiği için istenmeyen çok sayıda madde atmosfere hızla karışmaktadır, bu karışmada İklim özelliklerinin olumlu ve olumsuz etkileri bilinmektedir (Garipağaoğlu, 2013).

Atmosferin doğal yapısında bulunan maddelerin miktarlarının yükselmesi veya yapıya yabancı maddelerin girmesi sonucunda canlı ve cansız tüm ekosistemi farklı seviyelerde olumsuz etkileyen havaya kirli hava denir. Orman yangınları, volkanik patlamalar,

bataklıklarda anaerobik bakterilerin karmaşık organik maddeleri oluşturması esnasında ortaya çıkan karbon dioksit, metan, vb. gibi gazların atmosfere yayılması gibi doğal olaylar nedeni ile atmosfer hiç bir zaman tertemiz olmamıştır. Prehistorik devirde ateşin bulunması ile başlayan atmosferik kirlilik 20. yüzyılın ortalarından itibaren patlama noktasına varan endüstrileşme, kırsal alanlardan kentlere yönelik büyük insan göçü, hava kirlenmesi olayının boyutlarını büyütmüştür (Tufan Çetin ve Sümbül, 2010).

1. HAVA KİRLİLİĞİ

Hava kirliliği, insan sağlığı, canlı hayatına zarar verecek, eşya ve malzemelerin bozulmalarına, ekolojik dengenin bozulmasına neden olabilecek düzeyde katı, sıvı veya gaz formundaki kirleticilerin atmosferde bulunmasıdır. Hava kirliliği, volkanik aktiviteler, orman yangınları, depremler ve bataklıklar gibi doğal nedenlerle oluşabildiği gibi, sanayileşme, ısınma, ulaşım ve enerji üretimi gibi insan aktivitelerine bağlı da oluşabilmektedir. Nüfus artışı ve buna bağlı olarak artan şehirleşme ve sanayileşme eğilimi hava kirliliği sorununu beraberinde getirmektedir. Kuraklık, topoğrafik koşullar ve iklimsel özellikler de hava kirliliğinin düzeyini etkilemektedir (TMMOB Çevre Mühendisleri Odası, 2018).

Endüstriler ve enerji santralleri, yüksek miktarda Partikül Madde (PM), Azot Oksitler (NO_x), Kükürt dioksit (SO_2), karbon monoksit (CO), Hidrokarbonlar (HC), organik bileşik ve diğer kimyasalların atmosfere salınmasına ve hava kalitesinin azalmasına neden olur. Bu tesisler sadece yerel düzeyde insan ve çevre sağlığına zarar vermekle kalmaz, aynı zamanda bölgesel ölçekte asit yağmurları, ozon oluşumuna, ya küresel ölçekte ise iklim değişikliğine neden olarak dünyanın geleceği için yıkıcı sonuçlara sebep olabilir. Endüstriyel tesislerin enerji üretimi veya ürün prosesi sırasında hava kirliliğine neden olabilen kirletici emisyonları oluşabilmektedir.

Enerji üretimindeki hava kirliliğinin en büyük aktörü fosil yakıt kullanımıdır. 19. yüzyıldan beri kullanılmakta olan fosil yakıtlar insan ve çevre sağlığı açısından büyük tahribata neden olmuştur. Enerji ihtiyacı ulaşım sektöründe de kendini göstermektedir. Hava, deniz ve kara ulaşımı için gereken enerjinin çok büyük kısmı halen fosil yakıtlardan karşılanmaktadır. OECD verilerine göre, Türkiye'deki enerji ihtiyacının %88'i fosil yakıtlardan sağlanmaktadır (OECD, 2019)

Ulusal Hava Kalitesi İndeksi, EPA (Amerika Birleşik Devletleri Çevre Koruma Ajansı) Hava Kalitesi İndeksinin ulusal mevzuatımız ve sınır değerlerimize uyarlanması sonucu oluşturulmuştur. 5 temel kirletici için hava kalitesi indeksi hesaplanmaktadır. Bunlar; partikül maddeler (PM_{10}), karbon monoksit (CO), kükürt dioksit (SO_2), azot dioksit (NO_2) ve ozon (O_3) dur.

1.1 Hava Kirliliğine Neden Olan Faaliyetler

İç ya da dış ortamda soluduğumuz havanın, kimyasal, fiziksel veya biyolojik ajanlar ile doğal özelliğinin bozulması olarak tanımladığımız hava kirliliğini genel olarak iki ana nedenden dolayı ortaya çıkmaktadır.

Birincisi doğal kökenli kirliliktir. Burada en temel havayı kirleten kaynak, çöl tozları, volkanik patlamalar sonucunda ortaya çıkan toz, deniz tuzu gibi doğal kaynaklardan köken alan çoğunlukla toz ya da daha teknik olarak ifade etmek gerekirse partikül madde kirliliğidir. Bu kaynaklardan oluşan toz bulutları atmosfere karışmakta ve rüzgar ile uzak mesafelere kadar taşınabilmektedir.

İkincisi ise insan kaynaklı kirliliktir (Antropojenik kaynaklı). Ulaşım, sanayi ve santrallerde enerji üretimi için kullanılan fosil yakıtlar, madencilik tesisleri ve endüstriyel tesisler, evlerde ısınma ve yemek yapma amaçlı kömür ve odun yakılması, inşaat faaliyetleri ve yollardan kaynaklanan tozlar, atık ve anızların yakılması, bazı endüstriyel tarım faaliyetleri gibi insanların faaliyetleri sonucunda ortaya çıkan hava kirliliği de insan kaynaklı nedenlerdir.

Özellikle sanayiden kaynaklanan kirleticiler; iklim değişikliği ve asit yağmurlarının yanı sıra ciddi sağlık sorunlarına da neden olurlar. Bacalardan çıkan ve saç telinden daha ince olduğundan göremediğimiz partikül maddeler kana karışarak sağlık sorunlarına neden olmaktadır (Anonim 2019a).

1.2 Partikül Maddeler

$PM_{2.5}$ sağlık açısından çok tehlikelidir çünkü solunduğunda akciğerler içindeki gaz alışverişi ile kana karışabilir.

Partikül maddeler (birincil partikül maddeler) kirlilik oluşturan kaynaklardan doğrudan havaya yayılabilir veya atmosferik olaylar sonucunda sanayi kaynaklı diğer gazlarla birleşerek ikincil partikül maddeler ortaya çıkabilir ve hava hareketleriyle kilometrelerce uzaklara taşınabilir. Saç telinden bile ince olan ve (2,5-10) mikrometre çapındaki partikül maddelerin temel kaynakları sanayi tozları, topraktan kaynaklanan tozlar (çiftçilik, madencilik, yollar vb.), inşaat ve yıkım, kömür ve petrol yanması, okyanus spreyi ve biyolojik kaynaklardır

Şekil 1. Partikül Madde ve Boyutları

1.3. Hava Kalitesi İndeksi

Hava Kalitesi İndeksi (HKİ) denilen sınıflama sistemi ile havadaki kirleticilerin konsantrasyonlarına göre hava kalitesini iyi, orta, kötü, tehlikeli vb. şeklinde derecelendirme yapılmaktadır. Dünyanın pek çok ülkesinde indeks hesaplanmasında kullanılan yöntem ve kriterler, kendi ülkelerinde uygulanan hava kalitesi standartlarına uygun şekilde oluşturulmuştur.

Belli bir bölgedeki hava kalitesinin karakterize edilmesi için ülkelerin kendi sınır değerlerine göre dönüştürdükleri ve kirlilik sınıflandırılmasının yapıldığı bu indekse Hava Kalitesi İndeksi (HKİ) (Air Quality Index/AQI) adı verilmektedir. İndeks belirli kategorilerde farklı tanım ve renkler kullanılarak ifade edilmekte ve ölçümü yapılan her kirletici için ayrı ayrı düzenlenmektedir.

Ulusal Hava Kalitesi İndeksi, EPA Hava Kalitesi İndeksini ulusal mevzuatımız ve sınır değerlerimize uyarlayarak oluşturulmuştur. 5 temel kirletici için hava kalitesi indeksi hesaplanmaktadır. Bunlar; partikül maddeler (PM_{10}), karbon monoksit (CO), kükürt dioksit (SO_2), azot dioksit (NO_2) ve ozon (O_3) dur (Avşar, E., Alp, K.&Toröz, İ., 2015).

Tablo 3. EPA Hava Kalitesi indeksi

Hava Kalitesi İndeksi (AQI) Değerler	Sağlık Endişe Seviyeleri	Renkler	Anlamı
Hava Kalitesi İndeksi bu aralıkta olduğunda..	*..hava kalitesi koşulları..*	*..bu renkler ile sembolize edilir..*	*..ve renkler bu anlama gelir.*
0 - 50	İyi	Yeşil	Hava kalitesi memnun edici ve hava kirliliği az riskli veya hiç risk teşkil etmiyor.
51 - 100	Orta	Sarı	Hava kalitesi uygun fakat alışılmadık şekilde hava kirliliğine hassas olan çok az sayıdaki insanlar için bazı kirleticiler açısından orta düzeyde sağlık endişesi oluşabilir.
101- 150	Hassas	Turuncu	Hassas gruplar için sağlık etkileri oluşabilir. Genel olarak kamunun etkilenmesi olası değildir.
151 - 200	Sağlıksız	Kırmızı	Herkes sağlık etkileri yaşamaya başlayabilir, hassas gruplar için ciddi sağlık etkileri söz konusu olabilir.
201 - 300	Kötü	Mor	Sağlık açısından acil durum oluşturabilir. Nüfusun tamamının etkilenme olasılığı yüksektir.
301 - 500	Tehlikeli	Kahverengi	Sağlık alarmı: Herkes daha ciddi sağlık etkileri ile karşılaşabilir.

Tablo 4. Ulusal Hava Kalitesi İndeksi Kesme Noktaları

İndeks	HKİ	SO_2 [µg/m³]	NO_2 [µg/m³]	CO [µg/m³]	O_3 [µg/m³]	PM10 [µg/m³]
		1 Sa. Ort.	1 Sa. Ort.	8 Sa. Ort.	8 Sa. Ort.	24 Sa. Ort.
İyi	0 – 50	0-100	0-100	0-5500	0-120	0-50
Orta	51 – 100	101-250	101-200	5501-10000	121-160	51-100
Hassas	101 – 150	251-500	201-500	10001-16000	161-180	101-260
Sağlıksız	151 – 200	501-850	501-1000	16001-24000	181-240	261-400
Kötü	201 – 300	851-1100	1001-2000	24001-32000	241-700	401-520
Tehlikeli	301 – 500	>1101	>2001	>32001	>701	>521

Tablo 5. İndeks Hesaplanan Parametrelerin Sınır Değerleri

Parametre	SO_2 [µg/m³]	NO_2 [µg/m³]	CO [µg/m³]	O_3 [µg/m³]	PM10 [µg/m³]
	1 Sa. Ort.	1 Sa. Ort.	8 Sa. Ort.	8 Sa. Ort.	24 Sa. Ort.
Ulusal Sınır Değer	350	250	10.000	120	50
AB Üye Ülkeleri Sınır Değeri	350	200	10.000	120	50

06.06.2008 tarih ve 26898 Resmi Gazetede yayımlanan Hava Kalitesi Değerlendirme ve Yönetimi Yönetmeliğin Hava Kalitesi Değerlendirme ve Yönetimi Yönetmeliğine göre kirleticiler ve limit değerleri Tablo 6'da gösterilmiştir.

Tablo 6. Hava Kalitesi Sınır Değerleri

İnsan Sağlığı ve Ekosistemin Korunması İçin Hava Kalitesi Sınır Değerleri				
Kirletici Parametreler	**Ölçüm Periyodu**	**Sınır Değerler**		**Uyum Takvimi**
		Ülkemizde Uygulanan (2018 Yılı)	**AB Üye Ülkelerde Uygulanan**	
Kükürtdioksit SO_2 (µg/m³)	Saatlik	380	350	1.1.2019
	Günlük	150	125	
	Uyarı Eşiği (3 ardışık saat)	500	500	
	Saatlik Aşım Sayısı	-	24/Yıl	
	Günlük Aşım Sayısı	-	3/Yıl	
	Yıllık (Ekosistem)	20	20	1.1.2014
Partikül Madde PM10 (µg/m³)	Günlük	60	50	1.1.2019
	Yıllık	44	40	
	Günlük Aşım Sayısı	-	35/Yıl	
Azotdioksit NO_2 (µg/m³)	Saatlik	260	200	1.1.2024
	Yıllık	44	40	
	Uyarı Eşiği (3 ardışık saat)	400	400	
	Saatlik Aşım Sayısı	-	18/Yıl	
Azotoksitler NOx (µg/m³)	Yıllık (Ekosistem)	30	30	1.1.2014
Karbonmonoksit CO (mg/m³)	8 saatlik Ortalama	10	10	1.1.2017
Ozon O_3 (µg/m³)	8 saatlik Ortalama	120	120	1.1.2022
	Bilgi Eşiği (saatlik)	-	180	

	Uyarı Eşiği (saatlik)	-	240	
Benzen C6H6 (µg/m³)	Yıllık	8	5	1.1.2021
Kurşun Pb (µg/m³)	Yıllık	0.6	0.5	1.1.2019
Arsenik As (ng/m³)	Yıllık	-	6	1.1.2020
KadmiyumCd (ng/m³)	Yıllık	-	5	2.1.2020
Nikel Ni (ng/m³)	Yıllık	-	20	3.1.2020
Benzoapiren B(a)p (ng/m3)	Yıllık	-	1	4.1.2020

2. GAZİANTEP İLİNDE HAVA KİRLİLİĞİ KONUSUNDA YAPILAN ÇALIŞMALAR

Gaziantep nüfusu ve endüstrisi hızla büyüyen büyük şehirlerimizden birisidir. İlde son 35 yılda kaydedilen hızlı değişim, tarihi ve kültürel zenginliğinin yanı sıra, bilim ve teknolojik gelişmelere açık bir kent olarak da adından söz ettirmektedir. İldeki nüfus artışı, sanayileşme ve teknolojik gelişmelere paralel olarak Hava Kalitesinde de doğal olarak değişim yaşanmaktadır.

Bölgede hava kirliliği konusunda Çevre ve Şehircilik Bakanlığı ve taşra teşkilatının yaptığı çalışmalarla üniversitelerde yapılan araştırma ve tez çalışmaları bulunmaktadır.

Bu kapsamda yapılan en geniş kapsamlı çalışmalardan biri "Kentlerde Hava Kalitesi Değerlendirme Sisteminin Geliştirilmesi (KENTAIR)" projesi kapsamında hazırlanan hava kalitesi değerlendirme raporlarıdır. Proje kapsamında, ön değerlendirmesi yapılan 7 ilden Adana, Gaziantep ve Mersin için çalışmalar yapılarak rapor hazırlanmıştır. Bu raporlarda kentin emisyon envanteri ısınma, sanayi ve trafik emisyonları için çıkarılmış, mevcut hava kalitesi değerlendirmeleri yapılmış ve öneriler getirilmiştir.
Gaziantep Belediyesi, Gaziantep Kent Konseyi tarafından hazırlanan Gaziantep İli Hava Kirliliği Değerlendirme Raporu'nda ilin emisyon kaynakları tanımlanarak hava kalitesi ölçüm istasyonu verileri değerlendirilmiş ve çözüm önerileri sunulmuştur.

Yapılan çalışma neticesinde elde edilen verilere göre Gaziantep'teki hava kirliliğinin öncelikli sebebinin ısınmadan kaynaklandığı, ikincil sebebinin motorlu taşıtlar olduğu belirlenmiştir. Ancak, ölçüm verilerine göre yönetmeliklerde belirtilen sınır değerlerin aşılmadığı görülmektedir. Çalışmada çözüm önerisi olarak, trafik kaynaklı emisyonlar için taşıtların emisyon ölçümlerinin gerçekleştirilesi ve bakımlarının zamanında yapılması, kısa mesafelerde araç kullanılmamasının, uzun mesafelerde toplu taşımanın

özendirilmesi, ısınma kaynaklı emisyonlarda kaliteli yakıt kullanılması ve temiz enerji kaynaklarına (rüzgar, güneş enerjisi vb.), sanayi kaynaklı emisyonlarda sanayicilerin bilinçlendirilmesi ve denetim ve kontrollerin sık ve standartlara uygun olarak yapılması sunulmuştur.

2.1. Gaziantep İli Hava Kalitesi Ve Ölçüm İstasyonu Verilerinin Değerlendirilmesi

Gaziantep İlinde 1 adet sabit hava kalitesi izleme istasyonu bulunmakta olup, istasyonda sürekli olarak kükürt dioksit (SO2) ve partiküller madde (PM10) parametreleri otomatik cihazla ölçülmektedir ve saatlik ortalama değerler olarak alınmaktadır.
İstasyonda ölçülen değerler öncelikle elektronik ağ sistemi sayesinde Çevre ve Şehircilik Bakanlığının veri toplama merkezine iletilmekte olup buradan da İl Müdürlüğünde de bulunan bilgisayar ve modem aracılığı ile bilgiler elektronik ortama aktarılmakta ve istenildiği zaman ulaşılabilecek nitelikte depolanmaktadır. Bu ölçümlere ait saatlik, günlük, haftalık ve aylık verilerin internet sitesinden www.havaizleme.gov.tr adresinden izlenmesi mümkündür.

Şekil 2. ve 3. Gaziantep Temiz Hava eylem Planı ve Gaziantep Hava Kalitesi Ölçüm İstasyonu

Tablo 7. Gaziantep İlinde Son Dokuz Yıllık Hava Kalitesi Ölçüm Değerleri

		OCAK	SUBAT	MART	NİSAN	MAYIS	HAZİRAN	TEMMUZ	AGUSTOS	EYLÜL	EKİM	KASIM	ARALIK	YILLIK ORTALAMA (µg/m³)
2007	SO2	103	46	23	6	3	3	3	189	7	10	27	69	41
	PM	149	135	99	67	141	75	70	75	92	138	141	-	107
2008	SO2	-	-	-	-	-	-	-	3	-	-	15	62	27
	PM	-	-	-	-	-	-	-	-	-	-	128	-	128
2009	SO2	61	12	10	9	8	8	8	11	8	11	23	29	17
	PM	-	137	85	68	54	72	46	46	46	113	122	120	83
2010	SO2	30	32	22	6	5	4	3	5	5	5	41	43	17
	PM	124	124	104	48	27	36	25	35	34	67	97	134	71
2011	SO2	42	32	25	4	2	4	4	4	6	7	27	53	18
	PM	143	120	95	96	68	54	66	63	88	112	122	183	101
2012	SO2	19	32	14	3	8	9	5	5	5	8	10	34	13
	PM	130	132	112	85	74	78	77	73	138	164	141	-	109
2013	SO2	25	12	10	7	7	7	6	8	9	15	16	23	12
	PM	102	103	94	134	58	44	41	47	46	58	96	94	76
2014	SO2	10	10	6	4	3	3	3	3	3	4	14	17	7
	PM	91	75	68	48	40	37	40	53	47	53	76	78	59
2015	SO2	30	32	20	7	6	4	5	3	5	6	9	8	11
	PM	78	76	59	43	47	37	38	42	104	58	78	76	60

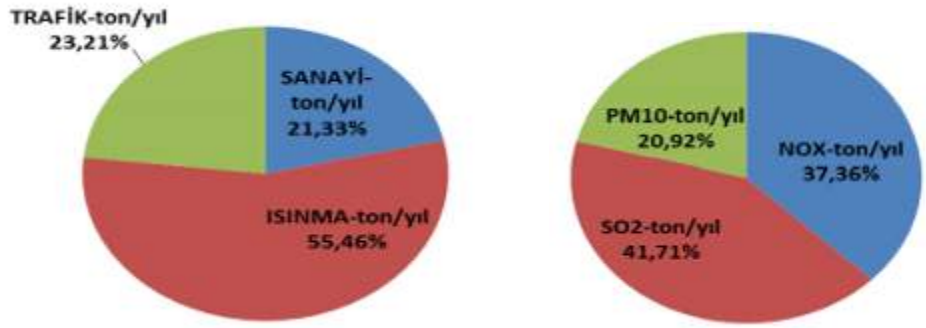

Şekil 4. ve 5. İl Genel Kirletici Dağılımı ve Kirleticilerin İl Genelinde Dağılım

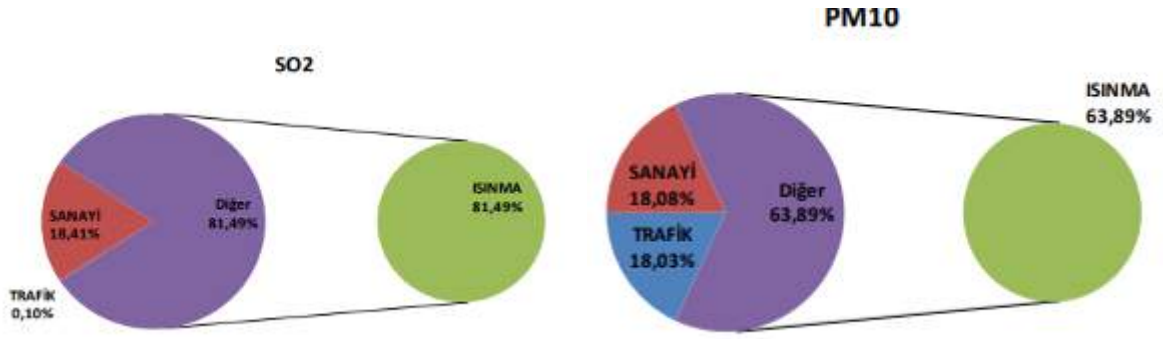

Şekil 6. ve 7. Gaziantep İli Toplam SO_x Emisyonlarının Dağılımı ve Gaziantep İli PM10 Emisyonları Dağılımı

Tablo 8. Gaziantep İlinde Hava Kalitesini Etkileyen Faktörler

Isınma	Yakıt Kalitesi	1	A
	Yakma Sistemleri		B
	Kışın, karasal iklime sahip olunmasından dolayı yılın 5 ayı ısınma ihtiyacı duyulması		C
Trafik	Taşıt Sayısı	2	A
	Motorlu Taşıtlarda Kullanılan Akaryakıt Kalitesi		B
Sanayi	Sanayi şehri olmasından dolayı sanayi tesisinin fazla olması	3	A
	Kirletici Vasfı Yüksek Olan Sanayi Tesislerinin Olması		B
Topoğrafik Durum, Nüfus ve Şehir Merkezinin Yapılanma Durumu	Nüfusun 1.9500.000 civarında olması	4	A
	İl Merkezinin Çanak Konumunda Olması		B
	Şehir Merkezinde Yoğun Yapılaşma Olması		C
Atmosferik ve Meteorolojik Şartlar	İnversiyonun Sık Olması	5	A
	Sıcaklığın Düşük Olması		B
	Rüzgâr Hızının Az Olması		C

➢ Gaziantep İli hava kalitesini etkileyen faktörler 1-5 arasında değerlendirilmiştir.

1 : Çok Önemli,
2 : Önemli,
3 : Az Önemli,
4 : Daha Az Önemli,
5 : Önemi Çok Az.

2.2. Şehirlerde Hava Kalitesinin İyileştirilmesi ve Kamuoyu Farkındalığının Artırılması Projesi

Ulusal düzeyde yürütülen hava yönetimi çalışmalarının yerel veriyle kuvvetlendirilmesiyle hava kalitesinin iyileştirilmesi ve bu alanda kamuoyu farkındalığı oluşturma amacıyla önerilmiştir.

Proje Süresi:

3 yıl; 2018-2021

Projenin Coğrafi Kapsamı:

Aydın, Denizli, İzmir, Manisa, Muğla, Uşak, Adana, Gaziantep, Hatay, Kahramanmaraş, Kilis, Mersin, Osmaniye, Amasya, Çorum, Giresun, Ordu, Samsun, Sinop, Sivas, Tokat, Afyon, Aksaray, Antalya, Burdur, Isparta, Karaman, Kayseri, Konya, Nevşehir ve Niğde

Proje Başlangıç Tarihi:

17 Aralık 2018

Proje Kapsamında:

- AB Direktifleri ile uyumlu olacak şekilde yerel veriyle birlikte ulusal emisyon envanteri raporlama kapasitesi artacaktır.
- Tüm paydaşların emisyon senaryoları, hava kalitesi modelleri, sektörel emisyon yönetim stratejileri konularında bilgi birikimleri artacaktır.
- Hava kirliliği ile mücadele yöntemleri konusunda kapasite arttırılacaktır.
- Kamuoyunun ve özellikle vatandaşlarımızın hava kalitesine ilişkin farkındalığı arttırılacaktır.
- Çevre ve Şehircilik Bakanlığının mevcut Hava Emisyon Yönetimi (HEY) Portalı için teknolojik gelişmeler ve diğer uygulama örnekleri ile sokak düzeyinde hava kalitesi modelleme çalışmaları için kapasite geliştirilmiş olacaktır.
- 31 ilin Temiz Hava Eylem Planları güncellenecektir.

3. HAVA KİRLİLİĞİNİN İNSAN SAĞLIĞI ÜZERİNE ETKİLERİ

Hava kirliliğinin yaygınlaşarak, bir halk sağlığı sorunu haline gelmesinin en önemli nedenleri kentleşme, ulaşım ve sanayileşmedir. Bu üç kaynak bir kısır döngü içinde birbirlerini etkilemektedir. Sanayileşmeyle birlikte endüstriyel tarım uygulamalarına geçiş kırsal işsizliği artırmış ve böylece kırdan kente göçü hızlanmıştır. Bunun bir sonucu olarak da kent büyüdükçe yaşayan insan sayısı artmakta, kentin konuşlandığı alan genişlemekte, ısınma kaynaklı kirletici miktarı artmaktadır. Kent büyüdükçe, buna bağlı olarak ulaşım ağı genişlemekte, araç sayısı artmakta, trafik yoğunlaşmakta kimi zaman çok yavaşlayıp durabilmekte, kullanılan yakıt miktarı ve egzoz emisyonları artmaktadır. Her üçünün birlikte artışı ise hava kirliliğinin yoğunlaşmasıyla sonuçlanmaktadır. (OECD, 2019)

Dünya Sağlık Örgütü (DSÖ) verilerine göre dünyada her yıl toplam 8 milyon insan iç ve dış ortam hava kirliliğinin yol açtığı hastalıklar nedeniyle erken ölmektedir. Bu ölümlerin 4,2 milyonu temelde sanayi, trafik ve ısınma kaynaklı dış ortamdaki hava kirliliği; 3,8 milyonu ise evin içinde yemek ve ısınma için yakılan yakıtlardan kaynaklanan iç ortam kirliliğine bağlı gerçekleşmektedir.

Türkiye'de de her yıl 34 binden fazla kişinin hava kirliliği nedeniyle erken öldüğü tahmin edilmektedir. Erken ölenlere başta akciğer kanseri olmak üzere hava kirliliğine bağlı olarak hastalananları, hastanede yatanları, ilaç kullananları ve işlerinden alıkonanları da ekleyecek olursak, hava kirliliğinin ülkemize maliyeti çok yüksektir.

Ortalama ağırlıkta bir insanın, ciğerlerinden her gün 12 m^3'ten (yaklaşık 15 kilogramdan) fazla hava geçmektedir. Bu miktar kişinin yaşına ve fiziksel aktivitesine göre farklılık göstermektedir. Solunumun kalitesi, insan metabolizmasının fonksiyonlarını yerine getirmede büyük bir etkendir. Her yıl 3,7 milyon kişi hava kirliliğin etkileri nedeniyle ölmekte ve bu tüm ölümlerin yüzde 5'ini oluşturmaktadır (Anonim, 2019b).

Hava kirliliğinin sağlık etkisi öksürük ve bronşitten, kalp hastalığı ve akciğer kanserine kadar değişmektedir. Kirliliğin olumsuz etkileri sağlıklı kişilerde bile gözlenmekle birlikte, bazı hassası gruplar daha kolay etkilenmekte ve daha ciddi sorunlar ortaya çıkmaktadır. Bu gruplardan biri yaşlılardır. Fizyolojik kapasitesi ve fizyolojik savunma mekanizması fonksiyonlarındaki azalma, kronik hastalıklardaki artma sebebiyle yaşlılar normal yaş gurubundaki halka nazaran hava kirliliğinden daha kolay etkilenmektedir. Küçük çocuklar, savunma mekanizması gelişiminin tamamlanmaması, vücut kitle birimi başına daha yüksek ventilasyon (soluk alıp verme) hızları ve dış ortamla daha sık temas sebebiyle daha fazla riske sahip diğer bir hassas gruptur. Yaş durumunun yanı sıra hava yolunda daralmaya yol açan hastalıklar da kirleticilere hassasiyeti artırmaktadır (Anonim 2016).

3.1 Solunum Sistemi Üzerine Etkileri

Etkiler şunları içerir: solunum bulgularında, enfeksiyonlarda artış; hava yolu tepkilerinde ve tahrişinde artış; akciğer iltihabı; solunumla ilişkili ölümlerde, hastane başvurularında ve hastanede tedavilerde artış; akciğer fonksiyonlarında azalma, astım atakları, kronik tıkayıcı akciğer hastalığında (KOAH) alevlenme ve akciğer kanseri riskinde artış gözlenmektedir.
Hava kirliliğine maruz kalma, yeni astım vakalarını tetikleyebilir; önceden var olan solunum hastalıklarını kötüleştirebilir ve aralarında KOAH, amfizem ve akciğer kanserinin de yer aldığı kronik hastalıkların gelişmesini veya ilerlemesini tetikleyebilir. KOAH, normal solumayı engelleyen ve yaşam tehdidi oluşturan bir akciğer hastalığıdır.

3.2 Kardiyovasküler Sistem Üzerine Etkileri

Etkiler şunları içerir: kalbin otonomik fonksiyonunda bozulma, kalp krizi (miyokard enfarktüsü), kalp kaynaklı göğüs ağrısı (angina pektoris); yükselmiş kan basıncı, damar sertleşmesi, hipertansiyon ve serebrovasküler iskemide artış gözlenmektedir.
Son yıllarda, farklı hava kirleticilerine maruz kalma ve kardiyovasküler etkiler arasında akut ve/veya kronik sonuçlar açısından- bağlantıyı güçlendiren önemli miktarda bilimsel kanıt ortaya konmuştur.

3.3 Sinir Sistemi Ve Serebrovasküler Sistem Üzerine Etkileri

Etkiler şunları içerir: nörogelişimsel hastalıklar, nöroinflamasyon,oksidatif stres, kan-beyin bariyerinde değişimler, baş ağrıları, anksiyete, inmeler, Alzheimer hastalığı ve Parkinson hastalığı.
Hava kirliliği bileşenlerinin karışımı, atmosfere yayılan cıva veya kurşun gibi ağır metaller de içerir. Bu metaller, yağmurla tekrar toprağa iletilene dek havada kalırlar. Ağır metallerin birçoğu insan vücudu ve özellikle çocuklar için nörotoksiktir.

3.4 Üreme Kapasitesi ve Çocuk Sağlığı Üzerine Etkileri

Etkiler şunları içerir: sperm kalitesinde düşüş, DNA parçalanması, düşük doğum ağırlığı, erken doğum ve gebelik yaşına göre küçük bebek doğumları.
Embriyo gelişiminde plasenta, çevresel açıdan tehlikeli birçok maddeye karşı bir bariyer olarak görev yapar; ancak hava kirliliğinin tüm bileşenlerine karşı koruyucu olamayabilir. Özellikle çocuklar, doğum öncesinde bile hava kirliliğine duyarlıdır. Sayıları giderek artan kanıtlar, yaşamın erken dönemlerinde hava kirliliğine maruz kalmanın, ileri yıllarda aralarında obezite, diyabet, göğüs ve prostat kanseri gibi hormonlarla ilintili kanserlerin de bulunduğu kronik hastalıklar geliştirme riskini artırdığını göstermektedir (Anonim 2015).

Tablo 1. Hava Kirleticileri ve Sağlık Etkileri

Kirletici	Ana Kaynağı	Sağlık Etkisi
Kükürtdioksit (SO_2)	Fosil Yakıt Yakılması, Taşıt Emisyonları	Solunum Yolu Hastalıkları
Azotoksitler (NO_x)	Taşıt Emisyonları, Yüksek Sıcaklıkta Yakma Prosesleri	Göz ve Solunum Yolu Hastalıkları
Partikül Madde	Sanayi, Taşıt Emisyonları, Fosil Yakıt Yakılması, Tarım ve İkincil Kimyasal Reaksiyonlar	Kanser, Kalp Problemleri, Solunum Yolu Hastalıkları, Bebek Ölüm Oranlarında Artış
Ozon (O_3)	Trafikten Kaynaklanan Azot Oksitler ve Uçucu Organik Bileşiklerin (VOC) Güneş Işığıyla Değişimi	Solunum Sistemi Problemleri, Göz ve Burunda İritasyon, Astım, Vücut Direncinde Azalma
Karbonmonooksit (CO)	Eksik Yanma Ürünü, Taşıt Emisyonları	Kandaki Hemeoglobin ile Birleşerek Oksijen Taşınma Kapasitesinde Azalma, Ölüm

Kaynak: ÇMO (2019), Hava Kirliliği Raporu 2018

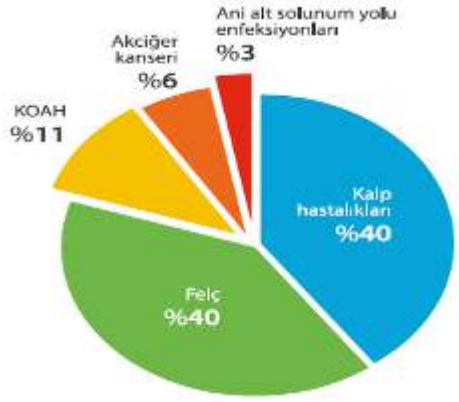

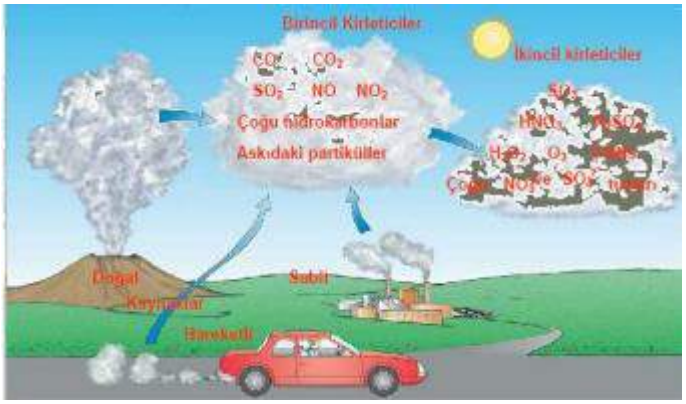

Şekil 2. ve 3. Hava Kirliliğinin Neden Olduğu Sağlık Sorunları (Dünya Sağlık Örgütü Hava Kirliliği Raporu/ 2016) ve Hava Kirleticilerinin Şematik Olarak Gösterilmesi

4. HAVA KİRLETİCİLERİNİN İNSAN SAĞLIĞI ÜZERİNE ETKİLERİ

Partikül Madde (PM_{10}, $PM_{2.5}$):
Havadaki partikül madde insan sağlığını etkileyen en önemli kirleticilerden biridir. Partikül boyutu ile sağlık üzerindeki olumsuz etkisi doğrusal olarak bağlantılıdır. PM'nin 10 µM'den büyük kısmı burun ve nazofarenkste tutulmaktadır.10 µM'den küçük kısmı bronşlarda birikirken 1-2 mikron çapındakiler alveollerde 0,1 mikron çapında olanlar ise alveollerden intrakapiller aralığa diffüze olmaktadır. Partikül maddeler civa, kurşun, kadmiyum gibi ağır metaller ile kanserojenik kimyasalları bünyelerinde bulundurabilmekte ve sağlık üzerinde önemli tehdit oluşturabilmektedirler.

Ozon (O_3): Ozon suda çözünmediğinden solunum sisteminin derinliklerine ulaşarak, akciğerlerdeki olumsuz etkilerini gösterir.

Azot Oksitler (NO_x): Azot oksitler (NOx) yüksek sıcaklıklarda (1200°C) oluşan pek çok türü renksiz ve kokusuzdur ve suda erimezler. Bu nedenle üst solunum yollarında elimine edilmeden solunum yollarının en uç noktalarına kadar inhale edilir ve buralarda olumsuz etkilerini gösterirler.

Kükürt dioksit (SO_2): Renksiz, yanmayan ve parlamayan bir gazdır. Burun ve farenkste irritasyona, ana hava yollarında spazma yol açabilir. Bu gaz suda çözüldüğünden, solunum yollarında uç noktalarına ulaşmadan büyük ölçüde burun ve farenkste elimine edilir.

Karbonmonoksit (CO): Renksiz, kokusuz bir gazdır ve yakıtlardaki karbon tam olarak yanmadığında oluşur. CO alveolar-kapilar membranda kolayca difüzyona uğrayarak hemoglobine bağlanarak kanda COHb oluşmasına yol açar. CO, O_2'ye oranla

Hemoglobine 200 kat daha kuvvetli bağlanır. Bundan dolayı da dokulara O_2 taşınmasını engelleyerek boğulmalara yol açar.

Uçucu Organik Bileşikler (UOB): Bu sınıfa çok sayıda kimyasal girer ve 300'ün üzerinde türü bulunmaktadır. Benzen, toluen, etilbenzen, ksilen, stiren en fazla sağlık riski oluşturan türlerdir. Kısa ve uzun dönemli olumsuz sağlık etkileri vardır.

Hidrokarbonlar: Yakıtların tam yanmaması sonucu ortaya çıkmasından dolayı CO_2'ye benzerler. Normal bulundukları düzeyde toksik etkileri gösterilememiştir.

Kurşun (Pb): Hava kirliliğine yol açan en önemli metaldir. Kurşun özellikle çocuklarda daha ciddi zehirlenmelere yol açmaktadır. Anemi, zeka geriliği ve davranış problemlerine neden olması yönünden önemlidir (Anonim 2019c).

2.3. HAVA KİRLİLİĞİNE KARŞI ALINABİLECEK ÖNLEMLER

- ✓ Hava kirliliğinin yoğun olduğu büyük illerimizde kaliteli ve temiz linyitin yakılması için gerekli tedbirler alınmalıdır.
- ✓ Kentsel ısınmada doğal gazın kullanımının artırılması ve yoğun hava kirliliği yaşanan illerimize doğal gazın götürülmesi gerekmektedir.
- ✓ Yakıtların tekniğe uygun olarak yakılabilmesi için kazanın, yakıtın yanma özelliğine göre standartlarına uygun olarak üretilmesi ve uygun yanma şartlarının sağlanması gerekmektedir.
- ✓ Kazan yakıcıların periyodik zamanlarda eğitilerek, uygun yakma kurallarını öğrenmeleri sağlanmalıdır.
- ✓ Büyük ısıtma sistemlerine filtre takma zorunluluğu getirilmelidir.
- ✓ Sadece uçucu kül için elektrofiltre bulunan termik santrallere desülfürizasyon tesislerinin de zorunlu olarak kurdurulması sağlanmalıdır.
- ✓ Bina projelerinde, baca ve kazanın konacağı yer standartlara uygun olmalı ve ısı yalıtımına önem verilmelidir.

SONUÇ

Ülkemizde hava kirliliği genel olarak ısınma, sanayi, madencilik ve motorlu taşıtlardan kaynaklanmaktadır. Bunların yanında büyük şehirlerimizde çarpık kentleşme, şehirlerin topografik yapısı, atmosferik şartlar ve meteorolojik parametreler, bina ve nüfus yoğunluğu gibi etkenler de özellikle kış sezonunda kirliliğin artmasına katkıda bulunmaktadır. Sınır değerlerin üzerinde konsantrasyona sahip olan kirleticilerin, insanlar ve çevre üzerinde olumsuz etkileri vardır (Anonim, 2017a).

Bu olumsuz etkileri en aza indirmek amacı ile yasal düzenlemere uyulması, hava kalitesinin korunması, halkın bilgilendirilmesi, çözümlerin üretilebilmesi ve gerekli

önlemlerin alınması bakımından Hava kalitesinin doğru bir şekilde belirlenmesi büyük önem taşımaktadır. Hava kirliliğinin ölçülmesi, tüm illerde hava kirliliği politikaları oluşturulması ve bu politikalar çerçevesinde illerin hava kalitesinin bir önceki yılın değerlerinden daha iyi durumlara getirilebilmesi amacıyla, Çevre ve Şehircilik Bakanlığı toplam 199 istasyondan oluşan Ulusal Hava Kalitesi İzleme Ağı oluşturmuştur. Bu istasyonlarının tamamında kükürtdioksit (SO_2) ve partikül madde (PM10) parametreleri, bazılarında ise partikül madde ($PM_{2.5}$), azotoksitler (NO, NO_2, NO_X), karbonmonoksit (CO) ve ozon (O_3) miktarı ölçülmektedir (Anonim, 2017a). Kirleticilerden insanların olumsuz yönde etkilenmemesi için en kısa sürede kirlilik seviyesinin bilinerek eyleme geçilmesi amacı ile ölçümler tam otomatik yöntemlerle yapılmakta ve sürekli olarak hava kalitesinin izlenmesi ve halkın bilgilendirilmesi sağlanmaktadır.

KAYNAKLAR

Anonim 2015. Türkiye'de Hava Kirliliği ve Sağlık Gerçekler, Veriler Ve Öneriler, Yayın Tarihi: Şubat 2015. Bu bilgi broşürü, Türkiye'den aşağıdaki hekim ve uzmanlık derneklerinin işbirliği ile yayınlanmıştır.

Anonim 2016. Gaziantep Temiz Hava Eylem Planı 2016-2019, Gaziantep Çevre Şehircilik İl Müdürlüğü.

Anonim 2019a. Toraks. https://www.toraks.org.tr/ halk/News

Anonim 2019b. https://www.who.int/airpollution/en/

Anonim 2019c. https://hsgm.saglik.gov.tr/tr/(Erişim Tarihi:30.09.2019).

Avşar, E., Alp, K.&Toröz, İ. 2015. Balıkesir İli Burhaniye İlçesi (İskele Mahallesi) Hava Kalitesinin Değerlendirilmesi. *BEÜ Fen Bilimleri Dergisi*. 4(1), 68-82

Çay, Y.& ÇELİK, E. (2015). Hava Kirliliğinin Doğal Gaz Kullanımı İle Değişimi, Sakarya İli Örneği, *Akademik Platform*, 1497-1504, ISITES Valencia –SPAİN

Çetin, T.Ö. & Sümbül, H. (2010). Hava kirliliğinin belirlenmesinde likenlerin kullanımı. *Mehmet Akif Ersoy Üniversitesi Fen Bilimleri Enstitüsü Dergisi.* 2: 73-85.

Garipağaoğlu, N. (2013). Tokat'ın Hava Kalitesinin Zamanla Değişimi ve Karadeniz Bölgesi İçerisindeki Durumu, *Tokat Sempozyumu 1-3 Kasım 2012 Tokat Bildiriler Kitabı*. Cilt: II s.9-32, Özyurt Matbaacılık, Ankara.

OECD. (2019, Şubat 1). OECD Çevresel Performans İncelemeleri Türkiye 2019.

TMMOB Çevre Mühendisleri Odası (2018). *Hava Kirliliği Raporu,* Çevre ve Şehircilik İl Müdürlüğü, (2017). Hava Kirliliği Verileri, Kırıkkale.

OBSERVATION OF PRIMARY PARAMETERS IN TWO-STAGE ANAEROBIC DIGESTERS UNDER UNSTEADY-STATE CONDITION

Merve AKCAKAYA
Environmental Engineering Department, Middle East Technical University
merve.akcakaya@metu.edu.tr

Sera TUNCAY
Environmental Engineering Department, Middle East Technical University
sera.tuncay@metu.edu.tr

Bulent ICGEN
Environmental Engineering Department, Middle East Technical University
bicgen@metu.edu.tr

ABSTRACT: Anaerobic digestion is a common sludge treatment method to produce biogas by microorganisms. Anaerobic digestion takes place through four stages as hydrolysis, acidogenesis, acetogenesis and methanogenesis. In single-stage anaerobic digesters, process failures often occur due to accumulation of volatile fatty acids. To overcome these problems, physical separation of acidogenesis and methanogenesis phase has led to the emergence of two-stage anaerobic digesters. Due to the complexity of the bioconversion processes, there are many factors affecting the performances of an anaerobic digesters. Those can be categorized as sludge characteristics and operational conditions. Among the operational conditions, temperature and pH are the most important parameters. For the characteristics of sludge, chemical oxygen demand (COD) and total nitrogen (TN) are also important parameters since they reflect the number of organics present in the sludge. The efficiency of anaerobic digestion can also be evaluated using COD, because its consumption shows the degradation taking place within an anaerobic digester. Therefore, in this study, weekly changes of primary parameters were investigated for 2 two-stage anaerobic digesters under unsteady-state condition. During the operation, pH, temperature, COD and TN values of the sludge were measured. It was observed that the values for each parameter fluctuated for the first 10 weeks. The values of the following weeks started to show same trend meaning that the digesters reached steady-state condition.

Keywords: Two-stage anaerobic digester, unsteady-state, COD, TN

Acknowledgement: This study was supported by TÜBİTAK 1001-Scientific and Technological Research Projects Funding Program (116Y181).

IDENTIFICATION AND EVALUATION OF TRAFFIC MANAGEMENT SCENARIOUS USING MICROSCOPIC SIMULATION IN MEKELLE

Hiluf Gebremariam Tetemke [1], Temesgen Destalem Yihdego [2] Melat Bereket Abraha [3]
[1] *Graduate student at Mekelle University, Mekelle, Ethiopia*
[2] *Bachelor Degree student at Adigrat University, Adigrat, Ethiopia*
[3] *Bachelor Degree student at Adigrat University, Adigrat, Ethiopia*

ABSTRACT: Transpiration system is an integral part of modern society. An increase in transportation demand is a serious problem for every city. As the number of vehicle and pedestrian grows the roads which were designed back are remaining the same.The Mekelle city roads are narrow and suffering traffic congestion. There could be two approaches to solve this peoblem. First and the most obevious approach is come up with modification and construction new rods. But for developing countires like Ethiopia, fund and land aquistion are serious concerns. The second approach is to manage existing tarffic with supply and demand taffic managmet is the economical and easily implementable. If traffic congestion are not solved, they could open door socioeconomic and safetey problem mainly on the residence. Studies neglected to consider how traffic mangmet could help to relax traffic conestion and assoiciated impacts at Mekelle city. The research study was aimed at investigatigation and evaluation traffic management scenarios using microscopic model at Mekelle city most busiest intersection and to select most suitable that can be adopt to reduce traffic congestion and other associated benefits such as reduction in in fuel consumption and motor vehicle emission. Three real-life implementaion tarfic managemet scenarios has been implemeted to solve those problems.The base case or do nothing was considered as control/reference for comparison success scenario. A model has been developed using microscopic simulation software SYNCRO version 9 and performance of the intersction has been found before and after implemtation of traffic mangment measure. The proposed of traffic mangemet scenarios was converting curb parking to effective tarffic lane, wavinig/shifting out of private vehicle to outside main road and providing traffic signal for Adi-Haqi Bridge and: lane addition, traffic signal timining optimizing, and wavinig/shifting out of private vehicle to outside main road for Adi-Shunduhun intersection. Result was extracted from the SYNCRO simulation output report the selection of the most decisive or most welcome scenario was based on set of measurement of effectiveness(Delay time, capacity, CO emission, queue length and fuel consumption). Based on the measurement of effectiveness criteria used the succeed scenario was recommended for implementation. The scenario or alternative congestion mitigation measurement being most effective were converting curb parking lane to effective lane and lane addition for Adi-Haqi Bridge and Adi-Shinduhun.

Keywords: Traffic congestion; Traffic management; Microscopic simulation; Measure of effectiveness; most welcome scenario

1. Introduction

Transport is crucial and necessary for modern life pattern. The freedom to move short and long distance creates horizons for personal development and professional activates, increases the opportunities for leisure and holidays, and allows better connection and understanding between people. Transpiration system is integral part of modern day society, designed to provide efficient and economic movement between the component parts of a country and offer maximum possible mobility to all citizens. According to (Leshem and Ritov, 2007), road transportation is a critical link between all the other modes of transportation and their proper functioning.

Unfortunately, the existing road networks, including the motorway system, is becoming explosively congested due to increase in the number of vehicles and inability to build new and larger motorway (David and Gregory, 2010). Congestion reduces city inhabitant quality of life and also has environmental adverse impact. The waste of energy in gridlocked traffic and the production of greenhouse gases and other pollutants are harmful to the urban areas. Perhaps most importantly, congestion has substantial economic costs. Decisions investment and jobs hinge depend on the quality of transportation infrastructure and the free flow of goods and people in and through our cities (UTTF, 2012).

Traffic congestion is the growing problem in Ethiopia. It is becoming acute for largest cities in Country including Mekelle. Mekelle has witnessed tremendous changes in the development of its economy. There exist rapid growing of population, both resident people and floating people. The city population is increasing 5% every year (CSA, 2013). The number vehicles are growing at a dramatically rate, even though road space remains stagnant, hence road capacity does not catch up with growth of vehicles. The road networks of Mekelle city are narrow. During the study the transport demand and capacity of facility were mismatched. This shows there is a need for concerted effort of improving the transport service in the city in order to increase accessibility and efficiency.

There could be two approaches to solve this problem of congestion. First and the most obvious solutions are to come up with infrastructure involving wider roads, flyovers, bypass and expressways. But for developing countries like Ethiopia, money and space are serious concerns. Second approach is to manage existing traffic, with the use of technology and by involving commuters in process which is traffic management.

In modern day, widening road is not the appropriate mitigation of road network particularly in mega city. Road expansion maybe encourages the development of real estate and businesses along the expressway. And new traffic flows added by those new settlers will offset some part of the benefits, which old road's users expected to have from upgrading of road at the beginning. So, it seems difficult to remove peak-hour traffic congestion only by enlarging the capacity of roads network. Enlarging the capacity of streets in old city for automotive traffic is widely opposed by local residents, since dwellings would be turn down by widening streets. Therefore, the growth of road capacity does not catch up with growth of vehicles and this mismatch could cause lots of vehicle blocked on narrow roads. There are three types of convergence

that appear when an new road is opened or an old road is improved: travelers who formerly chose alternative routes during peak hour turn to the new road (spatial convergence); travelers who formerly did not drive in peak hours start to travel during those periods (time convergence); and travelers who formerly did not travelling by vehicles switch to driving (modal convergence). So many drivers shift from those three types convergence to the new built or improved route, before long, its traffic capacity is reached and its top limit exceeded. This outcome is almost inescapable if peak hour traffic was slow already before the highway was improved (Downs, 2003).
This present study traffic management measures development and evaluation has not been done by else in Mekelle city before. There are some studies that have been done before with specific objectives investigation level of congestion and some optimization as scenarios of mitigation congestion. Even though, signal adjustment is method of alleviation traffic congestion impact on the road users, but there another strategy or instruments that are applicable traffic congestion potential avoidance. This study, in addition to traffic signal adjustment, has introduced several traffic management strategies towards reducing impact of traffic congestion on road users of Mekelle city.

2. Background

There is no unique definition of Traffic Management (TM), it differs upon the scholars. In generally, Traffic Management (TM) is the planning, monitoring, and control or influencing of traffic (TRKC, 2009).
Traffic management measures comprises different of intervention mainly in urban areas. Traffic management measures in principle aim at the following goals: to reduce traffic congestion; to improve road safety; to reduce environmental pollution and; to reduce energy consumption. Additional, traffic management (TM) is a management system and process conducted to improve traffic operations and safety through strategies that reduce demand or through operational improvement. Traffic management strategies are low-cost strategies, easily implemented in short period of time and cost-effective compared to more traditional capacity improvements, such as adding travel lanes, which takes several years to construct.
Congestion managements start by understanding the problem characteristics and causes. As (CMP, 2016) identifies the main cause of congestion to appear are: bottlenecks, traffic incidents, work zones, bad weather, poor traffic signal timing, and special events.
There are numerous measures that can be taken to alleviate urban traffic congestion. At a conceptual level, it is possible to identify and classify these measures according to three broad categories. The first category comprises measures that address the supply side of transport facilities (i.e., they are basically directed at increasing urban transport capacity). Measures in the second category are aimed at managing the demand side, specifically, in terms of encouraging efficient use of existing transport facilities (e.g., road space uncongested central areas). The third set of measures concerns the development of alternative urban structures conducive to the dispersal of economic activities and

improved physical integration between employment, amenities, and housing. Within the two main strategies (e.g., demand side and supply side), according to Dougherty (1994) there are more than 40 conventional and innovative congestion management measures, which are categories into nine strategic class: these are Land use and Zoning, Communications substitutes, Traveller information services, Economic measures, Administrative measures, Traffic operational measures, Preferential treatment, Public transport operations, Freight transport operations.

Table 1: Classification of Traffic Management Measures

Demand Side	Land use and zoning	• land use and zoning policy • site amenities and design
	Communications substitutes	• Telecommuting • Teleconferencing • Tele shopping
	Traveler information service	• pre-trip travel information • Regional rideshare matching
	Economic measures	• Congestion pricing • Parking pricing • Transportation allowances • Transit and rideshare financial incentive • Public transport pass program • Innovative Financing
	Administrative measures	• Transportation partnership • Trip reduction ordinances and Regulations • Alternative work schedules
Supply-Side	Traffic Operation measures	• Entrance ramp controls • Traveler information systems • Traffic signalization improvements • Incident management • Traffic maintenance during construction
	Preferential Treatment	• Bus lanes • Carpool lanes • Cycle and pedestrian facilities • Traffic signal pre-emption
	Public transport operations	• Express bus services • Park and ride services • Service improvements • public transport images

		• High capacity public transport vehicle
	Freight transport operations	• Urban goods movement • Intercity goods movement

(Source: Dougherty, 1994)

The software package SYNCHRO/SimTraffic incorporates both the analytical and micro-simulation models into the designing process. The analytical model is used in SYNCHRO to quickly evaluate the performance measures of different scenarios. The micro-simulation model is used in SimTraffic to provide better estimates of the performance measures (Li and Tarko, 2007).
SYNCRO version 9 software which is used for capacity analysis, coordination, signal modeling and to find signal timing. SYNCRO optimize cycle length, split times, offsets and phase sequence to minimize driver's stops and delay. The software can also provide a detailed summary report on analysis results like intersection capacity, level of service, volumes, timing, queue length, blocking problems, delay, fuel consumption and emission level.
For design and analysis of the signalized and non-signalized road intersections, many procedures or techniques are developed by researchers and traffic management companies (Freeman et al., 1999).

3. Study Area

For this study two main intersections were selected for further analysis in this study. Those are selected because privilege solution worthy. Those two selected intersection; Adi-Shinduhun and Adi-Haqi Bridge intersection were selected to be close as possible to scenarios developed and most congested intersection they were.
Adi-Haqi Bridge intersection was among most congested intersections of the city and high traffic accident where occurred. It is All-Way Stop Controlled intersection (AWSC).That intersection located at business area, which contains banks and insurance and it, is described as Center Business District (CBD) area. The Center of Business Districts are characterized by high traffic flow, high parking turnover, narrow short-block roadway and high pedestrian activity and the saturation flow of such areas are lower than other areas.
Adi-Shinduhun intersection was among most congested and very narrow intersection in city from traffic police witness. It is four-legged signalized intersection. In fact it serving arterial road class, but the geometry of link in the South-North approach is single in each direction. It deviated from local manual and international manual stated minimum lane required. Different manual covered that minimum lane required per direction is two, but it the existing road geometry is single lane.

(Source: Digital Google earth map)
Figure 1: (a). Adi-Haqi Bridge intersection, (b). Adi-Shinduhun intersection

4. Data Collection and Analysis

To achieve the objective of the investigation data's has been collected from primary and secondary sources. Primary data includes, traffic data, geometric data, signal timing or signing, whereas secondary data includes, registered vehicles in Mekelle city and the estimated population growth of the city.
The traffic data was collected at morning peak and evening peak hour for three days: Monday, Tuesday and Saturday. The three days were selected, because previous study conducted by city government shows high traffic was recorded on that days highly.
The traffic data depicted Figure 2 and 3 shows traffic volume of morning peak hour and evening peak hour. Fortunately the peak hour or highest hourly volume was recorded, on Monday from 7-8:00Am, on both study areas. Monday is market day, that why maximum traffic is collected on Monday.

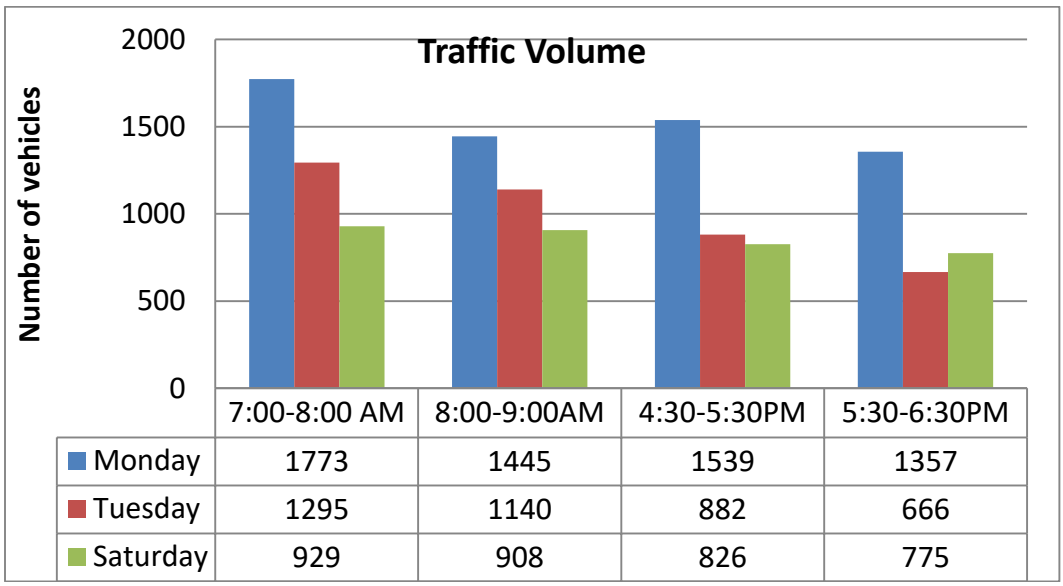

	7:00-8:00 AM	8:00-9:00AM	4:30-5:30PM	5:30-6:30PM
Monday	1773	1445	1539	1357
Tuesday	1295	1140	882	666
Saturday	929	908	826	775

Figure 2: Traffic data of Adi-Haqi Bridge intersection

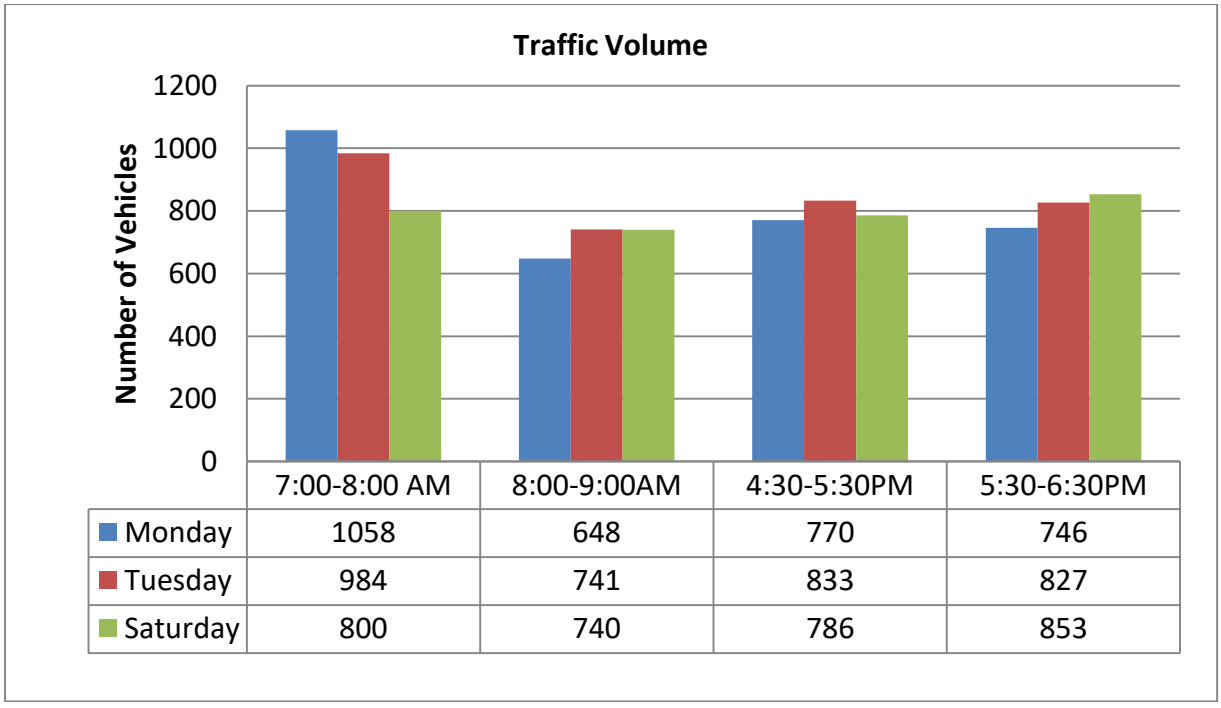

	7:00-8:00 AM	8:00-9:00AM	4:30-5:30PM	5:30-6:30PM
Monday	1058	648	770	746
Tuesday	984	741	833	827
Saturday	800	740	786	853

Figure 3: Traffic data of Adishinduhun intersection

5. Modeling and Scenario Development

After the data collection and analysis, a model is developed replicating the field condition. Volume at peak hour, modal split road inventory of study area the inputs required.

Traffic congestion mitigation strategies are the most important target of all transport decisions to balance the relationship between the demand and supply in a transport system so as to relax the traffic congestion. Urban traffic congestion mitigation measures encompass a set of strategies and techniques to reduce the impact of traffic congestion. Several mitigation strategies are available for mitigation of traffic congestion, using these strategies traffic congestion can be reduced on road user (OECD, 2004). There are many possible combinations to mitigate congestion; there is no single solution for congestion these solutions differs to place-to-place and site to site. The mitigation strategy selected should have the following criteria (OECD, 2004). The following rules were followed while developing scenarios for this study.

- Proven effectiveness in many studies congestion reduction
- The solution should be easy for implementation
- It should consider the minimum infrastructure modification
- It should interact and complement with other congestion mitigation programs

A. The alternative strategies forwarded for Adi-Haqi Bridge intersection were:

i. **Providing signal control:** Heavy traffic and money traffic accident occurred in intersection, since none signalized intersection is risky traffic safety. To reduce occurrence of traffic accident and minimize congestion effect traffic signal control has been implemented to as scenario mitigation of congestion

ii. **Converting parking lane to travel lane**: This study has implanted to convert curb parking lane to effective traffic lane in west bound approach. As it depicted in Figure 3 the west bound approach has single lane entry at boundary of intersection, however it has directional two lanes at upstream. At boundary intersection space of a traffic lane is occupied or reserved for on street (online) parking lane. For present study it was proposed to restrict on street parking, and to convert curb parking lane to effective lane.

Figure 3: Curb parking facility

iii. **Rerouting private vehicle:** This study has implemented waving out or shifting of private vehicle(Car and 4WD/Land Rovers) to uncongested to minor routes outside the system (outside Adi-Shinduhun intersection). Those private and semiprivate cars allowed them out from main road to minor roads join main road at the peak morning and

evening. Those private and semiprivate vehicles cause extra congestion and blocking problem, however their occupancy is very low. Then, private vehicle must be constrained to encourage public transportation. In order to attract more people to use the bus is necessary to introduce certain bus priority strategies. The main road will serve for High occupancy vehicle (HOV), and commercial vehicle.

B. The alternative strategies forwarded for Adi-Shinduhun intersection were:

i. Optimizing signal timing: The existing signal time plan is failed to accommodate for existing traffic demand. Seasonal signal time is necessary, since traffic demand varies season to season even month to month, because socio economic of commuters. The existing signal timing has taken long time without adjustment, even though it should have reviewed and updated periodically not longer than three or five years (MUCTD, 2010).

ii. Rerouting private vehicles: It is waving or shifting of private vehicle(Car and 4WD/Land Rovers) to uncongested to minor routes outside the system (outside Adi-Shinduhun intersection). Those private and semiprivate cars allowing them out from main road to minor road joins main road at the peak morning and evening. In order to attract more people to use the bus it is necessary to introduce certain bus priority strategies.

iii. Lane addition: The function of all road network pass through Adi-Shinduhun intersection was Arterial type. They are public routes. They connect trip origin to trip destination. The segments of South-North bound were single lane per direction; hence those segments even didn't meet the minimum lane number of urban arterial that in reference to AACRA standard. However, traffic management is searching strategies that could displace minimum infrastructure; at very minimum but the corridor should meet the minimum standard. Hence, adding a lane in South-North segment was proposed as congestion mitigation.

6. Evaluation of traffic management Scenarios

The measure of effectives varies from author to author, type control, purpose of evaluation. In principle traffic management goal is to exist fast, or less congested, energy efficient, environmental friendly transport system. To account to those goal and according to type control and simulation out the measure of effectiveness Delay time, fuel consumption and Co emission: Delay time, fuel consumption, queue length and capacity were chosen for Adi-Haqi Bridge and Adi-Shinduhun intersection sequentially.

i. Adi-Haqi Bridge intersection

Table 2: Simulated Measure of Effectives of Adi-Haqi Bridge intersection

Scenario(case)	Delay, sec	CO Emission, g/hr	Fuel consumption, l/hr
Do nothing	105	4160	239
Scenario-I	152	5565	299
Scenario-II	54	3140	169
Scenario-III	73	2800	151

Accordingly the analysis run and result of analysis are summarized in Table 2 it is surprising the performance measurement of if it were signal control, went from bad to worse the average control delay increased by 47 seconds (44.8%) compare to Do Nothing case. Hence signal control failed to reduce congestion adverse effect delay time.
For second scenario curb parking converting to traffic lane result analysis as depicted Table 2 the average delay time extremely decreased that is from 105 seconds to 54 seconds. Final waving out private vehicles scenario 3 analysis result shows moderate operation performance was gained. Intersection delay was changed from 105 second delay to 73 second if they were waved out private vehicle in most approach those right turn movements.
Finally, the best improvement in delay time was noticed in scenario two (2) followed by scenario three (3). As seen in Figure 4, the simulated delay time of Scenario two seen below others strategies simulated delay times cases.

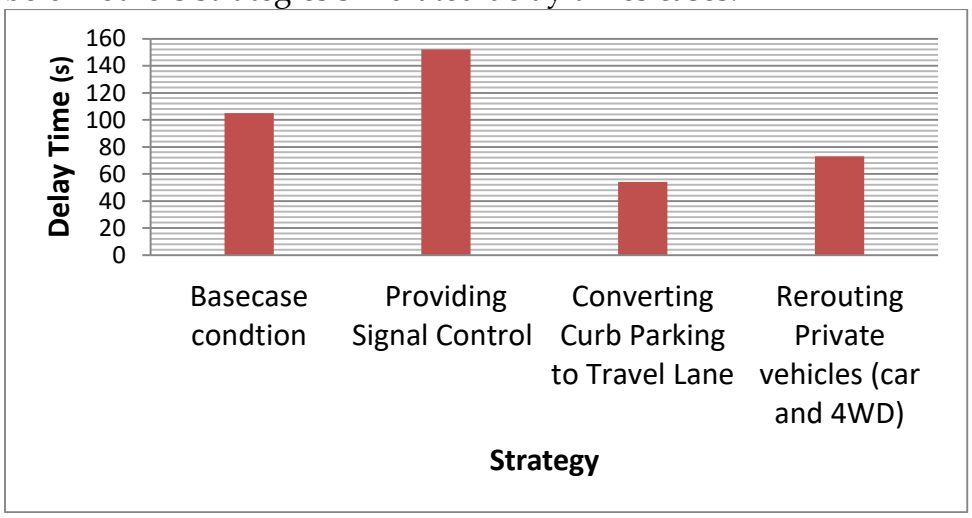

Figure 4: simulated delay time result

The estimated fuel consumption for do nothing case and scenarios case studied. As shown Table 2 considerable fuel consumption decrease noticed in case of scenario 2 (converting parking lane to effective lane) relative others. However scenario 1 didn't produce decrease fuel consumption, rather get worse or increased about 25.1%. The figures of fuel consumption shows the best result in terms of saving fuel consumption was obtained from scenario 2 with average percentage of 29.3 % compared to Do nothing case.

It is important to note fuel consumption from scenario 3(shifting private vehicle), was not used to compare for fuel consumption. Because some vehicle was waved out the main intersection that means that simulated figure fuel consumption is merely referred to those vehicle drives through main intersection, then it is not true fuel consumption depicted in Table 2 because it did not included energy consumed by vehicle shifted to the minor roads.

Among the objective of traffic management is to exist less pollution transportation system. To take account pollution effect, it has been considered, CO emission as measure of effectiveness.CO emission for the Do nothing case and scenario are presented in Table 2. It is clear from the Table that CO emission differ scenario to others.

As shown in figure considerable decrease noticed incase case of scenario 2 that converting curb parking lane to travel lane. However scenario 1(Providing signal control) went from bad to worse, as traffic signal implemented. Hence it didn't produce decrease CO emission. The figure showed in Table 2 the best result in terms of decreasing CO emission to be healthy environment was obtained from scenario 2(curb parking lane change to effective lane) with average percentage of 24.35% compared to Do nothing case.

ii. Adi-Shinduhun Intersection

For first scenario(Optimizing signal time) that is optimize signal timing result analysis as depicted Table 3 the average intersection delay time dropped by 8 seconds. For second scenario (shifting private vehicles to outside the study areas) the average delay time dropped by 18 seconds (16%). This shows moderate performance change of traffic operation is seen. Final lane addition scenario analysis result as seen in Table 3 shown better operation performance change was gained. Intersection delay was changed from 112 second to 60 seconds (46% dropped) after added single lane in South-North corridor. Finally, the best improvement in delay time was noticed in scenario 3 followed by scenario 2 where the graph of two scenarios were well below the graph of other scenarios as depicted Figure 5. As seen in Figure 5, the delay time seen continue to decrease from Do nothing (left) to land addition).

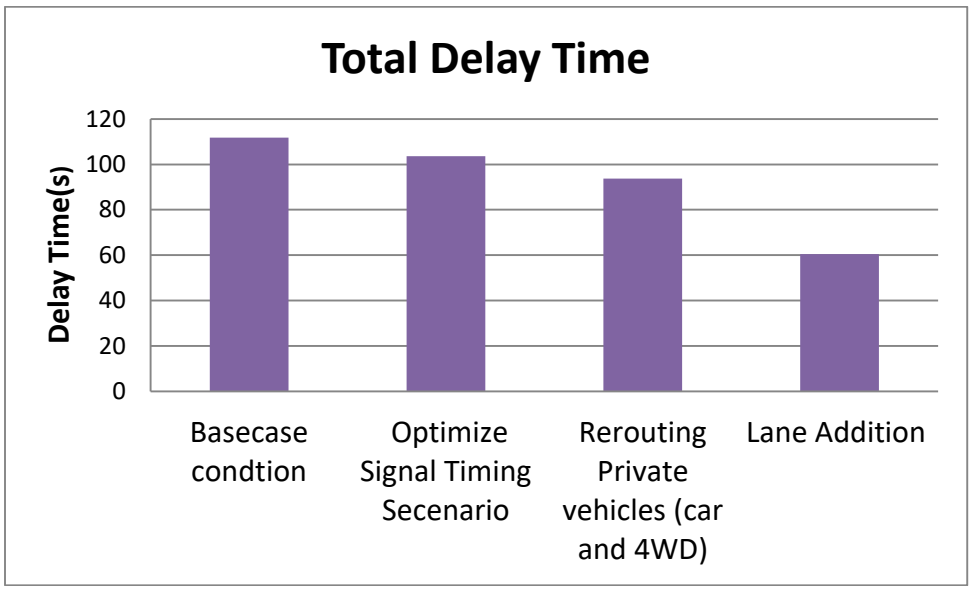

Figure 5: simulated delay time result

After implementation traffic management of noticeable improvement was gained from Scenario one (do nothing). Capacity of intersection increased by 12% (155vph) for the optimization signal time scenario compared to Do nothing case. The rerouting private vehicle to back street nearby main intersection didn't produce better change on capacity, instead it decreased by 10% compared to Do nothing. This is because of the closed intersection to Adi-Shinduhun are being activated during waving out scenario simulation. It produces effect on capacity of main intersection. In the other hand, for Do nothing condition, the minor intersections were not activated because it was too low volume where they use back street. Drastic increasing capacity has been observed, as lane addition scenario implemented as shown Table 3. The capacity increased by 55% compared to Do nothing condition.
The best improvement incapacity was noticed in Scenario 3 and followed scenario 1.

Table 3: Simulated Measure of Effectives of Adi-Shinduhun intersection

Scenario(case)	Delay, sec veh/hr	Capacity,	Queue length, m	Fuel consumption, l/hr
Do nothing	112	1320	343	131
Scenario-I	104	1475	314	124
Scenario-II	94	1179	284	94
Scenario-III	60	2054	191	75

Accordingly the analysis run and result of fuel used in all arms analysis result are summarized in Table 3.These shows estimated fuel consumption for do nothing case and scenarios studied. As shown in Table 3 result significance decrease noticed incase case of scenario three (lane addition). However scenario one (optimizing signal time) didn't

produce significance decrease fuel consumption. The figures shows the best result in terms of saving fuel consumption was obtained from scenario three (lane addition) with average percentage of 43% compared to Do nothing case.
It is important to note fuel consumption from scenario two (shifting private vehicle), was not used to compare for fuel consumption. Because some vehicle was waved out the main intersection, then it is not true fuel consumption depicted in Table 3.

SUMMARY AND CONCLUSIONS

The following conclusions are made according to the analysis:

- This study identification traffic congestion mitigation measures and evaluated using SYNCRO studio microscopic simulation.
- Delay, fuel consumption and CO emission; delay time, capacity, fuel consumption and queue length has been used to compare the effectiveness or success of traffic congestion mitigation with respect to base case or do nothing condition for Adi-Haqi Bridge and Adi-Shindihun intersection sequentially.
- The levels of service on the intersection were performing above their capacity for Adi-Haqi intersection with intersection delay 105 seconds. But, for signal providing scenarios intersection delay raised by 47seconds (45%). In converting curb parking lane to travel lane scenario the whole intersection delay dropped by 51 second (49%) that almost half for existing traffic operation performance. Likewise, the performance of third scenario rerouting or constrain of private vehicle like car, 4WD found moderate. Intersection delay changed from 105 second to 73 seconds after shifting of low volume vehicle to outside system. By looking at all performance measure possible scenarios, Scenario-II (Converting curb parking to traffic lane) is better to method to practice on selected intersection. And shifting of low occupancy vehicles (car and 4WD) is second best mitigation for selected Adi-Haqi Bridge intersection.
- Most traffic operation was operating with total delay 112 seconds at Adi-Shinduhun signalized intersection. The intersection delay a few change appeared that is 8 seconds after optimize signal time to the do nothing condition. Likewise, the performance of second scenario rerouting or constrain of private vehicle like car, 4WD found moderate performance seen. Final the lane addition scenarios, in fact it brought infrastructure modification, its performance found better than other scenarios. The intersection delay dropped from 112 seconds to 60 seconds after lane addition implemented South-North corridor a single lane to become two lanes per direction. By looking at all possible scenarios, Scenario-III (Lane addition) is better to method to practice on selected intersection. And shifting of low occupancy vehicles (car and 4WD) is second best mitigation for selected intersection.

REFERENCES

AACRA. (2003). Addis Ababa City Road Authority (AACRA): Geometric Design.

Abebe, Z. (2006). Urbanization for National Development in Ethiopia. Vision 2020 Ethiopia Forum held on May 2, 2006. Ethiopian Economic Association, Addis Ababa

Alaci, D.S.A. (2010). Regulating Urbanization in Sub-Saharan Africa through Cluster Settlements: Lessons for Urban Mangers in Ethiopia. Theoretical and Empirical Researches in Urban management 5(14).

Andy, H.F. Chow, Alex Santacreu, Ioannis Tsapakis, Garavig Tanasaranond and Tao Cheng. (2014). Empirical assessment of urban traffic congestion, *Journal of Advanced Transportation, J. Adv. Transp. 2014; 48:1000–1016.*

Belachew, M.H., Zeleke, D.A. (2015).Statistical Analysis of Road Traffic Car Accident in Dire Dawa Administrative City, Eastern Ethiopia. *Science Journal of Applied Mathematics and Statistics. Vol. 3, No. 6, 2015, pp. 250-256. doi: 10.11648/j.sjams.20150306.14.*

Byrne, G.E. & Mulhall, S.M. (1995) Congestion management data requirement and comparisons, Transportation Research Record: *Journal of the Transportation Research Board, No. 1499, pp. 28-36.*

Congestion Managmet Process (CMP).(2016). Congestion management process Technical Report. Metroplan Orlando, USA.

David, H., & Gregory, F. (2009). Gridlock and growth: The effect of traffic congestion on regional economic performance.

Downs, A. (2003). Still Stuck in Traffic: Coping with Peak-Hour Traffic Congestion. Washington, DC: Brookings Institution Press.

European Environment Agency (EEA). (2014) Noise in Europe 2014. European Environment Agency, Report 10/2014. Luxembourg: Publications Office of the European Union.

European Commission. (2015). Science for Environment Policy: Noise impacts on health.

E. O. Mogaka, Z. Ng'ang'a, J. Oundo, J. Omolo, and E. Luman. (2011).Factors associated with severity of road traffic injuries, Tika, Kenya, *Pan African Medical Journal, vol. 8, article 20, 2011.*

Emily, S., Mekamu, K. (2009). Urbanization and Spatial Connectivity in Ethiopia: Urban Growth Analysis Using GIS, Development Strategy and Governance Division, *International Food Policy Research Institute-Ethiopia Strategy Support Program 2, Ethiopia.*

FHWA. (2008). *Traffic Signal Timing Manual*: Kittelson and Associates, Inc, Wasninton, Dc, HWA-HOP-08-024.

FREEMAN, W., HO, K. & MCCHESNEY, E. An evaluation of signalized intersection system analysis techniques. Transportation Frontiers for the Next Millennium: 69th Annual Meeting of the Institute of Transportation Engineers, 1999.

Highway Capacity Manual (HCM). (2000).TRB, National Research Council, Washington, D.C.

Highway Capacity Manual (HCM). (2010).TRB, National Research Council, Washington, D.C.

Issa, Yazan. (2014). Reducing of Roads Congestion Using Demand Management Techniques, *International Journal of Computational Engineering Research (IJCER), vol. 04, no. 7, 2014.*

Jonkers, K., and Gorris, T. (2015) Intelligent Transport Systems and traffic management in urban areas. Policy Note 2020, CIVITAS WIKI Team, Netherland

Kibrom, G. (2005). Investigation into engineering properties of Mekele soils with an emphasis on expansive soils: MSc Thesis, Addis Ababa University, Ethiopia.

Kumar, A., Singh, R.R. (2017). Traffic Congestion and Possible Solutions in Urban Transportation System. *4th International conference on Emerging Trends in Engineering, Technology, Science and Management, ISBN: 978-93-8617154-2 New Delhi, India*

Leshem G & Ritov Y. (2007). Traffic Flow Prediction using Adaboost Algorithm with Random Forests as a Weak Learner. *International Journal of Intelligent Technology Vol. 2 No. 2 ISSN 1305-6417*

Levy, Jonathan I., Jonathan J. Buonocore, and Katherine von Stackelberg. (2010). Evaluation of the public health impacts of traffic congestion: a health risk assessment. Environmental Health 9(1): 65.

Lim Lan Yuan. A Case Study on Urban Transportation Development and Management in Singapore**.** National University of Singapore.

Lindley, J.A. (1987).Urban freeway congestion: quantification of the problem and effectiveness of potential solutions, ITE journal, 57(1), 27-32.

LI, W. & TARKO, A. P. (2007). Effective and Robust Coordination of Traffic Signals on Arterial Streets, Volume 1, Research Report. *Joint Transportation Research Program***,** 246.

Lomax, T., Turner, S., Shunk, G., Levinson, H.S., Pratt, R.H., Bay, P.N. and Douglas, G.B. (1997). Quantifying congestion, volume 1 & 2, NCHRP Report 398, Washington, DC: Transportation Research Board.

MUCD. (2009).*Manual on Uniform Traffic Control Device; for streets and Highway*. Federal Highway Administration Washington, D.C.

M. Aftabuzzaman. Measuring Traffic Congestion: A Critical Review, Institute of Transport Studies, Monash University, Melbourne, Victoria, Australia.

Nantulya, V.M. and Muli-Musiime. (2009).Uncovering the Social Determinants of Road Traffic Accidents, Chapter 15 in Challenging Inequities in Health: From Ethics to Action. In Timothy Evans, Margaret Whitehead, Finn Diderichsen, Abbas Bhuiya, and Meg Wirth. New York: Oxford University Press; pp. 211–225.

National Urban Planning Institute (NUPI). (2002). Urban Development and Implementation Problems in Ethiopia and Future Prosperity. Proceedings of the 2nd National Conference, 2002

Papaioannou p., and Georgiou, G. Are Traffic Demand Management (TDM) measures a solution for traffic problems in urban areas?: The Greek experience. Dept of Civil Engineering Aristotle University of Thessalonik, Greece.

PARK, B. (1998). Development of genetic algorithm-based signal optimization program for oversaturated intersections. Texas A&M University.
Peden, M., Scurfield, R., Sleet D. (2004). World report on road traffic injury prevention.
Rodrigue, J-P, Comtois, C., and Slack, B. (1997). Transportation and spatial cycles: evidence from maritime systems. *Journal of Transport Geography*, Vol. 5, 1997, pp. 87-98.
Rukunga, Kithunka Daniel. (2002). Towards A Strategy For The Reduction Of Urban Traffic Congestion: A Case Study of Nairobi Central Business District. MA. Thesis, University Of Nairobi, Kenya.
Sanjay Kumar Singh. (2012).Urban Transport in India: Issues, Challenges, and the Way Forward. *European Transport Issue 52, Paper no. 05, ISSN 1825-3997.*
Sengupta R. (2001). Sustainable Transport Pricing in India. Asian Institute of Transport Development, New Delhi, pp.80.
Singh, S.K. (2005). Review of urban transportation in India. *Journal of Public Transportation, vol. 8, no. 1, pp. 79-97*
SHUAIYU, C., HAO, X. & HONGCHAO, L. (2013). Timing oversaturated signals: what can we learn from classic and state-of-the-art signal control models. *Journal of Transportation Systems Engineering and Information Technology,* 13**,** 97-110
The Federal Democratic Republic Of Ethiopia, Ministry Of Transport, Ethiopian Roads Authority, (FDREMT). (2015).The Road Sector Development Program: Phase V, Addis Ababa.
Transport Research Knowledge Center (TRKC). (2009). Traffic Management for Land Transport, Directorate General for Energy and Transport, European Commission.
United Nations, Department of Economic and Social Affairs (UNDESA), (2014). World Urbanization Prospects: The 2014 Revision, Highlights. Working Paper No. ST/ESA/SER.A/352.
Urban Transportation Task Force (UTTF), Council of Ministers Responsible for Transportation and Highway Safety. (2012). The High Cost of Congestion in Canadian Cities, Canada.
Wheeler, N. and Figliozzi, M. (2011).Multi Criteria Freeway Performance Measures for Trucking in Congested Corridors, Transportation Research Record: Journal of the Transportation Research Board, Volume 2224
William L. Garrison. Historical Transportation Development. University of California, Berkeley, USA.
World Health Organization (WHO). (2005). Health Effects of Transport-related Air Pollution. WHO Regional Office for Europe, Copenhagen. 125-165.
World Health Organization (WHO). (2009). Global Status on Road safety: Time for action. Geneva; WHO .
World Health Organization (WHO). (2012). World Report on Road Traffic Injury Prevention.
World Health Organization (WHO). (2015). Economic Cost of the Health Impact of Air Pollution in Europe: Clean air, health and wealth. Copenhagen: WHO Regional Office for Europe.

SOLAR ASSISTED GROUND SOURCE HEAT PUMP MODELING AND SIMULATION FOR VAN REGION

Osman Seyit ÖZDAMAR
Iskenderun Technical University, Institute of Energy, Iskenderun, Hatay, Turkey
Van Yuzuncu Yıl University, Department of Mechanical Engineering, Tuşba, Van Turkey, seyitozdamar@gmail.com

Hazel SAĞLAM ÖZDAMAR
Van Yuzuncu Yıl University, Başkale Vocational School, Tuşba, Van Turkey, saglamhazel@gmail.com

Suha Orçun MERT*
Iskenderun Technical University, Department of Mechanical Engineering, Iskenderun, Hatay, Turkey, Iskenderun Technical University, Institute of Energy, Iskenderun, Hatay, Turkey, orcun.mert@iste.edu.tr, orcunmert@gmail.com

Tolga DEPCİ
Iskenderun Technical University, Department of Engineering Sciences, Iskenderun, Hatay, Turkey, tolga.depci@iste.edu.tr

ABSTRACT: The use of the Ground Source Heat Pump (TKIP) is increasing due to increasing energy prices, decreasing resources and environmental concerns. The operating principle of the system used in the heating and cooling of buildings, various engineering structures using the heat energy stored in the soil, as well as in the production of hot water is based on the principle of heat transfer. Especially in cold regions like Van, the need for heating is met with imported fossil fuels such as natural gas and coal. With the developing technology, the use of thermal energy storage systems, which is a new alternative energy source, is increasing. The aim of this study is to design a combined system consisting of TKIP and BTES systems to increase TKIP's performance coefficient (COP). In this study, the application of TKIP and BTES systems together in the regions with cold climatic conditions is modeled and calculated using MATLAB program. Different temperature distributions in the storage volume determined in the calculations of the designed system were calculated. In addition, heat losses, efficiency and heat draw values of the system were calculated. Calculations were made every month and also starting from May including the extraction of heat from the system. According to the results of each month, the most efficient and highest temperature values were determined in July and the lowest efficiency values and temperature values were determined in December. The highest yields were observed in May, while the highest yields were observed in July. It was determined that the maximum heat dissipation from the system was in January and December, and the maximum heat loss was observed in

these months. When the results were evaluated, it was found that TKIP and BTES systems are suitable for heating especially in cold climate regions with high solar potential or geothermal resources.

Key words: Thermal Energy Storage, Energy Efficiency, Ground Source Heat Pump

VAN BÖLGESİ İÇİN GÜNEŞ DESTEKLİ TOPRAK KAYNAKLI ISI POMPASI MODELLENMESİ VE SİMÜLASYONU

ÖZET: Toprak Kaynaklı Isı Pompasının (TKIP) kullanımı artan enerji fiyatları azalan, kaynaklar ve çevresel kaygılar sebebiyle gittikçe artmaktadır. Toprakta depolanan ısı enerjisini kullanarak binaların, çeşitli mühendislik yapıların ısıtılması ve soğutulmasında, ayrıca sıcak su üretiminde kullanılan sistemin çalışma prensibi, ısının taşınması esasına dayanmaktadır. Özellikle Van gibi soğuk bölgelerde ısınma ihtiyacı doğalgaz ve kömür gibi ithal fosil yakıtlarla karşılanmaktadır. Gelişen teknoloji ile birlikte yeni alternatif enerji kaynağı olan termal enerji depolama sistemleri kullanımı artmaktadır. Bu çalışmadaki amaç TKIP ve BTES sistemlerinden oluşan kombine bir sistem tasarlamak TKIP'ın performans katsayısını (COP) artırmaktır. Bu çalışmada soğuk iklim koşullarına sahip bölgelerde TKIP ve BTES sistemlerinin birlikte uygulanması modellenmesi ve MATLAB programı kullanılarak hesaplamaları yapılmıştır. Tasarlanan sistemin hesaplamalarında belirlenen depolama hacmindeki farklı sıcaklık dağılımları hesaplanmıştır. Ayrıca sistemin ısı kayıpları, verimi ve ısı çekim değerleri de hesaplanmıştır. Hesaplamalar her ay kendi içinde ve ayrıca Mayıs ayında başlanarak sistemden ısı çekilmesi de dâhil edilerek bir yıl zaman diliminin hesaplamaları yapılmıştır. Her ayı kendi içinde hesapladığımız sonuçlara göre en verimli ve en yüksek sıcaklık değerleri Temmuz ayındayken, en düşük verim değerleri ve sıcaklık değerleri ise Aralık ayında tespit edilmiştir. Bir yıl için yapılan hesaplamalarda ise en yüksek verim değerlerinin Mayıs ayındayken, en yüksek sıcaklık değerleri Temmuz ayında gözlemlenmiştir. Sistemden en çok ısı çekiminin Ocak ve Aralık aylarında olduğu, aynı zamanda en fazla ısı kaybının da bu aylarda olduğu tespit edilmiştir. Çıkan sonuçlar değerlendirildiğinde özellikle güneş potansiyeli veya jeotermal kaynakları fazla olan soğuk iklim bölgelerindeki ısıtma için TKIP ve BTES sistemlerinin uygun olduğu tespit edilmiştir.

Anahtar sözcükler: Termal Enerji Depolama, Enerji verimliliği, Toprak Kaynaklı Isı Pompası

GİRİŞ

Dünyadaki kontrol edilemeyen nüfus artışı ve tüketimin artmasına bağlı olarak sanayi ve endüstriyel üretim de artmaktadır. Bu durumdan dolayı gün geçtikçe artan sanayi ve endüstriyel üretime paralel olarak enerji tüketimindeki artış kaçınılmazdır. Dünyadaki enerji ihtiyacının büyük çoğunluğu fosil yakıtlar ile karşılanmaktadır. Fosil yakıtların günümüzde hızlıca tükenmesinden dolayı alternatif enerji kaynaklarına yönelik çalışmalar da artmıştır. Ülkemizde ithal kaynaklar olmasına rağmen en fazla tüketilen enerji kaynakları petrol, doğalgaz ve taşkömürü gibi fosil yakıtlardan karşılanmaktadır. 1900'li yılların son çeyreğinde çıkan ve tüm dünyanın etkilendiği enerji krizi sonrası, özellikle çevre dostu ve ekonomik olarak değerlendirilebilecek alternatif enerji kaynaklarına yönelik önemli Ar-Ge çalışmaları ve bütçeler ayrılmaya başlanmıştır (Anonim, 2004).

TKIP sistemlerinde tasarım yaparken en önemli faktörlerden biri boruların yerleşimin yapılacağı toprağın özellikleridir. Toprağın içeriği, nem miktarı ve çeşidi gibi etkenler ısı kapasitesini değiştirmektedir. Ayrıca toprak özellikleri mevsimsel olarak değiştiğinde, boruların etrafındaki toprağın fiziksel özellikleri bölgesel ve zamana bağlı olarak değişmektedir. Bu duruma örnek olarak ısı pompası sistemleri sıcak aylarda kullanımı durumunda, sıcak akışkan toprağa ısı vererek toprağın ısınmasına sebep olmaktadır. Buda toprağın nem miktarını düşürerek toprağın ısı tutma kapasitesini azaltmaktadır. Bu durum kış aylarında ısı pompası kullanım durumunda verimin düşmesine sebep olmaktadır. Diğer bir durum ise toprağın yeterince ısı depolayamadığı ve kış aylarındaki kullanımında topraktaki ısıyı almasından dolayı toprakta don olayları meydana gelmesidir (Çakmaz, 2007).

Şekil 1. Yenilenebilir Enerji Evi (Kıncay,2019)

TKIP sistemleri temelde topraktaki depolanan ısı enerjisini kullanır (Şekil 1). TKIP temel çalışma prensipleri toprağın altına döşenen borulardan akışkan geçirilerek bu akışkana topraktaki ısı enerjisinin aktarılmasıdır. Akışkan taşıdığı ısıyı ısı pompasında bulunan havaya aktarmaktadır. Bu sistemler TKIP tipindeki ısı değiştiricisinin başlangıcını oluşturmaktadır. TKIP sistemlerinde, topraktaki ısıyı en verimli şekilde almak için toprakaltı borular farklı şekillerde yerleştirilmektedir. Bu borular temel kısımda yatay ve dikey olmak üzere iki konumda yerleştirilir (Şekil 1). Yatay ısı değiştiricileri için toprağa açılan kuyu derinliği 1-3m arasında değişmektedir. Bu sistemlerin kurulumu ve maliyeti diğerlerine göre ucuz ve kolaydır. Konut ısıtması için de en uygun olan bu sistemdir. Toprağın 1-3 m arasındaki sıcaklığı derinlere göre daha azdır. Toprağın altına yatay olarak döşenen borular, topraktaki ısıl alışverişin en verimli şekilde olması için akışkanın temas yüzeyinin arttırılmasını gerektirir. Bu yüzden paralel, spiral veya serpantin gibi farklı şekillerde döşenir. Yatay ısı değiştiricili toprak kaynaklı ısı pompaları konut ısıtılması dışında soğuk bölgelerde yol ısıtılmasında da yaygın olarak kullanılmaya başlanılmıştır. Buna örnek olarak Arjantin, Amerika, Japonya, İzlanda ve İsviçre gibi ülkelerde 500.000 m2'lik yol ısıtılmasında kullanılmaktadır (Hepbaşlı ve Hancıoğlu, 2001).

YÖNTEM

Çalışmanın yapılacağı yer Van Yüzüncü Yıl Üniversitesi Zeve Kampüsü olarak seçilmiştir. Van bölgesinin güneş potansiyeli göz önüne alındığında bu potansiyel BTES kısmında termal enerji depolama olarak kullanılacaktır. Toprakta 5m*5m*5m bir alan olarak belirlenmiştir. Toprağın 2,5 metre derinliğine BTES borularının yerleştirildiği kabul edilmiştir. Bu boruların içerisinde sıcak aylarda (Mayıs-Haziran-Temmuz-Ağustos-Eylül) güneşten gelen ısı ile ısınan sıcak su gönderilmesi planlamıştır.

Bu sayede toprakta belirlenen alandan termal ısı depolanmasına bağlı olarak toprağın sıcaklık dağılımı incelenmiştir. Konutun ısıtılması gereken aylarda (Ekim-Kasım-Aralık-Ocak-Şubat-Mart-Nisan) sistemden TKIP yardımıyla ısı çekilmesi durumları incelenmiştir. Isı çekilmesi ve ısı kayıpları dâhil edildikten sonraki belirlenen depolama alanındaki sıcaklık dağılımı ve verim grafikleri elde edilmiştir.

Problemin Tanımı

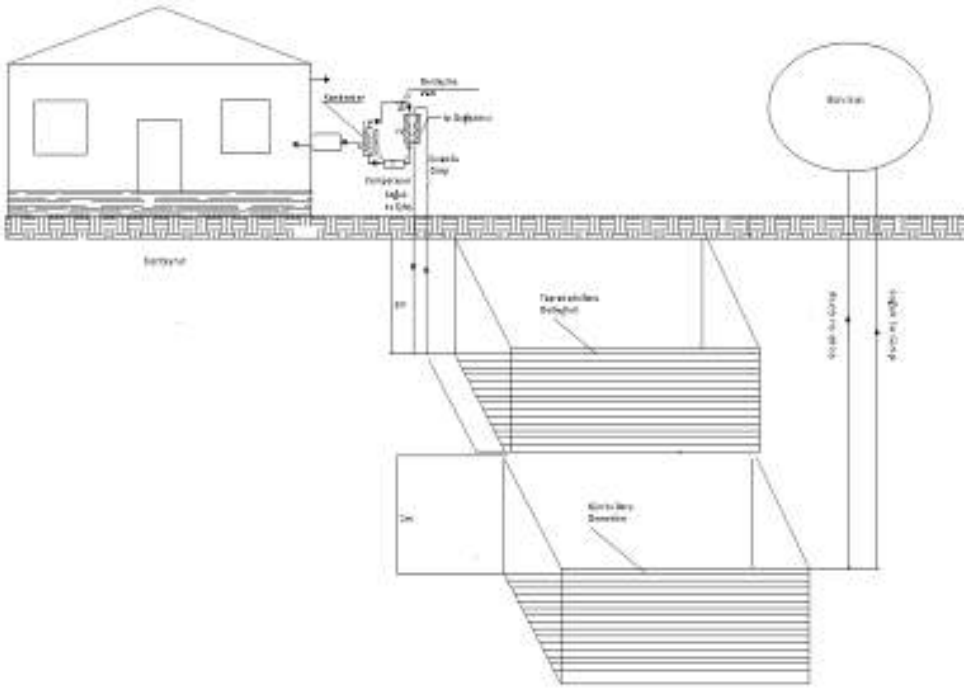

Şekil 2. Sistemin Genel Görünüşü.

Şekil 2.'de çalışmanın genel görünüşü verilmiştir. Matematiksel model bu şekilde verilen sistem için oluşturulmuştur. Problemin çözümünde ilk olarak iki boyutta çözümler yapılarak sonra üç boyuta geçilmiştir. Problemin çözümde kolaylıklar olması için kabuller yapılmıştır:

- Borular toprağın içerisinde aynı derinlikte ve aralarındaki mesafe sabittir,
- Boru içerisindeki suyun akışı laminardır.
- Borular içerisindeki suyun debisinin eşittir,
- Boru boyunca boru özellikleri aynıdır,
- Sistemin modellenmesi Kartezyen koordinatlardadır,
- Toprağın termodinamik ve diğer yapısal özellikleri her noktada aynıdır, konuma ve zamana bağlı olarak değişmemektedir,
- Topraktaki kütle geçişlerinden oluşan ısı kayıpları ihmal edilmiştir,
- Toprakta belirlenen bölgenin yalıtımında kullanılan malzemenin özellikleri her noktada aynıdır,

- Toprak sıcaklığı her noktada sabittir,
- Ay içeresinde güneşli günler peş peşedir,
- Isı geçişi iletim yoluyla olmaktadır.

Tasarım Adımları

Çalışmamanın tasarım adımları sırasıyla yapılmıştır, hesaplamalar ve tabloler sonucunda tablo 1 oluşturulmuştur. Oluşturulan tablodeki verilere göre MATLAB programında modelle yapılmıştır.

1. Konutun ısı kayıpları ve gerekli ısıl yükleri hesaplandı,
2. Yatay tip TKIP seçildi,
3. TKIP kurulacağı bölgenin toprak çeşidine göre ısıl direnç ve ısı iletim katsayıları belirlendi,
4. Boru secimi yapıldı,
5. Boru çapı belirlendi ve buna göre boru uzunluğu hesaplandı,
6. Isı pompası seçimi yapıldı,
7. Matematiksel model oluşturuldu
8. MATLAB'da Sonlu Elemanlar Yöntemi temel alınarak oluşturulan matematiksel model ile bir yıl için topraktaki sıcaklık dağılımı ve depolanmış ısıl enerji değerleri hesaplandı.
9. Aynı zamanda oluşturulan modelde toprakta depolanan enerjinin ısı çekme durumunda oluşan sıcaklık dağılımı ve elde edilen ısı miktarı hesaplandı.

Tablo 1 Sistem İçin Gerekli Veriler

Açıklama	Birim	Değer	Hesaplama
Boru malzemesi	-	PESCH40	Seçilir
Boru çapı	İnç	1	Seçilir
Boru direnci, R_b	m^oC/W	0,159	Tablo 2.3.
Toprak cinsi	-	Killi-Nemli	Kabul
Toprak direnci, R_t	m^oC/W	1,42	Tablo 2.3.
Ortalama yıllık hava sıcaklığı, $T_{orthava}$	^oC	9,4	Meteoroloji
Ortalama yıllık toprak sıcaklığı, $T_{orthava}$	^oC	15,2	Meteoroloji
Yüksek toprak sıcaklığı, $T_{maxtoprak}$	^oC	25	Tablo 3.6.
Düşük toprak sıcaklığı, $T_{mintoprak}$	^oC	7,2	Tablo 3.6.
Düşük toprak sıcaklığı, $T'_{mintoprak}$	^oC	15	Tahmin

Üniteye giren en düşük su sıcaklığı, T_{max}	°C	7	Kabul
Üniteye giren en yüksek su sıcaklığı, T_{min}	°C	70	Kabul
Isıtma çalışma faktörü, $F_ı$	-	0,134	Eş. 3.15
Ünitenin ısıtma performansı, $COP_ı$	-	3,2	Tablo 3.5.
Ünitenin ısıtma kapasitesi	Kw	21,4	Hesap
Boru uzunluğu	m	140	Eş. 3.18.
Boru kullanım şekli	-	Yatay	Seçilir
Gün Isısı Sistemi		30 Vakumlu	Seçilir
Yalıtım Malzemesi	XLPE	60 m^2	Seçilir
Boru içerisindeki akışkanın debisi	m^3/h	0,536	Hesaplama
Sirkülasyon Pompa Gücü	kW	0,8 kW	Hesaplama
Kontrol Mekanizması		Isı Sensoru	
		Basınç Sensoru	Seçilir

Toprak Özelliklerinin Belirlenmesi

Hesaplamalarda ısı transferi iletim yoluyla olduğu kabul edilmiştir. MATLAB da hesaplamalar yapılırken Van Yüzüncü Yıl Üniversitesi Zeve Kampüsü için toprak özellikler killi nemli toprak olarak kabul edilmiştir. Literatür taramalarında kuru killi toprak ve doygun nemli toprak için yapılan deneysel sonuçlar bulunmuştur. Bu değerlerin ortalamaları alınarak toprak için sabitler aşağıda listelenmiştir.

$k_t = \frac{1,7+0,5}{2} = 0.92\ W/mK$ Toprak ısı iletkenliği

$C_p = \frac{3,4+1,6}{2} = 2,5\ MJ/m^3K$ Toprak sabit hacimde ısı kapasitesi

$\alpha = \frac{0,5+0,31}{2} = 0,415\ 10^{-6} m^2/s$ Toprak ısıl geçirgenliği

$\Delta x = 6cm$ Nodlar arası mesafe

Tablo 2. Toprak Termodinamik Özellikleri (Marquez, 2016).

Toprak Tipi	**Isıl iletkenlik (W/mK)**			**Sabit hacimde ısı kapasitesi (MJ/m^3K)**	**Toprak ısıl geçirgenliği ($\frac{m^2}{s}$)**		
	Min.	Ort.	Maks.	Ort.	Min.	Ort.	Maks.
Kuru killi	0,4	0,5	1	1,6	0,25	0,31	0,68

Doygun killi	nemli	0,9	1,7	2,3	3,4	0,26	0,5	0,62

Sabit Değerlerin Belirlenmesi ve Hesaplanaması

Zaman aralığının hesaplamasında akışkanın toprak altı borularda tam bir döngüyü yapması için gerekli süre alınmıştır. Δt hesaplanması;

$$V_b = \pi x {r_b}^2 x {L'}_{top} \quad (1)$$

$r_b = 1{,}27\ cm$
${L'}_{top} = 140\ m$
${V_b} = \pi x {r_b}^2 x {L'}_{top} = \pi x (1{,}27 x 10^{-2} m)^2 x 140m \cong 0{,}071\ m^3$

$$\Delta t = \frac{V_b}{Q_p} = \frac{0.07 m^3}{0.4\ m^3/h} \cong 10\ dk \quad (2)$$

$V_b = \pi r_b^2 L_b = \pi x (1.25 x 10^{-2} m)^2 x 140m \cong 0.07 m^3$
$\Delta t = 10\ dk$ Zaman aralığı
Toprak için fourier sayısı aşağıda hesaplamıştır.

$$Fo = \frac{\alpha \Delta t}{(\Delta x^2)} = \frac{0{,}415\ 10^{-6} m^2/s * 600s}{(6 * 10^{-2} m)^2} \cong 0{,}069$$

Tasarımda toprakta belirlenen alanın duvarlarında 20 cm kalınlıkta polietilen köpük kullanılarak yalıtım yapılmıştır. Yalıtım malzemesinin özellikleri aşağıda listelenmiştir.

$k_y = 0{,}04 W/mK$ Yalıtım malzemesi ısı iletkenliği
$L_y = 20\ cm$ Yalıtım malzemesi kalınlığı

Diğer gerekli bir bilgi borular içerisindeki suyun debisi bilinmesi gerekmektedir. 8. adımda akışın laminar ve reynold sayısı 2000 olarak kabul edilmiştir. Buradan yapılan hesaplamalarda suyun debisi $\mathbf{0,536} \frac{\boldsymbol{m^3}}{\boldsymbol{h}}$ olarak hesaplanmıştır. Pompa gücü hesaplanıp ve piyasa araştırması yapıldığında aşağıdaki özelliklere sahip pompa seçimi yapılmıştır.

$P_p = 700\ W$ Kabul edilen sirkülasyon pompa gücü
$Q_p = 0.5\ m^3/h$ Kabul edilen borulardaki suyun debisi
Hesaplamalarda kolaylık olması için ilk olarak iki boyutta merkez kısım için hesaplamalar yapılmıştır. Sonraki kısımda derinlik için hesaplamalar yapılarak farklı derinlikler için ısı dağılımı hesaplanmıştır. Burada foruier değeri yeniden program tarafından hesaplanmıştır.

$\Delta z = 10\ cm$ Topraktaki derinlik aralığı
TKIP kısmında sisteme giriş yapan su sıcaklıkları Ankara için olan veriler kullanılmıştır.

Tablo 2. Şebeke Suyu Giriş Sıcaklıkları (Anonim, 2016b).

Aylara göre ilinin şebeke suyu sıcaklıkları	
Su sıcaklığı (℃)	**Su sıcaklığı (**℃)
Şubat	6,60
Mart	7,80
Nisan	10,70
Mayıs	14,50
Haziran	18,00
Temmuz	20,90
Ağustos	22,80
Eylül	21,60
Ekim	18,10
Kasım	14,60

MATLAB Hesaplamaları

Bu bölümde sistemin ısıtılması ve sistemden ısı çekilmesi durumları aylara göre hesaplanmış ve sonuçları incelenmiştir. Hesaplamaları Mayıs ayı başlangıç ayı olarak seçilmiş ve hesaplamalara bu ay itibari ile devam edilmiştir. Sistemden ısı çekilmesi Ekim-Nisan ayları arasında olup hesaplamalar mevsim sıcaklıklarına göre yapılmıştır. Mayıs ayının sonu itibari ile yapılan hesaplamaların sonuçları bir sonraki ayın başlangıç koşulu olarak kabul edilmiştir. Böylelikle sistem baştan başlatılmadan sürekliliği olan bir yıllık bir davranış gözlenmiştir. Ayrıca bu kısımda Ekim-Nisan ayları için sistemden çekebildiğimiz ısı miktarları hesaplanarak grafiğe dökülmüştür.

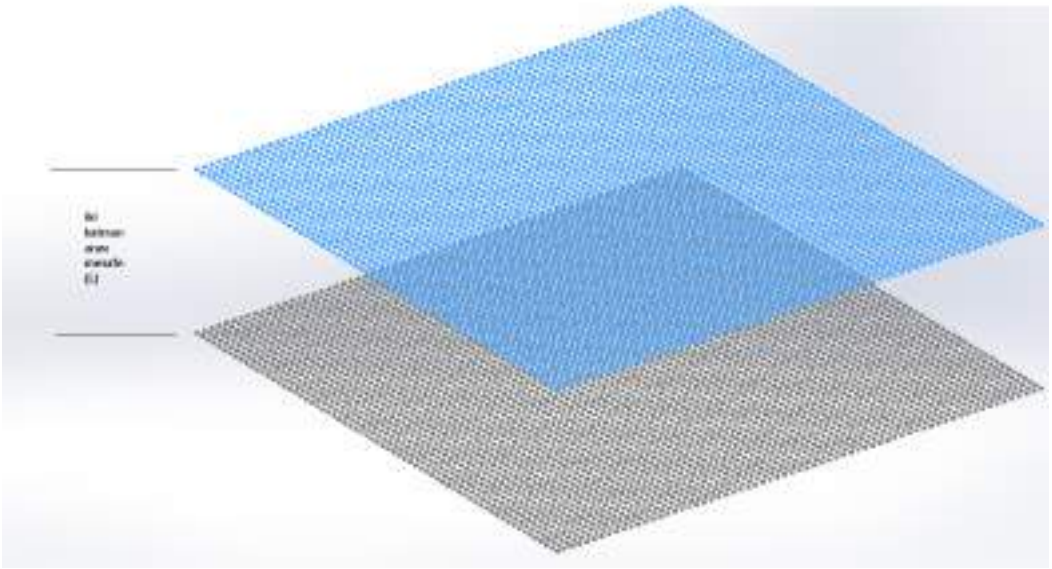

Şekil.2 Toprak katmanlarının 3 boyutta gösterimi.

BULGULAR

Bu çalışma iki ana bölümden oluşmaktadır. Toprak altına boruların yerleşimi iki farklı derinlikte olduğu kabul edilmiştir

Bu kısımda başlangıç sıcaklıkları yukarıdaki zaman adımı sonucunda ortaya çıkan sıcaklık profili baz alınarak oluşturulmuştur. BTES'in merkez yüzeyinin toprağa yakın olan bir üst katmanı TKIP sisteminin borularının döşendiği yüzey olarak seçilmiştir. Bu seçimde merkez yüzey sıcaklığının daha yüksek olması ve buradan çekilecek olan ısı miktarının daha fazla olması nedeniyle ve de merkeze en yakın katman olması itibariyle bu yüzey en uygun seçenek olarak belirlenmiştir. Boruların yerleşimdeki geometri ise daha yüksek verim elde edebilmek için BTES paralel olarak ve akış yönüne zıt akış biçiminde tanımlanmıştır. Bu yüzden yine yüzeylerde 67x67 nod sayısı ve 6 cm nod aralıkları devam ettirilmiştir. Burada farklı olarak sisteme giren suyun ilk sıcaklığı mevsimlere bağlı olarak şebeke su sıcaklıkları ile örtüşecek biçimde belirlenmiştir. Yine sisteme giriş ve sistemden çıkış yapan çevrim suyu sıcaklıkları farkı ile ısı pompasının verimi göz önüne alınarak sistemden farklı sürelerdeki ısı miktarları hesaplanmıştır

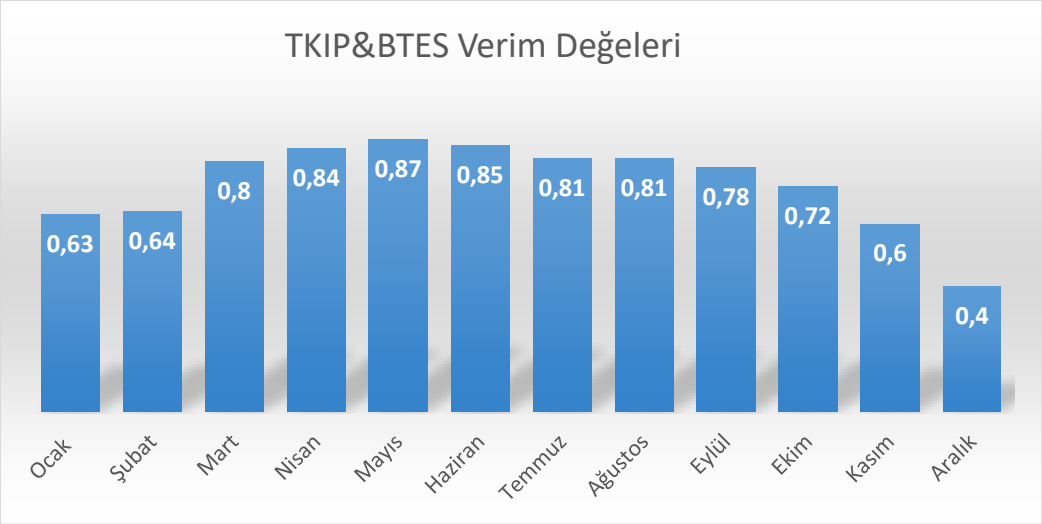

Şekil 3. TKIP ve BTES Durumunda Her Ayın Son Günündeki Verim Değerleri.

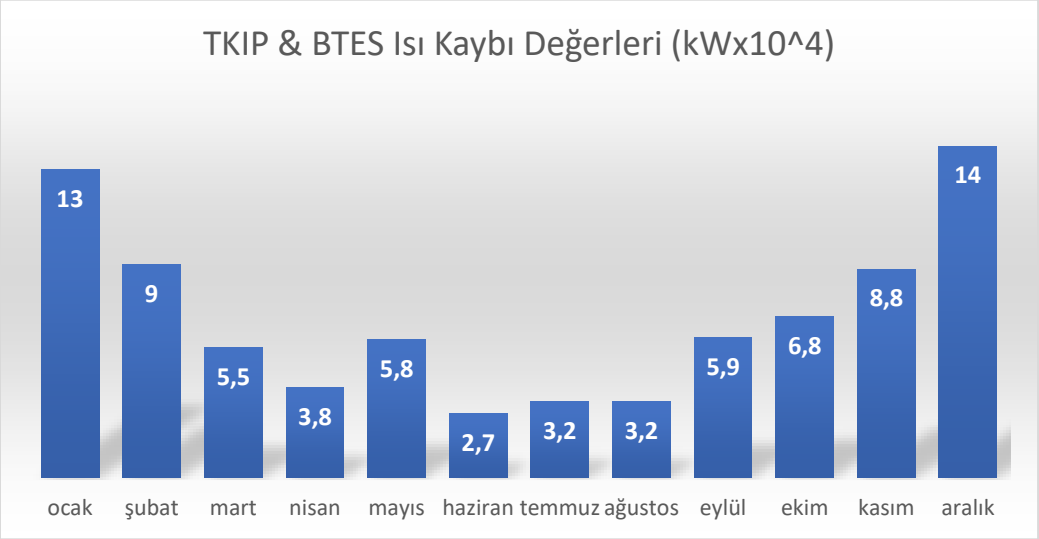

Şekil 4. TKIP & BTES Durumunda Her Ayın Son Günündeki Isı Kaybı Değerleri

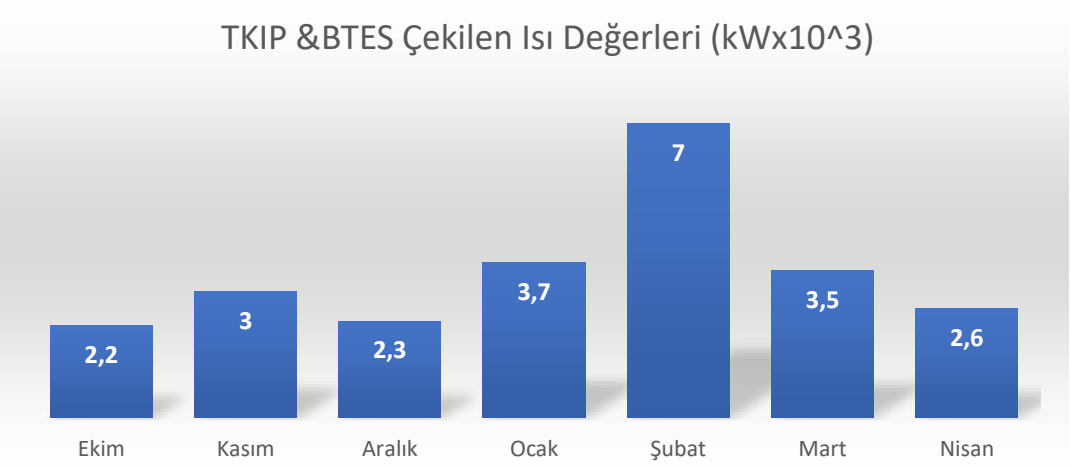

Şekil 5 TKIP & BTES Durumunda Her Ayın Son Günündeki Sistemden Çekilen Isı Değerleri.

Ekim ayından itibaren Nisan ayına kadar öncekine ek olarak mevsimsel koşullara bağlı olarak sistemden ısı çekerek buna bağlı değişimler de hesaplamıştır. Yine gün bazlı olarak bir ay için sistemden çekilen toplam ısı ve sistemden kaybedilen toplam ısı hesaplamalarının sonuçları yansıtılmıştır. Bu sonuçlara bakıldığında Aralık ayında sistemden çekilen ısı 24kW'a yaklaşan bir değerle maksimum olmuştur. Nisan ayı için ise 2.7kW'a yaklaşan bir değer ile minimum aylık değer hesaplanmıştır. Değerler de beklendiği üzere hava sıcaklığının düşmesi ile artarak ve yine hava sıcaklığının artması ise düşerek beklenilen değerlere yakın bir davranış göstermiştir. Ekim ayı ve özellikle Kasım ayında sistemden çekilen toplam ısının bir miktar parabolik davranış gösterdiği görülmektedir. Bunun sebebi ise ısı çekmeye başladığımız ilk aylarda sistemin sıcaklık değerlerinin yüksek olmasından, akışkanın sıcaklığının yüksek sıcaklık değerlerine

hızlıca ulaşmasıdır. İlerleyen aylarda sistemimizde depolanan ısının azalmasına bağlı olarak sistemimizden çekilen toplam ısı değerleri lineer bir davranışa yönelmiştir.

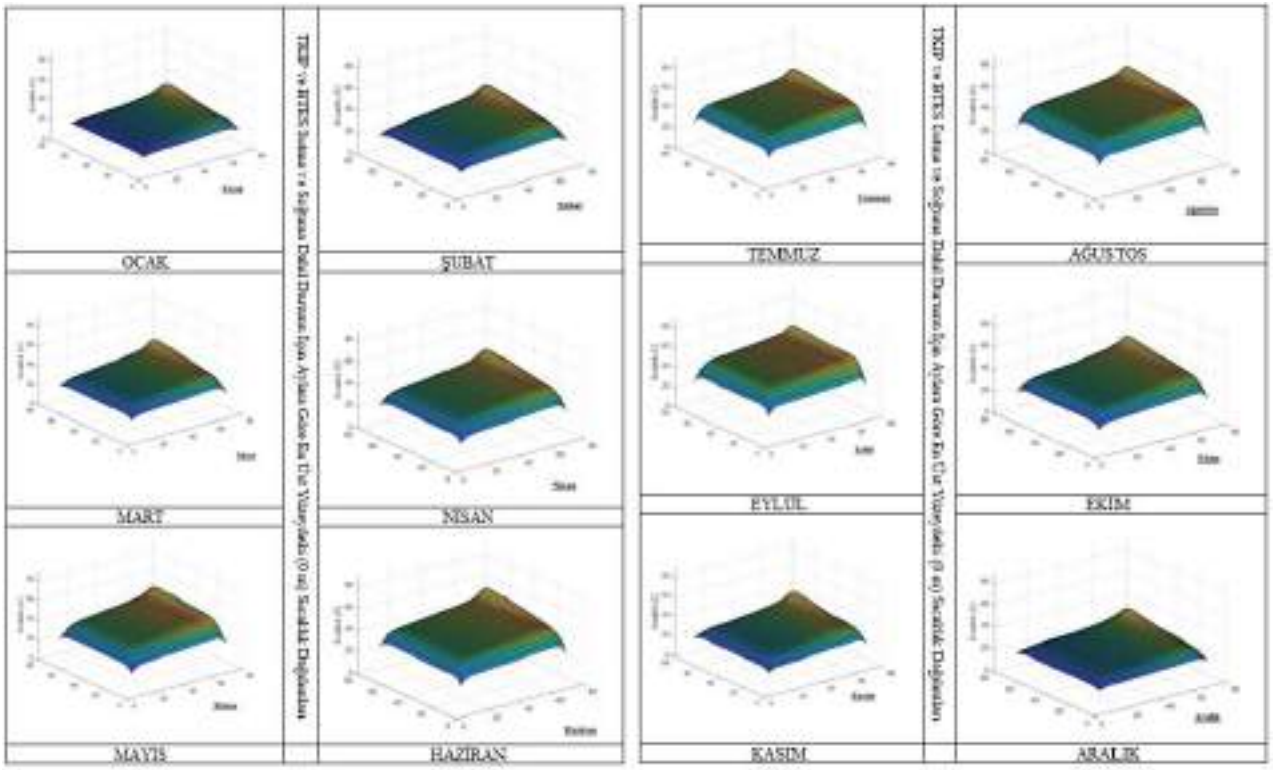

Şekil 6. TKIP& BTES Isıtma, Soğuma ve Isı Çekimi Durumu İçin Aylara Göre Merkez Yüzeydeki (-2,5 M) Sıcaklık Dağılımları

SONUÇ

Ortaya çıkan sonuçlar doğrultusunda sistemin çalıştırılmaya başlandığı ilk aylarda verimli bir şekilde ısı depolama sağlanabilmiştir. Daha sonrasında ise modellemesi yapılan hacmin yeterli olmaması nedeniyle bu verimin giderek düştüğü gözlemlenmiştir. Benzer şekilde ısı çekimi süresince sistemden verimli ve yeterli bir bicimde ısı çekmeyi başlandığı gözlemlenmiştir. Isı çekiminin yapıldığı aylarda kullanılması planlanan ısı pompasını COP değerlerinin karşılaştırılması yapıldığında BTES uygulamalı sistemin daha yüksek değerlere sahip olduğu tespit edilmiştir. Belirlenen konutun ısıtılması için gerekli ısı miktarının sistemden karşılandığı hesaplanmıştır. Çıkan sonuçlar değerlendirildiğinde çekilen ısının belirlenen konutun ısıtılması için yüzde yüz aktartılabilmesi durumunda yeterli olacağı görülmüştür. Fakat dünyada ki hiçbir ısı transfer sistemi yüzde yüz verime sahip değildir. Bu yüzden konutun için ısıtılması için gerekli çekilen ısının yetersizliği söz konusudur Hesaplamalar yapılırken kabul edilen ihmallerde göz önüne alındığında COP değerinin, sistemde depolanan ısı enerjisinin ve ısı çekimi değerlerinin düşmesi beklemektedir. Bu değerleri iyileştirmek için oluşturulan modele göre sistemimizde birtakım iyileştirmeler yapılması gerekmektedir. Modellemesinin yapıldığı TKIP ve BTES uygulamaları soğuk iklime sahip ancak güneş alan veya jeotermal kaynaklara yakın bölgelerde kullanım için gayet uygun sistemlerdir. Hesaplar dâhilinde verilen aralıkta yeterli ısı enerjisi üretilememesinin temel nedeni seçtiğimiz sistem hacminin küçük olmasından kaynaklanmaktadır. Yukarıdaki verim artış yöntemlerinin uygulanması dâhilinde oldukça TKIP ve BTES'in akılcı ve çevreci sistemler olduğu ispatlanmıştır.

KAYNAKLAR

Andújar Márquez, J., Martínez Bohórquez, M., & Gómez Melgar, S. 2016. Ground thermal diffusivity calculation by direct soil temperature measurement. ***Application to very low enthalpy geothermal energy systems, Sensors,* 16** (3): 306.

Anonim , 2015b, İllere göre şebeke suyu sıcaklıkları. ***http://www.svsltd.com.tr/gunes3.htm.*** SVS Enerji Sistemleri, İstanbul. Erişim tarihi: 01.04.2018

Anonim, 2004. Toprak Kaynaklı Isı pompası, uygulamaları ve hesaplamaları ile ilgili bilgiler, ***http://www.dicle.edu.tr/Contents/c1bc26e3-4692-4a8e-933e-04ef617ac1df.doc.*** Dicle Üniversitesi, Diyarbakır. Erişim Tarihi 14.04.2019

Çakmaz, T., 2007**.** ***Termal Enerjinin Yeraltında Depolanması ve Toprak Kaynaklı Dikey Borulu Isı Pompalı Sistemler İçin Ekserji Analizi*** (doktora tezi, basılmamış) YTU, Fen Bilimleri Enstitüsü, İstanbul.

Çengel Y., Boles M.A.,2002. The Second Law of Thermodynamics, Chap.5. ***Thermodynamic An Engineering Approach***, 4th ed. Mc Graw Hill, Boston, England.

Demir, H., 2006. ***Toprak Kaynaklı Isı Pompası Ve Toprak Isı Değiştiricilerinin Optimizasyonu ve Geliştirilmesi*** (doktora tezi, basılmamış). Yıldız Teknik Üniversitesi, Fen Bilimleri Enstitüsü, İstanbul.

Hepbaşlı A. ve Hancıoğlu E. 2001 Toprak Kaynaklı (Jeotermal) Isı pompalarının tasarımı, testi ve fizibilitesi. ***V. Ulusal Tesisat Mühendisliği Kongresi ve Sergisi.*** 3-6, Ekim, Konya: 521-564.

Incropera, F, P., Dewitt, P.,1996. Fundamentals of Heat and Mass Transfer Internal 4th ed, , Chap.8. ***Internal Flow***, Willey, United States of America, 340.

Kıncay, O., 2019. Isı pompaları .***http://www.yildiz.edu.tr /~okincay/dersnotu /IsiPompasi.pdf***, Yıldız Teknik Üniversitesi, İzmir Erişim Tarihi 15.06.2018

Miles, L. 1994 , Heat pump theory and services. **Delmar Publishers Inc.**

SEASONAL ENERGY STORAGE MODELING AND SIMULATION IN COLD CLIMATE CONDITIONS (VAN REGION)

Hazel SAĞLAM ÖZDAMAR
Van Yuzuncu Yıl University, Başkale Vocational School, Tuşba, Van Turkey
saglamhazel@gmail.com

Osman Seyit ÖZDAMAR
Iskenderun Technical University, Institute of Energy, Iskenderun, Hatay, Turkey
Van Yuzuncu Yıl University, Department of Mechanical Engineering, Tuşba, Van Turkey
seyitozdamar@gmail.com

Suha Orçun MERT*
Iskenderun Technical University, ISTE, Department of Mechanical Engineering, Iskenderun, Hatay,
Iskenderun Technical University, Institute of Energy, Iskenderun, Hatay, Turkey
Turkey
orcun.mert@iste.edu.tr, orcunmert@gmail.com

Tolga DEPCİ
Iskenderun Technical University, ISTE, Department of Engineering Sciences, Iskenderun, Hatay, Turkey
tolga.depci@ iste.edu.tr

ABSTRACT: Today, the most widely used types of energy are electricity and heat energy and are mostly supplied from fossil fuels. However, due to the reasons such as depletion of fossil fuels, increasing prices and damages to the environment, the importance given to energy storage methods and R & D studies are increasing. It aims to eliminate the time difference between the time when the energy is needed and its use by storing waste energy or renewable energy resources that are limited as a result of the use of energy through energy storage methods. Especially in our country, the importance of storage of renewable energy sources and produced energy is increasing day by day in order to reduce domestic dependency and to reduce dependence on foreign sources. In this study, UTES (Underground Thermal Energy Storage), which is one of the thermal energy storage (TED) methods, is modeled for Van Region by MATLAB program. The aim of this study is to investigate the performance of using an isolated zone defined by day heat system as TED. The area where thermal energy will be stored is determined as 5x5x5m soil area on Van Yüzüncü Yıl University Campus. In order to protect the stored heat, it was assumed that the volume was covered with 20 cm thick XLPE (Crosslinked Polyethylene) insulation. In the central part of the area (-2.5m), 140 m long U shaped underground pipes were designed. The temperature distribution in the soil was calculated by using the Finite Element Method (SEM) in MATLAB. The calculations were made for two different time conditions. The first part

was applied for the whole year starting from May. Thus, temperature distribution, heat loss and yield calculations were made for one-year time period according to 3D months in soil. In the other part, it was evaluated independently each month. The highest yields were observed in May, while the highest yields were observed in July. It was found that the maximum heat loss from the system was in January and December, and the maximum heat loss was observed in these months.

Key words: Thermal Energy Storage, Energy Efficiency, UTES, Finite Element Method

SOĞUK İKLİM KOŞULLARINA SAHİP (VAN BÖLGESİ) BÖLGELERDE MEVSİMSEL ENERJİ DEPOLAMA MODELLENMESİ VE SİMÜLASYONU

ÖZET: Günümüzde en çok kullanılan enerji çeşitleri elektrik ve ısı enerjisidir ve çoğunlukla da fosil yakıtlardan sağlanmaktadır. Fakat fosil yakıtların tükenmesi, artan fiyatları ve çevreye verdiği zararlar gibi nedenlerden dolayı enerji depolama yöntemlerine verilen önem ve Ar-Ge çalışmaları artmaktadır. Enerji depolama yöntemleri ile enerjinin kullanımı sonucunda oluşan atık enerjiyi veya zamanı kısıtlı olan yenilenebilir enerji kaynaklarını depolayarak enerjiye ihtiyaç duyulduğu zaman ile kullanımı arasındaki zaman farkı gidermeyi amaçlamaktadır. Özellikle ülkemizde yerli kaynaklarının sınırlı olması ve dışa bağımlığı azaltmak için yenilenebilir enerji kaynakları ve üretilen enerjinin depolanmasının önemi gün geçtikçe artmaktadır. Bu çalışmada Termal Enerji Depolama (TED) yöntemlerinin biri olan yeraltında termal enerji depolama olan UTES (Underground Thermal Energy Storage) yöntemi MATLAB programıyla Van Bölgesi için modellenmiştir. Bu çalışmanın amacı gün ısı sistemi ile tanımlı izole edilmiş bir bölgenin TED olarak kullanılmasının performansının incelenmesidir. Termal enerjinin depolanacağı alan Van Yüzüncü Yıl Üniversitesi Kampüsü'nde 5x5x5m toprak alanı olarak belirlenmiştir. Depolanan ısının korunması için hacmin etrafının 20 cm kalınlığında XLPE (Çapraz Bağlı Polietilen) yalıtım ile kaplandığı kabul edilmiştir. Alanın merkez kısmında (-2,5m) 140 m uzunluğunda U şeklinde toprak altı borularının tasarımı yapılmıştır. Toprak içerisindeki sıcaklık dağılımının hesabı Sonlu Elementler Metodu (SEM) ile MATLAB programında yapılmıştır. Çalışmada hesaplamalar iki farklı zaman koşulu için yapılmıştır. İlk kısımda Mayıs ayından başlanılarak tüm yıl için uygulanmıştır. Böylece bir yıllık zaman dilimi için toprak içerisindeki 3B aylara göre sıcaklık dağılımı, ısı kaybı ve verim hesapları yapılmıştır. Diğer kısımda ise her ay bağımsız olarak değerlendirilmiştir. Bir yıl için yapılan hesaplamalar da ise en yüksek verim değerlerinin Mayıs ayındayken, en yüksek sıcaklık değerleri Temmuz ayında gözlemlenmiştir. Sistemden en fazla ısı kaybının ise Ocak ve Aralık aylarında olduğu, aynı zamanda en fazla ısı kaybının da bu aylarda olduğu tespit edilmiştir.

Anahtar sözcükler: Termal Enerji Depolama, Enerji verimliliği, UTES, Sonlu Elementler Metodu

GİRİŞ

Günümüzde en çok kullanılan enerji çeşitleri elektrik ve ısı enerjisidir ve çoğunlukla da fosil yakıtlardan sağlanmaktadır. Fakat fosil yakıtların tükenmesi, artan fiyatları ve çevreye verdiği zararlar gibi nedenlerden dolayı enerji depolama yöntemlerine verilen önem ve Ar-Ge çalışmaları artmaktadır. Son zamanlarda TED sistemlerinin kullanılması gelişmiş ülkelerde yaygınlaşmaya başlamıştır. TED yöntemlerinden biri olan yeraltında termal enerji depolama UTES (Underground Thermal Energy Storage) n çok tercih edilen yöntemlerdendir. Isınmada yaygın olarak kullanılan yöntemlerle karşılaştırıldığında bu yöntemlerin tercih edilmesine bağlı olarak fosil yakıt tüketimindeki azalma ile sonuçlanması sera gazlarının salınımında ciddi bir düşüş olacağı göz ardı edilmemelidir (Yılmazoğlu, 2010).

BTES birden fazla uygulama ve modellenmesi ile ilgili literatürde birçok çalışma bulunmaktadır. BTES metodu genellikle akifer bulundurmayan jeolojik olarak dengeli ve bozulmalarını olmadığı bölgelerde kullanılmaktadır. Bu metot diğerlerine göre daha küçük ölçekli konutların ısıtılmasında ve soğutulmasında kullanılmaktadır. Tekniğin temel çalışma prensibi toprağın altı ve üstü arasındaki sıcaklık farkından kaynaklı ısı taşınımına dayanmaktadır. Örnek olarak Türkiye'nin doğusunda bulunan Van bölgesi kış aylarında -30^{o}C'lere kadar düşmektedir. Fakat Van bölgesinin jeolojik yapısı incelendiğinde jeotermal bakımdan, orta entalpi bakımından zengin bir bölge olduğu tespit edilmiştir. Buda yeraltı toprak sıcaklarının 10^{o}C ile 15^{o}C arasında olmasını sağlamaktadır. Kanallarda termal enerji depolamanın temel prensibi yeraltı ve üstündeki sıcaklık farkından yararlanarak, bu farkı ısıtma ve soğutmada kullanmaktır. Genel olarak çalışma prensibi; ısıtma veya soğutma yapılacak olan yapının ısıl yükleri hesaplanır. Bu hesaplamalara göre ısı yüklerini karşılayacak sondajlar açılır ve sondaj derinliği kadar yalıtım özelliği olmayan ve korozyona karşı dirençli polietilen borular yerleştirilir. Boruların yerleştirilmesi sırasında düzgün olması için boruların alt kısmına ağırlık yerleştirilir. Burada dikkat edilmesi gereken sondajlar arasında ısı etkileşimi olmaması için aralarındaki mesafenin 10 m olacak şekilde yerleşimleri yapılır. Boru ile toprak arasında ısıl direnci en aza indirgemek için dolgu malzemesi enjeksiyonu yapılır. Bu sayede boru ile toprak arasındaki temas maksimum düzeye çıkartılır. Isıtma aylarında soğuk bir akışkan borular içerisinde dolaştırılır ve akışkanın sıcaklığı yükseltilerek ısıtılması istenilen konuta verilir. Aynı işlem soğutma aylarında ise sıcak olan akışkan borularda dolaştırılarak akışkanın sıcaklığı düşürülür. Bu teknikte dikkat edilmesi gerekenlerden biri sistemin sürekli olarak ısıtma için kullanılması durumunda topraktan çekilen ısı miktarı, toprağa verilen ısı miktarını geçerse toprak sıcaklığı zamana bağlı olarak düşmeye başlayacaktır. Bu durumu önlemek için sıcak aylarda güneş enerjisi veya atık ısı kaynağı gibi kaynaklardan elde edilen sıcak akışkan borularda dolaştırılarak toprak sıcaklığı ve verimi artırılmış olur (Özsoy, 2015).

Bu çalışmada Termal Enerji Depolama (TED) yöntemlerinin biri olan yeraltında termal enerji depolama olan UTES (Underground Thermal Energy Storage) yöntemi MATLAB programıyla Van Bölgesi için modellenmiştir. Bu çalışmanın amacı gün ısı sistemi ile tanımlı izole edilmiş bir bölgenin TED olarak kullanılmasının

performansının incelenmesidir. Termal enerjinin depolanacağı alan Van Yüzüncü Yıl Üniversitesi Kampüsü'nde 5x5x5m toprak alanı olarak belirlenmiştir. Depolanan ısının korunması için hacmin etrafının 20 cm kalınlığında XLPE (Çapraz Bağlı Polietilen) yalıtım ile kaplandığı kabul edilmiştir. Alanın merkez kısmında (-2,5m) 140 m uzunluğunda U şeklinde toprak altı borularının tasarımı yapılmıştır. Toprak içerisindeki sıcaklık dağılımının hesabı Sonlu Elementler Metodu (SEM) ile MATLAB programında yapılmıştır. Çalışmada hesaplamalar iki farklı zaman koşulu için yapılmıştır. İlk kısımda Mayıs ayından başlanılarak tüm yıl için uygulanmıştır. Böylece bir yıllık zaman dilimi için toprak içerisindeki 3B aylara göre sıcaklık dağılımı, ısı kaybı ve verim hesapları yapılmıştır.

YÖNTEM

Modellemenin temelini SEM metodu oluşturmaktadır. BTES kısmı için toprağa verilen ısının hesaplanması gerekmektedir. Meteorolojiden alınan verilerde günün belli saatleri için Van bölgesindeki güneşten gelen radyasyon ölçülmüştür. Fakat verilenin değişken olmasından dolayı aylar için günlük güneşten gelen ortalama radyasyon değerleri hesaplanmıştır. Tabloda ayrıca aylara göre güneşlenme süresi ve günlük güneşlenme sürelerinin ortalama değerleri hesaplanmıştır.

Güneşten Gelen Enerjinin ve Gün Sayılarının Hesaplanması

BTES kısmı için toprağa verilen ısının hesaplanması gerekmektedir. Meteorolojiden alınan verilerde günün belli saatleri için Van bölgesindeki güneşten gelen radyasyon ölçülmüştür. Fakat verilenin değişken olmasından dolayı aylar için günlük güneşten gelen ortalama radyasyon değerleri hesaplanmıştır. Tabloda ayrıca aylara göre güneşlenme süresi ve günlük güneşlenme sürelerinin ortalama değerleri hesaplanmıştır.

Tablo 1. Güneşten Gelen Aylara Göre Radyasyon Değerleri (MGM, 2016).

Aylar	**Güneşten gelen ortalama radyasyon miktarı (W/hm²)**	**Aylık ortalama güneşli gün sayısı (gün)**	**Günlük ortalama güneşlenme süresi (saat)**
Ocak	11.9	19.1	4.6
Şubat	17.7	21.1	5.4
Mart	19.9	17.8	6.0
Nisan	26.4	17.7	7.3
Mayıs	27.4	19.9	9.3
Haziran	30.6	24.8	11.7
Temmuz	31.9	28	12.1
Ağustos	27.6	28.7	11.4
Eylül	25.6	27.6	9.8
Ekim	18.9	21.6	7.1

Kasım	15.6	21	5.5
Aralık	11.7	20.2	4.2

Güneşten gelen radyasyon gün ısısı yöntemi ile depolanmıştır. Suda depolanan enerji toprak altı boruları yardımıyla toprakta termal enerji depolanması için kullanılmıştır. Günlük sisteme verilecek olan toplam ısı miktarı aylara göre aşağıdaki eşitliklerden hesaplanmıştır (Anonim, 2016c).

$$Q_k = R * F * s * \eta_k \quad (1)$$

Hesaplamalarda aşağıdaki fiziksel özelliklere sahip gün ısısı sistemi kullanıldığı kabul edilip ve hesaplamalar bu değerlere göre yapılmıştır. Aylara göre kolektörde toplanan ortalama günlük ısıl enerji miktarı Tablo 2. de gösterilmiştir.

R : Tablo 3.8 aylara göre ortalama güneşten gelen radyasyon miktarı (W/m^2)
F : 30 ^{o} eğimli güneş kolektörü için eğim faktörü 1,03
s : 1,76 m^2
η_k : 0,7

Tablo 2. deki veriler termal enerji depolama hesaplamalarında kullanılacaktır. Su depolama hacmi 300 lt olarak seçilmiştir.

Tablo 2. Kolektörde aylara göre günlük ortalama hesaplanan ısı enerji miktarı.

	Ocak	**Şubat**	**Mart**	**Nisan**	**Mayıs**	**Haziran**
Q_k (kW/g)	15.0	26.3	29.7	39.3	40.71	45.5
	Temmuz	**Ağustos**	**Eylül**	**Ekim**	**Ekim**	**Kasım**
Q_k (kW/g)	47.5	41.1	38.2	28.1	23.3	17.4

Sabit Değerlerin Hesaplanması

Zaman aralığının hesaplamasında akışkanın toprak altı borularda tam bir döngüyü yapması için gerekli süre alınmıştır. Δt hesaplanması

$$V_b = \pi x {r_b}^2 x {L'}_{top} \quad (2)$$

$r_b = 1{,}27\ cm$
${L'}_{top} = 140\ m$
${V_b} = \pi x {r_b}^2 x {L'}_{top} = \pi x (1{,}27 x 10^{-2} m)^2 x 140 m \cong 0{,}071\ m^3$

$$\Delta t = \frac{V_b}{Q_p} = \frac{0.07 m^3}{0.4\ m^3/h} \cong 10\ dk \quad (3)$$

$V_b = \pi r_b^2 L_b = \pi x(1.25x10^{-2}m)^2 x140m \cong 0.07m^3$
$\Delta t = 10\ dk$ Zaman aralığı

Toprak için fourier sayısı aşağıda hesaplamıştır.

$$Fo = \frac{\alpha \Delta t}{(\Delta x^2)} = \frac{0{,}415\ 10^{-6} m^2/s * 600s}{(6 * 10^{-2}m)^2} \cong 0{,}069$$

Tasarımda toprakta belirlenen alanın duvarlarında 20 cm kalınlıkta polietilen köpük kullanılarak yalıtım yapılmıştır. Yalıtım malzemesinin özellikleri aşağıda listelenmiştir.

$k_y = 0{,}04 W/mK$ Yalıtım malzemesi ısı iletkenliği
$L_y = 20\ cm$ Yalıtım malzemesi kalınlığı

Diğer gerekli bir bilgi borular içerisindeki suyun debisi bilinmesi gerekmektedir. 8. adımda akışın laminar ve Reynold sayısı 2000 olarak kabul edilmiştir. Buradan yapılan hesaplamalarda suyun debisi $\mathbf{0,536}\frac{\boldsymbol{m^3}}{\boldsymbol{h}}$ olarak hesaplanmıştır. Pompa gücü hesaplanıp ve piyasa araştırması yapıldığında aşağıdaki özelliklere sahip pompa seçimi yapılmıştır.

$P_p = 700\ W$ Kabul edilen sirkülasyon pompa gücü
$Q_p = 0.5\ m^3/h$ Kabul edilen borulardaki suyun debisi

Hesaplamalarda kolaylık olması için ilk olarak iki boyutta merkez kısım için hesaplamalar yapılmıştır. Sonraki kısımda derinlik için hesaplamalar yapılarak farklı derinlikler için ısı dağılımı hesaplanmıştır. Burada foruier değeri yeniden program tarafından hesaplanmıştır.

$\Delta z = 10\ cm$ Topraktaki derinlik aralığı

Boru Boyunca Sıcaklık Dağılımını

Başlangıç için boru içerisindeki akışkanın konuma göre sıcaklık değişiminin belirlenmesi gerekmektedir. Toprak altında gömülü bulunan borulardan geçen akışkan yataydaki konuma bağlı olarak zamanla sıcaklığı değişmektedir. Şekil 2. boru boyunca akışkanın sıcaklık ve ısı değişimini temsili olarak gösterimidir.

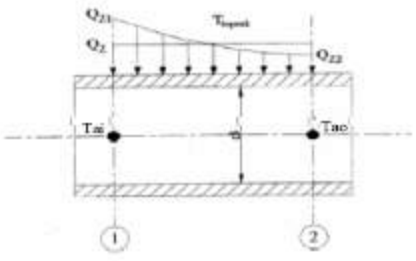

Şekil 1. Boru boyunca akışkandaki sıcaklık ve ısı değişimin (Demir, 2006).

Akışkanın boru boyunca sıcaklık değişimi hesaplanırken; boru içerisindeki akışın iç ve laminar akış olması ve sabit yüzey sıcaklığı durumları için Eş. 4 düzenlenirse (Incopera, 1996);

$$\frac{\Delta T_o}{\Delta T_i} = \frac{T_{fo} - T_s}{T_{fi} - T_s} = \exp\left(-\frac{P\Delta L}{\dot{m}_w c_{pw}}\bar{h}\right) \quad (4)$$

Eş. 4 de T_{fo} eşitlenecek şekilde düzenlenirse;

$$T_{fo} = \exp\left(-\frac{P\Delta L}{\dot{m}_w c_{p_w}}\bar{h}\right)(T_{fi} - T_s) + T_s \quad (5)$$

Bu çalışmada ısı transferinin verimli olması için akışın laminar olduğu kabul edilmiştir. Laminar ve tamamıyla gelişmiş koşullarda sabit yüzey sıcaklığı için Nussellt sayısı 3.66 olarak kabul edilmiştir.

$$Nu_d = \frac{\bar{h}D}{k} \quad (6)$$

$\bar{h}$ değeri hesaplarsak;
$Nu_d = 3.66$
$D = 2.54x10^{-2}\ m$
$k = 613x10^{3} W/mK$

$$\bar{h} = \frac{Nu_d k}{D} = \frac{3.66x613x10^{3} W/mK}{2.54x10^{-2}} \cong 8.1x10^{5} W/m^2K$$

$\bar{h}$ değerinin hesaplamasından sonra Eş. 3.5 de bilinen değerler hesaplanıp genel hali aşağıda hesaplamalardan sonra oluşturulmuştur.

$$\exp\left(-\frac{P\Delta L}{\dot{m}_w c_{p_w}}\bar{h}\right) = f \quad (7)$$

$P = \pi D = \pi x 2.54x10^{-2} = 7.62\ x10^{-2}\ m$
$\Delta L = 6x10^{-2} m$
$\dot{m}_w = 0.4m^3/h = 0.4x10^{-3}\ kg/h$
$c_{p_w} = 0.001152\ kWh/kgK$
$\bar{h} \cong 8.1x10^{5} W/m^2K$
$T_{fi} = 70℃$
T_s=10℃

$$f = \exp\left(-\frac{7.62\ x10^{-2}\ mx6x10^{-2}m}{0.4x10^{-3}\ kg/hx0.001152\ kWh/kgK}\ x8.1x10^{5} W/m^2K\right) \cong 0.97$$

Eş. 7'de f yerine konulursa;

$$T_{fo} = 0.97\ (T_{fi} - T_s) + T_s \qquad (8)$$

Programda Eş.8'den boru boyunca geçen akışkanın sıcaklık değişimini hesaplamakta kullanılmıştır

BTES Matlap Hesaplamaları

Hesaplamalara iki boyutta merkez yüzey seçilerek başlanmıştır. Merkez yüzeyinin yaklaşık 4m*4m yüzey alanına sahip olduğu kabul edilerek ve bu alanı çevreleyen 20 cm kalınlığında bir yalıtım yüzeyinin olduğu varsayılmıştır Buna dayanarak 6 cm aralıklarla 67*67 nodun uygun bir biçimde tüm yüzey alanının istenilen hassasiyette kapladığı bir çalışma alanı oluşturulmuştur. Sol alt köşenin hemen bir sağındaki noddan itibaren sıcak su girişinin yapıldığı varsayılıp bu nodun sağında ve solunda toprak yüzey nodlarının bulunduğu kabul edilmiştir. Giriş suyu sıcaklığı gün ısı sistemi yardımıyla ısıtılan sıcak su değerleridir. Sıcak su girişi 70 ^oC olarak kabul edilmiştir. Sıcak su girişinin yapıldığı 1. noddan 66. noda kadar akışın devam ettiği düşünülerek 67. sınır nodunun yine sınır toprak nodu olduğu kabul edilmiştir. Aşağıdaki Şekil 2 nodların yerleşimi gösterilmiştir.

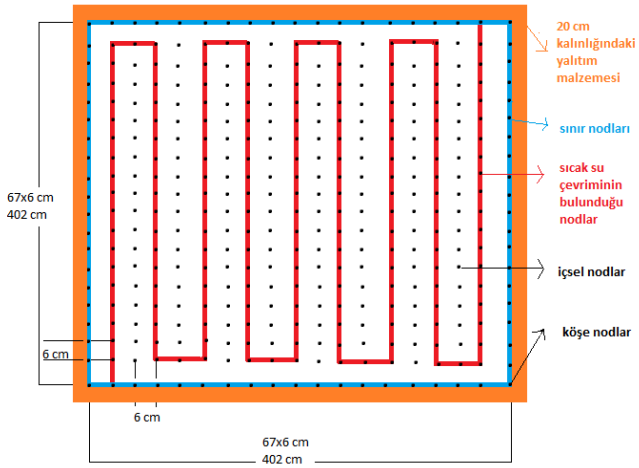

Şekil 2. Yüzey kesitinde 67x67 nodun yerleşim gösterimi.

İlk olarak başlangıç toprak sıcaklığı 10 ℃ olarak kabul edilmiştir. Toprak altı boru boyunca suyun konuma bağlı olarak sıcaklık değişimi ise Eş. 8'den hesaplandı. Nodun bir sonraki zaman SEM metodları kullanılarak giriş nodunda itibaren bir sonraki nodu komşuluklarındaki toprak sıcaklıkları hesaplanarak adım adım ilerlemektedir. Sağ üst köşe çıkış nodu sıcaklığı ve sol alt köşe nodu farkı baz alınaraktan sisteme aktarılan o yüzey için toplam ısı miktarı belirlenmiştir. Sonrasında ise merkez yüzeyin bir sonraki zaman için bütün nodlardaki sıcaklık değerleri hesaplanması ile bir üst yüzeyin sıcaklık değerleri yine SEM yardımıyla hesaplanmıştır. Sistemin toplam yüksekliği 5m olup merkez yüzeyinden toprak yüzeyine olan mesafenin de- 2,5 m olduğu göz önüne alınarak toplam 25 üst yüzey katmanı olduğu kabul edilmiştir. Böylelikle sistemde üçüncü boyutta sıcaklık ve ısı değerleri hesaplanmıştır.

Zaman adımlarının süresi ve sayısı hesaplanırken bir günün 24 saatten oluştuğu ve gün içerisinde güneşlenme saati ve gece süreleri göz önüne alınıp, sisteme giriş yapan suyun sistemde tam bir döngü yapması için gerekli olan süre temel alınmıştır. Sisteme giriş yapan suyun sistemde tam bir döngü yapması için gerekli olan 10 dk aynı zamanda adım süresi olarak da belirlenmiştir

Güneşli süre zarfında kaç kez döngü oluşturabileceği göz önüne alınarak toprağın ısınması için toplam kaç kere döngü yapabileceği de ısıtma zaman adım sayısı olarak belirlenmiştir. Mevsimlere göre akşam saatleri temel alınarak soğutma kısmı içinde soğutma adım sayısı belirlenmiştir.

Gün ışığının olmadığı zamanlarda ise sistem soğuma durumuna geçmiştir. Bu soğumanın etkisi hesaplanırken, soğumanın tüm yüzeylerde, yalıtım malzemesi sıcaklığına bağlı olarak ve soğuma süresi adımları boyunca ısı kayıpları hesaplandı Hesaplamalarda soğumanın sınırlara aynı anda etki etki ettiği dikkate alınmıştır.

BULGULAR

Bütün bu hesaplamalarının sonucunda bütün yüzeylerde sıcaklık değerleri oluşturulmuştur. Sınırdaki nodların sıcaklıkları ve sınır nodlarının yüksekliği ve aralığı doğrultusunda hesaplanan yüzey alanları baz alınaraktan ve sınır nodu ile toprak sıcaklığına bağlı olarak hesaplanan yalıtım sıcaklığı farkı ile, bütün yüzey nodlarının kaybettiği ısı miktarları ve bunların toplamı sistemimizin kaybettiği toplam ısı miktarı olarak ortaya çıkmıştır.

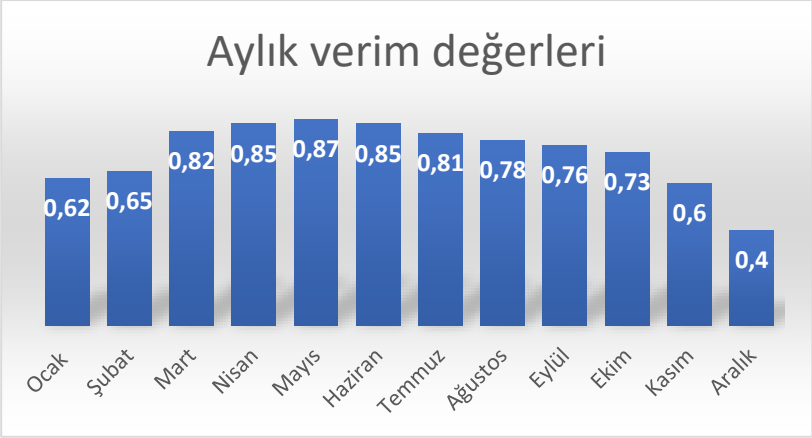

Şekil 3. BTES durumunda her ayın son günü için verim değerleri

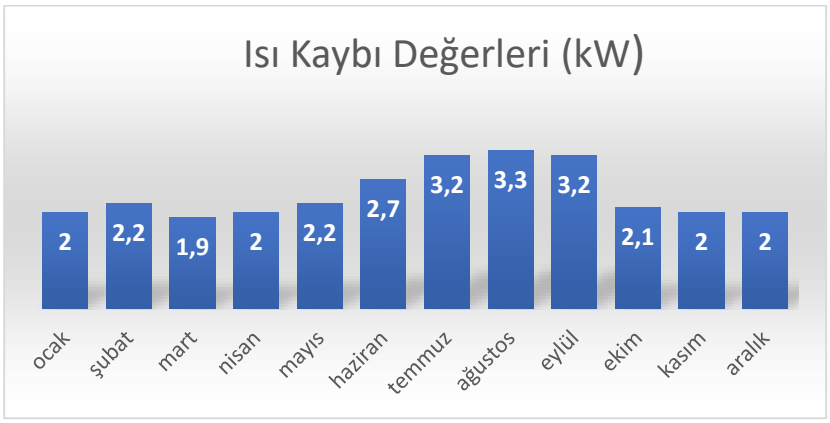

Şekil 4. BTES durumunda her ayın son günü için ısı kaybı değerleri

Genel olarak toprağın ısıya doyması ile gün geçtikçe verim değerleri lineer olarak azalmaktadır. Verimin düşmesi ve ısı kaybının artmasındaki en büyük etken çeper nodların sıcaklılarının yükselmesi ile ısı kaybındaki artıştır. Aynı zamanda sıcaklığı artan bir kütlenin zamana bağlı olarak ısı çekmesi de azalmaktadır. Özellikle kış aylarında verimin yıl içerisindeki en düşük değerleri gözlemlenmektedir. Bunun sebebi kış aylarında güneşte gelen radyasyonun az olması ile birlikte ısı kaybının da çevre koşullarına bağlı olarak artmasıdır. Görüldüğü üzere günlere bağlı olarak ısı kayıpları lineer olarak artmaktadır. En yüksek verimler de beklendiği gibi yaz aylarında gözlenmiştir. Bunun sebepleri ise güneşten gelen radyasyon miktarının artması ve aynı zamanda toprak sıcaklığının yükselmesi ile ısı kayıplarının azalmasıdır.

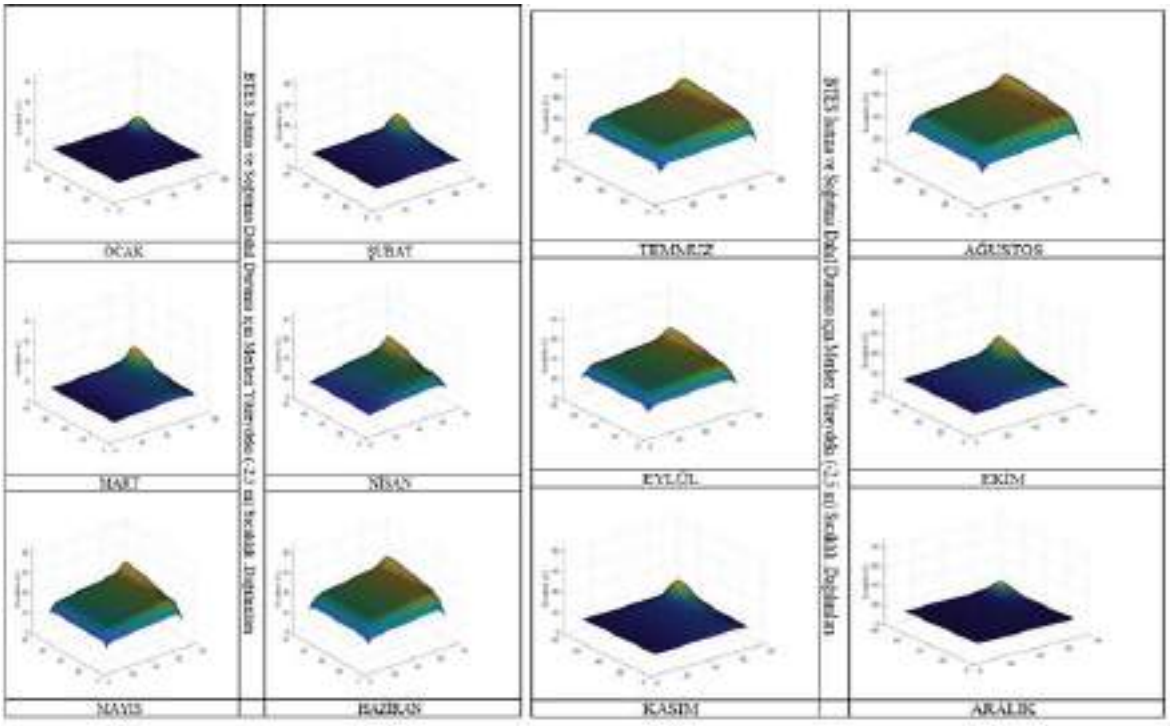

Şekil 5. BTES Sadece Isıtma Durumu İçin Merkez Yüzeydeki (-2,5 M) Sıcaklık Dağılım

SONUÇ

Matematiksel model oluşturulurken akışkanın geçtiği güzergah gerçeğe yakın olması amaçlanarak, ısıl dağılım yalnızca düz bir plaka olarak değil Şekil 2. deki gibi zikzak biçiminde tasarlanmıştır. Ayrıca soğumanın gerçekleştiği anlarda, soğuma kenarlardan sırasıyla değil de, aynı anda gerçekleştiği kabul edilerek model oluşturulmuştur. Bu yaklaşımlar daha gerçekçi sonuçlar elde edilmesine yardımcı olmuştur. Oluşturulan sistemde sadece ısınma ve ısınma anındaki soğumaların yanı sıra, aynı zamanda güneşlenme süresi bitiminde ortaya çıkan soğuma evresi de dikkate alınmıştır. Bütün bunlara ek olarak model, üçüncü boyut içinde incelemeye olanak sağlaması düşünülerek katmanlara ayrılarak, katmanlardaki sıcaklık dağılım hesaplamaları da yapılmıştır.
Modelleme sonuçlarına bakıldığında en yüksek sıcaklık değerleri Temmuz ayında ve Haziran ayında görülmüştür. En düşük sıcaklıklar ise güneşten gelen radyasyon miktarının azalmasına bağlı olarak aralık ayında tespit edilmiştir. Termal enerji depolanmasının ve sıcaklık değerlerinin Ağustos ayından sonra fazla değişim olmadığı hesaplanmıştır. Bu aydan sonraki sisteme verilen ısı enerjisinin sistemdeki mevcut ısıyı korumak için sistemde harcanmıştır.

KAYNAKLAR

Anonim, 2004. Toprak Kaynaklı Isı pompası, uygulamaları ve hesaplamaları ile ilgili bilgiler, ***http://www.dicle.edu.tr/Contents/c1bc26e3-4692-4a8e-933e-04ef617ac1df.doc.*** Dicle Üniversitesi, Diyarbakır. Erişim Tarihi 14.04.2019

Anonim, 2016c. Güneş enerjisi kollektör hesabı ve tesisat bağlantıları. ***https://www.tesisat.org/gunes-enerjisi-kollektor-hesabi-ve-tesisat-baglantilari.html***. Tesisat Bilgi ve Haber Portalı. Erişim Tarihi 10.01 2019

Cruickshanks, Frank B., O. Anderson, and James Bardsley.,2007. Borehole sealing in a coaxial heat exchanger by bentonite treatment. ***Report Prepared for Environment Canada, Climate Change Division (Atlantic Region), Halifax***, Dartmouth, Canada

Çengel Y., Boles M.A.,2002. The Second Law of Thermodynamics, Chap.5. ***Thermodynamic An Engineering Approach***, 4th ed. Mc Graw Hill, Boston, England.

Demir, H., 2006. ***Toprak Kaynaklı Isı Pompası Ve Toprak Isı Değiştiricilerinin Optimizasyonu ve Geliştirilmesi*** (doktora tezi, basılmamış). Yıldız Teknik Üniversitesi, Fen Bilimleri Enstitüsü, İstanbul.

Incropera, F, P., Dewitt, P.,1996. Fundamentals of Heat and Mass Transfer Internal 4th ed, , Chap.8. ***Internal Flow***, Willey, United States of America, 340.

Özsoy, A., 2015. Güneş enerjisinin ısıtma amaçlı mevsimlik depolanması ve ısı pompası destekli. ***Süleyman Demirel Üniversitesi Fen Bilimleri Enstitüsü Dergisi,***, 19(2): 55-59.

Uzun, M.H., 2010 ***Güneş Enerjisi Depolama Olanakları ve Bir Yöntemin Değerlendirilmesi*** (yüksek lisans tezi, basılmamış). Trakya Üniversitesi, Fen Bilimleri Enstitüsü, Trakya.

Yılmazoğlu, M Mustafa Zeki., 2010. Isı enerjisi depolama yöntemleri ve binalarda uygulanması. ***Politeknik Dergisi*** ,13.1: 33-42.

EXTRACTED OF AMORPHOUS SILICA FROM INDUSTRIAL RAW MATERIALS TO USE AS AN ADDITIVE FOR THE DRILLING MUD

Mustafa Göktan AYDIN
Iskenderun Technical University, Department of Petroleum and Natural Gas Engineering, Hatay, Turkey
goktan.aydin@iste.edu.tr

Tolga DEPCİ
Iskenderun Technical University, Department of Engineering Science, Hatay, Turkey
tolga.depci@ iste.edu.tr

Süha Orçun MERT
Iskenderun Technical University, Department of Mechanical Engineering, Hatay, Turkey

Ersin BAHÇECİ
Iskenderun Technical University, Department of Metallurgical and Material Engineering, Hatay, Turkey
ersin.bahceci@iste.edu.tr

ABSTRACT: Due to rapid industrialization, drilling operation has been intensively increased. In order to make cost effective drilling operations, some additives, nano or microsize materials/ore, have been added into drilling mud. In the present study, amorphous silica as an additive was extracted from the industrial raw materials (pumice, diatomite, pyrophyllite and quartzite) with high silica content by alkaline treatment method. Chemical and morphologies properties of the industrial raw materials and the extracted amorphous silica were determined by, XRD, ATR, XRF, SEM and BET. Comparison of the results showed that highly pure amorphous silica (SiO_2 ratio 98%), having a remarkable surface area (>300 m^2/g) with meso-pore structure could produce regardless of the starting materials.

Key words: amorphous silica, pumice, quartzite, diatomite, pyrophylite

INTRODUCTION

In a drilling activities for oil and gas, one of the main components to lift cuttings to the surface, stabilizing the wellbore and subsurface pressures, soften the cutting surface, cool and lubricate the all systems is drilling mud. Due to rapid industrialization, new oil and gas fields have been extensively researched and especially difficult subsurface environments and rigid part of the earth's crust are started to investigated. Therefore, formulation of the drill mud has been modified and while doing so, drilling operation is tried to cost effective [1-6]. Recently, Afolabi et al. [7,8] developed the new model to predict the fluid loss of the water based drilling fluid. They use as an additive

commercial silica particle which enhance the properties of the drilling muds, especially the preserve the fluid loss.
In the present study, amorphous silica was extracted from industrial raw materials, pumice, diatomite, pyrophyllite and quartzite to evaluate as an additive for drilling mud. Different novel and advanced materials like SiC, Si_3N_4, etc. are produced using amorphous SiO_2 [9-11]. Generally, amorphous silica is synthesized by sol–gel method [12] and precipitation method [13] and low-temperature alkali extraction method [14]. Our research group prefers the use low-temperature alkali extraction method due to its simplicity and efficiency [15,16]. The pumice, diatomite, pyrophyllite and quartzite as industrial raw materials were used, since they are abundant, cheap and easy to obtain in Turkey.

METHODS

Materials

The industrial raw materials with high silicium oxide content were chosen as starting materials. Pumice and diatomite from Van, Turkey, Quartzite and pyrophyllite from Malatya, Turkey were brought into our laboratory. All samples were crushed and ground to 80–85 mass% passing 180 µm. NaOH, H_2SO_4 and HCl (from Merck) were used for alkali extraction method.

Methods

Mourhly et al., [14] and our past studies [15,16] 300 ml of 3 molarities NaOH in a 500 ml 3 neck flask equipped with a reflux condenser was prepared and 5 gr of the sample was added into the flask. The mixture was continuously stirred at 100 °C for 14 hours to dissolve the silica and produce sodium silicate. After that, the solid part was removed by filter paper and the liquid part was titrated with H_2SO_4 (5M) while being stirred vigorously until obtaining a silica gel which was occurred at pH 7 until the silica gel was occurred. The silica gel was kept at room temperature for 24 hours and then washed several times to remove the sulphate salt. The gel form was put into the furnace at 80°C for 24 hours.

The obtained solid material was put into the flask which contained hydrochloric acid HCl (1M) solution and stirred at 110°C for 3 hours to remove the soluble minerals Al and K. The liquid and solid separation was done using centrifuge and the solid part was washed with distilled water at several times and dried at 110°C overnight and then sintered at 800 °C for two hours. All experiments were duplicated and the same procedure was followed for each industrial raw material.

Characterization of the Ore and Amorphous Silica

Chemical composition, structure and morphological properties of the industrial raw materials and the extracted amorphous silica was determined by Spectro XEPOS, Rigaku Miniflex 600 with Cu Kα (40 kV, 15 mA, λ=1.54050 Å) XRD, Perkin Elmer

Spectrum One FTIR-ATR and Leo Evo-40x VP Electron Microscope (Inonu University, Central Research Lab) and BET (Inonu University, Chemical Engineering Lab)

RESULTS AND FINDINGS

The XRD patterns of the industrial raw materials and the extracted amorphous silica were presented in Figure 1. P-SiO_2, D-SiO_2, Pyr-SiO_2 and Q-SiO_2 refer to amorphous silica samples were extracted, pumice, diatomite, pyrophyllite and quartzite, respectively. The comparison studies of the XRD patterns showed that the amorphous SiO_2 were extracted from the materials and there is no difference observed depending on the starting materials. The detected strong broad hump between 15 and 30° at 2θ values indicates the amorphous silica [14,15,17].

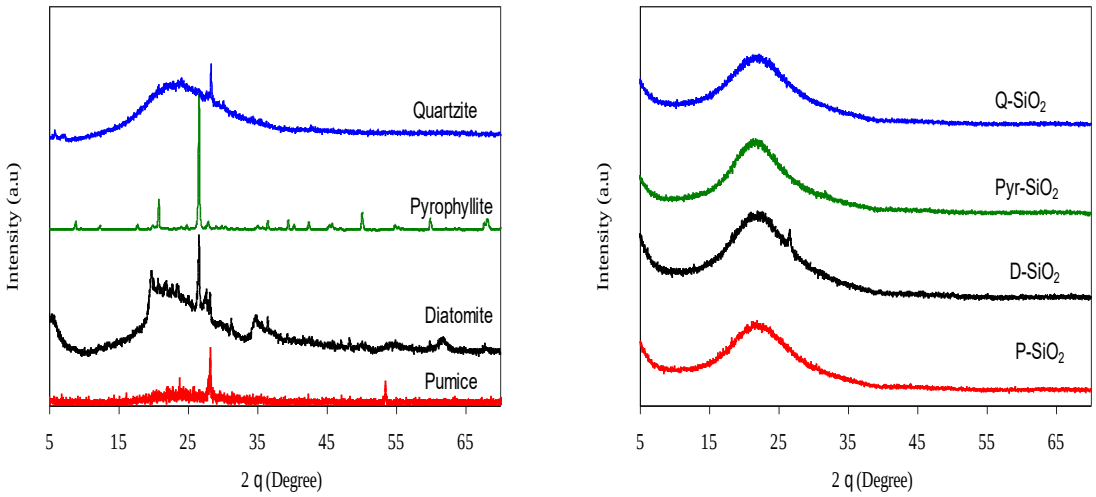

Figure 1. XRD Patterns of the Ores and Extracted Amorphous Silica

The IR spectra of the industrial raw materials and the amorphous silica materials are presented in Figure 2. The same result was observed in the IR spectra. The extracted amorphous silica process shows starting materials-independent character. All IR bands belonging to amorphous silica are nearly same and the vibrations were recorded at 1054 cm^{-1} and 792 cm^{-1}, representing the stretching-vibrations of Si-O-Si, which are characteristic bands of the amorphous SiO_2 [18].

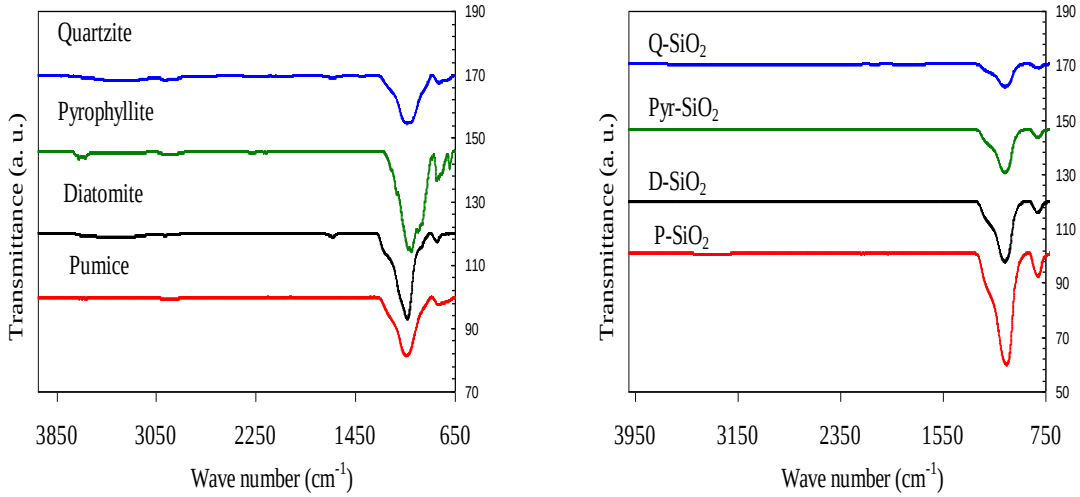

Figure 2. IR spectra of Ores and Extracted Amorphous Silica

In terms of the XRD and IR spectra results, the main composition of the extracted materials are silica and their structures are amorphous. The elemental composition of the extracted materials (Table 1) showed that the main composition was SiO_2, supporting to XRD and IR results. It means that amorphous silica was easily extracted from pumice, diatomite, pyrophyllite and quartzite by the alkaline method.

Table 1. Elemental analysis of the Ores and Extracted Amorphous Silica

Sample	Pumice	Diatomite	Pyrophyllite	Quartzite	P-SiO_2	D-SiO_2	Pyr-SiO_2	Q-SiO_2
SiO_2	74.01	71.10	59.53	91.5	98.12	98.74	98.68	99.1
TiO_2	0.22	0.08	0.71	0.21	n/a	n/a	n/a	n/a
Al_2O_3	14.7	11,48	30.14	3.12	0.06	0.23	0.4	0.08
Fe_2O_3	2.66	3,98	0.64	1.43	n/a	n/a	n/a	n/a
MgO	0.31	0.12	0.16	0.16	n/a	n/a	n/a	n/a
CaO	0.75	0,85	0.24	n/a	n/a	n/a	n/a	n/a
Na_2O	1.44	0,58	0.65	n/a	0.35	n/a	0.210	n/a
K_2O	4.5	1,20	1.89	2.18	0.54	n/a	0.14	0.22

The morphological structure of the raw materials and the amorphous silica materials were identified using SEM. The SEM images (Figure 3) show that the obtained materials have glassy structure and small particle size (agglomeration was seen due to the low resolution).

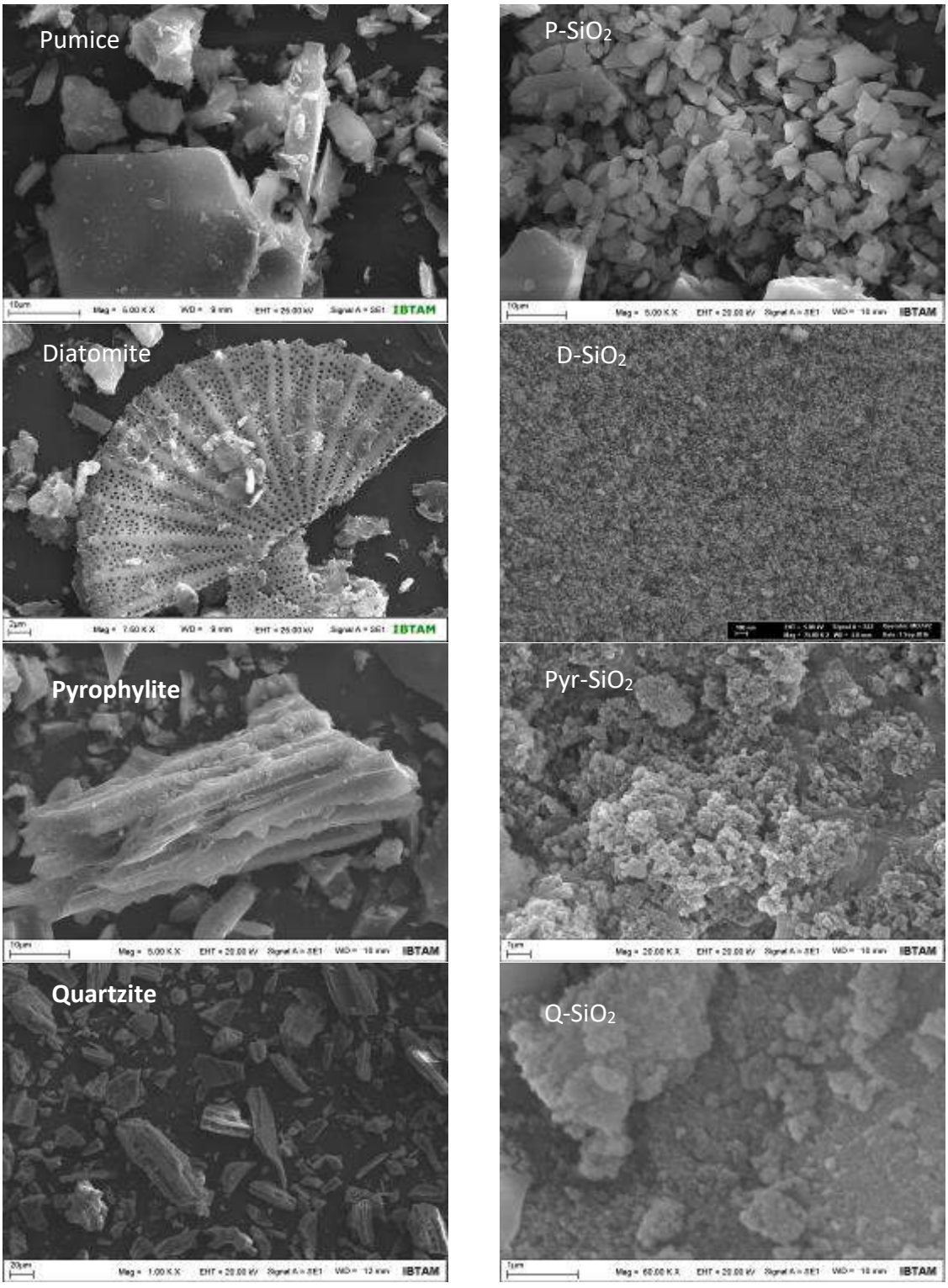

Figure 3. SEM images of the Ores and Extracted Amorphous Silica

In order to detect small particle size in the SEM images, the surface areas of the extracted amorphous silica materials were determined using BET. The BET results indicates that the obtained amorphous silica materials have remarkable surface area. The small size and remarkable surface area can make the amorphous silica to form

very good dispersion in the drilling mud and caused the filling gaps to prevent the fluid loss.

Table 2. BET Surface Area of the Ores and Extracted Amorphous Silica

	Pum.	Diat.	Pyro.	Quar.	P-SiO_2	D-SiO_2	Pyr-SiO_2	Q-SiO_2
BET Surface Area, m2/g	2.97	62.8270	1.68	0,82	358.27	333.75	318.43	348.56

CONCLUSION

The experimental results showed that the highly pure amorphous silica (> 98 % content SiO_2) could be extracted from the local and cheap silica rich industrial raw materials by alkaline treatment methods. Depending on the particle size and the remarkable surface area (> 300 m^2/g), the obtained silica might be a good candidate as an additive for drilling mud. Since, usage of the silica might be reducing the permeability of the mud cake and fluid loss.

RECOMMENDATIONS

As know that to improve the drilling fluid properties with cost effective way, some additives are mixed with drilling mud. Research should be done to improve the related properties of drilling mud by adding the obtained amorphous silica in different ratio.

REFERENCES

[1] Abdo, J., & Haneef, M. D. (2012). Nano-enhanced drilling fluids: pioneering approach to overcome uncompromising drilling problems. *Journal of Energy Resources Technology*, *134*(1), 014501.
[2] Sehly, K., Chiew, H. L., Li, H., Song, A., Leong, Y. K., & Huang, W. (2015). Stability and ageing behaviour and the formulation of potassium-based drilling muds. *Applied Clay Science*, *104*, 309-317.

[3] Mahmoud, O., Nasr-El-Din, H. A., Vryzas, Z., & Kelessidis, V. C. (2016, February). Nanoparticle-based drilling fluids for minimizing formation damage in HP/HT applications. In *SPE International Conference and Exhibition on Formation Damage Control*. Society of Petroleum Engineers.
[4] Afolabi, R. O., Orodu, O. D., Efeovbokhan, V. E., & Rotimi, O. J. (2017). Optimizing the rheological properties of silica nano-modified bentonite mud using overlaid contour plot and estimation of maximum or upper shear stress limit. *Cogent Engineering*, *4*(1), 1287248.
[5] Vryzas, Z., & Kelessidis, V. C. (2017). Nano-based drilling fluids: A review. *Energies*, *10*(4), 540.

[6] Singh, S. K., Ahmed, R. M., & Growcock, F. (2010, January). Vital role of nanopolymers in drilling and stimulations fluid applications. In *SPE Annual Technical Conference and Exhibition*. Society of Petroleum Engineers.

[7] Afolabi, R. O. (2018). A new model for predicting fluid loss in nanoparticle modified drilling mud. *Journal of Petroleum Science and Engineering*, *171*, 1294-1301.
[8] Afolabi, R. O., Orodu, O. D., & Seteyeobot, I. (2018). Predictive modelling of the impact of silica nanoparticles on fluid loss of water based drilling mud. *Applied Clay Science*, *151*, 37-45.
[9] Farooq, A., Al-Jowder, R., Narayanaswamy, R., Azzawi, M., Roche, P. J., & Whitehead, D. E. (2013). Gas detection using quenching fluorescence of dye-immobilised silica nanoparticles. *Sensors and Actuators B: Chemical*, *183*, 230-238.
[10] Arce, V. B., Gargarello, R. M., Ortega, F., Romañano, V., Mizrahi, M., Ramallo-López, J. M., ... & Mártire, D. O. (2015). EXAFS and DFT study of the cadmium and lead adsorption on modified silica nanoparticles. *Spectrochimica Acta Part A: Molecular and Biomolecular Spectroscopy*, *151*, 156-163.
[11] Gao, X., Yu, Q. L., & Brouwers, H. J. H. (2015). Characterization of alkali activated slag–fly ash blends containing nano-silica. *Construction and Building Materials*, *98*, 397-406.
[12] Fan, W., & Gao, L. (2006). Synthesis of silica hollow spheres assisted by ultrasound. *Journal of colloid and interface science*, *297*(1), 157-160..
[13] Monshizadeh, M., Rajabi, M., Ahmadi, M. H., & Mohammadi, V. (2015). Synthesis and characterization of nano SiO2 from rice husk ash by Precipitation method. In *3rd National Conference on Modern Researches in Chemistry and Chemical Engineering* (pp. 1-4).
[14] Mourhly, A., Khachani, M., Hamidi, A. E., Kacimi, M., Halim, M., & Arsalane, S. (2015). The synthesis and characterization of low-cost mesoporous silica SiO2 from local pumice rock. *Nanomaterials and Nanotechnology*, *5*, 35.
[15] Sarikaya, M., Depci, T., Aydogmus, R., Yucel, A., & Kizilkaya, N. (2016, October). Production of Nano Amorphous SiO2 from Malatya Pyrophyllite. In *IOP Conference Series: Earth and Environmental Science* (Vol. 44, No. 5, p. 052004). IOP Publishing.
[16] Bahceci, E., Aylikci, V., Gonullu, M. P., Ates, H., Celik, A. G., Depci, T. (2018, May). Adsorption of methylene blue on mesoporous nano silica obtained from quartzite. , *IV Internatıonal Conference on Engineering and Natural Sciences (ICENS)* (Page 55 – 61)
[17] Sarikaya, M., Deniz Turan, M., Aydogmus, R., Yucel, A., Kizilkaya, N., & Depci, T. (2017). Extraction of meso-pores amorphous SiO2 from van pumice. *Current Physical Chemistry*, *7*(4), 301-304.
[18] Yang, J., & Wang, E. G. (2006). Reaction of water on silica surfaces. *Current Opinion in Solid State and Materials Science*, *10*(1), 33-39.

USABILITY OF DIATOMITE AS ADDITIVE MATERIAL IN WATER-BASED DRILLING MUDS

Mustafa Göktan AYDIN
Department of Petroleum and Natural Gas Engineering, İskenderun Technical University, Hatay, TURKEY
goktan.aydin@iste.edu.tr

Tolga DEPCİ
Department of Engineering Science, Iskenderun Technical University, Hatay, TURKEY
tolga.depci@iste.edu.tr

Volkan AYLIKCI
Iskenderun Technical University, Department of Metallurgical and Material Engineering, Hatay, Turkey
volkan.aylikci@iste.edu.tr

ABSTRACT: One of the most important components in drilling operations is drilling mud. It is known that water based drilling mud is the most important control parameter in the progress of drilling operations. Various chemicals, different additives and polymers are mixed into the drilling mud to maintain flow characteristics (gel strength and filtration) parameters for the drilling mud at the desired levels. These substances are obtained by chemical processes, procurement, etc. and these causes increase the cost of drilling. In recent years, many studies have been carried out to reduce these costs and natural materials (sepiolite, diatomite) are prefered as additives. In this study, diatomite is used as water based drilling mud additive material. Diatomite reserves are abundant in our country and are relatively cheaper than other chemical additives. The diatomite sample was obtained from Kahramankazan district of Ankara province (40 ° 13′54 ″ N 32 ° 41′2 ″ D). Within the scope of the study, the Spud type drilling muds were prepared according to API 13-A standard and Bentonite and Diatomite were added to drilling mud. Sludge samples in different proportions (3-10%) were prepared. The rheological and filtration properties of the prepared samples were made according to API 13B-1 standard. According to the analysis results, only diatomite added sludge samples did not meet the values specified in the standards. The samples prepared with bentonite were found to provide most of the values specified in the standard as long as 6% and more were added. When diatomite and bentonite were used together, it was determined that 9% and more by weight met the relevant standard. As a result of the study, it was determined that only diatomite cannot be used as an additive in drilling mud. When used with bentonite, it has been found to have a positive effect.

Key words: Diatomite, Drilling Mud, Gel Strength, Bentonite, Drilling

DİATOMİTİN SU BAZLI SONDAJ ÇAMURLARINDA KATKI MALZEMESİ OLARAK KULLANILABİLİRLİĞİ

ÖZET: Sondaj operasyonlarında en önemli bileşenlerin başında sondaj çamuru gelmektedir. Su bazlı sondaj çamurunun sondaj operasyonlarının ilerlemesinde en önemli kontrol parametresi olduğu bilinmektedir. Sondaj çamuru için akış özelliklerinin (jel mukavemeti ve filtrasyon) istenilen seviyelerde tutulması için sondaj çamuruna çeşitli kimyasallar, farklı katkı maddeleri ve polimerler karıştırılmaktadır. Bu maddelerin kimyasal işlemler ile elde edilmesi, temin edilmesi vs. gibi sebepler sondaj maliyetini arttırmaktadır. Son yıllarda bu maliyetlerin azaltılması için birçok çalışma yapılmakta olup, doğal malzemeler (sepiyolit, diatomit) katkı malzemesi olarak değerlendirilmektedir. Bu çalışmada, su bazlı sondaj çamuru katkı malzemesi olarak doğal bir kayaç olan diatomit kullanılmıştır. Ülkemizde diatomit rezervleri bol miktarda bulunmakta olup diğer kimyasal katkı maddelerine göre göreceli olarak daha ucuzdur. Diatomit örneği Ankara iline bağlı Kahramankazan ilçesinden (40 ° 13′54 ″ N 32 ° 41′2 ″ D) temin edilmiştir. Çalışma kapsamında Spud tipi sondaj çamurları API 13-A standardına göre hazırlanmış ve sondaj çamuruna Bentonite ve Diatomite eklenmiştir.. Ağırlıkça farklı oranlarda (%3-10) çamur numuneleri hazırlanmıştır. Hazırlanan numunelerin reolojik ve filtrasyon özellikleri API 13B-1 standardına göre yapılmıştır. Analiz sonuçlarına göre sadece diatomit katkılı çamur numunelerinin standartlarda belirtilen değerleri karşılamadığı saptanmıştır. Bentonit ile hazırlanan numunelerin ise ağırlıkça %6 ve daha fazla katkılandığı sürece standartta belirtilen değerlerin çoğunu sağladığı görülmüştür. Diatomit ve bentonitin birlikte kullanıldığı numuneler incelendiğinde ağırlıkça %9 ve fazlasının ilgili standardı sağladığı belirlenmiştir. Çalışma neticesinde sadece diatomitin sondaj çamurlarında katkı malzemesi olarak kullanılamayacağı belirlenmiştir. Bentonit ile birlikte kullanıldığı zaman ise olumlu yönde etki gösterdiği belirlenmiştir.

Anahtar sözcükler: Diatomit, Sondaj Çamuru, Jel Mukavemeti, Bentonit, Sondaj

GİRİŞ

Sondaj çamurları inhibitiv ve inhibitiv olmayan iki ana başlık altında toplanmaktadır. Dünyada ve ülkemizdeki sondaj faaliyetleri incelendiğinde en çok kullanılan sondaj çamur türlerinin Spud, Lignosülfonat ve Polimer tip çamur oldukları görülmektedir. Bu sondaj çamurlarının sondaj operasyonlarının ilerlemesinde başlıca kontrol parametrelerinden birisi olduğu bilinmektedir. Dolayısı ile sondaj çamurunun önemi de giderek artmaktadır.[1]

Sondaj operasyonları için sondaj çamurunun; Filtrasyon, pH, Viskozite(Görünür, Plastik), Jel Kuvveti, Kopma noktası (Yield Point) ve Çamur yoğunluğu gibi özelliklerinin sondaj operasyonunun optimum şartlarda ilerlemesi için belirlenen değerlerde olması gerekmektedir. Sondaj çamurunun kuyu içerisinde dolaşımı sırasında bu özelliklerinin değerlerinin değiştiği bilinmektedir. Değişen değerleri istenilen seviyelere çekmek için sondaj çamuru içerisine çeşitli kimyasal katkı maddeleri katılmaktadır. Bu katkı malzemeleri sondaj maliyetini arttırdığı için günümüzde sondaj maliyetini düşürmek adına rezervi daha bol olan, ekonomik

açıdan daha ucuz endüstriyel ham maddeler veya çeşitli zararsız atıklar araştırmacılar için daha değerli hale gelmiştir.[2]

Çalışma kapsamında, diatomitlerin sondaj çamuru içerisinde katkı malzemesi olarak kullanılması araştırılmıştır. Diatomit, ülkemizde bol miktarda rezervi bulunan bir kayaçtır. Ekonomik olarak ucuz olması nedeniyle sondaj çamuru katkı malzemesi olarak kullanılmasının sondaj maliyetini düşüreceği düşünülmektedir. Kullanılan diatomitlerin boyutu 80 µm altındadır.

Diatomitin, volkanik aktivitelerin fazla olduğu bölgelerde bulunan tatlı ve tuzlu su haznelerinde fotosentez olayının yoğun olarak gerçekleştiği derinliklerde yaşayan tek hücreli alg türü olan diatome iskeletlerinin yanısıra kil, kum, volkanik kül ve diğer organik kalıntılardan oluşan bir kayaçtır. Diatomitin ana yapısını $SiO_2.nH_2O$ oluşturmaktadır. Diatomitlerin kimyasal bileşimleri ortam şartlarına göre değişmektedir. Sertliği içeriğine uygun olarak 4,5-6 arasında değişmekte olup kırılgan yapısı ve tanelenebilmesi nedeniyle sertlik 1,5' e kadar düşmektedir. Diatomiti oluşturan diatome iskelet kalıntıları 5-1000 µm boyutları arasında değişim gösterirken ağırlıklı olarak ortalama boyutları 50-100 µm arasında olmaktadır. Diatomitte boşluklu iskeletlere sahip diatomeler ve diatome taneleri arasında kalan boşluklar toplam poroziteyi oluşturmaktadırlar. Diatomitin boşluk değeri %95'e kadar çıkabilmektedir. Sahip oldukları poroz yapısının fazla miktarda olması nedeniyle ağırlıklarının neredeyse 3 katına kadar su emebildikleri bilinmektedir. Diatomitler birçok kimyasallara dayanıklıdır. Fakat yüksek sıcaklıklarda kuvvetli bazlardan etkilenir.[3-5]

YÖNTEM

Kimyasal yapısı SiO_2 (%72), Al_2O_3 (%12) ve Fe_2O_3 (%3) 'den oluşmakta olan diatomitin yüzey alanı 63 m^2/g'dır. Deneyler için kullanılan diatomit örneği Kahramankazan, Ankara'dan temin edilmiştir (Şekil 1).

Şekil 1. Deneylerde Kullanılan Diatomit Örneği

Deneyler için Amerikan Petrol Enstitüsü (API) 13-A standartına göre önce bentonit, diatomit ve bu numunelerin birlikte katkılanacağı Spud tip su bazlı sondaj çamurları hazırlanmıştır. Hazırlanan çamur numuneleri ağırlıkça farklı oranlarda (%3-10) bentonit ve diatomit içermektedir. Hazırlanan numunelerin ölçümleri API 13B-1 standardına göre yapılmış olup sırasıyla pH, Çamur Ağırlığı, Görünür Viskozite, Plastik Viskozite, Kopma Noktası (Yield Point), 10sn ve 10dk Jel Mukavemeti ve Sıvı Kaybı analizleri yapılmıştır [6,7]. Analizler esnasında ölçümler hata payı dikkate alınarak oda şartlarında üçer defa yapılıp ortalama değer kabul edilmiştir.

BULGULAR

Çalışma kapsamında Diatomit için elde edilen sonuçlar Tablo 1'de gösterilmiştir. Kodlama sistemi; katkılanan madde- ağırlıkça katkılanma oranı olarak belirlenmiştir. Örneğin D-3 ağırlıkça %3'lük diatomit içeren numune anlamına gelmektedir.

Tablo 1. Farklı Oranlarda Katkılanan Diatomit Numunesi İçin Elde Edilen Deney Verileri

Katkı Maddeleri	Numune Kodu	Konsantrayon	pH	MW	300 rpm	600 rpm	AV	PV	YP	10 saniye Jel	10 dakika Jel	Filtrasyon 7.5 dk.
Diatomit	D-3	21.64 g Diatomit 700 mLSu	7,4	8,5	2	3	1,5	1	1	1,5	2,5	300
	D-4	28.85 g Diatomit 700 Ml Su	7,57	8,6	2	3	1,5	1	1	1,5	1,5	340
	D-5	36.05 g Diatomit 700mL Su	7,48	8,7	2,5	3	1,5	0.5	2	1,7	1	340
	D-6	43.28 g Diatomit 700mL Su	7,30	8,7	2	3	1,5	1	1	1,5	1,5	330
	D-7	50.47 g Diatomit 700mL Su	7,28	8,7	2,5	3	1,5	0,5	2	1,5	1,3	335
	D-8	57.68 g Diatomit 700mL Su	7,34	8,8	2	3	1,5	1	1	1,5	1	325
	D-9	64.89 g Diatomit 700mL Su	7,32	8,9	2	3,5	1,75	1,5	0,5	1	0,5	320
	D-10	71.20 g Diatomit 700mL Su	7,30	9,0	2	3	1,5	1	1	1	1,5	320

Tabloda ağırlıkça farklı oranlarda hazırlanan diatomit katkılanmış su bazlı sondaj çamuru numunelerinin API 13B-1 standartına göre yapılmış olan ölçüm sonuçları görülmektedir. Kaydedilen ölçüm sonuçlarına göre sadece diatomit katkılı su bazlı sondaj çamuru numunelerinin standardı karşılamadığı görülmektedir.

Ölçülen filtrasyon değerlerinin tüm katkı değerleri için çok yüksek miktarda olduğu görülmektedir. Sondaj operasyonlarında sondaj çamurunun filtrasyon (sıvı kaybı) oldukça önemli bir parametredir. Sondaj çamurunda ki sıvı kaybının fazla olması çamur sirkülasyonunu olumsuz etkilemektedir. Poroz yapısının %95 oranlarında olmasından dolayı ağırlığının yaklaşık 3 katı kadar su emebilen diatomitin bünyesine aldığı suyu yeterince muhafaza edemediği görülmüş ve sondaj çamuru için tek başına kullanılmasının mümkün olmadığı saptanmıştır.

Sondaj operasyonu için en önemli parametrelerden biri olan jel mukavemeti değerlerine bakıldığında 10 saniye ve 10 dakika olmak üzere iki tip jel mukavemetinin ölçüldüğü görülmektedir. Kuyu içerisinde ki sondaj çamurunun sirkülasyonunun durduğu sırada çamurun yüzeye taşıdığı kırıntıları bünyesinde tutması jel mukavemetiyle doğrudan ilişkilidir. Sirkülasyonu durdurulan sondaj çamurunun jel kuvveti istenilen seviyeden düşük ise yüzeye taşıdığı kırıntılar kuyu tabanına iner ve sondaj operasyonu bu durumdan olumsuz etkilenir. Sadece diatomit katkılanarak hazırlanan su bazlı sondaj çamuru numunelerinin her birinde jel mukavemetinin 10 saniyelik ve 10 dakikalık değerleri incelendiğinde jel mukavemeti değerlerinin standardı karşılamadığı görülmüştür.

Sondaj operasyonları için önemli bir diğer parametre olan viskozite, sıvının akmaya karşı gösterdiği direnç olarak bilinmektedir. Viskozitesi yüksek sondaj sıvıları daha çok katı madde taşımaktadır. Ancak viskozitesi yüksek akışkanlar yüksek sürtünme kuvvetlerinden dolayı pompalanması için daha fazla motor gücü gerekmektedir.

Viskozite değeri ile 3 değer hesaplanması mümkündür. Bu değerler; Plastik Viskozite, Görünür Viskozite ve Akma Noktası (Yield Point). Plastik Viskozite (PV) sondaj çamuruna katkılanan katı madde içeriği arttıkça artmaktadır. Bu tip durumlarda sondaj çamurunun seyreltilmesi gerektiği bilinmektedir [8]. Diatomit katkısı ile hazırlanan numuneler için bu değerler standartın çok altında olduğundan seyreltme işlemi yapılmasına gerek olmadığı görülmektedir. Sonuçlar bu tip çamurun operasyonu olumsuz etkileyeceğini göstermiştir. Söz konusu numuneler Görünür Viskozite (AV) için incelendiğinde standart değerlerin karşılanmadığı görülmektedir. Viskozite değeri ile hesaplanan değerlerin sonuncusu Akma Noktasıdır (YP). Akma noktası sondaj çamurunun kesintileri yüzeye taşıyabilme kabiliyetini göstermektedir. Akma noktasının yüksek değerlerde olması yüksek basınç kaybına yol açtığından sondaj operasyonları için bu değerin kuyu durumuna ve şartlarına gore iyi hesaplanması gerekmektedir. Sondaj operasyonunun verimi ve ekonomik olarak uygunluğu için viskozite değerinin dikkatli bir şekilde hesaplanması gerekmektedir. Diatomit katkılanarak hazırlanan su bazlı sondaj çamuru numunelerinin her birinde (%3-10 katkılı numunelerin tümü) viskozitenin standartın çok altında olduğu görülmüştür. Bu durum sadece diatomit katkısı ile yapılacak çamurun kuyu içerisinde yeterli katı miktarını taşıyamayacağını göstermiştir.

Sadece diatomit katkılanarak hazırlanan su bazlı sondaj çamurunun ölçüm değerleri incelendiğinde tek başına bir katkı maddesi olarak kullanılamayacağı saptanmıştır. Bu sebeple önce aynı ağırlık oranlarında bentonit katkılanmış sondaj çamuru numuneleri

ile diatomitin bentonit ile birlikte ağırlıkça %3-10 değerlerinde katkılandığı su bazlı sondaj çamuru numuneleri hazırlanmıştır. Bu numunelerin ölçüm sonuçları ile diatomitin bentonit ile kullanıldığında söz konusu parametreler üzerinde oluşturduğu etkiler incelenmiştir.

Yapılan ölçümlerin sonuçları aynı parametreler için incelendiğinde Bentonit katkılanarak hazırlanan suz bazlı sondaj çamuru numunelerinden ağırlıkça %6-10 arasındaki numunelerin sondaj çamuru için standartların çoğunu sağladığı görülmekte olup bahsedilen numunelerden elde edilen deney verileri Tablo 2'de gösterilmiştir.

Tablo 2. Farklı Oranlarda Katkılanan Bentonit Numunesi İçin Elde Edilen Deney Verileri

Katkı Maddeleri	Numune Kodu	Konsantrasyon	pH	MW	300 rpm	600 rpm	AV	PV	YP	10 saniye Jel	10 dakika Jel	Filtraayon 7.5 dk.
Bentonit	B-6	43.28 g Bentonit 700mL Su	8,65	8,70	35	51	25,5	16	19	7	9	9
	B-7	50.47 g Bentonit 700mL Su	9,00	8,80	49	77	38,5	28	21	10	13	7
	B-8	57.68 g Bentonit 700mL Su	9,00	9,10	42	67	33,5	25	17	8	10	9
	B-9	64.89 g Bentonit 700mL Su	9,21	9,10	33	53	26,5	20	13	7	8,5	6
	B-10	71.20 g Bentonit 700mL Su	9,25	9,20	92	138	69	46	46	22	27	6

Sondaj operasyonlarında sondaj çamuru kuyu içerisinde sürekli sirkülasyon halindedir. Çamur, kuyu içerisinde dolaşırken birçok farklı katı madde içeriğine sahip formasyon ile temas ettiği için bünyesine karışan maddelerin özelliklerinden etkilenir. Bu durum yüzeyde hazırlanan sondaj çamurunun kontrol parametrelerinin sürekli değişmesine sebep olur. Operasyonların verimli bir şekilde devam edebilmesi için parametrelerinde değişiklik gösteren sondaj çamuruna birçok kimyasal katkı maddesi katıldığı bilinmektedir. Farklı katkı maddelerinin çamura katılması sondaj maliyetini arttırmaktadır. Bu sebeple sondaj operasyonlarının maliyeti düşürmek için ucuz yeni katkı maddeleri arayışı bulunmaktadır. Çalışma kapsamında ülkemizde rezervi bok miktarda bulunan ve ucuz bir kayaç olan diatomitin su bazlı sondaj çamuruna bentonit ile beraber katkılanarak kullanılabilirliği ölçülmüştür. Elde edilen ölçüm sonuçlarına göre ağırlıkça eşit olmak üzere hazırlanan %3-10 katkı maddesi içerikli Bentonit-Diatomit numunelerinden ağırlıkça %9 ve %10 katkı oranlarında ki numunelerin ilgili standartları sağladığı görülmüştür. Elde edilen veri sonuçları Tablo 3'de gösterilmektedir.

Tablo 3. Eşit Oranlarda Katkılanan Diatomit-Bentonit Numuneleri İçin Elde Edilen Deney Verileri

Katkı Maddeleri	Numune Kodu	Konsantrasyon	pH	MW	300 rpm	600 rpm	AV	PV	YP	10 saniye Jel	10 dakika Jel	Filtrasyon 7.5 dk.
Bentonit + Diatomit	DB-9	32,44 g Bentonit 32,44 g Diatomit 700 mLSu	8,05	8,90	18,50	31	15,5	12,50	6	4	2,5	11
	DB-10	35,60 g Bentonit 35,60 g Diatomit 700 mLSu	8,15	8,95	32	54	27	22	10	6	6,5	8

Ağırlıkça eşit miktarlarda diatomit ve bentonit katkılanarak hazırlanan %3-10 oranlarında ki su bazlı sondaj çamurlarının deney verileri incelendiğinde bentonit için belirlenen API standartlarını %9 ve %10 oranlarında katkı maddesi içeren numunelerin sağladığı görülmüştür. İlgili karşılaştırmaların yapıldığı bentonit standartları Tablo 4'de verilmektedir.

Tablo 4. API Standartlarına Göre Bentonitin Fiziksel Özellikleri

Özellik	Standart
Viskometre kadranı okuması 600 r/min	Minimum 30
Filtrat Hacmi	Maksimum 15,0 ml
75 µm'den büyük çapta kalıntı	Maksimum kütle oranı 4,0 %

SONUÇ VE ÖNERİLER

Çalışma kapsamında sondaj operasyonları için hayati önem taşıyan sondaj çamurunun maliyetini düşürmek için ülkemizde rezervi bol bulunan ve ekonomik açıdan göreceli olarak düşük maliyetli olan diatomit, önce tek başına ardından bentonit ile beraber su bazlı sondaj çamuru içerisine katkılanmıştır. Hazırlanan numunelerin analizleri esnasında ölçümlerin hata payı dikkate alınarak oda şartlarında üçer defa yapılıp ortalama değer kabul edilmiştir.

Deneysel veriler ışığında Diatomitin tek başına sondaj çamuruna katkı malzemesi olarak kullanılamayacağı belirlenmiştir. Diatomitin, bentonit ile beraber sondaj çamuruna katkılandığı durumlarda belirli ağırlık oranlarında olumlu etkilerinin olduğu gözlenmiştir. Günümüzde sondaj maliyetlerinin artmasının büyük bir kısmının sondaj çamuruna katılan kimyasal katkı maddelerinden kaynaklandığı düşünüldüğünde tek başına olmasa da diatomitin bentonit ile %9-10 ağırlık oranlarında kullanılmasının uygun olabileceği önerilmektedir. Bu ağırlık oranlarında

hazırlanan diatomit ve bentonit katkılı numunelerin standartların başta filtrasyon olmak üzere birçoğunu karşıladığı görülmüştür.

KAYNAKLAR

[1] Kök, O. E., Tanrıverdi, İ., & Erdoğan, Y. (2018). Usage of Vermiculite as Additive Material in Water-Based Drilling Muds. *Natural and Engineering Sciences*, *3*(2), 179-186.

[2] ALTUN, G., OSGOUEI, A. E., & SERPEN, U. SU BAZLI SEPİOLİT ÇAMUR ÖZELLİKLERİNİN ZORLU SONDAJ KOŞULLARINDA DENEYSEL OLARAK İNCELENMESİ.

[3] UYGUN, A. (1976). DİATOMİT Jeolojisi, ve yararlanma olanakları. *Bilimsel Madencilik Dergisi*, *15*(5), 31-38.

[4] Al-Sabagh, A. M., El-Awamri, A. A., Abdou, M. I., Hussien, H. A., El Fatah, H. A., & Rasmy, W. E. (2016). Egyptian diatomite as high fluid loss squeeze slurry in sealing fractures and high permeable formation. *Egyptian Journal of Petroleum*, *25*(3), 409-421.

[5] Mohamedbakr, H., & Burkitbaev, M. (2009). Elaboration and characterization of natural diatomite in Aktyubinsk/Kazakhstan. *The Open Mineralogy Journal*, *3*, 12-16.

[6] American Petroleum Intitute (1990) 13A. Specification for drilling fluid materials. USA.

[7] Caenn, R., & Chillingar, G. V. (1996). Drilling fluids: State of the art. *Journal of Petroleum Science and Engineering*, *14*(3-4), 221-230.

[8] ASME Shale Shaker Committee. (2011). *Drilling fluids processing handbook*. Elsevier.

AN ANALYSIS FOR THE PERFORMANCE OF A MULTICORE CPU FOR NUMERICAL SIMULATIONS WITH SEVEN POINT STENCIL CONFIGURATION

Recep BAKAR
Material Science and Engineering Department
Koc University
rbakar18@ku.edu.tr

Najeeb AHMAD
Computer Engineering Department
Koc University
nahmad16@ku.edu.tr

ABSTRACT: Simulations with seven-point simulations have been commonly used in engineering applications in many industries. Computational performance of simulations is very significant. The faster the results are found, the better it is in terms of time and cost. The objective of this study is to evaluate the performance of a reservoir simulation based on seven-point stencil configuration on Intel KNL, a multicore CPU, using different data formats, problem sizes, and vectorization modes. Four fundamental cases in terms of problem sizes were used on KNL with changing data formats namely CSR and SELL and with four different vectorization modes such as AVX, AVX2, AVX512, and no vectorization mode. In the simulated cases, the best performance was obtained with the number of processes equal to the number of KNL cores for all configurations. Also, SELL with AVX-512 vectorization mode resulted in the best performance for problem sizes occupying less than 50% of High Bandwidth Memory, followed by AVX2 and AVX. The performance of both SELL and CSR decreased with the problem size approaching to the memory of HBM. On the other hand, CSR AVX-512 was the best among CSR with all vectorization modes and marginally better than SELL AVX. With further usage of HBM, the best performance was obtained using CSR with AVX vectorization mode. However, generally, the performance of both CSR and SELL with any vectorization mode went down as problem size increased, but the rate of decline in performance was more for SELL than CSR. Among CSR with different vectorization modes, the performance of CSR-AVX degraded the least with increasing problem sizes. Finally, this study investigates, to the best of our knowledge, for the first time, the performance of SELL and CSR with different vectorization modes for numerical simulations with big problem sizes approaching and exceeding the size of the HBM.

Key words: Seven-point stencil simulations, Matrix-vector multiplication, PETSc, vectorization modes, simulation on multicore CPU

INTRODUCTION

Numerical Reservoir Simulation has been quite popular since the 1960s and still plays an important role in applications for the oil and gas industry in which conventional and unconventional reservoirs account for a significant amount of oil and gas. Not only successful and meaningful reservoir simulations are required but also the operational and computational cost of the simulations is trivial. Furthermore, multi-phase flows in porous media, reservoir management, reservoir characterization, production mechanism and many more operations in the oil and gas industry are currently depending on numerical reservoir simulations in order to have the best hydrocarbon recovery from the fields. Since both the conventional and unconventional reservoirs are composed of natural fractures and/or man-made fractures, there has been a great effort for understanding the mathematical modeling of porous media flow especially with fracture systems for a long period of time. In the last decade, the interest in modeling flow in fractured reservoirs has been also extensively increased by the exploration and development of unconventional shale resources from which the production of hydrocarbons is through natural fractures and hydraulic fractures.
The fractures in a petroleum reservoir system can be created by natural forces such as folding, faulting, and subsidence of geologic structures over a long period of time and/or by man-made interventions like multi-stage hydraulic fracturing and water injection. Fig. 1. shows as examples of outcrops of fractured rocks.

Fig. 4. Examples of outcrops of fractured rocks (Dichiarante et al. 2016), (Imber et al. 2014).

Since the 2000s, there have been significant studies in the enhanced oil and gas recovery methods for unconventionals like shale gas/oil reservoirs. As mentioned before, multistage hydraulic fracturing has been the fundamental way of producing hydrocarbons from these shale reservoirs in which the tight shale matrix is broken into smaller pieces to form larger surface areas of contact thanks to microfractures. What the multi-stage hydraulic fracturing creates is defined as a dual-porosity environment in the vicinity of the hydraulic fracture. Fig. 2 represents an example of a schematic of a multi-stage hydraulic fracturing in an unconventional reservoir. As it can be seen from Fig. 2, there is a high density of microfractures located around the wellbore and created by the stress changes caused by hydraulic fracture stimulation.

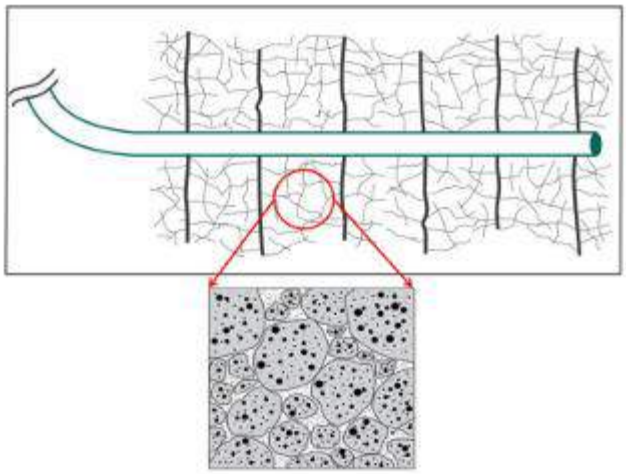

Fig. 5. An idealized schematic of multi-stage hydraulic fracturing in unconventional reservoirs (Torcuk, 2013).

A lot of heterogeneity and anisotropy in term of reservoir properties such as permeability and porosity are introduced by the existence of these fractures. Therefore, flow characterization in these naturally or man-made fractured reservoirs has been in the center of attention for many researchers. Matrix is a rock in which a fracture or a fracture network is located and, in general, fractures have much greater permeabilities and porosities than the matrix. So, these fractures significantly account for the reservoir permeability and porosity and they help hydrocarbon flow in the reservoir. All these fractures, as well as matrix blocks, can be in different sizes and shapes, which accounts for heterogeneity and complicates the flow characterization and modeling from these fractured reservoirs. Therefore, for modeling fluid flow in fractured reservoirs, the effect of both matrix and fractures must be considered. There have been numerous studies regarding the development of dual porosity modeling for the flow in fractured reservoirs since 1960s (Barenblatt et al., 1960; Warren and Root, 1963; Kazemi, 1969; De Swaan, 1976; Kazemi et al., 1992; Lim and Aziz, 1995; Rodriguez-Roman and Camacho, 2005; Gerami et al., 2007; Ranjbar and Hassanzadeh, 2011; De Souza et al., 2014; Zhang, 2015; Wu et al., 2019). In this study, we consider a 3D single phase pseudo-steady state flow from the matrix to natural fractures and then to a hydraulic fracture which is also the wellbore. We mainly focus on the performance of KNL, a multi-core processor, in a dual-porosity reservoir with different problem sizes and vectorization modes. First, we give the formulation for 3D single phase pseudo-steady state flow in a dual-porosity reservoir supported by a uniform set of matrix blocks. Then the effect of problem sizes and vectorization modes of the KNL on its simulation performance has been investigated. Finally, we present a discussion on the work done and give the conclusion of the work.

MATHEMATICAL MODELING

In our study, the concept of dual porosity modeling is composed of a continuum of interconnected fractures and a set of cubic matrix blocks embedded in the fractures.

However, in nature, the matrix block size and properties change. As shown in Fig. 3, Naturally fractured dual-porosity reservoirs are generally idealized as a set of uniform matrix blocks with the geometric shapes of cube or sphere or slab.

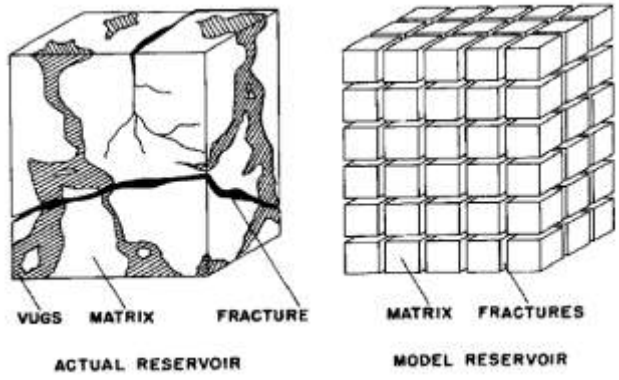

Fig. 6. Idealization of a dual-porosity medium with uniform cubic matrix blocks (Warren and Root, 1963).

In order to account for the fluid flow between the matrix and the fracture with uniform matrix block idealization in fractured reservoirs, a transfer function is added to the continuity equation. The Eq. 1 accounts for the continuity equation for the single phase, slightly compressible, 3D flow in a dual-porosity media with uniform size, homogeneous and isotropic matrix is given by:

$$\nabla \cdot \frac{k_{f,eff}}{\mu} \nabla p_f - \tau + \hat{q} = (\phi c_t)_f \frac{dp_f}{dt} \quad (1)$$

Where $k_{f,eff}$ accounts for the effective permeability of the formation, μ is viscosity, p_f stands for the pressure in the fracture, τ is the transfer function between the fracture and matrix, $\hat{q}$ is the oil rate per unit rock volume, ϕ_f is the fracture porosity and c_{tf} stands for the total compressibility.

The diffusivity equation for dual porosity modeling includes the conservation of mass in the fracture. The transfer function in Eq. 1, accounts for the volume of fluid transferred from matrix to the fracture per unit rock volume per unit time. Having the conservation of mass principle in the matrix system, it can be written as:

$$\tau = \sigma \frac{k_m}{\mu} \left(p_f - p_m\right) \quad (2)$$

Where, σ is the shape factor, k_m stands for the permeability of the matrix and p_m is defined as the pressure in the matrix. The governing equation for the flow in the matrix is given by the Eq. 3 as follows,

$$\sigma \frac{k_m}{\mu} \left(p_f - p_m\right) = (\phi c_t)_m \frac{dp_m}{dt} \quad (3)$$

Where, ϕ_m is the porosity in the matrix and c_{tm} accounts for the compressibility in the matrix. Also, the shape factor, σ, for a cubic matrix block with dimensions L_x , L_y and L_z can b calculated using the Eq. 4,

$$\sigma = 4\left[\frac{1}{{L_x}^2} + \frac{1}{{L_y}^2} + \frac{1}{{L_z}^2}\right] \quad (4)$$

Eventually, the seven-point stencil configuration which was showed by the Fig. 4 was used for these flow equations to be solved. The set of linear equations then were solved for the pressure values in the fractures and this was followed by calculation of pressure values in the matrix using the following equations 5 and 6.

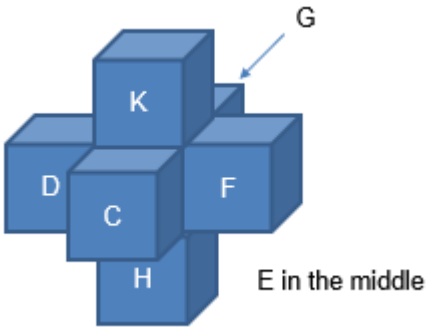

Fig. 4. Seven-Point Stencil Configuration

$$H_{i,j,k}p_{fi,j,k-1}^{n+1} + C_{i,j,k}p_{fi,j-1,k}^{n+1} + D_{i,j,k}p_{fi-1,j,k}^{n+1} + E_{i,j,k}p_{fi,j,k}^{n+1} + F_{i,j,k}p_{fi+1,j,k}^{n+1} + G_{i,j,k}p_{fi,j+1,k}^{n+1} + K_{i,j,k}p_{fi,j,k+1}^{n+1} = R_{i,j,k} \quad (5)$$

$$P_{m_i}^{n+1} = \frac{\left(0.006328\sigma k_m \mu P_{f_i}^{(n+1)} + \frac{\phi_m c_{tm} P_{m_i}^{n}}{\Delta t}\right)}{\frac{\phi_m c_{tm}}{\Delta t} + \frac{0.006328\sigma k_m}{\mu}} \quad (6)$$

BACKGROUND AND MODEL IMPLEMENTATION

For this particular reservoir simulation, the partial differential equations representing the mathematical model are discretized, resulting in a large sparse linear system of the form Ax = b. This system is then solved using one of the many available solver algorithms. Preconditioned Krylov subspace method-based algorithms (Saad Y., 2003) are popular algorithms to iteratively solve such large sparse systems. In cases where parallel preconditioners like Jacobi preconditioners can be used in the iterative solver to speed up convergence, sparse matrix-vector multiplication (SpMV) generally turns out to be the most time-consuming operation. Thus, the overall performance of the simulation depends on the optimal execution of the SpMV on given execution platform. This, in turn, depends on the input matrix representing the linear system and its storage format which directly affects SpMV performance on a given machine architecture. Unfortunately, no single matrix storage format gives the best SpMV performance on all architectures. For this reason, many matrix storage formats have

been proposed by researchers (Dongarra J., 2000; Liu W. et al., 2015; Kourtis K. et al., 2011).

In order to analyze the performance of multicore CPU for reservoir simulation, we chose a versatile scientific computing library, namely Portable Extensible Toolkit for Scientific computation (PETSc) (Balay S et al., 2019) for implementation of our mathematical model. The reason for this selection is the ease with which PETSc allows to switch between solver algorithms, preconditioners and matrix storage formats as well as the popularity of PETSc for applications based on partial differential equations. For the selection of the multicore CPU platform for this analysis, we based our decision on the observation that the operations used in sparse linear solvers generally have low arithmetic intensity. Thus, achieving higher memory bandwidth becomes the main optimization goal for achieving higher performance on such systems. The Intel Xeon Phi Knights Landing (KNL) processor is one of the first manycore processors that offer up to 72 cores, up to 16 GB of high bandwidth memory (HBM) and up to 384 GB of DDR4 memory (HCM). The higher number of cores along with higher capacity of HBM and HCM memories makes KNL a good candidate for implementation of large scientific simulations like reservoir simulation.

Brief PETSc Overview

PETSc library is a hierarchical collection of objects including solvers, preconditioners and parallel data structures that can be composed together to build a custom application. The library is designed for parallel execution of applications using MPI communication library. The library has been also enhanced to use manycore architectures like GPUs (Minden V., 2013). The parallel data structures offered by PETSc include vectors (Vec) and matrices (Mat). These data structures employ MPI for parallel implementation on CPUs while utilizing GPU libraries like cuSPARSE (NVIDIA cuSPARSE library, 2019) and VienaCL (Rupp K. et al., 2016) for GPU implementation. Linear solvers provided by PETSc are based on Krylov subspace methods and encapsulated in KSP class. Examples include Generalized Minimum Residual (GMRES), Conjugate Gradient (CG), Bi-conjugate Gradient (Bi-CG) and Bi-CGStab, Minimal Residual (MINRES), to name a few. The PC class provides various preconditioners. Some examples of preconditioners are Additive Schwarz, Jacobi, Block Jacobi, LU, ILU, SOR, and AMG. In addition, PETSc also provides interfaces to external solvers and preconditioners. For a complete list of linear solvers and preconditioners including external packages supported by PETSc, refer to (ANL; 2019). PETSc also supports non-linear solvers those are built on top of linear solvers and provided as SNES class. Other classes provided by PETSc include TS, DM, IS and TAO for time stepping, data management, index sets and optimization respectively.

Intel Knights Landing (KNL) processor

Architectural overview

The Intel Knights Landing manycore processor is a member of Intel Xeon Phi family supporting up to 72 cores with other variants having 64 or 68 cores. It is an improved

standalone version of its predecessor Knights Corner (KNC) processor that could only be used as a PCIe-connected device. From an architectural point of view, KNL is designed as a matrix of tiles, each tile containing two cores sharing 1 MB L2 cache and 2 Vector Processing Units (VPUs) per core (4 VPUs per tile). Tiles are interconnected with fast 2D mesh interconnect for accessing other processor L2 caches and HBM and HCM memory and for I/O operations.
Fig. 5. shows an architectural block diagram of KNL. For a 72-core machine, 36 of the available tiles are used while the rest are disabled during manufacturing. Similarly, for the 64 core and 68 cores machines, 32 and 34 tiles are used respectively. With hyperthreading enabled, each core can run up to 4 hyperthreads. The KNL processor employs two types of memories, namely a high capacity DDR4 memory (HCM) and a high bandwidth MCDRAM memory (HBM). MCDRAM is integrated on-chip and is composed of 8 devices, each with a capacity of 2 GB. MCDRAM is accessible to the cores through fast EDC interfaces (one per 2GB device) and can achieve a bandwidth of the order of 450 GB/sec. MCDRAM can be configured in one of the three memory modes, as discussed in the next sub-section. Cores can access off-chip HCM through six DDR4 channels, each channel supporting 64 GB giving a total capacity of up to 384 GB.

MCDRAM Memory modes

As previously discussed, MCDRAM, at boot-time, can be configured in one of the three memory modes, namely (i) Cache mode (ii) Flat mode and (iii) Hybrid mode. In cache mode, MCDRAM acts as a cache for the DDR memory. In flat mode, MCDRAM acts as addressable memory in same address space as DDR while in the hybrid mode, part of MCDRAM acts as a cache for DDR while the rest acts as addressable memory. In hybrid mode, it is possible to configure 25% or 50% of MCDRAM to act as a cache while the rest then acts as addressable memory. KNL memory modes are depicted in Fig. 6.

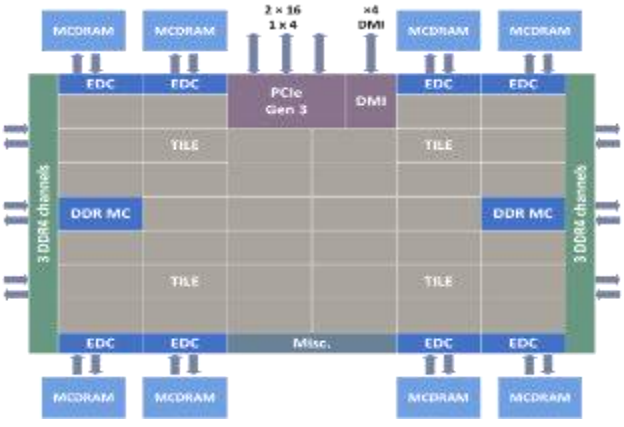

Fig. 7. Intel KNL processor block diagram (Jeffers J et al., 2016)

Cluster modes

Due to the presence of multiple tiles, memory access times for different cores are different, a phenomenon known as Non-uniform Memory Access (NUMA). To

mitigate this issue, KNL offers three cluster modes that can be employed by the user based on the application needs. These modes are (i) all-to-all, (ii) quadrant (also has hemisphere variation) and (iii) sub-NUMA clustering (SNC4) (also has SNC2 variation). On KNL, a distributed tag directory (DTD) is used to maintain cache coherency with two tag directories (TDs) per tile. These tag directories are used to identify location and state of a given cache line on the chip. In all-to-all mode, memory addresses are uniformly distributed among all tag directories resulting in data access latencies for various cores. In practice, this mode is either used when all DDR slots are not populated or for troubleshooting. In quadrant mode, tiles are divided into four quadrants, with each quadrant mapped to one of the four groups of memory controllers. Memory accesses within a quadrant are guaranteed to be served by the memory controller mapped to that quadrant. Hemisphere mode is a variant of this mode with tiles equally divided into two instead of four parts. In SNC4 mode, in addition to dividing the tiles into four equal parts, the four parts are also exposed as separate NUMA nodes. In SNC2 mode which is otherwise similar to SNC4, the number of NUMA nodes is 2. KNL cluster modes are depicted in Fig. 7.

Vectorization in KNL

To take advantage of data that can be processed in parallel, Intel provides Single Instruction Multiple Data (SIMD) instruction types for their processors in which single instruction operates on multiple data items. It started with Multi-Media extensions (MMX) in 1997 (with 64-bit SIMD registers), later followed by streaming SIMD extensions (SSE, with 128-bit SIMD registers) and its variants (SSE2, SSE3, SSE4) and subsequently Advanced Vector extensions (AVX, AVX2 with 256-bit SIMD registers). In recent years, Intel has introduced AVX-512 instructions, also supported by Intel KNL processor. AVX-512 use 512-bit SIMD registers supporting operations on 16 integers, 16 single-precision or 8 double-precision floating point data. In addition, in comparison to its predecessor AVX2, AVX-512 also supports more scalar types, better scatter-gather as well as more efficient math operations. For backward compatibility, any Intel processor supporting AVX-512 instructions also supports previous vectorization instructions including SSE, AVX, and AVX2. Programmer can choose vectorization instructions to be used for their code using Intel compiler switches. In this study, we also study the effect of vectorization mode on the simulation performance as discussed later.

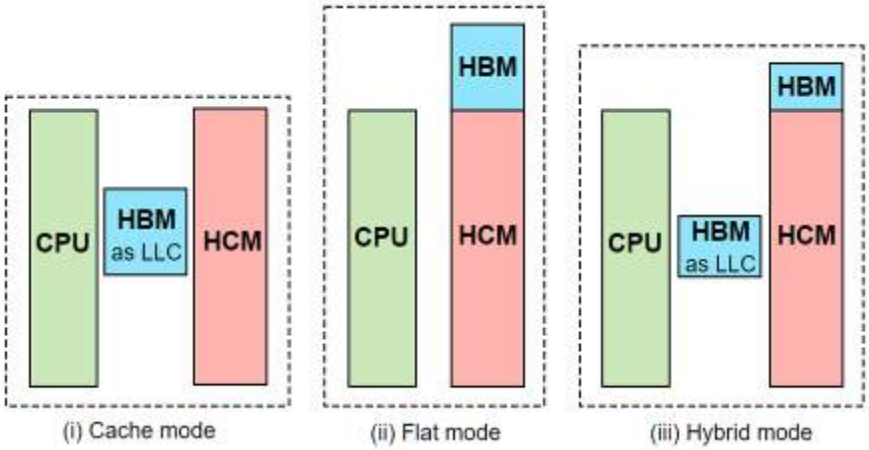

Fig. 8. KNL memory modes

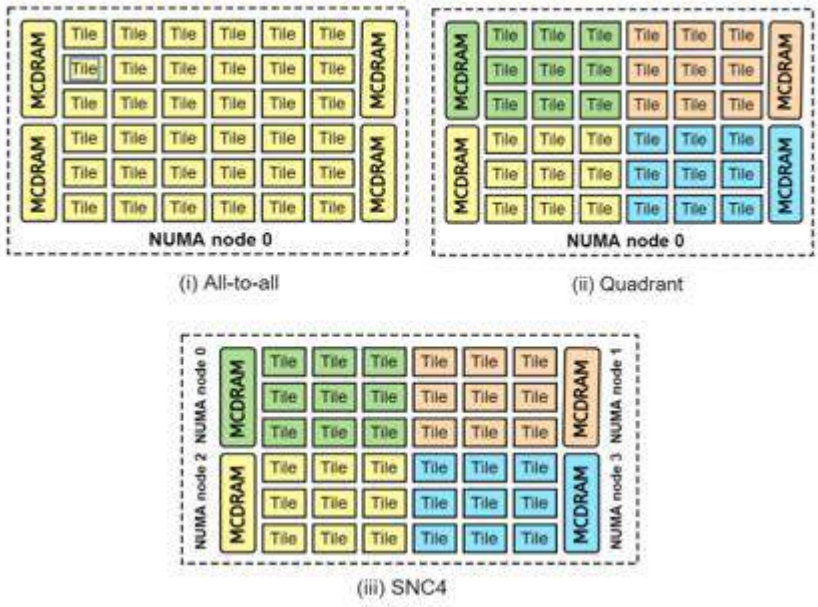

Fig. 9. KNL clustering modes

CSR and SELL Sparse Matrix Storage Formats

In scientific simulations, the matrix representing the system is generally very large and its number of rows and columns can be in the order of millions. However, most of the data entries in the matrix are zero, thus constituting a sparse matrix. In order to save data storage space, zeroes are generally not stored and are implicitly represented by the data storage format that only stores non-zero entries.

Compressed Sparse Row (CSR) format is one of the popular sparse matrix storage formats that uses three arrays to represent sparse matrix, a data array storing matrix non-zeroes row-wise (val), an array that stores positions of the first element of each row (ia) and an array storing column number of each non-zero (ja). Fig. 8. depicts CSR format for a sparse matrix where colored boxes show non-zero entries of the matrix and white boxes indicate zero entries. The corresponding val, ja and ia vectors are also

depicted. CSR is one of the most common sparse matrix storage format used in practice.

The sparsity pattern of the input matrix in conjunction with the matrix storage format and the machine architecture affect the performance of computational kernels like SpMV (Vuduc RW, 2003). With regard to matrix storage format, ELLPACK format has been designed to achieve better performance on vector processors like Intel KNL. The idea is to make the row length of the stored matrix uniform that equal to the maximum row length in the matrix and pad the rows with lesser row length with zeros on the right. This makes better utilization of the SIMD vectorization units in modern vector processors like Intel KNL thus improving throughput. However, if there is large variance between maximum row length and normal row lengths, the storage format can result in large storage overheads. To strike a balance between storage efficiency and vectorization performance, a variant of ELLPACK known as Sliced ELLPACK (SELL) is proposed by Monakov et al (Monakov A et al., 2010). The SELL format first slices input matrix into multiple submatrices, each containing the same number of adjacent matrix. Each of these submatrices is then represented in ELLPACK format. The result is better storage efficiency as maximum row length in each slice is different giving different row lengths for different slices.

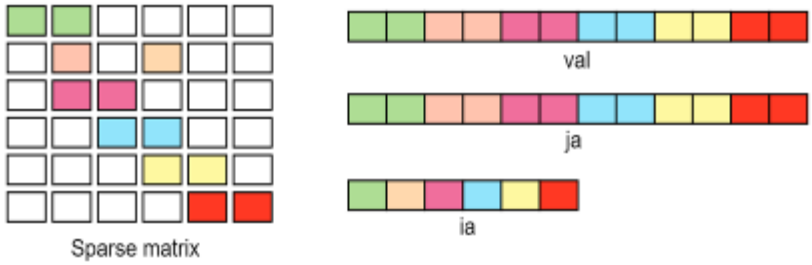

Fig. 10. Compressed Sparse Row (CSR) sparse matrix storage format

Fig. 9. shows how SELL format stores the sparse matrix. It uses three arrays, one for storing values (val), an array to store column index of the non-zero values (colidx), an array to store the start of each slice in the matrix (sptr) and an array to store row lengths in each slice (rlen).

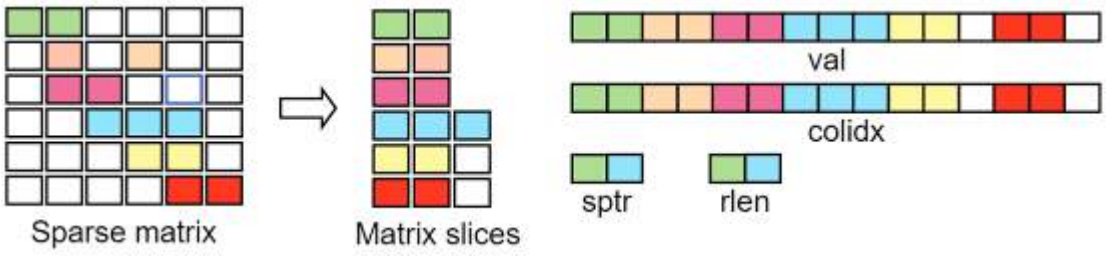

Fig. 11. Sliced ELLPACK sparse matrix storage format

Model Implementation

For the implementation of our reservoir simulation model, we used PETSc framework. We chose Krylov sub-space method based GMRES as the linear solver for our system,

which is a good choice for any general symmetric or non-symmetric system (Couturier R et al., 2012). For preconditioning, we used Jacobi preconditioner that has a better parallel efficiency and enabled our simulation to converge. The implementation is validated and tested by simulating a reservoir for a duration of one year (365 days). The hardware and software used for our implementation are given in Table 1 and 2 respectively.

Table 1. List of software used

Operating system	Ubuntu LTS 16.04, Release 16.04.3
Compiler	Intel ICC version 18.0.0
MPI library	Intel MPI version 2018
PETSc library	Version 3.10.4

Table 2. Specifications of hardware used

CPU	Intel Xeon Phi 7250 @ 1.4 GHz
Code Name	Knights Landing (KNL)
Number of cores	68 (272 hyperthreads)
DDR4	96 GB
MCDRAM	16 GB

ANALYSIS METHODOLOGY, RESULTS, AND DISCUSSION

In (Zhang H et al., 2018), the authors analyze the performance of an optimized SpMV kernel based on SELL format which they implemented in PETSc library. They have a comparison their SpMV kernel performance in SELL format against widely used CSR format on Intel KNL machine under different vectorization modes. They use a reaction-diffusion chemical simulation on 2D rectangular grid (5-point stencil) for their evaluation. For their implementation, they intentionally choose a grid size (2048 x 2048 for single node) that makes all data fit into the MCDRAM memory. Their results show SpMV in SELL format achieves better performance than CSR format under all vectorization modes, with AVX512 achieving the best performance. In our analysis of SpMV performance for our 3D reservoir simulation model (7-point stencil), we chose to evaluate simulation performance (SpMV performance) as the grid size is gradually increased to give a data size from less than 50% of MCDRAM memory to more than 50% of the DDR memory and see whether SELL data format still performs the best for all data sizes and vectorization modes. For this purpose, we configured KNL memory mode as cache and cluster mode as the quadrant. Different simulation grid sizes and the corresponding size of data are listed in Table 3. For each of the CSR and SELL data formats, we used AVX, AVX2, AVX512, and no-vectorization (novec) modes for our analysis.

Table 3. Simulation grid and data sizes used

S.No.	Grid size	Data size as percentage of MCDRAM size (16 GB)	Data size as percentage of DDR size (96 GB)
1.	200 x 200 x 200	26%	4%
2.	300 x 300 x 300	88%	14.5%
3.	500 x 300 x 200	96%	16%
4.	800 x 400 x 400	390%	65%

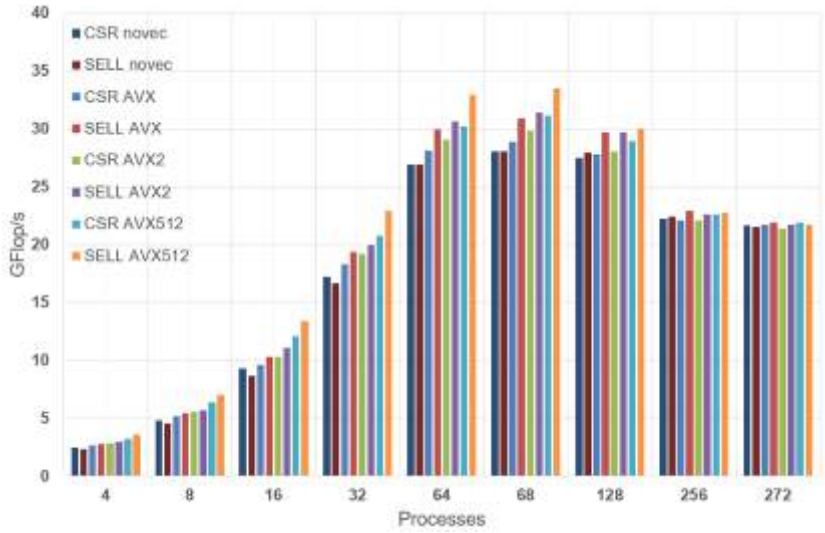

Fig. 12. SpMV performance for grid size 200 x 200 x 200

Figures 10, 11, 12 and 13 show SpMV performance comparison in CSR and SELL formats for the four simulation configurations shown in Table 3 with varying number of MPI processes and different vectorization modes. For all simulation configurations, it is observed that for a given data format and vectorization mode, the best performance is observed when the number of MPI processes equals the number of processor cores on our KNL machine (68 cores) and the performance gradually decreases if the number of MPI processes is increased or decreased from this number. Also, it is observed that in case of no vectorization, CSR format performs better than SELL format for a given processor configuration and all simulation configurations (Table 3). Comparing the performance of SELL format under different vectorization modes for a given process configuration, we notice that AVX512 always gives best performance against AVX, AVX2 and no vectorization modes. For CSR format on the other hand, AVX512 vectorization gives the best performance only for the first simulation configuration (grid size 200 x 200 x 200) while for the rest of the configurations, AVX stands as the best performant for a given process configuration. Comparing the performance of SELL against CSR, when simulation data size is less than 50% of the MCDRAM size (last level cache size), SELL format performs better than CSR for a given processor configuration and vectorization mode. This behavior, however, changes when simulation data size increase beyond 50% of the MCDRAM size and we see CSR performing better than SELL format for given process configuration and vectorization mode. An interesting observation from these results

is that for the simulation configurations where data size is less than the MCDRAM size, while the rest of data formats with a given vectorization and process configuration show rapid decline in performance as data size is increased, CSR with AVX and no-vectorization give almost consistent performance. Also, for data sizes exceeding 50% of the MCDRAM size and a given process configuration, CSR with AVX vectorization gives the best performance.

This can be explained by the fact that as the data size approaches MCDRAM size, MCDRAM channels become saturated and efficiency of feeding the wider vectorization units, performing AVX2 and AVX512 operations drop. Apparently, the hardware can still efficiently feed vectorization units for AVX operations in CSR format even when data size approaches MCDRAM capacity.

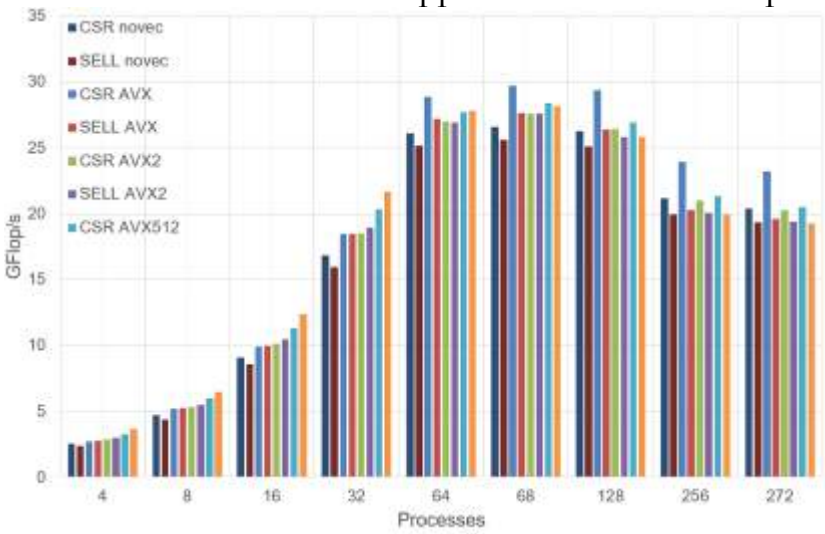

Fig. 13. SpMV performance for grid size 300 x 300 x 300

Considering the case when data size is more than the MCDRAM size, we notice a considerable performance deterioration (compared with when data size is less than MCDRAM size) for all data formats and vectorization modes for a given process configuration (Fig. 11). This deterioration is particularly higher for SELL format than for CSR format, with CSR along with AVX giving the best performance. From these results, we can conclude that when data size is considerably less than MCDRAM capacity (50% or less), SELL along with AVX512 vectorization gives promising results compared with CSR and other vectorization modes. However, as the problem size increases and approaches MCDRAM capacity and beyond (50% and more), CSR along with AVX vectorization becomes a better choice in terms of SpMV and consequently the simulation performance.

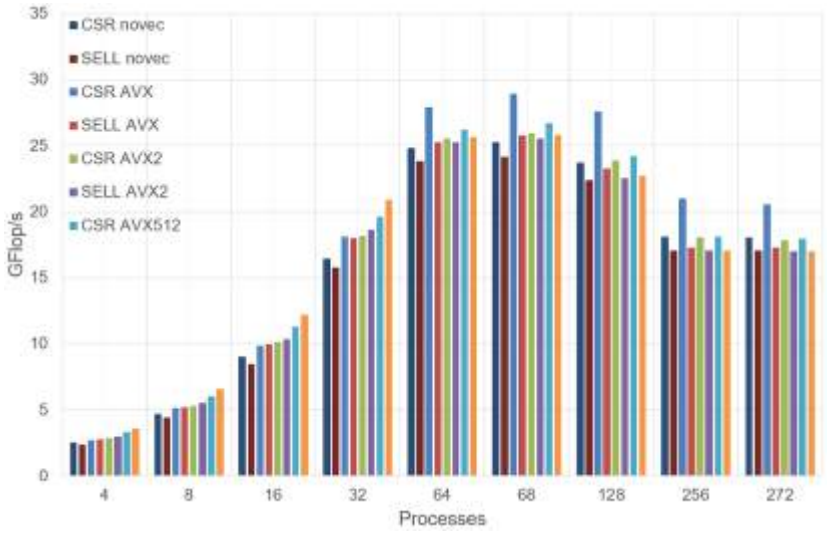

Fig. 14. SpMV performance for grid size 500 x 300 x 200

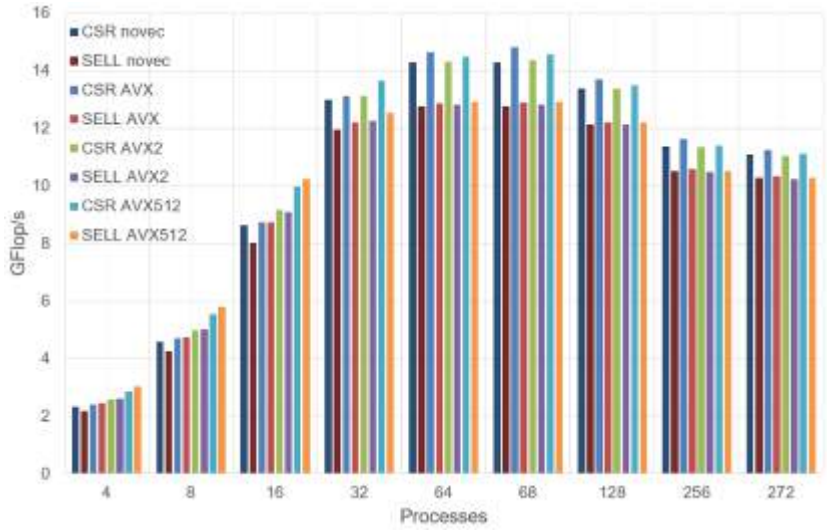

Fig. 15. SpMV performance for grid size 800 x 400 x 400

CONCLUSIONS

In this study, the performance of a dual porosity, single-phase, 3D single phase reservoir simulation is evaluated using various problem sizes, vectorization modes, and sparse matrix storage formats. The simulation is implemented using PETSc library and evaluated on Intel Knights Landing (KNL) multicore CPU, which offers one of the highest numbers of processor cores and high bandwidth memory for efficient data access. Intel KNL belongs to process family that is one of the first to use Intel AVX512 vectorization allowing 512-bit SIMD operations. Two sparse data storage formats, CSR and SELL, first one being a popular data format while the second designed for the vectorized processors are used in this evaluation. The high bandwidth memory is configured as cache memory and problem size is varied so that the simulation data size ranges from less than 50% of high bandwidth memory to more than 50% of the high capacity DDR memory. Different vectorization modes used for the evaluation are AVX, AVX2, AVX512 and no vectorization. The results show that for all data formats

and vectorization modes, the best performance is achieved when the number of MPI processes is equal to the number of processor cores on KNL (68 cores in our case). Also, when the data size is less than 50% of high bandwidth memory capacity, SELL format along with AVX512 vectorization gives the best performance. Moreover, CSR format along with AVX vectorization shows the least performance variation when data size is varied up to high bandwidth memory capacity. CSR along with AVX vectorization is also the best performing combination for problem sizes exceeding 50% of the HBM capacity. For the case when simulation data size exceeds high bandwidth memory capacity, performance of SELL format degrades considerably compared with CSR format under all vectorization modes, with CSR along with AVX vectorization giving the best performance. In conclusion, performance of reservoir simulation on a multicore CPU given a sparse data storage format and vectorization mode is dependent on the problem size. While the vectorization friendly SELL format with AVX512 performs best for smaller problem sizes easily fitting into HBM, CSR with AVX vectorization is good choice for problem sizes with data approaching or exceeding the HBM capacity.

Acknowledgments. The authors thank Professor Didem Unat at Koç University for her guidance and providing the resources used for this research.

REFERENCES

ANL. (2019). Summary of Sparse Linear Solvers Available from PETSc [Internet]. Available from: https://www.mcs.anl.gov/petsc/documentation/linearsolvertable.html.

Balay S, Abhyankar S, Adams M, Brown J, Brune P, Buschelman K, et al. (2019). PETSc Users Manual.

Barenblatt, G.I., Zheltov, I.P., and Kochina, I.N. (1960). Basic concepts in the theory of seepage of homogeneous liquids in fissured rocks: Journal of Applied Mathematics, v. 24, 1286-1303.

Couturier R, Domas S. (2012). Sparse systems solving on GPUs with GMRES. Journal of Supercomputing.

De Souza, Grazione & Souto, Helio. (2014). Numerical Reservoir Simulation of Naturally Fractured Reservoirs. Presented at XXXV Ibero-Latin American Congress on Computational Methods in Engineering, At Fortaleza, Ceará, Brazil.

De Swaan O., A. (1976). Analytic Solutions for Determining Naturally Fractured Reservoir Properties by Well Testing. Society of Petroleum Engineers. doi:10.2118/5346-PA.

Dichiarante, A.M., Holdsworth, R.E., McCaffrey, K.J.W., Dempsey, E.D., Selby, D., Conway, A., and Wilson, R. (2016). A reassessment of the brittle deformation history, age and attribute analysis from the Orcadian Basin, Scotland: implications for offshore Devonian fractured reservoirs.

Dongarra J. (2000). Sparse Matrix Storage Formats. Available from: http://www.netlib.org/utk/people/JackDongarra/etemplates/node372.html

Gerami, S., Pooladi-Darvish, M., Morad, K. et al. (2007). Type Curves for Dry CBM Reservoirs With Equilibrium Desorption. Presented at the Petroleum Society's 8th CIPC/58th Annual Technical Meeting, Calgary, 12-14 June. Paper2007-011.

Imber, J., Armstrong, H., Clancy, S., Daniels, S., Herringshaw, L., McCaffrey, K., Rodrigues, J., Trabucho-Alexandre, J., and Warren, C. (2014). Natural fractures in a United Kingdom shale reservoir analog, Cleveland Basin, northeast England, AAPG Bulletin, 98, 2411-2437.

Jeffers J, Reinders J, Sodani A. (2016). Intel Xeon Phi Processor High Performance Programming: Knights Landing Edition [Internet]. Elsevier Science.

Kazemi, H. (1969). Pressure Transient Analysis of Naturally Fractured Reservoirs with Uniform Fracture Distribution. Society of Petroleum Engineers. doi:10.2118/2156-A.

Kazemi, H., Gilman, J.R. and Elsharkawy, A.M. (1992). Analytical and Numerical Solution of Oil Recovery From Fractured Reservoirs With Empirical Transfer Functions (includes associated papers 25528 and 25818). SPE Res Eng 7 (2): 219-227. http://dx.doi.org/10.2118/19849-PA.

Kourtis K, Karakasis V, Goumas G, Koziris N. (2011). CSX: An Extended Compression Format for SpMV on Shared Memory Systems. In: Proceedings of the 16th ACM Symposium on Principles and Practice of Parallel Programming. New York, NY, USA: ACM.

Lim, K.T., and Aziz, K. (1995). Matrix-fracture transfer shape factors for dual-porosity simulators. Journal of Petroleum Science and Engineering, v. 13, issue 3–4, 169-178. ISSN 0920-4105. https://doi.org/10.1016/0920-4105(95)00010-F.

Liu W, Vinter B. (2015). CSR5: An Efficient Storage Format for Cross-Platform Sparse Matrix-Vector Multiplication.

Minden V, Smith B, Knepley MG. (2013). Preliminary Implementation of PETSc Using GPUs: GPU Solutions to Multi-scale Problems in Science and Engineering [Internet]. Berlin, Heidelberg: Springer Berlin Heidelberg.

Monakov A, Lokhmotov A, Avetisyan A. (2010). Automatically Tuning Sparse Matrix-Vector Multiplication for GPU Architectures: High Performance Embedded Architectures and Compilers. Berlin, Heidelberg: Springer Berlin Heidelberg.

NVIDIA. (2019). cuSPARSE library. https://docs.nvidia.com/cuda/cusparse/index.html.

Ranjbar, E. and Hassanzadeh, H. (2011). Matrix-fracture transfer shape factor for modeling flow of a compressible fluid in dual-porosity media. Adv. Water Resour. 34 (5): 627-639. http://dx.doi.org/10.1016/j.advwatres.2011.02.012.

Rodriguez-Roman, J., & Camacho Velazquez, R. (2005). Decline Curve Analysis Considering Non-Laminar Flow in Two Porosity Systems. Society of Petroleum Engineers. doi:10.2118/74388-PA.

Rupp K, Tillet P, Rudolf F, Weinbub J, Morhammer A, Grasser T, et al. (2016). ViennaCL-Linear Algebra Library for Multi- and Many-Core Architectures. SIAM Journal of Scientific Computing.

Saad Y. (2003). Iterative Methods for Sparse Linear Systems, Second Edition. Society for Industrial and Applied Mathematics.

Torcuk, M. A. (2013). Analytical solutions for multiple-matrix in fractured reservoirs: application to conventional and unconventional reservoirs. http://hdl.handle.net/11124/78950.

Vuduc RW. (2003). Automatic Performance Tuning of Sparse Matrix Kernels. Ph.D. Thesis.

Warren, J. E., & Root, P. J. (1963). The Behavior of Naturally Fractured Reservoirs. Society of Petroleum Engineers. doi:10.2118/426-PA.

Wu, Yu-Shu & Pruess, Karsten. (2019). A Physically Based Numerical Approach for Modeling Fracture-Matrix Interaction in Fractured Reservoirs.

Zhang. Z. (2015). PRODUCTION DATA ANALYSIS OF NATURALLY FRACTURED RESERVOIRS: A DENSITY-BASED APPROACH. Master's Thesis, John and Willie Leone Family Department of Energy and Mineral Engineering, Graduate School of the Pennsylvania State University, Pennsylvania, United States of America.

Zhang H, Mills RT, Rupp K, and Smith BF. (2018). Vectorized Parallel Sparse Matrix-Vector Multiplication in PETSc Using AVX-512. In: Proceedings of the 47th International Conference on Parallel Processing. New York, NY, USA.

A STUDY ON THE INTERACTION BETWEEN CALIXARENE DERIVATIVES AND BOVINE SERUM ALBUMIN

Bahar YILMAZ
Karamanoğlu Mehmetbey Üniverstesi
bahar.kmu@gmail.com

Mevlüt BAYRAKCI
Karamanoğlu Mehmetbey Üniverstesi
mevlutbayrakci@gmail.com

ABSTRACT: The interaction between water-soluble phosphate-derived calixarene compounds (pCLX4 and pCLX8) and bovine serum albumin (BSA) was investigated by emission and absorption spectrophotometry, Spectrophotometric results showed that pCLX4 and pCLX8 gradually quenched the fluorescence of BSA. This situation explained that there is an interaction between BSA and calixarene derivatives. And this interaction was shown that calixarene structures play an important role in the transport of protein-based drugs.

Key words: Calixarene, BSA, Fluorescence, Absorbance, Emission

KALİKSAREN TÜREVLERİ VE SIĞIR SERUM ALBÜMİNİ ARASINDAKİ ETKİLEŞİM ÜZERİNE BİR ÇALIŞMA

ÖZET: Suda çözünebilen fosfat türevli kaliksaren bileşikleri (pCLX4 ve pCLX8) ve sığır serum albümini (BSA) arasındaki etkileşim emisyon ve absorpsiyon spektrofotometresi ile araştırılmıştır. Spektrofotometrik sonuçlar, pCLX4 ve pCLX8'in BSA'nın floresansını yavaş yavaş söndürdüğünü göstermiştir. Bu durum BSA ve kaliksaren türevleri arasında bir etkileşim olduğunu açıkladı. Ve bu etkileşim, kaliksaren yapılarının protein temelli ilaçların taşınmasında önemli bir rol oynadığını göstermiştir.

Anahtar sözcükler: Kaliksaren, BSA, Floresans, Absorbans, Emisyon

GİRİŞ

Supramoleküler kimya, moleküller arasındaki ve içerisindeki etkileşimleri inceleyen bilim dalıdır. Son yıllarda başta fizik, kimya ve biyoloji alanları olmak üzere önemli bir yere sahiptir (Shinkai, 1993). Supramoleküler kimya, "moleküler reseptör" ve "substrat" olarak anılan supromoleküler türleri ele alır. Yani reseptör tarafından subratın bağlanması supramolekülleri oluşturur ve bağlanma prosesi molekülün yapısını doğrulamayı sağlar (Bayrakci, 2012). Makrosiklik bileşiklerin, köprülü yapıya sahip olmaları ve molekül içi boşluklar içermeleri reseptör olarak kullanılabilmelerini sağlar. Bu makrosiklik bileşikler arasında crown (taç) eterler, kriptantlar,

siklodekstrinler ve kaliksarenler en fazla ilgi çekenlerdir (Bayrakci ve ark., 2011). Kolay türevlendirilebildiklerinden dolayı kaliksarenler en çok tercih edilen makrosiklik bileşiklerdir. Kaliksarenler, fenol ve formaldehitin bazik ortamda kondensasyonu ile oluşturulmaktadır. Ayrıca, değişik moleküllerle kompleks yapabilme özelliğine sahip, metilen köprüleriyle fenolik birimlerin birbirlerine bağlanmasını sağlayarak hidrofobik bir boşluk oluşturabilen makrosiklik bileşiklerdir (Ertul ve ark., 2010). Kaliksarenler doğal olarak suda çözünmezler ve sulu çözeltide meydana gelen substrat-bağlanma çalışmaları için uygun değildirler. Kaliksarenlerin kullanım alanlarını genişletmek için suda çözünen kaliksaren türevlerinin sentezlenmesi gereklidir. Suda çözünen kaliksarenler ilaç çözünürlüğü ve kontrollü ilaç salınımı gibi birçok alanda kullanılmaktadır. Bu nedenle suda çözünür fonksiyonel gruplar (fosfo, sülfo ve nitro gibi gruplar) ile kaliksaren molekülleri türevlendirilmektedir (Bayrakci ve ark., 2012). Çeşitli ilaçların dağılımının, serbest konsantrasyonunun ve metabolizmasının, kan akışındaki ilaç-protein etkileşimlerinden etkilenmektedir. Bu tip bir etkileşim kemoterapötik işlem sırasında ilacın stabilitesini ve toksisitesini de etkileyebilir. Serum albüminler plazmadaki en bol bulunan proteinlerdir. Dolaşım sisteminin başlıca çözünebilir protein bileşenleri olarak, birçok fizyolojik fonksiyona sahiptirler (Hu et al., 2005). Kolloid ozmotik kan basıncına katkıda bulunurlar ve temel olarak kan pH'ının korunmasından sorumludurlar. Ayrıca ilaçların yerleştirilmesinde ve etkinliğinde baskın bir rol oynamaktadırlar (Wang et al., 2007). Birçok ilaç ve biyoaktif moleküller, başta albümin proteini olmak üzere taşıyıcı olarak işlev gören diğer serum bileşenlerine bağlanabilir. Bu nedenle ilacın serum albümine olan afinitesini bilmek önemlidir. Spektroskopik çalışmalar, kimyasal ve biyolojik sistemlerin reaktivitesinin incelenmesi için güçlü birer yöntemdir ve bu yöntemlerle bir proteinin spektrumunu yüksek güvenilirlikle analiz etmek mümkündür (Hu et al., 2005). Bu çalışmada, BSA proteini ile kaliksaren türevleri arasındaki etkileşimin floresans ve absorbans spektrumu kullanılarak aydınlatılması amaçlanmaktadır.

YÖNTEM

Sentez

Kaliksarenlerin O-fosfonik asit türevlerinin sentezi, daha önceki literatür çalışmaları (Bayrakci, 2012) göz önünde bulundurularak sentezlendi ve karakterize edildi.

Spektroskopik Çalışmalar

Molekül ve protein arasındaki etkileşimleri absorbsiyon ve emisyon çalışmaları ile incelemek için, BSA ile artan konsantrasyondaki fosfonatlı kaliksaren molekülünün absorbans ve emisyon ölçümleri alındı (shimadzu 1800, hitachi 7200).

BULGULAR

Sentez ve Karakterizasyon

Sentezi yapılan fosfanatlı kalikaren (pCLX[n]) moleküllerinin yapısal karakterizasyonu ^{1}H-NMR ve FT-IR (ATR) ile aydınlatıldı.

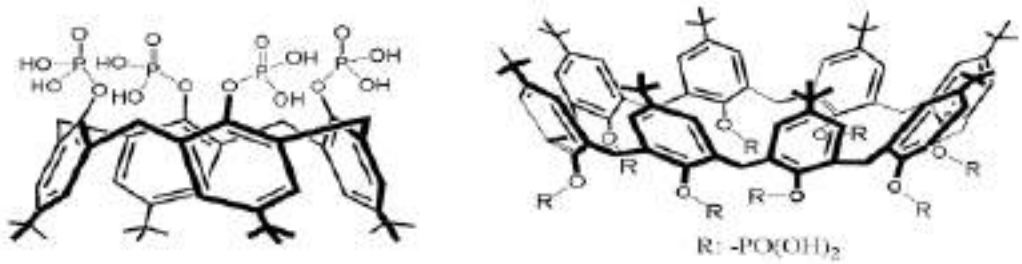

Şekil 1. 25,26,27,28-Tetrakis(dihidroksifosfonoksi)-5,11,17,23-tetra-terbütilkaliks[4]are ve Oktakis-O-(dihidroksifosforil)-p-ter-bütilkaliks[8]aren

Absorpsiyon ve Emisyon Çalışmaları

BSA ile farklı konsantrasyondaki pCLX4 ve pCLX8 arasındaki emisyon ve absorpsiyon çalışmaları su içerisinde oda sıcaklığında gerçekleştirildi ve sonuçlar şekil 2 ve şekil 3'de gösterildi. BSA proteinin absorbans ölçümlerinde 280 nm dalga boyunda gösterdiği pik pCLX4 ve pCLX 8 eklendiğinde kaybolmamış aksine daha da artmıştır. Bu durum pCLX[n] ile BSA arasındaki ilişkinin BSA'nın moleküler konformasyonunu değiştirmediğini, hidrojen bağ ve iyonik etkileşimin protein-molekül birleşimi için eşit derecede önemli güçlere sahip olduğunu öne sürmüştür (Wang et al., 2007).

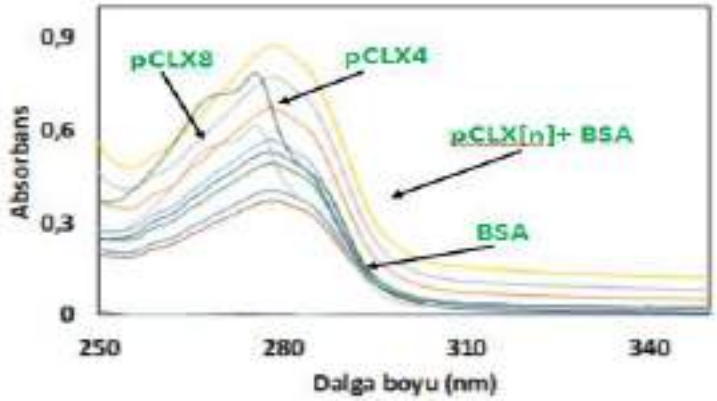

Şekil 2. BSA Varlığında pCLX4, pCLX8 ve BSA ile Etkileşimlerinin Absorpsiyon Spektrumları

Absorpsiyon spektrumlarındaki değişimleri destekleyebilmek amacıyla aynı karışımların emisyon spektrumları da alınmıştır. Şekil 3'de gösterildiği gibi 340 nm'de BSA proteini kuvvetli floresans spektrumu gösterirlerken, artan konsantrasyonda pCLX4 ve pCLX8 eklediğinde floresansın artan konsantrasyon ile kademeli olarak azaldığı ve kaybolduğu gözlenmiştir.

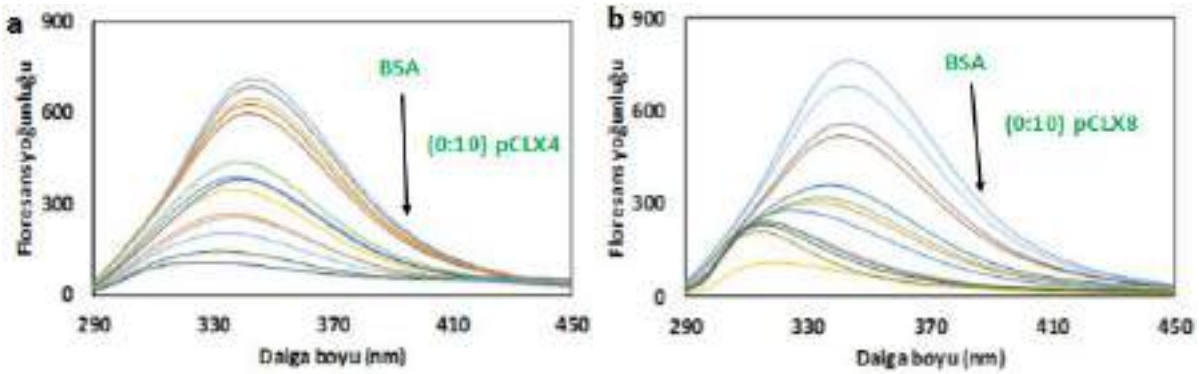

Şekil 3. BSA Varlığında Farklı Konsantrasyondaki; a) pCLX4 ve b) pCLX8 Moleküllerinin Emisyon Spektrumları

SONUÇ

İlaçların ya da aktif moleküllerin proteinlerle etkileşim çalışması başta eczane, farmakoloji ve biyokimya alanları olmak üzere birçok alanda önem taşımaktadır (Hu et al., 2005). Bu çalışmada, kaliksaren türevlerinin BSA ile etkileşimi, absorbans ve emisyon ölçümü içeren spektrofotometrik yöntemlerle incelenmiştir. Deney sonuçları, BSA moleküllerinin ikincil yapısının, pCLX4 ve pCLX8 varlığında değiştiğini göstermiştir. Ayrıca kaliksaren türevleri tarafından BSA'nın floresans özelliğinin söndürülmesi aralarında etkileşim olduğunu kanıtlamıştır. Sentezlenen bu kaliksaren türevlerinin, başta plazma proteinleri temelli ilaçlar olmak üzere benzer yapıdaki moleküllerin taşınmasında aktif olarak kullanılabileceği tespit edilmiştir.

KAYNAKLAR

Bayrakcı, M. (2012). Suda çözünebilen kaliksfosfonatlarin sentezi, antibakteriyel özelliklerinin incelenmesi ve furosemit, niklosamit ve nifedipin gibi bioaktif moleküllerin çözünürleştirilmesinde kullanimi (Doctoral dissertation, Selçuk Üniversitesi Fen Bilimleri Enstitüsü).

Bayrakcı, M., Ertul, S., & Yilmaz, M. (2011). Phase solubility studies of poorly soluble drug molecules by using O-phosphorylated calixarenes as drug-solubilizing agents. *Journal of Chemical & Engineering Data*, 57(1), 233-239.

Bayrakcı, M., Ertul, Ş., & Yılmaz, M. (2012). Solubilizing effect of the p-phosphonate calix [n] arenes towards poorly soluble drug molecules such as nifedipine, niclosamide and furosemide. *Journal of Inclusion Phenomena and Macrocyclic Chemistry*, 74(1-4), 415-423. https://doi.org/ 10.1007/s10847-012-0135-7

Ertul, Ş., Bayrakcı, M., & Yilmaz, M. (2010). Removal of chromate and phosphate anion from aqueous solutions using calix [4] aren receptors containing proton switchable units. *Journal of hazardous materials*, 181(1-3), 1059-1065. https://doi.org/10.1016/j.jhazmat.2010.05.121

Hu, Y. J., Liu, Y., Shen, X. S., Fang, X. Y., & Qu, S. S. (2005). Studies on the interaction between 1-hexylcarbamoyl-5-fluorouracil and bovine serum albumin. *Journal of Molecular Structure*, 738(1-3), 143-147. https://doi.org/10.1016/j.molstruc.2004.11.062

Shinkai, S. (1993). Calixarenes-the third generation of supramolecules. *Tetrahedron*, 49(40), 8933-8968. https://doi.org/10.1016/S0040-4020(01)91215-3

Wang, Y. Q., Zhang, H. M., Zhang, G. C., Tao, W. H., & Tang, S. H. (2007). Interaction of the flavonoid hesperidin with bovine serum albumin: A fluorescence quenching study. *Journal of Luminescence*, *126*(1), 211-218.

ELECTROCHEMICAL PROPERTIES OF CARBON SUPPORTED $Cu_2Mo_6S_8$ NANOSTRUCTURES

Meriç KARAKIŞ, Karamanoglu Mehmetbey University, Faculty of Engineering, Department of Energy Systems Engineering, Karaman, Turkey

Adem SARILMAZ, Karamanoglu Mehmetbey University, Faculty of Engineering, Department of Metallurgical and Materials Engineering, Karaman, Turkey

Faruk ÖZEL, Karamanoglu Mehmetbey University, Faculty of Engineering, Department of Metallurgical and Materials Engineering, Karaman, Turkey

Gamze KARANFİL, Karamanoglu Mehmetbey University, Faculty of Engineering, Department of Energy Systems Engineering, Karaman, Turkey, gamzekaranfil86@gmail.com

ABSTRACT: In this study, it is aimed to synthesize alternative, more economical and more efficient catalysts to the platinum catalyst which constitutes a large part of the proton exchange membrane (PEM) fuel cell cost and which has activation problems in the oxygen reduction reaction in the PEM fuel cell cathode electrode. For this purpose, the chevrel phases which exhibited remarkable electrocatalytic activities in the oxygen reduction reaction were synthesized as carbon supported and electrochemical properties were investigated to determine their use as catalyst in PEM fuel cell cathode reactions. Carbon supported-$Cu_2Mo_6S_8$ chevrel phase catalysts were synthesized at high temperatures by solid state synthesis conditions. The synthesis experiments were performed at different temperatures and times to optimize the production parameters. Optimization studies revealed that the most suitable production parameters were 24 hours and 1000˚C. CV and RDE measurements were performed to investigate the use of $Cu_2Mo_6S_8$ chevrel phase catalysts produced as PEM fuel cell cathode catalyst.

Key words: Energy, Catalyst, Chevrel phases, $Cu_2Mo_6S_8$

Acknowledgments

This work is supported by Karamanoglu Mehmetbey University BILTEM (Scientific and Technological Research and Application Center) and TUBITAK (The Scientific and Technological Research Council of Turkey) under project number 118M662.

INVESTIGATION OF THE EFFECT OF BREAD MOLD ON SOIL BASED MICROBIAL FUEL CELL

Gamze KARANFİL
Karamanoglu Mehmetbey University, Faculty of Engineering, Department of Energy Systems Engineering, Karaman, Turkey, gamzekaranfil86@gmail.com

ABSTRACT: Microbial fuel cells (MFCs) have attracted a lot of attention as a mode of converting organic waste into electricity. In this study, a soil-based microbial fuel cell that generates bioelectricity by biodegradation of food waste is developed. Bread mold was used as organic waste. The electric properties of the soil based-MFC were investigated along with the influence of using of vermicompost. It is observed that the power and lifetime of the soil based-MFC was increased by using of vermicompost. This developed soil based-MFC is a simple cell to generate electricity from organic waste.

Key words: Energy, Microbial Fuel Cell, Mold, Soil, Compost

INTRODUCTION

Rapid urbanization has accrued the necessity for reliable and sustainable energy sources (Sophia and Sreeja, 2017). The energy generation technologies which uses the reliable and sustainable energy sources is required to overcome with the growing energy request, the depletion of fossil fuels and environmental pollution. These energy generation technologies are related to natural energy sources as solar energy, wind energy and bio-energy (Wetser et al., 2015).

Another problem that is as important as the energy is solid organic waste. Solid organic wastes represent an important resource of environmental pollution world-wide. From a global perspective, organic wastes should be seen as a valuable resource that can be profitable and that fits the concept of energy from waste (Khudzari et al, 2016). Like all fungi, molds produce energy by using heterotrophy from the organic matter they live in, not through photosynthesis. Typically, the molds secrete hydrolytic enzymes essentially from the hiphal ends.

Microbial fuel cells (MFCs) convert the chemical energy stored in organic matter directly into electrical energy, thanks to the action of electrochemically active microorganisms (Castresana et al., 2019). There are some researches of MFCs to generate electricity from organic wastes, wastewaters, marine sediments and rice paddy fields. Besides, MFC in hybrid composting method by reutilizing kitchen waste as a raw material were proposed (Moqsud et al., 2013).

The aim of this study is to develop a soil based-microbial fuel cell that generates electricity through the usage of bread mold and to investigate the influence of using of vermicompost.

Microbial Fuel Cells

Microbial Fuel Cells (MFCs) were first successfully created in 1911 by Michael Potter (Wang et al., 2013). A typical MFC consists of anode and cathode compartments separated by a proton exchange membrane. Soil based-MFCs with living plants are also a way to get green energy. The bioelectrochemical principle of the soil based-MFCs is similar to typical MFCs. The anode captures the electrons from microbes and electrons arrive the cathode via the external circuit. This cycle can theoretically produce sustainable electricity (Guan et al., 2019). A shematic structure of soil based-MFC is given in Figure 1.

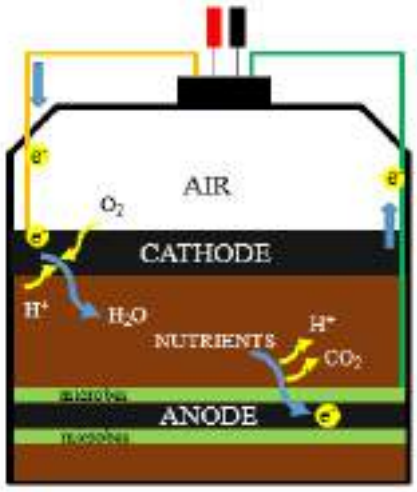

Figure 1. A schematic structure of soil based MFC

METHODS

The mixture soil, vermicompost, bread mold and water were placed in Mudwatt Microbial Fuel Cell Kit (FuelCell Store). The kit hosted a soil based-MFC, which consisted of an anode and a cathode electrode at a parallel distance of 2.5 cm from each other. The anode was immersed in the soil and the titnium wire was connetted to the cathode which was exposed to air. The anode (Green, 8 cm diameter and 0.5 cm thickness) and the cathode (Orange, 8.5 cm diameter and 1 cm thickness) were graphite fiber felt. A small circuit board with a capacitor and LED were visible indicators that electricity is being produced. Besides, the MudWatt Explorer App was used to convert the number of blinks into current produced (in microWatts (µW)) from LED light. Measurements were performed once a day for 15 days. In order to investigate the effect of vermicompost, the same system was installed without compost and measured. The design of soil based-MFC was given in Figure 2.

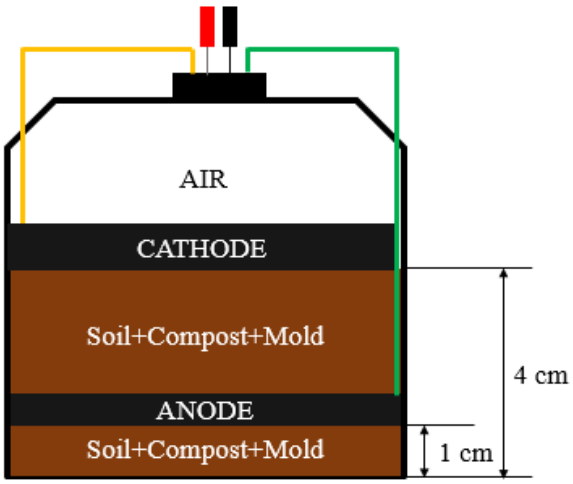

Figure 2. The design of soil based-MFC

RESULTS AND FINDINGS

Figure 3 shows the changes in the power of the soil based-MFCs over the 15-day experiment. Several abrupt power changes were observed. The power drop phenomenon happened because the carbon source limited the metabolism of bacteria within the anaerobic zone of the soil based-MFC. In other saying, whenever the organic matters begin depleting, the electricity production would decrease due to the low microbial metabolism happening in the soil based-MFC (Khudzari et al., 2016). In order to determine the electrical production potential of bread mold, the soil based-MFC system was established only as soil and soil+vermicompost. However, neither of these soil based-MFC systems produced electricity. In addition, the same soil based-MFC system was established without the addition of compost to investigate the effect of vermicompost. The results showed that the non-composted soil based-MFC system produced lower power generation and did not work after 3 days. Both soil based-MFC systems started to work at the end of the 3rd day and the maximum power generation for composted and non-composted soil based-MFC systems for 15 days was 193 µW and 40 µW, respectively.

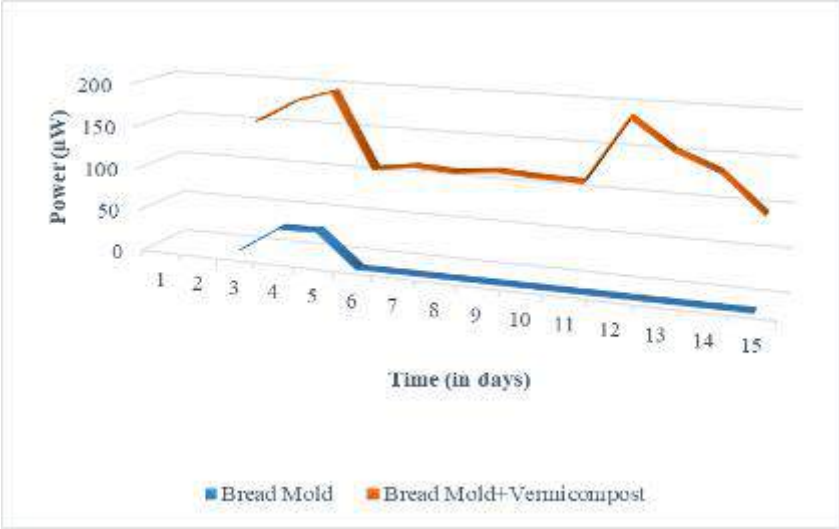

Figure 3. Changes in power over time of the soil-based MFC operated with/without vermicompost

CONCLUSION

In this study, bread mold was used in the soil based-MFC for bioelectricity generation. The peak power generated in the soil based-MFC was around 193 µW with bread mold when vermicompost was mixed with the soil. The power became 4.8 times higher when vermicompost was used. The organic content added by compost provides additional capacity to produce bioelectricity. The organic waste can be used for enhancing the power production in the soil based-MFCs. The the soil based-MFC using compost proved to be a good way for green electricity production as well as to recycle organic waste to continue a healthy and pollution free environment.

RECOMMENDATIONS

In this study, the potential of bread mold, which is one of the most discarded foods in the world, to be used in electricity production in soil based microbial fuel cell was investigated. The results showed that mold produced in bread contributes to electricity production. In the following studies, it is aimed to examine the potentials of molds formed in other organic wastes.

REFERENCES

Castresana, P. A., Martinez, S. M., Freeman, E., Eslava, S., Lorenzo, M. D. (2019). Electricity generation from moss with light-driven microbial fuel cells. *Electrochimica Acta, 298, 934-942.*

Guan, C.Y., Tseng, Y. H., Tsang, D. C. W., Hu, A., Yu, C. P., Wetland plant microbial fuel cells for remediation of hexavalent chromium contaminated soils and electricity production, *Journal of Hazardous Materials. 365, 137–145.*

Khudzari, J. Md., Tartakovsky, B., Raghavan, G.S.V. (2016). Effect of C/N ratio and salinity on power generation in compost microbial fuel cells. *Waste Management, 48, 135–142.*

Moqsud, M. A., Omine, K., Yasufuku, N., Hyodo, M., Nakata, Y. (2013). Microbial fuel cell (MFC) for bioelectricity generation from organic wastes. Waste Management 33, 2465–2469.

Sophia, A. C., & Sreeja, S. (2017). Green energy generation from plant microbial fuel cells (PMFC) using compost and a novel clay separator. *Sustainable Energy Technologies and Assessments, 21, 59–66.*

Wang, C. T., Liao, F. Y., Liu, K. S. (2013). Electrical analysis of compost solid phase microbial fuel cell. International Journal of Hydrogen Energy, 38, 11124-11130.

Wetser, K., Liu, J., Buisman, C., Strick, D. (2015). Plant microbial fuel cell applied in wetlands: Spatial, temporal and potential electricity generation of Spartina anglica salt marshes and Phragmites australis peat soils. *Biomass and Bioenergy, 83, 543-550.*

THE EFFECT OF DEEP EUTECTIC SOLVENT ON COPPER RECOVERY FROM COPPER SMELTING SLAG

Mehmet Ali Topçu
Karamanoğlu Mehmetbey University, Engineering Faculty, Metallurgical and Materials Engineering, Karaman, Turkey, topcumali@kmu.edu.tr

Aydın RÜŞEN
Karamanoğlu Mehmetbey University, Engineering Faculty, Metallurgical and Materials Engineering, Karaman, Turkey, aydinrusen@kmu.edu.tr

ABSTRACT: Copper smelting slag which forms during the smelting stage of concentrated ore in pyrometallurgical copper production includes remarkable amount of copper. Up to now, copper recovery has been extracted from copper smelting slag with hydrometallurgical routes by using various leaching agents based on acids or bases. Considering the negative effect of these solvents on human health and environment, the search for new solvents with less environmental damage continues. Therefore, in this work, a new generation solvent was investigated for copper recovery from copper smelting slag. For this work, 50 mL of deep eutectic solvent was prepared by mixing choline chloride and urea with 1:2 molar ratio. Reaction duration in the range of 2, 8, 16, 32, 48 and 72 hours and solid-to liquid ratio in the range of 1/10, 1/20, 1/30 and 1/40 was chosen as experimental variable at 95 ^{o}C reaction temperature and 600 rpm stirring speed. According to the experimental results, copper recovery from smelting slag increased with increasing reaction duration in deep eutectic solvent and maximum copper recovery was obtained as 80.84% after 72 hours of leaching. Also, experimental results showed that copper recovery increased with decreasing solid-to liquid ratio and highest copper recovery was achieved as 83.60% after leaching with 1/40 solid-to liquid ratio.

Key words: Smelting Slag, Copper Recovery, Deep Eutectic Solvents, Hydrometallurgy

INTRODUCTION

Sulphidic copper ores is generally used for copper production in pyrometallurgical production which includes concentration, smelting, converting and refining stages. In smelting stage, concentrated $CuFeS_2$ is melted under neutral atmosphere at 1200 – 1300 ^{o}C and two liquid phases, namely matte with a high copper content and a huge amount of smelting slag with a 0.7 – 2.3% of copper content. (Gorai and Jana, 2003; Rüşen et al., 2013) Copper smelting slag contains large amount of iron oxide (FeO and Fe_2O_3) and silica (SiO_2) phases. Expect the main phases, copper smelting slag includes small amount of Al_2O_3, CaO and MgO oxides and other metals such as Cu, Co, Zn and Ni. (Sridhar et. al., 1997; Davenport et. al., 2002). Due to the environmental risk and economic point of view, these copper smelting slags must be disposed (Ahmed et. al., 2012; Murari et al., 2015) Until today, many studies have been performed to recover

metals from copper smelting slag by using hydrometallurgical and/or pyrometallurgical methods. Hydrometallurgical methods are frequently used when evaluating the copper smelting slag because these methods are relatively more economical and environmentaly friendly than pyrometallurgical method. (Arslan and Arslan, 2002; Yang et al., 2010; Zhai et al., 2011; Dimitrijević et al., 2017) However, due to the negative effects of acid-based solvents on human and environment, many studies have been started for environmentally sensitive solvents.

Recently, Abbott et al., (2003) showed a new solvent, namely deep eutectic solvents which have extraordinary solving properties and prepared by two components which are cheap, renewable and biodegradable to form a eutectic mixture. Choline chloride is the most favourite component due to its low cost, biocompatibility and nontoxic structure. (Zhang et al. 2012) Nowadays, there is increasing interest in hydrometallurgical processes for DESs which prepared with ChCl and hydrogen bond donors such as urea, ethylene glycol and malonic acid due their low cost and dissolving properties. According to previous studies (Abbott et. al., 2009; Bakkar 2014), the solubility of metal oxides such as ZnO, Cu_2O and PbO in electric arc furnace was quite high in DES based on ChCl and urea. Also, it is stated that DESs provide a suitable environment for the removal of metals from the leach liquor by electro-wining. A recent study on metal recovery by using the choline chloride-urea mixture was conducted by Rüşen and Topçu (2017). In their study on zinc and lead recovery from zinc-lead leach residues showed that zinc and lead recovery increased with increasing reaction temperature and zinc and lead recovery was obtained as 55% and 47%, respectively.
In this study, the effect of reaction duration and solid-to liquid ratio on copper recovery from copper smelting slag was investigated by using a deep eutectic solvent.

METHODS

Leaching and characterization experiments were performed by using copper smelting slag from Eti Bakır Inc., Turkey. Chemical analyses of copper smelting slag were conducted by Inductively Coupled Plasma Mass Spectrometer (ICP – MS) in chemistry laboratory of Eti Bakır Inc. Mineralogical characterization of copper smelting was investigated by using X-Ray Diffractometer with Cu Kα radiation at 30 kV at a scanning rate of 0.4^o min^{-1} at Karamanoğlu Mehmetbey University.

Table 1. Chemical Composition of Copper Smelting Slag (wt.)

Elements	Fe_{Total}	SiO_2	Cu	Zn	Pb	Al_2O_3
Amount (wt%)	36.7	36.1	0.88	3.3	0.1	2.2

According to the XRD analysis, the copper smelting slag was composed of mainly Fayalite ($2FeO.SiO_2$) and magnetite (Fe_3O_4) phases. As stated previous studies (Rüşen et. al., 2012 Rüşen et. al., 2013; Rüşen et. al., 2016), copper is found in different structures as copper metallic copper, matte inclusions of various copper percentage

and complex (Cu–Fe–Zn) sulphides. Also copper smelting slag was included small amount of Al_2O_3 and CaO.

Choline chloride (>98%) and urea (>99%) was used without purification to prepare deep eutectic solvent. Choline chloride and urea were mixed in a glass baker with stoichiometric eutectic molar ratio 1:2, respectively and heated slowly to 90 ^oC on hot plate until a homogenous colourless liquid was obtained. The prepared deep eutectic solvent was shown in Figure 1.

Figure 1. The Prepared Deep Eutectic Solvent and Leach Liquor Obtained After Leach Process at 95 ^oC Reaction Temperature, 1/20 Solid-to Liquid Ratio and 48 Hours.

All leaching experiments were carried out by using constant volume of DES (50 ml) in closed three-necked glass flask on temperature controlled heater. Reaction duration and solid-to liquid ratio was chosen as experimental variable. Reaction duration and solid-to liquid ratio was selected in the range of 2, 8, 16, 32, 48 and 72 hours, and 1/10, 1/20, 1/30 and 1/40 g/L, respectively. After leaching experiments, the solid and liquid parts were separated from each other by filtration system. The obtained leach liquor was diluted 0.1 M HCl and analyzed by using Perkin Elmer PinAccle 900T model Atomic Absorption Spectroscopy.

As described before (Kılıçel and Karapınar, 2018), Cu hollow cathode lamps were used as radiation source. The most sensitive wavelengths (nm) and lamp current (mA) used for specification of the analytes were Cu 324.8 and 15. An air/acetylene flame was used for absorbance measurements of Cu. Diluted standard solutions were used to build calibration curve for method validation within linear range. Finally, the correlation coefficient was obtained as 0.9992571.

RESULTS AND FINDINGS

Effect of Reaction Duration

Effect of reaction duration on copper recovery from copper smelting slag with DES was investigated at 95 ^oC reaction temperature, 1/20 solid-to liquid ratio and 600 rpm stirring speed. Experimental results are shown in Fig 2.

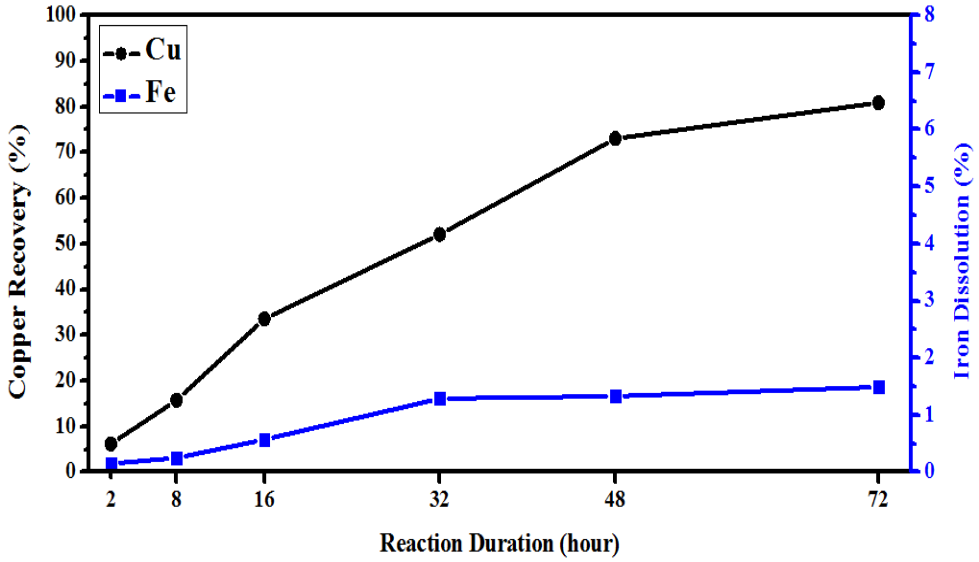

Figure 2. The Effect of Reaction Duration on Copper Recovery.

As seen in Fig. 2, copper recovery from copper smelting slag increased with increasing reaction duration in deep eutectic solvent and 80.84% of recovery rate was achieved after the reaction duration of 72 hours. Although very low copper recoveries were obtained at less reaction durations, the copper recovery was increased significantly after 16 hours of reaction duration. According to the experimental results, only 7.84% of increment was gained after reaction duration of 48 hours. Since the increase in copper recovery after this point is very low, it can be said that reaction duration of 48 hours was enough for copper recovery from copper smelting slag by using deep eutectic solvent.

On the other hand, Fig. 2 represents that iron dissolution from copper smelting slag remains very low and it does not changed with the reaction duration. Consequently, deep eutectic solvent can be used for copper recovery from copper smelting slag without dissolution of iron.

Effect of Solid-to Liquid Ratio

Effect of solid-to-liquid ratio on copper recovery from copper smelting slag with DES reagent was investigated as selected 1/10, 1/20, 1/30 and 1/40 solid-to liquid ratio at 95 ^{o}C reaction temperature, 48 hours reaction duration and 600 rpm stirring speed. Experimental results are shown in Fig 3.

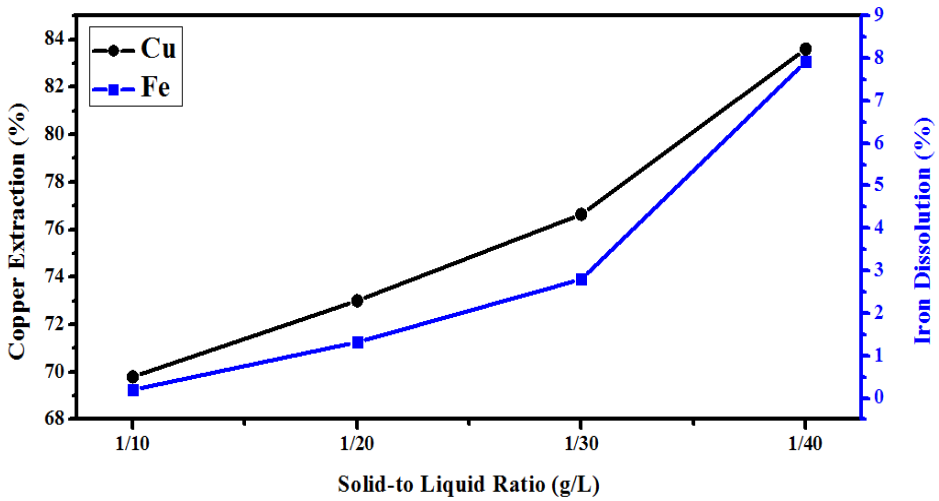

Figure 3. The Effect of Solid-to Liquid Ratio on Copper Recovery.

According to the experimental results, even significant copper recovery was obtained at high solid-to liquid ratio, copper recovery increased gradually with decreasing solid-to liquid ratio in DES solution. As seen in Fig. 3, approximately 70% of copper recovery was obtained at 1/10 of solid-to liquid ratio where 5 grams of smelting slag was added to 50 mL DES. After this point, 13.80% of a rising in copper recovery was observed and the highest copper recovery was obtained as 83.60% at 1/40 of solid-to liquid ratio where 1.25 grams of smelting slag was added to %0 mL DES. As illustrated in Fig. 3, iron dissolution increased with decreasing solid-to liquid ratio and the highest iron dissolution was obtained 7.92% after leaching experiment at 1/40 of solid-to liquid ratio. Considering the economic effect and low iron dissolution, it can be said that 1/20 of solid-to liquid ratio is sufficient for copper recovery from copper smelting slag.

CONCLUSIONS

In this study, use of a deep eutectic solvent formed with choline chloride and urea was investigated for copper recovery from copper smelting slag. According to the characterization studies, copper smelting slag includes huge amount of iron and silica. Apart from these metals, the slag consists of 0.8%Cu and 3.3% Zn. Fayalite including FeO and SiO_2 was detected as the major mineralogical structure of copper smelting slag. Also, little amount of other oxides (Al_2O_3 and CaO) were determined. Before the leaching experiments, deep eutectic solvent was prepared successively. Leaching experiments showed that the higher reaction duration and lower solid-to liquid ratio has great effect on copper recovery. The highest copper recovery was obtained as 83.60% at 95 ^oC, 48 hours and 1/40 solid –to liquid ratio. But considering the economic effect, the leaching condition for copper recovery was proposed as 95 ^oC, 48 hours and 1/20 solid –to liquid ratio.

ACKNOWLEDGEMENT

The authors gratefully acknowledge the Karamanoğlu Mehmetbey University Scientific Research Projects (BAP) Coordinating Office for support with grant number KMU-BAP-17-M-18

REFERENCES

Abbott, A. P., Capper, G., Davies, D. L., Rasheed, R. K., & Tambyrajah, V. (2003). Novel solvent properties of choline chloride/urea mixtures. *Chemical Communications*, (1), 70-71.

Abbott, A. P., Collins, J., Dalrymple, I., Harris, R. C., Mistry, R., Qiu, F., ... & Wise, W. R. (2009). Processing of electric arc furnace dust using deep eutectic solvents. *Australian journal of chemistry*, *62*(4), 341-347.

Ahmed, I. M., Nayl, A. A., & Daoud, J. A. (2016). Leaching and recovery of zinc and copper from brass slag by sulfuric acid. *Journal of saudi chemical society*, *20*, S280-S285.

Arslan, C., & Arslan, F. (2002). Recovery of copper, cobalt, and zinc from copper smelter and converter slags. *Hydrometallurgy*, *67*(1-3), 1-7.

Bakkar, A. (2014). Recycling of electric arc furnace dust through dissolution in deep eutectic ionic liquids and electrowinning. *Journal of hazardous materials*, *280*, 191-199.

Davenport, W. G., King, M. J., Schlesinger, M. E., & Biswas, A. K. (2002). *Extractive metallurgy of copper*. Elsevier.

Dimitrijević, M., Urošević, D., Milić, S., Sokić, M., & Marković, R. (2017). Dissolution of copper from smelting slag by leaching in chloride media. *Journal of Mining and Metallurgy B: Metallurgy*, *53*(3), 407-412.

Gorai, B., & Jana, R. K. (2003). Characteristics and utilisation of copper slag—a review. Resources, Conservation and Recycling, *39*(4), 299-313.

Kılıçel, F., & Karapınar, H. S. (2018). Determination of trace elements contents of some spice samples by using FAAS. *Asian Journal of Chemistry*, 30(7), 1551 – 1558.

Murari, K., Siddique, R., & Jain, K. K. (2015). Use of waste copper slag, a sustainable material. *Journal of Material Cycles and Waste Management*, *17*(1), 13-26.

Ruşen, A., Geveci, A., Topkaya, Y. A., & Derin, B. (2012). Investigation of effect of colemanite addition on copper losses in matte smelting slag. *Canadian Metallurgical Quarterly*, *51*(2), 157-169.

Rusen, A., Derin, B., Geveci, A., & Topkaya, Y. A. (2016). Investigation of Copper Losses to Synthetic Slag at Different Oxygen Partial Pressures in the Presence of Colemanite. *JOM*, *68*(9), 2316-2322.

Rusen, A., Geveci, A., Topkaya, Y. A., & Derin, B. (2016). Effects of some additives on copper losses to matte smelting slag. *JOM*, *68*(9), 2323-2331.

Rusen, A., & Ali Topcu, M. (2017). Investigation of Various Metal Recoveries from Zinc Plant Leach Residue by Choline-Chloride Agent. Current Physical Chemistry, 7(4), 273-280.

Sridhar, R., Toguri, J. M., & Simeonov, S. (1997). Copper losses and thermodynamic considerations in copper smelting. Metallurgical and Materials Transactions B, *28*(2), 191-200.

Yang, Z., Rui-lin, M., Wang-dong, N., & Hui, W. (2010). Selective leaching of base metals from copper smelter slag. *Hydrometallurgy*, *103*(1-4), 25-29.
Zhai, X. J., Li, N. J., Zhang, X., Yan, F. U., & Jiang, L. (2011). Recovery of cobalt from converter slag of Chambishi Copper Smelter using reduction smelting process. *Transactions of Nonferrous Metals Society of China*, *21*(9), 2117-2121.
Zhang, Q., Vigier, K. D. O., Royer, S., & Jerome, F. (2012). Deep eutectic solvents: syntheses, properties and applications. *Chemical Society Reviews*, *41*(21), 7108-7146.

THE EFFECT OF REACTION TIME ON COPPER RECOVERY FROM ANODE SLIME BY USING BMIMBF4 (1-BUTYL-3-METHYLIMIDAZOLIUM TETRAFLUOROBORATE) IONIC LIQUID

Mehmet Ali TOPÇU
Karamanoğlu Mehmetbey University, Department of Metallurgical and Material Engineering, Karaman, Turkey, topcumali@kmu.edu.tr

Aydın RÜŞEN
Karamanoğlu Mehmetbey University, Department of Metallurgical and Material Engineering, Karaman, Turkey, aydinrusen@kmu.edu.tr

Özkan KÜÇÜK
Şeyh Edebali University, Department of Metallurgical and Material Engineering, Bilecik, Turkey, ozkan.kucuk@bilecik.edu.tr

ABSTRACT: In this study, the use of 1-butyl-3-methyl-imidazolium tetraflouroborate ($BmimBF_4$) ionic liquid, a new environmentally sensitive solvent, is investigated for copper recovery from anode slime which have high amount of copper. The anode slime was supplied from a company where secondary sources uses to produce copper, and includes 23% Cu, 17% Pb and 20.5% Sn. The effect of reaction time was investigated in the range of 1 – 48 hours with leaching experiments conducted under conditions of %50 $BmimBF_4$, 50 ^oC temperature and 1/20 g/mL solid/liquid ratio in the presence of $BmimBF_4$. According to the preliminary results, although the copper recovery increased slightly with increasing reaction time, the leaching efficiency was limited to 10%. Studies for the recovery of precious metal from anode slime with BF_4 continue with investigation of the effects parameters such as temperature, ionic liquid concentration, solid/liquid ratio and oxidant addition in order to increasing leaching efficiency.

Key words: Ionic Liquid, $BmimBF_4$, Anode Slime, Leach, Copper Recovery

$BMİMBF_4$ (1-BÜTİL-3-METİL-İMİDAZOLYUM TETRAFLOROBORAT) İYONİK SIVISI KULLANILARAK ANOT ÇAMURUNDAN BAKIRGERİ KAZANIMINDA LİÇ SÜRESİNİN ETKİSİ

ÖZET: Bu çalışmada, yüksek bakır içeriğine sahip anot çamurlarından bakır metalini kazanmak için çevreye duyarlı yeni bir çözücü olan 1-bütil-3-metil-imidazolyum tetrafloroborat ($BmimBF_4$) iyonik sıvısının kullanımı araştırılmaktadır. İkincil atıklardan üretim yapan bir firmadan tedarik edilen ve %23 Cu, %17 Pb, %20,5 Sn temel kimyasal kompozisyonuna sahip anot çamuru başlangıç malzemesi olarak kullanılmıştır. %50 $BmimBF_4$ iyonik sıvı konsantrasyonu, 50^oC sıcaklık ve 1/20 g/mL

katı/sıvı oranı şartları altında yapılan deneylerde $BmimBF_4$ varlığında bakır metalinin geri kazanımında sürenin etkisi 1 – 48 saat aralığında incelenmiştir. Elde edilen ilk sonuçlara göre reaksiyon süresinin artışıyla bakır kazanımı bir miktar artış gösterse de liç verimi %10 ile sınırlı kalmıştır. BmimBF4 ile anot çamurundan değerli metal kazanımına yönelik çalışmalar liç veriminin arttırılması amacıyla sıcaklık, iyonik sıvı konsantrasyonu, katı/sıvı oranı ve oksidant ilavesi gibi parametrelerin etkilerinin araştırılmasıyla devam etmektedir.

Anahtar sözcükler: İyonik Sıvı, $BmimBF_4$, Anot Çamuru, Liç, Bakır Geri Kazanımı

GİRİŞ

Anot çamuru bakır üretim tesislerinde elektroliz aşamasında oluşan bir yan üründür. Bu atık yüksek oranda değerli metaller (Au, Ag, Cu, Se, Te ve platin grubu metaller)içerdiğinden bu atığın geri kazanımı ekonomik olarak önem arz etmektedir. Bu atıklar üzerine yapılan geri kazanım çalışmaları sadece pirometalurjik, sadece hidrometalurjik, veya piro-hidrometalurjik olarak her iki geri kazanım sürecini de içeren şekilde olabilmektedir. Anot çamuru içindeki bakır üretim sürecine bağlı olarak metalik, oksitli, sülfürlü veya selenyum ve tellür ile karmaşık yapılar oluşturmuş halde bulunabilir. Ayrıca, elektroliz aşamasında hücreden uzaklaştırılırken yıkama şekline bağlı olarak %20'ye kadar suda çözünebilen bileşiklere sahip olabilir. Anot çamurunun değerlendirilmesinde ilk işlem olarak içerisinde yüksek oranda bulunan bakır sülfürik asit ile liç edilerek uzaklaştırılmaktadır. Sülfürik asitte çözünebilir formda bakır bileşikleri oluşturmak için anot çamuru genellikle 300 ^oC civarında oksitleyici kavurma işlemine tabii tutulur. Böylece, sülfürik asit ile liç işlemi sonrasında yapıda çözünmeden kalan zenginleştirilmiş değerli metaller daha sonra geri kazanılmak üzere "Dore metal" olarak adlandırılan bir alaşım haline getirilir. Bu genel geri kazanım metodu Dönmez vd. (1988) tarafından Sarkuysan Elektrolitik Bakır Sanayi ve Ticaret A.Ş.'den temin ettikleri anot çamuru için uygulanmıştır. H_2SO_4 çözeltisi kullanarak yapıdaki bakırı %99.67 oranında geri kazanan yazarlar, çözünürlüğe etki eden en önemli parametrelerin kavurma (300 ^oC) ve liç reaksiyonu (70 ^oC) sıcaklığının olduğunu belirtmişlerdir. Bakırın tamamına yakını anot çamurundan alındıktan sonra kalan katının Altın ve Gümüş gibi değerli metallerin kazanımı için uygun olduğunu bildirmişlerdir. Benzer şekilde, Amer (2003) 0,25 M H_2SO_4 çözeltisinde 85 ^oC 'de 90 dk. liç işlemi sonunda yaklaşık %90 oranında bakır kazanılabileceğini bildirmiştir. Kılıç vd. (2013) Sarkuysan Elektrolitik Bakır Sanayi ve Ticaret A.Ş.'den temin ettikleri ağırlıkça %25 oranında bakır ve %4,68 oranında Selenyum içeren anot çamurundan bu iki metali kazanmak içinH_2SO_4 ortamında bakırsızlaştırma ve sonrasında NaOH çözeltisinde Selenyumun çözündürülmesini sağlayan iki kademeli hidrometalurjik prosedür uygulamışlardır. Bu çalışmada, en iyi bakır kazanımını %94 oranında 2M H_2SO_4 çözeltisi içerisinde 2 L/dk oksijen akış hızında 80 ^oC de 120 dk. Boyunca liç ederek elde etmişlerdir.

Yukarıda özetlenen çalışmalara bakıldığında, günümüzde anot çamurundan bakır geri kazanımı için uygulanan hidrometalurjik yöntemlerde çözücü olarak sülfürik asit (H_2SO_4) kullanıldığından çevresel etkiler başta olmak üzere birçok dezavantaja sahiptir. Öte yandan düşük buhar basıncı, elektrokimyasal kararlılık, tutuşmazlık, çözücülük ve termal kararlılık gibi birçok üstün özelliğe sahip "green solvent" olarak adlandırılan iyonik sıvılar araştırmacılar tarafından çeşitli cevher ve atıklardan metal kazanımı üzerine denenmeye başlanmış ve ilgi çekici sonuçlar elde edilmiştir.

İyonik sıvıların ilk defa cevherlerden metal eldesi/kazanımı amacıyla kullanımı McCluscey vd. tarafından 2002 yılında yapılmış ve çözücü olarak 1-butil-3-metilimidazolyum tetraflor borat ([Bmim]BF_4) iyonik sıvısının $Fe(BF_4)_3$ oksidantı varlığında kullanılmıştır. Çalışmada, kalkopirit cevherinden %90'a varan oranlarda bakır kazanımının 100 °C sıcaklıkta 8 saatlik liç sonrasında elde edilebileceği belirtilmiştir.2004 yılında Whitehead vd. (2004) tarafından gerçekleştirilen çalışmada 1-bütil-3-metil-imidazolyum hidrojen sülfat ($bmim^+HSO_4^-$) iyonik sıvısına tiyoüre ve oksidant olarak demir(III) sülfat eklenerek altın (Au) ve gümüş (Ag) kazanımı için seçici liç işlemi uygulanmıştır. Cevherden bakır kazanımı üzerine yapılan ilk çalışma ise yine Whitehead vd. (2007) tarafından 2007 yılında gerçekleştirilmiştir. Çeşitli iyonik sıvıları (1-alkil-3-metil-imidazolyum ve buna benzer türevlerini) sülfidik bakır, altın ve gümüş cevherlerinin liç edilmesi için kullanmışlar ve metallerin ekstrakt (çıkarım) verimliliğini sıcaklık, oksidant ve alkali zincir uzunluğu gibi çeşitli değişkenler için incelemişlerdir. Çözelti içindeki artan iyonik sıvı konsantrasyonu ve sıcaklık ile bakır çıkarım verimliliğinin %87'ye kadar çıkarılabileceğini ortaya koymuşlardır. Dong vd. (2009) tarafından yapılan bir çalışmada $BmimHSO_4$ ve onun sulu çözeltileri ile kalkopirit konsantresi 50-90 ^oC aralığında liç işlemine tabii tutulmuş ve araştırmacılar, çözeltideki iyonik sıvı konsantrasyonunun %10'dan %100'e çıkarılması ile kazanılan bakır oranının %52'den %88'e kadar arttığını gözlemlemişlerdir. Huang vd. (2014) elektrik ve elektronik ekipmanlarında kullanılan ve ağırlıkça yaklaşık %20 bakır içeren baskılı devre kartlarındaki bakırı geri kazanmak için bu artık malzemeleri $bmimHSO_4$ ile liç etmişlerdir. Deneysel verilerin ışığında neredeyse %100'e varan (%99,92) bakır kazanımıyla en uygun liç şartlarını; %80 (v/v) iyonik sıvı, 10 mL %30 H_2O_2, 1:25 (g/L) katı/sıvı oranı, 70 ^oC liç sıcaklığı ve 2 saat liç zamanı olarak belirlemişlerdir. Son yıllarda, Rüşen ve Topçu (2017, 2018) tarafından yapılan çalışmalarda ise %60 $EmimHSO_4$ iyonik sıvı konsantrasyonu, 95^oC sıcaklık, 2 saat süre ve 1/20katı/sıvı oranı (g/mL) şartları altında hiçbir oksidant ilavesi olmaksızın %50'nin üzerinde bakır geri kazanım oranı (Rüşen & Topçu 2017) elde edilmiş, [Bmim]HSO_4 iyonik sıvısı ile %60iyonik sıvı konsantrasyonu, 50 ^oC sıcaklık, 2 saat süre ve 1/25 g/mLkatı/sıvı oranı şartlarında %87,52 bakır geri kazanımı değerine ulaşılmıştır.

İyonik sıvılar ile cevher veya ikincil kaynaklardanbakır geri kazanımı üzerine gerçekleştirilen çalışmalara bakıldığında kısa alkil zincirli metil imidazolyum (1-butil-3met-imidazolyum; bmim+X-) temelli iyonik sıvıların su ile karışılabilirlik (hidrofobiklik) veyaviskozite gibi fiziksel özelliklerinin metal kazanımı açısından daha avantajlı olduğu belirtilmektedir. Bu sebeple, bu çalışmada kısa alkil zincir yapısına sahip olan ve daha önce anot çamuru üzerine herhangi bir uygulaması

bulunmayan $BmimBF_4$ iyonik sıvısı çözücü olarak tercih edilmiştir. Bu çalışmada, $BmimBF_4$ iyonik sıvısının varlığında yüksek bakır içeriğine sahip anot çamurlarından bakır metalinin geri kazanımında sürenin etkisi 1 – 48 saat aralığında incelenmiştir.

YÖNTEM

Bakır üretiminde oluşan atıklar içerisinde elektro-saflaştırma aşamasında ortaya çıkan bakır anot çamuru Altın, Gümüş, Bakır, Selenyum ve Tellür gibi değerli metalleri içerdiğinden yüksek ekonomik değere sahip önemli endüstriyel atıklar arasında yer almakta olup altın, gümüş ve bakır açısından ikincil kaynak olarak görülmektedir. Bu çalışmada kullanılan anot çamuru ikincil atıklardan yola çıkarak bakır tel üretimi yapmakta olan bir işletmeden temin edilmiştir. Daha önceki çalışmalarda (Rüşen & Topçu 2017, 2018) gerçekleştirilen analizlere göre anot çamurunun temel kimyasal kompozisyonu%23 Cu, %17 Pb, %20,5 Sn'den oluşmaktadır. Mineralojik yapı analizine göre ise anot çamurunun ana fazlarını $PbSO_4$, SnO_2 ve CuO bileşikleri oluşturmaktadır. Bu bileşikler dışında $BaSO_4$ ve $SbAsO_4$ bileşiklerine de rastlanmıştır.

Çalışmada kullanılan $BmimBF_4$ (>% 99) Merck firmasından ticari olarak satın alınmış ve hacimsel olarak %50 saf su karıştırılarak deneylerde kullanılmıştır. 5 gram anot çamuru 100 mL çözücüye (%50 BmimBF4 - %50 saf su karışımı) ilave edilip 50 ^oC'de ve 600 rpm hızla karıştırma hızında 1 – 48 saat aralığındaki sürelerde liç işlemine tabii tutulmuştur. Filtrasyon sonrasında filtre keki ve zengin liç çözeltisi birbirinden ayrılmış ve elde edilen çözelti 0.1 M HC1 ile seyreltilmiştir. Zengin liç çözeltisi Perkin ElmerPinAccle 900T model atomik absorpsiyon spektroskopisi (AAS) kullanılarak içerdiği bakır miktarı tayin edilmiştir.

BULGULAR

$BmimBF_4$ iyonik sıvısının varlığında anot çamurlarından bakır metalinin geri kazanımında sürenin etkisi 1, 2, 4, 8, 12, 24, 30, 36 ve 48 saatlik liç deneyleri ile incelenmiştir. Yapılan deneylerde diğer parametreler; %50 $BmimBF_4$ iyonik sıvı konsantrasyonu, 50^oC sıcaklık, 1/20 g/mL katı/sıvı oranı ve 600 rpm karıştırma hızı olarak sabit tutulmuştur. Deneyler sonucunda elde edilen bakır geri kazanım oranları Şekil 1'de verilmiştir.

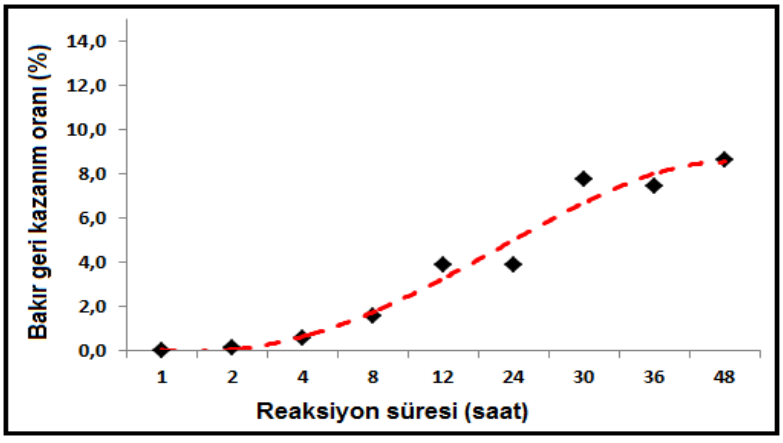

Şekil 1. Reaksiyon süresinin anot çamurundan bakır geri kazanımı üzerine etkisi

Şekil 1'den görüleceği üzere, deneysel çalışmalarda kullanılan %50 BmimBF4 iyonik sıvı konsantrasyonuna sahip çözeltinin anot çamuru içerisinde yaklaşık %23 oranında ve farklı formlarda (metalik, oksit ve kompleks halde) bulunan bakırı beklenen seviyede çözme yeteneğine sahip olmadığı anlaşılmaktadır. Anot çamurlarından bakırın geri kazanımına yönelik önceki çalışmalar (Rüşen & Topçu 2017, 2018) temel alındığında süre dışında liç sistemini etkileyen diğer parametrelerdeki (iyonik sıvı konsantrasyonu, sıcaklık ve katı/sıvı oranı) değişimin liç verimini doğrudan artıracak veya azaltacak yönde önemli etkilere sahip parametreler olduğu bilinmektedir. Özellikle iyonik sıvıların konsantrasyonlarındaki artışlar viskoziteyi arttırmakta iken sıcaklığın artışı çözelti viskozitesini azaltacak yönde etki etmektedir,bununla beraber her iki parametredeki artış bakır çözünürlüğünde bir artışa sebep olarak liç verimini yükseltebilmektedir. Bu sebeple, diğer parametrelerin incelenmesiyle beraber $BmimBF_4$ varlığında bakır geri kazanım oranlarının artacağı öngörülmektedir.

Literatürde $BmimBF_4$'ün atıklardan metal geri kazanımı üzerine herhangi bir çalışmaya rastlanmamış olupcevherlerden metal ekstraksiyonu üzerine yapılmış çalışmalara nadiren rastlanmaktadır. Daha önce bahsedildiği üzere bu konuda literatüre giren ilk çalışma McCluscey vd. tarafından 2002 yılında yapılmış ve çözücü olarak 1-butil-3-metilimidazolyum tetraflor borat ($[Bmim]BF_4$) iyonik sıvısının $Fe(BF_4)_3$ oksidantı varlığında kullanılmasıyla kalkopirit cevherinden %90'a varan oranlarda bakır kazanımının 100 °C sıcaklıkta 8 saatlik liç sonrasında elde edilebileceği belirtilmiştir. Bu sebeple, $BmimBF_4$ iyonik sıvısı ile anot çamuru liçi deneylerinde çözeltiye farklı oksidantlarilave edilerek liç veriminin arttırılması yönünde çalışmalar yapılması önem arz etmektedir. Böylece, bakır geri kazanımında önemli oranlarda artış elde edilebileceği düşünülmektedir.

Bu konudaki bir diğer çalışma 2007 yılında Whitehead vd. tarafından gerçekleştirilmiş olup $BmimBF_4$ iyonik sıvısı sülfidik bakır, altın ve gümüş cevherlerinin liç edilmesi için kullanılmış ve metallerin ekstrakt (çıkarım) verimliliğini sıcaklık, oksidant ve alkali zincir uzunluğu gibi çeşitli değişkenler için incelemişlerdir. İyonik sıvılarda katyon değişkeni dışında bir diğer değişken grubunu da anyonlar oluşturmaktadır. Yapılan bu çalışmada, Cl, BF_4, $N(CN)_2$, HSO_4 ve CH_3SO_3 anyonları Bmim katyonu ile kullanılmış ve metal extraksiyonlarında en iyi kazanımların sülfat (HSO_4) anyonları ile yapılabileceği ifade edilmiştir. BmimBF4 iyonik sıvısının çözme kabiliyetlerinin bakır için sınırlı ancak altın için daha yüksek olduğunu belirtmişlerdir. Literatürde verilen sonuçlara dayanılarak, tarafımızdan yapılan çalışma kapsamında çözeltilerde yaptırılacak altın analizleri sonucunda geri kazanım verimlerinin bakıra oranla çok daha yüksek olması beklenmektedir.

SONUÇ

Bu çalışmada, ikincil atıklardan bakır tel üretimi yapan bir firmadan tedarik edilen %23 Cu içerikli anot çamuru başlangıç malzemesi olarak kullanılarak BmimBF4

çözücüsünün anot çamurundanbakır geri kazanımı üzerinereaksiyon süresinin etkisi 1 – 48 saat aralığında incelenmiştir. %50 iyonik sıvı konsantrasynu, 50oC reaksiyon sıcaklığı, 1/20 katı/sıvı oranı (g/mL) ve 600 rpm karıştırma hızında48 saat liç süresinde yapılan deney sonucunda %10 civarında bakır geri kazanımı elde edilebilmiştir. Bu düşük orandaki bakır kazanımın yükseltilebilmesi ve altın ve gümüş gibi diğer değerli metallerde yüksek geri kazanım oranlarına ulaşılabilmesi için başta oksidant ilavesi olmak üzere liç sistemini etkileyen diğer parametrelerin araştırılmasına devam edilmektedir.

TEŞEKKÜR

Bu çalışma, Türkiye Bilimsel ve Teknolojik Araştırma Kurumu (TÜBİTAK) tarafından Tübitak-116M057 nolu projesi ile desteklenmiştir.

KAYNAKLAR

Amer, A. M. (2003). Processing of copper anodic-slimes for extraction of valuable metals. *Waste Management*, *23*(8), 763-770.

Dong, T., Hua, Y., Zhang, Q., & Zhou, D. (2009). Leaching of chalcopyrite with Brønsted acidic ionic liquid. *Hydrometallurgy*, *99*(1-2), 33-38.

Dönmez, B., Celik, C., Colak, S., & Yartaşi, A. (1998). Dissolution optimization of copper from anode slime in H_2SO_4 solutions. *Industrial & engineering chemistry research*, *37*(8), 3382-3387.

Huang, J., Chen, M., Chen, H., Chen, S., & Sun, Q. (2014). Leaching behavior of copper from waste printed circuit boards with Brønsted acidic ionic liquid. *Waste management*, 34(2), 483-488.

Kilic, Y., Kartal, G., & Timur, S. (2013). An investigation of copper and selenium recovery from copper anode slimes. *International Journal of Mineral Processing*, *124*, 75-82.

Rogers, R. D. (2002). Ionic liquids: industrial applications to green chemistry. In *ACS symposium series*. American Chemical Society.

Rüşen, A., & Topçu, M. A. (2017). Optimization of gold recovery from copper anode slime by acidic ionic liquid. *Korean Journal of Chemical Engineering*, *34*(11), 2958-2965.

Rüşen, A., & Topçu, M. A. (2018). Investigation of an alternative chemical agent to recover valuable metals from anode slime. *Chemical Papers*, *72*(11), 2879-2891.

Whitehead, J. A., Lawrance, G. A., & McCluskey, A. (2004). 'Green'leaching: recyclable and selective leaching of gold-bearing ore in an ionic liquid. *Green Chemistry*, *6*(7), 313-315.

Whitehead, J. A., Zhang, J., Pereira, N., McCluskey, A., & Lawrance, G. A. (2007). Application of 1-alkyl-3-methyl-imidazolium ionic liquids in the oxidative leaching of sulphidic copper, gold and silver ores. *Hydrometallurgy*, *88*(1-4), 109-120.

EFFECT OF TEOS AS CROSS-LINKER ON INTERFACE GFP EXPRESSED IN *E.Coli*/TiO_2 AT BIO-BASED SOLAR CELLS

Numan ECZACIOGLU, Department of Bioengineering, Karamanoğlu Mehmetbey University, Karaman, Turkey, numaneczacioglu@gmail.com

Erdi AKMAN, Nanotechnology R&D Laboratory, Karamanoğlu Mehmetbey University, Karaman, Turkey, erdiakman@kmu.edu.tr

Yakup ULUSU, Department of Bioengineering, Karamanoğlu Mehmetbey University, Karaman, Turkey, yakupulusu@yahoo.com

Savas SÖNMEZOĞLU, Department of Metallurgical and Materials Engineering, Karamanoğlu Mehmetbey University, Karaman, Turkey, svssonmezoglu@kmu.edu.tr

ABSTRACT: The microorganisms coating surface of the photoanodes via using some connection molecules as an interfacial layer modification and optimization plays an important role for the solar cells to obtained efficiency and performance in the biogenic photovoltaic technologies area. In this work, genetically engineered *E.coli* cells which heterologously expressed the green fluorescent protein (GFP) were used as a semiconductor in the presence and absence of tetraethyl orthosilicate (TEOS) which is a linker interface. Bio-based solar cell (BSCs) application was carried out by combining TEOS with bio-sensitizer. The coating on photoanode surface with TEOS linked GFP expressed in *E.coli* cells, showed better performance than cells employing without-TEOS.

Key words: Tetraethyl orthosilicate (TEOS) cross-linker, Green fluorescent protein (GFP), Bio-based solar cell (BSCs)

INTRODUCTION

In recent years, lots of solar cell systems are continue to designed, made and modulate as a photovoltaic device by scientist to solve the energy consumption problem (Akman et al., 2020 and Akin et al., 2018). With increasing interest in carbon-neutral energy production, photovoltaic (PV) technology is gaining more attention as a potentially approach to sustainable energy production (Lewis, 2007). The use of light-sensitive materials (synthetic and natural) has been an important step in the development of photovoltaic materials and bio-based solar cell (BSCs) (Srivastava et al., 2018). Fabrication of dye-sensitive solar cells (DSSCs) using some synthetic molecules such as ruthenium complexes is an important milestone (Thavasi et al., 2009). Because the ruthenium complexes are toxic and expensive, the interest in BSCs developed using natural dye pigments has increased. Although natural dye pigments are low cost and

environmentally friendly, they have disadvantages such as being complex in content, low in stability because of fast biodegradable (Mohammadpour et al., 2015).

Nature contains a series of photoactive proteins that collect solar energy and synchronize their functions to make photosynthesis very efficient. Among these proteins green fluorescent protein (GFP), a natural light activated protein, photon-induced electron ejection by some light-activated proteins, holds high promise for BSCs (Acikgoz et al., 2014). It is easy and inexpensive to clone and express of the GFP in the *E.coli BL21(DE3)plysE* cells. And also, a-helix containing the chromophore is located inside the barrel structure makes GFP very stable under a variety of conditions (Li et al., 1998).
In this present study, we report the TEOS linked GFP expressed in *E.coli BL21(DE3)plysE* cells can be used for particularly effective at harvesting light to built highly efficient bio-solar cells.

METHODS

Preparation of GFP/Cells

Production of the GFP expressed in *E.coli* BL21(DE3)plysE was carried out by following our previously published literature procedure (Acikgoz et al., 2014). Briefly, the plasmid vector carrying GFP gene was transformed into the *E.coli* BL21(DE3)plysE competent cells using heat shock. Then the cells were grown and inducted with IPTG. After GFP containing cells were collected and suspended in Tris HCl buffer, they were used as a layer in solar cell.

Preparation of TEOS solution

The gel solution was prepared by in-situ of TEOS with 0.11 mL tetraethyl orthosilicate, 0.15 mL ammonia in 5 mL ethanol. The solution was then stirred at room temperature for 2 hours.

Solar cells assembly

The preparation of working electrodes, TiO_2 paste and iodure-based redox electrolyte were manufactured in our previous studies (Akin et al., 2018 and Ozturk et al., 2017). After the TiO_2 pastes are prepared these TiO_2 electrodes were immersed in GFP/cells and TEOS/GFP/cells functionalized solution and kept at RT for 12 h. Then ten times spin-coating process (at 3000 rpm for 30 s) was carried out to cover the surface of the GFP/cells/TiO_2 films with pure cells solution. In the next step, GFP/cells and TEOS/GFP/cells covered TiO_2 electrode and Pt-CE were assembled into a sandwich type cell with a drop of I^-/I_3^- redox electrolyte (Akin et al., 2018).
The solar cells layers shown in Figure 1. The difference between A and B is presence and absence of TEOS as a linker molecule on the GFP expressed in *E.coli* BL21(DE3)plysE surface.

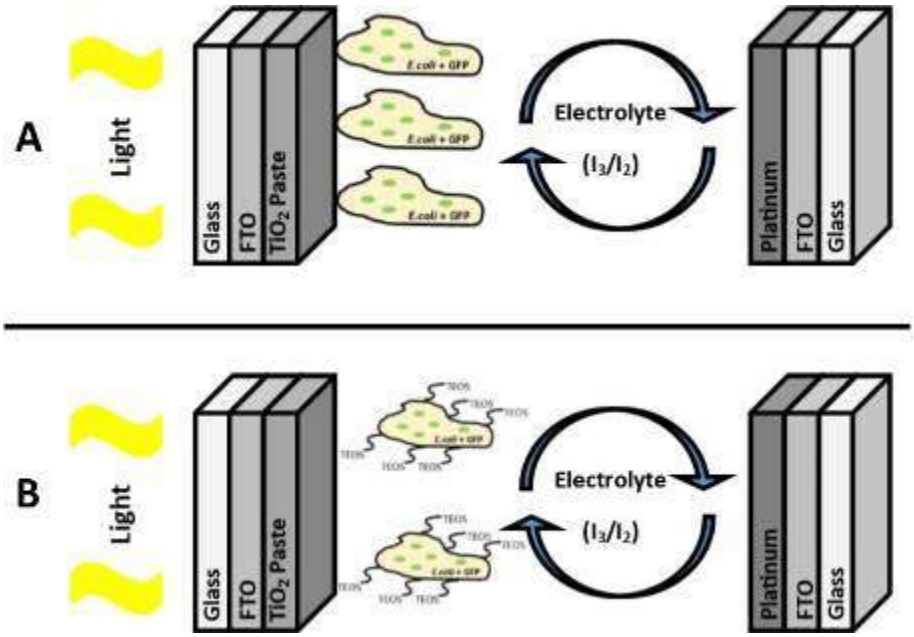

Figure 16. The solar cell layer; A. GFP expressed in *E.coli* BL21(DE3)plysE, B. TEOS linked GFP expressed in E.coli BL21(DE3)plysE

RESULTS AND FINDINGS

Current density−voltage (J−V) curve of the devices are represented in Figure 2, and the resulting photovoltaic parameters are summarized in Table 1. *E.coli*+GFP and TEOS + *E.coli*+GFP devices under optimized fabrication conditions executed a PCE of 0.032 % and 0.074 %, respectively. The efficiency value of the TEOS + *E.coli*+GFP device was about more than twice better than that of the *E.coli*+GFP devices. Further, TEOS + *E.coli* + GFP device all photovoltaic parameters such as Jsc, Voc and FF were better than *E.coli* + GFP devices. These results show that TEOS linker material is suitable for bio-based solar cell applications.

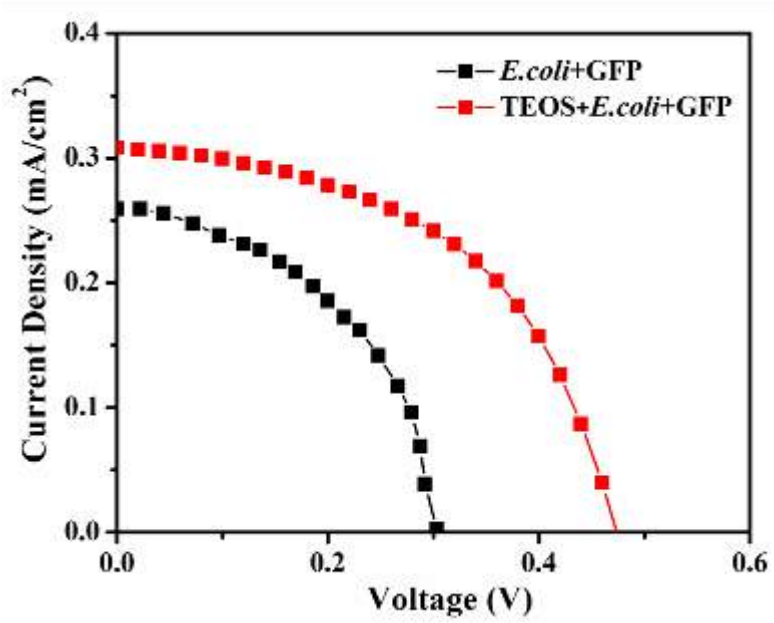

Figure 17. The J-V characteristics of the devices.

Table 1. Photovoltaic parameters of devices

Samples	Voc (V)	Jsc (mA/cm2)	FF	n (%)
E.coli+GFP	0.30	0.258	0.42	0.032
TEOS +*E.coli*+GFP	0.47	0.306	0.51	0.074

CONCLUSION

In conclusion, our results showed that surface treatment of TiO_2 nanoparticle with TEOS could enhance the significant gains in efficiency in the TiO_2/GFP expressed in *E.coli* BL21(DE3)plysE interface. This result shows that TEOS has the potential to be considered as an efficient linkage molecule on the interface between GFP expressed in *E.coli* BL21(DE3)plysE and TiO_2.

REFERENCES

Acikgoz, S., Ulusu, Y., Akin, S., Sonmezoglu, S., Gokce, I., & Inci, M. N. (2014). Photoinduced electron transfer mechanism between green fluorescent protein molecules and metal oxide nanoparticles. *Ceramics International*, 40(2), 2943-2951.

Akin, S., Ulusu, Y., Waller, H., Lakey, J. H., & Sonmezoglu, S. (2017). Insight into Interface Engineering at TiO2/Dye through Molecularly Functionalized Caf1 Biopolymer. *ACS Sustainable Chemistry & Engineering*, 6(2), 1825-1836.

Akman, E., Altintas, Y., Gulen, M., Yilmaz, M., Mutlugun, E., & Sonmezoglu, S. (2020). Improving performance and stability in quantum dot-sensitized solar cell through single layer graphene/Cu_2S nanocomposite counter electrode. *Renewable Energy*, 145, 2192-2200.

Lewis, N. S. (2007). Toward cost-effective solar energy use. *Science,* 315(5813), 798-801.
Li, X., Zhao, X., Fang, Y., Jiang, X., Duong, T., Fan, C., ... & Kain, S. R. (1998). Generation of destabilized green fluorescent protein as a transcription reporter. *Journal of Biological Chemistry*, 273(52), 34970-34975.
Mohammadpour, R., & Janfaza, S. (2015). Efficient nanostructured biophotovoltaic cell based on bacteriorhodopsin as biophotosensitizer. *ACS Sustain Chem Eng* 3: 809–813.
Ozturk, T., Gulveren, B., Gulen, M., Akman, E., & Sonmezoglu, S. (2017). An insight into titania nanopowders modifying with manganese ions: A promising route for highly efficient and stable photoelectrochemical solar cells. *Solar Energy*, 157, 47-57.
Srivastava, S. K., Piwek, P., Ayakar, S. R., Bonakdarpour, A., Wilkinson, D. P., & Yadav, V. G. (2018). A biogenic photovoltaic material. *Small*, 14(26), 1800729.
Thavasi, V., Lazarova, T., Filipek, S., Kolinski, M., Querol, E., Kumar, A., ... & Renugopalakrishnan, V. (2009). Study on the feasibility of bacteriorhodopsin as bio-photosensitizer in excitonic solar cell: a first report. *Journal of nanoscience and nanotechnology*, 9(3), 1679-1687.

PRODUCTION OF GLASS FIBER REINFORCED PHOTOVOLTAIC COMPOSITE PANEL AND INVESTIGATION OF ITS ELECTRICAL PROPERTIES

Serkan ERDEM
Firat University, Engineering Faculty, Department of Mechanical Engineering
serdem@firat.edu.tr

Ahmet YILDIZ
Firat University, Engineering Faculty, Department of Mechatronic Engineering
ayildiz@firat.edu.tr

Mete Onur KAMAN
Firat University, Engineering Faculty, Department of Mechanical Engineering
mkaman@firat.edu.tr

Mustafa GÜR
Firat University, Engineering Faculty, Department of Mechanical Engineering
mgur@firat.edu.tr

ABSTRACT: In this study, flexible photovoltaic panel design was made by encapsulating photovoltaic modules using resin doped composite material and electrical properties were investigated. With this method, the photovoltaic modules are connected to each other by suitable interconnection technologies and taken into the fiber reinforced composite material. Thus, instead of standard photovoltaic panel design; The design of photovoltaic panels suitable for the surfaces can be changed according to the location. With this study, instead of multi-layer different encapsulation of photovoltaic panels available in the market, composite coating was realized as a single block. After the encapsulation with laminated composite material, a certain degree of bending of the panel was achieved without damaging the photovoltaic modules due to the flexible properties of the coating obtained. In addition, the current, voltage, power and efficiency values of the flat and concave composite photovoltaic panel were designed and manufactured. The results showed that the resin doped composite material is suitable for encapsulation process, has superior performance in terms of module reliability and meets the requirements for electrical production.

Key words: Photovoltaic panel, encapsulant, glass fiber, composite, electrical efficiency

CAM FİBER TAKVİYELİ FOTOVOLTAİK KOMPOZİT PANEL ÜRETİMİ VE ELEKTRİKSEL ÖZELLİKLERİNİN İNCELENMESİ

ÖZET: Bu çalışmada reçine katkılı kompozit malzeme kullanılarak fotovoltaik modüllere kapsülleme yapılarak esnek fotovoltaik panel imalatı yapılmış ve elektriksel özellikleri incelenmiştir. Bu yöntemle fotovoltaik modüller uygun ara bağlantı teknolojileri ile birbirine bağlanarak reçine katkılı kompozit malzeme içerisine alınmıştır. Böylece standart fotovoltaik panel tasarımı yerine; montaj yerine göre değişebilen yüzeylere uygun fotovoltaik panellerin tasarımı gerçekleştirilmiştir. Yapılan bu çalışma ile piyasada mevcut olan fotovoltaik panellerde çok katmanlı farklı kapsülleme yerine tek blok halinde kompozit kaplama gerçekleştirilmiştir. Reçine katkılı kompozit malzeme ile kapsülleme yapıldıktan sonra elde edilen kaplamanın esnek özelliği nedeniyle fotovoltaik modüllere zarar verilmeden belli bir oranda panelin eğilmesi sağlanmıştır. Ayrıca, tasarımı ve imalatı gerçekleştirilen kapsüllenmiş kompozit düzlem levhaya konkav özelliği kazandırılmış fotovoltaik panelin elektriksel olarak akım, gerilim, güç ve verim değerleri belirlenmiştir. Elde edilen sonuçlar reçine katkılı kompozit malzemenin kapsülleme işlemi için uygun olduğu, modül güvenilirliği açısından üstün performanslara sahip olduğunu ve elektriksel üretim açısından gerekli şartları sağladığını göstermiştir.

Anahtar sözcükler: Fotovoltaik panel, kapsülleme, cam fiber, kompozit, elektrikel verimlilik

GİRİŞ

Günümüzde ülkeler gerekli olan enerjilerini birincil enerji kaynağı olan kömür, gaz ve petrol şeklindeki fosil yakıtlar yoluyla sağlanmaktadır. Fosil yakıt kaynakları hızlı bir şekilde azalmakta, çevreye zarar vermekte ve küresel iklim değişikliğine neden olmaktadır. Bu nedenle yenilenebilir olmayan kaynaklardan sürdürülebilir yenilenebilir enerji kaynaklarına geçiş bir zorunluluk olarak karşımıza çıkmaktadır (Yıldız vd., 2019). Yenilenebilir enerji kaynakları güneş, rüzgar, biyokütle, jeotermal, deniz, hidroelektrik gibi enerjileri içeresine almakta olup, bunlar içerisinde güneş enerjisinin her yerde bulunması nedeniyle güneş enerjisi sistemleri önem kazanmaktadır. Bu bağlamda özellikle yenilenebilir enerji sistemlerinden güneş enerjisi ile elektrik üreten fotovoltaik pil sistemleri son yıllarda hızlı bir büyüme göstermiştir.

Fotovoltaik piller güneş enerjisini doğrudan elektrik enerjisine dönüştüren sistemler olarak kullanılmaktadır (Yıldız and Dandıl, 2019). Fotovoltaik sistemlerin verimli ve uzun ömürlü olarak kullanımı önemli olup bu yönde yapılan çalışmalar son yıllarda artmıştır. Fotovoltaik modül yapımında uygun malzemelerin seçiminin verime etkisi ile ilgili çalışmalar yapılarak kullanılan malzemelerin verim üzerine etkisi araştırılmıştır. Bu doğrultuda fotovoltaik modül üzerine yapılan araştırmalardan bir bölümü de fotovoltaik modülünün performansına etki eden kapsülleme malzemesine odaklanmıştır. Fotovoltaik panellerin yapısal performansı, fotovoltaik hücrelerinin ve modüllerin dış çevrenin etkisinden izole eden koruyucu kaplama ile

sağlanabilmektedir (Mickiewicz vd., 2011). Kaplamalardaki tasarım problemleri fotovoltaik panellerin ömürlerinin azalmasına neden olmaktadır. Bu nedenle fotovoltaik modüllerin kapsüllenmesi için farklı polimerler üzerinde araştırmalar yapılmıştır (Wohlgemuth and Cunningham, 2008, Chaturvedi vd., 2013). Fotovotovoltaik modüller, bir ön camdan arka tabakaya doğru bir düzene göre tasarlanmaktadır. Buna göre bir modül; ön cam, kapsülleme ve arka kapaktan oluşmaktadır (Şekil 1). Modül etrafına genellikle alüminyum bir çerçeve uygulanır.

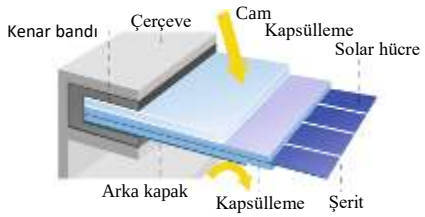

Şekil 1. Fotovoltaik Modül Tasarım Düzeni (Kopecek and Libal, 2018)

Fotovoltaik panellerin gerçek çalışma koşullarında çalışması durumunda verim düşüşü ve panelin bozulmasına etki eden parametreler üzerine birçok çalışmalar yapılmıştır (Ndiaye vd., 2013, Ottersböcket vd., 2017). Panelin çalışması sırasındaki bozulmasına etki eden parametrelerden biri panelin arka yüzey kaplaması ile ilişkilidir. Arka tabaka ve kapsülleme hatası nedeniyle modüle nem nüfuz eder. Dış ortam koşullarında kapsüllemenin zarar görmesi önemli ölçüde güç kaybına neden olabilmektedir (Kempe vd., 2007). Fotovoltaik panellerde kullanılan malzemeye ve fotovoltaik sistemin çalışma şartlarına bağlı olarak kısa süre ve uzun süre içinde bozunmalar meydana gelmektedir.

Son yıllarda fotovoltaik panellerdeki bozulmalar üzerine yapılan çalışmalarda fotovoltaik panelin uzun süre kullanılabilirliği ve maliyetler dikkate alınarak problem tespit edilmekte ve çözüm önerileri getirilmektedir. Fotovoltaik panellerde kullanılan kapsülleyici malzemenin renk bozulması üzerine de çalışmalar yapılmıştır (Munoz vd., 2011). Ayrıca arka tabakada oluşan boşluklar, kaplamadaki kusurlar, çatlaklar, modül lehim bağlantı ve eklem hataları da çalışılan diğer konular arasındadır (Dhere and Raravikar, 2001, Han vd., 2012). Araştırmalar fotovoltaik panellerdeki bozulmaların sıcak ve nemli iklim ile ilişkili olduğunu, ayrıca bu parametrelerin verim üzerinde de önemli etkilerinin olduğunu ortaya koymuştur (Gxasheka vd., 2005). Kempe (2006), fotovoltaik panellerin alt yüzeylerinde tabaka ile güneş pili arasındaki ara yüzeyde küçük su damlacıklarının oluşabileceğini, bu durumun ise korozyona neden olabileceğini ve hatta fotovoltaik panelin verimini ve ömrünü etkileyebileceğini ortaya koymuştur. Benzer şekilde arka yüzey kaplama kusurlarının fotovoltaik panelin ömür verimini etkilediğine yönelik çalışmalarda kaplamanın önemi vurgulanmıştır (Czanderna and Pern, 1996, Van Dyk vd., 2005).

Bu çalışmada, dış ortam koşullarına uygun fotovoltaik modüllerden oluşan panellerin güvenli ve verimli bir şekilde kullanımını sağlayacak şekilde fotovoltaik modüllerden oluşan panellere reçine esaslı kompozit malzeme ile kapsülleme yapılmıştır. Yapılan tasarım sonucunda elde edilen esnek düzgün yüzeyli ve konkav fotovoltaik panellerin

dış ortam şartlarına bağlı olarak akım, gerilim, güç ve verim olarak elektriksel özelliği araştırılmıştır.

YÖNTEM

Fotovoltaik modüllerin mekanik stabilitesini sağlamak ve panelin dış etkilere karşı korumasını sağlamak için modüllerin yüzeyleri uygun bir malzeme ile kaplanmaktadır. Bu çalışmada da 16 modülden oluşan fotovoltaik panelde modüllerin seri şekilde elektriksel bağlanışı yapılmış ve fotovoltaik modüller reçine esaslı kompozit malzeme ile kapsüllenmiştir. Reçine esaslı kompozit malzeme teknolojisi savunma, otomotiv ve havacılık sektörlerinde son yıllarda artan bir oranla kullanılmaktadır (Marsh, 2003). Reçine esaslı matris malzemesi ile çapraz dokuma fiber kumaşlarının birleştirilmesi sonucu kaplamaya ısıl, mekanik ve elektriksel özellikler açısından büyük bir fayda sağlanır. Bu özellikleri nedeniyle fotovoltaik paneller için bu kapsülleyiciler, uzun ömürlü bir kaplama malzemesi olarak fotovoltaik teknolojisinde alternatif bir kaplama malzemesi olabilecektir. Elde edilen reçine esaslı kapsülleyiciler elastik bir özelliğe sahiptir. Benzer hacimli izotropik malzemelere göre hem daha hafif hem de daha mukavemetlidirler. İnce kesitleri nedeniyle eğilme yükü altında sehim davranışı sergilerler. Böylece esnek olmalarından dolayı montaj edilecek yere göre daha rahat uyum sağlayabilirler.

Fotovoltaik Kompozit Panel Üretimi

Üretim vakum infüzyon yöntemiyle sıcaklık kontrollü kompozit üretim tezgâhında gerçekleştirilmiştir (Şekil 2).

Şekil 2. Sıcaklık Kontrollü Kompozit Üretim Tezgahı

Öncelikle tezgah üzerine, fotovoltaik kompozit panelin üretim sonrasında tezgah üzerinden rahatça ayrılabilmesini sağlayan ayırıcı film (release film) serilir (Şekil 3). Ayırıcı film ile tezgâha çift taraflı bant ile yapıştırılır. Ayırıcı film üzerine, birbirleriyle bağlantıları yapılmış olan hücreler güneşe bakacak olan yüzleri üretim tezgahına bakacak şekilde yerleştirilir. Güneş hücrelerinin üzerine dört tabaka 200 gr/m^2 cam kumaşlar serilir (Şekil 4). Matris malzemesi olarak epoksi reçine kullanılmıştır.

Şekil 3. Ayırıcı Film Üzerine Güneş Hücrelerinin Serilmesi

Şekil 4. Güneş Hücrelerinin Üzerine Cam Fiberlerin Serilmesi

Fotovoltaik kompozit panel üretildikten sonra panelin sarf malzemelerinden ayrılmasını sağlayacak olan soyma kumaşı (peel ply) kumaşların üzerine yerleştirilir. Daha sonra ise soyma kumaşı üzerine reçinenin rahatlıkla akmasını sağlayan infüzyon filesi (mesh) koyulur (Şekil 5).

Şekil 5. Güneş Hücrelerinin Üzerine Cam Fiberlerin Serilmesi

Son olarak Şekil 6.a'da görüldüğü gibi çift taralı bant ile temas edecek şekilde vakum naylonu serilir ve sonunda vakum torbasına pompa yardımıyla reçine emdirilir (Şekil 6.b). Reçinenin donması için 24 saat beklenip soyma kumaşı ve ayırma filmi çıkarılarak fotovoltaik kompozit panel üretilmiş olur.

a) **b)**

Şekil 6. Sisteme a)Vakum Naylonunun Yerleştirilmesi, b) Reçine Verilmesi

Fotovoltaik paneli oluşturan 16 adet polikristal 156 mm boyutlarında modüller kalaylı bakır şeritler ile yüksek sıcaklıkta lehimleme işlemi kullanılarak elektriksel olarak bağlanmıştır. Modüllerin birbirine bağlanması sırasında akım kaybını azaltacak şekilde modülleri panellere dönüştürürken enerji aktarım kaybını en aza indirecek şekilde mevcut çalışmalar da dikkate alınarak bağlantı gerçekleştirilmiştir (Söderström vd., 2013). Böylece uygun birleştirme yöntemiyle modüllerden oluşturulan panel cam fiber epoksi kompozit malzeme içerisine yerleştirilerek dış etkilere dayanıklı bir yapı oluşturulmuş ve yüzeye göre esneklik özelliği kazandırılmıştır (Şekil 7).

Şekil 7. Reçine Esaslı Kompozit Malzeme ile Kapsüllenmiş Fotovoltaik Panel

Uygulanan bu yöntem ile reçine esaslı kompozitin malzemenin kullanılması ile farklı sayıdaki modüllerden oluşturulan panele mekanik dayanım kazandırılmıştır. Böylece modüllerin tüm yüzeylerinin uygun bir şekilde kapsüllenmesi nedeniyle fotovoltaik

panelin etkisi altında rüzgar, kar, yağmur, nem gibi dış yük kuvvetlerinden korumuş olunacak ve fotovoltaik panelin ömürleri uzayacaktır. Ayrıca, geliştirilen bu kapsülleme yöntemiyle çok sayıdaki modüllerden oluşan panellerin alüminyum bir çerçeveyle ve cam yüzey ile kaplanmasına gerek olmayacaktır. İlave olarak gemi, uçak, otomobil vb. araçların çeşitli eğik yüzeylerine uygun bir şekilde modüller kompozit ile kapsüllenerek, üretilen panellerin esnek ve kolay bir şekilde bu tip yüzeylere montajı sağlanabilecektir. Böylece ağırlık, montaj sistemi ve maliyetteki azalmalar ile mevcut çerçeveli kullanımlara göre daha rekabetçi bir çözüm oluşturulmuştur.

Tablo 1. Fotovoltaik Modülün Teknik Özellikleri

Standart ışıma	1000 W/m^2
Standart sıcaklık	25 °C
Maksimum güç (P_{max})	4.5 W
Maksimum güç akımı (I_{mp})	8.8 A
Maksimum güç gerilimi (V_{mp})	0.54 V
Serilerdeki modül sayısı	16

Şekil 8. Eğrisel Yüzeye Sahip (Konkav) Fotovoltaik Panel

Panelin oluşturulmasında kullanılan modüllerin teknik özellikleri Tablo 1 de verilmiştir. Reçine esaslı kompozit malzeme ile kapsüllenen fotovoltaik panel için güneş ışınımına bağlı olarak akım, gerilim, güç ve verim değerleri incelenmiştir. Bu amaçla panelin akım ve gerilim özelliklerini belirlenmek için Elazığ iklim şartlarında dış atmosferik koşullarda deneysel çalışmalar yapılmıştır.

Panel üzerindeki deneyler 2019 Eylül ayı içerisinde gerçekleştirilmiştir. Panel Elazığ enlem açısı 38^o'ye ayarlanmıştır. Esnek özelliğinden yararlanılarak panel, düzlem ve eğrisel yüzey (konkav) formatında kullanılmıştır (Şekil 8). Deneylerde güneş ışınım, dış hava sıcaklıkları, akım ve gerilim değerleri ölçülmüştür. Her iki panel için aynı ışınım şiddeti dikkate alınarak ölçümler yapılmıştır. Fotovoltaik panelde yapılan deneylerde güneş ışınımı piranometre ve sıcaklık değerleri dijital termometre ile

ölçülmüştür. Ayrıca fotovoltaik panelin akım-gerilim değerlerini tespit etmek için multimetre kullanılmıştır (Şekil 8). Fotovoltaik panelin üretebileceği maksimum güç;

$$P_{max} = I_{max}.V_{max} \quad (1)$$

şeklinde ifade edilir (Yıldız and Dandıl, 2019). Burada I_{max} akım, V_{max} ise maksimum güç için gerekli gerilimi ifade eder. Fotovoltaik panelin verimi ise aşağıdaki eşitlik ile tespit edilebilir.

$$n_c = (I_{max}.V_{max})/ (G.A_c) \quad (2)$$

G ölçülen güneş ışınım şiddeti (W/m²) ve A_C güneş modüllerinin alanıdır (m²).

BULGULAR

16 adet modülden oluşan fotovoltaik panelin reçine esaslı kompozit malzeme ile kaplanmasından sonra elde edilen esnek düz yüzeyli ve konkav yüzeyli paneldeki akım ve gerilim değerleri belirlenmiştir. Yapılan çalışmalardan 25 Eylül 2019 tarihinde ölçülen ışınım ve sıcaklık değerleri Şekil 9′ da verilmiştir. Şekilde çevre sıcaklılarının ve ışınımın öğlen saatlerinde maksimum değer aldığı görülmektedir.

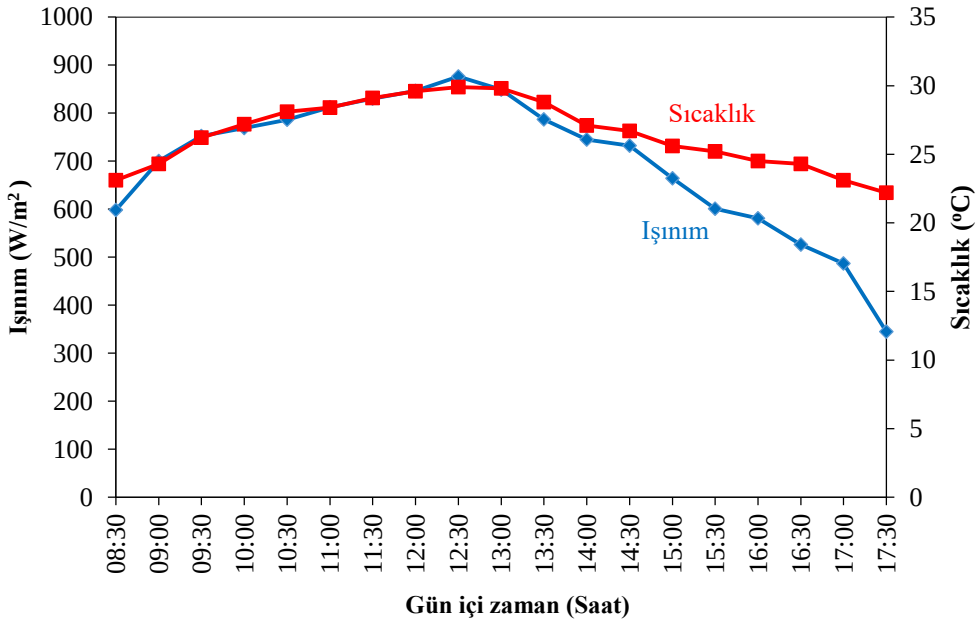

Şekil 9. Dış Atmosfer Şartlarında Ölçülen Sıcaklık ve Işınım Değerleri

Aynı ışınım şartları altında düzlem ve konkav yüzeyli fotovoltaik panelin akım ve gerilim değerleri ölçülmüştür. Her iki yüzey için elde edilen değerlerden düz yüzeyli fotovoltaik panele göre konkav yüzey için yüzde mertebesinde daha fazla artış elde edilmiştir. Bu nedenle grafikte sadece konkav yüzey için ölçülen sonuçlar verilmiştir.

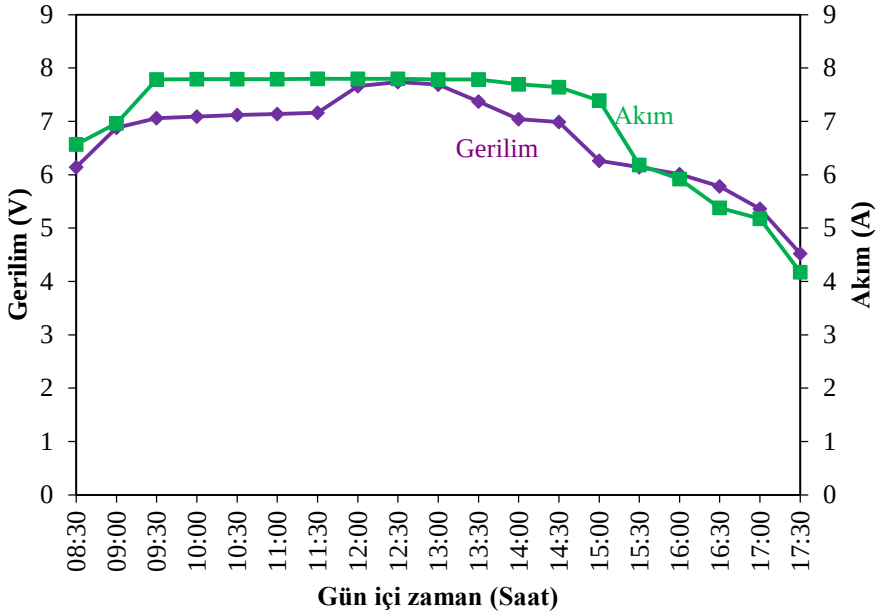

Şekil 10. Deneyler Sırasında Ölçülen Akım Gerilim Değerleri

Buna göre akım ve gerilimin güneş radyasyonu ile ilişkili olduğu görülmektedir. Akım ve gerilim değerleri çok değişmemekle birlikte maksimum gerilimin en yüksek güneş radyasyonunda elde edildiği görülmektedir. Ayrıca, yüksek ışınım değerleri için, üretilen akımın daha yüksek olduğu söylenebilir. Reçineli kompozit ile kapsüllenmiş fotovoltaik panel için hesaplanan güç değerlerinin günün saatlerine göre değişimi ise Şekil 11'de verilmiştir. Günün saatlerine göre gücün değiştiği, dolayısıyla güneş radyasyonununartışına bağlı bağlı olarak fotovoltaik panel gücünün arttığı görülmüştür. Dolayısıyla radyasondaki artışın, fotovoltaik panelden elde edilen güç üzerinde olumlu bir etkiye sahip olduğu ifade edilebilir.

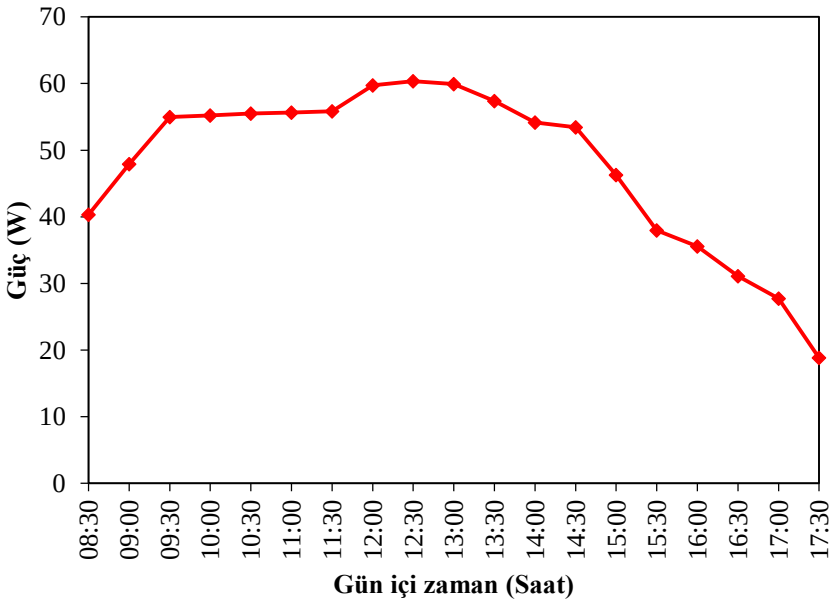

Şekil 11. Fotovoltaik Panelden Elde Edilen Güç

Şekil 12' de fotovoltaik panelin günün saatlerine ve dolayısıyla güneş ışınımına bağlı olarak verim değişimini gösterilmiştir. Buna göre fotovoltaik panelin veriminin yüksek güneş ışınımında arttığı ve düşük radyasonda düştüğü görülmektedir.

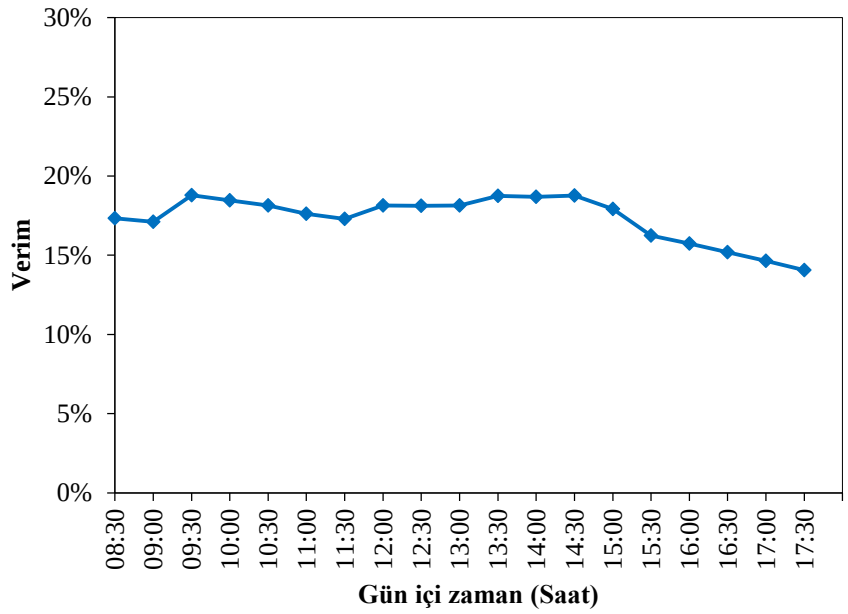

Şekil 12. Fotovoltaik Panel Verimi

SONUÇ

Bu çalışmada, fotovoltaik modüller reçine esaslı kompozit malzeme ile kapsüllenmiş ve fotovoltaik panellerin oluşturulması için yeni bir yaklaşım getirilmiştir. Böylece geleneksel olarak oluşturulan tasarıma göre modülün kapsüllenmesi ile modülün alt ve üst bölgelerindeki tabakalar kullanılmamakta ve daha az malzeme ve işçilik ile gerekli tasarım sağlanmaktadır. Bu kapsülleme yöntemiyle üst bölgede cam kullanılmamakta ve alüminyum çerçeveye ihtiyaç duyulmamaktadır.

Kapsülleme bir bütünlük içinde bir blok halinde yapıldığı için panel içerisine yağmur ve nem gibi problem oluşturacak etkenlerden de korunmuş olacaktır. Böylece tasarım ile fotovoltaik sistemlerin uzun ömürlü verimli ve ekonomik olarak çalışması sağlanacaktır. Ayrıca, bu yöntem ile panelin kullanacağı yüzeye göre modüller kapsülleneceği için eğri yüzeyler dahil olmak üzere her yüzeye uygun olarak kapsülleme yapılabilecektir. Ayrıca, kompozit malzemenin elastikiyeti nedeniyle panel levhası esnek yapıda olacak ve montaj yüzeyine uygun olarak belli bir oranda levhanın eğilmesine imkan olabilecektir.

Ayrıca yapılan çalışmada, reçine esaslı kompozit malzeme ile kapsüllenmiş modüllerden düzgün yüzeyli ve konkav yüzeyli fotovoltaik panel oluşturulduktan sonra akım, gerilim, güç ve verim değerleri incelenmiştir. Günün saatlerine dolayısıyla güneş radyasununa bağlı olarak fotovoltaik panelden elde edilen elektriksel özelliklerde değişimler olmuştur. Güneş radyasyonundaki artış ile fotovoltaik panelde elde edilen güçte ve verimde artış olduğu görülmüştür. Konkav yüzeyli panelde elde edilen elektriksel özelliklerin düzgün yüzeyli panele göre çok az bir iyileşme olmakla birlikte bu değerlerin genel olarak birebirine yakın olduğu gözlenmiştir.

Böylece fotovoltaik modüllerin çalışmada belirtildiği reçine esaslı bir kompozit malzeme ile kapsüllenmesi ile oluşturulan panellerin mevcut panellere göre daha kullanışlı, ekonomik, esnek yapılı ve sağlam yapılı olarak elektrik enerjisi üretiminde kullanılması mümkün olabilecektir.

TEŞEKKÜR

Yazarlar solar hücrelerin temini ve birleştirmeleri konusunda yardımlarından dolayı Emre BAY, Ali Ekber AKYOL ve Mehmet EMLEK'e teşekkür eder.

KAYNAKLAR

Chaturvedi, P., Hoex B., & Walsh, T.M. (2013). Broken metal fingers in silicon wafer solar cells and PV modules. *Solar Energy Materials & Solar Cells*, 108, 78-81.

Czanderna, A.W., & Pern, F.J. (1996). Encapsulation of PV modules using ethylene vinyl acetate copolymer as a pottant: A critical review. *Solar Energy Materials and Solar Cells*, 43(2), 101-181.

Dhere, N.G., & Raravikar, N.R. (2001). Adhesional shear strength and surface analysis of a PV module deployed in harsh coastal climate. *Solar Energy Materials and Solar Cells*, 67(1-4), 363-367.

Gxasheka, A.R., Van Dyk, E.E., & Meyer, E.L. (2005). Evaluation of performance parameters of PV modules deployed outdoors. *Renewable Energy*, 30(4), 611-620.

Han, X., Wang, Y., Zhu, L., Xiang, H., & Zhang, H. (2012). Mechanism study of the electrical performance change of silicon concentrator solar cells immersed in de-ionized water. *Energy Conversion and Management*, 53(1), 1-10

Kempe, M. D. (2006). Modeling of rates of moisture ingress into photovoltaic modules. *Solar Energy Materials and Solar Cells*, 90(16), 2720-2738.

Kempe, M.D., Jorgensen, G.J., Terwilliger, G.J., McMahon, T.J., Kennedy, C.E., & Borek, T.T. (2007). Acetic acid production and glass transition concerns with ethylene-vinyl acetate used in photovoltaic devices. *Solar Energy Materials & Solar Cells*, 91, 315–329

Kopecek, R. & Libal, J. (2018). Towards large-scale deployment of bifacial photovoltaics. *Nature Energy*, l3, 443-446.

Marsh, G., (2003). Next step for automotive materials, *Materials Today*, 6(4), 36-43.

Munoz, M.A., Alonso-García, M.C., Vela, N., & Chenlo, F. (2011). Early degradation of silicon PV modules and guaranty conditions. *Solar Energy*, 85(9), 2264-2274.
Mickiewicz, R., Doble, B., Li, D., Christian, T., Lloyd, J., Stoke,s A., Voelker, C., Winte,r M., Ketola, B., Norris, A., & Shephard, N. (2011). Effect of encapsulation modulus on the response of PV modules to mechanical stress. *Procedings of 26th European Photovoltaic Solar Energy Conference and Exhibition*. Hamburg.
Ndiaye, A., Charki, A., Kobi, A., Kébé, C.M.F., Ndiaye, P.A., & Sambou, V. (2013). Degradations of silicon photovoltaic modules: A literature review. *Solar Energy*, 96, 140-151.
Ottersböck, B., Oreski, G., & Pinter, G. (2017). Comparison of different microclimate effects on the aging behavior of encapsulation materials used in photovoltaic modules. *Polymer Degradation and Stability*, 138, 182-191.
Söderström, T., Papet, P., & Ufheil, J. (2013). Smart wire connection technology. *In the 28th European Photovoltaic Solar Energy Conference*.
Wohlgemuth, J. & Cunningham, D. (2008). Using accelerated tests and field data to predict module reliability and life time, *Proceedings of 23rd European Photovoltaic Solar Energy Conference and Exhibition*.Valencia.
Van Dyk, E. E., Chamel, J. B., & Gxasheka, A. R. (2005). Investigation of delamination in an edge-defined film-fed growth photovoltaic module. *Solar Energy Materials and Solar Cells*, 88(4), 403-411.
Yıldız, A., Dandıl, B., Çakmak, G. (2019). The effect on the efficiency of the photovoltaic panel used for the charging of mobile phones of the solar radiation in Elazig, Turkey. *International Journal of Renewable Energy and Technology*, 10(4), 301-314.
Yıldız, A. & Dandıl, B. (2019). Investigation of the effect of panel temperature on effıciency of organic photovoltaic panel, OEMT'2019:*4th International Organic Electronic Material Technology Conference*, Dubai.

ELEMENT ENRICHMENTS OF KARABOĞAZ FORMATION (ADIYAMAN) ORGANIC-RICH ROCKS

Veysi KOÇ
Batman University, Graduate School of Natural and Applied Sciences, Geological Engineering
veysikoc5@gmail.com

Derya KOCA
Batman University, Faculty of Engineering-Architecture, Petroleum and Natural Gas Engineering
derya.koca@batman.edu.tr

ABSTRACT: Organic-rich rocks that are deposited in anoxic environment accumulate some of the minerals and elements that are of economic importance. In this study, the distributions and enrichments of organic matter, major and trace elements of organic-rich rocks Adıyaman region were investigated. 13 rock samples were collected from Karaboğaz Formation and pyrolysis analysis, ICP analysis and XRD analysis were performed on these rock samples. As a result of pyrolysis analysis, samples have a carbonated lithology and are ranging from 0,76 to 7,09 % C_{org}, with a 2,72 % average. As a result of ICP analyzes, organic-rich limestone samples of Karabogaz Formation are enriched with Si, Ca, Na, P, Cr, Ni, Sc, Ba, Co, Rb, Sr, U, V, W, Mo, Cu, Pb, Zn, As, Cd, Sb, Hg and Se elements. Element enrichments of samples studied are compared with the element enrichments of Namibia (Africa) Coastal Shelf Sediments, Peruvian Shelf Sediments, Mediterranean and Black Sea Sapropels, Cenomanian/Turonian Gubbio Anoxic Sediments and Cenomanian/Turonian Demerara Anoxic Sediment. And consequently, Cr, P, Fe, Co, Sb, Zn, V, Cu, Ba, Pb and Zr were more enriched than other depositional environment. These element enrichments in Karaboğaz Formation samples is thought to be related to the redox conditions of the depositional environment, the C_{org} amount of rocks, and the various factors associated with the element relationship with C_{org}.

Key words: Major and trace element enrichments, Karaboğaz Formation, organic matter, redox conditions, oil source rock

KARABOĞAZ FORMASYONU (ADIYAMAN) ORGANİKÇE ZENGİN KAYAÇLARDA ELEMENT ZENGİNLEŞMELERİ

ÖZET: Anoksik ortam koşullarında depolanmış organikçe zengin sedimanter kayaçlar, ekonomik yönden önemli olan bazı mineral ve elementleri bünyesinde biriktirirler. Bu çalışmada Adıyaman bölgesi Karaboğaz Formasyonun organik maddece zengin kayaçlarının, organik madde içeriği, majör element ve iz element dağılımları ve zenginleşmeleri incelenmiştir. Arazi çalışması sırasında Karaboğaz Formasyonundan 13 adet kayaç numunesi alınmıştır. Bu kayaç numuneleri üzerinde Piroliz analizi, ICP analizi ve XRD analizi yapılmıştır. Yapılan bu analizler sonucunda Karaboğaz Formasyonu karbonatlı bir litolojiye sahip olduğu, % 0,76-7,09 arasında değişen ve ortalaması % 2,72 olan C_{org} olduğu belirlenmiştir. Karaboğaz Formasyonundan alınan organik maddece zengin kireçtaşı örnekleri üzerinde yapılan ICP analizi sonucunda, Si, Ca, Na, P, Cr, Ni, Sc, Ba, Co, Rb, Sr, U, V, W, Mo, Cu, Pb, Zn, As, Cd, Sb, Hg ve Se elementlerinin zenginleştikleri tespit edilmiştir. Zenginleşen ana ve iz elementler, anoksik-öksinik koşullarda depolanmış olan Namibya (Afrika) Kıyısal Şelfi Sedimanları, Peru Şelfi Sedimanları, Akdeniz ve Karadeniz Sapropelleri, Senomaniyen/Turoniyen Gubbio Anoksik Sedimanları ve Senomaniyen/Turoniyen Demerara Yükselimi Anoksik Sedimanlarına ait element zenginleşmeleri ile karşılaştırılmıştır. Bunun sonucunda Cr, P, Fe, Co, Sb, Zn, V, Cu, Ba, Pb ve Zr elementlerinin diğer ortamlara göre daha fazla zenginleşme gösterdikleri tespit edilmiştir. Karaboğaz Formasyonundaki bu element zenginleşmelerinin depolanma ortamının redoks koşullarına, kayaçların C_{org} miktarına, C_{org} ile element ilişkisine bağlı çeşitli faktörlerle ilişkili olduğu düşünülmektedir.

Anahtar sözcükler: Ana ve iz element zenginleşmeleri, Karaboğaz Formasyonu, organik madde, redoks koşullar, petrol kaynak kaya

AN APPLICATION AREA OF 4-D MATRIX

Celile YÜZBAŞI
Gaziantep Üniversitesi
celileyuzbasi@gmail.com

Doç.Dr. Necati Olgun
Gaziantep Üniversitesi
olgun@gantep.edu.tr

ABSTRACT: In this study we will focus on 4-D matrices and their application. The operation of the tomography device which has an important place in the health sector as the application area of 4-D matrices was examined. Our aim is to be able to interpret the images of 4-D matrices taken at different time intervals on tomography, which is the field of application, with the help of 4-D matrices. For this purpose, we examined tomographies taken at different time intervals.

Key words: matrix, tomography, matlab

4-D MATRİSLERİN BİR UYGULAMA ALANI

ÖZET: Biz bu çalışmada 4-D matrisler ve uygulama alanı üzerinde duracağız. 4-D matrislerin uygulama alanı olarak sağlık sektöründe önemli bir yeri bulunan tomografi cihazının işleyişi incelendi. Amacımız 4-D matrislerin uygulama alanı olan tomografi üzerindeki farklı zaman aralıklarında çekilmiş olan görüntülerini,4-D matrisler yardımıyla elde ettiğimiz sayısal değerler üzerinden yorum yapabilmektir. Bunun için de farklı zaman aralıklarında çekilmiş olan tomografileri inceledik

Anahtar sözcükler: matris, tomografi, matlab

GİRİŞ

Matris, her alanda kullandığımız uygulama alanı çok geniş olan matematiksel bir kavramdır. Matematikte matris dikdörtgen bir sayılar tablosu, çarpılabilir soyut miktarlar tablosudur. Dizeyler daha çok doğrusal denklemleri tanımlamak, doğrusal dönüşümlerde çarpanların takibi ve iki parametreye bağlı verilerin kaydedilmesi amacıyla kullanılırlar. Dizeylerin toplanabilir, çıkartılabilir, çarpılabilir ve bölünebilir olmaları, doğrusal cebir ve dizey kuramının temel kavramı olmalarını sağlamıştır. Doğrusal denklemler sisteminin ilk matris kullanılarak açıklanıp çözülmesi özellikle kare matrislerle determinant kullanımı dahil M.Ö 300 – M.S 200 yılları arasında yazılmış olan JİU ZHANG , SUAN SHU (Matematik Sanatında Dokuz Bölüm) adlı eserde bulunduğu anlaşılmıştır. Bundan sonra Matris kavramı 2000 yıl kadar sonra 1693'de 'Seki Kowa' adlı Japon matematikçi ve Batı Avrupa da ilk defa 1693'de Alman

matematikçisi Leibniz tarafından ortaya atılmış ve ilk determinant kullanılarak pratik çözüm olarak Cramer 'in kuralı 1750'de Gabriel Cramer tarafından gösterilmiştir. Matris terimi isim olarak ilk defa J.J.Syvester adlı İngiliz matematikçisi tarafından kullanılmıştır.[Leon,, Kaplan]
Günlük hayattaki kullanım örnekleri:

* 20 katlı ve her katında 5 daire bulunan bir apartmanda oturanların isimleri , 20x5 lik bir matris ile gösterilebilir.

* Paralel ve meridyenler bir matris halinde gösterilip, her ülkenin konumu matrisle ifade edilebilir.

Bu örnekler genişletilebilir.

Örneğin :
Bir sinemada, birinci sırada oturan insanların yerleri A ile gösterilir. Bunların baştan kaçıncı sırada oturduklarını ifade etmek için A'nın yanına 1,2,… sayıları getirilir. Bu koordinat olarak bilinir ama bunu a_{11} olarak gösterdiğimizde(ya da A_1), 1. sıra 1. sütunda oturtan kişi olarak anlarız. Bütün salon bu şekilde bir matris haline getirilebilir. Bir sınıf, otopark, yani yer bulma kavramının gerekli olduğu durumlarda kullanılır.

Tanım: $(F,+,*)$ bir cisim olsun. 4 - boyutlu $4*4*1*2$ tipindeki bir matris F cismi üzerinde aşağıdaki gibi tanımlanır:

$$M_{4*4*1*2} = \{(a_{ijkl}) \mid (a_{ijkl}); i = 1,2,3,4 : j = 1,2,3,4; k = 1,2,3,4; l = 1,2,3,4\}$$

olsun.

Bu matrisin görüntüsü aşağıdaki gibi olacaktır.

$$\left[\begin{bmatrix} a_{1111} & a_{1211} & a_{1311} & a_{1411} \\ a_{2111} & a_{2211} & a_{2311} & a_{2411} \\ a_{3111} & a_{3211} & a_{3311} & a_{3411} \\ a_{4111} & a_{4211} & a_{4311} & a_{4411} \end{bmatrix}, \begin{bmatrix} a_{1112} & a_{1212} & a_{1312} & a_{1412} \\ a_{2112} & a_{2212} & a_{2312} & a_{2412} \\ a'_{3112} & a_{3212} & a_{3312} & a_{3412} \\ a_{4112} & a_{4212} & a_{4312} & a_{4412} \end{bmatrix}\right]$$

Şekil 1.

UYGULAMA ALANI

Bu bölümde 4-D matrislerinin uygulama alanı üzerinde duracağız. Sağlık sektöründe önemli bir yer taşıyan tomografinin 4-D matrisler yardımıyla önceki ve sonraki alınan verilerini karşılaştırarak aynı anda çözüm almayı hedefledik. Öncesinde tomografinin işleyişine bir bakalım :

Bilgisayarlı Tomografi

Bilgisayarlı tomografinin temel problemi, kesit boyunca geçen x-ışınlarından toplanan verileri kullanarak insan vücudunun bir kesitinin görüntüsünü resmetmektir. x-ışınları taramalarının analizi ile bir insan vücudunu kesitsel resmetmek görüntünün

sayısal gösterimi için tutarsız lineer sisteme yol açar. x-ışınlarından toplanan veriler bir bilgisayar ile analiz edilir ve bu kesit bir video monitörde gösterilir.

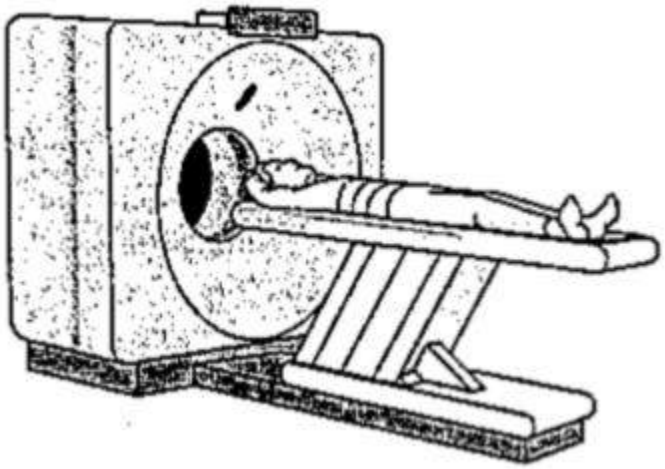

Şekil 2. X-Işın Tomografisine Hazırlanan Bir Hasta (Anton ve Rorres,1994)

Şekil 3. Bir Hasta Kafatasının Bilgisayar Destekli Tomografi Görüntüsü (Anton ve Rorres,1994)

Şekil 2. deki görüntü oluşumunda çıkan data işlenip, matris formuna dönüştürülüyor. Görüntüde oluşan değişimler Matlab programıyla inceleniyor.
Matlab programı tomografi görüntüsündeki sorunlu bölgenin matris formatını farklı zaman aralıklarla kontrol etmemizi sağlayıp, değişim sonucu hakkında yorum yapmamızı sağlıyor.
Matlab programı kullanılarak matrislerin arasındaki farkları, boyut olarak artmış, azalmış veya değişmemiş kararını veren kod;

```
clear; clc;
m=input('1.Matris Sütun Sayisi= ')
n=input('1.Matris Satir Sayisi= ')
for i=1:m;
   for j=1:n;
      a(i,j)=input('1.Matris Elemanlari= ');
   end
end
a=reshape(a,m,n)
for l=1:m;
            r(l)=input('1.Matris Esitligi= ');
end

for v=1:m;
                    for c=1:n;
                       q(v,c)=input('2.Matris Elemanlari= ');
   end
end
q=reshape(q,v,c)
for p=1:m;
   z(p)=input('2.Matris Esitligi= ');
end


b=r';
h=z';
o=[a b];
u=[q h];
k=rref(o);
d=rref(u);


for t=1:n;
f(1,t)= k(t,end);
f2(1,t)=d(t,end);
end
f
f2
A1='Artmis %';
A2='Azalmis %';
A3='Degismemis %';


x=abs( ((f(1,1)-f2(1,1))/f(1,1))*100)
y=abs( ((f(1,2)-f2(1,2))/f(1,2))*100)
z=abs( ((f(1,3)-f2(1,3))/f(1,3))*100)
```

```
if(x<3 && y<3 && z<3) disp(A3)
else
for t=1:n;

   if ( f(1,t) == f2(1,t) ) disp(A3)
   end
      if ( f(1,t) > f2(1,t) ) disp(A2)
      end
         if ( f(1,t) < f2(1,t) ) disp(A1)
         end
end
end
```

ÖRNEK 1)

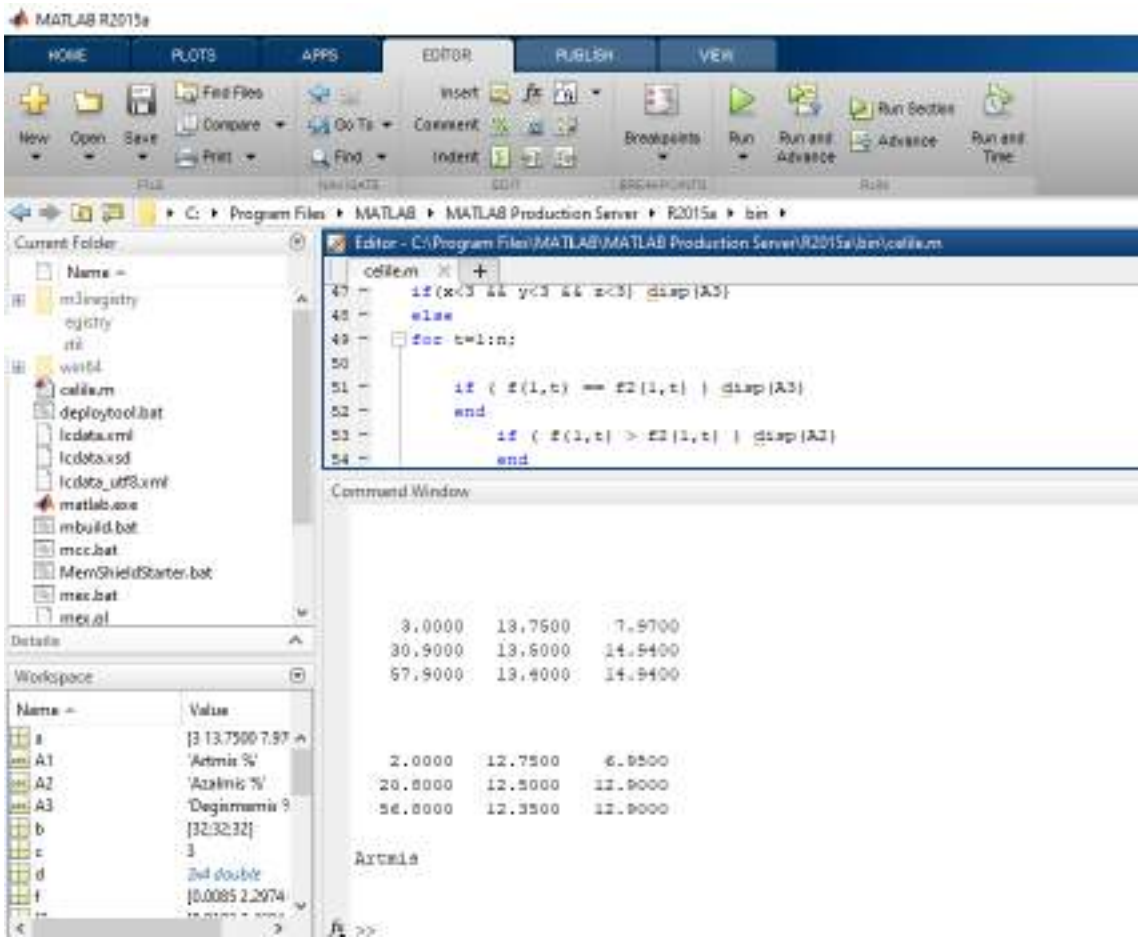

Şekil 4.

Hastadan alınan ilk data;

$$\begin{bmatrix} 3 & 18.75 & 7.97 & \vdots & 32 \\ 30.9 & 13.5 & 14.94 & \vdots & 32 \\ 57.9 & 13.4 & 14.94 & \vdots & 32 \end{bmatrix}$$

Hastadan alınan sonraki data;

$$\begin{bmatrix} 2 & 12.75 & 6.95 & \vdots & 32 \\ 20.8 & 12.5 & 12.9 & \vdots & 32 \\ 56.8 & 12.35 & 12.9 & \vdots & 32 \end{bmatrix}$$

Alınan bu iki matrisleri Matlab koduna verdiğimiz zaman sonuç artmış olarak çıkıyor.

ÖRNEK 2)

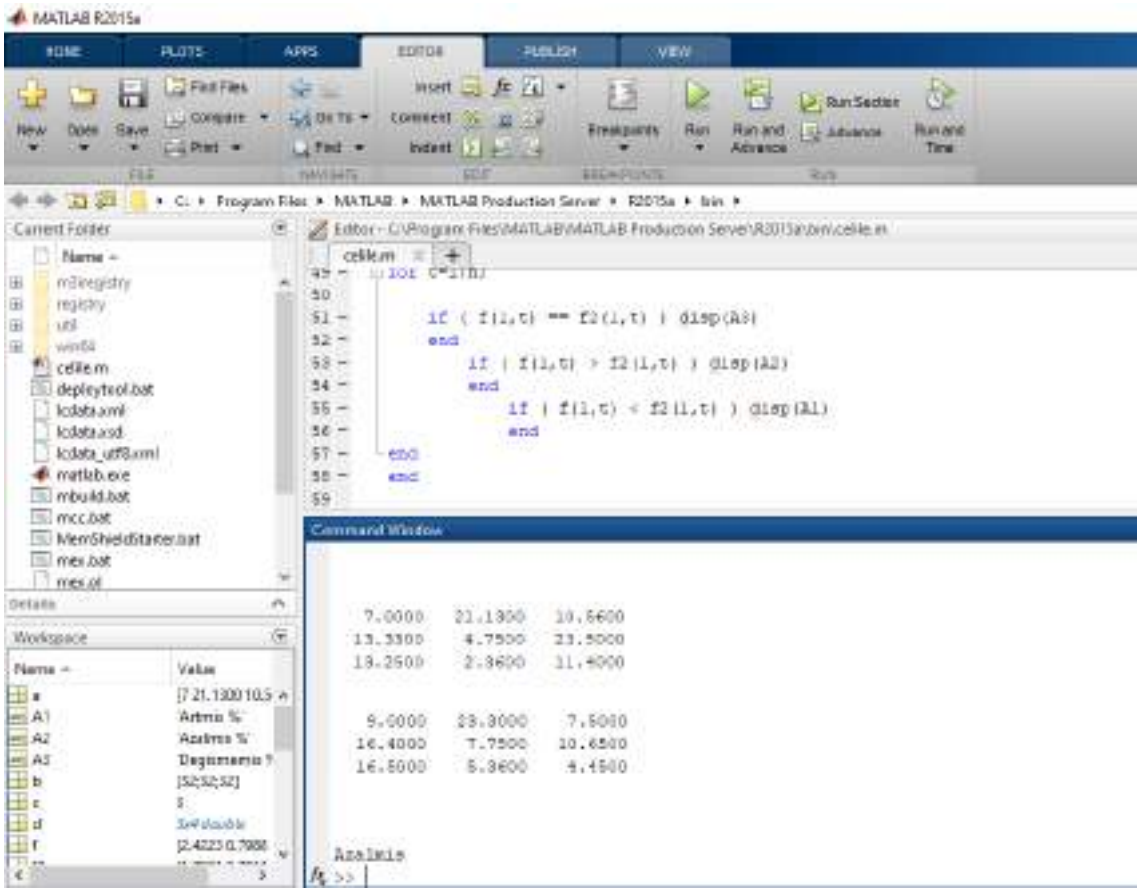

Şekil 5.

Hastadan alınan ilk data;

$$\begin{bmatrix} 7 & 21.13 & 10.56 & \vdots & 32 \\ 13.33 & 4.75 & 23.5 & \vdots & 32 \\ 13.25 & 2.36 & 11.4 & \vdots & 32 \end{bmatrix}$$

Hastadan alınan sonraki data;

$$\begin{bmatrix} 9 & 23.3 & 7.5 & \vdots & 32 \\ 16.4 & 7.75 & 10.65 & \vdots & 32 \\ 16.50 & 5.36 & 4.45 & \vdots & 32 \end{bmatrix}$$

Alınan bu iki matrisleri Matlab koduna verdiğimiz zaman sonuç azalmış olarak çıkıyor.

ÖRNEK 3)

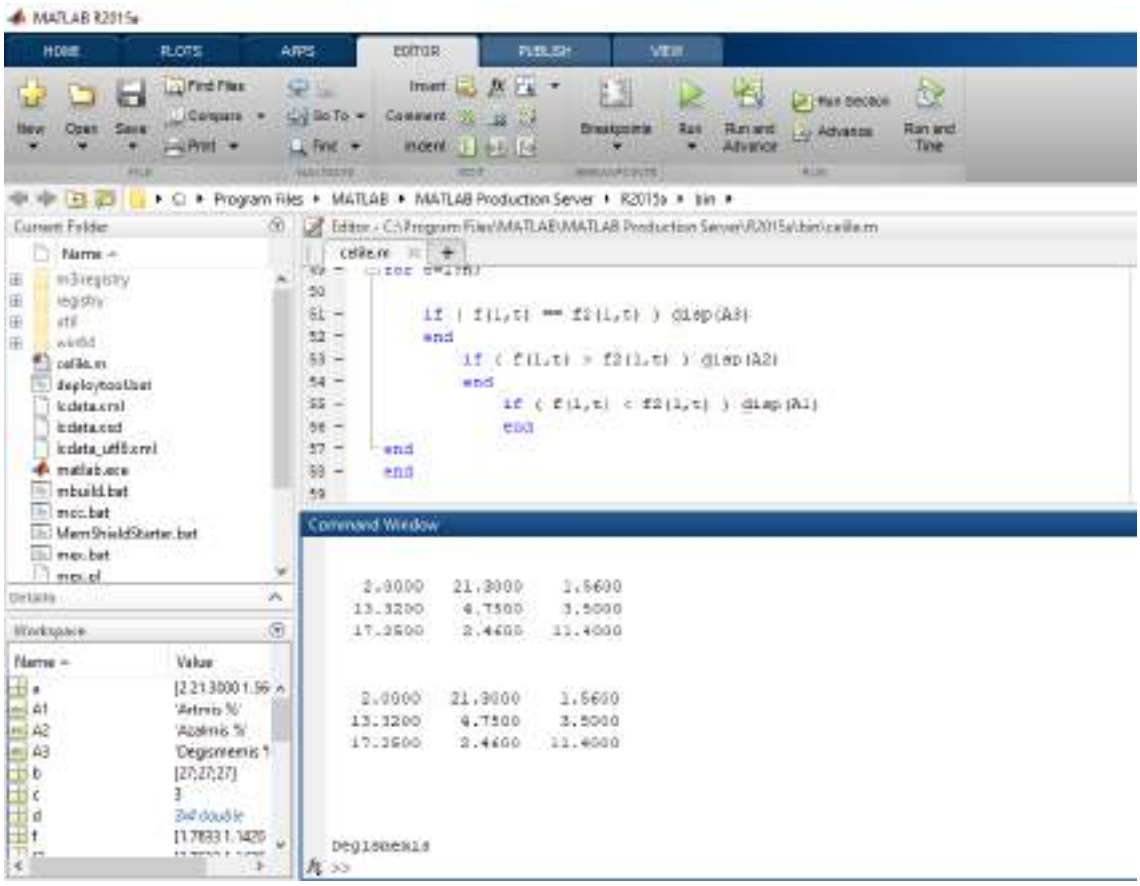

Şekil 6.

Hastadan alınan ilk data;

$$\begin{bmatrix} 2 & 21.3 & 1.56 & \vdots & 27 \\ 13.32 & 4.75 & 3.5 & \vdots & 27 \\ 17.25 & 2.46 & 11.4 & \vdots & 27 \end{bmatrix}$$

Hastadan alınan sonraki data;

$$\begin{bmatrix} 2 & 21.3 & 1.56 & \vdots & 27 \\ 13.32 & 4.75 & 3.5 & \vdots & 27 \\ 17.25 & 2.46 & 11.4 & \vdots & 27 \end{bmatrix}$$

Alınan bu iki matrisleri Matlab koduna verdiğimiz zaman sonuç değişmemiş olarak çıkıyor.

YÖNTEM

Bu makale de amacımız 4-D matrislerin uygulama alanı olan tomografi üzerindeki farklı zaman aralıklarında çekilmiş olan görüntülerini, 4-D matrisler yardımıyla elde ettiğimiz sayısal değerler üzerinden yorum yapabilmektir. Bunun için de farklı zaman aralıklarında çekilmiş olan tomografileri inceledik. Bu tomografilerin datalarını aynı anda Matlab'da çözdüğümüzde bize tomografi sonucunda hastalığın 'ARTMIŞ' , 'AZALMIŞ' veya 'DEĞİŞMEMİŞ' olduğu sonucunu verdi. Bizde bu sonuçlardan yola çıkarak hastalığın seyri hakkında yorumda bulunabildik.

SONUÇ

Makalemizde çalıştığımız konuda sonuç olarak aldığımız yanıt : 'ARTMIŞ' , 'AZALMIŞ' veya 'DEĞİŞMEMİŞ' olup farklı zamanlarda çekilen tomografinin aynı anda çözümlenip yorum yapılabilir hale getirilmiş olmasıdır.

KAYNAKLAR

Anton H, Rorres C. Elementary Linear Algebra, Binder Ready Version: Applications Version. John Wiley & Sons; 1994 Nov 4.

Kaplan, T. (2011). Lineer Denklem Sistemleri ve Uygulama Alanları . *Yüksek Lisans Tezi , Atatürk Üniversitesi*

Leon, Steven J., Ion Bica, and Tiina Hohn. *Linear algebra with applications*. New York: Macmillan, 1980.

Works, Math. "Using Matlab." *The Math Works Inc* (1996).

NEUTROSOPHIC DESICION TREE

Ahmed HATIP
Gaziantep University
kollnaar5@gmail.com

Necati OLGUN
Gaziantep University
olgun@gantep.edu.tr

ABSTRACT: In this research, we present neutrosophic decision-making, which is an extension of the classical decision-making process by expanding the data to cover the non-specific cases ignored by the classical logic which, in fact, supports the decision-making problem. The lack of information besides its inaccuracy is an important constraint that affects the effectiveness of the decision-making process, and we will rely on the decision tree model, which is one of the most powerful mathematical methods used to analyze many decision-making problems where we extand it according to the neutrosophic logic by adding some indeterminate data (in the absence of probability) or by substituting the classical probabilities with the neutrosophic probabilities (in case of probability). We call this extended model the neutrosophic decision tree, which results in reaching the best decision among the available alternatives because it is based on data that is more general and accurate than the classical model.

Key words: Decision-making process, Neutrosophic logic, Neutrosophic Decision-making, Neutrosophic Expected Monetary Value (NEMV).

INTRODUCTION

In our life, there is three kinds of logic. The first is classical logic which is gives the form "true or false, 0 or 1" to the values. The second is fuzzy logic was first advanced by Dr. Lotfi Zadeh in 1960s. It recognize more than true and false values, which are considered simple. With fuzzy logic, propositions can be represented with degrees of truth and falseness. And the third is neutrosophic logics which is an extension fuzzy logic in which indeterminacy is included *I*. Since the world is full of indeterminacy, the Neutrosophic found their place into contemporary research. Neutrosophic Science means development and applications of Neutrosophic Logic / Set / Measure / Integral / Probability etc. and their applications in any field. It is possible to define the Neutrosophic Measure and consequently the Neutrosophic Integral and Neutrosophic Probability in many ways, because there are various types of indeterminacies, depending on the problem we need to solve. Indeterminacy is different from randomness. Indeterminacy can be caused by physical space materials and type of construction, by items involved in the space, or by other factors.
Florentin Smarandanche introduced the notion of neutrosophy as a new branch of philosophy in 1980. After he introduced the concept of neutrosophic logic and

neutrosophic set where each proposition in neutrosophic logic is approximated to have the percentage of truth in a subset *T*, the percentage of indeterminacy in subset *I* and the percentage of falsity in a subset *F* where *T, I, F* are subset of [-,0,1,+] so that this neutrosophic logic is called an extension of fuzzy logic especially to intuitionistic fuzzy logic.
For more explanation, we can give these simple examples:

First Example of Indeterminacy: If there are two candidates A and B for presidency, and the probability that A wins is 0.46, it does not mean that the probability that B wins is 0.54 , since there may be blank votes (from the voters not choosing any candidate) or black votes (from the voters that reject both candidates). For example, the probability that B wins could be 0.45 , while the difference 1-0.46-0.45=0.09 would be the probability of blank and black votes together. Therefore we have a neutrosophic probability: NP(A)=(0.46, 0.09, 0.045).

Second Example of Indeterminacy: If a meteorology center reports that the chance of rain tomorrow is 60%, it does not mean that the chance of not raining is 40%, since there might be hidden parameters (weather factors) that the meteorology center is not aware of. There might be an unclear weather, for example, cloudy and humid day, that some people can interpret as rainy day and others as non-rainy day. The ambiguity arouses indeterminacy.
Third Example of Indeterminacy: Probability in a soccer game. Classical probability is incomplete, because it computes for a team the chance of winning, or the chance of not winning, nut not all three chances as in neutrosophic probability: winning, having tie game, or losing.
Fourth Example of Indeterminacy: An urn with two types of votes: A-ballots and B-ballots, but some votes are deteriorated, and we can't determine if it's written A or B. Therefore, we have indeterminate votes. In many practical applications, we may not even know the exact number of indeterminate votes, of A-ballots, or of B-ballots. Therefore, the indeterminacy is even bigger
In fact neutrosophic sets is the generalization of classical sets, neutrosophic groups, neutrosophic ring, neutrosophic fields, neutrosophic vector spaces … etc.
Using the idea of neutrosophic theory, Vasantha Kanadasamy and Florentin Samarandanche studied neutrosophic algebraic structures in by inserting an indeterminate element I in the algebraic structure and then combine (I) with each element of the structure with respect to corresponding binary operation.
The indeterminate element I is such that if * is ordinary multiplication $I * I = I^2 = I$, $I * I \dots * I = I^n = I$ and I^{-1} the inverse of I is not defined and hence does not exist. Moreover, if * is ordinary addition, then $I * I \dots * I = nI$ for $n \epsilon I$ [1]. They call it neutrosophic element and the generated algebraic structure. Is then termed as neutrosophic algebraic structure.
In 1995, Florentin Smarandache introduced the "neutrosophic set theory" to handle the indeterminate and inconsistent information that exist commonly in real situations.
Neutrosophic logic has wide applications in science, engineering, politics, economics, etc. Therefore, neutrosophic structures are very important and a broad area of study.

By doing this, we move from the classical form that gives a determinant value of benefits to the neutrosophic form that doesn't do that, but gives a range of expected values of benefits.

NEUTROSOPHIC DESCION TREE

We know from the definition of the Classical Decision Tree that it is a graphic in the form of a tree gives options and is used in choosing options in the case of one scale. Its root starts from the left and its branches spreads into the right showing the options and the possibilities of the natural cases (events). It is considered to be a suitable method to make a decision if one is not sure, and it is one of the strong mathematical methods that is used analyzing many problems.
The Neutrosophic Decisions Tree is the Classical Decision Tree with adding some indetermination to the data or by exchanging the classical probabilities with neutrosophical probabilities.
Building the neutrosophic tree of decisions without including the probabilities is considered to be a suitable option when the decision makers don't have enough information that can make them estimate the probability of the events that built up the tree of decisions. It is also suitable at analyzing the best or the worst options away from probabilities. This theory agrees with the concept of the classical tree of decision. However, what the neutrosophic logic adds to the tree of decision without probabilities is that the expected benefit that matches each option, which is usually evaluated by the decision makers according to their expertise or by related skills, will be evaluated more accurately and generally with less possible mistakes.
From another side, we may see that the expected values of the benefits whether good or bad are agreed on by some experts but others disagree. Therefore, the best solution to face this problem that absolutely affects the quality of the taken decision is to take the expected benefits with adding and reducing a value range between (0) and another determinate value, for example (a). (0) which represents the minimum value in this range means that there is no disagreement on the expected values among the experts or with the decision makers. (a) Which represents the maximum value in this range means that there is a disagreement among the experts or between them and the decision makers about the expected values of benefits and (a) is the highest estimated value.
Therefore, we will present the expected value of benefits with adding and reducing the range [0,a] not forgetting that all the various opinions about the expected values will be contained in the [0,a] range. So that, the expected value of benefits will become a range of values containing all the opinions.
For example, we can consider three options d_1, d_2 and d_3 by the best and the worst expectations as it is clarified in the following table:

Table1. The worst expectations

	High turnout	**Low turnout**

d_1	$A \pm i_1$	$B \pm i_2$
d_2	$C \pm i_3$	$D \pm i_4$
d_3	$E \pm i_5$	$F \pm i_6$

A, B, C, D, E, F : Represents the determinate part of the expected values.
$i_1 , i_2 , i_3 , i_4 , i_5 , i_6$: Represents the indeterminate part of the expected part.
$i_k \in [0, a_k] : k = 1,2,3,4,5,6$
Therefore, analyzing the tree of neutrosophic decisions from the tree of classical decisions when studying the Optimistic and Pessimistic and The Caution Approach for choosing the best alternative.

CONCLUSION

Dealing with the samples of the decision making process according to the Neutrosophic logic provides us with a comprehensive and complete study for the problem that we are studying. So that, we don't miss any data just because it is undetermined clearly. This makes us to choose the best option .
The existence of indeterminacy in the problem actually affects the process of taking the suitable decision. Therefore, the undetermined values can't be ignored/neglected while studying in order to get more accurate results that leads us to the best options.
Nowadays, the classical logic is not sufficient to deal with all the data that we study. Therefore, we had to expand the data of the study and name it accurately to get more real possibilities and, therefore, make decision more accurate. And here appears the role of the Neutrosophic logic that generalizes the classical logic and gives us a wider horizon in interpreting the data of the study and expand it and then make correct decisions with the least possible mistakes.

REFERENCES

[1] W.B. Vasantha Kandasamy and F. Smarandache. Neutrosophic Rings, Hexis, Phoenix, Arizona, 2006. URL: http://fs.gallup.unm.edu/NeutrosophicRings.pdf.

[2] L. A. Zadeh. Fuzzy Sets. Inform. Control 8, 1965.

[3] A. Kharal. A Neutrosophic Multicriteria Decision Making Method , National University of Sciences and Technology (NUST), Islamabad, Pakistan,2011.

[4] p. Majumdar. Neutrosophic Sets and its applications to Decision Making, computational intelligence for big data
analysis , Adaptation , leaning and optimization , vol19 , springer , Cham .pp 97-115, 2015.

[5] S. Pramanik, sh. Dalapati, sh. Alam and T. Kumar Roy. TODIM method for group decision making under bipolar neutrosophic set environment, pons asbl, 2018.

[6] F. Smarandache. Introduction to Neutrosophic measure neutrosophic integral and neutrosophic probability, Sitech – Education, 2013.

[7] A. A. Salama and F. Smarandache. Neutrosophic Crisp Set Theory, Education Publishing, Columbus, 2015.

USE OF TEA WASTE BASED ADSORBENTS FOR THE REMOVAL OF CATIONIC DYE FROM AQUOUS SOLUTIONS

Ayten ATEŞ
Department of Chemical Engineering, Engineering Faculty, Sivas Cumhuriyet University, Sivas, Turkey
ates@cumhuriyet.edu.tr

Tülay OYMAK
Department of Analytical Chemistry, Faculty of Pharmacy, Sivas Cumhuriyet University, Sivas, Turkey
tulayoymak@cumhuriyet.edu.tr

Yasemin MERT
Department of Chemical Engineering, Engineering Faculty, Sivas Cumhuriyet University, Sivas, Turkey
jasmin.iron@hotmail.com

ABSTRACT: Raw tea waste (RTW) was activated by microwave irradiation (RTW-A-MW) and pyrolyzed at 500 ^{o}C in N_2 (RTW-A-P500) in the presence of phosphoric acid. RTW, RTW-A-MW and RTW-A-P500 were tested as adsorbent for the adsorption of methylene blue (MB) from aqueous solution. The effect of factors on adsorption efficiency and potential mechanism was carried out. Adsorption capacity of MB onto adsorbents with the MB concentration, contact time and increasing pH were studied. The adsorption efficiency for three adsorbents with contact time increased and reached a stable state within 120 min. Whereas the Langmuir isotherm model was found to be the best isotherm models to elucidate the adsorption mechanism of acid activated samples, the Freundlich isotherm model described well for RTW. The maximum adsorption capacities calculated by the Langmuir model for RTW, RTW-A-MW and RTW-A-P500 were 142.8, 41.6 and 53.8 mg g^{-1}, respectively. The adsorption capacity of RTW is higher than activated ones, which might be due to its cellulosic content.

Key words: Raw tea waste, acid activation, pyrolysis, methylene blue, adsorption.

SULU ÇÖZELTİLERDEN KATYONIK BOYA GİDERİMİNDE ÇAY ATIĞI TEMELLİ ADSORBENTLERİN KULLANIMI

ÖZET: Ham çay atığı (HÇ), fosforik asit varlığında mikrodalga ışınımı ile (HÇ-A-MW) aktive ve N_2 atmosferinde 500 ° C'de piroliz (HÇ-A-P500) edilmiştir. HÇ, HÇ-A-MW ve HÇ-A-P500 örneklerinin her biri, metilen mavisinin (MM) sulu çözeltiden adsorpsiyonu için adsorbent olarak test edilmiştir. Adsorpsiyon çalışma koşullarının adsorpsiyon etkinliğine ve mekanizmasına etkisi incelenmiştir. Adsorbentlerin MM adsorpsiyon kapasitesi, MM derişimi, temas süresi ve pH artışı ile arttı. Üç adsorbent

için adsorpsiyon verimi artan adsorpsiyon süresi ile arttı ve 120 dakika sonra stabil kaldı. Langmuir izoterm modeli, asitle aktive edilmiş HÇ örneklerinin adsorpsiyon mekanizmasını açıklamak için en iyi izoterm modeli oluştururken, Freundlich izoterm model HÇ örneği için iyi uyum göstermiştir. Langmuir modeli ile belirlenmiş HÇ, HÇ-A-MW ve HÇ-A-P500 örnekleri için maksimum MM adsorpsiyon kapasiteleri sırasıyla 142.8, 41.6 ve 53.8 mg g^{-1}'dır. HÇ'in yüksek adsorpsiyon kapasitesi, yapısında yer alan selülozun varlığın bir sonucu olabilmektedir.

Anahtar sözcükler: Ham çay atığı, asit aktivasyonu, piroliz, metilen mavisi, adsorpsiyon

GİRİŞ

Tarımsal artıklardan ve su bitkilerinden elde edilen biyokütle, bol, ucuz ve sürdürülebilir bir hammadde olup, yüksek enerji içeriği ile enerji kaynağı olarak umut vaat etmektedir (Islam, Benhouria, Asif ve Hameed, 2015) . Biyokütleyi enerjiye dönüştürmek için biyokimyasal ve termokimyasal teknikler yaygın olarak kullanılmakta olup, termokimyasal yöntemler daha yüksek verime ve tam olmayan dönüşüme sahip olduğundan çok daha etkilidir (Tripathi, Sahu ve Ganesan, 2016). Bu nedenle, katı karbonlu bir biyokömür üretmek için oldukça ılımlı bir sıcaklıkta oksijence sınırlı atmosferde hidrotermal karbonizasyon ve piroliz gibi termokimyasal yöntemlere odaklanılmaktadır. Düşük maliyetli biyokütlenin biyokömüre dönüşümü, katı atık giderimi ile birlikte enerji üretimine de katkı sağlamaktadır. Üretilen biyokömürler toprak kalitesini artırmak için de kullanılabilmektedir (Lee, Cheng, Wong ve Wang, 2018). Üretilen biyokömürün yapısal özellikleri ve gözenek karakteristikleri, fonksiyonel aktif merkezleri ve yüksek hidrofobiklik özellikleri, biyokömürün boyalar (Sewu, Boakye ve Woo, 2017), fenoller (Zheng ve diğerleri, 2017), ağır metaller (Zhou ve diğerleri, 2016), böcek ilaçları (Vithanage, Mayakaduwa, Herath, Ok ve Mohan, 2016) ve antibiyotik kirleticileri (Lonappan, Rouissi, Kaur Brar, Verma ve Surampalli, 2018) etkin ve verimli bir şekilde gideriminde adsorbent olarak kullanımına imkan sağlamaktadır. Özellikle, biyokömürün aktif merkez doğası ve karakteristikleri, uygulanan kimyasala, ısıl muamele sıcaklığına, gaz akış hızına ve termokimyasal dönüşüm teknoloji ile ilişkilidir (Tan ve diğerleri, 2015).

Talaş (G. Ding, Wang, Chen ve Zhao, 2016), yabani otlar (Güzel, Sayğılı, Akkaya Sayğılı, Koyuncu ve Yılmaz, 2017), mısır sapları (Lian ve diğerleri, 2016) ve ceviz ağacı ahşabı (Z. Ding ve diğerleri, 2016) gibi bitki atıklarından üretilen biyokömürler metilen mavisi (MM) gibi tehlikeli katyonik boyaları atık sudan uzaklaştırmak için etkin, ekonomik ve çevresel olarak güvenli adsorbentler olarak kullanılabilmektedir. Özellikle, baskın selüloz yapısına sahip lignoselülozik bitkisel kaynaklardan üretilen biyokömürler, adsorbent olarak etkili bir kullanıma sahiptir(Ahmed, Okoye, Hummadi ve Hameed, 2019).

Çay atığı, çay hasadının yanlış yapılması sonucu yüksek miktarda üretilmekte olup, bu atık farklı alanlarda kullanılabilir. Bunlardan biri de, sulu çözeltilerden kirlilikleri uzaklaştırmak için etkin bir adsorbent olarak kullanımıdır (Nasuha, Hameed ve Din, 2010). Çay atığı ile boya endüstrisi atık suyunun arıtımı daha önce, farklı çalışmalarda incelenmiştir(Hameed, 2009; Liu, Fan ve Li, 2018; Nasuha ve Hameed, 2011; Uddin, Islam, Mahmud ve Rukanuzzaman, 2009). Ayrıca, çay atıklarından üretilmiş biyokömürün adsorpsiyon kabiliyeti asit ile muamele edilerek artırılmakla birlikte mikrodalga (MW) ışınımı teknolojisinin uygulanması çok umut verici sonuçlar verebilmektedir (Ania, Parra, Menéndez ve Pis, 2005). Bu nedenle, son zamanlarda, mikrodalga enerjisi hem araştırma hem de endüstriyel işletmelerde birçok uygulama alanında yaygın bir şekilde kullanmaktadır. Mikrodalga enerjisinin kullanılması karbonlu malzemelerin özelliklerini çok değiştirmesine rağmen, biokütleden üretilmiş biyokömür üzerine mikrodalganın etkisi üzerine az çalışma bulunmaktadır. Nabais ve ark.(2004) aktif karbon elyaflarının mikrodalga ısıtma vasıtasıyla yüzey kimyası modifikasyonu üzerinde çalışmış ve bunun çok etkili bir yöntem olduğunu bildirmiştir (Nabais, Carrott, Carrott ve Menéndez, 2004). Biyokütleden biyokömür üretimi ile ilgili literatürde birçok çalışma rapor edilmiş olmasına rağmen, fosforik asit varlığında mikrodalga enerjisi ile işleme tabi tutulmuş atık çaydan hazırlanan biyokömür ile ilgili herhangi bir çalışma bulunmamaktadır. Bir aktivasyon ajanı olarak fosforik asit, lignoselülozik ürünlerden kirletmeyen özellik ve suya ekstraksiyonla eliminasyon kolaylığı gibi bazı avantajlar sunmaktadır (Puziy, Poddubnaya, Martínez-Alonso, Suárez-García ve Tascón, 2005; Suárez-García, Martínez-Alonso ve Tascón, 2002). Girgis ve El-Hendawy (2002) fosforik asidin parçacık şişmesi ve biyolojik kütlenin kısmen çözülmesi, bağ parçalanması ve termal bozunmaya dirençli yeni polimerik yapıların yeniden düzenlenmesi ile botanik yapı üzerinde fiziksel ve kimyasal değişiklikler yaptığını rapor etmiştir (Girgis ve El-Hendawy, 2002). H_3PO_4'in bir kimyasal aktive edici ajan olarak kullanılması durumunda, gözenek boyutu dağılımlarının daha heterojen olacağı belirtilmiştir (Molina-Sabio ve Rodríguez-Reinoso, 2004). Ayrıca, üretilen biyokömürün özellikleri, H_3PO_4 derişimine, adsorplama oranına ve aktivasyon için kullanılan gaz türü gibi hazırlanma koşullarına güçlü bir şekilde bağlı olduğu rapor edilmiştir.

Bu nedenle çalışmada, ham çay atığı fosforik asit varlığında mikrodalgada aktive edilmiş ve fosforik asit varlığında 500 ^oC'de piroliz edilmiştir. Ham çay atığı, mikrodalgada aktive edilmiş çay atığı ve piroliz edilmiş çay atığı detaylı olarak karakterize edilmiş ve üç örnek metilen mavisinin sulu çözeltilerden uzaklaştırılmasında test edilmiştir. Örneklerin adsorpsiyon kapasitesi üzerine, çözeltilerin başlangıç pH değerinin, başlangıç metilen mavisi derişiminin ve temas süresinin etkisi belirlenmiş ve değerlendirilmiştir.

YÖNTEM

Malzemeler

Ham çay atığı (HÇ), Karadeniz Bölgesi Salarha-Rize'de bulunan bir çay fabrikasından elde edilmiştir. HÇ ilk önce 0.25 mm ila 0.5 mm arasında değişen partikül boyuna öğütüldü ve gece boyunca 80 °C'de bir fırında kurutuldu. HÇ, ağırlık olarak yaklaşık % 3.8 kül, % 7.2 nem ve % 70.3 uçucu madde içermesine ek olarak % 18.6 sabit karbon, % 31.0 holoselüloz, % 25.6 lignin, % 13.9 özütleyici ve %2.0 yağ içermektedir (Uzun, Apaydin-Varol, Ateş, Özbay ve Pütün, 2010).
Metilen mavisi (MM) için bir stok çözeltisi hazırlanmış ve istenilen derişimdeki MM, bu stok çözeltiden distile su ile seyreltme ile hazırlanmıştır. Çözeltilerin başlangıç pH'ı HCl ve NaOH çözeltileri ile Chebios 640 Lab pH metre kullanılarak ayarlanmıştır.

Ham Çayın Asit Aktivasyonu, Pirolizi ve Karakterizasyonu

Ham çayın H_3PO_4 ile asit aktivasyonu için, 2 g HÇ, bir teflon beher içinde 6 g ağırlıkça % 85 H_3PO_4 (Merck) ile karıştırılmış ve 30 saniye süreyle mikrodalga (MW) (Cem Mars 6) radyasyonu ile muamele edilmiştir. MW ekipmanının giriş gücü 900 W ve kullanılan mikrodalga frekansı 2,45 GHz'dir Asit içinde MW muamelesinden sonra, numune 80 °C'de fırında kurutulmuştur. Elde edilen aktive edilmiş HÇ örneği, HÇ-A-MW olarak kısaltıldı, burada A, fosforik asidi göstermektedir. Benzer olarak, H_3PO_4 ile HÇ 3:1 oranında karıştırılmış ve 500 °C'de Protherm fırında saf N_2 (80 cm^3 min^{-1}) akışı altında 1 saat boyunca piroliz edilmiştir. Bu örnek HÇ-A-P500 olarak kısaltılmış olup, burada A piroliz sırasında asidin varlığını göstermektedir. Fosforik asit varlığında üretilen tüm numuneler, fosfat türlerinin uzaklaştırılması için birkaç kez distile suyla yıkanmıştır. Örneklerin element bileşimleri (C, H, N, S ve O) taramalı elektron mikroskobu (SEM, TESCON, MIRAIII) üzerine yerleştirilmiş bir enerji dağıtıcı spektrofotometre (EDS) (Oxford Inst. INCA) ile belirlenmiştir. Numunelerin X ışını kırınımı (XRD) desenleri, monokromotografik olmayan Cu Kα1 radyasyonu (40 kV, 40 mA, λ = 1.5Å) kullanılarak bir RigakuSmartLab X-ışını difraktometresine kaydedildi. Tarama 2θ'ın 5-65 ° aralığında yapıldı. Tüm numunelerin yüzey morfolojileri EDS (Oxford Inst. INCA) ile donatılmış bir emisyon taramalı elektron mikroskobu (TESCON-Mira III XMU) kullanılarak incelendi. Brunauer-Emmett-Teller (BET) spesifik yüzey alanları (SBET), toplam gözenek hacimleri ve gözenek çapları bir gaz sorpsiyon analiz cihazı (AUTOSORB 1C, QuantachromeCorp.,) kullanılarak tayin edilmiştir.
Adsorpsiyon Deneyleri
HÇ, HÇ-A-MW ve HÇ-A-P500 örneklerinin MM adsorpsiyonu çalışmaları kesikli deney sistemde gerçekleştirilmiştir. MM adsorpsiyonunda; çözelti başlangıç pH (4-10)'ı, MM başlangıç derişimi ve adsorpsiyon süresi parametrelerinin etkileri incelenmiştir. Adsorpsiyon işleminin ardından çözelti içerisindeki MM derişimi, UV spektrofotometresinde (Shimadzu UV-1800) 664 nm dalga boyunda ölçülmüştür. Adsorbentin denge durumunda adsorpladığı MM adsorpsiyon kapasitesi (qe) ve % adsorplama yüzdesi Eşitlik 1 ve Eşitlik 2 kullanılarak hesaplanmıştır.

$$q_e = \frac{(C_o - C_e)V}{m} \quad [1]$$

Uzaklaştırma yüzdesi;

$$(R,\%) = \frac{C_0 - C_e}{C_0} x100 \quad [2]$$

Co, çözeltideki MM başlangıç derişimi (mg/L); Ce, denge durumunda çözeltideki MM derişimi (mg/L); V, çözelti hacmi (mL); m, adsorbent miktarı (g); R, adsorplanan MM derişim yüzdesidir. Tüm sorpsiyon deneyleri için 2 g L^{-1} adsorbent derişimi kullanıldı. Ön adsorpsiyon deneyleri için 3 saatlik bir denge süresi seçildi.

BULGULAR

Örneklerin Karakterizasyonu

HÇ, HÇ-A-MW ve HÇ-A-P500 örneklerinin elementel analiz bileşimi sonuçları Tablo 1'de listelenmiştir. HÇ, ağırlıkça % 60.4 C, % 3.7 N ve % 34.4 O'nun yanı sıra Al, S, Cl, K, Ca, Na ve Mg'nin küçük yüzdelerinden oluşmaktadır. HÇ'in asit pirolizi, örneğin karbon içeriğini önemli miktarda artırmıştır. Ancak, asitte MW ile muamele, piroliz sırasında fosforik asidin ayrışmasından salınan oksijen türleri ile karbonun kısmen oksidasyonu ve MW'de düşük sıcaklıkta (180 °C) piroliz sırasında karbon türünün kısmen oksidasyonu sonucu örneğin karbon içeriğini HÇ-A-P500 kıyasla daha düşük oranda artırmıştır.

Tablo 1. EDS ile belirlenmiş HÇ, HÇ-A-MW ve HÇ-A-P500 örneklerinin elementel bileşimi

Örnek	C	N	S	O	Na	Mg	Al	Cl	K	Ca	Si	P	S
HÇ	60.4	3.7	0.1	34.4	0.02	0.05	0.20	0.2	0.8	0.20	-	-	-
HÇ-A-MW	63.4	4.4	-	31.6	-	-	0.02	0.03	0.02	-	0.4	0.10	0.1
HÇ-A-P500	78.2	-	-	20.5	-	-	-	0.04	-	0.08	1.0	0.2	-

Ham ve muamele edilmiş örneklerin XRD desenleri incelendiğinde, HÇ örneğinin 2θ'ın 22.5° 'de karakteristik pik ve 15° ve 16.5°'de omuzlar gösterdiği gözlenmiş olup, bu kristal yapıdaki selüloz I'i göstermektedir (Dourado, Gama, Chibowski ve Mota, 1998). MW'de HÇ'ın asitle muamele edilmesi ve HÇ'in asit piroliz sonrasında, asit varlığında karbonun kısmen oksidasyonu nedeniyle selüloz pikinin tamamen kaybolmasına neden olmuştur.

Örneklerin yüzey morfolojisinin taramalı elektron mikrografları, Şekil 1'de gösterilmektedir. HÇ'nin yüzeyi büyük ölçüde pürüzsüzdür ve daha az çatlak ve boşluğa sahiptir. HÇ'in fosforik asidin varlığında, MW ile muamelesi düzensiz ve heterojen yüzey morfolojisine neden olmuştur. HÇ-A-MW'in yüzeyi açık bir şekilde MW ısıtma ve fosforik asit ile aktivasyon yoluyla pürüzlü bir yüzey morfolojisi göstermektedir (Prahas, Kartika, Indraswati ve Ismadji, 2008). Fosforik asit varlığında HÇ'nin pirolizi, pürüzlü ve gözenekli yüzey morfolojileri ile düzlemsel bir doku oluşturmaktadır.

Örneklerin N_2 adsorpsiyonu -desorpsiyonu izotermlerinden ve gözenek boyut dağılım eğrilerinden belirlenen yüzey alanı ve gözenek özellikleri Tablo 2'de gösterilmiştir. HÇ örneğinin yüzey alanı ve ortalama gözenek çapı sırasıyla 10.4 m^2g^{-1} ve 55.6 Å'dir. HÇ'ın asit varlığında pirolizi, ortalama gözenek çapının azalmasıyla artan mikro-gözeneklilik nedeniyle yüzey alanını önemli miktarlarda arttırmaktadır. Bununla birlikte, asit varlığında MW ile aktivasyon, gözenek özelliklerinin önemsiz değişikliklerle, HÇ-A-MW'in yüzey alanını hafifçe arttırmaktadır. Literatürde (Hoseinzadeh Hesas, Wan Daud, Sahu ve Arami-Niya, 2013), atıkların asit aktivasyonunun, yapısal bozulma ve yüzeyde defektlerin oluşumuyla homojen olmayan mikro yapı oluşumuyla homojen olmayan mikroyapı ile yüzey alanında önemli miktarda artışa neden olduğu rapor edilmiş olup bu çalışmada asidin varlığı mikro yapıyı önemli miktarda artırmıştır.

Tablo 2. Örneklerin yüzey alanı ve gözenek boyut dağılımı.

Örnek	S_{BET}[a] (m^2g^{-1})	V_{Toplam}[b] (cm^3g^{-1})	V_{Mikro} (cm^3g^{-1})	Dp (Å)[c]
HÇ	10.4	0.03	0.004	55.6
HÇ-A-P500	931	1.08	0.374	23.4
HÇ-A-MW	18.5	0.02	0.005	19.2

[a] Çok noktalı BET ile belirlenmiş yüzey alanı; [b] *P/Po* = 0.99'da hesaplanmış toplam yüzey alanı; [c]DR ile ortalama gözenek çapı.

Adsorpsiyon Sonuçları

pH'ın etkisi

HÇ, MÇ-A-MW ve HÇ-A-P500 adsorbentlerinin MM adsorpsiyonu üzerine çözelti başlangıç pH değerlerinin etkisi Şekil 2'de gösterilmiştir. Maksimum MM uzaklaştırma yüzdesi, HÇ için pH=6, HÇ-A-MW ve HÇ-A-P500 için pH=8 bulunmuştur. Çözelti pH ile MM giderim yüzdesi arasındaki ilişki MM ve adsorbentler arasındaki elektrostatik etkileşimle ilişkilendirilebilir (El-Shafey, Ali, Al-Busafi ve Al-Lawati, 2016). MM'nin adsorpsiyonunda adsorbentin zeta potansiyeli önemli bir işleve sahiptir. HÇ ve HÇ-A-MW'in izoelektrik nokta değerlerindeki pH değerlerinin değeri 1.5 iken, HÇ-A-P500 örneğinin değeri pH=2'de bulunmuş olup, izoelektrik noktanın üzerinde adsorbent yüzeyleri negatif olarak yüklenmekte olup, katyonik MB moleküllerini adsorplayabilmektedirler.

Adsorpsiyon izotermleri

pH incelemesi sonucunda, adsorpsiyon izotermi incelemesi pH=8 değerinde gerçekleştirilmiştir. Şekil 3'de gösterilen adsorpsiyon süresine bağlı olarak derişim verilerine Langmuir, Freundlich ve Temkin modelleri uygulanmıştır. Model denklemleri aşağıda listelenmiştir**.**

Langmuir sioterm denkleminin doğrusallaştırılmış denklemi

$$\frac{Ce}{qe} = \frac{1}{bqm} + \frac{Ce}{qm} \qquad (3)$$

Freundlich izotherm denklemi doğrusal şekli

$$\ln qe = \ln k_F + (1/n)\ln Ce \quad (4)$$

Temkin izoterm denkleminin doğrusal şekli

$$qe = \frac{RT}{b_T}\ln K_T + \frac{RT}{b_T}\ln Ce \quad (5)$$

Denklem (3)-(5)'de C_e dengedeki derişimi (mg L^{-1}); q_e denge süresinde adsorpsiyon kapasitesi (mg g^{-1}); q_m maksimum adsorpsiyon kapasitesi (mg g^{-1}); b is adsorpsiyon kapasitesi ile ilgili Langmuir sabiti; k_F Freundlich sabiti (L mg^{-1}); n adsorpsiyon "şiddeti"; K_T denge bağlanma sabiti (L mg^{-1}); b_T Temkin izoterm sabiti; R ideal gaz sabiti (8.314J mol^{-1} K^{-1}); T sıcaklık (K); B_T=RT/b_T adsorpsiyon ısısı terimi (J mol^{-1}).

Üç adsorpsiyon izoterm modelinin deneysel verilere uygulamasını sonucu bulunan parametreler ve regresyon katsayıları sonuçları Tablo 3'de gösterilmiştir. Regresyon katsayıları değerlerine göre, HÇ için Freundlich model ve asitte MW aktivasyon ve piroliz sonucu üretilen örneklerde ise Langmuir izoterm model deneysel verileri daha iyi tanımlamaktadır. İzotermler, MM'nin aktive edilmiş HÇ örneklerinde tek konum mekanizması ile yürüdüğünü göstermektedir.

Langmuir izoterminden bulunan 1/n değeri her üç adsorbent için de 0.5'den küçük olup bu, MM'nin yüzeyde kolayca adsorplandığını göstermektedir.

Temkin izoterm model, adsorbatın yüzey kaplama hızı azaldıkça, adsorpsiyon ısısının azaldığını varsaymaktadır (Kallel ve diğerleri, 2016). Temkin izoterm model elektrostatik etkileşim ile gerçekleşen kimyasal adsorpsiyonu tanımlamakta olup, HÇ ve HÇ-A-MW örnekleri için yüksek R^2 değeri ile deneysel verilere uyum göstermektedir. B_T değerlerinin 8 kJ/mol'den düşük olması, MM adsorpsiyonun yüzeyde fiziksel adsorpsiyon ile yürüdüğünü göstermektedir.

Tablo 3. MM uzaklaştırması için adsorbentlerin adsorpsiyon izoterm sabitleri

Örnek	Langmuir			Freundlich			Temkin		
	qm (mg g^{-1})	b (Lmg^{-1})	R^2	k_F ((mg g^{-1}) (mg $L^{-1})^{-n}$)	n	R^2	b_T (J mol^{-1})	A_T (L g^{-1})	R^2
HÇ	142.8	0.04	0.952	14.3	1.9	0.988	39.3	0.14	0.995
HÇ-A-MW	41.6	0.16	0.977	2.8	3.4	0.958	4.8	0.86	0.959
HÇ-A-P500	53.8	0.10	0.999	14.3	3.8	0.944	9.4	289.4	0.826

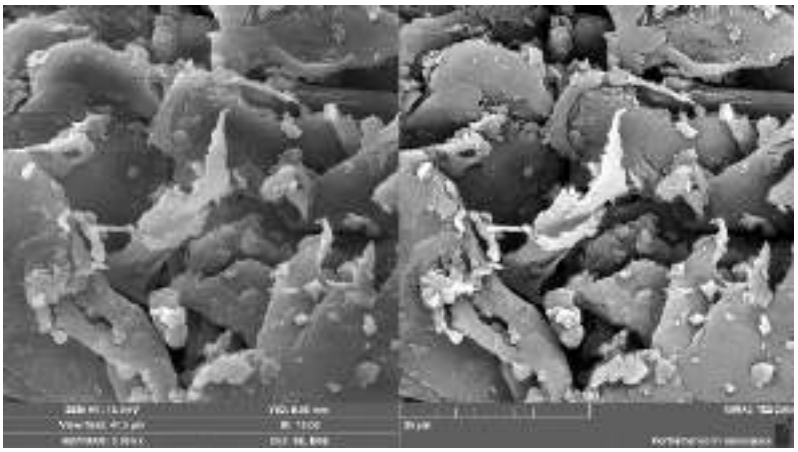

HÇ

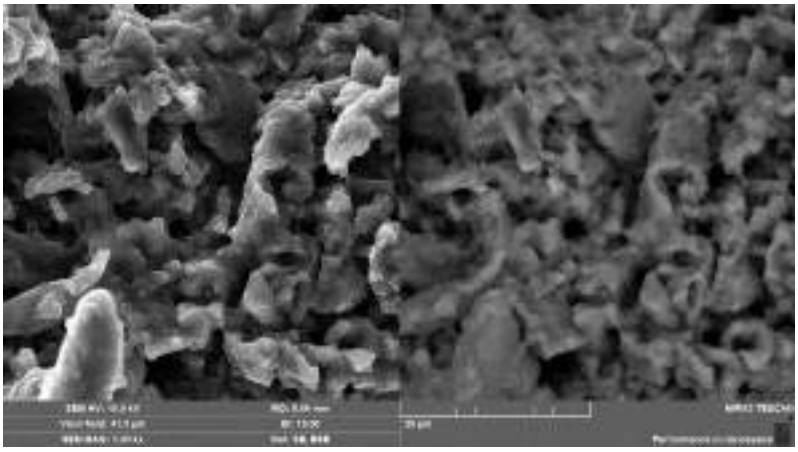

HÇ-A-MW

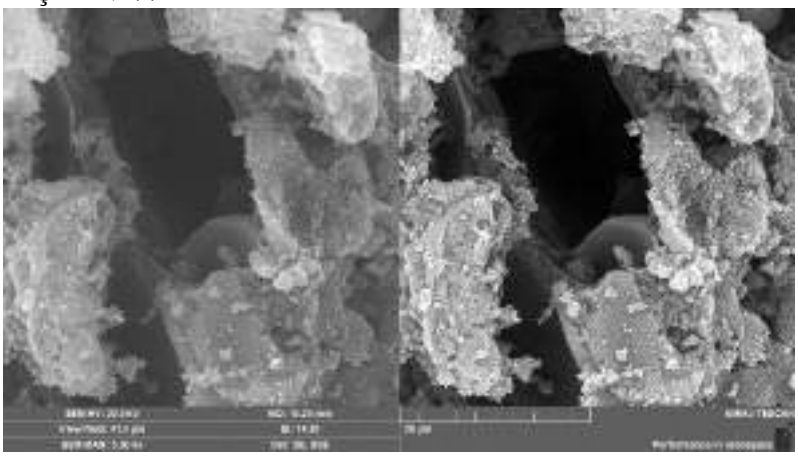

HÇ-A-P500

Şekil 1. HÇ, HÇ-A-MW ve HÇ-A-P500 örneklerinin SEM görünümleri

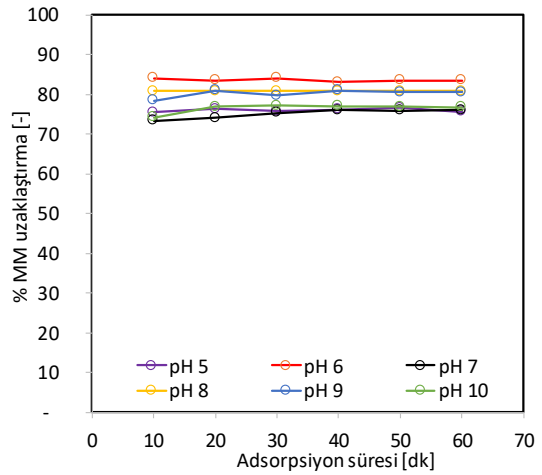

(a) HÇ

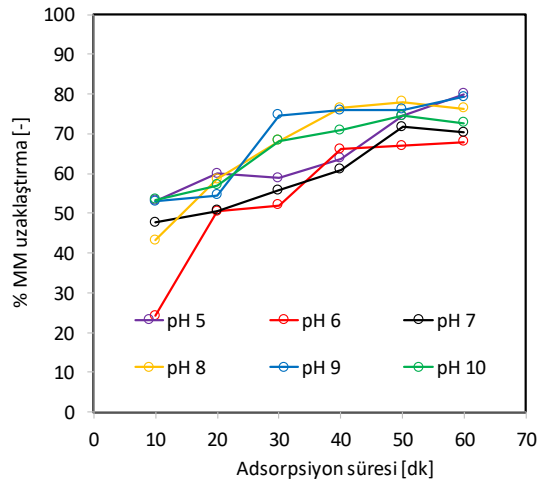

(b)HÇ-A-MW

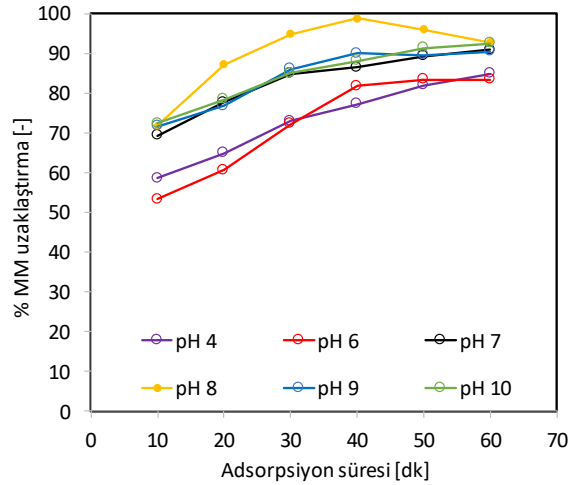

HÇ-A-P500

Şekil 2. Farklı pH değerlerinde adsorpsiyon yüzdesinin fonksiyonu olarak adsorbentlerin MM uzaklaştırma yüzdeleri

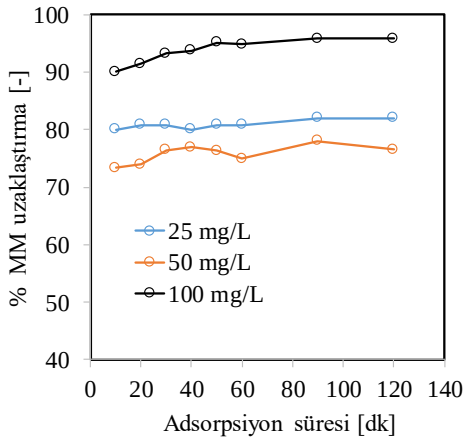

HÇ

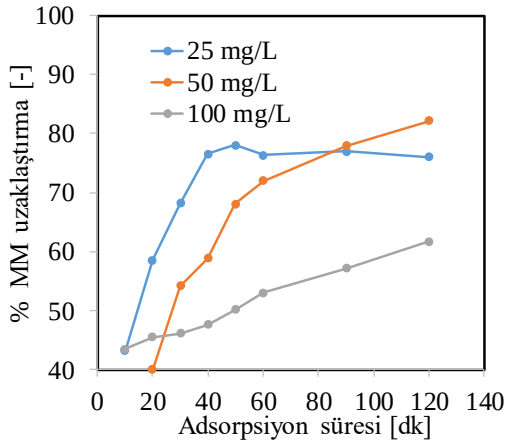

HÇ-A-P500

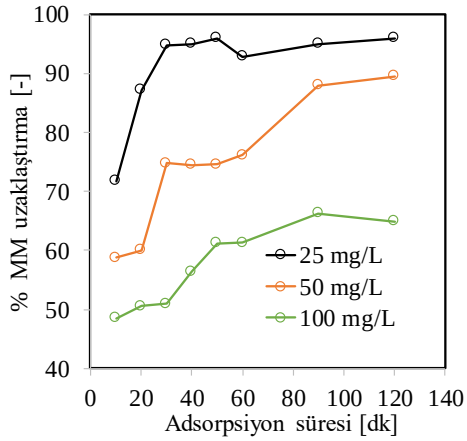

HÇ-A-P500

Şekil 3. MM başlangıç derişimin fonksiyonu olarak adsorpsiyon süresi ile adsorbentlerin % MM uzaklaştıra yüzdeleri

SONUÇ

Ham çay (HÇ) örneğinin fosforik asit varlığında mikrodalga (MW) ile aktive edilmiş ham çay (HÇ-A-MW) ve 500 ^{o}C'de pirolizi ile üretilmiş biyokömür örnekleri üretilmiştir. MW aktivasyonu HÇ'in karbon içeriğinde ve yüzey alanında artışa neden olmaktadır. Benzer olarak, HÇ'in asit varlığında pirolizi karbon içeriğini artırırken, yapıda mikro gözeneklerin oluşumuyla, yüzey alanında yüksek miktarda artışa neden olmuştur. XRD sonuçları, HÇ'in yapısındaki selülozun MW'de asit aktivasyonu ve asit piroliz ile amorf karbona dönüştüğünü göstermiştir. Örneklerin metilen mavisi (MM) adsorpsiyon sonuçlarına göre, Langmuir izoterminden sağlanan maksimum adsorpsiyon kapasitesi HÇ için 142. 8 mg g^{-1} bulunmuştur. HÇ-A-MW ve HÇ-A-P500 örneklerinin maksimum adsorpsiyon kapasiteleri sıra ile 41.6 ve 53.8 mg g^{-1} olarak bulunmuştur. HÇ örneğinin yüksek adsorpsiyon kapasitesi, yapısında yer alan selüloz ve ligninin varlığının bir sonucu olabilmektedir. HÇ-A-P500 örneğinin yüksek yüzey alanının aksine düşük MM adsorpsiyon kapasitesi, MM molekülerinin gözeneklere difüzyon probleminin olmasının bir sonucu olabilmektedir.

TEŞEKKÜR

Bu çalışma Sivas Cumhuriyet Üniversitesi Bilimsel Araştırma Fonu (M-657) tarafından desteklenmiştir.

KAYNAKLAR

Ahmed, M. J., Okoye, P. U., Hummadi, E. H. ve Hameed, B. H. (2019). High-performance porous biochar from the pyrolysis of natural and renewable seaweed (Gelidiella acerosa) and its application for the adsorption of methylene blue. *Bioresource Technology*. doi:10.1016/j.biortech.2019.01.054

Ania, C. O., Parra, J. B., Menéndez, J. A. ve Pis, J. J. (2005). Effect of microwave and conventional regeneration on the microporous and mesoporous network and on the adsorptive capacity of activated carbons. *Microporous and Mesoporous Materials*. doi:10.1016/j.micromeso.2005.06.013

Ding, G., Wang, B., Chen, L. ve Zhao, S. (2016). Simultaneous adsorption of methyl red and methylene blue onto biochar and an equilibrium modeling at high concentration. *Chemosphere*. doi:10.1016/j.chemosphere.2016.08.037

Ding, Z., Wan, Y., Hu, X., Wang, S., Zimmerman, A. R. ve Gao, B. (2016). Sorption of lead and methylene blue onto hickory biochars from different pyrolysis temperatures: Importance of physicochemical properties. *Journal of Industrial and Engineering Chemistry*. doi:10.1016/j.jiec.2016.03.035

Dourado, F., Gama, F. M., Chibowski, E. ve Mota, M. (1998). Characterization of cellulose surface free energy. *Journal of Adhesion Science and Technology*, *12*(10), 1081–1090. doi:10.1163/156856198X00740

El-Shafey, E. I., Ali, S. N. F., Al-Busafi, S. ve Al-Lawati, H. A. J. (2016). Preparation and characterization of surface functionalized activated carbons from date palm leaflets and application for methylene blue removal. *Journal of Environmental Chemical*

Engineering, *4*(3), 2713–2724. doi:10.1016/j.jece.2016.05.015
Girgis, B. S. ve El-Hendawy, A. N. A. (2002). Porosity development in activated carbons obtained from date pits under chemical activation with phosphoric acid. *Microporous and Mesoporous Materials*, *52*(2), 105–117. doi:10.1016/S1387-1811(01)00481-4
Güzel, F., Sayğılı, H., Akkaya Sayğılı, G., Koyuncu, F. ve Yılmaz, C. (2017). Optimal oxidation with nitric acid of biochar derived from pyrolysis of weeds and its application in removal of hazardous dye methylene blue from aqueous solution. *Journal of Cleaner Production*. doi:10.1016/j.jclepro.2017.01.029
Hameed, B. H. (2009). Spent tea leaves: A new non-conventional and low-cost adsorbent for removal of basic dye from aqueous solutions. *Journal of Hazardous Materials*. doi:10.1016/j.jhazmat.2008.04.019
Hoseinzadeh Hesas, R., Wan Daud, W. M. A., Sahu, J. N. ve Arami-Niya, A. (2013). The effects of a microwave heating method on the production of activated carbon from agricultural waste: A review. *Journal of Analytical and Applied Pyrolysis*. doi:10.1016/j.jaap.2012.12.019
Islam, M. A., Benhouria, A., Asif, M. ve Hameed, B. H. (2015). Methylene blue adsorption on factory-rejected tea activated carbon prepared by conjunction of hydrothermal carbonization and sodium hydroxide activation processes. *Journal of the Taiwan Institute of Chemical Engineers*, *52*, 57–64. doi:10.1016/j.jtice.2015.02.010
Kallel, F., Chaari, F., Bouaziz, F., Bettaieb, F., Ghorbel, R. ve Chaabouni, S. E. (2016). Sorption and desorption characteristics for the removal of a toxic dye, methylene blue from aqueous solution by a low cost agricultural by-product. *Journal of Molecular Liquids*, *219*, 279–288. doi:10.1016/j.molliq.2016.03.024
Lee, D. J., Cheng, Y. L., Wong, R. J. ve Wang, X. D. (2018). Adsorption removal of natural organic matters in waters using biochar. *Bioresource Technology*. doi:10.1016/j.biortech.2018.04.016
Lian, F., Cui, G., Liu, Z., Duo, L., Zhang, G. ve Xing, B. (2016). One-step synthesis of a novel N-doped microporous biochar derived from crop straws with high dye adsorption capacity. *Journal of Environmental Management*. doi:10.1016/j.jenvman.2016.03.043
Liu, L., Fan, S. ve Li, Y. (2018). Removal behavior of methylene blue from aqueous solution by tea waste: Kinetics, isotherms and mechanism. *International Journal of Environmental Research and Public Health*. doi:10.3390/ijerph15071321
Lonappan, L., Rouissi, T., Kaur Brar, S., Verma, M. ve Surampalli, R. Y. (2018). An insight into the adsorption of diclofenac on different biochars: Mechanisms, surface chemistry, and thermodynamics. *Bioresource Technology*. doi:10.1016/j.biortech.2017.10.039
Molina-Sabio, M. ve Rodríguez-Reinoso, F. (2004). Role of chemical activation in the development of carbon porosity. *Colloids and Surfaces A: Physicochemical and Engineering Aspects* içinde . doi:10.1016/j.colsurfa.2004.04.007
Nabais, J. M. V., Carrott, P. J. M., Carrott, M. M. L. R. ve Menéndez, J. A. (2004). Preparation and modification of activated carbon fibres by microwave heating. *Carbon* içinde . doi:10.1016/j.carbon.2004.01.033
Nasuha, N. ve Hameed, B. H. (2011). Adsorption of methylene blue from aqueous solution onto NaOH-modified rejected tea. *Chemical Engineering Journal*.

doi:10.1016/j.cej.2010.11.012
Nasuha, N., Hameed, B. H. ve Din, A. T. M. (2010). Rejected tea as a potential low-cost adsorbent for the removal of methylene blue. *Journal of Hazardous Materials*, *175*(1–3), 126–132. doi:10.1016/j.jhazmat.2009.09.138
Prahas, D., Kartika, Y., Indraswati, N. ve Ismadji, S. (2008). Activated carbon from jackfruit peel waste by H3PO4 chemical activation: Pore structure and surface chemistry characterization. *Chemical Engineering Journal*, *140*(1–3), 32–42. doi:10.1016/j.cej.2007.08.032
Puziy, A. M., Poddubnaya, O. I., Martínez-Alonso, A., Suárez-García, F. ve Tascón, J. M. D. (2005). Surface chemistry of phosphorus-containing carbons of lignocellulosic origin. *Carbon*. doi:10.1016/j.carbon.2005.06.014
Sewu, D. D., Boakye, P. ve Woo, S. H. (2017). Highly efficient adsorption of cationic dye by biochar produced with Korean cabbage waste. *Bioresource Technology*, *224*, 206–213. doi:10.1016/j.biortech.2016.11.009
Suárez-García, F., Martínez-Alonso, A. ve Tascón, J. M. D. (2002). Pyrolysis of apple pulp: Chemical activation with phosphoric acid. *Journal of Analytical and Applied Pyrolysis*. doi:10.1016/S0165-2370(01)00160-7
Tan, X., Liu, Y., Zeng, G., Wang, X., Hu, X., Gu, Y. ve Yang, Z. (2015). Application of biochar for the removal of pollutants from aqueous solutions. *Chemosphere*. doi:10.1016/j.chemosphere.2014.12.058
Tripathi, M., Sahu, J. N. ve Ganesan, P. (2016). Effect of process parameters on production of biochar from biomass waste through pyrolysis: A review. *Renewable and Sustainable Energy Reviews*. doi:10.1016/j.rser.2015.10.122
Uddin, M. T., Islam, M. A., Mahmud, S. ve Rukanuzzaman, M. (2009). Adsorptive removal of methylene blue by tea waste. *Journal of Hazardous Materials*, *164*(1), 53–60. doi:10.1016/j.jhazmat.2008.07.131
Uzun, B. B., Apaydin-Varol, E., Ateş, F., Özbay, N. ve Pütün, A. E. (2010). Synthetic fuel production from tea waste: Characterisation of bio-oil and bio-char. *Fuel*, *89*(1), 176–184. doi:10.1016/j.fuel.2009.08.040
Vithanage, M., Mayakaduwa, S. S., Herath, I., Ok, Y. S. ve Mohan, D. (2016). Kinetics, thermodynamics and mechanistic studies of carbofuran removal using biochars from tea waste and rice husks. *Chemosphere*. doi:10.1016/j.chemosphere.2015.11.002
Zheng, H., Guo, W., Li, S., Chen, Y., Wu, Q., Feng, X., … Chang, J. S. (2017). Adsorption of p-nitrophenols (PNP) on microalgal biochar: Analysis of high adsorption capacity and mechanism. *Bioresource Technology*. doi:10.1016/j.biortech.2017.05.025
Zhou, L., Liu, Y., Liu, S., Yin, Y., Zeng, G., Tan, X., … Huang, X. (2016). Investigation of the adsorption-reduction mechanisms of hexavalent chromium by ramie biochars of different pyrolytic temperatures. *Bioresource Technology*, *218*, 351–359. doi:10.1016/j.biortech.2016.06.102.

SYNHESIS AND CHARACTERIZATION OF ZnO PARTICLES

Ayten ATEŞ
Department of Chemical Engineering, Engineering Faculty, Sivas Cumhuriyet University, Sivas, Turkey
ates@cumhuriyet.edu.tr

ABSTRACT: A novel and easy route for preparing different size particles of zinc oxide is a mild sol–gel synthesis. ZnO particles were prepared by reacting zinc acetate dihydrate with NaOH in water at 50−60 °C and at varied pH (4, 6 and 9). The ZnO samples were characterized by scanning electron microscopy (SEM), X-ray diffraction (XRD) analysis and N_2 adsorption-desorption. pH and calcination temperature during preparation of ZnO affected significantly its particle size. ZnO particles synthesised involved mostly wurtzite structure as well as amorphous crystal structure. Surface areas of ZnO prepared are close to commercial ZnO. The surface area of ZnO prepared at pH 4 is higher than those of samples synthesised at higher pH values due to formation of micropores. ZnO prepared at pH 9 has particles with 20- 50 μm as well as aggregation of small crystallites (almost 10 μm). At higher calcination temperature (> 250 ^oC), no aggregation occurs and tiny single crystallite particles are obtained.

Key words: ZnO, sol- gel, calcination, pH

ZnO PARTİKÜLLERİNİN SENTEZİ VE KARAKTERİZASYONU

ÖZET: Farklı boyutlardaki çinko oksit parçacıklarını hazırlamak için yeni ve kolay bir yol ılımlı koşullarda sol-jel sentez yöntemidir. ZnO partikülleri, çinko asetat dihidratın NaOH ile sulu çözeltisinde 50−60 °C'de ve çeşitli pH (4, 6 ve 9) değerlerinde reaksiyonu ile hazırlanmıştır. . ZnO örnekleri taramalı elektron mikroskobu (SEM), X-ışını kırınımı (XRD) analizi ve N_2 adsorpsiyonu-desorpsiyonu ile karakterize edilmiştir. ZnO'nun hazırlanması sırasında pH ve kalsinasyon sıcaklığı, partikül büyüklüğünü önemli ölçüde etkilemektedir. Sentezlenen ZnO partikülleri, çoğunlukla wurtzite yapısının yanı sıra amorf kristal yapısını da içerir. Hazırlanan ZnO örneklerinin yüzey alanları ticari ZnO'ya yakındır. pH 4'te hazırlanan ZnO'nun yüzey alanı, mikro gözeneklerin oluşumu nedeniyle daha yüksek pH değerlerinde sentezlenen örneklerden daha yüksektir. pH 9'da hazırlanan ZnO, 20-50 μm partiküllerin yanı sıra küçük kristallerin (~ 10 μm) agregasyonuna sahiptir. Daha yüksek kalsinasyon sıcaklığında (> 250 ^oC), topaklaşma oluşmamakta ve küçük tek kristalli partiküller elde edilmektedir

Anahtar sözcükler: ZnO, sol-jel, kalsinasyon, pH

GİRİŞ

Çinko oksit (ZnO) yüksek yüzey alanı, yüksek elektron haraketliliği ve yüksek hassasiyet gibi üç eşsiz özelliğe ile ilgi çekmektedir. ZnO çok önemli II-VI yarı iletkenlerinden biri olarak bilinmekte olup, teknolojinin farklı alanlarında geniş bir şekilde uygulanmaktadır (Turgut, Duman ve Keskenler, 2015). ZnO partikülleri, katalizör uygulamalarına ek olarak güneş hücreleri, gaz sensörleri, anistatik kaplamalar, uzay endüstrisi gibi yaygın araştırma ve endüstriyel uygulamalar için gerekli olan optik, elektrik ve manyetik özelliklere sahiptir (Stefan, Ghica, Nistor, Maraloiu ve Plugaru, 2017).
Farklı boyut ve şekillerde ZnO'nun hazırlanması literatürde rapor edilmiştir (Eilers ve Tissue, 1995; Hu ve diğerleri, 2001; Jézéquel, Guenot, Jouini ve Fiévet, 1995; Milošević ve Uskoković, 1993; Nishizawa ve Yuasa, 1998; Zhou, Deng, Yi ve Liu, 1999). Nano boyutlu ZnO partiküllerini sentezlemek için çeşitli yöntemler rapor edilmektedir (Babu ve Hong, 2015). Örneğin gaz yoğunlaşması, poliol ortamında hidroliz, polimerik prekürsör yöntemi, aerosol sprey pirolizi, hidrotermal yöntem, sol-jel işlemi ve katı hal mikrodalga ayrışma yöntemi (Eilers ve Tissue, 1995; Hu ve diğerleri, 2001; Jézéquel ve diğerleri, 1995; Milošević ve Uskoković, 1993; Nishizawa ve Yuasa, 1998; Zhou ve diğerleri, 1999) şeklinde sıralanabilir . Bu yöntemlerden, sol-jel yöntemi yüksek yüzey alanlı parçacık üretmek, stokiometrinin mükemmel kontrolü, bileşim modifikasyonu, düşük maliyetli bir proses, ucuz ekipman gerekliliği gibi imkanla sunduğundan dolayı tercih edilmiştir (Aydin, El-Nasser, Aydin, Al-Ghamdi ve Yakuphanoglu, 2015; Wang ve diğerleri, 2015).
Bu çalışmada farklı pH (4, 5 ve 9) değerlerinde çinko asetat dihidratın NaOH ile sulu çözeltisinde 50−60 °C'de sol-jel yöntemi ile ZnO partikülleri sentezlenmiş ve XRD, N_2 adsorpsiyonu- desorpsiyonu ve SEM yöntemleri ile karakterize edilmiştir.

YÖNTEM

ZnO'in Hazırlama Yöntemi

1 M NaOH'in 5 ml, 0. 1 M $ZnAc_2.2H_2O$'in 25 ml'e eklenmiştir. HNO_3 ile pH 4 ve 6' ya ayarlanmıştır. Bir örnek ise doğal pH'ında (pH=9.2) bırakılmıştır. 60 C^o'de karışım1 saat karıştırılmıştır. Örnekler oda sıcaklığında 7 gün boyunca kurumaya bırakılmıştır. Kurumuş örnekler 250 oC'de 5 saat kalisne edilmiştir.

ZnO'in Karakterizasyonu

Sentezlenmiş ZnO örneklerinin kristal yapısı X-ışını kırınımı (XRD) (Rigaku SmartLab) ile analiz edilmiştir. ZnO örneklerinin yüzey alanı, gözenek hacmi ve gözenek boyut dağılımı yüksek çözünürlüklü yüzey alanı ölçüm cihazında (Quantachrome, AUTOSORB 1C) 77 K'de belirlenmiştir. Adsorpsiyon öncesinde örneklere 150 ^oC'de 1.3 Pa'a ulaşıncaya kadar vakum uygulanmıştır. Bu koşullarda örnek 8 saat tutulmuştur. Yüzey alanı, gözenek hacmi ve mikro gözenek hacmi sırayla çok noktalı BET (Brunauer, Emmett and Teller), t- plot ve DR (Dubinin–Radushkevic) yöntemleri ile belirlenmiştir. Gözenek boyut dağılımı ise Kelvin denklemini temel alan Barrett, Joyner, Halenda (BJH) yöntemi ile belirlenmiştir. Toplam gözenek hacmi (V_T), adsorpsiyonun ve desorpsiyonun aynı anda gerçekleştiği nokta olana P/P^o = 0.99'da

adsorplanmış hacim olarak alınmıştır. Tüm örnekler aynı yöntemlere göre analiz edilmiştir.
ZnO örneklerinin yüzey morfolojisi taramalı elektron mikroskobu (SEM, TESCAN, MIRA 3) ile örneklerin altın kaplaması sonucu görüntülenmiştir.

BULGULAR

$ZnAc_2.2H_2O$ ve NaOH kullanılarak sol- jel yöntemi ile farklı pH'larda ZnO katalizörleri sentezlenmiş ve 250 ^oC'de kalsine edilmiştir. Ticari ve sol-jel ile sentezlenmiş katalizörlerin XRD görünümleri Şekil 1'de verilmiştir. Ticari ile karşılaştırıldığında, sentezlenmiş ZnO'in pH'a bağlı olmaksızın pik şiddetleri düşük ve ticari ZnO'e ek bazı pikler gözlenmektedir. Pik şiddetleri kalsinasyon sıcaklığın 500 ^oC'e çıkarılmasıyla artırılabilir ve aynı zamanda yapıdaki bazı eser pikler de artan kalsinasyon sıcaklığı ile azaltılabilir. ZnO'in erime sıcaklığının düşük olması nedeniyle, düşük sıcaklıkta kalsine edilmiştir. Ayrıca, MDI-Jade (MDI-Jade 6) programı ile yapılan faz analizleri, ZnO partikülleri, çoğunlukla wurtzite kristal yapısına sahip olduğunu göstermiştir.
Ticari ve sol- jel ile üretilmiş farklı pH'da hazırlanmış ve 250 ^oC'de kalsine edilmiş ZnO örneklerininn N_2 adsorpsiyonu-desorpsiyonu izotermi ve diferansiyel gözenek boyut dağılımı Şekil 2'de verilmiştir. İzotermlerden hesaplanmış yüzey alanı, gözenek hacmi ve ortalama gözenek çapı verileri Tablo 1'de listelenmiştir. pH'a bağlı olmaksızın her üç örneğin de N_2 adsorpsiyonu-desorpsiyonu izotermi ve ticari ZnO'e benzerlik göstermektedir. Yüzey alanları da ticari ZnO'e yakındır. Tablo 1'den görülebileceği gibi pH artışı gözenek çapının artmasına neden olarak yüzey alanında azalmaya neden olmaktadır.

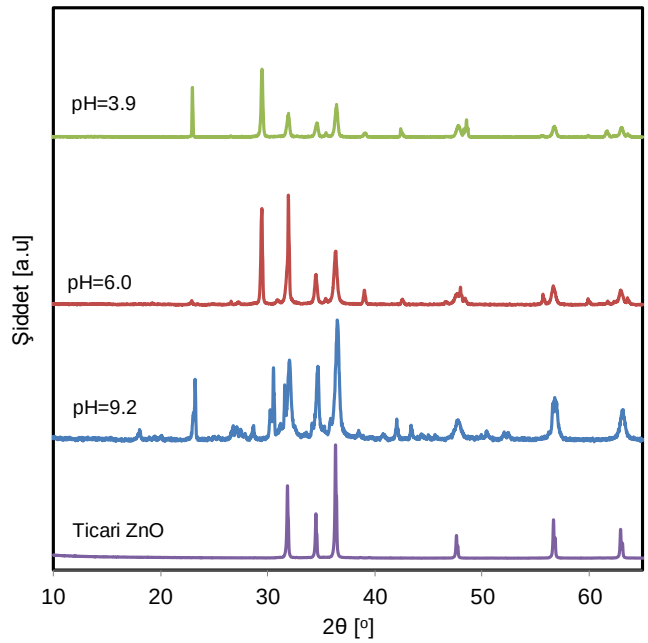

Şekil 1. Ticari ve sol- jel ile üretilmiş farklı pH'da hazırlanmış ve 250 ^oC'de kalsine edilmiş ZnO katalizörlerinin XRD görünümleri

Tablo 1. Ticari ve sol- jel ile üretilmiş farklı pH'da hazırlanmış ve 250 °C'de kalsine edilmiş ZnO örneklerinin yüzey alanı, gözenek hacmi ve ortalama gözenek çapı.

Örnek	SA[a] ($m^2.g^{-1}$)	V_T[b] ($cm^3.g^{-1}$)	D[c] (Å)
Ticari ZnO	9.7	0.04	167
ZnO-pH=9.2	7.1	0.07	213
ZnO-pH=6.0	8.7	0.02	49.8
ZnO-pH=3.9	13.4	0.02	-

[a] Çok noktalı BET yöntemi kullanılarak hesaplanmış yüzey alanı; [b] P/P^o = 0.99'da adsorplanmış hacim; [c] DFT ile belirlenmiş ortalama gözenek çapı.

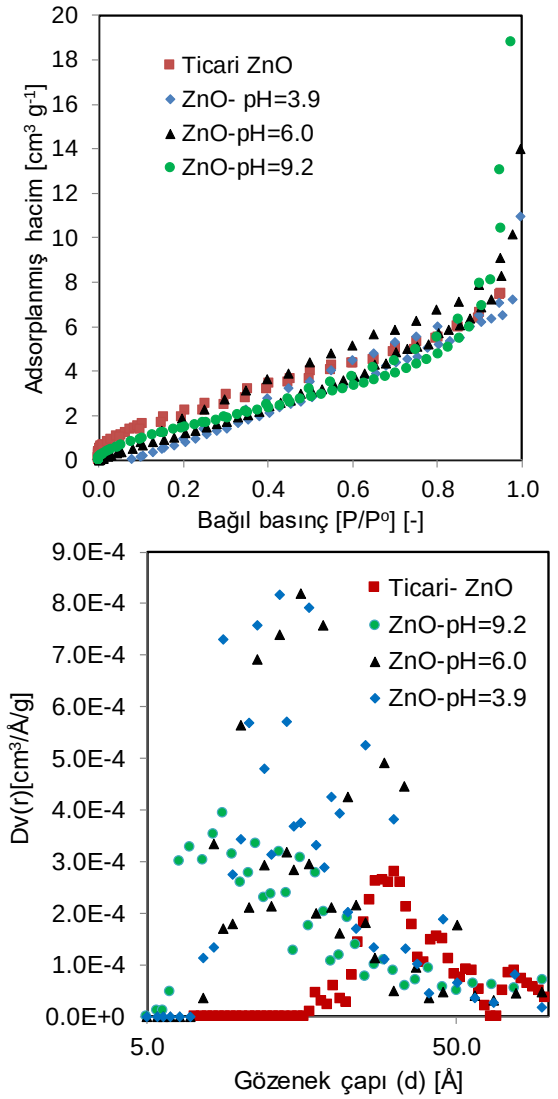

Şekil 2. Ticari ve sol- jel ile üretilmiş farklı pH'da hazırlanmış ve 250 °C'de kalsine edilmiş ZnO örneklerinin N_2 adsorpsiyonu-desorpsiyonu izotermi ve diferansiyel gözenek boyut dağılımı

Çözeltinin doğal sentezlenmiş pH değerinde (pH=9) ZnO örneğinin SEM görüntüsü Şekil 3'de gösterilmiştir. XRD verileri ile birlikte değerlendirildiğinde, ZnO örneği tam olarak kristallenmemiş olup, yapıda amorf yapılar bulunmaktadır. Bu nedenle pH 4 değerinde sentezlenmiş örnekte nano boyutlu tam kristallinmiş yapı gözlenmiş olup, bu yapı kalsinasyon sıcaklığının 350 ^{o}C'e artışı ile daha da belirginleşmektedir.

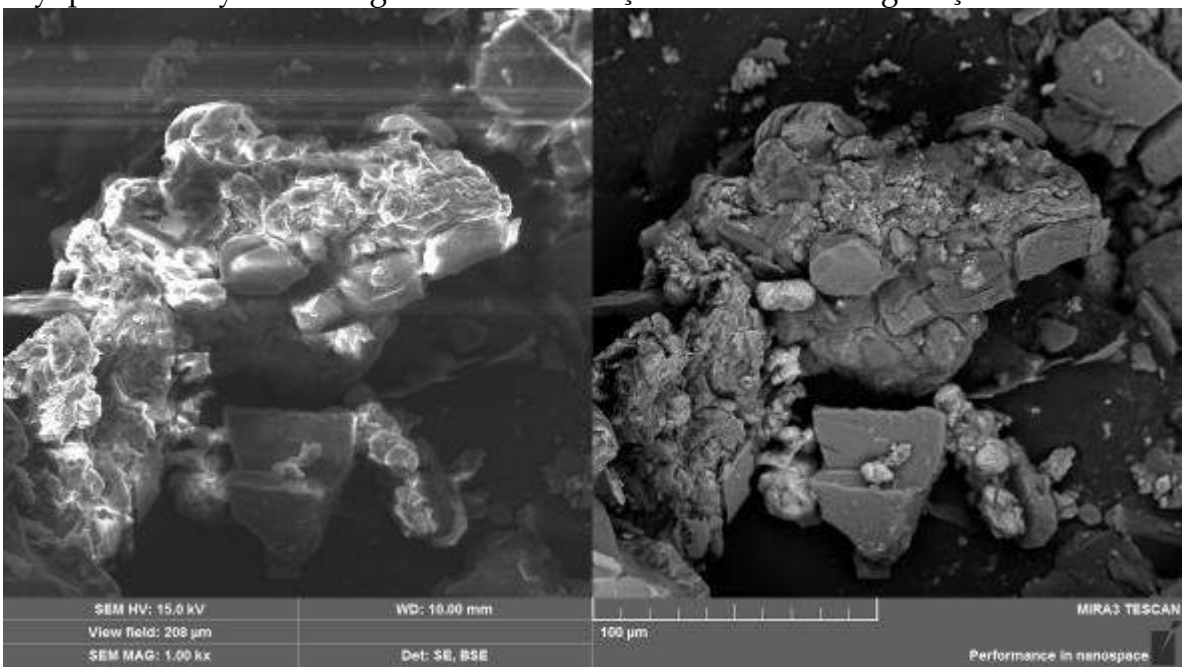

Şekil 3. Çözelti doğal pH değerinde sentezlenmiş ZnO örneğinin SEM görüntüsü

SONUÇLAR

Sol-jel yöntemi kullanılarak NaOH kullanılarak çinko asetat dihidrattan hekzagonal wurtzite faz yapısına sahip ZnO örneği sentezlenmiştir. XRD ve SEM sonuçları, hekzagonal wurtzite kristal yapısındaki ZnO partikülleri pH 6'da ve 350 ^{o}C'de 5 saat kalsinasyon ile gerçekleşmektedir.

TEŞEKKÜR

Çalışma Sivas Cumhuriyet Üniversitesi Bilimsel Araştırma Fonu (CUBAP) (M-742) ve TUBITAK (213M398)'ın desteği ile gerçekleştirilmiş olup, her iki kuruma desteklerinden dolayı teşekkür ederim.

KAYNAKLAR

Aydin, H., El-Nasser, H. M., Aydin, C., Al-Ghamdi, A. A. ve Yakuphanoglu, F. (2015). Synthesis and characterization of nanostructured undoped and Sn-doped ZnO thin films via sol-gel approach. *Applied Surface Science* içinde (C. 350, ss. 109–114). doi:10.1016/j.apsusc.2015.02.189

Babu, E. S. ve Hong, S. K. (2015). Effect of indium concentration on morphology of ZnO nanostructures grown by using CVD method and their application for H2 gas sensing. *Superlattices and Microstructures*, *82*, 349–356. doi:10.1016/j.spmi.2015.02.029

Eilers, H. ve Tissue, B. M. (1995). Synthesis of nanophase ZnO, Eu2O3, and ZrO2 by gas-phase condensation with cw-CO2 laser heating. *Materials Letters*, *24*(4), 261–265. doi:10.1016/0167-577X(95)00112-3

Hu, J. Q., Ma, X. L., Xie, Z. Y., Wong, N. B., Lee, C. S. ve Lee, S. T. (2001). Characterization of zinc oxide crystal whiskers grown by thermal evaporation. *Chemical Physics Letters*. doi:10.1016/S0009-2614(01)00720-5

Jézéquel, D., Guenot, J., Jouini, N. ve Fiévet, F. (1995). Submicrometer zinc oxide particles: Elaboration in polyol medium and morphological characteristics. *Journal of Materials Research*, *10*(1), 77–83. doi:10.1557/JMR.1995.0077

Milošević, O. ve Uskoković, D. (1993). Synthesis of BaTiO3 and ZnO varistor precursor powders by reaction spray pyrolysis. *Materials Science and Engineering: A*, *168*(2), 249–252. doi:10.1016/0921-5093(93)90736-X

Nishizawa, H. ve Yuasa, K. (1998). Preparation of highly oriented ZnO thin film under hydrothermal conditions. *Journal of Materials Science Letters*. doi:10.1023/A:1006601831316

Stefan, M., Ghica, D., Nistor, S. V., Maraloiu, A. V. ve Plugaru, R. (2017). Mn 2+ ions distribution in doped sol–gel deposited ZnO films. *Applied Surface Science*, *396*, 1880–1889. doi:10.1016/j.apsusc.2016.02.167

Turgut, G., Duman, S. ve Keskenler, E. F. (2015). The influence of Y contribution on crystallographic, topographic and optical properties of ZnO: A heterojunction diode application. *Superlattices and Microstructures*, *86*, 363–371. doi:10.1016/j.spmi.2015.08.002

Wang, L. W., Wu, F., Tian, D. X., Li, W. J., Fang, L., Kong, C. Y. ve Zhou, M. (2015). Effects of Na content on structural and optical properties of Na-doped ZnO thin films prepared by sol-gel method. *Journal of Alloys and Compounds*, *623*, 367–373. doi:10.1016/j.jallcom.2014.11.055

Zhou, Z., Deng, H., Yi, J. ve Liu, S. (1999). New method for preparation of zinc oxide whiskers. *Materials Research Bulletin*. doi:10.1016/S0025-5408(99)00183-X.

EFFECT OF AGITATION ON THE PROCESS OF BI METHANIZATION OF SLUDGE FROM LOW-TEMPERATURE WASTEWATER TREATMENT PLANTS

Soukaina AITLAHYANE

Laboratoire génie de l'Environnement, Faculté des sciences et techniques, Université Sultan Moulay Slimane, Béni Mellal

Laboratoire génie de l'Environnement, Equipe de recherche Hydr gie traitement olo et épuration des eaux et changement climatiques, Ecole Hassania des Travaux Publics, aitlahyanesoukaina@gmail.com

Zehor AITYACINE

Laboratoire génie de l'Environnement, Faculté des sciences et techniques, Université Sultan Moulay Slimane, Béni Mellal, azehor@yahoo.fr

Brahim LEKHLIF

Laboratoire génie de l'Environnement, Equipe de recherche Hydrologie traitement et épuration des eaux et changement climatiques, Ecole Hassania des Travaux Publics. lekhlif.brahim@ehtp.ac.ma

Hafida HANINE

Laboratoire de biointerface et biofilm Faculté des sciences et techniques, Université Sultan Moulay Slimane, Béni Mellal, Morocco. hanine1960@gmail.com

ABSTRACT: Wastewater treatment is one of the major environmental problems, particularly in developing countries such as Morocco. Their discharge into the natural environment has negative impacts on water resources and the environment. They are therefore purified to reduce the concentration of the main pollutants. Often biological remediation is used when wastewater contains biodegradable organic pollutants. This generally leads to treated water that can be discharged into the environment reused, or used as wastewater sludge. In the case of domestic or municipal water, this sludge has a fermentable character, which can have negative impacts on the environment especially when it is discharged directly into the environment. This sludge is subjected to various aerobic or anaerobic treatments to reduce the fermentable fraction. Anaerobic treatment seems more attractive because it makes it possible to eliminate organic matter, produce biogas and compost at the same time.

In this work, an experimental study was conducted on the anaerobic digestion of sewage sludge in two reactors at ambient temperature, operating with and without agitation, in order to evaluate the effect of the latter on the biological process.

Keywords: Bio-methanization, ambient temperature, agitation, sludge, COD, pH.

INTRODUCTION

Some solid wastes have a fermentable organic fraction which is an environmental problem. Their injection in the environment could be a real threat. Nevertheless, this organic character can be used wisely, by valorizing its potential in value-added products when subjected to anaerobic biological treatment, which, in addition to reducing negative effects (emission of bad odors, methane, mercaptans, etc.), makes it possible to produce biogas and sludge mineralization for soil amendment. This solid waste includes sludge from wastewater treatment plants. They are often disposed of in landfills or dumped into the natural environment. In Morocco, their quantity is estimated at 435.600 tones /year **(Elamin s. d.)**, and have a fermentable organic fraction between 50% and 70% **(eva bouille s. d.)** ;this is a good source for anaerobic biogas production, consisting mainly of methane 60 to 75%**(eva bouill e. d.)**, the equivalent of 128,000 tons of CH_4 per year .

The anaerobic biological bio-methanization treatment takes place in four stages (Figure 1). The first step is the hydrolysis of organic matter, such as proteins, fats, cellulose and starch.... These polymers such as amino acids, fatty acids and simple sugars are broken down into monomers.

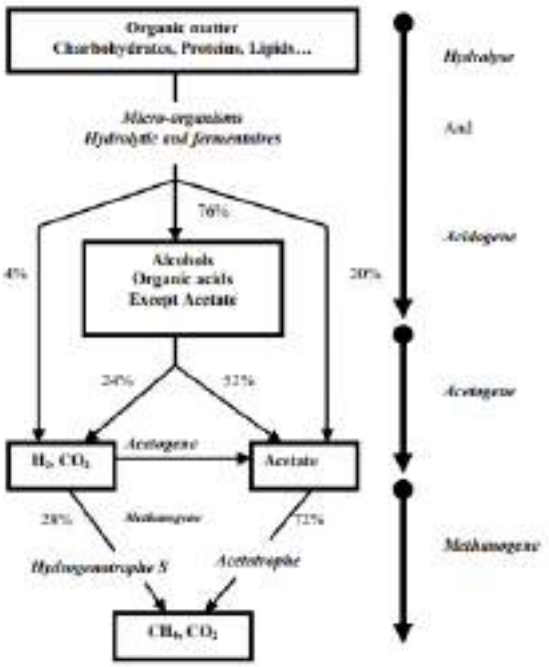

Figure 1. Diagram of the trophic chain of methanogenesis and its different stages (Moletta, 1993)

The second step is acidogenesis, during which the hydrolytes are oxidized to organic acids (e. g. lactates), alcohol (ethanol) or volatile fatty acids (propionate, butyrate and valerate).

In the third step, the resulting acidogenesis compounds are transformed into methane precursor products: acetic acid, carbon dioxide (CO_2) and hydrogen (H_2).

The fourth step biomethanization, which is done by two ways. One, it called hydrogenotrophic using hydrogenotrophic bacteria that draw their needs from the couple H_2/CO_2. These Bacteria get their energy from the reduction of carbon dioxide by hydrogen to produce methane according to the following reaction

$4H_2 + CO_2 \rightarrow CH_4 + 2H_2O$ (Reaction 1)

The other way called acetoclast where the strict anaerobic bacteria known as acetates, which extract their needs from the acetates, use acetate as their only carbon source (Reaction 2).

$CH_3COOH \rightarrow CH_4 + CO_2$ (Reaction 2)

The anaerobic process is a complex process Controlled by physico-chemical conditions such as the nature of the substrate, temperature, pH, agitation, etc. for instance, psychophilic digestion is optimal between in a temperature range around 6and 15°C, while mesophilic digestion in a range between 30-35°; for thermophilic anaerobic digestion, it is favored and most effective in temperatures above 45° because the reaction is accelerated by heat. However, anaerobic digestion is often used at mesophilic conditions, a compromise between performance and energy costs due to heating and especially because of its greater stability (LASKRI Nabila , Dépollution des déchets riches en matière organique (boues de station d'épuration et déchets d'abattoir) Par digestion anaérobie s. d.).

The anaerobic fermentation takes place in a pH range between 5.5 and 8 for all phases. For the acidogenesis phase, it is between 5.5 and 6.5 (Souza et al. 2012), for acetogenesis, it is near neutrality .For methanogens, the pH range is between 6 and 8 (Gourdon s. d.).

Agitation plays an important role in the anaerobic metabolic process. It ensures a good mixture, which improves the contact between the purifying bacteria and the sludge (Borole et al. 2006). Many studies have shown the importance of agitation on the fermentation process ; in the first hand JOHAN LINDMARK (Lindmark, Eriksson, et Thorin 2014) evaluated the effect of mixing by comparing tress régimes of mixing 150 RPM, 25 RPM and continuous mixing ; The results show that the biogas production is better with a speed of 25 RPM which reaches 240 Nml , while the speed of 150 RPM give a lower production of biogas ; the author found that strong agitation inhibits the anaerobic fermentation process.

In the second hand HAJJI(Hajji et Rhachi 2016) studied the influence of agitation on biogas production by comparing two reactors with and without agitation; he found a biogas production rate of a reaches a value of about 0.61m3/for a reactor of 40 rpm, then in the reactor without agitation the final volume of the final biogas is reduced to reduce up to 62%, most of these methanisation plants operate at temperatures of 37 or 55 °C, however MINDELE UKONDALEMBA(Ukondalemba et al. 2016) studied an anaerobic digestion with recirculation (type of agitation) of juice in the hydrolysis phase and acidogens at an ambient temperature of 25°C, results showed that 83% of the COD transformed into biogas.

This study aimed at studying the biomethanization of sludge from a wastewater treatment plant at ambient temperature. The objective is to evaluate the effect of agitation (agitated versus no agitated reactors) on the anaerobic biological process by comparing two identical reactors.

MATERIEL AND METHODS

Origin and characterization of the substrate

The sludge samples collected from a sludge wastewater treatment plant of the ONEE ("National Office of Water and Electricity ") of BOUREREG in Rabat-Morocco. This station receives discharges at an average rate = 86.4 m^3/d, and a peak flow rate = 259.2 m^3/d; these discharges have the following characteristics: COD = 15.1 Kg/d, BOD_5 = 9.0 Kg/d, mean TSS = 16.2 Kg/d. It is a station that produces between 7 kg/d to 10 m3/d of fresh liquid sludge in the open air on drying beds and then stocked.

Before their use, the dry sludge (Picture 1) was crushed and screened to generate small particles for better homogenization of the medium. To do this, the samples were spread on rectangular plates covered with filter paper, in the open air, then ground and sieved to obtain a homogeneous powder with a grain size of less than 2mm.

Photo 1. Dry raw and crushed sludge

Sludge characterization

Before use, the dry sludge (Picture 1) was crushed and sieved to obtain a homogeneous powder with a grain size of less than 2mm. Masses of 5 g of these sludge are added to 125 ml of distilled water. The mixture is then agitated every 15 min and then rested every 15 min for one hour (Imane s. d.) .

The mixture is recovered to determine the following parameters:

- The hydrogen potential (pH) is measured by using a multi-Parameter probe.

- The suspended matter has a centrifugation method,

- The electrical conductivity,

- Dissolved oxygen,

- Organic matter

- The chemical oxygen demand (COD) was determined according to the standard method (AFNOR T-101)[12]

- Metal measurement: ICP-AES

Batch digester operation

The experimental system (Figure 2) used for the anaerobic digestion of sludge consists of two opaque plastic tanks each with a volume of 30 L. Each tank was filled with 1,350 kg of dry sludge at a rate of (50 g/L). The tests were conducted at an average ambient temperature of 18°C for 40 days. In the reactor, agitation is ensured by using a mechanically controlled agitation motor with a speed of 40 rpm (Kalloum, Khelafi, et Djaafri s. d.).

The follow-up was made by daily samples of 50 ml from the reactors. The test was run during the month of February.

Figure 2 . Reactor for methanogenic digestion

RESULTS AND FINDINGS

Physical and Chemical Characteristics of Sludge

Table 1 presents the characteristics of the sludge from the BOUREGREGREG wastewater treatment plant.

Table 1 . Physical and chemical characteristics of the sludge from the BOUREGREGREG wastewater treatment plant

pH	Electrical conductivity (mS/cm)	Temperature (°C)	Dryness	COD (gO2/l)	Dry volatile matter (DVC)	Dissolved oxygen O2 mg/l
6,82	2,74	18	89,03%	10,89	63%	8,72

Elements	Cd	Ca	Cr	Cu	Fe	K	Mg	Mn	Na	Ni	Zn	Co	P	Pb	Ba	Al
Concentrations	3,023	71720	28,65	157,7	15470	1301	8808	252,4	1087	18,65	1652	4,077	--	138,5	518,6	7125

Unit	ppm	ppm	ppm	ppm	ppm	ppm	ppm	ppm	ppm	ppm	ppm	ppm	ppm	ppm	mg/L	mg/L

These results show that the sludge has a COD of 10.89 g/l, and contains a number of metals of significant concentrations, in this case Ca (71720 mg/L), Fe (15470 mg/L), Mg (8808 mg/L), Al (7125 mg/L) and to a lesser extent K (1301 mg/L), Na (1087 mg/L) and Zn (1652 mg/L). The organic matter content is 63%. The typology of this sludge is similar to that of domestic or municipal wastewater treatment plants (Choo-Kun s. d.) (Mehrez, Kalloum, et Khelifi s. d.) .

The evolutions of the different parameters of monitoring are presented in Figure 3. The analysis of some parameters shows differences indicating different kinetics of the biomethanization process in the two reactors.

The Temperature Variation

The temperature data shows a same trend between the two samples. The values vary between 15°C and 20°C. However, it is noted that temperature was higher in the agitated reactor.

The pH Variation

The pH profile shows two phases: the first probably corresponding to the hydrolysis and acetogenesis phase; the pH increases from 6.82 to 5.8 in the unagitated bioreactor and from 6.82 to 6.2 in the agitated bioreactor (Zhai et al. 2015) (Kalloum, Khelafi, et Djaafri s. d.), the second corresponding to the biomethanization phase; the pH increases from 5.8 to 6.5 in the unagitated bioreactor and from 6.2 to 7.5 in the agitated bioreactor. The agitated bioreactor has good pH conditions. This can be explained by a better use of volatile fatty acids (VFAs) by heterotrophic bacteria following their contact with the substrate enhanced by agitation process , as was highlighted by many authors (Mehrez, Kalloum, et Khelifi s. d.)(Monou et al. 2009). It can also be explained by the effects of agitation in favour of the emission of gases formed during the various stages of anaerobic fermentation, including in particular acidic materials: CO2, volatile fatty acids, H2S, etc. The partial hydrogen pressure is particularly important in the process. Excessively high hydrogen content prevents the conversion of intermediate products from being converted. As a result, organic acids accumulate and prevent the formation of methane (Wandrey et Aivasidis , 1983 Zur Reaktionstechnik der anaeroben Fermentation.pdf s. d.) ; Hydrogen sulphide has an inhibiting effect on methane formation. The inhibition thresholds encountered in methanogenic bacteria

vary according to the type of substrate and physicochemical conditions and range from 50 to 1000 mg/L.

The Variation of COD

The COD decreases for both bioreactors. This decrease is relatively more significant for the agitated bioreactor. The abatement rates achieved after 40 days are 60% and 81% respectively for the unagitated and agitated bioreactors. This difference is probably due to agitation, which on the one hand allows the organic matter and the purifying microorganisms present in solution to be mixed, as pointed out HAOQIN ZHOU AND ZHIYOU (Zhou et Wen - 2019 - Solid-State Anaerobic Digestion for Waste Manageme.pdf s. d.), and on the other hand to facilitate the liberation and disengagement that can remain trapped in the solid raw material HAOQIN ZHOU AND ZHIYOU (Zhou et Wen - 2019 - Solid-State Anaerobic Digestion for Waste Manageme.pdf s. d.), such as hydrogen formed during the acetogenesis step and H2S which can be generated by sulfate-reducing bacteria, both inhibitors of bacterial activity and particular for methanogenic bacteria with respect to hydrogen).

The work done by S. KALLOUM (Kalloum et Iddou - Utilisation du procédé de la digestion anaérobie p.pdf s. d.) by using manual agitation showed a significant reduction in the COD of sludge to conclude that anaerobic digestion is an efficient s method for the reduction of organic pollution and that the most of the organic matter that is present in the digester is biodegradable. SAMANTHA CRISTINA PINHO (Pinho et al. 2004) has confirmed that the agitation rate plays an important role in the solubilization of suspended organic matter. As well as the acceleration of the degradation of the COD in suspension. The same results were reported by I. MEHREZ (Mehrez, Kalloum, et Khelifi s. d.) T. Ahmed (Ahmed et al. s. d.) .

Variation of dissolved oxygen

The dissolved oxygen concentration values reflect the correct performance of anaerobic digestion in both bioreactors. By the third day, this concentration decreases below the value required for anaerobic conditions. It then reaches an average concentration of 0.3 mg/l. this value is comparable to what is being reported by other authors (Botheju - 2011 - Oxygen Effects in Anaerobic Digestion – A Review.pdf s. d.).

Variation of Conductivity

Electrical conductivity data showed an increase throughout the anaerobic fermentation process. This could be due to the appearance of small species of high ionic mobility and/or mineralization of the environment. This is more pronounced in the case of the agitated bioreactor. EL HAFIANE (el hafiane. d.) reported that

conductivity increases from the inlet to the outlet of the reactor, indicating progressive mineralization of the medium.

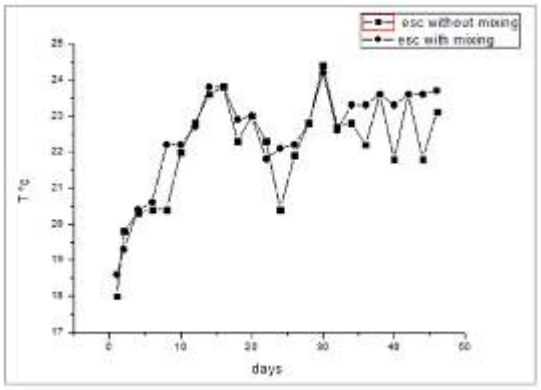

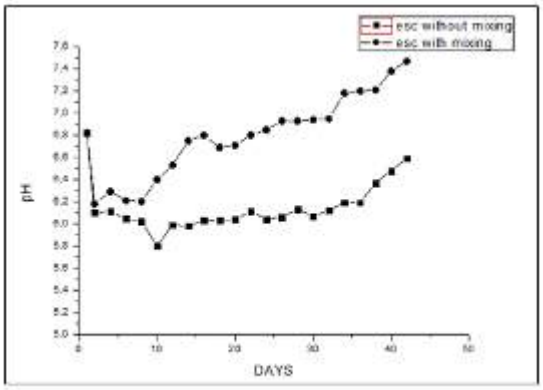

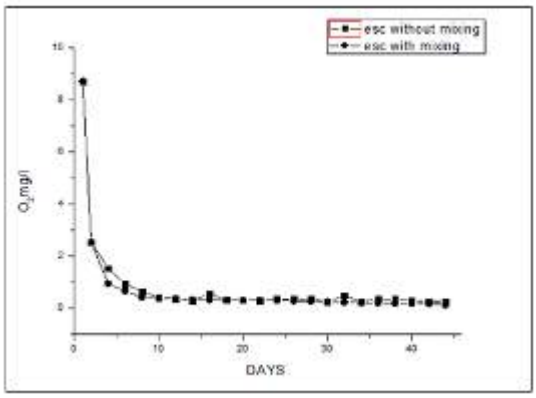

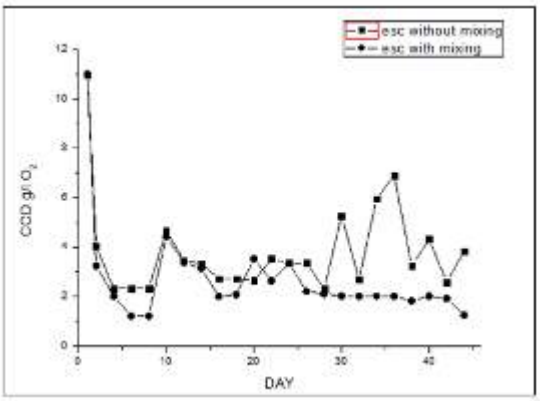

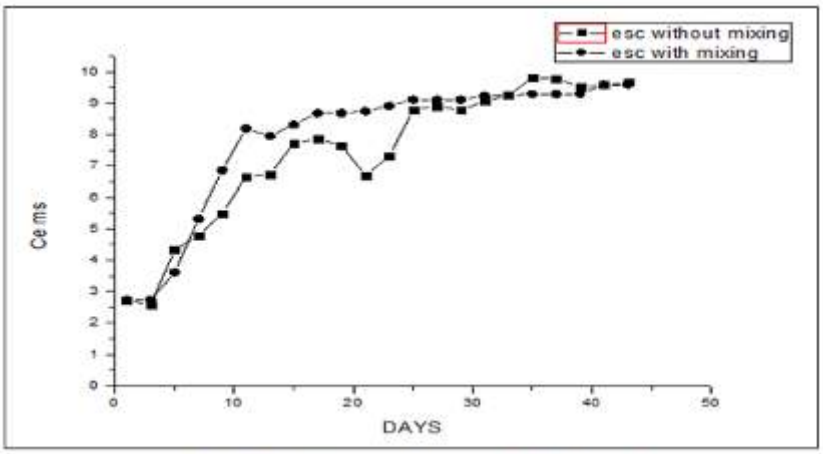

Figure 3 : Variation of the different monitoring parameters

CONCLUSIONS

The comparative psychrophilic anaerobic fermentation tests between two unagitated and agitated bioreactors have shown conclusive results regarding the role of agitation.

Indeed, the monitoring parameters: pH, COD, temperature, conductivity highlighted the effect of agitation. The anaerobic fermentation processes are to the advantage of the agitated reactor. The agitation promotes the homogenization of the reactor and a good mixing between the substrate and the purifying bacteria. It also makes it possible to break the layer of solid products that can float on the surface of the solution and thus prevent the escape of certain gases such as AGV, CO2, H2, H2S, which by their presence also make the medium acid and/or inhibit the activity of certain bacteria including methanogenic bacteria.

REFERENCE

Ahmed, TAHRI et al. « PRODUCTION DE BIOGAZ A PARTIR DU DECHET DE LA POMME DE ». : 6.

Borole, Abhijeet P et al. 2006. « Methane Production in a 100-L Upflow Bioreactor by Anaerobic Digestion of Farm Waste ». Applied Biochemistry and Biotechnology 129: 10.

Botheju - 2011 - «Oxygen Effects in Anaerobic Digestion – A Review.pdf ».

Choo-Kun, Marlène. « Intégration de la méthanisation des boues dans une filière alternative de traitement des eaux usées basée sur le procédé A/B: Vers la station d'épuration à énergie positive ». : 171.

EL HAFIANE, «Performances d'un système anaérobie à deux phases dans.pdf ».

Elamin, Pr AFILAL Mohamed. « Potentiel des déchets organiques et valorisation énergétique au Maroc ». : 12.

Eva BOUILLE 2004. « VA ». http://hmf.enseeiht.fr/travaux/CD0405/beiere/4/html/binome3/boue_met.htm (18 juillet 2019).

Gourdon, R. « Aide à la définition des déchets dits biodégradables, fermentescibles, méthanisables, compostables ». : 153.

Hajji, A, et M Rhachi. 2016. « Effet de l'agitation sur la digestion anaérobie des déchets ménagers et assimilés en régime mésophile ». : 8.

Imane, Melle HAMDANI. « Gestion des boues des stations d'épuration au Maroc : Quantification, caractérisation et options de traitement et de valorisation ». : 116.

Kalloum et Iddou -« Utilisation du procédé de la digestion anaérobie p.pdf ».

Kalloum, S, M Khelafi, et M Djaafri. « Etude de l'influence du pH sur la production du biogaz à partir des déchets ménagers ». : 5.

LASKRI Nabila , «Dépollution des déchets riches en matière organique (boues de station d'épuration et déchets d'abattoir) Par digestion anaérobie ».

Lindmark, Johan, Per Eriksson, et Eva Thorin. 2014. « The Effects of Different Mixing Intensities during Anaerobic Digestion of the Organic Fraction of Municipal Solid Waste ». Waste Management 34(8): 1391-97. https://linkinghub.elsevier.com/retrieve/pii/S0956053X14001469 (19 juillet 2019).

Mehrez, I, S Kalloum, et O Khelifi. « Study of Biogas Production from Lagooning Sludge by Anaerobic Digestion ». : 6.

Monou, M., N. Kythreotou, D. Fatta, et S.R. Smith. 2009. « Rapid Screening Procedure to Optimise the Anaerobic Codigestion of Industrial Biowastes and Agricultural Livestock Wastes in Cyprus ». Waste Management 29(2): 712-20. https://linkinghub.elsevier.com/retrieve/pii/S0956053X0800189X (30 juillet 2019).

Pinho, Samantha Cristina et al. 2004. « Influence of the Agitation Rate on the Treatment of Partially Soluble Wastewater in Anaerobic Sequencing Batch Biofilm Reactor ». Water Research 38(19): 4117-24. https://linkinghub.elsevier.com/retrieve/pii/S0043135404004129 (30 juillet 2019).

Souza, Milena Alves de et al. 2012. « Anaerobic Bio-Digestion of Concentrate Obtained in the Process of Ultra Filtration of Effluents from Tilapia Processing Unit ». Revista Brasileira de Zootecnia 41(2): 242-48. http://www.scielo.br/scielo.php?script=sci_arttext&pid=S1516-35982012000200002&lng=en&tlng=en (19 juillet 2019).

Ukondalemba, Léonard Mindele et al. 2016. « [VALORIZATION OF ORAGANIC HOUSEHOLD WASTE AND SEPTIC TANK SLUDGE BY ANAEROBIC DIGESTION] ». 20(2): 10.

Eva BOUILLE 2004. « Valorisation des boues de la station d'épuration en biogaz ». http://hmf.enseeiht.fr/travaux/CD0405/beiere/4/html/binome3/biogaz.htm (18 juillet 2019).

Wandrey et Aivasidis , 1983 « Zur Reaktionstechnik der anaeroben Fermentation.pdf ».

Zhai, Ningning et al. 2015. « Effect of Initial PH on Anaerobic Co-Digestion of Kitchen Waste and Cow Manure ». Waste Management 38: 126-31. https://linkinghub.elsevier.com/retrieve/pii/S0956053X15000082 (19 juillet 2019).

Zhou et Wen - 2019 - «Solid-State Anaerobic Digestion for Waste Manageme.pdf ».

TREND ANALYSIS OF MONTHLY MEAN STREAMFLOW DATA WITH MANN-KENDALL AND INNOVATIVE ŞEN METHOD IN PAMUKLUK RIVER DILAVER BRIDGE STATION

Yavuz AVŞAROĞLU
Harran University, Faculty of Engineering, Civil Engineering Department
yavuzavsaroglu@gmail.com

Veysel GÜMÜŞ
Harran University, Faculty of Engineering, Civil Engineering Department
gumus@harran.edu.tr

Oğuz ŞİMŞEK
Harran University, Faculty of Engineering, Civil Engineering Department
oguzsimsek@harran.edu.tr

ABSTRACT: In this study, the trend of monthly mean streamflow values of D26A008 streamflow gauge station (named as " Pamukluk Deresi Dilaver Köprüsü") in Tigris Basin, which is one of the most important basin of Turkey, is determined by non-parametric Mann-Kendall and Innovative Trend Analysis (ITA) methods. Trend slopes are determined by Sen's trend slope method. The results of the study show that according to Mann-Kendall test, a significant decreasing trend in March and a significant increasing trend in August are detected. The highest decreasing slope is calculated as -1.0765 m^3/s/decade in March with Sen's slope method. According to ITA method, generally there is no change in low streamflow values, but a decreasing trend is observed in average and high streamflow values. Also, the result of ITA analysis for the monthly and annual mean streamflow values, generally increasing trends are determined in October, November, August and September, and generally decreasing trend is observed In April, May and June.

Key words: Tigris basin, trend analysis, Mann-Kendall method, Innovative Trend Analysis

PAMUKLUK DERESİ DİLAVER KÖPRÜSÜ İSTASYONU AKIM DEĞERLERİNİN MANN-KENDALL VE YENİLİKÇİ ŞEN YÖNTEMLERİYLE TREND ANALİZİ

ÖZET: Bu çalışmada, Türkiye'nin en önemli havzalarından biri olan Dicle Havzası'nda bulunan D26A008 numaralı "Pamukluk Deresi Dilaver Köprüsü" akım gözlem istasyonuna ait aylık ortalama akım değerlerinin trendi parametrik olmayan Mann-Kendall testi ve Yenilikçi Şen yöntemi (Innovative Trend Analysis-ITA) ile belirlenmiştir. Trend eğimleri Sen'in trend eğim metodu ile belirlenmiştir. Çalışma sonucunda, Mann-Kendall testine göre, mart ayında azalan, ağustos ayında ise artan yönde anlamlı trend varlığına rastlanmıştır. Sen'in trend eğim metoduna göre elde en yüksek azalma miktarı, mart ayında -1.0765 m3/s/10yıl olarak bulunmuştur. ITA yöntemine göre düşük akım değerlerinde genel olarak bir değişim olmadığı, ancak orta ve yüksek akım değerlerinde bir azalma eğilimi gözlenmiştir. Aylık ve yıllık ortalama akım değerlerine göre ise ekim, kasım, ağustos ve eylül aylarında genel olarak artan yönde; nisan, mayıs ve haziran aylarında ise genel olarak azalan yönde bir eğilim görülmüştür.

Anahtar sözcükler: Dicle havzası, trend analizi, Mann-Kendall yöntemi, Yenilikçi Şen yöntemi

GİRİŞ

Sera gazı emisyonları düzenli bir şekilde artmakta ve küresel ısınma ile hidrolojik ve meteorolojik olaylar üzerinde iklim değişikliğinin etkisi belirgin bir şekilde görülmektedir. Taşkın ve kuraklık gibi olağanüstü durumlara karşı su yönetiminde önlemler alabilmek için hidrolojik ve meteorolojik verilerin eğilimlerinin bilinmesi gerekmektedir. Hidro-meteoroloji verilerin eğilimlerinin belirlenesinde parametrik olmayan yani veri setinin herhangi bir dağılıma uyma zorunluluğu aramayan testlerin başında gelen Mann-Kendall (MK) (Mann, 1945, Kendall, 1975) dünyada farklı bölgelerde sıklıkla kullanılmaktadır (Yenigün ve ark, 2008, Gocic ve Trajkovic, 2013; Ahmad ve ark., 2015; Ahmadi ve ark., 2018; Hadi ve Tombul, 2018, Gümüş, 2019). Bu testin yanında trendlerin eğimlerinin belirlenmesinde yine parametrik olmayan Sen'in trend eğim metodu da (Sen, 1968) kullanılmaktadır (Yenigün ve ark, 2008, Gümüş, 2019).

Öte yandan, Şen (2012) tarafından önerilen 1: 1 düz çizgi (45 °) yapısı ile kullanılan Yenilikçi Şen yöntemi (Innovative Trend Analysis-ITA) yöntemi, diğer trend yöntemlerinden farklı olarak monotonik trend değeri vermek yerine daha açıklayıcı bir yaklaşım ortaya koymaktadır. Son yıllarda sıklıkla kullanılana bu yöntem verilerin trendlerini değer bazlı ve grafiksel olarak ortaya koymaktadır. Örneğin, Sonali ve

Kumar (2013), ITA yöntemi dahil olmak üzere farklı trend analizi yöntemlerini kullanarak Hindistan'daki sıcaklık trendlerini tespit etmiştir. Ayrıca, Saplıoğlu ve ark. (2014), Türkiye'nin batı Akdeniz havzasındaki akımları, Dabanlı ve ark. (2016) ise Türkiye'deki Ergene havzasındaki hidro-meteorolojik kayıtların trendlerini Mann-Kendall testi ve ITA yöntemleri ile belirlemişlerdir.

Bu çalışma kapsamında, Dicle Havzası'nda yer alan D26A008 numaralı "Pamukluk Deresi Dilaver Köprüsü" istasyonuna ait aylık akım verileri kullanılarak aylık ve yıllık ortalama değerlerin parametrik olmayan Mann-Kendall ve sonuçları grafiksel olarak veren ITA yöntemine göre yapılmıştır. Ayrıca trend eğimleri Sen'in trend eğim metoduna göre belirlenmiştir.

ÇALIŞMA ALANI

Bu çalışmada Dicle Havzası'nda bulunan ve DSİ (Devlet Su İşleri) tarafından işletilen D26A008 numaralı "Pamukluk Deresi Dilaver Köprüsü" isimli akım gözlem istasyonuna ait aylık ortalama akım verileri kullanılarak trend analizi yapılmıştır (Şekil 1). Kullanılan bu istasyona ait veri aralığı 1974-2015 yılları arasında olup, istasyon 40°14'0" (D) - 37°40'0" (K) koordinatlarında bulunmaktadır. D26A008 istasyonu 702 m yükseklikte bulunmakta ve 648 km²'lik bir yağış alanını temsil etmektedir.

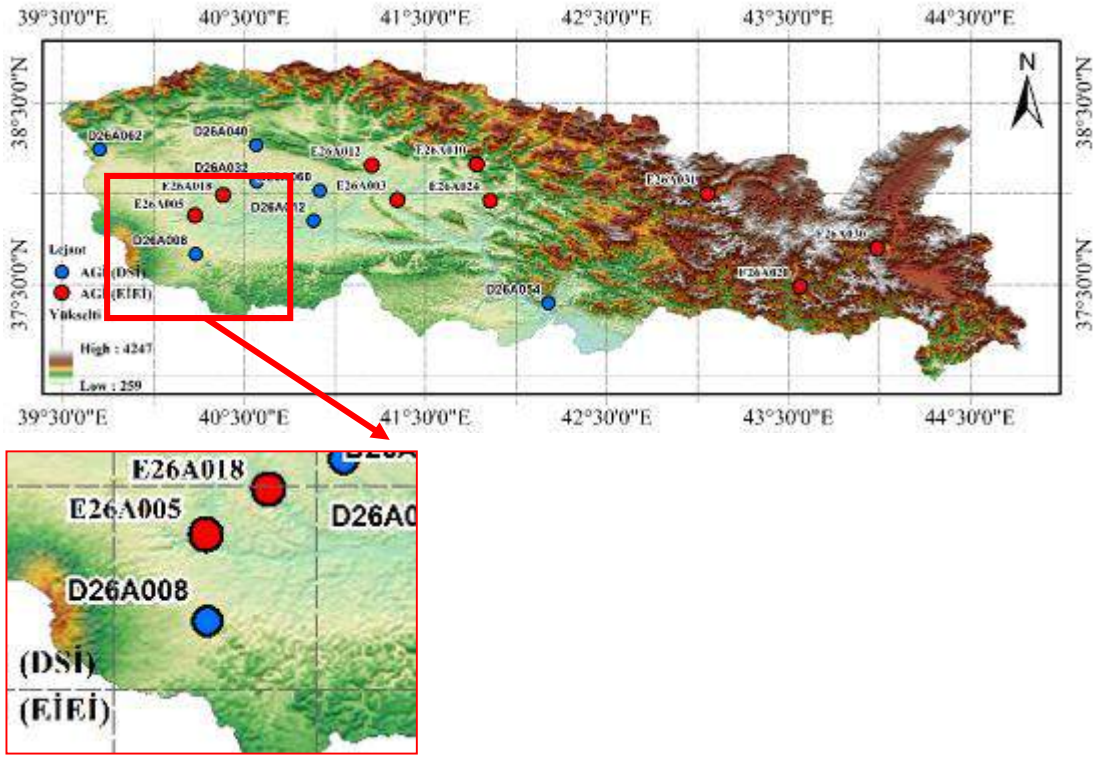

Şekil 1. Çalışma Alanı

YÖNTEM

Hidrolojik büyüklükler (yağış, akış) zaman içinde rasgele değişen karakterde olduğundan sürekli bir azalma veya artma eğiliminin araştırılması özel yöntemler kullanmayı gerektirir (Helsel ve Hirsch, 1992).

Veri setinin herhangi bir dağılıma uyma zorunluluğu olmaması nedeniyle, parametrik olmayan testlerin kullanılması parametrik testlere oranla daha uygundur. Parametrik olmayan trend testlerinin uygulanabilmesi için ise zaman serisinin iç bağımlılığının yani seri korelasyonun olmaması gerekmektedir. Von Storch ve Navarra (1995) trend varlığını belirlemek için kullanılacak testi uygulanmadan önce iç bağımlılığın zaman serisinden kaldırılması için "pre-whitening" yöntemini önermektedir. Bu çalışma kapsamında Salas (1980) tarafından önerilen yöntem ile iç bağımlılık etkisi giderilmiştir.

İç bağımlılık etkisi giderilmiş akım verilerine Mann-Kendall (Mann, 1945; Kendall, 1948) ve ITA (Şen, 2012) yöntemleri ile trend analizi yapılmış, trend eğimleri Sen'in trend eğim metoduna (Sen, 1968) göre belirlenmiştir.

BULGULAR

Diyarbakır-Mardin yolunun 8. km'sinde bulunan ve DSİ tarafından işletilen D26A008 numaralı istasyonun, 1974-2015 yılları arasındaki 42 yıla ait akım değerlerinin aylık zamansal değişimleri Şekil 2'de verilmiştir. Buna göre mart ayı, akımın en fazla geldiği ay olarak, ağustos ayı ise akımın en az geldiği ay olduğu görülmektedir. Ayrıca D26A008 numaralı istasyonumuzda ekim, kasım, haziran, temmuz, ağustos ve eylül aylarında, ölçüm alınan derenin kuru olduğu, yani akım değerinin 0 olduğu yıllar belirlenmiştir. Buna göre, en fazla kuru yıl 14 yıl ile ağustos ayında, en yüksek akım değeri 18.76 m^3/s ile 1976 yılının nisan ayında ölçülmüştür. Ayrıca Şekil 2'ye göre, en yüksek doğrusal eğim -0.145 ile mart ayında, en düşük eğim değeri ise 0.0003 ile temmuz ayında belirlenmiştir.

Trend analizi yapılmadan önce akımlarda iç bağımlılık etkisinin belirlenebilmesi için Salas ve ark. (1980) tarafından önerilen yöntem ile iç bağımlılığın olup olmadığı belirlenmiş ve iç bağımlılık belirlenen verilerde iç bağımlılık etkisi giderilmiştir. Salas ve ark. (1980) yöntemine göre elde edilen seri korelasyon değerlerinin veriler için dağılımı Şekil 3'te verilmiştir. Buna göre, D26A008 istasyonunda ağustos ve eylül aylarında iç bağımlılık belirlenmiş ve iç bağımlılık etkisi giderilmiştir. Tablo 1'de, iç bağımlılık etkisi giderilmiş verilere ait parametrik olmayan Mann-Kendall yöntemiyle elde edilen trend analizi sonuçları ile, Sen'in trend eğim metodu ile elde edilen trend eğimleri verilmiştir. Aynı sonuçların grafiksel gösterimleri Şekil 4'te verilmiştir. Buna

göre, mart ayında %95 güven aralığında azalan, ağustos ayında ise artan yönde anlamlı trend varlığına rastlanmıştır. Nisan ayında ise sadece Mann-Kendall yöntemine göre ve %90 güven aralığında azalan yönde trend belirlenmiştir.

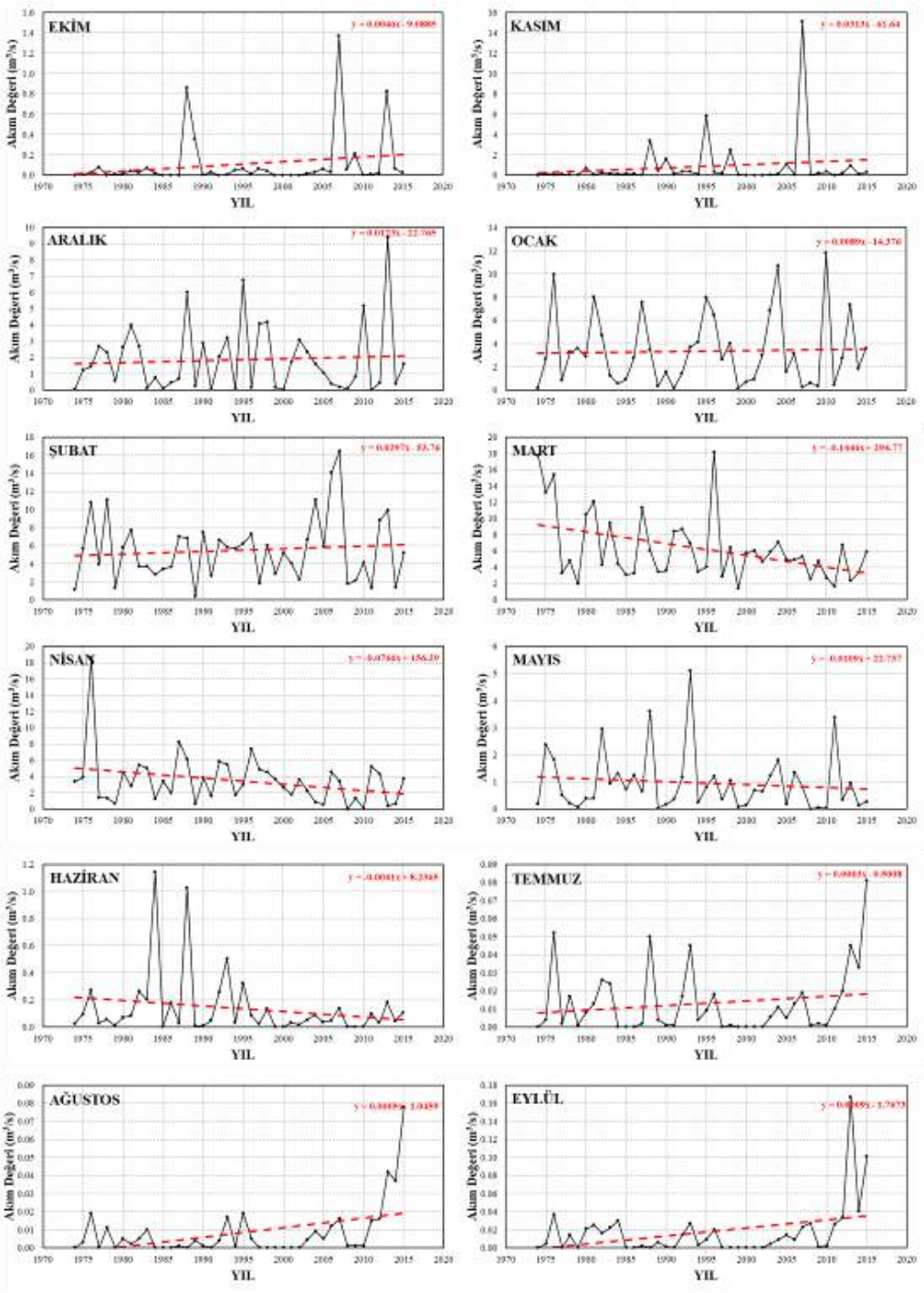

Şekil 2. Akım Değerlerinin Zamansal Değişimi

Tablo 1. Trend Analizi Sonuçları

Dönem	Mann-Kendall (Z)	Trend Eğimi ($m^3/s/yıl$)	Anlamlı Trend
Ekim	1.395	0.00043	Yok
Kasım	0.954	0.00164	Yok
Aralık	-0.249	-0.00236	Yok
Ocak	0.022	0.00155	Yok
Şubat	0.195	0.00514	Yok
Mart	***-2.233***	-0.10765	***Var (↓) %95***
Nisan	**-1.647**	-0.04411	**Var (↓) %90**
Mayıs	-1.062	-0.00610	Yok
Haziran	-0.932	-0.00073	Yok
Temmuz	1.048	0.00006	Yok
Ağustos	***2.242***	0.00009	***Var (↑) %95***
Eylül	1.001	0.00017	Yok
Yıllık Ort.	-0.650	-0.00866	Yok

Şekil 5'te ise Sen'in trend eğim metoduna göre, aylara göre elde edilen trend eğim değerleri 10 yıllık sürede değişimi verilmiştir. Buna göre 10 yıllık en yüksek azalma miktarı, mart ayında -1.0765 m^3/s olarak bulunmuş ve bu değerin elde edilen doğrusal trend değerleri ile paralel olduğu belirlenmiştir.

Akım değerlerinin trendinin belirlenmesi için parametrik olmayan Mann-Kendall yönteminin yanında ITA yöntemi de kullanılmıştır. Bu bağlamda, tüm akım değerlerinin ITA yöntemine göre sonuçları Şekil 6'da verilmiştir. Buna göre, yaklaşık olarak 0-5 m^3/s arasında olan düşük akım değerlerinde genel olarak bir değişim olmadığı, ancak 5-12 m^3/s arasındaki orta akım değerlerinde ve 12-20 m^3/s arasındaki yüksek akım değerlerinde bir azalma eğilimi gözlenmektedir.

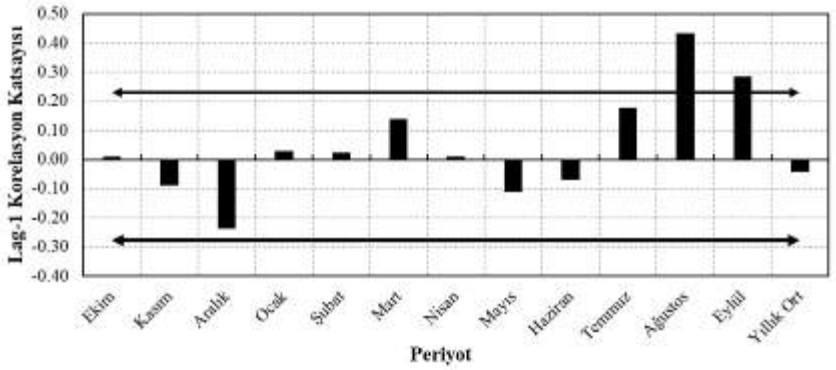

Şekil 3. Seri Korelasyon Sonuçları

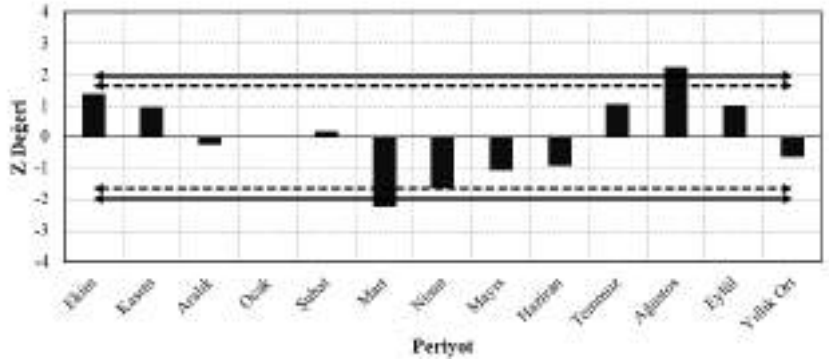

Şekil 4. Akım Değerlerinin Trend Analizi Sonuçları

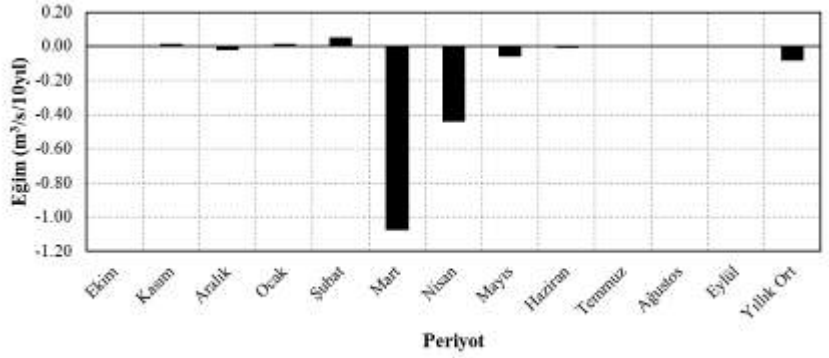

Şekil 5. Akım Değerlerinin Trend Eğim Değerleri

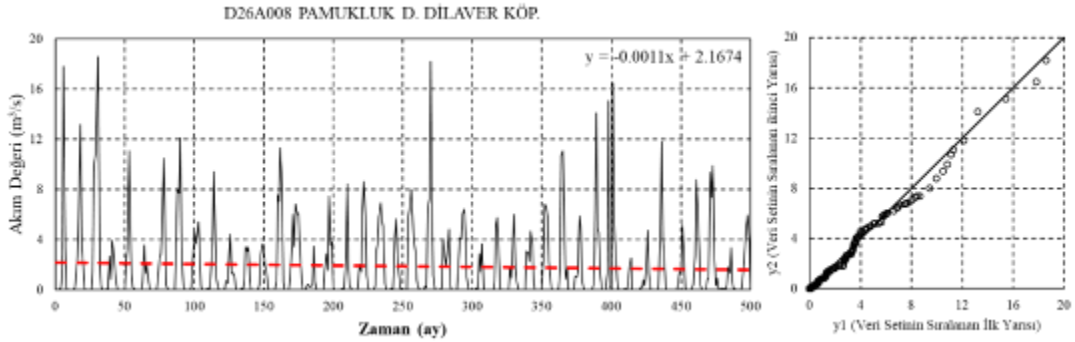

Şekil 6. Tüm akım değerlerinin ITA yöntemi ile trend analizi

Şekil 7'de ITA yöntemine göre aylık akım değerlerinin analizi verilmiştir. Buna göre, ekim, kasım, ağustos ve eylül aylarında genel olarak artan yönde; nisan, mayıs ve haziran aylarında ise genel olarak azalan yönde bir eğilim görülmüştür. Şekil 7'ye göre, aralık ayında 3 m^3/s'nin, ocak ayında 4 m^3/s, şubat ayında 6 m^3/s üstündeki değerlerde bir artma, mart ayında 5 m^3/s'nin üzerindeki değerlerde ise bir azalma eğilimi belirlenmiştir. Temmuz ayı ve yıllık ortalama için genel olarak akım değerleri 45º'lik çizgi üzerinde olduğu, yani herhangi bir trend varlığının olmadığı sonucuna varılmıştır.

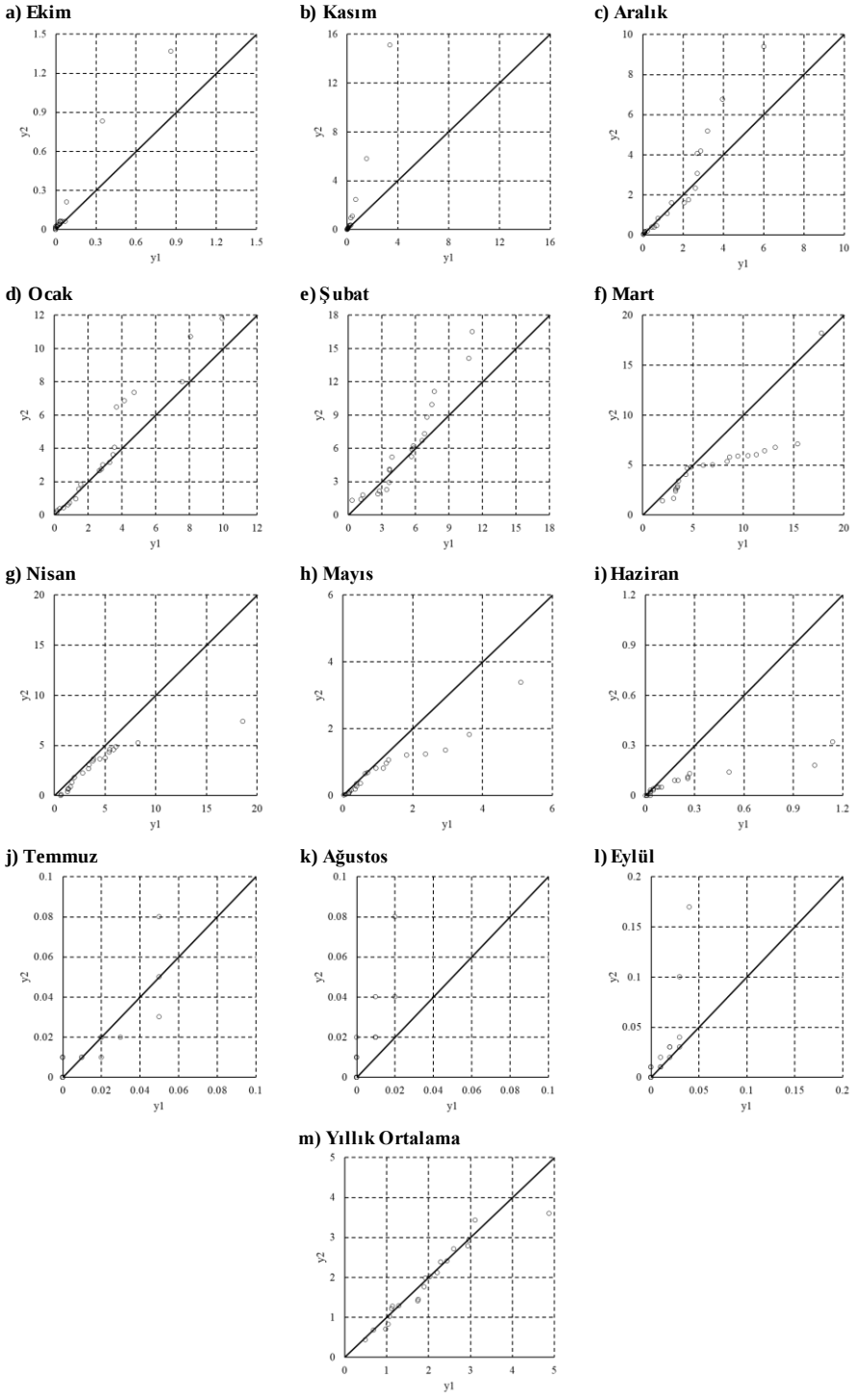

Şekil 7. D26A008 İstasyonuna Ait Akımların Aylara Göre ITA Yöntemi İle Trend Analizi

SONUÇLAR

Bu çalışmada Dicle Havzası'nda yer alan D26A008 numaralı "Pamukluk Deresi Dilaver Köprüsü" istasyonuna ait aylık akım verileri kullanılarak, aylık ve yıllık ortalama değerlerin trend analizi parametrik olmayan Mann-Kendall ve ITA yöntemlerine göre yapılmıştır. Ayrıca trend eğimleri Sen'in trend eğim metoduna göre belirlenmiş ve elde edilen sonuçlar aşağıda kısaca özetlenmiştir. Buna göre;

- En yüksek doğrusal eğim -0.145 ile mart ayında, en düşük eğim değeri ise 0.0003 ile temmuz ayında belirlenmiştir.
- Akımlarda iç bağımlılığın olup olmadığı belirlenmiş ve iç bağımlılık belirlenen verilerde iç bağımlılık etkisi giderilmiştir.
- MK yöntemine göre, mart ayında %95 güven aralığında azalan, ağustos ayında ise artan yönde anlamlı trend varlığına rastlanmıştır. %90 güven aralığında ise nisan ayında azalan yönde anlamlı trend varlığına rastlanmıştır.
- Sen'in trend eğim metoduna göre elde edilen eğim değerleri incelendiğinde 10 yıllık en yüksek azalma miktarı mart ayında -1.0765 m^3/s olarak bulunmuş ve bu değerin elde edilen doğrusal trend değeri ile paralel olduğu belirlenmiştir.
- ITA yöntemine göre tüm akım değerleri beraber değerlendirildiğinde yaklaşık olarak 0-5 m3/s arasında olan düşük akım değerlerinde genel olarak bir değişim olmadığı, ancak 5-12 m3/s arasındaki orta akım değerlerinde ve 12-20 m3/s arasındaki yüksek akım değerlerinde bir azalma eğilimi gözlenmiş, aylık ve yıllık ortalama değerler ayrı ayrı değerlendirildiğinde ise ekim, kasım, ağustos ve eylül aylarında genel olarak artan yönde; nisan, mayıs ve haziran aylarında ise genel olarak azalan yönde bir eğilim görülürken temmuz ayı ve yıllık ortalama için genel olarak akım değerleri 45o'lik 1:1 çizgisi üzerinde olduğu, yani herhangi bir trend varlığının olmadığı sonucuna varılmıştır.

TEŞEKKÜR

Bu çalışma Harran Üniversitesi Bilimsel Araştırma Projeleri Koordinasyon Birimi (HÜBAP) tarafından desteklenmiştir (Proje No:18196).

KAYNAKLAR

Ahmad, I., Tang, D., Wang, T., Wang, M. & Wagan, B. (2015). *Precipitation trends over time using Mann–Kendall and Spearman's rho tests in Swat River basin, Pakistan*. Advances in Meteorology, 2015, 1–15.

Ahmadi, F., Nazeri Tahroudi, M., Mirabbasi, R., Khalili, K. & Jhajharia, D. (2018). *Spatiotemporal trend and abrupt change analysis of temperature in Iran*. Meteorological Applications, 25(2), 314–321.

Gocic, M. & Trajkovic, S. (2013). *Analysis of changes in meteorological variables using Mann–Kendall and Sen's slope estimator statistical tests in Serbia*. Global and Planetary Change, 100, 172–182.

Gumus, V. (2019). *Spatio-temporal precipitation and temperature trend analysis of the Seyhan–Ceyhan River Basins, Turkey*. Meteorological Applications, 26(3), 369-384.

Hadi, S.J. & Tombul, M. (2018). *Long-term spatiotemporal trend analysis of precipitation and temperature over Turkey*. Meteorological Applications, 25, 445–455.

Helsel, D. R., & Hırsch, R. M. (1992). *Statistical methods in water resources* (Vol. 49). Elsevier.

Kendall, M. G. (1948). *Rank correlation methods*, Griffin: London, England. 160s.

Mann, H. B. (1945). *Econometrica*: Journal of the Econometric Society: 245-259.

Salas, J. D., Delleur, J.W., Yevjevich, V.M. & Lane, W.L. (1980). *Applied Modeling of Hydrologic Time Series*, Water Resources Publications: Littleton, Colorado, USA, 484s

Sen, P. K. (1968). *Estimates of the regression coefficient based on Kendall's tau*. Journal of the American statistical association, 63(324): 1379-1389.

Şen, Z. (2012*). Innovative trend analysis methodology*. Journal of Hydrologic Engineering, 17(9): 1042-1046.

Von Storch, H. & Navarra, A. (1995). *Analysis of Climate Variability-Applications of Statistical Techniques*. Springer-Verlag, New York; 334s.

CARBON FOOTPRINT ANALYSIS OF A RESIDENTIAL BUILDING

Adem ATMACA

Energy Systems Engineering, Faculty of Engineering, University of Gaziantep, 27310 Gaziantep, Turkey, aatmaca@gantep.edu.tr

ABSTRACT: The construction sector which consumes more than 40% of the global energy is one of the largest contributors to CO_2 emissions. There is an urgent need to evaluate the regional environmental impacts and related carbon footprint (CFP) of residential buildings globally. This paper contains a review of the related studies by assessing the construction materials, daily energy consumption of the habitants, maintenance of the building, and destruction stages in a 50-year of life cycle. It is seen that, the emissions of the buildings should be decreased by around 10% by the implementation of some basic low-carbon strategies. The results show that the emissions considerably depend on the behavioral factors of residents of a country.

Keywords; Carbon footprint, CO_2 emissions, life cycle, residential buildings, energy consumption.

1. INTRODUCTION

The carbon dioxide emissions in the World have increased to a record of 37 billion metric tons in 2017. Energy efficiency in construction sector has been one of the most important governmental concerns due to the climate change problem (Christopher and Weber, 2008). Energy depletion in residential buildings in Europe reduced by 9% between 2001-2011. However, energy use in residential buildings in Turkey has been increased by around 50% in this period. Around 32% of the energy is consumed by buildings in Turkey.

Calculating the CFP involves analyzing products' life cycle, carbon emissions of the related activities, maintenance, and destruction stages of the building. Evaluating the ecological impact of a construction over its lifetime is a complicated implementation as it demands evaluation of all its parts and life cycle phases (Yalcintas, 2005). Life cycle carbon emissions assessment ($LCCO_2A$) is a basic version of LCA that is only associated with the calculation of emissions related to different stages of the life cycle.

The CFP is a hot topic in the academic world in recent years. Present studies are mostly focused on the utilization of energy and CO_2 emissions related to the manufacturing of building materials, the use stage and demolition of the constructions. However, there are relatively few studies about detailed CFP analysis of residential buildings.

2. LITERATURE REVIEW

LCA approaches have been progressively considered by investigators to assist with decision-making for various strategies and to reduce constructions' ecological impacts for the last 30 years (Fava, 2006; Singh et al., 2011; Buyle et al., 2013; Manish, 2017). Ceullar and Azapagic (2012) studied three construction types in the United Kingdom. LC phases are measured, containing construction of the building, operation and destruction after 50 years. They found that the operational stage has the biggest impact to the amount of energy use.

studied on a building constructed in Taiwan. The energy use intensity (EUI) of the construction is 33.01 kWh/m^2y. The day-to-day energy use is the largest contributor to the CFP, and has the highest CFP at about 60.7% of the total.

The literature survey indicated that carrying out detailed LCCFP assessment of residential buildings have a great effect on the control of global warming (Table 1).

Table 1

Detailed literature survey.

Reference	**Country**	**Lifetime (year)**	**Building type**	**LC CO_2 emissions (kg CO_2/m^2/year)**	**LC embodied energy (GJ/m^2/year)**	**LC total energy (GJ/m^2/year)**
Adalberth (1997a)	Sweden	50	Residential	-	2.9-3.6	27.3-31.6
Newton et al. (2000)	UK	80	-	-	5.2	115
Adalberth et al. (2001)	Sweden	50	Residential	30	2.2-9.8	21.9-32.7

Suzuki & Oka (1998)	Japan	40	Residential	110.7	-	-
Keoleian et al. (2001)	USA	50	Residential	4.1	5.7	64
Treloar et al (2001)	Australia	40	Residential	-	-	10.7-18.4
Chulsukon et al. (2002)	USA	50	Residential	-	4.3	88.2
Yohanis & Norton (2002)	UK	25	Commercial	-	9.5	-
Marceau and Gajda (2002)	USA	100	Residential	32	-	
Thormark (2002)	Sweden	50	Residential	-	7.2	74.5
Lippke et al. (2004)	USA	75	Residential	21.5-43	2	34.2
Mithraratne & Vale (2004)	New Zealand	100	Residential	-	4.8	47.6
Winistorfer et al. (2005)	USA	75	Residential	-	2.2	37.1
Norman et al. (2006)	Canada	50	Residential	77.7-107.3	1.07-0.94	-
Itard (2007)	China	50	Residential	-	-	200
Holden & Gjerde (2007)	New Zealand	50	Residential	-	10.7	214
Asif et al. (2007)	Scotland	-	Residential	16	1.51	-
Citherlet and Defaux (2007)	Switzerland	-	Residential	10-27	-	0.58

Fay et al. (2008)	Australia	50	Residential	-	14.1	470
Xing et al. (2008)	China	50	Commercial	-	-	0.78-0.89
Kellenberger and Althaus (2009)	Switzerland	80	Residential	-	-	43.1
Kahhat et al. (2009)	USA	50	Residential	-	3.5	70.5
Perkins et al. (2009)	Australia	60	Residential	7-20	-	362.4
Utama and Gheewala (2009)	Indonesia	40	Residential	-	0.9	26
Shukla et al. (2009)	India	40	Residential	-	4.75	-
Blengini (2009)	Italy	40	Residential	67	-	0.99
Aste et al. (2010)	Italy	50	Residential	-	4	80
Deng et al. (2011)	China	50	Residential	63.3	4.3	115.2
Dodoo et al. (2011)	Sweden	50	Residential	-	2.2	36-88
Monteiro and Freire (2011)	Portugal	50	Residential	13	-	182
Ceullar and Azapagic (2012)	UK	50	Residential	69.9	-	-

Iyer and Wong (2012)	Australia	50-100	Commercial	131	-	39.1
Gong et al. (2012)	China	50	Residential	150	-	17.8
Asdrubali et al. (2013)	Italy	50	Residential	53.5	-	-
Bastos et al. (2014)	Portugal	75	Residential	12-19.7	62-66	190-352
Stephan and Stephan (2014)	Lebanon	50	Residential	-	18.8	544
Giordano et al. (2015)	Italy	50	Residential	-	6.4	26
Atmaca & Atmaca (2015)	Turkey	50	Residential	79	6.3	145-264
Dong and Ng (2015)	Hong Kong	-	Residential	12.7	-	-
Roh et al., (2016)	Korea	50	Residential	50.6	-	-
Motuziene et al., (2016)	Lithuania	100	Residential	28.6	-	72.2
Pal et al., (2017)	Japan	50	Residential	24.8	-	-
Andrić et al., (2017)	Portugal	50	Residential	-	-	24.84
Estokova et al. (2017)	Slovakia	100	Residential	36.2	5.67	-
Roh and Tae (2018)	Korea	50	Residential	49.4	-	-
Bojana et al. (2019)	Sweden	100	Residential	2	-	-

The CO_2 emissions values of studies across different geographic regions of the world are interpreted and shown in Table 2. The average CO_2 emission values per year for residential buildings in America, Asia, Europe and Oceania are evaluated to be 38.7, 65.9, 31.2 and 69.1 $kgCO_2/m^2/year$ respectively.

The CFP results studied by various studies all around the World are presented in Figure 1.

Table 2

The CFP values of studies across different geographic regions of the world.

Continent	**Reference**	**Country**	**Life cycle**	**CFP ($kgCO_2/m^2/year$)**
America	Keoleian et al., (2001)	USA	50	4.1
	Marceau and Gajda (2002)	USA	100	32
	Lippke et al. (2004)	USA	75	32.2
	Norman et al. (2006)	Canada	50	92.5
	Ortiz Rodriguez (2010)	Columbia	50	32.7
			Average	38.7
Asia	Deng et al. (2011)	China	50	63.3
	Gong et al. (2012)	China	50	150
	Dong and Ng (2015)	Hong Kong	50	12.4
	Roh et al. (2016)	Korea	50	50.6
	Roh and Tae (2018)	Korea	50	49.4
	Pal et al. (2017)	Japan	50	24.8
	Suzuki and Oka (1998)	Japan	40	110.7
			Average	65.9
Europe	Adalberth et al. (2001)	Sweden	50	30
	Asif et al. (2007)	Scotland	50	16
	Citherlet and Defaux (2007)	Switzerland	50	18.5
	Bribian et al. (2009)	Spain	48	35
	Blengini (2009)	Italy	40	67

	Monteiro and Freire (2012)	Portugal	50	13
	Bastos et al. (2014)	Portugal	75	16
	Atmaca & Atmaca (2015)	Turkey	50	39
	Motuzien˙e, et al. (2016)	Lithuania	100	28.6
	Estokova et al. (2017)	Slovakia	100	36.2
	Bojana et al. (2019)	Sweden	100	2
	Ceullar & Azapagic (2012)	UK	50	69.9
	Gustavsson & Joelsson (2012)	Sweden	50	12.6
	Asdrubali et al. (2013)	Italy	50	53.5
			Average	31.2
Oceania	Perkins et al. (2009)	Australia	60	13.5
	Iyer & Wong (2012)	Australia	50-100	124.7
			Average	69.1
			World Average	**43.9**

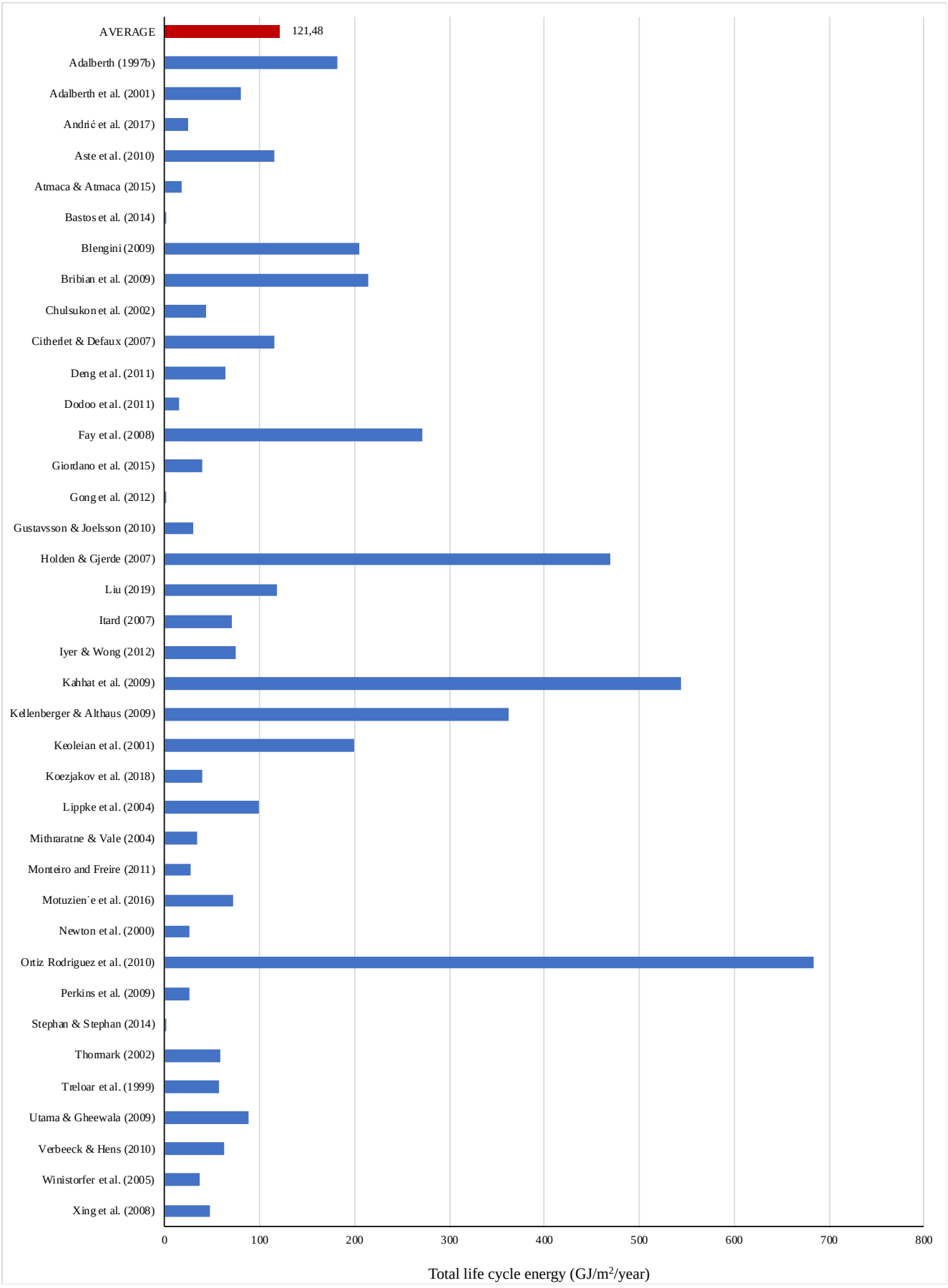
AVERAGE
121,48
Adalberth (1997b)
Adalberth et al. (2001)
Andrić et al. (2017)
Aste et al. (2010)
Atmaca & Atmaca (2015)
Bastos et al. (2014)
Blengini (2009)
Bribian et al. (2009)
Chulsukon et al. (2002)
Citherlet & Defaux (2007)
Deng et al. (2011)
Dodoo et al. (2011)
Fay et al. (2008)
Giordano et al. (2015)
Gong et al. (2012)
Gustavsson & Joelsson (2010)
Holden & Gjerde (2007)
Liu (2019)
Itard (2007)
Iyer & Wong (2012)
Kahhat et al. (2009)
Kellenberger & Althaus (2009)
Keoleian et al. (2001)
Koezjakov et al. (2018)
Lippke et al. (2004)
Mithraratne & Vale (2004)
Monteiro and Freire (2011)
Motuzien˙e et al. (2016)
Newton et al. (2000)
Ortiz Rodriguez et al. (2010)
Perkins et al. (2009)
Stephan & Stephan (2014)
Thormark (2002)
Treloar et al. (1999)
Utama & Gheewala (2009)
Verbeeck & Hens (2010)
Winistorfer et al. (2005)
Xing et al. (2008)
0
100
200
300
400
500
600
700
800
Total life cycle energy (GJ/m²/year)

Fig. 1. Total LC energy consumption values calculated by various studies.

3. CONCLUSIONS

This study conducted a detailed assessment of published papers, collected life cycle energy consumption and related CFP studies from around the world. Figure 2 represents the percentages of life cycle CFP results obtained from different studies all around the world.

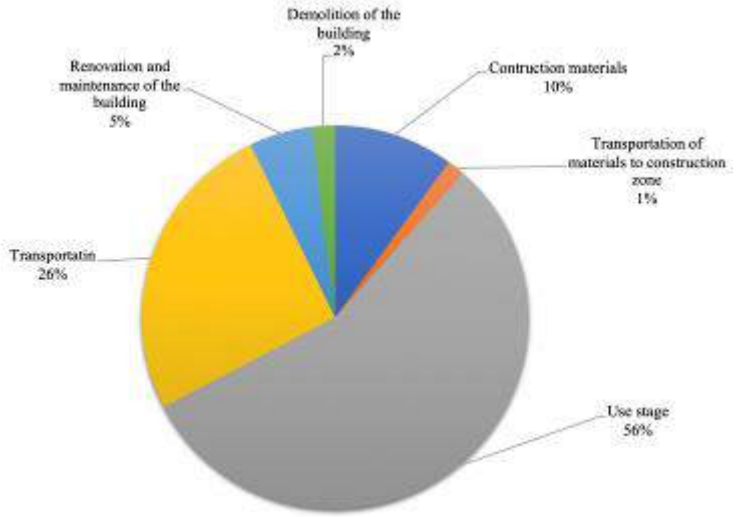

Fig. 2. CFP percentages of different stages of the construction.

Life cycle CO_2 emissions of a construction should be prevented by reducing the operating energy considerably. Decreasing the requirements for daily energy consumption is the most important aspect. The total life cycle CFP of the residential building found to be 56.45 tonCO_2/year which is higher compared to the other European Union countries. It is found that the life-cycle CO_2 emissions of the building constructed in Turkey is about 30% higher than the average CO_2 emissions of residential buildings constructed in European countries. The CFP of construction materials of the building has been calculated to be 5.65 tonCO_2/year which contributes 10.02 % of the total CFP. CFP in the use stage of the construction is accounted for the largest share. The daily energy use of the inhabitants is the main contributor to the CFP, representing 81.32% of the life cycle CFP. Construction of energy-efficient households will obviously reduce all life-cycle emissions significantly. Enhancing energy efficiency and reducing the dependency on fossil fuels to decrease energy demand, and ecological impacts will be the foremost concerns of construction industry in the near future (Atmaca and Atmaca, 2016a; Atmaca, 2018, Atmaca and Atmaca, 2016b, Atmaca et al., 2018). The investigations showed that CFP of a building notably depends on the behavioral factors of the habitants of a country.

REFERENCES

Adalberth, K., Almgreen, A., Petersen, E.H., 2001. Life cycle assessment of four multifamily buildings. Int. J. Low Energy Sustain. Build. 2,1–21

Adalberth, K.,1997a. Energy use during the life cycle of buildings: a method, Build.Environ. 32(4),317–320.

Adalberth, K.,1997b. Energy use during the life cycle of single unit dwellings: examples, Build. Environ 32(4),321–329.bcit

Andrić, I., Pina, A., Ferrão, P., Fournier, J., Lacarrière, B., Corre, O.L., 2017. Assessing the feasibility of using the heat demand-outdoor temperature function for a long-term district heat demand forecast. Energy Procedia 140,486-494.

Asdrubali, F., Baldassarri, C., Fthenakis, V., 2013. Life cycle analysis in the construction sector: guiding the optimization of conventional Italian buildings. Energy Build 64,73–89.

Asif, M., Muneer T., Kelley R., 2007. Life cycle assessment: a case study of a dwelling home in Scotland. Building and Environment 42,1391–1394.

Aste, N., Adhikari R.S., Buzzetti M.,2010. Beyond the EPBD: the low energy residential settlement Borgo Solare. Appl Energy 87(2),629–42.

Atmaca, A., Atmaca, N.,2016a. Comparative life cycle energy and cost analysis of post-disaster temporary housings. Applied Energy 171,429–443.

Atmaca, A., Atmaca, N., 2016b. Determination of correlation between specific energy consumption and vibration of a raw mill in cement industry. Anadolu University Journal of Science and Technology A- Applied Sciences and Engineering 17(1),209-219.

Atmaca, A., Yumrutaş, R., 2015. The effects of grate clinker cooler on specific energy consumption and emissions of a rotary kiln in cement industry. International Journal of Exergy 18(3),367-386.

Atmaca, A., 2018. Sustainable life span prediction of shelters constructed in refugee camps in Turkey. Energy, Ecology and Environment 3(1),5-12.

Atmaca, A., Atmaca, N., 2015. Life cycle energy (LCEA) and carbon dioxide emissions (LCCO2A) assessment of two residential buildings in Gaziantep, Turkey. Energy Build 102,417–431.

Atmaca, N., Atmaca, A., Aljumaili, M., Özçetin, A.İ., 2018. Strength and shrinkage properties of self-compacting concretes incorporating waste PVC dust. The International Journal of Energy & Engineering Sciences 3(1),47-57.

Bastos, J., Batterman, S.A., Freire, F., 2014. Life-cycle energy and greenhouse gas analysis of three building types in a residential area in Lisbon. Energy and Buildings 69,344–353.

Blengini, G.A., 2009. Life cycle of buildings, demolition and recycling potential: a case study in Turin, Italy. Build Environ 44,319–330.

Bojana, P., Myhren, J.A., Zhang, X, Wallhagen, M., Eriksson, O., 2019. Life Cycle Assessment of Building Materials for a Single-family House in Sweden. Energy Procedia 158,3547–3552.

Buyle, M., Braet, J., Audenaert, A.,2013. Life cycle assessment in the construction sector: a review. Renewable & Sustainable Energy Reviews 26,379–88.

Chau, C.K., Yik, F.W.H., Hui, W.K., Liu, H.C., Yu, H.K., 2007. Environmental impacts of building materials and building services components for commercial buildings in Hong Kong. Journal of Cleaner Production 15,1840–1851.

Christopher, L., Weber, H.S.,2008. Quantifying the global and distributional aspects of American household carbon footprint. Ecological Economics 66,379-391.

Chulsukon, P. 2002. Development and analysis of a sustainable low energy house in a hot and humid climate, Ph.D. Thesis. TX, USA: Texas A &M University, College Station.

Citherlet, S., Defaux, T., 2007. Energy and environmental comparison of three variants of a family house during its whole life span. Build Environ 42,591–598.

Cuellar-Franca, R.M., Azapagic, A., 2012. Environmental impacts of the UK residential sector: life cycle assessment of houses. Build Environ 54,86–99.

Deng, W., Prasad, D., Osmond, P., Li, F.T., 2011. Quantifying life cycle energy and carbon footprints of China's residential small district. Coll Publ 6(4),96–111

Dodoo, A., Gustavsson, L., Sathre, R., 2011. Building energy-efficiency standards in a life cycle primary energy perspective. Energy Build 43(7),1589–97.

Dong, Y., Ng, S.T., 2015. A life cycle assessment model for evaluating the environmental impacts of building construction in Hong Kong. Building and Environment 89,183–191.

Estokova, A., Vilcekova, S., Porhincak, M., 2017. Analyzing embodied energy, global warming and acidification potentials of materials in residential buildings. Procedia Engineering 180,1675 – 1683.

Fava, J.A., 2006. Will the next 10 years be as productive in advancing life cycle approaches as the last 15 years? Int J Life Cycle Assess 11,6–8.

Fay, R., Treloar, G., Iyer-Raniga, U., 2008. Life-cycle energy analysis of buildings: a case study. Building Research and Information 28,31–41.

Giordano, R., Serra, V., Tortalla, E., Valentini, V., Aghemo, C., 2015. Embodied Energy and Operational Energy Assessment in the Framework of Nearly Zero Energy Building and Building Energy Rating. Energy Procedia 78,3204–9.

Gong, X., Nie, Z., Wang, Z., Cui, S., Gao, F., Zuo, T., 2012. Life cycle energy consumption and carbon dioxide emission of residential building designs in Beijing: a comparative study. J Ind Ecol 4,576–587.

Gustavsson, L., Joelsson, A., 2010. Life cycle primary energy analysis of residential buildings. Energy Build 2,210–220

Holden, G., Gjerde, M., 2007. Urban Sustainability: Comparative Value of Building-Top Apartments. In International Conference on Whole Life Urban Sustainability and its Assessment.

Itard, L., 2007. Comparing environmental impacts from energy and materials embodied in buildings and used during their service life. Proceedings of Building Simulation 3-6 September, Beijing, China,1954–1961.

Iyer, R.U., Wong, J.P.C., 2012. Evaluation of whole life cycle assessment for heritage buildings in Australia. Build Environ 47,138–149.

Kahhat, R., Crittenden, J., Sharif, F., Fonseca, E., Li, K., Sawhney, A., Zhang, P., 2009. Environmental impacts over the life cycle of residential buildings using different exterior wall systems. J Infrastruct Syst 15(3),211–21.

Kellenberger, D., Althaus, H., 2009. Relevance of simplifications in LCA of building components. Build Environ 44(4),818–25.

Keoleian, G., Blanchard, S., Reppe, P., 2001. Life-cycle energy, costs, and strategies for improving a single-family house, J. Ind. Ecol. 4(2),135–156.

Koezjakov, A., Urge-Vorsatz, D., Crijns-Graus, W., van den Broek, M., 2018. The relationship between operational energy demand and embodied energy in Dutch residential buildings, Energy & Buildings 165,233–245.

Lippke, B., Wilson, J., Perez-Garcia, J., Bowyer, J., Meil, J., 2004. CORRIM: life-cycle environmental performance of renewable building materials. For Prod J 54(6),8–19.

Liu, HY., 2019. Building a dwelling that remains carbon-neutral over its lifetime: A case study in Kinmen. Journal of Cleaner Production 208,522-529.

Liu, H.Y., 2017. From Low Carbon Building to No Carbon House -Low to No- Use of a Single family House in Kinmen as an Example. Article in Chinese and English. Angle Publishing, Taipei, Taiwan.

Manish, K.D., 2017. Life cycle embodied energy analysis of residential buildings: A review of literature to investigate embodied energy parameters. Renewable and Sustainable Energy Reviews 79,390–413.

Marceau, M.L., Gajda, J., 2002. Partial environmental life cycle inventory of an insulating concrete form house compared to a wood frame house. Portland cement association research & development SERIAL No. 2464.

Mithraratne, N., Vale, B., 2004. Life cycle analysis model for New Zealand houses. Build Environ 39(4),483–92.

Monteiro, H., Freire, F., 2011. Environmental life-cycle impacts of a single-family house in Portugal: assessing alternative exterior walls with two methods. Gazi Univ. J. Sci. 24(3),527–534.

Monteiro, H., Freire, F., 2012. Life cycle assessment of a house with alternative exterior walls: comparison of three impact assessment methods. Energy Build. 47,575–583.

Motuzien˙e, V., Rogo˘za, A., Lapinskien˙e, V., Vilutien˙e, T., 2016. Construction solution for energy efficient single-family house based on its life cycle multi-criteria analysis: A case study. Journal of Cleaner Production 112,532–541.

Newton, P., Tucker, S., Ambrose, M., 2000. Housing form, energy use and greenhouse gas emission. In: Williams K, Burton E, Jenks M, editors. Achieving Sustainable Urban form, 2000. London: SPON Press.

Norman, J., MacLean, H.L., Asce, M., Kennedy, C.A., 2006. Comparing high and low residential density: life-cycle analysis of energy use and greenhouse gas emissions. J Urban Plan Dev. 32,10–21.

Ortiz-Rodríguez, O., Castells, F., Sonnemann, G., 2010. Life cycle assessment of two dwellings: one in Spain, a developed country, and One in Colombia, a country under development. Sci Total Environ 408(12),2435–43.

Pal, S.K., Takano, A., Alanne, K., Siren, K., 2017. A life cycle approach to optimizing carbon footprint and costs of aresidential building. Building and Environment 123,146-162.

Perkins, A., Hamnett, S., Pullen, S., Zito, R., Trebilcock, D., 2009. Transport, housing and urban form: the life cycle energy consumption and emissions of city centre apartments compared with suburban dwellings. Urban Policy Res 27(4),377–96.

Roh, S., Tae, S., Suk, S.J., Ford, G., Shin, S., 2016. Development of a building life cycle carbonemissions assessment program (BEGAS 2.0) for Korea′s green building index certi-fication system. Renew Sustain Energy Rev 53,954–65.

Roh, S., Tae, S., 2017. An integrated assessment system for managing life cycle CO2emis-sions of a building. Renewable and Sustainable Energy Rev 73,265–75.

Scheuer, C., Keoleian, G.A., Reppe, P., 2003. Life cycle energy and environmental performance of a new university building: modeling challenges and design implications. Energy Build 35,1049–1064.

Shukla, A., Tiwari, G.N., Sodha, M.S., 2009. Embodied energy analysis of adobe house. Renew Energy 34(3),755–61

Stephan, A., Stephan, L., 2014. Reducing the total life cycle energy demand of recent residential buildings in Lebanon. Energy 74,618–37.

Suzuki, M., Oka, T., 1998. Estimation of life cycle energy consumption and CO2 emission of office buildings in Japan. Energy Build 28.

Thormark, C., 2002. A low energy building in a life cycle its embodied energy, energy need for operation and recycling potential. Build. Environ. 4,429–435.

Treloar, G.J., Fay R., Ilozor, B., Love, P., 2001. Building materials selection: greenhouse strategies for built facilities. Facilities 3,139–150.

Utama, A., Gheewala S.H., 2009. Indonesian residential high rise buildings: a life cycle energy assessment. Energy Build 41(11),1263–8.

Verbeeck, G., Hens, H., 2010. Life cycle inventory of buildings: a contribution analysis. Build Environ 45(4),964–7.

Winistorfer, P., Chen, Z., Lippke, B., Stevens N., 2005. Energy consumption and greenhouse gas emissions related to the use, maintenance, and disposal of a residential structure. Wood Fiber Sci 37,128–39.

Xing, S., Xu, Z., Jun, G., 2008. Inventory analysis of LCA on steel and concrete construction office buildings. Energy Build 7,1188–1193.

Yalcintas, M., Akkurt, S., 2005. Artificial neural networks applications in building energy predictions and a case study for tropical climates. Int J Energy Res 29,891–901.

Yohanis, Y.G., Norton B., 2002. Life-cycle operational and embodied energy for a generic single-storey office building in the UK. Energy 27(1),77–92.

EVALUATION OF FIN DESIGN IN TERMS OF HEAT TRANSFER IN PLATE HEAT EXCHANGERS

Doğan Engin ALNAK

Sivas Cumhuriyet University, Technology Fac., Automotive Eng. Dept.

dealnak@cumhuriyet.edu.tr

Koray KARABULUT

Sivas Cumhuriyet University, Sivas Vocational High Sch., Electric and Energy Dept.

kkarabulut@cumhuriyet.edu.tr

ABSTRACT: In plate heat exchangers, the use of fins is an important application to increase the turbulance of the flow and the heat transfer surface area. In the present study, heat transfer enhancements of circular and triangle fins with fin heigth of 2 mm and pressure drops have been numerically investigated in plate heat exchangers. The fins are mounted on the flat plate channel. The numerical computations have been carried out by solving a steady, three-dimensional Navier-Stokes equation and an energy equation by using Ansys-Fluent software program. Air has been employed as working fluid. The study has been performed at Re=400 and inlet temperatures, inlet velocities of cold and hot air are fixed as 300 K, 600 K and 1.338 m/s, 0.69 m/s, respectively. This study displays new fin geometries for plate fin heat exchangers and the employed fin types in this work to increase the heat transfer rate have not still been researched in the reached literature. The results represent that while an increment with 4.18% is obtained in cold fluid temperature for plate heat exchanger with circular fin according to flat plate duct at counter flow, this enhancement value is 4.77% for plate heat exchanger with triangle fin. The heat transfer augments and turbulence kinetic energy (TKE) variations for different fin heights and also velocity, temperature and pressure contour distributions have been analyzed for parallel and counter flow arrangements.

Key words: plate heat exchanger, fin, heat transfer

PLAKALI ISI DEĞİŞTİRİCİLERDE KANATÇIK TASARIMININ ISI TRANSFERİ AÇISINDAN DEĞERLENDİRİLMESİ

ÖZET: Plakalı ısı değiştiricilerde, kanatçık kullanımı akışın türbülansını ve ısı transfer yüzey alanını artırmak açısından önemli bir uygulamadır. Bu çalışmada, plakalı ısı değiştiricilerde 2 mm kanatçık yükseklikli dairesel ve üçgen kanatçıkların ısı transferi artışları ve basınç düşüşleri sayısal olarak incelenmektedir. Kanatçıklar, düz plakalı kanala yerleştirilmektedir. Sayısal hesaplamalar, Ansys-Fluent bilgisayar programının kullanılmasıyla zamandan bağımsız, üç boyutlu Navier-Stokes ve enerji denklemlerinin çözülmesiyle yapılmıştır. Çalışma akışkanı olarak hava kullanılmıştır. Çalışma, Re=400'de gerçekleştirilmekte olup giriş sıcaklıkları, soğuk ve sıcak havanın giriş hızları sırasıyla 300 K, 600 K ve 1.338 m/s, 0.69 m/s olarak sabit alınmıştır. Bu çalışma, plakalı ısı değiştiricileri için yeni kanatçık geometrilerini sergilemektedir ve ısı transferini artırmak için kullanılan kanatçık tipleri ulaşılan literatürde henüz araştırılmamıştır. Sonuçlar, ters akışta kanatçıksız kanala göre dairesel kanatçıklı plakalı ısı değiştiricisinde soğuk akışkan sıcaklığında %4.18' lik bir artış elde edildiğini gösterirken, bu artış değeri üçgen kanatçıklı plakalı ısı değiştiricisi için %4.77 olmaktadır. Farklı kanatçık yükseklikleri için ısı transferi artışları ve türbülans kinetik enerji (TKE) değişimleri ve ayrıca hız, sıcaklık ve basınç konturü dağılımları parallel ve ters akış düzenlemeleri için analiz edilmiştir.

Anahtar sözcükler: plakalı ısı değiştiricisi, kanatçık, ısı transferi

GİRİŞ

Sınırlı enerji kaynakları ve artan çevre kirliliği günümüzde enerjinin tasarruflu ve verimli kullanılmasına yönelik çalışmaların artırılmasını gerekli kılmaktadır. Enerji tasarrufu, başta insan olmak üzere teknik bir problemdir. Teknik problemler ise teknolojik bakımdan bilinmekte olup bu problemlerin üstesinden gelmek için sistematik bir yaklaşım geliştirilmesi gereklidir. Bu amaçla, konuyla ilgili araştırmacılar enerjiyi daha faydalı kullanabilecek yeni makineler tasarlamakta veya var olan makinelerde iyileştirme çalışmaları yapmaktadırlar. Bu sayede, enerjinin maliyeti düşmekle birlikte hem kaynakların kullanım süreleri uzamakta hem de çevre kirliliğine olan olumsuz katkı azalmaktadır (Karabulut, 2011).

Birçok mühendislik uygulamasında önemli ve çok karşılaşılan işlemlerden birisi de farklı sıcaklıklarda iki veya daha çok akışkan arasındaki ısı değişimidir. Bu değişimin yapılabilmesi için gerekli olan cihaz, termik santrallarda, kimya endüstrisinde, iklimlendirmede, taşıtlarda ve elektronik cihazlar vb. gibi birçok alanda kullanılan ısı değiştiricisidir (Shah,1981). Isı değiştiricilerinde ısı transferini artırmak için genellikle kullanılan yöntemlerden birisi kanatçıklar yani genişletilmiş yüzeyler kullanılmasıdır. Kanatçıklı yüzeyler sayesinde yüzey alanı ve akışın türbülansı artırılarak taşınımla ısı ve kütle transferi artırılmış olur. Kanatçıklı yüzeylerin en önemli kullanım alanları olarak ise gaz türbini motorlarındaki türbin kanatçıklarının soğutulması ve üretim

tesislerindeki çeşitli ısı değiştiricileri gösterilebilir. Bununla birlikte, kanatçıkların gerektiği şekilde kullanılmaması ısı geçişini artırmak yerine azaltıcı etki gösterebilir. Bu nedenle, kanatçık malzemesinin türünün, yüzeye monte biçiminin ve özellikle şeklinin ısı transferini artıracak şekilde değerlendirilmesi gerekmektedir. Bu amaçla, plakalı ısı değiştiricilerde ısı transferi ve akış yapılarını değerlendirmek için birçok deneysel ve sayısal çalışma yapılmıştır. Tauscher ve Mayinger (1991) yaptıkları çalışmada plaka tipi ısı değiştiricilerde, çeşitli kurulumlarla oluşturdukları genişletilmiş yüzeylerle ısı aktarımının artırılmasını laminer ve düşük türbülanslı akış şartlarında deneysel ve sayısal olarak incelemişlerdir. Çalışmada, kanatçıkların türbülans oluşturucu etkisi nedeniyle ısı aktarımının arttığı gözlemlenirken, artış için en uygun kurulum belirlenerek, deneysel sonuçların sayısal sonuçlarla uyumu ayrıca incelenmiştir. Lee ve ark. (2001) laminer akış şartlarında plakalı ısı değiştiricisi kanallarının optimum şekillendirilmesi ve düzenlenmesi üzerine çalışmışlardır. Uzaklık, hacim, açı ve eğim olmak üzere bu çalışmada dört adet boyutsuz geometrik parametre kullanmışlardır. Ayrıca, plakalı ısı değiştiricilerinin basınç düşüşü ve ısı transfer özelliklerini de incelemişlerdir. Buyruk ve Karabulut (2017), 2 mm kanatçık yükseklikli 30^o ve 60^o kanatçık açılı ve akışa dik yatay yönde 10 mm ötelenmiş dikdörtgensel kanatçıkların ısı transferi potansiyeli ve basınç düşüşü özelliklerini sayısal olarak incelemişlerdir. Farklı bir çalışmada Buyruk ve Karabulut (2013), 4 mm kanatçık yüksekliği ve yatay eksenle arasında 30^o ve 90^o olmak üzere farklı kanatçık açılarına sahip plakalı kanatçıklı ısı değiştiricileri için ısı transferi artışını sayısal olarak değerlendirmişlerdir. Wang ve ark. (2009) düz ve tırtıklı kanatçıklara sahip plakalı ısı değiştiricileri için akış ve ısı transferi özelliklerinin analizini gerçekleştirmişlerdir. Düşük Reynolds sayıları için her iki kanatçıklı ısı değiştiricileri için sayısal simülasyonlar FLUENT bilgisayar programı kullanılarak yapılmıştır. Gupta ve ark. (2009), sayısal olarak üçgen kanatçıklı plakalı tip bir ısı değiştiricisinde ısı transferi artışı için bir çift kanatçık tip vorteks üretecini kullanarak ısı değiştirgecinin akış yapısı ve performans özelliklerini araştırmışlardır. Ayrıca, kanatçık çiftinin yüksekliklerini değiştirerek, ısı transferi artış oranına etkisini belirlemişlerdir. Zhu ve Li (2008) dikdörtgen, çubuk, oluklu ve dalgalı olmak üzere dört kanatçık tipi için laminer akış rejiminde, kanatçık kalınlığını da dikkate alarak akış yapısı ve ısı transferi üzerinde ısıl giriş ve çıkış etkilerini üç boyutlu sayısal olarak değerlendirmişlerdir. Buyruk ve Karabulut (2018) iç zikzak-düz-dış zikzak ve dış zikzak-düz-dış zikzak olmak üzere farklı geometrik şekillere ve 2 mm kanatçık yükseklikli ve yatayla 10 mm kaydırılmış düzene ve 30^o ve 90^o kanatçık açılı plakalı ısı değiştiricilerinin ısı transferi ve basınç düşüşü performanslarını araştırmışlardır. Ters akış durumunda kanatçıksız kanalla karşılaştırıldığında dış zikzak-düz-dış zikzak kanatçıklı plakalı ısı değiştiricisi için ısı transferinde %10'luk artış elde edilirken, 90^o kanatçık açılı ısı değiştiricisinde ise %8' lik bir artış elde etmişlerdir.

Literatürde ulaşılan çalışmalar değerlendirildiğinde, plakalı ısı değiştiricilerindeki kanatçık düzenlemelerinin ısı transferini iyileştirdiği görülmektedir. Bununla birlikte, hem bu çalışmada incelenen kanatçık şekillerinin henüz değerlendirilmediği hem de enerji verimliliğinin artırılmasının öneminin daha iyi anlaşıldığı günümüzde kanatçık üzerine daha yoğun araştırmalar yapılması gerekliliği göz önünde bulundurularak bu

çalışmada özgün kanatçık şekilleri değerlendirilmiştir. Bu amaçla, düz kanala yerleştirilen dairesel ve üçgen kanatçıkların plakalı ısı değiştiricilerinin ısı transferi, kanal içerisindeki akış yapısı, türbülans kinetik enerji değişimleri ve basınç düşüşü özellikleri sayısal olarak incelenmiştir. Çalışmada ayrıca, kanatçık yüksekliğinin soğuk akışkan sıcaklığı üzerindeki etkisi de değerlendirilmiştir. Bununla birlikte, farklı Re sayılarının Nu sayısı üzerindeki etkisi araştırılırken hız, sıcaklık ve basınç konturu dağılımları görselleştirilmiştir.

YÖNTEM

Sayısal çalışma üç boyutlu, zamandan bağımsız, birleşik (iletim ve taşınım) ısı transferi yaklaşımıyla çözülmüştür. Birleşik ısı transferi analizini çözmek için sonlu hacimler yöntemi (FLUENT programı) kullanılmıştır.

Kullanılan kanatçıklar, laminer akışta türbülansa neden olduğundan sayısal hesaplamalarda seçilen kanatçıklı geometriler için standart k-ε türbülans modelinin uygun olduğu belirlenmiş ve kullanılmıştır.

Geometri boyunca akış ve ısı transferinin çözümlemesi, zamandan bağımsız olarak kütlenin, momentumun ve enerjinin korunumu kanunlarından elde edilen kısmi türevli denklemlerin çözümlenmesi esasına dayanmaktadır (Wang ve ark. 2009; Fluent, 2003).

Süreklilik denklemi

$$\frac{\partial u}{\partial x}+\frac{\partial v}{\partial y}+\frac{\partial w}{\partial z}=0 \tag{1}$$

Momentum

x momentum denklemi

$$\rho\left(u\frac{\partial u}{\partial x}+v\frac{\partial u}{\partial y}+w\frac{\partial u}{\partial z}\right)=-\frac{\partial p}{\partial x}+\mu\left(\frac{\partial^2 u}{\partial x^2}+\frac{\partial^2 u}{\partial y^2}+\frac{\partial^2 u}{\partial z^2}\right) \tag{2}$$

y momentum denklemi

$$\rho\left(u\frac{\partial v}{\partial x}+v\frac{\partial v}{\partial y}+w\frac{\partial v}{\partial z}\right)=-\frac{\partial p}{\partial y}+\mu\left(\frac{\partial^2 v}{\partial x^2}+\frac{\partial^2 v}{\partial y^2}+\frac{\partial^2 v}{\partial z^2}\right) \tag{3}$$

z momentum denklemi

$$\rho\left(u\frac{\partial w}{\partial x}+v\frac{\partial w}{\partial y}+w\frac{\partial w}{\partial z}\right)=-\frac{\partial p}{\partial z}+\mu\left(\frac{\partial^2 w}{\partial x^2}+\frac{\partial^2 w}{\partial y^2}+\frac{\partial^2 w}{\partial z^2}\right) \tag{4}$$

Enerji denklemi

$$u\frac{\partial T}{\partial x}+v\frac{\partial T}{\partial y}+w\frac{\partial T}{\partial z}=\left(\frac{k}{\rho c_p}\right)\left(\frac{\partial^2 T}{\partial x^2}+\frac{\partial^2 T}{\partial y^2}+\frac{\partial^2 T}{\partial z^2}\right) \quad (5)$$

Bu denklemlerde, ρ yoğunluk, μ dinamik viskozite, p basınç, k ısıl iletkenlik, T sıcaklık, c_p özgül ısı ve u,v,w ise sırasıyla x, y ve z yönlerindeki hızlardır.

Kullanılan standart k-ε türbülans modelinde, k' türbülans kinetik enerji, ε disipasyon terimi ve ϕ viskoz kaybolma terimi kullanılmaktadır.

Daimi akış için türbülans kinetik enerjisi denklemi

$$\frac{\partial(\rho u k')}{\partial x}+\frac{\partial(\rho v k')}{\partial y}+\frac{\partial(\rho w k')}{\partial z}=\frac{\partial}{\partial x}\left(\frac{\mu_t}{\sigma_k}\frac{\partial k'}{\partial x}\right)+\frac{\partial}{\partial y}\left(\frac{\mu_t}{\sigma_k}\frac{\partial k'}{\partial y}\right)+\frac{\partial}{\partial z}\left(\frac{\mu_t}{\sigma_k}\frac{\partial k'}{\partial z}\right)+\mu_t\phi-\rho\varepsilon \quad (6)$$

Türbülans viskozitesi

$$\mu_t=C_\mu.\rho.\frac{k'^2}{\varepsilon} \quad (7)$$

Türbülans kinetik enerji

$$k'=\frac{1}{2}\left(\overline{u'^2}+\overline{v'^2}+\overline{w'^2}\right) \quad (8)$$

Viskoz kaybolma terimi

$$\phi=2\mu\left[\left(\frac{\partial u}{\partial x}\right)^2+\left(\frac{\partial v}{\partial y}\right)^2\right]+\mu\left(\frac{\partial v}{\partial x}+\frac{\partial u}{\partial y}\right)^2 \quad (9)$$

Türbülans kinetik enerji kaybolma denklemi

$$\frac{\partial(\rho u\varepsilon)}{\partial x}+\frac{\partial(\rho v\varepsilon)}{\partial y}+\frac{\partial(\rho w\varepsilon)}{\partial z}=\frac{\partial}{\partial x}\left(\frac{\mu_t}{\sigma_\varepsilon}\frac{\partial\varepsilon}{\partial x}\right)+\frac{\partial}{\partial y}\left(\frac{\mu_t}{\sigma_\varepsilon}\frac{\partial\varepsilon}{\partial y}\right)+\frac{\partial}{\partial z}\left(\frac{\mu_t}{\sigma_\varepsilon}\frac{\partial\varepsilon}{\partial z}\right)+C_{1\varepsilon}\mu_t\frac{\varepsilon}{k'}\phi-C_{2\varepsilon}\rho\frac{\varepsilon^2}{k'} \quad (10)$$

C_μ , $C_{1\varepsilon}$, $C_{2\varepsilon}$, σ_k ve σ_ε katsayıları sabit olup C_μ = 0.09, $C_{1\varepsilon}$ = 1.44, $C_{2\varepsilon}$ = 1.92, σ_k=1 ve σ_ε =1.3'dür.

Reynolds sayısı

$$Re=\frac{V_\infty.D_h}{\nu} \quad (11)$$

Burada, D_h kanalın hidrolik çapıdır.

$$D_h=\frac{4A_c}{P}=\frac{4(H_2.W)}{2(H_2.W)} \quad (12)$$

A_c kanalın kesit alanı, P ise kanalın çevre uzunluğudur.

Sınır şartı ve Nusselt sayısı aşağıdaki şekilde verilmiştir.

$$-k\left(\frac{dT}{dn}\right)_{yüzey}=h(T_\infty-T_s) \text{ ve } Nu=\frac{h.D_h}{k} \quad (13)$$

h yüzey ısı taşınım katsayısıdır.

Basınç düşüşü aşağıdaki şekilde hesaplanabilir

$$\Delta P_L = f.\frac{L}{D_h}.\frac{\rho.V_m^2}{2} \quad (14)$$

ΔP_L akış yönünde kanaldaki basınç düşüşü, *f* ise sürtünme faktörüdür.

Kanat malzemesinin ısıl iletkenliği kanal boyunca ısıl değişimi etkilediğinden ısı transferini artırmada kanatçık malzemesinin seçimi önemli bir faktördür. Bu nedenle, kanal malzemesi olarak yüksek ısıl iletkenliğe sahip, ucuz ve hafif olan alüminyum seçilmiştir. Kanatçıkların kanal yüzeyi ile bir bütün olarak üretildiği varsayılarak, kanatçıklar ve yüzey arasındaki ısıl direnç ihmal edilmiştir.

Şekil 1'de üç boyutlu düz kanal geometrisinin perspektif görünüşü gösterilmekte iken, Şekil 2a ve Şekil 2b'de ise sırasıyla sayısal hesaplamalarda kullanılan dairesel ve üçgen kanatçıklı modellere ait dikdörtgensel kanal geometrileri gösterilmektedir. Ayrıca, bu şekiller üzerinde sınır şartları da belirtilmiştir. Şekil 2a ve Şekil 2b'de kanatçıkların daha iyi görselleştirilebilmesi için kanalların ters çevrilmiş görüntüsü gösterilmektedir.

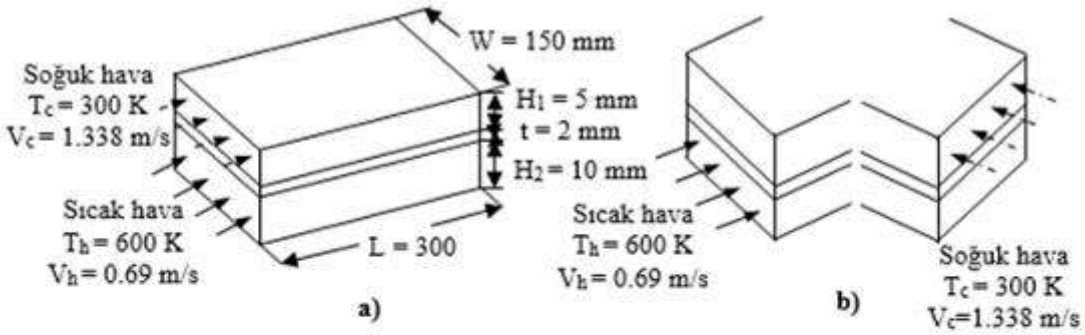

Şekil 1. Düz Kanal İçin Perspektif Görünüş a) Paralel Akış b) Ters Akış

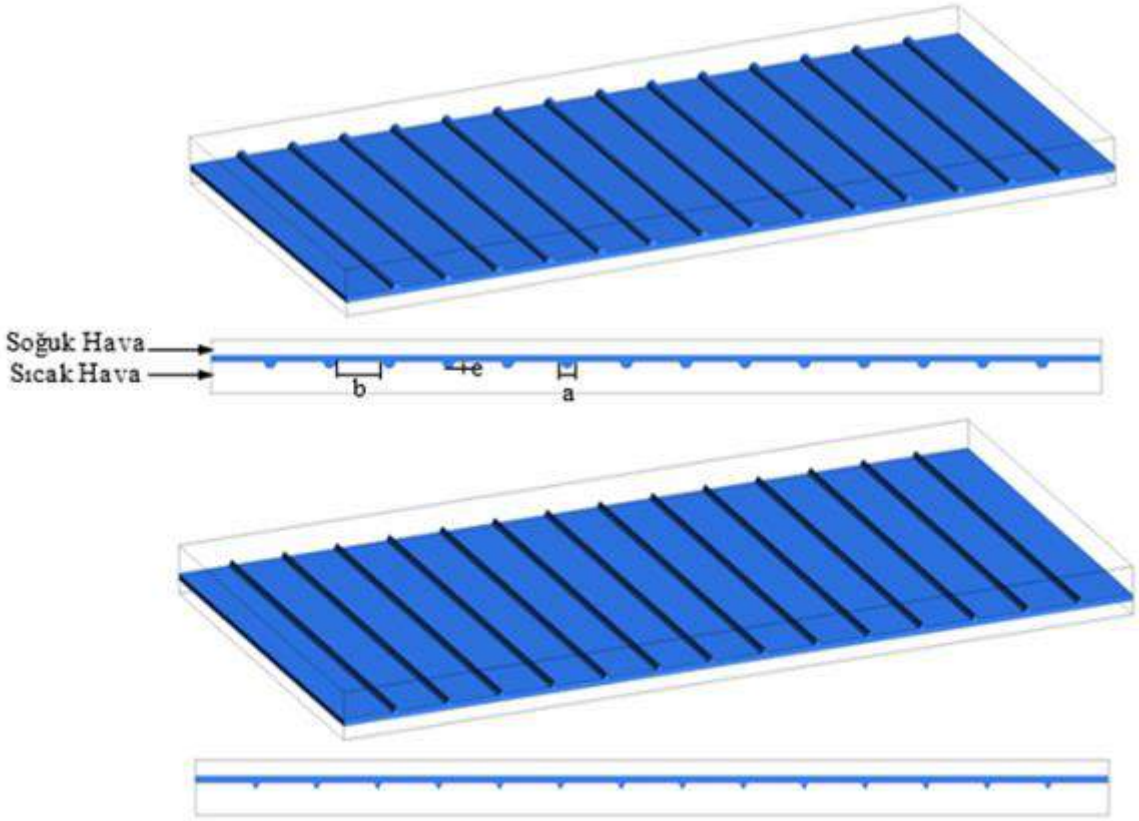

Şekil 2. Sayısal Hesaplamalarda Kullanılan Kanatçıklı Dikdörtgensel Kanal Modelleri A) Dairesel Kanatçıklı B) Üçgen Kanatçıklı

Geometrik özellikler olarak, kanatçık şekli: dairesel ve üçgen kanatçık yüksekliği (e): 2 ve 4 mm, kanatçık aralığı (b): 20 mm, kanatçık genişliği (a): 2 mm, kanal boyu (L): 300 mm, kanal genişliği (W): 150 mm, üst kanal yüksekliği (H_1): 5 mm, alt kanal yüksekliği (H_2): 10 mm, katı yüzey kalınlığı (t): 2 mm, Reynolds sayısı: 200, 400, 750, 1000, sıcak akışkan sıcaklığı (T_h): 600 K, soğuk akışkan sıcaklığı (T_c): 300 K, sıcak hava giriş hızı (V_h): 1.338 m/s, soğuk hava giriş hızı (V_c): 0.69 m/s' dir.

Çalışma, belirtilen şu sınır şartları altında yapılmıştır: a) akış üç boyutlu, zamandan bağımsız ve laminerdir, b) kullanılan akışkan sıkıştırılamazdır, c) kanatçık ve kanal malzemesi olarak alüminyum kullanılmıştır, d) tabakalar arası ısıl temas tamdır, e) kanalın alt ve üst bölümü için kullanılan akışkan havadır, f) akışkanın ısıl özellikleri sabittir, g) hem akışkan hem de katı malzeme için ısı üretimi söz konusu değildir.

BULGULAR VE SONUÇLAR

Şekil 3' de sunulan çalışma, Buyruk ve Karabulut, (2018) ve Kayatas ve Ilbas (2005) tarafından yapılan çalışmalarla karşılaştırılmıştır. Şekil 3' den de görülebildiği gibi çalışmanın sonuçları birbirleriyle uyumlu olup, bu nedenle sunulan çalışmanın doğru ve kabul edilebilir olduğu söylenebilmektedir. Bununla birlikte, çalışmada görülen sıcaklık farklılıklarının ağ yapısından kaynaklandığı öngörülmektedir.

Sunulan çalışmanın ağ bağımsızlık testinin sonuçları, soğuk akışkanın sıcaklık değişimi dikkate alınarak b=20 mm, e=2 mm ve Re=1000 için dairesel kanatçıklı kanal için Şekil 4' de verilmektedir. Akışkanın sıcaklık değişimi, kanal kesitinde 1,510.466 adet ağ elemanının olduğu durumla, 1,661.512 adet ağ elemanının olduğu durum karşılaştırıldığında aradaki farkın %0.02' den daha az olduğu görülmüştür. Bu nedenle, kanal kesitinde toplam 1,510.466 adet ağ elemanının yeterli olduğu sonucuna varılmıştır. Bununla birlikte, çalışmada üçgen kanatçıklı kanal için 1,511.822 adet ağ elemanı kullanılırken, düz kanal için bu değer 1,380.371' dir.

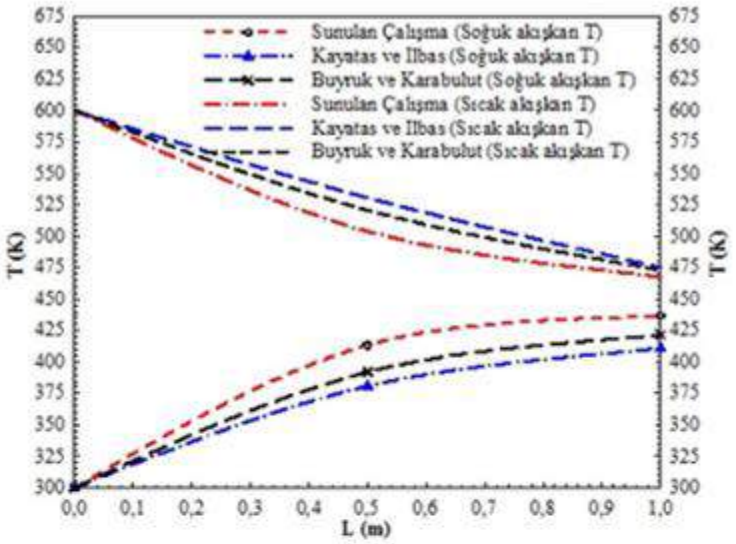

Şekil 3. Sunulan Çalışmanın Sonuçlarının Karşılaştırılması

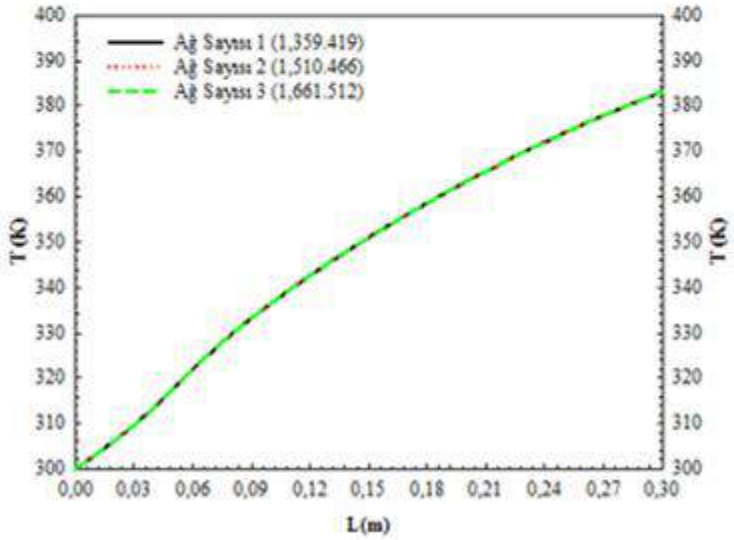

Şekil 4. Ağ Elemanı Sayısına Soğuk Akışkanın Sıcaklık Değişimi

Şekil 5' de düz kanal, 2 mm kanatçık yüksekliği (e) ve 20 mm kanatçık aralığına (b) sahip dairesel ve üçgen kanatçıklı kanallar için kanal boyunca sıcak akışkanın sıcaklık değişimleri gösterilmektedir. Paralel akış için girişte sıcak ve soğuk akışkan arası sıcaklık farkının yüksek olması nedeniyle yaklaşık 0.23 m kanal mesafesine kadar sıcak akışkanın sıcaklık değerleri ters akışa göre daha düşük değerlerdedir. Bununla birlikte, bu mesafeden sonra (L=0.23 m) ters akış için akışkanlar arası sıcaklık farkı artmakta ve paralel akışa göre daha düşük sıcak akışkan sıcaklık değerleri elde edilmektedir. Kanal girişi ve çıkışı arasındaki sıcaklık farkı değerlendirildiğinde; ters akışta, paralel akışa göre sıcak akışkan için daha düşük sıcaklık değerleri elde edilmektedir. Bu durum, ısı transferinin ters akışta daha fazla olması nedeniyledir. Dairesel kanatçıklı kanal için 600 K sıcaklıkta kanala giriş yapan sıcak akışkan, 516.11 K sıcaklık değeri ile kanaldan çıkış yaparken bu değer ters akış için 512.83 K olmaktadır. Kanatçıksız düz kanalda ise kanal çıkışında sıcak akışkan paralel akışta

539 K değerinde iken, ters akış için ise 538.4 K olmaktadır. Sıcaklıktaki bu azalma değeri, aynı zamanda kanatçığın ısı transferini artırmadaki önemini göstermektedir.

Kanal boyunca düz, dairesel ve üçgen kanatçıklı kanallara ait soğuk akışkanın sıcaklık değişimleri paralel ve ters akış için Şekil 6' da verilmektedir. Üçgen kanatçıklı kanalda, dairesel kanatçıklı kanala göre akışkanda daha fazla türbülans etkisi oluşturulması nedeniyle her iki akış yönü için daha yüksek soğuk akışkan çıkış sıcaklık değerlerine ulaşılmaktadır. Bununla birlikte, paralel akışta kanatçıksız kanala göre dairesel kanatçıklı kanalda soğuk akışkan sıcaklığında %4' lük bir artış elde edilirken, üçgen kanatçık için bu artış değeri %4.57 olmaktadır. Ters akış durumunda ise bu artış değeri, dairesel kanatçıklı kanal için %4.18 iken, üçgen kanatçıklı kanal için %4.77'dir.

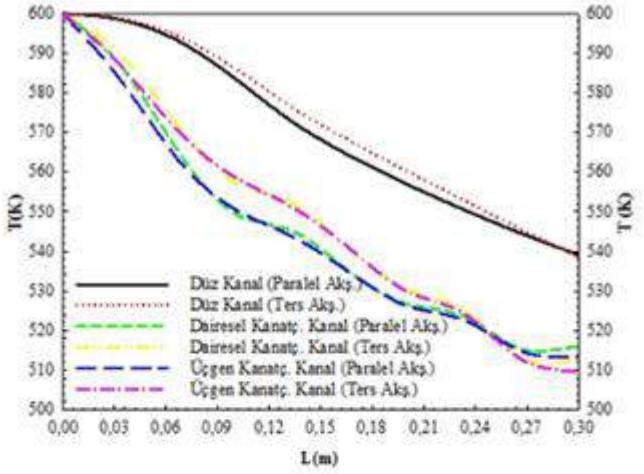

Şekil 5. Sıcak Akışkanın Kanal Boyunca Sıcaklık Değişimi (e=2 mm, Re=1000)

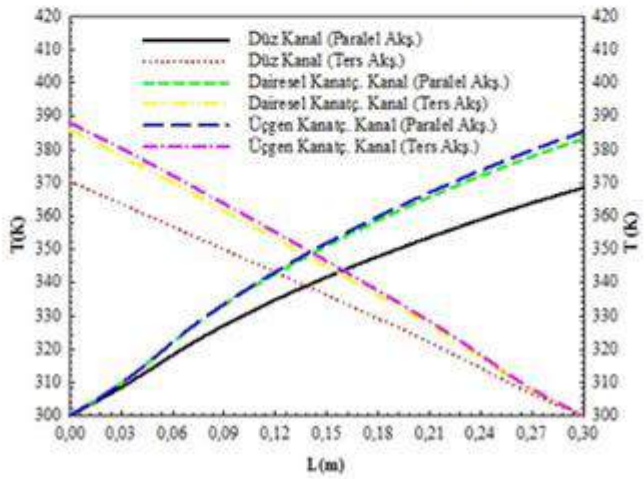

Şekil 6. Soğuk Akışkanın Kanal Boyunca Sıcaklık Değişimi (e=2 mm, Re=1000)

Şekil 7a, b' de sırasıyla paralel ve ters akışta soğuk akışkana ait kanal yüzeyi boyunca Re=400 ve Re=1000 için Nu sayısının değişimi gösterilmektedir. Paralel akışta kanal çıkışına doğru, sıcak ve soğuk akışkanlar arası sıcaklık farkının azalması nedeniyle Nu sayısı kanal çıkışına doğru azalmaktadır. Bununla birlikte, ters akışta ise kanal girişine doğru sıcaklık farkının artması sonucu Nu sayısı değerleri kanal girişine doğru artış

göstermektedir. Artan Re sayısı değerleriyle ısı transferindeki iyileşme nedeniyle her iki akış yönü için de Nu sayısı değerlerinde artış gözlemlenmektedir. Ayrıca, Re sayısının 400 değerinde her üç kanal şekli için kanal girişlerinde görülen noktasal Nu sayısı artışının gelişen ısıl sınır tabaka nedeniyle olduğu düşünülmektedir. Bunun yanı sıra, en yüksek Nu sayısı değerlerine düz kanala kanatçık eklenmesiyle birlikte elde edilen akış karışmasının daha fazla olduğu üçgen kanatçıklı kanalda ulaşılmaktadır.

Şekil 8'de paralel ve ters akış için dairesel kanatçıklı kanalda kanatçık yüksekliği değişiminin (e=2 mm ve e=4 mm) soğuk akışkanın sıcaklık değişimi üzerindeki etkisi verilmektedir. Artan kanatçık yüksekliği ile hem ısı transfer yüzey alanı hem de akışın türbülansı artmaktadır. Bu nedenle, daha yüksek soğuk akışkan sıcaklık değerleri elde edilmektedir. Ters akışta e=4 mm kanatçık yüksekliği için soğuk akışkanın kanaldan çıkış sıcaklığı, e=2 mm' ye göre %2.75 daha fazladır.

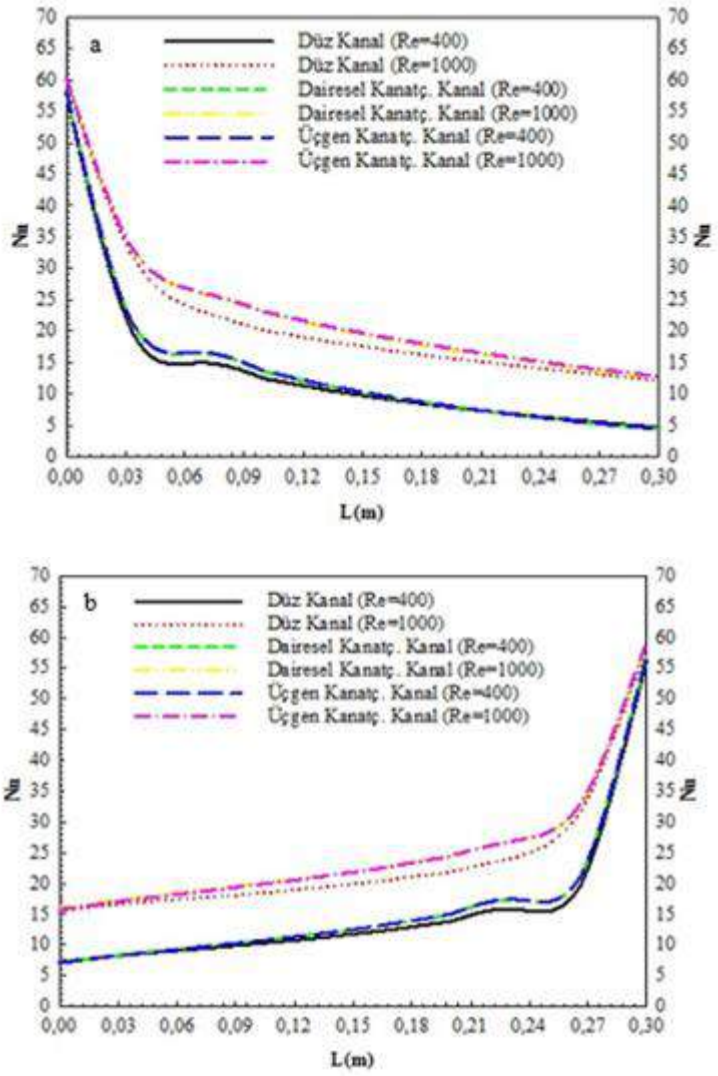

Şekil 7a) Paralel b) Ters akışta farklı Re sayılarında Soğuk Akışkanın Nu Sayısı Değişimleri

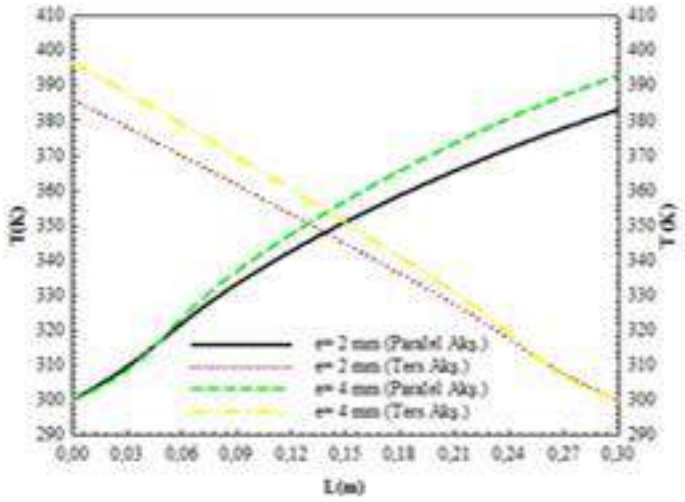

Şekil 8. Dairesel Kanatçıklı Kanalda Farklı Kanatçık Yükseklikleri İçin Soğuk Akışkanın Sıcaklık Değişimi (Re=1000)

Şekil 9′ da sıcak akışkanın geçtiği kanal boyunca düz kanal ve farklı kanatçık yüksekliklerine sahip dairesel ve üçgen kanatçıklı kanallar boyunca türbülans kinetik enerjinin değişimi gösterilmektedir. Bir akımın, türbülans kinetik enerjisi onun ne kadar türbülanslı olduğunu göstermektedir. Şekil 9' dan da kolaylıkla görülebildiği gibi en düşük türbülans kinetik değerleri düz kanal için elde edilirken, kanala kanatçıkların eklenmesiyle akışın türbülans kinetik enerjisi artmaktadır. Kanatçıklı kanallar içinde en yüksek türbülans kinetik enerji değeri, akış karışmasının da fazla olduğu 4 mm kanatçık yükseklikli üçgen kanatçıklı kanal düzenlemesi için elde edilirken, en düşük değer 2 mm kanatçık yükseklikli dairesel kanatçıkta görülmektedir. Bununla birlikte, kanal içerisinde türbülans kinetik enerjinin arttığı kısımlar kanatçık nedeniyle kesit daralmasının olduğu kısımlar olurken, kanatçığın ön ve arka kısımlarındaki kanatçık aralıkları ise kinetik enerjinin azaldığı kısımları oluşturmaktadır.

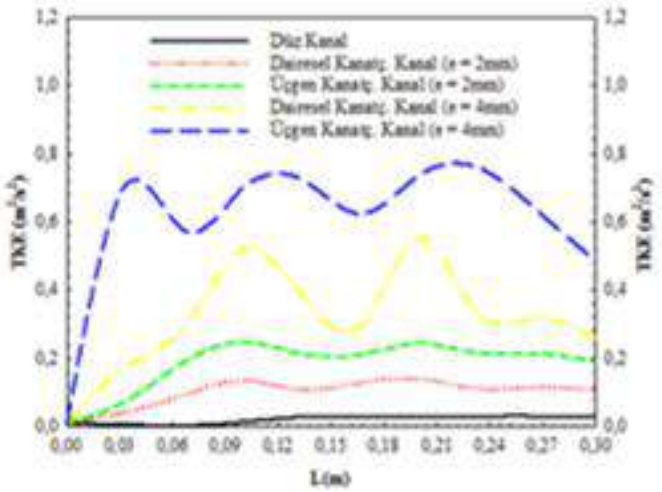

Şekil 9. Kanal Boyunca Türbülans Kinetik Enerji Değişimi (Re=1000)

Şekil 10' da sırasıyla düz kanal, dairesel kanatçıklı ve üçgen kanatçıklı kanallara ait paralel ve ters akış olmak üzere kanal boyunca hız dağılımları gösterilmektedir. Düz kanala göre, özellikle kanatçıklı kanallarda hız değişiminin daha fazla olduğu kontur dağılımından görülebilmektedir. Bununla birlikte, kanatçıklara çarparak duran akışkan, kanatçığın alt kısmı boyunca hızlanarak kanatçık aralıklarına ve kanalın alt kısmına doğru yönlenmektedir. Bunun yanı sıra, üçgen kanatçıklı kanallarda, dairesel kanatçıklı kanallara göre kanatçık aralıklarında daha yüksek akışkan hız değerleri elde edilmektedir. Ayrıca, ters akış durumunda paralel akışa göre kanal sonunda akışkanlar arası sıcaklık farkı daha fazla olduğundan moleküler hareketlenme nedeniyle kanal sonunda daha yüksek hız değerleri elde edilmektedir.

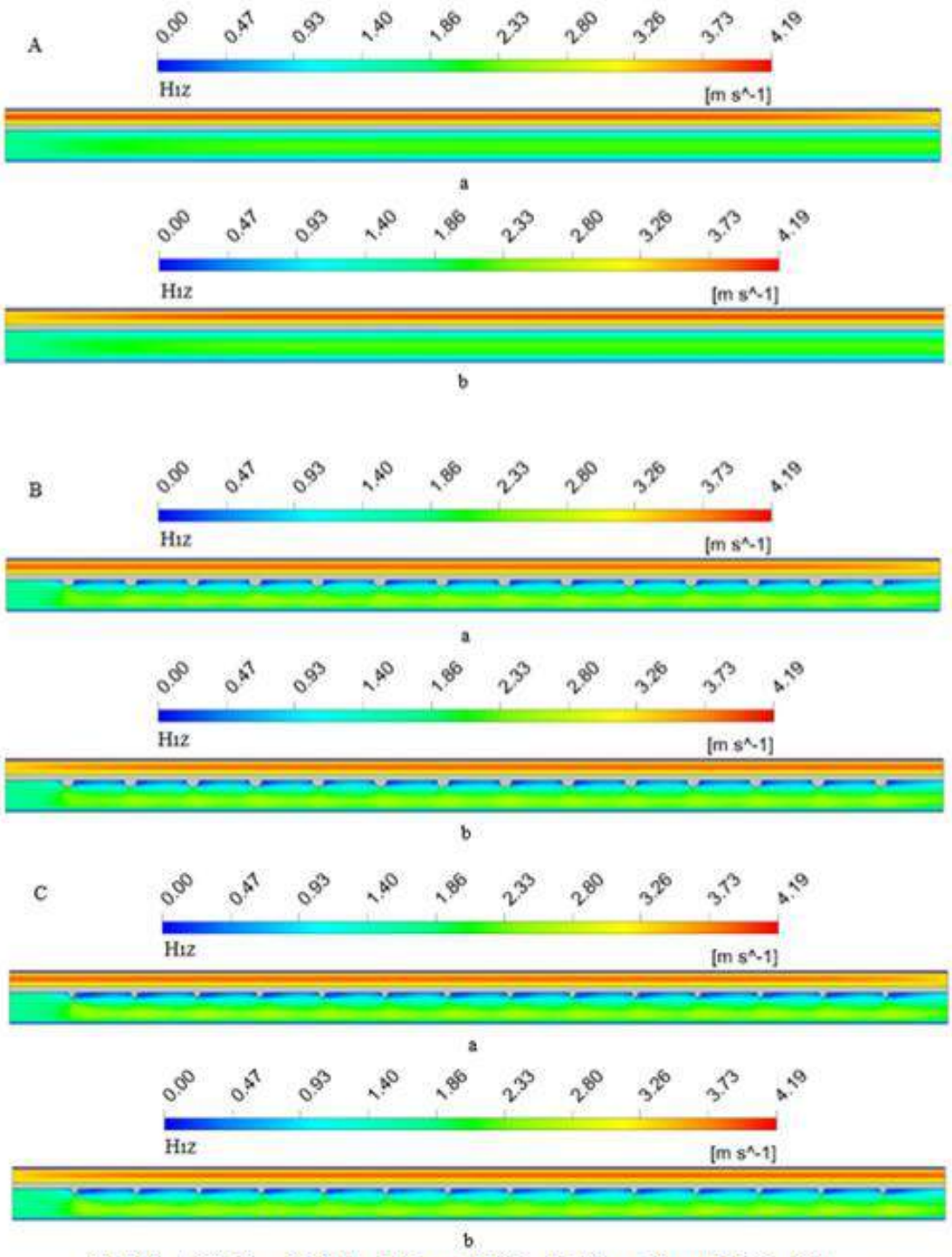

Şekil 10. A-Düz Kanal B-Dairesel Kanatçıklı Kanal C-Üçgen Kanatçıklı Kanal Boyunca Hız Konturu Dağılımı a-Paralel Akış b-Ters Akış

Paralel ve ters akışta düz, dairesel ve üçgen kanatçıklı kanallar için kanal boyunca akışkan sıcaklık konturu dağılımları Şekil 11' de verilmektedir. Düz kanala kanatçıkların eklenmesiyle Şekil 11' de de görüldüğü gibi hem sıcak akışkan hem de soğuk akışkan için akışkanın sıcaklık değişimi artmaktadır. Özellikle üçgen kanatçıklı kanal için sıcaklık değişiminin dairesel kanatçıklı kanala göre daha fazla olduğu sıcaklık konturu dağılımımdan görülebilmektedir. Ayrıca, ters akış durumunda ısı

transferinin daha fazla olması akışkanların sıcaklık değişiminin daha fazla olmasını sağlamaktadır.

Şekil 12' de düz, dairesel ve üçgen kanatçıklı kanallara ait paralel ve ters akışta kanal boyunca basınç konturu dağılımları sergilenmektedir. Akışkanların kanal boyunca basınç değişimi artmakla birlikte, kanatçıkların olduğu kanallarda daha fazla basınç değişimi elde edildiği basınç konturu dağılımlarından görülebilmektedir. Bu durum kanatçıkların akışa karşı oluşturdukları direnç sebebiyledir.

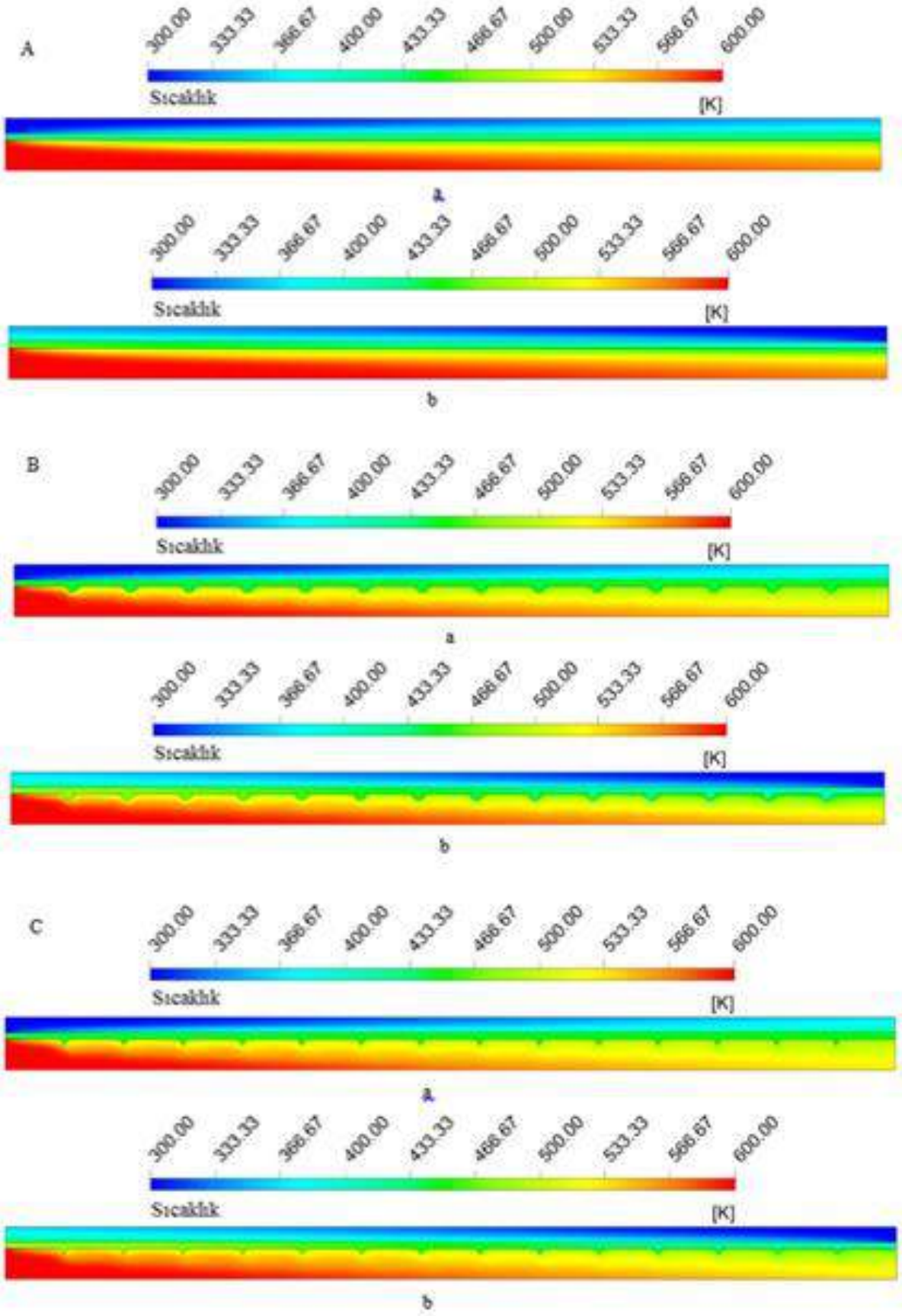

Şekil 11. A-Düz Kanal B-Dairesel Kanatçıklı Kanal C-Üçgen Kanatçıklı Kanal Boyunca Sıcaklık Konturu Dağılımı a-Paralel Akış b-Ters Akış

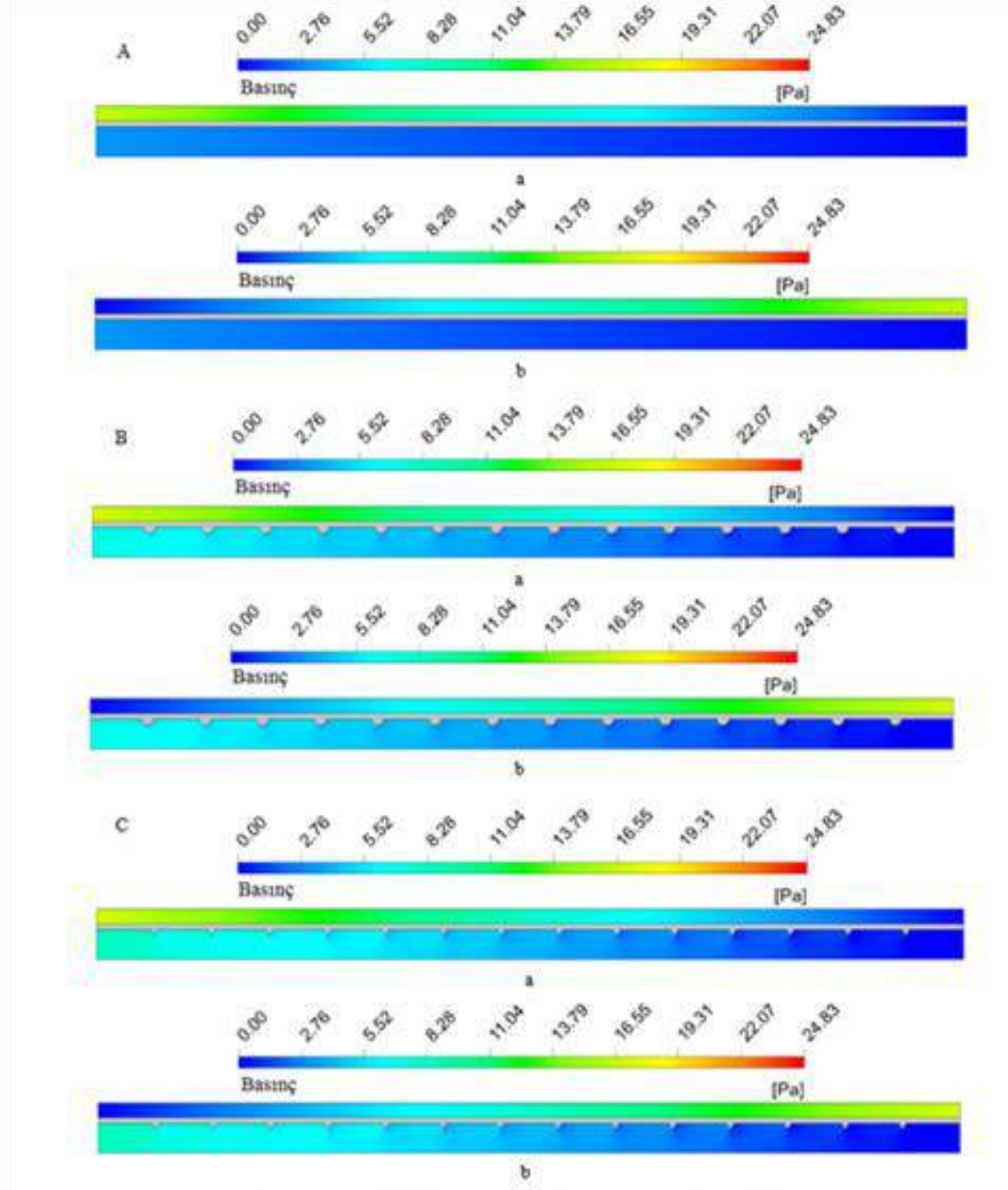

Şekil 12. A-Düz Kanal B-Dairesel Kanatçıklı Kanal C-Üçgen Kanatçıklı Kanal Boyunca Basınç Konturu Dağılımı a-Paralel Akış b-Ters Akış

Tablo 1' de Re=1000 değerinde b=20 mm ve e=2 mm için kanatçıkların bulunduğu sıcak akışkanın geçtiği kanal boyunca akışkanın basınç düşüşü değişimleri gösterilmektedir. Kanatçıklar, ısı transferi değerini artırırken akışa karşı direnç oluşturdukları için kanal boyunca basınç düşüşünü artırmaktadırlar. Her iki kanatçık

tipi için de kanatçıksız düz kanala göre daha yüksek basınç düşüşü değerleri elde edilmektedir ki bu da gereksinim duyulan pompalama gücünü artırıcı etki yapmaktadır. Bu nedenle, plakalı ısı değiştiricilerde kanatçık kullanımıyla ısı transferi artırılırken basınç düşüşü etkisi de göz önünde bulundurulmalıdır.

Tablo 1. Plakalı Isı Değiştiricilerin Basınç Düşüşleri

Kanal Tipi	ΔP (Pa)
Düz	3.215
Dairesel Kanatçıklı	7.205
Üçgen Kanatçıklı	8.632

SONUÇ

Bu çalışmada, dairesel ve üçgen kanatçıklı kanallara sahip ısı değiştiricilerinin ısı transferi, akış yapısı ve basınç düşüşü özellikleri üç boyutlu, zamandan bağımsız ve sayısal olarak çözülmüştür. Sayısal çalışma, ANSYS-FLUENT bilgisayar programının kullanılmasıyla gerçekleştirilmiştir. Çalışmada ayrıca kanatçık yüksekliğinin etkisi de dikkate alınmış ve paralel ve ters akış şartları altında kanal boyunca hız, sıcaklık ve basınç dağılımı konturları incelenmiştir. Kanatçıklar, kanal içerisinde ısı transferi yüzeylerini artırmalarının yanı sıra akışın türbülansını da artırmaktadırlar. Bu nedenle, çalışmada farklı kanatçık tiplerine sahip kanalların farklı kanatçık yüksekliklerinde türbülans kinetik enerji değişimleri de değerlendirilmiştir. Ayrıca, çalışmada düşük Re sayılarında kanatçıkların ısı transferi ve basınç düşüşü üzerindeki etkilerinin belirlenmesi amaçlanmıştır. Kanatçıklı kanalların basınç değişimi değerleri incelendiğinde türbülans kinetik enerji değeri fazla olan üçgen kanatçıklı kanalın daha fazla basınç düşüşüne sebep olduğu görülmüştür.

Ayrıca, çalışmada artan Re sayısı değerleriyle ısı transferindeki iyileşme nedeniyle her iki akış yönü için de Nu sayısı değerlerinde artış gözlemlenmektedir. Bunun yanı sıra, en yüksek Nu sayısı değerlerine düz kanala kanatçık eklenmesiyle birlikte elde edilen akış karışmasının daha fazla olduğu üçgen kanatçıklı kanalda ulaşılmaktadır. Artan kanatçık yüksekliği ile hem ısı transfer yüzey alanı hem de akışın türbülansı artmaktadır. Bu nedenle, daha yüksek soğuk akışkan sıcaklık değerleri elde edilmektedir. Ters akışta e=4 mm kanatçık yüksekliği için soğuk akışkanın kanaldan çıkış sıcaklığı, e=2 mm' ye göre %2.75 daha fazladır. Bununla birlikte, paralel akışta kanatçıksız kanala göre dairesel kanatçıklı kanalda soğuk akışkan sıcaklığında %4' lük bir artış elde edilirken, üçgen kanatçık için bu artış değeri %4.57 olmaktadır. Ters akış durumunda ise bu artış değeri, dairesel kanatçıklı kanal için %4.18 iken, üçgen kanatçıklı kanal için %4.77'dir.

Bununla birlikte, hem bu çalışmada incelenen kanatçık şekillerinin henüz değerlendirilmediği hem de enerji verimliliğinin artırılmasının öneminin daha iyi

anlaşıldığı günümüzde kanatçık üzerine daha yoğun araştırmalar yapılması gerekliliği göz önünde bulundurularak bu çalışmada özgün kanatçık şekilleri değerlendirilmiştir. Sonuç olarak, elde edilen bu verilerin ışığında bu çalışmadaki kanatçıkların plakalı ısı değiştiricilerin tasarımında ve optimizasyonunda doğrudan kullanılabileceği düşünülmektedir.

KAYNAKLAR

ANSYS Inc. (2003). ANSYS FLUENT User's Guide, Fluent, ANSYS Press, Netherland.

Buyruk, E., Karabulut, K., Karabulut, Ö. O. (2013). Three-dimensional numerical investigation of heat transfer for plate fin heat exchangers, Heat and Mass Transfer, 49, 817-826.

Buyruk, E., Karabulut, K. (2017). Plakalı kanatçıklı ısı değiştiricilerde kanat açısının ısı transferine olan etkisinin üç boyutlu sayısal olarak incelenmesi, Çukurova Üniversitesi Mühendislik Mimarlık Fakültesi Dergisi, 32, 49-62.

Buyruk, E., Karabulut, K. (2018). Enhancement of heat transfer for plate fin heat exchangers considering the effects of fin arrangements, Heat Transfer Engineering, 39, 1392-1404.

Gupta, M., Kasana, K. S., Vasudevan, R. (2009). A numerical study of the effect of flow structure and heat transfer of a rectangular winglet pair in a plate fin heat exchangers, Journal of Mechanical Engineering Science, 223, 2109-2215.

Karabulut, Ö, O. (2011). Kanatçıklı yüzeylerde ısı aktarımının üç boyutlu sayısal olarak incelenmesi, *Sivas Cumhuriyet Üniversitesi, Fen Bilimleri Enstitüsü*, Yüksek Lisans Tezi, 156s.

Lee, K., Kim, W., Si, J. (2001). Optimal shape and arrangement of staggered pins in the channel of a plate heat exchanger, *International Journal of Heat and Mass Transfer*, *44*, 1373–1378.

Shah, R.K. (1981). Classification of heat exchangers in heat exchangers, thermo-hydraulic fundamentals and design, S. Kakaç, A.E Berges and F. Mayinger (Ed.), Wiley, New York.

Tausher, R., Mayinger, F. (1991). Heat transfer enhancement ın a plate heat exchanger with rib-roughened surfaces. *Heat Transfer Enhancement of Heat Exchangers*, 207-221.

Wang, Y. Q., Dong, Q. W., Liu, M. S., Wang, D. (2009). Numerical study on plate fin heat exchangers with plain fins and serrated fins at low reynolds number, *Chemical Engineering&Technology*, *32*, 1219-1226.

Zhu, Y. H., Li, Y. Z. (2008). Three dimensional numerical ınvestigation on the laminar flow and heat transfer in four basic fins of plate fin heat exchangers, *Transactions of ASME Journal of Heat Transfer*, *130*, 1-8.

INVESTIGATION OF HEAT TRANSFER FROM HEATED SURFACES BY USING IMPINGING AIR JET

Koray KARABULUT

Sivas Cumhuriyet University, Sivas Vocational High Sch., Electric and Energy Dept.

kkarabulut@cumhuriyet.edu.tr

Doğan Engin ALNAK

Sivas Cumhuriyet University, Technology Fac., Automotive Eng. Dept.

dealnak@cumhuriyet.edu.tr

ABSTRACT: In this study, it is aimed to investigate the heat transfer from microchips used in computers by using impingement air jet. The cooling of surfaces with copper plate having different surface patterns as reverse circle, reverse triangle and rampart and constant heat flux of 1000 W/m^2 in rectangular ducts has been numerically investigated by using air jet and the optimum pattern has been determined among three shapes in terms of heat transfer. Numerical calculations have been carried out to solve Navier Stokes and enrgy equations by k-ε turbulance model as three dimensional and steady using Ansys-Fluent program. While the side, lower and upper surfaces of the rectangular ducts where the pattern surfaces are in it have been adiabatic, the constant heat flux has been only applied to the patterned surfaces. Air with 300 K inlet temperature has been used as the jet fluid. The jet-plate distance (H/D_h) evaluated in the study is 4, 6 and 12, and the range of Re numbers used is 4000-10000. When the results obtained have been compared with the numerical and experimental results of the study in the literature, they have been found to be in agreement with each other. The results have been shown as mean Nu number and surface temperature variations for different patterned surfaces. Furthermore, streamline and temperature distribution contours of the jet flow along the channel have been analyzed. It has been determined that the mean Nu number value obtained at Re=8000 and H/D_h=12 for the reverse patterned surfaces has been 21.9% higher than that obtained for the rampart surface.

Key words: impinging air jet, microchip cooling, heat transfer

ÇARPAN HAVA JETİ KULLANILARAK ISINMIŞ YÜZEYLERDEN OLAN ISI TRANSFERİNİN İNCELENMESİ

ÖZET: Bu çalışmada, bilgisayarlarda kullanılan mikroçiplerden olan ısı transferinin çarpan hava jeti kullanılarak araştırılması amaçlanmıştır. Dikdörtgen kesitli kanallar içerisindeki ters daire, ters üçgen ve sur şeklinde olmak üzere farklı yüzey desenlerine ve 1000 W/m^2 sabit ısı akısına sahip bakır plakalı yüzeylerin çarpan hava jeti kullanılarak soğutulması sayısal olarak incelenerek, üç desen arasında ısı transferi bakımından en uygun olanı belirlenmiştir. Sayısal hesaplamalar, üç boyutlu ve zamandan bağımsız olarak Navier Stokes ve enerji denklemlerinin k-ε türbülans modeli ile Ansys-Fluent programı kullanılarak çözülmesiyle yapılmıştır. Desenli yüzeylerin içerisinde bulunduğu dikdörtgen kesitli kanalların yan, alt ve üst yüzeyleri adyabatik iken yalnızca desenli yüzeylere sabit ısı akısı uygulanmıştır. Jet akışkanı olarak 300 K giriş sıcaklıklı hava kullanılmıştır. Çalışmada değerlendirilen jet-plaka arası uzaklık (H/D_h) 4, 6 ve 12 olup, kullanılan Re sayısı aralığı ise 4000-10000' dir. Ulaşılan sonuçlar, literatürde bulunan çalışmanın sayısal ve deneysel sonuçlarıyla karşılaştırıldığında birbirleriyle uyum içerisinde oldukları görülmüştür. Sonuçlar, farklı desenli yüzeyler için ortalama Nu sayısı ve yüzey sıcaklık değişimleri olarak gösterilmiştir. Ayrıca, jet akışın kanal boyunca akım çizgisi ve sıcaklık dağılımı konturları analiz edilmiştir. Ters daire desenli yüzeyler için Re=8000 ve H/D_h=12' de elde edilen ortalama Nu sayısı değerinin, sur desenli yüzey için elde edilenden %21.9 daha fazla olduğu belirlenmiştir.

Anahtar sözcükler: çarpan hava jeti, mikroçip soğutma, ısı transferi

GİRİŞ

Elektronik sistemlerin uygun şekilde tasarımı ve güvenli çalışma şartlarının sağlanabilmesinde ısı transferinin çok büyük bir önemi vardır. Mikroelektroniklerin keşfedilmesi ile elektronik elemanların hacminin küçülmesi, daha hızlı devreler ve artan kapasite ile elektronik devrelerin ısı üretim miktarı artmıştır. Bunun sonucu olarak, yalnızca hava soğutması kullanılarak yeterli ve gerekli soğutma performansının sağlanamayacağı belirlenmiştir. Bununla birlikte, yüksek ısı akılı elektronik elemanların soğutulmasında çarpan hava jetlerinin kullanılması ısı transferinin artışı yönünde etki etmektedir (Narumanchi ve ark., 2003; Kercher ve ark., 2003). Konu ile ilgili olarak yapılan çalışmalar incelendiğinde, Popovac ve Hanjalic (2007) yaptıkları çalışmada ısıtılmış kübik bir plakanın soğutulmasında çarpan jet akışın etkisini araştırmışlardır. Bunun yanı sıra, merkez noktası küp etrafı olmak üzere akış yapılarını incelemişler ve küpün soğutulması ile çevresindeki akış yapıları arasında doğrudan bir bağlantı olduğunu saptamışlardır. Carlomagno ve Ianiro (2014) çarpan jet akış yapısı ve ısı transferi üzerinde Re sayısı ve jet plaka arası uzaklığının değişiminin etkisini incelemişlerdir. Bunun için parçacık görüntülemeli hız ölçüm tekniğinden (PIV) faydalanmışlardır. Bununla birlikte, PIV sonuçlarını ileri hesaplama yöntemleriyle de kıyaslamışlardır. Alnak ve ark. (2018) ısıtılmış üçgen desenli yüzeylerin türbülanslı akış koşulları altında hava jeti akışı ile soğutulmasını sayısal

olarak incelemişlerdir. Sabit jet plaka arası uzaklıkta Nu sayısı üzerinde Re sayısı etkisinin oldukça fazla olduğunu belirlemişlerdir. Bir diğer çalışmalarında, Alnak ve ark. (2019) sabit ısı akılı dikdörtgen desenli yüzeylerin çarpan hava jeti ile soğutulmasını analiz etmişlerdir. Boyutsuz jet plaka arası uzaklığın (H/D_h) 4 olduğu durum için Re sayısının 4000' den 10000' e artışı ile ortalama Nu sayısında %59.28' lik artış sağlamışlardır. Bu çalışmalardan farklı olarak yapılan diğer araştırmalarda ise, aynı sınır şartlarında bulunan çarpan hava jeti etkisi altındaki sur ve dikdörtgen desenlere ve ters daire ve düz daire desenlere sahip farklı bakır plakalı yüzeylerin ısı transferi ve akış özellikleri birbirleriyle kıyaslanarak sonuçları analiz edilmiştir (Karabulut ve Alnak, 2019; Karabulut, 2019). Belarbi ve ark. (2018) kişisel bilgisayar işlemcisinin soğutma performansında iyileşme sağlamak amacıyla dikdörtgen kesitli mini kanallı soğutucu bloğun hava jeti çarpması altındaki ısıl ve aerodinamik performanslarını deneysel olarak incelemişler ve en iyi soğutma performansının Y/D=0.606 (jet yüksekliği/çap) oranında elde edildiğini gözlemlemişlerdir.

Bu çalışmada da gelişmiş teknolojinin en küçük elemanı olup, özellikle bilgisayar sistemlerinde yoğun olarak karşılaştığımız mikroçiplerin soğutma performanslarının iyileştirilmesini araştırmak amacıyla bir tarafı açık, üç tarafı kapalı dikdörtgen kesitli kanallar içerisindeki ters daire, ters üçgen ve sur şeklinde olmak üzere üç farklı desene sahip bakır plakalı yüzeylerin çarpan hava jeti ile soğutulmasının sayısal olarak incelenmesi gerçekleştirilmiş olup, birbirleriyle kıyaslanarak üçünün kullanılması halinde ısı transferi bakımından en uygun geometrik desen yapısının bulunması amaçlanmıştır. Sayısal inceleme, zamandan bağımsız, üç boyutlu enerji ve Navier-Stokes denklemlerinin k-ε türbülans modeli ile Ansys-Fluent bilgisayar programının kullanılarak çözülmesiyle yapılmıştır. Sunulan çalışmada, literatürde var olan çalışmalar göz önüne alınarak, 50x200 mm boyutlarında ve jet-plaka arası uzaklığın etkisini değerlendirmek amacıyla farklı kanal yüksekliklerinde dikdörtgen kesitli kanallar kullanılmış olup, çarpan jet akışkanı olarak ise 300 K kanal giriş sıcaklığına sahip hava kullanılmıştır. Sayısal hesaplamalarda kullanılan jet akışkanı olan havanın kinematik viskozitesi $\nu=15.89\ 10^{-6}$ m^2/s, yoğunluğu $\rho=1.1614$ kg/m^3, özgül ısısı $c_p=1.007$ kj/kgK, ısı iletim katsayısı $k=26.3\ 10^{-3}$ W/mK olarak alınmıştır. Jet-desenli plakalar arası uzaklıklar (H/D_h), ters daire, ters üçgen ve sur olmak üzere desenlerin geometrik şekilleri ve jet akışkanı olan havanın kanala giriş hızları (Re sayısı) değişken parametreler olarak değerlendirilmiştir. Tüm incelemelerde, desenli yüzeyler sabit 1000 W/m^2' lik ısı akısıyla ısıtılmaktadır. Çalışılan jet Re sayısı aralığı 4000-10000 iken jet plaka arası uzaklıkları ise 4, 6 ve $12D_h$' dır. Ayrıca, sunulan çalışma, literatürde var olan çalışmanın sayısal ve deneysel sonuçları ile kıyaslanmış ve sonuçların birbirleriyle uyumlu ve tutarlı oldukları belirlenmiştir. Elde edilen sonuçlar, ters daire, ters üçgen ve sur olmak üzere üç farklı desenli yüzeyin her biri için ortalama Nu sayısı ve yüzey sıcaklık değişimleri olarak sunulmuş ve birbirleriyle kıyaslanarak değerlendirilmiştir. Bununla birlikte, çalışmada jet akışın kanal boyunca sıcaklık, akım çizgisi konturu dağılımları da analiz edilmiştir.

YÖNTEM

Bu çalışmada, üç boyutlu ve zamandan bağımsız olarak farklı geometrik şekilli desenli plakalı yüzeyler üzerindeki jet akışın zorlanmış taşınım ısı transferinin çözümü Ansys-Fluent bilgisayar programının kullanılmasıyla sayısal olarak elde edilmiştir.

Süreklilik ve momentum denklemleri için hesaplamanın durdurulacağı yakınsaklık ölçeği 10^{-6} iken, bu değer enerji denklemi için 10^{-7}' ye sabitlenmiştir. Simülasyonlarda dörtyüzlü (tetrahedral) ağ yapısı kullanılmıştır. Bununla birlikte, literatürdeki çalışmalardan elde edilen sonuçlar da dikkate alınarak bu çalışmadaki sayısal hesaplamalarda kanaldaki jet akışın çözümlemesinde standart k-ε türbülans modeli kullanılmıştır.

Kanal boyunca akış ve ısı transferinin çözümüne aşağıda açıklandığı gibi gövde kuvvetinin olmadığı kararlı akış koşullarında türbülanslı akış için zaman ortalamalı kütle, momentum ve enerjinin korunumu denklemlerinden üretilen kısmi türevli diferansiyel denklemlerin çözümü ile ulaşılmıştır (Ansys, 2003).

Süreklilik denklemi

$$\frac{\partial \bar{u}}{\partial x}+\frac{\partial \bar{v}}{\partial y}+\frac{\partial \bar{w}}{\partial z}=0 \qquad (1)$$

x momentumu denklemi

$$\left[\bar{u}\frac{\partial \bar{u}}{\partial x}+\frac{\partial \overline{(u')^2}}{\partial x}\right]+\left[\bar{v}\frac{\partial \bar{u}}{\partial y}+\frac{\partial \overline{(u'v')}}{\partial y}\right]+\left[\bar{w}\frac{\partial \bar{u}}{\partial z}+\frac{\partial \overline{u'w'}}{\partial z}\right] = -\frac{1}{\rho}\frac{\partial \bar{p}}{\partial x}+\nu\left(\frac{\partial^2 \bar{u}}{\partial x^2}+\frac{\partial^2 \bar{u}}{\partial y^2}+\frac{\partial^2 \bar{u}}{\partial z^2}\right) \qquad (2.1)$$

y momentumu denklemi

$$\left[\bar{u}\frac{\partial \bar{v}}{\partial x}+\frac{\partial \overline{(v')^2}}{\partial x}\right]+\left[\bar{v}\frac{\partial \bar{v}}{\partial y}+\frac{\partial \overline{(v'v')}}{\partial y}\right]+\left[\bar{w}\frac{\partial \bar{v}}{\partial z}+\frac{\partial \overline{v'w'}}{\partial z}\right] = -\frac{1}{\rho}\frac{\partial \bar{p}}{\partial y}+\nu\left(\frac{\partial^2 \bar{v}}{\partial x^2}+\frac{\partial^2 \bar{v}}{\partial y^2}+\frac{\partial^2 \bar{v}}{\partial z^2}\right) \qquad (2.2)$$

z momentumu denklemi

$$\left[\bar{u}\frac{\partial\bar{w}}{\partial x}+\frac{\partial\overline{(w')^2}}{\partial x}\right]+\left[\bar{v}\frac{\partial\bar{w}}{\partial y}+\frac{\partial\overline{(w'v')}}{\partial y}\right]+\left[\bar{w}\frac{\partial\bar{w}}{\partial z}+\frac{\partial\overline{w'w'}}{\partial z}\right]$$
$$=-\frac{1}{\rho}\frac{\partial\bar{p}}{\partial z}+\nu\left(\frac{\partial^2\bar{w}}{\partial x^2}+\frac{\partial^2\bar{w}}{\partial y^2}+\frac{\partial^2\bar{w}}{\partial z^2}\right) \quad (2.3)$$

burada $\overline{u'}$, $\overline{v'}$, $\overline{w'}$ ortalama dalgalı hız bileşenleridir (m/s).

Enerji denklemi

$$\left[\bar{u}\frac{\partial\bar{T}}{\partial x}+\bar{v}\frac{\partial\bar{T}}{\partial y}+\bar{w}\frac{\partial\bar{T}}{\partial z}\right]+\frac{\partial\overline{(u'T')}}{\partial x}+\frac{\partial\overline{(v'T')}}{\partial y}+\frac{\partial\overline{(w'T')}}{\partial z}=\left(\frac{k}{\rho c_p}\right)\left(\frac{\partial^2\bar{T}}{\partial x^2}+\frac{\partial^2\bar{T}}{\partial y^2}+\frac{\partial^2\bar{T}}{\partial z^2}\right) \quad (3)$$

Eşitlik 1, 2 ve 3' de ρ yoğunluk (kg/m^3), ν kinematik viskozite (m^2/s), p basınç (N/m^2), k ısıl iletkenlik (W/m K), $\bar{T}$ ortalama sıcaklık (K), c_p akışkanın özgül ısı kapasitesi (J/kgK), $\bar{u},\bar{v},\bar{w}$ x, y ve z koordinatlarındaki ortalama hız bileşenlerini belirtmektedir (m/s).

Daimi akış türbülans kinetik enerjisi denklemi

$$\frac{\partial(\rho uk')}{\partial x}+\frac{\partial(\rho vk')}{\partial y}+\frac{\partial(\rho wk')}{\partial z}$$
$$=\frac{\partial}{\partial x}\left(\frac{\mu_t}{\sigma_k}\frac{\partial k'}{\partial x}\right)+\frac{\partial}{\partial y}\left(\frac{\mu_t}{\sigma_k}\frac{\partial k'}{\partial y}\right)+\frac{\partial}{\partial z}\left(\frac{\mu_t}{\sigma_k}\frac{\partial k'}{\partial z}\right)+\mu_t\phi-\rho\varepsilon \quad (4)$$

Türbülans viskozitesi

$$\mu_t=C_{\mu'}\rho\frac{k'^2}{\varepsilon} \quad (5)$$

Çalışmada kullanılan k-ε türbülans modelindeki, ε türbülans dağılımı (m^2/s^3), k' türbülans kinetik enerji (m^2/s^2) ve ϕ viskoz yayılım terimini (m^2/s^3) göstermektedir.

Türbülans kinetik enerji

$$k'=\frac{1}{2}\left(\overline{u'^2}+\overline{v'^2}+\overline{w'^2}\right) \quad (6)$$

Viskoz yayılım terimi

$$\phi = 2\mu\left[\left(\frac{\partial \bar{u}}{\partial x}\right)^2 + \left(\frac{\partial \bar{v}}{\partial y}\right)^2 + \left(\frac{\partial \bar{w}}{\partial z}\right)^2\right] + \mu\left[\left(\frac{\partial \bar{v}}{\partial x} + \frac{\partial \bar{u}}{\partial y}\right)^2 + \left(\frac{\partial \bar{w}}{\partial y} + \frac{\partial \bar{v}}{\partial z}\right)^2 + \left(\frac{\partial \bar{u}}{\partial z} + \frac{\partial \bar{w}}{\partial x}\right)^2\right] \quad (7)$$

Eşitlik 7′ deki μ dinamik viskozitedir (kg/s m).

Türbülans kinetik enerji kaybolma denklemi

$$\frac{\partial(\rho\bar{u}\varepsilon)}{\partial x} + \frac{\partial(\rho\bar{v}\varepsilon)}{\partial y} + \frac{\partial(\rho\bar{w}\varepsilon)}{\partial z} = \frac{\partial}{\partial x}\left(\frac{\mu_t}{\sigma_\varepsilon}\frac{\partial \varepsilon}{\partial x}\right) + \frac{\partial}{\partial y}\left(\frac{\mu_t}{\sigma_\varepsilon}\frac{\partial \varepsilon}{\partial y}\right) + \frac{\partial}{\partial z}\left(\frac{\mu_t}{\sigma_\varepsilon}\frac{\partial \varepsilon}{\partial z}\right) + C_{1\varepsilon}\mu_t\frac{\varepsilon}{k'}\phi - C_{2\varepsilon}\rho\frac{\varepsilon^2}{k'} \quad (8)$$

Model sabitleri olan C_μ, $C_{1\varepsilon}$, $C_{2\varepsilon}$, σ_k ve σ_ε standart k-ε türbülans modelinde kullanılan genel saptanmış değerlerdir (Fluent, 2003). Bu sabitlerin değerleri, birçok türbülanslı akış için çok sayıda veri uyumuyla sağlanmıştır.

Re sayısı aşağıda verilen denklem ile hesaplanmaktadır

$$\mathrm{Re} = \frac{V_\infty D_h}{\nu} \quad (9)$$

Eşitlik 9′ da D_h jet girişinin hidrolik çapıdır (m) ve V_∞ ise kanal girişindeki jet akışkanının ortalama hızıdır (m/s).

$$D_h = \frac{4A_c}{P} = \frac{4(aW)}{2(a+W)} \quad (10)$$

Bu denklemde, A_c ve P sırasıyla jet girişinin kesit alanı (m^2) ve çevre uzunluklarıdır (m).

Nu sayısı, taşınımla ısı geçişinin iletimle ısı geçişine oranı olarak değerlendirilir.

$$-k\left(\frac{\partial T}{\partial n}\right)_{yüzey} = h(T_\infty - T_s) \text{ ve } Nu = \frac{hD_h}{k} \quad (11)$$

Burada h yüzey üzerindeki yerel ısı taşınım katsayısını (W/m^2K), n ise yüzeye dik yönü belirtmektedir. Bununla birlikte, ortalama ısı taşınım katsayısı h_m ve Nu sayısı aşağıdaki gibi hesaplanmaktadır.

Ortalama ısı taşınım katsayısı, h_m ve ortalama Nusselt sayısı, Nu_m,

$$h_m = \frac{1}{L}\int_0^L h dx \text{ ve } Nu_m = \frac{h_m D_h}{k} \quad (12)$$

Çalışmada kullanılan desenli yüzeylerin yer aldığı kanalların boyutlarının da olduğu perspektif görünüşleri ve sınır şartları Şekil 1' de gösterilmektedir. Çalışmada kullanılan jet püskürtücünün hidrolik çapı (D_h) 9.9 mm iken, kanalın boyu (L) ve genişliği (W) ise sırasıyla 200 mm ve 50 mm' dir. Jet püskürtücüden çıkan akışkanın giriş hız aralığı 6.23-15.58 m/s iken jet girişinde uniform hız profili bulunan dikdörtgen püskürtücünün boyutları 5.5x50 mm' dir. Kanal yükseklikleri ise $4D_h$, $6D_h$, ve $12xD_h$' dır. Kanal boyutlarına bağlı olarak üç farklı kanal içerisinde beşer adet ters daire, ters üçgen ve sur desenli yüzeyler bulunmakta iken iki desen arası uzaklık Dh, sırasıyla desenin genişlik ve yüksekliği ise $2D_h$ ve D_h' dır. Bununla birlikte, bu çalışma belirtilen şu kabuller altında gerçekleştirilmiştir: a) Kanallar için akış alanı üç boyutlu, zamandan bağımsız ve türbülanslıdır, b) Desenli yüzeylerin soğutulması için kullanılan jet akışkanı sıkıştırılamaz özellikli havadır, c) Desenli yüzeylere uygulanan sabit ısı akısı 1000 W/m^2' dir, d) Jet akışkanın ısıl özelikleri sabittir ve e) Jet akışkanı ve desenli yüzeyler için ısı üretimi yoktur.

BULGULAR VE SONUÇ

Bu çalışmanın sayısal sonuçları, H/D_h=6 ve Re=6000 ve 8000 değerleri için Kılıç ve ark., (2017)' nın deneysel ve sayısal olarak yaptıkları çalışmanın Nu sayısı sonuçlarıyla karşılaştırılmış ve Şekil 2' de verilmiştir. Karşılaştırma amacıyla Kılıç ve ark., (2017)' nin çalışmalarında kullandıkları 200x50 mm boyutlu düz bir bakır plaka yüzeyi kullanılmıştır. Re=6000 için jet çarpma bölgesindeki Nusselt sayısı değeri incelendiğinde, bu çalışmanın sayısal sonucu ile Kılıç ve ark., (2017)' nın deneysel sonucu arasındaki sapma %3.99 iken her iki çalışmanın sayısal sonuçları arasındaki sapma değerinin %1 olduğu görülmüştür. Bununla birlikte, Re sayısının 8000 olduğu değer için çarpma bölgesinde türbülans yoğunluğunun artmasına bağlı olarak Kılıç ve ark., (2017)' nın deneysel sonuçları ile bu çalışmanın sayısal sonuçları arasındaki sapma miktarı artarak %9.15 olmaktadır. Buna karşın, aynı bölgede sayısal sonuçlar arasındaki sapma değeri ise %1.02'dir. Elde edilen bu sonuçlara göre, bu çalışmanın sayısal sonuçlarının Kılıç ve ark., (2017)' nın deneysel ve sayısal sonuçlarıyla karşılaştırılabilir ve sayısal çalışmanın makul ve uygun olduğu düşünülmektedir.

Desenli yüzeylerin ortalama Nu sayısı üzerinde ağ sayısının etkisini belirlemek amacıyla H/D_h=4 ve Re=4000′ de desenli yüzeyler için yapılan ağ bağımsızlık testleri sonucunda sırasıyla ters daire ve sur desenli yüzeyler için 3,338.659 ve ters üçgen desenli yüzey için ise 3,476.017 adet ağ elemanının yeterli olduğu belirlenmiştir.

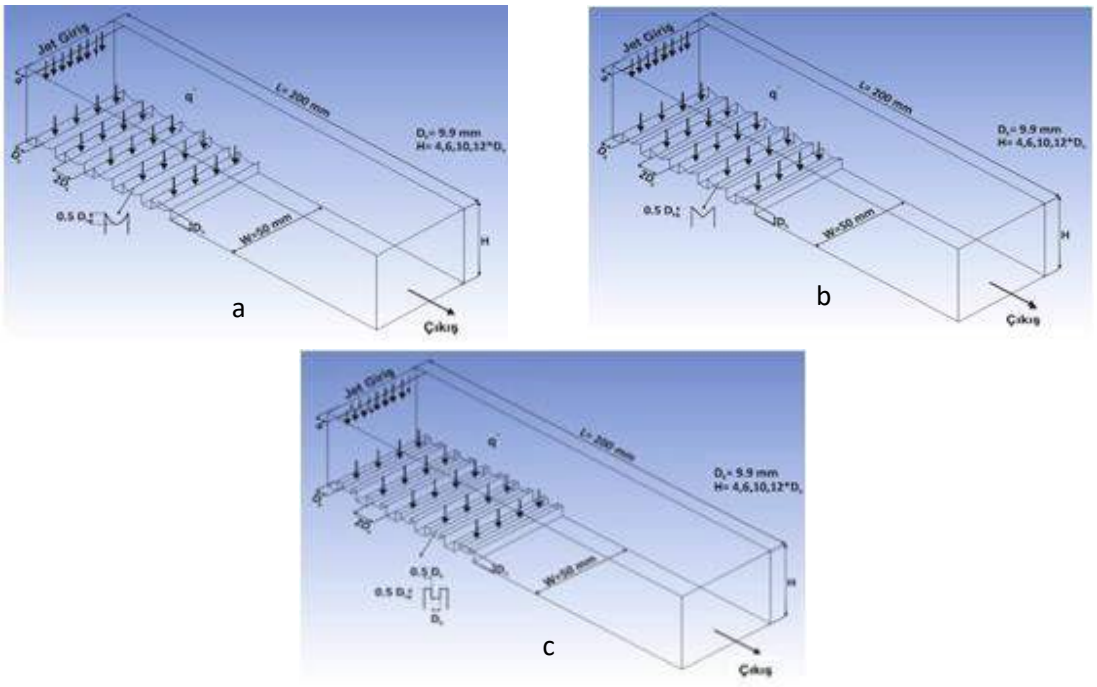

Şekil 1. (a)-Ters daire (b)-Ters üçgen (c)-Sur Desenli Yüzeylere Sahip Kanalların Perspektif Görünüşleri

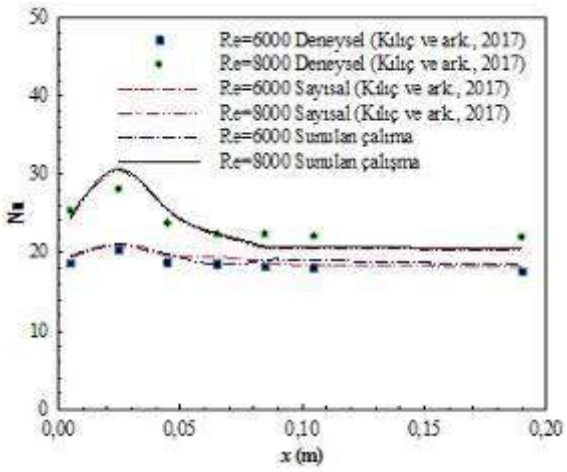

Şekil 2. Sunulan Çalışmanın Sonuçlarının Kılıç ve ark. (2017)′ nın Sonuçlarıyla Karşılaştırılması

Ters daire, ters üçgen ve sur desenli bakır plakalı yüzeylere ait ortalama Nu sayısının H/D_h=6 ve 12 için farklı Re sayılarına göre değişimi sırasıyla Şekil 3A, B ve C' de gösterilmektedir. Her üç desenli yüzey için beşer adet olmak üzere kanal girişlerinden çıkışlarına doğru eşit uzaklık ve boyutlarda desenler bulunmaktadır. Şekil 3 A, B ve C' deki ortalama Nu sayıları beş farklı desenin her biri için tüm yüzey boyunca elde edilen ortalama değerlerdir. Her üç desenli yüzeyin olduğu kanalda desenlerin sol alt taraflarında oluşan yeniden dolaşım bölgeleri jet akışı yönlendirmektedir. Buna bağlı olarak, en yüksek ortalama Nu sayısı değerleri Desen 2 için elde edilmektedir. Ayrıca, akışın desenli yüzeyler üzerindeki ve desen aralarındaki hareketine paralel olarak en yüksek ortalama Nu sayısı değerlerine ters daire desenli yüzeyler üzerinde ulaşılırken, en düşük Nu sayısı değerlerine sur desenli yüzeylerde ulaşılmaktadır. H/D_h=12 ve Re=8000 için ters daire desenli yüzeyler için ortalama Nu sayısı değeri ters üçgen desenli yüzeylerden %3.09 daha fazla iken ters üçgen desenli yüzeyler için sur desenli yüzeylere göre bu değerin %21.97 daha fazla olduğu tespit edilmiştir. Aynı zamanda, Re sayısının artışına bağlı olarak Nu sayısı değerlerinde artışlar elde edilmektedir. Bunun yanı sıra, jet etkisinin ve buna bağlı olarak kanal içerisindeki türbülans etkisinin azalması nedeniyle en düşük Nu sayısı değerlerine her üç desen şekli için de Desen 5' de ulaşılmaktadır. Bununla birlikte, jet plaka arası uzaklığın (H/D_h) artışı, jet akışın yüzeyler üzerindeki etkisinin azalmasına neden olarak soğutma etkisini azaltmaktadır. H/D_h=6 ve Re=8000 için ters daire desenli yüzeyler için elde edilen Nu sayısı değeri, sur desenli yüzeyden %22.6 daha fazla iken aynı Re sayısı değerinde H/D_h=12 için bu değer %21.9 değerine düşmektedir.

Şekil 4A, B ve C' de sırasıyla ters daire, ters üçgen ve sur desenli yüzeylere ait olmak üzere farklı Re sayılarında ve H/D_h uzaklıklarında desenlerin ortalama yüzey sıcaklıklarının değişimleri gösterilmektedir. Sıcaklık değerleri kıyaslandığında en yüksek yüzey sıcaklık değerleri sur desenli yüzey için elde edilirken, en düşük yüzey sıcaklık değerlerine ise ters daire desenli yüzeylerde ulaşılmaktadır. Bununla birlikte, H/D_h oranının artması hem jet akışın yüzeyler üzerindeki etkisinin hem de kanal içerisindeki türbülans etkisinin azalmasına neden olarak yüzey sıcaklık değerlerini artırmaktadır. Ayrıca, ters daire ve ters üçgen desenli yüzeyler için H/D_h=6' da kanal içerisinde meydana gelen yeniden dolaşım bölgelerinin jet akışı yönlendirmesi nedeniyle Desen 1 ile olan temasının azalması sonucu düşük Re sayılarında (4000, 6000) Desen 5' e göre daha yüksek sıcaklık değerleri elde edilmektedir.

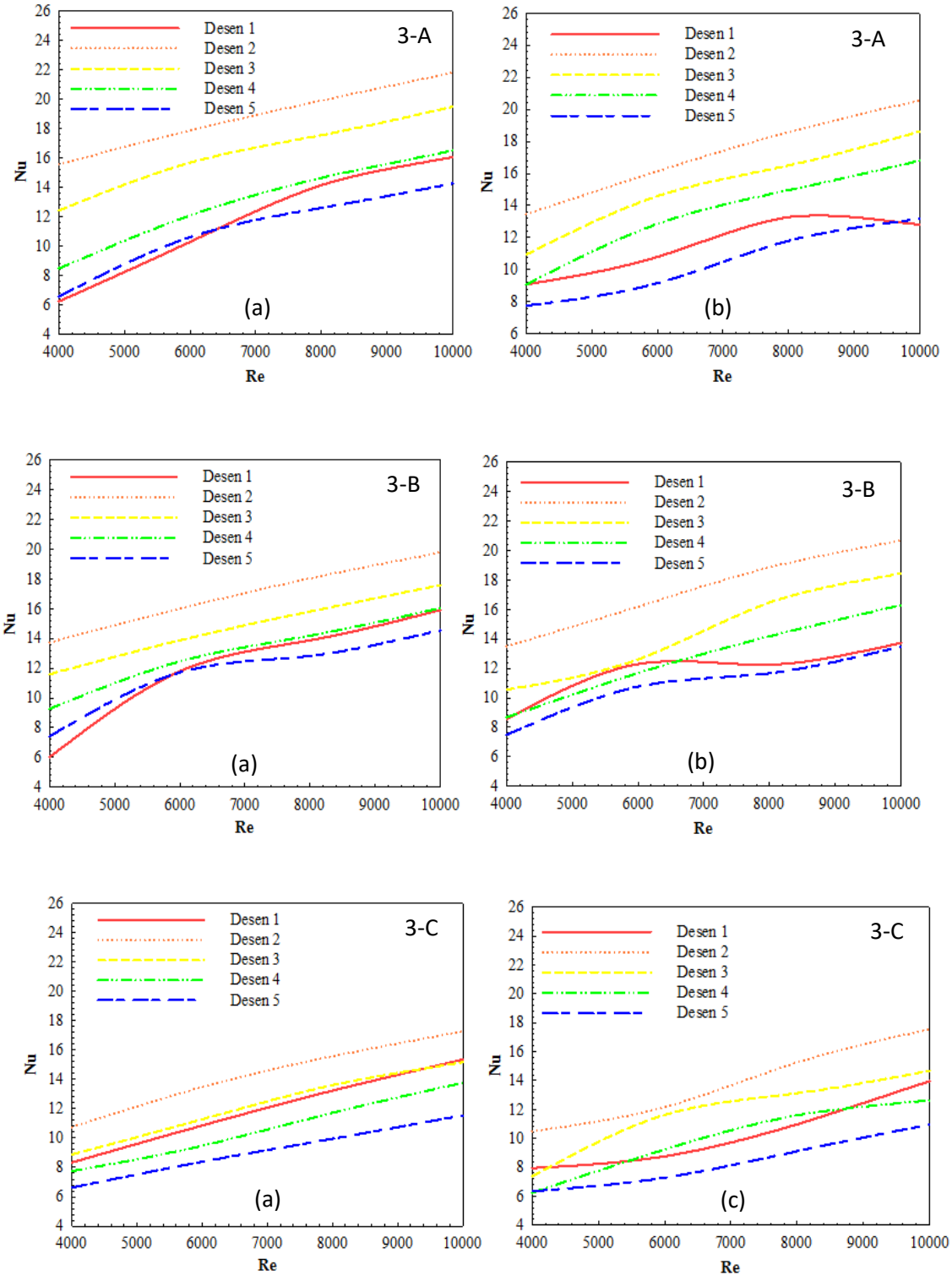

Şekil 3. A-Ters daire B-Ters üçgen C-Sur Desenli Yüzeylerde H/D_h (a)-6 (b)-12 İçin Desen Yüzeyleri Boyunca Ortalama Nu Sayısının Re Sayısı İle Değişimi

Şekil 5A, B ve C' de H/D_h=4 ve Re=4000 için sırasıyla ters daire, ters üçgen ve sur desenli yüzeylere sahip kanallardaki a-akım çizgisi ve b-sıcaklık dağılımı konturları gösterilmektedir. Şekillerden de görülebileceği gibi kanalların sol alt taraflarında

birinci desenlerin yanında oluşan yeniden dolaşım bölgesi jet akışı ikinci desene doğru yönlendirmektedir. Bununla birlikte, jet akışın desen aralıklarına giremediği ve özellikle kanal sonuna doğru desenli yüzeylerden ayrıldığı kısımlarda yeniden dolaşım bölgeleri oluşmaktadır. Bu kısımlar, hareketliliğin azaldığı ve akışın kendi içinde akış sirkülasyonunu sürdürdüğü kısımlardır. Bu nedenle, sıcaklık konturu dağılımlarından da görülebileceği gibi bu kısımlarda sıcaklık değerleri artış göstermektedir.

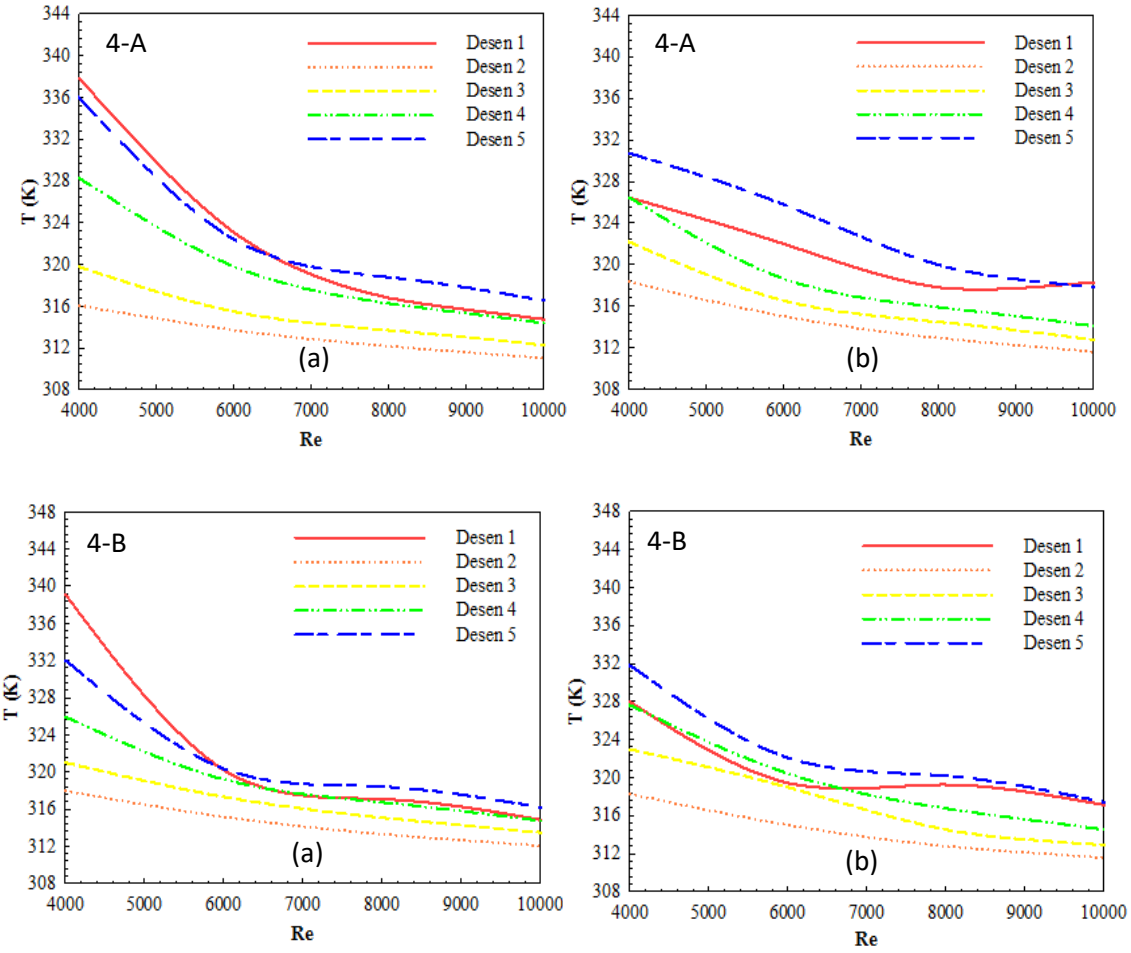

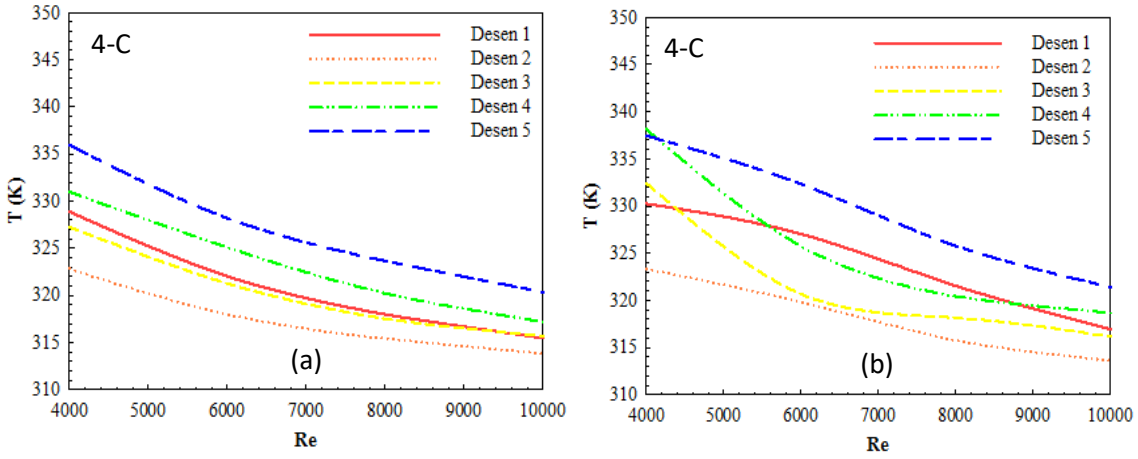

Şekil 4. A-Ters Daire B-Ters Üçgen C-Sur Desenli Yüzeylerde H/D_h (a)-6 (b)-12 İçin Desen Yüzeyleri Boyunca Ortalama Sıcaklığın Re Sayısı İle Değişimi

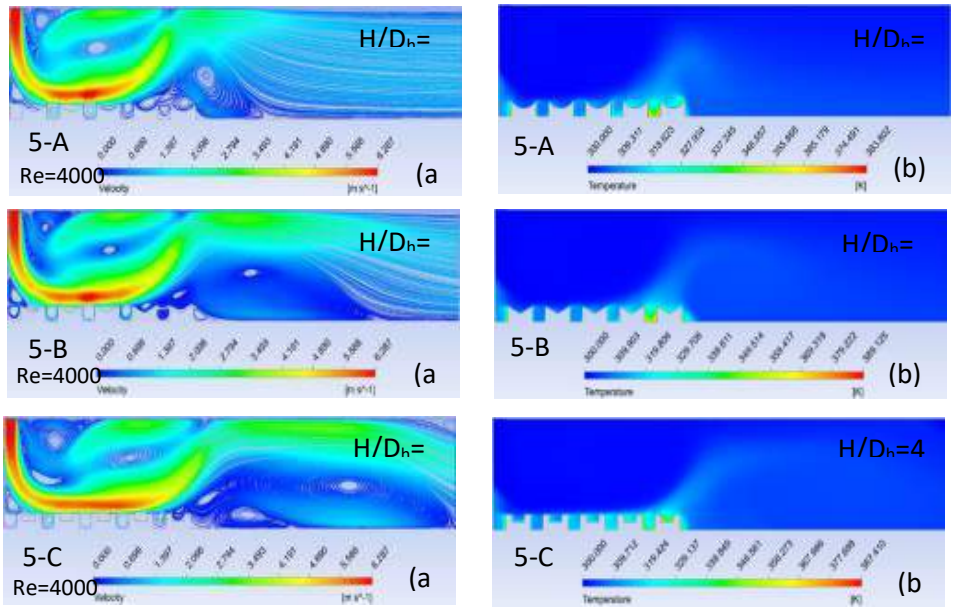

Şekil 5 A-Ters Daire B-Ters Üçgen C-Sur Desenli Yüzeyler İçin (a)-Akım Çizgisi (b)-Sıcaklık Konturu Dağılımları

SONUÇ

Bu çalışmada bir tarafı açık, üç tarafı kapalı dikdörtgen kesitli kanallar içerisindeki ters daire, ters üçgen ve sur şeklindeki desenlere sahip bakır plakalı yüzeylerin çarpan hava jeti ile soğutulması sayısal olarak incelenmiştir. Buna göre, çalışmadan elde edilen sonuçlar aşağıdaki gibi özetlenmiştir:

Genel itibariyle, Re sayısının artışıyla Nu sayısı artmakla birlikte özellikle Desen 1 için yeniden dolaşım bölgelerinin jet akışı yönlendirmesine bağlı olarak Nu sayısı değerlerinde dalgalanmalar görülebilmektedir. Ayrıca, yeniden dolaşım bölgeleriyle jet akışın yönlenmesi sonucu her üç desenli yüzey için en yüksek Nu sayısı değerlerine Desen 2 için ulaşılmaktadır. Bununla birlikte, en yüksek ortalama Nu sayısı değerlerine ters daire desenli yüzeyler üzerinde ulaşılırken, en düşük Nu sayısı değerleri ise sur desenli yüzeyler için elde edilmektedir.

Sıcaklık değerleri kıyaslandığında en yüksek yüzey sıcaklık değerlerine sur desenli yüzeylerde görülürken, en düşük yüzey sıcaklık değerlerine ise ters daire desenli yüzeylerde ulaşılmaktadır. Jet akışın desen aralıklarına giremediği ve özellikle kanal sonuna doğru desenli yüzeylerden ayrıldığı kısımlarda yeniden dolaşım bölgeleri oluşmaktadır. Sıcaklık konturu dağılımlarından da görülebileceği gibi bu kısımlarda sıcaklık değerleri artış göstermektedir.

Sonuç olarak, jet akışıyla desenli yüzeyler üzerindeki ısı transferi jet akışın Re sayısına, H/D_h oranına ve özellikle desenli yüzeylerin geometrik şekillerine önemli ölçüde bağlıdır. Bununla birlikte, bu çalışmada kullanılan yüzey geometrilerinin mikroçip gibi çeşitli elektronik devrelerde kullanılabilecek yüzey geometrileri düşünülerek tasarlandığından bu gibi elektronik tasarımların soğutma uygulamalarında kullanım alanlarının olabileceği düşünülmektedir.

KAYNAKLAR

ANSYS Inc. (2003). ANSYS FLUENT User's Guide, Fluent, ANSYS Press, Netherland.

Alnak, D.E., Karabulut, K., Koca, F. (2018). Desenli yüzeylerde hava jeti akışı için taşınım ısı transferi ve akış özelliklerinin incelenmesi, Geleceğin dünyasında bilimsel ve mesleki çalışmalar, Ekin basım yayın dağıtım, (s.191-217). Bursa-Türkiye.

Alnak, D. E., Karabulut, K., Koca, F. (2019). Investigation of heat transfer from heated square patterned surfaces in a rectangular channel with an air jet impingement. European Journal of Engineering and Natural Sciences (EJENS), 3, 78-86.

Belarbi, A. A., Beriache, M., Bettahar, A. (2018). Experimental study of aero-thermal heat sink performances subjected to impinging air flow. International Journal of Heat and Technology, 36, 1310-1317.

Carlomagno, G. M., Ianiro. A. (2014). Thermo-fluid-dynamics of submerged jets impinging at short nozzle-to-plate distance: a review. Experimental Thermal and Fluid Science, 58, 15-35.

Karabulut, K., Alnak, D.E. (2019). Değişik şekilde tasarlanan isıtılmış yüzeylerin hava jeti çarpmalı soğutulmasının araştırılması. Pamukkale Üniversitesi Mühendislik Bilimleri Dergisi, Baskıdaki makale, PAJES-58812. doi: 10.5505/pajes.2019.58812.

Karabulut, K. (2019). Heat transfer improvement study of electronıc component surfaces usıng air jet impıngement. Journal of Computational Electronics, Article in Press, doi: 10.1007/s10825-019-01387-3.

Kercher, D. S., Lee, J. B., Brand, O., Allen, M. G., Glezer, A. (2003). Microjet cooling devices for thermal management of electronics. IEEE Transactions on Components and Packaging Technologies, 26, 359-366.

Kılıç, M., Çalışır, T., Başkaya, S. (2017). Experimental and numerical study of heat transfer from a heated flat plate in a rectangular channel with an impinging air jet. Journal of Brazilian Society of Mechanical Sciences and Engineering, 39, 329-344.

Narumanchi, S. V. J., Amon, C.H., Murthy, J.Y. (2003). Influence of pulsating submerged liquid jets on chip-level thermal phenomena. *Journal of Electronic Packaging, 125*, 354-361.

Popovac, M., Hanjalic, K. (2007). Large-eddy simulation of flow over a jet impinged wall mounted cube in a cross stream. *International Journal of Heat and Fluid Flow, 28,* 1360-1378.

DESIGN OF EFFICIENT HEAT INTEGRATION BY PINCH AND EXERGY HYBRID METHODOLOGY

Ozben KUTLU

Ege University, Department of Chemical Engineering

ozben.kutlu@ege.edu.tr

Zehra OZCELIK

Ege University, Department of Chemical Engineering

zehra.ozcelik@ege.edu.tr

ABSTRACT: Energy efficiency has been taken a crucial attention by growth in energy demand, and economic crisis across the globe. In energy-intensive industrial sectors such as petrochemical industry and cement plant, more realistic process integration is required. Pinch and exergy are suggested as two powerful analytical methods among efficient process integrations. Pinch analysis is used into a general methodology for design of thermal processes, whereas exergy analysis is a tool that has been widely used to analyze the energy efficiency of industrial processes. The hybrid methodology of these analyses considers heat integration including other forms of recoverable exergy. However, different analysis techniques were applied to various industrial applications. In this study, the analysis techniques of the hybrid methodology applications were investigated, and a case study in the petrochemical plant was presented to demonstrate the efficiency of the hybrid methodology. As a result of the potential scenario, the external heating duty required could be completely eliminated by increasing in number of heat exchanger. Even though the average exergetic efficiency of whole heat exchangers is calculated as 73%, the applicability of scenario is significantly related with the economic evaluation of process.

Key words: energy efficiency, pinch analysis, exergy, process integration, heat exchanger network

INTRODUCTION

Nowadays, process integration (PI) is crucial methodology to use energy and water efficiently. It can be applied at both grassroots design of process and retrofitting the existing facility. Waste sources (energy, process water or wastewater) can be identified

according to minimum area, equipment and utility, and their recovering potential is determined. PI can be undertaken with following aims;

- Minimize energy consumption,
- Increase production yield,
- Reduce operating problems,
- Increase plant controllability,
- Enable the plant flexibility with respect to the plan,
- Minimize undesirable plant emissions.

Pinch analysis being a part of PI, is a thermodynamic approach. Even though beginning of Pinch analysis applications were aimed in energy saving in industry, nowadays it has been employed to solve general waste problems by using both heat and mass integration (Klemes et al., 2018). In the process of heat integration, energy demand and source is matched up (Linnhoff and Flower, 1978), and Heat Exchanger Network (HEN) is created by including multiple heat exchanger. Whereas HEN at grassroots design permits the freest choice in the design options and equipment dimensions, its aim at existing facility is both the improvement of capacity, product quality and safety, and the decrease in the operating costs and emissions by using available utility.

Heat integration consist of four phase; these are data extraction, targeting, initial design and optimization. In the first phase (data extraction), process streams and utilities is identified and divided by hot and cold streams. Hot process stream is defined for a stream being cooled forward to the outlet, while cold process stream stands for a stream being heated. In the second phase (targeting), minimum number of equipment, heat transfer area and optimum heat recovery are calculated in accordance with utility consumption. After that, the utility exchangers are placed on the streams, and then a heat exchanger network that satisfies the previously defined performance target, is established. In the last phase, the maximum energy recovery obtaining from third phase is economically simplified and improved according to minimum temperature difference (ΔT_{min}). As a results of high ΔT_{min}, the energy cost increases while investment cost decreases (Akgun and Ozcelik, 2017). For that reason, economical trade-offs should be taken into account during ΔT_{min} selection.

A graphical technique, i.e. T-H diagram, is carried out for determining heat cascade. The Composite Curves (T-H diagram) are generated by dividing the temperature axis into intervals depending on the supply and target temperatures of hot and cold streams, and to add together the heat load in each temperature interval (Gundersen, 2013). The curve identifies energy targets and Pinch point where the design is starting from. The design includes several principles that offer guidance in constructing a feasible and near optimal HEN. Whereas there is an endothermic zone with a heat deficit above the pinch point, an exothermic zone where cooling is needed presents below the point (Zoughaib, 2017). Furthermore, Pinch point divides the heat exchanger network into two distinct regions (heat source and sink), and therefore the heat does

not transfer across the Pinch point. Loops should also be avoided in the heat integration system.

One of the disadvantage of the Pinch analysis is to remain unsolvable for threshold problems that are considerable common in applications. Moreover, the pinch analysis cannot be applicable, if a system consists of not only heat exchangers. Exergy analysis is a much more powerful thermodynamic tool in these cases (Wall and Gong, 1996). Contrary to energy, exergy is exempt from the law of conservation. In reality, exergy input consistently exceeds exergy output owing to exergy destruction, i.e. irreversibility. (Cengel and Boles 1994). Since exergy analysis can identify quality of the energy, it enables to make complex thermodynamic systems operates more efficiently (Ahmadi et al., 2018). Therefore, combination of pinch and exergy analysis could be an appropriate tool for simultaneous study of heat and power. Even though previous applications were carried out in Combined Heat and Power systems, several methods and approaches have been developed. In this study, the analysis techniques of the hybrid methodology applications were summarized, and a case study in the petrochemical plant was presented to demonstrate the efficiency of the hybrid methodology.

HYBRID INDUSTRIAL APPLICATIONS

Pinch analysis deals with the quantity and quality of energy and targets to reduce the loss of energy. The power of using second law insights to prescribe improved designs in HEN, and the advantage of this approach over pinch technology has been clearly demonstrated (Wall and Gong, 1999).

Exergy Composite Curve (ECC) as a novel diagram where its axes are Carnot factor and enthalpy was introduced in the late 20th century (Umeda and Harada, 1979; Linnhoff and Dhole, 1992). After that, a new methodology referred to as Extended Pinch Analysis and Design (ExPAnD) was developed by a team at the Norwegian University of Science and Technology (Klemes et al. 2018). This study presented a procedure for utilizing pressure-based exergy at sub-ambient cooling (Aspelund et al., 2007). After following this study, ECC was improved again, and then the temperature-based exergy component in setting exergy targets was focused. For a constant heat capacity flow rate, mCp, the difference of exergy of a fluid between two state was derived as following equation (1);

$$\Delta X = \dot{m}c_p\left[T_2 - T_1 - T_0 \ln\frac{T_2}{T_1}\right] = \dot{m}c_p(T_2^{ex(T)} - T_1^{ex(T)}) \quad (1)$$

In a new Exergy Pinch Analysis, the exergetic temperatures (T^{ex}) at the equation replaced in time as the Carnot factor (Marmolejo-Correa and Gundersen, 2013). In recent years, a new numerical approach called the Exergy Problem Table Algorithm

(Ex-PTA) for exergy targets was eventually proposed by Hamsani et al. (2017). In the light of these information, some different techniques applied for various pinch and exergy analysis in industrial applications was summarized in Table 1. While researches about hybrid methodology have been going on day by day, it is foreseen that a direction of growing interest is tending to the Work and Heat Exchanger Network– WHEN synthesis (Klemes et al. 2018).

Table 1. Some techniques applied for various pinch and exergy analysis (Bandyopadhyay et al. 2019)

Reference	Technique applied	Application
Umeda et al. (1979)	Heat availability diagram	A basic chemical processing system comprising of a reactor subsystem and a distillation subsystem
Ishida and Kawamura (1982)	Enthalpy-direction factor diagram	Methanol synthesis, steam power generation system
Linnhoff and Dhole (1992)	Exergy Composite Curve (ECC) and Exergy Grand Composite Curve (EGCC)	Ethylene production process
Dhole and Zheng (1995)	Combined Pinch and Exergy Representation (CPER)	Closed cycle gas turbine (CCGT) system
Homsak and Glaviic (1995)	Temperature vs. power availability diagram	Evaporative process with two pressure exchangers
Staine and Favrat (1996)	Extended Composite Curves	Combined-cycle power plant
Sorin and Paris (1997)	PA integrated with exergy load distribution method	Hydrogen production by methane reforming
Feng and Zhu (1997)	Temperature level (U)-enthalpy (H) diagram	Combined power plant
Anantharaman et al. (2006)	Energy level Composite Curves	Methanol synthesis process
Aspelund et al. (2007)	Extended Pinch Analysis and Design (ExPAnD)	Liquefaction of natural gas to LNG
Ataei and Yoo (2010)	Combined Pinch and Exergy Analysis (CPEA)	Steam power plant
Ghorbani et al. (2012)	Exergy Grand Composite Curve (EGCC)	Refrigeration cycle in NGL recovery plant
Marmolejo-Correa and Gundersen (2012)	Exergetic temperature approach	LNG processes
Arriola-Medellín et al. (2014)	Exergy Composite Curve (ECC)	Steam power plant
Thibault et al. (2015)	Combining Pinch and Exergy Analysis in parallel step through MILP algorithm	Brewery process

Ghannadzadeh and Sadeqzadeh (2017b)	Exergy aided Pinch Analysis	Chlorine-caustic soda production process
Bühler et al. (2018)	PA and Exergy Analysis applied separately	Milk processing factory
Rashidi and Yoo (2018)	Exergy-Pinch (EXPA) Analysis	Kalina power-cooling cycle
Hamsani et al. (2018)	Exergy Problem Table Algorithm (Ex-PTA) - Extended Pinch Analysis and Design (ExPAnD)	Low temperature heat exchanger network
Mehdizadeh-Fard (2018)	Combined Pinch and Exergy Analysis (CPEA)	Natural gas refinery
Mehdizadeh-Fard (2019)	PA followed by Advanced Exergy Analysis (AEA)	Natural gas refinery

Some of the most recent combined pinch and exergy analysis were carried out in a steam power plant (Arriola-Medellin et al., 2014); chemical production plant (Ghannadzadeh and Sadeqzadeh, 2017a; Burre et al. 2019); methanation process in coal-gas industry (Wang et al., 2019); and diesel hydrotreating unit (Bandyopadhyay et al 2019). The results of the hybrid methodology for some industrial applications was summarized in Table 2.

Table 2. Results of exergy and pinch analysis for some industrial applications (Klemes et al. 2018)

Reference	Application	Results
Ghorbani et al. 2012	Natural gas liquids recovery plant	Refrigeration exergy efficiency increased from 26% to 28%, with a 170 kWe reduction in work
Modarresi et al. 2012	Bioethanol production	Increased heat integration up to 45MW
Arriola-Medellin et al. 2014	Steam power plant	Identified power efficiency increase from 29.48% to 30.30%
Kamalinejad et al. 2014	Liquefied Natural Gas Cycle	Shaft work reduced from 1479.36 kJ/kg to 1158.8 kJ/kg
Ghannadzadeh and Sadeqzadeh 2017a	Ethylene oxide production	Minimum cold utility requirement reduced from 602MW (normal Heat Pinch) to 578MW (Heat and Exergy Pinch)
Ghannadzadeh and Sadeqzadeh 2017b	Chlorine-caustic soda production process	Total cold energy reduced from 13.0 MW to 0.4 MW
Mehdizadeh Fard 2018	Natural Gas refinery	78% improvement in exergetic efficiency and a 36% reduction in energy consumption

DESCRIPTION of CASE STUDY

As a petrochemical plant, ethylene oxide/ethylene glycol plant was investigated with respect to minimum energy requirement (MER) and minimization of utility usage (Gündoğdu and Ceylan, 2016). The annual capacity of plant is 89,000 tonnes, and main raw materials are ethylene, oxygen, and methane. Furthermore, process water, demineralized water, process air, nitrogen, steam, and cooling water was used as auxiliary substances. In the process, ethylene and pure oxygen are firstly mixed and passed through a multitubular catalytic reactor to produce ethylene oxide selectively. Than ethylene oxide and water are reacted at high pressure due to produce ethylene glycols, mainly monoethylene and diethylene glycols. The plant can be investigated at five sections; (1) ethylene oxide reaction and recovery (2) ethylene oxide purification,

(3) glycol reaction and dehydration, (4) glycol purification and (5) glycol bleed recovery section. The simplified flowsheet of one section is shown in Figure 1 (Petkim, 2011). For the case study, the heat exchangers, reboilers, heaters, condensers and coolers in whole process were involved in pinch analysis. The external cold and hot utilities required are calculated as 53253.74 kW and 50483.36 kW, respectively. While a lot of reboiler and condenser are used, only three heat exchanger exist in entire plant. The recovered energy from these exchangers is found as 39457.71 kW that is about 38% of total utilities.

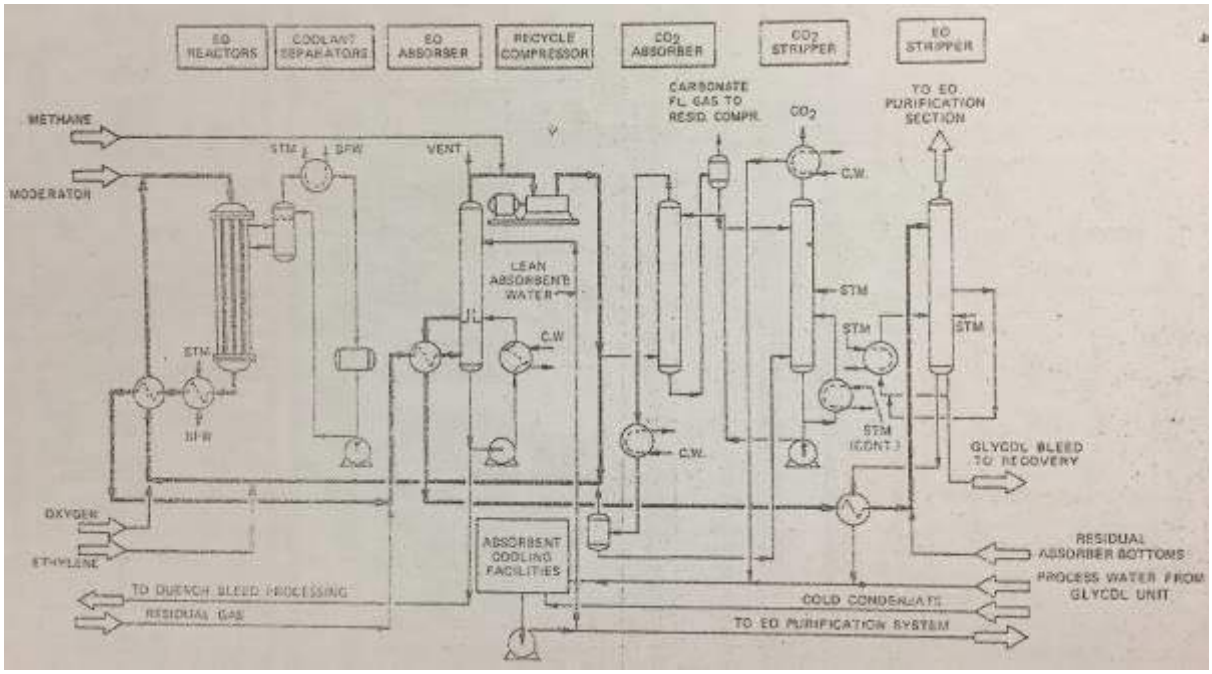

Figure 1. Simplified flowsheet of ethylene oxide reaction (Petkim, 2011)

As a result, fourteen hot and fourteen cold process streams were defined for HEN. The supply (T_s) and target temperatures (T_T) of process streams were shown in Table 3. At the beginning of alternative HEN design, the problem table for these streams was extracted by using mass flow rates, supply temperatures (T_s) and target temperatures (T_T). Then, the heat capacity flow rates (CP) and heat loads of all streams (ΔH) were calculated by following equations;

$$CP = m*Cp \quad (2)$$

$$\Delta H = CP*\Delta T \quad (3)$$

Table 3. Problem table of case study

Streams	CP (kW/K)	Ts (^{0}C)	T_T (^{0}C)	Streams	CP (kW/K)	Ts (^{0}C)	T_T (^{0}C)
Hot 1	104.79	260	110	Cold 1	104.81	53	152

Hot 2	22.50	109	69	Cold 2	6.25	109	110
Hot 3	5.97	98	85	Cold 3	6.71	109	110
Hot 4	2.67	53	45	Cold 4	421.5	38	107
Hot 5	424.50	140	71	Cold 5	3.29	140	141
Hot 6	2.66	140	40	Cold 6	32.19	140	141
Hot 7	8.09	126	38	Cold 7	0.72	140	141
Hot 8	0.83	35	21	Cold 8	1.36	53	54
Hot 9	0.80	35	21	Cold 9	111.98	94	190
Hot 10	44.98	229	179	Cold 10	68.42	171	172
Hot 11	67.54	229	180	Cold 11	26.55	169	170
Hot 12	9.77	71	50	Cold 12	111.02	171	172
Hot 13	7.44	125	40	Cold 13	6.25	170	171
Hot 14	0.70	120	40	Cold 14	10.83	172	173

RESULTS AND FINDINGS

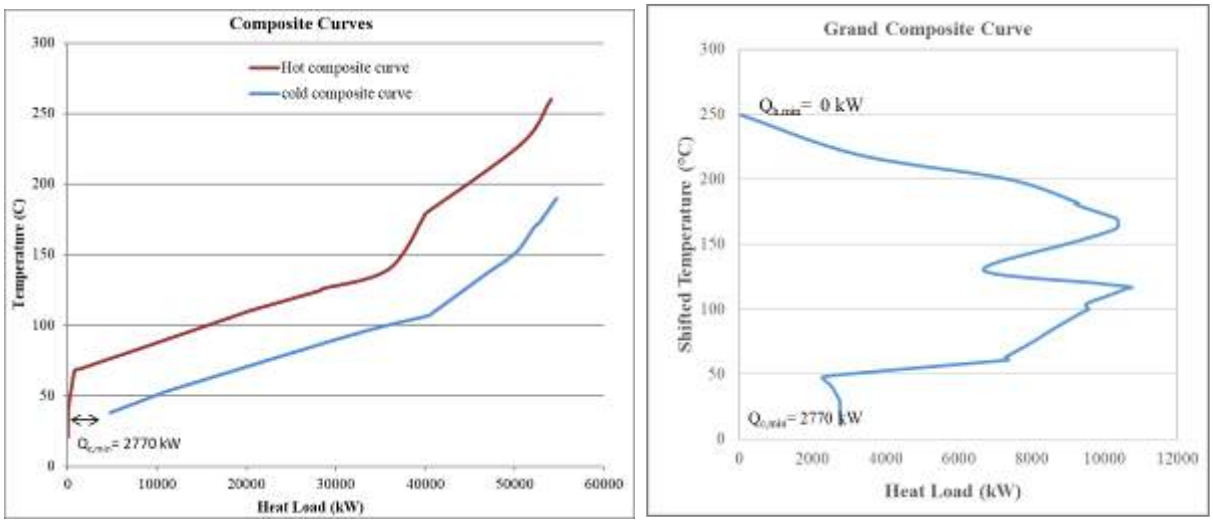

Figure 2. Composite and grand composite curves

Whereas the optimum value for ΔT_{min} is generally selected in the range of 3 to 40 °C, it is unique for each network (Keshavarzian et al., 2015). In this case study, ΔT_{min} was assumed as 20°C, and then the composite curve and grand composite curve were drawn by using cascade algorithm (Figure 2). There is no heat transfer between streams at 250°C, and therefore the pinch point was found as 250°C. On the other hand,

there existed a threshold problem due to the absence of hot utility, and no grid diagram for above the pinch was present. When considering the grid diagram below pinch point, ΔT_{min} around some exchangers was violated because of existing less temperature difference than ΔT_{min}. To provide heat flow from hot to cold stream, appropriate streams with suitable temperatures was rearranged, but this little breach for minimum temperature assumption was no problem for new heat exchanger network design; same cold utility requirement was therefore provided. As a result of pinch analysis, eleven coolers and seventeen heat exchangers were calculated in HEN design. Whereas energy in hot streams were completely saving, and total cold utility requirement is reduced to 2770 kW. Final flowsheet of alternative HEN design was created by using Aspen Plus (Figure 3).

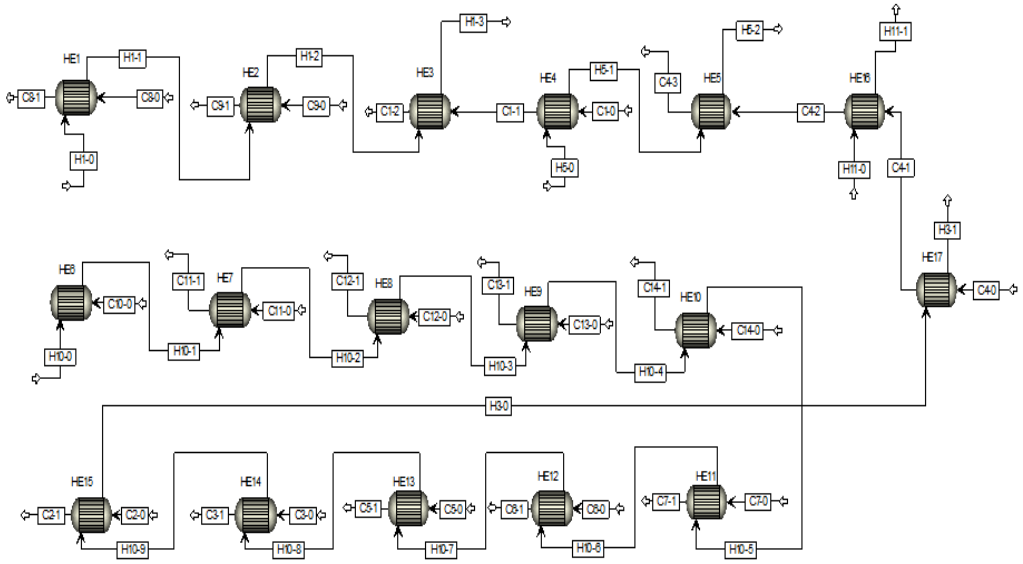

Figure 3. HEN design in alternative facility

Analogous to the Heat Pinch Composite Curve diagram is the original Exergy Pinch diagram where the Carnot factor (η_c) replaces the temperature scale on the y-axis (Klemes et al. 2018). The Carnot factor, is a well-known factor based on Carnot's application of the second law of thermodynamics and is defined in equation 4.

$$\eta_c = 1 - \frac{T_0}{T} \qquad (4)$$

In all cases, the hot stream heat capacity is assumed constant, and T_0 as the reference temperature of the system, is taken as 25°C. Generally, part of the exergy loss from the hot side is gained by the cold side of the heat exchanger. In the case study, physical exergy was examined related to heat exchangers. A heat exchanger exergy loss was determined from the difference between the exergy source (hot stream) and exergy sink (cold stream). Therefore, the ratio of them was found as each exergy efficiency. According to pinch and exergy methodology, the Exergy Composite Curve and Carnot Grand Composite Curve were created too (Figure 4), and therefore the exergy efficiency for each heat exchanger in the alternative HEN design was calculated (Table 4).

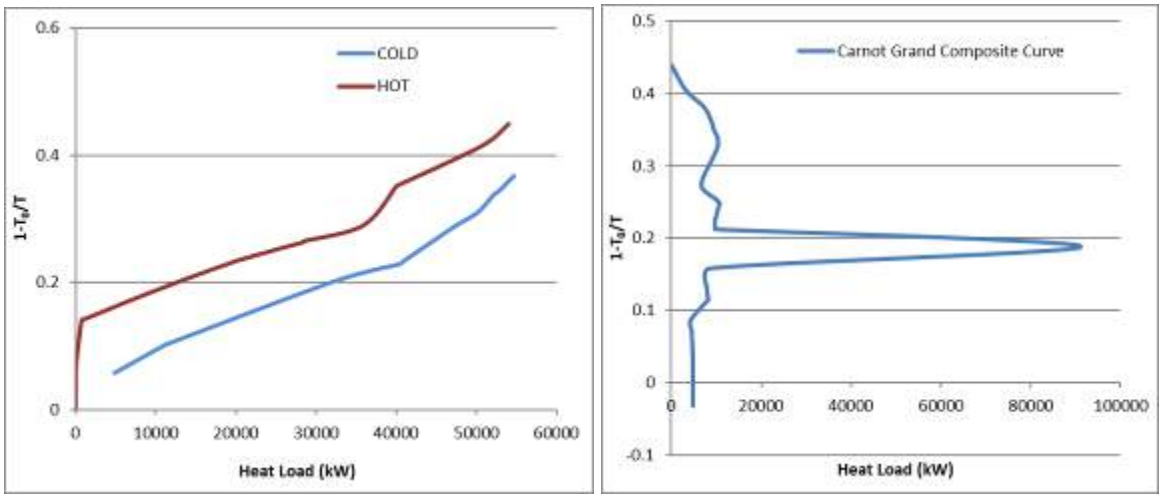

Figure 4. Exergy Composite Curve and Carnot Grand Composite Curve

Table 4. Exergy and Exergetic Efficiency Data for alternative HEN design

	ΔE (kW)	η_{ex}		ΔE (kW)	η_{ex}
HEX-1	2.35	83.99	**HEX-11**	0.47	38.23
HEX-2	873.12	81.80	**HEX-12**	0.32	98.17
HEX-3	190.57	86.07	**HEX-13**	0.31	83.15
HEX-4	710.86	49.81	**HEX-14**	0.05	98.57
HEX-5	1363.21	75.43	**HEX-15**	0.96	75.54
HEX-6	48.90	51.16	**HEX-16**	1231.04	0.59
HEX-7	0.25	98.06	**HEX-17**	334.62	41.00
HEX-8	0.01	99.98			
HEX-9	0.41	87.80			
HEX-10	0.01	99.84			

As a result of the combination of pinch and exergy analysis, total exergy loss is reduced from 5007 kW to about 4752 kW, and the average exergetic efficiency of HEN is calculated as 73 %. At this point, fifth heat exchanger has the highest exergy loss (1364 kW), and it causes to about 29% of the total exergy loss. As looking at the efficiency of this exchanger, it is observed that it has moderate exergetic efficiency among the exchangers.

Other high exergy loss (1231 kW) occurs in sixteenth exchanger, which connects eleventh hot stream to fourth cold stream. While its exergy loss results in approximately 26% of the total exergy loss, the lowest exergetic efficiency in HEN is also observed sixteenth exchanger (0.59%). This is a crucial problem, and so it should certainly be interfered to this exchanger for providing less exergy loss. Possible solutions to prevent undesirable loss may be to change the configuration of heat exchanger or thickness of isolation.

CONCLUSION

After the improvement, more energy was recovered and exergy losses were minimized. The number of heat exchangers were increased to seventeen. Whereas energy in hot streams were completely saving, and energy saving cold was calculated as 95%. By using this retrofitting, exergy was saved by the rate of 5%, too. When hot utility requirement was eliminated completely by increasing heat exchanger numbers, the importance of retrofitting for existing plant was therefore presented. Because the improvement of 5% for a plant at this capacity leads to the increase in annual profit, similar retrofitting alternatives should also be taken into account.

REFERENCES

Ahmadi, M.H., Alhuyi Nazari, M., Sadeghzadeh, M., et al. (2018) Thermodynamic and economic analysis of performance evaluation of all the thermal power plants: A review. *Energy Sci Eng.* :1–36. https://doi.org/10.1002/ese3.223

Akgun, N., Ozcelik, Z. (2017) Debottlenecking and Retrofitting by Pinch Analysis in a Chemical Plant. *American Journal of Energy Engineering* 5(5): 39–49. doi: 10.11648/j.ajee.20170505.13

Anantharaman, R., Abbas, O.S., Gundersen, T., (2006). Energy Level Composite Curvesda new graphical methodology for the integration of energy intensive processes. *Appl. Therm. Eng.* 26 (13), 1378–1384 DOI: 10.1016/j.applthermaleng.2005.05.029

Arriola-Medellín, A., Manzanares-Papayanopoulos, E., Romo-Millares, C., (2014). Diagnosis and redesign of power plants using combined pinch and exergy analysis. *Energy* 72, 643–651, https://doi.org/10.1016/j.energy.2014.05.090

Aspelund, A., Berstad, D.O., Gundersen, T. (2017) An Extended Pinch Analysis and design procedure utilizing pressure based exergy for subambient cooling. *Appl. Therm. Eng.* 27:2633–49 https://doi.org/10.1016/j.applthermaleng.2007.04.017

Ataei, A., Yoo, C., (2010). Combined pinch and exergy analysis for energy efficiency optimization in a steam power plant. *Int. J. Phys. Sci.* 5 (7), 1110–1123

Bandyopadhyay, Alkilde, O.F., Upadhyayula, S. (2019) Applying pinch and exergy analysis for energy efficient design of diesel hydrotreating unit, *Journal of Cleaner Production* 232: 337–349 https://doi.org/10.1016/j.jclepro.2019.05.277

Bühler, F., Nguyen, T.V., Jensen, J.K., Holm, F.M., Elmegaard, B., (2018). Energy, exergy and advanced exergy analysis of a milk processing factory. *Energy* 162, 576–592. https://doi.org/10.1016/j.energy.2018.08.029

Burre, J., Bongartz, D., Mitsos, A., (2019) Production of Oxymethylene Dimethyl Ethers from Hydrogen and Carbon Dioxide—Part II: Modeling and Analysis for OME3–5, *Ind. Eng. Chem. Res.* 58:5567−5578 https://doi.org/10.1021/acs.iecr.8b05577.

Cengel, Y.A., Boles, M.A. (1994) Thermodynamics: An Engineering Approach, *McGraw-Hill*, 2nd Edition, 388-391.

Dhole, V.R., Zheng, J.P., (1995). Applying combined pinch and exergy analysis to closed-cycle gas turbine system design. *J. Eng. Gas Turbines Power* 117, 47–52 https://doi.org/10.1115/1.2812780

Feng, X., Zhu, X.X., (1997). Combining pinch and exergy analysis for process modifications. *Appl. Therm. Eng.* 17 (3), 249–261 https://doi.org/10.1016/S1359-4311(96)00035-X

Ghannadzadeh, A., Sadeqzadeh, M. (2017a) Combined pinch and exergy analysis of an ethylene oxide production process to boost energy efficiency toward environmental sustainability, *Clean Techn. Environ. Policy* 19:2145–2160 https://doi.org/10.1007/s10098-017-1402-5.

Ghannadzadeh, A., Sadeqzadeh, M. (2017b) Exergy aided pinch analysis to enhance energy integration towards environmental sustainability in a chlorine-caustic soda production process. Appl Therm Eng 125:1518–29. https://doi.org/10.1016/j.applthermaleng.2017.07.052

Ghorbani B, Salehi GR, Ghaemmaleki H, Amidpour M, Hamedi MH. (2012) Simulation and optimization of refrigeration cycle in NGL recovery plants with exergy-pinch analysis. J Nat Gas Sci Eng;7:35–43. https://doi.org/10.1016/j.jngse.2012.03.003

Ghorbani, B., Salehi, G.R., Ghaemmaleki, H., Amidpour, M., Hamedi, M.H., (2012). Simulation and optimization of refrigeration cycle in NGL recovery plants with exergy-pinch analysis. *J. Nat. Gas Sci. Eng.* 7, 35–43. https://doi.org/10.1016/j.jngse.2012.03.003

Gundersen, T., (2013) Heat Integration: Targets and Heat Exchanger Network Design, *in Handbook of Process Integration (PI)*, Woodhead Publishing, Editor: Jiří J. Klemeš, 129-167.

Gündoğdu, G., Ceylan, Z. (2016) Exergo-Pinch application on a petrochemical plant, Ege University, Department of Chemical Engineering Diploma Project.

Hamsani, M.N., Liew, P.Y., Walmsley, T.G. (2017) A new numerical approach for exergy targets and losses determination in sub-ambient processes. Chem. Eng. Trans. 61:1225–31. https://doi.org/10.3303/CET1761202

Hamsani, M.N., Walmsley, T.G., Liew, P.Y., Wan Alwi, S.R. (2018) Combined Pinch and exergy numerical analysis for low temperature heat exchanger network. Energy 153:100–12. https://doi.org/10.1016/j.energy.2018.04.023

Homsak, M., Glavic, P., (1996). Pressure exchangers in pinch technology. *Comput. Chem. Eng.* 20 (6-7), 711–715 https://doi.org/10.1016/0098-1354(95)00204-9

Ishida, M., Kawamura, K., (1982). Energy and exergy analysis of a chemical process system with distributed parameters based on the enthalpy-direction factor diagram. *Ind. Eng. Chem. Process Des. Dev.* 21 (4), 690–695 https://doi.org/10.1021/i200019a025

Kamalinejad M, Amidpour M, Naenian MM. (2014) Optimal synthesis of cascade refrigeration in liquefied natural gas cycles by pinch-exergy. Journal of Oil, Gas and Petrochemical Technology 1:29–44 DOI: 10.22034/JOGPT.2014.4779

Keshavarzian, S., Verda, V., Colombo, E., Razmjoo, P. (2015) Fuel saving due to pinch analysis and heat recovery in a petrochemical company. Proceedings of ECOS 2015 - The 28th International Conference on Efficiency, Cost, Optimization, Simulation and Environmental Impact of Energy Systems, June 30-July 3, Pau, France.

Klemeš, J.J., Varbanov, P.S., Walmsley, T.G., Jia, X. (2018) New directions in the implementation of Pinch Methodology (PM), *Renewable and Sustainable Energy Reviews* 98: 439–468, https://doi.org/10.1016/j.rser.2018.09.030

Linnhoff, B., Dhole, V.R. (1992) Shaftwork targets for low-temperature process design. *Chem. Eng. Sci.* 47(8):2081–2091 https://doi.org/10.1016/0009-2509(92)80324-6

Linnhoff, B., Flower, JR., (1978) Synthesis of Heat Exchanger Networks. II. Evolutionary Generation of Networks with Various Criteria of Optimality, *AIChE J*; 24 (4): 633–642 https://doi.org/10.1002/aic.690240412

Marmolejo-Correa, D., Gundersen, T., (2012). A new procedure for the design of LNG processes by combining Exergy and Pinch Analyses. In: *The 25th International Conference on Efficiency, Cost, Optimization and Simulation of Energy Conversion Systems and Processes*, vol. 24.

Marmolejo-Correa, D., Gundersen, T., (2013) New graphical representation of exergy applied to low temperature process design. *Ind Eng Chem Res,* 52:7145–56. https://doi.org/10.1021/ie302541e

Mehdizadeh Fard M, Pourfayaz F, Mehrpooya M, Kasaeian AB. (2018) Improving energy efficiency in a complex natural gas refinery using combined pinch and advanced exergy analyses. *Appl Therm Eng* 137:341–55. https://doi.org/10.1016/j.applthermaleng.2018.03.054

Mehdizadeh-Fard, M., Pourfayaz, F., (2019). Advanced exergy analysis of heat exchanger network in a complex natural gas refinery. *J. Clean. Prod.* 206, 670–687 https://doi.org/10.1016/j.jclepro.2018.09.166

Modarresi A, Kravanja P, Friedl A. Pinch and exergy analysis of lignocellulosic ethanol, biomethane, heat and power production from straw. Appl Therm Eng 43:20–8. https://doi.org/10.1016/j.applthermaleng.2012.01.026

Petkim (2011) Operating education book of ethylene oxide/ethylene glycol (EO/EG) plant, 1–126.

Rashidi, J., Yoo, C., (2018). Exergy, exergo-economic, and exergy-pinch analyses (EXPA) of the kalina power-cooling cycle with an ejector. *Energy* 155, 504–520 https://doi.org/10.1016/j.energy.2018.04.178

Sorin, M., Paris, J., (1997). Combined exergy and pinch approach to process analysis. *Comput. Chem. Eng.* 21, S23–S28 https://doi.org/10.1016/S0098-1354(97)87473-X

Staine, F., Favrat, D., (1996). Energy integration of industrial processes based on the pinch analysis method extended to include exergy factors. *Appl. Therm. Eng.* 16 (6), 497–507 https://doi.org/10.1016/1359-4311(95)00036-4

Thibault, F., Zoughaib, A., Pelloux-Prayer, S., (2015). A MILP algorithm for utilities predesign based on the Pinch Analysis and an exergy criterion. *Comput. Chem. Eng.* 75, 65–73. https://doi.org/10.1016/j.compchemeng.2014.12.010

Umeda, T., Harada, T., Shiroko, K. A. (1979) A thermodynamic approach to the synthesis of heat integration systems in chemical processes. *Comput Chem Eng* 3(1–4):273–282 https://doi.org/10.1016/0098-1354(79)80046-0

Wall, G., Gong, M. (1999) Exergy Analysis Versus Pinch Technology, *Efficiency, Costs, Optimization, Simulation and Environmental Aspects of Energy Systems (ECOS'96)*, June 25-27, STOCKHOLM, 451–455.

Wang, C, Guang, C, Zhang, Z.S., Gao, J., (2019) Design and optimization of heat exchange network and exergy analysis for methanation process of coal-gas, *Latin American Applied Research* 49 (1):47-54.

Zoughaib, A. (2017) Energy Integration of Continuous Processes: From Pinch Analysis to Hybrid Exergy/Pinch Analysis, *in From Pinch Methodology to Pinch-Energy Integration of Flexible Systems*, ISTE Press – Elsevier, 1-53.

A LITERATURE REVIEW ON THE USE OF MACHINE LEARNING ALGORITHMS IN HEALTH

Tuba ADAR
Atatürk University, Department of Industrial Engineering, Erzurum, Turkey
tuba.adar@atauni.edu.tr

Elif KILIÇ DELİCE
Atatürk University, Department of Industrial Engineering, Erzurum, Turkey
elif.kdelice@atauni.edu.tr

ABSTRACT: Machine learning is a sub-branch of artificial intelligence that provides solutions to many difficult problems such as image, picture and voice recognition by learning from examples instead of creating solutions using coded ready instructions. It is possible to analyze and interpret very large-scale patient data stored in a computer environment with machine learning algorithms. One of the most important usage areas of machine learning which is used in many fields in recent years is the health sector. The aim of this study is to reveal for which purposes and in which diseases machine learning methods applied in the field of health is used with literature research. As a result of the literature research, it was found that the most frequently discussed issue in the field of health studies using machine learning algorithms is the subject of early detection/diagnosis. Early diagnosis is very important to reduce risk and prolong patient life in diseases requiring long-term treatment and having risk of death. Therefore, studies on the use of machine learning algorithms in the field of early detection/diagnosis will increase day by day. However, continuing to use machine learning algorithms in health will reduce the workload of doctors and provide patients with better quality health care.

Key words: machine learning, health applications, diagnosis, algorithms.

SAĞLIK ALANINDA MAKİNE ÖĞRENME ALGORİTMALARININ KULLANILMASINA YÖNELİK BİR LİTERATÜR TARAMASI

ÖZET: Makine öğrenmesi, kodlanmış olan hazır talimatları kullanarak çözüm üretmek yerine örneklerden öğrenerek, görüntü, resim ve ses tanıma gibi birçok zor probleme çözüm getiren yapay zekânın bir alt dalıdır. Bilgisayar ortamında saklanan büyük boyuttaki hasta verilerinin analiz edilmesi ve yorumlanması makine öğrenmesi

algoritmaları ile mümkündür. Son yıllarda birçok alanda kullanılan makine öğrenmesinin en önemli kullanım alanlarından biri de sağlık sektörüdür. Bu çalışmanın amacı sağlık alanında uygulanan makine öğrenmesi yöntemlerinin hangi amaçla ve hangi hastalıklarda kullanıldığını literatür araştırması ile ortaya koymaktır. Yapılan literatür araştırması sonucunda, makine öğrenmesi algoritmaları kullanılarak sağlık alanında yapılan çalışmalarda en çok ele alınan konunun erken tanı/teşhis konusu olduğu ortaya çıkmıştır. Uzun süreli tedavi gerektiren ve ölüm riski içeren hastalıklarda, riski azaltmak ve hastanın yaşam süresini uzatmak için erken tanının çok önemli bir yere sahiptir. Bu nedenle makine öğrenme algoritmalarının erken tanı/teşhis alanında kullanılması ile ilgili yapılan çalışmalar gün geçtikçe artacaktır. Bununla birlikte makine öğrenme algoritmalarının sağlık alanlarında kullanılmaya devam edilmesi ile hem doktorların iş yükleri azaltılacak hem de hastalara daha kaliteli sağlık hizmeti sağlanacaktır.

Anahtar sözcükler: makine öğrenmesi, sağlık uygulamaları, teşhis, algoritmalar.

GİRİŞ

Makine öğrenmesi (yapay öğrenme), eldeki verileri en iyi temsil eden modeli ve parametrelerini bulmak amacıyla geliştirilen algoritmaları içerir. Makine öğrenmesi, çeşitli algoritmalar ve yöntemler ile veride bazı kalıpları arar ve bu kalıplara karşılık gelen etiketlere bakarak önce öğrenir, daha sonra deneyimlerinden yararlanarak çıkarım yapabilen sistemler geliştirmeye imkân sağlar. Bu imkânı, çeşitli matematiksel ve istatistiksel yöntemlerin kullanıldığı birçok algoritma ile sağlamaktadır. Bu yöntem ve algoritmaların bir veya bir kaçı bir arada kullanılarak model(ler) oluşturulur ve bu modellerin bir kısmı tahmin ve kestirim bir kısmı da sınıflandırma için kullanılır.

Makine öğrenmesi yöntemleri yüksek boyutlu ve çeşitli biyomedikal verilerin analizi için sundukları objektif algoritmalar ile hastalıkların teşhisi konusunda yüksek performans göstermektedir. Çok büyük miktardaki verinin elle işlenmesi ve analizinin yapılması mümkün değildir. Bununla birlikte çoğu zaman geçmişteki veriler kullanılarak gelecek için tahminde, çıkarımda bulunmak mümkündür. Bu çıkarımları yapabilmek için makine öğrenmesi yöntemleri kullanılır. Makine öğrenmesinin kullanıldığı sistemler, karar destek sistemleridir. Karar destek sistemleri kullanım alanına bağlı olarak çeşitlilik göstermektedir. Sağlık alanındaki uygulamalarda klinik karar destek sistemleri kullanılmaktadır. Sağlık verilerinin karmaşıklığı karşısında geleneksel veri analiz yöntemleri yetersiz kalabilmektedir. Bu sebeple karmaşık yapıların anlaşılması, çözümlenebilmesi için makine öğrenmesi yöntemlerine başvurulur. Sağlık alanı, makine öğrenmesi yöntemlerinin sınırlı kullanıldığı ancak çok önemli kullanım potansiyeli olan alanlardan biridir.

Bu amaçla, bu çalışmada Türkiye'de sağlık alanında makine öğrenmesi algoritmaları kullanılarak yapılan çalışmalar incelenmiştir. İnceleme sonucunda, sağlık alanında hangi konuda daha fazla çalışma bulunduğu tespit edilmeye çalışılmıştır.

Çalışmanın geri kalanı şu şekilde oluşturulmuştur: literatür taraması bölümünde Türkiye'de mevcut olan makine öğrenmesi çalışmaları incelenmiş ve çalışmalar yapıldıkları alanlara göre gruplandırılmıştır. Sonuç ve tartışma bölümünde ise literatür incelemesi sonucunda elde edilen bilgiler görselleştirilmiş ve sonuçlar tartışılmıştır.

LİTERATÜR TARAMASI

Literatür taraması kapsamında; makine öğrenme algoritma çalışmaları aşağıda yer alan başlıklar halinde verilmiştir:

Kanserler

Meme Kanseri

Sarikoç vd. (2013), meme kanserinin prognozunda yaygın olarak uygulanan bir yöntem olan östrojen reseptörü (ER) durum değerlendirmesi için bir hastanın tümör örneği üzerinde yapılan testler doktorların öznel kararlarına bağlıdır. Buradan yola çıkarak, çalışmada nesnel bir karar modeli ile hastalığın ER prognozuna ulaşmak için bir makine öğrenme aracının, fonksiyonel ağaçların (FTs) kullanımı tanıtılmıştır. Bu amaçla, her biri invaziv duktal karsinom hastasının biyopsi numunesinden gelen 27 görüntü dosyası taranmış ve ışık mikroskobu ile yakalanmıştır.

Kaya (2013) çalışmasında, meme kanserinin tanısında kaba set (RS) ve aşırı öğrenme makinesi (ELM) yöntemleri kullanılmıştır. Gereksiz öznitelikler, RS yaklaşımıyla veri setinden atılmış ve ELM ile sınıflandırma işlemi, geri kalan özellikler kullanılarak gerçekleştirilmiştir. Kaliforniya Üniversitesi Irvine makine öğrenme veritabanından türetilen Wisconsin Göğüs Kanseri veri seti (WBCD), önerilen hibrit modeli test etmek için kullanılmış ve RS + ELM modelinin başarı oranı% 100 olarak belirlenmiştir. Ayrıca, bu çalışmada meme kanseri tanısı için en uygun özellikler WBCD'den belirlenmiştir.

İşeri (2014), yapılan araştırmalarda radyologların mikrokireçlenme (MC, Microcalcification) vakalarını tespit etmekte zorlandıklarını ve yüzde yetmişlik bir doğrulukla çalıştıkları vurgulamış ve çalışmasında mamogram görüntüleri üzerinde MC bölgelerinin tespitini yapmak için makine öğrenmesi yöntemlerini kullanarak bir çalışma yapmıştır. Yapılan çalışmada gri seviye eş oluşum matrisi temelli doku, dalgacık dönüşümü temelli ayrıştırma, iki boyutlu eşit genişlikli ayrıştırma ve çoklu pencere temelli istatistiki analiz kullanılarak farklı özellik çıkartım yöntemleri ile MC desenlerinin karakteristik özellikleri sayısal yöntemlerle analiz edilmiş olup çok katmanlı ileri beslemeli yapay sinir ağı olarak bilinen sınıflandırıcı ve destek vektör

makinesi kullanılarak bir makine öğrenmesi yaklaşımı geliştirilmiştir. Çalışmanın sonunda MATLAB yazılım geliştirme ortamı kullanılarak grafik arayüze sahip BCDS ismi verilen MC temelli meme kanseri teşhis yazılımı geliştirilmiştir.

Takci (2016), meme kanserinde mamografik görüntüleri yorumlamada radyologların yaşadığı görüş ayrılıkları nedeniyle daha güvenilir sonuçlar veren bilgisayar destekli karar verme mekanizmalarına ihtiyaç duyulduğunu ifade etmiştir. Bu amaçla, yapılan çalışmalarda destek vektör makineleri, yapay sinir ağları ve karar ağaçları gibi makine öğrenme yöntemleri kullanan bilgisayar destekli karar verme mekanizmaları geliştirilmiştir. Bu çalışmada ise, daha önce meme kanseri teşhisinde kullanılmamış olan üç farklı centroid sınıflayıcının kullanımı önerilmektedir. Bu tercihin en önemli nedeni centroid sınıflayıcıların yüksek performanslı sınıflayıcılar olmasıdır. Centroid sınıflayıcılar Wisconsin meme kanseri veri seti üzerinde test edilmiş olup en yüksek sınıflandırma doğruluğunu %99,04 ile Euclidian tabanlı centroid sınıflayıcı vermiştir. Centroid sınıflayıcılar kendi arasında karşılaştırıldıktan sonra diğer makine öğrenmesi yöntemleri ile de karşılaştırılmış ve sonuçlar raporlanmıştır.

Durak (2017) çalışmasında gereksiz biyopsiden kaçınarak meme kanserinin erken teşhisini makine öğrenmesi yöntemleriyle araştırmıştır. Önceki çalışmalarda teşhis için tümör bilgilerini içeren değişkenler kullanılırken yapılan bu çalışmada daha çok kültürel ve fiziksel etkisi olan değişkenlerle çalışılmıştır. Aynı veri seti üzerinde iki farklı uygulama yapılmıştır. İlki veri setinin eğitim ve test seti olarak ayrılarak SPSS.18 Moduler programında yapılmış uygulamadır. İkincisi ise k-kat çapraz doğrulama ile Weka'da yapılan uygulamadır. Kullanılan makine öğrenmesi yöntemlerinden Lojistik Regresyon (%78) ve Naive Bayes (%78) en iyi sonucu vermiştir. Bunlardan sonra sırasıyla Destek Vektör Makineleri (%76), Karar Ağacı C5.0 algoritması (%76), ve Yapay Sinir Ağları (%74) modelleri gelmektedir. 3 kat çapraz doğrulama yapıldığı durumda en iyi sınıflandırma doğrulunu veren yöntemler sırasıyla, Karar Ağacı C5.0 algoritması (%76), Lojistik Regresyon (%73), Destek Vektör Makineleri (%73), Yapay Sinir Ağları (%73) ve Naive Bayes (%73) olarak bulunmuştur.

Taşdemir (2018), görüntü işleme ve makine öğrenmesi yöntemiyle erken meme kanseri teşhisi üzerinde çalışmıştır. Sistemin performansını değerlendirmek için, gerçeklenen sınıflandırıcılar; rastgele orman, lojistik regresyon, k-en yakın komşular (k-NN), naive Bayes, karar ağacı, destek vektör makinesi (SVM), Adaboost, radyal temelli fonksiyon ağı (RBF-NN), çok katmanlı algılayıcı (MLP), konvolüsyonel sinir ağı (CNN) kullanılmıştır.

Sevli (2019), çalışmada her biri 30 adet özellik içeren ve 569 örnekten oluşan Wisconsin Üniversitesi göğüs kanseri veri setini, beş farklı makine öğrenmesi tekniği ile sınıflandırmıştır. Veriler rastgele olarak eğitim ve test setlerine ayrılmıştır. Destek vektör makinesi, Naïve Bayes, rastgele orman, K en yakın komşu ve lojistik regresyon metotları ile gerçekleştirilen eğitim sürecinin ardından confusion matrisleri ve roc eğrileri oluşturulmuştur. Her bir tekniğin başarısı karşılaştırılmıştır. Bu karşılaştırmanın sonucunda lojistik regresyonun %98.24 doğruluk ile en başarılı yöntem olduğu ortaya konmuştur.

Cilt kanseri

Yıldız (2019) çalışmasında, cilt kanseri türü olan melanom için otomatik tanı koyabilecek bir sistem önerilmektedir. Melanom tanısı için tasarlanan C4Net derin sinir ağ modeli ile beraber literatürde ön plana çıkmış AlexNet, GoogLeNet, ResNet, VGGNet derin öğrenme algoritmaları ve Yapay sinir ağları, En yakın komşu algoritması ve Destek vektör makinesi gibi geleneksel makine öğrenmesi algoritmalarını da kapsayan detaylı bir deneysel çalışma yapılmıştır. Gerçekleştirilen deneysel çalışmalarda melanom tanısı için tasarlanan C4Net derin sinir ağ modeli diğer yöntemlere göre daha yüksek doğrulukta sınıflandırma başarısı göstermiştir.

Bağırsak kanseri

Toraman vd. (2019), kolon kanserinin tespiti için kullanılan yöntemlerden biri olan biyokimyasal değişiklikleri gösterme yeteneğine sahip Fourier dönüşümlü kızılötesi (FTIR) spektroskopisi olduğunu ancak kanser hastalarını FTIR sinyalleri kullanarak sağlıklı bireylerden ayırmak için yapılan çalışmaların en büyük zorluğunun, kanser hastaları ve sağlıklı deneklerin sinyallerinin benzer olması olduğunu ifade etmiştir. Bu zorluğun üstesinden gelmek için FTIR sinyalinin alan ve yükseklik oranlarının yanı sıra çeşitli istatistiksel özelliklerin önerildiği bir yöntem önermiştir. Kan örnekleri (plazma) 30 kolon kanseri hastası ve 40 sağlıklı kişiden toplanmış ve FTIR ölçümleri yapılmıştır. Her FTIR sinyalinden beş yükseklik oranı, beş alan oranı ve altı istatistiksel özellik içeren toplam 16 özellik elde edildi. 16 özellik, çok katmanlı algılayıcı sinir ağı ve çapraz doğrulama kullanan destek vektör makineleri ile sınıflandırılmış ve performansları karşılaştırılmıştır.

Diğer Kanser Çalışmaları

Cüvitoğlu (2017), kanser konusunda daha etkili ilaç ikililerini olası tüm kombinasyonlar içinden tanımlayabilmek için, ilaç uygulanmış gen ifadesi ve biyolojik ağ verilerini kullanan bir sınıflandırma yöntemi geliştirmiştir. Farklı biyolojik verilerden türetilmiş altı öznitelik ile üç farklı makine öğrenmesi yöntemi, Yapay Sinir Ağları (YSA), Destek Vektör Makineleri (DVM) ve Rasgele Orman (RO), eğitilmiştir. Yöntem, içinde hem etkili hem de etkisiz ilaç birleşimlerini bulunduran iki farklı ilaç verisi üzerinde sınanmıştır.

Çakmak (2017), küçük hücreli dışı akciğer kanseri hastalarının radyoterapi verileri kullanılarak makine öğrenmesi yöntemleriyle tümör kontrol olasılığı hesaplanmıştır. Radyoterapiyi etkileyen birçok parametre olması ve hastaların her biri kişisel özellikleri bakımdan birbirinden farklı olması gibi nedenlerden dolayı, tümörün radyoterapiye vereceği yanıt her hasta için farklıdır. Çalışmada, radyasyon onkolojisindeki hasta verilerinin makine öğrenmesi yöntemleriyle sınıflandırılması ve çıkarım yapılması amaçlanmıştır. Çalışma kapsamında Karadeniz Teknik Üniversitesi Tıp Fakültesi Farabi Hastanesi Radyasyon Onkolojisine 2012-2015 yılları arasında gelen hastaların verileri kullanılmıştır. Bu kapsamda, destek vektör makineleri (DVM) ve yapay sinir ağları (YSA) ile tümörün radyoterapiye verdiği yanıtlar sınıflandırılması ve bunların karşılaştırılması ele alınmıştır. Bu çalışmada 30 hasta verisi kullanılarak DVM ve YSA makine öğrenmesi yöntemleri yardımıyla iki farklı

karar destek sistemi modeli geliştirilmiştir. DVM modeli için %90 duyarlılık, %100 özgüllük değeri elde edilmiş; YSA modeli için % 80 duyarlılık, % 100 özgüllük değeri elde edilmiştir. Bu çalışmada SVM modelinin %90 duyarlılıkla en başarılı sonucu verdiği görülmüştür.

Albayrak (2018), görüntüleme cihazlarının gelişmesi ile birlikte kanser ve ona bağlı hastalıkların görüntülenmesi, takibi ve Bilgisayar Destekli Teşhis (BDT) sistemlerinin de yardımıyla tedavi edilebilmesinin mümkün hale geldiğini vurgulamıştır. Çalışmasında, histopatolojik görüntülerin bölütlenmesi ve sınıflandırılmasını ele almıştır. Süperpiksel bölütleme yöntemlerinden SLIC, SLIC-DBSCAN, ERS ve TPRS algoritmalarının yüksek çözünürlüklü histopatolojik görüntülerde hücresel yapıların bölütlenmesindeki başarım performansları elde edilmeye çalışılmıştır. Histopatolojik görüntülerin sınıflandırılması bölümünde ise hem mitozlu hücrelerin hem de lenf nodlarında yer alan tümörlü bölgelerin özellikle son dönemde oldukça popüler olan evrişimsel sinir ağları yöntemi ile tespiti gerçekleştirilmiştir. Özellikle mitozlu hücrelerin tespitinde geleneksel şekil, renk, doku ve istatistiksel tabanlı özellik çıkarma yöntemleri ile ESA yöntemi karşılaştırılarak performans analizi gerçekleştirilmiştir. Elde edilen sonuçlar incelendiğinde ESA modelinin geleneksel yöntemlerden daha başarılı sonuç verdiği gözlemlenmiştir. Son olarak, Istanbul Medipol Universitesi Hastanesi, İstanbul Teknik Üniversitesi ve Yıldız Teknik Üniversitesi işbirliğiyle rahim ağzı kanseri öncü lezyonlarının derecelendirilmesi ile ilgili literatürde yer alan en geniş veri kümelerinden biri oluşturulmuş ve sınıflandırılmıştır. Elde edilen sınıflandırma başarısı iki patolog tarafından oluşturulan referans verilerle karşılaştırılarak analiz edilmiştir.

Nörolojik Hastalıklar

Parkinson

Aydın (2017) çalışmasında, Parkinson Hastalığı (PH) verilerine Makine Öğrenmesi algoritmalarını uygulamış ve karar kaynaştırma ve sınıflandırıcı seçimi yöntemlerine dayalı olarak VIBES isminde yeni bir topluluk öğrenme algoritması geliştirmiştir. Önerilen algoritma ve diğer makine öğrenmesi algoritmaları, UCI veritabanından seçilen 33 adet benchmark veri kümesine ve PhysioNet veritabanından elde edilen Parkinson verikümesine uygulanmıştır. Ayrıca, çoğunluk oylamalı topluluk öğrenicilerde oluşturulan topluluğun gerçek hata oranını tahmin etmek için de veri uyarlamalı bir yöntem geliştirilmiştir. Parkinson veri kümesi kullanılarak öznitelik oluşturmak için Fast Fourier Dönüşümü (FFD), Dalgacık dönüşümü (Haar, sym2, coif2, db2, db3, db4, db5, db6, db7, dmey, bio3.3 ve gaus2) ve Hilbert-Huang Dönüşümü (HHD) kullanılmıştır. Bu sinyal dönüşüm yöntemleri içerisinden HHD ile oluşturulmuş öznitelik kümesi üzerinde hem VIBES algoritması hem de diğer Makine Öğrenmesi algoritmaları yüksek doğruluk oranları vermiştir. Sonuç olarak literatürde daha önce yapılan 6 çalışmadan daha yüksek oranda sınıflandırma doğruluğu elde edilmiştir.

Kurt (2018), makine öğrenmesi yöntemleri kullanılarak sesin müzikal öznitelikleri ile Parkinson hastalığının tespiti konusuna yönelmiştir. Parkinson hastalığının ülkemizde ve dünyada Alzheimer hastalığından sonra en yaygın görülen, sinir sistemini etkileyen motor becerileri (yazma, denge, yutkunma, vb.), konuşma zorluğu, ses kısıklığı, düşünme ve davranış fonksiyonların kısmen veya tamamen kaybolmasına neden olan ve gündelik yaşantıyı olumsuz yönde etkileyen nörodejeneratif (sinir sisteminde geri dönüşü olmayan) hastalıklardan biri olduğunu vurgulamış ve konuşma ve ses bozukluklarının, Parkinson hastalığı sürecinin erken teşhisinde başvurulan en belirleyici semptomlar olduğunu ifade etmiştir. Bu amaçla çalışmada sesin müzikal özelliklerinin Parkinson hastalığının teşhisindeki etkisini incelemiştir. Bu doğrultuda, Parkinson hastası ve sağlıklı bireylerden alınan ham ses kayıtlarından sesin ritim, ton, tını, perde ve dinamiklik gibi özellikleri çıkartılarak yapay öğrenme algoritmaları ile hangi özelliklerin hastalığı teşhis etmede daha başarılı olduğu araştırılmıştır.

Gürel (2019), parkinson hastalığının (PD) en önemli semptomlarından birinin, ağız, dil, boğaz, ses tellerinin fiziksel bir bozukluğu nedeniyle konuşmada güçlük çeken konuşma bozukluğu olduğunu vurgulamış ve Vokal kord ölçümlerinden makine öğrenmesi yöntemleri kullanarak Parkinson hastalığının teşhisi üzerine çalışmıştır. Hastalardan alınan ve sağlıklı gönüllülerden kaydedilen vokal kord işaretlerinin zaman, frekans ve zaman-frekans domenlerinde istatistiksel parametreler yardımıyla özellik vektörleri çıkarılmış ve bu vektörler PD tanısı için makine öğrenmesi (ML) temelli sınıflayıcı modellere girdi olarak uygulanmıştır. Buna ek olarak, PD teşhisine ilişkin ilk kez bu çalışmada kullanılan noktalar-arası eğimi hem zaman hem de frekans domeninde uygulanıp elde edilen yeni işaretin Ki-Karesi ve entropisi hesaplanarak gerçekleştirilen sınıflandırma deneyleri tekrarlandığında özellikle işaretlerin frekans domeninde sınıflayıcı modeller çok daha yüksek TCC oranlarını sağlamıştır. Sonuç olarak, hastaların ses işaretlerine ait frekans alt-bantlarında istatistiksel parametrelerle ve ses işaretlerinin eğimi alınıp Ki-Kare ve entropi uygulandığında elde edilen özellik vektörlerinden ML yöntemleri yardımıyla PD'nin teşhisinin yüksek başarı oranlarında gerçekleştirilmesi mümkün olmuştur.

Badem (2019) çalışmasında, Parkinson hastalığının ses sinyalleri üzerinden sınıflandırılmasında, KYK, ROS, DVM, NB ve KA makine öğrenmesi tekniklerinin başarımının araştırılması amaçlanmıştır. Bu amaç için literatüre yeni sunulan yüksek boyutlu öznitelik ve örnekleme sahip PDC veri seti kullanılmıştır. Gerçekleştirilen deneysel çalışmalarda, oldukça yüksek doğruluk değerleri elde edilmiştir. Ayrıca, kullanılan yöntemler istatiksel olarak karşılaştırılmıştır.

Diğer Nörolojik Hastalıklar

Kaya ve Tekin (2012) çalışmasında, epileptik EEG işaretlerinin sınıflandırılmasında aşırı öğrenme makinesi (ELM) kullanılmıştır. ELM, tek gizli katmanlı ileri beslemeli

bir yapay sinir ağı modelidir. Ayrık dalgacık dönüşümü ile elde edilen istatistik özellikler ELM ile sınıflandırma işlemine tabi tutulmuştur. İki farklı veri kümesi için elde edilen başarı sonuçları %100 (A-D veri seti) ve %100 (A-E veri seti) olarak gözlenmiştir.

Çentik (2013) çalışmasında, Uykuda Periyodik Hareket Bozukluğu (UPHB), Polisomnografi (PSG) kaydındaki bacak Elektromiyografisi (EMG) haricindeki diğer kanallar kullanılarak, dijital sinyal işleme yöntemleri ve makine öğrenmesi yöntemleri ile analiz edilmiştir. Çalışma UPHB hastalığı teşhisi konulmuş farklı yaş ve cinsiyetten 153 bireyin, PSG kayıtları kullanılarak gerçekleştirilmiştir. Çalışma ekibi tarafından dijital sinyal işleme ve makine öğrenmesi yöntemlerini kullanan bir yazılım geliştirilmiştir. Bu yazılım hasta kayıtlarını (PSG) 2, 5, 30 ve 60 saniyelik epok (bölüt) sürelerine parçalayarak analiz etmekte ve elde edilen sonuçları karşılaştırmaktadır. Veritabanında saklanan öznitelikler, farklı makine öğrenmesi algoritmaları kullanılarak UPHB sınıflandırılmıştır.

İsenkul (2016), insan beyninin farklı imge örüntüleri arasındaki farklılık ve benzerliklere nasıl adapte olduğunu araştırmıştır. bu çalışma alanının aradığı cevaplar arasındadır. Görme sisteminde ilk girdinin alındığı Katman 4'e girdi olarak gelen görsel alandaki bilgi, belirli örüntülere duyarlı, RBF ağı gibi doğrusal olmayan bir gösterim sistemine dönüştürülerek komşu alan ve üst katmanlara iletilir. Çalışmada, Katman 4'ün imge gösterim kapasitesinin ölçülmesi ve retinal girdilerin (orijinal resimlerin) filtrelenmesiyle özetlenebilecek beynin talamus yapısı çıktı gösterimlerine göre karşılaştırılabilir performansının değerlendirilmesi amaçlanmıştır. Çalışma kapsamında, bir Katman 4 benzetim modeli (Favorov ve Kursun, 2011) kullanılarak, gösterimin doğal resimlerin uzamsal dönüşümlerine ve hareket izine olan hassasiyeti incelenmiş, kümeleme ve sınıflandırma problemlerindeki Katman-4 gösteriminin başarımları analiz edilmiştir.

Şeker (2017) çalışmasında, iyi – kötü koku verilerine ilişkin, beynin elektriksel aktivitesini inceleyebilmek için kullanılan elektro-fizyolojik yöntemlerden biri olan Elektroensefalogram (EEG) işaretlerinin analizi ve sınıflandırılması yapılmıştır. Sınıflandırıcı olarak WEKA veri madenciliği programına ait çok katmanlı algılayıcılar, k-en yakın komşuluk, naive bayes ve rastegele orman algoritmaları kullanılmıştır. Diferansiyel gelişim algoritması ile kanal seçimi yapılıp sınıflandırma işlemleri tekrarlanmış ve sonuçlar karşılaştırılmıştır. Tüm kanalların ve seçilen 5 kanalın kullanıldığı aşamada, sınıflandırma sonuçlarına bakıldığında en iyi algoritma RO algoritması çıkmış ve başarım oranları sırasıyla %99.19 ve %97.58 elde edilmiştir.

Uçar (2017) çalışmasında, uykuda solunumun durmasına bağlı olarak ortaya çıkan Obstrüktif Uyku Apne (OSA) hastalığının teşhisinde kullanılan ancak teşhis sırasında hastaya birçok rahatsızlık veren polisomnografi (PSG) cihazına alternatif yeni bir yaklaşım geliştirilmiştir. Bu yaklaşım ile PSG'ye alternatif, hastaya daha az rahatsızlık veren ve PSG kadar güvenilir bir cihazın oluşturulabileceği ispatlanmıştır. Çalışmada, 10 bireyden alınan Fotopletismografi (PPG) sinyali kullanılmıştır. Teşhis için PPG sinyali ve bu sinyalden türetilen Kalp Hızı Değişkeni (HRV) kullanılarak yapay zeka tabanlı teşhis algoritması tasarlanmıştır. Çalışma için PPG'den 46, HRV'den 40 adet olmak üzere toplam 86 özellik çıkarılmıştır. Çıkarılan özellikler, F-score özellik seçme

yöntemleriyle 2 defa azaltılmış ve sınıflandırılmıştır. Sınıflandırma sonuçlarına göre uyku evreleme 11 özellik ile, %84,93 duyarlılık, %97,40 özgüllük ve %91,09 sınıflandırma doğruluk oranı ile topluluk sınıflandırıcısı yardımıyla başarı ile sınıflandırılmıştır. Solunum skorlama işlemi, 86 özellik ile, %87,78 duyarlılık, %95,46 özgüllük ve %92,54 doğruluk oranı ile başarıyla gerçekleştirilmiştir.

Işık (2017), motor hareket hayali özelinde sinyal özellikleri, bu sinyallerin beyinde salındığı yerler ve oluşumu esnasında görülen olaya ilişkin senkronizasyon (ERS) ve olaya ilişkin desenkronizasyon (ERD) konularını ele almıştır. Makine öğrenmesi yöntemleri (Doğrusal Ayırtaç Analizi (LDA), Karar Destek Makinaları (SVM) ve K En Yakın Komşuluk (KNN)) ile motor hareket hayali tabanlı mobil beyin bilgisayar arayüzü tasarımı yapmıştır.

Demirhan (2018), otizm spektrum bozukluğu (OSB) hastalığının teşhisi için klinik yöntemlerin yanında teşhis süresini kısaltmak ve başarımı artırmak için makine öğrenmesi yöntemlerinin kullanımının önemli olduğunu ifade etmiştir ve çalışmasında OSB ergen tarama verileri kullanılarak destek vektör makineleri (DVM), k-en yakın komşu (kNN) ve rastgele orman (RO) makine öğrenmesi yöntemleriyle OSB durumunun hızlı ve doğru olarak teşhis edilmesine yönelik analizler yapmış ve bu yöntemlerin performansları karşılaştırmıştır. DVM, kNN ve RO yöntemleri kullanılarak 10-kat çapraz doğrulama ile yapılan ikili sınıflandırma işlemi sonucunda sırasıyla %95, %89 ve %100 doğruluk oranlarına erişilmiştir. Ayrıca, RO yöntemi ile yapılan sınıflamadan % 100 duyarlılık ve belirlilik değerleri elde edilmiştir.

Başçıl (2019) çalışması, SAM32RFO Elektroensefalografi (EEG) cihazı ve 10/20 sistemine sahip EEG kepi kullanılarak, 10 katılımcıdan belli bir düzen içerisinde kayıtlanmış olan EEG üzerinde ortaya çıkan beyin sinyallerinin çene hareketleri ile ilişkisinin değerlendirilmesi amacıyla yapılmıştır. Çalışma 03/09/2018-03/10/2018 tarihleri arasında ilgili üniversitenin Elektrik-Elektronik Mühendisliği Bölümünde, 10 katılımcıdan (3 kadın, 7 erkek) EEG sinyallerinin kayıtlanarak bilgisayar ortamına aktarılması ile tamamlanmıştır. Verilerin değerlendirilmesinde, standart sapma değişimlerinden faydalanılarak olasılıksal sinir ağı modeli (PNN) kullanılmıştır. Elde edilen sonuçlar yüzde olarak sunulmuştur. 21-35 yaş aralığındaki sağlıklı katılımcıların, her bir döngüsü 10 saniye süren ve bu süre boyunca (dudaklar kapalı, diş gıcırdatma ve vücut hareketi olmaksızın) yaklaşık 20 kez sağa ya da 20 kez sola doğru çene hareketleri yapabildiği görülmüştür. Çıkarılan tüm özelliklerin bilgisayar ortamındaki makine öğrenme algoritmaları yardımıyla incelenmesi sonucunda, sağ ve sol çene hareketleri sırasında beyinde oluşan iki farklı EEG sinyalinin, birbirlerinden %90,14 oranında farklı olarak belirlenebildiği bulunmuş ve beyin haritalama üzerindeki çıkarımlarda bu oranı desteklemiştir. Çenenin sağa veya sola hareketi ile oksipital, frontal ve temporal loblarda delta dalgalarına rastlanmıştır.

Dolaşım ve Solunum Sistemi Hastalıkları

Akciğer

Aykanat (2018), çalışmasında, 1.630 denekten elektronik stetoskop ile kaydedilen 17.930 ses ve metin verisinden oluşan bir veri kümesinde, konvolüsyonel sinir ağları (CNN), destek vektör makineleri (SVM), k en yakın komşuluk (k-NN) ve Gaussian Bayes (GB) algoritmaları kullanarak, solunum seslerinin ve akciğer hastalıklarının sınıflandırılmasını amaçlamıştır. Geleneksel ve elektronik stetoskobu karşılaştırmak için 3 uzman doktor, 100 sesi değerlendirmiştir.

Örenç (2019), Kronik Obstrüktif Akciğer Hastalığı (KOAH)'nda kullanılan mevcut spirometre ve polisomnografi (PSG) cihazının bireylere bazı zorluklar yaşattığını belirtmiş ve bireye daha az sıkıntı oluşturan ve bu cihaz kadar verimli bir şekilde çalışabilen bir sistem geliştirmiştir. Bu durumdan dolayı fotopletismografi sinyali kullanılarak zaman ekseninde 26 adet özellik çıkartılmıştır. Makine öğrenmesi modelleri olan k – En Yakın Komşu Algoritması, Olasılıksal Yapar Sinir Ağları ve Destek Vektör Makine olmak üzere toplamda 3 adet sınıflandırma algoritması kullanılmıştır. Ayrıca 8 KOAH'lı hasta ve 6 kişilik sağlıklı bireye ait veriler kullanılmıştır. Sınıflandırma algoritma performanslarını değerlendirebilmek için doğrululuk oranı, özgüllük, duyarlılık ve F-ölçümü gibi parametreler kullanılmıştır. Her 3 makine öğrenmesi modelinde de elde edilen sonuçlar en az doğruluk oranı %80 olup bazı algoritmalara göre tüm verilerin doğruluk oranı %100 doğru sınıflandırılmış, duyarlılık 1, özgüllük 1 ve F-ölçümü 1 olarak tespit edilmiştir.

Kalp

Toprak (2004) çalışmasında, makine öğrenmesi yoluyla tıp alanında cerrahi müdahelelerde kalp krizi riskinin (kardiyak risk) tespit edilmesi konusunda hekimlerin karar vermesinde onlara yardımcı olmak ve de onlar olmadan kendi başına öğrenebilen ve karar verebilen bir sistemin tasarlanması amaçlanmıştır. Bu amaca ulaşmak için genetik algoritma ve yapay sinir ağı tekniklerinden yararlanılmıştır.

Aydın (2011) çalışmasında, aritmi hastalarının tedavi süreçlerine yardımcı olmak amacıyla öğrenmeye dayalı bir sistem geliştirilmiştir. Bu sistem, lokasyondan bağımsız olarak hastanın bazı metabolik parametrelerini alarak bu verileri uzak bir sunucu üzerindeki veritabanında depolamaktadır. Depolanan bu veriler bir uzman tarafından etiketlendikten sonra veri ambarına aktarılmaktadır. Veri ambarındaki bu veriler daha sonra makine öğrenmesi sınıflandırıcısı tarafından eğitim verileri olarak kullanılmaktadır. Geliştirilen Sistemde, makine öğrenmesi algoritması olarak k en yakın komşuluk (kNN) algoritması kullanılmıştır. kNN algoritmasının seçilme sebebi düşük bias'a sahip nonlineer bir fonksiyon olmasındandır. Bu nedenle yapılan tahminlerde yüksek oranda doğruluk sağlanmaktadır.

Oktay (2011) çalışmasında, çeşitli tıbbi imgeler için nesne saptama ve kontur bulma işlemlerini farklı önsel bilgilerin eklenmesi ile gerçekleştiren makine öğrenmesi tabanlı yöntemler sunulmuştur. Geliştirilen ilk yöntem, global şekil ve imge bilgisi ile ekokardiyogramlardan ve kalp MR imgelerinden iç ve dış sol karıncık konturlarını bulmaktadır. Geliştirilen diğer bir yöntem ise kalp duvarının hareketi, görünüş ve

uzaklık gibi çeşitli lokal önsel bilgilerle, sol karıncığın geometrik şeklini birleştirerek ekokardiyogramlardan kontur bulmaktadır. Bir başka yöntem de, bel omurga MR imgelerinden lomber omurlar arasındaki disklerin konumlandırılması için geliştirilmiştir. Bu yöntem, disklerin lokal özellikleri ile lomber eğrinin global şeklini birleştirmektedir. Son olarak, MR kalp imgelerinden sol karıncığın yeri bulunmuş ve kalp duvarlarını gösteren skor imgeleri oluşturulmuştur. Geliştirilen yöntemlerin etkinliği, gerçek tıbbi imgeler ve sentetik imgeler kullanılarak gösterilmiştir.

Kocamaz (2012), tıp bilişimi alanında tele tıp uygulamaları ile hastaların tıbbi görüntüleri ve laboratuvar analizleri gibi anlık olmayan verilerin dijital olarak saklanabildiği gibi uzak mesafelere de gönderildiğini ifade etmiştir. Çalışmasında ise, bir kişiden alınan çeşitli yaşamsal veri ve parametrelerin GPRS teknolojisi aracılığı ile sunucuya gönderilmesi ve gönderilen verinin makine öğrenmesi algoritmaları kullanılarak değerlendirilmesi ile uzman bir sistem tasarımı gerçekleştirilmesini hedeflemiştir. Tasarlanan sistem iki kısımdan oluşmaktadır. Birinci kısım veri toplama ve iletim cihazıdır. Bu cihazın amacı verileri bir sensör, dönüştürücü ile veya sensör modülleri ile elde edilen analog verileri elektronik filtre işleminden geçirilmesi, bu verilerin dijital forma dönüştürülmesi, sunucuya belirli bir formatta, güvenli, veri kaybına izin vermeyecek veri transfer oranı ile iletilmesini sağlamaktır. Böylece kişi her an gözlem altında tutulabilecektir. Kişinin izlenmesi için klinik ortamda olması gerekmeyecektir. İkinci kısımda ise gelen veri ve parametreler sunucu tarafında veri tabanına kaydedilir ve kaydedilen veriler makine öğrenmesi algoritmaları ile sınıflandırılır. Kişinin durumunun kritik veya normal şeklinde sınıflandırılması ile kişiye hızlı müdahale imkânı sağlanmış olacaktır.
Kalbin korunması için nabız, kandaki oksijen saturasyonu, sinyal kalitesi, sinyal genliği gibi parametrik değerler ve pletismogram işaretlerinin izlenmesi konusunda uygulama yapılmıştır. Örnek çalışmanın kalp pletismogram veri ve parametreleri üzerinde gösterilmesinin nedeni; kalbin korunması için bu parametrelerinin sürekli izlenmesi ve kaydedilmesinin önem arz etmesidir.

Kartal (2015), kalp ameliyatı sırasında ya da kalp ameliyatı geçirdikten kısa bir süre sonra hastaya ait hayati riskin sınıflandırmaya dayalı makine öğrenmesi teknikleri kullanılarak belirlenmesini amaçlamıştır. Çalışmada kullanılan veri seti Acıbadem Maslak Hastanesi'nden temin edilmiştir. Naive Bayes Sınıflandırıcı, k-En Yakın Komşu Algoritması, Logistik Regresyon Analizi, ID3 ve C4.5 Karar Ağacı Algoritmaları kullanılarak farklı modeller oluşturulmuştur. Modellerin performansları karşılaştırılmıştır. Veri analizleri R dilinde yazılan kodlarla gerçekleştirilmiştir.

Kaya (2017) Erken karıncık kasılması (EKK)'nın ektopik kalp vuruları ile ortaya çıkan en yaygın kardiyak aritmilerinden biri olduğunu ifade etmiş ve aritmilerin algılanması kalple ilgili olabilecek problemlerin önceden tahmininde önemli rol oynadığını vurgulayarak çalışmasında, ilk olarak işarete ait zaman serilerini kullanarak EKK

vurusunun sınıflandırılmasını gerçekleştirmiştir. Bu aritmilerin sınıflandırılması için bir vuruluk işarete ait yeni öznitelikler çıkarılmıştır. Öznitelikler, boyut indirgeme algoritmaları kullanılarak daha küçük boyutlara düşürülmüştür. Deneyler, k-en yakın komşu algoritması, yapay sinir ağları, karar ağaçları ve destek vektör makinesi sınıflandırıcıları kullanılarak gerçekleştirilmiştir. Bulgular, doğruluk, duyarlılık, kesinlik, özgünlük ve çalışma süreleri bakımından değerlendirilmiştir. Çalışmada yapılan testlerde kullanılan veriler bu alanda standart hale gelmiş olan MIT-BIH aritmi veri tabanından alınmıştır.

Cihan (2018), Kardiyovasküler hastalıklar içerisinde ölümcül sonuçları olan en yaygın klinik tipin koroner arter hastalığı olduğunu vurgulamış ve Kaliforniya Üniversitesi, Irvine (UCI) veri kümesi koleksiyonundan alınan Cleveland, Macaristan, İsviçre ve VA Long Beach kalp hastalığı veri kümeleri üzerinde Rastgele Orman Algoritması kullanarak koroner arter hastalığı riski analizi yapmıştır. Veri analizi aşamasında, belirtilen tüm veri kümeleri incelenmiştir. Ancak, sınıflama modeli daha az eksik veri içermeleri ve dengeli bir dağılıma sahip olmaları nedeniyle Cleveland ve Macaristan veri kümeleri üzerinde kurulmuştur. Veri analizi, kardiyoloji alanında uzman bir hekimin rehberliğinde grafiksel ve istatistiksel yöntemlerle yapılmıştır. Uygulanan sınıflama modeli sonucunda, Cleveland veri kümesi üzerinde %86,13 doğruluk oranı ve Macaristan ve Cleveland veri kümelerinin birleştirilmesi ile elde edilen 596 hasta kaydından oluşan veri kümesi üzerinde ise %80 doğruluk oranı elde edilmiştir. Ayrıca, modelin uygulandığı her iki veri kümesinde de göğüs ağrısı tipi ve egzersizle tetiklenen ST depresyonu sınıflama açısından en önemli iki değişen olarak saptanmıştır.

Takci (2018) çalışmasında, kalp krizi geçirmeyi öngören en iyi makine öğrenme yöntemi ve en iyi özellik seçim algoritmasının belirlenmesi amaçlanmıştır. Bu amaçla, Statlog (Heart) veri setinde optimum parametrelere sahip birçok makine öğrenme yöntemi ve çeşitli özellik seçim yöntemleri kullanılmıştır ve değerlendirilmiştir. Deneysel sonuçlara göre, en iyi makine öğrenme algoritması doğrusal çekirdekli destek vektörlü makine algoritmasıdır, en iyi özellik seçim algoritması ise reliefF metodudur. Bu çift en yüksek% 84.81 doğruluk değerini vermiştir.

Kodal vd. (2018) çalışmasında, elektrokardiyogram (EKG) sinyallerindeki zemin gezinme gürültüsünün giderilmesi ve yüksek frekanslı gürültünün temizlenmesi amacıyla dalgacık analizi kullanılmıştır. Gürültüsü temizlenen sinyalde QRS zirvelerini belirlemek için Destek Vektör Makineleri ve Naive Bayes algoritmaları kullanılmıştır. QRS zirvelerinin bulunmasında, MIT-BIH aritmi veri tabanında verilen QRS zirvelerinin konum bilgileri kullanılmıştır. QRS zirvelerini doğru belirlemede Destek Vektör Makineleri algoritması Naive Bayes algoritmasından daha yavaş sonuç vermesine rağmen %99.46 duyarlılık, %100 seçicilik ve %0.54 hata değerlerine ulaşmıştır.

Göğüs hastalıkları

Yahyaoui (2017) çalışmasında, göğüs hastalıklarını teşhis etmek için destek vektör makinaları (SVM), K-en yakın komşular (K-NN) ve Basit Bayes sınıflandırma (NB) metotları kullanılmıştır. Ayrıca, ilk kez uyarlamalı destek vektör makina metodunun (ASVM) göğüs hastalıkları teşhisindeki performansı da değerlendirilmiştir. Bu metot, SVM tekniğinin en uygun eşik değerini bulacak şekilde geliştirilmesine dayanmaktadır. Kullanılan bu yaklaşımlar Diyarbakır Göğüs Hastalıkları Hastanesi'nden alınan deneysel veri seti kullanılarak ve daha önceki çalışmalarda kullanılan sinir ağları yöntemleri ile karşılaştırılarak değerlendirilmiştir. Yapılan çalışmada elde edilen sonuçlar, kullanılan metotların, özellikle de ASVM metodunun başarım etkisinin yüksek olduğunu göstermiştir.

Kan basıncı

Ertuğrul ve Sezgin (2018), Arteriyel kan basıncı (ABP)'yi elektrokardiyogram (ECG) ve fotopletismograf (PPG) sinyallerinden aşırı bir öğrenme makinesi (ELM) ve zaman-frekans alanındaki ECG ve / veya PPG sinyallerinin istatistiksel özellikleri ile tahmin etmek için basit ve etkili bir yaklaşım önermiştir. Önerilen yaklaşımı değerlendirmek ve uygulamak için, UCI tarafından yayınlanan ve paylaşılan Kolsuz Kan Basıncı Tahmin Veri Seti kullanılmıştır. ELM ve bazı popüler makine öğrenme yöntemleri ile her konu için kelepçesiz ABP'yi tahmin etmek için çıkarılan özellikler kullanılmıştır.

Böbrek Hastalıkları

Saçlı (2018), böbrek taşı türünün belirlenmesinde mevcut metotlara mikrodalga frekansında elektromanyetik dalgalardan faydalanan yeni bir alternatif geliştirmeyi amaçlamıştır. Böbrek taşlarının elektromanyetik özelliklerinin sınıflandırılması ise makine öğrenmesi algoritmaları (Artificial Neural Network and K-Nearest Neighbourhod) ile yapılmıştır.

Erdursun (2019), çalışmasında Kronik Böbrek Hastalığı(KBH) veri seti üzerinde analiz yapılmıştır. Çorum Hitit Üniversitesi Erol Olçok Eğitim ve Araştırma Hastanesinde 216 hastadan elde edilen veriler kullanılmıştır. Veriler üzerinde makine öğrenmesi yöntemleri uygulanmış ve hastalık sınıflandırılması yapılmıştır. Uzman görüşü alınarak, hastalara tanı koymak için kullanılan bazı değişkenler veri kümesinden çıkarılarak geriye kalan değişkenlerle analiz yapılmıştır.

Diyabet Hastalığı

Bozkurt vd. (2014) çalışmasında, Pima Indian Diabetes veri seti 8 farklı sınıflandırıcı ile sınıflandırılmıştır. Veriler California Üniversitesi Irvine Machine Learning Repository'nin web sitesinden alınmıştır. Bir sınıflandırıcı olarak, 6 farklı sinir ağı [olasılıksal sinir ağı (PNN), öğrenme vektör nicelemesi, ileriye dönük ağlar, ileriye dönük ağlar, dağıtılmış zaman gecikmeli ağlar (DTDN) ve zaman gecikmeli ağlar], yapay bağışıklık sistemi ve Gini karar ağaçlarından algoritma kullanılmıştır. Sınıflandırıcının performans oranları doğruluk, duyarlılık ve özgüllük olarak ayrı ayrı

incelenmiştir ve tüm sınıflandırıcıların başarı oranları sunulmaktadır. Bu 8 sınıflandırıcı arasında en iyi doğruluk ve özgüllük değerleri DTDN ile elde edilmiştir.

Akyol vd. (2016), şeker hastalığına bağlı olarak retinada ortaya çıkan hasarlanmaların sonucu körlüğe neden olan bir hastalık olan Diyabetik retinopatinin, erken evre (nonproliferatif) ve ileri evre (proliferative) olmak üzere iki aşaması olduğunu belirtmiştir. Görme kaybının önüne geçilebilmesi için erken evre DR bulgularının erken tanı ve teşhisi gerektiğinden dolayı bu çalışmada, erken evre DR lezyonlarından olan sert eksuda bölgelerinin otomatik olarak tespitinde kullanılmak üzere bir karar destek sistemi tasarlanmıştır. Bu sistem, anahtar nokta çıkarımı, özellik çıkarımı, görsel sözlük ve sınıflandırma aşamalarını içermektedir. Sistem performansı, publik (herkese açık) DIARETDB1 retinal görüntü dataseti üzerinde test edilmiştir. Deneysel sonuçların elde edilmesinde, Yapay Sinir Ağları, Rastgele Orman ve Karar Ağacı algoritmaları kullanılmıştır.

Adem (2017) çalışmasında, oftalmologların teşhis işlerini kolaylaştırma ve zaman kaybının önlenmesi için diyabetik retinopati hastalığının otomatik teşhisi ve sınıflandırılmasına odaklanılmıştır. Bu amaç için, retina görüntülerindeki anatomik yapılar olan optik disk ve damar bölgelerinin tespit edilerek görüntüden göz ardı edilmesi sağlanmıştır. Optik disk tespiti için sırasıyla HSV renk uzayı, adaptif histogram eşitleme, Gama dönüşümü, Canny kenar bulma algoritması ve çembersel Hough dönüşümü, damar bölütlemesi için ise sırasıyla RGB renk uzayı, adaptif histogram eşitleme, Gabor ve Top-hat dönüşümü yöntemleri uygulanmıştır. Anatomik bölgelerin tespit edilerek retina görüntüsünden göz ardı edilmesinden sonra eksuda ve hemoraji lezyonlarının tespit edilmesi için manüel eşikleme ve ateşböceği / parçacık sürü optimizasyonu temelli iteratif eşikleme yöntemleri kullanılmıştır. Eşikleme yöntemleri sonucu eksudalı toplam piksel sayısı, eksudalı bölge sayısı, hemorajili toplam piksel sayısı ve hemorajili bölge sayısından oluşan öznitelik veri seti doğrusal regresyon, çok katmanlı algılayıcı, çapsal tabanlı fonksiyon sinir ağı ve destek vektör makinesi temelli sınıflayıcılara giriş olarak kullanılarak diyabetik retinopati teşhisi ve sınıflandırılması gerçekleştirilmiştir. Sınıflandırma doğruluğu açısından sınıflayıcı performanslarını değerlendirmek için farklı kombinasyonlar kullanılarak farklı deneyler yapılmıştır. Gerçekleştirilen deneyler parçacık sürü optimizasyonu temelli destek vektör makinesi yaklaşımın ateşböceği temelli olan yaklaşımlardan daha yüksek toplam doğru sınıflandırma başarı oranlarına ulaştığını göstermiştir. Sonuç olarak, hasta yoğunluğundan dolayı yaşanabilecek muhtemel karışıklıkların önüne geçerek oftalmologlara ön-tanı imkânı veren teşhis destek sisteminin gerçekleştirilmesi sağlanmıştır.

Oğuztürk (2018) çalışmasında, Türkiye'deki diyabetli ve diyabetik olmayan hastaların sağlık profillerini veri seti olarak kullanmış, hastaların 10 farklı özelliğini giriş değişkeni olarak seçmiş ve deneklerin diyabetik durumunu 7 farklı makine öğrenmesi algoritması kullanarak tahmin etmiştir. Çalışmada toplam 2657 adet denekten 1860 adedi algoritmanın eğitimi için kullanılmış olup, kalan 797 veri adedi ise algoritmanın test edilmesi için ayrılmıştır. Diyabet tahmin modelinin geliştirilebilmesi için açık

kaynak kodlu Orange programı kullanılmıştır. Algoritmanın doğruluğunu optimize edebilmek için farklı kombinasyonlar, gizli düğüm sayısı ve beklenti maksimizasyonu (EM) iterasyonları uygulanmıştır. Yapay sinir ağı algoritmasının, %97.2'lik doğru tahmin başarısıyla en iyi başarıyı elde ettiği tespit edilmiştir. İkinci ve üçüncü en iyi başarı ise %96.9 ve %96'lık doğru tahmin başarı oranlarıyla lojistik regresyon ve random forest ile elde edilmiştir.

Özkaya (2018), aida simülatörü üzerinde kan şekeri tahmini için makine öğrenmesi algoritmalarının kıyaslanmasını ele almıştır. Tahminler, destekçi vektör makinesi, karar ağacı, Gauss sürec̈i, K-en yakın komşu, rastgele orman ve sinir ağları bulanık ve tekrarlayan yapay sinir ağları algoritmalarıyla gerçekleştirilmiş.

Bel Bölgesi Hastalıkları

Ünal (2015) çalışmasında, radyolog, uzman ve doktorların bel bölgesi rahatsızlıklarının teşhisine yardımcı olması amacıyla bir bilgisayar destekli teşhis (BDT) sistemi geliştirilmiştir. Bu sistem ile bel bölgesi rahatsızlıklarından bel fıtığı, dejeneratif disk, omur kayması (spondilolysthesis), lomber spinal stenoz, rahatsızlıkları teşhis edilmektedir. Çalışmada kullanılan bel bölgesi axial ve sagittal MR görüntüleri Selçuk Üniversitesi Tıp Fakültesi Hastanesi Radyoloji bölümünden alınmıştır. Ayrıca, California Üniversitesi Uluslararası Irvine Makine Öğrenme Veritabanından (UCI) alınan bel bölgesine ait vertebral veri kümesi de ayrı bir özellik vektörü olarak sınıflandırma aşamasında kullanılmıştır. Elde edilen veri kümelerinin sınıflandırılması işlemi için Destek Vektörü Makineleri (DVM), Çok Katmanlı Perseptron (MLP), LVQ sinir ağları (LVQ-NN), Radyal Tabanlı Fonksiyon Sinir Ağları (RTFA), k-en yakın komşu (K-NN) sınıflandırma algoritmaları uygulanmıştır.

Tümer (2018), makine öğrenmesi algoritmaları için kullanılan WEKA ile anlık gelen veri işleme için kullanılan Siddhi aracını birleştirerek bir akıllı sistem geliştirilmiştir. Çalışma verisi olarak sağlık alanından bel fıtığı (Hernia) ve bel kayması (Spondylolisthesis) teşhisinde kullanılabilecek Nesnelerin İnterneti verileri seçilmiştir. Sistem, WEKA kütüphanesini kullanarak Destek Vektör Makineleri, J48 Karar Ağacı, Yapay Sinir Ağları, Naif Bayes, Rastgele Orman, jRip, kYıldız ve Basit Lojistik makine öğrenmesi algoritmalarını başarı ve performans üzerinden karşılaştırılmıştır.

Göz Hastalıkları

Hacıefendioğlu (2012), genellikle göz içi sıvısının göz kanallarından boşalamadığı durumlarda ortaya çıkar ve göz içindeki basıncın(GİB) artması ile göz arkasındaki sinirlerin bu basınçtan ötürü zarar görmesi şeklinde gelişen Glokom hastalığının körlüğe kadar götüren bir hastalık olduğunu ifade etmiştir. Bu amaçla, hastalığın göz sinirleri hasar görmeden önce teşhis edilebilmesi için Pamukkale Üniversitesi Göz Hastalıkları Anabilim Dalından alınan hasta bilgiler ve makine öğrenmesi sınıflandırma yöntemlerinden Destek Vektör Makineleri, Yapay Sinir Ağları ve Karar Ağaçları kullanılarak glokom hastalığı başlangıç safhasında teşhisi için sınıflandırma

yapılmış ve birbirleri ile karşılaştırılmıştır. Adı geçen makine öğrenmesi yönetmelerinin performansları X-Validation ile belirlenmiş ve en yüksek sınıflandırma başarısının Destek Vektör Makineleri ile elde edileceği görülmüştür.

Açıl (2019), çalışmasında iris yapısını kullanarak cinsiyet tahmini yapmıştır. 750 kadın ve 750 erkek olmak üzere her kişinin sağ ve sol iris görüntüleri kullanılarak toplamda 3000 görüntü üzerinde uygulama gerçekleştirilmiştir. İris görüntülerine öznitelik çıkarma yöntemi olarak doku analiz yöntemleri, gemoterik features çıkartma, gabor filtresi, dalgacık dönüşüm, fourier dönüşümü uygulanmıştır. Her bir öznitelik çıkartma yöntemiyle öznitelik kümleri oluşturulmuş ve sınıflandırma başarım değerleri karşılaştırılmıştır. Sonuç olarak, %91 başarım oranı ile en iyi öznitelik alt kümesi non-liner dönüşüm yapılmış özniteliklerden elde edilmiştir.

Kadın ve çocuk hastalıkları

Yılmaz (2016), kardiotogram verisinden fetal iyilik halinin belirlenmesi için bir karar destek sistemi önermiştir. Sistem En Küçük Kareler Destek Vektör Makineleri ve Temel Bileşen Analizi üzerinde temellendirilmiştir. Temel Bileşen Analizi yöntemi ile kardiotokogram veri kümesinin boyutu indirgenmiştir. Özellik boyutu indirgenen veri kümesi üzerinde En Küçük Kareler Destek Vektör Makineleri kullanılarak sınıflandırma işlemi gerçekleştirilmiştir. Önerilen karar destek sisteminin başarımı UCI Makine Öğrenmesi Ambarlarından alınan kardiotokogram veri kümesi üzerinde 10-katlı Çapraz Doğrulama tekniği kullanılarak incelenmiştir. Deneysel sonuçlar önerilen sistemin %98,74 sınıflandırma doğruluğuna, %98,86 duyarlılık oranına ve %98,73 özgüllük oranına sahip olduğunu göstermiştir.

Cömert (2017), fetal sağlık durumunun belirlenmesi amacıyla gebelik dönemi ve doğum sırasında yaygın şekilde kullanılan bir gözetim tekniği olan Kardiyotokografi (KTG)'nin düşük pozitif tahmin değeri, yüksek yanıltıcılık oranı, yorumlanmadaki öznellik, yeniden üretilebilirlik değerindeki tutarsızlık ve yüksek seviyede gözlem içi ve gözlemciler arası anlaşmazlık seviyesi gibi çeşitli problemlere sahip olduğunu ifade etmiştir. Bu problemlerin üstesinden gelmek üzere bilgisayar destekli KTG analizi ile KTG işaretlerini morfolojik, doğrusal, doğrusal olmayan, frekans ve zaman-frekans alanlarında analiz edilmesini sağlayan bir yazılım geliştirilmiştir. KTG işaretlerinin normal ve hipoksik olarak sınıflandırılmasını sağlamak üzere yapay sinir ağı, aşırı öğrenme makinesi, destek vektör makinesi, radyal tabanlı fonksiyon ağı gibi çeşitli makine öğrenmesi tekniklerinin kullanılması sağlanmıştır.

Bulut (2017), çocuklarda obeziteye yakalanma riskini hesaplayan bir erken uyarı sisteminin geliştirilmesini amaçlamıştır. Makine öğrenmesi kolektif öğrenme algoritmaları kullanılarak yapay ve özgün bir klinik karar destek sistemi (KKDS) geliştirilmiştir. Obeziteye neden olan faktörler hazırlanan anket içerisine yerleştirmiştir. Devlet hastanelerinden ve okullarından alınan resmi izinlerle anketler çocuklara uygulanmış ve elde edilen verilerle güvenilir bir eğitim seti oluşturulmuştur. k En Yakın Komşuluk algoritmasının geliştirilmiş versiyonları Oylama, Bagging, Boosting ve Rastsal Altuzaylar yöntemlerinde tekil öğrenici olarak kullanılmıştır. Eğitim seti üzerinde yapılan öğrenme ve çapraz geçerleme işlemlerinde algoritmalara ait yüksek doğruluk oranları elde edilmiş ve en başarılı yöntemin

0,839'lık MCC (Matthews Correlation Coefficient) değeriyle Rastsal Altuzaylar olduğu görülmüştür.

Göker ve Tekedere (2019), çocukluk çağı dikkat eksikliği ve hiperaktivite bozukluğunun öngörülmesine yönelik çocuk psikiyatristlerinin alan uzmanlığı doğrultusunda tanı çıkarımı yapabilen bir dinamik uzman sistem tasarımı geliştirmiştir. Çalışmanın konusu gereksinim analizi yapılarak çocukluk çağının en sık görülen psikiyatrik bozukluklarından olan dikkat eksikliği ve hiperaktivite bozukluğu olarak seçilmiştir. Nitelikler alan uzmanları (çocuk psikiyatristleri) tarafından belirlenirken, kayıtlar Gazi Hastanesi Çocuk Ruh Sağlığı ve Hastalıkları Anabilim Dalından alınan kliniksel hasta verilerinden oluşmaktadır. Geliştirilen sistemin çıkarım mekanizması kısmında Naive Bayes algoritması kullanılarak, kural tabanının dinamik olarak yenilenmesinin sağlanması çalışmanın en önemli ayırt edici özelliğidir. Bu sayede sistem, daha önceden kayıtlı olmayan yeni bir durum ile karşılaştığında; mevcut kurallardan faydalanarak yeni kuralın hangi sınıfa ait olduğunu tahmin edebilmektedir. Gerçek veriler ile sistem eğitilmiş ve performansı test edilmiştir. Çalışmanın sonucunda, accuracy 88.62%, precision 89.2%, recall 88.6%, f-measure 88.6% ve ROC area değeri 89.8 % bulunmuştur.

Genetik Çalışmalar

Yengi ve İlhan Omurca (2016), gen dizilimlerinin sınıflandırılmasının, hastalıkların ön görülebilmesi veya teşhis edilebilmesinde çok önemli rol oynadığını ancak bütün gen dizilimi üzerinde sağlıklı bir sınıflandırma yapılabilmesi için gerekli bilgiyi içeren genlerin (özelliklerin) özellik azaltma algoritmaları ile ayıklanması gerektiğini ifade etmiştir. Çalışmada, özellikleri azaltmak için sezgisel arama teknikleri, özellik azaltma yaklaşımları (filter, wrapper, vb.) gibi farklı yöntemler analiz edilerek ön işleme adımının daha etkin bir şekilde gerçekleştirilmesi; bunun sonucunda elde edilen veri kümelerinin LR (Lojistik Regresyon) ve SVM (Destek Vektör Makineleri) gibi güçlü sınıflandırma araçları ile daha etkin şekilde sınıflandırılması hedeflenmiştir.

Pashei (2017), DNA dizileri miktarında ki olağanüstü artış nedeniyle, genlerin doğru tespit edilmesi için geliştirilen yöntemlerin başarısının, uçbirleştirme bölgelerinin kesin olarak tanımlanmasına bağlı olduğunu belirtmiştir. Uçbirleştirme yeri tespiti için çok sayıda makine öğrenmesi yöntemi kullanmıştır. Çalışmasında, uçbirleştirme tespitinde Markov kodlama yöntemleri kullanan RF'nin, en başarılı sınıflandırma yaklaşımı olan SVM'den üstün olup olmadığını araştırmıştır. Ayrıca uçbirleştirme yeri tespiti için SVM ve ikinci dereceden Markov modelini kullanan başka bir DNA kodlama yöntemi önermiştir.

Turgut (2017) çalışmasında, meme kanseri ile alakalı mikrodizi verileri kullanılarak makine öğrenmesi yöntemleriyle sınıflandırma yapılmıştır. Bu veriler 122'si hasta 11'i sağlıklı olan toplam 133 bireye ait 1919 protein çeşidi bilgisinin bulunduğu 1. veri ve 46'sı hastalığın tekrarladığı 51'i tekrarlamadığı toplam 97 bireye 24481 protein çeşidinin bilgisinin bulunduğu 2. veridir. Uygulamalar Python programlama dili kullanılarak gerçekleştirilmiştir. Uygulanan makine öğrenmesi algoritmaları DVM, YSA, K-EYK, Karar Ağaçları, Rastgele Orman, Lojistik Regresyon, Adaboost ve Gradyan Boosting Makinesi'dir. İlk veri için, herhangi bir öznitelik indirgeme metodu

uygulanmadan önce %99.23 ile lojistik regresyon yöntemi, ikinci veri için rastgele orman yöntemi %67.42 ile en yüksek sonuçları vermiştir. RLR ve YÖE öznitelik indirgeme metotları 50 adet en iyi öznitelikle sınıflandırma yapılacak şekilde uygulandıktan sonra ilk veride DVM, iki yöntemde de %99.23 ile en yüksek doğruluk oranıyla; ikinci veride ise RLR'de %87.87 ile, YÖE'de %88.82 ile yine DVM en iyi oranla sınıflandırma yapmıştır.

Pashei (2017), başarılı bir hastalık teşhisi için, sınıflandırma ile alakalı az sayıda ayrımcı gen seçmek gerektiğini ve mikrodizi veri analizinde gen seçiminin hem sınıflandırma doğruluğunu arttırdığı hem de klinik ortamda işleme süresini azalttığını vurgulamıştır. Bu nedenle, başarılı bir hastalık teşhis sistemi geliştirmek için genlerin minimum bir alt kümesini belirlemede, melez doğadan esinlenmiş optimizasyon algoritmaların ve farklı sınıflayıcılara dayanan kanser sınıflandırmasında yüksek derecede ayırıcı gen seçimi için iki yaklaşım önermiştir. Dört klinik veri kümesindeki deneysel sonuçlar ve istatistiksel analiz, önerilen yöntemin, ateş böceği, karınca koloni, yarasa arama, genetik algoritma, armoni araştırması, hızlı korelasyon tabanlı süzgeç ve korelasyon tabanlı özellik alt küme seçimi gibi yaklaşımlara göre önemli derecede daha iyi sınıflandırma performansı elde ederken çok küçük bilgi grubu genleri ürettiğini göstermektedir. Önemli bir tümör baskılayıcı mikroRNA olan MiR-145, birçok kanser çeşidinde downregüle edildiğini ve tümörün başlatılması, progresyonu, metastazı, invazyonu, reküransı ve kemoradyolojik direncinde önemli rollere sahip olduğunu göstermiştir.

Burakgazi (2017), çalışmasında RNA dizileme verileri üzerinde makine öğrenmesi yöntemlerini kullanarak meme kanseri hastalarının alt tipini tayin etmeyi amaçlamıştır. Önemli genler, kat değişikliği ve t-testi istatistiksel yöntemleri uygulanarak seçilmiştir. Destek vektör makinesi ve Rastgele orman modelleri, hasta numunelerinin %70'lık kısmından elde edilen genlerle eğitilmiştir. Modellerin tahminleme performansı, daha önce kullanılmayan test verileri üzerinde ölçülmüştür. Meme kanseri alt tip sınıflandırmasına hangi genlerin daha fazla etkisi olduğunu bulmak için, her bir alt tipi en iyi sınıflandıran genler analiz edilmiştir. Bu genlerin ilgili oldukları biyolojik aktiviteler, ağ tabanlı bir analiz ve gen zenginleştirme analizi uygulayarak bulunmuştur.

Işık (2018), over ya da akciğer kanseri olduğu tespit edilen bir hastanın kanser alt-türünü tespit edebilecek belirli sayıdaki biyoişaretin makine öğrenmesi yöntemleriyle bulunmasını amaçlamıştır. mRNA gen ekspresyon ve protein seviyesi bilgileri kullanılarak kısıtlı sayıda öz-nitelik seçilmiş, bu öz-niteliklerle gözetimli makine öğrenmesi metotları eğitilmiş, bu modeller ile yeni gelen bir hastanın kanser alt-türü tahmin edilmiştir. Destek vektör makineleri ve rastgele orman algoritmaları, yeni kanser hastalarının kanser alt-türlerini ortalama %87 ile %95 arasında değişen doğruluk dereceleriyle sınıflandırabilmiştir.

Candan vd. (2019), mikro dizi verisinde kanser teşhisi için makine öğrenmesi yöntemlerini kullanmanın, zaman ve doğruluk açısından avantajları olduğunu ifade etmiş ve çalışmasında, akciğer ve beyin kanseri veri setleri üzerinde makine öğrenmesi sınıflandırma yöntemleri ile performans analizi yapmıştır. Aynı veriler genetik algoritma ile öznitelik seçimine tabii tutulmuş ve öznitelik seçimi yapılmış verilerin

performans analizleri tekrar inlecelenip sonuçlar tablolar ile desteklenerek yorumlanmıştır. Makine öğrenmesi sınıflandırma yöntemlerinden Naive Bayes, Bayes NET, kNN, Random Forest ve LSVM kullanılmıştır.

Kılıçarslan vd. (2019), mikrodizi verilerine dayanan veri madenciliği analizi ile hastalık teşhisinin mümkün olduğu ancak ve mikrodizilerin yüksek boyutlu olması ve çok sayıda gereksiz öznitelik içermesinin analiz aşamasında zorluk çıkardığını ifade etmiştir. Bu nedenle çalışmada, prostat kanseri mikrodizi veri kümesi üzerinde öznitelik boyut azaltılması amacıyla Temel bileşenler analizi (TBA) ve Parçacık sürü optimizasyonu (PSO) kullanılmıştır. Bu sayede hastalıkları etkileyen genler tespit edilmiştir. Boyutu azaltılmış veri kümeleri Destek Vektör Makinesi ve k-En Yakın Komşuluk sınıflayıcı yöntemlerine giriş olarak verilmiş ve sınıflandırma başarı sonuçları değerlendirilmiştir. Sonuç olarak PSO boyut azaltma yöntemi ile prostat kanserinde etkin genler belirlenmiş ve 50 öznitelik ile %95.77 başarı elde edilmiştir.

Sağlık hizmetleri

Amasyalı (2008), ilaç tasarımının çok emek ve uzun zaman isteyen ve buna bağlı olarak çok büyük maliyetler içeren bir sektör olduğunu ifade etmiştir. Bu sürecin ve maliyetin önemli bileşenlerinden birinin olası ilaç moleküllerinin seçilmesi işlemi olduğu ve bu seçim işleminin sınıflandırma, kümeleme, özellik seçimi/çıkarımı, regresyon (eğri uydurma) problemlerinden bir ya da birkaçını içerdiğini belirtmiştir. Bu probleme çözüm üretmek amacıyla, ilaç tasarım süre ve maliyetini azaltacak makine öğrenmesi metotları geliştirilmiştir. Sınıflandırma problemleri için Cline adı altında bir algoritma ailesi tasarlanmıştır. Cline karar ağacı ve karar ormanları algoritmaları ClineToolbox adlı bir yazılımla kullanıcıların hizmetine sunulmuştur. Kümeleme problemleri için Clusline adı altında bir algoritma ailesi geliştirilmiş ve mevcut algoritmalarla çeşitli kümeleme performans kriterlerine göre yarışan sonuçlar elde edilmiştir. Çalışma sonunda bir veri kümesi üzerinde bir algoritmanın performansı veri kümesinin çeşitli özelliklerine bakarak tahmin edilebilen bir model geliştirilmiştir.

Ghahremanlou (2012), maksimal ve N-Ex değişkenlerini kullanarak doğru VO2max (bir kişinin çalışan kaslara esansiyel yakıt (oksijen) sağlama yeteneğinin ve kasların hareket oluşturmak için bu yakıtı kullanma verimliliğinin bir göstergesi) tahmin modelleri geliştirmektir. VO2max tahmin modellerinin geliştirilmesinde Destek Vektör Makineleri (SVM), Yapay Sinir Ağları (YSA), Çoklu Doğrusal Regresyon (MLR) ve Genel Regresyon Sinir Ağları (GRNN) gibi makine öğrenme yöntemleri kullanılmaktadır.

Bulut ve Bucak (2014) çalışmasında, bir gencin makine öğrenmesi ve veri madenciliğinde sınıflandırma algoritmaları kullanarak uyuşturucu bağımlısı olma olasılığını tespit etmek amaçlanmıştır. Çalışmada özel bir veri seti kullanılmıştır ve aynı zamanda psikometri ve istatistiklere odaklanılmıştır.

Köse (2015) çalışmasında, sağlık alanında sahtecilik ve suistimal vakalarını, ilgili vakaya dâhil olan aktör ve metâlardan (sağlık hizmeti, ilaç, vb.) bağımsız olarak tespit edebilen, anormal davranışların parçalı doğasını dikkate alan ve yeni sahtecilik türleri için kolaylıkla adapte edilebilen özgün bir uygulama çerçevesi önerilmiştir.

Çalışmada, etkileşimli makina öğrenmesi yöntemi kullanılarak uzman bilgisi gerekli tüm alanlarda çalışmaya aktarılmıştır. Alan uzmanları, senaryo hikâyelerini yazarak 6 farklı sahtecilik ve suistimal davranış türü tanımlamışlardır. Önerilen uygulama çerçevesi, gerçek ilaç reçete verileri üzerinde altı farklı sahtecilik ve suistimal davranışı için reçetedeki tüm aktör ve metâları kapsayacak şekilde deneysel süreçlerden geçirilmiştir. Her deneyin Area Under Curve (AUC) ve maliyet etkinlik derecesi ölçülmüştür. Önerilen model ile hem proaktif; hem de retrospektif tespite ve analize imkân sağlayan eFAD™ adında bir ürün geliştirilmiş ve alan uzmanlarının eFAD tarafından tespit edilen şüpheli işlemlerin delillerini inceleyerek nihai karar hızlıca ulaşmaları sağlanmıştır.

Çınaroğlu (2017), kişi başı sağlık harcamasının tahmini amacıyla bir çoklu regresyon modeli oluşturmuştur. Farklı hiperparametre değerleri belirlendiğinde elde edilen Lasso Regresyon, Rastgele Ağaç Regresyonu ile Destek Vektör Makinesi Regresyon performans sonuçları karşılaştırılmıştır. Çalışmada hiperparametre değeri olarak Lasso Regresyon için lamda (λ) değeri, Rastgele Ağaç Regresyonu için ağaç sayısı, Destek Vektör Regresyonu için epsilon değeri esas alınmıştır. Sonuçlar 5 ile 50 arasında değişen "k" parça çapraz geçerlilik uygulanarak performe edildiğinde makine öğrenmesi regresyon yöntemlerine ait performans sonuçlarının R^2, RMSE ve MAE değerleri bakımından istatistiksel olarak anlamlı farklılıklar gösterdiği ($p<0.001$) tespit edilmiştir. Tahmin performanslarına ait yüzey ve çubuk grafikleri ile istatistiksel test sonuçları incelendiğinde farklı hiperparametre değerlerine göre Rastgele Ağaç Regresyonun ($R^2 > 0.7500$, RMSE ≤ 0.6000 ve MAE ≤ 0.4000) daha iyi tahmin sonuçlarına sahip olduğu belirlenmiştir.

Eren (2019), insan aktivitelerinin tespitinin kişiye özel günlük kalorilerin hesaplanması, kişinin gerçekleştirdiği hareketlere göre sağlık durumunun analizi gibi sağlık uygulamaları olarak veya yaşlı insanların bulundukları ortamda gerçekleştirdiği hareketler ile gözetlenmesi, insan pozisyon takibi ve çeşitli güvenlik uygulamalarında kullanıldığını ifade etmiş ve çalışmasında, bir insan aktivite tespit sistemi tasarımı gerçekleştirmiştir. WISDM (Wireless Sensor Data Mining) ham veri seti kullanılarak, sürekli zamanlı dalga öznitelikleri ve Saklı Markov Modellerine dayalı öznitelikler çıkarılmış ve bu özniteliklerin insan aktivite tanımlamadaki etkileri incelenmiştir. Kurulmuş olan makine öğrenmeleri algoritmaları kullanılarak gerçek zamanlı bir uygulama örneği çalışma kapsamında gerçekleştirilmiştir.

Sakarya (2019), son zamanlarda yaygın ve ayak taban siğili olan hastalara uygulanmaya başlanan kriyoterapi ve immünoterapi tedavi yöntemlerinin siğil tedavisinde başarılı olup olmayacağını makine öğrenmesi yöntemleri (NaiveBayes, Lojistik Regresyon, K-yakın Komşuluk, Karar Ağacı, Destek Vektör Makineleri, Aşırı Öğrenme Makinesi, Çok Katmanlı Algılayıcı) ile tedavi uygulanmadan önce tahmin etmeye çalışmıştır. Seçilen siğil tedavi yönteminin başarısı duyarlık, belirleyicilik ve genel başarım ölçütlerine göre belirlenmiştir. Sonuç olarak, Çok Katmanlı Algılayıcı yöntemi ile literatürdeki mevcut az sayıdaki çalışmadan çok daha yüksek bir doğrulukla tercih edilen siğil tedavi yönteminin başarılı olup olamayacağını tahmin edilebilmiştir.

Görür (2019), makine öğrenmesi algoritmalarını uygulayarak 1-boyutlu hareketler içeren yardımcı teknolojileri kontrol etmek için glossokinetik potansiyel (GKP) tabanlı dil-makine arayüzü geliştirmiştir. GKP sinyalleri, dil hareket bilgilerini içeren elektrik sinyalleridir. Tez çalışmasında GKP sinyalleri, deneysel düzenler içinde dil ucunun yanak duvarlarıyla teması sırasında kafa derisine yerleştirilen elektrotlarla ölçülmüştür. Çalışma ile engelli insanlara yardımcı cihazları doğal, rahatsızlık vermeyen, hızlı ve güvenilir bir şekilde kontrol etmeye hizmet etmek amaçlanmıştır. Çalışmada, geleneksel makine öğrenmesi algoritmaları ve konvolüsyonel yapay sinir ağı kullanarak sırasıyla %99 ve %100'e ulaşan sınıflandırma doğrulukları elde edilmiş ve yöntemlerin karşılaştırmalı analizi yapılmıştır.

Biyomedikal

Bağcı (2016), protez-biyonik ellerin işlevselliğini arttırmak için yapılabilecek şeylerden biri olan EMG sinyallerinin analiz edilmesi konusunu ele almıştır. Sinyaldeki gürültülerden arındırmak için frekans band genişliğinin yüksek tutulması sinyalin bütünlüğünü bozan detayların dahil edeceği gibi düşük tutulması ise sinyal için önemli olan detayların kaybolarak karakteristiğinin bozulmasına neden olabileceğini vurgulamış ve doğru sinyal analizi için akıllı algoritmaların kullanılmasının şart olduğunu ifade etmiştir. Çalışmasında, EMG sinyallerinin temsil yeteneği en yüksek olan dalgacık tipi ve ayrıştırma derecesini kestirmeye çalışmıştır. Ayrıca en iyi sınıflandırmanın hangi metodla yapılacağını araştırmıştır. Protez-biyonik ellerin işlevselliğini arttırmak amacıyla gündelik hayatta nesneleri tutmaya/kavramaya yarayan ve sıklıkla kullanılan 6 temel el hareketine ait EMG sinyallerinden oluşan 900 örnek verilik bir veri seti kullanılmıştır. EMG sinyallerine ait temsil yeteneği en güçlü olan öznitelik vektörünü elde etmek için Markov geçiş matrisi elemanları ve Ayrık Dalgacık Dönüşümü analizi kullanılmıştır. Elde edilen öznitelik vektörüne çeşitli makine öğrenmesi algoritmalarıyla sınıflandırma performans analizleri uygulanmıştır.

BULGULAR

Bu çalışmada, Türkiye'de makine öğrenmesi algoritmaları kullanılarak sağlık alanında yapılan 68 çalışma incelenmiştir. Bu çalışmalar, Kanserler, nörolojik hastalıklar, dolaşım ve solunum sistemi hastalıkları, böbrek hastalıkları, diyabet hastalığı, bel bölgesi rahatsızlıkları, göz hastalıkları, kadın-çocuk hastalıkları, gen dizilimi/genetik hastalıklar, sağlık hizmetleri ve biyomedikal şeklinde gruplandırılmıştır. Hangi alanda/konuda daha fazla çalışma yapıldığını daha anlaşılır hale getirmek amacıyla, bu gruplar Şekil 1'de verilen grafikle gösterilmiştir. Bu grafik incelendiğinde, sağlık alanları içerisinde makine öğrenmesi algoritmaları ile en fazla çalışmanın dolaşım ve solunum sistemleri hastalıkları alanında yapıldığı görülmektedir.

Şekil 1. Makine Öğrenmesi Algoritmaları ile Çalışılan Sağlık Alanları

Dolaşım ve solunum sistemi hastalıkları içerisinde en fazla kalp rahatsızlıkları konusunda çalışma yapılmıştır. Ardından akciğer ve göğüs hastalıkları gelmektedir (Şekil 2).

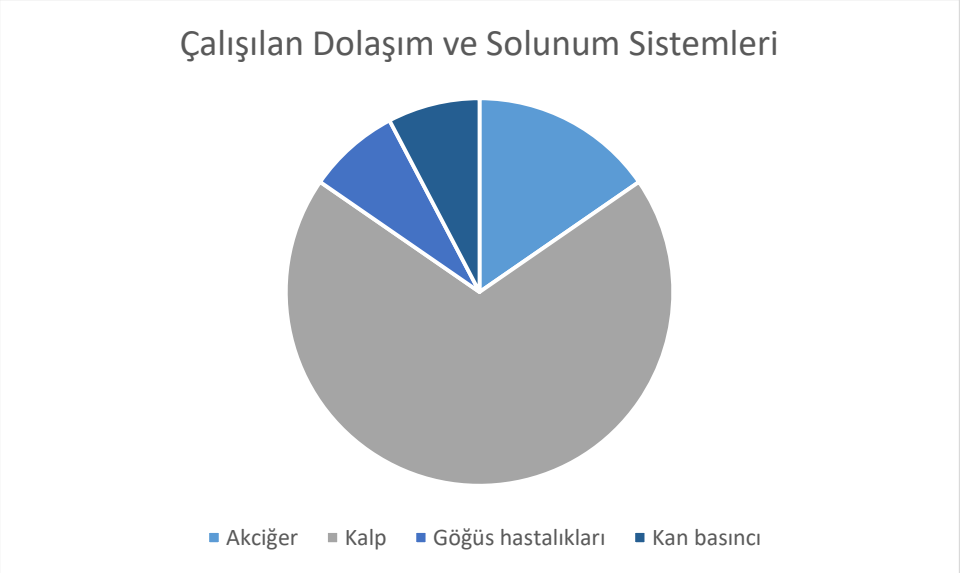

Şekil 2. Dolaşım ve Solunum Sistemleri

Solunum ve dolaşım sistemlerinden sonra gelen, en fazla çalışılan sağlık alanlarında kanserler ve nörolojik hastalıklar yer almaktadır. Kanser türlerinden en fazla hangisi üzerinde çalışma yapıldığı Şekil 3'te gösterilmiştir.

Şekil 3. Çalışılan Kanser Türleri

En fazla ele alınan kanser türleri şu şekildedir: meme kanseri, diğer kanser çalışmaları, cilt kanseri ve bağırsak kanseri. Makine öğrenmesi algoritmaları kullanılarak Türkiye'de Nörolojik hastalıklar ile ilgili olarak en fazla Parkinson hastalığı üzerinde çalışma yapılmıştır.

SONUÇLAR ve TARTIŞMA

Sağlık verilerinin karmaşıklığı karşısında geleneksel veri analiz yöntemleri yetersiz kalabilmektedir. Bu sebeple karmaşık yapıların anlaşılması, çözümlenebilmesi için makine öğrenmesi yöntemlerine başvurulur. Sağlık alanı, makine öğrenmesi yöntemlerinin sınırlı kullanıldığı ancak çok önemli kullanım potansiyeli olan alanlardan biridir. Çalışma sonucunda elde edilen bilgiler ışığında makine öğrenmesi algoritmaları kullanılarak sağlık alanında en fazla çalışma solunum ve dolaşım sistemleri hastalıkları, nörolojik hastalıklar ve kanserler konusunda yapılmıştır.

Sağlık alanında çok fazla çalışma yapılmasına rağmen Şekil 2'de görüldüğü üzere belli başlı hastalıklara/konulara daha çok yönelme olmuştur. Örneğin, diyabet, Parkinson hastalıkları ve kanser teşhisi konuları üzerinde çok fazla çalışma yapılmıştır. Kanser türleri içerisinde en fazla çalışılanı meme kanseridir. Bugün dünyada her 10 kadından ikisi meme kanserine yakalanmakta ve meme kanserine bağlı ölümler tüm kanser grupları arasında ikinci sırada olmaktadır. Meme kanseri özellikle kadın sağlığını

tehdit eden, ağrılı vücut değişkenliği yaratan önemli bir sağlık sorunudur. Görülme sıklığı ve içerdiği risk açısından konunun çok fazla çalışıldığı düşünülmektedir.

Uzun süreli tedavi gerektiren ve ölüm riski içeren hastalıklarda, riski azaltmak ve hastanın yaşam süresini uzatmak için erken tanının çok önemli bir yere sahiptir. Bu nedenle makine öğrenme algoritmalarının erken tanı/teşhis alanında kullanılması ile ilgili yapılan çalışmalar gün geçtikçe artacaktır. Bununla birlikte makine öğrenme algoritmalarının sağlık alanlarında kullanılmaya devam edilmesi ile hem doktorların iş yükleri azaltılacak hem de hastalara daha kaliteli sağlık hizmeti sağlanacaktır.

KAYNAKLAR

Açıl, T. (2019). Güncel makine öğrenmesi teknikleri ile iris görüntülerinden cinsiyet analizi, Yüksek Lisans Tezi, İskenderun Teknik Üniversitesi, Fen Bilimleri Enstitüsü, Hatay.

Adem, K. (2017). Görüntü işleme ve makine öğrenmesine dayalı diyabetik retinopati hastalığı teşhisi ve sınıflandırılması, Doktora Tezi, Gaziosmanpaşa Üniversitesi, Fen Bilimleri Enstitüsü, Tokat.

Akyol, K, Bayır, Ş, Şen, B. (2016). Detection of hard exudates in diabetic retinopathy retinal images by utilizing visual dictionary and classifier approaches. *Mugla Journal of Science and Technology, 2 (1),* 1-6.

Albayrak, A. (2018). Histopatolojik görüntülerin makine öğrenmesi yöntemleri ile analizi, Doktora Tezi, Yıldız Teknik Üniversitesi, Fen Bilimleri Enstitüsü, İstanbul.

Amasyalı, M.F. (2008). Yeni makine öğrenmesi metotları ve ilaç tasarımına uygulamaları, Doktora Tezi, Yıldız Teknik Üniversitesi, Fen Bilimleri Enstitüsü, İstanbul.

Aydın, F. (2011). Kalp ritim bozukluğu olan hastaların tedavi süreçlerini desteklemek amaçlı makine öğrenmesine dayalı bir sistemin geliştirilmesi, Yüksek Lisans Tezi, Trakya Üniversitesi, Fen Bilimleri Enstitüsü, Edirne.

Aydın, F. (2017). Parkinson hastalıkları verilerinin makine öğrenmesi yöntemleriyle araştırılması, Doktora Tezi, İstanbul Aydın Üniversitesi, Fen Bilimleri Enstitüsü, İstanbul.

Aykanat, M. (2018). Enhancing machine learning algorithms in healthcare with electronic stethoscope, Ph.D. Thesis, Ankara Yıldırım Beyazıt University, Department of Electrical and Computer Engineering, Ankara.

Badem, H. (2019). Parkinson hastalığının ses sinyalleri üzerinden makine öğrenmesi teknikleri ile tanımlanması. *Ömer Halisdemir Üniversitesi Mühendislik Bilimleri Dergisi, 8 (2),* 630-637.

Bağcı, D. (2016). Biyonik el kontrolü için EMG işaretlerininin makine öğrenmesi yöntemiyle sınıflandırılması, Yüksek Lisans Tezi, Yalova Üniversitesi, Fen Bilimleri Enstitüsü, Yalova.

Başçıl, M . (2019). EEG üzerinde ortaya çıkan beyin dalgalarının çene hareketleri ile ilişki. *Bozok Tıp Dergisi, 9 (3),* 45-49.

Bozkurt, M. R., Yurtay, N., Yilmaz, Z., & Sertkaya, C. (2014). Comparison of different methods for determining diabetes. *Turkish Journal of Electrical Engineering & Computer Sciences*, *22*(4), 1044-1055.

Bulut, F . (2017). Obezite riski altındaki çocukların örnek tabanlı sınıflandırıcı topluluklarıyla tespiti. *Gazi Üniversitesi Mühendislik-Mimarlık Fakültesi Dergisi, 32 (1).*

Bulut, F., & Bucak, İ. Ö. (2014). An urgent precaution system to detect students at risk of substance abuse through classification algorithms. *Turkish Journal of Electrical Engineering & Computer Sciences*, *22*(3), 690-707.

Burakgazi, Y. (2017). Identification of breast cancer sub-types by using machine learning techniques, M.Sc. Thesis, Dokuz Eylül University, Department of Computer Engineering, İzmir.

Candan, H, Durmuş, A, Harman, G. (2019). Genetik Algoritma Ve Sınıflandırıcı Yöntemler İle Kanser Tahmini. *Veri Bilimi, 2 (1) ,* 30-34.

Cihan, Ş. (2018). Koroner arter hastalığı riskinin makine öğrenmesi ile analiz edilmesi, Yüksek Lisans Tezi, Kırıkkale Üniversitesi, Fen Bilimleri Enstitüsü, Kırıkkale.

Cömert, Z. (2017). Kardiyotokografi işaretlerinin analizi ve makine öğrenmesi teknikleri ile sınıflandırılması, Doktora Tezi, İnönü Üniversitesi, Fen Bilimleri Enstitüsü, Malatya.

Cüvitoğlu, A. (2017). Prediction of synergistic drug combinations by using machine-learning methods, M.Sc. Thesis, Dokuz Eylül University, Department of Computer Engineering and Computer Science and Control, İzmir.

Çakmak, I. (2017). Makine öğrenmesi yöntemleriyle tümör kontrol olasılığının hesaplanması, Yüksek Lisans Tezi, Karadeniz Teknik Üniversitesi, Sağlık Bilimleri Enstitüsü, Trabzon.

Çentik, G. (2013). Makine öğrenmesi yöntemlerinin polisomnografik verilere uygulanması, Doktora Tezi, Trakya Üniversitesi, Fen Bilimleri Enstitüsü, Edirne.

Çınaroğlu, S. (2017). Sağlık harcamasının tahmininde makine öğrenmesi regresyon yöntemlerinin karşılaştırılması. *Uludağ University Journal of The Faculty of Engineering, 22 (2),* 179-200.

Demirhan, A. (2018). Performance of machine learning methods in determining the autism spectrum disorder cases. *Mugla Journal of Science and Technology, 4 (1),* 79-84.

Durak, M.N. (2017). Makine öğrenmesi sınıflandırma yöntemleri ile meme kanserinin erken teşhisi, Yüksek Lisans Tezi, Yıldız Teknik Üniversitesi, Fen Bilimleri Enstitüsü, İstanbul.

Erdursun, M.İ. (2019). Kronik böbrek hastalığının makine öğrenmesi yöntemleriyle analizi, Yüksek Lisans Tezi, Kırıkkale Üniversitesi, Fen Bilimleri Enstitüsü, Kırıkkale.

Eren, K.K. (2019). Makine öğrenmesi yöntemleri ile insan aktivite tespit sistemi tasarımı, Yüksek Lisans Tezi, Kocaeli Üniversitesi, Fen Bilimleri Enstitüsü, Kocaeli.

Ertuğrul, Ö. F., & Sezgin, N. (2018). A noninvasive time-frequency-based approach to estimate cuffless arterial blood pressure. *Turkish Journal of Electrical Engineering & Computer Sciences*, *26*(5), 2260-2274.

Ghahremanlou, N.S. (2012). Prediction of maximum oxygen uptake from maximal and non-exercise variables using machine learning methods, M.Sc. Thesis, Çukurova University, Department of Computer Engineering and Computer Science and Control, Adana.

Göker, H, Tekedere, H. (2019). Dynamic Expert System Design for the Prediction of Attention Deficit and Hyperactivity Disorder in Childhood. *Bilişim Teknolojileri Dergisi, 12 (1),* 33-41.

Görür, K. (2019). Makine öğrenmesi algoritmaları kullanılarak glossokinetik potansiyel tabanlı dil-makine arayüzü tasarımı, Doktora Tezi, Sakarya Üniversitesi, Fen Bilimleri Enstitüsü, Sakarya.

Gürel, B.Z. (2019). Vokal kord ölçümlerinden makine öğrenmesi yöntemleri kullanarak Parkinson hastalığının teşhisi, Yüksek Lisans Tezi, Tokat Gaziosmanpaşa Üniversitesi, Fen Bilimleri Enstitüsü, Tokat.

Hacıefendioğlu, Ş. (2012). Makine öğrenmesi yöntemleri ile glokom hastalığının teşhisi, Yüksek Lisans Tezi, Selçuk Üniversitesi, Fen Bilimleri Enstitüsü, Konya.

Işık, H. (2017). Motor imagery based mobile brain computer interface design using machine learning techniques, M.Sc. Thesis, İstanbul Technical University, Department of Mechatronics Engineering, İstanbul.

Işık, Z. (2018). Kanser alt-türlerinin sınıflandırılması için RNA-sekanslama ve RPPA verilerinin karşılaştırılması. *Dokuz Eylül Üniversitesi Mühendislik Fakültesi Fen ve Mühendislik Dergisi, 20 (59)* , 606-621.

İsenkul, M.E. (2016). Korteks tabanlı imge gösterim kapasitelerinin uzamsal dönüşümler ve makine öğrenmesi yöntemleriyle ölçülmesi, Doktora Tezi, İstanbul Üniversitesi, Fen Bilimleri Enstitüsü, İstanbul.

İşeri, İ. (2014). Mamogram görüntülerinden makine öğrenmesi yöntemleri ile meme kanseri teşhisi, Doktora Tezi, Sakarya Üniversitesi, Fen Bilimleri Enstitüsü, Sakarya.

Kartal, E. (2015). Sınıflandırmaya dayalı makine öğrenmesi teknikleri ve kardiyolojik risk değerlendirmesine ilişkin bir uygulama, Doktora Tezi, İstanbul Üniversitesi, Fen Bilimleri Enstitüsü, İstanbul.

Kaya, E. (2018). Machine learning techniques for surface electromyography based hand gesture recognition, M.Sc. Thesis, İstanbul Technical University, Department of Control and Automation Engineering, İstanbul.

Kaya, Y, Tekin, R. (2012). Epileptik Nöbetlerin Tespiti için Aşırı Öğrenme Makinesi Tabanlı Uzman Bir Sistem. *Bilişim Teknolojileri Dergisi, 5 (2),* 33-40.

Kaya, Y. (2013). A new intelligent classifier for breast cancer diagnosis based on a rough set and extreme learning machine: RS+ ELM. *Turkish Journal of Electrical Engineering & Computer Sciences*, *21*(Sup. 1), 2079-2091.

Kaya, Y. (2017). Makine öğrenmesi teknikleri ile aritmi tespiti ve yeni öznitelikler ile başarımın artırılması, Doktora Tezi, Karadeniz Teknik Üniversitesi, Fen Bilimleri Enstitüsü, Trabzon.

Kılıçarslan, S, Adem, K, Cömert, O. (2019). Parçacık Sürü Optimizasyonu Kullanılarak Boyutu Azaltılmış Mikrodizi Verileri Üzerinde Makine Öğrenmesi Yöntemleri ile Prostat Kanseri Teşhisi. *Düzce Üniversitesi Bilim ve Teknoloji Dergisi, 7 (1),* 769-777.

Kocamaz, A.F., 2012. Makine öğrenmesi tabanlı bir uzman sistem tasarımı, Doktora Tezi, Trakya Üniversitesi, Fen Bilimleri Enstitüsü, Edirne.

Kodal Sevindir, H, Çetinkaya, S, Yazıcı, C. (2018). Makine öğrenmesi algoritmaları ve dalgacık dönüşümü ile EKG sinyalinden özellik çıkarımı. *Balıkesir Üniversitesi Fen Bilimleri Enstitüsü Dergisi, 20 (1),* 94-109.

Köse, İ. (2015). İnteraktif makine öğrenmesi kullanılarak, aktör-metâ ilişkisinin analizi ile sağlık geri ödeme sistemlerinde proaktif suistimal tespiti modeli, Doktora Tezi, Gebze Teknik Üniversitesi, Fen Bilimleri Enstitüsü, Gebze.

Kurt, İ., 2018. Makine öğrenmesi yöntemleri kullanılarak sesin müzikal öznitelikleri ile Parkinson hastalığının tespiti, Yüksek Lisans Tezi, Trakya Üniversitesi, Fen Bilimleri Enstitüsü, Edirne.

Oğuztürk, G. (2018). Diyabet hastalığının makine öğrenmesi algoritmaları ile en iyi doğru tahmininin elde edilmesi, Yüksek Lisans Tezi, Kırıkkale Üniversitesi, Fen Bilimleri Enstitüsü, Kırıkkale.

Oktay, A.B. (2011). Önsel bilgi kullanılarak tıbbi görüntülerde makine öğrenmesi tabanlı kontur bulma ve nesne konumlandırma, Doktora Tezi, Gebze Teknik Üniversitesi, Gebze Yüksek Teknoloji Enstitüsü, Kocaeli.

Örenç, S. (2019). Kronik obstrüktif akciğer hastalığı teşhisi için makine öğrenmesi temelli yeni bir yöntem geliştirilmesi, Yüksek Lisans Tezi, Sakarya Üniversitesi, Fen Bilimleri Enstitüsü, Sakarya.

Özkaya, D. (2018). Comparison of machine learning algorithms for blood glucose prediction on aida simulator, M.Sc. Thesis, Boğaziçi University, Department of Biomedical Engineering, İstanbul.

Pashei, E. (2017). Meta-analysis of microRNA and gene selection using machine learning, Ph.D. Thesis, Yıldız Technical University, Department of Computer Engineering, İstanbul.

Pashei, E., 2017. Splice site prediction using machine learning, Ph.D. Thesis, Yıldız Technical University, Department of Computer Engineering, İstanbul.

Saçlı, B., 2018. Machine learning aided kidney stone classification with electromagnetic properties, M.Sc. Thesis, İstanbul Technical University, Department of Electronics and Communication Engineering, İstanbul.

Sakarya, M. (2019). Seçilen siğil tedavi yönteminin farklı makine öğrenmesi algoritmaları ile başarımının tahmin edilmesi, Yüksek Lisans Tezi, Zonguldak Bülent Ecevit Üniversitesi, Fen Bilimleri Enstitüsü, Zonguldak.

Sarikoc, F., Kalinli, A., Akgün, H., & Öztürk, F. (2013). An automated prognosis system for estrogen hormone status assessment in breast cancer tissue samples. *Turkish Journal of Electrical Engineering & Computer Sciences*, *21*(4), 1199-1221.

Sevli, O (2019). Göğüs Kanseri Teşhisinde Farklı Makine Öğrenmesi Tekniklerinin Performans Karşılaştırması, Avrupa Bilim ve Teknoloji Dergisi , (16) , 176-185.

Şeker, M., 2017. İyi–kötü kokular ile ilişkili EMOTIV-EPOC tabanlı EEG kayıtlarının makine öğrenmesi yöntemleri ile sınıflandırılması, Yüksek Lisans Tezi, Dicle Üniversitesi, Fen Bilimleri Enstitüsü, Diyarbakır.

Takci, H. (2016). Centroid sınıflayıcılar yardımıyla meme kanseri teşhisi. *Gazi Üniversitesi Mühendislik-Mimarlık Fakültesi Dergisi, 31 (2).*

Takci, H. (2018). Improvement of heart attack prediction by the feature selection methods. *Turkish Journal of Electrical Engineering & Computer Sciences*, *26*(1), 1-10.

Taşdemir, S.B.Y. (2018). Early prognosis of breast cancer using image processing and machine learning, M.Sc. Thesis, Abdullah Gül University, Department of Electrical and Computer Engineering, Kayseri.

Toprak, M.Ş. (2004). Tıp alanında makine öğrenmesi uygulaması, Yüksek Lisans Tezi, Selçuk Üniversitesi, Fen Bilimleri Enstitüsü, Konya.

Toraman, S., Girgin, M., Üstündağ, B., & Türkoğlu, İ. (2019). Classification of the likelihood of colon cancer with machine learning techniques using FTIR signals obtained from plasma. *Turkish Journal of Electrical Engineering & Computer Sciences*, *27*(3), 1765-1779.

Turgut, S. (2017). Makine öğrenmesi yöntemleri kullanarak kanser teşhisi, Yüksek Lisans Tezi, İstanbul Üniversitesi, Fen Bilimleri Enstitüsü, İstanbul.

Tümer, E.D., 2018. Nesnelerin interneti ortamındaki veriler kullanılarak makine öğrenmesi algoritmaları ile tahminleme ve gerçek zamanlı veriler üzerinde karmaşık olay işleme, Yüksek Lisans Tezi, Ege Üniversitesi, Fen Bilimleri Enstitüsü, İzmir.

Uçar, M.K. (2017). Obstrüktif uyku apne teşhisi için makine öğrenmesi tabanlı yeni bir yöntem geliştirilmesi, Doktora Tezi, Sakarya Üniversitesi, Fen Bilimleri Enstitüsü, Sakarya.

Ünal, Y. (2015). Makine öğrenmesi yöntemleriyle bel bölgesi rahatsızlıklarının tanısı, Doktora Tezi, Selçuk Üniversitesi, Fen Bilimleri Enstitüsü, Konya.

Yahyaoui, A. (2017). Göğüs hastalıklarının teşhis edilmesinde makine öğrenmesi algoritmalarının kullanılması, Doktora Tezi, Sakarya Üniversitesi, Fen Bilimleri Enstitüsü, Sakarya.

Yengi, Y, İlhan Omurca, S. (2016). Lojistik Regresyonun Özellik Azaltma Teknikleri ile Gen Dizilimlerinin Sınıflandırılmasındaki Başarısı. *Türkiye Bilişim Vakfı Bilgisayar Bilimleri ve Mühendisliği Dergisi, 8 (1),* 1-12.

Yıldız, O. (2019). Derin öğrenme yöntemleriyle dermoskopi görüntülerinden melanom tespiti: Kapsamlı bir çalışma. *Gazi Üniversitesi Mühendislik-Mimarlık Fakültesi Dergisi, 34 (4),* 2241-2260.

Yılmaz, E. (2016). Kardiotokogram verisinden fetal iyilik halinin belirlenmesi için bir karar destek sistemi. *Uludağ University Journal of The Faculty of Engineering, 21 (2)* , 331-340.

A LITERATURE REVIEW ON THESIS STUDIES REGARDING MACHINE LEARNING IN TURKEY

Tuba ADAR

Atatürk University, Department of Industrial Engineering, Erzurum, Turkey

tuba.adar@atauni.edu.tr

Elif KILIÇ DELİCE

Atatürk University, Department of Industrial Engineering, Erzurum, Turkey

elif.kdelice@atauni.edu.tr

ABSTRACT: Machine learning is an application of artificial intelligence (AI) that provides the ability to learn for systems automatically and from experience. It focuses on the development of computer programs that can access data and use what they have learned for themselves. Since machine learning, which includes computer algorithms modelling the problem according to the data of that problem, is one of the fields that have been studied intensively recently, there are many approaches and algorithms in this regard. Some of these approaches are capable of prediction and estimation, and some of them are capable of classification. The main objective is to provide machines with the ability to process collected data using computerized intelligence tools to collect data with senses similar to human senses and then to make predictions and make decisions at the same level as humans. It focused on many subjects such as natural language processing, cognitive computation, information presentation, image processing, pattern recognition, and has applications in many fields such as healthcare, finance, marketing, quality control, computer networks. In this study, the thesis studies conducted on machine learning issues in Turkey were examined. The aim of the study is to examine in which fields thesis studies are conducted and which machine learning algorithms are used in general. For this purpose, 146 thesis studies are discussed. It was consequently found that the most thesis was made in the field of health and K-nearest neighbors, Support vector machines, Decision trees, Naive Bayes algorithms were used frequently.

Key words: machine learning, field of application, algorithms, thesis studies.

TÜRKİYE'DE MAKİNE ÖĞRENMESİ İLE İLGİLİ YAPILAN TEZ ÇALIŞMALARINA YÖNELİK BİR LİTERATÜR TARAMASI

ÖZET: Makine öğrenmesi, sistemlere otomatik olarak ve deneyimlerden öğrenme yeteneği sağlayan yapay zekânın (YZ) bir uygulamasıdır. Verilere erişebilen ve kendileri için öğrendiklerini kullanabilen bilgisayar programlarının geliştirilmesine odaklanır. Ele alınan problemi, o probleme ait verilere göre modelleyen bilgisayar algoritmalarını içeren makine öğrenmesi, son zamanlarda yoğun çalışılan alanlardan biri olduğu için, konu ile ilgili önerilmiş birçok yaklaşım ve algoritma mevcuttur. Bu yaklaşımların bir kısmı tahmin ve kestirim bir kısmı da sınıflandırma yapabilme yeteneğine sahiptir. Temel amaç, makinelere insani duyulara benzer duyularla veri toplama ve daha sonra tahminleri yürütmek ve insanlarla aynı seviyede kararlar almak için bilgisayarlı zekâ araçlarını kullanarak toplanan verileri işleme becerisi sunmaktır. Doğal dil işleme, bilişsel hesaplama, bilgi sunumu, görüntü işleme, örüntü tanıma gibi birçok konuya odaklanmıştır ve sağlık hizmetleri, finans sektörü, pazarlama, kalite kontrol, bilgisayar ağları gibi birçok alanda uygulaması mevcuttur. Bu çalışmada Türkiye'de makine öğrenmesi konusu ile alakalı yapılan tez çalışmaları incelenmiştir. Çalışmanın amacı, tez çalışmalarının daha çok hangi alanda olduğunu, genel olarak hangi makine öğrenmesi algoritmalarının kullanıldığını incelemektir. Bu amaç doğrultusunda 146 tez çalışması ele alınmıştır. Sonuç olarak; sağlık alanında en fazla tez yapıldığı ve K-en yakın komşu, Destek vektör makineleri, Karar ağaçları, Naive Bayes algoritmalarının sıklıkla kullanıldığı tespit edilmiştir.

Anahtar sözcükler: makine öğrenmesi, uygulama alanları, algoritmalar, tez çalışmaları.

GİRİŞ

Yapay zekânın bir alt dalı olan makine öğrenmesi, çeşitli algoritmalar ve yöntemler ile veride bazı kalıpları arar ve bu kalıplara karşılık gelen etiketlere bakarak önce öğrenir, daha sonra deneyimlerinden yararlanarak çıkarım yapabilen sistemler geliştirmeye imkân sağlar. Bu imkânı, çeşitli matematiksel ve istatistiksel yöntemlerin kullanıldığı birçok algoritma ile sağlamaktadır. Bu algoritmalar, veri setindeki örnek olayları inceleyerek, bu olayların meydana geliş biçimlerini öğrendikten sonra problem üzerinde genelleme yapma yeteneği kazanır. Büyük veri yığınları içerisinde fark edilmesi zor olan yapıları bulup ortaya çıkarırken, algoritmalar sayesinde olayların meydana gelmesini sağlayan etkenleri ve etkenlerin etki şekillerini öğrenip herhangi bir yeni olay meydana gelmeden önce bu olayı tahmin edebilirler. Bu gibi durumlara şunlar örnek olarak verilebilir: Bir yıl sonraki enerji ihtiyacının ne kadar olacağı, bir uçağın ne kadar gecikeceği, gün içinde yağmur yağışı olup olmayacağı vb. (Shalev-Shwartz and Ben-David, 2014; Keskin 2018).

Yapay zekâ, insanlar gibi hedeflere ulaşma becerisine sahip olan akıllı makineler üretme bilimi ve mühendisliğidir. Makine öğrenmesi, insanların nasıl öğrendiğini de taklit eden bir yapay öğrenme biçimidir. Sinir ağları alanında, derinlemesine ağların üçten fazla katmana, yani birden fazla gizli katmana sahip olduğu alan ise derin

öğrenme alanıdır. Şekil 1'de makine öğrenmesinin yapay zekâ-derin öğrenme ile ilişkisi ve makine öğrenmesinde yaygın olarak kullanılan öğrenme türleri gösterilmiştir.

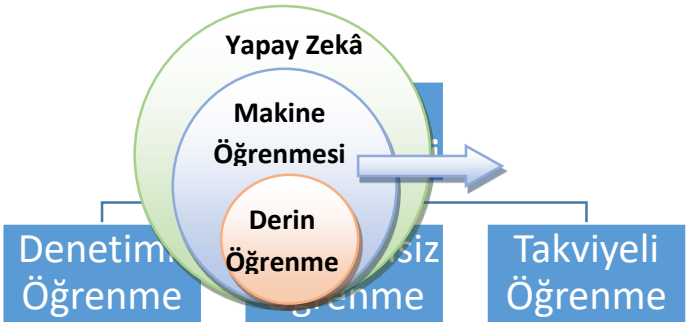

Şekil 1. Makine Öğrenmesi ve Öğrenme Türleri

Denetimli öğrenme: Girdi verisi veya eğitim verisi önceden belirlenmiş bir etikete sahiptir; Doğru / Yanlış, Olumlu / Olumsuz vb. Bir fonksiyon veya sınıflandırıcı, test verilerinin etiketini tahmin etmek için kurulur ve eğitilir. Sınıflandırıcı uygun bir doğruluk seviyesi elde etmek için uygun şekilde ayarlanmış (parametre değerleri ayarlanmıştır). Regresyon ve sınıflandırma, denetimli öğrenme türleridir.

Denetimsiz öğrenme: Girdi verileri veya eğitim verileri etiketlenmemiştir. Bir sınıflandırıcı, eğitim veri kümelerindeki mevcut modeller veya kümeler çıkartılarak tasarlanır. Kümeleme ve boyut indirgeme, denetimsiz öğrenme türleridir.

Takviyeli öğrenme: Algoritma, duruma göre eylemi haritalandırmak için eğitilir, böylece ödül veya geri bildirim sinyali en üst düzeye çıkarılır. Sınıflandırıcı doğrudan eylemi seçecek şekilde programlanmamıştır, ancak bunun yerine en çok ödüllendirici eylemleri deneme yanılma yoluyla bulmak için eğitilmiştir (Das ve Behera, 2017).

Bu öğrenme türleri içerisinde birçok algoritma mevcuttur. Bu algoritmaların, problem türüne göre etkinlik derecesi değişmektedir. İncelenen çalışmalarda en çok bahsi geçen algoritmalar şu şekildedir: K-En Yakın Komşu Algoritması (KNN), Karar Ağacı Algoritmaları (Sınıflandırma ve karar ağacı (CART)), Bayes Algoritmaları (Naive Bayes, Gaussian Naive Bayes), Destek Vektör Makinası (SVM), Kümeleme Algoritmaları (K-Means, K-Medians, vb.)

Bu çalışmanın amacı, makine öğrenmesi algoritmaları kullanılarak Türkiye'de yapılan tez çalışmalarının incelenmesi ve bu algoritmaların uygulama alanlarının sınıflandırılmasıdır. Bu sayede makine öğrenmesi algoritmalarının hangi alanda daha çok uygulandığı tespit edilmiş olacaktır.

Çalışmanın geri kalanı şu şekilde oluşturulmuştur: literatür taraması bölümünde Yöktez'de mevcut olan tez çalışmaları incelenmiş ve çalışmalar yapıldıkları alanlara göre gruplandırılmıştır. Sonuç ve tartışma bölümünde ise literatür incelemesi sonucunda elde edilen bilgiler görselleştirilmiş ve sonuçlar tartışılmıştır.

LİTERATÜR TARAMASI

Yöktez'de, Türkiye'de makine öğrenmesi ile alakalı yapılan toplamda 146 tane tez çalışması bulunmaktadır. Bu çalışmalar, yapıldıkları alanlara göre ayrılmıştır:

Ekonomi Alanında Yapılan Çalışmalar

Çizer (2018), çalışmasında kredi risk analizi konusunu ele almış ve kredi talebinde bulunan müşterileri kredi taleplerinin değerlendirilmesinde geri ödeme durumunu etkileyen faktörlerin objektif kararlar verilerek belirlenmesini hedeflemiştir. Bu doğrultuda, makine öğrenmesi tekniklerinden karar ağacı analizi, destek vektör makineleri analizi, bulanık mantık ve genetik algoritma analizi ve yapay sinir ağları analizi uygulamıştır. Yaptığı analizlerin sonuçları içerisinde test verilerini %76 doğruluk oranı ile en yüksek oranda sınıflandıran yöntemin yapay sinir ağları yöntemi olduğunu gözlemlemiştir.

Namlı (2018), çalışmasında filmlerin vizyona girmeden önce gişe hasılatının tahmin edilmesi için makine öğrenmesi esaslı sınıflandırma metodolojileri kullanılmıştır. Sınıflandırma modellerinin oluşturulmasında; makine öğrenmesi esaslı yöntemlerden Yapay Sinir Ağları ve Destek Vektör Makinaları, bileşik makine öğrenmesi esaslı yöntemlerden ise Torbalama algoritması gişe hasılatının tahmin edilmesi probleminin çözümünde uygulanmıştır. Çalışmada, hem bireysel sınıflandırma algoritmaları ile bileşik makine öğrenmesi algoritmasının sınıflandırma probleminin çözümündeki başarıları karşılaştırılmış hem de algoritmaların parametre değerlerinin eniyilenmesinin modellerin performansına etkisi araştırılmıştır.

Kalaycı (2018), makine öğrenmesi yöntemleri ile kredi risk analizi konusunu ele almıştır ve Türkiye'deki KOBİ müşterilerinin verilerini analiz ederek ileri bir tarihte durumun problemli kredi olup olmayacağını tahmin etmiştir. Makine öğrenmesi tekniklerinden, lojistik regresyon (LR), karar ağaçları (KA), destek vektör makineleri (DVM), sinir ağları (SA), rastgele orman algoritması (ROA) ve son olarak da meyilli hızlandırma (MH) yöntemleri kullanılmıştır. Gerçekleştirilen deneylerde en iyi başarımı %83,05 başarı ile MH algoritması vermiştir.

Uzel (2018) çalışmasında, Türk Lirası'nın ABD Doları karşısındaki döviz kurunun değişim yönünün tahmin edilmesi için çevrimiçi makine öğrenmesi kullanılarak modeller oluşturulmuş ve model başarımları FOREX piyasalarında alım-satım benzetimi ile gösterilmiştir. Modellerin eğitim sürecinde; döviz kuru zaman serisi sembolik temsile dönüştürülmekte, içinde örüntüler bulunarak örüntü bazında olasılık dağılımı çıkarılmakta ve bu olasılıklar kullanılarak kurun değişim yönü tahmin edilmektedir.

Aktepe 2018, çalışmasında farklı makine öğrenmesi tekniklerinden yararlanarak kripto para piyasalarında fiyat tahminlemesi yapmış ve kar getirebilecek algoritmalara ulaşmayı amaçlamıştır. Çalışmada, kurların Açılış-Yüksek-Düşük-Kapanış fiyat verisinden yararlanarak doğrusal modeller ve karar ağacı bazlı modeller kurulmuştur.

Kanmaz (2018), Borsa İstanbul'da bulunan farklı sektörlerdeki şirketlere ait fiyat verileri ile bu şirketlerle ilintili olan finansal haberlerde kullanılan ifadeler arasındaki ilişkiyi incelemiştir. Bu çalışmada, duygu analizi, doğal dil işleme ve finansal haberlerin bireysel hisse senedi performansları üzerindeki etkisi basit ve yeni bir yöntemle incelenmiştir. Duygu analizi, pay piyasasında halka açık bir şekilde işlem gören şirketlerin hisse senedi fiyatlarının günlük performansına göre, bu firmalara ait finansal piyasalarda yer alan haberlerin pozitif veya negatif olacak şekilde otomatik etiketlenmesi suretiyle makine öğrenmesi yöntemi kullanılarak yapılmıştır.

Çelikel (2018), örnek olay incelemesi olarak sosyal medya kaynaklarından Twitter platformu ile borsa verisi olarak İstanbul Borsası ve Bloomberg'deki Pegasus Havayolları A.Ş. ve Türk Hava Yolları A.O'ya ait verilerinden faydalanmıştır. Twitter üzerinden elde edilen tweetlerin borsa verileri ile korelasyonu incelenmiştir. Twitter'dan günlük ve aylık bazda Phyton programlama dili ve Tweett Scraper kullanılarak belirlenen tarih aralığında dataların çekilmesi sağlanmıştır. Ön işleme aşamasında bu dataların temizlenmesi ve manuel olarak oluşturulan pozitif ve negatif sözlüklerden faydalanılarak tweetlerin pozitif ve negatif olarak etiketlenerek sözlük tabanlı yaklaşımla duygu analizi sağlanmıştır. İkinci aşamada ise Borsa İstanbul ve Bloomberg kaynaklı ham verilerin etkili, etkisiz ve gürültülü verilerin temizlenmesi sağlanmıştır. R Studio programı aracılığıyla test ve eğitim aşamalarında regresyon algoritmaları kullanılarak analiz edilmiştir.

Öz (2019), makine öğrenmesi uygulamaları ile online ihale fiyatlarını etkileyen faktörler üzerine deneysel çalışmalar yapmıştır. Çalışmada, akıllı telefon piyasasında yapılan online ihalelerde son fiyat belirleyicileri analitik olarak incelenmektedir. Bu kapsamda 444 adet ihale ve 676 adet ŞSA satış verileri güncel makine öğrenme algoritmaları ile analiz edilmiştir.

Tozlu (2019) çalışmasında, ticari kredi başvurularında şirket bilançoları üzerinde gerçekleştirilen aktarma-arındırma işlemlerinin makine öğrenmesi yöntemleri kullanılarak basitleştirilmesini ele almıştır. Deneylerde LGBM, XGBoost, Catboost, karar ağacı, rastgele orman ve yığılmış genelleme yöntemleri kullanılmıştır.

Bulut (2019), tarımsal kredi limitlerinin tespit edilmesinde kullanılan değişkenler ile kredi kullanan şahıslara ait bazı demografik özelliklerin, kredilerin vadesinde tahsil edilmesine ne ölçüde etkide bulunduğunu tespit etmeyi amaçlamıştır. Amaç doğrultusunda bazı makine öğrenmesi algoritmaları kullanılarak, kredi tahsisinde kullanılan değişkenleri içeren bir model geliştirilmesi ve bu modelin kredilerin vadesinde tahsil edilip edilemeyeceğini en iyi şekilde öngörmesi hedeflenmiştir. Doğrusal Ayırma Analizi ve Lojistik Regresyon algoritmaları tarafından geliştirilen modellerin, eşik değerin altında doğru sınıflandırma yapabildiği görülmüştür. K en yakın komşu, Naive Bayes ve Yapay Sinir Ağları algoritmaları tarafından ortaya konulan modellerin eşik değerin üzerinde ve eşit düzeyde doğru sınıflandırma yapabildiği gözlenmiştir. En yüksek düzeyde doğru sınıflandırma yapabilen tahmin modeli, Karar Ağacı algoritmasınca geliştirilmiştir.

Demirel (2019), makine öğrenmesi ve derin öğrenme ışığında hisse senetlerinin açılış ve kapanış fiyatlarının tahmin edilmesini amaçlamıştır. Bu kapsamda tahminleme modeli oluşturabilmek adına Çok Katmanlı Algılayıcılar (ÇKA) ve Destek Vektör

Makineleri (DVM) gibi klasik makine öğrenimi yöntemleri ve Uzun Kısa Dönemli Hafıza (UKVH) yöntemi gibi derin öğrenme algoritmaları kullanılmıştır. Çalışmanın sonucunda ÇKA ve UKVH ağlarının DVM'lerine göre daha tutarlı tahminler yaptığı tespit edilmiştir.

Enerji Alanında Yapılan Çalışmalar

İşyapar (2013), çalışmasında abone gruplarını temsil eden yük profillerinin sınıflandırılması ile özel tarife tasarımı, yük tahmini ve kaçak elektrik kullanımının tespiti gibi uygulamaların yapılabileceği ve bu alanda karşılaşılan problemlere çözüm üretebileceğini vurgulamıştır. Bu amaçla, Türkiye'de faaliyet gösteren bir enerji dağıtım şirketinin abonelerine ait verilerinin veri madenciliği ve makine öğrenmesi teknikleri kullanılarak sınıflandırılmasını ele almıştır.

Alamin (2016), elektrik tüketimini hızlı ve güvenirliği yüksek şekilde tahmin etmek amacıyla, Bellek üzerinde çalışan veri tabanları ile makine öğrenmesi konusunu ele almıştır. Python ve Aerospike bellek veritabanında makine öğrenmesi teknikleri ile Londra Hanehalkı SmartMeter Enerji Tüketimi verileri kullanılarak elektrik tüketimi tahmin edilmiştir. Ayrıca çalışmada, Python kullanarak makine öğrenmesi için grafiksel kullanıcı arayüzü önerilmiştir.

Keçeli (2016), çalışmasında sosyal olayların Türkiye günlük enerji tüketimine etkilerini araştırmıştır. Çalışmada sosyal olayların enerji tüketimine etkisini incelemek için sosyal olayların yer verildiği kaynaklar araştırılmış ve gazete haberlerinde sıkça sosyal olaylara yer verildiği görülmüştür. Bu olayların haber metinlerden öğrenilebileceği kabul edilerek çalışmada sosyal olay kavramı, günlük gazete haberlerine indirgenerek Türkiye'de çok satılan gazetelerin birinin günlük haberlerinden yararlanılmıştır. Bu çalışmada üç-seviyeli bir makine öğrenme altyapısı kullanılmıştır; haber kategorileri, haberlerin enerji tüketim etkileri (haber puanları) ve günlük enerji tüketim etkileri çalışmada modellenmiş iç içe çalışan üç ayrı problemdir. Bu problemlerin her biri için çeşitli denetimli, tek etiketli makine öğrenme modelleri önerilmiş ve birçok makine öğrenme algoritması ile test edilmiştir.

Aksoy (2018), çalışmasında ilgili verileri kullanarak, derin öğrenme yöntemleri ve makine öğrenme yaklaşımları yardımıyla kısa vadeli rüzgâr gücü üretim tahmini yapmıştır. Bursa'nın Harmanlık ilçesindeki rüzgâr gücü üretim tesisindeki 8 türbin ele alınmıştır. Çalışmada "Çoklu Doğrusal Regresyon", "Destek Vektör Regresyon", "K-En Yakın Komşu " ve "Karar Ağacı Regresyonu" gibi farklı regresyon yöntemleri ile güvenilir tahmin algoritmaları oluşturulmuştur. Derin öğrenme yöntemi ise Python programında optimum konfigürasyonu kurmak ve rüzgar güç üretimini tahminlemek için kullanılmıştır.

İnşaat Alanında Yapılan Çalışmalar

Mbarak (2017), kritik zemin parametrelerinin belirlenmesinde, drenajsız kayma mukavemeti, elastisite modülü ve limit basınç paramatrelerini tahmin edebilmek için,

"Doğrusal Regresyon", "Random Forest" ve "Gradient Boosting" gibi makine öğrenimi algoritmalarını kullanan regresyon modellerinin geliştirilmesini amaçlamıştır. Çalışma sonunda, en iyi performansı gösteren modeller literatürdeki korelasyon denklemleri ile karşılaştırılmıştır.

Yarmatov (2017), mevcut karayolu üstyapılarının bakımı, onarımı ve yenilenmesi gibi çalışmaların önem kazanmaya başladığını ifade etmiştir. Çalışmada, karayolların üstyapısındaki bozulma derecelerine göre yol yüzey durumunun tahmin edilmesi için yol yüzey durumunu gösteren indeks modellenmiştir. Bu metodoloji, farklı makine öğrenmesi algoritmalarını birleştiren bir hibrid tekniğin uygulanmasını içermektedir.

Eğitim Alanında Yapılan Çalışmalar

Ünsal (2011) çalışmasında, mesleki teknik eğitim sürecinde başarılı ve başarısız olmuş bireylere ait toplanan verilere bir makine öğrenmesi tekniği olan Naive Bayes algoritması uygulanarak, sistemin geçmişte yapılan başarılı ve başarısız alan seçimlerini öğrenerek bu seçimler hakkında tecrübe kazanmasını sağlayan bir yazılım geliştirilmiştir. Geliştirilen yazılım ile mesleki alan seçim sürecinde bulunan bireyden alınan verilere göre birey için en uygun mesleki alanın sistem tarafından önerilmesi amaçlanmıştır.

Yıldız (2014), uzaktan eğitimdeki öğrencilerin yılsonu akademik performanslarının önceden tahmin edilmesi ve bu tahmin sonucunda elde edilecek bilginin kullanılmasıyla gerekli önlemlerin alınmasının çok önemli olduğunu ifade etmiştir. Bu amaçla çalışmasında, uzaktan eğitimdeki öğrencilerin ilk 6 haftalık öğretim yönetim sistemi verilerini kullanarak, yılsonu akademik performanslarını tahmin etmeye yönelik yeni bir matematiksel model geliştirmiştir. Klasik bulanık ve uzman görüşüne dayanılarak oluşturulan bulanık modeller kurulmuş, sonrasında genetik algoritma kullanılarak bulanık modele ait üyelik fonksiyon aralıkları optimize edilmiştir. Daha sonrasında kümeleme yöntemleri kullanılarak bulanık mantık ile birlikte melez bir model oluşturulmuştur

Özkan (2015) çalışmasında, makine öğrenmesinin sınıflandırma yöntemlerinden destek vektör makineleri ve k-en yakın komşu algoritması incelenmiştir. Bu yöntemler kullanılarak vakıf üniversitelerinin izleyen yıl ya da yıllarda kontenjanlarını doldurup doldurmayacağının tahmin başarısı araştırılmıştır.

Demirhan (2015) çalışmasında, makine öğrenmesi algoritmaları kullanılarak eğitim alanında bir veri kümesi üzerinde doygunluk ve karmaşıklık analizi gerçekleştirilmiştir. Weka'nın sahip olduğu LWL, J48, JRIP, Part, LMT, Baggıng, Random Forest, IBK, MultiLayer Perceptron, Voted Perceptron, SMO, Naïve Bayes sınıflandırma algoritmaları veri kümeleri üzerinde çalıştırılmıştır. Karmaşıklık analizinde verinin lineer olduğu durumlarda Voted perceptron algoritması en iyi sonuçları vermiştir. Sınıflandırma gücü yüksek IBK algoritması ve destek karar makineleri (SVM) ile yapılan deneylerde eğitim verisi ile aşırı uyum (overfitting) durumu ortaya çıkmıştır.

Karabıyık (2018) çalışmasında, akademik yayınlar için makine öğrenmesi tabanlı arama motoru tasarlanması ve uygulanması konusunu ele almıştır. Arama motorunun

sadece akademik yayınları bulması için kısıtlayıcı bir ağ örümceği tasarlanmıştır. Yapılan uygulamada arama sonuçlarının en doğru şekilde bulunabilmesi için metin sınıflandırma işlemi gerçekleştirilmiştir. Bu alanda en çok kullanılan sınıflandırıcılardan olan Sade Bayes ve Destek Vektör Makineleri sınıflandırıcıları uygulanarak elde edilen sonuçlar karşılaştırılmıştır. Aynı test verisi uygulandığında Sade Bayes sınıflandırıcıda %80, Destek Vektör Makineleri sınıflandırıcısında ise %70 başarı oranı elde edilmiştir.

Çiftçi (2018), Gazi Üniversitesi öğrencilerinin eğitmenleri hakkındaki değerlendirmelerini içeren bir veri seti üzerinde çalışmış, çeşitli öznitelik indirgeme algoritmaları ve farklı makine öğrenme algoritmalarıyla eğitmenlerin performanslarını tahmin etmiştir. Öznitelik indirgeme algoritmaları arasında en iyi sonucu Genetik Algoritma vermiş ve bu sayede daha az öznitelik kullanarak Tahmin Doğruluğu Performansı (TDP) arttırılmıştır. Kullanılan sınıflandırma algoritmaları arasında ise en doğru tahmin oranına Derin Öğrenme algoritması ulaşmıştır.

Çevre Alanında Yapılan Çalışmalar

Garip (2017), ülkelerin CO2 emisyonlarının takip edilmesi ve gelecek yılların CO2 emisyonlarının planlanmasının çevre için önem arz ettiğini belirtmiştir. Çalışmasında, OECD ülkelerindeki CO2 emisyonları makine öğrenmesi yöntemleri ile tahmin edilmiştir. Literatürde farklı alanlar için tahminlerde başarılı sonuçlar verdiği bilinen makine öğrenme metotlarından M5P, çok katmanlı algılayıcı ve destek vektör makinesi yöntemleri kullanılarak CO2 emisyonu tahmin edilmiştir. 34 adet Ekonomik İşbirliği ve Kalkınma Örgütü (OECD) ülkelerinden yüksek CO2 salınımına sahip ülkelerden A.B.D, Japonya, Kanada, Avustralya, Güney Kore, Almanya, İtalya, Fransa, Türkiye ve Meksika için tahminler gerçekleştirilmiştir. Bu metotların sonuçları farklı metriklere göre karşılaştırılmış ve performans değerlerine bakıldığında destek vektör makinesinin CO_2 tahmininde oldukça başarılı sonuçlar ürettiği görülmüştür.

Bilgili (2018), denizcilik sektöründe kullanılan gemi sevkini sağlayan yakıtların yanma sürecinde oluşturduğu gaz emisyonlarının, insan sağlığına ve çevreye çok ciddi zararları olduğunu vurgulamıştır. Çalışmasında, gemi emisyonlarının tahmini, azaltılması ve kontrol altına alınması amacıyla, öncelikle dokuz kuru yük gemisinin günlük raporlarından elde edilen verilerle toplam emisyon miktarları hesaplanmış, ardından bu veriler regresyon analizine sokulmuştur. Regresyon analizinin güvenilirliği yeterli bulunmadığından ikinci kısımda gemilerin günlük raporlarından alınan veriler kullanılarak yapay sinir ağlarında modelleme yapılmış ve en iyi sonucu veren yapay sinir ağı yöntemi tespit edilmiştir. Üçüncü kısımda ise elde edilen en iyi yapay sinir ağı yöntemi Atlantik ve Pasifik Okyanusları'nda kuzey ve güney olmak üzere iki farklı rotaya ocak ve haziran ayları için uygulanmış ve böylece her iki okyanus ve zaman dilimi için de farklı sürelerle farklı deniz ve hava koşullarına sahip bu rotalarda oluşan emisyon miktarları tahmin edilmiştir.

Fen Alanında Yapılan Çalışmalar

Kimya

Sümbül (2008), öncelikle bağlanma yüzeyindeki amino asitleri yüzeyin geri kalan kısmından ayıran özellikleri araştırmış, daha sonra bu özelliklerin muhtemel bağlanma amino asitlerinin makine öğrenmesi ile tahmininde kullanılmasını ele almıştır. İncelenen özellikler kullanılarak birer makine öğrenmesi metodu olan destek vektör makinesi ve çoklu kernel öğrenmesi metodları ile muhtemel bağlanma amino asitleri tahmin edilmeye çalışılmıştır.

Yoldaş (2011), çalışmasında Hidrofibisti yüzeylerin PCP benzeri bileşiklerin bağlanma eğilimlerine etkisini makine öğrenmesi yöntemlerini kullanarak tahmin etmiştir. Çalışmadaki amaç, moleküllerin hidrofobisiti yüzeyindeki noktaların sayısını azaltmaktır. Bu nedenle bu özellik küresel örgütlemeli harita ve k-ortalama kümeleme kullanılarak modellenmiştir. Bağlanma eğilimlerini öngörmek amacıyla destek vektör regresyonu ve kısmi en küçük kareler regresyonu kullanılmıştır.

Acı (2016), karbon nanotüplerin atomik koordinatlarını tahmin etmek için yedi adet tahmin modeli (İleri Beslemeli (İBYSA), Fonksiyon Uydurma (FUYSA), Kaskat Bağlantılı (KBYSA) ve Genelleştirilmiş Regresyon Yapay Sinir Ağları (GRYSA) ile Destek Vektör Regresyonu (DVR), Sınıflama ve Regresyon Ağacı (SRA) Çoklu Regresyon Analizi (ÇRA)) geliştirmiştir. Önerilen modeller ile atomik koordinatların hesaplanma süresini günlerden dakikalara düşürmeyi amaçlamaktadır.

Türkoğlu (2017), Bazik Oksijen Fırını (BOF) ile çelik üretimi işleminin, karbon içeriğini düşürmeyi ve sıcaklığı yükseltmeyi amaçlayan oldukça karmaşık, birçok fazlı fizik ve kimyasal reaksiyon içeren bir işlem olduğunu ifade etmiştir. Proses esnasında BOF içerisine üflenen oksijen miktarı BOF refrakter kaplamasının ömrünü, üretim maliyetlerini ve istenen kalitede çelik üretimi yapılabilmesini etkileyen en önemli kontrol parametresi olduğu için çalışmasında, BOF ile çelik üretimi sürecinde dinamik üfleme aşamasında üflenen oksijen miktarını makine öğrenmesi algoritmaları ile tahminleme modeli geliştirmiştir. En iyi tahminleme modelinin bulunabilmesi için, Doğrusal Regresyon, Çok katmanlı Algılayıcı(MLP), K-En Yakın Komşu (KNN), Aşırı Öğrenme Makinesi (ELM) ve Destek Vektör Makineleri (SVM) tabanlı Sıralı Minimal Optimizasyon (SMO) Regresyonu algoritmalarının Weka ve MATLAB kullanılarak karşılaştırılması yapılmıştır.

Ardıç (2018), ışık spektrum verisinden madde özelliklerinin tahmini için makine öğrenmesi tekniklerini kullanmıştır. Çalışmada farklı sıvı çözeltilerin emilim spektrumları üzerinde kısmi en küçük kareler, gradyan destekli regresyon, rastgele ormanlar, evrişimsel sinir ağları ve uzun kısa-süreli bellek modelleri eğitilerek belirli bir molekülün yoğunluğu tahmin edilmiştir.

Ulutaş (2018), protein parçacık seçiminin proteinlerin üç boyutlu yapılarının tahmin edilmesindeki önemli adımlardan biri olduğunu belirtmiş ve doğru parçacık yapılarının seçilmesinin üç boyutlu yapının doğru tahmin edilmesi için gerekli olduğunu ifade etmiştir. Bu amaçla iki protein parçacığının üç boyutlu yapılarının birbirine benzer olup olmadığını tahmin eden çeşitli yapay öğrenme yöntemleri geliştirmiştir. Çalışmada, üç ve dokuz amino asitlik parçacıkların yapısal benzerlik tahmini için çeşitli sınıflandırma ve regresyon modelleri eğitilmiş ve optimize edilmiştir. Bunlar arasında lojistik regresyon, AdaBoost, karar ağacı, en yakın komşu,

sade Bayes, rastgele orman, destek vektör makinası ve çok-katmanlı algılayıcı bulunmaktadır.

Biyoloji

Ataş (2011), çalışmasında dokulu gıdaların sınıflandırılmasında hiperspektral görüntüleme ve makine öğrenmesi konusunu ele almıştır. Amaç, bu yöntemleri kullanarak pul biberleri temiz biberlerden, hızlı ve tahribatsız bir şekilde ayırabilecek bir bilgisayarla görü sistemi geliştirmektir. Doğrusal Ayrımsallık Sınıflandırıcısı (DAS), Destek Vektör Makineleri (DVM) ve Yapay Sinir Ağları (YSA) modelleri sınıflandırıcı olarak kullanılmıştır.

Güneş (2017), günümüzde gıda kaynaklı hastalıkların, genellikle patojenik mikroorganizmalar veya kanserojen toksinler içeren gıda ürünlerinin tüketilmesinden kaynaklandığını ifade etmiştir. Gıda güvenliği problemlerinin çözümünde bilgisayarlı görmeye dayalı tahribatsız çözüm yöntemleri önemli bir gereklilik olduğu için çalışmada hiperspektral görüntüleme teknolojisi kullanılarak aflatoksin ve yüzey küf kontaminasyonuna sahip incirlerin yüksek başarımla tespit edilmesine yönelik özgün yöntemler geliştirilmiştir. Aflatoksin ve yüzey küf yaklaşımı için hiperspektral görüntülerin sınıflandırılmasına yönelik etkili algoritmalar geliştirilmiştir. Ayrıca yeni bir yöntem önerilmiş ve bu yöntem ile eğitim kümesi için gerekli olan etiketli örnek sayısı minimum düzeye indirgenerek etiketleme maliyeti düşürülmüştür.

Demir (2018), arı kanatları üzerindeki kavşak noktalarına göre arı türlerinin sınıflandırılmasını amaçlamıştır. Destek Vektör Makineleri (DVM), Yapay Sinir Ağları (YSA), K-Ortalama (K-Means) ve K-en Yakın Komşu (KNN) algoritmaları, sınıflandırma yöntemi olarak kullanılmıştır. Veri boyutunu azaltmak için Kaba Kuvvet Yöntemi (BFM) , İleri Sıralı Seçim (SFS) ve Lineer Discirimant Analiz (LDA) yöntemlerinden yararlanılmıştır. Arı alt türlerinin sınıflandırılmasında en yüksek başarı, K-Means yöntemi ile %50, DVM yöntemi ile % 71, KNN yönteminde ile %55,3 ve YSA ile %82,7 olarak gözlemlenmiştir.

Balta (2018) çalışmasında, Makine Öğrenmesinde yaygın kullanılan Yapay Sinir Ağları, K-NN, K-Means, Naive Bayes, ve Karar Ağacı Sınıflandırma (ID3) yöntemlerinin, ekolojik verilerde ne şekilde kullanılabileceğinin anlaşılması amacıyla iki adet örnek veri kümesi, bu yöntemler kullanılarak değerlendirilmiştir.

Öztürk (2018), makine öğrenmesi ve görüntü işleme tekniklerini kullanarak, drone ile farklı bitki çeşitlerinden ortaya çıkan yaprakların şekilsel olarak sınıflandırmasını yapmıştır. Bu çalışmadaki amaç, insansız hava araçları vasıtasıyla otonom bir şekilde yaprak çeşitlerini tanıyarak tarımda kimyasal ve biyolojik iyileşmenin önünü açmaktır. İlaveten, drone görüntülemesi sayesinde bitkisel hastalıklar ve böceklenme gibi ortaya çıkabilecek sorunlar daha önceden fark edilerek gerekli tedbirlerin alınmasını kolaylaştırmaktadır. Sınıflandırmaların başarıya ulaşması için Watershed algoritması uygulanmıştır. Her bölümde de, temel olarak görüntünün işlenmesi, özelliklerin cıkartılması, özelliklerin öğretilerek SVM ile sınıflandırma yapılmıştır.

Fizik

Abuzarifa (2018) çalışmasında, tek bir görüntü üzerinde yerçekimi yönü tespit etmek amacıyla, klasik görüntü geometrisine dayalı yöntemlerle makina öğrenmesine dayalı

yöntemler gerçeklenip karşılaştırılmıştır. Ayrıca çalışmada yeni bir yöntem önerilmiştir. Önerilen metod ve Derin sinir Ağları, gürültülü okumalar direkt kullanılarak oluşturulmuş geniş bir veri seti üzerinde eğitilmiştir, deneysel sonuçlar ayrıntılı olarak sunulmuştur.

Ağ Güvenliği/Güvenlik Alanında Yapılan Çalışmalar

Özhan (2013) çalışmasının amacı, günümüz bilgisayar sistemlerinin sağlıklı çalışabilmesi için önemli bir süreç olan ağ güvenliğini artırmaktır. Bu amaçla ağ güvenliğini sağlamada temel unsur olan güvenlik duvarları, daha önce araştırmacılar tarafından çok az denenmiş yapay zekânın alt dalı olan makine öğrenmesi yöntemleri ile analiz edilmiş ve güvenliği artırıcı bir model oluşturulmaya çalışılmıştır. Bu amaca ek olarak güvenliği artırmada yeni yöntemlerin alternatif çözümler sunabileceği de gösterilmeye çalışılmıştır.

Topuz (2014), çalışmasında makine öğrenmesi algoritmalarının ve yaklaşımlarının, veri kümesi içinde beklenmeyen davranış olarak tanımlanan anomalinin tespit edilmesinde nasıl kullanılacağını göstermiştir.

Kaytan (2016) çalışmasında, öncelikle bilgi güvenliğine yönelik tehditler açıklanmış; bu tehditlere karşı savunma yöntemleri ve öneriler sunulmuştur. Oltalama web sitelerinin tespit edilmesine yönelik olarak iki uygulama gerçekleştirilmiştir. Birinci uygulamada Yapay Sinir Ağı modeli ile oltalama web sitelerinin tespit edilmesine yönelik sınıflandırma uygulaması gerçekleştirilmiştir. İkinci uygulamada ise Aşırı Öğrenme Makinesi modeli ile oltalama web sitelerinin tespit edilmesine yönelik sınıflandırma uygulaması gerçekleştirilmiştir.

Kaya (2017) çalışmasında, gerçekleştirilen deneylerle saldırı tespit sistemlerinde en sık kullanılan makine öğrenmesi tekniklerinden Bayes ağları, destek vektör makinesi, karar ağaçları, yapay sinir ağları ve k en yakın komşu algoritmasının performans analizi yapılmış ve saldırı türlerine göre doğruluk, seçicilik, duyarlılık, kesinlik, F-Ölçütü değerleri incelenerek en başarılı sınıflandırıcılar belirlenmiştir.

Yıldırım (2017), günümüzde her gün binlerce sistemin otomatik araçlarla yapılan ve uzman saldırganların çeşitli yöntemler kullanarak gerçekleştirdiği saldırılara maruz kaldığını ifade etmiştir. Yapılan bu çalışmada, bilgisayar ağlarındaki anomali (düzensizlik) tespitinde kullanılan makine öğrenmesi yöntemlerinden bazıları incelenmiştir. Bu alanda en çok tercih edilen veri setlerinden KDD cup'99 ve NVD veri setleri üzerindeki başarı oranları karşılaştırılacak ve performans analizleri yapılmıştır.

Özdağ (2017) çalışması kapsamında, özellik seçim yöntemi olarak bilgi kazanımı ve özellik çıkarım yöntemi olarak da temel bileşen analizi kullanılarak doğruluk oranları üzerindeki etkileri gözlemlenmiştir. Saldırı tespiti için makine öğrenmesi algoritmalarından Yapay Bağışıklık Sistemi (YBS) kullanılmıştır. YBS'nin öğrenme sürecinde etkinliğini arttırmak için geleneksel detektör üretim tekniklerine ek olarak genetik algoritma kullanılarak hibrid bir çözüm geliştirilmiştir. YBS ile geliştirilmiş modelin, eğitim ve test aşamalarında KDD Cup 99 veri seti kullanılmıştır.

Akar (2017), araç içi kontrol ağları uygulamaları için Makine Öğrenmesi metotlarını kullanan anomali tabanlı araç içi saldırı tespit motorunu (IVADE) önermektedir. Araçtan araca ağlarda (V2V) ve araçtan altyapıya ağlarda (V2I) Kooperatif Farkındalık Mesajı (CAM) içeriği olarak paylaşılan ve aracın konum, hız ve yön bilgisini içeren Hareket Verisine yönelik veri bozma saldırılarını tespit etmeyi amaçlamaktadır. Algoritmanın işlevselliği, Şerit Takip Asistanı (LKA) sistemine ait modelin sinyal ölçümleri ve kontrol işlemleri için Elektronik Kontrol Birimleri (ECU) ile bir CAN haberleşme hattı üzerine simülasyonu uygulanarak doğrulanmıştır. IVADE'de uygulanan makine öğrenmesi özellikleri, araç içi ağdaki CAN ağı üzerindeki mesajların veri alanlarından toplanmış, otomotiv sistemlerine özgü dinamik sistem davranışı bilgileriyle desteklenmiş ve Karar ağaçları ile öğrenilmiştir.

Büber (2017), "Oltalama Saldırıları" nın, insanların zafiyetlerinden faydalanarak kullanıcıların gizli bilgilerini elde etmeyi amaçlayan, kişi ve kurumları tehdit eden siber saldırı türlerinden birisi olarak tanımlamış ve bu saldırıların neden olduğu maddi kayıpların azaltılabilmesi için kullanıcıların bilinçlendirilmesinin yanı sıra bu tip saldırıları tespit etme yeteneğine sahip uygulamalara ihtiyaç duyulduğunu vurgulamıştır. Bu amaçla, çalışmasında, Oltalama Saldırılarının karakteristik özniteliklerinin açıklanmasının ardından bu saldırıların tespit edilmesine yönelik Makine Öğrenmesi tabanlı bir sistem önerilmiştir. Oluşturulan sistem üzerinde birçok test uygulanmış ve elde edilen başarı oranlarına ilişkin değerlendirmeler yapılmıştır. Gerçekleştirilen testler sonucunda test edilen algoritmalar arasından Rastsal Orman algoritmasının en yüksek başarı değerine sahip olduğu görülmüştür.

Kapar (2018), kimlik Avı saldırısında kullanılan web sitelerinin makine öğrenmesi algoritmaları yardımıyla tespiti ve uygulaması konusunu ele almıştır. Çalışmada Lojistik Regresyon, KNN ve Naive Bayes algoritmaları kullanılarak, PhishTank ve Google arama sonuçlarında elde edilen URL setleri üzerinde modeller eğitilmiştir. Lojistik Regresyon algoritmasının diğer algoritmalara göre daha başarılı olduğu tespit edilmiştir.

Peynirci (2018), son kullanıcının, tipik güvenlik yetersizliğine bağlı olarak, kötücül yazılımın Google Play Store veya herhangi bir resmi olmayan uygulama mağazasında yayımlanmadan önce tespit edilmesinin hayati bir öneme sahip olduğunu vurgulamıştır. Çalışmasında, makine öğrenmesi teknikleri kullanarak yeni bir Android kötücül yazılım tespit metodolojisi yanında yeni bir öznitelik seçim metodolojisi ortaya koymuştur.

Kurt (2019), makine öğrenmesi algoritmalarının aynı ağ verileri üzerindeki performanslarını karşılaştırarak geliştirilmekte olan saldırı tespit sistemlerine referans kaynak oluşturmayı amaçlamıştır. Çalışmada, büyük veri teknolojisi Apache Spark kullanılarak KDD Cup'99 verilerinin tamamı makine öğrenmesi algoritmalarından Lojistik Regresyon, Destek Vektör Makineleri, Naive Bayes ve Rastgele Orman üzerinde koşturulmuş; sonuçlar karşılaştırmalı olarak analiz edilmiştir.

Akpınar (2019), otomasyon uygulamalarında yaygın bir kullanıma sahip olan, Ethernet tabanlı gerçek zamanlı EtherCAT protokolü için Snort saldırı tespit sistemi üzerinde bilinen ve bilinmeyen saldırıları tespit eden bütüncül bir yapı ve makine öğrenmesi teknikleriyle anomali tespiti olmak üzere ikisi kural biri anomali tespitine

dayanan 3 farklı yaklaşım sunmaktadır. Sistem, geliştirilen önişlemci yardımıyla, bilinen saldırılar için güvenli düğüm yaklaşımı, bilinmeyen saldırılar için ise saha veri yolu tekrar periyodunu tespit ederek istatistiksel tekniklerle ve özgün çözümlerle kural tabanlı olarak saldırı tespitini kapsamaktadır. k-NN ve SVM GA tekniklerinin olay tespitinde başarılı sonuç verdikleri belirlenmiştir.

Khalifa (2019), yasadışı gizli iletişimleri engellemek için steganalize olan ihtiyacın arttığını ifade etmiş ve eş oluşum matrisini, frekans alanı dönüşümlerini, ilk üç momenti ve Geri Yayılımlı Sinir Ağlarını (GYSA) kullanarak hareketsiz görüntülerdeki gizli bilgileri tespit etmek için bir steganaliz sistemi sunmuştur. Görüntünün gizli bilgi içerip içermediğini belirlemek için bir GYSA sınıflandırıcısı kullanılmıştır.

Duygu Analizi/Metin Sınıflama Alanında Yapılan Çalışmalar

Doğrusöz (2007) çalışmasında, veri madenciliğinin bir alt dalı olan metin madenciliği kapsamında metin sınıflama algoritmalarının matematiksel modelinin incelenmesi ve bir uygulamasının yapılması ele alınmıştır. Literatürde bu konu ile alakalı olan çalışmalar incelenmiş ve sonuçlar yorumlanmıştır. Ayrıca, algoritma performanslarının sayısal sonuçları verilerek özellik seçim algoritmalarının sınıflama yüzdesini ne ölçüde etkilediği tartışılmıştır.

Çetingöz (2011), "anahtar ifade"nin, bir metnin içeriğini özetleyen anlamsal kelime ya da kelimeler topluluğu olduğunu ve anahtar ifade ile bir metnin tamamının okunmasına gerek kalmayacak şekilde metnin içeriği hakkında fikir sahibi olunabileceğini vurgulamıştır. Çalışmasında, Türkçe haber metinlerinden elde edilen eğitim ve test verilerini ve açık kaynak kodlu yazılım algoritmasını kullanarak uygulama geliştirmiştir.

Güldan (2014), olumsuz aldatıcı tüketici yorumlarını tespit edebilmek üzere, çoklu sınıflayıcılı sistemler kullanılarak bir model önerilmiş ve önerilen model otel yorumları ile ilgili olarak hazırlanmış veri setinde uygulanmıştır. Önerilen modelde, beş sınıflayıcı (libLinear, libSVM, ardışık minimal optimizasyon (SMO), Random Forest ve J48'dir. LibSVM ve libLinear, Destek Vektör Makinelerinin (DVM)) kullanılmıştır.

Güvenç (2016), doğal dil işleme konusunda makine öğrenmesi yöntemleri ile anahtar kelime çıkarma ve metin özetlemeyi ele almıştır. Word2Vec ve PageRank algoritmalarını kullanarak anahtar kelime çıkartmak için yeni ve etkili bir yöntem önermiştir. Elde ettikleri sonuçlara göre, önerdikleri özetleme algoritmaları haber metinleri üzerinde en iyi sonucu verirken kısa öyküler için daha az optimal sonuç vermektedir.

Onan (2016) çalışması kapsamında, görüş madenciliği, bir metin sınıflandırma problemi olarak ele alınarak makine öğrenmesi yöntemleri aracılığıyla etkin görüş sınıflandırma yöntemleri geliştirilmiştir. Geliştirilen yöntemlere dayalı yeni bir sınıflandırma mimarisi önerilmiştir. Bu mimari ile geliştirilen yöntemler etkin bir

şekilde birleştirilerek mevcut ve geliştirilen yöntemlerin bireysel performanslarına kıyasla daha iyi başarım elde edilmiştir.

Taşpınar (2017), çalışmasında gözetimli öğrenme algoritmalarını ve sosyal medya uygulaması Twitter verilerini kullanarak, mikro blog (Twitter) verilerinde kavram tanıma/çıkarma işlemi yapmıştır. Verilen 140 karakter içinden kişi, organizasyon, lokasyon, ürün, olay ve karakter bilgileri tahmin edilmeye çalışılmıştır. Veri kümesi olarak 2016 yılında yapılan NEEL konferansı verileri kullanılmıştır. Önerilen sistemin sonuçları da aynı konferanstaki sonuçlarla karşılaştırılmıştır.

Başkaya (2017) çalışmasında yapılan ilk uygulama, makine öğrenmesi teknikleri ile haber metinlerinin farklı öznitelik ve terim ağırlıklandırma yöntemleriyle sınıflandırılması, yöntemlerin verimliliğinin ve başarısının test edilmesidir. İkinci uygulama ile yine makine öğrenmesi teknikleriyle duygu analizi çalışması yapılarak, Twitter gönderilerini içeren farklı iki veri seti pozitif, negatif ve nötr sınıflarla etiketlenmiş ve Parçacık Sürü Optimizasyonu tabanlı K-En Yakın Komşu Algoritması ile sınıflandırılmıştır. Daha önce aynı veri kümeleri üzerinde önerilen guguk kuşu algoritması ile karşılaştırıldığında önerilen yöntemin daha başarılı sonuçlar verdiği gözlemlenmiştir.

Altan (2018), metin sınıflandırma problemine makine öğrenmesi yöntemleriyle çözüm getirmiştir. Metin sınıflandırma işlemi sırasında; doğal dil işleme teknikleriyle metni temsil eden değerler belirlenirken sınıflandırma aşamasında farklı makine öğrenmesi algoritmaları birleştirilerek sınıflandırıcı topluluğunun başarıları gözlenmiştir. Öznitelik vektörü olarak kelimeler, cümle birimleri ve varlık isimlerinin birlikte kullanılmasının başarıyı olumlu etkilediği görülmüştür.

Ayata (2018), Türkçe ve İngilizce twitter duygu sınıflandırması için makine öğrenmesi ve doğal dil işleme tekniklerinin uygulanmasını göstermiştir. Cümle bazında duygu çözümlemesi ile kullanıcıların bir ürün, kişi vb. hakkında yazdığı mesajların olumlu, olumsuz veya nötr sınıflarından hangisini taşıdığını belirleme işlemi yapılmıştır. Çalışmada Türkçe tweet duygu çözümlemesi, sektöre dayalı duygu çözümlemesi, İngilizce tweet duygu çözümlemesi ve politik yönelim tahminlemesi yapılmıştır.

Monhamady (2018), çalışmasında verilen bir web sayfası metninden şirket ismini otomatik olarak tespit eden iki aşamalı yeni bir makine öğrenmesi yöntemi geliştirmiştir. İlk aşamada verilen bir kelimenin şirket ismi olup olmadığını tahmin eden bir sınıflandırma yöntemi geliştirilmiştir. Doğal dil işleme teknikleri ile ve metinsel verilerdeki örüntülerin incelenmesi sonucu öznitelikler çıkarılmıştır. Bu öznitelikler daha sonra Naive Bayes, karar ağacı ve rastgele orman gibi sınıflandırma yöntemlerine girdi parametresi olarak aktarılmıştır. İkinci aşama içinse kural tabanlı bir sınıflandırma yöntemi geliştirilmiştir.

Alnawas (2019), Arap Irak lehçesinde Duygu Analizi çalışması gerçekleştirmiştir. Çalışmada veriler toplandıktan sonra, karmaşıklığı en aza indirmek ve metin biçimini standartlaştırmak için veri kümelerinden gereksiz terimler çıkarılmıştır. Özellikler çıkarılmıştır ve bir duygu tahmin modeli oluşturmak için oluşturulan vektörler dört makine öğrenme algoritmasıyla eğitilmiştir.

Işık (2019) çalışmasında, öncelikle müşteri yorumlarının analiz yöntemleri ile incelenmesi gerçekleştirilmiştir. Yazılı metin içerisinde bulunan içerikler sayesiyle bilgi keşfi adına analiz çalışmalar yapılmıştır. Bu bağlamda gerçekleştirilen bu çalışmada müşteri yorumların sınıflandırılması için Naive bayes, lojistik regresyon ve destek vektör makinesi algoritmaları kullanılmış ve yorumlar üzerindeki model performansları karşılaştırılmıştır.

Yüz / Ses / El jesti Tanıma Alanında Yapılan Çalışmalar

Turhal (2016), çalışmasında yüz resimlerinden yaş ve cinsiyet tahmini yapmıştır. Temelde iki farklı problem olan yaş ve cinsiyet tahmini bu çalışmada tek bir problem olarak ele alınmıştır. Bu iki problemi en iyi tanımlayacak minimum sayıda özniteliğin belirlenmesi ve elde edilen öznitelik kümesinin sınıflandırılması sonucunda minimum hesaplama sürelerinde maksimum doğruluk değerlerinin üretilmesi ana hedef olarak belirlenmiştir. Çalışmada kullanılan örüntülerdeki yüz bölgelerinin tespitinde, literatürde bulunan birçok çalışmada yaygın olarak tercih edilmiş Viola-Jones algoritması kullanılmıştır.

Karabina (2017) çalışmasında, otomatik konuşmacı tanıma çalışmalarında kullanılması amacı ile yeni bir veri seti oluşturulmuştur. TIMIT veri seti ve çalışma kapsamında oluşturulan veri seti üzerinde derin öğrenme ağının da dâhil edildiği bir dizi yapay zekâ tekniği ile konuşmacıların cinsiyet, yaş, boy ve kilolarının tahmini sağlanmıştır. Bu özelliklerin otomatik tahmininin çağrı merkezleri, e-ticaret ile meşgul kurumlar ve adli makamlar gibi kurumlar için fayda sağlayacağı düşünülmüştür.

Kutlugün (2017) çalışmasında, ses sentezlemenin bir çeşidi olan metinden konuşma sentezleme konusu ele alınmıştır. Uygulamada düz metin türlerinin monoton, robotik bir ses biçimi olarak seslendirilmesi yerine, metinleri gruplara ayırarak farklı metin türlerinin kendi alanlarına uygun olduğu düşünülen farklı ses biçimleri şeklinde seslendirilmesinin daha doğal olacağı düşünülmüştür.

Sarı (2017) çalışmasında, iki farklı ses veri seti oluşturularak bu veri tabanları üzerinden metinden bağımsız konuşmacı tanıma uygulaması geliştirilmiştir. Öznitelik vektörü işlemlerine geçmeden önce ses kaydı ön işlemlerden geçirilmiş, sonrasında öznitelik vektörü olarak MFCC katsayıları elde edilmiştir. Sınıflandırma işlemi için makine öğrenmesi yöntemlerinden MLP (Multi Layer Perceptron- Çok Katmanlı Algılayıcı) ağları ve vektör niceleme algoritması kullanılmıştır.

Çelen (2017) çalışmasında, konuşma ve konuşma dışı şeklinde iki sınıfla ifade edilen test verisinde konuşma var olarak işaretlenen pencerelerdeki veriler birleştirilip hızlandırılmış ses verisi üretilmiştir. Hızlandırılmış ses verisi konuşma sentezleme programları ile metine dökülüp sistemin başarımı ölçülmüştür. Bu çalışma ile görülmüştür ki çeşitli yöntemler kullanılarak konuşmalar, insan beyninin anlayabileceği sınırlara kadar hızlandırılabilmektedir. Hızlı dinleme sistemlerini test etmek için konuşma tanıma yöntemleri kullanılan bir sistem geliştirilmiştir.

Öztel (2018), kısmi ve tam yüz görüntüleri üzerinde makine öğrenmesi yöntemleriyle yüz ifadesi tespiti yapmıştır. Yazar tarafından geliştirilen ilk uygulamada, yüz görüntülerinden duygu tespiti için literatürdeki çalışmalardan farklı olarak sadece göz

ve kaşların bulunduğu bölgeler kullanılarak sınıflandırma yapılmış ve yüksek başarım elde edilmiştir. Önerilen bu yöntem sayesinde yüz ifadesi tespitleri alt yüz kapanmalarından veya ağız hareketlerinden etkilenmeyecek, gürbüz özniteliklerin seçimi ile daha az öznitelikle sınırlı kaynaklara sahip cihazlarda çalışabilecek niteliktedir.

Dabanoğlu (2018), altı temel ifadeden oluşan, mutluluk, üzüntü, korku, tiksinme, şaşırma ve öfke ifadelerinin, makine öğrenmesi yardımıyla, kişiden bağımsız olarak gerçek zamanlı videodan tanınmasını amaçlamıştır. Yüz ifadesi tanımada en başarılı bulunan yöntem ve veri seti, gerçek zamanlı videodan alınan görüntüler üzerinde denenmiştir. Elde edilen sonuçlara göre, dört sınıftan (ifadesiz, mutluluk, şaşırma ve üzüntü) oluşan veri seti, Destek Vektör Makineleri sınıflandırıcı kullanılarak en yüksek tanıma oranı olan %85,37 tanıma doğruluğuna ulaşılmıştır. İncelenen temel altı yüz ifadesi içerisinde diğer sınıflarla en az karıştırılan iki duygu ise şaşırma ve mutluluk olarak gözlemlenmiştir.

Kaya (2018), çalışmasında geliştirilen el jestlerini tanıma sistemi için Türk İşaret Dili'ndeki rakamların jestlerini veri seti olarak kullanmıştır. Statik el hareketlerinin tanınabilmesi için toplamda 11 farklı el jesti için kas sinyalleri toplanmış. Sekiz farklı kanaldan aynı anda sinyaller toplandığı ve toplanan sinyallerin basit eşikleme yöntemiyle sınıflandırılması mümkün olmadığı için el jestlerinin tanımlanmasında makine öğrenmesi tekniklerine başvurulmuş. Çalışma kapsamında dört adet sınıflandırma algoritması uygulanmış ve el jesti tanımlama performansları karşılaştırılmıştır. Bu algoritmalar k-En Yakın Komşu, Karar Ağacı, Destek Vektör Makinesi ve Yapay Sinir Ağları sınıflandırma algoritmalarıdır. Son olarak, Yapay Sinir Ağları algoritması el jestlerini sınıflandırmak için uygulanmıştır. Elde edilen sonuçlara göre, en yüksek başarımlı sınıflandırma oranı olan 0.87'ye Destek Vektör Makinesi algoritması ile ulaşılmıştır.

Alp (2018), videodan insan aktivitelerinin otomatik tespit edilmesi ve sınıflandırılmasının son yıllarda oldukça fazla miktarda araştırmacının üzerinde çalıştığı aktif bir araştırma konusu olduğunu vurgulamış ve çalışmasında Weizmann ve KTH veri kümelerine ait olan videolar ile çeşitli makine öğrenmesi yöntemleri kullanarak aktivite sınıflandırma çalışması yapmıştır. Bu çalışmalar kapsamında hem özniteliklerin çıkarımında, hem de akış sınıflandırmada iki farklı yaklaşım ele alınmıştır. Öznitelik çıkarımında, el ile özniteliklerin çıkarılması ve derin ağlar kullanılarak özniteliklerin çıkarılması-yaklaşımları kullanılmıştır.

Spor Alanında Yapılan Çalışmalar

Al-Asadi (2018), çalışmasında futbol takımı yönetimi için makine öğrenmesi yöntemlerinden faydalanan yeni bir karar destek sistemi önermiştir. Bu karar destek sisteminin başlıca hedefi takımdaki her oyuncu için kişisel yeteneklerini temel olarak en uygun pozisyonu belirlemek ve istenen formasyona göre en iyi takımı oluşturmaktır. Ayrıca, bir sezon için 17359 oyuncu içeren FIFA futbol oyunu verileri analiz edilmiş ve bunun için sınıflandırma ve regresyon problemleri için makine öğrenmesi teknikleri kullanılmıştır (linear and logistic regression, random forest, neural network and k nearest neighbor). Son olarak top sürme becerisini belirlemek için dört farklı algoritma kullanılmıştır (linear regression, logistic regression, random

forest and neural network). En iyi sonucu 17 performans niteliği kullanılarak % 99.90 doğruluk değeriyle rastgele orman algoritması vermiştir.

Sosyal Alanda Yapılan Çalışmalar

Orakcı (2017), çalışmada; suçun tanımından ve suç bilimi olan kriminolojinin ilgi alanlarından yola çıkarak, veri madenciliği ve makine öğrenmesi tekniklerinin suç analizinde nasıl kullanılabileceğini açıklamıştır. İki tekniğin birlikte kullanımı; yapılan analizlerden elde edilen bulgular doğrultusunda değerlendirilmiştir. Bu bağlamda ilk olarak, Federal soruşturma Bürosu tarafından oluşturulan, Ulusal Vaka Tabanlı Raporlama Sistemi kullanılarak; tecavüz, cinayet ve adam kaçırma vakaları üzerinde analizler gerçekleştirilmiştir. Daha sonra; terörist grupların gerçekleştirdiği eylemlerin ayrıntılı bilgisinden oluşan Küresel Terörizm Veritabanı kullanılarak terörist grubu tahmin sistemi geliştirilmiştir.

Belek (2018), çalışmasında güvenli yolu tespit ederek insanların bir yerden başka bir yere giderken daha güvenli bir şekilde gitmesini sağlamak için suçları analiz ederken gerçek ortamda harita üzerinde makine öğrenimi yöntemleri kullanılarak güvenli yol planlaması yapmıştır. Çalışmada, K-Means, K-Median, K-Medoid, X-Means, Expectation-Maximization yöntemleri gerçek suç verileri üzerinde kullanılmıştır.

Şahinarslan (2019), çalışmasında farklı makine öğrenmesi algoritmaları ile nüfus tahmini yapmıştır. Bunun için altı farklı makine öğrenmesi algoritması seçilmiştir; Light Gradyan Artırma (Light Gradient Boosting, LightGBM), Doğrusal Regresyon, Ridge Regresyon, Üstel Düzeltme yöntemlerinden biri olan Holt-Winters, Bütünleşik Otoregresif Hareketli Ortalama (Autoregressive Integrated Moving Average, ARIMA) ve Prophet tahmin modeli. 262 farklı ülkenin 1960-2017 yılları arasındaki 1595 farklı demografik göstergesi kullanılarak modeller eğitilmiştir. Makine öğrenmesi algoritmaları Python programlama dili ile Jupyter program arayüzü kullanılarak eğitilmiştir. Ayrıca, eğitilen modeller ile 2017 yılı toplam Türkiye nüfusu tahmin edilmiştir.

Ulaşım Alanında Yapılan Çalışmalar

Akı (2017), sürücü uykululuğunun görüntü işleme ve makine öğrenmesi teknikleri ile gerçek zamanlı olarak tespit edilerek sürücünün uyarılmasını sağlayan bir sistemin tasarlanması ve gerçekleştirilmesidir. Çalışmada veri tabanı oluşturmak için dört gönüllünün gerçek zamanlı kamera görüntüsü verileri kullanılmıştır. Oluşturulan veri setleri ile beş farklı makine öğrenme algoritmasının sınıflandırma performansları birbiriyle kıyaslanmıştır.

Soylu (2018) çalışmasında, yüksek hızlarda ve doğrulukta trafik sınıflandırma yapabilmek için makine öğrenmesi tabanlı ve donanım üzerinde gerçeklenen trafik sınıflandırma yöntemleri incelenmiştir. Çalışmanın ana katkısı olarak paralel boru hatlı (pipeline) mimariler üzerinde uygulanan yüksek hızlarda ve doğrulukta sınıflandırma yapabilen makine öğrenmesi tabanlı Genişletilmiş Simple CART (E-SC) mimarisinin önerilmesidir.

Gülaçar (2018), çalışmasında veri tahmini yapan bir tahmin modülü oluşturmuştur. Çalışmalar için İstanbul Büyükşehir Belediyesi (İBB) Trafik Kontrol Merkezi (TKM) tarafından D100 karayolu üzerine yerleştirilmiş, VITAL platformuna bağlı, hız ölçümü

yapan sensörlerin ölçtüğü araç hız verileri kullanılmış ve sensörlerin 30 dakika sonraki hızlarının asgari hata ile tahmin edilmesi hedeflenmiştir. Veri kümesi üzerinde regresyon işlemi için Karar Ağacı Regresyon (KAR), Gradient Boosting Regresyon (GBR), K-Nearest Neighbours Regresyon (KNN), Kernel Ridge Regresyon (KRR), Random Forest Regresyon (RFR), Destek Vektör Regresyon (DVR) yöntemleri uygulanmıştır. Tahminlerin doğruluk değeri ise Root Mean Square Error (RMSE) yöntemi ile değerlendirilmiştir. Sınıflandırma işlemi için ise Karar Ağacı Sınıflandırıcı (KAS), Gradient Boosting Sınıflandırıcı (GBS), K-Nearest Neighbours Sınıflandırıcı (KNN), Random Forest Sınıflandırıcı (RFS), Destek Vektör Sınıflandırıcı (DVS) yöntemleri uygulanmıştır.

Karataş (2018), araç sürüş verilerinden makine öğrenmesi tekniklerini kullanarak sürücü sınıflandırma konusunu ele almıştır. Sürücü kümeleme deneylerinde Dynamic Time Warping ve geliştirdikleri Dynamic Distance Warping veri dönüşüm metodları uygulanarak farklı mesafe metriklerine göre hiyerarşik sürücü kümeleme işlemi gerçekleştirilmiştir.

Sağlık Alanında Yapılan Çalışmalar

Sağlık alanında yapılan 44 tez çalışması, Şekil 2'de görüldüğü üzere kanser, parkinson, diyabet çalışmaları, böbrek, akciğer, kalp hastalıkları, gen dizilimi, bel bölgesi rahatsızlıkları, göz hastalıkları, kadın-çocuk hastalıkları, diğer nörolojik çalışmalar, biyomedikal çalışmalar, tümör kontrol ve diğer sağlık çalışmaları şeklinde gruplandırılmıştır. Dağılıma bakılacak olursa, kalp rahatsızlıkları, gen dizilimi ve kanser konuları üzerinde diğerlerine göre daha fazla durulduğu görülmektedir.

Şekil 2. Sağlıkta Makine Öğrenmesi Çalışma Alanları

Diğer Çalışmalar

İş Gücü Tahmini

Yurdakurban (2018), yazılım projelerinde iş gücü tahmini için makine öğrenmesi yöntemlerini karşılaştırmıştır. Karar Ağacı, Naive Bayes ve Çoklu Regresyon analizi modellerini baz almıştır ve her üç model aynı eğitim veri kümesiyle eğitilmiş ve aynı test veri kümesiyle test edilmiştir. Elde edilen sonuçlar karşılaştırıldığında, Çoklu

Regresyon Analizi modelinin en doğru tahminleme sonucunu elde ettiği görülmüştür. İkinci sırada Karar Ağacı, son sıradaysa Naive Bayes modeli yer almıştır.

Oyun Modelleme

Şirin (2012), eksik bilgi oyunlarında rakip modelleme problemine ilişkin bir makine öğrenmesi yaklaşımı sunmuştur. Popüler bir örnek olan Texas Usulü Poker, önerilen metodların gerçeklenmesi için kullanılmıştır. Bu çalışmada, rakip modelleme problemi bir sınıflandırma problemi olarak ele alınmıştır. Oyunun her bir fazı için değişik bir sınıflandırıcı içeren bir mimari önerilmiştir. Sınıflandırıcı olarak Yapay Sinir Ağları, K-En Yakın Komşu (KYK) ve Destek Vektör Makineleri yöntemleri kullanılmıştır. Belirli bir oyuncuyu modellemede %88 doğru tahmin oranıyla KYK yönteminin daha başarılı olduğu gözlenmiştir.

Doğal Taş Sınıflandırma

Temiz (2018), çalışmasında doğal taş karolarına ait resimlerden görüntü işleme teknikleri yardımıyla renk ve yüzey hakkında bilgi verecek öznitelikler çıkarmış ve daha sonra bu öznitelikleri kullanarak elde ettiği veri setini çeşitli yapay zekâ ve veri madenciliği teknikleriyle sınıflandırmıştır. Veri setlerinin sınıflama performansı, Yapay Sinir Ağları (YSA), Destek Vektör Makineleri (Support Vector Machine-SVM), k En Yakın Komşu (k- Nearest Neighbour-k-NN), Karar Ağaçları (Decision Tree-KA), Naive Bayes (NB) gibi çeşitli yöntemler kullanılarak karşılaştırılmıştır.

Objektif Karar Verme

Bilgilioğlu (2018), kararlara etki eden kriterlerin sayısı arttıkça, kriterlerin sıralanması ve ağırlık değerlerinin hesaplanmasının daha karmaşık hale geldiğini ifade ederek, özellikle mekânla ilişkili karar analizlerinde, gerek veri yoğunluğu, gerekse kriterlerin fazlalığının problemi daha karmaşık hale getirdiğini belirtmiştir. Bu problemin çözümüne yönelik, Coğrafi Bilgi Sistemleri (CBS) ve Karar Destek Sistemleri (KDS) temellerine dayalı Mekânsal Karar Destek Sistemleri (MKDS) yöntemleri geliştirmiştir. Çalışmada, envanter bilgilerine dayalı MKDS'lere yapay zeka tekniklerinden makine öğrenmesi tekniğinin entegre edilmesi ve bu sistemlerinin otomatikleştirilmesi amaçlanmıştır. Bu amaçla makine öğrenmesinde öne çıkan denetimli öğrenme algoritmalarından Yapay Sinir Ağları, Destek Vektör Makineleri, CHAID ve Karar Ağacı algoritmalarından ID3, C4.5, CART ve Rastgele Orman algoritmaları Aksaray ili taşınmaz değer haritasının üretiminde kullanılmış ve performansları değerlendirilmiştir.

Uydu Görüntü Analizi

Çınar (2019), uzaktan algılama teknolojisindeki son gelişmeler ile yeryüzü hakkında elde ettiğimiz verinin kalitesinin önemli bir biçimde arttığını ve uydu görüntüleri ile yeryüzü hakkında önemli veriler sağladığını ifade etmiştir. Çok kanallı optik görüntülerin destek vektör makineleri, komşuluk bileşen analizi, karar ağaçları, derin öğrenme, k en yakın komşu, lineer diskriminant gibi gelişmiş makine öğrenmesi teknikleri ile sınıflandırılması hedeflenmiştir ve bu metotların performansları analiz

edilmiştir. Bu sınıflandırmanın, arazi kullanımı ve değişim analizi gibi uygulamaların hayata geçirilmesine olanak sağlamak hedeflenmiştir.

Piksel Hatalarının Tespiti

Çelik (2019), LCD piksel hatalarının tespiti problemine, bir nesne tespiti problemi olarak yaklaşmış ve makine öğrenmesi temelli üç yöntem önermiştir. Birinci yöntem GLCM öznitelikleri ve SVM sınıflandırıcı kullanmaktadır. İkinci yöntemde CNN sınıflandırıcı kullanılmıştır. Üçüncü yöntem ise piksel hatalarının tespiti için tümleşik, tek aşamalı, CNN tabanlı bir nesne tespit mimarisi kullanmaktadır. En iyi tespit sonuçları tümleşik ve tek aşamalı olan CNN tabanlı bir nesne tespit mimarisi kullanıldığı yöntemle elde edilmiştir.

Konum Tahmini

Hassan (2017) çalışmasında, çoğu akıllı telefonda yaygın olarak bulunan Wi-Fi sinyallerini kullanarak makine öğrenmesi yaklaşımlar ile konum tahmini için alternatif bir servis sunulmuştur. ELM, ANN, SVM ve Regresyon gibi makine öğrenmesi yöntemler ile Wi-Fi parmak izi kullanılarak konum belirlemenin gerçekleştirilebileceği gösterilmiştir.

Girişimcilik Niyet Tahmini

Oruç (2019), girişimcilik yöneliminin kaynaklarını araştırmak, teori ve hipotezleri bir araya toplayarak faktörleri bir arada veri olarak kullanmak ve girişimcilik niyetini tahmin eden bir model önermeyi amaçlamıştır. Makine öğrenmesi kullanarak şimdiye kadar araştırılmış olan girişimcilik niyeti faktörlerinin bir arada kullanılmasıyla, en geçerli tahmin yöntemini geliştirmeye çalışmıştır. Ayrıca, Türkiye içerisinde özellikle kişilerin iş anlamında aktif olabileceği süreç olduğu varsayılarak 18-55 yaş arasındaki bireylerin girişimcilik niyetini etkileyen faktörleri belirleyerek bu faktörlerin birlikte analiz edilmesini sağlamıştır.

Risk Tahmini

Sayın (2019), Çoklu Ayraç Analizi, Lojistik Model, Sinir Ağları, Destek Vektör Makineleri, Karar Ağaçları ve Karar Ormanları algoritmaları ile finans dışı şirketlerin süreklilik risklerinin belirlenmesini amaçlamıştır. Araştırmada R istatistik dilinden ve ilgili R Makine Öğrenmesi model kütüphanelerinden faydalanılmaktadır. Eldeki örneklem çerçevesinde, bir Breiman Karar Ağacı modelinin en başarılı süreklilik riski öngörüsü modeli olduğu ve bu modelin sade ve kolay anlaşılır yapısından ötürü pratikte de faydalı olabileceği öngörülmektedir.

Hiperspektral Görüntüleme

Tekcan (2018), hiperspektral görüntülerin makine öğrenmesi ile spektral-uzamsal sınıflandırılmaları üzerinde çalışmıştır. Spektral bilgilerin yanında hiperspektral görüntüden elde edilecek uzamsal özelliklerin de hiperspekral görüntü sınıflandırmada kullanılması amaçlanmıştır. Elde edilen spektral-uzamsal öznitelikler Destek Vektör Makineleri ve Evrişimsel Sinir Ağları ile sınıflandırma yapılmıştır. Sınıflandırma deneyleri Indian Pines, Pavia University ve Salinas veri kümeleri ile yapılmıştır.

Yazılım Geliştirme

Aktaş (2018), çalışmasında yazılım geliştiricilere ve test uzmanlarına hata eğilimli sınıfları öngörme, hataların kaynakları hakkında bilgi vererek tasarım kusurlarını ortadan kaldırma ve bakım maliyetlerini azaltma konularında yardımcı olmak amacıyla nesneye yönelik sistemlerde kusurlu sınıfların öngörülmesi için makine öğrenmesi temelli bir yöntem oluşturmuştur. Önerilen yaklaşımlar ile sistemdeki hataya eğilimli sınıfları %70'ine kadar bulabilmektedir. Bununla birlikte, hataya yatkın sınıfların belirlenmesinde hangi metriklerin etkili olduğu incelendi, bunların projelere göre farklılıklar gösterdiği tespit edilmiştir.

Rıhtım (2018) çalışmasında, eski teknolojilerle, yeni teknolojinin birleştirilerek kullanılmasına olanak sağlayan, verilerin daha efektif bir biçimde kullanılarak, kullanıcılara performanslı bir kullanıcı deneyimi yaşamalarına olanak sağlayacak bir arama motoru tasarımı makine öğrenmesi teknikleri ile yapılmıştır.

Algoritmaların İncelenmesi ile İlgili Yapılan Çalışmalar

Acı (2009), çalışmasında Bayes, K-En Yakın Komşu Metotları ve Genetik Algoritma Kullanılarak Hibrit Sınıflama ve Kestirim Eniyileme Tabanlı Sınıflama Metodunda K-En Yakın Komşu Metodundan Faydalanılması konularında araştırma yapılmıştır. Öğrenmeyi zorlaştıran verilerin elenmesi ile en iyi sınıflamayı yapmak amaçlanmıştır. Test işlemleri, University of California Irvine (UCI) makine öğrenmesi veri kümelerinin en bilinenlerinden beşi olan Iris, Breast Cancer, Glass, Yeast ve Wine ile yapılmıştır.

Pekel (2018), probleme yaklaşımlarına göre farklılık gösteren (sınıflandırma, tahmin, kümeleme) ve bu yüzden farklı problemlerde farklı başarılara sahip olan birçok makine öğrenmesi yöntemi bulunduğunu vurgulamış ve dört temel sınıflandırma algoritmasını (Karar Ağacı, Destek Vektörü Makineleri, Naive Bayes, Yapay Sinir Ağları) sunmuş ve hazır veri setindeki performanslarını karşılaştırmıştır. Naive Bayes Algoritmasının, veri setinde uygulanan diğer sınıflandırma yöntemlerinden daha iyi performans (%70,29) gösterdiği tespit edilmiştir.

Keskin (2018), literatürde her birinin kendi içinde karmaşık bir teoriye sahip oldukları görülen, Karar Ağacı, Naive Bayes, Rastgele Orman ve K-en yakın komşu sınıflandırma algoritmalarını R programında yazılan kodlar yardımıyla, farklı veri tiplerine uygulanması ile daha anlaşılır ve açık bir şekilde sunmayı hedeflemiştir. Ayrıca gerçek bir veri kümesi üzerinden, son dönemlerde makine öğrenmesi yöntemleri için son kullanıcı dostu yeniliklerle ön plana çıkan KNIME programı yardımıyla yukarıda bahsedilen dört makine öğrenme sınıflandırma algoritmasının bir performans karşılaştırması yapılmıştır.

Büyük Veri Analizi

Yardımcı (2011), çalışmasında makine öğrenmesi teknikleri ile kullanıcıya bilgiyi filtrelemesinde veya analiz etmesinde kolaylık sağlayan bir sistem sunulması amaçlanmıştır.

Hallaç (2014) çalışmasında, büyük veri ve bulut bilişim teknolojileri, büyük veri üzerinde paralel algoritmaların çalıştırılması ve dağıtık makine öğrenmesi algoritmalarının büyük veriye uygulanması incelenmiştir.

Erdem (2017) çalışmasında, büyük verinin işlenmesi ve analiz edilmesi için geliştirilen Apache Spark teknolojisi kullanılarak farklı büyük veriler üzerinde sınıflandırma, kümeleme ve aykırı değer algılama işlemlerinin yapılması amaçlanmıştır. Bu amaçla, makine öğrenmesi algoritmalarını içeren Apache Spark'ın MLlib kütüphanesinden faydalanılmıştır. Bu çalışmada kullanılan MLlib kütüphanesinde yer alan Naïve Bayes, K-means ve Gaussian Mixture yöntemleri ile büyük verilerin başarılı bir şekilde analiz edilmesi sağlanmış algoritmaların çalışma süreleri farklı veri boyutları kullanılarak tespit edilmiştir.

Keskin (2018), bulut servisi üzerinde büyük veri araçları kullanılarak büyük veride keşifçi veri analizi, büyük veri görselleştirmesi ve büyük veride makine öğrenmesi uygulamaları gerçekleştirmiştir. Uygulamada Amazon Web Servisi Elastic Map Reduce, Apache Hadoop, Apache Hive, Apache Spark ve R Studio kullanılmıştır. Makine öğrenmesi literatüründe yer alan ve sık kullanılan algoritmalar ele alınmış ve uygulama içinde performansları karşılaştırılmıştır.

Kavuncu (2018), internet üzerinden veya çevrimdışı olarak elde edilen büyük verinin saklanmasının oldukça zor olduğunu ve düzenlenerek bir araya getirilen verilerin makine öğrenmesi ve derin öğrenme yöntemler ile anlamlandırılarak yeni veya öngörülemeyen veriler için doğru tahminlerde kullanılabileceğini ifade etmiştir. Çalışmasında, derin öğrenme yöntemi ve diğer makine öğrenmesi yöntemleri gerçek görüntülerden oluşan CIFAR-10 ve MNIST veri setleri üzerinde uygulanmıştır.

Çelebi (2018), büyük bilgi tabanları üzerinde çıkarım yapmak için yaklaşım sunmuştur. Bu yaklaşımlar, bilgi tabanını bir çizge olarak ele almakta ve bu çizgenin karakteristiğini elde etmek için öznitelikler oluşturmaktadır. Öznitelikler ise, makine öğrenmesi modellerini eğitmek için kullanılmaktadır. Çalışma kapsamında biyolojik ve biyomedikal bilgi ağlarında varlıklar arasında yeni ilişkileri keşfetmek için bilgi çizgeleri kullanarak makine öğrenmesi temelli melez bir yaklaşım önerilmiştir.

Baysal (2019), geleneksel yöntemlerle işlenemeyecek boyut ve çeşitlilikteki veriler için geliştirilmiş olan dağıtık veri yönetim ve analiz araçlarını kullanarak makine öğrenmesi uygulamaları geliştirmiştir. Uygulamalar Google Cloud hizmeti kullanılarak oluşturulmuş Spark kümesi üzerinde pyspark kütüphaneleri kullanılarak gerçekleştirilmiştir. Çalışmada iki farklı veri seti kullanılarak makine öğrenmesi uygulamaları gerçekleştirilmiştir.

Tüketici/Müşteri Tercihleri

Ceylan (2018), çamaşır yumuşatıcı kategorisinde, tüketicilerin marka alım tercihlerinin sınıflandırmaya dayalı makine öğrenmesi teknikleri kullanılarak belirlenebilmesini amaçlamıştır. Extreme Gradient Boosting ve Naive Bayes Sınıflandırma algoritmaları kullanılarak modellenmiştir. Veri analizi sırasında SQL ve R programı kullanılmıştır.

Günay (2018), çalışmasında makine öğrenmesi teknikleri ile telekomünikasyon sektöründeki müşterilerin üyelikten çıkıp çıkmayacağını tahmin etmiştir. Konu ile ilgili geçmişte yapılan çalışmalar incelendiğinde en çok kullanılan yöntemler bulunmuş ve algoritmaların performansı ölçülmüştür. Bununla birlikte Lojistik Regresyon ve Naive Bayes yöntemleri kullanılarak yeni bir yöntem önerilmiştir. Bu

yeni yöntemin tahmin başarısının Naif Bayes ve Lojistik Regresyon yöntemlerinden daha yüksek olduğu görülmüştür.

BULGULAR

Çalışmada Türkiye'de makine öğrenmesi algoritmaları kullanılarak yapılan tez çalışmaları incelenmiştir. Bu amaçla ele alınan 146 tez çalışması ekonomi, enerji, inşaat, eğitim, sosyal, çevre, fen, ağ güvenliği/güvenlik, duygu analizi/metin sınıflandırma, el/yüz/jest tanıma, spor, ulaşım, sağlık ve diğer alanlar olmak üzere gruplandırılmıştır. Ayrıca, en çok hangi alanda çalışma yapıldığını daha anlaşılır bir şekilde ortaya koymak amacıyla Şekil 3'te görüldüğü üzere grafiklendirilmiştir.

Şekil 3. Türkiye'de Makine Öğrenmesi Çalışma Alanları

Şekil 3'teki grafiği incelediğimiz zaman, bahsi geçen alanlar içerisinde en çok çalışma sağlık alanında yapılmıştır. Ardından diğer alanlarda yapılan çalışmalar gelmekte ve ağ güvenliği, duygu analizi/metin sınıflandırma konularında da çokça çalışma bulunduğu anlaşılmaktadır. 'Diğer alanlar' diye ifade edilen alanda yapılan çalışmaları daha ayrıntılı incelemek amacıyla Şekil 4'te verilen grafik oluşturulmuştur.

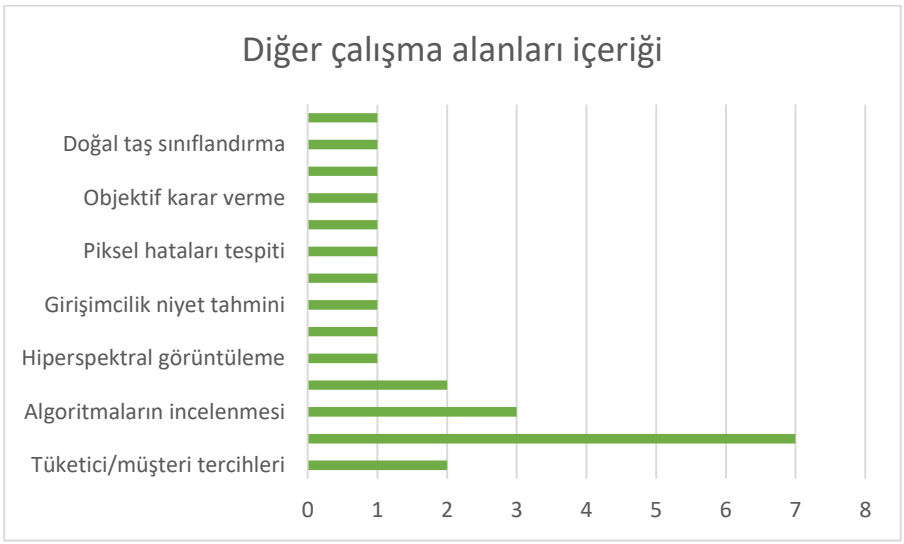

Şekil 4. Diğer Çalışma Alanları

Diğer çalışma alanları içerisinde en çok 'Büyük verinin özetlenmesi, sınıflandırılması' konusu üzerinde durulmuştur. Problem türüne göre değişen algoritma türlerine eleştirel bir gözle bakılan, algoritmaların performanslarının kıyaslandığı ve tartışıldığı çalışmalar ikinci sırada yer almaktadır. Bunun sebebi, makine öğrenmesi ile alakalı çok fazla algoritma bulunmasıdır.

SONUÇLAR ve TARTIŞMA

Çalışma sonucunda elde edilen bilgiler ışığında makine öğrenmesi algoritmaları kullanılarak en fazla çalışma sağlık alanında yapılmıştır. Sağlık verilerinin karmaşıklığı karşısında geleneksel veri analiz yöntemleri yetersiz kalabilmektedir. Bu sebeple karmaşık yapıların anlaşılması, çözümlenebilmesi için makine öğrenmesi yöntemlerine başvurulur. Sağlık alanı, makine öğrenmesi yöntemlerinin sınırlı kullanıldığı ancak çok önemli kullanım potansiyeli olan alanlardan biridir. Sağlık alanında çok fazla çalışma yapılmasına rağmen Şekil 2'de görüldüğü üzere belli başlı hastalıklara/konulara daha çok yönelme olmuştur. Örneğin, diyabet, Parkinson hastalıkları ve kanser teşhisi konuları üzerinde çok fazla çalışma yapılmıştır. Buradan da anlaşılacağı üzere veri tabanına erişim sağlanabilecek ayrıca ölüm riski taşıyan diğer hastalıklar da ele alınabilir. Diğer önemli alanlardan olan enerji, eğitim, fen vb. alanlarda çok fazla çalışma yapılmamıştır. Bu anlamda literatüre katkı sağlamak amacıyla gelecek çalışmalar bu alanlarda yapılabilir.

Çalışmanın amacı doğrultusunda, tez çalışmalarının daha çok hangi alanda olduğunu, genel olarak hangi makine öğrenmesi algoritmalarının kullanıldığı incelenmiştir. Sonuç olarak; sağlık alanında en fazla tez yapıldığı ve K-en yakın komşu, Destek

vektör makineleri, Karar ağaçları, Naive Bayes algoritmalarının sıklıkla kullanıldığı tespit edilmiştir.

KAYNAKLAR

Abuzarifa B.Z.T.T.T. (2018). Estimation of gravity direction using a machine learning model trained on imperfect imu data, M.Sc. Thesis, Gebze Technical University, Department of Computer Engineering, Gebze.

Acı, M. (2009). Development of a hybrid classification method for machine learning, M.Sc. Thesis, Çukurova University, Department of Computer Engineering and Computer Science and Control, Adana.

Acı, M. (2016). Prediction of carbon nanotube atomic coordinates based on machine learning algorithms, Ph.D. Thesis, Çukurova University, Department of Computer Engineering and Computer Science and Control, Adana.

Akar, A. (2017). Machine learning based anomaly detection technique for in-vehicle networks, M.Sc. Thesis, Çankaya University, Department of Electronic and Communication Engineering, Ankara.

Akı, M.O. (2017). Sürücü uykululuğunun gerçek zamanlı görüntü işleme ve makine öğrenmesi teknikleri ile tespitine yönelik bir sistem tasarımı ve uygulaması, Doktora Tezi, Trakya Üniversitesi, Fen Bilimleri Enstitüsü, Edirne.

Akpınar, K.O. (2019). Ethercat tabanlı bir SCADA sisteminde kural ve makine öğrenmesine dayalı saldırı ve anomali tespiti, Doktora Tezi, Sakarya Üniversitesi, Fen Bilimleri Enstitüsü, Sakarya.

Aksoy, F. (2018). Short-term forecasting of wind power production using machine learning and deep learning methods, M.Sc. Thesis, İstanbul Technical University, Department of Electrical Engineering, İstanbul.

Aktaş, F. (2018). Nesneye yönelik sistemlerde kusurlu sınıfların öngörülmesi için makine öğrenmesi temelli bir yöntem oluşturulması, Yüksek Lisans Tezi, İstanbul Teknik Üniversitesi, Fen Bilimleri Enstitüsü, İstanbul.

Aktepe, Ç. (2018). Algorithmic trading on cryptocurrency markets using machine learning techniques, M.Sc. Thesis, Boğaziçi University, Department of Industrial Engineering, İstanbul.

Alamin, M. (2016). Power consumption estimation using in-memory database computation, M.Sc. Thesis, Kadir Has University, Department of Information Technology, İstanbul.

Al-Asadi, M.A.M. (2018). Decision support system for a football team management by using machine learning techniques, M.Sc. Thesis, Selçuk University, Department of Computer Engineering, Konya.

Alnawas, A.D.M. (2019). Sentiment analysis in Iraqi Arabic dialects based on distributed representations of sentences and machine learning approach, Ph.D.

Thesis, Gazi University, Department of Computer Engineering and Computer Science and Control, Ankara

Alp, E.C. (2018). Makine öğrenmesi yöntemleriyle akan görüntülerden otomatik aktivite sınıflandırma, Yüksek Lisans Tezi, Ankara Üniversitesi, Fen Bilimleri Enstitüsü, İstanbul.

Altan, S.N. (2018). Metin sınıflandırma için makine öğrenmesi tekniklerine dayalı bir yöntem geliştirme, Yüksek Lisans Tezi, Ege Üniversitesi, Fen Bilimleri Enstitüsü, İzmir.

Ardıç, E. (2018). Machine learning techniques for the estimation of material properties from light spectrum data, M.Sc. Thesis, Gebze Technical University, Department of Computer Engineering, Gebze.

Ataş, M. (2011). Hyperspectral imaging and machine learning of texture foods for classification, Ph.D. Thesis, Middle East Technical University, Department of Computer Engineering and Computer Science and Control, Ankara.

Ayata, D. (2018). Applying machine learning and natural language processing techniques to twitter sentiment classification for turkish and english, M.Sc. Thesis, İstanbul Technical University, Department of Computer and Control Engineering, İstanbul.

Balta, A. (2018). Makine öğrenmesi teknikleri ile ekolojik verilerin değerlendirilmesi, Yüksek Lisans Tezi, Fırat Üniversitesi, Fen Bilimleri Enstitüsü, Elazığ.

Başkaya, F. (2017). Kısa metinlerden sosyal duygu sınıflandırma için makine öğrenmesi tabanlı yöntemlerin geliştirilmesi, Yüksek Lisans Tezi, Fırat Üniversitesi, Fen Bilimleri Enstitüsü, Elazığ.

Baysal, E. (2019). Dağıtık veri yönetim ve işleme mimarisi kullanılarak makine öğrenmesi uygulamaları gerçekleştirilmesi, Yüksek Lisans Tezi, Sakarya Üniversitesi, Fen Bilimleri Enstitüsü, Sakarya.

Belek, Y.U. (2018). Safe path planning with machine learning, M.Sc. Thesis, İstanbul University, Department of Computer Engineering, İstanbul.

Bilgili, L. (2018). Gemi yaşam döngüsünde operasyonel gaz emisyonlarının makine öğrenmesi yöntemiyle tahmini, Doktora Tezi, Yıldız Teknik Üniversitesi, Fen Bilimleri Enstitüsü, İstanbul.

Bilgilioğlu, S.S. (2018). Makine öğrenmesi teknikleri ile mekansal karar destek sistemlerinin geliştirilmesi: Aksaray ili örneği, Doktora Tezi, Aksaray Üniversitesi, Fen Bilimleri Enstitüsü, Aksaray.

Bulut, M.A., 2019. Kredi analizinde makine öğrenmesi kullanımı: Tarımsal kredilerde uygulama örneği, Doktora Tezi, Eskişehir Osmangazi Üniversitesi, Sosyal Bilimler Enstitüsü, Eskişehir.

Büber, E. (2017). Oltalama saldırılarında kullanılan URL'lerin makine öğrenmesi teknikleri ile tespit edilmesi, Yüksek Lisans Tezi, Marmara Üniversitesi, Fen Bilimleri Enstitüsü, İstanbul.

Ceylan, T. (2018). Perakende sektöründe makine öğrenmesine dayalı yaklaşımlar, Yüksek Lisans Tezi, Yıldız Teknik Üniversitesi, Fen Bilimleri Enstitüsü, İstanbul.

Çelebi, R. (2018). Biyomedikal bilgi çizgeleri için makine öğrenmesi tabanlı anlamsal bağ tahmini, Yüksek Lisans Tezi, Ege Üniversitesi, Fen Bilimleri Enstitüsü, İzmir.

Çelen, P.D. (2017). Makine öğrenmesi tekniği ile konuşma kayıtlarının hızlandırılması, Yüksek Lisans Tezi, Gazi Üniversitesi, Fen Bilimleri Enstitüsü, Ankara.

Çelik, A. (2019). LCD piksel hatalarının makine öğrenmesi yöntemleri ile tespiti, Yüksek Lisans Tezi, Kocaeli Üniversitesi, Fen Bilimleri Enstitüsü, Kocaeli.

Çelikel, A.D. (2018). Stock value prediction using machine learning and text mining, M.Sc. Thesis, Kadir Has University, Department of Management Information Systems, İstanbul.

Çetingöz, M. (2011). Makine öğrenmesi ile Türkçe haber metinlerinde anahtar ifade çıkarımı, Yüksek Lisans Tezi, Trakya Üniversitesi, Fen Bilimleri Enstitüsü, Edirne.

Çınar, A.M. (2019). Çok kanallı optik görüntülerin makine öğrenmesi teknikleri ile sınıflandırılması ve analizi, Yüksek Lisans Tezi, Erciyes Üniversitesi, Fen Bilimleri Enstitüsü, Kayseri.

Çiftçi, F. (2018). Öznitelik seçme ve makine öğrenmesi yöntemleriyle eğitmen performansının tahmin edilmesi, Yüksek Lisans Tezi, Anadolu Üniversitesi, Fen Bilimleri Enstitüsü, Eskişehir.

Çizer, E.B. (2018). Makine öğrenmesi teknikleriyle kredi risk analizi, Yüksek Lisans Tezi, Marmara Üniversitesi, Fen Bilimleri Enstitüsü, İstanbul.

Dabanoğlu, M.B. (2018). Makine öğrenmesi ile gerçek zamanlı videodan yüz ifadesi analizi, Yüksek Lisans Tezi, Karadeniz Teknik Üniversitesi, Fen Bilimleri Enstitüsü, Trabzon.

Das, K., & Behera, R. N. (2017). A survey on machine learning: concept, algorithms and applications. *International Journal of Innovative Research in Computer and Communication Engineering*, *5*(2), 1301-1309.

Demir, H. (2018). Makine öğrenmesi yöntemleri ile arı alt türlerinin sınıflandırılması, Yüksek Lisans Tezi, Düzce Üniversitesi, Fen Bilimleri Enstitüsü, Düzce.

Demirel, U. (2019). Hisse senedi fiyatlarının makine öğrenmesi yöntemleri ve derin öğrenme algoritmaları ile tahmini, Yüksek Lisans Tezi, Gümüşhane Üniversitesi, Sosyal Bilimler Enstitüsü, Gümüşhane.

Demirhan, T. (2015). Makine öğrenmesi algoritmalarının karmaşıklık ve doygunluk analizinin bir veri kümesi üzerinde gerçekleştirilmesi, Doktora Tezi, Trakya Üniversitesi, Fen Bilimleri Enstitüsü, Edirne.

Doğrusöz, A. (2007). Makine öğrenmesi teknikleri ile metinlerin otomatik olarak sınıflandırılması, Yüksek Lisans Tezi, Yıldız Teknik Üniversitesi, Fen Bilimleri Enstitüsü, İstanbul.

Erdem, Y. (2017). Büyük verinin makine öğrenmesi yöntemleri ile apache spark teknolojisi kullanılarak sınıflandırılması, Yüksek Lisans Tezi, Karabük Üniversitesi, Fen Bilimleri Enstitüsü, Karabük.

Garip, E. (2017). OECD ülkelerindeki karbondioksit (co2) emisyonunun makine öğrenmesi ile tahmin edilmesi, Yüksek Lisans Tezi, İstanbul Medeniyet Üniversitesi, Fen Bilimleri Enstitüsü, İstanbul.

Ghahremanlou, N.S. (2012). Prediction of maximum oxygen uptake from maximal and non-exercise variables using machine learning methods, M.Sc. Thesis, Çukurova University, Department of Computer Engineering and Computer Science and Control, Adana.

Gülaçar, H. (2018). Nesnelerin interneti platformları için makine öğrenmesi tabanlı bir tahmin modülü, Yüksek Lisans Tezi, İstanbul Teknik Üniversitesi, Fen Bilimleri Enstitüsü, İstanbul.

Güldan, S. (2014). Makine öğrenmesi yöntemleriyle gerçek olmayan tüketici yorumlarının tespiti, Yüksek Lisans Tezi, İstanbul Kültür Üniversitesi, Fen Bilimleri Enstitüsü, İstanbul.

Günay, M. (2018). Makine öğrenmesiyle müşteri kayıplarının tahmini, Yüksek Lisans Tezi, İstanbul Üniversitesi, Fen Bilimleri Enstitüsü, İstanbul.

Güneş, A. (2017). Hiperspektral görüntüleme ve makine öğrenmesi teknikleri ile küflü kuru incirlerin tahribatsız olarak tespiti, Doktora Tezi, Süleyman Demirel Üniversitesi, Fen Bilimleri Enstitüsü, Isparta.

Güvenç, B. (2016). Machine learning methods in natural language processing, M.Sc. Thesis, Boğaziçi University, Computer Engineering and Computer Science and Control, İstanbul.

Hallaç, İ.R. (2014). Büyük veri analizinde dağıtık makine öğrenmesi algoritmalarının kullanılması, Yüksek Lisans Tezi, Fırat Üniversitesi, Fen Bilimleri Enstitüsü, Elazığ.

Hassan, Y.A.H. (2017). Improving indoor positioning system by using wi-fi fingerprint with machine learning methods, M.Sc. Thesis, Siirt University, Department of Electrical and Electronics Engineering, Siirt.

Işık, M. (2019). Müşteri yorumları üzerinde metin analitiği çalışmaları ve yorumların makine öğrenmesi algoritmaları ile modellenmesi, Yüksek Lisans Tezi, İstanbul Medeniyet Üniversitesi, Lisansüstü Eğitim Enstitüsü, İstanbul.

İşyapar, M.T. (2013). Classification of electricity customers based on real consumption values using data mining and machine learning techniques and its corresponding applications, M.Sc. Thesis, Middle East Technical University, Department of Computer Engineering and Computer Science and Control, Ankara.

Kalaycı, S. (2018). Makine öğrenmesi yöntemleri ile kredi risk analizi, Yüksek Lisans Tezi, İstanbul Teknik Üniversitesi, Fen Bilimleri Enstitüsü, İstanbul.

Kanmaz, M. (2018). The effect of financial news on bist stock prices: A machine learning approach, M.Sc. Thesis, Middle East Technical University, Department of Economics, Ankara.

Kapar, F. (2018). Phıshıng saldırısında kullanılan web sitelerinin makine öğrenmesi algoritmaları yardımıyla tespiti ve uygulaması, Yüksek Lisans Tezi, Van Yüzüncü Yıl Üniversitesi, Fen Bilimleri Enstitüsü, Van.

Karabıyık, M.A. (2018). Akademik yayınlar için makine öğrenmesi tabanlı arama motoru tasarlanması ve uygulanması, Yüksek Lisans Tezi, Süleyman Demirel Üniversitesi, Fen Bilimleri Enstitüsü, Isparta.

Karabina, A. (2017). Konuşmacı tanımada makine öğrenmesi tekniklerinin kullanımı, Yüksek Lisans Tezi, Ondokuz Mayıs Üniversitesi, Fen Bilimleri Enstitüsü, Samsun.

Karataş, B. (2018). Araç sürüş verilerinden makine öğrenmesi tekniklerini kullanarak sürücü sınıflandırma, Yüksek Lisans Tezi, TOBB Ekonomi ve Teknoloji Üniversitesi, Fen Bilimleri Enstitüsü, Ankara.

Kavuncu, S.K. (2018). Makine öğrenmesi ve derin öğrenme: Nesne tanıma uygulaması, Yüksek Lisans Tezi, Kırıkkale Üniversitesi, Fen Bilimleri Enstitüsü, Kırıkkale.

Kaya, Ç. (2017). Saldırı tespit sistemlerinde makine öğrenmesi tekniklerinin kullanılması: Karşılaştırmalı performans analizi, Yüksek Lisans Tezi, Gazi Üniversitesi, Fen Bilimleri Enstitüsü, Ankara.

Kaya, E. (2018). Machine learning techniques for surface electromyography based hand gesture recognition, M.Sc. Thesis, İstanbul Technical University, Department of Control and Automation Engineering, İstanbul.

Kaytan, M. (2017). Web tabanlı oltalama saldırılarının makine öğrenmesi yöntemleri ile tespiti, Yüksek Lisans Tezi, İnönü Üniversitesi, Fen Bilimleri Enstitüsü, Malatya.

Keçeli, H. (2016). Haber kaynaklarından makine öğrenmesi ile Türkiye genelinde zaman bazlı elektrik enerjisi tüketim modeli, Yüksek Lisans Tezi, Türk Hava Kurumu Üniversitesi, Fen Bilimleri Enstitüsü, Ankara.

Keskin, A.K. (2018). Makine öğrenmesi sınıflandırma algoritmalarının incelenmesi, Yüksek Lisans Tezi, Sinop Üniversitesi, Fen Bilimleri Enstitüsü, Sinop.

Keskin, M.V. (2018). Büyük veride makine öğrenmesi uygulaması, Yüksek Lisans Tezi, Yıldız Teknik Üniversitesi, Fen Bilimleri Enstitüsü, Kocaeli.

Khalifa, I.A.K. (2019). Still image steganography detection based on machine learning techniques, M.Sc. Thesis, Siirt University, Department of Computer Engineering and Computer Science and Control, Siirt.

Kurt, E.M. (2019). Apache spark ve makine öğrenmesi algoritmaları ile ağ saldırısı tespiti, Yüksek Lisans Tezi, Kocaeli Üniversitesi, Fen Bilimleri Enstitüsü, Kocaeli.

Kutlugün, M.A. (2017). Gözetimli makine öğrenmesi yoluyla türe göre metinden ses sentezleme, Yüksek Lisans Tezi, İstanbul Sabahattin Zaim Üniversitesi, Fen Bilimleri Enstitüsü, İstanbul.

Mbarak, W.K. (2017). Using machine learning approaches to construct correlations for cohesive soils using in-situ and laboratory data, M.Sc. Thesis, Boğaziçi University, Department of Civil Engineering, İstanbul.

Monhamady, K.K. (2018). Developing machine learning methods for business intelligence, M.Sc. Thesis, Abdullah Gül University, Department of Electrical and Computer Engineering, Kayseri.

Namlı, Ö.H. (2018). Film endüstrisinde makine öğrenmesi algoritmaları ile yeni ürünlerin gelir tahmini, Yüksek Lisans Tezi, İstanbul Üniversitesi, Fen Bilimleri Enstitüsü, Endüstri Mühendisliği Anabilim Dalı, İstanbul.

Onan, A. (2016). Görüş sınıflandırma için makine öğrenmesi algoritmalarına dayalı bir yöntem tasarımı ve gerçekleştirimi, Doktora Tezi, Ege Üniversitesi, Fen Bilimleri Enstitüsü, İzmir.

Orakçı, M. (2017). Veri madenciliği ve makine öğrenmesi kullanılarak suç analizi, Yüksek Lisans Tezi, Gazi Üniversitesi, Bilişim Enstitüsü, Ankara.

Oruç, S.N. (2019). Prediction of entrepreneurial intentions by using machine learning, M.Sc. Thesis, Bahçeşehir University, Department of Entrepreneurship and Innovation Management, İstanbul.

Öz, E. (2019). Empirical Studies on Price Determinants of Online Auctions with Machine Learning Applications, Ph.D. Thesis, Middle East Technical University, Department of Economics, Ankara.

Özdağ, F.S. (2017). Makine öğrenmesi yöntemiyle ağ ataklarının tespiti, Yüksek Lisans Tezi, İstanbul Üniversitesi, Fen Bilimleri Enstitüsü, İstanbul.

Özhan, O. (2014). Makine öğrenmesi ile uzaktan eğitim öğrencilerinin performanslarının değerlendirilmesi, Doktora Tezi, İstanbul Üniversitesi, Fen Bilimleri Enstitüsü, İstanbul.

Özkan, T.K. (2015). Makine öğrenmesi yöntemleri ile vakıf üniversiteleri doluluk tahminlemesi, Doktora Tezi, Marmara Üniversitesi, Sosyal Bilimler Enstitüsü, İstanbul.

Öztel, İ. (2018). Kısmi ve tam yüz görüntüleri üzerinde makine öğrenmesi yöntemleriyle yüz ifadesi tespiti, Doktora Tezi, Sakarya Üniversitesi, Fen Bilimleri Enstitüsü, Sakarya.

Öztürk, M. (2018). Makine öğrenmesi ve görüntü işleme tekniklerini kullanarak drone ile yaprak sınıflandırma, Yüksek Lisans Tezi, İstanbul Teknik Üniversitesi, Fen Bilimleri Enstitüsü, İstanbul.

Pekel, E. (2018). Farklı makine öğrenmesi algoritmalarının karşılaştırılması, Yüksek Lisans Tezi, Ondokuz Mayıs Üniversitesi, Fen Bilimleri Enstitüsü, Samsun.

Peynirci, G. (2018). Malware detection for the android platform using machine learning techniques, Ph.D. Thesis, Yaşar University, Department of Computer Engineering, İzmir.

Rıhtım, M.F. (2018). Makine Öğrenmesi Bazlı Arama Motoru, Yüksek Lisans Tezi, Beykent Üniversitesi, Fen Bilimleri Enstitüsü, İstanbul.

Sarı, Y. (2017). Ses kayıtlarındaki insan seslerinin makine öğrenmesi yöntemleriyle tanınması ve sınıflandırılması, Yüksek Lisans Tezi, Karabük Üniversitesi, Fen Bilimleri Enstitüsü, Karabük.

Sayın, G. (2019). Halka açık finans dışı şirketlerde süreklilik riskinin makine öğrenmesi ile öngörülmesi, Doktora Tezi, İstanbul Aydın Üniversitesi, Sosyal Bilimler Enstitüsü, İstanbul.

Shalev-Shwartz, S., and Ben-David, S., (2014). Understanding Machine Learning: From Theory to Algorithms, *Cambridge University Press,* Cam.

Soylu, T. (2018). Makine öğrenmesi yöntemleri kullanılarak FPGA tabanlı gerçek zamanlı yeni bir trafik sınıflandırma mimarisi tasarımı, Doktora Tezi, Trakya Üniversitesi, Fen Bilimleri Enstitüsü, Edirne.

Sümbül, F. (2008). Determination of protein-protein binding sites using machine learning tools, M.Sc. Thesis, Boğaziçi University, Department of Chemical Engineering, İstanbul.

Şahinarslan, F.V. (2019). Makine öğrenmesi algoritmaları ile nüfus tahmini: Türkiye örneği, Yüksek Lisans Tezi, İstanbul Teknik Üniversitesi, Sosyal Bilimler Enstitüsü, İstanbul.

Şirin, V. (2012). Machine learning methods for opponent modeling in games of imperfect information, M.Sc. Thesis, Middle East Technical University, Department of Computer Engineering and Computer Science and Control, Ankara.

Taşpınar, M. (2017). A feature based simple machine learning approach with word embeddings to named entity recognition on tweets, M.Sc. Thesis, Galatasaray University, Department of Computer Engineering, İstanbul.

Tekcan, F.M. (2018). Makine öğrenmesi ile hiperspektral görüntü sınıflandırma, Yüksek Lisans Tezi, İstanbul Üniversitesi, Fen Bilimleri Enstitüsü, İstanbul.

Temiz, M. (2018). Doğal taş karolarının görüntü işleme ve makine öğrenmesi teknikleri ile sınıflandırılması, Yüksek Lisans Tezi, Sivas Cumhuriyet Üniversitesi, Sosyal Bilimler Enstitüsü, Sivas.

Topuz, M.D. (2014). Makine öğrenmesi algoritmaları ve anomali tespiti, Yüksek Lisans Tezi, Bahçeşehir Üniversitesi, Fen Bilimleri Enstitüsü, İstanbul.

Tozlu, İ. (2019). Simplifying balance sheet adjustment process in commercial loan applications using machine learning methods, M.Sc. Thesis, İstanbul Technical University, Department of Computer Engineering, İstanbul.

Turhal, U. (2016). Yüz resimlerinden çoklu makine öğrenmesi yaklaşımları ile yaş ve cinsiyet bilgisinin tespit edilmesi, Yüksek Lisans Tezi, Yalova Üniversitesi, Fen Bilimleri Enstitüsü, Yalova.

Türkoğlu, S. (2017). Developing oxygen amount prediction model of basic oxygen furnace steelmaking process with machine learning algorithms, M.Sc. Thesis, Çukurova University, Department of Computer Engineering and Computer Science and Control, Adana.

Ulutaş, A.E. (2018). Protein fragment selection using machine learning, M.Sc. Thesis, Abdullah Gül University, Department of Electrical and Computer Engineering, Kayseri.

Uzel, E. (2018). Makine öğrenmesi ile FOREX piyasalarında alım satım kararları uygulaması, Yüksek Lisans Tezi, Atılım Üniversitesi, Sosyal Bilimler Enstitüsü, Ankara.

Ünsal, Ö. (2011). Mesleki alan seçimlerinin makine öğrenmesi algoritması kullanılarak belirlenmesi, Yüksek Lisans Tezi, Gazi Üniversitesi, Bilişim Enstitüsü, Ankara.

Yardımcı, T. (2011). Makine öğrenmesi teknikleri ile RSS besleme yönetimi, Yüksek Lisans Tezi, Gazi Üniversitesi, Bilişim Enstitüsü, Ankara.

Yarmatov, B. (2017). Hibrid makine öğrenmesi teknikleri ile yol yüzey durumunun modellenmesi, Yüksek Lisans Tezi, Süleyman Demirel Üniversitesi, Fen Bilimleri Enstitüsü, Isparta.

Yıldırım, M.Z. (2017). Makine öğrenmesi yöntemleri ile network üzerinde saldırı tespiti, Yüksek Lisans Tezi, Karabük Üniversitesi, Fen Bilimleri Enstitüsü, Karabük.

Yıldız, O. (2014). Makine öğrenmesi ile uzaktan eğitim öğrencilerinin performanslarının değerlendirilmesi, Doktora Tezi, İstanbul Üniversitesi, Fen Bilimleri Enstitüsü, İstanbul.

Yoldaş, M. (2011). Predicting the effect of hydrophobicity surface on binding affinity of pcp-like compounds using machine learning methods, M.Sc. Thesis, Middle East Technical University, Department of Computer Engineering and Computer Science and Control, Ankara.

Yurdakurban, V. (2018). Yazılım projelerinde iş gücü tahmini için makine öğrenmesi yöntemlerinin karşılaştırılması, Yüksek Lisans Tezi, İstanbul Teknik Üniversitesi, Fen Bilimleri Enstitüsü, İstanbul.

PASSIVE THERMAL MANAGEMENT OF A SIMULATED BATTERY PACK AT DIFFERENT DISCHARGE RATES

Serkan COŞKUN, Sivas Cumhuriyet Üniversitesi Enerji Bilimi ve Teknolojisi Anabilim Dalı, serkancoskn0@gmail.com

Ümit Nazlı TEMEL, Sivas Cumhuriyet Üniversitesi, Mühendislik Fakültesi Makine Mühendsiliği Bölümü, untemel@cumhurieyet.edu.tr

ABSTRACT: In this study, a thermally enhanced energy storage material is obtained through increasing the low thermal conductivity of the RT-44 organic phase change material (PCM) with a phase change temperature of 41-44 °C by 227.5% via the addition of 7% graphene nanoplatelets (GNP). The thermal management of the obtained 7% GNP / RT-44 composite in a simulated battery pack was examined in terms of temperature rise prevention and maximum temperature difference criteria. At 1.30W and 2.75W heating rates, both RT-44 and 7% GNP / RT-44 passive thermal protection have been found to keep the maximum temperature of the battery pack below 50^{o}C during the entire heating period. For a battery pack operating at 3.90 W, it was found that the duration of maximum temperature staying below 50 °C was increased 9.1 times than the unprotected battery pack and 2.3 times than the RT-44 protected battery pack. It was determined that the maximum temperature difference across the battery pack can be kept below 5 °C for both RT-44 and 7%GNP/RT-44, which is a critical value for thermal protection of battery. However, RT-44 has been shown to be unsuccessful in contrast to 7% GNP/RT-44 in terms of maximum temperature and temperature difference in discharge/cooling cycles.

Key words: battery pack, thermal management, phase change material, nanoparticle

FARKLI DEŞARJ HIZLARINDA ÇALIŞTIRILAN SİMÜLATİF BİR BATARYA PAKETİNİN PASİF TERMAL KORUNUMU

ÖZET: Bu çalışmada; faz değişim sıcaklığı 41-44 ^{o}C arasında olan RT-44 organik faz değişken malzemesinin düşük ısıl iletkenlik problemi, içerisine katkılanan %7 Grafen nanoyaprak (GNP) sayesinde %227.5 civarında arttırılarak termal olarak iyileştirilmiş bir enerji depolama malzemesi elde edilmiştir. Elde edilen %7 GNP/RT-44 kompozitinin simülatif bir pil paketi içerisindeki termal yönetimi, sıcaklık artışını önleme ve maksimum sıcaklık farkı kriterleri açısından incelenmiştir. 1.30W ve 2.75W ısıtma hızlarında gerek RT-44 gerekse de %7 GNP/RT-44 pasif termal korumasının simülatif batarya paketi maksimum sıcaklığını tüm ısıtma süresince 50^{o}C'nin altında tutuğu belirlenmiştir. 3.90W ısıtma hızında çalışan simülatif pil paketi için maksimum

sıcaklığın 50 °C'nin altında kalma süresinin korumasız pil paketine göre 9.1 kat, RT-44 korumalı pil paketine göre 2.3 kat uzatıldığı tespit edilmiştir. Pil paketi boyunca maksimum sıcaklık farkının hem RT-44 hem de %7 GNP/RT-44 koruması için kritik değer olan 5 °C'nin altında tutulabildiği belirlenmiştir. Bununla birlikte RT-44'ün ısıtma/soğutma çevrimlerinde maksimum sıcaklık ve sıcaklık farkı açısından %7 GNP/RT-44'ün aksine başarısız olduğu gösterilmiştir.

Anahtar sözcükler: pil paketi, termal koruma, faz değişken malzeme, nanoparçacık

GİRİŞ

Lityum-iyon piller; yüksek enerji yoğunluğu ve özgül gücü, yüksek deşarj voltajı ve uzun şarj/deşarj çevrim ömrü gibi avantajlarından dolayı güç gerektiren sistemler için en uygun güç kaynaklarından birisidir(Jarrett & Kim, 2011)(Lin, Xu, Chang, & Liu, 2015). Gerekli güç gereksinimini sağlamak için Lityum-iyon piller seri ve paralel bağlanarak pil paketi haline getirilmektedirler. Pil hücrelerinin deşarj edilmesi sırasında gerek ohmic gerekse de kimyasal enerji dönüşümüne bağlı olarak önemli miktarda ısı üretimi gerçekleşmektedir. Pil içerisinde üretilen ısı, pilin çalışması sırasında önemli derecede sıcaklık artışına maruz kalmasına sebep olmaktadır (Hémery, Pra, Robin, & Marty, 2014)(Qu, Li, & Tao, 2014). Yüksek çalışma sıcaklığı Lityum iyon pillerin en önemli dezavantajı olup, pil paketi içerisinde termal dengesizlik, performans ve kapasite kaybı, şarj/deşarj ömrünün kısalması ve patlama riski gibi birtakım olumsuzluklara neden olmaktadır (Duan & Naterer, 2010). Lityum-iyon pil paketlerinden faydalanma veriminin arttırılabilmesi için optimum çalışma sıcaklığının 20°C-50°C aralığında, paket boyunca hücreler arasındaki sıcaklık farkının 5°C'den düşük tutulması gerekmektedir. Bu durum, lityum-iyon paketlerinin, çalışması sırasında termal olarak korunmasını gerektirmektedir.

Literatürde pil paketlerini termal olarak korumak amacıyla farklı yöntemler kullanılmıştır. Sıvı ve hava soğutmalı aktif soğutma sistemlerinin; sistem karmaşıklığı, maliyet, ek güç gereksinimi (fan veya pompa) ve pil paketi içerisinde düzgün sıcaklık dağılımı sağlayamama gibi dezavantajlara sahip oldukları belirlenmiştir(Zichen Wang, Zhang, Jia, & Yang, 2015)(Ling, Wang, Fang, Gao, & Zhang, 2015)(L. Fan, Khodadadi, & Pesaran, 2013)(Sabbah, Kizilel, Selman, & Al-Hallaj, 2008). Son yıllarda, Faz Değişken Malzeme(FDM) kullanımına dayalı pasif termal koruma yöntemleri araştırmacıların ilgi odağı olmuştur. Organik FDM'ler (parafinler), yüksek enerji depolama kabiliyetlerine ek olarak zehirli ve aşındırıcı etki içermemesi, düşük maliyet gibi birtakım avantajlarından dolayı uygulamalarda en çok tercih edilen FDM türüdür (Sharma, Tyagi, Chen, & Buddhi, 2009)(Yuan, Li, Zhang, Cao, & Yang, 2016). Organik FDM'lerin Lityum-iyon pillerin termal korumasında kullanılabileceği fikri ilk defa Al-Hallaj ve arkadaşları (Hallaj & Selman, 2000) tarafından önerilmiştir. Bununla birlikte organik FDM'lerin bilinen en önemli dezavantajı ısıl iletkenliklerinin düşük olmasıdır. Lityum-iyon pillerin termal yönetiminde FDM ve batarya arasındaki temas sıcaklığını kontrol etmek önemlidir.

Temas sıcaklığı ve pilde üretilen ısının FDM içerisine transfer edilmesi, FDM ısıl iletkenliği ile doğrudan ilişkilidir (Bahiraei, Fartaj, & Nazri, 2017). Bu nedenle organik FDM'lerin yüksek enerji depolama ve düşük ısıl iletkenlik kabiliyetleri arasındaki çelişkiyi çözmek için termal olarak geliştirilmesi gerekmektedir. Organik FDM'lerin ısıl iletkenliklerinin arttırmak için içerisine yüksek ısıl iletkenliğe sahip birçok malzeme katılmıştır (Cui, 2012)(Zhou & Zhao, 2011)(Zhou & Zhao, 2011)(Zhou & Zhao, 2011). Batarya paketi termal korunumu için böyle bir FDM kompozitinin kullanılması durumunda, kompozit bütününün ısı absorblama verimi artacağından paket içerisinde daha homojen bir ısı dağılımı elde edilecektir (Rao & Wang, 2011). Bu olay aynı zamanda, pil paketinin optimum sıcaklıkta tutulma süresini uzatacaktır.

Metal köpükler; yüksek ısıl iletkenlik, gözenekli yapısı nedeniyle FDM kompozitlerin katı iskeletini oluşturmak için kullanılmışlardır (Bhattacharya, Calmidi, & Mahajan, 2002)(Giuliano, Prasad, & Advani, 2012)(Baby & Balaji, 2013). Batarya paketinin termal korumasında Alüminyum köpük/FDM kompoziti kullanıldığında koruma yapılmayan pakete göre maksimum sıcaklık %50 oranında azaltılmıştır (Khateeb, Amiruddin, Farid, Selman, & Al-Hallaj, 2005)(Kizilel et al., 2008). Benzer sonuçlar Cu/FDM kompozitleri için de elde edilmiştir(Li, Qu, He, & Tao, 2014)(Rao, Huo, Liu, & Zhang, 2015). Son yıllarda genişletilmiş grafit/FDM kompozitleri; yüksek ısıl iletkenlik, düşük ağırlık, korozyona karşı direnç ve kullanım kolaylığı açısından batarya paketlerinin termal korumasında yaygın olarak tercih edilmiştir. R Zhao ve arkadaşları (R. Zhao, Gu, & Liu, 2017) metal köpüklerde görülen sıvı FDM sızıntısı probleminin, genişletilmiş grafit matrisi tarafından oluşturulan güçlü kılcal kuvvetler sayesinde önlendiğini tespit etmişlerdir. G. Jiang (Jiang, Huang, Liu, & Cao, 2017) genişletilmiş grafit/FDM kompozitinin, batarya paketi boyunca maksimum sıcaklığı önemli ölçüde azalttığını, maksimum sıcaklık farkını ise 1-2 ^{o}C civarında tuttuğunu belirlemişlerdir. Köpük/FDM kompozitleri her ne kadar batarya paketlerinde etkin koruma sağlasa da köpük gözeneklerine emdirilen FDM miktarının sınırlı oluşu etkin koruma süresini önemli ölçüde kısaltmaktadır. Batarya paketlerinin pasif termal korunumu için önerilen diğer yöntem FDM içerisine metal parçaların ilave edilmesidir. Zhao ve arkadaşları (J. Zhao, Lv, & Rao, 2017) batarya paketinin termal korunmasında FDM içerisine yerleştirilen metal ısı borularının etkilerini deneysel olarak incelemişlerdir. Batarya paketinin 50 ^{o}C'nin altında çalışma süresinin sadece FDM kullanılması durumuna göre önemli derecede arttığını belirlemişlerdir. Benzer olarak Wang ve arkadaşları (Zhiwei Wang, Zhang, & Xia, 2017), FDM/kanatçık yapılarının batarya paketlerinin çalışma süresini sadece FDM kullanılmasına göre belirgin derecede uzattığını bildirmişlerdir. Buna karşılık FDM içerisine metal parçaların eklenmesinin sistem ağırlık/hacmini önemli derecede artırması ve sıvı FDM'nin kristalleşeme problemleri bu yöntemin önemli eksiklikleridir.

Son yıllarda nanoteknoloji alanındaki gelişmelere bağlı olarak sentezlenen nanoparçacıkların ısıl iletkenliği iyileştirmek için FDM içerisine belirli kütle bölüntülerinde katkılanmasına yönelik çalışmalar gerçekleştirilmiştir. Karbon tabanlı nanoparçacıkların; düşük yoğunluk, yüksek ısıl iletkenlik gibi özelliklerinden dolayı

FDM termal iyileştirmesinde diğer metal/metaloksit nanoparçacıklara göre daha iyi sonuçlar verdiği ortaya çıkarılmıştır. Bununla birlikte farklı şekillerdeki karbon tabanlı nanoparçacıkların FDM ısıl iletkenliğinin iyileştirilmesinde farklı etkilere sahip olduğu gözlemlenmiştir. Özellikle levha biçiminde şekil yapısına sahip nanoparçacıkların FDM ısıl iletkenliğini artırmada daha etkin olduğu belirlenmiştir(L. W. Fan et al., 2013)(Liu, Su, Tang, & Fang, 2016). Karbon tabanlı nanoparçacıkların FDM'lerin termal iyileştirilmesine yönelik birçok çalışma olmasına rağmen iyileştirilmiş kompozitlerin batarya paketlerinin termal yönetiminde kullanılması henüz yeni bir konudur. Bu nedenle bu çalışma levha şekline sahip Grafen nanoyaprak parçacıklar (GNP) katkılanarak iyileştirilmiş FDM kompozitinin bir batarya paketinin pasif termal korumasında uygulanmasına odaklanmıştır. Çalışmada öncelikle %0, %3,%5 ve %7 kütle bölüntülerinde GNP ile katkılanan FDM kompozitlerinin termal özellikleri karakterize edilmiştir. Daha sonra en iyi termal özelliklere sahip GNP/FDM kompozitinin simülatif bir pil paketinin termal korumasındaki performansı elde edilerek sadece FDM ve doğal taşınım durumuyla karşılaştırılmıştır.

MATERYAL VE METOD

GNP/FDM Kompozitlerinin Hazırlanması ve Termal Özelliklerinin Belirlenmesi

Çalışmada enerji depolama malzemesi olarak 41-44 ^{o}C aralığında erime sıcaklığına sahip bir organik FDM olan RT-44 (Rubitherm Tech., Germany) kullanılmıştır. RT-44'ün ısıl iletkenliğini arttırmak için kullanılan GNP nanoparçacıklar, 150 m^2/g yüzey alanına ve 6-8 nm plaka kalınlığına sahip olup, Skyspring Nanomaterials şirketinden (USA) temin edilmiş ve herhangi bir ön işleme maruz bırakılmaksızın kullanılmıştır.

GNP/RT-44 kompozitlerini hazırlamak için eritme ve karıştırma işlemleri uygulanmıştır. Öncelikle bir cam kap içerisine konulan katı haldeki RT-44, ısıtma plakası üzerinde ısıtılarak tamamen eriyik hale getirilmiştir. Daha sonra eriyik RT-44 içerisine kütlece %0 (FDM), %3, %5 ve %7 bölüntülerini sağlayacak miktarda GNP eklenmiştir. Sıvı RT-44 içerisinde GNP nanoparçacıkların homojen dağılımlarını sağlamak için elde edilen karışım, 30 dakika boyunca 750 W (Sonics & Materials INC, ABD) gücündeki ultrasonik karıştırma cihazıyla karıştırma işlemine maruz bırakılmıştır.

Elde edilen homojen karışımların ısıl iletkenlikleri, geçici doğrusal ısı kaynağı prensibine çalışan KD2 Pro cihazı (Decagon Devices Inc, USA) ile ölçülmüştür. KD2 Pro cihazına uygun katı faz ölçüm numuneleri ortasında 2.4 mm çapında ve 100 mm uzunluğunda bir mil bulunan, 30 mm çapındaki ve 120 mm uzunluğundaki silindir biçimindeki bir kalıp kullanılarak gerçekleştirilmiştir. Ölçüm numuneleri kalıp içerisine dökülen sıvı haldeki karışımın oda koşullarında katılaşması sonucunda elde edilmiştir. KD2 Pro cihazı bir mikro kontrol birimi ve iğneden oluşmaktadır. İğne hem

ısıtıcı olarak hem de sıcaklık sensörü olarak çalışmakta olup, bir zaman periyodunda ısıtıcı boyunca geçen akım sırasındaki sıcaklık değişimini belirlemektedir. Ölçülen sıcaklıkların zaman periyodu için analiz edilmesi sonucunda ısıl iletkenlik katsayısı belirlenmektedir. Katı faz ölçümleri 20 ^{o}C ortam sıcaklığında cihaza ait katı faz ölçüm iğnesi (TR1) aracılığıyla, sıvı faz ölçümleri 50 ^{o}C ortam sıcaklığında sıvı ölçüm iğnesi (KS1) aracığıyla gerçekleştirilmiştir. Isıl iletkenlik ölçümleri bir iklimlendirme kabini içerisinde gerçekleştirilmiş olup her bir numune en az beş kez ölçülmüş ve ortalama değerler sonuç olarak verilmiştir. Cihazın ölçüm hassasiyeti 0.2-4W/mK aralığı için ±10%, 0.1-0.2W/mK aralığı için ise ±0.02W/mK'dir.

Elde edilen numunelerin erime sıcaklık ve gizli ısıları Diferansiyel Taramalı Kalorimetre (DSC-60 Shimadzu Corporation, Japonya) (DTK) cihazı aracılığıyla ölçülmüştür. Hazırlanan kompozitlerden çıkarılan toz parçacıkların hassas bir elektronik terazide kütle duyarlı olarak 5mg kütlesinde tartılıp, özel bir alüminyum kap içerisine konulması ve preslenmesi suretiyle DTK numuneleri hazırlanmıştır. Tüm kompozitler için DTK sıcaklık artış hızı 20 ^{o}C'den başlayıp 80 ^{o}C'ye ulaşıncaya kadar 2 ^{o}C/dakika olarak ayarlanmıştır. Her bir kompozit için ölçümler en az üç kez gerçekleştirilmiş olup ortalama değerler sonuç olarak verilmiştir. DTK cihazının kalorimetrik hassasiyet ve sıcaklık doğruluğu ±.1% ve ±0.1^{0}C'dir.

Simülatif Pil Paketinin Termal Performans Testleri

Şekil 1 simülatif bir pil paketi için kurulmuş olan deney düzeneğini göstermektedir. Deneysel düzenek; bir pil paketi, DC güç kaynağı, ısıl çiftler, veri toplama birimi ve bilgisayardan oluşmaktadır. Güvenlik ve kolaylık açısından pil paketinde gerçek Lityum-iyon piller yerine elektrikli ısıtıcılar kullanılarak simülatif bir pil paketi oluşturulmuştur. Pil yerine kullanılan elektrikli ısıtıcıların boyutları silindir biçimindeki 18650 Lityum-iyon pillerle (18mm çapında 65mm yüksekliğinde) aynı seçilmiştir. Simüle edilmiş pil paketinde, ısıtıcılar arasındaki etkileşimleri incelemek için, on iki ısıtıcı 4S3P (dört seri 3 paralel) biçiminde bir alüminyum kap içerisine Şekil 1'de gösterildiği gibi dikey olarak monte edilmiştir. Komşu ısıtıcılar arasındaki mesafe 36 mm olarak ayarlanmış olup böylelikle ısıtıcı başına 9 mm RT-44 (veya %7GNP/RT-44) düşmesi sağlanmıştır. Eriyik hale getirilen RT-44 veya %7 GNP/RT-44 kompozitleri, sıvı halde alüminyum kap içerisine dökülmüş ve oda sıcaklığında soğumaya bırakılarak pasif termal korumalı pil paketleri oluşturulmuştur. Sıcaklık ölçümleri ± 0.5 ^{o}C hassasiyete sahip J tipi ısıl çiftler aracılığıyla gerçekleştirilmiştir. Isıl çiftler Şekil 1'de gösterildiği gibi belirli ısıtıcı yüzeylerine ve RT-44 (veya GNP/RT-44) soğutma ortamı içerisine ısıtıcı yarı yüksekliğinde olacak biçimde bağlanmış ve isimlendirilmiştir. Isıl çiftler tarafından ölçülen sıcaklık verileri bir veri toplayıcı (Agilent 34970A) ile 30 saniye aralıklarla toplanarak bilgisayara kaydedilmiştir.

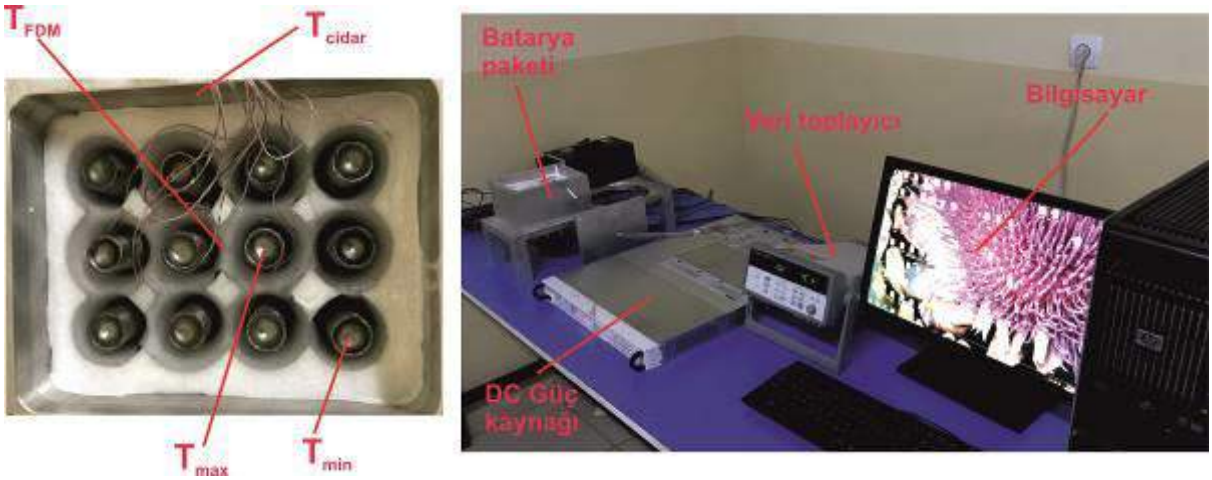

Şekil 1. Simültif Pil Paketi İçin Deneysel Düzenek

BULGULAR VE DEĞERLENDİRMELER

GNP/RT-44 kompozitlerinin katı haldeki (20 ^{o}C) ve sıvı haldeki (50 ^{o}C) ısıl iletkenlik ölçümleri ve ısıl iletkenlikte sağlanan yüzdelik iyileşme oranları Şekil 2'de verilmiştir. RT-44 organik faz değişken malzemesinin katı hal ısıl iletkenliği 0.364 W/mK iken sıvı haldeki ısı iletkenliği 0.153 W/mK olarak ölçülmüştür. Bu durum katılaşma sırasında kristalleşmeye bağlı olarak nanoparçacık/nanoparçacık ve nanoparçacık/RT-44 ara yüzünde daha etkin bir temas alanının oluşmasıyla ilişkilendirilebilir. RT-44 içerisine eklenen GNP kütle bölüntüsünün artmasına bağlı olarak ısıl iletkenlikte doğrusal bir artış olduğu görülmektedir. Bununla birlikte katı numunenin ısıl iletkenliğindeki artış, sıvı numuneye göre nanoparçacık kütle bölüntüsünün daha güçlü bir fonksiyonudur. Bu durum ısıl iletkenlikte görülen artışın eğiminden açıkça görülmektedir. En yüksek nanoparçacık kütle bölüntüsü eklenerek oluşturulan %7 GNP/RT-44 kompozitinin ısıl iletkenlikleri sırasıyla katı ve sıvı hal için 1.192 W/mK ve 0.357 W/mK olarak ölçülmüştür.

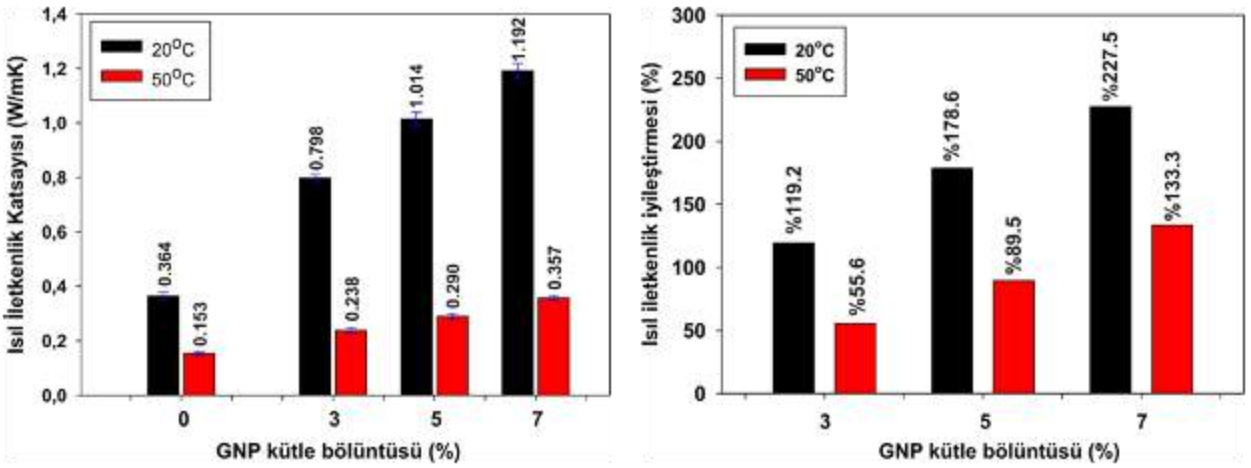

Şekil 2. GNP Kütle Bölüntüsüne Bağlı Isıl İletkenlik Katsayıları ve Isıl İletkenlik İyileştirmeleri

RT-44'e kıyasla, eklenen GNP miktarına bağlı olarak ısıl iletkenlikte elde edilen yüzdelik iyileşmeler hesaplanmış ve Şekil 2'nin sağ tarafında verilmiştir. Kütlece %3 GNP eklenen katı ve sıvı kompozitlerin ısıl iletkenliklerinde sağlanan iyileşmeler sırasıyla %119.2 ve %55.6 iken, en yüksek bölüntüye sahip %7 GNP/RT-44 kompoziti için bu iyileşmeler sırasıyla %227.5 ve %133.3 olarak belirlenmiştir. RT-44 içerisine eklenen GNP kütle bölüntüsünün artmasına bağlı olarak ısıl iletkenlikteki iyileşmenin gerek katı hal gerekse de sıvı hal için arttığı açıktır. Bununla birlikte eklenen GNP miktarının artmasına bağlı olarak katı kompozitlerin ısıl iletkenlik iyileşmelerinin sınırlanmaya başladığı görülmektedir. Buna ilave olarak %7 GNP/RT-44 kompozitinin sıvı halinde eklenen nanoparçacık miktarının kompozit akıcılık özelliğini de önemli ölçüde engellemeye başladığı gözlemlenmiştir. Bu nedenle çalışmada en yüksek kütle bölüntüsüne, dolayısıyla en yüksek ısıl iletkenliğe sahip kompozit olarak %7GNP/RT-44 belirlenmiştir.

Organik FDM'lerin uygulamada kullanılmasını cazip kılan özelliği onların enerji depolama yetenekleridir. Isıl iletkenliklerinin düşük olması ise uygulamada etkin bir biçimde kullanılmalarının önündeki en önemli engeldir. Bu noktada, içerisine GNP ekleyerek ısıl iletkenliğini arttırdığımız GNP/RT-44 kompozitlerinin enerji depolama yeteneklerinin bu durumdan nasıl etkilendiğinin de belirlenmesi gerekmektedir. DTK analizleri, RT-44 ve GNP/RT-44 kompozitlerinin erime sıcaklıkları ve gizli ısılarını belirlemek için gerçekleştirilmiştir. Şekil 3'de DTK analizleri sonucunda elde edilen termogram eğrileri RT-44 ve GNP/RT-44 kompozitleri için aynı grafik üzerinde verilmiştir. Termogram eğrilerinin benzer bir değişim göstererek ekzoterm tepesi oluşturdukları görülmektedir. Ekzoterm tepesinin taban çizgisinden ayrılma ve tekrar birleşme noktaları erime başlangıç ve erime sonlanma sıcaklıkları ile ilişkilidir. Gerek RT-44 gerekse de GNP/RT-44 kompozitleri için elde edilen termogram eğrilerinin analiz edilmesi sonucunda GNP eklentisinin, erime başlangıç ve sonlanma sıcaklıkları üzerinde herhangi bir etkisinin olmadığı belirlenmiştir.

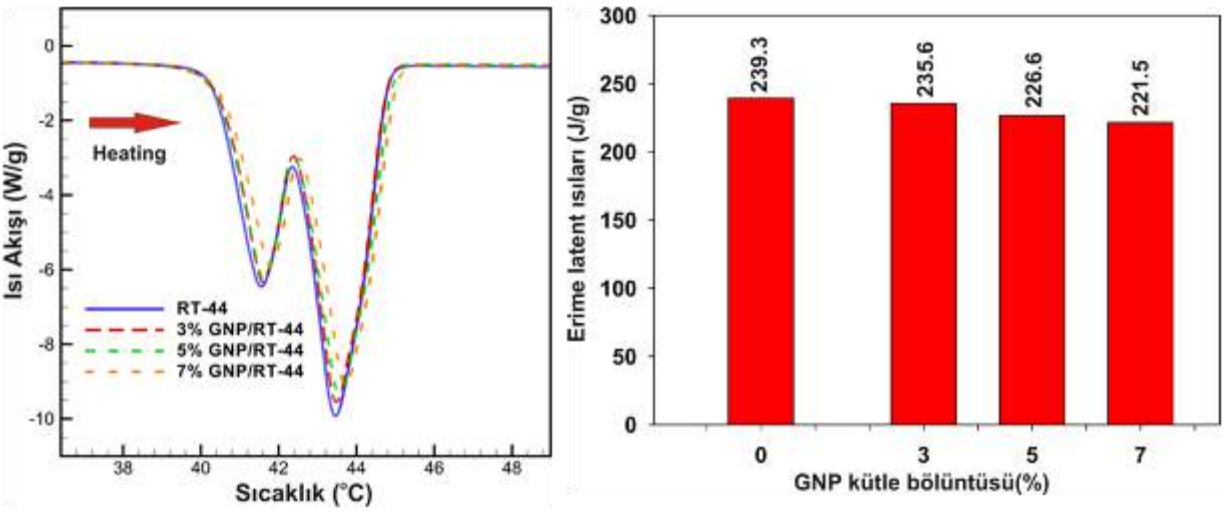

Şekil 3. GNP Kütle Bölüntüsüne Bağlı Termogram Eğrileri ve Erime Gizli Isıları

Bununla birlikte ekzoterm tepesi ile taban çizgisi arasında kalan alan gizli ısının bir göstergesi olup eklenen GNP kütle bölüntüsüne bağlı olarak gizli ısıların azaldığı görülmektedir. Bu sonuç, enerji depolama yeteneğine sahip RT-44 içerisine bu yetenekten yoksun GNP nanoparçacıklar eklenmesi için olağan bir durumdur. Ekzoterm eğrilerinin analiz edilmesi sonucunda elde edilen gizli ısı değerleri Şekil 3'ün sağ tarafında verilmiştir. RT-44'ün erime gizli ısısı 239.3 J/g olarak ölçülmüş olup içerisine %7 GNP eklenmesi durumunda %7.5 kötüleşme göstererek 221.5 J/g değerine düşmüştür. %7 GNP eklenen RT-44 kompozitinin gram başına enerji depolama kapasitesinin hatırı sayılır biçimde 200 J/g üzerinde olmasına ek olarak ısıl iletkenlikte elde edilen en yüksek iyileşme, onun simülatif batarya paketinde soğutma ortamı olarak kullanılmasının uygun olduğu sonucunu doğurmuştur.

Batarya paketlerinin deşarjı sırasında paket içerisindeki maksimum sıcaklık en önemli tasarım parametresi olup, bu sıcaklığın mümkün olduğunca 50 ^{o}C'nin altında olması istenilen durumdur. Oluşturulan simülatif pil paketi içerisindeki maksimum sıcaklığa sahip hücrenin sıcaklık-zaman değişimi herhangi bir koruma olmaması durumu için Şekil 4'te verilmiştir. 1.30W ısıtma hızında 100 dakika sonunda maksimum sıcaklığın 50 ^{o}C sınır değerinin altında olduğu görülmektedir. Özellikle ısıtma işleminin sonuna doğru batarya paketinin çevre ile termal dengeye gelmeye başlaması nedeniyle sıcaklık artışının yavaşladığı görülmektedir. Bununla birlikte ısıtma hızının 2.75W ve 3.90W'a çıkarılması durumunda sıcaklık artışının parabolik artışını devam ettirdiği ve kısa bir süre içerisinde 50 ^{o}C'yi geçtiği görülmektedir. Öyle ki 2.75W ve 3.90W deşarj hızlarında 50 ^{o}C'yi geçme süreleri sırasıyla 13.9 ve 8.7 dakika olarak belirlenmiştir.

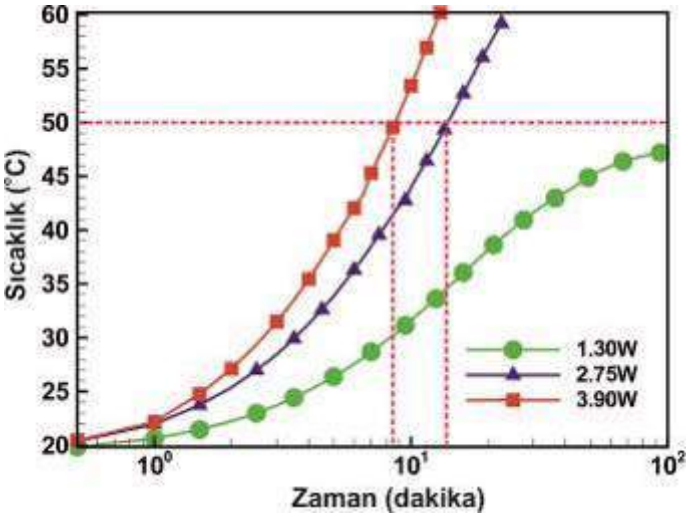

Şekil 4. Pil Paketindeki Maksimum Sıcaklık Hücresinin Sıcaklık-Zaman Değişimi

Bu süreyi uzatabilmek için RT-44 ve %7 GNP/RT-44 kullanımına dayanan pasif termal koruma sistemlerine sahip simülatif batarya paketlerinin performans test sonuçları Şekil 5'de verilmiştir. Simülatif batarya paketi için maksimum sıcaklığa sahip hücre, düşük ısı yayılım yeteneği nedeniyle paket orta bölgesinde olduğu belirlenmiştir. Tam tersi olarak minimum sıcaklığa sahip hücrelerin de pil paketinin dış bölgesine yerleşmiş hücrelerde olduğu belirlenmiştir. Şekil 5, paket içerisindeki farklı noktaların sıcaklıklarının zamana göre değişimini göstermektedir. %7 GNP/RT-44 kompozitinin soğutma ortamı olarak kullanılması durumunda, RT-44 kullanılmasına göre maksimum sıcaklık artışının yavaşlatıldığı, cidar sıcaklık artışının ise hızlandırıldığı görülmektedir. Bu durum paket içerisindeki sıcaklık farklılığının daha dar bir bölgeye sıkışmasından net olarak anlaşılmaktadır. Bu farklılığın nedeni olarak ısıl iletkenlikte sağlanan iyileşme sayesinde ısıtıcı üzerinde açığa çıkan ısıl enerjinin daha etkin bir biçimde ısıtıcıdan uzaklaştırılması gösterilebilir. RT-44 pasif termal korumalı pil paketinde faz değişiminin başlamasıyla sıcaklık değişiminde meydana gelen yavaşlama belirli bir andan itibaren yerini sabit sıcaklık düzlüğüne bırakmaktadır. Bu durum RT-44 içerinde meydana gelen konvektif akımlar etkisiyle ısı transferinin efektif biçimde gerçekleşmeye başlamasıyla ilişkilidir. %7 GNP/RT-44 pasif termal korumasında faz değişiminin başlamasıyla sıcaklık değişiminde RT-44'e nazaran daha etkin bir yavaşlama olmasına rağmen sabit sıcaklık düzlüğü oluşmamaktadır. Bu durum nanoparçacık eklentisiyle ilişkili viskozite artışı yüzünden konvektif akımların bastırılması yüzündendir.

RT-44 ve %7 GNP/RT-44 pasif termal korumasına sahip simülatif batarya paketlerinin 100 dakika sonundaki maksimum sıcaklık hücresi açısından karşılaştırılmasına ait bulgular aşağıdaki biçimde sıralanabilir; i) 1.30W ısıtma hızında RT-44 pasif termal korumasına sahip batarya paketinin maksimum sıcaklık hücresi 37.5 ^{o}C iken %7 GNP/RT-44 pasif termal korumasında bu değer 33.8 ^{o}C'dir, ii) 2.75W ısıtma hızı ve RT-44 pasif termal korumasında maksimum sıcaklık hücresi 49.6^{o}C iken %7 GNP/RT-

44 korumasında maksimum sıcaklık hücresi 44.9^{o}C civarındadır, iii) 3.90W ısıtma hızında RT-44 pasif termal korumalı paketin maksimum sıcaklık hücresi 52.8^{o}C'ye ulaşırken, %7 GNP/RT-44 pasif korumalı paketin maksimum sıcaklık hücresi 52^{0}C'ye ulaşmaktadır. Özellikle 3.90W ısıtma hızında RT-44 ve %7 GNP/RT-44 kompoziti için maksimum sıcaklıklarının birbirine yaklaştığı görülmektedir.

Pil paketleri için maksimum sıcaklık hücresinin 50^{o}C'ye ulaşma süresi etkin kullanım süresi olarak değerlendirilmektedir. RT-44 ve %7 GNP/RT-44 pasif termal korumalı simülatif batarya paketlerinde 1.30W ve 2.75W ısıtma hızlarında maksimum sıcaklık hücresi 50^{o}C'nin altında kalarak etkin koruma sağlamaktadır. Buna karşılık 3.90W ısıtma hızında her iki koruma sisteminde de 50^{o}C sınır değerinin aşıldığı görülmektedir. Herhangi bir koruma yapılmayan paket için 3.90W ısıtma hızında etkin kullanım süresinin 8.7 dakika olduğundan daha önce bahsedilmişti. RT-44 pasif termal korumaya sahip pil paketinde bu sürenin 34.8 dakikaya çıktığı belirlenmiştir. Etkin kullanım süresinde elde edilen iyileşmenin pil üzerinde açığa çıkan ısının hem duyulur ısı hem de gizli ısı olarak RT-44 tarafından depolanması sayesinde gerçekleştiği söylenebilir. RT-44 pasif termal korumalı batarya paketinin 3.90W ısıtma hızında etkin kullanım süresini, koruma yapılmayan batarya paketine kıyasla 4 kat arttırdığı belirlenmiştir. Bununla birlikte %7 GNP/RT-44 pasif termal korumasında, ısıl iletkenliğin arttırılması nedeniyle pil civarında biriken ısının soğutma ortamının daha uzak bölgelerine aktarılması ve kompozitin bütününe yayılması, etkin kullanım süresi daha da uzayarak 78.9 dakikaya ulaşmaktadır. Bu durumda %7 GNP/RT-44 korumasının 3.90W ısıtma hızında çalışan simülatif bir batarya paketinde, etkin kullanım süresini RT-44 termal korumalı sisteme göre 2.3 kat, koruma yapılmayan batarya paketine göre ise 9.1 kat arttırdığı söylenebilir.

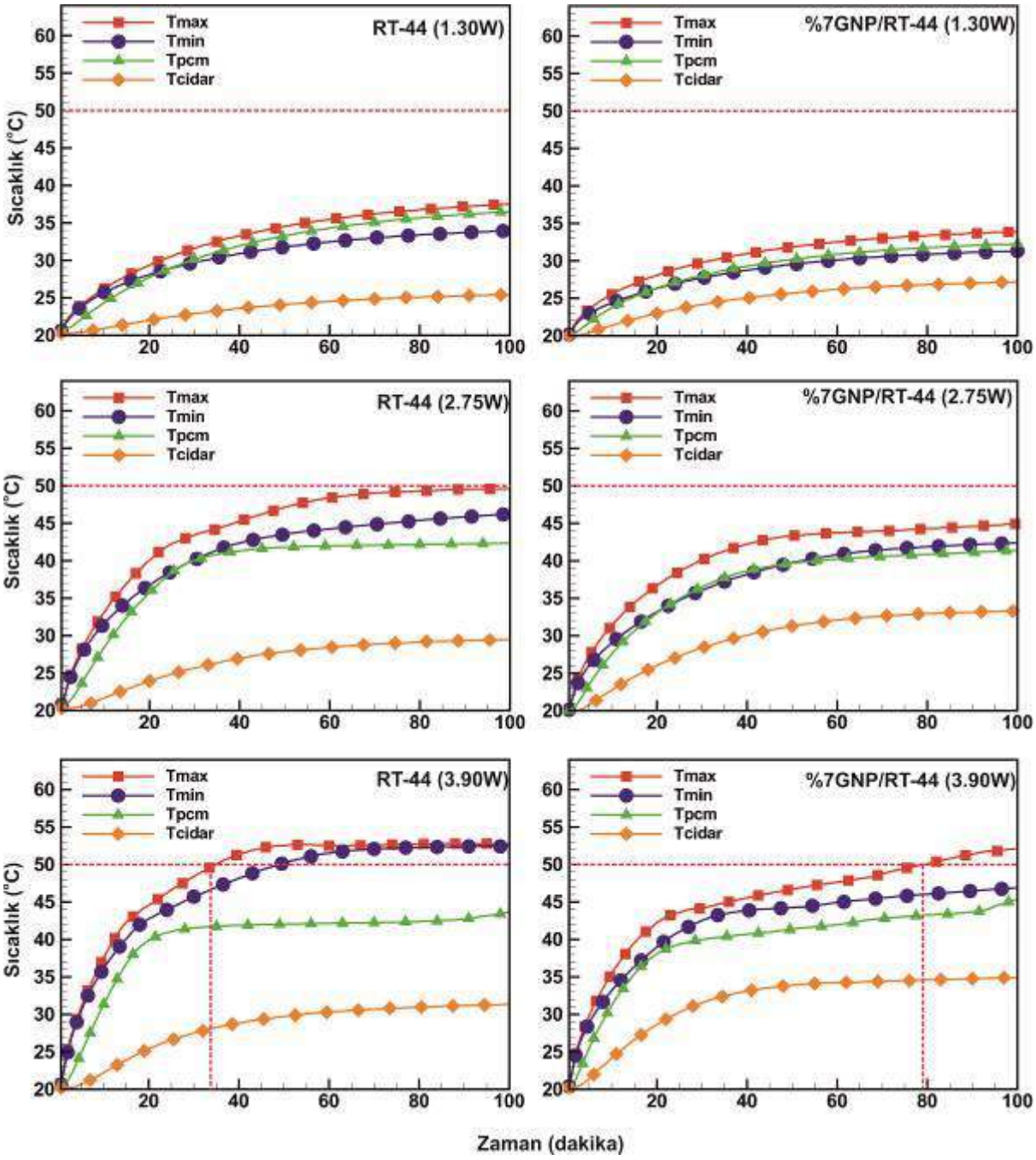

Şekil 5. Pil Paketindeki Farklı Noktaların Sıcaklık-Zaman Değişimi

Pil paketi içerisindeki maksimum sıcaklık farkının ($\Delta T_{max}=T_{max}-T_{min}$) zamana göre değişimi Şekil 6'da verilmiştir. İdeal pil paketlerinde pil hücreleri arasındaki maksimum sıcaklık farklılığının 5^oC'nin altında olması istenmektedir. Genel olarak tüm ısıtma hızları için maksimum sıcaklık farkının her iki yöntem için de 5^0C'nin altında olduğu görülmektedir. Maksimum sıcaklık farkının gerek RT-44 gerekse de %7 GNP/RT-44 kullanılması durumunda 1.30W deşarj hızı için sürekli artış gösterdiği görülmektedir. Bu durum 1.30W ısıtma hızında çalışma süresi boyunca faz değişiminin henüz başlamamış olması nedeniyle gerçekleşmektedir. Bununla birlikte

artan ısıl iletkenliğe bağlı olarak %7 GNP/RT-44'de maksimum sıcaklık farkı beklenen şekilde daha da azalmıştır. Faz değişiminin oluşmaya başladığı durumlarda (2.75W ve 3.90W ısıtma hızları) maksimum sıcaklık farkının zamana göre değişiminin farklı davranış gösterdiği görülmektedir. Bu durumlarda faz değişiminin öncelikle batarya paketinin iç bölgesindeki hücreler etrafında daha sonra da dış bölge civarındaki hücrelerde gerçekleştiği söylenebilir. Bu nedenle faz değişiminin başlamasıyla maksimum sıcaklık hücresinin artışının yavaşlamasına, bu esnada minimum hücrenin artışına devam etmesine bağlı olarak sıcaklık farkının azaldığı söylenebilir. Faz değişiminin sonlanmasının ardından maksimum sıcaklık hücresindeki artışın hızlanmasıyla sıcaklık farkının tekrar artışa geçtiği görülmektedir. RT-44 kullanımına dayalı pasif termal korumada maksimum sıcaklık hücresinin 50^{o}C'nin üzerine çıkması (3.90W deşarj hızı) durumunda oluşan sabit sıcaklık platosu, maksimum sıcaklık farkının son olarak önemli derecede azalmasına neden olmuştur. Bununla birlikte sabit sıcaklık platosunun %7 GNP/RT-44 korumasında görülmemesi, maksimum sıcaklık farkının artışına devam etmesine neden olmuştur. Öyle ki %7GNP/RT-44 pasif termal korumasında 3.90W deşarj hızında 90 dakikadan itibaren maksimum sıcaklık farkının 5^{0}C'nin üzerine çıktığı görülmektedir.

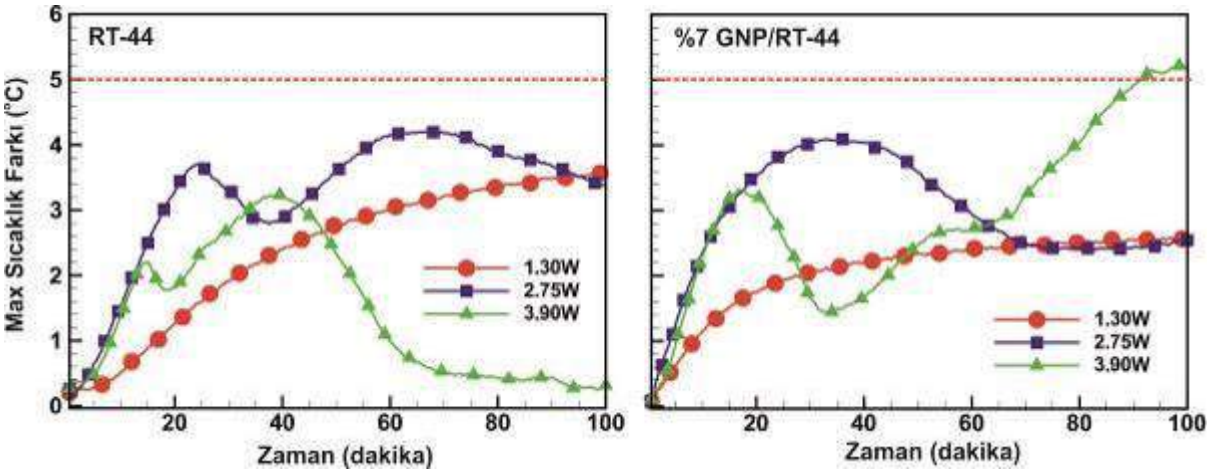

Şekil 6. Pil Paketindeki Hücreler Arası Maksimum Sıcaklık Farkı

Geçici çalışan pil paketlerinde önceki ısıtma/soğutma çevriminin sonrakilere olan etkisini belirlemek için beş ısıtma/soğutma çevrimi gerçekleştirilmiştir. Her bir çevrim için 30 dakika ısıtma ve sonrasında 30 dakika soğutmadan oluşan bir senaryo benimsenmiştir. Simülatif pil paketinin beş ısıtma/soğutma çevrimi süresince termal davranışı Şekil 7'de verilmiştir. RT-44 pasif termal korumasında 1.30W ve 2.75W deşarj hızları için maksimum sıcaklık 50 ^{o}C'nin altında kalırken 3.90W deşarj hızında maksimum sıcaklığın ikinci ısıtma itibariyle 50 ^{o}C'nin üzerine çıktığı belirlenmiştir. Buna karşılık %7 GNP/RT-44 pasif termal korumasının beş ısıtma/soğutma çevrimi boyunca ve üç farklı ısıtma hızı için sıcaklığı 50 ^{o}C'nin altında sınırlamayı başardığı görülmüştür. %7 GNP/RT-44 pasif termal korumasının RT-44 korumasına nazaran

maksimum sıcaklıkta 1.30W, 2.75W ve 3.90W deşarj hızları için sırasıyla 2.73°C, 3.98°C ve 5.41°C azalma sağladığı görülmüştür.

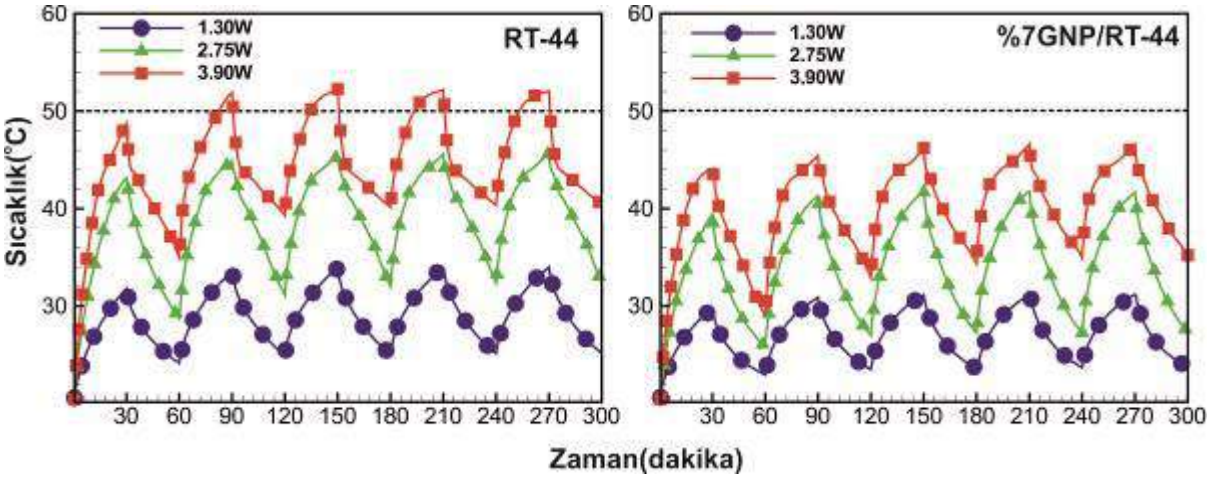

Şekil 7. Pil Paketi İçin Beş Istma/Soğutma Çevrimi Boyunca Maksimum Sıcaklık Değişimi

Benzer biçimde beş ısıtma/soğutma çevrimi sırasında pil paketi içerisindeki maksimum sıcaklık farkının zamana göre değişimi Şekil 8'de verilmiştir. RT-44 pasif termal korumasında 2.75W ve 3.90W deşarj hızlarında maksimum sıcaklık farkının ikinci ısıtmadan itibaren 5°C'nin üstüne çıktığı görülmektedir. Buna karşılık %7 GNP/RT-44 pasif termal korumasının, tüm ısıtma hızları için maksimum sıcaklık farkını 5 °C'nin altında tuttuğu belirlenmiştir. %7 GNP/RT-44 pasif termal korumasının RT-44 korumasına nazaran maksimum sıcaklık farkında 1.30W, 2.75W ve 3.90W deşarj hızları için sırasıyla 0.39 °C, 3.25 °C ve 3.13 °C azalma sağladığı görülmüştür.

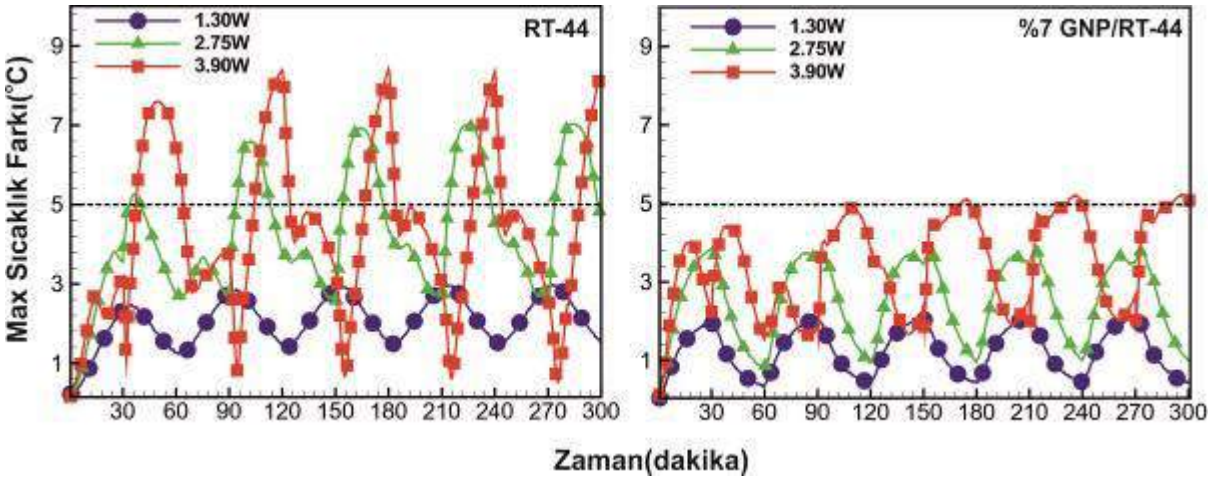

Şekil 8. Pil Paketi İçin Beş Istma/Soğutma Çevrimi Boyunca Maksimum Sıcaklık Farkı Değişimi

SONUÇ VE TARTIŞMA

Bu çalışmada, düşük ısıl iletkenliğe sahip organik RT-44 faz değişken malzemesinin ısıl iletkenliği iyileştirilerek bir pil paketinin pasif termal korumasındaki kullanılabilirliği araştırılmıştır. %7 GNP/RT-44 kompozitinin ısıl iletkenliğinde sırasıyla katı ve sıvı hal için %227.5 ve %133.3 iyileşme sağlanmıştır. Isıl iletkenlikte elde edilen iyileşmeye karşılık gizli ısıdaki %7.5 kaybın göz ardı edilebileceği belirlenmiştir.

1.30W ve 2.75W ısıtma hızlarında çalışan simülatif batarya paketi için maksimum sıcaklık kısıtlama iyileştirmesi %7 GNP/RT-44 kullanılması durumunda RT-44'e göre 3.7 ^{o}C-4.7 ^{o}C aralığındadır. %7 GNP/RT-44 kompozitinde sabit sıcaklık platosunun oluşmaması nedeniyle 3.90W ısıtma hızında çalışan batarya paketi için bu iyileşme 0.8 ^{o}C'ye düşmektedir. 1.30W ve 2.75W ısıtma hızlarında çalışan batarya paketinde, gerek RT-44 gerekse de %7 GNP/RT-44, tüm ısıtma işlemi süresince etkin koruma sağlamaktadır. RT-44, 3.90W ısıtma hızında etkin kullanım süresini, koruma yapılmayan batarya paketine kıyasla 4 kat arttırmaktadır. Buna karşılık %7 GNP/RT-44, 3.90W ısıtma hızında çalışan simülatif bir batarya paketinde, etkin kullanım süresini RT-44 termal korumalı sisteme göre 2.3 kat, koruma yapılmayan batarya paketine göre ise 9.1 kat arttırmaktadır. Tüm ısıtma işlemleri için her iki koruma sistemi de maksimum sıcaklık farkını 5^{o}C'nin altında tutabilmektedir. Ardışık ısıtma/soğutma çevrimleri süresince maksimum sıcaklık ve maksimum sıcaklık farkı kriterleri açısından %7 GNP/RT-44 pasif termal koruması RT-44'e nazaran iyi bir

performans sergilemektedir. Bu sonuçlar ışığında %7 GNP/RT-44 kompozitinin pil paketlerinde termal koruma ortamı olarak kullanılabileceği sonucuna varılmıştır.

TEŞEKKÜR

Bu çalışma Cumhuriyet Üniversitesi Bilimsel Araştırma Projeleri Komisyonu (CÜBAP) tarafından M-622 nolu proje ile desteklenmiştir.

KAYNAKLAR

Baby, R., & Balaji, C. (2013). Experimental investigations on thermal performance enhancement and effect of orientation on porous matrix filled PCM based heat sink. *International Communications in Heat and Mass Transfer*, *46*, 27–30. https://doi.org/10.1016/j.icheatmasstransfer.2013.05.018

Bahiraei, F., Fartaj, A., & Nazri, G. A. (2017). Experimental and numerical investigation on the performance of carbon-based nanoenhanced phase change materials for thermal management applications. *Energy Conversion and Management*. https://doi.org/10.1016/j.enconman.2017.09.065

Bhattacharya, A., Calmidi, V. V., & Mahajan, R. L. (2002). Thermophysical properties of high porosity metal foams. *International Journal of Heat and Mass Transfer*, *45*(5), 1017–1031. https://doi.org/10.1016/S0017-9310(01)00220-4

Cui, H. T. (2012). Experimental investigation on the heat charging process by paraffin filled with high porosity copper foam. *Applied Thermal Engineering*, *39*, 26–28. https://doi.org/10.1016/j.applthermaleng.2012.01.037

Duan, X., & Naterer, G. F. (2010). Heat transfer in phase change materials for thermal management of electric vehicle battery modules. *International Journal of Heat and Mass Transfer*. https://doi.org/10.1016/j.ijheatmasstransfer.2010.07.044

Fan, L., Khodadadi, J. M., & Pesaran, A. A. (2013). A parametric study on thermal management of an air-cooled lithium-ion battery module for plug-in hybrid electric vehicles. *Journal of Power Sources*, *238*, 301–312. https://doi.org/10.1016/j.jpowsour.2013.03.050

Fan, L. W., Fang, X., Wang, X., Zeng, Y., Xiao, Y. Q., Yu, Z. T., … Cen, K. F. (2013). Effects of various carbon nanofillers on the thermal conductivity and energy storage properties of paraffin-based nanocomposite phase change materials. *Applied Energy*. https://doi.org/10.1016/j.apenergy.2013.04.043

Giuliano, M. R., Prasad, A. K., & Advani, S. G. (2012). Experimental study of an air-cooled thermal management system for high capacity lithium-titanate batteries. *Journal of Power Sources*, *216*, 345–352. https://doi.org/10.1016/j.jpowsour.2012.05.074

Hallaj, S. Al, & Selman, J. R. (2000). A Novel Thermal Management System for Electric Vehicle Batteries Using Phase-Change Material. *Journal of The Electrochemical Society*. https://doi.org/10.1149/1.1393888

Hémery, C. V., Pra, F., Robin, J. F., & Marty, P. (2014). Experimental performances of

a battery thermal management system using a phase change material. *Journal of Power Sources*, *270*, 349–358. https://doi.org/10.1016/j.jpowsour.2014.07.147

Jarrett, A., & Kim, I. Y. (2011). Design optimization of electric vehicle battery cooling plates for thermal performance. *Journal of Power Sources*, *196*(23), 10359–10368. https://doi.org/10.1016/j.jpowsour.2011.06.090

Jiang, G., Huang, J., Liu, M., & Cao, M. (2017). Experiment and simulation of thermal management for a tube-shell Li-ion battery pack with composite phase change material. *Applied Thermal Engineering*. https://doi.org/10.1016/j.applthermaleng.2017.03.107

Khateeb, S. A., Amiruddin, S., Farid, M., Selman, J. R., & Al-Hallaj, S. (2005). Thermal management of Li-ion battery with phase change material for electric scooters: Experimental validation. *Journal of Power Sources*. https://doi.org/10.1016/j.jpowsour.2004.09.033

Kizilel, R., Lateef, A., Sabbah, R., Farid, M. M., Selman, J. R., & Al-Hallaj, S. (2008). Passive control of temperature excursion and uniformity in high-energy Li-ion battery packs at high current and ambient temperature. *Journal of Power Sources*. https://doi.org/10.1016/j.jpowsour.2008.04.050

Li, W. Q., Qu, Z. G., He, Y. L., & Tao, Y. B. (2014). Experimental study of a passive thermal management system for high-powered lithium ion batteries using porous metal foam saturated with phase change materials. *Journal of Power Sources*. https://doi.org/10.1016/j.jpowsour.2014.01.006

Lin, C., Xu, S., Chang, G., & Liu, J. (2015). Experiment and simulation of a LiFePO4 battery pack with a passive thermal management system using composite phase change material and graphite sheets. *Journal of Power Sources*, *275*, 742–749. https://doi.org/10.1016/j.jpowsour.2014.11.068

Ling, Z., Wang, F., Fang, X., Gao, X., & Zhang, Z. (2015). A hybrid thermal management system for lithium ion batteries combining phase change materials with forced-air cooling. *Applied Energy*, *148*, 403–409. https://doi.org/10.1016/j.apenergy.2015.03.080

Liu, L., Su, D., Tang, Y., & Fang, G. (2016). Thermal conductivity enhancement of phase change materials for thermal energy storage: A review. *Renewable and Sustainable Energy Reviews*. https://doi.org/10.1016/j.rser.2016.04.057

Qu, Z. G., Li, W. Q., & Tao, W. Q. (2014). Numerical model of the passive thermal management system for high-power lithium ion battery by using porous metal foam saturated with phase change material. *International Journal of Hydrogen Energy*, *39*(8), 3904–3913. https://doi.org/10.1016/j.ijhydene.2013.12.136

Rao, Z., Huo, Y., Liu, X., & Zhang, G. (2015). Experimental investigation of battery thermal management system for electric vehicle based on paraffin/copper foam. *Journal of the Energy Institute*, *88*(3), 241–246. https://doi.org/10.1016/j.joei.2014.09.006

Rao, Z., & Wang, S. (2011). A review of power battery thermal energy management. *Renewable and Sustainable Energy Reviews*, *15*(9), 4554–4571. https://doi.org/10.1016/j.rser.2011.07.096

Sabbah, R., Kizilel, R., Selman, J. R., & Al-Hallaj, S. (2008). Active (air-cooled) vs. passive (phase change material) thermal management of high power lithium-ion packs: Limitation of temperature rise and uniformity of temperature distribution. *Journal of Power Sources*, *182*(2), 630–638. https://doi.org/10.1016/j.jpowsour.2008.03.082

Sharma, A., Tyagi, V. V., Chen, C. R., & Buddhi, D. (2009). Review on thermal energy storage with phase change materials and applications. *Renewable and Sustainable Energy Reviews*. https://doi.org/10.1016/j.rser.2007.10.005

Wang, Zhiwei, Zhang, H., & Xia, X. (2017). Experimental investigation on the thermal behavior of cylindrical battery with composite paraffin and fin structure. *International Journal of Heat and Mass Transfer*, *109*, 958–970. https://doi.org/10.1016/j.ijheatmasstransfer.2017.02.057

Wang, Zichen, Zhang, Z., Jia, L., & Yang, L. (2015). Paraffin and paraffin/aluminum foam composite phase change material heat storage experimental study based on thermal management of Li-ion battery. *Applied Thermal Engineering*, *78*, 428–436. https://doi.org/10.1016/j.applthermaleng.2015.01.009

Yuan, Y., Li, T., Zhang, N., Cao, X., & Yang, X. (2016). Investigation on thermal properties of capric–palmitic–stearic acid/activated carbon composite phase change materials for high-temperature cooling application. *Journal of Thermal Analysis and Calorimetry*. https://doi.org/10.1007/s10973-015-5173-0

Zhao, J., Lv, P., & Rao, Z. (2017). Experimental study on the thermal management performance of phase change material coupled with heat pipe for cylindrical power battery pack. *Experimental Thermal and Fluid Science*. https://doi.org/10.1016/j.expthermflusci.2016.11.017

Zhao, R., Gu, J., & Liu, J. (2017). Optimization of a phase change material based internal cooling system for cylindrical Li-ion battery pack and a hybrid cooling design. *Energy*, *135*, 811–822. https://doi.org/10.1016/j.energy.2017.06.168

Zhou, D., & Zhao, C. Y. (2011). Experimental investigations on heat transfer in phase change materials (PCMs) embedded in porous materials. *Applied Thermal Engineering*, *31*(5), 970–977. https://doi.org/10.1016/j.applthermaleng.2010.11.022

EFFECTS OF NATURAL GAS ENRICHMENT WITH HYDROGEN ON ENGINE PERFORMANCE IN A COMPRESSION IGNITION ENGINE

Müjdat FIRAT, Dept. of Automotive Engineering, Technology Faculty, Firat University, 23119, Elazig, Turkey, mfirat@firat.edu.tr

ABSTRACT: In the present study investigates the effect of hydrogen addition to natural gas on engine performance in a compression ignition engine. This study is aimed to develop the 1-D model of a four-stroke compression ignition engine for predicting the effect of natural gas enrichment with hydrogen on engine performances. AVL BOOST was used as a simulation tool to analyze the engine performance for different blends of natural gas and hydrogen. Various hydrogen fractions (10% and 20%) are examined. Results showed that natural gas enrichment with hydrogen leads in general to an improved gaseous fuel combustion and engine performance. The results indicated that when natural gas enrichment with hydrogen were used, the brake specific fuel consumption decreased up to 30% and effective efficiency increased up to 10% compared to those of natural gas fuel.

Key words: Natural gas, Hydrogen, Engine performance, Modeling

SIKIŞTIRMA ATEŞLEMELİ BİR MOTORDA HİDROJENLE ZENGİNLEŞTİRİLMİŞ DOĞALGAZ KULLANIMININ MOTOR PERFORMANSINA ETKİLERİ

ÖZET: Bu çalışmada sıkıştırma ateşlemeli bir motorda hidrojen eklenmiş doğalgaz kullanımının motor performansı üzerine etkileri incelenmiştir. Bu çalışma, hidrojenle zenginleştirilmiş doğalgazın dört zamanlı sıkıştırma ateşlemeli bir motorda kullanımının motor performansı üzerine etkilerini incelemek için 1-Boyutlu bir model geliştirmeyi amaçlamaktadır. Farklı oranlarda hidrojen doğalgaz karışımının motor performansına etkilerinin incelenmesi için AVL-BOOST sayısal yazılımı kullanılmıştır. Farklı hidrojen oranları (%10 ve %20) araştırılmıştır. Sonuçlar hidrojenle zenginleştirilmiş doğalgaz yanmasının gaz yakıt yanmasını ve motor performansını geliştirdiğini göstermiştir. Ayrıca, hidrojenle zenginleştirilmiş doğalgaz kullanıldığında özgül yakıt tüketiminin %30'a kadar azaldığı ve efektif verimin %10'a kadar artığı görülmüştür.

Anahtar sözcükler: Doğalgaz, Hidrojen, Motor performansı, Modelleme

GİRİŞ

Enerji ihtiyacında artan talebe karşılık fosil yakıtların gittikçe azalmasından dolayı özellikle içten yanmalı motorlarda alternatif yakıt arayışları artış göstermektedir. Bu arayış neticesinde son yıllarda umut verici sonuçlar elde edilen alternatif yakıtlardan biriside doğalgazdır. Doğalgaz daha iyi motor performansı daha düşük emisyon üretimi, uygun fiyat ve ulaşılabilirlik gibi avantajları sebebiyle içten yanmalı motorlarda kullanılmaktadır (Choi vd. 2016). Doğalgazın düşük yanma hızı ve fakir yanma durumunu gidermek için, doğalgaz farklı gaz yakıtlarla desteklenmektedir. Bu destekleme için en iyi alternatiflerden biriside hidrojendir. Hidrojenin daha geniş yanma limiti ve daha yüksek yanma hızıyla, doğalgaz için çevrimsel değişimler giderilmektedir. Bu şekilde özellikle ısıl verim artırılırken motor performansı iyileştirilebilmektedir (Lounici vd. 2014). Hidrojenle zenginleştirilmiş doğalgazın içten yanmalı motorlarda kullanımı ile ilgili olarak literatürde farklı çalışmalar görülmektedir (Imran vd.(2018), Kalsi ve Subramanian (2017)). Zhou vd. (2014) hidrojen-metan karışımının bir dizel motorda kullanılmasının, yanma karakteristikleri ve kirletici emisyonlar üzerine etkilerini analiz etmişlerdir. Farklı hidrojen oranları ve motor yükleri için gerçekleştirilen çalışmada yüksek hidrojen oranlarda ve %30 motor yüklerinde motor performansının yükseldiği, CO ve HC emisyonlarının düştüğü gözlenmiştir. Ayrıca %30 hidrojen oranında ve yüksek motor yüklerinde NOx emisyonlarının azaldığı gözlenmiştir. Lounici vd. (2014) hidrojenle zenginleştirilmiş doğalgazın ikinci yakıt olarak kullanıldığı çift yakıtlı bir motoru deneysel olarak incelemişlerdir. Hidrojen katkısının özellikle düşük yüklerde kirletici emisyonları düşürdüğü gözlenmiştir. Ayrıca %10 hidrojen kullanımı durumunda özgül yakıt tüketiminin ciddi oranda düştüğü, motor performansı bakımından önemli bir sonuç olarak sunulmuştur. Ouchikh vd. (2019) deneysel olarak yürüttükleri çalışmada çift yakıtlı bir dizel motorunda zenginleştirilmiş doğalgaz kullanımını araştırmışlardır. Çalışma 1500 motor devrinde farklı motor yüklerinde (%30-%70) ve farklı hidrojen oranlarında (%10,%20 ve %30) gerçekleştirilmiştir. Çalışmanın sonucunda hidrojen katkısı durumunda özgül yakıt tüketiminde azalma görülürken termal verimde artış gözlenmiştir.

İncelenen literatür ışığında, doğalgazla çalışan motorlar için hidrojenle zenginleştirilmiş doğalgaz kullanımı konusunda eksikler görülmüş ve bu çalışmanın konusu belirlenmiştir. Çalışma kapsamında %10 ve %20 oranlarında hidrojenle zenginleştirilmiş doğalgazın sıkıştırma ateşlemeli bir motorda kullanımı araştırılmıştır. Sonuçlar özellikle motor performansı bakımından tartışılmıştır.

YÖNTEM

Bu çalışma kapsamında tek silindirli sıkıştırma ateşlemeli bir motorda hidrojenle zenginleştirilmiş doğalgaz kullanımı 1-Boyutlu sayısal model kullanılarak analiz edilmiştir. Analizler AVL-BOOST yazılımı kullanılarak gerçekleştirilmiştir (AVL, 2018). AVL-BOOST çok geniş aralıkta içten yanmalı motorların modellenmesinde kullanılmaktadır. Bu yazılım ile iki ve dört zamanlı motorlar, tek silindirli ve çok silindirli motorlar ve farklı amaçlı endüstriyel motorların emme ve egzoz hatlarındaki tüm bileşenleriyle birlikte çevrim bazında termodinamik analizi yapılabilmektedir (Iliev, (2015), Petranović vd. (2018)). Çalışmada kullanılan bir boyutlu model Şekil 1'de görülmektedir. Model üzerinde E1 tanımlanan motoru ve genel özelliklerini, C1 silindiri, MP1 ve MP2 ölçüm noktalarını, SB1 ve SB2 ise sistem sınırlarını ifade etmektedir. Her bir bileşen için birçok özellik ve sınır şartı tanımlanarak tam çevrim analizleri gerçekleştirilmektedir. Motor geometrik verileri, piston hareketleri, supap profilleri, yakıt miktarı, enjeksiyon zamanı ve süresi gibi bir çok parametre giriş verisi olarak tanımlanarak analizler yapılmıştır. Yanma analizleri için Vibe 2-Zone yanma modeli kullanılmıştır. Bu modelde yanmış ve yanmamış bölgelere göre çözüm yapılmaktadır. Bu ayrım ise sıcaklık değişimine göre termodinamik ifadelerle yapılmaktadır. Ayrıca NOx emisyonları için iyi bilinen Zeldovich mekanizması tercih edilmiştir. Analizler için kullanılan motorun teknik özellikleri Tablo 1'de verilmiştir.

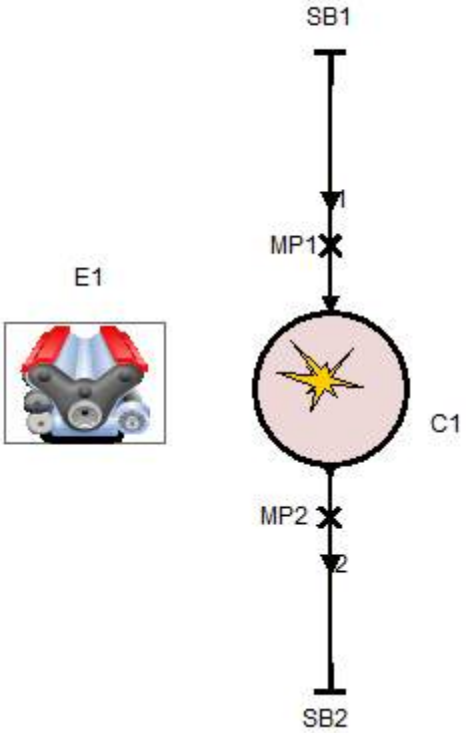

Şekil 1. AVL-BOOST Tam Çevrim Analiz Modeli

Tablo 1. Motorun Teknik Özellikleri

Silindir sayısı	1

Motor tipi	4 zamanlı, sıkıştırma ateşlemeli, direk enjeksiyon
Çap (mm)	95.4
Strok (mm)	88.9
Hacim (cm^3)	625
Sıkıştırma oranı	18.1
Enjeksiyon zamanı	14^o KMA üst ölü noktadan önce
Motor devri (d/d)	1500

Bu çalışma kapsamında hidrojen ile zenginleştirilmiş doğalgazın sıkıştırma ateşlemeli bir motorda kullanılması amaçlanmıştır. Bu amaçla doğalgaz tüm bileşenleriyle birlikte tanımlanmış ve belirli oranlarda hidrojen tanımlamaları yapılmıştır. Kullanılan doğalgazın bileşenleri Tablo 2'de görülmektedir. Yakıtın doğru tanımlanması için AVL-BOOST içerisinde yeni bir yakıt kütüphanesi oluşturulmuştur. Hazırlanan kütüphanenin hidrojen oranı değiştirilerek tüm analizlerde kullanılmıştır. Çalışma kapsamında %100 doğalgaz, %90 doğalgaz-%10 hidrojen ve %80 doğalgaz-%20 hidrojen oranları için analizler gerçekleştirilmiştir.

Tablo 2. Doğalgaz Bileşenleri

Bileşen	%
Metan (CH_4)	90.65
Etan (C_2H_6)	6.8
Propan (C_3H_8)	1.8
Bütan (C_4H_{10})	0.7
Pentan (C_5H_{12})	0.05

BULGULAR

Bu çalışma kapsamında farklı oranlarda hidrojenle zenginleştirilmiş doğalgazın, doğalgazla çalışan sıkıştırma ateşlemeli bir motorda kullanılması araştırılmıştır. Tamamen doğalgazın yakıt olarak kullanıldığı durumun yanında, %10 ve %20 oranlarda hidrojen eklenmesinin özellikle motor performansı üzerindeki etkileri araştırılmıştır.

Şekil 2'de farklı oranlarda hidrojen kullanılmış durumlar için silindir içi basıncın krank mili açısına (KMA) bağlı değişimi görülmektedir. Her üç durum için benzer eğilimler elde edilmekle birlikte, hidrojen oranı arttıkça silindir içi basınçta artış gözlenmiştir. Doğalgazın eksik yanma sınırları ve düşük alev hızının hidrojenle

birlikte geliştirildiği düşünülürse silindir içi basınçtaki artış bu bakımdan olumlu karşılanmaktadır. Silindir içi basınçtaki artışın motor performansına etki edeceği düşünülmektedir. Özellikle yanmanın başladığı krank açılarında ani basınç yükselişlerinin görülmemesi hidrojen katkısının yanmayı olumsuz etkilemediği sonucunu vermektedir.

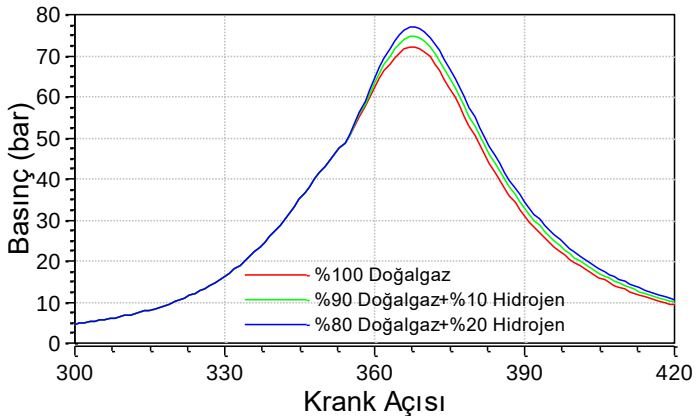

Şekil 2. Silindir İçi Basıncın Hidrojen Oranına Bağlı Değişimi

Hidrojen oranına bağlı olarak ısı salınım oranında meydana gelen değişimler Şekil 3'de görülmektedir. Şekilde hidrojen oranı arttıkça ısı salınım oranınında arttığı görülmektedir. Ayrıca hidrojen yüzdesine bağlı olarak ısı salınımının birkaç KMA öne çekildiği görülmekte olup, yanma hızının ifade edilmesi bakımından önemli bir sonuçtur. Krank açısı başına ısı salınımını ifade eden ısı salınım oranı, enjekte edilen yakıtların ısıl değerleri ile de ilgilidir. Doğalgazın alt ısıl değerinin yaklaşık 50MJ/kg, Hidrojenin alt ısıl değerinin ise yaklaşık 120MJ/kg olduğu düşünülürse ısı salınımdaki artış açıklanabilmektedir.

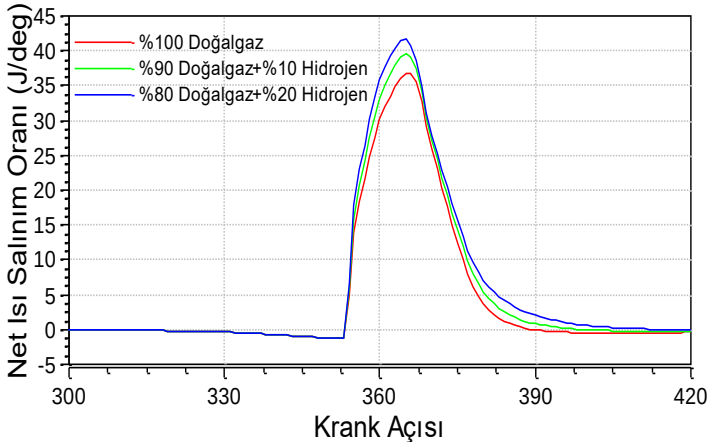

Şekil 3. Isı Salınım Oranının Hidrojen Oranına Bağlı Değişimi

Şekil 4'de silindir içi sıcaklığın hidrojen oranına bağlı olarak değişimi görülmektedir. Silindir içi sıcaklık yanma oluşumuna göre değişmekle birlikte yanma için önemli bir

göstergedir. Elde edilen şekilde, hidrojen katkısına bağlı olarak silindir içi sıcaklığının da arttığı görülmektedir. Doğalgazın düşük yanma hızı ve fakir yanma sınırlarının hidrojenle geliştirilmesinin bir sonucu olarak yanma sonu sıcaklıklarının da arttığı görülmektedir.

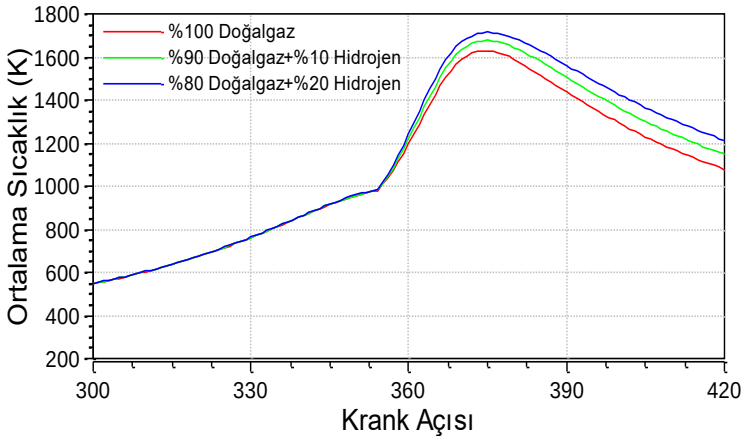

Şekil 4. Silindir İçi Ortalama Sıcaklığın Hidrojen Oranına Bağlı Değişimi

İçten yanmalı motorlar için en önemli performans parametrelerinden bir diğeri ise özgül yakıt tüketimidir. Doğalgazla çalışan bir motorda hidrojen katkısının özgül yakıt tüketimine etkisi Şekil 5'de görülmektedir. Birim güç başına yakıt tüketiminin hidrojen oranına bağlı olarak azaldığı çalışma kapsamında elde edilen önemli bir sonuçtur. Hidrojenle zenginleştirilmiş doğalgaz kullanımı durumunda özgül yakıt tüketimin yaklaşık %30 oranında düştüğü gözlenmiştir. Bu sonuç daha önceki grafikleri doğrulamakla birlikte enjekte edilen yakıtın yanma veriminin de iyileştiğini gösteren bir sonuç olarak değerlendirilmiştir.

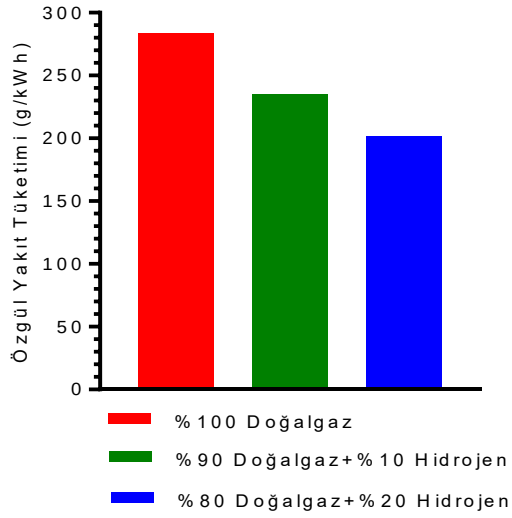

Şekil 5. Özgül Yakıt Tüketiminin Hidrojen Oranına Bağlı Değişimi

Şekil 6'da efektif verimin hidrojen oranına bağlı değişimi görülmektedir. Efektif verim motor performansını gösteren önemli bir parametredir. Şekil 5'de görülen özgül yakıt tüketiminin düşüşüne bağlı olarak, efektif verim hidrojen oranıyla birlikte artış göstermektedir. Bu artış %20 hidrojen katkısı durumunda yaklaşık %10 olarak gerçekleşmektedir. Doğalgaz yanmasının olumsuz yönlerinin hidrojen katkısıyla giderilmesi neticesinde motor performansının artacağı bu grafikte görülmektedir.

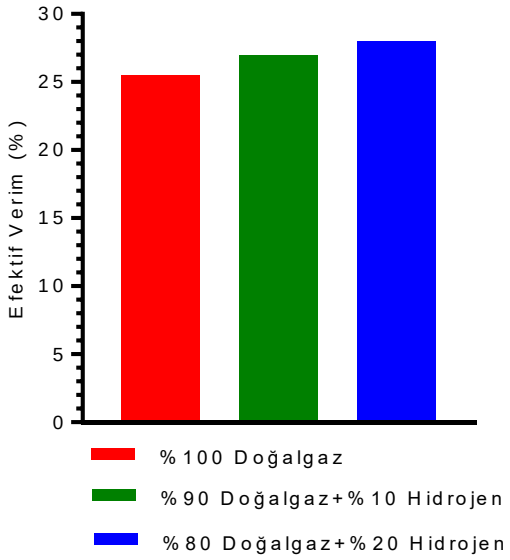

Şekil 6. Efektif Verimin Hidrojen Oranına Bağlı Değişimi

SONUÇ

Sıkıştırma ateşlemeli bir motorda hidrojenle zenginleştirilmiş doğalgaz kullanımın motor performansına etkileri bu çalışma kapsamında 1-Boyutlu termodinamik çevrim analizi ile araştırılmıştır. AVL-BOOST yazılımının kullanıldığı çalışmada %100 doğalgaz kullanımının yanında %10 ve %20 oranlarında hidrojen katkısının performans karakteristikleri üzerine etkileri incelenmiştir. Çalışmada elde edilen temel sonuçlar aşağıda sıralanmıştır.

Doğalgazla çalışan bir motorda hidrojenle zenginleştirilmiş doğalgaz kullanımın silindir içi basıncı yaklaşık %7 oranında arttırdığı görülmüştür.

Hidrojen oranı artıkça silindir içi sıcaklık ve ısı salınım oranının artış gösterdiği görülmüş ve hidrojen katkısının doğalgaz yanmasını iyileştirdiği düşünülmüştür.

Hidrojen oranına bağlı olarak, %10 hidrojen oranında özgül yakıt tüketimin yaklaşık %18, %20 hidrojen kullanımında ise yaklaşık %30 oranında azaldığı görülmüştür.

Doğalgaza hidrojen katkısının efektif verimi etkilediği görülürken, %20 hidrojen oranında efektif verimin yaklaşık %10 artış gösterdiği elde edilmiştir.

Elde edilen sonuçların, deneysel verilerle desteklenmesi ve geliştirilmesi durumunda doğalgazla çalışan içten yanmalı motorlar için umut verici sonuçların ortaya çıkarılması mümkün olabilecektir. Bundan sonraki çalışmaların, deneysel bulguların ortaya çıkarılmasına yoğunlaşması önerilmektedir.

KAYNAKLAR

AVL-BOOST Manuel, 2018.

Choi, M. Song, J., & Park, S. (2016). Modeling of the fuel injection and combustion process in a CNG direct injection engine. *Fuel, 179,* 168–178.

Iliev, S. (2015). A Comparison of Ethanol and Methanol Blending with Gasoline Using a 1- D Engine Model. *Procedia Engineering, 100,* 1013 – 1022

Imran, S., Korakianitis, T., Shaukat, R., Farooq, M., Condoor, S., & Jayaram S. (2018). Experimentally tested performance and emissions advantages of using natural-gas and hydrogen fuel mixture with diesel and rapeseed methyl ester as pilot fuels. *Appl Energy, 229*, 1260-1268.

Kalsi, S.S., & Subramanian, K. (2017). Experimental investigations of effects of hydrogen blended CNG on performance, combustion and emissions characteristics of a biodiesel fueled reactivity controlled compression ignition engine (RCCI). *Int J Hydrogen Energy, 42,* 4548-4560.

Lounici, M.S., Boussadi, A., Loubar, K., & Tazerout, M. (2014). Experimental investigation on NG dual fuel engine improvement by hydrogen enrichment. *Int J Hydrogen Energy, 39*, 21297-21306.

Ouchikh, S., Lounici, M.S., Tarabet, L., Loubar, K., & Tazerout, M. (2019). Effect of natural gas enrichment with hydrogen on combustion characteristics of a dual fuel diesel engine. *Int J Hydrogen Energy, 44*,13974-13987.

Petranović, Z., Sjerić, M., Taritaš, I., Vujanović, M.,& Kozarac, D. (2018). Study of advanced engine operating strategies on a turbocharged diesel engine by using coupled numerical approaches. *Energy Conversion and Management, 171*, 1–11.

Zhou, J., Cheung, C.,& Leung, C. (2014). Combustion, performance and emissions of a diesel engine with H_2, CH_4 and H_2-CH_4 addition. *Int J Hydrogen Energy, 39*,4611-4621.

EXPERIMENTAL AND NUMERICAL MODELING OF A LOW FROUDE NUMBER FREE HYDRAULIC JUMP

Mehmet PARMAKSIZ, Harran University, Faculty of Engineering, Civil Engineering Department, mhmtprmksz@gmail.com

Veysel GÜMÜŞ, Harran University, Faculty of Engineering, Civil Engineering Department, gumus@harran.edu.tr

Oğuz ŞİMŞEK, Harran University, Faculty of Engineering, Civil Engineering Department, oguzsimsek@harran.edu.tr

ABSTRACT: Hydraulic jump defined as a rapid transition from the supercritical to the subcritical flow regime. In hydraulic jump a large amount of energy is absorbed during this transition. Knowledge of the characteristics of the hydraulic jump is important in the design of these stilling basin structures and in terms of the safe transfer of water to the downstream side. In this study, the characteristics of hydraulic jumps having Froude number 2.54 are experimentally measured and the obtained experimental results are compared with numerically model. Computational Fluid Dynamics (HAD) methods based on finite volume method are used in the numerical model. Standard k-ε (SKE), Renormalization Group k-ε (RNG), Shear Stress Transport k-ω (SST) and Reynold Stress Models (RSM) are used for the identification of turbulence in numerical modelling, and VOF method is used to determination of free surface profile. Grid convergence index method is also used for determination of the mesh density. As a result of the study, SKE model is found most successful model to determine the free surface profile of the free hydraulic jump.

Keywords: Free hydraulic jump, turbulence models, computational fluid dynamics (CFD), open channel flows

DÜŞÜK FROUDE SAYISINDA MEYDANA GELEN SERBEST HİDROLİK SIÇRAMANIN DENEYSEL VE SAYISAL MODELLEMESİ

ÖZET: Hidrolik sıçramada akım kritik üstü (sel rejimi) akımdan kritik altı (nehir rejimi) akıma hızlı bir geçiş sağlar ve bu geçiş esnasında meydana gelen sıçrama bölgesinde ciddi miktarda bir enerji sönümlenir. Hidrolik sıçramanın karakteristiklerinin bilinmesi bu enerji kırıcı yapıların tasarımında ve suyun güvenle mansap tarafına aktarılması açısından önemlidir. Bu çalışma kapsamında laboratuvar ortamında Froude sayısının 2,54 olduğu akımda meydana gelen hidrolik sıçramanın karakteristik yapısı deneysel olarak ölçülmüş ve elde edilen deneysel bulgular sonlu hacimler yöntemine dayalı Hesaplamalı Akışkanlar Dinamiği (HAD) yöntemleri ile sayısal olarak modellenmiştir. Sayısal modellemede türbülansın tanımlanması için Standart k-ε (SKE), Renormalization Group k-ε (RNG), Shear Stress Transport k-ω

(SST) ve Reynold Stress Model (RSM), serbest su yüzünün belirlenmesinde ise VOF yöntemi kullanılmıştır. Ağ hassasiyetinin uygunluğu için de ağ yakınsama indeksi yöntemi ile belirlenmiştir. Çalışma sonucunda, serbest hidrolik sıçramanın su yüzü profilini belirlemede en başarılı türbülans kapatma modelinin SKE türbülans kapatma modeli olmuştur.

Anahtar Kelimeler: Serbest hidrolik sıçrama, türbülans modelleri, hesaplamalı akışkanlar dinamiği (HAD), açık kanal akımları

1. GİRİŞ

Hidrolik sıçrama, açık kanallarda kritik üstü akımdan (Froude>1) kritik altı akıma (Froude<1) ani ve hızlı geçiş olarak tanımlanır. Bu geçiş, yüzey dalgaları, enerji yayılımı ve havanın sürüklenmesine bağlı olarak büyük çaplı türbülansa sebep olur, buna bağlı olarak da önemli bir enerji kaybı meydana gelir. Şekil 1-A, bir sel baskını sırasında menfez girişindeki bir hidrolik sıçramayı, Şekil 1-B ise taşkın sırasında baraj dolusavak mansabında meydana gelen hidrolik sıçramayı göstermektedir. Bir taşkın sırasında dolusavak mansap bölgesinde akım çok yüksek hızlara erişebilmekte ve buna bağlı olarak dolusavağa ve etrafındaki yapılara zarar verebilmektedir. Ancak, hidrolik sıçrama sırasında çok fazla enerji kaybı meydana geldiğinden ve akım kritik altı akıma dönüştüğünden bu yapılara zarar gelmesi engellenebilmektedir. Hidrolik sıçramanın yapısı ve enerji kaybının belirlenebilmesi için fiziksel modellemeler yapılmakta ve ayrıca gelişen teknolojiyle birlikte bu modellemeler sayısal olarak yapılabilmektedir. Geçmiş çalışmalar incelendiğinde, sıçramanın fiziksel modellemesi ile ilgili yapılan çalışmalar uzun yıllardır devam etmektedir (Pillai ve ark., (1989), Hager ve Li, (1992), Liu ve ark., (2004), Özbay, (2008), Alikhani ve ark., (2010), Padulano ve ark. (2017)). Günümüzde ise serbest su yüzüne sahip farklı türdeki açık kanal akımlarının sayısal modellemesi başarı ile yapılmaktadır (Gharangik ve ark., (1991), Carvalho ve ark., (2008), Chippada ve ark., (1994)). Sıçrama ile ilgili çalışmalar incelendiğinde ise, Gümüş (2013), batık hidrolik sıçramanın deneysel ve sayısal modellemesini yapmışlar, çalışmalar üç farklı türbülans kapatma modeli ile modelleme yapılmış ve sıçrama karakteristikleri belirlenmiştir. Ma (2004) yine batık hidrolik sıçramanın su yüzü profilini belirlemek için sayısal modelleme yapmıştır. Serbest hidrolik sıçramanın modelleme çalışmaları incelendiğinde ise Gümüş ve ark. (2012)'de kayar kapak sonrası meydana gelen serbest hidrolik sıçramanın su yüzü profili sayısal olarak belirlenmiştir.

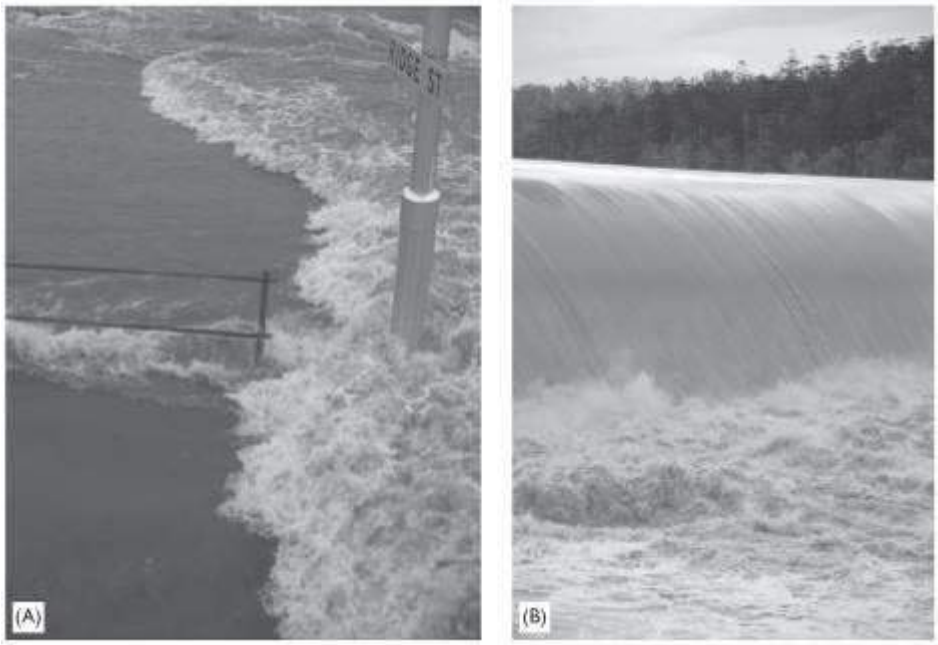

Şekil 1. Farklı Bölgelerde Meydana Gelen Serbest Hidrolik Sıçrama

Bu çalışma kapsamında laboratuvar ortamında hidrolik sıçrama membasında Froude sayısının 2.54 olduğu akımda oluşan hidrolik sıçramanın karakteristikleri deneysel olarak ölçülmüş ve elde edilen deneysel bulgular Hesaplamalı Akışkanlar Dinamiği (HAD) yöntemleri ile farklı türbülans modelleri kullanılarak sayısal olarak modellenmiştir. Çalışma kapsamında, serbest hidrolik sıçramanın karakteristikleri deneysel ve sayısal olarak değerlendirilmiş ve deneysel veriler sayısal modelin doğrulanmasında kullanılmıştır.

2. DENEYLER

Deneyler, Harran Üniversitesi Mühendislik Fakültesi İnşaat Mühendisliği Bölümü Hidrolik Laboratuvarında bulunan 400x35x35 cm boyutundaki açık kanal modelinde yapılmıştır (Şekil 2). Oluşturulmak istenilen hidrolik sıçramanın yapısının ayarlanması için kanal memba kısmına bir kayar kapak yerleştirilmiş ve kanal sonuna bir savak yerleştirmek suretiyle Fr=2.54 akım şartında sıçrama oluşturulmuştur.

Şekil 2. Deneyde Kullanılan Açık Kanal Modeli

Sıçramanın türünün belirlenmesinde esas parametre sıçrama öncesi kesitteki Froude sayısıdır. Froude sayısı Denklem 1'deki gibi hesaplanır.

$$Fr_1 = \frac{V}{\sqrt{gh_1}} \qquad (1)$$

Burada V akımın ortalama hızını, h_1 su derinliğini, g ise yerçekimi ivmesini simgelemektedir.

3. YÖNTEM

3.1 Temel Denklemler

Serbest hidrolik sıçrama türbülanslı bir akım olup, akımın çözülebilmesi amacıyla kullanılacak temel denklemler süreklilik ve Reynolds Ortalamalı Navier-Stokes (RANS) denklemleridir. Bu denklemler sırasıyla Denklem 2 ve Denklem 3'te verilmiştir.

$$\frac{\partial u_i}{\partial x_i} = 0 \qquad \textbf{(2)}$$

$$\rho\left(\frac{\partial u_i}{\partial t} + u_j \frac{\partial u_i}{\partial x_j}\right) = \rho g_i - \frac{\partial p}{\partial x_i} + \mu \frac{\partial^2 u_i}{\partial x_j^2} + \frac{\partial}{\partial x_j}(\tau_{ij}) \qquad \textbf{(3)}$$

Süreklilik ve RANS denklemlerinde bulunan u_i ortalama hız bileşenlerini, p ortalama basıncı, μ akışkanın dinamik viskozitesini, ρ akışkanın yoğunluğunu, ρg_i yerçekiminin sebep olduğu kütlesel kuvveti, t zamanı, τ_{ij} ise türbülans (Reynolds) gerilmelerini ifade etmektedir. Türbülans yani Reynolds gerilmeleri Boussinesq yaklaşımına göre Denklem 4'teki gibi ifade edilir:

$$\tau_{ij} = -\rho\overline{u_i' u_j'} = \mu_t\left(\frac{\partial u_i}{\partial x_j} + \frac{\partial u_j}{\partial x_i}\right) - \frac{2}{3}\delta_{ij}\rho k \qquad \textbf{(4)}$$

Burada, u_i' ve u_j' türbülans hız sapınçları ve μ_t türbülans viskozitesi olup δ_{ij} Kronecker deltadır (i=j için δ_{ij}=1).

RANS denklemlerinde üç boyutlu akışta bir basınç, üç hız, altı türbülans kayma gerilmesi bileşeni ile toplam 10 bilinmeyen bulunur. Buna karşılık her bir doğrultu için birer toplam üç RANS denklemi ve bir süreklilik denklemi bulunmaktadır. Bilinmeyen sayısından az yani dört denklem bulunduğundan denklem sistemi çözülememektedir. Bu sorunun çözümü için araştırmacılar tarafından farklı türbülans kapatma modelleri geliştirilmiştir. Bu çalışma kapsamında Standart k-ε (SKE) (Launder ve Spalding, 1972), Renormalization Group k- ε modeli (RNG) (Yakhot ve ark., 1992), Shear Stress Transport k-ω (SST) (Menter, 1994) ve RSM (Reynolds Stress Model-Reynold Gerilme Modeli) (Launder ve ark., 1975) olmak üzere toplam dört farklı türbülans modeli kullanılmıştır. Serbest su yüzeyinin belirlenmesinde Akışkan hacimler yöntemi (Volume of Fluid-VOF) yöntemi (Hirt ve Nichols, 1981) kullanılmıştır.

4. ARAŞTIRMA BULGULARI ve TARTIŞMA

4.1 Çözüm Bölgesi ve Sınır Şartları

Serbest hidrolik sıçramanın meydana geldiği dikdörtgen kesitli açık kanal akımının sayısal modeli için kullanılan çözüm bölgesi ve sınır şartları Şekil 3'te verilmiştir. x, y koordinat sisteminin orijini, çözüm bölgesinin sol alt köşesi olarak alınmıştır. Şekilde verilen çözüm bölgesi toplam beş alt bölgeye ayrılmış ve çözüm bölgesinin üst sınırı ve çıkış bölgesi sınır şartı p=0, kanal tabanında ve savak yüzeyinde sıfır-hız sınır şartı, yani u=0, v=0 olarak tanımlanmıştır. Giriş sınır şartı olarak v hızı sıfır olarak alınmış olup, yatay hız bileşeni u değeri ise 1.618 m/s olarak hesaplanmıştır. Giriş sınırında başlangıç şartı olarak F=1 alınmıştır. Bunun anlamı ise bu sınır su ile dolu su girişi buradan olacak demektir. Çözüm bölgesinin tamamı başlangıçta tamamen boş kabul edilmiş olup F=0 olarak tanımlanmıştır.

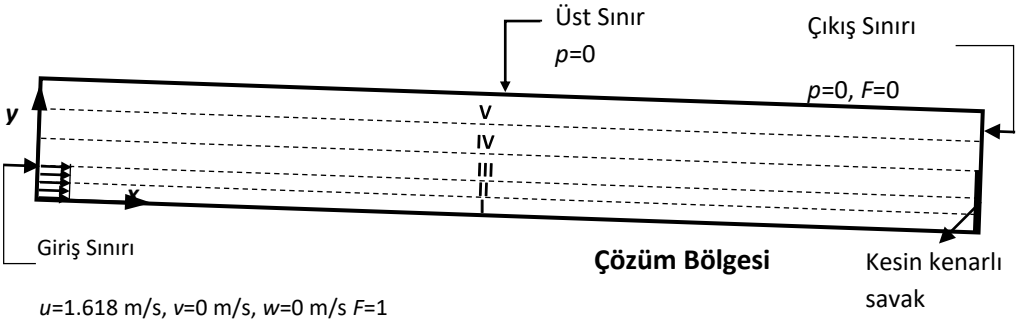

Şekil 3. Sayısal çözüm bölgesi, başlangıç ve sınır şartları

4.2 Ağ Yapısının Belirlenmesi

Çalışma kapsamında oluşturulan modelin çözüm bölgesinde hesaplama ağı beş alt bölgeye ayrılmış ve ağ yapısının sayısal çözüm değerleri üzerindeki etkisi incelenmiştir. Ağ yapısı etkisi ile meydana gelecek ayrıklaştırma hatasının belirlenebilmesi için üç farklı yoğunlukta hesaplama ağı oluşturulmuş ve ağ yapısının her bir alt bölgesindeki eleman sayısı yaklaşık olarak %25 ve %50 oranında arttırılarak üç farklı yoğunluktaki hesaplama ağları oluşturulmuştur. Tablo 1'de sayısal hesaplamalarda kullanılan üç farklı yoğunluktaki ağ yapısı için eleman sayıları verilmiştir.

Ağ yapısının sıklığının yeterliliği yani sayısal çözümün ağ yapısından bağımsız olup olmadığının belirlenebilmesi için Ağ Yakınsama İndeksi (Grid Convergence Index-GCI) (Roache, 1998) yöntemi ile oluşturulan Ağ 1 (Kaba), Ağ 2 (Orta) ve Ağ 3 (İnce) değerlendirilmiştir. Yapılan hesaplamalar sonucunda nümerik çözümde elde edilen hesaplama hassasiyetinin ağ yoğunluğundan bağımsızlaştığı anlaşılmaktadır

Tablo 1. Farklı yoğunluktaki hesaplama ağlarına ait bölgesel eleman sayıları

Bölge	**Ağ 1** (Kaba)	**Ağ 2** (Orta)	**Ağ 3** (İnce)
1	8x200	10x250	12x300
2	6x200	7x250	8x300
3	12x200	15x250	18x300
4	33x200	42x250	50x300
5	20x200	25x250	30x300

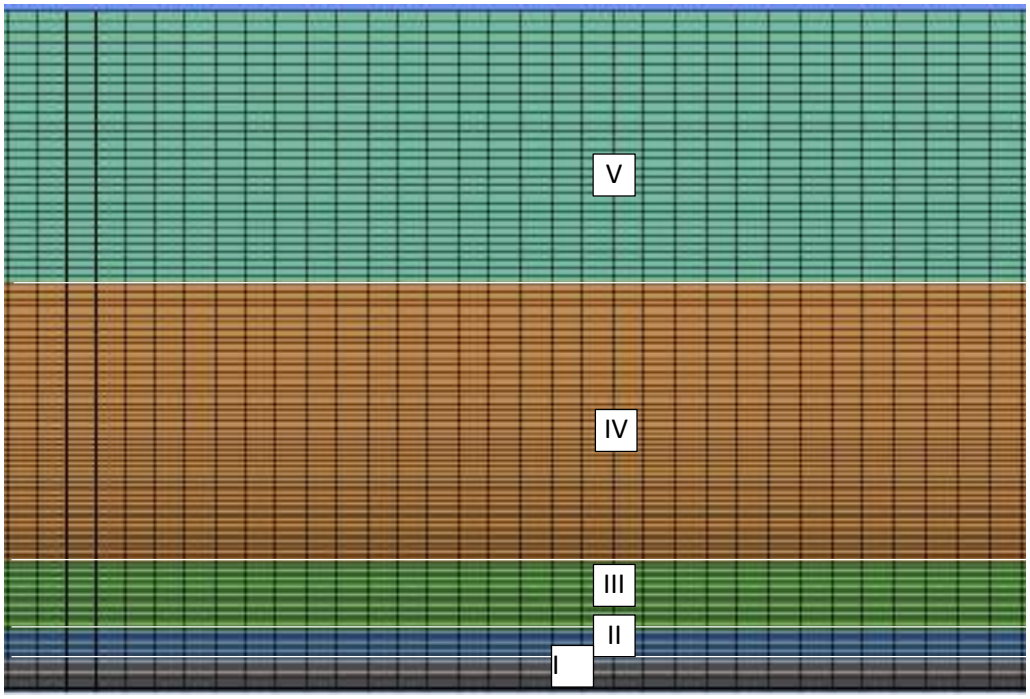

Şekil 4. Hesaplama Ağı

4.3. Sayısal Modelleme

Bu çalışma kapsamında düşük Froude sayısına sahip akım şartlarında oluşan serbest hidrolik sıçramanın akım özellikleri detaylı bir şekilde değerlendirilmiştir. Dört farklı türbülans modeli ile elde edilen sayısal bulgular ve deneysel bulgular literatürdeki çalışmalar ile karşılaştırılmıştır.

4.3.1. Serbest su yüzü profili (Fr_1=2.54)

Serbest hidrolik sıçramanın meydana geldiği açık kanal akımın su yüzü profili deneysel olarak ölçülmüş ve sayısal olarak farklı türbülans kapatma modelleriyle yapılan çözüm sonuçları Denklem 5 ve 6'da sırasıyla verilen Ortalama Karesel Hata (OKH) ve Ortalama Mutlak Göreceli Hata (OMGH) parametrelerine göre karşılaştırılmıştır. Karşılaştırma sonucunda hesap edilen OKH ve OMGH değerleri Tablo 2'de verilmiştir. Buna göre, en az OKH ve OMGH değerinin elde edildiği SKE modelinin kullanılan diğer modellere kıyasla az bir farkla da olsa daha başarılı olduğu ve tüm modeller genel olarak serbest su yüzünü belirlemede başarılı olduğu belirlenmiştir.

$$\mathrm{OKH} = \frac{1}{N}\sum_{n=1}^{N}(u_d - u_h)^2 \qquad \textbf{(5)}$$

$$\text{OMGH} = \frac{1}{N}\sum_{n=1}^{N}\left(\frac{|u_d - u_h|}{u_d}\right) \quad \textbf{(6)}$$

Tablo 2. OKH ve OMGH değerleri

	OKH (cm^2/s^2)	**OMGH (%)**
SKE	**0.3140**	**7.9815**
RNG	0.3350	8.0853
RSM	0.3274	8.0045
SST	0.3726	8.1268

SKE, RNG, SST ve RSM türbülans kapatma modelleri ile elde edilen su yüzü profillerinin grafiksel karşılaştırılması Şekil 5'de verilmiştir. Buna göre, SST dışında tüm modellerin sıçrama bölgesi geometrisini hesaplamada başarılı olduğu, bunun yanında sıçrama sonrası derinliğin hesaplanmasında ise deneysel sonuçlar ile ele alınan tüm türbülans modelleriyle elde edilen sayısal sonuçların birbirine benzer olduğu görülmektedir. Yani SST türbülans kapatma modeli hidrolik sıçramanın gerçekleştiği bölgeyi diğer modeller kadar başarılı modelleyememiştir.

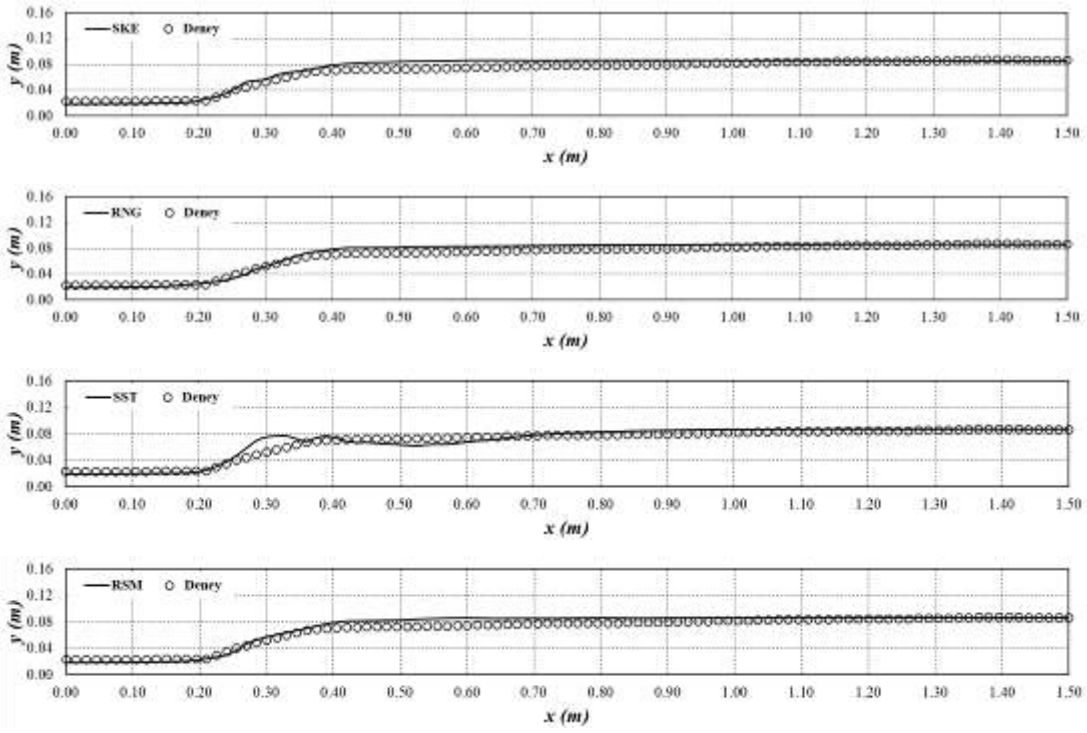

Şekil 5 Sayısal ve deneysel su yüzü profilleri

4.3.2. Sayısal Hız profilleri (Fr_1=2.54)

En başarılı model olan SKE modeliyle sayısal olarak hesaplanan hız profilleri Şekil 6'da verilmiştir. Buna göre, sıçrama öncesi (x=10 cm) oluşan hız profillerinin ortalama hız değerleri 1.6 m/s civarında olup benzer bir profil sergilemektedir. Sıçramanın başladığı noktadan 10 cm uzaklıkta bulunan x=30 cm kesiti için kanal tabanına yakın olan bölgede yaklaşık 1 m/s civarında maksimum hıza sahip bir jet akımı oluşturduğu ve su yüzeyine yakın bölgede ise düşük bir hız değeri aldığı görülmektedir. Kanal sonuna doğru ilerledikçe su derinliğinin artmasına paralel olarak maksimum hızın azaldığı görülmektedir. Ayrıca SKE modelinde jet akımının yaklaşık x=65 cm'de klasik açık kanal akım profiline yakın bir profil sergilediği ve çalışma alanının sonuna doğru ise açık kanal akım profili sergilediği yani sıçrama etkisinden kurtulduğu görülmektedir. Buna göre, sıçrama bölgesinin içinde yer aldığı çalışma alanı için SKE türbülans kapatma modeli ile hesaplanan sayısal hız profillerinin yapısı incelendiğinde, SKE modelinin sıçrama sonlandıktan sonra hız profillerini vermede McCorquodale ve Khalifa (1983) sonuçlarına benzer bir yapı sergilediği ve buna bağlı olarak su yüzü profilinin hesaplanmasında benzer bir şekilde hız profilini de belirlemede başarılı olduğu görülmüştür.

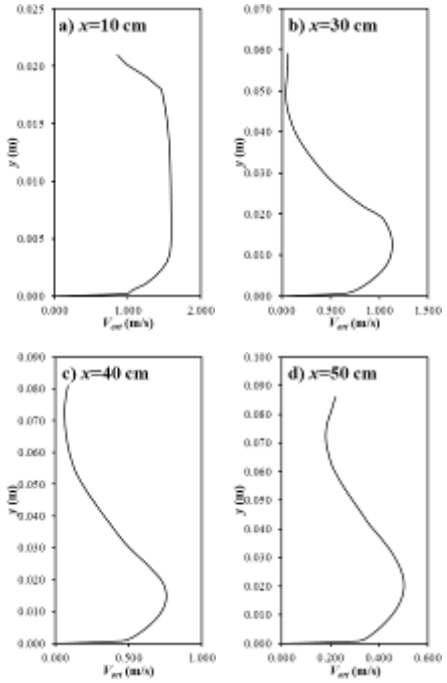

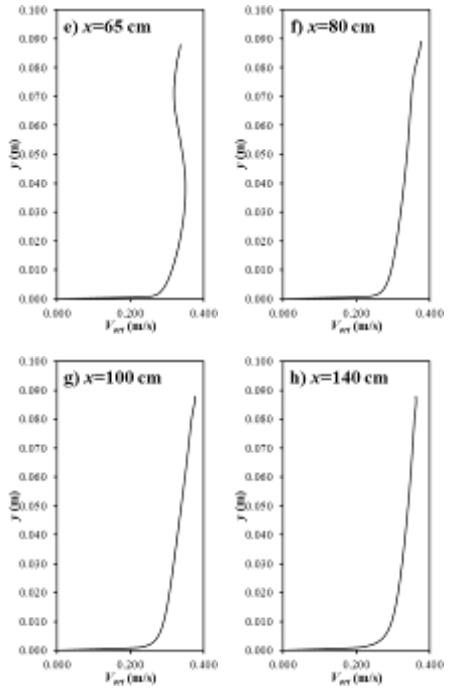

Şekil 6. SKE modeli ile elde edilen ortalama akım hız profilleri

5. SONUÇ

Bu çalışmada laboratuvar ortamında hidrolik sıçrama öncesi kesitte Froude sayısı 2.54 olan akım durumunda meydana gelen hidrolik sıçramanın karakteristikleri deneysel ve sayısal olarak modellenmiştir. Farklı türbülans modelleri kullanılarak elde edilen sayısal model sonuçları deneysel bulgular ile karşılaştırılmıştır. Buna göre;

- Sayısal model sonuçları üzerinde etkisinin olduğu bilinen ağ yapısının sıklığının yeterliliği, yani sayısal çözümün ağ yapısından bağımsız olup olmadığının belirlenebilmesi için GCI yöntemi değerlendirilmiş ve nümerik çözümde elde edilen hesaplama hassasiyetinin ağ yoğunluğundan bağımsızlaştığı belirlenmiştir.

- Serbest su yüzünün belirlenmesinde, SST dışında tüm modellerin sıçrama bölgesi geometrisini hesaplamada başarılı olduğu, bunun yanında sıçrama sonrası derinliğin hesaplanmasında ise deneysel sonuçlar ile ele alınan tüm türbülans modelleriyle elde edilen sayısal sonuçların birbirine benzer olduğu görülmüştür.

- Sayısal hız profillerine göre, sıçrama bölgesinin içinde yer aldığı çalışma alanı için SKE türbülans kapatma modeli ile hesaplanan profillerin yapısının literatür ile uyumlu olduğu, yani su yüzü profillerini belirlemede başarılı olan modelin hız profillerini hesaplamada da başarılı olduğu belirlenmiştir.

Çalışma kapsamında elde edilen bulgulara göre, serbest hidrolik sıçrama gibi değişken bir yapıya sahip karmaşık bir akım türünün uygun ağ yapısı ve türbülans modeli ile başarılı bir şekilde belirlenebileceği sonucuna varılmıştır.

TEŞEKKÜR

Bu çalışma Harran Üniversitesi Bilimsel Araştırma Projeleri Koordinasyon Birimi (HÜBAP) tarafından desteklenmiştir (Proje No:19118).

KAYNAKLAR

Alikhani, A., Behrozi-Rad, R., and Fathi-Moghadam, M., 2010. Hydraulic jump in stilling basin with vertical end sill. International Journal of Physical Sciences, 5(1):25-29.

Carvalho, R. F., Lemos, C. M., & Ramos, C. M. (2008). Numerical computation of the flow in hydraulic jump stilling basins. Journal of Hydraulic Research, 46(6), 739-752.

Chippada, S., Ramaswamy, B., & Wheeler, M. F. (1994). Numerical simulation of hydraulic jump. International Journal for Numerical Methods in Engineering, 37(8), 1381-1397.

Gharangik, A. M., & Chaudhry, M. H. (1991). Numerical simulation of hydraulic jump. Journal of hydraulic engineering, 117(9), 1195-1211.

Gümüş, V., Aköz, M. S. ve Kırkgöz, M. S. (2013). Kapak Mansabında Batmış Hidrolik Sıçramanın Deneysel ve Sayısal Modellenmesi. İMO-Teknik Dergi, 24(2): 6379-6397.

Gümüş, V., Aköz, M. S., Şımşek, O., Soydan, N. G. ve Kırkgöz, M. S. (2012). Experimental and Numerical Modeling of Free Hydraulic Jump Downstream of a Gate. 10th International Congress on Advances in Civil Engineering, Ankara-Turkey.

Hager, W. H., and Li, D., 1992. Sill-controlled energy dissipator. Journal of Hydraulic Research, 30(2):165-181

Hirt, C. W., and Nichols, B. D. (1981). "Volume of fluid (Vof) method for the dynamics of free boundaries." J. Comput. Phys., 39(1), 201–225.

Launder, B. E., and Spalding, D. B. (1972). Lectures in mathematical models of turbulence, Academic, New York.

Launder, B. E., Reece, G. J., and Rodi, W. (1975). "Progress in the development of a Reynolds-stress turbulence closure." J. Fluid Mech., 68(3), 537.

Liu, M., Rajaratnam, N., and Zhu, D. Z., 2004. Turbulence structure of hydraulic jumps of low Froude numbers. Journal of Hydraulic Engineering, 130(6):511-520.

Ma, F., Hou, Y. ve Prinos, P., "Numerical calculation of submerged hydraulic jump", Journal of Hydraulic Research, 39(5), 1-11, 2002.

McCorquodale, J. A., & Khalifa, A. (1983). Internal flow in hydraulic jumps. Journal of Hydraulic Engineering, 109(5), 684-701.

Menter, F. R. (1994). "2-equation Eddy-viscosity turbulence models for engineering applications." AIAA J., 32(8), 1598–1605.

Özbay, Ö., 2008. Şüt Kanallarına Yerleştirilen Farklı Tip Enerji Kırıcı Blokların İncelenmesi. Yüksek Lisans Tezi, Fen Bilimleri Enstitüsü, Fırat Üniversitesi, Elazığ.

Padulano, R., Fecarotta, O., Del Giudice, G., and Carravetta, A., 2017. Hydraulic Design of a USBR Type II Stilling Basin. Journal of Irrigation and Drainage Engineering:04017001

Pillai, N. N., Goel, A., ve Dubey, A. K., 1989. Hydraulic jump type stilling basin for low Froude numbers. Journal of Hydraulic Engineering, 115(7):9899

Roache, P. J. (1998). "Verification of codes and calculations." AIAA J., 36(5), 696–702.

Yakhot, V., Orszag, S. A., Thangam, S., Gatski, T. B., and Speziale, C. G. (1992). "Development of turbulence models for shear flows by a double expansion technique." Phys. Fluids A, 4(7), 1510–1520.

LIFE CYCLE ASSESSMENT OF SOLAR PHOTOVOLTAIC ELECTRICITY GENERATION POWER PLANT: A CASE STUDY OF KAYSERİ TURKEY

Nesrin KAYATAŞ DEMİR

Department of Energy Systems Engineering, Erciyes University, 38039 Kayseri, Turkey

nkayatas@erciyes.edu.tr

Melike ÖZATA

Department of Energy Systems Engineering, Erciyes University, 38039 Kayseri, Turkey

Melikeozata9652@gmail.com

Akif TAŞKIN

Graduate School of Natural and Applied Sciences, Erciyes University, 38039 Kayseri, Turkey, taskinakif@gmail.com

ABSTRACT: Energy related topics essentially occupy the world with respect to the environmental, economic, political and security affairs. Generation of electricity is primary factor of environmental impacts in global scale. Regardless of whether the power source is renewable or non-renewable environmental impacts of the electricity generation technique must be analyzed to obtain sustainable development. Life cycle assessment is useful tool to evaluate the environmental energy relation of a system or product during its lifetime. In this study, environmental and energy impacts of 55 MWp capacity solar photovoltaic power plant, installed in Kayseri Organized Industrial Zone, are analyzed. SimaPro PhD 8.4.1.0 software is used for calculations. Inventory data is collected from the power plant, Ecoinvent database and literature. Three different functional units are selected such as 1kWh electricity delivered to the grid, number panels and panel installed area. CML-IA Baseline, version 3.04 and Cumulative Energy Demand, version 1.09 are used for environmental and energy calculations, respectively. Results show that; 8.30E-02 kg CO2 eq/kWh, 1.61E+02 kg CO_2 eq/m^2 and 7.37E+02 are calculated in terms of global warming potential and total cumulative energy demand calculated as 2.66E+09.

Key words: Climate change, life cycle assessment, solar energy, sustainable development.

INTRODUCTION

Energy based problems have been playing crucial role around the world since the last decades. Increase in the energy demand leads to the social, economic and environmental problems. Global interest concentrated to solve these problems to provide sustainable development. Electricity and heat production are the largest contributor on the total CO_2 emissions by sector in the global range with 49.04 % (Our World in Data, 2017). Gross electricity generation trend in the world has been tending to use renewable energy sources but non-renewable energy source use such as coal and natural gas is still mainly occupying the world electricity production by power source (International Energy Agency, 2019). There are several electricity generation technologies with the advantages and disadvantages according to the power source, efficiency, environmental impact and economic factors. Among the renewable energy sources solar energy has been attracting the attention in terms of the clean and sustainable characteristics. In 2018, electricity generation from solar energy expanded rapidly and the growth of the electricity generation from renewable energy sources was provided mainly by the solar energy with 40% share (BP Statistical Review of World Energy, 68th Edition, 2019). Table 1 gives information about the status of the electricity generation methods of the Turkey. Table 1 illustrates that solar energy shares 6.11 % of total installed power with 6430 power plants (Turkish Electricity Transmission Corporation, 2019).

Increase in the electricity production accelerates the formation of environmental impacts, therefore these impact values must be calculated and analyzed to provide sustainable development (A.F. Sherwani, J.A. Usmani, Varun, 2010). All the energy generation methods generate the environmental impacts in different loads through operation, manufacturing, installation, decommissioning and recycling stages. Life cycle assessment (LCA) is useful approach to calculate the environmental and energy impacts of the electricity generation technologies (R. Turconi, A. Boldrin, T. Astrup, 2013). In this study, environmental and energy analysis of 55 MWp capacity solar power plant are performed. Inventory data is gathered from the power plant, Ecoinvent database and literature. Collected data is compiled by SimaPro PhD 8.4.1.0 LCA software. 1kWh electricity delivered to the grid, number panels and panel installed area are selected as functional units.

Table 1. Distribution of Primary Energy Sources in Turkey

Power Source	**Power Plant**	**Installed Power (MW)**	**Installed Power (%)**
River	545	7854.7	8.69

Asphaltite Coal	1	405	0.45
Waste Heat	76	339.6	0.38
Dam	122	20582.4	22.77
Biomass	158	706.8	0.78
Natural Gas	328	26035.8	28.80
Fuel Oil	15	487.2	0.54
Solar	6430	5528.1	6.11
Import Coal	14	8938.9	9.89
Geothermal	48	1335.5	1.48
Lignite	48	10101	11.17
LNG	1	2	0.00
Wind	259	7270	8.04
Hard Coal	4	810.8	0.90
Total	8.051	90403.4	100

METHODS

In this work, environmental and energy life cycle analysis of 55 MWp capacity solar power plant is carried out by considering the IS0 14040 and ISO 14044 standards (ISO, 1997), (ISO, 2006). Goal of this study is to calculate environmental and energy impacts of 55MWp capacity solar photovoltaic power plant installed in Kayseri. Within this scope, field researches are performed on the power plant and life cycle inventory data are collected from plant area, literature, technicians and Ecoinvent database with respect to the system boundaries. System boundary is selected according to the site-specific data to analyze the impacts properly and given as follows:

- Panel, electronics, inverter and auxiliary components production and operation,
- Plant construction,
- 1 kWh electricity delivery to the grid.

In a typical LCA study functional unit must be defined to normalize and compare the results with other systems. For this work, functional units are selected as 1 kWh electricity output, number of panels and panel installed area. Moreover, to obtain more precise results in consideration of system boundaries some assumptions are made as follows:

- Lifetime of the plant is 25 years,

- Decrease in the efficiency about 1% per year,
- Inverter maintenance per 6 months,
- All panels are accepted as multi-Si panels,
- Panel cleaning: 10 cleaners works with distilled water to clean 1MW panel per day.

CML-IA Baseline and Cumulative Energy Demand impact methods are used for the impact assessments and characterization factors are selected according to these impact methods. Inventory data are gathered according the Table 2. Installed power, area, panel capacity, number of panels, inverter type and annual generated electricity are given in the Table 2, separately. Canadian Solar, Solar Frontier, Hanwha and Hanwha Tracker panels are used. ABB and Huawei brand inverters are assembled on the plant. The solar power plant consists of four different locations as given in the following table. In a typical LCA model data have some uncertainties. In this study, SimaPro PhD is run Monte Carlo analysis to define the uncertainties on the results and following parameters are considered;

- Impact assessment method,
- Fixed number of runs,
- Stop factor.

In this work impact assessment method is selected as CML-IA Baseline, number of runs 1000 times and stop factor as 0.005 for uncertainty analysis. Moreover, uncertainty results are not used for comparison because of the considered one system as solar power plant.

Table 2. Characteristics of Solar Power Plant

	Installed Power (MWp)	Area (m^2)	Panel Capacity (W)	Number of Panels	Inverter	Annual Electricity Production (kWh)
Plant 1	6.8	120,000	255W Canadian Solar	26,496	6 ABB PVS800	10,829,701
Plant 2	11.5	265,000	170W Solar Frontier	67,640	10 ABB PVS800	19,500,000
Plant 3	32.4	515,000	305 W 310W Hanwha	104,652	27 ABB PVS800	50,000,000

Plant 4	4.2	68,000	345W Hanwha	12,258	68 HUAWEI SUN2000 60-KTL-MO	8,000,000
Total	55	968,000	-	211,046	111	88,329,701

RESULTS AND FINDINGS

Electricity generation is calculated by considering the 1% loss in the efficiency. Generated electricity results per years are given in the Table 3, Table 4 and Table 5.

Table 3. Annual Energy Production of Solar Power Plant in 25 Years

	First Year	2	3	4	5	6	7	8
Plant 1	1.083E+07	1.072E+07	1.061E+07	1.051E+07	1.040E+07	1.030E+07	1.020E+07	1.009E+07
Plant 2	1.950E+07	1.931E+07	1.911E+07	1.892E+07	1.873E+07	1.854E+07	1.836E+07	1.818E+07
Plant 3	5.000E+07	4.950E+07	4.901E+07	4.851E+07	4.803E+07	4.755E+07	4.707E+07	4.660E+07
Plant 4	8.000E+06	7.920E+06	7.841E+06	7.762E+06	7.685E+06	7.608E+06	7.532E+06	7.457E+06
Total	8.833E+07	8.745E+07	8.657E+07	8.571E+07	8.485E+07	8.400E+07	8.316E+07	8.233E+07

Table 4. Annual Energy Production of Solar Power Plant in 25 Years (Continued)

	9	10	11	12	13	14	15	16
Plant 1	9.993E+06	9.893E+06	9.794E+06	9.696E+06	9.599E+06	9.503E+06	9.408E+06	9.314E+06
Plant 2	1.799E+07	1.781E+07	1.764E+07	1.746E+07	1.728E+07	1.711E+07	1.694E+07	1.677E+07

Plant 3	4.614E+07	4.568E+07	4.522E+07	4.477E+07	4.432E+07	4.388E+07	4.344E+07	4.300E+07
Plant 4	7.382E+06	7.308E+06	7.235E+06	7.163E+06	7.091E+06	7.020E+06	6.950E+06	6.880E+06
Total	8.151E+07	8.069E+07	7.988E+07	7.908E+07	7.829E+07	7.751E+07	7.674E+07	7.597E+07

Table 5. Annual Energy Production of Solar Power Plant in 25 Years (Continued)

	17	18	19	20	21	22	23	24	25	Total
Plant 1	9.221E+06	9.129E+06	9.038E+06	8.947E+06	8.858E+06	8.769E+06	8.681E+06	8.595E+06	8.509E+06	2.298E+08
Plant 2	1.660E+07	1.644E+07	1.627E+07	1.611E+07	1.595E+07	1.579E+07	1.563E+07	1.548E+07	1.532E+07	4.137E+08
Plant 3	4.257E+07	4.215E+07	4.173E+07	4.131E+07	4.090E+07	4.049E+07	4.008E+07	3.968E+07	3.928E+07	1.061E+09
Plant 4	6.812E+06	6.744E+06	6.676E+06	6.609E+06	6.543E+06	6.478E+06	6.413E+06	6.349E+06	6.285E+06	1.697E+08
Total	7.521E+07	7.446E+07	7.371E+07	7.298E+07	7.225E+07	7.152E+07	7.081E+07	7.010E+07	6.940E+07	1.874E+09

Table 6 gives information about the impact categories according to the CML-IA Baseline methods. All the impact results are divided to the total energy generation and delivered to the grid as 1.874E+09 to compare the results with other energy generation technologies. Thus, emissions per kWh values are calculated. GWP per kWh is 8.30E-02 kg CO_2 eq/kWh as given in the Table 6. It means that for every kWh electricity delivered to the grid emits 8.30E-02 kg CO_2 emissions to the atmosphere.

Table 6. Total Impacts and Emissions per kWh of Solar Power Plant

Impact category	**Unit**	**Total**	**Emissions per kWh**
Abiotic depletion	kg Sb eq/kWh	4.77E+03	2.54E-06
Abiotic depletion (fossil fuels)	kWh	4.88E+08	2.61E-01
Global warming (GWP100a)	kg CO_2 eq/kWh	1.56E+08	8.30E-02

Ozone layer depletion (ODP)	kg CFC-11 eq/kWh	2.75E+01	1.47E-08
Human toxicity	kg 1.4-DB eq/kWh	1.53E+08	8.15E-02
Fresh water aquatic ecotoxicity	kg 1.4-DB eq/kWh	1.33E+08	7.12E-02
Marine aquatic ecotoxicity	kg 1.4-DB eq/kWh	5.99E+11	3.20E+02
Terrestrial ecotoxicity	kg 1.4-DB eq/kWh	5.10E+05	2.72E-04
Photochemical oxidation	kg C_2H_4 eq/kWh	5.10E+04	2.72E-05
Acidification	kg SO_2 eq/kWh	9.35E+05	4.99E-04
Eutrophication	kg PO_4 eq/kWh	3.75E+05	2.00E-04

Impacts values are divided to the panel areas and panel numbers to calculate the emissions per m^2 and emissions per panel and given in the Table 7 and Table 8, respectively.

Table 7. Emissions per m^2 of Solar Power Plant

Impact category	**Unit**	**Impacts per m^2**
Abiotic depletion	kg Sb eq/m^2	4.92E-03
Abiotic depletion (fossil fuels)	kWh/ m^2	1.82E+03
Global warming (GWP100a)	kg CO_2 eq/m^2	1.61E+02
Ozone layer depletion (ODP)	kg CFC-11 eq/m^2	2.84E-05
Human toxicity	kg 1.4-DB eq/m^2	1.58E+02
Fresh water aquatic ecotox.	kg 1.4-DB eq/m^2	1.38E+02
Marine aquatic ecotoxicity	kg 1.4-DB eq/m^2	6.19E+05
Terrestrial ecotoxicity	kg 1.4-DB eq/m^2	5.27E-01

Photochemical oxidation	kg C_2H_4 eq/m^2	5.27E-02
Acidification	kg SO_2 eq/m^2	9.66E-01
Eutrophication	kg PO_4 eq/ m^2	3.88E-01

Table 8. Emissions per Panel of Solar Power Plant

Impact category	**Unit**	**Total**
Abiotic depletion	kg Sb eq/panel	2.26E-02
Abiotic depletion (fossil fuels)	kWh/panel	2.31E+03
Global warming (GWP100a)	kg CO_2 eq/panel	7.37E+02
Ozone layer depletion (ODP)	kg CFC-11 eq/panel	1.30E-04
Human toxicity	kg 1.4-DB eq/panel	7.24E+02
Fresh water aquatic ecotoxicity	kg 1.4-DB eq/panel	6.32E+02
Marine aquatic ecotoxicity	kg 1.4-DB eq/panel	2.84E+06
Terrestrial ecotoxicity	kg 1.4-DB eq/panel	2.42E+00
Photochemical oxidation	kg C_2H_4 eq/panel	2.42E-01
Acidification	kg SO_2 eq/panel	4.43E+00
Eutrophication	kg PO_4 eq/panel	1.78E+00

Table 9 provides information about the energy demand of the solar power plant throughout lifetime as 25 years. Values on the table mean that consumed energy according to the source as non-renewables and renewables. Figure 1 represent the Sankey diagram of the provides information about the GWP of the solar power plant in percentage values. Figure provides the information about the contribution of every sub-unit processes on GWP. Thickness of the diagram defines the magnitude of the contribution on GWP of the unit process. This figure guides researchers to determine the hot points of the system by evaluating the percentages. According to the figure multi-Si photovoltaic panel and mounting process share the 68.7% and 27.2% of the total GWP emissions, respectively.

Table 9. Cumulative Energy Demand of Solar Power Plant

Impact category	**Unit**	**Total**
Non-renewable, fossil	kWh	4.89E+08
Non-renewable, nuclear	kWh	7.04E+07
Non-renewable, biomass	kWh	1.37E+05
Renewable, biomass	kWh	2.11E+07
Renewable, wind, solar, geothermal	kWh	2.01E+09
Renewable, water	kWh	7.24E+07
Total		2.66E+09

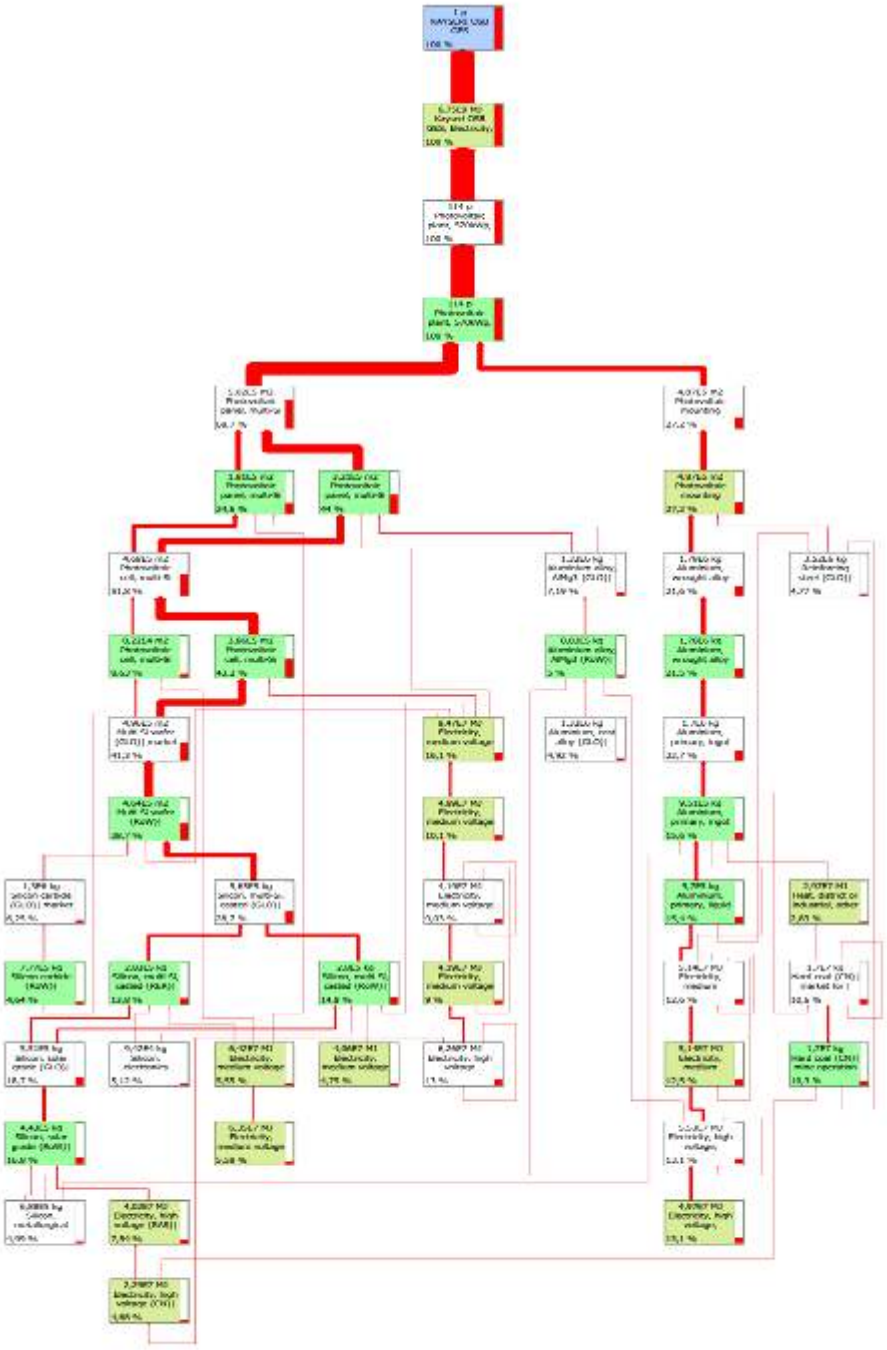

Figure 1. GWP Impact Analysis of Solar Power Plant (%)

Monte Carlo Analysis

Lognormal distribution of the uncertainty is given in the Figure 2 with the 95% confidence interval for GWP indicator. Mean, median, standard deviation and coefficient of variability for all impact categories are given in the Table 10. Figure 3 represents the uncertainty range as bar charts for each impact category. T lines define

the 95% confidence interval and the magnitude of the T lines show the uncertainty range per impact category.

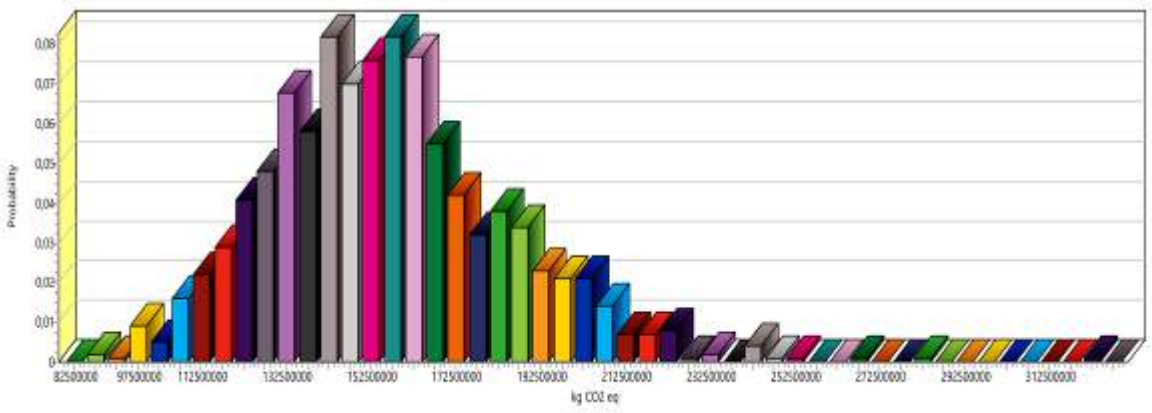

Figure 2. Lognormal Distribution of GWP Impact

Table 10. Uncertainty Data per Impact Category

Impact category	**Unit**	**Mean**	**Median**	**SD**	**CV %**
Abiotic depletion	kg Sb eq	4.78E+03	4.65E+03	9.78E+02	20.48
Abiotic depletion (fossil fuels)	MJ	1.75E+09	1.72E+09	3.33E+08	18.99
Acidification	kg SO_2 eq	9.40E+05	9.22E+05	1.79E+05	19.07
Eutrophication	kg PO_4 eq	3.74E+05	3.40E+05	1.52E+05	40.57
Fresh water aquatic ecotox.	kg 1.4-DB eq	1.35E+08	1.26E+08	4.52E+07	33.49
Global warming (GWP100a)	kg CO_2 eq	1.56E+08	1.51E+08	2.86E+07	18.13
Human toxicity	kg 1.4-DB eq	1.54E+08	1.46E+08	4.37E+07	28.32
Marine aquatic ecotoxicity	kg 1.4-DB eq	6.03E+11	5.72E+11	1.73E+11	28.66
Ozone layer depletion (ODP)	kg CFC-11 eq	2.73E+01	2.69E+01	5.89E+00	21.55
Photochemical oxidation	kg C_2H_4 eq	5.12E+04	5.00E+04	1.02E+04	19.91

Terrestrial ecotoxicity	kg 1.4-DB eq	5.12E+05	4.98E+05	1.11E+05	21.64

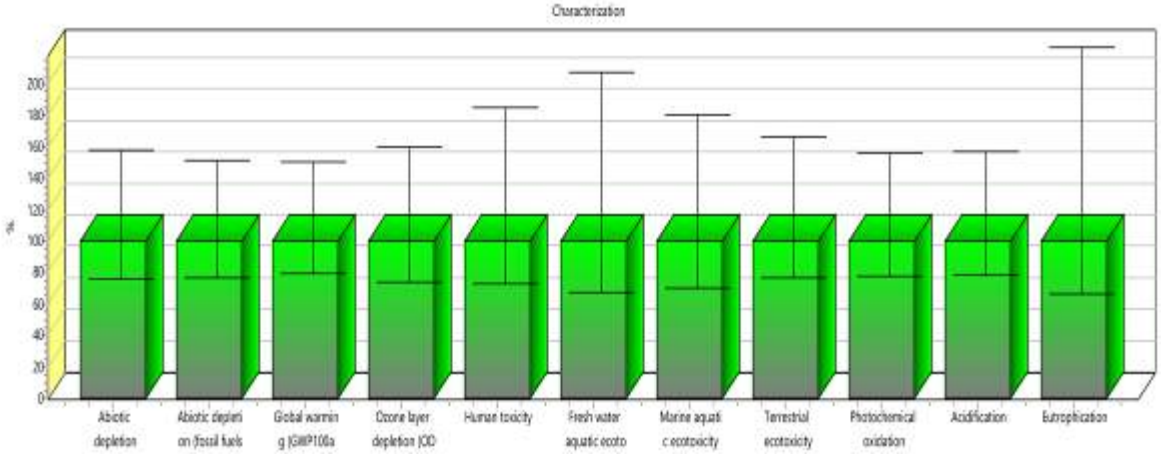

Figure 3. Uncertainty Data per Impact Category as Bar Chart

CONCLUSION

Energy and environment related problems principally deal with the sustainable development concerns on global scale. These problems must be analyzed to determine the magnitude of the problems. Life cycle assessment approach is a useful methodology to define the environmental and energy impacts of a system or a product. In this study environmental and energy analysis of 55 MWp solar photovoltaic power plant are performed. SimaPro LCA software is used to compile the inventory data. Inventory data is collected from the literature, Ecoinvent database and field researches. System boundary and assumptions are defined according to the goal of the study. 1kWh electricity delivered to the grid, panel area in m^2 and number of panels selected as functional units. Results show that GWP of the power plant is calculated as 1.56E+08 kg CO_2 eq/kWh. Moreover, GWP values for individual electricity generation technologies and calculated value for this study are given in the Table 11. According to Table 11 results of this study are in acceptable range and proven by the literature works.

Table 11. Mean Global Warming Potential (GWP) of Energy Generation Technologies

Energy Generation Technology	Mean Global Warming Potential (GWP)

	kgCO_2/kWh
Lignite	1.054
Coal	0.088
Oil	0.073
Natural Gas	0.049
Biomass	0.045
Nuclear	0.029
Hydro	0.026
Wind	0.026
Photovoltaic	0.085
Photovoltaic (This Study)	0.083

This study can be a guide for investors, municipalities or researchers in the field of sustainable production of electricity.

RECOMMENDATIONS

The authors acknowledge the financially support of Erciyes University Scientific Research Projects Funding Department (ERU-BAP) (Grant No: FDK-2016-6871). Authors also thank to the Administration of Kayseri Organized Industrial Zone for providing the LCI data used in this study.

REFERENCES

A.F. Sherwani, J.A. Usmani, Varun. (2010). Life cycle assessment of solar PV based electricity generation systems: A review. *Renewable and Sustainable Energy Reviews, 14,* 540-544. doi: 10.1016/j.rser.2009.08.003.

BP Statistical Review of World Energy, 68th Edition. (2019). Retrieved 2019, from https://www.bp.com/content/dam/bp/business-sites/en/global/corporate/pdfs/energy-economics/statistical-review/bp-stats-review-2019-full-report.pdf

CO_2 and Greenhouse Gas Emissions. (2018). Retrieved 2019, from https://ourworldindata.org/co2-and-other-greenhouse-gas-emissions.

Electricity Information 2019 Overview, International Energy Agency. (2019). Retrieved 2019, from https://www.iea.org/statistics/electricity/

Installed power report of Turkey, Turkish Electricity Transmission Corporation. (2019). Retrieved 2019, from https://www.teias.gov.tr/sites/default/files/2019-09/KURULU%20G%C3%9C%C3%87%20%C4%B0NTERNET%20%28A%C4%9EUSTOS%20AYI%20SONU%20%C4%B0T%C4%B0BAR%C4%B0%20%C4%B0LE%29.pdf

ISO 14040: Environmental management - life cycle assessment - principles and framework. (1997). Geneve (Switzerland): ISO.

ISO 14044: Environmental management, life cycle assessment, requirements and guidelines. (2006). Geneve (Switzerland): ISO.

R. Turconi, A. Boldrin, T. Astrup. (2013). Life cycle assessment (LCA) of electricity generation technologies: Overview, comparability and limitations. *Renewable and Sustainable Energy Reviews, 28,* 555-565. doi: 10.1016/j.rser.2013.08.013.

THE PROPERTIES OF HYBRID FIBER REINFORCED SELF-COMPACTING CONCRETE WITH DIFFERENT TYPE MICRO FIBER

Kazim TURK, Inonu University,Engineering Faculty, Department of Civil Engineering, Malatya, Turkey, kazim.turk@inonu.edu.tr

Esma ATALAY, Inonu University,Engineering Faculty, Department of Civil Engineering, Malatya, Turkey, esmaatalayinsaat@gmail.com

ABSTRACT: In this study, six different fiber reinforced self-compacting concrete (FRSCC) mixtures were adopted; one types of single reinforced mixtures with only macro steel fiber, three types of binary reinforced mixtures with (75% macro steel+25% micro steel fiber) and (1% macro steel fiber+25% PVA) and (1% macro steel fiber+25% PP), two types of ternary reinforced mixtures with (75% macro steel fiber+25% micro steel fiber+25% PVA) and (75% macro steel fiber+25% micro steel fiber+25% PP), were prepared to investigate the effect of different type micro fiber on the mechanical properties of FRSCC. For this reason, all FRSCC mixtures had water/binder ratio of 0.23 and total binder content of 900 kg/m^3. Portland cement (PC) and fly ash (FA) were used as binders. The mixtures obtained as a result of workability tests (slump-flow and T_{50}) were cured in water at 20 ± 3 ° C at 28 days. Hardened specimens were subjected to compressive strength and tensile strength and four-point bending tests. Finally, it was observed that the addition of micro steel fiber and macro steel fiber together into mixtures had a negative effect on the workability properties of FRSCC specimens. Moreover, while the addition of micro steel fiber and macro steel fiber together into mixtures decreased flexural strength and the capacity of energy absorbtion, the addition of PVA synthetic fiber into mixtures had more positive effect than PP synthetic fiber on the flexural strength and the capacity of energy absorbtion of specimens.

Key words: Synthetic fiber, Micro steel fiber, Macro steel fiber, Hybrid fiber, SCC

FARKLI TİP MİKRO LİF İÇEREN KARMA LİF TAKVİYELİ KENDİLİĞİNDEN YERLEŞEN BETONUN ÖZELLİKLERİ

ÖZET: Bu çalışmada, altı farklı lif takviyeli kendiliğinden yerleşen beton (LTKYB) karışımı benimsendi; sadece makro çelik lifli bir tip tek takviyeli karışım, üç tip ikili takviyeli karışım (% 75 makro çelik +% 25 mikro çelik lif) ve (% 1 makro çelik lif +% 25 PVA) ve (% 1 makro çelik lif) +% 25 PP), iki tip üçlü takviyeli karışım (% 75 makro çelik elyaf +% 25 mikro çelik elyaf +% 25 PVA) ve (% 75 makro çelik elyaf +% 25 mikro çelik elyaf +% 25 PP); farklı tip mikro lifin LTKYB'nin mekanik özellikleri üzerindeki

etkisini araştırmak için hazırlanmıştır. Bu nedenle, tüm LTKYB karışımları, 0.23 su / bağlayıcı oranına ve toplam 900 kg / m3 bağlayıcı içeriğine sahipti. Bağlayıcı madde olarak Portland çimentosu (PÇ) ve uçucu kül (UK) kullanılmıştır. İşlenebilirlik testleri (çökme-yayılma ve T_{50}) sonucunda elde edilen karışımlar 20±3 ^{0}C sıcaklıktaki suda 28 gün kür edilmiştir. Kür edilen numunelere basınç dayanım testi ve dört notalı eğilmede çekme dayanımı testleri uygulanmıştır. Sonuç olarak, karışıma makro çelik lif ile birlikte mikro lif eklenmesinin işlenebilirlik özelliklerini olumsuz etkilediği gözlemlenmiştir. Ayrıca, makro çelik lif ile birlikte mikro çelik lifin karışıma eklenmesinin, numunelerin eğilme dayanımını ve enerji yutma kapasitesini azalttığı görülürken, mikro sentetik liflerden PVA lifinin eğilme dayanımı ve enerji yutma kapasitesi üzerinde PP lifine kıyasla daha olumlu bir etkiye sahip olduğu tespit edilmiştir.

Anahtar sözcükler: Sentetik lif, Mikro çelik lif, Makro çelik lif, Karma lif, KYB

GİRİŞ

Kendiliğinden yerleşen beton, dünyada ilk defa 1980'lerin ikinci yarısında Japonya'da deprem bölgelerindeki sık donatılı betonarme elemanlarda sıkıştırma işlemine gerek olmadan yerleşebilen beton ihtiyacından dolayı geliştirilmiştir (Okamura ve Quchi, 1999). Bileşimlerinde kullanılan hiperakışkanlaştırıcı katkı ile elde edilen düşük su/bağlayıcı oranı ile birlikte hem yüksek dayanıma hem de üstün dayanıklılığa sahip olması nedeniyle KYB'ler yüksek performanslı betonlar sınıfına girebilmektedir (Özkul, M.,H., 2002 ile Sağlam ve ark. 2005). EFNARC'a (2005) göre, bir karışımın KYB olma şartı için, işlenebilirlik testlerine (çökme-yayılma, T_{50}, V-hunisi, L-kutusu, U-kutusu gibi) ait sınır değerlerin sağlanması gerekmektedir.

Lif takviyeli beton ile ilgili ilk çalışmalar ise 1950 ve 1960'larda çelik lif takviyeli betonun mekanik davranışını anlamak amacıyla yapılmıştır (Hannant, D. J., 1987). Birden çok süreksiz lif tipinin karışıma dahil edilmesi ile geleneksel beton matrisinin birleşiminden elde edilen lif takviyeli betona karma lif takviyeli beton denilmektedir (Ding, Y.N., You, Z., Jalali, S., 2010 ile Sukontasukkul, P., Jamsawang, P.,2012). Karma lif takviyeli kompozitte, bir tip lif varlığı diğer lif özelliklerini faydalı kıldığı için daha ilgi çekici mühendislik özellikler sunar (Mobasher, B., Li Cheng, Y.,1996 ile Akcay, B.,2012). Karma lif takviyeli çimento esaslı kompozitlerde uzun ve çekme dayanımı yüksek makro lifler büyük çatlakları, kısa ve çekme dayanımı düşük olan mikro lifler ise çatlak başlaması ve ilerlemesini kontrol amacıyla kullanılırlar (ARAL,M.,2006). Sentetik ve çelik lifin bir arada kullanılması durumunda, çelik lifler yüksek süneklik sağlarken ve betondaki çatlak yayılımını azaltırken, polipropilen lifler ise betondaki parçalanmayı hafifletebilirler (Rodrigues, J. P. C., Laím, L., Correia, A. M.,2010). Şekil değiştirme sertleşmesi gösteren çimento esaslı kompozitte sentetik lif olarak en çok polivinil alkol (PVA) lifleri kullanılmaktadır (Jin-Cheng Liu, Kang Hai Tan.,2017).

Bu çalışmada, mikro lifin karma lif takviyeli KYB'nin işlenebilirlik özellikleri üzerine etkisini belirlemek için çökme-yayılma ve T_{50} testleri gerçekleştirilirken, mekanik özelliklere etkisini incelemek amacıyla da elde edilen karışımlardan üretilen 28 günlük lif takviyeli KYB numuneleri üzerinde basınç dayanımı ile dört noktalı eğilmede çekme dayanımı testleri yapılmıştır.

DENEYSEL PROGRAM

Deneysel program 2 aşamadan oluşmuştur. Birinci aşamada, taze haldeki lif takviyeli karışımların çökme-yayılma ve T_{50} ölçümleri yapıldı. İkinci aşamada ise, lif takviyeli karışımlarla hazırlanan numunelerin 28 günlük basınç ve eğilmede çekme dayanımları tespit edildi.

Malzemeler

Bu çalışmadaki bütün karışımlarda bağlayıcı malzeme olarak, CEM I 42.5 R Portland Çimentosu (PC) ile uçucu kül (UK) mineral katkısı kullanıldı. Bağlayıcılara ait kimyasal ve fiziksel özellikler Tablo 1'de verilmiştir. 0-5 ve 5-10 mm elek aralığına sahip iki farklı tipte agrega kullanılırken, yüksek oranda su azaltıcı özelliğine sahip hiperakışkanlaştırıcı olarak ise Sika Yapı Kimyasalları A.Ş. tarafından temin edilmiş ve özgül ağırlığı 1.06 olan ViscoCrete Hi-Tech 51 kullanıldı. 0-5 ve 5-10 mm agregalarına ait su emme değerleri sırasıyla, %2.2 ve %0.3, özgül ağırlık değerleri ise sırasıyla, 2.49 ve 2.63 olarak bulunmuştur. Karışımlarda makro çelik lif 3D 65/35 ve mikro çelik lif OL 6/.16 kullanılırken, sentetik olarak ise PVA ve PP mikro lifleri tercih edildi. Bu liflere ait özellikler Tablo 2'de sunulmuştur.

Tablo 1. Portland Çimentosu ve Uçucu Külün Kimyasal Özellikleri

Çimentolu Malzemeler	Kompozisyon (%)									Özgül Ağırlık (g/cm^3)	Yüzey Alanı (cm^2/g)	İncelik (<45 m) (%)
	SiO_2	Al_2O_3	Fe_2O_3	CaO	MgO	SO_3	K_2O	Na_2O	LOI			
PC	19.41	5.58	3.67	58.85	2.12	3.16	0.69	0.61	6.07	3.06	4891	1.1
UK	63.04	21.63	6.77	1.07	-	0.10	-	-	2.6	2.3	-	21

Tablo 2. Makro ve Mikro Liflerin Özellikleri

Lif Adı	Lif Türü	Uzunluk (mm)	Narinlik	Çekme Dayanımı (MPa)	Elastisite Modülü (GPa)	Yoğunluk (g/cm^3)

3D 65/35	Çelik Lif	35	65	1345	200	7.8
OL 6/16	Çelik Lif	6	40	3000	200	7.2
PVA	Sentetik Lif	8	200	1600	41	1.3
PP	Sentetik Lif	6	-	350	-	0.91

Karışım Oranları

Sadece makro çelik lif içeren 1 adet tek lifli karışım, %75 makro çelik lif ve %25 mikro çelik lif ile %1 makro çelik lif ve ayrı ayrı %25 PVA ile %25 PP sentetik lif içeren toplam 3 adet ikili lif karışımı ve %75 makro çelik lif ve %25 mikro çelik lif ve ayrı ayrı %25 PVA ile %25 PP sentetik lif içeren toplam 2 adet üçlü lif karışımı olmak üzere toplam 6 adet lif takviyeli kendiliğinden yerleşen beton karışımı tasarlanmıştır Tablo 3'te agregaların doygun kuru yüzey alındığı lif takviyeli beton karışım oranları verilmiştir.

Tablo 3. Karışım Oranları (kg / m³)

Karışım Adı	PÇ	UK	Su	Çelik Lif		Sentetik Lif		Agrega		Akışkanlaştırıcı
				3D 65/35	OLI 6/16	PVA	PP	0-5 mm	5-10 mm	
TKLF	600	300	204	80	0	0		952.0	168.0	16
MAK1.00+PVA0.25	600	300	204	80	0	3.25	0	918.5	162.1	20
MAK1.00+PP0.25	600	300	204	80	0	0	2.38	922.6	162.8	18
MAK0.75+MİK0.25	600	300	204	60	20	0	0	949.5	167.6	19
MAK0.75+MİK0.25 +PVA0.25	600	300	204	60	20	3.25	0	914.0	161.3	22
MAK0.75+MİK0.25 +PP0.25	600	300	204	60	20	0	2.38	914.0	161.3	22

*TKLF: Tek Lif Katkılı, MAK: Makro Çelik Lif, MİK: Mikro Çelik Lif, PVA: Polivinil Alkol Lifi, PP: Polipropilen Lifi, İsimlendirmedeki rakamlar karışım içindeki yüzdece lif oranını belirtmektedir.

Numunelerin Hazırlanması

Karışımlara kendiliğinden yerleşen beton için esas alınan işlenebilirlik testleri olarak çökme-yayılma ve T_{50} yapıldı. Tüm karışımlara özellikle çökme-yayılma değerlerinin EFNARC'ın belirlediği sınırlar (650-800 mm) içerisinde kalması için yeteri miktarda hiperakışkanlaştırıcı katıldı. Karışımların hepsinde homojenliği sağlamak amacıyla karıştırılma süreleri sabit tutuldu. Agregalar ve çelik lifler karışım suyunun 2/3 oranıyla 3 dakika karıştırıldı. Daha sonra çimento, uçucu kül, yüksek oranda su azaltıcı özelliğine sahip hiperakışkanlaştırıcı ve karışım suyunun kalan 1/3 oranıyla 15 dakika karıştırıldı. Sentetik lifler topaklanmayı önlemek amacıyla 7. dakikada azar azar eklendi. Basınç dayanımı testi için 100 x 100 x 100 mm^3 küp numuneler, dört noktalı eğilmede çekme dayanımı testi için 400 x 100 x 100 mm^3 prizma numuneler 28 gün kür edildi.

Test Yöntemleri

Taze Beton İçin İşlenebilirlik Testleri

KYB hazırlanırken EFNARC'a [4] göre, bir karışımın KYB olma şartlarından olan çökme-yayılma ve T_{50} testleri yapıldı. Çökme-yayılma testinde düz bir plaka üzerinde kesik koni doldurularak dik bir şekilde yukarıya kaldırıldı. Çökme-yayılma çapı birbirine dik iki boyutun ortalamasıyla belirlendi ve T_{50} süresine bakıldı (Şekil 1).

(a) (b)

Şekil 1. İşlenebilirlik Testleri : a) T_{50} , b) Çökme-Yayılma Çapı

Sertleşmiş Beton İçin Basınç ve Eğilme Dayanımı Testleri

Lif takviyeli KYB karışımların dayanım testlerinde her bir karışım için, basınç dayanımının belirlenmesinde 100 x 100 x 100 mm^3 boyutundaki 3 küp numunenin ortalaması kullanıldı, dört noktalı eğilmede çekme dayanımının belirlenmesinde ise 400 x 100 x 100 mm^3 boyutundaki 2 prizma numunenin ortalaması kullanıldı (Şekil 2).

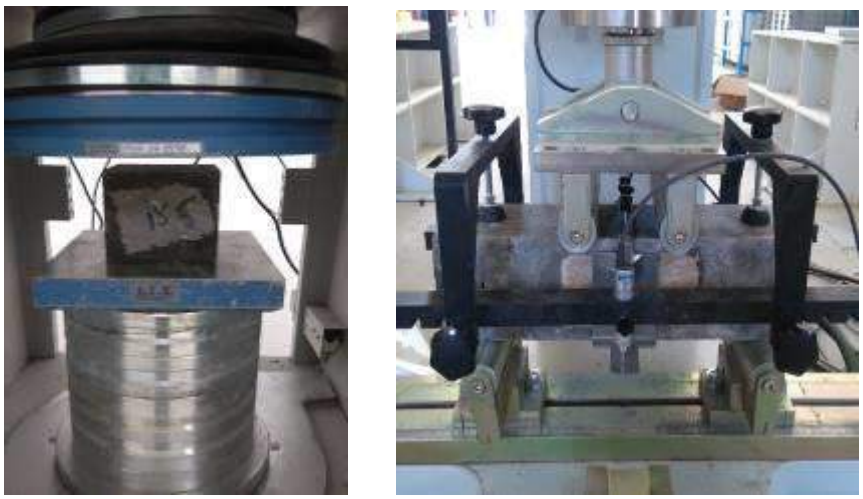

(a) (b)

Şekil 2. Sertleşmiş Beton Testleri : a) Basınç Dayanımı, b) Dört Noktalı Eğilmede Çekme Dayanımı

BULGULAR ve TARTIŞMA

Taze Beton Özellikleri

Tek ve karma lif takviyeli KYB karışımlarının taze haldeki özelikleri Tablo 4'te verilmiştir. Tüm karışımların çökme-yayılma değerleri EFNARC'ın belirlediği sınırlar (650-800 mm) içerisinde kalmıştır. Lif takviyeli KYB karışımlarının işlenebilirlik testlerinden elde edilen bulgulara bakıldığında, tek lifli KYB karışımına kıyasla hem çelik hem de sentetik mikro liflerin karışıma dahil edilmesinin işlenebilirlik özellikleri üzerinde olumsuz bir etkiye sahip oldukları tespit edilmiştir. Mikro lif içeren karışımlara bakıldığında, mikro çelik lifler ile sentetik lifler karşılaştırıldığında hem PVA hem de PP lifler karışımların işlenebilirlik özellikleri üzerinde daha fazla negatif etkiye sahip olduğu tespit edilmiştir. Sentetik lifler kendi arasında karşılaştırıldığında ise PVA lifin PP lifine göre karışımların işlenebilirliğini daha fazla azalttığı gözlemlenmiştir.

Tablo 4. T_{50} Süreleri ve Çökme-Yayılma Çapları

Karışım Adı	T_{50}(s)	Çökme-Yayılma Çapı (mm)
TKLF	5	730

MAK1.00+PVA0.25	7	660
MAK1.00+PP0.25	6	720
MAK0.75+MİK0.25	7	720
MAK0.75+MİK0.25+PVA0.25	7	660
MAK0.75+MİK0.25+PP0.25	6	710

Basınç ve Eğilmede Çekme Dayanımı

Tek ve farklı tip sentetik lif içeren ikili ve üçlü karma lif takviyeli KYB karışımlarına ait mekanik özellikler Tablo 5'te verilmiştir. Lif takviyeli KYB karışımlarının mekanik özelliklerinin belirlenmesi için gerçekleştirilen testlerden elde edilen bulgulara bakıldığında, tek lifli karışımlara kıyasla, mikro çelik lifin basınç dayanımının gelişimi üzerinde azda olsa olumlu bir etkiye sahip olduğu görülürken, sentetik liflerin basınç dayanımını %4 ile %10 arasında azalttığı bulunmuştur. Sentetik liflerin basınç dayanımı üzerindeki etkisi incelendiğinde ise PP lifinin PVA lifine göre basınç dayanımı üzerinde daha fazla olumsuz etkiye sahip olduğu tespit edilmiştir (Bakınız Tablo 5). Mikro çelik liflerin basınç dayanımını arttırması mikro çatlakları köprüleyerek mikro çatlak oluşumunu ertelemesine ve çatlakların yayılmasını önlemesine dayandırılabilir (Haddadou ve ark.,2014).

Dört noktalı eğilme deneyinden elde edilen eğilmede çekme dayanımı bulguları incelendiğinde ise tek lifli karışıma kıyasla, KYB karışımına çelik mikro lif ilave edilmesinin eğilmede çekme dayanımını azalttığı tespit edilmiştir. Çünkü makro çatlakları köprüleyen makro liflerin mikro liflerle yer değiştirilerek azalmasının sonucu olarak çekme dayanımı azalmıştır. Bu benzer bulgu Haddaou ve arkadaşları (2014) tarafından da bulunmuştur. Bunun yanında, hem tek lifli hem de makro çelik ve mikro çelik liften oluşan ikili karışımlara sentetik liflerin dahil edilmesinin eğilmede çekme dayanımını arttırdığı gözlemlenmiştir. Sentetik lifler kendi arasında kıyaslandığında ise PVA lifi PP lifine göre daha yüksek performans sergilemiştir. Böylece karışıma ikinci ve/veya üçüncü lif olarak sentetik lif eklenmesine bağlı olarak açığa çıkan sinerjinin çekme dayanımını arttırdığı sonucuna varılabilir.

Tablo 5. Lif Takviyeli KYB Karışımlarına ait Dayanım Değerleri

Karışım Adı	Basınç Dayanımı (MPa)	Eğilmede Çekme Dayanımı (MPa)	Sehim (mm)
TKLF	96.10	10.15	
MAK1.00+PVA0.25	92.40	11.39	1.16
MAK1.00+PP0.25	86.45	10.24	0.64
MAK0.75+MİK0.25	96.75	9.49	1.26

MAK0.75+MİK0.25+PVA0.25	90.45	10.04	1.86
MAK0.75+MİK0.25+PP0.25	87.60	9.74	1.46

Yük-Sehim Eğrileri

Tekli, ikili ve üçlü lif içeren KYB karışımlardan üretilen 100*100*400 mm^3 prizma numunelerin sehim kontrollü dört noktalı eğilme testi sonucu elde edilen yük-açıklık ortası sehim eğrileri Şekil 4'te gösterilmiştir. Tablo 5'te verilen açıklık ortası sehim değerleri maksimum eğilme dayanımına karşılık gelen sehimdir. Şekil 4'te görüldüğü gibi, bu çalışmaya konu olan bütün lif takviyeli KYB karışımlarına ait numunelerin yük-sehim eğrileri maksimum yükten sonra yavaş yavaş azalarak sehim-sertleşmesi davranışı sergilemiştir. Tekli, ikili ve üçlü lif içeren KYB karışımlarının yük-sehim eğrileri altında kalan alan dikkate alındığında, %1 makro çelik lif ile %0.25 PVA sentetik lif içeren karışımlardan üretilen numunelerin en fazla enerji absorbe ettiği tespit edilmiştir. Tüm eğrilerden, makro lifin azalmasıyla birlikte yük-sehim eğrileri altında kalan alanın da azaldığı görülmüştür. Makro çelik lif mikro çatlakların oluşumu üzerinde önemli bir etkiye sahip olmamasına rağmen, eğrinin maksimum yük sonrası kısmının oluşmasında etkilidir. Dolayısıyla, yüksek oranda makro lif içeren karışımlarda yük-sehim eğrisi altında kalan alan genelde daha fazla olmaktadır. Benzer sonuçlar aynı zamanda Haddou ve ark. (2014) ile Naaman ve Reinhardt (1995) tarafından yapılan çalışmalarda bulunmuştur. Sadece %1 makro çelik lif içeren karışım ile %0.75 makro çelik lif ve %0.25 mikro çelik lif içeren karışıma PVA veya PP sentetik lif ilave edilerek elde edilen ikili ve üçlü lif kombinasyonundan oluşan karışımlara ait numunelerin yük-sehim eğrileri altında kalan alan incelendiğinde, PVA eklenmesinin numunelerin absorbe ettiği enerji bakımından daha olumlu etkiye sahip olduğu görülmüştür. Bunun yanında, fazla miktarda makro çelik lif içeren tek lifli karışımlar ile PVA içeren ikili ve üçlü karışımlara ait numuneler çok daha düktil davrandılar.

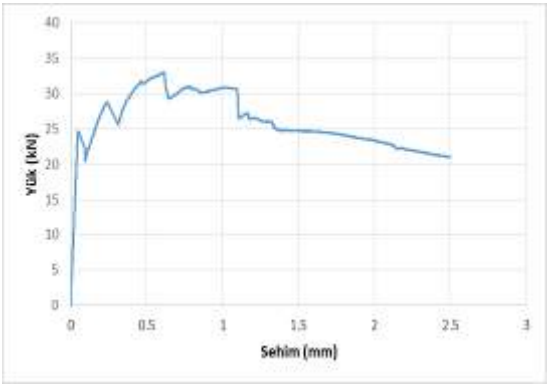

(a)

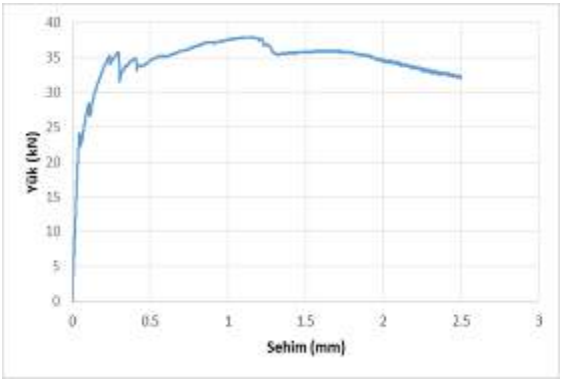

(b)

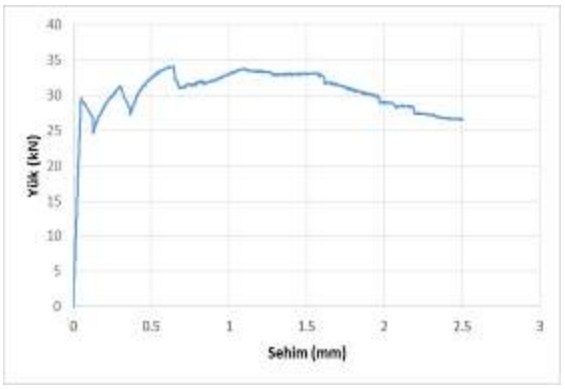

(c)

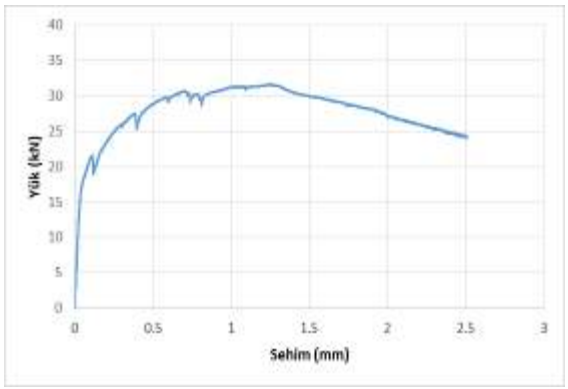

(d)

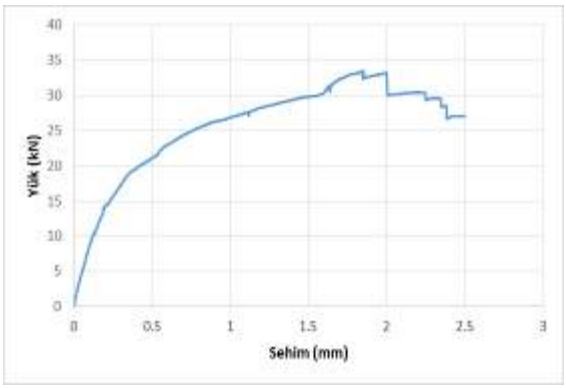

(e)

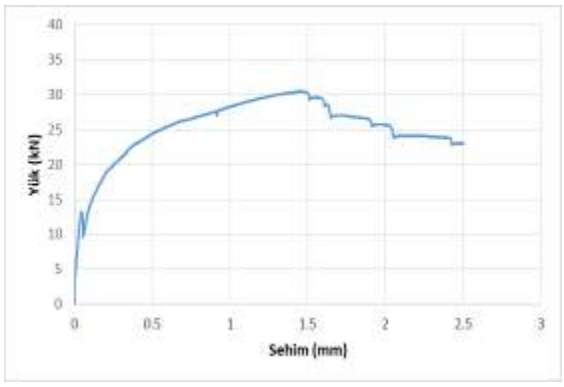

(f)

Şekil 4. Yük-Sehim Grafikleri: a) TKLF, b) MAK1.00+PVA0.25, c) MAK1.00+PP0.25, d) MAK0.75+MİK0.25, e) MAK0.75+MİK0.25+PVA0.25, f) MAK0.75+MİK0.25+PP0.25

Şekil 5'te görüldüğü gibi, fazla sayıda çatlak oluşumunun daha çok sentetik lif içeren KYB karışımlarına ait numunelerde olduğu görülürken, PVA lifi içeren ikili ve üçlü lif kombinasyonuna sahip karışımlardan (MAK1.00+PVA0.25 ve MAK0.75+MİK0.25+PVA0.25) elde edilen numunelerde tipik çoklu çatlak oluşumu gözlemlenmiştir. Bunun yanında, sadece makro ve mikro çelik lif içeren ikili KYB karışımları (MAK0.75+MİK0.25) ile PP içeren üçlü lif kombinasyonuna sahip karışımlardan (MAK0.75+MİK0.25+PP0.25) üretilen numunelerde daha az sayıda çatlak oluşmuştur.

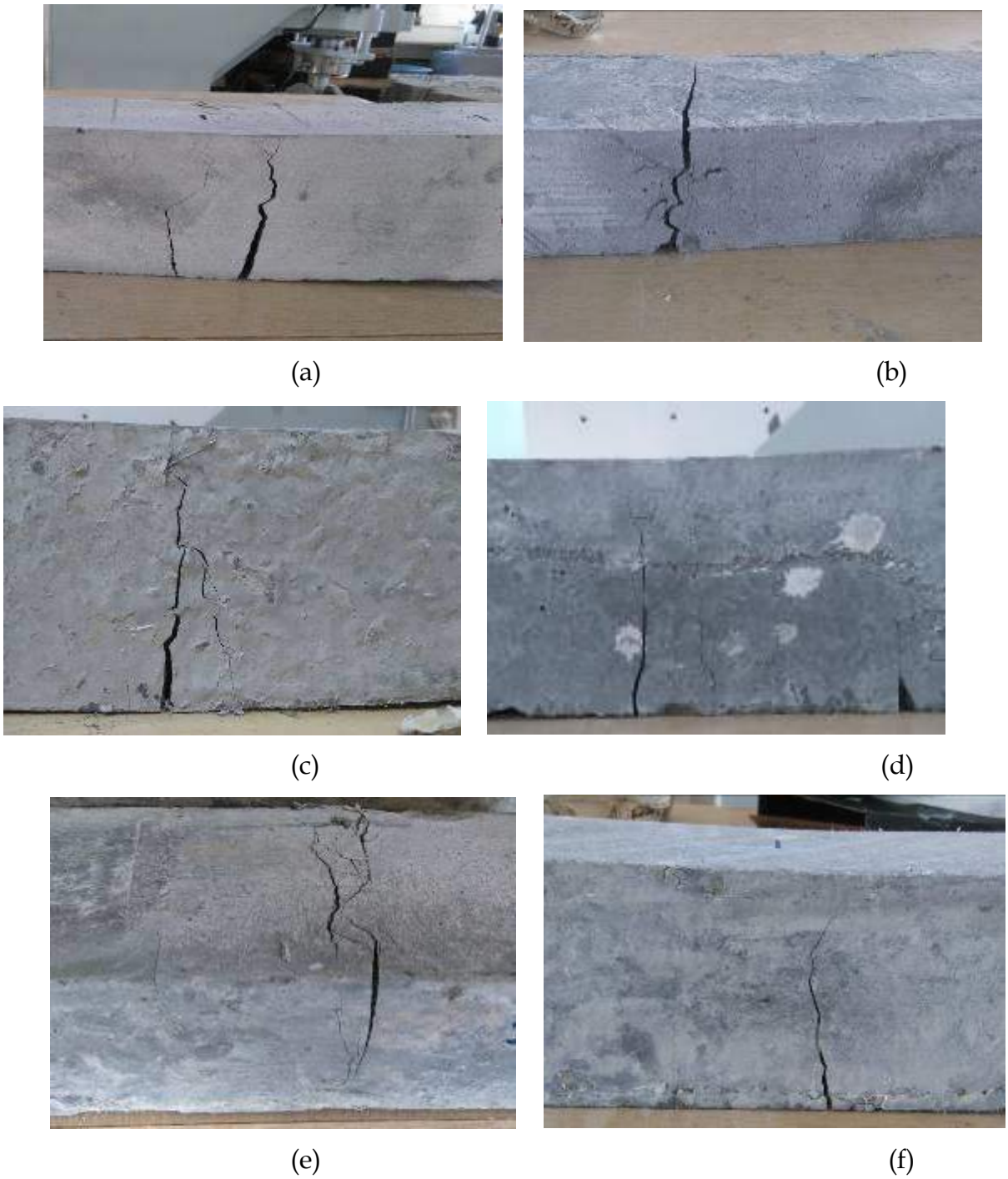

Şekil 3. Eğilme Testlerinden Sonraki Görüntüler: (a) TKLF, b) MAK1.00+PVA0.25, (c) MAK1.00+PP0.25, d) MAK0.75+MİK0.25, e) MAK0.75+MİK0.25+PVA0.25, f)MAK0.75+MİK0.25+PP0.25

SONUÇ

Bu çalışmada yürütülen deneylerden elde edilen bulgular dikkate alındığında aşağıdaki sonuçlara varılabilir:

1- Tek lifli KYB karışımına kıyasla, karışıma hem mikro çelik lifin hem de sentetik lifin katılmasının işlenebilirlik özelliklerini olumsuz etkilediği gözlemlenmiştir. Sentetik lifler kendi arasında karşılaştırıldığında ise, PVA lifinin PP lifine göre işlenebilirlik üzerinde daha olumsuz bir etkiye sahip olduğu tespit edilmiştir.

2- Lif takviyeli KYB karışımlarına mikro çelik lifin eklenmesinin, basınç dayanımında azda olsa bir artışa neden olduğu gözlemlenirken, sentetik liflerin karışıma eklenmesinin basınç dayanımını düşürdüğü bulunmuştur. Bunun yanında, sentetik lifler kendi arasında kıyaslandığında ise, PP lifinin PVA lifine göre basınç dayanımı üzerinde daha fazla olumsuz bir etkiye sahip olduğu tespit edilmiştir.

3- Lif takviyeli KYB karışımlarına mikro çelik lifin eklenmesinin, eğilme dayanımını düşürdüğü tespit edilmiştir. Ancak, sentetik liflerin karışımlara eklenmesinin hem ikili lif hem de üçlü lif içeren karışımlarda eğilme dayanımını arttırdığı gözlemlenmiştir. Bunun yanında, mikro çelik lif içeren ikili lif takviyeli KYB karışımlarına sentetik lif eklenmesinin eğilme dayanımı performansını iyileştirdiği görülürken, PVA lifinin PP lifine göre eğilme dayanımı performansını daha olumlu etkilediği bulunmuştur.

4- Tüm lif takviyeli KYB karışımlarına ait numunelerin sehim-sertleşmesi davranışı gösterdiği tespit edilmiştir. Tekli, ikili ve üçlü lif içeren KYB karışımlarının yük-sehim eğrileri altında kalan alan dikkate alındığında, mikro çelik lifin eklenmesiyle yük-sehim eğrisinin altında kalan alanın azaldığı gözlemlenmiştir. Bunun yanında, sadece makro çelik lif ile hem makro hem de mikro çelik lif içeren ikili lif takviyeli KYB karışımlarına sentetik lif eklenmesinin enerji yutma kapasitesini iyileştirdiği görülürken, PVA lifinin PP lifine göre karışımların enerji yutma kapasitesini daha olumlu etkilediği bulunmuştur.

5- Lif takviyeli KYB karışımlarından üretilen numunelerin dört noktalı eğilme deneyi sonrası oluşan çatlak durumu incelendiğinde, sentetik lif içeren KYB karışımlarında, mikro çelik lif içeren ikili lif kombinasyonuna sahip karışımlarına kıyasla daha fazla sayıda çatlak gözlemlenmiştir. Bunun yanında, sentetik lif içeren bu karışımlarda ise, PVA lifi içeren ikili ve üçlü lif takviyeli numunelerde tipik çoklu çatlak oluşumu tespit edilmiştir.

TEŞEKKÜR

Bu çalışmada, İnönü Üniversitesi Bilimsel Araştırma Projesi Birimine verdiği finansal destekten dolayı minnettarız. (Proje numarası: FYL-2017-844)

REFERANSLAR

Okamura ve Quchi, 1999. Self Compacting Concrete. *Development Present Use and Future.Proceedings of the First International RILEM Symposium(pp 3-14).* Edited by A. Skarendahland 6. Peterson.

Özkul, M.,H., 2002. Beton teknolojisinde bir devrim: Kendiliğinden yerleşen-sıkışan beton, *52, 64-71*.

Sağlam, R.,A., Parlak, N., Doğan, A., Ü. ve Özkul, M.,H., 2005. Kendiliğinden yerleşen betonda çimento katkı uyumu, *6.Ulusan Beton Kongresi(s. 213-224)*. İTÜ, İstanbul, 1618 Kasım 2005.

EFNARC, 2005. European guidelines for self-compacting concrete, Specification and Production and Use, Association House, UK, (www.efnarc.org).

Hannant, D. J., 1987.Fiber cements and fiber concrete. *Chichester*, UK, Wiley.

Ding, Y.N., You, Z., Jalali, S., 2010. "Hybrid fiber influence on strength and toughness of RC beams". *Compos Struct, 92, 2083–9*.

Sukontasukkul, P., Jamsawang, P.,2012. Use of steel and polypropylene fibers to improve flexural performance of deep soil–cement column. *Constr Build Mater, 29, 201–5*.

Mobasher, B., Li Cheng, Y.,1996. Mechanical properties of hybrid cement based composites. *ACI Materials Journal, 93(3), 284–92.*

Akcay, B.,2012. Experimental investigation on uniaxial tensile strength of hybrid fibre concrete. *Compos: Part B, 43, 766–78.*

ARAL,M.,2006. Karma lif içeren çimento esaslı kompozitlerin mekanik davranışı: Bir-optimum tasarım, İSTANBUL TEKNİK ÜNİVERSİTESİ FEN BİLİMLERİ ENSTİTÜSÜ *Yüksek Lisans Tezi*.

Rodrigues, J. P. C., Laím, L., Correia, A. M.,2010. Behaviour of fiber reinforced concrete columns in fire. *Compos. Struct., 95, 1263–1268, 2010.*

Jin-Cheng Liu, Kang Hai Tan.,2017. Fire resistance of strain hardening cementitious composite with hybrid PVA and steel fibers. *Construction and Building Materials 135 (2017) 600-611*.

Haddadou,N., Chaid, R.,Ghernouti, Y., &Adjou, N. (2014). The effect of hybrid steel fiber on the properties of fresh and hardened self-compacting concrete. J *Build Mater Struct*, 1, 65-76

Naaman, A.E., & Reinhardt, H.W. (1995). Characterization of high performance fiber reinforced cement composites (HPFRCC2). *In: Second International Workshop*, Ann Arbor, USA.

SOME PROPERTIES OF HYBRID FIBER REINFORCED SELF-COMPACTING CONCRETE CONTAINING BINARY AND TERNARY MINERAL ADMIXTURE

Kazim TURK, Inonu University,Engineering Faculty, Department of Civil Engineering, Malatya, Turkey, kazim.turk@inonu.edu.tr

İzzeddin DONMEZ, Inonu University,Engineering Faculty, Department of Civil Engineering, Malatya, Turkey, izzeddin.dnmz@gmail.com

ABSTRACT: It has been known that the addition of single or hybrid reinforced fibers to self-compacting concrete (SCC) improves the mechanical properties such as bending toughness, tensile strength, ductility. To able to exhibit the expected performance of SCC mixtures with fiber, filling ability into framework and the passing ability between obstacles with no segregation and no bleeding have a key role. In this study, the effect of mineral admixture type as well as the use of mineral admixture as binary and ternary blends of fly ash (FA) and blast furnace slag (BFS) on the fresh and hardened properties of SCC with/out hybrid fiber was investigated. The passing ability of SCC mixtures with binary and ternary blends of FA and BFS was measured by J-ring test while the filling ability and viscosity was obtained using by slump-flow and T_{500} tests. According to the results of experiment, the use of mineral admixture by mass of 35% instead of cement provided the workability properties of all mixtures. Mixture with ternary blends of FA and BFS had the best passing ability in fiber reinforced mixtures while the mixtures with binary blend of FA or only cement had the highest slump-flow diameter. SCC mixtures with BFS had in general better mechanical properties whilst FA induced little decrease in the strength of mixtures. The compressive strength of the mixtures with hybrid reinforced fiber at 7 days was higher than that of the mixtures with no fiber while 28-day compressive strength for some mixtures exhibited decreasing in proportion of 2-4%. The properties such as bending toughness, flexural tensile strength, ductility improved when the fiber was added into mixtures.

Key words: hybrid fiber reinforced self-compacting concrete, mineral admixture, workability, compressive strength, four-point flexural test

İKİLİ VE ÜÇLÜ MİNERAL KATKI İÇEREN KARMA LİF TAKVİYELİ KENDİLİĞİNDEN YERLEŞEN BETONUN BAZI ÖZELLİKLERİ

ÖZET: Kendiliğinden yerleşen betona (KYB) tekli veya karma olarak ilave edilen liflerin; eğilme tokluğu, çekme dayanımı, süneklilik gibi mekanik özellikleri geliştirdiği bilinmektedir. Lifli KYB karışımlarının, beklenen performansı gösterebilmesi için terleme ve segregasyon oluşmadan, kalıpları doldurma ve engeller

arasından geçiş gibi işlenebilirlik özellikleri kilit rol oynar. Bu çalışmada, tek tip lif kombinasyonuna sahip karma lifli ve lifsiz karışımlar üzerinde, mineral katkı türü ile uçucu kül (UK) ve yüksek fırın cürufunun ikili ve üçlü harmanlama olarak kullanımının taze ve sertleşmiş karma lif takviyeli KYB özellikleri üzerinde etkisi incelenmiştir. Uçucu kül ve yüksek fırın cürufu (YFC) içeren ikili ve üçlü bağlayıcı sistemli karışımların doldurma kabiliyeti ve viskozitesi çökme-yayılma ve T_{500} testleriyle belirlenirken, engeller arasından geçiş kabiliyeti ise J-halkası testiyle ölçülmüştür. Deney sonuçlarına göre, çimento yerine ağırlıkça %35 mineral katkı kullanımı, tüm karışımların işlenebilirlik özelliklerini geliştirmiştir. En yüksek yayılma çapına, UK ve portland çimentosu (PC) içeren karışımlar ulaşırken, lifli karışımlar arasında en iyi geçiş kabiliyetini üçlü bağlayıcı içeren karışım sergilemiştir. YFC içeren karışımlar genel olarak daha iyi mekanik özelliklere sahipken, UK ise karışımlrın dayanımlarında bir miktar azalmaya neden olmuştur. Karma lif kullanılan tüm karışımların 7 günlük basınç dayanımları lifsizlerden yüksek çıkarken, 28 günlük basınç dayanımı bazı karışımlarda %2-4 oranlarında düşüş göstermiştir. Lif varlığında, eğilme tokluğu, eğilmede çekme dayanımı, süneklik, düktilite gibi özellikler oldukça geliştirmiştir.

Anahtar sözcükler: karma lifli kendiliğinden yerleşen beton, mineral katkı, işlenebilirlik, basınç dayanımı, dört-noktalı eğilme testi

GİRİŞ

Kendiliğinden yerleşen beton, kendi ağırlığı altında akabilen ve yerleşebilen, donatılar arasında geçerek kalıpları tamamen doldurabilen, tüm bunları stabil durumu bozulmadan yapan bir beton türüdür (Okamura, H., 1997). Kendiliğinden yerleşen yüksek performanslı beton ise yeterli derecede işlenebilirliğe, yüksek mukavemete ve iyi dayanıklılığa sahip beton olarak tanımlanmaktadır (Worrell vd., 2001). Bu gereklilikleri yerine getiren bir beton oluşturmak için, yüksek miktarda bağlayıcı dozajına, süper akışkanlaştırıcıya (SP), viskozite düzenleyici katkı (VDK) veya UK, YFC gibi amorf yapıya sahip mineral katkılara ihtiyaç vardır (Safiuddin, M., 2008). KYB'nin olumsuz özelliklerinde birisi yüksek hacimde portland çimentosuna (PC) ihtiyaç duymasıdır. Çimento sektörünün Dünya'da en yüksek üçüncü karbondioksit emisyonuna yol açan sektör olduğu düşünülürse, betona talebin her geçen gün artmasıyla bu olumsuzluk daha önemli bir hal alır (Initiative, C. S., 2009). KYB'de portland çimentosu kullanımını sınırlandırmanın bir yolu, uçucu kül, doğal puzolan, kireç taşı tozu gibi mineral katkıları(MK) çimentoyla yer değiştirerek ikame etmektir (Erdoğan, T. Y., 1997). Bu gibi MK'ların kullanımı, betonun işlenebilirlik ve mekanik özelliklerini geliştirdiği gibi endüstriyel atık kategorisindeki UK, YFC, silis dumanı gibi malzemeler değerlendirilerek çevresel ayak izini azaltır.

UK betonun işlenebilirliğini ve uzun dönem basınç dayanımını arttırmaktadır. UK küresel taneli şekillere sahip olduğu için ve çimentoya kıyasla su ihtiyacının daha az

olması sebebiyle, sadece çimento içeren bir karışımla aynı çökme-yayılma değerini elde etmek için daha az suya ve akışkanlaştırıcıya ihtiyaç duyar (Turk, K. 2012), (Bouzoubaa, N., & Lachemi, M. 2001). YFC, çimentoya yakın bir kimyasal bileşime sahiptir. Dünyada yılda yaklaşık 250 milyon ton cüruf üretilir ve beton üretiminde 90 milyon tonu kullanılır. Ayrıca YFC; düşük hidratasyon ısısı, yüksek sülfat ve asit direnci, daha iyi işlenebilirlik ve düşük geçirgenlik gibi avantajlara da sahiptir (Öner vd., 2003).

Günümüzde yapılan araştırmalar sonucunda, betona katılan liflerin betonda çatlak oluşumunu önemli ölçüde azalttığı, betonun şekil değiştirme kapasitesini, tokluğunu, çarpma ve çekme dayanımını arttırdığını ve sünekliği yüksek betonlar elde etmeyi mümkün kıldığı görülmüştür (Bunsell, A.R., 1988). Lif takviyeli betonlarda, tek çeşit ve karma lif olmak üzere iki tip uygulama vardır. Tek tip lif kullanımı betonun özelliklerini sınırlı bir düzeye getirebilir. Bununla birlikte, betona iki veya daha fazla sayıda farklı lif tipinin eklenmesiyle daha gelişmiş mühendislik özellikleri sunulabilir; çünkü bir lifin varlığı diğer lifin sağlayacağı özelliklerin daha verimli kullanılmasını sağlar (Rossi, P. 1997).

Bu çalışmada, mineral katkı türünün, ikili ve üçlü bağlayıcı sistemlerde lifli ve lifsiz karışımların işlenebilirlik ve mekanik özelliklerini nasıl etkilendiğinin araştırılması hedeflenmiştir.

DENEYSEL ÇALIŞMA

Malzemeler

Çimento

Tüm karışımlarda, Elazığ SEZA Çimento firmasına ait, TS-EN 197-1:2012 standartına uygun CEM I 42,5 R çimentosu kullanılmıştır. Çimentoya ait fiziksel özellikler ve kimyasal bileşim Tablo 1'de verilmektedir.

Tablo 1. Bağlayıcı Malzemelere Ait Kimyasal Bileşenler

Kimyasal Kompozisyon (%)	**PC**	**UK**	**YFC**
SiO_2	19.41	63.04	32.37
Al_2O_3	5.58	21.63	10.00
Fe_2O_3	3.67	6.77	1.33

CaO	58.85	1.07	32.94
MgO	2.12	-	9.77
SO_3	3.16	0.10	0.7
Na_2O	0.61	2.79	0.42
K_2O	0.69	-	0.83
Kızdırma kaybı	6.07	2.68	0
$SiO_2+Al_2O_3+Fe_2O_3$	28.66	91.44	43.7
Özgül ağırlık (gr/cm^3)	3.17	2.35	2.86
Blaine (cm^2/gr)	-	2900	4085
45 µm elek bakiyesi (%)	-	19	0.8
28 günlük puzolanik aktivite (%)	-	81	72.9

Çalışmada, 0-5 mm ve 5-10 mm olmak üzere iki tip, kalker esaslı kırma agrega kullanılmıştır. Agregaların fiziksel özellikleri ve elek analizleri Tablo 2'de verilmiştir.

Tablo 2. Agregalara Ait Özellikler

Agrega	Özgül ağırlık (gr/cm^3)	Su emme (%)	İncelik modülü	Elek boyutu, mm - % Geçen							
				0.125	0.25	0.5	1	2	4	8	16
Kırma kum	2.58	2.26	4.10	10	13	18.4	25.6	45.5	78.1	99.5	100
Kırma taş	2.63	0.3	4.09	-	-	1.7	1.9	2.4	5.3	78.5	100

Mineral Katkılar

İsken-Sugözü enerji santraline ait uçucu kül ve Karabük'te bulunan Karçimsa fabrikasına ait öğütülmüş yüksek fırın cürufu kullanılmıştır. Malzemelere ait özellikler Tablo 1'de verilmiştir.

Akışkanlaştırıcı

Beton karışımlarında TS EN 934-2 standardına uygun, modifiye polikarboksilat esaslı, yoğunluğu 1,06 gr/cm^3 olan hiper akışkanlaştırıcı Sika ViscoCrete Hi-Tech 51 modeli tercih edilmiştir.

Lif

Lifli beton karışımlarında çelik lif olarak, Dramix 3D 65/35 makro lif ve Dramix OL 6/.16 mikro lif kullanılmıştır. Sentetik lif olarak ise polipropilen kullanıldı. Liflere ait özellikler Tablo 3'de belirtilmiştir.

Tablo 3. Çelik ve Sentetik Liflerin Özellikleri

Lif Adı	Lif türü	Uzunluk (mm)	Narinlik	Çekme dayanımı (MPa)	Elastisite modülü (GPa)	Yoğunluk (g/cm^3)
3D 65/35	Çelik lif	35	65	1345	200	7.8
OL 6/16	Çelik lif	6	40	3000	200	7.2
PP	Sentetik lif	6	-	350	-	0.91

Beton Karışımları

Deneysel çalışmalar için, EFNARC'ın kendiliğinden yerleşen betonlar için hazırladığı kılavuzdaki öneriler dikkate alınarak ve İnönü Üniversitesi Yapı Malzemesi Laboratuvarı'nda yapılan benzer çalışmaların deneysel verilerinden faydalanılarak karışım reçetesi oluşturulmuştur (). Tüm karışımlarda su/bağlayıcı oranı (0,22), agrega karışım oranları sabit ve toplam bağlayıcı miktarı (850 kg/m^3) sabit tutulmuştur. Kontrol karışımı hariç karışımlarda kimyasal katkı dozajı 6,5 kg/m^3'dür. Mineral katkı olarak kullanılan uçucu kül ve yüksek fırın cürufu, çimentoyla ağırlıkça yer değiştirilerek kullanılmıştır. Lifli karışımlarda ise 60 kg/m^3 makro lif, 20 kg/m^3 mikro lif ve 2,36 kg/m^3 sentetik lif içeren, tek tip lif kombinasyonlu karma lifli betonlar hazırlanmıştır. Bir adet kontrol karışımı, 3 adet; mineral katkı ikameli lifsiz karışım, 3 adet; mineral katkı ikameli lifli karışım olmak üzere toplam 7 adet karışım hazırlanmıştır. Karışım oranları Tablo 4'da verilmektedir.

Tablo 4. Beton Karışım Oranları

							Agrega (kg/m^3)	Çelik lif (kg/m^3)		

Karışım Adı	PC (kg/m³)	UK (kg/m³)	YFC (kg/m³)	Su (kg/m³)	S/B	SA (%)	Kırmakum 0-5 mm	Kırmataş 5-10 mm	3D 65/35	OL 6/.16	PP lif (kg/m³)	SA (kg/m³)
C850	850	-	-	190	0,22	0,9	926	397	-	-	-	7,75
U300	550	300	-	190	0,22	1,18	876	375	-	-	-	6,5
Y300	550	-	300	190	0,22	1,18	910	390	-	-	-	6,5
U150Y150	550	150	150	190	0,22	1,18	893	382	-	-	-	6,5
U300-KL	550	300	-	190	0,22	1,18	853	365	60	20	2,36	6,5
Y300-KL	550	-	300	190	0,22	1,18	886	380	60	20	2,36	6,5
U150Y150-KL	550	150	150	190	0,22	1,18	870	372	60	20	2,36	6,5

Deneysel Yöntem

Deneysel çalışmalarda toplam bağlayıcı miktarı 850 kg/m³ seçilmiştir. İnce agrega/toplam agrega oranı 0,30'dur. Kontrol karışımı dışındaki karışımlarda toplam mineral katkı dozajı 300 kg/m³'dür ve akışkanlaştırıcı oranı sabittir. Mineral katkı türünün ikili ve üçlü sistemlerde, karışımların işlenebilirlik ve mekanik özelliklerini nasıl etkilediği araştırılmıştır. Testler sırasıyla, işlenebilirlik ve sertleşmiş beton testleri olarak iki bölümde gerçekleştirilmiştir. İşlenebilirlik testleri olarak; çökme-yayılma çapı, T_{500} süresi, J-halkası yayılma çapı (SF_J), T_{500j} süresi ve J-halkası geçiş yeterliliği (PJ) değerleri ölçülmüştür. Sertleşmiş beton testlerinde ise 7 ve 28 günlük 100x100x100 mm'lik küp numunelere basınç dayanımı testi ve 100x75x400 mm prizmatik numunelere dört noktalı eğilme testleri gerçekleştirilmiştir.

Beton karışımları hazırlanırken, 100 lt hazneye sahip pan tipi mikser kullanıldı. Karıştırma metodu olarak sırasıyla şu işlemler uygulanmıştır:

- Agrega ile varsa lifler kuru olarak 15 sn. karıştırıldı.

• Karışım suyunun 2/3'si eklenerek karıştırmaya 3 dk. daha devam edildi.

• Çimento ve mineral katkılar eklenerek 2 dk. karıştırıldı.

• Kalan karışım suyu, akışkanlaştırıcıyla birlikte karışıma eklendi ve 8,5 dakika karıştırma işlemine devam edildi.

Taze Beton Deneyleri

İşlenebilirlik deneyleri EFNARC Komitesi'nin önerilerine göre yapılmıştır (EFNARC, 2002),(EFNARC, 2005). Betonda oluşan tiksotropik davranış, kıvam kaybı vb. gibi değişkenliklerin en aza indirilebilmesi için her bir karışımın çökme-yayılma ve J-halkası deneylerine ayrı numuneler üretildi ve karıştırma işlemi bitince, mümkün olduğunca zaman kaybetmeden işlenebilirlik testleri gerçekleştirildi.

Betonun doldurma kabiliyetinin ve stabilitesinin incelendiği Çökme-yayılma testinde, deney aletleri hafif nemli biz bezle silindikten sonra, karışımı temsil edecek numune çökme konisine doldurulduk. Koni doldurulduktan sonra, 30 sn. içerisinde dikey olarak kaldırıldı ve en büyük yayılma çapı ve ona dik doğrultudaki çap ölçülüp aritmetik ortalaması alındı. Çökme konisinin kaldırıldığı an ile betonun 500 mm yayılma çapına ulaştığı an arasında geçen T_{500} süresi kaydedildi. Betonun donatılar arasından geçiş kabiliyetini belirlemek için yapılan J-halkası deneyinde, en büyük yayılma çapı ve ona dik çapın aritmetik ortalaması alınarak J-halkası yayılma çapı belirlenmiştir. Halkanın merkezindeki ile halkanın hemen dışındaki 4 nokta arasındaki yükseklik farklarının ortalaması alınarak J-halkası geçiş yeterliliği ölçülmüştür (Tablo 7).

(a) (b)

Şekil 1 İşlenebilirlik Testlerine Ait Çökme-Yayılma ve J-Halkası Deneyi Fotoğrafları (a) Mineral Katkı ve Lif İçermeyen Kontrol Karışımı (C850) (b) Uçucu Kül ve Yüksek Fırın Cüruflu Karma Lifli Karışım (U150Y150-KL)

Sertleşmiş Beton Deneyleri

Bu bölümde, karışımların 7 ve 28 günlük basınç ve 4 noktalı eğilme deneyi gerçekleştirilmiştir.

Basınç dayanımı testleri, her dayanım sınıfı için 3 adet 100x100x100 mm küp numuneler kullanılarak, TS EN 12390 – 3 standardına uygun olarak 0,6 MPa/sn yükleme hızında yapıldı.

4 noktalı eğilme deneyi, her sınıfta 2 adet 100x75x400 mm numuneler üzerinde, ASTM C1609 stardartına uygun olarak gerçekleştirilmiştir. Açıklık ortasındaki net deplasmanlar ölçülmüştür.

BULGULAR VE TARTIŞMA

Taze Beton Özellikleri

Tüm karışımlara ait Çökme-yayılma ve J-halkası deney sonuçları Tablo 5, Şekil 2 ve Şekil 3'te verilmiştir. Uçucu kül ve yüksek fırın cürufunun tekli ve ikili kullanımda, işlenebilirlik üzerine etkilerinin daha net gözlemlenebilmesi için karışımların S/B, toplam bağlayıcı miktarı, agrega karışım oranları, akışkanlaştırıcı katkı dozajı gibi parametreleri sabittir ancak Kontrol karışımının kendiliğinden yerleşen beton özelliği gösterebilmesi için akışkanlaştırıcı dozajı bir miktar fazla tutulmuştur. Lifsiz karışımlarda, uçucu külün, PC ile ağırlıkça %35 yer değiştirilmesiyle oluşturulan U300 karışımı incelendiğinde, en yüksek yayılma çapı ve en düşük T_{500} süresi değerlerine sahip olduğu görülür. Bunun sebebi uçucu külün Blaine özgül yüzey alanının PC ve YFC'den daha düşük olmasına ve UK partiküllerinin küresel şekillerinin sürtünmeyi azaltarak hareket kabiliyetini arttırmasına bağlanabilinir (Ramachandran, V. S., 1996). U300 karışımının J-halkası sonuçlarına bakılırsa, yine en iyi geçiş kabiliyeti özelliğine sahip olduğu görülür çünkü UK düşük özgül ağırlığından dolayı, belirli bir ağırlıkta daha yüksek hamur hacmine sahiptir. Böylelikle daha kohezif ve plastisitesi yüksek

bir beton oluşumuna imkan sağlayarak kaba parçacıklarla tutunma kuvvetini arttırır (Yahia vd., 2005). Karma lifli karışımların sonuçları değerlendirilirse, yayılma çapı ölçülerinin büyükten küçüğe sıralaması yapılırsa, U300-KL(UK-PC) > Y300-KL(YFC-PC) > U150Y150-KL(UK-YFC-PC) olduğu görülmektedir. UK ve YFC içeren ikili harmanlamaya sahip karma lifli karışım, liflerin en homojen yayıldığı karışımdır (Şekil 1 (b)). Bu karışımın en düşük J-halkası yükseklik farkına sahip olması ile homojenliği arasında ters orantılı bir ilişki kurabiliriz. Bu karışımın, en stabil lifli karışım olması ve engeller arasından geçiş yeteneğinin daha üstün olmasının sebebi, farklı tane boyutu dağılımlarına sahip UK ve YFC'nin birlikte kullanılmasının daha kararlı bir tanecik iskeleti oluşturmasına ve bu sayede viskozitenin artışına yol açmasıyla ve de UK ile YFC'nin fiziko-kimyasal özelliklerinin uyumlu etkileşimiyle açıklayabiliriz (Yahia vd., 2005).

Tablo 5. Karışımlara Ait İşlenebilirlik Deneyleri Sonuçları

Karışım Adı	Çökme-Yayılma		J-halkası	
	Çap (mm)	T_{500} (sn)	Çap (mm)	h_2-h_1 (mm)
C850	695	5,4	620	7
U300	890	2,1	880	3,2
Y300	730	4,7	710	9,7
U150Y150	865	2,4	860	8,2
U300-KL	695	6,8	655	22,7
Y300-KL	690	8,1	622	45,2
U150Y150-KL	675	8,7	640	20,7

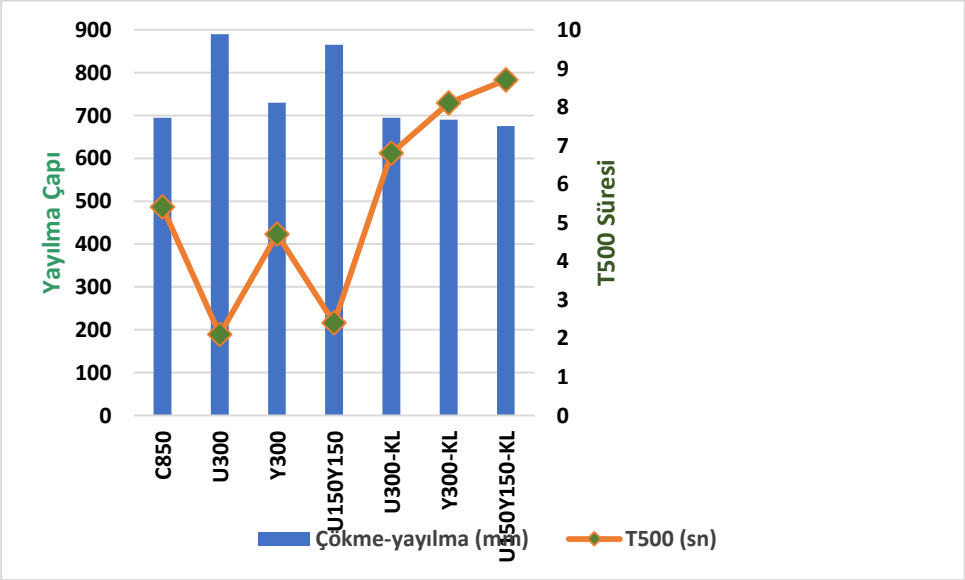

Şekil 2 Karışımların Çökme-Yayılma ve T_{500} Değerleri

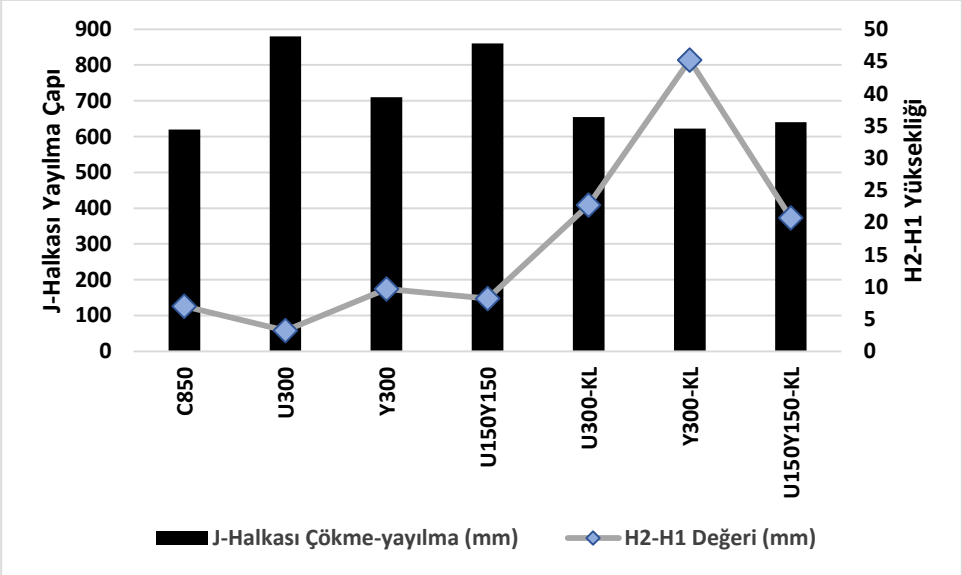

Şekil 3 Karışımların J-Halkası Yayılma ve Yükseklik Farkı Değerleri

Sertleşmiş Beton Özellikleri

Basınç Dayanımı

Karışımlara ait 7 ve 28 günlük basınç dayanımları Tablo 6.'da gösterilmiştir. Basınç dayanımı sonuçları incelenirse, 7 ve 28 günlük dayanımda en yüksek değer, kontrol karışımına aittir. Aynı mineral katkı içeriğine sahip, lifli ve lifsiz karışımların basınç

dayanımları kıyaslandığında, 7 günlük dayanımlarda, lifli karışımların mukavemeti daha yüksek iken, 28 günlük dayanımlarda, U300-KL hariç diğer lifli karışımların basınç dayanımları lifsizlere göre %2-5 mertebelerinde daha düşük çıkmıştır. Basınç dayanımları, mineral katkı etkisinde incelenecek olursa, lifli ve lifsiz karışımlarda en yüksek dayanım, PC ve YFC içeren ikili sistem karışımlardan elde edilmiştir. Çimentoya mineral katkı olarak yalnız uçucu külün ikame edildiği karışımların dayanım değerleri en düşük çıkmıştır.

Tablo 6. Karışımlara Ait Basınç Dayanımı Değerleri

Karışım Adı	Basınç Dayanımı (MPa)	
	7 gün	28 gün
C850	86,7	108,7
U300	64,4	86,7
Y300	81,3	100
U150Y150	78,2	98
U300-KL	69,4	93,3
Y300-KL	83,8	98,5
U150Y150-KL	82,07	94

Dört Noktalı Eğilme Deneyi

Dört noktalı eğilme deneyi sonuçları Tablo 7'de verilmiştir. Deney sonuçlarına göre tüm lifli karışımların eğilmede çekme dayanımları lifsizlere oranla oldukça yüksektir. Lif kullanımı, çatlama sonrası eğilme tokluğunu ve düktiliteyi arttırmıştır. YFC kullanılan karışımların eğilme dayanımları daha yüksek çıkmıştır. Lifli karışımlarda oluşan çoklu çatlakların daha net gözlemlenebilmesi için fotoğraf düzenleyici bir program kullanılarak çatlaklar belirginleştirilmiştir (Şekil 3).

Tablo 7. Dört Noktalı Eğilme Deney Sonuçları

	P	*f*	δ

Karışım Adı	(KN)		(MPa)		(mm)	
	7 gün	28 gün	7 gün	28 gün	7 gün	28 gün
C850	17,66	19,85	9,42	10,59	-	-
U300	15,55	15,74	8,28	8,39	-	-
Y300	21,8	23,77	11,62	12,67	-	-
U150Y150	15,9	17,88	8,48	9,54	-	-
U300-KL	35,3	40,2	18,71	21,4	2	0,71
Y300-KL	36,07	48,76	19,24	26	1,02	0,38
U150Y150-KL	32,7	40,67	17,4	21,7	1,37	0,96

(a)

(b)

(c)

Şekil 3 Karma Lifli Numunelerin 28 Günlük Eğilme Testi Sonrası Çatlak Oluşumları (a) U150Y150-KL (b) Y300-KL (c) U300-KL

SONUÇLAR

Yapılan çalışmada, endüstriyel atık olan uçucu kül ve yüksek fırın cürufu içeren ikili ve üçlü bağlayıcı sistemlerde, 60 kg/m^3 makro, 20 kg/m^3 mikro, 2,36 kg/m^3 polipropilen lif içeren karma lifli ve lifsiz karışımların işlenebilirlik ve mekanik özellikleri test edilmiştir. Elde edilen sonuçlar aşağıdaki gibi özetlenebilir:

1. Karışıma mineral katkı ilavesi kontrol karışımına kıyasla akışkanlaştırıcı ve su ihtiyacını azaltmıştır.

2. UK ve PC'li karma lif içeren karışımın Çökme-yayılma değeri aynı karışımın lifsiz haline göre %22 azalırken, YFC ve PC'li karışım %6, YFC UK PC'li karışım %22 azalmıştır.

3. Bazı karışımlar EFNARC'ın belirlediği 550 – 850 mm yayılma çapı aralığını aşmıştır ancak herhangi ayrışma ya da segregasyon problemiyle karşılaşılmadı.

4. Deney sonuçlarına göre ağırlıkça %35 mineral katkı ikamesi betonun işlenebilirlik ve mekanik özelliklerini olumlu etkilemiştir. 7 ve 28 günlük basınç dayanımında kontrol numunesine en yüksek değere sahiptir.

5. Mineral katkılı karışımlar arasında YFC PC karışımı en iyi mekanik özellikleri göstermiştir. UK ise dayanımları bir miktar düşürmüştür.

6. Hacimce %1 çelik lif ve %0.25 sentetik lif kullanımı, lifsiz karışımlara kıyasla, eğilme dayanımlarını ve 7 günlük basınç dayanımlarını arttırmıştır.

7. Lifsiz karışımlarda en üstün doldurma ve geçiş kabiliyeti UK PC karışımıdır. Lifli karışımlarda ise UK PC en iyi doldurma özelliğine sahipken UK YFC PC en başarılı geçiş yeteneğine sahiptir. Bunun sebebi YFC ve UK'nın tane dağılımı açısından daha başarılı bir iskelet oluşturarak sinerjik etki göstermesine dayandırılabilinir.

8. Lifli karışımların Yük – Sehim grafikleri incelenirse tüm karışımlar ilk çatlaktan sonra pekleşme (Strain-Hardening) sergilemiştir. Karma lifli karışımların eğilme tokluklarının yüksek olduğu grafik altında kalan alandan anlaşılabilir.

TEŞEKKÜR

Bu çalışmada, İnönü Üniversitesi Bilimsel Araştırma Projesi Birimine verdiği finansal destekten dolayı minnettarız. (Proje numarası: FYL-2017-889)

KAYNAKLAR

Okamura, H. (1997). Self-compacting high-performance concrete. *Concrete international*, *19*(7), 50-54.

Worrell, E., Price, L., Martin, N., Hendriks, C., & Meida, L. O. (2001).

Safiuddin, M. (2008). Development of self-consolidating high performance concrete incorporating rice husk ash.

Initiative, C. S. (2009). Cement industry energy and CO2 performance: getting the numbers right. *World Business Council for Sustainable Development*.

Erdoğan, T. Y. (1997). *Admixtures for concrete*. Middle East Technical University Press.

Bouzoubaa, N., & Lachemi, M. (2001). Self-compacting concrete incorporating high volumes of class F fly ash: Preliminary results. *Cement and concrete research*, *31*(3), 413-420.

Turk, K. (2012). Viscosity and hardened properties of self-compacting mortars with binary and ternary cementitious blends of fly ash and silica fume. *Construction and Building Materials*, *37*, 326-334.

Öner, M., Erdoğdu, K., & Günlü, A. (2003). Effect of components fineness on strength of blast furnace slag cement. *Cement and Concrete Research*, *33*(4), 463-469.

Bunsell, A.R., (1988). Fiber Reinforcement for Composite Materials, Vol:2 Composite Materials Series, Elseiver Science, The Netherlands

Rossi, P. (1997). High performance multimodal fiber reinforced cement composites (HPMFRCC): the LCPC experience. *Materials Journal*, *94*(6), 478-783.

Ramachandran, V. S. (1996). *Concrete admixtures handbook: properties, science and technology*. William Andrew.

Yahia, A., Tanimura, M., & Shimoyama, Y. (2005). Rheological properties of highly flowable mortar containing limestone filler-effect of powder content and W/C ratio. *Cement and concrete Research*, *35*(3), 532-539.

EFNARC, S. (2002). Guidelines for self-compacting concrete. *London, UK: Association House*, *32*, 34.

Bibm, C., & Ermco, E. (2005). EFNARC. *The European Guidelines for Self-Compacting Concrete. Specification, Production and Use*.

PERFORMANCE ANALYSIS OF DIFFERENT MACHINE LEARNING ALGORITHMS FOR THE DETECTION OF SCHIZOPHRENIA WITH EEG SIGNALS

Zülfikar ASLAN*

Fen Bilimleri Enstitüsü, Dicle Üniversitesi, Diyarbakır, Türkiye

zulfikaraslan27@gmail.com

Mehmet AKIN

Elektrik-Elektronik Mühendisliği, Mühendislik Fakültesi, Dicle Üniversitesi, Diyarbakır

makin@dicle.edu.tr

ABSTRACT: In this study, performance of different machine learning algorithms in automatic detection of Schizophrenia disease is analyzed by using EEG signals of 84 individuals from 39 healthy and 45 diseased patients. The raw data utilized in the study is composed of single dimension arrays of size 122280 extracted from each channel of the EEG signal. Primarily, feature extraction from raw EEG signal is performed by using standard statistical methods and Relative Wavelet Energy (RWT) method. Obtained data is classified by using Naive Bayes, SVM (Support Vector Machine), MLP (Multi-Layer Perceptron), KNN (K Nearest Neighbors) and Random Forest machine learning algorithms and their classification performances are analyzed. Afterwards, because of the low number of samples in the dataset, a resampling is performed over the final version of the data. With these settings, classification performance is observed to rise to %95.

Key words: Relative Wavelet Energy, EEG, Schizophrenia, Machine Learning

EEG SİNYALLERİNDE ŞİZOFRENİ TESPİTİNDE FARKLI MAKİNA ÖĞRENME ALGORİTMALARININ PERFORMANS ANALİZİ

ÖZET: Bu çalışmada 39 sağlıklı ve 45 şizofreni hastasına ait toplam 84 bireyin EEG sinyalleri kullanılarak, şizofreni hastalığının otomatik olarak tespitinde farklı makine öğrenme algoritmalarının başarımları analiz edilmiştir. Çalışmamızda kullanılan ham veri EEG kanallarından alınan sinyali temsil eden 122280 uzunluğunda tek boyutlu dizilerden oluşmaktadır. Öncelikle ham EEG sinyalinden standart istatistiksel yöntemler kullanılarak ve Göreceli Dalgacık Dönüşümü Enerjisi (RWT) metoduyla

özellik çıkarımı yapılmıştır. Elde edilen yeni veri Naive Bayes, Destek Vektör Makinaları (SVM), Çok Katmanlı Algılayıcı (MLP), k En Yakın Komşu (KNN) ve Random Forest makine öğrenme algoritmalarıyla ile sınıflandırılmış ve metotların başarımları analiz edilmiştir. Random Forest algoritmasıyla 90% civarında bir sınıflandırma başarımı elde edilmiştir. Sonrasında veri sayısının az olmasından dolayı, verinin son haline Resampling işlemi uygulanmıştır. Bu şartlar altında başarım oranının 95% 'e kadar yükseldiği gözlemlenmiştir.

Anahtar sözcükler: Göreceli Dalgacık Dönüşümü Enerjisi, EEG, Şizofreni, Makine Öğrenme

GİRİŞ

İnsan kafa derisi üzerinde kaydedilen elektroensefalogram (EEG) sinyalleri, çok yönlü elektriksel aktivitenin senkron bileşenlerinin bir göstergesidir. Artan klinik uygulama ve EEG çalışması, EEG'nin çeşitli davranışsal, patolojik ve ilaç modellerini ortaya koyabildiğini göstermektedir. Günümüzde, EEG beyin fonksiyonlarının çalışılmasında, beyin hastalığında tedavinin ve teşhiste çok faydalı ve önemli bir bölüm olmuştur. Bu nedenle, beyin hastalığında beyin dalgasının özelliklerini araştırmak ve sonuçları erken tanı, tedavi, rehabilitasyon ve öngörme dahil klinik uygulamalarda kullanmak önemlidir. Klinik uygulama şizofreni, depresyon ve normal sağlıklı kişiler arasında (Chen et al. 2000) olduğu EEG ritimlerine dayanarak farklılaşmanın mümkün olduğunu göstermektedir. Başka bir deyişle, bu ritimler, bilgisayarın farklı hastalıkları otomatik olarak tanıması için özellikler olabilir (Li and Fan 2005).

Şizofreni, dünya nüfusunun yaklaşık % 0,4-0,6'sını etkileyen şiddetli ve kalıcı bir psikiyatrik hastalıktır. Etkilenen bireyler sıklıkla geç ergenlik veya erken yetişkinlik döneminde klinik olarak dikkat çekmektedir. Amerikan Psikiyatri Birliği (DSMIV) ' nin tanı kriterlerine göre (American Psychiatric Association 2000), hastalar sağlıklı bireylere göre düşüncelerde, etkilerde, ilişkilerde algı ve zorluklarda rahatsızlıklar göstermektedir. Şizofreni sıklıkla olumlu ve olumsuz belirtilerle tanımlanmaktadır. Olumlu belirtiler arasında sanrılar, işitsel halüsinasyonlar ve düşünce bozukluğu vardır ve genellikle psikozun belirtileri olarak kabul edilir. Olumsuz belirtiler, normal özelliklerin veya yeteneklerin kaybı veya yokluğu, konuşma yoksulluk ve motivasyon eksikliğidir. Şizofreni hastaları diğer insanlardan daha düşük iş, evlilik ve bağımsız yaşam oranlarına sahiptir (Sabeti et al. 2011).

Şizofreni, bazılarında, ancak hepsinde değil, beyin fonksiyonlarında bir rahatsızlığı temsil ettiğinden, belirli beyin bölgelerinin veya sinir devrelerinin yer aldığını varsaymak mantıklıdır. Nöropsikolojik çalışmalar, şizofreni hastalarında prefrontal ve temporal kortekste kortikal gri maddenin azaldığına dair kanıtlar bulmuştur. Örneğin; serebral beyaz cevher elyaf yolu değişimleri, amigdale, hipokampus ve entorinal

korteks ve talamus gibi limbik sistem yapılarının hacminin azalması ve bazal ganglion çekirdeklerinin hacminin artması gibi kanıtlar bulmuşlardır. Ayrıca, nöroanatomik çalışmalar, prefrontal ve limbik sistem fonksiyonlarının bozulmasının şizofreni hastalarında gözlenen pozitif ve negatif semptomlara ve bilişsel bozulmalara yol açtığını öne sürmektedir. Klinik, nöroanatomik, nöropsikolojik ve nörogörüntüleme yaklaşımları hastalığın daha iyi anlaşılmasına katkıda bulunmuş olsa da, altta yatan mekanizmalar hakkında daha kesin bir bilgi hala gereklidir (Sadock and Sadock 200AD).

Son zamanlarda, şizofrenik hastaların EEG sinyallerinin analizine çok önem verilmiştir. Bazı araştırmalarda, şizofrenik hastaların ve kontrol katılımcılarının EEG sinyallerine doğrusal olmayan yöntemler uygulanmıştır (Jeong et al. 1998; Koukkou et al. 1993; Röschke, Fell, and Beckmann 1995). Sonuçlar, iki grup arasındaki dinamik süreçte farklılıklar göstermiştir. Hornero ve arkadaşları (Hornero et al. 2006) katılımcılardan zaman serileri oluşturmak için rastgele boşluk tuşuna basmalarını istedi. Sonuçlar şizofreni hastaları tarafından oluşturulan zaman serilerinin kontrol grubundan daha düşük bir karmaşıklığa sahip olduğunu göstermiştir. Başka bir testte ise, rastgele sayı üretimi için (Rosenberg et al. 1990) katılımcılardan bir ila on kez bir sayı seçmeleri istenmiştir. Sayıların üretici bir kuraldan yoksun olması, yani mümkün olduğunca rastgele olması gerekiyordu. Şizofreni hastalarının daha fazla tekrarlanma eğiliminde olduğunu buldular. (Pressman, Peledu, and Geva 2000) şizofreni hastalarında çalışma hafızası görevi sırasında senkronizasyon değişim yeteneğinin olmadığını göstermişlerdir. Beyin aktivitesinde, özellikle önden ve geçici kanallar (Cherif et al. 2004), şizofreni hastalarının sağlıklı katılımcılarla karşılaştırıldığında, göz fiksasyon işlerinde anormallik gösterdiğini belirtmiştir. (Gaser et al. 1999) şizofreni hastalarında yapısal beyin değişikliklerini betimlemiştir. Ayrıca, (Keil et al. 1998) şizofrenik hastalarda ritmik parmak salınımları göstermiştir. (Paulus, Geyer, and Braff 1999), şizofreni ve kontrol grubu olan hastalarda ikili yanıt almak için bir uyarıcının 500 rastgele sağ veya sol görüntüsünü öngörmekten oluşan basit bir seçim görevi gerçekleştirmiştir. Karşılıklı ve çapraz karşılıklı bilgi uyguladıktan sonra, hastalar tarafından oluşturulan yanıt dizilerinin kontrol grubundakilerden daha yüksek derecede bir bağımlılık gösterdiğini göstermişlerdir.

Bu çalışmada 39 sağlıklı ve 45 şizofreni hastaya ait toplam 84 bireyden elde edilen 16 kanallı EEG sinyali kullanılmıştır. EEG sinyalinden şizofreni hastalığının tespiti için üç farklı özellik çıkarım yöntemi kullanılmıştır. Öncelikle ham EEG sinyalinden standart istatistiksel metotlar ve Göreceli Dalgacık Enerjisi metodu kullanılarak bir özellik seti çıkarılmıştır. Elde edilen bu sette özellik değerlerinin sayısı çok fazla olduğundan sonraki aşamada "Best First Search" algoritması kullanılarak bu özellikler arasında en uygun olan özellikler seçilmiş ve özellik sayısı daha makul değerlere getirilmiştir. Elde edilen özellikler bu haliyle Naive Bayes, SVM, MLP, KNN ve Random Forest makine öğrenme algoritmaları kullanılarak sınıflandırma başarımları performansları analiz edilmiştir. Veri setindeki birey sayısının az olmasından dolayı makine öğrenme algoritması sonuçlarını iyileştirmek adına "Resampling" metodu uygulanmış ve sınıflandırma başarımını olumlu olarak etkilediği gözlemlenmiştir. Veri setindeki örnek (sample) sayısı, dengeli bir şekilde dağılmadığı ve bu durum makine öğrenmesi metotlarının eğitimini zorlaştırdığı için, veri setini daha dengeli

yapma amaçlı çoğaltma (oversampling) ve azaltma (undersampling) işlemleri yapılarak, veri seti normal ve hastalıklı bireylerin dağılımını dengeleyecek şekilde resampling işlemine tabi tutulmuştur.

Veri Seti

Bu çalışmada kullanılan EEG kayıtları, benzer şizofrenik bozukluğa sahip 45 çocuğa ait şizofreni hastalığını içermektedir. Ruh Sağlığı Araştırma Merkezi (MHRC) uzmanları tarafından tüm hastaların tanıları doğrulanmıştır. MHRC muayenesi yapılan hastaların hiçbirisi kemoterapi görmemiştir. Hastaların en büyüğü de 14 yaşında ve en küçüğü 10 yıl 8 aylıktır. Kontrol grubu (sağlıklı örnekler) ise en büyüğü 13 yaş 9 aylık ve en küçüğü 11 yaş olan 39 sağlıklı öğrenciden oluşmaktadır. Her iki gruptaki çocukların ortalama yaşı 12 yıl 3 aydır (Borisov et al. 2005). Bireyler rahat, gözleri kapalı ve uyanık iken kafalarına bağlı 16 elektrot ile EEG kayıtları alınmıştır. Her kanaldan alınan veri 7680 uzunluğunda tek boyutlu bir dizi yapısındadır. Bir bireye ait tüm kanallardan alınan EEG kaydı 122280 uzunluğunda tek boyutlu bir dizi yapısındadır.

YÖNTEM

45 şizofreni hastası ve 39 sağlıklı bireylerden alınan EEG verisi 16 kanallıdır. Ham EEG verisi üzerinden öncellikle standart istatistiksel özellik çıkarımları (entropi, ortalama, maksimum, standart sapma, güç yoğunluğu gibi) yapılmıştır. Sonrasında göreceli dalgacık enerji yöntemi ile elde edilen özellik veri seti, eldeki özellik veri seti ile birleştirilmiştir. Özellik sayısının oldukça fazla olmasından dolayı özellik seçimi için "Best First Search" algoritması kullanılmıştır. Elde edilen özellik değerleri Naive Bayes, SVM, MLP, KNN ve Random Forest makine öğrenme algoritmalarıyla başarımları hesaplanmış ve analiz edilmiştir. Şekil 1'de bu çalışmada yapılan işlem süreçleri gösterilmektedir.

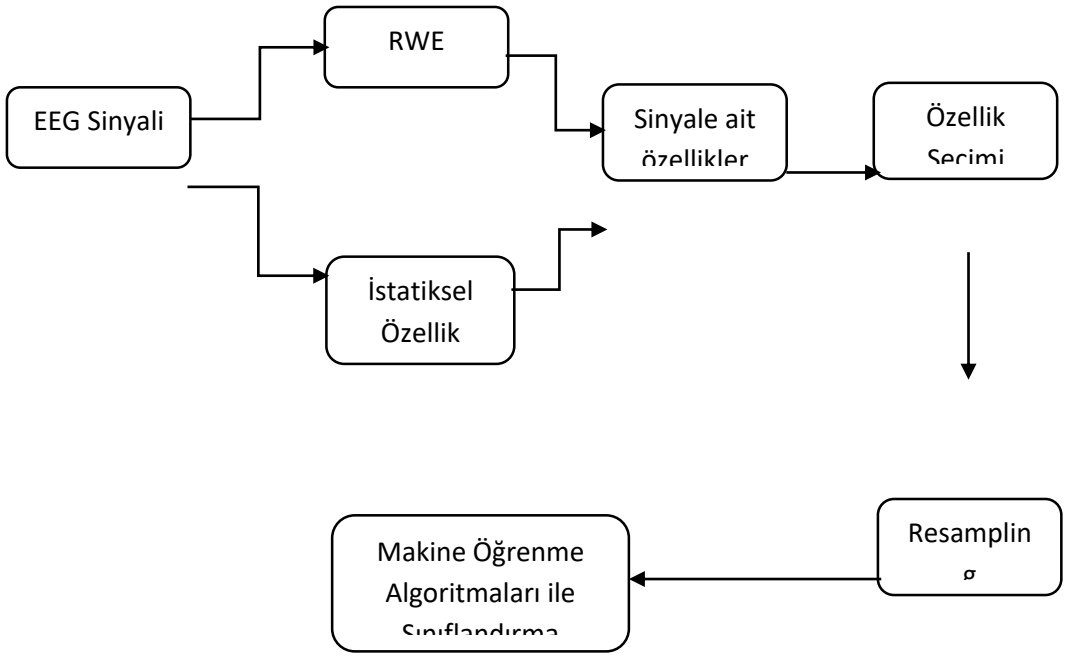

Şekil 1. Bu çalışmada uygulanan metot ve yöntemlere ait süreçler.

Göreceli Dalgacık Dönüşümü Enerjisi (Relative Wavelet Energy)

Dalgacık katsayılarının farklı ölçeklerdeki entropileri, katsayıların taşıdığı bilgi içeriğini ortaya çıkarmak için ölçülür. Dalgacık entropisi, sinyalin düzen / düzensizlik derecesinin bir ölçüsüdür ve doğrusal olmayan sinyallerin gizli dinamik özelliklerini gösterir(Rosso et al. 2006; Rosso, Martin, and Plastino 2002). Verilen ayrık sinyal x (n) anında k ve j ölçeğinde dönüştürülür. Yüksek frekans bileşenli dalgacık katsayısı Dj (k) 'ye ve düşük frekanslı bir bileşen dalgacık katsayısı Aj (k) sahiptir. Dj (k) ve Aj (k) sinyal bileşeninde bulunan bilgilerin frekans bantları aşağıdaki şekilde elde edilir.

$$\left.\begin{array}{l} D_j(k): [2^{-(j+1)} f_s \, , 2^{-j} f_s] \\ A_j(k): [0, 2^{-(j+1)} f_s] \end{array}\right\}$$

Where j=1,2,3,……,J (1)

fs örnekleme frekansıdır. (1,…, N) 'den farklı ayrışma seviyesindeki enerji, dalgacık ayrıntı katsayıları Dj (k) ve dalgacık yaklaşık katsayısı Aj (k)' nin enerjisidir.

Her ayrışma seviyesindeki enerji,

$$E_j = \sum_k |D_j(k)|^2 \quad (2)$$

$$E_{N+1} = \sum_k |A_j(k)|^2 \quad (3)$$

Ortalama dalgacık Enerjisi detay katsayıları

$$\bar{E}_j = \frac{1}{N_j}\sum_j |D_j(k)|^2 \quad (4)$$

Nj, j seviyesindeki dalgacık ayrıntı katsayılarının sayısıdır.

$$\bar{E}_{N+1} = \frac{1}{N_j}\sum_j |A_j(k)|^2 \quad (5)$$

Ortalama dalgacık Enerjisi yaklaşık katsayıları,

Daha sonra, dalgacık ayrışmasından sonra sinyalin toplam enerjisi,

$$E_{total} = \sum_{j=1}^{N+1} \bar{E}_j \quad j = 1,2,\ldots,N+1 \quad (6)$$

Böylece göreceli dalgacık enerjisi (RWE),

$$\rho_j = \frac{\bar{E}_j}{E_{total}} \quad (7)$$

$\sum_j \rho_j = 1$ ve dağılım ρ_j zaman ölçeği yoğunluğu olarak düşünülebilir. Bu, farklı frekans bantlarındaki sinyal enerjisi dağılımını karakterize etmek için bilgi sağlar (Kumar, Dewal, and Anand 2012).

Özellik Seçimi

Özellik seçimi, "the curse-of-dimensionality" olarak adlandırılan problemle mücadele etmek için kullanılmıştır (Elder and Pregibon 1996). Önceki çalışmalar, eğitim örneklerinin sayısının özellik vektörlerinin sayısından daha küçük olması durumunda sınıflandırıcının zayıf sonuçlar verme eğiliminde olduğunu göstermiştir (Lotte et al. 2007). Bu çalışmada 84 bireye ait özellik vektörlerinin boyutu oldukça fazladır. Bu nedenle sınıflandırıcının performansını iyileştirmek için geliştirilebilecek önemli özellikleri belirlemek hayati önem taşımaktadır. Bu çalışmamızda "Best First Search" algoritması kullanılarak özellik seçimi yapılmış ve özellik vektörünün boyutu makul değerlere indirgenmiştir. Elde edilen özellik değerlerinin makine öğrenme algoritmalarıyla elde edilen başarımları gözlenmiş ve sonuçlar oldukça tatmin edici bulunmuştur.

Naive Bayes

Naive Bayes algoritması belirli bir veri kümesindeki değer kombinasyonlarını ve frekansları sayarak bir olasılık kümesini hesaplayan sınıflandırma algoritmasıdır. Bu algoritma temelde Bayes teoremini kullanır ve sınıf değişkeninin değeri göz önüne alındığında tüm özniteliklerin bağımsız olduğunu varsayar. Bu koşullu bağımsızlık varsayımı nadiren gerçek dünyadaki uygulamalarda geçerlidir, dolayısıyla niteleme saftır, ancak algoritma çeşitli denetlenen sınıflandırma problemlerinde hızla öğrenme eğilimindedir ve iyi performans göstermektedir (Dimitoglou, Adams, and Jim 2012).

$$P(A|B) = \frac{P(B|A)P(A)}{P(B)} \quad (8)$$

Önsel olasılık, Bayes teoremine öznellik katmaktadır. Başka bir şekilde ifade edecek olursak P(A) , A olayı ile ilgili henüz hiçbir veri elde edilmeden A olayı hakkında edinilen bilgidir. Diğer taraftan P(B | A) ardıl olasılıktır çünkü veri elde edildikten sonra, A olayının gerçekleşmiş olduğu durumlarda B olayının gerçekleşme olasılığı hakkında bilgi verir (Pawlak 2003).

Destek Vektör Makinaları (SVM)

Bir SVM, bir çekirdek işlevi K (·, ·), toplamlarından oluşan iki sınıflı bir sınıflandırıcıdır (Cristianini, Shawe-Taylor, and others 2000).

$$f(x) = \sum_{i=1}^{L} \alpha_i t_i K(x, x_i) + d\,, \quad (9)$$

Burada ti ideal çıktılardır, $\sum_{i=1}^{L} \alpha_i t_i$ ve αi> 0. Vektörler xi destek vektörleri olup, bir optimizasyon işlemi vasıtasıyla belirlenen eğitim setinden elde edilmiştir (Collobert and Bengio 2001). İdeal çıktı, sırasıyla, karşılık gelen destek vektörünün sınıf 0 veya sınıf 1'de olup olmadığına bağlı olarak 1 veya -1'dir. Sınıflandırma için, sınıf kararı, f(x) değerinin bir eşiğin üstünde veya altında olup olmadığına dayanır. Çekirdeğin K (·, ·) bazı özellikleri (Mercer koşulu) olması için sınırlandırılmıştır, böylece K (·, ·) aşağıdaki gibi ifade edilebilir:

$$K(x, y) = b(x)^t b(y), \quad (10)$$

Burada b(x), (x' in var olduğu) giriş alanından muhtemel sonsuz boyutlu bir SVM genişleme alanını ifade eder. SVM eğitim sürecinin odağı sınıflar arasındaki sınırı modellemektir. Ayrılabilir bir veri kümesi için, SVM optimizasyonu genişleme

alanındaki maksimum sınırla bir hiper düzlemi seçer (Cristianini, Shawe-Taylor, and others 2000). Sınırları yatan eğitim setinden gelen veri noktaları, denklem (10) 'da ki destek vektörleridir (Campbell et al. 2006).

Çok Katmalı Algılayıcı (MLP)

Yapay sinir ağları (RP Lippmann 1987), özellikle dikkate alınan görevin altında yatan istatistiklerin iyi anlaşılmadığı durumlarda kullanılır ve girdi ile çıktılar arasındaki karmaşık dönüşümleri öğrenir . Sinir ağları konuşma işleminde kullanımı gittikçe yaygınlaşmaktadır (Farrell, Mammone, and Assaleh 1994; Morgan, D. P., & Scofield 1991) ve sadece yakın zaman önce konuşmacı tanıma için düşünülmüştür (Freund and Mason 1999; Latifoğlu et al. 2008).

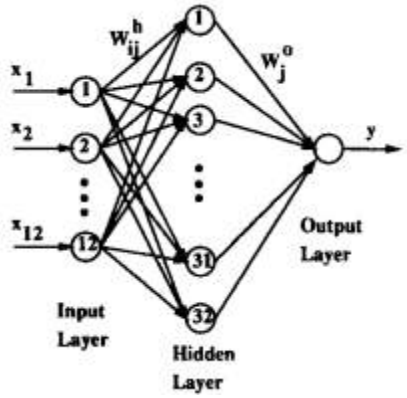

Şekil 2. Tek gizli katmanlı MLP

Şekil 2' de bir gizli katman, bir giriş katmanı ve bir çıktı katmanı içeren bir MLP gösterilmiştir. MLP, perceptron adı verilen basit nöronların bir ağıdır. Tek bir perceptronun temel konsepti 1958'de Rosenblatt tarafından ortaya atılmıştır. Perceptron, giriş ağırlıklarına göre doğrusal bir kombinasyon oluşturarak ve daha sonra bazı doğrusal olmayan aktivasyon fonksiyonu ile çıktıyı koyarak, çok sayıda gerçek değerli girdiden tek bir çıktı hesaplar. Matematiksel olarak bu, şu şekilde yazılabilir:

$$y = \varphi(\sum_{i=1}^{n} w_i x_i + b) = \varphi(w^T x + b) \quad (11)$$

Bir ileri beslemeli ağ tarafından gerçekleştirilen, Lineer olmayan aktivasyon fonksiyonlarına sahip tek bir gizli katman ve doğrusal bir çıkış katmanı için uygulanacak hesaplamalar matematiksel olarak aşağıdaki gibi yazılabilir:

$$x = f(s) = B\varphi(As + a) + b \quad (12)$$

Burada *s* bir girdi vektörü ve *x* bir çıkış vektörüdür. *A* birinci tabakanın ağırlık matrisi, *a* birinci tabakanın ön gerilim vektörüdür. *B* ve *b*, sırasıyla, ikinci katmanın ağırlık matrisi ve önyargı vektörüdür. *φ* işlevi, elemanlı bir doğrusal olmama durumunu belirtir. MLP'nin denetlenen öğrenme problemi, geri yayılım algoritması (McClelland and Rumelhart 1988)ile çözülebilir. Algoritma iki aşamadan oluşur. İleri geçişte verilen girdilere karşılık gelen tahmini çıktılar Denklem(12)' de olduğu gibi değerlendirilir. Geriye doğru geçişte, maliyet fonksiyonunun farklı parametrelere göre kısmi türevleri şebeke boyunca geri yayılır. Farklılaşma zinciri kuralı, ileri geçişte olanlar gibi geriye doğru geçiş için çok benzer hesaplama kuralları verir. Ağ ağırlıkları daha sonra gradyan tabanlı optimizasyon algoritması kullanılarak uyarlanabilir. Ağırlıklar birleşinceye kadar tüm süreç yinelenir (Haykin 1994).

En Yakın k Komşu Sınıflandırma Algoritması (KNN)

En basit sınıflandırma tekniklerinden biri, en yakın k komşu sınıflandırıcısıdır. Bir girdi özellik vektörü X'in sınıflandırılması, en yakın k eğitim vektörlerini uygun bir mesafe metrik değerine göre belirleyerek yapılır. Vektör X daha sonra, bu en yakın komşuların çoğunluğunun ait olduğu sınıfa atanır (Latifoğlu et al. 2008; Sengur 2008). KNN algoritması, en yakın komşuluklarda bir mesafe fonksiyonu ve bir oylama fonksiyonuna dayanmaktadır, kullanılan metrik Öklid uzaklığıdır. En yakın k komşu sınıflandırıcısı, optimum değerler k (Duda, Hart, and Stork 1998) için iyi bir performans sergilediği söylenen klasik parametrik olmayan denetimli sınıflandırmasıdır.

Çoğu öğreticili öğrenme algoritması gibi, KNN algoritması bir eğitim aşamasından ve bir test aşamasından oluşur. Eğitim aşamasında, veri noktaları n-boyutlu bir alanda verilir. Bu eğitim veri noktalarında, sınıflarını belirten onlarla ilişkili etiketler bulunur. Test aşamasında, etiketlenmemiş veriler verilir ve algoritma etiketlenmemiş noktaya en yakın k (en önceden sınıflandırılmış) veri noktalarının listesini oluşturur. Algoritma daha sonra o listenin çoğunluğunun sınıfını döndürür (Hall 1998; Morgan, D. P., & Scofield 1991) . En yakın k komşu algoritması aşağıdaki adımlardan oluşmaktadır (El-Dahshan, Hosny, and Salem 2010) :

1.Uygun bir mesafe metriğini belirleyin.

2.Eğitim aşamasında: P tüm eğitim verilerini P çiftlerine (seçilen özelliklere göre) depolayın, burada $P = \{(y_i, c_i), i = 1, ..., n\}$, y_i bir eğitim modeli Eğitim verileri seti, c_i karşılık gelen sınıf ve n, eğitim kalıpları miktarıdır.

3.Test aşamasında: Yeni özellik vektörü ile depolanan tüm özellikler (eğitim verileri) arasındaki mesafeleri hesaplayın.

4. En yakın komşular seçilir ve yeni örneği sınıf için oy kullanmaları istenir. Test aşamasında verilen doğru sınıflandırma algoritmanın doğruluğunu değerlendirmek için kullanılır. Eğer bu tatmin edici değilse, makul bir doğruluk düzeyi elde edilinceye kadar k değeri ayarlanabilir.

Random Forest

Rastgele Orman, ayrılmamış sınıflandırma ağaçlarının bir toplamıdır. Hızlı çalışır ve genelde birçok ağaç tabanlı algoritma üzerinde önemli bir performans gelişimi sergiler. Rastgele Orman'daki sınıflandırma ağaçları, tahmini değişkende bölünmeleri belirlemek için kullanılan Gini düğüm kriterini kullanarak tekrarlanır şekilde oluşturulmuştur. Bir ağaç düğümünün bölünmesi, veride bulunan belirsizliği ve dolayısıyla yanlış sınıflandırmanın olasılığını azaltacak şekilde değişken üzerinde yapılır. Bir ağaç düğümünün ideal bölünmesi, Gini değeri sıfır olduğunda oluşur. Bölme işlemi, birden fazla ağaçtan oluşan bir "orman" oluşturulana kadar devam eder. Sınıflandırma, ormandaki her ağaç en popüler sınıf için bir birim oy kullandığında oluşur. Rastgele Orman, daha sonra ormandaki tüm ağaçlar üzerinde en çok oy alan sınıflandırmayı seçer. Her bir sınıflandırma, verinin rasgele bir alt kümesi aracılığıyla yaratılmış bağımsız olarak oluşturulmuş ağaçlardan oluşan ve aşırı montajdan kaçınarak son bir orman tarafından üretildiği için budama gerekli değildir. Genelleme hata oranları, ormandaki ağaçların mukavemetine ve aralarındaki korelasyona bağlıdır. Ormandaki ağaç sayısı arttıkça bu hata oranı bir sınıra yaklaşır.

Rastgele Orman'ın bir diğer avantajı test seti hatasının tarafsız bir tahminini elde etmek için çapraz doğrulama veya ayrı bir test setinin bulunmamasıdır. Test setinin doğruluğu, çantadan çıkma (OOB) örnekleri çalıştırarak Rastgele Orman 'da dahili olarak tahmin edilmiştir. Rastgele Orman 'da yetişen her ağaç için, vakaların yaklaşık üçte biri çantanın dışındadır (önyükleme örneğinin dışında). Çantanın dışındaki (OOB) örnekler, OOB olmayan veriler üzerinde yetişen ağaç için bir test seti olarak kullanılabilir.

Rasgele Orman algoritması şu şekilde özetlenebilir:

1. Bir sayı n, toplam değişken sayısı N'den (genellikle n~√N) çok daha küçük olarak belirtilmiştir.

2. Her derinlikteki ağaç budama olmadan eğitim setinin bir önyükleme örneği üzerinde yetiştirilir

3. Her düğümde, N değişkeninin dışındaki n'ler rastgele seçilir

4. Bu n değişken üzerindeki en iyi bölünme, Gini düğüm impurity kriterini kullanarak belirlenir.

Oranın azaltılması, ormandaki ağaçların mukavemetlerini ve aralarındaki ilişkiyi azaltır. Arttırılması her ikisini de artırır. OOB hata oranını kullanarak uygun değer bir n değeri bulunabilir. Bu, rastgele ormanların hassas olduğu tek ayarlanabilir parametredir. Rasgele Orman ' da ki her ağaç için hesaplama karmaşıklığı $\sqrt{N}\, S \log(S)$, burada S eğitim vakalarının sayısıdır. Bu nedenle, gözlemlerin orta sayıda olduğu çok sayıda değişken işleyebilir (Emanet 2009).

BULGULAR

39 sağlıklı ve 45 şizofreni hastası bireylerden alınan 16 kanallı EEG kayıtlarından her bir kanal ve tüm kanallardan alınan sinyaller için vektörler oluşturulmuştur. Her bir kanal verisi 7680 uzunluğunda tek boyutlu bir veriden oluşmaktadır. Verilere öncelikle standart istatistiksel(ortalama, güç yoğunluğu, maksimum değer, entropi

gibi) özellik çıkarımları uygulanmıştır. Bu özellikler, sinyal verisine uygulanan Göreceli Dalgacık Enerji (RWE) metodu ile elde edilen özellik değerleri ile birleştirilerek sınıflandırma işlemi için gerekli olan özellik değerleri elde edilmiştir. Ancak elde edilen özellik değerlerinin çok fazla olmasına karşılık, veri sayısının (birey sayısı) az olması sınıflandırma başarımlarının doğru olarak ölçülemeyeceği gözlemlenmiştir. Bu nedenle mevcut özellik değerlerinin makul bir sayıya indirgenebilmesi için "Best First Search" algoritması kullanılarak bu özellik değerleri üzerinden özellik seçim işlemi uygulanmıştır. Bu işlemden sonra özellik sayısının daha makul bir değerde olduğu gözlemlenmiş ve uygulanan makine öğrenme algoritmalarıyla sınıflandırılma işleminde başarılı sonuçlar elde edildiği görülmüştür. Tablo 1' de tüm kanallar ve her bir kanal için, beş farklı sınıflandırıcı ile elde edilen başarım değerleri ve elde edilen özellik sayıları görülmektedir. Burada Naive Bayes, SVM, KNN, MLP ve Random Forest makine öğrenme algoritmaları kullanılarak başarın performansları analiz edilmiştir.

Tablo 1. Tüm kanallar ve her bir kanal için sınıflandırma algoritmalarıyla elde edilen başarım sonuçları.

	Tüm kanallar	**C3**	**C4**	**CZ**	**F3**	**F4**	**F7**	**F8**	**O1**	**O2**	**P3**	**P4**
Naive Bayes	89,3%	84,5%	79,8%	72,6%	78,6%	82,2%	73,8%	70,2%	85,6%	88,1%	83,3%	77,4%
SVM	86,9%	75,0%	75,0%	73,8%	76,2%	79,7%	77,4%	71,1%	76,2%	82,1%	77,4%	73,8%
MLP	82,1%	71,4%	70,2%	72,5%	72,7%	73,8%	60,7%	59,5%	79,7%	75,0%	75,0%	70,0%
KNN	78,4%	70,3%	82,0%	72,5%	63,1%	72,6%	67,9%	59,5%	58,2%	72,1%	75,6%	77,1%
Random Forest	90,5%	77,4%	80,8%	83,3%	79,8%	77,4%	76,2%	77,4%	81,0%	85,7%	79,8%	77,4%
Özellik Sayısı	75	21	15	23	20	17	11	13	49	49	31	30

Tablo1' de görüldüğü üzere özellikle Random Forest ile başarım oranı 90% civarındadır. Burada görüldüğü üzere tüm kanallardan elde edilen özelliklerle elde edilen başarım oranlarının daha yüksek olduğu gözlemlenmiştir. Veri sayısı (birey sayısı) az olduğundan mevcut özelliklere Resampling işlemi uygulanarak başarım oranının yükseltilmesi hedeflenmiştir. Tablo 2.'de Resampling işlemi sonucu elde edilen başarım oranları gösterilmektedir. Tablo 2 incelendiğinde elde edilen başarı oranlarında önemli bir artış olduğu görülmektedir. Başarım oranı en yüksek 95,2% olarak elde edilmiştir.

Tablo 2. Resampling işlemi sonucu elde edilen başarım sonuçları.

	Tüm kanallar	C3	C4	CZ	F3	F4	F7	F8	O1	O2	P3	P4
Naive Bayes	92,9%	84,5%	83,4%	79,7%	75,0%	77,3%	82,2%	59,6%	91,7%	95,2%	85,7%	84,5%
SVM	95,2%	78,6%	75,0%	79,7%	77,2%	75,0%	84,5%	55,9%	90,4%	94,1%	86,9%	78,6%
MLP	95,2%	85,7%	84,5%	85,6%	94,1%	78,6%	84,5%	82,0%	92,8%	92,9%	89,3%	91,7%
KNN	94,1%	84,5%	87,8%	77,3%	78,5%	83,3%	85,6%	86,9%	88,0%	84,3%	89,2%	84,4%
Random Forest	92,9%	91,7%	91,7%	91,7%	91,7%	89,3%	91,6%	88,1%	95,2%	96,4%	94,1%	94,0%
Özellik sayısı	75	21	15	23	20	17	11	13	49	49	31	30

Şekil 3'de Resampling işlemi öncesi ve Şekil 4' de Resampling işlemi sonrası farklı beş makine öğrenme algoritması kullanılarak elde edilen sonuçların grafiği gösterilmektedir.

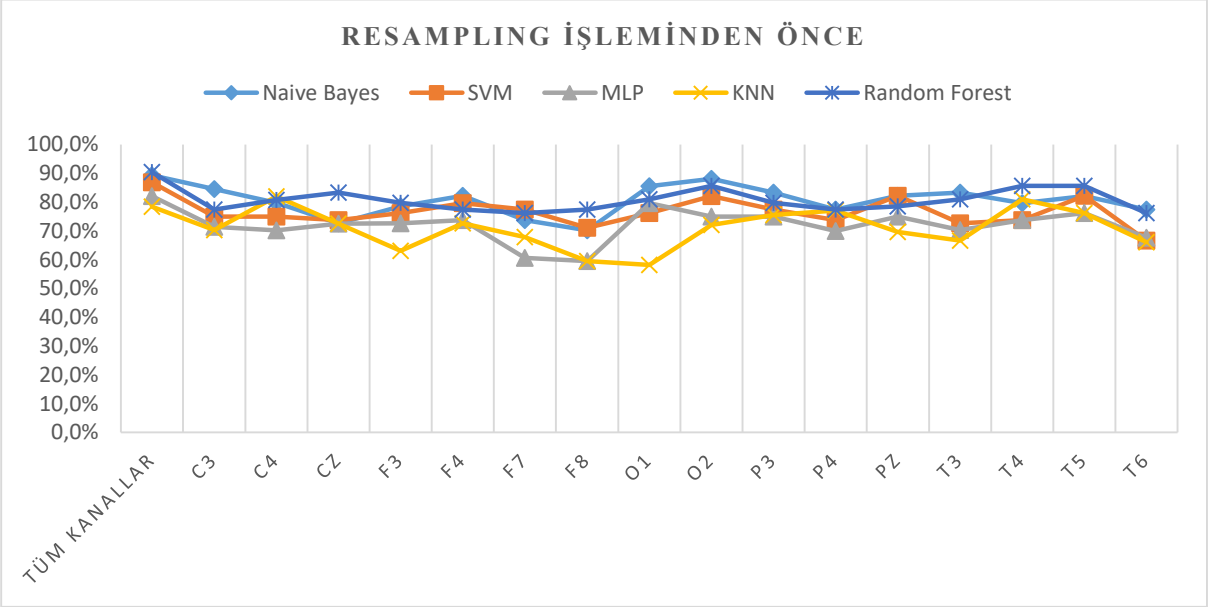

Şekil 3. Resampling işlemi öncesi farklı sınıflandırma algoritmaları için elde edilen başarım grafiği.

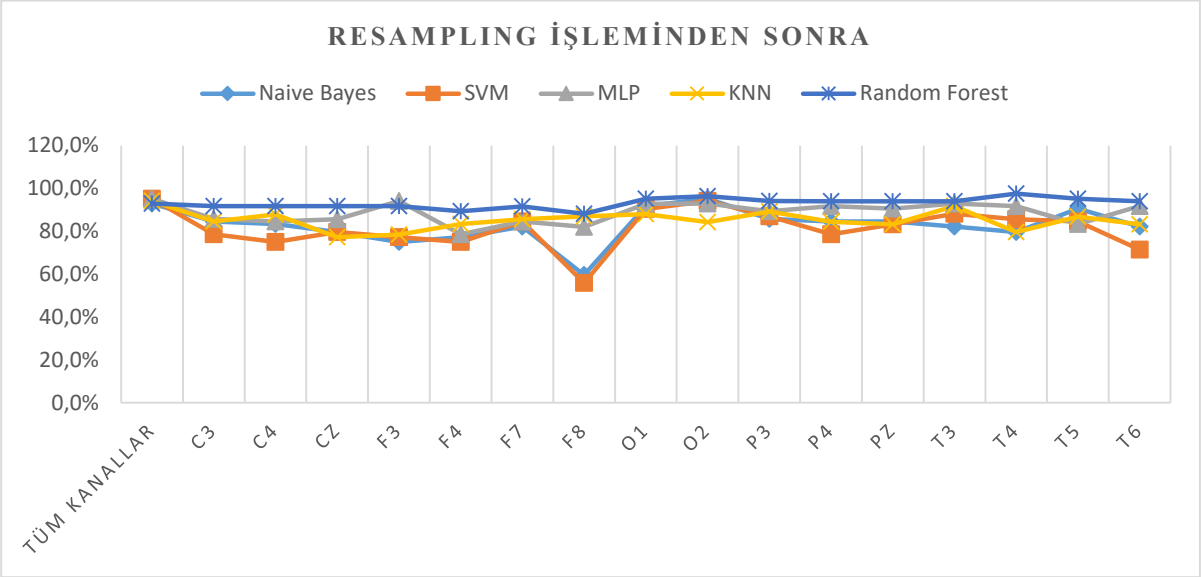

Şekil 4. Resampling işlemi sonrası farklı sınıflandırma algoritmaları için elde edilen başarım grafiği.

SONUÇ

Bu çalışmada şizofreni hastası ve sağlıklı bireylere ait EEG kayıtları Göreceli Dalgacık Enerjisi ve standart istatistiksel hesaplama metotları ile analiz edilmiştir. Bu analiz sonucu elde edilen özellik seti, farklı beş sınıflandırma algoritmasıyla sınıflandırılarak, ilgili özelliklerin hastalığı ayırt edici özelliğe sahip olup olmadıkları incelenmiştir. Sonuç olarak, kullanılan sınıflandırma işleminde, resampling işlemi yapılmadan önce tüm kanallardan alınan veri ile başarım 90% civarında elde edilmektedir. Ancak verinin sayısının az olmasından ve verinin daha dengeli olarak dağılımını gerçekleştirmek için, mevcut özellik seti korunarak resampling işlemi uyguladıktan sonra başarım oranının 95%' e kadar çıktığı gözlemlenmiştir. Bu yaptığımız çalışmada ilgili analiz metotlarının EEG sinyalinden, tanı amaçlı olarak kullanılabilecek önemli özellik değerleri elde ettiğini göstermiştir. Farklı sınıflandırma algoritmalarıyla elde edilen sınıflandırma başarımları analiz edildiğinde, genel olarak bir bireye ait tüm kanallardan alınan kayıtlar ele alındığında tüm sınıflandırıcılar için başarım oranlarının birbirine yakın olduğu görülmektedir. Ancak kanal bazında elde edilen başarım oranları farklılık göstermektedir. Sonraki çalışmalarda, bu çalışmadaki metot ve yöntemler göz önüne alınarak, şizofreni hastalığının tespiti veya buna benzer alanlarda klinik çalışanlara yardımcı olabilecek sistemlerin geliştirilmesinin mümkün olduğu görülmektedir.

KAYNAKLAR

American Psychiatric Association. 2000. American Journal of Critical Care *Diagnostic*

and Statistical Manual of Mental Disorders, 4th Ed. DSM-IV-TR.

Borisov, S. V., A. Ya Kaplan, N. L. Gorbachevskaya, and I. A. Kozlova. 2005. "Analysis of EEG Structural Synchrony in Adolescents with Schizophrenic Disorders." *Human Physiology*.

Campbell, William M, Douglas E Sturim, Douglas A Reynolds, and Alex Solomonoff. 2006. "SVM Based Speaker Verification Using a GMM Supervector Kernel and NAP Variability Compensation." In *2006 IEEE International Conference on Acoustics Speech and Signal Processing Proceedings*, , I--I.

Chen, X S, J J Wang, F Y Lou, and others. 2000. "A Comparative Study of Positive and Negative Schizophrenics Using BEAM." *Acta Universitatis Medicinalis Secondae Shanghai* 20: 547–49.

Cherif, R., A. Nait-Ali, J.F. Motsch, and M.O. Krebs. 2004. "A Parametric Analysis of Eye Tremor Movement during Ocular Fixation, Applied to Schizophrenia."

Collobert, Ronan, and Samy Bengio. 2001. "SVMTorch: Support Vector Machines for Large-Scale Regression Problems." *Journal of machine learning research* 1(Feb): 143–60.

Cristianini, Nello, John Shawe-Taylor, and others. 2000. *An Introduction to Support Vector Machines and Other Kernel-Based Learning Methods*. Cambridge university press.

Dimitoglou, George, James A Adams, and Carol M Jim. 2012. "Comparison of the C4. 5 and a Na{\"\i}ve Bayes Classifier for the Prediction of Lung Cancer Survivability." *arXiv preprint arXiv:1206.1121*.

Duda, Richard O, Peter E Hart, and David G Stork. 1998. "Pattern Classification (2nd Ed .)." *Computational Complexity*.

El-Dahshan, El Sayed Ahmed, Tamer Hosny, and Abdel Badeeh M. Salem. 2010. "Hybrid Intelligent Techniques for MRI Brain Images Classification." *Digital Signal Processing: A Review Journal*.

Elder, J, and D Pregibon. 1996. "A Statistical Perspective on KDD." *Advances in knowledge discovery and data mining*.

Emanet, Nahit. 2009. "ECG Beat Classification by Using Discrete Wavelet Transform and Random Forest Algorithm." In *2009 Fifth International Conference on Soft Computing, Computing with Words and Perceptions in System Analysis, Decision and Control*, , 1–4.

Farrell, Kevin R, Richard J Mammone, and Khaled T Assaleh. 1994. "Speaker Recognition Using Neural Networks and Conventional Classifiers." *IEEE Transactions on speech and audio processing* 2(1): 194–205.

Freund, Yoav, and Llew Mason. 1999. "The Alternating Decision Tree Learning Algorithm." In *Icml*, , 124–33.

Gaser, Christian et al. 1999. "Detecting Structural Changes in Whole Brain Based on Nonlinear Deformations Application to Schizophrenia Research." *NeuroImage*.

Hall, M. 1998. "Correlation-Based Feature Selection for Machine Learning." Waikato Uni.

Haykin, Simon. 1994. "A Comprehensive Foundation." *Neural Networks*.

Hornero, Roberto et al. 2006. "Variability, Regularity, and Complexity of Time Series Generated by Schizophrenic Patients and Control Subjects." *IEEE Transactions on Biomedical Engineering*.

Jeong, Jaeseung et al. 1998. "Nonlinear Analysis of the EEG of Schizophrenics with Optimal Embedding Dimension." *Medical Engineering and Physics*.

Keil, Andreas, Thomas Elbert, Brigitte Rockstroh, and William J. Ray. 1998. "Dynamical Aspects of Motor and Perceptual Processes in Schizophrenic Patients and Healthy Controls." *Schizophrenia Research*.

Koukkou, M. et al. 1993. "Dimensional Complexity of EEG Brain Mechanisms in Untreated Schizophrenia." *Biological Psychiatry*.

Kumar, Yatindra, Mohan Lal Dewal, and Radhey Shyam Anand. 2012. "Relative Wavelet Energy and Wavelet Entropy Based Epileptic Brain Signals Classification." *Biomedical Engineering Letters*.

Latifoğlu, Fatma, Kemal Polat, Sadik Kara, and Salih Güneş. 2008. "Medical Diagnosis of Atherosclerosis from Carotid Artery Doppler Signals Using Principal Component Analysis (PCA), k-NN Based Weighting Pre-Processing and Artificial Immune Recognition System (AIRS)." *Journal of Biomedical Informatics*.

Li, Ying Jie, and Fei Yan Fan. 2005. "Classification of Schizophrenia and Depression by EEG with ANNs." In *Annual International Conference of the IEEE Engineering in Medicine and Biology - Proceedings*,.

Lotte, F. et al. 2007. "A Review of Classification Algorithms for EEG-Based Brain-Computer Interfaces." *Journal of Neural Engineering*.

McClelland, James L., and David E. Rumelhart. 1988. "A Simulation-Based Tutorial System for Exploring Parallel Distributed Processing." *Behavior Research Methods, Instruments, & Computers*.

Morgan, D. P., & Scofield, C. L. 1991. "Neural Networks and Speech Processing." *In Neural Networks and Speech Processing* Springer(Boston, MA.): (pp. 329-348).

Paulus, Martin P., Mark A. Geyer, and David L. Braff. 1999. "Long-Range Correlations in Choice Sequences of Schizophrenic Patients." *Schizophrenia Research*.

Pawlak, Zdzisław. 2003. "A Rough Set View on Bayes' Theorem." *International Journal of Intelligent Systems* 18(5): 487–98.

Pressman, A., A. Peledu, and A. B. Geva. 2000. "Synchronization Analysis of Multi-Channel EEG of Schizophrenic during Working-Memory Tasks." In *21st IEEE Convention of the Electrical and Electronic Engineers in Israel, Proceedings*,.

Röschke, Joachim, Jürgen Fell, and Peter Beckmann. 1995. "Nonlinear Analysis of Sleep EEG Data in Schizophrenia: Calculation of the Principal Lyapunov Exponent." *Psychiatry Research*.

Rosenberg, Stewart et al. 1990. "Random Number Generation by Normal, Alcoholic and Schizophrenic Subjects." *Psychological Medicine*.

Rosso, O. A. et al. 2006. "EEG Analysis Using Wavelet-Based Information Tools." *Journal of Neuroscience Methods*.

Rosso, O. A., M. T. Martin, and A. Plastino. 2002. "Brain Electrical Activity Analysis Using Wavelet-Based Informational Tools." *Physica A: Statistical Mechanics and its Applications*.

RP Lippmann. 1987. "An Introduction to Computing with Neural Nets." *IEEE ASSP Magazine*.

Sabeti, M., S. D. Katebi, R. Boostani, and G. W. Price. 2011. "A New Approach for EEG Signal Classification of Schizophrenic and Control Participants." *Expert Systems with Applications*.

Sadock, Benjamin J., and Virginia A. Sadock. 200AD. Lippincott Williams & Wilkins Publishers *Comprehensive Textbook & Psichiatry*.

Sengur, Abdulkadir. 2008. "An Expert System Based on Principal Component Analysis, Artificial Immune System and Fuzzy k-NN for Diagnosis of Valvular Heart Diseases." *Computers in Biology and Medicine*.

ECOLOGICAL CONDUCTIVE YARN PRODUCTION METHOD FOR ELECTRONIC TEXTILES

Özgü ÖZEN
Suleyman Demirel University, Engineering Faculty, Textile Engineering Dept. Isparta
ozgu.ozen.91@gmail.com

Demet YILMAZ
Suleyman Demirel University, Engineering Faculty, Textile Engineering Dept. Isparta
demetyilmaz@sdu.edu.tr

Kerim YAPICI
Suleyman Demirel University, Engineering Faculty, Chemical Engineering Dept. Isparta
kerimyapici@sdu.edu.tr

ABSTRACT: In recent years, with the advancement of technology and the fact that electronic products have become an indispensable part of our lives, it has been become one of the most researched subjects on conductive textiles. Although many methods have been proposed for obtaining textiles conducting electrical current, most of them are not environmentally friendly in terms of water consumption and chemical waste. In this context, the study aimed to develop a new environmentally friendly conductive textile production method which is an alternative to the methods used in the production of conductive textiles. In the proposed method, it is provided to make each fiber conductive before yarn and fabric formation. The high stability graphene based nanosuspension is applied to viscose fibers to provide conductivity. Following the application process, yarn production was realized. In the proposed method, as in the impregnation method, there is no need to remove the remaining solution after passing the textile material through a conductive solution or soaking in the solution and drying after application. With the proposed method, conductive yarn having electrical resistance values ranging between 1.51-5.86 MΩ / cm was obtained. In addition, yarn production with tensile properties required for textile surface production was realized.

Key words: conductive yarns, smart textiles, reduced graphene oxide, new environmental approach

INTRODUCTION

Wearable electronics has become an important field of study in recent years with the advancement of technology and the widespread use of electronic products. Wearable electronics are defined as textiles such as fibers, filaments and yarns as well as woven, knitted or nonwoven surface fabrics that may interact with the environment or the user (Stoppa and Chiolerio 2014). In recent years, the use of conductive textiles for electronic products has attracted considerable attention (Gregory et al., 1989). Due to their rigid structure, electronic devices deform quickly under any influence. However, textile structures have high stability against deformations. However, due to their porous structure, they are breathable and have soft properties (Weng et al. 2016). These features are advantageous in terms of garment comfort. Due to the opportunities provided by textile materials, the combination of textile structures with electronic circuits or elements allows the simultaneous fulfillment of the expected properties of both textiles and electronics.

Conductive textiles have the potential to be used mostly in health, military and aviation fields, but especially with the widespread use of electronics such as mobile phones and computers; It has started to find its place in daily life with examples such as clothes that follow body functions, sportswear activities, jackets integrated with mp3 player, touch screen clothes (Aniolczyk et al. 2004; Ermes and Pärkkä, 2008). As a result of the increase in the usage areas in social life, with the intense interest in conductive textile samples, studies on obtaining these products have increased. Copper, silver, stainless steel, metals such as gold, iron compounds such as FeCl3, silver salts such as AgNO3, conductive polymers such as polyaniline, polyacetylene, polyphenylene, polythiophene, materials such as carbon powder, carbon nanotube and graphene it is used.

In order to provide electrical conductivity to textile structures, researchers use various methods. These methods; production of fibers from metal sheets or tapes (Anderson and Seyam 2002), production of conductive core yarns based on the placement of conductive wires in the core of yarn and coating with staple fibers (Ueng and Cheng 2001), fiber extraction from conductive polymers (Pormfret et al. 1999), fibers of metals (Lu et al. 1996; Rossi et al. 2005), coating metal oxides or salts with conductive carbon or self-conducting polymers (Rossi et al. 1999; Mazzoldi et al 2002) using various methods, passing textile yarns and fabrics through a solution containing conductive material impregnation of the material (Molina et al. 2013a; Molina et al. 2013b). Among these methods, the impregnation method is more preferred because of its applicability to textile processes and its easy and simple process.

The impregnation method, which is used as a common method in the production of conductive textiles as well as in dyeing and finishing processes, causes problems such as the consumption of large amounts of water and waste water and thus the formation of chemical waste. The rapid depletion of the already limited water resources and the

high amount of chemical wastes generated cause environmental problems. Therefore, sustainable, environmentally friendly materials and methods are needed. In this study, it is aimed to develop a new alternative to the methods used in the production of conductive textiles. In this method, it is provided to make each fiber conductive before yarn and fabric formation. First, a certain concentration of solution is prepared with a material having electrical conductivity. Then, while the fibers forming the yarn are in the open state, a certain amount of the prepared solution is applied to the fiber bundle in a controlled manner. Solution is applied to each fiber. Then yarn and fabric are obtained. Thus, as in the impregnation method, there is no need to discard the remaining solution after passing the textile material through a conductive solution or soaking.

METHODS

In this study, reduced graphene oxide was used as conductive material and viscose fiber was used as yarn raw material. Viscose fibers are also known as 'artificial silk nedeniyle because they give bright and soft properties to textile fabrics. Viscose fibers were preferred in this study due to their characteristics such as absorbing more moisture and being more compatible with human body (Özgüney et al. 2006).

In recent years, many studies have been carried out on the application of graphene based nanomaterials to textile fabrics in order to obtain conductive textile structures. Graphene; It is a two dimensional carbon allotrope with the thickness of an atom formed by the arrangement of carbon atoms in a hexagonal structure in one plane (Çakmak et al. 2017). Due to its two-dimensional structure, flexibility shows superior mechanical, electrical, thermal, optical and opticalelectronic properties (Qu et al. 2014). It is also preferred by researchers because it is reliable in terms of environment and human health and easy to produce and process (Molina et al. 2013a; Molina et al. 2013b; Karimi et al. 2016; Sahito et al. 2016). In the studies, graphite particles are first synthesized by the Hummer method and graphene oxide (GO) suspensions prepared at certain concentrations are applied to woven or knitted fabrics by impregnation method at certain temperatures and durations (Gu and Zhao 2011). GO impregnated and dried fabrics are then subjected to reduction using a certain reducing agent such as $NaBH_4$, N_2H_4, $C_6H_8O_6$, $Na_2S_2O_4$ and NaOH under the specified temperature and time. The two-step process of impregnation and subsequent reduction is not practical and environmentally friendly, since it is not a simple and easily applicable process and requires the use of reducing agents with toxic properties. Both impregnation and reduction processes result in high water consumption and waste water generation. In this study, a more environmentally friendly reducing agent such as PSS was obtained and reduced GO was obtained by a single step process and thus a more environmentally friendly material was used.

Nanosuspension containing reduced graphene oxide (rGO) for conductive yarn production was controlled to the fiber bundle by a specially designed feed system. After the nanosuspension is applied, the fiber bundle is spun into a yarn. In this way, it is ensured that the nanosuspension penetrates not only the outer region of the yarn but also the inner region. In the method, there is no need to discard the unused solution. Therefore, this method minimizes the problem of chemical waste occurring in impregnation methods.

Analyzes

In this study, the effect of different feed rates on electrical conductivity was investigated and optimum feed amount was determined. In addition, electrical conductivity, strength and elongation properties of yarns treated with reduced graphene oxide (rGO) nanosuspension were investigated. The electrical conductivity of the yarns was realized by using a multimeter device with 2 end points method, and the resistance values representing the inverse conductivity of the yarns were obtained. As the resistance value decreases, the conductivity increases. For resistance measurements, 10 measurements were taken and average values were calculated. The strength and elongation values of the yarn were measured on the Uster Tensorapid tester. The measurement distance of the specimens for strength and elongation values is 500 mm and the average values were determined by taking 10 measurements from the yarns.

RESULTS AND FINDINGS

Electrical Resistance Results

The application of graphene to the viscose fiber bundle was started primarily by investigating the appropriate feed amount and increased from 30000 mL / h to 80000 mL / h. Electrical conductivity could not be measured in the experiments carried out at 50000 mL / h and below, and it was determined that this situation would be caused by insufficient solution. it was observed that the resistance values decreased and the electrical conductivity increased when feeding amount increased from 50000 mL / h to 70000 mL / h. At feed rates above 70000 mL / h, resistance values have tended to increase and conductivity has started to decrease. This is thought to be due to the aggregation of graphene nanoparticles. It was found that the highest resistance and the lowest conductivity values were obtained at 80000 mL / h, which is the highest feed amount. However, the lowest resistance and highest conductivity were observed at 70000 mL / h feed amount. As can be seen from the results listed in Table 1, it was observed that the variation in resistance values decreased with increasing feed amount except 60000 mL / h feed amount and more homogeneously distributed measurement results were obtained.

Table 1. Resistance Results of Viscose / rGO / PSS Yarns Produced at Different Feed Rates

Feed Rates (mL/h)	Average Resistance (MΩ/cm)	Standard Deviation	CV (%)
50000	3,63	1,22	0,34
55000	2,08	0,98	0,47
60000	2,25	1,49	0,66
65000	2,05	0,63	0,31
70000	1,57	0,40	0,26
75000	2,05	0,34	0,17
80000	5,86	0,67	0,11

Strength and Elongation at Break Results

With the method developed in the study, rGO nanosuspension was applied to viscose fibers. In order to determine whether the yarns have sufficient strength and elongation properties to be used in fabric production processes such as weaving and knitting, the tensile properties of the obtained yarns were analyzed. The nanosuspension was not applied and the strength and tensile elongation properties of the yarns produced under the same conditions were examined and the results were compared. When the strength results of the yarns were examined, it was determined that viscose-free viscose yarns had values between 16,206 RKM and graphene-containing yarns between 14,013-17,783 RKM. Therefore, it is considered that the strength values of these yarns are comparable to each other. After graphene application, it was observed that the strength values of the yarns tended to increase and decrease depending on the feed amount. When the break elongation results of the yarns were examined, a similar tendency was found to the yarn strength. It was observed that the rupture elongation values of viscose yarns with rGO nanosuspension applied 14,960% and 11,800-14,960% of rGO applied yarns were observed. Consequently, it has been concluded that the conductive yarns produced by the alternative method have yarn flexibility comparable to viscose yarns. On the other hand, it was determined that the elongation at break values tended to increase and decrease as rGO feed amount increased.

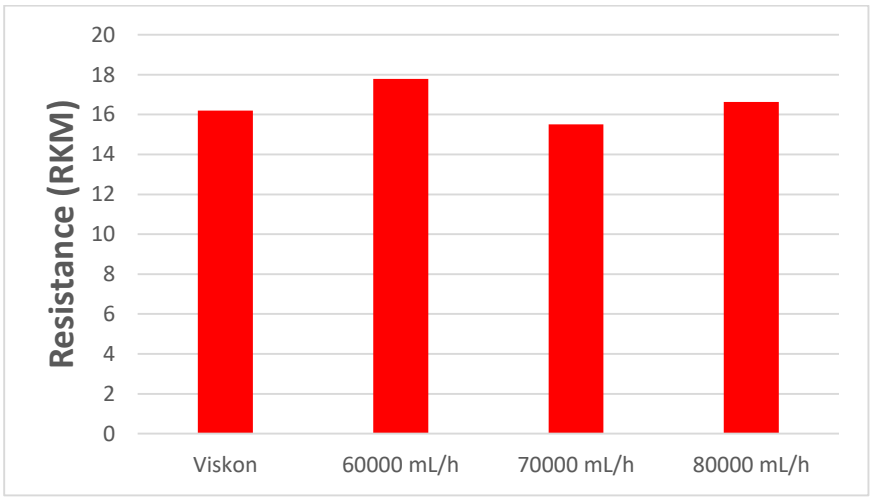

Figure 2. Yarn Strength Results of Viscose Yarns Applied to rGO Nanosuspension

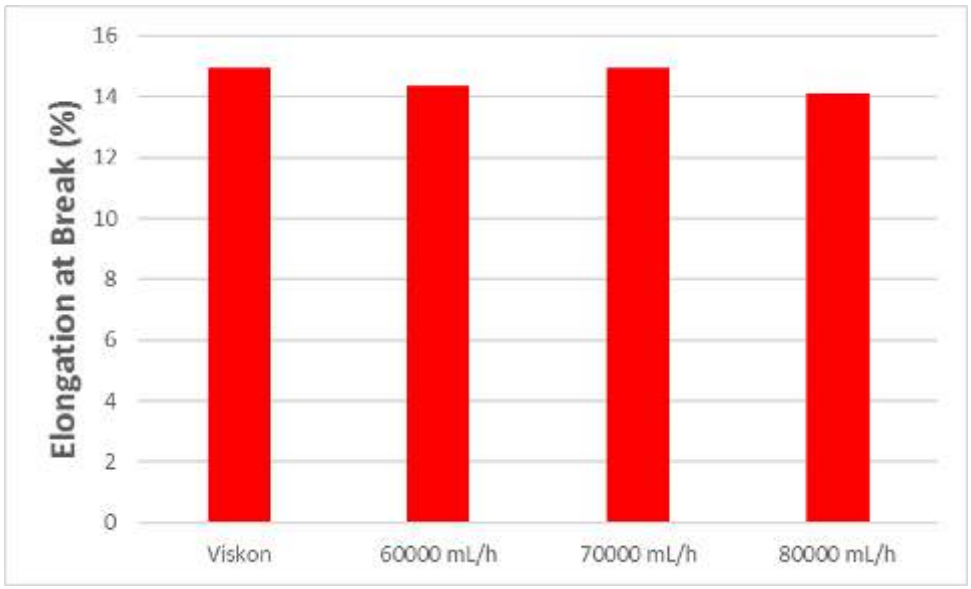

Figure 3. Breaking Elongation Results of rGO Nanosuspension Applied Viscose Yarns

CONCLUSION

Electronic textiles (e-textiles), which emerged from the merger of textiles with electronics, have become a major field of study with high added value, making life easier and brought by the age of technology. In the field of health; to be able to remotely control the health status of patients without fatigue, blood pressure, respiration, etc. In addition to the vital elements such as measuring body functions, determining the life functions and places of the soldiers in the military field, the garments with mp3 player or touch screen that make daily life easier and more enjoyable are no longer a dream, and nowadays can be produced. Although the

majority of these products are still in the experimental stage, production has become a source of inspiration for many fields of study and is still under investigation. Many methods are used to obtain conductive textiles. Although these methods meet the expected conductivity performances according to their application areas (fabric antennas, sensors, etc.), they still have some problems in terms of being a low cost, simple and easy to apply method, maintaining electrical stability against various effects and user comfort. Therefore, there is a need to develop alternative new methods. In this study, an alternative method was developed based on making a conductive solution and conducting each fiber forming the textile structure before yarn and fabric production. In the developed method, water consumption and wastewater formation problems caused by the use of less conductive solution compared to other existing methods have been tried to be minimized. As the conductive material, reduced graphene oxide (rGO) produced by a single step process was used. By the alternative method, rGO-containing nanosuspension was applied to viscose fibers and the conductivity values of the yarns were determined by two-end point method and electrical resistance values were found to vary between 1,51-5,86 MΩ / cm depending on the conductor solution feed amount. It was determined that the strength and elongation properties of the yarns were comparable to those of nanosuspension non-applied viscose yarns.

RECOMMENDATIONS

With the development of technology, textile, space, health, such as areas have come a long way, although rapidly depleting energy sources, is highly thought-provoking. Therefore, sustainable and innovative methods are needed. In particular, the chemicals used in the textile sector are highly harmful to the environment and therefore the ecosystem is damaged. For this reason, it is very important to use environmentally friendly materials and methods that are safe for human health. The study is in the initial stage and it is considered that there is a need to conduct experiments with different materials in order to increase the conductivity by decreasing the resistance values and to evaluate the performance and garment comfort related properties of the surfaces to be obtained from the yarns.

ACKNOWLEDGEMENT

This study was carried out by Süleyman Demirel University Scientific Research Projects Management Unit with the support of FYL-6955.

REFERENCES

Anderson, K. S. A. M., & Seyam, A. M. (2004). The road to true wearable electronics. *TEXTILES MAGAZINE*, *31*(1), 17-22.

Aniołczyk, H., Koprowska, J., Mamrot, P., & Lichawska, J. (2004). Application of electrically conductive textiles as electromagnetic shields in physiotherapy. *Fibres & Textiles in Eastern Europe*, (4 (48)), 47-50.

Çakmak, N. K., Temel, Ü. N., & Yapıcı, K. (2017). Grafen oksit-su nanoakışkanlarının reolojik davranışlarının incelenmesi. *Cumhuriyet Science Journal*, *38*(4), 176-183.

De Rossi, D., Della Santa, A., & Mazzoldi, A. (1999). Dressware: wearable hardware. *Materials Science and Engineering: C*, *7*(1), 31-35.

De Rossi, D., Carpi, F., Lorussi, F. E. D. E. R. I. C. O., Paradiso, R., Scilingo, E. P., & Tognetti, A. (2005). Electroactive fabrics and wearable man-machine interfaces. *Wearable electronics and photonics*, 59-80.

Ermes, M., Pärkkä, J., Mäntyjärvi, J., & Korhonen, I. (2008). Detection of daily activities and sports with wearable sensors in controlled and uncontrolled conditions. *IEEE transactions on information technology in biomedicine*, *12*(1), 20-26.

Gu, W. L., & Zhao, Y. N. 2011. Graphene Modified Cotton Textiles, In Advanced Materials Research, 331, 93-96.

Gregory, R. V., Kimbrell, W. C., & Kuhn, H. H. (1989). Conductive textiles. *Synthetic Metals*, *28*(1-2), 823-835.

Karimi, L., Yazdanshenas, M. E., Khajavi, R., Rashidi, A., & Mirjalili, M. (2016). Functional finishing of cotton fabrics using graphene oxide nanosheets decorated with titanium dioxide nanoparticles. *The Journal of The Textile Institute*, *107*(9), 1122-1134.

Lu, G., Li, X., & Jiang, H. (1996). Electrical and shielding properties of ABS resin filled with nickel-coated carbon fibers. *Composites Science and Technology*, *56*(2), 193-200.

Mazzoldi, A., De Rossi, D., Lorussi, F., Scilingo, E. P., & Paradiso, R. (2002). Smart textiles for wearable motion capture systems. *AUTEX Research Journal*, *2*(4), 199-203.

Molina, J., Fernández, J., Del Rio, A. I., Bonastre, J., & Cases, F. (2013). Chemical and electrochemical study of fabrics coated with reduced graphene oxide. *Applied Surface Science*, *279*, 46-54.

Molina, J., Fernández, J., Inés, J. C., Del Río, A. I., Bonastre, J., & Cases, F. (2013). Electrochemical characterization of reduced graphene oxide-coated polyester fabrics. *Electrochimica Acta*, *93*, 44-52.

Özgüney, A. T., Körlü, A. E., Bahtiyari, İ., & Bahar, M. (2006). Viskon Liflerinin Fiziksel Özellikleri ve Makromolekülerüstü Yapısı. *Tekstil ve Konfeksiyon*, *2*(2006), 100-104.

Stoppa, M., & Chiolerio, A. (2014). Wearable electronics and smart textiles: a critical review. *sensors*, *14*(7), 11957-11992.

Pomfret, S. J., Adams, P. N., Comfort, N. P., & Monkman, A. P. (1999). Advances in processing routes for conductive polyaniline fibres. *Synthetic metals*, *101*(1-3), 724-725.

Qu, L., Tian, M., Hu, X., Wang, Y., Zhu, S., Guo, X., ... & Tang, X. (2014). Functionalization of cotton fabric at low graphene nanoplate content for ultrastrong ultraviolet blocking. *Carbon*, *80*, 565-574.

Sahito, I. A., Sun, K. C., Arbab, A. A., Qadir, M. B., Choi, Y. S., & Jeong, S. H. (2016). Flexible and conductive cotton fabric counter electrode coated with graphene nanosheets for high efficiency dye sensitized solar cell. *Journal of Power Sources*, *319*, 90-98.

Stoppa, M., & Chiolerio, A. (2014). Wearable electronics and smart textiles: a critical review. *sensors*, *14*(7), 11957-11992.

Ueng, T. H., & Cheng, K. B. (2001). Friction core-spun yarns for electrical properties of woven fabrics. *Composites Part A: Applied Science and Manufacturing*, *32*(10), 1491-1496.

Weng, W., Chen, P., He, S., Sun, X., & Peng, H. (2016). Smart electronic textiles. *Angewandte Chemie International Edition*, *55*(21), 6140-6169.

A RESEARCH ON SOUND WAVES AND FIRE EXTINGUISHING SYSTEMS

Mustafa ALTIN

Konya Teknik Üniversitesi, Teknik Bilimler M.Y.O., İnşaat Bölümü, Konya, maltin@ktun.edu.tr

Sümeyye Hasibe KARA

Konya Teknik Üniversitesi, Mühendislik ve Doğa Bilimleri Fakültesi, İnşaat Mühendisliği Bölümü, Konya, hasibesumeyyekara@gmail.com

ABSTRACT: Fire, like an earthquake, is an event that is unclear where and when it will occur, resulting in disaster and is usually a chain of neglect. Fires are mostly resulted from by unpredictable situations such as electricity leakage, gas leakage and neglect. Late-intervention fires can result in loss of life and property. Therefore, early intervention is very important. When a fire occurs, it should be detected as quickly as possible, people should be evacuated and the fire should be intervened. In this study; the basic features of sound have been examined, investigations have been conducted on fire extinguishing systems that use sound waves unlike conventional fire extinguishing systems, and recommendations have been made for the extinguishing mechanism. This mechanism aims to intervene in the fire immediately and without the need for human evacuation.

Key Words: Sound waves, Fire Extinguishing, Frequency, Active Fire Extinguishing Systems

SES DALGALARI VE YANGIN SÖNDÜRME SİSTEMLERİ ÜZERİNE BİR ARAŞTIRMA

ÖZET: Yangın aynı deprem gibi nerede ve ne zaman olacağı belli olmayan, felaketle sonuçlanan ve genellikle ihmaller zinciriyle oluşan bir olaydır. Yangınlar çoğunlukla elektrik kaçağı, gaz kaçağı, ihmal vb. gibi öngörülemeyen durumlardan kaynaklanır. Geç müdahale edilen yangınlar ise can ve mal kaybına neden olabilir. Bundan dolayı erken müdahale çok önemlidir. Bir yangın meydana geldiğinde mümkün olduğunca çok çabuk tespit edilmeli, insanlar tahliye edilmeli ve yangına müdahale edilmelidir. Bu çalışmada; sesin temel özellikleri irdelenmiş, geleneksel yangın söndürme sistemlerinden farklı olarak ses dalgaları kullanan yangın söndürme sistemleri üzerine araştırmalar yapılmış ve söndürme mekanizması için önerilerde bulunulmuştur. Bu mekanizma ile yangına anında ve insan tahliyesine gerek kalmadan müdahale edilmesi amaçlanmaktadır.

Anahtar sözcükler: Ses dalgaları, Yangın söndürme, Frekans, Aktif yangın söndürme önlemleri

GİRİŞ

Yangın, gerekli önlemler alınmadığı takdirde can ve mal kaybına sebep olan önemli bir afettir. Gelişen teknoloji ve sanayileşmenin artması, nüfusun giderek çoğalmasına paralel olarak toplu yerleşim bölgelerinin fazlalaşması, yangın riskinin ve buna bağlı olarak yangının maddi ve manevi zararlarının artışına sebep olmaktadır. Bu sebeple yangın güvenliği adına tüm önlemler alınmalıdır (Ali M. A., 2017). Yangın güvenliği; ölüm, yaralanma ya da maddi hasara neden olan bir yangının çıkma olasılığını azaltmaya yönelik önlemler bütünüdür. Bu önlemler, canlıların yangın yerinden kolaylıkla uzaklaşmaları ve olaydan olabildiğince az zararla kurtulabilmelerini sağlamayı da amaç edinir. Yangın güvenliği önlemleri inşaat sürecinde ele alınabildiği gibi, var olan bir yapıya daha sonra da uygulanabilmektedir (Gültek M., 2005).

Yangın güvenliğinde öncelik yangının hızlı algılanması ve yangına hızlı müdahale edilmesi konularına verilmelidir. Bu tarz istekleri karşılayan sistemlere yangın algılama sistemleri denir. Binalara bu sistemlerin tesis edilmesi gerekmektedir. Yangın güvenliği ile ilgili bu sistemler sayesinde yangın hızlı olarak algılanmakta ve hızlı müdahale edilerek oluşacak maddi ve en önemlisi manevi kayıpların önüne geçilebilmektedir (Gültek M., 2005).

Yangın güvenliğinde ikinci sırayı yangın söndürme sistemleri alır. Geleneksel yangın söndürme sistemleri gerek yangın bölgesindeki ekipmanlara zarar vermesi gerekse insan sağlığı için risk oluşturması bakımından dezavantajlıdır. Ayrıca yangın olması durumunda müdahale için insan gücüne ihtiyaç duyar (Gültek M., 2005).

Geniş bir kullanım alanına sahip olan sesin değişik alanlarda kullanımı her geçen gün daha da artmaktadır. Son yıllarda ortaya çıkan kullanım alanlarından biri ise yangın söndürme sistemlerinde sesin kullanımıdır. Geleneksel yangın söndürme sistemlerinin dezavantajlarını bertaraf etmek adına ses dalgalarının kullanımı yangın söndürme sistemlerine yeni bir soluk getirecektir.

Sesin yangın söndürme sistemlerinde kullanımı dünyada yok denecek kadar azdır. Bununla ilgili yapılan çalışmalardan ilki; DARPA' nın (Amerikan Savunma Bakanlığı İleri Araştırma Projeleri Ajansı) yangını akustik yöntemlerle söndürecek bir alet geliştirmesidir. Bu proje ile yangın başlar başlamaz hızla söndürmenin en iyi yolu bulunmaya çalışılmıştır. Sonuç olarak ses ile yangın söndürmek son deneylere göre mümkün görülmüştür. Yangın söndürücü iki güçlü hoparlör ve belirli frekansta verilen ses sayesinde yanma işlemi bozulmakta ve yangının bileşenlerinden olan oksijen kesilerek yangının sönmesi mümkün olmaktadır. Şekil 1 ve Şekil 2 de yapılan deneysel çalışmalara ait görüntüler yer almaktadır. Ses dalgaları ilk olarak hava akış hızını artırmakta, hız yükseldikçe alev sınır tabakasında incelme olmaktadır. Yanma sıcaklığı sesin ısıyı düzenli dağıtmasıyla azalmakta, yanma işlemi zorlaşmakta ve yangın sönmektedir. Ancak, günlük uygulamalarda yangınları söndürmek için pratik bir aygıt henüz geliştirilememiştir (URL 3, 2012).

Şekil 1. Belli Frekanstaki Ses Dalgalarının Gönderimi (URL 3, 2012)

Şekil 2. Saniyeler içerisinde alevin söndürülmesi (URL 3, 2012)

Yapılan çalışmalardan bir diğeri ise; Viet Tran ve Seth Robertson' ın nesneleri etkileyenin mekanik ses dalgası olduğu düşüncesi ile geliştirmiş olduğu dalga söndürücüdür. Tran ve Robertson yanan malzeme ve çevresindeki oksijeni, ses dalgaları ile ayırt ederek ve bu ikisi arasındaki reaksiyonu durdurarak yangını söndürmeyi hedeflemişler. 30 ve 60 Hertz arasında düşük frekansların yangınlara etki eden en etkili frekans olduğunu tespit etmişlerdir. Böylece yangında ses dalgalarına odaklanarak bir ses üreteci, bir amplifikatör, güç kaynağı ve tüp bir kartondan oluşan dalga söndürücüyü üretmişlerdir. Bu teknolojinin en önemli avantajlarından biri herhangi bir kimyasal madde ya da suya gerek duymadan yangınla müdahalenin mümkün olmasıdır. Ancak dalga söndürücü sadece kimyasal kaynaklı küçük alevler üzerinde test edilmiştir. Geniş bir uygulama yelpazesi için kullanılacak teknolojinin geliştirilebileceğini belirtmişlerdir. Örneğin, benzer bir cihazın küçük yangınları durdurmak için mutfak davlumbazına monte edilebileceğini ya da uzay istasyonlarındaki yangınları söndürmek için astronotlar tarafından kullanılabileceğini belirtmişlerdir (URL 2, 2015).

Yangın

Yanma; yanıcı madde ve gazların hızlı oksidasyonuyla ısı ve ışık üretimidir. Başka bir ifade ile yanma, malzemenin hidrojenden kurtulması ve oksijenin emilimini sağlayan sıcaklık ve akkor hale gelme olayıdır (İplikçi E., 2006).

Yanmanın başlayabilmesi için, yanıcı madde, oksijen ve ısının bir arada bulunması gerekir. Yanma süreci bu üç bileşen olmadan meydana gelmez (Şekil 3). Yangın bileşenleri olan yanıcı maddenin cinsi, miktarı ve dağılımı, oksijen veya havanın oranı, hava büyüklüğü, rüzgârın varlığı ve ısı transferi gibi faktörler yangının yayılmasını etkilemektedirler. Yangının başlangıç, gelişme ve sonuç safhalarında ayrı ayrı davranış biçimleri ve tehlikeler oluşmaktadır (URL 1, 2005).

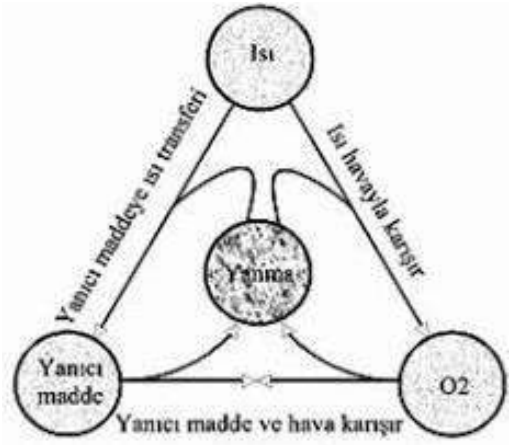

Şekil 3. Yangın üçgeni (İplikçi E., 2006)

Ses Kavramı

Ses dediğimiz olgu, hareketin meydana getirdiği bir üründür. Diğer bir değişle ses, bir objenin (cismin) titreşimleriyle oluşan bir enerji türüdür. Hareket eden her hangi bir madde havada titreşimler oluşturur, bu titreşimlerin yarattığı etki sestir. Titreşim ise, bir cismin yaptığı ileri, geri, küçük ve çok hızlı harekettir (Yılmaz S., 2008). Sesin oluşması için titreşim ve iletken madde gerekmektedir. Ses dalgaları her türlü iletken maddeler üzerinde değişik hızlarda yol alır (Olesik S., 2000). Ancak iletken maddelerin sesi iletebilecek nitelikte esnek olması şarttır. Bir nesnenin her titreşmesinde, titreşimin bir kısmı sese dönüşerek bir parça enerji kaybına neden olur. Sesin yol alabilmesi için

bir ortam gereklidir. Bu ortam katı, sıvı, ya da gaz olabilir. Ses dalgası ortamda sıkışıklık ve seyreklik bantları oluşturarak ilerler. Sıkışıklık bantları ortam basıncına göre artmış, seyreklik bantları ise azalmış basınç alanlarını ifade eder. Birbiri ardına gelen iki sıkışıklık bandının pik noktaları arasındaki mesafe dalga boyu (l), dalganın birim zamandaki tekrarlama sayısı ise frekans (f) olarak tanımlanır. Sesin ortamdaki hızı (V) ses dalgasının dalga boyu ile frekansının çarpımına eşittir (V = l × f) (Yılmaz S., 2008).

Sesin Özellikleri

Sesin Tizliği

Sesin tiz veya pes oluşunu belirlemek için sesin frekansları kullanılır. Bir sesin tizliği, o sesin dalgasının frekansı ile ölçülür. Bunun hesaplanması için sesin saniyedeki frekansı bulunur. Frekanslar yükseldikçe ses incelir alçaldıkça ses kalınlaşır. Şekil 4de seslerin dağılım şekilleri görülmektedir (Yılmaz S., 2008).

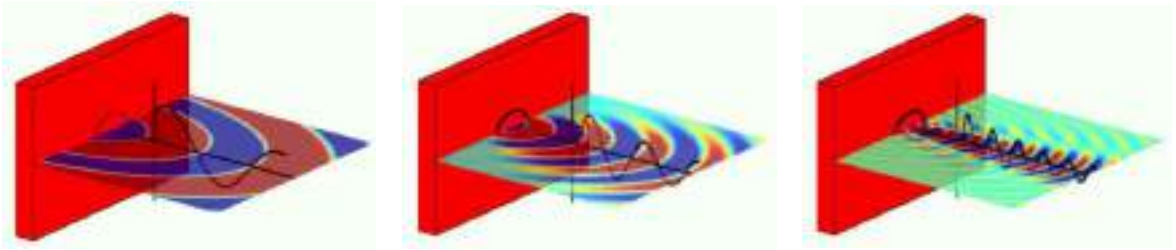

a. Pes sesler **b. Midi sesler** **c. Tiz Sesler**

Şekil 4. Seslerin dağılım şekli (Özen A., 2012)

Sesin Gürlüğü (Desibel Oranı)

Sesin gürlüğü titreşim genişliğine bağlıdır, ses dalgalarının genliği arttıkça, sesin yüksekliği artar. Ses şiddeti desibel (dB) cinsinden ölçülür. Frekansı 30 Hz' den az ve 15.000 Hz' den fazla olan seslerin duyulması sesin şiddeti ve yüksekliğine bağlıdır (Yılmaz S., 2008).

Sesin Şiddeti

Sesin şiddeti; santimetre kare basına düşen güç olarak tanımlanmaktadır. Şiddet belirli bir alanda belirli bir sürede akan enerji akımını ifade eder. Birimi watt/cm^2/sn'dir. Tanısal US cihazlarının şiddeti 1-40 miliwatt arasında değişmektedir (Yılmaz S., 2008).

Hiper Sonik Ses

Günümüzde kullanılmakta olan geleneksel hoparlörler sadece bir noktaya yayın yapacak şekilde odaklanamazlar. Yaptıkları yayını etki mesafesinde bulunan tüm kişiler duyabilirler. Hiper Sonik Ses (HSS) ise normal ses dalgası gibi her yöne yayılmayıp, lazer ışını gibi doğrusal olarak hareket eder. Ultrasonik ses bir insana çarptığında yavaşlar ve dalgalar değişerek bir araya gelir. Yayının tam karşısında duran bir kişi sesleri bir kulaklıktan duyuyormuş gibi dinler. Yayının karşısındaki kişi alanın dışına çıktığında hiçbir şey duyamaz. Böylelikle kişiye özel ses iletimi gerçekleştirilebilir (Yılmaz S., 2008).

Sesin havadaki yayılma hızı 332 m/s' dir. Sıcaklık arttıkça sesin hızı da artar. Sıcaklık artışı moleküllerin titreşim hızlarını arttırır, dolayısıyla sesin yayılma hızının artmasına sebep olur. Sıcaklıktaki bir derece artışa karşın 0,6 m/s' lik bir hız artışı görülür. 20°C' de ses, havada 344 m/s hızla hareket eder (Yılmaz S., 2008).

Bazı ortamlarda sesin yayılma hızı değerleri Tablo 1'de verilmiştir.

Tablo 1. Bazı ortamlarda sesin yayılma hızı değerleri (Yılmaz S., 2008)

Ortam	Sesin Yayılma Hızı (m/s)
Hava	332
Su	1454
Tahta	3828
Demir	5103
Taş	5971

Ses dalgasının dalga boyu sesin hızı kullanılarak hesaplanabilir. Hızın frekansa oranı dalga boyuna eşittir. (Yılmaz S., 2008). Ses kaynağından çıkıp yayılan ses dalgaları sert bir yüzeye çarptığında doğrultusunu ve yönünü değiştirir. Bu olaya sesin yansıması denir. Sesin yansıma özelliğinden yararlanılarak uzaklıklar ölçülebilir. Ayrıca sesin yansıma özelliğinden denizdeki balık sürülerinin yerleri, okyanus derinlikleri, uçakların yüksekliği ve bazı maddelerdeki bozukluklar tespit edilebilir. Ses dalgaları bir yüzeye çarpıp yansıyarak tekrar duyulmasına yankı denir. Yankı olayı dağ yamaçlarında, boş odalarda, spor salonları gibi yerlerde gerçekleşir; küçük kapalı yerlerde (3-5 m mesafeden) fark edilmez. Yankı olayının gerçekleştiğinin anlaşılabilmesi için ses kaynağı ile sesin çarptığı engel arasındaki uzaklık hava

ortamında en az 17 m olmalıdır. Şekil 5'de da görüleceği gibi ses kaynağından yayılan ses dalgaları hem doğrudan hem de farklı yüzeylerdeki yansımaları - yankılanmaları sonucu kulağa gelir. Ses kaynağı ile yüzey arasındaki uzaklık 17 m' den daha az olursa kaynaktan yayılıp kulağa gelen ses ile yankılanma - yansıma sonucu kulağa gelen ses birbirinden ayırt edilemez (Yılmaz S., 2008).

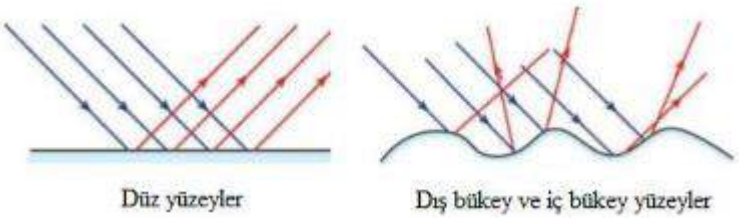

Şekil 5. Farklı yüzeylerde sesin yansıması (Arslan M. A., 2018)

Sesin Kırılması

Ses kırılması, ses dalgalarının bir engelle karşılaştığında yön değiştirmesi olayına denir. Engelin boyutları ve dalganın boyuna göre farklılık gösterir. Sesin dalga boyu eğer bir engelin boyutlarından büyükse kırılma olayı meydana gelir. Kırılma genellikle düşük frekanslarda söz konusu olup, köşe, kolon, kiriş ve duvarlar gibi engellerde bükülerek uzaklaşır ya da dağılır. Yansıtıcı özelliğe sahip, küçük, üniform ve düz yüzeylerde ise istenmeyen kırılma etkileri oluşabilir (Arslan M. A., 2018).

Sesin Soğrulması

Ses kaynağından çıkan ses dalgaları katı bir yüzeye (engele) çarptığında ses dalgalarının bir kısmı yüzey tarafından soğrulur, bir kısmı iletilir, bir kısmı da yüzey tarafından yansıtılır. Ses dalgaları katı yüzeye çarptığında bir kısmı soğrulduğu için yüzeyin diğer tarafına iletilen ses dalgalarının şiddeti azalır. Maddelerin sesi soğurma özellikleri farklıdır. Sert yüzeyli cisimlerin sesi soğurma özelliği olmayıp sesi yansıtırken, yumuşak ve pürüzlü yüzeyler ise sesi daha fazla soğurur (Özen A.,2012).

Sesin Farklı Ortamlarda Yayılması

Ses katı, sıvı ve gazlarda farklı hızlarda yayılır ve aynı zamanda ses bir ortamdan diğer bir ortama kolaylıkla ve iyi bir şekilde geçemez. Bir tuğla duvara vurulduğu zaman çok az miktarda ses enerjisi havada diğer ortama geçebilir, ses enerjisinin büyük bir kısmı duvardan geri yansır. Boş alanlarda ve özellikle tünellerde ses dalgaları eko yaparak tekrar geri yansır. Eko bazı durumlarda çok ise yaramasına rağmen bazı durumlarda sıkıntıya yol açar. Kütüphane, restaurant ve bunun gibi topluluk alanları sessiz olmalıdır. Bu nedenle bu tür alanlar yumuşak ve engebeli malzemelerle yapılmalıdır. Bunun nedeni bu tür malzemelerin ses dalgaları emmesidir. Bunun yanında konser alanları, konferans salonları gibi alanlar sert ve pürüzsüz malzemeler kullanılarak yapılmalıdır. Böylelikle ses dalgalı emilmeden salonun her tarafına eşit

olarak yayılabilir. Bazı düz pürüzsüz malzemelerle yapılmış alanlarda eko oluşmaz. Bunun nedeni çok yüksek frekanslarda ses titreşimlerinin ultra ses üretmesidir. Havada ses dalgaları görünmez fakat bunların bıraktığı etki görülür. Buna örnek olarak bir plakaya vurulduğu zaman plakada bir titreşim meydana gelir. Burada plakanın titreşimi aynı zamanda plakanın etrafındaki havada da titreşim meydana gelmesi anlamına gelir. Havadaki bu küçük titreşim hareketi (ses dalgası) çok hızlı bir şekilde havada tüm yönlere doğru yayılır (Yılmaz S., 2008).

Ses ile İlgili Ekipmanlar

Müzikal enstrümanlar, işitme yardımcıları, sonar sistemler ve yayın ekipmanları ses oluşturan veya sesi kullanan ekipmanlardır. Bunların çoğu mikrofon ve hoparlör gibi elektro akustik dönüştürücü olarak kullanırlar (Özen A., 2012).

Mikrofon

Mikrofon, ses dalgalarını elektriksel titreşimlere çeviren, elektro akustik bir cihazdır. Bir ses dalgasındaki titreşimlerin elektriksel benzeri olan sinyali üretmeye yarayan birçok fiziksel prensip vardır. Bunlar, bağlantı direncinin değişimi, piezoelektrik, elektromanyetik ve manyetostriksiyon prensiplerini içine alır. Bütün bu prensipler ve diğerleri yıllarca denenmiş, ancak sonunda piezo-elektrik, elektromanyetik, elektrostatik ve kapasitif prensipleri uygulamaya konmuştur (Özen A., 2012). Bütün mikrofonlar ses dalgalarına tepki gösteren çeşitli şekillerde yapılmış diyafram veya benzeri bir elemana sahiptir. Mikrofona gelen ses dalgaları diyaframa çarpar ve ses basıncındaki değişikliklere göre diyafram içe veya dışa doğru hareket ederek mekanik titreşim yapar. Bu titreşimler sonucunda mikrofonun çıkış uçlarında bir gerilim meydana gelir. Çıkış uçlarında meydana gelen gerilim, hareket eden parçanın hızı veya titreşimlerinin genliği ile orantılıdır (Özen A., 2012).

Hoparlör

Hoparlör, elektrik akımı değişimlerini ses titreşimlerine çeviren alettir. 1920 yıllarında elektrikli ses dalgalarının kaydedilip yayınlanmasına imkân sağlayan buluşlar ortaya çıktı. Bu buluşların neticesinde ilk hoparlör 1924-1925 yıllarında yapılmıştır. Chester W. Rice ve Edward W. Kellogg tarafından yapılan çalışmalar hoparlörü geliştirdi. Bu iki bilim adamının ortaya çıkardığı sistem, günümüzde önemli değişikliğe uğramamıştır (Özen A., 2012).

Çalışma şekillerine göre elektrodinamik, magnetostatik, elektrostatik ve elektromanyetik hoparlör olmak üzere dört tip hoparlör vardır. Hareketli bobinli hoparlörler, daire veya elips biçiminde bir diyaframdan meydana gelir. Diyafram ortası ve kenarları boyunca dizilen yaylarla metal bir çerçeveye asılıdır. Diyaframın ortasında sıkıca tutturulmuş silindir şeklinde bir çekirdek ve üstüne sarılı bir ses bobini bulunur. Bobin ve çekirdek bir mıknatısın kutupları arasına yerleştirilmiştir. Mıknatıs olarak günümüzde yumuşak demirden kalıcı mıknatıslar veya seramik maddeler kullanılmaktadır (Özen A., 2012).

YÖNTEM

Ses ile yangın söndürme amacı ile bir dizi deneyler gerçekleştirilmiştir. Şekil 6'da gösterilen deney düzeneği hazırlanmıştır. Deney düzeneğinde şehir elektrik şebekesinden aldığımız enerji kaynağını, frekanslarını istediğimiz gibi değiştirebildiğimiz bir PZT seramik piezoelektrik transdusere bağlayarak ve çıkış olarak piezoelektrik (kristal) hoparlör ile ses frekans devresi tamamlanmıştır. Yangın için ateş kaynağı olarak mum ve çakmak ayrı ayrı kullanılmıştır. İlk olarak hoparlöre 10 cm mesafede mum yerleştirilmiş ve tranduser ile frekans ayarlarını değiştirerek yangın söndürülmesi denenmiştir. Frekans aralıkları değiştirilirken mum sönmüş ve değerleri kaydedilmiştir. Frekans değerleri düşük değerlerde iken mum sönmemiş, frekans değerleri yükseltildiğinde alevlerin arttığı gözlemlenmiştir. Mesafe 15 cm ve 20 cm mesafelere taşınarak deneyler tekrarlanmıştır. Mesafeye göre frekanslarda değişimler olduğu sonucuna gözlemlenmiştir. Aynı deneyler çakmak ateşi ile tekrarlanmış ve buradaki frekanslarda farklılıklar olduğu tespit edilmiştir. Deneysel çalışmaların farklı ateş kaynakları ve farklı mesafelerde yangını söndürme frekansları tespit edildiğinde söndürülebileceği düşünülmektedir.

a.Enerji kaynağı b. Piezoelektrik transduser c. Piezoelektrik hoparlör d. Ateş kaynağı

Şekil 6. Deney düzeneği

SONUÇ ve ÖNERİLER

Günümüzde ses frekansları tarım, tıp, yer tespiti, sanayi, temizlik sektörü gibi birçok uygulama alanında kullanılmaktadır. Ses dalgaları kullanılarak yangın söndürme sistemlerinin geliştirilmesi ile zaman, maliyet, can kaybı ve/veya mal güvenliği açısından geleneksel yangın söndürme sistemlerine kıyasla oldukça avantajlıdır. Ses bombası ile orman yangınlarının söndürülme örnekleri, ses ile ciddi yangınların söndürülebileceğini de gündeme taşımıştır. Orman yangınları gibi doğal afetlerde ve büyük yangınlarda itfaiye birimlerinin ulaşamadığı yerlerde insansız hava araçları ile yangının türüne bağlı olarak ses frekansları ile yangınlara müdahale edilebileceği söylenebilir. Bu sistemlerin yeni bilimsel çalışmalarla desteklenmesi, özellikle yapay zeka tekniklerine adapte edilerek bir sonuca ulaşılabileceği düşünülmektedir. Bu motivasyondan hareketle bilgisayar teknolojileri ve yazılımları kullanılarak özellikle uzman sistemler, yapay sinir ağları uygulamaları ile geliştirilerek çalışmaların hızlandırılmasının uygun olacağı kanısına varılmıştır.

KAYNAKLAR

Ali M. A. (2017). Cam Lif Takviyeli Betonun Yangın Dayanımlarının Çeşitli Parametreler Açısından İrdelenmesi. Yüksek Lisans Tezi. *Selçuk Üniversitesi Fen Bilimleri Enstitüsü*. Konya.

Arslan M. A. (2018). Şekillendirilebilir Isı ve Yalıtım Malzemesinin Geliştirilmesi ve Analizi. Doktora Tezi, *Gazi Üniversitesi Fen Bilimleri Enstitüsü*. Ankara.

Gültek M. (2005). Yangın Güvenliği Çerçevesinde Atriumlu Alışveriş Merkezlerinin Mevzuat Değerlendirmesi ve Örnek Projeler Aracılığı ile Kaçış Yollarının Simülasyonu. Doktora Tezi. *Gazi Üniversitesi Fen Bilimleri Enstitüsü*. Ankara.

Heat Transfer (2005). http//www.firesafetyinfo.org/Environment

İplikçi E. (2006). Binalarda Yangın Güvenlik Önlemlerinin Analizi ve Yangın Güvenlikli Bina Tasarımına İlişkin Performans Kriterlerinin Ortaya Konulması. Yüksek Lisans Tezi. *Gazi Üniversitesi Fen Bilimleri Enstitüsü*. Ankara. Sayfa 5.

Olesik S. (2000). SOUND: "Science Projects." Simon de Pinna, Raintree Steck-Vaughn Publishers: Austin. 36-37.

Özen A. (2012). Ses Kaynağının Yönünün Bulunması ve Kaynağın Kamera ile Takibi. Yüksek Lisans Tezi. *Marmara Üniversitesi Fen Bilimleri Enstitüsü*. İstanbul.

Ses Dalgalarıyla Yangın Söndüren Cihaz- Teknofone (2015). http://www.teknofone.com/ses-dalgalariyla- yangin-sonduren-cihaz-38047/

Sesle Yangın Söndürmek- Bilim ve Teknoloji (2012). https://www.bilim-teknoloji.com/sesle-yangin-sondurmek/

Yılmaz S. (2008). Reflektör Antenin Ses Dalgaları Üzerindeki Etkisinin Araştırılması. Yüksek Lisans Tezi. *Mustafa Kemal Üniversitesi Fen Bilimleri Enstitüsü*. Hatay.

GEMİ KAYNAKLI EMİSYONLARIN HESAPLANMASI; İSTANBUL HAYDARPAŞA LİMANI UYGULAMASI

Mahmut AVCI, Yıldız Teknik Üniversitesi Gemi İnşaatı ve Denizcilik Fakültesi, avcim@yildiz.edu.tr

Tarık KOÇAL, Yıldız Teknik Üniversitesi Gemi İnşaatı ve Denizcilik Fakültesi, tkocal@yildiz.edu.tr

Kaan ÜNLÜGENÇOĞLU, Yıldız Teknik Üniversitesi Gemi İnşaatı ve Denizcilik Fakültesi, kunlu@yildiz.edu.tr

ÖZET: Sanayileşmenin artmasıyla ticareti yapılan yüklerin çeşitlenip, miktarının arttığı günümüzde, taşımacılık geçmişte hiç olmadığı boyutlara ulaşmıştır. Taşımacılık sektöründe, düşük maliyet, taşınan mal miktarı ve güvenlik en önemli unsurlardır. Bu sebeplerden dolayı dünyadaki yük taşımacılığının büyük bir çoğunluğu deniz yoluyla yapılmaktadır. Deniz taşımacılığı diğer taşımacılık türlerine göre daha çevrecidir. Ancak uluslararası ticaret hacminin ve dolayısıyla gemi sayılarının artışı, gemi kaynaklı emisyon miktarlarını arttırmıştır. Bu açıdan bakıldığında gemi emisyonları konusu irdelenmesi gereken önemli bir konudur.

Uluslararası Denizcilik Örgütü özellikle SOx, NOx, PM ve CO2 emisyonlarında gemilere sınırlandırmalar getirmektedir. Gemi kaynaklı emisyonların uluslararası kurallar ile sınırlandırılması, gemilerin emisyon takibi ve değerlendirilmesi açısından denizcilik sektörünün yeni teknolojilerle tanışmasını ve büyük bir revizyona gitmesini zorunlu hale getirmiştir. Gemi kaynaklı emisyonların özellikle liman bölgelerinde yüksek değerlerde olduğu, şehir merkezine yakın noktalarda bulunan limanlar için bu emisyonların liman çevresinde yaşayan insanların sağlığını olumsuz yönde etkilediği bilinmektedir.

Marmara bölgesi ve çevresindeki limanlar, İstanbul ve Çanakkale Boğazları, Türkiye için gemi trafiğinin en yoğun olarak yaşandığı bölgelerdir. Bu nedenle bu çalışmada İstanbul Boğazında önemli bir noktada, kent ile iç içe geçmiş durumda bulunan Haydarpaşa Limanı seçilmiştir. 2019 yılı Mart, Nisan ve Mayıs ayları boyunca Haydarpaşa Limanına gelen gemilerin; tipi, inşa yılı, gros tonajı, ana makine güçleri ve devirleri, yardımcı makine güçleri, limana geliş sayıları ve seyir, manevra ve limanda kalış süreleri dikkate alınarak literatürde yer alan emisyon tahmin yöntemleri kullanılarak, geliştirilen web tabanlı veri toplama yazılımı ile NOx, CO2, SO2, VOC, CO ve PM emisyonları hesaplanmıştır.

Anahtar kelime: Gemi kaynaklı emisyon, liman emisyonları, küresel ısınma.

IMPACT OF SVC DEVICES ON POWER SYSTEM LOSSES IN POWER SYSTEM WITHOUT RENEWABLE ENERGY SOURCES

Katarina KECOJEVIĆ
University of Montenegro, Faculty of Electrical Engineering
katarinakecojevic@gmail.com

Ognjen LUKAČEVIĆ
University of Montenegro, Faculty of Electrical Engineering
ognjen.lukacevic96@gmail.com

Martin ĆALASAN
University of Montenegro, Faculty of Electrical Engineering
martinc@t-com.me

ABSTRACT: This paper deals with the investigation of the effect of the SVC devices location on the power system losses in power grid. For these purposes the standard IEEE 9-test bus system was used, while all calculations were carried out in program package GAMS. The optimal value of power losses before and after installation of SVC device shows that the position and power of the SVC device greatly influence the amount of losses in the system.

Key words: SVC, optimal allocation, IEEE 9-test bus system

INTRODUCTION

Flexible AC transmission systems, so-called FACTS devices, can help reduce power flow on overloaded lines. These devices will help in case of power system overload and in case of high power system losses.Furthermore, just like reserach conducted by Mathur and Rajiv demonstrate, the usage of FACTS devices will improve the system stability and security.

SVC is one of the most used parallel FACTS devices nowdays. The main motivations in developing SVCs were for enhancing the operational flexibility of the compensator during large disturbances and for reducing the steady-state losses.

Many recent studies have focused on FACTS devices allocation in power system considering the voltage stability and power system losses. In Shaik and Reddy's

research, a systematic method for finding optimal location of SVC is proposed to improve voltage profile of a power system under normal conditions and under contingency conditions with Artificial Bee Colony (ABC) Algorithm. On the other hand, Belazzoug & Boudour proposed a new technique for the optimal location and design of two kinds of FACTS devices (SVC and TCSC) handling the minimization of transmission losses in electrical network. Using the proposed scheme, the type, the location and the rating of FACTS devices are optimized simultaneously. Similarly, in *FACTS devices allocation for preventive/corrective control against voltage collapse under deregulated power system*, an approach for optimal allocation of FACTS devices under deregulated power systems is presented. In mentioned paper the overall problem is formulated as a mixed integer nonlinear programming problem is solved using hybrid Particle Swarm Optimization. The effectiveness of the proposed approach is demonstrated on modified IEEE 14 bus test system. In *Improvement of voltage stability and reduce power system losses by optimal GA-based allocation of multi-type FACTS devices* a Genetic Algorithm (GA) is presented. Proposed algorithm is tested on IEEE 30 bus power system for optimal allocation of multi-type FACTS devices. Pisica, Bulac, Toma & Eremia presented in their paper *Optimal SVC placement in electric power systems using a genetic algorithms-based method*, a genetic algorithm that tries to identify the optimal location and size of an SVC device. In above mentioned paper, a multi-criteria function is developed, comprising of both operational objectives and investment costs. The computer program is run on a 13 nodes test system, assessing improvements in voltage profile and reducing power losses.

Unlike the available literature researches, in this paper will be observed the impact of SVC devices on power losses observing IEEE 9-test bus system. All testing will be performed by using CONOPT solver embedded in program General algebric Modeling System - GAMS, unlike literature approaches which are dominantly based on the usage of metaheuristic methods.

This paper will be organized in 4 parts. At first, the problem formulation will be given. Secondly, progam GAMS and the IEEE 9-test bus system will be shortly described. The third part will give the optimisation results, obtained in the GAMS, for testing the impact of SVC devices on power losses. Final remarks and conclusion are given in section Conclusion.

PROBLEM FORMULATION

The goal of this paper is to show the influence of SVC on total power loss depending on its location. Therefore, the objective function in optimization process is function which describes the power system losses. The optimal function (OF), is formulated as follows:

$$OF = \sum_{\substack{i,j \in Nb \\ i \neq j}} \left[g_{ij} / 2(V_i^2 + V_j^2 - 2V_iV_j \cos(\delta_j - \delta_i)) \right], \quad (1)$$

where *Nb* is the number of branches of the network; V_i and V_j are the nodal voltages of bus i and bus j respectively; g_{ij} is the conductance of the line *ij*, and δ_j and δ_i are phase angles in the busses *j* and *i*.

The balance equations of active and reactive power in buses are formulated as follows:

$$\sum_g P_{i,t}^g - P_{i,t}^L(i) = \sum_j P_{i,j,t}, \quad (2)$$

$$\sum_g Q_{i,t}^g - Q_{i,t}^L(i) = \sum_j Q_{i,j,t}, \quad (3)$$

where $P_{i,j,t}$ and $Q_{i,j,t}$ represent active and reactive power trough branches, respectively. For the node in which we connect the SVC, (3) will be slightly different. There will be another member on the left side of equality, which is the power of the SVC device Q_{SVC}.

Active and reactive power are formulated as follows:

$$P_{ij} = G_{ij}U_i^2 - U_iU_j[G_{ij}cos(\theta_i - \theta_j - \delta_{ij}) + B_{ij}sin(\theta_i - \theta_j - \delta_{ij})],$$
$$Q_{ij} = -U_i^2(B_{ij} + \frac{B_{Cij}}{2}) - U_iU_j[G_{ij}\sin(\theta_i - \theta_j - \delta_{ij}) + B_{ij}\cos(\theta_i - \theta_j - \delta_{ij})]. \quad (4)$$

PROGRAM GAMS AND IEEE 9-BUS TEST SYSTEM

In this paper the results were obtained using the General Algebraic Modeling System - GAMS program. The GAMS is a modeling tool for mathematical programming and optimization purpose. Like Soroudi said in *Power System Optimization Modeling in GAMS*, it can be used for solving different types of optimization problems. Its efficiency over metaheuristics methods is shown in Ćalasan, Nikitović and Mujović's paper.

In this paper, IEEE 9-bus test system is used as a test network. Graphical view of this network is given in Figure 1. This network consists of three generators and 9 buses.

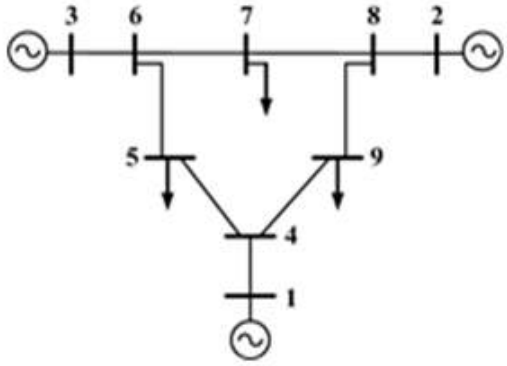

Figure 1. IEEE 9-test bus system

RESULTS

In order to see the impact of SVC devices on power system losses, in this paper, the production of generators, when there are no SVC devices in power network, was optimized. These results are presented in Table 1. After that, all nodes of this network were tested in order to find the optimal value of SVC's reactive power which minimize power system losses. All obtained results are presented in Table 1, too. In this way, the SVC device was found to be optimally located in the ninth node. Also, in this case the minimal value of power losses is 2.242996 MW, which is lower value in comparison with power losses for power network without SVC device for 0.072801 MW. The corresponding optimal value of SVC's reactive power is 28.50485 MVAr.

Table 1. Power losses with and without SVC device in IEEE 9-bus test system

	Power losses [MW]	
without SVC	2.3157972	
Location of SVC in node:	Power losses [MW]	Optimal Q_{SVC} [MVAr]
4	2.3029419	28.3526
5	2.3082493	7.81084
6	2.3157972	32.73094
7	2.3033475	16.99262
8	2.3157972	34.88944
9	**2.242996**	**28.50485**

The optimal value of SVC's reactive power can be also found by testing different values of SVC devices connected in certain node. In Table 2 and on Figure 2 the impact of SVC's reactive power on power losses is presented for node 9. It can be seen that the optimal value of SVC's reactive power is around 30MVAr, what corresponds to results presented in Table 1.

Table 2. Impact Of Q_{SVC} On Power Losses For Node 9

Q_{SVC} [MVAr]	Power losses [MW]	Q_{SVC} [MVAr]	Power losses [MW]
-35	2.641907	10	2.26999
-30	2.579082	15	2.25625
-25	2.521648	20	2.248227
-20	2.469735	25	2.24388
-15	2.423244	30	2.243156
-10	2.382042	35	2.246002
-5	2.346289	40	2.252367
0	2.315797	45	2.266664
5	2.290399	50	2.289301

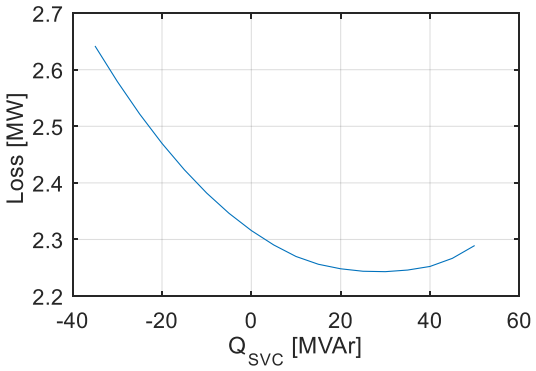

Figure 2. Impact Of Q_{SVC} On Power Losses For Node 9

CONCLUSION

In this paper, program GAMS has been used for finding the optimal placement and sizing of SVC for minimizing power system losses. The proposed approach has been implemented on IEEE 9-bus system without renewable energy sources. It is shown that by using SVC device and with optimal location of SVC device the power losses can be reduced significantly. In the future work, the impact of the optimal location of SVC devices on power losses, in presence of renewable power source, will be observed.

REFERENCES

Mohan Mathur R. & Varna Rajiv K. (2002). Thyristor-Based FACTS Controllers for Electrical Transmission

Systems, *Wiley-IEEE Press, 1 edition.*

Shaik M. R. & Reddy A. S. (2016). Optimal placement and sizing of FACTS device to overcome contingencies

in power systems, *2016 International Conference on Signal Processing, Communication, Power and*

Embedded System (SCOPES), Paralakhemundi, pp. 838-842.

Belazzoug M. & Boudour M. (2010). FACTS placement multiobjective optimization for reactive power system

compensation, *7th International Multi- Conference on Systems, Signals and Devices, Amman, pp. 1-6.*

Wibowo R. S, Priyadi A, Soeprijanto A. & Yorino N. (2011). FACTS devices allocation for

preventive/corrective control against voltage collapse under deregulated power system, *TENCON 2011 -*

2011 IEEE Region 10 Conference, Bali, pp. 918-922.

Baghaee H. R, Jannati M, Vahidi B, Hosseinian S. H & Rastegar H. (2008). Improvement of voltage stability

and reduce power system losses by optimal GA-based allocation of multi-type FACTS devices, *11th*

International Conference on Optimization of Electrical and Electronic Equipment, Brasov, pp. 209-214.

Pisica I, Bulac C, Toma L. & Eremia M. (2009). Optimal SVC placement in electric power systems using a

genetic algorithms based method, *IEEE Bucharest PowerTech, Bucharest, pp. 1-6.*

Soroudi A. (2017). Power System Optimization Modeling in GAMS, *Springer*.

Ćalasan M, Nikitović L. & Mujović S. (2019). *J. Renewable Sustainable Energy 11, 046301;doi:*

10.1063/1.5113902 11, 046301-1.

BENEFITING FROM RAINWATER POTENTIAL in HOUSINGS

Ramazan VAROL, Department of Energy Systems Engineering, Recep Tayyip Erdogan University, 53100 Rize, Turkey, ramazanvaroll@gmail.com

Burak MARKAL, Department of Energy Systems Engineering, Recep Tayyip Erdogan University, 53100 Rize, Turkey, burak.markal@erdogan.edu.tr

ABSTRACT: Water is the most basic requirement for the survival, but incorrect and / or unnecessary usage will result in the problem of depletion of clean water resources in the future. In housings (in bathrooms and toilets), by utilizing rainwater potential instead of clean drinking water coming from plumbing line, both efficient use of clean water resources and reduction of energy consumption can be achieved. In this context, in this study, for the province of Rize, where rainfall potential is high, the calculation of the usage of rain water in houses is made. As an example, a five-storey and fifteen flats residence was selected in Rize province and the potential of rainwater collected on the roof in terms of domestic usage was evaluated according to the annual rainfall regime. The column diagram of the rain water collection system was drawn and the cost analysis was made to calculate the depreciation time.

Key words: the usage of rainwater, importance of water, cost analysis.

KONUTLARDA YAĞMUR SUYU POTANSİYELİNDEN FAYDALANMA

ÖZET: Su, canlılığın devamı için en temel gereksinimdir ancak yanlış ve/veya gereksiz kullanım sonucunda gelecekte temiz su kaynaklarının tükenmesi problemi ortaya çıkacaktır. Konutlarda banyo ve tuvaletlerde, sıhhi tesisat hattından gelen temiz içme suyu yerine yağmur suyu potansiyelinden yararlanılarak hem temiz su kaynaklarının verimli kullanılması hem de enerji tüketiminin azaltılması sağlanabilir. Bu kapsamda, bu çalışmada, yağış potansiyelinin fazla olduğu Rize ili için, yağmur suyunun konutlarda kullanılmasıyla ilgili hesaplama yapılmıştır. Örnek olarak, Rize ilinde beş katlı ve on beş daireli bir konut seçilmiş ve yıllık yağış rejimine bağlı olarak çatıda toplanan yağmur suyunun evsel kullanım açısından potansiyeli değerlendirilmiştir. Yağmur suyu toplama sisteminin kolon şeması çizilmiş ve maliyet analizi yapılarak amortisman süresi hesaplanmıştır.

Anahtar sözcükler: yağmur suyu kullanımı, suyun önemi, maliyet analizi

GİRİŞ

Su, canlılar açısından en önemli doğal kaynaklardan biri olup, biyolojik yaşamın sürekliliğinin sağlanması ve çeşitliliğinin korunması bakımından vazgeçilmezdir. Yeryüzünün yaklaşık olarak dörtte üçü sularla çevrili olup, Alparslan vd. (2008) tarafından belirtildiği üzere dünyadaki suyun %97'si denizlerde, %2'si kutuplarda, %1'i ise karada bulunmaktadır. Yeryüzündeki herhangi bir su kaynağında bulunan su, güneş ışınlarına maruz kaldığında, bir başka ifade ile ısındığında, buharlaşarak atmosfere ulaşır ve soğuk tabakalarla etkileşmesi durumunda, yağmur veya kar olarak tekrar yer yüzene düşer. Bu döngü yaşam boyunca sürüp gitmektedir ancak gereksiz kullanım, plansız nüfus artışı, küresel kirlilik ve benzeri sebeplerle ilgili döngü zarar görmektedir (Alparslan vd., 2008). Alparslan vd. (2008) ve Şahin ve Manioğlu (2011) tarafından da belirtildiği üzere temiz su kaynaklarında yaşanan ve yukarıda bahsedilen problemlerden dolayı ülkeler sürdürülebilir su politikaları uygulamak zorunda kalmaktadır.

Ülkeler su potansiyeline göre sınıflandırıldığında, yılda kişi başına düşen ortalama kullanılabilir su miktarı 1000 m^3'ten az olanlar, su fakiri; 1.000-3.000 m^3 arasında olanlar su sıkıntısı çeken; 3.000-10.000 m^3 arasında olanlar suyun yeterli olduğu, 10.000 m^3'ten fazla olanlar ise su zengini ülkeler olarak adlandırılmaktadır (Alparslan vd.,2008; Şahin ve Manioğlu, 2011).Ülkemizde ise kişi başına düşen kullanılabilir su miktarı yılda 1.500 - 1.600 m^3 olup, su sıkıntısı çeken ülke konumunda bulunmaktayız. Gelecek yirmi yıl içinde ise bu değerin 1042 m^3/yıl'a düşüp, ülkemizin su fakiri ülkeler arasına gireceği beklenilmektedir (Eren vd.,2016; URL-3, 2019). İlgili veriler ve ön görüler ülkemizde su yönetiminin kritik öneme sahip olduğunu belirtmektedir.

Şehirlerdeki temiz su, deniz, gölet ve/veya akarsulardaki suyun çeşitli işlemlerden geçirilerek kullanıma hazır hale getirilmesiyle elde edilmektedir. Kullanım arttıkça, su arıtma tesislerinin ve/veya su depolarının kapasiteleri artırılmakta, böylece ilk yatırım maliyeti ve harcanan enerji miktarı artmaktadır. Bu sebeple, su kaynaklarının daha verimli kullanılmasına katkı sunmak adına evlerde klozet ve helalarda temiz arıtılmış içme suyu yerine yağmur suyu kullanılarak temiz su tüketiminin azaltılmasına katkı sunulabilir. Bu kapsamda yapılan çalışmalardan bazıları aşağı özetlenmiştir:

Yaman (2009) sunmuş olduğu çalışmada, Siemens Gebze Organize Sanayi Bölgesi'nde yeşil bina kapsamında, su korunumuna yönelik yapılan girişimler hakkında bilgi vermiştir. Bu kapsamda, çatıdan toplanan yağmur suyunun yangın sulama tertibatında ve tüm alan içerisinde kullanım suyu olarak değerlendirilmesi, bina dışında ise peyzaj sulamasında kullanılması sağlanmıştır. Erengezgin (2009) yaptığı

çalışmada, Diyarbakır Güneş Evi'nde çatılardan toplanarak su deposuna gelen yağmur suyu ile evsel atık su arıtımından elde edilen suyun, karbon filtreden geçirilerek bahçe sulamasında ve tuvalet rezervuarlarında kullanılmasına yönelik çalışma yapmıştır. Şahin ve Manioğlu (2011) tarafından ise Borusan Oto İstinye Tesisleri'nde çatılardan toplanan yağmur sularının, tuvalet rezervuarlarında, araç yıkamada, bahçe sulamada ve yangın deposunda kullanıldığı belirtilmiştir. Ayrıca, URL-1 (2019)'da, Bursa Gaz Genel Müdürlük Binası'nın çatısındaki yağmur suları ile binanın çevresindeki drenaj sularının biriktirilip filtrelerden geçirilerek depolandığı ve depolanan suyun, yeşil alanların sulanması ve tuvalet rezervuarlarında kullanılmakta olduğu belirtilmektedir.

Bayar (2006), Karabük ili için yapmış olduğu çalışmada, sarnıçlarda toplanan yağmur sularının, dokuz bloklu bir sitenin tuvalet temizliğinde kullanılabilirliğini incelemiş ve amortisman süresinin on iki yıl olacağını belirlemiştir. Eren vd., (2016) Sakarya Üniversitesinin kampüsü içerisinde bulunan binaların çatılarında toplanan suyun yeşil alanların sulanmasındaki kullanılabilirliğini incelemiştir. Kılıç ve Abuş (2018), bir konutun çatısında toplanan yağmur suyunun konut dışı olan su ihtiyaçlarında kullanım potansiyelini incelemiştir. Bu incelemede, su ihtiyacı, su potansiyeli ve maliyet hesabı yapılmıştır.

Yukarıdaki paragraflarda, su yönetiminin önemi vurgulanmış ve temiz su kaynaklarının daha verimli kullanılmasına yönelik yapılan çalışmalar özet halinde verilmiştir. Bu kapsamda, bu çalışmada, Rize ilinde, beş kat ve on beş daireden oluşan bir apartman seçilerek, çatıda toplanacak yağmur sularının banyo ve tuvaletlerde kullanımına yönelik hesaplama yapılmıştır. İlgili tesisatın kurulum maliyeti, ilin su potansiyeli, ihtiyaç duyulan su miktarı ve amortisman süresi hesaplanmıştır.

YÖNTEM VE BULGULAR

Yıllık Yağış Potansiyelin Hesaplanması

Rize ili için yıllık yağış potansiyeli dikkate alınarak elde edilebilecek maksimum yağmur suyu miktarı hesaplanacaktır. Bu kapsamda, URL-4 (2019)'da belirtilen hesaplama prosedürü dikkate alınmıştır. İlgili hesaplama için gerekli olan tanımlama ve veriler aşağıda maddeler halinde verilmiştir:

- Yağmur toplama alanı (YTA): Toplam çatı alanı (470 m^2)
- Yağmur yağış miktarı (YYM): Meteoroloji Genel Müdürlüğünden alınan yıllık yağış miktarı (2296.1l/m^2).
- Çatı katsayısı (ÇK): Alman standartlarına (DIN 1989) göre belirlenen katsayı (0.8). Çatı katsayısı çatıya düşen yağmurun tamamından verim alınamayacağını belirtmektedir.

- Filtre etkinlik katsayısı (FEK):Alman standartlarına (DIN 1989) göre belirlenen katsayı (0.9). Çatıda elde edilen yağmur suyunun, görünen katı maddelerden ayrıştırılması için geçirilen ilk filtrenin verimlilik katsayısıdır. Suyun bir miktarının buradan geçemeyeceğini belirten katsayıdır.

Yıllık yağış potansiyel hesabı = Yağmur toplama alanı x Yağış miktarı x Çatı katsayısı x Filtre etkinlik katsayısı (1)

Tablo 1. Rize İli için yıllara bağlı (1928 - 2018) olarak gerçekleştirilen ortalama akış değerleri (URL-2., 2019)

Aylar	Ocak	Şubat	Mart	Nisan	Mayıs	Haziran	Temmuz	Ağustos	Eylül	Ekim	Kasım	Aralık	Yıllık
Yağış Miktarı Ortalaması (mm)	234.1	185.8	161.3	95.9	96.3	133.1	152.1	194.6	253.1	294.0	256.9	238.9	2296.1

Bu çalışma kapsamında, Rize ilinde on beş daireli bir konut seçilmiştir. Yağmur toplama alanı olarak 470 m^2'lik bir çatı alanı belirlendi. Rize ili için ortalama yıllık yağış miktarı (1918-2018 yılları arasındaki) 2296.1 mm (2296.1 l/ m^2) olarak ölçülmüştür (URL-2 2019). Alman standartları tarafından belirlenen çatı katsayısı ve filtre etkinlik katsayısı ele alınarak hesaplama yapılmıştır. Bu veriler doğrultusunda çatının kapladığı alana düşen yıllık yağış potansiyel hesabı aşağıdaki gibidir:

Yıllık yağış potansiyel hesabı = 470 m^2 x 2296.1 l/ m^2 x 0.8 x 0.9 = 777000.24 litre = 777 m^3

Yıllık İhtiyaç Duyulan Su Tüketiminin Belirlemesi

Yağmur suyu, konutlarda kullanım suyu olarak, kimyasal dezenfeksiyondan geçmeden tuvalet rezervuarlarında kullanılabilmektedir. Konutlarda su kullanımın önemli bir bölümü (yaklaşık %30) tuvalet rezervuarlarında kullanılmaktadır. Bu kapsamda, tuvalet ve banyolardaki rezervuarlarda yağmur suyu kullanılarak şebeke suyundan tasarruf sağlanmış olacaktır. Örnek olarak 15 daireli bir konut seçilmiştir. Her bir dairede, gerçek uygulamalara bağlı kalarak, 4 litre ile tam yıkama yapabilen rezervuarlı klozet ve 13 litrelik rezervuarlı alaturka hela tesisatı kullanıldığı düşünülmüştür. Böylece, tek bir daire için alaturka hela ve klozeti kapsayacak şekilde ortalama su tüketimi 8.5 litre olarak belirlenmiştir. Tek kişinin günlük ortalama 2 kez

tuvalet rezervuarını kullanacağı düşünüldüğünde, kişi başına düşen su tüketimi günlük 17 litre olacaktır. Her bir dairede 4 kişinin yaşayacağı düşünülmüş ve böylece tek bir dairedeki tuvalet rezervuarları için gerek duyulan su tüketiminin 68 litre olacağı belirlenmiştir.

- Apartmanın günlük su tüketimi miktarı: 68 litre/daire x 15 daire = 1020 Litre = 1.02 m^3
- Apartmanın aylık su tüketimi miktarı:1.02 m^3x 30 = 30.6 m^3
- Apartmanın yıllık su tüketimi miktarı: 30.6 m^3 x 12 = 367.2 m^3
- Tesisatta kullanılacak su deposu hacmi belirlenirken, apartmanın aylık su tüketimi ihtiyacı dikkate alınmıştır. Bu kapsamda, 37.5 m^3 hacimli su deposu seçilmiştir.
- Çatı yüzeyine düşen yağmurun su deposuna iletilmesi gerekmektedir. Bunun için çatıda yağmur suyu boru çapı hesabı yapılmıştır (MMO, 2008). İlgili hesaplama için Makine Mühendisleri Odasının Sıhhi tesisat proje hazırlama esasları ve iki yüz on sayılı kitabındaki hesaplama prosedürü dikkate alınmıştır. Yapılan hesap sonucunda beş adet 100 mm çaplı yağmur suyu borusu gerektiği belirlenmiştir.

Su deposu ve rezervuarlara giden su hattı için kolon şeması çizilmiştir. Şekil 1'de verilen kolon şeması dikkate alınarak yağmur suyundan kaynaklı ek maliyet hesabı yapılmış ve Tablo 2'de verilmiştir:

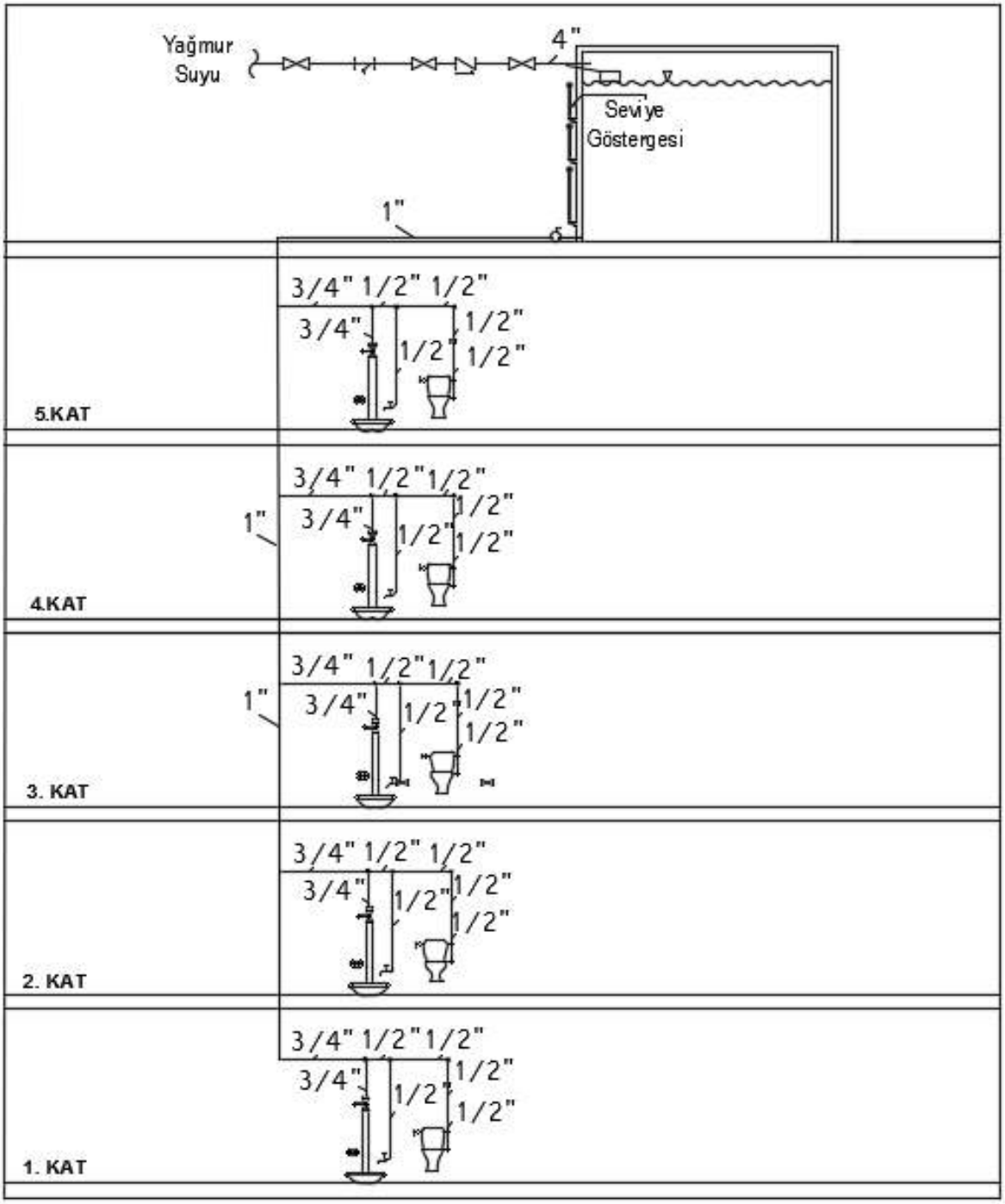

Şekil 1.Tesisat kolon şeması

Tablo.2 Yağmur Hasadının Sistem Maliyeti

Ürün	Özellik / Ölçü	Birim	Miktar	Maliyet (TL)
Prizmatik Modüler Galvanizli Su Deposu	37.5	m^3	1	23.255,98

Polipropilen Temiz Su Borusu	1/2 "	m	40	213,16
Polipropilen Temiz Su Borusu	3/4 "	m	30	267,38
Polipropilen Temiz Su Borusu	1 "	m	40	359,09
PVC Yağmur Suyu Borusu	100 mm	m	30	608,33
Küresel Vana	100 mm	Adet	3	1.442,79
Küresel Vana	25 mm	Adet	1	45,69
Flatör	100 mm	Adet	1	1.916,03
Pislik Tutucu	100 mm	Adet	1	1.387,89
Geri Tepme Ventili	100 mm	Adet	1	658,34
	Toplam (KDV Hariç) = 30.354,68 TL			
	Toplam (KDV Dahil) = 35.818,52 TL			

(Not: Yukarıdaki fiyatlara montaj bedeli de dahildir.)

Yukarıda belirtildiği üzere, yıllık olarak tasarruf edilen su miktarı 367.2 m^3'tür. Rize Su ve Kanalizasyon İşleri Müdürlüğü meskenler su satış fiyatı 2019 yılı için (şebeke suyu ücreti KDV dahil) 3,24 TL / m^3 olarak belirlenmiştir (URL-5., 2019). Bu şekilde, tasarruf edilen tutar, yıllık olarak, 1.189,73 TL olarak hesaplanmıştır. Bu tutar üzerinden değerlendirildiğinde, amortisman süresi yaklaşık 30 yıl olup, su fiyatlarındaki yıllık enflasyon artışı da hesaba katıldığında (yaklaşık %10 olarak alınmıştır) amortisman süresi yaklaşık 14 yıl olacaktadır.

SONUÇ

Bu çalışmada, yağmur suyunun konutlarda kullanımına yönelik inceleme yapılmıştır. Rize ilinde on beş daireden oluşan beş katlı bir apartman seçilmiştir. Hesaplamalarda gerçek meteorolojik veriler kullanılmıştır. Yağmur suyundan faydalanmak için gerekli tesisat çizimi, hesabı ve maliyet analizi yapılmıştır. Yapılan çalışmadan elde edilen sonuçlar aşağıda belirtilmiştir:

- Yağmur suyu, konutlarda tuvalet ve banyolardaki rezervuarlarda kullanılabilir. Böylece, temiz su kaynaklarının daha verimli kullanılmasına ve ülke ekonomisine katkı sunulabilir.
- Su fiyatları enflasyona bağlı olarak zaman içinde artmaktadır ve bir binanın ortalama ömrü yaklaşık 50 yıl olarak kabul edilir. Bu açıdan değerlendirildiğinde, yağmur suyundan faydalanmak, konut sahiplerine ekonomik olarak avantaj sunacaktır.
- Sisteme yerleştirilen su deposunda biriken yağmur suları binalarda bahçe sulama ve apartman temizliği kapsamında da kullanılabilir.

KAYNAKLAR

Şahin, N., & Manioğlu G. (2011). *Binalarda yağmur suyunun kullanılması*. Tesisat Mühendisliği, 125: 21-32.

Alparslan N., Tanık A & Dölgen D**.** (2008). *Türkiye'de Su Yönetimi Sorunlar ve Öneriler*. Türk Sanayicileri ve

İşadamları Derneği (TÜSİAD) Yayın No: T/2008-09/469.

DIN. (1989). *Regenwassernutzungsanlagen.* Deutsches Institut Normung DIN: German.

YAMAN, C. (2009) "*Siemens Gebze Tesisleri Yeşil Bina*", IX. Ulusal Tesisat Mühendisliği Kongresi, İzmir.

ERENGEZGİN, Ç. (2009) "*Diyarbakır Güneş Evi*", Yapı Dergisi Yapıda Ekoloji Eki.

Makine Mühendisler Odası (2008); *Sıhhi Tesisat Proje Hazırlama Esasları* TMMOB Makina Mühendisleri Odası Yayın No 122,135

Kılıç, M. Y., & Abuş, N. M. (2018). *Bahçeli Bir Konut Örneğinde Yağmur Suyu Hasadı*, Bursa Uludağ Üniversitesi, Mühendislik Fakültesi, Çevre Mühendisliği Bölümü, Bursa

Bayar, E**.** (2006). *Karabük İlinde Yağış Sularının Depolanarak Değerlendirilmesinde Maliyet Analizi*, Yüksek Lisans Tezi, Zonguldak Kara Elmas Üniversitesi, Fen Bilimler Enstitüsü, Zonguldak

Eren B., Aygün A., Likos S., & Damar İ. A**.** (2016). *Yağmur Suyu Hasadı: Sakarya Üniversitesi Esentepe Kampüsü Potansiyelinin Değerlendirilmesi*., Uluslararası Mühendislik ve Teknoloji Araştırmaları Dergisi.

URL-1. (2019). *Bursa gaz'a yeşil bina sertifikası.*http://www.milliyet.com.tr/bursagaz-a-yesil-bina-sertifikasi-bursa-yerelhaber-1991153/ [Erişim: 21.09 2019].

URL-2. (2019). https://www.mgm.gov.tr/ veri değerlendirme /il istatistik.= RİZE [Erişim: 22 09 2019].

URL-3. (2019). *Yağmur suyu filtreleme ve depolama sistemi.* http://www.sfr.com.tr/yagmur-suyu-hasati-s6.html [Erişim: 22 09 2019].

URL-4**. (**2019) Su Tema https://sutema.org/gelecegin-suyu/cati-suyu-hasadi.19.aspx [Erişim: 21.09.2019].

URL-5. (2019) *Rize Belediyesi Su ve Kanalizasyon İşleri Müdürlüğü* http://www.rize.bel.tr/ [Erişim 28.09.19].

INVESTING THE EFFICIENCY OF GENERATING ENERGY USING SOLAR WIND TECHNOLOGY

Mohammed QADDOORI HAMMOODI
University of Gaziantep, Aircraft and space science engineering
qaddormohammed@gmail.com

Sohayb ABDULKERIM
University of Gaziantep, Aircraft and space science engineering
karim@gantep.edu.tr

ABSTRACT: In this research, an attempt to investigate the possibility of converting the solar energy into electricity using Solar Updraft Tower SUT, also called solar wind or solar chimney plants. Literature showed that it is attracting interest in off-grid desert locations where conventional photovoltaic technology faces some difficulties due to dust and the lack of water for cooling or cleaning the panels. In addition, other advantages come from the fact that SUT are fueled by hot air rather than direct sunlight, which means it has the capability to generate power in the night since the components or ground surface are stored thermal energy during the daylight. The working principle depends on the fact that sunlight penetrates the semi-transparent wall, hence the solar radiation is converted to heat due to the greenhouse effect and air flows upwards the chimney. This continuous airflow spins a vertical axis turbine located at the top and at the smallest cross-section of the chimney. The nighttime difference in temperature between the ground and the air allows this effect to continue. In order to experiments the feasibility of SUT, a small scale prototype has been designed and then manufactured at an in-house workshop using low-cost material. The dimensions of the tower were semi pyramid 60x20x100. At the top of the tower, a vertical axis turbine was installed and connected directly to a DC generator. The power of the generator was 100 Watts. Measurements have been conducted in order to evaluate the productivity and the efficiency compared to the capital and the operating costs. The initial results have shown a promising technique with respect to the simplicity of the technique and ot its low costs and its superiority to its competitive in some circumstances.

Key words: Solar Power, Vertical axis wind turbine, chimney

CRITICAL THICKNESS CALCLATION OF A SLAB REACTOR FOR TRIPLET ANISOTROPIC SCATTERING

Halide KÖKLÜ, Gaziantep University, koklu@gantep.edu.tr

Okan ÖZER, Gaziantep University, ozer@gantep.edu.tr

ABSTRACT: Critical thickness is calculated for triplet anisotropic scattering in plane geometry one-speed neutron transport equation. The value of the critical slab thickness is investigated numerically by using the P_N method of the first type Legendre polynomial and also second type of the Chebyshev polynomial U_N methods. The eigenfunctions, normalization and orthogonally relations are used to derive for this type of scattering of critical thickness values. By making this calculation the well-known Mark boundary condition is used for this method. As a difference from previous studies, the scattering function is expanded to f_3 that is the tetra anisotropic scattering term. So, the critical thickness results are found for corresponding different secondary neutron number (c) in tetra anisotropic scattering. It is shown that our results are in agreement with the existing literature.

Key words: Critical Thickness, Neutron Transport Theory, Chebyshev Polynomials

INTRODUCTION

The neutron transport equation is the general form of the describing the behavior of the neutrons in a reactor core. The equation includes position, velocity and time variables with seven unknown parameter. For this reason some approximations are assumed and the steady-state neutron transport equation for one speed plane system can be written as (R, 1979),

$$\mu \frac{\partial \psi(x,\mu)}{\partial x} + \psi(x,\mu) = \frac{c}{2}\int_{-1}^{1} f(\mu,\mu')\psi(x,\mu')\,d\mu' \qquad (1)$$

where μ' is the direction of the scattering, $f(\mu,\mu')$ is the scattering function and defines the scattering probability of neutrons, $\psi(x,\mu)$ is the number of the neutrons at position x- and direction μ with distance measured in units of mean free path (mfp), c is the number of secondary neutrons per collision related with the material cross sections by the equation $c\sigma_t = \upsilon\sigma_f + \sigma_s$. Here σ_f is the fission cross section and σ_s is the scattering cross section, υ is the number of neutrons per fission. The distance

measured for neutrons is in units of total mean free path, "mfp". The scattering function in Eq. (1) is expanded with the Legendre polynomials (Mika, 1961) as

$$f(\mu,\mu') = \sum_{n=0}^{N} (2n+1) f_n P_n(\mu) P_n(\mu') \tag{2}$$

where $P_n(\mu)$ and $P_n(\mu')$ are Legendre polynomials and f_n is the scattering coefficient. The scattering function defines the probability of scattering then the sum of these scatterings must equal to one. Therefore the interval values of f_n must be determined for every scattering situation.

The reactor core critical thickness calculations are very complicated for real media and very hard to solve in neutron transport equation. By making this calculation for triplet anisotropic scattering, we have taken into account more scattering probabilities.

P_N SOLUTION OF THE NEUTRON TRANSPORT EQUATION FOR TRIPLET ANISOTROPIC SCATTERING

The series expansion of the scattering function given in Eq. (2) for triplet anisotropic scattering can be written as,

$$f(\mu,\mu') = f_0 P_0(\mu) P_0(\mu') + 3 f_1 P_1(\mu) P_1(\mu') + 5 f_2 P_2(\mu) P_2(\mu') + 7 f_3 P_3(\mu) P_3(\mu') \tag{3}$$

Legendre moments of the flux is defined as (Sahni D C, 1995)

$$\phi_n(x) = \int_{-1}^{1} P_n(\mu') \psi(x,\mu') d\mu' \tag{4}$$

If the scattering function in Eq. (3) is defined in Eq. (1) with the definition of the Legendre moments,

$$\mu \frac{\partial \psi(x,\mu)}{\partial x} + \psi(x,\mu) = \frac{c}{2}\left[P_0(\mu) f_0 \phi_0(x) + 3P_1(\mu) f_1 \phi_1(x) + 5P_2(\mu) f_2 \phi_2(x) + 7P_3(\mu) f_3 \phi_3(x)\right] \tag{5}$$

The angular flux can be expanded in terms of the Legendre polynomials (Lewis EE, 1984)

$$\psi(x,\mu) = \sum_{n=0}^{\infty} \frac{2n+1}{2} \phi_n(x) P_n(\mu) \tag{6}$$

One can insert the Eq. (6) into Eq. (5) by multiplying the resulting equation with $P_m(\mu)$ and integrating over $\mu \in (-1,1)$. The recursion relation

$$\mu P_n(\mu) = \frac{1}{2n+1}\left[(n+1) P_{n+1}(\mu) + n P_{n-1}(\mu)\right] \tag{7}$$

and the orthogonality of the Legendre polynomials

$$\int_{-1}^{1} P_m(x)P_n(x)dx = \begin{cases} 0 & m \neq n \\ \dfrac{2}{2n+1} & m = n \end{cases} \tag{8}$$

are used in this application (F,1967): After some algebra, one can obtain the moments $\phi_n(x)$ in general form as

$$\begin{aligned} &(n+1)\frac{d\phi_{n+1}(x)}{dx} + n\frac{d\phi_{n-1}(x)}{dx} + (2n+1)(1 - cf_n\delta_{n0} + cf_n\delta_{n1} + cf_n\delta_{n2} \\ &+cf_n\delta_{n3})\phi_n(x) = 0, \qquad n = 0,1,2,....,N \end{aligned} \tag{9}$$

The kronecker delta is defined as $\delta_{nm} = \begin{cases} 1, & n = m \\ 0, & n \neq m \end{cases}$ A well-known ansatz for the solutions of Eq. (9) is employed of the form (Davison & Sykes, 1957),

$$\phi_n(x) = A_n(v)e^{-\sigma_t x/v} \tag{10}$$

where A_n is the eigenfunctions corresponding to v eigenvalues. We represent a method and corresponding computer code to get all eigenvalues for tetra anisotropic scattering. Using Eq. (10) in Eq. (9), a system of equations is obtained for the analytic expressions of $A_n(v)$

$$A_1(v) = vA_0(v)(1 - cf_0) \tag{11}$$

$$A_2(v) = \frac{3vA_1(v)(1 - cf_1) - A_0(v)}{2} \tag{12}$$

$$A_3(v) = \frac{5vA_2(v)(1 - cf_2) - 2A_1(v)}{3} \tag{13}$$

$$A_4(v) = \frac{7vA_3(v)(1 - cf_3) - 3A_2(v)}{4} \tag{14}$$

The general form of Eq. (11-14) may be given by

$$\begin{aligned} &(n+1)A_{n+1}(v) + nA_{n-1}(v) + (2n+1)(1 - cf_n\delta_{n0} + cf_n\delta_{n1} + cf_n\delta_{n2} \\ &+cf_n\delta_{n3})vA_n(v) = 0, \qquad n = 0,1,2,...,N \end{aligned} \tag{15}$$

As shown in Eq. (15) the analytical solution of the $A_n(v)$ gives the eigenvalues by solving $A_{n+1}(v) = 0,$ for any c. The discrete eigenvalues v_k and eigenfunctions of the neutron flux are included in the equation of criticality. If c is equal 1, one pair of roots is imaginary ($\pm\infty$i), other pairs are in the range [-1, +1]. If c is between 0 and 1, all roots are imaginary but one pair of them is greater than 1. If c is greater than 1, one pair of roots are pure imaginary, and the other pairs are in the range [-1, +1]. After determining the discrete eigenvalues v_k the general solution of the flux moments in the Eq. (15) can be written for odd numbers of N

$$\phi_n(x)=\sum_{k=1}^{\frac{N+1}{2}}\beta_k A_n(\nu_k)\left[e^{\sigma_t x/\nu_k}+(-1)^n e^{-\sigma_t x/\nu_k}\right] \qquad (N+1)/2<k\le(N+1) \quad (16)$$

where β_k are the coefficients comes from the linear combinations of the solutions corresponding to each ν_k eigenvalues, and they are determined from the boundary conditions of the system using the parity relation of $A_n(-\nu)=(-1)^n A_n(\nu)$. Therefore, the general solution to Eq. (1) for the neutron angular flux can be found by replacing the flux moments Eq. (16) into Eq. (6),

$$\psi(x,\mu)=\sum_{n=0}^{\infty}\sum_{k=1}^{\frac{N+1}{2}}\frac{2n+1}{2}\beta_k A_n(\nu_k)\left[\left(1+(-1)^n\right)\cosh(\frac{\sigma_t x}{\nu_k})+\left(1-(-1)^n\right)\sinh(\frac{\sigma_t x}{\nu_k})\right]P_n(\mu) \quad (17)$$

U_N SOLUTION OF THE NEUTRON TRANSPORT EQUATION FOR TRIPLET ANISOTROPİC SCATTERING

Starting with the flux function in U_n is shown as (Öztürk, 2011)

$$\psi(x,\mu)=\frac{2}{\pi}\sqrt{1-\mu^2}\sum_{n=0}^{N}\phi_n(x)U_n(\mu) \qquad (18)$$

Substituting Eq.(18) and then Eq.(3) into Eq.(1), and using the repetition correlation of the Type II Chebyshev polynomials $2\mu U_n(\mu)=U_{n+1}(\mu)+U_{n-1}(\mu)$ and the orthogonally relation $\int_{-1}^{1}U_m(\mu)U_n(\mu)(1-\mu^2)^{1/2}d\mu=\begin{cases}0, & m\neq n\\ \pi/2, & m=n\end{cases}$ are used.

$$\frac{\sqrt{1-\mu^2}}{\pi}\sum_{n=0}^{N}\frac{d\phi_n(x)}{dx}U_{n+1}(\mu)+\frac{\sqrt{1-\mu^2}}{\pi}\sum_{n=0}^{N}\frac{d\phi_n(x)}{dx}U_{n-1}(\mu)+\frac{2}{\pi}\sqrt{1-\mu^2}\sum_{n=0}^{N}\phi_n(x)U_n(\mu)$$
$$=\frac{c}{2}\int_{-1}^{1}\left(f_0P_0(\mu)P_0(\mu')+3f_1P_1(\mu)P_1(\mu')+5f_2P_2(\mu)P_2(\mu')+7f_3P_3(\mu)P_3(\mu')\right)\left(\frac{2}{\pi}\sqrt{1-\mu^2}\sum_{n=0}^{N}\phi_n(x)U_n(\mu)\right)d\mu' \qquad (19)$$

Eq. (19) is multiplied with $U_m(\mu)$ and integrated between (-1, 1). The integrals are solved for the different n and m values, the orthogonally properties of the Type II Chebyshev polynomials are used for solving Eq. (19). One obtains

$$
\begin{aligned}
m=0,&\quad \frac{d\phi_1(x)}{dx}+2\phi_0(x)-2cf_0\phi_0(x)=0\\
m=1,&\quad \frac{d\phi_0(x)}{dx}+\frac{d\phi_2(x)}{dx}+2\phi_1(x)-2cf_1\phi_1(x)=0\\
m=2,&\quad \frac{d\phi_1(x)}{dx}+\frac{d\phi_3(x)}{dx}+2\phi_2(x)-\frac{2}{3}cf_0\phi_0(x)+\frac{2}{3}cf_2\phi_0(x)-2cf_2\phi_2(x)=0\\
m=3,&\quad \frac{d\phi_2(x)}{dx}+\frac{d\phi_4(x)}{dx}+2\phi_3(x)-\frac{4}{5}cf_1\phi_1(x)+\frac{4}{5}cf_3\phi_1(x)-2cf_3\phi_3(x)=0
\end{aligned}
\tag{20}
$$

and it is so on. The solution of Eq. (20) can be found by a new proposal flux moment equation, as following

$$\phi_n(x)=G_n(v)\exp(x/v) \tag{21}$$

Replacing Eq. (21) into Eq. (20), the following results are found.

$$
\begin{aligned}
&G_1(v)=-2vG_0(v)-2cvf_0G_0(v)\\
&G_2(v)=-2vG_1(v)-G_0(v)+2cvf_1G_1(v)\\
&G_3(v)=-2vG_2(v)-G_1(v)+\frac{2}{3}cvf_0G_0(v)-\frac{2}{3}cvf_2G_0(v)+2cvf_2G_2(v)\\
&G_4(v)=-2vG_3(v)-G_2(v)+\frac{4}{5}cvf_1G_1(v)-\frac{4}{5}cvf_3G_1(v)+2cvf_3G_3(v)
\end{aligned}
\tag{22}
$$

As a result, by using the eigenvalues v_k, a general expression for the flux moment can be written as,

$$\phi_n(x)=\sum_{k=1}^{N+1/2}\beta_k G_n(v_k)\left[\exp(\sigma_t x/v_k)+(-1)^n\exp(-\sigma_t x/v_k)\right] \qquad n=1,2,3,,,,,N \tag{23}$$

The Eq. (23) is substituted into Eqn. (18). So the resultant equation is obtained as,

$$\psi(x,\mu)=\frac{2}{\pi}\sqrt{1-\mu^2}\sum_{n=0}^{N}\sum_{k=1}^{N+1/2}\beta_k G_n(v_k)\left[\left(1+(-1)^n\right)\cosh(\frac{x}{v})+\left(1-(-1)^n\right)\sinh(\frac{x}{v})\right]U_n(\mu_k) \tag{24}$$

CRITICALITY CONDITIONS

The aim in criticality problem is to solve the equation of transport related with the number of secondary neutrons "c". In this study eigenvalues corresponding to the case c > 1 are used. Eq. (17) shows that neutron flux expression obtained by P_N method. Half slab thickness is obtained by applying Mark boundary condition to the Eq. (17). Mark maintains the continuity of neutron flux along the boundaries encircled in a vacuum. He used the idea of continuity of the angular flux, and for the special values of μ. It is showed that the angular flux from the boundary is equal to zero. Here, Mark-type boundary condition is used (Yaşa, Anli, & Güngör, 2006)

$$\psi(a,\mu_m)=0, \qquad 1\le m\le (N+1)/2 \tag{25}$$

Here, μ_m is the root of the Legendre polynomials that can be found from $P_{N+1}(\mu_m)=0$. Then, the criticality equation can be obtained by using Eq. (18) in the Mark boundary condition given in Eq. (25)

$$\sum_{n=0}^{\infty}\sum_{m,k=1}^{\frac{N+1}{2}}\frac{2n+1}{2}\beta_k A_n(\nu_k)\left[\left(1+(-1)^n\right)\cosh(\frac{\sigma_t a}{\nu_k})+\left(1-(-1)^n\right)\sinh(\frac{\sigma_t a}{\nu_k})\right]P_n(\mu_m)=0 \qquad (26)$$

Eq. (25) can also be written in a matrix form as $\left[M_m^k(a)\right]\mathrm{B_k}=\left[0\right]$, where $\mathrm{B_k}$ is a vector with elements β_k and $\left[M_m^k(a)\right]$is a square matrix with elements$\left[(N+1)/2\right]^2$. The determinant of $\left[M_m^k(a)\right]$ must be equal to zero for the criticality condition for a non-trivial solution of Eq. (26).

By applying same procedure for P_N method the critical thickness equation can be obtained for U_N method.

NUMERICAL RESULTS

We can calculate the critical thickness by using Eq. (26) for Mark boundary condition. The neutron transport equation with triplet anisotropic scattering has three scattering terms. It means that three different scattering coefficients must have been added to general transport equation. The maximum value of the literature study are used for the linear, quadratic and triplet anisotropic scattering coefficients (f_1=0.3, f_2=0.2 and f_3=0.142 respectively) (Yildiz, 1998, Rashis,2013).

It is seen from the Table 1., the critical thickness results of P_N method for changing number of secondary neutrons "c" show that the critical thickness decreases with increasing c values, as expected. Then the critical thickness values are tabulated with fixed c values for isotropic, linear, quadratic pure quadratic, triplet, and pure triplet anisotropic scattering types. So the changing in critical thickness is observed from the Tables 2,3,4,5 (1.01, 1.1, 1.5, and 2.0 respectively). Legendre polynomial solutions are solved up to thirteenth order, however the convergence is observed up to three digits in the results. In literature, slab critical thickness solutions are done for strongly anisotropic scattering by C. Yıldız (1998). In his study, the solutions have been done up to fifteenth order with P_N method, and the convergence was obtained up to three digits. ; In Table 6 the critical thickness values are tabulated for U_N method. In Table 7 four different scattering types are showed for fixed and changing c values with U_N method.

In literature, the solutions of the critical thickness for neutron transport equation are done in plane geometry for triplet anisotropic scattering with F_N method by G. Türeci (Türeci, 2015) (as shown in Table 8). We compared pure triplet anisotropic critical thickness values of our calculations with the literature study done by G. Türeci in order to see the compatibility of our method. To obtain the critical thickness values as shown in Table 8, the peak order of P_{13} in our results and the peak order of F_3 in G. Türeci results were used.

Table 1. Critical half-thickness for triplet anisotropic scattering in P_N method

c	P_1	P_3	P_5	P_7	P_9	P_{11}	P_{13}
1.01	10.0384	9.82526	9.81031	9.80604	9.80423	9.80329	9.80222
1.05	4.07718	3.83286	3.81531	3.81064	3.80868	3.80767	3.80709
1.10	2.68134	2.43080	2.40904	2.40381	2.40166	2.40057	2.39994
1.20	1.71227	1.47377	1.44256	1.43586	1.43331	1.43203	1.43130
1.40	1.05213	0.852709	0.809563	0.798604	0.794817	0.793103	0.792162
1.60	0.774859	0.607738	0.562009	0.547607	0.542141	0.539718	0.538471
1.80	0.61747	0.474534	0.430248	0.414186	0.407336	0.404099	0.402421
2.00	0.51481	0.39021	0.34864	0.33215	0.32447	0.32055	0.31843

Table 2. Critical half-thickness for different scattering types for c=1.01

Scattering types	P_1	P_3	P_5	P_7	P_9	P_{11}	P_{13}
Isotropic	8.49356	8.34635	8.33616	8.33309	8.33175	8.33104	8.33064
Lin.ans.	10.0384	9.83575	9.82133	9.81695	9.81505	9.81404	9.81297
Pure quadratic	8.49356	8.34750	8.32548	8.32258	8.32133	8.32068	8.32032
Quadratic	10.0384	9.82195	9.80846	9.80378	9.80201	9.80109	9.80012
Pure triplet	8.49356	8.34868	8.33784	8.33466	8.33329	8.33257	8.33214
Triplet	10.0384	9.82526	9.81031	9.80604	9.80423	9.80329	9.80222

Table 3. Critical half-thickness for different scattering types for c=1.1

Scattering types	P_1	P_3	P_5	P_7	P_9	P_{11}	P_{13}
Isotropic	2.30869	2.13534	2.12100	2.11734	2.11580	2.11501	2.11454
Lin.ans.	2.68134	2.44941	2.43108	2.42613	2.42402	2.42292	2.42227
Pure quadratic	2.30869	2.11492	2.09910	2.09586	2.09383	2.09305	2.09260
Quadratic	2.68134	2.42299	2.40329	2.39831	2.39624	2.39517	2.39455
Pure triplet	2.30869	2.14065	2.12481	2.12097	2.11938	2.11857	2.11809
Triplet	2.68134	2.43080	2.40904	2.40381	2.40166	2.40057	2.39994

Table 4. Critical half-thickness for different scattering types for c=1.5

Scattering types	P_1	P_3	P_5	P_7	P_9	P_{11}	P_{13}
Isotropic	0.78001	0.64949	0.62089	0.61223	0.60904	0.60762	0.60686

Lin.ans.	0.89092	0.71651	0.68261	0.67284	0.66925	0.66759	0.66689
Pure quadratic	0.78001	0.63423	0.59956	0.58880	0.58483	0.58311	0.58222
Quadratic	0.89092	0.69594	0.65485	0.64278	0.63840	0.63646	0.63544
Pure triplet	0.78001	0.65802	0.62654	0.61727	0.61389	0.61240	0.61161
Triplet	0.89092	0.70879	0.66356	0.65065	0.64603	0.64399	0.64292

Table 5. **Critical half-thickness for different scattering types for c=2.0**

Scattering types	**P_1**	**P_3**	**P_5**	**P_7**	**P_9**	**P_{11}**	**P_{13}**
Isotropic	0.45343	0.36197	0.33477	0.32350	0.31817	0.31545	0.31396
Lin.ans.	0.51481	0.39320	0.36065	0.34775	0.34184	0.33887	0.33728
Pure quadratic	0.45345	0.35219	0.32014	0.30656	0.29993	0.29647	0.29455
Quadratic	0.51481	0.38020	0.34204	0.32651	0.31919	0.31543	0.31338
Pure triplet	0.45345	0.36889	0.33939	0.32745	0.32186	0.31902	0.31748
Triplet	0.51481	0.39021	0.34864	0.33215	0.32447	0.32055	0.31843

Table 6. Critical thickness for tetra anisotropic in U_N method

c	**U_1**	**U_3**	**U_5**	**U_7**	**U_9**	**U_{11}**	**U_{13}**
1.01	8.69353	9.83803	9.80774	9.80570	9.80387	9.80316	9.80021
1.05	3.53097	3.84589	3.81216	3.81029	3.80830	3.80753	3.78888
1.1	2.32211	2.44054	2.40531	2.40346	2.40124	2.40042	2.39980
1.2	1.48287	1.47617	1.43793	1.43548	1.43280	1.43185	1.43115
1.4	0.911174	0.846959	0.803447	0.797894	0.79412	0.79288	0.79201
1.6	0.671047	0.599463	0.555151	0.546368	0.54118	0.53941	0.53833
1.8	0.534744	0.465747	0.423289	0.412533	0.40612	0.40366	0.40227
2.0	0.445836	0.381598	0.341897	0.33064	0.32306	0.31999	0.31825

Table 7. Critical thickness for different scattering types in U_N method

c	**Scattering types**	**U_1**	**U_3**	**U_5**	**U_7**	**U_9**	**U_{11}**	**U_{13}**
1.01	Isotropic	7.35564	8.35915	8.33360	8.33306	8.33139		8.33044

	Lin.ans.	8.69353	9.84411	9.81891	9.81654	9.81469	9.81389	9.81181
	Pure quadratic	7.35564	8.34963	8.32294	8.32257	8.32099	8.32064	8.32006
	Quadratic	8.69353	9.83133	9.80561	9.80339	9.80169	9.80094	9.79827
	Pure triplet	7.35564	8.36457	8.33504	8.33467	8.33290	8.33252	8.33192
	Triplet	8.69353	9.83803	9.80774	9.80570	9.80387	9.80316	9.80021
1.1	Isotropic	1.99938	2.14732	2.11715	2.11744	2.11537	2.11495	2.11441
	Lin.ans.	2.32211	2.45596	2.42788	2.42571	2.42363	2.42275	2.42215
	Pure quadratic	1.99938	2.14732	2.09947	2.09548	2.09340	2.09300	2.09248
	Quadratic	2.32211	2.42298	2.400006	2.39788	2.39587	2.39500	2.39444
	Pure triplet	1.99938	2.1555	2.13050	2.12115	2.11891	2.11853	2.11795
	Triplet	2.32211	2.44054	2.40531	2.40346	2.40124	2.40042	2.39980
1.5	Isotropic	0.675511	0.649014	0.614898	0.612239	0.608157	0.60759	0.60663
	Lin.ans.	0.771558	0.709976	0.677860	0.671952	0.668670	0.66733	0.66653
	Pure quadratic	0.675511	0.631454	0.592975	0.58851	0.58386	0.58303	0.58197
	Quadratic	0.771558	0.686091	0.649633	0.641482	0.637795	0.63613	0.63528
	Pure triplet	0.675511	0.659725	0.619508	0.61753	0.61284	0.61242	0.61137
	Triplet	0.771558	0.701373	0.656974	0.649678	0.645208	0.64373	0.64277
2.0	Isotropic	0.392699	0.358758	0.329089	0.322756	0.316880	0.31525	0.31357

Lin.ans.	0.445836	0.385204	0.355760	0.346055	0.340912	0.33836	0.33704
Pure quadratic	0.392699	0.346906	0.314049	0.30528	0.29848	0.29611	0.29410
Quadratic	0.445836	0.369567	0.336717	0.324224	0.318115	0.31473	0.31310
Pure triplet	0.392699	0.367502	0.332642	0.32703	0.32031	0.31893	0.31712
Triplet	0.445836	0.381598	0.341897	0.330261	0.323061	0.31999	0.31824

Table 8. Critical 2a Thickness for Pure Triplet Anisotropic Scattering

c	P_N Method	U_N Method	R. G. Türeci [19]
1.1	4.23866	4.237817	4.2430863
1.3	1.891516	1.890154	1.8924836
1.5	1.227636	1.225680	1.2252848
1.7	0.90406	0.901579	0.8986480
2.0	0.643614	0.640628	0.6322023

CONCLUSION

In this study, we examine the critical half-thickness of the slab by changing scattering types with P_N and U_N method. We have been seeking an answer for the question what are the effects of anisotropic scattering on the critical thickness. In previous studies, this effect was investigated for each scattering type individually. In contradistinction, this study presents the results from isotropic to triplet anisotropic scattering calculations that are applied simultaneously. Comprehensive and comparative results of all scattering types provided in this study, offers a good source for further studies and researches.

We have extended the neutron scattering function up to f_3, called as triplet anisotropic scattering. It is quite difficult to obtain the analytical solutions for this kind of scattering. When the number of terms in scattering function is increased, the equation becomes more complicated. In this study, finding the eigenvalues of the neutron transport equation was the first step. Then they are substituted into neutron flux equation to obtain the critical thickness by using a computer code. The thickness required for the criticality depends on the scattering parameters in the solutions. In our solutions, the Legendre polynomials are used since it provides suitable and rapid direct results. The critical half-thickness of the uniform-medium slab for one-energy

group with triplet anisotropic scattering is computed by using the well-known and widely used boundary conditions which is Mark boundary condition. The critical thickness decreases by increasing the number of secondary neutrons c as expected. The deviation between each scattering coefficients is getting smaller by increasing the order of anisotropic scattering. Hence, critical thickness results are converging which means less difference between the values of each next orders scattering results.

REFERENCES

Case K M and Zweifel P F, (1967) Linear *Transport Theory*, New York: Addison Wesley.

Davison, B., & Sykes, J. B. (1957). Neutron Transport Theory. *Zeitschrift Fur Naturforschung - Section A Journal of Physical Sciences*. https://doi.org/10.1515/zna-1957-1219

Duderstadt, J. J., & Martin, W. R. (1979). *Transport theory* New York: Addison Wesley

Lewis EE, M. W. (Wiley/ N. Y. (1984). *Computational methods of neutron transport*. Wiley/ New York.

Mika, J. (1961). Neutron transport with anisotropic scattering. *Nucl. Sci. and Engineering*, *11*, 415.

Öztürk, H. (2011). Modified UNmethod for the reflected critical slab problem with forward and backward scattering. *Kerntechnik*. https://doi.org/10.3139/124.110126

Rashis, P. A. H., (2013)"Investigation of the solution by using P_N method of transport equation for triplet anisotropic scatterıng" Ms Thesis, Publication of Kahramanmaraş of Sütçü Imam University, Kahramanmaraş, , 35-50 .

Sahni D C, D. E. B. and S. N. G. (1995). Real criticality eigenvalues of the one-speed linear transport operator. *Transp. Theory Statist. Phys*, *24*, 1295–1317.

Türeci, R. G. (2015). Solving the criticality problem with the reflected boundary condition for the triplet anisotropic scattering with the modified FNmethod. *Kerntechnik*.

Yaşa, F., Anli, F., & Güngör, S. (2006). Eigenvalue spectrum with chebyshev polynomial approximation of the transport equation in slab geometry. *Journal of Quantitative Spectroscopy and Radiative Transfer*. https://doi.org/10.1016/j.jqsrt.2004.12.017

Yildiz, C. (1998). Variation of the critical slab thickness with the degree of strongly anisotropic scattering in one-speed neutron transport theory. *Annals of Nuclear Energy*. https://doi.org/10.1016/S0306-4549(97)00114-X.

DETERMINATION OF STIFFNESS PARAMETERS IN FINITE ELEMENT ANALYSIS OF INTERFERENCE FIT

Fatih GÜVEN

Akdeniz University, Mechanical Engineering Department, Antalya, Turkey

fatihguven@akdeniz.edu.tr

ABSTRACT: Shrink fit is one of the joining methods used for torque transmission between a shaft and a hub. In this joining method, the outside diameter of shaft is slightly greater than the inner diameter of hub. After mounting of parts, a contact pressure originates between contacting surfaces. The pressure is the basis of torque transmission that results in a frictional force resisting against relative movement of parts. This kind of joints have a non-linear problems because of the friction and deformation of surfaces in contact. The pressure could be computed theoretically via thick walled vessel formulations. Another solution is finite element analysis that utilizes the penalty method and the augmented Lagrange method. In this method, contact parameters should be carefully specified to get contact pressure between mating surfaces correctly. Contact stiffness is one of the important parameters that affect the accuracy of solution. Another important parameter is the size of elements used to constitute finite element model. In this study, a sample shrink fitted assembly with specified dimension and Young's modulus was considered to investigate effect of contact parameters on contact pressure distribution. Contact stiffness value and size of elements were considered to examine their effects on contact pressure. Results showed that the smaller the elements, the smaller the contact stiffness. Elements size should be specified according to contact stiffness that should have a value between 0.1 and 1.0 in order to balance accuracy of solution and time required.

Key words: Contact stiffness, Lagrange, Penalty method, FEA

SIKI GEÇME BAĞLANTILARIN SONLU ELEMANLAR ANALİZİNDE KATILIK PARAMETRELERİNİN BELİRLENMESİ

ÖZET: Sıkı geçme bağlantılar mil ve göbek arasında moment iletiminde kullanılan bağlantı şekillerindendir. Milin boyutunun göbek deliğinden büyük olmasından dolayı yapılan montaj sonunda temas yüzeylerinde bir basınç meydana gelmektedir. Oluşan bu basınç moment iletiminin temelidir. Sıkı geçme bağlantılar, temas mekaniğinde sürtünmeye dayalı temas koşullarından dolayı doğrusal olmayan çözüm gerektirmektedir. Teorik hesaplamaları kalın cidarlı tüpler teorisine dayanmaktadır.

Sonlu elemanlar çözümlerinde penaltı yöntemi veya genişletilmiş Lagrange yöntemi kullanılmaktadır. Bu yöntemlerde temas basıncının doğru bir şekilde elde edilebilmesi için temas değişkenlerinin doğru bir şekilde tanımlanması gerekmektedir. Temas eden yüzeylerin katılık değeri çözümün doğruluğu açısından son derece önem arz etmektedir. Bir diğer önemli husus ise kullanılan elemanların boyutudur. Bu çalışma kapsamında örnek bir sıkı geçme bağlantının sonlu elemanlar yöntemi ile temas basıncı analizleri yapılmıştır. Temas eden elemanlardaki değişkenler ile elastik direnç değerinin temas basıncı üzerinde etkileri incelenmiştir. Yapılan çalışmalar ve değerlendirmeler sonucunda Genişletilmiş Lagrange yönteminde eleman boyutu küçüldükçe seçilmesi gereken temas katılığı değerlerinin de küçüldüğü görülmüştür.

Anahtar sözcükler: FEA, Lagrange, Penaltı yöntemi, Temas katılığı

GİRİŞ

Moment iletimi için kullanılan sıkı geçme mil-göbek bağlantıları, kalın cidarlı tüpler teorisine dayanarak Lame bağlantıları ile hesaplanmaktadır (Budynas ve Nisbett, 2006; Niemann, Winter ve Hoehn, 2005). Denklem (1)'de görülen bu hesap yöntemi standartlarda da kullanılmaktadır (DIN 7190-1:2017, 2017). Zhang vd. (2000) yaptığı çalışmanın sonuçlarını, sıkı geçme bağlantılarında temas basıncının temeli olarak görülen Lame bağlantıları ile elde bulduğu sonuçları kıyaslamış ve oluşan temas basıncının beklenenden %78 daha fazla olduğunu belirtmiştir. Bu önemli fark, Zhang vd.nin bu çalışmasında göbek cidar kalınlığının mil çapına oranının küçük olmasından kaynaklanmaktadır. İç basınca maruz kalan cidarlı kaplarda ince ve kalın cidarlı olarak hesaplamalar değişmektedir (Campos ve Hall, 2019). Bundan sonra sıkı geçme bağlantılar ifadesi sadece kalın cidarlı tüpler teorisine uyan mil-göbek bağlantılarını ifade etmekte kullanılacaktır. Şekil 1'de bir sıkı geçme bağlantıya ilişkin büyüklükler görülmektedir.

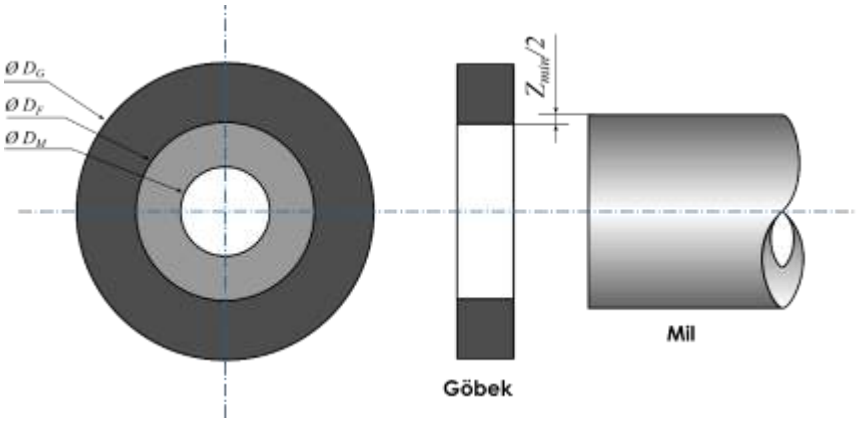

Şekil 1. Sıkı geçme bağlantılarında boyutlar

$$p = \frac{Z_{min}}{D_F\left[\frac{1}{E_G}\left(\frac{D_G^2 + D_F^2}{D_G^2 - D_F^2} + \nu_G\right) + \frac{1}{E_M}\left(\frac{D_F^2 + D_M^2}{D_F^2 - D_M^2} - \nu_M\right)\right]} \quad (1)$$

Bu denlmem aynı malzemeden imal edilmiş mil-göbek çiftinde milin dolu olduğu özel durum için $E_G = E_M = E$ olmak üzere Denklem (2)'deki hali almaktadır.

$$p = \frac{Z_{min}}{\frac{D_F}{E}\left(\frac{D_G^2 + D_F^2}{D_G^2 - D_F^2}\right) + 1} \quad (2)$$

Yukarıdaki denklem temas uzunluğu boyunca temas basıncının değişmediğini kabul etmektedir. Ancak yapılan çalışmalar, sıkı geçme bağlantılarında temas basıncı, temas uzunluğunun merkezinden uçlarına doğru arttığı ve doğrusal olmadığı göstermiştir (Özel, Temiz, Aydin ve Şen, 2005).

Temas mekaniği doğrusal olmayan çözüm gerektirdiğinden çözümlemelerde sonlu elemanlar yönteminden faydalanılmaktadır. Sonlu elemanlar yöntemi ile temas mekaniği problemi çözümlemelerinde kullanılan iki temel yaklaşım Penaltı yöntemi ve Lagrange çarpanları yöntemidir. Bu iki yöntem arasındaki fark Denklem (3)'de verilen toplam potansiyel enerji ifadesinde, temas elemanlarının potansiyel enerjisinin Π_c çözümüne ilişkin yaklaşımdır.

$$\Pi = \Pi_b + \Pi_c = \frac{1}{2}\int_V \varepsilon^T \sigma dV - \int_S u^T F dS + \Pi_c \quad (3)$$

Potansiyel enerjisi sıfıra yaklaştırılması problemin çözümünü vermektedir. Dolayısıyla Denklem (3)'ün bilinmeyen yer değiştirme vektörü olan u'ya göre türevinin sıfıra eşitlenmesi ile Denklem (4) elde edilmektedir.

$$\delta\Pi = \delta\Pi_b + \delta\Pi_c = \frac{\partial(\Pi_b + \Pi_c)}{du}\delta u = 0 \quad (4)$$

Penaltı yaklaşımı ile elde edilen çözümler ekonomik yönüyle kabul görürken sayısal hatalar içerebilmektedir. Buna karşın Lagrange çarpanı yöntemi daha fazla çözüm zamanına ihtiyaç duymakla birlikle iyi sonuçlar vermektedir (Zahavi ve Barlam, 2000). Temas çözümlerine her iki yöntemin avantajlarından faydalanmak üzere genişletilmiş Lagrange çarpanı yöntemi kullanılmaktadır.

Temas Problemlerinde Kullanılan Bağıntılar

Penaltı Yöntemi

Bu yöntemde gerçekte olmamasına karşın temas eden elemanlar arasında hayali bir geçirgenlik olduğu varsayılır (Wriggers, Van ve Stein, 1990). Bu yönteme göre temas elemanlarının potansiyel enerji çözümünün birinci türevi alınarak Denklem (5) ile belirlenir.

$$\delta\Pi_c = f_n\delta g_n + f_t\delta g_t = k_n g_n \delta g_n + \mathrm{sgn}(g_t)\,\mu_d k_n g_n \delta g_t \qquad (5)$$

Bu ifadede k_n ve k_t sırasıyla normal ve teğetsel yöndeki penaltı değerini, g_n ve g_t yine sırasıyla normal ve teğetsel yöndeki geçirgenlik değerini ve μ_d dinamik sürtünme katsayısını ifade etmektedir.

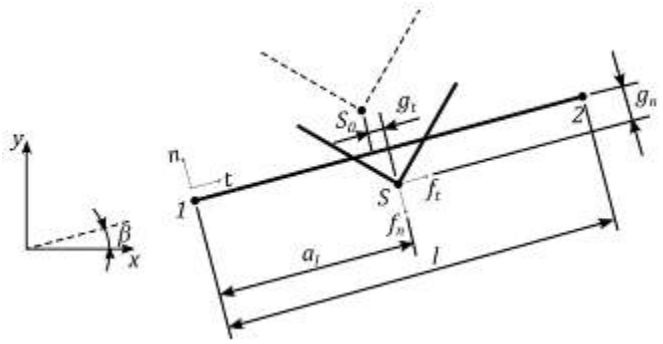

Şekil 2. Penaltı yönteminde elamanlar ve önemli büyüklükler

Genişletilmiş Lagrange çarpanı yöntemi

Bu yöntem Lagrange yöntemine penaltı fonksiyonunun eklenmesi ile geliştirilmiştir. Potansiyel enerjinin azaltılması için Denklem (6)'da görülen potansiyel enerji ifadesi sıfıra eşitlenir.

$$\Pi(u,\Lambda) = \Pi_b(u) + \Lambda^T g + \frac{1}{2} g^T k g \qquad (6)$$

Bu ifadede Λ^T, Lagrange çarpanı olarak karşımıza çıkmaktadır.

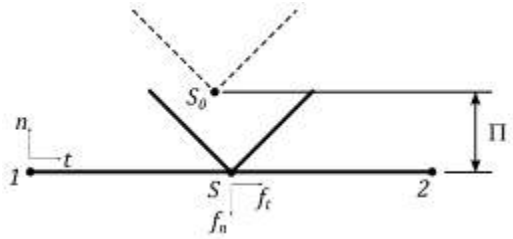

Şekil 3. Lagrange yönteminde elamanlar ve önemli büyüklükler

Sonlu Elemanlar Yönteminde Temas Problemleri

Sonlu elemanlar yönteminde normal doğrultudaki temas kuvveti F_n; x_p bağımsız temas yüzeylerindeki iki düğüm arasındaki mesafe ve k_n temas katılığı olmak üzere Denklem (7)'da verilmiştir.

$$F_n = k_n x_p \tag{7}$$

Temas katılığı artıkça geçirgenlik azalmaktadır. Temas katılığının sonsuz değeri için herhangi bir geçirgenlik olmamakla birlikte sayısal açıdan mümkün olmamaktadır. Dolayısıyla x_p nin küçük değerleri için doğru sonuçlar elde etmek mümkündür. Genişletişmiş Lagrange çarpanı yönteminde Denklem (7)'da verilen ifadeye Lagrange çarpanı λ eklenerek Denklem (8) elde edilmektedir. Bu çarpanın eklenmesinden dolayı genişletişmiş Lagrange çarpanı yöntemi temas katılığı değerine daha az hassasiyet göstermektedir.

$$F_n = k_n x_p + \lambda \tag{8}$$

Rijit cisimlerin teması incelenirken penaltı yöntemi önerilirken, diğer temas türlerinde genişletişmiş Lagrange çarpanı yönteminin kullanılması daha uygundur. Ağ yapısının aşırı bozunumu iterasyon sayısının artmasına neden olmaktadır. Çok noktalı koşul (MPC) yöntemi birleşik veya ayrılmaz yapıdaki temas durumu için uygun bir seçimdir. Sonlu elemanlar yönteminde başarılı sonuçlar elde edilebilmesi için doğrusal olmayan temas problemlerinde temas katılığı, geçirgenlik toleransı gibi temas algoritmasına ilişkin değerlerin belirlenmesi gerekmektedir. Penaltı yöntemi ve Genişletilmiş Lagrange yöntemi kıyaslandığından penaltı yöntemi iyi bir yakınsama sunarken seçilen temas katlığı değerine çok hassastır. Genişletilmiş Lagrange yöntemi geçirgenliğin fazla olduğu durumlarda daha fazla iterasyona ihtiyaç duymasına karşın seçilen temas katılığı değerine daha az hassastır. Temas analizlerinde kullanılan tanımlar aşağıda verilmiştir.

Temas algılama

Sonlu elemanlar yöntemi ile çözüm yaparken temas eden elemanların belirtilmesi gerekir. Çözüm yazılımlarının teması algılamak ve yakınsamayı hızlandırmak için seçenekler sunmaktadır. Penaltı ve genişletilmiş Lagrange çarpanı yöntemlerinde Gauss bütünleşim noktası kullanılmaktadır. Analiz esnasında elemanların durumuna göre temas algılanmaması durumunda serbest cisim hareketi meydana gelebilir. Bir sönüm katsayısı ile iki parça arasındaki izafi hareket engellenebilmektedir. Pinball yarıçapının genişletilmesi ile daha geniş bir alanda temas algılanması sağlanabilir.

Geçirgenlik toleransı

Genişletilmiş Lagrange çarpanı yöntemi kullanılması durumunda geçirgenlik toleransı tanımlanması gerekmektedir. Geçirgenlik toleransı pozitif bir boyutsal değer ya da 0 ila 1 arasında bir katsayı olarak formülasyona dâhil edilmektedir (ANSYS, 2004).

Arabağ bakımı

Sürtünmesiz, sürtünmeli veya pürüzlü temas koşullarının analizinde temas yüzeylerinin bakım yönteminin de belirtilmesi gerekir. Aralarında açıklık bulunan iki elemanın temas durumu incelenirken analiz başlangıcında temas halindeymiş gibi davranması sağlanabilir.

Katılık değerleri

Temas eden elamanların ve temas bölgesinin katılık değerleri sonlu elemanlar çözümü açısından hesaplanmalıdır. Hesaplamalara elastiklik modülünün 0.01 ila 10 arasında pozitif bir değerle çarpımı olarak katılmaktadır. Değerler küçüldükçe yakınsama kolaylaşsa da daha fazla geçirgenlik olmaktadır.

Çözüm esnasında temas katılığı değerlerinin güncellenmesi gerektiğine karar verilmesi durumunda Penaltı yöntemi ya da genişletilmiş Lagrange çarpanı yöntemi kullanılması durumunda gerilme ve geçirgenliğe bağlı olarak (geçirgenliği azaltmak için) her bir iterasyon için temas katılığını azaltma, artırma veya sabit tutma seçeneklerinden biri kullanılabilir.

YÖNTEM

Çalışma kapsamında örnek bir modelde farklı eleman ve düğüm sayıları için temas parametrelerin yakınsama ve doğruluk üzerine olan etkileri incelenmiştir. Eksenel simetrik sıkı geçme bağlantı yarım model olarak oluşturulmuştur. Modelde 4 düğümlü dörtgen elemanlar kullanılmıştır. Modele ilişkin büyüklükler Şekil 4'te görülmektedir. Örnek modelde geçme çapı $D_F = 30$ mm, göbek dış çapı $D_G = 90$ mm, mil uzunluğu $L_M = 120$ mm ve temas uzunluğu $L = 50$ mm'dir. Mil ve göbek arasında geçme sıkılığı $Z = 0.08$ mm olarak tanımlanmıştır. Ağ yapısı korunacak şekilde eleman boyutu 0.5, 1 ve 2 mm için analizler tekrarlanmıştır. Her bir eleman boyutu için genişletilmiş Lagrange yöntemi ile temas katılığı değeri elastik direnç değerinin 0.125, 0.5 ve 1.0 katı için temas basıncının değişimi incelenmiştir. Sonlu elemanlar çözümlerinde seçilen malzemenin elastik direnci 210 GPa ve Poisson oranı 0.3 olarak belirlenmiştir.

Analizlerde temas uzunluğu boyunca temas basıncındaki değişim incelenmiştir. Sonlu elemanlar yöntemiyle elde edilen sonuçlar daha önce bahsedilen kalın cidarlı basınçlı kaplar teorisine dayanan teorik hesaplamalarla kıyaslanmıştır. Simetri ekseni referans

alınarak modelden elde edilen sonuçların doğrulaması teorik hesaplamalarla yapılmıştır.

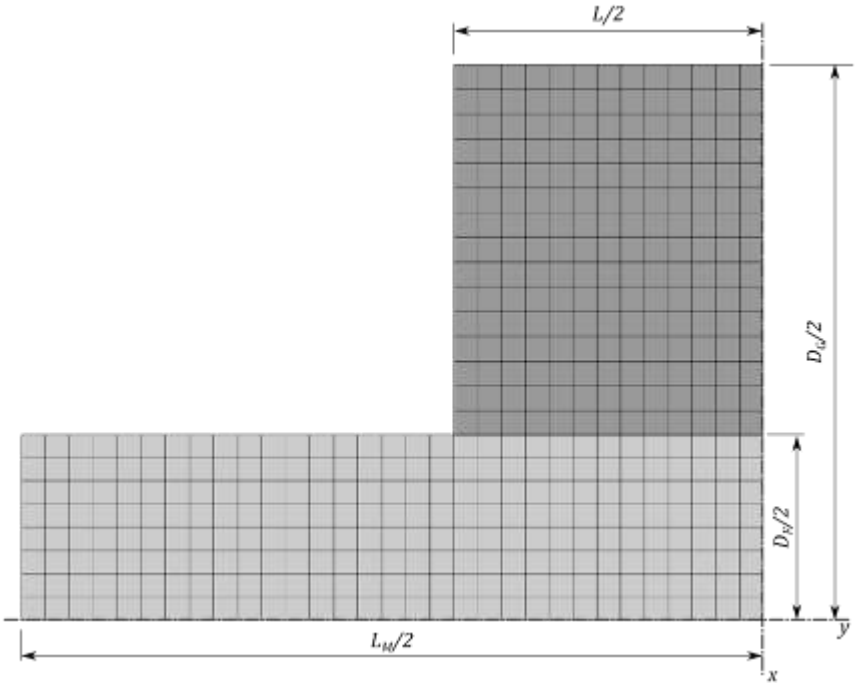

Şekil 4. Sonlu elemanlar modeli ve önemli büyüklükler

BULGULAR

Yapılan analizler sonucunda elde edilen temas basıncı değerlerinin temas uzunluğu boyunca değişimi normal farklı katılık değerleri için incelenmiştir. Farklı eleman boyutları için elde edilen değerler burada sunulmuştur. Şekil 4'te eleman boyutu 0.5 mm ve daha küçük olan modelin temas uzunluğu boyunca temas basıncındaki değişimi görülmektedir. Şekilde verilen normal katılık değerleri (FKN) malzemenin elastik direnç değerine oranıdır. Yatay sabit çizgi ise kalın cidarlı basınçlı kaplar teorisine göre hesaplanmış teorik temas basıncını göstermektedir. Şekilde görülen noktalar ilgili düğüm noktasının koordinatına denk gelmektedir. 0 koordinatı referans alınmıştır. Buna göre teorik değere en yakın basınç dağılımı elastik direncinin 0.125 katına denk gelen 26250 değeri için elde edilmiştir. Sıkı geçme bağlantının her iki ucunda oluşan basınç artışları bağlantının doğasından kaynaklanmaktadır ve sonlu elemanlar modeli ile uyum içindedir.

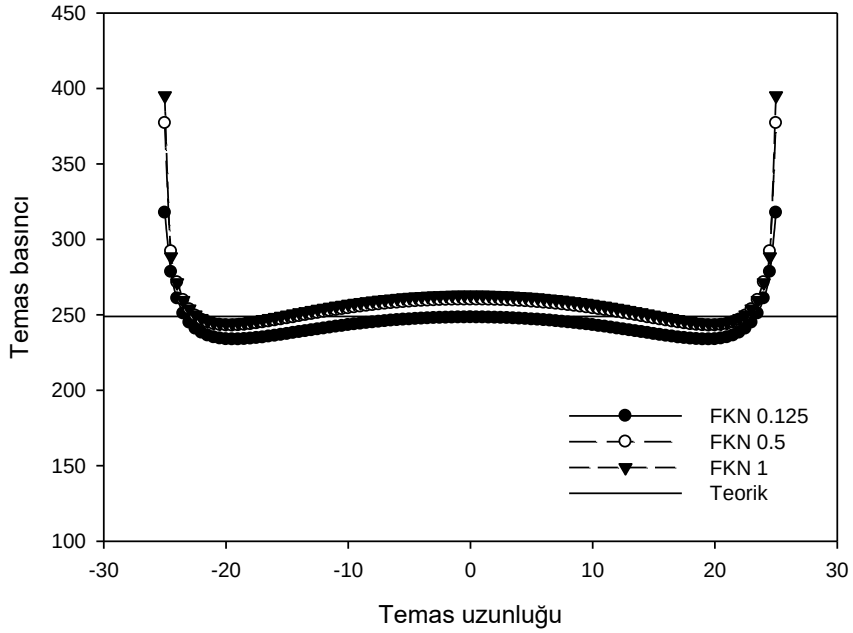

Şekil 4. Eleman boyutu 0.5 mm için temas basıncının değişimi

Benzer şekilde Şekil 5'te boyutu 1 mm den küçük ve Şekil 6'da ise 2 mm küçük olan elemanlar kullanılarak elde edilen basınç dağılımları görülmektedir. 1 mm eleman boyutu için en yakın referans değer elastik direncin 0.5 katı için elde edilmiştir. 2 mm eleman boyu için bu değer 1.0 olmaktadır.

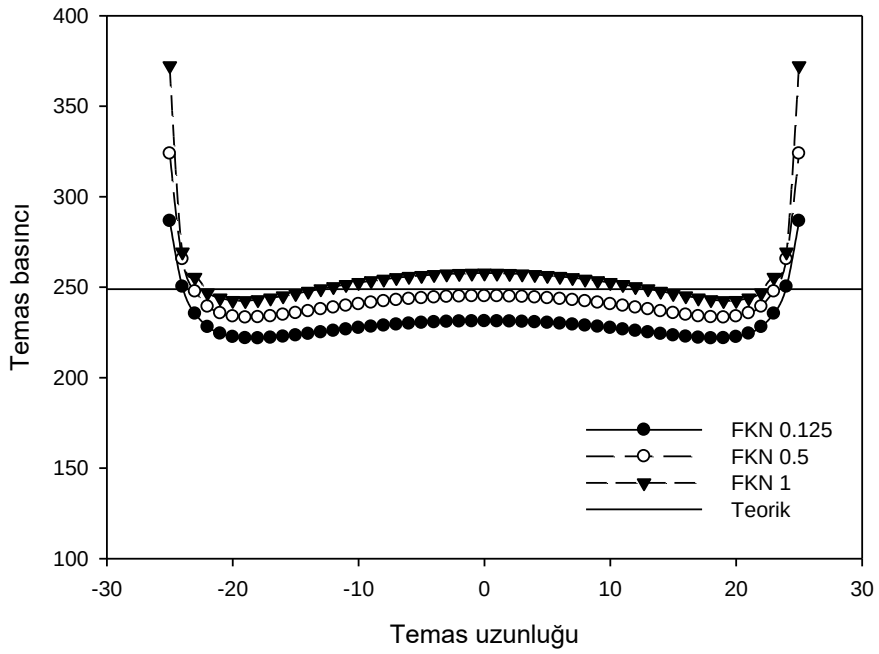

Şekil 5. Eleman boyutu 1 mm için temas basıncının değişimi

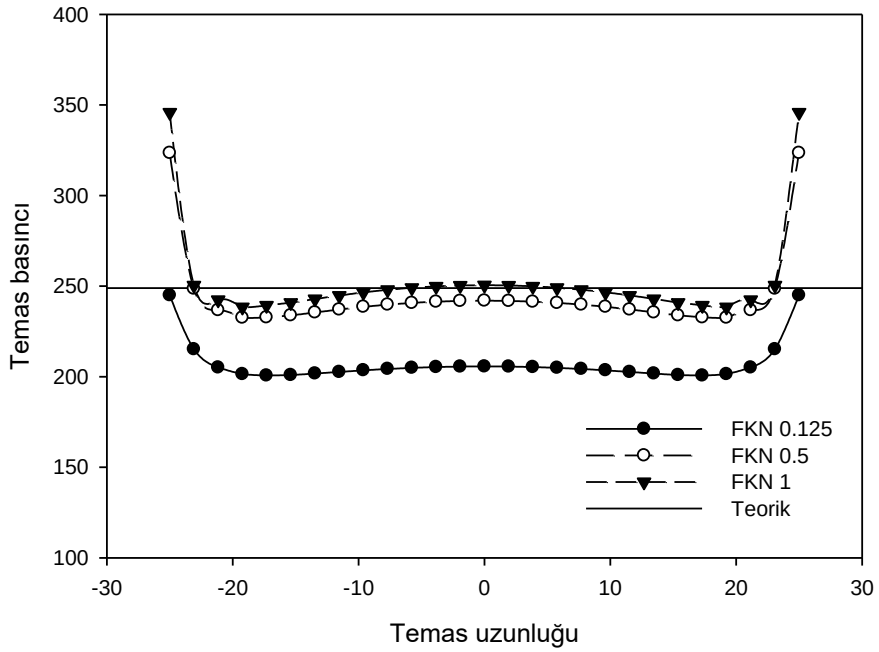

Şekil 6. Eleman boyutu 2 mm için temas basıncının değişimi

Yapılan çalışmalar ve bulgular neticesinde temas katılığı değerinin sonlu sıkı geçme bağlantıların sonlu elemanlar yöntemi çözümlerinden elde edilen sonuçlar üzerinde etkili olduğu görülmüştür. Elastik direnç değerinin ve eleman boyutunun temas katılığını önemli ölçüde etkilediği görülmektedir. Eleman boyutu artıkça yüksek temas katılığı değerlerinin tercih edilmesi gerekmektedir. Ancak bu değerin elastik direnç değerinin tam katından daha fazla olması çözüm hatalarını artıracağından eleman boyutunun küçültülmesi yoluna gidilmelidir. Sıkı geçme bağlantılar özelinde temas katılığının elastik direncin 0.1 katından daha düşük olmasını gerektirecek kadar küçük eleman boyutu işlem süresini ve maliyetini artıracağından tercih edilmemelidir. Aynı koşullar altında asimetrik çözüm daha az iterasyonla çözüme ulaşmaktadır. Bu çalışmada 4 düğümlü elemanlar kullanılmıştır. Modelin 8 düğümlü elemanlar kullanılarak oluşturulduğu çözüm için 0.5 mm eleman boyutunda 4 düğümlü veya 8 düğümlü elemanlar arasındaki fark %0.01'den daha küçüktür.

SONUÇ

Örnek bir sıkı geçme bağlantıda farklı eleman boyutları için sonlu elemanlar çözümünde kullanılan temas katılığının temas basıncı üzerine olan etkileri incelenmiştir. Yapılan çalışma ve değerlendirmeler sonucunda aşağıdaki sonuçlar ortaya çıkmıştır.

Sonlu elemanlar yöntemi kullanılarak sıkı geçme bağlantıların temas analizinde Penaltı ve genişletilmiş Lagrange yöntemleri kullanılması uygundur.

Temas katılığı değerinin elastik direnç değerine tamamen bağlı olduğu bilinmektedir. Genişletilmiş Lagrange yöntemi kullanılarak yapılan analizlerde eleman boyutunun etkisi görülmüştür. Eleman boyutu küçüldükçe seçilmesi gereken temas katılığı değerleri de küçülmektedir.

Eleman boyutu küçüldükçe işlem süresi artacağından temas katılığının elastik direncin 0.1 katından daha küçük ve hassas sonuçlar elde edilmesi adına elastik direncin tam katından büyük olmayacak şekilde modelin oluşturulması önemlidir.

KAYNAKLAR

ANSYS. (2004). *ANSYS Contact Technology Guide*. Canonsburg: Ansys Inc.

Budynas, R. G. ve Nisbett, J. K. (2006). *Shigley's Mechanical Engineering Design*. *McGraw-Hill* (8. bs.). New York: McGraw-Hill.

Campos, U. A. ve Hall, D. E. (2019). Simplified Lamé's equations to determine contact pressure and hoop stress in thin-walled press-fits. *Thin-Walled Structures*, *138*(September 2018), 199–207. doi:10.1016/j.tws.2019.02.008

DIN 7190-1:2017. (2017). *Pressverbände - Teil 1: Berechnungsgrundlagen Und Gestaltungsregeln Für Zylindrische Pressverbände*.

Niemann, G., Winter, H. ve Hoehn, B.-R. (2005). *Maschinenelemente Band I: Konstruktion und Berechnung von Verbindungen, Lagern, Wellen*. *Springer* (4. bs.). Berlin Heidelberg: Springer.

Özel, A., Temiz, Ş., Aydin, M. D. ve Şen, S. (2005). Stress analysis of shrink-fitted joints for various fit forms via finite element method. *Materials and Design*, *26*(4), 281–289. doi:10.1016/j.matdes.2004.06.014

Wriggers, P., Van, T. V. ve Stein, E. (1990). Finite element formulation of large deformation impact-contact problems with friction. *Computers & Structures*, *37*(3), 319–331.

Zahavi, E. ve Barlam, D. M. (2000). *Nonlinear Problems in Machine Design*. CRC Press.

Zhang, Y., McClain, B. ve Fang, X. D. (2000). Design of interference fits via finite element method. *International Journal of Mechanical Sciences*, *42*(9), 1835–1850. doi:10.1016/S0020-7403(99)00072-7.

PROBLEMS AND SUGGESTIONS FOR SUSTAINABLE RENEWABLE SOLAR ENERGY COOPERATIVING

Ahmet HAMZAOĞLU

Electric-Electronic Engineering, Hakkari University

ahmethamzaoglu@hakkari.edu.tr

Ali ERDUMAN

Electric-Electronic Engineering, Hakkari University

alierduman@hakkari.edu.tr

ABSTRACT: Depending on the increase in demand for the use of energy production resources, problems such as diversification of production, transmission of produced energy to the consumer, storage of produced and unavailable energy, complexity of the energy system and difficulty of management are observed in central production systems. One of the methods used to overcome the problems is the use of on-site production systems. On-site production systems provide advantages such as reducing transmission losses and meeting load on-site. The cooperative model used in the installation of on-site production systems is expressed as renewable energy cooperative. Since renewable energy cooperatives are established through the merger of producers, they can provide advantages in terms of reducing energy production costs and ensuring the sustainability of the enterprise. In this study, the technical components necessary for the development of renewable energy cooperatives were examined according to solar energy production management. According to the types of solutions for the technical problems identified on the basis of solar energy source, the things to be done are listed.

Key words: sustainability, renewable energy sources, solar energy, solar energy cooperatives

SÜRDÜRÜLEBİLİR YENİLENEBİLİR GÜNEŞ ENERJİ KOOPERATİFÇİLİĞİ ÖNÜNDEKİ PROBLEMLER VE ÇÖZÜM ÖNERİLERİ

ÖZET: Enerji üretim kaynaklarının kullanımına olan talebin artmasına bağlı olarak merkezi üretim sistemlerinde; üretimin çeşitlendirilmesi, üretilen enerjinin tüketiciye iletilmesi, üretilip kullanılamayan enerjinin depolanması, enerji sisteminin karmaşıklaşması ve yönetimin zorlaşması gibi konularda problemler görülmektedir.

Problemlerin aşılmasına yönelik kullanılan yöntemlerden birisi de yerinde üretim sistemlerinin kullanılmasıdır. Yerinde üretim sistemleri iletim kayıplarının azaltılması ve yükün yerinde karşılanması gibi avantajlar sağlamaktadır. Yerinde üretim sistemi için gerekli olan sermaye tüketici tarafından bizzat karşılanabildiği gibi tüketicilerin birleşip kooperatifleşmesiyle de karşılanabilmektedir. Yerinde üretim sistemlerinin kurulmasında kullanılan kooperatifçilik modeli yenilenebilir enerji kooperatifçiliği olarak ifade edilmektedir. Yenilebilir enerji kooperatifleri üreticilerin birleşmesi ile kurulduğundan enerji üretim maliyetlerinin azaltılması ve işletmenin sürdürülebilirliğinin sağlanması açısından avantaj sağlayabilmektedir. Bu çalışma kapsamında yenilenebilir enerji kooperatifçiliğin geliştirilmesi için gerekli olan teknik bileşenler güneş enerjisi üretim yönetimine göre incelenmiştir. Güneş enerjisi kaynağı bazında tespit edilen teknik problemlerin çözümüne yönelik çeşitlerine göre yapılması gerekenler sıralanmıştır.

Anahtar sözcükler: sürdürülebilirlik, yenilenebilir enerji kaynakları, güneş enerjisi, güneş enerji kooperatifçiliği

GİRİŞ

Dünya genelinde enerjiye olan talep 1971 ile 2017 yılları arasında 2.5 kat artmış ve 5519 Mtoe 'den 13972 Mtoe değerine ulaşmıştır (Fallis, 2013). Enerjiye olan talebin artması kaynakların çeşitlendirilmesi ve yeni olan kaynakların üretime katılması ile mümkün olmaktadır. Günümüzde yeni kaynakların enerji sistemlerine katılımında; enerji üretim maliyetlerinin azaltılması, enerji iletim ve dağıtım kayıplarının azaltılması, düşük karbon salınımlı ve daha verimli sistem gereksinimleri gibi kazanımlar etkili olmuştur. Aynı zamanda toplam kurulu güç içerisinde yerinde üretim tesislerin payı giderek artmaktadır (Bauwens, Gotchev, & Holstenkamp, 2016). Yerinde üretim tesislerinin çevreci olması, bölgesel kaynakları kullanması ve düşük karbon salınımları gibi kazanımları yenilenebilir enerji kaynaklarının daha çok tercih edilmesini sağlamaktadır. Yenilenebilir enerji kaynakları hidroelektrik, rüzgar, güneş, biyoenerji, gel git enerjisi gibi kaynaklar olup bölgesel analizler sonucunda o bölge için uygun kaynak seçilmektedir. Bu kaynakların enerji üretiminde kullanılmasında; kamu üretimi, yap işlet devret, özel sektör girişimi veya kooperatifçilik gibi faklı ekonomik modeller kullanılmaktadır. Kullanılan yöntemlerden biri olan enerji kooperatifçiliği; o bölgede oturan enerji kullanıcılarının üretime katılımını sağlaması, bölgesel refah seviyesinin yükseltmesine katkı sağlaması, sürdürülebilir ekonomiye uygun olması vb. nedenlerden dolayı devletler ve yerel yönetimler tarafından desteklenmektedir (Viardot, 2013). Bu bağlamda yenilenebilir enerji kooperatifi; kooperatif ortaklarının hepsinin aynı dağıtım bölgesinde elektrik abonesi olması ve en az 7 kişinin bir araya gelmesiyle oluşan kooperatif modelidir. Kooperatifi oluşturan ortaklar özel kişiler olabileceği gibi, tüzel kişilerden de oluşabilir. Yenilebilir enerji kooperatifçiliği dünya genelinde 1974 yılında yaşanan petrol krizinden sonra ortaya çıkmıştır (Derneği YD, 2017). Günümüze gelindiğinde ise elde edilen nemanın üyelerine paylaştırıldığı ve çok

katılımcılı bir hal almıştır. Şekil 1'den de görüldüğü gibi birçok yenilenebilir enerji kooperatifi ortaya çıkmıştır.

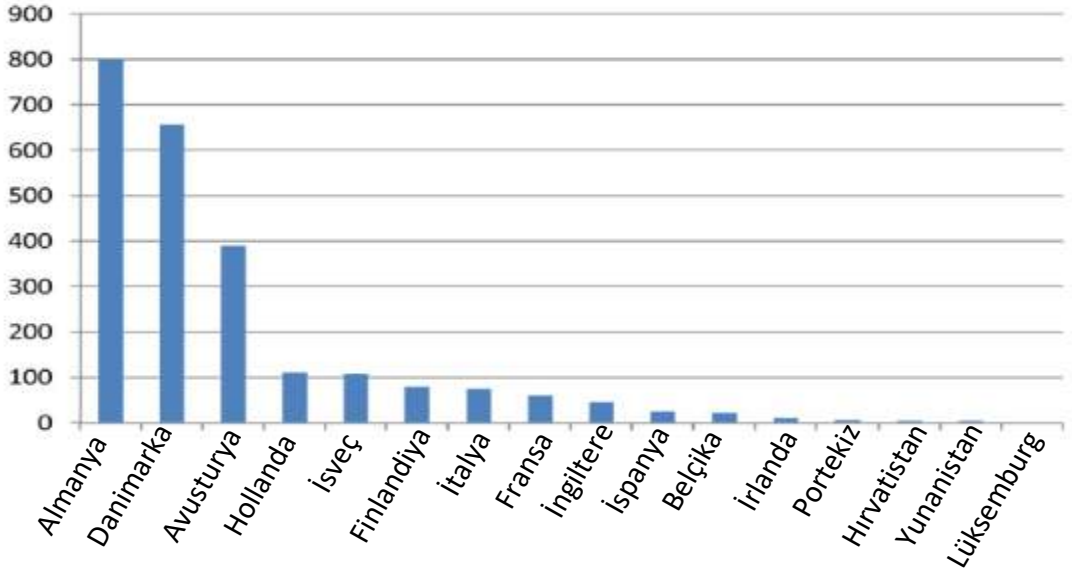

Şekil 1. Yedi Avrupa Ülkesinde Kurulu Yaklaşık Yenilenebilir Enerji Kooperatif Sayıları (Bauwens, Gotchev, & Holstenkamp, 2016).

Almanya, Danimarka, Hollanda gibi ülkeler yenilenebilir enerji kooperatifçiliği konusunda başı çekmektedir. Almanya'da görülen büyümenin başlıca nedeni önümüzdeki birkaç 10 yılda enerji kaynaklarının tamamını yenilenebilir enerjiden karşılamayı planlamaları gelmektedir. Almanya'da 2015 yılı itibariyle bireylerin ve kooperatiflerin elektrik üretimi toplam üretimin %47'si olarak hesaplanmıştır (Derneği YD, 2017) Türkiye'de ise yenilenebilir enerji kooperatifçiliği 2012'den itibaren yasal olarak tanımlanmış ve 2016 yılından itibaren lisanssız elektrik üretimin desteklenmesiyle hız kazanmıştır (Çetinkaya, 2014). Uluslararası Kooperatifler Birliği'nin bir işletmenin kooperatif olabilmesi için belirlediği temel 7 ilke vardır. Bu ilkeler tüm kooperatifler için geçerlidir ve her kooperatifin bünyesinde bulunması gereklidir. Bu ilkeler: gönüllü ve açık üyelik, ortakların demokratik kontrolü, ortakların ekonomik katılımı, özerklik ve bağımsızlık, eğitim öğretim ve bilgilendirme, kooperatifler arası bilgilendirme, topluma karşı sorumluluktur.

Yenilenebilir enerji kooperatifçiliğin geliştirilebilmesi politik, ekonomik, sosyal ve teknik birçok parametrenin birlikte değerlendirilmesi mümkün olacaktır. Türkiye'de yenilenebilir enerji kooperatifi kurulabilmesi 2 Ekim 2013 tarihli ve 28783 sayılı Resmi Gazetede yayınlanan " Elektrik Piyasasında Lisanssız Elektrik Üretimine İlişkin Yönetmelik" in 5. Maddesi ile olası kılınmıştır. Bu çalışma kapsamında yenilenebilir enerji kooperatiflerin kurulumunda güneş enerjisine göre ortaya çıkabilecek teknik problemler ve bunların çözüm yöntemleri incelenmiştir.

Güneş enerji pazarı güneşlenmenin yoğun olduğu Afrika, Orta doğu, Asya, Hindistan ve Çin'de giderek büyümektedir (Costa, Diniz, & Kazmerski, 2016). Türkiye'de güneş enerjisi kullanımında son yıllarda önemli atılımlar yapmaktadır. Güneş enerji santrallerinin doğru planlanması santrallerin geri dönüşümünü doğrudan etkilemektedir. Durusu ve Erduman'ın yapmış olduğu çalışmada santrallerin geri dönüşüm sürelerini etkileyen başlıca parametreler; kurulum ve işletme maliyetleri olarak belirlenmiştir (Durusu & Erduman, 2018). Kurulum parametreleri içinde ise en büyük payı santrallerde kullanılan güneş panelleri almıştır. Güneş panellerinin verimli çalışması bu açıdan önem kazanmaktadır. Güneş enerjisi panellerinin verimini etkileyen parametreler yapısal ve çevresel olarak ikiye ayrılabilir. Yapısal parametreler konusunda Green ve arkadaşlarının yapmış olduğu çalışmada üretimde kullanılan yöntem ve teknikler hakkında ayrıntılı bilgi verilmiştir. Bu yapılardan üretimde kullanılan malzemeler (Si, GaAs InP, CIGS,CdTe vb.) , üretim teknikleri (Monokristal, Polikristal, İnce film vb.) olarak örneklendirilebilir (Green, Emery, Hishikawa, Warta, & Dunlop, 2016). Çevresel değişkenler; sıcaklık, nem, ışınım miktarı, gölgelenme, bulutluluk etkisi, yağmur, kar ve kirlilik olarak sınıflandırılabilmektedir (Akdemir, Durusu, Erduman, & Nakir, 2018; Costa et al., 2016; Kaldellis & Kapsali, 2011; Maghami et al., 2016; Romero-Fiances, Muñoz-Cerón, Espinoza-Paredes, Nofuentes, & De La Casa, 2019). Yapılan bu çalışlardan görüldüğü gibi çevresel etkiler ve bunlarının değişimleri sonucunda güneş enerji panelleri fabrika koşullarında vermiş oldukları verim değerlerinin altında çalışmaktadırlar. Literatürde bu konu üzerine birçok örnek bulmak mümkündür. Asad Ullah ve arkadaşları kirlilik ve açı ilişiklisini incelemiş ve Pakistan'da yaptıkları çalışmada %40 kirliliğe sahip bir panelin 100 gün sonunda üretim değerlerinin 0^0 de % 26, 35^0 de %18,4 ve 90^0 de % 13,5 kadar azaldığı tespit edilmiştir (Ullah, Imran, Maqsood, & Butt, 2019). Negash ve arkadaşlarının Ethiopia'da yaptığı çalışmada ise faklı yerleşim açılarında kirliliğe bağlı kayıplarının % 25,45 ile % 12,54 arasında değiştiğini deneysel olarak tespit etmişlerdir.

Çalışmanın bundan sonraki bölümünde dağıtım sistemi ve yenilenebilir enerji kaynaklarının sisteme entegrasyonunda ortaya çıkan problemler güneş enerjisine bağlı yenilenebilir enerji kooperatifleri için etkileri ve çözüm önerileri sıralanmıştır.

Yenilenebilir Enerji Kooperatifçiliği İçerisinde Güneş Enerji Sistemini Etkileyen Değişkenler

Yenilenebilir enerji kooperatifleri kurulumunda faklı yenilenebilir enerji kaynakları tercih edilebilmektedir. Başlıca yenilenebilir enerji kaynakları ise rüzgar, güneş, hidro, jeotermal, biyokütle, dalga enerjisi ve hidrojen enerjisi olarak sınıflandırılmaktadır. Bu kaynakların şebekeye bağlantısında kendi üretim modellerine göre bağlantı kısıtlar oluşturabilmektedir. Bu çalışmada güneş enerji santrallerinin kısıtları ve bu kısıtlara yönelik çözüm önerileri getirilecektir. Güneş enerji santrallerin kurulumundaki kısıtlar meteorolojik, çevresel ve elektrifikasyon yapısı ve santral teknolojisi bileşenleri olarak dört ana başlıkta toplanabilmektedir.

Meteorolojik Değişkenler

Güneş enerjisine bağlı olarak kurulacak enerji santrallerinin kurulması düşünülen yerin üretim kapasitesinin hesaplanmasında doğrudan etkisi olduğu için meteorolojik değişkenlerin analiz edilmesi büyük önem taşımaktadır. Meteorolojiye bağlı değişkenler; güneşlenme süresi, güneş radyasyonun miktarı, rüzgar, sıcaklık, nem vb. olarak sınıflandırılabilmektedir. Günlük güneşlenme süresi o bölgede güneşin gökyüzünde görülebildiği süre olarak tanımlanmaktadır. Güneşlenme süresinin artması güneşten alınabilecek enerjinin artması anlamına gelmektedir ve güneş enerji santralleri günlük güneşlenme süresilerin uzun olduğu yerlere kurulması yatırım geri dönüşüm sürelerin kısaltmaktadır. Güneşlenme süresini etkileyen değişkenler ise; bulutluluk, bakı ve gündüz süresi olarak tanımlanmaktadır.

Tablo 1. Güneşlenme Süresini Etkileyen Faktörler ve Çözüm Önerileri

Güneşlenme Süresini Etkileyen Faktörler	Santral Üzerindeki Olumsuz Etkisi	Çözüm Önerileri
Bulutluluk	Santral kurulumunun planladığı yerdeki bulutluluğun fazla olması panel verimini düşürecek buna bağlı olarak enerji üretimi azalacaktır.	Santral kurulumu yapılacak bölgelerde aylık ve yıllık bulutluluk ölçümleri yapılarak kurulum için bulutluluğun az olduğu bölgeler tercih edilmelidir.
Bakı	Dağlık bölgelerde santrallerin güneşe karşı konumlarına bakı etkisi denir. Güneş yönünde kurulmayan santraller gölgede kalacağı için üzerlerine düşen ışınım azalacak ve üretim düşecektir.	Bakı etkisinin azaltılması için Kuzey yarım kürede santraller güneye bacak şekilde güney yarım kürede ise kuzeye bakacak şekilde konumlandırılması gerekmektedir.
Gündüz Süresi	Güneşin doğup batma anına kadar geçen süre olan gündüz süresi santrallerin kurulumu süresinde dikkat edilmelidir. Gündüz süresinin az olduğu yerlerde güneşten	Gündüz süresi santralin kurulumunda dünyada üzerindeki konumuyla alakalı olduğu için mümkün olduğu kadar ekvatora yakın bölgelerde

	faydalanma azalacağı için üretim miktarı da düşecektir.	kurulum yapılması gerekmektedir.
Güneş ışınımı	Bir bölgenin güneş enerjisi potansiyeline dair en önemli meteorolojik değişken ölçümü güneş ışımasıdır. Güneş enerjisi üretiminde güneş ışınımının düşük olduğu yerlerde üretim yapılması sistemi verimlilik açısından olumsuz etkilemektedir.	Kurulum yapılacak bölgenin güneş ışınım değerleri piranometre yardımıyla ölçülerek ortalama yıllık ışınım değeri çıkarılıp elde edilen sonuçlara göre kurulum yapılacak bölge belirlenmelidir.
Rüzgar	FV paneller güneş enerjisinden elektrik üretimi yaparken ortaya ısı enerjisi de çıkar. Isı enerjisi ile birlikte ısınan panelin verimliliği azalır ve bu durum üretimi olumsuz etkiler.	Rüzgar ölçümleri sonucunda rüzgar varlığının olduğu bölgelerde güneş enerji santralleri kurulumunun yapılması panellerin doğal yollarla soğutulmasını sağlayarak verimliliği arttıracaktır.
Sıcaklık	Güneş enerjisi kurulumunda sıcaklık değişkeni üretim miktarını doğrudan etkilediği için kurulum yapılacak bölgenin sıcaklık açısından uygun seviyede olmaması üretimdeki verimliliği olumsuz etkilemektedir.	Güneş enerji santrali kurulacak bölgenin sıcaklık ölçümü yapılarak panel verimini olumsuz etkilemeyecek bölgelerde kurulum yapılmalıdır.
Nispi nem	FV panellerin üzerine gelen ışınlar en fazla havadaki nem tarafından emilir, sıçratılır veya yansıtılır. Bu durum panelin güneşlenme süresini azaltır ve verimliliği düşürür.	FV panellerin kurulumu planlamasında nem miktarının belirli periyotlarla ölçülerek nemin az olduğu bölgeye kurulumun yapılması panel verimliliği açısından önem arz etmektedir.

Çevresel Değişkenler

Güneş enerji santrallerin kurulması düşünülen bölgenin coğrafi konumuna bağlı olarak çevresel değişkenlikler gözükebilmektedir. Bu değişkenler ise; bölgenin coğrafi yapısı, bölgenin kirlenme, bitki örtüsü yapısı, yüzey eğimi olarak tanımlanmaktadır.

Tablo 2. Çevresel Değişkenlerin Santral Üzerindeki Etkisi ve Çözüm Önerileri

Çevresel Değişkenler	Santral Üzerinde Olumsuz Etkisi	Çözüm Önerileri
Kirlenme	Panel üzerinde oluşan toz, kuş pisliği vb. değişkenlerden dolayı panelin enerji üretim değeri azalmaktadır.	Panelin kurulacağı bölgenin önceden izleme modelleri ile izlenerek kirlenme periyotlarının belirlenmesi, panellerin temizlenmesi için gerekli düzenek ve personelin maliyete katılması, santrallerin kuş göç ve yaşam alanlarından uzaklara kurulması gerekmektedir.
Bitki örtüsü	Çok ağaçlıklı ve eğimin düşük olduğu yerlerde ağaçların panelleri gölgelemesi sebebi ile enerji üretimi azalmaktadır. Ayrıca panellerin faklı gölgelenmeleri iç sirküle akımlar oluşturmaktadır.	Panellerin kurulum aşamasında bitki örtüsü analiz edilerek panellerin gölgelenmeye en az maruz kalacak yerleşim planı ile konumlandırılması, göllenme boyları önceden hesap edilerek panellerin ekstra yükseltilmesi, faklı göllenmelerin panellerde sirküler akımları oluşturmasını engellenmesi içinse blokaj diyotları projeye konulması gerekmektedir.
Yüzey eğimi	Bölgenin eğinin yüksek olması panellerin gelen ışınımı tam dik olarak almamasına ve nu durum verimin düşmesine sebep olmaktadır.	Panellerin üretim noktası için optimal eğim açısı hesaplanmalı ve bölgeler için çıkartılan değerlere dikkat edilme fazla açılarda açıyı düşürmek için teraslama yapılmalı

		düşük eğimlerde ise konstrüksyioına uygun eğim için gerekli ekstra yükseltmeler yapılmalı bu eklemeler ayrıca kurulum maliyetlerine eklenmelidir. Panellerin eğimi bölgesel olarak değişmesine rağmen genel olarak arazinin ortalama eğiminin %10 eğimli olmasına dikkat edilmelidir.

Elektrifikasyon Altyapısı

Yenilenebilir enerji kaynakları güç sistemi içerisinde iletim ve dağıtım noktalarında bağlanabilmektedir. Bu bağlantılar lisanslı ve lisansız olarak yapılabilmektedir. Genel olarak Elektrifikasyon alt yapısına bağlantılarda iletim ve dağıtım bölgesine göre özel şartları olabilmektedir. Bu şartların neler olduğu kurulması düşünülen bölgesel iletim ve dağıtım sistemi yöneticilerinden ayrıca talep edilmelidir. Genel olarak enerji sistemi üzerinde kurulması düşünülen yenilenebilir enerji kaynakları için dikkate edilmesi gerekenler; bağlantı noktasına olan uzaklığı, bağlantı noktasında olan trafoların yüklenebilirlik değeri, enerji aktarım sisteminde kullanılan iletken tipleri ve kapasiteleri, enerji koruma ve koordinasyon sistemleri ile ölçme sistemleri olarak sınıflandırılmaktadır.

Santral Teknoloji Bileşenleri

Santral teknoloji bileşenleri ise; PV santrallerinde kullanılan panel tipleri verimlilikleri, DC/AC dönüşümünde kullanılan dönüştürücü tipleri, santral içi kablaj, santral içi koruma ve topraklama sistemleri olarak sınıflandırabilmektedir.

Tablo 3. Santral Teknoloji Değişkenlerinin Sistem Üzerindeki Etkileri ve Çözüm Önerileri

Santral Teknoloji Bileşenleri Değişkenler	Santral Üzerine Olumsuz Etkisi	Çözüm Önerileri
Panel Tipleri	FV santral kurulumunda kullanılan panel türünün verimliliğe	Kurulum yapılacak bölgenin coğrafi ve meteorolojik özelliklerine bağlı olarak en uygun

	doğrudan etkisi olduğu bilinmektedir. Sıcaklık, nem vs. gibi değişkenlere bağlı olarak panel verimleri değişmektedir.	panel seçiminin yapılması verimlilik açısından önem arz etmektedir.
DC/AC Dönüştürücü Tipleri ve Topolojileri	FV santrallerden elde edilen DC enerjinin başka bir hatta iletilmesi aşamasında yaşanan kayıplarda dönüştürücü tipi de etkendir.	FV santrallerdeki paneller kendi içlerinde gruplandırılarak her gruba uygun dönüştürücü kullanılması grup içerisindeki sistemsel arızaların tüm tesisi etkilemesini engelleyecektir.
Santral İçi Koruma Sistemleri	Enerji üretimi ve iletimi aşamasında sahadaki koruma teçhizatlarının eksikliği veya bakımdan uzak olması işletmeyi maddi anlamda büyük kayıplara götürebilir.	Santrallerde kullanılan sistem koruma teçhizatlarının bakımlarının veya kullanılma ömrü tamamlanmış ise değişimlerinin gerçekleştirilmesi işletmenin küçük çıktılarla büyük zararlardan kurtaracaktır.
Kablolama	Üretilen enerjinin yeraltı ve havai hatlarda iletilmesi ve bu aşamada doğru iletkenlerin seçilmemesi sistemsel arızaları ve enerji kayıplarını beraberinde getirecektir.	Ülkemizde iletim ve dağıtımdaki enerji kayıplarının %14 civarlarında olduğu gerçeği, işletmelerde kullanılacak iletkenlerin işletmeye en uygun olmasını zorunlu hale getirmektedir. Bu sayede kısa mesafelerde iletim ve dağıtım kayıplarının azaltılması mümkün hale gelecektir.
Topraklama	Kurulması planlanan FV sistemdeki tüm elektriksel teçhizatın topraklamalarının yapılmaması veya tek	FV sistemlerde her elektriksel alet veya teçhizat için ayrı ayrı topraklama noktaları oluşturulması ve sistemin

	bir topraklama hattına bağlanarak sistemin korunması ciddi riskler taşımaktadır.	bu şekilde topraklanması bölgesel oluşabilecek arızaların tüm sistemi etkilemesini engelleyerek üretim sisteminin verimliliğini etkilemeyecektir.

Türkiye şartlarında yenilenebilir enerji kooperatifçiliği adı altında şirket kurmak ve lisans almaktan muaf tutulan kooperatiflerin kuruluşunu şöyle sıralayabiliriz; en az 7 tüzel veya gerçek kişiden oluşabilecek ortaklık, ortakların bir araya gelmesiyle tüzüğün oluşturulması, ana sözleşmenin kooperatifçilik genel müdürlüğüne gönderilmesi, kooperatif ortakları tarafından seçtikleri yenilenebilir enerji kaynağı ile nerede üretim yapılacağının belirlenmesi, güneş enerjisi paneli kurulumu yapılacak arazi için bulundukları ilin gıda tarım ve hayvancılık il müdürlüğünden marjinal tarım arazisi yazısının alınması, yine kurulum yapılacak arazi için 'çevresel etki değerlendirme gerekli değildir' kararının çevre ve şehircilik il müdürlüklerinden alınması, bu aşamaya kadar hazırlanan tüm belgeler ile o bölgedeki elektrik dağıtım şirketine başvurulması, dağıtım şirketine başvuru sonrası müteakip 90 gün içinde tesis projesi ve bağlantı hattı onay için TEDAŞ'a sunulur, projenin onayı ile birlikte kurulum yapılacak bölgedeki belediyeden imar izni alınır ve son olarak yenilenebilir enerji sistem kurulumu gerçekleştirilir.

SONUÇ

Yenilenebilir, sürdürülebilir, çevreci ve tükenmeyen enerji kavramlarının son yıllarda dünyada yükselen bir trende sahip olmasıyla birlikte enerji yatırımcıları ve tüzel kişiler yenilenebilir enerji kaynaklarına ve buna bağlı enerji tüketicilerinin örgütlenmesiyle oluşan kooperatifçilik kavramına yönelmişlerdir. Bu çalışmayla birlikte yenilenebilir enerji kaynaklarından olan güneş enerjisi önündeki teknik problemler incelenerek çözüm önerileri sunulmuştur. Bununla birlikte yenilenebilir güneş enerji kooperatifçiliği kavramı ortaya konarak kooperatifleşmenin önündeki teknik problemler ve kooperatifleşme süreci araştırılıp gerekli olan bilgiler derlenerek özet halinde sunulmuştur. Sistem kurulum maliyeti ve enerji karlılığı sağlayan enerji kooperatiflerinin ülkemizde yaygınlaşması ile enerji iletim-dağıtım sistemlerinde görülen birçok teknik kaybın önüne geçildiği tespit edilmiştir. Son olarak yenilenebilir enerji kooperatifçiliğinde güneş enerji santrallerinin kurulum ve işletme şemasındaki planlamacı ve üreticiler için muhtemel teknik problemler ve çözüm önerileri verilmiştir.

BİLGİLENDİRME

Bu çalışma, Hakkari Üniversitesi Bilimsel Araştırma Projeleri Koordinatörlüğü'nün FM19BAP18 numaralı projesi ile desteklenmiştir.

KAYNAKLAR

Fallis, A. (2013). *Journal of Chemical Information and Modeling*, *53*(9), 1689-1699.

Bauwens, T., Gotchev, B., & Holstenkamp, L. (2016). Energy Research & Social Science What drives the development of community energy in Europe ? The case of wind power cooperatives, *13*, 136–147.

Viardot, E. (2013). The role of cooperatives in overcoming the barriers to adoption of renewable energy. *Energy Policy*, *63*, 756-764.

Derneği, Y. D. (2017). Enerji Kooperatifleri El Kitabı.

Bauwens, T., Gotchev, B., & Holstenkamp, L. (2016). Energy Research & Social Science What drives the development of community energy in Europe ? The case of wind power cooperatives, *13*, 136–147.

Çetinkaya, H. B. (2014). Proceeding book, 72–75.

Costa, S. C. S., Diniz, A. S. A. C., & Kazmerski, L. L. (2016). Dust and soiling issues and impacts relating to solar energy systems: Literature review update for 2012-2015. *Renewable and Sustainable Energy Reviews*, *63*, 33–61. https://doi.org/10.1016/j.rser.2016.04.059

Durusu, A., & Erduman, A. (2018). An Improved Methodology to Design Large-Scale Photovoltaic Power Plant. *Journal of Solar Energy Engineering, Transactions of the ASME*, *140*(1). https://doi.org/10.1115/1.4038589

Green, M. A., Emery, K., Hishikawa, Y., Warta, W., & Dunlop, E. D. (2016). Solar cell efficiency tables (version 47). *Progress in Photovoltaics: Research and Applications*, *24*(1), 3–11. https://doi.org/10.1002/pip.2728

Akdemir, H., Durusu, A., Erduman, A., & Nakir, I. (2018). Effect of energy management of a grid connected photovoltaic/ battery/load system on the optimal photovoltaic placement on a national scale: The case of Turkey. *Journal of Solar Energy Engineering, Transactions of the ASME*, *140*(2). https://doi.org/10.1115/1.4039077

Costa, S. C. S., Diniz, A. S. A. C., & Kazmerski, L. L. (2016). Dust and soiling issues and impacts relating to solar energy systems: Literature review update for 2012-2015. *Renewable and Sustainable Energy Reviews*, *63*, 33–61. https://doi.org/10.1016/j.rser.2016.04.059

Kaldellis, J. K., & Kapsali, M. (2011). Simulating the dust effect on the energy performance of photovoltaic generators based on experimental measurements. *Energy*, *36*(8), 5154–5161. https://doi.org/10.1016/j.energy.2011.06.018

Maghami, M. R., Hizam, H., Gomes, C., Radzi, M. A., Rezadad, M. I., & Hajighorbani, S. (2016). Power loss due to soiling on solar panel: A review. *Renewable and Sustainable Energy Reviews*, *59*, 1307–1316. https://doi.org/10.1016/j.rser.2016.01.044

Romero-Fiances, I., Muñoz-Cerón, E., Espinoza-Paredes, R., Nofuentes, G., & De La Casa, J. (2019). Analysis of the performance of various pv module technologies in Peru. *Energies*, *12*(1). https://doi.org/10.3390/en12010186

Ullah, A., Imran, H., Maqsood, Z., & Butt, N. Z. (2019). Investigation of Optimal Tilt Angles and Effects of Soiling on PV Energy Production in Pakistan. *Renewable Energy*, *139*, 830–843. https://doi.org/10.1016/j.renene.2019.02.114.

MECHANICAL PROPERTIES OF STEAM CURED CONCRETE INCORPORATING QUARRY DUST

Didar Yasin NAJMADDIN

G. Directory of Projects/Ministry of Higher Education and Scientific Research-KRG/Iraq,

didar.najmaddin@mhe-krg.org

Ayşe Yeter GÜNAL

Civil Engineering Department, Gaziantep University, Turkey

agunal@gantep.edu.tr

ABSTRACT: Steam curing at atmospheric pressure is an important technique for obtaining high early strength values in concrete production. It also aids in faster and safer construction as sufficient strength is attained in short period and maintained without any other form of curing. Concrete type, as well as curing period and temperature, is an important parameter in the steam-curing process. The strength development depends on steam curing cycle. The parameters involved in a steam curing cycle include a delay period, a gradual increase to a temperature where it is to be maintained for a specific curing period followed by gradual cooling. Quarry dust has been identified as possible replacement for sand in concrete works. Crushed rock aggregate quarrying generates considerable volumes of quarry fines, often termed "quarry dust". The finer fraction is usually smaller than 5mm in size. In this study, samples of concrete were made using varying contents of quarry dust as fine aggregate. The quantity of quarry dust was varied from 0% to 60% against quarry dust at intervals of 10%. For each mix, specimens were standard-cured in a water bath of room temperature and steam-cured at 70◦C maximum temperature over 24 h. And the specimens tested for compressive and flexural strength of the concrete and the results were satisfactory.

Keywords: Compressive strength, Flexural strength, Steam curing, Quarry dust.

A STUDY TO FABRICATE ENVIRONMENTALLY-FRIENDLY CONDUCTIVE TEXTILES

Burak SÖGÜT

Suleyman Demirel University Graduate School Of Natural And Applied Sciences

sogutburak93@gmail.com

Kerim YAPICI

Suleyman Demirel University, Engineering Faculty, Chemical Engineering Dept. Isparta

kerimyapici@sdu.edu.tr

Demet YILMAZ

Suleyman Demirel University, Engineering Faculty, Textile Engineering Dept. Isparta

demetyilmaz@sdu.edu.tr

ABSTRACT: It is a threat to both nature and human health because it causes pollution in the chemicals used in textile products and waste water. For this reason, materials that do not harm the ecosystem should be selected and such chemicals should be made legally mandatory. In this study, the effect of reduced graphene oxide nanosuppression on electrical conductivity, consisting of a single process instead of impregnation and reduction processes, which would cause less damage to the environment in terms of water consumption and waste formation, was examined.

Key words: Conductive textiles, conductive materials, pollution, graphene, reduced graphene oxide, nanomaterials

ÇEVRE DOSTU İLETKEN TEKSTİLLERİN ÜRETİMİNE YÖNELİK BİR ÇALIŞMA

ÖZET:

Tekstil ürünlerinde kullanılan kimyasal maddeler ile atık sularında kirliliğe neden olması sebebiyle hem doğaya hem de insan sağlığını tehdit oluşturmaktadır. Bu nedenle kullanılan kimyasalların ekosisteme zararı olmayan malzemeler seçilmeli ve bu tarz kimyasalların yasal olarak zorunlu hale getirilmesi gerekmektedir. Bu çalışmada da, emdirme ve indirgeme işlemleri yerine tek bir işlemden oluşan, su tüketimi ve atık oluşumu açısından çevreye daha az zarar oluşturacak indirgenmiş

grafen oksit nanosüspansiyon uygulamasının elektriksel iletkenliğe etkisi incelenmiştir.

Anahtar sözcükler: İletken tekstiller, iletken malzemeler, grafen, indirgenmiş grafen oksit, çevre kirliliği, nanomalzemeler

GİRİŞ

Teknolojinin hızla ilerlemesi ile birlikte insan ihtiyaçları çeşitlenerek artmış ve bu durum yeni ve pratik pek çok ürünün geliştirilmesini sağlamıştır. Tekstil sektöründe de bu ihtiyaçlara cevap verebilmek amacıyla değişik yapı ve özelliklerde malzemeler kullanılarak, çeşitli tekniklerle farklı yapılarda ürünlerin üretilmesine yönelik çalışmalar artmış ve sonuçta değişik yapı ve özellikte tekstil ürünleri üretilmeye başlanmıştır. Günümüzde özellikle elektronik ürünlere olan ilgi ve beraberinde kullanımın artması ile birlikte elektronik sistemlerle normal tekstil yapılarının bir araya gelmesi üzerine çalışmalar yoğunlaşmaktadır. Bu özelliklerinden ötürü, "elektronik fonksiyonelliğe ve aynı zamanda da tekstil özelliklerine sahip malzemeler" elektronik tekstil olarak tanımlanmaktadır. Elektronik tekstillerin özellikle elektronik tıp adıyla sağlık, askeri, savunma alanları ile günlük yaşamda kullanımları dikkat çekmektedir. Mobil telefon veya mp3 çalarlar ile bağlantı kurarak müzik dinlemeye ve iletişim kurmaya olanak sağlayan giysiler, kalp atışlarını kontrol edebilen yatak çarşafları elektronik tekstillere verilebilecek örneklerdir. Elektronik bir tekstil yapısının elde edilebilmesi için öncelikle iletken özelliğe sahip lif, iplik veya kumaş yapısının elde edilmesi gerekmektedir. İletkenlik özelliğinin tekstil yapılarına kazandırılması için pek çok yöntem bulunmaktadır. Ancak, kolay bir proses olma ve tekstil endüstrisinde de uygulanabilme açısından emdirme ve kaplama yöntemleri bu yöntemler içerisinde yaygın kullanıma sahiptir. Bununla birlikte, iletkenliğin kazandırılması için gümüş, karbon tozu, karbon nanotüp, altın, bakır gibi iletken özelliğe sahip malzemeler kullanılmaktadır. Belirli düzeyde iletkenliğe sahip tekstil materyalleri ile elektronik tekstil örnekleri geliştirilmesine rağmen, ilk geliştirilen örneklerin hafiflik, yumuşaklık, esneklik, eğilme-bükülme gibi özellikler açısından yetersiz olma, yüksek maliyet gerektirme yanında yıkama, sürtme, eğme sonucunda iletkenlikte kayıp ve düşük stabilite gibi önemli problemleri bulunmaktadır. Bu nedenle, elektronik tekstil ürünler henüz yaygın kullanıma sahip değildir. Yüksek iletkenlik yanında elektriksel kararlılık, esneklik, hafiflik, kolay temin edilebilme ve endüstriyel proseslere uygunluk gibi özelliklere olan ihtiyaç sebebiyle farklı malzeme ve yöntemlerin geliştirilmesi konusunda çalışmalar yapılmaktadır. İletkenliğin tekstil malzemelerine kazandırılması için adı geçen yeni malzemeler içerisinde en dikkat çekenlerden biri de grafendir. Grafen, hekzagonal (bal peteği) kafes düzleminde düzenli karbon atomlarının sp2 hibritleşmesi yaptığı tek katmanlı bir yapıdır. İki-boyutlu (2D) ve tek atom kalınlığında olması ve kuvvetli bağ yapısı ile eşsiz moleküler bir yapı olan grafen, çok iyi elektrik, elektrokimyasal, optik, termal ve mekanik özelliklere sahiptir (Yazıcı vd., 2016; Ersoy vd., 2015).

Grafenin tekstil kumaşlarına uygulanması amacıyla yapılan çalışmalarda, Hummers metodu ile grafen oksit (GO) sentezlenmekte ve daha sonra emdirme yöntemi ile tekstil kumaşlarına aplike edilmektedir. Özellikle iletkenliğin arttırılması amacıyla grafen içerikli nanosüspansiyon tekstil kumaşlarına belirli sıcaklık ve sürede 1, 5, 10, 20, 40 gibi değişen sayılarda uygulanmakta ve kumaşlar belirli sıcaklık ve sürede kurutma işleminden geçirilmektedir. Emdirme-ön kurutma-kurutma işlemleri sonrasında, $NaBH_4$, N_2H_4, $C_6H_8O_6$, $Na_2S_2O_4$ ve NaOH gibi çeşitli indirgenler kullanarak indirgeme işlemi ve takiben yıkama, kurutma işlemleri yapılmaktadır. Emdirme, kurutma, indirgeme, yıkama ve kurutma gibi işlemlerden oluşan emdirme yöntemi, hem işlem maliyeti hem de su ve kimyasal madde tüketimi açısından yeterince çevreci değildir. Dolayısıyla, halen kolay uygulanabilir, ve su tüketimi, kimyasal atık oluşumu, kurutmadan kaynaklı enerji maliyeti gibi etkileri mümkün olduğunca azaltacak, düşük maliyetli üretim proseslerine ihtiyaç bulunmaktadır.

Bilindiği gibi, tekstil ürünlerinin özelliklerini geliştirmek için yıkama, boyama, yumuşatma, haşıl sökme vb. çeşitli terbiye işlemleri yapılmaktadır. Bununla birlikte, son yıllarda tüketicinin tekstil ürünlerinden beklediği özellikleri karşılamak için fonksiyonel özelliklere yönelik çeşitli apre işlemleri yapılmaktadır. Yapılan bu işlemler, su, kimyasal madde tüketimini beraberinde getirmektedir. Günümüzde üretim yapan endüstrilerin su tüketimi ve atık su değerleri değerlendirildiğinde, tekstil sektörü 1000-5000 m^3/gün arasında değişen miktar ile en başta gelmektedir (Balcı, 2016). Atık su hacmine ve atılan su içerisinde bulunan kimyasal maddeler incelendiğinde, tekstil sektörü diğer sektörler bakımından çevre kirliliğinde en büyük kirletici durumunda olduğu ortaya çıkmaktadır (Vandevivere vd., 1998). Tekstil prosesleri içerisinde özellikle boyama, baskı ve apre gibi işlemlerden oluşan terbiye prosesi yüksek miktarda su tüketimi ve atık su oluşumuna neden olmaktadır. Bununla birlikte, elyaftan son ürüne kadar olan prosesler içerisinde son işlem olan terbiye prosesinde meydana gelen proses hatalarının düzeltilmesi için ekstra işlemlerin yapılması gerekmekte ve bu da terbiye işlemlerin su tüketimi ve kimyasal atık oluşumu açısından etkilerini daha da arttırmaktadır. Yapılan araştırmalarda, 1 kg tekstil ürünü için 40 L atık suyun oluştuğu belirlenmiştir. Atık suların içerisinde; yumuşatıcı malzemeler, Pentaklorofenoller, Etilklorofosfatlar vb. toksik bileşenler, nişasta, sentetik reçine, NH_4^+ ve $ZnCl_2$ gibi çeşitli kimyasallar, asit ağır metaller, pigmentler, tuzlar, ağır metaller ve boyalar bulunmaktadır (Biroğlu, 2012). Bu maddeler içerisinde spesifik iyonlar, yağ ve hidrokarbonlar, Cl iyonu, fenol bileşikleri toprakta ciddi sorun yaratabilecek kimyasal atıklardır. Tekstil su atıklarının kirletici içeriğine bakıldığında, atık suyun biyolojik oksijen miktarı 80- 6000 mg/L, kimyasal oksijen miktarı 150- 12000 mg/L, toplam klor miktarı 1000- 1600 mg/L, toplam askıda kalan katı madde 15- 8000, toplam çözünmüş katı madde 2900- 3100 mg/L ve atık sudaki renk miktarı 50- 2500 Pt- Co olarak tespit edilmiştir (Arslan vd., 2016). Atık suların içerdiği kimyasal maddelerin yeraltı ve yer üstünde yaşayan her türlü biyolojik canlılar üzerinde oluşturduğu tehditleri yanında temiz su kaynakları, hava, toprak gibi canlı hayatının yapıtaşlarına olan olumsuz etkileri nedeniyle atık su oluşumunun azaltılması ve oluşan atık suyun da filtrelenmesi gerekmektedir. Dolayısıyla, günümüzde tekstil başta olmak üzere her türlü endüstri dalında canlılar ve çevre ile

daha dost teknolojilerin kullanılmasına ihtiyaç bulunmaktadır. Daha çevreci malzeme ve yöntemler kullanılmalıdır.

Son yıllarda iletken tekstil üretiminde, gümüş vb. metalik nanopartiküller, karbon nanotüp, karbon tozu ve grafen tabanlı nanomalzemeler kullanılmaktadır. Grafen sentezlenmesinde, uygulanan iki ana yöntem bulunmaktadır. Bunlar sırası ile tabandan tepeye; kimyasal buhar depolama (CVD), SiC üzerinde epitaksiyel büyüme, ark boşalması vb. ve tepeden tabana; grafit oksitin kimyasal eksfoliasyonu ve grafitin ultrasonik ve/veya mekanik parçalayıcılı karıştırıcı yardımı ile sıvı faz eksfoliasyon prosesleridir. Tabandan tepeye prosesler ile yüksek saflıkta, yapısal düzenli, kırışıklıklardan bağımsız ve geniş alanlı grafen eldesi mümkün olmasına karşın, kütlesel ölçekte üretilmesi oldukça maliyetlidir. Buna karşın, tepeden tabana yöntemler ile düşük maliyette ve geniş ölçekte grafen üretilme potansiyeli daha yüksektir.Grafit oksitin eksfoliasyonu/indirgenmesi, diğer üretim yöntemleri ile kıyaslandığında basit ve düşük maliyette oluşu potansiyel olarak ölçeklendirilebilir olmasına olanak sağlamaktadır (Zhong vd., 2015).

Grafenin tekstil malzemelerinin elektriksel iletkenliğin arttırılması amacıyla genellikle Hummers metodu ile elde edilen ve çeşitli konsantrasyonlarda hazırlanan grafen oksitin (GO) tekstil kumaşlarına emdirilmekte, ön kurutma ve kurutma işlemleri sonrasında $NaBH_4$, N_2H_4, $C_6H_8O_6$, $Na_2S_2O_4$ ve NaOH gibi çeşitli indirgenler kullanarak indirgeme işlemi yapılmaktadır. Kimyasal indirgeme işlemi kompleks olduğu gibi yüksek miktarda kimyasal madde ve su tüketimi yanında kullanılan kimyasal maddelerin toksit olması nedenleriyle çevreyle dost değildir (Javed vd., 2014; Cai vd., 2017). Bununla birlikte, kimyasal indirgeme sonrasında yapılan kurutma işlemleri, son ürünün özelliklerini olumsuz etkileyebilmektedir (Javed vd., 2014). Bu nedenle, çevre ile dost, tehlikeli kimyasal maddeleri içermeyen, tek adımlı üretim proseslerine ihtiyaç bulunmaktadır (Javed vd., 2014; Ramadoss vd., 2015; Woltornist vd., 2015; Cai vd., 2017; Karim vd., 2017). Bu çalışmada da, emdirme ve indirgeme işlemleri yerine tek bir işlemden oluşan ve su tüketimi ve atık oluşumu açısından çevreye daha az yük oluşturacak bir grafen uygulamasının elektriksel iletkenliğe etkisinin incelenmesi amaçlanmıştır. Çalışmada, indirgenmiş grafen oksit (rGO) kullanılarak indirgeme işleminin elimine edilmiştir.

YÖNTEM

Bu çalışma kapsamında indirgenmiş grafen oksit (rGO) nanosüspansiyonu, viskon ipliklerine aplike edilmiş ve elektriksel iletkenlik özelliğindeki değişim incelenmiştir. rGO'nun ipliklere uygulanabilmesi için tekstil sektöründe de kullanabilmek açısından tekstil işletmelerinde kullanılan bobin boyama yöntemi tercih edilmiştir. Şekil 1'de görüldüğü gibi, viskon iplikleri bir bobin üzerine sarılmıştır. Hazırlanan bobin ve rGO bir tüp içerisine konulmuştur. Uygulama sırasında rGO nanosüspansiyonun tüm ipliklere uygulanabilmesi için tüp Gyrowash numune yıkama makinasına yerleştirilerek nanosüspansiyonun hareket etmesi sağlanmıştır. Daha sonra, tekstil

işletmelerinde kullanılan viskon ipliği bobin boyama işlem şartları esas alınarak, 60 °C'de 30 dakika viskon ipliğinin rGO nanosüspansiyonu ile muamele etmesi sağlanmıştır. Uygulama sonrasında bobinler oda sıcaklığında 24 saat kurumaya bırakılmıştır. Çalışmada ayrıca, tekstil ürünlerin kullanımları sırasında yapılan yıkama işleminin elektriksel iletkenlik özelliğine etkisini belirlemek amacıyla bobinler 49 °C'de 90 dakika yıkanmıştır. Söz konusu yıkama şartları, 10 yıkamaya eşdeğer olarak kabul edilmektedir. İpliklerin elektriksel iletkenlik özelliği iki-uç nokta yöntemiyle multimetre cihazı kullanılarak gerçekleştirilmiş olup, ölçüm sonucunda iletkenliğin tersini ifade eden direnç değerleri elde edilmiştir. Direnç değeri azaldıkça, iletkenlik artmaktadır. Direnç ölçümleri 10 defa tekrarlanıp ortalama değer alınmıştır.

(a) (b)

Şekil 1. rGO nanosüspansiyon uygulanmamış (a) ve uygulanmış (b) viskon iplik bobin görüntüleri

BULGULAR

Bobin boyama işlemi ile indirgenmiş grafen oksit (rGO) nanosüspansiyon aplike edilen viskon ipliklerin elektriksel iletkenlik özelliğini sembolize eden elektriksel direnç değerleri Çizelge 1'de verilmiştir. Direnç değerleri incelendiğinde, bobin boyama işlemi sonrasında ipliklerin 248 kilo.ohm seviyesinde direnç değerine sahip olduğu ve yıkama işlemi sonrasında ipliklerin direnç değerinin 1170 kilo.ohm'a yükseldiği gözlemlenmiştir. Elde edilen bu sonuç, 10 yıkama sonrasında bile ipliklerin iletkenlik özelliğini halen sağladığı gözlemlenmiştir.

Çizelge 1. Emdirme İşlemi ve Yıkama Sonrası Elektriksel Direnç Değerleri

	Yıkama öncesi	**Yıkama sonrası**
Direnç (MΩ)	0,248	1,17

ÖNERİLER

Çalışmada, tek adımlı bir proses ile elde edilen indirgenmiş grafen oksit (rGO) kullanılarak daha çevreci bir prosesden oluşan uygulama ile belirli düzeyde iletkenliğe sahip iplik üretimi gerçekleştirilmiştir. Elde edilen ipliklerin ve bu ipliklerden elde edilen tekstil kumaşlarının performans özelliklerinin de incelenmesi gerekmektedir. Ayrıca, elde edilen iplikler elektronik cihazların neden olduğu elektromanyetik dalgalara karşı koruyucu tekstil ürünlerinde kullanımı mümkün olmakla birlikte sensör, enerji depolama gibi farklı kullanımlar için elektriksel iletkenlik özelliğinin iyileştirilmesi konusunda çalışmaların yapılması gerektiği düşünülmektedir.

TEŞEKKÜR

Bu çalışma Süleyman Demirel Üniversitesi Bilimsel Araştırma Projeleri Koordinasyon Birimince Desteklenmiştir. Proje Numarası: 7354.

KAYNAKLAR

Arslan, S., Eyvaz, M., Gürbulak, E., Yüksel, E. (2016). *A Review of State-of-the-Art Technologies in Dye-Containing Wastewater Treatment – The Textile Industry Case*, E. Kumbasar, A. Korlu (Eds.), Textile Wastewater Treatment. Retrieved from https://www.intechopen.com/books/textile-wastewater-treatment/a-review-of-state-of-the-art-technologies-in-dye-containing-wastewater-treatment-the-textile-industr

Balcı, E (2016). *Tekstil atık sularının membran proseslerle arıtımı ve endüstriyel su geri kazanımı*. Yüksek Lisans Tezi, Gebze Teknik Üniversitesi, Fen Bilimleri Enstitüsü, Gebze

Biroğlu, N. (2012). *Bir tekstil atık suyunun koagülasyon – flokülasyon – membran filtrasyon süreçleri ile arıtılabilirliğinin incelenmesi*. Yüksek Lisans Tezi, Osmangazi Üniversitesi, Fen Bilimleri Enstitüsü, Eskişehir.

Cai, G., Xu, Z., Yang, M., Tang, B., Wang, X. 2017. '*Functionalization of Cotton Fabrics Through Thermal Reduction of Graphene Oxide', Applied Surface Science,* 393, 441-448.

Ersoy M.S., Dönmez U., Yildiz K., Salan T., Yazici M., Tiyek İ., Alma M.H., (2015), *Graphene Applied Textile Materials for Wearable E-Textiles, 5th International Istanbul Textile Congress 2015: Innovative Technologies "Inspire To Innovate, pp. 82-86, 11th -12th September 2015, Istanbul Technical University, Istanbul, Turkey.*

Javed, K., Galib, C. M. A., Yang, F., Chen, C. M., Wang, C. 2014. '*A New Approach to Fabricate Graphene Electro-Conductive Networks on Natural Fibers by Ultraviolet Curing Method', Synthetic Metals*, 193, 41-47.

Karim, N., Afroj, S., Tan, S., He, P., Fernando, A., Carr, C., Novoselov, K. S. 2017. '*Scalable Production of Graphene-Based Wearable E-Textiles', ACS Nano*, 11(12), 12266-12275.

Ramadoss, A., Saravanakumar, B., Kim, S. J. 2015. *'Thermally Reduced Graphene Oxide-Coated Fabrics for Flexible Supercapacitors and Self-Powered Systems', Nano Energy,* 15, 587-597.

Vandevivere P.C., Bianchi R., Verstrate W., (1998), *"Treatment and Reuse of Wastewater from the Textile Wet Processing Industry: Review of Emerging Technologies", Journal of Chemical Technology and Biotechnology, 72(4)*, 289-302.

Woltornist, S. J., Alamer, F. A., McDannald, A., Jain, M., Sotzing, G. A., & Adamson, D. H. 2015. *Preparation of conductive graphene/graphite infused fabrics using an interface trapping method. Carbon*, 81, 38-42.

Yazıcı, M., Tiyek, İ., Ersoy, M. S., Alma, M. H., Dönmez, U., Yıldırım, B., Salan, T., Karataş, Ş., Uruş, S., Karteri, İ., ve Yıldız, K., (2016), *Modifiye Hummers Yöntemiyle Grafen Oksit (GO) Sentezi ve Karakterizasyonu, Gazi Üniversitesi Journal of Science Part C*, 4(2), 613-623.

Zhong, Y. L., Tian, Z., Simon, G. P., Li, D. 2015. *Scalable Production of Graphene Via Wet Chemistry: Progress and Challenges, Materials Today*, 18(2), 73-78.

STOCHASTIC CHINESE POSTMAN PROBLEM AND AN APPLICATION

Özlem ÇOMAKLI SÖKMEN, Erzurum Technical University, ozlem.sokmen@erzurum.edu.tr

Mustafa YILMAZ, Ataturk University, mustafay@atauni.edu.tr

ABSTRACT: Arc routing problems are problems used to determine the shortest path or paths returning to the starting vertex by traversing all arcs or edges on a graph at least once. Chinese Postman Problem (CPP), one of the arc routing problems; can be defined as the problem of returning to the starting point after a postman traverses all connections on the defined network. Since various factors such as weather conditions, traffic density, traffic accidents, construction and repair works change the arrival time between the two vertices, CPP was applied on a sample problem with a chance constrained stochastic programming approach in this study. In this study, the objective function coefficients are considered as random variables. The mathematical model formed was solved by using GAMS programming language.

Key words: stochastic chinese postman problem, arc routing problem, chance constrained programming

STOKASTİK ÇİNLİ POSTACI PROBLEMİ VE BİR UYGULAMA

ÖZET: Ayrıt rotalama problemleri, bir çizge üzerinde yer alan tüm ayrıtlardan en az bir kere geçilerek başlangıç düğümüne dönen en kısa yol veya yolların belirlenmesinde kullanılan problemlerdir. Ayrıt rotalama problemlerinden biri olan Çinli Postacı Problemi (CPP) ise; tanımlanan ağ üzerindeki tüm bağlantıların bir postacı tarafından ziyaret edilerek, başlangıç noktasına dönülmesi problemi olarak tanımlanabilir. Hava koşulları, trafik yoğunluğu, trafik kazaları, yapım ve onarım çalışmaları gibi çeşitli etkenler iki düğüm arasındaki varış süresini değiştirdiğinden dolayı bu çalışmada bir örnek problem üzerinde üzerinde şans kısıtlı stokastik programlama yaklaşımı ile CPP uygulanmıştır. Çalışmada amaç fonksiyonu katsayıları rasgele değişkenler olarak ele alınmıştır. Oluşturulan matematiksel model GAMS programlama dili kullanılarak çözüme ulaştırılmıştır.

Anahtar sözcükler: stokastik çinli postacı problemi, ayrıt rotalama problemi, şans kısıtlı programlama

GİRİŞ

Çinli Postacı Problemi (CPP) ilk kez 1962 yılında Mei-Ko Kwan tarafından incelenmiştir. Problemde bir postacının postaneden aldığı mektupları mümkün olan en kısa yoldan (Euler tur) şehrin tüm caddelerine dağıtması ve bu işlemden sonra postaneye geri dönmesi amaçlanmaktadır. (Ahujava vd., 1993, Eiselt v.d., 1995a). ÇPP; çöplerin toplanması, sokakların temizlenmesi, su ve gazete dağıtımı, mektup dağıtımı, cadde ve otobanlarda kar ve buz kontrolleri, okul servisleri ve polis devriye araçlarının rotalanması, kar temizleme çalışmaları ve etkili web sitesi kullanılabilirliğinin tespiti gibi birçok alanda kullanılabilmektedir (Thimbleby, 2002).

Deterministik araç rotalama probleminin bazı elemanları rassal olduğunda gerçek hayat problemlerine daha yakın olan Stokastik Araç Rotalama Problemi (SARP) ortaya çıkmaktadır. Rassal elemanlar ziyaret edilecek müşteri kümesi, müşteri talepleri veya müşteriler arasındaki seyahat zamanları olabilir (İşleyen 2008). Gerçek hayat problemlerinde iki merkez arasındaki ulaşım süresi hava koşulları, trafik yoğunluğu, trafik kazaları gibi çeşitli nedenlerden ötürü büyük ölçüde değişmektedir. Bu nedenle bu çalışmada iki düğüm arasındaki varış süresini temsil eden amaç fonksiyonu katsayıları normal dağılıma sahip rassal değişkenler olarak ele alınmış ve problem şans kısıtlı stokastik programlama kullanılarak çözüme kavuşturulmuştur. İlgili literatür incelendiğinde daha önce Stokastik Çinli Postacı Problemi (SCPP) ile ilgili bir çalışma yapılmadığı görülmektedir. Literatürde SARP üzerine yapılan çalışmaların bir kısmı ise Tablo 1'de özetlenmiştir.

Tablo 1. Literatür Araştırması

Yazar(lar) ve Yayın Yılı	Problem Tipi	Çözüm Yöntemi
Gendreau *et al.* (1996)	Stokastik Müşteri ve Talepli ARP	Tabu Arama Algoritması
Hvattum *et al.* (2004)	SARP	Sezgisel Algoritma
Frazolli and Bullo (2004)	SARP	Dağınık Algoritmalar
Mak and Guo (2004)	Stokastik Talepli ve Esnek Zaman Kısıtlı ARP	Genetik Algoritma
Chepuri and Homem-De-Mello (2005)	Stokastik Talepli ARP	

		Sezgisel Algoritma
Bianchi *et al.* (2006)	Stokastik Talepli ARP	Metasezgisel
İşleyen (2008)	Stokastik Talepli ARP	Sezgisel Algoritma
Shen *et al*. (2009)	SARP	Tabu Sezgiseli
Li *et al.* (2010)	Zaman Pencereli, Stokastik Seyehat ve Servis Süreli ARP	Tabu Sezgiseli
Taş *et al.* (2014)	Zaman Pencereli ve Stokastik Seyehat Süreli ARP	Markov Karar Süreçleri
Miranda and Conceição (2016)	Zaman Pencereli, Stokastik Seyehat ve Servis Süreli ARP	Metasezgisel

YÖNTEM

Şans Kısıtlı Stokastik Programlama

Rassal parametrelere sahip bir problemde kısıtların belirli dağılımlara ait olasılık seviyelerinin izin verdiği ölçüde bozulmasına olanak sağlayan stokastik programlamaya şans kısıtlı programlama denir. Problemin stokastik yapısı doğrusal kısıtın beklenen değeri ve kısıtın bozulma genişliği ile birleştirilerek deterministik hale getirilir ve simpleks yöntemle çözülebilir (Sawyer and Lin 1998). Şans kısıtlı doğrusal programlama modeli,

$$\text{maks(min)}Z(x) = \sum_{j=1}^{n} c_j \, . \, x_j$$

$$P\left[\sum_{j=1}^{n} a_{ij} . x_j \leq b_i\right] \leq 1 - u_i, \quad i = 1, 2, 3, \ldots, m \qquad (1)$$

$$u_i \in (0,1) \qquad i = 1, 2, 3, \ldots, m$$

şeklinde tanımlanır. c_j, a_{ij} ve b_i model parametreleridir ve bunlardan en az bir tanesi rassal değişkenlerdir. Modelde u_i önceden belirlenen olasılıkları göstermektedir ve x_j karar değişkenleri deterministik yapıdadır (Taha 2000). Modeldeki stokastik parametreler belirli bir dağılıma sahip olmalı ve u_i olasılık seviyeleri belirlenmelidir. Bu bilgilerle model deterministik hale getirilerek çözülmektedir. (Aksaraylı ve Pala 2015).

Katsayıları Normal Dağılıma Sahip Rasgele Değişkenler Olan Şans Kısıtlı Modeller

Katsayıları rassal değişken olan doğrusal programlama problemlerinde, genellikle katsayıların normal dağılım özelliği gösterdiği varsayılmaktadır. Bu varsayım altında (1) modeli ile verilen şans kısıtlı stokastik doğrusal programlama probleminde c_j, a_{ij} ve b_i'ler normal dağılım özelliği gösteren rasgele değişkenlerdir.

Katsayıları normal dağılım özelliği gösteren şans kısıtlarının belirlenmesi

1) Yalnız a_{ij} katsayıları rasgele değişken,
2) Yalnız b_i katsayıları rasgele değişken,
3) Yalnız c_j katsayıları rasgele değişken,
4) a_{ij} ve b_i katsayılarının her ikisi de rasgele değişken,

şeklinde dört durum ile incelenebilir. Bu dört durum kullanılarak diğer durumlar bulunabilir. (Hulsurkar *et al.*1997).

Bu çalışmada iki düğüm arasındaki varış süresini temsil eden amaç fonksiyonu katsayıları (c_j) rasgele değişken olarak ele alındığı için bu bölümde üçüncü durum üzerinde durulmuştur.

Durum 3: Yalnız c_j Katsayıları Rasgele Değişken ise;

c_j katsayıları normal dağılıma sahip rasgele değişkenler olduğundan z (x), amaç fonksiyonu da normal dağılım özelliği gösterecektir. z (x)'in ortalaması,

$$E\big(z\,(x)\big) = \sum_{j=1}^{n} (c_j)\, x_j \qquad (2)$$

olacaktır. Böylece E-modele (beklenen değer modeline) sahip deterministik amaç fonksiyonu;

$$\text{maks (min) } E(z(x)) = \sum_{j=1}^{n} c_{j\,.}\, x_j \qquad (3)$$

biçimine dönüşecektir (Hulsurkar *et al.* 1997).

Stokastik Çinli Postacı Problemi

CPP, tanımlanan ağ üzerinden tüm bağlantıların; tek bir postacı tarafından, mektupların dağıtılıp toplanması için ziyaret edilerek, başlangıç noktasına dönmesi problemi olarak tanımlanabilir. Bu problem türünde iki düğüm arasındaki varış süresini gösteren amaç fonksiyonu katsayı değerleri rasgele değişken olarak ele alındığında problem SCPP'ye dönüşmektedir. Problemde rassallığı oluşturan amaç fonksiyonu katsayılarının normal dağıldığı kabul edilmektedir.

Bir G = (V, E) grafı ele alındığında; ayrıt (i, j) i ve j düğümleri arasında bir bağlantı kurmaktadır. CPP için matematiksel model, parametre ve değişkenler aşağıda sunulmuştur (Yılmaz *et al.* 2017). Bu modelde amaç fonksiyonu katsayılarının beklenen değerleri alınarak, amaç fonksiyonu deterministik hale dönüştürülmüştür. Böylece model; beklenen değer modeline sahip deterministik amaç fonksiyonlu SCPP modeline dönüşmüştür.

Parametre ve değişkenler;

x_{ij} = *i'* den *j'* ye giderken (*i,j*) ayrıtından geçilme sayısı,

x_{ji} = *j'* den i' ye giderken (*j,i*) ayrıtından geçilme sayısı,

C_{ij} = (*i,j*) ayrıtının uzunluğu,

V = Şebekedeki tüm düğümlerin kümesi,

E = Şebekedeki tüm ayrıtların kümesi,

n = Şebekedeki toplam düğüm sayısı.

$$\text{Min } E(z(x)) \sum_{i=1}^{n} \sum_{j=1}^{n} c_{ij}\, x_{ij} \qquad (4)$$

Kısıtları altında,

$$\sum_{j=1}^{n} x_{ij} - \sum_{j=1}^{n} x_{ji} = 0 \qquad i = 1,2,\dots,n \qquad \forall_i \in V \tag{5}$$

$$x_{ij} + x_{ji} \geq 1 \qquad \forall (i,j) \in E \tag{6}$$

$$x_{ij}, x_{ji} \geq 0 \quad \text{ve tamsayı.} \tag{7}$$

(4), en kısa uzunluğu hedefleyen beklenen değer modeline sahip deterministik amaç fonksiyonunu; (5), akışı sağlayan süreklilik kısıtlarını, (6) her bir ayrıttan herhangi bir yönde en az bir kez geçilmesi gerektiğini; (7) nolu kısıt ise, tüm değişkenlerin pozitif tamsayı olması gerektiğini belirtmektedir.

Uygulama

Bu çalışmada 7 düğümlü bir SCPP ele alınmıştır. Hava koşulları, trafik yoğunluğu, trafik kazaları, yapım ve onarım çalışmaları gibi etmenler iki düğüm arasındaki varış süresini değiştirdiğinden dolayı amaç fonksiyonunda mesafe yerine süreler kullanılmıştır. Trafiğin durumuna göre önceden belirlenen aralıklarda rassal sayılar üretilmiş ve beklenen değerleri alınmıştır. ARENA 9.0 programının "Input Analyzer" sekmesi kullanılarak amaç fonksiyonu katsayıları değerlerinin normal dağılıma uyduğu tespit edilmiştir. Böylece c_j amaç fonksiyonu katsayıları; normal dağılıma uygun rasgele değişkenler olarak ele alınmış, beklenen değer modeline sahip deterministik amaç fonksiyonu elde edilerek modele eklenmiştir. Problemde her ayrıttan en az bir kez geçilerek en kısa turun oluşturulması amaçlanmıştır. Örnek problemin matematiksel modeli aşağıda verilmiştir.

$$\text{Min } E(z(x)) = 13.1x_{12} + 5.92x_{13} + 21.7x_{15} + 13.1x_{21} + 7.65x_{23} + 14.5x_{24} + 21.8x_{25} + 5.92x_{31} + 7.65x_{32} + 11.5x_{34} + 19.8x_{37} + 14.5x_{42} + 11.5x_{43} + 11.1x_{45} + 5.3x_{46} + 21.7x_{51} + 21.8x_{52} + 11.1x_{54} + 7.88x_{56} + 5.3x_{64} + 7.88x_{65} + 8.86x_{67} + 19.8x_{73} + 8.86x_{76}$$

Kısıtları altında

$$\sum_{j=1}^{n} x_{ij} - \sum_{j=1}^{n} x_{ji} = 0 \qquad i = 1,2,\dots,n \qquad \forall_i \in V$$

$$x_{ij} + x_{ji} \geq 1 \qquad \forall (i,j) \in E$$

$$x_{ij}, x_{ji} \geq 0 \text{ ve tamsayı}$$

BULGULAR

Bu çalışmada; iki düğüm arasındaki varış süresini temsil eden, amaç fonksiyonu katsayıları olan rassal değişkenlerin dağılımını bulmak için ARENA 9.0 programının "Input Analyzer" modülü kullanılmıştır. Şebekede bulunan tüm yollar için elde edilen varış sürelerinin genel olarak (0.96 – 0.99 güven düzeyinde) normal dağılım özelliği gösterdiği tespit edilmiştir. Örnek olarak (3-4) yolu için ARENA 9.0 programının "Input Analyzer" modülünden elde edilen normal dağılıma uygunluk grafiği Şekil 1'de gösterilmiştir. (3-4) yolu için varış süresinin 0.99 güven düzeyinde normal dağılıma uyduğu tespit edilmiş ve bu yol için varış süresinin ortalaması (μ) 11.5 ve standart sapması (σ) 4.47 olarak bulunmuştur.

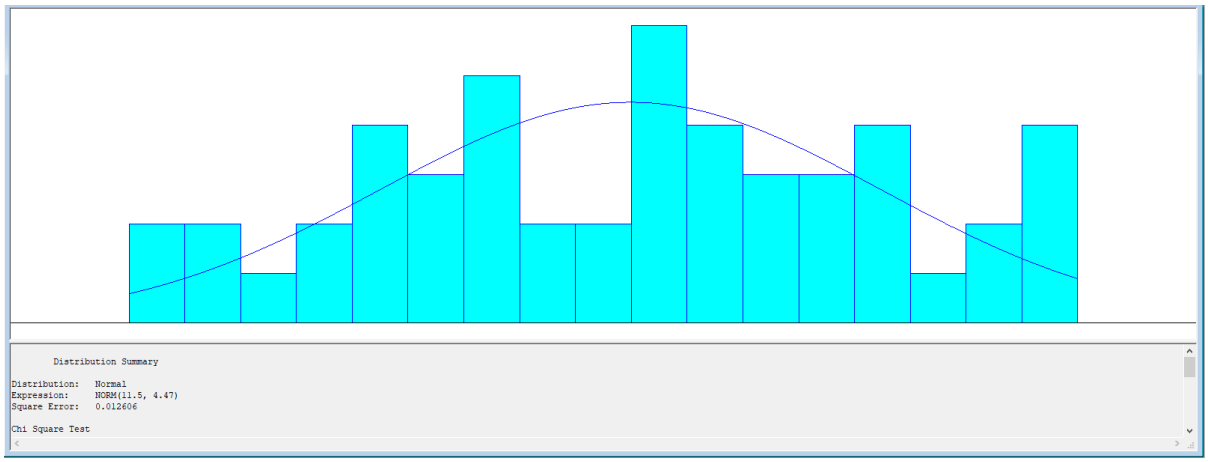

Şekil 1. (3-4) Yolu Normal Dağılıma Uygunluk Grafiği

GAMS Programında problem çözülerek optimum rota ve süre bulunmuştur. Optimum rota: R = 1–3–4–2–3–7–6–4–5–2–1–5–6–4–3–1 ve amaç fonksiyonu değeri Min E(z(x)) =171.830 olarak bulunmuştur.

SONUÇ VE ÖNERİLER

Gerçek hayat problemlerinin birçoğunda veriler tam olarak bilinemediği için belirsizlik söz konusu olmakta ve bu sebepten ötürü katsayılar rasgele değişken olarak ortaya çıkmaktadır. Bu çalışmada amaç fonksiyonu katsayıları rasgele değişkenler olan SCPP ele alınmıştır. Gerçek hayat problemlerinde iki düğüm arasındaki varış süresi çeşitli sebeplerden dolayı sabit olmadığı için amaç fonksiyonunda mesafe yerine süreler kullanılmıştır. ARENA 9.0 programının "Input Analyzer" modülü kullanılarak bu katsayıların normal dağılıma uyduğu belirlenmiştir. E-modele sahip

deterministik amaç fonksiyonu eklenerek model çözüme kavuşturulmuştur. İlgili literatür incelendiğinde daha önce SCPP ile ilgili bir çalışma yapılmadığı görülmektedir. Rotalama problemleri için harcanan paralar ve yanlış planlamalardan kaynaklı israflar göz önünde bulundurulduğunda bu alanda yapılan çalışmaların önemi görülmektedir. Gelecek çalışmalarda, CPP'nin farklı türlerinda amaç fonksiyonu katsayıları rasgele değişkenler olarak ele alınarak gerçek hayat problemlerine uygulanabilir. Ayarıca rasgele değişkenler olan katsayıların farklı dağılıma sahip olması durumu ele alınarak problem yeniden çözülebilir.

KAYNAKLAR

Ahuja, R. K., Magnanti, T. L., Orlin, J. B., & Weihe, K. (1995). Network flows: theory, algorithms and applications. *ZOR-Methods and Models of Operations Research*, *41*(3), 252-254.

Aksaraylı, M., & Pala, O. (2015). Şans Kısıtlı Stokastik Programlama Yaklaşımı İle Ofis Ürünleri Üretim Sistemi Modellemesi. *15. Üretim Araştırmaları Sempozyumu*.

Bianchi, L., Birattari, M., Chiarandini, M., Manfrin, M., Mastrolilli, M., Paquete, L., ... & Schiavinotto, T. (2006). Hybrid metaheuristics for the vehicle routing problem with stochastic demands. *Journal of Mathematical Modelling and Algorithms*, *5*(1), 91-110.

Chepuri, K., & Homem-De-Mello, T. (2005). Solving the vehicle routing problem with stochastic demands using the cross-entropy method. *Annals of Operations Research*, *134*(1), 153-181.

Eiselt, H. A., Gendreau, M., & Laporte, G. (1995). Arc routing problems, part I: The Chinese postman problem. *Operations Research*, *43*(2), 231-242.

Frazzoli, E., & Bullo, F. (2004, December). Decentralized algorithms for vehicle routing in a stochastic time-varying environment. In *2004 43rd IEEE Conference on Decision and Control (CDC)(IEEE Cat. No. 04CH37601)* (Vol. 4, pp. 3357-3363). IEEE.

Gendreau, M., Laporte, G., & Séguin, R. (1996). Stochastic vehicle routing. European Journal of Operational Research, 88(1), 3-12.

Hulsurkar, S., Biswal, M.P. ve Sinha, S.B. (1997). Fuzzy Programming Approach to Multi-Objective Stochastic Linear Programming Problems. *Fuzzy Sets and Systems 88*,173-181.

Hvattum, L. M., Lokketangen, A., & Laporte, G. (2004). A heuristic solution method to a stochastic vehicle routing problem. In Proceedings of TRISTAN V—The Fifth Triennial Symposium on Transportation Analysis.

İşleyen, S. K. (2008). *Lojistik Yönetim Sistemlerinde Stokastik Talepli Araç Rotalama Problemi* (Doctoral dissertation, Doktora Tezi, Gazi Üniversitesi, Fen Bilimleri Enstitüsü, Ankara).

Li, X., Tian, P., & Leung, S. C. (2010). Vehicle routing problems with time windows and stochastic travel and service times: Models and algorithm. *International Journal of Production Economics*, *125*(1), 137-145.

Mak, K. L. ve Guo, Z. G. (2004), "A Genetic Algorithm for Vehicle Routing Problems with Stochastic Demand and Soft Time Windows", Proceedings of the 2004 IEEE Systems and Information Engineering Design Symposium, Virginia, USA.

Miranda, D. M., & Conceição, S. V. (2016). The vehicle routing problem with hard time windows and stochastic travel and service time. *Expert Systems with Applications*, *64*, 104-116.

Sawyer, C. S., & Lin, Y. F. (1998). Mixed-integer chance-constrained models for ground-water remediation. *Journal of water resources planning and management*, *124*(5), 285-294.

Shen, Z., Ordónez, F., & Dessouky, M. M. (2009). The stochastic vehicle routing problem for minimum unmet demand. In *Optimization and logistics challenges in the enterprise* (pp. 349-371). Springer, Boston, MA.

Taha, H.A. (2000).Yöneylem Araştırması, 1.basım, Literatür Yayıncılık, İstanbul.

Taş, D., Gendreau, M., Dellaert, N., Van Woensel, T., & De Kok, A. G. (2014). Vehicle routing with soft time windows and stochastic travel times: A column generation and branch-and-price solution approach. *European Journal of Operational Research*, *236*(3), 789-799.

Thimbleby, H. (2003). Explaining code for publication. *Software: Practice and Experience*, *33*(10), 975-1001

Yılmaz, M., Çodur, M. K., & Yılmaz, H. (2017). Chinese postman problem approach for a large-scale conventional rail network in Turkey. *Tehnički vjesnik*, *24*(5), 1471-1477.

DETERMINATION OF OPTIMUM TIGHTENING TORQUE FOR TIE ROD WITH SPECIAL CONNECTION TYPES

Emre Azim HASANOĞLU
ZF Lemförder Aks Modülleri San. Tic. A.S.
emre.hasanoglu@zf.com

Buğra Yiğit ÇETİN
ZF Lemförder Aks Modülleri San. Tic. A.S.
bugra.cetin@zf.com

İlker CANBAZ
ZF Lemförder Aks Modülleri San. Tic. A.S.
ilker.canbaz@zf.com

ABSTRACT: Tie rod is the part of the steering mechanism in a vehicle. It provides the mechanical connection between knuckle and steering rack. Tie Rods consist of two different components which are called as Inner Tie Rod and Outer Tie Rod. During a conventional Tie Rod assembly, these two components are fastened each other with nut to transfer the applied loads from steering gear to the wheel. For this reason, the tightening torque regulations play important role to ensure the safety and sustainability of the connection. Differently from the most common connection type which is assemblied with the nut, some of car manufacturers demands the special type of connection between Inner Tie Rod and Outer Tie Rod because of their assembly process. Therefore, it is crucial to identify the suitable tightening regulations for connection type mentioned. In this study, the optimum tightening torque is determined by using an experimental and numerical methods. At first, the special connection type is evaluated with the standard nut tightening regulation. The experimental investigation shows that the standard tightening torque value does not comply with special connection type. Therefore, the numerical simulations are performed to define the optimum tightening torque. For this purpose, nonlinear structural finite element analysis method is developed to simulate the special connection screwing process. HyperMesh, Abaqus and HyperView are used for finite element analysis. Stress dispersion and the amount of plastic deformation especially on the thread area of special connection are evaluated by considering different tightening torque values. The defined torque value from numerical study is validated with tightening test experimentally. Consequently, optimum tightening torque which ensures safety and durability for the steering system is identified.

Key words: Steering Components, Tie Rod, Tightening Torque, Vehicle Safety

FALL-CONE TESTS ON A CLAYEY SOIL TREATED WITH ROCK POWDER-SEWAGE SLUDGE ASH MIXTURES

Yunus UÇUR, Ali Fırat ÇABALAR

Department of Civil Engineering, University of Gaziantep

ucuryunus@gmail.com, cabalar@gantep.edu.tr

ABSTRACT: The study presents a series of fall-cone tests on a clayey soil treated with rock powder and sewage sludge ash mixtures. The clay used during the tests were obtained from the University of Gaziantep campus, and was found to have 34.22% liquid limit, 28.32% plastic limit, and 5.90% plasticity index, respectively. The fall cone results on the clean clay was compared with the results on the mixtures with different proportions. According to results obtained from the fall-cone tests, the plasticity index of the mixtures were found to be less than the clean clay samples by addition of the wastes. For example, plasticity index values are 3.19% and 3.61% for the mixtures of 15% rock powder-clayey soil and 15% sewage sludge ash-clayey soil, respectively. Undrained shear strength parameter was also calculated during the study. Maximum undrained shear strength value of the clean clay was found to be 2.945 kPa at a moisture content of 31.81%. Considering all the mixtures, the clay with 20% rock powder, and the clay with 15% sewage sludge ash had the greatest undrained shear strength values, which were 16.337 kPa and 13.971 kPa respectively.

Keywords: fall-cone test, clay, sewage sludge ash, rock powder.

INTRODUCTION

In recent years, use of solid wastes have been studied by many researchers in order to minimize the environmental problems raised due to the greenhouse gas emission, clean air and water requirements. One of the application areas for different solid wastes generated in urban and industry transformation projects is civil engineering including geotechnical engineering discipline. For example, the clay described as a problematic soil could be improved by using various types of solid wastes (Cabalar et al., 2016).

While there are numerous investigations focusing on the use of recycled asphalt shingles, crushed concrete aggregates, crushed ceramic and bricks only in various

geotechnical applications (Warner and Edil, 2012; Zhu et al., 2012; Cabalar and Karabash, 2015), the performance of clay soils using both rock powder and sewage sludge ash has not been previously reported. Therefore, the present study aims to investigate the effects of these waste materials on the response of a clay tested in British fall cone testing apparatus.

EXPERIMENTAL STUDY

Three different materials were used in the experimental studies, rock powder, sewage sludge ash (SSA), and clay. The rock powder primarily include limestone powder with high percentage of $CaCO_3$ (calcium carbonate). Its water absorption was observed to be quite low. The SSA mainly include sulphur, and observed to have a high water absorption. The clay samples used during the experimental studies were quarried in the University of Gaziantep campus (LL=34, PL=28; PI=6). These three materials have been tested at different mixture ratios. The mixtures used during the tests are presented in Table 1 as follows. Figure 1 presents the SEM pictures of the materials used during the experimental studies.

Table 1. Mixtures for the specimen tested during the experimental studies

Series 1	Series 2		Series 3
SSA(%)	Rock powder (%)	SSA (%)	Rock powder (%)
5	5	20	5
10	10	15	10
15	15	10	15
20	20	5	20
25	-	-	25

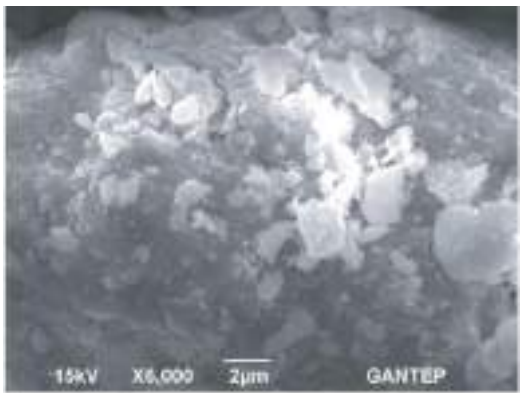

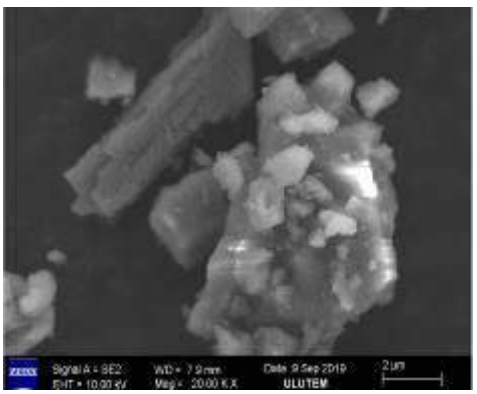

(a) (b)

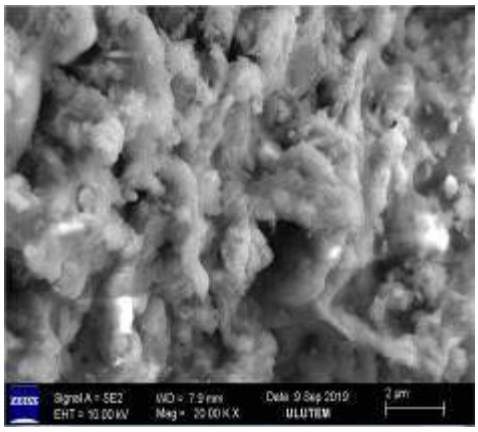

(c)

Figure 1. SEM pictures of the (a) clay, (b) rock powder, and (c) SSA used during the experimental studies.

RESULTS AND DISCUSSION

According to the results obtained at the end of the experimental works, plastic limit values were found to increase significantly by SSA additions (from 28% to 41%), though those were found to be almost same by rock powder additions (from 28% to 30%). Similar results were found in liquid limit values. On the other hand, there is no systematic change observed in the undrained shear strength values (Table 2).

Table 2. Testing results

Specimen	Plastic limit (%)	Liquid limit (%)	Undrained shear strength (kPa)
Clean clay	28	34	1.4
Clay with 5% rock powder	29	39	1.5
Clay with 10% rock powder	26	35	1.4
Clay with 15% rock powder	30	34	1.7

Clay with 20% rock powder	28	37	1.6
Clay with 25% rock powder	30	35	1.7
Clay with 5% SSA	29	40	1.4
Clay with 10% SSA	35	40	1.4
Clay with 15% SSA	39	42	1.7
Clay with 20% SSA	36	45	1.7
Clay with 25% SSA	41	46	1.6
Clay with 5% rock powder & 20% SSA	35	44	1.3
Clay with 10% rock powder & 15% SSA	35	41	1.5
Clay with 15% rock powder & 10% SSA	34	39	1.5
Clay with 20% rock powder & 5% SSA	31	36	1.7
Rock powder	na	29	1.5

CONCLUSIONS

Response of a clay treated with both rock powder and sewage sludge ash was investigated experimentally by using British fall-cone device. The observations made in the investigation reveals that addition of rock powder only was not found to be very effective on the Atterberg's limit tests, although SSA addition affected substantially the behaviour of the clay tested. The authors' interpretation is that there is a requirement for a research on the influence of curing time on the testing results.

REFERENCES

Cabalar AF, Karabash Z (2015) Stabilizing California bearing ratio of a subgrade soil using waste tire and cement addition. J Test Eval ASTM 43(6):1279–1287

Cabalar, A.F., Abdulnafaa, M.D., Karabash, Z. (2016). Influences of various construction and demolition materials on the behavior of a clay. Environmental Earth Sciences, 75, 9, 841.

Warner JD, Edil TB (2012) An evaluation of reclaimed asphalt shingles for beneficial reuse in roadway construction. J ASTM Int 1(9):146–167

Zhu J, Wu S, Zhong J, Wang D (2012) Investigation of asphalt mixture containing demolition waste obtained from earthquake damaged buildings. Constr Build Mater 29:466–475.

FABRIC PRODUCTION FROM TEXTILE FABRIC WASTES

Özge Yurtaslan, Bursa Teknik Üniversitesi, Mühendislik Fak., Lif ve Polimer Mühendisliği Bölümü, Bursa, Türkiye, ozge.yrtsln@gmail.com

Şule Altun Kurtoğlu, Artisan Teknik Danışmanlık ve Ar-Ge, Bursa, Türkiye, slaltun54@gmail.com

Demet Yılmaz, Süleyman Demirel Üniversitesi, Mühendislik Fak., Tekstil Mühendisliği Bölümü, Isparta, Türkiye, demetyilmaz@sdu.edu.tr

ABSTRACT: The textile industry, which is one of the most prominent industrial areas in the world and in Turkey, has become significant in which environmental studies are intensified due to energy intensive processes and wastes. Cotton is one of the main raw materials of textile industry and thus has significant environmental impacts through the whole life cycle. Recycling is one of the most suitable methods to minimize these impacts. In this study, for the purpose of evaluating cotton-weighted waste fabrics, fiber blends were prepared with opened fabric wastes and yarn produced by OE-rotor method and woven fabric characteristics were evaluated.

Key words: Green marketing, recycling, fabric wastes, textile wastes, cotton wastes, carbon footprint.

TEKSTİL ATIKLARINDAN KUMAŞ ÜRETİMİ

ÖZET: Dünyada ve Türkiye'de önemli sanayi kollarından biri olan tekstil sektörü, enerji yoğun prosesleri ve oluşturduğu atıklar ile çevresel çalışmaların yoğunlaştırıldığı alanlardan biri haline gelmiştir. Tekstil üretiminin temel hammaddelerinden olan pamuk, tüm yaşam döngüsü boyunca önemli çevresel etkilere sahip doğal bir elyaftır. Bu çevresel etkileri minimize etmede en etkili yöntemlerden biri ise, geri kazanımdır. Bu çalışmada, pamuk ağırlıklı atık kumaşların değerlendirilmesi amacıyla kumaş atıklarının açılması sonucu elde edilen liflerin farklı atık lifleri ile elyaf harmanları hazırlanmış ve OE-rotor yöntemi ile iplik ve dokuma kumaşlar üretilmiş ve performans özellikleri değerlendirilmiştir.

Anahtar sözcükler: Yeşil pazar**,** geri kazanım, kumaş atıkları, tekstil atıkları, pamuk atıkları, karbon ayakizi.

GİRİŞ

Çevresel problemler günümüzde küresel bir boyut kazanmış ve dünyanın herhangi bir yerindeki bir fabrikanın salgıladığı sera gazı, tüm canlıları etkileyen bir konu haline gelmiştir. Çevre ile ilgili problemlerin küreselleşmesi ile birlikte, çözüm metotları da küreselleşmiş ve tüm dünya ülkelerinin yer aldığı platformlarda; enerji, hammadde, atık, katı sıvı gaz emüsyonları, sürdürülebilirlik, ekosistem, endüstriyel simbiyoz, küresel ısınma, karbon ayakizi, ozon tabakası incelmesi, temiz üretim vb. konular tartışılmaya başlanmıştır. Birleşmiş Milletler İklim Değişikliği Çerçeve Sözleşmesi, Kyoto Protokolü ve ozon tabakasını incelten maddelere karşı oluşturulan yaklaşık 200 ülkenin taraf olduğu Montreal Protokolü bu kapsamda ilk akla gelen örneklerdir [1]. Adı geçen protokoller ve sözleşmeler, şu anda dünyada bu protokollere taraf olan ve olmayan ülkelerle birlikte Türkiye'nin de çevre politikalarının belirlenmesinde önemli bir rol oynamaktadır.

Çevre ile ilgili hareketlerin yakın geçmişine bakıldığında, bu hareketlerin 1960'lı yıllardan itibaren önce bölgesel olarak başladığı, daha sonra küresel boyuta ulaştığı görülmektedir. Çevre kirliliğinin insan ve diğer canlıların hayatını tehdit eden boyutlara ulaşması, 1960'lı yılların aktif politik ortamı ve 1969'daki Santa Barbara petrol saçılması gibi kazalar, çevre ile ilgili konulara duyarlı grupların oluşmasına zemin hazırlamış ve bu konuda bir kamuoyu oluşmasını tetiklemiştir. Şu anda Detox kampanyası ile tekstil firmalarını temiz üretim yapmaya zorlayan Greenpeace çevre örgütü de, bu ortam içerisinde 1971 yılında kurulmuştur. 1980 ve 1990'lı yıllar asit yağmurları, ozon incelmesi gibi yeni sorunları gündeme getirmiş ve bilinçli/yeşil tüketicinin ilk örnekleri görülmeye başlanmıştır. 2000'li yıllarda ise küresel ısınma ve iklim değişikliğinin etkilerinin somut olarak görülmeye başlanması ile birlikte bireysel bazda çevreye duyarlı tüketicilerin çevre sorunları ile mücadele etmek için yeşil ürünlere yönelmesi, Avrupa Birliği (AB) gibi oluşumların örneğin kamu ihalelerinde yeşil ürünleri tercih etmesi gibi etkenler yeşil pazar payını artırmıştır [2]. AB Komisyonunun 2012 yılında yaptırdığı bir ankette, katılımcıların %56'sı zaman zaman, %26'sı ise sık sık çevre dostu ürünleri satın aldığını söylemiştir. Aynı ankette, katılımcıların %38'i ürünün çevresel etkisinin satın almalarını etkileyen çok önemli bir kriter olduğunu belirtmiştir [3]. 1975 yılında American Marketing Association (AMA), Yeşil Pazar (Green Marketing) terimini kullanmıştır. Günümüzde, çevreci pazarlama (environmental marketing), ekolojik pazarlama (ecological marketing), sürdürülebilir pazarlama (sustainability marketing) gibi farklı isimler alan ama temelde aynı kriterlerden oluşan özel bir alan gelişmektedir. Bu pazar, İskandinav ülkeleri, Avrupa Birliği ülkeleri ve Amerika Birleşik Devletlerinde %30'un üzerinde oranlara ulaşmaktadır, aynı pazarın Çin'de de hızla büyümekte olduğu göz ardı edilmemelidir [4]. Dünyada çevresel konuların önem kazanması ile birlikte "döngüsel ekonomi" olarak adlandırılan farklı bir ekonomik anlayış da gündeme gelmeye başlamıştır. Döngüsel ekonomi, ürün, malzeme ve kaynakların mümkün olduğunca uzun süre ekonomi içerisinde tutulabildiği ve atık minimizasyonunun temel alındığı bir

kavramdır. Diğer ifade ile "üret, kullan imha et" yerine, "kaynak verimliliğine dikkat ederek üret, uzun süre kullan ve geri dönüştür" prensibini esas almaktadır. Dolayısıyla, döngüsel ekonomi ile yeni bir anlayışa geçilmeye başlanmıştır. Avrupa Birliği bu konuda bir eylem planı hazırlamıştır. Öte yandan, tekstil sektöründe de döngüsel ekonominin esasını oluşturan verimli kaynak kullanımı ve geri kazanım kavramları önemli hale gelmiştir. Özellikle, tekstil sektöründeki gün geçtikçe artan küresel yarış, üreticileri artan kalitede ve rekabet edilebilir fiyatta ürünler üretmeye zorlamaktadır. Ancak, hammadde fiyatları, enerji ve işgücü maliyetleri her geçen yıl artan şekilde yükselmektedir. Örneğin, pamuk ipliği üretiminde, hammadde maliyeti genel olarak toplam iplik üretim maliyetinin %50'sinden fazlasını oluşturmaktadır [5]. Yüksek hammadde maliyetlerinin yanısıra enerji ve işgücü maliyetleri konusunda yapılabilecek iyileştirmelerin de mevcut teknoloji içerisinde sınırlı olması nedeniyle atık minimizasyonu ve atık geri kazanımı önem kazanmaktadır. Pamuk ipliği üretiminde hammadde maliyetlerini azaltmaya yönelik olarak yürütülen araştırmalarda ilk çözüm olarak, harman hallaç ve tarak makinelerindeki işlemler sırasında yüksek temizleme veriminin sağlanması ve telef miktarının azaltılması hedeflenmiştir. İkinci çözüm ise, elyaf atıklarından geri kazanımıdır [6].

Tekstil çevre ve atık problemlerinin gelişimi

Küresel ekonominin önem kazandığı bu çağda, istenen kalitedeki tekstil ürününün çevreye duyarlı bir şekilde üretilmesi, firmaların hayatta kalabilmelerinin temel şartlarından biri haline gelmiştir [7].

Dünyada kişi başına düşen lif tüketimi, nüfus ve gelir düzeyindeki artışa bağlı olarak 2016 yılı itibari ile 13 kg'a ulaşmış olup, 2050 yılında bu rakamın 20 kg'a ulaşacağı tahmin edilmektedir [8]. Bilindiği gibi, son yıllarda sezonlar haftalara kadar inmiş, ucuz ve düşük kalitedeki ürünler tüketimi önemli ölçüde artırmıştır. Lüks moda trendlerini taklit eden düşük maliyetli ürünler (fast fashion), örneğin İngiltere gibi ülkelerde pazarın 1/5'ini oluşturmaya başlamıştır [9]. Yüksek tüketim beraberinde yüksek tekstil atığını da getirmektedir. ABD'de, her yıl 11 milyon ton civarında kullanılmış tekstil atığı oluşmaktadır [10]. Tekstil atıkları ayrıca, dünyada ortalama olarak çöplüklerde %5 civarında bir yer kaplamaktadır [11]. Gelişmiş ülkelerin önümüzdeki dönemlerde en önemli hedefleri, tekstil atıklarının geri kazanım oranlarını mevcut durumdan (%15-30) daha iyi oranlara (~%50) yükseltebilmektir [10].

Pamuk elyafı polyester ile beraber günümüzde tekstil sanayisinin en temel ve stratejik iki hammaddesinden biri olma özelliğini korumaktadır. 2016/2017 yılı verilerine göre dünya toplam pamuk lif tüketimi 24.13 Milyon ton civarındadır. 2024 yılında bu rakamın 30.4 milyon tona ulaşması beklenmektedir [12]. Tekstilde temel ve vazgeçilemez lif olan pamuk aynı zamanda buğday ve pirinç ile birlikte, en geniş sulama alanına sahip üç bitkiden biridir ve temiz su kaynaklarının en önemli tüketicilerindendir. Örneğin, dördüncü büyük pamuk üreticisi olan Pakistan'da

sulama için yeraltı sularının %31'i çekilmektedir [13]. Pamuk lifi üretiminde, dünyada 7000-29000 m^3 arasında su kullanılmaktadır. Ayrıca, pamuk lif üretimi için ekili alanların yaklaşık %2.4 gibi küçük bir oranı kullanılmasına rağmen, dünyada kullanılan pestisitlerin %11'i pamuk üretiminde kullanılmaktadır. Pamuk bitkisi üretiminin başlıca çevresel etkileri olarak, gübreler nedeniyle ötröfikasyon oluşumu, aşırı sulama nedeniyle toprakta tuzlanma oluşumu, pestisitler nedeni ile vahşi hayatın zarar görmesi, yeraltı sularının ve yüzey sularının kirlenmesi, su tablalarının yer değiştirmesi, yeraltı ve yerüstü sularının azalması verilebilir [14-15]. Türkiye, pamuk üretiminde lider ilk 6 ülke içerisinde yer alırken, su kaynakları (kendi içerisinde) en düşük olan 2. ülkedir. Ayrıca, Türkiye'de kullanılan pestisitlerin %29'u pamuk üretimi için kullanılmaktadır. Bu durum, özellikle Çukurova Bölgesinde vahşi hayata önemli zararlar vermektedir [16-17]. Türkiye'de kullanılan gübreler genellikle azot esaslıdır, azot esaslı gübreler taşınarak su kütlelerine ulaşmaktadır. Türkiye'de bir ton pamuk üretimi için 0.004 ton azot su kütlelerine karışmaktadır [18-19]. Pamuk ipliği üretimi, lif üretiminde kullanılan pestisit, gübre ve aşırı su tüketimi yanında enerji yoğun bir proses olması nedeni ile de çok önemli çevresel etkilere yol açmaktadır. Pamuk lifi ve ipliğinin eldesi sırasında ortaya çıkan bu çevresel etkileri azaltmanın en önemli yolu, hammadde geri kazanımıdır.

Atık geri kazanımının çevresel boyutu

Geri kazanım süreci, ürünün tasarlandığı aşamada başlamaktadır. Genel bir tanım olarak eko tasarım, bir ürünün tüm yaşam döngüsü göz önüne alınarak tasarlanmasıdır. Eko tasarımda, çevresel etkinin azaltılması, etik ve sosyal ihtiyaçların gözetilmesi, aynı zamanda ürünün fonksiyonel ve estetik özelliklerinin geliştirilmesi hedeflenmektedir [20]. Günümüzde EkoTasarım (Ecodesign), Çevreye Duyarlı Tasarım (Environmentally Conscious Design), Yeşil Mühendislik (Green Engineering), Beşikten Beşiğe Tasarım (CradletoCradle Design) gibi birçok kavram kullanılmaktadır. Bu kavramların aralarında farklılıklar olmasına rağmen uygulamada, kavramlar çoğu zaman birbirlerinin yerine kullanılabilmektedir [21]. Eko tasarım, çevreye ve kurumsal imaja gelebilecek potansiyel zararları engelleme, malzeme ve enerji girdilerinde azalma, atık, emisyon ve toksik maddelerin azalımı, çevresel standartlara uyum, yasalar ve yönetmeliklere uyum gibi çevre ile bağlantılı avantajların yanı sıra, yenilikçi ürün geliştirme ve maliyetlerin azalması gibi imkanlar da sağlamaktadır. Geri kazanılmış malzeme kullanımı, eko tasarımın önemli araçlarından biridir. Yapılan çeşitli Yaşam Döngüsü Değerlendirme (YDD) çalışmalarında, orijinal ürün yerine geri kazanılmış ürün kullanımının çevresel etkiyi önemli ölçüde düşürdüğü görülmüştür. Özellikle en yaygın olarak kullanılan iki lif olan pamuk ve polyesterde, bu düşüşler çok önemli boyutlardadır. Örneğin, bir kg orijinal iplik yerine kullanılmış tekstil atıklarının geri kazanılması ile elde edilen iplik kullanıldığında, pamuk için 65 kWh, polyester için 90 kWh'lık kazancın elde edildiği belirlenmiştir [22]. Bir başka çalışmada ise orijinal ve geri kazanılmış pamuktan elde edilmiş kıyafetlerin karbon ayak izi değerleri karşılaştırılmış ve 1 kg pamuklu giysi için bu değer orijinal üründe 42 kg CO_2 eq iken, geri kazanılmış üründe 22 kg CO_2 eq olarak bulunmuştur [23].

Günümüzde geniş ticari hacme sahip olan küresel ölçekli firmaların da maliyet avantajının yanısıra özellikle çevresel kaygılar nedeniyle geri dönüştürülmüş malzeme kullanımına yöneldiği görülmektedir. Marks&Spencer 2025'e kadar ürünlerinin en az %25'ini, %25 oranında geri kazanılmış malzeme kullanarak üretmeyi hedeflemektedir [24]. Levi's, 2020 yılına kadar ürettiği pantolonlardan hammaddeleri geri kazanarak yeni pantolonlar üretmeyi planlamaktadır [25]. H&M, üretimlerinde %20 oranında geri kazanılmış hammadde kullanarak giysi ürettiğini belirterek, gelecekte bu oranı %100'e çıkarmaya çalışacağını beyan etmektedir [26].

Pamuk ipliği üretiminde geri kazanım süreci

Elyaf geri kazanım kavramı ve uygulaması, sanayi devriminden bu yana tekstil endüstrisinin önemli bir bölümünü oluşturmuştur [27]. Pamuk ipliği üretiminde, açma, temizleme ve karıştırma işlemlerinden eğirme aşamasına kadar olan süreçte elyaf ve iplik atıkları meydana gelmektedir. Oluşan atıkların içerisinde yaklaşık olarak %50 oranında iyi lif bulunmaktadır. Dolayısıyla, işlenen hammaddenin neredeyse yarısı kaybedilmektedir (Şekil 1). Telef ve telefteki iyi lif oranının yüksek olması nedeniyle teleften iyi kalitede iplik üretimi mümkün olabilmektedir. Ancak, bu durum öncelikle birincil hammadde kalitesi ve geri kazanımda kullanılacak makinelere bağlıdır [6, 28-29].

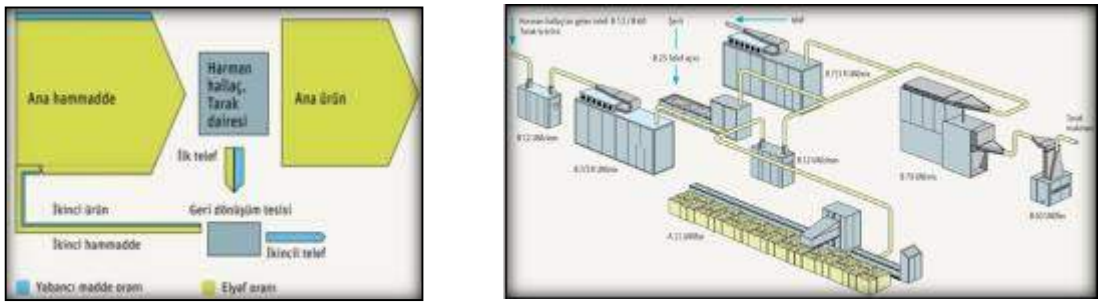

(a) (b)

Şekil 1. Telef değerlendirme için örnek bir proses akışı (a) ve geri kazanım tesisi (b) [30]

Eğirme prosesindeki işlemler içerisinde en fazla elyaf telefi, başta tarama ve taramayı takiben harman hallaç ve tarak makinalarında gerçekleşmektedir. Ürün kalitesi konusundaki ihtiyaçlar doğrultusunda tarama işleminde, belirli oranlarda kısa lifler uzaklaştırılmaktadır. Harman hallaç ve tarak makinelerinde ise hammaddenin özellikle temizlenmesi ve açılması sırasında lifler kirliliğe neden olan yabancı maddelerle birlikte kaybedilmektedir. Farklı teknik gelişmelere rağmen, harman hallaç makinelerinin oluşturdukları atıklar, büyük oranda lif içermektedirler [6, 31].

Tekstil atıklarının neredeyse tamamının geri kazanımı mümkündür [32]. Türkiye özelinde, tekstil atıklarının önemli bir kısmı iplik üretim proseslerinde hammadde olarak değerlendirilmektedir. Özellikle ring iplikçilik sistemine kıyasla, daha kısa uzunluktaki elyafın da üretime dahil edilebilmesi nedeni ile OE-rotor iplikçilik sisteminde geri dönüştürülmüş lifler büyük bir oranda üretimde kullanılabilmektedir [33].

Geri kazanılan veya geri dönüşüm lifleri ile gerçekleştirilen eğirme işlemi hammadde tasarrufu yanında atık liflerin endüstriyel döngüye yeniden kazanımını sağlamaktadır (Çizelge 1). %100 orijinal pamuktan elde edilen iplik üretiminde; hammadde maliyeti, toplam maliyetin %50'sini oluştururken, %50 geri dönüşüm pamuk ve %50 orijinal pamuktan oluşan karışımlı harmandan iplik üretiminde ise toplam maliyetin %33.5'ini oluşturduğu belirtilmektedir [34]. Dolayısıyla, hammadde ile ilgili tasarruf üretim maliyetlerini önemli oranda azaltmaktadır.

Çizelge 1. Örnek bir işletme için telef yönetimi ve hammadde kullanımın tasarruf açısından değerlendirilmesi [30]

	Ekonomik değeri
Bir yılda işlenen hammadde miktarı	10.000 ton
Harman hallaç ve tarak dairesinden çıkan toplam telef	800 ton
Geri kazanılabilir telef	360 ton
Bir kg hammadde fiyatı (ABD$)	1.32
Yıllık hammadde tasarrufu (ABD$)	475.000

Geri dönüşüm liflerin ve elde edilecek ipliğin kalitesi, aslında ipliğin üretim süreci ile ilgilidir [6, 31]. Eğirmede geri kazanılmış liflerin yeniden kullanımını ele alan birçok yayınlanmış makale mevcuttur. Çalışmalarda OE-rotor eğirme prosesi ile rotor iplikler üretilmiştir. Yapılan ilk çalışmalarda Wulfhorst (1984), geri kazanılan elyafın birincil hammadde ile %20'ye kadar harmanlaması sonucunda, harman kalitesinde değişiklik olmadığı sonucuna varmıştır [35]. Bruggeman (1998) eklenecek ikincil hammaddenin oranının dikkatli bir şekilde belirlenmesi gerektiğini belirtmiştir [28]. Son yıllarda yapılan çalışmalar incelendiğinde, genellikle çeşitli elyaf teleflerinin kullanılmamış pamuk liflerine çeşitli oranlarda harman hallaç ve I.pasaj cer makinesinde karıştırıldığı ve çoğunlukla Ne 5/1 ve Ne 20/1 numara aralığında OE-rotor iplikler üretildiği görülmektedir [36, 39]. Çalışmalar özellikle, karışım oranının çeşitli iplik özelliklerine etkisi yanında açma silindir türü, hızı, rotor hızı, düze türü gibi optimum OE-rotor iplik makine parametrelerinin belirlenmesi konularında yoğunlaşmaktadır. Kullanılan telef türü, karışım oranı ve iplik numarasına bağlı olarak uygun rotor iplik eğirme parametreleri değişmekle birlikte [36-40] özellikle belirli karışım oranına kadar (%20-25 arasında) iplik ve kumaş özelliklerinin telef içermeyen ipliklerle benzer

olduğu tespit edilmiştir [35-36, 40-42]. Ancak bu oran %25'i aştığında özellikle düzgünsüzlük, tüylülük, mukavemet ve kopma uzaması gibi iplik kalite özelliklerinde düşüş yaşandığı gözlenmiştir. Üretime eklenen telefin türü de (pnomofil, şapka, brizör, cer telefi), en az eklenen telef oranı kadar önemlidir. Özellikle daha temiz ve uzun lif içermesi nedeniyle pnomofil teleflerinin daha iyi özellikler sağladığı tespit edilmiştir [36]. Cer makinesinde yapılan karışımdan ziyade harman hallaç dairesinde yapılan karıştırmanın daha homojen bir lif dağılımı sağladığı ve böylece daha düşük düzgünsüzlük değerlerine ulaşıldığı görülmüştür [37, 43]. İplik özelliklerinin incelendiği çalışmalarda telef lifleri çoğunlukla birincil pamuk lifleri ile karıştırılırken denim kumaş [42, 44] ve çorap eldesi [38] için geri dönüşüm polyester ile, battaniye üretimi için ise polyester ve akrilik lifleri ile birlikte belirli oranlarda harmanlanmıştır. Elde edilen denim [42, 44], battaniye [38, 45-46] gibi ürünlerde yırtılma mukavemeti, ısıl konfor gibi özellikler değerlendirilmiştir. Çalışmalarda geri dönüşüm elyaftan üretilen battaniyelerin kabul edilebilir seviyede mukavemet değerleri [45] ve alternatif olabilecek seviyede iyi konfor özelliği sağlaması [46] ve daha düşük maliyetli olması nedenleriyle geri dönüşüm lif içermeyen orijinal battaniyelere alternatif olarak kullanılabileceği belirtilmiştir [45-46]. %20 oranında geri dönüşüm pamuk lifi içeren karışımdan elde edilen denim kumaşlarda yırtılma mukavemetinin düşük olduğu tespit edilmiş ve lif mukavemeti arttırılarak kumaş performansının iyileştirilebileceği belirtilmiştir [42]. Çoraplarda ise geri dönüşüm lif içerikli çorapların termal iletkenliği ve soğurganlık değerlerinin daha düşük, termal direnç ve su buharı geçirgenliği değerlerinin ise daha yüksek olduğu belirlenmiştir [38].

Türkiye tekstil geri kazanım sektörü hakkında kısa bilgiler

Türkiye'de, telef geri kazanım sektörü önemli bir sektör olmasın rağmen atık yönetimi konusunda toplumsal duyarlılığın sağlanması, Ar-Ge çalışmaları, tekstil atıklarının yüksek katma değerli ürünlere çevrilmesi konularında ilave çalışmalar yapılmasına ihtiyaç bulunmaktadır. Türkiye'de atıkların önemli bir bölümü iplik üretiminde kullanılmaktadır. Geri kazanılmış hammaddeden iplik üretiminde, Uşak ili lider durumdadır ve sektöründe %75 oranında bir paya sahiptir. Türkiye'de pamuk teleflerinin geri kazanımında en yaygın yöntem OE rotor iplikçiliğidir. Türkiye'de teleflerin geri kazanılması ile elde edilen başlıca ürünler ve üretim oranları aşağıda verilmiştir [21], [38].

- Dolgu (%22)
- Keçe (%13)
- Battaniye (%13)
- Triko-örgü (%13)
- Dokuma kumaş (ev tekstil ve giyim) (%12)
- İplik (%9)
- Çorap (%6)
- Ayakkabı (%4)

- Kilim, yorgan, yastık (%4)
- Halı (%3)'dır.

Türkiye'deki pamuk geri kazanım sektörünün en önemli sorunları ise, kalın ve düşük kalitede, katma değeri düşük iplik üretimi ve ürün çeşitliliğinin az olmasıdır [47]. Dünyada son yıllarda telef/atık geri kazanımı yeni bir boyut kazanmış ve atıklardan yüksek katma değerli ürün eldesi önem kazanmıştır [48]. Yukarıda da bahsedildiği gibi, günümüzün önemli tekstil firmaları üretimlerinde geri kazanılmış hammadde kullanmaya başlamıştır ve gelecekte de bu oranı artıracaklarını beyan etmişlerdir. Bu pazardan pay alabilmek için Türkiye'de bulunan firmaların Ne 20 bandının üzerine çıkmaları, ürün performansını ve çeşitliliğini iyileştirmeye yönelik Ar-Ge çalışmaları yapmaları önemlidir.

Bu çalışmada, pamuk ağırlıklı atık kumaşlardan elde edilen liflerin farklı atık lifleri ile hazırlanan harmanları kullanarak OE-rotor yöntemi ile iplik ve dokuma kumaşlar üretilmiş ve performans özellikleri değerlendirilmiştir.

YÖNTEM

Mekanik açma işleminden geçirildikten sonra elyaf haline getirilen dokuma telefleri ile farklı elyaf karışımları oluşturulmuştur. Orijinal pamuk ve geri dönüşüm polyester (rPET) lifleri kullanılarak harmanlar elde edilmiştir. Oluşturulan harmanlara ait bilgiler, Çizelge 1'de gösterilmektedir.

Çizelge 2. Açılan dokuma teleflerine ait harmanlar

	Harman No	**1. Elyaf**	**2. Elyaf**	**3. Elyaf**	**Açıklama**
Açma telef harmanları	1	60%	25%	15%	Pamuk açma + pamuk/sentetik açma + rPET
	2	80%	20%	-	Pamuk açma + siyah rPET

Açma işleminden geçirilen dokuma kumaş telef liflerinin SEM görüntüleri alınarak, gerçekleştirilen mekanik açma işleminin elyaf morfolojisine olan etkileri de incelenmiştir. Oluşturulan harmanlar ile Ne 8/1 numara OE-Rotor iplikler üretilmiştir. Telef içeren ipliklerin düzgünsüzlük, ince-kalın yer, neps ve tüylülük özellikleri Uster Tester 3'de, mukavemet ve kopma uzaması özellikleri Uster Tensorapid test cihazlarında test edilmiştir. Bununla birlikte, üretilen bu ipliklerden numune dokuma tezgahında kumaşlar üretilip, aşınma (ISO 12947-2) ve boncuklanma

(ASTM D4970, 2000) direnci ile asidik (ISO 105 E04) ve bazik ter (ISO 105 E04) haslığı, yıkama haslığı (ISO 105 C06), su haslığı (ISO 105 E01), kuru (ISO 105 X12) ve yaş sürtme (ISO 105 X12) haslığı gibi çeşitli renk haslıklarından oluşan fiziksel testleri yapılmıştır.

BULGULAR

Açma işlemi sonrası elyaf görüntüleri

Açma makinesinde 6 aşamalı açma işleminden geçirilen dokuma kumaş teleflerinden her açma işlemi sonrası numuneler alınmış ve taramalı elektron mikroskobunda (SEM) mekanik açma işleminin elyaf morfolojisine olan etkileri incelenmiştir (Şekil 2). Lif görüntüleri incelendiğinde, mekanik açma işleminden geçirilen dokuma kumaş teleflerine ait liflerin açma işlemi sonrasında liflerin uç kısımlarında hasarların oluştuğu gözlemlenmektedir.

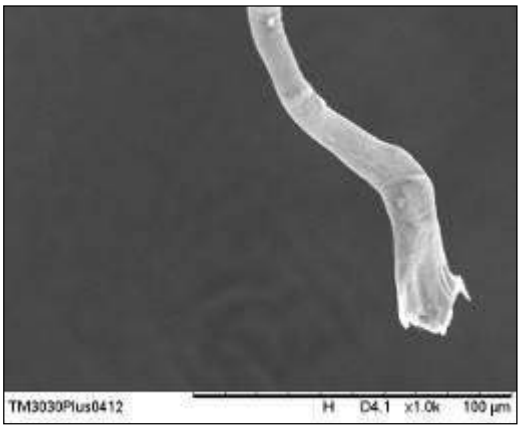

(a)

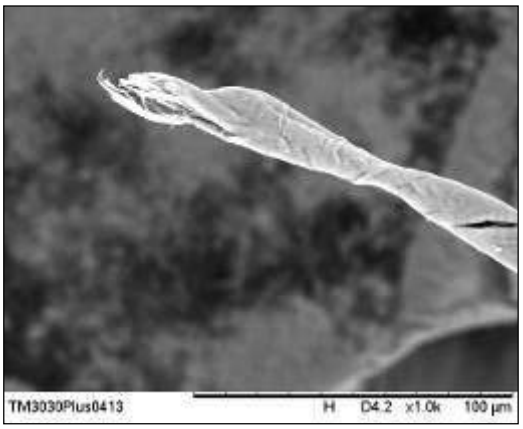

(b)

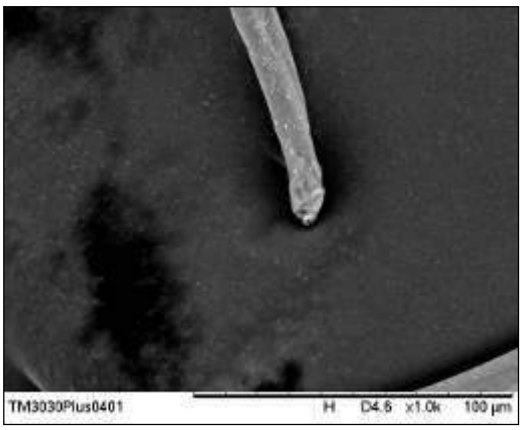

(c)

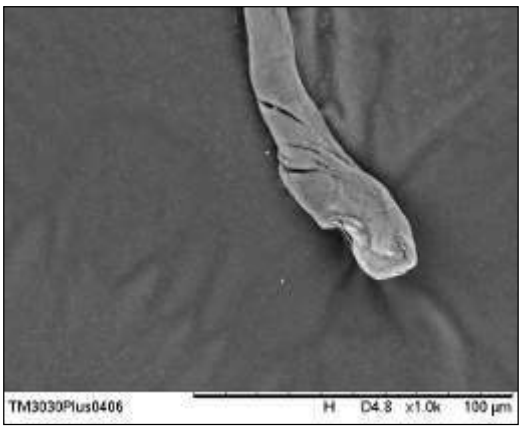

(d)

Şekil 2. 6 aşamalı açma işlemine tabi tutulan dokuma teleflerine ait elyafların SEM görüntüleri (a: İşlem görmemiş, b: 1 defa açma işleminden geçen lif, c: 3 defa açma işleminden geçen lif ve d: 6 defa açma işleminden geçen lif)

İplik özelliklerine ait sonuçlar

Mekanik açma işleminden geçirildikten sonra elyaf haline getirilen dokuma telefleri ile oluşturulan farklı harman karışımlarından elde edilen Ne 8/1 numara OE-rotor ipliklerin düzgünsüzlük (CVm), hata (ince yer, kalın yer ve neps) ve iplik tüylülüğü sonuçları Çizelge 3 ve mukavemet ve kopma uzaması sonuçları Çizelge 4'de verilmektedir. Üretilen iplikler, Uster Dünya İstatistikleri ile değerlendirmelere tabi tutularak ipliklerin uluslararası platformda kalite değerleri değerlendirilmiştir. Uster İstatistiklerinde oluşturulan harman içeriğinin bulunmaması nedeni ile %100 pamuk elyafından elde edilen Ne 8/1 numara dokuma ipliklerine ait %5, %50 ve %95 kalite grubuna ait değerler ile karşılaştırma yapılmıştır (Çizelge 5). İpliklerin sonuçları incelendiğinde, kumaş teleflerinin açılmasından elde edilen lifler ile oluşturulan harmanlardan elde edilen ipliklerin yüksek iplik düzgünsüzlüğü ve iplik hatalarına sahip olduğu belirlenmiştir. İplik tüylülüğü açısından ise oldukça düşük iplik tüylülüğü değerlerine sahip olduğu gözlenmiştir. Öte yandan, açma işleminden geçirilmiş dokuma teleflerinden elde edilen ipliklerin mukavemet ve kopma uzaması özellikleri açısından iyi değerler sağladığı tespit edilmiştir.

Çizelge 3. Açılan dokuma teleflerini içeren OE-rotor ipliklere ait Uster Tester 3 sonuçları

Harman No	CVm (%)	İnce yer (-%50)	Kalın yer (+%50)	Neps (+%280)	Toplam İplik Hataları	Tüylülük (H)
1	21,93	82	1411	794	2287	5,12
2	16,65	15	324	208	547	5,25

Çizelge 4. Açılan dokuma teleflerini içeren OE-rotor ipliklere ait Uster Tensorapid sonuçları

Harman No	Kopma kuvveti (N)	Mukavemet (cN/tex)	Kopma uzaması (%)	Kopma işi (N.cm)
1	5,69	7,71	10,13	17,33
2	5,89	7,98	9,12	16,32

Çizelge 5. Uster istatistiklerinin %5, 50 ve %95 kalite grubuna göre iplik özelliklerine ait değerler

İplik özelliği	%5	%50	%95
CVm (%)	11,3	12,8	14,4
İnce yer (-%50)	0	1	6
Kalın yer (+%50)	5	17	57
Neps (+%280)	1	4	18
Toplam iplik hataları	6	22	81
Tüylülük (H)	5,5	7	8,8
Mukavemet (cN/tex)	15,6	13,1	11,2
Kopma uzaması (%)	8,9	7,4	6,1

Kumaş özelliklerine ait sonuçlar

Oluşturulan harmanlardan Ne 8/1 numara OE-rotor iplik üretimini takiben bu ipliklerden numune dokuma tezgahında 2/2 panama örgü türünde dokuma kumaş numuneleri üretilmiştir. Telef içerikli iplikler, atkı ve çözgü yönünde kullanılmıştır. Çeşitli fiziksel ve haslık testleri gerçekleştirilmiştir (Çizelge 6-7). Dokunan kumaşların fiziksel performans özellikleri değerlendirildiğinde; aşınma direncinin yeterli, boncuklanma direnci değerinin ise istenen değerin bir derece altında olduğu gözlemlenmiştir. Telef içerikli ipliklerden elde edilen kumaşların lif uzunluğunun kısa olması ve liflerin açma işleminden dolayı deforme olmasından dolayı aşınma ve boncuklanma direnci açısından daha kötü değerler vermesi beklenmektedir. Ancak, ipliklerin özellikle iplik tüylülüğü, mukavemet ve kopma uzaması açısından kabul edilebilir değerler sağlaması telef içerikli ipliklere ait kumaşların aşınma ve boncuklanma direnci özelliklerinin istenilen değerlerin bir derece altında değerler vermesini sağladığı düşünülmektedir. Haslık performanslarında yıkama, su ve kuru sürtme haslıklarının sağlandığı, asidik, bazik ve yaş sürtme haslıklarının ise istenilen değerin altında olduğu belirlenmiştir.

Çizelge 6. Dokuma kumaş telefi içerikli OE-rotor ipliklere ait dokuma kumaşların fiziksel özelliklerine ait sonuçlar

	Gramaj (g/m^2)	Aşınma (Tur)	Boncuklanma (Derece)

İstenen değer		±5%	MİN 10000	3
Harman No	1	307	Kopma yok	2/3
	2	305	Kopma yok	2/3

Çizelge 7. Dokuma kumaş telefi içerikli OE-rotor ipliklere ait dokuma kumaşların renk haslığı ve boyutsal çekme özelliklerine ait sonuçlar

		Ter Haslığı		**Yıkama Haslığı**	**Su Haslığı**	**Sürtme Haslığı**	
		Asidik	**Bazik**			**Kuru**	**Yaş**
İstenen değer		MİN 3/4C, 3/4S	MİN 3/4C, 3/4S	MİN 3/4C, 3/4S	MİN 3C, 3S	MİN 4S	MİN 3/4S
Harman no	1	4C, 2/3S	4C, 2/3S	4C, 3/4S	4C, 3/4S	4S	2/3S
	2	4C, 2/3S	4C, 2/3S	4C, 3/4S	4C, 3/4S	4S	2/3S

SONUÇLAR

Kumaş atıklarının değerlendirilmesinin amaçlandığı bu çalışmada, kumaş telefleri mekanik açma işlemi ile lif haline getirilmiş ve genel olarak %80 açılmış telef lifleri %20 geri dönüşüm polyester liflerinden oluşan harmanlar oluşturulmuştur. Çalışmada, iplik tüylülüğü ve gerilme özellikleri açısından yeterli özelliklere sahip Ne 8/1 numara OE-rotor iplik üretiminin mümkün olduğu belirlenmiştir. Elde edilen iplikler atkı ve çözgü ipliği kullanılarak dokuma kumaş üretimi yapılmış ve fiziksel ve renk haslığı özellikleri açısından istenilen değerlerin bir derece altında özelliklerin elde edildiği tespit edilmiştir. Çalışmada, atkı ve çözgü yönünde telef içerikli ipliklerin kumaş üretiminde kullanılmasından yola çıkarak özellikle atkı veya çözgü yönünde daha iyi iplik özelliklerine sahip iplikler kullanılarak kumaş özellikleri açısından daha iyi değerlere sahip kumaş üretiminin mümkün olduğu düşünülmektedir. Dolayısıyla, kumaş atıklarının açma işleminden geçirilerek uygun harman içerikleri oluşturularak iplik ve kumaş üretiminde değerlendirilebileceği sonucuna ulaşılmış olup, bu durumunda çevre kirliliğinin azalması ve var olan hammadde kaynaklarının daha verimli olarak kullanılabileceği düşünülmektedir.

ÖNERİLER

Önemli bir tekstil ve hazır giyim üreticisi, ithalatçısı ve ihracatçısı olan Türkiye'de tekstil atıkları uzun yıllardır geri kazanılmaktadır ve bu konuda önemli bir bilgi alt

yapısı da mevcuttur. Sektörün son yıllarda bilinçlendiği de görülmektedir. Özellikle son yıllarda ince numaralarda üretim yapan, kurumsallaşmış firmalar da bulunmaktadır. Ancak, sektörün %80'den fazlası kurumsallaşmamış firmalardan oluşmaktadır. Recycle sertifikası dahil olmak üzere, ekolojik sertifikalar konusunda yeterli bilgiye sahip değillerdir ve mühendis çalıştırma oranı düşüktür. Tüm bunların sonucu olarak, elde edilen ürünler özellikle üst segmente yönelik üretim yapan firmaların standartlarını karşılayamamaktadır. Ayrıca, sektör OE-rotor iplik üretiminde yoğunlaşmış ve gelişmekte olan teknik tekstil pazarının önemli bir aracı olan dokusuz yüzey üretimi ihmal edilmiştir. Günümüzde bilindiği gibi geri dönüştürülmüş elyaf kullanımı, farklı ekolojik etiketlerde teşvik edilmekte/zorunlu tutulmaktadır. Bu durum da geri dönüşüm sektörüne önemli avantajlar sunmaktadır. Geri dönüşüm sektörünün bu avantajlardan faydalanması, yeni pazarlara ulaşabilmesi, ihracat odaklı çalışabilmesi için;

- Sektörün kurumsallaşması
- Mühendis, teknik personel sayısının artırılması
- Ar-Ge çalışmalarına yönelinmesi
- Sektördeki eğilimlerin ve teknolojik yeniliklerin takip edilmesi
- Ürün çeşitliliğinin artırılması önerilebilir.

TEŞEKKÜR

Bu çalışma, Bilim, Sanayi Ve Teknoloji Bakanlığı-Bilim Ve Teknoloji Genel Müdürlüğü tarafından desteklenen San-Tez projesi çerçevesinde gerçekleştirilmiştir (Proje No: 0999.STZ.2015).

KAYNAKLAR

[1] İklim Değişikliği Çerçeve Sözleşmesi. Kyoto Protokolü ve Türkiye. http://www.dsi.gov.tr/docs/iklimdegisikligi/iklim_degisikligi_cerceve_sozlesmesi_ve_turkiye.pdf?sfvrsn=2 (12.10.2015).

[2] Green Public Procurement. http://ec.europa.eu/environment/gpp/index_en.html (12.10.2015).

[3] Attitudes of Europeans towards building the single market for green products. FlashEurobarometer367.
http://ec.europa.eu/public_opinion/flash/fl_367_sum_en.pdf (01.10.2015).

[4] Zhu, Q., & Sarki J. (2015). Green Marketing and Consumerism in China: Analyzing the Literature Working Paper. *WP1-2015*, *Worcester Polytechnic Institute [US]*, 1-46.
http://www.wpi.edu/Images/CMS/Business/WP1-2015_Green_Marketing.pdf

[5] Klein, W., (2011). Stalder H. Rieter İplikçilik El Kitabı.

[6] Leifeld, F. (1996). Récupération de déchets de coton: un procédé de filature lucratif. *ITB Filature et Tissage/Maille*, *3*, 96.

[7] Bouchraiet, R., Azzouz, B., Ben Hassen, M., & Saklı, F. (2016). Modeling cotton/ natural bast fibers blends: graphic and statisctical analyses of cotton-flax blended yarns produced on ring and rotor spinning machines. *International Journal of Applied Research on Textile*, 4(1), 62-75.
[8] Saurer. The fiber year 2015/2016, *Oerlikon Cooperation AG*, 2016,
[9] Sustainable Clothing Action Plan , Şubat 2010. http://www.defra.gov.uk/environment/business/products/roadmaps/clothing/index.htm (07.12.2015).
[10] Department for environment, Food and Rural Affairs "Sustainable Clothing Action Plan" 2011.
https://www.gov.uk/government/uploads/system/uploads/attachment_data/file/69193/pb13206-clothing-action-plan-100216.pdf (01.10.2015).
[11] TextileExchange, 2012.
http://farmhub.textileexchange.org/farm-library/farm-fiber-report (01.10.2018).
[12] OECD-FAO Agricultural Outlook 2015-2024. *Commodity Snapshots: Cotton 2015*, 1-148 (07.12.2015)
[13] Quick Facts and Statistics for Textile and Product Waste 2012.
http://www.purewaste.org/media/pdf/textile-product-waste-fast-facts.pdf
(07/12/2015)
[14] Soth, J., Grasser, C., & Salerno, R. (1999). The impact of cotton on fresh water resources and ecosystems. *A Preliminary Synthesis, WWF International*, 1-48.
[15] Cherrett, N., Barrett, J., Clemett, A., Chadwick, M., & Chadwick, M.J. (2005). Ecological footprint and water analysis of cotton. *Hemp and Polyester*, Stockholm Environment Institute, 73.
[16] Uluatam, S.S. (1994). Protection measures for environmental problems due to water development in the southeastern anatolia project region. *Improvement of Water and Soil Resources, Ankara,* State Hydraulic Works III, 1119-1130,.
[17] Harmancioglu, N., Alpaslan, N., & Boelee, E. (2001). Irrigation, health and environment: A review of literature from Turkey. Colombo, Sri Lanka: *International Water Management Institute (IWMI),* IWMI Working Paper, 6, 21.
[18] Chapagain, A.K., Hoekstra, A.Y., Savenije, H.H.G., & Gautam, R. (2006). The water footprint of cotton consumption: An assesment of the impact of worldwide consumption of cotton products on the water resouces in the cotton producing countries. *Ecological Economics*, *60*, 186-203.
[19] Yilmaz, I., Akcaoz, H., & Ozkan, B. (2005). An anaylsis of energy use and input costs for cotton production in Turkey. *Renewable Energy*, *30*, 145-155.
[20] Niinimki, K. (2006). Ecodesign and textiles. *Research Journal of Textile and Apparel*, 10(3), 67-75.
[21] Kasap, G.Ç., & Peker, D. (2011). An environmentalist approach: green design. *Business and Economics Research Journal*, *2*(2), 101-116.
[22] Woolridge, A.C., Ward, G.D., Phillips, Collins, M., Gandy, S. (2006). Life cycle assessment for reuse/recycling of donated waste textiles compared to use of virgin material: An UK energy saving perspective Resources. *Conservation and Recycling*, *46*, 94-103.

[23] Defra Contract Reference: WRT152, Oakdene Hollins Ltd, Salvation Army Trading Company Ltd, "Recycling of Low Grade Clothing Waste". Nonwovens Innovation & Research Institute Ltd.
http://docplayer.net/25633310-Recycling-of-low-grade-clothing-waste.html (07.12.2015)

[24] https://corporate.marksandspencer.com/documents/plan-a/plan-a-2025-commitments.pdf (07.12.2015)
[25] http://www.levistrauss.com/unzipped-blog/2015/07/embracing-the-circular-economy (07.12.2015)
[26] https://about.hm.com/en/sustainability/get-involved/recycle-your-clothes.html (07.12.2015)
[27] Richard, H. (2000). Recycling textile and plastic waste. *Recycling and Recovery Strategies*, Woodhead Publishing Limited, 1–3.
[28] Bruggeman, J.P. (1998). Traitements mécaniques des déchets et des cotons charges. *l'industrie textile*, *1128*, Décembre, 1049-1051.
[29] Hanafy, I. *(*1997). Fabric from cotton waste. *The Indian Textile Journal*, 16-18.
[30] Klein, W. (2014). Kısa Lif İplikçilik Teknolojisi. *Rieter El Kitabı*, Rieter Machine Works Ltd., Cilt 2.
[31] Specklin, F.P. (1994). Environnement et gestion des d´echets. *L'industrie Textile*, *1254*, 52–570.
[32] Wang, Y. (2010). Fiber and textile waste utilization. *Waste Biomass Valorization*, Şubat, *1*,135–143.
[33] Merati, A. A., & Okamura, M. (2004). Producing medium count yarns from recycled fibers with friction spinning. *Textile research journal*, *74*(7), 640-645.
[34] Wanassi, B., Azzouz, B., & Hassen, M. B. (2016). Value-added waste cotton yarn: Optimization of recycling process and spinning of reclaimed fibers. *Industrial crops and products*, *87*, 27-32.
[35] Wulfhorst, B. (1984). The technological and economic aspects of the recycling of wastes in modern cotton mills. *Foreign edition with English supplement*, *8*, 741-743.
[36] Khan, K., & Rahman, H. (2015). Study of Effect of Rotor Speed, Combing-Roll Speed and Type of Recycled Waste on Rotor Yarn Quality Using Response Surface Methodology. *Journal of Polymer and Textile Engineering*, *2*(1), 47-55.
[37] Khan, M. K. R., Hossain, M. M., & Sarker, R. C. (2015). Statistical analyses and predicting the properties of cotton/waste blended open-end rotor yarn using Taguchi OA design. *International Journal of Textile Science*, *4*(2), 27-35.
[38] Gun, A. D., Alan, G., & Macit, A. S. (2016). Thermal properties of socks made from reclaimed fibre. *The Journal of The Textile Institute*, *107*(9), 1112-1121.
[39] Repon, M. R., Al Mamun, R., Reza, S., Das, M. K., & Islam, T. (2016). Effect of Spinning Parameters on Thick, Thin Places and Neps of Rotor Spun Yarn. *Journal of Textile Science and Technology*, *2*(03), 47.
[40] Mohamed Taher, H., Bechir, A., Mohamed, B. H., & Faouzi, S. (2009). Influence of spinning parameters and recovered fibers from cotton waste on the uniformity and hairiness of rotor spun yarn. *Journal of Engineered Fibers and Fabrics*, *4*(3), 155892500900400304.

[41] Halimi, M. T., Hassen, M. B., & Sakli, F. (2008). Cotton waste recycling: Quantitative and qualitative assessment. *Resources, Conservation and Recycling*, *52*(5), 785-791.
[42] Borman, T., & Sun, D. (2016). Recycled jean: property comparison to standard jean. *Journal of Fashion Technology and Textile Engineering*, *4*(2), 1000136.
[43] Pınarlık, G., & Şenol, M. (2012). İkincil kullanım tekstil liflerinden yapılan open-end rotor ipliklerinin özellikleri. *I. Ulusal Geri Kazanım Kongre ve Sergisi*, Uşak, 169-174.
[44] Telli, A., & Babaarslan, O. (2017). The effect of recycled fibers on the washing performance of denim fabrics. *The Journal of The Textile Institute*, *108*(5), 812-820.
[45] Alan, G., Koçlu, A., & Yüksekkaya, M. (2012). Geri dönüşüm hammaddeden üretilmiş olan battaniyelerin kopma mukavemeti performansının incelenmesi üzerine bir çalışma. *I. Ulusal Geri Kazanım Kongre ve Sergisi*, Uşak, 276-297.
[46] Celep, G., & Yüksekkaya, M. (2012). Geri dönüşüm liflerden ve orijinal liflerden üretilen battaniyelerin ısıl konfor özelliklerinin incelenmesi. *I. Ulusal Geri Kazanım Kongre ve Sergisi*, Uşak, 157-162.
[47] Altun, Ş. (2012). Tekstil üretim ve kullanım atıklarının, geri kazanımı, çevresel ve ekonomik etkileri. Rapor, Uşak Ticaret ve Sanayi Odası, Uşak.
[48] Meyabadi, T.F., & Dadashian, F. (2012). Optimization of enzymatic hydrolysis of waste cotton fibers for nanoparticles production using response surface methodology. *Fibers Polymers,* 13 (3), 313–321.

ENERGY VALORIZATION OF OIL PALM AGRO-RESIDUES BY AIR-DOWNDRAFT GASIFICATION: TECHNICAL AND ECONOMIC ANALYSIS

Juan C. SOLARTE-TORO

Instituto de Biotecnología y Agroindustria, Universidad Nacional de Colombia Sede Manizales – Km 07 vía al Magdalena. Colombia. Email: jcsolartet@unal.edu.co

Mariana ORTIZ-SANCHEZ

Instituto de Biotecnología y Agroindustria, Universidad Nacional de Colombia Sede Manizales – Km 07 vía al Magdalena. Colombia. Email: mortizs@unal.edu.co

Leonardo A. ALONSO-GÓMEZ

Grupo de Investigación, Ciencia, Tecnología e Innovación Agroindustrial. Universidad de Los Llanos, Villavicencio, Colombia. Email: lalonso@unillanos.edu.co

Carlos A. CARDONA-ALZATE

Instituto de Biotecnología y Agroindustria, Universidad Nacional de Colombia Sede Manizales – Km 07 vía al Magdalena. Colombia. Email: ccardonaa@unal.edu.co ; Corresponding author

ABSTRACT: The application of renewable resources has been encouraged to diversify the energy matrix and decrease the environmental impact caused by the oil-based energy production. In this way, oil palm waste gasification has been proposed as alternative to produce electricity. Therefore, this paper aims to evaluate oil palm rachis and petiole (OPRP) as suitable feedstock to be gasified analyzing its fuel properties. For this purpose, a 10-kW pilot-scale air-downdraft gasifier was used. As results, syngas with a H_2/CO ratio of 0.57 and LHV of 5.46 MJ/Nm3 was produced. The carbon conversion and cold gas efficiency were 94.98% and 72.94%, respectively. The energy balance of the process leads to establish energy losses of 6.45%. Moreover, an electricity cost range of 0.614 USD/kWh - 0.286 USD/kWh was obtained, which can be only compared with those prices found in off-grid zones. Moreover, CO_2 emissions are lower than those derived from combustion processes. Finally, the OPRP gasification is a promising alternative to produce renewable energy in a decentralized way (including off-grid zones, where the electricity prices are higher).

Key words: Biochar, Biomass gasification, Electricity generation, Syngas, Waste valorization

INTRODUCTION

A reliable, efficient and affordable electricity generation and supply for both rural and urban communities are one of the most important commitments acquired by countries to ensure a sustainable progress (Anco S. Blazev, 2015; Ang, Choong, & Ng, 2015). In accordance with the U.S Energy Information Administration (EIA), globally 24TWh of electricity were produced in 2017 with an annual increase of 1.9% in The Organization for Economic Co-operation and Development countries (OECD) countries and 1.0% in non-OECD countries (US Energy Information Administration, 2017). This energy production was carried out using different energy sources such as fossil fuels (i.e., coal, natural gas, petroleum), renewables (i.e., hydropower, biomass, wind, solar) and nuclear processes (BP, 2017). Nevertheless, 65% of the net electricity generated was obtained using fossil fuels, which have been classified as the main cause of environmental issues such as global warming and natural resources pollution (Renewable energy policy network for the 21st century (REN21)., 2018). Therefore, electricity generation using renewable energy sources as raw material must be increased to diversify the energy matrix as well as reduce the oil-based energy production in the world.

Renewable electricity generation has been used to supply the energy demand in different sectors (e.g., residential, industrial, transport and so forth). Moreover, the electricity derived from renewable resources has been implemented in regional energy developing plans as well as a surplus in the grid capacity of a wide variety of countries in rural and urban zones. Biomass is a renewable energy source that can be processed to generate electricity through different ways in energy vectors such as bioethanol, biogas and syngas as well as used directly in combustion chambers (Solarte-Toro, Chacón-Pérez, & Cardona-Alzate, 2018). In comparison to the energy derived from sunlight and wind, electricity generation from biomass has been developed on low, middle and high scale (Kitzler, Pfeifer, & Hofbauer, 2011; Surendra, Takara, Hashimoto, & Khanal, 2014).

Thermochemical paths (i.e., combustion and gasification) have been the main technologies used to produce electricity for both industrial and residential sectors. Combustion releases the energy content of the feedstock in form of heat through its degradation in presence of an oxidizing agent (e.g., air) (Overend, 2009). Instead, gasification comprises the conversion of carbonaceous materials in a partially oxidized environment to produce char, tars and a mixture of gases composed by hydrogen (H_2), carbon monoxide (CO), carbon dioxide (CO_2) and methane (CH_4) as well as other low molecular weight hydrocarbons. This gas mixture is known as syngas (Brown, 2011; Molino, Chianese, & Musmarra, 2016). Air, steam and oxygen are the main gasifying agents used to upgrade biomass in the above-mentioned products (Couto, Rouboa, Silva, Monteiro, & Bouziane, 2013; Gil, Corella, Aznar, & Caballero, 1999). On industrial level, combustion and gasification have been employed to produce heat and power simultaneously in cogeneration systems to supply part of the energy

requirements of chemical facilities (Islas, Manzini, Masera, & Vargas, 2019). The main advantage of the thermochemical conversion routes can be associated to the environmental friendliness of the processes due to the waste reduction and management. The gasification of biomass produces lower amount of CO_2, NO_x, SO_x, dioxins and furans than the direct combustion (Dong et al., 2018). Thus, gasification has been outlined as a striking technology to be implemented at different scales as base process to produce energy vectors, chemical compounds and direct usable power.

The gasification process has been classified considering crucial aspects such as oxidizing agent (i.e., air, steam and oxygen), and gasifier configuration (i.e., downdraft, updraft, fluidized bed, entrained bed).

Coal, petcoke, lignocellulosic biomass and municipal solid waste (MSW) are the main feedstocks used to be gasified and produce syngas (Solarte-Toro et al., 2018). The last two feedstocks have been widely studied in low scale applications while coal and petcoke are mainly used in chemical plants. The lower heating value (LHW) of the syngas changes based on the type of employed feedstock. Biomass produces a syngas with a LHV between 4 - 7 MJ/Nm^3, which can be used for generation purposes (Couto et al., 2013). Moreover, the updraft and downdraft gasifiers are the most common used configurations at these scales. Biomass and MSW are also common raw materials used in middle and low scale, which are used mainly for power generation and management of residues from agro-industrial processes, forest and waste.

The gasification process has been widely researched as alternative to produce electricity in different regions. Moreover, this technology has been studied to be used on industrial scale applications as well as an important stage in the steam and power generation in chemical facilities. The increased biomass production from industrialized crops (e.g., oil palm, rice, sugarcane) have boosted the search of alternatives for their proper management without considering the direct disposal into landfills or incineration. In this sense, this investigation focusses in evaluate the oil palm rachis and petiole (OPRP) as suitable feedstock to be gasified analyzing economical aspects, syngas properties, and mass and energy balances of the OPRP gasification using a pilot-scale air-downdraft gasifier.

METHODS

Oil Palm Waste Characterization

OPRP samples were obtained from an oil palm crop located in Cundinamarca, Colombia. The leaflets of the oil palm frond were removed and left in the field. Therefore, only the rachis and petiole of the frond was used as feedstock in the gasification process. The elemental composition (i.e., C, H, O, and N), as well as the volatile and fixed carbon content of this raw material were determined prior to the

experimental pilot-scale gasification. These parameters were used to calculate the OPRP fuel properties (i.e., heating value) and other important characteristics such as the alkalinity index. For this purpose, OPRP samples were dried using a convective furnace (Thermolab DiEs TH53) and milled using a knives mill (Thomas-Wiley mill) to reduce their particle size until ASTM 40 sieve (i.e., 0.42 mm). Then, the volatile matter (ASTM E872 – 82), fixed carbon (ASTM E870 – 82), and the ultimate analysis (ASTM D5373- 16) were determined. Finally, the high heating value (HHV) of the samples was calculated using the empirical correlation proposed by Nhuchhen and Salam (2012) and the experimental data obtained from the proximate analysis.

Experimental Set-Up Of The Air-Downdraft Gasification Of Oil Palm Rachis And Petiole

The Power Pallet system (i.e., gasifier) with a peak power production capacity of 10 kW manufactured by the company All Power Labs industry (USA) was used to perform the gasification of the OPRP. This system is composed by an Imbert-style downdraft gasifier, pre-heating air and feedstock system, spark fired industrial engine Kubota model DG972 and electrical generator Mecc-alte ECO3N-4. This system uses air as gasifying agent and no-compression stage is involved during the operation. Therefore, the gasification system operates at a lower pressure than the atmospheric (i.e., 78 kPa). Different flows of solids and gaseous components can be identified in the gasification equipment, which allows understanding in a better way the conversion of the OPRP samples into syngas and subsequently, power. A detailed flow diagram of the gasifier is presented in Figure 18

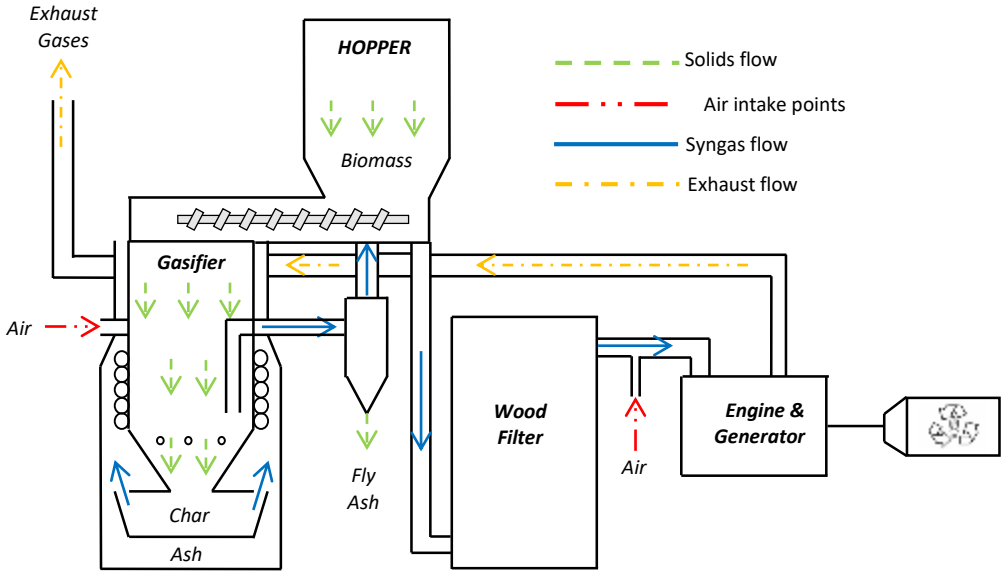

Figure 18. Process Flow Diagram Of A Downdraft Gasifier.

The gasification equipment presented in Figure 18 can be classified as an auto-thermal gasifier since it does not require an external heat source to maintain the endothermic

reactions that characterize the reduction zone of the process (Akay & Jordan, 2011; Molino et al., 2016). In addition, the equipment is powered by vacuum pressure. Nevertheless, the characterization of the syngas can be performed after the wood filter, before being used as fuel in the engine to produce electricity. As presented in Figure 18, there are three types of flows: the solids flow is related to the feedstock use and its degradation to syngas, which is mixed with air prior to enter the engine to generate electricity and exhaust gases. Additionally, the syngas flow starts in the gasifier and ends in the engine, whereas the exhaust gas flow is expelled from the gas engine and released to the atmosphere.

Before the operation of the gasifier, the conditioning of the raw material must be carried out to avoid operational problems associated to the feeding of the raw material into the equipment (e.g., bridging, rat-holing, binding). The conditioning stage involved two stages: i) feedstock drying until a moisture content below 20% and ii) dried feedstock chipping to obtain a particle size between 1.27 and 3.81 cm using a two-step milling process. The first milling step was carried out using a band saw Dewalt Dw739 and the second one was performed manually. This step was done to increase the energy efficiency of the process as well as to guarantee the correct size of the raw material.

Operation Run And Process Description

The feedstock was placed inside the hopper before turning-on the gasifier. The equipment was sealed and insured to avoid disrupting the system vacuum. Then, the equipment was started and the OPRP chips are conveyed through a horizontal auger to the reactor. A level switch sensor is coupled with the auger to control the raw material entering the reaction. This control is performed through an on-off system. Afterward, a torch and 50-ml gasoline were used to start with the first phase of combustion. As consequence, the temperatures inside the gasifier were increased until reaching a reduction temperature above 800°C. The syngas generated in the gasifier is transported to a cyclone in order to remove fly-ash. Additionally, this syngas was used to heat-up the inlet air to the process as well as to remove moisture from the raw material in the drying bucket. This “heat integration” is performed to increase the energy efficiency of the process and reduce the syngas temperature before using it as fuel in the gas engine. Simultaneously to the syngas generation, char, ash and tars were produced as main by-products. Char is collected through a vibratory grater, which separates the biochar fraction from the ash fraction. The produced tars in the process are removed from the syngas using a stratified wood filter. The first level of the filter contains big pieces of wood (average particle size of 5 - 10 cm), the second level has smaller pieces of wood (3 - 5 cm), the third level is filled with shavings from the furniture industry, and the last level consists of a foam filter. At the same time, the air flow rate was measured using a rotameter. Finally, the relative cold and clean syngas is combusted in the gas engine to produce electricity and from this process, exhaust gaseous (composed mainly by CO_2 and H_2O) are released.

Measurement Of The Syngas Composition

The syngas composition was measured using a portable gas analyzer (Gasboard—3100P, Wuhan, China), which records the volumetric composition of O_2, CO, CO_2, H_2, CH_4 and light hydrocarbons such as ethane and propane (C_nH_m). The determination of the gas composition was performed continuously throughout the gasification. However, the syngas composition was recorded every 5 seconds in the gas analyzer memory. In order to avoid any damage of the gas analyzer, the syngas was conducted through a cleaning system composed by a water column, an activated carbon bed and coalescing filter.

Temperature Profile Estimation

The temperature profiles into the gasifier were measured using four (4) K-type thermocouples located at different heights from the top of the gasifier. Two of these thermocouples are located at 540 mm and 630 mm from the top of the gasifier allowing the registration of the temperature at the reduction zone (usually called as "throat" or "restriction") and the temperature at the bottom of the reduction zone (above the grate basket), respectively. The other two thermocouples were located at 400 mm and 900 mm from the top of the reactor. The temperature profiles were recorded every two minutes throughout the operation using a FLUKE 50S K/J thermometer. The temperatures profile of the OPRP gasification was measured to compare the reached temperatures inside the reactor to the temperatures reported for other raw materials. Moreover, the temperature profile was determined aiming to evidence the relation of the temperature inside of the gasifier and the final product composition

Assessment Of The OPRP Gasification From A Technical, Energy, Economic And Environmental Perspective.

The gasification of biomass to produce electricity is a process widely studied and analyzed in the open literature for different raw materials (Atnaw, Kueh, & Sulaiman, 2014; García, Morales, Quintero, Aroca, & Cardona, 2017; Yoon, Son, Kim, & Lee, 2012). The technical, energy, economic and environmental assessment of this process still can be complemented through the calculation of other indicators or applying different approaches. In this paper, the mass and energy balances of the gasification experience are used as input data to evaluate the performance of the process in terms of efficiency, carbon conversion and energy losses. Moreover, the economic context of Colombia off-grid zones as well as information related to the gasifier (i.e., equipment cost,

depreciation and maintenance) are used to calculate the electricity cost and the electricity yield of the OPRP gasification.

Performance Of The Gasification Process

The performance of the OPRP gasification process was evaluated through the calculation of the global mass and energy balances. Then, the LHV of the syngas and biochar were calculated. In addition, parameters such as gas yield, carbon conversion efficiency and cold gas efficiency were estimated to compare with other results reported in the literature using oil palm residues as well as lignocellulosic materials. The mass balance was performed weighting the amount of ash and char produced after the gasification process. These fractions were separated through the grate basket located at the bottom of the gasifier. On the other hand, the syngas mass flow was estimated using the so-called nitrogen-based method, which correlates the nitrogen composition before and after of the gasification process as well as the inlet volumetric flow in normal conditions of air. Thus, Equation (1) was used to calculate the syngas flow (Nm^3/h) in dry basis is given below:

$$\dot{Q}_{Syngas} = \dot{Q}_{Air} * \frac{\%N_{2,\,Air}}{\%N_{2,\,Syngas}} \qquad \text{Eq. (1)}$$

Where $\dot{Q}_{Air}$ is the inlet air flow rate (Nm^3/h), $\%N_{2,\,Air}$ and $\%N_{2,\,Syngas}$ are the volume percentage of nitrogen in air and syngas, respectively. This information was used to calculate the dry gas yield of the process as the ratio between the mass flow of syngas and feedstock. Afterward, the LHV of the syngas and the HHV of biochar were estimated as follows:

$$LHV_{Syngas} = 10.79\, x_{H_2} + 12.62\, x_{CO} + 35.62\, x_{CH_4} \qquad \text{Eq. (2)}$$

$$HHV = 20.7999 - 0.3214\left(\frac{VM}{FC}\right) + 0.0051\left(\frac{VM}{FC}\right)^2 - 11.227\left(\frac{Ash}{VM}\right) + 4.4953\left(\frac{Ash}{VM}\right)^2 - 0.7723\left(\frac{Ash}{VM}\right)^3 + 0.0383\left(\frac{Ash}{VM}\right)^4 + 0.0076\left(\frac{FC}{Ash}\right) \qquad \text{Eq. (3)}$$

Where in Equation. (2), the x_{H_2}, x_{CO} and x_{CH_4} are the mole fractions of the syngas and the LHV of the syngas is given in MJ/Nm^3. Moreover, Equation. (3) describes the HHV in terms of volatile matter (VM), fixed carbon (FC) and ash content. Once these values have been calculated, the global energy balance of the gasification process can be

estimated. The results obtained from the energy balance are presented in a Sankey diagram (See Figure 6, Section 3.3). Finally, the carbon conversion efficiency and the cold gas efficiency of the process were calculated using the Equations (4) and (5):

$$\eta_C = \frac{\dot{m}_{Syngas}\left(0.273\, w_{CO_2} + 0.749\, w_{CH_4} + 0.428\, w_{CO}\right) + \dot{m}_{Biochar}\, w_C + \dot{m}_{Tar}\, w_C}{\dot{m}_{Feedstock}\, w_C} \quad \text{Eq. (4)}$$

$$\eta_{Cold\ gas\ efficiency} = \frac{LHV_{Syngas}\, \dot{m}_{Syngas}}{LHV_{Feedstock}\, \dot{m}_{Feedstock}} \quad \text{Eq. (5)}$$

Where $\dot{m}_{Syngas}$, $\dot{m}_{Char}$, $\dot{m}_{Tar}$ and $\dot{m}_{Feedstock}$ are the mass flow rate of the syngas, char, tar and feedstock obtained in the gasification process. w_{CO_2}, w_{CH_4}, w_{CO} and w_C are the mass fractions of CO_2, CH_4, CO and C, respectively. Finally, the electrical output of the equipment was calculated according to the gasifier specifications.

Economic Assessment Of Syngas, Biochar And Electricity Generation

The calculation of the costs associated to the syngas production, biochar and electricity is not widely reported in the open literature. Nevertheless, different approaches have been employed to calculate the net incomes from the syngas and biochar sales (Yao, You, Ge, & Wang, 2018). Moreover, other studies have been focused on the estimation of the economics of gasification facilities considering real costs associated to the equipment acquisition, maintenance and operational investments (Sobamowo & Ojolo, 2018). In this sense, the economic parameters related to the syngas and biochar generation as well as the equipment cost are given before to the electricity production costs. Yao et al. reported the following equations to perform an economic evaluation of the syngas and biochar production through biomass gasification.

The net incomes from the syngas and char sales can be calculated using the Equation (6):

$$Incomes = P_{Biochar} * \dot{m}_{Biochar} + P_{Syngas} * \dot{m}_{Syngas} \quad \text{Eq. (6)}$$

Where $P_{Biochar}$ and P_{Syngas} are the unit price of biochar and syngas, respectively. These prices can be calculated using the reported costs for biochar and syngas by Yoder et al., (Yoder, Galinato, Granatstein, & Garcia-Pérez, 2011) and Wang et al., (Wang, Mao, Sui, & Jin, 2015), which are expressed per unit of energy. Therefore, the HHV of each

product is used to express the prices on a material basis. The calculation of $P_{Biochar}$ and P_{Syngas} is showed below:

$$P_{Biochar} = f_{Biochar} * HHV_{Biochar} \quad \text{Eq. (7)}$$

$$P_{Syngas} = f_{Syngas} * HHV_{Syngas} \quad \text{Eq. (8)}$$

Where $f_{Biochar}$ and f_{Syngas} are the unit price per mega-joule of biochar and syngas, which have the following values: $2.528x10^{-3}$ USD/MJ and $6.78X10^{-3}$ USD/MJ, respectively. Moreover, $HHV_{Biochar}$ and HHV_{Syngas} are the high heating values of the main products, which were calculated in the section 2.3.1.

The electricity production cost was calculated considering the electrical output of the equipment and the costs associated to the raw material, depreciation, labor and maintenance. The equipment was purchased from the All Power Labs industry (i.e., 33,000 USD) and the depreciation calculation was carried out considering a salvage value of 15% and applying a straight-line method for a 10-year period. The OPRP cost was calculated as 17.50 USD/ton considering the raw material conditioning and transportation costs necessary to cover a 200 km distance. The calculated price was similar with those reported by Tan et al., (2016). The operating labor cost was calculated considering the current legal monthly minimum wage (SMMLV) for a Colombian worker, which is 282.26 USD/month. On the other hand, the maintenance cost was calculated as 6% of the fixed capital investment. Finally, operating times s of 8 h and 24 h for electricity generation were considered to perform the calculations. Costs associated to oversizing, administration and utilities costs are not reflected in this preliminary economic evaluation.

RESULTS AND FINDINGS

OPRP Feedstock Analysis As Fuel For Biomass Gasification

The results obtained from the proximate and ultimate analysis of the OPRP are showed in Table 4. According to the proximate analysis, the OPRP has a high amount of ash in comparison to other raw materials used as feedstock in thermochemical conversion applications, which can cause troubles during its processing. On the other hand, the ratio between the volatile matter and fixed carbon is 5.46, which is higher than the maximum ratio recommended for gasification processes (i.e., 3 – 4) (All Power Labs, 2015). This ratio can be used to estimate qualitatively the temperatures reached during the process. In fact, high ratios indicate that lower temperatures will be reached in the gasification process (i.e., lower than 900°C). Therefore, the co-gasification of OPRP with coal or any other raw material could increase the temperatures inside the gasifier

and stimulate the gas-solid reactions in the reduction zone of the gasifier (Rong et al., 2015). Nevertheless, the proximate analysis of the OPRP is quite similar to *Pinus patula* and coffee cut-stems, which have been successfully used in the gasification process (García, Betancourt, & Cardona, 2017). Thus, OPRP can be used in the process without major drawbacks. In addition, the heating value of the OPRP is similar as those reported for several raw materials, which allows expecting a considerable increase in the temperature during the gasification (at least 800°C).

Table 4. Proximate And Ultimate Analysis Of The Oil Palm Rachis And Petiole (OPRP) Samples.

Proximate analysis (%w/w, db.)*		**Ultimate analysis (%w/w, db.)**	
Moisture	11.71 ± 0.52	Carbon	44.53
Fixed Carbon	14.72 ± 0.91	Hydrogen	5.75
Volatile matter	80.45 ± 0.12	Oxygen	49.41
Ash	4.81 ± 1.12	Nitrogen	0.31
HHV (MJ/kg)	18.56	**Empirical formula**	$C_6H_{9.23}O_5$

*Proximate analysis was performed by triplicate. db. dry basis

The ultimate analysis of the OPRP samples allows calculating the H/C and O/C ratios, which were 1.54 and 0.83, respectively. These ratios are comparable to the results obtained for different raw materials such as sugarcane bagasse, rice husks, *Pinus patula*, coffee cut-stems and so forth, which ranges from 0.6 to 1.2 in the O/C case and 1.4 to 1.6 in the H/C case (García, Betancourt, et al., 2017; García, Peña, Betancourt, & Cardona, 2017). In fact, the HHV of different feedstocks decrease when the O/C ratio decreases as well as increase at high H/C ratios, which support the torrefaction as thermochemical pretreatment (Bach & Skreiberg, 2016; Brown, 2011). In addition, OPRP has a HHV value lower than other fuels such as anthracite, coal, lignite and peat, which are derived from the non-renewable resources exploitation (P. Tan, Zhang, Xia, Fang, & Chen, 2015). The above is caused by the high oxygen content in the OPRP in comparison to the other fuels, hindering the conversion of OPRP into value-added products (Basu, 2010). In this way, the results obtained from the proximate and ultimate analysis allows identifying the OPRP as a potential raw material to be used as feedstock in gasification processes.

Pilot-Scale Of OPRP Gasification

The experimental results obtained from the OPRP gasification in terms of syngas composition and temperature profile inside the gasifier were analyzed. On the other hand, the CO, CO_2, CH_4 and H_2 gases were correlated with the reduction of

temperature to evaluate its effect in the volumetric yields of the syngas. The concentration profiles from the OPRP gasification are showed in Figure 19.

The variation of each gas in the syngas remains relatively constant once the temperatures inside of the gasifier have stabilized. Nevertheless, the CO composition decreases from 30% to 20% at the end of the operation. This behavior is related to the gas-solid reactions given in the reduction zone, where a decrease in the temperature affects the product gas composition. The other gases (i.e., H_2, CO_2, CH_4 and N_2) had a similar behavior during all the operation time. At the end of the gasification, the gas composition changed abruptly due to the change in the gasifier temperatures and more than 85% of the raw material was consumed. The mean syngas composition obtained from Figure 19 was CO (21.01% vol.), CO_2 (15.91% vol.), CH_4 (4.46%), H_2 (11.87%) and N_2 (46.65%) in dry basis. The obtained profile for each gas as well as the mean composition is similar to other gasification experiences reported in the literature (Atnaw, Sulaiman, & Yusup, 2013; García, Moncada, Aristizábal M., & Cardona, 2017). In fact, common values for the gas composition obtained using an air-downdraft gasifier are CO (15 – 20% vol.), CO_2 (10 – 15% vol.), CH_4 (0.5 – 2% vol.) and H_2 (15 – 20% vol.), which have been reported for several raw materials (Ouadi, Brammer, Kay, & Hornung, 2013), (Brown, 2011; Martínez, Mahkamov, Andrade, & Silva Lora, 2012). Once the syngas composition was determined, an analysis of the possible application ranges of this gas is developed in terms of the H_2/CO ratio.

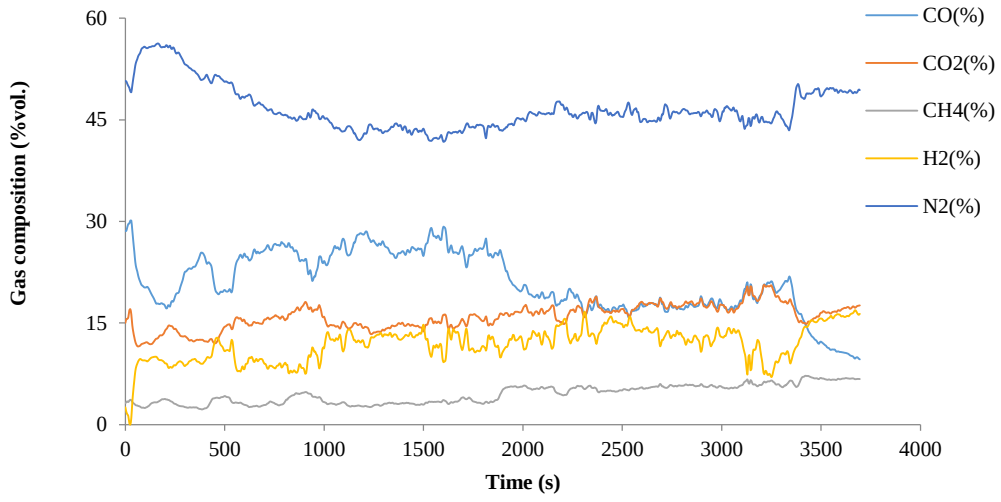

Figure 19. Syngas Composition Change With The Operation Time Of The Oil Palm Rachis And Petiole Gasification

The H_2/CO ratio is considered a critical parameter to determine the application range of the syngas since some chemical reactions need different amounts of reactants to obtain products such as gasoline, methanol, ammonia and methane. In this way, the H_2/CO ratio of the obtained gas from the OPRP gasification was 0.56 in volume basis,

which is appropriate to obtain gasoline as well as heat and power (i.e., electricity) (Brown, 2011). Therefore, the syngas can be used directly in the above-mentioned applications. However, it is necessary to increase the H_2/CO ratio through the water – gas shift reaction until a ratio between 0.6 and 2.0 in order to promote the application of the syngas to produce other products such as methanol. Nevertheless, the volumetric concentration of nitrogen, which dilutes the hydrogen and carbon monoxide in the syngas, limits the application range of the gas produced from the air-downdraft gasification process. Therefore, the syngas obtained from the air-downdraft OPRP gasification only can generate electricity. This statement can be corroborated calculating the HHV and LHV of the syngas. In fact, the mean HHV and LHV were 5.85 MJ/Nm^3 and 5.46 MJ/Nm^3, respectively. These values are in agreement with the reported data by Atnaw et al., (2013) for a similar raw material. In addition, these values also are in agreement with the reported data in different experiences using an air-downdraft gasifier (Waldheim, L. Nilsson, 2001).

In the same way, the temperature profile into the gasifier during the operation run is presented in Figure 20. The recorded temperatures in the gasifier show more clearly the start-up, steady state and shut down of the equipment. The temperatures at the restriction of the reduction zone (T_tred) and the temperature at the bottom of the reduction zone (T_bred) are quite similar since these are very close with a temperature ranging between 650°C – 825°C. The behavior obtained for T_tred and T_bred are very similar with the reported profiles by the All Power Labs industry for other raw material as softwood chips, walnut shells and wood pellets (All Power Labs, 2009a, 2009b). Nevertheless, the range of temperatures reached is very different due to the feedstock composition differences. On the other hand, the T_pyro thermocouple measured a temperature range between 550°C - 750°C achieving a mean value of 616°C. The trend of this thermocouple was like the above-mentioned temperatures. In addition, the temperature recorded at the bottom of the gasifier, T_syngas, has a lower temperature, which is about 242°C. The temperatures profile during the gasification experience shows that the process was stable in more than 70% of the operation time.

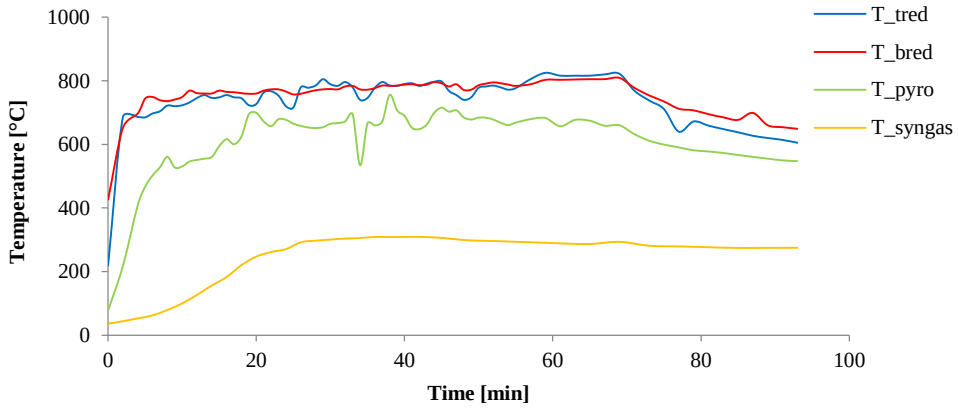

Figure 20. Temperature Profile Recorded In The Gasification Experience

The relation between the temperatures recorded in the reduction zone and the compositional change of each gas was determined. This behavior can be observed in Figure 21 (a - d), where the CO, H_2 and CH_4 molar composition increase with the reduction temperature while the CO_2 composition decreases. In general, the CO composition varies from 10.06% to 28.57% in a temperature range from 600°C to 850°C. The CO_2 composition decreases from 18.17% to 12.33% in the same temperature range. Moreover, H_2 and CH_4 vary from 8.5% to 15% and 2.5% to 6.5%, respectively. This behavior can be explained from the thermodynamic point of view analyzing the reactions given in the reduction zone.

R_1	Boudouard	$C + CO_2 \leftrightarrow 2CO$	$\Delta H = 172$ kJ/mol
R_2	Water – Gas	$C + H_2O \leftrightarrow CO + H_2$	$\Delta H = 131$ kJ/mol
R_3	Hydrogasification	$C + 2H_2 \leftrightarrow CH_4$	$\Delta H = -74.8$ kJ/mol
R_4	Steam Reforming	$CH_4 + H_2O \leftrightarrow CO + 3H_2$	$\Delta H = 206$ kJ/mol
R_5	Water – Gas shift	$CO + H_2O \leftrightarrow CO_2 + H_2$	$\Delta H = -41.2$ kJ/mol

The reactions R_1, R_2 and R_4 are highly endothermic, whereas the reactions R_3 and R_5 are slightly exothermic (Khartchenko & Kharchenko, 2010). Therefore, high temperatures are necessary to promote the formation of the products, as is the case of the CO, H_2 and CH_4, which are the main combustible components of the syngas. In the CO_2 case, which is present in the reactions R_1 and R_5, the CO_2 acts as reactant and product, respectively. The reaction R_1 has an activation energy higher than the reaction R_5, which favors the CO_2 disappearance. Therefore, high temperatures increase the equilibrium constant value favoring the formation of the products. Thus, the decrease in the relative concentration of CO_2 is explained in terms of the increase in the production of other permanent gases, mainly CO and H_2 with the temperature.

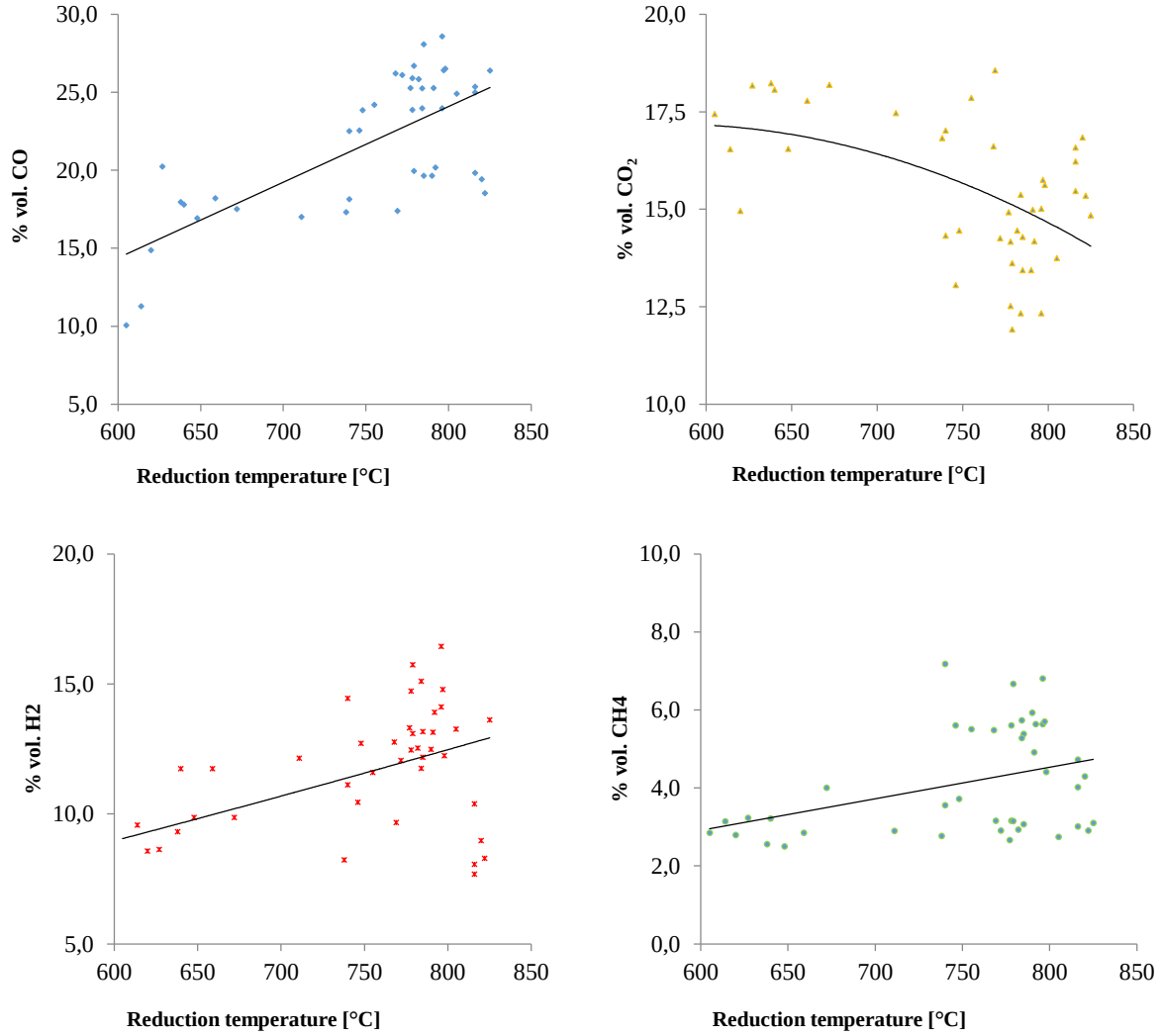

Figure 21. Effect Of The Reduction Zone Temperature In The Syngas Composition

The scattering plot in Figure 4 shows a large dispersion of the experimental data obtained from the OPRP gasification. An increasing tendency can be observed in the H_2, CH_4 and CO case. This is because the direct relation of these products and the reduction temperature due to the reduction zone is characterized to be endothermic. Nevertheless, other important aspects related to the mass and energy transfer between the gaseous phase and solid phase inside of the gasifier influence highly the final syngas composition and its production rate. For this reason, a more deeply study of the biochar must be done considering variables such as surface area, char reactivity, char porosity, char H/O ratio, pressure and residence time. In this work, these variables were not studied to explain the behavior showed in Figure 4. Even so, the above mentioned information can be supported by the studies performed by Sulaiman et al., (2015).

Mass And Energy Balance Of The Pilot Scale Air-Downdraft Gasification

The global mass and energy balance of the OPRP gasification was estimated using the available data from the procedures described in the methodology (see, section 2.2). Furthermore, the proximate analysis of the produced char was performed to calculate its heating value to complete the overall energy balance. The measured air inlet flow rate was 110 lpm (6.6 Nm^3/h) at 15°C and 101.325 kPa. Thus, the calculated mean syngas flow was 11.52 Nm^3/h. Moreover, the raw material consumption was calculated as the ratio between the load used and the time required to exhaust it completely. The overall mass balance of the OPRP gasification is showed in Figure 22.

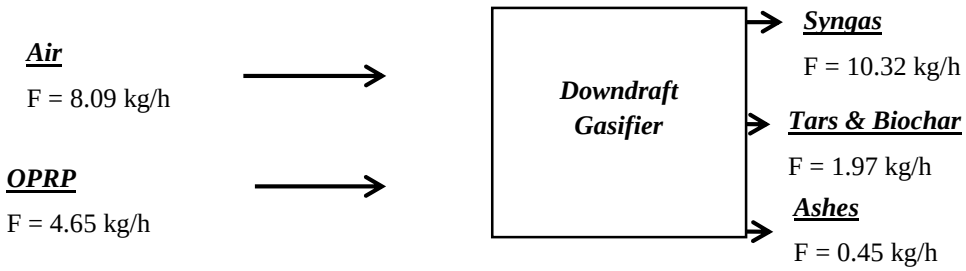

Figure 22. Overall Mass Balance Of The OPRP Gasification In A Downdraft Gasifier

A summary of the operating parameters and experimental results obtained in the OPRP gasification with a moisture content of 10% is showed in Table 5. Operation Parameters And Results Obtained From The OPRP GasificationTable 5. The results presented in this table are compared to those reported by Atnaw et al., (2014).

Table 5. Operation Parameters And Results Obtained From The OPRP Gasification

Parameter	This work	Atnaw et al., (2014).
Total operation time (min)	93	118
Moisture content (% wet basis)	9.68	22.00
Initial weight of feed (kg)	11.20	12.00
Average initial air flow rate (lpm)	110	180
Air fuel ratio (kg air/kg fuel)	1.74	2.07
Equivalence ratio (ER)	0.35	0.44
Average pyrolysis zone temperature (°C)	620	456

Average reduction zone temperature (°C)	755	510
Average fuel gas output (lpm)	191.9	281.2
Average HHV of fuel gas (MJ/Nm^3)	5.46	4.95
Amount of char obtained (g)	1200	620
Amount of ash obtained (g)	700	N.R
Syngas yield (kg syngas/kg raw material)	2.22	N.R
Carbon conversion efficiency (%)	94.98	93.94
Cold gas efficiency (%)	72.94	70.54

From Table 5, it can be evidenced a higher carbon conversion efficiency and cold gas efficiency in the gasification experience than the reported results by Atnaw et al., (2013) which can be attributed to the low equivalence ratio employed. In accordance with the mass balance expressed in **Figure 22**, the char and ash flow is about 1.97 kg/h from which 0.77 kg/h are biochar (see, Table 5). Therefore, 1.27 kg/h could be attributed to the tar flow. However, this value is excessive when this flow is compared to the literature (Atnaw, Kueh, et al., 2014). This can be explained due to the tars flow was calculated as the difference between all inputs and outputs, without consider the accumulation of ashes inside of the gasifier (Chern, Walawender, & Fan, 1989).

On the other hand, the obtained biochar was characterized in terms of volatile matter and fixed carbon content and then, the calculation of the heating value was performed. The amount of volatile matter was 15.93%, ash 16.95% and fixed carbon 67.11%. These results suggest that the char produced from the OPRP gasification has a lower LHV that other types of chars obtained from wood gasification (Fryda & Visser, 2015). In this way, the HHV of the produced biochar using the equation proposed by Nhuchnen et al., (2012) was 17.25 MJ/kg. Nevertheless, the calorific value of the biochar produced from the OPRP gasification can be compared to coal extracted from opencast mining, which can vary between 15 MJ/kg to 26 MJ/kg (P. Tan et al., 2015). Finally, the produced ashes were characterized in terms of mineralogical composition to calculate the alkali index of the raw material and determine the possible clinker formation during the gasification process. Table 6 shows the oxides composition of these ashes.

Table 6. Oxides Composition Of The Gasified Oil Palm Rachis And Petiole

Item	SiO_2	MgO	Mn_2O_3	Fe_2O_3	Al_2O_3	CaO	Na_2O	K_2O	**Total SiO_2 + Fe_2O_3 + Al_2O_3**

%w/w, db.*	80.78	3.78	0.05	1.22	0.24	7.82	0.21	5.91	82.24

*db. dry basis.

Ashes from the OPRP gasification have a high amount of silica oxides, which can be used to produce other value-added products such as additives for concrete or high purity silica (Fernandes et al., 2016). The share of SiO_2, Fe_2O_3 and Al_2O_3 shows that these ashes can be used to produce additives for the cement industry. However, aspects related to their crystallinity index must be evaluated to ensure this option (Fernandes et al., 2016). The content of K_2O and Na_2O is 6.12%. This value is low in comparison to other raw materials employed in gasification processes such as switchgrass and rice straw, which have a K_2O and Na_2O content of 12.18% and 13.26%, respectively. Thus, the alkali index of the OPRP calculated was 0.059 kg/MJ. This result suggests that the formation of clinker and slagging is improbable since these problems only appears with alkali index higher than 0.17 kg/MJ due to high amounts of ash as well as K_2O and Na_2O decrease the fusion temperatures of other mineral oxides.

The global energy analysis of the gasification system was also performed. For this, the energy content of the raw material and the gasification products were considered. A graphical method to show the energy balance of the gasification process is the Sankey diagram, which shows the global energy analysis of a process. This diagram is showed in Figure 23**.** The syngas can be classified as the main product of the gasification process. However, the produced biochar has the potential to generate a relevant amount of energy. Both syngas and biochar can produce an energy flow of 80.75 MJ/h, which in comparison with the energy content of the OPRP accounts an energy efficiency of 93.56%.

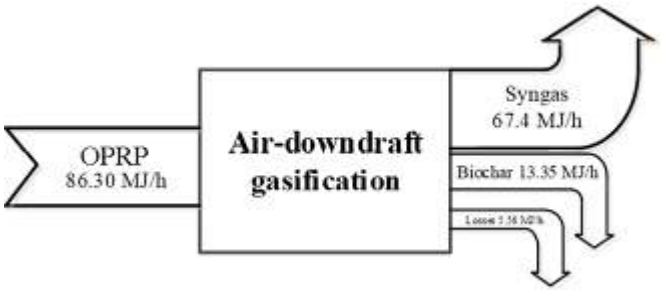

Figure 23. Sankey Diagram Of The Oil Palm Rachis And Petiole Gasification Process.

The gasification process is a conversion pathway to add value to the OPRP waste because the syngas can be used as a versatile energy vector or chemical platform. Moreover, the produced biochar can be used as soil enhancer or heat source in boilers for steam generation. The losses associated to the gasification process are about of 5.56 MJ/h, which can be attributed to the heat losses in the equipment and the

irreversibility produced in the chemical reactions inside of the gasifier. The efficiency of the gasification process only considering the generated syngas is about 78.09%, which is similar to the energy efficiency reported by García et al. (2017) using *Pinus Patula* as raw material (i.e., 79.9%). The Sankey diagram showed in Figure 23 does not take into account the energy flow that can be obtained from the tars production. Nevertheless, this fact can be explained due to the low amount of tars produced in the gasification process and this compound does not have a well-established used at industrial or agricultural level in contrast with the syngas and biochar. On the other hand, Antonopoulos et al., (2012) analyzed the energy balance of a downdraft gasifier using olive wood as raw material. The energy efficiency only considering the syngas as energy vector reported by these authors was 82.31%, which is a similar value to the obtained in this work. Therefore, the energy efficiency of the air-downdraft gasification process for softwood and hardwood raw materials varies from 75% to 85%, which indicates high-energy conservation in the gasification process.

Economic Perspective

The economic assessment of the syngas (for electricity generation) and biochar generation using the OPRP as raw material was performed. The incomes calculated from the mass flows of syngas and biochar are $4.57x10^{-1}$ USD/h and $3.36x10^{-2}$ USD/h, respectively. Moreover, the total incomes by period (i.e., 1 period = 8000 h) are 3921.50 USD/period. These results were calculated from the unit price of biochar and syngas, which were $4.36x10^{-2}$ USD/kg biochar and $3.97x10^{-2}$ USD/Nm^3, respectively. The results obtained from this analysis are similar compared to the reported data from Yao et al., (2018), who reported that the biochar price varies from 0.017 USD/kg to 0.009USD/kg, whereas the syngas price varies from 0.057 USD/kg to 0.077 USD/kg. Nevertheless, the ER is a function of the amount of air employed in the gasification process. Therefore, the ideal amount of air that must be employed in a gasification process varies as a function of the elemental composition of the raw material. One aspect that can affect the quality and price of the biochar is the equivalence ratio (ER), which determines the amount of air used during the gasification process. In this work, the ER used was 0.35, which is close to the optimum ER for gasification experiences (i.e., 0.25). Therefore, the quality and price of the generated syngas is acceptable for electricity generation.

On the other hand, the electricity generation costs were calculated considering two operation periods: The first scenario is considering an electricity generation for 8 hours and the second scenario is considering 24 hours. The summary of the main costs estimated to calculate the unit price of the electricity production costs as well as the total electricity generated for a year are presented in Table 7.

Table 7. Annualized Costs And Unit Cost Of The Electricity Generation

Feature	Electricity generation for 8 h		Electricity generation 24 h	
	USD/year	**Share (%)**	**USD/year**	**Share (%)**
Raw material	216.98	3.42	651.45	7.34
Operating Labor	1045.33	16.48	3136.22	35.36
Maintenance	2277.04	35.89	2277.04	25.67
Depreciation	2805.45	44.21	2805.45	31.63
Total cost	6344.33	100	8869.22	100
Electricity generated (MWh)	10.33	-	31.62	-
Electricity unit cost (USD/kWh)	0.614	-	0.286	-

The results given in Table 7 shows that the fixed capital costs are the most influential cost in the economic analysis. This can be explained due to the low costs associated to the raw material and labor costs. The unit costs for the 8 h period is higher than the unit cost of the electricity generation for a 24 h period. This can be explained since the depreciation cost was calculated using a straight-line method, which considers a constant rate of depreciation. The unit electricity prices are comparable to the current electricity production costs using diesel as energy source. In fact, the electricity generated using this energy source in off-grid zones varies between 0.219 USD/kWh – 0.292 USD/kWh.

Table 8. Comparison Between Gases Emissions After The Combustion Of Syngas, OPRP And Biodiesel/Diesel

Units (mg/Nm^3)	**Syngas combustion**	**Direct use OPRP**	**Biodiesel/Diesel**
CO_2	108.48	166.90	193.24
CO	3.45	8.50	5.5.
SO_x	0.13	0.44	0.89
NO_x	0.27	0.76	1.14
PM	N.R.	N.R.	1.40

The information presented in Table 8 leads to establish that the transformation of OPRP into syngas through a gasification process impacts favorably the environment

due to the lower carbon dioxide emissions. On the other hand, the use of biodiesel/diesel has higher pollutant emissions than the use of syngas due to the difference in chemical composition of both fuels. Therefore, the use of syngas for electricity generation purposes is recommended.

CONCLUSION

The gasification technology is a promising thermochemical alternative to upgrade biomass and produce electricity as well as value-added products. Nevertheless, the syngas application range depends on the gas quality in terms of heating value and H_2/CO ratio. In the specific case of an air-downdraft gasifier, the syngas produced only can be used for electricity generation. Raw materials with high availability such as the oil palm waste can be profiled as potential feedstock to be used in gasification processes to reduce waste management problems and supply electricity in off-grid zones. According to the results obtained, the use of OPRP as raw material and the implementation of the gasification plant is promising. However, more research must be performed to elucidate the feasibility of this process in different rural and urban contexts.

CONFLICT OF INTERESTS.

The authors declare that they do not have potential conflict of interests.

FINANCIAL SUPPORT

This work was supported by the Departamento Administrativo de Ciencia, Tecnología e Innovación (Colciencias, grant number 761 Jóvenes Investigadores).

REFERENCES

Akay, G., & Jordan, C. A. (2011). Gasification of fuel cane bagasse in a downdraft gasifier: Influence of lignocellulosic composition and fuel particle size on syngas composition and yield. *Energy and Fuels*, *25*(5), 2274–2283. https://doi.org/10.1021/ef101494w

All Power Labs. (2009a). Instrumented softwood chip run 091609.

All Power Labs. (2009b). Instrumented walnut shell run 082409.

All Power Labs. (2015). Biomass Feedstock Requirements. In *Power pallet technicians manual* (pp. 1–20).

Anco S. Blazev. (2015). *Energy Security for The 21st Century*. CRC Press.

Ang, B. W., Choong, W. L., & Ng, T. S. (2015). Energy security: Definitions, dimensions and indexes. *Renewable and Sustainable Energy Reviews*, *42*, 1077–1093. https://doi.org/10.1016/j.rser.2014.10.064

Antonopoulos, I. S., Karagiannidis, A., Gkouletsos, A., & Perkoulidis, G. (2012). Modelling of a downdraft gasifier fed by agricultural residues. *Waste Management*, *32*(4), 710–718. https://doi.org/10.1016/j.wasman.2011.12.015

Atnaw, S. M., Kueh, S. C., & Sulaiman, S. A. (2014). Study on tar generated from downdraft gasification of oil palm fronds. *The Scientific World Journal*, *2014*, 1–8. https://doi.org/10.1155/2014/497830

Atnaw, S. M., Sulaiman, S. A., & Yusup, S. (2013). Syngas production from downdraft gasification of oil palm fronds. *Energy*, *61*, 491–501. https://doi.org/10.1016/j.energy.2013.09.039

Atnaw, S. M., Sulaiman, S. A., & Yusup, S. (2014). Influence of fuel moisture content and reactor temperature on the calorific value of Syngas resulted from gasification of oil palm fronds. *The Scientific World Journal*, *Article ID*, 9 pages. https://doi.org/10.1155/2014/121908

Bach, Q.-V., & Skreiberg, Ø. (2016). Upgrading biomass fuels via wet torrefaction: A review and comparison with dry torrefaction. *Renewable and Sustainable Energy Reviews*, *54*, 665–677. https://doi.org/10.1016/j.rser.2015.10.014

Basu, P. (2010). *Biomass Gasification and Pyrolysis: Practical Design*. Elsevier Inc.

BP. (2017). BP Statistical Review of World Energy. In *BP Statistical Review of World Energy*. London, UK.

Brown, R. C. (2011). *Thermochemical Processing of Biomass: Conversion into Fuels,Chemicals and Power*. https://doi.org/10.1002/9781119990840

Chern, S. M., Walawender, W. P., & Fan, L. T. (1989). Mass and energy balance analyses of a downdraft gasifier. *Biomass*, *18*(2), 127–151. https://doi.org/10.1016/0144-4565(89)90089-9

Couto, N., Rouboa, A., Silva, V., Monteiro, E., & Bouziane, K. (2013). Influence of the biomass gasification processes on the final composition of syngas. *Energy Procedia*, *36*, 596–606. https://doi.org/10.1016/j.egypro.2013.07.068

Dong, J., Tang, Y., Nzihou, A., Chi, Y., Weiss-Hortala, E., Ni, M., & Zhou, Z. (2018). Comparison of waste-to-energy technologies of gasification and incineration using life cycle assessment: Case studies in Finland, France and China. *Journal of Cleaner Production*, *203*, 287–300. https://doi.org/10.1016/j.jclepro.2018.08.139

Fernandes, I. J., Calheiro, D., Kieling, A. G., Moraes, C. A. M., Rocha, T. L. A. C., Brehm, F. A., & Modolo, R. C. E. (2016). Characterization of rice husk ash produced using different biomass combustion techniques for energy. *Fuel*, *165*, 351–359. https://doi.org/10.1016/j.fuel.2015.10.086

Fryda, L., & Visser, R. (2015). Biochar for Soil Improvement: Evaluation of Biochar from Gasification and Slow Pyrolysis. *Agriculture*, *5*(4), 1076–1115. https://doi.org/10.3390/agriculture5041076

García, C. A., Betancourt, R., & Cardona, C. A. (2017). Stand-alone and biorefinery pathways to produce hydrogen through gasification and dark fermentation using Pinus Patula. *Journal of Environmental Management*, *203* part *2*, 695–703.

https://doi.org/10.1016/j.jenvman.2016.04.001

García, C. A., Moncada, J., Aristizábal M., V., & Cardona, C. A. (2017). Techno-economic and energetic assessment of hydrogen production through gasification in the Colombian context: Coffee Cut-Stems case. *International Journal of Hydrogen Energy*, *42*(9), 5849–5864. https://doi.org/10.1016/j.ijhydene.2017.01.073

García, C. A., Morales, M., Quintero, J., Aroca, G., & Cardona, C. A. (2017). Environmental assessment of hydrogen production based on Pinus patula plantations in Colombia. *Energy*, *139*, 606–616. https://doi.org/10.1016/j.energy.2017.08.012

García, C. A., Peña, Á., Betancourt, R., & Cardona, C. A. (2017). Energetic and environmental assessment of thermochemical and biochemical ways for producing energy from agricultural solid residues: Coffee Cut-Stems case. *Journal of Environmental Management*. https://doi.org/10.1016/j.jenvman.2017.04.029

Gil, J., Corella, J., Aznar, M. P., & Caballero, M. A. (1999). Biomass gasification in atmospheric and bubbling fluidized bed: Effect of the type of gasifying agent on the product distribution. *Biomass and Bioenergy*, *17*(5), 389–403. https://doi.org/10.1016/S0961-9534(99)00055-0

Islas, J., Manzini, F., Masera, O., & Vargas, V. (2019). Solid Biomass to Heat and Power. In *The Role of Bioenergy in the Bioeconomy*. https://doi.org/10.1016/B978-0-12-813056-8.00004-2

Khartchenko, N. V, & Kharchenko, V. M. (2010). *Advanced energy systems* (2nd editio). CRC Press, Taylor and Francis.

Kitzler, H., Pfeifer, C., & Hofbauer, H. (2011). Pressurized gasification of woody biomass—Variation of parameter. *Fuel Processing Technology*, *92*(5), 908–914. https://doi.org/10.1016/J.FUPROC.2010.12.009

Martínez, J. D., Mahkamov, K., Andrade, R. V., & Silva Lora, E. E. (2012). Syngas production in downdraft biomass gasifiers and its application using internal combustion engines. *Renewable Energy*, *38*(1), 1–9. https://doi.org/10.1016/j.renene.2011.07.035

Molino, A., Chianese, S., & Musmarra, D. (2016). Biomass gasification technology: The state of the art overview. *Journal of Energy Chemistry*, *25*(1), 10–25. https://doi.org/10.1016/j.jechem.2015.11.005

Nhuchhen, D. R., & Abdul Salam, P. (2012). Estimation of higher heating value of biomass from proximate analysis: A new approach. *Fuel*, *99*, 55–63. https://doi.org/10.1016/j.fuel.2012.04.015

Ouadi, M., Brammer, J. G., Kay, M., & Hornung, A. (2013). Fixed bed downdraft gasification of paper industry wastes. *Applied Energy*, *103*, 692–699. https://doi.org/10.1016/j.apenergy.2012.10.038

Overend, R. P. (2009). Direct Combustion of Biomass. In E. E. Shpilrain (Ed.), *Renewable energy sources charged with energy from the sun and originated from Earth-Moon interaction* (Volume 2, pp. 74–101). Encyclopedia of Life Support Systems.

Renewable energy policy network for the 21st century (REN21). (2018). Renewables

2017 global status report. *Paris: Renewable Energy Policy Network for the 21st Century*, 325. https://doi.org/978-3-9818911-3-3

Rong, L., Maneerung, T., Ng, J. C., Neoh, K. G., Bay, B. H., Tong, Y. W., … Wang, C. H. (2015). Co-gasification of sewage sludge and woody biomass in a fixed-bed downdraft gasifier: Toxicity assessment of solid residues. *Waste Management*, *36*, 241–255. https://doi.org/10.1016/j.wasman.2014.11.026

Sobamowo, G. M., & Ojolo, S. J. (2018). Techno-Economic Analysis of Biomass Energy Utilization through Gasification Technology for Sustainable Energy Production and Economic Development in Nigeria. *Journal of Energy*, *2018*, 1–16. https://doi.org/10.1155/2018/4860252.

Solarte-Toro, J. C., Chacón-Pérez, Y., & Cardona-Alzate, C. A. (2018). Evaluation of biogas and syngas as energy vectors for heat and power generation using lignocellulosic biomass as raw material. *Electronic Journal of Biotechnology*, *33*, 52–62. https://doi.org/10.1016/j.ejbt.2018.03.005

Sulaiman, S. A., Balamohan, S., Moni, M., Atnaw, S. M., & Mohamed, A. (2015). Feasibility study of gasification of oil palm fronds. *Journal of Mechanical Engineering and Sciences*, *9*, 1744–1757. https://doi.org/10.15282/jmes.9.2015.20.0168

Surendra, K. C., Takara, D., Hashimoto, A. G., & Khanal, S. K. (2014). Biogas as a sustainable energy source for developing countries: Opportunities and challenges. *Renewable and Sustainable Energy Reviews*, *31*, 846–859. https://doi.org/10.1016/j.rser.2013.12.015

Tan, J. P., Jahim, J. M., Harun, S., Wu, T. Y., & Mumtaz, T. (2016). Utilization of oil palm fronds as a sustainable carbon source in biorefineries. *International Journal of Hydrogen Energy*, *41*(8), 4896–4906. https://doi.org/10.1016/j.ijhydene.2015.08.034

Tan, P., Zhang, C., Xia, J., Fang, Q. Y., & Chen, G. (2015). Estimation of higher heating value of coal based on proximate analysis using support vector regression. *Fuel Processing Technology*, *138*, 298–304. https://doi.org/10.1016/j.fuproc.2015.06.013

US Energy Information Administration. (2017). Annual energy outlook 2017 with projections to 2050. In *US Energy Information Administration*. https://doi.org/DOE/EIA-0383(2012) U.S.

Waldheim, L. Nilsson, T. (2001). Heating value of gases from biomass gasification. In *IEA Bioenergy Agreement, Task 20 - Thermal Gasification of Biomass*.

Wang, J., Mao, T., Sui, J., & Jin, H. (2015). Modeling and performance analysis of CCHP (combined cooling, heating and power) system based on co-firing of natural gas and biomass gasification gas. *Energy*, *93*, 801–815. https://doi.org/10.1016/j.energy.2015.09.091

Yao, Z., You, S., Ge, T., & Wang, C. H. (2018). Biomass gasification for syngas and biochar co-production: Energy application and economic evaluation. *Applied Energy*, *209*(July 2017), 43–55. https://doi.org/10.1016/j.apenergy.2017.10.077

Yoder, J., Galinato, S., Granatstein, D., & Garcia-Pérez, M. (2011). Economic tradeoff between biochar and bio-oil production via pyrolysis. *Biomass and Bioenergy*, *35*(5),

1851–1862. https://doi.org/10.1016/j.biombioe.2011.01.026

Yoon, S. J., Son, Y. Il, Kim, Y. K., & Lee, J. G. (2012). Gasification and power generation characteristics of rice husk and rice husk pellet using a downdraft fixed-bed gasifier. *Renewable Energy*, *42*, 163–167. https://doi.org/10.1016/j.renene.2011.08.028.

DETAILED COMPARISON OF HYDROGEN CONCENTRATION MODELLING IN DIFFERENT METAL MATRICES

Burak BAL, Abdullah Gul University, burak.bal@agu.edu.tr

Syed Faiz ALI, Abdullah Gul University, faiz.ali@agu.edu.tr

Fasih Munir MALIK, Abdullah Gul University, fasih.malik@agu.edu.tr

ABSTRACT: The hydrogen concentration contours are analyzed using an iterative modeling approach. The contours in 4 different metal matrices are modeled and analyzed with respect to variance in diffusivity in BCC and FCC crystal lattice structures in the presence of an edge dislocation and under static external loading. The effect of alloying elements on iron in allowing the hydrogen to enter the tensile region is discussed. The contours of hydrogen are modeled and studied in both near-by edge dislocation and far away from the dislocation.

Key words: Hydrogen embrittlement, hydrogen diffusion, finite element modeling, modelling, crystal structure

INTRODUCTION

Hydrogen Embrittlement (HE) is a well-known phenomenon and holds its vitality in terms of affecting the mechanical properties of various metals (Tiwari et al, 2000). The HE phenomenon was first studied by Johnson almost a century back (Johnson, 1875) and since then it has widely being studied by numerous material-scientists and other experts.

HE is a phenomenon which hydrogen atoms to diffuse into the metals degrade mechanical properties (Luo et al, 2013). This imperfection incepted in metals causes hindrance to the dislocation movements inside the metals. Dislocations movement is an essential driving force for material to exhibit the plastic deformation. Hydrogen interstitials restricting the plastic deformation leads the material to the brittle behavior (Bal et al, 2016). Hence, it reduces the ductility of the material and therefore, allowing failure to occur without any observable warning as necking does not take place. Often, hydrogen atoms diffuse into the metals during the manufacturing process, at higher stress levels, at elevated temperature levels, and in enriched hydrogen concentrations. Secondly, the HE causes the fracture-stress to decrease and the material undergoes fracture at lower stress (Symons, 1998).

It is of vital importance to be aware of hydrogen concentration in the metal matrix, being induced due to the diffusion of hydrogen in metal matrix under certain

conditions, in order to predict the HE mechanism active at time (Bal, 2017). The experimental approach to measure or to calculate the diffused hydrogen concentration in a metal matrix is expensive, and therefore values the non-expensive approach of using computational power to simulate the diffused hydrogen concentration.

Over the years, different mechanisms describing the HE phenomenon have been proposed including Hydrogen Enhanced Localized Plasticity (HELP), Hydrogen Induced Decohesion (HID), and Stress-Induced Hydride Formation and Cleavage (SIHFC).

HELP mechanism in HE substantiates the lowering of interaction energy between dislocation movement and the hindrance. This allows the localized induced plasticity in the material. Therefore, the intrinsic material flow stress is lower in hydrogen concentrated region of in non-homogeneously distributed hydrogen bearing metal. The position of material flow stress therefore, depends on the position (Beachem, 1972).

HID mechanism deals with the concentration of hydrogen at crack tip. The dislocation movement carries the hydrogen to the crack tip. To point it here, the dislocation movement is not needed to instigate the localized fracture other than to serve as carrier of hydrogen. The micro crack introduced by hydrogen joins the already cracked vertex and propagation takes place. The hydrogen that is carried to crack tip increases the hydrostatic stress. This weakens the interatomic bonds at crack tip by separating the crystal along a crystallographic plane (Geng et al, 1999).

SIHFC mechanisms occurs due to the concentration of hydride ions at the localized stress regions such as crack tips. It is an iterative fracture which means that the hydride induced stress at crack tips propagates the crack and ultimately the brittle fracture takes place. It is also well established that in this mechanism the plastic deformation also occurs, therefore; the brittle fracture rendered by hydride induced stress is dependent on strain rate (Office of Naval Research, 1989).

THEORY

The carrier mobility of hydrogen plays a vital role in deciding the HE active mechanism. Therefore, to define the hydrogen contours around the dislocation is necessary as the hydrogen induced stress field depends on the distribution of hydrogen in vicinity of dislocation (Bal, 2017). In this paper the different materials which are prone to hydrogen embrittlement are modeled in finite element analysis program to model the hydrogen concentration around the dislocation and also far away from the dislocation.

Once the hydrogen is diffused into the material, in this case metals, it finds it place in either the interstitial lattice sites or the reversible trap sites (Taha & Sofronis, 2001). The positional placement of hydrogen depends on the lattice sites and the trap binding energy (Liang et al, 2004). Due the presence of outside introduced hydrogen the expansion causes the volumetric strain in the hydrogen occupied augment. The

vacancies at micro structural level offers the room to hydrogen and therefore, hydrostatic region at the edge dislocation, specifically, holds a vital importance of hydrogen surroundings as it is the potential point of fracture or the point of inception for fracture (Bal, 2017).

In this paper, the hydrogen contours around the edge dislocation in different metals have been modeled with respect to hydrogen concentration at distant and nearby positional displacement (burger vector). The modeling is conducted with zero flux boundary conditions and with singularity considered at the edge dislocation augment. The diffusion of hydrogen is set to be based on static external parameters i.e. observed without any external parametric influence. Iterative approach is adopted in modeling the hydrogen contours. COMSOL Multiphysics, Finite Element Analysis, software is used to model the results.

CALCULATIONS

The diffused hydrogen in metal, fits the normal interstitial sites due to the low potential energy property of interstitial sites. In general, hydrogen tends to get attracted to the augment with greater binding energy, relatively (Taha & Sofronis, 2001). Once, the interstitial sites get filled then hydrogen fills the vacant places like grain boundaries, dislocation, or voids.

The partial derivative of concentration with respect to time is defined as Flux (**J**). The **J** is proportional to the gradient of chemical potential as defined by the following equations:

$$\frac{\partial}{\partial t}\int_{\Omega} c \, d\Omega + \frac{\partial}{\partial t}\int_{\partial\Omega} J \, . \, ndS = 0 \quad (1)$$

$$J = -m\Delta\mu \quad (2)$$

Hence,

$$J = -\frac{Dc}{RT}\Delta\mu \quad (3)$$

In equation 1, **J** is the flux, **c** is the hydrogen concentration, and **n** is the outward normal vector to surface $\partial\Omega$..

In equation 2, **D** is the diffusion coefficient of hydrogen, **R** is the universal gas constant, **μ** is the chemical potential, and **T** is the temperature. The negative sign denotes the flow in field from high potential region to low potential region of hydrogen.

The flux **J** is therefore, the prime means of activating the hydrogen diffusion, hydrogen concentration and hydrogen coefficient in the metal matrix.

$$J = -D\Delta c - \frac{D<V_H>}{RT} c\Delta \frac{\sigma_{kk}}{3} \quad (4)$$

The equation 3 is formulated after substitution of **μ initial** and **μ stressed**. Where $\mathbf{V_H}$ is partial molar volume of hydrogen and $\boldsymbol{\sigma_{kk}}$ is the applied stress. Therefore, the final equation defining the diffusion in terms of flux **J** is as follows:

$$\frac{\partial c}{\partial t} = -\Delta J \quad (5)$$ Hence,

$$\frac{\partial c}{\partial t} = D\Delta^2 c - \frac{D<V_H>}{RT}\{c\Delta^2 \frac{\sigma_{kk}}{3} + \Delta c\Delta \frac{\sigma_{kk}}{3}\} \quad (6)$$

The change in flux **J** is defined as partial derivative of concentration with respect to time, displacing form higher concentrated region to the lower concentrated region. For further details of the calculations refer to (Barrera et al, 2016). Equations 1 to 6 are retrieved from (Barrera et al, 2016).

METHODOLOGY

The Finite Element Analysis (FEM) is used to model the hydrogen concentration contours in the vicinity of edge dislocation in the metal matrices, provided the static external parametric influence. COMSOL Multiphysics is used to model the results. The properties of metals that are modeled are given in the table below.

Table 1. Properties of Metal Matrices

Material	**AISI-4130**	**X-750**	**Iron**	**Aluminum-7050**
Burger's Vector (B)	2.580×10^{-10}	2.580×10^{-10}	2.478×10^{-10}	$3.64\times e^{-10}$
Partial Molar Volume of Hydrogen (VH) [m^3/mol]	2.00×10^{-6}	1.72×10^{-6}	2.66×10^{-6}	1.65×10^{-6}
Shear Modulus (G) [Pa]	8.077×10^{10}	8.256×10^{10}	8.600×10^{10}	2.70×10^{10}
Young's Modulus (E) [Pa]	2.1×10^{11}	2.13×10^{11}	2.00×10^{11}	1.17×10^{10}

Poisson's Ratio (v)		0.300	0.290	0.300	0.33
Diffusion Coefficient (D) [m^2/s]		1.41×10^{-8}	4.20×10^{-15}	7.02×10^{-9}	2.2×10^{-14}
Molar Volume of Metal Matrix (VM)		1.183×10^{-6}	6.87×10^{-6}	7.11×10^{-6}	1.08×10^{-5}

Table 2. Constants Used In Equations

T [K]	**Co [mol/×m^3]**	**R [J/(mol×K)]**	**NA [1/mol]**	**Kb [m2×kg/(s2×K)]**
298	1	8.134	6.022×10^{23}	1.38×10^{-23}

RESULTS

As shown in the figure 1 below the AISI-4130 metal matrix observed the hydrogen concentration contours in compressive and tensile region. The sign of burger vector for metal is positive demonstrated. In the tensile region there appears to be only one contour expanding away from the edge dislocation. To the nearest of edge dislocation, the value of concentration is 17.83mol/ m^3 which represents the highest value for hydrogen concentration. As we move away from the center of dislocation the hydrogen concentration decreases.

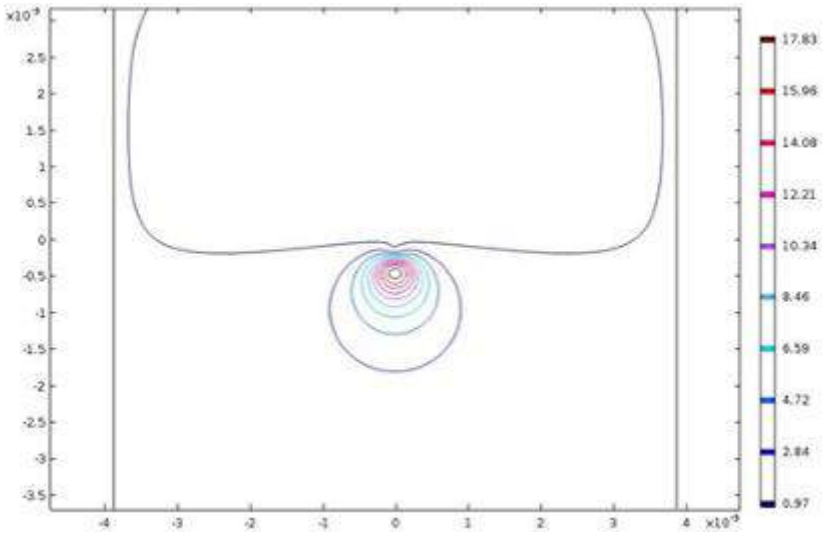

Figure 1. The hydrogen contours around the edge dislocation in AISI-4130 [c(mol/m^3)]

As shown in the figure 2 below the hydrogen contours in metal X-750 are present in both tensile and compression region. Like AISI-4130 the X-750 also shows only one contour in tensile region. It is to be noted that the demonstrated burger vector for the X-750 shows the positive sign. The highest concentration of hydrogen is at near edge dislocation in the compression region which is 12.25 mol/m^3. The concentration of hydrogen decreases as we move further from the dislocation center.

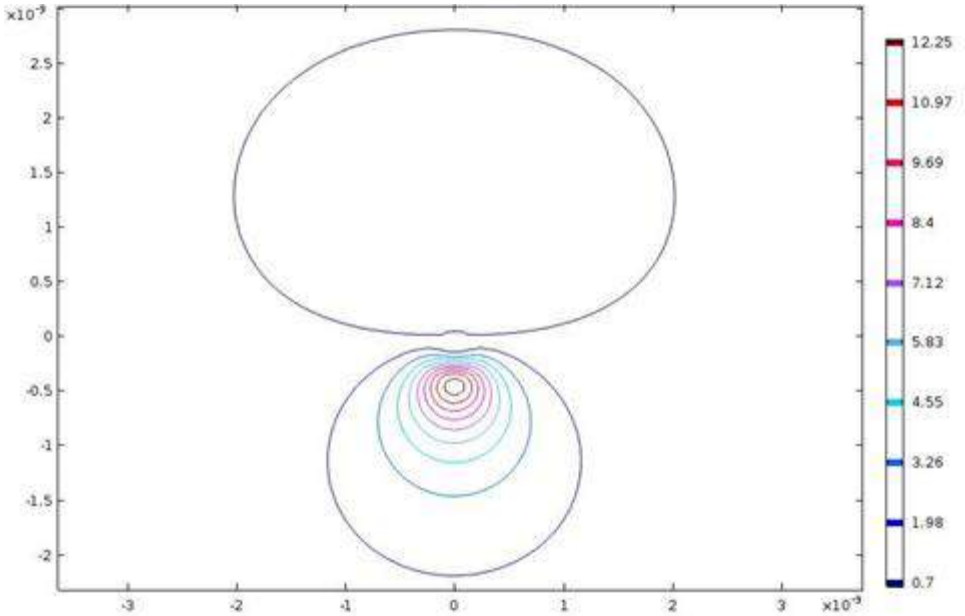

Figure 2. The hydrogen contours around the edge dislocation in X-750 [c(mol/m^3)]

As shown in the figure 3 below, in iron matrix there is no hydrogen contour present in the tensile region. The concentration of hydrogen is highest near the edge dislocation in iron is 57.16 mol/ m^3 and the concentration of hydrogen decreases as we move further from the dislocation.

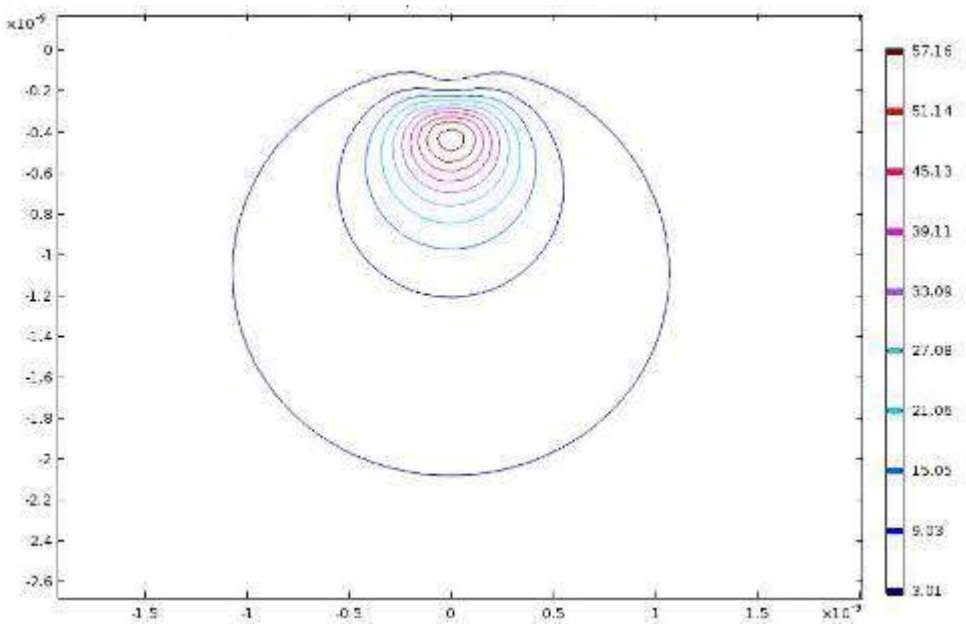

Figure 3. The hydrogen contours around the edge dislocation in Iron [c(mol/ m^3)]

As shown in the figure 4 below, the aluminum metal also holds the hydrogen contours in both; compressive and tensile region. The highest value of concentration in the compression region is nearly 2.31 mol/ m^3, which is near to the edge dislocation and the concentration decreases further from the dislocation center. The partial molar volume of aluminum was not found in the literature. Therefore, the authors used the partial molar volume of FCC crystal structure of 316L stainless-steel (Ilin.D, 2014).

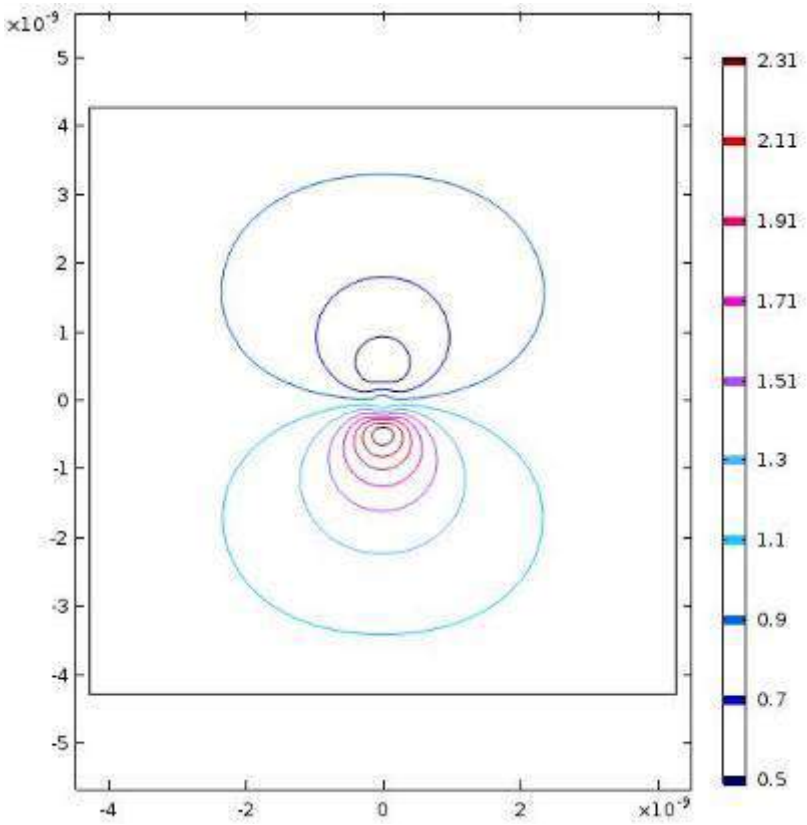

Figure 4. The hydrogen contours around the edge dislocation in Alumunium-7050 [c(mol/m^3)]

DISCUSSIONS

In this study the hydrogen distribution appeared to be symmetric with respect to edge dislocation plane in all 4 metals. This is primarily a result of symmetric hydrostatic stress field of hydrogen (Bal, 2017). The highest concentration was observed near the edge dislocation in the metal matrices which in accordance to the study conducted by (Bal, 2017) in niobium metal matrix. Except iron, the other metals held the hydrogen concentration in tensile region and compression region. The iron, however; restricted hydrogen to compression region only. The iron has the highest concentration around the edge dislocation whereas aluminum-7050 has the lowest hydrogen concentration around the edge dislocation in the compressive region.

The close-packed structures i.e. FCC in aluminuim-7050 case, the diffusivity of hydrogen is low as compared to BCC structures like iron has. This makes them more resistive as less hydrogen is induced fluxed in the metal matrix system causing the hydrostatic stress at the defect sites. The results in this study show the Aluminum having the lowest hydrogen concentration in the compressive region while Iron observing the highest concentration of hydrogen at near the dislocation in the compressive region due to the FCC and BCC structures, as described by (Hirata. K et al, 2018), of the lattices, respectively under static external influence.

The results of iron diffusion are also in agreement with the study by (Evers et al, 2013) which states that in the ideally dissolved hydrogen in iron matrix the hydrogen is considered almost unperturbed in the lattice sites. And the other hydrogen has the interactions with the lattice defects and cannot be considered as diffused hydrogen. These interaction keeps the hydrogen strongly bounded to the lattice defects. In this study the iron results showed the iron mobility restricted to the compressive region only. Due to the edge dislocation the defect site is in under compression and agrees with the finding of Stefan Evers et al of hydrogen strongly bounded to the lattice defects and hence not diffusing to tensile region.

The AISI-4130 is the alloy steel having the highest concentration of chromium alloying of up to 1.1%. In the results the AISI-4130 showed around 78% less highest concentration contour than to iron. This agrees with the (Grabke & Riecke, 2000) who state in their study the lowering effect of alloying elements of hydrogen diffusivity in the matrix. AISI-4130 is BCC structure at the room temperature; and therefore, the crystal lattice structure is not effective in lowering the hydrogen diffusivity in matrix unlike Alumunium-7050 which is FCC.

CONCLUSIONS

The hydrogen concentration is investigated in this paper using iterative modeling approach. The hydrogen concentration contours are modeled around the edge dislocation in 4 metal matrices. The hydrogen concentration contours around the edge dislocations are modeled for AISI 4130, Iron, X-750, and Aluminuim-7050 meatal matrices. The paper concludes on the following points observed in the analysis:

The highest concentration is observed at the edge dislocation and decreases with the burger vectors away from the edge dislocation.

The hydrogen distribution remained symmetric with respect to edge dislocation plane in all 4 matrices.

Except Iron, all the metal matrices observed the concentration presence in both regions: tensile and compression.

All 4 metal matrices showed the highest concentration near the edge dislocation which is in the compressive region.

The impurity lowers the hydrogen diffusivity in the iron matrix.

The FCC structure has the lower hydrogen diffused in lattice system compared to BCC structures.

REFERENCES

B. Bal, I. Sahin, A. Uzun, and D. Canadinc, "A new venue toward predicting the role of hydrogen embrittlement on metallic materials,". *Metallurgical and Materials Transactions A, vol. 47, no. 11, pp. 5409–5422, 2016.*

Barrera, E Tarleton, H W Tang, and A C F Cocks. Modelling the coupling between hydrogen diffusion and the mechanical behavior of metals. *Computational Materials Science, 122:219–228, 2016*

B. Bal, "Numerical Investigation of the Role of Volumetric Transformation Strain on the Relaxation Stress and the Corresponding Hydrogen Interstitial Concentration in Niobium Matrix," *Advances in Materials Science and Engineering, vol. 2017, Article ID 2036516, 7 pages, 2017*

D. Beachem, "A new model for hydrogen-assisted cracking (hydrogen 'embrittlement')," *Metallurgical and Materials Transactions, vol. 3, pp. 437–451, 1972.*

Dmitrii Ilin. Simulation of hydrogen diffusion in fcc polycrystals. Effect of deformation and grain boundaries: effect of deformation and grain boundaries. *Mechanics [physics.med-ph]. Université de Bordeaux, 2014. English. ffNNT : 2014BORD0157ff. fftel-01136181f*

Evers, S., Senöz, C., & Rohwerder, M. (2013). Hydrogen detection in metals: a review and introduction of a Kelvin probe approach. *Science and Technology of Advanced Materials, 14(1), 014201. doi: 10.1088/1468-6996/14/1/014201*

G. P. Tiwari, A. Bose, J. K. Chakravartty et al., "A study of internal hydrogen embrittlement of steels," *Materials Science and Engineering A, vol. 286, no. 2, pp. 269–281, 2000.*

Hirata, K. Iikubo, S. Koyama, M. Tsuzaki, K. and Ohtani, H. "First-Principles Study on Hydrogen Diffusivity in BCC, FCC, and HCP Iron". *Metallurgical and Materials Transactions1543-1940 https://doi.org/10.1007/s11661-018-4815-9 10.1007/s11661-018-4815-9, 2018*

H.J. Grabke, E. Riecke. "ABSORPTION AND DIFFUSION OF HYDROGEN IN STEELS". *Max-Planck-Institut für Eisenforschung GmbH, Postfach 140444, 40074 Düsseldorf, Germany. 34(6)331, 2000.*

M. Symons, "The effect of carbide precipitation on the hydrogen-enhanced fracture behavior of alloy 690,". *Metallurgical and Materials Transactions A, vol. 29, no. 4, pp. 1265–1277, 1998.*

Mechanisms of hydrogen related fracture. *Office of Naval research. (1989).*

Taha and P. Sofronis, "A micromechanics approach to the study of hydrogen transport and embrittlement," *Engineering Fracture Mechanics, vol. 68, no. 6, pp. 803–837, 2001.*

W. H. Johnson, "On some remarkable changes produced in iron and steel by the action of hydrogen and acids," *Proceedings of the Royal Society of London, vol. 23, pp. 168–179, 1875.*

W.T. Geng, A.J. Freeman, R. Wu, C.B. Geller, J.E. Raynolds Embrittling and strengthening effects of hydrogen, boron, and phosphorus on a 5-nickel grain boundary. *Phys Rev B 60(10):7149–7155. (1999)*

Y. Liang, P. Sofronis, and R. Dodds, "Interaction of hydrogen with crack-tip plasticity: effects of constraint on void growth," *Materials Science and Engineering. A, vol. 366, no. 2, pp. 397– 411, 2004.*

Y. Qi, H. Luo, S. Zheng, C. Chen, and D. Wang, "Effect of immersion time on the hydrogen content and tensile properties of A350LF2 steel exposed to hydrogen sulfide environments," *Corrosion Science, vol. 69, pp. 164– 174, 2013.*

EVALUATION OF DESICCANT DRYING SYSTEM DESIGNED FOR DRYING FOOD WITH LOW TEMPERATURE IN DIFFERENT CLIMATE CONDITIONS

Kamil Neyfel ÇERÇİ, Osmaniye Korkut Ata University, kcerci@osmaniye.edu.tr

Ertaç HÜRDOĞAN, Osmaniye Korkut Ata University, ehurdogan@osmaniye.edu.tr

ABSTRACT: The moisture content of foods and seeds must be reduced to a certain level in food drying or seed breeding. The drying air must be at low temperature in order to preserve the color, taste, vitamin content and structure of foods during drying, to obtain high quality dried food and to maintain germination of seed separated products. However, drying air at low temperature causes an increase in drying time. In addition, in areas with high humidity, drying time increases and molds can develop and leads to loss of quality and product in foods. At the same time, mitotoxins formed as a result of mold can cause health problems such as mutagen, carcinogen, teratogen, tremorgen. In order to avoid these problems, drying time should be reduced. Modern and energy saving drying systems with low drying air temperature have been interest of many researchers to maintain product quality and save energy. In this study, a drying system that include two dehumidification processes (desiccant rotor and heat pump) were designed for drying food at low temperature and moisture content to reduce drying times. For this purpose, a model of the designed drying system was developed and system was evaluated for different climatic conditions.

Key words: Food Drying, Desiccant Wheel, Heat Pump, Solar Energy

DÜŞÜK SICAKLIKTA GIDA KURUTMAK İÇİN TASARLANAN NEM ALMALI BİR KURUTMA SİSTEMİNİN FARKLI İKLİM ŞARTLARI İÇİN DEĞERLENDİRİLMESİ

ÖZET: Gıda kurutulmasında veya tohum ıslahında gıdaların ve tohumlarının nem içeriğinin belirli bir oranın altına düşürülmesi gerekmektedir. Gıdaların, kurutma esnasında renginin, tadının, vitamin içeriği ve yapısının korunarak, kaliteli kurutulmuş gıda eldesi ve tohumluk olarak ayrılan ürünlerde çimlenme özelliğinin muhafazası için kurutma havasının düşük sıcaklıkta olması gerekmektedir. Fakat kurutma havasının düşük sıcaklıkta olması, kurutma zamanının uzamasına neden olmaktadır. Ayrıca nem oranı yüksek olan bölgelerde, kurutma süresi uzamakta ve bunun neticesinde küfler gelişebilmektedir. Küflenmenin kalite ve ürün kayıplarına sebep olmasının yanı sıra oluşan mitotoksinler mutajen, kanserojen, teratojen, tremorgen gibi sağlık sorunlarına neden olabilmektedir. Bu sorunların önüne geçebilmek için kurutma zamanını azaltmak gerekmektedir. Ürün kalitesini korumak

ve enerji tasarrufu sağlamak için modern ve enerji tasarrufu sağlayıcı düşük sıcaklıklı kurutma sistemleri birçok araştırmacının ilgi alanı olmuştur. Bu çalışmada tasarlanan kurutma sistemiyle iki nem alma işleminin (nem alıcı rotor ile ısı pompası) aynı anda kullanılması sağlanarak düşük sıcaklıkta, nem içeriği düşük hava ile kısa kurutma süreleriyle gıda kurutulması amaçlanmıştır. Bu amaç doğrultusunda, tasarlanan kurutma sisteminin bir modeli oluşturulmuş ve farklı iklim şartları için değerlendirilmiştir.

Anahtar sözcükler: Gıda Kurutma, Nem Alıcı Rotor, Isı Pompası, Güneş Enerjisi

GİRİŞ

Gıdalar için kurutma, içerisindeki nemin değişik metotlarla alınarak, bozulmasına neden olan etkenlerin ortadan kaldırılması, bir başka ifade ile gıdadaki nemin uzaklaştırılması olarak tanımlanabilir. Gıdadaki serbest nem ve ürün içindeki bağlı nem alınırken en uygun olan kurutma yöntemini seçmek, günümüz enerji ve ekoloji dengeleri açısından oldukça önemli hale gelmiştir. [1]. Birçok kurutma yöntemi arasında en sık kullanılanı, tabii kurutma olarak da isimlendirilen günışığında kurutmadır. Güneş enerjisi ile kurutma yapan birçok sistemde enerjiye para ödenmezken bu yöntemle kurutulan ürünlerin orijinal şeklini ve dokusunu (tekstür), taze iken sahip olduğu rengini ve vitamin içeriğini kaybetme eğilimi vardır. Ayrıca kurutma hızının hava şartlarına çok bağlı olması ve hava şartlarının değişiminin kontrol edilmesinin mümkün olmaması, düzgün dağılımlı ürün kalitesinin önüne geçmektedir [2]. Kurutma zamanı, kurutma havası sıcaklığının artması ile kısalmasına rağmen kurutulan ürünlerdeki renk ve tat değişimi, vitamin içeriğindeki değişim ve yapısal bozukluklar (ısıl gerilmelerden kaynaklanan çatlamalar vb.) sıcaklık arttıkça daha fazla gerçekleşmektedir. Özellikle kivi, yerfıstığı gibi ürünler kurutma sıcaklığına çok duyarlıdır. Kurutma sıcaklığı 35 °C üzerine çıktığı zaman yerfıstığının iç yapısında çatlama ve tat değişimi meydana gelmektedir [3]. Gıda kalitesi üzerine artan bu talepler kurutmada yenilikçi fikirlerin gelişmesine sebep olmuştur. Bu yenilikçi fikirler arasında en önemlileri ısı pompalı ve nem almalı (desisif) kurutuculardır. Bu kurutucuların kurutma uygulamalarında kullanılmasındaki avantajlar, sürekli kurutmayı sağlamak (gece-gündüz), kuru havadan dolayı kurutma miktarını arttırmak, daha üniform bir kurutmayı sağlamak ve özellikle ısıya duyarlı ürünler için ürün kalitesini arttırmak olarak sıralanabilir [4]. Bu avantajlar göz önünde bulundurulduğu zaman, ürün kurutma işleminin düşük neme sahip kurutma havası ile gerçekleştirilmesi büyük önem arz etmektedir. Bu amaçla literatürde kurutma havasından nem uzaklaştırmak için sadece ısı pompası kullanımına dayalı farklı çalışmalar mevcuttur [5-10]. Isı pompalı kurutma sistemlerinde kurutma havasından nem alınabilmesi için nemli hava çiğ noktası sıcaklığı altına kadar ısı pompasının buharlaştırıcısı üzerinden geçirilerek soğutulmakta ve havanın taşıdığı nemin yoğuşması sağlanarak düşük neme sahip kurutma havası elde edilebilmektedir. Fakat sadece buharlaştırıcı ile nem alma işlemi sonucu, ısı pompası sisteminin etkinlik katsayısının düşük olmasına neden olacak ve dolayısıyla ihtiyaç duyulan enerji artacaktır. Bir başka ifadeyle kurutma havası neminin düşük değerlere indirilmesi

işleminin sadece ısı pompası buharlaştırıcısıyla yapılması enerji tüketiminin fazla olması anlamına gelmektedir. Bu anlamda nem alma işleminde buharlaştırıcıya düşen yükü azaltabilmek ve sistem performansını arttırabilmek için nemin bir kısmının farklı ekipmanlarla da alınabilmesinin sağlanması gerekmektedir. Kurutma uygulamalarında buharlaştırıcı yükünü azaltmaya alternatif yöntemler olarak katı ve sıvı nem alıcılar gösterilmektedir [4]. Özellikle düşük sıcaklıkta nem alıcı materyallerin rejenerasyonu enerji verimliliği açısından çok faydalı olmakta ve herhangi bir sistemden atık ısı ya da yenilenebilir enerji kullanımı nem alıcı sistemlerdeki çalışma maliyetini düşürmektedir [4].

Bu çalışmada, ısı pompası ve nem alıcı döner rotorun birlikte kullanıldığı düşük sıcaklıklı hibrit bir kurutma sistemi tasarlanarak, sistemin bir modeli oluşturulmuş ve farklı iklim şartlarına göre termodinamik analizler gerçekleştirilmiştir. Bu analizler doğrultusunda buharlaştırıcı yükü, sulu bataryanın yükü, kompresörün tükettiği güç, sistemin nem alma performans katsayısı, buharlaştırıcı ve nem alıcı rotordan alınan nem miktarlarının değişimi incelenmiştir.

SİSTEMİN TANITIMI VE MODELLENMESİ

Şekil 1'de tasarlanan sistemin genel görünüşü verilmiştir. Şekilden de görüldüğü gibi sistemde iki hava kanalı (proses ve rejenerasyon) bulunmaktadır. Bu hava kanallarına, sistemin amacına uygun olarak çeşitli ekipmanlar (nem alıcı rotor, buharlaştırıcı, yoğuşturucu, fan, kurutma kabini, su bataryası) yerleştirilmiştir.

Proses hava kanalına fan vasıtasıyla giren dış hava (1 noktası) öncelikle ısı pompasının buharlaştırcısı üzerinden geçirilmektedir (2→3). Burada hem hava içerisindeki nem yoğuşturularak (üzerinden geçen havanın çiğ noktası sıcaklığının altına kadar soğutma gerçekleştirilerek sağlanacaktır) daha kuru bir hava elde edilmekte, hem de sıcaklığı düşmektedir. Ele alınan sistem düşük sıcaklıkta kurutma için düşünülmüştür. Kuru hava daha sonra nem alıcı rotor üzerinden geçirilerek nemi daha da aşağılara düşürülmekte (3→4) ve kuru, ancak daha yüksek sıcaklıkta (<35 °C) hava elde edilebilmektedir (4 noktası). Aynı anda bir miktar sıcak hava (rejenerasyon havası) ters yönden nem alıcıya gönderilerek (8 noktası) proses havasından çekilen nem, nem alıcı rotor üzerinden uzaklaştırılmaktadır (8→9). Proses havası içerisindeki nemin alınması işlemi iki aşamada (buharlaştırıcı ve nem alıcı rotor) gerçekleştirilmektedir. Bunun iki ana sebebi şu şekilde açıklanabilir. Nem alıcı rotorlarda, nem alma kapasitesini etkileyen en önemli parametrelerden biri rejenerasyon sıcaklığıdır. Rejenerasyon sıcaklığı, rotor üzerinde alınan nemin buharlaştırılarak tamamen uzaklaştırılabilmesi için gerekli olan hava sıcaklığıdır. Düşük rejenerasyon sıcaklığı daha az nem alınması anlamına geldiğinden kurutmanın gerçekleştirilmesi için gerekli çok düşük nem, ısı pompasının buharlaştırıcısı ile sağlanacaktır. Nem alıcı rotorlarda, nem alma kapasitesini etkileyen bir diğer önemli parametre ise giriş havası şartlarıdır (nem ve sıcaklık). Aynı nem değeri için sıcaklığın düşmesi, nem alma kapasitesini artırmaktadır. Nem alıcıdan 4 noktasında kuru bir şekilde çıkan hava, kurutma kabinine gönderilmekte ve ürün üzerindeki nem uzaklaştırılarak kurutma prosesi tamamlanmaktadır (5 noktası). Döner nem alıcıda,

proses havasından çekilen nemin (3→4) uzaklaştırılması için sıcak rejenerasyon havası kullanılmaktadır. Rejenerasyon kanalına emilen dış hava, (1 noktası) ısı pompasının yoğuşturucusu üzerinden geçerek ısınmaktadır (6→7). Isınan hava daha sonra, nemi uzaklaştırmak için gerekli olan sıcaklığı sağlamak amacıyla güneş kollektörleri vasıtasıyla ısıtılan sıcak suyun kullanıldığı su bataryası üzerinden geçirilerek ısıtılmaktadır (7→8). 8 noktasında nem alma ünitesine giren rejenerasyon havası, nem alıcıdaki nemi üzerine alarak soğumakta ve dışarı atılmaktadır (9 noktası).

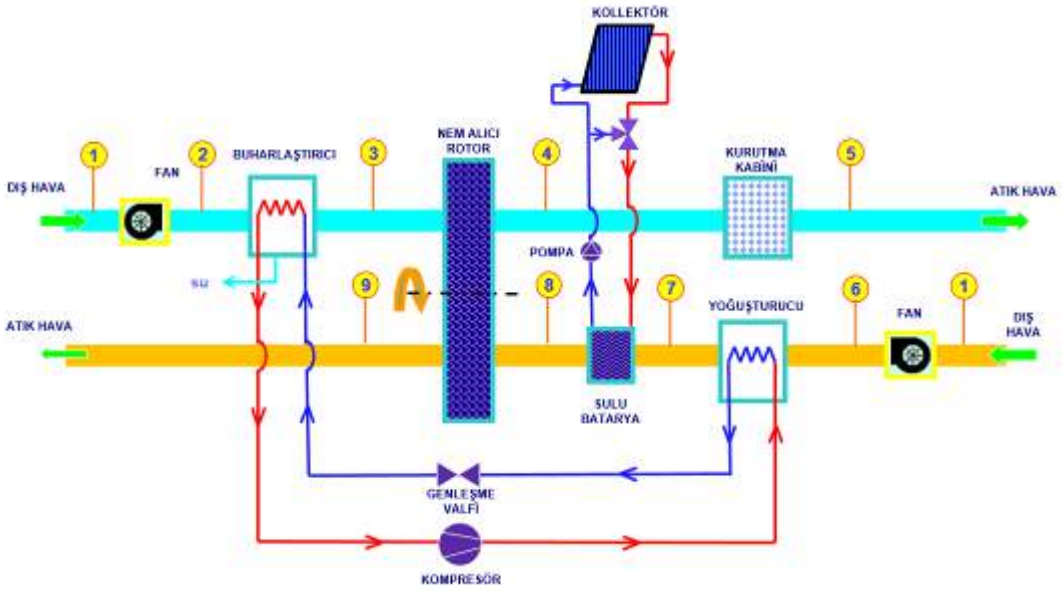

Şekil 1. Sistemin genel görünüşü

Sistemdeki ana bileşenler kompresör, yoğuşturucu, buharlaştırıcı, genleşme valfi, nem alıcı rotor, kurutma kabini ve güneş kollektörlü ısıtıcıdır (su bataryası). Bu çalışmada, evaporatörde gerçekleşen ısı transferi ($\dot{Q}_b$) gizli ve duyulur ısı transfer mekanizmaları ile gerçekleşmiştir.

$$\dot{Q}_b = \dot{Q}_d + \dot{Q}_g \quad (1)$$

$$\dot{Q}_b = \dot{m}_{ph} \cdot (h_2\text{-}h_3) \quad (2)$$

$$T_b = T_3\text{-}\Delta T_b \quad (3)$$

Burada$\dot{Q}_d$ duyulur ısı transfer miktarı (kW), $\dot{Q}_g$ buharlaşmadan kaynaklı gizli ısı transfer miktarı (kW), $\dot{m}_{ph}$ proses havasının kütlesel debisi (kg/sn), h_2 ve h_3 sırasıyla 2 ve 3 noktasındaki entalpi (kJ/kg) değerleridir. T_b buharlaşma sıcaklığıdır (°C), ΔT_b buharlaşma sıcaklığı ve 3 noktasının arasındaki sıcaklık farkıdır (°C).

Sistemde bulunan yoğuşturucuda gerçekleşen ısı transfer miktarını hesaplamak için Eşitlik (4), (5) ve (6)'den faydalanılmıştır. Yoğuşturucuya rejenerasyon havası 6 noktasından girmekte ve 7 noktasından çıkmaktadır. Bu esnada yoğuşturucudan rejenerasyon havasına ısı atılmaktadır.

$$COP_{SM} = \frac{\dot{Q}_b}{\dot{W}_k} \quad (4)$$

$$\dot{Q}_y = \dot{m}_{rh} \cdot (h_7\text{-}h_6) \quad (5)$$

$$T_y = T_7 + \Delta T_y \quad (6)$$

Burada $\dot{Q}_y$, yoğuşturucunun ısı transfer miktarını vermektedir (kW). T_y yoğuşma sıcaklığı (°C), ΔT_y yoğuşma sıcaklığı ve 7 noktasının arasındaki sıcaklık farkıdır (°C). COP_{SM} ise soğutma makinesinin performans katsayısıdır [11].

Sistemde kullanılan su bataryası, güneşten elde ettiği ısıyı ($\dot{Q}_k$ (kW)), 7 noktasındaki rejenerasyon havasına vererek, nem alıcı rotor girişindeki rejenerasyon sıcaklığının elde edilmesini sağlamaktadır. Su bataryasının ısı transfer miktarını hesaplamak için gerekli eşitlikler aşağıda verilmiştir [12];

$$\eta_k = -11.235 \cdot \left(\frac{T_m\text{-}T_o}{\dot{q}}\right)^2 - 3.4165 \cdot \left(\frac{T_m\text{-}T_o}{\dot{q}}\right) + 0.728 \quad (7)$$

$$\dot{Q}_k = \eta_k \cdot F \cdot \dot{q} \quad (8)$$

$$\dot{Q}_k = \dot{Q}_{sb} \quad (9)$$

$$\dot{Q}_{sb} = \dot{m}_{rh} \cdot (h_8\text{-}h_7) \quad (10)$$

Burada η_k kollektör verimini (%), T_m sisteme giren/çıkan suyun ortalama sıcaklığı (K), T_o dış ortam havasının sıcaklığı (K), $\dot{q}$ güneş ışınım akısı (W/m^2), F güneş kollektörünün yüzey alanı (m^2), $\dot{Q}_{sb}$ rejenerasyon havasını katı nem alıcı rotora girmeden önce istenilen sıcaklığa çıkarılması için aktarılan ısı transfer miktarı (kW), $\dot{m}_{rh}$ ise rejenerasyon havasının kütlesel debisidir (kg/sn).

Nem alıcı rotordan proses hava kanalında çıkan havanın özellikleri (4 noktası) aşağıdaki eşitlikler yardımıyla belirlenmiştir [13,14,15].

$$F_{1,i} = \frac{-2865}{(T_i+273.15)^{1.49}} + 4.344 \cdot \left(\frac{W_i}{1000}\right)^{0.8624} \quad (11)$$

$$F_{2,i} = \frac{(T_i+273.15)^{1.49}}{6360} - 1.127 \cdot \left(\frac{W_i}{1000}\right)^{0.07969} \quad (12)$$

$$\eta_{F1} = \frac{F_{1,2}\text{-}F_{1,1}}{F_{1,3}\text{-}F_{1,1}} \quad (13)$$

$$\eta_{F2} = \frac{F_{2,2}\text{-}F_{2,1}}{F_{2,3}\text{-}F_{2,1}} \quad (14)$$

$$\Delta F_1 = F_{1,3}\text{-}F_{1,1} \quad (15)$$

$$\Delta F_2 = F_{2,3}\text{-}F_{2,1} \quad (16)$$

$$\eta_{F1} = a1 + a2 \cdot \dot{V} + a3 \cdot \Delta F_1 + a4 \cdot \dot{V}^2 + a5 \cdot \dot{V} \cdot \Delta F_1 + a6 \cdot \Delta F_1{}^2 + a7 \cdot \dot{V}^3 + a8 \cdot \dot{V}^2 \cdot \Delta F_1 + a9 \cdot \dot{V} \cdot \Delta F_1{}^2 + a10 \cdot \Delta F_1{}^3 + a11 \cdot \dot{V}^3 \cdot \Delta F_1 + a12 \cdot \dot{V}^2 \cdot \Delta F_1{}^2 + a13 \cdot \dot{V} \cdot \Delta F_1{}^3 + a14 \cdot \Delta F_1{}^4 \quad (17)$$

$$\eta_{F2} = b1 + b2 \cdot \dot{V} + b3 \cdot \Delta F_2 + b4 \cdot \dot{V}^2 + b5 \cdot \dot{V} \cdot \Delta F_2 + b6 \cdot \dot{V}^3 + b7 \cdot \dot{V}^2 \cdot \Delta F_2 \quad (18)$$

Burada, $F_{1,1}$ ve $F_{2,1}$ nem alıcı rotora proses kanalından giren havanın (3 noktası) karakteristik potansiyelleridir. $F_{2,1}$ ve $F_{2,2}$ nem alıcı rotorda proses kanalından çıkan havanın (4 noktası) karakteristik potansiyelleridir. $F_{1,3}$ ve $F_{2,3}$ nem alıcı rotora rejenerasyon kanalından giren havanın (8 noktası) karakteristik potansiyelleridir. η_{F1} ve η_{F2} nem alıcı rotorun verimlilik faktörleridir. ΔF_1 ve ΔF_2 karakteristik potansiyel farklarıdır. $\dot{V}$ hacimsel debidir (m^3/h). η_{F1} ve η_{F2} değerlerinin hesaplanmasında kullanılan sabitler Tablo 1'de verilmiştir.

Tablo 1. η_{F1} ve η_{F2} değerlerinin hesaplanmasında kullanılan sabitler [15]

Eşitlik 17	a1=0.03235, a2=-0.002886, a3=6.734, a4=8.204×10^{-6}, a5=0.0004009,
	a6=-41.55, a7=-6.929×10^{-09}, a8=-5.047×10^{-06}, a9=0.006358,
	a10=101.8, a11=4.071×10^{-09}, a12=7.24×10^{-07}, a13=-0.01002, a14=-87.73
Eşitlik 18	b1=1.744, b2=-0.00882, b3=-0.4722, b4=2.556×10^{-05}, b5=-0.002296,
	b6=-2.227×10^{-08}, b7=2.299×10^{-06}

Kurutucu kabine giren proses havası ile ürün arasında ısı ve kütle transferi gerçekleşmektedir. Üründen uzaklaştırılan nem miktarını ve kabinden çıkan havanın özelliklerini belirlemek için aşağıdaki eşitlikler kullanılmıştır [16,17].

$$G = V \cdot \rho \quad (19)$$

$$h_c = 413.5 \cdot G^{0.37} \quad (20)$$

$$\dot{m}_{kh} = (h_c \cdot (T_4\text{-}T_{4s}))/(\rho_y \cdot h_{fg} \cdot s) \quad (21)$$

$$\dot{m}_{kh} = \dot{m}_{ph} \cdot (w_5\text{-}w_4) \quad (22)$$

Burada V havanın hızı (m/s), ρ havanın yoğunluğu (kg/m^3), h_c ısı transfer katsayısı (W/m^2K), G ise kabine giren havanın kütle akış hızıdır (kg/m^2sn). $\dot{m}_{kh}$ sabit kuruma hızı (kg/m^2s), ρ_y ürün yığın yoğunluğu (kg/m^3), s ise ürün kalınlığıdır (m). T_4 ve T_{4s} sırasıyla kurutma kabinine giren havanın kuru ve ıslak termometre sıcaklıklarıdır (°C).

Bu çalışma kapsamında tasarlanan kurutma sisteminin performansını (COPs) belirlemek için Eşitlik 23 ve 24 kullanılmıştır [18].

$$COP_s = \frac{\dot{m}_{pa} \cdot h_{fg} \cdot (W_1 - W_4)}{\dot{W}_c} \quad (23)$$

$$COP_s = \frac{\dot{m}_{pa} \cdot (h_1 - h_4)}{\dot{W}_c} \quad (24)$$

BULGULAR VE TARTIŞMA

Bu çalışmada, tasarlanan nem almalı kurutma sisteminin modellenmesi yapılmıştır. Modelin oluşumu için gerekli çözümlemeler için, MATLAB yazılımı kullanılmıştır. Hesaplamalarda, Tablo 2'de verilen giriş parametreleri göz önünde bulundurulmuştur. Analizlerde ürün olarak düşük sıcaklıklarda (<35 °C) kurutulması uygun olan yerfıstığı ürünü seçilmiştir [19,20]. Tablo 3'de sistemin farklı dış hava koşullarındaki performansının araştırılabilmesi amacıyla ele alınan Osmaniye, Mersin ve Antalya illerinin yaz sezonu dış hava dizayn şartları verilmiştir. Bu iller Türkiye'de yerfıstığının yetiştiği iller arasından seçilmiştir [21].

Tablo 2. Analizlerde kullanılan giriş parametreleri

Parametre	**Değer**
Buharlaştırıcı çıkışında çiğ noktası sıcaklığı (°C)	14
Buharlaştırıcı çıkışında rölatif nem (%)	95
Proses havasının hacimsel debisi (m^3/h)	600
Rejenerasyon havasının hacimsel debisi (m^3/h)	600
Su bataryasında giriş/çıkış ortalama sıcaklığı (°C)	55
Nem alıcı rotora rejenerasyon havasından giriş sıcaklığı (°C)	70
Ürünün yığın yoğunluğu (kg/m^3)	480
Ürün kalınlığı (mm)	5
Tepsinin taban alanı (m^2)	1
Buharlaşma sıcaklığı ve 3 noktası arasındaki sıcaklık farkı (°C)	3
Yoğuşma sıcaklığı ve 7 noktası arasındaki sıcaklık farkı (°C)	3
Yoğuşma sıcaklığı (°C)	55

Tablo 3. Analizleri yapılan illerin dış hava dizayn şartları [22]

İller	Kuru Termometre Sıcaklığı (°C)	Yaş Termometre Sıcaklığı (°C)	Mutlak Nem ($g_ş/kg_{kh}$)
Osmaniye	38	26	16.26
Mersin	35	29	23.03
Antalya	39	28	19.41

Şekil 2'de buharlaştırıcı yükü, su bataryası yükü, kompresörün tükettiği güç parametrelerinin Osmaniye, Mersin ve Antalya illerinin iklim koşulları için hesaplanmış değerleri verilmiştir. Şekilden, nem alıcı rotorun 70 °C rejenerasyon sıcaklığında çalıştığı durumda, hem 35°C'den düşük sıcaklıkta, hem de olabildiğince kuru hava elde edilmesi istendiği için dış hava koşullarına bağlı olarak tüm illerde buharlaştırıcı yükünün ($\dot{Q}_b$) değişim gösterdiği ve en yüksek değerini Mersin ili, en düşük ise Osmaniye ilinde meydana geldiği görülmüştür. Mevcut iller arasında Mersin ili en yüksek nem miktarına sahiptir. Bu sebeple Mersin ilinde istenilen düşük nem değerinin elde edilebilmesi için buharlaştırıcı yükünün diğer illere göre daha yüksek olmuştur. Buna bağlı olarak en düşük buharlaştırıcı yükü mutlak nemi en düşük olan Osmaniye ilinde gözlemlenmiştir. Bu durum aynı zamanda Osmaniye ilinde kompresörün tükettiği gücün en düşük olması durumunu da açıklamaktadır.

Şekil 3'de farklı iklim şartlarına göre sırasıyla sistemdeki buharlaştırıcıdan ve nem alıcı rotordan alınan nem miktarlarının değişimi verilmiştir. Nem alıcı rotorun 70 °C rejenerasyon sıcaklığında çalıştığı durumda, istenilen kurutma havası şartlarının elde edilmesi için mutlak nem miktarı en yüksek olan Mersin ilinde buharlaştırıcıdan en çok nem alma işlemi gerçekleştirilmiştir. Buharlaştırıcıdan en az nemin alındığı il ise Osmaniye ilidir. Çünkü dış ortamın nem miktarının az olması buharlaştırıcıdan daha az nem alınmasına dolayısıyla kompresörün daha az enerji tüketmesine sebep olmuştur. Nem alıcı rotora proses havasından giren havanın şartları ve rejenerasyon sıcaklığının aynı olması durumuna rağmen illere göre nem alıcı rotorun nem alma performansı farklılık göstermiştir. Nem alıcı rotordan en çok nem Osmaniye ili iklim koşullarında alınmıştır. Çünkü Osmaniye ilinde diğer illere göre proses giriş şartları ve rejenerasyon sıcaklığı aynı olmasına rağmen dış ortamın mutlak neminin daha düşük olması nem alıcı rotorun rejenerasyon kanalından daha çok nem alınmasına sebep olmuştur. Mersin ilinde ise bu değer en düşüktür.

Şekil 4'de farklı iklim koşullarına göre istenilen kurutma havası şartlarının sağlanması için sistemin nem alma performans parametresinin ($COP_{s.}$) değişimi incelenmiştir. Sistemde nem alıcı rotorda alınan nem miktarı dış hava şartına bağlı olarak fazla bir değişim göstermemektedir (Şekil 3). Şekil 4'den görüldüğü gibi, Mersin ilinde sistemin performans parametresi en yüksek değerdedir. Bunun sebebi, yüksek dış hava neminden dolayı proses havasından uzaklaştırılan nem miktarının fazla olmasıyla buharlaştırıcı yükünün ($\dot{Q}_b$) kompresörün tükettiği güce ($\dot{W}_k$) oranla daha çok olmasından dolayıdır.

Şekil 5'de sırasıyla Osmaniye (a), Mersin (b) ve Antalya (c) illerinin iklim koşulları göz önünde bulundurularak tüm noktalar için hesaplanan değerlerin psikrometrik diyagram üzerinde değişimleri gösterilmiştir. Dış iklim şartlarına göre sistemdeki noktaların değişimi psikrometrik diyagram üzerinden de görülebilmektedir. Mersin ilinde diğer illere kıyasla istenilen kurutma havası şartları için buharlaştırıcıdan alınan nem miktarı daha fazla olduğu gözlemlenmektedir.

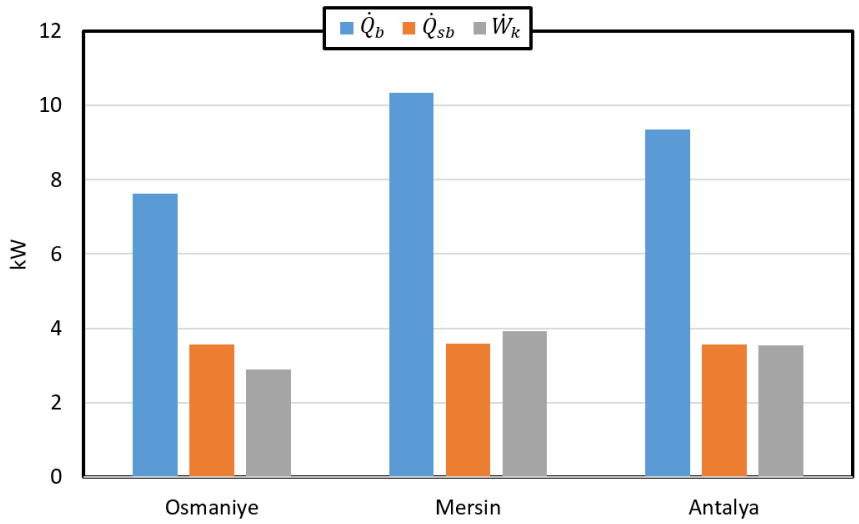

Şekil 2. Buharlaştırıcı, su bataryası yükü ve kompresörün tükettiği gücün illere göre değişimi

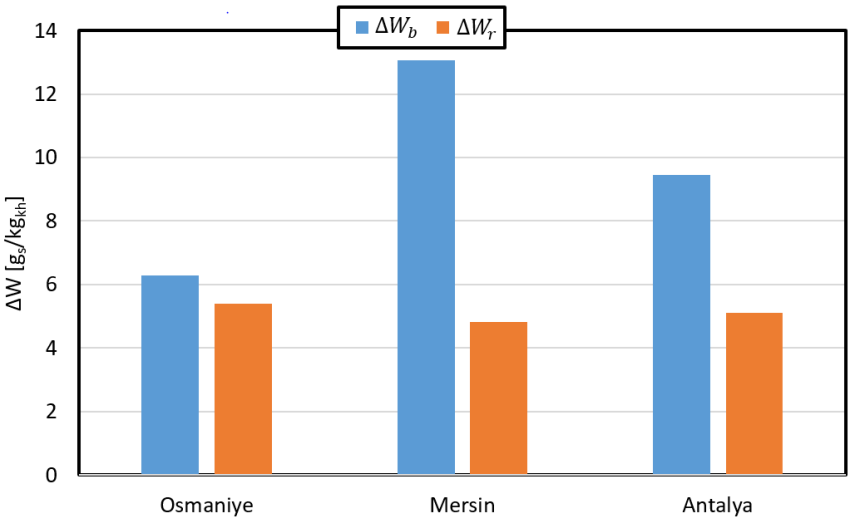

Şekil 3. Farklı iklim koşullarına göre sırasıyla buharlaştırıcı ve nem alıcı rotordan alınan nem miktarları

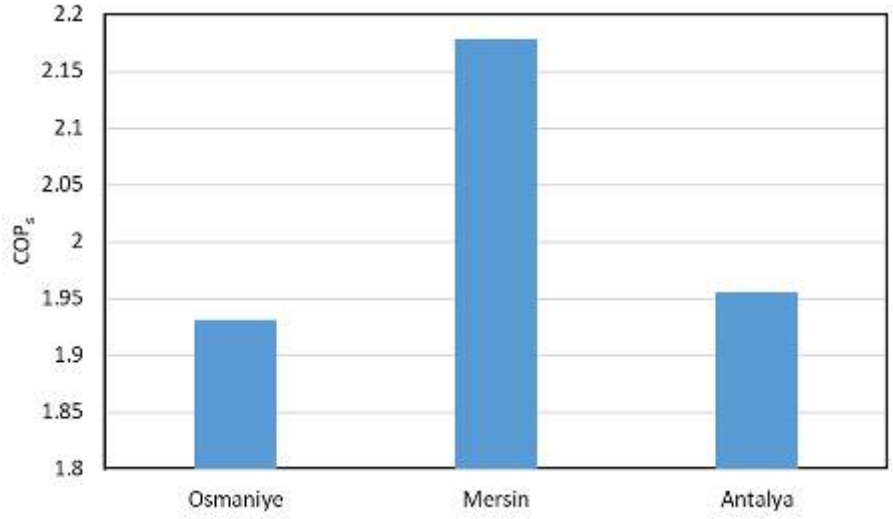

Şekil 4. Farklı iller için COP_s'nin değişimi

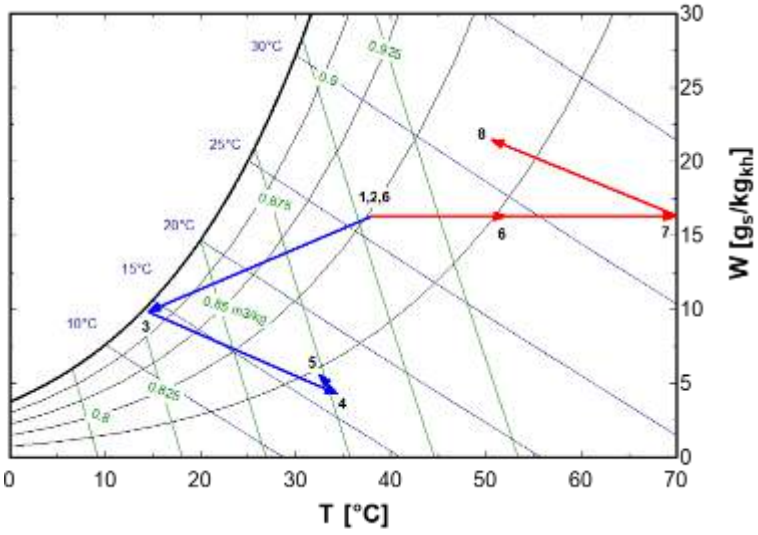

(a)

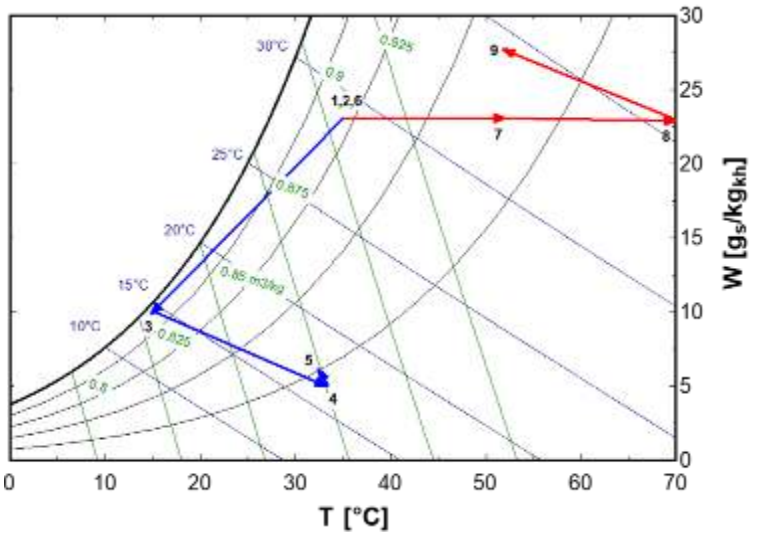

(b)

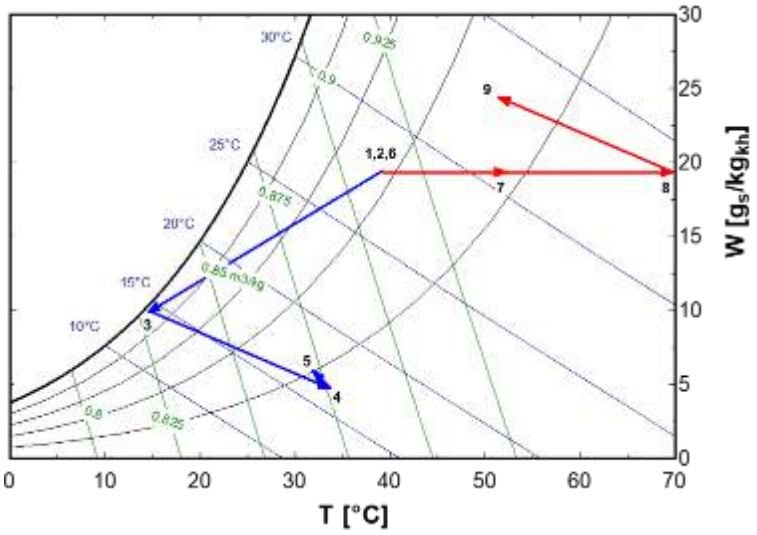

(c)

Şekil 5. Osmaniye (a), Mersin (b) ve Antalya (c) iklim koşullarında sistemdeki tüm noktaların psikrometrik diyagram üzerindeki gösterimi

SONUÇ

Bu çalışmada, tasarlanan düşük sıcaklıkta nem almalı bir kurutma sisteminin farklı iklim koşullarına göre performans analizleri gerçekleştirilmiştir. Analizlerde en yüksek mutlak nem değerine sahip olan Mersin ili için buharlaştırıcı yükü, dolayısıyla kompresörün tükettiği güç yüksek çıkmıştır. En düşük mutlak nem değerine sahip olan Osmaniye ilinde ise buharlaştırıcı yükü ve kompresörün tükettiği güç değeri en düşüktür. Osmaniye ilinde dış hava mutlak nem değerinin düşük olması sebebiyle, aynı rejenerasyon sıcaklığı ve rotora proses kanalından giren hava şartlarında, nem alıcı rotorun nem alma performansı en yüksek olarak bulunmuştur. Sistemin performans katsayısına bakıldığında ise en yüksek değer Mersin ili için elde edilmiştir.

TEŞEKKÜR

Bu çalışma Osmaniye Korkut Ata Üniversitesi Bilimsel Araştırma Projeleri Birimi (OKÜBAP) tarafından OKÜBAP-2018-PT3-015 numaralı proje kapsamında desteklenmiştir. Desteklerinden dolayı OKÜBAP'a teşekkür ederiz.

KAYNAKLAR

[1] Ceylan,I., Aktaş, M., (2008). Isı pompası destekli bir kurutucuda fındık kurutulması. Gazi Üniv. Müh. Mim. Fak. Der., (C:23, No 1), 215-222.

[2] Nagaya, K., Li, Y., Jin, Z., Fukumuro, M., Ando, Y., Akaishi, A., (2006). Low-temperature desiccant-based food drying system with airflow and temperature control. Journal of Food Engineering, 75, 71-72.

[3] Butts, C.L., Williams, E.J., Sanders, T.H. (2002). Algorithms for automated temperature controls to cure peanuts. Postharvest Biology and Technology, 309-316.

[4] Misha, S., Mat, S., Ruslan, M.H., Sopian, K., (2012). Review of solid/liquid desiccant in the drying applications and its regeneration methods. Renewable and Sustainable Energy Reviews, 16, 4686-4707.

[5] Chua, K. J., Chou, S. K., Ho, J. C., Hawlader, M. N. A., 2002, "Heat pump drying: recent developments and future trends", Drying Technology, 1579-1610.

[6] Colak, N., Hepbasli, A., 2009, A review of heat pump drying: Part 1 – Systems, Models and Studies. Energy Conversion and Management, 2187-2199.

[7] Colak, N., Hepbasli, A., 2009, A review of heat-pump drying (HPD): Part 2 – Applications and performance assessments. Energy Conversion and Management, 2187-2199.

[8] Lee, K. H., Kim O. J., 2009, Investigation on drying performance and energy savings of the batch-type heat pump dryer. Drying Technology, 565-573.

[9] Zhang, J., Zhang, H.H., He, Y.L., Tao, W.Q., 2016. A comprehensive review on advances and applications of industrial heat pumps based on the practices in China. Applied Thermal Energy, 178, 800-825.

[10] Liu, S., Li, X., Song, M., Li, M., Li, H., Sun, Z. (2018). Experimental investigation on drying performance of an existed enclosed fixed frequency air source heat pump drying system. Applied Thermal Engineering, 130, 735-744.

[11] Van Schijndel, A. W. M., Qiao, Z., Yang, Y. (2012). 777777Y700 Sustainable Building and System Modelling, Case Study.

[12] Hürdoğan, E., Yılmaz, T., Büyükalaca, O. (2010). Akdeniz kıyı bölgesi için adsorbsiyonlu güneş enerjisi destekli iklimlendirme sistemi. Tesisat Dergisi, Sayı: 172, 150-158.

[13] Jurinak, J.J. (1982). Open-cycle Solid Desiccant Cooling – Component Models and System Simulation, Ph.D. Thesis, University of Wisconsin, Madison.

[14] Panaras, G., Mathioulakis, E., Belessiotis, V., Kyriakis, N. (2010). Experimental Validation of a Simplified Approach for a Desiccant Wheel Model, Energy and Buildings, 42, 1719-1725.

[15] Çerçi, K.N., Hürdoğan, E., KARA, O. (2019). Katı Nem Alıcı Bir Rotorun Farklı Çalışma Şartları için Modellenmesi. Çukurova Üniversitesi Mühendislik Mimarlık Fakültesi Dergisi, 34(2), ss. 267-277.

[16] Fellows, P., Food Processing Technology. Woodhead Publishing Ltd., Cambridge, England, 2000.

[17] Cemeroğlu, B., Gıda Mühendisliğinde Temel İşlemler, Gıda Teknolojisi Derneği Yayınları, Ankara, 2010.

[18] Antonellis, S.D., Intini, M., Joppolo, C.M., Romano, F. (2016). On the control of desiccant wheels in low temperature drying processes. International Journal of Refrigeration, 70, 171-182.

[19] Rotimi, D. (2009). Some Physical Properties of Groundnut Grains. Research Journal of Applied Sciences, Engineering and Technology, 1(2), 10-13.

[20] Beasley, E.O. Dickens, J.W. (1963). Engineering research in peanut curing, Tech. N.C. Agricultural Experiment Station., 155.

[21] Kadiroğlu, A. Yerfıstığı yetiştiriciliği. Batı akdeniz tarımsal araştırma enstitüsü müdürlüğü, Antalya, 2018.

[22] "Alarko-carrier/teknik destek" Erişim adresi: https://www.alarko-carrier.com.tr/tr/TeknikDestek/DisHavaTasarimSicakliklari.pdf, Erişim Tarihi: 18.01.2017.

MANUFACTURING OF A FINNED TYPE SOLAR AIR COLLECTOR AND INVESTIGATION OF ITS PERFORMANCE IN OSMANIYE CLIMATE CONDITIONS

Doğan Burak SAYDAM
Osmaniye Korkut Ata University
dburaksaydam@gmail.com

Kamil Neyfel ÇERÇİ
Osmaniye Korkut Ata University
kcerci@osmaniye.edu.tr

Ertaç HÜRDOĞAN
Osmaniye Korkut Ata University
ehurdogan@osmaniye.edu.tr

Coşkun ÖZALP
Osmaniye Korkut Ata University
coskunozalp@osmaniye.edu.tr

ABSTRACT: Turkey is a country with high solar energy potential due to its geographical location. Solar energy is an important renewable energy source because it can be evaluated with different processes and equipments. Solar air collectors are one of the devices used to obtain heat energy from the sun. Due to the simple technology for installation and low equipment costs, solar collectors are usually used in space heating applications and drying processes (textiles and food). There are several types of absorber plates which are formed in different types to improve the heat transfer coefficient between the absorber plate and the air in the solar collectors. One of most important of these applications is the finned absorber plate. The main objective is to increase the heat transfer between the absorber and the air. In this study, a solar air collector, where fins are created by giving obstacles to the collector absorber plate, was designed, manufactured and experimentally tested . in the climatic conditions of Osmaniye province. The experiments were carried out for two consecutive days and collector thermal efficiency was calculated using temperature, humidity and radiation data measured at different points on the collector. At the end of the study, it was observed that the air temperature of the designed solar collector could be increased by 35 ^{o}C and average collector efficiency was approximately 45%.

Key words: Solar Air Collector, Solar Energy, Osmaniye, Thermal Efficiency

KANATÇIKLI TİP BİR HAVALI GÜNEŞ KOLEKTÖRÜNÜN İMALATI VE OSMANİYE İKLİM ŞARTLARINDA PERFORMANSININ İNCELENMESİ

ÖZET: Türkiye, coğrafi konumundan dolayı yüksek güneş enerji potansiyeline sahip bir ülkedir. Güneş enerjisi, farklı proses ve ekipmanlar ile değerlendirilebiliyor olmasından dolayı önemli bir yenilenebilir enerji kaynağıdır. Havalı güneş kolektörleri güneşten ısı enerjisi elde etmek için kullanılan araçlardan birisidir. Kurulumlarının basit teknolojiye sahip olması ve ekipman maliyetlerinin düşük olmasından dolayı güneş kolektörleri tekstil, gıda gibi alanlarda kurutma ve mahal ısıtma uygulamalarında sıklıkla kullanılmaktadır. Havalı güneş kolektörlerinde bulunan yutucu plaka ile hava arasındaki ısı transfer katsayısını iyileştirmek için farklı tiplerde oluşturulmuş birçok yutucu plaka tipi bulunmaktadır. Bu uygulamalardan önemli olanlardan bir tanesi de kanatçıklı yutucu plakadır. Yutucu plaka üzerine yerleştirilen kanatçıklar ile yutucu plaka ile hava arasındaki ısı transferinin artırılması temel amaçtır. Bu çalışmada, kolektör yutucu plakasına engeller verilerek kanatçık oluşturulan bir havalı güneş kolektör tasarlanmış, imal edilmiş ve Osmaniye ili iklim koşullarında deneysel olarak test edilmiştir. Deneyler kesintisiz iki gün süre ile yapılmış ve kolektör üzerinde farklı noktalarda ölçülen sıcaklık, nem ve ışınım verileri kullanılarak kolektör ısıl verimi hesaplanmıştır. Yapılan çalışma sonunda, tasarımı yapılan güneş kolektöründe, hava sıcaklığında 35 ^{o}C'lik artış elde edilebileceği ayrıca ortalama kolektör veriminin yaklaşık %45 olduğu görülmüştür.

Anahtar sözcükler: Havalı Güneş Kolektörü, Güneş Enerjisi, Osmaniye, Isıl Verim

GİRİŞ

Sanayi devrimi, kentleşmeyi, sanayileşmeyi, ekonomik ve sosyal modernleşmenin bir baskın yolu olarak açığa çıkartmıştır. Buna bağlı olarak dünyadaki nüfus artışı ve sanayileşmenin etkisi ile enerji gereksinimi de her geçen gün artmaya devam etmektedir [1]. Fosil kaynakların yeterli olmayışı ve çevreye verdiği zararlar göz önüne alındığında alternatif enerji kaynaklarına yönelim artmaktadır. Alternatif enerji kaynaklarından biri olan güneş enerjisinden de temiz yollarla ısı ve güç elde etmek mümkündür. Güneş enerjisinden ısı elde etmede yaygın olarak kullanılan uygulamalardan birisi havalı güneş kolektörleridir. Havalı güneş kolektörleri, kolay kurulum ve düşük maliyetlere sahip cihazlar olmanın yanında bakım maliyetlerinin de çok düşük olmasından dolayı tercih edilmektedirler. Kurutma, iklimlendirme sistemleri, seralar ve damıtma sistemleri gibi birçok uygulamada, ısı ihtiyacını havalı güneş kolektörleri ile karşılaşmak mümkündür [2,3]. Temelde havalı güneş kolektörlerinin çalışma prensibi; güneşten gelen ışınımı cam tabakası altından akan akışkana ileterek akışkan ile ısı transferi gerçekleştirerek akışkanın sıcaklığı artırmaktır. Hava kolektörleri içerisinde yaygın olarak düz plaka kullanılmaktadır. Düz plakalı kolektörlerin yutucu plakası ile akışkan olarak kullanılan hava arasındaki düşük konvektif ısı transfer katsayısı nedeniyle ısıl verimleri düşüktür [4]. Havalı

güneş kolektörlerinin ısıl performansı toplayıcı malzemesinin şekline, boyutuna ve içerisinde bulunan kanatçık yapılarına bağlıdır. Literatürde, çeşitli şekil ve boyutlara sahip farklı malzemeler kullanılarak performans iyileştirmesi sağlanabildiği belirtilmiştir. Emici plaka ve hava arasındaki ısı transfer katsayısını iyileştirme yöntemlerinin bazıları, oluklu bir emici plaka, matris tipi emici plaka, V tipi emici plaka kullanımıdır[5].

Havalı güneş kolektörlerinde farklı yutucu plakalar ile ısıl verim analizi, enerji analizi, kolektörlerin imalat ve tasarımı ile ilgili literatürde birçok çalışma görmek mümkündür [6-12]. Karsli [8], kolektör içerisinde bulunan emici plaka üzerine farklı açılarda kanatlar vererek kolektörün verimliliğini birinci ve ikinci yasa verimine göre incelemiştir. Verimler %20-80 arasında değişmiş ve en yüksek kolektör verimliliği 75° kanat açısına sahip kolektörde çıkmıştır. Fudholi ve Sopian [9], kurutma uygulamalarında yoğun olarak kullanılan güneş kolektörlerin enerji ve ekserji analizi üzerine bir çalışma yapmışlardır. Çalışmada iç mekan testlerinde, düz plakalı havalı güneş kolektörünün enerji ve ekserji verimleri sırasıyla % 30 ile % 79 ve % 8 ile % 61 arasında değiştiğini gözlemlenmiştir. Gürel ve ark. [10] yaptıkları çalışmada, dünyada farklı uygulamalarda mahal ısıtmasında kullanılan havalı güneş kolektörlerini incelemişlerdir. Yazarlar havalı güneş kolektörlerinin kargo depoları, hangarlar, kapalı otoparklar, hayvan barınakları gibi hacimlerin ön ısıtması veya direk ısıtılmasında kullanılabileceğini göstermişlerdir.

Bu çalışmada, engelli tip kanatçık modeline sahip bir havalı güneş kolektörünün imalatı yapılarak, performansı Osmaniye iklim şartlarına göre deneysel olarak incelenmiştir.

YÖNTEM

Tasarımı yapılan kanatçıklı havalı güneş kolektörünün imalat aşamaları Şekil 1'de yer almaktadır. Havalı güneş kolektörü Osmaniye Korkut Ata Üniversitesi'nin Makine Metal Bölümü atölyelerinde imal edilmiştir. Kasası pleksiglastan yapılmış 195x95x12 cm ölçülerindeki (1,70 m^2) kolektör içerisine engellerin bulunduğu plaka yerleştirmeden önce ısı kayıplarının azaltılması amacıyla alt ve yan yüzeyleri alüminyum kaplı camyünü ısı yalıtım malzemesiyle kaplanmıştır (Şekil 1-a). Akışkanın kolektör içerisinde daha fazla dolaşmasını sağlamak ve bu sayede ısı transferini artırmak için alüminyum plaka üzerine yine alüminyumdan imal edilen engeller yerleştirilmiştir (Şekil 1-b). Daha sonra plaka üzerine kolektöre dış ortam havasının kolektöre girebilmesi için kolektör giriş ağzı ve emici plaka içerinde dolaşan havanın kolektörden çıkabilmesi için kolektör çıkış ağzı eklenmiştir (Şekil 1-c). Engellerin ve hava giriş çıkış ağzının oluşturulmasından sonra plaka, emiciliği yüksek kolektör boyası ile boyanmıştır (Şekil 1-d). Bu sayede kolektör yüzeyine düşen ışınımdan maksimum oranda faydalanmak hedeflenmiştir. Boya işleminin ardından plaka kurumaya bırakılmış ve kuruduktan sonra yüzeye, geçirgenliği yüksek kolektör camı montajı yapılmıştır. Montajlanan cam ile kolektör yüzeyi arasında birleşim

yerlerinden meydana gelebilecek hava sızıntılarının önlenmesi amacıyla hava geçişinin olduğu tüm bağlantı noktaları ve alanlar silikon kullanılarak kapatılmıştır (Şekil 1-e). Silikonun kurumasının ardından kolektör, deneylerin gerçekleştirileceği Osmaniye Korkut Ata Üniversitesi Mühendislik Fakültesi çatısına güneşten maksimum fayda sağlayabilmesi için yüzeyi güneye bakacak şekilde yerleştirilmiştir (Şekil 1-e). Ek olarak havalı güneş kolektörü içerisinden geçecek olan havanın sirkülasyonunu sağlamak için 170W gücünde 650 m^3/saat (maks.) debiye sahip hız kontrollü radyal tip bir fan kullanılmıştır. Şekil 2'de ise deneylerin yapıldığı kolektörün son hali yer almaktadır.

(a) (b) (c)

(d) (e) (f)

Şekil 1. Kanatçıklı havalı güneş kolektörün imalat aşamaları

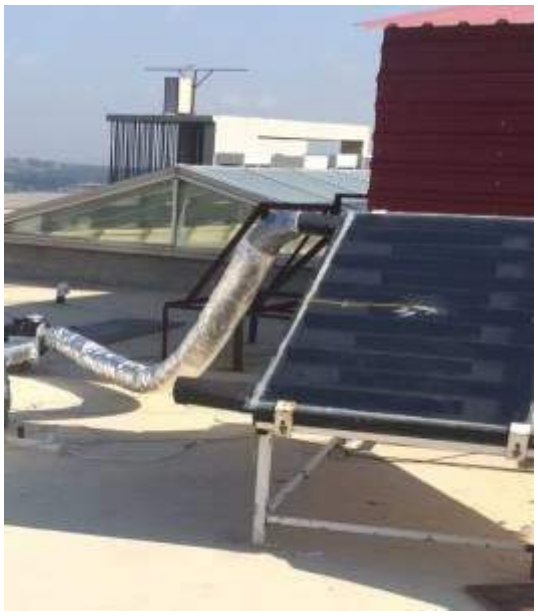

Şekil 2. Kanatçıklı havalı güneş kolektörünün son halinin görünüşü

Güneş kolektörüne giren taze hava, kolektör içinde ısınarak bir fan yardımıyla sistemden çekilmektedir. Sistemin performansını belirleyebilmek amacıyla sistem üzerinde farklı notlarda ölçümler gerçekleştirilmiştir. Deney düzeneğinde farklı parametrelerin (sıcaklık, nem, hava hızı) ölçülmesi ve anlık olarak belirli aralıklarla (15 dk) kaydedilebilmesi için bilgisayar destekli bir veri toplama ünitesi kullanılmıştır. Tablo 1'de sistem üzerinde farklı bölgelerde yapılan ölçümlerde ve analizlerde kullanılan cihazlar yer almaktadır.

Tablo 1. Ölçümlerde ve Analizlerde Kullanılan Cihazlar

Cihaz	**Ölçüm Parametreleri**	**Hassasiyet**
TESTO 435	Hava Hızı	0.1 m/s
COLE PARMER Isıl Eleman Çifti	Sıcaklık	0.1 °C
EPLUSE Nem Ölçer	Rölatif nem	2-3 %
IOTECH PD3001Veri Kaydedici	Veri kayıt	16 bit
FRONIUS Işınım Ölçer	Işınım	±%5

İmalatı yapılan kanatçıklı güneş kolektöründe havaya aktarılan enerji miktarını hesaplamak için aşağıdaki eşitlik kullanılmıştır.

$$\dot{Q} = \dot{m}.C_p.(T_g - T_ç) \quad (1)$$

Burada, ṁ, kolektörden geçen havanın kütlesel debisi (kg/s), C_p havanın özgül ısısı (J/kgK), T_g ve $T_ç$ sırasıyla kolektör hava giriş ve çıkış sıcaklıklarıdır (°C). Kolektörden geçen havanın kütlesel debisi ise Eşitlik 2 kullanılarak belirlenmiştir.

$$\dot{m} = \rho . V A_ç \quad (2)$$

Eşitlikte ρ havanın yoğunluğu (kg/m³), V hava akış hızı (m/s), $A_ç$ ise kolektörün çıkış kesit alanı (m²)'dır.

Havalı güneş kolektörün ısıl verimi (η_c) Eşitlik 3 ile hesaplanmıştır.

$$\eta_c = \frac{\dot{m} . C_p . (T_g - T_ç)}{I . A_k} \quad (3)$$

Burada, I kolektör yüzeyine gelen güneş ışınımı (W/m²), A_k ise güneş ışınımının direkt olarak vurduğu yutucu plaka yüzey alanıdır (m²) [13,14].

BULGULAR VE TARTIŞMA

Bu çalışmada, engelli tip kanatçık modeline sahip bir havalı güneş kolektör imal edilmiş ve deneysel olarak incelenmiştir. Birbirini takip eden iki günde (13 ve 14 Eylül 2019 tarihlerinde) gerçekleştirilen deneylerde, farklı noktalarda ölçülen sıcaklık, ışınım ve nem değerlerinin zamana göre değişimi gözlemlenmiştir. Deneyler sabah 07:30'da başlanmış ve kesintisiz bir şekilde iki gün devam ettirilmiştir. Sistem debisi deney süresince sabit tutulmuş ve kütlesel debi 0,0264 kg/s olarak hesaplanmıştır. Şekil 3'de kolektörün farklı noktalarından ölçülen sıcaklıkların ve ışınımın zamana göre değişimleri verilmiştir. Düşük sıcaklıkta kolektöre giren ortam havası kolektörden ısınarak çıkmaktadır. Sıcaklıkların gün içerisinde ışınımın etkisi ile değiştiği de açık bir şekilde görülmektedir. Kolektör çıkış sıcaklığının deneyler boyunca 25°C ile 60 °C arasında değiştiği ve kolektörün giriş ve çıkış noktaları arasında en fazla 35 °C' lik bir sıcaklık artışı yapılabildiği yine Şekil 2 incelendiğinde görülmektedir. Işınım gece saatlerinde 0 W/m² ile en düşük öğle saatlerinde ise 945 W/m² ile en yüksek değerlere ulaşmıştır. Bulutlanmanın etkisi ile ışınımda sürekli bir dalgalanma olduğu yine şekillerden görülmektedir. Şekil 3'den ayrıca kolektör giriş sıcaklığı arttıkça ışınımın da etkisi ile kolektör cam yüzey sıcaklığının da arttığı görülmektedir. Şekil 4'de rölatif nem ve ışınımın zaman ile değişimini gösteren grafik yer almaktadır. Şekilden, deneyler boyunca kolektör giriş (dış hava) ve çıkışındaki havanın rölatif nem değerinin, dış hava sıcaklığı ve ışınıma bağlı olarak değişim gösterdiği ve kolektörde ısınan havanın rölatif neminin düştüğü görülmektedir. Rölatif nem özellikle sabah ve gece saatlerinde yüksek (%95), gün içerisinde ise özellikle öğlen saatlerinde düşük (%15) değerdedir.

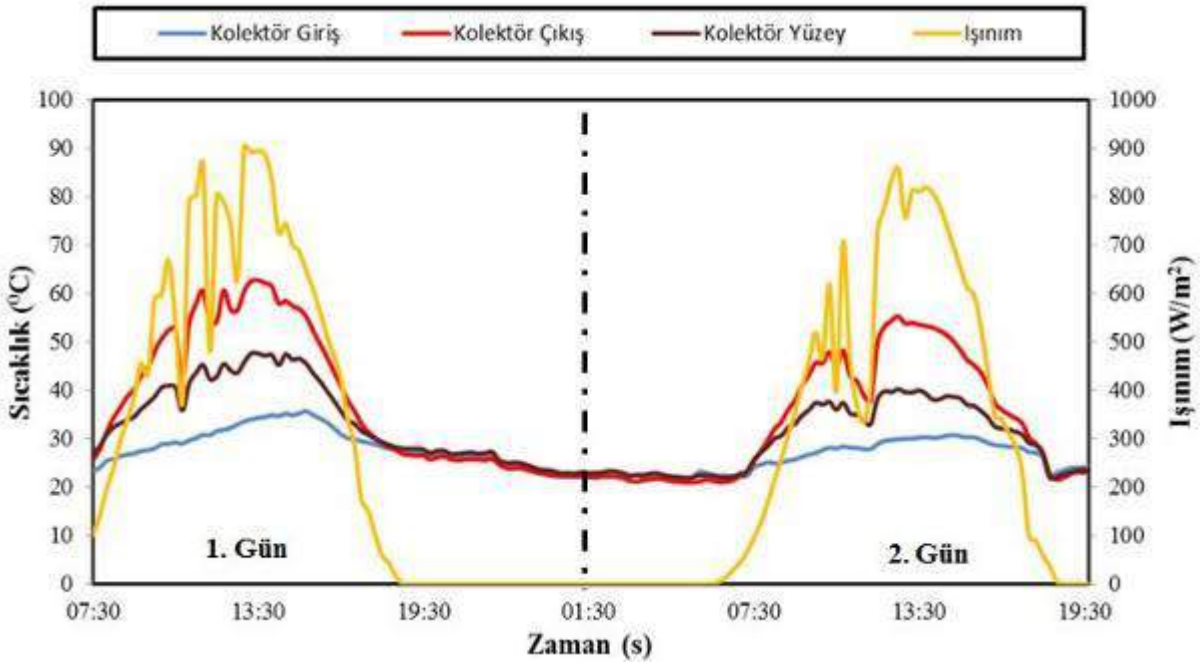

Şekil 3. Sıcaklık ve Işınımın Zaman Göre Değişimi

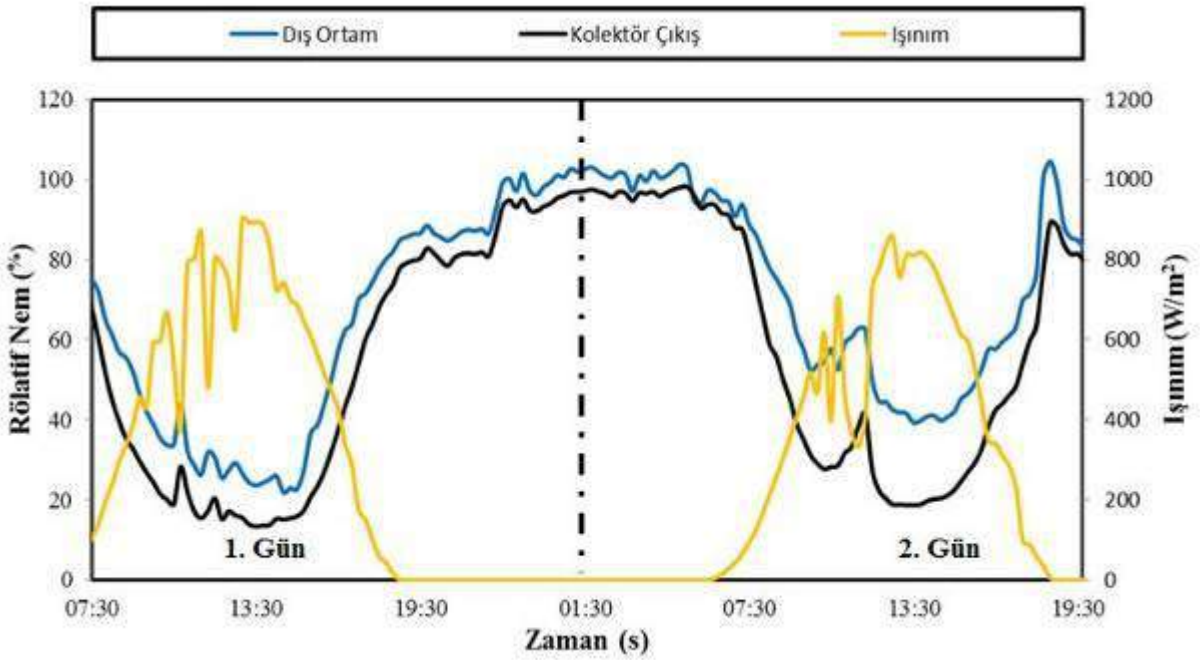

Şekil 4. Rölatif Nemin ve Işınımın Zamana Göre Değişimi

Şekil 5'de kolektör veriminin, zamana göre değişimi yer almaktadır. Şekilden bulutlanmanın etkisi ile ışınımdaki dalgalanmanın kolektör verimini de etkilediği görülmektedir. Deneyler boyunca kolektör verimi en yüksek %67 değerine ulaşmış ve iki günlük deney süresince ortalama verim ise %44,6 olarak hesaplanmıştır.

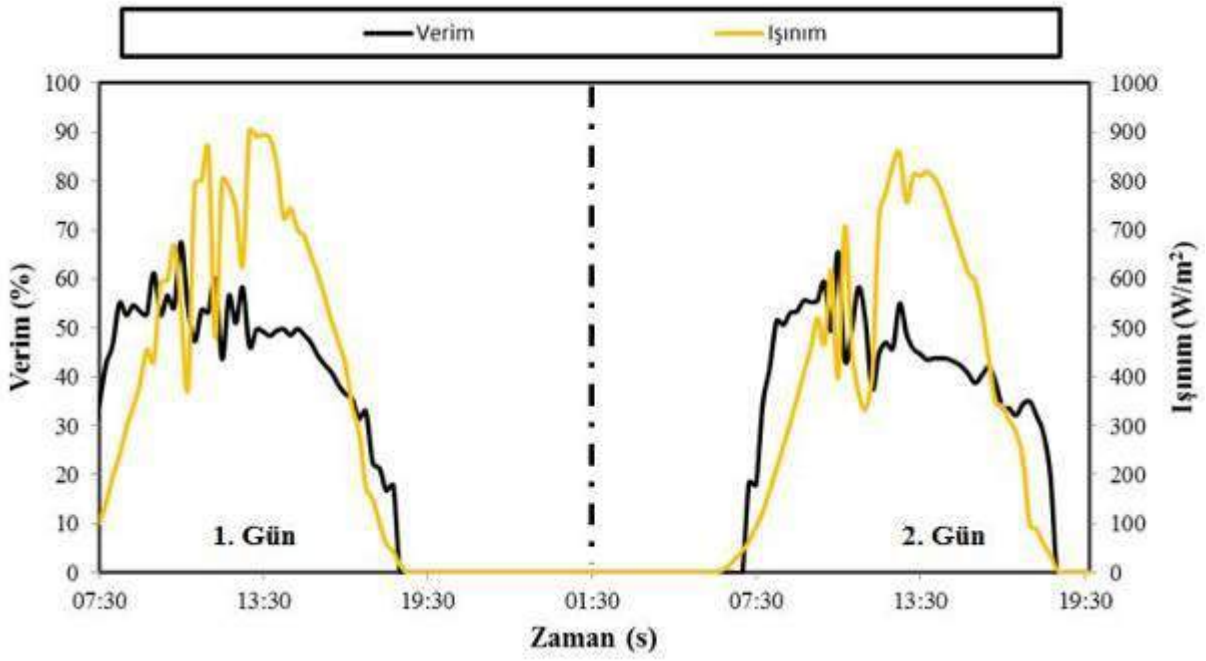

Şekil 5. K**olektör Veriminin ve Işınımın Zamana Göre Değişimi**

SONUÇ

Bu çalışmada, engelli tip kanatçık modeline sahip bir havalı güneş kolektörünün imalatı Osmaniye Korkut Ata Üniversitesi atölyelerinde yapılmış ve Osmaniye iklim şartlarına göre farklı noktalarda gerçekleştirilen sıcaklık, nem ve ışınım ölçümleriyle deneysel olarak incelenmiştir. Birbirini takip eden iki günlük deneylerden, kolektör çıkış sıcaklığının deneyler boyunca 25°C ile 60 °C arasında değiştiği ve kolektörün giriş ve çıkış noktaları arasında hava sıcaklığında 35 °C' lik artış gerçekleşebileceği görülmüştür. Elde edilen sonuçlardan ayrıca kolektör veriminin dış ortam şartlarına özellikle de ışınıma bağlı olarak değişim gösterdiği, en yüksek %67 değerine ulaştığı ve iki günlük deney süresince ortalama verimin yaklaşık %45 olduğu görülmüştür.

KAYNAKLAR

[1] Özalp , C., Saydam, D. B., Çerçi, K. N., Hürdoğan, E., & Moran, H. (2019). Evaluation of a sample building with different type building elements in an energetic and environmental perspective. Renewable and Sustainable Energy Reviews, 115, https://doi.org/10.1016/j.rser.2019.109386.

[2] Ural, T. (2019). Experimental performance assessment of a new flat-plate solar air collector having textile fabric as absorber using energy and exergy analyses. Energy, 188, https://doi.org/10.1016/j.energy.2019.

[3] Hu, J., Zhang, G. (2019). Performance improvement of solar air collector based on airflow reorganization: A review. Applied Thermal Engineering, 155, 592–611. https://doi.org/10.1016/j.applthermaleng.2019.04.021

[4] Hu, j., Liu, K., Guo, M., Zhang, G., Chu, Z., Wang M. (2019). Performance improvement of baffle-type solar air collector based on first chamber narrowing. Renewable Energy, 135, 701-710.

[5] Akpinar, E., K., Koçyiğit, F. (2010) Energy and exergy analysis of a new flat-plate solar air heater having different obstacles on absorber plates. . Applied Energy, 87, 3438–3450. doi:10.1016/j.apenergy.2010.05.017

[6] Daş, M. Akpınar, E., K.. (2018). Farklı Tip Güneş Kollektörlerinin Isıl Verim Değerlerinin Hesapsal Zekâ Yöntemleriyle Tahmin Edilmesi. Harran Üniversitesi Mühendislik Dergisi, 2, 43-48.

[7] Karsli, S. (2007). Performance analysis of new-design solar air collectors for drying applications. Renewable Energy, 32,1645–1660. doi:10.1016/j.renene.2006.08.005.

[8] Karsli, S. (2007). Performance analysis of new-design solar air collectors for drying applications. Renewable Energy, 32,1645–1660. doi:10.1016/j.renene.2006.08.005..

[9] Fudholi, A., Sopian, K. (2019). A review of solar air flat plate collector for drying application. Renewable and Sustainable Energy Reviews 102, 333–345. https://doi.org/10.1016/j.rser.2018.12.032

[10] Gürel, A. E., Yıldız, G., Ceylan, İ. (2019). Havalı güneş kolektörlerinin hacim ısıtma uygulamalarında kullanımı. 14. Ulusal Tesisat Mühendisliği Kongresi, İzmir, 1866-1875.

[11] Ho, C.D., Yeh, H.M., Cheng, T.W., Chen, T.C., Wang , R.C.(2009) The influences of recycle on performance of baffled double-pass flat-plate solar air heaters with internal fins attached. Applied Energy, 86, 1470–1478. doi:10.1016/j.apenergy.2008.12.013.

[12] K., Shukla. A., Sharma. A., Kumar. A., Jain, A. (2016). Thermal energy storage based solar drying systems: A review, Innovative Food Science and Emerging Technologies, 34, 86–99. https://doi.org/10.1016/j.ifset.2016.01.007

[13] Çerçi, K., Süfer, Ö., Söyler , M., Hürdoğan , E., & Özalp , C. (2018). Thın Layer Dryıng Of Zucchını In Solar Dryer Located In Osmanıye Regıon. Tehnıčkı Glasnık, 79-85. [17] Nimrotham , C., Songrakorp ,.

[14] Oztop. H.F., Bayrak. F., Hepbaslı. A. (2013). Energetic and exergetic aspects of solar air heating (solar collector) systems. Renewable and Sustainable Energy Reviews, 21, 59–83,. http://dx.doi.org/ 10.1016/j.rser.2012.12.019.

A COMPARISON OF HEURISTIC SEARCH ALGORITHMS IN AUTOMATIC DETECTION OF SCHIZOPHRENIA

Zülfikar ASLAN*

Fen Bilimleri Enstitüsü, Dicle Üniversitesi, Diyarbakır, Türkiye, zulfikaraslan27@gmail.com

Mehmet AKIN

Elektrik-Elektronik Mühendisliği, Mühendislik Fakültesi, Dicle Üniversitesi, Diyarbakır, makin@dicle.edu.tr

ABSTRACT: In this study, heuristic search algorithms, which are extensively used in the literature for search and feature selection purposes, are compared in terms of their performance in automatic detection of schizophrenia. Our study considers the most commonly used algorithms, namely, Genetic Algorithm, Particle Swarm Optimization (PSO), Evolutionary Search and Ant Colony Optimization Search, for the task of feature selection. The utilized data consists of 16-channel EEG recordings of a total of 84 individuals from 39 healthy and 45 schizophrenia patients. Feature extraction is done by using Relative Wavelet Energy (RWE) method. The number of extracted features being high in contrast to low number of samples diminishes the classification performance. Therefore, a feature selection strategy is adopted by using heuristic search algorithms in order to improve the classification performance. The new set of features are then used to feed the Support Vector Machine (SVM) machine learning algorithm to perform a classification and consequently compare performance of heuristic search algorithms. The best performance is observed to be 90,5% by the PSO heuristic search algorithm.

Key words: Heuristic Algorithm, EEG, Schizophrenia, Machine Learning

OTOMATİK ŞİZOFRENİ TESPİTİNDE SEZGİSEL ARAMA ALGORİTMALARININ KARŞILAŞTIRILMASI

ÖZET: Bu çalışmada literatürde arama ve özellik seçimi için yaygın olarak kullanılan sezgisel arama algoritmalarının, otomatik olarak şizofreni tespitindeki başarımları karşılaştırılmaktadır. Çalışmamızda, literatürde en yaygın olarak kullanılan Genetik Algoritma, Parçacık Sürü Optimizasyon (PSO), Evrimsel Arama ve Karınca Kolonisi Optimizasyonu Arama algoritmaları özellik seçimi için kullanılmıştır. 39 sağlıklı ve 45 şizofreni hastasına ait toplam 84 bireye ait 16 kanallı EEG sinyalleri kullanılmıştır. Öncelikle ham EEG sinyalinden, Göreceli Dalgacık Dönüşümü (RWE) kullanılarak özellik çıkarımı yapılmıştır. Elde edilen özellik veri setinin, özellik değerlerinin fazla

olması ve denek sayısının az olması sınıflandırma işleminin başarımını olumsuz etkilemektedir. Bu nedenle başarım oranını arttırmak adına farklı sezgisel arama algoritmaları kullanılarak özellik seçimi yapılmıştır. Elde edilen yeni özellik veri seti Destek Vektör Makinası (SVM) makine öğrenme algoritması ile sınıflandırılarak, kullanılan sezgisel arama algoritmaları için elde edilen başarımlar karşılaştırılmıştır. En iyi başarım oranı PSO sezgisel arama algoritmasıyla 90,5% olarak elde edilmiştir.

Anahtar sözcükler: Sezgisel Algoritma, EEG, Şizofreni, Makine Öğrenmesi

GİRİŞ

Şizofreni hastalığı, dünya genelinin yaklaşık % 0,4-0,6'sını etkileyen önemli bir psikiyatrik hastalıktır. Bu hastalığa sahip bireyler genellikle geç ergenlik veya erken yetişkinlik döneminde klinik olarak dikkat çekmektedir. Amerikan Psikiyatri Birliği (DSMIV) ' nin bu hastalığın tanı kriterleri şunlardır; (American Psychiatric Association 2000), şizofreni hastaları sağlıklı bireylere göre ilişkilerde, düşüncelerde, etkilerde ve algıda ciddi rahatsızlıklar göstermektedir. Şizofreni genellikle olumsuz ve olumlu belirtilerle göstermektedir. Olumlu belirtiler arasında sanrılar, işitsel halüsinasyonlar ve düşünce bozukluğu bulunmaktadır. Olumsuz belirtiler, normal özelliklerin veya yeteneklerin kaybı veya yokluğu, konuşma ve dikkat eksikliğidir. Şizofreni hastaları diğer insanlara göre daha düşük evlilik, iş ve bağımsız yaşam oranlarına sahiptir (Sabeti et al. 2011).

Şizofreni, bazılarında hastalarda, beyin fonksiyonlarında bir rahatsızlığı temsil ettiğinden, belirli beyin bölgelerinin veya sinir devrelerinin etkilediğini varsaymak mantıklıdır. Nöropsikolojik çalışmalar, şizofreni hastalarında kortikal gri maddenin prefrontal ve temporal kortekste azaldığına dair kanıtlar bulmuştur. Örneğin; serebral beyaz cevher elyaf yolu değişimleri, amigdale, hipokampus ve entorinal korteks ve talamus gibi limbik sistem yapılarının hacminin azalması ve bazal ganglion çekirdeklerinin hacminin artması gibi kanıtlar bulmuşlardır. Ayrıca, nöroanatomik çalışmalar, prefrontal ve limbik sistem fonksiyonlarının bozulmasının şizofreni hastalarında gözlenen pozitif ve negatif semptomlara ve bilişsel bozulmalara sebep olduğunu iddia etmektedir. Klinik, nöroanatomik, nöropsikolojik ve nörogörüntüleme gibi yaklaşımlar hastalığın daha iyi anlaşılmasına katkıda bulunmuş olsa da, altta yatan mekanizmalar hakkında daha kesin bir bilgi hala gereklidir (Sadock and Sadock 200AD).

Son zamanlarda, şizofrenik hastalara ait EEG sinyallerinin incelenmesine önem verilmiştir. Bazı araştırmalarda, şizofrenik hastaların ve sağlıklı bireylerin EEG sinyallerine doğrusal olmayan yöntemler uygulanmıştır (Jeong et al. 1998; Koukkou et al. 1993; Röschke, Fell, and Beckmann 1995). Sonuçlar, iki grup arasındaki değişken süreçte farklılıklar göstermiştir. Hornero ve arkadaşları (Hornero et al. 2006) katılımcılardan zaman serileri oluşturmak için rastgele boşluk tuşuna basmalarını istemiştir. Şizofreni hastaları tarafından oluşturulan zaman serilerinin sağlıklı gruptan elde edilen değerlerden daha düşük bir karmaşıklığa sahip olduğunu göstermiştir. Başka bir testte ise, rastgele sayı üretimi için (Rosenberg et al. 1990) katılımcılardan bir

ile on kez bir sayı seçmeleri istenmiştir. Sayıların üretici bir kuraldan yoksun olması, yani mümkün olduğunca rastgele olması gerekiyordu. Şizofreni hastalarının sağlıklı bireylere göre daha fazla tekrarlanma eğiliminde olduğunu göstermişlerdir. (Pressman, Peledu, and Geva 2000) şizofreni hastalarında çalışma hafızası görevi sırasında senkronizasyon değişim yeteneğinin olmadığını göstermişlerdir. Beyin aktivitesinde, özellikle önden ve geçici kanallar (Cherif et al. 2004), şizofreni hastalarının sağlıklı katılımcılarla karşılaştırıldığında, göz fiksasyon işlerinde anormallik gösterdiğini bildirmişlerdir. (Gaser et al. 1999) şizofreni hastalarında yapısal beyin değişikliklerini tasvir etmişlerdir. Ayrıca, (Keil et al. 1998) Şizofreni hastalarında, ritmik parmak salınımları olduğunu göstermiştir

Bu çalışmada 39 sağlıklı ve 45 şizofreni hastaya ait toplam 84 bireye ait 16 kanallı EEG verisi kullanılmıştır. EEG sinyalinden şizofreni hastalığının tespiti için öncelikle ham EEG sinyalinden Göreceli Dalgacık Dönüşümü yöntemi ile özellik çıkarımı yapılmıştır. Ancak elde edilen özellik veri setinin boyutu oldukça fazla olduğundan sonrasında özellik seçim işlemi gerçekleştirilmiştir. Özellik seçimi için literatürde yaygın olarak kullanılan sezgisel arama algoritmalarından Genetik Algoritma, PSO, Evrimsel Arama ve Karınca Kolonisi Optimizasyonu kullanılmıştır. Veri setindeki birey sayısı az olduğundan bu durum başarım oranını olumsuz etkilemektedir. Bu nedenle makine öğrenme algoritması başarımlarını arttırmak için "Resampling" metodu uygulanmış ve makine öğrenme algoritması başarımını olumlu olarak etkilediği görülmüştür. Veri setindeki örnek (sample) sayısı, dengeli bir şekilde dağılmadığında makine öğrenmesi metotlarının eğitimini zorlaştırmaktadır. Bunun için, veri setini daha dengeli yapmak amacıyla çoğaltma (oversampling) ve azaltma (undersampling) işlemleri uygulanmış, veri seti hastalıklı ve normal bireylerin dağılımını dengeleyecek şekilde resampling işlemine tabi tutulmuştur. Her bir sezgisel arama algoritması sonucu elde edilen yeni özellik veri setleri SVM makine öğrenme algoritması kullanılarak sınıflandırılmıştır. Farklı sezgisel arama algoritmalarıyla elde edilen başarım oranları karşılaştırılmıştır.

Veri Seti

Bu çalışmada kullanılan EEG kayıtları, benzer şizofrenik bozukluğa sahip 45 çocuğa ait şizofreni hastalığını ve 39 sağlıklı bireye ait bilgileri içermektedir. Ruh Sağlığı Araştırma Merkezi (MHRC) uzmanları tarafından tüm hastaların şizofreni olduğuna dair tanıları tespit edilmiştir. MHRC muayenesi yapılan bu şizofreni hastaların tamamı kimyasal tedavi görmemiştir. Hastaların en büyüğü de 14 yaşında ve en küçüğü 10 yıl 8 aylıktır. Sağlıklı bireyler ise en büyüğü 13 yaş 9 aylık ve en küçüğü 11 yaş olan 39 sağlıklı öğrenciden oluşmaktadır. Her iki gruptaki çocukların ortalama yaşı 12 yıl 3 aydır (Borisov et al. 2005). Bireyler rahat, gözleri kapalı ve uyanık iken kafalarına bağlı 16 elektrot ile EEG kayıtları alınmıştır. Bir bireye ait tüm kanallardan alınan EEG kaydı 122280 uzunluğunda tek boyutlu bir dizi yapısındadır. Her kanaldan alınan veri 7680 uzunluğunda tek boyutlu bir dizi yapısındadır.

YÖNTEM

Bu çalışmada 45 şizofreni hastası ve 39 sağlıklı bireylerden oluşan toplam 84 bireye ait 16 kanallı EEG verisi kullanılmıştır. Her bireye ait EEG verisi 122280 uzunluğunda tek boyutlu bir dizidir. Öncelikle ham EEG verisi üzerinden göreceli dalgacık enerji yöntemi kullanılarak özellik çıkarımı işlemi yapılmıştır. Elde edilen yeni özellik veri setinin boyutunun oldukça fazla olduğu gözlemlenmiştir. Özellik sayısının oldukça fazla olmasından dolayı özellik seçimi için Genetik Algoritma, PSO, Evrimsel Arama ve Karınca Kolonisi Optimizasyonu sezgisel arama algoritmaları kullanılmıştır. Her sezgisel algoritma ile elde edilen özellik veri seti, SVM makine öğrenme algoritması kullanılarak sınıflandırılmıştır. Her sezgisel arama algoritması için elde edilen sınıflandırma başarımları karşılaştırılmıştır. Şekil1 'de yapılan çalışmaya ait işlem süreçleri gösterilmektedir.

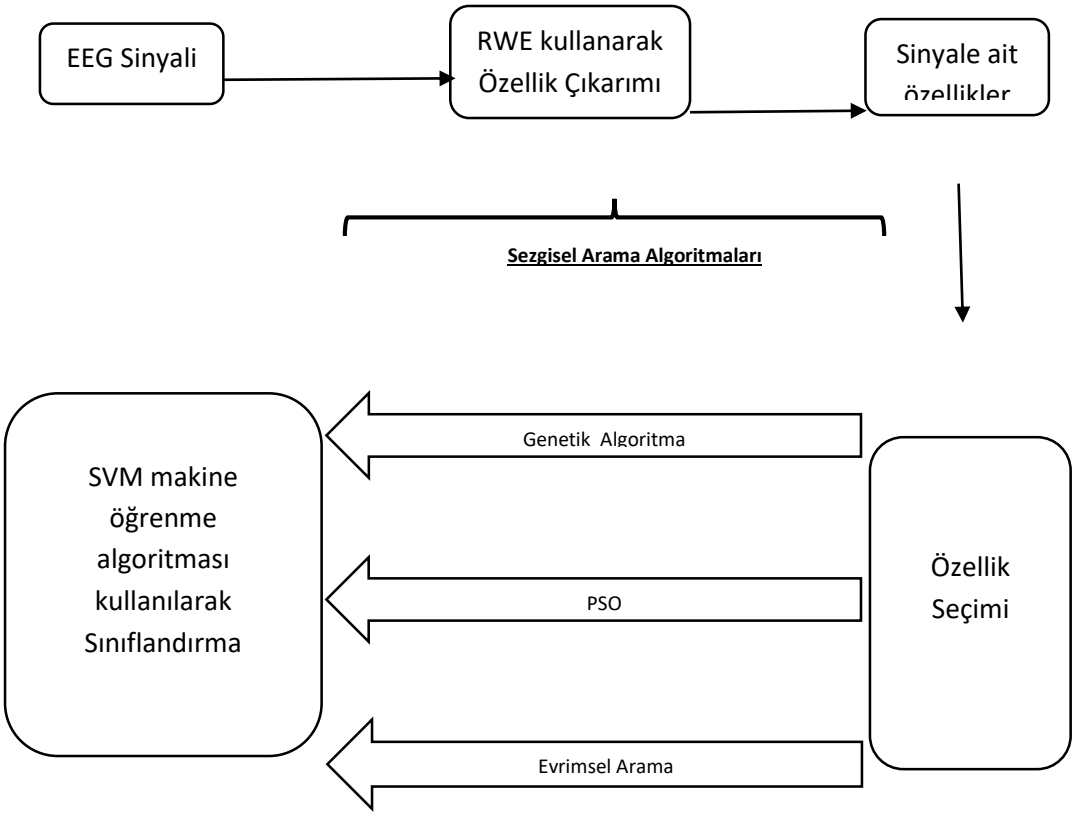

Şekil 1. Bu çalışmada uygulanan işlem süreçleri.

Destek Vektör Makinaları (SVM)

Destek Vektör Makinaları, İki grup sınıflandırma problemini çözmek için Vapnik ve Cortes tarafından bulunmuştur. SVM, EEG sinyal sınıflandırması, kanser tanımlaması, biyoinformatik, nöbet tahmini, yüz tanıma ve konuşma bozukluğu gibi birçok alanda uygulanmaktadır. Destek Vektörü Makine teknikleri (Byun and Lee 2002), Şekil2' de gösterildiği gibi Doğrusal olarak ayrılabilir, Doğrusal olarak ayrılmaz ve Doğrusal olmayan ayrılabilir olarak üç tipe ayrılmaktadır.

Şekil 2. SVM sınıflandırıcı türleri.

SVM, verileri iki grup arasında ayırmak için en büyük kenar boşluğuna sahip optimum hiper düzlemi oluşturmak için kullanılır. İki boyutlu veriler için, tek hiper düzlem, verileri +1 veya -1 gibi iki gruba ayırmak için yeterlidir. Veri noktalarını, üç boyutlu verilere için ayırmak için iki hiper düzlem gerekmektedir. SVM, örnek verileri hedef kategorilere göre ayırmak için hiper düzlem oluşturur. İki boyutlu veriler için, olası birçok lineer ayırıcı (hiper düzlem) vardır ve maksimum marjin genişliğine sahip olan optimum hiper düzlemi bulması gerekir. H1 ve H2 çizgileri, uygun değer hiper düzleme (düz çizgi) paralel olarak çizilir ve hiper düzlem ile veri noktaları arasındaki mesafeyi işaretler. Noktalı çizgiler (AC) arasındaki mesafeye kenar boşluğu denir. Hiper düzlemde H1 ve H2 bulunan örnek veri noktalarının bazıları Destek Vektörleri (SVM' ler) olarak adlandırılır, Şekil3' de gösterilmektedir. Kenar boşluğu genişliğini hesaplamak için bu SVM' ler önemlidir (Bhuvaneswari and Kumar 2013).

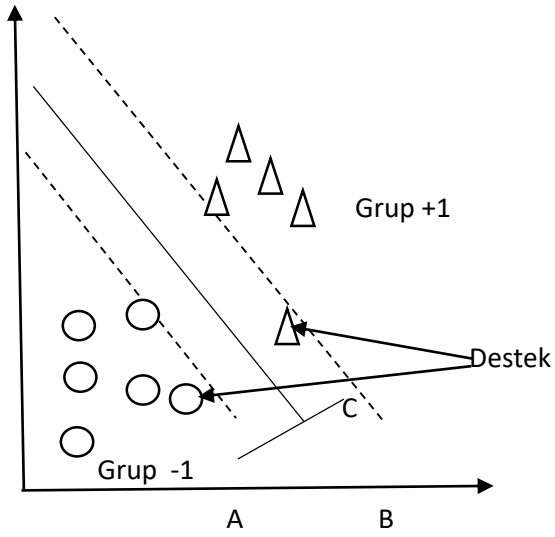

Şekil 3. Lineer olarak ayrılabilir SVM.

Genetik Arama Algoritması

Genetik algoritma (GA), Darwinist evrim ve genetiğe dayanan bir optimizasyon metodolojisidir (Eiben, Smith, and others 2003). Geleneksel gradyan tabanlı optimizasyon teknikleri, çok boyutlu bir optimizasyon yüzeyinde tek bir çözümü yinelemeli bir şekilde rafine ederek optimum bir nokta arar. Öte yandan, GA paralel olarak bir dizi aday çözüm koleksiyonu üzerinde çalışmaktadır. Bu yaklaşımla, GA, ilk optimum tahmin etrafında yerel bir optimumda sıkışıp kalma olasılığı daha yüksek olan, genel olarak uygun olan noktayı geleneksel tekniklerden daha fazla bulma olasılığına sahiptir. GA bir optimizasyon problemlerine olası bir çözümü temsil eden bireyler, bir başlangıç nüfusu ile başlar. Evrim süreci seçim, geçiş ve mutasyona aşamalarından oluşmaktadır. "En güçlü olanın hayatta kalması" ilkesine göre, GA bir dizi yinelemeli hesaplamadan sonra en uygun çözümü elde eder. Çaprazlama ve mutasyon operatörleri nüfusun çeşitliliğini korumaktadır. GA, geniş arama alanını etkin bir şekilde ele alabilir, keşif ve sömürünün birleşimi ile yerel optimal çözümlerden kaçınabilir (Huang and Wang 2006).

PSO Arama Algoritması

Parçacık sürüsü optimizasyon konsepti ilk olarak, 1995 yılında, kuşların sürü hareketi veya yiyecek bulmak için balık sürüsü gibi sosyal sistem davranışına dayanarak,

Kennedy ve Eberhart (Eberhart and Kennedy 1995a, 1995b) tarafından tanıtılmıştır. Sürüdeki her bireye parçacık denir. Sürünün i. parçacığı, konumu için X_i ve hızı için V_i vektörleri ile temsil edilir. Parçacık, P_i vektöründe en iyi kişisel performansını, kişisel en iyi (pbest) konumunu ve en iyi parçacığın kümesinde, global en iyi (gbest) konumunu P_g vektöründe kaydettiren bir belleğe sahiptir. Parçacık sürüsü optimizasyon algoritması, her yinelemede, her parçanın hızını en iyi performansı olan P_i'ye ve P_i en iyi pozisyonu olan Pg'ye doğru değişimini içerir. Böylece orijinal versiyonda parçacıklar, aşağıdaki formüle göre hareket eder:

$$V_i^{t+1} = V_i^t + c_1 \text{Rand}()(P_i - X_i^t) + c_2 \text{Rand}()\left(P_g - X_i^t\right), X_i^t = X_i^t + V_i^{t+1} \quad (1)$$

c_1 ve c_2 parametreleri bilişsel ve sosyal öğrenme oranlarıdır. Bu iki oran, sürünün en iyi performansının hafızasının bireyin hafızasına göreceli etkisini kontrol eder ve her bir öğrenme hızına eşit ağırlık vermek için genellikle aynı değerde seçilir. c_1 ve c_2 parametrelerine ek olarak, orijinal algoritmanın uygulanması, ayrıca arama alanına (X_{max} ve X_{min}) ve hıza (V_{max}) sınır koyulmasını gerektirmektedir (Shirvany et al. 2013).

Evrimsel Arama Algoritması

Önerilen evrimsel arama algoritması, doğal seleksiyon ve genetik mekaniğine dayanan biyolojik sistemlerin evrimsel davranışını taklit eden genetik algoritma kavramından kaynaklanmaktadır (Goldberg 1989). Temel çalışması, geçit ve mutasyon gibi genetik operatörleri kullanarak yavruları çoğaltmaktır, evrim süreci, popülasyondaki en uygun yavru üretilinceye kadar devam eder (Ng et al. 1994).

Karınca Kolonisi Optimizasyonu Arama Algoritması

Gerçek karınca kolonilerinde, dolaylı bir iletişim aracı olarak bir koku maddesi olan bir feromon kullanılır. Bir besin kaynağı bulunduğunda, karıncalar yolu işaretlemek için bir miktar feromon bırakır. Dökülen feromonun miktarı, yiyecek kaynağının uzaklığına, miktarına ve kalitesine bağlıdır. Rasgele hareket eden izole edilmiş bir karınca atılan bir feromonu tespit ederken, yolunu izlemeye karar vermesi çok muhtemeldir. Karıncanın kendisi belli miktarda feromon bırakacak ve bu nedenle bu belirli yoldaki feromon izini belirgin hale getirecektir. Buna göre, daha fazla karınca tarafından kullanılan yolun izlenmesi daha cazip olacaktır. Dorigo ve diğ. ark. (Dorigo and Di Caro 1999) bu konsepti benimsemiş ve zor kombinasyonlu optimizasyon problemlerini çözmek için gerçek karınca kolonileri davranışına dayanan yapay bir algoritma önermiştir (Khushaba et al. 2008).

BULGULAR

Toplam 84 bireye ait 16 kanallı EEG verisi, 39 sağlıklı ve 45 şizofreni hastasına aittir. Her bir bireye ait EEG verisi 122280 uzunluğunda tek boyutlu bir dizi yapısındadır ve her bir kanaldan alınan veri ise 7680 uzunluğunda tek boyutlu bir dizi yapısındadır. Bu çalışmada öncelikle veri boyutunun yüksek olmasından ve başarım oranını etkileyen önemli bir faktör olmasından dolayı ham veri üzerinden özellik çıkarımı işlemi gerçekleştirilmiştir. Özellik çıkarım işlemi için ham EEG sinyaline Göreceli Dalgacık Enerjisi metodu uygulanmıştır. Elde edilen veri setine özellik seçim işlemi uygulanarak sınıflandırma başarımını olumlu etkileyecek özelliklerin ön plana çıkarılması hedeflenmiştir. Bu amaçla, sezgisel arama algoritmalarının literatürde en çok kullanılanları tercih edilmiştir. Elde edilen özellik veri setleri SVM makine öğrenme algoritması kullanılarak sınıflandırılmıştır. Kullanılan sezgisel arama algoritmalarının sınıflandırma sonucu elde edilen başarımları karşılaştırılmıştır. Her bir sezgisel arama algoritması ile elde edilen özellik değerleri ve sınıflandırma başarımları Tablo1'de ve Şekil2'de gösterilmektedir. Tablo1' de görüldüğü üzere en iyi başarım PSO sezgisel arama algoritması ile 90,5% olarak elde edilmişti.

Sezgisel Arama Algoritması	Özellik Sayısı	Başarım Oranı
Genetik Arama	350	88,1%
PSO	336	90,5%
Evrimsel Arama	689	89,3%
Karınca Kolonisi Optimizasyonu	510	85,7%

Tablo 1. Farklı sezgisel arama algoritmalarıyla özellik seçimi sonucu elde edilen özellik sayıları ve başarım oranları.

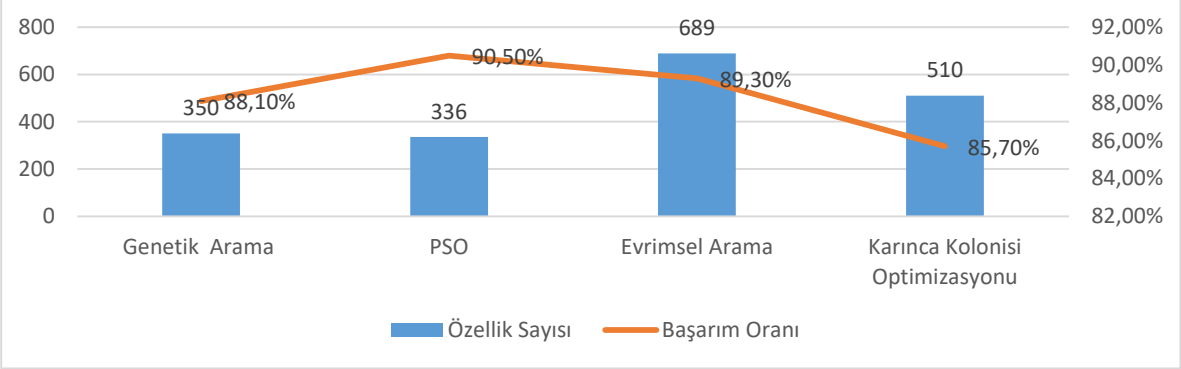

Şekil 4. Farklı sezgisel arama algoritmalarıyla özellik seçimi sonucu elde edilen özellik sayıları ve başarım oranları.

SONUÇ

Bu çalışmada şizofreni hastası ve sağlıklı bireylere ait 16 kanallı EEG kayıtları kullanılmıştır. Öncelikle ham EEG verisi üzerinde özellik çıkarımı yapmak için Göreceli Dalgacık Enerjisi yöntemi kullanılmıştır. Elde edilen özellik veri setinin boyutunun fazla olması makine öğrenme algoritmasının sınıflandırma performansını olumsuz etkilemektedir. Bu nedenle en son elde edilen özellik veri setine özellik seçim işlemi uygulanmıştır. Özellik seçimi için literatürde çok fazla kullanılan sezgisel arama algoritmalarından; Genetik Algoritma, Parçacık Sürü Optimizasyonu, Evrimsel Arama ve Karınca Kolonisi Optimizasyonu kullanılmıştır. Her bir sezgisel arama algoritmasıyla elde edilen özellik veri setleri, SVM makine öğrenme algoritması ile sınıflandırılarak başarımları karşılaştırılmıştır. Kullanılan sezgisel arama algoritmalarından en iyi başarım PSO ile 90,5% olarak elde edilmiştir. Bu yaptığımız çalışmada sezgisel arama algoritmalarının EEG sinyalinden, tanı amaçlı olarak kullanılabilecek önemli özellik değerleri elde edebildiği gözlemlenmiştir. Farklı sezgisel arama algoritmalarıyla elde edilen sınıflandırma başarımları analiz edildiğinde, PSO en az sayıda özellik ile en iyi başarım sonucunu vermiştir. Bu çalışmada sezgisel arama algoritmalarıyla özellik seçimi yapıldıktan sonra elde edilen özellik veri setinin hastalığa ait anlamlı bilgiler taşıdığı görülmektedir. İleriki çalışmalarda, şizofreni hastalığının tespiti veya buna benzer alanlarda klinik çalışanlara yardımcı olabilecek sistemlerin bu çalışmadaki metot ve yöntemler dikkate alınarak geliştirilebilir.

KAYNAKLAR

American Psychiatric Association. 2000. American Journal of Critical Care *Diagnostic and Statistical Manual of Mental Disorders, 4th Ed. DSM-IV-TR*.

Bhuvaneswari, P, and J Satheesh Kumar. 2013. "Support Vector Machine Technique for EEG Signals." *International Journal of Computer Applications* 63(13).

Borisov, S. V., A. Ya Kaplan, N. L. Gorbachevskaya, and I. A. Kozlova. 2005. "Analysis of EEG Structural Synchrony in Adolescents with Schizophrenic Disorders." *Human Physiology*.

Byun, Hyeran, and Seong-Whan Lee. 2002. "Applications of Support Vector Machines for Pattern Recognition: A Survey." In *International Workshop on Support Vector Machines*, , 213–36.

Cherif, R., A. Nait-Ali, J.F. Motsch, and M.O. Krebs. 2004. "A Parametric Analysis of Eye Tremor Movement during Ocular Fixation, Applied to Schizophrenia."

Dorigo, Marco, and Gianni Di Caro. 1999. "Ant Colony Optimization: A New Meta-Heuristic." In *Proceedings of the 1999 Congress on Evolutionary Computation-CEC99 (Cat. No. 99TH8406)*, , 1470–77.

Eberhart, Russell, and James Kennedy. 1995a. "New Optimizer Using Particle Swarm

Theory." In *Proceedings of the International Symposium on Micro Machine and Human Science*,.

———. 1995b. "Particle Swarm Optimization." In *Proceedings of the IEEE International Conference on Neural Networks*, , 1942–48.

Eiben, Agoston E, James E Smith, and others. 2003. 53 *Introduction to Evolutionary Computing*. Springer.

Gaser, Christian et al. 1999. "Detecting Structural Changes in Whole Brain Based on Nonlinear Deformations Application to Schizophrenia Research." *NeuroImage*.

Goldberg, David E. 1989. "Genetic Algorithms in Search, Optimization, and Machine Learning, Addison Wesley, Reading, MA." *SUMMARY THE APPLICATIONS OF GA-GENETIC ALGORITHM FOR DEALING WITH SOME OPTIMAL CALCULATIONS IN ECONOMICS*.

Hornero, Roberto et al. 2006. "Variability, Regularity, and Complexity of Time Series Generated by Schizophrenic Patients and Control Subjects." *IEEE Transactions on Biomedical Engineering*.

Huang, Cheng-Lung, and Chieh-Jen Wang. 2006. "A GA-Based Feature Selection and Parameters Optimizationfor Support Vector Machines." *Expert Systems with applications* 31(2): 231–40.

Jeong, Jaeseung et al. 1998. "Nonlinear Analysis of the EEG of Schizophrenics with Optimal Embedding Dimension." *Medical Engineering and Physics*.

Keil, Andreas, Thomas Elbert, Brigitte Rockstroh, and William J. Ray. 1998. "Dynamical Aspects of Motor and Perceptual Processes in Schizophrenic Patients and Healthy Controls." *Schizophrenia Research*.

Khushaba, Rami N, Ahmed Al-Ani, Akram AlSukker, and Adel Al-Jumaily. 2008. "A Combined Ant Colony and Differential Evolution Feature Selection Algorithm." In *International Conference on Ant Colony Optimization and Swarm Intelligence*, , 1–12.

Koukkou, M. et al. 1993. "Dimensional Complexity of EEG Brain Mechanisms in Untreated Schizophrenia." *Biological Psychiatry*.

Ng, Sin Chun, Chi Yin Chung, S I Leung, and Andrew Luk. 1994. "An Evolutionary Search Algorithm for Adaptive IIR Equalizer." In *Proceedings of IEEE International Symposium on Circuits and Systems-ISCAS'94*, , 53–56.

Pressman, A., A. Peledu, and A. B. Geva. 2000. "Synchronization Analysis of Multi-Channel EEG of Schizophrenic during Working-Memory Tasks." In *21st IEEE Convention of the Electrical and Electronic Engineers in Israel, Proceedings*,.

Röschke, Joachim, Jürgen Fell, and Peter Beckmann. 1995. "Nonlinear Analysis of Sleep EEG Data in Schizophrenia: Calculation of the Principal Lyapunov Exponent." *Psychiatry Research*.

Rosenberg, Stewart et al. 1990. "Random Number Generation by Normal, Alcoholic and Schizophrenic Subjects." *Psychological Medicine*.

Sabeti, M., S. D. Katebi, R. Boostani, and G. W. Price. 2011. "A New Approach for EEG

Signal Classification of Schizophrenic and Control Participants." *Expert Systems with Applications*.

Sadock, Benjamin J., and Virginia A. Sadock. 200AD. Lippincott Williams & Wilkins Publishers *Comprehensive Textbook & Psichiatry*.

Shirvany, Yazdan et al. 2013. "Application of Particle Swarm Optimization in Epileptic Spike EEG Source Localization." *Applied Soft Computing* 13(5): 2515–25.

EFFECT OF STEEL FIBER ON LOAD CARRYING CAPACITY OF REINFORCED CONCRETE CORBELS

Mehmet Eren GÜLŞAN
Department of Civil Engineering, Gaziantep University
gulsan@gantep.edu.tr

Necip Altay EREN
Department of Civil Engineering, Gaziantep University
altayeren@gantep.edu.tr

Abdulkadir ÇEVİK
Department of Civil Engineering, Gaziantep University
akcevik@gantep.edu.tr

ABSTRACT: Corbels are significant structural elements in construction sector and it is critical connection region between beams and columns or walls, especially in industrial buildings. Therefore its mechanical behavior directly influences the safety of the related structure. Use of steel fiber as secondary reinforcement in reinforced concrete corbels is a good option to achieve ductility without any loss in load carrying capacity. This study investigates mechanical behavior of steel fiber reinforced concrete (SFRC) corbels. A detailed research was carried out on SFRC corbels. Experimental works of SFRC corbels were carried out for the study. As a result of experimental work, mechanical outputs of SFRC corbels were interpreted and rules were proposed for the prediction of failure mode and crack pattern of SFRC corbels. Experimental results show how steel fiber affects the load carrying capacity of corbels.

Keywords: Steel Fiber Reinforced Concrete, Corbels, Load Carrying Capacity

INTRODUCTION

Corbels are significant structural elements used in precast construction and especially in industrial building sector. It transfers the load coming from the beam to the column or wall to which it is connected. Since it provides the beam-column connection, its strength, ductility and functionality are more critical as compared to other structural elements. For the experimental part of the study, 24 corbels were prepared. Various parameters were changed to observe the mechanical behavior of related corbels. Those parameters were compressive strength, reinforcement rebar ratio, steel fiber ratio and

shear span to effective depth ratio. Two values were considered for cubic compressive strength of corbels which were nearly 30 MPa and 50 MPa. Two types reinforcement rebars were used in the corbels. These were (2-φ 10) and (2-φ 12). Moreover, two diffrent shear span were selected for tests. These were 100 mm and 130 mm. Steel fiber reinforced concrete (SFRC) is concrete made of hydraulic cement containing fine or fine and coarse aggregate and discontinuous discrete steel fibers and SFRC corbels containing diffrent percentages of steel fibers (0%, 1% and 1.5%) as volumetric. In tension, SFRC fails only after the steel fiber breaks or is pulled out of the cement matrix shows a typical fractured surface of SFRC. Steel fibers intended for reinforcing concrete are defined as short, discrete lengths of steel having an aspect ratio (ratio of length to diameter) from about 20 to 100, with any of several cross-sections, and that are sufficiently small to be randomly dispersed in an unhardened concrete mixture using usual mixing procedures (ACI 544.1R-96 Report, 2002).

The addition of steel fibers provides a number of significant behavioral enhancements to concrete. In compression, steel fibers do not significantly affect the ascending curve of the compressive stress-strain response, but they cause the descending post-peak response curve to decline in a shallower fashion than the curve of plain concrete, resulting in an increased ductility and toughness (Fanella and Naaman, 1985). The peak compressive strength is not significantly affected; experiments have observed a maximum strength gain of only 15% (Fanella and Naaman, 1985; ACI 544.1R-96 Report, 2002; Thomas and Ramaswamy, 2007). However, the peak strain increases perceptibly with the addition of steel fibers. The addition of steel fibers has a much more noticeable effect on the tensile behavior of the composite. In typical fiber volume contents the material exhibits strainsoftening behavior; however, the degradation in load-carrying capacity is slower than that of plain concrete. This results in the composite having greater ductility and energy absorption capabilities than plain concrete. In addition, because the fibers bridge the cracks in the composite and aid in the transfer of forces across the cracks, crack widths are less than those of plain concrete. If reinforcing bars are present, multiple cracks can form, even for a strain-softening material. There will be more cracks at a shorter spacing and smaller widths than the equivalent structure constructed from plain concrete (Deluce, 2011).

1.MIX DESIGN FOR SFRC CORBELS:

In the concrete mix design, coarse aggregate (crushed gravel and maximum size is 10mm), fine aggregate (fine sand and size interval is 0-4 mm), cement and water whose weight ratios are 2.78: 1.5: 1: 0.48, respectively were used for the concrete class of 50 MPa. 42.5R Portland cement was used for the production. Hooked end type steel fibers (ZP 305 type of Bekaert-Dramix steel fibers) were used for the preparation of SFRC corbels. Length and diameter of the steel fiber is 30 mm and 0.55 mm, respectively (aspect ratio is 54.5). Since steel fiber reduces the workability of the concrete, superplasticizer was added to mix with an amount of 0.45% of the cement weight. Amounts of ingredients are given for 1 m^3 concrete in Table 1.

Table 1 Ingredient Amounts for the Production of 1 m³ Concrete (*fc u* is 50 MPa)

Coarse Agg. (kg)	Fine Agg. (kg)	Cement (kg)	Water (kg)	w/c ratio	Steel fiber (kg)
1110	600	400	190	0.48	78,4 (1%) 117,6 (1.5%)

For the production of the other concrete class (*fcu* is 30 MPa), same ingredients and same weight ratios were used except water/cement ratio (w/c) and cement type. 0.55 was selected as w/c ratio and 32.5R Portland cement was used. Related amounts of ingredients are shown in Table 2.

Table 2 Ingredient Amounts for the Production of 1 m³ Concrete (*fc u* is 30 MPa)

Coarse Agg. (kg)	Fine Agg. (kg)	Cement (kg)	Water (kg)	w/c ratio	Steel fiber (kg)
1110	600	400	220	0.55	78,4 (1%) 117,6 (1.5%)

2.TESTING PROCEDURE:

Corbels were tested with a 500 kN capacity loading frame. Corresponding samples were also tested to measure the compressive strength and tensile strength. Compressive strength and tensile strengths were tested in a 2000 kN capacity concrete press machine. Geometry of experimented corbels, cubic compressive strength results, shear span and steel fiber ratio are shown in table 3.

Table 3 Designation and Properties of Experimented Corbels

Designation	**Cubic Compressive Strength (*fcu*) (MPa)**	**Steel Fiber Ratio (*vf*) (%)**	**Diameter of Main Reinforcement (φ) (mm)**	**Shear Span (*a*) (mm)**
30-0-10-100	30	0	10	100

30-1-10-100	30	1	10	100
30-1.5-10-100	30	1.5	10	100
30-0-12-100	30	0	12	100
30-1-12-100	30	1	12	100
30-1.5-12-100	30	1.5	12	100
30-0-10-130	30	0	10	130
30-1-10-130	30	1	10	130
30-1.5-10-130	30	1.5	10	130
30-0-12-130	30	0	12	130
30-1-12-130	30	1	12	130
(Table 3 Continue)				
30-1.5-12-130	30	1.5	12	130
50-0-10-100	50	0	10	100
50-1-10-100	50	1	10	100
50-1.5-10-100	50	1.5	10	100
50-0-12-100	50	0	12	100
50-1-12-100	50	1	12	100
50-1.5-12-100	50	1.5	12	100
50-0-10-130	50	0	10	130
50-1-10-130	50	1	10	130
50-1.5-10-130	50	1.5	10	130
50-0-12-130	50	0	12	130
50-1-12-130	50	1	12	130
50-1.5-12-130	50	1.5	12	130

The thickness of corbels is 150 mm. That is, cross sections of both column and corbels are 150mm x 150 mm square section. Load was transferred from the loading frame to the corbel by the 15 mm thickness loading plate. Loading plate was produced from a transmission steel to transfer the load effectively. While one of the roller supports allows to rotation in the transverse direction, the other is not. Corbel loading tests were carried out as displacement controlled mode. Therefore, post-peak behavior of corbels could be observed and load-displacement curve could be obtained. Corbels were loaded monotonically. The loading rate of corbels is 0.3 mm/minute. A typical implemented corbel test is shown in Fig. 1 and Fig. 2.

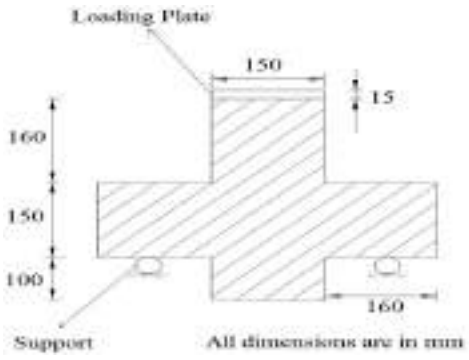

Figure 1 Dimensions of Experimented Corbels

Figure 2 Test Configuration and Set-up for Corbels

3.RESULTS OF CORBELS TESTS:

3.1 LOAD CARRING CAPACITIES:

Results of load carrying capacities of experimented corbels are listed in Table 4. Measurements of tensile strengths (*fct*), cylindrical compressive strengths (*fc*), effective depth (*d*), reinforcement ratio (*As/bh*) and ultimate load carring capacity of corbels are also listed in the same table 4.

Table 4 Measured Outputs of Experimented Corbels

Designation	Cubic Compressive Strength (*fcu*) (MPa)	Splitting Tensile Strength (*ft*) (MPa)	Effective Depth (*d*) (mm)	Reinforcement Ratio (ρ %)	Ultimate Load Per Corbel (kN)
30-0-10-100	24	1.9	124	0.851	57.22
30-1-10-100	22.3	2.5	124	0.851	71
(Table 4 Continue)					
30-1.5-10-100	25.5	3.1	122	0.851	79.67
30-0-12-100	25	2.0	124	1.216	63.53
30-1-12-100	22.3	2.3	124	1.216	73.4
30-1.5-12-100	25.5	3.1	127	1.216	87.01

30-0-10-130	24	1.9	123	0.851	37.57
30-1-10-130	22.3	2.5	124	0.851	52.6
30-1.5-10-130	25.5	3.1	123	0.851	58.35
30-0-12-130	25	2.0	125	1.216	48.65
30-1-12-130	22.3	2.3	127	1.216	56.15
30-1.5-12-130	25.5	3.1	124	1.216	59.79
50-0-10-100	39	2.8	122	0.851	65.91
50-1-10-100	40	3.7	120	0.851	110.58
50-1.5-10-100	42.5	4.5	123	0.851	125.13
50-0-12-100	38.5	2.8	124	1.216	68.06
50-1-12-100	38	3.6	122	1.216	121.78
50-1.5-12-100	42.5	4.2	124	1.216	127.54
50-0-10-130	39	2.8	123	0.851	55.52
50-1-10-130	40	3.7	124	0.851	78.8
50-1.5-10-130	42.5	4.5	125	0.851	86.59
50-0-12-130	38.5	2.8	128	1.216	57.65
50-1-12-130	38	3.6	122	1.216	89.18
50-1.5-12-130	42.5	4.2	125	1.216	89.13

3.2 INTERPRETATION OF EXPERIMENTAL RESULTS:

As a result of experiments, the following conclusions can be drawn:

3.2.1 EFFECT OF STEEL FIBER ON LOAD CARRING CAPACITY OF CORBELS:

Load carrying capacities of SFRC corbels increase with the increment in the compressive strength of the concrete (Figs. 3-10). This increment is also indirectly related with increment of tensile strength with the compressive strength. However, it is also important to note that the rate of increment is increased when the steel fiber percentage increases since the rate of increment of tensile strength becomes higher as the fiber percentage increases for the same compressive strength. As a result, compressive strength of concrete is effective on the load carrying capacity of corbels. However, its effect is also connected with tensile strength of the concrete.

Effect of steel fiber percentage (*vf* %) is directly related with splitting tensile strength of concrete. Whenever the steel fiber percentage increases the tensile strength of the concrete, the increment in the load carrying capacity of corbels can be observed clearly (Figs. 3-10). The increment in the capacity is pronounced more as compared to the sample without steel fiber to the same sample with steel fiber. However, a general conclusion can be made that the load carrying capacity of a corbel is increased with steel fiber percentage increment. The increase in the load carrying capacity of SFRC corbels becomes smaller as the steel fiber percentage increases (Figs. 3-10). This situation can be explained with the sudden increment in the tensile strength when the steel fiber is added to plain concrete.

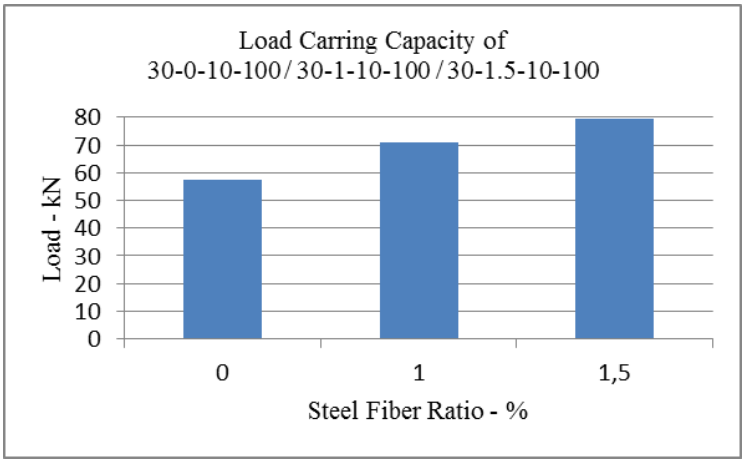

Figure 3 Load Carrying Capacities of Experimented Corbels
(Compressive Strength=30MPa, Rebar =2-φ10, Shear Span=100mm)

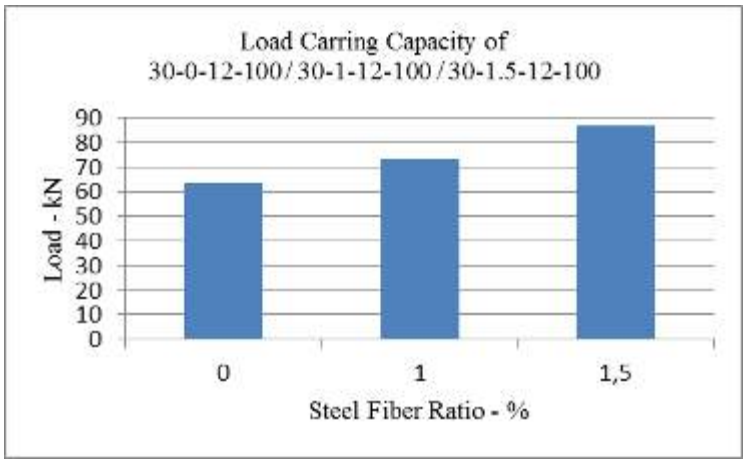

Figure 4 Load Carrying Capacities of Experimented Corbels

(Compressive Strength=30MPa, Rebar=2-φ12, Shear Span=100mm)

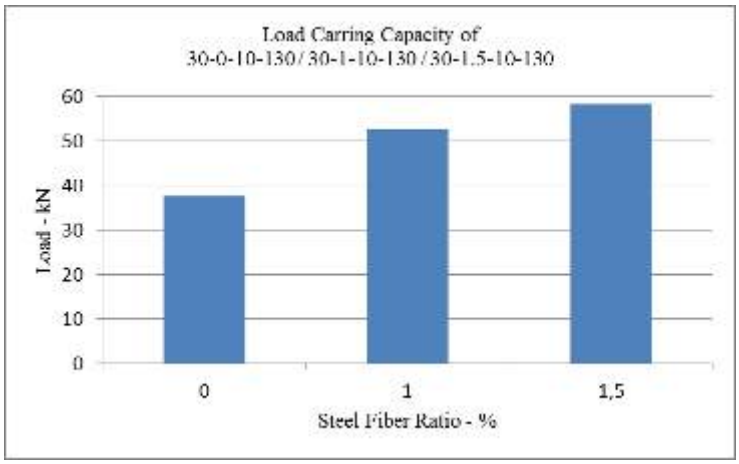

Figure 5 Load Carrying Capacities of Experimented Corbels

(Compressive Strength=30MPa, Rebar=2-φ10, Shear Span=130mm)

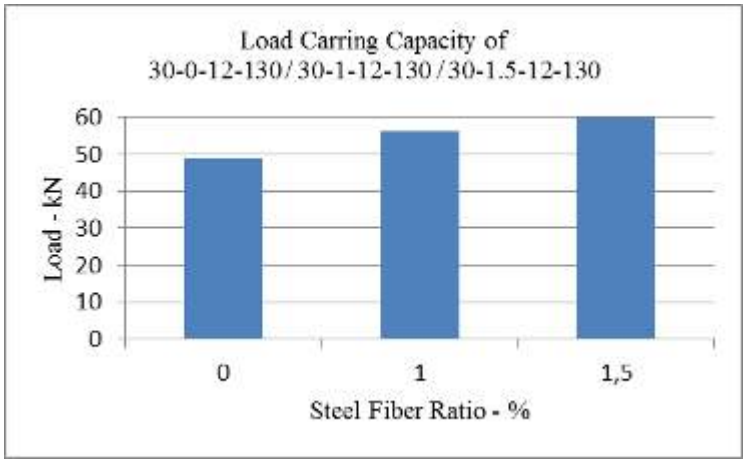

Figure 6 Load Carrying Capacities of Experimented Corbels

(Compressive Strength=30MPa, Rebar =2-φ12, Shear Span=130mm)

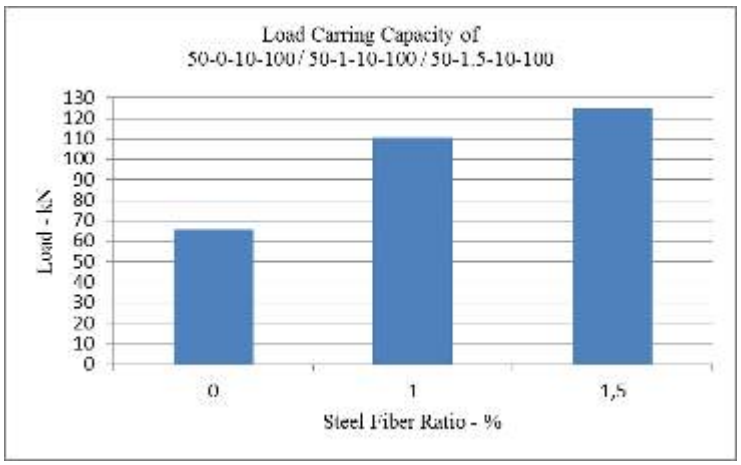

Figure 7 Load Carrying Capacities of Experimented Corbels

(Compressive Strength=50MPa, Rebar=2-φ10, Shear Span=100mm)

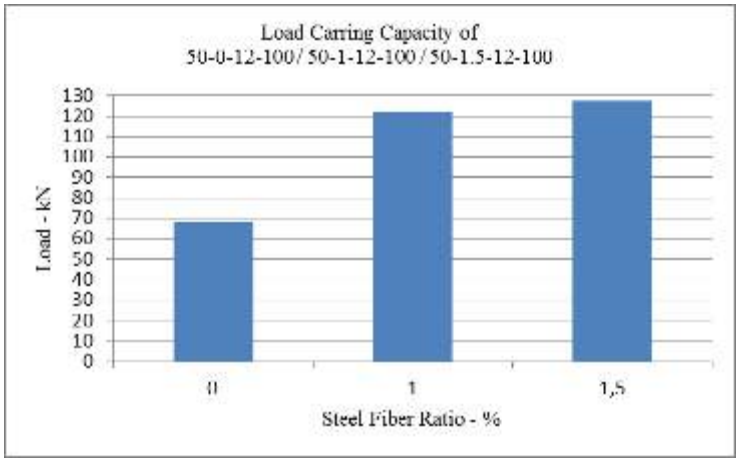

Figure 8 Load Carrying Capacities of Experimented Corbels

(Compressive Strength=50MPa, Rebar =2-φ12, Shear Span=100mm)

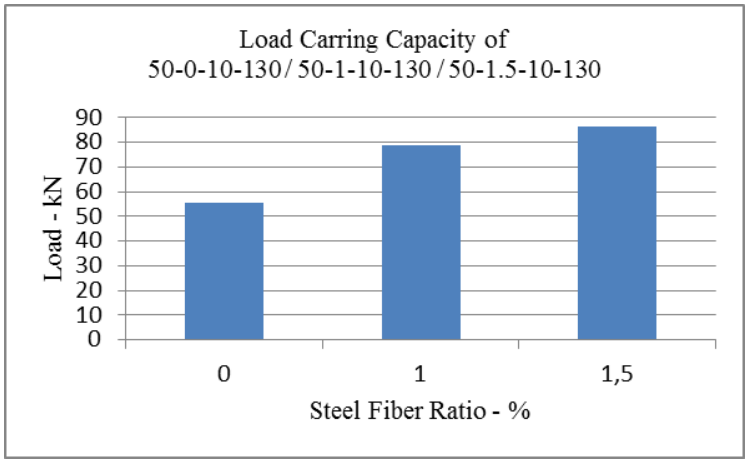

Figure 9 Load Carrying Capacities of Experimented Corbels

(Compressive Strength=50MPa, Rebar=2-φ10, Shear Span=130mm)

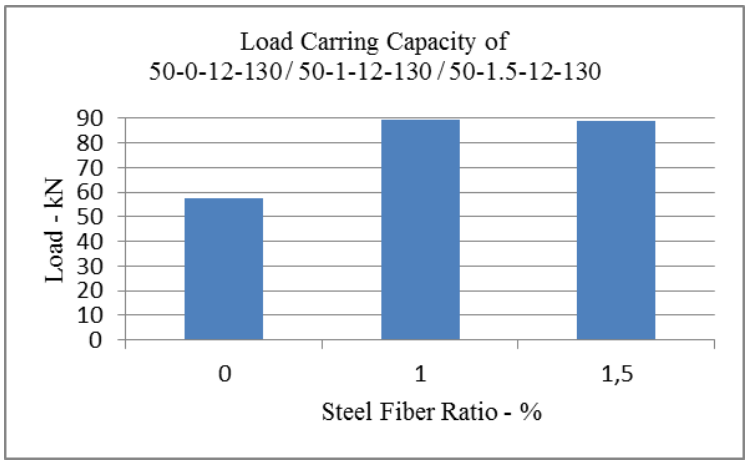

Figure 10 Load Carrying Capacities of Experimented Corbels

(Compressive Strength=50MPa, Rebar=2-φ12, Shear Span=130mm)

CONCLUSION

Although corbels are important structural elements and widely used frequently in construction industry little research has been carried so far as compared to other structural members. This study contributes effects of compressive strength on SFRC corbels' load carring capacity. Results of experimental works carried out on the corbels in this study are summarized in the following paragraphs.

Use of steel fibers in reinforced concrete corbels leads to considerable advantages. The most apparent benefits are to satisfy ductile behavior and to increase the load carrying capacity. These outputs prove that steel fibers can be used as secondary reinforcement instead of horizontal stirrups. However, use of steel fibers does not guarantee ductile behavior since this behavior is also dependent on shear span, reinforcement ratio and compressive strength of concrete. Therefore, if a designer designs a SFRC corbel, he or she has to be careful about selection of class of concrete, diameter of main reinforcement and shear span values as well as steel fiber percentage amount.

Another advantage of use of steel fiber in the corbel is about the crack widths. Crack widths of SFRC corbels are much smaller as compared to corbels without steel fiber. Reduction in crack widths leads to longer service life of corbels. Moreover, it facilitates effective and successful repairing operation in the case of a possible rehabilitation process.

In this study, experimental works were carried out for SFRC corbels. Detailed research was implemented on SFRC corbels to clarify all uncertainties on the mechanical behavior and ultimate load carrying capacities. Load capacity of corbels depend on shear span reinforced rebar ratio and steel fiber ratio. Therefore, if a designer designs a SFRC corbel, he or she has to be careful about selection of class of concrete, diameter of main reinforcement and steel fiber ratio. Experimental results carried out on SFRC corbels show that compressive strength is effective parameter on the load carrying capacities of SFRC corbels. Load carrying capacity and failure mode of SFRC corbel can be regulated by altering of this parameter. The following inference was recommended to designers and engineers about mechanical behavior corbels:

- Whenever steel fiber amount increases, the load carrying capacity of SFRC corbels increases. However, the rate of increase decreases as the fiber amount becomes higher and higher.

REFERENCES

Abdel-Hafez, A. M., Ahmed, M. M., Diab, H., Drar, A. A. M. (2012). Shear Behaviour of high strength fiber reinforced concrete corbels. Journal of Engineering Sciences. 40(4), 969-987.

Abdul-Wahab, H. M. (1989). Strength of reinforced concrete corbels with fibers. ACI Structural Journal. 86(1). 60- 66.

ACI. American Concrete Institute. (1999). Static flexural analysis of beams containing bars and fibers, Design considerations for steel fiber reinforced concrete. ACI Committee 544, Detroit.

ACI. American Concrete Institute. (2002). State-of-the-Art Report on Fiber Reinforced Concrete. ACI 544.1R-96..

ACI. American Concrete Institute. (1999). Building code requirements for structural concrete (ACI 318-99) and commentary (318R-99), Farmington Hills, Michigan.

ASCE. American Society of Civil Engineers. (1998). Minimum design load for buildings and other structures. ASCE 7-98. Washington, D. C., 352 pp.

Alameer, M. (2004). Effects of fibres and headed bars on the response of concrete corbels. M.Sc. Thesis. McGill University, Montreal, Canada.

Asensio E. C. (2012). On Shear Behavior of Structural Elements Made of Steel Fiber Reinforced Concrete. Ph.D. Thesis. Universitat Politecnica De Valencia.

Bergmeister, K., Novak, D., Pukl, R. and Cervenka, V. (2009). Structural assessment and reliability analysis for existing engineering structures, theoretical background. Structure and Infrastructure Engineering. 5(4), 267-275.

Campione G., Mendola L. L., Papia M. (2005). Flexural behavior of concrete corbels containing steel fibers or wrapped with FRP sheets. Materials and Structures. 38,617-625.

Campione, G. (2009a). Flexural response of FRC corbels. Cement and Concrete Composites. 31(3), 204-210.

Campione, G. (2009b). Performance of steel fibrous reinforced concrete corbels subjected to vertical and horizontal loads. Journal of Structural Engineering. 135(5),519-529.

Cevik, A., Gulsan., M. E. (2013). Modelling ultimate load capacity of steel fibre reinforced concrete corbels: Part1. Formulation. Fibre Concrete, Cezech Republic, Prague.

Ersoy, U., Özcebe, G. and Tankut, T. (2006). Reinforced concrete. Ankara: Middle East Technical University Press.

Fanella, D. A., Naaman, A. E. (1985). Stress-strain properties of fiber reinforced mortar in compression. ACI Journal Proceedings. 82(4), 475-483.

Fattuhi, N. I. (1987). Sfrc corbel tests. ACI Structural Journal. 84(2), 119-123.

Fattuhi, N. I. and Hughes, B. P. (1989b). Ductility of reinforced concrete corbels containing either steel fibers or stirrups. ACI Structural Journal. 86(6), 644-651.

Fattuhi, N. I. (1990a). Column-load effect on reinforced concrete corbels. Journal of Structural Engineering. 116(1), 188-197.

Fattuhi, N. I. (1990b). Strength of SFRC corbels subjected to vertical load. Journal of Structural Engineering. 116(3), 701–718.

Fattuhi, N. I. (1994a). Strength of FRC corbels in flexure. Journal of Structural Engineering. 120(2), 360-377.

Fattuhi, N. I. (1994b). Reinforced corbels with plain and fibrous concretes. ACI Structural Journal. 91(5), 530-536.

Fattuhi, N. I. (1994c). Reinforced corbels made with high strength concrete and various secondary reinforcements. ACI Structural Journal. 91(4), 376-383.

Gulsan., M.E. (2015). Stochastic finite element based reliability analysis of steel fiber reinforced concrete (SFRC) corbels. Ph.D. Thesis. University of Gaziantep, Gaziantep, Turkey.

TSE. Turkish Standart Institute. (2000). Design and construction rules for reinforced concrete structures. TSE 500, Ankara.

Waschbeton. (2013). Precast structures company. http://www.waschbeton.com.

NUMERICAL INVESTIGATION OF FLOW CHARACTERISTICS OF 90°PIPE BEND FITTING USING NANOFLUID

Nehir TOKGOZ*

Department of Energy Systems Engineering, Osmaniye Korkut Ata University Osmaniye, Turkey

nehirtokgoz@osmaniye.edu.tr

Mehmet Tahir ERDINC

Department of Mechanical Engineering, Osmaniye Korkut Ata University Osmaniye, Turkey mehmettahirerdinc@osmaniye.edu.tr

Onder KASKA

Department of Mechanical Engineering, Osmaniye Korkut Ata University Osmaniye, Turkey onderkaska@osmaniye.edu.tr

Muruvvet AVCI

Department of Energy Systems Engineering, Osmaniye Korkut Ata University Osmaniye, Turkey

muruvvet.oku @gmail.com

ABSTRACT: In this study, flow characteristics and pressure drops are investigated numerically by passing nanofluids through the fittings 90° pipe bend commonly used in installations. Aluminum, copper and titanium-based nanoparticles were added homogeneously to water to obtain nanofluids. Five different concentrations of Al_2O_3 (%0.3, %0.5, %1, %2, %3). The Reynolds number was determined as Re = 500 and Re = 5000 to examine the structure of the flow through the fittings under both turbulent and laminar conditions. The results obtained by using water were confirmed with the literature results and nano-fluid calculations were started. In order to determine the most accurate numerical model; the laminar model, k- ϵ Standard turbulence model and k- ω Standard turbulence model were used. It was observed that as the concentration increased for all nanofluids, local losses increased due to the increase in viscosity. When different turbulence models are examined, it is seen that the most suitable model for Reynolds number, Re = 500 is the laminar model for T. The most suitable model for the Reynolds number, Re=5000 for elbow fitting is k- ϵ Standard model.

Key words: nanofluid, pressure drop, local loss coefficient, turbulence model

90º DİRSEK TESİSAT BAĞLANTI ELEMANIN AKIŞ ÖZELLİKLERİNİN NANOAKIŞKAN KULLANARAK SAYISAL OLARAK İNCELENMESİ

ÖZET: Sunulan bu çalışmada, tesisatlarda yaygın olarak kullanılan 90°dönümlü dirsek bağlantı parçasının içerisinden nanoakışkan geçirilerek akış karakteristikleri ve basınç düşüşleri sayısal olarak incelenmiştir. Alüminyum esaslı nanoparçacıkların temel akışkan olarak belirlenen suya ilave edilmesiyle homojen bir nanoakışkan elde edildiği kabul edilmiştir. Konsantrasyonun akış yapısı ve basınç kaybı üzerine etkisini incelemek için beş farklı konsantrasyonda Al_2O_3 (%0.3, %0.5, %1, %2, %3) nanoakışkanı ele alınmıştır. Bağlantı parçasından geçen akışın yapısını hem türbülanslı hem de laminar şartlar altında incelemek için Reynolds sayısı Re=500 ve Re=5000 olarak belirlenmiştir. Su kullanılarak elde edilen sonuçlar literatür sonuçları ile doğrulanıp, nanoakışkan hesaplamalarına geçilmiştir. En doğru sayısal modeli tespit edebilmek için laminar model, k- ϵ Standard türbülans modeli ve k- ω Standard türbülans modeli kullanılmıştır. Konsantrasyon arttıkça viskozitenin artmasına bağlı olarak yerel kayıpların arttığı görülmüştür. Farklı türbülans modelleri incelendiğinde Reynolds sayısı, Re=500 için laminar model olduğu görülmüştür. Reynolds sayısı, Re=5000 için en uygun modelin k- ϵ Standard modelin en iyi sonucu verdiği ortaya konulmuştur.

Anahtar sözcükler: nanoakışkan, basınç kaybı, yerel kayıp katsayısı, türbülans modeli

GİRİŞ

Günümüzde ısı transferine yönelik araştırma ve çalışmaların temel amacı; enerjinin etkin ve verimli bir şekilde kullanılmasıdır. En iyi enerji mevcut mantığı ile enerji tüketen cihazların verimliliğini arttırmak için geniş kapsamlı çalışmalar devam etmektedir.Isı transferini iyileştirmeye yönelik çalışmalar ekonomik açıdan çok önemli bir parametre olan enerjinin, etkin ve verimli bir şekilde kullanılmasına olanak sağlamıştır. Bu çalışmalar ile ısı değiştiricililerin daha verimli, daha düşük maliyetli, daha hafif ve daha küçük ebatlı tasarlanarak enerjinin daha etkin kullanılması hedeflenmektedir. Isı transferini iyileştirmeye yönelik çalışmalar genelde aktif, pasif, karma yöntemler kullanılarak elde edilir. Pasif yöntemler dış güç kullanılmasını gerektirmeyen yöntemlerdir. Genişletilmiş yüzeyler, bobinli borular buna örnek verilebilir. Aktif yöntemlerde bir dış güç kaynağına ihtiyaç duyulur. Yüzey ve akışkan titreşimi, elektrostatik alanlar buna örnek verilebilir. Karma yöntemler ise aktif ve pasif yöntemlerden iki ya da daha fazlası bir arada kullanılır (Bergles,1983). İş yapan akışkanının (temel akışkan) ısı transferi etkinliğini artırmak için içerisine mikro veya nano boyuttaki katı parçacıklar ilave edilerek yeni akışkan elde edilmesi pasif yöntemlerden biridir. Bu yöntemlerin amacı ısı transferini iyileştirmeye yönelik olsa da birçok dezavantajı da beraberinde getirmektedir. Buna santrallerde boru

sistemlerinde yorulmalara, akışkanlarda çökelme ve tortulaşmalara sebep olması örnek gösterilebilir (Şahin,vd., 2006). Bu da performansı düşürüp, ısı değiştiricilerinin boyutlarını ve maliyetini artırdığı için ısı transferine yönelik çalışmalarda yeni arayışların doğmasına sebep olmuştur. Araştırmacılar son yıllarda nanoparçacık boyutunun, konsantrasyonun, viskozitesinin, yoğunluğunun ve ısıl iletkenliğinin ısı transfer mekanizması üzerine etkilerini içeren birçok çalışma yapmışlardır. Bu kapsamda teorik ve deneysel çalışmalar yapılmıştır ve yapılmaya da devam edilmektedir. Araştırmaların genel sonucu nanoakışkanların ısı transferini artırdığı iddia edilse de deney sonuçları her zaman bunu doğrulamamaktadır. Mohamad vd. yaptıkları çalışmalarda temel akışkana nano parçacık eklenmesinin (akışkanın yoğunluğuna kıyasla) kaldırma kuvveti ve doğal konveksiyonu azaltacağını savunmuştur. Ayrıca nano parçacıkların eklenmesi sonucu etkin viskozite artacağından bununda zorlanmış taşınım ve basınç düşüşünü olumsuz etkileyeceğini ve bu parçacıkların yüzeylere çarpması sonucu erozyonların artabileceği belirtmiştir (Mohamad vd., 2015).

Çalışmaların çoğunda ısı değiştiricileri, bina ısıtması ve otomotiv soğutması gibi çeşitli uygulamalarda kullanılmaktadır. Günlük hayatta düşünüldüğünde borularda ve boru proje sistemlerinde, bağlantı elemanlarında kullanılan akış da ısı transferi açısından çok önemlidir. Burada oluşan yerel kayıplar ve basınç kayıpları sistemlerin uygun tasarlanması için gerekli bir parametredir. Enerjideki kayıpları içeren en temel etkenler; boru içerisindeki akışın durumu, borunun boyutu, malzemesi gibi fiziksel özellikleri, boru içerisinde akan akışın yön değiştirmesine sebep olan geometrik faktörler sayılabilir. Basınç dağılımlarının ve yerel kayıpların belirlenmesinde bağlantı elemanlarının eğrilik çapları, içerdiği akışın durumu, giriş hızı gibi parametreler çok önemlidir. Akışkan boru içerisinde aktığı zaman, akışkanın akışkanlığı ve türbülans nedeniyle de bazı kayıplar verir. Kayıpların olması verimlilik açısından ve maliyet açısından istenmeyen bir durumdur.

Sunulan bu çalışmada, tesisatlarda yaygın olarak kullanılan 90° dönümlü dirsek bağlantı malzemesinin nanoakışkan kullanılan tesisatlarda kullanılması durumunda oluşturdukları basınç farkları ve buna bağlı olarak meydana getirdikleri yerel kayıp katsayıları sayısal olarak incelenmiştir. Nanoakışkanın ısı transferini arttırmada önemli bir parametre olduğu göz önüne alınarak bağlantı parçaları içerisinden farklı konsantrasyonda nanoakışkan geçirilerek suya göre bağıl yerel kayıp katsayıları hesaplanmıştır. Temel akışkan su seçilerek içerisine Al_2O_3 için beş farklı hacim konsantrasyonunda nano parçacık ilave edilmiştir.. Seçilen nanoakışkanın termofiziksel özellikleri daha önce yapılan deneysel çalışmalardan alınmıştır. Bağlantı elemanı Ansys- Fluent programında çizilip, modellenerek çözümlemeleri yapılmıştır. Yerel kayıpların hesaplanmasında laminar model, k- ϵ Standard model, k- ω Standard türbülans modeli kullanılmıştır. Hesaplamalar önce su kullanılarak yapılmış ve elde edilen sonuçlar literatürde yaygın olarak kullanılan Çengel ve arkadaşalrının (Çengel vd., 2008) sonuçlarıyla mukayese edilerek doğrulamıştır. Nanoakışkan kullanılarak elde edilen sonuçlar ise su temel alınarak yorumlanmıştır. Hangi modelin daha uygun olduğu bulunmuştur.

ÖNCEKİ ÇALIŞMALAR

Vajiha vd. bu çalışmalarında kütlece %60 etilen glikol ve %40 su karışımı içinde süspansiyon haline getirilmiş alüminyum oksit nanopartiküllerin özgül ısı ve yoğunluğunun ölçümlerini incelemişlerdir. Amaçları nanoakışkanların akışkanlar dinamiğini ve ısı transfer özelliklerini belirlemektir. Bunu yaparken farklı hacim konsantrasyonları için bir çok farklı sıcaklıkta ölçümler alığ, elde ettikleri deney sonuçlarını da sıcaklık ve partikül hacmi konsantrasyonunun bir fonksiyonu olarak geliştirmişlerdir. Çalışmalarının sonucunda elde ettikleri korelâsyonların, endüstriyel ısı eşanjörleri, bina ısıtması ve otomotiv soğutması gibi çeşitli uygulamalarda $AI_2 0_3$ nanoakışkanının ısı transfer performansını ve pompalama gücü gereksiniminin incelenmesinde kullanılabileceği sonucuna varmışlardır (Vajiha vd., 2008). Sridhara ve Satapathy soğutma teknolojisinde verimi artırmak için çalışmalar yapmışlardır. Metalik veya metalik olmayan nanometre boyutlu katı partikülleri, su, yağ, dizel, etilen glikol, vb. gibi ısı transfer akışkanlarına ekleyerek yeni ısı transferi akışkanları elde etmişlerdir. Yeni nanoakışkanları baz sıvılarla karşılaştırmışlar ve önemli ölçüde daha yüksek termal iletkenliğe sahip olduğunu görmüşlerdir. Özellikle Al_2O_3 nanopartikül esaslı nano sıvıları incelemişler ve bu nano sıvıların ısıl iletkenliğinin artırılması, viskozitesi gibi konularını ele almışlardır. Termal iletkenlikte artışın %2 ile %36 arasında olduğunu görmüşlerdir (Sridhara ve Satapathy, 2011) . Farsani ve Nodooshan 90° kare kesitli yatay bir tüpte zorlanmış ısı transferini sayısal yöntemlerle incelemişlerdir. Çalışma sıvısı olarak Al_2O nanoakışkanını ele alıp sonlu hacimler yöntemini kullanmışlardır. Araştırmacılar elde ettikleri sonuçlara göre, nanoakışkanın hacim konsantrasyonu ve Reynolds saysının artmasıyla dirsek içerisindeki ısı transferinin arttığını görmüşlerdir. Aynı zamanda boru içerisindeki iç bükey yüzey, ısı transferi açısından dış bükey yüzeyden daha büyük bir etkiye sahip olduğunu ortaya koymuşlardır. (Farsani vd., 2015). Barik vd. 90° dirsek bağlantı parçasından Al_2O, Ti_2O ve CuO nanoakışkanlarını geçirip sonlu hacimler yöntemi kullanarak ısı transferini hesaplamışlardır. Reynolds sayısını 2500 ve 6000 arasında değiştirip, k- ϵ türbülans modelinde çözümlemeler yapmışlardır. Barik ve arkadaşları yaptıkları sayısal çalışmalar sonucunda nanoakışkanların hacim fonksiyonlarının değişiminin ısı transferini önemli ölçüde arttığını görmüşlerdir. Ayrıca ısı transferinin Reynolds sayısı ile de arttığını gözlemlemişlerdir. Araştırmacılar dirsek bağlantı parçasının dış duvar olarak tanımladıkları bölgede ikincil bir akış olduğunu görüp, buradaki kinetik enerjinin iç duvardan daha yüksek olduğunu belirtmişlerdir. Ayrıca ısı transferiyle beraber hesapladıkları Nusselt sayısının mevcut literatürün bir kısmı ile doğrulamışlardır. Diğer nanoakışkanlara karşı ısı transferindeki en fazla artışın CuO nanoakışkanında olduğunu görmüşlerdir (Barik vd., 2016). Huminic ve arkadaşı sarmal borularda, spiral kıvrımlı borularda ve diğer kavisli borularda temel akışkan ve nanoakışkan kullanılması durumunda gerçekleşen ısı transferi ve akış özelliklerini hakkında yayınlanmış makaleleri derlemişlerdir. Huminic vd. yaptıkları derleme çalışmalarının sonunda ısı transferi açısından en kapsamlı çalışmaların kavisli borularda yapıldığını görmüşlerdir. Nusselt sayısı ve sürtünme faktörü açısından en kapsamlı çalışmanın ise sarmal borularda olduğunu görmüşlerdir. Nanoakışkanların ısı transfer katsayılarının temel akışkandan daha yüksek olduğunu belirtip kavisli

boruların termohidrodinamik performanslarının nanoakışkan kullanımı ile artırılabileceğini söylemişlerdir. Ayrıca nanoakışkanların sürtünme faktörü ve basınç düşüşünün de çok yüksek olduğunu vurgulamışlardır. Araştırmacılar yaptıkları çalışmalar sonucunda ısı transferi ve akış özelliklerini incelemek için özellikle kavisli borularda daha fazla çalışmaya ihtiyaç duyulduğunu belirtmişlerdir (Huminic vd., 2016). Dutta vd. 90° dirsek bağlantı parçası için yüksek Reynolds sayılarında akışkanın özelliklerini incelemişlerdir. Akışı tek fazlı olarak ele almışlar ve k- ϵ türbülans modelini kullanmışlardır. Akış ayrılma bölgelerini birincil ve ikincil akış ayrılma bölgesi olarak tanımlamışlar ve hız vektörlerinin dağılımlarını göstermişlerdir. Dutta ve arkadaşları araştırmalarından elde ettikleri sonuçlara göre; Reynolds sayısı arttıkça bağlantı parçasının iç ve dış bükümlerinde hız profilinin etkileri artıp azalarak tam gelişmiş şeklini elde ettiğini görmüşlerdir. Reynolds sayısının çok yüksek değerlerinde ise bağlantı parçasının eğriliğinin etkisinin azaldığı sonucuna ulaşmışlardır (Dutta vd., 2016). Vasa vd. 180° üçgen kesitli bir U bağlantı parçasında Al_2O nanoakışkanın farklı konsantrasyonlarında ısı transfer karakteristiklerini sayısal olarak incelemişlerdir. Reynolds aralığını 5000 ile 30000 arasında değiştirip türbülanslı akış durumunu ele almışlardır. Vasa ve arkadaşları elde ettikleri sonuçlara göre hem Reynolds sayısının hem de nanoakışkanın hacim fonksiyonu arttıkça bağlantı parçasının ısı transferinde de önemli bir artış olduğunu gözlemlemişlerdir (Vasa vd., 2017). Çelen ve arkadaşları 180° kavisli kare kanal içerisinden Al_2O nanoakışkanı geçirip üç boyutlu bir laminar akışın sayısal incelemesini yapmışlardır. Kanal yüksekliği, Dean sayısı, hacim fonksiyonunun akışkanın akış ve ısı transferi üzerine etkisini incelemişlerdir. Araştırmacılar elde ettikleri sayısal sonuçlara göre, kavisli kare kanal kullanıldığında ısı transferinin % 59.0 oranında arttığını, bu kanal içerisinden nanoakışkan geçirildiğinde ise yine ısı transfer katsayısının % 30.8 oranında arttığını görmüşlerdir. Ayrıca nanoakışkanların hacim oranı, Dean sayısı ve kanal yüksekliği arttıkça ısı transfer katsayısının ve basınç düşüşünün arttığı sonucuna ulaşmışlardır (Çelen vd., 2017). Das, uzun vadeli kararlı bir nanoakışkan hazırlanmasının, ısı transferi uygulamalarında daha iyi kullanılacağını, sürdürülebilirlik ve verimlilik açısından da temel gerekliliklerden biri olduğunu düşünmüştür. Termal iletkenliği etkileyen katı hacim fraksiyonu, farklı baz sıvılar, sıcaklık, parçacık boyutu, pH, yüzey aktif maddeler ve nanoakışkan gelişiminde termal iletkenliğin arttırılmasına ilişkin çeşitli mekanizmalar da dahil olmak üzere çeşitli faktörleri tartışmıştır. Ayrıca melez nanoakışkanların sentezi, hazırlama yöntemleri, ısıl iletkenlik ve sorunları da göz önüne almıştır. Efektif parametrelerin termofiziksel özelliklere etkisi hakkında literatürde birçok çelişkili sonuç olduğunu görmüştür. Das yaptığı geniş çaplı çalışmalar sonucunda tüm parametrelerin, herhangi bir nano akışın termofiziksel etkisini önemli derecede etkilediği ve melez nano akışkanın, normal nano akışkandan daha iyi ısıl iletkenlik özelliği sergilediği bulmuştur (Das, 2017).

MATERYAL VE YÖNTEM

Akışı analiz edebilmek için sonlu hacimler metodu kullanarak çözüm yapan Ansys-Fluent paket programı kullanılmıştır. 3 boyutlu olarak çizilen geometri önce Gambit programı aracılığıyla ağlara bölünmüştür. Problemin çözüm aşamaları Şekil 1'de sunulmuştur. Çözüm Reynolds Sayısı, Re=500 ve 5000 için yapılarak hem laminer hem de türbülanslı akış yapısı ortaya konulmaya çalışılmıştır. Basınç için standart durumu ele alınmıştır. Momentum, enerji için ikinci dereceden upwind diskritizasyonu kabul edilmiştir. Viskoz çözüm modeli için farklı Reynolds sayılarına bağlı olarak laminar model, k- ϵ standard modeli, k- ω standard modeli olmak üzere üç çözüm modeli kullanılmıştır. Hangi modelin uygun olduğu belirlenmiştir. Model çözümlenmesi sırasında başlangıç şartları hız girişine göre alınmıştır. Yakınsama kriteri 10^{-5} olarak alınmıştır. Çalışmada kullanılan geometriler çok karmaşık olmadığından ve enerji denklemleri çözümlenmediğinden yakınsama kriteri kabul edilebilir (10^{-3}-10^{-4}) değerlerin üzerinde seçilerek çözümün hassas olması sağlanmıştır. Çözümde kullanılan türbülans modellerinin denklemlerine ve temel denklemlere Avcı (Avcı, 2019)'nın yapmış olduğu tez çalışmasından ulaşılabilir.

Şekil 1. Problemin Çözüm Aşaması

Modellenen parçanın 3D görüntüsü ve sınır şartları Şekil 2'de sunulmuştur. Dirseğin giriş ve çıkış çapı 0,2 m, uzunlukları 5 m olarak alınmıştır. Akışa uniform hız girişi tanımlanmış olup, çıkış etkilerinin ihmal edilebilmesi için çıkış uzunluğu yeterince uzun alınmıştır (25D).

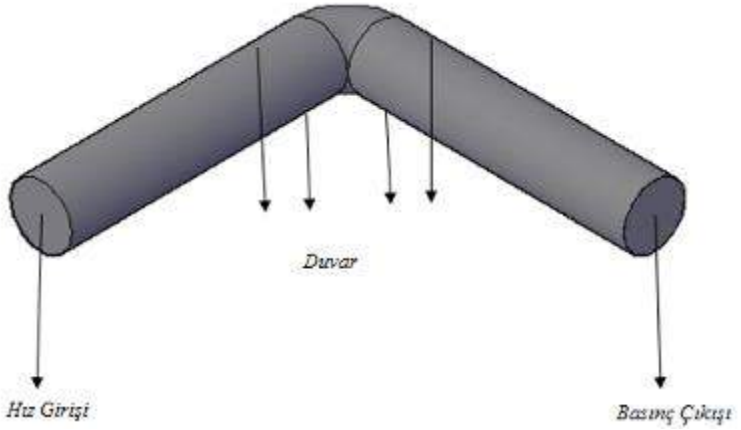

Şekil 2. 90° Dönümlü Dirsek Bağlantı parçasının Modeli ve Sınır şartları

Nanoakışkanın Termofiziksel Özellikleri

Çalışmada Al_2O_3-su nanoakışkan kullanılmıştır. Nanoakışkanlar suya aynı boyut ve hacimde olduğu varsayılan nanoparçacıkların eklenmesi ve homojen bir karışım elde edilmesiyle oluşturulmuştur. Konsantrasyon açısından beş farklı konsantrasyonda Al_2O_3 (%0.3, %0.5, %1, %2, %3), kullanılmıştır. Her bir konsantrasyon için ayrı ayrı hesaplama yapılmıştır. Kullanılan nanoakışkanların fiziksel özellikleri daha önce literatürde yapılan deneysel çalışmalardan alınarak aşağıdaki çizelgede özetlenmiştir.

Çizelge 1. 20 °C'de Alüminyum Oksidin Fiziksel Özellikleri (Özbey vd., 2011)

Akışkanlar	**Fiziksel Özelikler**			
	Yoğunluk,ρ (kg/m³)	**Özgül ısı, C_p, (j/kg K)**	**Dinamik Viskozite, μ (kg /ms)**	**Isı İletim Katsayısı,k (W/m K)**
Su	998.2	4182.0	0.001003	0.6
Su+%0.3 Al_2O_3	1005.80	4145.20	0.0010862	0.608334
Su+%0.5 Al_2O_3	1011.87	4110.86	0.00117021	0.619223
Su+%1.0 Al_2O_3	1028.20	4036.67	0.00139827	0.644465
Su +%2.0 Al_2O_3	1055.48	3925.80	0.0019319	0.685893
Su+%3.0 Al_2O_3	1083.60	3810.77	0.0025689	0.728339

BULGULAR VE TARTIŞMA

Bu bölümde Al_2O_3 nanoakışkanın farklı hacim konsantrasyonlarından elde edilen sonuçlara yer verilmiştir. Giriş hızına göre akışın tam gelişmiş olduğu yer tespit edilip iki farklı yüzey atılarak basınçlar hesaplanmıştır. Belirli noktalarda elde edilen basınç farkları ile yerel kayıp katsayısı değerleri hesaplanmış, her bir nanoakışkan konsantrasyonu için detaylı çizelgeler, hız ve basınç dağılımları oluşturulmuştur. Basınç farkları ile hesaplanan yerel kayıp katsayısı literatürde türbülanslı akış için kabul görmüş (Çengel vd., 2008) yerel kayıp katsayıları ile kıyaslanmıştır. Bu katsayı 90° dönümlü dirsek bağlantı parçası için 0.9 dur. Yapılan çözümlemede su için kayıp katsayısı K_k=0.923 olarak hesaplanmıştır. Çengel vd. tarafından yapılan çalışmayla mukayese edildiğinde aradaki fark yaklaşık %2.5 mertebesindedir.

Bu çalışmada bağlantı malzemelerinden su yerine nanoakışkan geçirilmesi durumundaki yerel kayıp katsayıları hesaplanmıştır. Yerel kayıp katsayı hesabında kullanılan hız değerleri Reynolds sayısından çekilerek hesaplanmıştır. Çözümlemeler sonucunda hangi modelin referans alınan kaynağa en yakın sonuçlar verdiği tespit edilerek uygun türbülans modeline karar verilmiştir. Aradaki farkın büyüklüğünü ortaya koymak adına kullanılan modellerin hepsi için sonuçlar ayrı ayrı çizelge ve grafikler halinde sunulmuştur. Reynolds=500 için elde edilen sonuçlar çizelge 2'de sunulmuştur.

Çizelge 2. Dirsek Bağlantı Parçası Reynolds Sayısı, Re =500 Laminar Model (Al_2O_3)

Akışkanlar	Hesaplanan Değerler			
	1.Yüzey Basıncı	2.Yüzey Basıncı	Basınç Farkı (Pa)	K_k
Su	0.01591929	0.013034998	0.002884294	0.917
Su+%0.3 Al_2O_3	0.01834248	0.015000208	0.003342276	0.925
Su+%0.5 Al_2O_3	0.02138785	0.017512256	0.003875595	0.930
Su+%1.0 Al_2O_3	0.02995296	0.024529777	0.005423183	0.946
Su+%2.0 Al_2O_3	0.05581891	0.045707114	0.010111798	0.970
Su+%3.0 Al_2O_3	0.09615476	0.078735195	0.017419569	0.996

Çizelge 4.1'de görüldüğü gibi konsantrasyon arttıkça yerel kayıp katsayısı da artmaktadır. Dirsek bağlantı parçasında akış, köşeli bir dönüş ile yönünü 90° değiştirmeye zorlamaktadır. Bu durum akışın enerjisini düşürerek basınç kaybıyla sonuçlanmaktadır. Düşük konsantrasyonlardaki kayıpta artış gözle görülür seviyede olmasa da hacim konsantrasyonunun 10 katı değerde artması ile yerel kayıp katsayısı hemen hemen 1 değerine kadar ulaşmıştır. Yerel kayıp katsayısındaki bu artış, viskozite ve yoğunluktaki artış ile doğrudan ilişkilendirilebilir. Reynolds Sayısı=5000 için farklı türbülans modelleri kullanılarak elde edilen sonuçlar Çizelge 3 ve 4 'de verilmiştir.

Çizelge 3. Dirsek Bağlantı Parçası Reynolds Sayısı, Re=5000 k - ϵ Standard Model (Al_2O_3)

Akışkanlar	Hesaplanan Değerler			
	1.Yüzey Basıncı	2.Yüzey Basıncı	Basınç Farkı (Pa)	(K_k)
Su	0.9926023	0.7023890	0.2902132	0.923
Su+%0.3 Al_2O_3	1.1547027	0.8170479	0.3376547	0.935
Su+%0.5 Al_2O_3	1.3326982	0.9430386	0.3896596	0.935
Su+%1.0 Al_2O_3	1.8609949	1.3164114	0.5445835	0.949
Su+%2.0 Al_2O_3	3.4815586	2.4635568	1.0180018	0.977
Su+%3.0 Al_2O_3	5.9953484	4.2420979	1.7532505	1.002

Çizelge 3 ve 4 ’de görüldüğü gibi nanoakışkan hacim konsantrasyonundaki artışla birlikte yoğunluk ve viskozitenin artması beklenen bir durumdur. Reynolds sayısı ve bununla doğrudan ilişkili olarak hızdaki artış ile birlikte akışın yönünü köşeli olarak 90° zorlamasından kaynaklanan enerji kayıpları birlikte ele alındığında basınç farkında ve yerel kayıp katsayısı değerinde bir artış görülmüştür. Düşük konsantrasyonlarda gözle görülür bir değer artışı olmasa da yüksek konsantrasyonlarda yerel kayıp katsayısı değerinin 1’i geçtiği görülmektedir. Yerel kayıp katsayı değeri hesaplanırken suyun yoğunluğunun referans değer alındığı göz önünde bulundurmalıdır.

Çizelge 4. Dirsek Bağlantı Parçası Reynolds Sayısı, Re=5000 k - ω Standard Model (Al_2O_3)

Akışkanlar	Hesaplanan Değerler			
	1.Yüzey Basıncı	2.Yüzey Basıncı	Basınç Farkı (Pa)	(K_k)
Su	1.1895039	0.8473607	0.3421431	1.088
Su+%0.3 Al_2O_3	1.3856059	0.9870186	0.3985872	1.104
Su+%0.5 Al_2O_3	1.5993963	1.1394007	0.4599956	1.103
Su+%1.0 Al_2O_3	2.2466016	1.600466	0.6461356	1.127
Su+%2.0 Al_2O_3	4.1772389	2.975771	1.2014677	1.153
Su+%3.0 Al_2O_3	7.1952977	5.125992	2.0693054	1.183

Çizelge 4’de görüldüğü gibi akışın türbülanslı bölgede oluşu, nanoakışkan hacim konsantrasyonuna bağlı olarak hızdaki, yoğunluktaki, viskozitedeki artışlardan ötürü basınç farkında ve yerel kayıp katsayısında ciddi artışlar görülmektedir. Saf su değerinde yerel kayıp katsayısının literatürde olması gereken (Çengel vd., 2008) değerden daha fazla çıkması çözümlemede kullanılan türbülans modelinin k - ω Standard model olması ile ilişkilendirilebilir. Hacim konsantrasyonunun artışı ile yerel kayıp katsayısı değerindeki bu fazla artış çözümlemedeki k - ω Standard model uygun olmadığını göstermektedir. Akış yapısını daha iyi açıklayabilmek için simetri eksenlerine tanımlanan yüzeylerdeki hız ve basınç dağılımları Şekil 3 ve Şekil 4 ’de verilmiştir.

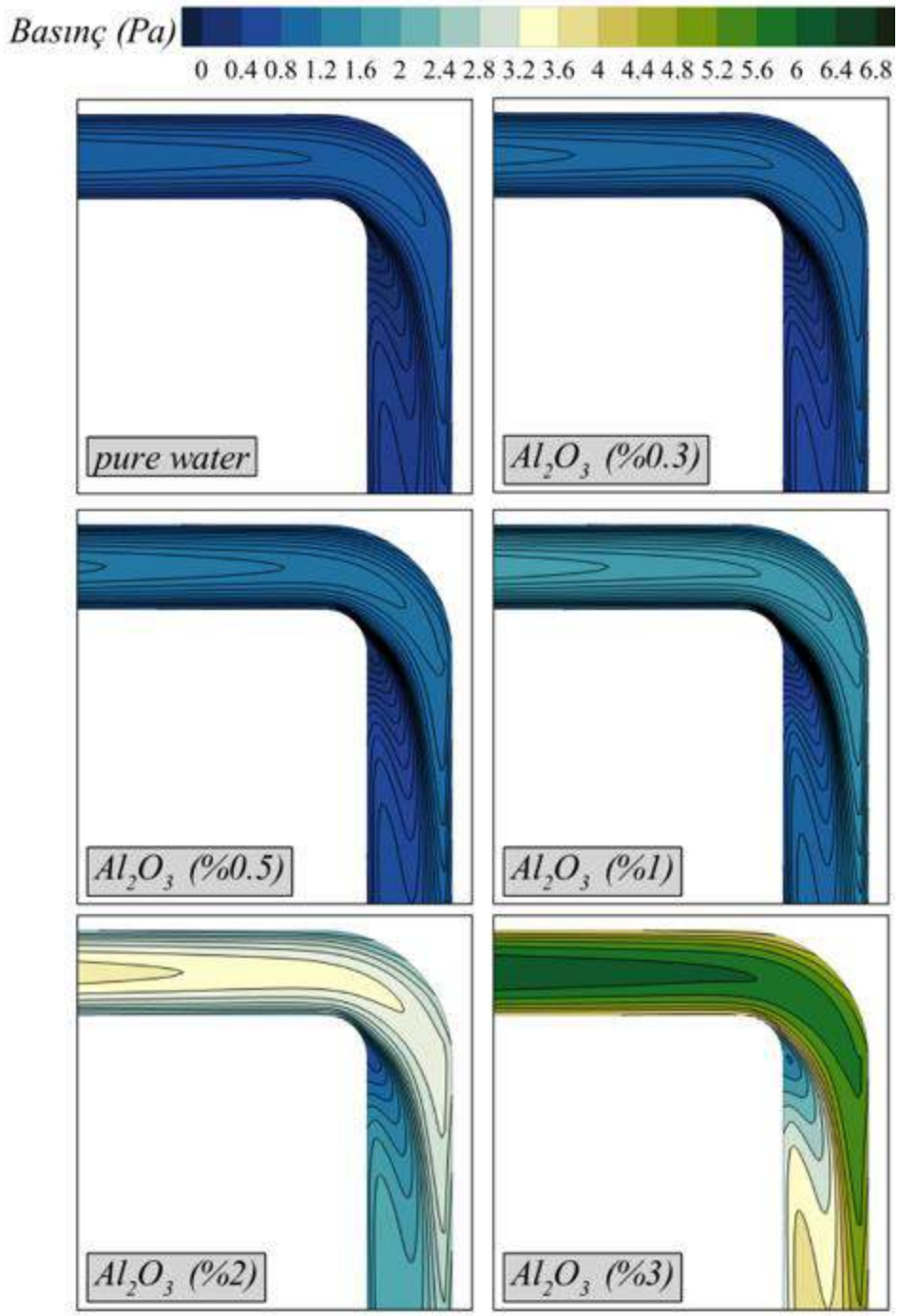

Şekil 3. Dirsek Bağlantı Parçası Reynolds Sayısı, Re=5000 için basınç dağılımı (Al_2O_3)

Artan konsantrasyonun basınç dağılımı üzerine etkisi Şekil 3'de verilmiştir. Daha önce verilen çizelgelerde belirtildiği gibi nanoakışkanın konsantrasyonunun artması sonucu basınç dağılımı da değişmektedir. Dirseğin içerisinden geçerken 0.4 Pa mertebesinde olan basınç en yüksek konsantrasyon değeri olan %3'e çıktığında 6.8 Pa mertebesine kadar çıkmıştır. Dağılım olarak bütün şekillerde geometrinin tamamının verilmediği sadece akış için önemli olan yerlerin yakınlaştırılarak sunulduğu göz önünde bulundurulmalıdır. Akışkanın dirsekten tam dönerken alt bölgesinde kalan

kısmında, iç tarafta akış ayrılmasından kaynaklanan girdaplı akıştan dolayı basıncın diğer bölgelere göre çok fazla düştüğü açıkça görülmektedir.

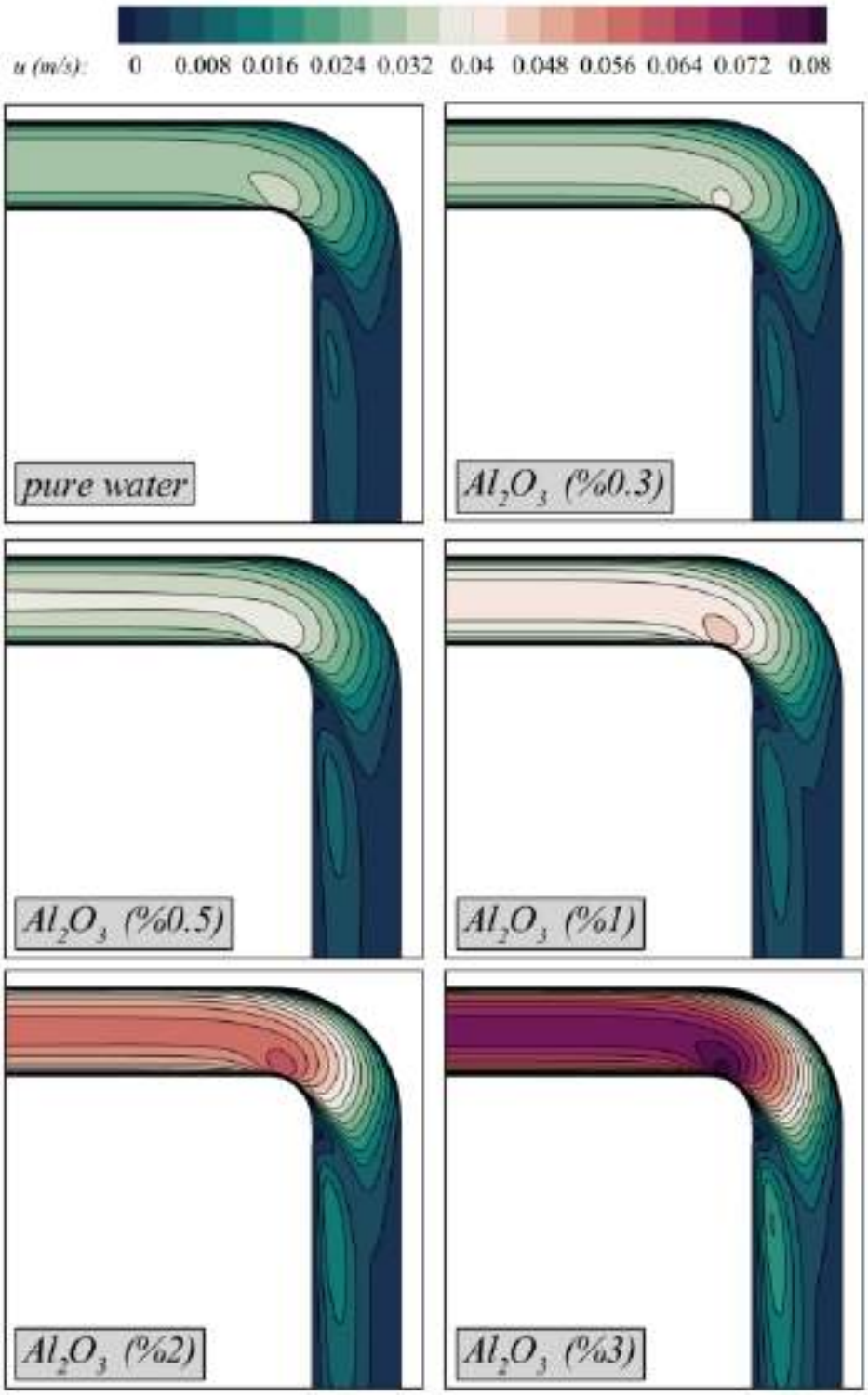

Şekil 4. Dirsek Bağlantı Parçası Reynolds Sayısı, Re=5000 için hız dağılımı (Al_2O_3)

Şekil 4 incelendiğinde dirsek bağlantı parçası için Al_2O_3 nanoakışkanında konsantrasyon artışı ile birlikte hız değerlerinin artığından dolayı hız dağılımının

sıklaştığı görülmüştür. Düşük konsantrasyon değerinde 0.008 m/s olan hız değeri konsantrasyon değerinin artışı ile birlikte yaklaşık 10 katı değerine çıkarak 0.08 m/s mertebesine kadar ulaşmıştır. Bu da Reynolds sayısı Re=5000 değerinde akışın türbülanslı bölgede olmasıyla ilişkilendirilebilir. Basınç dağılımında olduğu gibi, akışkanın dirsekten tam dönerken alt bölgesinde kalan kısmında hızın diğer bölgelere göre çok fazla düştüğü açıkça görülmektedir.

SONUÇ

Bu dirsek tesisat bağlantı parçalarının içerisinden su yerine nanoakışkan geçirilmesi durumunda oluşan basınç kayıp karakteristiği ve yerel kayıp katsayıları sayısal olarak incelenmiştir. Nanoakışkanların konsantrasyonu arttıkça yerel kayıp katsayısı değerinin ve basınç farkının nasıl etkilendiği incelenmiştir. Bağlantı parçalarının içerisinden geçirilen nanoakışkanların enerji verimliliği açısından basınç karakteristikleri ve yerel kayıpları nasıl etkilediği amaçlanmıştır. Al_2O_3 nanoakışkan kullanılarak çözülen modelde hacim konsantrasyonlarındaki artışa bağlı olarak dinamik viskozitenin artışı ile birlikte basınç farkının da arttığı görülmüştür. Sayısal çözümlemelerde laminar model, k- ϵ Standard türbülans modeli ve k- ω Standard türbülans modeli olmak üzere dört farklı model kullanılmıştır. Düşük Reynolds sayısı olan Re=500 için en uygun laminar model görülmüştür. Reynolds sayısı Re=5000 için k - ϵ Standard modelin uygun sonuçları verdiği doğrulanmıştır. Bunun nedeni k - ϵ Standard modelin yüksek türbülanslarda başarılı sonuçlar veren bir model olmasındandır.

AÇIKLAMA

Sunulan bu çalışma Mürüvvet AVCI'nın Dr. Nehir TOKGÖZ danışmalığında bitirdiği yüksek lisans tezinin bir parçasıdır.

KAYNAKLAR

Avcı, M. ., Tesisat Bağlantı Parçalarının Akış Karakteristiklerinin Nanoakışkan Kullanılarak Sayısal Olarak İncelenmesi, Osmaniye Korkut Ata Üniversitesi Fen Bilimleri Enstitüsü, Yüksek Tezi, Osmaniye, 2014.

Barik, A., Satapathy P., Sahoo S., CFD study of forced convective heat transfer enhancement in a 90 bend duct of square cross section using nanofluid, Indian Academy of Science, (7), 795-804, 2016.

Bergles, A.E., Augmentation of Heat Transfer. Heat Exchanger Design Handbook. Hemisphere Publishing Co, Washington DC, 1983.

Çelen, F., Evran Ö., Turgut O., Tigli B., Numerical study of flow and heat transfer in a curved square duct with longitudinal triangular rib using al_2o_3 /water nanofluid , Athens Journal of Technology and Engineering, Gazi Üniversitesi, 1-21, 2017.

Çengel Y., Cimbala J.M.,Akışkanlar Mekaniği Temelleri ve Uygulamaları, İzmir Güven Kitabevi, İzmir, 2008.

Das, K.S., A Review Based on The effect and mechanism of thermal conductivity of normal nanofluids and hybrid nanofluids, Journal of Molecular Liquids, 240 (2017) 420–446, 2017.

Dutta, P., Saha K., Nandi N., Pal N., Numerical study on flow separation in 90° pipe bend under high Reynolds number by k-ε modelling, Engineering Science and Technology, an International Journal 19 (2016), 904–910, 2016.

Farsani, A., Nodooshan A., Numerical investigation of nanofluids flow and heat transfer in 90° elbow with square cross-section, 37 (2), 162-172, 2015.

Huminic G., Huminic A., Heat transfer and flow characteristics of conventional fluids and nanofluids in curved tubes: A review, Renewable and Sustainable Energy Reviews, 58 (2016), 1327–1347, 2016.

Mohamad, A.A., Myth About nano-fluid heat transfer enhancement, International Journal of Heat and Mass Transfer, 86 (2015), 397–403, 2015.

Özbey, M., Namlı, L., Özcan, H., 2011. Nanoakışkanların helisel dönen akımında ısı transferinin sayısal ve deneysel incelenmesi. TÜBİTAK MAG 1001 projesi, 108M119.

Sridhara, V., Satapathy, N.L., Mujumdar, A.S., AI_2O_3 -based Nanofluids: a Review, Nanoscale Research Letters, India, 2011.

Şahin, B., Çomaklı, K., Yılmaz, M., Çomaklı, Ö., Nanoakışkanlarla ısı transferinin iyileştirilmesi, Mühendis Makine, 559 (2006), 29-34, 2006.

Vajjiha, R.S., Debendra K.D., Measurements of specific heat and density of AI_2O_3nanofluid, AIP Conference Proceedings, 6 (8), 361-370, 2008.

Vasa, A., Barik A., Nayak B., Turbulent convection heat transfer enhancement ın a 180-degree U-bend of triangular cross-section using nanofluid, Materials Science and Engineering, 225 (2017), India , 2017.

HEAT TRANSFER ANALYSIS IN CYLINDRICAL CORRUGATED CHANNEL WITH CFD METHOD

Nehir TOKGOZ*

Department of Energy Systems Engineering, Osmaniye Korkut Ata University Osmaniye, Turkey, nehirtokgoz@osmaniye.edu.tr

Mehmet Tahir ERDINC

Department of Mechanical Engineering, Osmaniye Korkut Ata University Osmaniye, Turkeymehmettahirerdinc@osmaniye.edu.tr

Onder KASKA

Department of Mechanical Engineering, Osmaniye Korkut Ata University Osmaniye, Turkey onderkaska@osmaniye.edu.tr

Çağrı KUTLU

Department of Architecture and Built Environment, University of Nottingham, NG7 2RD, UK, cagri.kutlu@nottingham.ac.uk

ABSTRACT: There have been many studies about heat transfer enhancement method and one of them is corrugated channel. In this work, heat transfer enhancement performance of cylindrical corrugated channel is numerically investigated. Ansys Fluent which uses finite volume method is used to solve continuity, momentum, turbulence and energy equations. For different Reynolds number values,to see heat transfer enhancement regions, field synergy principle is used. As a result of the calculations, it was seen that the cylindrical corrugated channels thin the thermal boundary layer, reduce the angle between the temperature gradientand the velocity vector, ie improve the heat transfer.

Key words: Heat transfer, cylindrical corrugated, computational fluid dynamics, field synergy.

SİLİNDİRİK OLUKLU KANALLARDA ISI TRANSFERİNİN HESAPLAMALI AKIŞKANLAR DİNAMİĞİ İLE İNCELENMESİ

ÖZET: Literatürde birçok ısı transferi iyileştirme yöntemleri mevcut olup, bu yöntemlerden biri de kanallarda oluklar oluşturmaktır. Bu çalışma da silindirik oluklu bir kanalda ısı transferi iyileştirme performansı sayısal olarak incelenmiştir. Sonlu hacimler metodu ile çalışan Ansys Fluent programı kullanılarak süreklilik, momentum, türbülans ve enerji denklemleri çözülmüştür. Farklı Reynolds sayıları için silindirik oluklu kanalda ısı transferi iyileştirmesinin gösterimi için alan sinerji prensibi (field synergy principle) dağılımı gösterilmiştir. Yapılan hesaplamalar sonucunda silindirik oluklu kanalların ısıl sınır tabakayı inceltiği, hız vektörü ile sıcaklık gradyanı arasındaki açıyı azalttığı yani ısı transferinin iyileştirdiği görülmüştür.

Anahtar sözcükler: Isı transferi, silindirik oluklu kanal, hesaplamalı akışkanlar dinamiği, alan sinerji.

GİRİŞ

Geçmişte yaşanan ve yakın gelecekte yaşanması beklenen enerji krizleri, çoğu ülkeyi enerjiyi daha verimli kullanmak için enerji yönetimi politikaları oluşturmaya zorlamıştır. Bundan dolayı, araştırmacılar enerji sistemlerinin optimizasyonuna odaklanmaya başlamışlardır. Isı değiştiricileri gıda, kimya, metal endüstrisi gibi pek çok endüstriyel uygulamalarda önemli bir role sahiptir. Örneğin, araçlarda, motorun ısı üretmesi için uygun şekilde çıkarılması gerekir. Benzer şekilde, elektronik ekipmanın aşırı ısınmayı önlemek için soğutma amacıyla kullanılan bir sisteme ihtiyacı vardır. Isıtma, iklimlendirme ve havalandırma sistemlerinin yanı sıra, bazı diğer endüstriyel uygulamalar, farklı ısı transfer mekanizmalarını içerir.Isı değiştiricilerinde minimum basınç kaybında maksimum ısı transferi beklenmektedir. Isı ve momentum transferinde iyileştirmeler yapmak ve ayrıca oluklar gibi yüzeylerdeki modifikasyonların ilgili mekanizmalar üzerindeki etkisini anlamak için bilimsel bilgiye ihtiyaç vardır. Bunun için literatürde farklı tip ısı değiştiricileri ve kanallar çalışılmaktadır. Dışardan enerjiye ihtiyaç duyulmadan ısı transferini arttırdıkları için ısı değiştiricilerinde farklı tip oluklu kanallar kullanılmaktadır. Fakat geometri değişikliği akışta çalkantılar meydan getirip ısı transferini iyileştirirken aynı zamanda basınç kaybının artmasına ve bunun neticesinde de pompa gücünün artmasına sebep vermektedir. Oluklu kanallar da çeşitli mühendislik uygulamalarında kullanılmaktadır. Bu kanallarlailgili ve bunların optimum geometrilerini belirlemek için literatürde birçok çalışma bulunmaktadır.

ÖNCEKİ ÇALIŞMALAR

Reynolds sayısının, geometrik parametrelerin ve akışkan özelliklerinin spiral oluklu tüplerin ısıl performansları üzerindeki etkileri sayısal olarak Jinet ve arkadaşları tarafından çalışılmıştır [1]. Elde edilen sonuçlar, artan oluk derinliği ile hem uzunlamasına girdap uzunluğunun (longitudinal vorticity length) hem de ikincil akış hızının arttığını göstermiştir. Ayrıca, ısı transfer katsayısı ve Nusselt sayısı, perde sayısı arttıkça düşer. Öte yandan, saha büyüdükçe, Nusselt sayısı ve ısı transfer katsayısı azalmaktadır.

Fabbri [2], laminer akış koşulları altında düz ve oluklu duvarlardan oluşan bir kanalda taşınımla ısı transferini araştırmıştır. Optimize edilmiş oluklu profilin ısı transfer hızının Reynolds sayısı ve Prandtl sayısının bir fonksiyonu olarak arttığı bulunmuştur. Wang ve ark. [3] helisel oluklu boruların türbülanslı akış yapıları üzerindeki etkilerini ve farklı oluklarda ısı aktarım ve direnç özelliklerinin oranını bildirmiştir. Elde ettiği sonuçlar, girdap akışının büyüklüğünün, oluk adımlarının azalması ve oluk yüksekliğinin artmasıyla arttığını göstermiştir.

Dikdörtgen kesitli oluklu mikrokanalların akış ve ısı transferi, sayısal olarak Mohammed ve ark. [4] tarafından çalışılmıştır. Oluklu mikro kanalların ısıl verimlerinin aynı kesitler için düz mikro kanallardan daha iyi olduğu belirtilmiştir. Oluklu mikro kanallar boyunca basınç kayıpları, ısı transfer iyileştirmesinden daha düşüktür.

Xiang [5], oluklu bir yüzey boşluğunun faz kayma açısı$\Phi = 0°$olan sinüzoidal kanallar için ısı transferi iyileştirme ve akış karakteristiği üzerindeki etkileri üzerine araştırmalar yapmışlardır. Çalışmalarında, akış özellikleri ve farklı faz açılarının ısı transferi iyileştirme üzerine etkilerini incelemişlerdir.

Oluklu kanallarla ilgili daha detaylı bilgiler [6-10] numaralı referanslardan elde edilebilir. Tokgöz [7] çalışmasında dairesel oluklu kanaldaki akış, Parçacık Hız Görüntü (PIV) tekniği ve hesaplamalı akışkanlar dinamiği (HAD) kullanılarak Reynolds sayısının bir fonksiyonu olarak deneysel ve sayısal olarak incelenmiştir. Çalışmasında olukların momentum transferini arttırdığı görülmüştür. Bu çalışmada bu oluklu kanalların ısı transfer mekanizması incelenmiştir.

MATERYAL VE YÖNTEM

Akış ve ısı transferi analizleri için gerekli olan denklemler Ansys-Fluent paket programı ile çözülmüştür.Underrelaxation faktörleri basınç denklemleri için 0,3, momentum denklemleri için 0,7 enerji denklemi için 1, gövde kuvveti ve yoğunluğu için ise 1,0 değerleri seçilmiştir. Süreklilik ve momentum denklemlerinin yakınsama değeri 10^{-6} ve enerji denkleminin yakınsama değeri ise 10^{-9} alınmıştır. Momentum denklemlerinin çözümünde SIMPLEalgoritması kullanılmıştır. Türbülans modeli standart k-ε seçilmiştir. Bunlarla ilgili denklemler Ref. [7]'de verilmiştir. Şekil 1'de HAD yöntemiyle çözümlemesi yapılan kanalın geometrisi verilmiştir.

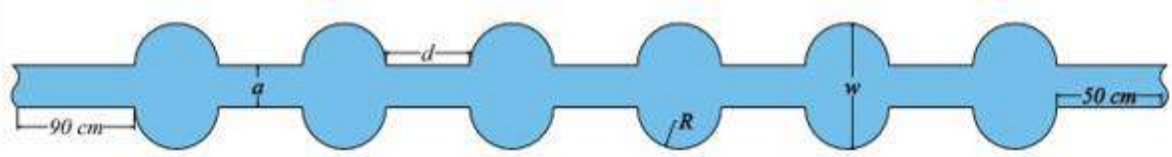

Şekil 5. Çözümlemesi Yapılan Dairesel Oluklu Kanal Geometrisi [7]

Akışın tam gelişmesini sağlamak için oluklu bölüme girmeden önce 90cm, çıkış etkilerinin ihmal edilebilmesi içinde çıkışa 50 cm uzunluğunda oyuksuz bölüm bırakılmıştır. En boy oranı (aspect ration), a/R=1 içinhesaplamalar yapılmıştır.

Hesaplama alanın girişine üniform bir u_0 hızı ve T_0 sıcaklığı verilmiştir.

Duvardaki sınır şartında kaymama ve sabit duvar sıcaklığı verilmiştir:

$$u = v = 0 \text{ ve } T = T_w \quad (1)$$

Ortalama hızlar, belirlenen Reynolds Sayısından eşitlik 2 yardımıyla hesaplanmıştır.

$$\mathrm{Re} = \frac{\rho_f \bar{u} D_h}{\mu_f} \quad (2)$$

Burada hidrolik çap iki plaka arasındaki yüksekliğin, a iki katı alınarak hesaplanmıştır (D_h=2a). $\rho_f$akışkanın yoğunluğu, μ_f de akışkanın dinamik viskozitesidir.

Alan sinerji(koordinasyon) hesaplamalarında ise Guo ve ark. [11]'nın taşınımla ısı transferi için sunmuş olduğu yöntem kullanılmıştır.Hız vektörü ile sıcaklık gradyanı arasındaki açının azalmasıyla ısı transferinde iyileştirme olacağını belirtilmiştir. Konuyla ilgili birçok çalışma yapılmıştır [12-20]. Şekil 2'de sıcaklık gradyanı ile hız vektörü arasındaki açı(β)ile hız gradyanı ile hız vektörü arasındaki açı(α) ve gösterilmiştir [19].

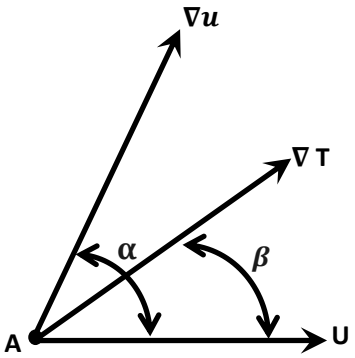

Şekil 2. Sıcaklık gradyanı ile hız vektörü arasındaki açı(β)ile hız gradyanı ile hız vektörü arasındaki açı(α)'nın kanal içerisinde bir noktada gösterimi [19].

Bu çalışmada sinerji açıları α ve β aşağıdaki eşitlikler yardımıyla hesaplanmıştır [16]:

$$\alpha = \arccos\left(\frac{\left|u\frac{\partial u}{\partial x}+v\frac{\partial u}{\partial y}+w\frac{\partial u}{\partial z}\right|}{\sqrt{u^2+v^2+w^2}\sqrt{\left(\frac{\partial u}{\partial x}\right)^2+\left(\frac{\partial u}{\partial y}\right)^2+\left(\frac{\partial u}{\partial z}\right)^2}}\right) \quad (3)$$

$$\beta = \arccos\left(\frac{\left|u\frac{\partial T}{\partial x}+v\frac{\partial T}{\partial y}+w\frac{\partial T}{\partial z}\right|}{\sqrt{u^2+v^2+w^2}\sqrt{\left(\frac{\partial T}{\partial x}\right)^2+\left(\frac{\partial T}{\partial y}\right)^2+\left(\frac{\partial T}{\partial z}\right)^2}}\right) \quad (4)$$

BULGULAR VE TARTIŞMA

Isı transferi iyileştirme çalışmaları çoğunlukla, ısı transferi geliştirme mekanizmasını tamamen açıklamayan sürtünme faktörüne ve Nusselt sayısına odaklanmıştır [16]. Şekil 3'te dört farklı Reynolds sayısı için sıcaklık gradyanı ile hız vektörü arasındaki açı β'nın dağılımı gösterilmiştir. Burada açının sıfır olması ısı transferinin çok iyi olduğunu göstermektedir. Olukların hemen başında akış ayrılmalarından dolayı ısı transferi iyileşmekte ancak derinlik (en/boy oranına göre) fazla olduğundan dolayı olukların iç kısımlarında ısı transferi iyi olmamaktadır. Reynolds sayısı arttıkça akışkanın olukların çıkışında β açısı azalmakta yani ısı transferi artmaktadır. Şekil 4'te de dört farklı Reynolds sayısı için hız gradyanı ile hız vektörü arasındaki açı α'nın dağılımı verilmiştir. Bu şekilde açının sıfır olması basınç kaybının çok fazla olduğunu göstermektedir. Burada da oluklar içerisindeki girdaplardan dolayı basınç kaybı artmaktadır. Oluklar içerindeki türbülanstaki yoğunluğun artması, yüksek momentum transfer hızı geliştirildiğinden ısı transferi artmıştır. Boşlukların girişinde, yüksek Reynolds sayılarının etkisiyle, sık sık atma girdapları nedeniyle çekirdek ve uyanık akış bölgeleri arasında daha enerjik bir akış vardır. Boşlukların keskin köşeleri, türbülanslı kinetik enerjinin büyüklüğü yani ısı transferi ve basınç kaybı üzerinde ek bir etkiye sahiptir. Hem ısı transferi hem de basınç kaybı, oluklu kanalda keskin kenarlar nedeniyle düz kanaldan daha yüksektir. Olukların tekrarlanmasından dolayı, girdaplı akış yapılarının büyüklüğü akış yönlerinde kademeli olarak artar ve buna bağlı olarak türbülans yoğunluğu ile birlikte akışkan karışımı ve momentumu da artar ve aynı zamanda ayrılan akış bölgelerinin boyutunu azaltır. İyileştirme çalışmalarında amaç sıcak ve soğuk akışkan arasındaki karışımın artırılmasıdır. Akış karıştırma ve türbülans yoğunluğunu artıran oluklu kanalarda ısıl performansı iyileştirir. Bununla birlikte, mevcut geometrik modifikasyonların ilave kanal boyunca basınç düşüşünü arttıracağı da dikkate alınmalıdır. Oluklu kanalın ekseni üzerindeki akış yönünde hız dağılımının incelenmesi, paralel kanalın plakaları üzerinde daire şeklindeki oluklu malzemenin kullanılmasının, eksen üzerinde bir harmonik hız dağılımı geliştirdiğini ortaya koymaktadır.

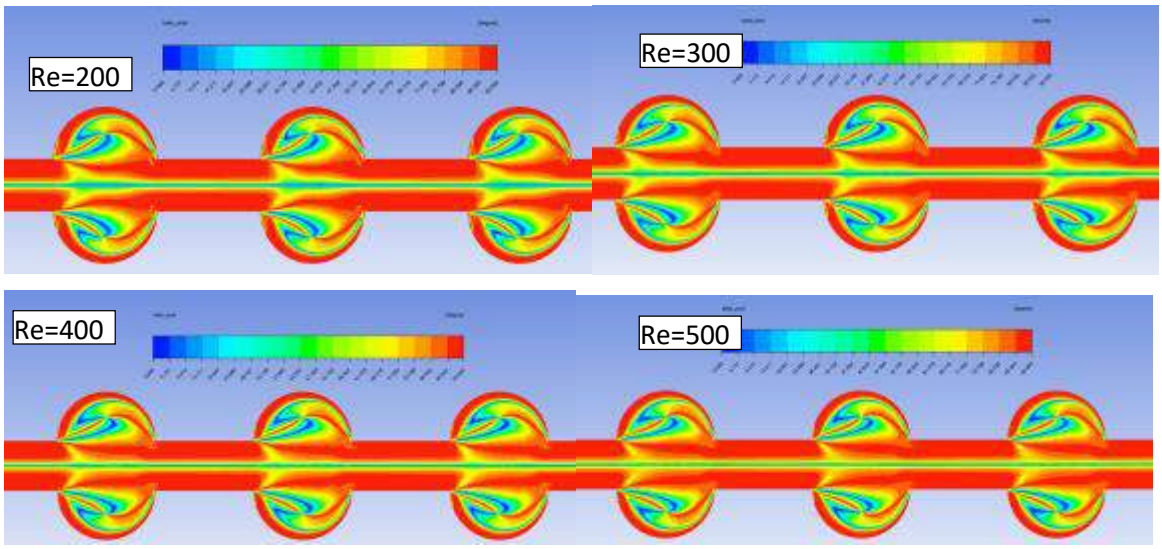

Şekil 3. β açısının dört farklı Reynolds sayısı için dağılımı

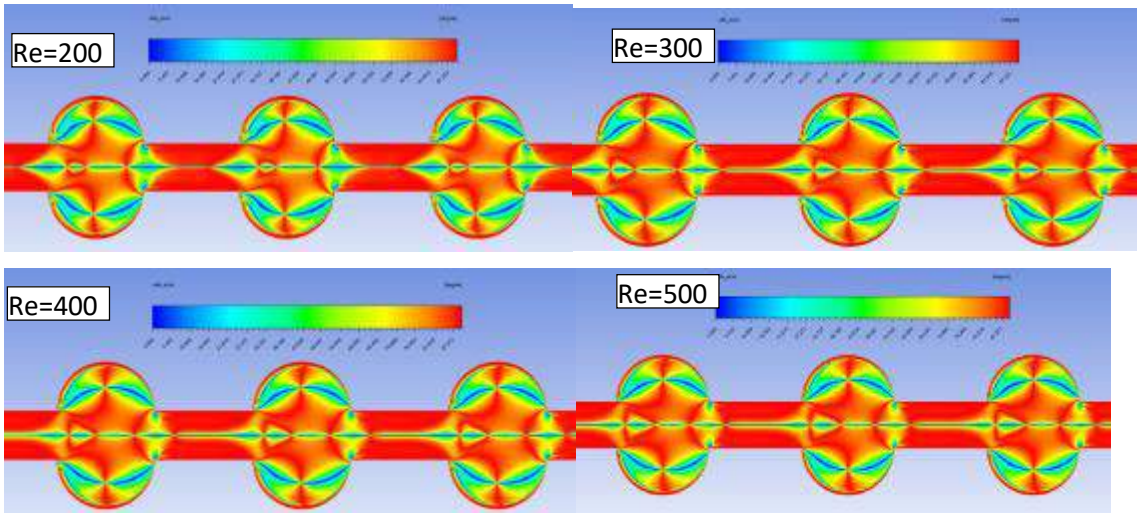

Şekil 4. α açısının dört farklı Reynolds sayısı için dağılımı

SONUÇ

Isı transferi uygulamalarının gerekli olduğu endüstriyel uygulamalarda, termal ve hidrodinamik alanlar arasındaki etkileşime bağlı olan doğru tasarım ve optimizasyon çalışmalarını bir arada yürütmek ve bu etkileşimlerin sonuçlarını doğru bir şekilde değerlendirmek kaçınılmazdır. Oluklu kanallar termal enerjiyi aktarmak için kullanılan ve elektronik cihazların soğutulmasında yaygın olarak kullanılan termal cihazlardır. Bu nedenle, ısı transferindeki mekanizmaların incelenmesi bu kanallarda enerji tasarrufu için büyük önem taşımaktadır. Isı değiştirici olarak kullanılan oluklu kanalların akış özelliklerinin ayrıntılı bir analizi, tasarım parametrelerini belirleyerek bu kanalların optimizasyonunu sağlanmalıdır. Bu çalışmada en boy oranı (aspect ratio), a/R=1 olan bir silindirik oluklu kanalda ısı transferi alan sinerji prensibine göre

sayısal olarak incelenmiştir. Oluklar içerindeki akışın karıştırması ve türbülanstaki yoğunluğun artması, yüksek momentum transfer hızı gelişmesini sağlamakta ve ısı transferi ve basınç kaybını artırmaktadır.Olukların iç kısımlarında ısı transferinin iyileştirilmesi gerektiği görülmüş olup, ileriki çalışmalarda en/boy oranının her iki açıya etkisinin incelenmelidir. Ayrıca farklı en/boy oranlarına göre basınç kayıp katsayısı, Nusselt sayısı ve ısıl iyileştirme performansını incelenmelidir.

KAYNAKLAR

[1] Z.-j. Jin, F.-q. Chen, Z.-x. Gao, X.-f. Gao, J.-y. Qian, Effects of pitch and corrugation depth on heat transfer characteristics in six-start spirally corrugated tube, International Journal of Heat and Mass Transfer, 108 (2017) 1011-1025.

[2] G. Fabbri, Heat transfer optimization in corrugated wall channels, International journal of heat and mass transfer, 43 (2000) 4299-4310.

[3] W. Wang, Y. Zhang, B. Li, H. Han, X. Gao, Influence of geometrical parameters on turbulent flow and heat transfer characteristics in outward helically corrugated tubes, Energy conversion and management, 136 (2017) 294-306.

[4] H. Mohammed, P. Gunnasegaran, N. Shuaib, Numerical simulation of heat transfer enhancement in wavy microchannel heat sink, International Communications in Heat and Mass Transfer, 38 (2011) 63-68.

[5] J.-X. Yin, G.-J. Li, Z.-P. Feng, Numerical investigation of effects of plate spacing on flow and heat transfer in sinusoidal channels, Re Kexue yu Jishu(Journal of Thermal Science and Technology)(China), 4(2) (2005) 123-129.

[6] S. Eiamsa-ard, P. Promvonge, Numerical study on heat transfer of turbulent channel flow over periodic grooves, International Communications in Heat and Mass Transfer, 35(7) (2008) 844-852.

[7] Tokgoz, N. (2019). Experimental and numerical investigation of flow structure in a cylindrical corrugated channel. International Journal of Mechanical Sciences, 157, 787-801.

[8] H. Mohammed, A.M. Abed, M. Wahid, The effects of geometrical parameters of a corrugated channel within out-of-phase arrangement, International Communications in Heat and Mass Transfer, 40 (2013) 47-57.

[9] Tokgoz, N., Tunay, T., & Sahin, B. (2018). Effect of corrugated channel phase shifts on flow structures and heat transfer rate. Experimental Thermal and Fluid Science, 99, 374-391.

[10] Tokgoz, N., & Sahin, B. (2019). Experimental studies of flow characteristics in corrugated ducts. International Communications in Heat and Mass Transfer, 104, 41-50.

[11] Guo, Z. Y., Li, D. Y., Wang, B. X., A novel concept for convective heat transfer enhancement, Int. J. Heat Mass Transfer, 1998.

[12] He, Y. L., Tao, W. Q., Convective Heat Transfer Enhancement: Mechanisms, Techniques, and Performance Evaluation, Adv. Heat Transf., 46, 2014.

[13] Saha, P., Biswas, G., Sarkar, S., International Journal of Heat and Mass Transfer Comparison of winglet-type vortex generators periodically deployed in a plate-fin heat exchanger – A synergy based analysis, Int. J. Heat Mass Transfer, 74, 292–305, 2014.

[14] Erdinç, M. T., Yılmaz, T., Cihan, E., Ünal, Ş., Isı transferi problemlerinin Ansys Workbench ile hızlı analizi ve kaydırılmış levhada örnek uygulama, 20. Ulusal Isı Bilimi ve Tekniği Kongresi, Balıkesir, 1424–1430, Eylül 2015.

[15] Tao, W., He, Y., Field synergy principle and its applications in enhancing the convective heat transfer and improving the performance of pulse tube refrigerator (1), Hsi-An Chiao Tung Ta Hsueh/Journal Xi'an Jiaotong Univ., 2002.

[16] Zhai, Y. L., Xia, G. D., Liu, X. F., Li, Y. F., Heat transfer in the microchannels with fan-shaped reentrant cavities and different ribs based on field synergy principle and entropy generation analysis, Int. J. Heat Mass Transfer, 68, 224–233, 2014.

[17] Tao, W. Q., Guo, Z. Y., Wang, B. X., Field synergy principle for enhancing convective heat transfer - Its extension and numerical verifications, Int. J. Heat Mass Transfer, 45 (18), 3849–3856, 2002.

[18] Guo, Z. Y., Tao, W. Q., Shah, R. K., The field synergy (coordination) principle and its applications in enhancing single phase convective heat transfer, Int. J. Heat Mass Transf., 48 (9), 1797–1807, 2005.

[19] Wei, L., Zhichun, L., Tingzhen, M., Zengyuan, G., Physical quantity synergy in laminar flow field and its application in heat transfer enhancement, Int. J. Heat Mass Transf., 52 (19–20), 4669–4672, 2009.

[20] Erdinç, M. T., Yeni bir sıvı-sıvı plakalı ısı değiştiricisinin sayısal ve deneysel olarak incelenmesi, Osmaniye Korkut Ata Üniversitesi Fen Bilimleri Enstitüsü, 2019.

STARCH CONVERSION IN CORN MALTOSE SYRUP PRODUCTION: DETERMINATION OF OPTIMUM REACTION AND PROCESS CONTROL PARAMETERS

Sema Nur Çinçik, MSc., Gaziantep University, cinciksema@gmail.com

Assist. Prof. Dr. Fatih BALCI, Gaziantep University, fbalci@gantep.edu.tr

Prof. Dr. Mustafa BAYRAM, Gaziantep University, mbayram@gantep.edu.tr

ABSTRACT: In the maltose syrup production, one of the critical processing stage is the starch conversion process. During this process, the reaction time and enzyme concentrations are two important parameters to obtain the standard sugar spectrum. The purpose of this study is; i) to find optimum reaction time and enzyme concentrations during the starch conversion process, ii) to determine process control and dynamic parameters during the starch conversion process in the maltose syrup production. The different amounts of beta and alpha-amylase enzymes (0.10, 0.15, 0.20 and 0.25 ml of β-amylase; 0.03, 0.05, 0.07 and 0.09 ml of α-amylase) were used to determine the optimum concentrations and time. pH, Brix and the concentrations of sugars (dextrose, maltose, maltotriose (DP3) and high sugars (DPN)) were determined. It was found that the enzyme concentration, ratios of the enzyme used and reaction time significantly affect the starch conversion process. The mixture containing 0.20 ml β-amylase and 0.05 ml α-amylase was determined as the optimum value ($P \leq 0.05$). It was found that the maximum process gains were obtained at Run 1, 13, 9 and 13 for dextrose, maltose, DP3 and DPN, respectively.

Key words: process control; gain value; stach conversion; corn maltose syrup; α-amylase; β-amylase.

EARTHQUAKE ANALYSIS OF A SCHOOL PROJECT WITH TBDY 2018

Nihat ATMACA, Civil Engineering Department, atmaca@gantep.edu.tr
Adem ATMACA, Energy Systems Engineering Department, aatmaca@gantep.edu.tr
Seydi KILÇIK, Civil Engineering Department, infokilcikoglu@gmail.com

ABSTRACT: As a result of developing technology and increasing knowledge levels, updates are made in earthquake regulations (codes). The new building earthquake regulation of Turkey has been published on 18 March 2018. There are especially two methods in this new code: Linear and nonlinear methods. In this study, project of a school that is located in Gaziantep province of Turkey analysed by TDY 2007 regulation on buildings in earthquake zones is compared with the new Turkish earthquake code by using linear calculation methods. SAP 2000 software was used for the calculations and program outcomes were used for comparison. Base shear forces, maximum forces and structure rotation moments findings are calculated. The obtained results show that the new earthquake codes are designed in a safer way.

Key words: 2018 Turkish earthquake code, SAP 2000, Base shear forces, 2007 regulation on buildings in earthquake zones

INTRODUCTION

TDY 2007 earthquake regulation consists of four earthquake zones. N the other hand, earthquake zone areas aren't defined in the new earthquake regulation TBDY 2018. The new regulation focused on the specific site of earthquake risk and ground behaviour. Therefore the related results can be obtained with locational earthquake datas. There are some other revisions in TBDY 2018.

The main purpose of this study is to show the differences between the TDY 2007 and TBDY 2018 earthquake regulation of the Turkey and their structural analysis results. A school project with different structural design configurations analysed for this purpose. The linear calculation method is carried on by equivalent seismic load method according to the TDY 2007 and TBDY 2018 earthquake regulations for frames with shear walls and reinforcement concrete columns models with SAP2000 software.

HISTORY OF EARTHQUAKE REGULATIONS IN TURKEY

In Turkey, the first earthquake regulations are taken with some revisions from Italy in 1940. This revised regulation was modified as a result of severe earthquakes, changing material and structural techniques and technological developments. In order to fulfil the requirements of the earthquake regulations, the labour of the buildings must also comply with the project. Earthquake performance was found to be incompatible with the regulations or significant design deficiencies at the time of construction of many buildings. For example, when a project designed and constructed in 1987 is examined, it does not comply with the 1975 ABYYHY rules in terms of design. It is seen that the structure was designed according to the rules of 1968 ABYYHY or it contains big deficiencies according to 1975 ABYYHY. (Ellul F et al., 2003)

Earthquake regulations used in turkey are:

- 1940 - Italian Building Instructions for Construction in Earthquake Districts,
- 1944 - Earthquake Districts Provisional Building Instructions,
- 1949 - Turkish Ground Movement Region Building Regulation,
- 1953 - Regulation on Structures to Be Built In Ground Movement Regions,
- 1962- Regulation on structures in disaster zones (ABYYHY),
- 1968 - Regulation on structures in disaster zones (ABYYHY),
- 1975 - Regulation on structures to be built in disaster zones (ABYYHY),
- 1998 - Regulation on structures in disaster zones (ABYYHY),
- 2007 - Regulation on buildings in earthquake zones (DBYBHY),
- 2018 - Turkey building earthquake regulation (TBDY) (Alyamaç and Erdoğan, 2005).

TDY 2007 AND TBDY 2018 EARTHQUAKE REGULATIONS IN TURKEY

The structural models of the study are designed with linear and non-linear methods according to the TDY 2007 and TBDY 2018 earthquake regulations. Linear earthquake calculation used as equivalent earthquake load method. There are many differences in the parameters used in model designs. Information on these parameters are shown below (Figures 1 and 2).

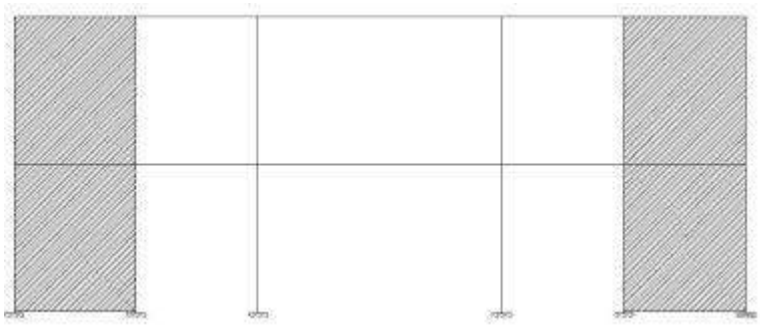

Figure 1.Frames with Shear Walls and Reinforcement Concrete Columns Side View

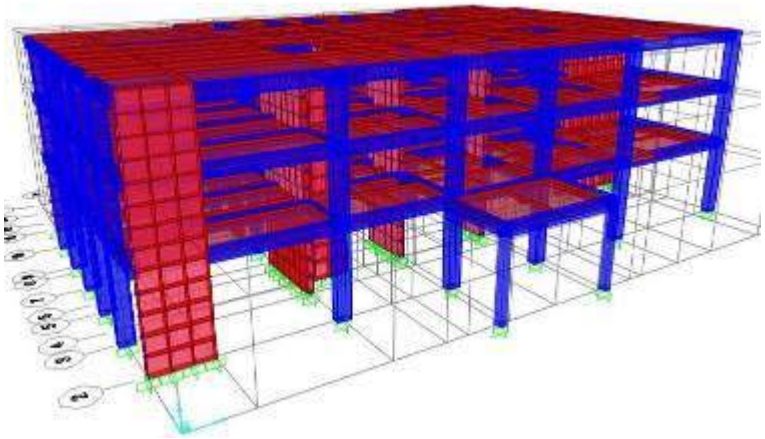

Figure 2. Frames with Shear Walls and Reinforcement Concrete Columns 3D View

GENERAL DIFFERENCES BETWEEN TDY 2007 AND TBDY 2018 EARTQUAKE REGULATIONS IN DESIGN METHODS

There are many differences between the two regulations. While earthquake zones exist in the previous earthquake regulation, the new regulation examines the site specific earthquake risk and ground behaviour. There are also changes related to earthquake ground motion. In the 2007 earthquake regulation, the acceleration coefficient was taken as the only value according to the region where the structure is located. The new regulation takes different values for the short and long period coefficients. There are differences in definitions of ground classes. In the previous regulation the ground class was divided into 4 classes (Z_1, Z_2, Z_3, and Z_4). In the new regulation the ground class is divided into 5 classes. (Z_A, Z_B, Z_C, Z_D, Z_E, Z_F).There is also a change in the building importance coefficient. The building importance coefficient used in the previous earthquake regulation changed to 1.4 value 1.5. The new regulation includes criteria for earthquake design classes and building height classes. One of the most important changes in the new regulation is the use of the coefficient of behaviour and the coefficient of strength (D).

PARAMETERS USED IN EARTHQUAKE REGULATIONS TDY 2007

In this study, project of a school building that is located in Gaziantep city was used. The school is located in the 3rd earthquake zone according to the 2007 earthquake regulation. The ground class was taken as Z_2 from the ground survey report. Since the structure is located in the 3rd earthquake zone, the effective ground acceleration coefficient A_o= 0.2 is taken from Table 2.2 of the 2007 earthquake regulation. The building significance coefficient is 1.4 for school building. The structural behaviour coefficient is R=7 for the frames with shear walls and reinforcement concrete columns system.

PARAMETERS USED IN TBDY 2018 EARTHQUAKE REGULATION

According to 2018 earthquake regulations, S_S = 0.395, S_1 = 0.143 values were determined according to the location of the school building. Soil class is determined as Z_C according to soil survey report. The structural behaviour coefficient is R=7 for the frames with shear walls and reinforcement concrete columns system. The building importance coefficient 1.5 is taken from Table 3.1 of the 2007 earthquake regulation.

$S_{DS}=S_S * F_S = 0.395*1.3=0.513$

$S_{D1}=S_1 * F_1 = 0.143*1.5=0.215$

RESULTS AND FINDINGS

The results of the calculations according to TDY 2007 and TBDY 2018 earthquake regulations are in Figures 3-6 as 4 different evaluations: structure displacement, maximum force generated in the structure, base shear force and structure rotation moment.

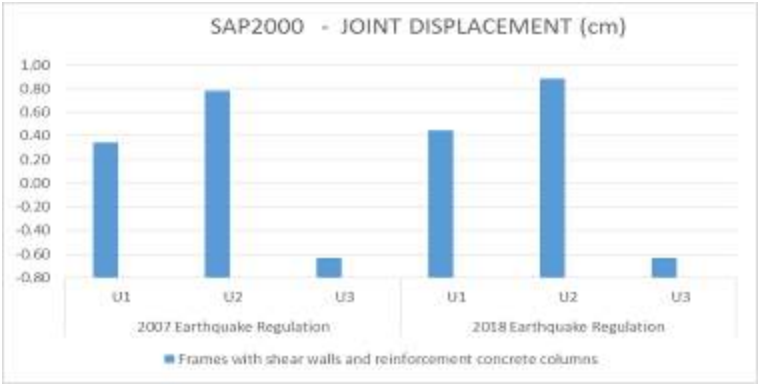

Figure 3. Joint Displacement

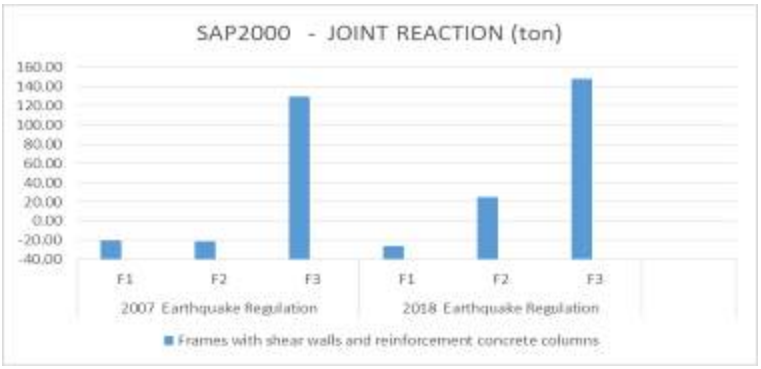

Figure 4. Joint Reaction

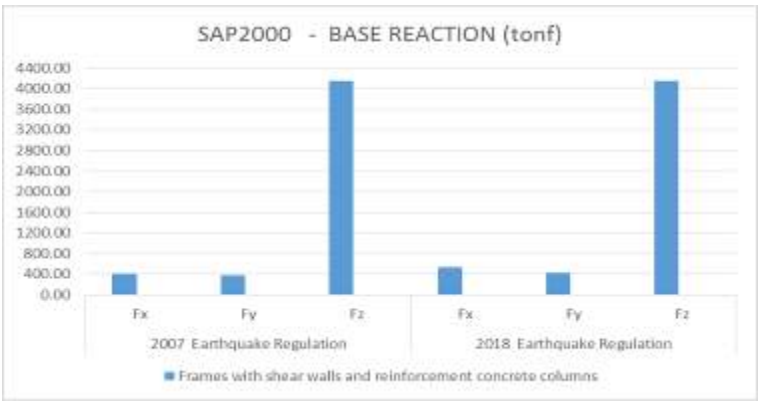

Figure 5. Base Reaction

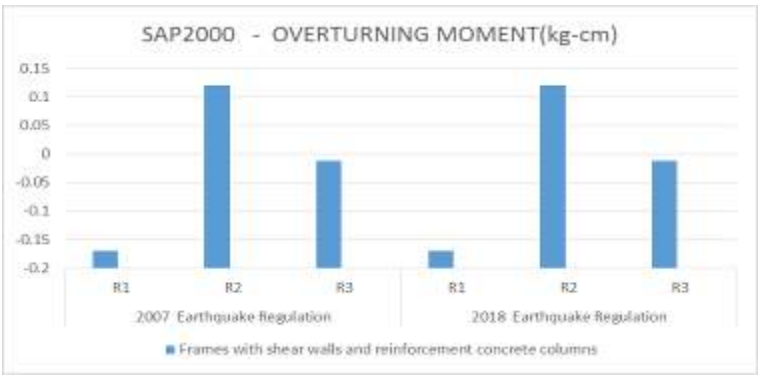

Figure 6. Overturning Moment

CONCLUSIONS

The findings of this study display many differences between TBDY 2018 earthquake regulation and TDY 2007 earthquake regulation. The differences are mainly based on the change in some coefficients such as building importance, structural behaviour, acceleration coefficient and soil safety coefficients. Structural analysis results exhibit that these parameters have a significant impact on the calculations of structural systems. In conclusion;

- The joint displacement in TBDY 2018 and TDY 2007 earthquake regulations are 0.44cm and 0.34cm in X direction respectively. The joint displacement in TBDY 2018 and TDY 2007 earthquake regulations are 0.88 cm and 0.78 cm in Y direction respectively. The displacement results of the TBDY 2018 earthquake regulation are higher than the 2007 earthquake regulation results.
- TBDY 2018 Shear force results provides higher than TDY 2007 earthquake regulations. The 2007 earthquake results are 20.2 ^{t} in the X direction and 21.24 ^{t} in Y direction. TBDY 2018 earthquake regulation shear force results are 25.91 ^{t} in X direction and 24.93 ^{t} in Y direction.
- The base reaction values of TDY 2007 earthquake regulations are 408, 75 ^{t} in X direction and 377.99 ^{t} in Y direction. The base reaction values of the TBDY 2018 regulations are 541.96 ^{t} in X direction and 425.95 ^{t} in the Y direction.
- The overturning moment results both regulation results are very close to each other as -0.17 rad in X direction and 0.12 rad in Y direction.

These findings provide us that TBDY 2018 earthquake regulations stay in more safer side than the TDY 2007 earthquake regulations. Results provides that building design with TBDY 2018 earthquake regulation is , the analysis of this building with 2007 earthquake regulation will be safer.

REFERENCES

Ellul, F., Dina, D., 2003. The Bingol, Turkey Earthquake of the 1st of May 2003, University of Bath Architecture and Civil Engineering Department, England, pp. 10-38.

Alyamaç, K. E. and Erdoğan, A. S. (2005) 'Geçmişten Günümüze Afet Yönetmelikleri ve Uygulamada Karşılaşılan Tasarım Hataları', Deprem Sempozyumu, pp. 707–715.

Deprem, N. A. et al. (2018) 'Resmî Gazete', 30364(1).

Türkiye Deprem Yönetmeliği, Mart, (2007), Deprem Bölgelerinde Yapılacak Binalar Hakkında Yönetmelik", Bayındırlık ve Ġskan Bakanlığı, Ankara

Ge, B. and Hükümler, E. L. (2007) 'Deprem bölgelerinde de yapilacak binalar hakkında yönetmelik'.

Türkiye Bina Deprem Yönetmeliği, Mart, (2018), DEPREM ETKİSİ ALTINDA BİNALARIN TASARIMI İÇİN ESASLAR.

CALCULATION OF HEAT CONDUCTIVITY VALUES OF SOME METALS BY USING ANN

Medine ATMACA, Department of Mathematics, Gaziantep University, mdntmc12@gmail.com

Assoc.Prof.Dr. Necati OLGUN, Department of Mathematics, Gaziantep University, olgun@gantep.edu.tr

ABSTRACT: There are 4 main layers of Neuro fuzzy artificial intelligence systems which have a wide range of application area. These are fuzzification, analysis, function and defuzzification layers. It is very important to calculate accurately the heat thranfer coefficient of materials in thermodynamic problems. In order to calculate the heat transfer coefficient by using theoretical and experimental methods, the inner and outher side temperatures, material thickness, humidity of the environment and surface orea of the material are the basic factors. In this study, the thermal conductivity of aluminum and brass materails have been calculated by using artificial neural networs methodology. The heat transfer consuction coefficient generated by the formulation has been compared with the experimantal results and the correlation coefficient has been checked. The generated formulation will be very useful fort he researchers.

Key words: ANN, Artificial neural networks, Heat consyction coefficiecnt, Aluminum, Brass.

BAZI METALLERİN ISI İLETİM KATSAYISININ YSA METODU İLE BELİRLENMESİ

ÖZET: Oldukça yaygın bir kullanıma sahip olan Yapay Sinir Ağları (YSA) yöntemi 4 ana katmandan oluşmaktadır. Bunlar, Bulanıklaştırma, Analiz, Fonksiyon ve Berraklaştırma katmanlarıdır. Termodinamik problemlerinde ısı iletim katsayısının doğru hesap edilmesi oldukça önemlidir. Isı iletim katsayısının deneysel ve teorik olarak hesaplanmasında; iç ve dış ortam sıcaklığı, malzeme kalınlığı, ortam nem koşulları ve kesit yüzey alanı gibi birçok faktör etkilidir. Bu çalışmada, aluminyum ve pirinç alaşımlı malzemeler için ısı iletim katsayısı bulanık yapay sinir ağları yöntemi kullanılarak tespit edilmiştir. Ortaya çıkan yeni formülle elde edilen ısı iletim katsayısı değerleri deneysel ısı iletim katsayısı değerleri ile karşılaştırılmış ve korelasyon katsayısı kontrol edilerek birbiri ile uyumlu çıkan sonuçlar elde edilmiştir. Bu sonuçlar sayesinde pratik olan bu formül araştırmacıların kullanımına sunulmuştur.

Anahtar Kelimeler: YSA, Bulanık Mantık, Isı iletim katsayısı, Aluminyum, Pirinç.

GİRİŞ

Kinetik teorisine göre doğada bulunan bir maddeyi oluşturan moleküllerin ortalama kinetik enerjileri o maddenin sıcaklığı ile doğru orantılıdır. Bir bölgedeki moleküllerin ortalama kinetik enerjileri yüksek olan ortam içerisindeki bölgede sıcaklık yüksektir. moleküller arası enerji iletimi Katılarda yüksek sıcaklıktan düşük sıcaklığa doğru maddenin ve moleküllerin yapısını oluşturan kafeslerin titreşimleri ile olur. Sıvılarda ise moleküllerin birbirini takip eden çarpışmaları ile olur. (Altun, Ö. & Böke, E., 2009). Isı iletim katsayısının doğru hesap edilmesi oldukça önemlidir. bu katsayının deneysel ve teorik hesabındaki önemli faktörler iç ve dış ortam sıcaklığı ,malzeme kalınlığı, kesit yüzey alanı, ve ortam nem koşullarıdır. Isı iletim katsayısının hesaplanmasında deneysel ve teorik hataların ortaya çıkmasının yanı sıra harcanan zaman ve maliyet kaybının da çıkması kaçınılmazdır. Isı iletim katsayısının hesap edilmesinde alternatif bir yaklaşım olarak YSA Metodu kullanılarak ortaya çıkan yeni formülle elde edilen ısı iletim katsayısı değerleri deneysel ısı iletim katsayısı değerleri ile karşılaştırılmış ve korelasyon katsayısı kontrol edilmiştir.

YÖNTEM

Isı Transferi

Termodinamiğin 2. Yasasına göre iki ortam arasında sıcaklık farkı varsa ısı yüksek sıcaklıktaki ortamdan düşük sıcaklıktaki ortama geçer. Isı transferi sistemi üç başlık altında incelenmelidir. Bunun nedeni ısınım geçişinin ortam sıcaklıklarındaki farka bağlı olduğu kadar, ortam ve yüzeylerinin özelliklerine de bağlı olmasından kaynaklanmaktadır.

İletim

İletimle (kondüksiyon) ısı geçişi bir cismin birbirinden farklı olan sıcaklıktaki bölgeleri arasında, birbiriyle temas halinde olan parçacıklardan yüksek enerji seviyesinde bulunan parçacıklardan, düşük enerji seviyesinde bulunan parçacıklara doğru geçen enerji katı, sıvı ve gaz ortamlarında gerçekleşebilmesidir.

Fourier Isı İletim Yasası

Yukarıdaki şekilde görüldüğü gibi iki boyutlu oldukça büyük düz bir levha örnek olarak alınsın. T_1 ve T_2 levha yüzey sıcaklıkları ($T_1 > T_2$) A levhanın yüzey alanını göstersin. Sıcaklık geçişi T_1 (sıcak yüzeyinden T_2 (soğuk) yüzeyine doğru olacak ve zamanla değişmeyecektir. Deneylere göre ısı geçişi;

$$q = A\frac{T_1 - T_2}{L}$$

şeklinde olmalıdır. Yukarıda da gösterildiği gibi, katı bir cisimden ısı geçiş hızı levha kalınlığı L ile ters orantılı A yüzeyi ve (T_1-T_2) sıcaklık farkı ile doğru orantılıdır. Yukarıdaki ifadenin içerisine orantı kat sayısı k yerleştirilirse,

$$q = -kA\frac{(T_2 - T_1)}{L}$$

şeklindeki ifade elde edilir. Isı iletim katsayısı malzemenin bir özelliğidir ve k olarak ifade edilir. Termodinamiğin 2.yasası gereği ısı iletim katsayısı sıcaklığın azaldığı yönündedir. Bu nedenle sıcaklık farkı ile ısı akısı ters işaretlidir. Pozitif yönde ısı geçişi elde etmek için yukarıda bulunan ifadenin önüne (-) işareti konulur. Isı iletim katsayısı olan k'nın boyutu SI birim sisteminde W/mK veya W/m^{o}C'dır.

Taşınım

Katı yüzey ile akışkan yüzey arasında gerçekleşen ısı transferinin bir çeşidi olan taşınım (konveksiyon) katılarda olmaz, sadece hareket halinde olan akışkan(sıvı ya da gazlarda) olur. (TURAN, O. 2018).

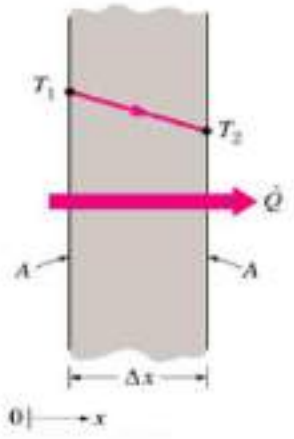

Şekil 1. Düzlem bir duvarın her iki yüzeyinde taşınım sınır şartı

Işınım

Işınım olarak adlandırılan sonlu sıcaklığa sahip bir cisim tarafından elektromanyetik dalgalar şeklinde yayılan enerji ile ısı transferi için bir ortam gerekliliği bulunmamaktadır. Hatta ışınım ile ısı transferi boşlukta daha etkin olarak gerçekleşmektedir. Ancak iletim ve taşınımda ısı transferi için bir ortama ihtiyaç duyulmaktadır. Tüm maddeler ışınımı farklı seviyelerde soğurur, yayar veya geçirirler. (TURAN, O. 2018).

Genel olarak ısı transferi mekanizmaları Şekil 2.'deki gibi belirtilebilir.

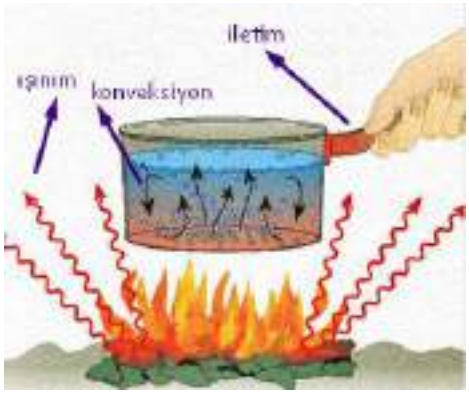

Şekil 2. Isı Transferi Mekanizmaları

Sinirsel Bulanık Sistem (Neuro-Fuzzy)

Yapay sinir ağları, Bulanık sinirsel ağlar ve bulanık sistemlerin birleşiminden oluşan sinirsel bulanık sistem yapay zekâ tekniklerinden birisidir. Bulanık mantık yaklaşımı, karar almada çok iyi sonuçlar verir. Ancak bu süreç içerisindeki kural oluşturmayı kendiliğinden gerçekleştiremez. Yapay sinir ağlarının öğrenme yeteneği, bulanık mantığın insan gibi karar verme ve uzman bilgisi sağlama kolaylığı gibi üstünlüklerinin birleştirilmesi düşüncesine dayanmaktadır. Sinirsel bulanık mantık yaklaşımı, bu yolla bulanık denetim sistemlerine, sinir ağlarını öğrenme ve hesaplama gücü verilebilir. Sinir ağlarına da uzman bilgisi sağlama yeteneği ve karar verme yeteneği de edindirilmektedir. (Çoban, M.A., 2012).

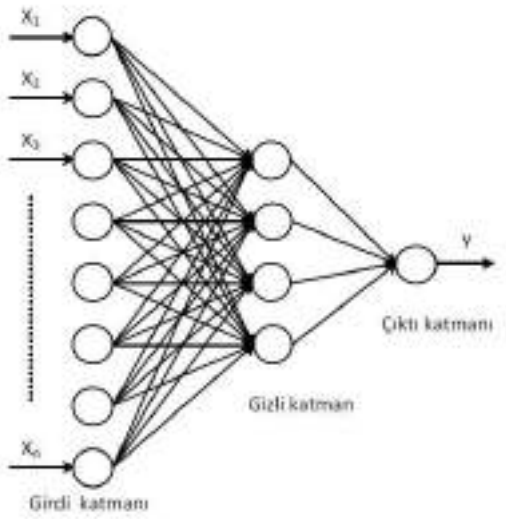

Şekil 4. Biyolojik ve Nöral Hücre

BULGULAR
Deneysel Veriler

Bu çalışmada alüminyum ve pirinç alaşımlı malzemelerin ısı iletim katsayısının bulanık yapay sinir ağları yöntemi kullanılarak tespit edilmiştir. Isı iletim katsayılarının zamana bağlı olarak değişimi incelendi. Deney numunesi olarak kullanılan pirinç ve alüminyum alaşımı 50 W güç girişi altında 70 °C sabit rezistans sıcaklığı altındadır. Bulunan veriler tablo oluşturularak gözlemlendi. Bu çalışma kapsamında alüminyum ve pirinç alaşımlı malzemeler için belirli sıcaklıklardaki ısı iletim katsayısı değerleri Özçelik vd. (2017)'de bulunan deneysel verilerden alınmıştır. Söz konusu malzemelerin her katmandaki girdileri sıcaklık değerleri, ve ölçüm süreleridir. Isı iletim katsayısı değeri ise çıktıdır.

FORMÜLLERDEN ÇIKAN ISI İLETİM KATSAYISI DEĞERLERİ

Ağın çıktı değerleri sunulan girdiye bağlı olarak hesaplanılır. Çıktı verileri eğitim verilerinden yola çıkılarak elde edilmeye çalışılır. Girdi hesaplamadaki en önemli husus çıktı değerlerinin en düşük hata ile tahmin edilmeye çalışılmasıdır.Ayrıca YSA 'nın en temel kuralı da budur.

Tablo 3. Sistem için tasarlanan Alüminyum malzemesi Girdi ve Çıktı Tablosu

Ölçüm Süresi (Dakika)	T1	T2	T3	T4	T5	T6	T7	T8	T9	T10	Deneysel	YSA
5	17,1	16,6	16,6	16,1	17,1	17,1	17,6	18,6	25,4	25,4	796,18	796,1859
10	17,1	17,1	16,6	16,1	17,6	18,1	19,5	22	39,6	40	306,22	302,28
15	17,1	17,1	16,6	16,6	17,6	19	20,5	24,9	42,5	42,5	202,42	204,35
20	17,1	17,1	17,1	16,6	17,6	20,5	22,5	27,3	44,4	43,9	175,63	165,24
25	17,6	17,6	17,1	17,1	18,1	21,5	23,4	28,3	44,4	45,4	175,63	165,24
30	17,6	17,6	17,1	17,1	18,6	22	23,9	28,8	44,4	44,9	175,63	165,24
35	17,6	17,6	17,1	16,6	18,6	22,5	24,4	29,3	44,4	44,9	175,63	165,24
40	18,1	17,6	17,1	17,1	18,6	22,5	24,9	29,3	44,4	44,4	175,63	165,24
45	17,6	17,6	17,1	17,1	18,6	22	24,9	28,8	43,5	43,9	175,63	165,24
50	17,6	17,6	17,6	17,1	18,6	22,5	24,4	29,3	43,5	43,5	175,63	165,24

55	18,1	17,6	17,6	17,1	18,6	22,5	24,9	29,3	43	43,5	175,63	165,24
60	18,1	18,1	17,6	17,6	19	22,5	24,9	29,3	43	43	175,63	165,24

Tablo 4. Sistem için tasarlanan Pirinç malzemesi Girdi ve Çıktı Tablosu

Ölçüm Süresi (Dakika)	T1	T2	T3	T4	T5	T6	T7	T8	T9	T10	Deneysel	YSA
5	17,6	17,6	17,6	17,1	18,1	17,6	18,6	19	26,9	33,7	568,69	568,69
10	18,1	18,1	18,1	17,6	18,6	18,6	19,5	21,5	37,4	68,4	274,54	271,25
15	18,1	18,1	18,1	17,6	18,6	19	20,5	24,4	41,5	43	147,44	145,36
20	18,1	18,1	18,1	17,6	18,6	20	21,5	25,9	43,5	44,4	134,95	130,96
25	18,1	18,1	18,1	18,1	19	20,5	22,5	26,4	43,5	45,4	134,95	130,96
30	18,1	18,1	18,1	18,1	19	21	23	27,3	44,4	45,4	126,38	118,56
35	18,1	18,1	18,1	18,1	19	21	23	27,3	43,9	45,4	126,38	118,56
40	18,6	18,6	18,1	18,1	19	21	23	27,3	43,9	45,9	126,38	118,56
45	18,6	18,6	18,1	18,1	19,5	21	23	27,3	43,9	45,9	126,38	118,56
50	18,6	18,6	18,6	18,6	19	21	23	27,3	43,5	44,9	126,38	118,56
55	18,6	18,6	18,6	18,1	19,5	21	23,4	27,3	43	48,3	126,38	118,56
60	18,6	18,6	18,6	18,1	19,5	21	23	27,3	43,5	48,8	126,38	118,56

Eğitim verilerini kullanarak gerekli öğrenmeyi sağlayan YSA daha sonra öğrenme setindeki örneklerin ağa uygulanması ile öğrenme işlemini gerçekleştirir. YSA 'nın test eğitim verilerinin ağa uygulanması ile belli bir hata değeriyle tahmin etme işlemi Ysa'nın öğrenme yeteneğini gösterir. Öğrenmede ağırlıklar rastgele atanır. öğrenmeye bağlı olarak YSA 'nın eğitilmesi işleminde de ağırlıklar çıkışa bağlı olarak sistemli bir Şekilde öğrenme gerçekleştirildikten sonra güncellenecektir. İleri beslemeli YSA'da hata istenilen düzeyin altına indiğinde veya belli bir iterasyon sayısı tamamlandığında öğrenme ve ağın eğitimi bitmiş olur. YSA ile ısı iletim katsayısının tahmin edilmesi için Neuro Solution programı kullanılmıştır. Isı iletim Katsayısı tahmini için sırası ile

aşağıdaki aşamalar test edilmiştir. Eğitim verileri daha iyi bir sonuç elde edilmesi için Neuro Solutionda normalize edildi. Şekil 8 ve 9 da görüldüğü gibi ısı ıletim katsayısı tahmini için elde edilen grafiklerde sonuçların yakınsadığı görülmüştür.

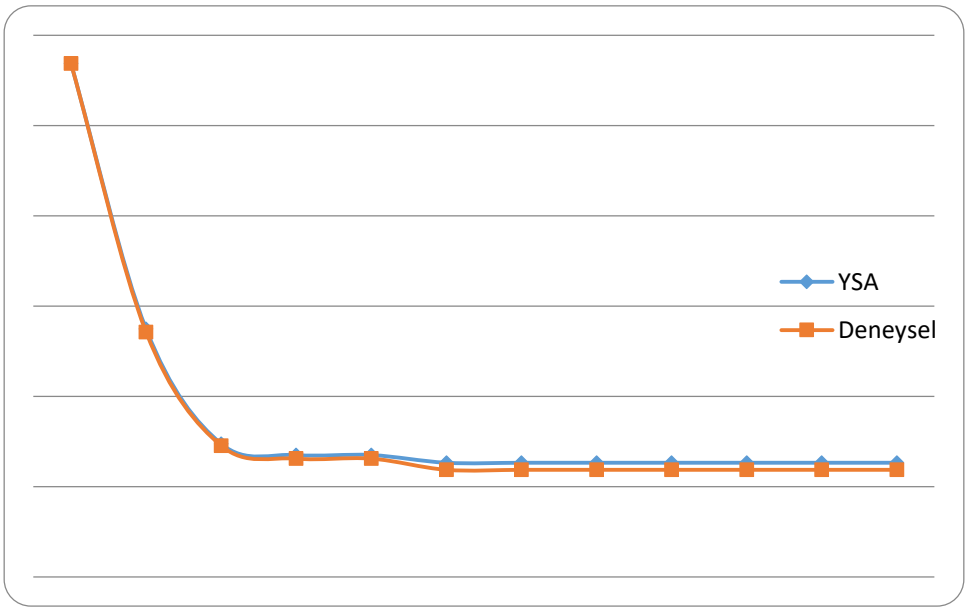

Şekil 8. Alüminyum Malzemesi için YSA-Deneysel Sonuçlar

Eğitimin deney verileri ile tamamlanmasından sonra, ağın güvenilirliğini sınamak amacıyla, eğitim kümesinden gerçek çıkış ile yapay sinir ağının hesaplamış olduğu çıkış karşılaştırılarak elde edilen YSA çıkışı ile Eğitim verisinin çıkışı grafiksel olarak görsel bi şekilde gösterilmiştir. Yani ısı iletim katsayısı başarılı bir şekilde tahmin edilmiştir.

Eğitim sonucu tahmin edilen ısı iletim katsayısı değeri mavi çizgi ile YAS deneysel ısı iletimi değerleri ise sistemde kırmızı çizgi ile gösterilmektedir.

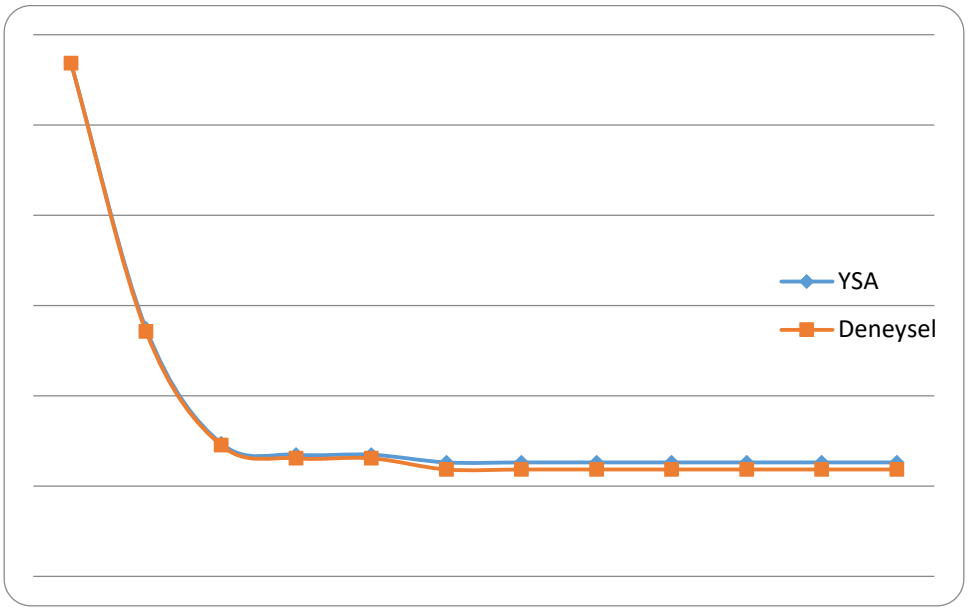

Şekil 9. Pirinç Malzemesi için YSA-Deneysel Sonuçlar

SONUÇ

Termodinamik problemlerinde ısı iletim katsayısının doğru hesap edilmesi oldukça önemlidir. Bu çalışmamızda Isıl İletim Katsayısı Bulanık Mantık İle Modellenmesi 25 deneysel veri kullanılarak yapılmıştır. Isı iletim katsayısının deneysel ve teorik olarak hesaplanmasında; iç ve dış ortam sıcaklığı, malzeme kalınlığı, ortam nem koşulları ve kesit yüzey alanı gibi birçok faktör etkilidir. Bu çalışmada, alüminyum ve pirinç alaşımlı malzemeler için ısı iletim katsayısı bulanık yapay sinir ağları yöntemi kullanılarak tespit edilmiştir. Ortaya çıkan yeni formülle elde edilen ısı iletim katsayısı değerleri deneysel ısı iletim katsayısı değerleri ile karşılaştırılmış ve korelasyon katsayısı kontrol edilerek birbiri ile uyumlu çıkan sonuçlar elde edilmiştir. Bu sonuçlar sayesinde pratik olan bu formül araştırmacıların kullanımına sunulmuştur.

KAYNAKÇA

Altun, Ö. & Böke, E. (2009). Isıl Engelleyici Kaplamaların Etkin Isı İletim Katsayısının Teorik Olarak Belirlenmesi, Eskişehir Osmangazi Üniversitesi Mühendislik Mimarlık Fakültesi Dergisi, 22 (2) 139-152.

Civalek, Ö., Çatal, H.H., (2004). Geriye Yayılma Yapay Sinir Ağı Kullanarak Elastik Kirişlerin Statik ve Dinamik Analizi, DEÜ Mühendislik Fakültesi Fen ve Mühendislik Dergisi, 6(1),1-16.

Çoban, M.A., (2012). Konut Yapımında Kullanılan Farklı Duvar tipleri için Toplam Eşdeğer Sıcaklık Farklarının(TESF) Bulanık Sinirsel Denetim Metoduyla Tahmini Olarak Elde Edilmesi, Gaziantep Üniversitesi Matematik Bölümü.

Ergezer, H., Dikmen, M., Özdemir, E., 2003, Yapay Sinir Ağları ve Tanıma Sistemleri, Pivolka, s. 14-17

Özçelik (2017)Teskon Termodinamik Sempozyumu

TURAN, O., (2018) Ders Notları, Bilecik Şeyh Edebali Üniversitesi Makine ve İmalat Mühendisliği Bölümü.

UNDERGRADUATE INDUSTRIAL CONTROL LABORATORY EXPERIMENTAL SETUP: PART 3 LIQUID LEVEL CONTROL WITH PLC

Cengiz TEPE, Ondokuz Mayıs University, Electrical and Electronics Engineering Department, cengiztepe1@gmail.com

Mehmet Serdar ÇELİK, Ondokuz Mayıs University, Electrical and Electronics Engineering Department, mehmetserdar.celik@omu.edu.tr

Mustafa ÖZÇELİK, Ondokuz Mayıs University, Electrical and Electronics Engineering Department, ozcelikm.emin@gmail.com

İlyas EMİNOĞLU, Ondokuz Mayıs University, Electrical and Electronics Engineering Department, ilyaseminoglu@hotmail.com

ABSTRACT: Liquid level control systems controlled by PLC (Programmable Logic Controller) are one of the widely used applications in industry and commercial products. To implement this process control by PLC will make a significant contribution to the future professional life of Electical and Electronics, Control, Mechatronic and Machine Engineering departments students. For this purpose, through a commercial PLC and HMI (Human Machine Interface) display, a experimental setup was designed and implemented to control 50 cm height tank liquid level. PID (Proportional - Integral - Derivative) block in the PLC software was used as the controller. Liquid level was measured using a magnetic liquid level sensor, which provides level information as a 4-20 mA current output. The level information in the range of 4-20 mA is converted to the voltage value in the range of 0-10 V by the signal converter and read from the analog input of PLC. Direct current bilge pump was used as actuator and driven by L298 direct current motor driver. Disturbance can be applied to the system by a drain valve. The liquid level data, which is the instant output value of the process, is displayed both on the HMI display with a bar and numerically. Thanks to this study using industrial devices, the students are given the ability to implement an industrial application besides providing theoretical knowledge.

Key words: level control, experimental setup, PLC, industrial, education

LİSANS ENDÜSTRİYEL KONTROL LABORATUVARI DENEY DÜZENEĞİ: BÖLÜM 3 PLC İLE SIVI SEVİYE DENETİMİ

ÖZET: PLC ile denetlenen sıvı seviye denetim sistemleri, endüstride ve ticari ürünlerde yaygın olarak kullanılan uygulamalardan bir tanesidir. Elektrik - Elektronik, Kontrol, Mekatronik ve Makine Mühendisliği bölümü öğrencilerinin bu prosesi tanımaları ve bu prosesin PLC (Programmable Logic Controller) aracılığıyla nasıl denetlenebileceğini öğrenmeleri, gelecek meslek hayatları için öğrencilere ciddi katkılar sunacaktır. Bu amaçla, ticari bir PLC ve HMI (Human Machine Interface) ekran aracılığı ile, 50 cm yüksekliğe sahip tanktaki sıvı seviyesini denetleyen bir deney seti gerçeklenmiştir. Denetleyici olarak PLC yazılımı içerisindeki PID (Proportional – Integral - Derivative) bloğu kullanılmıştır. Sıvı seviye ölçümü, seviye bilgisini 4-20 mA akım çıkışı olarak veren manyetik sıvı seviye sensörü kullanılarak gerçekleştirilmiştir. 4-20 mA aralığındaki seviye bilgisi, sinyal dönüştürücü ile 0-10 V aralığındaki gerilim değerine dönüştürülmüş ve PLC analog girişinden okunmuştur. Eyleyici olarak doğru akım sintine pompası kullanılmış olup, L298 doğru akım motor sürücüsü ile sürülmüştür. Sisteme bir vana yardımıyla bozucu etki uygulanabilmektedir. Prosesin anlık çıkış değeri olan sıvı seviye bilgisi, HMI ekran üzerinden hem bir bar ile hem de sayısal olarak gösterilmiştir. Endüstriyel cihazlar kullanılarak yapılan bu çalışma sayesinde öğrencilere teorik bilgi vermenin yanında, endüstriyel bir uygulamayı gerçekleştirme becerisi kazandırılmıştır.

Anahtar kelimeler: seviye denetimi, deney düzeneği, PLC, endüstriyel, eğitim

GİRİŞ

Sıvı seviye denetimi endüstriyel sistemlerde ve ticari ürünlerde sıklıkla uygulanmaktadır ve çeşitli uygulama yolları gerçekleştirilmiştir. En basit sıvı seviye uygulaması su tankındaki sıvı seviyesinin mekanik olarak şamandıralar vasıtasıyla algılanmasıdır. Sıvıya göre yoğunluğu daha düşük olan şamandıra, sıvı seviyesi arttıkça sıvı yüzeyine yükselir. İlk seviye uygulamalarında şamandıralar kablo, makara ve dişliler ile birlikte çalışırken günümüzde manyetik yöntemler kullanan şamandıralar da kullanılmaktadır (Şahbazlı, 2017). Önceden belirli bir seviyeyi ya da belirli bir aralığı algılayan sıvı seviye uygulamaları şamandıralı seviye şalterleri, ultrasonik şalterler ve kapasitif problar gibi algılayıcılar ile kolaylıkla gerçekleştirilebilir (Milli Eğitim Bakanlığı, 2009). Mekanik seviye şalteri (A) ve iletken elektrotlara (B) ait bir görsel Şekil 1'de verilmiştir.

Şekil 6. Belirli Bir Seviyeyi Algılamak İçin Kullanılan Mekanik Seviye Şalteri (A) ve Aralık Algılamada Kullanılan İletken Elektrotlar (B)
Noktasal olarak değişken ve hassas ölçüm gerektiren uygulamalar için oransal manyetik sıvı seviye sensörü, radar ya da ultrasonik sensör kullanılabilmektedir.

Günümüz endüstriyel uygulamalarının yaklaşık %90'ında denetim, PID (Proportional-integral-derivative) algoritmasıyla gerçekleştirilmektedir (Astöm & Hagglund, 2006). Sistemler, ticari PID cihazları ile ya da PLC (programmable logic controller) cihazlarında koşturulan PID algoritmalarıyla denetlenebilir.

Sıvı seviye denetimi, endüstride ve ticari ürünlerde sıklıkla kullanılmasının yanında kontrol yöntemlerinin anlaşılması, geliştirilmesi ve uygulanmasında kullanılabilecek pratik bir sistemdir. Çalışmanın amacı, Ondokuz Mayıs Üniversitesi Elektrik Elektronik Mühendisliği bölümünde verilen Kontrol Sistemleri Laboratuvarı dersini alan öğrencilerin, gelecek iş hayatlarına adapte olmalarını kolaylaştırmak ve endüstride sıklıkla kullanılan bu gibi sistemlere aşina olmalarını sağlamaktır. Bu amaçla, günümüzde bazı firmalar tarafından üretilen ticari deney setleri bulunmaktadır. Ticari deney setleri üreten Feedback Instruments, Kent Ridge Instruments, Çokesen Elektronik ve Ulus Otomasyon firmalarına ait sıvı seviye deney setleri mevcuttur. Şekil 2'de Kent Ridge Instruments firmasına ait sıvı seviye deney setinin görseli paylaşılmıştır.

Şekil 7. Ticari Sıvı Seviye Denetimi Deney Seti Örneği (Kent Ridge Instruments, 2019)

Sıvı seviye denetimi akademik çalışma ve kaynaklarda da kendine sıklıkla yer bulmuştur. Erdemir (2006) çalışmasında, üniversite kontrol laboratuvarı için doğrusal olmayan sistemlerin kontrol yazılımlarının üzerinde denenebileceği web tabanlı bir deney seti yapmayı amaçlamıştır ve tasarladığı deney seti üzerinde PID, bulanık mantık, aç-kapa denetim gibi farklı denetim yöntemlerini uygulamıştır. Adiyan (2012) gerçekleştirdiği çalışmasında motor sürücüsü içinde yer alan PID denetleyicisi ile, potansiyometreye bağlı bir şamandıra ve santrifüj pompa kullanarak sıvı seviye sistemini denetlemiştir. Ulu (2010) gerçekleştirdiği çalışmasında kontrol deneylerinde kullanılması için geliştirilmiş bir sıvı seviye sistemini PID denetimi ile MATLAB® paket programı üzerinden gerçek zamanlı olarak denetlemiştir. Literatüre yansıyan bir başka çalışmada sıvı seviyesi PLC içerisindeki PID denetleyici ile denetlenmiştir ve denetleyici parametreleri röle geribesleme yöntemiyle otomatik olarak ayarlanmıştır (Dandan, Zhiyun, Meng, Yue & Chen, 2015). Bir diğer çalışmada PID ve bulanık mantık temelli denetleyicilerle kimyasal endüstrisinde kullanılacak endüstriyel bir sıvı seviye denetim düzeneği tasarlanmıştır (Bu, Li, Chen & 2016). Benzer biçimde Popescu (2018) tarafından gerçekleştirilen çalışmada da sıvı seviye denetimi için PID ve bulanık mantık tabanlı denetleyiciler karşılaştırılmıştır.

Bu çalışma ile, Elektrik Elektronik Mühendisliği bölümü Kontrol Sistemleri dalı öğrencilerinin endüstride sıklıkla kullanılan sıvı seviye denetimini gerçekleştirebilmeleri, bu sistemde kullanılan endüstriyel sensör ve denetleyicileri kullanabilmeleri amaçlanmıştır. PLC ile gerçekleştirilen bu çalışmada PID denetimi kullanılmış olup diğer denetim yöntemlerinin de düzenekte denenmesi mümkündür. Teorik kontrol eğitiminin endüstriyel yansımalarını gören öğrencilerin özgüvenlerinin ve ilgilerinin arttırılması planlanmıştır.

DENEYSEL ÇALIŞMA

Sıvı Seviye Deney Düzeneği Tasarımı ve Gerçeklemesi

Bu çalışmada tasarlanan ve gerçeklenen deney düzeneğinin öbek çizgesi Şekil 3'te ve deney düzeneği Şekil 4'te verilmiştir. Deney düzeneğinde kullanılan devre elamanları Tablo 1'de gösterilmiştir.

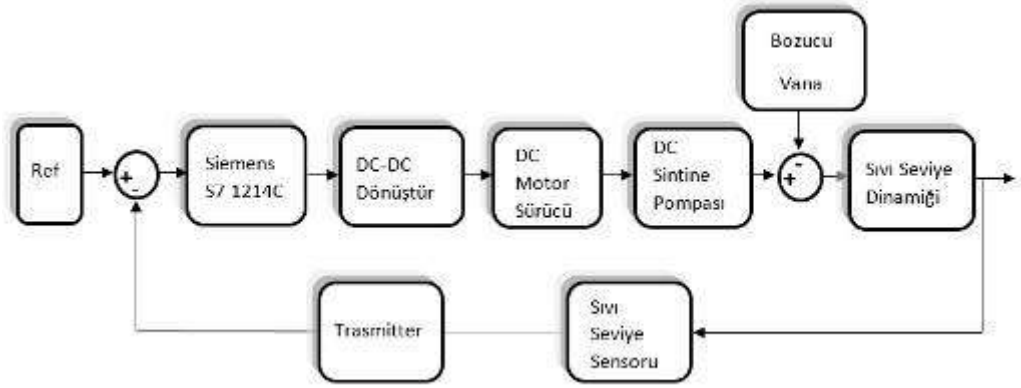

Şekil 3. Sıvı Seviye Sistemi Blok Diyagramı

Şekil 4. Sıvı Seviye Sistemi Genel Görünümü

Tablo 1. Sıvı Seviye Sisteminde Kullanılan Malzemeler

Malzemeler	Harflendirme
Siemens S7 1214C PLC	A
KTP700 Basic HMI	B

4-20ma to 0-10V Transmitter	C
Manyetik Sıvı Seviye Sensörü	D
DC-DC Dönüştürücü	E
DC Motor Sürücü	F
12V, 24V DC Kaynak	G
12V DC Sintine Pompası	H

Manyetik Sıvı Seviye Sensörü

Manyetik sıvı seviye sensörü (Şekil 5) 12 volt ile beslenmektedir. Çıkışı ise 4-20 mA arasında sıvı seviyesine göre değişmektedir. Kullanılan PLC modeli analog giriş olarak 0-10 V arasını kabul etmektedir. Bu nedenle 4-20 mA değerini 0-10 V değerine dönüştüren trandüser kullanılmıştır. Sensör bağlantı şeması Şekil 9'da gösterilmiştir.

Şekil 5. Manyetik Sıvı Seviye Sensörü

DC-DC Dönüştürücü

Şekil 6' daki dönüştürücü 900 kHZ değerlerine kadar çalışabilmektedir. Dönüştürücünün V_{IN} girişine PLC Q0.0 çıkışından gelen 24 V'luk PWM sinyali bağlanır. V_{OUT} çıkışından ise doğru akım (DC) motor sürücüsüne gidecek 5V'luk PWM alınır. GND hem PLC hem de DC motor sürücüsü toprağı ile kısa devre edilir.

Şekil 6. Dc-Dc Dönüştürücü

Su Pompası

Şekil 7′ de doğru akım sintine pompası gösterilmiş olup pompa 12 V ile beslenmektedir. Pompa 500 GPH (galon per hour) değerinde sıvı pompalamaktadır ki bu değer 1890 saat başına litre hacmine denktir. Su pompasının bağlantı şeması Şekil 14′te gösterilmiştir.

Şekil 7. Su Pompası

L298n Motor Sürücü

Şekil 8′deki L298n motor sürücüsü 2 tane dc motoru 2A ve 35V değerlerine kadar sürebilmektedir. 12V besleme gerilimi yapılmıştır. ENA girişine dönüştürücüden gelen PWM sinyali bağlanmıştır. Pompa ise OUT1 çıkışına bağlanmıştır. IN1 girişine kartın üzerindeki 5V′luk çıkış ve IN2 ‘ye ise topraktan bağlantı yapılarak yön bilgisi girilmiştir. Bağlantı şeması Şekil 9′da gösterilmiştir.

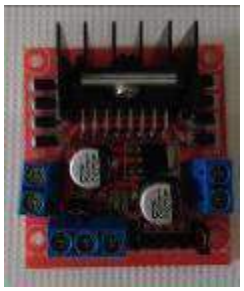

Şekil 8. L298n Motor Sürücüsü

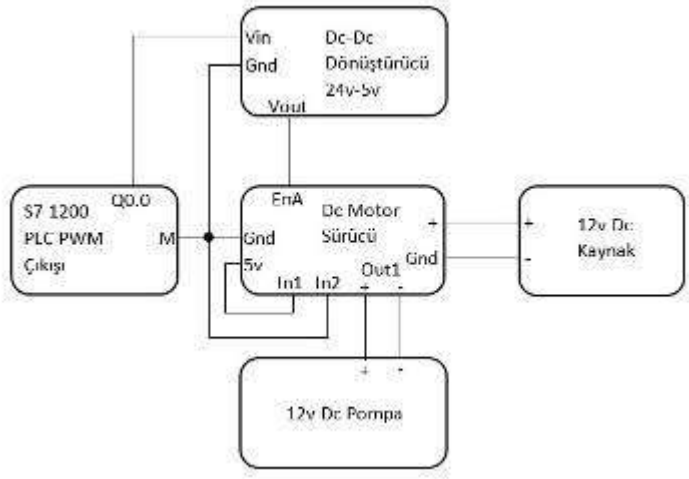

Şekil 9. Motor Sürücü Bağlantıları

Transdüser (Dönüştürücü)

Şekil 10'da A potu 3, B potu 7, D potu ise 3 olarak ayarlandığında 4-20mA giriş değeri 0-10V çıkış değerine çevrilmektedir. Dönüştürücünün bağlantı şeması Şekil 11'de gösterilmiştir.

Şekil 10. Transdüser

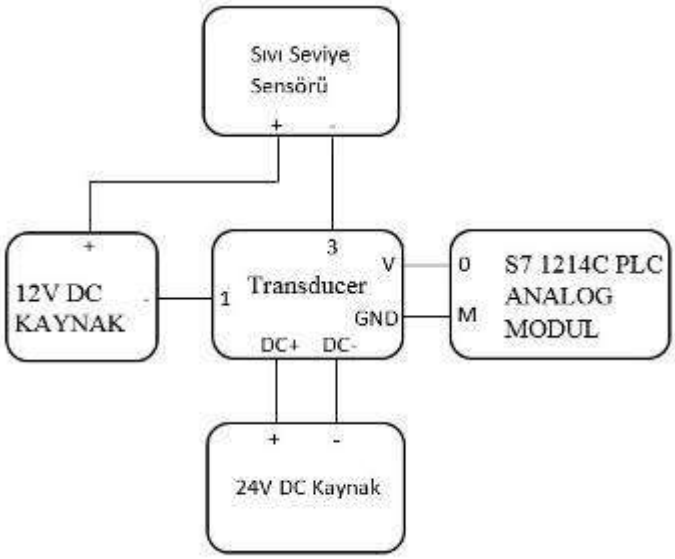

Şekil 11. Transdüser Bağlantıları

PLC Programı

Şekil 12 ve Şekil 13'de gözüktüğü gibi Network 1 ve Network 2 Program Blocks altında bulunan Main Block içerisinde iken PID bloğu Cyclic Interrupt içerisindedir. Transdüser 0-10 V çıkış vermeye ayarlandığından NORM_X bloğunda MAX değer olarak 10V değerinin sayısal karşılığı olan 27648 değeri girilmiştir.

NORM_X bloğu analog gerilim geldiğinde sayısal karşılığı olan değeri 0-27648 arasındaki konumuna göre yüzdeliğe çevirmektedir. SCALE_X bloğu ise yüzdelik değeri 0-50 arasına çevirir.

HMI ekranda sıvı seviyesi tam sayı olarak gösterilmek istenmiştir. Çünkü kullanılan manyetik sıvı seviye sensörü 1 cm hassasiyetinde çalışmaktadır. Bunun için SCALE_X bloğu çıkışı tam sayı olacak şekilde ayarlanmıştır. PID bloğu girişinde ise reel sayı girilmesi için CONV bloğu ile sıvı seviye değişkeni reel sayı tipine dönüştürülmüştür.

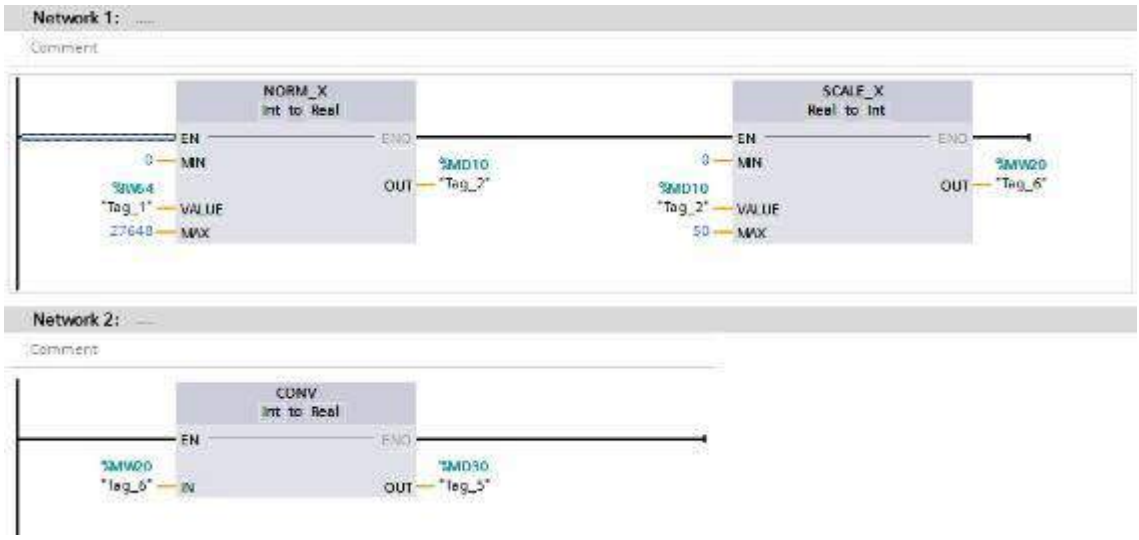

Şekil 12. Ladder Diyagramı

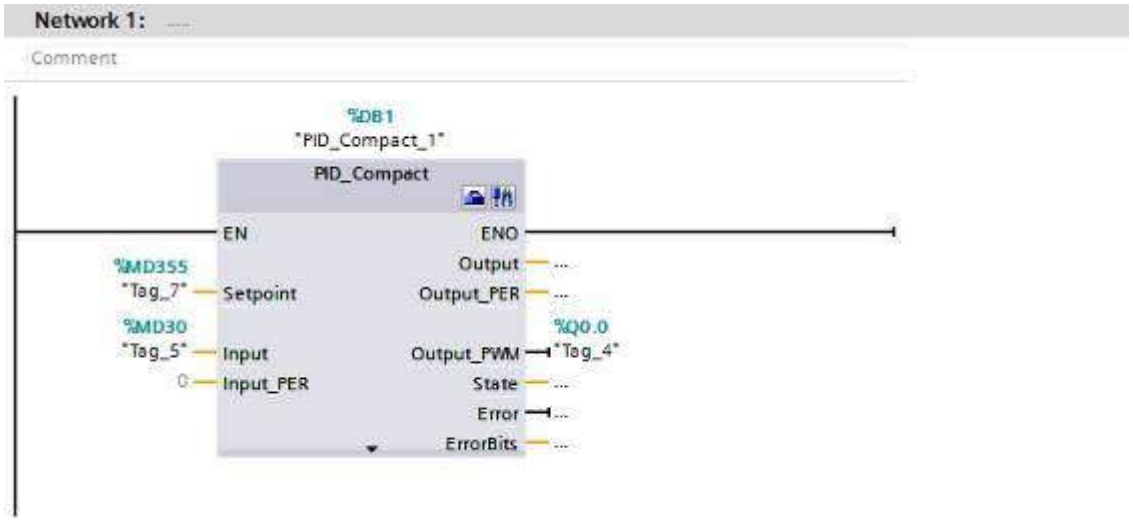

Şekil 13. PID bloğunu içeren Cyclink Network

PLC Tag Tablosu

PLC hafızası içerisinde yardımcı röleler ve donanımsal çıkışların adresleri Tablo 2'de gösterilmiştir.

Tablo 2. PLC Etiket ve Adresleri

Etiketler	PLC Adres	Açıklamaları
Tag_1	%IW64	Manyetik sıvı seviye sensörünün bağlı olduğu sinyal dönüştücüden çıkan 0-10 V arası analog değerin okunduğu PLC adresi
Tag_2	%MD10	0-10 V analog değerin 0-27648 sayısal değerleri arasında ve yüzdeliğe çevrilmiş değerini tutan PLC adresi
Tag_4	%Q0.0	Motor sürücüsüne gönderilmek üzere Dc-Dc düşürücüye bağlı bulunan PLC PWM çıkış adresi
Tag_5	%MD30	0-50cm arası tam sayı değerin reel sayı karşılığını tutan PLC adresi
Tag_6	%MW20	Yüzdeliğe çevrilmiş seviye bilgisinin 0-50cm arasına ölçeklenmiş değerini tutan PLC adresi
Tag_7	%MD355	PID blok girişinde setpoint değerini tutan PLC adresi

HMI Ekran

Şekil 14. HMI Ekran Tasarımı

HMI Tag Tablosu

Tablo 3. PLC Etiket ve Adresleri

Etiketler	HMI Adres	Açıklamaları
Tag_6	%MW20	HMI ekranda anlık değeri gösterilen proses çıkışını yani sıvı seviyesini tutan PLC adresi
Tag_7	%MD355	HMI ekrandan girilen setpoint değerini tutan PLC adresi

BULGULAR

Gerçeklenen sistemde ticari bir manyetik sıvı seviye sensörü kullanılmıştır. Kullanılan sensör, seviye bilgisini ±1 cm hassasiyet ile algılamaktadır. Bu sapma sistemin denetimini de zorlaştırmaktadır. Denetim başarımının artması için daha hassas manyetik sıvı seviye sensörleri ya da ultrasonik sensörler kullanılabilir. Şekil 4'te paylaşılan düzenekteki tank sıvı seviyesi PLC aracılığıyla PID denetim yöntemi kullanılarak denetlenmiştir. Öncelikle sistemin yalnızca oransal denetim kullanıldığındaki davranışı incelenmiştir. PID denetleyicinin integral elemanı sabiti ve türev elemanı sabiti sıfır iken, oransal eleman sabitine 29 değeri verilmiştir. Tank tamamen boş iken 10 cm referans değeri HMI ekrandan girilmiştir. Sistem çıkışına ait grafik Şekil 15'de paylaşılmıştır. Beklendiği üzere yalnızca oransal denetim kullanıldığında sistemde kalıcı hal hatası oluşmuştur. Bu hatayı ortadan kaldırabilmek için denetleyiciye integral elemanı da eklenmiştir.

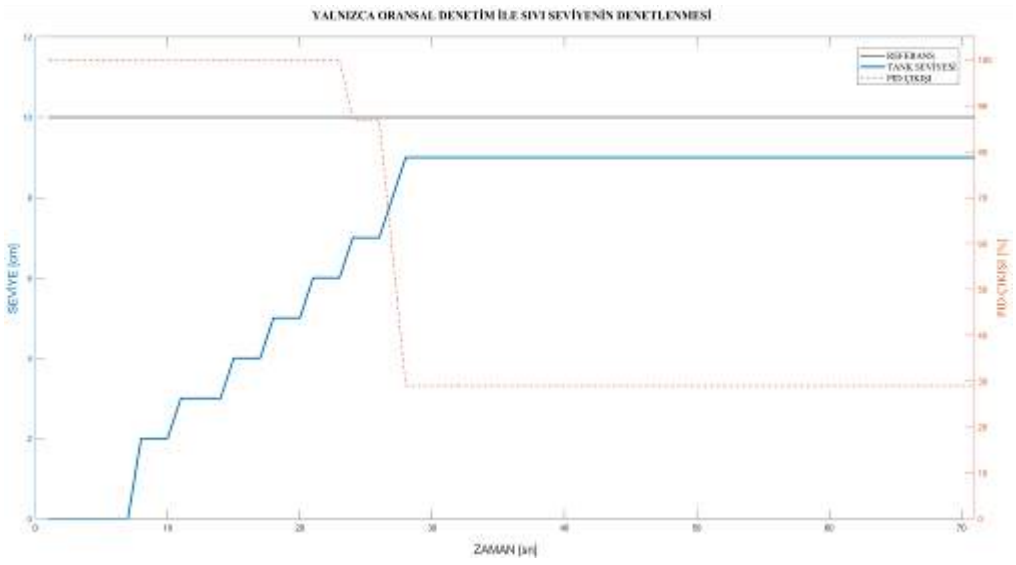

Şekil 15. Yalnızca Oransal Denetim Kullanıldığında Sistem Davranışı (K_P = 29)

Oransal eleman katsayısı 8,47 ve integral eleman katsayısı 31,12 yapılmıştır. Denetleyici parametreleri PLC'deki otomatik katsayı ayarı aracı (auto-tuning) ile bulunmuştur. Tank tamamen boşken HMI üzerinden referans değeri 10 cm girilmiştir. Sistem davranışı kaydedilmiştir ve Şekil 16'da paylaşılmıştır. Şekilde de görüldüğü üzere yalnızca oransal denetim kullanıldığında ortaya çıkan kalıcı durum hatası ortadan kaldırılmıştır. Sistemin oturma zamanı yaklaşık 50 saniyedir ve aşım %10 altındadır. Yaklaşık 270. saniyede boşaltma vanası açılarak sisteme bozucu uygulanmıştır. Sistem bozucunun neden olduğu tepkiyi yaklaşık 100 saniyede ortadan kaldırmıştır ve sistem 10 cm'ye oturmuştur. Sistemde kullanılan sensörün hassasiyeti nedeniyle seviye ±1 cm hata ile okunabilmektedir.

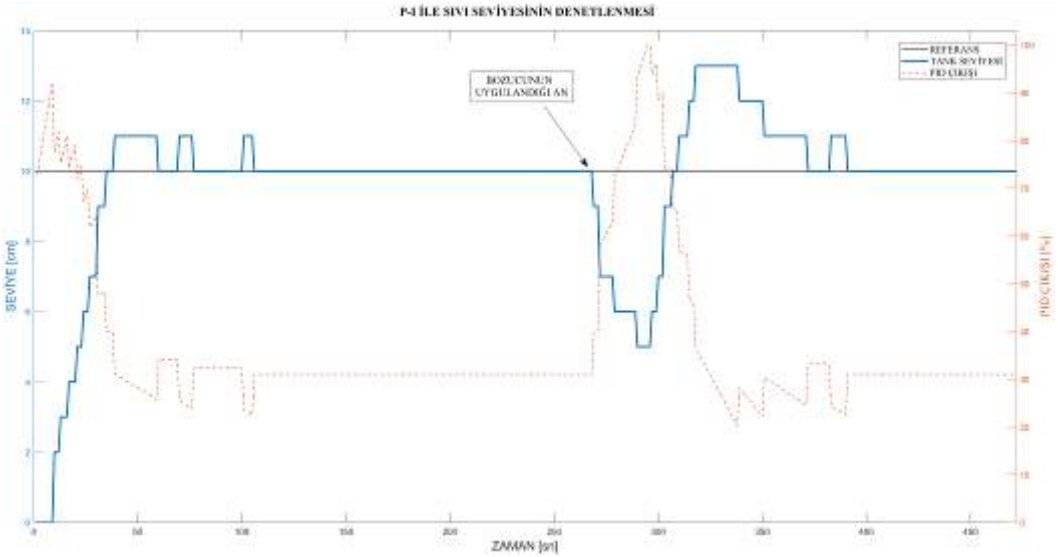

Şekil 16. P-I Denetim Kullanıldığında Sistem Davranışı (K_P = 8,47 ; K_I =31,12)

Son olarak denetleyiciye türev elemanı da eklenmiştir ve P-I-D denetimi gerçekleştirilmiştir. Tank tamamen boşken HMI ekrandan 10 cm referans değer girilmiştir. Denetleyici katsayıları otomatik katsayı ayarı ile bulunmuştur. Oransal eleman sabiti 10, integral eleman sabiti 32,4 ve türev eleman sabiti 8,2 olarak verilmiştir. Şekil 17'de denetime ait sonuçlar paylaşılmıştır. Şekilde de görüldüğü üzere P-I-D denetimde denetleyici çıkışı, referans değerin altına ve üstüne geçtiğinde denetleyici büyük tepkiler vermektedir. Bunun nedeni sisteme eklenen türev elemanının ani hata değişimlerine gösterdiği tepkilerdir. Sistem oturduktan sonra sensör hassasiyetinin düşüklüğü nedeniyle seviyedeki ufak değişimler de türev elemanının tepkisinin artmasına neden olmaktadır. Sistem yaklaşık olarak 60 saniyede oturmuştur ve aşım %10 altında kalmıştır. 360. Saniyede sisteme bozucu uygulanmıştır. Denetleyici bozucunun etkisini yaklaşık olarak 50 saniyede ortadan kaldırmıştır.

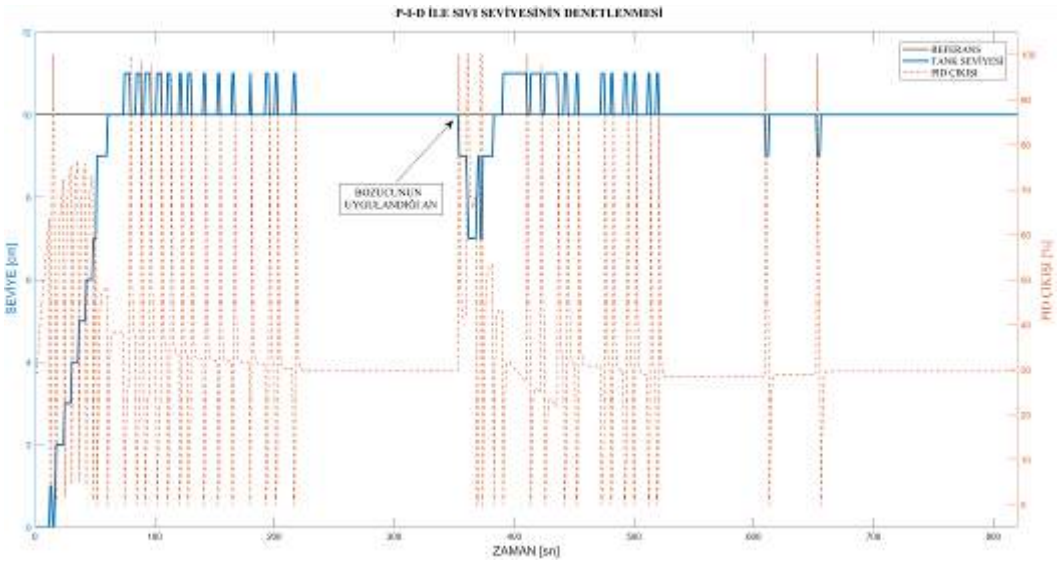

Şekil 17. P-I-D Denetim Kullanıldığında Sistem Davranışı (K_P =10 ; K_I =32,4 ; K_D =8,2)

SONUÇ

Bu çalışmada ile endüstride ve ticari ürünlerde sıkça kullanılan sıvı seviye denetiminin, Elektrik-Elektronik, Makine, Kontrol ve Mekatronik Mühendisliği öğrencileri tarafından daha iyi kavranması ve gerçeklenmesi için bir deney düzeneği tasarlanmıştır. Tasarlanan düzenek geliştirilmeye müsaittir. Öğrenciler bu düzenek üzerinde geri besleme, bozucu etkileri, ölçüm gürültüleri, PLC kullanma ve programlama, PID denetimi, endüstriyel sensörler, motor sürücüleri gibi pek çok değerli kontrol mühendisliği konusu hakkında fikir edinmişlerdir.

Bu çalışmanın amacı, iş hayatlarında kontrol alanında çalışacak öğrencilerin endüstride karşılaşılan bu prosese aşina olması ve seviye denetim yöntemleri hakkında fikir sahibi olmaları olduğundan, çalışma sonuçları tatmin edicidir. Uygulamanın, uygulamayı gerçekleştiren öğrencilerin Kontrol Mühendisliği için cesaretlendirilmesi ve özendirilmesinde etkili olduğu görülmüştür.

TEŞEKKÜR

Bu çalışma Ondokuz Mayıs Üniversitesi tarafından Bilimsel Araştırma Projesi kapsamında desteklenmektedir

(PYO.MUH.1906.17.002).

ÖNERİLER

Bu çalışma daha hassas manyetik sıvı sensörü, ultrasonik sensör ya da radar ile aynı denetleyici kullanılarak tekrarlanabilir. Böylece sistem denetiminin daha iyi gerçekleştiği görülebilir. Ayrıca çalışmada kullanılan PID denetleyicisinin yanında bulanık mantık gibi daha gelişmiş denetim yöntemleri kullanılabilir ve karşılaştırması yapılabilir.

KAYNAKLAR

Adiyan, A. (2012). *Sıvı seviye kontrolü için SCADA sistem tasarımı* (Master's thesis). Dokuz Eylül Üniversitesi, İzmir, Türkiye.

Aström K.J. & Hagglund T. (2006). *Advanced PID control* (2nd ed.). Connecticut, USA: ISA Publication.

Bu, B., Li, C., & Chen, M. (2016). Based on PLC fuzzy control algorithm in the application of level control. In *Proceedings - 2016 IEEE International Symposium on Computer, Consumer and Control, IS3C 2016* (pp. 698–701). Institute of Electrical and Electronics Engineers Inc. https://doi.org/10.1109/IS3C.2016.179

Dandan, Z., Zhiyun, Z., Meng, Y., Yue, H., & Chen, G. (2015). Application of relay feedback auto-tuning algorithm in a liquid level PID control system. In *Proceedings of the World Congress on Intelligent Control and Automation (WCICA)* (Vol. 2015-March, pp. 4313–4315). Institute of Electrical and Electronics Engineers Inc. https://doi.org/10.1109/WCICA.2014.7053438

Erdemir, G. (2016). *Kaskat bağlı sıvı seviye akış sisteminin web tabanlı gerçek zamanda zeki kontrolü* (Master's thesis). Marmara Üniversitesi, İstanbul, Türkiye.

Kent Ridge Instruments. (2007, May 31). *Coupled-tank control apparatus.* Retrieved from http://www.kri.com.sg/ctank.html

Milli Eğitim Bakanlığı. (2009). *Endüstriyel otomasyon teknolojileri - seviye ölçümü.* Retrieved from http://www.megep.meb.gov.tr/mte_program_modul/moduller_pdf/Seviye%20%C3%96l%C3%A7%C3%BCm%C3%BC.pdf

Popescu, M. (2019). Comparative Study of PID and Fuzzy Level Control using Delta v Distributed System. In *Proceedings of the 10th International Conference on Electronics, Computers and Artificial Intelligence, ECAI 2018*. Institute of Electrical and Electronics Engineers Inc. https://doi.org/10.1109/ECAI.2018.8679011

Şahbazlı, R. (2017). *Su tanklarında sıvı seviye kontrol sisteminin geliştirilmesi* (Master's thesis). Retrieved from https://adudspace.adu.edu.tr:8080/xmlui/bitstream/handle/11607/3217/Rufet%20SAHBAZLI.pdf?sequence=1&isAllowed=y

Ulu, C. (2010). MATLAB tabanlı sıvı seviye denetim sistemi tasarımı (Master's thesis). Dumlupınar Üniversitesi, Kütahya, Türkiye.

HEAT TRANSFER AND VARIABLE SPECIFIC HEATS OF WORKING FLUID IN OTTO CYCLE

Okan OZER, Department of Engineering Physics, Engineering Faculty, University of Gaziantep, 27310, Gaziantep-TURKEY, ozer@gantep.edu.tr

ABSTRACT: An analyze of an air-standard Otto cycle with variable specific heats of working fluid and the heat transfer loss is studied in the framework of finite-time thermodynamics. The relations among the power output, the thermal efficiency and the compression ratio are presented numerically and graphically. The effects of variable specific heats of working fluid and the heat transfer loss on the cycle performance are presented. A brief conclusion is presented.

Key words: Otto cycle, Heat transfer, Variable specific heat.

ANALYSIS OF EFFECTS OF DYNAMIC TIME OF USE PROGRAM ON INDUSTRIAL ELECTRICITY CONSUMPTION

Nurettin BEŞLİ

Harran University, Şanlıurfa, Turkey, nbesli@harran.edu.tr

Nusret MUTLU

Southeastern Anatolia Project Regional Development Administration, Şanlıurfa, Turkey, nmutlu@gap.gov.tr

Yilmaz DAGTEKİN

Harran University, Şanlıurfa, Turkey, yilmazdagtekin@hotmail.com

ABSTRACT: Serious problems in energy supply security have brought the concept of demand side management to the forefront. An important component of demand side management is Demand Response(DR). Time of Use(ToU) program is a basic price-based DR program that is also used in Turkey. The more precise form of ToU program is Dynamic Time of Use(dToU) program. This article aims to develop a method for implementing ToU and dToU programs on industrial energy consumption. For this purpose, three industrial users with different load curves and price elasticity matrix are selected. These users represent the three sectors with the highest energy consumption in Sanliurfa Organized Industrial Zone. On these users, ToU and dToU programs were applied for four selected representative days with the help of a MATLAB code. The price advantage results of dToU and ToU programs obtained from this analysis are compared.

Key words: Demand response, Price elasticity matrix, Industrial energy consumption, Time of Use, Dynamic Time of Use

INTRODUCTION

The classical electricity grid approach is based on meeting the increasing demand. In parallel with the increase in demand, new power plant and grid investments were made to meet the demand. The California energy crisis, that took place between 2000-2001 in the United States, led to a significant change in electricity market management approach. After this crisis, an approach that aims to reduce the new power plant and grid investments by reflecting the risks of fluctuations in the amount and price of electricity generation on both supply and demand side was adopted. This approach

brought the concept of Demand Side Management (DSM) into prominence. DSM is basically divided into two categories as Energy Efficiency (EE) and Demand Response (DR). EE is an approach that enables efficient and effective use of energy on the user side. DR, on the other hand, is an approach aimed at balancing the electricity supply and demand by taking into account all the parties of the electricity market (supply side, demand side and transmission network etc.)(Salman 2017). The most important tool for DR implementation is the advanced metering infrastructure that provides bidirectional communication of the supply and demand side of the network(Commision 2008).

Privatization of distribution companies and establishment of the Turkish Energy Markets Operations Company (EPİAŞ) are important steps for liberalization of the Turkey's electricity market. Establishment of day ahead market and intraday market accelerated the liberalization on the supply side. These developments have created an important infrastructure for DR implementation(Beşli and Dağtekin 2015). The implementation of DR programs in Turkey is still very new. Although there are several studies on the basis of individual customers, the expected progress on the basis of customer groups has not been achieved yet(Vingerhoets, Schmitt et al. 2016). Turkey Ministry of Energy and Natural Resources, has set the goal of ensuring the participation of at least 40% of all electricity consumers to DR programs by year 2035(EPDK 2018).

Deciding which DR program to implement depends on user type and behavior. Although load shifting and load shedding are much easier for domestic and commercial users, it is not easy to bring together and manage consumers in a number and power that can affect the grid. For industrial consumers, load shedding and load shifting operations are more difficult and limited in percentage than domestic and commercial consumers. However, it is clear that for a small number of industrial consumers the effect of very low percentages of load shedding or load shifting will have much greater impact on the grid. For example, 50% price advantage can be achieved with ToU application in metal industry(Shoreh, Siano et al. 2016). How industrial consumers can be classified and how they will participate in DR programs are important questions that have been tried to be solved in recent years.

Time of Use(ToU) program is the most basic form of price-based programs. ToU tariff includes 3 usage zones during the day. These are off-peak, mid-Peak use and on-peak times. ToU program is also used for many years in Turkey. However, it is not a healthy approach to keep time zones constant throughout the year. In the Dynamic Time of Use (dToU) program, peak, mid-peak use and off-peak times vary depending on the change in peak usage during certain time periods of the year. The dToU program is a DR program implemented in various countries(Azman, Abdullah et al. 2017). In the dToU program, one day can also be divided into half-hour segments. Thus, it is more sensitive to reflect peak time prices to consumers(Wang and Li 2015).

The DR application tries to enable the consumer to regulate the load curve through load shift, load shedding, incentive and penalty payment methods. In this way, the energy consumed during peak hours is reduced, thus contributing to the reliability of the electricity supply. There are many researches on the implementation of DR programs for industrial users. Algorithms have been developed to program loads in accordance with ToU program(Q., D. et al. 2013). In order to analyze the effects of clustered users on the network, logarithmic, exponential and linear modeling was applied to the grid model by applying various scenarios(Aalami, Parsa Moghaddam et al. 2015). Methodologies have been developed to find a consumer baseline curve for DR implementation in clustered users with similar load curves(Song, Li et al. 2018).

In this study, it is aimed to reveal the price advantage of ToU and dToU programs on electricity bills of industry users with similar load curve. With this study, it has been tried to contribute to the search for a collective model for the implementation of DR programs for industrial users. In this study, three users' load curves have been selected that represent the three sectors with the highest energy consumption in Şanlıurfa Organized Industrial Zone. ToU and dToU programs were applied to users with the help of a MATLAB code by selecting four representative days in the selected year. As a result of the analysis, annual saving rates on the electricity bills of the users were compared. It has been tried to develop a common model for the implementation of these DR programs to industrial users.

PROBLEM FORMULATION

Price Elasticity Model For DR Implementation

Electricity is a commodity that can be priced according to time zones during the day. In this respect, the change in price over time can be defined by the price elasticity model, which is a basic economic definition(Qu, Hui et al. 2018). The basic formula of price elasticity is:

$$E = \frac{P_0}{D_0} \cdot \frac{\Delta D}{\Delta P} \qquad (1)$$

Here;

P_o: Indicates the base price.

D_o: Indicates the base demand.

ΔP: Indicates the change in price.

ΔD: Indicates the change in demand.

A Price Elasticity Matrix (PEM) is created that represents the behavior of consumption in each time zone relative to the price change to consumption in another time zone. PEM is a 24x24 matrix(Gutiérrez-Alcaraz, Tovar-Hernández et al. 2016). The elasticity coefficients in the diagonals of PEM represent self-elasticity and shows the effect of price change on demand in the same time zone. The self-elasticity coefficient formula is as follows:

$$E_{i,i} = \frac{P_0}{D_0} \cdot \frac{\Delta D(t_i)}{\Delta P(t_i)} \quad (2)$$

Elasticity coefficients in other parts of PEM represent cross-elasticity and show the effect of price change in another time zone on demand. The cross-elasticity coefficient formula is as follows:

$$E_{i,j} = \frac{P_0}{D_0} \cdot \frac{\Delta D(t_i)}{\Delta P(t_j)} \quad (3)$$

Since the price increase in the same time zone will affect demand negatively, the self-elasticity coefficient is always negative. The cross-elasticity coefficient is zero or positive, as price increases in another time zone will reduce demand. PEM matrix and base consumption curve must be calculated accurately in order to accurately calculate a consumer's response to the DR program.

Economic Model For DR Implementation

Various economic models have been developed to calculate the economic benefit to the consumer through the implementation of DR programs. In this study, the economic model presented in (Mohajeryami, Schwarz et al. 2015), rearranged according to different representative load curves and ToU and dToU program scenarios. The hourly demand for a user can be calculated as follows:

$$d(i) = d_0(i) \cdot \left[1 + \frac{E(i) \cdot (p(i) - p_0(i) + \lambda \cdot R(i))}{p_0(i)}\right] \quad (4)$$

Here;

p_o: Indicates the base price

d_o: Indicates the base demand

E: Coefficient of Elasticity

λ: The coefficient representing the actual value of the symbolic reward or incentive payment.

R: Indicates the incentive payment made by the Distribution Company for every kWh demand reduction.

If self-elasticity and cross-elasticity parameters are added in this model, considering incentive payment and price sensitivity, the economic model of DR program will be as follows(Mohajeryami, Schwarz et al. 2015):

$$d(i) = d_0(i) + E(i) \cdot \frac{d_0(i)}{p_0(i)} \cdot \left(p(i)\text{-}p_0(i) + \lambda \cdot R(i)\right) + \sum_{\substack{j=1 \\ j \neq i}}^{24} E(i,j) \cdot \frac{d_0(i)}{p_0(j)} \cdot \left(p(j)\text{-}p_0(i,j) + \lambda \cdot R(j)\right) \quad (5)$$

Selection of Representative User Load Curves

The three sectors with the highest annual energy consumption in the Sanliurfa Organized Industrial Zone are Yarn (56%), Oil-gin (17%) and Building materials-plastic pipes (14%) respectively. To represent these sectors, three representative users with different behaviors were selected for the analysis.

The first user (K-1), symbolizes a yarn and textile factory. Hourly electricity consumption of the plant varies between 395-854 kWh. This operation is not very keen on reducing and shifting load. The load curve and PEM of the User K-1 are shown in Fig. 1.

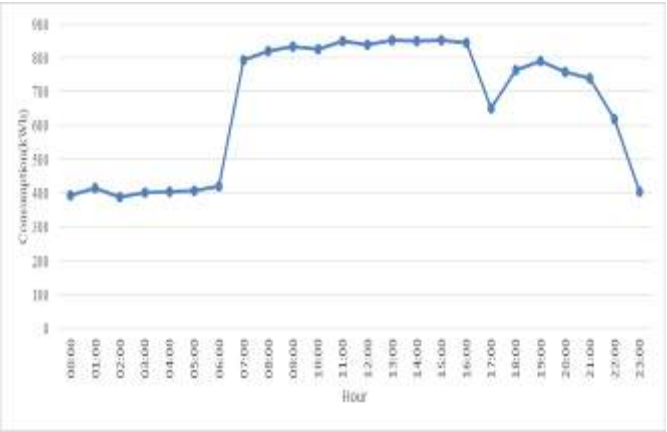

	Peak	**Off-Peak**	**Mid-Peak**
Peak	-0.1	0.005	0.01
Off-Peak	0.005	-0.1	0.03
Mid-Peak	0.01	0.03	-0.1

Fig. 1. K-1's load curve and PEM

The second user (K-2) symbolizes an oil and gin factory. Hourly electricity consumption of the facility varies between 266-388 kWh. This operation is willing to reduce load and shift. The load curve and PEM of the User K-2 are shown in Fig. 2.

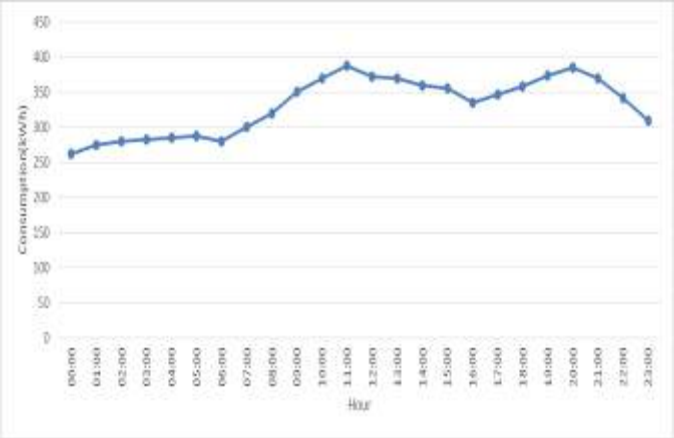

	Peak	Off-Peak	Mid-Peak
Peak	-0.2	0.01	0.008
Off-Peak	0.01	-0.2	0.005
Mid-Peak	0.008	0.005	-0.2

Fig. 2. K-2's load curve and PEM

The third user(K-3) symbolizes a building materials factory. Hourly electricity consumption of the plant varies between 656-1125 kWh. This plant is very eager to reduce and shift load. The load curve and PEM of the User K-3 are given in Fig. 3.

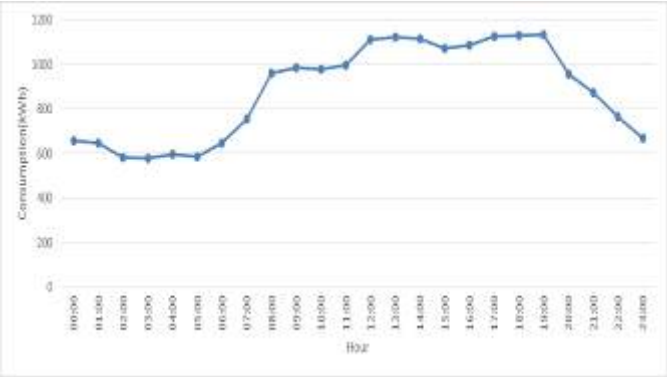

	Peak	Off-Peak	Mid-Peak
Peak	-0.3	0.02	0.009
Off-Peak	0.02	-0.3	0.007
Mid-Peak	0.009	0.007	-0.3

Fig. 3. K-3's load curve and PEM

Selection of Representative Days

In order to implement the DR program, the hourly price curve of that day needs to be known. This study represents four days in Turkey were selected by examining the electricity consumption by 2018,((TEIAS) 2018). Selected representative days (RD) and their characteristics are shown in Table 1:

Table 1. Selected Representative Days

Representative Day	Definition	Date	Total Energy Consumption of Turkey (MWh)
RD-1	Winter Lowest Consumption	7.10.2018	634.962
RD-2	Winter Highest Consumption	18.01.2018	888.033
RD-3	Summer Lowest Consumption	3.06.2018	653.851
RD-4	Summer Highest Consumption	3.08.2018	977.870

Then price signals have been identified for each representative day by examining Turkey's electricity consumption curve on these days. The price signal without DR is constant and assumed to be the price of mid-peak time.

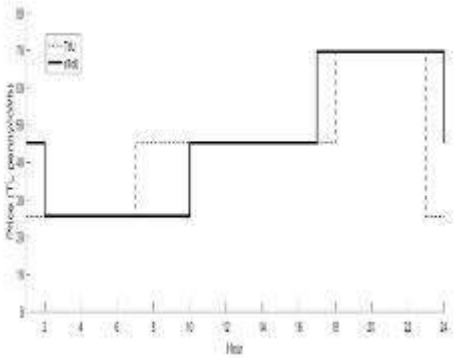

Fig. 4. (a) Price signal for the day RD-1

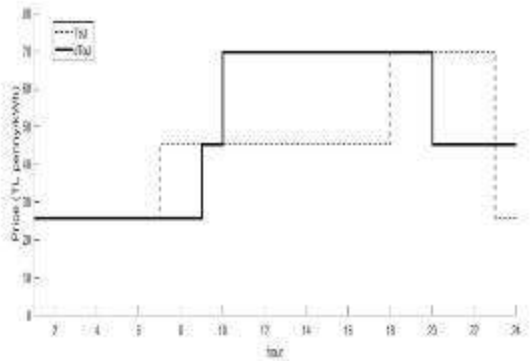

Fig. 4. (b) Price signal for the day RD-2

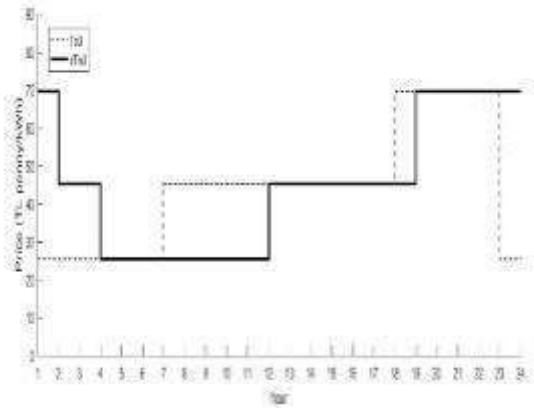

Fig. 4. (c) Price signal for the day RD-3

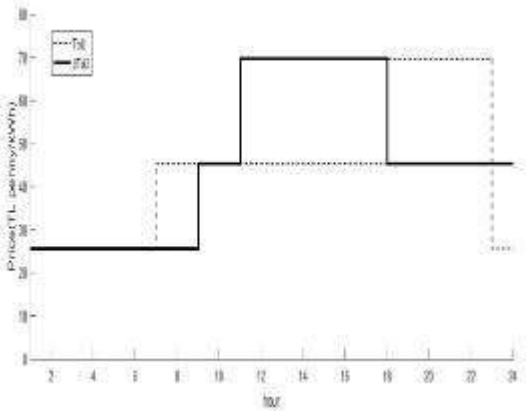

Fig. 4. (d) Price signal for the day RD-4

The price signal scenarios selected for each representative day were applied to three users and shown in Fig. 4. It is assumed that the distribution company makes 15.8 kr/kwh incentive payment to users for load reductions only during the peak period. However, Distribution companies or aggregators may demand program participation fee from consumers according to program size and installed power in order to participate in DR program. In the USA, the participation price is around $60-$120 per month for medium-sized industrial users(Woolf, Malone et al. 2013). Therefore, it is assumed that the program participation price of 500 TL per month for ToU tariff and 550 TL per month for dToU tariff will be paid by the user. In this study, it is also assumed that there is no production loss as a result of the use of DR.

TEST RESULTS AND DISCUSSION

DR programs applied to all users with the help of the code arranged according to the price signal scenarios described in the previous section. The results are shown below.

Analysis Results for User K-1

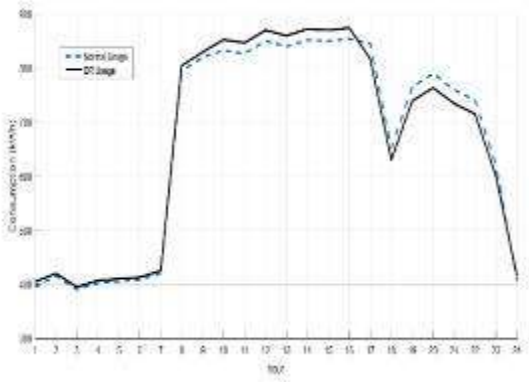

Fig. 5. (a) Analysis results on RD-1 day for user K-1

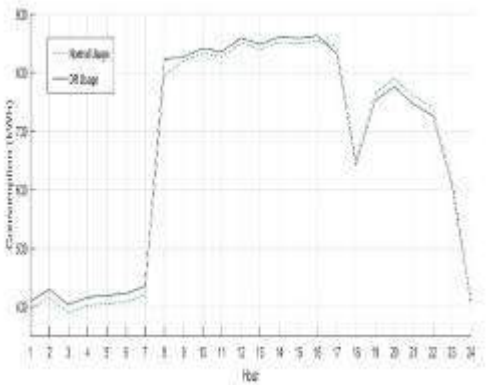

Fig. 5. (b) Analysis results on RD-2 day for user K-1

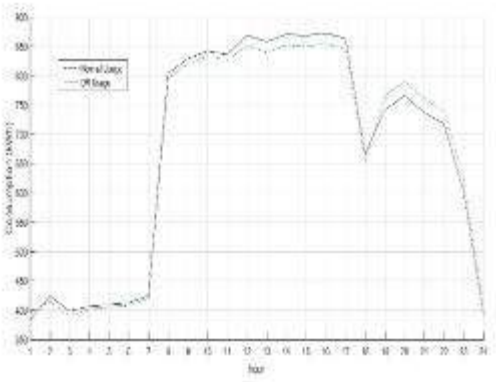

Fig. 5. (c) Analysis results on RD-3 day for user K-1

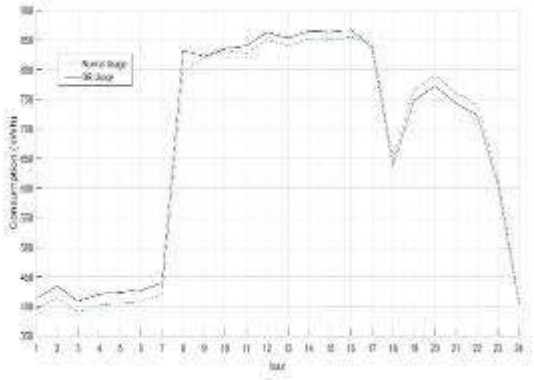

Fig. 5. (d) Analysis results on RD-4 day for user K-1

As seen in Fig. 5, the shape of the load curve has changed slightly since the K-1 user is not willing to shift the load. The electricity bill reduction rate of RD-3 and RD-4 is higher than RD-1 and RD-2. Accordingly, it can be said that the K-1 user reacts more to the ToU and dToU programs during the summer representative days.

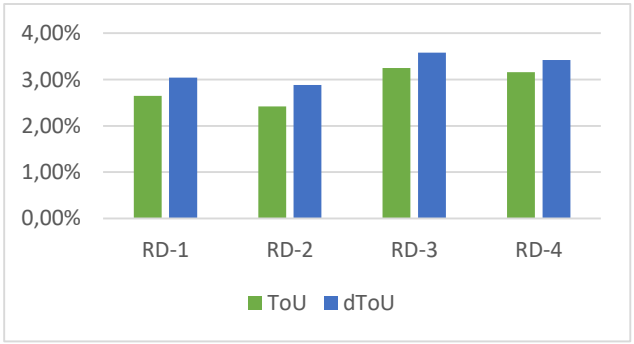

Fig. 6. Electricity bill reduction rates of K-1 for all RDs

Fig. 6. shows electricity bill reduction rates of K-1 for all RDs. Here, K-1 reduces electricity bills between 2.42% and 3.25% in ToU program and between 2.89% and 3.58% in dToU program. Therefore, switching from ToU to dToU is not profitable for this user.

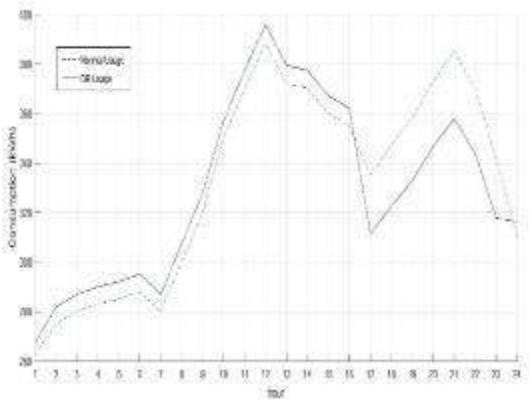

Fig. 7. (a) Analysis results on RD-1 day for user K-2

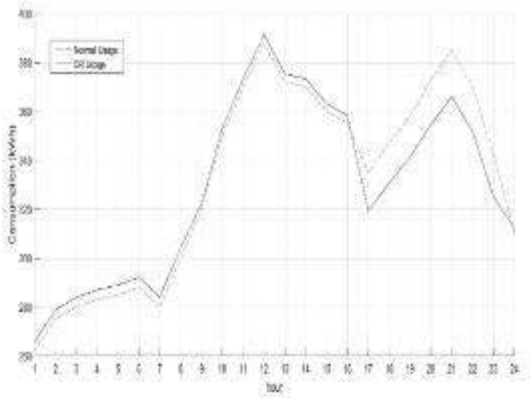

Fig. 7. (b) Analysis results on RD-2 day for user K-2

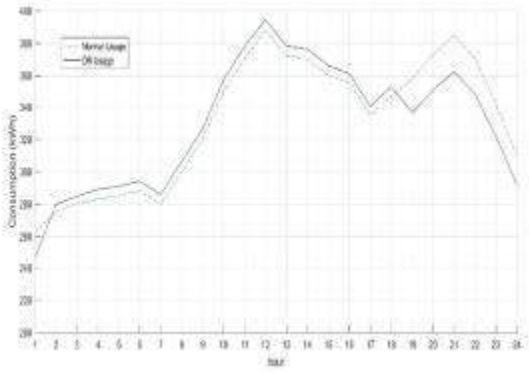

Fig. 7. (c) Analysis results on RD-3 day for user K-2

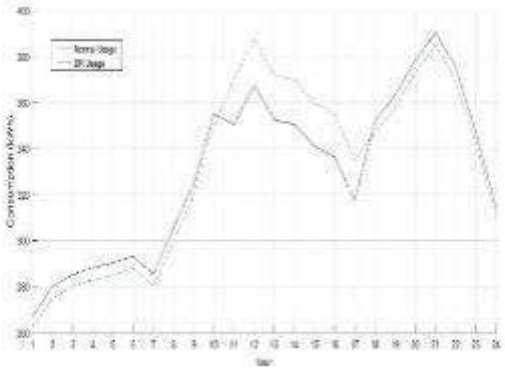

Fig. 7. (d) Analysis results on RD-4 day for user K-2

As shown in Fig. 7, the shape of the load curve has changed since the K-2 user is willing to shift the load. The electricity bill reduction rate in RD-2 and RD-4 is higher than RD-1 and RD-3. Accordingly, it can be said that the K-2 user reacts more to the ToU and dToU programs on summer representative days. The difference between the dToU program and the ToU program is around 2%.

Fig. 8. Electricity bill reduction rates of user K-2 for all RDs

Fig. 8. shows the electricity bill reduction rates of K-2 for all RDs. Here, K-1 reduces its electricity bill between 4.04% - 4.48% in ToU program and 5.94% - 6.75% in dToU program. Therefore, switching from ToU to dToU is profitable for this user.

Analysis Results for User K-3

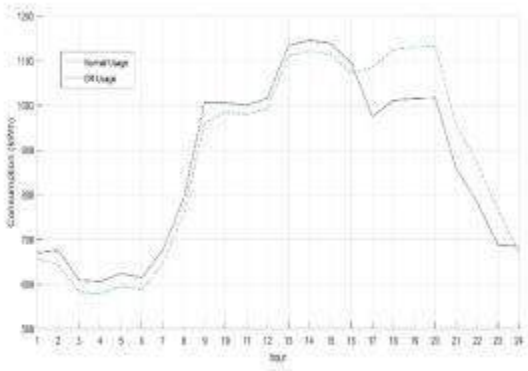

Fig. 9. (a) Analysis results on RD-1 day for user K-3

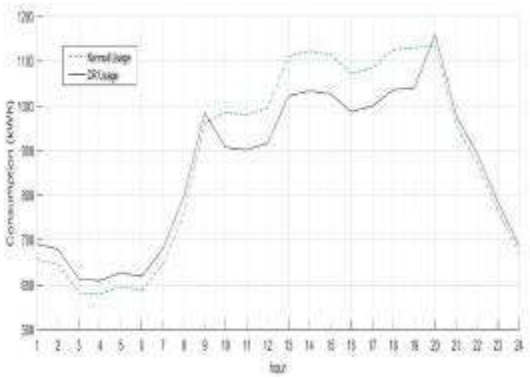

Fig. 9. (b) Analysis results on RD-2 day for user K-3

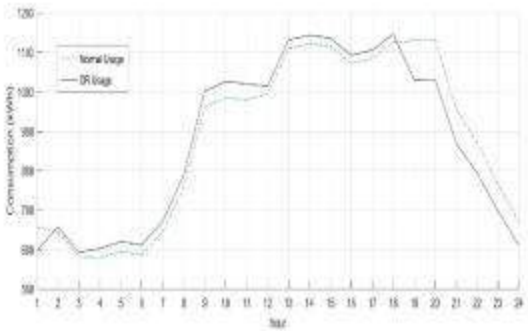

Fig. 9. (c) Analysis results on RD-3 day for user K-3

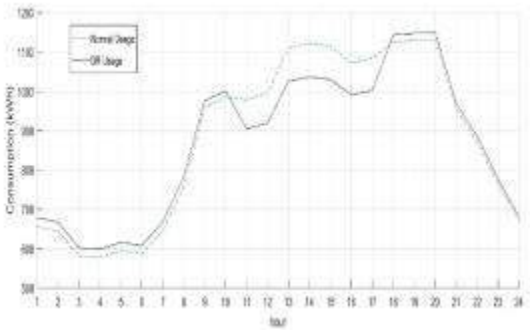

Fig. 9. (d) Analysis results on RD-4 day for user K-4

As seen in Fig. 9, user K-3 is very keen to shift the load, so the shape of the load curve has changed significantly. The electricity bill reduction rate in RD-2 and RD-4 was higher than RD-1 and RD-3. Accordingly, it can be said that user K-3 gives the best response to ToU and dToU programs on high energy consumption days. The difference between the dToU program and the ToU program is about 3%.

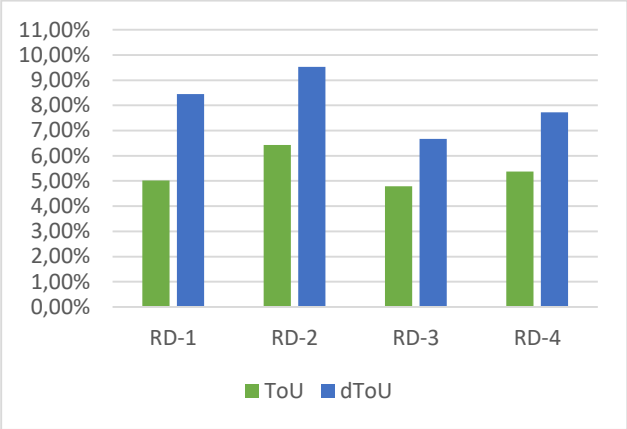

Fig. 10. Electricity bill reduction rates of user K-3 for all RDs

Fig. 10. shows the electricity bill reduction rates of K-3 for all RDs. Here, K-3 reduces its electricity bill between 4.79% - 6.43% in ToU and 6.68% - 9.4% in dToU. Therefore, switching from ToU to dToU is very profitable for this user.

Comparison of All Users

Fig. 11. shows the annual savings rates of users after deducting all expenses that explained in previous section.

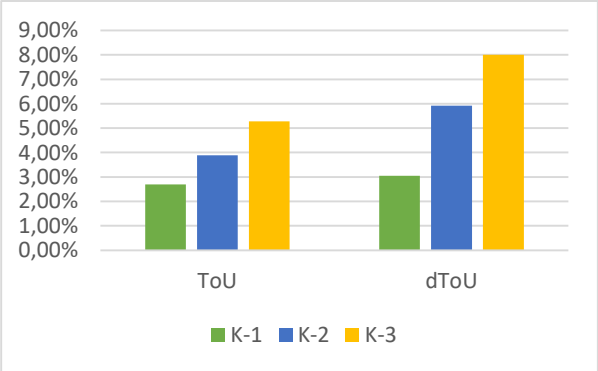

Fig. 11. Comparison of all users' annual electricity bill reduction rates

As shown in Fig. 11., users can reduce electricity bills between 2.70%-5.28% in ToU program and 3.05%-8.05% in dToU program implementation compared to standard pricing. In dToU program, which intervenes in the price signal very little, the amount of savings can be increased to 8% for the most demanding users. In winter and summer high energy consumption days (RD-2 and RD-4), it is seen that users provide higher reducing advantage electricity bill with DR. The main reason for this is the higher hourly energy prices on the days of high energy consumption.

CONCLUSIONS

DR implementation is a very important tool for balancing energy demand and ensuring system reliability. Turkey is in the process of electricity market liberalization. In the coming years, widespread implementation of DR is inevitable. In this study, the price advantage of the users transitioning to ToU and dToU programs is examined. For this purpose, three users representing the three most energy consuming sectors in Sanliurfa Organized Industrial Zone are selected. After simulating DR programs according to the load curve and the Price Elasticity Matrix of each user, an average electricity bill reduction of 5% in ToU program and 8% in dToU program annually is achieved. The annual electricity bill of Sanliurfa organized industrial zone is 151.466.550 TL and the energy consumption of these three sectors corresponds to approximately 87% of total consumption. Considering these three types of consumers as clusters, the annual cost savings can be calculated as 4.408.000 TL for ToU program and 5.809.000 TL for dToU program.

In order to implement DR more effectively in industry, industrial consumers must be clustered according to their load curves and PEMs. PEM matrices can be accurately identified by analyzing the production processes of all consumers. For this purpose, it would be more appropriate for the Energy Management Department established within Organized Industrial Zones to actively engage in these activities.

For industrial energy users, ToU and dToU programs are easier to implement and can reduce electricity bills substantially. However, the most precise DR program is Real Time Pricing. For the implementation of Real Time Pricing, advanced metering infrastructure and algorithms are required. Also, users should reach sufficient level of awareness. While further researches are carried out on the Real Time Pricing, implementation of dToU program can be the first stage for smooth transitioning to the Real Time Pricing program in Turkey. Various supporting systems such as electrical storage, heat storage, cogeneration and trigeneration systems can be also employed by users for adapting DR programs more effectively.

ACKNOWLEDGEMENTS

This research was partially supported by Southeastern Anatolia Project Regional Development Administration within the scope of “Utilization of Renewable Energy Sources and Increasing Energy Efficiency in South-eastern Anatolia Region Project”. The authors are thankful for supporting this research.

REFERENCES

Aalami, H. A., et al. (2015). "Evaluation of nonlinear models for time-based rates demand response programs." International Journal of Electrical Power & Energy Systems **65**(0): 282-290.

Azman, N. A. M., et al. (2017). "Enhanced Time of Use Electricity Pricing for Industrial Customers in Malaysia." Indonesian Journal of Electrical Engineering and Computer Science **Vol. 6**.

Beşli, N. and Y. Dağtekin (2015). Demand Response: A Way to Balance Production and Consumption of Energy for Turkey. 9th International Conference on Electrical and Electronics Engineering(ELECO). Bursa, TURKEY, IEEE.

Commision (2008). Advanced Metering Infrastructure. U.S.A., U.S. Department of Energy.

EPDK (2018). Türkiye Akıllı Şebekeler 2023 Vizyon ve Strateji Belirleme Projesi Sonuç Raporu. Ankara, EPDK**:** 96.

Gutiérrez-Alcaraz, G., et al. (2016). "Effects of demand response programs on distribution system operation." International Journal of Electrical Power & Energy Systems **74**: 230-237.

Mohajeryami, S., et al. (2015). Including the behavioral aspects of customers in demand response model: Real time pricing versus peak time rebate. 2015 North AAmerican Power Symposium (NAPS).

Q., A. S., et al. (2013). Load scheduling with maximum demand and time of use pricing for microgrids. 2013 IEEE Global Humanitarian Technology Conference: South Asia Satellite (GHTC-SAS), IEEE**:** 234-238.

Qu, X., et al. (2018). "Price elasticity matrix of demand in power system considering demand response programs." IOP Conference Series: Earth and Environmental Science **121**: 052081.

Salman, S. K. (2017). Introduction to the Smart Grid: Concepts, Technologies and Evolution. U.K., The Institution of Engineering and Technology.

Shoreh, M. H., et al. (2016). "A survey of industrial applications of Demand Response." Electric Power Systems Research **141**: 31-49.

Song, T., et al. (2018). "A Cluster-Based Baseline Load Calculation Approach for Individual Industrial and Commercial Customer." Energies **12**(1).

TEIAS, T. E. T. C. (2018). "Turkey electricity production and consumption statistics." 2019, from https://ytbsbilgi.teias.gov.tr/ytbsbilgi/frm_istatistikler.jsf.

Vingerhoets, P., et al. (2016). Demand Response Status And Initiatives Around The World, The Global Smart Grid Federation.

Wang, Y. and L. Li (2015). "Time-of-use electricity pricing for industrial customers: A survey of U.S. utilities." Applied Energy **149**: 89-103.

Woolf, T., et al. (2013). A Framework for Evaluating the Cost-Effectiveness of Demand Response.

COLD-BONDING METHOD IN ARTIFICIAL AGGREGATE PRODUCTION

Nihat ATMACA, Gaziantep University, Civil Engineering Department, atmaca@gantep.edu.tr

ABSTRACT: Agregate occupies 70-75% of the volume of concrete. It is produced artificially or found naturally inorganic granular material and used as a constructional material. Production of artificial aggregate as an alternative of natural aggregate is one of the most popular theme in construction materials literature last two decades. In production of artificial aggregate, either sintering or cold bonding methods are widely used common methods. The use of pelletized artificial aggregates as an alternative construction material in light weight concrete production is the main topic of this paper. This paper aims to summarize manufacturing processes of Light Weight Artificial Aggregate and its impacts on concrete properties.

Key words: pelletization, cold bonded, light weight artificial aggregate

INTRODUCTION

Concrete is a main and most widely used material in civil engineering applications. It has serious effects on environmental pollution and energy consumption [Atmaca, N. et al., 2017]. The main constituents of concrete are cement, water, admixtures and aggregate. Agregate occupies 70-75% of the volume of concrete. It is produced artificially or found naturally inorganic granular material mostly used as a constructional material. In production of artificial aggregate, either sintering or cold bonding methods can be used. The cold bonding method process is used as to produce artificial aggregate by pelletization. Pelletization process is used to manufacture artificial lightweight coarse aggregate using fly ash and it depends on the size of particles and their distribution, the wettability of particles and moisture content, along with the process related parameters [K.I. Harikrishnan and K. Ramamurthy, 2006].

The main objective of the waste management is to reduce environmental pollution by reusing and recycling of waste materials. The usage of waste materials is a significant research area in concrete as a cement or aggregate replacement ingredient. In cold-bonding process, fly ash is used as a waste material in concrete production. Fly ash as a waste material is the byproduct of coal-fired power plants that improves cementitious properties when mixed with water and cement. Fly ash in concrete is widely used in order to increase strength of concrete, improve workability properties of fresh state of concrete and reduce water demand, shrinkage and permeability of the finished hardened state of concrete. There are two main benefits of Light Weight

Artificial Aggregate (LWAA). On one hand it gives an enhancement in concrete properties, on the other hand it has an important advantage with environmental aspect.

COLD - BONDED AGGREGATE PRODUCTION

Pelletization is a common method of non-pressure agglomeration techniques used in LWAA production. LWAA production process has three main sections and three steps. The sections are Pelletization disc, switch board and water reservoir. Pelletization disc has an engine and a feeder apart from disk.

The three steps are as follows:

First step is the mixing 90% of Fly ash class (F) with 10% of Portland Cement by weight though moisturing by water spraying (by using 18-20% of total binder weight). The process will continue for 10 min at ambient temperature in a pelletization disc with a diameter of 800 mm and depth of 350 mm as seen in Fig 1.

The disc revived at a constant velocity and a slope angle in order to get a homogeneous fresh pellets. This ***second step*** will carry on to get a sufficient stiffness of fresh pellets on account of agglomeration.

The third final step is the curing process for fresh pellets. It is quite important to cure the pellets in sealed plastic bags for 28 days under self-curing conditions. The curing temperature is 20 ^{o}C and relative humidity is 70% in self-curing conditions. The hardened LWAA has been obtained at the end of the curing process.

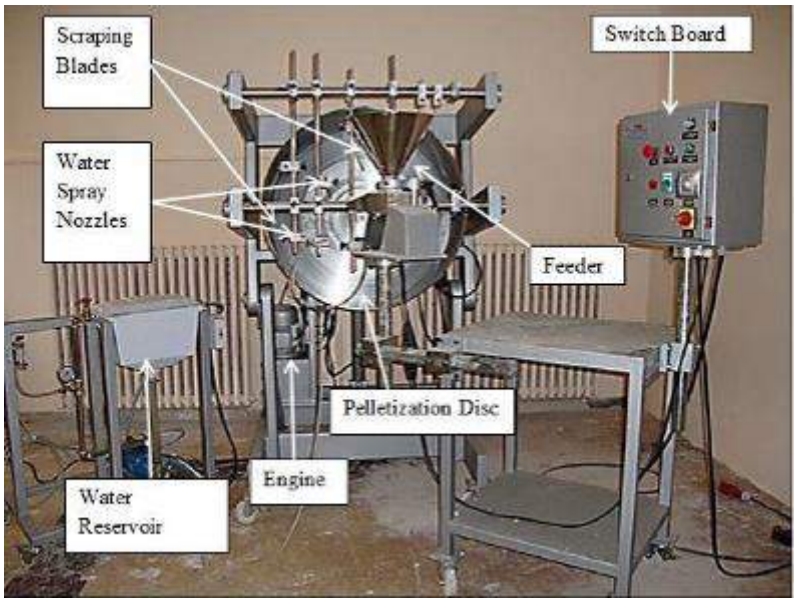

Figure.1 Pelletization Disc and Sections

RAW MATERIALS USED IN LWAA CASE STUDIES

There are variety of raw materials, binders and additives used by researchers in Literature. But Fly ash is most commonly used material in cold-bonded light weight aggregate production. It is due to availability in huge amounts throughout the world as a waste material. In addition to fly ash, waste water treatment sludge, ground granulated blast furnace slag, rice husk ash and very different waste materials are used in Literature. Some special additives have also been used in many different researches in order to get specific performance requirements.

An experimental design procedure is performed by using cementitious materials and LWAA. Chemical composition and some physical properties of cementitious materials Portland Cement (PC) and Fly Ash (FA) is shown in Table 1.

Table 1 Chemical Composition and Physical Properties of Cementitious Materials

Item	PC	FA
CaO (%)	62.12	2.24
SiO_2 (%)	19.69	57.2
Al_2O_3 (%)	5.16	24.4
Fe_2O_3 (%)	2.88	7.1
MgO (%)	1.17	2.4
SO_3 (%)	2.63	0.29
K_2O (%)	0.88	3.37
Na_2O (%)	0.17	0.38
Loss on ignition (%)	2.99	1.52
Specific gravity	3.15	2.04
Blaine Fineness (m^2/kg)	394	379

Water absorption and specific gravity for LWAA are found about 19.2% and 1.33g/cm^3 respectively, according to ASTM C 127. It is possible to apply sieve test analysis and draw gradation curves of LWAAs according to TS 802 before concrete mix design. Additionaly, the crushing strength test of LWAAs was performed as BS 812, part 110 (Fig. 2).

Figure.2 LWAA, PC and FA samples

RESULTS AND FINDINGS

The compressive strength, splitting tensile strength and sorptivity tests have been applied by using LWAA as aggregate replacement material.

The compressive strength values for 28 days are given in Table 1 and Fig. 3. There is a 15% decrease in compressive strength values.

The splitting tensile strength values for 28 days are given in Table 1 and Fig. 4. There is a noticeable decrease in compressive strength values. The reduction percentage is 24%.

The sorptivity values for 28 days are given in Table 1 and Fig. 5. There is a remarkable increase in compressive strength values. The increase in sorptivity values is about 52%.

Table 2 Test Results with respect to different percentegas of LWAAs

MIX ID	Comp.Strength 28days (MPa)	Splitting 28 days (MPa)	Sorptivity 28 days ($mm/min^{1/2}$)
LWAA0	64.1	4.5	0.077
LWAA10	62.2	3.9	0.083
LWAA20	57.2	3.7	0.091
LWAA30	56.7	3.5	0.1064
LWAA40	54.1	3.4	0.1171

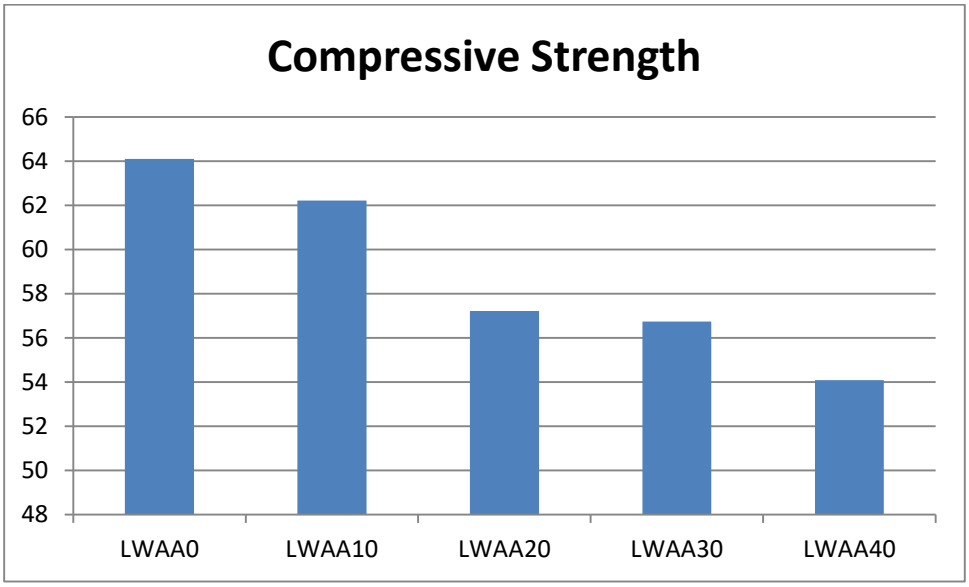

Figure 3. Compressive Strength with LWAA

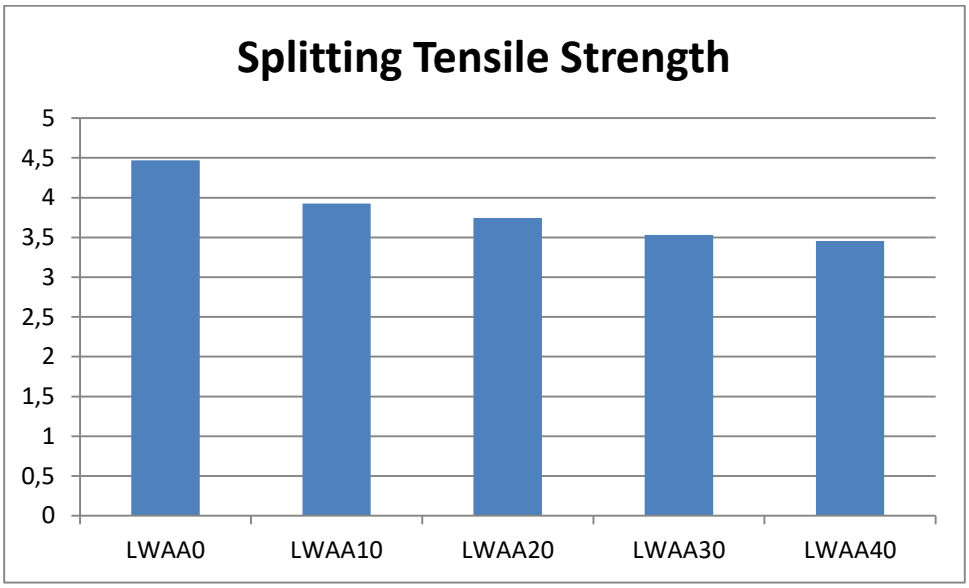

Figure 4. Splitting Tensile Strength with LWAA

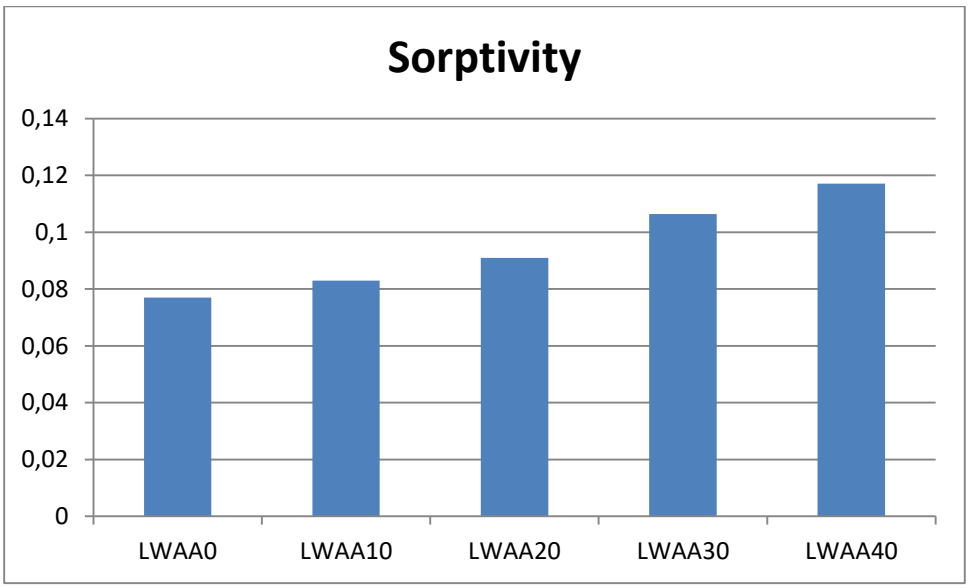

Figure 5. Sorptivity with LWAA

The results confirm that compressive strength and splitting tensile strength values are decreasing with an increase in LWAA ratios. However, Sorptivity increases with an increase in LWAA percentages.

There are lots of parameters that effect experimental results directly. Speed of revolution and duration of pelletization can be given as an examples of this type of parameters.

CONCLUSION

On the bases of experimental analysis, compressive and splitting tensile strength values decreases with an increase of LWAA percentages. But there is an increasing tendency with an increasing LWAA percentages.

There are some important parameters such as angle of pelletizer disc, moisture content, speed of revolution and duration of pelletization have an influence on the pelletization of fly ash aggregates. The relative influence of the factors given above and their interaction effects on the strength, water absorption and size growth of fly ash aggregates should be investigated severally.

The main conclusion that can be drawn from this study is preserving of natural sources. Saving energy consumption and converting waste materials into value-added products are also very important results of this present study.

REFERENCES

ATMACA, N., ABBAS, M. L., & ATMACA, A. (2017). Effects of nano silica on the gas permeability durability and mechanicalproperties of high strength lightweight concrete. *Construction and Building Materials, 147*, 17–26.

ASTM C127. American Society for Testing and Materials, Standard test method for specific gravity and absorption of coarse aggregate, *Annual Book of ASTM Standard*, 2007.

Harikrishnan, K.I. and Ramamurthy, K. (2006). Influence of pelletization process on the properties of fly ash aggregates. *Waste Management, 26-8,* 846-852.

TS 802, Design of concrete mixtures, *Institute of Turkish Standards*, Ankara, 2009.

BS 812, Part 110, Methods for determination of aggregate crushing value (ACV), *British Standarts*, 1990.

ENERGY ANALYSIS OF A SOLAR-ASSISTED HEAT PUMP DRYING SYSTEM WITH ENERGY STORAGE TANK

Hatem Hasan Ismaeel, Bardarash Technical Institute, Duhok Polytechnic University, Duhok, Iraq, bardarashi77@gmail.com

Recep Yumrutaş, Department of Mechanical Engineering, Gaziantep University, Gaziantep, Turkey, yumrutas@gantep.edu.tr

ABSTRACT: The drying process in the industrial applications consumes a great amount of energy. There are many types of drying applications in the industry. This study has developed the Solar-Assisted Heat Pump Drying (SAHPD) system with underground Thermal Energy Storage (TES) tank. In this study, long-term performance parameters of the new drying system are investigated. The SAHP drying system consists of a drying unit, a heat pump, flat plate solar collectors, a spherical underground TES tank to be used for corn drying. Duhamel's superposition and similarity transformation techniques for TES tank and multiple expressions for other components in an analytical model of the drying system are used. The performance parameters used as Coefficient of Performances for the heat pump (COP) and system (COPs), Specific Moisture Evaporation Rate (SMER), annual variation of water temperature in the TES tank, energy fractions for energy charging and extraction from the system. A program in MATLAB has been prepared using the expressions for the drying system in order to find its performance parameters. The results of this study reveal that the SAHPD system attains periodic operation time in 5th year onwards for 10 years of operation.

Key words: Heat pump drying, corn drying, energy storage, solar energy

INTRODUCTION

The world population is increasing from day to day that makes difficult to access affordable and healthy basic foods, such as fresh and normal corn throughout the year in the World. There are many reasons for preserving of the corn during long term in many years. One of the most important reasons to store corn successfully is the moisture content. The high levels of moisture leads to storage problems including insect and fungal infestation, germination, and respiration (Mrema et al., 2011). Temperature is another major factor which affects corn wastage. From a biological perspective corn grains are active and respire during storage and in order to eliminate these problems corn drying is required (Mrema et al., 2011). Decreasing moisture levels within stored crops is requirement and is attainable via drying process for agricultural products and food (Leon et al, 2002). There are many types of drying systems which are used for food or agricultural products drying. Natural drying, heat

pump drying (Fatouh et al., 2006; Xu et al., 2016; Erbay and Hepbasli, 2014), infrared drying (Nowak and Lewicki, 2004; Wang et al., 2014; Aktaş et al., 2016), solar air heater drying (Turgut and Onur, 2000; Koyuncu, 2006; Momin et al., 2002), drying by burning of fossil fuels and solar assisted heat pump drying systems can be given as some examples for the drying systems (Naemsai et al., 2019; Wang et al., 2019).

Systems that are more efficient in drying compared to conventional ones should be used to save energy and decrease pollution. Solar assisted heat pump drying systems are more efficient than the conventional drying systems. When solar energy and heat pump are used together for food drying, performance of the system will be higher than the conventional drying systems. However, previous studies indicate that there are inadequate studies related to solar assisted heat pump drying (HPD) systems and ground source HPD systems. Mohanraj and Chandrasekar (2009) investigated chili drying via an experimental study on indirect forced convection solar dryer integrated with different sensible heat storage materials. Performance of a forced convection mixed mode solar dryer with thermal energy storage was experimentally analyzed by (Baniasadi et al., 2017). During the experiments, they found that fresh apricot slices can be dried at different working conditions. Another experimental study was conducted by (Şevik et al., 2013) using a solar assisted heat pump drying system with flat plate collectors for drying of mushroom. System coefficients performance (COP) were calculated as values in a range from 2.1 to 3.1 using experiment results. They also found SMER values between 0.26 and 0.92 kg kW^{-1} h^{-1}. Qiu et al. (2016) performed an experimental study to obtain performance and operation mode analysis of a heat recovery and thermal storage solar-assisted heat pump drying system. They have shown that coefficient of performance of the drying system ranged from 3.21 to 3.49, and that payback periods for drying radish, pepper, and mushroom in the life span of the system were 6 years, 4 years, and 2 years, respectively.

After displayed the literature on drying system we can say the underground TES application can be used to store energy acquired from the flat plate solar collectors. The utilization of the stored energy by the heat pump in drying applications should be considered a priority due to fluctuation of fossil fuels prices, environmental impact and anticipated depletion of conventional fossil fuels. Application of the solar assisted heat pump drying system by storing of solar energy during whole year in the form of thermal energy makes the greater system thermal performance than the other types of the systems.

Due to the multiple advantages, a theoretical model for a solar assisted heat pump corn drying system with underground TES tank is developed in the present study. The drying system comprises of drying unit, solar collectors, an underground TES tank and a heat pump. Thermal analysis for each component of the drying system is obtained, and they are combined with each other to obtain a mathematical model for the new drying system. A computational model based on the mathematical model has

been developed, and a program prepared in MATLAB is executed by using different input data to find performance parameters for the drying system. These parameters are temperature of water in the TES tank, Coefficient of performance of the heat pump (COP) and system (COPs), Specific Moisture Evaporation Rate (SMER) and energy fractions.

DESCRIPTION OF THE DRYING SYSTEM

The corn drying system under study is an environment friendly drying system. Since, it uses great amount of its energy from solar energy charged in the TES tank. The scheme of the drying system is shown in Fig.1. The system consists of four main parts which are corn dryer unit, a heat pump, flat plate solar collectors and an underground TES tank. The system is considered to be installed in Gaziantep (37.1 ^{o}N), Turkey.

The most important part of the drying system is dryer unit. Since drying evaporating of water in the corn is performed in the drier unit. Wet product enters to the drier unit from the top of it, and moves slowly towards to bottom of the drier. At the same time, fresh air comes to heating channel, and it is heated by the condenser. The hot air is pumped by a fan from bottom of the drier unit, and moves toward top of the unit by contacting to the product. During this process, water in the product is evaporated, and exit to outside with the air.

Heat pump is another essential part of the drying system. It works as a heat transformer from the TES tank to the drier unit. Ground source heat pumps (GSHP) are much more efficient than the air source heat pumps. Therefore, the GSHP coupled with the TES tank supplies higher energy for less temperature fluctuations. Heat is absorbed from the water in the TES tank by the refrigerant flow through evaporator of the heat pump cycle. The energy extracted and transferred by the compressor is rejected from the condenser of the heat pump to the drying air. The heat pump operates in order to correspond heating requirement of the corn and evaporating of the water present in the corn during all times of year.

Flat plate solar collectors are considered to be used in the drying system. They absorb solar energy, and charge it to the TES tank throughout the entire year. They operate when they exposed to useful solar energy. Otherwise, water in the cycle between collectors and the TES tank will not be circulated.

The TES tank is heart of the drying system. Spherical tank is considered to store solar energy as a sensible heat in the water presented as a storage medium in the tank, and buried under the ground. It stores solar energy by circulating water between collectors and the tank during all seasons, and gives the stored energy to the drying unit during whole year by using the heat pump. Bigger volume is necessary for long term storage

of energy so that much more solar energy can be stored, and to get benefit from it particularly in low temperatures. Therefore, large scale TES tank is used to collect more solar heat needed for corn drying process.

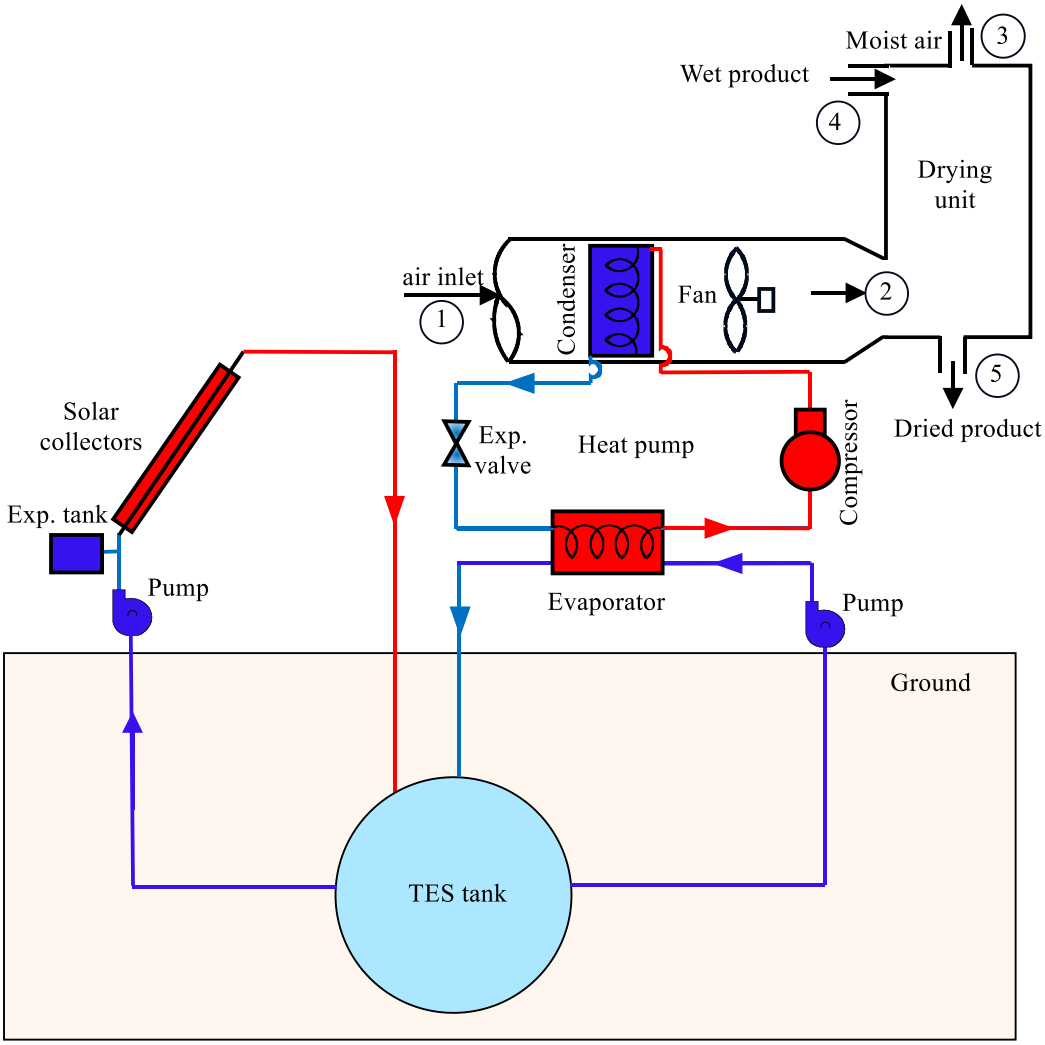

Figure 1. Schematic of the drying system with underground TES tank.

SYSTEM MODELING

Energy expressions or energy model for each component of the system is defined to obtain mathematical modeling of the drying system. These models are for the drying unit, ground coupled heat pump, underground TES tank, and solar collectors. Mathematical modeling will be obtained by combining these expressions. In this section, the expressions will be given in detail.

Energy requirement of the dryer unit

The dryer unit is used to evaporate moisture from wet corn, which is shown in Fig. 1. There are four main interactions in the drying unit; influx of drying air from condenser to drying chamber, exit of moist air after evaporation of moisture from the drying unit, input of wet corn from top of the dryer and output of dried corn with moisture lowered to the desired level.

Mass and energy balances may be formulated for the dryer unit by using as control volume. Mass balances for the dryer unit may be expressed for product or corn, dry air and water as:

$\dot{m}_{p_4} = \dot{m}_{p_5} = \dot{m}_p$ for the product and $\dot{m}_{a_2} = \dot{m}_{a_3} = \dot{m}_a$ for the air

$\omega_2 \dot{m}_a + \dot{m}_{w_4} = \omega_3 \dot{m}_a + \dot{m}_{w_5}$ for the water (1)

or Eq. (1) can be rearranged as follows:

$\dot{m}_w = \dot{m}_{w_4} - \dot{m}_{w_5} = \dot{m}_a(\omega_3 - \omega_2)$ (2)

The dryer unit is assumed to be insulated. Under this assumption, an energy balance may be expressed for the drying chamber as follows:

$\dot{m}_a h_2 + \dot{m}_p h_{p_4} + \dot{m}_{w_4} h_{w_4} = \dot{m}_a h_3 + \dot{m}_p h_{p_5} + \dot{m}_{w_5} h_{w_5}$ (3)

Where $\dot{m}_w$, $\dot{m}_{w_4}$, $\dot{m}_{w_5}$, and ω are mass flow rate for evaporated water from the product, mass flow rate of water in the product at state 4, mass flow rate of water in the product at state 5, and humidity ratio respectively.

The enthalpy of the moist air is equal to total individual partial enthalpies of the dry air and water vapor. Thus, the moist air enthalpy may be formulated (ASHRAE, 1997) as:

$h = h_a + \omega h_g$ (4)

Where h_g refers to the specific enthalpy of saturated water vapor, and h_a refers to the specific enthalpy of dry air at the mixture temperature. The specific enthalpy of the dry air is**:**

$h_a = C_{p_a} T_{mo}$ (5)

The enthalpy of the moist air may be given as the following (Alves-Filho, 2015).

$h = 1.006\, T_{mo} + (2501 + 1.86\, T_d)\omega$ (6)

Where T_d is dry-bulb temperature of the moist air. The specific enthalpy of the product or corn in the energy balance may be written as below:

$(h_{p_5} - h_{p_4}) = C_{p\ wheat}(T_5 - T_4)$ (7)

Therefore Eq. (3) can be written as following expression:

$$\dot{m}_a(h_2\text{-}h_3) = \dot{m}_p\, C_{p\,wheat}(T_5\text{-}T_4) + \dot{Q}_{evap} \quad (8)$$

Heat transfer caused by phase change is:

$$\dot{Q}_{evap} = \dot{m}_w\, h_{fg} \quad (9)$$

Where h_{fg} refers to latent heat of vaporization of water at the average temperature, $T_{av} = (T_4 + T_5)/2$, $\dot{m}_w$ is mass flow rate for evaporated water from moist corn, $\dot{m}_p$ is mass flow rate for dry corn, T_4 and T_5 are corn temperatures before and after drying process respectively.

The offered specific heat of corn by (Kazarian and Hall, 1962).

$$C_{p_{wheat}} = 1465 + 3560\left(\frac{M_P}{1+M_P}\right) \quad (10)$$

Where, M_p refers to moisture content of corn on a dry basis (kg water/kg solid), and $M_P = (\frac{W_4\text{-}W_5}{W_5})$. W_4 refers to pre-drying weight, W_5 refers to post-drying weight. Another equation is used to find the weight of the material after drying process as follows (Mrema et al., 2011)**:**

$$W_5 = W_4\text{-}\left[W_4\frac{(MC_4\text{-}MC_5)}{100\text{-}MC_5}\right] \quad (11)$$

Where MC_4 and MC_5 are moisture contents on wet basis of the product at states 4 and 5, respectively.

Power requirement of the fan

Fresh air is firstly is taken from atmosphere by a fan, and it is heated by the condenser of the heat pump, then sent to the dryer unit to evaporate water from the moist corn. The fan is necessary for this operation. Pressure loss should be firstly calculated to find energy requirement of the fan. For that reason, pressure loss of air flowed over an air-cooled condenser is calculated. The heat exchanger geometry is given in Table 1 and used for condenser design. By neglecting entrance and exit losses, the pressure drop across the condenser for air side is computed (Kays and London, 1984)

$$\Delta P = G^2 \cdot \frac{v_1}{2}\left[(1+\sigma^2)\left(\frac{v_2}{v_1}\text{-}1\right) + f\cdot\frac{A_o}{A_c}\cdot\frac{v_m}{v_1}\right] \quad (12)$$

Where v_1 and v_2 are specific volumes of air before and after drying respectively, v_m is average specific volume for air, j_H and St are Calburn factor, and Stanton number respectively. f is estimated from a figure adopted by (Kays and London, 1984). f is used to find the air side pressure drop for the compact tube-fin heat exchanger. The hourly power input to the fan for the air cooled condenser can be calculated by:

$$\dot{W}_{fan}(t) = \Delta P(t)\,\dot{V}_a(t) \quad (13)$$

Remaining steps and correlations for overall heat transfer coefficient and other parameters may be found in (Akers et al., 1958; Kays and London, 1984; ASHRAE, 2000; Icropera and De Witt, 2006).

Energy demand of the heat pump

Heat pump are device which extract heat from a source at low temperature, and transfer it to a hotter sink (ASHRAE, 1997). In the drying system, ground source heat pump extracts heat from the TES tank, and supplies the heat to cold drying air. The heat supplied by the heat pump condenser to the drying air may be expressed as a function of condenser temperature;

$$\dot{Q}_H(t) = (UA)_{he}[T_h(t)\text{-}T_c] \quad (14)$$

Where $(UA)_{he}$ and $T_h(t)$ are UA value and temperature for the condenser, and T_c represents the average temperature of air entering to condenser and that is leaving condenser.

The heat absorbed by the drying air is given as;

$$\dot{Q}_H(t) = \dot{m}_a C_{p_a}[T_2\text{-}T_a(t)] \quad (15)$$

The heated air is used to dry the moist corn or to evaporate the water present in the corn. After heating the air, it is flowed through the dryer unit. Therefore, energy requirement of the dryer unit can be expressed as;

$$\dot{Q}_H(t) = \dot{m}_p\, C_{pw}\,(T_5\text{-}T_4) + \dot{m}_w\, h_{fg} \quad (16)$$

Coefficient of Performance of heat pump (COP) and system (COP_s), work consumption of the compressor and Specific Moisture Evaporation Rate (SMER) are very important for the heat pump drying system as they may serve as indicators for system performance. Therefore, expressions related with these parameters should be obtained. COP may be given as a function of Carnot efficiency, η_c:

$$COP = \eta_c \left(\frac{T_h(t)}{T_h(t)\text{-}T_w(t)}\right) \quad (17)$$

Then, Eqs. (14) and (15) can be combined, and solved for T_h, then the result of T_h inserted in Eq. (17), which eventually gives:

$$COP = \eta_c \left(\frac{u(\phi_c+1)+\phi_2\text{-}\phi_a(t)}{u\phi_a+\phi_2\text{-}\phi_a(t)\text{ -}u\phi_w(t)}\right) \quad (18)$$

Where u in Eq. (18) is a parameter obtained when equating heat transfer Eq. (14) with (15), ϕ_c, ϕ_a, ϕ_2 and ϕ_w are dimensionless average air temperatures before and after condenser, ambient air temperature, air temperature pre-dryer, and water temperature in the TES tank respectively.

$$u = \frac{(UA)_{he}}{\dot{m}_a C_{p_a}} = \frac{T_2\text{-}T_a(t)}{T_h(t)\text{-}T_c} \quad (19)$$

By using definition of COP for the heat pump, work requirement of the compressor for the heat pump is known as:

$$W_c(t) = \frac{\dot{Q}_H(t)}{COP} \quad (20)$$

When Eqs. (18) and (15) are inserted into Eq. (20), the dimensionless work for the compressor, w, will be derived as below:

$$w(\tau) = \frac{[\phi_2-\phi_a(\tau)][\, u\phi_c+\phi_2-\phi_a(\tau)\, -u\phi_w(\tau)]}{\eta_c[u(\phi_c+1)+\phi_2-\phi_a(\tau)]} \quad (21)$$

Coefficient of performance for the system can be expressed as;

$$COP_s = \frac{\dot{Q}_H(t)}{W_c(t)+W_f(t)} \quad (22)$$

For a drying system, the most suitable efficiency parameter is the Specific Moisture Evaporation Rate (SMER) (ASHRAE, 1999) that is defined as the energy needed to take away 1 kg of water (Alves-Filho, 2015). So, SMER is recorded as the heat pump dryer efficiency.

$$SMER = \frac{\dot{m}_w}{E_{in}} = \frac{\dot{m}_w}{\dot{W}_c(t)+\dot{W}_f} \quad (23)$$

Where $E_{in}, \dot{W}_c(t)$, and $\dot{W}_f$ are the total energy, hourly compressor work, and hourly fan power input to the ground heat pump drying system.

Solution of TES tank problem

Storage tank is the heart of the drying system since solar energy will be stored in the TES tank, and the stored energy will be extracted and transferred to drying air in all seasons by the heat pump. At the same time, ground around the tank is used as a storage medium. Therefore, unsteady heat transfer problem around the tank should be solved to perform energy analysis for the interaction between both of solar collectors and heat pump with TES tank.

TES tank considered in this study is spherical and located in deep earth. The tank is filled with water, and fully mixed. As a result, its temperature will change with time, $T_w(t)$. Water temperature is initially assumed to be equal to the deep ground temperature T_∞. It is assumed that the earth around the tank has a homogeneous structure and constant thermal properties. Schematic representations of the spherical TES tank and energy balance for the tank are shown in Figure 2.

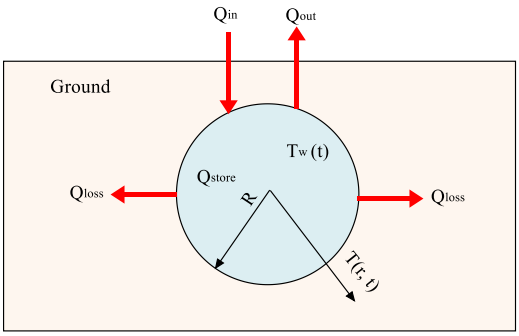

Figure 2. Schematic of the underground TES tank problem.

Unsteady heat transfer problem around the tank is given by a differential equation, initial and boundary conditions in the spherical coordinate system:

$$\frac{\partial^2 T}{\partial r^2} + \frac{2}{r}\frac{\partial T}{\partial r} = \frac{1}{\alpha}\frac{\partial T}{\partial t} \quad (24)$$

$$T(R,t) = T_w(t) \quad (25)$$

$$T(\infty,t) = T_\infty \quad (26)$$

$$T(r,0) = T_\infty \quad (27)$$

Some of the energy charged to the tank is stored in the tank as a sensible heat, and the remaining will be transferred to the surrounding earth as a conduction heat loss. The energy balance equation can be expressed as:

$$Q = \rho_w c_w V_w \frac{dT_w}{dt} - kA\frac{\partial T}{\partial r}(R,t) \quad (28)$$

Where V_w, ρ_w and c_w are volume of the water present in the tank, density and specific heat of the water in the tank. R, A and k are radius, surface area of the tank, and thermal conductivity of the surrounding earth.

The unsteady conduction heat transfer problem given by Eqs. (24-28) is transferred into dimensionless form by using dimensionless variables is presented in (Yumrutas and Ünsal, 2012). Then, dimensionless problem formulation will be obtained. All steps for the solution of the problem are given in (Yumrutas and Ünsal, 2012), therefore, only solution is presented in this section.

$$\phi_w(\tau_n) = \frac{q(\tau_n) + \left[\frac{P}{\Delta\tau} + \frac{1}{\sqrt{\pi\Delta\tau}}\right]\phi_w(\tau_{n-1}) - \sum_{i=1}^{n-2}\frac{\phi_w(\tau_{i+1}) - \phi_w(\tau_i)}{\sqrt{\pi\Delta\tau(n-i)}}}{1 + \frac{P}{\Delta\tau} + \frac{1}{\sqrt{\pi\Delta\tau}}} \quad (29)$$

Equation (29) is used to find the hourly dimensionless temperature of water in TES tank. The term $q(\tau)$ in Eq. (57) refers to the net dimensionless heat input rate to the tank [30].The input heat rate, $q(\tau)$, is the difference between dimensionless useful solar energy and energy extracted by the heat pump. It was expressed in (Yumrutas and Ünsal, 2000; Yumrutas and Ünsal, 2012) as:

$$q(\tau) = q_u(\tau) - q_H(\tau) + \frac{w(\tau)}{\gamma} \quad (30)$$

Where $q_u(\tau)$ is the dimensionless useful solar energy charge rate to the tank, q_H and $w(\tau)$ are the dimensionless heat demand of the drying unit, and heat pump work, respectively, and γ is a dimensionless parameter ($4\pi Rk/\dot{m}_a(t)\, C_{p_a}$).

Useful solar energy collection rate to the TES tank

Solar collectors are used to absorb solar energy and to charge it to the tank. The solar energy charge rate, $\dot{Q}_u(t)$ is calculated by using the formula given by (Duffie and Beckman, 1991);

$$\dot{Q}_u(t) = \eta_{fc}(t)\, A_{col}\, I_T(t) \quad (31)$$

Where η_{fc} is the flat plate solar collector efficiency, and A_{col} is the collector area. The collector efficiency variation with respect to dimensionless factor, $[T_w(t)-T_a(t)]/I_T(t)$ was obtained from the experimental study by Yumrutas and Kaşka (Yumrutas and Kaşka, 2004), and it is also used in the present study;

$$\eta_{fc}(t) = 0.72\text{-}6.4\left[\frac{T_w(t)-T_a(t)}{I_T(t)}\right] \quad (32)$$

Where $T_w(t)$ is the temperature of the water in the TES tank and $T_a(t)$ is the ambient air temperature. $I_T(t)$ in Eqs. (31-32) is the hourly solar radiation coming to the collector surface. Calculation procedure for finding $I_T(t)$ is given in (Duffie and Beckman, 1991).

INPUT DATA FOR THE DRYING SYSTEM

A computer code in MATLAB has been developed for numerical calculations. In this section, main input data for finding performance parameters for the drying system are outlined. The input data are for dryer unit, heat pump, TES tank, ground around the tank, and solar collectors. The data and information for the main components of the drying system are given in the following subsections.

Drying unit

Energy requirement of the dryer unit is necessary throughout all seasons on hourly basis. Mass flow rate of the wet corn is selected basically as 30 kg h^{-1}, which can be changed to find its effect on performance of the drying system. The inlet air temperature to dryer unit, T_2 , and outside design air temperature for Gaziantep, T_o, are set as 55 ℃ depending on (Sundaram, et al., 2016; KCD dryer, 2019), and -9 ℃, respectively. For design conditions, "u" value in Eq. (19) is 1.7. Ambient air temperature, $T_a(t)$, is heated up by the heat pump condenser to reach design temperature (55 ^oC), and is blown to the dryer unit by a fan to evaporate water existing in the corn. The wet corn temperature, T_4, and drying corn temperature, T_5, are taken as 20 ℃ and 45 ℃, respectively. Moisture contents of moist corn, MC_4, and drying corn, MC_5, have been considered as 25% and 15% respectively, according (www.gov.mb.ca/agriculture, 2019). Hourly humidity ratio has been evaluated by using EES (Engineering Equation Solver) program depending on hourly ambient air temperature for Gaziantep, at atmospheric pressure, while relative humidity of 30% is taken in this study based on (Strommen, 1980; Magnussen and Strommen, 1981). Pressure drop through the drying unit is neglected since it is very low in relation to compressor work. EES program is also used to calculate hourly power input to the blower or fan.

Heat pump

Heat is absorbed by the evaporator of the heat pump from the underground TES tank, and some amount of energy is added to the working fluid by the compressor. Heat is rejected to drying air to evaporate water in the corn. Expressions for energy requirement and COP of the heat pump are derived in previous sections. A practically reasonable Carnot efficiency (CE) value was used basically as 0.4 in the present study. Zogou and Stamatelos (1998) expressed that CE values range between 0.30 and 0.50 for small electric heat pumps, and accordingly three CE values of 0.30, 0.40 and 0.50 were taken in this study. In the present study, CE value was set at 0.4, and tank volume was set at 100 m^3 for all calculations unless another CE and tank volume is used.

The TES tank and its surrounding structure

Water in the TES tank is assumed fully mixed. Specific heat and density of the water are 4.18 kJ/kg°C, and 1000 kg/m^3, respectively. Temperature of the water at the beginning of operation is taken as equal to deep earth temperature of 15 ^oC. Solar energy is charged to the water if there is useful solar energy during whole year. Some of the stored energy is absorbed by the heat pump, and some is lost to the earth surrounding the tank, and the remaining part is stored as a sensible heat in the TES tank. In this study, limestone is basically considered as an earth surrounding the tank since it is the prevalent geo-structure of Gaziantep. To investigate effect of the earth type on the performance of the system, three types of earth are considered; limestone, granite and coarse graveled. Thermophysical properties of the earths are given in (Ozisik, 1985), and illustrated in Table 2. Tank volume is selected as 100 m^3 in all calculations unless another volume is used.

Solar collectors

In this study, flat plate solar collectors are used to collect useful solar energy in TES tank. They are assumed to be directed toward the south, and their tilt angle is taken as latitude angle (37.1°N) of Gaziantep, Turkey since highest solar energy is collected when the slope angle is equal to the latitude angle for yearly operation (Elminir et al., 2006). Useful solar energy charge to the underground TES tank given by Eq. (31) is calculated by using Eqs. (32) and other equations given by (Duffie and Beckman, 1991). Hourly solar radiation values and ambient air temperatures are used in the numerical calculations. The values of the hourly solar radiation on horizontal surface and ambient air temperature were taken from Gaziantep Meteorological Station. Effect of solar energy collection rate on performance of the drying system is investigated. During the calculations of the model, collector area as an input data is set at 20 m^2 if another collector area is not used.

COMPUTATION PROCEDURE FOR THE DRYING SYSTEM

In order to examine performance of corn drying system, a computation procedure is developed by using interrelated analytical models and expressions for each system component. The drying system consists of four main components; drying unit, heat pump, solar collectors and TES tank. The current drying system is a solar-assisted heat pump drying system with the TES tank. The numerical computation is prepared by using MATLAB, and is explained in this section.

The computation procedure passes through several stages. Firstly, heating load for drying unit has been calculated through Eqs. (3-9). Both hourly heating requirement of the drying unit and corn mass flow rate are considered to be constant. Secondly, since ambient air temperature changes hourly, mass or volume flow rate of the air will change. The power input required by the fan is calculated by using Eqs. (12) through (13) and others correlations which presented in (Akers et al., 1958; Kays and London, 1984; ASHRAE, 2000; Icropera and De Witt, 2006). Thirdly, hourly useful solar energy, $\dot{Q}u(t)$, is computed by using Eq. (31) in addition to Eq. (32) which is recommended by (Yumrutas and Kaşka, 2004). Collector efficiency in Eq. (32) is computed by using hourly solar radiation rates on tilted surfaces, TES tank temperature, and outside air temperature. Solar energy gain is later transformed into dimensionless form using dimensionless expressions referred to in (Yumrutaş and Ünsal, 2012). Next, new hourly water temperature in TES tank has been estimated through Eq. (29) by utilizing net energy charge rate to TES tank expressed in Eq. (30). Finally, hourly, monthly and annual values of water temperature in TES tank, COP, COPs, SMER and energy fractions have been computed. These computations were done on an hourly basis for sufficient number of years until the annual temperature distribution of the water in the TES tank reaches annually periodic operating conditions.

RESULTS AND DISCUSSION

It is necessary to find performance parameters for the drying system in order to know whether the system within which the parameters operate are efficient or not. The performance parameters are: temperature of water in TES tank, coefficient of performance for the heat pump (COP) and system (COPs), energy ratio, and specific moisture evaporation ratio (SMER). They have been computed by executing a computer program in MATLAB and using drying system parameters such as Carnot efficiency, type of ground, collector area, and TES tank volume. In the calculations, limestone is used as a geological structure, and Carnot efficiency (CE), collector area, volume of TES tank are set as, 0.4, 20 m^2 and 100 m^3, respectively, unless other values of these input parameters are used. Results obtained from the numerical computations are presented in figures, and discussed in this section.

Each earth surrounding TES tank gives different performance parameters because of different thermophysical properties. Variation of water temperature in the TES tank is a type of performance parameter. Hence, every performance parameter depends on storage temperature. For that reason, Fig. 3 depicts the individual effects of the three selected types of ground on temperature variation of water in TES tank during fifth year of operation by using these input parameters; collector area (20 m^2), Carnot efficiency factor (40%), storage volume (100 m^3), and mass flow rate of cooked corn (30 kg h^{-1}). The reasons behind selecting these parameters are discussed in the following figures. It is observed from Fig. 4 that water temperatures have higher values during summer months and lower values during winter season when the TES tank is surrounded by the coarse graveled earth. But, water temperatures for granite have lower values in summer and higher values in winter. Limestone gives medium temperature values that are between coarse graveled and granite, which accordingly give medium performance parameters. Granite and coarse graveled earth types do not present widely as a geological structure around Gaziantep City, Turkey. All figures depict limestone ground since it is widely present in Gaziantep, unless another type is given in this study.

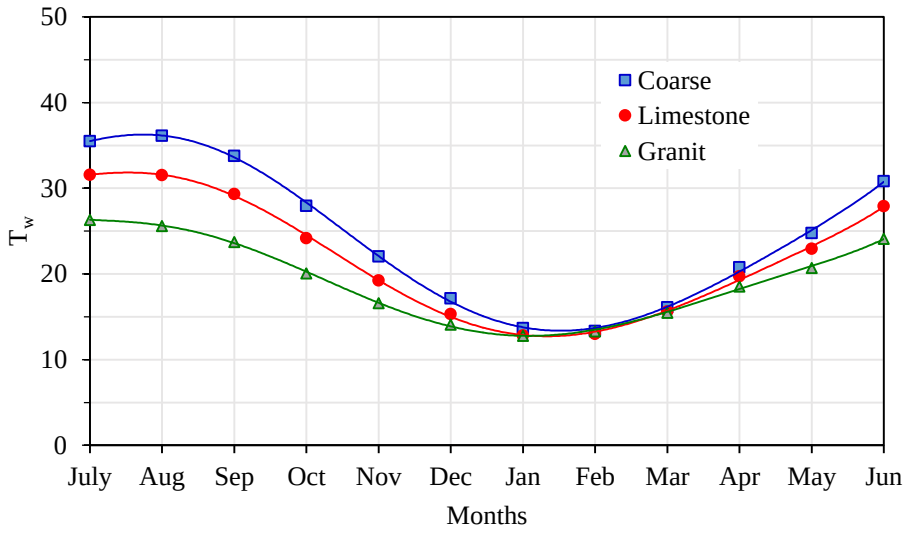

Fig. 3. Effect of earth type on annual temperature variation of water in the TES tank during fifth year of operation (Ac = 20 m^2, CE = 40%, V = 100 m^3, W_4=30 kg h^{-1}).

Annual temperature variation of water in the TES tank for the first, second, third and fifth year of operation is shown in Fig. 4. It is seen from the figure that water temperature varies rapidly during the first few years. After that this variation decreases, and the drying system reaches the annual periodic operation in fifth year of operation onwards. It can be concluded that the number of periodical operation is equal to 5 years. That is, energy input to the TES tank is equal to heat loss from the tank, and energy balance takes place from fifth year of operation.

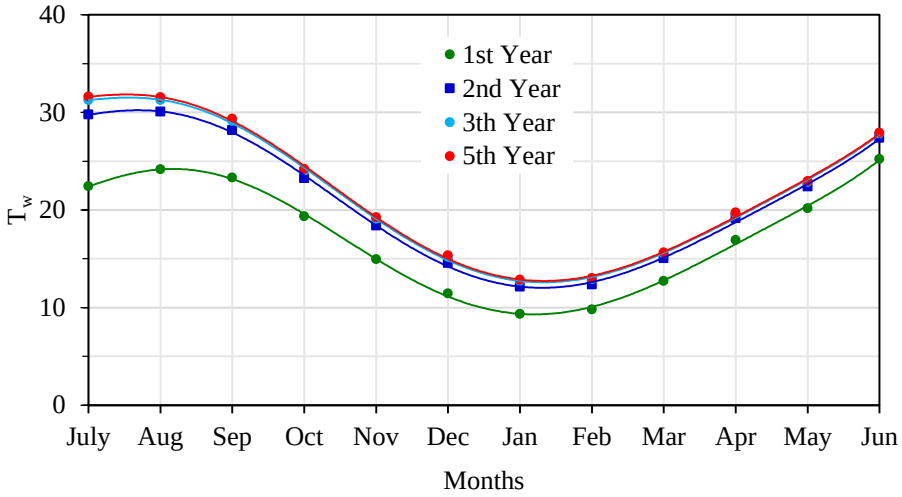

Fig.4. Annual temperature variation of water in the TES tank for September (Limestone, Ac=20 m², CE=40%, V=100 m³, W_4=30 kg h^{-1})

In order to define collector area for selected load or mass flow rate of cooked corn, Fig.5 illustrates three different collector areas which are 20, 25 and 30 m². It is known that higher collector area gives higher water temperature. This indicates that there is a proportional relationship between collector area and water temperature in TES tank. An important point is that the selection of collector area should provide reasonable temperature for the water in TES tank. It is known that minimum collector area should be selected for reasonable performance parameters and three selected areas were suitable. When the collector area decreases below 20 m², water temperature approaches 0 °C especially for first year of operation, and consequently gives lower performance parameters of COP, COPs and SMER. Therefore, the suitable collector area is 20 m².

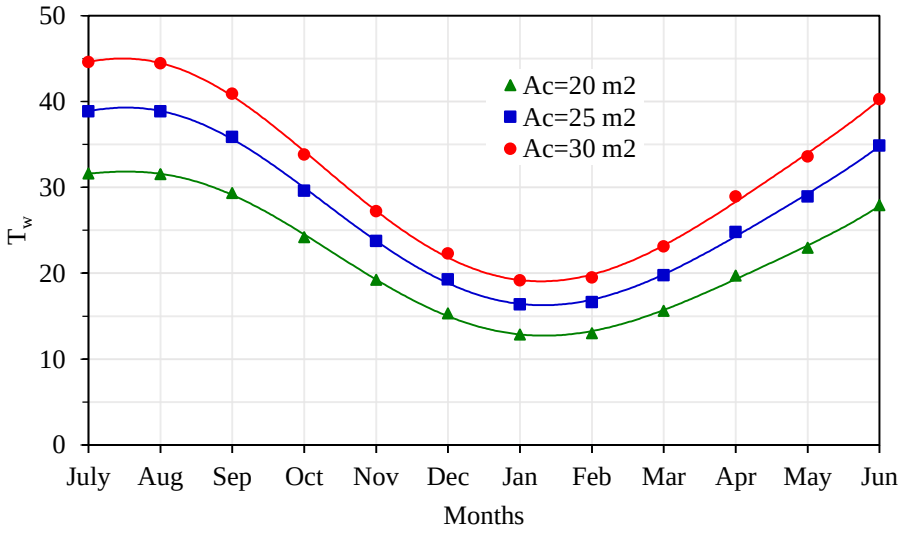

Fig. 5. Effect of collector area on annual temperature of water in the TES tank during fifth year of operation (limestone, CE = 40%, V = 100 m³, W_4=30 kg h^{-1})

Performance parameters are important for the drying system. The parameters are water temperature in the tank, SMER and COPs. Impact of collector area upon variation in water temperature during fifth year is discussed in Fig.6. The effects of collector area on COPs and SMER are illustrated in Figs. 6 and 7. for three different collector areas which are 20, 25 and 30 m^2 for year 5 of operation. It can be noticed that the COP and SMER increases with the collector area because of increasing energy charging to the TES tank. It is important to select a reasonable collector area in order to have a reasonable SMER and COP. It is seen from the figures 6 and 7 that COPs ranged between 4.24 and 5.06, and SMER ranged between 5.49 and 6.56 for the collector area 20 m^2. These are reasonable values for the periodic operation. Accordingly, collector area is selected to be 20 m^2. The results for the COP are in agreement with (Yumrutaş and Ünsal, 2012). Because of these reasonable values of COP and SMER, collector area is selected as 20 m^2 for the other input data used in this study.

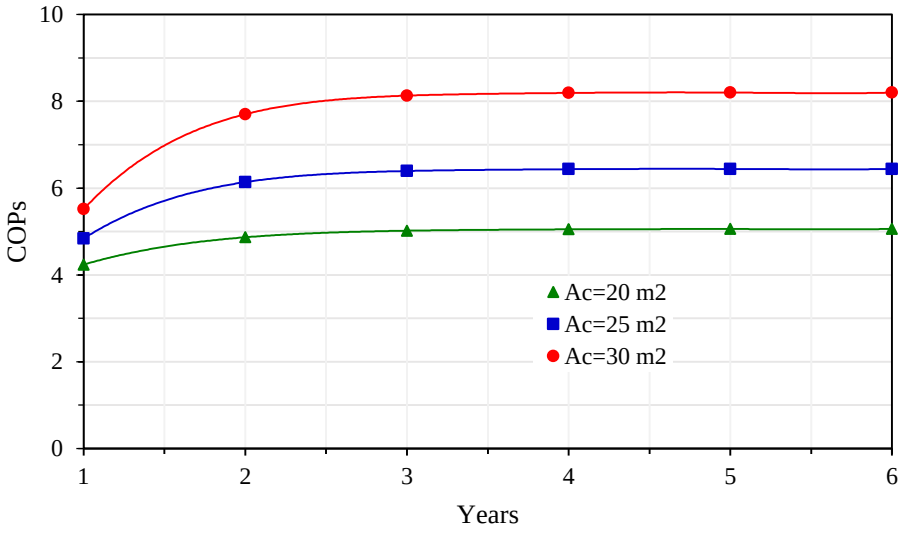

Fig. 6. Effect of collector area on heat pump COPs (limestone, CE = 40%, V = 100 m^3, W_4=30 kg h^{-1})

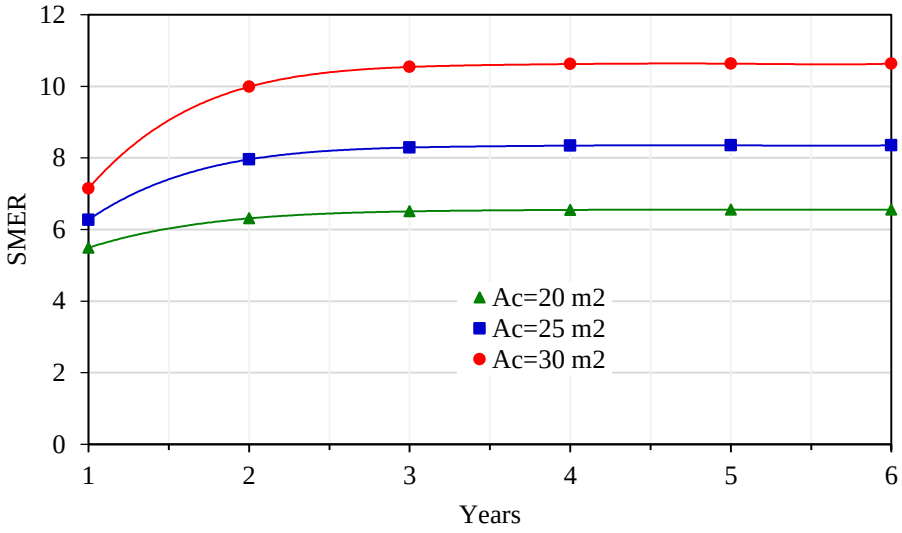

Fig. 7. Effect of collector area on SMER (limestone, Ac=20 m^2, CE = 40%, V = 100 m^3, W_4=30 kg/h)

The effect of another significant parameter which is drying air teperature, T_2, on system performance is showed in Fig. 8. Three different tempeartures are selected according to (www.gov.mb.ca/agriculture, 2019) which are 55, 60, and 65 °C. This figure indicates that when T_2 is set at higer values as in 60 and 65 °C the heat pump COP is decreased. The reason is that the heat pump is supplied heat to drying air, T_2, when drying air temperature is high the heat pump needs to more power input by compressor, accordingly COP is go down. In the calculations the default T_2 is considered 55 C°.

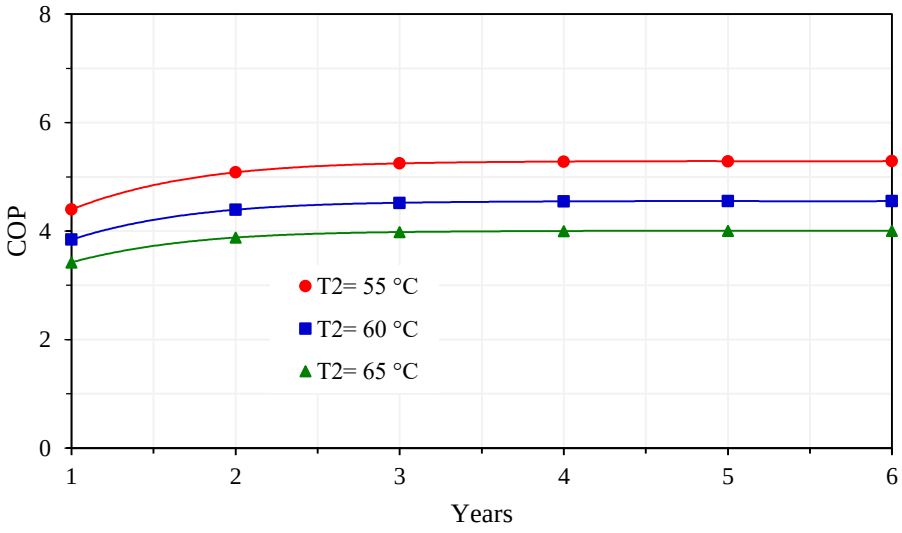

Fig.8. Effect of T_2 on COP (limestone, Ac=20 m^2, CE = 40%, V = 100 m^3, W_4=30 kg h^{-1})

Heating load for the drying unit that must be provided hourly during the year is considered constant and that load is divided into two parts; sensible and latent heat. The biggest part of the load of wet corn is the latent. In order to evaporate the moisture present in the wet corn, more heat is required. There are some factors such as moisture content of corn at inlet and outlet states of corn. Moisture content of initial state of corn should be considered to be within reasonable values. Therefore, the effect of moisture content existing in moist corn on performance parameters of water temperature in TES tank is shown in Fig. 9. Three different moisture contents with values of 20, 25, and 30 % for the moist corn at initial state are selected in the analysis. As it is clear from the figure, when the moisture content, MC_4 increased to 30%, T_w decrease, accordingly the other performance parameters such as COP, COPs, and SMER will be decreased because these performance parameters have inversely relations with T_w. However, moisture content of 25 % is practical value according to (www.gov.mb.ca/agriculture, 2019) and suitable for energy saving for the drying system. Therefore, moisture content at inlet state of corn is selected as 25 % for all calculations in this study.

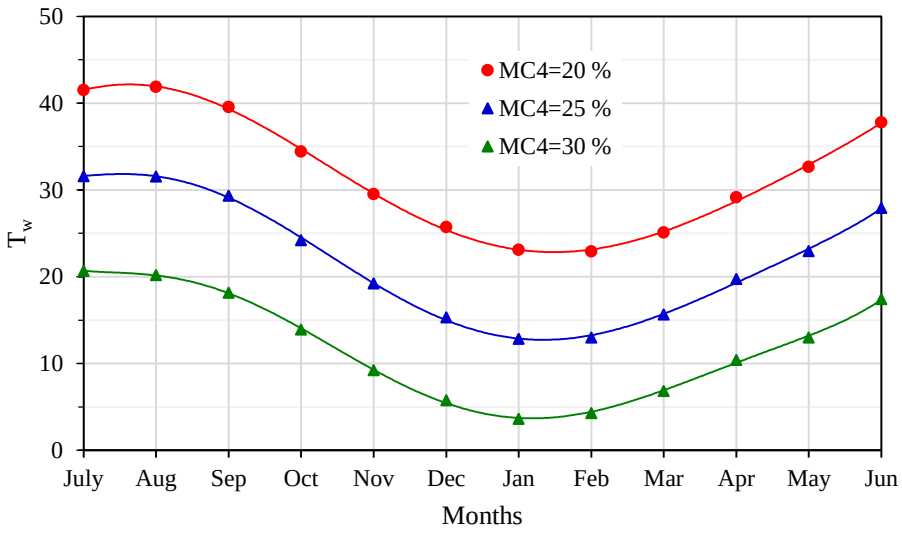

Fig. 9. Effect of entering moisture content of corn on annual temperature of water temperature in the TES tank during fifth year of operation (limestone, Ac=20 m², CE = 40%, V= 100 m³, W_4=30 kg h^{-1}).

It is important to make annual energy balance for the drying system. The energy supplied to the drying system consists of solar energy, heat pump work and fan power. The energy supplied to the system should be equal to total useful energy or load for the dryer unit, partially stored energy in the TES tank, energy lost to the surrounding earth. Energy fractions are defined as the ratio of each energy component to the total energy supplied to the system. Figure 10 shows energy fractions during the fifth year of operation for the first, second and fifth year of operation. It is seen from the figure that solar energy increases, compressor work decreases, and fan power stays constant throughout years. At the same time, both stored and lost energy decrease, and load increases with the years. It is observed that there is no stored energy during the fifth

year operation, that is, the system operates periodically in fifth year of operation onwards.

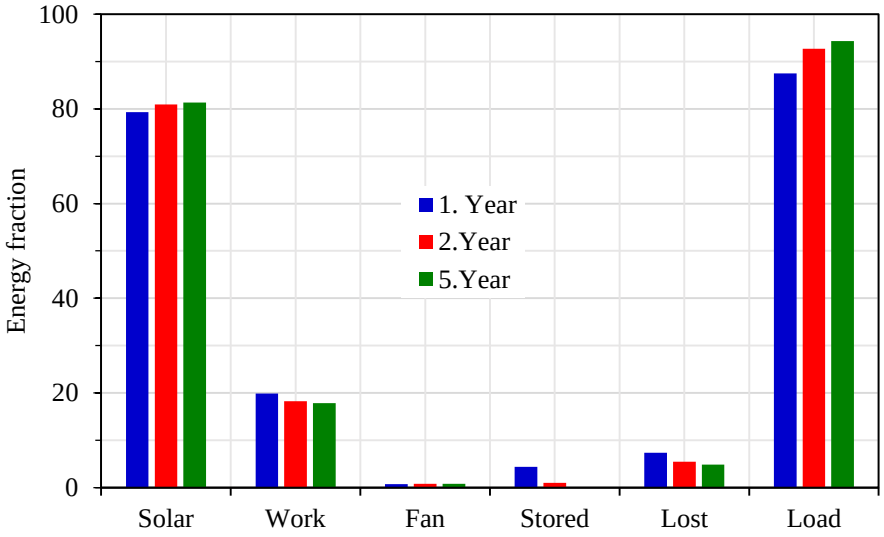

Fig. 10. Effect of years on energy fraction (limestone, Ac=20 m^2, CE = 40%, V = 100 m^3, W_4=30 kg h^{-1})

CONCLUSIONS

1- The system reach to periodic operation in fifth year onwards for 10 years of operation.
2- Earth type around the underground TES tank has a great effect on the drying system performance.
3- When corn mass flow rate and Carnot Efficiency are selected as 30 kg h^{-1} and 40 %, more suitable collector area and TES tank volume are obtained as 20 m^2 and 100 m^3, respectively. For these values, the performance parameters of the COP, COPs and SMER are obtained as 5.29, 5.06 and 6.56 respectively, when the drying system reaches periodic operation from fifth year onwards.
4- Moisture content of corn at initial state has inversely relation while collector area has a proportional relation with performance parameters.
5- Drying air temperature, T_2, has significant effect on performance parameters.
6- Total energy input to the drying system supplied by solar energy, compressor work and fan power are 81.35 %, 17.83 %, and 0.8 % respectively during the fifth year of operation.

TABLES

Table 1. Input design parameters for compact heat exchanger used as a condenser (Kays and London, 1984).

Parameter	Value
Tube outside diameter, D_o	17.17 (mm)
Fin pitch	305 (1/ m)
flow passage hydraulic diameter, D_h	3.48 (mm)
Fin thickness, t	0.4064 (mm)
Free flow area/frontal area, σ	0.481
Heat transfer area/total volume, α	554 m^2/m^3
Fin area/total area, A_f/A	0.95

Table 2. Characteristics of the ground structures (Ozisik, 1985).

Ground type	Conductivity (W/m K)	Diffusivity (m^2/s)	Specific heat (J/kg K)	Heat capacity (kJ/m^3K)
Limestone	1.3	5.75×10^{-7}	900	2250
Granite	3.0	14.00×10^{-7}	820	2164.8
Coarse	0.519	1.39×10^{-7}	1842	3772

REFERENCES

Aktaş, M., Şevik, S., & Aktekeli, B. (2016). Development of heat pump and infrared-convective dryer and performance analysis for stale bread drying. *Energy Conversion and Management*, *113*, 82-94.

Alves-Filho, O. (2015). *Heat pump dryers: Theory, design and industrial applications*. CRC Press.

Akers, W. W., Deans, H. A., & Crosser, O. K. (1958). Condensing heat transfer within horizontal tubes. *Chem. Eng. Progr.*, *54*.

Baniasadi, E., Ranjbar, S., & Boostanipour, O. (2017). Experimental investigation of the performance of a mixed-mode solar dryer with thermal energy storage. *Renewable energy*, *112*, 143-150.

Erbay, Z., & Hepbasli, A. (2014). Advanced exergoeconomic evaluation of a heat pump food dryer. *Biosystems engineering*, *124*, 29-39.

Fatouh, M., Metwally, M. N., Helali, A. B., & Shedid, M. H. (2006). Herbs drying using a heat pump dryer. *Energy Conversion and Management*, *47*(15-16), 2629-2643.

Mrema, G. C., Gumbe, L. O., Chepete, H. J., & Agullo, J. O. (2012). *Rural structures in the tropics: design and development*. Food and Agriculture Organization of the United Nations.

Leon, M. A., Kumar, S., & Bhattacharya, S. C. (2002). A comprehensive procedure for performance evaluation of solar food dryers. *Renewable and Sustainable Energy Reviews*, *6*(4), 367-393.

Xu, C., Xu, G., Zhao, S., Dong, W., Zhou, L., & Yang, Y. (2016). A theoretical investigation of energy efficiency improvement by coal pre-drying in coal fired power plants. *Energy conversion and management*, *122*, 580-588.

Nowak, D., & Lewicki, P. P. (2004). Infrared drying of apple slices. *Innovative Food Science & Emerging Technologies*, *5*(3), 353-360.

Wang, Y., Zhang, M., Mujumdar, A. S., & Chen, H. (2014). Drying and quality characteristics of shredded squid in an infrared-assisted convective dryer. *Drying technology*, *32*(15), 1828-1839.

Duffie, J. A., & Beckman, W. A. (1991). Solar Engineering of Thermal Processes, New York: John Wiley& Sons.

Handbook, ASHRAE Fundamentals: American Society of Heating, Refrigerating and Air Conditioning Engineers, Atlanta, USA, 1997.

Handbook, ASHRAE Systems and Equipment: American Society of Heating, Refrigerating, and Air- Conditioning Engineers, Atlanta, USA, 2000.

https://www.gov.mb.ca/agriculture/crops/production/grain-corn/print,corn-harvesting-and-storage.html; [accessed 30 July 2019].

Icropera, F. P., and De Witt, D. P. (2006). Fundamentals of Heat and Mass Transfer, Sixth Edition, John Wiley and Sons, Inc. USA.

Kazarian, E. A., and Hall, C. W. (1962). Thermal properties of grain (Doctoral dissertation, Michigan State University of Agriculture and Applied Science. Dept. of Agricultural Engineering).

Kays, W. M., & London, A. L. (1984). Compact heat exchangers. 3rd ed. Blacklick, Ohio, USA, McGraw Hill

Koyuncu, T. (2006). Performance of various design of solar air heaters for crop drying applications. *Renewable Energy*, *31*(7), 1073-1088.

KCD dryer continuo's mixed flow. Operation manual, www.kongskilde.com, kcd-mk4_man-gb_117012512.; 2019 [accessed 30 July 2019].

Momin, A. M. E., Saini, J. S., & Solanki, S. C. (2002). Heat transfer and friction in solar air heater duct with V-shaped rib roughness on absorber plate. *International journal of heat and mass transfer*, *45*(16), 3383-3396.

Mohanraj, M., & Chandrasekar, P. (2009). Performance of a forced convection solar drier integrated with gravel as heat storage material for chili drying. *Journal of Engineering Science and Technology*, *4*(3), 305-314.

Magnussen, O. M. and Strommen, I. (1981). Heat pump drying of heavily salted codfish, Nordic Refrigeration Meeting, Copenhagen, May 21–23 (in Norwegian).

Naemsai, T., Jareanjit, J., & Thongkaew, K. (2019). Experimental investigation of solar-assisted heat pump dryer with heat recovery for the drying of chili peppers. *Journal of Food Process Engineering*, e13193.

Ozisik, M. N. (1985). Heat transfer: a basic approach, McGraw-Hill, New York.

Qiu, Y., Li, M., Hassanien, R. H. E., Wang, Y., Luo, X., & Yu, Q. (2016). Performance and operation mode analysis of a heat recovery and thermal storage solar-assisted heat pump drying system. *Solar Energy*, *137*, 225-235.

Sundaram, P., Sudhakar, P., & Yogeshwaran, R. (2016). Experimental studies and mathematical modeling of drying wheat in fluidized bed dryer. *Indian Journal of Science and Technology*, *9*(36), 1-8.

Strommen, I. (1980) Drying of heavily salted codfish, Ph.D. Thesis, The Norwegian Institute of Technology, Division of Refrigeration Engineering, Trondheim, Norway (in Norwegian).

Şevik, S., Aktaş, M., Doğan, H., & Koçak, S. (2013). Mushroom drying with solar assisted heat pump system. *Energy Conversion and Management*, *72*, 171-178.

Turgut, O., & Onur, N. (2000). Design and performance of a special solar collector and its application to drying of agricultural products. *Gazi Üniversitesi Fen Bilimleri Enstitüsü Dergisi*, *13*(3), 639-648.

Wang, Y., Li, M., Qiu, Y., Yu, Q., Luo, X., Li, G., & Ma, X. (2019). Performance analysis of a secondary heat recovery solar-assisted heat pump drying system for mango. *Energy Exploration & Exploitation*, 0144598718823937.

Yumrutaş, R., & Ünsal, M. (2012). Energy analysis and modeling of a solar assisted house heating system with a heat pump and an underground energy storage tank. *Solar Energy*, *86*(3), 983-993.

Yumrutaş, R., & Ünsal, M. (2000). Analysis of solar aided heat pump systems with seasonal thermal energy storage in surface tanks. *Energy*, *25*(12), 1231-1243.

Yumrutas, R., & Kaska, Ö. (2004). Experimental investigation of thermal performance of a solar assisted heat pump system with an energy storage. *International journal of energy research*, *28*(2), 163-175.

Zogou, O., & Stamatelos, A. (1998). Effect of climatic conditions on the design optimization of heat pump systems for space heating and cooling. *Energy Conversion and Management*, *39*(7), 609-622.

Nomenclature

A	tank surface area (m^2)
A_o	outside area of condenser (m^2)
A_{col}	collector area (m^2)

c_{pa} specific heat of air (kJ kg^{-1} K^{-1})

$C_{p_{wheat}}$ specific heat of wheat (kJ kg^{-1} K^{-1})

G mass velocity for air across condenser (kg m^{-2} s^{-1})

h specific enthalpy of the moist air (kj kg^{-1})

h_g specific enthalpy of saturated water vapor (kj kg^{-1})

h_a specific enthalpy of dry air at the mixture temperature (kj kg^{-1})

h_4 specific enthalpy of dry wheat pre drying (kj kg^{-1})

h_5 specific enthalpy of dry wheat after drying (kj kg^{-1})

h_{fg} latent heat of vaporization of water at the average temperature (kj kg^{-1})

I_T hourly solar radiation on tilted surface (W m^{-2})

k thermal conductivity of earth (W m^{-1} K^{-1})

$\dot{m}_a$ mass flow rate of dry air (kg s^{-1})

$\dot{m}_w$ amount of evaporated water from moist wheat (kg s^{-1})

$\dot{m}_{w_4}$ mass flow rate of water in wheat pre-drying (kg s^{-1})

$\dot{m}_{w_5}$ mass flow rate of water in wheat after drying (kg s^{-1})

$\dot{m}_p$ mass flow rate of dry corn (kg s^{-1})

M_p moisture content of corn on a dry basis (kg water kg^{-1} solid)

MC_4 moisture content pre drying on wet basis (%)

MC_5 moisture content after drying on wet basis (%)

P dimensionless parameter [-]

q dimensionless heat transfer to the tank [-]

Q heat transfer to the tank (W)

$\dot{Q}_H$ condenser heating load (W)

$\dot{Q}_{evap}$ latent heat of evaporation water from moist wheat (W)

$\dot{Q}_u$ solar energy rate (W)

q_u dimensionless useful solar energy charge rate to the tank, $q_u = \frac{\dot{Q}_u}{4\pi RKT_\infty}$ [-]

q_H dimensionless condenser heat load, $q_H = \frac{\dot{Q}_H}{4\pi RKT_\infty}$ [-]

r radial distance from the tank centre (m)

R tank radius (m)

t time (s)

T earth temperature (K)

T_a ambient air temperature (K)

T_o outside design air temperature (K)

T_d dry bulb temperature of moist air (K)

T_2 condenser outlet temperature (K)

T_4 undried wheat temperature (K)

T_5 dried wheat temperature (K)

T_w water temperature in the tank (K)

T_c average temperature of air pre and after condenser (K)

T_h condenser temperature (K)

T_∞ deep ground temperature (K)

u dimensionless parameter for design condition [-]

$(UA)_{he}$ product of heat transfer coefficient and area for heat pump condenser (W K^{-1})

V volume of the tank (m^3)

$\dot{V}_a$ volume flow rate for air (m^3 kg^{-1})

w dimensionless compressor work [-]

$\dot{W}_c$ compressor input power (W)

$\dot{W}_f$ fan input power (W)

W_4 weight of wheat pre-drying (kg h^{-1})

W_5 weight of wheat after drying (kg h^{-1})

Greek letters

α thermal diffusivity of earth (m^2 s^{-1})

η_c Carnot efficiency [-]

η_{fc} flat plate solar collector efficiency [-]

ϕ dimensionless temperature for earth [-]

ϕ_1 dimensionless condenser inlet air temperature [-]

ϕ_c dimensionless average temperature for air pre and after condenser [-]

ϕ_w dimensionless water temperature in the tank [-]

ϕ_2 dimensionless air supply temperature pre-dryer [-]

γ dimensionless parameter [-]

ρ_w water density (kg m^{-3})

Δp pressure drop of air across condenser (Pa)

σ free flow area/frontal area for condenser [-]

f parameter estimated from a figure [-]

v_1 specific volume for air pre-condenser (m^3 kg^{-1})

v_2 specific volume for air after condenser (m^3 kg^{-1})

v_m average specific volume for air (m^3 kg^{-1})

ω humidity ratio for moist air (kg water kg^{-1} dry air)

ω_2 humidity ratio for moist air pre drying process (kg water kg^{-1} dry air)

ω_3 humidity ratio for moist air after drying process (kg water kg^{-1} dry air)

Acronyms

COP coefficient of performance of heat pump

COPs coefficient of performance of whole system

CE Carnot Efficiency

HPD Heat Pump Drying

GSHP Ground Source Heat Pump

SMER specific moisture evaporation rate (kg kW^{-1} h^{-1})

SAHP Solar-Assisted Heat Pump

TES thermal energy storage

HPD heat pump drying

AN OVERVIEW ABOUT THE USAGE OF NANOFLUIDS IN HEAT TRANSFER ENHANCEMENT STUDIES

Nehir TOKGOZ, Osmaniye Korkut Ata University, Engineering Faculty, Energy Systems Engineering, Osmaniye, nehirtokgoz@osmaniye.edu.tr

ABSTRACT: The lack of effective and productive use of energy is one of the most important problems of today's world. The applications in energy efficiency have started to become widespread day by day due to depletion of fossil fuels. In this context, the enhancement studies of heat exchangers which are used for transporting heat in industry have been conducting expeditiously. The major target of this subject is to design more efficient, economic and compact devices. Improving techniques which can be categorized into three groups like active, passive and combined methods have gained new dimensions with developing technologies. Especially, passive procedures are preferable because of not requiring energy from an external source. One of the passive methods is either the addition of a liquid into main fluid or enhancing main fluid with solid particles. Nanofluid is chosen as main fluid in aforementioned systems and nanoparticles are mixed with that nanofluid. Thus, the heat transfer properties of original liquid are improved greatly and it seems to be ideal for practical applications. This paper focuses on the heat transfer and surface volume improvements, advancements in thermal conductivity and Brownian movement of nanofluids. Although, many researchers claim that nanofluids have positive effects on heat transport, conflicting results have arisen by the reasons of unclear heat transfer mechanisms and single phase-double phase approach need to insert an English abstract into this section by taking into account exactly the same format. The abstract should not exceed the 300-word limitation. If your translation does exceed the given limitation, you should arrange your wording to keep within the 300-word limit. You may need to insert an English abstract into this section by taking the word limit into account.

Key words: heat transfer enhancement, nanofluid, single phase, two phase

NANO AKIŞKANLARIN ISI TRANSFERİ İYİLEŞTİRME ÇALIŞMALARINDA KULLANILMASINA GENEL BAKIŞ

ÖZET: Enerjinin etkin ve verimli kullanılmaması günümüzün en önemli problemlerinden biridir. Özellikle fosil yakıtların tükenmek üzere olması neticesinde her alanda giderek artan enerji verimliliği uygulamaları günden güne yaygınlaşmaktadır. Bu çerçevede endüstride ısıyı taşımak için kullanılan ısı değiştiricileri iyileştirme çalışmaları da hızla devam etmektedir. Isı transferi iyileştirme çalışmalarının en önemli amacı daha verimli, daha az maliyetle daha kompakt cihazların tasarlanmasıdır. Aktif, pasif ve birleşik sistemler olmak üzere üç

sınıfa ayrılan iyileştirme teknikleri gelişen teknolojiyle yeni boyutlar kazanmaktadır. Özellikle dışardan herhangi bir enerjiye ihtiyacı duymayan pasif iyileştirme teknikler çok fazla tercih edilmektedir. Bu yöntemlerden biri de temel akışkana ilave edilen sıvılar veya katı partiküllerle iyileştirme yapmaktır. Nano sıvılar olarak adlandırılan bir temel akışkan içine nano boyutlu parçacıkların karışımı, orijinal sıvının ısı transfer özelliklerini büyük ölçüde artırdıklarından pratik uygulamalar için idealdir gibi görülmektedir. Bu makale, ısı transferinin arttırılması, ısıl iletkenlikteki iyileşme, yüzey hacim oranındaki artış, Brownian hareketi, vb. gibi nano sıvıların özellikleri üzerine yapılan çalışmaları ele almaktadır. Birçok araştırmacı nano akışkan kullanılmasının ısı transferini çok büyük oranda artırdığını iddia etse de transfer mekanizmalarının tam olarak belirlenmemiş olması ve tek faz-çift faz yaklaşımından dolayı çelişkili sonuçlar ortaya çıkmaktadır.

Anahtar sözcükler: Isı transferi iyileştirmr, nanoakışkan, tek faz, çift faz

GİRİŞ

Isı transferini iyileştirme teknikleri en genel halde aktif ve pasif teknikler olarak sınıflandırılmaktadır. (Bergles, 1983). Aktif teknikte yüzey titreşimi veya dışarıdan verilmesi gereken elektriğe ihtiyaç duyulurken pasif tekniklerde iyileştirme yüzey geometrisi ve akışkan hareketinin değiştirilmesiyle yapılabilmektedir. İş yapan akışkanının (temel akışkan) ısı transferi etkinliğini artırmak için içerisine katı parçacıklar ilave edilerek yeni akışkan elde edilmesi pasif yöntemlerden biridir. Temel akışkanın içerisine mikro boyuttaki parçacıkların eklenmesi ile yapılan iyileştirme çalışmaları ilk olarak Maxwell tarafından uzun yıllar önce teorik olarak ortaya konulmuştur (Maxwell, 1891). Kullanılan parçacıkların boyutları yeterince küçük olmadığından ve kararsız yapılarından dolayı birçok dezavantajı da beraberinde getirmiştir (basınç kayıpları, tıkanma tortulaşma gibi). Son yıllarda gelişen teknolojiyle temel akışkanların içerisine ilave edilen mikro boyuttaki parçacıkların yerini nano boyuttaki parçacıklara bırakmaktadır. Nanoparçacıklar aynı hacimsel konsantrasyonda mikro parçacıklara kıyasla daha fazla yüzey alanına sahip olduklarından ısı transferini daha fazla artırabilmektedirler (Murshed vd., 2008). Endüstride yaygın olarak kullanılan saf su, motor yağı, etilen glikol gibi temel akışkanların içerisine 100 nm den daha küçük, ısıl iletkenlikleri yüksek, metalik veya metal olmayan katı parçacıklar ilave edilerek nanoakışkan adı verilen yeni akışkanlar elde edilerek iyileştirme çalışmalarında kullanılmaya başlanmıştır. Nanoakışkan ifadesi ilk olarak doksanlı yıllarda Choi ve arkadaşları (Choi vd., 1995) tarafından ortaya konulmuştur. Nanoakışkanların ısı iletim katsayılarının geleneksel akışkanlara göre çok daha yüksek olması, basınç düşümünü çok fazla artırmaması, yüksek ısı transfer performanslarından dolayı daha küçük boyutlarda ısı değiştirici yapma imkânları sunmaktadır. Isı iletimdeki artışı araştırmacılar (Keblinski vd., 2002) nanoparçacıkların Brownian hareketi, parçacık/sıvı ara yüzeyindeki akışkan tabakası, nanoparçacıklardaki ısı aktarım mekanizması ve nanoparçacık kümelenmesinin etkisi olarak sıralamışlardır. Nanoakışkanların termofiziksel özellikleri ve ısı transfer mekanizmaları üzerine etkileri bilim adamları tarafından farklı yaklaşım ve metodalar

la çözülmeye çalışılsa da günümüzde hala kesinleşmiş bilgiler mevcut değildir. Nanoakışkanlar son yıllarda birçok araştırmacının ilgi odağı haline gelmiştir. Nanoakışkanların ilgi odağı haline gelmesinin en önemli sebebi, akışkanın içerisine küçük yüzdelerde ilave edilen nanoparçacıklar sayesinde termal iletkenliğin çok fazla artması ve buna karşılık basınç düşüsün artmasına yok denecek kadar az etkili olmasıdır. Termo-fiziksel özelliklerinden ve basınç düşüşü artırmamasından dolayı özellikle ısı transferi iyileştirme çalışmalarında çok fazla tercih edilir duruma gelmiştir. Isı transfer uygulamalarında sürdürülebilirlik ve verimlilik açısından kararlı nanoakışkanların hazırlanması çok önemlidir. Sunulan bu çalışmanın temel amacı nanoakışkanların termofiziksel özellikleri üzerine yapılan deneysel ve nümerik araştırmaları özetleyen kapsamlı bir derleme yapmaktır. Ayrıca termal iletkenlik, vizkozite gibi termofiziksel özellikleri etkileyen; farklı temel akışkanlar, hacim konsantrasyonu, parçacık boyutu, sıcaklık gibi parametrelerin etkisi tartışılmaktadır. Termofiziksel özellikler üzerinde etkili olan bu parametrelerle ilgili literatürde çok çelişkili sonuçlar bulunmaktadır. Dolayısıyla yapılan çalışma bu alanda çalışan araştırmacılar için yaralı olacaktır. Çalışmalar sonucunda tek nanoparçacık yerine hibrit nanoparçacıklar la nanoakışkan hazırlamanın kararlılık açısından daha zor olduğunu ortaya koymuştur. Bu nedenle, daha iyi termal iletkenlik elde etmek için tercih edilen hibrid nanaoakışkanların mekanizmaları hakkında daha derin bilgi ve anlayış gerekmektedir.

ÖNCEKİ ÇALIŞMALAR

Yeni bir teknoloji olmasından kaynaklı nanoparçacıkların özellikleriyle ilgili çok fazla bilgi bulunmamaktadır. Bunun için nanoparçacıkların konsantrasyonunun ölçümüne dair çalışmalar yapan Kostic vd. (Kostic vd., 2006) geliştirdikleri teknik ile nanoakışların yoğunluğunu ölçmüşlerdir. Yoğunluğu belli saf suyun konsantrasyonunu ölçerek doğruladıkları teknikle nanoakışların yoğunluğunu karşılaştırmışlardır. Yaptıkları ölçümler sonucunda geliştirdikleri ölçüm tekniğinin küçük konsantrasyonlar için ölçüm belirsizliğinin büyük ve kabul edilemez, ancak, daha yüksek konsantrasyonlar için doğru ve kabul edilebilir olduğu sonucuna ulaşmışlardır. Bu nedenle düşük konsantrasyonlar için büyük hacim oranları önermişlerdir. Şahin vd. (Şahin vd., 2006) ısı transferinin yoğun olarak kullanıldığı endüstriyel sistemlerde iyileştirme için nanoakışkanların çok büyük potansiyele sahip olduğunu ifade etmişlerdir. Nanoakışkanların ısı transferini iyileştirme üzerine etkilerini, parçacıkların karmaşık hareketleri sonucu enerji transferi, termal iletkenliği artırmaları, basınç düşümünü ihmal edilebilir düzeyde artırmaları gibi sebeplere açıklamışlardır.

Kulkarni vd. (Kulkarni vd., 2007) süspansiyon halinde metalik nanoparçacıkler içeren nanoakışkanları, temel akışkanın termal iletkenliğini önemli miktarda arttırdığı göstermek için yaptıkları çalışmalarında ilk olarak SiO_2, Al_2O_3 ve CuO içeren nanoakışkanların çeşitli sıcaklıktaki farklı hacim yüzdelerindeki özelliklerini incelemiş, sıcaklık ve parçacık çapının viskozite üzerine etkisini araştırmışlardır. Çalışmalarının sonucunda nanoakışların viskozitesinin konsantrasyonun bir fonksiyon olduğu ve konsantrasyonla arttığı sonucuna ulaşmışlardır. Parçacık boyutu

arttıkça viskozitenin azaldığını ve ısı transfer katsayısının artığını ortaya koymuşlardır. Yoğunluğa bağlı olarak viskozitenin arttığını ve konsantrasyon arttıkça basınç kaybının da arttığı sonucuna ulaşmışlardır.

Artuç (Artuç, 2007) farklı boyutlarda bakır ve gümüş parçacık ilavesi ile elde ettiği nanoakışkanların kullanımının ısı transferi üzerindeki etkileri incelemiş; öğütme ve yoğunlaştırma gibi belirli yöntemlerle nanoakışkanlar hazırlamıştır. Artuç, elde ettiği sonuca göre ısıl iletkenliğin nanoakışkanların hacimsel değerinin artışıyla arttığını belirlemiştir. Belirli bir artış değerinden sonra ise doyuma ulaştığını görmüştür. Nanoakışkanlar da ısı iletimini etkileyen faktörlerin boyut, hacimsel oran, sıcaklık, nanoparçacığın ısı iletim katsayısı gibi faktörler olduğu sonucuna varmıştır.

Kütlece %60 etilen glikol ve %40 su karışımı içinde süspansiyon haline getirilmiş alüminyum oksit nanoparçacıkların özgül ısı ve yoğunluğunun ölçüldüğü çalışmada nanoakışkanların akış karakteristikleri ve ısı transfer özelliklerini belirlemek amaçlanmıştır. Vajjha vd. (Vajjha vd. ,2008) farklı hacimsel konsantrasyonları için bir dizi sıcaklıkta ölçümler yapıp, elde ettikleri deney sonuçlarını da sıcaklık ve parçacık hacmi konsantrasyonunun bir fonksiyonu olarak belirlemişlerdir. Çalışmalarının sonucunda, ısı değiştiricileri, bina ısıtması ve otomotiv soğutması gibi çeşitli uygulamalarda Al_2O_3 nanoakışkanının ısı transfer performansının ve pompalama gücü gereksiniminin incelenmesinde kullanılabilecek korelasyonlar elde etmişlerdir. Araştırmacı aynı temel akışkanla yapmış olduğu başka bir çalışmasında (Vajjha vd., 2009) akışkanın içerisine alüminyum oksit Al_2O_3, antimon-kalay oksit ve çinko oksit (ZnO) nanoparçacıkları içeren üç farklı nanoparçacık ilave etmiştir. İlk olarak temel akışkanın yoğunluğu için bir ölçüm alınmış, sonra nanoakışkanların farklı hacmi konsantrasyonu için 0 ° C ila 50 ° C sıcaklık aralığında yoğunluk ölçümlerini incelemişlerdir. Yaygın olarak kullanılan teorik denklemler ile ölçüm sonuçları karşılaştırıldığında en iyi uyum Al_2O_3, ve antimon-kalay oksit içeren nanoakışkan için elde edilirken en fazla sapmanın ZnO nanoakışkanı için belirlenmiştir.

Bianco vd. (Bianco vd., 2009) çalışmalarında, sabit ve homojen ısı akısına tabi tutulan bir dairesel tüp içindeki su- Al_2O_3 içeren nanoakışkanı sayısal olarak incelemişlerdir. Tek ve çift faz model kullandıkları çalışmalarının sonucunda iki model arasında ortalama ısı transfer katsayısındaki maksimum fark yaklaşık %11 olduğu ve nanoakışlar için taşınım ısı transfer katsayısı temel akışkanınkinden daha büyük olduğu sonucuna ulaşmışlardır. Ayrıca ısı transferinin arttırılması parçacık hacmi konsantrasyonuyla birlikte arttığını, ancak bunun kayma gerilmesini de arttırdığını belirlemişlerdir.

Gedik, (Gedik, 2009) nanoakışkanları, metal veya ametal nanoparçacıkların bir akışkanla süspansiyonu olarak tanımlanmış ve ısı transferini arttırmaya olan etkisini deneysel incelemiştir. Al2O3- su ve CuO-su nanoakışkanlarının dairesel bir boruda türbülanslı akışta zorlanmış taşınımla ısı transferini ve basınç düşüşünü incelemiştir. Nanoparçaçıklı akışkanın, ısı transferini arttırmaya yönelik katkısı belirli hacimsel oranlarda meydana geldiği ve daha büyük hacimsel oranlarda bir etkisinin olmadığı sonucuna ulaşmıştır.

Ding vd. (Ding vd. 2009) klasik soğutucular yerine nanoakışkanların ısı transferini artırması nedeniyle, alternatif bir soğutucu olarak kabul etmişler ve böylece gerekli

soğutma akışkanı gücünü azaltmışlardır. Laminer akış koşulları altında taşınımla ısı transferinin sayısal modellemesini yaparak artan nanoparçacık hacminin duvar kayma gerilmesi üzerindeki etkisi olduğu ve nanoparçacıkların hacim konsantrasyonun artmasıyla hem ısı transfer katsayısının hem de duvar kayma geriliminin arttığı sonucuna ulaşmışlardır.

Kakaç ve Pramuanjaroenkij (Kakaç ve Pramuanjaroenki, 2009) zorlanmış taşınımla ısı transferinin nanoakışkanlarla iyileştirilmesi üzerine yapılmış olan önemli makaleleri incelemişlerdir. Nanoakışkanların ısı transferi iyileştirme tekniklerinde son gelişmeler olmasına rağmen, nano parçacıkların ısı transfer mekanizmaları ve akış karakteristiklerini anlamak için daha fazla deneysel ve teorik çalışmalara ihtiyaç olduğunu ve yapılacak çalışmalarda parçacık ve temel akışkan arasındaki kayma hızı, nanoakışkanların ısı transfer performansı üzerinde önemli rol oynadığından nanoakışkanları tek değil iki fazlı akış olarak incelenmesi gerektiğini belirtmişlerdir.

Ontiveros vd. (Ontiveros vd., 2010) kaynama üzerine nanoakışkanların etkisini araştırmak parçacık görüntülemeli hız yöntemini (PIV) kullanarak deneysel çalışma yapmışlardır. Kabarcıkların hidrodinamik davranışındaki değişiklikleri de gözlemlemişlerdir. Duvar sıcaklığı ve nanoakışkanın konsantrasyonu arasında bir ilişki olduğunu da vurgulamışlardır. PIV sonucu elde edilen nanoakışkanınn hız profili şekil 1 de gösterilmiştir.

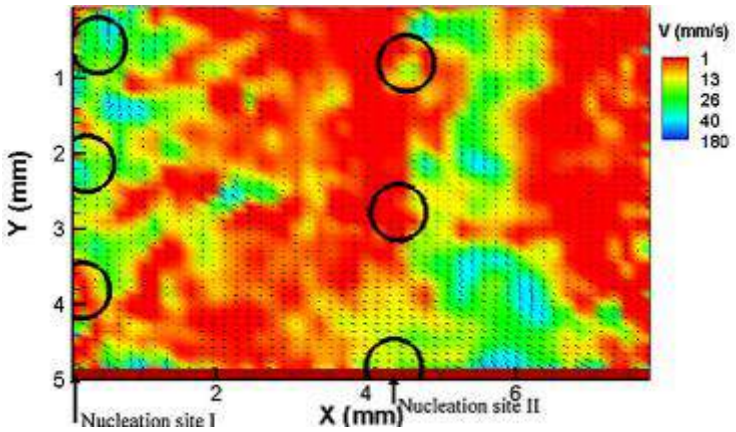

Şekil 1. Nanoakışkanın (%0.002 konsantrasyonlu) Hız Profili (ontiveros vd., 2010)

Özerinç (Özerinç, 2010) çalışmasında, nanoakışkanların yüksek ısıl iletim katsayıları sebebiyle ısı transferini arttırmada önemli rol oynadığını fakat ısıl iletim katsayısı artışına sebep olan mekanizmaların tam olarak anlaşılmadığını söylemiştir. Nanoakışkanları teorik ve deneysel olarak incelemiştir. Deneysel çalışmalarda, ısıl iletim katsayısına etki eden hacimsel parçacık oranı, parçacık boyutu ve sıcaklık ele almıştır. Nanoakışkanların kullanılmasının ısı transferini arttırdığı sonucuna varmıştır.

Timofeeva vd.(2011) nanoakışkanlar da viskozite, ısıl iletkenlik ve soğutma verimliliği gibi kavramların incelemişlerdir. Tek fazlı sıvılar için soğutma verimliliği ölçümlerini analiz edip, ısı transferi için önemli olan nanoakışkanların özelliklerini

belirlemişlerdir. Nanoakışkanlar için çok değişkenliği şematik gösterimleri Şekil 2 de sunulmuştur. Nanoparçacıkların temel akışkan içinde ki konsantrasyonun ısı transferini artırmak için en etkili parametre olduğunu ortaya koymuşlardır.

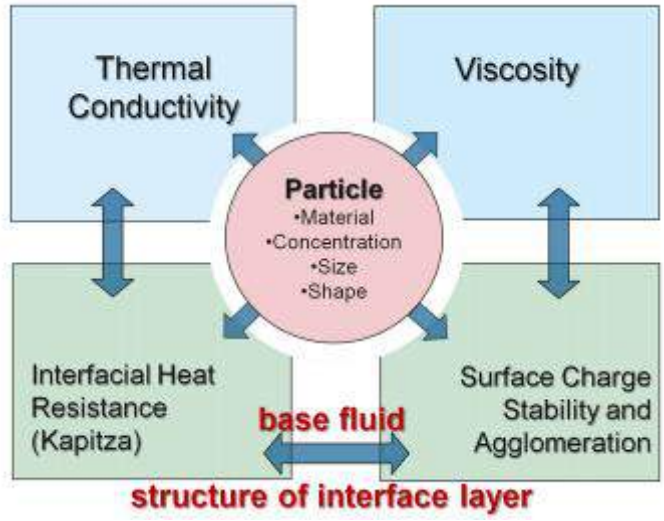

Şekil 2. Nanoakışkan Sisteminin Çok değişkenliğinin Şematik Gösterimi (Timofeeva vd., 2011)

Demir vd. (Demir vd.,2011) sabit duvar sıcaklığına sahip yatay bir boru içinde, TiO_2 ve Al_2O_3 nanoparçacıkları içeren nanoakışların zorlanmış taşınım akışlarını sayısal olarak incelemişlerdir. Deneysel veriler ile TiO_2 modelini doğrulamış ve modelinin doğrulanmasından sonra Al_2O_3 için çalışma yapmışlardır. Nanoparçacık konsantrasyonunun ve Reynolds sayısının duvar kayma gerilmesi, Nusselt sayısı, ısı transfer katsayısı ve basınç düşüşü üzerindeki etkilerini incelemiş, nanoparçacıkların ilavesi ile ısı transferinin arttığını tespit etmişlerdir.

Abu-Nada ve Oztop (Abu-Nada ve Oztop, 2011) sonlu hacim yöntemini kullanarak, Al_2O_3- su nanoakışının ısı transferi artırma üzerine etkisini sayısal olarak incelemişlerdir. Nanoakışkanın etkin termal iletkenliğini ve viskozitesini sırasıyla Maxwell-Garnetts ve Brinkman modelleriyle hesaplamışlardır. Çözümleri, farklı Rayleigh sayıları ve nanoakışların farklı hacim fonksiyonları için yerel ve ortalama Nusselt sayıları ve hız profilleri ile sunmuşlardır. Temel akışkana Al_2O_3 nanoparçacığının eklenmesinin ortalama Nusselt sayısını arttırdığını ve ısı transferinin aynı Rayleigh sayısı için geometri parametresinin artmasıyla arttığını görmüşlerdir.

Ahmed vd. (Ahmed vd., 2011) oluklu kanal üzerinden bakır-su nanoakışkanının ısı transferi ve basınç düşüşü özelliklerini sayısal olarak incelemişlerdir. Elde ettikleri sonuçlara göre ısı transferinin, Reynolds sayısı ve nanoparçacık hacim fonksiyonu arttıkça arttığı ancak basınç düşüşünde de hafif bir artış olduğunu görmüşlerdir. Farklı konsantrasyonlar için sayısal sonuçlardan elde edilen akım çizgileri ve izoterm eğrileri Şekil 3'de gösterilmiştir.

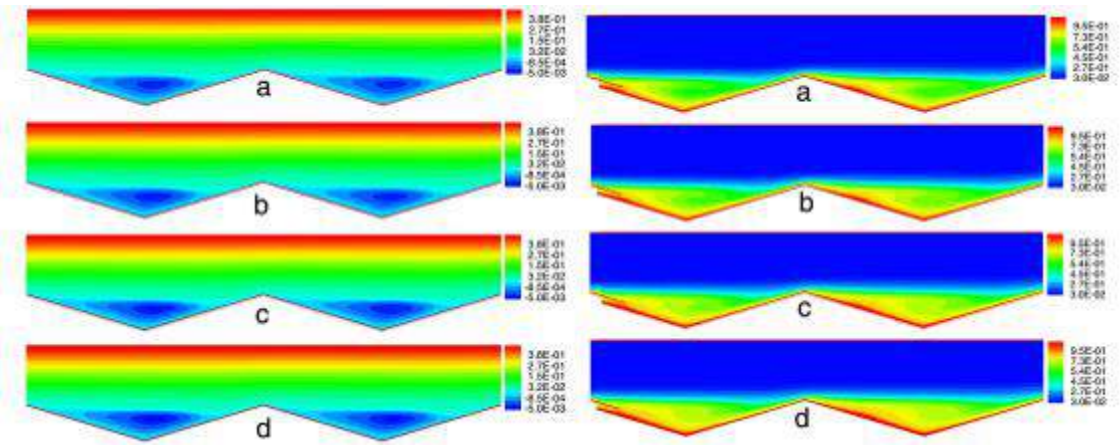

Şekil 3. Farklı Konsantrasyonlar İçin Akım Çizgileri ve İzoterm Eğrileri(Ahmed vd., 2011)

Saterlie vd. (Saterlie vd., 2011) bakır bazlı nanoakışkanların dağılma özelliklerini ve termal iletkenlik performansını incelemişlerdir. %0.55 ve %1 oranlarında bakır nanoparçacıklı akışkanlar hazırlayıp bakır parçacıkların temel akışkan içerisindeki tanecik boyutu dağılımını belirlemişlerdir. Bakır nanoparçacıkların su içinde homojen bir şekilde dağılmasını sağlamak için bir dağıtıcı madde olan sodyum dodesilbenzensülfonat (SDBS) kullanmışlardır. Termal iletkenlikteki artışın bakır nanoparçacıkların boyutuyla doğrudan ilişkili olduğunu görmüşlerdir.

Hosseini vd. (Hosseini vd., 2011) termal iletkenlik, viskozite, yoğunluk ve özgül ısı gibi nano akışkanların fiziksel özellikleri hakkında mevcut tüm formül ve korelasyonları gözden geçirip sınıflandırmışlardır. Yaptıkları çalışmalar ile nano sıvıların fiziksel özelliklerine parçacık konsantrasyonu, parçacık ve baz sıvısının fiziksel özellikleri, sıcaklık gibi birçok faktörün etki ettiğini görmüşlerdir. Tüm korelasyonun parçacık boyutu ve kullanılan parçacığın özelliğine bağlı olduğunu yüksek parçacık hacmi konsantrasyonunda viskozite, yoğunluk ve özgül ısının etkinliğinin daha belirgin olduğunu ortaya koymuşlardır.

Sasmito vd. (Sasmito vd., 2011) yaptıkları çalışma ile pasif iyileştime teknikleri için kullanılan geometri etkisini (Şekil4) ve nanoparçacık ilavesini birleştirerek ısı transferini arttırmayı amaçlamışlardır. Al_2O_3-su ve CuO_2 süspansiyonları içeren akışkanların akış davranışı ve ısı transfer performansını inceleyip düz tüp içinde akan suyun akış davranışlarıyla karşılaştırmışlardır. Elde ettikleri sonuçlara göre %1'e kadar olan nanoparçacık ilavesinin ısı transfer performansını önemli ölçüde artırdığını daha fazlasının ise ısı transfer performansını bozma eğiliminde olduğunu görmüşlerdir.

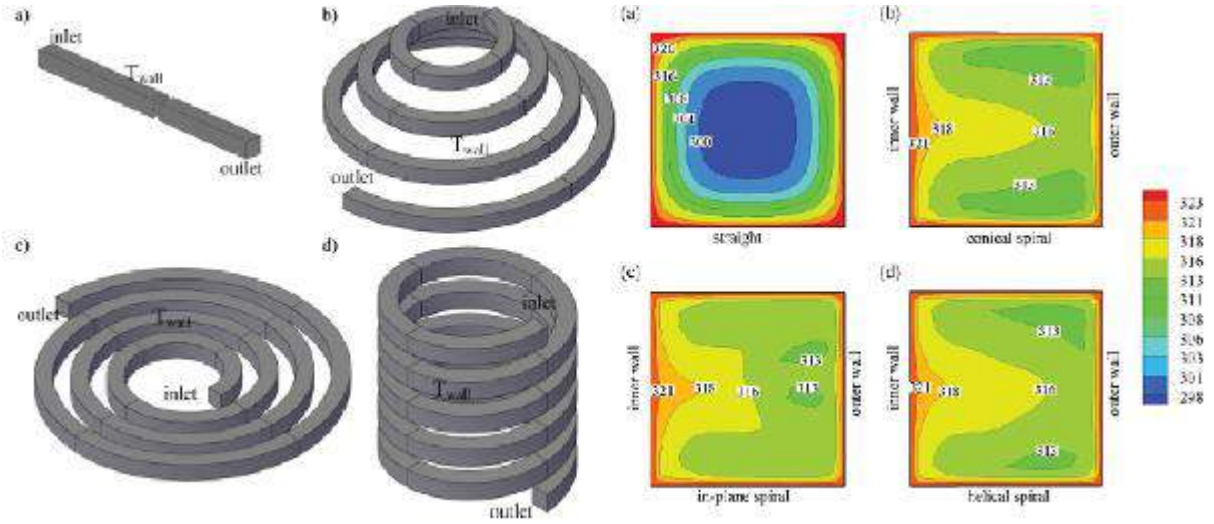

Şekil4. (a) Düz tüp,(b)Konik Spiralli Tüp, (c) Sıralı Spiralli Tüp,(d) Helisel Spiralli Tüp ve Sıcaklık Dağılımları, (Sasmito vd., 2011)

Bianco vd. (Bianco vd., 2011) sabit duvar ısı akısı verilen kare bir tüp içindeki bir $Al_2 0_3$ –su nanoakışkanın türbülanslı zorlanmış taşınım akışını sayısal olarak modellemişlerdir. Optimal çalışma koşulunu bulmak için entropi üretim analizi de yaparak sonuçları nümerik hesaplamalarla karşılaştırmışlardır. Optimum Reynolds sayısını, minimum entropi oluşumunu belirlemiş ve sonuçların birbiriyle uyum içerisinde olduğunu görmüşlerdir.

Ahmed vd. (Ahmed vd.,2011)iki boyutlu dalgalı kanaldaki laminer akışta bakır-su nanoakışkanının ısı transferini sayısal olarak incelemişlerdir. Dalgalı kanalın genliği arttıkça sürtünme katsayısının ve Nusselt sayısının da arttığını görmüşlerdir. Buna ek olarak, ısı transferindeki artışın ağırlıklı olarak dalga boyundan (L_w) ziyade nanoparçacık hacim konsantrasyonuna, dalgalı duvarın genlik derecesine ve Reynolds sayısına bağlı olduğunu bulmuşlardır.

Mohammed vd. (Mohammed vd., 2012) türbülanslı nanoakış akışının termal ve hidrodinamik özellikleri sayısal olarak inceledikleri çalışmalarında dikdörtgen, üçgen ve trapez şeklinde olmak üzere üç farklı oluk şekli olan kanal geometrisi ve farklı hacim konsantrasyonlarında farklı nanoakışları ($Al_2 0_3$, CuO, $Si0_2$, Zn0) incelemişlerdir. Sonuçta dikdörtgen yiv-üçgen oluğun, diğer yiv oyuğu şekilleri arasında en yüksek Nusselt sayısına sahip olduğunu, $Si0_2$ nanoakışının diğer nanoakış türlerine kıyasla en yüksek Nusselt sayısına sahip olduğunu ve Nusselt sayısının nanoparçacık hacim konsantrasyonu, Reynolds sayısı ve en/boy oranı arttıkça arttığını nanoparçacık çapının arttıkça da azaldığını belirtmişlerdir.

Nazififard vd. (Nazififard vd., 2012) tipik bir basınçlı su reaktörünün alt kanalında $Al_2 0_3$ –su nanoakışının türbülanslı zorlanmış taşınım akışını sayısal olarak analiz etmişler ve elde ettikleri sonuçlara göre nanoparçacık hacim konsantrasyonları ile ısı transferinin arttığını ve en yüksek ısı transferinin her konsantrasyon için, en yüksek Reynolds sayısına karşılık geldiğini görmüşlerdir. Alt kanalındaki $Al_2 0_3$ –su

nanoakışının basınç düşümünün ise hacim konsantrasyonu arttıkça arttığını ortaya koymuşlardır. Analiz sonucu elde edilen tütbülans yoğunluğu şekil 5 verilmiştir.

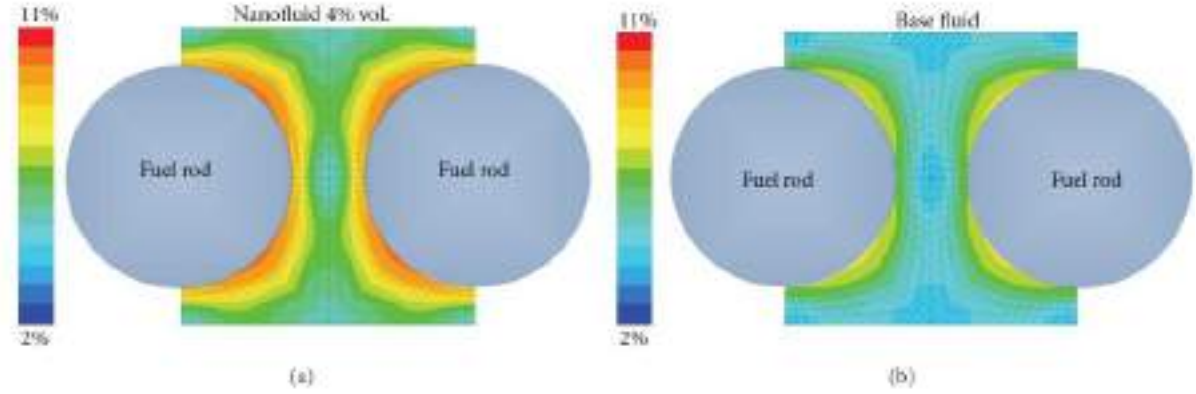

Şekil 5: Nanoakışkan ve Suyun Türbülans Yoğunluğu

Gavtash vd. (Gavtash vd., 2012) Nanoparçacık yoğunluğunun ve boyutunun ısı transferi üzerine etkisini sayısal olarak incelemişler ve parçacık konsantrasyonu arttıkça ve parçacık yarıçapı azaldıkça ısı transferinin düştüğü sonucuna varmışlardır.

Fathinia vd. (Fathinia vd., 2012) iki boyutlu bir kanaldaki türbülanslı zorlanmış akışı farklı yükseklik oranları için sayısal olarak incelemişlerdir. Sonuçta, hacim fonksiyonun %4 ve nanoparçacık çapının 20 nm olduğu SiO_2 nanoparçacık kullanılan kanalda ısı transferinin %114 oranında arttığını tespit etmişlerdir.

Manay vd. (Manay vd.,2012) mikrokanalların içerisinde nanoakışkanlar kullanılarak elde edilen kararlı ve homojen yapının cidarlarda tıkanmaya yol açmayacağını ve aynı zamanda türbülans sağlayarak, ısıl iletkenliklerinin yüksek olması ile daha iyi bir ısı transferi elde edileceğini belirtikleri çalışmalarında parçacıkların varlığının kanallar içerisinde basınç düşümüne neden olabileceğini söylemişlerdir. Kanal yüzeyi ile nanoakışkan arasındaki sıcaklık farkını azaltarak ısıl direncin azalmasını ve sonuç olarak soğutma sanayide yaygın olarak kullanılan mikro kanallarda nanoakışkan kullanılmasının ısı transferini iyileştireceğini belirtmişlerdir.

Naraki vd. (Naraki vd.,2013) otomobil radyatörünün ısı transfer performansını, geleneksel ε-NTU tekniğine göre hesapladığı toplam ısı transfer katsayısını kullanarak deneysel olarak değerlendirmişlerdir. Elde ettikleri sonuçlara göre, nanoakışkanların ısı transfer katsayısının suya kıyasla %9'a daha fazla olduğunu ortaya koymuşlardır. Ayrıca, nanoparçacık konsantrasyonunun arttırılmasının, hava hızını ve nanoakışkanın ısı transfer katsayısını arttırdığını görmüşlerdir Giriş sıcaklığının artırılmasıyla da ısı transfer katsayısının düştüğünü kaydetmişlerdir.

Kabeel vd. (Kabeel vd., 2013) su-AL_2 0_3 nanoakışkanını kullanarak plakalı ısı eşanjörü için ısı transfer özelliklerini incelemişlerdir. Nanoparçacık konsantrasyonunun arttırılmasıyla hem ısı transfer katsayısında hem de aktarılan güçte belirgin bir artış gözlenlenmiştir. Reynolds sayısı ve nanoakış konsantrasyonun artmasıyla basınç düşüşü ve bunun sonucu olarak da pompala gücünün arttığını belirtmişlerdir.

Mohammed vd. (Mohammed vd., 2013) dairesel çift borulu ısı eşanjörüne yerleştirilen engellerin ısı transferi üzerine etkisini sayısal yöntemler ile incelemişlerdir. Farklı Reynolds sayısı aralığı, farklı hacim konsantrasyonları, farklı çaplardaki nanoparçacıklarına sahip nanoparçacıkların (Al_2O_3, CuO, SiO_2, ZnO) kullanıldığı çalışma sonucunda nanoparçacık çapının küçülmesi ve hacim fonksiyonun artmasıyla Nusselt sayısının arttığını görmüşlerdir.

Ho ve Chen (Ho ve Chen, 2013) bir kanalda soğutucu olarak suyun yerine Al_2O_3 –su nanoakışkanın kullanıldığı zorlanmış taşınımda ısı transferini araştırmak için deneyler yapmışlardır. Kanalların hidrolik ve termal performanslarını, pompalama güçlerini gösteren sonuçları değerlendirip saf su ile karşılaştırmışlardır ve ortalama ısı transfer katsayısının %35 ve %72 oranında arttığını görmüşlerdir.

Tiwari vd. (Tiwari vd., 2013) deneysel araştırmalarını, CeO_2-su nanoakışkanını kullanan plakalı ısı eşanjöründeki ısı transferi ve basınç düşüşü üzerine yapmışlardır. Nanoakışkanların optimum konsantrasyonda ısı transferini iyileştirirken basınç düşüşünde ihmal edilebilir bir artış olduğunu belirtmişlerdir.

Duangthongsuk vd. (Duangthongsuk vd., 2013) Al_2O_3 – su içeren nanoakışkanı kullanarak yaptıkları deney sonucunda, nanoakışkanların ısı transfer katsayısının suyunkinden düşük olduğunu ve konsantrasyon yüksek olduğunda azalma eğiliminde olduğunu görmüşlerdir.

Bedir (Bedir, 2013) nanoakışkanın hacim oranının artmasıyla ısı transfer katsayısının ve basınç kaybının arttığını saptamıştır. Yaptığı çalışmada uniform ısı akılı bir boruda CuO ve Al_2O_3 içeren iki farklı nanoakışkanın zorlanmış türbülanslı akışını ve ısı transfer karekteristiklerini sayısal olarak incelemiştir. Her iki nanoakışkan tipinde de suya göre ısı transferinin arttığı sonucuna varmıştır. CuO-su nanoakışkanın ısı transfer yüzeyi daha büyük olduğu için Al_2O_3-su nanoakışkanına göre ısı transfer katsayısındaki artış daha fazla olduğunu söylemiştir.

Elçioğlu (Elçioğlu,2013) ısıl iletkenliklerinden dolayı ısı transfer uygulamalarında üstünlükleri olduğu kabul edilen nanoakışkanların viskozitesinin iş yapan akışkandan daha yüksek olmasından dolayı çeşitli dezavantajları olduğunu belirtmiştir. Pompa gücünü direk olarak etkileyen viskozitenin artışı işletme maliyet artışlarını da beraberinde getirmektedir. Bu nedenle nanoakışkan viskozitesini teorik, deneysel ve istatistiksel analizler ile incelemiştir. Tez çalışmasının sonucunda Al_2O_3–su nanoakışkanının viskozitesinin parçacık boyutu ile arttığını, değişen sıcaklıklık ile üstel azaldığını göstermiş ve nanoakışkan viskozitesi ve bağıl viskozite için birer korelasyon ifade etmişlerdir.

Azari vd. (Azari vd., 2014) çalışmalarında, homojen ve sabit ısı akısı altında dairesel bir tüpte Al_2O_3 - su nano akışkanının laminer taşınım ısı transfer katsayısının tek fazlı (CP-SP) model, değişken fiziksel özellikler tek fazlı (VP-SP) model ve ayrı parçacıklar iki fazlı model de dahil olmak üzere üç farklı model geliştirmişlerdir. Elde ettikleri simülasyon sonuçlarına göre, nanoakışkanların termal performansının baz sıvının termal performansından daha yüksek olduğunu ve parçacık hacmi konsantrasyonu ve Reynolds sayısı ile ısı transferinin arttığını ve VP-SP modeli ve iki fazlı model durumunda yüksek ısı transfer katsayıları hesaplamışlardır.

Borazjani vd. (Borazjani vd., 2014) karşıt akışlı bir ısı eşanjörün de $AL_2\ O_3$ – su içeren nanoakışların zorlanmış taşınımını sayısal olarak incelemişlerdir. Nanoakışının hidrodinamik ve termal davranışlarını incelemek için yaptıkları çalışmalarının sonucunda, Reynolds sayısının artmasıyla ısı akısının ve basınç düşüşünün arttığını ve ayrıca, ısı eşanjörünün iç borusunda temel akışkanına (su) $AL_2\ O_3$ nanoparçacıkların eklenmesi, enerji verimliliği oranının arttırdığını ve pompalama gücünün azalttığını belirlemişlerdir.

Teymur (Teymur, 2015) nanoakışkanların sabit basınç grandyanı altında izotermal olmayan kanalda ki akışını incelemiştir. Çalışmasının sonucunda hacimsel konsantrasyonun arttıkça nanoakışkan viskozitesinin arttığını ve viskozitenin artmasıyla da akış hızının azalıp böylece gerilmenin de arttığını görmüştür. Ayrıca hacimsel konsantrasyonun artışı da hız profilinin ve basınç gradyanın artmasına neden olduğunu belirtmiştir.

Mohamad (Mohamad,2015) nanoakışkanların ısı transferi iyileştirmek için kullanılmasının fizik kurallarına çokta uygun olmadığını belirttiği makalesinde temel akışkana nanoparçacık eklenmesinin (akışkanın yoğununa kıyasla) kaldırma kuvveti ve doğal konveksiyonu azaltacağını savunmuştur. Ayrıca nanoparçacıkların eklenmesi sonucu etkin viskoziteyi artıracağı bununda zorlanmış taşınım ve basınç düşüşünü olumsuz etkileyeceğini ve bu parçacıkların yüzeylere çarpması sonucu erozyonların artabileceği belirtmiştir.

SONUÇ

Bu makale de ısı transferini iyileştirmek için nanoakışkanların kullanımı üzerine deneysel, sayısal ve analitik olarak son zamanlarda yapılan çalışmalar derlenmiştir. Çalışmaların bir kısmında nanoakışkanlar tek fazlı ele alınırken bir kısmında iki fazlı olarak ele alınmıştır. Parçacık boyutu, viskozite, termal iletkenlik ve daha birçok termofiziksel özelliğin ısı transfer mekanizması ve akış karakteristikleri üzerine etkisi araştırmacılar tarafından incelenmiştir. Genel bulgular ısı transferini artırmak için nanoakışkanlar kullanılması yönünde olsa da araştırmacıların bazıları nanoakışkanların ısı transferini artırmadığı hatta azalttığını belirtmişlerdir (Mohamad,2015). Bu bağlamda nanoakışkanların ısı transferini iyileştirmesi konusunda devam eden tartışmalar söz konusudur (Haddad vd., 2012). Sayısal sonuçların çoğunda geleneksel akışkanlara göre nanoakışkanların ısı transferini artırdığı iddia edilse de deney sonuçları her zaman bunu doğrulamamaktadır. Nano parçacıkların ısı transfer mekanizmaları ve akış karakteristiklerini anlamak için daha fazla deneysel ve teorik çalışmalara ihtiyaç olduğunu ve yapılacak çalışmalarda parçacık ve temel akışkan arasındaki kayma hızı, nanoakışkanların ısı transfer performansı üzerinde önemli rol oynadığından nanoakışkanların tek değil iki fazlı akış olarak incelenmesi gerekmektedir.

KAYNAKLAR

Bergles, A.E., 1983. Augmentation of Heat Transfer. Heat Exchanger Design Handbook. Hemisphere Publishing Co., Washington DC.

Maxwell, J.C., A treatise on electricity and magnetism, unabridged 3rd ed., Clarendon Press, Oxford, UK, 1891.

Murshed, S.M.S., Leong, K.C., Yang, C., Thermophysical and elektrokinetic properties of nanofluids-A critical review, Applied Thermal Engineering, 28, 2109-2125, 2008.

Choi, S.U.S., Eastman, J.A., Enhancing thermal conductivity of fluids with nanoparticles, ASME International Mechanical Engineering Congress& Exposition, San Fransisco, CA. 1995.

Eastman, J. A., Choi, S. U. S., Yu, W., Thompson, L. J., Anomalously increased effective thermal conductivity of ethylene glycol-based nanofluids containing copper nanoparticles, Appl. Phys. Lett., 78, 718-720, 2001.

Keblinski, P., Phillpot, S.R., Choi, S.U.S., Eastman, J.A., Mechanisms of heat flow in suspensions of nano-sized particles (nanofluids), International Journal of Heat and Mass Transfer, 855–863, 2002

Kostic, M., Vijay Kumar Sankaramadhi, and Kalyan Chaitanya Simham. "New educational lab: Measurement and uncertainty evaluation of nanofluid particle concentration using volumetric flask method." *American Society for Engineering Education*. 2006.

B.Şahin, K.Çomaklı, M.Yılmaz, Ö.Çomaklı, Nanoakışkanlarla ısı transferinin iyileştirilmesi, Mühendis Makina, Sayı: 559, 2006, 29–34

KULKARNI, Devdatta P.; NAMBURU, Praveen K.; DAS, Debendra K. Comparison of Heat Transfer and Fluid Dynamic Performance of Nanofluids.

Artuç, M. (2007), Nanoakışkanların Isıl İletkenliklerinin Ölçülmesi, Hacettepe Üniversitesi Fen Bilimleri Enstitüsü, Yüksek Lisans Tezi, Ankara

VAJJHA, Ravikanth S.; DAS, Debendra K. Measurements of Specific Heat and Density of Al 2 O 3 Nanofluid. In: *AIP Conference Proceedings*. AIP, 2008. p. 361-370.

VAJJHA, R. S.; DAS, D. K.; MAHAGAONKAR, B. M. Density measurement of different nanofluids and their comparison with theory. *Petroleum Science and Technology*, 2009, 27.6: 612-624.

Bianco, V., Chiacchio, F., Manca, O., & Nardini, S. (2009). Numerical investigation of nanofluids forced convection in circular tubes. *Applied Thermal Engineering*, *29*(17), 3632-3642.

Gedik, G. (2009) Nanoakışkanların Isı Transferi ve Basınç Düşüşünün Belirlenmesi, *Atatürk Üniversitesi Fen Bilimleri Enstitüsü, Yüksek Lisans Tezi*, Erzurum

Ding, Z. W., Cheah, S. C., & Saeid, N. H. (2009, December). Parametric study of heat transfer enhancement using nanofluids. In *Energy and Environment, 2009. ICEE 2009. 3rd International Conference on* (pp. 294-298). IEEE.

Kakaç, S., & Pramuanjaroenkij, A. (2009). Review of convective heat transfer enhancement with nanofluids. *International Journal of Heat and Mass Transfer*, *52*(13), 3187-3196.

Dominguez-Ontiveros, E., Fortenberry, S., & Hassan, Y. A. (2010). Experimental observations of flow modifications in nanofluid boiling utilizing particle image velocimetry. *Nuclear Engineering and Design*, *240*(2), 299-304.

Özerinç, S., (2010), Heat transfer enhancement with nanofluids, Orta Doğu Teknik Üniversitesi Fen Bilimleri Enstitüsü, Yüksek Lisans tezi, Ankara

Timofeeva, E. V., Yu, W., France, D. M., Singh, D., & Routbort, J. L. (2011). Nanofluids for heat transfer: an engineering approach. *Nanoscale research letters*, *6*(1), 182.

Demir, H., Dalkilic, A. S., Kürekci, N. A., Duangthongsuk, W., & Wongwises, S. (2011). Numerical investigation on the single phase forced convection heat transfer characteristics of TiO 2 nanofluids in a double-tube counter flow heat exchanger. *International Communications in Heat and Mass Transfer*, *38*(2), 218-228.

Abu-Nada, E., & Oztop, H. F. (2011). Numerical analysis of Al2O3/water nanofluids natural convection in a wavy walled cavity. *Numerical Heat Transfer, Part A: Applications*, *59*(5), 403-419.

Ahmed, M. A., Shuaib, N. H., Yusoff, M. Z., & Al-Falahi, A. H. (2011). Numerical investigations of flow and heat transfer enhancement in a corrugated channel using nanofluid. *International Communications in Heat and Mass Transfer*, *38*(10), 1368-1375.

Saterlie, M., Sahin, H., Kavlicoglu, B., Liu, Y., & Graeve, O. (2011). Particle size effects in the thermal conductivity enhancement of copper-based nanofluids. *Nanoscale research letters*, *6*(1), 217.

Hosseini, S. S., Shahrjerdi, A., & Vazifeshenas, Y. (2011). A review of relations for physical properties of nanofluids. *Australian Journal of Basic and Applied Sciences*, *5*(10), 417-435

Sasmito, A. P., Kurnia, J. C., & Mujumdar, A. S. (2011). Numerical evaluation of laminar heat transfer enhancement in nanofluid flow in coiled square tubes. *Nanoscale research letters*, *6*(1), 376.

Bianco, V., Nardini, S., & Manca, O. (2011). Enhancement of heat transfer and entropy generation analysis of nanofluids turbulent convection flow in square section tubes. *Nanoscale research letters*, *6*(1), 252.

Ahmed, M. A., Shuaib, N. H., & Yusoff, M. Z. (2012). Numerical investigations on the heat transfer enhancement in a wavy channel using nanofluid. *International Journal of Heat and Mass Transfer*, *55*(21), 5891-5898.

Mohammed, H. A., Al-Shamani, A. N., & Sheriff, J. M. (2012). Thermal and hydraulic characteristics of turbulent nanofluids flow in a rib–groove channel. *International Communications in Heat and Mass Transfer*, *39*(10), 1584-1594.

Nazififard, M., Nematollahi, M., Jafarpur, K., & Suh, K. Y. (2012). Numerical simulation of water-based alumina nanofluid in subchannel geometry. *Science and Technology of Nuclear Installations*, *2012*.

Gavtash, B., Hussain, K., Layeghi, M., & Lafmejani, S. S. (2012). Numerical simulation of the effects of nanofluid on a heat pipe thermal performance. *World Academy of Science, Engineering and Technology*, *68*, 549-555.

Fathinia, F., Parsazadeh, M., & Heshmati, A. (2012, December). Turbulent Forced Convection Flow in a Channel over Periodic Grooves Using Nanofluids. In *Proceedings of World Academy of Science, Engineering and Technology*(No. 72, p. 1217). World Academy of Science, Engineering and Technology (WASET)

Manay, E., Sahin, B., Akyürek, E.F., Comaklı, Ö., Mikrokanallarda Nanoakışkanların Kullanımı, Mühendis ve Makine, Cilt: 53, Sayı: 627, 2012, 38-42.

Haddad, Z., Oztop, H. F., Abu-Nada, E., & Mataoui, A. (2012). A review on natural convective heat transfer of nanofluids. *Renewable and Sustainable Energy Reviews*, *16*(7), 5363-5378.

Peyghambarzadeh, S. M., Hashemabadi, S. H., Naraki, M., & Vermahmoudi, Y. (2013). Experimental study of overall heat transfer coefficient in the application of dilute nanofluids in the car radiator. *Applied Thermal Engineering*, *52*(1), 8-16.

Kabeel, A. E., El Maaty, T. A., & El Samadony, Y. (2013). The effect of using nano-particles on corrugated plate heat exchanger performance. Applied Thermal Engineering, 52(1), 221-229.

Mohammed, H. A., Hasan, H. A., & Wahid, M. A. (2013). Heat transfer enhancement of nanofluids in a double pipe heat exchanger with louvered strip inserts. *International Communications in Heat and Mass Transfer*, *40*, 36-46.

Ho, C. J., & Chen, W. C. (2013). An experimental study on thermal performance of Al 2 O 3/water nanofluid in a minichannel heat sink. *Applied Thermal Engineering*, *50*(1), 516-522.

Tiwari, A. K., Ghosh, P., & Sarkar, J. (2013). Heat transfer and pressure drop characteristics of CeO 2/water nanofluid in plate heat exchanger. *Applied Thermal Engineering*, *57*(1), 24-32.

Duangthongsuk, W., Yiamsawasd, T., Selim Dalkilic, A., & Wongwises, S. (2013). Pool-Boiling Heat Transfer Characteristics of Al2O3-Water Nanofluids on a Horizontal Cylindrical Heating Surface. *Current Nanoscience*, *9*(1), 56-60.

Bedir, Ö. (2013), Sabit Isı Akılı Yatay Bir Boruda Türbülanslı Akışta Nanoakışların Sayısal İncelenmesi, Atatürk Üniversitesi Fen Bilimleri Enstitüsü, Yüksek Lisans Tezi, Erzurum

Elçioğlu, E.B., Experimental and theoretical investigations on alümina–water nanofluid viscosity with statistical analysis, Ortadoğu Teknik Üniversitesi Fen Bilimleri Enstitüsü, Yüksek lisans Tezi, Ankara, 2013.

Azari, A., Kalbasi, M., & Rahimi, M. (2014). CFD and experimental investigation on the heat transfer characteristics of alumina nanofluids under the laminar flow regime. *Brazilian Journal of Chemical Engineering*, *31*(2), 469-481.

Borazjani, M. S., Bamdad, M., & Hashemi, R. (2014). Numerical investigation on the single phase forced convection heat transfer characteristics of Al2o3 nanofluids in a

double-tube counter flow heat exchanger. *International Journal of Basic Sciences and Applied Research*, *3*, 266-273.

Teymur, B. (2015),İzotermal Olmayan Kanal Akışında Nanoakışkanların Sayısal Olarak İncelenmesi, Osmaniye Korkut Ata Üniversitesi Fen Bilimleri Enstitüsü, Yüksek Lisans Tezi

Mohamad, A. A. (2015). Myth about nano-fluid heat transfer enhancement. International Journal of Heat and Mass Transfer, 86, 397-403.

MECHANICAL PROPERTIES OF STEAM CURED CONCRETE INCORPORATING QUARRY DUST

Didar Yasin NAJMADDIN
G. Directory of Projects/Ministry of Higher Education and Scientific Research-KRG/Iraq, didar.najmaddin@mhe-krg.org

Ayşe Yeter GÜNAL
Department of Civil Engineering, Gaziantep University, Turkey, agunal@gantep.edu.tr

ABSTRACT: The research deals with reusing waste material in engineering application and performance of alternative method of curing for gaining hardened concrete. Steam curing at atmospheric pressure is an important technique for obtaining high early strength values in concrete production. It also aids in faster and safer construction as sufficient strength is attained in short period and maintained without any other forms of curing. Concrete types, as well as curing period and temperature are important parameters in the steam-curing process. The strength development depends on steam curing cycle. The parameters involved in a steam curing cycle include a delay period, a gradual increase to a temperature where it is to be maintained for a specific curing period followed by gradual cooling. Quarry dust has been identified as possible replacement for sand in concrete works. Crushed rock aggregate quarrying generates considerable volumes of quarry fines, often termed "quarry dust". The finer fraction is usually smaller than 5mm in size. In this study, samples of concrete were made using varying contents of quarry dust as fine aggregate. The quantity of quarry dust was varied from 0% to 60% against quarry dust at intervals of 10%. For each mix, specimens were standard-cured in a water bath of room temperature and steam-cured at 70◦C maximum temperature over 24 h. And the specimens tested for compressive and flexural strength of the concrete and the results were satisfactory.

Key words: Quarry dust (waste material), Steam curing, Compressive strength, Flexural strength

INTRODUCTION

In recent years, using waste materials were developed in engineering applications. Concrete is one of the most common construction materials. Cast-in-situ concrete and precast concrete are two techniques that housing developers and construction workers

often adopt. However, precast concrete members have been increasingly utilized in civil engineering construction in recent years due to their advantages: reliable quality assurance, simple production process, faster construction speed, and environmentally friendly building operations. Currently available information indicates that the technique of steam curing is the most frequently employed technique among various production processes of prefabricated members. The benefits of steam curing (SC) are as follows: simple process, convenient operation, production with high early strength, short production cycle, and superior economic benefits. The steam curing process includes the following four stages: the pre-curing stage, the heating stage, the thermostatic stage, and the cooling stage. (Long, and Omran, 2012). The advantages of utilization of by-products or aggregates obtained as waste materials are pronounced in the aspects of reduction in environmental load & waste management cost, reduction of production cost as well as improving the quality of concrete. Quarry dust has been used for different activities in the construction industry such as road construction and manufacture of building materials such as light weight aggregates, bricks, and tiles. The present research deals with the influence of different replacement proportion of sand with quarry dust and type of curing on the properties of hardened concrete. This research is planned to study the effects of quarry dust addition in water cured (WC) and steam cured (SC) concrete and to assess the rate of compressive and flexural strength development. The aim and objectives of this research is; 1) to use quarry dust as the fine aggregate to decreases the cost of concrete production. 2) to investigate some properties of quarry dust and the suitability of those properties to enable quarry dust to be used. 3) to observe the effect of steam curing in concrete with partially replaced quarry dust.

EXPERIMENTAL PROGRAM & METHODOLOGY

The experimental program consists of casting and testing of cubes and prisms, to study the compressive strength and flexural strength by replacement of natural fine aggregate with quarry dust aggregate, for 0%, 10%, 20%, 30%, 40%, 50% and 60% of quarry dust, for each point change in compressive strength and flexural strength is studied with steam curing.

Cube and Prism Specimens Description

In this study cubes were tested with compressive strength machine at the rate of 500kN/min. In all cubes the cross section was 150*150*150 mm .Also beams were tested with flexural strength machine at the rate of 5.0mm/min. In all beams, the cross section was 150mm wide and 150 mm in depth, the overall length was 500mm with clear span 400mm.The beams were tested under a point load at the center of the beam.

Properties of materials

Cement

The cement which is used from Mass Company, it was ordinary Portland cement (OPC) type-1.The chemical composition and physical properties are shown in Table 1 and table 2.Its properties are conformed to the ASTM C150-00.

Table 1. Chemical properties of cement

Chemical Requirements	**ASTM C150-00**
	TEST RESULT
Sulfate Content(as S03) %	2.43
loss on ignition (Lol) %	1.30
Calcium Oxide (Cao) %	64.23
Magnesium Oxide (as Mgo) %	1.65

Table 2. Physical properties of cement

Physical requirements		**ASTM C150-00**
		TEST RESULT
initial setting time	min	130
Final setting time	hour	3:05
(Blaine) Finesse	cm^2/g	3780
Soundness(expansion)	mm	0.0
Compressive strength is not less than(MPa)	3 days	15
	28 days	43.5

Quarry Dust

The quarry dust is the residue of particles in the size range of 0 – 4.75mm. Table 3 shows the properties of quarry dust. And the sieve analysis of the aggregate is shown in figure 1.

Table 3. Properties of quarry dust

properties	Quarry dust
Specific gravity	2.62
water absorption	2.1%
density	1720 kg/m3

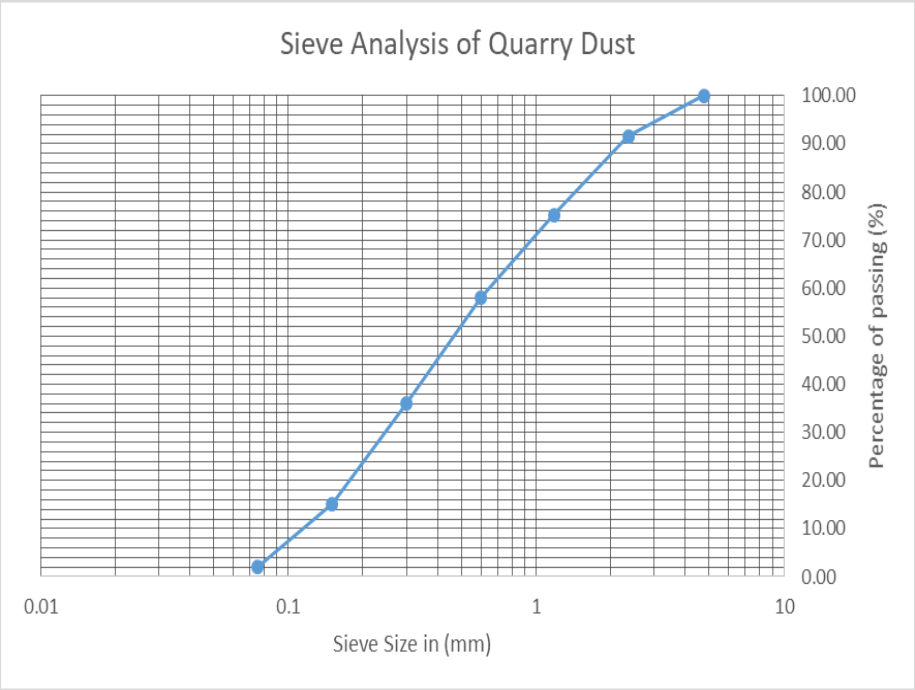

Figure1. Sieve analysis of quarry dust

Fine Aggregate

The fine aggregate was river sand. Its properties are shown in table 4 below and its sieve analysis is shown in figure 2.

Table 4. Properties of fine aggregate

Properties	Fine aggregate
Specific gravity	2.66
water absorption	1.15 %
Density	1650 kg/m^3

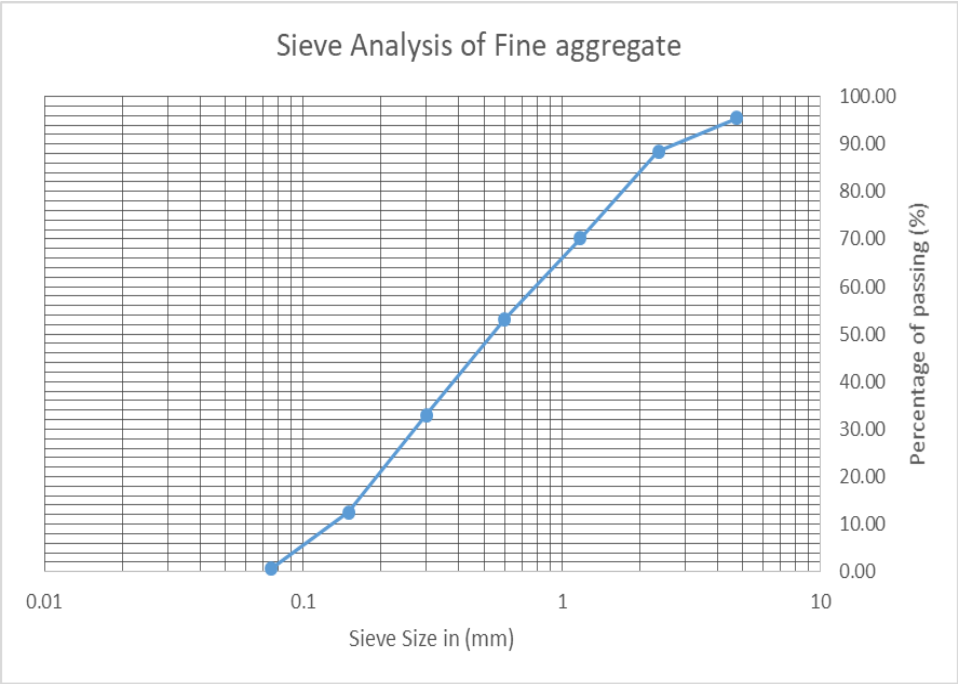

Figure 2. Sieve analysis of fine aggregate

Coarse Aggregate

The coarse aggregate was natural aggregate with maximum size of 22mm. Its properties are shown in table 5 below and its sieve analysis is shown in figure3.

Table 5. Properties of coarse aggregate

Properties Coarse aggregate	Coarse aggregate
Specific gravity	2.71
water absorption	0.63%
density	1673 kg/m3

Figure 3. Sieve analysis of coarse aggregate

Water

Ordinary drinking water was used for mixing and curing of concrete.

Concrete Mix Design

In this study M25 grade is used for mix design. The mixing procedure is important for obtaining the required workability. The amount of material used for one meter cubic is specified in table 6 for replacement of Quarry dust (0%, 10%, 20%, 30%, 40%, 50% and 60%).

Table 6: Mix proportion

Replacement %	**water kg/m³**	**Cement kg/m³**	**Fine Agg. kg/m³**	**Quarry dust kg/m³**	**Coarse Agg. kg/m³**
0%	200	550	636	0	1230
10%	200	550	569	67	1230
20%	200	550	502	134	1230
30%	200	550	435	201	1230
40%	200	550	368	268	1230
50%	200	550	301	335	1230
60%	200	550	234	402	1230

Curing Process

Two different methods of curing were applied in this research for each series, namely standard water curing (WC) and steam curing (SC). As usual, in WC the concrete samples are demolded 24 h after casting and then kept in water at 20 ± 2 C until the date of testing. However, in steam-curing condition, fresh specimens within the molds were placed in the steam chamber in which they were subjected to the heat treatment cycle shown in Figure 4. In this research, the steam curing cycle had a total duration of 24 h including 2 h of preheating, 3 h of heating until reach the maximum temperature which is selected as 70 ± 1 C and keeping the temperature stable for 17 h and finally cooling of the chamber which takes 1 h. The humidity in steam curing chambers was about 95 ± 2%. The samples were demolded and placed in water at 20 chambers was about 95 ± 2%. The samples were demolded and placed in water at 20 ± 2 C till the age of testing.

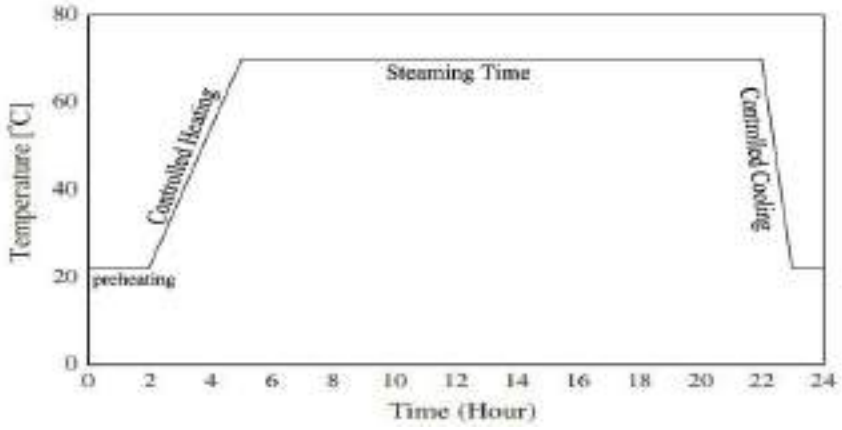

Figure 4. Steam Curing Cycle

Hardened properties of concrete

Compressive Strength

Compressive strength of concrete depends on many factors such as water-cement ratio, cement strength, quality of concrete material, and quality control during production of concrete etc. Test for compressive strength is carried out on cube. Various standard codes recommends concrete cube as the standard specimen for the test. American Society for Testing Materials ASTM C39/C39M provides Standard Test Method for Compressive Strength of cube test of specimens cubes of 15 cm X 15 cm X 15 cm .For most of the works cubical molds of size 15 cm x 15cm x 15 cm are commonly used. This concrete is poured in the mold and tempered properly so as not to have any voids. After 24 hours these molds are removed and test specimens are put in water for curing. These specimens are tested by compression testing machine after1, 3, 14 days curing or 28 days curing. Load should be applied gradually at the rate of 140 kg/cm2 per minute till the Specimens fails. Load at the failure divided by area of

specimen gives the compressive strength of concrete. Then comparison was done between the companion concretes in SC and WC.

Flexural Strength

The flexural test on concrete can be conducted using center point load test (ASTM C293).According to ASTM the size of the specimen is 150mm width, 150mm depth and the length should not be at least three times the depth of the specimen. The size of the mold 150mm width, 150mm depth, and span of 500mm for the specimen. The test should be conducted on the specimen immediately after taken out of the curing condition so as to prevent surface drying which decline flexural strength. Place the specimen on the loading point. The hand finished surface of the specimen should not be in contact with loading points. This will ensure an acceptable contact between the specimen and loading points. Center the loading system in relation to the applied force. Loading the specimen continuously without shock till the point of failure at a constant rate of 400 Kg/min for 150mm specimen, stress increase rate 0.06+/-0.04N/mm2.

RESULT AND DISCUSSION

Development of Compressive Strength with age

The variations of compressive strengths of concrete with steam cured and water cured concrete for different replacement of quarry dust on concrete presented in Figures 5 and 6. It may be concluded from the Figure 5 that increasing quarry dust content in replacement of sand causes an increase in compressive strength values. Furthermore, at all quarry dust replacement levels, compressive strength of steam cured specimens is more than the water-cured specimen. As illustrated in Figure 5 increase in compressive strength occurred with increasing the level of replacement of quarry dust. Early age (1 and 3 days) and later age (14 and 28 days) compressive strength values of SC concretes were very close to each other, while significant differences were observed for WC cured concretes. The highest 1 day compressive strength of 41.62 MPa was observed for SC at 60% quarry dust while the lowest was observed at WC at 0% quarry dust replacement as 12.05 MPa. SC showed higher enhancement in compressive strength development than WC. However, for later ages compressive strength was not significantly different between the WC and SC The experimental results indicated that by increasing percentage of Quarry dust, the compressive strength of the concretes is increased. The results is also achieved by Pratik Deogekar, Ashwini Jain, Sudhanshu Mishra, Prakash Nanthagopalan according to them the increase in early compressive strength for the steam cured concrete over the normal cured concrete With the progress of time, the difference in compressive strength between steam cured concrete and normal cured concrete was seen to reduce implying that a greater percentage of the 28 day compressive strength was attained in case of steam curing after 0.5 days than in case of normal cured concrete. (Deogekar et al , 2013).

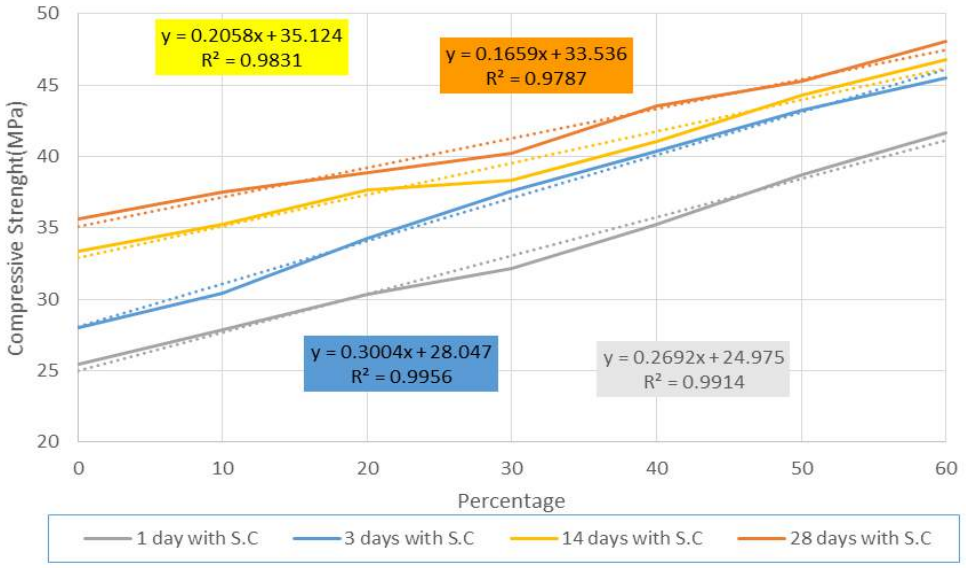

Figure 5. Compressive strength subjected to steam curing (SC) at different ages

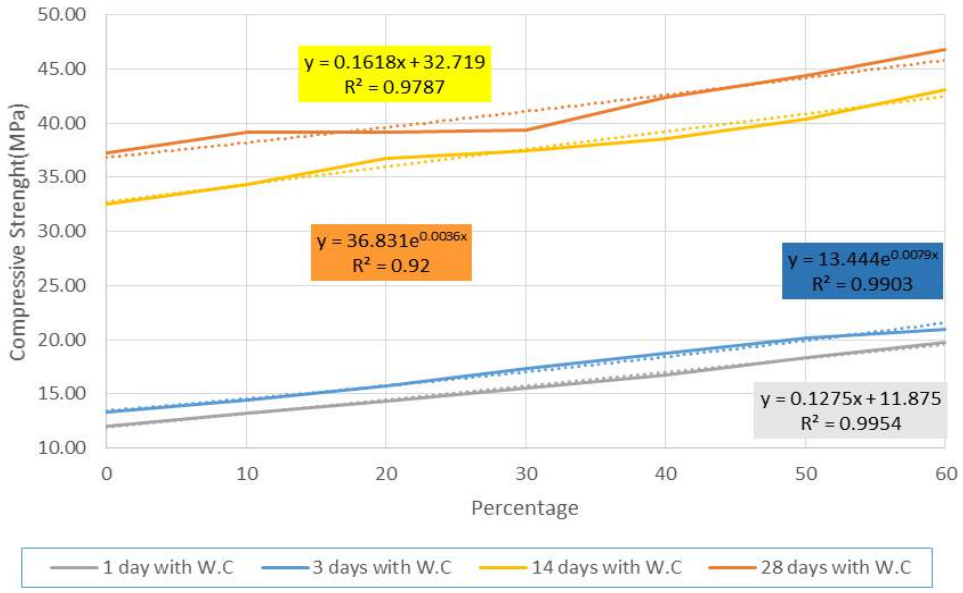

Figure 6. Compressive strength subjected to water curing (WC) at different ages

Development of Strength for Flexural strength

Figure 7 and 8 Show how the concrete develop strength with age for Steam cured concrete and water cured concrete. The use of quarry dust improved the flexural strength results from control at nearly all testing ages for water and steam curing. The concretes subjected to steam curing had higher flexural strength than Water curing which is illustrated in figure 7 and 8.The steam-cured concretes showed 48.8 % higher 3-day flexural strength than their Water-cured s due to the increasing the hydration in concrete by applying steam curing .Steam-cured concretes achieved higher flexural strength than those from water-cured concretes at all ages of curing. At Early age (3 days) the strength development of the steam cured concrete is about 45-50% higher than W and at later ages (14 and 28 days) compressive strength values of SC and WC concretes were very close to each other.

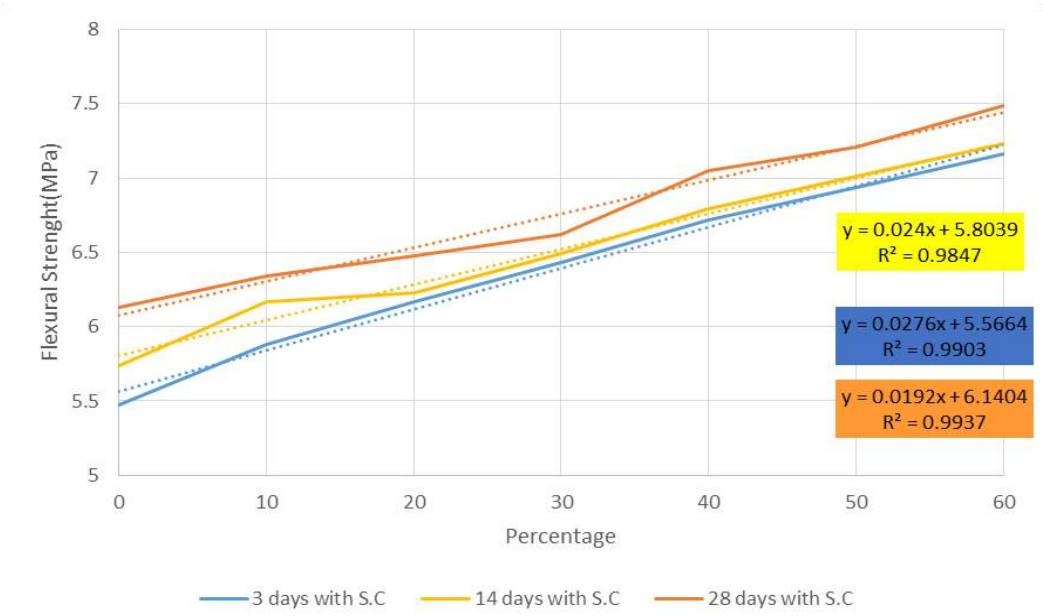

Figure 7. Flexural strength subjected to steam curing (SC) at different ages

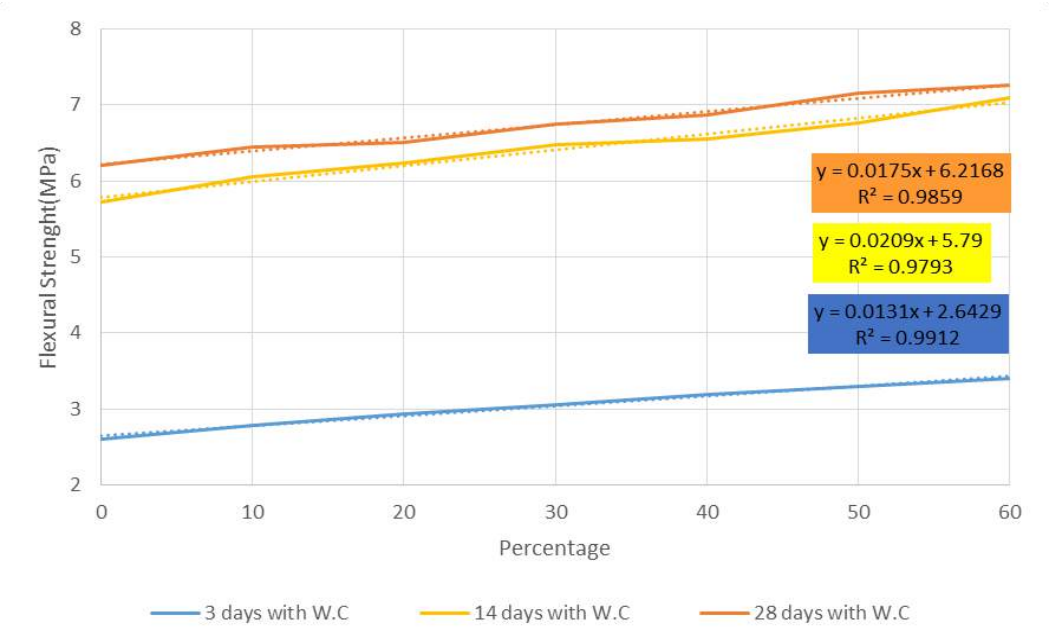

Figure 8. Flexural strength subjected to water curing (WC) at different ages

CONCLUSION

Based on the results presented in this study, the following conclusions can be drawn:-

1) As a result of steam curing had significant high early strength especially at 1 day. However, when comparing later age compressive strength development of the concretes, it was observed that water cured concretes had equal rate of strength development. Steam cured concrete displayed higher performance than water cured in terms of early age compressive strength and flexural strength.

2) By increasing the quarry dust content in the concrete leads to increase the compressive and flexural strength.

3) One of the ways to improving sustainability is to reduce the human consumption of natural resources. In order to protect the natural resources such as river sand, this study has identified quarry dust, which is a waste product from stone crushing industry and available almost free-of-cost, as partial replacement for river sand.

REFERENCES

Saul, A. G. A. (1951). Principles underlying the steam curing of concrete at atmosphericpressure. *Magazine of Concrete Research, 2(6)*, 127-140.

Bentur, I. S. (1978). Short-term steam-curing and concrete later-age strength. *Matériaux et Construction,* 93-96.

Poon, C. S., Kou, S. C., & Chan, D. (2006). Influence of steam curing on hardened properties of recycled aggregate concrete. *Magazine of concrete research, 58(5),* 289-299.

Chandana Sukesh, K. B. (2013). Partial Replacement of Sand with Quarry Dust in Concrete. *International Journal of Innovative Technology and Exploring Engineering (IJITEE)*, 5.

Long, G., He, Z., & Omran, A. (2012). Heat damage of steam curing on the surface layer of concrete. *Magazine of Concrete Research*, *64*(11), 995-1004.

Hanson, J. (1963). *Optimum steam curing procedure in precasting plants.* ACI J. Proc.

Higginson, E. C. (1961). Effect of Steam Curing on the Important Properties of Concrete. *Journal Proceedings*, 281-298.

M., A. S. (2011). Characteristic studies on the mechanical properties of quarry dust addition in conventional concrete. *Journal of Civil Engineering and Construction Technology Vol. 2(10)*, 218-235.

Mir, A. H. (2015). Improved Concrete Properties Using Quarry Dust as Replacement for Natural Sand. *International Journal of Engineering Research and Development*, 46-52.

Oztekin, E. (1984). Determination of heat treatment cycle for cements. *Turkish cement manufacturers' association*, 24-26.

Ilangovana, R., Mahendrana, N., & Nagamanib, K. (2008). Strength and durability properties of concrete containing quarry rock dust as fine aggregate. *ARPN Journal of Engineering and Applied Sciences*, *3*(5), 20-26.

R-87, A. 5. (1992). *Accelerated Curing of Concrete at Atmospheric.* ACI Manual of Concrete.

Rao, K. S. (2016). Strength Characteristics of Quarry Dust in Replacement of Sand. *International Conference on Advanced Material Technologies (ICAMT)-2016*, 7.

Rao, K. S. (2016). Study on Compressive Strength of Quarry. *http://dx.doi.org/10.1155/2016/1742769*, 5.

Mindess, S., Young, J. F., & Darwin, D. (1981). Concrete Prentice-Hall. *Englewood Cliffs, NJ*, *481*.

Türkel, S., & Alabas, V. (2005). The effect of excessive steam curing on Portland composite cement concrete. *Cement and Concrete Research*, *35*(2), 405-411.

Erdem, T. K., Turanli, L., & Erdogan, T. Y. (2003). Setting time: an important criterion to determine the length of the delay period before steam curing of concrete. *Cement and Concrete Research*, *33*(5), 741-745.


9 789757 375470